

Conformations of α - and β -D-Glucopyranose from an Empirical Force Field

K LAVS KILDEBY, STEEN MELBERG * and KJELD RASMUSSEN

Chemistry Department A, The Technical University of Denmark, Building 207, DK-2800 Lyngby, Denmark

Conformations of the pyranose ring are studied, using convergent energy minimisation in a simple force field. Parameters for the force field are adapted from similar studies on different classes of substances.

The global minima of the α - and β -anomers of D-glucopyranose are found; the energy difference is 0.26 kcal mol⁻¹ and the anomer equilibrium at 300 K is $\alpha:\beta=0.39:0.61$, in agreement with experimental results.**

The calculated ring geometry is in good agreement with results from crystal structure determinations, but side chain orientations are not well reproduced due to neglect of the crystal forces. The short anomeric bond is not represented by the present force field.

The present work is part of an endeavour to investigate the possibility of using energy minimisation in an empirical force field, with parameters adapted from several sources, to determine equilibrium conformations of molecules too large to handle by *ab initio* or even semi-empirical methods. Similar work using the same methods and programmes has recently been reported for tris(diamine) chelates of transition metal ions.¹ This research programme is a prerequisite to the development of a consistent force field (CFF)² for wide classes of compounds.

Two simple sugars were chosen for four main reasons. Firstly, reliable experimental data are available for comparison with calculated structures and, in subsequent work, vibrational frequencies. Secondly, the number of different atoms, and therefore of the necessary energy parameters, is limited. Thirdly, the adaptation

of a satisfactory provisional force field for monosaccharides would open possibilities of calculating conformations and other properties of substituted saccharides and oligosaccharides, which are not readily accessible with experimental methods. Fourthly, no theoretical conformational analysis of sugars is yet available, in which all degrees of freedom are allowed to relax.

The favoured conformations of D-glucopyranoses in aqueous solution and in crystal phases have been determined from NMR studies^{3,4} and from diffraction analysis.⁵⁻⁹ Angyal^{10,11} has derived interaction energies for the chair conformations of aldopyranoses from experimental data obtained from the equilibria of cyclitols and sugars. Rao *et al.*¹² have calculated the potential energies of only non-bonded interactions for the two chair and six boat conformers of α -D-glucopyranose. For the $4C_1$ and $1C_4$ conformers those calculations were further developed to include non-bonded, electrostatic and angle bending terms.¹³

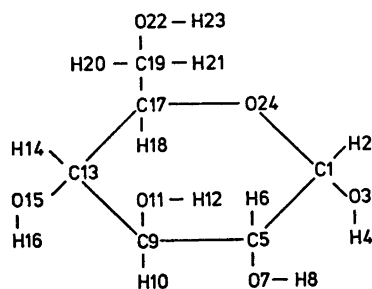


Fig. 1. Constitution and atom numbering of α -D-glucopyranose.

* To whom correspondence should be addressed.

** 1 kcal = 4.184 kJ.

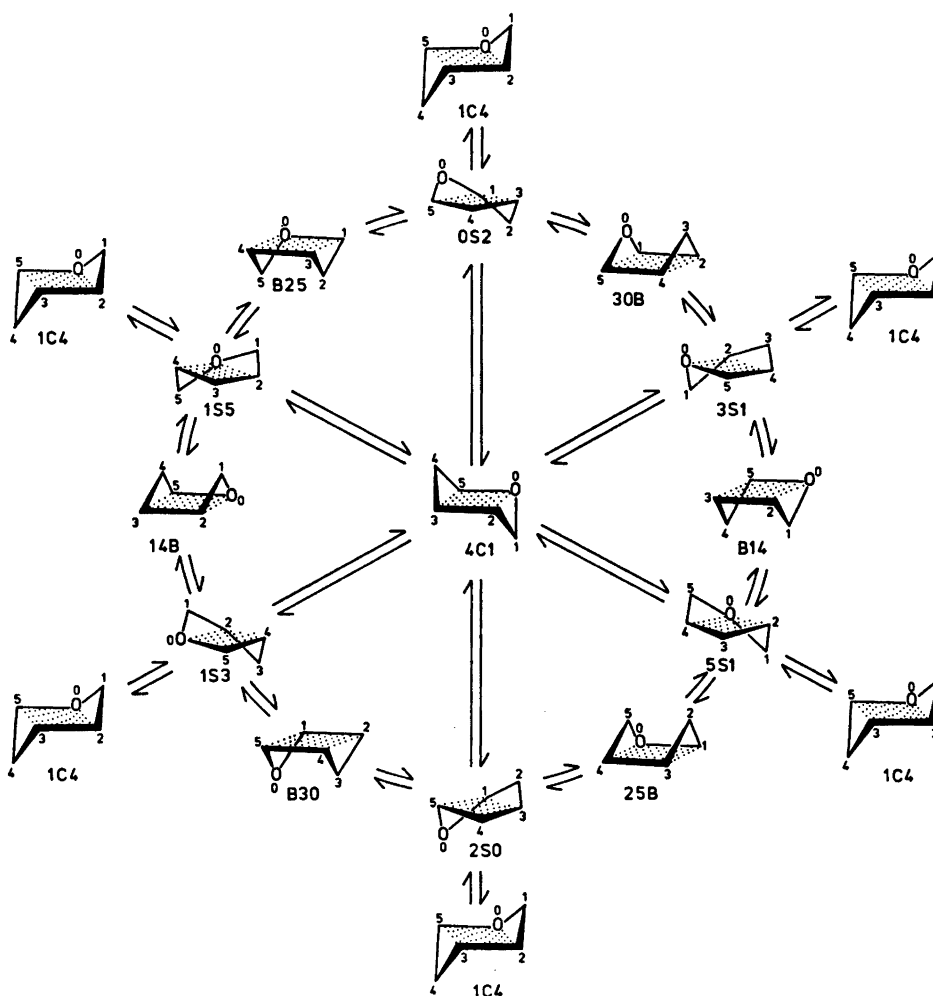


Fig. 2. Conformers of the pyranose ring.¹⁵

The computational methods and programmes used here were developed from the CFF system of Lifson and Warshel² and will be documented elsewhere.¹⁴

CALCULATIONS

Nomenclature of ring conformers. Our calculations deal with the six-membered ring system of α - and β -D-glucose. The constitution, with atom numbering for later reference, is shown in Fig. 1. The various stable and metastable basic geometries of the pyranose ring will be termed *C* for chair, *B* for boat, and *S* for skew-

boat. Our nomenclature of *ring* conformations follows Stoddart,¹⁵ whose proposal we consider more logical than the traditional one of Reeves.¹⁶ The ring atoms are numbered 0–5, starting on the oxygen and proceeding clockwise to end on the carbon carrying the primary alcohol group. A reference plane is defined by four ring atoms. If alternative choices of such four atoms are possible, as in certain *C* and *S* conformers, the carbon of lowest number is left out of the plane. Ring atoms lying above and below the plane are indicated before and behind the basic geometry symbol. These rules provide an easily memorised shorthand for the two *C*, six *B*,

and six S ring conformers. For the overall absolute configuration D, the unfolded sphere representation in Fig. 2 shows how the pyranose ring may attain all fourteen ring conformations through pseudorotation.

Initial conformations. In cyclohexane, C and S conformers would be equilibrium conformations, *i.e.* minima on the potential energy surface, and B conformers would be saddle points. (It is meaningless to talk about maxima on a potential energy surface covering *all* degrees of freedom.)

In our calculations on α - and β -D-glucopyranose, we did not *a priori* exclude the possibility that a local minimum conformation might be found close to a B conformer. Therefore we performed energy minimisation of all fourteen ring conformers. The various choices of side group orientations are described later.

Cartesian atomic coordinates were measured on scale models and used directly for input.

Potential energy functions. A reasonable force field should reproduce a maximum of observables with a minimum of parameters. We selected ours through an initial series of calculations on α -D-glucopyranose, composing the trial force fields from the following energy terms.²

Bond deformation:

$$E_b = \sum_{\text{bonds}} \frac{1}{2} K_b (b - b_0)^2 \quad \text{I}$$

Valence angle deformation:

$$E_\theta = \sum_{\text{angles}} \frac{1}{2} K_\theta (\theta - \theta_0)^2 \quad \text{II}$$

$$E_{UB} = \sum_{\text{angles}} \{ \frac{1}{2} F (d - d_0)^2 + F' (d - d_0) \} \quad \text{III}$$

Torsional deformation:

$$E_\phi = \sum_{\text{torsions}} \frac{1}{2} K_\phi (1 + \cos 3\phi) \quad \text{IV}$$

Non-bonded interactions:

$$E_{nb} = \sum_{i < j} \{ A_{ij} \exp (-B_{ij} r_{ij}) - C_{ij} / r_{ij}^6 \} \quad \text{V}$$

$$E_{nb} = \sum_{i < j} \varepsilon_{ij} \left[\left(\frac{r_{ij}^*}{r_{ij}} \right)^{12} - 2 \left(\frac{r_{ij}^*}{r_{ij}} \right)^6 \right] \quad \text{VI}$$

$$E_{cl} = \sum_{i < j} q_i q_j / r_{ij} \quad \text{VII}$$

In our first trial force field, FF1, we used terms I, II, IV, and V, with 46 parameters; in FF2 I, II, III, IV, VI, and VII, with 61 param-

eters; and in our final choice, FF3, I, II, IV, and V, with 46 parameters.

Parameters. We required parameters for interactions between atoms C, O, and H. A ready-made set for this purpose is not found in the literature, so in addition to the assumptions implicit in the choice of energy functions, we had to make assumptions as to numerical values of parameters.

For FF1 we selected parameters from optimised (CFF)^{17,18,22} and non-optimised^{18,20,21,23} force fields. As the results were not satisfactory we changed three key parameters, b_0 for C—C, C—O, and O—H. The results (see below) were still not sufficiently good and we then used the more complicated FF2, with parameters optimised on lactams.^{17,18,24} For our alcohol- and ether-type O we used parameters optimised for N where possible, and otherwise parameters optimised for C. The results were rather disappointing, wherefore we resorted to the simpler FF3, using parameters developed without optimisation for coordination compounds of amines and amino acids.²⁵ Parameters for O were selected as above. Also here we changed the three bond energy parameters mentioned above. Parameter values for the three force fields are shown in Table 1.

Selection of force field. Tests of force fields were carried out through comparison of calculated conformations of α -D-glucopyranose with crystal structure data obtained by Brown and Levy.⁶ Neutron diffraction data are well suited for this purpose, because they allow for determination of H atoms. Our test calculations were made on the same ring conformer as that found in the crystal, the 4C1.

Our calculations are, with our present programmes, limited to molecules in a hypothetical gaseous state, and thus do not allow for crystal forces. This shortcoming is serious only for exocyclic torsional angles, as will be shown below.

In Table 2 we show deviations for the anomeric bond, mean deviations and mean square root deviations for bonds and valence angles, and all absolute deviations and mean square root deviations in endocyclic, hybrid, and exocyclic torsional angles. It is clearly seen from Table 2 that there is no reason to prefer the 61-parameter FF2 to the 46-parameter FF1 and FF3. It is also seen that, apart from the

Table 1. Energy function parameters. Units are chosen to give energy in kcal mol⁻¹, with distances in Å. All θ_0 were set to 1.911 rad. Values marked with an asterisk are those changed from original ones to give better fits; the final values are shown. F' values marked \square were set to $F' = -0.1 F'_0$. For torsional terms, X and Y can be C, O, and H.

Type	FF1		FF2		FF3		Ref.	Ref.	Ref.
	K_b	b_0	K_b	b_0	K_b	b_0			
C-C	224	1.52*	224	1.46	720	1.52*	17	25	25
C-O	324	1.42*	522	1.46	863	1.42*	17	25	25
C-H	574	1.10	574	1.10	720	1.09	17	25	25
O-H	810	0.97*	810	0.98	806	0.97*	19	25	25
	K_θ		K_θ	F	F'	d_0			
C-C-O	43.2		43.2	75.0	-1.608	2.50	24	25	25
C-C-O	58.0		42.0	101.0	-24.75 \square	2.45	24	25	25
C-C-H	54.0		54.0	86.4	-0.699	2.20	24	25	25
C-O-C	80.0		43.2	75.0	-1.608	2.50	24	25	25
C-O-H	58.0		62.8	52.0	-9.36 \square	1.80	24	25	25
O-C-O	50.0		43.2	75.0	-1.608	2.50	24	25	25
O-C-H	40.0		60.2	82.0	-15.58 \square	1.90	24	25	25
H-C-H	76.4		76.4	5.58	-0.099	1.80	24	25	25
	K_ϕ		K_ϕ						
X-C-C-Y	1.25*		2.82				24	25	25
X-O-C-Y	2.33		3.0				24	25	25
	$A \times 10^{-4}$	B	C						
C---C	92.4	4.6	599.9				$A \times 10^{-4}$	B	C
C---O	43.3	4.6	461.6				23.70	4.32	287.8
C---H	7.79	4.6	165.8				21.21	4.44	244.0
O---O	21.7	4.6	368.9				3.14	4.20	121.1
O---H	3.83	4.6	124.1				18.64	4.55	200.0
H---H	0.829	4.6	46.8				2.81	4.32	99.2
							0.66	4.08	49.2
				$\epsilon^* \times 10^3$	r^*	q			
C--				19.6	4.22	-0.28			
O--				193.6	3.60	-0.30			
H--				4.489	2.94	0.14			

Table 2. Selection of energy function parameters through deviations of calculated from measured ⁶ internal coordinates. For bonds are shown: Deviations for the anomeric bond, mean deviations $\sum(b_{\text{calc}} - b_{\text{meas}})/24$ and mean square root deviations $(\sum(b_{\text{calc}} - b_{\text{meas}})^2/24)^{1/2}$; for bond angles: mean deviations $\sum(\theta_{\text{calc}} - \theta_{\text{meas}})/42$ and mean square root deviations $(\sum(\theta_{\text{calc}} - \theta_{\text{meas}})^2/42)^{1/2}$; for torsions: absolute deviations $|\phi_{\text{calc}} - \phi_{\text{meas}}|$ and mean square root deviations.

	FF1	FF2	FF3
Bond lengths, Å			
C1-O3	0.036	0.097	0.037
Mean dev.	0.0062	0.0359	0.0026
Mean sq. rt. dev.	0.0108	0.0476	0.0107
Valence angles, °			
Mean dev.	0.1	-0.6	0.1
Mean sq. rt. dev.	1.4	4.4	1.5
Endocyclic torsions, °			
O24-C1-C5-C9	3.1	4.4	3.5
C1-C5-C9-C13	4.9	11.7	4.9
C5-C9-C13-C17	1.8	9.0	0.0
C9-C13-C17-O24	1.5	0.1	0.9
C13-C17-O24-C1	2.0	8.6	1.8
C17-O24-C1-C5	0.5	7.5	0.4
Mean sq. rt. dev.	2.7	7.8	2.6
Hybrid torsions, °			
O24-C1-C5-O7	0.3	9.6	0.4
C1-C5-C9-O11	4.7	20.8	4.4
C5-C9-C13-O15	0.4	17.7	0.5
C9-C13-C17-C19	0.5	7.9	0.3
C17-O24-C1-O3	1.7	19.2	1.4
Mean sq. rt. dev.	2.3	15.9	2.1
Exocyclic torsions, °			
H4-O3-C1-C5	17.8	23.3	16.2
H8-O7-C5-C1	39.1	38.7	38.3
H12-O11-C9-C5	11.7	15.6	9.8
H16-O15-C13-C9	40.9	40.1	31.5
O22-C19-C17-C13	10.9	5.8	12.5
H23-O22-C19-C17	36.0	34.6	35.8
Mean sq. rt. dev.	29.1	29.2	26.6

anomeric centre at C1, the structure is well represented by FF1 and FF3. A choice between them can be made only from mean deviations of bonds, and we should therefore look for other types of observables. Different types of experiments ^{3,4,26} show that β -D-glucopyranose is more stable than the α configuration. We therefore minimised also a conformation of the 4C1 ring conformer of β -D-glucopyranose in FF1 and FF3. The result was $E_{\alpha} - E_{\beta} = -0.06$ kcal mol⁻¹ in FF1 and $E_{\alpha} - E_{\beta} = 0.88$ kcal mol⁻¹ in FF3, both cases referring to minimisation of the conformations found in crystals, ^{6,9} and not

to the global minima described later. It may also be mentioned that preliminary calculations showed that vibrational frequencies are better reproduced by FF3 than by FF1.

Local and global minima of the glucopyranoses. We therefore used FF3 for a detailed analysis of the fourteen conformers of α -D-glucopyranose, and for determination of the global minima of the α and β configurations. Input conformations were measured on models as described above, and minimisation was considered finished when the norm of the energy gradient became less than 10⁻⁶ kcal mol⁻¹ Å⁻¹.

Table 3. Endocyclic torsional angles in degrees and equilibrium energies in kcal mol⁻¹ of fourteen conformers of α -D-glucopyranose.

Initial conformer	4C1 init.	fn.	1C4 init.	fn.	0S2 init.	fn.	30B init.	fn.	3S1 init.	fn.	B14 init.	fn.	5S1 init.	fn.
O24-C-C5-C9	-63.4	-57.8	36.1	58.0	27.6	27.2	-5.4	25.2	-31.1	-24.9	-62.0	-62.3	-55.0	-62.1
C1-C5-C9-C13:	51.0	55.7	-42.2	-53.5	-74.5	-61.7	-65.5	-63.5	-36.5	-35.1	8.0	28.1	9.3	26.4
C5-C9-C13-C17	-54.7	-55.1	48.6	50.3	39.4	32.1	66.8	36.9	75.1	58.9	48.1	27.3	66.0	28.4
C9-C13-C17-O24	62.7	56.6	-55.4	-50.2	28.7	29.6	5.2	25.1	-35.4	-20.1	-63.6	-57.0	-64.6	-55.6
C13-C17-O24-C1	-69.6	-60.1	58.2	55.8	-74.0	-68.6	-61.7	-67.6	-34.5	-43.6	14.2	24.3	32.8	21.2
C17-O24-C1-C5	74.8	60.7	-52.5	-60.2	37.5	37.2	59.8	39.4	76.5	68.7	51.8	34.1	33.7	36.4
Final conformer	4C1		1C4		0S2		30B		3S1		B14		5S1	
E_{total}	1.982		3.846		7.582		8.018		9.271		10.247		9.927	
E_b	0.345		0.427		0.471		0.497		0.563		0.543		0.516	
E_θ	0.884		2.097		1.233		1.411		1.502		3.186		3.051	
E_ϕ	0.168		0.709		3.866		3.908		4.839		4.767		4.568	
E_{nb}	0.585		0.613		2.012		2.202		2.367		1.751		1.792	
Initial conformer	25B init.	fn.	2S0 init.	fn.	B30 init.	fn.	1S3 init.	fn.	14B init.	fn.	1S5 init.	fn.	B25 init.	fn.
O24-C1-C5-C9	-66.5	-19.0	-32.1	-20.8	7.7	37.4	29.9	37.7	49.0	34.3	54.5	64.4	55.3	63.8
C1-C5-C9-C13	69.6	63.2	73.8	63.3	45.7	23.9	36.8	23.6	7.3	27.9	-23.7	-26.7	-56.7	-25.3
C5-C9-C13-C17	-22.3	-46.4	-38.5	-44.6	-57.2	-61.8	-76.1	-61.7	-74.2	-62.7	-38.3	-31.7	-3.8	-33.2
C9-C13-C17-O24	-32.1	-12.3	-37.9	-13.9	5.9	37.3	25.7	37.3	67.2	33.2	86.4	62.9	66.2	63.4
C13-C17-O24-C1	44.1	61.0	72.0	61.0	58.5	25.8	44.1	25.7	-1.6	31.0	-53.1	-27.0	-70.3	-26.7
C17-O24-C1-C5	4.6	-43.4	-37.8	-41.7	-73.0	-66.0	-82.0	-66.2	-57.3	-68.1	-21.2	-35.1	6.4	-35.5
Final conformer	25B		2S0		B30		1S3		14B		1S5		B25	
E_{total}	10.365		9.708		7.923		7.870		7.509		8.095		8.608	
E_b	0.527		0.555		0.506		0.489		0.462		0.483		0.468	
E_θ	2.139		2.310		1.920		1.749		1.339		1.467		1.615	
E_ϕ	5.130		4.898		3.667		3.696		3.669		4.078		4.281	
E_{nb}	2.569		1.945		1.830		1.836		2.039		2.067		2.244	

Table 4. Determination of the exocyclic torsions of α -D-glucopyranose, tO22, tH16, tH12 and tH8, tH4, tH23, in degrees.

tH4	tH8	tH12	tH16	tO22	tH23	E_{total}
179.3	-62.5	175.7	60.4	179.1	179.9	1.637
179.3	-62.5	175.6	60.6	67.3	-179.6	1.983
179.2	-62.5	175.8	60.4	-60.8	179.8	1.739
179.3	-62.6	64.4	-64.5	179.0	179.9	1.663
179.2	-62.7	64.5	-64.9	67.1	-179.6	2.042
179.2	-62.7	64.4	-64.5	-60.9	179.8	1.762
179.3	-62.6	64.3	-166.1	-177.1	179.7	2.223
179.3	-62.6	64.2	60.4	179.1	179.9	1.649
179.3	-62.6	64.4	-64.5	179.0	179.9	1.663
179.3	-62.4	-60.2	60.3	179.1	179.9	1.694
179.3	-62.5	-60.2	-64.6	178.9	179.9	1.690
179.3	-62.5	175.7	60.4	179.1	179.9	1.637
179.3	-175.9	175.5	60.4	179.1	179.9	1.696
179.2	-169.5	70.8	60.4	179.1	179.9	2.117
179.3	-175.9	-60.1	60.3	179.1	179.9	1.737
179.3	62.2	175.8	60.4	179.0	179.9	1.766
179.2	62.2	64.3	60.4	179.0	179.9	1.773
179.3	62.2	-60.0	60.4	179.0	179.9	1.828
179.3	-62.5	175.7	60.4	179.1	179.9	1.637
179.3	-62.6	64.2	60.4	179.1	179.9	1.649
179.3	-62.4	-60.2	60.3	179.1	179.9	1.694
63.9	-62.8	175.8	60.4	179.0	179.9	1.811
63.9	-175.9	175.5	60.4	179.0	179.9	1.887
179.3	-62.5	175.7	60.4	179.1	179.9	1.637
179.3	-62.5	175.7	60.4	177.0	64.0	1.688
179.4	-62.5	175.8	60.4	-179.6	-62.4	1.626

RESULTS

Bond lengths and valence angles were found to be independent of ring conformation. Therefore it will be sufficient to list endocyclic torsions for description of ring conformations. Results for the fourteen *B*, *C*, and *S* conformers are shown in Table 3. For each conformer two sets of torsional angles are given. The first set designated "init.", applies to values calculated from the initial conformation specified by cartesian coordinates measured on models; the second set, "fin.", applies to the final conformation.

It is clearly seen that *C* and *S* conformers correspond to local minimum energy conformations, and that each *B* conformer during minimisation changes to one of the two *S* conformers which are its nearest neighbours on the topological map (Fig. 2). The differences between minimum conformations of the same

ring conformer, *e. g.* 1S3, are due to different exocyclic conformations.

Global minimum of α -D-glucopyranose. Table 3 shows that all *S* conformers have much higher energy than *C* conformers, and that 4C1 has the lowest energy of all. This is in accordance with crystal structure⁵⁻⁷ and NMR^{3,4} data. In the following search for the global minimum, therefore, the ring conformer 4C1 was retained while the exocyclic torsions were changed from one input to the next. We still allow all 72 degrees of freedom to relax.

A shorthand for exocyclic torsions is introduced: H4-O3-C1-C5, H8-O7-C5-C1, H12-O11-C9-C5, H16-O15-C13-C9, O22-C19-C17-C13, and H23-O22-C19-C17 will be named tH4, tH8, tH12, tH16, tO22, and tH23, respectively. A torsional angle A-B-C-D is defined through a Newman projection:

Table 5. Determination of the exocyclic torsions of β -D-glucopyranose, in degrees.

tH4	tH8	tH12	tH16	tO22	tH23	E_{total}
-179.2	-64.4	175.8	60.5	-179.5	-62.4	1.385
62.3	-64.4	175.7	60.5	-179.5	-62.5	1.407
-179.3	-175.8	175.6	60.5	-179.5	-62.4	1.364
62.3	-175.8	175.5	60.5	-179.5	-62.5	1.401
-64.3	-175.6	175.5	60.5	-179.5	-62.5	1.523
-179.3	-175.8	175.5	60.5	179.2	179.9	1.365
-179.3	-175.8	175.5	60.5	177.3	64.1	1.414
-179.3	-175.8	175.6	60.5	-179.5	-62.4	1.364
-179.2	-64.6	64.2	-167.3	-55.2	-62.7	1.922
-179.2	-64.6	64.3	-64.5	-60.7	179.8	1.494

ϕ is the angle through which A-B must be rotated around B-C to cover C-D when looking from B towards C; the sign is positive if the sense of rotation is positive, *i.e.* anticlockwise.

With the assumed threefold potential around a C-O or C-C bond, any ring conformer will give rise to $3^6 = 729$ distinct conformations. It would be futile to minimise all, and the less favourable conformations must be excluded in a stepwise way.

A series of test calculations starting with exocyclic torsions close to the values found in the crystal phase⁸ and changing tH4 and tH8 one after the other by $\pm 60^\circ$ gave a series of local minima.

These tests suggested that it would be acceptable to consider only first-neighbour exocyclic groups when determining the most favourable value of a specific exocyclic torsion. For the following twenty-one calculations a provisional value for tH4 of 180° was used.

O22-C19-C17-C13. tO22 is primarily influenced by tH16. For tH16 = -60° a sterically unfavourable situation occurs for tH12 = 180° . This led us to choose the first set of six runs shown in Table 4. It is seen that tO22 = 180° is most favourable.

H16-O15-C13-C9. tH8 was fixed at -60° to influence tH12 as little as possible. The second set of six runs in Table 4 shows that tH16 = 60° is the best choice.

H8-O7-C5-C1 and H12-O11-C9-C5. For tH8 and tH12 all nine possibilities were investigated, as shown in the third set of Table 4. tH8 = -60° and tH12 = 180° were selected.

H4-O3-C1-C5. tH4 = -60° is sterically unfavourable, but the possibility of tH4 = 60° can be excluded only on inspection of the two next runs. Therefore tH4 = 180° is still preferred.

H23-O22-C19-C17. The three last runs lead to the conclusion that tH23 = -60° in the global minimum of α -D-glucopyranose.

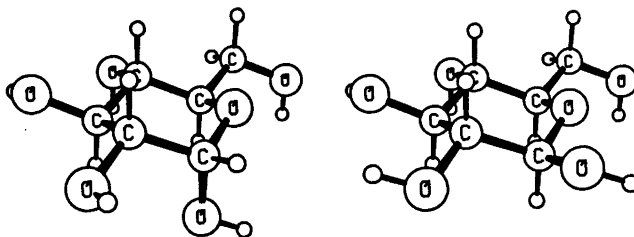


Fig. 3. Global minima of glucopyranoses drawn by ORTEP. Left: α -D-glucopyranose; right: β -D-glucopyranose.

Table 6. Continued.

C9-C13-H14	108.3(0.2)	109.0	0.7		108.9	
C9-C13-C17	111.2(0.1)	109.8	-1.4	109.8(0.2)	109.8	0.0
O15-C13-H14	109.8(0.2)	108.3	-1.5		108.3	
O15-C13-C17	110.9(0.1)	110.4	-0.5	108.2(0.2)	110.4	2.2
C13-O15-H16	107.0(0.3)	111.5	4.5		111.5	
H14-C13-C17	108.3(0.2)	109.2	0.9		109.2	
C13-C17-C19	111.6(0.1)	110.4	-1.2	114.9(0.2)	110.5	-4.4
C13-C17-H18	109.8(0.2)	109.4	-0.4		109.5	
C13-C17-O24	108.7(0.1)	110.2	1.5	107.6(0.2)	109.8	2.2
C19-C17-H18	109.0(0.2)	108.5	-0.5		108.7	
C19-C17-O24	108.1(0.1)	108.8	0.7	107.1(0.3)	108.9	1.8
C17-C19-O22	110.4(0.1)	110.5	0.1	111.9(0.3)	110.5	-1.4
C17-C19-H20	109.0(0.3)	109.6	0.6		109.6	
C17-C19-H21	109.0(0.3)	110.1	1.1		110.1	
H18-C17-O24	109.6(0.2)	109.5	-0.1		109.4	
C17-O24-C1	113.8(0.1)	113.4	-0.4	112.7(0.2)	112.6	-0.1
O22-C19-H20	110.1(0.2)	108.7	-1.4		108.7	
O22-C19-H21	110.5(0.3)	109.2	-1.3		109.2	
C19-O22-H23	107.7(0.3)	111.0	3.3		111.0	
H20-C19-H21	107.9(0.4)	108.7	0.8		108.7	
Mean dev.			0.2			0.2
Mean sq. rt. dev.			1.6			1.8
			$ \phi_{\text{calc}} - \phi_{\text{meas}} $			$ \phi_{\text{calc}} - \phi_{\text{meas}} $
Endocyclic torsions,°						
O24-C1-C5-C9	-54.1(0.2)	-57.0	2.9	-53.7(0.3)	-57.8	4.1
C1-C5-C9-C13	51.2(0.1)	55.4	4.2	50.8(0.4)	54.8	4.0
C5-C9-C13-C17	-53.2(0.1)	-55.4	2.2	-53.4(0.4)	-54.8	1.4
C9-C13-C17-O24	57.5(0.2)	57.0	0.5	59.8(0.3)	57.4	2.4
C13-C17-O24-C1	-62.2(0.2)	-60.3	1.9	-66.3(0.3)	-61.8	4.5
C17-O24-C1-C5	61.0(0.2)	60.3	0.7	62.8(0.3)	62.1	0.7
Mean sq. rt. dev.			2.4			3.2
Hybrid torsions,°						
O24-C1-C5-O7	-179.6(0.2)	-177.7	1.9	-175.0(0.2)	-178.2	3.2
C1-C5-C9-O11	172.0(0.1)	175.6	3.6	170.5(0.3)	175.0	4.5
C5-C9-C13-O15	-175.3(0.1)	-177.1	1.8	-173.1(0.3)	-176.6	3.5
C9-C13-C17-C19	176.6(0.1)	177.2	0.6	179.0(0.3)	177.5	1.5
C17-O24-C1-O3	-60.6(0.1)	-62.2	1.6	179.4(0.2)	-177.9	2.7
Mean sq. rt. dev.			2.1			3.2
Exocyclic torsions,°						
H4-O3-C1-C5	163.1(0.3)	179.4	16.3		-179.3	
H8-O7-C5-C1	100.4(0.2)	-62.5	162.9		-175.8	
H12-O11-C9-C5	165.9(0.3)	175.8	9.9		175.6	
H16-O15-C13-C9	-134.2(0.2)	60.4	165.4		60.5	
O22-C19-C17-C13	170.3(0.1)	-179.6	10.1	59.1(0.4)	-179.5	121.4
H23-O22-C19-C17	143.9(0.2)	-62.4	153.7		-62.4	
Mean sq. rt. dev.			114.0			

Global minimum of β -D-glucose. β -D-Glucopyranose differs from the α form only in the configuration around the anomeric centre at C1. We determined the global minimum of the 4C1 conformer of the β anomer by variation of tH4 for two values of tH8, and of tH23. This led to the first eight of ten runs shown in Table 5. The first run corresponds to the global minimum of the α -anomer, except of course for the anomeric centre. For the two last runs input coordinates were taken from crystal structure data.^{8,9}

The internal coordinates of the global minima are given in Table 6. Computer-produced model drawings are shown in Fig. 3. Cartesian coordinates may be obtained from the authors.

DISCUSSION

Comparison with crystal structure analyses. Table 6 shows a comparison of our results with data from one crystal structure determination for each anomer. Only one, the neutron diffraction study of the α -anomer by Brown and Levy,⁶ gives reliable values for hydrogen positions and internal coordinates dependent thereon. This study was carried through to an R value of 0.060. The X-ray diffraction structure of the 1:1 complex of α -D-glucopyranose with urea⁷ was refined to $R=0.041$. The older X-ray diffraction study of the β -anomer⁸ is not extremely accurate, $R \sim 0.25$; the more recent one⁹ was refined to $R=0.043$. For both anomers, we thus have good experimental structures for comparison.

We transformed all fractional coordinates to cartesian, from which we calculated the internal coordinates including the standard deviations. These operations were done with a programme supplied by Professor John A. Schellman, University of Oregon, and modified by Dr. Svetozar R. Niketić, University of Beograd.

For bond lengths and valence angles our calculated values are in good agreement with the experimental values, with the length of the anomeric bond C1–O3 as a notable exception.

Endocyclic and hybrid torsional angles are well reproduced, exocyclic not. This is understandable since the orientations of the side-groups depend very much on crystal forces, which are not taken into account in our method.

The anomeric effect. An abnormally short C1–O3 bond was observed in the earliest structure determinations of pyranose.⁵ Berman *et al.* showed in a compilation²⁷ that this anomeric property is common to the whole class of substances. The term "anomeric effect" is due to Lemieux²⁸ who defined it as an effect favouring axial orientation for certain substituents on the anomeric carbon atom.

Ab initio calculations on model substances²⁹ suggest that the relatively electronegative O24 has attracted electronic charge from C1, depopulating a C1 2p orbital, and thus forced a measure of double bond character upon the C1–O3 bond.

In the context of our calculations, the anomeric effect does not show up at all. This means that our force field, in order to reproduce it, would have to supply different energy function parameters for at least the C1–O3 bond. Although this would be a minor task with our programme, we have refrained from it, because we intend to proceed to more complex molecules involving glycosidic linkages. It is known¹⁸ that glycosidic substituents modify the anomeric effect markedly, and we prefer to handle the inconsistency in a larger context.

Distribution of potential energy. The contributions to the energy from bond and angle deformations, and torsional and non-bonded interactions, vary from one conformer to another in an unsystematic manner, even within the same basic ring conformer. This is borne out by data in Table 3. The explanation is that any strain introduced by a local change of geometry will, during relaxation, be distributed on all energy terms. This emphasizes the necessity of allowing for relaxation of all degrees of freedom. This is not always observed in similar work, where bonds and often even angles are kept fixed.

The manifold of minima. With any C and S ring conformer there is associated a multitude of local energy minimum conformations, corresponding to different values of exocyclic torsional angles. They lie close on the energy scale, characteristically less than 1 kcal mol⁻¹ apart; for 4C1, *e.g.*, the basic ring conformer studied in greatest detail, the largest energy difference between local minima encountered was 0.60 kcal mol⁻¹. At equilibrium, therefore, the local minima would be almost equally populated.

The saddle points between them would be of the order of the torsional potential height, 1.5 or 2.4 kcal mol⁻¹ (Table 1) and, at ordinary temperature, the equilibrium would be quickly established. Therefore each basic ring conformer represents almost a continuum of conformations, and the same statistical weight can thus be assigned to each basic ring conformer.

Equilibrium distributions. The *S* conformers of α -D-glucopyranose have 6–9 kcal mol⁻¹ higher energies than the global minimum (Tables 3 and 4), and will therefore not be populated at ordinary temperature. The energy difference between the two *C* conformers, 1*C*4 and 4*C*1, will be of the order of 2 kcal mol⁻¹. The precise value cannot be given, as the most favourable exocyclic torsions were not determined for the 1*C*4 conformer. Neglecting a change in volume arising from a change of conformer from 1*C*4 to 4*C*1, the enthalpy difference equals the energy difference. Any entropy difference would arise from differences in the vibrations of lowest frequencies and from differences in moments of inertia. These differences are assumed to be small (in aqueous solution the rotational term is largely quenched), and the entropy difference therefore negligible. We can then equate free enthalpy difference with energy difference. As the two conformers are given the same statistical weight, the equilibrium ratio of 1*C*4 to 4*C*1 will be $\sim 1:25$. Presumably this holds also for the β anomer, and both anomers will to a good approximation be represented by their 4*C*1 conformers. Therefore the free enthalpy difference between the two anomers will be 0.262 kcal mol⁻¹, and their equilibrium ratio at 300 K will be $\alpha : \beta = 0.39 : 0.61$. This should be compared with kinetic and NMR studies^{26,3,4} which show a ratio of $\alpha : \beta = 0.36 : 0.64$.

Comparison with earlier calculations. As mentioned before, our calculations seem to be the first to include relaxation of all degrees of freedom, which is imperative for attainment of minimum energy conformation. Also in other respects, earlier investigations employed methods basically different from ours. The most serious difference was the introduction of an extra energy term for the anomeric effect in order to improve specifically the agreement with experimentally derived free enthalpies. With this addition Angyal¹⁰ and Vijayalakshmi and Rao¹³ were able to calculate $\alpha : \beta$ equilibrium

ratios of 0.36 : 0.64 and 0.38 : 0.62, respectively. To avoid circular argument, we did not use such adjustment.

CONCLUSIONS

We have calculated equilibrium conformations of α - and β -D-glucopyranoses by truly convergent energy minimisation using a simple force field with parameters adapted from studies of different classes of compounds.

The simple force field cannot reproduce the anomeric effect, but does give the correct anomer distribution at equilibrium.

Calculated ring geometries conform to those found in crystal structure analysis, but orientations of side chains do not. This is due to a basic limitation in our approach, which at present can handle only isolated molecules. The extension of our programme to treat crystal structures is a major project, which has now been initiated.

The force field used here will be employed and augmented in studies of glycosidic linkages and other substitutions of pyranose rings.

An optimisation procedure for fitting energy function parameters simultaneously to conformations and vibrational spectra determined experimentally is being developed.

Acknowledgements. We wish to thank The Weizmann Institute of Science, Rehovot, Israel and the Danish Natural Science Research Council for assisting in the transfer and further development of the original CFF programme. KK thanks Tribute to the Danes through Scholarship in Israel for a grant. KjR acknowledges travel aid from the Johanne Louise & Ditlev Berg Foundation. We thank Mrs. Birgit Rasmussen for technical assistance in all phases of the work.

REFERENCES

1. Niketić, S. R., Rasmussen, K., Woldbye, F. and Lifson, S. *Acta Chem. Scand. A* 30 (1976) 485.
2. Lifson, S. and Warshel, A. *J. Chem. Phys.* 49 (1968) 5116.
3. Rudrum, M. and Shaw, D. F. *J. Chem. Soc.* (1965) 52.
4. Lemieux, R. U. and Stevens, J. D. *Can. J. Chem.* 44 (1966) 249.
5. McDonald, T. R. R. and Beevers, C. A. *Acta Crystallogr.* 5 (1952) 654.
6. Brown, G. M. and Levy, H. A. *Science* 147 (1965) 1038.

7. Snyder, R. L. and Rosenstein, R. D. *Acta Crystallogr. B* 27 (1971) 1969.
8. Ferrier, W. G. *Acta Crystallogr.* 16 (1963) 1023.
9. Chu, S. S. C. and Jeffrey, G. A. *Acta Crystallogr. B* 24 (1968) 830.
10. Angyal, S. J. *Aust. J. Chem.* 21 (1968) 2737.
11. Angyal, S. J. *Angew. Chem. Int. Ed. Engl.* 8 (1969) 157.
12. Rao, V. S. R., Sundararajan, P. R., Ramakrishnan, C. and Ramachandran, G. N. In Ramachandran, G. N., Ed., *Conformation of Biopolymers II*, Academic, New York 1967, p. 721.
13. Vijayalakshmi, K. S. and Rao, V. S. R. *Carbohydr. Res.* 22 (1972) 413.
14. Niketić, S. R. and Rasmussen, K. *The Consistent Force Field: A Documentation*, Lecture Notes in Chemistry, Springer, Heidelberg. *To be published.*
15. Stoddart, J. F. *Stereochemistry of Carbohydrates*, Wiley-Interscience, New York 1971, p. 54 ff.
16. Reeves, R. E. *Adv. Carbohydr. Chem.* 6 (1951) 107.
17. Karplus, S. and Lifson, S. *Biopolymers* 10 (1971) 1973.
18. Vijayalakshmi, K. S. and Rao, V. S. R. *Carbohydr. Res.* 29 (1973) 427.
19. Warshel, A., Levitt, M. and Lifson, S. *J. Mol. Spectrosc.* 33 (1970) 84.
20. Rao, V. S. R., Vijayalakshmi, K. S. and Sundararajan, P. R. *Carbohydr. Res.* 17 (1971) 341.
21. Sundararajan, P. R. and Rao, V. S. R. *Biopolymers* 8 (1969) 313.
22. Rasmussen, K. *Conformations and Vibrational Spectra of Tris(diamine) Chelate Complexes*, Thesis, The Technical University of Denmark, Copenhagen 1970, p. 76 ff.
23. Ramachandran, G. N., Venkatachalam, C. M. and Krimm, S. *Biophys. J.* 6 (1966) 849.
24. Schellmann, J. A. and Lifson, S. *Biopolymers* 12 (1973) 315.
25. Buckingham, D. A., Maxwell, I. E., Sargeson, A. M. and Snow, M. R. *J. Am. Chem. Soc.* 92 (1970) 3617.
26. Bates, F. J., Ed., *Polarimetry, Saccharimetry and the Sugars*, Nat. Bur. Stand. (U.S.), *Circ. C440* (1942), p. 436.
27. Berman, H. M., Chu, S. S. C. and Jeffrey, G. A. *Science* 157 (1967) 1576.
28. Lemieux, R. U. In Mayo, P. de, Ed., *Molecular Rearrangements*, Interscience, New York 1963, Part 2, p. 713.
29. Jeffrey, G. A., Pople, J. A. and Radom, L. *Carbohydr. Res.* 38 (1974) 81.

Received July 1, 1976.

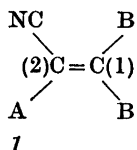
Photoelectron Spectra of Some Simple Push-pull Ethylenes

D. BETTERIDGE,^a L. HENRIKSEN,^b J. SANDSTRÖM,^c I. WENNERBECK^c and M. A. WILLIAMS^a^aDepartment of Chemistry, University College of Swansea, Swansea SA2 8PP (Wales),^bChemical Laboratory II, The H.C. Ørsted Institute, DK-2100 Copenhagen, Denmark and ^cDivision of Organic Chemistry, Chemical Center, University of Lund, P.O.B. 740, S-220 07 Lund 7, Sweden

The photoelectron spectra of a number of push-pull ethylenes with alkylthio, alkylseleno, and dialkylamino groups as electron donors and cyano groups as electron acceptors have been studied together with those of some simpler reference compounds containing either the donor or the acceptor groups. Band assignments have been made utilizing qualitative orbital interaction schemes, symmetry arguments, and CNDO/2 calculations. The band with lowest IP in all cases is ascribed to a delocalized π -orbital, and the second band in the molecules with donor groups to the antisymmetric combination of the donor atom p_z orbitals. The effect of ring size when the donor atoms are included in cyclic systems is also discussed.

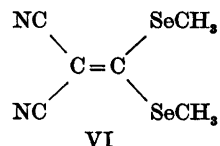
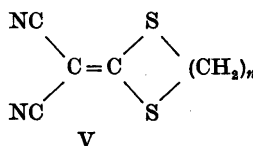
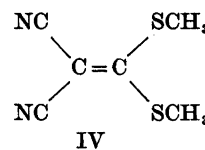
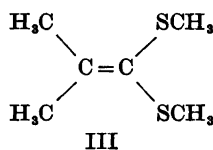
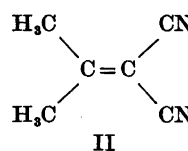
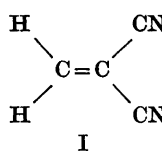
The powerful stabilizing influence of donor and acceptor groups interacting across a carbon- π -framework, which has been termed the push-pull effect, was elegantly demonstrated when Gompper and Seybold¹ succeeded in preparing a stable push-pull substituted cyclobutadiene.

Doubly push-pull substituted ethylenes in which at least one acceptor group is a cyano function and the donor groups contain sulfur, selenium or nitrogen atoms (*I*) are convenient models for studies of the push-pull effect. These compounds are readily accessible, and the substituents are well suited for the push-pull interaction.

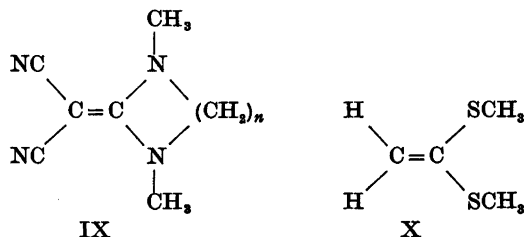
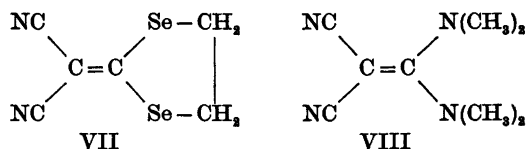
A = CN, CO₂R, CONR₂, CORB = SR, SeR, NR₂

dipole moments⁵) and dynamic physical properties (activation barriers for internal rotations).^{6–8} Also the chemical properties reflect this interaction. Thus the central double bond undergoes neither oxidation nor reduction under mild conditions.⁹ Nucleophiles attack at C(1)¹⁰ and electrophiles at C(2)¹¹ and in both cases the reaction course leads to substitution rather than to addition showing the resistance toward disruption of the push-pull system.

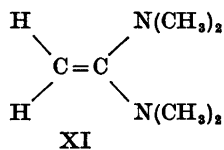
In order to obtain further information about the effect of push-pull substituents on the electronic structure, and especially on basis orbital participation in the molecular orbitals, photoelectron spectra (PES) of a number of simple push-pull ethylenes have been studied (I–IX).

a, $n = 3$ b, $n = 2$ c, $n = 1$

The push-pull interaction in *I* has been evidenced by several previous investigations of their static (UV-² and IR-spectra^{3,4} and



a, $n=2$
b, $n=3$



The compounds chosen are a series of 1,1-dicyanoethylenes with sulfur (IV and V), selenium (VI and VII) or nitrogen (VIII and IX) atoms as electron donors. For comparison, two 1,1-dicyanoethylenes (I and II) and one 1,1-bismethylthioethylene (III) have also been studied. Bock *et al.*¹³ have recently described and interpreted the PES of some ethylenes with alkoxy, alkylthio, and dimethylamino substituents, and these form a suitable series of reference compounds for our study.

EXPERIMENTAL

Preparative part. All compounds have been prepared by literature methods: I,¹³ II,¹⁴ III,¹⁵ IV,⁹ Va,⁹ Vb,⁹ Vc,¹⁶ VI,¹⁷ VII,¹⁷ VIII,¹⁸ IXa¹⁸ and IXb.⁵

Instrument part. The spectra were obtained with a photoelectron spectrometer with a magnetic electron-energy analyzer, which has been described elsewhere.^{19,20} The samples were heated to give a pressure of 1.3 Pa, and the temperature (°C) of the heating flange at this point for the different samples was: I:53; II:19; III:19; IV:90; Va:100; Vb:160; Vc:102; VI:65; VII:101; VIII:131; IXa:167; IXb:100.

Calibration was carried out with the $P_{3/2}$ and $P_{1/2}$ peaks of argon and xenon. The experimental values quoted relate to vertical ionization potentials and have an accuracy of ± 0.05

eV for well defined peaks and ± 0.1 eV for broad bands.

CNDO/2 calculations. These have been performed without d -orbitals for sulfur, using a revised version²¹ of the original program.²² No calculations have been performed on the selenium compounds. The geometries of all systems treated except those of Vb and Vc are given in Ref. 5. The geometry of the dithiolane ring in Vb is assumed to be the same as in ethylene trithiocarbonate,²³ where it is somewhat twisted, and the geometry of the dithietane ring in Vc is taken from the structure of an adduct from 3-diazobutanone and carbon disulfide.²⁴ The $(NC)_2C=CX_2$ part of the molecules are placed in the XY plane.

RESULTS AND DISCUSSION

The schematic molecular orbital diagram for the combination of the π orbitals of a 1,1-dicyanoethylene moiety and the p_x orbitals of the donor atoms (Fig. 1) is used as a basis for the following discussion.

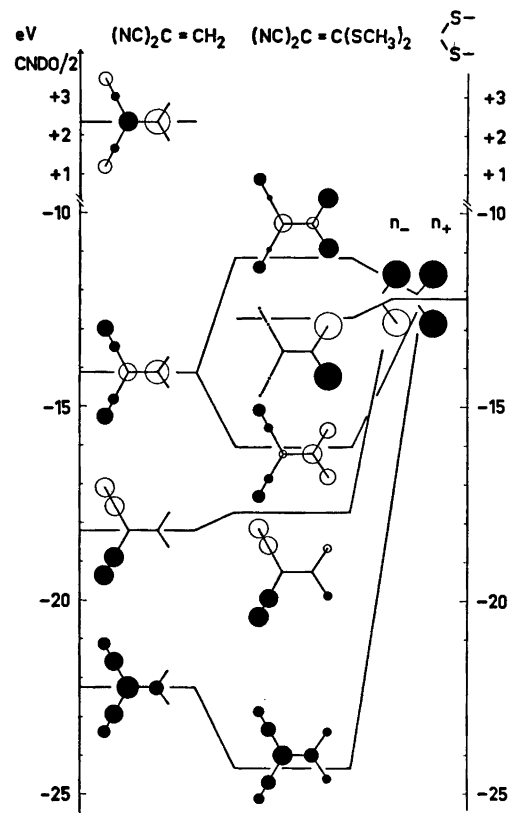


Fig. 1. Molecular orbital diagram for the π orbitals of $(NC)_2C=CX_2$.

Compounds I–III have been studied as reference systems. The PES of *cis*- and *trans*-1,2-dicyanoethylene have been analyzed by Bock and Stafast.²⁵ Both compounds show a first peak typical of ionization from a π -orbital at 11.15 eV, *i.e.* with somewhat higher IP than the π -orbital in ethylene (10.51 eV²⁶). The coupling of the C \equiv N and C=C π -orbitals alone should raise the highest occupied MO (HOMO), but charge displacement to the cyano groups and interaction with the LFMO of the cyano groups will lower the C=C π -orbital, and the net result is a lowering of the HOMO. The same effect is observed in I, though the coupling here is less efficient since it results in cross-conjugation. Its PES displays a first peak at 11.29 eV with a short progression of spacings of ca 1400 cm⁻¹, indicating ionization from a π -orbital mainly localized in the C=C bond. According to the calculations, this orbital is an antibonding combination of the bonding C=C π -orbital and the symmetric C \equiv N p_x orbital combination with the largest contribution from the C=C bond. The following peak, centered at 13.5 eV, is quite broad and probably contains several ionizations. After the present work was concluded, the PES of I was published²⁷ with essentially the same interpreta-

tion as the one given above.

The PES of II is rather similar to that of I, only with the first peak appearing at 10.21 eV. This difference can be ascribed to the inductive and hyperconjugative effect of the methyl groups, in agreement with calculations.

1,1-Bismethylthio-2-methylpropene (III) displays four well resolved peaks at 8.12, 8.77 (sharp), 9.84, and 10.66 eV, followed by a group of strongly overlapping bands. The spectrum is rather similar to that of 1,1-bismethylthioethylene¹² (X), and the interpretation of the first two peaks is the same as that given by Bock *et al.*¹² The first peak is ascribed to ionization from a π -orbital, which is an antibonding combination of the C=C π -orbital and the symmetric combination of the sulfur p_x orbitals, the second peak to the asymmetric combination of the sulfur p_x orbitals, and the fourth peak to the bonding combination of these orbitals. The first of these orbitals is referred to in the following as n_1 , the second as n_- , and the third as n_+ . The difference of 1.89 eV between n_- and n_+ is then a measure of the interaction between the sulfur p_x orbitals and the C=C π -orbitals. The different effect of methyl substitution in the dicyanoethylenes and bismethylthioethylenes is worth noticing.

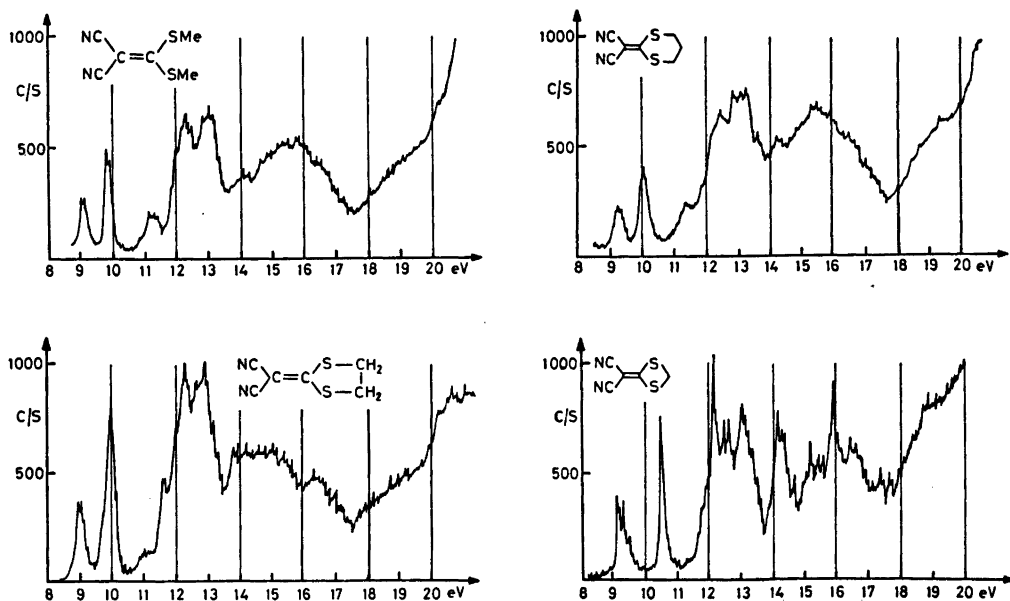


Fig. 2. UV photoelectron spectra of IV, Va, Vb, and Vc.

In the first set of compounds, two methyl groups lower the IP of the highest π -orbital with *ca.* 1.1 eV, whereas in the methylthio compounds the two first bands are virtually unaffected by methyl substitution. This is in agreement with simple perturbation arguments based on the energy differences between the interacting groups.²⁸

The PES of 1,1-bismethylthio-2,2-dicyanoethylene (IV) displays three resolved bands at 9.16, 9.89 (sharp), and 10.20 eV followed by a series of overlapping bands (Fig. 2). Symmetry arguments, the shape of the band, and the calculations all agree in assigning the first band to ionization from an antibonding combination of the π_1 orbital in the $S_2C=C$ part and the symmetric combination of the p_z orbitals in the CN groups (Fig. 1), and the second band to the n_- orbital. The third band is according to the calculations ascribed to a σ -orbital with strong contribution from the sulfur atoms. The introduction of sulfur lowers the π_1 IP in IV relative to that in II by 1.05 eV.

The six-membered cyclic analog Va has a spectrum rather similar to that of IV, the main difference being a shift of the second band by 0.14 eV to higher IP. The five-membered analog Vb has a higher IP for the third band (11.55 eV) and shows a barely resolved vibrational structure in the first band with a spacing of *ca.* 1200 cm^{-1} , which is reasonable for ionization from an orbital with considerable C=C bond character. The IR spectrum of Vb has a strong band at 1480 cm^{-1} , which is assigned to a vibration dominated by C=C stretching.³

The first band in the spectrum of the compound with the four-membered ring, Vc, shows

a clear vibrational structure with a spacing of 1250 cm^{-1} . The corresponding IR band appears at 1505 cm^{-1} and has more C=C stretching character than the analogous bands in Vb.³ The lack of fine structure in the first band in IV and Va may be due to flexibility and the existence of several conformers. It has been shown by dipole moment measurements that IV exists as an equilibrium mixture of the *Z,Z*, the *E,Z*, and possibly also the *E,E* conformations.⁵

The second band of Vc is sharper than in any of the analogous compounds, indicating ionization from an orbital with insignificant bonding character. Its IP is also higher (10.50 eV) than in IV, Va and Vb (9.89–10.03 eV). In the latter compounds the n_- orbital can interact in an antibonding fashion with the antisymmetric combination of the $2p_z$ orbitals on the neighbouring carbon atoms, and to some extent also with combinations of the hydrogen $1s$ orbitals of suitable symmetry, which raises the energy of the n_- orbitals in these compounds. Such interactions are demonstrated by the CNDO/2 calculations. In an alternative but equivalent description n_- interacts with combinations of the C–H bond orbitals of suitable symmetry. In Vc the atoms of the CH_2 group are in the nodal plane of the n_- orbital and no interaction is possible, which probably accounts for the high IP.

The seleno compounds VI and VII have spectra rather similar to those of the sulfur analogs (Fig. 3), but with lower IP:s of the three first bands, which are assigned similarly, *i.e.* π_1 , n_- , and σ_{C-Se} , respectively. This reflects the difference in IP of the sulfur and selenium atoms (IP for $S(^3P_2)$: 10.35 eV, for $Se(^3P_2)$: 9.75 eV).²⁹ The first band is shifted 0.31 eV from IV to

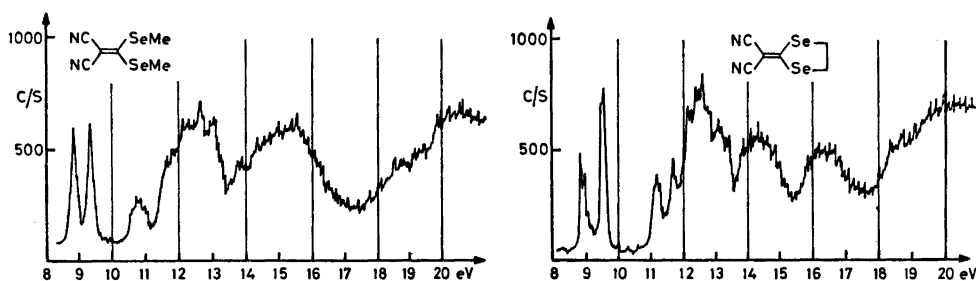


Fig. 3. UV photoelectron spectra of VI and VII.

VI, and 0.06 eV from Vb to VII. For the second band the corresponding shifts are 0.50 and 0.40 eV and the third band 0.47 and 0.40 eV, respectively. The larger shifts for the second and third band are in agreement with ionization from orbitals with dominating S(Se) character. In Vb and VII non-planarity of the ring causes some mixing of the S(Se) outer-shell p_z orbitals with other orbitals. This diminishes the proportion of S(Se) basis orbitals in the first two molecular orbitals relative to the non-cyclic analogs IV and VI, which probably accounts for the smaller effect of replacement of sulfur by selenium in the cyclic compounds. It may also explain the differences in intensities of the π_1 bands in VI and VII. The areas of the first two bands in VI are almost equal, suggesting a considerable mixing of the Se p_z and C=C π orbitals.

In the spectra of the 1,1-dicyano-2,2-diamino compounds VIII, IXa and IXb (Fig. 4), two bands appear at low IP, followed by a system of poorly resolved bands above 11 eV. In VIII and also in IXb the second band is sharper than the first, but both bands are considerably broader than the first two bands in the sulfur and selenium analogs.

The assignment is analogous to the one given for the compounds IV to VII, in agreement with calculations and also with the analysis of the PES of 1,1-bisdimethylaminoethylene (XI) given by Bock *et al.*¹² Also in this case introduction of the cyano groups causes a lowering of the two highest orbitals (Table 1). This effect, however, is not brought out by the calculations, which may be ascribed to a general tendency of the CNDO/2 method to underestimate the electron-withdrawing effect of cyano groups.^{30,31} The experimental IP:s for the first band are 7.5 eV for XI and 8.21 for VIII, and the calculated values are 10.49 *versus* 10.14 eV. For the second band, at 8.2 eV for XI and at 9.17 eV for VIII, the calculated values of 11.77 and 12.14 eV fall in the right order, but the difference is strongly underestimated.

The conformations of the diamines VIII, IXa and IXb are rather different. As discussed before,⁵ the dimethylamino groups in VIII, and also in XI, cannot be in the molecular plane for steric reasons but are probably twisted around the =C-N bond by an angle of *ca.* 20° in the same sense. In IXa and IXb the amino trigonal planes and double bond plane are probably much more coincident, as evidenced

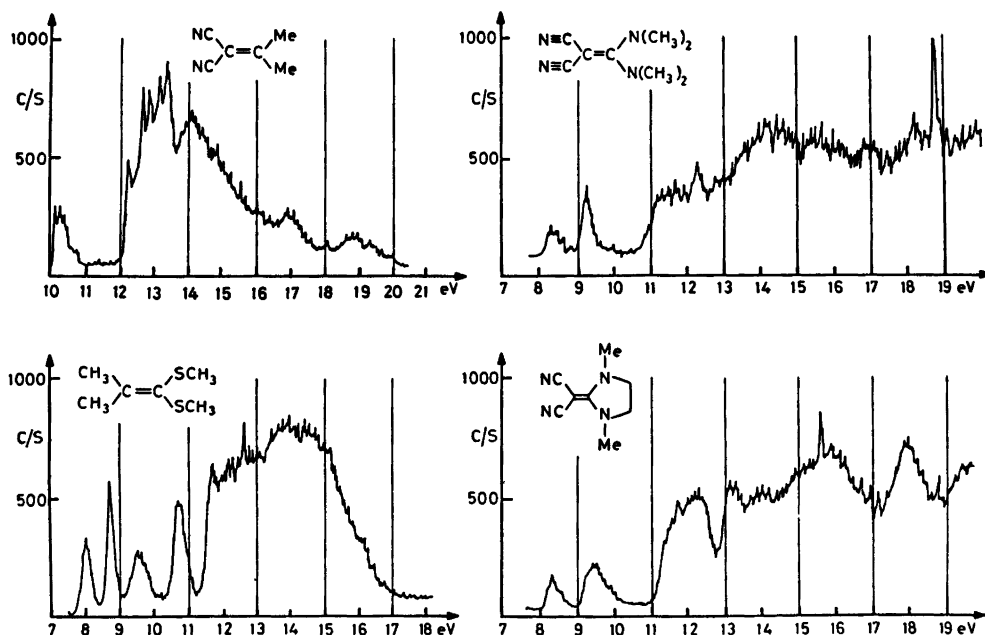


Fig. 4. UV photoelectron spectra of II, III, VIII, and IXa.

Table 1. Experimental and calculated ionization potentials together with band assignments.

Compound	IP (exp) eV	IP (calc) eV	Orbital type
I	11.29 (1400 cm ⁻¹)	14.10	$\pi (B_2)$
	13.0	15.92	$\sigma (B_2)$
II	10.21 (1100 cm ⁻¹)	12.52	$\pi (B_2)$
	12.23	15.16	$\sigma (B_2)$
III	8.12	10.58	$\pi (B_2)$
	8.74	11.98	$n_- (A_2)$
	9.54	11.98	σ
	10.66	13.08	n_+
IV	9.16	11.15	$\pi (B_2)$
	9.89	12.70	$n_- (A_2)$
	11.20	12.71	σ
	12.02	13.30	σ
Va	9.18	11.38	$\pi (B_2)$
	10.03	11.83	$n_- (A_2)$
	11.39	12.34	σ
	12.35	13.27	σ
Vb	8.88 (1200 cm ⁻¹)	11.26	$\pi (B_2)$
	9.94	12.66	$n_- (A_2)$
	11.55	12.76	σ
	12.16	13.97	σ
Vc	9.08 (1250 cm ⁻¹)	11.51	$\pi (B_2)$
	10.50	12.99	$n_- (A_2)$
	11.92	11.51	σ
	12.1	14.58	σ
VI	8.85		$\pi (B_2)$
	9.39		$n_- (A_2)$
	10.73		
	11.59		
VII	8.82		$\pi (B_2)$
	9.54		$n_- (A_2)$
	11.15		
	11.63		
VIII	8.21	10.15	$\pi (B_2)$
	9.17	12.14	$n_- (A_2)$
	11.04	13.90	σ
	11.29	14.03	σ
IXa	8.20	9.81	$\pi (B_2)$
	9.51	12.73	$n_- (A_2)$
	11.47	13.78	σ
IXb	11.88	14.35	σ
	8.11	9.73	$\pi (B_2)$
	9.33	12.86	$n_- (A_2)$
	11.26	12.59	σ
X	8.2 ^a	11.42	$\pi (B_2)$
	8.8 ^a	12.19	$n_- (A_2)$
XI	7.5 ^a	10.49	$\pi (B_2)$
	8.2 ^a	11.77	$n_- (A_2)$
	10.3 ^a	14.51	σ
	12.5 ^a	14.59	σ

^a From Ref. 12.

by an X-ray crystallographic study of an analog of IXa.²² This conformational difference has only a very small effect on the first band and more important effects on the second band.

The low IP of the latter band in VIII may be due to an antibonding interaction of the n_- orbital with a combination of N-C(H₃) bond orbitals of the right symmetry. Such an effect

is also indicated by the calculations.

The general broadness of PES "lone pair" bands in compounds containing nitrogen compared to those of analogous sulfur compounds may be attributed to a generally more bonding character of nitrogen "lone pairs", which reflects the better overlaps between carbon and nitrogen orbitals than between carbon and sulphur orbitals (Figs. 2 and 4).

Conclusion. The experimental IP's show that the position of the π_1 orbital is greatly affected by substituents. Replacement of H by CN results in an increase in the π_1 IP of 1–1.3 eV. For the series $(\text{CN})_2\text{C}=\text{CX}_2$, the lowering of the π_1 IP relative to $\text{X}=\text{H}$ (ΔIP) is:

X	H	CH ₃	SCH ₃	SeCH ₃	N(CH ₃) ₂
ΔIP	0	1.1	2.1	2.4	3.1

The replacement of two methyl groups bonded to X by $(\text{CH}_2)_n$, where $n=1-3$, has comparatively little effect on the π_1 energy. The series given above may be taken as a measure of relative donor efficiency toward a carbon π system. The same order of donor efficiency of CH_3S and CH_3Se has previously been suggested on the basis of force constants.⁴

The calculated electron distribution in π_1 is in good agreement with reactivity data, which show C₁, X, and the cyano nitrogen atom to be centra of reactivity towards electrophiles.^{11,32}

Acknowledgements. Two of the authors (J.S. and I.W.) gratefully acknowledge financial support by the Swedish Natural Sciences Research Council. D.B. and M.A.W. are grateful for support from the Agricultural Research Council and the Science Research Council for grants for instrumentation. M.A.W. is grateful to the T. and E. Williams Trust for a maintenance grant.

REFERENCES

- Gompper, R. and Seybold, G. *Angew. Chem.* 80 (1968) 804.
- Wennerbeck, I. *Acta Chem. Scand.* 27 (1973) 258.
- Henriksen, L., Nielsen, P. H., Borch, G. and Klæboe, P. *Spectrochim. Acta A* 31 (1975) 373.
- Henriksen, L., Nielsen, P. H., Borch, G. and Klæboe, P. *Spectrochim. Acta A* 31 (1975) 1371.
- Ericsson, E., Marnung, T., Sandström, J. and Wennerbeck, I. *J. Mol. Struct.* 24 (1975) 373.
- Kessler, H. *Chem. Ber.* 103 (1970) 973.
- Wennerbeck, I. and Sandström, J. *Org. Magn. Reson.* 4 (1972) 783.
- Kalinowski, H.-O. and Kessler, H. *Top. Stereochem.* 7 (1973) 295.
- Jensen, K. A. and Henriksen, L. *Acta Chem. Scand.* 22 (1968) 1107.
- Gompper, R. and Töpfl, W. *Chem. Ber.* 95 (1962) 2871.
- Henriksen, L. and Autrup, H. *Acta Chem. Scand.* 24 (1970) 2629.
- Bock, H., Wagner, G., Wittel, K., Sauer, J. and Seebach, D. *Chem. Ber.* 107 (1974) 1869.
- Rosenberg, A. and Devlin, J. P. *Spectrochim. Acta* 21 (1965) 1613.
- Cope, A. C. and Hoyle, K. E. *J. Am. Chem. Soc.* 63 (1941) 733.
- Schuijl, P. J. W., Brandsma, L. and Arens, J. F. *Recl. Trav. Chim. Pays-Bas* 85 (1966) 1263.
- Dittmer, D. C., Simmons, H. E. and Vest, R. D. *J. Org. Chem.* 29 (1964) 497.
- Jensen, K. A. and Henriksen, L. *Acta Chem. Scand.* 24 (1970) 3213.
- Ericsson, E., Sandström, J. and Wennerbeck, I. *Acta Chem. Scand.* 24 (1970) 3102.
- Betteridge, D., Baker, A. D., Bye, P., Hasannudin, S. K., Kemp, N. R. and Thompson, M. J. *Electron Spectrosc. Rel. Phenom.* 4 (1974) 163.
- Bye, P. and Betteridge, D. J. *Electron Spectrosc. Rel. Phenom.* 7 (1975) 355.
- Nelander, B. *Theor. Chim. Acta* 25 (1972) 382.
- Santry, D. P. and Segal, G. A. *J. Chem. Phys.* 47 (1967) 158.
- Klewe, B. and Seip, H. M. *Acta Chem. Scand.* 26 (1972) 1860.
- Kapecki, J. A., Baldwin, J. E. and Paul, I. C. *Tetrahedron Lett.* (1967) 5307.
- Bock, H. and Stafast, H. *Chem. Ber* 105 (1972) 1158.
- Baker, A. D., Baker, C., Brundle, C. R. and Turner, D. W. *Int. J. Mass. Spectrom. Ion. Phys.* 1 (1968) 285.
- Stafast, H. and Bock, H. *Tetrahedron* 32 (1976) 855.
- Dewar, M. J. S. In *The Molecular Orbital Theory of Organic Chemistry*, McGraw-Hill, New York 1969, Chapter 6.
- Taylor, H. S. and Glasstone, S. *A Treatise on Physical Organic Chemistry*, Part I, D. Van Nostrand Co., 3rd Ed., New York 1942, p. 287.
- Brownlee, R. T. C. and Taft, R. W. J. *Am. Chem. Soc.* 92 (1970) 7007.
- Brownlee, R. T. C. and Taft, R. W. J. *Am. Chem. Soc.* 90 (1968) 6537.
- Abrahamsson, S., Rehnberg, G., Liljefors, T. and Sandström, J. *Acta Chem. Scand.* B 28 (1974) 1109.
- Henriksen, L. *To be published.*

Received July 12, 1976.

Rare Earth Carboxylates. 26. The Geometry of the Mononuclear Tris(oxydiacetato)cerate(III) Complex in the Solid State

JÖRGEN ALBERTSSON and INGA ELDING

Inorganic Chemistry and Physical Chemistry 1, Chemical Center, University of Lund, P.O.B. 740, S-220 07 Lund 7, Sweden

The crystal structure of the compound $\text{Na}_3[\text{Ce}(\text{C}_4\text{H}_4\text{O}_6)_3] \cdot 2\text{NaClO}_4 \cdot 6\text{H}_2\text{O}$ has been determined at 123, 163, and 295 K using X-ray intensity data collected with a four-circle single crystal diffractometer. The space group is $R\bar{3}2$ with $Z=3$. The unit cell dimensions are $a=9.805(1)$ and $c=28.545(1)$ Å at 295 K. Layers, parallel to the ab -plane, containing the tris(oxydiacetato)cerate(III) complexes and the perchlorate ions, interspaced with layers containing the water molecules and the sodium ions build up the structure. A slightly distorted tricapped trigonal prism of carboxylate and ether oxygen atoms surrounds the nine-coordinated cerium ion. The geometry of the complex is compared to the geometry of the tris(oxydiacetato)cerate(III) complex in the triclinic compound $\text{Na}_3[\text{Ce}(\text{C}_4\text{H}_4\text{O}_6)_3] \cdot 9\text{H}_2\text{O}$.

In a not too diluted water solution containing the trivalent cerium ion and the tridentate ligand oxydiacetate in the molar ratio 1:3, the predominant species is the tris(oxydiacetato)cerate(III) complex.¹ Solution X-ray diffraction has shown that nine donor oxygen atoms forming a tricapped trigonal prism (TCTP) surround the lanthanoid ion.² The symmetry of the complex in water solution is D_3 . The distortion of the coordination polyhedron from the D_{3h} symmetry of a regular TCTP depends on ligand constraints which cause the triangular faces to be slightly rotated relative to one another.³

The sodium salts of the tris(oxydiacetato)cerate(III) complex can be prepared by slow evaporation of a water solution at room temperature. In the simple sodium salt, the triclinic $\text{Na}_3[\text{Ce}(\text{C}_4\text{H}_4\text{O}_6)_3] \cdot 9\text{H}_2\text{O}$ (TCDG), the symmetry of the complex ion is degraded to C_1

by the packing forces.⁴ The most predominant of these forces are the coordination of the outer carboxylate oxygen atoms to the sodium ions and the hydrogen bonds between the water molecules and both the outer and inner carboxylate oxygen atoms of the complex.⁵ However, if sodium perchlorate is present in the mother liquor, a double salt, the trigonal $\text{Na}_3[\text{Ce}(\text{C}_4\text{H}_4\text{O}_6)_3] \cdot 2\text{NaClO}_4 \cdot 6\text{H}_2\text{O}$ (CDG), is formed,³ in which the complex retains the D_3 symmetry in the solid state.

The present investigation aims at comparing the geometry of the tris(oxydiacetato)cerate(III) complex in the triclinic and the trigonal phases. The results of both X-ray and neutron diffraction studies on the triclinic TCDG-phase have been published previously,^{4,5} as well as the results of X-ray studies on the trigonal "CDG-phase" formed by the lanthanoid ions neodymium(III), gadolinium(III), and ytterbium(III).^{3,6} To obtain the actual bond distances and bond angles in CDG, we have now investigated this compound with X-ray diffractometry. Due to the potential low temperature applications of CDG as a magnetic coolant and thermometer⁷ the effect of cooling on the structure was also investigated by collecting data at 123 and 163 K besides room temperature, 295 K.

EXPERIMENTAL

Data collection. Crystals of CDG were prepared as described in Ref. 6. Table 1 gives information concerning the collection and reduction of the intensity data sets and the refinements based on them. The method employed in the data

Table 1. Data collection and reduction of CDG. The least-squares refinements.

	Crystal 1		Crystal 2	
Crystal size (mm ³)	0.09 × 0.11 × 0.17		0.05 × 0.09 × 0.10	
Radiation	Graphite monochromated CuK α		Graphite monochromated CuK α	
ω -Interval (°) (ω -2 θ scan)	0.80 + 0.50 tan θ		0.75 + 0.40 tan θ	
θ -Interval (°)	5-70		5-70	
Minimum number of counts in a scan	3000		3000	
Maximum recording time (min)	3		3	
μ (CuK α) (cm ⁻¹)	139.3		139.3	
Range of the transmission factor	0.28-0.42		0.34-0.58	
Temperature (K)	295	163	295	123
Number of measured reflexions	642	1162	1193	1233
Number of reflexions given zero weight [$I < 3\sigma_c(I)$]	11	29	—	—
Number of reflexions skipped due to collision	—	—	27	14
Number of independent reflexions used in the final refinements, m	598	583	594	592
Number of parameters refined, n	77	77	77	77
$R = \sum(F_o - F_c) / \sum F_o $	0.023	0.029	0.028	0.028
$R_w = \{\sum w(F_o - F_c)^2 / \sum w F_o ^2\}^{1/2}$	0.031	0.040	0.036	0.035
$S = \{\sum w(F_o - F_c)^2 / (m-n)\}^{1/2}$	0.995	0.908	0.865	0.881
C_1 (weighting function)	0.0005	0.0009	0.0005	0.0005
C_2 " "	0.5	2.0	0.5	0.5
$g \times 10^{-4}$ (extinction)	0.116	0.134	0.077	0.207
Mosaic spread (")	4.99×10^3	4.34×10^3	7.57×10^3	281×10^3
Domain size (cm)	0.18×10^{-4}	0.21×10^{-4}	0.12×10^{-4}	0.32×10^{-4}

collection has been described in Ref. 4 and the low temperature apparatus in Ref. 8. To certify that the derived model of CDG and its interatomic distances and angles are typical of that material duplicate measurements on two different crystals were performed. Fluctuations in the intensities in three reference reflexions were mostly within 8 % for crystal 1 and 12 % for crystal 2 and they could be described by polynomials of the second degree which were used for scaling the data sets. The values of I and $\sigma_c(I)$ were corrected for Lorentz, polarization, and absorption effects. $\sigma_c(I)$ is based on counting statistics. The expression used in the polarization correction was $p = (1 + \cos^2 2\theta_M \cos^2 2\theta) / (1 + \cos^2 2\theta_M)$ with $\theta_M = 13.3^\circ$.

Unit cell and space group. CDG, Na₃[Ce(C₄H₉O₅)₃].2NaClO₄.6H₂O, F.W. = 958.28, crystallizes in the trigonal system with space group R32. The unit cell dimensions at the different temperatures were determined with least-squares refinement of θ -values for about 40 reflexions, measured on the diffractometer with CuK α_1 radiation as described in Ref. 8 ($\lambda = 1.54051 \text{ \AA}$). The following unit cell dimensions were obtained.

	295 K	163 K	123 K
$a/\text{Å}$	9.8052(9)	9.7405(11)	9.7117(79)
$c/\text{Å}$	28.5452(14)	28.4540(17)	28.4531(118)
$V/\text{Å}^3$	2376.7	2337.9	2324.1

The unit cell contains three formula units.⁴

Refinements. The parameters used as starting values in the least-squares refinements of CDG were those for the non-hydrogen atoms in the neodymium structure in Ref. 3. The function $\sum w(|F_o| - |F_c|)^2$ was minimized with weights calculated using the equation $1/w = \sigma_c^2/4|F_o|^2 + C_1|F_o|^2 + C_2$. C_1 and C_2 are adjustable constants. An isotropic extinction correction was also included. After a few cycles of refinements R had converged to 0.056. Anomalous dispersion for Ce and Cl was included and resulted in $R = 0.093$. The other absolute configuration was then tried with the unaveraged data and one cycle of refinement gave $R = 0.027$. This absolute configuration was chosen as a model of CDG in crystal 1. CDG in crystal 2 appears to have the same absolute configuration as in crystal 1.

Only one of the hydrogen atoms of the water

Table 2. Atomic parameters with estimated standard deviations in parentheses for CDG at 295, 163 and 123 K. The H atoms were not refined.

Atom	295 K			163 K			123 K		
	x	y	z	x	y	z	x	y	z
Ce	0	0	0	0	0	0	0	0	0
Cl	1/3	-1/3	0.0956(1)	1/3	-1/3	0.0968(1)	1/3	-1/3	0.0962(1)
Na(1)	0.0371(5)	-1/3	1/6	0.0321(5)	-1/3	1/6	0.0359(5)	-1/3	1/6
Na(2)	0	0	0.2001(1)	0	0	0.1977(1)	0	0	0.1980(1)
O(1)	-0.2615(6)	-0.2615(6)	0	-0.2604(7)	-0.2604(7)	0	-0.2638(7)	-0.2638(7)	0
O(2)	-0.0374(5)	-0.1978(5)	0.0599(1)	-0.0372(6)	-0.1991(6)	0.0595(1)	-0.0341(5)	-0.1974(5)	0.0597(1)
O(3)	-0.1709(6)	0.4153(5)	0.1008(1)	-0.1743(6)	0.4183(6)	0.1015(2)	-0.1693(6)	0.4153(6)	0.1021(2)
O(4)	0.1773(6)	-0.4177(14)	0.1134(2)	0.1732(7)	-0.4203(13)	0.1141(2)	0.1735(6)	-0.4195(13)	0.1135(2)
O(5)	1/3	-1/3	0.0465(3)	1/3	-1/3	0.0469(3)	1/3	-1/3	0.0470(3)
O(6)	0.1412(7)	-0.0793(7)	0.1432(1)	0.1424(7)	-0.0788(7)	0.1416(2)	0.1434(7)	-0.0776(7)	0.1425(1)
C(1)	-0.2921(8)	0.3839(8)	0.0324(2)	-0.2955(9)	0.3869(10)	0.0324(2)	-0.2932(10)	0.3878(10)	0.0328(3)
C(2)	-0.1536(12)	-0.3298(5)	0.0669(1)	-0.1576(15)	-0.3322(7)	0.0671(2)	-0.1520(14)	-0.3315(7)	0.0670(2)
H(1)	-0.3852	-0.4096	0.0495	-0.3900	-0.4131	0.0491	-0.3870	-0.4148	0.0501
H(2)	-0.3061	-0.4738	0.0158	-0.3089	-0.4771	0.0156	-0.3066	-0.4784	0.0161
H(W)	0.1157	-0.1073	0.1144	0.0963	-0.1056	0.1142	0.1072	-0.1082	0.1158

molecule could be located in a difference synthesis. This atom, hydrogen bonded to O(2), and the methylene hydrogen atoms were included in the structure factor calculations with their isotropic temperature factors fixed at 5.0 Å². Attempts to refine these coordinates were not successful.

The parameter shifts in the last cycle of refinements were within 10 % of the estimated standard deviations, except for Ce β_{11} in the 123 and 163 K structures (12 and 20 %, respectively), O(1) β_{23} in the 123 K structure (30 %), and O(1) β_{11} in the 295 K structure of crystal 1 (22 %). Final difference maps were featureless.

The scattering factors for Ce were taken from Cromer *et al.*⁹ those for Na, Cl, O, and C from Hanson *et al.*¹⁰ and those for H from Stewart *et al.*¹¹ The anomalous dispersion corrections were taken from Cromer and Liberman.¹² Tables 2 and 3 list the final positional parameters with estimated standard deviations and the thermal parameters, respectively. Lists of structure factors are available on request from the authors.

Probability plot analysis. As intensity measurements at 295 K were made with two different crystals, a probability plot of the measured structure factors was performed according to Abrahams and Keve.¹³ Ordered values of $\delta m_i = (|F(1)_i| - K|F(2)_i|) / [(\sigma^2 F(1)_i + K^2 \sigma^2 F(2)_i)]^{1/2}$ are compared with the values expected for a normal distribution with zero mean and unit variance. K is a scale factor such that $\sum (\delta m_i)^2$ is a minimum. Fig. 1a shows that the plot is linear with slope 0.48 and intercept -0.03. A half-normal probability plot of the positional and thermal coordinates (a δp -plot: $\delta p_i = \frac{|p(1)_i| - |p(2)_i|}{[(\sigma^2 p(1)_i + \sigma^2 p(2)_i)]^{1/2}}$) is shown in Fig. 1b. This comparison results in a straight line with slope 0.97 and intercept 0.06 indicating that the systematic differences between the two determinations are very small. Together the δm - and δp -plots indicate that the systematic errors are comparable or smaller than the random errors and that the values assigned to $\sigma(F)$ are larger than the correct ones (see p. 162 in Ref. 13). δR -plots comparing model with experiment were also made for each of the two 295 K structures (Fig. 1c and d). The slopes are somewhat smaller than the S -values (Table 1): 0.93 for crystal 1 and 0.80 for crystal 2. They indicate that the $\sigma(F)$'s are overestimated by 8 and 25 %, respectively. As the slope of the δm -plot is still lower than the slopes of the δR -plots, there also appears to be an underestimation of $\Delta F_i = |F(1)_i| - K|F(2)_i|$ in the δm -plot. Parameters from crystal 1 only are given in this paper for the 295 K structure of CDG as this determination seems to be better than that of crystal 2.

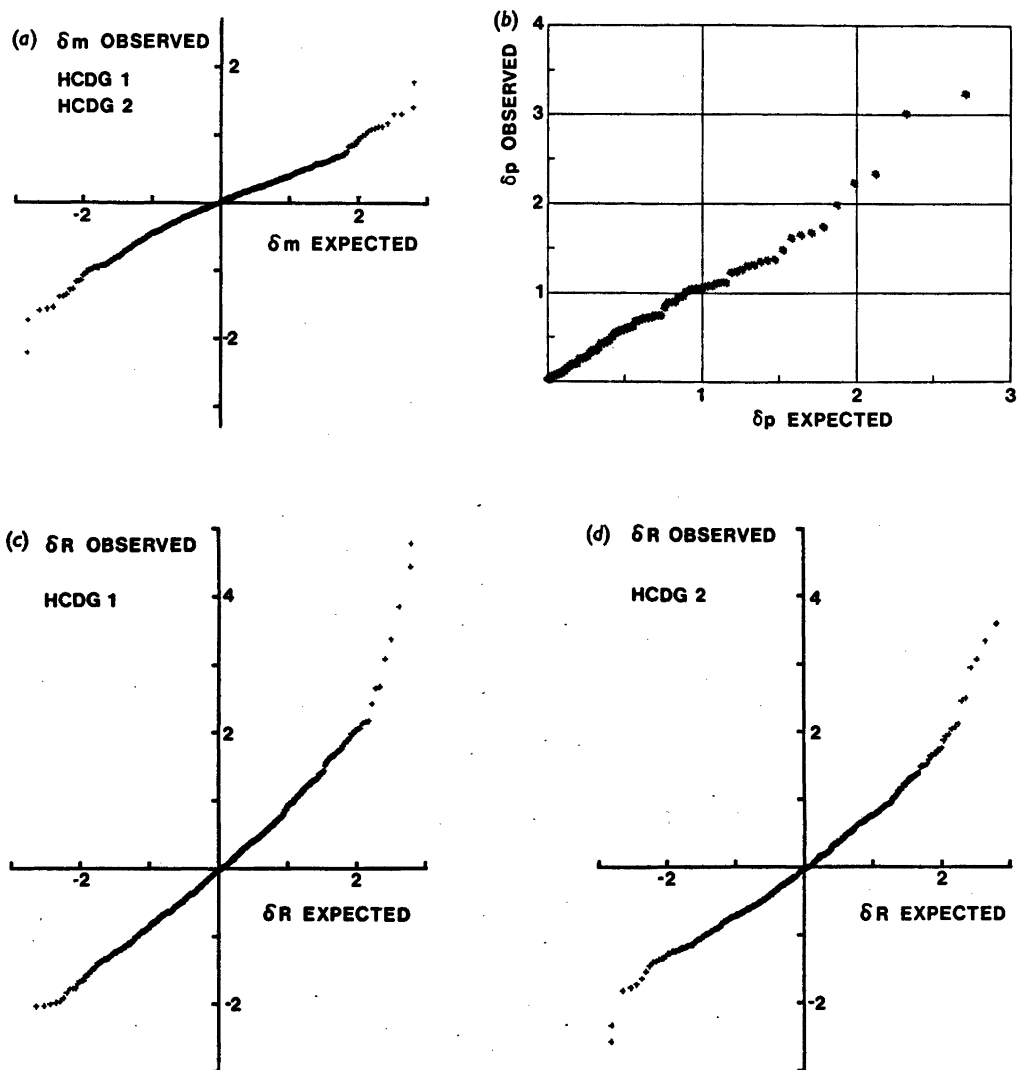


Fig. 1. Probability plot analysis of data and models of CDG at room temperature: (a) a δm -plot comparing the data sets for crystal 1 (HCDG1) and crystal 2 (HCDG2); (b) a δp -plot comparing the models derived from crystals 1 and 2; (c) a δR -plot comparing the model with experiment for crystal 1; (d) the same for crystal 2.

DISCUSSION

A description of the structure has been given in Refs. 3 and 6. The structure is composed of layers, perpendicular to c containing the mononuclear tris(oxydiacetato)cerate(III) complexes and the perchlorate ions alternating with layers containing the sodium ions and the water molecules. In Ref. 3 projections of the cerium

layer including the perchlorate ion and the sodium layer are shown. Figs. 2–4 show stereoscopic pairs of drawings of the cerium complex, part of the sodium layer, and the vicinity of the water molecule including the perchlorate ion, respectively. Table 4 gives selected interatomic distances and angles with estimated standard deviations. The room temperature values in Table 4 are slightly at

Table 3. Thermal parameters with standard deviations ($\times 10^3$). The form of the temperature factor is $\exp(-\beta_{11}h^2 - 2\beta_{12}hk \dots)$.

	β_{11}	β_{22}	β_{33}	β_{12}	β_{13}	β_{23}
A. 295 K						
Ce	992(10)	992(10)	43(1)	496(5)	0	0
Cl	1665(29)	1665(29)	97(2)	833(15)	0	0
Na(1)	2186(63)	1530(59)	193(6)	765(30)	28(8)	56(15)
Na(2)	1268(40)	1268(40)	100(3)	634(20)	0	0
O(1)	1265(115)	1265(115)	103(7)	459(67)	-29(19)	29(19)
O(2)	1575(62)	1424(58)	95(4)	713(52)	-19(13)	69(13)
O(3)	2059(90)	1713(63)	150(5)	928(61)	89(17)	249(16)
O(4)	1767(73)	2218(126)	229(8)	527(115)	74(19)	-92(44)
O(5)	4028(240)	4028(240)	107(9)	2014(120)	0	0
O(6)	2205(133)	2071(119)	105(4)	1075(119)	1(17)	55(16)
C(1)	1716(103)	1245(87)	131(8)	537(79)	107(24)	60(23)
C(2)	1363(128)	1264(69)	98(5)	689(94)	103(22)	58(14)
B. 163 K						
Ce	820(14)	820(14)	25(1)	410(7)	0	0
Cl	1166(32)	1166(32)	55(3)	583(16)	0	0
Na(1)	1593(64)	1240(68)	101(5)	620(34)	16(8)	32(15)
Na(2)	999(51)	999(51)	61(4)	500(26)	0	0
O(1)	969(150)	969(150)	81(8)	650(82)	19(21)	-19(21)
O(2)	1201(75)	1167(73)	60(5)	637(64)	5(16)	34(16)
O(3)	1506(97)	1300(73)	91(6)	680(69)	69(18)	142(17)
O(4)	1207(72)	1465(114)	106(6)	554(99)	30(16)	25(35)
O(5)	2138(162)	2138(162)	58(9)	1069(81)	0	0
O(6)	1464(121)	1405(112)	64(5)	632(111)	-31(18)	43(17)
C(1)	1097(107)	1090(111)	71(8)	390(89)	69(25)	18(25)
C(2)	1137(151)	973(85)	63(6)	638(117)	74(27)	47(17)
C. 123 K						
Ce	932(12)	932(12)	29(1)	466(6)	0	0
Cl	1377(33)	1377(33)	72(2)	688(16)	0	0
Na(1)	1809(65)	1421(69)	133(5)	711(35)	35(8)	70(16)
Na(2)	1116(48)	1116(48)	77(4)	558(24)	0	0
O(1)	1271(152)	1271(152)	89(8)	485(87)	-19(24)	19(24)
O(2)	1383(73)	1207(67)	71(4)	691(61)	14(14)	87(14)
O(3)	1738(95)	1566(76)	135(6)	914(69)	130(18)	221(18)
O(4)	1387(72)	1676(119)	155(6)	568(107)	58(17)	17(38)
O(5)	3028(206)	3028(206)	79(9)	1514(103)	0	0
O(6)	1935(140)	1832(126)	78(5)	975(125)	-20(18)	34(17)
C(1)	1748(136)	1337(119)	111(9)	700(106)	92(29)	39(28)
C(2)	1400(163)	1240(88)	81(6)	701(114)	92(25)	44(17)

variance with what may be expected from the values in Table 4 of Ref. 3. The probability-plot analysis indicates, however, that the present investigation of CDG must be looked upon as more accurate than the neodymium and ytterbium studies presented in Ref. 3.

The coordination polyhedron. As is the case in TCDG,⁴ the cerium ion in CDG is surrounded

by a distorted TCTP of carboxylate and ether oxygens (Fig. 2). To compare the distortions of the two polyhedra in CDG and TCDG, respectively, a number of quantities are collected in Table 5. The geometry of the coordination polyhedron in CDG is almost unchanged in the temperature interval 123–295 K. The triangular faces of the trigonal prism are only

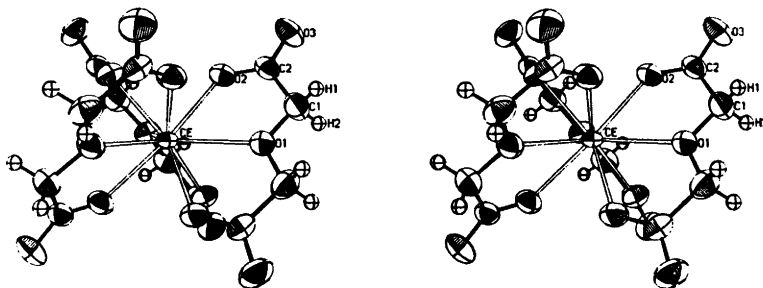


Fig. 2. The tris(oxydiacetato)cerate(III) complex. The thermal ellipsoids for the non-hydrogen atoms are scaled in Figs. 2–4 to include 50 % probability.

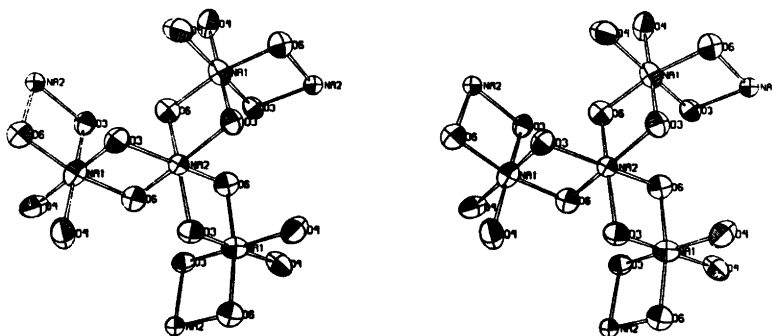


Fig. 3. The coordination around the sodium ions.

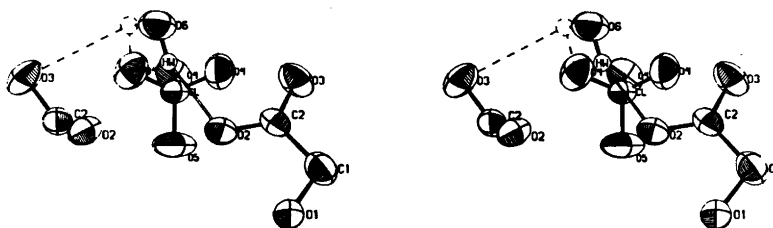


Fig. 4. The hydrogen bond O(6)–H(W)···O(2) and the perchlorate ion.

approximately equilateral in TCDG where the symmetry of the polyhedron is C_1 . The edge is about 0.1 Å longer in TCDG than in CDG. The equatorial triangle has approximately the same edge length in CDG and TCDG. The height of the trigonal prism, measured as the distance between the centroids of the triangular faces in TCDG, is about 0.1 Å larger

in CDG than in TCDG. In TCDG the two triangular faces of the prism are tilted 2 and 5°, respectively, to the equatorial plane and 5° to each other. The rigid oxydiacetate ligands cause the triangular faces of the prism to be rotated relative to one another. The resulting torsion angles are calculated by method 1 as given by Dymock and Palenik.¹⁴ The average

Table 4. Selected interatomic distances (Å) and angles (°) with e.s.d.'s in CDG at 295, 163, and 123 K. The superscripts (i)–(v) indicate the following equivalent sites in the structure:

(i)	$y, x, -z$	(iii)	$-y, x-y-1, z$
(ii)	$y-x, -x, z$	(iv)	$-y, x-y, z$
		(v)	$1+y-x, -x, z$

	295 K	163 K	123 K
A. The cerium coordination polyhedron; distance			
Ce–O(1)	2.564(6)	2.537(7)	2.564(7)
Ce–O(2)	2.471(4)	2.461(4)	2.457(4)
O(1)–O(2)	2.602(5)	2.579(6)	2.615(6)
O(1)–O(2 ⁱⁱ)	3.096(5)	3.068(6)	3.063(6)
O(2)–O(2 ⁱⁱ)	3.091(7)	3.092(9)	3.075(8)
O(2 ⁱ)–O(2 ⁱⁱ)	3.476(7)	3.446(8)	3.444(7)
B. The ligand; distance			
O(1)–C(1)	1.423(7)	1.436(9)	1.435(9)
C(1)–C(2)	1.541(11)	1.532(13)	1.542(13)
C(2)–O(2)	1.241(7)	1.258(10)	1.249(9)
C(2)–O(3)	1.234(6)	1.247(8)	1.246(7)
Angle			
C(1)–O(1)–C(1 ⁱ)	116.4(8)	113.6(8)	117.4(8)
O(1)–C(1)–C(2)	110.3(6)	108.9(6)	110.1(6)
C(1)–C(2)–O(2)	116.5(5)	116.9(6)	117.0(6)
C(1)–C(2)–O(3)	117.9(6)	118.4(8)	118.0(7)
O(2)–C(2)–O(3)	125.3(8)	124.6(9)	124.6(9)
Dihedral angle			
O(1)–C(1)–C(2)–O(2)	–4.2(0.9)	–5.8(1.1)	–4.6(1.1)
O(1)–C(1)–C(2)–O(3)	171.0(0.6)	171.3(0.8)	168.3(0.7)
C(1 ⁱ)–O(1)–C(1)–C(2)	–176.6(0.6)	–176.3(0.7)	–176.5(0.7)
C. The sodium coordination; distance			
Na(1)–O(3)	2.589(6)	2.549(6)	2.529(6)
Na(1)–O(4)	2.455(9)	2.451(9)	2.427(9)
Na(1)–O(6)	2.270(6)	2.269(6)	2.266(6)
Na(1)–Na(2)	3.593(3)	3.526(3)	3.539(4)
Na(2)–O(3)	2.355(4)	2.334(5)	2.346(5)
Na(2)–O(6)	2.497(5)	2.476(6)	2.459(6)
D. The perchlorate ion; distance			
Cl–O(4)	1.420(5)	1.439(6)	1.433(6)
Cl–O(4) ^a	1.455(5)	1.452(6)	1.452(6)
Cl–O(5)	1.401(8)	1.420(8)	1.399(8)
Cl–O(5) ^a	1.463(10)	1.445(9)	1.441(9)
Angle			
O(4)–Cl–O(4 ⁱⁱⁱ)	107.9(2)	109.0(2)	108.8(2)
O(4)–Cl–O(5)	111.0(2)	110.0(2)	110.1(2)
E. The water molecule and possible hydrogen bonds; distance			
O(6)–H(W)	0.86	0.87	0.83
H...O(W)O(2)	2.03	1.94	2.00
O(6)...O(2)	2.835(6)	2.799(6)	2.806(6)
O(6)...O(3 ^{iv})	3.198(8)	3.155(8)	3.142(8)
O(6)...O(4 ^v)	3.290(14)	3.232(13)	3.239(13)
O(6)...O(2 ^{iv})	3.191(6)	3.155(7)	3.175(7)

Table 4. Continued.

Angle			
O(6)–H(W)···O(2)	154.3	169.3	164.9
O(2)···O(6)···O(3 ^{iv})	97.5(2)	99.1(2)	98.2(2)
O(2)···O(6)···O(4 ^v)	94.5(2)	95.7(2)	94.4(2)
O(2)···O(6)···O(2 ^{iv})	61.4(2)	62.2(2)	61.5(2)

^a Values corrected for thermal motion, O(4) and O(5) riding on Cl.

torsion angle in TCDG is about the same as the angle in CDG. The difference in height between the prisms is, thus, compensated by the difference in the length of the edges of the triangular faces.

The six cerium-carboxylate oxygen bond distances within the trigonal prism are 2.471 Å at room temperature. The average value in TCDG is 2.477 Å. The three equatorial cerium-ether oxygen bond distances are 2.564 Å in CDG and 2.583 Å in TCDG (average value). The equatorial bonds are significantly longer than the prismatic bonds. The symmetry requires the cerium ion to be in the equatorial plane of the CDG polyhedron. Also in the polyhedron of symmetry C_1 in TCDG, the cerium ion is located in the equatorial plane. The quotient between the equatorial and prismatic bond distances, ρ in Table 5, has the same value in both structures. The angle θ in Table 5 is calculated as the angle between the line connecting the cerium ion and the centroid of a triangular face and the bond between cerium and a carboxylate oxygen in this triangle. The regular TCTP of symmetry D_{3h} is described by the parameters ρ and θ .¹⁵ The

distortions of the polyhedra in TCDG and CDG from the symmetry D_{3h} are small making it possible to use ρ and θ for an approximate description. The value of θ for a hard sphere model with $\rho = 1.04$ is 42.6°. Kepert¹⁶ has shown that a more stable structure is obtained for nine independent real ligand atoms by increasing the hard sphere value of θ about 3°. The values of θ for the CDG and TCDG complexes formed by three tridentate ligands are 46.3 and 48.2°, respectively, corresponding to increases from the hard sphere value of 3.7 and 5.6°.

The ligands. The oxydiacetate ion is approximately planar in CDG as can be seen from the dihedral angles (Table 4 B). Its conformation is, however, slightly different in CDG and TCDG at 295 K. The dihedral angles corresponding to, e.g., O(1)–C(1)–C(2)–O(2) are in TCDG ligand 1: –12.5 and 10.8°, ligand 2: 2.7 and –3.2°, ligand 3: 6.0 and –14.9°. Its value is $\pm 4.2^\circ$ in CDG at 295 K. Most interatomic distances (bonded and non-bonded) less than 2.50 Å appear to be longer at 123 and 163 K than at 295 K as the geometries of the ligand at the different temperatures are uncorrected for thermal motion.

Table 5. A comparison of the coordination polyhedra in CDG and TCDG.⁴ The various quantities are defined in the text.

Quantity	TCDG(295 K)		CDG		
	Range	Average	295 K	163 K	123 K
Edge of the prismatic triangles (Å)	3.10–3.22	3.20	3.09	3.09	3.08
Edge of the equatorial triangle (Å)	4.38–4.53	4.47	4.44	4.39	4.44
Height of the prism (Å)	—	3.30	3.42	3.39	3.40
Tilt angles (°)	2, 5, 5	—	—	—	—
Torsion angle (°)	19.2–21.7	20.1	20.5	20.3	18.6
ρ	1.02–1.05	1.04	1.04	1.03	1.04
θ (°)	45.5–50.7	48.2	46.3	46.5	46.3

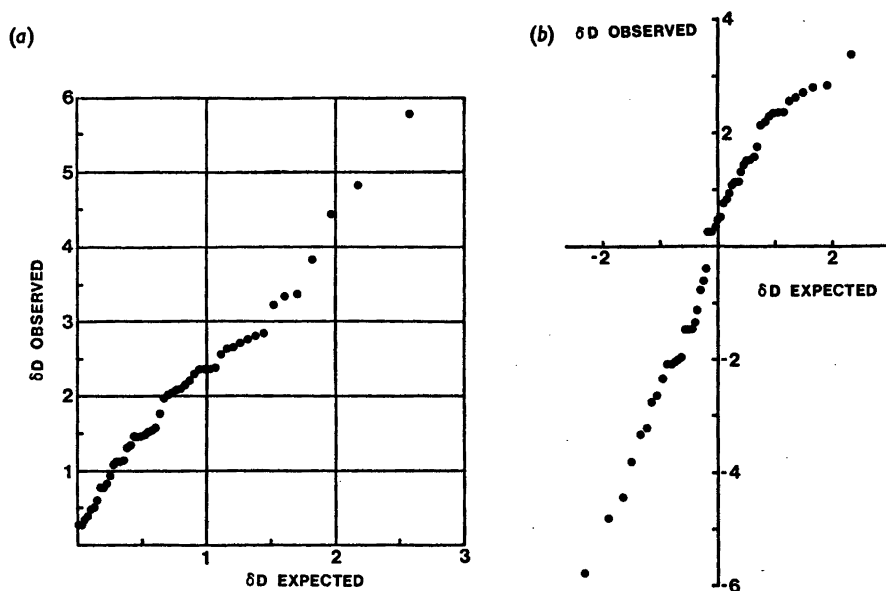


Fig. 5. A δd probability plot comparison of the bond distances and angles in the oxydiacetate ligands in CDG and TCDG at 295 K: (a) half-normal, (b) full-normal.

The oxydiacetate bond distances and bond angles within the cerium complexes in TCDG and CDG are compared at 295 K in Fig. 5. Both half-normal (a) and full-normal (b) probability plot comparisons of interatomic distances less than 2.50 Å are shown.^{16,17} The non-linear plots with intercepts 0.33 and 0.10, respectively, indicate differences between the ligands in the two structures. The distance C(1)–C(2) is 1.541 Å in CDG but the corresponding average value is 1.507 Å in TCDG. The angle O(1)–C(1)–C(2) is smaller in TCDG (average value 107.9°) than in CDG (110.3°). The angle C(1)–O(1)–C(1ⁱ) has also a smaller value in TCDG (average value 112.5°) than in CDG (116.4°). On the average, the geometry of the ligands of TCDG are more in agreement with the geometry of the oxydiacetate residues in the alkali hydrogen salts¹⁸ than is the ligand in CDG.

The hydrogen bonds. The only hydrogen bond distance in the structure is between O(6) and O(2), 2.84 Å at room temperature. The water hydrogen atom found in the difference synthesis is located between these two atoms. There is a possibility for an interaction between the

other water hydrogen atom and either of the oxygen atoms O(3) and O(4). The distances at 295 K are O(6)–O(3^{iv}), 3.20 Å, and O(6)–O(4^v), 3.29 Å. In Fig. 4 the hydrogen atom not found has been drawn dotted in a position where its distances to O(3^{iv}) and O(4^v) are about the same. As no peak corresponding to this hydrogen atom was found in the difference synthesis it might be disordered.

Acknowledgements. We thank Professor I. Leden and Dr. Å. Oskarsson for helpful discussions. The Swedish Natural Science Research Council gave financial support, which is gratefully acknowledged.

REFERENCES

1. Grenthe, I. and Tobiasson, I. *Acta Chem. Scand.* 17 (1963) 2101.
2. Hansson, E. *To be published.*
3. Albertsson, J. *Acta Chem. Scand.* 24 (1970) 3527.
4. Elding, I. *Acta Chem. Scand. A* 30 (1976) 649.
5. Albertsson, J. and Elding, I. *Acta Crystallogr. B* 32 (1976) 3066.
6. Albertsson, J. *Acta Chem. Scand.* 22 (1968) 1563.

7. Albertsson, J., Chen, P. Y. and Wolf, W. P. *Phys. Rev. Sect. B* 11 (1975) 1943.
8. Danielsson, S., Grenthe, I. and Oskarsson, Å. *J. Appl. Crystallogr.* 8 (1975) 14.
9. Cromer, D. T., Larson, A. C. and Water, J. T. *Acta Crystallogr.* 17 (1964) 1044.
10. Hanson, H. P., Herman, F., Lea, J. D. and Skillman, S. *Acta Crystallogr.* 17 (1964) 1040.
11. Stewart, R. F., Davidson, E. R. and Simpson, W. T. *J. Chem. Phys.* 42 (1965) 3175.
12. Cromer, D. T. and Liberman, D. *J. Chem. Phys.* 53 (1970) 1891.
13. Abrahams, S. C. and Keve, E. T. *Acta Crystallogr. A* 27 (1971) 157.
14. Dymock, K. R. and Palenik, G. J. *Inorg. Chem.* 14 (1975) 1220.
15. Kepert, D. L. *J. Chem. Soc.* (1965) 4736.
16. De Camp, W. H. *Acta Crystallogr. A* 29 (1973) 148.
17. Albertsson, J. and Schultheiss, P. M. *Acta Crystallogr. A* 30 (1974) 854.
18. Albertsson, J., Herbertsson, H. and Grenthe, I. *Acta Crystallogr. B* 29 (1973) 1855 and 2839.

Received June 21, 1976.

The Catalytic Effect of Silver Salts upon the Rate of Isomerization of Triphenylmethyl Isocyanide to Triphenylmethyl Cyanide in Acetonitrile

ARVE MARTINSEN

Department of Chemistry, University of Bergen, N-5014 Bergen-Univ., Norway

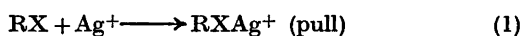
Triphenylmethyl isocyanide, Ph_3CNC , isomerizes very slowly in acetonitrile to triphenylmethyl cyanide, Ph_3CCN . The first order rate constant at 35.0°C is $6.1 \times 10^{-7} \text{ s}^{-1}$. The isomerization reaction is efficiently catalyzed by minute amounts of silver nitrate and silver perchlorate, the latter salt being the better catalyst.

The rate increase caused by the silver(I) catalysts is directly proportional to their concentrations. It is proposed that the rate determining step involves a cyclic intermediate involving the silver(I) ion.

Among the various methods for the preparation of alkyl isocyanides, the reaction between alkyl halides and silver cyanide^{1,2} or onium dicyanoargentates^{3,4} is well established. However, when using silver cyanide, the alkyl isocyanide formed is usually contaminated by the corresponding cyanide⁵ which seriously limits the generality of this synthetic method. There are, however, no reports of such limitations when onium dicyanoargentates are used as reagents.

Organic reactions assisted by silver(I) ions are quite common and studies by Kornblum⁶⁻⁹ and Kevill and Pocker¹⁰⁻¹² are repeatedly quoted. From kinetic studies on reactions of alkyl halides and silver nitrate the determined order in the alkyl halides is 1, while the order in the silver nitrate varies between 1.5 and 2.¹⁰⁻¹⁴ These variations are explained by an electrophilic pull by the silver ion on the outgoing halide atom, eqn. 1, and a nucleophilic push by the nitrate ion on the central carbon atom, eqn. 2. The reaction order appears to be

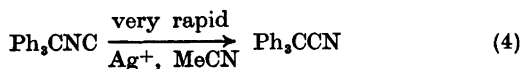
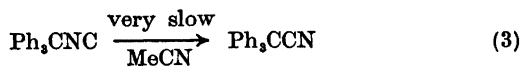
somewhat dependent upon the applied silver nitrate concentration.



The silver(I) ion, having its $4d$ orbitals filled while the $5s$ and $5p$ orbitals are vacant, can readily be coordinated by electron-rich ligands and at the same time exert a stabilization due to back bonding from its d -orbitals to vacant or antibonding orbitals in the ligands. The silver(I) ion may even coordinate with strained σ -bonds in bicyclic ring systems exerting a catalytic effect upon the rearrangements of these systems as shown by Paquette.¹⁵

Recently Austad and Songstad¹⁶ reported rates of isomerization of triphenylmethyl isocyanide to the corresponding cyanide in acetonitrile at various temperatures on samples of triphenylmethyl isocyanide synthesized from triphenylmethyl chloride and onium dicyanoargentates. However, we have been unable to reproduce their results from samples of triphenylmethyl isocyanide synthesized from *N*-triphenylmethyl formamide and 4-methylphenyl sulfonyl chloride,¹⁷ a synthetic route which avoids the use of silver species.

Actually, we have found that triphenylmethyl isocyanide, synthesized by this method, is isomerizing extremely slowly in pure acetonitrile, eqn. 3, but that the isomerization is efficiently catalyzed by silver ions from added silver nitrate or silver perchlorate, eqn. 4.



In this work we have therefore performed a kinetic study on the effect of silver(I) ions upon the rate of isomerization to evaluate the mechanism of this reaction and to obtain further information on when silver species can be employed as reagents toward alkyl halides for the synthesis of alkyl isocyanides.

Silver nitrate and silver perchlorate are well suited as sources of the silver(I) ion in acetonitrile since the dissociation constants of these salts are 9×10^{-8} M and 4.3×10^{-4} M, respectively.¹⁰ In the concentration range applied in the present study, $< 1.5 \times 10^{-4}$ M, these salts can thus be considered fully dissociated. In acetonitrile the silver(I) ion is solvated by four acetonitrile molecules when the concentration is less than 0.5 M.¹⁸ In this solvent the silver(I) ion should thus be formulated as $[\text{Ag}(\text{MeCN})_4]^+$.

EXPERIMENTAL

Solvents. Acetonitrile, Baker Analyzed Reagent, was distilled from phosphorus pentoxide and finally from calcium hydride¹⁹ and stored

on Linde 3 Å molecular sieves in a dry box under nitrogen. Cyclohexane and hexane were distilled from sodium. Formamide was distilled in vacuum prior to use.

Materials. Silver nitrate, Merck, *p.a.* grade, was dried at 120°C for 2 h. Anhydrous silver perchlorate, K & K Laboratories, was used without further purifications. *N*-Triphenylmethylformamide was prepared from triphenylmethyl chloride and formamide,²⁰ m.p. 203–204°C (MeCN). Triphenylmethyl isocyanide was prepared by two routes:

Method A. From *N*-triphenylmethylformamide and 4-methylphenylsulfonyl chloride in pyridine,¹⁷ m.p. 132–133°C (hexane).

Method B. Purified triphenylmethyl chloride and tetramethylammonium dicyanoargentate yielded an impure product.¹⁹ However, by addition of a trace amount of tetraphenylarsonium iodide to the reaction mixture immediately after the reaction was completed to complex catalytic amounts of silver species, the desired product was obtained, m.p. 131–132°C (hexane).

Tetramethylammonium dicyanoargentate was prepared from freshly prepared silver cyanide and dried tetramethylammonium chloride,³ m.p. 194–195°C (MeCN). Tetraphenylarsonium iodide was prepared as reported by Songstad and co-workers.²¹

Kinetic studies. The rate studies were performed with a Unicam SP 200 Infrared Spectrophotometer by following the disappearance of the isocyanide peak at 2126 cm^{-1} employing liquid IR cells with a cell length of 0.1 cm. The initial concentration of the substrate was 2.0×10^{-2} M in all runs. The logarithmic rate plots were linear throughout each run. When

Table 1. Rates of isomerization of triphenylmethyl isocyanide, RNC, to triphenylmethyl cyanide at 35°C at various concentrations of silver nitrate. The initial concentration of the isocyanide is 2.0×10^{-2} M.

$[\text{AgNO}_3] \times 10^6/\text{M}$	$k_{\text{obs}}/\text{s}^{-1}$	$k_1'K_A/\text{l s}^{-1} \text{mol}^{-1}$
0	$(6.1 \pm 0.4) \times 10^{-7}$	
1	$(3.2 \pm 0.2) \times 10^{-6}$	
2	$(8.8 \pm 0.4) \times 10^{-6}$	
5	$(7.2 \pm 0.4) \times 10^{-6}$	
10	$(2.3 \pm 0.1) \times 10^{-4}$	31 ± 3
20	$(5.3 \pm 0.3) \times 10^{-4}$	
50	$(1.5 \pm 0.1) \times 10^{-3}$	
160	$(3.8 \pm 0.5) \times 10^{-3}$	
0 ^a	$(3.5 \pm 0.2) \times 10^{-4}$	
0 ^b	$(1.3 \pm 0.1) \times 10^{-6}$	
0 ^c	3.34×10^{-4}	
5.0×10^{-5} Me ₄ NAg(CN) ₂	$(1.7 \pm 0.1) \times 10^{-6}$	
2.5×10^{-5} M AgNO ₃ + 2.3×10^{-5} M Ph ₄ AsCl	$(1.8 \pm 0.1) \times 10^{-4}$	

^a With excess AgCN at 25°C. ^b Determined from triphenylmethyl isocyanide prepared by route B. ^c From Ref. 16 at 35°C.

Table 2. Rates of isomerization of triphenylmethyl isocyanide to triphenylmethyl cyanide at 35 °C at various concentrations of silver perchlorate. The initial concentration of the isocyanide is 2.0×10^{-3} M.

$[\text{AgClO}_4] \times 10^6/\text{M}$	$k_{\text{obs}}/\text{s}^{-1}$	$k_1'K_A/1 \text{ s}^{-1} \text{ mol}^{-1}$
0	$(6.1 \pm 0.4) \times 10^{-7}$	
3	$(4.6 \pm 0.2) \times 10^{-6}$	
6	$(1.4 \pm 0.1) \times 10^{-4}$	
10	$(4.9 \pm 0.2) \times 10^{-4}$	53 ± 5
20	$(9.1 \pm 0.4) \times 10^{-4}$	
40	$(1.9 \pm 0.1) \times 10^{-3}$	
60	$(2.5 \pm 0.5) \times 10^{-3}$	

the concentration of the added silver salts exceeded $\sim 10^{-4}$ M the rates were too fast to be determined accurately by the technique employed.

RESULTS AND DISCUSSION

The observed rates of isomerization at 35 °C in acetonitrile are listed in Tables 1 and 2. In pure acetonitrile, triphenylmethyl isocyanide, synthesized from *N*-triphenylmethylformamide and 4-methylphenyl sulfonyl chloride in pyridine, Method A, is isomerizing very slowly and with a first order rate constant of $6.1 \times 10^{-7} \text{ s}^{-1}$. The catalysis exerted by silver(I) ions is pronounced even for concentrations of silver salts of only 1×10^{-3} M, *i.e.* 5×10^{-3} % of the concentration of the organic substrate. At this concentration of the catalyst the rate of isomerization is five times as high as the uncatalyzed reaction (Tables 1 and 2).

In Fig. 1 the observed rate constants are plotted *versus* the concentration of added silver nitrate and silver perchlorate. For concentrations of the silver salts above $\sim 3 \times 10^{-4}$ M, the observed rate constants are seen to be linearly related to the concentration of the silver salts fitting a rate equation $k_{\text{obs}} = a + b[\text{AgX}]$. The lack of linearity at very low concentrations of silver salt may be due to several factors. First of all, these low concentrations are considerably below the purification limit of the solvent. Furthermore, since the ratio between the concentration of the substrate and the silver catalyst in this non-linear region is more than 7×10^3 , undetectable contaminations in the substrate may be the cause of the non-linearity observed. For concentrations of

silver salts above $\sim 1 \times 10^{-4}$ M, the rates of isomerization were too rapid to be determined accurately by the technique employed. The possible deviation from linearity at high concentrations may thus be due to experimental error.

The results obtained in the present study suggest that the isomerization reaction studied takes place by an unassisted path, eqn. 3, with a first order rate constant k_1 , along with an $\text{S}_{\text{N}}1$ Ag^+ assisted step, eqns. 5 to 7.

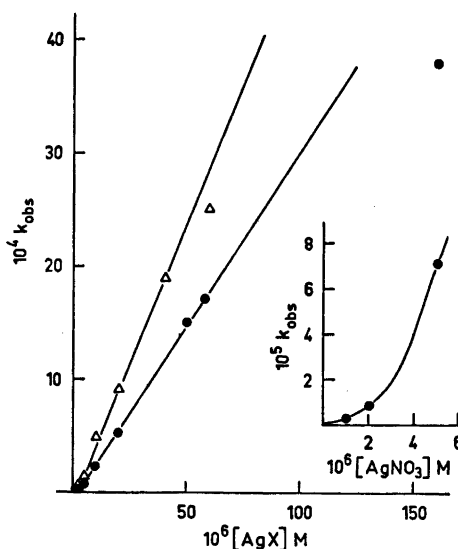
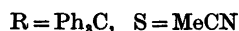
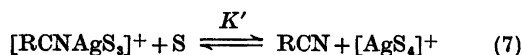
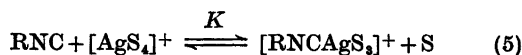


Fig. 1. The effect of added silver salts upon the observed rate constant, k_{obs} , for the isomerization of triphenylmethyl isocyanide to triphenylmethyl cyanide in acetonitrile at 35.0 ± 0.1 °C. Filled circles, silver nitrate. Triangles, silver perchlorate.



The first step in the assisted reaction, eqn. 5, is supposed to be the displacement of a solvent molecule from the silver tetraacetonitrile ion followed by the intramolecular isomerization, eqn. 6. The final step in the sequence is the regeneration of the silver tetraacetonitrile ion together with the product, triphenylmethyl cyanide, eqn. 7. The latter step, being in principle an acid-base equilibrium, is set up very rapidly and is displaced completely to the right since triphenylmethyl cyanide is assumed to be a considerably weaker base toward the silver(I) ion than is the acetonitrile molecule.

Assuming the second step, eqn. 6, to be the rate determining one, the following rate equation is obtained:

$$k_{\text{obs}} = k_1 + k_1' \frac{K_a[\text{AgX}]}{1 + [\text{RNC}]} \quad (8)$$

where $\text{X} = \text{ClO}_4^-$, NO_3^- and $K_a = K[\text{MeCN}]^{-1}$. Eqn. 8 conforms with the linearity observed provided $K_a[\text{RNC}] \ll 1$, and we thus obtain:

$$k_{\text{obs}} = k_1 + k_1' K_a[\text{AgX}] \quad (9)$$

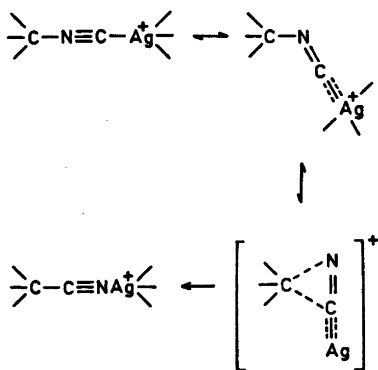
Table 3. The effect of water upon the rate of isomerization of triphenylmethyl isocyanide to triphenylmethyl cyanide at 35 °C in acetonitrile. The initial concentration of the isocyanide is 2.0×10^{-2} M.

$[\text{H}_2\text{O}] \times 10^2/\text{M}$	$k_{\text{obs}}/\text{s}^{-1}$
1.49	$(6.4 \pm 0.4) \times 10^{-7}$
14.9	$(8.3 \pm 0.5) \times 10^{-7}$
149	$(6.3 \pm 0.3) \times 10^{-7}$
820	$(6.9 \pm 0.4) \times 10^{-7}$
5.8×10^{-5} M H_2O + 5.8×10^{-5} M AgNO_3	$(1.7 \pm 0.2) \times 10^{-5}$

Addition of water along with silver nitrate causes the same catalytic effect as if the silver nitrate had been added alone, Table 3. The presence of water due to the hygroscopic nature of the solvent and silver perchlorate does not affect the rates. However, added tetraphenylarsonium chloride to a sample of the substrate and silver nitrate, (Table 1), shows a marked reduction of the expected rate acceleration due to the silver nitrate. This may be due to a complexing of the halide ion with the silver(I) ion forming traces of AgCl or preferably AgCl_2^- .^{22,23} The rates reported by Austad and Songstad¹⁶ for an uncatalyzed isomerization are too high compared to the results obtained in this paper. They also reported a rate depression by anions and assumed this to be caused by a salt effect due to the nucleophilic anions. In the light of the present work it now seem reasonable to assign these rate decelerations to a complexing of the added anions with impurities of silver(I) species in their employed triphenylmethyl isocyanide. From their reported rate constant, $3.35 \times 10^{-4} \text{ s}^{-1}$, and the results obtained in the present study one can estimate a concentration of approximately 1.4×10^{-5} M of active catalytic silver species in their applied reaction mixture, amounting to a contamination of 0.07 % (in mol) of the substrate. From Table 1 it can be seen that this contamination cannot be the pure tetramethylammonium dicyanoargentate alone since a concentration of 5×10^{-5} M of this salt only doubles the observed rate compared to the rate observed for the uncatalyzed isomerization.

Isocyanides are known to form stable complexes with the silver(I) ion although few of these complexes have been characterized.²⁴⁻²⁶ However, the silver nitrate-triphenylmethyl isocyanide complex has been isolated in poor yield in acetonitrile at -20 °C, while attempts to isolate the silver perchlorate complex have failed.²⁷ A preequilibrium step *via* the silver(I) isocyanide complex is therefore proposed.

In triphenylmethyl isocyanide the central carbon atom is surrounded by three phenyl groups. The silver(I) ion is attached to four acetonitrile solvent molecules¹⁸ and for steric reasons the most possible attacking site is on the lone pair of the isocyanide carbon atom (Scheme 1).



Scheme 1.

In the complex formed a stabilization due to back donation from silver d^{10} orbitals to the antibonding orbitals of the isocyanide carbon atom is to be expected.^{28,29} The negatively charged surroundings of the cyano groups in the solvent molecules will tend to increase this back donation due to their interactions with the electron rich d^{10} sphere of the silver(I) ion. It is assumed that this back donation will cause the isocyanide nitrogen atom to be sp^2 hybridized and the C-NC bond angle approaches 120° , Scheme 1. Once formed, the isocyanide group in this complex will collapse to the product *via* an intermediate cyclic three center ion, with negligible separation of the alkyl and cyanide group in the transition state. This should be consistent with a synchronous mechanism as proposed by Casanova *et al.*²⁸ and calculated by Schaefer *et al.*^{30,31} for similar uncatalyzed systems. Casanova and co-workers²⁸ found that *p*-substituted aryl isocyanides isomerize synchronously and unaffected by the substituents and for the isomerization of methyl isocyanide to methyl cyanide Schaefer and co-workers^{30,31} calculated a transition state with a C-NC bond angle of 106° .

Yamada and co-workers³² have shown that isocyanides may isomerize *via* a radical mechanism with racemization. A radical mechanism for the reaction studied is excluded as shown by Austad and Songstad.¹⁶ Moreover, the enhanced rate reported when they added tetraphenylarsonium perchlorate or lithium perchlorate strongly supports a transition state with a charged alkyl carbon atom. The marked increase in the observed rates from silver

nitrate ($k_1'K_A=31 \text{ l s}^{-1} \text{ mol}^{-1}$) to silver perchlorate ($k_1'K_A=53 \text{ l s}^{-1} \text{ mol}^{-1}$) as catalyst supports a mechanistic route *via* a rate determining step with a positively charged intermediate as proposed. The perchlorate ion as a counter ion will be able to stabilize a positively charged transition state better than the nitrate ion. Songstad and Austad¹⁶ could not isolate any triphenylmethyl azide when ionic azide was added to the reaction medium. Thus a long lived and stable carbenium ion can be excluded.³³

The results reported in this paper suggest that the difficulties in preparing silver alkyl isocyanide complexes and in isolating alkyl isocyanides by applying silver compounds may be due to an isomerization of the isocyanide group which is catalyzed by the silver(I) ion. In other words, the initial product may be the desired complex or the alkyl isocyanide which then isomerizes to the corresponding cyanide in either case. One known exception to this is 4,4',4''-trinitrotriphenylmethyl isocyanide which can be obtained from the corresponding bromide and silver cyanide.³ Furthermore, the reported stability of diphenylmethyl isocyanide and 4,4'-dimethyldiphenylmethyl isocyanide prepared *via* onium dicyanoargentates³ suggests that the synthetic application of these silver salts is quite useful for alkyl substrates which do not readily ionize, or, when a silver complexing ion like ionic iodide is added to the reaction mixture.

Acknowledgement. The author is indebted to J. Songstad for fruitful discussions.

REFERENCES

1. Gautier, A. *Ann. Chim. (Paris)* 7 (1869) 203, 215, 233.
2. Hartley, E. G. A. *J. Chem. Soc.* 109 (1916) 1296.
3. Engemyr, L. B., Martinsen, A. and Songstad, J. *Acta Chem. Scand.* 28 (1974) 255.
4. Songstad, J., Stangeland, L. J. and Austad, T. *Acta Chem. Scand.* 24 (1970) 355.
5. Guilmard, H. *Ann Chim. Phys.* 14 (1908) 311.
6. Kornblum, N., Fishbein, L. and Smiley, R. A. *J. Am. Chem. Soc.* 77 (1955) 6261.
7. Kornblum, N., Smiley, R. A., Blackwood, R. K. and Iffland, D. J. *J. Am. Chem. Soc.* 77 (1955) 6269.
8. Kornblum, N., Willard, J. J. and Hardies, D. E. *J. Am. Chem. Soc.* 88 (1966) 1704.

9. Kornblum, N. and Hardies, D. E. *J. Am. Chem. Soc.* **88** (1966) 1707.
10. Kevill, D. N. and Pocker, Y. *J. Am. Chem. Soc.* **87** (1965) 4760.
11. Kevill, D. N. and Pocker, Y. *J. Am. Chem. Soc.* **87** (1965) 4771.
12. Kevill, D. N. and Pocker, Y. *J. Am. Chem. Soc.* **87** (1965) 4778.
13. Hammond, G. S., Hawthorne, M. F., Waters, J. H. and Greybill, B. N. *J. Am. Chem. Soc.* **82** (1960) 704.
14. Kevill, D. N. and Held, L. *J. Org. Chem.* **38** (1973) 4445.
15. Paquette, L. A. *Acc. Chem. Res.* **4** (1971) 280.
16. Austad, T. and Songstad, J. *Acta Chem. Scand.* **26** (1972) 3141.
17. Alexandrou, N. E. *J. Org. Chem.* **30** (1965) 1335.
18. Balasubrahmanyam, K. and Janz, G. J. *J. Am. Chem. Soc.* **92** (1970) 4189.
19. Austad, T., Songstad, J. and Stangeland, L. *J. Acta Chem. Scand.* **25** (1971) 2327.
20. Brederbeck, H., Gompper, R. and Theilig, G. *Chem. Ber.* **87** (1954) 537.
21. Austad, T., Songstad, J. and Åse, K. *Acta Chem. Scand.* **25** (1971) 331.
22. Luehrs, D. C., Iwamoto, R. T. and Kleinberg, J. *Inorg. Chem.* **5** (1966) 201.
23. Alexander, R., Ko, E. C. F., Mac, Y. C. and Parker, A. J. *J. Am. Chem. Soc.* **89** (1967) 3703.
24. Klages, F. and Moenkmeier, K. *Chem. Ber.* **85** (1952) 109.
25. Cotton, F. A. and Zingales, F. *J. Am. Chem. Soc.* **83** (1961) 351.
26. Minghetti, G., Flavio, B. and Massobrio, M. *Inorg. Chem.* **14** (1975) 1974.
27. Martinsen, A. *To be published.*
28. Casanova, Jr., J., Werner, N. D. and Schuster, R. E. *J. Org. Chem.* **31** (1966) 3473.
29. Vogler, A. In Ugi, I., Ed., *Isonitrile Chemistry*, Academic, New York 1971, p. 217.
30. Liskow, D. H., Bender, C. F. and Schaefer, III, H. F. *J. Chem. Phys.* **57** (1972) 4509.
31. Liskow, D. H., Bender, C. F. and Schaefer, III, H. F. *J. Am. Chem. Soc.* **94** (1972) 5178.
32. Yamada, S., Takashima, K., Sato, T. and Terashima, S. *Chem. Commun.* (1969) 811.
33. Martinsen, A., Austad, T. and Songstad, J. *Acta Chem. Scand.* **29** (1975) 661.

Received May 6, 1976.

The Crystal Structure of Magnesium *p*-Nitrosophenolate Hexahydrate. The Influence of Hydrogen Bonding on Conjugation in the *p*-Nitrosophenolate Ion

H. J. TALBERG

Department of Chemistry, University of Oslo, Oslo 3, Norway

The crystal structure of magnesium *p*-nitrosophenolate hexahydrate, $\text{Mg}(\text{C}_6\text{H}_4\text{O}_2\text{N})_2 \cdot 6\text{H}_2\text{O}$, has been determined from X-ray diffraction data collected at -165°C and refined by least squares methods.

The space group is $P2_1/c$ with cell dimensions $a = 10.579(1) \text{ \AA}$, $b = 6.242(1) \text{ \AA}$, $c = 13.198(3) \text{ \AA}$ and $\beta = 106.97(1)^\circ$ at -165°C . The final R factor was 3.7 % and the estimated standard deviations in bond lengths are about 0.001 \AA and in angles 0.1° .

In the anion the C-N, C-O and N-O bond lengths differ about 0.020 \AA and the C-C bond lengths differ from 0.005 to 0.012 \AA from corresponding bonds in the sodium salt. The anion has a less pronounced *p*-quinonoid character in the present structure than in the sodium salt. This is probably due to a greater, respectively lesser, ability of the crystal field in stabilizing charge in the phenoxide-oxygen atom than in the nitroso-oxygen atom in the title compound and the sodium salt.

The anions in the two salts are compared as to gross atomic populations determined from both INDO calculations and by *L*-shell refinement. Also, the two anions are compared by difference syntheses. Finally, some features of the UV and UV-KCl spectra of the title compound, the sodium and the potassium salt are discussed.

The present structure determination of magnesium *p*-nitrosophenolate hexahydrate (I) is part of a series of structural investigations of *C*-nitroso compounds and oximes derived from these. Previously the tautomeric isomer of *p*-nitrosophenol, *p*-benzoquinone monoxime (II), and the salts potassium *p*-nitrosophenolate monohydrate (III) and sodium *p*-nitrosophenolate trihydrate (IV) have been investigated.¹⁻³

A characteristic feature of oximidoketones like (II) is the diversity in colour shown by the salts obtained from alkaline solutions.⁴ In the present case (III) is green, (IV) is red while (I) is reddish green. Seventy years ago Hantzsch attributed the diversity in colour to structural differences in the anion;⁴ salts having the characteristic blue or green colour of *C*-nitroso compounds should comprise anions having a "nitroso-phenoxide" structure $\text{O}=\text{N}-\text{C}=\text{CH}-\text{CH}=\text{C}-\text{O}^-$, colourless salts should comprise anions having an "oxime-ketone" structure $^- \text{O}-\text{N}=\text{C}-\text{CH}=\text{CH}-\text{C}=\text{O}$ while red salts should comprise anions having the formal charge delocalized to both oxygen atoms.

Unfortunately the poor crystal quality prevented high accuracy in the structure investigation of (III);³ consequently the question whether the anion has a less predominant *p*-quinonoid (or "oxime-ketone") structure in the green potassium salt than in the red sodium salt could not be answered. However, the differences in hydrogen bonding to and coordination about the phenoxide oxygen atom and the nitroso group atoms in the two salts indicate that this is actually the case.

As the reddish green magnesium salt forms crystals of high quality and shows characteristic differences from both the potassium and the sodium salt in the UV, UV-KCl, and IR-KBr spectra it was decided to determine the structure of this salt in order to compare the anion structure with that found in (IV).

EXPERIMENTAL

Well-formed tabular crystals were grown by evaporation of an aqueous solution prepared by adding *p*-benzoquinone monoxime (purified by sublimation) to 0.004 M magnesium carbonate. Traces of unsolved magnesium carbonate were present during the evaporation. A preliminary film investigation showed systematic absences consistent with the space group $P2_1/c$. Determination of unit cell parameters and intensity measurements were done using a crystal of dimensions $0.55 \times 0.40 \times 0.08$ mm. The crystal was mounted with the *b* axis tilted somewhat away from the goniometer spindle axis.

All measurements were made on a SYNTEX $P\bar{1}$ diffractometer with graphite monochromatized $MoK\alpha$ radiation and equipped with an Enraf-Nonius liquid nitrogen cooling device (modified by H. Hope). The temperature at the crystal site was -165°C . Cell constants were determined by least squares treatment of measurements of 15 general reflections. Three-dimensional data were collected using the $\omega-2\theta$ scan technique. The scan speed varied between 2.0 and $6.0^\circ/\text{min}$, and the total time for background counts at the scan limits $2\theta(\alpha_1) - 0.8^\circ$ and $2\theta(\alpha_2) + 1.0^\circ$ was 0.7 of the time of integration. A quadrant of reciprocal space was examined. All reflections having 2θ less than 45° were measured; between 45 and 70° only reflections having integrated counts larger than a preset value during a 2 s scan over the peak were measured. The intensity of three test reflections measured for every 50 reflections showed no significant change during the measurements. Out of 3254 unique reflections 2884 had intensities larger than $2.5\sigma(I)$. They were regarded as observed. $\sigma(I)$ is the estimated standard deviation of the intensity based on counting statistics adding 1% uncertainty due to experimental fluctuations. The atomic scattering factors for the heavy atoms were those of Doyle and Turner⁵ and for hydrogen those of Stewart *et al.*⁶ Core and valence electron scattering factors used in an *L*-shell refinement were those given by Stewart.⁷ All programs except for the ORTEP program⁸ and the MULTAN program⁹ applied during the structure investigation are described in Ref. 10. The UV spectra were recorded on a CARY MODEL 14 spectrophotometer with variable slit and a scan speed of 7 \AA s^{-1} .

CRYSTAL DATA

Magnesium *p*-nitrosophenolate hexahydrate, $Mg(C_6H_4O_2N)_2 \cdot 6H_2O$, space group $P2_1/c$ (No. 14). Dimensions of the unit cell at -165°C : $a = 10.579(1) \text{ \AA}$, $b = 6.242(1) \text{ \AA}$, $c = 13.198(3) \text{ \AA}$ and $\beta = 106.97(1)^\circ$. $V = 834.1 \text{ \AA}^3$, $M = 376.61$,

$$F(000) = 396, D_{\text{calc}}(-165^\circ\text{C}) = 1.499 \text{ g cm}^{-3}$$

$$\mu = 0.175 \text{ mm}^{-1}.$$

STRUCTURE DETERMINATION

The structure was solved by direct methods^{9,10} and refined by full-matrix least-squares technique. Initial positional parameters for all hydrogen atoms were calculated from stereochemical considerations. The final refinement including all atoms and all the observed reflections converged with a conventional *R* factor of 0.037, a weighted R_w factor of 0.039 and a goodness of fit *S* of 2.9. Using 2266 reflections with $\sin \theta/\lambda$ greater than 0.45 the refinement yielded $R = 0.034$, $R_w = 0.032$ and $S = 1.9$. The scale factor increased from 0.138(1) to 0.144(2) and the e.s.d.'s in the bond lengths changed from 0.0012–0.0015 to 0.0010–0.0012 \AA . Further, and as with the sodium salt, (IV), all the C–C bonds and the C–N bond lengthened while the C–O and the N–O bond shortened. The change was 2.5σ in the

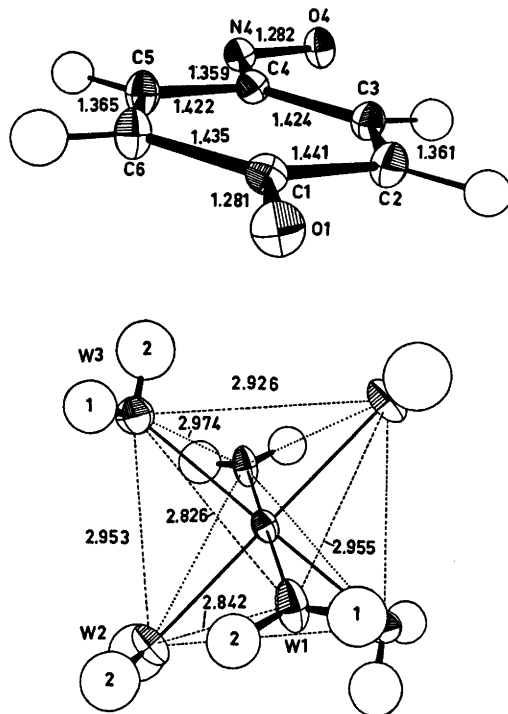


Fig. 1. 50% probability ellipsoids and numbering of atoms. a, anion; b, cation.

Table 1. Fractional atomic coordinates and thermal parameters ($\times 10^5$) for nonhydrogen and ($\times 10^3$) for hydrogen atoms. The anisotropic temperature factors are expressed as: $\exp -2\pi^2(U_{11}h^2a^{*2} + U_{22}k^2b^{*2} + U_{33}l^2c^{*2} + 2U_{12}hka^*b^* + 2U_{13}hla^*c^* + 2U_{23}klb^*c^*)$. Estimated standard deviations in parentheses.

Atom	<i>x</i>	<i>y</i>	<i>z</i>	U_{11}	U_{22}	U_{33}	U_{12}	U_{13}	U_{23}
Mg	0	0	0	101(2)	107(2)	177(2)	-7(2)	40(2)	-2(2)
OW1	2664(08)	29248(14)	6881(07)	148(4)	146(4)	332(5)	-33(3)	120(3)	-65(3)
OW2	19964(08)	-5706(15)	7140(07)	121(3)	146(4)	324(5)	-1(3)	20(3)	-4(3)
OW3	4430(08)	10932(14)	-13459(07)	194(4)	194(4)	194(4)	-70(3)	42(3)	5(3)
O1	13302(07)	-196(13)	33154(06)	124(3)	184(4)	202(3)	8(3)	57(3)	-2(3)
O4	73858(07)	215(13)	39652(07)	134(3)	171(4)	320(4)	-12(3)	65(3)	-12(4)
N4	65944(09)	-15194(15)	39917(07)	136(4)	161(4)	197(4)	8(3)	46(3)	-7(3)
C1	25619(10)	-3547(16)	34462(08)	133(4)	150(5)	137(4)	0(3)	41(3)	-9(3)
C2	34171(10)	13652(17)	33306(09)	152(4)	136(4)	207(5)	15(4)	58(4)	22(4)
C3	47353(10)	10402(18)	35045(08)	137(4)	141(4)	189(5)	-1(4)	50(4)	11(4)
C4	52935(10)	-10264(17)	37921(08)	122(4)	141(4)	156(4)	14(3)	41(3)	-6(4)
C5	44497(11)	-27516(18)	38709(09)	169(5)	128(4)	247(5)	18(4)	72(4)	10(4)
C6	31267(11)	-24470(18)	37035(09)	162(4)	134(4)	250(5)	-7(4)	81(4)	7(4)

Atom	<i>x</i>	<i>y</i>	<i>z</i>	<i>B</i>	Atom	<i>x</i>	<i>y</i>	<i>z</i>	<i>B</i>
H2	301(1)	279(2)	316(1)	1.5(2)	H3	529(1)	217(2)	342(1)	1.8(2)
H6	257(1)	-358(2)	378(1)	2.1(3)	H5	488(1)	-415(2)	404(1)	1.8(2)
H1W1	-20(2)	343(3)	92(1)	2.9(3)	H2W1	92(2)	358(3)	77(1)	2.4(3)
H1W2	231(2)	-175(3)	78(1)	4.6(4)	H2W2	253(2)	48(3)	87(1)	4.0(4)
H1W3	-10(2)	87(3)	-189(1)	3.7(4)	H2W3	74(2)	231(3)	-146(1)	2.6(3)

C—O bond length and 3.5σ in the C2—C3 bond length. A list of structure amplitudes is available from the author. Final parameters from the refinement with all the observed reflections are given in Table 1.

Magnitudes and directions of the principal axis of the vibrational ellipsoids are indicated in Fig. 1. The r.m.s. discrepancy between the atomic vibrational tensor component obtained in the structure determination and those calculated from a rigid body analysis was 0.0006 Å² in the anion. The translational r.m.s. amplitudes of vibration along the principal axes are 0.12, 0.11, and 0.11 Å and the r.m.s. librational amplitudes are 4.7, 2.0, and 1.4°. The largest increase in bond lengths was 2.7σ when adjusting the coordinates according to this libration.

Bond lengths and angles with their estimated standard deviations calculated from the correlation matrix are given in Table 2. Deviations from a least-squares plane through the benzene ring atoms are given in Table 3.

The final difference Fourier or X—X map of the anion in the benzene ring plane is shown

in Fig. 7. A similar map for the sodium salt is also shown.

In both cases the synthesis was calculated using the reflections having $\sin \theta/\lambda$ less than 0.45 and positional and temperature parameters from the refinement with the reflections having $\sin \theta/\lambda$ greater than 0.45. The scale factor used was from a refinement with reflections at $\sin \theta/\lambda$ less than 0.45 and with the other parameters fixed at their "high" angle values. This choice of scale factor is justified *a posteriori* by the reasonable appearance of the maps.^{11a}

Both the electron density in (0.15–0.50 e Å⁻³) and the position of (in the middle of the bonds and in lone pair positions) the well defined and sharp residual peaks are in good conformity with what has been found in very accurate work with other organic compounds.^{11a}

Thus, it seems reasonable to assume only small systematic errors in the intensities. A normal probability plot using observed and calculated structure factors shows absence of systematic errors not absorbed by the models.^{11b}

An *L*-shell refinement⁷ of the anionic atoms

Table 2. Bond lengths (Å) and angles (°). Estimated standard deviations in parentheses. Differences in length and angle value between corresponding bonds and angles in (I) and (IV) are also given. Bond lengths in the anion. Values obtained in refinement with all observed reflections are given on the first line and libration corrected bond lengths from the same refinement are given on the second line, while values obtained in a refinement using only reflections with $\sin \theta/\lambda$ greater than 0.45 are given on the third line.

	(I)	(I)–(IV)		(I)	(I)–(IV)
O1–C1	1.2807(12)	0.0221(17)	C3–C4	1.4235(15)	–0.0051(21)
	1.2816	0.0221		1.4273	–0.0044
	1.2770(10)	0.0216(16)		1.4247(11)	–0.0064(16)
O4–N4	1.2823(12)	–0.0208(16)	C4–C5	1.4218(15)	–0.0066(21)
	1.2856	–0.0196		1.4256	–0.0052
	1.2811(11)	–0.0176(15)		1.4240(12)	–0.0053(18)
N4–C4	1.3589(13)	0.0187(18)	C5–C6	1.3651(15)	0.0075(21)
	1.3600	0.0188		1.3662	0.0076
	1.3594(11)	0.0184(16)		1.3681(12)	0.0085(18)
C1–C2	1.4405(15)	–0.0089(21)	C6–C1	1.4351(15)	–0.0120(21)
	1.4445	–0.0074		1.4388	–0.0113
	1.4449(12)	–0.0067(18)		1.4378(12)	–0.0133(18)
C2–C3	1.3608(15)	0.0072(21)	sum of differences:		0.0021(59)
	1.3619	0.0072			0.0078
	1.3675(12)	0.0098(18)			0.0090(49)

Bond angles in the anion

	(I)	(I)–(IV)
O1–C1–C2	120.7(1)	–0.4(1)
O1–C1–C6	121.1(1)	–0.8(1)
C6–C1–C2	118.2(1)	1.3(1)
C1–C2–C3	121.0(1)	–0.8(1)
C2–C3–C4	120.3(1)	–0.3(1)
C3–C4–C5	119.0(1)	0.5(1)
C4–C5–C6	121.2(1)	–0.3(1)
C5–C6–C1	120.1(1)	–0.7(1)
C3–C4–N4	125.1(1)	0.3(1)
C5–C4–N4	115.9(1)	–0.8(1)
C4–N4–O4	117.2(1)	0.1(1)

Distances in the $\text{Mg}(\text{H}_2\text{O})_6^{2+}$ ion

Mg···OW1(a)	2.0218
Mg···OW2(a)	2.0770
Mg···OW3(a)	2.0801
OW1(a)···OW2(a)	2.8416(12)
OW1(a)···OW2(b)	2.9546(12)
OW1(a)···OW3(a)	2.9735(12)
OW1(a)···OW3(b)	2.8262(12)
OW2(a)···OW3(a)	2.9264(12)
OW2(a)···OW3(b)	2.9526(12)

Distances and angles involving hydrogen atoms

	O–H	H···O(N)	O···O(N)	O–H···O(N)	H–O–H
OW1–H1···O1(c)	0.73(2)	2.02(2)	2.743(1)	173.6(1.8)	113.7(1.7)
OW1–H2···O4(d)	0.79(2)	1.94(2)	2.726(1)	175.3(1.6)	
OW2–H1···O4(e)	0.80(2)	2.05(2)	2.831(1)	156.2(1.3)	117.7(1.7)
OW2–H2···N4(d)	0.85(2)	2.08(2)	2.904(1)	165.1(1.7)	
OW3–H1···O1(f)	0.79(2)	2.02(2)	2.807(1)	172.8(1.9)	101.8(1.6)
OW3–H2···O1(g)	0.85(2)	1.86(2)	2.708(1)	178.1(1.5)	
	C–H		C–C–H		C–C–H
C2–H	0.98(1)	C1–C2–H	116.9(8)	C4–C5–H	115.3(8)
C3–H	0.95(1)	C3–C2–H	122.0(8)	C6–C5–H	123.5(8)
C5–H	0.98(1)	C2–C3–H	120.7(8)	C5–C6–H	121.3(9)
C6–H	0.95(1)	C4–C3–H	118.9(8)	C1–C6–H	118.5(9)

Table 2. Continued.

Other intermolecular contacts		Dihedral angles in the anion	
OW1...OW1(f)	3.120	C3-C4-N4-O4	3.4(2)
		C5-C4-N4-O4	-177.5(1)
		C2-C1-O1(f)...OW3	98.6(1)
		C2-C1-O1(g)...OW3	-26.6(1)
		C2-C1-O1...OW1	-148.6(1)
		C5-C4-N4...OW2	-9.6(1)
		C4-N4-O4...OW2	-13.9(1)
		C4-N4-O4...OW1	-167.1(1)
Symmetry codes			
(a): x	y	z	(b): $-x$
(d): $-x+1$	$y-\frac{1}{2}$	$\frac{1}{2}-z$	(e): $-x+1$
(g): x	$-y+\frac{1}{2}z-\frac{1}{2}$		(f): $-x-y+1$
			$-z$

Table 3. Atomic coordinates, l, m , and deviations, n , of atoms from a least-squares plane through the benzene ring atoms C1, C2, C3, C4, C5, and C6. The coordinate system is orthogonal and its unitary vectors L, M, and N (with a length of 1 Å) are defined by the following equations:

$$\begin{aligned} \mathbf{L} &= -0.0271\mathbf{a} - 0.1486\mathbf{b} + 0.0128\mathbf{c} \\ \mathbf{M} &= -0.0936\mathbf{a} + 0.0490\mathbf{b} - 0.0147\mathbf{c} \\ \mathbf{N} &= 0.0164\mathbf{a} + 0.0342\mathbf{b} + 0.0768\mathbf{c} \end{aligned}$$

The origo, which is the center of gravity, has coordinates $x=0.3931$, $y=0.9304$ and $z=0.3608$. N is normal to the plane.

	l	m	n
C1	0.2348	1.3972	0.0171
C2	-1.1038	0.8657	-0.0111
C3	-1.3258	-0.4768	-0.0041
C4	-0.2311	-1.3864	0.0135
C5	1.0942	-0.8720	-0.0073
C6	1.3318	0.4723	-0.0080
O1	0.4346	2.6616	0.0550
O4	-1.5236	-3.2321	0.1024
N4	-0.3411	-2.7408	0.0330
H2	-1.842	1.516	0.013
H3	-2.208	-0.822	-0.038
H5	1.805	-1.547	-0.039
H6	2.213	0.816	0.008

using the reflections having $\sin \theta/\lambda$ less than 0.65 \AA^{-1} yielded $R=0.041$ and $R_w=0.042$ for the present structure and $R=0.037$ and $R_w=0.040$ for the sodium salt structure. The R factors from a normal refinement on the same data sets were not different from those of the refinement with all data. The adjusted 7 gross atomic populations are listed in Table 4 together with results from INDO 12 calculations.

Acta Chem. Scand. A 31 (1977) No. 1

DISCUSSION

Interionic structural features. A general view of the structure is shown in Fig. 2. The structure comprises separate $\text{Mg}(\text{H}_2\text{O})_6^{2+}$ ions with the magnesium atom located in the inversion centres at $x=0$. Consequently, there are only three independent water molecules (as in (IV)). The cation structure resembles closely that usually found in the magnesium aquo ions; *i.e.* a regular octahedral coordination and an average length of the coordination contacts of 2.05 \AA .¹³ The W1 and W2 water molecules belong to Class 1, type D of Ferraris and Franchini-Angela (see Ref. 13) having e_1 values *i.e.* values of the angle between the coordination contact direction and the plane of the water molecule, of 3 and 7°, respectively. Probably

Table 4. Gross atomic populations. Estimated standard deviations are given in parentheses. The INDO calculations were performed using the l and m coordinates in Table 3 as input parameters ($n=0$). INDO calculations using coordinates for the anion in (IV) as input parameters yielded nearly identical results.

Atom	(I)	(IV)	INDO
O1	8.39(3)	8.36(3)	8.55
O4	8.31(3)	8.33(3)	8.38
N4	7.27(3)	7.20(3)	6.98
C1	5.90(3)	5.91(4)	5.70
C2	6.05(4)	6.01(4)	6.15
C3	5.84(4)	5.92(4)	5.94
C4	6.06(4)	6.02(4)	6.06
C5	5.95(4)	5.94(4)	5.95
C6	5.97(4)	5.93(4)	6.16

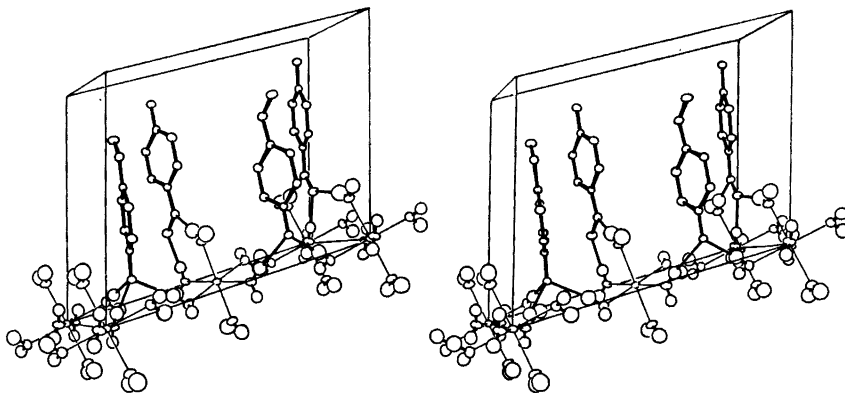


Fig. 2. A stereoscopic illustration of the structure. Anion hydrogen atoms are not shown for clarity.

the $W3$ molecule is a Class 1', type J water molecule as e_1 is 32° in this case.

All the six water protons are engaged in hydrogen bonding to anion atoms. The length of the $O \cdots H - OW$ bonds are in the usual range,¹³ the average value being 2.76 Å.

Fig. 3 shows the coordination about the anion terminal atoms in (I) and (IV).³ In both structures there are six contacts to the anion; *i.e.* one for each lone pair. The nitroso group atoms are acceptors in four hydrogen bonds in (IV)³ and three in the present structure. However, the nitrogen atom is an acceptor in both structures. On the other hand the phenoxide oxygen atom accepts only one hydrogen atom in (IV) and even three in (I). The coordination around $O4$ is tetrahedral in (IV) and trigonal in (I) whereas the opposite is the case for $O1$. Apparently the ability of the crystal field to stabilize negative charge is greater at $O1$ than at $O4$ as to the title compound and less so at $O1$ than at $O4$ as to the sodium salt. Thus, the contribution of the "oxime-ketone" or *p*-quinonoid VB structure to resonance in the anion should be expected to be less in (I) than in (IV).

The p-nitrosophenolate ion. A comparison between bond lengths in (I) and (IV) clearly shows that the above expectation is realized. The C–O and the C–N bond is about 0.020 Å longer and the N–O bond 0.021 Å shorter in (I) than in (IV). Accordingly, the C–C "double" bonds are 0.007 Å longer and the C–C "single" bonds from 0.005 to 0.012 Å shorter in (I) than

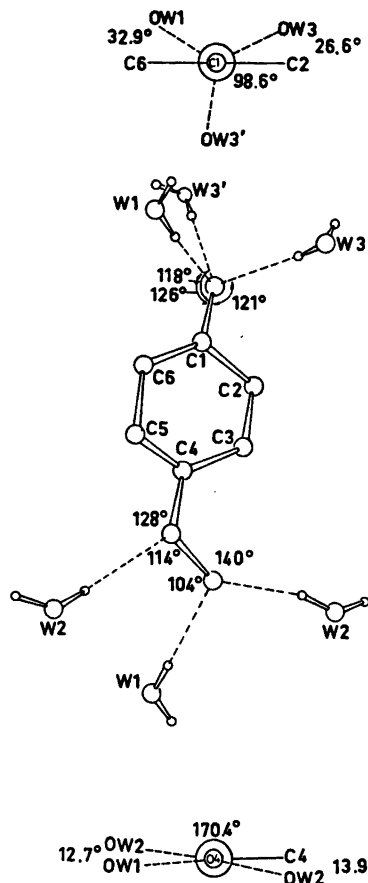


Fig. 3. The coordination about the anion.

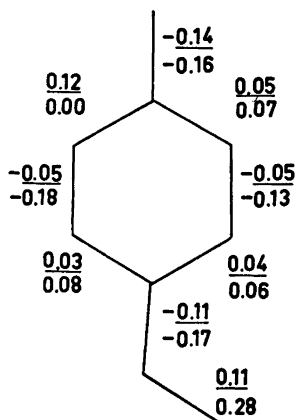


Fig. 4. Differences between "observed" bond orders. The underlined figures are the differences between the anion in (I) and the anion in (IV), while the other figures are the differences between (IV) and the acid (II).

in (IV). All the differences but that of the C3 - C4 bond are significant.

Craven *et al.*¹⁴ have found that when the exocyclic C-O bonds in the barbiturates are engaged in a hydrogen bond, this bond is lengthened by approximately 0.010 Å. A shift in the C-O bond in the *p*-nitrosophenolate ion about twice this value may be caused by

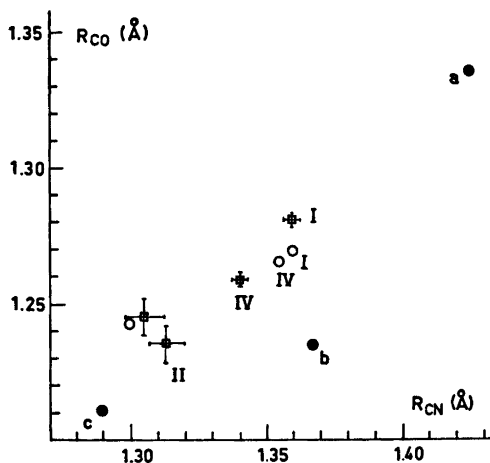


Fig. 5. A plot of the C-O bond length against the C-N bond length in (I), (II), (IV), *p*-nitrosophenol (a), anion (b), and *p*-benzoquinone monoxime (c). □, observed point (2.5σ indicated with bars); ○, calculated point (CNDO/2); ●, calculated point (MINDO/3).

several factors. First, and perhaps most important, is the fact that the nitroso oxygen atom is less engaged in hydrogen bonding in (I) than in (IV). This has probably a similar, but of course smaller, lengthening effect on the C-O bond as that caused by ionization. Further, a sodium ion contact has been replaced by a hydrogen bond. A sodium ion contact may probably be considered less effective in lengthening the bond than hydrogen bonding, as a lithium ion contact is considered about as effective as a hydrogen bond in this respect.¹⁵ Finally, the change from a trigonal to a tetrahedral coordination may induce a slight shift in the hybridization of the phenoxide oxygen atom. The minor changes in conjugation in the ring is probably mainly caused by the transfer of charge between the oxygen atoms.

This analysis indicates that the change in the N-O bond length is about the same as

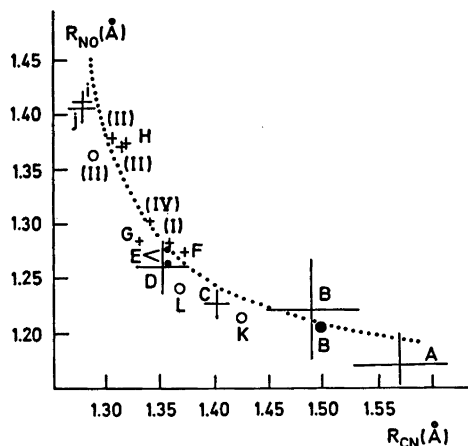


Fig. 6. A plot of the N-O bond length against the C-N bond length in the *C*-nitroso compounds whose structure is determined with some accuracy and in some selected oximes. Names and references for the compounds A, B, C, D, and G are given in Table 5 in Ref. 3, E is tetramethylammonium benzonitrosolate;²¹ F, *N,N,N',N'*-tetramethyl-4-nitroso-1,3-phenylenediamine;²² H, i, and j are the references 3, 14 and 13 in Ref. 1; K, *p*-nitrosophenol and L, *p*-nitrosophenolate. The graph is for $R_{NO} - R_{NO}^0 = k / (R_{CN}^0 - R_{CN}^0)$ with $R_{NO}^0 = 1.150$ Å, $R_{CN}^0 = 1.233$ Å and $k = 0.016$ Å². CNO angles (°): A, 121(2); B, 113(1) and 113.0; C, 115(1); D, 116; E, 117; F, 116.3(2); (I), 117.2(1); (IV), 117.1(1); G, 116.4(1); H, 111.7(2); (II), 112.3(2); (II), 112.8(2) and 112.3; i, 112.0(2); j, 110.2(2) and 110.7(2); K, 113.0; L, 117.1.

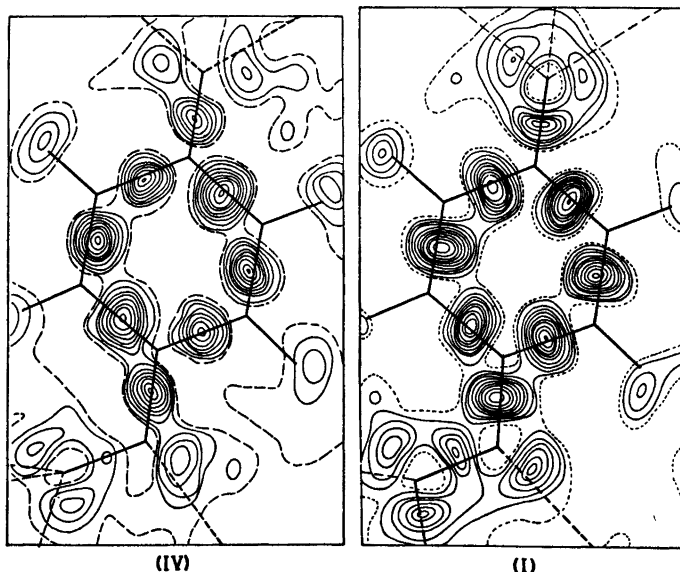


Fig. 7. Final difference Fourier syntheses in the least-squares plane through the benzene ring atoms in (I) and (IV). The dotted line runs through points of $0.0 \text{ e } \text{Å}^{-3}$, and the differences between the contours are $0.05 \text{ e } \text{Å}^{-3}$.

Table 5. Wave length ($m\mu$) of some transitions in the UV and UV-KCl absorption spectra of (I), (II), (III) and (IV) and the number of hydrogen bonds to the nitroso group atoms, n , and to the phenoxide oxygen atom, m . Molecular extinction coefficients are shown in parentheses.

Compound in the solid state	Nitroso band ($n_{\text{NO}^- - \pi^*}$)		2nd band (charge transfer band, $\pi - \pi^*$)		3rd band ($\pi - \pi^*$)	
	λ_{max} (e)	n	λ_{max} (KCl) (log e)	m	λ_{max} (KCl) (log e)	
(II)			305 (strong) or 360 (weak)	1		
(IV)	535	4	354	1	260	
(I)	560	3	387	3	255	
(III)	610	1?	337	1	265	
Compound in solution						
(II) in water			310	(3.9)		
(I), (III), (IV) in water	500	(100)	400	(4.2)	255	(3.7)
(III) in acetone	610	(35)	410	(4.2)		
<i>p</i> -nitrosophenol in water	735	(35)				

in the C-O bond length towards a similar change in the environment.

A shift in the resonance equilibrium between the two main VB structures is more directly expressed by changes in bond orders than by

changes in bond lengths. Fig. 4 shows the bond order differences between (I) and (IV). The bond orders are calculated using a linear bond order-bond length relationship.¹⁶ The differences between (IV) and the acid (II) is shown

for comparison. The differences are fairly consistent with a decrease in the weight of the *p*-quinonoid VB structure from 83 % in the acid (II) to 55 % in (IV) to 44 % in (I).

In Fig. 5 the C–O bond length is plotted against the C–N bond length in (II), (IV) and (I). Some calculated points are also shown; both CNDO/2¹⁷ calculations using the *l* and *m* coordinates in Table 3 as input parameters ($n=0$), and MINDO/3¹⁸ calculations with bond length and angle optimization (fixing the CNO angle at the observed value and the C–H bond length at 1.0 Å) have been performed. The plot indicates roughly a linear relationship between the two bond lengths. Evidently the change in conjugation caused by a slight change in the environment is comparable with that caused by ionization.

A plot of C–N bond lengths against N–O bond lengths is shown in Fig. 6. Apparently a hyperbola having asymptotes at $R_{\text{NO}}=1.150$ Å and $R_{\text{CN}}=1.233$ Å might pass through nearly all the indicated areas formed by an 2.5σ uncertainty allowance in the bond lengths. Thus, in those compounds having the largest conjugation over the CNO fragment the sum of the C–N and the N–O bond lengths appears to be less than elsewhere along the curve. According to VSEPR theory¹⁹ this should promote larger CNO angles in these compounds than in the other. The values observed seem to indicate that this expectation is realized to some extent.

A value of $117.1(1)^\circ$ for the CNO angle in the present structure is in good conformity with the values found in the compounds having a similar degree of conjugation over the CNO fragment. In nitrosates the angles are in the range 116 – 117° . Other factors may also influence this angle and hydrogen bonding is probably of particular importance. It is therefore surprising that all anion bond angles *but* the CNO angle are significantly different from those of the anion in (IV). The differences are shown in Table 2. As to the benzene ring angles, the angle at C1 and C4 is larger while the other angles are smaller in (I) than in (IV). It appears that $\Delta C1 \sim -2\Delta C2 \sim -2\Delta C6$ and $\Delta C4 \sim -2\Delta C3 \sim -2\Delta C5$, Δ denoting the C–C–C angle differences. Whereas the average benzene ring angle differs 1.7° from 120° in (IV) it differs only

0.9° from 120° in the present structure. This is in accordance with the change in bond lengths towards a more benzenoid (or “nitroso-phenoxide”) structure when passing from (IV) to (I).

The anion has the same weakly expressed boat form as in (IV) although to a somewhat greater extent.

The charge distribution in the anion. This subject has previously been discussed to some extent.³ The *L*-shell refinement gives adjusted gross atomic populations that lend support to the result of the CNDO/2 and the INDO calculations of a nearly equal distribution of negative charge between the two oxygen atoms. Further there is a rather good accordance between theory and experiment as to the charge distribution in the benzene ring. The comparison is made in Table 4. Comparing (I) and (IV) one detects a striking resemblance between the two anions. The differences are in the range 0.01 – 0.08 e and far from significant.

The UV and UV-KCl absorption spectrum of the p-nitrosophenolate ion. The λ_{max} values for the three transitions of least energy of the anion in the three salts and in water and acetone solution are given in Table 5. Some values for the acid (II) and its tautomer are shown for comparison.

Generally the spectrum bear strong resemblance with that of other *p*-substituted nitrosobenzenes.²⁰ However, contrary to what has been found for these the weak $n_{\text{NO}^-} - \pi^*$ transition seems not to be coupled with the 2nd transition so that a blue shift in the first follows a red shift in the second. CNDO/2 calculations on *isolated* species indicate that the more the “oximeketone” or *p*-quinonoid structure dominates the longer the wave length of the second ($\pi - \pi^*$) transition and the shorter the wave length of the weak transition.

The two transitions are also strongly dependent upon the crystal field. It is interesting to note that the weak transition gets an increasing blue shift when the number of hydrogen bonds to the nitroso group atoms increases. The diversity in colour is then probably caused both by hydrogen bonding *per se* and the shift it induces in the resonance equilibrium between the two main VB structures.

REFERENCES

1. Talberg, H. J. *Acta Chem. Scand. A* 28 (1974) 910.
2. Talberg, H. J. *Acta Chem. Scand. A* 28 (1974) 593.
3. Talberg, H. J. *Acta Chem. Scand. A* 29 (1975) 919.
4. Hantzsch, A. *Ber. Dtsch. Chem. Ges.* 42 (1909) 966.
5. Doyle, P. A. and Turner, P. S. *Acta Crystallogr. A* 24 (1970) 2232.
6. Stewart, R. F., Davidson, E. R. and Simpson, W. T. *J. Chem. Phys.* 42 (1965) 3175.
7. Stewart, R. F. *J. Chem. Phys.* 53 (1970) 205.
8. Johnson, C. K. *ORTEP*, Report ORNL-3795, Oak Ridge National Laboratory, Oak Ridge 1965.
9. Germain, G., Main, P. and Woolfson, M. M. *Acta Crystallogr. A* 27 (1971) 368.
10. Groth, P. *Acta Chem. Scand.* 27 (1973) 1837.
11. a. Griffin, J. F. and Coppens, P. *J. Am. Chem. Soc.* 97 (1975) 3496; b. Abrahams, S. C. and Keve, E. T. *Acta Crystallogr. A* 27 (1971) 157.
12. Pople, J. A., Beveridge, D. L. and Dobosh, P. A. *J. Chem. Phys.* 47 (1967) 2026.
13. Ferraris, G. and Franchini-Angela, M. *Acta Crystallogr. B* 28 (1972) 3572.
14. Craven, B. M., Cusack, C., Gartland, G. L. and Vizzini, E. A. *J. Mol. Struct.* 16 (1973) 331.
15. Enders-Beumer, A. and Harkema, S. *Acta Crystallogr. B* 29 (1973) 682.
16. Stals, J. *Rev. Pure Appl. Chem.* 20 (1970) 1.
17. Pople, J. A. and Segal, G. A. *J. Chem. Phys.* 44 (1966) 3289.
18. Bingham, R. C., Dewar, M. J. S. and Lo, D. H. *J. Am. Chem. Soc.* 97 (1975) 1285.
19. Gillespie, R. J. *J. Chem. Educ.* 47 (1970) 18.
20. Nakamoto, K. and Rundle, R. E. *J. Am. Chem. Soc.* 78 (1956) 1117.
21. Vetter, G., Kopf, J. and Klar, G. *Z. Naturforsch. B* 28 (1973) 293.
22. Talberg, H. J. *Acta Chem. Scand. A* 30 (1976) 829.

Received June 1, 1976.

The Coefficients for Isothermal Transport. I. Cation Exchange Membrane and Electrodes Reversible to a Common Anion

KATRINE SEIP FØRLAND,^a TORMOD FØRLAND^b and SIGNE KJELSTRUP RATKJE^{c*}

^a Laboratory of Inorganic Chemistry, The Norwegian Institute of Technology, The University of Trondheim, N-7034 Trondheim-NTH, Norway, ^b Laboratory of Physical Chemistry, The Norwegian Institute of Technology, The University of Trondheim, N-7034 Trondheim-NTH, Norway and ^c Department of Chemistry, The University of Trondheim, N-7000 Trondheim, Norway

Isothermal transport processes across a membrane, placed between anion reversible electrodes, is described by a set of relations between fluxes and forces. The fluxes are transfer of neutral components and current. The forces are gradients in chemical potential for the neutral components, and a gradient in electric potential that can be measured between defined electrodes. Thus the presentation deals only with measurable quantities. The number and kind of components used to describe the system, conform with the phase rule. The forces used in the flux equations are therefore independent.

Restrictions of the system, such as the selectivity of the electrodes and of the membrane, and the charge of the ions composing the salts, lead to relations between the transport coefficients in addition to the Onsager reciprocal relations.

Methods for experimental determination of the transport coefficients are discussed.

1. INTRODUCTION

Irreversible thermodynamics is used for describing transport processes in membranes in various contexts.^{1–10} When treating electrolyte solutions, commonly single ion components are used. The basic fluxes and forces are ionic fluxes and gradients in electrochemical potential of ions, and the electric current is expressed as the sum over all charges carried by the ionic fluxes.^{3–5} General thermodynamic objections can be raised to the definitions of single ion quantities, and thus to their use.

* Present address: Laboratory of Physical Chemistry, The Norwegian Institute of Technology, The University of Trondheim, N-7034 Trondheim-NTH, Norway.

An alternative treatment considering only measurable quantities, presented previously,¹ is used in a wider context in this paper. The components of the system are the components in terms of the phase rule, and the electric current is treated as one of the basic fluxes of the system. In this way a more exact and general description of the transport processes is obtained. The physical interpretations of the coupling phenomena on this basis are limited to the macroscopic phenomenological level.

The importance of the analysis is seen when the description of the transport processes is developed for a cation exchange membrane placed between anion reversible electrodes. New information about the phenomenological coefficients is then obtained. Finally experimental conditions consistent with the theoretical treatment are outlined.

2. TRANSPORTS IN AN ION EXCHANGE MEMBRANE PLACED BETWEEN ELECTRODES REVERSIBLE TO A COMMON ANION

The system considered consists of two solutions separated by a cation exchange membrane and an anion reversible electrode in each solution. Each solution contains two electrolytes with a common anion. In our example the electrolytes are HCl and NaCl, and Ag/AgCl electrodes are used. The system is illustrated in Fig. 1.

The system is assumed to be isothermal. Any enthalpy change by the transport across

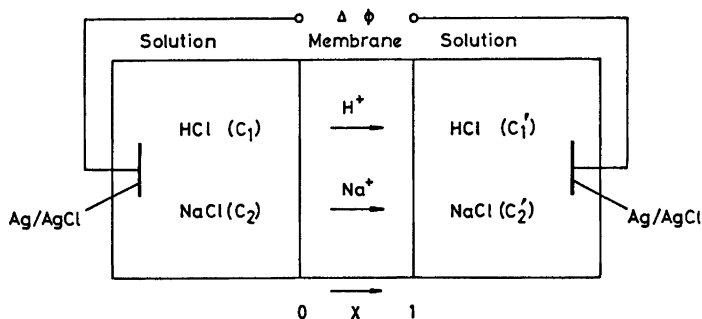
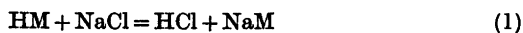


Fig. 1. A cation exchange membrane separating two solutions of HCl and NaCl. The electrodes are reversible to the Cl^- ion.

the electrolyte-membrane phase boundary is assumed to have no significant effect on the mass fluxes, *i.e.* temperature gradients are negligibly small.

In terms of the phase rule, the system contains the four components HCl, NaCl, H_2O and HM, where HM denotes the membrane in the hydrogen form. For the case of diffusive flows Hanley⁶ discussed why the membrane must be included among the components. The membrane in the sodium form, NaM, is not a component in terms of the phase rule. Assuming local equilibrium inside the membrane, NaM can be expressed by the other components in the equilibrium equation:



Thus it is always possible to avoid the component NaM, when describing a membrane consisting of X mol of HM and $(1-X)$ mol of NaM. The membrane may be considered to contain:

$$\begin{aligned} X \text{ mol HM} + (1-X) \text{ mol} [\text{HM} + \text{NaCl} - \text{HCl}] &= \\ = 1 \text{ mol HM} + (1-X) \text{ mol NaCl} - & \\ (1-X) \text{ mol HCl} & \end{aligned} \quad (2)$$

Mass fluxes to be considered need therefore only be J_{HCl} , J_{NaCl} , $J_{\text{H}_2\text{O}}$ and J_{HM} . According to Prigogine⁷ any reference velocity can be used to define isothermal diffusion at mechanical equilibrium. Our system is assumed to undergo only negligible changes in macroscopic kinetic energy. This means that the flux of HM, J_{HM} , can be chosen equal to zero and the other fluxes can be given relative to J_{HM} .

One may note that the amount of HM on the right hand side of eqn. (2) is always 1 mol (1 equiv.). This means that the reference, HM, is constant for all membrane compositions. The reference is also equivalent to the membrane matrix as a reference for both stationary and non-stationary flow. The membrane matrix was chosen as the reference in the "black box" description of membrane transport processes.^{3,4}

The set of flux equations. When diffusion takes place across a membrane while a current passes through the system, the changes taking place are described by fluxes of the neutral components, J_{HCl} , J_{NaCl} , $J_{\text{H}_2\text{O}}$ and the electric current, I . The second postulate of irreversible thermodynamics gives the following relations between fluxes and forces for an isothermal system:

$$J_{\text{HCl}} = J_1 = -L_{11}\nabla\mu_1 - L_{12}\nabla\mu_2 - L_{13}\nabla\mu_3 - L_{14}\nabla\phi \quad (3)$$

$$J_{\text{NaCl}} = J_2 = -L_{21}\nabla\mu_1 - L_{22}\nabla\mu_2 - L_{23}\nabla\mu_3 - L_{24}\nabla\phi \quad (4)$$

$$J_{\text{H}_2\text{O}} = J_3 = -L_{31}\nabla\mu_1 - L_{32}\nabla\mu_2 - L_{33}\nabla\mu_3 - L_{34}\nabla\phi \quad (5)$$

$$I = J_4 = -L_{41}\nabla\mu_1 - L_{42}\nabla\mu_2 - L_{43}\nabla\mu_3 - L_{44}\nabla\phi \quad (6)$$

where L_{ij} are called phenomenological coefficients.

The fluxes in the above equations are obtained by measuring the electric current and composition changes in the solutions over time. The forces can be obtained by measuring dif-

ferences in chemical or electric potential over very small differences in the space coordinates. Chemical potentials are measured by standard methods. The electric potential is measured by inserting minute electrodes reversible to the chloride ion. (If the chloride content of the membrane is equal to zero, a minute quantity of electrolyte should be in contact with each electrode). These electrodes carry no current and are not assumed to disturb the transport processes significantly, as any change in membrane properties will be only over a very limited region.

One cannot insert electrodes without introducing additional components in the system. When electrodes reversible to the chloride ion are Ag/AgCl electrodes, the additional components are Ag and AgCl. The transfer of these components is connected to the transfer of charge in a simple way:

$$J_{\text{Ag}} = I \text{ and } J_{\text{AgCl}} = -I$$

Correspondingly there is a transfer of volume from left to right equal to $I(V_{\text{Ag}} - V_{\text{AgCl}})$, where V_{Ag} and V_{AgCl} are the molar volumes of Ag(s) and AgCl(s), respectively.

The components Ag and AgCl are separate phases, they are not present in any of the other phases. This means that the gradients in their chemical potential are equal to zero unless there is a pressure gradient in the system. With a pressure gradient, ∇P , the gradients in chemical potential for the two components are:

$$\nabla \mu_{\text{Ag(s)}} = V_{\text{Ag}} \nabla P \text{ and } \nabla \mu_{\text{AgCl(s)}} = V_{\text{AgCl}} \nabla P$$

The contribution to the gradient in electric potential from these components is equal to:

$$(V_{\text{AgCl}} - V_{\text{Ag}}) \nabla P \text{ [cf. eqn. (26)]}$$

By subtracting this term from the measured electric potential gradient, $\nabla \phi_{\text{obs}}$, one obtains the gradient $\nabla \phi$ in eqns. (3-6):

$$\nabla \phi = \nabla \phi_{\text{obs}} - (V_{\text{AgCl}} - V_{\text{Ag}}) \nabla P$$

In this way one avoids operating with additional components in the basic set of equations.

The eqns. (3-6) describe the transport processes in the system on a macroscopic phenomenological level, they are not based on any model assumption. This description is as close to physical reality as can be obtained by a rigorous

thermodynamic method. A description in terms of volume flows^{3,4,8} is also independent of model assumptions, but is less precise than the present approach.

The gradients in chemical and electric potential in the system are assumed to be only across the membrane, *i.e.* no diffusive film will be considered. Any pressure gradient in the membrane is included in the gradients in chemical potential.

The gradients in chemical potential are linearly dependent through the Gibbs-Duhem equation. When energy contributions due to changes in dipole orientation are negligible, the equation does not contain gradients in electric potential. For an isothermal system where $\nabla \mu_i$ include pressure gradients, the equation takes the form:

$$\sum_i n_i \nabla \mu_i - V \nabla P = 0$$

The chemical potentials of HM and NaM can be expressed by the chemical potentials of HCl, NaCl and H₂O and P by application of the Gibbs-Duhem equation and the membrane exchange equilibrium restriction, eqns. (1,2). Conversely the chemical potentials of HCl and NaCl can be expressed by the chemical potentials of HM, NaM and H₂O and P . This means that μ_1 and μ_2 are well-defined functions anywhere in the membrane even when the content of Cl⁻ ions in the membrane is negligible.

Transference numbers and diffusion coefficients. According to the Onsager reciprocal relations, $L_{ij} = L_{ji}$. The coefficient L_{44} may be interpreted as the electrolytic conductance of the membrane. The coefficients L_{14} , L_{24} and L_{34} may be identified by means of a Hittorf experiment. In the Hittorf experiment all gradients in chemical potential are equal to zero, and the following information is obtained:

$$\left(\frac{J_1}{I} \right)_{\nabla \mu_i = 0} = \frac{L_{14}}{L_{44}} = t_1 \quad (7)$$

$$\left(\frac{J_2}{I} \right)_{\nabla \mu_i = 0} = \frac{L_{24}}{L_{44}} = t_2 \quad (8)$$

$$\left(\frac{J_3}{I} \right)_{\nabla \mu_i = 0} = \frac{L_{34}}{L_{44}} = t_3 \quad (9)$$

With electrodes reversible to the Cl⁻ ion, the cation fluxes through the membrane are equal to the fluxes of the respective neutral com-

ponents through the system, $J_1 = J_{\text{HCl}} = J_{\text{H}^+}$ (in membrane) and $J_2 = J_{\text{NaCl}} = J_{\text{Na}^+}$ (in membrane). Therefore t_1 is equal to the ionic transference number of the H^+ ion, $t_1 = t_{\text{H}^+}$, and similarly $t_2 = t_{\text{Na}^+}$. The t_3 is the transference number of neutral water and does not represent any transfer of charges.

The gradient in electric potential, $\nabla\phi$, may be eliminated in the mass flux equations. The eqns. (7–9) may be substituted in eqn. (6).

$$\nabla\phi = -t_1\nabla\mu_1 - t_2\nabla\mu_2 - t_3\nabla\mu_3 - (I/L_{44}) \quad (10)$$

Substituting this expression in eqns. (3–5) gives:

$$J_1 = -(L_{11} - t_1L_{14})\nabla\mu_1 - (L_{12} - t_2L_{14})\nabla\mu_2 - (L_{13} - t_3L_{14})\nabla\mu_3 + t_1I$$

$$J_2 = -(L_{21} - t_1L_{24})\nabla\mu_1 - (L_{22} - t_2L_{24})\nabla\mu_2 - (L_{23} - t_3L_{24})\nabla\mu_3 + t_2I$$

$$J_3 = -(L_{31} - t_1L_{34})\nabla\mu_1 - (L_{32} - t_2L_{34})\nabla\mu_2 - (L_{33} - t_3L_{34})\nabla\mu_3 + t_3I$$

For convenience the equations may be written in the abbreviated form:

$$J_1 = -l_{11}\nabla\mu_1 - l_{12}\nabla\mu_2 - l_{13}\nabla\mu_3 + t_1I \quad (11)$$

$$J_2 = -l_{21}\nabla\mu_1 - l_{22}\nabla\mu_2 - l_{23}\nabla\mu_3 + t_2I \quad (12)$$

$$J_3 = -l_{31}\nabla\mu_1 - l_{32}\nabla\mu_2 - l_{33}\nabla\mu_3 + t_3I \quad (13)$$

when the current, I , is equal to zero, eqns. (11–13) represent a homogeneous set of equations with a symmetric matrix. The number of equations is reduced by one, and the number of coefficients is reduced from sixteen to nine, compared with eqns. (3–6). The diffusion coefficients l_{ij} are independent of the kind of electrodes one may use for measuring $\nabla\phi$ and independent of the transference numbers.

Eqn. (14) gives the relations between the diffusion coefficients, as obtained from pure diffusion experiments, and the phenomenological coefficients, as obtained from experiments involving mixed diffusion and electric transport.

$$l_{ij} = L_{ij} - \frac{L_{4j}L_{14}}{L_{44}} \quad i, j = 1, 2, 3 \quad (14)$$

When the Onsager reciprocal relations $L_{ij} = L_{ji}$ are valid, the relations $l_{ij} = l_{ji}$ are also valid, as can be seen from eqn. (14)

It is essential for the following derivation that all the forces in eqns. (11–13) are independent. For many kinds of membrane transports the fluxes may be interdependent. For such cases the Onsager reciprocal relations need not be valid, unless the forces are independent.⁹ We will show that the gradients in chemical potential in eqns. (11–13) can be changed independent of one another.

Application of the phase rule to the membrane-electrolyte system. Equilibrium is assumed between the membrane and the solution at the phase boundaries, in agreement with the first postulate of local equilibrium in irreversible thermodynamics. The phase rule:

$$F = C - Ph + 1 \quad (\text{at constant temperature})$$

may be applied to a region extending across a phase boundary, in order to determine the number of independent intensive variables or degrees of freedom. The number of components, C , is equal to 4, and the number of phases, Ph , is equal to 2. This gives the number of degrees of freedom, F , equal to 3. One can, e.g., change the chemical potentials μ_1 , μ_2 and μ_3 independently at both sides of the membrane, while μ_4 (μ_{HM}) and the pressure are dependent variables. Thus the potential differences $\Delta\mu_1$, $\Delta\mu_2$ and $\Delta\mu_3$ over the membrane are also independent variables.

We will now consider stationary state for the system. At any position inside the membrane, the gradients in chemical potential are then determined by the composition and the pressure of the electrolytes on the two sides of the membrane. The gradient $\nabla\mu_1$ is mainly a function of the difference $\Delta\mu_1$ over the membrane, but modified by $\Delta\mu_2$ and $\Delta\mu_3$:

$$\nabla\mu_1 = f_1(\Delta\mu_1, \Delta\mu_2, \Delta\mu_3)$$

Thus $\nabla\mu_1$ at a given position in the membrane can be changed by changing $\Delta\mu_1$, while $\nabla\mu_2$ and $\nabla\mu_3$ are kept constant by slight adjustments of $\Delta\mu_2$ and $\Delta\mu_3$. Similarly $\nabla\mu_2$ and $\nabla\mu_3$ are mainly functions of $\Delta\mu_2$ and $\Delta\mu_3$, respectively, and each can be changed independent of the others.

Transport coefficients for a cation exchange membrane. We will consider the same kind of system as discussed above. We will, however, make the restriction that the membrane is a perfect cation exchange membrane. That means

$$t_1 + t_2 = 1$$

or stated in an equivalent way

$$L_{14} + L_{24} = L_{44} \tag{15}$$

The current, I , can be expressed by the fluxes J_1 and J_2

$$I = J_1 + J_2 \tag{16}$$

Combining eqn. (16) with eqns. (11 and 12) we have

$$(l_{11} + l_{21})\nabla\mu_1 + (l_{12} + l_{22})\nabla\mu_2 + (l_{13} + l_{23})\nabla\mu_3 = 0 \tag{17}$$

This equation is valid for any value of $\nabla\mu_1$, $\nabla\mu_2$ and $\nabla\mu_3$. Because these forces are independent variables, we can conclude that

$$l_{i1} + l_{21} = 0 \quad i = 1, 2, 3 \tag{18}$$

Further, since all forces in eqns. (3–6), $\nabla\mu_1$, $\nabla\mu_2$, $\nabla\mu_3$ and $\nabla\phi$ are independent variables and since $J_1 + J_2 = I$, we obtain in a similar way:

$$L_{i1} + L_{21} = L_{41} \quad i = 1, \dots, 4 \tag{19}$$

The eqns. (19) are valid when there are three independent mass fluxes across a cation exchange membrane, and electric charge is transported by two univalent cations between electrodes reversible to a common anion. The eqns. (18) are independent of the kind of electrodes used.

The l_{ij} and L_{ij} coefficients are functions of local composition, P and T , i.e. they are gradient independent. Followingly the eqns. (18,19) are also valid for a system that is not in stationary state.

It should be noted that by assuming $L_{13} = 0$ and $\nabla\mu_3 = 0$, eqns. (3,4) become identical with the Nernst-Planck flux equation. When $L_{13} = 0$, eqns. (19) give $L_{11} = L_{14}$ and $L_{22} = L_{24}$, and the following expressions for eqns. (3,4) are obtained:

$$J_1 = -L_{14}(\nabla\mu_1 + \nabla\phi)$$

$$J_2 = -L_{24}(\nabla\mu_2 + \nabla\phi)$$

The single ion chemical potential is defined as:

$$\mu_1 = \mu_{HCl} = \mu_{H^+} + \mu_{Cl^-}$$

$$\mu_2 = \mu_{NaCl} = \mu_{Na^+} + \mu_{Cl^-}$$

With chlorine reversible electrodes, the emf of the cell, $\Delta\phi$, is defined as equal to the so-

called electric potential difference, $\Delta\psi$ minus the difference in the chemical potential of Cl^- , $\Delta\mu_{Cl^-}$, between the electrodes (two immeasurable quantities). Thus the relation between the gradients would be:

$$\nabla\phi = \nabla\psi - \nabla\mu_{Cl^-}$$

The electrochemical potential of an ion is defined:

$$\tilde{\mu}_j = \mu_j + z_j\psi \quad (z_j \text{ is the charge of the ion})$$

Using these definitions and remembering that $J_1 = J_{H^+}$ (in membrane) and $J_2 = J_{Na^+}$ (in membrane), one obtains the well-known form of the Nernst-Planck flux equation:

$$J_{H^+} = -L_{14}(\nabla\mu_{H^+} + \nabla\psi) = -L_{14}\nabla\tilde{\mu}_{H^+}$$

$$J_{Na^+} = -L_{24}(\nabla\mu_{Na^+} + \nabla\psi) = -L_{24}\nabla\tilde{\mu}_{Na^+}$$

In this way the assumptions behind the Nernst-Planck equation are shown. Assuming a zero value for L_{13} means assuming the same mobility for $\nabla\phi = 0$ and for transport in an electric field without concentration gradients. The same assumption about mobilities is inherent when the concept of electrochemical potential is used in the single ion terminology. Assuming a zero value for $\nabla\mu_3$ ($\nabla\mu_{H_2O}$) is probably close to reality for dilute aqueous solutions.

Generalization of the derivation. The above derivation can be extended to an n -component system containing ions with different charges.

For a system of n components one can choose one of the components as the reference component, thus the flux of this component is equal to zero. For an isothermal two-phase system there are $n - 1$ independent intensive variables. With an electric current passing through the system, there are n independent forces (including the gradients in chemical potential and the gradient in electric potential) and n fluxes (including the mass fluxes J_1, \dots, J_{n-1} and the electric current $J_n = I$). The fluxes may be linearly dependent:

$$\sum_{i=1}^{i=n} \alpha_i J_i = 0 \tag{20}$$

where α_i is called a coupling coefficient. The set of coupling coefficients expresses the interdependence of the fluxes. (For the system just dealt with, $HCl-NaCl-H_2O-HM$, $\alpha_1 = 1$, $\alpha_2 = 1$,

$\alpha_3=0$ and $\alpha_4=-1$. For a system HCl-CaCl₂-H₂O-HM one would have $\alpha_1=1$, $\alpha_2=2$, $\alpha_3=0$ and $\alpha_4=-1$ using a cation exchange membrane and anion reversible electrodes.)

Since all forces are independent, the phenomenological coefficients must also be linearly related:

$$\sum_{i=1}^{i=n} \alpha_i L_{ij} = 0 \quad j = 1, \dots, n \quad (21)$$

Similarly one will have for the diffusion coefficients:

$$\sum_{i=1}^{i=n-1} \alpha_i J_{ij} = 0 \quad j = 1, \dots, n-1 \quad (22)$$

The values of the coupling coefficients are determined by the selectivity of the electrodes, the selectivity of the membrane (*e.g.* cation- or anion exchange membrane) and the charges of the ions migrating through the membrane.

A set of coupling coefficients can be used to express any kind of interdependence between fluxes. Take for example the system HCl-NaCl-H₂O-HM. If all transport of water molecules is connected only to the transport of components 1 and 2, this can be expressed by eqn. (23)

$$\alpha_1 J_1 + \alpha_2 J_2 = J_3 \quad (23)$$

where α_1 and α_2 are the number of water molecules transported together with component 1 and 2, respectively. This will give eqns. (24) relating coefficients connected to transport of water:

$$\alpha_1 L_{1i} + \alpha_2 L_{2i} = L_{3i} \quad i = 1, \dots, 4 \quad (24)$$

In a set of equations describing n fluxes caused by n forces, there are n^2 coefficients. Owing to the Onsager reciprocal relations the number of independent coefficients is only $\frac{1}{2}n(n+1)$. For a system described by eqn. (20) where the n relations given in eqn. (21) are valid, the number of independent coefficients will be reduced to $\frac{1}{2}n(n-1)$. This means that $\frac{1}{2}n(n-1)$ independent transport coefficients must be determined experimentally in order to obtain a complete description of isothermal transport of mass and charge across a cation exchange membrane between anion reversible electrodes. When cation reversible electrodes are used, one will arrive at the same number of independ-

ent coefficients. This will be shown in a subsequent paper.

Commonly transport processes in membranes are described by treating the ionic species as components (see Meares *et al.*⁴ for further references). Some problems inherent in the ionic description will be discussed in a subsequent paper, where the methods will be compared.

3. EXPERIMENTAL DETERMINATION OF THE PHENOMENOLOGICAL COEFFICIENTS, L_{ij}

Experimental conditions consistent with the preceding theoretical treatment are outlined below. Returning to the previously considered example, we will discuss the experiments needed to determine six independent coefficients of a cation exchange membrane. For all the experiments the vector fluxes are assumed to be perpendicular to the surface of the membrane. This allows us to replace gradients by one-dimensional differentials in the set of flux equations (3-6). Further, the differentials are replaced by differences over a unit length of membrane thickness. The difference can be made sufficiently small to allow the use of average values for transport coefficients over the composition interval considered.

The coefficients L_{14} , L_{24} , L_{34} and L_{44} . The electrolytic conductance of the membrane, L_{44} , can be obtained by standard methods of conductance measurements. A Hittorf experiment gives either t_1 or t_2 . When L_{44} is known, L_{14} and L_{24} are obtained applying eqns. (7,8,15).

The coefficient L_{34} can be obtained in three alternative ways:

1. The coefficient L_{34} can be obtained by measuring the flux of water, J_3 , when a known current passes through the system with identical electrolytes on both sides of the membrane (electroosmosis). When L_{44} is known, L_{34} is obtained applying eqn. (9).

2. Alternatively, under the same conditions, one can measure the volume flow, J_v , which can be expressed by the equation:

$$J_v = J_1 \bar{V}_1 + J_2 \bar{V}_2 + J_3 \bar{V}_3 + I(V_{Ag} - V_{AgCl})$$

where the last term is the transfer of volume due to changes in the electrodes. The \bar{V}_i is the known molar volume of the component i in the electrolyte. When L_{44} and t_1 (and t_2) are known, one obtains the transference number for water applying eqns. (7-9), and hence $L_{34} = t_3 L_{44}$.

$$t_3 \bar{V}_3 = (J_v/I) \Delta \mu_i = 0 - (t_1 \bar{V}_1 + t_2 \bar{V}_2) - V_{Ag} + V_{AgCl}$$

3. One can obtain L_{43} and thus L_{34} by measuring the electric potential difference with identical electrolytes on both sides,

but different pressures (streaming potential). A pressure difference leads to a difference in chemical potential:

$$\Delta\mu_1 = \bar{V}_1 \Delta P \quad (25)$$

With Ag/AgCl electrodes the transfer of charge corresponds to a transfer of Ag(s) and AgCl(s) in addition to the components HCl, NaCl, H₂O. With different pressures at the two electrodes eqn. (10) is extended by the two additional components transferred:

$$\Delta\phi_{\text{obs}} = -t_1 \Delta\mu_1 - t_2 \Delta\mu_2 - t_3 \Delta\mu_3 - t_{\text{Ag}} \Delta\mu_{\text{Ag}} - t_{\text{AgCl}} \Delta\mu_{\text{AgCl}} - (I/L_{44})$$

where t_{Ag} and t_{AgCl} are defined similarly as t_1 , t_2 and t_3 , i.e. the number of moles transferred per faraday. For the present electrodes $t_{\text{Ag}} = +1$ and $t_{\text{AgCl}} = -1$, which gives:

$$\Delta\phi_{\text{obs}} = (-t_1 \bar{V}_1 - t_2 \bar{V}_2 - t_3 \bar{V}_3 - V_{\text{Ag}} + V_{\text{AgCl}}) \Delta P - (I/L_{44}) \quad (26)$$

The measurement of $\Delta\phi_{\text{obs}}$ is carried out at practically zero current, and thus one obtains:

$$(\Delta\phi_{\text{obs}}/\Delta P)_{I=0} = -t_1 \bar{V}_1 - t_2 \bar{V}_2 - t_3 \bar{V}_3 - (V_{\text{Ag}} - V_{\text{AgCl}})$$

from which t_3 can be found when all the other quantities are known, and hence $L_{34} = t_3 L_{44}$.

The coefficients L_{11} , L_{12} and L_{22} can all be obtained from a pure diffusion experiment when L_{14} , L_{24} and L_{44} are known. When I is equal to zero, eqn. (11) is reduced to:

$$J_1 = -l_{11} \Delta\mu_1 - l_{12} \Delta\mu_2 - l_{13} \Delta\mu_3$$

which combined with eqn. (18) gives:

$$J_1 = -l_{11} (\Delta\mu_1 - \Delta\mu_2) - l_{12} \Delta\mu_3 \quad (27)$$

The experiment can be arranged in such a way that $\Delta\mu_3 = 0$ (the vapour pressure over both solutions is the same), or one can correct for the small term $l_{13} \Delta\mu_3$, when measuring J_1 for known differences $\Delta\mu_1$ and $\Delta\mu_2$ which gives l_{11} . Using eqn. (14) and the known values of L_{14} , L_{24} and L_{44} , one obtains the coefficients L_{11} , L_{12} and L_{22} .

The coefficient L_{12} (the difference between L_{14} and L_{11}) is probably very small. Therefore it may be an advantage to determine this coefficient directly.

One method for direct determination of L_{12} is by means of the experiment illustrated in Fig. 2. The potential across membrane 1 is measured using electrodes reversible to H⁺. Membrane 2 (on the left hand side of the small volume) is of a very small area. This will give a high current density in the membrane, preventing H⁺ ions from diffusing to the left.

With a closed circuit, the concentrations in the small volume will change rapidly by combined diffusion and electric transport between the small and the large volume, until steady state is obtained. At steady state the electric transport of H⁺ ions across membrane 1 is just counterbalanced by the diffusion of H⁺ ions. There is no net transfer of this species, and $J_{\text{HCl}} = J_1 = 0$.

Using H⁺ reversible electrodes, the emf of the cell, $\Delta\phi'$, is equal to the sum of the following contributions:

1. The emf of the cell with Cl⁻ reversible electrodes, $\Delta\phi$, as given by eqn. (3) when $J_1 = 0$.

$$\Delta\phi = -\frac{1}{L_{14}} (L_{11} \Delta\mu_1 + L_{12} \Delta\mu_2) - \frac{L_{13}}{L_{14}} \Delta\mu_3$$

which combined with eqn. (17) gives:

$$\Delta\phi = -\Delta\mu_1 + \frac{L_{12}}{L_{14}} (\Delta\mu_1 - \Delta\mu_2) - \frac{L_{13}}{L_{14}} \Delta\mu_3$$

2. The emf of the cell H|(HCl, NaCl)_I|Cl, $\Delta\phi'' = -\mu_{\text{HCl}_I} + \text{constant}$. Here H and Cl mean electrodes reversible to H⁺ and Cl⁻, respectively, and the number I refers to the electrolyte on the left hand side of membrane 1.

3. The emf of the cell Cl|(HCl, NaCl)_{II}|H, $\Delta\phi''' = +\mu_{\text{HCl}_{II}} + \text{constant}$. The meaning of H and Cl is the same as above, and the number II refers to the electrolyte on the right hand side of membrane 1.

The emf of the cell with H⁺ reversible electrodes is then.

$$\Delta\phi' = \Delta\phi + \Delta\phi'' + \Delta\phi''' = \Delta\phi + (\mu_{\text{HCl}_{II}} - \mu_{\text{HCl}_I}) = \Delta\phi + \Delta\mu_1$$

$$\Delta\phi' = \frac{L_{12}}{L_{14}} (\Delta\mu_1 - \Delta\mu_2) - \frac{L_{13}}{L_{14}} \Delta\mu_3$$

By suitable choice of electrolyte compositions $\Delta\mu_3$, and thus the last term, can be made very small. When L_{13} and L_{14} are known, the last term can be corrected for, and L_{12} is found by measuring $\Delta\phi'$.

The coefficients L_{13} , L_{23} and L_{33} . The remaining coefficients, L_{13} , L_{23} and L_{33} can be obtained from two independent measurements of water flux.

In the pure diffusion experiment described on the basis of eqn. (27) one can measure J_3 in addition to J_1 . From eqns. (11,13,18) one obtains the ratio between the fluxes:

$$\left(\frac{J_3}{J_1}\right)_{I=0, \Delta\mu=0} = \frac{l_{31}}{l_{11}}$$

Thus l_{31} can be found after determining l_{11} . When L_{14} , L_{24} and L_{34} are known, L_{12} and L_{22} are obtained applying eqns. (14,19).

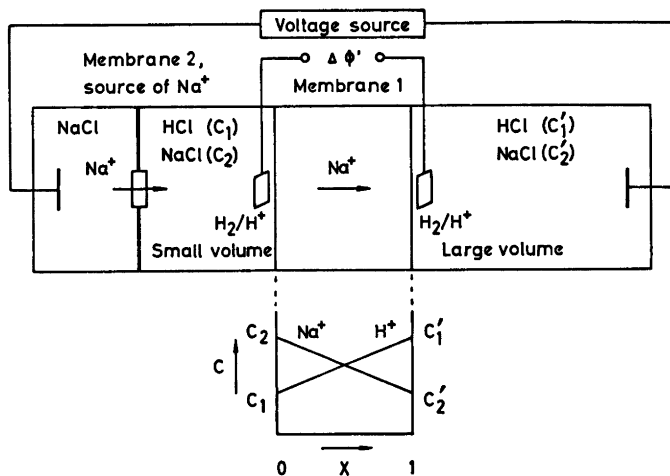


Fig. 2. Experimental arrangement for determining L_{12} . The electrodes are reversible to the H^+ ion.

The coefficients L_{13} and L_{23} may be obtained more conveniently, however, in a different way. We define two new symbols:

$$r_1 = \frac{L_{13}}{L_{34}} \quad \text{and} \quad r_2 = \frac{L_{23}}{L_{24}}$$

Introducing these symbols one obtains from eqn. (19):

$$r_1 L_{14} + r_2 L_{24} = L_{43} \quad (28)$$

or with eqns. (7,9)

$$r_1 t_1 + r_2 t_2 = t_3$$

The transference numbers t_1 and t_2 as functions of composition are known from the Hittorf experiment. From measurements of t_3 as a function of t_1 (or of composition) one can thus find r_1 and r_2 as functions of composition, yielding L_{13} and L_{23} when L_{14} and L_{24} are known.

For several systems t_3 was found to be an approximately linear function of t_1 .^{10,11} This means that r_1 and r_2 can be interpreted as a constant number of water molecules coupled to the electric transport of components 1 and 2, respectively. Eqn. (28) is the same as eqn. (24) when i is 4 and when $\alpha_1 = r_1$ and $\alpha_2 = r_2$. Thus the restriction given by eqn. (23) must lead to eqn. (28). Eqn. (28), however, involves only the electric transport of the components 1 and 2. It does not give any information about diffusional transport, and the more general eqn. (23) is not proved valid by the above experiment.

The coefficient L_{33} can be obtained by measuring the flux of water through the mem-

brane at zero current with identical electrolytes, but different hydrostatic pressure on the two sides of the membrane. The flux of water is then given by eqn. (13) combined with eqn. (25):

$$J_3 = -l_{31} \bar{V}_1 \Delta P - l_{32} \bar{V}_2 \Delta P - l_{33} \bar{V}_3 \Delta P$$

Eqn. (18) is used to eliminate l_{32} :

$$J_3 = -l_{13} (\bar{V}_1 - \bar{V}_2) \Delta P - l_{33} \bar{V}_3 \Delta P$$

A reshuffling of the above equation gives:

$$l_{33} = -\frac{1}{\bar{V}_3} \left(\frac{J_3}{\Delta P} \right) - l_{13} \left(\frac{\bar{V}_1 - \bar{V}_2}{\bar{V}_3} \right)$$

When the molar volumes, L_{13} , L_{14} , L_{34} and L_{44} are known, L_{33} is obtained by applying eqn. (14).

4. CONCLUSION

The description of transport phenomena given in this paper has several advantages:

Only measurable quantities are used for describing the transport phenomena. The mathematical description is as close to the physical processes as possible by a rigorous thermodynamic method.

The choice of components is in accordance with the phase rule. The flux equations contain independent forces, both for the case when electric energy is introduced into the system, and for the pure diffusion process.

The description is independent of the structure of the system. It can be used for non-electrolytes as well as for electrolytes. The equations are also applicable to transport of molten salts through membranes.

For a perfect cation (or anion) exchange membrane the transport coefficients are related by equations of general validity in addition to the Onsager reciprocal relations. This reduces the complexity of the system. All transport coefficients can be obtained directly from measured relations between the basic fluxes and forces.

Assumptions behind approximate flux equations can be analysed as shown by the interpretation of the Nernst-Planck flux equations. Thus the validity of the approximations can be tested experimentally.

REFERENCES

1. Førland, T. In Sundheim, B. R., Ed., *Fused Salts*, McGraw-Hill, New York 1964, p. 111.
2. Førland, T. and Østvold, T. *J. Membrane Biol.* 16 (1974) 101.
3. Katchalsky A. and Curran, P. F. *Nonequilibrium Thermodynamics in Biophysics*, Harvard University Press, Cambridge, Mass. 1965, p. 133.
4. Meares, P., Thain, J. F. and Dawson, D. G. In Eisenman, G., Ed., *Membranes*, Dekker, New York 1972, Vol. 1, Chapter 2.
5. Miller, D. G. *J. Phys. Chem.* 70 (1966) 2639; 71 (1967) 616.
6. Hanley, H. *J. Chem. Educ.* 44 (1967) 717.
7. Prigogine, I. *Introduction to Thermodynamics of Irreversible Processes*, 3rd Ed., Interscience, New York 1967, p. 36.
8. Katchalsky, A. *Pure Appl. Chem.* 16 (1968) 229.
9. DeGroot, S. R. and Mazur, P. *Non-equilibrium Thermodynamics*, North-Holland Publ. Co., Amsterdam 1962, p. 67.
10. Paterson, R. and Gardner, C. R. *J. Chem. Soc. A* (1971) 2254.
11. Winger, A. G., Ferguson, R. and Kunin, R. *J. Phys. Chem.* 60 (1956) 556.

Received March 18, 1976

Preparation of Tetramethylammonium Selenosulfate. Infrared and Raman Spectra of Tetramethylammonium Selenosulfate and Thiosulfate

PETER KLÆBOE,^a ARVE MARTINSEN^b and JON SONGSTAD^b

^a Department of Chemistry, University of Oslo, Oslo, Norway and ^b Department of Chemistry, University of Bergen, N-5014 Bergen-Univ., Norway

Selenium-free tetramethylammonium selenosulfate in high yield can be prepared easily from the corresponding sulfite and elemental selenium in methanol. Tetramethylammonium selenosulfate, like the corresponding thiosulfate, is rather soluble in warm methanol, only limitedly soluble in ethanol and appears insoluble in both acetone and acetonitrile.

The selenosulfate ion acts as an electrophile and thus as a selenating agent toward both triphenylphosphine and ionic cyanide, but only in solvents in which the tetramethylammonium salt is soluble. Toward alkyl halides the selenosulfate ion is a powerful nucleophile and the facile preparation of some tetramethylammonium "seleno-Bunte" salts, $\text{Me}_4\text{N}^+\text{RSeSO}_3^-$, is described.

The infrared and Raman spectra of tetramethylammonium selenosulfate and thiosulfate together with the assigned fundamentals are presented. As anticipated, the selenosulfate ion probably possesses the thionic structure with C_{3v} symmetry similar to that of the thiosulfate ion.

In an aqueous solution of a metal sulfite, preferably the very soluble potassium salt, elemental selenium readily dissolves, particularly at elevated temperatures^{1–5} and the following equilibrium is established:

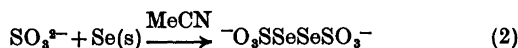


Due to the positive temperature dependence of the equilibrium constant for eqn. 1,⁶ salts of the selenosulfate ion have been most difficult to obtain in pure form since selenium will precipitate along with the desired selenosulfate upon cooling of the reaction mixture. The first selenosulfate, K_2SeSO_3 , was prepared by

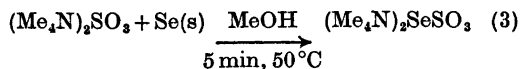
Rathke,⁷ but his synthetic route led to an impure product.⁸ As shown by Janickis and co-workers,⁹ potassium selenosulfate can be stored for years when properly purified.

SYNTHESIS OF TETRAMETHYL-AMMONIUM SELENOSULFATE

We have looked for improved synthetic routes for the preparation of pure salts of the selenosulfate ion. An attempt to use the reaction of elemental selenium with tetramethylammonium sulfite or tetraphenylarsonium sulfite in acetonitrile failed. The product of the reaction was not the expected selenosulfate, but the diselenotetrathionate,¹⁰ although oxygen was carefully excluded during the reaction:



The reaction between onium sulfites and selenium in warm methanol was far more successful. From tetramethylammonium sulfite a selenosulfate of high purity was obtained rapidly in high yield, (usually more than 70 %), eqn. 3:



Due to the low solubility of this salt in cold methanol, it crystallized rapidly from the reaction mixture prior to the formation of elemental selenium. Cold ethanol, 0 °C, was

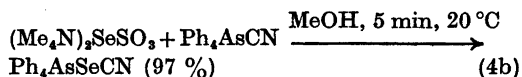
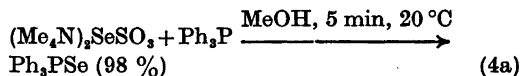
used to remove from the crystalline product unreacted tetramethylammonium sulfite and sulfate, the latter compound formed by possible oxidation of the sulfite. (Separate experiments showed that both these two salts are soluble in cold ethanol.) When tetraphenylarsonium sulfite was employed, the corresponding selenium-free selenosulfate was rapidly obtained in a similar way. However, pure samples of tetraphenylarsonium selenosulfate could not be obtained since the solubility of this salt does not allow the product to be washed with any of the usual protic and aprotic solvents to remove unreacted tetraphenylarsonium sulfite and possibly sulfate.

Tetramethylammonium selenosulfate is a colourless crystalline compound which decomposes slowly in moist air, but can be stored for months without decomposition when stored in a closed bottle. When dissolved in methanol, water or warm ethanol, the equilibrium according to eqn. 1 is set up immediately and red selenium is precipitated. As in aqueous solution, the temperature coefficient of the equilibrium constant in methanol, eqn. 1, is positive, but the large difference in solubility of tetramethylammonium selenosulfate in methanol at 50 °C and at room temperature is the probable cause for the facile formation of the selenium-free selenosulfate. At 25 °C, some 30 % of a 0.02 M solution of tetramethylammonium selenosulfate in methanol is decomposed, a little less than in distilled water of pH 6.0. At 50 °C considerably less is decomposed in methanol, allowing the salt to be crystallized from this solvent without extensive losses. (See Experimental Part.) In refluxing acetone and acetonitrile, tetramethylammonium selenosulfate appears quite insoluble. No selenium was precipitated during the attempt to dissolve the salt in these two solvents, but in acetonitrile the solution turned very slowly yellow, presumably due to traces of tetramethylammonium diselenotetrathionate, according to eqn. 2.

REACTIONS

Tetramethylammonium selenosulfate as electrophilic agent (selenating agent). Tetramethylammonium selenosulfate is deselenated quantitatively and very rapidly by both triphenyl-

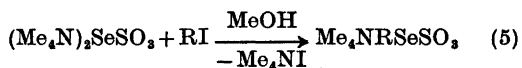
phosphine and ionic cyanide in methanol according to eqns. 4a and 4b:



The latter reaction provides a simple test of the purity of the compound by measuring the amount of ionic selenocyanate, SeCN^- , formed, by recording the IR spectrum,¹¹ after transfer of the reaction mixture to acetonitrile.

In acetonitrile and in acetone, no yield of triphenylphosphine selenide, eqn. 4a, could be obtained, and the formation of ionic selenocyanate, eqn. 4b, was exceedingly slow, presumably due to the negligible solubility of the salt in these solvents. Tetramethylammonium selenosulfate can thus only be applied as a selenating agent in a solvent in which it is soluble. Tetramethylammonium thiosulfate could similarly only form ionic thiocyanate with ionic cyanide in protic solvents. (See Experimental Part.)

Tetramethylammonium selenosulfate as nucleophilic agent. Formation of "seleno-Bunte" salts from alkyl iodides, RI. Tetramethylammonium selenosulfate dissolves without decomposition in methanolic solutions of methyl iodide and 4-nitrobenzyl iodide, forming very rapidly the corresponding Se-alkyl selenosulfates, "seleno-Bunte" salts, in high yield according to eqn. 5:



The organic iodides are favourable compared to the bromides and the chlorides since, due to their higher reactivity, their reaction with the selenosulfate ion takes place during the mixing of the reagents preventing the decomposition of the selenosulfate ion to take place according to eqn. 1. Furthermore, the very limited solubility of tetramethylammonium iodide in methanol allows this product from the reaction to be easily removed from the reaction mixture.

A number of well-characterized "seleno-Bunte" salts have previously been prepared

from the selenosulfate ion, made *in situ* according to eqn. 1, and alkyl and activated aryl iodides.¹²⁻¹⁶ However, since the decomposition of organic selenosulfates is known to be catalyzed by both acid, base and heat,¹⁶⁻¹⁸ pure tetramethylammonium selenosulfate in methanol appears superior to potassium selenosulfate prepared *in situ* for the synthesis of "seleno-Bunte" salts.

The readiness by which the reaction between tetramethylammonium selenosulfate and alkyl iodides takes place clearly indicates that the selenosulfate ion is a very powerful nucleophile. This is not surprising in view of the fact that the selenosulfate ion is very easily oxidized.^{1,12-21} The high yield of "seleno-Bunte" salts from alkyl halides and potassium selenosulfate, prepared *in situ*,¹²⁻¹⁶ suggests that the sulfite ions present cannot compete with the selenosulfate ions for the organic substrate. Since

the thiosulfate ion is only three times as reactive as the sulfite ion toward methyl iodide in methanol,²¹ it is conceivable that the selenosulfate ion is more nucleophilic than is the thiosulfate ion, a conclusion which fits nicely into the generally accepted pattern of the relative nucleophilicity of divalent selenium and sulfur species toward polarizable substrates: $\text{NCSe}^- > \text{NCS}^-$, $\text{R}_2\text{Se} > \text{R}_2\text{S}$, $\text{PhSe}^- > \text{PhS}^-$, $\text{O}_3\text{SSe}^{2-} > \text{O}_3\text{SS}^{2-}$.²¹

SPECTROSCOPIC STUDIES

Tetramethylammonium thiosulfate was prepared in approximately the same way as the corresponding selenosulfate (see Experimental Part). Therefore, non-hygroscopic salts of these two ions without crystal water or small polarizing cations were available for the spectroscopic study. Accordingly, the spectra of these com-

Table 1. Infrared and Raman spectral data for tetramethylammonium thiosulfate below 1200 cm^{-1} .^a

Infrared Nujol	KBr	Raman Solid	Interpretation
1195 vw		1197 w	$\text{N}(\text{CH}_3)_4^+$
1168 vw	1176 m		$\text{N}(\text{CH}_3)_4^+$
1160 w	1160 m		
1132 vs	1140 vs	1124 m	ν_4, E
1118 s	1125 s		
1092 w			
1050 vw	1048 w		
1020 w	1024 m	1033 w	
	1007 s		
996 s	998 s	996 m	ν_1, A_1
960 m	951 s		
950 s	945 s	955 m	$\text{N}(\text{CH}_3)_4^+$
918 w	918 w		$\text{N}(\text{CH}_3)_4^+$
866 vw			
845 w			
		757 s	$\text{N}(\text{CH}_3)_4^+$
665 w	674 s		
653 s	677 s	653 vs	ν_2, A_1
640 w	657 s		
610 w	616 w		
	547 m		
533 m	538 m	537 w	ν_5, E
	536 m		
462 m	454 w	460 s	$\text{N}(\text{CH}_3)_4^+$
435 vw	431 vw	436 vs	ν_3, A_1
370 vw	370 w ^b	378 w	
331 vw	335 w ^b	322 s	ν_6, E
	324 w ^b	190 vw	
		95 vs	lattice

^a Abbreviations: s, strong; m, medium; w, weak and v, very. ^b Polyethylene (Rigidex) pellet.

Table 2. Infrared and Raman spectral data for tetramethylammonium selenosulfate below 1200 cm^{-1} .^a

Infrared Nujol	KBr	Raman Solid	Interpretation
	1191 m	1198 vw	$\text{N}(\text{CH}_3)_4^+$
	1150 s		
1140 vs	1128 vs	1139 vw	ν_4, E
1091 vw			
	1051 w		
1041 m	1042 m	1032 m, br	
1019 s	1011 s, sh		
	1004 s	994 m	ν_1, A_1
996 vs	996 s		
959 s	950 s	954 w	$\text{N}(\text{CH}_3)_4^+$
949 s	944 s		$\text{N}(\text{CH}_3)_4^+$
921 w	917 w		
845 w		754 s	$\text{N}(\text{CH}_3)_4^+$
650 w	652 s	639 s	ν_2, A_1
638 vs	644 s		
616 m			
	595 m		
540 m	550 w		
538 w	530 w, sh	528 vw, br	ν_5, E
522 m	526 m		
462 m	454 w	457 m	$\text{N}(\text{CH}_3)_4^+$
302 vw	300 w ^b	300 vs	ν_3, A_1
281 vw	278 w ^b	277 s	ν_6, E
	250 vw ^b	242 w	
	225 vw ^b	227 w	
		205 vw	
		117 w	
		88 s	lattice

^a Abbreviations: s, strong; m, medium; w, weak; v, very; sh, shoulder and br, broad. ^b Polyethylene (Rigidex) pellet.

Table 3. Fundamental frequencies^a for the thiosulfate and the selenosulfate ions in their tetramethylammonium salts.

$\text{S}_2\text{O}_3^{2-}$	SeSO_3^{2-}	No.	Species	Assignment
996	996	ν_1	A_1	S—O stretch
653	638	ν_2	A_1	S—O bend
436 ^b	300 ^b	ν_3	A_1	S—S (S—Se) stretch
1132	1140	ν_4	E	S—O stretch
533	522	ν_5	E	S—O bend
322 ^b	277 ^b	ν_6	E	SO_3 rock

^a Infrared bands from the nujol spectra, except when noted. ^b Bands observed in the Raman spectra.

pounds are to a good approximation expected to give a superposition of the cation $\text{N}(\text{CH}_3)_4^+$ and the anion SSO_3^{2-} or SeSO_3^{2-} spectra. The thiosulfate ion has been investigated in a number of compounds by X-ray²²⁻²⁵ and spectro-

scopic²⁶⁻²⁸ methods and is known to belong to point group C_{3v} .³⁰

The observed infrared and Raman lines below 1200 cm^{-1} for tetramethylammonium thiosulfate and selenosulfate, respectively, are

listed in Tables 1 and 2. Tentative interpretations of the major infrared and Raman lines are presented. As apparent, a number of the observed bands can with reasonable confidence be attributed to the cation $N(CH_3)_4^+$ since they are present in a number of salts containing this ion.³¹⁻³³ More interesting for the present work are the bands attributed to the anions, and in Table 3 the fundamentals assigned to the thiosulfate and the selenosulfate groups are listed. The thiosulfate modes agree well with the results of earlier work.²⁶⁻²⁸ With C_{3v} symmetry the fundamentals divide themselves between the symmetry species $3 A_1$ and $3 E$. Since no Raman polarization ratios can be obtained from the solid state spectra, the A_1 and E fundamentals cannot be distinguished with certainty. In most cases the A_1 modes give rise to the most intense Raman bands in the spectra. Also, the degenerate S—O stretch (E) will generally be at higher frequencies than the totally symmetric ones (A_1) while the opposite will be the case for the S—O bending modes.

In the selenosulfate ion we have no guide-lines from previous work. Particularly, the molecular structure of this ion is unknown, but an X-ray crystallographic determination of tetramethylammonium selenosulfate is presently being carried out. As apparent from Table 3 the various vibrations ν_1 , ν_2 , ν_4 and ν_5 are only slightly displaced from the thiosulfate to the selenosulfate ions. This fact strongly suggests C_{3v} molecular symmetry also in the selenosulfate group, since lower symmetry (e.g. C_s) would lead to splitting of the doubly degenerate E modes contrary to the observations (Tables 1 and 2). More definite conclusions regarding the structure could be extracted from the spectra only when Raman polarization data become available. The lowest A_1 fundamental involving mainly S—Se stretch was assigned to the very intense Raman band at 300 cm^{-1} having weak counterparts in the infrared. This value agrees with the suggested S—Se stretching frequency in the selenopentathionate ion.³⁵

The shift of the S—Se stretch (436) compared to the S—S stretch (300 cm^{-1}) is much larger than caused by the increased atomic mass of the atom, only. A considerable weakening of the S—Se force constant (compared to S—S) is in agreement with the chemical

experience of the weak S—Se bond in the selenosulfate ion. Finally, the lowest E fundamental is attributed to the intense Raman band at 277 cm^{-1} with weak IR counterparts. Again, the large shift from the thiosulfate ion frequency at 322 cm^{-1} is not surprising because of the increased mass and weaker S—Se bond compared with the S—S bond.

The conclusion arrived at in the present study with regard to the structure of the selenosulfate ion conforms with results from recent infrared spectra of sodium and potassium selenosulfate.^{36,37} The selenosulfate complexes, $Zn(en)_2SeSO_3$ and $Cu(en)_2SeSO_3$, (en = ethylenediamine), have been shown by X-ray methods to be isostructural with the corresponding thiosulfate complexes.³⁹⁻⁴⁰

EXPERIMENTAL

Solvents: Merck's *Methanol zur Analyse* was used without further purification since separate experiments showed that the decomposition of tetramethylammonium selenosulfate in this solvent according to eqn. 1 was the same as in a solvent batch distilled from magnesium methoxide, $Mg(OCH_3)_2$.

Acetonitrile, *Baker Analyzed Reagent*, was distilled from phosphorus pentoxide, P_2O_5 , and finally from calcium hydride, CaH_2 . The solvents applied in the present study were carefully flushed with dry oxygen-free nitrogen.

All operations with solutions of salts of the selenosulfate ion, the thiosulfate ion and the sulfite ion were carefully performed under nitrogen.

Tetramethylammonium sulfite, $(Me_4N)_2SO_3$. To 20.1 g tetramethylammonium iodide, *Fluka purum*, carefully washed with acetonitrile and diethyl ether, in 200 ml methanol was added 14.8 g freshly prepared silver sulfite. The slurry was stirred at room temperature for 3 h, filtered, and stirred for still 1 h after the addition of 1 g of silver sulfite. After filtration and removal of the solvent in vacuum, the product was repeatedly dissolved in methanol and azeotropically dried with benzene to remove traces of water and silver compounds. The final product was slightly greyish suggesting some silver species to be present. All attempts to crystallize the product from the usual protic and aprotic solvents failed. [Yield 10.3 g (90 %)]. An IR spectrum (nujol) showed that the amount of tetramethylammonium sulfate (made in a similar way from silver sulfate) present was negligible. However, an absorption in the 3500 cm^{-1} region suggested the presence of residual water.

Tetramethylammonium selenosulfate, $(Me_4N)_2SeSO_3$. To 10.3 g tetramethylammonium sulfite

dissolved in 100 ml methanol was added an equivalent amount of black selenium powder. No reaction was found to take place at room temperature. However, at reflux temperature nearly all selenium was consumed during 5 min and a slightly yellow solution was obtained. The solution was rapidly filtered and the product immediately separated as white needles (yield 8.9 g). After addition of 100 ml ethanol to the mother liquor, an additional amount of 2.0 g pure salt was obtained. Total yield 10.9 g, 78 %. M.p. 171 °C (dec.). (Found: C 30.82; H 7.36; N 9.51. Calc. for $C_8H_{24}N_2O_3SSe$: C 31.26; H 7.87; N 9.12.) The salt could be recrystallized from methanol at reflux temperature in more than 70 % yield. The melting point and IR spectrum (in the 4000–650 cm^{-1} region) was unaltered after this purification.

Tetramethylammonium thiosulfate. This salt was made analogous to tetramethylammonium selenosulfate, from tetramethylammonium sulfite and elemental sulfur. However, if sulfur was used in excess or even in an equivalent amount, the product obtained was slightly yellow, a colour which could not be removed by repeated crystallizations from methanol or by washings with carbon disulfide. When tetramethylammonium sulfite was used in 5 % excess, these difficulties were not encountered. Since the solubility of this salt in cold methanol is considerable, the volume was reduced to 50 ml prior to filtration and crystallization. From 10.3 g tetramethylammonium sulfite and 1.2 g sulfur the yield of crude product was 7.8 g. The salt was crystallized from 50 ml methanol yielding 5.4 g pure product, 57 % based upon the added amount of sulfur, m.p. 238–240 °C. The salt appeared non-hygroscopic. (Found: C 36.48; H 9.15; N 11.34; S 24.92. Calc. for $C_8H_{24}N_2O_3S_2$: C 36.89; H 9.29; N 10.76; S 24.63.)

Decomposition of tetramethylammonium selenosulfate in protic solvents. (1) *Methanol at reflux temperature:* 5.9 g, 0.019 mol, dissolved in 100 ml methanol at reflux temperature, (0.19 M solution), gave 0.253 g, 0.0032 mol, selenium, 17 %. (2) *Methanol at 25 °C:* 0.307 g, 1×10^{-3} mol, dissolved in 50 ml methanol, (0.02 M solution) was stirred at 25 °C for 30 min and filtered. Yield of selenium 0.0281 g, 35 %. (3) *Distilled water, pH 6, at 25 °C:* 0.307 g, 1×10^{-3} mol, dissolved in 50 ml water, (0.02 M solution) was stirred at 25 °C for 30 min and filtered. The precipitated selenium was washed with methanol and finally with ether. Yield of selenium 0.0333 g, 42 %.

Reactions of tetramethylammonium selenosulfate. 1. *Ionic cyanide.* To 10 ml 0.02 M solution of tetraphenylarsonium cyanide in methanol was added 0.0163 g tetramethylammonium selenosulfate. The salt dissolved immediately with no formation of selenium. The solution was evaporated to dryness, dissolved in acetonitrile and the amount of tetraphenylarsonium selenocyanate, $Ph_4AsSeCN$, formed determined

by liquid IR. Found: 97 ± 2 %. Similar experiments employing 0.0142 g tetramethylammonium thiosulfate gave 97 ± 2 % of the theoretical amount of ionic thiocyanate, SCN^- . When these experiments were performed in acetonitrile, less than 5 % ionic selenocyanate and thiocyanate could be detected after 1 h.

2. *Triphenylphosphine.* To 0.524 g triphenylphosphine, Ph_3P , 2×10^{-3} mol, dissolved in 20 ml methanol was added an equivalent amount of tetramethylammonium selenosulfate, 0.614 g. The salt dissolved immediately without formation of selenium. The reaction mixture was stirred for 15 min at room temperature whereupon triphenylphosphine selenide, Ph_3PSe , started to separate. After 12 h in the refrigerator 0.670 g triphenylphosphine selenide, m.p. 187–188 °C, (189 °C⁴¹) was obtained, 98 %. In ethanol, 5 min at reflux temperature was necessary to obtain a quantitative yield of triphenylphosphine selenide. In acetonitrile, no yield of triphenylphosphine selenide could be detected after 24 h at room temperature.

3. *Alkyl iodides, RI.* To 4×10^{-3} mol of the alkyl iodide, RI, in 25 ml methanol was added an equivalent amount of tetramethylammonium selenosulfate. The salt dissolved immediately with only slight reddish colouration of the reaction mixture which disappeared after a few minutes. After 5 min at room temperature all ionic selenosulfate was consumed (no colour due to elemental selenium was observed when 1 ml of the reaction mixture was added to 10 ml of water). The reaction mixture, turbid due to precipitated tetramethylammonium iodide, was set aside for 2 h in the refrigerator and then filtered. The mother liquor was three times dissolved in a minimum amount of methanol, cooled and filtered to ensure a complete removal of tetramethylammonium iodide. The salts were finally recrystallized from acetonitrile, if necessary with some diethyl ether added.

R=Me: White microcrystalline compound with obnoxious odour which could not be removed by repeated purifications. The salt appears hygroscopic, yield 54 %. M.p. (acetonitrile/diethyl ether): 171 °C (dec.). (Found: C 24.29; H 5.96; N 5.44. Calc. for $C_8H_{14}NO_3SSe$: C 24.19; H 6.09; N 5.64.)

R=4-Nitro-benzyl, NO₂-C₆H₄-CH₂: Slightly yellowish compound, m.p. (acetonitrile) 175–177 °C (dec.). 74 % yield. (Found: C 35.30; H 5.37; N 7.64. Calc. for $C_{11}H_{15}N_2O_5SSe$: C 35.77; H 4.92; N 7.59.)

Instrumental. The IR spectra were recorded with Perkin-Elmer model 225 (1400–200 cm^{-1}) and 180 (1400–180 cm^{-1}) spectrometers. The solid samples were investigated in KBr pellets CsI and polyethylene (Rigidex) pellets, and Nujol mulls between CsI plates.

A Coderg model T 800 triple monochromator spectrometer equipped with a Spectra Physics model 170–03 argon ion laser was employed for the Raman recordings, using the 5145 Å

line for excitation. The samples were filled into capillary tubes and recorded with ca. 80 mW power after the plasma lines were removed with an interference filter. Improved spectra were recorded with the aid of a spinning sample holder (Coderg) permitting the use of 250 mW laser power. Most of the Raman spectra were recorded with spectral slit widths of ca 2–3 cm⁻¹.

Acknowledgement. One of the authors (PK) is grateful to Professor W. Zeil, Tübingen, in whose laboratory parts of this work were done and for the hospitality shown him during his sabbatical leave 1975–1976. Financial support from NTNF is acknowledged.

REFERENCES

- Janickis, J. and Zelionkaitė, V. *Zh. Obshch. Khim.* 25 (1955) 841.
- Janickis, J. *Zh. Neorg. Khim.* 2 (1957) 1341.
- Klebanov, G. S. and Ostapkevich, N. A. *Zh. Prikl. Khim. (Leningrad)* 33 (1960) 1957.
- Kitaev, G. A. and Terekhova, T. S. *Zh. Neorg. Khim.* 15 (1970) 48.
- Kitaev, G. A. and Fofanov, G. M. *Zh. Prikl. Khim. (Leningrad)* 43 (1970) 1694.
- Chizhikov, D. M. and Shehastlivyi, V. P. *Selenium and the Selenides*, Collets Ltd., London 1968, p. 107.
- Rathke, B. J. *Prakt. Chem.* 95 (1865) 1.
- Foerster, F., Lange, F., Drossback, O. and Seidel, W. *Z. Anorg. Chem.* 128 (1923) 245.
- Zelionkaitė, V., Janickis, J. and Liksiene, R. *Chem. Abstr.* 58 (1963) 6444c.
- Austad, T. *Acta Chem. Scand. A* 29 (1975) 71.
- Austad, T., Songstad, J. and Åse, K. *Acta Chem. Scand.* 25 (1971) 331.
- Price, T. S. and Jones, L. M. *Proc. Chem. Soc. London* 24 (1908) 134.
- Price, T. S. and Jones, L. M. *J. Chem. Soc.* 95 (1909) 1729.
- Twiss, D. F. *J. Chem. Soc.* 105 (1914) 1674.
- Günther, W. H. H. and Mautner, H. G. *J. Med. Chem.* 7 (1964) 229.
- Klayman, D. L. *J. Org. Chem.* 30 (1965) 2454.
- Günther, W. H. H. *J. Org. Chem.* 31 (1966) 1202.
- Klayman, D. L. In Klayman, D. L. and Günther, W. H. H., Eds., *Organic Selenium Compounds*, Wiley, New York 1973, pp. 94 and 151.
- Pacaukas, E. I. and Janickis, J. *Chem. Abstr.* 56 (1962) 9877b.
- Janickis, J. *Acc. Chem. Res.* 2 (1969) 316.
- Pearson, R. G., Sobel, H. and Songstad, J. *J. Am. Chem. Soc.* 90 (1968) 319.
- Sandor, E. and Csordas, L. *Acta Crystallogr.* 14 (1961) 237.
- Taylor, P. G. and Beevers, C. A. *Acta Crystallogr.* 15 (1962) 341.
- Nardelli, M. and Fava, G. *Acta Crystallogr.* 15 (1962) 477.
- Nardelli, M., Fava, G. and Giraldi, G. *Acta Crystallogr.* 15 (1962) 227.
- Agarwala, U., Rees, C. E. and Thode, H. *G. Can. J. Chem.* 43 (1965) 2802.
- Wilkins, C. H. and Muller, F. A. *Anal. Chem.* 24 (1952) 1253.
- Freedman, A. N. and Straughan, B. P. *Spectrochim. Acta A* 27 (1971) 1455.
- Siebert, H. *Z. Anorg. Allg. Chem.* 275 (1955) 210 and 225.
- Bannister, A. J., Moore, L. F. and Padley, J. S. In Nickless, G., Ed., *Inorganic Sulfur Chemistry*, Elsevier, Amsterdam 1968, p. 167.
- Nakamoto, K. *Infrared Spectra of Inorganic and Coordination Compounds*, Wiley-Interscience, New York 1970.
- Ferraro, J. R. *Low-Frequency Vibrations of Inorganic and Coordination Compounds*, Plenum, London 1971.
- Ellestad, O. H., Klæboe, P. and Songstad, J. *Acta Chem. Scand.* 26 (1972) 1721.
- Ellestad, O. H., Klæboe, P., Tucker, E. E. and Songstad, J. *Acta Chem. Scand.* 26 (1972) 1724.
- Clark, E. R. and Collett, A. J. *J. Chem. Soc. A* (1969) 1594.
- Kalyakina, A. V. and Pelyukpashidi, R. I. *Chem. Abstr.* 79 (1973) 132488f.
- Ostapkevich, N. A., Pakhomova, N. V. and Morozova, A. V. *Chem. Abstr.* 80 (1974) 77697s.
- Schulman, V. M. and Varand, V. L. *Izv. Akad. Nauk SSSR* 1 (1965) 1389; *Chem. Abstr.* 64 (1966) 2989f.
- Podberezsakaya, N. V. and Borisov, S. V. *Zh. Strukt. Khim.* 12 (1971) 1114.
- Podberezsakaya, N. V., Borisov, S. V. and Bakakin, V. V. *Zh. Strukt. Khim.* 12 (1971) 840.
- Songstad, J. and Stangeland, L. J. *Acta Chem. Scand.* 24 (1970) 804.

Received May 13, 1976.

Molecular Structure of Gaseous Pyridazine and 3,6-Dichloropyridazine by Electron Diffraction

ARNE ALMENNINGEN,^a GUDMUND BJØRNSSEN,^a TOR OTTERSEN,^b RAGNHILD SEIP^a and TOR G. STRAND^a

^aDepartment of Chemistry and ^bDepartment of Pharmacy, University of Oslo, Oslo 3, Norway

For pyridazine (C_{2v} symmetry), the microwave R_s coordinates of the ring atoms are known except for the a coordinate of the C3 and C6 atoms. This missing coordinate was determined to be 0.013(2) Å from the electron diffraction data, and the following previously undetermined thermal average parameters (R_a) and standard deviations were obtained: $R(N-C) = 1.341(2)$ and $R(C3-C4) = 1.393(2)$ Å, and $\angle(NNC) = 119.3(1)$ and $\angle(NCC) = 123.7(1)^\circ$. The same results, but with higher standard deviations, were obtained from only the electron diffraction data.

For 3,6-dichloropyridazine (C_{2v} -symmetry) the following thermal average parameters were determined: $R(N-N) = 1.339(8)$, $R(C-N) = 1.334(9)$, $R(C3-C4) = 1.373(8)$, $R(C4-C5) = 1.377(9)$ and $R(C-Cl) = 1.717(3)$ Å, and $\angle(NNC) = 118.6(2)$, $\angle(NCC) = 124.6(3)$, and $\angle(CCl) = 120.0(5)^\circ$.

A series of structure determinations of 3,6-pyridazinediones and other substituted pyridazines where the pyridazine moiety mostly exists as a monolactam or dilactam have previously been reported.¹ It seemed of interest to compare these results to the structure of the basic diazabenzene itself. For pyridazine, the R_s coordinates of the ring atoms are known from microwave spectroscopy except for the a coordinate of the C3 and C6 atoms, which was too small to be determined,² and only two of the five parameters necessary to describe the ring could be given. An attempt to determine the crystal structure of 3,6-dichloropyridazine at -165 and 19°C failed because of large structural disorder.³

The chemistry of the parent ring and its derivatives has attracted considerable inter-

est,^{4,5} and a number of theoretical calculations^{4,6} have been performed for the pyridazine molecule.

Given the large interest in the pyridazines, an electron diffraction study on pyridazine and 3,6-dichloropyridazine was started in the hope of establishing a satisfactory structural model of the heterocycle.

STRUCTURE INVESTIGATION

Pyridazine from Koch-Light Laboratories LTD was applied without further purification. 3,6-Dichloropyridazine was synthesized⁷ and recrystallized by sublimation (20 mmHg, 25°C).

The diffraction photographs (Table 1) were treated as usually,⁸ and the molecular intensities were modified by $s/|f_c|^2$. The average molecular intensities and standard deviations are illustrated in Fig. 1. Scattering factors for the atoms were computed from the atomic potentials.⁹ Using $\Delta s = 0.125 \text{ \AA}^{-1}$ for the data of the longest camera distance and $\Delta s = 0.25 \text{ \AA}^{-1}$ for the other data, the average correlation was calculated, and elements p_1 and p_2 for the non-diagonal part of the weight matrix¹⁰ of -0.60 and 0.110 , and of -0.60 and 0.115 were applied for the longest and the shorter camera distances, respectively.

Root mean-square amplitudes of vibration and the correction terms between the thermal average distances, R_a , and the electron diffraction distances, R_d ,¹¹ were computed.¹² For pyridazine, a force field for benzene¹³ was modified until the result agreed satisfactorily

Table 1. Experimental parameters and constants for the diagonal part of the weight matrix (s_1 , s_2 , w_1 , w_2) for the intensities of 3,6-dichloropyridazine and pyridazine.

Nozzle temp. °C	Camera distance mm	Electron wave-length, Å	Number of plates	s (min) Å ⁻¹	s (max) Å ⁻¹	s_1 Å ⁻¹	s_2 Å ⁻¹	w_1 Å ²	w_2 Å ²
3,6-Dichloropyridazine									
100	480.66 ^a	0.06458	6	1.50	19.75	5.0	12.0	0.80	0.07
	200.03 ^a	0.06458	4	7.25	41.75	8.5	25.0	2.20	0.01
Pyridazine									
75	578.55 ^b	0.05852	5	1.50	13.25	2.5	9.0	10.00	0.06
	188.78 ^b	0.05849	5	4.00	35.00	7.0	25.0	0.30	0.02
	120.65 ^a	0.06458	5	8.25	46.00	10.0	25.0	0.64	0.01

^aData from the Oslo apparatus for an accelerating voltage of about 35 kV. ^bData from the Balzer apparatus for an accelerating voltage of about 42 kV.

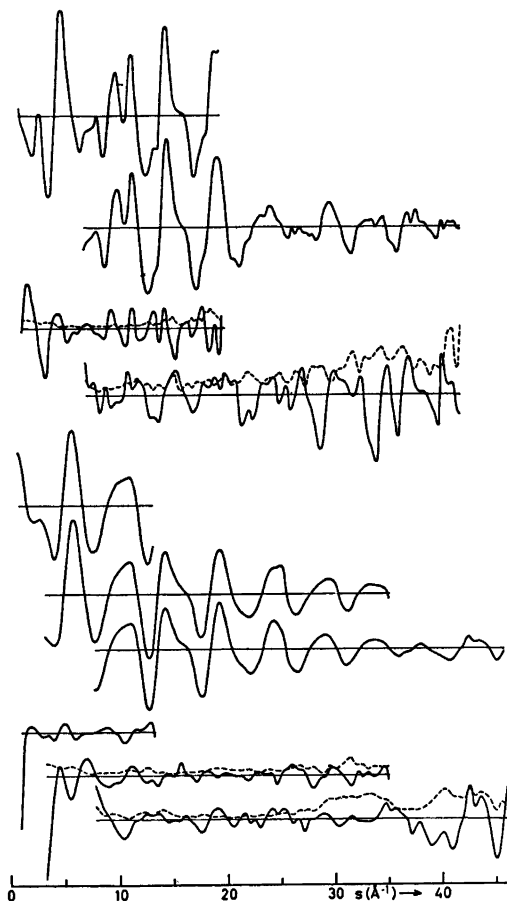


Fig. 1. $s/|f_c|^2$ -modified average experimental intensities for the different camera distances (Table 1) of 3,6-dichloropyridazine (upper

curves) and pyridazine. The standard deviations of the average intensities (broken curves), and the differences between the experimental intensities and the intensities calculated from the parameters of Table 3 multiplied by a factor of four are given below the average intensities. The standard deviations of the average 58 cm intensities of pyridazine were of the order of one fifth of the differences and are not included.

to the normal frequencies.¹⁴ This force field was further modified for 3,6-dichloropyridazine. The results are given in Table 2.

The initial least-squares refinements for 3,6-dichloropyridazine converged and after background adjustments, the results given in Table 3, A were obtained. For this refinement a non-diagonal weight matrix was applied, and the independent geometrical parameters were $R(1,2)$, $R(2,3)$, $R(3,4)$, $\Delta R = R(4,5) - R(3,4)$ and $\angle(6,1,2)$ for the pyridazine ring, and $R(3,7)$, $R(4,8)$, $\angle(4,3,7)$ and $\angle(3,4,8)$ for the position of the hydrogen and the chlorine atoms. The C_{2v} symmetric model was satisfied by the R_α distances. The vibrational amplitudes were fixed on the calculated values. The correlation coefficients of the parameters with absolute values larger than 0.4 for this refinement are given in the upper left part of Table 4. Starting this refinement with the ring parameters later obtained for pyridazine, the iteration returned to the given results. Attempts to vary some of the vibrational amplitudes along with the geometrical parameters showed strong correlation with some of the distances and gave less reasonable results both for the amplitudes themselves and for the distances.

Table 2. Calculated root mean-square amplitudes of vibration, $u = [\langle \Delta z^2 \rangle]^{1/2}$, and correction terms between the thermal average distances R_α and the electron diffraction distances R_a , $D = R_\alpha - R_a = u^2/R - [\langle \Delta v^2 \rangle + \langle \Delta \psi^2 \rangle]/2R$ for 3,6-dichloropyridazine and pyridazine.

Distance	3,6-Dichloro- pyridazine 100 °C		Pyridazine 75 °C	
	u , Å	D , Å	u , Å	D , Å
1-2	0.0456	-0.0036	0.0454	-0.0016
2-3	0.0459	-0.0025	0.0450	-0.0017
3-4	0.0460	-0.0021	0.0458	-0.0016
4-5	0.0460	-0.0038	0.0459	-0.0017
3-7	0.0430	-0.0110	0.0770	-0.0127
4-8	0.0769	-0.0127	0.0769	-0.0117
1...3	0.0553	-0.0028	0.0548	-0.0002
1...4	0.0609	-0.0008	0.0599	0.0007
1...5	0.0545	-0.0009	0.0538	-0.0002
1...7	0.0676	-0.0042	0.0994	-0.0032
1...8	0.0936	-0.0043	0.0930	-0.0021
1...9	0.0953	-0.0044	0.0946	-0.0031
1...10	0.0712	-0.0065	0.1026	-0.0053
3...5	0.0551	-0.0027	0.0548	-0.0002
3...6	0.0603	-0.0029	0.0605	0.0006
3...8	0.0983	-0.0062	0.0977	-0.0052
3...9	0.0941	-0.0061	0.0936	-0.0031
3...10	0.0635	-0.0032	0.0943	-0.0024
4...7	0.0712	-0.0054	0.0950	-0.0058
4...9	0.0984	-0.0080	0.0974	-0.0054
4...10	0.0663	-0.0036	0.0919	-0.0035
7...8	0.1505	-0.0019	0.1521	-0.0030
7...9	0.1130	-0.0036	0.1239	-0.0042
7...10	0.0667	0.0006	0.1205	-0.0036
8...9	0.1589	-0.0052	0.1549	-0.0028

For pyridazine, several models were initially tried without obtaining a converging iteration. The iteration would not converge, neither for a ring structure close to the final ring structure of 3,6-dichloropyridazine nor by fixing the N-N and the C4-C5 distances on the microwave R_s values.³ However, after fixing the coordinates of the ring atoms on the known microwave R_s values,² the missing α coordinate of the C3 and C6 atoms was determined by the least-squares method as the only independent geometrical parameter of the pyridazine ring, and from this result a converging model was obtained, and background adjustments were carried out. Results of the final refinement of this type are given in Table 3, B, where a non-diagonal weight matrix was applied. The parameters for the position of the hydrogen atoms were fixed on values obtained separately

in earlier refinements (Table 3, C), and the amplitudes of vibrations were fixed on the calculated values. The value obtained for the α coordinate of the atoms C3 and C6 was 0.0130(21) Å and the corresponding R_α ring structure with C_{2v} symmetry satisfying the microwave coordinates are given. From this result for the ring structure the results of refinement C was obtained with $R(1,2)$, $R(2,3)$, $R(3,4)$, ΔR and $\angle(6,1,2)$ as independent geometrical parameters, again with the hydrogen parameters fixed on the given values and applying a diagonal weight matrix. The corresponding refinement for a non-diagonal weight matrix would not converge. The given standard deviations, however, were estimated by starting from the values of Table 3, C, and varying all the geometric parameters and the scale factors simultaneously for a non-diagonal weight matrix by forcing the least-squares changing vector to be zero. The corresponding elements of the correlation matrix of the parameters with absolute value larger than 0.4 are given in the lower, right part of Table 4.

Then the best estimate of the structures is the result given in Table 3, A for 3,6-dichloropyridazine and the result in Table 3, B with parameters for the position of the hydrogen atoms of Table 3, C for pyridazine. These results are included in Fig. 2 and the atomic coordinates in the principal axis of rotation system for these structures are given in Table 5. Experimental radial distribution functions are compared to calculated ones in Fig. 2.

DISCUSSION

The least-squares standard deviations are based upon the assumptions that the electron diffraction data are without systematic errors and that the applied vibrational amplitudes and D -values are correct. For pyridazine, also the applied microwave R_s coordinates should be correct and the R_s and R_α structures should be identical. The calculated u - and D -values are probably sufficiently accurate. The microwave R_s coordinates may be close to the equilibrium coordinates within a standard deviation of 0.001 Å or better. The D -values, especially of the ring distances, are small and as effects from anharmonic vibrations on these

Table 3. Thermal average structures, R_{α} , for 3,6-dichloropyridazine (A) and pyridazine (B, C). For the scale factors, K , and the weighted R -factors, $R = 100[\sum_i w_i(I_{\text{exp}} - I_{\text{calc}})^2 / \sum_i w_i I_{\text{exp}}^2]^{1/2}$, the camera distances in cm are given in parenthesis. Contributions of 0.001 R due to uncertainties in the electron wave length are included in the standard deviations.

	A	B ^c	C
$R(1,2)$	1.3394(78)	1.3300(13)	1.3317(67)
$R(2,3)$	1.3343(90)	1.3414(20)	1.3406(45)
$R(3,4)$	1.3733(84)	1.3931(21)	1.3960(51)
ΔR^a	0.0034(139)		-0.0206(163)
$R(4,5)$	1.3767(86)	1.3754(14)	1.3754(117)
$R(3,7)$	1.7166(28)		
$R(4,8)$	1.1087(269)		1.0639(160)
$\angle(6,1,2)$	118.60(21)	119.29(3)	119.29(12)
$\angle(4,3,7)$	120.00(51)		124.59(185)
$\Delta(\text{CCH})^b$			-1.87(701)
$\angle(3,4,8)$	120.97(450)		122.72(578)
$\angle(2,3,4)$	124.56(27)	123.66(1)	123.70(28)
$\angle(3,4,5)$	116.84(25)	117.05(3)	117.01(23)
$K(48), K(58)$	191.7(48)	198.7(22)	200.3(23)
$K(20), K(19)$	178.0(47)	198.9(21)	200.5(22)
$K(12)$		200.5(26)	200.7(28)
$R(48), R(58)$	7.1	3.63	3.45
$R(20), R(19)$	20.6	6.96	7.04
$R(12)$		9.32	9.06

^a $\Delta R = R(4,5) - R(3,4)$. ^b $\Delta(\text{CCH}) = \angle(3,4,8) - \angle(4,3,7)$. ^cThe only independent geometrical parameter was the a coordinate of atom C3 and C6, which converged to the value of 0.0130(21) Å.

Table 4. Correlation coefficients of the parameters for 3,6-dichloropyridazine (upper left part) and pyridazine (figures with asterisk) for the least-squares refinements A and C of Table 3. Only coefficients with an absolute value larger than 0.4 are given.

	$R(3,7)$	$R(1,2)$	$R(2,3)$	$R(3,4)$		
$\angle(4,3,7)$	-0.450		0.525	-0.653	-0.809*	$R(2,3)$
$\angle(6,1,2)$			-0.469	0.617	0.443*	$R(3,4)$
ΔR			-0.434	-0.820	-0.964*	ΔR
$R(3,4)$			-0.651	0.663*	-0.856*	$\angle(6,1,2)$
$R(2,3)$		-0.558	-0.740*			$\angle(4,3,7)$
			$\Delta(\text{HCC})$	$R(2,3)$	$R(3,4)$	$R(1,2)$

Table 5. Atomic coordinates in principal axis of rotation system for most abundant isotopes corresponding to the structures of Table 3 (C_{2v} symmetries).

Atom	3,6-Dichloropyridazine		Pyridazine		Ref. 2	
	b	a	a	b	a	b
N1	1.1330	0.6697	1.1832	0.6650	1.1830	0.6650
C5	-1.2633	0.6884	-1.2270	0.6877	-1.2277	0.6877
C6	-0.0382	1.3084	0.0136	1.3212		1.3212
H9	-2.2019	1.2793	-2.1454	1.2227		
Cl10,H10	0.0564	3.0228	0.1531	2.3748		

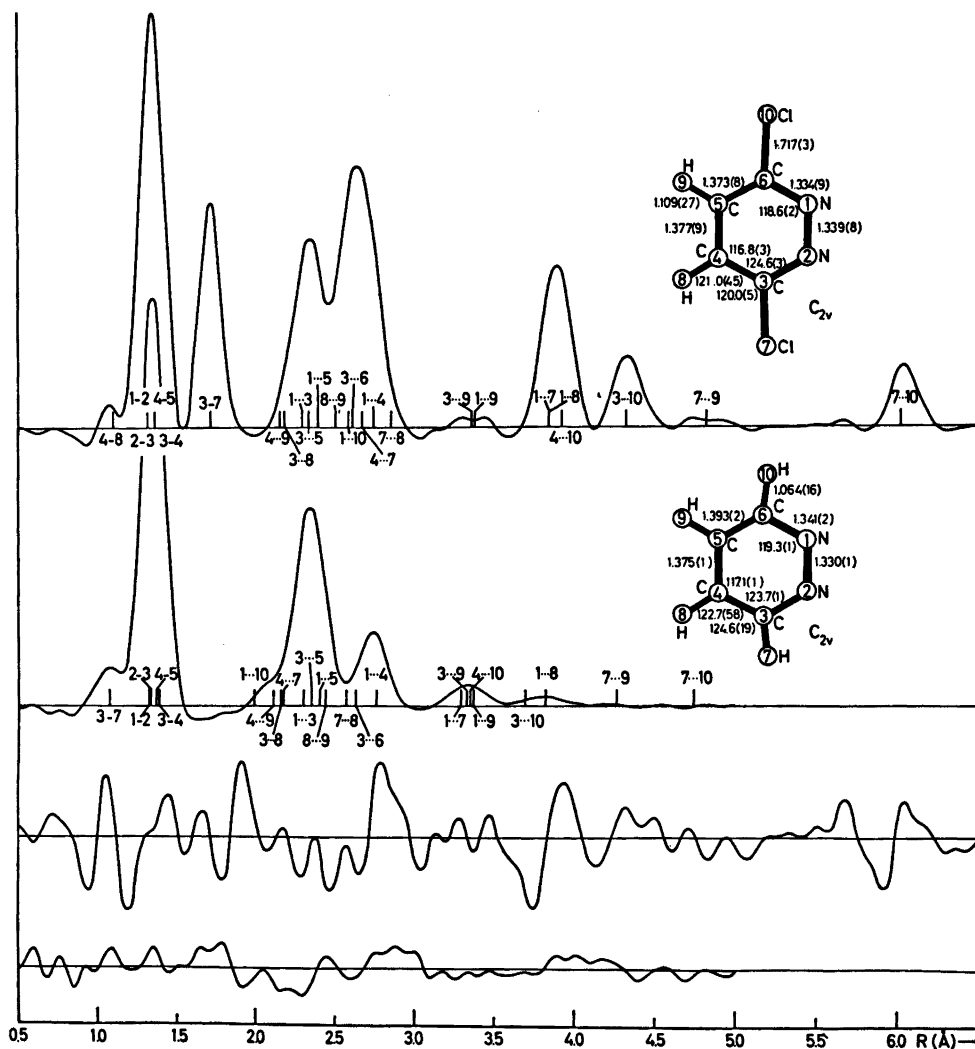


Fig. 2. Experimental radial distribution functions of 3,6-dichloropyridazine and pyridazine for damping functions of $\exp(-0.0015s^2)$. Calculated intensities were added inside $s = 4 \text{ \AA}^{-1}$ for 3,6-dichloropyridazine and $s = 2 \text{ \AA}^{-1}$ for pyridazine. The two lower curves are the differences between the experimental and calculated functions for 3,6-dichloropyridazine and pyridazine, respectively, multiplied by a factor of four. The best estimates of the R_α structures are included in the figure.

distances probably are small, also the R_α distances should be close to the equilibrium distances.

Correcting the least-squares standard deviations by including $0.001 R$ should take care of systematic errors in the electron diffraction data due to the uncertainty in the electron wave length. However, other types of systematic errors could make the calculated u -

values inconsistent with the data and through the high correlation between u -values and distances that exists in these molecules lead to errors in the distances not accounted for by the given standard deviations. These values may therefore be too small by an uncertain amount and should be used with caution.

There is definitely a least-squares minimum for the pyridazine ring structure of Table 3, B

also when the constraints of the microwave R_s coordinates are removed, as shown by the good agreement between the parameters of Table 3, B and C.

Comparing the rings of pyridazine and 3,6-dichloropyridazine the C3–C4 bond has decreased by 0.020(8) Å and the angle (6,1,2) is smaller by 0.7(2)° in 3,6-dichloropyridazine with minor changes in the other parameters. As the given standard deviations might be too small these changes are probably not significant.

The C4–C5 bond of 1.375(1) Å is shorter than the normal aromatic bond of benzene of 1.397 Å. The bond order of this bond is 1.79, whereas the other bonds in the ring seem to have a normal aromatic bond order of 1.67.^{6a} Similar short C–C bonds are indicated in pyrimidine.^{15,16}

The only bond lengths changing upon protonation of the N2 atom of pyridazine are the C–N bonds which both are shortened to 1.314(5) in pyridazine hydrochloride.¹ In relation to the angles of pyridazine, the angle N1,N2,C3 of pyridazine hydrochloride is increased to 125.8(3)° and the angle N2,N1,C6 is decreased to 115.8(3)° with no significant changes in the other angles.

REFERENCES

- Ottersen, T. *Acta Chem. Scand. A* 29 (1975) 637, and references therein.
- Werner, W., Dreizler, H. and Rudolph, H. D. *Z. Naturforsch. Teil A* 22 (1967) 531.
- Ottersen, T. *Unpublished results.*
- Castle, R., Ed., *Heterocyclic Compounds* 28, Wiley, New York 1973.
- Ottersen, T. *Acta Chem. Scand.* 27 (1973) 797.
- a. Gropen, O. and Skancke, P. N. *Acta Chem. Scand.* 24 (1970) 1768; b. Almløf, J., Roos, B., Wahlgren, V. and Johansen, H. *J. Elect. Spectrosc. Relat. Phenom.* 2 (1973) 51.
- Mizzoni, R. H. and Spoerri, P. E. *J. Am. Chem. Soc.* 76 (1954) 2201.
- Andersen, B., Seip, H. M., Strand, T. G. and Stølevik, R. *Acta Chem. Scand.* 23 (1969) 3224.
- a. Yates, A. C. *Comput. Phys. Commun.* 2 (1971) 175; b. Stewart, R. F., Davidson, E. R. and Simpson, W. T. *J. Chem. Phys.* 42 (1965) 3175; c. Strand, T. G. and Bonham, R. A. *J. Chem. Phys.* 40 (1964) 1686.
- Seip, H. M., Strand, T. G. and Stølevik, R. *Chem. Phys. Lett.* 3 (1969) 617.
- Morino, Y., Kuchitsu, K. and Oka, T. *J. Chem. Phys.* 36 (1962) 1108.
- a. Gwinn, W. D. *J. Chem. Phys.* 55 (1971) 477; b. Stølevik, R., Seip, H. M. and Cyvin, S. *Chem. Phys. Lett.* 15 (1972) 263.
- Seip, H. M. *Private communication.*
- Stidham, H. D. and Tucci, J. V. *Spectrochim. Acta Part A* 23 (1967) 2233.
- Wheatley, P. J. *Acta Crystallogr.* 13 (1960) 80.
- Furberg, S. and Aas, J. B. *Acta Chem. Scand. A* 29 (1975) 714.

Received June 10, 1976.

Conformational Analysis. XIII. The Structure of Gaseous 1,1,2,3,3-Pentachloropropane, $(\text{CHCl}_2)_2\text{CHCl}$, as Determined by Electron Diffraction and Compared with Molecular Mechanics Calculations

SJUR GRINDHEIM^a and REIDAR STØLEVIK^b

^a Department of Chemistry, University of Oslo, Blindern, N-Oslo 3, Norway and ^b Department of Chemistry, University of Trondheim, NLHT, Rosenborg, N-7000 Trondheim, Norway

1,1,2,3,3-Pentachloropropane has been studied at a nozzle temperature of 83°C. One conformer, which contains no parallel (1:3) Cl...Cl interaction, was detected. Results are presented with error limits (2σ). The following values for bond lengths (r_g) and bond angles (\angle_α) were obtained: $r(\text{C}-\text{C})=1.523(18)$ Å, $r(\text{C}-\text{Cl})=1.776(4)$ Å, $\angle\text{CCC}=113.8^\circ(1.6)$, $\angle\text{C}_2\text{C}_1\text{X}=111.8^\circ(1.0)$, $\angle\text{C}_1\text{C}_2\text{X}=109.8^\circ(1.2)$. The conformer has torsion angles close to staggered values. An average torsional force constant was estimated by combining information from vibrational spectroscopy and electron diffraction. Vibrational frequencies, u and K values, have been computed.

The diffraction data are consistent with the results obtained from molecular-mechanics calculations, which predict ca. 95 % of the stable conformer.

According to the molecular-mechanics calculations the lowest rotational barriers, involving transitions between enantiomeric forms of the stable conformer, are 7–9 kcal/mol.*

The results are compared with those of 1,1,2,2,3,3-hexachloropropane.

Six energetically different conformers have to be considered as shown in Table 1. The conformers 2, 3, and 4 exist as enantiomeric pairs.

From IR spectra and coupling constants derived from NMR spectra Dempster *et al.*¹ concluded that PCP (1,1,2,3,3-pentachloropropane) exists in conformation 4 in the liquid phase. Conformer 4 is the only one which does not possess parallel (1:3) Cl...Cl interactions.

CALCULATIONS OF CONFORMATIONAL ENERGIES, GEOMETRIES, TORSIONAL BARRIERS, AND FORCE CONSTANTS

The energy model corresponds to molecular-mechanics calculations, including atom-atom potentials² and valence force constants as described in Ref. 3, and applied in subsequent

Table 1. Staggered conformers of 1,1,2,3,3-pentachloropropane ($\text{C}_1\text{C}_2\text{C}_3$).

Conformer	ϕ_{12}° (deg.)	ϕ_{23}° (deg.)	Symmetry
1 XHX HCCCH XXX	0	0	C_s
2 XHX XCCCH HXX	120	0	C_1
XHX HCCCH XXH	0	120	
3 HHX XCCCH XXX	-120	0	C_1
HHX HCCCH XXX	0	120	
4 XHH XCCCH HXX	120	120	C_1
XHH XCCCH XXH	-120	-120	
5 XHX XCCCH HXH	120	-120	C_s
6 HHH XCCCH XXX	-120	120	C_s

* 1 kcal=4.184 kJ.

Table 2. Calculated conformational energy parameters for 1,1,2,3,3-pentachloropropane.

Conformer	1	2	3	4	5	6
ΔE (kcal/mol) ^a	6.9	2.5	3.3	0	4.7	3.2
Composition (%) ^b	0	3	1	95	0	1
ϕ_{1-2} (°) ^c	0.7	115.8	-139.0	115.2	-129.3	-136.8
ϕ_{2-3} (°) ^c	-0.7	-20.7	2.8	123.5	129.3	136.8
\angle CCC (°)	120.4	117.1	116.7	112.9	113.8	113.9
$F_{\phi}(1-2)$ ^d	0.55	0.36	0.39	0.31	0.42	0.34
$F_{\phi}(2-3)$ ^d	0.55	0.45	0.30	0.37	0.42	0.34
$F_{\phi\phi}$ ^e	-0.08	-0.07	-0.21	-0.08	-0.31	-0.20

^a Conformational energy $\Delta E = E - E(4)$. ^b Assuming equal vibrational partition functions and 83 °C. ^c Torsion angles (see also Table 1). ^d Diagonal torsional force constants in m dyn Å (rad)⁻². ^e Non-diagonal element.

papers (conformational analysis I–XI). In minimizing the energy the geometry was constrained as explained below. Results corresponding to energy minima are shown in Table 2, and further details are given elsewhere.⁴ The deviations from exact staggered forms are found by comparing ϕ values in Tables 1 and 2.

Dempster *et al.*⁵ have determined the rotational barrier for the transition 4 (120, 120°) → 4 (−120, −120°). The experimental NMR value is $\Delta H^* = 6.7 \pm 1.0$ kcal/mol. In the same paper⁵ the authors propose a mechanism which can be indicated as follows (approximate values of the torsion angles are given): 4(120, 120°) → transition state (180, 180°)* → 4 (−120, −120°). However, the calculated barrier heights are shown in Table 3. The proposed mechanism corresponds to a barrier height of 15.5 kcal/mol. The following mechanism: 4 (120, 120°) → (180, 120°)* → 6 (240, 120°) → (240, 180°)* → 4 (240, 240°) ≡ 4 (−120, −120°) includes two

barrier heights of 8.4 kcal/mol, which is comparable with the experimental value. Our mechanism includes conform 6 having one parallel (1:3) Cl⋯Cl interaction, while the first mechanism was proposed in order to avoid the parallel (1:3) Cl⋯Cl interaction.⁵ Although the calculated barrier heights are uncertain values the error is hardly as large as 7 kcal/mol.

CALCULATION OF VIBRATIONAL QUANTITIES

Valence force constants, except for the torsional part were taken from works of Schachtschneider⁶ and Snyder.⁷ The final force-constant values used in this work are found in Ref. 4. An average torsional force constant has been adjusted to fit the diffraction data as described below. The normal-coordinate program described by Gwinn⁸ was used in computing vibrational frequencies. The fit between observed¹ and calculated⁴ frequencies

Table 3. Torsional barriers (kcal/mol) within 1,1,2,3,3-pentachloropropane. The energy values have been obtained by adjusting all geometry variables except for the ϕ -values being ± 60 , ± 180 °. The exact values of ϕ corresponding to conformational minima are found in Table 2.

ϕ_{1-2} ϕ_{2-3}	−120°	−60°	0°	60°	120°	180°
180°	8.4	21.4	8.4	18.4	8.6	15.5
120°	3.2(6)	13.0	3.3(3)	7.7	0(4)	8.4
60°	13.0	36.3	16.5	33.9	14.3	21.4
0°	3.3(3)	16.5	6.9(1)	10.0	2.5(2)	8.4
−60°	7.7	33.9	10.0	29.7	8.6	18.4
−120°	0(4)	14.3	2.5(2)	8.6	4.7(5)	8.6

Table 4. Mean amplitudes of vibration (u in Å) calculated for Cl...Cl internuclear distances with $F_\phi = 0.27, 0.43, \text{ and } 0.54 \text{ mdyn } \text{Å} (\text{rad})^{-2}$ at 83 °C.

Distance (r)	$r(\text{Å})$	0.27	0.43	0.54
$X_1 \cdots X_2$ (<i>a:anti</i>)	4.36	0.0724	0.0723	0.0722
$X_1 \cdots X_2$ (<i>g:gauche</i>)	3.28	0.158	0.145	0.141
$X_2 \cdots X_3$ (<i>g:gauche</i>)	3.26	0.160	0.148	0.143
$X_2 \cdots X_3$ (<i>g:gauche</i>)	3.32	0.160	0.147	0.143
$X_1 \cdots X_3$ (<i>a a</i>)	5.10	0.102	0.101	0.101
$X_1 \cdots X_3$ (<i>a g</i>)	4.75	0.168	0.156	0.152
$X_1 \cdots X_3$ (<i>a g</i>)	4.92	0.153	0.142	0.139
$X_1 \cdots X_3$ (<i>g g</i>)	4.03	0.255	0.218	0.204

is satisfactory for calculating mean amplitudes of vibration. However, the important frequencies below 562 cm^{-1} have not been observed.¹

Mean amplitudes of vibration (u) and perpendicular amplitude correction coefficients (K) were computed as described in Ref. 9. Some of these quantities are sensitive to the values of the torsional force constants.⁴ The average torsional force constant $F_\phi = F_\phi(1-2) = F_\phi(2-3)$ corresponding to the best value as estimated from the diffraction data, was used. The values of the torsional frequencies calculated with $F_\phi = 0.43 \text{ mdyn } \text{Å} (\text{rad})^{-2}$ and $F_{\phi\phi} = 0$ are 74 and 82 cm^{-1} , while the lowest non-torsional frequencies are 99, 154, 170, 203, 275, 322, 344, 418 and 568 cm^{-1} . Final u - and K values for all internuclear distances are found in Ref. 4. Only the most important u values for Cl...Cl distances are shown in Table 4.

EXPERIMENTAL AND DATA REDUCTION

A commercial sample of PCP was obtained. The purity was better than 99 %.

Electron-density photographs were made at a nozzle temperature of 83 °C in the Balzer¹⁰ apparatus¹¹ under conditions summarized below.

Nozzle-to-plate distance (mm)	500	250.0
Electron wave length (Å)	0.05852	0.05853
Number of plates	3	4
Range of data, in s (Å ⁻¹)	1.25–15.625	2.25–30.50
Data interval Δs (Å ⁻¹)	0.125	0.250
Uncertainty in s -scale (%)	0.14	0.14

The electron wavelength was determined by calibration against ZnO and benzene.²⁰ The data were reduced in the usual way¹² to yield an intensity curve for each plate. Average curves for each set of distances were formed. A composite curve was then made by connecting the two average curves after scaling. The final experimental intensity curve is shown in Fig. 1. The intensities have been modified by $s/|f'_{\text{Cl}}|^{-2}$. Scattering amplitudes (f') were calculated by the partial-wave method¹³ using Hartree-Fock atomic potentials.¹⁴ The radial distribution (RD) curve¹² is shown in Fig. 2.

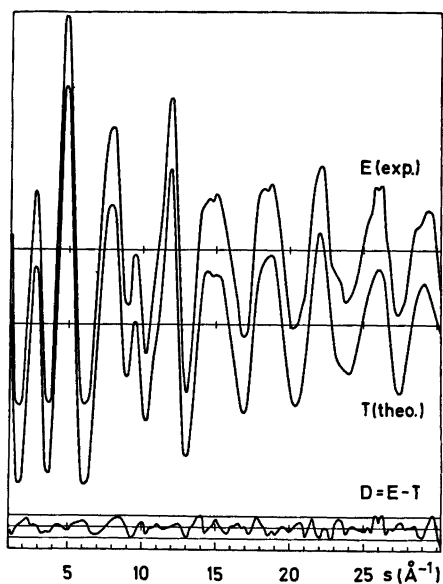


Fig. 1. Experimental (E) and theoretical (T) intensity curves for 1,1,2,3,3-pentachloropropane, and $D = E - T$, corresponding to final least-squares parameters. The straight lines give the experimental uncertainties as ± 3 times the standard deviations.

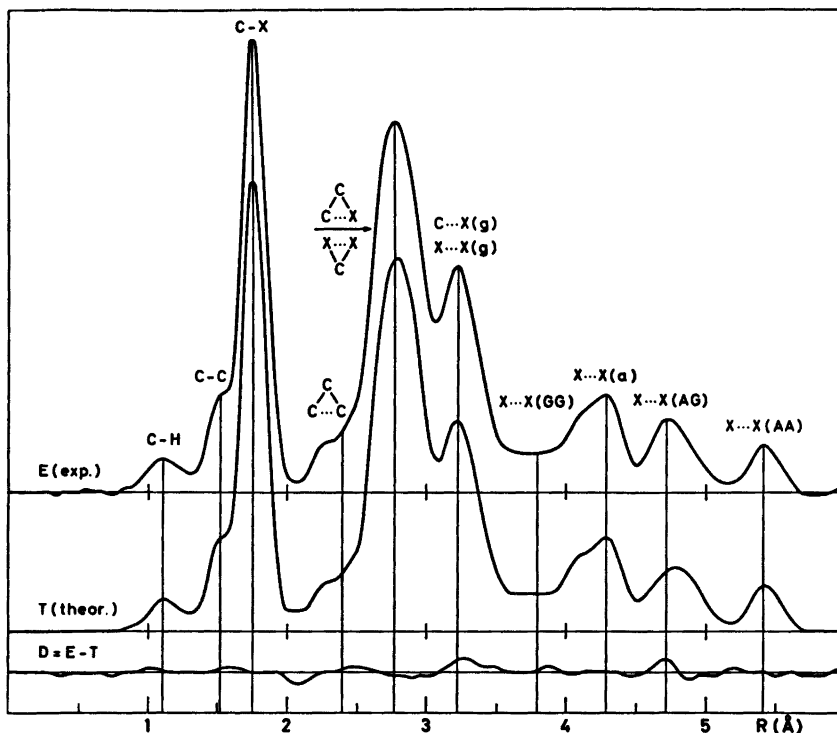


Fig. 2. Experimental (E) and theoretical (T) RD curves for 1,1,2,3,3-pentachloropropane at 83 °C. The curves were computed from the intensities in Fig. 1 with an artificial damping constant of 0.002 Å².

STRUCTURE ANALYSIS

According to the calculated energies, 95 % of conformer 4 is expected in the conformational mixture at 83 °C. It was assumed that only intensities corresponding to conformer 4 had to be included in the least-squares analysis.¹² It was assumed that the group C₁-C₂(XH)-C₃ and the two C-CHX₂ groups possess C_s symmetry, all C-H bonds have equal lengths, all C-X bonds have equal lengths, and the C-C bonds have equal lengths. The geometrical model is then defined in terms of the following average parameters: $r(\text{C-H})$, $r(\text{C-C})$, $r(\text{C-X})$, $\angle \text{CCC}$, $\angle \text{C}_2\text{C}_1\text{H}$, $\angle \text{C}_1\text{C}_2\text{H}$, $\angle \text{C}_2\text{C}_1\text{X}$, $\angle \text{C}_1\text{C}_2\text{X}$, the torsion angles ϕ_{2-1} and ϕ_{2-3} and $\angle(\text{XC}_1\text{X})^*$ which is the projection of the angle XC₁X on a plane perpendicular to the C₂-C₁ axes. Non-bonded distances were computed as dependent parameters, restricted under the constraints of geometrically consistent r_α parameters,^{15,16} by

including vibrational correction terms $D = r_\alpha - r_a$ for all distances.

The following parameter correlation coefficients (ρ) had values of $|\rho|$ greater than 0.4: $\rho[\angle \text{C}_2\text{C}_1\text{X}/r(\text{C-C})] = -0.75$, $\rho(\phi_{1-2}/\angle \text{C}_2\text{C}_1\text{X}) = 0.42$, $\rho[\angle(\text{XC}_1\text{X})^*/r(\text{C-C})] = -0.64$, $\rho[\angle(\text{XC}_1\text{X})^*/\angle \text{C}_2\text{C}_1\text{X}] = 0.93$, and $\rho[\angle(\text{XC}_1\text{X})^*/\phi_{1-2}] = 0.45$.

Determination of the torsional force constant

In previous papers (Conf. anal. I-XII) it has been shown that information about the torsional force constants can be obtained from the diffraction data. Assuming the harmonic force field, two diagonal elements $F_\phi(1-2)$, $F_\phi(2-3)$, and the non-diagonal element $F_{\phi\phi'}$ have to be determined (see Table 2). Determination of all three elements is not possible from diffraction data alone. However, an

Table 5. Structure parameters for conformer 4 of 1,1,2,3,3-pentachloropropane. Bond lengths (r_a) in Å, bond angles (\angle_α) and torsion angles (ϕ) in deg. Standard deviations in parenthesis.

$r(\text{C}-\text{X})$	1.774(2)	$\angle \text{CCC}$	113.8(0.8)
$r(\text{C}-\text{C})$	1.521(9)	$\angle \text{C}_2\text{C}_1\text{X}$	111.8(0.5)
$r(\text{C}-\text{H})$	1.115(-) ^a	$\angle \text{C}_1\text{C}_2\text{X}$	109.8(0.6)
ϕ_{1-2}	112.3(0.9)	$\angle \text{C}_2\text{C}_1\text{H}$	109.4(-) ^c
ϕ_{2-3}	123.8(1.1)	$\angle \text{C}_1\text{C}_2\text{H}$	107.3(-) ^c
$\angle \text{HC}_1\text{X}$	106.6(0.6) ^b	$\angle (\text{XC}_1\text{X})^*$	123.3(0.8) ^d
$\angle \text{HC}_2\text{X}$	108.3(1.8) ^b	$\angle \text{XC}_2\text{X}$	109.5(0.2) ^b

^a Estimated from the RD curve in Fig. 2. ^b Dependent angle. ^c Values from molecular-mechanics calculations. ^d Defined in text above.

average value $F_\phi = F_\phi(1-2) = F_\phi(2-3)$ for conformer 4 was estimated. The best fit between theoretical and experimental intensities was obtained for $F_\phi = 0.43$ mdyn Å (rad)⁻², with error limits¹⁷ of ca. 20 %. The estimated value is not considered significantly different from those calculated for conformer 4 in Table 2. The calculated $F_{\phi\phi'}$ value of Table 2 is indirectly supported by the agreement found for the diagonal elements.

RESULTS

Structural parameters from the final least-squares refinements and standard deviations corrected for correlation in the experimental data¹⁸ are given in Table 5. In the final refinements all intensities were given equal weight. Calculated vibrational parameters, u and K values, were included. The agreement between

intensity curves in Fig. 1 shows that the calculated values of the vibrational parameters⁴ are reasonable.

The structure parameters obtained for conformer 4 by molecular-mechanics calculations are: $\angle \text{CCC} = 112.9^\circ$, $\angle \text{C}_2\text{C}_1\text{X} = 112.4^\circ$, $\angle \text{C}_1\text{C}_2\text{X} = 111.0^\circ$, $\angle (\text{XC}_1\text{X})^* = 121.6^\circ$, $\phi_{1-2} = 115.2^\circ$, and $\phi_{2-3} = 123.5^\circ$. The agreement with experimental values in Table 5 is fair. Both sets of values show that $\angle \text{C}_2\text{C}_1\text{X} > \angle \text{C}_1\text{C}_2\text{X}$, $\angle (\text{XC}_1\text{X})^* > 120^\circ$, $\phi_{1-2} < 120^\circ$ (staggered), and $\phi_{2-3} > 120^\circ$ (staggered).

DISCUSSION

The lack of agreement between theoretical and experimental RD curves at ca. 4.75 Å might be an indication that more than one conformer ought to be included in the analysis. Intensity contributions from conformer 2, and later on conformers 3 and 6, corresponding to 2, 5, 10, and 20 % did not lead to a better fit. The diffraction data are thus consistent with the results obtained from the molecular-mechanics calculations.

The results for *PCP* are compared with those of *HCP* (1,1,2,2,3,3-hexachloropropane).¹⁹ Both molecules exist in the gas phase as conformers without parallel (1:3) Cl...Cl interactions. The results are given in Table 6.

Since the parameters $r(\text{C}_1-\text{X})$ and $r(\text{C}_2-\text{X})$ were treated as one independent variable within *PCP*, 1.776 Å is an average value approximately equal to $[4r(\text{C}_1-\text{X}) + r(\text{C}_2-\text{X})]/5$. This

Table 6. The results for *PCP* compared with those for *HCP*.

Parameter	X H H			X X H		
	XC(1)C(2)C(3)X	H X X		XC(1)C(2)C(3)X	H X X	
$r_g(\text{C}_1-\text{X})$ (Å)	(1.776)			1.780(5)		
$\angle_\alpha \text{C}_2\text{C}_1\text{X}$ (°)	111.8(0.5)			111.4(0.4)		
$\angle_\alpha \text{C}_1\text{C}_2\text{X}$ (°)	109.8(0.6)			108.8(0.4)		
$r_g(\text{C}_2-\text{X})$ (Å)	(1.776)			1.752(9)		
$\angle_\alpha \text{CCC}$ (°)	113.8(0.8)			108.0(1.0)		
$r_g(\text{C}-\text{C})$ (Å)	1.523(9)			1.558(8)		
ϕ_{1-2} (°)	112.3(0.9)			116.2(0.7)		
ϕ_{2-3} (°)	123.8(1.1)			116.2(0.7)		
$\angle (\text{XC}_1\text{X})^*$ (°)	123.3(0.8)			120.5(0.8)		
F_ϕ [mdyn Å (rad) ⁻²]	0.43			0.86		

relation ⁴ is based on the assumption that the vibrational parameters for the two bond types are equal. Substituting $r(C_1-X)=1.780 \text{ \AA}$ from *HCP* in the above relation, the value $r(C_2-X)=1.760 \text{ \AA}$ was obtained with $\sigma=0.022 \text{ \AA}$. The values of $r(C_2-X)$ within *PCP* and *HCP* thus are not significantly different. Statistically the parameters $r(C-C)$ and $\angle CCC$ are significantly different within the two compounds, and both conformers have torsion angles close to staggered values, but significantly different from 120° (staggered). The two conformers have nearly equal values of the C_2C_1X angles as well as the C_1C_2X angles. The main conclusion of this comparison must be that the effect of having one heavy Cl atom at the centre of *PCP*, as compared with two symmetrically substituted Cl atoms at the centre of *HCP*, is of little importance to the values of structural parameters within the terminal groups. However, the effect on the $r(C-C)$ and $\angle CCC$ values is pronounced. The values of the torsional force constants are very different for the two conformers, while both molecules exist in nearly staggered conformations.

According to the molecular-mechanics calculations the lowest rotational barriers, involving transitions between enantiomeric forms of the stable conformers, are 7–9 kcal/mol within *PCP* and 14–15 kcal/mol within *HCP*. The ratio between these values is roughly equal to the ratio between the experimentally estimated torsional force constants.

Acknowledgements. We are grateful to Kristen Brøndhaugen for recording the diffraction photographs. Financial support from Norges almenvitenskapelige forskningsråd is gratefully acknowledged.

REFERENCES

1. Dempster, A. B., Price, K. and Sheppard, N. *Spectrochim. Acta A* 27 (1971) 1579.
2. Abraham, R. J. and Parry, K. J. *J. Chem. Soc. B* (1970) 539.
3. Stølevik, R. *Acta Chem. Scand. A* 28 (1974) 327.
4. Grindheim, S. *Thesis*, University, Oslo 1975.
5. Dempster, A. B., Price, K. and Sheppard, N. *J. Magn. Reson.* 16 (1974) 235.
6. Schachtschneider, J. H. and Snyder, R. G. *Vibrational Analysis of Polyatomic Molecules IV*. Project No. 31450, Technical Report No. 122-63 of Shell Development Company.

7. Snyder, R. G. *J. Mol. Spectrosc.* 28 (1960) 273.
8. Gwinn, W. D. *J. Chem. Phys.* 55 (1971) 477.
9. Stølevik, R., Seip, H. M. and Cyvin, S. J. *Chem. Phys. Lett.* 15 (1972) 263.
10. Zeil, W., Haase, J. and Wegmann, L. *Z. Instrumentenk.* 74 (1966) 84.
11. Bastiansen, O., Graber, R. and Wegmann, L. *Balzer's High Vacuum Report* 25 (1969) 1.
12. Andersen, B., Seip, H. M., Strand, T. G. and Stølevik, R. *Acta Chem. Scand.* 23 (1969) 3224.
13. Peacher, J. and Willis, J. C. *J. Chem. Phys.* 46 (1967) 4809.
14. Strand, T. G. and Bonham, R. A. *J. Chem. Phys.* 40 (1964) 160.
15. Morino, Y., Kuchitsu, K. and Oka, T. *J. Chem. Phys.* 36 (1962) 1108.
16. Kuchitsu, K. *J. Chem. Phys.* 49 (1968) 4456.
17. Fernholt, L. and Stølevik, R. *Acta Chem. Scand. A* 28 (1974) 963.
18. Seip, H. M. and Stølevik, R. In Cyvin, S. J., Ed., *Molecular Structures and Vibrations*, Elsevier, Amsterdam 1972.
19. Fernholt, L. and Stølevik, R. *Acta Chem. Scand. A* 29 (1975) 651.
20. Tamagawa, K., Iijima, T. and Kimura, M. *J. Mol. Struct.* 30 (1976) 243.

Received August 3, 1976.

Short Communications

Structural Studies on the Rare Earth Carboxylates. 27. The Crystal Structure of Erbium Tris(oxydiacetato)erbate Hexahydrate, Containing Eight- and Nine-coordinated Erbium Ions

INGA ELDING

Physical Chemistry 1, Chemical Center, University of Lund, P.O.B. 740, S-220 07 Lund 7, Sweden

In lanthanoid compounds with bidentate carboxylate ligands, the coordination number of the lanthanoid ion most often is nine for the largest and eight or nine for the smallest ions. The earlier reported lanthanoid compounds with the tridentate oxydiacetate ligand have the mononuclear nine-coordinate tris(oxydiacetato)lanthanoidate(III) complex through the whole lanthanoid series.¹⁻³ When preparing oxydiacetate compounds of composition M_2L_3 , several phases were found. The crystals formed in the first part of the lanthanoid series were not stable, but the erbium compound, isostructural with the terbium one, could be investigated with X-ray diffraction methods.

Single crystals of erbium oxydiacetate were prepared by dissolving erbium hydroxide in a water solution of oxydiacetic acid (molar ratio 2:3) and evaporating at room temperature at pH 5–7. Addition of solutions of erbium chloride or sodium hydroxide to the solution resulted in identical crystals.

The crystal data are: $\text{Er}[\text{Er}(\text{C}_4\text{H}_7\text{O}_5)_3]_3 \cdot 6\text{H}_2\text{O}$; F.W. 918.8. Orthorhombic system; space group $C222_1$; $a=8.744(1)$, $b=17.685(2)$, and $c=14.922(1)$ Å. $Z=4$; $D_m=2.32$ and $D_x=2.41$ g cm^{-3} . $\mu(\text{CuK}\alpha)=142$ cm^{-1} . Elemental analyses for Er, C, and H gave: Er 39.5; C 17.1; H 3.20. Calc. for $\text{Er}_2\text{C}_{12}\text{H}_{24}\text{O}_{36}$: Er 39.9; C 17.2; H 2.88. The unit cell dimensions were determined from powder photographs recorded at 23°C by a Guinier-Hägg camera.

The reflexions $hk0-hk12$ were recorded at room temperature with nonintegrated Weissenberg multiple-film technique using Ni-filtered $\text{CuK}\alpha$ -radiation. A pink crystal, tabular b , with approximate dimensions $0.2 \times 0.2 \times 0.1$ mm³ was used. The intensities of 1041 independent reflexions were estimated visually by com-

parison with a calibrated scale and corrected for Lorentz, polarization and absorption effects.

A three-dimensional vector map revealed the erbium ions in two fourfold positions, resulting in a false mirror plane at $z=1/4$ in the difference map based only on erbium. The two images of the structure were slightly resolved by placing an oxygen atom in one of the highest peaks apart from the mirror plane. The atomic coordinates and temperature factors together with the interlayer scale factors were refined using a least-squares programme, minimizing $\sum w(|F_o| - |F_c|)^2$, and with weights according to Cruickshank.⁴ The final value of R was 0.10 and of R_w 0.13. The atomic parameters and temperature factors are given in Table 1. The scattering factors were taken from Refs. 5–7. The Er scattering factor was corrected for anomalous dispersion.

The structure is composed of layers parallel to the ac -plane in which the coordination polyhedra around the two nonequivalent erbium ions are held together through coordination to Er(2) of outer carboxylate oxygen atoms of the tris(oxydiacetato)erbate complex around Er(1). Each Er(1) ion is thus linked to four Er(2) and *vice versa*, Fig. 1. Between these layers there seem to be only van der Waals forces. An indication of a fourth water oxygen in a fourfold position (which would give 7 H_2O in the formula) was obtained in the first difference map, but in later calculations this peak was both weakened and located too close to C(3), 2.4 Å. Furthermore, the temperature coefficient of the tentative atom refined to high values. Therefore it was excluded from this model of erbium oxydiacetate.

The Er(1) ion is nine-coordinated, surrounded by a distorted tricapped trigonal prism (TCTP) of carboxylate and ether oxygen atoms. The coordination is similar to that in the other oxydiacetates.¹⁻³ The distances from the erbium ion to the six carboxylate oxygens are in the range 2.33–2.36 Å (mean 2.35 Å) and the distances to the ether oxygens significantly longer, 2.49–2.50 Å. Compared to the cerium-oxygen distances in the other investigated oxydiacetates,³ the former distance is 0.12 Å shorter, compatible with the decrease in ionic radius of 0.15 Å between cerium and erbium, while the latter distance is only 0.07 Å shorter. Using the same parameters as those defined in Table 5 of Ref. 3 to describe the TCTP polyhedron of Er(1) we obtain: $\rho=1.06$; $\theta=47.8^\circ$, torsion of prism 16.3° ; tilt of triangular

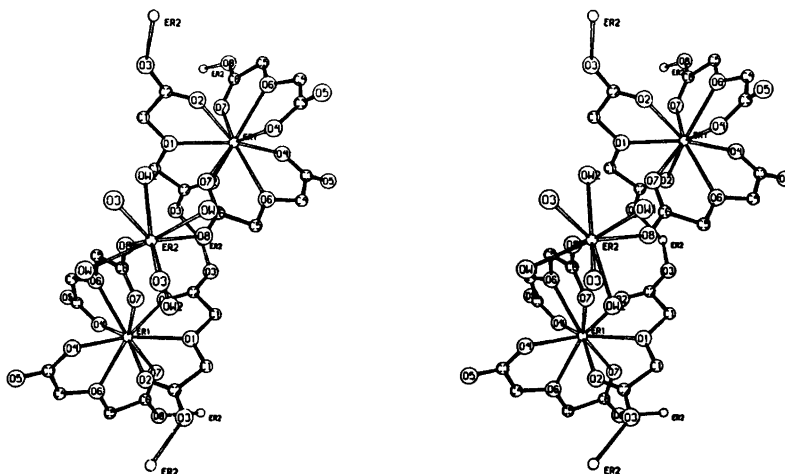


Fig. 1. A stereoscopic pair of drawings showing the coordination around the erbium ions looking down the a -axis. b is to the right and c upwards.

Table 1. Atomic parameters with estimated standard deviations in parentheses. B denotes the isotropic temperature factor.

Atom	$x/a (\times 10^4)$	$y/b (\times 10^4)$	$z/c (\times 10^4)$	$B (\text{Å}^2)$
Er(1)	0	1151(1)	2500	a
Er(2)	5078(2)	0	0	a
O(1)	0	-263(15)	2500	3.3 (5)
O(2)	1727(27)	518(13)	3420(17)	3.2 (4)
O(3)	2849(23)	-416(11)	4172(15)	2.6 (3)
O(4)	-1877(22)	2093(10)	2298(13)	2.4 (3)
O(5)	-3134(45)	3063(20)	1628(27)	5.9 (8)
O(6)	116(24)	1865(8)	1061(13)	2.5 (3)
O(7)	1798(19)	732(10)	1429(13)	2.1 (3)
O(8)	2939(24)	796(13)	119(16)	3.4 (4)
C(1)	1050(64)	-691(30)	3095(36)	6.1 (11)
C(2)	1893(26)	-114(13)	3628(19)	2.1 (4)
C(3)	-1812(39)	2624(19)	1748(25)	2.8 (6)
C(4)	-706(40)	2557(19)	1043(26)	4.4 (6)
C(5)	1025(36)	1692(17)	386(24)	3.2 (6)
C(6)	2008(37)	1014(19)	674(25)	3.1 (6)
OW(1)	5921(21)	1148(10)	655(14)	2.6 (3)
OW(2)	4169(27)	-265(12)	1486(17)	3.7 (4)
OW(3)	4208(34)	2258(17)	1434(21)	5.3 (5)

^a The anisotropic thermal parameters, calculated from the expression $\exp [-(h^2\beta_{11} + 2hk\beta_{12} + \dots)]$, are for Er(1): $\beta_{11} = 0.0047(4)$, $\beta_{22} = 0.0014(1)$, $\beta_{33} = 0.0021(3)$, $\beta_{12} = 0$, $\beta_{13} = 0.00020(2)$, $\beta_{23} = 0$ and for Er(2): $\beta_{11} = 0.0031(4)$, $\beta_{22} = 0.0016(1)$, $\beta_{33} = 0.0018(3)$, $\beta_{12} = 0$, $\beta_{13} = 0$, $\beta_{23} = 0.00034(1)$.

faces to the equatorial plane: 3° , to each other: 5° ; height of trigonal prism: 3.15 Å; edge of prismatic triangle: 2.99–3.07 Å, of equatorial triangle: 4.30–4.34 Å.

The Er(2) ion is eight-coordinated, surrounded by a distorted square antiprism of

oxygen atoms, four of which are outer carboxylate oxygens (O(3) and O(8)), belonging to the four nearest Er(1)-polyhedra, and the others the water oxygen atoms OW(1) and OW(2) (cf. Fig. 1). The distances from the erbium ion to the oxygen atoms of the poly-

hedra are in the range 2.31–2.40 Å (mean 2.36 Å). The value of θ (angle between the erbium-oxygen bonds and the pseudo eightfold rotation inversion axis) is in the range 53.7–59.7° (mean 56.7°), in agreement with that found in erbium glycolate (Table 7 in Ref. 8). The distances along the edges of the square planes are in the range 2.78–2.80 Å, and the distance between these planes 2.59 Å. They are almost parallel with the a -axis and tilted 0.5° to each other.

The distances and angles within the ligand molecules are not far from those found in the other lanthanoid oxydiacetate compounds. The two halves of the ligand containing O(1)–O(3) and C(1), C(2) are planar and the angle between them is 5°. In the other ligand the half containing O(7) and O(8) is planar while the other is more twisted (dihedral angles O(6)–C(5)–C(6)–O(8): –179°, O(6)–C(4)–C(3)–O(5): –151°). Apparently, O(5) has refined to a somewhat erroneous location.

The OW(3) water oxygen atom is not coordinated to erbium. It is within hydrogen bond distance from O(5) (2.74 Å), O(4) (2.80 Å), and OW(1) (2.74 Å).

As this structure contains both eight- and nine-coordinated erbium ions, erbium seems to have a preference for eight-coordination when it is not forced by the ligands to adopt nine-coordination as in the tris(oxydiacetato)erbate complex.

Acknowledgements. I thank Dr. J. Albertsson for many helpful discussions. The Swedish Natural Science Research Council gave financial support.

1. Albertsson, J. *Acta Chem. Scand.* 24 (1970) 3527.
2. Elding, I. *Acta Chem. Scand. A* 30 (1976) 649.
3. Albertsson, J. and Elding, I. *Acta Chem. Scand. A* 31 (1977) 21.
4. Cruickshank, D. W. J. In Pepinsky, R., Robertson, J. M. and Speakman, J. C., Eds., *Computing Methods and the Phase Problem in X-Ray Crystal Analysis*, Pergamon, Glasgow 1961, p. 45.
5. Cromer, D. T., Larson, A. C. and Water, J. T. *Acta Crystallogr.* 17 (1964) 1044.
6. Hanson, H. P., Herman, F., Lea, J. D. and Skillman, S. *Acta Crystallogr.* 17 (1964) 1040.
7. Cromer, D. T. and Liberman, D. *J. Chem. Phys.* 53 (1970) 1891.
8. Hansson, E. *On the Structure of Solid Rare Earth Oxalates and Malonates*, Thesis, Lund 1973.

Received July 6, 1976.

Preparation and Structure of Stoichiometric δ -NbN

A. NØRLUND CHRISTENSEN

Department of Inorganic Chemistry, Aarhus University, DK-8000 Aarhus C, Denmark

The cubic phase of niobium nitride, δ -NbN, can be obtained in a reaction between niobium and nitrogen. A rod pressed isostatically from niobium powder was heated by induction in pure nitrogen gas at 2.0 MPa in an ADL MP crystal growth furnace. For experimental details see Ref. 1. The sample was 15 cm long and 10 mm in diameter. When the sample was red-hot, a violent and fast exothermic reaction between niobium and nitrogen started. The sample became incandescent and measurements with a disappearing filament pyrometer indicated that the temperature was at least 1800 °C. After approximately 20 s, the whole volume of the sample had reacted with nitrogen and the temperature of the specimen dropped to the level determined by the power of the induction heater.

A Guinier powder pattern obtained with a Guinier de Wolff camera with $\text{CuK}\alpha_1$ radiation ($\lambda = 1.54051$ Å) and germanium ($a_{\text{Ge}} = 5.6576$ Å) as an internal standard showed that a sample treated as described above was cubic δ -NbN with $a = 4.394(3)$ Å. It was recently reported,¹ that zone melting of a specimen of δ -NbN at pressures up to 2 MPa resulted in a sample containing γ -NbN with the composition $\text{NbN}_{0.84(1)}$, and β -Nb₂N with the composition $\text{NbN}_{0.46(1)}$. A determination of the composition of δ -NbN is reported below.

A neutron diffraction powder pattern of δ -NbN was measured with a double axis neutron spectrometer at the DR3 reactor at Risø. The pattern was obtained with an incident neutron wave length of 0.998 Å, reflected from a (002) plane of a Be crystal. The collimations in front of and behind the sample were defined by Soller slits to be 21 and 30', respectively. The pattern was obtained for scattering angles (2θ) from 20 to 102° in steps of 0.2° and could be indexed with a cubic unit cell with $a = 4.39$ Å.

The structure of the compound was refined using the Rietveld refinement programs^{2,3} for powder profile intensities. The scattering lengths⁴ (in 10^{-12} cm) were: $b_{\text{Nb}} = 0.711$, and $b_{\text{N}} = 0.940$.

The intensities of the diffraction pattern had contributions from 18 reflections. Two of these, (400) and (440), had an additional scattering contribution from an unidentified impurity.

δ -NbN is isostructural with NaCl, space group $Fm\bar{3}m$, No. 225, with niobium in site 4a, and nitrogen in site 4b. The variable parameters used in the refinements are: Two isotropic temperature factors, an occupancy factor for

hedra are in the range 2.31–2.40 Å (mean 2.36 Å). The value of θ (angle between the erbium-oxygen bonds and the pseudo eightfold rotation inversion axis) is in the range 53.7–59.7° (mean 56.7°), in agreement with that found in erbium glycolate (Table 7 in Ref. 8). The distances along the edges of the square planes are in the range 2.78–2.80 Å, and the distance between these planes 2.59 Å. They are almost parallel with the a -axis and tilted 0.5° to each other.

The distances and angles within the ligand molecules are not far from those found in the other lanthanoid oxydiacetate compounds. The two halves of the ligand containing O(1)–O(3) and C(1), C(2) are planar and the angle between them is 5°. In the other ligand the half containing O(7) and O(8) is planar while the other is more twisted (dihedral angles O(6)–C(5)–C(6)–O(8): –179°, O(6)–C(4)–C(3)–O(5): –151°). Apparently, O(5) has refined to a somewhat erroneous location.

The OW(3) water oxygen atom is not coordinated to erbium. It is within hydrogen bond distance from O(5) (2.74 Å), O(4) (2.80 Å), and OW(1) (2.74 Å).

As this structure contains both eight- and nine-coordinated erbium ions, erbium seems to have a preference for eight-coordination when it is not forced by the ligands to adopt nine-coordination as in the tris(oxydiacetato)erbate complex.

Acknowledgements. I thank Dr. J. Albertsson for many helpful discussions. The Swedish Natural Science Research Council gave financial support.

1. Albertsson, J. *Acta Chem. Scand.* 24 (1970) 3527.
2. Elding, I. *Acta Chem. Scand. A* 30 (1976) 649.
3. Albertsson, J. and Elding, I. *Acta Chem. Scand. A* 31 (1977) 21.
4. Cruickshank, D. W. J. In Pepinsky, R., Robertson, J. M. and Speakman, J. C., Eds., *Computing Methods and the Phase Problem in X-Ray Crystal Analysis*, Pergamon, Glasgow 1961, p. 45.
5. Cromer, D. T., Larson, A. C. and Water, J. T. *Acta Crystallogr.* 17 (1964) 1044.
6. Hanson, H. P., Herman, F., Lea, J. D. and Skillman, S. *Acta Crystallogr.* 17 (1964) 1040.
7. Cromer, D. T. and Liberman, D. *J. Chem. Phys.* 53 (1970) 1891.
8. Hansson, E. *On the Structure of Solid Rare Earth Oxalates and Malonates*, Thesis, Lund 1973.

Received July 6, 1976.

Preparation and Structure of Stoichiometric δ -NbN

A. NØRLUND CHRISTENSEN

Department of Inorganic Chemistry, Aarhus University, DK-8000 Aarhus C, Denmark

The cubic phase of niobium nitride, δ -NbN, can be obtained in a reaction between niobium and nitrogen. A rod pressed isostatically from niobium powder was heated by induction in pure nitrogen gas at 2.0 MPa in an ADL MP crystal growth furnace. For experimental details see Ref. 1. The sample was 15 cm long and 10 mm in diameter. When the sample was red-hot, a violent and fast exothermic reaction between niobium and nitrogen started. The sample became incandescent and measurements with a disappearing filament pyrometer indicated that the temperature was at least 1800 °C. After approximately 20 s, the whole volume of the sample had reacted with nitrogen and the temperature of the specimen dropped to the level determined by the power of the induction heater.

A Guinier powder pattern obtained with a Guinier de Wolff camera with $\text{CuK}\alpha_1$ radiation ($\lambda = 1.54051$ Å) and germanium ($a_{\text{Ge}} = 5.6576$ Å) as an internal standard showed that a sample treated as described above was cubic δ -NbN with $a = 4.394(3)$ Å. It was recently reported,¹ that zone melting of a specimen of δ -NbN at pressures up to 2 MPa resulted in a sample containing γ -NbN with the composition $\text{NbN}_{0.84(1)}$, and β -Nb₂N with the composition $\text{NbN}_{0.46(1)}$. A determination of the composition of δ -NbN is reported below.

A neutron diffraction powder pattern of δ -NbN was measured with a double axis neutron spectrometer at the DR3 reactor at Risø. The pattern was obtained with an incident neutron wave length of 0.998 Å, reflected from a (002) plane of a Be crystal. The collimations in front of and behind the sample were defined by Soller slits to be 21 and 30', respectively. The pattern was obtained for scattering angles (2θ) from 20 to 102° in steps of 0.2° and could be indexed with a cubic unit cell with $a = 4.39$ Å.

The structure of the compound was refined using the Rietveld refinement programs^{2,3} for powder profile intensities. The scattering lengths⁴ (in 10^{-12} cm) were: $b_{\text{Nb}} = 0.711$, and $b_{\text{N}} = 0.940$.

The intensities of the diffraction pattern had contributions from 18 reflections. Two of these, (400) and (440), had an additional scattering contribution from an unidentified impurity.

δ -NbN is isostructural with NaCl, space group $Fm\bar{3}m$, No. 225, with niobium in site 4a, and nitrogen in site 4b. The variable parameters used in the refinements are: Two isotropic temperature factors, an occupancy factor for

Table 1. Results from neutron diffraction on a sample of δ -NbN.

	Site	Occupancy	B (\AA^2)
18 reflections; $R = 9.4$ %			
Nb	4a	1.0	0.6(2)
N	4b	1.00(4)	0.3(1)
16 reflections; $R = 3.7$ %			
Nb	4a	1.0	0.77(9)
N	4b	0.98(2)	0.26(5)

Table 2. Observed and calculated intensities for δ -NbN. Reading from left to right, the columns are: h k l I_{obs} I_{calc} .

1	1	1	6594	5971	5	1	1	8665	3144
2	0	0	163434	162989	3	3	3	2888	1048
2	2	0	157627	160406	4	4	0	65090	38216
3	1	1	5464	5734	5	3	1	2120	2811
2	2	2	67621	70289	6	0	0	15914	17045
4	0	0	71704	39061	4	4	2	63658	68178
3	3	1	9083	3860	6	2	0	60591	61886
4	2	0	120513	123773	5	3	3	2693	2674
4	2	2	102576	102404	6	2	2	60143	57092

nitrogen, a scale factor, three half-width parameters, a zero point parameter, and a unit cell parameter, giving a total of nine parameters. The results of the refinement including the 18 reflections are listed in Table 1. When the two reflections (400) and (440) were omitted from the refinements, the R -factor dropped from 9.4 to 3.7 % (see Table 1). The values of the occupancy factor and the two isotropic temperature factors obtained in the refinement with 16 reflections are not significantly different from the values obtained in the refinement with the 18 reflections. In Table 2 are listed the observed and calculated intensities from the refinement with the 18 reflections.

The investigation shows that the composition of the sample is $\text{NbN}_{0.98(2)}$, or that the sample is stoichiometric within experimental errors. It is interesting to note that the cubic phase, δ -NbN, with a stoichiometric composition thus can be made by direct reaction of a rod made from niobium powder and pure nitrogen at a pressure of 2 MPa. The temperature at the synthesis is mainly determined by the heat of reaction for the exothermic process and the preparation is completed in a period of time less than 1 min.

When a rod of stoichiometric δ -NbN was zone melted in an ambient nitrogen gas pressure of 2 MPa, it was observed that the molten zone expanded or boiled in the moment it was formed. This is because nitrogen gas is released

from the melt. The composition of the zone melted material is between $\text{NbN}_{0.5}$ and $\text{NbN}_{0.6}$,¹ when the material is zone melted at an ambient nitrogen gas pressure of 2 MPa. In order to prepare crystals of δ -NbN by zone melting it is most likely necessary to increase the ambient nitrogen gas pressure to 10 or 20 MPa.

Acknowledgements. The author is indebted to Mrs. B. Lebech and Dr. O. W. Dietrich, Department of Physics, Risø, for assistance in measuring the neutron diffraction powder pattern.

- Christensen, A. N. *Acta Chem. Scand. A* 30 (1976) 219.
- Rietveld, H. M. *Program F418-Fortran IV Version*, Reactor Centrum Nederland, Petten (N. H.), The Netherlands.
- Rietveld, H. M. *J. Appl. Crystallogr.* 2 (1969) 65.
- Bacon, G. E. *Acta Crystallogr. A* 28 (1972) 357.

Received December 6, 1976.

Preparation of Single Phases and Single Crystals of Niobium–Germanium Compounds

SVEND ERIK RASMUSSEN

Department of Inorganic Chemistry, Aarhus University, DK-8000 Aarhus C, Denmark

Niobium-germanium compounds were prepared by floating zone melting of niobium-germanium mixtures. Compounds with a β -W-like structure (A15) and composition Nb_xGe were prepared as single phases for $6 \geq x \geq 4$. Small single crystals were found. Single crystals of Nb_6Ge_3 of volume 30 mm^3 were prepared by peritectic melting. Sintering of niobium-germanium mixtures leads to formation of both an A15 phase and of Nb_6Ge_3 also at compositions where one of the phases disappears on melting and re-solidification.

The formation of niobium-germanium compounds has been investigated by several authors. Carpenter and Searcy¹ reported a compound of stoichiometry Nb_3Ge and of A15 structure. They also described a compound NbGe_3 . Geller² pointed out that the lattice constant for Nb_3Ge reported in Ref. 1 indicated a deviation from stoichiometry. Reed *et al.*³ found that the stability range of the A15 structure is from $\text{Nb}_{6.29}\text{Ge}$ to $\text{Nb}_{4.52}\text{Ge}$. They found transition temperatures for superconductivity from 4.9 K to 5.5 K. Carpenter⁴ also studied the composition range of the A15 structure. His results agree with those of Reed *et al.* Matthias *et al.*⁵ achieved a more stoichiometric Nb_3Ge A15 phase with a critical temperature of 17 K by rapid quenching of a melt of Nb and Ge. Gavaler⁶ used sputtering techniques to fabricate films of Nb_3Ge which exhibit superconductivity above 21.4 K. Müller⁷ published a phase diagram for NbGe covering the region 60–100 atomic % Nb. Heller⁸ gave a slightly more complete phase diagram.

In the composition range 50–100 atomic % Nb the phase of A15 structure and one other

niobium-germanium compound, Nb_6Ge_3 , are generally encountered. Nb_6Ge_3 crystallizes in the tetragonal system. Nowotny *et al.*⁹ determined its structure from powder photographs. Jagner and Rasmussen¹⁰ redetermined the structure using single crystal X-ray diffraction, and Larsen and Rasmussen¹¹ confirmed their results by single crystal neutron diffraction.

As most structural investigations in the Nb–Ge system have been carried out using powder methods the present work aims at investigating the possibilities of producing single crystals of Nb–Ge compounds in order to get improved crystallographic description of these compounds. As a first attempt to grow single crystals, the conditions for producing single phase samples were investigated.

EXPERIMENTAL

Powder mixtures of nominally 99.8 % Nb and 99.99 % Ge were pressed into nearly cylindrical rods of 12 mm diameter and 100–130 mm length by isostatic pressing at a force of $4 \times 10^5 \text{ N}$. The rods were sintered in an A.D. Little model MP furnace in a helium atmosphere at 1000–1300 °C by inductive heating. Afterwards a molten zone of width ~ 10 –15 mm was passed through the sample at a speed of about 10 mm/h. All operations were crucible free. The temperature of the molten zone was estimated at intervals using a pyrometer. Fairly large crystals (30 mm^3) of nominal composition Nb_6Ge_3 were grown in the following manner: Rods of compositions Nb_6Ge_3 and NbGe were sintered in the usual way. A piece of NbGe of width 15 mm was inserted in the Nb_6Ge_3 rod and melted, and the molten zone was passed through the sample. Samples of NbGe composition melt peritectically, the melt being in equilibrium with solid Nb_6Ge_3 .

Table 1. Phases observed in experiments of sintering and/or zone melting mixtures of niobium and germanium.

Initial composition	Phases after sintering	Phases after zone melting	
		Surface layer	Core
12Nb + Ge	Nb + unknown phase		
12Nb + Ge			A15, Nb
9Nb + Ge	Nb ₅ Ge ₃ , Nb		
9Nb + Ge		Nb, NbO	A15, Nb ₅ Ge ₃
6Nb + Ge	Nb ₅ Ge ₃ , A15, Nb		A15, Nb ₅ Ge ₃ , Nb
6Nb + Ge			A15
5Nb + Ge			A15
4.5Nb + Ge			A15
4Nb + Ge			A15
5Nb + 3Ge + (Nb + Ge)	Nb ₅ Ge ₃		Nb ₅ Ge ₃ , A15
Peritectic melting			Nb ₅ Ge ₃
3Nb + Ge	A15, Nb ₅ Ge ₃	A15, Nb ₅ Ge ₃	A15, Nb ₅ Ge ₃

Although helium of high purity was used, a thin layer of NbO was invariably formed at the surface of part of the sample, always on the part which was melted first.

After the zone melting we cut the rods perpendicular to the cylinder axis in several pieces and took samples partly from the surface and partly from the interior by filing with a diamond file. The powder obtained was examined using a Guinier-de Wolff powder camera. The plane surfaces of a number of samples were ground and polished and examined by metallographic methods. The chemical composition was established by X-ray fluorescence analysis. Typical results are given in Tables 1 and 2.

The formation of Nb-Ge phases was also examined using a high temperature X-ray powder diffractometer, PW 1158. Tantalum sample holders were employed and the samples were surrounded by a helium atmosphere.

Diffractograms were taken at temperatures ranging from 25 °C to 1800 °C. A surface layer of NbO and NbO₂ was invariably formed during heating and as the linear absorption coefficient for Nb towards CuK α radiation is

1277 cm⁻¹ even a thin oxide layer obscures observations of reactions in the bulk of the sample. The lattice constant of Nb was determined as a function of temperature. When a vacuum of $P \leq 2 \times 10^{-5}$ Torr was obtained and the temperature was above 1000 °C, the formation of niobium oxides was avoided. The following lattice constants were found for Nb: $a = 3.3027$ Å (296 K), 3.329 Å (1268 K), 3.345 Å (1738 K).

RESULTS AND DISCUSSION

According to the phase diagram by Müller and Heller⁸ the A15 phase melts peritectically at 1910 °C and Nb₅Ge₃ is formed by incongruent melting. It is also reported that Nb₅Ge₃ melts congruently at 2065 °C. We have not been able to confirm this supposition. Nb₅Ge₃ should also be formed at peritectic melting of phases of composition NbGe. The latter observation is in agreement with the way in which we prepared large crystals of Nb₅Ge₃. This compound has a narrow composition range as shown by the X-ray single crystal analysis of Jagner and Rasmussen¹⁰ on a crystal formed from an experiment where the initial composition was 3Nb + Ge and a neutron crystallographic investigation by Larsen and Rasmussen¹¹ on a large crystal from the peritectic formation as described in EXPERIMENTAL. In both investigations excellent agreement was found between observed and calculated structure factors assuming a stoichiometric composition. The Nb₅Ge₃ phase is formed readily at sintering processes also in concentration ranges where

Table 2. X-Ray fluorescence analysis for niobium at various sections in a rod after zone melting. Initial composition: 5Nb + Ge: 86.49 wt % Nb.

Zone travel (mm)	Wt % Nb
12	86.8
14	86.9
38	86.1
40	87.0
61	88.8
63	86.9

Table 3. Phases identified by powder diffractometry at various temperatures. The sample holder was a tantalum boat.

Initial composition	T/K	Phases identified	Lattice constants (Å)
3Nb, Ge	1278	Nb ₅ Ge ₃ (NbO, NbO ₂)	
3Nb, Ge	1483	A15 Nb ₅ Ge ₃ (NbO, NbO ₂)	5.169
6Nb, Ge	787	Nb, Ge	
6Nb, Ge (a)	2000	hexagonal phase	a = 5.346 c = 5.021
6Nb, Ge (a) after cooling	296	hexagonal phase	a = 5.286 c = 4.977
6Nb, Ge after heating to 2473 K	296	hexagonal phase	a = 5.292 c = 4.972

it is not stable at equilibrium conditions. The lattice constants vary slightly according to the composition of the matrix in which the compound is formed (Table 4).

According to the evidence from the X-ray powder diagrams, the A15 phase is formed as a single phase or at least nearly so at the zone melting process when the compositions of the rods are in the interval Nb₅Ge to Nb₄Ge. For a given rod, *e.g.* of initial composition Nb₅Ge, the X-ray fluorescence analysis showed that no significant change in composition accompanied the travel of the molten zone. It is therefore probable that equilibrium was established during the zoning process. Single crystals of volume $\sim 10^{-3}$ mm³ were found in runs where initial compositions were Nb₄Ge, Nb₅Ge and Nb₆Ge, respectively. These crystals

have been subject to single crystal X-ray investigations which will be reported in a forthcoming publication in collaboration with R. G. Hazell. For compositions $5/3 \leq x \leq 3$ of Nb_xGe the A 15 phase is formed together with Nb₅Ge₃. The latter compound is formed in smaller or greater amounts by sintering processes at temperatures between 500 °C and the melting points in the range $5/3 \leq x \leq 9$.

In the sintering processes the A15 phase was invariably formed together with the Nb₅Ge₃ phase. It is therefore unlikely that a pure A15 phase of stoichiometry Nb₅Ge can be formed by sintering. The A15 phase of this composition is not stable and apparently it has to be prepared by techniques which prevent equilibrium from being established (Matthias *et al.*¹⁵, Gavalier¹⁶).

Table 4. Lattice constants of A15 compounds and of Nb₅Ge₃.^a

Initial comp.	Phases after zone melting	A15 a, Å	Nb ₅ Ge ₃ a, Å	c, Å
12Nb, Ge	A15, Nb	5.177		
9Nb, Ge	A15, Nb ₅ Ge ₃	5.178		
6Nb, Ge	A15 (Nb ₅ Ge ₃)	5.167		
5Nb, Ge	A15	5.170		
4.5Nb, Ge	A15	5.170		
4Nb, Ge	A15	5.170		
3Nb, Ge	A15, Nb ₅ Ge ₃	5.166	10.162	5.144
5Nb, 3Ge	Nb ₅ Ge ₃ , A15	5.167	10.173	5.141
Peritectic melting	Nb ₅ Ge ₃		10.170	5.139

^a Average standard deviation ~ 1 part in 2000.

Because of the presence of niobium oxides in the samples examined by high temperature X-ray diffractometry, it is difficult to draw definite conclusions from these experiments except in one case. When a mixture of composition $6\text{Nb} + 1\text{Ge}$ is heated in a tantalum sample holder, a hexagonal phase is formed which remains on cooling (Table 3). We checked that it was not due to a thin surface layer by taking a Guinier diagram of the bulk of the sample. We did not observe this hexagonal phase in any of the experiments using the crucible free technique.

The lattice constant of the A15 phase depends to some extent on the composition of the matrix in which it is formed (Table 4). The variation is so small, however, that the lattice constant cannot be used for estimating analytical compositions. The precision of our measurements is not high enough for this purpose.

T. Claeson *et al.*¹² measured critical temperatures of superconductivity of Nb_3Ge_3 crystals. Similar measurements were carried out on A15 phases too. We hope to report on these measurements later.

Acknowledgements. I thank B. Lundtoft for excellent technical assistance. She carried out the majority of the experimental work reported. I am grateful to the Danish Science Research Council for having covered the cost of the high temperature powder diffractometer.

REFERENCES

1. Carpenter, J. H. and Searcy, A. W. *J. Am. Chem. Soc.* 78 (1956) 2079.
2. Geller, S. *Acta Crystallogr.* 9 (1956) 885.
3. Reed, T. B., Gatos, H. C., LaFleur, W. S. and Roddy, J. T. In Brock, G. E., Ed., *Metallurgy of Advanced Electronic Materials*, Interscience, New York 1963, p. 71.
4. Carpenter, J. H. *J. Phys. Chem.* 67 (1963) 2141.
5. Matthias, B. T., Geballe, T. H., Willens, R. H., Corenzwit, E. and Hull, G. W. *Phys Rev.* 139 (1965) A 1501.
6. Gavaler, J. R. *Appl. Phys. Lett.* 23 (1973) 480.
7. Müller, A. *Z. Naturforsch. Teil A* 25 (1970) 1659.
8. Heller, W. *Z. Metallkd.* 64 (1973) 124.
9. Nowotny, H., Searcy, A. W. and Orr, J. E. *J. Phys. Chem.* 60 (1956) 677.
10. Jagner, S. and Rasmussen, S. E. *Acta Crystallogr. B* 31 (1975) 2881.

11. Larsen, F. K. and Rasmussen, S. E. *In preparation.*
12. Claeson, T., Ivarsson, J. and Rasmussen, S. E. *J. Appl. Phys. In press.*

Received July 21, 1976.

NMR and IR Studies on Cyclic Sulfites. VIII. Sulfites Substituted at the Axial Position of Carbon Atom 5

PER ALBRIKTSEN * and TORE THORSTENSON

Department of Chemistry, University of Bergen, N-5014 Bergen-Univ., Norway

NMR and IR studies on three cyclic sulfites substituted at carbon 5 with the substituent occupying the *axial* position have been performed. The conformation is discussed on the basis of the spectral properties, examining the molecules in both a polar and a non-polar solvent. For these molecules an equilibrium is proposed between two chair forms (axial and equatorial S=O bond) and a twisted one.

NMR, IR, and dipole moment measurements on trimethylene (TM) sulfites substituted at carbon 5 have been reported.¹⁻⁹ It has been found that the equatorially substituted sulfites exist in the chair conformation with preferentially axial S=O group.⁶ The axially substituted 5-methyl- and 5-*tert*-butyl-TM sulfites have been examined^{2,6} and found to exist in an equilibrium between two chair conformations with the S=O bond situated in the axial or equatorial position. The preference for the S=O axially as compared to the S=O equatorially oriented is estimated to be 3.5 kcal/mol.^{2,3}

SPECTRAL ANALYSIS

The 5-phenyl- and 5-*tert*-butyl-TM sulfites constitute an [AB]₂C system with respect to the aliphatic ring protons. The appearances of the two spectra seem very similar (Fig. 1). Three main regions are due to the protons in position 4 and 6 (bands A and B, respectively), and the protons in position 5 (band C). The

proton in equatorial position 5 comes to resonance at lower frequency for the 5-*tert*-butyl substituted sulfite as compared to the 5-phenyl substituted one due to the difference in the shielding effects of the two substituents.

The protons in 4 (or 6) position are differently shielded by the S=O group. The lower field region is assigned to the axial protons. From the quartet structure of band A and B one large coupling constant (~ 12.0 Hz) is assigned to the 2J_4 (2J_6) coupling.

The fully computer analyzed 60 and 100 MHz spectra, with CCl₄ as solvent, and 60 MHz with CH₃CN as solvent resulted in good correlation between calculated and experimental spectra. The final r.m.s. values obtained were better than 0.06 when 7 to 9 of the 9 possible parameters were allowed to vary and about 40 transitions were fitted.

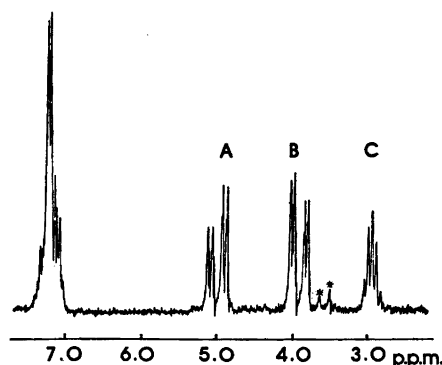
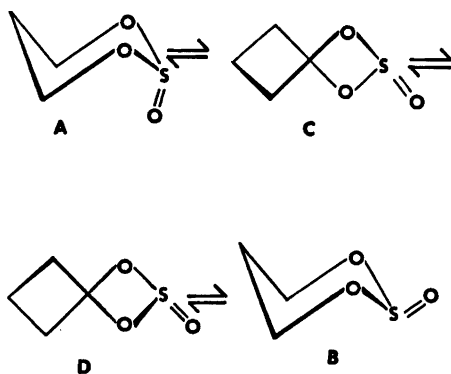


Fig. 1. The 60 MHz spectrum of axial 5-phenyl-trimethylenesulfite. (Solvent: CCl₄). An asterisk indicates impurity.

* Present address: Rafinor A/S & Co., N-5154 Mongstad, Norway.

RESULTS AND DISCUSSION

TM sulfite and some 5 equatorially substituted TM sulfites have been shown to exist in the chair conformation with the S=O group occupying the axial position in the ring.^{5,6} Other substituted cyclic sulfites are found to exist in non-chair conformations^{3,7,10} or in chair conformation with the S=O group in the equatorial position.¹⁰ Albriktsen⁶ has suggested that 5-methyl-TM sulfite with axial substituent exists in an equilibrium between two chair conformations with ax. and eq. S=O group, in which at most 2 % of the conformer with equatorial S=O group exists.



An NMR and IR study has been reported³ for 5-*tert*-butyl-TM sulfite with axial substituent. It has been concluded that the molecule exists in an equilibrium between two chair conformers A and B. Albriktsen⁶ has found that J_{4esa} is in the range 4.2–4.6 Hz in chair

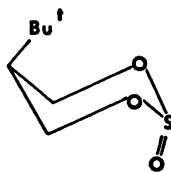
forms with an axial S=O group. Supposing an equilibrium as reported³ we will have A→B ($J_{4esa} \rightarrow J_{4ase}$) and excluding substituent effects on the coupling constants, a 4a5e coupling of 4.6 Hz for 5-*tert*-butyl-TM sulfite is possible for conformer B alone (Table 1).

Wucherpennig¹⁰ has calculated the dihedral angles for the conformers C and D. Applying Karplus plot, he calculated the corresponding coupling constants for the 4a5e coupling to be 6–7 Hz. From Table 1, it is evident that an equilibrium involving only the forms A and B is not probable.

Changing the solvent from a nonpolar to a polar one, J_{4ase} increases with only 0.15 Hz; the J_{4ese} , however, is increasing with approximately 2.1 Hz. The latter will have contribution from J_{4asa} (~12 Hz in conformer B) by an A→B transition. This comparatively small increase in J_{4ase} and the great increase in J_{4ese} may then be suggestive of a comparatively greater contribution from conformer B in a more polar medium, as anticipated from the dipole moment values for the different conformers,¹⁰ Table 2. Dipole moment measurements which have been performed¹¹ are also suggestive of a conformational equilibrium. The most probable equilibrium will consequently be one with contribution from all the symmetric forms; A, B, C, and D.

Looking at Table 3 concerning 5-phenyl-TM sulfite, no significant change in J_{4ase} is observed when changing the solvent. J_{4ese} , however, is changed from 3.2 to 4.5 Hz when increasing the polarity of the solvent. This suggests

Table 1. Spin-spin coupling constants (Hz) calculated from 60 and 98 MHz spectra of 5-*tert*-butyl-TM sulfite.



Solvent	2J_4	${}^3J_{4ese}$	${}^3J_{4ase}$	${}^4J_{4ese}$	${}^4J_{4asa}$	${}^4J_{4esa}$
CH ₃ CN ^a	-12.02	6.80	5.10	1.73	-0.20	-0.07
CCl ₄ ^b	-12.21	4.74	4.95	1.45	-0.15	-0.01

^a 60 MHz. ^b 98 MHz.

Table 2. Calculated dipole moment values for the different conformers of TM sulfite.¹⁰

Conformer	μ (D)
A	3.55 exp.
B	5.22 exp.
C	4.5 calc.
D	4.5 calc.

a conformational equilibrium, when the concentration of species with equatorial S=O bond grows increasing the polarity of the solvent.

If an equilibrium $S=O(a) \rightleftharpoons S=O(e)$ exists, the observed coupling constants can be expressed by eqn. 1

$$J_{4e5c}^{obs} = nJ_{4e5c} + (1-n)J_{4a5a} \quad (1)$$

By assuming ⁵ $J_{4e5c} = 2.73$ and $J_{4a5a} = 12.08$ and excluding substituent effects, we find that 5 % of conformer B is present in CCl_4 and 19 % in CH_3CN . The magnitude of J_{4a5a} may suggest contribution from the twisted conformers C and D in the equilibrium. The effect from the equatorial S=O bond may be the reason why J_{4a5a} is comparatively great since this coupling constant is 2.61 Hz in unsubstituted TM sulfite.⁶

It is known that the orientation of the electrons of a β -substituent may cause changes in a geminal coupling.¹² It is possible that such an effect also influences the vicinal coupling. The *gem*-coupling ³ J_4 decreases from -11.50 Hz in CCl_4 as solvent, to -12.22 Hz in CH_3CN .

However, the change in J_{4a5c} from unsubstituted TM sulfite to the molecule in discussion, is so large that we cannot exclude the participation of twisted forms in the equilibrium.

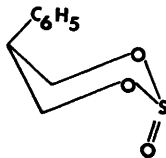
INFRARED SPECTRA

Several cyclic sulfites have been examined by IR spectroscopy.^{2-4,10,13} TM sulfite shows a strong absorption at 1190 cm^{-1} , and this frequency has been assigned to an *axial* S=O stretching vibration in a 6-membered ring.² *trans*-4,6-Dimethyl-TM sulfite has been proposed to exist in chair conformation with equatorial S=O bond.¹⁰ This molecule has a S=O absorption at 1240 cm^{-1} . This absorption has then been assigned an *equatorial* S=O bond in a 6-membered ring. Maroni and Tisnes⁹ have found an IR absorption at 1218 cm^{-1} for 4,5,6-trimethyl-TM sulfite. Furthermore, an absorption at 1224 cm^{-1} for *cis*-4,6-dimethyl-TM sulfite has been reported.⁹ These were assigned to a *twisted* conformer.

The nature of the solubility mechanism implies that polar conformers are to be favoured in a polar medium. The IR spectra of all the three molecules, 5-methyl-, 5-phenyl-, and 5-*tert*-butyl-TM sulfite with axial substituent show considerable changes at approximately 1200 cm^{-1} when changing the solvent from a nonpolar to a polar one (Fig. 2).

The intensity of the absorption at $\sim 1230\text{ cm}^{-1}$ is greatly increased at the expense of the one at $\sim 1200\text{ cm}^{-1}$ in the polar medium. This may also be suggestive of a conformational

Table 3. Spin-spin coupling constants (Hz) calculated from 60 and 98 MHz spectra of 5-phenyl-TM sulfite.



Solvent	² J_4	³ J_{4e5c}	³ J_{4a5c}	³ J_{4e5c}	³ J_{4a5a}	³ J_{4e5a}
CH_3CN	-12.22	4.50	3.80	1.83	-0.66	-0.16
CCl_4	-11.48	3.22	3.79	1.58	-0.20	-0.25
CCl_4^a	(-11.59)	(3.15)	(3.85)	(1.49)	(-0.21)	(-0.31)

^aNumbers in parentheses refer to 98 MHz spectra.

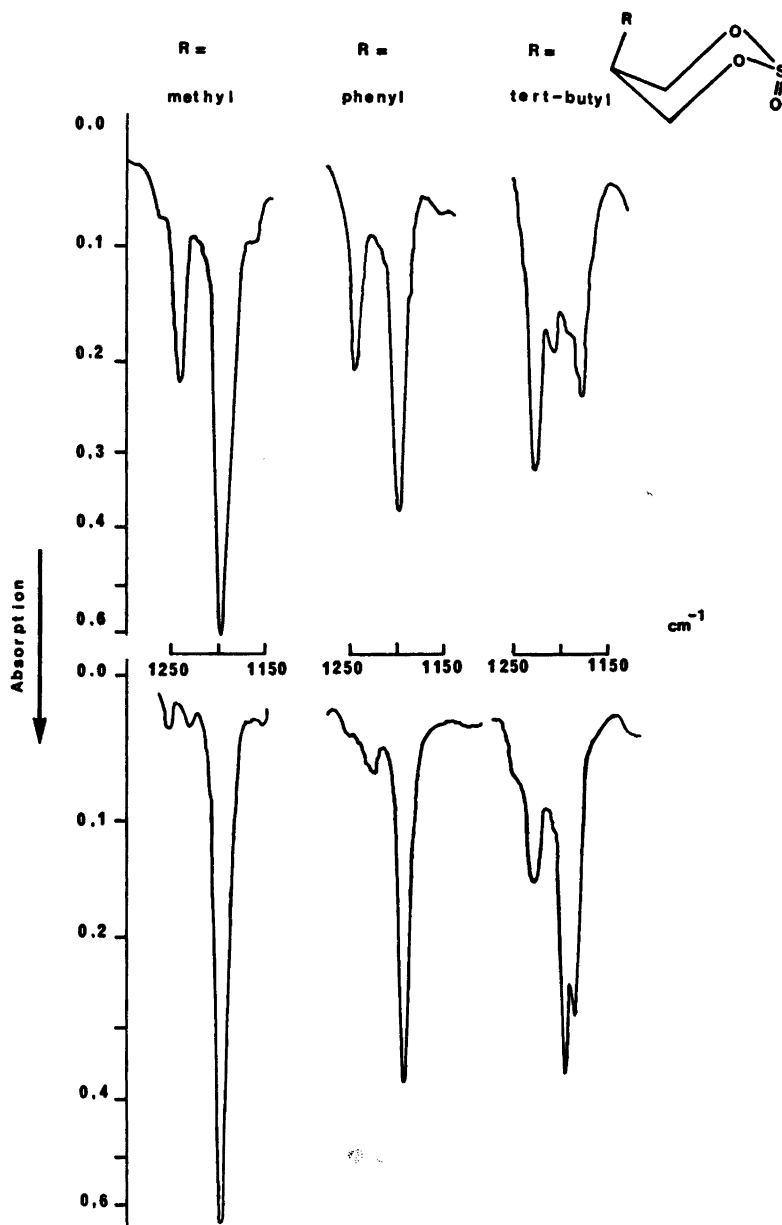


Fig. 2. The IR spectra of axial 5-substituted TM sulfites. (Solvents: Acetonitrile, upper spectra; 1,1,2,2-tetrachloroethane, lower spectra).

equilibrium with participation of a conformer with equatorial S=O bond.

In all cases examined (neat and in the two solvents) the IR spectra of 5-*tert*-butyl-TM sulfite with axial substituent show an absorp-

tion at ~ 1210 cm^{-1} . A weak shoulder is found at 1205 cm^{-1} in the spectrum of 5-phenyl-TM sulfite in acetonitrile as solvent. These absorptions are probably due to twisted conformers. Both the 1210 and the 1230 cm^{-1} peaks of

5-*tert*-butyl-TM sulfite are stronger in the more polar solvent which was to be expected due to the higher dipole moment of both the chair form with eq. S=O bond and the twisted ones. From the IR spectra it also seems conceivable that the contribution from the chair conformer with eq. S=O bond increases more than the contribution from the twisted conformer when changing to the more polar solvent.

EXPERIMENTAL

The 2-substituted 1,3-propane-diols were all prepared from the corresponding diethylmalonates by reduction with lithium aluminium hydride according to the method of Eliel *et al.*¹³

The cyclic sulfites were prepared according to the following method: The appropriate diol was dissolved in dry chloroform (ca. 20 % w/w) with two equivalents of pyridine. 1.02 equivalents of thionyl chloride, dissolved in three times its volume of chloroform, was added dropwise under stirring. The temperature was kept at 0 °C for about 3 h. The reaction mixture was filtered, and the filtrate was washed with a 2 % NaHCO₃ solution, 0.1 N HCl and water, respectively. The solution was dried over MgSO₄ prior to distillation.

The purity of the compounds was checked by NMR spectra and GLC analyses. The isomers of 5-methyl-TM sulfite (92 % S=O (a) 8 % S=O (e)) were separated by GLC on an Aerograph Autoprep A-700 with a 2.1 m × 6.0 mm column packed with 10 % PDEAS and 10 % Carbowax on Chromosorb W, OMCS A/W, 45/60 Mesh. The isomers of 5-phenyl-TM sulfite [84 % S=O (a) and 16 % S=O (e)] were separated by dissolving the crude product in ethanol. Since the isomer with axial phenyl group was negligibly soluble, it was filtered off at ca. 0 °C and recrystallized from ethanol as long white needles. (M.p. 60–62 °C). The isomers of 5-*tert*-butyl-TM sulfite (57 % S=O (a) and 43 % S=O (e)) were separated by cooling the crude product to -10 °C. The isomer with the axial substituent was then purified by GLC.

The NMR spectra were recorded in 5 mm O.D. sample tubes, and a small quantity of TMS was added to serve as reference and locking substance. The solvents used were CCl₄ and CH₃CN of spectroscopic purity. Dry nitrogen was bubbled through the solution to remove traces of oxygen.

The spectra were recorded by a JEOL JNM-C-60H instrument operating at 60 MHz (ca. 27 °C) and on a Varian HA-100 operating at 98 MHz (ca. 35 °C). All spectra were recorded in an internal lock mode with frequency sweep at 1.5 Hz/cm and calibrated every 5 Hz using a frequency counter. The counters were accurate

to 0.1 Hz for a 10 s count. The line position was taken as average of several spectra and is assumed to be accurate to about 0.05 Hz.

The IR spectra were recorded on an Unicam SP 200G instrument. Polystyrene was used for calibration. The spectra were recorded as 0.1 M solutions in CCl₄ and CH₃CN using cells with 0.1 mm path length.

REFERENCES

1. Van Woerden, H. F. and White, R. F. M. *Chem. Ind. London* (1963) 1956.
2. Van Woerden, H. F. and Havinga, E. *Rec. Trav. Chim. Pays-Bas* 86 (1967) 341.
3. Van Woerden, H. F. and Havinga, E. *Rec. Trav. Chim. Pays-Bas* 86 (1967) 353.
4. Cazaux, M. M. L. and Maroni, P. *Tetrahedron Lett.* (1969) 3667.
5. Albriktsen, P. *Acta Chem. Scand.* 25 (1971) 478.
6. Albriktsen, P. *Acta Chem. Scand.* 26 (1972) 1783.
7. Albriktsen, P. *Acta Chem. Scand.* 26 (1972) 3678.
8. Cazaux, L. and Maroni, P. *Bull. Soc. Chim. Fr.* 2 (1972) 785.
9. Maroni, P. and Tisnes, P. *Bull. Soc. Chim. Fr.* 2 (1972) 780.
10. Wucherpfennig, W. *Justus Liebig's Ann. Chem.* 737 (1970) 144.
11. Wood, G., McIntosh, J. M. and Miskow, M. H. *Can. J. Chem.* 49 (1971) 1202.
12. Pople, J. A. and Bothner-By, A. A. *J. Chem. Phys.* 42 (1965) 1339.
13. Eliel, E. L. and Knoeber, M. C. *J. Am. Chem. Soc.* 90 (1968) 3444.

Received June 14, 1976.

Étude de la Conductivité Ionique des Solutions Solides

$\text{Li}_{1-x}\text{Ta}_3\text{O}_{8-x}\text{F}_x$ et $\text{Li}_{1-x}\text{Ta}_{3-x}\text{W}_x\text{O}_8$

JEAN-MAURICE REAU, GUY MAGNIEZ, JEAN-PIERRE CHAMINADE, MICHEL POUCHARD et PAUL HAGENMULLER

Laboratoire de Chimie de Solide du C.N.R.S., Université de Bordeaux I, 351 Cours de la Libération, 33405 Talence, France

La conductivité des ions lithium au sein des solutions solides $\text{Li}_{1-x}\text{Ta}_3\text{O}_{8-x}\text{F}_x$ et $\text{Li}_{1-x}\text{Ta}_{3-x}\text{W}_x\text{O}_8$ ($0 \leq x \leq 1$) a été étudiée en fonction des compositions. Des corrélations ont été établies entre propriétés électriques et structurales.

The conductivity of the lithium ions in the $\text{Li}_{1-x}\text{Ta}_3\text{O}_{8-x}\text{F}_x$ and $\text{Li}_{1-x}\text{Ta}_{3-x}\text{W}_x\text{O}_8$ ($0 \leq x \leq 1$) solid solutions has been investigated. Electrical and structural data are correlated.

L'utilisation d'accumulateurs à électrolytes solides de capacité élevée est l'une des solutions de choix envisagée pour résoudre le problème du stockage de l'énergie soit pour ajuster la fourniture d'énergie primaire à la consommation soit à bord d'engins mobiles. L'obtention d'électrolytes solides qui soient des isolants électroniques, mais comportant une forte mobilité ionique, constitue l'étape préliminaire indispensable. Les études effectuées actuellement sur de tels matériaux ont porté principalement sur la zircone stabilisée, les alumines β et β'' ou les composés halogénés de l'argent.^{1a} Celles-ci ont d'ailleurs abouti à la mise au point d'un générateur électrochimique utilisant l'action du sodium sur le soufre.⁷ Des considérations énergétiques et massiques ont orienté nos recherches vers le lithium plus léger et susceptible de donner des tensions plus élevées que le sodium.

A défaut de réseaux dans lesquels les ions Li^+ pourraient jouir d'une mobilité bidimensionnelle comme au sein des alumines β et β'' , quelques structures particulières où les ions Li^+ sont susceptibles de migrer au sein de tunnels ont fait l'objet de nos recherches.

Le réseau de la variété de haute température β du tantalate de lithium LiTa_3O_8 isotype de $\text{LiNb}_3\text{O}_{15}\text{F}^8$ est formé de blocs constitués d'une bipyramide dont la base pentagonale est associée par des arêtes communes à cinq octaèdres adjacents.⁹ Les blocs liés par des sommets communs laissent apparaître des cavités qui constituent des tunnels parallèles à l'axe \vec{b} dans lesquels peuvent s'insérer les atomes de lithium (Fig. 1). Pour placer les quatre atomes de lithium de la maille élémentaire, nous disposons de six sites de coordinence 12 [positions (4j) et (2d)] et de deux sites plus petits de coordinence 9 [position (2f)]. Compte tenu de cette structure il semblait raisonnable d'envisager pour $\text{LiTa}_3\text{O}_8\beta$ une possibilité de conduction ionique due au déplacement du lithium dans les tunnels. Nous avons donc entrepris dans la première partie de ce travail l'étude des propriétés de transport de $\text{LiTa}_3\text{O}_8\beta$.

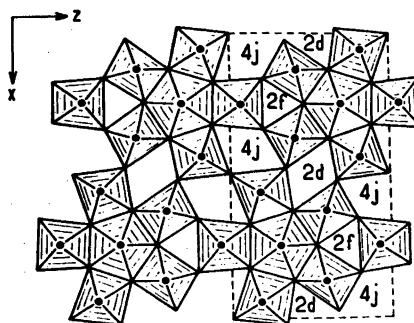


Fig. 1. Projection de la structure de $\text{LiTa}_3\text{O}_8\beta$ sur le plan (010).

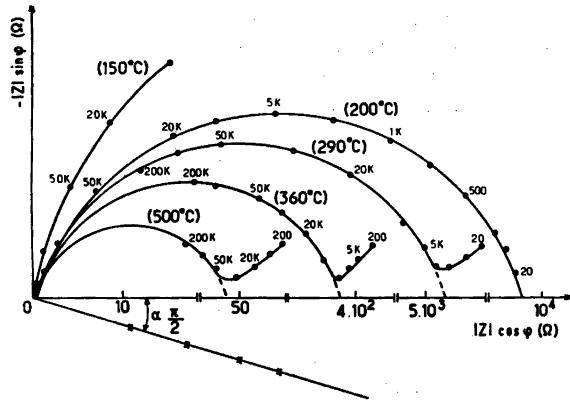


Fig. 2. Diagramme d'impédance complexe de $\text{LiTa}_3\text{O}_8\beta$ à diverses températures.

Nous avons montré dans un mémoire antérieur¹⁰ que $\text{LiTa}_3\text{O}_8\beta$ formait avec la variété haute température de l'oxyfluorure $\text{Ta}_2\text{O}_7\text{F}^{11}$ une solution solide $\text{Li}_{1-x}\text{Ta}_3\text{O}_{8-x}\text{F}_x$ ($0 \leq x \leq 1$) sans lacune de miscibilité. Le passage de $\text{Ta}_2\text{O}_7\text{F}$ à LiTa_3O_8 correspond au remplissage progressif de tunnels du réseau par des ions Li^+ . L'étude des propriétés électriques de $\text{Li}_{1-x}\text{Ta}_3\text{O}_{8-x}\text{F}_x$, entreprise dans une seconde partie, devait permettre de déterminer l'évolu-

tion des propriétés de transport au sein de cette solution solide en fonction du taux de lithium inséré. Cette étude a ensuite été étendue à une seconde solution solide que nous avons mise en évidence entre $\text{LiTa}_3\text{O}_8\beta$ et Ta_2WO_8 ,¹² de formule $\text{Li}_{1-x}\text{Ta}_{3-x}\text{W}_x\text{O}_8$ ($0 \leq x \leq 1$).

Les mesures électriques ont été effectuées en courant alternatif entre 20 Hz et 200 kHz par la méthode des impédances complexes.¹³ Nous avons montré au cours d'études précédentes^{14a17} que c'est là une méthode de choix pour l'étude des propriétés électriques des électrolytes sol-

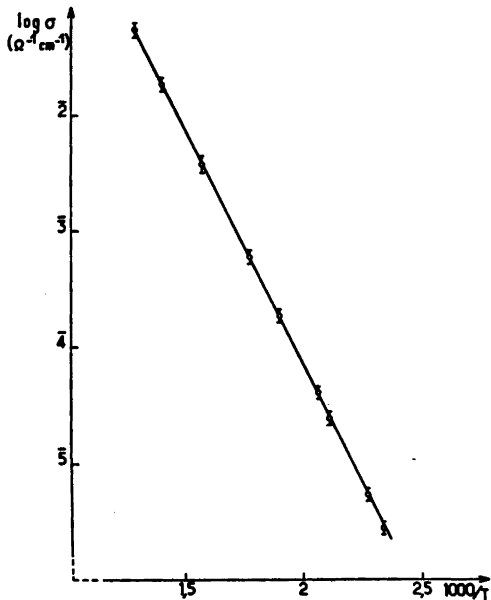


Fig. 3. Variation de $\log \sigma$ en fonction de l'inverse de la température absolue pour $\text{LiTa}_3\text{O}_8\beta$ (compacité 90 %).

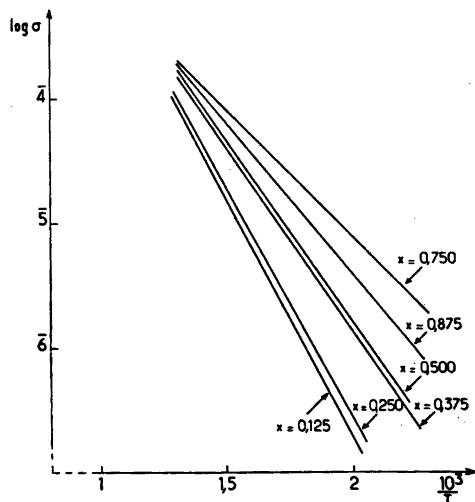


Fig. 4. Variation de $\log \sigma$ en fonction de l'inverse de la température absolue pour diverses compositions de la solution solide $\text{Li}_{1-x}\text{Ta}_3\text{O}_{8-x}\text{F}_x$ (compacité 70 %).

ides. Elle permet en effet de séparer dans l'interprétation des mesures le rôle de l'électrolyte solide proprement dit de celui des électrodes et de déterminer ainsi avec précision la résistance ohmique du matériau.

ETUDE DES PROPRIETES ELECTRIQUES DE $\text{LiTa}_3\text{O}_8\beta$

Les divers échantillons utilisés de $\text{LiTa}_3\text{O}_8\beta$ sont des pastilles frittées à 1450 °C de compacité égale à 90 %, des électrodes d'or ont été déposées par évaporation sous vide. Les mesures électriques sont effectuées entre 25 et 500 °C.

Nous avons représenté dans le plan complexe de la Fig. 2 l'impédance de l'ensemble électrolyte-électrodes. Pour chaque température le diagramme d'impédance est formé de deux arcs de cercle: le premier est relatif à l'électrolyte proprement dit, le second concerne les phénomènes au voisinage des électrodes.

La Fig. 3 donne la variation avec l'inverse de la température de la conductivité électrique σ déduite des valeurs de Z obtenues par extrapolation des premiers cercles à angle de déphasage nul. Dans le domaine de température considéré σ est de la forme $\sigma = nq\mu_0 \exp(-\Delta E/kT)$ où n représente le nombre de porteurs de charge q et de mobilité $\mu = \mu_0 \exp(-\Delta E/kT)$. L'énergie d'activation obtenue est: $\Delta E = 0,78$ eV. Pour une même compacité ce matériau possède donc des propriétés électriques voisines de celles de la hollandite $\text{K}_{1,60}\text{Mg}_{0,80}\text{Ti}_{7,2}\text{O}_{18}$ qui comporte comme $\text{LiTa}_3\text{O}_8\beta$ une structure à tunnels.¹⁸

Ces résultats sont rassemblés au Tableau 1.

Tableau 1. Conductivité à 300 °C et énergie d'activation des phases $\text{LiTa}_3\text{O}_8\beta$ et $\text{K}_{1,6}\text{Mg}_{0,8}\text{Ti}_{7,2}\text{O}_{18}$.

$\Omega^{-1} \text{ cm}^{-1}$	$\text{LiTa}_3\text{O}_8\beta$	$\text{K}_{1,6}\text{Mg}_{0,8}\text{Ti}_{7,2}\text{O}_{18}$
$\sigma(300 \text{ °C})$ ($\Omega^{-1} \text{ cm}^{-1}$)	6×10^{-4}	4×10^{-4}
ΔE (eV)	0,78	0,78

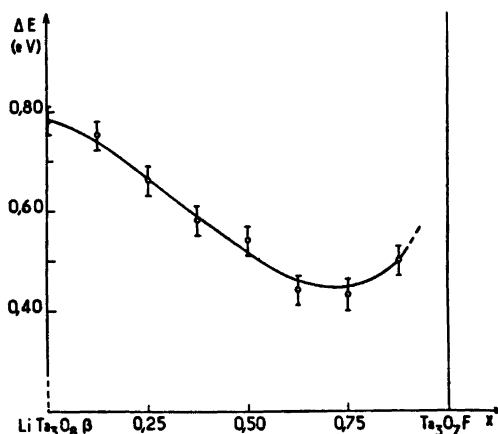


Fig. 5. Variation de l'énergie d'activation en fonction de x au sein de la solution solide $\text{Li}_{1-x}\text{Ta}_3\text{O}_{8-x}\text{F}_x$.

ETUDES DES PROPRIETES ELECTRIQUES DE LA SOLUTION SOLIDE $\text{Li}_{1-x}\text{Ta}_3\text{O}_{8-x}\text{F}_x$ ($0 \leq x \leq 1$)

Les divers échantillons utilisés de la solution solide $\text{Li}_{1-x}\text{Ta}_3\text{O}_{8-x}\text{F}_x$ ont été frittés en tubes scellés de platine à 1250 °C. Même à cette température, la compacité des pastilles frittées obtenues n'excède pas 70 %.

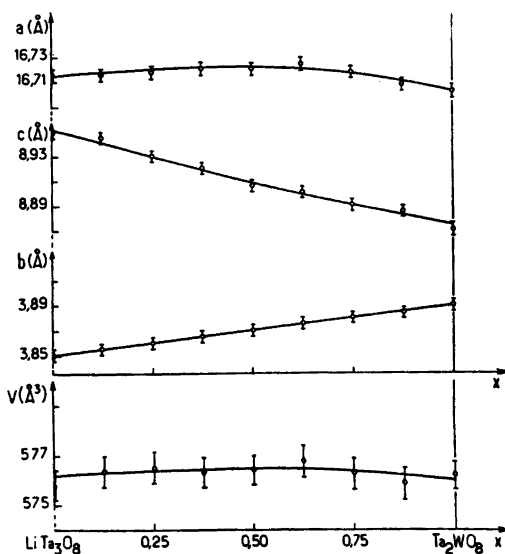


Fig. 6. Evolution avec x des paramètres cristallins de la solution solide $\text{Li}_{1-x}\text{Ta}_{3-x}\text{W}_x\text{O}_8$.

Nous avons représenté à la Fig. 4 la variation de $\log \sigma$ en fonction de l'inverse de la température absolue pour diverses valeurs de x à même compacité. Dans le domaine de température étudié (de 25 à 500 °C) σ est toujours de la forme $A - \Delta E/kT$.

La Fig. 5 donne la variation de l'énergie d'activation ΔE , qui s'avère en fait indépendante de la compacité, en fonction de x . Elle laisse apparaître un minimum, $\Delta E_m \approx 0,43$ eV pour $x \approx 0,75$, qui coïncide d'ailleurs avec un maximum de conductivité pour tout le domaine de température considéré. Le remplacement de l'oxygène par le fluor dans le réseau de $\text{LiTa}_3\text{O}_8\beta$ associé à la diminution progressive du taux de lithium inséré dans les tunnels entraîne donc dans un large domaine de composition ($0 \leq x \leq 0,75$) une mobilité plus grande pour les ions Li^+ .

ETUDE DES PROPRIETES ELECTRIQUES DE LA SOLUTION SOLIDE $\text{Li}_{1-x}\text{Ta}_{3-x}\text{W}_x\text{O}_8$ ($0 \leq x \leq 1$)

Les pastilles frittées ont été préparées à 1300 °C sous courant d'oxygène.

La Fig. 6 donne l'évolution des paramètres de la maille quadratique de $\text{Li}_{1-x}\text{Ta}_{3-x}\text{W}_x\text{O}_8$ et du volume élémentaire en fonction de x . Cette

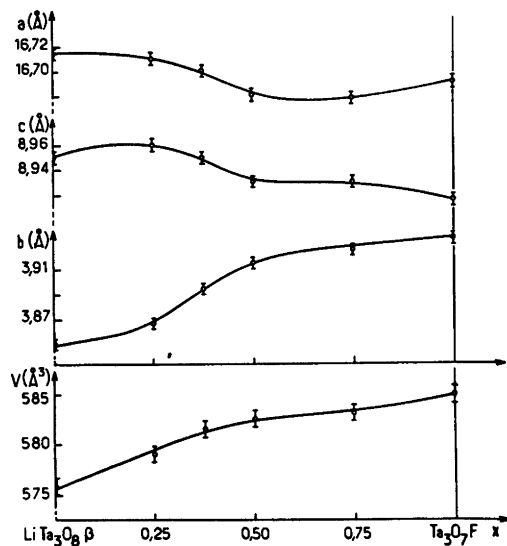


Fig. 7. Evolution avec x des paramètres cristallins de la solution solide $\text{Li}_{1-x}\text{Ta}_{3-x}\text{F}_x$.

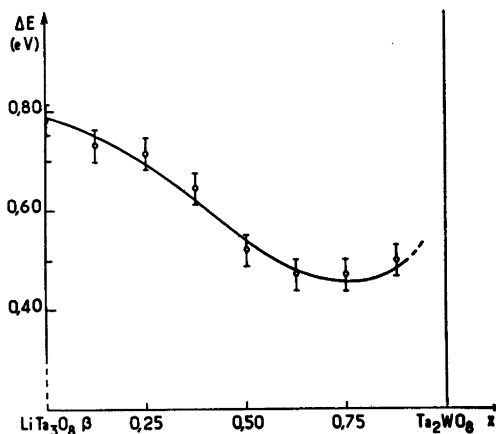


Fig. 8. Variation de l'énergie d'activation en fonction de x au sein de la solution solide $\text{Li}_{1-x}\text{Ta}_{3-x}\text{W}_x\text{O}_8$.

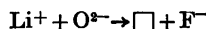
évolution est beaucoup plus régulière que celle décrite par certains d'entre nous pour la solution solide $\text{Li}_{1-x}\text{Ta}_3\text{O}_{8-x}\text{F}_x$ (Fig. 7).¹⁰

La conductivité correspond comme celle de l'oxyfluorure à un mécanisme activé. Nous avons représenté à la Fig. 8 la variation de l'énergie d'activation en fonction de x au sein de la solution solide $\text{Li}_{1-x}\text{Ta}_{3-x}\text{W}_x\text{O}_8$. Elle laisse apparaître, comme pour $\text{Li}_{1-x}\text{Ta}_3\text{O}_{8-x}\text{F}_x$ un minimum correspondant à $x \approx 0,75$: l'énergie d'activation est alors $\Delta E \approx 0,46$ eV.

Le remplacement du tantale +V par le tungstène +VI associé à une diminution progressive du taux de lithium inséré entraîne donc également pour $0 \leq x \leq 0,75$ une mobilité plus grande des ions Li^+ . La substitution du tungstène +VI au tantale +V dans $\text{LiTa}_3\text{O}_8\beta$ a les mêmes conséquences sur le plan des propriétés électriques que celle de la substitution du fluor à l'oxygène.

DISCUSSION DES RESULTATS OBTENUS

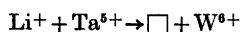
Le remplacement de l'oxygène par le fluor dans $\text{LiTa}_3\text{O}_8\beta$ correspond au mécanisme de substitution:



Il y a donc au sein de la solution solide $\text{Li}_{1-x}\text{Ta}_{3-x}\text{O}_{8-x}\text{F}_x$ à la fois augmentation avec x du nombre de lacunes de lithium et diminution

du potentiel négatif qui caractérise la liaison ion lithium-réseau, dans la mesure où celui-ci s'enrichit en fluor moins chargé que l'oxygène.

Pour la substitution du tungstène +VI au tantale +V dans LiTa_xO_5 , le mécanisme est le suivant:



Pour $\text{Li}_{1-x}\text{Ta}_{9-x}\text{W}_x\text{O}_8$ il y a donc simultanément augmentation avec x du nombre de lacunes de lithium comme dans le cas des oxyfluorures et augmentation de la covalence des blocs qui constituent le réseau, l'ion W^{6+} étant plus petit et plus chargé que l'ion Ta^{5+} ($r_{\text{W}^{6+}} = 0,62 \text{ \AA}$, $r_{\text{Ta}^{5+}} = 0,68 \text{ \AA}$). Il en résulte que l'ion Li^+ est moins attiré également par le réseau au fur et à mesure que x croît.

On peut donc attribuer les diminutions d'énergie d'activation observées dans les deux solutions solides pour $0 \leq x \leq 0,75$ à la fois à l'augmentation du nombre de lacunes disponibles pour les ions lithium dans le réseau et à l'affaiblissement des forces de liaison du lithium. Ce résultat est d'autant plus significatif que le nombre de porteurs diminue.

Pour $x = 0,75$ le huitième seulement des sites du lithium est occupé. Au-delà non seulement la conductivité diminue, ce qui pourrait s'expliquer par le très petit nombre de porteurs, mais on enregistre un accroissement de l'énergie d'activation. La compréhension de ce dernier phénomène nécessiterait la connaissance précise de la distribution du lithium entre les sites (4j) (2d) et (2f). Cette dernière étude est entreprise par ailleurs.

Ce travail fait partie d'un projet commun au Laboratoire de Chimie du Solide du C.N.R.S. à Bordeaux et au Laboratoire Arrhenius de l'Université de Stockholm avec l'aide financière du Centre National de la Recherche Scientifique (CNRS) et du Conseil National de la Recherche Scientifique Suédoise (NFR) (ATP franco-suédoise "Stockage chimique de l'énergie").

BIBLIOGRAPHIE

- Whittingham, M. S. et Huggins, R. A. *J. Chem. Phys.* 54 (1971) 414.
- Whittingham, M. S. et Huggins, R. A. *J. Electrochem. Soc.* 1 (1971) 118.
- Boilot, J. P., Thery, J. et Collongues, R. *Mater. Res. Bull.* 8 (1973) 1143.
- Patterson, J. W., Bugrew, E. C. et Rapp, R. A. *J. Electrochem. Soc.* 114 (1967) 752.
- Deportes, C., Robert, G. et Forestier, M. *Electrochim. Acta* 16 (1971) 1003.
- Kvist, A. et Josefson, A. *Z. Naturforsch. Teil A* 23 (1968) 625.
- Gratch, S., Petrocelli, J. V., Tischer, R. P., Minck, R. W. et Whalen, T. J. *7th International Energy Conversion Engineering Conf.* 729008 (1972).
- Lundberg, M. *Acta Chem. Scand.* 19 (1965) 2274.
- Chaminade, J. P. et Pouchard, M. *Ann. Chim. (Paris)* 10 (1975) 75.
- Chaminade, J. P. *Thèse de doctorat es Sciences Physiques*, Université de Bordeaux I, Bordeaux 1974.
- Jahnberg, L. et Andersson, S. *Acta Chem. Scand.* 21 (1967) 615.
- Roth, R. S. et Waring, J. L. *J. Res. Nat. Bur. Stand. Sect. A* 70 (1966) 281.
- Bauerle, J. F. *J. Chem. Phys. Solids* 30 (1969) 2657.
- Reau, J. M., Claverie, J., Campet, G., Deportes, C., Ravaine, D., Souquet, J. L. et Hammou, A. *C. R. Acad. Sci. Sér. C* 280 (1975) 325.
- Reau, J. M., Lucat, C., Campet, G., Portier, J. et Hammou, A. *J. Solid State Chem.* 17 (1976) 123.
- Lucat, C., Campet, G., Claverie, J., Portier, J., Reau, J. M. et Hagenmuller, P. *Mater. Res. Bull.* 11 (1976) 167.
- Delmas, C., Fouassier, C., Reau, J. M. et Hagenmuller, P. *Mater. Res. Bull. En cours de parution.*
- Moali, J. *Communication privée.*
- Ahrens, L. H. *Geochim. Cosmochim. Acta* 2 (1952) 155.

Reçu le 1 juin 1976.

The Electrophilic Nature of *o*-Nitrobenzenesulfonyl and *o*-Nitrobenzeneselenenyl Halides. A Kinetic Study

TOR AUSTAD*

Department of Chemistry, University of Bergen, N-5014 Bergen-Univ., Norway

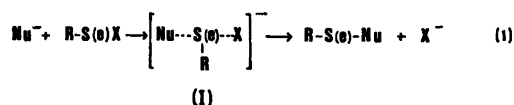
Kinetic measurements on the reaction between *o*-nitrobenzenesulfonyl chloride and 12 different nucleophiles, and some further studies involving nucleophilic substitution on *o*-nitrobenzeneselenenyl halides, have been performed in methanol using stopped-flow and conventional spectrophotometry. The kinetic plots showed the reactions to be of second order, first order in each of the reactants. The electrophilic nature of divalent sulfur and selenium has been discussed on the basis of these results and previously published kinetic data for substitutions on *o*-nitrobenzeneselenenyl halides. The proton basicity of the nucleophile was found to be of negligible importance in determining the reactivity toward S(II), confirming the statement that S(II) should be characterized as a soft electrophilic center. Regarding Se(II) as electrophilic center, the data suggest that monodentate nucleophiles form a transition state of the type: Nu---Se---X, *i.e.*, only one donor atom is bonded to the Se atom, while bidentate dithio nucleophiles appear to form a transition state where both of the donor atoms are bonded to the Se atom. A mechanism involving nucleophilic attack *trans* to the leaving group is suggested on the basis of leaving group effects and solvent effects on the rates of reaction.

During the last twenty years numerous papers dealing with kinetic studies of nucleophilic substitutions on divalent sulfur have been

published (for a review see Refs. 1–4). However, prior to 1974 no kinetic studies concerning nucleophilic substitution on divalent selenium and tellurium have been reported. Such reactions are known to be very fast. In recent studies we found that the pentathionate ions of the above-mentioned elements, *i.e.*, $S(S_2O_3)_2^{2-}$, $Se(S_2O_3)_2^{2-}$, and $Te(S_2O_3)_2^{2-}$ do react with ionic cyanide in acetonitrile at such a rate that it is possible to follow the reaction kinetically applying IR-spectroscopy.^{5,6} In a previous paper we have found that *o*-nitrobenzeneselenenyl halides, *o*-NO₂PhSeX, react with a large number of nucleophiles in methanol, and kinetic experiments have been carried out by means of the stopped-flow technique.⁷

In the present paper we wish to report the results of a kinetic study of the reaction between *o*-nitrobenzenesulfonyl chloride, *o*-NO₂PhSOCl, and various nucleophiles in methanol, and some further results from experiments concerning nucleophilic substitutions on *o*-NO₂PhSeX, X = Cl and Br. By comparing these rate constants with those obtained earlier under identical conditions for the reactions of the same nucleophiles with *o*-NO₂PhSeBr,⁷ we hope to gain some further knowledge about the electrophilic nature of S(II) and Se(II).

The bulk of information concerning nucleophilic substitution on S(II)^{3,4} and Se(II)^{5–8} points to an attack of the nucleophile *trans* to the leaving group, followed by synchronous bond formation and bond breaking, eqn. (1).



* Present address: Rogaland Regional College, Dept. of Science and Engineering, N-4000 Stavanger, Norway.

(I) is to be considered as the transition state. In the present reactions the organic moiety is *o*-nitrophenyl, and the position *trans* to the leaving group is already occupied through an intramolecular interaction.^{9,10} In a foregoing paper we have suggested two possible reaction mechanisms.⁷

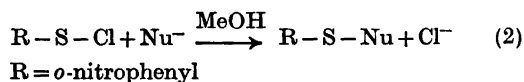
RESULTS

The stability of *o*-NO₂PhSCl in pure methanol was tested by measuring the absorbance at $\lambda_{\text{max}} = 395 \text{ nm}$ ¹¹ applying a spectrophotometer. The absorbance was found to be the same after 5 days at room temperature, which suggests that the reaction between the present sulfenyl chloride and methanol is very slow. The disappearance of the substrate due to solvolysis may then be disregarded when calculating the rate constant of the reaction between *o*-NO₂PhSCl and the various nucleophiles.

Likewise, *o*-NO₂PhSeX, (X = Cl and Br), was found to be stable against solvolysis during the kinetic runs in methanol.

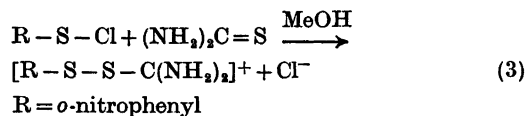
Kinetic studies on S(II). The products of the reaction between the various nucleophiles and

o-NO₂PhSCl have been synthesized, and the melting point, the recrystallization medium, and the analysis of each compound are listed in Table 1.



In most cases, except for ionic cyanide and di-*O*-ethylmonoselenophosphate, thio nucleophiles were applied. One of the nucleophiles, *i.e.*, di-*O*-ethylmonoselenophosphate, forms a yellowish-red, oily product. The other products of reaction (2) form quite stable yellowish-green solid compounds.

In the case of the neutral nucleophile, thiourea, the reaction product is a salt, eqn. (3).



In all the reactions studied, excellent second order kinetics were observed. Furthermore, the reactions were first order in each of the reactants. The rate of reaction was followed at

Table 1. Products of the reaction between various nucleophiles and *o*-nitrobenzenesulfenyl chloride.

No.	Compound (R = <i>o</i> -nitrophenyl)	M.p. °C	Recrystallized from	Found % S	Calc. % S
1	$\text{R-S-S-C} \begin{array}{c} \parallel \\ \text{S} \\ \parallel \\ \text{NC}_5\text{H}_{10}^a \end{array}$	154	chloroform	29.6	30.5
2	$\text{R-S-S-C} \begin{array}{c} \parallel \\ \text{S} \\ \parallel \\ \text{N}(\text{Me})_2 \end{array}$	157	chloroform	34.2	35.0
3	$\text{R-S-S-P} \begin{array}{c} \parallel \\ \text{S} \\ \parallel \\ (\text{Me})_2 \end{array}$	200	chloroform	34.1	34.4
4	$\text{R-S-S-P} \begin{array}{c} \parallel \\ \text{S} \\ \parallel \\ (\text{OEt})_2 \end{array}$	53	ether	28.2	28.3
5	R-S-S-Ph	52	ether	24.1	24.3
6	$\text{R-S-S}_2\text{O}_3\text{Ph}_4\text{As}$	164–166	acetonitrile/ether	14.6	14.8
7	$\text{R-S-S-SO}_2\text{-Ph}$	158–160	chloroform	29.2	29.3
8	$\text{R-S-S-SO}_2\text{-CH}_3$	85	ether	35.0	36.2
9	$\text{R-S-Se-P} \begin{array}{c} \parallel \\ \text{O} \\ \parallel \\ (\text{OEt})_2 \end{array}$	oil	—	—	—
10	R-S-CN	116–117	benzene	18.3	17.7
11	$\text{R-S-S-C}(\text{NH}_2)_2\text{Cl}$	178	methanol	23.9	24.1
12	R-S-SCN	95 ^b	carbon tetrachloride	—	—

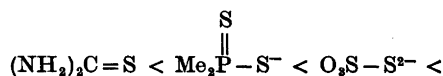
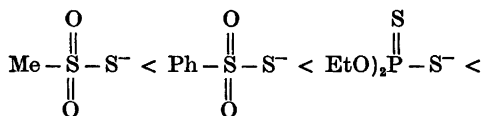
^a NC₅H₁₀ = piperidinyl. ^b Lit.²⁸ 93–94 °C.

Table 2. Pseudo-first-order rate constant (k') and second-order rate constant k_2 [S(II)] for the reaction between *o*-nitrobenzenesulfonyl chloride and different nucleophiles in methanol at 25 °C. The column to the right gives the second-order rate constants, k_2 [Se(II)] toward *o*-nitrobenzeneselenenyl bromide.

No.	Nucleophile	[Nu]/10 ⁻² M	k'/s^{-1}	k_2 [S(II)]/M ⁻¹ s ⁻¹	k_2 [Se(II)]/M ⁻¹ s ^{-1a}
1	C ₅ H ₁₀ N-C(=S)-S ^{-b}	0.50	4.17 × 10 ⁻³	0.889	4 200
		1.00	9.20 × 10 ⁻³		
		2.00	17.7 × 10 ⁻³		
2	Me ₂ N-C(=S)-S ⁻	0.401	1.29 × 10 ⁻³	0.444	2 667
		0.785	3.30 × 10 ⁻³		
		1.57	8.12 × 10 ⁻³		
3	Me ₂ P(=S)-S ⁻	1.00	2.17 × 10 ⁻⁴	2.13 × 10 ⁻³	350
		2.00	4.18 × 10 ⁻⁴		
4	(MeO) ₂ P(=S)-S ⁻	2.00	4.06 × 10 ⁻⁵	2.02 × 10 ⁻³	35.3
		3.00	6.20 × 10 ⁻⁵		
		4.00	8.03 × 10 ⁻⁵		
5	(EtO) ₂ P(=S)-S ⁻	2.00	4.06 × 10 ⁻⁵	2.02 × 10 ⁻³	35.3
		3.00	6.20 × 10 ⁻⁵		
		4.00	8.03 × 10 ⁻⁵		
6	Ph-S ⁻	0.555	0.116	22.8	7 000
		1.114	0.258		
		2.78	0.712		
7	S ₂ O ₃ ²⁻	0.50	0.841 × 10 ⁻³	0.164	125
		0.78	1.30 × 10 ⁻³		
		1.00	1.60 × 10 ⁻³		
8	Ph-SO ₂ -S ⁻	2.60	1.42 × 10 ⁻⁵	5.58 × 10 ⁻⁴	3.25
		4.00	2.30 × 10 ⁻⁵		
		6.07	3.36 × 10 ⁻⁵		
9	CH ₃ -SO ₂ -S ⁻	4.33	2.26 × 10 ⁻⁵	5.38 × 10 ⁻⁴	2.82
10	(EtO) ₂ P(=O)-S ⁻				1.97
11	(iPrO) ₂ P(=O)-S ⁻				4.57
12	(NH ₂) ₂ C=S	3.485	6.60 × 10 ⁻⁴	1.85 × 10 ⁻²	53.3
		4.45	7.99 × 10 ⁻⁴		
		7.25	13.3 × 10 ⁻⁴		
13	(MeO) ₂ P(=O)-Se ⁻			4.67 × 10 ⁻³	120
		2.00	9.55 × 10 ⁻⁵		
		3.00	13.73 × 10 ⁻⁵		
14	(EtO) ₂ P(=O)-Se ⁻			4.67 × 10 ⁻³	160
		2.00	9.55 × 10 ⁻⁵		
		3.00	13.73 × 10 ⁻⁵		
15	(iPrO) ₂ P(=O)-Se ⁻			4.67 × 10 ⁻³	222
16	CN ⁻	0.50	2.60 × 10 ⁻³	6.75	994
		1.00	7.06 × 10 ⁻³		
		1.41	9.40 × 10 ⁻³		

^a Ref. 7. ^b C₅H₁₀N=piperidinyl.

410 nm applying stopped-flow or conventional spectrophotometry. The rate constants of the reaction between the various nucleophiles and *o*-NO₂PhSCl are tabulated in Table 2. It is seen that the nucleophilicity of the thio nucleophiles progressively increases in the order:



Acta Chem. Scand. A 31 (1977) No. 2

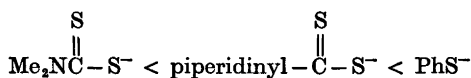


Table 2 further shows that the cyanide ion, No. 16, is a stronger nucleophile than the dithiocarbamates toward S(II), but is less nucleophilic than the thiophenolate ion.

Di-*O*-ethylmonoselenophosphate, No. 14, is more reactive than di-*O*-ethylthiophosphate, No. 5, but less reactive than dimethyldithiophosphate, No. 3, toward S(II).

The rate constants for three different types of nucleophiles, *i.e.*, (NH₂)₂C=S, Me₂NCS₂⁻, and CN⁻, have also been determined at different

Table 3. Pseudo-first-order rate constant (k') and second-order rate constant (k_2) for the reaction between *o*-nitrobenzenesulfonyl chloride and various nucleophiles in methanol at different temperatures.

Nucleophile	[Nu]/10 ⁻³ M	20 °C		25 °C		30 °C		35 °C		
		k'/s^{-1}	$k_2/M^{-1}s^{-1}$	$k_2/M^{-1}s^{-1}$	k'/s^{-1}	$k_2/M^{-1}s^{-1}$	k'/s^{-1}	$k_2/M^{-1}s^{-1}$	k'/s^{-1}	$k_2/M^{-1}s^{-1}$
(NH ₂) ₂ C=S	3.485	5.22 × 10 ⁻⁴	1.45 × 10 ⁻²	1.85 × 10 ⁻²	8.1 × 10 ⁻⁴	2.25 × 10 ⁻²	9.45 × 10 ⁻⁴	2.61 × 10 ⁻²		
	4.45	6.10 × 10 ⁻⁴			10.2 × 10 ⁻⁴		11.8 × 10 ⁻⁴			
	7.25	10.55 × 10 ⁻⁴			15.9 × 10 ⁻⁴		17.27 × 10 ⁻⁴			
S Me ₂ N-C-S ⁻	0.411	1.46 × 10 ⁻³	3.75 × 10 ⁻¹	4.44 × 10 ⁻¹	2.71 × 10 ⁻³	6.47 × 10 ⁻¹	2.89 × 10 ⁻³	8.09 × 10 ⁻¹		
	0.917	3.36 × 10 ⁻³			5.92 × 10 ⁻³		7.25 × 10 ⁻³			
	1.71	6.66 × 10 ⁻³			11.09 × 10 ⁻³		14.20 × 10 ⁻³			
CN ⁻	0.50	2.07 × 10 ⁻³	4.82	6.75	3.84 × 10 ⁻³	8.70	5.33 × 10 ⁻³	11.2		
	1.00	4.88 × 10 ⁻³			8.525 × 10 ⁻³		11.17 × 10 ⁻³			
	1.41	6.796 × 10 ⁻³			12.73 × 10 ⁻³		17.3 × 10 ⁻³			

temperatures, 20, 25, 30, and 35 °C, and the activation parameters have been calculated, Tables 3 and 4. Concerning these nucleophilic substitutions on *o*-NO₂PhSeCl, it is seen that the enthalpy of activation is rather similar while the entropy of activation is drastically increased when going from (NH₂)₂C=S to CN⁻.

Kinetic studies on Se(II). Kinetic studies have also been performed between the above-mentioned three nucleophiles and *o*-NO₂PhSeCl. The kinetic data and activation parameters are collected in the Tables 5 and 4, respectively.

The rate constants and the activation parameters for the reaction between *o*-NO₂PhSeBr and the same three nucleophiles are presented in Tables 6 and 4.

When the leaving group is changed from chloride to bromide, Tables 5 and 6 clearly show that the effect on the second order rate constant is rather small. At 30 °C the $k_2(\text{Cl})/k_2(\text{Br})$ ratios were found to be 1.20, 1.10, and 0.80 for (NH₂)₂C=S, Me₂NCS₂⁻, and CN⁻, respectively. Table 4 further shows that the activation parameters for the two thio nucleophiles are nearly unaffected by the change of the leaving group. The log $k_2 - 1/T$ correlation for the *o*-NO₂PhSeCl - CN⁻ reaction showed a curved plot, and activation parameters for this reaction have not been calculated.

The products of the reactions involving *o*-NO₂PhSeX as substrates have been described in the foregoing paper.⁷

log k₂[S(II)] - E° and log k₂[Se(II)] - log k₂[S(II)] relationships. With regard to nucleophilic substitution on *o*-NO₂PhSeCl, the anionic nucleophiles whose oxidation potentials, E° , are known, appear to conform to a rough linear relationship between log $k_2[\text{S(II)}]$ and E° , Fig. 1. However, one may notice that the point of the neutral thio nucleophile, (NH₂)₂C=S, appears to deviate markedly from this line.

Rate constants from the foregoing work⁷ for the reaction between the nucleophiles and *o*-NO₂PhSeBr are also listed in Table 2. In order to compare the electrophilic nature of S(II) and Se(II), the logarithm of the rate constants have been plotted against each other, Fig. 2. The figure shows that the log $k_2[\text{Se(II)}] - \log k_2[\text{S(II)}]$ plot of the thio nucleophiles splits up into two approximately parallel lines. The points for the monodentate nucleophiles lie on the lower line, while the points for

Table 4. Activation parameters for the reaction between *o*-nitrobenzenesulfonyl chloride, *o*-nitrobenzeneselenenyl chloride, and *o*-nitrobenzeneselenenyl bromide and various nucleophiles in methanol at 25 °C (R = *o*-nitrophenyl). 1 kcal = 4.184 kJ.

Nucleophile	ΔH^\ddagger kcal/mol	ΔS^\ddagger , cal/mol deg	ΔF^\ddagger kcal/mol
R-S-Cl + Nu ⁻ → RS-Nu + Cl ⁻			
(NH ₂) ₂ C=S	6.5	-45	19.9
Me ₂ N-C(=S)-S ⁻	8.8	-30	17.7
CN ⁻	8.3	-27	16.4
R-Se-Cl + Nu ⁻ → R-Se-Nu + Cl ⁻			
(NH ₂) ₂ C=S	3.5	-38	14.8
Me ₂ N-C(=S)-S ⁻	5.6	-24	12.7
R-Se-Br + Nu ⁻ → R-Se-Nu + Br ⁻			
(NH ₂) ₂ C=S ^a	3.3	-40	15.2
Me ₂ N-C(=S)-S ⁻	5.9	-23	12.8
CN ^{-a}	8.7	-16	13.4

^a Ref. 7.

Table 5. Pseudo-first-order rate constant (*k'*) and second-order rate constant (*k₂*) for the reaction between *o*-nitrobenzeneselenenyl chloride and various nucleophiles in methanol at different temperatures.

Nucleophile	[Nu]/ 10 ⁻² M	20 °C		25 °C		30 °C		35 °C	
		<i>k'</i> /s ⁻¹	<i>k₂</i> / M ⁻¹ s ⁻¹	<i>k'</i> /s ⁻¹	<i>k₂</i> / M ⁻¹ s ⁻¹	<i>k'</i> /s ⁻¹	<i>k₂</i> / M ⁻¹ s ⁻¹	<i>k'</i> /s ⁻¹	<i>k₂</i> / M ⁻¹ s ⁻¹
(NH ₂) ₂ C=S	1.00	0.696		0.80		1.04		1.19	
	2.10	1.284	61	1.41	66	1.708 ^a	73	2.03 ^a	87
	3.485	2.16		2.19		2.42		2.96	
$\begin{array}{c} \text{S} \\ \\ \text{Me}_2\text{N}-\text{C}-\text{S}^- \end{array}$	0.361			10.9		12.5		14.8	
	0.791			22.9	2 850	26.0	3 330	32.2	4 000
	1.264			35.5		40.9		48.3	
CN ⁻	0.50	3.08		3.50		3.93		6.03	
	1.00	6.73	672	7.48	750	8.93	888	12.1	1 200
	1.56	10.7		11.7		14.7		19.1	

^a [Nu] = 2.207 × 10⁻² M.

the bidentate nucleophiles lie on the upper line corresponding to about 10 times higher reactivity toward Se(II) at constant reactivity toward S(II). Fig. 2 further shows that di-*O*-ethylmonoselenophosphate, No. 14, behaves more like the bidentate dithio nucleophiles, and the reactivity of the cyanide ion appears to resemble the monodentate thio nucleophiles.

Solvent effect. Finally, some attempts were made to study the solvent effect on the reactions described above. The dipolar aprotic solvent acetonitrile was chosen because it has nearly the same dielectric constant as methanol, 36 and 33, respectively. The thiocyanate ion was applied as the nucleophile. For all the substrates studied, *i.e.*, *o*-NO₂PhSeX (X = Cl and Br) and

Table 6. Pseudo-first-order rate constant (k') and second-order rate constant (k_2) for the reaction between *o*-nitrobenzeneselenenyl bromide and various nucleophiles in methanol at different temperatures.

Nucleophile	[Nu]/ 10 ⁻³ M	20 °C		25 °C		30 °C		35 °C	
		k'/s^{-1}	$k_2/M^{-1} s^{-1}$	k'/s^{-1}	$k_2/M^{-1} s^{-1}$	k'/s^{-1}	$k_2/M^{-1} s^{-1}$	k'/s^{-1}	$k_2/M^{-1} s^{-1}$
(NH ₂) ₂ C=S ^a			48.9 ^b		53.3		60.5		66.9
$\begin{array}{c} \text{S} \\ \\ \text{Me}_2\text{N}-\text{C}-\text{S}^- \end{array}$	0.361	7.10		9.33		10.84		13.17	
	0.791	17.46	2 060	19.72	2 520	23.97	3 010	28.76	3 570
	1.264	25.3		31.68		37.36		44.38	
CN ^{-a}			500 ^b		994		1 110		1 460

^a Ref. 7. ^b Temp. 15 °C.

o-NO₂PhSCl, the reaction was too fast to be followed by means of the stopped-flow technique. Experimentally, we may then conclude that the second order rate constant of the reaction between the thiocyanate ion and the various substrates in acetonitrile is greater than $2 \times 10^6 \text{ M}^{-1} \text{ s}^{-1}$.

DISCUSSION

With regard to the thio nucleophiles, Table 2 shows that the relative order of reactivity toward S(II) and Se(II) is not quite the same. Fig. 2 further shows that the main reason for this disparity in reactivity toward S(II) and Se(II) is due to a higher nucleophilicity of the

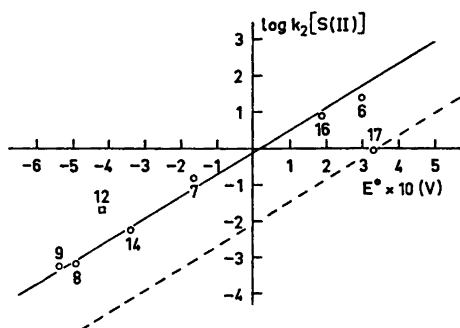


Fig. 1. Logarithm of the rate constants for the reaction of nucleophiles with *o*-nitrobenzenesulfenyl chloride as a function of the oxidation potential of the nucleophile. The numbers give the compounds as listed in Tables 2 and 7, and the E° -values correspond to those applied in Ref. 7.

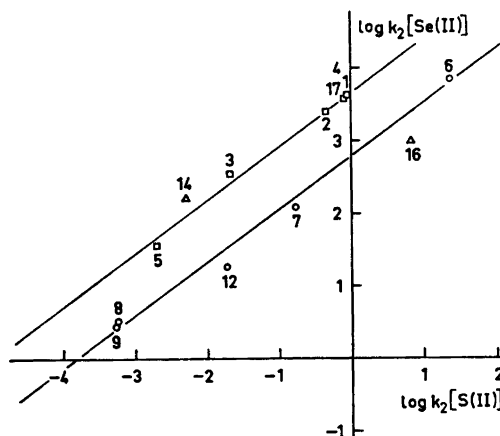
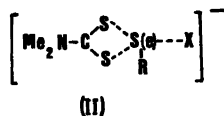


Fig. 2. Logarithm of the rate constants for the reaction of nucleophiles with *o*-nitrobenzeneselenenyl bromide as a function of the logarithm of the rate constants for the reaction of the same nucleophiles with *o*-nitrobenzenesulfenyl chloride. The numbers give the compounds as listed in Tables 2 and 7.

bidendate nucleophiles toward Se(II) at constant reactivity toward S(II).

The fact that the $\log k_2[\text{Se(II)}] - \log k_2[\text{S(II)}]$ correlation splits up into two lines may indicate that the mechanism, or the transition state, is not quite the same for the monodentate and the bidentate nucleophiles in their reactions with substrates of divalent sulfur and selenium. In the case of the monodentate nucleophiles, a transition state of the type (I), which is in agreement with previous studies, probably

occurs with both types of substrate. The bidentate dithio nucleophiles studied in this work have two equivalent donor sulfur atoms. Thus, we may for these suggest a transition state in which both of the donor atoms participate. If we consider the nucleophile, $\text{Me}_2\text{NCS}_2^-$, such a transition state may be represented by (II).



Generally, as central atom, the heaviest atom is the best complex former, and consequently a transition state of this type should be more favourable for Se(II) than for S(II). Thus, the enhancement in the reactivity of the bidentate nucleophiles toward Se(II) relative to S(II), considered in relation to the reactivity of the monodentate thio nucleophiles toward the same substrates, can be explained on the basis of a transition state of the type (II) in the case of Se(II) and a transition state of the type (I), eqn. (1), in the case of S(II).

The above explanation gains support from the crystallographic works by Husebye *et al.*¹²⁻¹⁴

Foss⁵ has suggested to describe the bonding in the transition state in nucleophilic substitution on S(II), Se(II), and Te(II) as a three-center four-electron bonding system. The parallellicity of the lines of the monodentate and the bidentate nucleophiles in Fig. 2 is an indication that the bonding in the transition states (I) and (II) is of the same type, *i.e.*, a three-center four-electron bonding system. The selenium *p*-orbital in the transition state for the reaction between the bidentate dithio nucleophile and selenenyl halides is assumed to overlap with orbitals of both of the donor atoms of the nucleophile. In the product, however, only one of the sulfur atoms may be bonded to the Se atom.

If the difference in the standard free energy changes for the reactions between *o*-NO₂PhSX and two of the nucleophiles is nearly equal to the difference in the standard free energy changes for the reactions between *o*-NO₂PhSeX and the same two nucleophiles, nucleophilic substitution reactions on Se(II) should be less selective than those on S(II) due to the higher rates of the former.¹⁶ This agrees with the

magnitude of the slope of the lines in Fig. 2, slope ≈ 0.72 , which is a value less than 1.

Furthermore, the slope of the lines in Fig. 2 can be related to the ability of the electrophilic centers to form a bonding system of the three-center four-electron type, which is believed to be $\text{S} < \text{Se} < \text{Te}$.⁸

The anionic nucleophiles appear to conform to a rough linearity in the $\log k_2[\text{S(II)}] - E^\circ$ plot, Fig. 1. Since the proton basicities of these differ widely, ($\text{p}K_a \approx -6$ and $\text{p}K_a = 7.5$ in the case of ¹⁷MeSO₂-S⁻ and ¹⁸Ph-S⁻, respectively), the relationship suggests that the proton basicity of the nucleophiles contributes very little in determining the reactivity toward S(II). Consequently, divalent sulfur should be characterized as a soft electrophilic center, in terms of the HSAB language.¹⁹ These findings accord with the conclusion of Kice and Large²⁰ that sulfenyl sulfur is a soft electrophilic center, comparable to peroxide oxygen. Ritter and Krueger¹⁸ have pointed out that although polarizability of the nucleophile is the dominant factor, basicity is also important in nucleophilic substitutions on the trithionate ion.

The present kinetic data also agree with the results of previous exchange reactions of Foss.^{21,22}

$$\log (k_{\text{Nu}}/k_{\text{H}_2\text{O}}) = \alpha E_{\text{a}} + \beta \text{H} \quad (4)$$

In the Edwards¹⁷ equation (4), the kinetic data for nucleophilic substitution on S(II) by anionic nucleophiles, Fig. 1, give $\alpha[\text{S(II)}]$ and $\beta[\text{S(II)}]$ values of ≈ 5.7 and ≈ 0 , respectively. The α and β values for Se(II) have previously been found to be ≈ 3.9 and ≈ 0.7 . Thus, the β values for S(II) and Se(II) are both

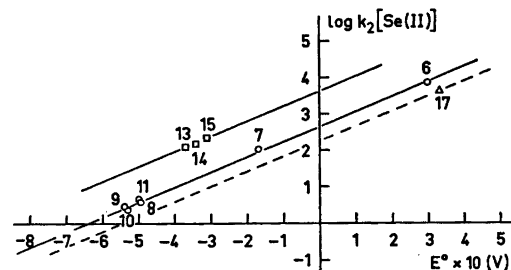


Fig. 3. Logarithm of the rate constants for the reaction of nucleophiles with *o*-nitrobenzeneselenenyl bromide as a function of the oxidation potential of the nucleophile. The numbers give the compounds as listed in Tables 2 and 7.

Table 7. Pseudo-first-order constant, k' , and second-order rate constant, k_2 , for the reaction between $\text{Et}_2\text{NCS}_2^-$ and $o\text{-NO}_2\text{PhSCl}$ and $o\text{-NO}_2\text{PhSeBr}$ in methanol at 25 °C. (R = *o*-nitrophenyl).

No.	Nucleophile	$[\text{Nu}]/10^{-3} \text{ M}$	$k'/10^{-3} \text{ s}^{-1}$	$k_2/\text{M}^{-1} \text{ s}^{-1}$
$\text{R-S-Cl} + \text{Nu}^- \rightarrow \text{R-S-Nu} + \text{Cl}^-$				
17	$\text{Et}_2\text{NCS}_2^-$	2.13	1.68	0.818
		2.76	2.26	
		4.55	3.74	
$\text{R-Se-Br} + \text{Nu}^- \rightarrow \text{R-Se-Nu} + \text{Br}^-$				
17	$\text{Et}_2\text{NCS}_2^-$	2.13	8.56	4 050
		2.76	11.1	
		4.55	18.3	

nearly zero, while the α value for S(II) is significantly higher than that for Se(II).

In order to verify if the bidentate dithio nucleophiles fit the $\log k_2 - E^\circ$ correlations of the other thio nucleophiles, Figs. 1 and 3, the rate constants for the reactions between $\text{Et}_2\text{NCS}_2^-$ and the substrates $o\text{-NO}_2\text{PhSCl}$ and $o\text{-NO}_2\text{PhSeBr}$ were determined, Table 7. The oxidation potential of $\text{Et}_2\text{NCS}_2^-$ has been determined by Gregg and Tyler;²³ the value found was +0.33 V. As is seen from Figs. 1 and 3, the point of $\text{Et}_2\text{NCS}_2^-$, No. 17, deviates markedly from the lines of the other anionic thio nucleophiles. Especially in the case of S(II) as electrophilic center, $\text{Et}_2\text{NCS}_2^-$ has a much lower rate constant than predicted from

Table 8. Oxidation potentials, $E^\circ[\text{S(II)}]$ and $E^\circ[\text{Se(II)}]$, for various bidentate dithio nucleophiles estimated on the basis of their rate constants towards $o\text{-NO}_2\text{PhSCl}$ and $o\text{-NO}_2\text{PhSeBr}$ and the dashed lines of Figs. 1 and 3, respectively.

Nucleophile	$E^\circ[\text{S(II)}]/\text{V}$	$E^\circ[\text{Se(II)}]/\text{V}$
$\text{C}_5\text{H}_{10}\text{N}-\text{C}(=\text{S})-\text{S}^-^a$	+0.34	+0.33
$\text{Me}_2\text{N}-\text{C}(=\text{S})-\text{S}^-$	+0.29	+0.28
$\text{Me}_2\text{P}(=\text{S})-\text{S}^-$	+0.065	+0.060
$(\text{EtO})_2\text{P}(=\text{S})-\text{S}^-$	-0.11	-0.19

^a $\text{C}_5\text{H}_{10}\text{N}$ = piperidinyl.

the E° value relative to the other thio nucleophiles. On the assumption that the slope of the line in the $\log k_2[\text{S(II)}] - E^\circ$ plot and in the $\log k_2[\text{Se(II)}] - E^\circ$ plot only depends on the electrophilic center, the oxidation potentials of the other dithio nucleophiles, except for $(\text{EtO})_2\text{PS}_2^-$, correspond very well with each other, Table 8.

Davis²⁴ has presented a theoretical and general justification of the Edwards equation, and he renamed this four-parameter equation the "Oxibase Scale". Davis suggested that this scale could be used in discussing kinetic data concerning nucleophilic substitutions on S(II). However, the experimental data from this work are not in line with this equation. Firstly, the proton basicity of the nucleophile appears to be of negligible effect in determining the reactivity towards S(II) and secondly, there appears to be a correlation between the rate constant and the oxidation potential that changes with the nature of the nucleophile. Thus, concerning S(II) and Se(II) as electrophilic centers, we may then conclude that a simple four-parameter equation analogous to the Edwards equation, is unsuitable in determining the reactivity of the nucleophiles listed in Table 2. Other parameters have to be included.

On the basis of the foregoing discussion, and together with previously published data for nucleophilic substitution on Se(II),⁷ the following conclusions may be drawn.

S(II) as electrophilic center. All types of nucleophiles discussed in this paper, *i.e.*, monodentate and bidentate nucleophiles, probably form a transition state of the type (I). The logarithms of the rate constants of the anionic monodentate nucleophiles, when plotted against their oxidation potentials, conform to a rough linearity. The bidentate dithio nucleophiles probably give a $\log k_2[\text{S(II)}] - E^\circ$ relationship different from that found for other anionic nucleophiles. Neutral nucleophiles, probably due to solvation effects, seem to deviate from these correlations.

Se(II) as electrophilic center. A transition state as pictured by (II) is suggested for the bidentate dithio nucleophiles, while a "normal" transition state of the type (I), appears to occur for the other nucleophiles of Table 2. The bonding in the two transition states (I) and (II) is probably basically of the same type,

i.e., based on a single p -orbital of the electrophilic center. Anionic seleno nucleophiles, *i.e.*, di- O -alkylmonoselenophosphates, monodentate thio nucleophiles, and bidentate dithio nucleophiles, form different parallel lines in the $\log k_2[\text{Se(II)}] - E^\circ$ plot. Neutral nucleophiles, probably due to solvation effects, seem to deviate from these correlations.

Activation parameters. The data in Table 4 show that for the two thio nucleophiles there is a decrease in ΔH^\ddagger and an increase in ΔS^\ddagger as the substrate changes from $o\text{-NO}_2\text{PhSCl}$ to $o\text{-NO}_2\text{PhSeCl}$. Thus, both ΔH^\ddagger and ΔS^\ddagger are more favourable in the case of the Se(II)-substrate. The decrease in ΔH^\ddagger is the largest factor in causing a higher reactivity of $o\text{-NO}_2\text{PhSeCl}$.

The decrease in ΔH^\ddagger for the thio nucleophiles, when going from $o\text{-NO}_2\text{PhSCl}$ to $o\text{-NO}_2\text{PhSeCl}$, points to a more stabilized transition state in the latter case, and furthermore, the increase in ΔS^\ddagger can be related to a more tight transition state in substitution reaction on S(II), relatively to Se(II).

When the leaving group was changed from chloride to bromide, only very small effects on the rate constants in substitution reactions on Se(II) were observed. Table 4 shows that the activation parameters of $(\text{NH}_2)_2\text{C}=\text{S}$ and $\text{Me}_2\text{NCS}_2^-$ are nearly unchanged when chloride is replaced with bromide.

Reaction mechanism. The rate constant of the $\text{SCN}^- - o\text{-NO}_2\text{PhSeBr}$ reaction in methanol at 25°C was observed to be $0.133 \text{ M}^{-1} \text{ s}^{-1}$.⁷ By means of Fig. 2 the rate constant of the $\text{SCN}^- - o\text{-NO}_2\text{PhSCl}$ reaction at the same condition can be estimated to $\approx 10^{-5} \text{ M}^{-1} \text{ s}^{-1}$. This means that when changing the solvent from MeOH to MeCN, the solvent effects on the rate constants can be given by the ratios

$$\frac{k_2[\text{Se(II)}]_{\text{MeCN}}}{k_2[\text{Se(II)}]_{\text{MeOH}}} > 1.5 \times 10^6$$

and

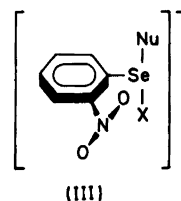
$$\frac{k_2[\text{S(II)}]_{\text{MeCN}}}{k_2[\text{S(II)}]_{\text{MeOH}}} > 2 \times 10^{10}$$

respectively. These tremendous increases in the rate constants observed in MeCN relatively to MeOH, cannot be attributed only to a different solvation of the thiocyanate ion in these solvents, because the thiocyanate ion is only

36 times more reactive toward methyl iodide in MeCN than in MeOH.²⁵ Some other factors associated with the substrates are probably involved.

The intramolecular three-center system, $\text{X}-\text{S(e)}\cdots\text{O}$, of the present substrates is probably maintained in solution, otherwise a higher reactivity of these substrates would be observed.⁷ Due to a strong solvation of the polar NO_2 -group in a protic solvent, such as MeOH, a nucleophilic attack *trans* to the leaving group is probably very hindered. In acetonitrile the NO_2 -group is not H-bonded to the solvent, and the nucleophile has only to push the oxygen atom of the nitro group slightly aside in order to get in contact with the chalcogen atom. Thus, supposing a nucleophilic attack *trans* to the leaving group, a large solvent effect is to be expected. A mechanism involving an attack at the chalcogen atom normal to the plane of the molecule would probably not lead to such a large solvent effect on the rate of reaction.

Thus, the present results together with previously published and discussed data,⁷ suggest the mechanism of the reaction between o -nitrobenzenesulfonyl and o -nitrobenzeneselenenyl halides and nucleophilic reagents to involve a nucleophilic attack *trans* or nearly *trans* to the leaving group, accompanied by a synchronous rotation about the chalcogen-carbon bond. The transition state may be represented by (III).



The above view concerning the solvation of $o\text{-NO}_2\text{PhS(e)X}$ in protic solvents may also explain the unusual stability of these compounds in protic solvents, relatively to the unsubstituted analogous.²⁶

o -Nitrobenzenesulfonyl (-selenenyl) substrates that have leaving groups with larger *trans* bonding-lengthening effects than Cl and Br, are expected to form a less stable intramolecular three-center system, $\text{X}-\text{S(e)}\cdots\text{O}$.⁸ The chalcogen-oxygen bond is then weakened, and in

solution a rotation about the chalcogen-carbon bond may occur, causing a higher reactivity of these types of substrates. This will be discussed in a later paper.²⁷

EXPERIMENTAL

Solvents. Methanol "Merck" *p.a.* was used without further purification. Acetonitrile was purified as reported by Coetzee.²⁹

Substrates. *o*-Nitrobenzenesulfonyl chloride "Fluka" *puriss.* was recrystallized from light petroleum (40–60°C). *o*-Nitrobenzeneselenenyl chloride was kindly provided by Mr. R. Eriksen.³⁰ *o*-Nitrobenzeneselenenyl bromide was synthesized from *o*-nitrophenyl selenocyanate and excess of bromine in dry chloroform.³¹ The product was recrystallized three times from light petroleum (40–60°C).

Nucleophiles. The following nucleophiles were employed: (Piperidyl) $\text{CS}_2\text{Na}\cdot 2\text{H}_2\text{O}$,³² $\text{Me}_2\text{NCS}_2\text{Na}\cdot 3\text{H}_2\text{O}$,³² $\text{Et}_2\text{NCS}_2\text{Na}\cdot 3\text{H}_2\text{O}$,³² $\text{Me}_2\text{PS}_2\text{Na}\cdot 2\text{H}_2\text{O}$,³³ $(\text{EtO})_2\text{PS}_2\text{NH}_4$,³⁴ PhSNa , $(\text{PhAs})_2\text{S}_2\text{O}_3$,⁷ $\text{Me}_4\text{NPhSO}_3\text{S}$, $\text{Me}_4\text{NMeSO}_3\text{S}$, $(\text{EtO})_2\text{P}(\text{O})\text{SeNa}$,³⁵ Ph_4AsCN ,³⁶ and $(\text{NH}_4)_2\text{C}=\text{S}$ ("Fluka" *puriss. p.a.*) Sodium thiophenolate was prepared *in situ* by dissolving equivalent amounts of thiophenol and sodium in methanol. $\text{Me}_4\text{N PhSO}_3\text{S}$ and $\text{Me}_4\text{N MeSO}_3\text{S}$ were prepared from the respective potassium salts and dry Me_4NCl in methanol. KCl separated and was filtered off. The solvent was removed in vacuum. $\text{Me}_4\text{NPhSO}_3\text{S}$ was recrystallized from methanol. M.p. 182°C. (Found: S 25.83. Calc. for $\text{C}_{16}\text{H}_{17}\text{NO}_3\text{S}_2$: S 25.88). $\text{Me}_4\text{NMeSO}_3\text{S}$ was recrystallized from acetonitrile. M.p. 275°C. (Found: S 34.75. Calc. for $\text{C}_6\text{H}_5\text{NO}_3\text{S}_2$: S 35.55).

Products. The compounds Nos. 1, 2, 3, and 4 of Table 1 were synthesized by the general procedure described by Foss³⁷ for preparing *o*-nitrobenzeneselenenyl sulfur compounds.

The compounds Nos. 7, 8, and 9 were prepared in a similar way, as above, using ethyl acetate and methanol, but in these cases the compounds did not crystallize spontaneously. Potassium or sodium salts of the nucleophiles and *o*-nitrobenzenesulfonyl chloride were used. The reaction mixtures were evaporated to dryness in vacuum, and the salts were separated from the products by means of chloroform in the case of Nos. 7 and 8 and ether in the case of No. 9.

The unsymmetrical disulfide, compound No. 5, was prepared by using acetic acid as solvent as proposed by Happer, Mitchell and Wright.³⁸ 2.20 g of thiophenol was dissolved in 8 ml of glacial acetic acid, and 3.77 g of *o*-nitrobenzenesulfonyl chloride was dissolved in 50 ml of glacial acetic acid. The thiol solution was added to the sulfonyl chloride solution, and the reaction mixture was stirred for 15 min at room temperature. The solvent was removed in vacuum, and the compound appeared as an

oily substance. On dissolving in diethyl ether and cooling in a dry-ice acetone bath, pure crystalline material was obtained, yield 4.07 g or 78%, based on the amount of sulfonyl chloride.

Compounds Nos. 10 and 12, Table 1, were prepared as reported previously.^{39,28} Compound No. 11 was synthesized in the same way as described for the analogous selenium compound.⁷

The tetraphenylarsonium salt of the *o*-nitrobenzenesulfonyl thiosulfate ion, compound No. 6, was prepared from *o*-nitrobenzenesulfonyl thiocyanate, sodium thiosulfate, and tetraphenylarsonium chloride according to the following procedure. 1.06 g of sulfonyl thiocyanate (5×10^{-3} mol) was dissolved in a mixture of 8 ml of ethyl acetate and 4 ml of methanol. 1.36 g of $\text{Na}_2\text{S}_2\text{O}_3 \cdot 5\text{H}_2\text{O}$ (5.5×10^{-3} mol) and 2.40 g $\text{Ph}_4\text{AsCl} \cdot \text{H}_2\text{O}$ (5.5×10^{-3} mol) were dissolved in about 25 ml of water. The sulfonyl thiocyanate solution was added to the aqueous salt solution under vigorous stirring for 5 min, during which the Ph_4As -salt of the *o*-nitrobenzenesulfonyl thiosulfate ion precipitated as a yellowish-green substance, which was filtered off, washed carefully with water, and drained. The compound was recrystallized from acetonitrile by the addition of some ether. Yield, 2.58 g, or 80% based on the amount of *o*-nitrobenzenesulfonyl thiocyanate.

The products of the reactions using *o*-nitrobenzeneselenenyl halides as substrates have been synthesized previously.⁷

Kinetics. The reaction between *o*-nitrobenzenesulfonyl chloride and the various nucleophiles was in most cases followed by measuring the decrease in the absorption at 410 nm with a Beckman spectrophotometer, using 1 cm thermostated cells. In the case of the two strongest nucleophiles, *i.e.*, Ph-S^- and CN^- , the rate was determined with a Durrum stopped-flow spectrophotometer. The kinetic runs were performed under pseudo-first order conditions, with excess of nucleophile. The substrate concentration was about $(2-4) \times 10^{-5}$ M. The plots of $\log(D_\infty - D_t)$ against time gave in all cases straight lines, and the pseudo-first order rate constants k' , were determined from these diagrams. The second-order rate constants, k_2 , were calculated from the slope of the best straight line through the origin in the $k' - [\text{Nu}]$ plots.

The rate of the reaction between *o*-nitrobenzeneselenenyl halides and the various nucleophiles was followed at $\lambda = 430$ nm applying the stopped-flow technique. The kinetic runs were performed under the same conditions as described earlier.⁷

The activation parameters were determined from the best straight line plots of $\log k_2$ against $1/T$.

Acknowledgement. The author wishes to thank Professor O. Foss for valuable discussions, and

Dr. S. Husebye for providing samples of the sodium dithiocarbamates and ammonium di-O-ethylthiophosphate.

REFERENCES

1. Foss, O. In Kharash, N., Ed., *Organic Sulfur Compounds*, Pergamon, New York 1961, Vol. 1, pp. 83–96.
2. Davis, R. E. In Nickless, G., Ed., *Inorganic Sulfur Chemistry*, Elsevier, Amsterdam—London—New York 1968, pp. 85–135.
3. Ciuffarin, E. and Fava, A. *Prog. Phys. Org. Chem.* 6 (1968) 81.
4. Kice, J. L. In Senning, A., Ed., *Sulfur in Organic and Inorganic Chemistry*, Dekker, New York 1971, p. 153.
5. Austad, T. *Acta Chem. Scand. A* 28 (1974) 935.
6. Austad, T. *Acta Chem. Scand. A* 28 (1974) 927.
7. Austad, T. *Acta Chem. Scand. A* 29 (1975) 895.
8. Foss, O. *Pure Appl. Chem.* 24 (1970) 31.
9. Hamilton, W. C. and La Placa, S. J. *J. Am. Chem. Soc.* 86 (1964) 2289.
10. Eriksen, R. and Hauge, S. *Acta Chem. Scand.* 26 (1972) 3153.
11. Yamabe, T., Nagata, S., Kikuzona, Y. and Fukui, K. *Bull. Chem. Soc. Jpn.* 48 (1975) 1349.
12. Husebye, S. and Helland-Madsen, G. *Acta Chem. Scand.* 24 (1970) 2273.
13. Husebye, S. *Acta Chem. Scand.* 27 (1973) 756.
14. Brøndmo, N. J., Esperås, S. and Husebye, S. *Acta Chem. Scand. A* 29 (1975) 93.
15. Husebye, S. and Helland-Madsen, G. *Acta Chem. Scand.* 23 (1969) 1398.
16. Leffler, J. E. and Grunwald, E. *Rates and Equilibria of Organic Reactions*, Wiley, New York and London 1963, p. 162.
17. Edwards, J. O. *J. Am. Chem. Soc.* 76 (1954) 1540.
18. Ritter, R. D. and Krueger, J. H. *J. Am. Chem. Soc.* 92 (1970) 2316.
19. Pearson, R. G. and Songstad, J. *J. Am. Chem. Soc.* 89 (1967) 1827.
20. Kice, J. L. and Large, G. B. *J. Am. Chem. Soc.* 90 (1968) 4069.
21. Foss, O. K. *Nor. Vidensk. Selsk. Skr.* (1945) No. 2.
22. Foss, O. *Acta Chem. Scand.* 1 (1947) 307.
23. Gregg, R. C. and Tyler, W. P. *J. Am. Chem. Soc.* 72 (1950) 4561.
24. Davis, R. E. In Nickless, G., Ed., *Inorganic Sulfur Chemistry*, Elsevier, Amsterdam—London—New York 1968, p. 85.
25. Austad, T., Engemyr, L. B. and Songstad, J. *Acta Chem. Scand.* 25 (1971) 3535.
26. Behaghel, O. and Seibert, H. *Ber. Dtsch. Chem. Ges.* 66 (1933) 708.
27. Austad, T. *Acta Chem. Scand. A* 30 (1976) 579.
28. Lecher, H. and Simon, K. *Ber. Dtsch. Chem. Ges.* 54 (1921) 632.
29. Coetzee, J. F. *Pure Appl. Chem.* 1967 429.
30. Eriksen, R. *Acta Chem. Scand.* 26 (1972) 1274.
31. Rheinboldt, H. In Houben-Weyl, *Methoden der organischen Chemie*, 4th Ed., Thieme, Stuttgart 1955, Band IX, p. 1164.
32. Gleu, K. and Schwab, R. *Angew. Chem.* 62 (1950) 320.
33. Kuchen, W., Strolenberg, K. and Metten, J. *Chem. Ber.* 96 (1963) 1733.
34. Ketelaar, J. A. A. and Gersmann, H. R. *Recl. Trav. Chim. Pays-Bas* 77 (1958) 973.
35. Foss, O. *Acta Chem. Scand.* 1 (1947) 8.
36. Andreades, S. and Zahnow, E. W. *J. Am. Chem. Soc.* 91 (1969) 4181.
37. Foss, O. *J. Am. Chem. Soc.* 69 (1947) 2236.
38. Happer, D. A. R., Mitchell, J. W. and Wright, G. J. *Aust. J. Chem.* 26 (1973) 121.
39. Austad, T. and Esperås, S. *Acta Chem. Scand. A* 30 (1976) 563.

Received July 5, 1976.

The Crystal Structure of Sodium Hexacyanochromate(II) Decahydrate, $\text{Na}_4[\text{Cr}(\text{CN})_6]\cdot 10\text{H}_2\text{O}$

EVERT LJUNGSTRÖM

Department of Inorganic Chemistry, University of Göteborg and Chalmers University of Technology, Fack, S-402 20 Göteborg 5, Sweden.

The crystal structure of sodium hexacyanochromate(II) decahydrate has been determined by single crystal X-ray methods using diffractometer data collected at -100°C . The crystals are monoclinic with $a = 9.866(4) \text{ \AA}$, $b = 11.502(4) \text{ \AA}$, $c = 9.152(4) \text{ \AA}$, $\beta = 98.30(3)^\circ$, and belong to space group $P2_1/n$. A final R value of 0.052 was obtained for 1210 independent reflections. The complex ion has nearly octahedral symmetry with mean Cr—C and C—N distances of 2.053(4) and 1.156(5) \AA , respectively.

As part of a systematic investigation of transition metal hexacyanides, the crystal structure of $\text{Na}_4[\text{Cr}(\text{CN})_6]\cdot 10\text{H}_2\text{O}$ has been determined. By correlating the M—C and C—N bond lengths and the geometries of the complex ions for various metals and oxidation states with other experimental data, such as IR and X-ray photoelectron spectra, and with molecular orbital calculations it should be possible to estimate the relative magnitudes of the σ and π contributions to the M—C(N) bonds. Structural data are now available for $\text{K}_4[\text{V}(\text{CN})_6]$,¹ $\text{Na}_4[\text{Cr}(\text{CN})_6]\cdot 10\text{H}_2\text{O}$, $\text{Na}_4[\text{Mn}(\text{CN})_6]\cdot 10\text{H}_2\text{O}$,² $\text{Na}_4[\text{Fe}(\text{CN})_6]\cdot 10\text{H}_2\text{O}$,² $\text{K}_3[\text{Cr}(\text{CN})_6]$,³ $\text{K}_3[\text{Mn}(\text{CN})_6]$,⁴ $\text{K}_3[\text{Fe}(\text{CN})_6]$,⁵ and $\text{K}_3[\text{Co}(\text{CN})_6]$.⁵

EXPERIMENTAL

The compound was prepared by a modification of the method due to Ludi.⁶ 2.5 g $\text{Na}_2[\text{Cr}(\text{CN})_6]$ and 1.7 g NaCN were dissolved in 10 ml 0.2 M NaOH and an amalgamated aluminum sheet was added. After a few minutes the solution turned red and hydrogen gas was evolved. Within 10 h dark green crystals of $\text{Na}_4[\text{Cr}(\text{CN})_6]\cdot 10\text{H}_2\text{O}$ suitable for single crystal X-ray work

developed on the aluminum sheet and on the walls of the vessel. The amalgamation of the aluminum sheet, which seems to be the critical step in this synthesis, was accomplished by first washing the aluminum sheet (ca. $7 \times 15 \times 0.1 \text{ mm}$) in CCl_4 , dipping it into a 0.1 M solution of $\text{Hg}(\text{NO}_3)_2$ for 30 s, and finally rinsing it in water. The above method is to the author's knowledge the only way by which large single crystals of this compound can be prepared.

$\text{Na}_2[\text{Cr}(\text{CN})_6]$ was prepared by passing a solution of $\text{K}_3[\text{Cr}(\text{CN})_6]$ through a Merck No. 1 ion exchange column saturated with sodium ions. The resulting solution was filtered and evaporated *in vacuo* at 50°C . $\text{K}_3[\text{Cr}(\text{CN})_6]$ was prepared according to Brauer.⁷

The chromium content was determined gravimetrically as PbCrO_4 by oxidation with boiling perchloric acid and subsequent precipitation with an aqueous solution of lead nitrate. The water content was determined by drying the compound over P_2O_5 with gentle heating using argon as protective atmosphere and measuring the loss in weight. The sodium content was determined gravimetrically as sodium uranyl zinc acetate by precipitation with uranyl zinc acetate saturated with the sodium salt. [Found: Cr 10.98; Na 20.0; H_2O 36.5. Calc. for $\text{Na}_4[\text{Cr}(\text{CN})_6]\cdot 10\text{H}_2\text{O}$: Cr 10.82; Na 19.15; H_2O 37.5].

The compound is very unstable in air due to loss of water of crystallization and oxidation of chromium to the trivalent state. Upon dissolution in water the compound is immediately oxidized and gives a yellow solution from which $\text{Na}_2[\text{Cr}(\text{CN})_6]$ can be crystallized. The compound is also sensitive to X-rays at room temperature.

Unit cell parameters were determined from Guinier powder photographs using $\text{CuK}\alpha_1$ radiation ($\lambda = 1.54050 \text{ \AA}$) and SiO_2 as an internal standard. The powder samples were prepared in a glove-box filled with humid argon to prevent oxidation and loss of crystal water, and were covered with mylar film during exposure in the Guinier camera. 23 lines were

indexed and the cell parameters were refined using the program POWDER.⁸ A number of lines could not be indexed owing to too large deviations from possible $\sin^2\theta$ values or to calculated and observed intensities not matching each other. These lines probably originated from decomposition products.

An attempt was made to record the IR spectrum of Na₄[Cr(CN)₆].10H₂O with the KBr disc technique. However, only the spectrum of the chromium(III) compound could be recorded and it is obvious that milling and exposure to infrared radiation caused rapid oxidation of the substance.

The crystal used in the investigation (approximate size 0.17 × 0.18 × 0.23 mm) was picked out from the vessel where it was grown, dried with a filter paper, covered with epoxy resin and mounted on a glass fibre. The intensities were collected with a SYNTEX P2₁ automatic four circle diffractometer using monochromatized CuK α radiation. The ω - 2θ scan method was used and the 2θ scan speed was allowed to vary between 2 and 15°/min depending on the intensity of the measured reflexion. Data were collected for $2\theta \leq 115^\circ$. During the data collection the crystal was cooled to -100°C using the SYNTEX LT1 low temperature device. Without cooling and an epoxy cover, the crystals lose their diffracting power in less than 30 min.

In order to minimize the expected radiation damage to the crystal no separate background counts were made. The scan range was instead increased slightly in order to obtain a representative background on each side of a reflexion. A profile analysis based on the Larsen-Lehmann method⁹ was then applied to the 96 step profile collected for each reflexion. It was thus possible to reduce the time required to collect the data by one third. The deterioration of the crystal appeared, however, to be slight since the periodically measured test reflexion did not show any significant decrease in intensity.

STRUCTURE DETERMINATION

1210 independent reflexions with $F_o^2 > 2.5 \sigma(F_o^2)$ were considered as being observed and were corrected for Lorentz, polarization and absorption effects. Na₄[Cr(CN)₆].10H₂O was found to be isomorphous with Na₄[Fe(CN)₆].10H₂O and Na₄[Mn(CN)₆].10H₂O.² The positional parameters of the manganese compound were used to start a series of least squares refinements. The refinement of an over-all scale factor, atomic coordinates and isotropic thermal parameters using the block diagonal approximation yielded an R -value of 0.065. On introduction of anisotropic thermal parameters and using full matrix least squares refinement an R value of 0.052 was obtained for 124 parameters ($R = \sum ||F_o| - |F_c|| / \sum |F_o|$). Throughout the refinement Cruickshank's weighting scheme¹⁰ [$w = (a + F_o + cF_o + dF_o^2)^{-1}$] was used with $a = 15.0$, $c = 0.015$ and $d = 0.0$. The scattering factors for Cr⁰, O, N, C, and Na⁺ were those of Doyle and Turner.¹¹ A difference synthesis calculated after the final cycle of refinement showed no peak higher than about 1.5 e/Å³. Such peaks were close to the oxygen atoms where the water hydrogen atoms would be expected to lie. No attempt was, however, made to locate the hydrogen atoms. Some crystallographic data are given in Table 1.

A list of observed and calculated structure factors is available from the author on request.

Table 1. Crystallographic data for Na₄[Cr(CN)₆].10H₂O.

Unit cell	monoclinic with $a = 9.866(4) \text{ \AA}$ $b = 11.502(4) \text{ \AA}$ $c = 9.152(4) \text{ \AA}$ $\beta = 98.30(3)^\circ$ $V = 1027.7(7) \text{ \AA}^3$
Formula weight	480.0
Density	$D_m = 1.54 \text{ g/cm}^3$ $D_x = 1.551 \text{ g/cm}^3$
Systematic absences	$h+l = 2n+1$ for $h0l$ $k = 2n+1$ for $0k0$
Space group	$P2_1/n$ (non-standard setting)
General positions	$\pm(x, y, z) \pm(\frac{1}{2} + x, \frac{1}{2} - y, \frac{1}{2} + z)$
Crystal habit	dark green prismatic crystals
$\mu(\text{Cu})$	61.7 cm^{-1}

RESULTS AND DISCUSSION

The final atomic coordinates and thermal parameters are given in Tables 2 and 3, respectively. Some distances and angles are given in Table 4. The basic building unit in the structure is the almost octahedral $\text{Cr}(\text{CN})_6^{4-}$ ion. Due to the center of symmetry there are three crystallographically different cyanide groups. The mean Cr—C and C—N distances are 2.053(4) and 1.156(5) Å, respectively. The deviations from linearity of the cyanide groups are significant and are probably due to packing effects.

The N(3) atoms are in contact with three sodium ions while the N(2) atoms are in contact

with one sodium ion. The N(1) atoms have relatively short distances to some water oxygen atoms and appear to be involved in weak hydrogen bonding. Each sodium ion is surrounded by two nitrogen atoms from cyanide groups and four water oxygen atoms forming a distorted octahedron. The sodium ions thus link the complex ions together, forming a three-dimensional network. A stereoscopic projection of the unit cell along [010] is shown in Fig. 1.

The strength of the metal-carbon σ -bond is expected to be dependent on the effective nuclear charge of the metal atom and thus to increase from V to Co. For the same reason the σ -contributions are expected to be stronger for the M(III) complexes than for the M(II) complexes. One effect of the σ -bond is to reduce the positive charge on the metal atom.

d - π^* donation should be favoured by a low positive charge on the metal atom and a large number of metal d -electrons. Back-donation leads to increased strength of the metal-carbon bond, decreased strength of the carbon-nitrogen bond, and an increased positive charge on the metal atom.

In all cases where bond lengths are known for both the formally di- and trivalent states of a given metal atom, the M(III)—C bond is longer than the M(II)—C bond. From a simple electrostatic approach considering σ -bonding only one would expect the reverse situation. The short M(II)—C bonds must therefore be due to a strong π -contribution.

Table 2. Atomic coordinates with estimated standard deviations.

Atom	<i>x</i>	<i>y</i>	<i>z</i>
Cr	0	0	0
Na1	0.5959(2)	0.3569(2)	0.0123(2)
Na2	0.7184(2)	0.1280(2)	0.4025(2)
C1	0.2043(6)	0.0122(4)	0.0743(6)
C2	0.4982(5)	0.3214(5)	0.4758(6)
C3	0.0435(5)	0.0189(4)	0.2118(7)
N1	0.3204(5)	0.0215(4)	0.1137(5)
N2	0.5040(5)	0.2207(4)	0.4672(6)
N3	0.9278(5)	0.0312(4)	0.3283(5)
O1	0.2967(4)	0.0376(3)	0.4439(4)
O2	0.6117(4)	0.0068(4)	0.2025(5)
O3	0.7663(4)	0.2782(4)	0.2142(5)
O4	0.1148(6)	0.2710(4)	0.3184(5)
O5	0.3866(4)	0.2793(3)	0.1004(5)

Table 3. Anisotropic thermal parameters ($\times 10^3$) with their standard deviations. The temperature factor is expressed as $\exp[-2\pi^2(h^2a^{*2}U_{11} + k^2b^{*2}U_{22} + l^2c^{*2}U_{33} + hka^*b^*U_{12} + hla^*c^*U_{13} + klb^*c^*U_{23})]$.

Atom	U_{11}	U_{22}	U_{33}	U_{12}	U_{23}	U_{13}
Cr	5.5(7)	6.6(7)	9.4(8)	-0.5(9)	6.6(11)	0(9)
Na(1)	15(1)	19(1)	24(1)	2(2)	4(2)	6(2)
Na(2)	14(1)	16(1)	20(2)	3(2)	7(2)	3(2)
C(1)	21(4)	10(3)	13(3)	0(4)	23(5)	-2(4)
C(2)	8(3)	22(4)	17(3)	5(4)	20(5)	6(5)
C(3)	6(3)	7(3)	21(3)	1(4)	3(5)	1(4)
N(1)	13(3)	29(3)	32(3)	2(4)	17(5)	-1(4)
N(2)	19(3)	15(3)	47(4)	-1(4)	20(5)	-4(5)
N(3)	17(3)	21(3)	14(3)	4(4)	13(5)	2(4)
O(1)	21(2)	18(2)	22(2)	-5(3)	15(4)	0(3)
O(2)	17(2)	47(3)	29(3)	5(4)	3(9)	19(4)
O(3)	24(2)	27(2)	47(3)	-6(4)	19(4)	-30(4)
O(4)	72(4)	24(3)	42(3)	-14(5)	6(5)	9(4)
O(5)	28(2)	21(2)	37(3)	-9(4)	14(4)	12(4)

Table 4. Some distances (Å) and angles (°) in $\text{Na}_4[\text{Cr}(\text{CN})_6] \cdot 10\text{H}_2\text{O}$. Standard deviations are given within parentheses. No superscript, atom in x, y, z ; ', atom in $\bar{x}, \bar{y}, \bar{z}$; '', atom in $\frac{1}{2} + x, \frac{1}{2} - y, \frac{1}{2} + z$; ''', atom in $\frac{1}{2} - x, \frac{1}{2} + y, \frac{1}{2} - z$.

Cr—C(1)	2.037(6)	C(1)—N(1)	1.155(8)
Cr—C(2)	2.065(6)	C(2)—N(2)	1.163(8)
Cr—C(3)	2.057(6)	C(3)—N(3)	1.150(8)
C(1)—Cr—C(2)	92.3(2)	C(1)—Cr—C(3)	90.5(2)
C(2)—Cr—C(3)	90.2(2)	Cr—C(1)—N(1)	178.1(5)
Cr—C(2)—N(2)	176.3(5)	Cr—C(3)—N(3)	177.6(5)
Na(1)—N(3)'''	2.509(5)	Na(1)—N(3)''	2.537(5)
Na(1)—O(1)	2.479(4)	Na(1)—O(3)	2.483(5)
Na(1)—O(4)	2.334(5)	Na(1)—O(5)''	2.489(5)
Na(2)—N(2)	2.515(5)	Na(2)—N(3)''	2.525(5)
Na(2)—O(1)'	2.385(4)	Na(2)—O(2)''	2.417(5)
Na(2)—O(3)''	2.532(5)	Na(2)—O(5)''	2.511(5)
Some short oxygen-nitrogen distances			
N(1)—O(2)'''	3.081(7)	N(1)—O(2)''	2.877(7)
N(1)—O(4)	2.997(7)	N(1)—O(5)''	3.042(7)

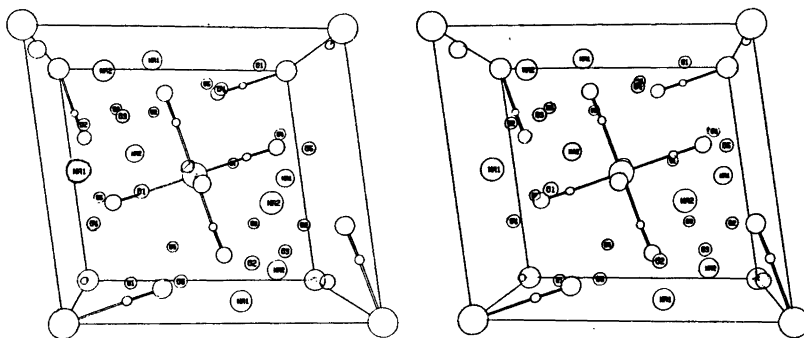


Fig. 1. Stereoscopic projection of the unit cell of $\text{Na}_4[\text{Cr}(\text{CN})_6] \cdot 10\text{H}_2\text{O}$ along [010]. The a axis is horizontal. The labels of the chromium, carbon and nitrogen atoms have been omitted for clarity.

Graphical representations of the metal-carbon and carbon-nitrogen bond lengths for the hexacyano compounds mentioned in the introduction of this paper are shown in Figs. 2–3. The differences in carbon-nitrogen bond lengths are not significant but there is a tendency for the C–N bonds to weaken when going from V(II) to Fe(II). This is also supported by a decrease in the ν (C–N) IR stretch frequency.¹ No such trend is observed for the M(III) complexes.

The observed bond lengths indicate that π -bonding is strongest in the Mn(II) and Fe(II) complexes. Here the π -contribution almost

compensates for the decreased effective nuclear charge when going from Co(III) to Fe(II) (both d^5 ground state configuration) or from Fe(III) to Mn(II) (both d^5). This is in good agreement with the results of semi-empirical molecular orbital calculations made by Alexander and Gray.^{12,13} When comparing Mn(III) and Cr(II) (both d^4) it is seen that the decreased nuclear charge is not fully compensated for by π -bonding and the π -bonding seems to be weaker than in the Fe(II) and Mn(II) complexes. The largest difference in M–C bond lengths for metals with the same electronic ground state configuration is observed between V(II) and

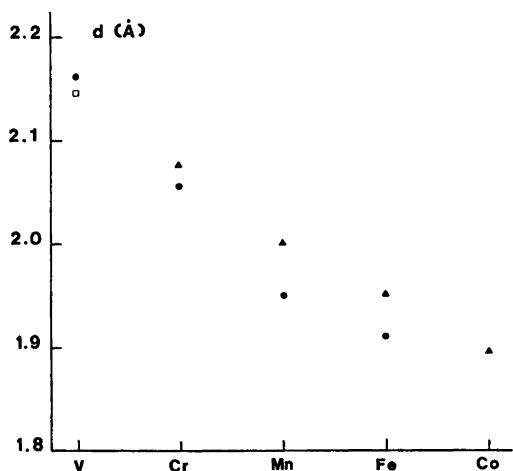


Fig. 2. Mean M-C bond lengths for some transition metal hexacyano complexes. ●, M(II)-C; ▲, M(III)-C. The seven-coordinated V(III) complex $K_4[V(CN)_7] \cdot 2H_2O$ is denoted by □.

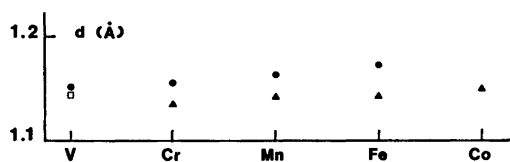


Fig. 3. Mean C-N bond lengths for some transition metal hexacyano complexes. ●, distance in M(II) complexes; ▲, distance in M(III) complexes. The seven-coordinated V(III) complex is denoted by □.

Cr(III) (both d^3). This means that the weakest π -contribution in the M(II) series is found in the V(II) complex. These observations are also supported by the tendency for the C-N bond length to increase when going from V(II) to Fe(II).

No structure of a hexacyano complex with V(III) is known but the structure of $K_4[V(CN)_7] \cdot 2H_2O$ has been solved,¹⁴ the complex ion having a pentagonal bipyramidal conformation. Although a comparison of bond lengths is not strictly relevant it is interesting to note that the V(III)-C bond is shorter than the V(II)-C bond. This also appears to indicate that the π -contribution in the V(II) complex is weaker than in the other M(II) complexes. The weak

bonding in the V(II) complex has been noted earlier.¹

An X-ray photoelectron investigation of transition metal hexacyanides confirms these conclusions.¹⁵

Acknowledgements. The author wishes to thank Professor A. Ludi for discussions concerning the preparation of the investigated compound. Many thanks are also due to Dr. S. Jagner for valuable comments and for revising the English text. A grant from the Swedish Natural Science Research Council (Contract No. 2286-18) is gratefully acknowledged.

REFERENCES

- Jagner, S. *Acta Chem. Scand. A* 29 (1975) 255.
- Tullberg, A. and Vannerberg, N.-G. *Acta Chem. Scand. A* 28 (1974) 551.
- Jagner, S., Ljungström, E. and Vannerberg, N.-G. *Acta Chem. Scand. A* 28 (1974) 623.
- Vannerberg, N.-G. *Acta Chem. Scand.* 24 (1970) 2335.
- Vannerberg, N.-G. *Acta Chem. Scand.* 26 (1972) 2863.
- Ludi, A. *Private communication.*
- Brauer, G. *Handbuch der Präparativen Anorganischen Chemie*, Ferd. Enke, Stuttgart 1962, Vol. II, p. 1202.
- Lindqvist, O. and Wengelin, F. *Ark. Kemi* 28 (1967) 179.
- Larsen, F. K. and Lehmann, M. S. *Acta Crystallogr. A* 30 (1974) 580.
- Cruickshank, D. W. J. *The Equations of Structure Refinements*, Glasgow 1964.
- Doyle, P. A. and Turner, P. S. *Acta Crystallogr. A* 24 (1969) 390.
- Alexander, J. J. and Gray, H. B. *Coord. Chem. Rev.* 2 (1967) 29.
- Alexander, J. J. and Gray, H. B. *J. Am. Chem. Soc.* 90 (1968) 2460.
- Towns, R. L. and Levenson, R. A. *Inorg. Chem.* 13 (1974) 105.
- Vannerberg, N.-G. *Chem. Scr.* 9 (1976) 122.

Received August 10, 1976.

Vibrational Spectra of the Tris(1,2-ethanediamine)rhodium(III) Cation. I. Normal Coordinate Analysis of the Parent Compound, Three Deuterated, and Four ^{15}N Substituted Species*

G. BORCH,^a P. H. NIELSEN^b and P. KLÆBOE^c

^a Chemistry Department A, The Technical University of Denmark, DK-2800 Lyngby, Denmark, ^b Chemical Laboratory II, The H.C. Ørsted Institute, DK-2100 Copenhagen, Denmark and ^c Department of Chemistry, University of Oslo, Oslo 3, Norway.

A normal coordinate analysis of the tris(1,2-ethanediamine)-rhodium(III) cation, the $N\text{-}d_{12}$, $C\text{-}d_{12}$ and $N,C\text{-}d_{24}$ deuterated, and the four corresponding ^{15}N substituted species has been accomplished as a 37 body problem (including all atoms). The complex with the three chiral five-membered rings in the more stable δ conformation and the same absolute configuration Δ as in $(+)\text{[Co(en)}_3\text{]}^{3+}$ was selected for the analysis among the four possible combinations of Δ,Δ absolute configuration with δ,Δ ring conformation; resulting in D_3 symmetry of the complex ion. By fitting 38 force constants in the GVFF (General Valence Force Field) approximation to reproduce more than 500 observed frequencies, the normal modes of vibration for the observed bands can be described in terms of the potential energy distribution (PED) between the symmetry coordinates. The force field and vibrational modes related to the Rh—N bonds and N—Rh—N angles are discussed in some detail.

A large amount of data has been collected on the vibrational spectra of metal chelates of 1,2-ethanediamine (en). However, the interpretation of these results is still very unsatisfactory and band assignments and interpretations are usually made without any assistance from normal coordinate calculations. A partial calculation considering only the nine skeletal atoms was performed by Ashley and Torrible¹ for Ti(en) tetrahalide complexes and used as a basis for assigning the IR spectrum in the region above 300 cm^{-1} . A more detailed cal-

ulation has been reported by Omura, Nakagawa and Shimanouchi² for the IR active species of several bis(en) metal chelates, but in this case the force constants were refined to fit the frequencies especially in the region below 600 cm^{-1} . Attempts to give detailed assignments of IR and Raman spectra based upon complete normal coordinate calculations have, to our knowledge, not been published.

In the present paper the results of a complete normal coordinate treatment of this ion and seven isotopically labelled species are discussed with special emphasis on the force constants and the vibrational modes involving the central part of the complex compounds. The IR and Raman spectra in the solid state and in solution including polarization measurements of the Raman bands of the parent molecule $[\text{Rh(en)}_3]^{3+}$ and the three deuterated species will be dealt with in separate papers.³ The shifts observed by ^{15}N isotopic substitution are also included here. Hence, this is the first of several papers concerning the vibrational characteristics of the $[\text{Rh(en)}_3]^{3+}$ cation.

STRUCTURE

By investigation of X-ray powder photographs of active racemates it was shown by Andersen *et al.*⁴ that $(+)\text{[Co(en)}_3\text{]}^{3+}$ and $(-)\text{[Rh(en)}_3\text{]}^{3+}$ have the same absolute configuration Δ . Since a three-dimensional analysis of $(+)\text{[Co(en)}_3\text{]Cl}_3\cdot\text{H}_2\text{O}$ ⁵ revealed the ligand conformation to be δ , i.e. that the

* Presented in parts at the Nordiske Kemikermøde, Umeå, Sweden, June 1971.

C-C direction within each chelate ring is approximately parallel to the threefold axis of the complex ion (*lel* arrangement), the same must necessarily be true for the rhodium complex in the solid state. The complex has accordingly the symmetry D_3 with the six nitrogen atoms of the three ligands bonded nearly octahedrally to the central rhodium atom. The present calculations have therefore been based upon a $A-(\delta\delta\delta)$, or $A-lel_3$, model for the $[\text{Rh}(\text{en})_3]^{3+}$ ion.

The Cartesian coordinates were constructed in the following way. The $[\text{Rh}(\text{en})_3]^{3+}$ ion was located in a three-dimensional coordinate system with the rhodium atom *in origo* and with the six nitrogen atoms placed upon the X, Y, and Z axes assuming N-Rh-N angles of 90° . The unknown coordinates were then calculated by a vector analytical method⁶ applied to one of the ligands only. Transcription of (x,y,z) coordinates to the trigonal coordinate system⁶ (x',y',z') proceeded *via* the orthonormal transformations

$$x' = (2/3)^{1/2}z - 6^{-1/2}y - 6^{-1/2}x$$

$$y' = -2^{-1/2}y + 2^{-1/2}x$$

$$z' = 3^{-1/2}z + 3^{-1/2}y + 3^{-1/2}x$$

and finally the coordinates obtained (x',y',z') were rotated $\pm 120^\circ$ around the Z' axis to give the coordinates of the two other ligands.

The average Rh-N distance in (+)-*trans*-1,2-cyclohexanediamine[rhodium (-)-*trans*-1,2-cyclohexanediamine]rhodium (III) nitrate trihydrate was found⁷ to be 2.08 Å. Since the Rh-N bond length was very close to 1.99 Å in both dimethylglyoxime^{8,9} and ethylenimine¹⁰ complexes, the rounded value of 2.00 Å was adopted in the present calculation. The values used for the ligand distances and bond angles are mostly standard values: $r(\text{N}-\text{H}) = 1.01$ Å, $r(\text{C}-\text{H}) = 1.09$ Å, $r(\text{C}-\text{C}) = 1.53$ Å, $r(\text{C}-\text{N}) = 1.47$ Å, $\angle\text{H}-\text{N}-\text{H} = \angle\text{H}-\text{C}-\text{H} = 111^\circ$, $\angle\text{Rh}-\text{N}-\text{C} = 105^\circ$, $\angle\text{N}-\text{C}-\text{C} = 111^\circ$, $\angle\text{Rh}-\text{N}-\text{H} = 115^\circ$, $\angle\text{N}-\text{C}-\text{H} = 107^\circ$, $\angle\text{Rh}-\text{N}-\text{C}-\text{C} = 33^\circ$.

NORMAL COORDINATE ANALYSIS

The normal coordinate analysis was performed as a 37-body problem using Wilson's GF matrix method as treated in the program of Schachtschneider and Snyder.¹¹ The potential

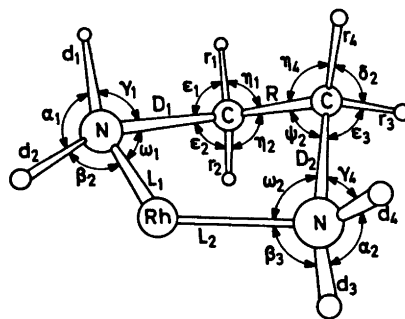


Fig. 1. Internal coordinates of the chelate ring I. Additional coordinates are: Torsion around the Rh-N bonds τ_1 and τ_3 , the N-C bonds τ_2 and τ_4 , and around the C-C bond Δ . Torsion around the Rh-N bonds (τ_1 and τ_3) have been defined as C-N-Rh-N torsion within a chelate ring. Torsion around the N-C bonds (τ_2 and τ_4) have been defined as Rh-N-C-N torsion, and around the C-C bond (Δ) as N-C-C-N torsion.

function employed was of the GVFF type originally developed for hydrocarbons,¹² extended to molecules containing the X-CH₂-CH₂-X moiety¹³⁻¹⁶ also present in $[\text{Rh}(\text{en})_3]^{3+}$. The internal coordinates of the chelate ring are shown in Fig. 1, while the internal NRhN deformation coordinates are separately given in Fig. 2. The symmetry coordinates listed in Table 1 were derived making use of the D_3 symmetry of the complex. The redundancies

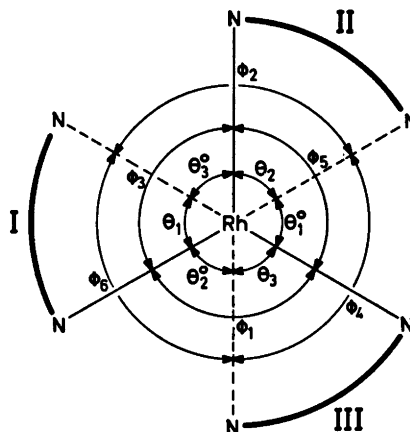


Fig. 2. The internal NRhN deformation coordinates. The numbers I, II, and III refer to the three chelate rings.

Table 1. Symmetry coordinates for the tris(1,2-ethanediamine)Rh(III) cation. The numbers I, II, and III refer to the chelate rings. The symbols used are defined in section (c) of this Table for the chelate ring I and similar expressions are used for the other chelate rings.

(a) Chelate rings

Species A_1

$$S_1 - S_{22} = [Sx(I) + Sx(II) + Sx(III)]/\sqrt{3} \quad (x = a, b, c, d, \dots, v)$$

Species A_2

$$S_1 - S_{20} = [Sx'(I) + Sx'(II) + Sx'(III)]/\sqrt{3} \quad (x = a, b, d, e, \dots, u)$$

Species E

$S_1 = [2Sa(I) - Sa(II) - Sa(III)]/\sqrt{6}$	$S_2 = [Sa'(II) - Sa'(III)]/\sqrt{2}$
$S_3 = [2Sb(I) - Sb(II) - Sb(III)]/\sqrt{6}$	$S_4 = [Sb'(II) - Sb'(III)]/\sqrt{2}$
$S_5 = [2Sc(I) - Sc(II) - Sc(III)]/\sqrt{6}$	
$S_6 = [2Sd(I) - Sd(II) - Sd(III)]/\sqrt{6}$	$S_7 = [Sd'(II) - Sd'(III)]/\sqrt{2}$
$S_8 = [2Se(I) - Se(II) - Se(III)]/\sqrt{6}$	$S_9 = [Se'(II) - Se'(III)]/\sqrt{2}$
$S_{10} = [2Sf(I) - Sf(II) - Sf(III)]/\sqrt{6}$	$S_{11} = [Sf'(II) - Sf'(III)]/\sqrt{2}$
$S_{12} = [2Sg(I) - Sg(II) - Sg(III)]/\sqrt{6}$	$S_{13} = [Sg'(II) - Sg'(III)]/\sqrt{2}$
$S_{14} = [2Sh(I) - Sh(II) - Sh(III)]/\sqrt{6}$	$S_{15} = [Sh'(II) - Sh'(III)]/\sqrt{2}$
$S_{16} = [2Si(I) - Si(II) - Si(III)]/\sqrt{6}$	$S_{17} = [Si'(II) - Si'(III)]/\sqrt{2}$
$S_{18} = [2Sj(I) - Sj(II) - Sj(III)]/\sqrt{6}$	$S_{19} = [Sj'(II) - Sj'(III)]/\sqrt{2}$
$S_{20} = [2Sk(I) - Sk(II) - Sk(III)]/\sqrt{6}$	$S_{21} = [Sk'(II) - Sk'(III)]/\sqrt{2}$
$S_{22} = [2Sl(I) - Sl(II) - Sl(III)]/\sqrt{6}$	$S_{23} = [Sl'(II) - Sl'(III)]/\sqrt{2}$
$S_{24} = [Sm(II) - Sm(III)]/\sqrt{2}$	$S_{25} = [2Sm'(I) - Sm'(II) - Sm'(III)]/\sqrt{6}$
$S_{26} = [2Sn(I) - Sn(II) - Sn(III)]/\sqrt{6}$	$S_{27} = [Sn'(II) - Sn'(III)]/\sqrt{2}$
$S_{28} = [So(II) - So(III)]/\sqrt{2}$	$S_{29} = [2So'(I) - So'(II) - So'(III)]/\sqrt{6}$
$S_{30} = [2Sp(I) - Sp(II) - Sp(III)]/\sqrt{6}$	$S_{31} = [Sp'(II) - Sp'(III)]/\sqrt{2}$
$S_{32} = [Sq(II) - Sq(III)]/\sqrt{2}$	$S_{33} = [2Sq'(I) - Sq'(II) - Sq'(III)]/\sqrt{6}$
$S_{34} = [2Sr(I) - Sr(II) - Sr(III)]/\sqrt{6}$	$S_{35} = [Sr'(II) - Sr'(III)]/\sqrt{2}$
$S_{36} = [Ss(II) - Ss(III)]/\sqrt{2}$	$S_{37} = [2Ss'(I) - Ss'(II) - Ss'(III)]/\sqrt{6}$
$S_{38} = [2St(I) - St(II) - St(III)]/\sqrt{6}$	$S_{39} = [St'(II) - St'(III)]/\sqrt{2}$
$S_{40} = [2Su(I) - Su(II) - Su(III)]/\sqrt{6}$	$S_{41} = [Su'(II) - Su'(III)]/\sqrt{2}$
$S_{42} = [2Sv(I) - Sv(II) - Sv(III)]/\sqrt{6}$	

(b) Symmetry coordinates involving NRhN deformation (δ NRhN)Species A_1

$$S_{23} = [\phi_1 + \phi_2 + \phi_3 + \phi_4 + \phi_5 + \phi_6]/\sqrt{6}$$

$$S_{24} = [\theta_1 + \theta_2 + \theta_3 + \theta_1^\circ + \theta_2^\circ + \theta_3^\circ]/\sqrt{6}$$

$$S_{25} = [\theta_1 + \theta_2 + \theta_3 - \theta_1^\circ - \theta_2^\circ - \theta_3^\circ]/\sqrt{6}$$

Species A_2

$$S_{21} = [\phi_1 - \phi_2 + \phi_3 - \phi_4 + \phi_5 - \phi_6]/\sqrt{6}$$

Species E

$$S_{43} = [2\phi_1 + 2\phi_2 - \phi_3 - \phi_4 - \phi_5 - \phi_6]/\sqrt{12}$$

$$S_{44} = [\phi_3 - \phi_4 + \phi_5 - \phi_6]/2$$

$$S_{45} = [2\theta_1 - \theta_2 - \theta_3 + 2\theta_1^\circ - \theta_2^\circ - \theta_3^\circ]/\sqrt{12}$$

$$S_{46} = [\theta_2 - \theta_3 + \theta_2^\circ - \theta_3^\circ]/2$$

Table 1. Continued.

(c) Local symmetry coordinates of the chelate ring I

Symmetry coordinate	Symbol	Description
$Sa(I) = (L_1 + L_2)/\sqrt{2}$	$\nu_s \text{RhN}$	Symm. RhN stretch
$Sa'(I) = (L_1 - L_2)/\sqrt{2}$	$\nu_{as} \text{RhN}$	Asym. RhN stretch
$Sb(I) = (D_1 + D_2)/\sqrt{2}$	$\nu_s \text{CN}$	Symm. CN stretch
$Sb'(I) = (D_1 - D_2)/\sqrt{2}$	$\nu_{as} \text{CN}$	Asymm. CN stretch
$Sc(I) = R$	ν_{CC}	CC stretch
$Sd(I) = (d_1 + d_2 + d_3 + d_4)/2$	$\nu_s \text{NH}$	Symm. NH stretch
$Sd'(I) = (d_1 + d_2 - d_3 - d_4)/2$	$\nu_s \text{NH}$	Symm. NH stretch
$Se(I) = (d_1 - d_2 + d_3 - d_4)/2$	$\nu_{as} \text{NH}$	Asym. NH stretch
$Se'(I) = (d_1 - d_2 - d_3 + d_4)/2$	$\nu_{as} \text{NH}$	Asym. NH stretch
$Sf(I) = (r_1 + r_2 + r_3 + r_4)/2$	$\nu_s \text{CH}$	Symm. CH stretch
$Sf'(I) = (r_1 + r_2 - r_3 - r_4)/2$	$\nu_s \text{CH}$	Symm. CH stretch
$Sg(I) = (r_1 - r_2 + r_3 - r_4)/2$	$\nu_{as} \text{CH}$	Asym. CH stretch
$Sg'(I) = (r_1 - r_2 - r_3 + r_4)/2$	$\nu_{as} \text{CH}$	Asym. CH stretch
$Sh(I) = (\omega_1 + \omega_2)/\sqrt{2}$	$\delta_s \text{RhNC}$	Symm. RhNC deformation
$Sh'(I) = (\omega_1 - \omega_2)/\sqrt{2}$	$\delta_{as} \text{RhNC}$	Asym. RhNC deformation
$Si(I) = (\psi_1 + \psi_2)/\sqrt{2}$	$\delta_s \text{NCC}$	Symm. NCC deformation
$Si'(I) = (\psi_1 - \psi_2)/\sqrt{2}$	$\delta_{as} \text{NCC}$	Asym. NCC deformation
$Sj(I) = (\alpha_1 + \alpha_2)/\sqrt{2}$	δNH_2	NH_2 deformation
$Sj'(I) = (\alpha_1 - \alpha_2)/\sqrt{2}$	δNH_2	NH_2 deformation
$Sk(I) = (\delta_1 + \delta_2)/\sqrt{2}$	δCH_2	CH_2 deformation
$Sk'(I) = (\delta_1 - \delta_2)/\sqrt{2}$	δCH_2	CH_2 deformation
$Sl(I) = (\beta_1 + \beta_2 + \beta_3 + \beta_4)/2$	$[Sl(I) + Sn(I)]/\sqrt{2} = \delta \text{NH}_2$	NH_2 deformation
$Sl'(I) = (\beta_1 + \beta_2 - \beta_3 - \beta_4)/2$	$[Sl'(I) + Sn'(I)]/\sqrt{2} = \delta \text{NH}_2$	NH_2 deformation
$Sm(I) = (\beta_1 - \beta_2 + \beta_3 - \beta_4)/2$	$[Sm(I) + So(I)]/\sqrt{2} = \rho \text{NH}_2$	NH_2 rock
$Sm'(I) = (\beta_1 - \beta_2 - \beta_3 + \beta_4)/2$	$[Sm'(I) + So'(I)]/\sqrt{2} = \rho \text{NH}_2$	NH_2 rock
$Sn(I) = (\gamma_1 + \gamma_2 + \gamma_3 + \gamma_4)/2$	$[Sl(I) - Sn(I)]/\sqrt{2} = \omega \text{NH}_2$	NH_2 wag
$Sn'(I) = (\gamma_1 + \gamma_2 - \gamma_3 - \gamma_4)/2$	$[Sl'(I) - Sn'(I)]/\sqrt{2} = \omega \text{NH}_2$	NH_2 wag
$So(I) = (\gamma_1 - \gamma_2 + \gamma_3 - \gamma_4)/2$	$[Sm(I) - So(I)]/\sqrt{2} = t \text{NH}_2$	NH_2 twist
$So'(I) = (\gamma_1 - \gamma_2 - \gamma_3 + \gamma_4)/2$	$[Sm'(I) - So'(I)]/\sqrt{2} = t \text{NH}_2$	NH_2 twist
$Sp(I) = (\varepsilon_1 + \varepsilon_2 + \varepsilon_3 + \varepsilon_4)/2$	$[Sp(I) + Sr(I)]/\sqrt{2} = \delta \text{CH}_2$	CH_2 deformation
$Sp'(I) = (\varepsilon_1 + \varepsilon_2 - \varepsilon_3 - \varepsilon_4)/2$	$[Sp'(I) + Sr'(I)]/\sqrt{2} = \delta \text{CH}_2$	CH_2 deformation
$Sq(I) = (\varepsilon_1 - \varepsilon_2 + \varepsilon_3 - \varepsilon_4)/2$	$[Sq(I) + Ss(I)]/\sqrt{2} = \rho \text{CH}_2$	CH_2 rock
$Sq'(I) = (\varepsilon_1 - \varepsilon_2 - \varepsilon_3 + \varepsilon_4)/2$	$[Sq'(I) + Ss'(I)]/\sqrt{2} = \rho \text{CH}_2$	CH_2 rock
$Sr(I) = (\eta_1 + \eta_2 + \eta_3 + \eta_4)/2$	$[Sp(I) - Sr(I)]/\sqrt{2} = \omega \text{CH}_2$	CH_2 wag
$Sr'(I) = (\eta_1 + \eta_2 - \eta_3 - \eta_4)/2$	$[Sp'(I) - Sr'(I)]/\sqrt{2} = \omega \text{CH}_2$	CH_2 wag
$Ss(I) = (\eta_1 - \eta_2 + \eta_3 - \eta_4)/2$	$[Sq(I) - Ss(I)]/\sqrt{2} = t \text{CH}_2$	CH_2 twist
$Ss'(I) = (\eta_1 - \eta_2 - \eta_3 + \eta_4)/2$	$[Sq'(I) - Ss'(I)]/\sqrt{2} = t \text{CH}_2$	CH_2 twist
$St(I) = (\tau_1 + \tau_2)/\sqrt{2}$	$\tau_s \text{RhN}$	Symm. RhN torsion
$St'(I) = (\tau_1 - \tau_2)/\sqrt{2}$	$\tau_{as} \text{RhN}$	Asym. RhN torsion
$Su(I) = (\pi_1 + \pi_2)/\sqrt{2}$	$\tau_s \text{NC}$	Symm. NC torsion
$Su'(I) = (\pi_1 - \pi_2)/\sqrt{2}$	$\tau_{as} \text{NC}$	Asym. NC torsion
$Sv(I) = \Delta$	τ_{cc}	CC torsion

Table 2. Valence force constants for the $[\text{Rh}(\text{en})_3]^{3+}$ cation.

Force type	Constants symbol	Group	Coordinate(s) involved	Atoms common to interacting coordinates	Value ^a Initial	Final	
Stretch	K_r	CH_2	C-H	-	4.55 ^b	4.706	
	K_d	NH_2	N-H	-	6.42 ^c	5.669	
	K_R	CH_2-CH_2	C-C	-	4.39 ^b	3.581	
	K_D	CH_2-NH_2	C-N	-	4.97 ^c	4.692	
Stretch-stretch	K'_L	RhN_6	Rh-N	-	2.31 ^d	1.607	
	F_r	CH_2	C-H, C-H	C	0.01 ^b	0.0398	
	F_d	NH_2	N-H, N-H	N	0 ^c	0.0307	
	F_{RD}	$\text{CH}_2-\text{CH}_2-\text{NH}_2$	C-C, C-N	C	0.10 ^b	0.391	
Bend	F'_{LL}	RhN_6	Rh-N, Rh-N, <i>cis</i>	Rh	0.05 ^d	0.250	
	F'_{LL}	RhN_6	Rh-N, Rh-N, <i>trans</i>	Rh	-	-0.0868	
	H_δ	CH_2	<HCH	-	0.55 ^b	0.554	
	H_α	NH_2	<HNH	-	0.64 ^c	0.547	
	H_η	CH_2-CH_2	<HCC	-	0.656 ^b	0.651	
	H_ϵ	CH_2-NH_2	<HCN	-	0.656 ^b	0.732	
	H_γ	CH_2-NH_2	<CNH	-	0.578 ^c	0.692	
	H_ψ	$\text{CH}_2-\text{CH}_2-\text{NH}_2$	<CCN	-	1.13 ^b	1.087	
	H_β	$\text{Rh}-\text{NH}_2$	<HNRh	-	0.19 ^e	0.458	
	H_ω	$\text{Rh}-\text{NH}_2-\text{CH}_2$	<RhNC	-	0.77 ^f	0.755	
	$H_\phi = H_\theta$	RhN_6	<NRhN	-	0.20 ^f	1.100	
	Stretch bend	$F_{R\eta}$	CH_2-CH_2	C-C, <HCC	C-C	0.328 ^b	0.301
		$F_{R\epsilon}$	$\text{CH}_2-\text{CH}_2-\text{NH}_2$	C-C, <HCN	C	0.079 ^b	0.101
		$F_{R\psi}$	$\text{CH}_2-\text{CH}_2-\text{NH}_2$	C-C, <CCN	C-C	0.42 ^b	0.250
$F_{D\epsilon}$		CH_2-NH_2	C-N, <HCN	C-N	0.36 ^c	0.473	
$F_{D\gamma}$		CH_2-NH_2	C-N, <HNC	C-N	0.16 ^c	0.385	
$F_{D\eta}$		$\text{CH}_2-\text{CH}_2-\text{NH}_2$	C-N, <HCC	C	-	0.141	
$F_{D\psi}$		$\text{CH}_2-\text{CH}_2-\text{NH}_2$	C-N, <CCN	C-N	0.42 ^b	0.466	
$F_{L\omega}$		$\text{Rh}-\text{NH}_2-\text{CH}_2$	Rh-N, <RhNC	Rh-N	-	0.216	
$F_{D\omega}$		$\text{Rh}-\text{NH}_2-\text{CH}_2$	C-N, <RhNC	C-N	-	0.0984	
Bend-bend		F_η	CH_2-C	<HCC, <HCC	C-C	-0.021 ^b	-0.0324
	F_ϵ	CH_2-N	<HCN, <HCN	C-N	-0.031 ^c	-0.0218	
	F_γ	NH_2-C	<HNC, <HNC	C-N	-0.05 ^c	-0.128	
	F_β	NH_2-Rh	<HNRh, <HNRh	N-Rh	-	0.0856	
	$F_\phi = F_\theta$	RhN_6	<NRhN, <NRhN	Rh-N	-	-0.200	
	$F'_\phi = F'_\theta$	RhN_6	<NRhN, <NRhN coplanar	Rh-N	-	0.200	
Torsion	f_η^t	CH_2-CH_2	<HCC, <CCH	C-C	0.127 ^b	0.0996	
	H_t	RhN_6	Rh-N	-	-	0.205	
	H_π	CH_2-NH_2	C-N	-	0.058 ^c	0.060	
	H_Δ	CH_2-CH_2	C-C	-	0.058 ^c	0.127	

^a In units of $\text{mdyn}/\text{\AA}$ (stretch constants) mdyn/rad (stretch-bend interaction constants) and $\text{mdyn}/\text{\AA}/(\text{rad})^2$ (bending and torsion constants). ^b Refs. 12 and 17. ^c Ref. 18. ^d Ref. 19. ^e Ref. 2. ^f Ref. 20.

$7A_1 + 4A_2 + 11E$ included here were in the calculations eliminated directly by the program. The initial force constants, based on values for similar molecules^{12,17-20} are listed in Table 2 for comparison with the final GVF constants. The calculated frequencies are given in Table 3, which also includes an approximate description of the vibrational modes based upon the PED (potential energy distribution) of each vibration among the symmetry coordinates. The PED

among the force constants, $K_h J_{\lambda_h} / \lambda^{11}$ was also calculated to estimate the significant force constants for each vibration, but are not listed in order to save space.

Treatment of $[\text{Rh}(\text{en})_3]^{3+}$ under the point group D_3 reduces the 105 normal modes of vibration to the irreducible representation $\Gamma = 18A_1(\text{R}) + 17A_2(\text{IR}) + 35E(\text{R}, \text{IR})$, where (R) and (IR) indicate the Raman and infrared active modes, respectively. The eight isotopic

species considered here accordingly give us potentially 144 A_1 , 136 A_2 , and 280 E frequencies, or a total of 560 frequencies which we have tried to fit to the minimum number of force constants in an internally consistent approximation.

Method of calculation. Since the experimental Raman data included semiquantitative depolarization ratios for many bands, it was decided to perform exploratory calculations of the A_1 block separately and obtain a fit of the calculated frequencies to those of the polarized Raman bands. The force field obtained was then transferred to species A_2 and E after having properly utilized the molecular symmetry, and a provisional assignment of approximately one half of the 560 fundamentals made. Least squares refinements of each species separately disclosed the presence of inconsistencies which led to the introduction of new interaction force constants and revision of the assigned fundamentals. An examination of the Jacobian elements indicated that several of these were very poorly determined while others were essential to insure satisfactory convergence. The following constraints were now made to the calculations. (i) The force constants were not allowed to deviate beyond some fixed limits found valid for similar molecules (*vide infra*). (ii) The final force field should as far as possible be truly convergent, *i.e.* obtained by allowing all force constants to vary simultaneously. (iii) The standard error (excluding NH/ND and CH/CD stretching) for each species (A_1, A_2, E) in any of the four isotopic molecules should not exceed a fixed limit (1 % intended). (iv) The number of force constants should be held as low as possible. With these constraints it was possible to assign almost all fundamentals and explain the significant bands in the observed spectra, by using a 38-parameter GVFF.

Force field related to RhN_6 . The approach developed here is based mainly upon the general considerations by Claassen²¹ to molecules of formula XY_6 and the results for hexamine complexes derived from Ru, Rh, Ir, and Os¹⁹ and Ni.²² The vibrations involving Rh–N stretching could only be fitted satisfactorily by including the three force constants K_L (Rh–N stretching), F_{LL} (bond with a bond at right angles to it), and F'_{LL} (bond with opposite

bond). No improvement was obtained by introducing different interaction force constants F_{LL} for interactions within a chelate ring and interaction between Rh–N bonds of two different chelate rings. The interaction force constants $F_{L\phi}$ and $F_{L\theta}$ were found to be small and omitted in the final calculations.

The force constants for N–Rh–N deformation were initially introduced with different values for deformation within a chelate ring and deformation between two rings. This was considered important since all equilibrium values for N–Rh–N angles were put equal to 90° which is a reasonable but nevertheless conjectural value, being at variance with an $A-(\lambda, \lambda, \lambda)$ (ob_3) isomer⁷ of the $[Rh(-chxn)_3]^{3+}$ cation. However, as the calculations proceeded it became clear that this distinction was not warranted and accordingly the constraint that all $H_\theta = H_\phi$ was introduced. To be consistent the interaction constants were constrained in the same way, *i.e.* all interactions involving deformation of the RhN_6 part of the chelate were considered equal whether the deformation occurs within a chelate ring or between two chelate rings. The force constants H_θ , F_θ , and F'_θ were now determined by trial and error. These constraints ensured convergence of the remaining force field (*vide supra*). The standard error of the final set did not exceed 1.1 % for each species (A_1, A_2, E) in any of the eight compounds.

The description of the low frequency modes in terms of PED on symmetry coordinates were not sufficient for an understanding of the vibrational spectrum of $[Rh(en)_3]^{3+}$ in this region. Accordingly, we finally calculated the elements of the transformation matrix L_x between the Cartesian displacement vector X and the normal coordinate vector Q .

RESULTS AND DISCUSSION

Some features considered to be of general interest will be pointed out from the results of the normal coordinate analysis. Nevertheless, in the following discussion it should be kept in mind that (i) the experimental frequencies used are not unambiguously classified to their species from the Raman polarization ratios and (ii) certain constraints have been imposed on the force field. Undoubtedly, these sources

of error are only partly counterbalanced by attempting alternative assignments of fundamentals in all cases of reasonable doubt and systematic attempts to evaluate the significance of the force field during the calculations as discussed above.

Potential constants. Let us compare the values of the initial and the final valence force constants listed in the last two columns of Table 2. The agreement is very satisfactory for force constants related to the ethylenediamine ligand provided allowance is made for the somewhat larger variation observed for interaction force constants than for pure stretch and bending constants. Appreciable changes are noted for some of the force constants involving the amino groups (*e.g.* K_d, H_α and F_γ), but this is easily understandable as a result of the coordination to Rh. The changes in K_R and K_D are mainly the result of the increase in K_{RD} following complex formation. From the overall pattern we may conclude this part of the force field to be essentially comparable to that of similar molecules.

Very similar changes have been observed for the Urey-Bradley force constants of bis(en) metal chelates³ compared with those found for unchelated aliphatic amines.¹⁰ Thus, for example, the value of the N-H stretching force constant was found to decrease from 6.3 mdyn/Å in amines to *ca.* 5.7 mdyn/Å in chelated 1,2-ethanediamine. In the GVFF developed here, K_D decreased from 6.42 mdyn/Å in aliphatic amines to 5.669 mdyn/Å in $[\text{Rh}(\text{en})_3]^{3+}$ in complete harmony. This behaviour is hardly coincidental but rather reflects a mutual consistency between the present and previous calculations.

An evaluation of the force field related to the central part of the $[\text{Rh}(\text{en})_3]^{3+}$ ion is much more difficult, since data suitable for comparison have not been reported. The differences between initial and final GVF constants (Table 2) for the RhN_6 group are therefore largely due to an unprecedented choice of the initial value rather than real discrepancies. From an assignment of five fundamentals for $[\text{Rh}(\text{NH}_3)_6]\text{Cl}_3$ in the low frequency region, assuming O_h symmetry and treating the NH_3 molecules as single masses, Griffith¹⁹ calculated the force constant for Rh-N stretch, K_L , to be 2.3–2.5 mdyn/Å and the interaction force

constant for two Rh-N *cis* bonds, F'_{LL} , to be 0.05 mdyn/Å. We have attempted to evaluate the force field in more detail using the GVF expressions given by Claassen²¹ with suitable approximations, but the derived force constants have in many cases complex solutions and are very dependent on the details of the sophistication. Such calculations have been successfully carried out by Müller *et al.*²² for the $[\text{Ni}(\text{NH}_3)_6]^{2+}$ ion indicating values of 0.87, 0.12, and 0.00–0.01 mdyn/Å for Ni-N stretch, *cis* Ni-N and *trans* Ni-N stretch-stretch interactions, respectively. The values obtained here for K_L , K_{LL} , and F'_{LL} of 1.607, 0.250, and -0.0868 mdyn/Å are considered quite reliable since they depend heavily upon the assignment of the fundamentals involving Rh-N stretching which in fact are some of those most reliable in the experimental material (*cf.* Schmidt and Müller²³).

From these results we conclude that K_L decreases somewhat from $[\text{Rh}(\text{NH}_3)_6]^{3+}$ to $[\text{Rh}(\text{en})_3]^{3+}$ but this trend does not necessarily reflect a weaker bond in the latter compound but may be due to an erroneous choice of the Rh-N bond length in our calculations. The value of F'_{LL} appears to increase to the fivefold value on changing the ligand from NH_3 to 1,2-ethanediamine, but if we consider instead the ratio K_L/F'_{LL} it compares favourably with $[\text{Ni}(\text{NH}_3)_6]^{2+}$. In short, the values are not unreasonable, but unsatisfactory for deductions regarding the detailed nature of the bonds in the complex.

The GVF constant for N-Rh-N deformation was found to be 1.10 mdyn Å/(rad)², considerably higher than the corresponding values for $[\text{Ni}(\text{NH}_3)_6]^{2+}$ ²² and for dimethylglyoxime chelates¹⁹ which are in the range 0.10–0.30 mdyn Å/(rad)². However, in the UBFF approximation the appropriate range for 1,2-ethanediamine chelates is 0.16–0.40 mdyn/Å (in-plane bending) and 0.53–0.90 mdyn Å (out-of-plane bending)³ suggesting the value obtained here to be significant. The numerical values of the interaction force constants F_ϕ and F'_ϕ and of the force constant for Rh-N torsion are also considerably higher than expected from other complex compounds²² and suggest a considerable stiffening of $[\text{Rh}(\text{en})_3]^{3+}$. The high values of the bending force constants H_β and H_ω and of the interaction

Table 3. Continued.

ν_{36}	3232	3245	10	10	$\nu_{\text{as}}\text{NH}(100)$	ν_{40}	2390	2397	14	10	ν_{36}	2390	2391	14	8
ν_{37}	3230	3250	10	30	$\nu_{\text{as}}\text{NH}(100)$	ν_{41}	2387	2397	14	10	ν_{37}	2387	2390	14	15
ν_{38}	3174	3150	5	5	$\nu_{\text{s}}\text{NH}(100)$	ν_{43}	2304	2339	8	10	ν_{38}	2304	2330	8	5
ν_{39}	3173	3145	5	5	$\nu_{\text{s}}\text{NH}(100)$	ν_{43}	2302	2279	8	8	ν_{39}	2302	2290	8	7
ν_{40}	2971	2968	0	10	$\nu_{\text{as}}\text{CH}(99)$	ν_{36}	2971	2972	0	6	ν_{40}	2971	2968	0	0
ν_{41}	2966	2964	0	0	$\nu_{\text{as}}\text{CH}(99)$	ν_{37}	2966	2966	0	4	ν_{41}	2211	2196	0	0
ν_{42}	2911	2906	0	5	$\nu_{\text{s}}\text{CH}(99)$	ν_{38}	2911	2907	0	2	ν_{42}	2127	2132	0	0
ν_{43}	2909	2890	0	0	$\nu_{\text{s}}\text{CH}(99)$	ν_{39}	2909	2905	0	8	ν_{43}	2123	2132	0	0
ν_{44}	1606	1607	5	3	$\delta\text{NH}_2(99)$	ν_{50}	1185	1187	7	10	ν_{44}	1196	1190	7	10
ν_{45}	1604	1607	5	3	$\delta\text{NH}_2(99)$	ν_{51}	1181	1187	6	10	ν_{45}	1183	1190	6	10
ν_{46}	1478	1469	0	2	$\delta\text{CH}_2(94)$	ν_{44}	1478	1474	0	3	ν_{46}	1074	1077	1	1
ν_{47}	1464	1459	1	1	$\delta\text{CH}_2(96)$	ν_{45}	1464	1467	1	1	ν_{47}	1066	1069	0	0
ν_{48}	1380	1374	1	2	$\nu\text{CH}_2(56), \omega\text{CH}_2(31)$	ν_{46}	1375	1385	1	1	ν_{48}	1004	1003	6	12
ν_{49}	1355	1357	1	1	$\omega\text{CH}_2(69), \nu\text{CH}_2(13)$	ν_{47}	1338	1352	2	2	ν_{49}	843	838	1	1
ν_{50}	1318	1310	0	5	$\omega\text{CH}_2(47), \nu\text{CH}_2(38)$	ν_{48}	1305	1307	0	0	ν_{50}	843	838	1	1
ν_{51}	1303	1305	3	5	$\nu\text{NH}_2(65), \nu\text{CH}_2(22)$	ν_{52}	1064	1058	4	4	ν_{51}	1155	1150	2	7
ν_{52}	1296	1293	3	4	$\nu\text{NH}_2(88)$	ν_{56}	959	962	5	8	ν_{52}	993	1003	3	12
ν_{53}	1242	1227	1	1	$\nu\text{CH}_2(54), \nu\text{NH}_2(33)$	ν_{49}	1256	1270	1	4	ν_{53}	894	893	1	0
ν_{54}	1181	1173	2	2	$\omega\text{NH}_2(77), \omega\text{CH}_2(14)$	ν_{55}	979	980	9	8	ν_{54}	959	929	4	4
ν_{55}	1167	1163	4	1	$\omega\text{NH}_2(80), \omega\text{CH}_2(14)$	ν_{57}	882	888	2	0	ν_{55}	978	980	13	15
ν_{56}	1065	1059	17	11	$\nu\text{CN}(92)$	ν_{53}	1062	1051	14	7	ν_{57}	818	828	1	11
ν_{57}	1028	1028	13	8	$\nu\text{CN}(92)$	ν_{54}	1034	1038	17	18	ν_{56}	1106	1103	5	1
ν_{58}	980	980	2	2	$\nu\text{CH}_2(86), \nu\text{NH}_2(12)$	ν_{58}	867	864	1	4	ν_{58}	1027	1027	21	18
ν_{59}	901	880	4	4	$\nu\text{CC}(61), \nu\text{CN}(15)$	ν_{59}	823	830	1	3	ν_{59}	768	765	1	1
ν_{60}	820	812	4	4	$\nu\text{CH}_2(59), \nu\text{NH}_2(37)$	ν_{60}	775	777	1	0	ν_{60}	788	790	0	0
ν_{61}	751	750	3	3	$\nu\text{NH}_2(93)$	ν_{62}	585	587	5	5	ν_{62}	639	645	4	4
ν_{62}	731	728	2	2	$\nu\text{NH}_2(64), \nu\text{CH}_2(35)$	ν_{63}	580	587	5	5	ν_{63}	573	570	2	7
ν_{63}	663	664	8	8	$\delta\text{NCC}(59), \delta\text{RhNC}(22)$	ν_{61}	648	650	6	7	ν_{61}	551	544	3	3
ν_{64}	507	506	13	9	$\nu\text{RhN}(64), \delta\text{RhNC}(14), \delta\text{NCC}(13)$	ν_{64}	475	475	10	11	ν_{64}	622	628	6	10
ν_{65}	435	445	7	4	$\delta\text{NRhN}(36), \delta\text{RhNC}(18), \nu_{65}$	ν_{65}	422	424	5	5	ν_{65}	420	413	6	4
ν_{66}	402	397	3	3	$\tau\text{RhN}(11), \tau\text{CC}(10)$	ν_{66}	397	390	3	0	ν_{66}	395	398	3	3
ν_{67}	359	357	7	4	$\delta\text{NCC}(26), \tau\text{CC}(25)$	ν_{67}	343	333	6	2	ν_{67}	337	328	5	2
ν_{68}	291	296	7	7	$\delta\text{NRhN}(41), \nu\text{RhN}(20)$	ν_{68}	274	273	5	5	ν_{68}	270	270	5	5
ν_{69}	173	184	3	3	$\nu\text{RhN}(86)$	ν_{69}	168	176	3	2	ν_{69}	165	170	3	1
ν_{70}	120	120	0	0	$\delta\text{NRhN}(87)$	ν_{70}	119	113	0	0	ν_{70}	118	120	0	5
					$\delta\text{NRhN}(48), \tau\text{RhN}(40)$										

^a The fundamentals of the tris(1,2-ethanediamine)rhodium(III) cation have been arranged according to their species with diminishing frequencies, those of the deuterated compounds to give, as far as possible, matching PED's. The stated PED's are only approximative and small contributions have been neglected. ^b Iteration based upon all eight isotopic species. ^c Solvent data used wherever available. ^d Shift following ¹⁵N substitution of all six nitrogen atoms. ^e The PED is defined as $x_{\text{ik}} = 100F_{\text{H}}/L_{\text{ik}}^{3/4}$.

force constant $F_L = 0.209$ mdyn/rad (cf.²² $[\text{Ni}(\text{NH}_3)_6]^{2+}$: 0.09 mdyn/rad) suggest a strong chelation of the ligand.

Normal modes mainly confined to the ligand. From the results given in Table 3 the following values seem to be typical for 1,2-ethanediamine bonded to Rh^{3+} : δCH_2 , 1470 cm^{-1} , ωCH_2 , 1370 cm^{-1} and 1330 cm^{-1} , tCH_2 , 1230 and 1330 cm^{-1} , and ρCH_2 , 820 and 980 cm^{-1} . The results of free 1,2-ethanediamine based upon *cis* C_{2v} symmetry,^{24,25} later proved incorrect,^{26,27} correspond to the following ranges: δCH_2 , 1445–1469, ωCH_2 , 1298–1318, tCH_2 , 880–1360, and ρCH_2 , 761–815 cm^{-1} . The only major discrepancy concerns the assignment of a tCH_2 mode to 880 cm^{-1} in free 1,2-ethanediamine²⁵ which appears to be too low. Previous assignments of the modes in $[\text{Rh}(\text{en})_3]^{3+}$ complexes have been based upon the results of *N*-deuteration^{28,29} using polarized radiation.³⁰

Our calculations confirm the coupling between the two amine groups of 1,2-ethanediamine to be much smaller, and the separation between the in-phase and the out-of-phase combination usually does not exceed 50 cm^{-1} . The following regions are typical for 1,2-ethanediamine chelated to Rh^{3+} : δNH_2 , 1600–1610 cm^{-1} , tNH_2 , 1290–1310 cm^{-1} , ωNH_2 , 1165–1185 cm^{-1} , and ρNH_2 , 730–780 cm^{-1} . As before, these regions apply only to modes which are reasonably localized; they may easily be displaced by 100 cm^{-1} upon coupling with neighbouring modes. The δNH_2 mode in $[\text{Rh}(\text{en})_3]^{3+}$ chelates has been attributed by other authors to bands in the 1500–1600 cm^{-1} region.^{28,29} This can hardly be correct since (i) the bands in this region (in contrast to the results described recently by Gouteron³⁰) disappear by removal of the coordinated water, (ii) the bands are not observed in solution (cf. Krishnan and Plane³¹) and (iii) these assignments disagree with the results of the normal coordinate analysis, which consistently place them above 1600 cm^{-1} .

The C–C and C–N stretching vibrations in $[\text{Rh}(\text{en})_3]^{3+}$ are coupled to other vibrations, but the C–N stretching modes are usually found in the region 1020–1070 cm^{-1} . Previous assignments have been based upon comparison with free 1,2-ethanediamine, and locate the modes in question within the region 1000–1100 cm^{-1} .^{28,29}

Normal modes mainly confined to the central RhN₆ region. The six rhodium-nitrogen stretching coordinates form a basis with the reduced representation: $A_1 + A_2 + 2E$ of the point group D_3 . Previous investigations^{28,30} have identified the symmetrical Rh–N stretching vibration of species A_1 as the very strong Raman band at ca. 545 cm^{-1} . Our calculations confirm this band to consist mainly of $\nu_5\text{RhN}$ (68%), but weakly coupled to the δNCC (11%) and δRhNC (14%) deformational modes. Inspection of the L matrix shows that stretching of the RhN bonds is followed by a closing of the RhNC angles and opening of the NCC angles in such a way that the distance between the rhodium atom and the midpoint of the C–C bond is almost unaltered. It should be noted that this band is unambiguously identified by the major shift on ^{15}N substitution (Table 3). It has recently been proposed³² that the other strong fundamental of species A_1 in the 280–320 cm^{-1} region of the Raman spectra of tris(ethylenediamine) complexes (*i.e.* ν_{17} at 272 cm^{-1}) should have substantial RhN stretching character. This is not confirmed by our calculations, which indicate the contribution of $\nu_5\text{RhN}$ to this band to be only 12%.

Our calculations show that two bands near 450 cm^{-1} in $[\text{Rh}(\text{en})_3]^{3+}$ attributed³⁰ to species A_2 and E can be assigned as the fundamentals ν_{33} and ν_{35} . The former of these arises from $\nu_{35}\text{RhN}$ (84%) coupled to δNCC (14%), *i.e.* corresponds to an almost pure Rh–N stretching vibration of species A_2 . This was previously assigned^{28–30} to bands at ca. 100 cm^{-1} higher frequencies.

One of the Rh–N stretching vibrations of species E was attributed²⁹ to a band near 500 cm^{-1} , but this band was assigned by Gouteron³⁰ to a ligand deformation. The major shifts observed on ^{15}N substitution (Table 3) leave no doubt that this band must arise mainly from Rh–N stretching. However, the calculations indicate that in addition to νRhN (64%) the PED contains δNCC (13%) and δRhNC (14%), and accordingly the fundamental comprises both proposals mentioned above. The other Rh–N stretching vibration of species E is calculated to lie around 290 cm^{-1} , which complies with a weak band in the spectrum of $[\text{Rh}(\text{en})_3]^{3+}$ but may very well need future revision since the ^{15}N shifts are not decisive.

The remaining fundamentals of this region show no features of special interest. However, it should be mentioned that the fundamental ν_{32} of species A_2 was previously attributed to Rh-N stretching²⁸⁻³⁰ while our calculations indicate mainly ring deformation coupled to CH_2 rocking. On successive removal of 1, 2, and 3 hydrogen atoms with KNH_2 this band is displaced towards higher frequencies.²³ Since coordination of ethylenediamine anions is undoubtedly much stronger than coordination of neutral ethylenediamine, this shift merely reflects the increase in force constants for δRhNC and δNCC following deprotonation.

Acknowledgement. This project was partially supported by grants from the Danish Natural Science Research Council and the Norwegian Research Council for Science and the Humanities.

REFERENCES

- Ashley, P. J. and Torrible, E. G. *Can. J. Chem.* 47 (1969) 167.
- Omura, Y., Nakagawa, I. and Shimanouchi, T. *Spectrochim. Acta A* 27 (1971) 2227.
- Borch, G., Klæboe, P. and Nielsen, P. H. *Spectrochim. Acta. To be submitted.*
- Andersen, P., Galsbøl, F. and Harnung, S. E. *Acta Chem. Scand.* 23 (1969) 3027.
- Iwata, M., Nakatzu, K. and Saito, Y. *Acta Crystallogr. B* 25 (1969) 2562.
- Corey, E. J. and Snee, R. A. *J. Am. Chem. Soc.* 77 (1955) 2505.
- Kuroda, R., Sasaki, Y. and Saito, Y. *Acta Crystallogr. B* 30 (1974) 2053.
- Cotton, F. A. and Norman, J. G., Jr. *J. Am. Chem. Soc.* 93 (1971) 80.
- Caulton, K. G. and Cotton, F. A. *J. Am. Chem. Soc.* 93 (1971) 1914.
- Lussier, R., Edwards, J. O. and Eisenberg, R. *Inorg. Chim. Acta* 3 (1969) 468.
- Schachtschneider, J. H. and Snyder, R. G. *Spectrochim. Acta* 19 (1963) 117.
- Snyder, R. G. and Schachtschneider, J. H. *Spectrochim. Acta* 21 (1965) 169.
- Borch, G., Henriksen, L., Nielsen, P. H. and Klæboe, P. *Spectrochim. Acta A* 29 (1973) 1109.
- Henriksen, L., Nielsen, P. H., Borch, G. and Klæboe, P. *Spectrochim. Acta A* 31 (1975) 373.
- Henriksen, L., Nielsen, P. H., Borch, G. and Klæboe, P. *Spectrochim. Acta A* 31 (1975) 191.
- Henriksen, L., Nielsen, P. H., Borch, G. and Klæboe, P. *Spectrochim. Acta A* 31 (1975) 1371.
- Schachtschneider, J. H. and Snyder, R. G. *Spectrochim. Acta* 19 (1963) 168.
- Dellepiane, G. and Zerbi, G. *J. Chem. Phys.* 48 (1968) 3573.
- Griffith, W. P. *J. Chem. Soc. A* (1966) 899.
- Bigotto, A., Costa, G., Galasso, V. and De Alti, G. *Spectrochim. Acta A* 26 (1970) 1939.
- Claassen, H. H. *J. Chem. Phys.* 30 (1959) 968.
- Müller, A., Schmidt, K. H. and Vandrish, G. *Spectrochim. Acta A* 30 (1974) 651.
- Schmidt, K. H. and Müller, A. *Inorg. Chem.* 14 (1975) 2183.
- Sabatini, A. and Califano, S. *Spectrochim. Acta* 16 (1960) 677.
- Diot, A. and Theophanides, T. *Can. J. Spectrosc.* 17 (1972) 67.
- Jouan, M. and Dao, N. Q. *C. R. Acad. Sci. Ser. C* 274 (1972) 1987.
- Jamet-Delcroix, P. S. *Acta Crystallogr. B* 29 (1973) 977.
- Watt, G. W. and Crum, J. K. *J. Am. Chem. Soc.* 87 (1965) 5366.
- James, D. W. and Nolan, M. J. *Inorg. Nucl. Chem. Lett.* 9 (1973) 319.
- Gouteron, J. *J. Inorg. Nucl. Chem.* 38 (1976) 63.
- Krishnan, K. and Plane, R. A. *Inorg. Chem.* 5 (1966) 852.
- Flint, C. D. and Matthews, A. P. *Inorg. Chem.* 14 (1975) 1219.

Received August 11, 1976.

Infrared and Raman Spectra of Some Three-coordinated Complexes of Divalent Tellurium

PETER KLÆBOE^a and OLAV VIKANE^b

^a Department of Chemistry, University of Oslo, Oslo 3, Norway and ^b Department of Chemistry, University of Bergen, N-5014 Bergen, Norway

The infrared and Raman spectra of crystalline samples of halo(ethylenethiourea)phenyltellurium(II) (halo = Cl, Br, I), halo(ethyleneselenourea)phenyltellurium(II) (halo = Br, I), halo(phenyl)thioureatellurium(II) (halo = Cl, Br), phenyldithiocyanato- and phenyldiselenocyanatotellurate(II) ions were recorded below 500 cm⁻¹. From these data the two fundamental stretching frequencies connected with the approximately linear X—Te—Y linkage were assigned. These frequencies were compared with those obtained from a simplified force constant calculation on the linear group.

Divalent tellurium most often forms four-coordinated complexes, but when a phenyl group is one of the ligands, the position *trans* to the phenyl group is vacant. Crystal structures of three-coordinated complexes of divalent tellurium are well known,¹⁻³ revealing that each molecule has a T-shaped geometry. Each tellurium atom is part of a nearly linear three-centre four-electron bonding system, comprising the tellurium atom and two ligand atoms. Nearly at right angle to the three-centre system, the tellurium atom is bonded to a phenyl carbon atom, so that the Te—C bond nearly bisects the angle of the three-centre system.

Very little information from infrared and Raman spectra is available on three-coordinated complexes of divalent tellurium. In two papers Hendra and Jovic^{9,10} report the infrared and Raman spectra of several square-planar complexes of divalent tellurium. The vibrational frequencies of these complexes are discussed in relation to the isoelectronic ICl₄⁻ ion.^{9,10} Recently, Wynne *et al.* reported the Raman spectra of a few dihaloaryltellurate(II) anions.¹¹

The present paper reports the infrared and Raman spectra of a series of three-coordinated complexes of divalent tellurium, whose crystal structures are already known.

EXPERIMENTAL

The syntheses of the present compounds (I—X, Table 1) have previously been reported.^{9,12-15} Elementary analyses on C, H, N, S, Cl, Br, and I were determined and melting points and densities were reported.

The far infrared spectra of the samples I—X were recorded on a Perkin-Elmer-Hitachi far infrared spectrometer, model FIS-3 through the courtesy of Dr. D. H. Christensen, the University of Copenhagen. Approximately 10–20 mg of the samples were mixed with 200 mg of polyethylene (Rigidex) and the pellets recorded in the region 500–50 cm⁻¹.

Table 1. Numbering and formula of the tellurium(II) compounds studied.

Number	Compound ^a	Ref.
I	C ₆ H ₅ Te(etu)Cl	7,14
II	C ₆ H ₅ Te(etu)Br	6,14
III	C ₆ H ₅ Te(etu)Br	6,14
IV	C ₆ H ₅ (etu)I	8
V	C ₆ H ₅ Te(esu)Br	7,15
VI	C ₆ H ₅ Te(esu)I	8
VII	[(CH ₃) ₄ N][C ₆ H ₅ Te(SCN) ₂]	5,13
VIII	[(CH ₃) ₄ N][C ₆ H ₅ Te(SeCN) ₂]	5,13
IX	C ₆ H ₅ Te(tu)Cl	3,12
X	C ₆ H ₅ Te(tu)Br	3,12

^a Here etu = ethylenethiourea (C₂H₆N₂CS), esu = ethyleneselenourea (C₂H₆N₂CS), and tu = thiourea (N₂H₄CS).

Table 2a. The far infrared (IR) and Raman (R) spectral data for halo(ethylenethiourea)phenyltellurium(II).

I ^a S, Cl ^b IR		II S, Br IR		III S, Br IR		IV S, I IR		Inter- pretation
R	R	R	R	R	R	R	R	
345 m	345 vw	365 w ^c 340 m	362 s 342 w	362 s 324 vw? 287 w	367 vs	360 s 324 vw?	357 s	
275 vw		255 w	251 w	273 m 245 w	255 w			
254 w	257 s	222 w	228 s	222 m	223 m	265 m 244 w 224 m	255 w 220 vw	S—Te—X asym. str.
	240 m	212 w				182 w,sh		
210 m	208 s	193 m	193 vs 170 vw	190 s,br 168 w	189 vs 170 w	172 s 102 s	170 vs 113 w	S—Te—X sym. str.
140 s,br	140 w,br	110 s	125 w,br	130 w 120 s 100 s	131 w 106 w 99 w	91 m	88 w	
75 m	90 w	75 m		75 m				
	60 w,sh		56 m		58 m		55 m	

^aRoman numerals refer to compounds listed in Table 1. ^bSubstituents (S—Te—hal) in approximately linear arrangement. ^cAbbreviations: s, strong; m, medium; w, weak and v, very.

Table 2b. The far infrared and Raman spectral data for halo(ethyleneselenourea)phenyltellurium(II).

V Se, Br IR		VI Se, I IR		Inter- pretation
R	R	R	R	
340 m		336 w		
269 m	270 vw	277 w 272 w	278 w	
247 m	248 w	219 m	222 vw	
210 m	220 vw?	212 w		
190 m	192 w	180 m	178 w	Se—Te—X asym. str.
170 s	169 m	150 s	152 vs	S—Te—X
130 w		133 w		sym. str.
99 s	93 w	100 m 84 m	94 w 77 w	
	70 w	74 w		

Table 2c. The far infrared and Raman spectral data for phenyldithio(diseleno)cyanotellurate(II).

VII S, S IR		VIII Se, Se IR		Inter- pretation
R	R	R	R	
			389 w	
272 w		272 w	254 w	
247 w	257 w	189 w	188 vw	S(Se)TeS(Se) asym. str.
219 vw	216 vs	138 vw	136 vs	S(Se)TeS(Se)
212 w	210 s	118 m	120 m	sym. str.
150 s	141 w			
100 s	100 w	101 m		
75 s		74 w		
	55 vw		66 w	

Table 2. Continued.

Table 2d. The far infrared and Raman spectral data for halo(thiourea)phenyltellurium(II).

IX S, Cl IR	R	X S, Br IR	R	Inter- pretation
		272 m		
252 w	257 m	242 s	242 vs	S-Te-X asym. str.
		222 m	219 w	
		194 m	191 m	
244 m	243 m	164 w	164 w	S-Te-X sym. str.
158 w				
118 s	110 w	125 m	130 vw	
99 s	94 w	99 s	98 w	
93 m		85 m	86 vw	
76 m		76 m	75 w	
	67 w	66 vw		
		57 w		
			48 m	

A Cary model 81 Raman spectrometer equipped with a Spectra Physics model 125 A helium-neon laser and a Coherent Radiation Laboratory model 52 G argon ion laser were employed for the Raman recordings. The 6328 and 5145 Å lines were used for excitation and interference filters employed to remove the plasma lines. The solid samples were filled into tubes with flat ends and placed against the hemispherical lens and illuminated in the 180° mode. Since most of the present compounds were somewhat coloured, the spectra obtained with the red laser (*ca.* 40 mW irradiation on the sample) were in most cases preferable to those recorded with the green light (100 mW on the sample).

In addition, the vibrational spectra of the ligands: ethylenethiourea, ethyleneselenourea, and thiourea were recorded in order to gain information regarding the ligand vibrational spectra.

RESULTS AND DISCUSSION

The observed infrared and Raman frequencies (in cm^{-1}) of the ten present tellurium(II) complexes are listed in Table 2. The bands interpreted as the asymmetric and symmetric stretching frequencies of the approximately linear X-Te-Y moiety have been listed in Table 2 and can be assigned with considerable confidence. Much more uncertain are the fundamental modes mainly connected with the X-Te-Y deformation and thus no attempts were made to assign them. Although the samples II and III contain the same molecular complex (with different crystal structure) the

spectra were somewhat different. However, as apparent, the assigned X-Te-Y vibrations were only negligibly displaced from sample II to III.

Obviously, the present tellurium(II) complexes with the large number of atoms (maximal 27 and minimal 18) should give rise to very complicated vibrational spectra because of the many fundamental modes expected. As a first approximation the normal modes may be divided into those characteristic of the ligands and those pertaining to stretching of the tellurium-ligand bonds. Also, it is generally assumed¹¹ that the ligand vibrations (phenyl, ethylenethiourea *etc.*) give rise to weaker bands (particularly in Raman) than those due to stretchings of the metal-ligand system, thus simplifying the interpretations. Finally, the pseudo-linearity of the three-centre bond makes it feasible to treat the system as a linear X-Te-Y three body problem of $C_{\infty v}$ symmetry. Apart from diatomic molecules the linear three-atomic molecules represent the simplest possible case, making force constant calculations very convenient.

In a linear molecule X-Te-Y the following relations can easily be derived:

$$\lambda_1 + \lambda_2 = k_1 \frac{1}{m_X} + k_2 \frac{1}{m_Y} + (k_1 + k_2 - 2k_1 k_2) \frac{1}{m_{Te}}$$

$$\lambda_1 \lambda_2 = (k_1 k_2 - k_{12}^2) \left(\frac{1}{m_X m_Y} + \frac{1}{m_Y m_{Te}} + \frac{1}{m_X m_{Te}} \right)$$

in which $\lambda_1 = 4\pi^2\nu_1^2c^2$, where ν_1 and ν_2 are the stretching frequencies, k_1 and k_2 are the diagonal stretching constants for the Te-X and Te-Y bonds, k_{12} is the interaction constant, and m_x , m_y and m_{Te} are the atomic masses. Since only two force constants can be determined from the two observed stretching bands and k_{12} is typically 10 % of k_1 and k_2 , k_{12} can to a first approximation be neglected. A simple set of force constants for the Te-S, Te-Se, Te-Cl, Te-Br, and Te-I were derived from the symmetric stretching modes (most reliable, since generally very intense in Raman) of selected model compounds. From compounds VII and VIII the Te-S and Te-Se stretching force constants were calculated to 0.89 and 0.84 mdyne/Å, respectively. Correspondingly the Te-halogen stretching constants were calculated from the reported values given by Hendra and Jovic.^{9,10} They gave the approximate values 245, 150, and 100 cm⁻¹ for the symmetric and 205, 160, and 130 cm⁻¹ for the asymmetric X-Te-X stretching frequencies in the case of Cl, Br, and I, respectively. The force constants 1.25, 1.06, and 0.74 mdyne/Å were obtained from these frequencies. However, much better agreement with the present data were obtained by reversing their symmetric and asymmetric stretching vibrations, for the Cl-Te-Cl case. When the low frequency band at 205 cm⁻¹ was used as the symmetric mode a force constant of 0.88 mdyne/Å was derived for Te-Cl. The calculated frequencies are listed in Table 3 and compared with the experimental values.

The agreement between the observed and calculated X-Te-Y stretching frequencies is in most cases satisfactory taking into account the severe simplifications: (a) the thiourea or ethylenethio(seleno)urea groups are neglected and the S or Se considered terminal atoms, (b) the existence of the phenyl group and the Te-C bond is neglected, (c) a simple diagonal force field is derived in which the stretching force constants are transferable within the series, and (d) the X-Te-Y arrangement is considered linear.

Obviously, the agreement between the observed and calculated frequencies could be greatly improved, e.g. by introducing the interaction constant k_{12} . Thus, it was found that by setting $k_{12} = 0.1$ mdyne/Å and maintaining k_1 and k_2 , the frequency difference between the symmetric and asymmetric stretches decreased (a factor of two for IX and X) without shifting the average value significantly. Because of the severe simplifications made and since the interaction constants in no case could be given a significant physical value, we did not proceed along this line.

At the outset of this work we hoped that the bond length variations within the series, carefully determined from the X-ray crystallographic studies, should manifest themselves in the vibrational spectra. It was found that the *trans* bond lengthening order of halogens on the Te-S or Te-Se bond decrease in the order I > Br ≥ Cl.⁸ The relative *trans* bond lengthening order of the ligands on the Te-halogen bond decrease in the order esu ~ tu >

Table 3. Observed and calculated X-Te-Y stretching vibrations.

Compound	Linkage	Obs ^a	Calc ^b	k_1 mdyn/Å	k_2 mdyn/Å
I	S-Te-Cl	254 210	264 236	0.89	0.88
II	S-Te-Br	222 193	257 178	0.89	1.06
III	S-Te-Br	222 189 ^c	257 178	0.89	1.06
IV	S-Te-I	265 172	250 130	0.89	0.74
V	Se-Te-Br	190 170	217 142	0.84	1.06
VI	Se-Te-I	180 150	197 133	0.84	0.74
VII	S-Te-S	247 216 ^c	268 218	0.89	0.89
VIII	Se-Te-Se	189 136 ^c	203 136	0.84	0.84
IX	S-Te-Cl	252 244	264 236	0.89	0.88
X	Se-Te-Br	242 164	257 178	0.89	1.06

^a IR data except when noted. ^b For calculations, see text; the interaction constant k_{12} is set equal to zero.

^c Raman data.

etu.⁷ From the well known relations between bond length—bond energy and stretching force constant, a bond lengthening should result in a smaller force constant and eventually lower Te—X(Y) stretching vibrations. No such systematic trends can be observed from the spectra.

Clearly, the fact that the “Te—X and Te—Y vibrations” are not localized modes, but can better be described as X—Te—Y symmetric and asymmetric stretches, makes such correlations more difficult. When the ligands have very different masses and/or are attached to the central atom with quite different bond strengths the two stretching vibrations become well localized (*e.g.* in H—C≡N or X—C≡N), and can be directly correlated with the bond distance or bond energy. In the present case much more sophisticated force constant calculations, not warranted by the observed spectra, would be necessary to correlate the X—Te—Y stretching vibrations with the bond distances.

The assigned X—Te—Y stretching modes (Tables 2 and 3) agree reasonably well with the values reported by other workers on similar complexes. A curious discrepancy is provided by compound IV in which the 172 cm⁻¹ band appears too high. However, a very intense Raman band was observed at this wave number (no other intense Raman band was detected at lower wave numbers) making an assignment to a symmetric S—Te—I vibration very likely.

Acknowledgement. We are grateful to Dr. D. H. Christensen, Copenhagen, for providing the far-IR spectra and to Mrs. J. Gustavsen for recording the Raman spectra. Financial support from NAVF is acknowledged.

REFERENCES

1. Foss, O. In Andersen, P., Bastiansen, O. and Furberg, S., Eds., *Selected Topics in Structure Chemistry*, Universitetsforlaget, Oslo 1967, 145.
2. Foss, O. *Pure Appl. Chem.* 24 (1970) 31.
3. Foss, O. and Husebye, S. *Acta Chem. Scand.* 20 (1966) 132.
4. Foss, O. and Marøy, K. *Acta Chem. Scand.* 20 (1966) 123.
5. Hauge, S. and Vikane, O. *Acta Chem. Scand. A* 29 (1975) 755.
6. Vikane, O. *Acta Chem. Scand. A* 29 (1975) 738.
7. Vikane, O. *Acta Chem. Scand. A* 29 (1975) 763.

8. Vikane, O. *Acta Chem. Scand. A* 29 (1975) 787.
9. Hendra, P. J. and Jovic, Z. *J. Chem. Soc. A* (1967) 735.
10. Hendra, P. J. and Jovic, Z. *J. Chem. Soc. A* (1968) 911.
11. Petragnani, N., Torres, L., Wynne, K. J. and Maxwell, W. J. *Organomet. Chem.* 76 (1974) 241.
12. Foss, O. and Hauge, S. *Acta Chem. Scand.* 13 (1959) 2155.
13. Hauge, S. and Vikane, O. *Acta Chem. Scand.* 27 (1973) 3596.
14. Vikane, O. *Acta Chem. Scand. A* 29 (1975) 150.
15. Vikane, O. *Acta Chem. Scand. A* 29 (1975) 152.

Received August 18, 1976.

An Investigation of the Molecular Structure and Conformation of Dipropyl Ether, $\text{CH}_3\text{—CH}_2\text{—CH}_2\text{—O—CH}_2\text{—CH}_2\text{—CH}_3$, in the Gas Phase

E. E. ASTRUP

Department of Chemistry, University of Oslo, Oslo 3, Norway

The molecular structure of dipropyl ether has been investigated in the gas phase by the electron diffraction method. Satisfactory agreement between experimental and theoretical data is obtained for an equilibrium mixture of 26(6) % *aaaa* and 74(6) % *g±aag±* conformers. However, also the *aaag* conformation alone gives an acceptable correspondence to the experimental data. Consequently, any proportion of a mixture of the *aaaa/g±aag±*, where the ratio 26:74 is maintained, and the *aaag* conformer will also be a solution to the problem. Despite this impossibility to obtain a unique solution it is concluded that strong attractive 1,4-CH...O interactions cannot be present. Independently of conformation the bond distances and valence angles are found to be the following: $r(\text{O—C})=1.404(6)$ Å, $r(\text{C—C})=1.524(8)$ Å, $r(\text{C—H})=1.116(6)$ Å, $\angle\text{COC}=116.1(3.6)^\circ$, $\angle\text{OCC}=109.1(1.5)^\circ$, $\angle\text{CCC}=113.5(1.8)^\circ$, $\angle\text{CCH}(\text{methyl})=114.7^\circ$, $\angle\text{HCH}(\text{methylene})=108.0^\circ$.

Earlier investigations of ring systems like 1,5,9,13-tetraoxacyclohexadecane^{1,2} and of polymer chains like poly(trimethyleneoxide)³ in the crystalline state have shown that each $-(\text{O—CH}_2\text{—CH}_2\text{—CH}_2)_n\text{—}$ unit prefers one unique conformation, where the dihedral angles $\delta(\text{COCC})$ are *anti* and $\delta(\text{OCCC})$ are *gauche*. From these observations it seems reasonable to assume that 1,4-CH...O interactions are present in molecules of this type.⁹

It was therefore of interest to investigate the molecular structure of simpler molecules in the gas phase by the electron diffraction method in order to see if the 1,4-CH...O *gauche* interaction is attractive also when no crystal forces are present. Among such model compounds 1,3-dimethoxypropane would be chemically

most similar, but also dipropyl ether would potentially have such interactions although the CH involved here is less acidic.

EXPERIMENTAL

The sample of dipropyl ether used in the experiment was delivered from Fluka.

The electron diffraction experiment was performed on a Balzers Eldigraph KDG2. The scattering diagram has been recorded at two different nozzle-to-plate distances, *i.e.* 579.85 and 250.12 mm. The wavelengths of the electrons were 0.05851 and 0.05855 Å, respectively. The pressure measured in the apparatus during the exposure was about 6×10^{-6} Torr. The sample was kept at approximately 0°C. Four selected photographic plates recorded at each nozzle-to-plate distance were used in the structure analysis. The intensity of the scattering was recorded on a photometer for each

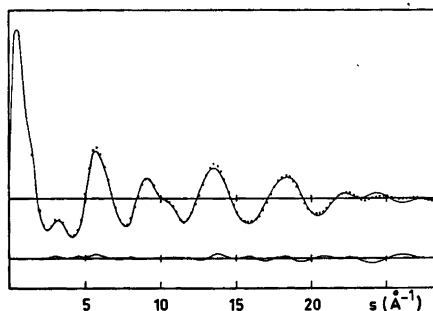


Fig. 1. Dipropyl ether. Theoretical molecular intensity curve. The dots show the experimental values. The lower curve shows the difference between the experimental and theoretical values.

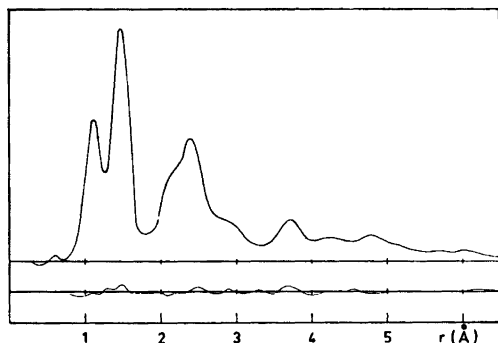


Fig. 2. Dipropyl ether. Experimental radial distribution curve. The lower curve shows the difference between the experimental values and the theoretical values for a conformational mixture of 26 % *aaaa* and 74 % *g±aag±* conformers. Artificial damping constant $k=0.0020 \text{ \AA}$.

0.25 mm of the photographic plate. Each plate was oscillated about the center of the diffraction diagrams and the intensity integrated over the arc. The data have been treated in the usual way.⁴

An empirical background has been subtracted on each plate before averaging the data. The molecular intensity curves from the 25 and the 58 cm nozzle-to-plate distances were scaled and combined to one experimental molecular intensity curve covering a scattering angle equivalent to $s=1.5 \text{ \AA}^{-1}$ to $s=30.25 \text{ \AA}^{-1}$ (Fig. 1). The mean values have been used in the overlap region. The intensities were modified by $s/|f_C'|/|f_O'|$, where $|f'|$ is the complex scattering amplitude^{5,6} for carbon and oxygen.

A least-squares procedure was used to refine the parameters estimated from the experimental radial distribution (RD) curve (Fig. 2). The calculations have been carried out on CDC 3300 and CDC 7400 (CYBER) computers.⁴

Table 1. Structure parameters for dipropyl ether obtained by least-squares refinement on the intensity data. Distances (r_a -values) are given in \AA , angles in degrees. The standard deviations given in parentheses have been corrected to take into account data correlation. The uncertainty arising from error in the electron wavelength is included. (For numbering system of the atoms see Fig. 3).

Conformation	B <i>aaaa</i>	C <i>ag±g±a</i>	D <i>g±aag±</i>	E <i>g±aag±</i>	F <i>aaaa</i>	G <i>aaag</i>
Distances						
O—C	1.404	1.404	1.404(4)	1.404	1.404(4)	1.404(6)
C—C	1.524	1.524	1.524(5)	1.524	1.524(5)	1.524(8)
C—H	1.116	1.116	1.116(4)	1.116	1.116(4)	1.116(6)
O...C(2)	2.390	2.380	2.390(10)	2.389	2.385(10)	2.391(17)
O...C(3)	} 3.763	} 3.740	} 3.036(22)	} 3.033	} 3.759(12)	} 3.762(20)
O...C(3)'						
C(1)...C(1)'	2.383	2.383	2.383(30)	2.383	2.383(28)	2.383(46)
C(2)...C(3)	2.551	2.525	2.536(13)	2.536	2.549(13)	2.548(20)
C(1)...C(2)'	3.697	} 2.983	} 3.697(12)	} 3.696	} 3.694(12)	} 3.698(18)
C(1)'\...C(2)	3.172					
C(1)...C(3)'	4.927	} 4.363	} 4.320(24)	} 4.371	} 4.925(31)	} 4.925(44)
C(1)'\...C(3)	4.516					
C(2)...C(2)'	4.424	3.901	4.762(31)	4.759	4.751(31)	4.764(52)
C(2)...C(3)'	5.874	} 5.004	} 5.174(41)	} 5.168	} 6.143(18)	} 5.231(81)
C(2)'\...C(3)	5.566					
C(3)...C(3)'	6.947	6.064	5.790(73)	5.124	7.454(31)	6.643(83)
Angles						
∠ COC	116.1	116.1	116.1(2.1)	116.1	116.1(2.1)	116.1(3.6)
∠ OCC	109.3	108.7	109.4(0.8)	109.2	109.1(0.8)	109.4(1.5)
∠ CCC	113.6	111.9	112.6(1.1)	112.1	112.6(1.1)	113.4(1.8)
∠ CCH(methyl)	114.7	114.7	114.7	114.7	114.7	114.7
∠ HCH(methylene)	108.0	108.0	108.0	108.0	108.0	108.0
β	90.3	} 72.4	0.0	0.0	0.0	0.0
β'	0.0		0.0	0.0	0.0	0.0
α	0.0	0.0	} 72.1(2.9)	71.8	0.0	75.0(6.0)
α'	0.0	0.0		-71.8	0.0	0.0

Table 2. Vibrational amplitudes (u -values) for dipropyl ether. The u -values are given in Å. The values are determined partly by trial and error, partly by refinements in separate cycles of a small number of parameters. Column I shows u -values for bond distances and distances over one angle, while column II and III show the u -values for *anti* and *gauche* distances, respectively.

Distances	I	II	III
O—C	0.043		
C—C	0.052		
C—H	0.070		
O···C(2)	0.063		
O···C(3)		} 0.098	} 0.110
O···C(3)'			
C(1)···C(1)'	0.069		
C(2)···C(3)	0.076		
C(1)···C(2)'		} 0.099	} 0.136
C(1)···C(2)'			
C(1)···C(3)'			
C(1)'···C(3)'		} 0.114	} 0.139
C(2)···C(2)'			
C(2)···C(3)'		0.113	0.140
C(2)'···C(3)		} 0.152	} 0.166
C(2)'···C(3)			
C(3)···C(3)'		0.200	0.221

STRUCTURE ANALYSIS

Approximate values for the structure parameters used in the least-squares refinement are determined from the experimental RD curve in Fig. 2.

The first two peaks in the RD curve correspond to the bond distances in the molecule. The peak at about 1.1 Å represents the fourteen C—H distances which are assumed to be of equal length. The peak at 1.5 Å is composed of contributions from the C—O and C—C bond distances. A possible difference between the bond lengths of the terminal C—C bond and the C—C bonds within the chain cannot be determined from the experimental data. The refinement of one average C—C bond distance results in a bond length of 1.524 Å (Table 1)

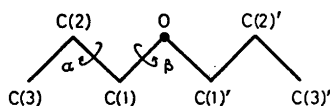


Fig. 3. Dipropyl ether. Model showing the numbering of the atoms and the torsion angles, α and β .

Acta Chem. Scand. A 31 (1977) No. 2

and a corresponding vibrational amplitude (u -value, Table 2) of 0.048 Å. From the magnitude of the u -value there is no indication of any change in the C—C bond length depending on position in the chain (Table 2).

The shoulder at about 2.1 Å represents non-bonded C···H and O···H distances. In the structure analyses it has been assumed that the plane through the hydrogen atoms in each methylene group is bisecting the CCC (OCC) valence angle. The largest contribution to the main peak at 2.4 Å comes from O···C and C···C distances over one angle. These broad peaks contain a large number of distances, many of these are contributing with about equal weight. However, large correlations between several distances and u -values make impossible the simultaneous refinement of the parameters. For this reason a great part of the vibrational amplitudes had to be adjusted by trial and error.

All the interatomic distances which are shorter than 2.6 Å, are independent of conformation. Fig. 4 reproduces the regions outside 2.6 Å in the theoretical RD curves, which show varying features dependent on the conformation of the dipropyl ether chain. In the structure analysis all *anti* conformations are fixed at exactly 180°, while the torsional angles of the *gauche* conformations are refined by a least-squares procedure.

The dipropyl ether chain may in principle have a number of different conformations depending on the torsion about the O—C(1), O—C(1)', C(1)—C(2) and C(1)—C(2)' bonds.

aaaa. The theoretical RD curve for the planar *aaaa* conformer (Fig. 4, curve F) shows two well-defined peaks, which are not present in the experimental RD curve. The area underneath the shoulder at about 3.0 Å is too small, while the peak at 3.7 is too large, due to the two O···C(3) and the two C(1)···C(2)' distances at 3.76 and 3.69 Å. Also the area underneath the peak at 4.8 is too large, because the two C(1)···C(3)' and the C(2)···C(2)' are of approximately the same length. This also goes for the C(2)···C(3)' distances at 6.1 Å in the all-*anti* conformer.

aaag. By rotating one of the methyl groups about the C(1)—C(2) bond (Fig. 4, curve G), a distribution of the interatomic distances is obtained which results in a fairly good agreement with the experimental curves. In this

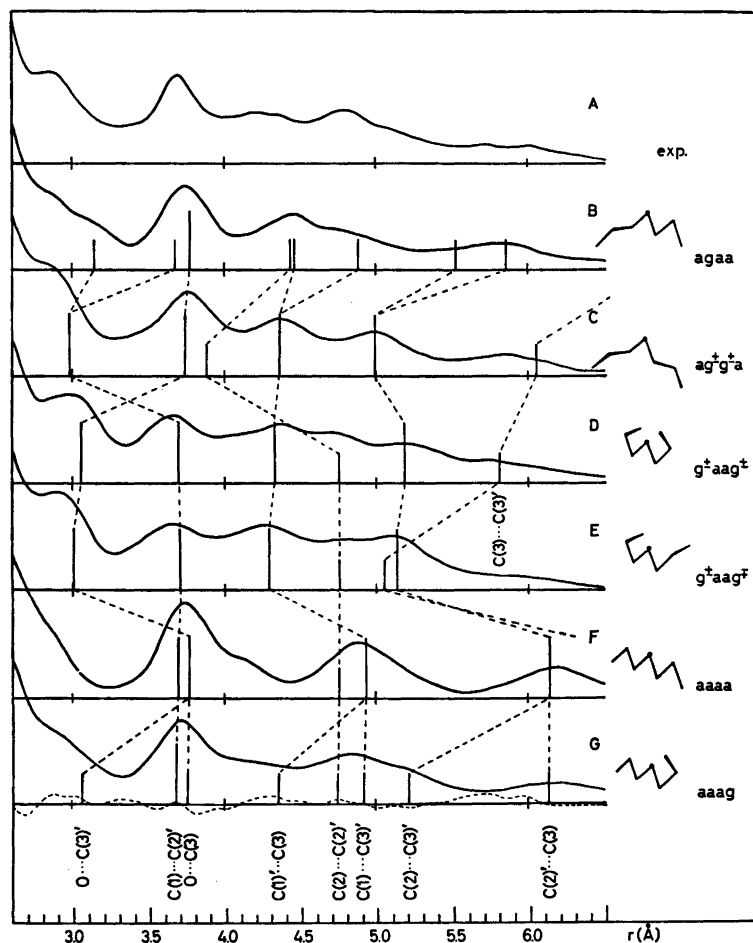


Fig. 4. Dipropyl ether. The outer part of the experimental (A) radial distribution curve compared with the corresponding part of the theoretical radial distribution curves for the conformers: *aaga* (B), *ag[±]g[±]a* (C), *g[±]aag[±]* (D), *g[±]aag[∓]* (E), *aaaa* (F), and *aag* (G). ($k=0.0020$ Å).

conformer there could be one 1,4-CH₃···O *gauche* interaction.

g[±]aag[±] and *g[±]aag[∓]*. Further, equal rotation of both methyl groups about the C(1)···C(2) bonds results in a *g[±]aag[±]* or a *g[±]aag[∓]* conformer. As may be seen from Table 1, the only pronounced difference in interatomic distances of these conformers is the length of the C(3)···C(3') distance, which is 5.79 Å in the former and 5.12 Å in the latter. This difference is shown in Fig. 4, curve D and E. None of these models, however, correspond satisfactorily to the experimental data. This means that two 1,4-*gauche* interactions between CH₃ and O can-

not be especially preferred, whether the methyl groups are on the same side or on opposite sides of the molecular plane.

agaa. Proceeding to the conformers arising from rotation about the O-C(1) bonds, the *agaa* conformer (Fig. 4, curve B) shows a theoretical RD curve, which is not in agreement with experimental data. The shoulder at 3.0 Å is too small due to the presence of only one C(1)···C(2') distance in this region, and the peak at 4.5 Å is too large due to the C(2)···C(2') and the C(1)'···C(3) distances.

ag[±]g[±]a. By equal rotation about both O-C(1) and O-C(1') the area of the shoulder

at 3.0 Å in the RD curve will increase due to the shortening of the C(1)···C(2)' distance from 3.70 to 2.98 Å in agreement with the experimental RD curve. The area underneath the peak at 3.7 Å will, however, change very little as the loss of the C(1)···C(2)' distance in this region compared to the *agaa* conformer, will be compensated by the gain of the C(2)···C(2)' distance. The fact that the C(1)···C(3)' and C(1)'···C(3) distances are equal in an *ag±g±a* conformer, results in a too well-defined peak at 4.4 Å.

ag±g±a. This conformer can be disregarded because of the too short distances between the methylene groups C(2)H₂ and C(2)'H₂.

As strong attractive 1,4-*gauche* CH···O interactions thus do not seem to be present in dipropyl ether, the molecule may well exist as an equilibrium mixture of more than one conformer. Based on the RD curves for the single conformations, theoretical radial distribution curves for mixtures of two conformations have been calculated. The bond distances, COC, CCH and HCH angles have been kept at fixed values during the refinement of the data and the CCC, OCC, the torsion angles, and the ratio of each conformer have been determined by a

least-squares procedure. Most of the single conformers have too large area underneath the peak at about 4.4 Å. Excepted are the *aaaa* conformer, which has a minimum in this region and the *aaag* conformer, which shows a fairly good agreement with experimental data. From this it might be expected that in the mixture of two conformers which gives the best fit to the experimental curve, one should be an *aaaa* conformer.

But as the *aaaa* conformer shows too large area at 3.7 Å and too small around 2.9 Å, the other conformer in the mixture must show the opposite effect in the mentioned regions (Fig. 5).

aaaa + *g±aag±*. The best agreement is obtained for a mixture of 26 % *aaaa* and 74 % *g±aag±* conformers. The peak at 3.0 Å which compared to the experimental data is too little for an all-*anti* conformer and too large for the *g±aag±* conformer, fits fairly well for the mixture of the two. A similar argument holds for the peak at 3.7 Å, while the lack of distances at 4.3 Å in the *aaaa* conformer is compensated for by C(1)···C(3)' distances in the *g±aag±* conformer. Taking into account the statistical population of the *gauche* conformer, the ratio

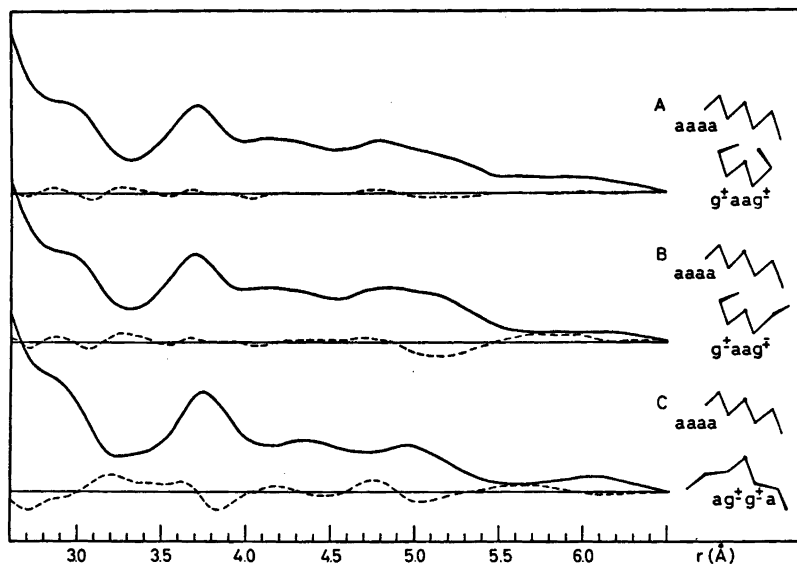


Fig. 5. Dipropyl ether. The outer part of the radial distribution curves for equilibrium mixtures of the conformers: 26 % *aaaa* + 74 % *g±aag±* (A), 28 % *aaaa* + 72 % *g±aag±* (B), and 18 % *aaaa* + 82 % *ag±g±a* (C). The broken lines show the difference between experimental and theoretical values. ($k=0.0020$ Å).

$aaaa/g^{\pm}aag^{\pm}$ means that the energies of the two conformers are approximately equal. During the refinements the carbon-oxygen skeleton of the *anti* conformer is assumed to be exactly planar, while the $\delta(\text{OCCO})$ of the $g^{\pm}aag^{\pm}$ conformer is found to be 72.1° (Fig. 5, curve A).

$aaaa + g^{\pm}aag^{\mp}$, $aaaa + ag^{\pm}g^{\pm}a$. Curve B and C show the best fit between experimental and theoretical data obtained for mixtures of $aaaa$ and $g^{\pm}aag^{\mp}$ conformers (28 and 72 %, respectively) and for $aaaa$ and $ag^{\pm}g^{\pm}a$ conformers (18 and 82 %). The theoretical RD curve for the mixture of $aaaa$ and $ag^{\pm}g^{\pm}a$ conformers clearly shows larger deviations from the experimental data than the two other conformational mixtures shown in Fig. 5. By comparison of curve A and B it is seen that the somewhat larger discrepancies in the region 5.0–6.0 Å for the $aaaa/g^{\pm}aag^{\mp}$ mixture compared to the $aaaa/g^{\pm}aag^{\pm}$ mixture corresponds nicely to the position of the $\text{C}(3)\cdots\text{C}(3')$ distance, which is 5.12 Å for the $g^{\pm}aag^{\mp}$ conformer and 5.79 Å for the $g^{\pm}aag^{\pm}$. These circumstances indicate that if both methyl groups in dipropyl ether are in *gauche* positions to the oxygen atom, there may be a preference for one *gauche* interaction on each side of the oxygen atom rather than two on the same side. If the proportions in the conformational mixture were purely statistical, the ratio of the $g^{\pm}aag^{\pm}$ conformer to the $g^{\pm}aag^{\mp}$ should be 1:1, which does not seem to be the case for dipropyl ether.

DISCUSSION

The conformational analysis of dipropyl ether in the gas phase does not result in an unequivocal solution of the problem. The only single conformation which gives a satisfactory agreement between theoretical and experimental data is the *aaag* conformer. However, a mixture of 26 % $aaaa$ and 74 % $g^{\pm}aag^{\pm}$ gives a good agreement and the smallest error of square residuals from the data refinement. Of course also a mixture of all three conformers will be an acceptable solution if the $aaaa/g^{\pm}aag^{\pm}$ ratio is maintained. In that case, however, it is impossible to determine the ratio of the *aaag* conformer to the mixture, as both solutions fit satisfactorily to the experimental curves and so does any ratio between them.

As already mentioned, in larger ring systems^{1,2} and polymer chains³ built up of $-(\text{O}-\text{CH}_2-\text{CH}_2-\text{CH}_2)-$ units, all the dihedral angles $\delta(\text{COCC})$ are found to be *anti* and all the $\delta(\text{OCCC})$ *gauche*. This seems to favour a 1,4- $\text{CH}\cdots\text{O}$ *gauche* interaction. This favourable *gauche* interaction is also observed in other ethers.^{7,8}

However, an NMR investigation of the conformations of aliphatic ethers by Dale *et al.*⁹ concludes that the 1,4- $\text{CH}\cdots\text{O}$ *gauche* interaction in monoethers is not attractive. The effect of the 1,4- $\text{CH}\cdots\text{O}$ interaction is further explained as being attractive only when the interacting hydrogen atom has an acidic character. This is the case for hydrogen atoms bonded to carbon atoms in α -position to oxygen. In unsubstituted monoethers the acidic character of the relevant hydrogen is missing, and the energy difference between *gauche* and *anti* conformers is found to be negligible.

It may be seen from Fig. 4 that a *gaag* conformer alone obviously does not give any satisfactory solution to the conformation problem of dipropyl ether. From this it may be concluded that there is no preference for 1,4- $\text{CH}\cdots\text{O}$ *gauche* interactions in this molecule and consequently the conformation is not comparable with the $-(\text{O}-\text{CH}_2-\text{CH}_2-\text{CH}_2)-$ units in larger ring systems and polymer chains, where all the dihedral angles $\delta(\text{COCC})$ are *anti* and $\delta(\text{OCCC})$ are *gauche*.

Based on the NMR results for monoethers,⁹ it should be expected that dipropyl ether should not show attractive 1,4- $\text{CH}\cdots\text{O}$ *gauche* interactions, in good agreement with this investigation. On the other hand, the conformer distributions found here are not in agreement with the statistical distribution, and so there must be other effects resulting in an exclusion or very small portion of some conformers or a dominance of others. Thus, in the experimental data there is no support for conformations with *gauche* CCOC dihedral angles being present, and also indications of the absence of the $g^{\pm}aag^{\mp}$ conformer.

Acknowledgements. The author is grateful to Professor J. Dale for suggesting this conformational problem and for valuable discussions and to Siv.ing. R. Seip for recording the experimental data.

REFERENCES

1. Borgen, G. and Dale, J. *Chem. Commun.* (1970) 1340.
2. Groth, P. *Acta Chem. Scand.* 25 (1971) 725.
3. Tadokoro, H., Takahashi, Y., Chatani, Y. and Kakida, H. *Makromol. Chem.* 109 (1967) 96.
4. Andersen, B., Seip, H. M., Strand, T. G. and Stølevik, R. *Acta Chem. Scand.* 23 (1969) 3224.
5. Strand, T. G. and Bonham, R. A. *J. Chem. Phys.* 40 (1964) 1686.
6. Peacher, J. and Wills, J. C. *J. Chem. Phys.* 46 (1967) 4809.
7. Astrup, E. E. *Acta Chem. Scand.* 27 (1973) 3271.
8. Astrup, E. E. and Aomar, A. M. *Acta Chem. Scand. A* 29 (1975) 794.
9. Dale, J. and Greig, D. G. T. *Acta Chem. Scand. B* 28 (1974) 697.

Received September 1, 1976.

An X-Ray Diffraction Study of Iodide and Bromide Complexes of Mercury(II) in Aqueous Solution

MAGNUS SANDSTRÖM and GEORG JOHANSSON

Department of Inorganic Chemistry, Royal Institute of Technology, S-100 44 Stockholm 70, Sweden

From X-ray scattering measurements on concentrated aqueous solutions of the mercury(II) halides the Hg–X bond lengths in the tetrahedral HgX_4^{2-} complexes have been determined to be 2.785(3) Å for the iodide and 2.610(5) Å for the bromide. The X-ray scattering data are consistent with the formation of mononuclear HgI_3^- or HgBr_3^- ions when the X/Hg mol ratio in the solutions is reduced below 4.0. The Hg–X bond lengths in the pyramidal HgI_3^- and HgBr_3^- complexes are estimated to be about 0.03 Å shorter than in the corresponding HgX_4^{2-} complexes. A model for the hydration of the HgX_4^{2-} complexes, which is consistent with the scattering data, is suggested.

As part of a series of X-ray investigations of the structures of the mercury(II) halide complexes in different solvents, aqueous solutions of mercury(II) chloride, bromide and iodide have been investigated. The first paper in this series was a study of mercury(II) iodide complexes in DMSO solution.¹

The low solubilities of the HgX_2 complexes in water do not allow accurate structure determinations of the lower halide complexes. The chloride solutions will be treated in the following paper.²

Previous work. Several investigations of the mercury(II) halide complexes in aqueous solutions, applying different methods,^{3,4} have been reported in the literature. Emf measurements on dilute solutions have shown that HgX^+ , HgX_2 , HgX_3^- and HgX_4^{2-} complexes are formed.^{5,6} The emf data give no evidence for the formation of polynuclear complexes at the low concentrations used. The stability constants show the ranges of stability of the iodide and bromide complexes to be well separated (Fig. 1),

which allows the preparation of solutions in which a specific complex can be dominant.

From X-ray scattering measurements on approximately 1 M solutions of mercury(II) with sodium iodide and bromide, van Eck^{7,8} concluded from the positions of peaks in the radial distribution functions (RDF), that the HgX_4^{2-} ions are probably tetrahedral but highly distorted. Within an HgX_4^{2-} tetrahedron all Hg–X bonds were found to be equal, but

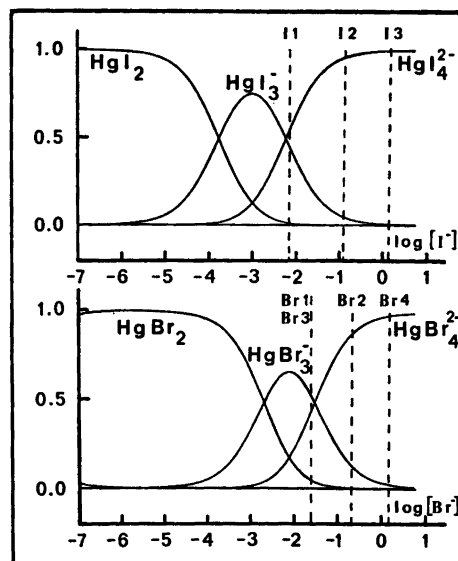


Fig. 1. Fraction of Hg bonded in the different halide complexes as a function of the free halide concentration. The calculated complex distributions of the solutions investigated, assuming the equilibrium constants to be valid, are indicated.

large differences seemed to occur between the X-X distances.⁸ A similar investigation was carried out by Furey⁹ on approximately 3 M mercury(II) iodide solutions. He concluded that the HgI₄²⁻ group is a regular tetrahedron with an Hg-I bond length of 2.80 Å. In a solution with an I/Hg ratio of 3.6, where HgI₃⁻ complexes should be present, he found the same tetrahedral coordination of iodide, which requires the sharing of iodide ions between mercury atoms.

Results from spectroscopic investigations support a regular tetrahedral structure for the HgX₄²⁻ complexes in solution.¹⁰⁻¹² In anhydrous TBP solutions Raman and IR spectra have been interpreted as indicating a planar symmetry for HgI₃⁻. For HgBr₃⁻ in TBP, however, a deviation from planarity occurred probably caused by solvent interactions.¹³

In DMSO X-ray scattering measurements have shown the HgI₂ complex to be approximately linear, HgI₃⁻ to have a pyramidal shape and HgI₄²⁻ to form a regular tetrahedron.¹

EXPERIMENTAL

The solutions were prepared by dissolving dried and weighed amounts of mercury(II) halide and sodium halide (Mallinckrodt, analytical reagent) in distilled water and diluting to a known volume. The compositions of the solutions investigated are given in Table 1.

The X-ray scattering was measured (at 25 ± 1 °C) from the free surface of the solutions in the way described in previous papers.¹⁵ MoK α radiation ($\lambda = 0.7107$ Å) was used. The scattered intensity was measured at discrete points between $\theta = 1^\circ$ and $\theta = 70^\circ$, where 2θ is the scattering angle. Intervals of 0.1° for $1^\circ < \theta < 10^\circ$ and 0.25° for $10^\circ < \theta <$

Table 1. Compositions of the solutions at 25 °C in mol l⁻¹.

Sol.	Hg	X	Na	H ₂ O
I1	3.453	12.20	5.297	27.89
I2	3.052	12.21	6.104	28.02
I3	2.693	12.18	6.792	28.63
Br1	1.923	6.520	2.675	44.61
Br2	1.630	6.521	3.261	44.62
Br3	3.600	12.21	5.010	34.58
Br4	2.700	12.21	6.809	34.93

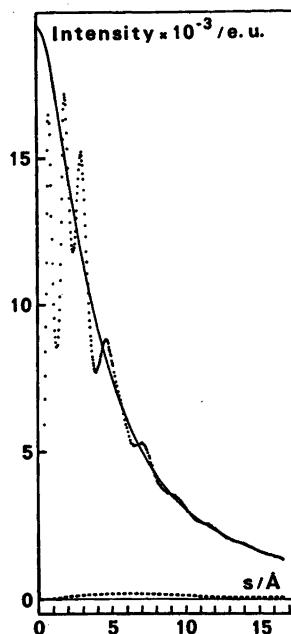


Fig. 2. Experimental normalized intensity values (dots), calculated structure-independent coherent scattering (line), and the incoherent scattering reaching the counter (dashed line), as a function of $s = (4\pi/\lambda) \sin \theta$ for solution I3.

70° were used. Usually 100 000 counts were taken for each point, which corresponds to a statistical error of about 0.3 %.*

DATA TREATMENT

All calculations were carried out by means of the KURVLR and PUTSLR programs.¹⁶ The measured intensities were corrected and normalized to a stoichiometric unit of volume, V , corresponding to the average volume per mercury atom in the solution. The normalization was done by comparing the observed intensities with the calculated sum of the independent coherent and the incoherent scattering in the high angle region. The double scattering¹⁷ was calculated and did not exceed 2 % for the iodide solutions and 3 % for the bromide solutions. The reduced intensities, $i(s)$, were obtained as described previously.¹⁵

* The intensity data can be obtained on request from the authors.

The scattering factors given by Cromer and Waber¹⁸ were used for all the atoms except H, for which Stewart's values¹⁹ were used. Anomalous dispersion corrections, $\Delta f'$ and $\Delta f''$, were taken from Cromer.²⁰ The values used for the incoherent radiation were those given by Cromer²¹ for O, Br and I, by Compton and Allison²² for H, and by Cromer and Mann²³ for the remaining atoms. Corrections were made for the Breit-Dirac factor,^{24,25} in the form appropriate for a radiation counter.²⁶

The reduced intensity curves, $i_{\text{obs}}(s)$, where $s = (4\pi/\lambda) \sin \theta$, were corrected for low-frequency additions by removing peaks in the RDF's below 1 Å, which could not be related to interatomic distances.¹⁶ From the reduced intensity values the electronic radial distribution functions, $D(r)$, were calculated.¹⁶ The modification function, $M(s)$, was $[f_{\text{Hg}}^2(0)/f_{\text{Hg}}^2(s)] \exp(-0.01s^2)$, and ρ_0 was calculated as $[(\sum_p f_p)^2 + (\sum_p \Delta f_p'')^2]/V$.

Intramolecular contributions to the intensities were calculated according to the expression:

$$i_{\text{calc}}(s) = \sum_{\substack{p \\ p \neq q}} \sum_q (f_p f_q + \Delta f_p'' \Delta f_q'') \\ [\sin(r_{pq}s)/(r_{pq}s)] \exp(-b_{pq}s^2)$$

Here r_{pq} is the average distance between the atoms p and q , and $b_{pq} = \frac{1}{2} \langle \Delta r^2 \rangle$ is a temperature coefficient, equal to half the mean square variation in r_{pq} . When the variation in r_{pq} is caused only by molecular vibrations, the amplitude of vibration equals Δr . Corresponding peak shapes were obtained from these intensities by a Fourier transformation carried out in the same way as for the experimental intensities. Intensity contributions from coordinated water molecules were calculated using the molecular scattering factor for H_2O , given by Narten.²⁷

The experimental intensities obtained for solution I3 are illustrated in Fig. 2. For all the solutions the reduced intensities, after multiplication by s , are shown in Fig. 3. Radial distribution curves, $D(r)$ and $D(r) - 4\pi r^2 \rho_0$, are given in Figs. 4 and 7.

Least squares refinements. Reduced intensities, i_{calc} , can be evaluated for assumed models of a solution, taking both intra- and intermolecular interactions into account.¹⁶ The parameters

defining such a model can be refined by minimizing the function $U = \sum w(s)[i_{\text{obs}}(s) - i_{\text{calc}}(s)]^2$, where $w(s)$ is a weighting function,^{16,28} and the i_{calc} values are evaluated for each experimental point in a selected s interval.

Usually only the intramolecular interactions will give significant contributions to the high-angle part of the intensity curve, which can therefore be used for the refinement of the corresponding parameters.

An intramolecular interaction can be characterized by three parameters: the distance, r_{pq} , the number of such distances, n , in a stoichiometric unit of volume, and a temperature coefficient, b_{pq} . The result of a refine-

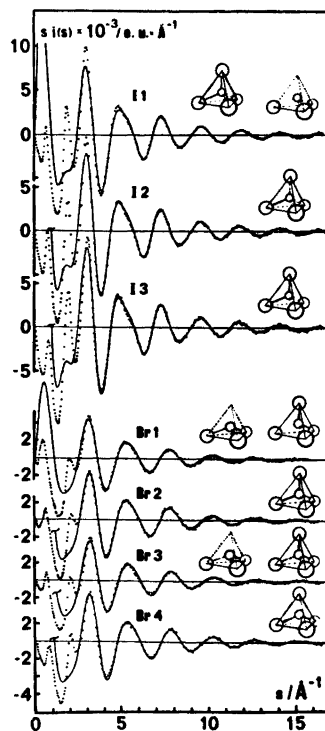


Fig. 3. Reduced intensity values, multiplied by s , (dots), for the solutions investigated. The solid lines give calculated $si(s)$ values for regular tetrahedral HgX_4^{2-} complexes with parameter values $b_{\text{Hg-X}} = 0.006 \text{ \AA}^2$, $b_{\text{X-X}} = 0.028 \text{ \AA}^2$, and $r_{\text{Hg-X}} = 2.785$ and 2.610 \AA for the iodide and bromide solutions, respectively. For solutions I1, Br1 and Br3 stoichiometric amounts of pyramidal HgX_3^- complexes are also included, with $r_{\text{Hg-X}} = 2.76$ and 2.58 \AA , respectively.

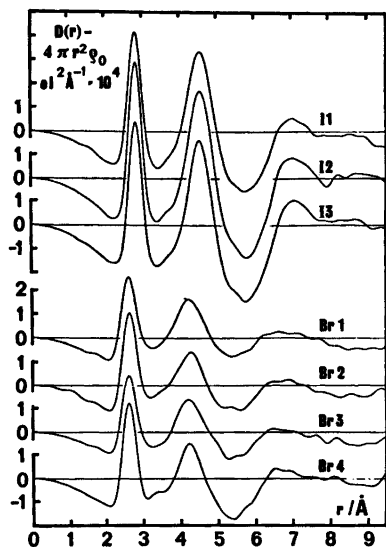


Fig. 4. $D(r) - 4\pi r^2 \rho_0$ functions for the solutions investigated.

ment will be meaningful only if all the significant contributions to the reduced intensities in the selected s interval are included in the model.²⁸ Moreover, the number of parameters which can be simultaneously refined is small due to the limited amount of information which is contained in the one-dimensional intensity curve.

Systematic errors^{15,17,28-35} which still can remain in the $i_{\text{obs}}(s)$ curve will in general have a much longer period in regard to s than those of the intramolecular interactions and will to a large extent be eliminated by the removal of spurious peaks at low distances in the RDF's.¹⁶ A check for systematic errors can be made by comparing results obtained from refinements carried out for different s intervals. In particular, by varying the lower s limit, systematic errors caused by intermolecular intensity contributions can be detected as they decrease rapidly with increasing s values.

RESULTS

For all the solutions in the present investigation, the RDF's show only two prominent peaks (Fig. 4). One corresponds to the Hg-X and the other to the X-X distances within the mercury halide complexes. These interactions are by far the dominant contributors

to the reduced intensity curves, with the exception of the innermost parts as is illustrated in Fig. 3. Therefore, accurate parameter values for these two types of intramolecular interactions can be determined by least squares refinements in which the low-angle parts of the intensity curves are not included.

A number of refinements were carried out using different weighting schemes and different s intervals and with various symmetry restrictions imposed on the allowed variations of the parameter values for the Hg-X and the X-X interactions. However, no significant differences between the results were found when i_{obs} values for $s > 3 \text{ \AA}^{-1}$ were used. A summary of the results of the least squares refinements is given in Tables 2 and 3. The standard deviations are those calculated in the least squares refinement process and do not include systematic errors. From the variation of the results with the different ranges of s values used, it seems that the systematic errors in the parameter values can be of about the same order of magnitude as the calculated standard deviations. All the refinement results given in the tables were obtained using a weighting function chosen to give each part of the $i(s)$ curve a weight corresponding approximately to its statistical accuracy and included a factor which compensated for the unequal spacing between the points caused by the constant $\Delta\theta$ values used during the intensity measurements.³

The RDF's and calculated peak shapes for solutions I2 and Br2 are shown in Fig. 7.

DISCUSSION

Intramolecular interactions. A simultaneous refinement of all six parameters used to describe the Hg-X and the X-X interactions leads to the results given in Table 2. The parameters r , n and b of the Hg-X interaction and the X-X distance are those most accurately determined. For X/Hg ratios of four and larger the number of X atoms bound to each mercury atom is found, within the estimated errors, to be four as expected for a tetrahedral complex. Similarly, the ratio between the X-X and the Hg-X distances is not significantly different from that expected for a regular tetrahedral symmetry.

Table 2. Results of least squares refinements of six independent parameters for the Hg–X and X–X interactions; r is the distance, n the number of distances per mercury atom, and b the temperature coefficient. For a regular tetrahedron the calculated ratio $r_{\text{Hg-X}}/r_{\text{X-X}}$ is $\sqrt{3}/8 = 0.6124$.

Sol.	Ratio X/Hg	$r_{\text{Hg-X}}/\text{Å}$	$n_{\text{Hg-X}}$	$b_{\text{Hg-X}}/\text{Å}^2$	$r_{\text{X-X}}/\text{Å}$	$n_{\text{X-X}}$	$b_{\text{X-X}}/\text{Å}^2$	$r_{\text{Hg-X}}/r_{\text{X-X}}$
I1	3.53	2.774(2)	3.5(1)	0.005(1)	4.55(1)	6(1)	0.03(1)	0.610(2)
I2	4.00	2.786(2)	3.9(1)	0.006(1)	4.55(1)	8(1)	0.04(1)	0.612(2)
I3	4.52	2.786(2)	3.9(1)	0.005(1)	4.55(1)	7(1)	0.03(1)	0.612(2)
Br1	3.39	2.597(2)	3.2(1)	0.006(1)	4.22(2)	9(2)	0.05(1)	0.615(4)
Br2	4.00	2.613(2)	3.9(1)	0.005(1)	4.26(1)	7(1)	0.04(1)	0.613(2)
Br3	3.39	2.594(3)	3.2(1)	0.006(1)	4.26(2)	9(2)	0.05(1)	0.609(4)
Br4	4.52	2.608(3)	3.9(1)	0.005(1)	4.25(2)	8(1)	0.04(1)	0.614(4)

Table 3. Results of least squares refinements of four independent parameters assuming tetrahedral HgX_4 groups; r is the Hg–X distance, m the number of HgX_4 complexes in a stoichiometric unit of volume, and b the temperature coefficient.

Sol.	$r_{\text{Hg-X}}/\text{Å}$	m	$b_{\text{Hg-X}}/\text{Å}^2$	$b_{\text{X-X}}/\text{Å}^2$
I2	2.785(2)	0.99(1)	0.006(1)	0.029(1)
I3	2.785(2)	0.98(2)	0.005(1)	0.025(2)
Br2	2.614(2)	1.01(2)	0.007(2)	0.028(2)
Br4	2.605(2)	1.00(2)	0.006(3)	0.029(3)

The number of Hg–X bonds for the solutions with X/Hg mol ratios less than four is of the magnitude expected if an HgX_3^- complex is assumed to be formed. This indicates that sharing of halide atoms between different complexes does not occur, and that, therefore, polynuclear complexes are not formed. However, the level of significance in these comparisons is relatively low as shown by the standard deviations given in Table 2. Because of the small contributions to the intensity curves of the X–X, compared to the Hg–X interactions, the standard deviations obtained for the number of X–X distances are high (Table 2). This parameter, therefore, cannot be used to differentiate between HgX_4^{2-} and HgX_3^- complexes.

A comparison of the RDF's between the solutions with $\text{X/Hg} \geq 4$ and those with $\text{X/Hg} < 4$, shows more clearly that polynuclear complexes are not formed in significant amounts. This is demonstrated in Fig. 5, which gives differences between the $D(r)$ –

$4\pi r^2 \rho_0$ functions for the following pairs of solutions: I2–I1, Br2–Br1 and Br4–Br3. The difference in areas of the Hg–X peaks corresponds to that expected if a mononuclear HgX_3^- complex is formed and peaks which could indicate the presence of polynuclear complexes, do not appear in the difference curves.

The results from the least squares refinements, given in Table 2, indicate a slight shortening of the Hg–X distances for X/Hg mol ratios below 4. By using the parameter values for the HgX_4^{2-} complexes, as given in Table 3, and assuming the relative amounts of HgX_3^- and HgX_4^{2-} to be given by the X/Hg mol ratios, estimates of the Hg–X bond lengths in HgX_3^- could be obtained from the distances in Table 2 and by least squares refinements on solutions I1, Br1 and Br3. The results indicated the Hg–I and the Hg–Br bond lengths in

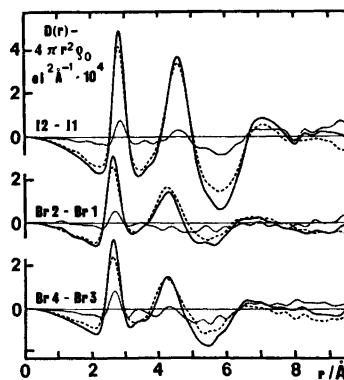


Fig. 5. Differences (dotted lines) between the $D(r) - 4\pi r^2 \rho_0$ functions for the solutions I2–I1, Br2–Br1, and Br4–Br3.

HgX₃⁻ to be 0.03(1) Å shorter than those in HgX₄²⁻. No shortening of the X–X distances, however, seems to occur. This is comparable to what was found for DMSO solutions,¹ where the Hg–I bond lengths were determined to be 2.80 and 2.73 Å in HgI₄²⁻ and HgI₃⁻, respectively.

Table 3 gives the results of the refinements for solutions with X/Hg mol ratios ≥ 4, when only four of the six parameter values are allowed to vary independently. For this refinement a regular tetrahedral HgX₄ group was assumed to occur and the number of such groups in the stoichiometric unit of volume, the temperature factors corresponding to the Hg–X and the X–X interactions, and the Hg–X bond lengths were independently varied. Since the ratio between the number of X–X and Hg–X distances is constant in the complex, the precision in the determination of the temperature factor of the X–X interaction will be higher (Table 3). With this exception the parameter values given in Table 3 do not differ from those given in Table 2.

The temperature factor of the Hg–X interaction corresponds to a root-mean-square value for the variation in the distance of about 0.10 Å. For the X–X interaction, the corresponding value is about 0.24 Å. This can be compared to the mean amplitude of vibration calculated for HgBr₃⁻ in TBP solution from observed vibrational frequencies, 0.0583 Å for Hg–Br and 0.1965 Å for Br–Br.³⁸

Intermolecular interactions. The parameter values obtained for the HgX_n complexes were used to calculate peak shapes for the intramolecular Hg–X and X–X interactions, which were subtracted from the RDF's. The resulting functions (Fig. 7) indicate a remaining structure in the solutions, which cannot be explained by merely introducing a continuous electron contribution or a continuous complex distribution around each HgX_n complex.¹⁶ Some of these remaining interactions occur at distances that are shorter than those expected for X–X contact distances. Thus, in HgX₄²⁻ solutions they can be explained only by contributions from X–H₂O or, to a smaller extent, from H₂O–H₂O and Na⁺–H₂O interactions. It was found that a simple model for the packing of water molecules around an HgX₄²⁻ complex could account for most of these effects. A layer

of water molecules, in an approximately close-packed arrangement (Fig. 6), was assumed to surround the HgX₄²⁻ complex. The distance of this layer from the center of the complex was refined in a least squares process, using appropriate parts of the reduced intensity curves. The halide-water distances obtained, Br⁻–H₂O in the range 3.4 to 3.6 Å and I⁻–H₂O 3.6 to 4.0 Å, are consistent with expected interatomic distances. The H₂O–H₂O distances within the layer could not, however, be separately adjusted, because their contributions to the intensity values were too small. The results of the refinement showed the long X–H₂O interactions to be much less distinct than the short ones. This indicates an arrangement in which the surrounding water molecules are in contact with the X atoms but do not have fixed positions on the surface of the HgX₄²⁻ complex.

The final model used to calculate theoretical intensities and RDF's consisted of an HgX₄²⁻ complex of tetrahedral symmetry or an HgX₃⁻ complex with an H₂O molecule in the fourth vertex, surrounded by a layer of water molecules (Fig. 6) outside of which the distribution of atoms was approximated by a continuous electron distribution. This is exemplified in Figs. 7 and 8 for the concentrated solution I2 (3.05 M Na₂HgI₄), where all water molecules as well as the sodium ions could be placed into this layer around the HgI₄²⁻ complex. The radius for the beginning of the even electron distribution, $R = 5.06$ Å, was estimated from the stoichiometric volume per Hg atom. For the more dilute solutions an average coordination of six water molecules around sodium and excess halide ions was also included. The contributions from residual water structure were approximated by assuming tetrahedral (H₂O)₆ groups.³⁹ An example is shown in Fig. 7 for the solution Br2 (1.63 M Na₂HgBr₄), where the radii chosen for the even electron distributions around the assumed species were 5.3 and 3.5 Å for the hydrated HgBr₄²⁻ and Na⁺ ions, and 3.2 Å for the H₂O groups, respectively.

Since the emergence of the continuum will not be sharp, a temperature factor, $\exp(-0.1 s^2)$, was included in all calculations.³⁹

As shown in Fig. 7, this model approximately accounts for the observed interactions up to

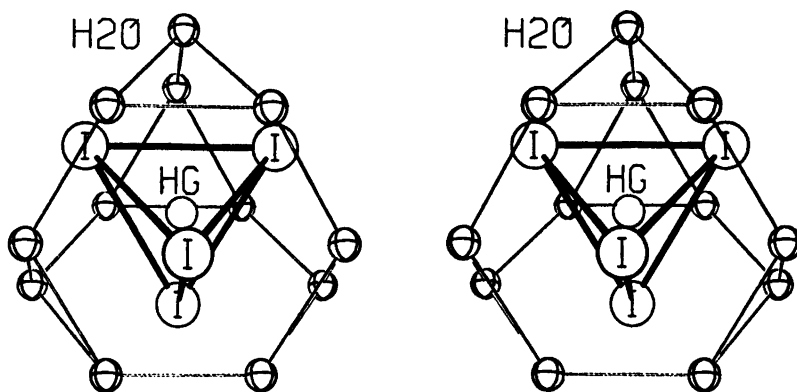


Fig. 6. The model used in the calculations for the packing of water molecules around an HgX_4^{2-} complex.

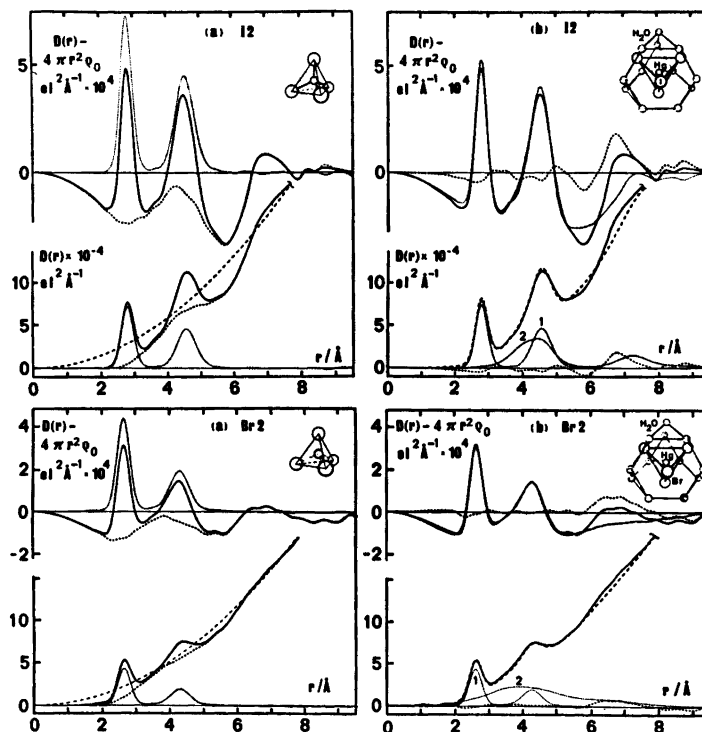


Fig. 7. Comparison between the experimental RDF's (solid lines) and (a) the peak shapes calculated for an HgX_4^{2-} tetrahedron (dotted lines), and (b) the calculated RDF's including both intra- and intermolecular interactions (dotted lines for the $D(r) - 4\pi r^2 \rho_0$ functions and long dashes for the $D(r)$ curves). The dotted lines marked 1 are the peak shapes for an HgX_4^{2-} tetrahedron and those marked 2 represent the interactions between the HgX_4^{2-} complex and its surrounding hydration layer. For solution Br2 this curve 2 also contains the interactions within the assumed $\text{Na}(\text{H}_2\text{O})_6^+$ and H_2O groups. The calculated RDF's also contain the contributions from an assumed even electron distribution around these species.

Differences between experimental and calculated curves are given by dashed lines (short dashes).

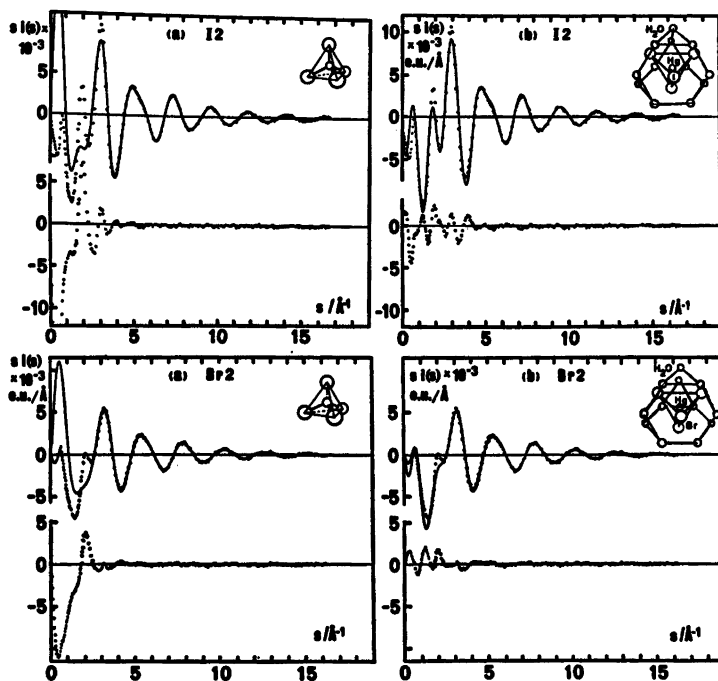


Fig. 8. Comparison between the experimental (dots) and calculated (solid lines) $s(s)$ values corresponding to the RDF's in Fig. 7.

The difference between experimental and calculated values is marked by dots below.

about 6 to 7 Å. The remaining interactions, which are too diffuse to allow an interpretation in terms of a specific structural model, probably result from the packing of the complexes not being completely random. This is supported by the observation that the remaining interactions become more pronounced as the concentration of the solution increases.

For the more concentrated solutions an attempt was made to relate the remaining interactions to possible restrictions in the free rotations of HgX_4^{2-} ions leading to preferred relative orientations of the groups. The model tried was based on the crystal structure of SnI_4 , modified in a way similar to that used in the investigations of liquid CCl_4 .⁴⁰ It became obvious, however, that such a model could not account for the observed interactions at the longer distances, and that the observed intermolecular interactions were too diffuse to be related to such a rigid model.

Conclusions and comparisons with other structure determinations. The bond lengths found for the HgI_4^{2-} and the HgBr_4^{2-} complexes, 2.785(3) and 2.610(5) Å, respectively, are similar to values found for tetrahedrally coordinated mercury in crystal structures.⁴¹⁻⁵² The comparatively low temperature factors obtained in the least squares refinements of the scattering data indicate that the Hg-X bond lengths in the aqueous solutions are more regular than is usually found in crystal structures.

The X-ray scattering data show, in an apparently conclusive way, that even in these concentrated solutions the HgI_3^- and the HgBr_3^- complexes formed for X/Hg mol ratios < 4, have no tendency to share X atoms which is in contrast to what is found in chloride solutions² and in the solid state where most mercury halides form infinite complexes^{41-44,51-53} and few compounds have been found to contain discrete groups.^{45-50,54}

Acknowledgements. The work has been supported by the Swedish Natural Science Research Council. Computer time was made available by the Computer Division of the National Swedish Office for Administrative Rationalization and Economy. We thank Mr. I. Duncan for linguistic help.

REFERENCES

- Gaizer, F. and Johansson, G. *Acta Chem. Scand.* 22 (1968) 3013.
- Sandström, M. *Acta Chem. Scand. A* 31 (1977) 141.
- Sillén, L. G. and Martell, A. E. *Stability Constants*, Spec. Publ. No. 17 (1964) and *Suppl.* No. 1, Spec. Publ. No. 25, The Chemical Society, London 1971.
- Deacon, G. B. *Rev. Pure Appl. Chem.* 13 (1963) 189.
- Sillén, L. G. *Acta Chem. Scand.* 3 (1949) 539.
- Arnek, R. *Ark. Kemi* 24 (1965) 531.
- van Panthaleon van Eck, C. L., Wolter, H. B. M. and Jaspers, W. J. M. *Recl. Trav. Chim. Pays-Bas* 75 (1956) 802.
- van Panthaleon van Eck, C. L. *Thesis*, Leiden 1958, see Gmelin *Handb. Anorg. Chem.* Hg-B2, Verlag Chemie Weinheim/Bergstr. 1967.
- Furey, D. A. *Thesis*, Kent State University 1967 (Access No. 68-6207, Univ. Microfilms, Ann Arbor, Mich.).
- Long, D. A. and Chau, J. Y. H. *Trans. Faraday Soc.* 58 (1962) 2325.
- Hooper, M. A. and James, D. W. *Aust. J. Chem.* 24 (1971) 1345.
- Macklin, J. W. and Plane, R. A. *Inorg. Chem.* 9 (1970) 821.
- Waters, D. N., Short, E. L., Tharwat, M. and Morris, D. F. C. *J. Mol. Struct.* 17 (1973) 389.
- Sandström, M. *To be published.*
- Johansson, G. *Acta Chem. Scand.* 25 (1971) 2787; 20 (1966) 553.
- Johansson, G. and Sandström, M. *Chem. Scr.* 4 (1973) 195.
- Warren, B. E. and Mozzi, R. L. *Acta Crystallogr.* 21 (1966) 459.
- Cromer, D. T. and Waber, J. T. *Acta Crystallogr.* 18 (1965) 104.
- Stewart, R. F., Davidson, E. R. and Simpson, W. T. *J. Chem. Phys.* 42 (1965) 3175.
- Cromer, D. T. *Acta Crystallogr.* 18 (1965) 17.
- Cromer, D. T. *J. Chem. Phys.* 50 (1969) 4857.
- Compton, A. H. and Allison, S. K. *X-Rays in Theory and Experiment*, van Nostrand, New York 1935.
- Cromer, D. T. and Mann, J. B. *J. Chem. Phys.* 47 (1967) 1892.
- Breit, G. *Phys. Rev.* 27 (1926) 362.
- Dirac, P. A. M. *Proc. R. Soc. London A* 111 (1926) 405.
- Dwiggins, C. W. and Park, D. A. *Acta Crystallogr. A* 27 (1971) 264.
- Narten, A. H. and Levy, H. A. *J. Chem. Phys.* 55 (1971) 2263.
- Sillén, L. G. *Acta Chem. Scand.* 16 (1962) 159.
- Warren, B. E. and Mozzi, R. L. *J. Appl. Crystallogr.* 3 (1970) 59.
- Milberg, M. E. *J. Appl. Phys.* 29 (1958) 64.
- Levy, H. A., Danford, M. D. and Narten, A. H. *Data Collection and Evaluation with an X-Ray Diffractometer Designed for the Study of Liquid Structure*, Report ORNL-3960, Oak Ridge National Laboratory, Oak Ridge 1966.
- Pirene, M. H. *The Diffraction of X-Rays and Electrons by Free Molecules*, Cambridge Univ. Press, London-New York 1946.
- Åberg, M. *Acta Chem. Scand.* 24 (1970) 2901.
- Cromer, D. T. *Acta Crystallogr.* 19 (1965) 224.
- Warren, B. E. *X-Ray Diffraction*, Addison-Wesley, Reading, Massachusetts 1969.
- Frey, M. and Monier, J. C. *Acta Crystallogr. B* 27 (1971) 2487.
- Leligny, H., Frey, M. and Monier, J. C. *Acta Crystallogr. B* 28 (1972) 2104.
- Sanyal, N. K., Goel, R. K. and Pandey, A. N. *Indian J. Phys.* 49 (1975) 546.
- Narten, A. H., Danford, M. D. and Levy, H. A. *Discuss. Faraday Soc.* 43 (1967) 97, see also Luck, W., Ed., *Structure of Water and Aqueous Solutions*, Verlag Chemie, Weinheim/Bergstr. 1974.
- Narten, A. H., Danford, M. D. and Levy, H. A. *J. Chem. Phys.* 46 (1967) 4875.
- Jeffrey, G. A. and Vlasse, M. *Inorg. Chem.* 6 (1967) 397.
- Hahn, H., Frank, G. and Klingler, W. *Z. Anorg. Allg. Chem.* 279 (1955) 271.
- Nyqvist, L. and Johansson, G. *Acta Chem. Scand.* 25 (1971) 1615.
- Fedorov, P. M. and Pakhomov, V. I. *Koord. Khim.* 1 (1975) 1140.
- Fedorov, P. M., Pakhomov, V. I. and Ivanova-Korfini, I. N. *Koord. Khim.* 1 (1975) 1569.
- Fenn, R. H. *Acta Crystallogr.* 20 (1966) 24.
- Fenn, R. H. *Acta Crystallogr.* 20 (1966) 20.
- Beurskens, P. T., Bosman, W. P. J. H. and Cras, J. A. *J. Cryst. Mol. Struct.* 2 (1972) 183.
- Harris, G. S., Inglis, F., McKechnie, J., Cheung, K. K. and Ferguson, G. *Chem. Commun.* 9 (1967) 442.
- Kamenar, B. and Nagl, A. *Acta Crystallogr. B* 32 (1972) 1414.
- Padmanabhan, V. M. and Ydava, V. S. *Acta Crystallogr. B* 25 (1969) 647.
- White, J. G. *Acta Crystallogr.* 16 (1963) 397.
- Brodersen, K. *Acta Crystallogr.* 8 (1955) 723.

Received August 30, 1976.

An X-Ray Diffraction and Raman Study of Mercury(II) Chloride Complexes in Aqueous Solution. Evidence for the Formation of Polynuclear Complexes

MAGNUS SANDSTRÖM

Department of Inorganic Chemistry, Royal Institute of Technology, S-100 44 Stockholm 70, Sweden

For concentrated mercury(II) chloride solutions ($C_{\text{Hg}} \geq 1 \text{ M}$), containing a large excess of chloride (mol ratios $\text{Cl}/\text{Hg} \geq 4.5$), the data are consistent with a dominant tetrahedral HgCl_4^{2-} complex with an $\text{Hg}-\text{Cl}$ bond length of $2.47(1) \text{ \AA}$. The vibration frequency $\nu_1(\text{HgCl}_3^-)$ is found to be $288 \pm 2 \text{ cm}^{-1}$.

For solutions with Cl/Hg mol ratios around three and $C_{\text{Hg}} \geq 0.5 \text{ M}$ polynuclear complexes occur, probably with distorted octahedral coordination and with double chlorine bridges between the mercury atoms. Structural models for these complexes consistent with the experimental data are proposed.

Dilute aqueous solutions of mercury(II) chloride complexes, which have been investigated by a variety of methods,¹⁻³ do not seem to contain polynuclear complexes in detectable amounts. A number of suggestions of polynuclearity³ has not been supported by later careful studies.^{1,4}

The distribution of chloride complexes, HgCl_n^{2-n} ($n=0, 1, 2, 3$, and 4), calculated with the use of equilibrium constants determined by emf methods in 0.5 M (Na)ClO_4 medium,⁵ is given in Fig. 1.

However, in more concentrated solutions polynuclear complexes could occur.³ The solubility of HgCl_2 increases rapidly as the temperature is raised — it is 0.265 M at 25°C ⁶ and 1.81 M at 100°C .⁷ From an ebullioscopic investigation it was proposed that for concentrations higher than 0.5 M the dominant complex, beside the monomeric HgCl_2 , is the trimeric Hg_3Cl_6 .⁸

Structure of the complexes in solution. An 0.23 M aqueous solution of HgCl_2 was studied by

X-ray diffraction in this work, but no accurate structure information of the complex could be obtained, since the relatively small effects are obscured by the water structure.

There is still some ambiguity of the structure of the HgCl_3^- complex in solution. Incomplete spectra have been reported for several organic solvents^{9-12, 44} and for a melt.¹³ It has not been possible to distinguish between the pyramidal C_{3v} or the planar D_{3h} symmetries on the basis of these spectra. Moreover, the possible coordination of a solvent molecule probably determines which structure the HgX_3^- complex assumes in different solvents.⁹

Pyramidal structures with C_{3v} symmetry have been found for the HgI_3^- and HgBr_3^- complexes in aqueous¹⁴ and DMSO^{15,16} solutions by X-

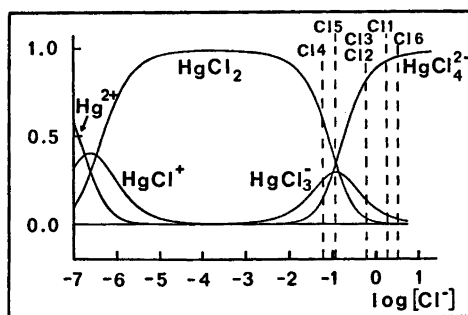


Fig. 1. Fraction of Hg bonded in the different chloride complexes as a function of the free chloride ion concentration. The calculated complex distributions of the solutions investigated by X-ray diffraction, assuming the equilibrium constants to be valid, are indicated.

ray diffraction. Preliminary results of X-ray and Raman studies of 1 M NaHgCl₃ in DMSO solution show that polynuclear complexes are not formed in any large amount.¹⁶ The bond length, 2.44 Å, found from the sharp Hg–Cl peak in the radial distribution function (RDF) is indicative of a pyramidal structure. Thus, by analogy, HgCl₃[–] probably also has C_{3v} symmetry in aqueous solution.

From X-ray scattering measurements on approximately 1 M aqueous solutions of mercury(II) and sodium chloride van Eck proposed that HgCl₄^{2–} is tetrahedral but highly distorted.¹⁷ He found an Hg–Cl bond length of 2.51 Å.

Raman studies of aqueous HgCl₄^{2–} solutions frequently are reported as a simple one-line spectrum.^{18–21} A complete assignment consistent with a tetrahedral T_d symmetry has been made for the spectra of crystalline [(CH₃)₄N]₂HgCl₄,²² which is isomorphous with the corresponding tetrahedral bromide.²³ An earlier study of HgCl₄^{2–} in a melt¹³ appears to lead to an incorrect assignment.²²

In the crystal structure of the salt (AH)₂HgCl₄·2H₂O (where A is the alkaloid perloine, C₂₀H₁₆N₂O₃) discrete HgCl₄^{2–} groups with an average Hg–Cl bond length of 2.50 Å occur. The slight deviation found from a regular tetrahedral structure is probably due to non-bonded compression.²⁴

EXPERIMENTAL

Dried and weighed amounts of mercury(II) chloride (Mallinckrodt, analytical reagent) and lithium or sodium chloride (Merck, suprapur) were dissolved in distilled water and diluted to a known volume. The compositions of the

Table 1. Compositions at 25 °C in mol l^{–1} of the solutions investigated by X-ray diffraction.

Sol.	Hg	Cl	Li	Na	H ₂ O	Ratio Cl/Hg
C11	1.000	5.83	3.827	–	48.1	5.83
C12	1.000	4.50	2.495	–	49.7	4.50
C13	0.999	4.50	–	2.499	52.7	4.50
C14	1.000	2.80	0.798	–	51.7	2.80
C15	5.000	15.00	5.002	–	35.2	3.00
C16	3.400	17.01	10.21	–	33.8	5.00

solutions investigated by X-ray diffraction are given in Table 1.

The diffracted intensity of MoKα radiation (λ=0.7107 Å) was measured at 25 ± 1 °C from the free surface of the solutions in the same way as described previously.¹⁴

Raman spectra were obtained with a Cary 82 Spectrophotometer using the 4880 Å Ar⁺–Kr⁺ laser excitation. Slit widths corresponded typically to 5 cm^{–1}. The solutions were contained in a quartz capillary.

DATA TREATMENT

The processing of the X-ray data was performed as described before.¹⁴ The additional scattering factors needed for Li(0) and Cl(0) were taken from the same sources as before.¹⁴ The calculated double scattering¹⁴ did not exceed 3 %. All curves are calculated for a stoichiometric unit of volume corresponding to one mercury atom.

Least squares refinements of parameters for intramolecular interactions¹⁴ in the mercury(II) chloride complexes were performed. A minimum was sought for the function $U = \sum_{s(1)}^{s(2)} w(s) [i_{\text{obs}}(s) - i_{\text{calc}}(s)]^2$. Due to the relatively larger influence of intermolecular intensity than in the iodide and bromide solutions,¹⁴ only the outermost parts of the reduced intensity curves, $i_{\text{obs}}(s)$, could be used. The contribution of the intramolecular Cl–Cl interaction is too small, however, to permit its parameters to be independently refined in these intervals.

Two models were used for the refinements: (a) allowing only for the Hg–Cl interaction and (b) a regular tetrahedral HgCl₄^{2–} complex where the temperature coefficient for the Cl–Cl interaction was kept constant at the mean value, $b_{\text{X-X}} = 0.028 \text{ Å}^2$, which was obtained for the HgBr₄^{2–} and HgI₄^{2–} complexes.¹⁴ This corresponds to a root-mean-square variation of 0.24 Å in the distance $r_{\text{Cl-Cl}}$, which can be compared to the mean amplitude of vibration 0.1932 Å, calculated for HgCl₃[–] in TBP solution from spectral data.²⁵ The parameters refined in the models are the distance, $r_{\text{Hg-Cl}}$, the number of Hg–Cl distances per mercury atom, $n_{\text{Hg-Cl}}$, and the temperature coefficient, $b_{\text{Hg-Cl}}$. For the solutions C14 and C15 no least-squares refinement results are given, since they contain mercury chloride complexes with several different Hg–Cl distances.

Table 2. Results of least squares refinements for an Hg-Cl interaction; r is the distance, n the number of distances per mercury atom, and b the temperature coefficient.

Sol.	Interval s_1 to s_2	$r/\text{\AA}$	n	$b/\text{\AA}^2$
Cl1	8-15	2.469(3)	4.3(3)	0.006(1)
Cl2	8-15	2.454(4)	4.0(4)	0.007(1)
Cl3	8-15	2.436(2)	3.3(2)	0.004(1)
Cl6	6-16	2.469(3)	3.7(3)	0.009(2)

RESULTS

X-Ray data. The addition of the intramolecular Cl-Cl interaction, which is the only difference between the refined models, gave slightly lower error square sums, U . However, no significant differences occurred in the parameter values for the two models (Table 2) in the same s interval. The standard deviations given are the ones calculated in the least squares process for a weighting function, $w(s)$, pro-

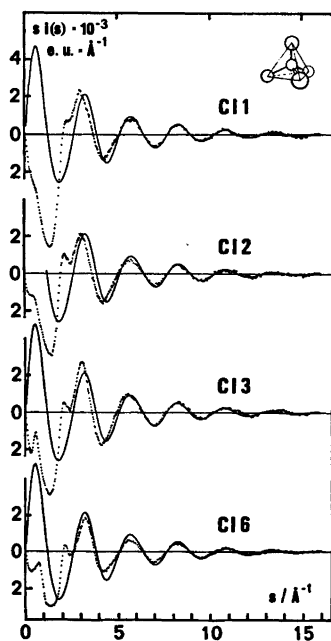


Fig. 2. Reduced intensity values, $i(s)$, multiplied by s , (dots), for the solutions containing an excess of chloride ions. The solid lines give calculated $si(s)$ values for a regular tetrahedral HgCl_4^{2-} complex.

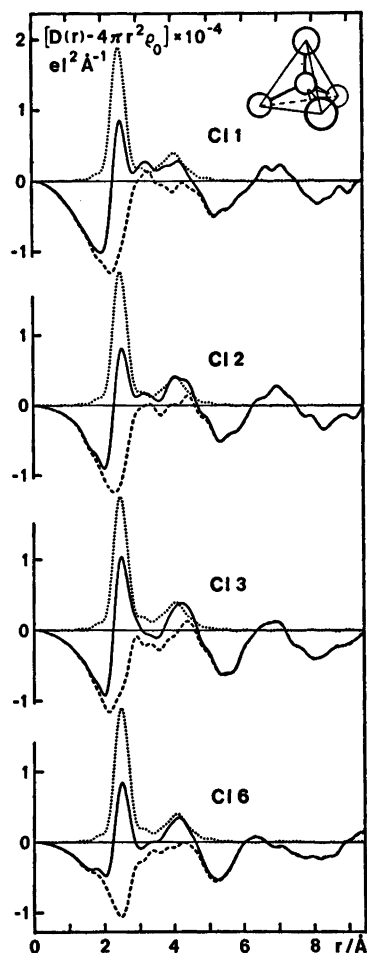


Fig. 3. Experimental $D(r) - 4\pi r^2 \rho_0$ functions for the solutions (solid lines), compared with peak shapes calculated for a regular HgCl_4^{2-} tetrahedron (dotted lines). The difference is shown by the dashed lines.

portional to $\cos \theta/I^2_{\text{corr}}$.¹⁴ The systematic errors seem to be of at least the same order of magnitude as estimated from the variation of the parameter values from refinements in various s intervals.¹⁴

Fig. 2 shows the experimental $si(s)$ curves compared with the calculated curves for a regular HgCl_4^{2-} tetrahedron for the solutions Cl1, Cl2, Cl3, and Cl6. The parameters used are $r_{\text{Hg-Cl}} = 2.47 \text{ \AA}$, $b_{\text{Hg-Cl}} = 0.006 \text{ \AA}^2$, $n_{\text{Hg-Cl}} = 4$ and $b_{\text{Cl-Cl}} = 0.028 \text{ \AA}^2$. The corresponding experimental $D(r) - 4\pi r^2 \rho_0$ functions and the peak

shapes for the HgCl_4^{2-} complex, obtained by Fourier transformation of the intensity curves,¹⁴ are shown in Fig. 3.

In solutions Cl4 and Cl5 (Fig. 7), with mol ratios $\text{Cl}/\text{Hg} \leq 3$, a minor peak at about 2.9 Å is observed in addition to the larger peaks at 2.44 and 2.45 Å, respectively. A large peak at 4.2 Å also occurs for both solutions.

Raman measurements. Two series of solutions were studied. In the first the Cl/Hg mol ratio was varied from 2 to 9, keeping the total mercury concentration, C_{Hg} , at 1 M in most of the solutions. The results are given in Table 3. In the second series the Cl/Hg mol ratio was kept constant at 3.0, while C_{Hg} was varied from 0.050 to 5.00 M. The spectra obtained are shown in Fig. 10.

DISCUSSION

X - Ray data

The peak at 2.4–2.5 Å, corresponding to Hg–Cl distances, is of approximately the same size for the solutions Cl1, Cl2, Cl3, and Cl6, but is smaller in the cases of solutions Cl4 and Cl5, which have much lower Cl/Hg mol ratios. However, the broad peak at 4 to 4.5 Å grows larger as the Cl/Hg mol ratio is reduced.

In the previous study of iodide and bromide complexes¹⁴ Na^+ was the cation. However, in this study Li^+ was used, except for solution Cl3, in order to avoid overlap between the peaks corresponding to the $\text{Na}^+ - \text{H}_2\text{O}$ and Hg–Cl distances.* The difference between the $D(r) - 4\pi r^2 \rho_0$ functions for solutions Cl3 (Na^+) and Cl2 (Li^+), which have the same mercury and chloride concentrations, demonstrates the effects of the strong $\text{Li}^+ - \text{H}_2\text{O}$ coordination²⁶ (Fig. 4). In this difference curve the $\text{Na}^+ - \text{H}_2\text{O}$ interactions give rise to a peak at 2.4 Å. In solution Cl3 the remaining water structure is less disturbed and this appears as broad peaks at about 2.8 and 4.5 Å.²⁷

The Cl– H_2O distances at about 3.1–3.2 Å^{26,28} and O–O distances at about 3.27 Å within a $\text{Li}(\text{H}_2\text{O})_4^+$ tetrahedron,²⁶ can explain the peaks found at about 3.2 Å in solutions Cl1, Cl2 and Cl6. This is demonstrated in Fig. 5, where the hydration model proposed for the

* This overlap probably also affects the parameter values obtained for solution Cl3 in Table 2.

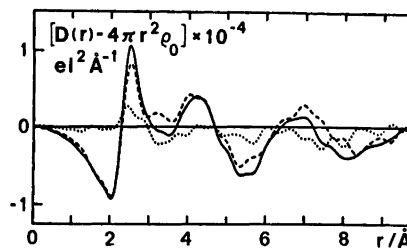


Fig. 4. The difference (dotted line) between $D(r) - 4\pi r^2 \rho_0$ functions for solutions Cl3 (solid line) and Cl2 (dashed line).

HgX_4^{2-} complexes in the preceding article,¹⁴ has been used for solution Cl1 together with independent $\text{Li}(\text{H}_2\text{O})_4^+$ and $\text{Cl}(\text{H}_2\text{O})_6^-$ groups.²⁶ The small amount of free residual water structure was approximately accounted for by assuming a tetrahedral arrangement in $(\text{H}_2\text{O})_6$ units.²⁷ Remaining interactions in the solution were approximated to even electron distributions around these groups.¹⁴ The radii used were 4.95, 3.4, 4.0 and 2.6 Å for the hydrated HgCl_4^{2-} , $\text{Li}(\text{H}_2\text{O})_4^+$, $\text{Cl}(\text{H}_2\text{O})_6^-$ and H_2O species, respectively. A much larger variation in the distances between the HgCl_4^{2-} complex and the water molecules in its surrounding hydration layer had to be assumed than for the bromide and iodide solutions, thus indicating a more irregular hydration sphere. This is probably an effect of the much stronger coordination of water by Li^+ than by Na^+ .²⁶

The described model gives a reasonable account of the experimental intensities and RDF's (Fig. 5). The Hg– H_2O interactions for the hydrated complex give a large and broad peak at about 4.1 Å, which overlaps the intramolecular Cl–Cl interactions. Thus, the direct use of the observed peaks at 4.2 and 4.1 Å in solutions Cl1 and Cl6, respectively, to detect irregularities in the structure of the tetrahedral HgCl_4^{2-} complex is of little value, especially as intramolecular Cl–Cl contacts also can contribute to this peak in the very concentrated solution Cl6. However, the temperature coefficients, $b_{\text{Hg-Cl}}$ (Table 2), are of the same magnitude as found for the HgI_4^{2-} and HgBr_4^{2-} complexes,¹⁴ which indicate all the Hg–Cl bond lengths to be equal. The subtraction of the peak shapes calculated for a regular HgCl_4^{2-} tetrahedron leaves a rather smooth background curve (Fig. 3). A regular tetrahedral

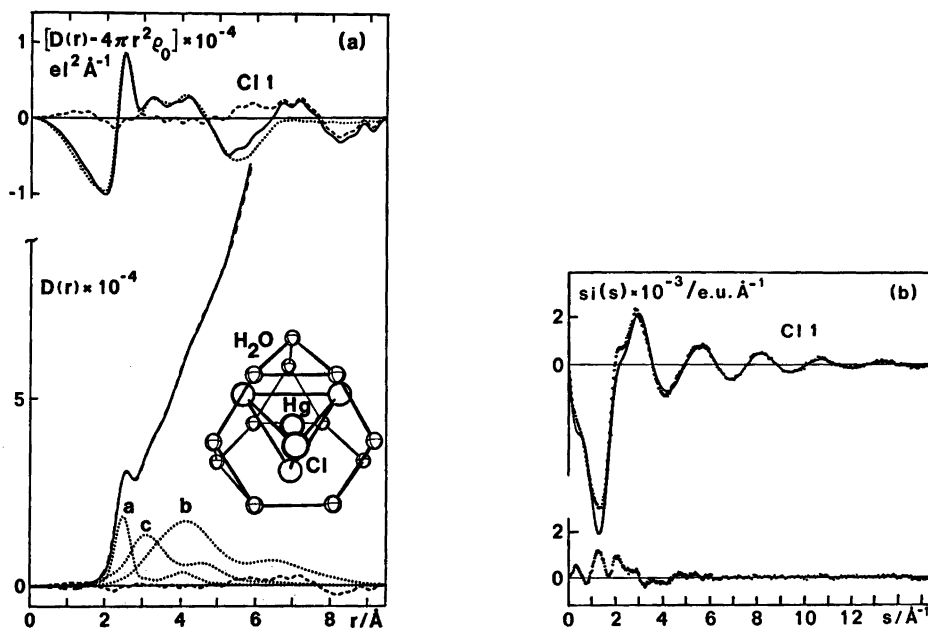


Fig. 5. (a) Comparison between the experimental RDF's for solution Cl1 (solid lines) and the calculated $D(r) - 4\pi r^2 \rho_0$ function (dotted curve) and $D(r)$ curve (long dashes almost coinciding with the solid line), containing both intra- and intermolecular interactions. The difference is shown by the dashed curves. The dotted curve, *a*, shows the peak shapes calculated for an HgCl_4^{2-} tetrahedron, *b* shows the interactions between the HgCl_4^{2-} complex and its surrounding hydration layer and *c* the peak shapes for the interactions within the $\text{Li}(\text{H}_2\text{O})_4^+$ and $\text{Cl}(\text{H}_2\text{O})_6^-$ groups and for the residual water structure. In addition, the calculated $D(r)$ curve contains contributions from the even electron distributions assumed to surround these groups. (b) Comparison between the corresponding experimental (dots) and calculated (solid lines) $si(s)$ curves. The difference is marked by dots below.

structure thus seems to be probable for the HgCl_4^{2-} complex.

Polynuclear complexes. The large peak at about 4.2 Å in solutions Cl4 and Cl5 with mol ratios $\text{Cl}/\text{Hg} \leq 3$ must, because of its size, be due to intramolecular Hg-Hg and Hg-Cl interactions, which means that polynuclear complexes are formed. However, at longer distances no pronounced peaks, indicating distinct intramolecular interactions, are present.

The two distances observed at about 2.4 and 2.9 Å in both solutions correspond approximately to Hg-Cl bond lengths found in crystal structures.³⁰⁻³⁹

Another indication of polynuclearity is the considerable solubility of mercury dichloride in these almost saturated solutions. If the equilibrium constants used to calculate the distribution of complexes (Fig. 1) are reasonably valid even for these concentrated solutions and

assuming no polynuclear complexes are formed, then the calculated concentrations of the HgCl_2 complex should amount to 0.55 M and 2 M in solutions Cl4 and Cl5, respectively. This greatly exceeds the solubility of HgCl_2 at 25 °C, which is 0.265 M.⁶

Comparisons with crystal structures. In most mercury(II) compounds the mercury atoms are joined by double chlorine bridges. Only in a few adducts of HgCl_2 double oxygen bridges are known to occur.^{36,40} The oxygen atoms then belong to strongly polar groups in the adduct molecules and have a high electron density which favours bridge-formation.^{40,41} In the aqueous solutions studied here, where chloride ions have been added to mercury dichloride, water molecules should not be expected to take part in any bridge formation.

Both distorted tetrahedral^{24,37-40} and distorted octahedral^{30-37,42-44} coordination around

mercury, have been observed in crystal structures. Tetrahedral coordination with double chloride bridges, which has been found in a few discrete dimeric complexes,³⁸⁻³⁹ does not seem to be consistent with the present scattering data since: (a) the Hg–Hg distances at about 3.9 Å would be too short to explain the observed peaks at 4.2–4.3 Å, (b) the area of the peak shapes calculated for a dimeric complex is too small to account for the large peaks observed and (c) this type of coordination seems to occur only when some of the non-bridging ligands are bulky.

A single chloride bridge between four-coordinated mercury atoms is found in very few compounds.^{22,27,44} In single-bridged chains short Hg–Hg distances of suitable length could occur. However, to explain the size of the observed peaks the chains must be rather long, since the average number of Hg-neighbours at about 4.2 Å around each Hg-atom including mononuclear complexes, seems to be approximately 1.5 and 1.8 in solution Cl4 and Cl5, respectively, as is shown in the subsequent calculations. These chains would then have to be rather flexible to account for the absence of pronounced peaks at longer distances in the RDF's.

A more probable structure is the distorted octahedral coordination around mercury, with two short bonds in an approximately linear arrangement which is found, for instance, in a number of complex halides, $MHgCl_3$ and $MHgCl_4$, and in hydrates of these, where M is an alkali or ammonium ion.^{31-35,44} In the crystals the double chloride bridges can be formed both by chlorine atoms in the linear $HgCl_2$ units and by other chloride ions with the $HgCl_2$ units perpendicular to the plane of the bridge (Fig. 6).

The Hg–Cl bond lengths in the linear $HgCl_2$ unit are fairly constant. With few exceptions they fall in the range 2.30 to 2.36 Å. They increase when the donor atoms of the other ligands have a high electron density, especially a negative charge.³⁹

Calculations of peak shapes for the polynuclear complexes. Peak shapes calculated for dinuclear complexes could not entirely account for the 4.2 Å peak in the RDF's of solutions Cl4 and Cl5. The use of a fragment of a double chain structure³⁰ (Fig. 6) to form a triangular trinuclear complex of octahedra with common

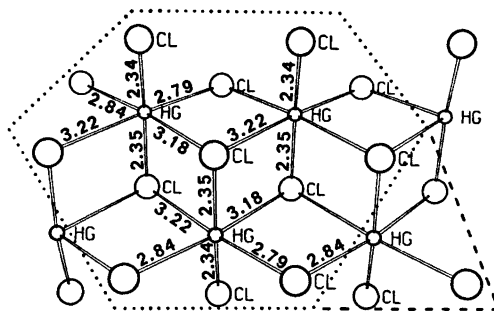


Fig. 6. The double chain, $(HgCl_3^-)_n$, from the crystal structure in Ref. 30. The Hg–Cl bond distances are given in Å. The trinuclear chain fragment used in the calculations for solution Cl4 is outlined by the dotted line, and the tetranuclear fragment used for solution Cl5 is contained within the dotted and dashed lines.

edges, gave a satisfactory agreement with the RDF's and intensity curves for solution Cl4. For solution Cl5 a tetranuclear chain fragment had to be assumed to account for the relatively larger 4.2 Å peak (Figs. 7 and 8). As shown in Fig. 7, complexes of higher nuclearity than three would be expected to give rise to peaks at larger distances in the RDF, where no distinct experimental peaks are found. However, frequent intermolecular interactions in this very concentrated solution (5 M $LiHgCl_3$) could not only obscure such effects but also give substantial contributions to the 4.2 Å peak. This, thus, prevents more definite conclusions about the average nuclearity.

The models used for the final calculations consisted of a trinuclear complex (0.25 M) and a tetranuclear complex (0.9 M) for solutions Cl4 and Cl5, respectively. The remaining amount of mercury, 25 and 28 %, respectively, was assumed to be present in pyramidal $HgCl_3^-$ complexes, with an assumed bond length of 2.45 Å. The peak shapes calculated for these ratios between linear $HgCl_2$ units in the polynuclear complexes and the pyramidal $HgCl_3^-$ complexes were found to reasonably account for the first Hg–Cl peak in the RDF's of the two solutions. The possible occurrence of some $HgCl_4^{2-}$ complexes instead of $HgCl_3^-$ will not affect the results significantly. As before $Li(H_2O)_4^+$ tetrahedra were assumed and for solution Cl4 the contributions from the residual free water structure were approximated by a

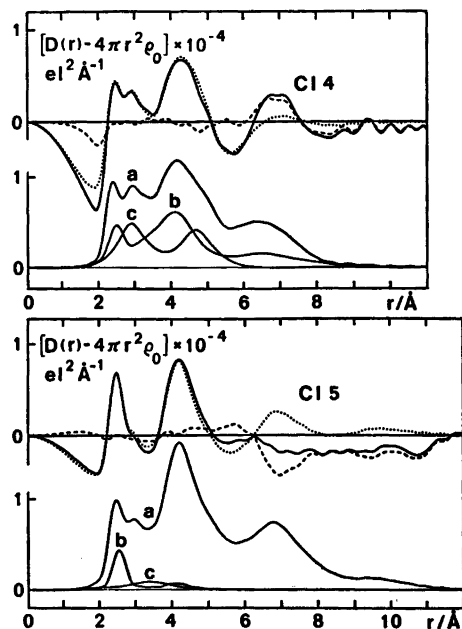


Fig. 7. The experimental $D(r) - 4\pi r^2 \rho_0$ functions (solid lines) for solutions Cl4 and Cl5, compared with the calculated $D(r) - 4\pi r^2 \rho_0$ curves (dotted lines), containing both intra- and intermolecular interactions. The difference is shown by the dashed line. The solid lines below are calculated peak shapes. For solution Cl4 they correspond to: a, the trinuclear complex (Fig. 6) of an average composition $\text{Hg}_3\text{Cl}_{8.3}(\text{H}_2\text{O})_{4.7}$ (0.25 M); b, the HgCl_3^- complex, with its surrounding hydration layer (0.25 M); and c, the $\text{Li}(\text{H}_2\text{O})_4^+$ tetrahedron (0.80 M) plus the residual water structure. For solution Cl5 they are: a, the tetranuclear complex $\text{Hg}_4\text{Cl}_{12}(\text{H}_2\text{O})_3$ (0.9 M); b, the HgCl_3^- complex (1.4 M); and c, the $\text{Li}(\text{H}_2\text{O})_4^+$ tetrahedron (5.0 M).

The calculated $D(r) - 4\pi r^2 \rho_0$ curves also contain contributions from the even electron distribution assumed around the complexes.

tetrahedral arrangement in $(\text{H}_2\text{O})_5$ groups,²⁷ which also gives a contribution to the experimental peak at 2.9 Å. The remaining diffuse interactions in the solutions were approximated as even electron distributions¹⁴ around the assumed complexes and molecules outside radii approximately corresponding to the radii of the species.

In the polynuclear complexes all bridging and linearly coordinated atoms were assumed to be chlorine. The octahedral coordination was completed by the remaining chloride ions and by

water molecules placed about 2.6 Å from the mercury atoms.^{35,46} Stoichiometric considerations then give average compositions for the polynuclear complexes corresponding to $\text{Hg}_3\text{Cl}_{8.3}(\text{H}_2\text{O})_{4.7}$ for solution Cl4 and $\text{Hg}_4\text{Cl}_{12}(\text{H}_2\text{O})_3$ for solution Cl5.

For solutions Cl2 and Cl3 (mol ratios Cl/Hg = 4.5) the peak at 4.2 Å is somewhat larger (Fig. 3) and the Hg-Cl bond length is slightly shorter (Table 2) than for solution Cl1 (mol ratio Cl/Hg = 5.8). These effects indicate that polynuclear complexes, containing roughly 10 to 20 % of the mercury atoms, are still present.

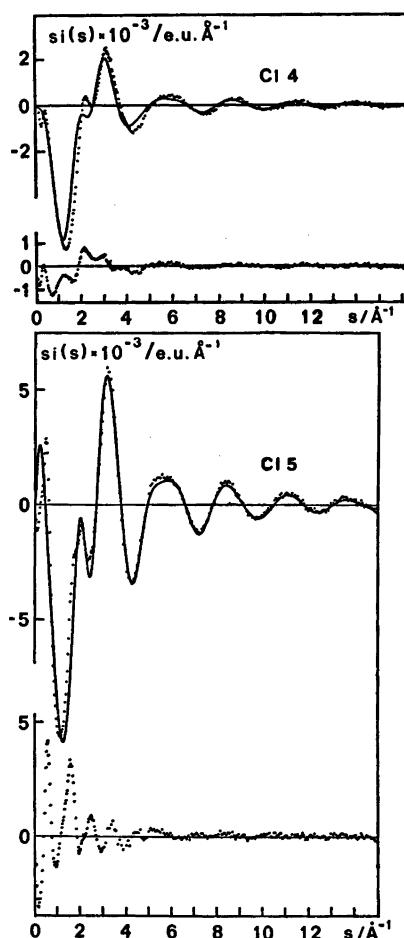


Fig. 8. Comparison between the experimental (dots) and calculated (solid lines) $si(s)$ curves corresponding to the RDF's in Fig. 7. The difference is shown separately underneath (dots).

Table 3. Raman frequencies found for some mercury(II) chloride solutions.

Sol.	C_{Hg}/M	Ratio: Cl to Hg	ν/cm^{-1}	
Cl1	1.00	9.0	270(s)	
	1.00	7.4	270.5(s)	
	1.00	5.83	270(s)	
	Cl6	5.00	5.00	270(vs)
	Cl2	1.00	4.50	270(s)
	Cl3	1.00	4.50	270(s)
Cl4	1.00	3.00	275(s), ~312(m,br)	
	1.00	2.80	~270(w), ~285(m,br), ~312(m,br)	
			~270(vw), ~288(w), 320(m)	
			322(m)	
			0.25	2.80
	0.23	2.00	322(m)	

Raman data

For the first series of solutions where the Cl/Hg mol ratio is varied from 2 to 9, the results in Table 3 show the ν_1 symmetrical stretching frequency to be $270 \pm 1 \text{ cm}^{-1}$ for the HgCl_4^{2-} complex and $322 \pm 1 \text{ cm}^{-1}$ for the HgCl_2 complex in good accordance with previously reported values.^{18-21,47} No other frequencies could be observed in these spectra. The results support the conclusions from the X-ray investigation that the HgCl_4^{2-} complex is dominating in the solutions Cl1, Cl2, Cl3 and Cl6. The presence of a minor amount of polynuclear complexes in solutions Cl2 and Cl3, as indicated by the X-ray data, is supported by the asymmetrical broadening towards higher wave-numbers observed for the Raman bands of these solutions.

For the second series of solutions with constant mol ratio Cl/Hg = 3, the principal shape of the Hg-Cl band should not change if the relative complex distribution remains the same. This would be the case if only mononuclear complexes are formed and the free chloride concentration is negligible. Fig. 9, calculated with the equilibrium constants in Ref. 5, shows that this should be approximately valid at least for concentrations $C_{\text{Hg}} > 0.5 \text{ M}$, but at lower concentrations, where the free Cl^- concentration cannot be neglected, the HgCl_2 complex would dominate.

The spectra of this series (Fig. 10) can be interpreted in the following way. At the lowest

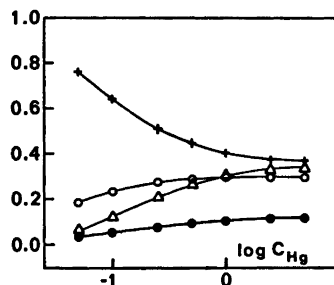


Fig. 9. Relative distribution of mercury(II) chloride complexes at constant mol ratio Cl/Hg = 3, as a function of the total mercury concentration, C_{Hg} . The curve with symbols + gives the ratio $[\text{HgCl}_2]/C_{\text{Hg}}$, the symbol O denotes $[\text{HgCl}_3^-]/C_{\text{Hg}}$, and Δ $[\text{HgCl}_4^{2-}]/C_{\text{Hg}}$. The free chloride ion concentration in mol/l is given by the curve marked with the symbol ●.

concentration studied, $C_{\text{Hg}} = 0.05 \text{ M}$, only the HgCl_2 band at 322 cm^{-1} can be seen. When the concentration is raised, first a band at $288 \pm 2 \text{ cm}^{-1}$ assigned to $\nu_1(\text{HgCl}_3^-)$ and then the band $\nu_1(\text{HgCl}_4^{2-})$ at 270 cm^{-1} start to contribute. No contributions from polynuclear complexes could be detected for concentrations $C_{\text{Hg}} < 0.5 \text{ M}$. At 0.5 M , however, two new bands at 305 ± 3 and $275 \pm 1 \text{ cm}^{-1}$ appear and become dominating at higher concentrations. These frequencies must arise from the polynuclear complexes observed by X-ray diffraction.

Raman and IR studies have been made of crystalline salts, $\beta\text{-NH}_4\text{HgCl}_2$ and $\beta\text{-ND}_4\text{HgCl}_2$, with the double chain structure (Fig. 6) proposed for the polynuclear complexes in solution.⁴⁴ Two Raman bands at 297 and 262 cm^{-1} and at 300 and 265 cm^{-1} , respectively, were found. They were assigned to the symmetrical terminating and bridging Hg-Cl frequencies, respectively. That the same assignments can be made for the two new bands observed for concentrated solutions is supported by the measured depolarization ratios $\rho = I_{\parallel}/I_{\perp}$. For the 0.23 M HgCl_2 solution $\rho = 0.14$ was obtained, which is comparable to the values found by Brill for the HgCl_2 complex in other solvents.⁴⁸ Approximately the same ρ -value was found for the band at 305 cm^{-1} , which thus should correspond to the symmetrical stretching frequency of the HgCl_2 unit. The other Hg-Cl frequencies observed have much lower depolarization ratios, which was helpful in determining the position of this band.

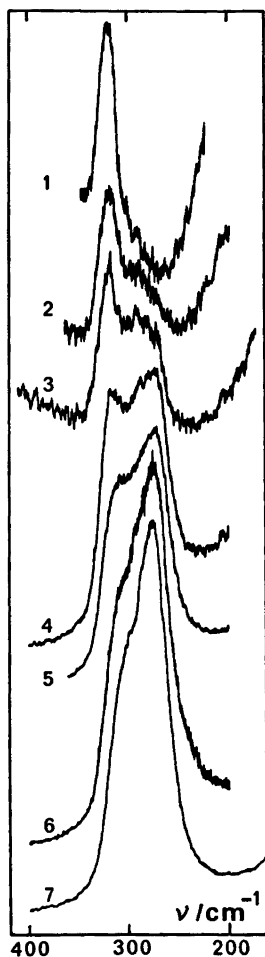


Fig. 10. The Raman bands observed for the series of solutions with constant mol ratio Cl/Hg=3. The total mercury concentrations were 0.050, 0.10, 0.25, 0.50, 1.00, 2.50, and 5.00 M for the solutions 1 to 7, respectively.

The relative intensity scales used for the curves 1 to 7 correspond approximately to the ratios 1:2:4:8:20:40:100, respectively.

CONCLUSIONS

The experimental data are consistent with a regular tetrahedral structure for the HgCl_4^{2-} ion with a bond distance of 2.47(1) Å. It has not been possible to obtain any direct information about the structure of the HgCl_3^- complex in aqueous solution.

In concentrated solutions with $C_{\text{Hg}} \geq 0.5$ M and a Cl/Hg mol ratio around three, polynuclear

Acta Chem. Scand. A 31 (1977) No. 2

complexes occur. The X-ray diffraction data are reasonably well explained by assuming the dominating complex to be tri- or tetranuclear fragments of a double chain structure with double chlorine bridges between the mercury atoms. The coordination around mercury in these complexes is that of a distorted octahedron with two shorter bonds forming a linear unit. Such a model is also compatible with the Raman frequencies observed.

Note added in proof. The crystal structure of Cs_2HgCl_6 contains distorted tetrahedral HgCl_4^{2-} ions, with an average bond length of 2.464 Å.⁴⁰

Acknowledgements. The author is greatly indebted to Dr. G. Johansson for his continuous interest in the work and many helpful suggestions and comments on the manuscript. I also wish to thank Professor K. Larsson for kindly putting the Laser Raman Spectrophotometer at my disposal and Mr. I. Duncan for linguistic help. This work has been supported by the Swedish Natural Science Research Council. Computer time was made available by the Computer Division of the National Swedish Office for Administrative Rationalization and Economy.

REFERENCES

1. Sillén, L. G. and Martell, A. E. *Stability Constants*, Spec. Publ. No. 17 (1964) and *Suppl. No. 1*, Spec. Publ. No. 25, The Chemical Society, London 1971.
2. Deacon, G. B. *Rev. Pure Appl. Chem.* 13 (1963) 189.
3. *Gmelin Handb. Anorg. Chem.* Hg-B2, Verlag Chemie, Weinheim/Bergstr. 1967.
4. Ciavatta, L. and Grimaldi, M. *J. Inorg. Nucl. Chem.* 30 (1968) 197.
5. Lindgren, B., Jonsson, A. and Sillén, L. G. *Acta Chem. Scand.* 1 (1947) 479.
6. Marcus, Y. *Acta Chem. Scand.* 11 (1957) 329.
7. Linke, W. F. *Solubilities of Inorganic and Metal-Organic Compounds*, Van Nostrand, New York 1958.
8. Bourion, F. and Royer, E. *Ann. Chim. (Paris)* 10 (1928) 263.
9. Waters, D. N., Short, E. L., Tharwat, M. and Morris, D. F. C. *J. Mol. Struct.* 17 (1973) 389.
10. Kecki, Z. *Spectrochim. Acta* 18 (1962) 1165.
11. Hooper, M. A. and James, D. W. *Aust. J. Chem.* 24 (1971) 1331 and 1345.
12. Reedijk, J. and Groeneveld, W. L. *Recl. Trav. Chim. Pays-Bas* 88 (1969) 655.
13. Janz, G. J. and James, D. W. *J. Chem. Phys.* 38 (1963) 905.
14. Sandström, M. and Johansson, G. *Acta Chem. Scand. A* 31 (1977) 132.

15. Gaizer, F. and Johansson, G. *Acta Chem. Scand.* 22 (1968) 3013.
16. Sandström, M. *To be published.*
17. van Panthaleon van Eck, C. L. *Thesis*, Leiden 1958, see also Ref. 3.
18. Rolfe, J. A., Sheppard, D. E. and Woodward, L. A. *Trans. Faraday Soc.* 50 (1954) 1275.
19. Davies, J. E. D. and Long, D. A. *J. Chem. Soc. A* (1968) 2564.
20. Delwaille, M.-L. *Bull. Soc. Chim. Fr.* (1955) 1294.
21. Saraf, J. R., Aggarwal, R. C. and Prasad, J. *Bull. Chem. Soc. Jpn.* 43 (1970) 264.
22. Herlinger, A. W. *Spectrosc. Lett.* 8 (1975) 787.
23. Kamenar, B. and Nagl, A. *Acta Crystallogr. B* 32 (1976) 1414.
24. Ferguson, G., Jeffreys, J. A. D. and Sim, G. A. *J. Chem. Soc. B* (1966) 454.
25. Sanyal, N. K., Goel, R. K. and Pandey, A. N. *Indian J. Phys.* 49 (1975) 546.
26. Narten, A. H., Vaslow, F. and Levy, H. A. *J. Chem. Phys.* 58 (1973) 5017.
27. Narten, A. H., Danford, M. D. and Levy, H. A. *Discuss. Faraday Soc.* 43 (1967) 97, see also Luck, W., Ed., *Structure of Water and Aqueous Solutions*, Verlag Chemie, Weinheim/Bergstr. 1974.
28. Licheri, G., Piccaluga, G. and Pinna, G. *J. Chem. Phys.* 64 (1976) 2437.
29. Kavanau, J. L. *Water and Solute-Water Interactions*, Holden Day, San Francisco 1964.
30. Authier-Martin, M. and Beauchamp, A. L. *Can. J. Chem.* 53 (1975) 2345.
31. Zvonkova, Z. V., Samodurova, V. V. and Vorontsova, L. G. *Dokl. Akad. Nauk SSSR* 102 (1955) 1115.
32. Sagisawa, K., Kitahama, K., Kiriya, H. and Kiriya, R. *Acta Crystallogr. B* 30 (1974) 1603.
33. Malčić S. S. *Bull. Inst. Nucl. Sci. Boris Kidrič* 9 (1959) 115.
34. Harmsen, E. J. *Z. Kristallogr.* 100 (1938) 208.
35. Brusset, H. and Madaule-Aubry, F. *Bull. Soc. Chim. Fr.* 10 (1966) 3122.
36. Biscarini, P., Fusina, L., Nivellini, G. D., Mangia, A. and Pelizzi, G. *J. Chem. Soc. Dalton Trans.* (1973) 159; (1974) 1846.
37. Brotherton, P. D. and White, A. H. *J. Chem. Soc. Dalton Trans.* (1974) 2698.
38. Glasser, D., Ingram, L., King, M. G. and McQuillan, G. P. *J. Chem. Soc. A* (1969) 2501.
39. Brotherton, P. D., Epstein, J. M., White, A. H. and Willis, A. C. *J. Chem. Soc. Dalton Trans.* (1974) 2341.
40. Brändén, C. I. *Ark. Kemi*, 22 (1964) 501.
41. Lindqvist, I. *Inorganic Adduct Molecules of Oxo-Compounds*, Springer, Berlin 1963.
42. Grdenić, D. *Arh. Kem.* 22 (1950) 14.
43. Grdenić, D. and Krstanović, I. *Arh. Kem.* 27 (1955) 143.
44. Barr, R. M. and Goldstein, M. *J. Chem. Soc. Dalton Trans.* (1974) 1180; (1976) 1593; *Inorg. Nucl. Chem. Lett.* 10 (1974) 33.
45. White, J. G. *Acta Crystallogr.* 16 (1963) 397.
46. McPhail, A. T. and Sim, G. A. *Chem. Commun.* 1 (1966) 21.
47. Allen, G. and Warhurst, E. *Trans. Faraday Soc.* 54 (1958) 1786.
48. Brill, T. B. *J. Chem. Phys.* 57 (1972) 1534.
49. Clegg, W., Brown, M. L. and Wilson, L. J. A. *Acta Crystallogr. B* 32 (1976) 2905.

Received August 31, 1976.

A Comparative *ab initio* Study of the Dicyanomethanide, Cyanonitromethanide, Dicyanamide and Cyanonitramide Anions

HARALD JENSEN, BERNT KLEWE and EGIL TJELTA *

Department of Chemistry, University of Oslo, Oslo 3, Norway

Results from geometry optimizations by use of *ab initio* methods and a double zeta basis set give results in good accordance with experimental findings for these four systems. The agreement in the trends when comparing effects of substitution is excellent. Neither optimization with a minimal basis nor MINDO/3 calculations reproduce geometries for systems like the present ones satisfactorily. The anion bond parameters are discussed in terms of qualitative bond concepts.

The structures of the dicyanomethanide (A), the cyanonitromethanide (B), the dicyanamide (C), and the cyanonitramide (D) anions have been determined in our laboratory by low temperature single crystal X-ray studies of the potassium salts.¹ The cyano as well as the nitro group are recognized as powerful electron withdrawing substituents thereby stabilizing the anions. All four systems are found to be essentially planar and they are therefore convenient for a study of the influence of the cyano and nitro group on the adjacent π -systems and *vice versa*. Furthermore, differences in structural parameters within the two pairs of isoelectronic ions demonstrate the influence of the nitrogen lone pair electrons as compared with those of the C—H bond.

The anion geometries as determined in the solid state are to some extent influenced by coordination forces and packing effects. *Ab initio* calculations may give information about structures of isolated anions. In the present paper standard calculations by use of the program MOLECULE² is presented. The cal-

culations were carried out in order to see how well the experimental geometries were reproduced. A recent account on *ab initio* calculations on anions may be found in Ref. 3 and references therein. References to structural findings relevant to the present species will mainly be given in the presentation of the crystal structures.¹

COMPUTATIONAL DETAILS AND GEOMETRY OPTIMIZING PROCEDURES

The calculations were performed on a CYBER-74 with the program MOLECULE² which solves the Roothaan-Hall equations for a Gaussian type basis. All results were calculated with a (7s3p/4s) basis⁴ contracted to (4,2/2). A scale factor of 1.2 was used for the exponents of the hydrogen basis set.^{5,6}

The symmetry requirements were C_{2v} for $\text{CH}(\text{CN})_2^-$ (A) and $\text{N}(\text{CN})_2^-$ (C), and C_s for $\text{CH}(\text{CN})(\text{NO}_2)^-$ (B) and $\text{N}(\text{CN})(\text{NO}_2)^-$ (D). The C—H distance was optimized in (A) and the same value was used for (B). All angles of the nitro groups were given the value 120° and both N—O bond lengths of one nitro group were kept equal. For the initial models experimentally determined bond length and bond angle values were applied, except for C—H for A (1.09 Å), the central angles for A and C (120°), and the cyano legs which were assumed to be linear. First the bonds of the cyano legs were optimized simultaneously. Then the C—H bond was refined for A. For B and D, the N—O bond and the bond between the central atom and the nitro group were optimized. Finally the central bond angle and the bending

* Present address: Institute of Occupational Health, Gydas vei 8, Oslo 3, Norway.

Table 1. Total energies, atomic and overlap populations.

CH(CN) ₂ ⁻ (A)			N(CN) ₂ ⁻ (C)		
Energy: -222.78937 a.u.			Energy: -238.75600 a.u.		
Atomic populations			Atomic populations		
	Gross	π		Gross	π
N1	7.467	1.312	N1	7.431	1.262
C1	6.031	0.880	N3	7.851	1.631
C3	6.183	1.614	C1	5.644	0.922
H	0.820				
Overlap populations			Overlap populations		
	Gross	π		Gross	π
N1-C1	1.587	0.470	N1-C1	1.597	0.468
C1-C3	0.724	0.097	C1-N3	0.724	0.105
C3-H	0.814				
CH(CN)(NO ₂) ⁻ (B)			N(CN)(NO ₂) ⁻ (D)		
Energy: -334.31507 a.u.			Energy: -350.25359 a.u.		
Atomic populations			Atomic populations		
	Gross	π		Gross	π
O1	8.489	1.676	O1	8.459	1.613
O2	8.510	1.684	O2	8.448	1.600
N1	7.400	1.217	N1	7.370	1.220
N2	6.849	1.084	N2	6.579	1.080
C1	6.072	0.901	N3	7.531	1.565
C2	5.899	1.437	C1	5.613	0.923
H	0.786				
Overlap populations			Overlap populations		
	Gross	π		Gross	π
N1-C1	1.512	0.498	N1-C1	1.594	0.480
C1-C2	0.322	0.046	C1-N3	0.392	0.087
C2-N2	0.642	0.210	N3-N2	0.468	0.139
N2-O1	0.367	0.170	N2-O1	0.408	0.190
N2-O2	0.288	0.162	N2-O2	0.448	0.192
C2-H	0.814				

of the cyano groups were adjusted. In every case the coupling between two parameters was included by assuming the energy to be a second order degree polynomial in the parameters and computing six points on the energy surface. The coupling was small in most cases.

RESULTS AND DISCUSSION

The total energies of the geometry optimization procedures and results of Mulliken population analyses are listed in Table 1. All occupied MO's are bound for the four anions. According to Koopmans' theorem, in which the ionization potential is approximated as the energy of the highest occupied orbital, the ionization potentials are 2.39, 3.68, 3.79, and 5.01 eV for A, B, C, and D, respectively. For all species these MO's are π orbitals with large net population on the central atom. The geometries are presented in Fig. 1, where experimental results in parentheses and the numbering of atoms also are given. As the strict symmetry of the anions in the crystalline phase is C₁, mean values are listed for the dicyano-substituted anions, the values of the C-C≡N angles have been ob-

tained by projecting the atoms into the least-squares planes of the anions, and the small twists of the nitro groups have been neglected. The parameters of the high angle X-ray refinements (sin θ/λ > 0.60–0.65 Å⁻¹) have been applied, the largest difference between "equivalent" bonds is 0.005 Å, and the estimated standard deviations in bond length values (excluding hydrogen) are 0.002 Å or less.

The anion geometries of the *ab initio* study are in good accordance with the X-ray results (Fig. 1). Bond lengths (neglecting C-H) and bond angles show discrepancies smaller than 0.02 Å and 5°, respectively. The agreement in the trends when comparing the effects of substitution is excellent except for the N-C≡N angles in the amide anions. According to the theoretical calculations, the introduction of a nitro group should result in an increased bending of the cyano leg. The X-ray results show the opposite, however. The other differences between the experimental and calculated shifts are 0.005 Å or less for comparable bond lengths and less than 1° for the central angles. It must be concluded that the applied double zeta basis set seems to give a satisfactory description of the structural variations within the present set of anions. Furthermore, the coordination forces and packing effects in the crystals do not seem to alter the anion geometries seriously.

Geometries resulting from *ab initio* calculations using minimal basis sets are frequently reported in the literature. For systems analogous to those presented, a warning should be given. In a theoretical study of nitromethane and its anion,⁷ a minimal basis set was used to establish an optimum geometry for a planar

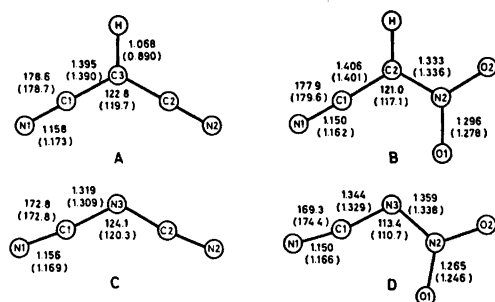


Fig. 1. Anion geometries. (Å and °, experimental values in parentheses.)

anion, even though the authors seemed to be well aware of the pitfalls in this procedure. The resulting geometry was unreasonable as compared with our findings for cyanonitromethanide (B).^{*} Accordingly the geometry of the nitromethanide anion was reoptimized with the present basis set. The results were as follows (values of Ref. 7 in parentheses): N—O = 1.331 (1.228) Å C—N = 1.298 (1.397) Å, C—H = 1.068 (1.090) Å, O—N—O = 120.3 (121)°. The total energy for the anion was 53.1 kJ/mol less for the optimal geometry than for the geometry of Ref. 7 calculated with the present basis set.

The semiempirical MINDO/3 program has recently become readily available.⁸ The parameters for C, H, O, and N have been successfully tested on a large number of species.⁹ The authors state, however, that for the bonds between atoms with lone pairs of electrons, the calculated values are much too small and that for nitriles the results of MINDO/3 are inferior to those of MINDO/2.⁹ Nevertheless, MINDO/3 calculations were carried out in order to see how well the geometries of the present anions were reproduced. Except for the somewhat large values for the central angles [129° for (A) and 127° for (B)], the geometries of the methanides were satisfactory. For the amides the calculations gave reasonable values for the bending of the cyano legs. However, the central angles were seriously in error [153° for (C) and 131° for (D)]. Furthermore, the N—N bond length of cyanonitramide (D) was 1.23 Å and the difference between the

N—O bond lengths of (B) and (D) was not reproduced, both being 1.26 Å. One must conclude that MINDO/3 is not suitable for systems like the present ones.

In the remaining part of the paper the results of the *ab initio* calculations will be discussed in terms of purely qualitative valence bond and electron pair repulsion concepts. In Fig. 2 the distributions of the negative charges of the anions are shown (to the extreme left) together with valence bond structures of importance in describing the resonance stabilized species. The charges are calculated from the gross atomic populations of Table 1 by subtracting the values for neutral atoms. Lacking structural information one might use the following two arguments in order to estimate the relative importance of the canonical forms in describing the ions as resonance hybrids. (1) Nitrogen is more electronegative than carbon, and the unsubstituted amide anion is more stable than the reactive methanide ion; thus A-III and B-III should be of less importance than C-III and D-III. (2) When properly oriented, the nitro group is known as a more powerful electron withdrawing substituent than the cyano group; accordingly B-II and D-II should be more important than B-I and D-I, respectively.

The results of the *ab initio* calculations support this simple description. Within the two isoelectronic pairs the charge density at the central atom is more negative for the amides [by 0.67 and 0.63 e for (A,C) and (B,D), respectively] and the nitro group reduces the charge density [by 0.28 (A,B) and 0.32 e (C,D)]. Furthermore, the gross overlap populations for the bonds between the cyano carbon and the central atoms decrease by introduction of the nitro group. For the bond lengths of the cyano legs one finds a slightly shorter "triple" bond and a somewhat longer bond to the central atom for the methanide as well as for the amide when one cyano group is substituted by the nitro group. The bond lengths of the nitro groups also reflect the relative importance of the canonical forms. The nitronate character of cyanonitromethanide (B-II) is predominant; the N—O bond being rather long and the N—C bond rather short. The observed N—O bond lengths in cyanonitramide (D) are similar to values reported for nitrates

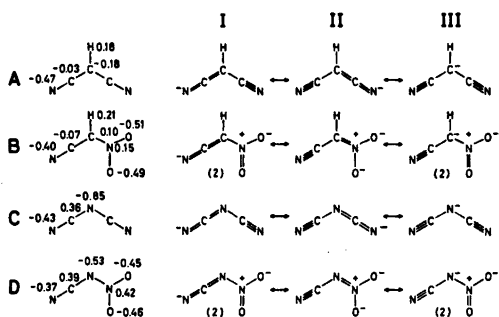


Fig. 2. Atomic charges and valence bond models.

^{*} Added in proof. However, see Ref. 15.

and far shorter than those of the trioxodinitrate anion,¹⁰ where the valence bond structure with a nitrogen nitrogen double bond corresponds most closely to the observed geometry. Accordingly, the N–N bond length of D is 0.074 Å longer than that of trioxodinitrate (X-ray values); the canonical forms having the negative charge at the central atoms contribute thus significantly in the resonance stabilization of the amides. The population analysis shows that although the gross atomic population of the central atom decreases when going from C to D, the π population remains nearly constant.

Finally, some aspects of the bond angle variations will be discussed. We have seen above that introduction of a nitro group causes a lengthening in the bond between the central atom and the other cyano group. The nitro group is also said to be the more electronegative of the two. According to the valence shell electron pair repulsion model the angle between the bonds from the central atoms to the substituents should therefore decrease, in agreement with our findings. A lone pair is said to take up more room on the surface of an atom than a bonding electron pair. The bond lengths to the central atoms of the amide anions indicate more non bonding electrons at the central nitrogen atom in the cyanonitramide (D) than in the dicyanamide (C). This would also tend to decrease the central angle. One would therefore expect a larger decrease in the central angle for the amide than for the methanide anion, when the nitro group replaces one of the cyano groups. The bond angle values support such arguments in contrast to results from the population analysis.

The influence of the lone pair electrons of the central nitrogen atom compared with that of the bonding electrons of the carbon hydrogen bond can be seen by comparing the bending of the cyano legs. Non linear R–C \equiv N arrangements are well known and have been explained in different ways.^{11–13} An *ab initio* study has also recently been published.¹⁴ According to Ref. 13 the sigma lone pair electrons can interact with the in-plane component of the carbon nitrogen multiple bond. If this interaction is bonding, a bend of the π system towards the lone pair will be favoured in order to increase the interaction. Although the

argumentation may be questioned, it predicts non-linearity of the cyano leg in the amide anions, in agreement with our findings. The *ab initio* calculations also give non linear C–C \equiv N arrangements. However, the deviations from linearity are small in these cases. Effects causing non linear C–C \equiv N groups are extensively discussed in Ref. 12.

Acknowledgements. We are indebted to Dr. Jan Almlöf for valuable comments. One of us (E. T.) is grateful to the Norwegian Research Council for Science and the Humanities for financial support.

REFERENCES

1. Klewe, B. and Tjelta, E. *To be submitted for publication in Acta Chem. Scand. A.*
2. Almlöf, J. USIP rep. 72–09, University of Stockholm, Stockholm 1972.
3. Williams, J. E., Jr. and Streitwieser, A., Jr. *J. Am. Chem. Soc.* 97 (1975) 2634.
4. Roos, B. and Siegbahn, P. *Theor. Chim. Acta* 17 (1970) 209.
5. Huzinaga, S. *J. Chem. Phys.* 42 (1965) 1293.
6. Dunning, T. H., Jr. *J. Chem. Phys.* 53 (1970) 2823.
7. Murrell, J. N., Vidal, B. and Guest, M. F. *J. Chem. Soc. Faraday Trans. 2*, 71 (1975) 1577.
8. Dewar, M. J. S., Metiu, H., Student, P. J., Brown, A., Bingham, R. C., Lo, D. H., Ramsden, C. A., Killmar, H., Weiner, P. and Bischof, P. K. *MINDO/3; Modified Intermediate Neglect of Differential Overlap*, Program 279, Quantum Chemistry Program Exchange, Indiana University, 1975.
9. Bingham, R. C., Dewar, M. J. S. and Lo, D. H. *J. Am. Chem. Soc.* 97 (1975) 1302.
10. Hope, H. and Sequeira, M. R. *Inorg. Chem.* 12 (1973) 286.
11. Hartman, A. and Hirshfeld, F. L. *Acta Crystallogr.* 20 (1966) 80.
12. Matthews, D. A., Swanson, J., Mueller, M. H. and Stucky, G. D. *J. Am. Chem. Soc.* 93 (1971) 5945.
13. Lee, P. L., Cohn, K. and Schwendeman, R. N. *Inorg. Chem.* 11 (1972) 1917.
14. Howell, J. M., Rossi, A. R. and Bissell, R. *Chem. Phys. Lett.* 39 (1976) 312.
15. Mezey, P. G., Kresge, A. J. and Csizmadia, I. G. *Can. J. Chem.* 54 (1976) 2526.

Received August 25, 1976.

Short Communication

Studies on Gold Complexes. III. The Standard Electrode Potentials of Aqua Gold Ions

L. H. SKIBSTED^a and JANNIK BJERRUM^b^a Chemistry Dept., Royal Veterinary and Agricultural University, DK-1871 Copenhagen V, Denmark and ^b Chemistry Dept. I, Inorganic Chemistry, H.C. Ørsted Institute, University of Copenhagen, DK-2100 Copenhagen Ø, Denmark

The hypothetical diauagold(I) and tetraaqua-gold(III) ions do not exist even in strong perchloric acid solution, and their standard electrode potentials are therefore not accessible to direct measurements. However, information about these potentials can be obtained by utilizing the knowledge of the standard potentials for a series of gold(I) and gold(III) complexes. A number of such potentials are tabulated in Table 1.

Some authors have assumed that linear relationships exist between these potentials and analogous potentials for other d^{10} and d^8 metal ions for which the potentials of the aqua ions are known.¹⁻³ However, standard potentials obtained by such correlations are open to criticism.⁴ More reliable results might be expected with the use of Edward's four-parameter equation⁵

$$(1/N) \log \beta_N' = \alpha E_n + \beta H$$

In this equation α and β are parameters for the metal ion and E_n and H parameters for the ligand. E_n is related to the oxidation potential of the ligand: $E_n = E^\circ(X^r, \frac{1}{2}X_2^{(2r-2)-}) - E^\circ(\text{ref.})$, and H is related to $\text{p}K_a$ for the corresponding Brønsted acid: $H = \text{p}K_a - \text{p}K_a(\text{ref.})$. Both of these parameters as well as the relative overall stability constants β_N' are usually defined with water and the aqua complex as reference. It then follows that: $\log \beta_N' = \log \beta_N + N \log 55$. In order to use the equation for Au(I) and Au(III) complexes β_N' were defined relative to the relevant chlorido complexes and E_n and H relative to $E^\circ(\text{Cl}^-, \frac{1}{2}\text{Cl}_2) = -1.36$ V and $\text{p}K_a(\text{HCl}) = -6.1$.⁶ The necessary ligand parameters were estimated from literature data⁵ and are tabulated in Table 2. A certain arbitrariness in the choice of the E_n and H parameters is apparent. The lack of spread in the Edwards plots, shown in Fig. 1, which is based partly on parameters resulting from accurate experiments and partly on rough estimates, provides some justification for the E_n and H values proposed in Table 2. Values for $\log \beta_N'$ are given in Table 1. The upper part in Fig. 1 is a plot of $\frac{1}{2} \log \beta_2'/H$ versus E_n/H for Au(I), and the lower part a plot of $\frac{1}{4} \log \beta_4'/H$ versus E_n/H for Au(III). Straight lines are obtained in both cases, α being equal to the slope of the lines. E_n/H for water has the value -0.28 (see Table 2), corresponding to $\frac{1}{2} \log \beta_2'/H = -1.70$ for Au(I) and $\frac{1}{4} \log \beta_4'/H = -1.90$ for Au(III). Inserting $H = 4.40$ for water, one calculates on this basis $\log \beta_2 \cong 11.5$ for Au(I),

Table 1. Standard electrode potentials at 25 °C of Au(I) and Au(III) complexes and their stability constants in aqueous solution.^a

Ligand	$E^\circ_{1,0}$	$\log \beta_2'$	$\log \beta_2^a$	$E^\circ_{3,0}$	$\log \beta_4'$	$\log \beta_4^b$
Cl ⁻	+1.154	0	11	+1.002	0	26
Br ⁻	+0.959	3.29	15	+0.854	7.50	34
SCN ⁻	+0.662	8.31	20	+0.636	18.55	45
I ⁻	+0.578	9.73	21	(+0.56)	22.4	49
NH ₃	+0.563	10.0	21	+0.325	34.3	60
(NH ₂) ₂ CS	+0.380	13.1	24			
S ₂ O ₃ ²⁻	+0.153	16.9	28			
Dpm ^c	+0.053	18.6	30			
CN ⁻	-0.48	27.6	39	(-0.10)	56	82
OH ⁻				(+0.48)	26.4	53

^a Calculated with $E^\circ[\text{Au}(\text{H}_2\text{O})_2^+, \text{Au}] = +1.83$ V. ^b Calculated with $E^\circ[\text{Au}(\text{H}_2\text{O})_4^{3+}, \text{Au}] = +1.52$ V.

^c Diphenylphosphinobenzene-*m*-sulfonate.

Table 2. Ligand parameters to Edwards' equation defined relative to the chloride ion.

Ligand	H	E_n	E_n/H
Br^-	-1.1	+0.27	-0.25
SCN^-	+5.3	+0.59	+0.11
I^-	-3	+0.82	-0.27
NH_3	+15.3	+0.60	+0.04
$(\text{NH}_3)_2\text{CS}$	+5.2	+0.94	+0.18
$\text{S}_2\text{O}_3^{2-}$	+7.8	+1.28	+0.16
CN^-	+15.5	+1.56	+0.10
OH^-	+21.9	+0.36	+0.02
H_2O	+4.4	-1.24	-0.28

Table 3. Softness parameter for some heavy metals.

	α	σ_K
Cd(II)	2.2	2.0
Cu(I)	3.4	2.3
Ag(I)	3.5	2.8
Tl(III)	4.6	3.4
Au(I)	6.5	4.4
Hg(II)	6.8	4.6
Au(III)	7.4	-

and $\log \beta_4 \approx 26.4$ for Au(III). These values combined with the standard electrode potentials for the relevant chlorido complexes yield the following estimate for the two aqua gold potentials: $E^\circ[\text{Au}(\text{H}_2\text{O})_2^+, \text{Au}] = 1.83$ V and $E^\circ[\text{Au}(\text{H}_2\text{O})_4^{3+}, \text{Au}] = 1.52$ V.

Previous estimates of the aqua gold(I) electrode potential range from 1.67 to 2.12 V.^{1,3,7,8} The present value of 1.83 V is further supported by other evidence which will be discussed in a forthcoming paper.⁹ The value of 1.52 V found for the aqua gold(III) electrode potential deviates less from values in the literature^{7,10} and is in good agreement with Latimer's⁷ estimate of 1.50 V. We therefore suggest that the stability constants given in Table 1 calculated on the basis of the present new values should replace constants already published by one of the present authors.⁸

The α coefficient in Edwards' equation is a measure of the softness¹¹ of the metal; in Table 3 the values for Au(I) and Au(III) obtained from Fig. 1 are compared with values of α for other metals¹¹ as well as with Klopman's¹² softness parameter σ_K which is derived from polyelectronic perturbation theory. The most remarkable result is that Au(III) is softer than Au(I) with Hg(II) having an intermediate softness.

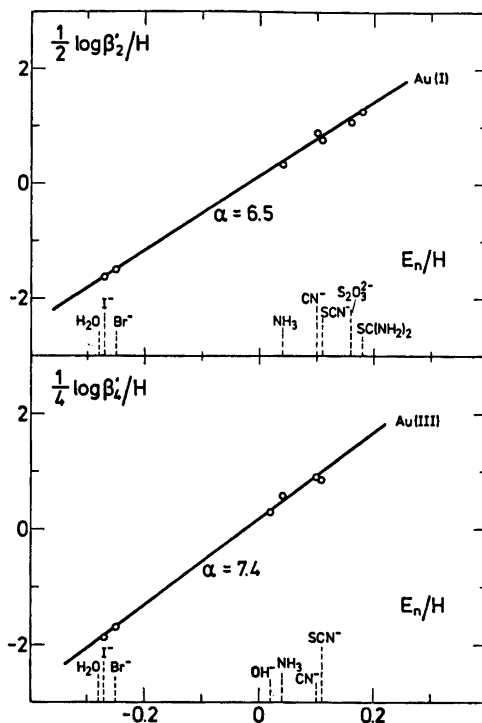


Fig. 1. Edwards' plots for Au(I) and Au(III).

- Ehrenburg, A. M. and Peshchevitskii, B. I. *Russ. J. Inorg. Chem.* 14 (1969) 1429.
- Jørgensen, C. K. and Pouradier, J. *J. Chim. Phys.* 67 (1970) 124.
- Hancock, R. D., Finkelstein, N. P. and Evers, A. *J. Inorg. Nucl. Chem.* 36 (1974) 2539.
- Pearson, R. G. *J. Chem. Educ.* 45 (1968) 581.
- Edwards, J. O. *J. Am. Chem. Soc.* 76 (1954) 1540.
- Robinson, R. A. *Trans. Faraday Soc.* 32 (1936) 743.
- Latimer, W. M. *The Oxidation Potentials*, 2nd Ed., Prentice-Hall, New York 1952, p. 192.
- Hawkins, C. J., Mønsted, O. and Bjerrum, J. *Acta Chem. Scand.* 24 (1970) 1059.
- Skibsted, L. H. and Bjerrum, J. *Indian J. Chem.* 54 (1977) *In press*.
- Finkelstein, N. P. and Hancock, R. D. *Gold Bull.* 7 (1974) 72.
- Bjerrum, J. *Essays on Analytical Chemistry. In Memory of Professor Anders Ringbom*, Pergamon, Oxford 1976.
- Klopman, G. *J. Am. Chem. Soc.* 90 (1968) 223.

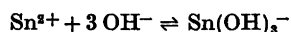
Received November 26, 1976.

Hydrolysis of the Tin(II) Ion, Sn^{2+} , in Alkaline Solution

WANDA MARK

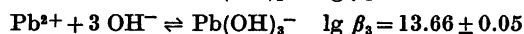
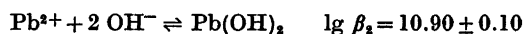
Department of Inorganic Chemistry, Chalmers University of Technology and the University of Göteborg, P.O. Box, S-402 20 Göteborg 5, Sweden

Emf methods have been used to study the complex formation between tin(II) ions and hydroxide ions in 3 M NaClO_4 at 25 °C. A fully automatic computer-operated system was used in the investigation which was mainly carried out through titration of strongly alkaline tin(II) solutions with perchloric acid. The experimental data could best be explained by the formation of the complex $\text{Sn}(\text{OH})_3^-$ only. The stability constant was obtained graphically and the data were corrected for experimental errors by the program LETAGROP. The value obtained for the equilibrium constant is:



$$\lg \beta_3 \pm 3\sigma = 24.58 \pm 0.04$$

The hydrolysis of tin(II) ions in acid medium has been studied by Tobias,¹ whose data could be explained by the formation of the complexes $\text{Sn}_2(\text{OH})_4^{2+}$, $\text{Sn}_3(\text{OH})_6^{2+}$ and SnOH^+ . The only attempt to investigate the complex formation of Sn^{2+} in hydroxide solutions has been made polarographically by Smrž.² By assuming that the only complex formed was $\text{Sn}(\text{OH})_3^-$ the stability constant for this complex was determined to be $\beta_3 = 4 \times 10^{24} \text{ M}^{-3}$. An investigation of the complex formation of lead(II) ions in alkaline solution, by Carell and Olin,³ gave the following results in 3 M NaClO_4 medium



The aim of the present work was to determine whether $\text{Sn}(\text{OH})_3^-$ is the only complex formed in alkaline tin(II) solutions or if $\text{Sn}(\text{OH})_2$ and possibly $\text{Sn}(\text{OH})_4^{2-}$ are also present. A preliminary investigation of this system by the author showed that the complex $\text{Sn}(\text{OH})_3^-$ is much stronger than $\text{Pb}(\text{OH})_3^-$ and that the constant

is of the same magnitude as that determined by Smrž.

Since most recent investigations on hydrolysis systems in solution have been performed in 3 M NaClO_4 at 25 °C this medium and temperature were employed in the present investigation.

List of symbols

A	total concentration of OH^-
a	free concentration of OH^-
B	total concentration of $\text{Sn}(\text{II})$
b	free concentration of $\text{Sn}(\text{II})$
Sn-Hg(G)	tin amalgam electrode used to generate Sn^{2+}
Sn-Hg(M)	tin amalgam electrode used to measure Sn^{2+}
RE	reference Ag, AgCl electrode
S	equilibrium solution
E_{Sn}	measured emf
$E_{0\text{Sn}}$	a constant in $E_{\text{Sn}} = E_{0\text{Sn}} + (RT \ln 10/2F) \lg b + E_j$
E_j	liquid junction potential, $E_j = 8[\text{OH}^-] \text{ mV}^4$
Z	average number of OH^- per $\text{Sn}(\text{II})$ in complexes
η	$\lg(B/b)$
β_n	formation constant of $\text{Sn}(\text{OH})_n^{(n-2)-}$ from Sn^{2+} and OH^-
A_0	the concentration of OH^- before titration
A_T	the concentration of OH^- in the titration solution
H_T	the concentration of H_3O^+ in the titration solution
δA_0	group parameter obtained by refining A_0

EXPERIMENTAL

Chemicals and analyses

Perchloric acid (Merck, *p.a.*) was standardized against thallium carbonate (BDH). Sodium perchlorate was prepared from sodium carbonate (Merck, *p.a.*) and perchloric acid, as described by Biedermann.⁵ Sodium hydroxide solutions were prepared from a 50% NaOH stock solution and standardized against potassium hydrogen phthalate. Tin(II) ions were generated by anodic oxidation of tin in tin amalgam by means of a constant current source. The tin amalgam used for the generation of Sn²⁺ was kept in a teflon dish which was immersed in the equilibrium solution during the electrolysis only, by an automatic lift arrangement (*cf.* Fig. 1). The procedure used was that described by Gobom and Kovács.⁶ Iodometric determination of the tin(II) content agreed well with the concentration calculated. Tin amalgam was prepared by dissolving 0.8% tin in mercury in a 0.1 M HClO₄ solution. The mixture was stirred violently for several hours and stored in an argon atmosphere.

Apparatus

A tin amalgam electrode was used to measure the concentrations of free Sn²⁺ in the equilibrium solutions. To prevent the platinum wire used for connection from coming into contact with the alkaline solutions the bottom of the titration vessel was drawn out into a U-formed tube into which the amalgam was poured. The platinum wire could then be immersed in the measuring amalgam from the outside of the vessel (*cf.* Fig. 1). A cell of the following type was used for the emf measurements:

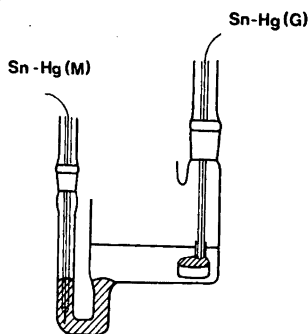
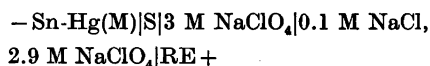


Fig. 1. Schematic representation of the titration vessel used in the experiments. The shaded areas represent tin amalgam.

The composition of the reference half cell used for the generation of tin(II) ions was the same as that for the measuring cell. The vessels used for the salt bridges and the reference electrodes were of the Wilhelm type.⁷ The cells were kept in a paraffin oil thermostat at 25.00 ± 0.01 °C in a room thermostated to 25.0 ± 0.1 °C.

The equilibrium solutions and the measuring amalgam in the tube were kept in an inert atmosphere by passing argon gas over the surfaces. The argon gas was taken from cylinders and purified by passage through a column of activated copper and then through four bottles containing 10% H₂SO₄, 10% NaOH, 3 M NaClO₄ and 3 M NaClO₄, respectively.

The emf's of the cell were measured with a digital voltmeter, HP 3450A, which had a sensitivity of 1 μV in the measuring range. The titrations were performed and controlled by a fully automatic computer-operated system developed at this department by Gobom and Kovács.⁸

Emf measurements

Tin(II) ions were generated electrolytically from the tin amalgam by means of a constant current source, using a current of 3.289 mA. This meant that the electrolysis had to proceed for 40 min to achieve a tin(II) ion concentration of 1.0 mM in a solution of 40 ml. When the electrolysis was carried out in alkaline solution it had to be done in steps of a few seconds to prevent precipitation of stannous oxide.

The tin(II) ions were generated stepwise in the alkaline solutions for 5 s in each step to avoid precipitation of stannous oxide around the generating amalgam electrode. This procedure thus took several hours. The alkaline tin(II) solutions were titrated with perchloric acid and attempts were made to reach an OH⁻ concentration close to the solubility limit of stannous oxide.

After each titration perchloric acid was added to the equilibrium solution in such an amount that $[\text{H}_3\text{O}^+] \approx 80$ mM. No tin(II) complexes are formed at this hydrogen concentration¹ and the emf's were measured at different tin(II) concentrations to enable the determination of E_{0Sn} . In some titrations the calculated values of E_{0Sn} were the same for different tin(II) concentrations, but the agreement was mostly not satisfactory and, moreover, the emf's drifted. This was probably due to the fact that the solubility range of stannous oxide had to be passed when the solutions were acidified and some precipitate might remain undissolved.

Due to the long time for generating Sn(II) ions in the alkaline solutions and to the difficulties in obtaining the E_{0Sn} values another way of performing the titrations was tried. The titrations were started in perchloric acid where the tin(II) ions were generated and the

emf's were measured in between the steps of the electrolysis in order to determine the constant E_{Sn} . The acid solutions were then titrated with sodium hydroxide solutions, but due to difficulties in dissolving the precipitated stannous oxide, it was doubtful if equilibrium was attained during the titrations. This method was therefore abandoned in favour of commencing with an alkaline solution.

Efforts were made to measure the free hydrogen concentration during the titrations but neither a glass electrode nor a hydrogen gas electrode did function in the alkaline equilibrium solutions.

Earlier experiments by the author had shown the main tin(II)-bearing species to be $\text{Sn}(\text{OH})_3^-$. To ensure that no polynuclear complexes were formed, titrations were performed in which a was kept constant and B was varied between 0.1 and 1.0 mM. The slope of the straight line obtained by plotting $\lg B = f(\lg b)$ was 0.98 which indicated that only mononuclear species had to be considered. The free OH^- concentrations, a , were calculated assuming $a = A - 3B$, i.e. that the ratio OH^-/Sn was 3:1 in the dominating tin(II) species.

Two series of titrations were performed. In one series the total OH^- concentration, A , ranged from 265 mM to ≈ 80 mM and in the other A ranged from 97 mM to ≈ 30 mM. To avoid variations in the activity factors no measurements were made in more concentrated hydroxide solutions. In each titration the total tin(II) concentration, B , was kept constant by electrolytic generation of tin(II) ions for every addition of perchloric acid. The different total tin(II) concentrations were: $B = 1.00, 0.50$ and 0.25 mM where 0.25 mM was the lowest total tin(II) concentration that led to satisfactory results. Due to the long time of electrolysis required to achieve a concentration of $B = 1.00$ mM it was not considered feasible to perform titrations at higher B .

A great number of titrations had to be carried out because of the practical difficulties encountered during the experiments. In many cases equilibrium was not attained even after 1 to 2 h, due to a slight amount of precipitate formed during the electrolysis. These experiments were rejected and in the titrations used for the calculations equilibrium was established within half an hour and no precipitate was detected during the generation of the tin(II) ions. To make sure that true equilibria were measured back-titrations were carried out in a few cases by addition of sodium hydroxide solution.

The measuring amalgam electrode proved to be unstable in alkaline solutions. Its potential oscillated about an equilibrium value and the deviation could reach ± 0.10 mV. The emf measurements were therefore performed in such a way that 25 readings were made on the digital voltmeter with an interval of 3 s. A mean value was calculated by the computer and printed out. After four such measurements the

printed emf's were compared and tested for equilibrium. If no equilibrium had been attained another group of four measurements was made, otherwise the titration was continued. In acid solutions the electrode potential was stable for several hours and oscillated only within ± 0.01 mV. The discrepancy between the behaviour of the electrode in the two different media may be attributable to the Frumkin effect. In 3 M NaClO_4 where the concentration of supporting electrolyte is high and kept constant, the ϕ_2 -potential of the electrode double layer (the outer Helmholtz plane) should be negative and have the same value in alkaline as in acid solutions.^{8,9} According to the expression $(2-j)\phi_2 = RT/F \ln ([\text{SnL}_j^{2-j}]/[\text{SnL}_j^{2-j}'])$ where j is the number of anionic ligands, $[\text{SnL}_j^{2-j}]$ and $[\text{SnL}_j^{2-j}']$ are concentrations in the solution and at the electrode double layer, respectively, the total tin(II) concentration at the electrode double layer will be much lower in alkaline solutions ($B = [\text{Sn}(\text{OH})_3^-]$) than in acid solutions ($B = [\text{Sn}^{2+}]$). Assuming the ϕ_2 -potential to be approximately -60 mV there will be a difference between the total tin(II) concentrations in the two cases with a factor 10^3 . The value of the exchange current density at the electrode will therefore most probably be much higher in acid solutions than in alkaline which explains the fact that more stable potentials are established in acid solutions.

INTERPRETATION OF DATA

Since the concentration of free ligand, a , is large compared to B and the complexes formed are mononuclear, the formulae given by Leden¹⁰ can be used, i.e. $\partial \eta / \partial \lg a = Z$ and $a = A - BZ$. The most probable complexes are $\text{Sn}(\text{OH})_2$, $\text{Sn}(\text{OH})_3^-$ and $\text{Sn}(\text{OH})_4^{2-}$. Since the dominating complex was assumed to be $\text{Sn}(\text{OH})_3^-$ the preliminary calculations were performed with $a = A - 3B$. The Z values obtained varied between 3.00 and 3.05. This could indicate the presence of $\text{Sn}(\text{OH})_4^{2-}$ in addition to $\text{Sn}(\text{OH})_3^-$ and if these two complexes are the only complexes formed, from the expression for the total tin(II) concentration $B = b + \beta_2 b a^2 + \beta_3 b a^3 + \beta_4 b a^4$ the equation $B b^{-1} a^{-3} = \beta_3 + \beta_4 a$ is obtained. By plotting $B b^{-1} a^{-3}$ as a function of a , a straight line would result if the hypothesis were valid. As this is not the case for any titration, the presence of $\text{Sn}(\text{OH})_4^{2-}$ was considered out of question. Moreover, the lines obtained for $\eta(\lg a)$ did not deviate towards higher values for $\Delta \eta / \Delta \lg a$ at high hydroxide concentrations.

Table 1. Preliminary values of A_0 and $E_{0\text{Sn}}$ compared to δA_0 and $E_{0\text{Sn}}$ calculated by LETAGROP for the best fit of the experimental data listed in Table 2.

$B \times 10^3$ M	$A_0 \times 10^3$ M	$\delta A_0 \times 10^3$ M	$E_{0\text{Sn}}$ (meas.)	$E_{0\text{Sn}}$ (calc.)
1.00	265.14	-1.04	-429.20	-429.97
1.00	97.52	-1.62	-428.43	-430.44

The presence of the complex $\text{Sn}(\text{OH})_2$ was tested by plotting $Bb^{-1}a^{-2}$ as a function of a , thus assuming that only $\text{Sn}(\text{OH})_2$ and $\text{Sn}(\text{OH})_3^-$ were formed. The graphs obtained were straight lines although the intercepts on the $Bb^{-1}a^{-2}$

axis varied, which was probably due to poor accuracy in the determination of the constants $E_{0\text{Sn}}$.

In most titrations the differences between calculated emf's when only $\text{Sn}(\text{OH})_3^-$ was taken into consideration and the measured emf's drifted, but in a way that could not be explained by the existence of $\text{Sn}(\text{OH})_2$. The best fit of the data was thus obtained for $\text{Sn}(\text{OH})_3^-$ as the only complex formed in the concentration ranges studied.

Data from seven titrations ($B=0.25, 0.50$ and 1.00 mM) for which $E_{0\text{Sn}}$ were determined most accurately were used to calculate the stability constant β_3 . For each titration the constant was obtained from the slope of the

Table 2. Emf data for two titrations, $B = 1.0$ mM, for tin(II) in alkaline solutions. The five columns give the values for added volume of titrator (ml), E_{Sn} (mV), A (mM), η (calc.), $\Delta E_{\text{Sn}} = E_{\text{Sn}}(\text{calc.}) - E_{\text{Sn}}(\text{exp.})$ (mV), respectively. The calculations are based on $\lg \beta_3 = 24.58$ and the A_0 and $E_{0\text{Sn}}$ values are those obtained by LETAGROP refinement.

$B = 1.0$ mM $A_0 = 264.1$ mM					$B = 1.0$ mM $A_0 = 95.90$ mM				
$H_T = 260.0$ mM $E_{0\text{Sn}} = -429.97$ mV $V_0 = 40$ ml					$H_T = 106.0$ mM $E_{0\text{Sn}} = -430.44$ mV $V_0 = 40$ ml				
0.0	-1191.94	264.10	22.832	-0.00	2.50	-1148.84	84.02	21.308	0.08
0.50	-1191.03	257.63	22.800	0.00	3.00	-1147.69	81.81	21.272	-0.02
1.00	-1190.11	251.31	22.767	-0.00	3.50	-1146.65	79.65	21.236	-0.00
1.50	-1189.18	245.15	22.734	-0.01	4.00	-1145.60	77.54	21.199	0.00
2.00	-1188.28	239.14	22.702	0.01	4.50	-1144.49	75.48	21.163	-0.04
2.50	-1187.35	233.27	22.669	0.00	5.00	-1143.43	73.46	21.126	-0.03
3.00	-1186.42	227.53	22.636	-0.00	5.50	-1142.34	71.49	21.089	-0.04
3.50	-1185.49	221.93	22.603	-0.00	6.00	-1141.24	69.56	21.052	-0.06
4.00	-1184.55	216.45	22.570	-0.01	6.50	-1140.24	67.67	21.014	0.04
4.50	-1183.60	211.10	22.537	-0.03	7.00	-1139.14	65.82	20.976	0.04
5.00	-1182.67	205.86	22.504	-0.02	7.50	-1138.00	64.02	20.938	0.01
5.50	-1181.75	200.74	22.470	0.01	8.00	-1136.92	62.24	20.900	0.05
6.00	-1180.82	195.74	22.437	0.03	8.50	-1135.77	60.51	20.861	0.03
6.50	-1179.86	190.84	22.403	0.02	9.00	-1134.59	58.81	20.822	-0.01
7.00	-1178.90	186.04	22.370	0.02	9.50	-1133.51	57.15	20.783	0.07
7.50	-1177.94	181.34	22.336	0.02	10.00	-1132.18	55.51	20.743	-0.10
8.00	-1176.98	176.75	22.302	0.03	10.50	-1131.14	53.92	20.703	0.04
8.50	-1176.00	172.24	22.268	0.03	11.00	-1129.89	52.35	20.662	-0.01
9.00	-1175.01	167.83	22.233	0.02	11.50	-1128.69	50.81	20.621	-0.01
9.50	-1174.03	163.51	22.199	0.03	12.00	-1127.44	49.30	20.579	-0.03
10.00	-1173.03	159.28	22.164	0.03	12.50	-1126.21	47.82	20.537	-0.03
10.50	-1172.03	155.13	22.129	0.03	13.00	-1125.01	46.37	20.494	0.03
11.00	-1171.01	151.06	22.093	0.02	13.50	-1123.68	44.95	20.450	-0.02
11.50	-1170.00	147.07	22.058	0.03	14.00	-1122.47	43.55	20.406	0.06
12.00	-1168.96	143.15	22.022	0.02	14.50	-1121.15	42.18	20.361	0.06
12.50	-1167.92	139.31	21.986	0.02	15.00	-1119.83	40.83	20.316	0.07
13.00	-1166.86	135.54	21.949	0.01	15.50	-1118.38	39.51	20.269	-0.02
13.50	-1165.80	131.85	21.912	0.01	16.00	-1117.02	38.21	20.222	0.01
14.00	-1164.75	128.22	21.875	0.04	16.50	-1115.65	36.93	20.174	0.05
14.50	-1163.65	124.66	21.838	0.02	17.00	-1114.10	35.68	20.125	-0.06
15.00	-1162.53	121.16	21.800	-0.00	17.50	-1112.60	34.45	20.075	-0.09
15.50	-1161.39	117.73	21.761	-0.04	18.00	-1111.12	33.24	20.024	-0.06
16.00	-1160.27	114.35	21.722	-0.03	18.50	-1109.64	32.05	19.971	-0.01
16.50	-1159.13	111.04	21.683	-0.04	19.00	-1108.11	30.88	19.918	0.04
17.00	-1157.99	107.79	21.643	-0.02					
17.50	-1156.82	104.59	21.603	-0.02					
18.00	-1155.63	101.45	21.562	-0.03					
18.50	-1154.42	98.36	21.520	-0.03					
19.00	-1153.18	95.32	21.478	-0.05					
19.50	-1151.93	92.33	21.435	-0.06					
20.00	-1150.66	89.40	21.392	-0.06					

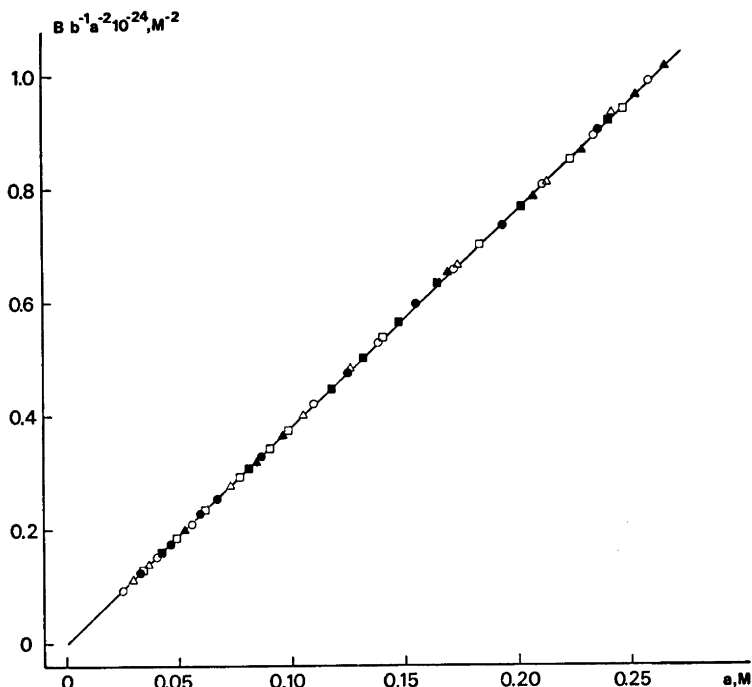


Fig. 2. Randomly chosen experimental data $Bb^{-1}a^{-2}=f(a)$ for titrations in strongly alkaline solutions as well as at lower hydroxide concentrations. The symbols denote the following total tin(II) concentrations: 2.5 mM (\blacktriangle , \triangle); 0.5 mM (\blacksquare , \square); and 1.0 mM (\bullet , \circ).

line $Bb^{-1}a^{-2}=f(a)$. For all these titrations the plotted lines passed through the origin and a mean value was calculated, giving $\lg \beta_3 \pm 3\sigma = 24.58 \pm 0.04$ where σ is the standard deviation in β_3 . In order to obtain a better fit of the data, the least squares program LETAGROP¹¹ was used in calculations based on $\lg \beta_3 = 24.58$. If the constant $\lg \beta_3$ was set to 24.58 the constants E_{osn} could be refined and also an allowance for analytical errors in A_0 could be made in each titration. The perchloric acid concentrations H_T , were kept constant, assuming that the experimental errors in determining the concentration of hydroxide solutions are larger than those in determining the acid concentrations.

The calculations were performed with two titrations for each B value in the two series. Since the accuracy of the data was not satisfactory for $B = 0.1$ mM these data were deleted.

The concentrations and group parameters for two titrations are given in Table 1. Fig. 2 shows the graphs $Bb^{-1}a^{-2}=f(a)$ for twelve titrations

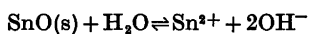
representing the two different titration series. The measured emfs are listed in Table 2 for the two titrations given in Table 1 together with concentrations and differences between the measured emfs and those calculated for $\lg \beta_3 = 24.58$.

DISCUSSION

According to Latimer & Hildebrand¹² tin(II) ions disproportionate in alkaline media. However, since the analyses of tin(II) were in good agreement with the tin(II) concentrations calculated from the generations of tin(II) ions, such a disproportionation tendency could not be detected.

The only complex found in the concentration ranges investigated was $\text{Sn}(\text{OH})_3^-$. This is in contrast to the $\text{Pb}^{2+} - \text{OH}^-$ system where both $\text{Pb}(\text{OH})_3^-$ and $\text{Pb}(\text{OH})_2$ could be detected. To test whether $\text{Sn}(\text{OH})_2$ is present at low hydroxide concentrations which were not investigated due to practical difficulties, the

solubility data for SnO(s) in alkaline and acid solutions obtained by Garrett and Heiks¹³ were used. The solubility product, K_{s0} , was calculated for stannous oxide dissolved in alkaline solutions, assuming that only $\text{Sn}(\text{OH})_2^-$ is present even at very low hydroxide concentrations. The complex formation constants reported by Tobias¹ were used for the same calculations in the acid solutions. Mean values were calculated and the results thus obtained were:



$\lg K_{s0} = -25.43$ (SnO dissolved in hydroxide)

$\lg K_{s0} = -25.4$ (SnO dissolved in acid)

Solubility products for SnO determined by polarographic measurements are reported by Smrž² and Kovalenko¹⁴ to be $\lg K_{s0} = -27.85$ and $\lg K_{s0} = 28.1$, respectively. Emf measurements were used by Prytz¹⁵ to determine K_{s0} in various ionic media and values of $\lg K_{s0}$ between -25.70 and -24.97 were obtained.

Acknowledgements. I wish to thank Professor Nils Ingri, University of Umeå, for introducing me to the problem and Professor Sture Fronæus, University of Lund, for valuable discussions. I am greatly indebted to Ing. Eva Lundqvist for skilful performance of the experiments, to Dr. Sylvia Gobom for placing the titration equipment at my disposal and to Dr. Susan Jagner for revising the English text. The work was supported by a grant from the Swedish Natural Science Research Council (Contract No. 2318) which is gratefully acknowledged.

REFERENCES

1. Tobias, R. S. *Acta Chem. Scand.* 12 (1958) 198.
2. Smrž, S. J. *Recl. Trav. Chim. Pays-Bas* 44 (1925) 580.
3. Carell, B. and Olin, Å. *Acta Chem. Scand.* 14 (1960) 1999.
4. Ingri, N., Lagerström, G., Frydman, M. and Sillén, L. G. *Acta Chem. Scand.* 11 (1957) 1034.
5. Biedermann, G. *Ark. Kemi* 9 (1956) 277.
6. Gobom, S. and Kovács, J. *Chem. Scr.* 2 (1972) 103.
7. Forsling, W., Hietanen, S. and Sillén, L. G. *Acta Chem. Scand.* 6 (1952) 901.
8. Fronæus, S., Johansson, R. and Östman, C.-O. *Chem. Scr.* 1 (1971) 52.
9. Fronæus, S. and Johansson, C. L. *Electroanal. Chem. Interfacial Electrochem.* 60 (1975) 29.
10. Leden, I. *Thesis*, Lund 1943, p. 14.
11. Brauner, P., Sillén, L. G. and Whiteker, R. *Ark. Kemi* 31 (1969) 365.
12. Latimer and Hildebrand, *Reference Book of Inorganic Chemistry*, Macmillan, New York.
13. Garrett, A. B. and Heiks, R. E. *J. Am. Chem. Soc.* 63 (1941) 562.
14. Kovalenko, P. N. *Zh. Neorg. Khim.* 3 (1958) 1065.
15. Prytz, M. Z. *Anorg. Chem.* 174 (1928) 355.

Received October 22, 1976.

The Crystal Structure of a Dimeric Cerium(IV) Sulfate



OVE LINDGREN

Department of Inorganic Chemistry, Chalmers University of Technology and the University of Göteborg, P.O. Box, S-402 20 Göteborg 5, Sweden

The crystal structure of $\text{Ce}_2(\text{OH})_2(\text{H}_2\text{O})_4(\text{SO}_4)_3$ has been determined from three-dimensional X-ray diffractometer data. The crystals are monoclinic, space group $A2/a$, with $a = 15.583(11)$ Å, $b = 13.448(13)$ Å, $c = 6.748(4)$ Å, $\gamma = 95.39(6)^\circ$ and $Z = 4$.

The positions of the cerium, sulfur and oxygen atoms were evaluated from a Patterson function and a subsequent electron density summation. Full matrix least-squares refinement based on 1425 reflexions yielded a final R value of 4.25 %.

The structure contains discrete $\text{Ce}_2(\text{OH})_2(\text{H}_2\text{O})_4^{4+}$ ions, in which the Ce(IV) atoms are connected by double OH^- bridges, the Ce—Ce and OH^- — OH^- distances being 3.769(3) and 2.481(14) Å, respectively. Cerium is eight-coordinated by two OH^- ions, two water molecules and four oxygen atoms belonging to sulfate groups, giving a distorted dodecahedral configuration with Ce—O distances of 2.223—2.406 Å (mean 2.328 Å). The $\text{Ce}_2(\text{OH})_2(\text{H}_2\text{O})_4^{4+}$ ions are linked through SO_4^{2-} ions to form a three dimensional network.

The oxygen coordination of some tetravalent metal ions has been a subject of study at this Department for several years. The work was commenced by Lundgren¹ who investigated some basic salts of Ce^{IV} , Th^{IV} , U^{IV} , Ti^{IV} , and Zr^{IV} , and was continued on essentially the same lines by Hansson² and Mark³ on Hf and Zr, by Lindqvist⁴ on Te and by Titze and Allard⁵ on Th and Np. The present author has studied the oxygen coordination of cerium in a cerium(III)sulfate,^{6a} basic and neutral cerium(IV) sulfates^{6b,6c} and a cerium(IV) chromate.^{6d} In this paper the investigation of the crystal structure of a dimeric basic cerium(IV) sulfate, viz. $\text{Ce}_2(\text{OH})_2(\text{H}_2\text{O})_4(\text{SO}_4)_3$, is reported.

EXPERIMENTAL

The commercially available compound, $\text{Ce}(\text{SO}_4)_2(\text{H}_2\text{O})_4$, (orthorhombic, space group $Fddd$, manufactured by Merck AG), was dissolved in 1 M H_2SO_4 . About 100 ml of the solution, still containing some undissolved salt, was transferred to a glass flask which was then sealed. After some months, small yellow prismatic crystals had formed. Oscillation and Weissenberg photographs showed the crystals to be monoclinic. Systematically absent reflexions, i.e.

$$hkl: k+l=2n+1$$

$$hk0: h=2n+1$$

indicated the space group to be Aa or $A2/a$.

Approximate cell dimensions were calculated from oscillation and Weissenberg photographs. Guinier X-ray powder photographs were taken using $\text{CuK}\alpha_1$ radiation and with $\text{Pb}(\text{NO}_3)_2$ ($a = 7.8566$ Å at 21°C)⁷ as an internal standard. The cell dimensions as calculated from these photographs with the programme POWDER⁸ are: $a = 15.583(11)$ Å, $b = 13.448(13)$ Å, $c = 6.748(4)$ Å and $\gamma = 95.39(6)^\circ$.

The crystal chosen for single crystal work had the approximate dimensions $0.08 \times 0.1 \times 0.08$ mm³. Ten layers, $hk0-hk9$, were recorded on a PAILRED single crystal diffractometer using graphite monochromatized $\text{MoK}\alpha$ radiation. The Lorentz and polarisation effects were corrected for, using the programme DATAP1,⁹ those reflexions for which $\sigma(I)/I > 0.3$ where $\sigma(I) = (I_t + I_b)^{\frac{1}{2}}$, I_t denoting total intensity and I_b background intensity, being discarded. The remaining 1425 symmetry independent reflexions were used in the refinement of the structure. However, to solve the structure only reflexions from the layers $hk0-hk4$ were considered necessary. Before the final refinement a correction was made for absorption with the programme DATAPA.⁹ The trans-

Table 1. Atomic coordinates and temperature factors for $\text{Ce}_2(\text{OH})_2(\text{H}_2\text{O})_4(\text{SO}_4)_2$. Estimated standard deviations are given in parentheses. The thermal parameters have been multiplied by 10^5 for Ce and by 10^4 for S and O. The temperature factor is of the form $\exp[-2\pi^2(h^2a^{*2}U_{11} + \dots + klb^*c^*U_{23})]$.

	<i>x</i>	<i>y</i>	<i>z</i>	U_{11}	U_{22}	U_{33}	U_{12}	U_{13}	U_{23}
Ce	0.08607(3)	0.10763(4)	-0.02215(6)	852(21)	722(21)	638(20)	714(26)	-3(37)	66(37)
S1	0.56723(14)	0.20905(16)	0.52131(32)	118(9)	83(8)	66(8)	136(13)	-25(14)	-22(14)
S2	1/4	0	0.27320(44)	121(14)	68(13)	75(12)	62(21)	0	0
O1	-0.0149(5)	0.2472(5)	0.5367(11)	160(32)	137(31)	150(31)	168(51)	-16(51)	-100(51)
O2	0.0517(6)	0.1460(7)	0.3031(12)	271(44)	249(44)	166(34)	323(73)	-11(60)	-160(61)
O3	0.1343(6)	0.2889(6)	0.4426(15)	196(38)	175(38)	395(50)	38(61)	163(70)	246(70)
O4	0.0943(5)	0.1453(6)	0.6409(11)	246(40)	194(38)	108(31)	393(61)	133(53)	101(52)
O5	0.3165(6)	0.0560(6)	0.3931(12)	209(38)	118(35)	214(36)	-11(58)	-98(58)	-88(55)
O6	0.2899(5)	0.4286(6)	0.6431(13)	128(35)	183(38)	276(40)	175(58)	62(58)	-62(61)
W1	0.1439(6)	0.4790(7)	0.2852(12)	344(48)	213(42)	120(34)	341(72)	82(60)	48(56)
W2	0.3949(5)	0.2555(6)	0.4642(14)	197(36)	103(32)	395(48)	63(54)	-8(70)	-128(66)
OH	0.0428(5)	0.4577(5)	0.6239(10)	115(31)	73(30)	154(31)	41(49)	-37(48)	32(50)

mission factors, ranging from 0.71 to 0.82, were calculated using a $6 \times 8 \times 6$ grid.

STRUCTURE DETERMINATION

A Patterson synthesis was calculated using the programme DRF.⁹ The interpretation, in terms of space group $A2/a$, gave positions for the cerium atom, one sulfur atom and the OH⁻ ion, all situated in the general positions of the space group. A subsequent three-dimensional Fourier synthesis based on these three atomic positions, clearly revealed the locations of the remaining nonhydrogen atoms. The final refinement with the full matrix programme LALS⁹ was based on all the 1425 recorded reflexions. The scattering factors used were those given

by Cromer and Waber,¹⁰ corrected for the real part of the anomalous dispersion, and the reflexions were weighted according to $w = 1/(80 + |F_o| + 0.001|F_o|^2)$. One scale factor, 34 positional parameters, and 70 anisotropic temperature factors were refined giving a conventional *R* value of 4.25 %.

Lists of observed and calculated structure factors are available on request from the author. The final atomic parameters are listed in Table 1.

DESCRIPTION AND DISCUSSION

Fig. 1 illustrates the structure viewed along the *c*-axis. The structure consists of $\text{Ce}_2(\text{OH})_2(\text{H}_2\text{O})_4$ ⁶⁺ ions and SO_4 ²⁻ ions joined in a three-

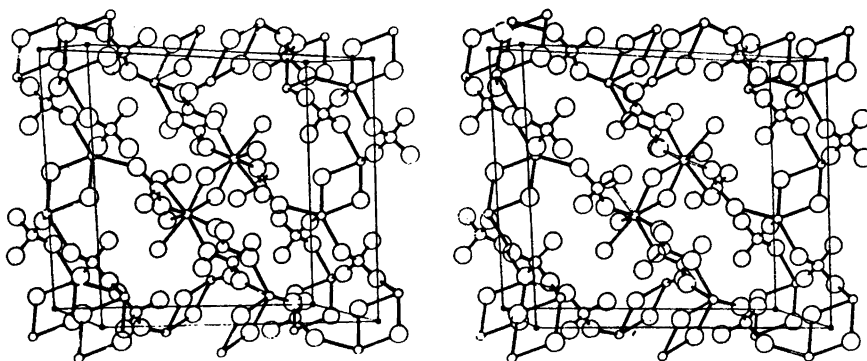


Fig. 1. Stereo drawing of $\text{Ce}_2(\text{OH})_2(\text{H}_2\text{O})_4(\text{SO}_4)_2$ viewed along the *c* axis. For clarity only two complete cerium-oxygen polyhedra are shown.

Table 2. Interatomic distances (Å) and angles (°).

Ce—Ce	3.769(3)	S1—O1	1.475(8)
OH ⁻ —OH ⁻	2.481(14)	—O2	1.464(9)
		—O3	1.446(9)
Ce—O1	2.337(8)	—O4	1.476(8)
—O2	2.329(8)	Average:	1.465
—O4	2.331(7)	S2—O5(×2)	1.465(9)
—O6	2.322(8)	—O6(×2)	1.481(9)
—W1	2.406(9)	Average:	1.473
—W2	2.386(8)	O1—O2	2.382(11)
—OH ⁻	2.289(7)	—O3	2.423(11)
—OH ⁻	2.223(7)	—O4	2.388(11)
Average:	2.328	O2—O3	2.402(13)
W1—O3	2.759(13)	—O4	2.374(11)
—O5	2.768(12)	O3—O4	2.383(12)
W2—O3	2.742(12)	Average:	2.392
—O5	2.749(11)	O5—O5	2.444(17)
O1—S1—O2	108.3(5)	—O6(×2)	2.412(12)
O1—S1—O3	112.1(5)	—O6(×2)	2.388(12)
O1—S1—O4	108.1(5)	O6—O6	2.384(17)
O2—S1—O3	111.2(5)	Average:	2.407
O2—S1—O4	107.8(5)		
O3—S1—O4	109.2(5)		
O5—S2—O5	113.0(7)		
O5—S2—O6(×2)	109.9(5)		
O5—S2—O6(×2)	108.3(5)		
O6—S2—O6	107.3(7)		

dimensional network, so that cerium is surrounded by eight oxygen atoms. Distances and angles with their standard deviations are listed in Table 2. No correction has been made for thermal motion.

Fig. 2. shows the bonding viewed in the y direction. The dimeric cerium complexes are arranged in a chain along the a -axis. Between them are SO_4^{2-} ions situated on the twofold axes. Only half of the oxygen atoms of these groups are involved in bonds to cerium.

The cerium—sulfate bonds, viewed in the x direction are illustrated in Fig. 3, a zigzag pattern being formed by cerium atoms and sulfate groups (S1). Two of the oxygen atoms

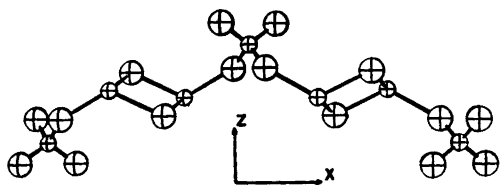


Fig. 2. The bonding viewed in the y direction showing the $\text{Ce}_2(\text{OH})_2^{4+}$ dimers linked by sulfate ions.

in the S1 group participate in the chain along the a -axis. A third oxygen atom, also bonded to S1, is coordinated to a cerium atom in a neighbouring zigzag chain.

Although the square Archimedean antiprism is the usual coordination polyhedron in known compounds with cerium(IV)—oxygen bonds, the eight oxygen atoms in this substance form a dodecahedron. Since they are of four different kinds: OH^- ions, water molecules, and sulfate oxygen atoms bonded to S1 or S2, it could be expected that there would be different bond lengths within the coordination polyhedron and that the cerium—hydroxide bond distances would be shorter than those of $\text{Ce}-\text{H}_2\text{O}$.

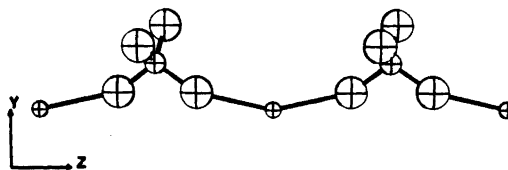


Fig. 3. The cerium-sulfate zigzag pattern viewed in the x direction.

This is, in fact, the case, the former being 2.223(7) and 2.289(7) Å, while the latter are 2.386(8) and 2.406(9) Å. The Ce–O(sulfate) bond lengths are intermediate between these two groups of Ce–O distances. Although three of the oxygen atoms in the S1 group are coordinated to cerium but only two of those in the S2 group are similarly coordinated, there is no significant difference between the Ce–O_S distances (mean Ce–O_{S1} = 2.332(8) Å; Ce–O_{S2} = 2.322(8) Å). The mean Ce–O distance is 2.328 Å. This value is close to those found in Ce₆O₄(OH)₄(SO₄)₆¹¹ (2.33 Å) and in Ce(CrO₄)₂·(H₂O)₂^{9d} (2.342 Å). Although the oxygen atoms in these structures form an antiprism, the mean Ce–O distances ought to be comparable, since a dodecahedron and an antiprism are nearly equivalent energetically. In CeOSO₄·H₂O^{6b} the corresponding mean is 2.364(5) Å, which is probably due to a different type of packing, a fact that is supported by the extremely short Ce–Ce distance: 3.568 Å (3.63 Å in cerium metal). In the cubically coordinated CeO₂¹² the mean Ce–O distance is 2.343(1) Å.

The average S–O distances in the sulfate groups are 1.465(9) Å for S1 and 1.473(9) Å for S2 and the mean O–O distances are 2.392(12) and 2.407(12) Å, respectively. These values agree well with mean S–O, 1.472 Å, and O–O, 2.404 Å, distances obtained in recently determined sulfate structures.¹³ The O–S1–O angles vary between 107.8 and 112.1°, the corresponding range in the O–S2–O angles being 107.3–113.0°. A higher irregularity is to be expected in the latter case, since only two of the oxygen atoms are bonded to cerium.

The unit cell contains two symmetrically independent water molecules, which form hydrogen bonds stabilizing the structure. These water molecules, W1 and W2, probably each form two hydrogen bonds, the W–O distances being short in each case, W1–O5: 2.768 Å, W1–O3: 2.759 Å, the O5–W1–O3 angle being 101.8°. For W2 the corresponding values are W2–O5: 2.749 Å, W2–O3: 2.742 Å, the O5–W2–O3 angle being 107.7°. All other short O–O distances are within the coordination polyhedron. Both O3 and O5 may thus act as acceptors in two hydrogen bonds and the fact that O3 and O5 are not coordinated to

cerium supports the theory that the hydrogen atoms of W1 and W2 are bonded to O3 and O5.

Acknowledgements. The author is very grateful to Professor G. Lindgren for many stimulating discussions during the work. He also wishes to thank Dr. S. Jagner for revising the English text. This investigation was supported by the Swedish Natural Science Research Council (Contract No. 2318).

REFERENCES

1. Lundgren, G. *Sven. Kem. Tidskr.* 71 (1959) 1.
2. Hansson, M. *Crystal Structure Investigations of some Zirconium and Hafnium Hydroxide Salts*, Diss., University of Gothenburg, Göteborg 1973.
3. Mark, W. *Crystal Structure Investigations on Complex Zirconium Compounds*, Diss., Chalmers University of Technology, Göteborg 1972.
4. Lindqvist, O. *The Oxygen Coordination of Tellurium(IV) and Tellurium(VI)*, Diss., University of Gothenburg, Göteborg 1973.
5. Allard, B. *The Coordination of Tetravalent Actinide Chelate Complexes with β-Diketones*, Diss., Chalmers University of Technology, Göteborg 1975.
6. a-d. Lindgren, O. *To be published.*
7. *International Tables for X-Ray Crystallography*, Kynoch Press, Birmingham 1959.
8. Lindqvist, O. and Wengelin, F. *Ark. Kemi* 28 (1967) 179.
9. The Programme Library of the Dept. of Inorg. Chem., Göteborg.
10. Cromer, D. T. and Waber, J. T. *Acta Crystallogr.* 18 (1965) 104.
11. Lundgren, G. *Ark. Kemi* 10 (1956) 183.
12. Magnéli, A. and Kihlberg, L. *Acta Chem. Scand.* 5 (1951) 578.
13. Nord, A. G. *On the Crystal Chemistry of Anhydrous Alkali Sulphates*, Diss., University of Stockholm, Stockholm 1974.

Received September 2, 1976.

The Crystal Structure of Cerium(IV) Dichromate Dihydrate, $\text{Ce}(\text{CrO}_4)_2(\text{H}_2\text{O})_2$

OVE LINDGREN

Department of Inorganic Chemistry, Chalmers University of Technology and the University of Göteborg, P.O. Box, S-402 20 Göteborg 5, Sweden

The crystal structure of $\text{Ce}(\text{CrO}_4)_2(\text{H}_2\text{O})_2$ has been determined by Fourier and least-squares analysis from film data taken with $\text{CuK}\alpha$ radiation. The compound crystallizes in the monoclinic space group $P2_1/m$ with $a = 6.5865(12)$ Å, $b = 10.6716(7)$ Å, $c = 5.6699(6)$ Å, $\beta = 92.59(1)^\circ$ and $Z = 2$.

A distorted bicapped trigonal prism is formed by the eight oxygens coordinated to the cerium atom which lies in a mirror plane. Two of the oxygens are water oxygens also situated in the mirror plane, while the other six belong to different chromate groups. The Ce—O bond distances vary between 2.232 and 2.575 Å, the average being 2.342 Å.

The structure was refined to a final R value of 8.4 %.

Investigations on the crystal structures of basic salts of some tetravalent elements (Ce^{IV} , Th^{IV} , U^{IV} , Ti^{IV} , Zr^{IV}) were started by Lundgren,¹ who made a general survey in the field. In connection with this, and also in order to study cerium-oxygen coordinations, investigations of crystal-line phases of the system CeO_2 — CrO_3 — H_2O were started. Crystals have been prepared by a number of methods, including hydrothermal hydrolysis and room temperature crystallisation from solutions of varying acidities. In this way it was possible to obtain several solid compounds, some of which were suitable for single crystal X-ray studies. The results from the crystal structure determination of one of these compounds, $\text{Ce}(\text{CrO}_4)_2(\text{H}_2\text{O})_2$, are reported below.

EXPERIMENTAL

Crystals of $\text{Ce}(\text{CrO}_4)_2(\text{H}_2\text{O})_2$ were prepared by dissolving freshly precipitated ceric hy-

drous oxide in concentrated chromic acid. Slow evaporation of this solution at room temperature, yielded crystals suitable for X-ray investigations. They were red, of trigonal prismatic shape and elongated along the c axis. The dimensions of the crystal chosen for data collection were $0.023 \times 0.070 \times 0.16$ cm.

$\text{Ce}(\text{CrO}_4)_2(\text{H}_2\text{O})_2$ forms monoclinic crystals. Guinier photographs calibrated with $\text{Pb}(\text{NO}_3)_2$ ² were taken, using $\text{CuK}\alpha_1$ radiation, and 44 lines were indexed. These were refined by means of the programme POWDER.³ The refined cell parameters with standard deviations (at 21 °C) are:

$$a = 6.5865(12) \text{ \AA}$$

$$b = 10.6716(7) \text{ \AA}$$

$$c = 5.6699(6) \text{ \AA}$$

$$\beta = 92.59(1)^\circ$$

$$V = 398.12 \text{ \AA}^3$$

A listing of the observed and calculated $\sin^2\theta$ values is available on request. The measured density, 3.37 g cm^{-3} , agrees with the calculated value, 3.40 g cm^{-3} , assuming a unit cell content of two formula units. The reflexions systematically absent were $0k0$ for $k = 2n + 1$, which indicates that the crystals belong to the space group $P2_1$ or $P2_1/m$.

Integrated multiple-film equi-inclination Weissenberg photographs $hk0$ — $hk4$ were recorded using Ni-filtered $\text{CuK}\alpha$ radiation. A total of 584 independent reflexions, which is about 32 % of those within the Cu-sphere, were obtained. The intensities were estimated visually using a scale prepared with a logarithmic wheel. The intra-level film ratios were calculated using the programme SCALE.⁴ Lorentz and polarisation corrections, as well as approximate inter-level scale factors based on exposure times, were then applied. The intensities were corrected for absorption in the later stages of the calculations, $\mu = 672 \text{ cm}^{-1}$.

Table 1. Atomic coordinates and temperature factors for $\text{Ce}(\text{CrO}_4)_2(\text{H}_2\text{O})_2$. Estimated standard deviations are given in parentheses. The thermal parameters have been multiplied by 10^4 for Ce and Cr and by 10^3 for O. The temperature factor is of the form $\exp[-2\pi^2(h^2a^{*2}U_{11} + \dots + klb^*c^*U_{23})]$.

Atom	<i>x</i>	<i>y</i>	<i>z</i>	U_{11}	U_{22}	U_{33}	U_{12}	U_{13}	U_{23}
Ce	0.04385(21)	0.25	0.22064	154(7)	141(7)	146(13)	0	-89(11)	0
Cr	0.25701(40)	0.04332(26)	0.74536(59)	128(13)	127(14)	138(26)	-13(17)	-51(24)	4(21)
O1	0.8401(23)	0.9014(14)	0.0092(33)	32(7)	27(7)	41(13)	-1(11)	6(13)	13(13)
O2	0.7749(18)	0.3866(12)	0.2649(28)	15(6)	17(6)	41(12)	0(9)	-11(11)	-9(11)
O3	0.5081(21)	0.9255(16)	0.2545(30)	19(6)	48(9)	26(11)	-16(11)	-10(11)	5(13)
O4	0.8570(20)	0.8891(12)	0.4833(31)	22(6)	16(6)	52(13)	-11(10)	-24(13)	23(13)
O5	0.4124(30)	0.25	0.2672(51)	16(8)	30(11)	76(22)	0	-16(18)	0
O6	0.1761(32)	0.75	0.1665(41)	31(9)	44(12)	8(15)	0	-14(16)	0

STRUCTURE DETERMINATION

The structure was determined using standard Patterson and Fourier techniques. A final refinement was carried out by the method of least squares. Scattering factors according to Cromer and Waber⁵ and Cruickshank's⁶ weighting scheme, $w = (a + |F_o| + c|F_o|^2 + d|F_o|^3)^{-1}$ with $a = 15$, $c = 0.013$ and $d = 0$ were used. A total of 66 parameters were refined from 584 reflexions. After three cycles all shifts were less than 1 % of the estimated standard deviations, and the *R* value was 8.4 %. The positional and thermal parameters are listed in Table 1. A list of observed and calculated structure factors can be obtained on request from the author.

DESCRIPTION AND DISCUSSION OF THE STRUCTURE

The chromate groups in $\text{Ce}(\text{CrO}_4)_2(\text{H}_2\text{O})_2$ are approximately layered since the *y*-coordinates of the chromium atoms differ only slightly from 0 and $\frac{1}{2}$. The cerium atoms and water molecules lie in the mirror planes between these layers. The main interatomic distances and angles, with their standard deviations, are quoted in Table 2. Fig. 1. shows a stereo drawing of the structure.

The oxygen coordination of cerium is eight-fold, cf. Fig. 2. Six of the oxygen atoms belong to six different chromate groups and the other two belong to water molecules. Four of the

Table 2. Interatomic distances (Å) and angles (°).

Ce - polyhedron				
Ce - O1	(2 ×)	2.232(16)	O1 - Ce - O1'	92.7(8)
- O2	(2 ×)	2.321(13)	O5 - Ce - O6	127.8(8)
- O4	(2 ×)	2.313(16)	O2 - Ce - O4	121.1(5)
- O5		2.430(20)	O2 - O2' - O4	90.5(4)
- O6		2.575(23)	O2 - O4 - O4'	89.5(4)
Average:		2.342	O5 - O1 - O6	106.6(6)
			O1 - O5 - O1'	71.8(9)
			O1 - O6 - O1'	69.0(8)
Chromate group				
Cr - O1		1.665(18)	O1 - Cr - O2	109.3(8)
- O2		1.685(13)	O1 - Cr - O3	109.7(8)
- O3		1.583(14)	O1 - Cr - O4	109.0(8)
- O4		1.636(16)	O2 - Cr - O3	109.0(8)
Average:		1.642	O2 - Cr - O4	111.1(7)
			O3 - Cr - O4	108.8(8)
Other distances in $\text{Ce}(\text{CrO}_4)_2(\text{H}_2\text{O})_2$				
O5 - O2		2.793(21)		
O6 - O3		2.905(22)		

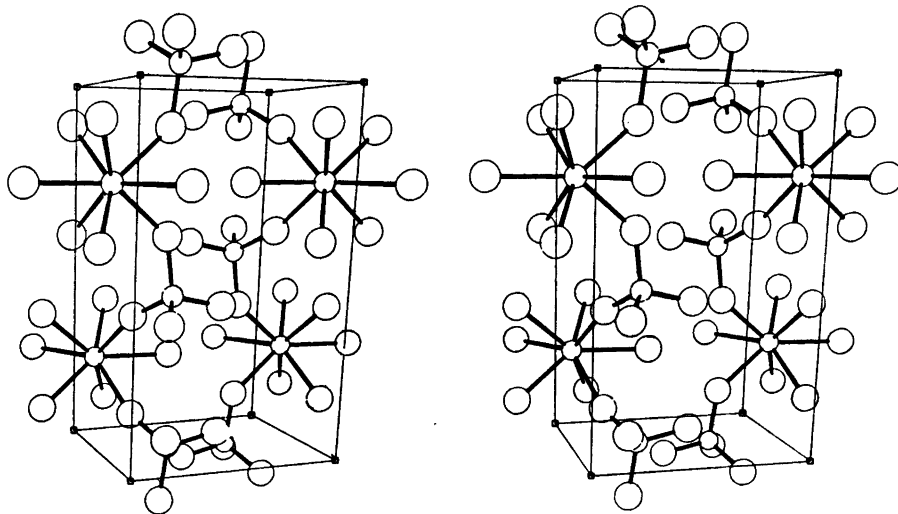


Fig. 1. A stereo drawing of the structure viewed approximately in the c -direction. The longest axis is the b axis.

chromate oxygens (O2, O2', O4, O4') are, for symmetry reasons, coplanar. They have Ce–O distances of 2.313 and 2.321 Å. The remaining two chromate oxygen atoms (O1, O1') and the two water molecules (O5, O6) form another but less regular cerium oxygen pyramid. The atoms O1 and O1' are at a distance of 2.232 Å from the cerium atom. The water molecules, on the other hand, are not equidistant from the cerium atom (2.430 and 2.575 Å) and the four oxygens O1, O1', O5 and O6 are not coplanar; the angle between the planes O1–O1'–O5 and O1–O1'–O6 is 158°. The configuration may be described as a distorted square antiprism or as

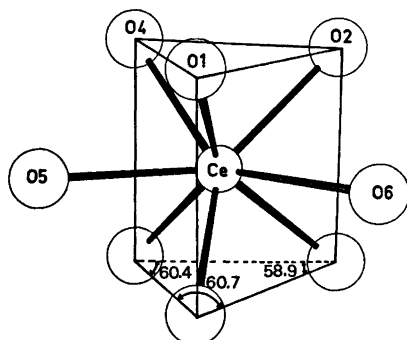


Fig. 2. A view of the coordination polyhedron.

Acta Chem. Scand. A 31 (1977) No. 3

a trigonal prism with water molecules on two faces, *cf.* Fig. 2. The average Ce–O distance is 2.342 Å.

The chromate group is bonded to three different Ce atoms with the fourth chromate oxygen O3 probably involved in hydrogen bonding to a water molecule, the O3–O6 and O3'–O6 distances being 2.905 Å. This is also reflected in the bond lengths within the chromate group, since the distances from the chromium atom to the three cerium-bonded oxygen atoms (mean 1.662 Å) are significantly longer than the fourth Cr–O distance (1.583 Å).

The other water molecule, O5, has six nearest neighbour oxygen atoms (two O1, two O2 and two O4) at distances less than 2.80 Å, the remaining O5–O distances being > 3.30 Å. O1 and O4 are bonded to the same Ce atom as O5 while the two O2 atoms are linked to another cerium atom. The protons of O5 are probably directed towards the O2 atoms, creating the possibility for hydrogen bonding.

Acknowledgements. The author would like to thank Professor Georg Lundgren for encouraging and valuable discussions concerning this work. Sincere thanks are also due to Dr. John Wood, who revised the English of this article.

This work has been financially supported by the Swedish Natural Science Research Council (Contract No. 2318).

REFERENCES

1. Lundgren, G. *Sven. Kem. Tidskr.* 71 (1959) 1.
2. *International Tables for X-Ray Crystallography*, Kynoch Press, Birmingham 1959, Vol. III, p. 122.
3. Lindqvist, O. and Wengelin, F. *Ark. Kemi* 28 (1967) 179.
4. The programme library of the Dept. of Inorg. Chem., Göteborg.
5. Cromer, D. T. and Waber, J. T. *Acta Crystallogr.* 18 (1965) 104.
6. Cruickshank, D. W. J. *The Equations of Structure Refinements*, Glasgow, October 1964.

Received October 8, 1976.

An X-Ray Investigation of Some Aqueous Zirconium(IV) Halide, a Hafnium(IV) Chloride, and Some Zirconium(IV) Perchlorate Solutions

MÄRTHA ÅBERG

Department of Inorganic Chemistry, Royal Institute of Technology, S-100 44 Stockholm 70, Sweden

The X-ray scattering from aqueous zirconium(IV) halide, hafnium(IV) chloride, and zirconium(IV) perchlorate solutions has been measured. The mol ratios $X/Zr=1$ and 2 ($X=Cl$ or Br) and $Cl/Hf=2$ have been studied. The mol ratio ClO_4/Zr has been varied from 1.7 to 4.3. The experimental data, excluding $X/Zr=1$, are consistent with the formation of a predominant tetranuclear complex, $[M_4(OH)_8(H_2O)_{16}]^{8+}$ ($M=Zr$ or Hf), with a structure similar to that of $[Zr_4(OH)_8(H_2O)_{16}]Cl_8 \cdot 12H_2O$ ($=ZrOCl_2 \cdot 8H_2O$) known from the solid state. Part of the halide ions are associated with the complex, and possible sites for these ions are discussed. For $X/Zr=1$ the scattering data indicate the formation of polymers, $[Zr_xO_x(OH)_{12-x}(H_2O)_{8+2x}]_n^{4+}$, built up from the discrete tetramers, $[Zr_4(OH)_8(H_2O)_{16}]^{8+}$, linked to each other through new O or double HO bridges in a random way.

Zr(IV) and Hf(IV) are known to undergo complicated hydrolysis even in very acidic aqueous solutions. The large amount of experimental results from solution chemistry studies of these metal ions has been reviewed by, *e.g.*, Solovkin and Tsvetkova,¹ Caletka,² Hala,³ and Larsen.⁴ From a compilation of published data Solovkin and Tsvetkova have concluded that there is no justification for the existence of the zirconyl ion, ZrO^{2+} , in aqueous solutions. The infrared⁵ and Raman⁶ spectra of some Zr(IV) salts also show no evidence for the presence of the $Zr=O$ group.

The predominant hydrolyzed complexes of Zr(IV) and Hf(IV) are polynuclear even in very dilute ($> 10^{-4} - 10^{-3}$ M) solutions of high acidity (1–2 M). Various experimental techniques such

as ultracentrifugation, spectrophotometry, potentiometry, light scattering, diffusion, and extraction have been utilized to characterize these complexes.⁷ Species such as $M_3(OH)_4^{6+}$ and $M_4(OH)_8^{8+}$ have been suggested, and in some investigations formation constants have been derived from the experimental data. The studies are complicated by the slowness with which the systems attain equilibrium.

Direct proofs for the existence of discrete polymeric species have been provided by Clearfield and Vaughan⁸ and by Mak⁹ through the determination of the crystal structure of $ZrOCl_2 \cdot 8H_2O$. This structure, which will be discussed more in detail below, is built up from the tetramers $[Zr_4(OH)_8(H_2O)_{16}]^{8+}$ linked to each other through chloride ions and water molecules. An X-ray diffraction study of aqueous solutions of zirconium and hafnium halides has been carried out by Muha¹⁰ to see whether or not the tetramer $[M_4(OH)_8(H_2O)_{16}]^{8+}$ remains intact when the compound $MOX_2 \cdot 8H_2O$ is dissolved. The results, which will also be discussed below, indicate that a tetramer with a structure similar to that in the solid state is the predominant complex in solution.

Thus, it has now been clearly shown that tetramers are the predominant polynuclear complexes for $Y/M=2$, where Y is a weak complexing anion like Cl^- , Br^- , or ClO_4^- . But very little is known about the structures of the species at other stages during the hydrolysis. In the present investigation zirconium perchlorate solutions with ClO_4/Zr mol ratios between 1.7 and 4.3 have been studied to see what structural

changes occur on acidification. No solutions with $X/Zr > 2.5$ ($X = Cl$ or Br) and a sufficiently high total concentration of Zr can be prepared because the solubility of $ZrOX_2 \cdot 8H_2O$ decreases as the amount of excess acid is increased. Also two zirconium halide solutions with $X/Zr = 1$, the minimum value obtainable, have been studied. Here higher complexes than tetramers are suggested to be the predominating species.⁴ As the data collected by Muha¹⁰ are not as accurate as those which can now be obtained, the scattering from some solutions with $X/M = 2$ has also been measured for comparison.

EXPERIMENTAL

Preparation and analysis of the solutions. Hydrous ZrO_2 (zirconium hydroxide) was precipitated by NH_3 from aqueous solutions of $ZrOCl_2 \cdot 8H_2O$ (*p.a.*). It was then dissolved in aqueous HCl , HBr , or $HClO_4$ of known concentrations. HfO_2 (*p.a.*) was melted with $Na_2B_4O_7 \cdot 10H_2O$ and the melt was then dissolved in HCl . Hydrous HfO_2 (hafnium hydroxide) was precipitated from the solution by NH_3 and was subsequently dissolved in aqueous HCl of known concentration. All solutions were allowed to stand on the water bath for about one month before measurements were performed.

The amount of Zr or Hf was determined by precipitation using NH_3 and ignition of the hydroxide to ZrO_2 or HfO_2 . The total amount of

anion present was determined by passing a portion of the solution, from which the metal ions had been removed by precipitation and filtration, through an H^+ -saturated cation exchanger. The free acid was then titrated with standardized $NaOH$. The densities of the solutions were determined pycnometrically.

The compositions of the solutions investigated are given in Table 1.

Measurements of the X-ray scattering. The diffractometer was the same as described previously.¹¹⁻¹³ $MoK\alpha$ radiation ($\lambda_{K\alpha} = 0.7107 \text{ \AA}$) was used for the measurements on the hafnium solution. For the zirconium solutions all scattering curves were measured with AgK radiation ($\lambda_{K\alpha} = 0.5608 \text{ \AA}$) to avoid fluorescence. A Philips X-ray generator PW 1130 was used. All measurements were carried out at $25^\circ C$.

The scattering was measured at discrete points from $\theta = 1^\circ$ up to $\theta = 70^\circ$, 2θ being the scattering angle. The opening slits used were $1/12$, $1/4$, and 1° . The scattering data were recalculated to a common slit width from measurements in overlapping regions. Usually 40 000 counts were taken for each point corresponding to a statistical error of 0.5%. For $\theta < \sim 20^\circ$ (or 6° for some solutions) points were measured at intervals of 0.1° and for $\theta > \sim 20^\circ$ (or 6°) intervals of 0.25° were used. All measurements were made twice.

Treatment of the intensity data. All calculations were carried out on an IBM 360/75 computer with the use of the KURVLR and PUTSLR programs.¹⁴

The measured intensity data were corrected for polarization in the sample and in the mono-

Table 1. Compositions of the solutions. The volume of a stoichiometric unit of solution containing one Zr(Hf) atom = V (\AA^3). n_{HO} = number of HO groups per Zr(Hf) atom as estimated from the analyses. I = halide solutions, II = perchlorate solutions.

Solution	I:1	I:2	I:3	I:4	I:5	II:1	II:2	II:3	II:4	II:5
Concentration in mol/l										
Hf	1.729									
Zr		2.598	3.822	3.124	3.269	2.663	2.880	3.007	2.445	2.074
Br				6.418	3.235					
Cl	3.485	4.974	4.003			4.462	6.689	8.409	8.649	8.925
O	55.52	55.18	57.58	51.98	56.02	67.00	70.94	73.05	72.96	72.59
H	107.61	104.95	103.87	97.89	102.21	92.12	83.53	75.21	75.59	74.41
Number of atoms in the unit of volume V										
Hf	1.000									
Zr		1.000	1.000	1.000	1.000	1.000	1.000	1.000	1.000	1.000
Br				2.055	0.990					
Cl	2.015	1.914	1.047			1.675	2.322	2.797	3.537	4.303
O	32.10	21.24	15.06	16.64	17.14	25.16	24.63	24.30	29.84	35.00
H	62.22	40.39	27.17	31.34	31.27	34.59	29.00	25.01	30.92	35.88
n_{HO}	1.985	2.086	2.953	1.945	3.010	2.325	1.678	1.203	0.463	-0.303
V	960.2	639.0	434.4	531.6	508.0	623.5	576.6	552.3	679.2	800.6

chromator by dividing by the factor $(1 + \cos 2\alpha \cos^2 2\theta)/(1 + \cos 2\alpha)$, where 2α is the scattering angle at the monochromator.¹⁴ Corrections for multiple scattering were applied, but they were almost negligible.¹⁴ The incoherent scattering passing through the monochromator was estimated in the way described previously.^{11,13,15}

For each solution the intensities were normalized to a stoichiometric unit of volume containing one Zr or Hf atom (Table 1). The scaling was done by comparing the observed intensities corrected for polarization and multiple scattering, $I_{\text{corr}}(s)$, where $s = 4\pi \sin \theta/\lambda$, with the calculated sum of the independent coherent and

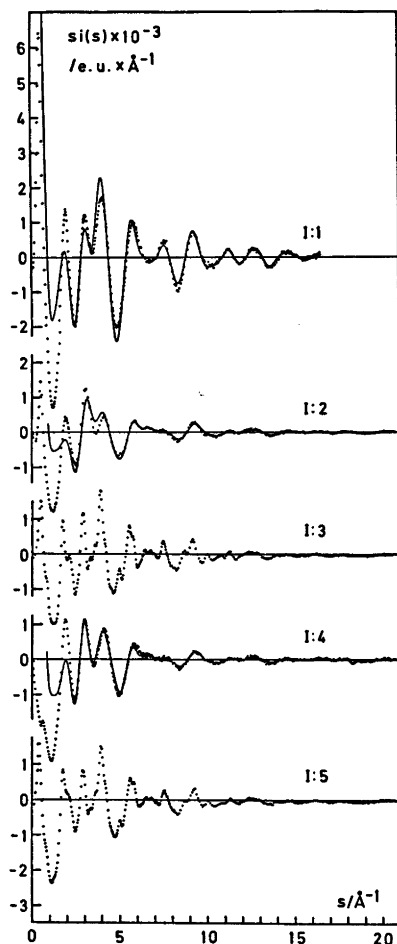


Fig. 1a. Reduced intensity functions, $i(s)$, multiplied by s for the halide solutions. The experimental values are given as dots. The full-drawn curves represent intramolecular contributions calculated with the use of parameters given by Mak,⁹ in Table 2, and in the text.

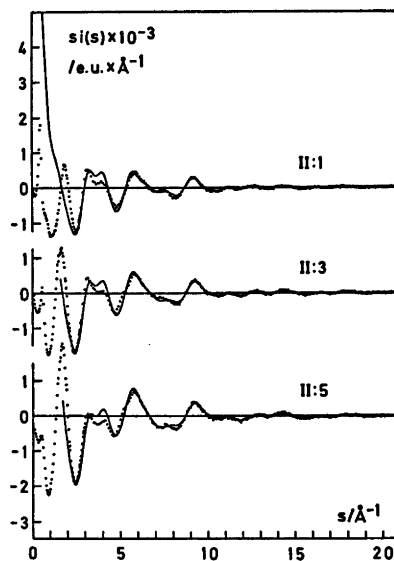


Fig. 1b. $si(s)$ functions for three of the perchlorate solutions. The full-drawn curves have been calculated with the use of parameters given by Mak⁹ and in the text.

the incoherent scattering in the high-angle region ($\theta > 55^\circ$).

The reduced intensity data, $i(s)$, were corrected for low-frequency additions resulting in spurious peaks below 1 Å in the radial distribution curves, which could not correspond to interatomic distances.¹⁴

From the reduced intensity values the electronic radial distribution functions were calculated:

$$D(r) = 4\pi r^2 \rho_0 + 2r/\pi \int_0^{s_{\text{max}}} si(s)M(s) \sin(rs) ds \quad (1)$$

The modification function, $M(s)$, was chosen to be $[f_{\text{Zr}}^2(0)/f_{\text{Zr}}^2(s)] \exp(-0.01s^2)$ and corresponding for Hf. ρ_0 is the average scattering density given by the square of the number of electrons per unit volume (V in Table 1). The observed $i(s)$ values were used for the integration, *i.e.*, no attempt was made to draw a smooth curve through the experimental points.

Theoretical pair interaction functions were calculated from:

$$i_{pq}(s) = \sum_{\substack{p, q \\ p \neq q}} [f_p(s)f_q(s) + \Delta f_p'' \Delta f_q''] \sin(r_{pq}s) \times (r_{pq}s)^{-1} \exp(-b_{pq}s^2) \quad (2)$$

Here r_{pq} is the distance between the atoms p and q and b_{pq} is a temperature factor related to the root mean square variation u_{pq} of the distance r_{pq} by $b_{pq} = u_{pq}^2/2$.

The Fourier inversion of $\sum i_{pq}(s)$ was made in the same way as that of the experimental reduced intensities.

The scattering factors, $f(s)$, used were those given by Cromer and Waber¹⁶ for Hf, Zr, Br, Cl, and O. For H the values given by Stewart *et al.*¹⁷ were used. Corrections for anomalous dispersion, $\Delta f'$ and $\Delta f''$, were taken from Cromer.¹⁸ Values for the incoherent radiation were taken from Cromer¹⁹ for Hf, Zr, Br, Cl, and O and from Compton and Allison²⁰ for H. They were corrected for the Breit-Dirac factor.

Tables of the normalized intensities and of the reduced intensity values for the investigated solutions are available from the author on request. The normalized intensities are corrected for incoherent radiation and the reduced intensity values corrected for spurious peaks below 1 Å. The reduced intensity values in the form $si(s)$ are also shown in Figs. 1a and 1b.

ANALYSIS OF THE DATA

Radial distribution curves, $D(r)$, are given in Figs. 2a and 2b, and $D(r) - 4\pi r^2 \rho_0$ functions are shown in Figs. 3a and 3b.

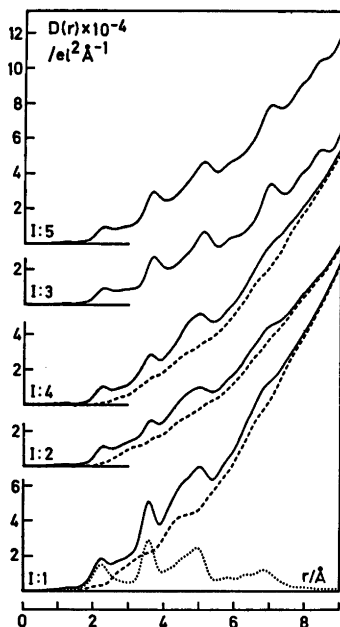


Fig. 2a. Radial distribution curves, $D(r)$, for the halide solutions. The dashed curves are the differences between the experimental functions and the calculated intramolecular contributions. The sum of the intramolecular contributions is also given separately for solution 1:1.

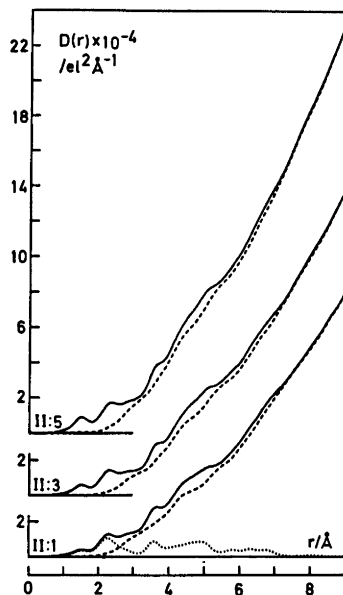


Fig. 2b. $D(r)$ curves for three of the perchlorate solutions. The sum of the intramolecular contributions is given separately for solution 11:1.

Early X-ray scattering data on aqueous solutions of $MOX_3 \cdot 8H_2O$ ($M = Zr$ or Hf , $X = Cl$ or Br) collected by Muha¹⁰ were explained by assuming the existence of a complex $[M_4(OH)_8(H_2O)_{16}]X_8$ with a structure similar to that which at that time was known from the solid state. But in the first crystal structure determination of $ZrOCl_3 \cdot 8H_2O$ made by Clearfield and Vaughan⁸ from two-dimensional data, only the Zr atoms were located with any degree of accuracy. Later on, a refinement of the structure based on three-dimensional data was carried out by Mak.⁹ He found the main features of the old structure to be correct, but the coordination polyhedron of O atoms about each Zr atom to be more closely related to the dodecahedron rather than the square antiprism suggested by Clearfield and Vaughan. The structure is built up from discrete $[Zr_4(OH)_8(H_2O)_{16}]^{8+}$ tetramers linked to each other through a network of Cl^- ions and water molecules. In the tetramer (Fig. 4) the Zr atoms are in a slightly puckered square configuration. Adjacent Zr atoms are joined through double HO bridges with one O atom above and the other below the mean square plane. The dis-

torted dodecahedron about each Zr atom is completed by terminal O atoms from four coordinated water molecules.

With the use of the positional parameters from the crystal structure determined by Mak the expected peak shapes for the tetramer $Zr_4O_8O_{16}$ (H atoms being omitted) were calculated. The temperature factors were assumed to be 0.003 \AA^2 for Zr–Zr interactions, 0.0065 \AA^2 for Zr–O interactions, and 0.01 \AA^2 for O–O interactions. The calculated peak shapes are shown in Fig. 5. Comparison with the functions $D(r) - 4\pi r^2 \rho_0$ in Figs. 3a and 3b and also with the $D(r)$ functions in Figs. 2a and 2b shows similar peaks to be present for all the solutions investigated, halide as well as perchlorate solutions, except the zirconium halide solutions with $n_{HO} = 3$. These two solutions behave differently and will be discussed separately.

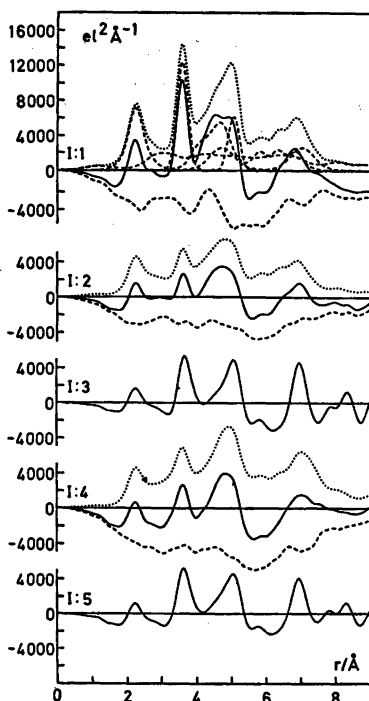


Fig. 3a. Functions $D(r) - 4\pi r^2 \rho_0$ (full-drawn) for the halide solutions and theoretical peak shapes for the $M_4O_8O_{16}X_8$ complex (dotted). The lower dashed curves are obtained when the calculated peak shapes are subtracted from the experimental $D(r) - 4\pi r^2 \rho_0$ curves. For solution I:1 the Hf–Hf, Hf–O, Hf–Cl, and light-atom interactions are drawn separately (upper dashed curves).

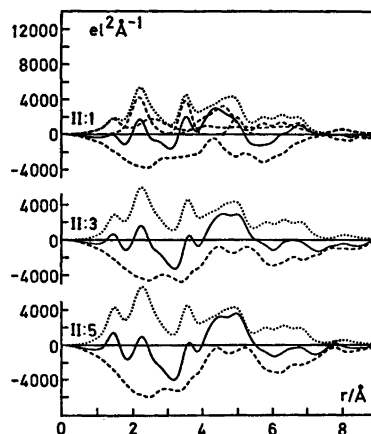


Fig. 3b. Functions $D(r) - 4\pi r^2 \rho_0$ for three of the perchlorate solutions and theoretical peak shapes for the $Zr_4O_8O_{16}$ and ClO_4^- complexes. For solution II:1 the Zr–Zr, Zr–O, and light-atom interactions are drawn separately (upper dashed curves).

Fig. 5 also shows the difference curve obtained when the sum of the intramolecular interactions within the $Zr_4O_8O_{16}$ group is subtracted from the experimental $D(r) - 4\pi r^2 \rho_0$ function for solution I:2. This curve represents the remaining interactions in the solutions. Broad peaks are found around 3.1, 4.6, and 7.0 Å. They contain contributions from the coordination of the Cl^- ions and from that part of the water structure which has not been broken down by the solute species. All intermolecular interactions will also contribute to the remaining structure of the solution.

The halide solutions with $n_{HO} = 2$

Analyses of the intramolecular interactions within the $M_4O_8O_{16}$ group ($M = Zr$ or Hf) for the three halide solutions with $n_{HO} = 2$ were made by least squares refinement procedures using the PUTSLR program.¹⁴ The experimental reduced intensity values, $i(s)$, were compared with $\sum i_{pq}(s)$ values calculated from eqn. (2). For each pair interaction a distance r_{pq} , a temperature factor b_{pq} , and a frequency factor n_{pq} were introduced as parameters that could be varied. A minimum was sought for the error square sum $U = \sum w(s)[i(s) - \sum i_{pq}(s)]^2$. The weighting function $w(s) = \cos \theta / I_{corr}^2(s)$ was chosen. With

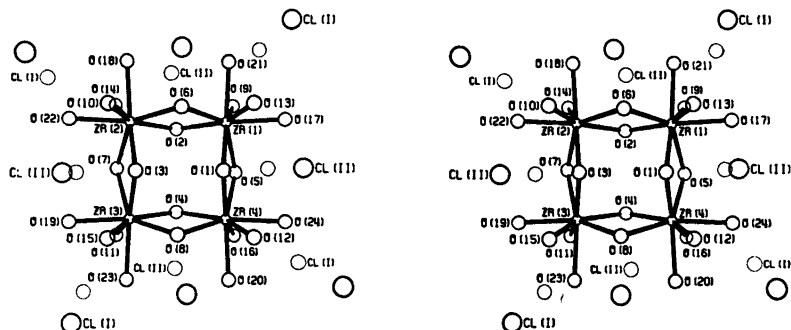


Fig. 4. A stereoscopic view of the tetranuclear complex $[\text{Zr}_4(\text{OH})_8(\text{H}_2\text{O})_{16}]^{8+}$ drawn with the use of the positional parameters given by Mak.⁹ The two chloride sites, Cl(I) and Cl(II), outside the complex are also shown.

this weighting function the contribution to U from each experimental point is inversely proportional to the square of its estimated standard deviation.

As the curves in Fig. 5 indicate that no significant deviations from the positional parameter values obtained by Mak.⁹ seem to occur for $\text{Zr}_4\text{O}_8\text{O}_{16}$ in solution 1:2, only the temperature factors for the interactions within the $\text{M}_4\text{O}_8\text{O}_{16}$ complex were adjusted by means of the least squares procedures. Experimental data for $s_{\min} < s < s_{\max}$, where $s_{\max} = 16 \text{ \AA}^{-1}$ (MoK radiation) or 20 \AA^{-1} (AgK radiation), were used, s_{\min} being varied from 6.5 to 10 \AA^{-1} . The average values obtained were: $b_{\text{M}-\text{M}} = 0.0030(1) \text{ \AA}^2$, $b_{\text{M}-\text{O}} = 0.0035(2) \text{ \AA}^2$, and $b_{\text{O}-\text{O}} = 0.0040(3) \text{ \AA}^2$.

With the use of the refined values of the temperature factors theoretical curves similar to those in Fig. 5 were calculated for the three halide solutions with $n_{\text{HO}} = 2$. The new difference

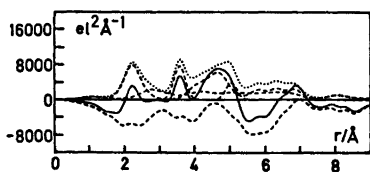


Fig. 5. Expected peak shapes for the tetramer $\text{Zr}_4\text{O}_8\text{O}_{16}$ calculated from the positional parameters given by Mak.⁹ The upper dashed curves represent Zr-Zr, Zr-O, and O-O interactions. The dotted curve gives the sum of all intramolecular interactions. The lower dashed curve is the difference between the $D(r) - 4\pi r^2 \rho_0$ for solution 1:2 (full-drawn curve) and the sum of the intramolecular interactions within the tetramer.

curves are shown in Fig. 6. Because of the high charge of the $[\text{M}_4(\text{OH})_8(\text{H}_2\text{O})_{16}]^{8+}$ complex it seems reasonable to assume that halide ions are arranged in a second coordination sphere outside the tetramer, probably being held in place by electrostatic forces. In the solid state many Zr-Cl distances are found in the regions $4.6-5.0$ and $7.0-7.3 \text{ \AA}$.⁹ The residual peaks at these r values have thus been assigned to M-X interactions. Further support for such an interpretation is given by the sizes of the peaks which correspond to about two M-X interactions/M atom in each of the two regions. In addition the difference curves in Fig. 6 indicate that for the zirconium bromide solu-

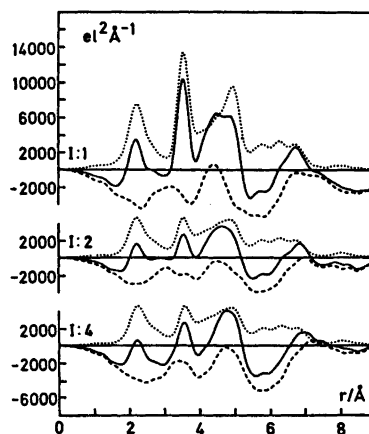


Fig. 6. Difference curves for the halide solutions with $n_{\text{HO}} = 2$ (dashed) obtained by subtracting the calculated peak shapes for the $\text{M}_4\text{O}_8\text{O}_{16}$ complex (dotted) from the experimental $D(r) - 4\pi r^2 \rho_0$ functions (full-drawn).

Table 2. Parameters for the halide ions. (X, Y, Z) are the positional parameters (\AA) in a coordinate system with the origin at the centre of the M_4 square and the x and y axes directed horizontally and vertically, respectively, (Fig. 4), r_{M-X} = $M-X$ distance (\AA), b = temperature factor (\AA^2), and n_{M-X} = frequency factor (number of $M-X$ distances/ M atom).

Solution	(X, Y, Z) ^a	r_{M-X}	$\begin{matrix} b_{X-X} \\ b_{M-O} \end{matrix}$
I:1	3.79, 0, ± 3.83	4.68	0.043 ^c
		6.99	
I:2	3.79, 0, ± 3.83	4.68	0.043 ^c
		6.99	
I:4	3.89(2), 0, $\pm 3.96(2)$ ^b	4.83	0.043(2) ^{bc}
		7.14	

^a Remaining parameter values are obtained from the S_4 point group symmetry. ^b These values were obtained from a least squares refinement series using experimental data for $2.2 \text{ \AA}^{-1} < s < 8.8 \text{ \AA}^{-1}$. ^c $n_{M-X} (= \frac{1}{2} n_{M-X}^{\max}) = 2$. Non-coordinated halide ions are assumed to be octahedrally surrounded by water molecules ($r_{Cl-O} = 3.1 \text{ \AA}$, $r_{Br-O} = 3.25 \text{ \AA}$, $b_{X-O} = 0.043 \text{ \AA}^2$) when parameters from this table are used for calculations of theoretical peak shapes.

tion the $M-X$ distances are longer than those for the two chloride solutions.

Preliminary theoretical peak shapes based on the rather irregular arrangement of halide ions in the positions II in the solid state (Fig. 4), four $M-X$ distances per M atom in each of the two regions, gave a rather good explanation of the experimental data when an occupancy factor of 0.5 was used. Therefore, the halide positions II were arranged more symmetrically, and a least squares refinement series was performed using data for the zirconium bromide solution. Three parameters were varied: two positional parameters and one temperature factor. The results are given in Table 2.

Theoretical peak shapes for the complexes $M_4O_8O_{16}X_8$ with the parameters for the halide ions taken from Table 2 are shown in Fig. 3a. They seem to give a satisfactory explanation of the experimental data for the zirconium halide solutions with $n_{HO} = 2$ (I:2 and I:4). But for the hafnium chloride solution (I:1) there is a residual peak at 4.3 \AA which is too pronounced to be due only to the highly damped intermolecular interactions. As this peak may be interpreted in many different ways, no additional structural

models including interactions at 4.3 \AA have been tested quantitatively.

For the positions I in the solid state (Fig. 4) the $Zr-Cl$ distances range from 4.9 to 10.2 \AA . Due to this spread no pronounced difference is obtained when these positions are included in the structural model for the solutions. For a more symmetrical arrangement of the positions I, there are for each Zr atom: two $Zr-Cl$ distances at about 4.7 \AA , four at about 7.0 \AA , and two at about 8.7 \AA which do not seem to be in very good agreement with the difference curves in Fig. 6. This means that the positions I alone do not give a satisfactory explanation of the experimental data and that no better agreement is obtained on adding these positions to a structural model including the positions II.

The perchlorate solutions

Because of the low atomic number of Zr the ClO_4 groups contribute relatively more to the X-ray scattering in the zirconium perchlorate solutions than in, e.g., the mercury perchlorate solutions investigated previously.¹³ For this reason, the distance and the temperature factor for the $Cl-O$ interaction in a tetrahedral ClO_4 group were refined in a series of least squares procedures. The temperature factor for the $O-O$ interactions was kept constant at 0.004 \AA^2 . Theoretical intensity values for the $Zr_4O_8O_{16}$ complex calculated with the same parameters, as were used for Fig. 6, were introduced as a constant background during the refinements. Experimental data for $s_{\min} < s < 20 \text{ \AA}^{-1}$ were used, and s_{\min} was varied from 4 to 10 \AA^{-1} . The average values obtained were: $r_{Cl-O} = 1.465(4) \text{ \AA}$ ($r_{O-O} = 2.40 \text{ \AA}$) and $b_{Cl-O} = 0.0031(3) \text{ \AA}^2$.

In a second step of the least squares refinements the temperature factors for the interactions within the $Zr_4O_8O_{16}$ complex were adjusted. Experimental data for $s_{\min} < s < 20 \text{ \AA}^{-1}$ with s_{\min} varying from 4 to 10 \AA^{-1} were used. The average values obtained were: $b_{Zr-Zr} = 0.0028(1) \text{ \AA}^2$, $b_{Zr-O} = 0.0037(3) \text{ \AA}^2$, and $b_{O-O} = 0.0046(5) \text{ \AA}^2$. Calculated peak shapes for the $Zr_4O_8O_{16}$ and ClO_4 complexes based on the refined structural parameters are given in Fig. 3b.

If it is assumed that the intermolecular interactions are very similar in the three halide solutions with $n_{HO} = 2$, differences between the experimental radial distribution curves will

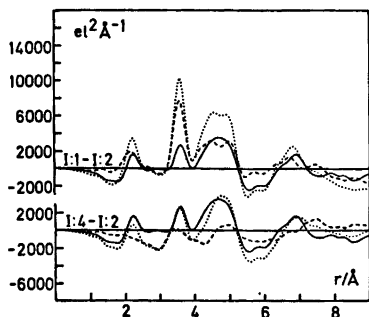


Fig. 7. Difference curves between the experimental radial distribution functions $D(r) - 4\pi r^2 \rho_0$ for the halide solutions with $n_{\text{HO}} = 2$ (dashed). The full-drawn curve is always subtracted from the dotted curve.

mainly reflect differences in the intramolecular interactions within the $M_4O_8O_{16}X_8$ complexes. Such difference curves obtained by subtracting the $D(r) - 4\pi r^2 \rho_0$ function for solution I:2 from those of the other two halide solutions with $n_{\text{HO}} = 2$ are shown in Fig. 7.

The difference curve for the chloride solutions has peaks in regions where the interactions involving the metal atoms are expected to occur according to the suggested structural model: 2.2 Å (M-O), 3.55 Å (M-M), 4-5 Å (M-O,

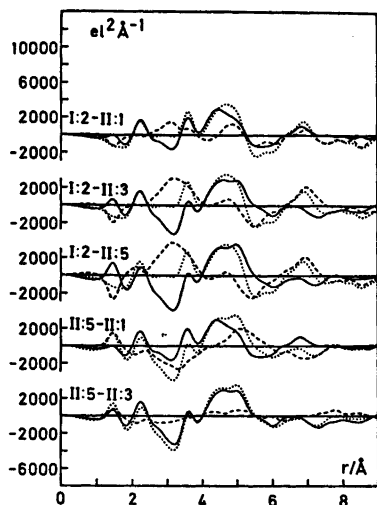


Fig. 8. Difference curves between the experimental radial distribution functions $D(r) - 4\pi r^2 \rho_0$ for solution I:2 and three of the perchlorate solutions (dashed) and for the perchlorate solutions (dashed).

M-Cl, M-M), and 6.2-7 Å (M-O, M-Cl) (compare Fig. 5) reflecting the higher scattering power of Hf compared to Zr.

The difference curve for the zirconium halide solutions has peaks in regions where the interactions involving the halide ions are expected to occur according to the suggested structural model: 3.4 Å (X-O), 4.5-5.2 Å (Zr-X, X-O, X-X), and 7-7.7 Å (Zr-X, X-O, X-X) reflecting the difference in scattering power between Br and Cl.

Difference curves calculated by subtracting the $D(r) - 4\pi r^2 \rho_0$ functions for the perchlorate solutions from that of solution I:2 (Fig. 8) show as main features (apart from the negative perchlorate peaks) peaks around 3.2 Å (Cl-O), 4.75 Å (Zr-Cl), and 7 Å (Zr-Cl) which strongly support the suggested structural models.

Difference curves calculated by subtracting the $D(r) - 4\pi r^2 \rho_0$ functions for the solutions II:1 to II:4 from that of solution II:5 (Fig. 8) show a broad peak at about 5 Å. This increases in size as the difference in the perchlorate concentration increases.

The halide solutions with $n_{\text{HO}} = 3$

On comparing the scattering curves in Fig. 1a it is obvious that the two halide solutions with $n_{\text{HO}} = 3$ behave quite differently from those with $n_{\text{HO}} = 2$. A structural change has occurred when the degree of hydrolysis has been increased. It is also seen from the scattering curves that the more hydrolyzed solutions seem to contain very large molecules. The Fourier inversions of the reduced intensity values (Figs. 2a and 3a) also have peaks at r values greater than 9 Å.

From a comparison between the $D(r) - 4\pi r^2 \rho_0$ curves for the two structurally different types of halide solutions (Fig. 9), the following characteristics of the structure of the large molecules may be deduced: (1) The first coordination sphere of O atoms around Zr is not changed. It still contains eight O atoms at the same Zr-O distances as in the complex $[\text{Zr}_4(\text{OH})_8(\text{H}_2\text{O})_{16}]^{8+}$. (2) The peak at 3.6 Å (for $n_{\text{HO}} = 2$) is higher and broader for the more hydrolyzed solutions. This means that in the large aggregates the number of Zr-Zr distances per Zr atom at 3.6 Å is larger than one. The peak sizes give

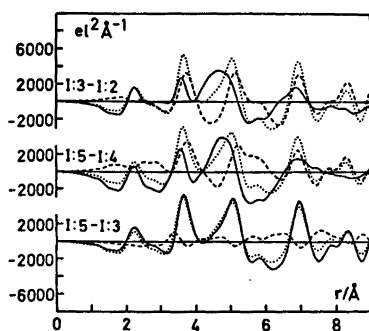


Fig. 9. Difference curves between the experimental radial distribution functions $D(r) - 4\pi r^2 \rho_0$ for the zirconium halide solutions (dashed).

about two such distances per Zr atom. The broadness of the peaks indicates a distribution of Zr-Zr distances in the region 3.55–3.75 Å. (3) The third peak in the $D(r) - 4\pi r^2 \rho_0$ curves has moved to higher r values as the degree of hydrolysis has been increased. Subtraction of the curve for the zirconium bromide (chloride) solution with $n_{\text{HO}}=2$ from that of the corresponding solution with $n_{\text{HO}}=3$ (Fig. 9) results in difference curves with a residual peak at about 5.15 Å (i.e. $3.65\sqrt{2}$ Å). Thus, if it is assumed that the second coordination sphere of O atoms about Zr is essentially the same, further hydrolysis of the tetramers gives large aggregates having more than 0.5 Zr-Zr distances per Zr atom in the region 5–5.15 Å. The peak sizes give about two such distances per Zr atom. (4) There is also a large peak at 6.95 Å which most probably is due mainly to Zr-Zr interactions. The size of the peak indicates about two Zr-Zr distances per Zr atom at a distance which is somewhat less than twice the mean shortest Zr-Zr distance in the large molecules (2×3.65 Å = 7.3 Å). (5) There is no clear indication of a coordination of halide ions in the second coordination sphere around Zr. This is seen from the featureless difference curve between the $D(r) - 4\pi r^2 \rho_0$ functions for the two halide solutions with $n_{\text{HO}}=3$ in Fig. 9.

The scattering curves for the two zirconium halide solutions with $n_{\text{HO}}=3$ are not similar to any of the diffraction patterns reported in the ASTM card index of the various modifications of ZrO_2 (cubic, tetragonal, or monoclinic).

Acta Chem. Scand. A 31 (1977) No. 3

Clearfield²¹ has discussed a probable mechanism for the hydrolytic polymerization of the species $[\text{Zr}_4(\text{OH})_8(\text{H}_2\text{O})_{16}]^{8+}$. The polymerization is suggested to occur by the formation of double HO bridges between tetramers, the new bridges being at right angles to those already present. The arrangement is supposed to be irregular when just adding HO^- to a solution containing tetrameric Zr(IV) complexes, but it is supposed to be ordered after refluxing the Zr(IV) solution.

The scattering curves for the two zirconium halide solutions with $n_{\text{HO}}=3$ may be explained by assuming randomly formed polymers according to Clearfield. The polymer drawn in Fig. 10 is one example of a complex containing about two Zr-Zr distances per Zr atom in each of the r regions around 3.65, 5.15, and 6.95 Å. It has, as a mean, $n_{\text{HO}}=3$.

DISCUSSION

Radial distribution curves give only one-dimensional representations of the structures of the three-dimensional complexes in a solution. Many structural models that give a good explanation of the experimental data may therefore be derived. But from the scattering curves obtained here it seems reasonable to assume that the complex $\text{M}_4\text{O}_8\text{O}_{16}$ with a structure known from the solid state⁹ is predominating in all the solutions investigated, halide as well as perchlorate solutions. The halide solutions with $n_{\text{HO}}=3$ are, of course, excepted. The intensity data are, however, not very sensitive to changes in the parameters of interactions including only light atoms. Thus, a small rearrangement of the coordinated water

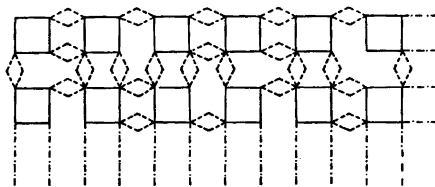


Fig. 10. A two-dimensional representation of a randomly formed polymer $[\text{Zr}_4(\text{OH})_{12}(\text{H}_2\text{O})_8]_n^{4+}$. The solid lined squares denote the original tetramers and the dashed lines represent new Zr-OH bonds formed by hydrolysis.

molecules in $M_4O_8O_{16}$ may not change the calculated curves significantly.

It seems unlikely that the halide ions which are not directly coordinated to the metal atom in the solid (Fig. 4) should enter the first coordination sphere in solution. In the crystal structure of, e.g., $Zr(CH_3COCHCOCH_3)_3Cl$, where Zr(IV) is seven-coordinated, the Zr-Cl bond length is 2.47 Å.²² The radial distribution curves (Figs. 2a and 3a) do not show any peaks in this region.

In the solid state two crystallographically different sites are occupied by the halide ions. They are called I and II in Fig. 4. With four halide ions statistically distributed over the eight II positions, the calculated difference curves in Figs. 2a and 3a show no pronounced peaks related to intramolecular interactions not included in the structural model for the zirconium halide solutions. For the hafnium chloride solution, however, there remains an unexplained peak at 4.3 Å which is too large to be related to highly damped intermolecular interactions only. This peak may be due to Hf-Cl and (or) Hf-O interactions within the second coordination sphere. Another explanation is that condensation into higher complexes has taken place. But there seems to be no reason to assume that complexes of higher nuclearity should occur in hafnium chloride than in zirconium halide solutions of the same degree of hydrolysis. Furthermore, when condensation occurs, the ultracentrifugation measurements indicate a higher average nuclearity for Zr.²³

It might be possible to get a still better agreement between experimental and calculated scattering data by trying more complicated structural models for the halide solutions ($n_{H_2O} = 2$) not necessarily based on or related to the halide positions I and II in the solid state. But the model including the II positions fractionally occupied seems to be the simplest one which adequately explains the scattering data. The contact distances to neighbouring O atoms are then 3.1–3.5 Å for the Cl^- and 3.2–3.6 Å for the Br^- ion. These values are roughly in agreement with the sum of the ionic radii.

Muha¹⁰ in his early investigation of the structure of aqueous solutions of $MOX_2 \cdot 8H_2O$ ($M = Zr$ or Hf , $X = Cl$ or Br) explained his

scattering data by assuming the existence of a complex $[M_4(OH)_8(H_2O)_{16}]X_8$. The structural parameters for the complex $M_4O_8O_{16}$ were taken from the old crystal structure determination by Clearfield and Vaughan.⁸ Nevertheless Muha found residual peaks of about equal size at 4.6 and 7.3 Å for a 2 molal hafnium bromide solution. These peaks were attributed to Hf-Br interactions. Several structural models were tested, but the one based on halide ions in positions II were found to give the best agreement between experimental and calculated data for the hafnium halide solutions. The data did not permit a definite conclusion concerning the average number of chloride ions associated with a $Hf_4O_8O_{16}$ complex to be drawn, but for the bromide solutions the halide sites seemed to be fractionally occupied.

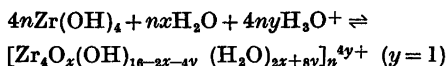
For the perchlorate solutions the difference curves in Fig. 3b are all very similar regardless of the degree of acidity. Thus it seems that the complex $Zr_4O_8O_{16}$ is formed rapidly when $HClO_4$ is added to hydrous ZrO_2 , giving $ClO_4/Zr = 2$, but that it remains intact on further acidification even after "equilibrating" the solutions for one month on the water bath. All the difference curves show broad peaks at about 2.9, 4.3, 5.25, 6.5, and 7.8 Å. The peak at 5.25 Å gets larger as the ClO_4/Zr ratio is increased. If the ClO_4 group enters the second coordination sphere around Zr the expected Zr-Cl distance would be about 5.25 Å. No quantitative analyses of the residual peaks were made due to the large number of ways for arranging ClO_4 about a $Zr_4O_8O_{16}$ complex.

The peak at 4.3 Å found in the difference curves of the hafnium chloride solution is seen also for the zirconium halide solutions, although of much smaller size. Thus, as a pronounced peak at this r value was found for the perchlorate solutions as well, it seems more likely that this peak is due mainly to M-O interactions from a second coordination sphere of water molecules rather than to interactions involving halide ions. Furthermore, the size of the peak is about the same for the zirconium bromide and chloride solutions.

For the most hydrolyzed perchlorate solution $n_{H_2O} = 2.3$. Although $n_{H_2O} > 2$ there seems to be no tendency towards formation of polymers, e.g., of the type suggested in Fig. 10. The difference curve for solution II:1 in Fig. 3b has

no unexplained peaks around 3.65, 5.15, and 6.95 Å. Instead, it is similar to the difference curves for the perchlorate solutions with lower degrees of hydrolysis (II:2–II:5).

A possible scheme for the formation of polymers with a random structure in the zirconium halide solutions with $n_{\text{HO}} = 3$ is:



The factor x takes into account the possible formation of an O bridge and a coordinated water molecule instead of a double HO bridge in and (or) between some tetramers. The coordination number of Zr is assumed to be eight.

Acknowledgements. I wish to thank Dr. Georg Johansson for his interest in this work, Civ. ing. Magnus Sandström for valuable help in handling the computer programs, and B. Sc. Ian Duncan for revising the English of the text.

The work has been financially supported by the Swedish Natural Science Research Council. Computer time has been made available by the Computer Division of the National Swedish Office for Administrative Rationalization and Economy.

REFERENCES

- Solovkin, A. S. and Tsvetkova, S. V. *Russ. Chem. Rev.* 31 (1962) 655.
- Caletka, R. *Chem. Listy* 58 (1964) 349.
- Hala, J. *U. S. At. Energy Comm., Accession No. 35508 Rept. No. UJV-1066/64.*
- Larsen, E. M. *Adv. Inorg. Chem. Radiochem.* 13 (1970) 1, and references therein.
- Hardy, C. J., Field, B. O. and Scargill, D. *J. Inorg. Nucl. Chem.* 28 (1966) 2408.
- Baglin, F. G. and Breger, D. *Inorg. Nucl. Chem. Lett.* 12 (1976) 173.
- Sillén, L. G. and Martell, A. (compilers) *Stability Constants of Metal-Ion Complexes*, Chem. Soc. Spec. Publ. No. 17 (1964); Suppl. No. 1, Spec. Publ. No. 25 (1971).
- Clearfield, A. and Vaughan, P. A. *Acta Crystallogr.* 9 (1956) 555.
- Mak, T. C. W. *Can. J. Chem.* 46 (1968) 3491.
- Muha, G. M. and Vaughan, P. A. *J. Chem. Phys.* 33 (1960) 194; Muha, G. M. *Univ. Microfilms L. C. Card No. Mic 60-1445, Diss. Abstr.* 20 (1960) 4292.
- Johansson, G. *Acta Chem. Scand.* 20 (1966) 553.
- Gaizer, F. and Johansson, G. *Acta Chem. Scand.* 22 (1968) 3013.
- Johansson, G. *Acta Chem. Scand.* 25 (1971) 2787.
- Johansson, G. and Sandström, M. *Chem. Scr.* 4 (1973) 195.
- Pocov, S. and Johansson, G. *Acta Chem. Scand.* 27 (1973) 2146.
- Cromer, D. T. and Waber, J. T. *Acta Crystallogr.* 18 (1965) 104.
- Stewart, R. F., Davidson, E. K. and Simpson, W. T. *J. Chem. Phys.* 42 (1965) 3175.
- Cromer, D. T. *Acta Crystallogr.* 18 (1965) 17.
- Cromer, D. T. *J. Chem. Phys.* 50 (1969) 4857.
- Compton, A. H. and Allison, S. K. *X-Rays in Theory and Experiment*, van Nostrand, New York 1935.
- Clearfield, A. *Rev. Pure Appl. Chem.* 14 (1964) 91.
- von Dreele, R. B., Stezowski, J. J. and Fay, R. C. *J. Am. Chem. Soc.* 93 (1971) 2887.
- a. Johnson, J. S., Kraus, K. A. and Holmberg, R. W. *J. Am. Chem. Soc.* 78 (1956) 26; b. Johnson, J. S. and Kraus, K. A. *Ibid.* 3937.

Received August 11, 1976.

The Crystal Structure of *trans*-Dichlorobis[(—)-1(*R*),2(*R*)-cyclohexanediamine]platinum(IV)-bis[(—)-1(*R*),2(*R*)-cyclohexanediamine]platinum(II) Tetrachloride. A Note on the Corresponding Bromide Compound

KARL PEDER LARSEN^a and HANS TOFTLUND^b

^a Department of Inorganic Chemistry, Aarhus University, DK-8000 Aarhus C, Denmark and

^b Department of Chemistry, Odense University, DK-5000 Odense, Denmark

The title compound is orthorhombic, *I*222 with $a = 24.268(4)$ Å, $b = 6.820(1)$ Å, $c = 5.158(1)$ Å, and $Z = 1$. The structure has been solved by conventional X-ray methods and refined by the method of least-squares to an *R*-value of 0.025 based on 1528 independent counter reflections. The structure consists of a stacking of chains parallel to the *c*-axis along which quadratic $[\text{Pt}(-\text{chxn})_2]^{2+}$ and tetragonal $[\text{Pt}(-\text{chxn})_2\text{Cl}_2]^{2+}$ alternate. The Pt—Cl and Pt—N distances are 2.324(2) Å and 2.056(4) Å, respectively. The cyclohexane ring has the chair conformation with the nitrogen atoms in equatorial positions.

Platinum(III) complexes containing amines and halogens as ligands are now generally believed not to exist. X-Ray investigations¹⁻⁷ have shown that these compounds more adequately are described as mixed-valence complexes of quadratically coordinated Pt(II) and octahedrally coordinated Pt(IV) linked together by unsymmetrical halide bridges. The compounds subjected to X-ray investigations until now, have all shown a certain degree of disorder revealed as continuous streaks in reciprocal space and interpreted as due to stacking faults. The initial X-ray examination of the present compound by film methods showed no sign of partial disorder. A complete three-dimensional X-ray analysis has therefore been undertaken in an attempt to clarify the structure of these mixed-valence Pt complexes. The analogous bromide $[\text{Pt}(-\text{chxn})_2\text{Br}_2][\text{Pt}(-\text{chxn})_2]\text{Br}_4$

with cell parameters $a = 23.80(2)$ Å, $b = 7.009(6)$ Å and $c = 5.373(4)$ Å is isostructural with the chloride.

EXPERIMENTAL

Preparations

Bis[(—)-1,2-cyclohexanediamine]platinum(II) chloride. To a boiling solution of 4.2 g potassium tetrachloroplatinate(II) (10 mmol) in 30 ml of water containing a few drops of ethanol was slowly added 2.51 g pure (—)-1,2-cyclohexanediamine (22 mmol). The precipitate which immediately separated was gradually dissolved during vigorous mechanical stirring and heating for 1 h. The reaction mixture was filtered and 2 ml conc. hydrochloric acid was added. After cooling in ice for 1 h the product was collected on a filter and washed with ethanol and dried in air. Yield: 4.3 g (87 %).

trans-Dichloro-bis[(—)-1,2-cyclohexanediamine]platinum(IV) chloride. 2 g of $[\text{Pt}(-\text{chxn})_2]\text{Cl}_2$ (4.05 mmol) was dissolved in 40 ml of water and chlorine gas was slowly bubbled through the solution until its colour began to change from light yellow to orange. Air was bubbled through the solution to remove the excess chlorine gas. The solution was filtered and evaporated in vacuum to approximately 5 ml and after addition of 1.0 ml conc. hydrochloric acid the mixture was cooled in ice for $\frac{1}{2}$ h. The crystalline product was collected on a filter and washed with ethanol. Yield: 1.7 g (74.3 %).

trans-Dichlorobis[(—)-1,2-cyclohexanediamine]platinum(IV) - bis[(—)-1,2-cyclohexanediamine]platinum(II) chloride. A 50 °C hot solution of 0.56 g *trans* $[\text{Pt}(-\text{chxn})_2\text{Cl}_2]\text{Cl}_2$ (1.0 mmol) in 12 ml water was added to a 50 °C hot

solution of 0.5 g [Pt(-chxn)₂]Cl₂ (1.0 mmol) in 6 ml of water. 10 ml of a saturated solution of lithium chloride in methanol was slowly added. The solution turned black and soon crystals with a metallic sheen commenced to separate. The mixture was cooled in ice and filtered after 1 h. The product was washed with ethanol and dried in air. Yield 0.8 g (75.5 %).

The black crystals of the compound dissolved in a minimum of hot water give an almost colourless solution, from which black crystals separate out on cooling. (Found: C 27.92; H 5.33; N 10.58; Cl 20.08; Pt 36.3. Calc. for [Pt(C₆H₁₄N₂)₂Cl₂][Pt(C₆H₁₄N₂)₂]Cl₄: C 27.22; H 5.66; N 10.82 Cl 19.92; Pt 36.8).

trans-Dibromobis[(-)-1,2-cyclohexanediamine]platinum(IV)-bis[(-)-1,2-cyclohexanediamine]platinum(II) bromide. To a solution of 0.5 g [Pt(-chxn)₂]Cl₂ (1.0 mmol) in 10 ml of water was added 2.2 ml of a saturated aqueous bromine solution (0.5 mmol). After 15 min 1 ml of a saturated ammonium bromide solution was added dropwise. Black crystals with a golden sheen separated. The mixture was cooled in ice and filtered after ½ h. The product was washed with ethanol and dried in air. Yield 0.55 g (83 %). Anal. [Pt(C₆H₁₄N₂)₂Br₂][Pt(C₆H₁₄N₂)₂]Br₂: C, H, N, Br, Pt.

X-Ray technique. Space groups were determined from Weissenberg and precession photographs using Cu and Mo radiation ($\lambda(\text{CuK}\alpha) = 1.5418 \text{ \AA}$, $\lambda(\text{MoK}\alpha) = 0.7107 \text{ \AA}$). Lattice parameters for the chlorine compound were obtained from a least-squares refinement of setting angles for 26 reflections with $18.9^\circ \leq 2\theta < 37.6^\circ$. Three-dimensional intensity data were collected with an automatic Picker four-circle instrument using graphite monochromatized MoK α radiation. The background-peak-background technique was used in a $\omega/2\theta$ scan, $t_{\text{background}} = 20 \text{ s.}$, scan rate = $2^\circ/\text{min}$. The crystal which had the linear dimensions $0.03 \times 0.35 \times 0.46 \text{ mm}^3$ bounded by {100}, {010} and {001} and was mounted in an arbitrary orientation. Data were collected out to $\sin \theta/\lambda \approx 0.9 \text{ \AA}^{-1}$ giving 3665 reflections which were reduced to 1529 independent reflections with $F_o^2 \geq 3\sigma(F_o^2)$. Data processing included absorption correction. A $4 \times 10 \times 12$ grid was used and the transmission factor varied between 0.0853 and 0.7578. Lattice parameters for the bromine compound were determined by film technique.

CRYSTAL DATA

[Pt(C₆H₁₄N₂)₂Cl₂][Pt(C₆H₁₄N₂)₂]Cl₄; M = 1059.6, orthorhombic. Unit cell: $a = 24.268(4) \text{ \AA}$, $b = 6.820(1) \text{ \AA}$, $c = 5.158(1) \text{ \AA}$, $V = 853.7 \text{ \AA}^3$, $D_m = 2.058 \text{ g cm}^{-3}$, $D_c = 2.061 \text{ g cm}^{-3}$, $Z = 1$. $\mu_{\text{MoK}\alpha} = 91.0 \text{ cm}^{-1}$. Systematic absences: hkl : $h + k + l = 2n + 1$. Space group: $I222$ (D_2^2 , No. 23); from structure analysis. [Pt(C₆H₁₄N₂)₂Br₂]-

Acta Chem. Scand. A 31 (1977) No. 3

[Pt(C₆H₁₄N₂)₂]Br₂; M = 1326.4. Crystal system: orthorhombic. Unit cell: $a = 23.80(2) \text{ \AA}$, $b = 7.009(6) \text{ \AA}$, $c = 5.373(4) \text{ \AA}$.

STRUCTURE DETERMINATION AND REFINEMENT

The structure was determined by the Patterson heavy atom method. The systematic absences indicated four possible space groups: $I222$, $I2_12_12_1$, $Imm2$ and $Immm$ of which the last two were impossible due to the lack of mirror planes in the *chxn* molecule. As $I2_12_12_1$ has only eightfold and fourfold point positions $I222$ was left as the most probable space group requiring the overall formula to be [Pt(-*chxn*)₂Cl]₂Cl₂ with $Z = 2$. This was confirmed by the three-dimensional Patterson map from which all non-hydrogen atoms could be found and which clearly showed the appearance of two half-weight chlorine atoms (point position 4(i)). Least-squares refinement of atomic coordinates, scale factor and isotropic temperature factors gave $R = 0.081$. Hydrogen atoms were inserted in fixed calculated positions with constant B -values of 3.0 \AA^2 , weighting was introduced and the (200) reflection removed because of probable extinction effects. Finally the z -coordinates of N and C₃ were allowed only to move half the calculated distance in the least-squares refinement as these parameters oscillated severely; this may be due to their closeness to $z = 0.0$. With anisotropic temperature factor parameters for non-hydrogen atoms final R and R_w values of 0.025 and 0.031, respectively, were obtained and a difference Fourier map showed no further atoms, the largest peak being less than 0.5 electron/ \AA^3 . Atomic coordinates are given in Table 1, temperature factor parameters in Table 2. A list of observed and calculated structure factors is available on request.

Data processing was performed with the programs DATAPP and DSORTH. Least-squares refinement was carried out with the full matrix program LINEX, the quantity minimized was

$$R_w = \sum w ||F_o| - k|F_c|| / \sum |F_o|, \text{ where}$$

$$w = 1/(\mu(F))^2$$

$$\mu(F) = [\sigma(F_o^2)_{\text{count}} + 1.02F_o^2]^{\frac{1}{2}} - |F_o|$$

Table 1. Atomic coordinates with standard deviations $\times 10^4$ in parentheses. Calculated hydrogen positions under the assumption of sp^3 hybridized atoms and distances N-H = 0.95 Å, C-H = 1.00 Å. The atom Cl₁ is disordered.

Atom	<i>x</i>	<i>y</i>	<i>z</i>	Atom	<i>x</i>	<i>y</i>	<i>z</i>
Pt	0	0	0	H ₁	0.056	0.299	0.138
Cl ₁	0	0	0.4505(4)	H ₂	0.067	0.263	-0.154
Cl ₂	0.5834(1)	0	0	H ₃	0.116	0.070	0.267
N	0.0634(2)	0.2019(5)	0.0115(79)	H ₄	0.167	0.345	0.094
C ₁	0.1150(2)	0.0954(7)	0.0763(10)	H ₅	0.167	0.240	-0.189
C ₂	0.1670(2)	0.2162(7)	0.0057(75)	H ₆	0.216	0.062	0.268
C ₃	0.2181(2)	0.0947(9)	0.0801(13)	H ₇	0.252	0.171	0.045

Table 2. Mean square vibration amplitudes u_{ij} with estimated standard deviations (both $\times 10^4$). The u_{ij} are defined by: $\exp[-2\pi^2(u_{11}a^{*2}h^2 + \dots + 2u_{12}a^*b^*hk + \dots)]$.

Atom	u_{11}	u_{22}	u_{33}	u_{12}	u_{13}	u_{23}
Pt	210(1)	130(1)	117(1)	0	0	0
Cl ₁	352(13)	297(11)	147(10)	-147(31)	0	0
Cl ₂	564(10)	269(6)	278(7)	0	0	33(46)
N	298(14)	170(10)	221(7)	-11(10)	54(29)	5(24)
C ₁	268(19)	205(15)	213(16)	-18(15)	-30(16)	-17(14)
C ₂	295(19)	256(17)	637(38)	-4(16)	96(134)	103(89)
C ₃	256(21)	400(27)	381(28)	-73(21)	-23(20)	26(24)

The atomic scattering factors used were those given by Cromer and Mann⁸ for Pt, Cl, N, and C. For hydrogen the scattering curve given by Stewart, Davidson and Simpson⁹ was used. No correction was made for anomalous dispersion. Interatomic distances and angles were calculated with the program ORFFE including variance-covariance matrix and cell parameter errors; drawings were made using ORTEP. Detailed references to the programs are given in Ref. 10.

RESULTS AND DISCUSSION

The title compound is to our knowledge the first described analogue to Wolfram's red salt¹¹ and Reihlen's green salt¹² Pt *etn*₄x₃.2H₂O (*etn* = ethylamine, x = Cl and Br).

Wolfram obtained his salt from [Pt *etn*₄]Cl₂.2H₂O by the action of hydrogen peroxide in hydrochloric acid. The same procedure with [Pt(-*chxn*)₂]Cl₂ (-*chxn* = (-)-1,2-cyclohexanediamine) yields the colourless sparingly soluble hydroxo-complex: [Pt(-*chxn*)₂OH]Cl₂.H₂O. Reihlen and Flohr¹² found that Wolfram's salt

Table 3. Interatomic distances and angles with standard deviations in parentheses.

Distance	Å	Angle	Degrees
Pt-Cl ₁	2.324(2)	N-Pt-Cl ₁	88.4(1.1)
Pt-Cl ₁ ⁱ	2.834(2)	N-Pt-N ⁱⁱ	83.7(0.2)
Pt-N	2.056(4)	Pt-N-C ₁	108.0(0.4)
N-C ₁	1.485(11)	N-C ₁ -C ₂	111.9(0.6)
C ₁ -C ₁ ⁱⁱ	1.521(9)	N-C ₁ -C ₁ ⁱⁱ	107.6(1.0)
C ₁ -C ₂	1.550(10)	C ₁ ⁱⁱ -C ₁ -C ₂	109.5(1.0)
C ₂ -C ₃	1.541(12)	C ₁ -C ₂ -C ₃	108.2(0.9)
C ₂ -C ₃ ⁱⁱ	1.534(14)	C ₂ -C ₃ -C ₃ ⁱⁱ	108.6(1.1)
Cl ₁ -Cl ₂	3.974(1)		
Cl ₂ -Cl ₂ ⁱⁱⁱ	4.050(4)		
Hydrogen bonds			
N...Cl ₂	3.274(31)		
N...Cl ₂ ^{iv}	3.366(31)		
H ₁ -Cl ₂	2.41		
H ₂ -Cl ₂ ^{iv}	2.44		
Dihedral angles			
(N-Pt-N ⁱⁱ)-(N ^v -Pt-N ^{vi})			11.5(3.7)
(N-Pt-N ⁱⁱ)-(C ₁ -C ₁ ⁱⁱ -C ₃ ⁱⁱ)			25.5(1.9)
(C ₁ -C ₁ ⁱⁱ -C ₃ ⁱⁱ)-(C ₁ -C ₂ -C ₃)			58.7(2.1)
Symmetry operations			
(i) <i>x, y, 1-z</i> ; (ii) <i>x, \bar{y}, \bar{z}</i> ; (iii) \bar{x}, y, z			
(iv) <i>x, \bar{y}, \bar{z}</i> ; (v) \bar{x}, \bar{y}, z ; (vi) \bar{x}, y, \bar{z}			

could be prepared directly by mixing aqueous solutions of [Pt(*etn*)₂]Cl₂ and *trans*[Pt(*etn*)₂]Cl₂. The same method is used by preparation of [Pt(-*chxn*)₂]Cl₂ and [Pt(-*chxn*)₂]Br₂.

It seems to be obvious that Wolfram's salt and the present salts contain platinum in the oxidation states +2 and +4, and not +3. As is the case for Wolfram's salt¹⁸ [Pt(-*chxn*)₂]Cl₂ is diamagnetic. The black-green crystals of the compound dissolved in a minimum of hot water give a colourless solution from which the black-green crystals of the original compound separate out on cooling. The crystals show a striking dichroism. They are black with polarized light having the electric vector along the *c*-axis and almost colourless with polarized light having its electric vector normal to the *c*-axis.

Description of the structure. The structure is interpreted in terms of chains of Pt(-*chxn*)₂ groups connected by chloride ions with the

Pt-Cl bonds parallel to the *c*-axis (Figs. 1 and 2). Film data showed no sign of disorder in the structure. But the appearance of two half-weight chloride ions attached to each platinum indicate stacking faults. A chain remains internally ordered but is displaced in the chain direction by one-half the repeat unit. Thus there is no crystallographic distinction between Pt(II) and Pt(IV). Each chlorine atom in the chain may be regarded as forming a covalent bond to a Pt(IV) with length 2.324 Å. This is significantly longer than the Pt(IV)-Cl distance in Wolfram's salt (2.26 Å).⁵ On the other hand the distance to the Pt(II) 2.834 Å compared with 3.13 Å for Wolfram's salt suggests a much stronger interaction between the two units in the (-)-1,2-cyclohexanediamine complex salt. It is interesting that [Pt(-*chxn*)₂]Cl₂ is nearly black (absorbs at all wavelengths in the visible region) whereas Wolfram's salt only absorbs at wavelengths less

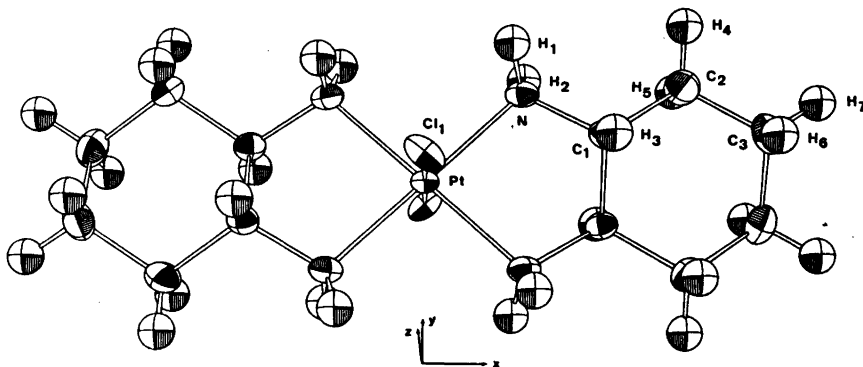


Fig. 1. Perspective drawing of *trans*-[Pt(-*chxn*)₂Cl₂]⁺² in *trans*-[Pt(-*chxn*)₂Cl₂][Pt(-*chxn*)₂]Cl₄. Thermal ellipsoids enclose 50 % probability (ORTEP II).

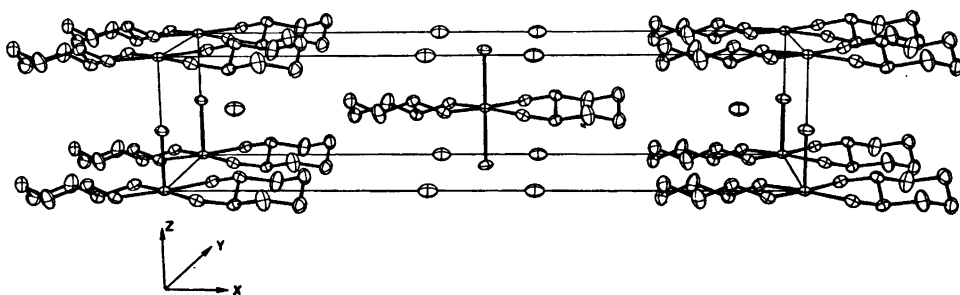


Fig. 2. Perspective drawing of *trans*-[Pt(-*chxn*)₂]Cl₂. Hydrogen atoms have been omitted for clarity.

than about 600 nm. Thus the charge transfer from Pt(II) to Pt(IV) along the chains appears at lower energy when the two oxidation states are in more similar environment.

As no correction was made for anomalous dispersion, the small differences in interatomic distances and angles between this structure and similar structures should not be regarded as significant.

The geometrical data for the coordinated (-)-1,2-cyclohexanediamine may also be affected by the disorder along the *c*-axis. The Pt-N distance which is a mean value between Pt(II)-N and Pt(IV)-N distances is close to other reported Pt-N distances.^{3,7} Angles and distances in (-)-1,2-cyclohexanediamine are within two standard deviations of those found in $AlCl_3[Co(+chxn)_2]Cl_3 \cdot 5H_2O$.¹⁴ However, the N-Pt-N angle in the five-membered chelate ring is significantly smaller than the analogous angle in the Co(III) complex.¹⁴

The absolute configuration of (-)-1,2-cyclohexanediamine is 1(*R*), 2(*R*).¹⁴ Thus in the Pt(-*chxn*)₂ unit the chelate rings have the conformations $\lambda\lambda$.

The fact that the Pt(-*chxn*)₂ unit is unable to perform any changes of conformation and is rather flat is probably the reason why a packing with such a short Pt-Cl-Pt distance can be achieved. Hydrogen bonds between the ionic chloride and the amino groups may also be of importance in this respect. In contrast to Wolfram's salt the present salt does not contain water of crystallization. This is quite remarkable as Wolfram's salt changes colour to pale yellow on dehydration.

Acknowledgements. The authors are indebted to F. Krebs Larsen and O. Lillelund for assistance in data collection and to Mrs. R. Hazell for useful discussions and advice on computing.

REFERENCES

- Hall, D. and Williams, P. P. *Acta Crystallogr.* **11** (1958) 624.
- Ryan, T. D. and Rundle, R. E. *J. Am. Chem. Soc.* **83** (1961) 2814.
- Craven, B. M. and Hall, D. *Acta Crystallogr.* **14** (1961) 475.
- Wallén, J., Brosset, C. and Vannerberg, N. G. *Ark. Kemi* **18** (1962) 541.
- Craven, B. M. and Hall, D. *Acta Crystallogr.* **21** (1966) 177.
- Browall, K. W., Kasper, J. S. and Inter-rante, L. V. *Acta Crystallogr. B* **30** (1974) 1649.
- Brown, K. L. and Hall, D. *Acta Crystallogr. B* **32** (1976) 279.
- Cromer, D. T. and Mann, J. B. *Acta Crystallogr. A* **24** (1968) 321.
- Stewart, R. F., Davidson, E. R. and Simpson, W. T. *J. Chem. Phys.* **42** (1965) 3175.
- Larsen, K. P. *Acta Chem. Scand. A* **29** (1975) 499.
- Wolfram, H. *Ueber aethylaminhaltige Platinbasen*, Diss., Königsberg 1900.
- Reihlen, N. and Flohr, E. *Ber. Dtsch. Chem. Ges.* **67** (1934) 2010.
- Jensen, K. A. *Z. Anorg. Allg. Chem.* **229** (1936) 252.
- Marumo, F., Utsumi, Y. and Saito, Y. *Acta Crystallogr. B* **26** (1970) 1492.

Received September 9, 1976.

The Molecular Structure of α -D-Talose

LARS K. HANSEN and ASBJØRN HORDVIK

Department of Chemistry, Institute for Mathematical and Physical Sciences, University of Tromsø, Box 790, N-9001 Tromsø, Norway

Crystals of α -D-talose $C_6O_6H_{12}$ are orthorhombic, space group $P2_12_12_1$, with unit cell dimensions $a=8.101(2)$ Å, $b=12.126(2)$ Å, $c=7.655(1)$ Å, and $Z=4$.

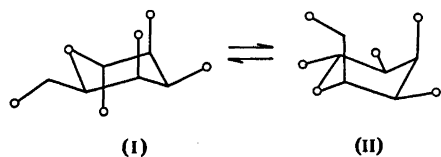
X-Ray intensity data were collected on a Siemens AED diffractometer using $MoK\alpha$ radiation and the five-value scan technique. The structure was solved by direct methods and refined by full-matrix least squares.

α -Talose occurs in the conversion form $1a2a3e4a5e$. The length of the anomeric C(1)–O(1) bond is $1.403(3)$ Å, and the C(1)–O(5)–C(5) angle is $113.7(2)^\circ$ with C(1)–O(5) = $1.438(3)$ Å and C(5)–O(5) = $1.434(3)$ Å.

In the crystal there is a complete set of hydrogen bonds; O(2)···O(4) = $2.654(3)$ Å is intramolecular with H(O2)···O(4) = 1.96 Å.

An analysis of the standard deviations in the C–C and C–O bond lengths as a function of the intensity threshold value has been carried out. The standard deviations increase by a factor of 1.5 for a change in the threshold value from $\sigma(I)$ to $10\sigma(I)$. Corresponding values for R are 0.078 and 0.026, and the numbers of reflections per parameter are 13.8 and 4.3, respectively.

The possible pyranose forms of α -D-talose are $1a2a3e4a5e$ (I) and $1e2e3a4e5a$ (II), II being formed from I through a conversion of the ring.



A stability scheme for the conversion forms of pyranoses was proposed by Reeves in 1950,¹ and the normal conformation of a series of pyranoses have been correctly predicted from this scheme.

However, in the case of α -talose the difference in stability between forms I and II is

too small for a prediction to be made, and a structure study of α -talose was therefore thought of interest.

Results from a preliminary X-ray investigation of α -D-talose have been reported.²

STRUCTURE ANALYSIS

Crystal data.

α -D-Talose, $C_6O_6H_{12}$; M.W. = 180.16

Space group $P2_12_12_1$

$a=8.101(2)$ Å, $b=12.126(2)$ Å, $c=7.655(1)$ Å

$V=751.97$ Å³

$D_c=1.591$ g/cm³, D_m (floatation) = 1.59 g/cm³

$Z=4$

$\mu=1.55$ cm⁻¹ ($MoK\alpha$)

All the X-ray measurements were carried out on a papertape controlled Siemens AED diffractometer using $MoK\alpha$ radiation ($\lambda=0.71069$ Å).

The unit cell dimensions were determined from the 2θ values of 16 high order reflections measured at room temperature, $t=22^\circ$ C. A least squares procedure gave the values quoted above.

The intensities of the reflections were measured by means of the five-value scan technique.³ 2961 independent reflections were measured within $\theta=42^\circ$.

Lp corrections were carried out in the usual way, but absorption corrections were considered unnecessary. The dimensions of the crystal used for the intensity collection were $0.2 \times 0.3 \times 0.4$ mm in the three axial directions.

The scattering factors for oxygen and carbon were taken from the *International Tables*.⁴ For hydrogen, the scattering factor curve given by Stewart *et al.*⁵ was used.

Table 1. Atomic coordinates in fractions of corresponding cell edges. The standard deviations given in parentheses refer to the last digits of the respective values.

Atom	<i>x</i>	<i>y</i>	<i>z</i>
O(1)	0.16055(25)	0.11857(15)	-.07331(21)
O(2)	0.04684(20)	0.11688(14)	0.38321(21)
O(3)	0.13025(20)	0.34071(13)	0.34129(24)
O(4)	0.35274(19)	0.17603(14)	0.46492(21)
O(5)	0.31694(17)	0.04293(11)	0.15639(19)
O(6)	0.67062(21)	0.01932(15)	0.07775(25)
C(1)	0.15583(27)	0.07540(18)	0.09663(28)
C(2)	0.08353(25)	0.16380(17)	0.21734(28)
C(3)	0.20314(27)	0.26040(16)	0.23022(28)
C(4)	0.37218(25)	0.22088(17)	0.29368(28)
C(5)	0.43391(27)	0.13315(17)	0.16523(28)
C(6)	0.59898(29)	0.08400(21)	0.21496(33)
H(11)	0.0934(28)	0.0088(17)	0.1064(29)
H(21)	-.0189(25)	0.1871(16)	0.1706(26)
H(31)	0.2167(25)	0.2913(16)	0.1171(26)
H(41)	0.4447(27)	0.2783(16)	0.2977(26)
H(51)	0.4395(28)	0.1635(17)	0.0521(27)
H(61)	0.6712(32)	0.1422(21)	0.2385(33)
H(62)	0.5936(31)	0.0381(21)	0.3238(36)
H(O1)	0.1865(40)	0.0741(25)	-.1324(41)
H(O2)	0.1281(31)	0.1187(21)	0.4407(31)
H(O3)	0.1909(33)	0.3841(22)	0.3601(36)
H(O4)	0.4371(30)	0.1836(19)	0.5165(32)
H(O6)	0.6072(33)	-.0076(21)	0.0330(38)

The structure was solved by direct methods (MULTAN)⁶ and refined by full matrix least squares (see Ref. 7). All the hydrogen atoms were found from a difference map.

Final atomic coordinates and temperature parameters are listed in Tables 1 and 2, respectively. The values there correspond to the refinement in which $3\sigma(I)$ was used as intensity threshold value. With this criterion 1556 out of 2961 measured reflections were accepted as observed. The value of *R* for this refinement is 0.047. The structure factor list is available on request.

The calculations mentioned above were carried out on a UNIVAC 1110 computer at the University of Bergen. The programs, with some exceptions, originate from the Weizmann Institute of Science, Rehovoth, Israel.

DISCUSSION

The conversion form of α -D-talose in the crystalline state is *1a2a3e4a5e*, cf. Fig. 1. One may query, however, whether it is the assumed stabilizing effect of the axial hydroxyl group on C(1) that has been decisive for the structure

Table 2. Temperature parameters $U_{ij}(\text{\AA}^2)$ for oxygen and carbon, and $U(\text{\AA}^2)$ for hydrogen. The expressions used are $\exp\{-2\pi^2(h^2a^{*2}U_{11} + \dots + 2hka^*b^*U_{13} + \dots)\}$ and $\exp\{-8\pi U(\sin^2\theta/\lambda^2)\}$. All values are multiplied by 10^4 . Standard deviations in parentheses refer to the last digits of the respective values.

Atom	U_{11}	U_{22}	U_{33}	U_{12}	U_{23}	U_{13}
O(1)	452(11)	358(9)	209(8)	103(9)	-63(8)	-65(8)
O(2)	240(8)	303(9)	276(9)	-48(7)	37(7)	28(7)
O(3)	261(8)	199(7)	417(10)	-40(7)	-99(8)	113(8)
O(4)	247(8)	376(9)	216(8)	-70(8)	36(7)	-59(7)
O(5)	217(7)	187(7)	256(8)	22(6)	-14(6)	-16(7)
O(6)	231(8)	315(9)	413(1)	55(8)	-70(8)	8(8)
C(1)	208(10)	204(10)	252(11)	16(9)	-26(9)	-58(9)
C(2)	175(9)	192(10)	233(10)	12(8)	12(9)	-12(8)
C(3)	203(9)	171(9)	206(10)	-6(8)	-5(8)	37(8)
C(4)	174(9)	182(9)	229(10)	-49(8)	16(8)	12(8)
C(5)	205(9)	216(11)	201(10)	18(8)	22(9)	19(9)
C(6)	197(10)	277(12)	309(13)	30(9)	-21(10)	-17(10)

Atom	<i>U</i>	Atom	<i>U</i>	Atom	<i>U</i>
H(11)	153(58)	H(51)	129(54)	H(O2)	237(72)
H(21)	31(47)	H(61)	295(70)	H(O3)	286(78)
H(31)	71(50)	H(62)	325(69)	H(O4)	156(62)
H(41)	75(51)	H(O1)	519(108)	H(O6)	287(90)

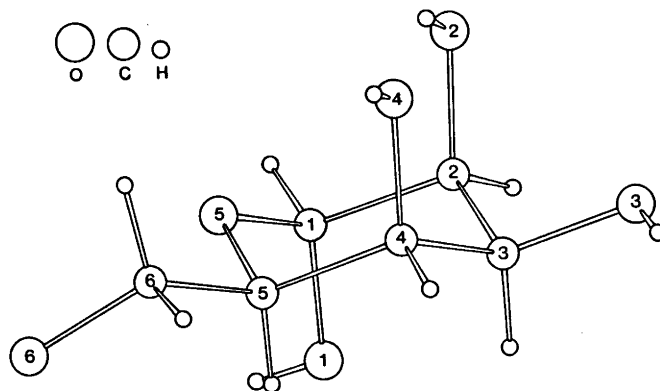


Fig. 1. The α -D-talose molecule with numbering of atoms.

in this case.⁸ There is namely, in the present structure as well as in the structure of methyl- β -D-ribofuranoside,^{9,10} methyl-1-thio- α -D-ribofuranoside¹¹ and methyl-1,5-dithio- β -D-ribofuranoside,¹¹ an intramolecular hydrogen bond between O(2) and O(4) which at least to some degree stabilizes the molecule. Thus, the possibility for such bonding should be taken into account when assessing the stabilities of the conversion forms of pyranoses. On the other hand, 5-thio- β -D-ribofuranoside occurs as *1e2e3a4e* in the crystal,¹² showing that molecular packing too may be of importance for the choice of conversion form.

Bond lengths and angles in the α -D-talose molecule, as derived from the coordinates in Table 1, are listed in Table 3. It is realized that a more realistic estimate of the standard deviations probably might be obtained by multiplying those given by a factor of two.¹³

The values in Table 3 are normal for pyranose molecules. One notes that C(1)–O(1) = 1.403(3) Å is shorter than the other C–O bonds in the molecule and that C(1)–O(5)–C(5) = 113.7(2)° is greater than the other bond angles in the pyranose ring.

In the crystal there is a complete set of hydrogen bonds, *cf.* Fig. 2. The lengths

Table 3. Bond angles $\angle(ijk)$ and bond lengths $D(ij)$ in α -D-talose. The standard deviations are 0.2° in bond angles and 0.003 Å in bond lengths.

i	j	k	$\angle(ijk)^\circ$	i	j	$D(ij)$ Å
C(2)	C(1)	O(1)	108.0	C(1)	C(2)	1.532
C(2)	C(1)	O(5)	110.3	C(2)	C(3)	1.523
O(1)	C(1)	O(5)	111.9	C(3)	C(4)	1.530
C(1)	C(2)	O(2)	109.8	C(4)	C(5)	1.533
C(1)	C(2)	C(3)	109.5	C(5)	C(6)	1.513
O(2)	C(2)	C(3)	112.5	C(1)	O(1)	1.403
C(2)	C(3)	O(3)	107.5	C(1)	O(5)	1.438
C(2)	C(3)	C(4)	110.4	C(2)	O(2)	1.423
O(3)	C(3)	C(4)	113.4	C(3)	O(3)	1.421
C(3)	C(4)	O(4)	108.2	C(4)	O(4)	1.428
C(3)	C(4)	C(5)	107.8	C(5)	O(5)	1.449
O(4)	C(4)	C(5)	111.1	C(6)	O(6)	1.434
C(4)	C(5)	O(5)	109.9			
C(4)	C(5)	C(6)	113.6			
C(6)	C(5)	O(5)	107.0			
C(5)	C(6)	O(6)	112.9			

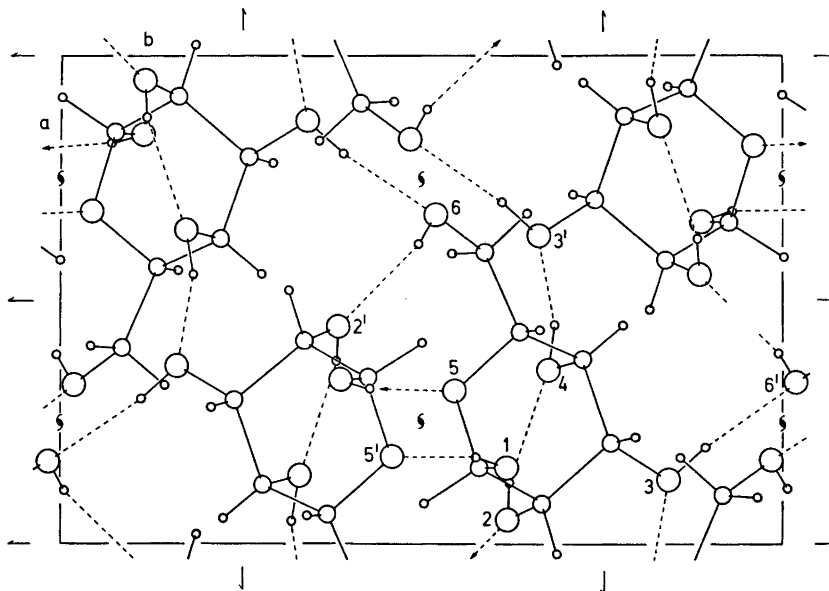


Fig. 2. The crystal structure of α -talose as seen along c . The $\text{O}\cdots\text{H}$ contacts in hydrogen bonds are indicated, and the oxygen atoms are numbered in accordance with the text.

of these are, $\text{O}(1)\cdots\text{O}(5')=2.855(3)$ Å, $\text{O}(2)\cdots\text{O}(4)=2.654(3)$ Å (this hydrogen bond is intramolecular with $\text{H}(\text{O}2)\cdots\text{O}(4)=1.96$ Å), $\text{O}(3)\cdots\text{O}(6')=2.771(3)$ Å, $\text{O}(4)\cdots\text{O}(3')=2.701(3)$ Å and $\text{O}(6)\cdots\text{O}(2')=2.837(3)$ Å.

An analysis of the standard deviations in the C—C and C—O bond lengths as a function of a preset intensity threshold value has been carried out. Some results from this analysis are listed in Table 4 and shown in Fig. 3. We realize that the trend shown in Fig. 3 cannot be generalized, but it is interesting to note that there in the present case is found to be an approximate linear relationship be-

tween the standard deviations and the threshold values for threshold values up to $10\sigma(I)$.

The changes in bond lengths as a result of the changes in intensity threshold value are all within one σ and thus almost negligible, and the standard deviations in C—C and C—O bond lengths increase by a factor of only 1.5 for a change in intensity threshold value from $\sigma(I)$ to $10\sigma(I)$. The corresponding numbers of reflections per parameter are 13.8 and 4.3, respectively.

Similar analyses have been carried out for L,D-alanyl-D,L-methionine and N-acetyl-phenylalanyl-L-tyrosine by Stenkamp and Jensen.¹⁴

Table 4. Average values of standard deviations in C—C and C—O bond lengths, R factors, and numbers of observed (N_o) and unobserved (N_u) reflections from refinements with different intensity threshold values ($n\sigma(I)$). 157 parameters have been refined.

	$\sigma(I)$	$2\sigma(I)$	$3\sigma(I)$	$4\sigma(I)$	$5\sigma(I)$	$10\sigma(I)$
$\bar{\sigma}(l)_{\text{C-C}}10^4$ Å	26.4	28.6	30.0	31.8	33.8	41.0
$\bar{\sigma}(l)_{\text{C-O}}10^4$ Å	23.7	26.0	27.1	28.6	30.3	36.6
R	0.078	0.061	0.047	0.040	0.036	0.026
N_o	2174	1743	1405	1194	1038	672
N_u	787	1218	1556	1767	1923	2289
$N_o/157$	13.8	11.1	9.0	7.6	6.6	4.3

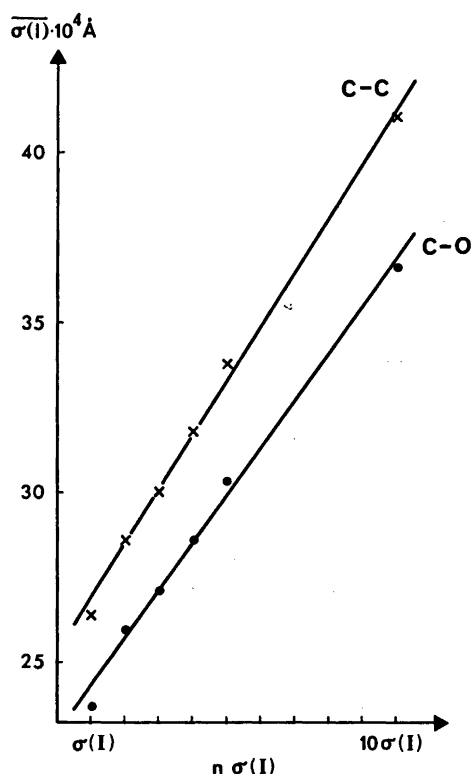


Fig. 3. The average standard deviations in C-C and C-O bond lengths in α -D-talose as a function of the intensity threshold value $n\sigma(I)$.

We have recently been informed that an independent structure study of α -D-talose has been carried out.¹⁵ The results from the two studies are in excellent agreement.

Acknowledgements. The authors wish to thank Dr. L. M. J. Verstraeten, Laboratory of Organic Chemistry, Institute of Agriculture, University of Louvain, Belgium, for a sample of α -D-talose. One of us (A.H.) is indebted to the Norwegian Research Council for Science and the Humanities for financial support.

REFERENCES

1. Reeves, R. E. *J. Am. Chem. Soc.* 72 (1950) 1499.
2. Hordvik, A. *Acta Chem. Scand.* 20 (1966) 1173.
3. Troughton, P. G. H. *Siemens Review XXXVII* (1970), Fourth Special Issue: X-Ray and Electron Microscopy News.

4. *International Tables for X-Ray Crystallography*, Kynoch Press, Birmingham 1968, Vol. III, p. 202.
5. Stewart, R. F., Davidson, E. R. and Simpson, W. T. *J. Chem. Phys.* 42 (1965) 3175.
6. Main, P., Woolfson, M. M. and Germain, G. *MULTAN - A Complete Program for the Automatic Solution of Crystal Structures*, Department of Physics, University of York, York, England, May 1971.
7. Hordvik, A. and Sæthre, L. *J. Acta Chem. Scand.* 26 (1972) 3114.
8. Furberg, S. *Acta Chem. Scand.* 14 (1960) 1357.
9. Hordvik, A. *Acta Chem. Scand. B* 28 (1974) 261.
10. James, V. J. and Stevens, J. D. *Carbohydr. Res.* 21 (1972) 334.
11. Girling, R. L. and Jeffrey, G. A. *Carbohydr. Res.* 18 (1971) 339.
12. Girling, R. L. and Jeffrey, G. A. *Acta Crystallogr. B* 29 (1973) 1162.
13. Hamilton, W. C. and Abrahams, S. C. *Acta Crystallogr. A* 26 (1970) 18.
14. Stenkamp, R. E. and Jensen, L. H. *Acta Crystallogr. B* 31 (1975) 1507.
15. Kanters, J. A., Roelofsen, G., Alblas, B. P. and Smits, B. A. A. *Third European Crystallographic Meeting, Zürich 1976*, Collected Abstracts, p. 240.

Received September 23, 1976.

The Cumulative Stability Constant of the Bis(1,2-ethanediamine) (1,3-propanediamine)cobalt(III) Complex Ion, $[\text{Co en}_2\text{tn}]^{3+}$

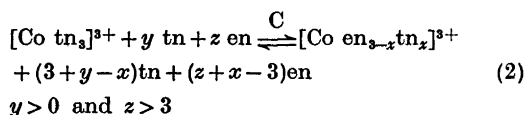
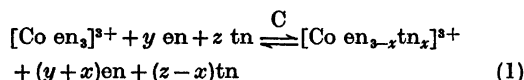
OLE BANG, KJELD RASMUSSEN* and FLEMMING WOLDBYE

Chemistry Department A, The Technical University of Denmark, Building 207, DK-2800 Lyngby, Denmark

The cumulative stability constant of $[\text{Co en}_2\text{tn}]^{3+}$ relative to $[\text{Co en}_3]^{3+}$ is measured in 1 M NaNO_3 at 298 K. The difference, $\log \beta_3(\text{Co en}_2\text{tn}^{3+}) - \log \beta_3(\text{Co en}_3^{3+})$, is -2.12 , giving $\log \beta_3(\text{Co en}_2\text{tn}^{3+}) = 46.95$. The corresponding figure for $[\text{Co en tn}_2]^{3+}$ is tentatively given as 44.3. Equilibrium was reached from both sides, using $[\text{Co en}_3]^{3+}$ and $[\text{Co tn}_3]^{3+}$ as reactants, excess of the diamines, and activated carbon as catalyst. The four product species, $[\text{Co en}_{3-x}\text{tn}_x]^{3+}$ ($x=0, 1, 2, 3$), were separated by a paper chromatographic procedure.

Whereas the cumulative stability constant β_3 of $[\text{Co en}_3]^{3+}$ (en = ethylenediamine = 1,2-ethanediamine) has long been known,^{1,p,233} attempts to determine β_3 of the robust but less stable $[\text{Co tn}_3]^{3+}$ (tn = trimethylenediamine = 1,3-propanediamine) using the Bjerrum cycle^{1,p,221} failed due to precipitation of cobalt(II) hydroxide at increased pH.

Equilibria in robust Co(III) complex systems can be established with activated carbon as catalyst.^{1,p,235ff} In the system $[\text{Co en}_{3-x}\text{tn}_x]^{3+}$ ($x=0, 1, 2, 3$), therefore, equilibrium conditions can be attained by adding carbon to a solution containing one of the terminal species of the series and excess amine:



* To whom correspondence should be addressed.

When the equilibrium is reached, further substitution will be quenched by removal of carbon, and if the concentrations of complexes and amines can be measured, β_3 can be calculated relative to β_3 of $[\text{Co en}_3]^{3+}$:

$$\frac{\beta_3(\text{Co en}_{3-x}\text{tn}_x^{3+})}{\beta_3(\text{Co en}_3^{3+})} = \frac{[\text{Co en}_{3-x}\text{tn}_x^{3+}]}{[\text{Co en}_3^{3+}]} \left(\frac{[\text{en}]}{[\text{tn}]} \right)^x \quad (3)$$

The amine concentrations can be found from

$$[\text{en}] = \frac{C_{\text{en}} - \sum_{x=0}^2 (3-x)[\text{Co en}_{3-x}\text{tn}_x^{3+}]}{1 + [\text{H}^+]K_{\text{enH}^+} + [\text{H}^+]^2K_{\text{enH}^+}K_{\text{enH}_2^+}} \quad (4)$$

and

$$[\text{tn}] = \frac{C_{\text{tn}} - \sum_{x=1}^3 [\text{Co en}_{3-x}\text{tn}_x^{3+}]}{1 + [\text{H}^+]K_{\text{tnH}^+} + [\text{H}^+]^2K_{\text{tnH}^+}K_{\text{tnH}_2^+}} \quad (5)$$

where C is the total amine concentration and K the acid dissociation constant, $-\log K_{\text{enH}^+} = 10.17$, $-\log K_{\text{enH}_2^+} = 7.49$, $-\log K_{\text{tnH}^+} = 10.62$ and $-\log K_{\text{tnH}_2^+} = 9.12$.² Measurement of $[\text{H}^+]$ can be done by potentiometry, and the complex species can be isolated quantitatively by a paper chromatographic method³ developed in this laboratory.

EXPERIMENTAL

Equilibria. Reactions were carried out in a closed vessel fitted with stirrer and glass and calomel electrodes (Radiometer G202B and K401), and placed in a thermostat at 298 K. pH was measured with a Radiometer PHM4. The glass electrode was selected on basis of linearity, which was measured with standard buffer solutions (0.025 M KH_2PO_4 + 0.025

Table 1. All concentrations are in mol l⁻¹.

	Complexes added [Co en ₃] ³⁺			[Co tn ₃] ³⁺	
C_{en}	0.344	0.0769	0.321	0.0225	0.0616
C_{tn}	2.953	3.529	3.626	2.697	2.233
pH corr.	11.74	11.99	12.09	11.67	11.99
[Co en ₃] ³⁺	0.0744	0.00981	0.0688	0.0166	0.0491
[Co en ₂ tn] ³⁺	0.0188	0.00776	0.0397	0.0059	0.0106
[Co entn ₂] ³⁺	—	0.00234	—	—	—
[en]	0.0810	0.0292	0.0348	0.0673	0.0872
[tn]	2.730	3.373	3.469	2.470	2.131
$[\beta_3(\text{Co en}_2\text{tn}^{3+})/\beta_3(\text{Co en}_3^{3+})] \times 10^3$	7.50	6.85	5.79	9.68	8.83
$[\beta_3(\text{Co entn}_2^{3+})/\beta_3(\text{Co en}_3^{3+})] \times 10^5$	—	1.79	—	—	—
$\log [\beta_3(\text{Co en}_2\text{tn}^{3+})/\beta_3(\text{Co en}_3^{3+})]$	-2.13	-2.16	-2.23	-2.02	-2.05
$\log [\beta_3(\text{Co entn}_2^{3+})/\beta_3(\text{Co en}_3^{3+})]$	—	-4.75	—	—	—

M Na₂HPO₄, pH=6.86; 0.01 M borax, pH=9.18; sat. Ca(OH)₂, pH=12.45). pH as measured in the reaction vessel was calibrated by measurements on 0.1, 0.01 and 0.001 F HCl at constant ionic strength $I=1$. This pH was corrected for influence of Na⁺ of the 1 M NaNO₃ medium.⁴

Stock solutions of amines were 1 M in NaNO₃ and, respectively, 0.591 M in en and 4.73 in tn.

Stock solutions were pipetted into the vessel, and a convenient pH of 10–12 established by addition of 1 M HNO₃. Total volume ranged from 13 to 67 ml. 1–1.4 mmol accurately weighed [Co en₃]Cl₃ or [Co tn₃]Cl₃ and 0.15–1.0 g activated carbon were added to the vessel. After stirring for 48 h pH was measured and carbon removed by filtration and washing.

Separations. The equilibrium solutions were concentrated at room temperature under a stream of air. When the original volume exceeded 35 ml, NaNO₃ was precipitated with abs. ethanol and removed prior to renewed evaporation. The concentrated solutions underwent chromatographic separation as described elsewhere.³ In the present case, two eluents were employed: 90% phenol:1-butanol:pyridine:benzene:acetone:water:80% acetic acid. No. 1, 30:14:14:14:14:0.5:0; No. 2, 30:14:14:14:14:1.5:2.5 by volume. Eluent No. 1 removed the bulk of the nitrates (48 h); No. 2 separated the complexes (48 h).

Analyses. Molecular weights of the complexes were obtained from Co analyses. The complexes were fumed to dryness with conc. H₂SO₄, diluted with H₂O, and Co(II) determined with excess EDTA and backtitration with Zn(II).⁵ The absolute molar amounts of complexes in the equilibrium mixtures were estimated from the weights and molecular weights of the chromatographic fractions and converted to concentrations by division with the total reaction volume. The data are presented in Table 1.

RESULTS AND DISCUSSION

Table 1 shows that equilibrium has been reached from both sides, and that $\log \beta_3(\text{Co en}_2\text{tn}^{3+}) - \log \beta_3(\text{Co en}_3^{3+}) = -2.12 \pm 0.08$. The corresponding value for $[\text{Co en tn}_2]^{3+}$, -4.75, is reasonable, though merely indicative, as only one determination was made. It is experimentally very difficult to obtain a better estimate, and hardly possible for $[\text{Co tn}_3]^{3+}$. Such experiments would require very high concentrations of tn and therefore large reaction volumes, which due to the salt medium would further complicate the chromatography.

Absolute values of β_3 may be estimated from a recent determination⁶ of $\beta_3(\text{Co en}_3)^{3+} = 49.07$ in 1 M KCl at 298 K. (Bjerrum's value¹, p. 233 of 48.69 was measured at 303 K.) This gives $\beta_3(\text{Co en}_2\text{tn}^{3+}) = 46.95$ and $\beta_3(\text{Co en tn}_2)^{3+} \approx 44.3$.

It may be relevant to compare our result with the measurements of Poulsen and Bjerrum² on $[\text{Ni en}_x]^{2+}$ and $[\text{Ni tn}_x]^{2+}$ complexes. In these labile systems, all consecutive stability constants could be measured, and from them we find that $\log \beta_3(\text{Ni tn}_3)^{2+} - \log \beta_3(\text{Ni en}_3)^{2+} = -6.27$. One-third of this value, -2.1, agrees well with our result, which suggests an intrinsic stability difference between six-membered and five-membered diamine chelate rings, to some extent independent of the metal and of the number of chelate rings.

REFERENCES

1. Bjerrum, J. *Metal Ammine Formation in Aqueous Solution*, Haase & Søn, Copenhagen 1941, reprint 1957.
2. Poulsen, I. and Bjerrum, J. *Acta Chem. Scand.* 9 (1955) 1407.
3. Bang, O., Engberg, A., Rasmussen, K. and Woldbye, F. *Acta Chem. Scand. A* 29 (1975) 749.
4. Radiometer, Copenhagen, Publ. 982-442.
5. Kiss, T. A. *Z. Anal. Chem.* 208 (1965) 334.
6. Bang, O. *Diss.*, Chemistry Department A, The Technical University of Denmark, Lyngby 1976.

Received September 7, 1976.

A Study of Radiation-induced Free Radicals in Thymine by Spin-unrestricted Molecular Orbital Calculations

ANDERS B. HEIBERG and HARALD H. JENSEN

Department of Chemistry, University of Oslo, Oslo 3, Norway

Two conflicting interpretations of the ESR spectrum of irradiated single crystals of thymine monohydrate have been elucidated by semi-empirical unrestricted Hartree-Fock calculations. Isotropic and anisotropic hyperfine splitting constants for the various radical species proposed have been obtained and compared with experimental values. The result of this comparison is thought to be clearly in favour of one particular of the two alternative interpretations.

The ESR spectrum due to radiation-induced free radicals in single crystals of thymine monohydrate was investigated independently by Henriksen and Snipes¹ and by Hüttermann.² At room temperature the spectrum was dominated by the 5-thymyl radical (radical (I) in Fig. 1) which gives rise to eight lines spread out over approximately 140 G. At 77° K both investigators found a spectrum of six lines superimposed on a very weak 5-thymyl radical pattern. However, their interpretations of the low-temperature spectrum did not agree. Whereas Henriksen and Snipes concluded that the six lines are due to two different radicals, one contributing a quartet and the other a doublet, Hüttermann attributed these lines to only one radical. In both cases specific suggestions were made as to the radical species involved. The 6-thymyl radical and the 2-oxo-4-hydroxy-5-methyl-4-pyrimidinyl radical [radicals (II) and (III) in Fig. 1] were proposed as the origin of the quartet and doublet, respectively. In the alternative interpretation the radical (IV) was made responsible for the sextet.

The main purpose of the present work is to elucidate this discrepancy by molecular orbital

calculations. Two different semi-empirical unrestricted Hartree-Fock (UHF) methods were applied to the radicals (I)–(IV) and to two additional radical candidates: the thymine anion [radical (V)] and the 2,4-dioxo-5-methyl-5-hydroxy-6-pyrimidinyl radical [radical (VI)]. Calculated values of the different elements of

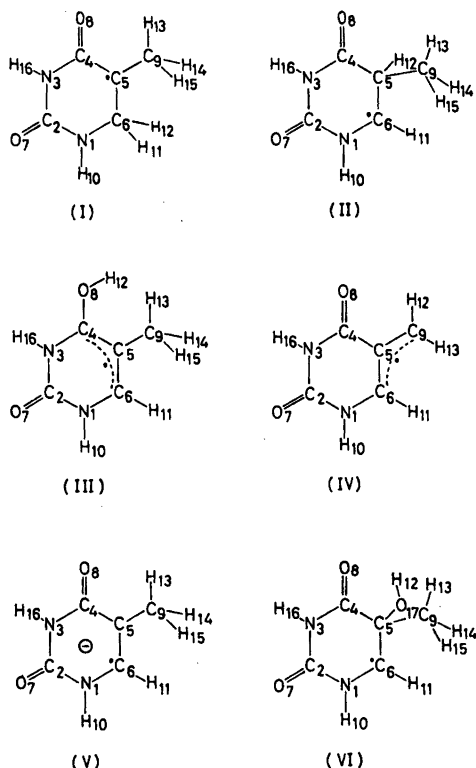


Fig. 1. Labelling of molecules and numbering of atoms.

the hyperfine splitting tensors are compared with the corresponding experimental data. In addition to the attempt to find support for any of the above conclusions it is also of general importance to gain systematic experience with the predictive abilities of the simpler Hartree-Fock methods in cases like the present one.

METHODS OF CALCULATION

The INDO method of Pople and coworkers⁹ was applied to all the radicals and the isotropic as well as the anisotropic components of the principal splitting constants were calculated.

In the INDO method all valence electrons are included and accordingly both π -electron and σ -electron components of the spin density distribution of a π -electron radical are evaluated. Pople and coworkers have developed an explicit procedure for obtaining isotropic hyperfine splitting constants from INDO wave functions before⁴ and after⁵ annihilation of the contaminating quartet spin component. In the present work isotropic splitting constants are obtained by this procedure. Results before and after annihilation will be labelled *sd* (single determinant) and *aa*, respectively.

Beveridge and McIver⁶ have established a method for calculating the anisotropic components of the principal splitting constants from an INDO wave function. The present calculations followed their scheme by use of a computer program written by one of us (A.B.H.).

In addition to the INDO method the Pariser-Parr-Pople (PPP) method^{7,8} for π -electron calculations was used when possible. A combination⁹ of the UHF formalism with and without annihilation^{10,11} and a special scheme for evaluation of semi-empirical parameters in the PPP approximation¹²⁻¹⁷ was employed in these calculations.

In the PPP calculations only π -electron spin densities were obtained, but they could be related to isotropic proton splitting constants by means of the empirical relations

$$A_{\text{H}} = Q \rho_{\text{C}^{\pi}} \quad (1)$$

$$A_{\text{H}(\text{CH}_3)} = Q^0 \rho_{\text{C}^{\pi}} \quad (2)$$

applicable to α - and methyl proton splitting constants, respectively.

In eqn. (1), which is the McConnell relation¹⁸ in its simplest form, A_{H} is the splitting constant of the α -proton and $\rho_{\text{C}^{\pi}}$ the spin density of the $2p_{\pi}$ -orbital of the carbon atom to which the proton is bonded. A value of the proportionality factor Q in the range -20 to -30 G usually gives good agreement between experimental A_{H} values and theoretical estimates of $\rho_{\text{C}^{\pi}}$.

In equation (2) $\rho_{\text{C}^{\pi}}$ is the π -electron spin density on the carbon atom to which the methyl group is attached. $A_{\text{H}(\text{CH}_3)}$ is the effective methyl proton splitting constant. Hence the formula is applicable only if the methyl group is rotating freely about the C-CH₃ bond. From the ESR spectra one may conclude that this has to be the case for all the radiation-induced thymine radicals.

The relation (2) was calibrated in the present work by a separate PPP calculation on the ethyl radical, leading to $Q^0 = 27.5$ G (π -electron spin density on CH₃: 0.97, observed splitting 26.87 G).

For each radical species one basic set of structural parameters was developed (Table 1) although additional calculations based on variation of geometry were also important in some cases. These basic geometries did all involve planar rings and roughly tetrahedral arrangements (bond angles 108–110°) around tetravalent carbon atoms. When possible bond lengths were obtained by repeated PPP calculations aiming at bond order-bond length selfconsistency.^{9,19} The results of this procedure are given to three decimal places in Table 1. In the case of radicals (II) and (VI) the values are based on PPP calculations on the open-chain system CHO-NH-CO-NH-CH₃.

Other bond lengths given in Table 1 are simply reasonable values, for instance the standard values recommended by Pople and Beveridge.²⁰ Most bond angles and also a few remaining bond lengths were chosen with some guidance from the results of a crystallographic investigation of thymine monohydrate.²¹ Thus the C5-C9 distance obtained the value 1.503 Å (Table 1) in the INDO calculations. In the PPP calculations the C5-methyl distance was set equal to 1.70 Å and the methylene group of radical (I) was treated as suggested by Flood and Skancke.¹⁷

Table 1. Structural parameters adopted for the basic calculations. The structure of radical (II) was also used for radical (VI) with the addition of: C5-O 1.43 Å, O-H 0.96 Å, \angle COH 109°.

	Radical (I)	(II)	(III)	(V)	(IV)
Bond lengths (Å)					
N1-C6	1.46	1.396	1.402	1.420	1.394
C6-C5	1.52	1.50	1.398	1.418	1.400
C5-C4	1.444	1.50	1.400	1.400	1.463
C4-N3	1.376	1.363	1.402	1.405	1.372
N3-C2	1.385	1.383	1.376	1.360	1.377
C2-N1 ^a	1.353	1.383	1.368	1.376	1.376
C2-O7	1.249	1.244	1.248	1.262	1.245
C4-O8	1.243	1.229	1.384	1.274	1.239
C5-C9	1.503	1.503	1.503	1.503	1.405
C6-H11	1.09	1.08	1.08	1.08	1.08
other C-H	1.09	1.09	1.09	1.09	1.08
N-H	1.01	1.01	1.01	1.01	1.01
O-H			0.96		
Bond angles (degrees)					
N1-C6-C5	108	120	122	122	122
C6-C5-C4	123	110	117	117	118
C5-C4-N3	117	124	118	118	116
C4-N3-C2	126	125	126	126	126
N3-C2-O7	122	122	122	122	122
C6-C5-C9	123		123	123	123
C5-C4-O8	126	126	126	126	126
C5-C9-H	109.5	109.5	109.5	109.5	120
H11-C6-H12	109				
C2-N1-H10	120	120	120	120	120
C4-N3-H16	120	120	120	120	120
N1-C6-H11		120	120	120	120
C4-O8-H12			109		
C9-C5-H12		109			
C2-N1-C6 ^a	131.1	127.6	122.1	120.3	120.3

^a The N1-C2 bond length and the C2-N1-C6 bond angle are both dependent variables. Their values are determined by the values of the other structural parameters.

RESULTS

The principal splitting constants from the INDO calculations are collected in Table 2, separated in their isotropic and anisotropic components. Experimental values are also included for comparison. Before treating each radical species in more detail, we will make some general comments.

Hyperfine splitting constants are usually discussed in terms of their magnitudes only because the signs are normally not obtained experimentally. The signs of the observed data in Table 2 have their basis in the calculated results. However, whenever the value of a

splitting constant is discussed in this paper only the magnitude is considered.

A large part of the isotropic splitting constants obtained from the INDO wave functions has been drastically reduced after annihilation. To be specific this is the case for all the constants which come out with a negative sign in the calculation (constants corresponding to a negative spin density value). Among these are all the α -proton splitting constants but— with the exception of the methyl protons in radical (III)— none of the out-of-plane protons. As can be seen from Table 2 the values before annihilation are close to or lower than the experimental ones. In view of this and in view

Table 2. Isotropic (A^{cont}) and anisotropic (A_1^{dip}) components of the principal splitting constants calculated by the INDO method. Experimental values are included for comparison. In some cases the agreement could be improved by changing the geometry (see text for details). All values are in G.

	First proton				Second proton			
	A^{cont}	A_1^{dip}	A_2^{dip}	A_3^{dip}	A^{cont}	A_1^{dip}	A_2^{dip}	A_3^{dip}
5-Thymyl radical (I)								
	Ring protons (H11,H12)				Methyl protons (H13, H14,H15)			
Exp.	40.0 ^a				21.7			
Calc., <i>sd</i>	31.6				22.3 ^b			
Calc., <i>aa</i>	26.5				19.2 ^b			
Quartet resonance								
	α -proton (H11)				β -proton (H12)			
Exp.	-28.3	6.2	-8.4	2.2	17.1	-2.4	3.4	-1.1
Calc., rad. (II) <i>sd</i>	-18.3	14.9	-12.0	-2.9	36.6	-2.9	4.1	-1.2
Calc., rad. (II) <i>aa</i>	-7.9	13.5	-11.3	-2.2	32.8	-2.3	4.1	-1.7
Doublet resonance								
	α -proton (H11)				Methyl protons ^b (H13,H14,H15)			
Exp.	-21.1	5.9	-6.1	0.1	small			
Calc., rad. (III) <i>sd</i>	-12.7	10.5	-8.6	-1.9	-7.4			
Calc., rad. (III) <i>aa</i>	-5.5	8.4	-6.9	-1.5	-3.1			
Calc., rad. (V) <i>sd</i>	-13.7	12.1	-9.8	-2.4	1.9			
Calc., rad. (V) <i>aa</i>	-6.0	10.8	-8.9	-1.9	2.9			
Calc., rad. (VI) <i>sd</i>	-17.7	14.7	-11.8	-2.9	0.3			
Calc., rad. (VI) <i>aa</i>	-7.7	13.3	-11.1	-2.2	0.9			
Sextet resonance								
	Ring proton (H11)				Methylene protons (H12,H13)			
Exp.	-11.3	4.0	-3.5	-0.5	-15.4	7.2	-7.0	-0.2
Calc., rad. (IV) <i>sd</i>	-12.1	9.2	-6.9	-2.3	-14.5	11.0	-8.7	-2.3
Calc., rad. (IV) <i>aa</i>	-5.3	7.4	-5.6	-1.8	-15.1	12.1	-10.2	-2.0
					-6.3	8.6	-6.8	-1.7
					-6.6	9.4	-7.9	-1.5

^a Mean value. ^b Mean value calculated by fitting the relation $A_H = B_0 + B_1 \cos^2 \theta$ to the splitting values obtained for one particular methyl proton when $\theta = 0^\circ$ and 90° and then averaging the resultant expression over all angles θ , θ being the dihedral angle of the proton.

of the fact that the α -splitting constants obtained after annihilation correspond to theoretical McConnell Q values that lie substantially lower than the empirical region -20 to -30 G ($A_{\alpha}^{\text{aa}}/eC^{\text{naa}}$ varying from -10 to -12 G), the standard procedure for obtaining isotropic α -proton splitting constants by INDO including annihilation⁵ seems inadequate.

On this basis only single determinant isotropic constants will be compared with experimental values in the following.

The calculated anisotropic components of the splitting constants are characterized by values substantially higher than the observed ones.

Furthermore annihilation only leads to a slight reduction. It therefore seems somewhat dubious to let the eventual rejection of certain radical candidates be too strongly based on the anisotropic components.

In Table 3 the main contributions to the computed spin density distributions are given. All radicals are regarded as π -electron radicals even if radical (II) and (VI) have unsymmetrical side groups. Only the π -part of the INDO spin densities at the conjugated atoms are given.

The 5-thymyl radical (I). This is the only radical that has been identified beyond doubt in irradiated thymine.^{1,2,22} The experimental

Table 3. Calculated π -electron spin densities at carbon, oxygen and nitrogen atoms together with INDO spin densities at hydrogen atoms. Some π densities smaller than 0.05 and hydrogen densities smaller than 0.006 are omitted. The methyl proton spin densities given correspond to a rotational conformation of the methyl group in which the plane defined by the C5-C9 and C9-H13 bonds is perpendicular to the ring plane.

Radical	Method	C4	C5	C6	C9	H11	H12	H13	H14	H15	N1	N3	O7	O8
(I)	PPP	<i>sd</i>	-0.06	0.81										0.20
	PPP	<i>aa</i>	0.01	0.79		0.059	0.058	0.080	0.022	0.022				0.13
	INDO	<i>sd</i>	-0.25	0.65		0.038	0.037	0.053	0.013	0.014				0.53
(II)	INDO	<i>aa</i>	-0.07	0.57										0.39
	INDO	<i>sd</i>		0.77	0.77	-0.034	0.068	-0.004	0.004	-0.002	0.13		0.07	
(III)	INDO	<i>aa</i>		0.76	0.76	-0.011	0.046	-0.001	0.004	-0.001	0.13		0.04	
	PPP	<i>sd</i>	0.54	-0.33	0.57						0.11	0.11		0.04
(V)	PPP	<i>aa</i>	0.43	-0.10	0.47						0.09	0.09		0.03
	INDO	<i>sd</i>	0.47	-0.24	0.53	-0.023	-0.002	-0.025	-0.008	-0.008	0.12	0.11		0.05
	INDO	<i>aa</i>	0.40	-0.07	0.45	-0.008	-0.001	-0.008	-0.003	-0.003	0.10	0.09		0.05
(VI)	PPP	<i>sd</i>	0.23	-0.03	0.60						0.06	0.05		0.12
	PPP	<i>aa</i>	0.20	0.07	0.56						0.05	0.04		0.09
	INDO	<i>sd</i>	0.07	0.03	0.62	-0.025		0.008	0.001	0.002	0.07	0.03		0.18
(IV)	INDO	<i>aa</i>	0.09	0.09	0.59	-0.008		0.009	0.002	0.002	0.06	0.03		0.12
	INDO	<i>sd</i>		0.76	0.76	-0.033	-0.003	-0.003	0.006	-0.002	0.14		0.08	
(IV)	INDO	<i>aa</i>		0.75	0.75	-0.011	-0.000	-0.001	0.005	-0.001	0.14		0.04	
	PPP	<i>sd</i>	0.03	-0.34	0.56						0.08		0.01	-0.07
	PPP	<i>aa</i>	0.01	-0.10	0.44	0.60					0.06		0.01	0.02
(IV)	INDO	<i>sd</i>	0.09	-0.23	0.52	0.62	-0.023	-0.027	-0.028		0.11		0.05	-0.14
	INDO	<i>aa</i>	0.03	-0.07	0.44	0.52	-0.007	-0.009	-0.009		0.09		0.03	-0.04

splitting constants are 36.2 and 43.8 G due to the methylene protons and 21.7 G due to the methyl protons.³ The splittings are isotropic.

According to the PPP calculations about 80 percent of the unpaired electron is located at atom C5 (Table 3). The relation (2) (with $Q^0 = 27.5$ G) then gives the following estimates of the methyl splitting constant: 22.2 G (*sd*) and 21.7 G (*aa*), in nice agreement with experiment.

The INDO calculations resulted in a somewhat different spin distribution (Table 3), but the methyl splitting (mean value given in Table 2) came out close to the PPP result.

The calculated methylene splittings are equivalent, as is to be expected from the symmetrical arrangement of the methylene protons. As Table 2 shows the splitting values are substantially smaller than those obtained experimentally. However, further calculations revealed that the methylene proton splittings are sensitive to changes in the conformation of the methylene group. Thus by rotating the fragment $>CH_2$ around an axis through C5 and N1 a separation of the splitting of the two methylene protons could be obtained. The mean value of the methylene proton splitting constants remained almost constant under this change of geometry. A rotation angle of 5° was needed to achieve the experimental split of 7.6 G.

Furthermore by allowing the HCH angle of the methylene group to decrease the methylene proton splitting could be considerably increased. A bond angle as low as 90° was required to bring the coupling constant up to the experimental value of around 40 G. This does not seem conformationally quite acceptable although a bond angle somewhat smaller than normal might be the result of creating the radical from a thymine molecule without altering its surroundings in the crystal.

The 6-thymyl radical (II). As discussed by Henriksen and Snipes¹ the observed isotropic splitting of the α -hydrogen (28.3 G) was surprisingly large. This surprise is accentuated by a preceding study of irradiated dihydrothymine²⁸ where the α -proton splitting of the 6-thymyl radical was only 17.4 G, a reasonable value for a conjugated $>\dot{C}-H$ fragment. Furthermore the β -proton splitting was also very different in the two cases, 17.1 G in the thymine case and 44.0 G in dihydrothymine.

Only INDO calculations could be performed on the 6-thymyl radical. As is seen from Table 2 the isotropic *sd*-results fit fairly well with the experimental dihydrothymine data, but not with the thymine data. This might indicate that only in the dihydrothymine case the 6-thymyl radical is actually formed. However, Henriksen and Snipes attributed the large differences in splitting constant values to differences in molecular geometry. It seemed important to test this possibility within the INDO calculations.

When the $C_5H_12CH_3$ fragment was rotated around an axis through the C4 and C6 positions, the calculated β -proton splitting varied in this way:

- 10°	43.7 G
0°	36.6 G
10°	28.1 G
20°	19.3 G

(Positive angle values define the rotation of the plane through C4, C5, C6 such that the β -proton is approaching the plane of the ring). According to these calculations ring puckering will easily be able to account for large variations in the splitting constant. This is in good agreement with the assumptions of Henriksen and Snipes.

The same authors based a possible explanation of the large α -proton splitting on a strong dependence of this splitting on the C5-C6-N1 bond angle. However, the present calculations give no support to this view. When the bond angle was shifted from 120 to 115° (compensated by small shifts in other bond angles of the ring), the splitting constant did only change very slightly from 18.3 to 18.9 G. Other variations of geometry were also tested but they did not give any increase of the α -splitting.

A look at the anisotropic constants in Table 2 reveals a rather bad agreement between experiment and calculation for the α -proton whereas the β -proton shows a very nice agreement.

Radical candidates for the doublet resonance: (III), (V) and (VI). From Table 2 radical (III) is seen to be the least satisfactory doublet candidate on the basis of the calculated isotropic splitting, but the best one when the anisotropic components are concerned. Radical

(VI) shows the opposite pattern and radical (V) is intermediate. However, it is seen that the calculated isotropic component is too small in all cases and the anisotropic ones are all too large.

In the doublet case all splitting constants but one have to be sufficiently small to escape detection in the ESR spectrum. The calculated isotropic component of the methyl protons of radical (III) is much too large from this point of view (Table 2) being more than half of the corresponding α -proton value. Table 3 shows how this is connected to a high negative spin population at atom C5. Furthermore the table shows that this population was even more negative in the PPP calculation whereas the spin population at atom C6, that in a sense is responsible for the low α -proton splitting, was about equal to the INDO value.

The Hüttermann radical (IV). When the six lines of the low temperature resonance were interpreted as being due to only one radical, Hüttermann² obtained the experimental splitting constants given in Table 2. As is seen from the table our INDO calculation on the radical postulated by Hüttermann to account for the sextet, radical (IV), gave isotropic *sd*-results in good agreement with experiment. Furthermore Table 3 shows that the PPP calculations gave spin populations at the carbon atoms C6, C5 and C9 that were similar to those from the INDO calculations. The populations at C6 and C9 were large enough for a McConnell *Q* value in the usual range (25–26 G before and 20–21 G after annihilation)¹⁸ and their relative magnitudes corresponded closely to the observed splittings.

The calculated anisotropic components of the principal splitting constants, as shown in Table 2, are larger than the observed values, but there is a qualitative agreement in relative magnitudes. The *aa*-values are slightly better than the *sd*-values.

DISCUSSION

The present calculations do not permit any definite conclusion as to which radical or radicals are actually formed in the thymine monohydrate crystal. There are several reasons for this. The MO methods used are too crude to give anything like really reliable predictions on a quantitative level. Furthermore when

all components of the calculated splitting constants are taken into account, there seems to be no satisfactory overall agreement with experiment for any of the investigated radicals.

Nevertheless, we feel that the present calculations are clearly in favour of the Hüttermann radical. The observed isotropic splittings attributed to this radical are in very good agreement with the INDO values (*sd*) as well as with the PPP spin densities *via* the McConnell relation. A comparison with the alternative quartet-doublet interpretation of Henriksen and Snipes permits us to make a few points that give further support to the Hüttermann radical. Firstly the very high isotropic α -proton coupling constant obtained for the postulated 6-thymyl radical inevitably casts some doubt on the validity of this interpretation. The anomaly of this constant is emphasized by the fact that the α -splitting observed for the 6-thymyl radical in *dihydrothymine* has a quite normal value. Our calculations on the 6-thymyl radical were unable to account for the large α -proton splitting constant. The splitting obtained was in fact very close to the value observed for the 6-thymyl radical in the dihydrothymine case. As far as the doublet resonance is concerned the accordance between experiment and calculated splitting constants is not especially good for any of the investigated radical candidates. On the basis of this we feel it justified to say that the quartet and doublet radicals are an unlikely alternative in the interpretation of the thymine monohydrate spectrum.

The anisotropic splitting constants do not support Hüttermann's conclusion in quite the same way. Their agreement with the experimental data is comparable to that found for the doublet radical candidate (III) and somewhat better than for the α -proton in the 6-thymyl radical. Considering the approximate nature of the computational method employed and the lack of experience with this method the discrepancy between observed and calculated values can hardly be said to represent a real argument against the Hüttermann radical. Thus we think it is right to say – as a conclusion – that our calculations point out rather unequivocally Hüttermann's spectral interpretation and radical identification as the most probable of the two alternatives considered.

REFERENCES

1. Henriksen, T. and Snipes, W. *Rad. Res.* **42** (1970) 255.
2. Hüttermann, J. *Int. J. Rad. Biol.* **17** (1970) 249.
3. Pople, J. A., Beveridge, D. L. and Dobosh, P. A. *J. Chem. Phys.* **47** (1967) 2026.
4. Pople, J. A., Beveridge, D. L. and Dobosh, P. A. *J. Am. Chem. Soc.* **90** (1968) 4201.
5. Beveridge, D. L. and Dobosh, P. A. *J. Chem. Phys.* **48** (1968) 5532.
6. Beveridge, D. L. and McIver, Jr., J. W. *J. Chem. Phys.* **54** (1971) 4681.
7. Pariser, R. and Parr, R. G. *J. Chem. Phys.* **21** (1953) 466; *Ibid.* **21** (1953) 767.
8. Pople, J. A. *Trans. Faraday Soc.* **49** (1953) 1375.
9. Fjeldstad, A. and Jensen, H. H. *Acta Chem. Scand.* **26** (1972) 1869.
10. Amos, T. and Snyder, L. C. *J. Chem. Phys.* **41** (1964) 1773.
11. Snyder, L. C. and Amos, T. *J. Chem. Phys.* **42** (1965) 3670.
12. Roos, B. and Skancke, P. N. *Acta Chem. Scand.* **21** (1967) 233.
13. Roos, B. *Acta Chem. Scand.* **21** (1967) 2318.
14. Fischer-Hjalmars, I. and Sundbom, M. *Acta Chem. Scand.* **22** (1968) 607.
15. Jensen, H. and Skancke, P. N. *Acta Chem. Scand.* **22** (1968) 2899.
16. Höjer, G. *Acta Chem. Scand.* **23** (1969) 2589.
17. Flood, E. and Skancke, P. N. *Acta Chem. Scand.* **27** (1973) 3069.
18. McConnell, H. M. *J. Chem. Phys.* **24** (1956) 764.
19. Skancke, A. and Skancke, P. N. *Acta Chem. Scand.* **22** (1968) 175.
20. Pople, J. A. and Beveridge, D. L. *Approximate Molecular Orbital Theory*, McGraw-Hill, New York 1970, p. 111.
21. Gerdil, R. *Acta Crystallogr.* **14** (1961) 333.
22. Pruden, B., Snipes, W. and Gordy, W. *Proc. Nat. Acad. Sci. U.S.A.* **53** (1965) 917.
23. Henriksen, T. and Snipes, W. *J. Chem. Phys.* **52** (1970) 1997.

Received September 9, 1976.

The Crystal Structure of D-Histidinato-L-histidinatocobalt(III) Bromide

NIELS THORUP

Chemistry Department B, Technical University of Denmark, DTH 301, DK-2800 Lyngby, Denmark

The crystal structure of the title compound has been determined by X-ray crystallographic methods. The crystals are monoclinic, space group $P2_1/c$, with 4 formula units in the unit cell of dimensions $a = 9.834(4)$ Å, $b = 15.104(11)$ Å, $c = 10.772(7)$ Å, and $\beta = 107.16(2)^\circ$. Intensity data were collected using an automatic equi-inclination diffractometer. The structure has been refined to an R value of 0.057. The cobalt atom is octahedrally coordinated to the amino nitrogen atom, an imidazole nitrogen atom, and a carboxylate oxygen atom of each histidinate group. The coordinating atoms of one histidinate group are in *cis* positions to the corresponding atoms of the other histidinate group, *i.e.*, the configuration is all-*cis*.

This paper reports the three-dimensional crystal structure analysis of D-histidinato-L-histidinatocobalt(III)bromide, $[\text{Co}(\text{C}_6\text{H}_9\text{N}_3\text{O}_2)_2]\text{Br}$. The histidinate ion is shown in Fig. 1 with its three metal binding sites indicated.

The preparation of this compound is described by Bagger, Gibson, and Sørensen.¹ They also present and discuss the visible and proton magnetic resonance spectra which suggest an all-*cis* arrangement of the histidinate groups. The present X-ray investigation was initiated to obtain verification of this configuration. Suitable single crystals were provided by Bagger *et al.*

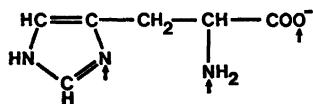


Fig. 1. Histidinate with metal binding sites indicated by arrows.

EXPERIMENTAL

Unit cell and space group. Crystal symmetry and space group were established from precession photographs applying Zr-filtered Mo-radiation. Preliminary unit cell dimensions were also determined from these photographs. Later, the cell dimensions were refined using diffractometer measurements. The observed density of the crystals, as found by the flotation method, is in fair agreement with the calculated value corresponding to four formula units per unit cell. The crystal data are given in Table 1.

Collection of intensity data. A crystal with dimensions approx. $0.1 \times 0.2 \times 0.2$ mm³ was mounted with the *b*-axis as rotation axis. The intensity measurements were made by means of an automatic equi-inclination diffractometer (Stoe & Cie, Darmstadt, BRD). MoK α -radiation was selected using a graphite monochromator. Harmonics were excluded by means of a pulse height discriminator in combination with the scintillation detector. The relative intensities of reflections $h0l$ through $h16l$ within a hemisphere of $\sin \theta/\lambda < 0.70$ Å⁻¹ were measured applying the ω -scan technique. Reflections having averaged net intensities less than three times their standard deviation, calculated from counting statistics, were considered unobserved. This criterion left a total of 2051 unique observations. The intensities were converted to structure factors by conventional Lp correction formulas ignoring the polarization in the

Table 1. Crystal data. Estimated standard deviations are given in parentheses.

Crystal system: Monoclinic (*b* unique)
 Space group: $P2_1/c$ (No. 14)
 $a = 9.834(4)$ Å, $b = 15.104(11)$ Å,
 $c = 10.772(7)$ Å,
 $\beta = 107.16(2)^\circ$, $M = 447.14$ g mol⁻¹, $Z = 4$,
 $D_m = 1.93$ g cm⁻³, $D_x = 1.94$ g cm⁻³,
 $\mu(\text{MoK}\alpha) = 37.4$ cm⁻¹.

monochromator of the incident beam. No correction for absorption was applied.

Computer programs. The programs V72 and REDIDAT, both written at this laboratory, calculated setting angles for the diffractometer and checked the consistency of diffractometer output data, respectively. The regular structure analysis was performed using the program system X-RAY.² Crystal structure illustrations were produced by the program ORTEP.³ All calculations were carried out on the IBM 370/165 computer and the RC 4000 computer, both situated at the Technical University of Denmark.

STRUCTURE DETERMINATION

A three-dimensional Patterson map was first calculated, but the interpretation of this was not straightforward, and, therefore, direct

methods were used to determine the positions of the heavy atoms, cobalt and bromine. The remaining non-hydrogen atoms were found in subsequent electron density maps in the usual heavy atom procedure. Atomic scattering factors for the neutral atoms were generated from the analytical functions given by Cromer and Mann.⁴

The structure thus obtained was then refined by a full matrix minimization of $\sum w(|F_o| - |F_c|)^2$, using first isotropic temperature factors for all atoms and later introducing anisotropic temperature factors for cobalt and bromine. The weighting scheme used was of the type: $1/w = 1 + ((F_o - b)/a)^2$, where a and b were given values minimizing the variation of $\langle w(|F_o| - |F_c|)^2 \rangle$ with F_o and $\sin \theta$. The actual values

Table 2a. Fractional coordinates and isotropic thermal parameters (\AA^2) with estimated standard deviations. The temperature factor is given by $\exp[-8\pi^2 U(\sin \theta/\lambda)^2]$.

Atom	x	y	z	U
Br	0.2194(1)	0.0130(1)	0.5441(1)	
Co	0.2122(1)	0.7289(1)	0.5332(1)	
C1	0.4295(8)	0.8385(6)	0.6535(7)	0.024(2)
C2	0.4407(8)	0.8277(6)	0.5156(7)	0.025(2)
C3	0.5473(9)	0.7530(6)	0.5157(8)	0.028(2)
C4	0.5105(8)	0.6701(6)	0.5719(8)	0.026(2)
C5	0.3752(9)	0.5707(7)	0.6230(8)	0.034(2)
C6	0.5991(10)	0.6038(7)	0.6354(9)	0.041(2)
C11	0.0110(8)	0.6906(6)	0.6513(7)	0.026(2)
C12	-0.0603(8)	0.7544(6)	0.5430(7)	0.024(2)
C13	-0.1454(9)	0.7024(6)	0.4230(8)	0.027(2)
C14	-0.0518(8)	0.6457(5)	0.3875(7)	0.024(2)
C15	0.1383(9)	0.5974(6)	0.3242(8)	0.026(2)
C16	-0.0937(9)	0.5823(6)	0.2756(8)	0.031(2)
N1	0.2979(6)	0.8029(5)	0.4298(6)	0.020(1)
N2	0.3721(7)	0.6490(4)	0.5669(6)	0.023(1)
N3	0.5084(9)	0.5409(6)	0.6651(8)	0.043(2)
N11	0.0533(7)	0.8078(4)	0.5104(6)	0.022(1)
N12	0.0956(7)	0.6567(4)	0.3969(6)	0.021(1)
N13	0.0288(8)	0.5532(6)	0.2502(7)	0.034(2)
O1	0.3230(5)	0.7991(4)	0.6747(5)	0.024(1)
O2	0.5221(6)	0.8777(5)	0.7359(5)	0.034(1)
O11	0.1399(6)	0.6684(4)	0.6556(5)	0.026(1)
O12	-0.0527(7)	0.6602(4)	0.7242(6)	0.033(1)

Table 2b. Anisotropic thermal parameters (\AA^2) with estimated standard deviations. The temperature factor is given by $\exp[-2\pi^2(h^2a^{*2}U11 + \dots + 2klb^*c^*U23)]$.

Atom	$U11$	$U22$	$U33$	$U12$	$U13$	$U23$
Br	0.0365(5)	0.0379(6)	0.0277(4)	0.0026(4)	0.0030(3)	0.0062(4)
Co	0.0139(4)	0.0190(6)	0.0117(4)	0.0007(5)	0.0029(3)	-0.0003(4)

DESCRIPTION AND DISCUSSION OF THE STRUCTURE

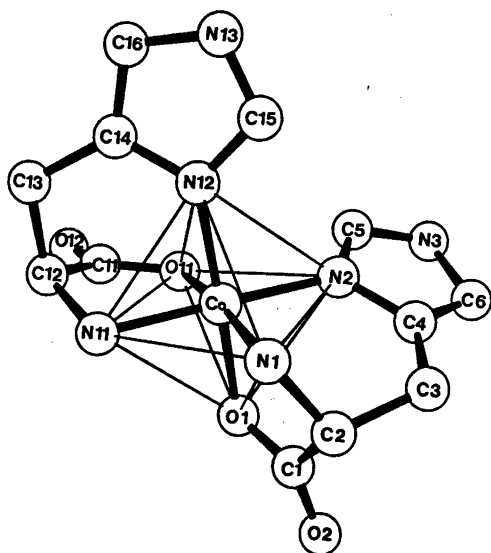


Fig. 2. The structure of the complex ion $[\text{Co}(\text{C}_6\text{H}_8\text{N}_3\text{O}_2)_2]^+$. The lower right histidinate has D configuration, the other one has L configuration. Thin lines show the coordination polyhedron.

of a and b were 20 and 45, respectively. The refinement terminated with residuals $R = 0.057$ and $R_w = 0.067$.

Hydrogen atoms have not been included in this structure determination. The final positional and thermal parameters are given in Tables 2a and 2b. A list of observed and calculated structure factors may be obtained from the author upon request.

Fig. 2 shows the structure of the complex ion $[\text{Co}(\text{C}_6\text{H}_8\text{N}_3\text{O}_2)_2]^+$. The cobalt atom is octahedrally coordinated to the amino nitrogen atom, an imidazole nitrogen atom, and a carboxylate oxygen atom of each histidinate group. One of these groups is D-histidinate and the other group is L-histidinate. The configuration is termed all-*cis*, because the coordinating atoms of one histidinate group are all in *cis* positions to the corresponding atoms of the other histidinate group.

Bond distances and angles are given in Tables 3 and 4. A comparison between the two histidinate groups shows that none of the corresponding bond lengths differ significantly (the difference is in each case less than twice its standard deviation). The corresponding bond angles within the histidinate groups are also equal. However, bond angles involving cobalt differ slightly (up to 4°). A small difference in metal-ligand bonding of the two histidinate ions is also seen when considering the imidazole rings. The distances from the cobalt atom to the least squares planes of the imidazole rings are 0.47 and 0.18 Å for D- and L-histidinate, respectively. Correspondingly, the Co-N2 and Co-N12 bonds make angles of 14.0 and 5.8° with their respective imidazole rings. Similar displacements of the metal atom with respect to the imidazole rings have been observed in other histidinate complexes.⁵

The major torsion angles of the two histi-

Table 3. Bond distances (Å) with estimated standard deviations.

Atoms	Distance	Atoms	Distance
Co-N1	1.937(7)	Co-N11	1.923(7)
Co-N2	1.930(7)	Co-N12	1.915(6)
Co-O1	1.912(5)	Co-O11	1.907(6)
C1-O1	1.282(11)	C11-O11	1.298(10)
C1-O2	1.221(9)	C11-O12	1.229(11)
C1-C2	1.531(12)	C11-C12	1.516(11)
C2-N1	1.484(9)	C12-N11	1.502(11)
C2-C3	1.539(12)	C12-C13	1.533(11)
C3-C4	1.482(13)	C13-C14	1.506(13)
C4-C6	1.370(13)	C14-C16	1.351(12)
C4-N2	1.383(11)	C14-N12	1.397(10)
N2-C5	1.324(12)	N12-C15	1.336(11)
C5-N3	1.332(12)	C15-N13	1.317(10)
N3-C6	1.402(15)	N13-C16	1.384(13)

Table 4. Bond angles (°) with estimated standard deviations.

Atoms	Angle	Atoms	Angle
N1—Co—N2	90.0(3)	N11—Co—N12	88.6(3)
N1—Co—O1	84.1(3)	N11—Co—O11	86.0(3)
N2—Co—O1	87.5(3)	N12—Co—O11	89.7(3)
N1—Co—N11	92.5(3)	N2—Co—O11	91.1(3)
N1—Co—N12	98.7(3)	N11—Co—O1	90.5(3)
N2—Co—N12	93.3(3)	O1—Co—O11	87.5(2)
N1—Co—O11	171.4(3)	N2—Co—N11	176.6(3)
N12—Co—O1	177.1(4)		
Co—N1—C2	106.3(5)	Co—N11—C12	105.7(5)
Co—N2—C4	126.9(6)	Co—N12—C14	126.0(6)
Co—N2—C5	123.5(6)	Co—N12—C15	127.6(5)
Co—O1—C1	114.7(5)	Co—O11—C11	114.3(5)
O1—C1—O2	124.6(8)	O11—C11—O12	123.9(7)
C2—C1—O1	114.8(6)	C12—C11—O11	114.6(7)
C2—C1—O2	120.4(8)	C12—C11—O12	121.4(7)
C1—C2—N1	107.8(7)	C11—C12—N11	108.3(6)
C1—C2—C3	108.8(6)	C11—C12—C13	109.7(7)
N1—C2—C3	109.6(7)	N11—C12—C13	109.6(7)
C2—C3—C4	111.8(8)	C12—C13—C14	112.4(6)
C3—C4—N2	122.3(7)	C13—C14—N12	123.9(7)
C3—C4—C6	128.8(8)	C13—C14—C16	127.0(7)
C4—N2—C5	107.4(7)	C14—N12—C15	105.7(6)
N2—C5—N3	110.1(9)	N12—C15—N13	110.7(8)
C5—N3—C6	108.7(8)	C15—N13—C16	108.8(8)
N3—C6—C4	104.8(8)	N13—C16—C14	105.9(7)
C6—C4—N2	108.9(8)	C16—C14—N12	108.9(8)

Table 5. Torsion angles (°) with estimated standard deviations in the histidinate groups. Designations and signs are in accordance with IUPAC-IUB conventions.*

Designation	Atoms	Angle (this study)	Angle (Ref. 5)	Angle (Ref. 7)
ψ^2	N1—C2—C1—O2	-163.3(8)	-167	
ψ^2	N11—C12—C11—O12	156.2(7)	167	154.6(5)
χ^1	N1—C2—C3—C4	-64.0(8)	-71	
χ^1	N11—C12—C13—C14	54.9(9)	64	-58.3(6)
$\chi^{2,1}$	C2—C3—C4—N2	28.2(10)	36	
$\chi^{2,1}$	C12—C13—C14—N12	-16.8(11)	-19	56.6(7)

inate ions are given in Table 5. Numerical differences between corresponding angles are rather small (7–12°). For comparison, the angles in D-histidinato-L-histidinatocobalt(II) dihydrate⁵ and in orthorhombic L-histidine⁷ are also included in Table 5. The conformations in the two cobalt complexes are very similar, whereas the conformation in histidine is quite different with respect to the angles χ^1 and $\chi^{2,1}$.

The packing of a unit cell is shown in Fig. 3. Apart from weak van der Waals interactions the structure seems to be held together by hydrogen bonds and electrostatic forces. Using Bondi's⁸ van der Waals radii for C, N, and O and Pauling's⁹ radius for Br⁻, the following contact distances are obtained: N···O, 3.07 Å; C···O, 3.22 Å; N···Br⁻, 3.50 Å; C···Br⁻, 3.65 Å. As apparent from Table 6, some intermolecular distances are fairly short and suggest

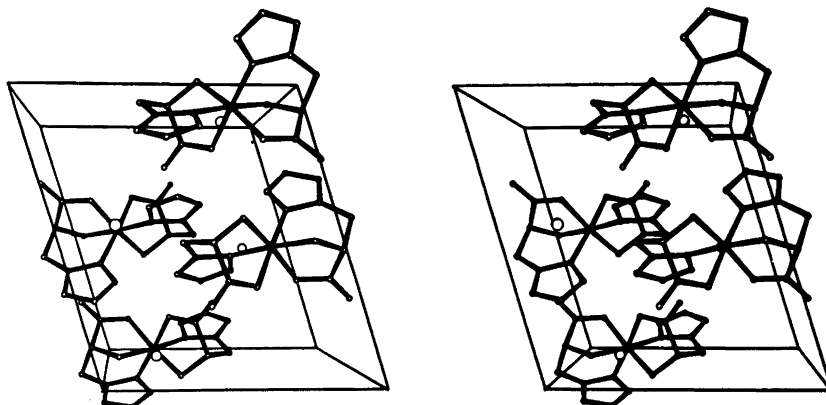


Fig. 3. Stereo view along b axis of the structure. Large spheres represent bromide ions.

hydrogen bonds $\text{N}-\text{H}\cdots\text{O}$ and possibly $\text{N}-\text{H}\cdots\text{Br}^-$. However, a detailed discussion of hydrogen bonds is hardly justifiable, since hydrogen atoms were not located. The close approach between Cl , which has no hydrogen attached, and Br^- can be accounted for by assuming an excess positive charge on Cl leading to considerable Coulomb interaction.

Table 6. Short intermolecular distances (\AA) with estimated standard deviations. The symmetry operations involved are: a, $(1-x, y-1/2, 3/2-z)$; b, $(x, 3/2-y, z-1/2)$; c, $(x, y+1, z)$; d, $(-x, y+1/2, 1/2-z)$; e, $(1-x, y+1/2, 3/2-z)$; and f, $(x, 1/2-y, z-1/2)$.

Atoms	Distance
$\text{N3}\cdots\text{O2(a)}$	2.738(12)
$\text{N1}\cdots\text{O11(b)}$	2.936(8)
$\text{N11}\cdots\text{O12(b)}$	2.987(9)
$\text{Cl5}\cdots\text{O1(b)}$	3.172(11)
$\text{Cl1}\cdots\text{Br(c)}$	3.342(8)
$\text{Cl6}\cdots\text{Br(d)}$	3.461(9)
$\text{N13}\cdots\text{Br(d)}$	3.437(7)
$\text{N13}\cdots\text{Br(f)}$	3.449(9)
$\text{N11}\cdots\text{Br(c)}$	3.472(7)
$\text{N3}\cdots\text{Br(e)}$	3.494(7)

REFERENCES

1. Bagger, S., Gibson, K. and Sørensen, C. S. *Acta Chem. Scand.* 26 (1972) 2503.
2. Stewart, J. M. *The X-RAY System*, Technical Report TR-192, University of Maryland 1972.
3. Johnson, C. K. *ORTEP*, Report ORNL-3794, Oak Ridge National Laboratory, Oak Ridge 1965.
4. Cromer, D. T. and Mann, J. B. *Acta Crystallogr. A* 24 (1968) 321.
5. Candlin, R. and Harding, M. M. *J. Chem. Soc. A* (1970) 384.
6. IUPAC-IUB Commission on Biochemical Nomenclature, *J. Mol. Biol.* 52 (1970) 1.
7. Lehmann, M. S., Koetzle, T. F. and Hamilton, W. C. *Int. J. Peptide Protein Res.* 4 (1972) 229.
8. Bondi, A. *J. Phys. Chem.* 68 (1964) 441.
9. Pauling, L. *The Chemical Bond*, Cornell University Press, Ithaca 1967, p. 151.

Received September 3, 1976

Preparation and Reactions of a Coordinatively Unsaturated Surface Compound of Cobalt(II) on Silica Gel

BERND REBENSTORF

Division of Inorganic Chemistry I, Chemical Center, University of Lund,
Box 740, S-220 07 Lund 7, Sweden

The preparation of a coordinatively unsaturated surface compound of cobalt(II) on silica gel is described. This surface compound adsorbs easily CO, C₂H₄, NO or H₂O at room temperature with an accompanying colour change. Stoichiometric measurements of the complex formation showed that two ligands can be adsorbed by one cobalt ion, which is thought to be connected to the silica gel surface by two oxygen ligands. Reactions catalysed by this cobalt(II) surface compound are the oxidation of CO with O₂ (air) and the oligomerization of C₂H₂. Polymerization of C₂H₄ was not observed.

Since Krauss and Stach¹ described a coordinatively unsaturated surface compound of chromium(II) on silica gel and stated that this compound is the polymerization center of the widely used Phillips process² for polymerization of ethylene, there has been some interest in surface compounds of transition metal ions, mainly those of chromium(II).³⁻⁵

Although some papers deal with cobalt(II) on silica gel a coordinatively unsaturated surface compound of this ion, comparable to that of chromium(II) has not been observed. The adsorption of different cobalt(II) complexes on ion exchanged silica gel was investigated by Burwell, Jr. *et al.*⁶ Subsequently Anderson⁷ described the change in the coordination sphere of cobalt(II) adsorbed on silica gel due to heat treatment up to 500 °C. Investigations of Kazansky *et al.*⁸ yielded surface compounds which adsorbed water or ammonia but gave only labile surface complexes of olefins.

EXPERIMENTAL

Silica gel "Merck 7733" was purified by heating in distilled water to 95 °C and additional

washing with distilled water. After drying at 150 °C in air for 3 h a solution of the cobalt(II) salt in water was added and the silica gel dried at 120 °C in air. The impregnated silica gel was heated in a quartz tube under vacuum and afterwards handled with exclusion of moisture and air.

Gravimetric measurements were carried out with the samples placed in a Schlenck tube equipped with a teflon stopcock. When the amount of adsorbed gas was measured after evacuating no correction was necessary for physisorbed gas. At a pressure of 760 Torr the correction was calculated from identical argon measurements assuming the physisorption of argon to be the same as that of CO. The error of the stoichiometric relation ranged from 5 to 10 % depending on the amount of adsorbed gas.

Cobalt(II) was analysed by dissolving the silica gel in a boiling solution of sodium hydroxide, acidifying the solution by hydrochloric acid after cooling, replacing the silica gel by filtering and determining the absorption at 630 nm of the thiocyanate complex in acetone. The error was within 2 %.

IR spectra were obtained on powdered samples mixed with paraffin oil under argon and placed between plates of calcium fluoride. The measurements were performed with a Perkin-Elmer 221 spectrophotometer and were accurate to within ± 2 cm⁻¹.

RESULTS

After impregnation, the silica gel is light pink but changes colour at 100 °C under vacuum to blue due to the change from Co(H₂O)₆²⁺ to Co(H₂O)₄²⁺ (with O_h and T_d symmetry at the Co²⁺ ion, respectively). This reaction is reversed by treatment with water as shown by the use of such silica gel as moisture indicator. Heating of the impregnated silica gel to tem-

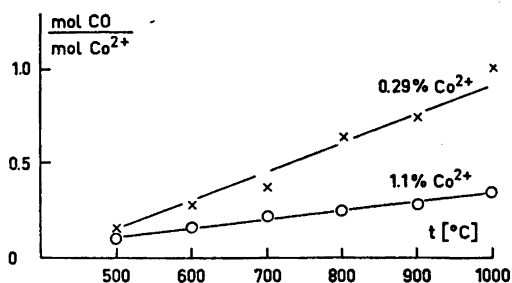


Fig. 1. CO adsorption at 0°C/1 Torr on samples impregnated with cobalt(II) chloride versus temperature of the vacuum heat treatment (1 Torr).

peratures between 300 and 500°C under vacuum results in an almost irreversible colour change to blue. This is due to the bonding of a cobalt(II) ion to the silica gel surface with loss of acid formed by the former anion of the cobalt salt and a proton from silanol groups at the surface. The hydrochloric or acetic acid so formed can be collected in a cold trap.

Further vacuum heating changes the colour to light blue and results in production of the coordinatively unsaturated cobalt(II) surface compound, which can be detected by adsorption of CO. Fig. 1 shows the adsorption of CO, determined by gravimetric measurements, for samples with different vacuum heat treatments. Adsorption of CO also gives rise to a colour change ranging from violet to brown⁹ depending on the amount of adsorbed CO.

As shown in Figs. 2 and 3 the cobalt concentration has a great influence with respect to the percentage of the cobalt(II) surface compound compared to the total analysed cobalt. This effect may be due to the different cobalt content of the silica gel particles resulting from chromatographic separation during the impregnation. This can result in the formation of small crystals of cobalt(II) salts on the surface during the heat treatment which cannot react as coordinatively unsaturated surface compounds.

The CO is released when heated under vacuum to 100°C, restoring the coordinatively unsaturated surface compound. C_2H_4 replaces CO and gives a colour change to red violet, but is not bonded more strongly than CO. Polymerization of C_2H_4 was not observed. Both ligands

Acta Chem. Scand. A 31 (1977) No. 3

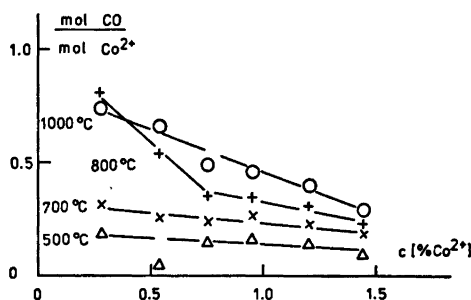


Fig. 2. CO adsorption at 0°C/1 Torr on samples impregnated with cobalt(II) acetate versus cobalt content. Different temperatures of vacuum heat treatment (1 Torr) as indicated.

are replaced when exposed to water with change of colour to blue.

To determine the stoichiometric relation between the ligands and the cobalt(II) surface compound, adsorption of NO was examined (colour change to brown). For this purpose NO is better suited than CO because it is adsorbed more strongly and so ensures that all coordinatively unsaturated surface sites have adsorbed ligands. As shown in Fig. 4, at low cobalt content two NO ligands are adsorbed per cobalt(II) ion but this ratio decreases with rising cobalt content due to the effect discussed previously. Adsorption of CO at 760 Torr is equal to the adsorption of NO under vacuum. CO and C_2H_4 adsorption under vacuum is lower than both NO and CO at 760 Torr, but is greater than a ratio of one ligand per cobalt ion at low cobalt content. Comparison of Figs. 2 and 4 reveals the influence of the vacuum

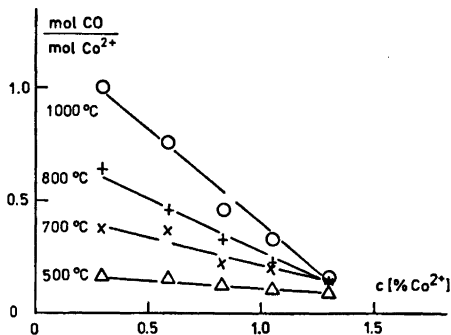


Fig. 3. The same as Fig. 2 but with samples impregnated with cobalt(II) chloride.

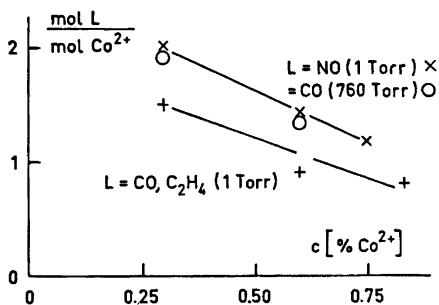


Fig. 4. NO, CO and C_2H_4 adsorption on samples impregnated with cobalt(II) chloride versus cobalt content. Vacuum heat treatment (10^{-2} Torr) at $1000^\circ C$.

during the heat treatment on the amount of adsorbed ligands: with a higher vacuum the yield of the coordinatively unsaturated cobalt(II) surface compound increases.

Adsorbed NO is not stable against O_2 (air), but reacts to form adsorbed NO_2 . The surface compound is then blue brown and is destroyed by water. Adsorption of N_2 , CO_2 and O_2 was not observed.

If the complex between water and the coordinatively unsaturated cobalt(II) surface compound is heated under vacuum, adsorption of CO at $0^\circ C$ begins after temperature treatment higher than $400^\circ C$. After this temperature treatment roughly 1.3 mol H_2O per cobalt is still adsorbed, which is within error just the same as shown for adsorbed NO in Fig. 4 for a sample with the same cobalt content

(0.59 %). The temperature of $400^\circ C$ fits well with results shown in Fig. 1 which means that in both cases the same reaction takes place. If the samples, which have adsorbed water, are heated in vacuum to temperatures used in the preparation, the coordinatively unsaturated compound is regained.

IR spectra of adsorbed CO and NO are shown in Figs. 5 and 6, with adsorbed CO exhibiting two peaks at 2184 and 2170 cm^{-1} and NO at 1875 and 1797 cm^{-1} . No frequency shift was observed on samples with different cobalt content (0.29, 0.59, 0.83 % Co). Only slight differences of the intensities were observed due to different cobalt contents.

The angles between the two ligands were calculated from the intensities of the IR absorptions according to Beck *et al.*¹⁰ The values from Figs. 5 and 6 for adsorbed CO are nearly 90° and for adsorbed NO 110° . For the latter, both the IR absorptions¹¹ and their intensities agree remarkably well with those of $(Co(NO)_2Cl)_2$:¹⁰ 1860 and 1795 cm^{-1} , angle 112° . On the basis of this comparison the symmetry of the complex between NO and the coordinatively unsaturated cobalt(II) surface compound is thought to be pseudo tetrahedral.

Catalysed reactions. In contrast to adsorbed C_2H_4 , adsorbed CO reacts with O_2 (air), revealing the light blue colour of the coordinatively unsaturated surface compound. However, at room temperature this reaction is quite slow: it takes about half an hour for full conversion of the adsorbed CO. Between 50 and $100^\circ C$

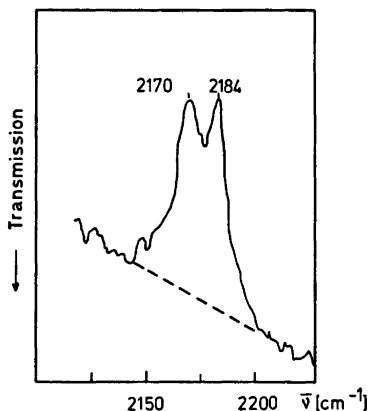


Fig. 5. IR spectrum of adsorbed CO. Samples as used in Fig. 4 (0.59 % Co).

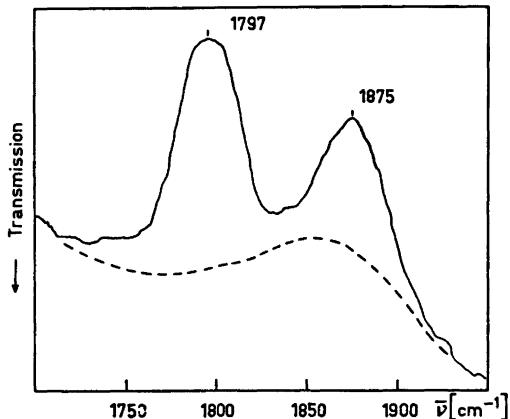


Fig. 6. IR spectrum of adsorbed NO. Samples as used in Fig. 4 (0.59 % Co).

(760 Torr) the conversion time decreases to some minutes and the evolved CO_2 was easily identified with barium hydroxide solution and by means of IR spectrophotometry.

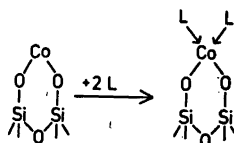
Adsorbed C_2H_2 changes the colour of the cobalt(II) surface compound to pink, almost like C_2H_4 , but reacts, in contrast to C_2H_4 , easily at 25°C to give a brown product. By means of mass spectroscopy benzene was detected as the main reaction product, but higher oligomers were also present.

DISCUSSION

A comparison of the heat treatment of the impregnated silica gel as described by Kazansky *et al.*⁸ with that used in this work, reveals that the temperatures used by Kazansky (500 and 700°C) were too low and could only give poor yields of the coordinatively unsaturated cobalt(II) surface compound (see Fig. 1).

The structure of the coordinatively unsaturated cobalt(II) surface compound may be approached in the following way. The angle between the two NO ligands (110°) and comparison with the structure of $[\text{Co}(\text{NO})_2\text{Cl}]_2$ ¹⁰ is strong evidence for a pseudo tetrahedral structure with symmetry C_{2v} . The angle of the two adsorbed CO molecules (90°) would lead to a pseudo square planar or distorted pseudo tetrahedral configuration with symmetry C_{2v} . Further evidence for such a structure is gained

by the colour (blue) and the stoichiometric relation between water and cobalt(II) (1.3:1)* of the water complex with the cobalt(II) surface compound. Thus on the basis that the structure of the water complex is pseudo tetrahedral (the same colour as the blue $\text{Co}(\text{H}_2\text{O})_4^{2+}$ complex) the cobalt ion must be bonded to the silica gel surface by two oxygen ligands. This is confirmed by the formation of hydrochloric or acetic acid during the vacuum heat treatment up to 500°C of the impregnated samples.



The structure and the reaction with ligands of the coordinatively unsaturated cobalt(II) surface compound on silica gel is schematically shown.

This model is the same as that of the coordinatively unsaturated surface compound of chromium(II) on silica gel reported by Krauss.¹² The comparison of both compounds in Table 1 reveals some common behaviour, but two main differences are obvious: the chromium(II) compound is easily oxidized by O_2 to chromium(VI) while the similar co-

* In view of the cobalt concentration influence discussed above, the real value is thought to be 2:1.

Table 1. Comparison of the chromium(II) and cobalt(II) coordinatively unsaturated surface compounds on silica gel.

	Chromium(II) ³⁻⁵	Cobalt(II)
Oxygen ligands from the silica gel surface	2	2
Stoichiometry of ligand adsorption	2, 3, 4,	2, ?,
Possible ligands	N_2 , CO_2 , CO , C_2H_4 , H_2O , NO (and others)	CO , C_2H_4 , NO , H_2O
IR absorptions at 20°C ^a		
for adsorbed CO	2186 cm^{-1}	$2184, 2170\text{ cm}^{-1}$
for adsorbed NO	$1865, 1747\text{ cm}^{-1}$	$1875, 1797\text{ cm}^{-1}$
Oxidation with O_2	easily to Cr^{6+}	none
Polymerization of C_2H_4	rapid reaction	none
Oligomerization of C_2H_2	yes	yes

^a IR data for chromium(II) were taken from Zecchina *et al.*⁴

balt(II) compound does not react in this way, and the chromium(II) polymerizes C_2H_4 extremely well while cobalt(II) gives a stable complex with adsorbed C_2H_4 . This comparison may give some further argument for an oxidative cycloaddition of two C_2H_4 molecules as the first step of the polymerization of C_2H_4 by a coordinatively unsaturated chromium(II) surface compound on silica gel.¹⁴

Acknowledgement. This work was made possible by a stipend from the Deutsche Forschungsgemeinschaft.

REFERENCES

1. Krauss, H. L. and Stach, H. *Inorg. Nucl. Chem. Lett.* 4 (1968) 393.
2. a. Clark, A., Hogan, J. P., Banks, R. L. and Lanning, W. C. *Ind. Eng. Chem.* 48 (1956) 1152; b. Clark, A. *Catal. Rev.* 3 (1969) 145.
3. a. Hogan, J. P. *J. Polym. Sci.* 8 (1970) 2637; b. Hierl, G. and Krauss, H. L. *Z. Anorg. Allg. Chem.* 402 (1973) 113; c. Krauss, H. L. and Rebenstorf, B. *Z. Anorg. Allg. Chem.* 402 (1973) 263; d. Krauss, H. L. and Weisser, B. *Z. Anorg. Allg. Chem.* 412 (1975) 82; e. Krauss, H. L., Rebenstorf, B. and Westphal, U. *Z. Anorg. Allg. Chem.* 414 (1975) 97; f. Krauss, H. L., Rebenstorf, B., Westphal, U. and Schneeweiss, D. In Delmon, B., Jacobs, P. A. and Poncelet, G., Eds., *Preparation of Catalysts*, Elsevier, Amsterdam 1976, p. 149.
4. a. Zecchina, A., Garrone, E., Ghiotti, G., Morterra, C. and Borello, E. *J. Phys. Chem.* 79 (1975) 966; b. Zecchina, A., Garrone, E., Ghiotti, G. and Coluccia, S. *J. Phys. Chem.* 79 (1975) 972; c. Zecchina, A., Garrone, E., Morterra, C. and Coluccia, S. *J. Phys. Chem.* 79 (1975) 978; d. Zecchina, A., Garrone, E., Ghiotti, G. and Coluccia, S. *J. Phys. Chem.* 79 (1975) 984.
5. a. Yermakov, Yu. and Zakharov, V. *Adv. Catal.* 24 (1975) 173; b. Kugler, E. L., Kokes, R. J. and Gryder, J. W. *J. Catal.* 36 (1975) 142; c. Kugler, E. L. and Gryder, J. W. *J. Catal.* 36 (1975) 152.
6. Burwell, Jr., R. L., Pearson, R. G., Haller, G. L., Tjok, P. B. and Chock, S. P. *Inorg. Chem.* 4 (1965) 1123.
7. Anderson, Jr., J. H. *J. Catal.* 28 (1973) 76.
8. a. Brotikovskii, O. I., Shvets, V. A. and Kazanskii, V. B. *Kinet. Katal.* 13 (1972) 1342, Engl. 1198; b. Borovkov, V. Yu. and Kazanskii, V. B. *Kinet. Katal.* 13 (1972) 1356, Engl. 1217; c. Kazansky, V. B., Borovkov, V. Yu. and Zhidomirov, G. M. *J. Catal.* 39 (1975) 205.
9. UV/VIS spectra will be published elsewhere.
10. Beck, W., Melnikoff, A. and Stahl, R. *Chem. Ber.* 99 (1966) 3721.
11. Connelly, N. G. *Inorg. Chim. Acta Rev.* 6 (1972) 47.
12. Krauss, H. L. *Proc. Int. Congr. Catal.* 5th, 1972, 1 (1973) 207.
13. Rebenstorf, B., *Diss.*, Freie Universität Berlin, Berlin 1975.

Received September 10, 1976.

Structural Investigations of Sulfonated 1,2-Nitrosonaphthol (\rightleftharpoons 1,2-Naphthoquinone Oxime) Ligands. Part VI. The Crystal Structure of Potassium 1,2-Naphthoquinone-1-oxime-7-sulfonate Monohydrate: $\text{KC}_{10}\text{H}_6\text{NO}_5\text{S}\cdot\text{H}_2\text{O}$

HEIKKI SAARINEN, JORMA KORVENRANTA and ELINA NÄSÄKKÄLÄ

Department of Inorganic Chemistry, University of Helsinki, SF-00100 Helsinki 10, Finland

The crystal structure of the title compound has been determined from three-dimensional X-ray diffraction data and refined by least-squares methods. The space group is $P2_1/c$, $a = 7.195(4)$, $b = 21.278(10)$, $c = 7.973(5)$ Å, $\beta = 104.27(5)^\circ$, $Z = 4$. The final R value was 0.070 for 1304 observed reflections and the estimated standard deviation in the bond lengths for the non-hydrogen atoms was in the range 0.007–0.016 Å. The CN(1.31 Å), NO(1.39 Å), CO(1.22 Å), and C3–C4(1.31 Å) bond lengths indicate that the organic anion exists in its tautomeric oxime form. The oxime group and the quinone oxygen are in the *anti* configuration. The potassium ions are linked together by a bridging water molecule, which is hydrogen-bonded to two sulfonate oxygens. A third hydrogen bond is formed between the oxime nitrogen and sulfonate oxygen atoms. The results are compared with those obtained earlier for similar ligands in free and metal-coordinated state.

In previous papers we have described the structures of some complexes of copper(II) with 1,2-nitrosonaphthol ligands.^{1–3} The X-ray studies indicated that the coordinated ligand anions are consistent with significant contributions from the quinone oxime structure. In fact, the compounds in question have been classified according to their tautomeric oxime names. Apart from the metal chelates, we have also reported the crystal structures of several uncoordinated sulfonic acid derivatives of 2-nitroso-1-naphthol.^{4–8} All these ligands were found to be very similar in structure, having a tautomeric 1,2-naphthoquinone-2-oxime form

in which the oxime group is in the *anti* configuration with respect to the quinone oxygen. However, this decision cannot be confidently assumed for compounds derived from 1-nitroso-2-naphthol. Although the quinonoid character of all the 1,2-isomers can already be predicted, the orientation of the oxime group with respect to the quinone oxygen in 1-nitroso-2-naphthol compounds is still fully in doubt.

In order to clarify this particular relationship we have now determined the crystal structure of potassium 1,2-naphthoquinone-1-oxime-7-sulfonate monohydrate. Being the first representative of a free 1-nitroso-2-naphthol type of ligand investigated by X-rays, it also makes possible a more detailed discussion of the structures of such molecules in free and metal-coordinated state.

EXPERIMENTAL

Crystal preparation. Potassium 1,2-naphthoquinone-1-oxime-7-sulfonate was prepared from potassium 2-naphthol-7-sulfonate (Koch Light, pure, and Pfaltz & Bauer, Inc.) by nitrosation with potassium nitrite in acidic solution cooled to 0 °C.⁹ After it was recrystallized from water, microcrystalline yellow needles were obtained, which on further recrystallization from a water-acetone (3:1) mixture grew to thin lath-shaped prisms. The formula weight of the product based on potentiometric neutralization titration was found to be 307 ± 2 .

Crystal data. The space group, from systematic absences, and initial unit cell parameters were determined from Weissenberg photographs

Table 1. Fractional atomic coordinates ($\times 10^4$) and anisotropic thermal parameters a ($\times 10^3$) for non-hydrogen atoms. Estimated standard deviations are given in parentheses.

Atom	X/a	Y/b	Z/c	U_{11}	U_{22}	U_{33}	U_{12}	U_{13}	U_{23}
C1	2889(13)	4403(4)	647(11)	35(6)	26(5)	22(4)	-6(4)	7(4)	-6(3)
C2	2645(14)	3995(4)	-959(11)	40(6)	24(5)	27(4)	-7(4)	7(4)	-3(4)
C3	2164(15)	4323(5)	-2625(13)	44(7)	43(6)	28(5)	-13(4)	9(4)	-13(4)
C4	1968(16)	4937(4)	-2699(12)	63(7)	32(5)	18(5)	-5(4)	0(4)	-1(4)
C5	1928(16)	5990(4)	-1460(13)	59(7)	28(5)	27(5)	8(4)	-1(5)	4(4)
C6	2180(13)	6390(4)	-52(11)	33(6)	33(5)	25(5)	0(4)	5(4)	4(4)
C7	2633(12)	6137(4)	1598(10)	31(6)	26(5)	19(4)	-2(3)	7(4)	-2(3)
C8	2824(13)	5502(4)	1885(10)	46(6)	16(4)	17(4)	-1(3)	8(4)	0(3)
C9	2650(14)	5080(4)	490(11)	52(6)	22(5)	20(4)	1(4)	6(4)	-4(3)
C10	2168(13)	5346(4)	-1224(10)	40(6)	25(4)	16(4)	-1(4)	9(4)	-1(3)
N	3406(12)	4049(3)	2030(9)	52(5)	25(4)	23(4)	1(3)	12(3)	-7(3)
O1	3680(11)	4375(3)	3577(8)	85(6)	24(4)	20(3)	4(3)	0(3)	1(2)
O2	2879(11)	3426(3)	-856(9)	87(6)	13(3)	44(4)	-2(3)	21(4)	-5(5)
S	2958(3)	6642(1)	3423(3)	39(1)	16(1)	21(1)	3(1)	3(1)	-1(1)
O3	2540(11)	7270(3)	2750(8)	72(5)	23(3)	33(4)	13(3)	-3(3)	-6(3)
O4	1714(11)	6408(3)	4440(8)	63(5)	37(4)	33(4)	-8(3)	19(3)	-10(3)
O5	4980(10)	6597(3)	4340(8)	54(5)	23(3)	28(3)	-8(3)	-6(3)	0(3)
K	3495(3)	2689(1)	2285(3)	58(2)	24(1)	31(1)	3(1)	12(1)	2(1)
O6	901(11)	2802(4)	4359(11)	33(5)	44(4)	62(5)	-1(3)	7(4)	-11(4)

^a The anisotropic thermal parameters are of the form $\exp[-2\pi^2(h^2a^{*2}U_{11} + k^2b^{*2}U_{22} + \dots)]$.

taken with $\text{CuK}\alpha$ ($\lambda = 1.5418 \text{ \AA}$) radiation. More accurate cell constants were obtained by least-squares procedure from powder photographs taken with a Hagg-Guinier camera using calcium fluoride as internal standard ($a = 5.4630 \text{ \AA}$). The density was determined by the flotation technique. The crystal data for $\text{KC}_{10}\text{H}_8\text{NO}_5\text{S}\cdot\text{H}_2\text{O}$ are:

$a = 7.195(4) \text{ \AA}$ FW = 309.34
 $b = 21.278(10) \text{ \AA}$ $D_o = 1.72 \text{ g cm}^{-3}$
 $c = 7.973(5) \text{ \AA}$ $D_c = 1.736 \text{ g cm}^{-3}$
 $\beta = 104.27(5)^\circ$ $Z = 4$
 $V = 1182.97 \text{ \AA}^3$ Space group $P2_1/c$ (No. 14)

Intensity data. The crystal selected for data collection had approximate dimensions $0.25 \times 0.1 \times 0.1 \text{ mm}$. Ni-filtered Cu radiation ($\text{CuK}\alpha$, $\lambda = 1.5418 \text{ \AA}$) was used with a Stoe-Güttinger diffractometer. Of the 1758 recorded

independent reflections from the levels $0kl - 6kl$, 1304 had intensities greater than twice the standard deviations calculated from counting statistics. The data were corrected for Lorentz and polarization factors, but extinction and absorption corrections were not applied [$\mu(\text{CuK}\alpha) = 57.25 \text{ cm}^{-1}$].

Structure determination. The structure was solved by direct methods with the X-RAY 72 program system.¹⁰ All non-hydrogen atoms were located from an E map, computed by use of 278 reflections with $|E| \geq 1.40$. Refinement was carried out by full-matrix least-squares methods, using first isotropic and then anisotropic temperature factors. The function to be minimized was $\sum w(|F_o| - |F_c|)^2$, where $w = 1/(35.0 + |F_o| + 0.044|F_o|^2)$. The atomic scattering factors for non-hydrogen and hydrogen atoms were taken from Refs. 11 and 12, respectively. When the R value ($R = \sum ||F_o| -$

Table 2. Fractional atomic coordinates ($\times 10^3$) for hydrogen atoms.^a

Atom	X/a	Y/b	Z/c	Atom	X/a	Y/b	Z/c
H(C3)	184(14)	409(5)	-358(14)	H(C8)	310(14)	524(5)	306(13)
H(C4)	189(14)	511(5)	-371(14)	H(O1)	400(14)	406(5)	438(14)
H(C5)	149(14)	612(4)	-275(13)	H1(O6)	-37(15)	259(5)	377(13)
H(C6)	226(14)	693(5)	-17(13)	H2(O6)	3(17)	302(5)	471(14)

^a Isotropic temperature factors for hydrogen atoms were set at 3.2 \AA^2 .

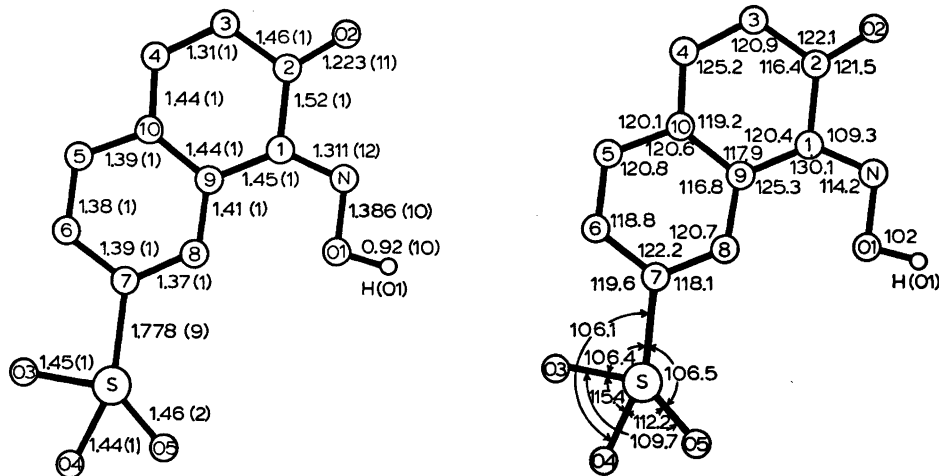


Fig. 1. Schematic representation of the anion showing bond lengths with their standard deviations (Å) and bond angles ($^{\circ}$). The e.s.d.'s in angles are in the range $0.4 - 0.9^{\circ}$.

$|F_c|/|\sum|F_o||$ was reduced to 0.090, a difference Fourier map was computed and all hydrogen atoms were located. The positional parameters of the hydrogen atoms were allowed to vary in subsequent least-squares refinements but their temperature parameters were kept fixed at $B = 3.2 \text{ \AA}^2$. After the last cycle the average shift/e.s.d. value of variable parameters for the non-hydrogen atoms was 0.06 and for the hydrogen atoms 0.24. The final R value was 0.070 for 1304 observed reflections.

The atomic coordinates and thermal parameters for the non-hydrogen atoms are given in Table 1 and the atomic coordinates for hydrogen atoms in Table 2. A list of the observed and calculated structure factors is obtainable on request from the authors.

RESULTS AND DISCUSSION

The dimensions of the organic anion of the present compound which can be seen in Fig. 1 generally well accord with those of the 1,2-naphthoquinone-2-oximes studied previously.⁴⁻⁶ The characteristic CO, CN, NO, C1-C2, and C3-C4 bond distances, together with the CNO bond angle of all these compounds, are listed in Table 3. It is evident that the molecules exist in their tautomeric naphthoquinone oxime forms. Table 3 shows that the CN and NO distances remain fairly constant around 1.31 and 1.38 Å, respectively. These values compare well with the average $\text{C}=\text{N}$ ($1.27 \pm$

0.02 \AA) and $\text{N}-\text{O}$ ($1.40 \pm 0.02 \text{ \AA}$) bond lengths collected by Chakravorty for several typical oximes.¹³ The average CNO bond angle in Table 3 (113°) is also consistent with the respective value 112° reported by Chakravorty. Additional evidence for the quinonoid character of these compounds is given by the average CO distance 1.21 \AA , which is closely equal to the $\text{C}=\text{O}$ bond lengths found in benzoquinone¹⁴ and naphthoquinone¹⁵ compounds, and the visibly long C1-C2 and short C3-C4 bond lengths (cf. Table 3). The quinonoid structure is not extended over the whole naphthalene carbon plane, however, as the C5-C10 carbon ring has maintained its aromatic character.

It is especially worthy of note that in the present compound the 1-oxime group and the quinone oxygen are in the *anti*-position, and are thus similar in their arrangement to the same groups in 1,2-naphthoquinone-2-oxime compounds. As we have pointed out earlier, both *anti* and *syn* configurations are found in benzoquinone oxime series.⁵

It is interesting to determine the magnitude of naphthalene *peri* effects on the orientation of the 1-oxime group. As can be seen from Fig. 1, the angle C9-C1-N (130°) is markedly larger than the angle C2-C1-N (109°), which together with the deviations of the N and O atoms from the naphthalene mean plane (Table 4) indicate a significant shift of the

Table 3. Characteristic bond distances (Å) and angles (°) of different 1,2-naphthoquinone oxime compounds.

Formula	qoH	CO	CN	NO	C3-C4	C1-C2	CNO	Ref.
Na(qoH).1½H ₂ O (mean)	I	1.20	1.31	1.35	1.34	1.52	111	4
H(qoH).H ₂ O	I	1.24	1.30	1.38	1.33	1.47	112	5
K(qoH).2H ₂ O	II	1.21	1.30	1.38	1.33	1.50	113	6
[Ni(H ₂ O) ₆](qoH) ₂ .4H ₂ O	III	1.21	1.31	1.37	1.33	1.49	113	7
KNa(qoH) ₂ .3H ₂ O (mean)	I	1.22	1.30	1.37	1.33	1.48	112	8
K(qoH).H ₂ O	IV	1.22	1.31	1.39	1.31	1.52	114	This work
[Cu(qo) ₂].2(CH ₃) ₂ CO	V	1.30	1.35	1.26	1.36	1.43	122	1
[Cu(qo) ₂].H ₂ O (mean)	VI	1.28	1.35	1.26	1.36	1.44	121	2
[Cu(qo)(H ₂ O) ₂].3H ₂ O	III	1.26	1.35	1.25	1.34	1.43	121	3

qoH = 2-nitroso-1-naphthol-5-sulfonate (I), 2-nitroso-1-naphthol-8-sulfonate (II), 2-nitroso-1-naphthol-4-sulfonate (III), 1-nitroso-2-naphthol-7-sulfonate (IV), 1-nitroso-2-naphthol (V), and 2-nitroso-1-naphthol (VI).

group away from the hydrogen on the 8-carbon atom.

The geometry of the sulfonate group attached to the 7-position of the naphthalene nucleus is as expected: the values of the C-S bond length (1.78 Å), the S-O distances (1.44–1.46 Å), the O-S-O angles (110–115°), and the C-S-O angles (106–107°) are all normal values frequently reported for several different sulfonate compounds.

The environment of the potassium ion is heteroatomic, being composed of six oxygen atoms and one nitrogen atom (Fig. 2). Two of these oxygen atoms are sulfonate oxygens, two are quinone oxygens, and the remaining two are water oxygens. In this way the same water molecule is connected with two adjacent

potassium ions. The bond contacts about the potassium ion fall in the range 2.79–3.05 Å (Table 5).

Table 4. The least-squares plane defined by the naphthalene carbon ring. Deviations (Å) of different atoms from the plane are given. X', Y', and Z' are orthogonal axes related to X, Y, and Z by $X' = X + Z \cos \beta$, $Y' = Y$, and $Z' = Z \sin \beta$. Plane C1-C10: $0.9946X' + 0.0960Y' + 0.0408Z' - 2.8570 = 0$

Atom	Distance	Atom	Distance	Atom	Distance
C1	0.003	C6	0.017	N	0.075
C2	0.009	C7	0.018	O1	0.084
C3	0.005	C8	-0.022	O2	0.043
C4	0.002	C9	-0.004	S	0.055
C5	-0.015	C10	-0.014		

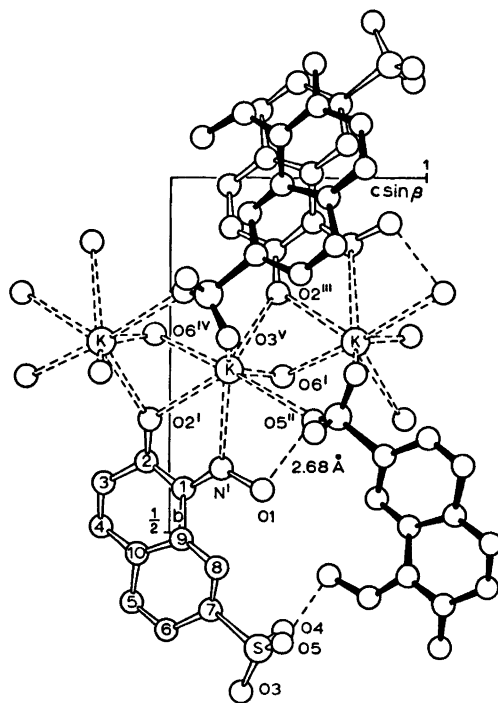


Fig. 2. Partial packing diagram of $KC_{10}H_6NO_6S \cdot H_2O$ as viewed down the a axis. Symmetry operations used in Fig. 2 and Table 5 are: I x, y, z II $1-x, 1-y, 1-z$ III $x, \frac{1}{2}-y, \frac{1}{2}+z$ IV $x, \frac{1}{2}-y, -\frac{1}{2}+z$ V $1-x, -\frac{1}{2}+y, \frac{1}{2}-z$.

Table 5. Interatomic distances (Å) of the potassium ion environment.

K-O2 ^I	2.89	K-N ^I	2.90	K-O6 ^I	2.79
K-O5 ^{II}	3.05	K-O2 ^{III}	2.90	K-O6 ^{IV}	2.81
K-O3 ^V	3.00				

The role of the water molecule in the structure is distinct: besides the K-O contact mentioned it also takes part in hydrogen bonding by accepting two hydrogen bonds from sulfonate oxygens. These bond lengths are both 2.86 Å. A third and somewhat shorter hydrogen bond is formed through the oxime hydrogen atom which is bound to the remaining sulfonate oxygen. Each sulfonate oxygen atom is thus active in hydrogen bonding. It may be noted that the last-mentioned $\text{NOH}\cdots\text{O}$ contact has always been found to be the shortest hydrogen bond in these compounds. Details of the hydrogen bonding can be found in Table 6 and the packing of the structure is illustrated in Fig. 2.

As mentioned above, the free 1,2-naphthoquinone oximes studied are clearly similar in structure, and the minor differences to be found in separate ligands (Table 3) are not significant. Due to the different positions of the substituents on the naphthalene carbon ring and to the different packing effects, exact similarity could hardly be expected.

Selected bond lengths and angles of the ligand anions coordinated to copper(II) ion are also included in Table 3. On comparing the bond distances with those of the free oximes supposed to exist in the alkali salts and in the salt of the nickel hexaaqua ion,⁴⁻⁶ some general observations can be made: (i) the N-O distance is significantly shortened from *ca.* 1.37 to *ca.* 1.26 Å on complex formation, (ii) the C-O

bond is significantly lengthened from *ca.* 1.21 to 1.28 Å, (iii) the C-N bond may be slightly lengthened (from *ca.* 1.31 to 1.35 Å, and (iv) the C-N-O angle is opened up by about 8° from the average free ligand value of 113°. Another result is that on complex formation the C1-C2 bond distance shortens to some extent and the C3-C4 bond is only slightly affected (Table 3).

Clearly, these alternations all lead to a resonance structure that can well be regarded as a metal-nitrosophthalato structure. On this view, it is understandable that unambiguous conclusions about the tautomeric form of these uncoordinated ligand acids are not possible merely from a consideration of structures of their metal chelates.

Acknowledgement. The financial support of the Science Research Council of Finland is gratefully acknowledged.

REFERENCES

1. Saarinen, H. and Korvenranta, J. *Acta Chem. Scand. A* 29 (1975) 409.
2. Korvenranta, J. and Saarinen, H. *Acta Chem. Scand. A* 29 (1975) 861.
3. Korvenranta, J. and Saarinen, H. *Finn. Chem. Lett.* (1975) 115.
4. Näsäkkälä, M., Saarinen, H. and Korvenranta, J. *Finn. Chem. Lett.* (1977) 42.
5. Saarinen, H., Korvenranta, J. and Näsäkkälä, M. *Finn. Chem. Lett.* (1977) 47.
6. Korvenranta, J., Saarinen, H., Näsäkkälä, E. and Näsäkkälä, M. *Finn. Chem. Lett.* (1977) 52.
7. Korvenranta, J., Saarinen, H. and Näsäkkälä, E. *Finn. Chem. Lett.* (1977). *In press.*
8. Näsäkkälä, M., Saarinen, H., Korvenranta, J. and Näsäkkälä, E. *Finn. Chem. Lett.* (1977). *In press.*
9. Mäkitie, O., Saarinen, H., Mattinen, H. and Seppovaara, K. *Suom. Kemistil. B* 43 (1970) 340.

Table 6. Hydrogen bonding details.

X-H \cdots Y	X \cdots Y Å	X-H Å	H \cdots Y Å	X-H \cdots Y (°)
O1-H(O1) \cdots O5 ^I	2.68	0.92	1.77	166
O6-H1(O6) \cdots O3 ^{II}	2.86	1.03	1.85	167
O6-H2(O6) \cdots O4 ^{III}	2.86	0.87	1.99	173

^I1-x, 1-y, 1-z

^{II}-x, - $\frac{1}{2}$ +y, $\frac{1}{2}$ -z

^{III}-x, 1-y, 1-z

10. X-Ray 72, Program System for X-Ray Crystallography, *Technical Report TR-192 of the Computer Science Center*, University of Maryland.
11. Cromer, D. T. and Mann, J. B. *Acta Crystallogr. A* 24 (1968) 321.
12. Stewart, R. F., Davidson, E. and Simpson, W. *J. Chem. Phys.* 42 (1968) 3175.
13. Chakravorty, A. *Coord. Chem. Rev.* 13 (1974) 1.
14. Trotter, J. *Acta Crystallogr.* 13 (1960) 98.
15. Gaultier, P. J. and Hauw, C. *Acta Crystallogr.* 18 (1965) 179.

Received September 23, 1976.

Equilibrium Studies of Chromium(III) Complexes.

III. The Complex Formation between Chromium(III) and Ethylenediaminetetraacetic Acid

PETER ANDERSEN, TORSTEN BERG and JENS JACOBSEN

Chemistry Department I, Inorganic Chemistry, H.C. Ørsted Institute, University of Copenhagen, DK-2100 Copenhagen Ø, Denmark

It has previously been shown that under the combined catalytic effect of Cr(II) and charcoal equilibrium between the mononuclear Cr(III) amines or Cr(III) ethylenediamine complexes is established within a few days. In the present work it has been shown that the Cr(III) complexes $[\text{Cr}(\text{NH}_3)_6]\text{Cl}_3$, $[\text{Cr}(\text{NH}_3)_5\text{Cl}_2(\text{H}_2\text{O})_2]\text{Cl}$ and $[\text{Cr}(\text{urea})_6]\text{Cl}_3$ react with EDTA in aqueous solution within a few hours using this catalyst to give the Cr(III) EDTA complex quantitatively.

From emf measurements with a mercury electrode in such solutions with $C_{\text{KCl}} = 0.60 \text{ M}$, $C_{\text{EDTA}} = 65 \text{ mM}$, $C_{\text{Cr}} = 5.0 \text{ mM}$ and $4.5 < \text{pH} < 9.5$ (22°C) the stability constant for the formation of the Cr(III) EDTA complex was found to be $10^{23.1} \text{ M}^{-1}$.

In recent papers we described a method by which it is possible to establish equilibrium between the mononuclear chromium(III) complexes with ethylenediamine¹ or ammonia² as ligands in aqueous solution within a few days at room temperature. The method is based on the combined catalytic effect of chromium(II) (1–2 % of the total chromium content) and charcoal, which must both be present. During the equilibration chromium(II) is continuously generated by electrolytic reduction so as to compensate for the amount of chromium(II) which is oxidized to chromium(III) by the medium, this oxidation being catalyzed by the charcoal. The emf was measured continuously during the equilibration using a mercury electrode, and from these emf measurements it was possible to determine the chromium(II) content of the solutions¹ as well as the gross stability constants.

We describe here a similar investigation of the chromium(III)-EDTA system (EDTA \equiv ethylenediaminetetraacetic acid $\equiv \text{H}_4\text{Y}$). Our intention was to find out whether it was possible, using this catalytic procedure, to establish equilibrium over a large pH range (4.5–9.5), and to see whether the mercury electrode worked satisfactorily under these conditions. EDTA is suitable for this purpose because of its high stability and because of the simplicity of the system involving only a few species (*vide infra*).

EXPERIMENTAL

Procedure. The experimental arrangement has been described by us previously.¹ Table 1 gives the experimental conditions and results of a single typical experiment (exp. 1 of Table 2): After the first *ca.* 6 h with an electrolysis current of *ca.* 20 mA the emf had dropped to between –1.1 and –1.2 V and this could subsequently be maintained by using 1–5 mA, giving $[\text{Cr}(\text{II})]/[\text{Cr}(\text{III})] \simeq 0.01–0.1$. From time to time the current was switched off in order to measure E and $[\text{Cr}(\text{II})]$ simultaneously as described previously.¹ At the same time a small sample was removed for analysis.

Table 2 gives the experimental conditions employed in a series of experiments involving various pH, initial Cr(III) compounds, times of equilibration, *etc.*

All experiments were performed at $22 \pm 1^\circ\text{C}$.

Chemicals and apparatus. All chemicals used were reagent grade or were analyzed by us. *cis*- $[\text{Cr}(\text{NH}_3)_2(\text{H}_2\text{O})_2\text{Cl}_2]\text{Cl}$,³ $[\text{Cr}(\text{NH}_3)_6]\text{Cl}_3$,⁴ $[\text{Cr}(\text{urea})_6]\text{Cl}_3 \cdot \text{H}_2\text{O}$,⁵ and $\text{CrSO}_4 \cdot 5\text{H}_2\text{O}$ ⁶ were prepared according to the literature methods and were analyzed for Cr, N, chloride, Cr(II)

Table 1. Experimental details for exp. 1 (Table 2). $C_{Cr} = 5.0$ mM (from $CrCl_3 \cdot 6H_2O$ heated at $90^\circ C$ for 5 min with the $Na_2H_2Y \cdot 2H_2O$ -solution), $C_{EDTA} = 65$ mM, $pH_{start} = 6.0$ (adjusted to this pH with 0.1 M $NaOH$), 50 mg charcoal, 0.60 M KCl , $22^\circ C$, 50 ml solution.

Meas- ure- ment	Total time h	Electrolysis mA	Current mA	Voltage V	Total amount of electricity C	pH	emf, E Hg. sat. calomel mV	$(\partial E/\partial t)_0$ mV min ⁻¹	Hydrogen vol. V_{H_2}	$[Cr(II)]_0$ from $(\partial E/\partial t)_0$ mM	$[Cr(II)]_0$ from V_{H_2} mM	$\log(K_{III}/K_{II})$ from $(\partial E/\partial t)_0$ V_{H_2}	$\log(K_{III}/K_{II})$ from V_{H_2}
	2.0	20	25	25	144	6.1	-611						
	6.0	16	28	28	360	6.2	-1171						
	6.5	4.0	8.5	8.5	367	6.2	-1158						
	7.5	3.3	7.7	7.7	379	6.2	-1143	2.1	0.34	0.50	0.56	9.32	9.26
	27.5	0.5	3.0	3.0	415	6.2	-1110	1.8	0.14	0.089	0.23	9.54	9.42
	29.0	1.0	3.9	3.9	420	6.3	-1128	1.7	0.28	0.48	0.46	9.19	9.21
	30.0	1.5	4.4	4.4	425	6.3	-1135	1.0					

Table 2. $\log K_{III}/K_{II}$ determined under different conditions. $C_{Cr} = 5.0$ mM, $C_{EDTA} = 65$ mM, 0.6 M KCl (except for exp. 14), $22^\circ C$, 50 ml solution.

Exp. No.	pH	Initial Cr(III) compound	$\log K_{III}/K_{II}$	Other experimental details different from those in exp. 1 (Table 1)
1	6.2	$CrCl_3 \cdot 6H_2O$ heated at $90^\circ C$ with EDTA	9.35	
2	6.2	as exp. 1	9.38	
3	6.3	as exp. 1	9.45	100 mg charcoal (100 mg was also used in exp. 3-10 and 14) 0.1 mM $< [Cr(II)] < 0.6$ mM in 5 E -measurements 0.08 mM $< [Cr(II)] < 0.3$ mM in 3 E -measurements electrolyzed for 4 days with 1117 C 0.01 mM $< [Cr(II)] < 0.7$ mM in 3 E -meas. with 1 day's interval
4	6.2	as exp. 1	9.38	pH variation
5	4.6	as exp. 1	9.42	
6	7.6	as exp. 1	9.39	
7	9.7	as exp. 1	9.34	0.03 mM $< [Cr(II)] < 0.5$ mM in 3 E -meas. per exp.
8	6.1	cis - $[Cr(NH_3)_3Cl_3(H_2O)_2]Cl$	9.47	Variation of initial Cr-compound, which was not heated with the EDTA-solution.
9	5.6	$[Cr(NH_3)_4Cl_3]$	9.58	0.04 mM $< [Cr(II)] < 0.7$ mM in 2 E -meas. per exp.
10	5.6	$[Cr(NH_3)_4Cl_3]$	9.42	After the second E -meas. of exp. 11 5.13 mg $CrSO_4 \cdot 5H_2O$ was added to the solution at $E = -1000$ mV: $[Cr(II)] = 0.43$ mM (calc.), 0.41 mM (from V_{H_2}), $E = -1145$ mV leading to $\log(K_{III}/K_{II}) = 9.47$
11	5.7	$[Cr(urea)_4Cl_3 \cdot H_2O]$	9.52	
12	6.2	The equilibrated sol. from exp. 4 as exp. 1	9.35	The solution had been left for 12 months, charcoal was removed, 2.41 mg $CrSO_4 \cdot 5H_2O$ was added giving $[Cr(II)] = 0.20$ mM (from V_{H_2}), $E = -1120$ mV
13	6.1	as exp. 1	9.60	6.83 mg $CrSO_4 \cdot 5H_2O$ was added giving $[Cr(II)] = 0.54$ mM (from V_{H_2}), $E = -1161$ mV (no charcoal)
14	5.6	as exp. 1	9.41	$C_{Cr} = 1.0$ mM, $C_{EDTA} = 5.0$ mM, 0.1 M KCl , $[Cr(II)] = 0.03$ mM
	6.2	Average exp. 1-13	9.41	in 2 E -meas.
			9.44	

and sulfate. All analyses agreed within 1–2 % (relative) with the formulae given. The charcoal used was a Norit W product, and purified redistilled mercury was used for the electrodes.

The emf and pH measurements were made with a Radiometer PHM 52, the G 202 C glass electrodes being tested in the relevant media according to Bjerrum.⁷ Visible spectra were recorded on a Cary 14 or a Bausch and Lomb Spectronic 505 spectrophotometer.

RESULTS

In the pH range investigated only two Cr(III)-EDTA complexes need to be taken into consideration, namely $\text{CrY}(\text{H}_2\text{O})^-$ and $\text{CrY}(\text{OH})^{2-}$ since the acid dissociation constants of Cr(HY) (H_2O) are $\text{p}K_{\text{S}_1}^{\text{III}}=1.95$ and $\text{p}K_{\text{S}_2}^{\text{III}}=7.39$ (0.1 M KCl, 20 °C)⁸ and $\text{CrY}(\text{OH})^{2-}$ takes up a second OH^- with “ $\text{p}K_{\text{S}_3}^{\text{III}}=12.25$.” Cr(II) exists as CrY^{2-} under our conditions, Cr(HY) (H_2O)⁻ having $\text{p}K_{\text{S}_1}^{\text{II}}=3.00$ and $\text{p}K_{\text{S}_2}^{\text{II}}>11$.¹⁰

In order to minimize pH changes during the electrolysis C_{EDTA} was chosen to be as high as 6.5×10^{-3} M, giving a reasonably high buffer capacity which was almost independent of pH between pH 5.5 and 8. A 0.6 M KCl medium was chosen as a compromise so as to ensure a medium of constant ionic strength and at the same time facilitate comparison of our results with stability constants from the literature, most of which have been determined for 0.1 M KCl. Table 1 shows that during the first 5–6 h with high electrolysis current the pH increased by 0.2 after which it was nearly constant and in no case increased more than 0.1 pH unit except in exp. 14 with $C_{\text{EDTA}}=5 \times 10^{-3}$ M (0.1 M KCl), where the pH increase was *ca.* 5 times as great. E does not, however, depend very much on pH in this pH range (see the following equation).

The ratio of the EDTA stability constants K^{III} and K^{II} for Cr(III) and Cr(II), respectively, is calculated from

$$\log \frac{K^{\text{III}}}{K^{\text{II}}} = \log \frac{[\text{CrY}(\text{H}_2\text{O})^-][\text{Cr}^{2+}]}{[\text{CrY}^{2-}][\text{Cr}^{3+}]}$$

$$= -\frac{E+652}{58.5} + \log \frac{\{C_{\text{Cr}} - [\text{Cr}(\text{II})]\}[\text{H}^+]}{[\text{Cr}(\text{II})]\{[\text{H}^+] + K_{\text{S}_2}^{\text{III}}\}}$$

“652” is the difference between the standard potentials of the $\text{Cr}^{2+} - \text{Cr}^{3+}$ couple and of the saturated calomel electrode (–410 mV¹¹ and 242 mV, respectively).

The calculated values of $\log(K^{\text{III}}/K^{\text{II}})$ are given in Tables 1 and 2. $\text{p}K_{\text{S}_3}^{\text{III}}$ was determined from spectral data for Cr(III)-EDTA solutions in 1 M KCl at various pH as 7.34 ± 0.06 to be compared with a value of 7.39 ± 0.02 (0.1 M KCl, 20 °C) determined by other workers.⁸

The rate of formation of $\text{CrY}(\text{H}_2\text{O})^-$ from $\text{Cr}(\text{NH}_3)_6^{3+}$ under a variety of conditions was followed spectrophotometrically. The reaction time for the formation of 90 % $\text{CrY}(\text{H}_2\text{O})^-$ is given in Table 3.

DISCUSSION

The average value of $\log K^{\text{III}}/K^{\text{II}}=9.4$ from Table 2 corresponds to a standard potential (*versus* the saturated calomel electrode) $E^{\circ}_{\text{SCE}} = -1204$ mV. Pecsok *et al.* determined $\log K^{\text{II}}=13.61$ in 0.1 M KCl at 20 °C and from polarographic measurements found $\log K^{\text{III}}/K^{\text{II}}=9.79$.¹⁰ The experiment 14 in 0.1 M KCl medium (Table 2) shows that $\log K^{\text{III}}/K^{\text{II}}$ in this medium is the same within experimental error as in 0.6 M KCl. Using $\log K^{\text{II}}=13.61$ this equilibrium determination of $\log K^{\text{III}}/K^{\text{II}}$ gives $\log K^{\text{II}}=23.1$ in good agreement with the previous determination¹⁰ (see Table 4). A comparison of the stability constant data for chromium(III), cobalt(III), and nickel(II) with

Table 3. Rate of formation of $\text{CrY}(\text{H}_2\text{O})^-$ (90 mol-%) under various catalytic conditions. $C_{\text{Cr}}=5.0$ mM, $C_{\text{EDTA}}=65$ mM, pH=5.5 (0.6 M KCl, 22 °C, 50 ml). $[\text{CrY}(\text{H}_2\text{O})^-]/C_{\text{Cr}}$ was measured spectrophotometrically.

Exp.	90 % $\text{CrY}(\text{H}_2\text{O})^-$ after	Catalytic conditions
a	< 4 h	100 mg charcoal, Cr(II) produced electrolytically (15–20 mA), daylight, exp. 10 (Table 2)
b	30 d	no charcoal, no Cr(II)
c	65 d	100 mg charcoal, no Cr(II)
d	83 d	as c but in the dark
e	163 d	as b but in the dark
f		addition of 1.2 mg $\text{CrSO}_4 \cdot 5\text{H}_2\text{O}$ (2 mol-%).
	After 1 day:	No detectable Cr(II) and 70 mol-% $\text{CrY}(\text{H}_2\text{O})^-$.

Table 4. Comparison of stability constants at room temperature for Cr(III), Co(III), and Ni(II) with ammonia (extrapolated values), en (= ethylenediamine) and EDTA.

	NH ₃ log K _s	log K _s	log β _s	en log K _s	log β _s	EDTA log K
Cr(III) ^{1,2,10}	1.6	1.5	13	6.4	19.5	23.1 ^a 23.4 ^b
Co(III) ^{7,12-15}	5.5	4.9	38	13.3	48.7	40.7
Ni(II) ^{7,14,17}	0.9	0.2	10	4.4	18.3	18.6 ^b
Medium	4.5 M NH ₄ Cl			1 M 1:1 salt		^a 0.6 M KCl ^b 0.1 M KCl

the ligands ammonia, ethylenediamine, and EDTA is given in Table 4.

The mercury electrode worked reproducibly within 1–2 mV under these conditions with varying [Cr(II)] and pH, and equilibrium was attained within 4–5 h irrespective of the initial Cr(III) compound. We also performed some experiments with charcoal-free solutions by adding known amounts of CrSO₄·5H₂O to a solution which had been equilibrated with charcoal and Cr(II) and then aged for 12 months (exp. 12), and also by adding Cr(II) to a thermally treated solution (exp. 13), both experiments giving results in agreement with the others in Table 2.

Table 3 shows that the rate of formation of CrY(H₂O)⁻ from the very robust Cr(NH₃)₆³⁺ in the presence of Cr(II) and charcoal is increased at least 400 times relative to the rate in solutions without Cr(II). Charcoal alone has only a small effect. Exposure to daylight has some effect and the lower rate of exp. c compared to exp. b (Table 3) is probably due to the light shielding effect of the charcoal. It was difficult to measure the effect of the few per cent Cr(II) alone because of the rapid oxidation to Cr(III) especially with charcoal present. Thus no Cr(II) could be detected after one day in charcoal-free solution starting with 2 % Cr(II) (as CrSO₄·5H₂O, exp. f). As exp. f shows, Cr(II) alone definitely shows a large catalytic effect in this system, in contrast to our observations in the ethylenediamine and ammonia systems.^{1,2}

REFERENCES

1. Andersen, P., Berg, T. and Jacobsen, J. *Acta Chem. Scand. A* 29 (1975) 381.
2. Andersen, P., Berg, T. and Jacobsen, J. *Acta Chem. Scand. A* 29 (1975) 599.

3. Andersen, P., Berg, T. and Jacobsen, J. *To be published.*
4. Schäffer, C. E. *Advances in the Chemistry of the Coordination Compounds*, MacMillan, New York 1961, p. 628.
5. Brauer, G. *Handbuch der präparativen anorganischen Chemie*, Enke Verlag, Stuttgart 1962, p. 1190.
6. Lux, J. and Illman, H. *Chem. Ber.* 91 (1958) 2148.
7. Bjerrum, J. *Metal Ammine Formation in Aqueous Solution*, Haase, Copenhagen 1941. Reprinted 1957.
8. Schwarzenbach, G. and Heller, J. *Helv. Chim. Acta* 34 (1951) 576.
9. Furlani, C., Morpurgo, G. and Sartori, G. *Z. Anorg. Allg. Chem.* 303 (1960) 1.
10. Pecsok, R. L., Shields, L. D. and Schaefer, W. P. *Inorg. Chem.* 3 (1964) 114.
11. Grube, G. and Breiting, G. *Z. Elektrochem.* 33 (1927) 112.
12. Bjerrum, J. and Rasmussen, S. E. *Acta Chem. Scand.* 6 (1952) 1265.
13. Woldbye, F. *Acta Chem. Scand.* 12 (1958) 1079.
14. Reilley, C. N., Scribner, W. G. and Temple, C. *Anal. Chem.* 28 (1956) 450.
15. Tanaka, N. and Ogino, H. *Bull. Chem. Soc. Jpn.* 38 (1965) 1054.
16. Poulsen, I. and Bjerrum, J. *Acta Chem. Scand.* 9 (1955) 1407.
17. Schwarzenbach, G., Gut, R. and Anderegg, G. *Helv. Chim. Acta* 37 (1954) 937.

Received October 15, 1976.

Crystal Structure Refinement of α -V₅As₃

ROLF BERGER

Institute of Chemistry, University of Uppsala, Box 531, S-751 21 Uppsala, Sweden

The crystal structure of α -V₅As_{2.74} has been refined on F^2 to an R -value of 2.7 % using X-ray single-crystal data. The symmetry is tetragonal, space group $I4/mcm$. The compound is arsenic-deficient and is isostructural with W₅Si₃. The cell dimensions are: $a=9.5031(4)$ Å and $c=4.8255(3)$ Å.

The V—As system contains three phases of composition approximating to V₅As₃. Two of these, β -V₅As₃ and γ -V₅As₃, are stable only at elevated temperatures,¹ while α -V₅As₃ also forms in silica-tube syntheses. The latter phase was first reported by Boller and Nowotny,² who, on the grounds of powder data only, assigned the structure to the W₅Si₃ type. A literature survey made by the author revealed that α -V₅As₃ is the only arsenide known to crystallize with this structure. The W₅Si₃ type is otherwise represented by the Group V and Group VI silicides and germanides, by the Group IV and Group V gallides and also by a few rare-earth compounds.

One striking feature of this structure type is the occurrence of infinite linear chains running along the c -axis of the tetragonal cell for both kinds of atom. The interatomic distance in these chains is only 2.41 Å in the case of α -V₅As₃, a remarkably short distance especially for arsenic. Short intermetallic distances are not uncommon in other metal-rich pnictides and chalcogenides. Close arsenic contacts are normally found only in arsenic-rich compounds, where, however, the As atoms never occur in a chain arrangement but form pairs or infinite networks.

Boller and Nowotny^{2,3} observed a homogeneity range extending towards the metal-rich side, and syntheses made by the author confirmed this and indicated that the lattice

dimension variations affect the c -axis to the greatest extent.¹ This naturally leads to the assumption that a vacancy mechanism involving the occupancy of sites in the chains must play an important role.

This paper presents a single-crystal X-ray refinement, together with microprobe analyses, in an attempt to clarify the atomic distribution and to produce accurate values for the atomic coordinates as well as for the interatomic distances.

EXPERIMENTAL

Vanadium (Materials Research Corp., 99.95 % pure) was arc-melted together with a specimen of the composition VAs_{0.88} (prepared by a two-zone synthesis⁴), in an atmosphere of purified argon. The final product contained V₂As,⁵ V₃As and only small amounts of α -V₅As₃. The latter formed rod-like crystals in the matrix.

A well-shaped single crystal in the form of a parallelepiped was selected for collecting the X-ray intensity data. Its dimensions were 42 × 47 × 83 μm, its greatest extension being along the c -axis. The equipment and the intensity-collecting procedure were the same as in earlier studies.^{1,4} Intensities were recorded up to $2\theta=85^\circ$, corresponding to $0 \leq h \leq 18$, $0 \leq k \leq 18$ and $0 \leq l \leq 9$. The instrumental stability, checked by three standard reflexions, was satisfactory.

Apart from Lp corrections, the single-crystal X-ray data were also corrected for absorption by a Gaussian grid method, the crystal being limited by faces of the forms {110} and {001}. The minimum and maximum transmission factors obtained were 0.272 and 0.326, using a calculated linear absorption coefficient of 345 cm⁻¹.

Powder diffraction films recorded for the arc-melted alloy showed weak and diffuse α -V₅As₃ lines, particularly diffuse in the case of $l=2$. Evidently, the composition of the α -V₅As₃ phase varied appreciably within the

sample, making it necessary to determine both the composition and the lattice parameters for the particular crystal used for collecting the intensity data.

For the lattice parameter determination a General Electric "Single Crystal Orienter" equipped with $\text{CuK}\alpha$ radiation was utilized. High-angle reflexions with a good α_1 to α_2 separation were measured for determining the Bragg angles. A least-squares refinement yielded the unit cell parameters (22 °C): $a = 9.5031(4)$ Å and $c = 4.8255(3)$ Å, assuming $\lambda(\text{CuK}\alpha_1) = 1.540598$ Å and $\lambda(\text{CuK}\alpha_2) = 1.544408$ Å. Corresponding four-circle data for $\lambda(\text{MoK}\alpha) = 0.710688$ Å were: $a = 9.500(2)$ Å and $c = 4.830(2)$ Å.

Microprobe analyses were performed on single crystals only, including the one used for the intensity recordings as well as for the lattice dimension determination. The single crystals were embedded in a silver cement, precautions being taken to align a crystal surface perpendicular to the electron beam, since the instrument (Cambridge) was not equipped with any tilting or rotating facilities. The preparation technique introduces an angular error which is hard to avoid. Pure vanadium and arsenic, the latter being surface-treated with aluminium, were used as standards. As an extra check, measurements were also performed on VAs single crystals, prepared by chemical transport. Selte *et al.*⁴ suggest a narrow range of composition of $\text{VAs}_{1.00 \pm 0.02}$, which is supported by the consistency of lattice parameter values given by various authors. A line sweep to investigate the homogeneity of the chosen area of a crystal face was followed by five spot measurements for each element. The microprobe intensity data were corrected for the effects of atomic number, fluorescence and absorption by the MK 13 program obtained from the Geological Survey of Sweden.⁷ The estimated relative accuracy was 5 %.

The numerical calculations were performed using IBM 370/155 and IBM 1800 computers. The crystallographic programs for the structure analysis are described in Ref. 8.

STRUCTURE REFINEMENT

The coordinates given by Boller and Nowotny² were used as the starting parameters for a series of full-matrix least-squares refinements, together with one scale factor and isotropic temperature factors. The space group $I4/mcm$ was assumed, and the scattering factors, including dispersion corrections, were taken from Ref. 9.

The agreement obtained after convergence was rather poor, with a conventional $R(F)$ of 0.12. A data survey revealed that the F_o/F_c

ratio was near unity for reflexions with odd l , while those with even l showed severe disagreement between F_o and F_c . Indeed, another refinement, restricted to reflexions with l odd, converged to $R(F) = 0.05$. These reflexions are insensitive to the occupation in the $z = 1/4$ plane. A difference Fourier map was calculated for this plane to find out whether there were other peaks than those corresponding to the special positions $4a$ and $4b$, but it only revealed that anisotropic thermal parameters were required. The introduction of these made $R(F)$ drop drastically.

The occupancies of the $4a$ and $4b$ positions were allowed to vary. Only the $4a$ position assigned to the arsenic atoms was affected significantly. Extinction effects were taken care of by a method devised by Coppens and Hamilton.¹⁰ The final refinements were made on F^2 rather than F so as to include reflexions with "negative intensities".¹¹ The equivalent (hkl) and (khl) reflexions were all included (845 refl.) and not averaged as in the early stages of refinement so as to take care of the extinction effects properly. The final agreement factors were $R(F^2) = 0.027$ and $R_w(F^2) = 0.044$, with the corresponding $R(F) = 0.028$, where

$$R(F^n) = \frac{\sum ||F_o^n| - |F_c^n||}{\sum |F_o^n|} \text{ and } R_w(F^n) = \left[\frac{\sum w(|F_o^n| - |F_c^n|)^2}{\sum w|F_o^n|^2} \right]^{1/2} \quad n = 1, 2$$

The weights were assigned according to $w^{-1} = \sigma_c^2(F_o^n) + (p_n|F_o^n|)^2$, with $p_2 = 0.02$. $\sigma_c(F_o^n)$ is

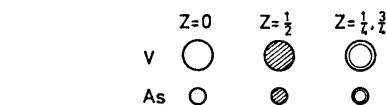
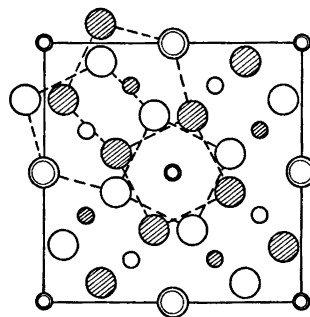


Fig. 1. The structure of $\alpha\text{-V}_5\text{As}_3$ projected on (001).

Table 1. Structure data for α -V₅As_{2.74}, including anisotropic thermal parameters U_{ij} ($\times 10^6$) Å². The form of the temperature factor is $\exp[-2\pi^2 a^{*2} (U_{11}h^2 + U_{22}k^2 + 2U_{12}hk) - 2\pi^2 U_{33}l^2 c^{*2}]$; $U_{13} = U_{23} = 0$. Standard deviations within brackets. Space group: $I4/mcm$ (No. 140).

Atom	Position	Occupancy (%)	x	y	z	U_{11}	U_{22}	U_{33}	U_{12}
V(1)	16k	100	0.07601(3)	0.22405(3)	0	520(10)	677(11)	1005(12)	77(7)
V(2)	4b	100	0	$\frac{1}{2}$	$\frac{1}{2}$	498(11)	U_{11}	467(19)	0
As(1)	8h	100	0.16458(2)	$x + \frac{1}{2}$	0	425(6)	U_{11}	880(11)	-33(6)
As(2)	4a	74.3(2)	0	0	$\frac{1}{2}$	503(15)	U_{11}	9580(84)	0

the standard deviation of F_o^n based on counting statistics, and p_n is an empirical factor accounting for instrumental errors. A ΔR normal probability plot¹² gave the slope 0.95 and an intercept of -0.10, which shows that the intensity material was not too heavily affected by systematic errors.

The structural parameters from the last F^2 refinement are given in Table 1. The structure factors can be obtained on request from the author.

DISCUSSION

In the least-squares refinement, three parameters are sensitive to the intensities of strong reflexions with even l : the anisotropic temperature factors, the extinction factor and the occupancy of the 4a and 4b positions. It is comforting to note that the refinement showed rather weak correlations between these parameters; the greatest correlation was 0.59 between the occupancy of 4a and the corresponding U_{11} . The refinement clearly showed that only the occupancy of the 4a position (arsenic) and not the 4b position (vanadium) is affected, entirely in line with expectations. The large apparent thermal motion of As(2) in the c -direction is probably an indication as to small random deviations from the value of $z = 1/4$

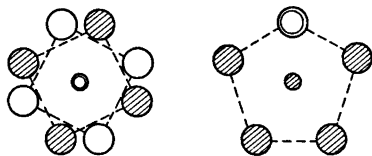


Fig. 2. Coordination polyhedra around arsenic, corresponding to the coordination numbers 8 (left) and 6 (right). Notation similar to Fig. 1.

Acta Chem. Scand. A 31 (1977) No. 3

caused by the vacancies. Unfortunately, there is an additional problem. It cannot be concluded with certainty from this study whether 4a is occupied to 74 % by arsenic as indicated by the refinement, or whether it has a mixed occupation of both kinds of atom so as to give the corresponding scattering power as suggested by Boller and Nowotny.⁸ A neutron diffraction study is planned in order to resolve this ambiguity. At the present stage, the composition is assumed to be V₅As_{2.74}, i.e. 55.4 % V and 44.6 % As. The microprobe analyses on the same crystal yielded 57.2 % V and 42.8 % As. In view of the experimental difficulties, these values agree very well - within 4 % - with the crystallographic data as interpreted in terms of arsenic vacancies only.

A projection of the α -V₅As₃ structure is shown in Fig. 1. The interatomic distances in α -V₅As_{2.74} are given in Table 2. As(2) coordinates eight vanadium atoms in a slightly irregular square antiprismatic arrangement (Fig. 2). In fact, no W₅Si₃-type compound

Table 2. Interatomic distances (Å) and coordination in α -V₅As_{2.74}. The maximum standard deviation obtained was 0.0006 Å. Distances shorter than 3.5 Å are listed.

V(1)-As(1)	2.520	As(1)-2V(2)	2.519
As(1)	2.529	2V(1)	2.520
2As(2)	2.551	2V(1)	2.529
V(1)	2.687	4V(1)	2.766
2As(1)	2.766	2As(1)	3.331
2V(1)	2.812		
2V(2)	2.976	As(2)-2As(2)	2.413
2V(1)	3.127	8V(1)	2.551
2V(1)	3.179		
V(2)-2V(2)	2.413		
4As(1)	2.519		
8V(1)	2.976		

presents a regular antiprism. As(1) has six vanadium neighbours at fairly even distances in an arrangement (Fig. 2) similar to what is found in the Nb_4As_3 type,¹³ but in $\alpha-V_5As_3$ there are four additional atoms only slightly further away. The V(2) atoms form a straight chain, extending infinitely in the *c*-direction. Such metal chains with short intermetallic distances are also found in the Cr_3Si structure type — V_3As being an example — a class of compounds often showing superconductivity explained by a Barisic-Labbé-Friedel linear-chain model, which exhibits strong transition metal *d*-electron overlap.¹⁴ It seems that very few investigations have been performed on the possibility of superconductivity among the W_6Si_3 -type compounds. Nb_6Ga_3 has a T_c of 1.35 K,¹⁵ while V_6Si_3 shows no superconducting behaviour down to 0.3 K.¹⁶ The V_6Si_3 structure type¹⁷ is another example of a crystal structure characterized by infinite linear metal chains with short intermetallic distances. Attempts to detect superconductivity above 1.5 K for the isostructural V_6Si_3 and Ti_6Ge_3 failed.¹⁸

Acknowledgements. The author wishes to thank Professor I. Olovsson for all the facilities provided and is indebted to Professor S. Rundqvist for his great interest in this work. Thanks are also due to Mr. T. Wennelin of the Institute of Geology, University of Uppsala, for his help with the microprobe analyses. The financial support by the Swedish Natural Science Research Council is gratefully acknowledged.

REFERENCES

- Berger, R. *Acta Chem. Scand. A* 30 (1976) 363.
- Boller, H. and Nowotny, H. *Monatsh. Chem.* 97 (1966) 1053.
- Boller, H. and Nowotny, H. *Monatsh. Chem.* 98 (1967) 2127.
- Berger, R. *Acta Chem. Scand. A* 28 (1974) 771.
- Berger, R. *Acta Chem. Scand. A* 29 (1975) 641.
- Selte, K., Kjekshus, A. and Andresen, A. F. *Acta Chem. Scand.* 26 (1972) 4057.
- Larkin, S. and Sturesson, E. Sveriges Geologiska Undersökning, Datasektionen, Stockholm 1974.
- Lundgren, J.-O., Ed., *Crystallographic Computer Programs*, Institute of Chemistry, University of Uppsala, Uppsala 1975, UUIC-B13-04-2.
- International Tables of X-Ray Crystallography*, Kynoch Press, Birmingham 1974, Vol. IV, pp. 71, 148.
- Coppens, P. and Hamilton, W. C. *Acta Crystallogr. A* 26 (1970) 71.
- Hirshfeld, F. L. and Rabinovich, D. *Acta Crystallogr. A* 29 (1972) 1643.
- International Tables of X-Ray Crystallography*, Kynoch Press, Birmingham 1974, Vol. IV, p. 293.
- Carlsson, B. and Rundqvist, S. *Acta Chem. Scand.* 25 (1971) 1742.
- Weger, M. *Physica* 55 (1971) 545.
- Havinga, E. E., van Maaren, M. H. and Damsma, H. *Phys. Lett. A* 29 (1969) 109.
- Ryder, E. J. *18th Calorimetry Conference*, Bartlesville, Okla. 1963.
- Spinat, P., Fruchart, R. and Herpin, P. *Bull. Soc. Fr. Mineral. Cristallogr.* 93 (1970) 23.
- Hallais, J. *Thesis*, Paris 1970.

Received October 15, 1976.

A Kinetic Study of the Reaction of Various *para*-Substituted *o*-Nitrobenzeneselenenyl Bromides with Thiourea and Benzenethiosulfonate as Nucleophiles

TOR AUSTAD

Rogaland Regional College, Department of Science and Engineering, Ullandhaug, N-4000 Stavanger, Norway

The rate of reaction of various *para*-substituted *o*-nitrobenzeneselenenyl bromides with thiourea and benzenethiosulfonate as nucleophiles has been measured in methanol at 25 °C using the stopped-flow technique. In all cases the kinetic plots showed the reaction to be of second order, first order in each of the reactants. For both of the nucleophiles, the reaction is markedly accelerated by electron-releasing groups in the *para* position of the substrate. Substituents that are able to act through mesomeric effects showed a correlation between $\log k_2$ and the Hammett σ values, while substituents that only act through σ -bonds, causing inductive effects, showed a relatively lower enhancement of reactivity. The slope in the Hammett plots for the former type of substituents was calculated to be $\rho = -1.2$ and $\rho = -0.34$ for thiourea and benzenethiosulfonate, respectively.

The electronic effects on the rate of reaction are discussed in terms of previous crystallographic studies of complexes of divalent selenium and tellurium, and previous kinetic studies on divalent sulfur. It is concluded that the present kinetic data are compatible with a transition state in which the bonding is of the three-center four-electron type.

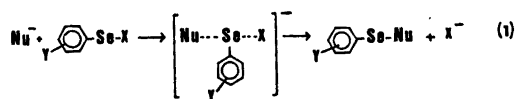
A large number of stable complexes with divalent selenium and tellurium as central atoms have been prepared, and the bonding in these complexes has been discussed by Foss and co-workers on the basis of X-ray crystallographic studies (for a review see Refs. 1–3). Furthermore, in 1962 Foss⁴ pointed out that complexes of Te(II) may be regarded as model substances for the transition state in nucleophilic displacement at divalent chalcogen atoms. The crystallographic data clearly suggest that the transition state is linear with bonds probably of the

three-center four-electron type, *i.e.*, one occupied bonding orbital involving all three atoms, one occupied non-bonding orbital with all or most of the electron density on the entering atom and the leaving atom, and one empty anti-bonding orbital.²

According to Foss,² kinetic studies involving nucleophilic substitution on S(II), and structural evidence concerning the bonding in complexes of Se(II) and Te(II), are compatible in the description of the reaction mechanism for nucleophilic substitution on divalent chalcogen atoms.

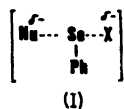
In the later years we have undertaken a kinetic study concerning nucleophilic substitutions on Se(II)^{5–9} and Te(II)¹⁰. The main purpose of this study is to find out if the kinetic data accord with the structural evidence in the description of the reaction mechanism. So far both structural and kinetic data point to the same reaction mechanism.

The present paper which may be regarded as part of this study, will deal with the timing of covalency changes in nucleophilic substitutions at divalent selenium and with the charge distribution around the selenium atom in the transition state relative to the ground state of the substrate. One way of studying this matter is through measurements of the effect of various substituents on the rate of a displacement reaction of the type:



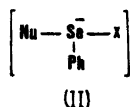
The sign and the magnitude of the ρ -value in the Hammett plot may tell something about the charge distribution around the selenium atom in the transition state.

A transition state that accords with the three-center four-electron bonding model, will probably give a ρ -value that is near zero.



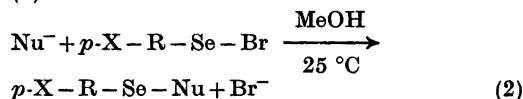
As indicated by (I), the non-bonding orbital of the three-center arrangement has most of its electron density on the outer atoms. Thus, the electron density around the selenium atom in the transition state is not very much different from the electron density around the selenium atom in the ground state.

Most of the existing kinetic work concerning nucleophilic displacement at divalent sulfur points to a synchronous displacement analogous to the S_N2 mechanism for sp^3 carbon. However, Ciuffarin *et al.*^{11,12} have found that special sulfonyl chlorides probably undergo a two-step reaction when reacted with amines in benzene. They suggested that the intermediate may either be an ion pair or an addition complex formed through the use of the sulfur d orbitals.^{11,12} If the displacement reaction is a two-step addition elimination process involving the selenium d orbitals, a negative charge on the selenium atom has to be stabilized. The Hammett plot should then give a large positive ρ -value. Such a transition state is pictured by (II).



RESULTS AND DISCUSSION

In the present work we have studied the reaction between various *para*-substituted *o*-nitrobenzeneselenenyl bromides and thiourea and benzenethiosulfonate as nucleophiles, reaction (2).



R = *o*-nitrophenyl
Nu = $(\text{NH}_2)_2\text{C}=\text{S}$ and PhSO_2S^-
X = CH_3O , CH_3 , H, F, Cl, and NO_2 .

Table 1 contains some data on the substrates. In the case of the neutral nucleophile, the product of reaction (2) is a salt. The rate measurements were performed in methanol at 25 °C applying a stopped-flow spectrophotometer.

Examination of the rate constants that are listed in Table 2 reveals that the rate for both of the nucleophiles obviously depends on the electron-withdrawing or electron-releasing character of the substituent attached to the aromatic ring. In both cases, electron-releasing substituents cause an increase in the rate. Furthermore, the effect of the substituents on the rate of reaction is somewhat stronger in the case of the neutral nucleophile.

The Hammett plot for the reaction between the various selenenyl bromides and thiourea is shown in Fig. 1. Hammett σ -values have been used.¹⁵ The correlation of CH_3O , F, Cl, and NO_2 , *i.e.*, substituents that are able to act through mesomeric effects, is rather good. On the other hand, substituents that only cause inductive effects through σ -bonds, *i.e.*, Me and H, deviate markedly from this correlation. This may suggest that σ^+ values rather than σ values should be used, but the $\log k_s - \sigma^+$ plot did not show satisfactory results. A more reasonable explanation may be to suggest that the Hammett plot splits into two lines, an upper line that contains the points of the substituents that

Table 1. Some data on the substrates, $p\text{-X} - \text{R} - \text{SeBr}$, used in this work, (R = *o*-nitrophenyl). Recrystallized from diethyl ether, unless otherwise stated.

X	M.p./°C	$\lambda_{\text{max}}^a/\text{nm}$
CH_3O	114 (113.7–114.5) ^b	396
CH_3	90 (86.2) ^c	427
H	65 ^d (64–65) ^e	417
F	68	427
Cl	102 (102.5–103.5) ^c	425
NO_2	118 ^f (118) ^g	400 ^h

^a Measured in methanol. ^b Ref. 13. ^c Ref. 14. ^d Recryst. from light petroleum (40–60 °C). ^e Ref. 15. ^f Recryst. from diethyl ether/benzene. ^g Ref. 16. ^h The spectrum showed a shoulder at this wavelength.

Table 2. Pseudo-first-order rate constant, k' , and second-order rate constant, k_2 , for the reaction between various *para* substituted *o*-nitrobenzeneselenenyl bromides and the two nucleophiles thiourea and benzenethiosulfonate in methanol at 25 °C. (R = *o*-nitrophenyl).

X	[Nu]/ 10 ⁻² M	k'/s^{-1}	$k_2/M^{-1} s^{-1}$
$p\text{-X-R-SeBr} + (\text{NH}_2)_2\text{C}=\text{S} \longrightarrow$			
$p\text{-X-R-Se-S-C}^+(\text{NH}_2)_2 + \text{Br}^-$			
CH ₃ O	0.675	2.57	342 ± 40
	1.17	4.08	
	2.11	6.28	
CH ₃	0.675	0.842	116 ± 8
	1.17	1.32	
	2.11	2.32	
H ^a	0.675	1.38	53.3
	1.17	2.24	
	2.11	3.50	
Cl	0.675	0.867	115 ± 15
	1.17	1.30	
	2.11	2.10	
NO ₂	0.675	0.184	24 ± 3
	1.17	0.281	
	2.11	0.498	
$p\text{-X-R-SeBr} + \text{PhSO}_2\text{S}^- \longrightarrow$			
$p\text{-X-R-Se-S-SO}_2\text{Ph} + \text{Br}^-$			
CH ₃ O	0.572	0.087	14.7 ± 0.5
	2.12	0.309	
	2.60	0.372	
CH ₃	0.572	0.038	6.3 ± 0.3
	2.12	0.132	
	2.60	0.158	
H ^a	0.572	0.077	3.25
	2.12	0.269	
	2.60	0.322	
Cl	0.572	0.0568	9.3 ± 0.6
	2.12	0.189	
	2.60	0.231	
NO ₂	0.572	0.0369	6.3 ± 0.3
	2.12	0.125	
	2.60	0.168	

^a Ref. 7.

operate through mesomeric effects, and a lower line that probably will contain points corresponding to substituents that cause only inductive effects on the aromatic ring. The sign and the magnitude of the slope of the line that fits the former substituents, $\rho = -1.2$, indicate that the transition state is stabilized by electron-donating substituents. Furthermore, substit-

Acta Chem. Scand. A 31 (1977) No. 3

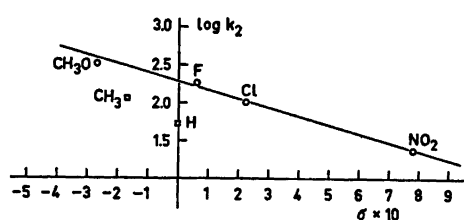


Fig. 1. Hammett plot for the reaction of various *para*-substituted *o*-nitrobenzeneselenenyl bromides and thiourea in methanol at 25 °C. σ -Values from Ref. 25.

uents that donate π -electrons to the electrophilic center appear to stabilize the transition state better than substituents that only donate electrons through σ -bonds.

Thiourea as nucleophile gives a neutral transition state complex. For the anionic nucleophile, benzenethiosulfonate, the transition state is a negatively charged complex. Even in this case the transition state is stabilized by electron-releasing groups in the *para* position, and the Hammett plot shows a similar trend as for thiourea, Fig. 2. The slope of the line through the points for the substituents that exert mesomeric effects, is, however, significantly less negative, $\rho = -0.34$. Furthermore, all substituents of this type give a higher rate than do Me and H. Thus, relatively to the unsubstituted *o*-nitrobenzeneselenenyl bromide, substituents that act through electron-withdrawing mesomeric effects also accelerate the reaction. This points to some electron donation from the selenium atom to the aromatic π -

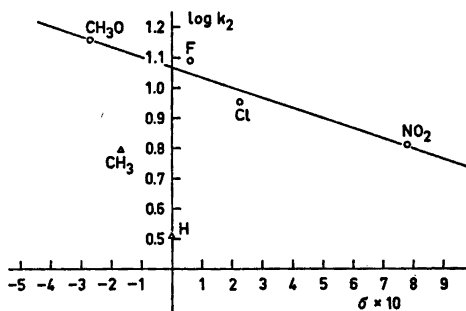


Fig. 2. Hammett plot for the reaction of various *para*-substituted *o*-nitrobenzeneselenenyl bromides and benzenethiosulfonate in methanol at 25 °C. σ -Values from Ref. 25.

orbitals in the transition state. However, the sign and the magnitude of the ρ value strongly indicate that only a small part of the negative charge is located on the Se atom in the transition state complex.

With regard to nucleophilic substitutions on S(II), a lot of papers dealing with the electronic distribution around the sulfur atom in the transition state have been published. The electronic effects on the rate of reaction have in some cases been reported to be almost nil,¹⁷ and in other cases a slightly positive ρ value has been found.^{18,19} Substitution reactions on S(II) in which both electron-releasing and electron-withdrawing groups in the *para* position accelerate the reaction have also been reported.^{20,21} This type of behaviour has been interpreted as indicating different degrees of bond formation and fission in the transition state.

In the foregoing discussion the electronic effects of the nitro group in the *ortho* position of the selenenyl bromides have been ignored. We are aware of the fact, however, that the ground state of the substrates is stabilized by an intramolecular linear three-center arrangement involving one of the oxygen atoms of the nitro group, the selenium atom, and the bromine atom.²² The electrophilic nature of these compounds has been discussed previously.⁹ A nucleophilic attack *trans* or nearly *trans* to the leaving group is probably very hindered due to a strong solvation of the polar nitro group.⁹ Thus, even though the nitro group is in the *meta* position relatively to the various substituents, electron donating groups probably make the nitro group more polar, and therefore more strongly solvated by methanol. This would lead to a slower reaction for substrates having electron-releasing groups in the *para* position. However, the opposite is really observed.

Electron donating groups in the *para* position may cause the selenium atom to be less electrophilic, and an equilibrium between intramolecularly bonded substrates and substrates which may undergo a rotation about the C-Se bond may be set up. The latter type of substrates are found to be much more reactive than the intramolecularly bonded substrates,⁹ and an equilibrium as above should lead to a much faster reaction. As shown by Table 2, there is a rather small difference between the rate con-

stants of the various substrates. A drastic change in the initial state of the substrates would probably lead to a much greater difference in the rate constants.

In summary then, we find that the electronic requirements of the present reactions are best discussed on the basis of factors that stabilize the transition state and not the initial state of the substrates. In this way, the data are in complete consistency with the three-center four-electron bonding model as suggested by Foss on the basis of crystallographic studies.

EXPERIMENTAL

Solvent. Methanol Merck *p.a.* was used without further purification.

Substrates. The *para*-substituted *o*-nitrobenzeneselenenyl bromides were prepared from the corresponding selenocyanates and excess of bromine in dry chloroform.¹⁵

The aromatic selenocyanates, except for 2,4-dinitrophenyl selenocyanate, were prepared from diazotized anilines and potassium selenocyanate.²³ 2,4-Dinitrophenyl selenocyanate was synthesized by reacting 1-chloro-2,4-dinitrobenzene with potassium selenocyanate in warm ethanol as described by Fromm and Martin.²⁴

Nucleophiles. Thiourea, $(\text{NH}_2)_2\text{CS}$, (Fluka, *puriss. p.a.*) and tetramethylammonium benzenethiosulfonate, $\text{Me}_4\text{N}^+\text{PhSO}_3\text{S}^-$,⁹ were employed.

Kinetics. The rate of the reaction between the nucleophiles and the various aromatic selenenyl bromides was followed by measuring the decrease in the absorption near the λ_{max} of the substrates, Table 1, with a Durrum stopped-flow spectrophotometer. The kinetic runs were performed under pseudo-first order conditions, with excess of nucleophile, and the substrate concentrations were about $(2-4) \times 10^{-5}$ M. The second order rate constants appeared to increase slightly as the concentration of the nucleophile decreased. The k_2 values given in Table 2 are the average values of the three individual k_2 values, $k'/[\text{Nu}]$.

In the case of the anionic nucleophile, PhSO_3S^- , the final optical density of the solution was not stable. An increase in the optical density was observed for the two most concentrated solutions, which points to a consecutive reaction between the product and the nucleophile. However, this reaction is much slower than the original displacement reaction, and it has no influence in the calculation of the rate constant of the first step. This second reaction was not studied any further.

The experimental part of this work was performed at the Department of Chemistry, University of Bergen.

REFERENCES

1. Foss, O. In *Selected Topics in Structure Chemistry*, Universitetsforlaget, Oslo 1967, pp. 145–173.
2. Foss, O. *Pure Appl. Chem.* 24 (1970) 31.
3. Vikane, O. *Ph. D. Thesis*, University of Bergen 1975.
4. Foss, O. *Acta Chem. Scand.* 16 (1962) 779.
5. Austad, T. *Acta Chem. Scand. A* 28 (1974) 935.
6. Austad, T. *Acta Chem. Scand. A* 29 (1975) 71.
7. Austad, T. *Acta Chem. Scand. A* 29 (1975) 895.
8. Austad, T. *Acta Chem. Scand. A* 30 (1976) 579.
9. Austad, T. *Acta Chem. Scand. A* 31 (1977) 93.
10. Austad, T. *Acta Chem. Scand. A* 28 (1974) 927.
11. Ciuffarin, E. and Guaraldi, G. *J. Am. Chem. Soc.* 91 (1969) 1745.
12. Ciuffarin, E. and Griselli, F. *J. Am. Chem. Soc.* 92 (1970) 6015.
13. Rheinboldt, H. and Perrier, M. *Bull. Soc. Chim. Fr.* 20 (1953) 484.
14. Rheinboldt, H. and Giesbrecht, E. *J. Am. Chem. Soc.* 72 (1950) 866.
15. Behaghel, O. and Seibert, H. *Ber. Dtsch. Chem. Ges.* 66 (1933) 708.
16. Behaghel, O. and Müller, W. *Ber. Dtsch. Chem. Ges.* 68 (1935) 1540.
17. Givens, E. N. and Kwart, H. *J. Am. Chem. Soc.* 90 (1968) 378.
18. Ciuffaring, E. and Fava, A. *Progr. Phys. Org. Chem.* 6 (1968) 81.
19. Di Nunno, L., Modena, G. and Scorrano, G. *Ric. Sci.* 36 (1966) 825.
20. Kice, J. L. and Anderson, J. M. *J. Org. Chem.* 33 (1968) 3331.
21. Brown, C. and Hogg, D. R. *Chem. Commun.* (1967) 38.
22. Eriksen, R. and Hauge, S. *Acta Chem. Scand.* 26 (1972) 3153.
23. Rheinboldt, H. In Houben-Weyl, *Methoden der organischen Chemie*, 4th Ed., Thieme, Stuttgart 1955, Band IX, p. 943.
24. Fromm, E. and Martin, K. *Justus Liebigs Ann. Chem.* 101 (1913) 171.
25. McDaniel, D. H. and Brown, H. C. *J. Org. Chem.* 23 (1958) 420.

Received September 30, 1976.

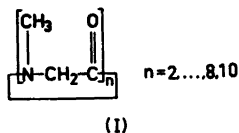
Short Communication

Crystal Conformation of Cyclohexasarcosyl $2\text{CH}_3\text{OH}$ at -156°C

P. GROTH

Department of Chemistry, University of Oslo, Oslo 3, Norway

With exception for the case $n=6$, the crystal structures of cyclic oligopeptides of sarcosine with the general formula I are known.^{1a–g}



For $n=2, 3, 4$, and 8 the conformations could be predicted on the basis of NMR-data.² For $n=5, 6, 7$, and 10 no conformational evidences are obtainable from NMR-spectroscopy. The crystal structure of cyclohexasarcosyl, $\text{C}_6\text{H}_{10}\text{N}_2\text{O}_2$, (crystallizing with two molecules of methanol per formula unit) is now reported.

The crystals belong to the orthorhombic system with space group $Pna2_1$ and cell dimensions $a=14.379(6)$ Å, $b=10.203(4)$ Å, $c=16.236(5)$ Å, and $Z=4$ ($D_m=1.35$ g cm⁻³, $D_x=1.36$ g cm⁻³).

With $2\theta_{\text{max}}=50^\circ$ and MoK α -radiation 2165 independent reflections were measured on an automatic four-circle diffractometer. The crystals are unstable at room temperature and data were therefore collected at -156°C . Using an observed–unobserved cutoff at $2.5\sigma(I)$, 1264 reflections were recorded as observed. No corrections for absorption or secondary extinction were applied (crystal size $0.3 \times 0.2 \times 0.3$ mm³).

The structure was solved by direct methods³ and refined by full-matrix least-squares technique.^{4*} Hydrogen atom positions were partly calculated and partly localized in difference Fourier maps (except for those of the methanol molecules which remained undetermined). Anisotropic temperature factors were introduced for O, N and C atoms and weights in least-

* All programs used (except those for phase determination) are included in this reference.

Table 1. Final fractional coordinates and thermal parameters with estimated standard deviations. The expression for anisotropic vibration is $\exp[-2\pi^2(h^2a^{*2}U11 + \dots + 2klb^*c^*U23)]$. Hm is bonded to Cm, HMm to CMm and HOM to Om.

ATOM	X	Y	Z	U11	U22	U33	U12	U13	U23
O1	.2104(3)	.8173(5)	.7773(8)	.0291(29)	.0429(32)	.0177(26)	-.0045(28)	.0026(24)	-.0035(26)
O2	.0878(4)	.9082(5)	1.0045(3)	.0267(32)	.0408(39)	.0325(33)	-.0189(30)	-.0010(27)	-.0041(28)
O3	.3481(3)	1.0146(5)	1.0759(3)	.0262(30)	.0262(32)	.0258(30)	-.0012(26)	.0029(23)	-.0001(27)
N1	.3782(4)	.7744(6)	.8893(3)	.0127(31)	.0315(45)	.0159(29)	-.0018(31)	-.0054(25)	-.0059(29)
N2	.1748(4)	.9853(6)	.8588(3)	.0207(36)	.0304(37)	.0119(30)	.0098(35)	-.0025(29)	-.0013(31)
N3	.1597(4)	1.0609(6)	1.0821(3)	.0272(34)	.0325(37)	.0135(30)	-.0075(31)	-.0009(30)	-.0012(32)
C1	.2775(5)	.8168(9)	.9158(5)	.0174(43)	.0298(50)	.0249(41)	.0045(42)	-.0016(36)	-.0072(41)
C2	.1828(7)	1.0671(10)	.9348(5)	.0245(55)	.0394(58)	.0175(45)	.0054(46)	-.0065(38)	-.0023(43)
C3	.2236(6)	1.1717(8)	1.0893(5)	.0267(45)	.0275(49)	.0169(39)	-.0010(39)	.0035(41)	-.0009(42)
CC1	.2211(5)	.8778(7)	.8446(4)	.0097(30)	.0325(46)	.0187(40)	-.0025(37)	.0007(32)	-.0002(37)
CC2	.1368(5)	1.0028(8)	1.0094(4)	.0176(42)	.0345(48)	.0266(42)	.0025(42)	.0048(35)	-.0001(40)
CC3	.3266(5)	1.1312(7)	1.0777(4)	.0302(40)	.0179(44)	.0017(38)	.0342(40)	-.0002(35)	-.0048(35)
CM1	.3066(8)	.6383(10)	.8763(7)	.0311(61)	.0295(60)	.0317(58)	-.0048(50)	-.0058(55)	-.0007(50)
CM2	.1146(7)	1.0367(11)	.7937(6)	.0172(47)	.0552(73)	.0222(48)	.0058(47)	-.0064(41)	-.0055(49)
CM3	.1245(7)	1.0028(11)	1.1684(5)	.0306(52)	.0424(65)	.0277(48)	-.0171(52)	.0002(42)	.0108(53)
OM	.4500(5)	1.2388(7)	.8284(4)	.0705(49)	.0516(43)	.0709(48)	-.0055(45)	.0165(36)	.0075(44)
CF	.3588(6)	1.2849(9)	.8399(5)	.0493(63)	.0672(82)	.0558(59)	.0212(55)	.0091(49)	.0106(54)

ATOM	X	Y	Z	B	ATOM	X	Y	Z	B
H11	.279(4)	.880(6)	.958(4)	2.0	H12	.248(3)	.734(6)	.937(3)	2.0
H21	.159(5)	1.145(7)	.923(4)	2.0	H22	.240(5)	1.071(7)	.947(4)	2.0
H31	.225(5)	1.230(8)	1.136(4)	2.0	H32	.211(4)	1.256(7)	1.053(3)	2.0
H41	.440(6)	.626(8)	.857(5)	2.0	H42	.342(9)	.682(14)	.838(8)	2.0
H43	.385(8)	.592(13)	.930(7)	2.0	H44	.071(8)	.975(10)	.768(6)	2.0
H45	.157(13)	1.078(18)	.750(12)	2.0	H46	.076(6)	1.111(13)	.817(8)	2.0
H47	.071(10)	1.053(13)	1.180(8)	2.0	H48	.177(4)	1.089(5)	1.282(3)	2.0
H49	.112(6)	.926(10)	1.154(6)	2.0	H07	.439(12)	1.153(17)	.858(11)	2.0

squares were calculated from the standard deviations in intensities, $\sigma(I)$, taken as

$$\sigma(I) = [C_T + (0.02 C_N)^2]^{\frac{1}{2}}$$

where C_T is the total number of counts and C_N the net count. The form factors used were those of Hanson *et al.*,⁵ except for hydrogen.⁶ The molecule has a pseudo centre of symmetry at $X_0 = 0.3789$, $Y_0 = 1.0012$, $Z_0 = 0.9774$. This fact was indeed reflected in large correlation coefficients between corresponding positional as well as thermal parameters. The refinement converged at $R_w = 8.5\%$ ($R = 9.1\%$) and some of the bond distances thus obtained were unreasonable. By introducing the extra symmetry in the least-squares refinement, the final R_w -value was 8.0% ($R = 8.9\%$) for 1264 observed reflections, and the bond distances and angles (given in Table 2) do not deviate significantly from normal values.^{1f} Final fractional coordinates (for half the molecule) together with thermal parameters are listed in Table 1. Positional parameters for the pseudo centrosymmetrically related atoms are given by $X' = 2X_0 - X$, $Y' = 2Y_0 - Y$, $Z' = 2Z_0 - Z$. A Fourier synthesis with $Pna2_1$ symmetry and phases corresponding to the parameters of Table 1 (and their pseudo-equivalents) were calculated. By averaging the mean values of pseudo-related peak coordinates no significant shifts in X_0 , Y_0 , Z_0 were obtained.

Table 2. Bond distances, bond angles and dihedral angles with estimated standard deviations.

DISTANCE (Å)		DISTANCE (Å)	
CC1 - N1	1.25(1)	CC2 - O2	1.21(1)
CC3 - N3	1.23(1)	N1 - CM1	1.43(1)
N2 - CM2	1.43(1)	N3 - CM3	1.48(1)
N1 - CC3'	1.34(1)	N2 - CC1	1.34(1)
N3 - CC2'	1.36(1)	N1 - C1	1.46(1)
N2 - C2	1.50(1)	N3 - C3	1.46(1)
C1 - CC1	1.54(1)	C2 - CC2	1.51(1)
C3 - CC3	1.55(1)	C7 - O7	1.42(1)
O7 - O3	2.76(1)		

ANGLE (°)		ANGLE (°)	
O1 - CC1 - C1	117.9(6)	O2 - CC2 - C2	122.8(7)
O3 - CC3 - C3	120.2(7)	O1 - CC1 - N2	122.7(7)
O2 - CC2 - N3	122.6(7)	O3 - CC3 - N1'	123.1(7)
CM1 - N1 - CC3'	124.0(7)	CM2 - N2 - CC1	118.7(7)
CM3 - N3 - CC2'	120.1(6)	CM1 - N1 - C1	120.1(7)
CM2 - N2 - C2	117.7(7)	CM3 - N3 - C3	116.3(6)
CC3' - N1 - C1	115.2(6)	CM1 - N2 - C2	122.9(6)
CC2' - N3 - C3	123.2(6)	N1 - C1 - CC1	112.0(6)
N2 - C2 - CC2	112.0(7)	N3 - C3 - CC3	112.7(6)
C1 - CC1 - N2	119.2(7)	C2 - CC2 - N3	114.6(7)
C3 - CC3 - N1'	116.6(6)	C7 - O7 - O3	93.3(5)
O7 - N3 - CC3	146.5(5)		

DIHEDRAL ANGLE (°)		
CC3' - CC3' - N1 - C1	168.5(6)	
CC3' - N1 - C1 - CC1	74.9(8)	
N1 - C1 - CC1 - N2	-137.6(7)	
C1 - CC1 - N2 - C2	13.5(10)	
CC1 - N2 - C2 - CC2	-75.1(9)	
N2 - C2 - CC2 - N3	169.5(6)	
C2 - CC2 - N3 - C3	-3.6(10)	
CC2 - N3 - C3 - CC3	-73.5(9)	
N3 - C3 - CC3 - N1'	168.5(6)	

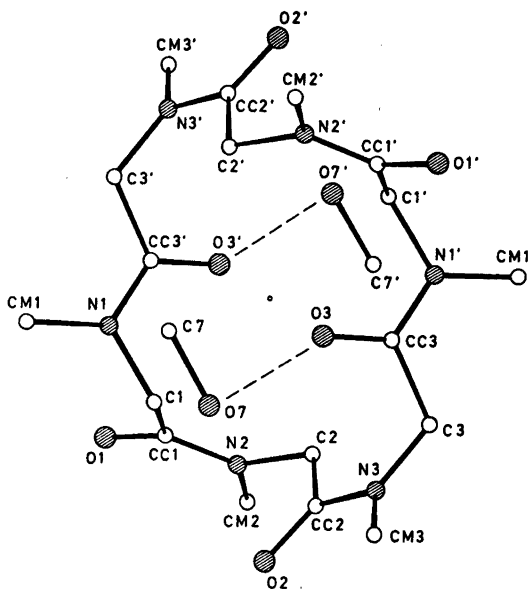


Fig. 1. Schematic drawing of the molecule.

The principal axes of the thermal vibration ellipsoids for oxygen, nitrogen, and carbon atoms were calculated from the temperature parameters of Table 1. Maximum r.m.s. amplitudes for the atoms of the cyclohexasarcosyl molecule range from 0.17 to 0.24 Å, while those of C7 and O7 are 0.30 Å.

Fig. 1 is a schematic drawing of the molecule where the pseudo centre of symmetry, the two methanol molecules, and the numbering of atoms is indicated. It may also be seen that the configuration of the six *N*-methyl amide groups has the sequence, *cis*, *cis*, *trans*, *cis*, *cis*, *trans*. Corresponding sequences for other cyclic peptides of sarcosine are given in Ref. 1g. It should be pointed out that no conformation with more *trans*- than *cis*-configurations has been observed. Another striking feature is the general occurrence of sequences of only *cis*- or only *trans*-amide configuration. The torsion angles $\phi(C-N)$ and $\psi(C-CC)$ of these compounds will be discussed elsewhere.⁷

A list of observed and calculated structure factors is available from the author.

Acknowledgement. The author would like to thank cand.real. K. Titlestad for preparing the crystals.

1. a. Groth, P. *Acta Chem. Scand.* 23 (1969) 3155; b. *Ibid.* 24 (1970) 780; c. *Ibid.* 27 (1973) 3217; d. *Ibid.* 27 (1973) 3419; e. *Ibid. A* 29 (1975) 38; f. *Ibid. A* 30 (1976); g. *Ibid. A* 30 (1976).
2. Dale, J. and Titlestad, K. *Chem. Commun.* (1969) 656.
3. Germain, G., Main, P. and Woolfson, M. M. *Acta Crystallogr. A* 27 (1971) 368.
4. Groth, P. *Acta Chem. Scand.* 27 (1973) 1837.
5. Hanson, H. P., Herman, F., Lea, J. D. and Skillman, S. *Acta Crystallogr.* 17 (1964) 1040.
6. Stewart, R. F., Davidson, E. R. and Simpson, W. T. *J. Chem. Phys.* 43 (1965) 3175.
7. Dale, J., Groth, P. and Titlestad, K. *Acta Chem. Scand.* To be published.

Received February 3, 1977.

Thermodynamics of Surface Phase Systems. VII. The Influence of Solid Surface Strain Changes on the Contact Angle Equilibrium and Some Further Comments on Adhesional Wetting Thermodynamics

JAN CHRISTER ERIKSSON

Division of Physical Chemistry, The Royal Institute of Technology, S-100 44 Stockholm 70, Sweden

A thermodynamic fundamental equation valid for equilibrium contact angle systems is derived that includes a term accounting for the effect of solid surface strain variations. Various contributions to the (mechanical) surface tension difference, $\Delta\gamma$, between the solid-vapor and solid-liquid interfaces are considered. It is concluded that stretching experiments are required in order to confirm the applicability of the approximate fundamental equation implicit in the Gibbs treatment which involves the assumption that surface strain effects are negligible. Some recent determinations of the temperature dependence of equilibrium contact angles are discussed in terms of entropy on basis of the fundamental equation given. It is furthermore concluded that separate measurements of the Gibbs surface excess of the liquid component at the solid-liquid interface are needed to precisely determine the interfacial energy and entropy of this interface.

It is generally accepted that the Gibbs fundamental equation for interfaces, *viz.*

$$dg_{\text{ex}}^s = -S_{(1)}^s dT - \sum_{i=2}^r \Gamma_{i(1)} d\mu_i \quad (1)$$

is valid without restrictions for plane liquid-gas and liquid-liquid interfaces. However, it appears to be less well recognized that the validity of this equation for solid-gas and solid-liquid interfaces is limited to cases of constant state of strain of the solid surface.¹⁻³ In eqn. (1) all symbols have their usual meaning, *i.e.*

g_{ex}^s = the excess surface free energy per unit area

$S_{(1)}^s$ = the surface phase entropy per unit area

$\Gamma_{i(1)}$ = the superficial density of component *i*

Subscript (1) denotes that a Gibbs type of surface phase with zero thickness is considered which is positioned in such a way as to make $\Gamma_1 = 0$. A more general equation applicable for some (but not all) solid-fluid interfaces is the following (binary system);

$$dg_{\text{ex}}^s = -S_{(1)}^s dT + (\gamma - g_{\text{ex}}^s) d\varepsilon_s - \Gamma_{2(1)} d\mu_2 \quad (2)$$

where the term involving the differential $d\varepsilon_s = dA/A$ relates to isotropic and homogeneous changes of the solid surface strain.² The validity of eqn. (2) is restricted to such plane solid surfaces for which the (mechanical) surface tension, γ , is a nontensorial property, *i.e.* to amorphous solid surfaces and to crystal faces with a sufficiently high degree of symmetry.⁴

For *fluid-fluid* interfaces the surface tension, γ , and the excess surface free energy per unit area, g_{ex}^s (that physically corresponds to the reversible *work of formation* of new surface area), are always equal, *i.e.*

$$\gamma = g_{\text{ex}}^s \quad (3)$$

and in this case eqn. (2) reduces to the fundamental eqn. (1). In general, for *solid-fluid* interfaces, however, γ and g_{ex}^s are not equal and the complete thermodynamic treatment should include separate set of equations for both these quantities. For interfaces of this kind, g_{ex}^s is

conveniently interpreted physically as the reversible *cleavage work* per unit area whereas γ , the surface tension (sometimes called surface stress) has a mechanical significance.

It is evident that the conclusions stated above which were discussed at length in number V and utilized in connection with insoluble surface films in number VI of this series of papers on surface phase thermodynamics² should have certain previously not observed consequences with respect to the detailed thermodynamic treatment of contact angle equilibrium. For instance, a clear distinction has rarely been made between γ - and g_{ex}^{s} -quantities for the solid-vapor and solid-liquid interfaces when deriving Young's equation and its nature of mechanical *and* physico-chemical equilibrium condition is often obscured (*cf.* Ref. 5). Moreover though considered by Gibbs, the problem concerning the effect of solid surface strain changes on the contact angle equilibrium has not received much attention later on.

When treating the contact angle equilibrium on inert solids, Gibbs¹ introduced a surface free energy quantity, q , called the superficial tension of the fluid in contact with the solid effectively as $q = g_{\text{ex}}^{\text{s}} - g_{\text{ex}}^{\text{l}}$ (for clean solid surface plus localized adsorbate) that relates specifically to matter at the interface which is "fluid or movable". He claimed that q is approximately unaffected by variations in the state of strain of the solid surface and he also attributed a mechanical significance to q as "the superficial tension of the fluid in contact with solid". In view of our previous conclusions (*cf.* Ref. 2) concerning the difference between the mechanical effects of localized and mobile adsorption and the influence of solid surface strain changes on adsorbate properties, the Gibbs procedure appears to be reasonable. Still, methods are desirable to test the adequacy of the approximation involved.

In order to elucidate the above-mentioned questions, a rigorous thermodynamic treatment of adhesional wetting is carried through in the present paper using eqn. (2) as the point of departure. The likewise rigorous thermodynamic analysis presented by Melrose³ of the interrelations between adhesional and immersionsal wetting is in some respects closely related to this treatment. Melrose, however, based his formalism on eqn. (1).

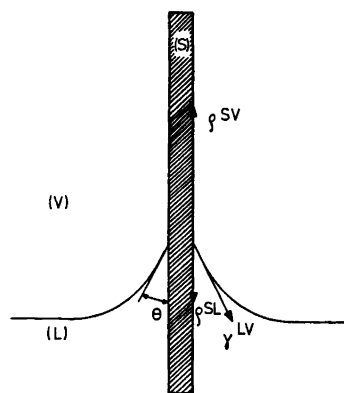


Fig. 1. Sketch of the equilibrium contact angle system studied. θ is the contact angle, q^{SV} and q^{SL} are the superficial tensions of the vapor and the liquid in contact with the solid surface and γ^{LV} is the surface tension of the liquid-vapor interface.

Description of the thermodynamic system studied. The system subject to investigation is a closed equilibrium contact angle system consisting of a pure rigid monocrystalline solid (component 1) with a high symmetry crystal face partly exposed to a pure liquid (component 2) and partly to the vapor of the same liquid (Fig. 1). Alternatively, the solid can be amorphous with a plane and smooth surface. According to the phase rule, this system has only *one* degree of freedom: the temperature T . However, at the outset we may formally consider the solid surface strain, ϵ_s , as a further independent variable though in conformity with Ref. 2 we shall limit the treatment to isotropic and homogeneous reversible strain variations from an approximately unstressed bulk phase state of the solid.

Throughout much of the present paper use will be made of the Gibbs surface phase convention with one dividing surface positioned at the solid surface in such a way that $\Gamma_1 = 0$ in order to completely define the thermodynamic interfacial properties (energy, entropy, mol numbers *etc.*). Thus the surface phase considered only contains component 2. In some connections below, however, it is really more convenient to make use of a Verschaffelt-Guggenheim kind of surface phase with two dividing surfaces, Σ' and Σ'' , located somewhere within the homogeneous phases as is shown in Fig. 2

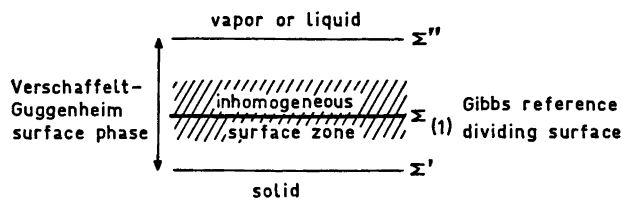


Fig. 2. Surface phase according to the Verschaffelt-Guggenheim convention defined by two dividing surfaces Σ' and Σ'' located within the homogeneous phases and according to Gibbs defined by the dividing surface $\Sigma_{(1)}$ positioned so as to make the superficial density of the solid component Γ_1 equal to zero.

(for further details cf. paper number I of this series, Ref. 6).

The vapor pressure of the liquid component is assumed to be low enough to warrant that pV -terms are negligible for condensed matter. Hence U (=energy) $\simeq H$ (=enthalpy), F (=Helmholtz free energy) $\simeq G$ (=Gibbs free energy), f (=molar Helmholtz free energy) $\simeq \mu$ (=chemical potential) etc. for all parts of the system except the vapor phase. It is also presupposed (though not strictly required) that the adsorption isotherm for the vapor on the solid surface has such a course that the adsorption can be limited at the saturation vapor pressure. This condition guarantees that the system studied actually constitutes what is normally called a contact angle system, i.e. $\theta \neq 0$.⁷

Definitions. In conformity with Gibbs' treatment of solid-fluid interfaces (Ref. 1, p. 315) and Ref. 2 the excess surface free energies per unit surface area of the S/V- and S/L-interfaces are defined by the expressions

$$g^{\text{SV}}_{\text{ex}} = F^{\text{SV}}_{(1)} - \Gamma^{\text{SV}}_{2(1)}\mu_2 \quad (4)$$

$$g^{\text{SL}}_{\text{ex}} = F^{\text{SL}}_{(1)} - \Gamma^{\text{SL}}_{2(1)}\mu_2 \quad (5)$$

Physically, $g^{\text{SV}}_{\text{ex}}$ and $g^{\text{SL}}_{\text{ex}}$ correspond to the reversible work per unit surface area of cleaving the crystal at constant temperature in the vapor and in the liquid, respectively. These in principle measurable quantities are not dependent, of course, on the exact choice of surface phase (Ref. 2).

Following Gibbs (Ref. 1, p. 328) we also introduce the *superficial tensions of the vapor and the liquid in contact with the solid surface*, ρ^{SV} and ρ^{SL} , at equilibrium. Their difference, $\rho^{\text{SV}} - \rho^{\text{SL}} = \Delta\sigma$ is called the *adhesion tension* in accordance with the nomenclature used by

Defay, Prigogine, Bellemans and Everett.⁸ Since the external force per unit length acting downwards on the (freely movable) three-phase junction is $\gamma^{\text{LV}} \cos \theta$ we obviously have (Fig. 1)

$$\Delta\sigma = \gamma^{\text{LV}} \cos \theta \quad (6)$$

where θ is the contact angle. This mechanical equilibrium condition is to be considered as the *operational* definition of $\Delta\sigma$. Evidently, the relation $\rho^{\text{SV}} - \rho^{\text{SL}} = \Delta\sigma$ is of little practical utility since ρ^{SV} and ρ^{SL} cannot be measured separately. In order to actually determine the *equilibrium* contact angle and hence the adhesion tension $\Delta\sigma$, it is a prerequisite, of course, that all the mass transfer needed for restructuring of the S/L-interface into S/V-interface and *vice versa* proceeds rapidly enough to warrant reversibility.

Young's equation. Next we shall show that the cleavage work interpretation of g^{ex} favourably may be utilized when deriving Young's equation. At constant temperature, the work required for reversible cleavage of the solid in the vapor phase must be the same as for first reversibly cleaving the solid in the liquid and then reversibly transferring the solid surface so formed to contact with the vapor. Thus it follows that

$$g^{\text{SV}}_{\text{ex}} - g^{\text{SL}}_{\text{ex}} = \Delta\sigma \quad (7)$$

since $\Delta\sigma$ is obviously equal to the reversible work per unit area needed at constant temperature for the transfer process. Making use of eqn. (6) we obtain

$$g^{\text{SV}}_{\text{ex}} - g^{\text{SL}}_{\text{ex}} = \gamma^{\text{LV}} \cos \theta \quad (8)$$

i.e. Young's equation. It constitutes a physico-chemical equilibrium condition that is fulfilled for the equilibrium contact angle only.

In principle at least, all the quantities involved in eqn. (8) are separately measurable. Often, it is incorrectly assumed^{9,10} that $g^{\text{SV}}_{\text{ex}}$ and $g^{\text{SL}}_{\text{ex}}$ (σ_{BS} and σ_{AS} in Gibbs' text) can not be measured separately and that only their difference, equal to the adhesion tension Δq , is an experimentally accessible thermodynamic variable. However, Bailey, Price and Kay¹¹ have actually succeeded in directly verifying eqn. (8) by measuring the reversible work of cleaving mica samples in the liquid and vapor phases of water, hexane, decane and by determining the corresponding contact angles.

It results from eqns. (4), (5) and (7) that Δq is related to the basic thermodynamic interfacial properties in the following way,

$$\Delta q = \Delta F_{(1)} - \Delta \Gamma_{2(1)} \mu_2 \quad (9)$$

where

$$\Delta F_{(1)} = F_{(1)}^{\text{SV}} - F_{(1)}^{\text{SL}} \quad (10)$$

$$\Delta \Gamma_{2(1)} = \Gamma^{\text{SV}}_{2(1)} - \Gamma^{\text{SL}}_{2(1)} \quad (11)$$

Hence, Δq equals the surface phase free energy difference per unit area between the S/V- and S/L-interfaces corrected for the free energy associated with the corresponding difference in superficial density of component 2.

The thermodynamic fundamental equation for an equilibrium contact angle system. Taking into consideration that T and μ_2 cannot be varied independently for two-component contact angle systems, eqn. (2) should be modified as follows for the S/V- and S/L-interfaces, respectively.

$$dg^{\text{SV}}_{\text{ex}} = -(S^{\text{SV}}_{(1)} - \Gamma^{\text{SV}}_{2(1)} s^{\text{L}}_2) dT + (\gamma^{\text{SV}} - g^{\text{SV}}_{\text{ex}}) d\varepsilon_s \quad (12)$$

$$dg^{\text{SL}}_{\text{ex}} = -(S^{\text{SL}}_{(1)} - \Gamma^{\text{SL}}_{2(1)} s^{\text{L}}_2) dT + (\gamma^{\text{SL}} - g^{\text{SL}}_{\text{ex}}) d\varepsilon_s \quad (13)$$

Here we have inserted the obvious relationship

$$d\mu_2 = -s^{\text{L}}_2 dT \quad (14)$$

Forming the difference between eqns. (12) and (13) and taking eqn. (7) into account, yields the resulting equation

$$d(\Delta q) = -(\Delta S_{(1)} - \Delta \Gamma_{2(1)} s^{\text{L}}_2) dT + (\Delta \gamma - \Delta q) d\varepsilon_s \quad (15)$$

where $\Delta \gamma$ is the surface tension difference $\gamma^{\text{SV}} - \gamma^{\text{SL}}$ and $\Delta S_{(1)}$ is defined analogously to $\Delta F_{(1)}$.

This equation is the thermodynamic fundamental equation for the kind of equilibrium contact angle system considered in this paper. It includes two derivatives of special interest, namely

$$\left(\frac{\partial(\Delta q)}{\partial \varepsilon_s} \right)_T = \Delta \gamma - \Delta q \quad (16)$$

$$\frac{d(\Delta q)}{dT} = -(\Delta S_{(1)} - \Delta \Gamma_{2(1)} s^{\text{L}}_2) + (\Delta \gamma - \Delta q) \frac{d\varepsilon_s}{dT} \quad (17)$$

Eqn. (16) is the counterpart in this connection to the well-known Shuttleworth equation⁴ valid for a pure solid surface whereas eqn. (17) gives the temperature coefficient of the adhesion tension. We should note, in particular, that in certain cases (*e.g.* using elastomers) it might well be feasible to obtain an experimental estimate of the partial derivative $(\partial(\Delta q)/\partial \varepsilon_s)_T$ and thus by using eqn. (16), also an estimate of $\Delta \gamma$.

Eqn. (17) is applicable for a free (unstressed) solid and it includes a correction term that accounts for the influence of the solid surface strain change associated with a change of temperature. The relative magnitude of this correction term is generally not known but can be obtained, in principle at least, on basis of stretching experiments and using eqn. (16). In this way the assumption implied in Gibbs' treatment concerning the approximate independence of Δq with respect to variations of the state of strain of the solid surface could actually be tested. The correction is likely to be small, however, on grounds that will next be discussed with reference to some oversimplified structural models of the S/V- and S/L-interfaces.

Discussion of the various contributions to $\Delta \gamma$. For a Vershaffelt-Guggenheim kind of surface phase that is bounded by two dividing surfaces, Σ' and Σ'' , positioned within the homogeneous phases, we have the following definition of γ ,

$$\gamma = \left(\frac{\partial F^s}{\partial A} \right)_{T, n^s_1, n^s_2} \quad (18)$$

where F^s , n^s_1 and n^s_2 are *total* surface phase quantities. Very schematically, we may picture the structures of the S/V- and S/L-interfaces as is shown in Fig. 3 with a mobile adsorption layer on top of a localized adsorption layer. Assuming that the adsorbent is inert it is possible to make a clearcut division of F^s in two

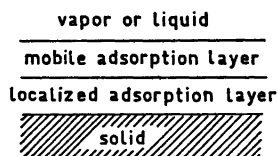


Fig. 3. Schematic interfacial structure of the S/V- and S/L-interfaces.

parts, $F^{s_0}_1$ for the pure solid surface and F^{s_2} for the adsorbate. Evidently, the $F^{s_0}_1$ -parts of F^s are the same for the S/V- and S/L-interfaces independently of ε_s and in such a case there is no resulting contribution to $\Delta\gamma$ due to the solid surface itself.

In general, F^{s_2} cannot be split in parts associated with the localized and mobile adsorption layers, respectively, in a similar straightforward way because the presence of the mobile adsorbate is likely to affect the thermodynamic properties of the localized adsorbate. Still, for the purpose of discussion we may suppose that it is possible to estimate $F^{s_2}(\text{loc})$ and $F^{s_2}(\text{mob})$ separately in some way such that

$$F^{s_2}(\text{loc}) + F^{s_2}(\text{mob}) = F^{s_2} \quad (19)$$

where the interaction free energy between the localized and mobile layers is ascribed to the mobile layer. Now, since the structures and thermodynamic properties of the S/V- and S/L-mobile adsorption layers must be rather different it is reasonable to assume that the corresponding localized adsorption layers are also somewhat different in the same respects. Though very little is actually known about these matters it is likely that the effect of solid surface strain changes on $F^{s_2}(\text{loc})$ is inherently small when the adsorbent-adsorbate interaction is comparatively weak (*cf.* Ref. 2). So, we might tentatively conclude, referring to eqn. (18), *i.e.*

$$\Delta\gamma = \frac{\partial}{\partial A} (F^{\text{SV}} - F^{\text{SL}}) = \frac{\partial}{\partial A} (F^{\text{SV}_2} - F^{\text{SL}_2}) \quad (20)$$

that for many such systems there can be a small contribution, $\Delta\gamma(\text{loc})$, to $\Delta\gamma$ arising from the two rather similar localized adsorption layers. For systems with filled localized adsorption layers, however, it is clear that $\Delta\gamma(\text{loc}) \approx 0$, because in such a case is $F^{\text{SV}_2}(\text{loc}) - F^{\text{SL}_2}(\text{loc}) \approx 0$.

Concerning the contribution to $\Delta\gamma$ from the mobile adsorption layers, it is evident that

Δq *i.e.* the difference between the superficial tensions of the vapor and the liquid in contact with the solid, in most cases constitutes the major contribution. However, there may also be a certain contribution, $\Delta\gamma(\text{mob})$, due to the change of the state of the mobile adsorption layers associated with a solid surface strain variation (*cf.* Ref. 2). This conclusion holds true, of course, irrespective of whether the mobile adsorption layers are in direct contact with the solid surface or if they are formed on top of localized adsorption layers. Consequently, there are reasons in favour of the assumption effectively stated by Gibbs that

$$\Delta\gamma - \Delta q \approx \Delta\gamma(\text{loc}) + \Delta\gamma(\text{mob}) \quad (21)$$

is a relatively small quantity and, in particular, since $d\varepsilon_s/dT$ normally is $10^{-5} - 10^{-4}/K$ for solids that the last term of eqn. (17) is often negligible. However, in order to ascertain this rather qualitatively based conclusion, experiments are needed aiming at the determination of the partial derivative $[\partial(\Delta q)/\partial\varepsilon_s]_T$ so that a comparison can be made of the relative magnitudes of $d(\Delta q)/dT$ and $[\partial(\Delta q)/\partial\varepsilon_s]_T d\varepsilon_s/dT$.

The temperature dependence of Δq and θ . In most cases the leading term in eqn. (17) presumably is

$$\Delta S_{(1)} - \Delta\Gamma_{2(1)}s^L_2 = S^{\text{SV}}_{(1)} - S^{\text{SL}}_{(1)} - (\Gamma^{\text{SV}}_{2(1)} - \Gamma^{\text{SL}}_{2(1)})s^L_2 \approx - \frac{d(\Delta q)}{dT} \quad (22)$$

Though formally (but not explicitly) included in the Melrose treatment,³ it appears that the implications of this term with respect to the temperature dependence of Δq and θ have not been elaborated previously. In this section we will indicate that on basis on eqn. (22) it is possible to qualitatively account entropy-wise for some observed $d(\Delta q)/dT$ -values.

For systems with comparatively weak adsorbent-adsorbate interaction and *extensive* adsorption on the solid surface from the vapor the following relations should hold because of the considerable density difference between the vapor and liquid phases

$$\Gamma^{\text{SV}}_{2(1)} \approx \Gamma^{\text{SV}}_2 \gg \Gamma^{\text{SL}}_{2(1)} \quad (23)$$

$$S^{\text{SV}}_{(1)} - S^{\text{SL}}_{(1)} \approx S^{\text{SV}}_2/A = \Gamma^{\text{SV}}_2 s^{\text{SV}}_2 \quad (24)$$

Also, the approximate eqn. (24) is applicable only so far as there is no large entropy effect on

the liquid adjacent to the solid due to the interaction with the solid surface. Consequently, from eqn. (22) we obtain

$$\frac{d(\Delta\varrho)}{dT} \equiv \gamma^{LV} \frac{d \cos \theta}{dT} + \frac{d\gamma^{LV}}{dT} \cos \theta \approx -\Gamma^{SV_2}(s^{SV_2} - s^{L_2}) \quad (25)$$

When the adsorption in contact with the vapor is mobile we normally expect that $s^{SV_2} - s^{L_2} > 0$ and thus that $d(\Delta\varrho)/dT$ is a negative quantity. Concerning the resulting sign of $d\theta/dT$ we find that no general statement can be made in this case; it will be determined by the sign of the sum of $\Gamma^{SV_2}(s^{SV_2} - s^{L_2})$ and $(d\gamma^{LV}/dT) \cos \theta$.

A common situation of particular interest is the case of low degree of adsorption at the solid-vapor interface. Then the approximations

$$\Gamma^{SV_2}, \Gamma^{SL_{2(1)}} \approx 0 \quad (26)$$

$$S^{SV_{(1)}} - S^{SL_{(1)}} \approx - (S^{SL_{(1)}} - S^{So_{(1)}}) = -S^{SL_{2(1)}} \quad (27)$$

may well be fulfilled. It follows from eqn. (22) that $d(\Delta\varrho)/dT \approx S^{SL_{2(1)}}$ under these circumstances. We can expect that $S^{SL_{2(1)}}$ normally is a positive quantity when the adsorbent-adsorbate interaction is weak compared with the cohesive interaction in the liquid. Then $d\theta/dT$ will be < 0 at least for $\theta < 90^\circ$. The naphthalene-water system studied by Jones and Adamson¹² between 10 and 80 °C appears to be of this kind with $\Delta\varrho$ close to zero and $d(\Delta\varrho)/dT = 0.13$ erg/cm², K. We note that $S^{SL_{(2)}}$ ($= -d\gamma^{LV}/dT$) for the liquid-vapor interface of water is of similar magnitude, ~ 0.15 erg/cm², K. The corresponding interfacial energy value for the naphthalene-water interface, $U^{SL_{2(1)}}$, as obtained on basis of eqn. (9) is 37 erg/cm².

When there is relatively strong adsorbent-adsorbate interaction, however, $S^{SL_{2(1)}}$ may become negative as a consequence of local ordering of the liquid at the interface. In such a case a negative value of $d(\Delta\varrho)/dT$ is predicted and a resulting positive sign of $d\theta/dT$ is possible for $\theta < 90^\circ$. The system CS₂ on monocrystalline ice studied by Adamson, Shirley and Kunichika¹³ is presumably of this latter kind with $d\theta/dT = 0.35^\circ/\text{K}$ within the temperature range -50 to -5 °C. This value would correspond to $S^{SL_{2(1)}} = -0.25$ erg/cm², K and is indicative of an ordering effect of the (polar) ice surface on

liquid CS₂. The corresponding $U^{SL_{2(1)}}$ -value is -94 erg/cm².

Evaluation of the thermodynamic properties of the S/L-interface. From a more fundamental point of view contact angle measurements are important in the first place because equilibrium contact angle data are needed for the evaluation of the basic thermodynamic properties of the S/L-interface. Thus, when $U^{SV_{2(1)}} = U^{SV_{(1)}} - U^{So_{(1)}}$, $S^{SV_{2(1)}} = S^{SV_{(1)}} - S^{So_{(1)}}$ and $\Gamma^{SV_{2(1)}}$ of the S/V-interface are known at the saturation vapor pressure through adsorption measurements and $\Delta\varrho$ and $d(\Delta\varrho)/dT$ have been determined, $S^{SL_{2(1)}} - \Gamma^{SL_{2(1)}}s^{L_2}$, $F^{SL_{2(1)}} - \Gamma^{SL_{2(1)}}\mu_2$ and $U^{SL_{2(1)}} - \Gamma^{SL_{2(1)}}u^{L_2}$ can all be obtained (approximately) by means of eqns. (22) and (9).

It appears, however, that adsorption and contact angle measurements must be supplemented with a separate determination of $\Gamma^{SL_{2(1)}}$ in order to enable the precise evaluation of $U^{SL_{2(1)}}$ and $S^{SL_{2(1)}}$. Possibly, such a determination can be carried out by measuring the volume change, ΔV , generally occurring at cleavage of the solid in the liquid. For a Verschauffelt-Guggenheim surface phase this volume change is given by the expression

$$\Delta V = V^{SL} - n^{SL_1}v^{S_1} - n^{SL_2}v^{L_2} \quad (36)$$

or, for a Gibbsian surface phase ($V^{SL}, n^{SL_1} = 0$)

$$\Delta V/\Delta A = -\Gamma_{2(1)}v^{L_2} \quad (37)$$

where ΔA is the surface area formed at cleaving. To the present author's knowledge no such experiments have ever been reported. In most cases, $\Gamma^{SL_{2(1)}}$ is presumably a rather small quantity but this is not to say that terms like $\Gamma^{SL_{2(1)}}s^{L_2}$ etc. always are negligible compared with $S^{SL_{2(1)}}$ etc.

CONCLUSIONS

The main conclusions of the formal investigation presented in this paper are:

(i) results of elastic stretching experiments are needed on the change of the equilibrium contact angle due to a surface strain variation in order to estimate the error involved when applying the fundamental equation for contact angle systems resulting from the Gibbs thermodynamic treatment;

(ii) when interpreting $\theta = \theta(T)$ data it is advantageous to base the discussion on the thermodynamic fundamental equation for contact angle systems and to carry it through in terms of interfacial entropy;

(iii) for the precise evaluation of the interfacial energy and entropy of the solid-liquid interface, the surface excess of the liquid component at this interface must be separately measured.

REFERENCES

1. Gibbs, J. W. *The Scientific Papers of J. Willard Gibbs, I*, p. 328.
2. Eriksson, J. C. *Surface Science* 14 (1969) 221 (V); *J. Colloid Interface Sci.* 37 (1971) 659 (VI).
3. Melrose, J. C. *J. Colloid Sci.* 20 (1965) 801.
4. Shuttleworth, R. *Proc. Phys. Soc. (London)* A 63 (1950) 444.
5. Johnson, Jr., R. E. *J. Phys. Chem.* 63 (1959) 1655.
6. Eriksson, J. C. *Ark. Kemi* 25 (1966) 331.
7. Derjaguin, B. V. and Zorin, Z. M. *Proc. 2nd Intern. Congr. Surface Activity*, Butterworths, London 1957, Vol. II, p. 145.
8. Defay, R., Prigogine, I., Bellemans, A. and Everett, D. H. *Surface Tension and Adsorption*, Longmans, London 1966, p. 14.
9. Johnson, Jr., R. E. and Dettre, R. H. In Matijević, E., Ed., *Surface and Colloid Science 2*, Wiley-Interscience, New York 1969, p. 85.
10. Adamson, A. W. and Ling, I. *Adv. Chem. Ser. 43* Am. Chem. Soc., Washington D. C. 1964.
11. Bailey, A. I., Prince, A. G. and Kay, S. M. *Spec. Discuss. Faraday Soc. 1* (1970) 118.
12. Jones, J. B. and Adamson, A. W. *J. Phys. Chem.* 72 (1968) 646.
13. Adamson, A. W., Shirley, F. P. and Kuni-chika, K. T. *J. Colloid Interface Sci.* 34 (1970) 461.

Received November 2, 1976.

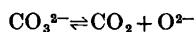
Thermodynamic Properties of the $O_2-O_2^- - O_2^{2-} - O^{2-}$ System in Molten Alkali Carbonates

B. K. ANDERSEN

Fysisk-Kemisk Institut, The Technical University of Denmark, DK-2800 Lyngby, Denmark

The chemical equilibrium properties of the system $O_2-O_2^- - O_2^{2-} - O^{2-}$ in molten alkali carbonates have been studied for various cation combinations (Li, Na, NaK, and LiNaK) in the temperature range 800 to 1200 K. The experimental method used was based on quenching of equilibrated melts followed by chemical analyses. The accuracy in some of the results is inferior because of the very severe corrosion in the "basic" carbonate melts. It was found that the stability of the peroxide and hyperoxide ions compared with that of the oxide ions increases with increasing cation "radius" and decreasing temperature.

It is well-known that the carbonate ions in molten alkali carbonates dissociate according to the reaction



In an oxygen atmosphere the oxide ions may be oxidized to peroxide and hyperoxide (super-oxide) ions. Therefore, the following redox equilibria are assumed to exist in these melts.



Only two of these equilibria are independent (*e.g.*, $R3 = R1 + R2$; $R4 = 2R1 - R2$). The corresponding standard equilibrium constants may be written

$$K^{\ominus}_1 = [a(O^{2-})/a(O_2^{2-})][p(O_2)/p^{\ominus}]^{\frac{1}{2}} \quad (1)$$

$$K^{\ominus}_2 = a(O_2^{2-})/[a(O_2^-)]^2[p(O_2)/p^{\ominus}] \quad (2)$$

$$K^{\ominus}_3 = a(O^{2-})/[a(O_2^-)]^2[p(O_2)/p^{\ominus}]^{\frac{3}{2}} \quad (3)$$

$$K^{\ominus}_4 = [a(O^{2-})]^2[a(O_2^-)]/[a(O_2^{2-})]^3 \quad (4)$$

No systematic thermodynamic investigation of the redox system $O_2-O_2^- - O_2^{2-} - O^{2-}$ in alkali carbonate melts has been carried out previously. However, some crude measurements which showed the importance of peroxide ions in "basic" alkali carbonate melts (see definitions and notations) were performed by the present author in the late sixties.^{1,2} Information on the equilibrium properties of the mentioned reactions is important in applications of oxygen electrodes in alkali carbonate melts. For this reason it was decided to carry out more accurate measurements.

Recently Appleby and Nicholson^{3,4} measured limiting oxygen reduction currents in "acid" $(Na,K)_2CO_3$ - and Li_2CO_3 -melts (see definitions and notations). No quantitative equilibrium data are given by these authors, but their results indicate the presence of both peroxide- and hyperoxide-ions in significant amounts in NaK-melts. They also conclude that hyperoxide-ions are not stable in Li-melts.

Studies of the system $O_2-O_2^- - O_2^{2-} - O^{2-}$ in other oxy-anionic melts are of interest. Lux *et al.*⁵ have investigated the formation of peroxides and hyperoxides by reactions between molten single cation alkali hydroxides and oxygen in the presence of water vapour at 683 and 733 K by means of an analytical method. In Li-melts neither O_2^{2-} -ions nor O_2^- -ions could be detected, in Na-melts there is evidence that mainly O_2^{2-} -ions are formed, whereas in K-, Rb-, and Cs-melts O_2^- -ions

are the main reaction products. However, no quantitative equilibrium data were given.

Later Goret ⁶ and Goret and Trémillon ⁷ did voltammetric studies of the $O_2-O_2^- - O_2^{2-} - O^{2-}$ -system in NaK-hydroxide melts at 500 K. This work also was of a qualitative nature only.

During the last decade Zambonin and co-workers have studied the redox chemistry and mechanisms of the same system in molten alkali nitrates. Zambonin ⁸ calculated the following "equilibrium constants" for the reactions R1 and R2 at 503 K

$$K_1' = [O^{2-}][O_2]^{1/2}/[O_2^{2-}] \approx 10^{-8} \text{ (mol kg}^{-1}\text{)}^{1/2}$$

and

$$K_2' = [O_2^{2-}][O_2]/[O_2^-]^2 \approx 5 \times 10^{-7}$$

where the brackets denote molality concentrations. The data given are those for the (Na,K)- NO_3 -system with 50 mol % Na. Desimoni *et al.*⁹ have determined Henry's law constants for oxygen solubility in the same system by means of rotating disk electrode voltammetry. They obtained the Henry's law constants 4.6×10^{-6} and 5.3×10^{-6} mol kg⁻¹ atm⁻¹ at 511 and 533 K, respectively. From the data given above the following "equilibrium constants" on a mol fraction/pressure basis are deduced (standard states are given later in this section): $K_1 \approx 5 \times 10^{-6}$, $K_2 \approx 1.3$, $K_3 \approx 6 \times 10^{-6}$, $K_4 \approx 2 \times 10^{-12}$. All data refer to a temperature of about 500 K. These data show clearly that when $p(O_2) \approx 101$ kPa and $x(O_2^-) < 0.03$ it follows that $x(O^{2-}) \ll x(O_2^{2-}) < x(O_2^-)$.

Because of the different solvent anions and especially because of the relatively low temperatures used in the works of Zambonin and coworkers it is difficult to estimate data for the corresponding equilibria in alkali carbonate melts from the information above. However, an attempt to do this will be discussed later.

In the present investigation an experimental method based on quenching followed by chemical analyses was adapted in order to study the $O_2-O_2^- - O_2^{2-} - O^{2-}$ -system in molten alkali carbonates.

Definitions and notations. The following definitions and notations are used:

a. Standard states are "pure" substances - $M_2O(l)$, $M_2O_2(l)$, $MO_2(l)$, and $O_2(g)$ - at the pressure 101.325 kPa.

b. All thermodynamic data refer to the stoichiometry used in the reactions R1-R4.

c. Data in parentheses refer to temperatures below the melting points of the respective alkali carbonates.

d. The general term "oxide" is used for oxide, peroxide, as well as for hyperoxide.

e. Anionic fractions of the "oxide" species, $x(i)$ are defined as $x(i) = n(i)/n$ where $n(i)$ is number of mol of ion i and $n = n(CO_3^{2-}) + n(O^{2-}) + n(O_2^{2-}) + \frac{1}{2}n(O_2^-)$.

f. Mol fraction of "oxide" = x_{ox}

$$x_{ox} = x(O^{2-}) + x(O_2^{2-}) + \frac{1}{2}x(O_2^-) \quad (5)$$

g. Apparent mol fraction of peroxide =

$$x^*(O_2^{2-}) = x(O_2^{2-}) + \frac{1}{2}x(O_2^-) \quad (6)$$

h. Relative amount of oxide, peroxide or hyperoxide = mol % oxide, peroxide or hyperoxide of total amount of "oxide"

$$Y(O^{2-}) = [x(O^{2-})/x_{ox}] \times 100 \text{ (mol \%)} \quad (7)$$

$$Y(O_2^{2-}) = [x(O_2^{2-})/x_{ox}] \times 100 \text{ (mol \%)} \quad (8)$$

$$\frac{1}{2}Y(O_2^-) = [\frac{1}{2}x(O_2^-)/x_{ox}] \times 100 \text{ (mol \%)} \quad (9)$$

i. Apparent equilibrium constants of reactions R1 and R3

$$K^*_1 = [x(O^{2-})/x^*(O_2^{2-})][p(O_2)/p^\ominus]^{1/2} \quad (10)$$

$$K^*_3 = x(O^{2-})/[2x^*(O_2^{2-})]^2[p(O_2)/p^\ominus]^{3/2} \quad (11)$$

j. Carbonate melts are denoted "acid" when they are under a relatively high CO_2 pressure (of the order 100 kPa) and "basic" when relatively large quantities of "oxide" have been added to the melts (typically 1-3 mol %) and the CO_2 pressure above the melts is negligible.

k. The symbol f is used for activity coefficient on mol fraction basis.

EXPERIMENTAL

Chemicals. The chemicals used in the present investigation were: Li_2CO_3 (Riedel-de Haën, Hannover, Chem. Pure), Na_2CO_3 , K_2CO_3 , Na_2O_2 (Riedel-de Haën, Hannover, P.A.), Li_2O and Na_2O (K & K Laboratories Inc., Plainview, N.Y. and Hollywood, California).

The alkali carbonates were dried in the following way: They were kept for a period of 24 h or more at about 470 K. Then the salts were slowly heated and melted in dry CO_2 atmosphere and CO_2 gas was bubbled through the melts for at least 12 h.

The gases used were supplied by A/S Dansk Ilt- & Brintfabrik, Copenhagen (O_2 and N_2) and Nordisk Kulsyrefabrik A/S, Copenhagen (CO_2). The gases were dried by passing through tubes with silica gel, "Anhydrone" ($MgCl_2$), and/or P_2O_5 . The gases O_2 and N_2 also passed tubes with "Carbosorb" (soda lime).

The alumina used for crucibles and tubes was the quality DEGUSSIT AL 23 (> 99.5 % Al_2O_3) supplied by Degussa, Frankfurt a.M.

Apparatus and procedure. A standard type resistance furnace as described by Motzfeldt¹⁰ was used in the experiments. This furnace made it possible to work in a controlled atmosphere at a rather constant temperature (within ± 0.2 K in the melt, when an appropriate temperature controlling system was applied).

Alkali oxide or alkali peroxide was added (usually 3.0 mol %) to the alkali carbonate melt (about 50 g) and the mixture was kept in an atmosphere of dry oxygen at constant pressure (about 101 kPa) until equilibrium was attained.* Stirring was achieved by bubbling oxygen through the melts.

Samples (about 5 g) were taken out by means of an alumina pipette and quenched to room temperature within a few seconds. This process was carried out as fast as possible under protection of an inert gas (nitrogen). Different quenching conditions, e.g., change in the cooling rate, did not have any influence on the results, and, therefore, the "oxide"-equilibria could be considered as sufficiently "frozen". The contents of "oxide" and apparent amount of peroxide in the samples were determined by means of volumetric analyses.** Special precautions had to be taken to prevent loss of active oxygen.

* Equilibrium in the total system was not attained since CO_2 formed by the dissociation of CO_3^{2-} -ions did escape. This process, however, is very slow and the influence on the $O_2-O_2^{2-}-O_2^{2-}-O_2^-$ equilibrium was neglected.

** *Determination of "oxide" content in alkali carbonates.* The samples were dissolved in hot water. Excess of $BaCl_2$ -solution was added and the precipitated $BaCO_3$ filtered off. The OH^- -content was determined by pH-metric titration in an inert atmosphere. 2 mol of OH^- -ions correspond to 1 mol of "oxide"-ions. When the concentrations of OH^- -ions were small the concentrations of CO_3^{2-} - and HCO_3^- -ions in the filtered solutions had to be taken into account.

*** *Determination of apparent peroxide content in alkali carbonates.* About 1 g of the pulverized sample was transferred very slowly to a vigorously stirred mixture prepared from 50 ml crushed ice and water, 20 ml 1:10 sulfuric acid, and 1 g pure boric acid. This mixture was titrated with standard 0.02 N $KMnO_4$ -solution. Since O_2^{2-} -ions react with water to form O_2^{2-} -ions, only the apparent contents of peroxide in the samples could be determined. Blind experiments confirmed the usefulness of this method.

The following alkali carbonate systems were investigated: Li_2CO_3 , Na_2CO_3 , $(Na,K)_2CO_3$ (56.0 mol % Na), and $(Li,Na,K)_2CO_3$ (the ternary eutectic melt - 43.5 mol % Li and 31.5 mol % Na). The melting points of these carbonates are 999, 1131, 983, and 670 K, respectively.

The container and the thermocouple protection tube were made of high purity alumina.

Two hours or less was sufficient time to attain equilibrium in the melts when Na_2O and Na_2O_2 were added. It was observed that addition of Na_2O and Na_2O_2 gave the same results, thus indicating the "oxide"-reactions to be reversible. When Li_2O was added to $(Li,Na,K)_2CO_3(l)$ the time to reach equilibrium was longer, probably because of the smaller solubility of Li_2O in carbonate melts.

RESULTS

In Fig. 1 the experimentally determined apparent equilibrium constants *versus* $1/T$ are shown for the Na-, NaK-, and LiNaK-systems. The total "oxide" concentration in the melts was about 3.0 mol %. Application of higher "oxide" concentrations was restricted because of the very severe corrosion taking place.¹¹ In the Li-containing melts the "oxide" concentrations had to be chosen equal to or less than the solubilities of Li_2O . When hyperoxide is present in significant amounts it should be remembered that $Y(O_2^{2-})$ is a function of x_{Ox} .

In the cases where Li-melts were investigated the peroxide contents at equilibrium were found to be less than that which could be determined by the analytical method used, that is, $Y(O_2^{2-}) < 0.2$ mol %.

The results in Fig. 1 were fitted to straight lines ($\log K^*_1 = b/T + a$) by least squares treat-

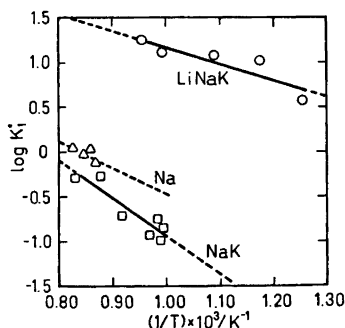


Fig. 1. Plots of $\log K^*_1$ versus $1/T$ for reaction R1 [$O_2^{2-} = O_2^{2-} + \frac{1}{2}O_2(g)$] in molten alkali carbonates. $x_{Ox} \approx 0.03$, $p(O_2) \approx 101$ kPa.

Table 1. Apparent equilibrium constants for the reaction R1 in molten alkali carbonates.

System (M)	log K* ₁	S.D.	Temperature range/K
Li	> 2.7	-	1000-1100
LiNaK	(-1800/T)+2.98	0.14	800-1050
Na	(-3000/T)+2.52	0.064	1150-1210
NaK	(-4250/T)+3.31	0.13	1000-1200

ments. The functions and standard deviations are tabulated in Table 1.

From the results of the chemical analyses only the oxide concentrations, $x(O^{2-})$, and the apparent peroxide concentrations, $x^*(O_2^{2-})$, are obtained. The following question now arises: What are the relative amounts of peroxide and hyperoxide ions in various melts under specified experimental conditions? If this question could be answered "real" thermodynamic data could be calculated for the reactions R1-R4. The following experimental method was used: The total "oxide" concentration and oxygen pressure [x_{ox} , $p(O_2)$] were changed from (0.03, 101 kPa) to (0.01, 101 kPa) or (0.03, 10.1 kPa) and the changes in the apparent equilibrium constants, K^*_{1} , were studied.

These measurements, which were of a semi-quantitative nature, showed that under the experimental conditions $x_{ox} \approx 0.03$ and $p(O_2) \approx 101$ kPa the ratio $x(O_2^{2-})/[1/2x(O_2^-)]$ is about 4/1 for the Na-system near 1150 K and about 1/1 for the NaK-system near 1100 K. Furthermore, calculations show that the ratio $x(O_2^{2-})/[1/2x(O_2^-)]$ probably does not change very much in the temperature range 1000-1200 K. For the LiNaK-system no measurable amounts of

Table 2. Standard equilibrium constants for the reaction R1 in molten alkali carbonates. Assumption: $f(O^{2-}) \approx f(O_2^{2-})$.

System (M)	log K [⊖] ₁				
	800 K	900 K	1000 K	1100 K	1200 K
Li	-	-	-	> 2.7	-
LiNaK	0.73	0.98	1.18	1.34	1.48
Na	-	-	(-0.39)	(-0.11)	0.12
NaK	-	-	-0.65	-0.25	0.07

Table 3. Standard equilibrium constants for the reaction R3 in molten alkali carbonates. Assumption: $f(i) = 1$.

System (M)	log K [⊖] ₃		
	1000 K	1100 K	1200 K
Na	(1.96)	(2.32)	2.65
NaK	0.63	1.07	1.49

O₂⁻-ions could be detected by the present method.

Using this information combined with the experimentally determined data for the apparent equilibrium constants (Table 1) the "true" standard equilibrium constants were calculated for the reactions R1 and R3 for the Na- and NaK-systems (Tables 2 and 3).

DISCUSSION

General. Tables 2 and 3 show clearly that the stability of the peroxide/hyperoxide ions increases with increasing cation "radius" (or decreasing cation ionic potential). The strength of the M-O bonding weakens when the distance between the centres of the atomic cores increases, and, therefore, the relative strength of the O-O bonding increases.

According to the literature¹² pure LiO₂ cannot be isolated and the only evidence for its existence is the similarity in the absorption spectra of the pale yellow solutions of Li, Na, and K on rapid oxidation of the metals in liquid ammonia at 195 K by oxygen.

Using (a) the statements above, (b) the experimental result that the hyperoxide concentration is small or negligible compared with the peroxide concentration in the LiNaK-system, (c) the qualitative results of Appleby and Nicholson⁴ and of Lux *et al.*,⁵ it seems to be well justified to assume that hyperoxide ions are not present in measurable amounts in "basic" alkali carbonate melts rich in Li⁺-ions.

It is now possible to calculate approximate thermodynamic data also for systems which have not been investigated experimentally (the Li-, LiNa(53.3 mol % Li)-, LiK(50.0 mol % Li)-, and K-systems). The calculations are based on the data in Tables 2 and 3 and the assump-

Table 4. Standard thermodynamic data for the reaction R1, $M_2O_2(l) = M_2O(l) + \frac{1}{2}O_2(g)$, in $M_2CO_3(l)$. Assumption: $f(O_2^{2-}) \approx f(O_2^{2-})$.

System (M)	$\Delta G^\ominus_1/kJ \text{ mol}^{-1}$ 1000 K	1100 K	1200 K	ΔS^\ominus_1 $J \text{ K}^{-1} \text{ mol}^{-1}$	$\log K^\ominus_1$ (1000 K)
Li	—	< -57	—	—	—
Li ^a	-68.2	-71.9	-76.2	≈ 40	3.56
LiNa ^a	-32.9	-37.2	-41.9	≈ 45	1.72
LiK ^a	-24.7	-31.4	-38.0	≈ 67	1.29
LiNaK	-22.6	-28.3	-34.0	57	1.18
Na	(7.5)	(2.3)	-2.8	≈ 52	(-0.39)
NaK	12.4	5.3	-1.6	70	-0.65
K ^a	(18.8)	(9.0)	0.1	≈ 93	(-0.98)

^a Calculated values (see Discussion).

tion that the O_2^{2-} -concentration is negligible in Li-containing systems. In these calculations deviations from ideal mixtures were to be neglected (or the differences between the excess functions of reactants and products are assumed to be small). Furthermore, extrapolations have to be made outside the experimentally investigated temperature and in some cases also below the normal melting points.

Tables 4 and 5 show increases in standard Gibbs free energy and entropy as well as standard equilibrium constants at 1000 K of the reactions R1 and R3 for all seven possible cation combinations. Except for the LiNaK- and NaK-systems the uncertainties in the entropy functions are large; the orders of magnitude, however, seem to be reasonable.

Table 6 shows the relative amounts of oxide-, peroxide-, and hyperoxide-ions in alkali carbonate melts with a total "oxide" concentration of 3.0 mol % and under an oxygen pressure of 101 kPa. The values for the systems not studied experimentally are calculated from the data in Tables 2 and 3.

Table 6 as well as Tables 4 and 5 shows again clearly how the stability of O_2^{2-} -ions compared with that of the O_2^{2-} - and/or O_2^- -ions decreases with increasing cation "radius". The stability of the O_2^{2-} -ions is slightly larger in the LiK-system than in the LiNaK-system at the same temperature. This may be due to the higher Li-content in the LiK-system. Except for the Li-system it is observed that the stability of the O_2^{2-} -ions increases with increasing temperature. The apparent anomaly observed in the case of the Li-system probably is due to uncertainties in the experimental data and the approximations used in the calculations. It is also noticed that the calculated relative amounts of O_2^{2-} -ions in the Li-system ($0.03 \text{ mol } \% < Y(O_2^{2-}) < 0.05 \text{ mol } \%$ in the temperature range 1000–1200 K) is consistent with the experimental statement that $Y(O_2^{2-}) < 0.2 \text{ mol } \%$.

This paper deals only with the thermodynamic aspects of the reactions R1–R4 and no attempts has been made to study the kinetics or the mechanisms of the mentioned pro-

Table 5. Standard thermodynamic data for the reaction R3, $2MO_2(l) = M_2O(l) + \frac{3}{2}O_2(g)$, in $M_2CO_3(l)$. Approximation: $f(i) \approx 1$.

System (M)	$\Delta G^\ominus_3/kJ \text{ mol}^{-1}$ 1000 K	1100 K	1200 K	ΔS^\ominus_3 $J \text{ K}^{-1} \text{ mol}^{-1}$	$\log K^\ominus_3$ (1000 K)
Na	(-38)	(-49)	61	≈ 117	(1.96)
NaK	-12	-23	-34	≈ 111	0.63
K ^a	(20)	(11)	0	≈ 103	(-1.06)

^a Calculated values (see Discussion).

Table 6. Relative amounts of oxide, peroxide, and hyperoxide ions in molten alkali carbonates containing 3.0 mol % "oxide".

 $p(O_2) \approx 101$ kPa.

System (M)	$Y(O^{2-}) - Y(O_2^{2-}) - \frac{1}{2}Y(O_3^{2-})$ /mol %			1100 K			1200 K		
	1000 K								
Li ^{a,b}	99.97	0.03	0.00	99.96	0.04	0.00	99.95	0.05	0.00
LiNa ^a	98.1	1.9	0.0	98.3	1.7	0.0	98.5	1.5	0.0
LiK ^a	95.1	4.9	0.0	96.9	3.1	0.0	97.8	2.2	0.0
LiNaK	94.0	6.0	0.0	95.7	4.3	0.0	96.8	3.2	0.0
Na	(25)	60	15)	(38	49	12)	51	39	10
NaK	10	45	45	22	39	39	37	32	32
K ^a	(0.9	8.5	91)	(2.9	7.9	89)	8.6	8.7	83

^a Calculated. ^b Experimentally determined: $Y(O_3^{2-}) < 0.2$ mol %.

cesses in molten carbonates. One possibility is, though it is not likely to be significant in "basic" carbonate melts, that the CO_3^{2-} -ions take part in the redox processes, e.g., $CO_3^{2-} + \frac{1}{2}O_2 = CO_2 + O_3^{2-}$.

Comparison with literature data. Thermodynamic data for the alkali oxides, peroxides, and hyperoxides are scarce — even at room temperature — and it is not possible to calculate or estimate data for the equilibrium properties of the reactions R1–R4 with any reasonable accuracy.

The results obtained in this investigation agree with the qualitative results given by Appleby and Nicholson^{3,4} for $(Na,K)_2CO_3$ - and Li_2CO_3 -melts and also with the information given by Lux *et al.*⁵ for single cation alkali hydroxides.

Using the equilibrium constants for the reactions R1 and R3 in NaK-melts at about 500 K calculated from experimental data published by Zambonin⁸ and by Desimoni *et al.*⁹ (see Introduction) together with estimated increases in standard entropy it is possible to calculate thermodynamic data for the reactions

R1 and R3 at higher temperatures (see Table 7). Comparing these results with the corresponding data obtained in this investigation (Tables 2–5) a rather good consistency is observed. The different oxy-anions in the two systems and an extrapolation over a temperature range of 500 to 700 K indicates, however, that this consistency may be fortuitous.

Ionic species in molten alkali carbonates. Most authors agree that molten alkali carbonates are almost completely ionized and that the predominant species are the planar CO_3^{2-} -ions and the M^+ -ions. Janz *et al.*^{14–16} also believe that "contact ion pairs" [like $(M+CO_3^{2-})^-$] may be of some importance. They suggest that these ions contribute to the mechanism of electrical transport.

In the presence of an O_2 atmosphere it seems likely, as assumed in this work, that O^{2-} -ions are oxidized to O_2^{2-} and O_3^{2-} -ions. The presence of O_3^{2-} -ions is demonstrated by the quenching experiments and analyses, but no definite proof has been given of the existence of O_3^{2-} -ions. The observed change in the apparent equilibrium constant, K^*_1 , by decreasing x_{Ox} or $p(O_2)$,

Table 7. Standard thermodynamic data for the reactions R1 and R3 in NaK-melts (50 mol % Na) calculated from experimental results of Zambonin⁸ and Desimoni *et al.*,⁹ and estimated standard entropy changes.

Reaction	ΔG^\ominus /kJ mol ⁻¹			log K^\ominus		
	500 K	1000 K	1200 K	500 K	1000 K	1200 K
R1	51.0	13.8	-0.4	-5.3	-0.7	0.0
R3	49.8	-14.6	-37.2	-5.2	0.8	1.6

however, indicates the presence of O_2^- -ions in some of the systems, and from an energetic point of view it seems likely that O_2^- -ions are stable in melts with negligible amounts of Li^+ -ions. The electro-analytical studies of Appleby and Nicholson described previously also strongly indicate the presence of O_2^- -ions in NaK-carbonate melts. Furthermore, Zambonin¹⁷ has used the paramagnetic property of hyperoxide ions to detect O_2^- -ions in molten NaK-nitrates by means of ESR spectroscopy in the corresponding quenched matrices.

O^- -ions may be present as intermediate species, but it is unlikely that these ions are stable. It is also assumed that other "oxide"-species such as O_3^- and O_3^{2-} do not play an important part as stable ions.

Various carbonate-oxygen or carbonate-"oxide" species such as CO_4^{2-} and CO_4^{4-} also seem possible. However, one should here remember the controversy in defining complexes in molten salts. From a thermodynamic point of view this author considers it to be well justified to assume that the stable species in "basic" alkali carbonate melts are limited to the following ones: Cations Li^+ , Na^+ , K^+ ; Anions CO_3^{2-} , O^{2-} , O_2^{2-} , O_2^- ; Molecules O_2 , CO_2 .

REFERENCES

1. Andersen, B. K. *Unpublished* (1969).
2. Andersen, B. K. *Proc. 3rd Int. Conf. Fuel Cells*, Brussels 1969, p. 87.
3. Appleby, A. J. and Nicholson, S. J. *Electroanal. Chem.* 38 (1972) App. 13.
4. Appleby, A. J. and Nicholson, S. J. *Electroanal. Chem.* 53 (1974) 105.
5. Lux, H., Kuhn, R. and Niedermaier, T. *Z. Anorg. Allgem. Chem.* 298 (1959) 285.
6. Goret, J. *Bull. Soc. Chim. Fr.* (1964) 1074.
7. Goret, J. and Trémillon, B. *Bull. Soc. Chim. Fr.* (1966) 67.
8. Zambonin, P. G. J. *Electroanal. Chem.* 33 (1971) 243.
9. Desimoni, E., Paniccia, F. and Zambonin, P. G. J. *Electroanal. Chem.* 38 (1972) 373.
10. Motzfeldt, K. In Bockris, J. O'M., MacKenzie, J. D. and White, J. L., Eds., *Physicochemical Measurements at High Temperatures*, Butterworths, London 1959, p. 313.
11. Andersen, B. K., *Ph.D. Thesis*, The Technical University of Denmark, Copenhagen 1975.
12. Cotton, F. A. and Wilkinson, G. *Advanced Inorganic Chemistry*, 2nd Ed., Interscience, New York 1967, p. 375.
13. Gmelin's *Handbuch der anorganischen Chemie*, 8th Ed., System-Nummer 20, 21 and 22, Verlag Chemie, Berlin and Weinheim 1937, 1960 and 1965.
14. Janz, G. J. and Lorenz, M. R. *J. Electrochem. Soc.* 108 (1961) 1052.
15. Janz, G. J. and Saegusa, F. *J. Electrochem. Soc.* 110 (1963) 452.
16. Ward, A. T. and Janz, G. J. *Electrochim. Acta* 10 (1965) 849.
17. Zambonin, P. G. J. *J. Phys. Chem.* 78 (1974) 1294.

Received June 8, 1976.

On the MnP Type Structure of RuSb and RhSb

KARI ENDRESEN,^a SIGRID FURUSETH,^a KARI SELTE,^a ARNE KJEKSHUS,^a
TROND RAKKE^a and ARNE F. ANDRESEN^b

^a Kjemisk Institutt, Universitetet i Oslo, Blindern, Oslo 3, Norway and

^b Institutt for Atomenergi, Kjeller, Norway

The crystal structures of RuSb and RhSb have been determined from powder neutron diffraction data. The results are used in reevaluation of a geometrical model for the relationship between the NiAs and MnP type structures.

Geometrical and bonding properties which affect the relation between the NiAs and MnP type crystal structures are discussed in Ref. 1 on the basis of structural data for phosphides and arsenides of the latter type. Hence, accurate structure determinations for the only hitherto known MnP type antimonides, RuSb² and RhSb,³ are of considerable interest. (The abbreviations *T*=transition element and *X*=non-metal from groups IV B to VI B are used throughout this text.)

EXPERIMENTAL

RuSb and RhSb were prepared by heating equi-atomic quantities of the elements [99.99 % Ru and Rh (Johnson, Matthey & Co.) and 99.9995 % Sb (Koch-Light Laboratories)] in crucibles of alumina inside evacuated, sealed silica tubes. Three heat treatments of 10–14 d duration at 850–1200 °C, interrupted by intermediate crushings, were necessary to obtain homogeneous samples. The samples were finally cooled to 600 °C over 2 d and then air-quenched.

Experimental details concerning X-ray and neutron diffraction measurements have been reported in Ref. 4.

RESULTS AND DISCUSSION

The unit cell dimensions and positional parameters for RuSb and RhSb, as derived by least squares treatments of powder X-ray (Guinier) and neutron diffraction data, are

listed in Table 1 together with the shortest interatomic distances. Both with respect to axial ratios and positional parameters, these compounds fall naturally in among the other compounds with MnP type structure listed in Refs. 1 and 5. As this result is not an *a priori* consequence of the geometrical model in Ref. 1, a critical reexamination of the model and its postulates is called for.

The main aspects of the model are recapitulated in Table 2, and only a few, particularly

Table 1. Unit cell dimensions, positional parameters, and shortest interatomic distances for RuSb and RhSb. [Space group *Pnma*, positions 4(c).]

Parameter	RuSb	RhSb
<i>a</i> (Å)	5.9608 (13)	5.9718 (7)
<i>b</i> (Å)	3.7023 (9)	3.8621 (7)
<i>c</i> (Å)	6.5797 (13)	6.3242 (9)
<i>x_T</i>	0.0053 (10)	0.0053 (19)
<i>z_T</i>	0.2037 (7)	0.1942 (12)
<i>x_X</i>	0.1992 (8)	0.1949 (15)
<i>z_X</i>	0.5808 (10)	0.5915 (14)
<i>T</i> – <i>X</i> (Å) × 1	2.614 (8)	2.589 (13)
<i>T</i> – <i>X</i> (Å) × 2	2.631 (6)	2.645 (9)
<i>T</i> – <i>X</i> (Å) × 2	2.680 (6)	2.712 (10)
<i>T</i> – <i>X</i> (Å) × 1	2.737 (8)	2.756 (12)
(<i>T</i> – <i>X</i>) _{av.} (Å)	2.662	2.677
<i>T</i> – <i>T</i> (Å) × 2	3.042 (8)	3.068 (16)
<i>T</i> – <i>T</i> (Å) × 2	3.258 (5)	3.125 (8)
<i>T</i> – <i>X</i> (Å)	4.258 (8)	3.976 (12)
<i>T</i> – <i>T</i> (Å)	3.702 (1)	3.862 (1)
<i>X</i> – <i>X</i> (Å)	3.193 (6)	3.238 (10)

Table 2. Geometrical model for conversion from NiAs to MnP type structure. Postulates (including empirical constraints) and consequences outlined in Ref. 1. (Axes and positional parameters expressed in terms of MnP type cell of setting *Pnma*.)

Postulate No.	Cue for content	Application, specification, elaboration, etc.	Mathematical formulation [Formula No.]	Matching numerical value
1	Coordination symmetry essentially retained			
2	Approx. equal size for <i>T</i> and <i>X</i>			
3	2 and 4 <i>T-T</i> contacts in NiAs and MnP type, respectively	Equal length of <i>T-T</i> contacts in MnP type	$z_T = \frac{1}{4} - \frac{1}{8} \left(1 + \frac{b^2}{c^2} - \frac{a^2}{c^2} \right)$ [I]	$0.181 < z_T < 0.195$
4	$(T-X)_{av}$, bond length unchanged from NiAs to MnP type with min. scatter in latter type	<i>T-X</i> bond lengths equalized two by two in MnP type	$x_X = \frac{1}{4} - \frac{1}{12} \left(-1 + \frac{b^2}{a^2} + \frac{c^2}{a^2} \right)$ [II]	$0.194 < x_X < 0.206$
			$x_X = \frac{1}{4} - \frac{1}{8} \left(-1 + 3 \frac{b^2}{a^2} + \frac{1c^2}{3a^2} \right)$ [III]	$0.152 < x_X < 0.202$
			$x_X = \frac{1}{4} - \frac{1}{8} \left(-1 + \frac{b^2}{a^2} + \frac{5c^2}{3a^2} \right)$ [IV]	$0.065 < x_X < 0.077$
			$x_X = \frac{1}{4} - \frac{1}{6} \left(-1 + \frac{b^2}{a^2} + \frac{c^2}{a^2} \right)$ [V]	$0.138 < x_X < 0.162$
		Scatter in <i>T-X</i> bond lengths in MnP type minimized		Calc. for CoP $x_X = 0.205$
5	<i>T</i> displaced mainly $\parallel \pm c$ in MnP type	$x_T \approx 0, z_T \neq \frac{1}{4}$		
6	<i>X</i> displaced mainly $\parallel \pm a$ in MnP type	$x_X \neq \frac{1}{4}, z_X \approx \frac{7}{12}$		
7	Limitations on axial proportions in MnP type	$\frac{c}{a} \approx 1.10$ $1.63 < \frac{c}{b} < 2.08$		
8	Negligible <i>X-X</i> bonding interaction	Shortest <i>X-X</i> distance $\sim 20\%$ longer than bonding <i>X-X</i>	x_X defined by: $\frac{5}{2}x_X^3 + \frac{3}{4}x_X \approx$ $\frac{3}{16} + \left(\frac{3}{2}z_T^3 - \frac{3}{4}z_T + \frac{3}{20} \right) \frac{c^3}{a^3}$ [VI]	
9	"Idealized" MnP type	$\frac{c}{a} = 1.10, \frac{c}{b} = \sqrt{3},$ $x_T = 0, z_T = 0.20$ $x_X = 0.20, z_X = \frac{7}{12}$		
10	Volume per formula unit unchanged from NiAs to MnP type			

relevant points will be considered further in the text. Post. 1 appears to have a superior function and is implicitly included in most of the other postulates. It carries information about the nature of the NiAs \rightarrow MnP type transition, which may be explored by means of group theory as has been done in Ref. 6. However, no quantitative deductions are made directly from this postulate in Ref. 1. The same applies to Post. 10 which merely states a particular requirement on second order phase transitions.

The contents of Posts. 3 and 8 are essential to the original quantitative development of the geometrical model.¹ Thus, "the strive" for establishing four $T-T$ contacts is considered as the initiator and driving force of the NiAs \rightarrow MnP type transition. Unfortunately, the understanding of the physical background for this statement has not proceeded beyond the rather vague indications in Ref. 1. In a similar manner the non-metal atoms may be regarded as the stoppers of the transformation process. In this case, however, the physical picture is more clear-cut since the size of X (*vide infra*) and the assumed non-bonding character of all $X-X$ distances will act as limitators for the deformation of the NiAs type atomic arrangement.

Formulae Nos. [II]–[V] in Table 2 (when combinations giving undetermined x_X are omitted) show that Post. 4 has much the same function as Post. 8, in that both provide mathematical expressions for the calculation of the parameter x_X . Granted that one is prepared to accept "the strive" for four $T-T$ contacts as a reasonable cause of the MnP type deformation, one may equally well accept that the X atoms adjust their positions to equalize the $T-X$ bond lengths. However, complete equalization of the four crystallographically independent $T-X$ distances is incompatible with T positions defined according to formula No. [I], and this constraint can only be achieved on returning to the NiAs type symmetry. The unattainableness of the requirement in Post. 4 is also reflected in formulae Nos. [II]–[V], which are obtained by equalizing the $T-X$ bond lengths two by two, resulting in different mathematical expressions and numerical values for the parameter x_X . On relinquishing the strict requirement for equal $T-X$ distances

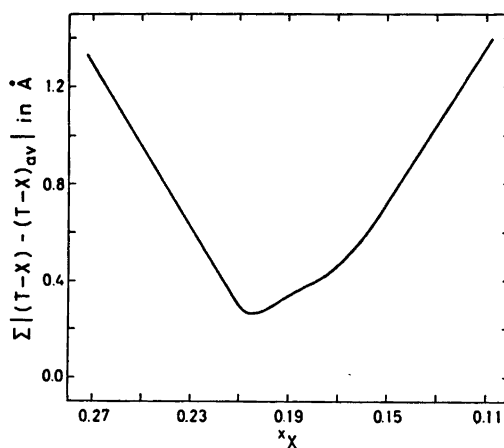


Fig. 1. Scatter in $T-X$ bond lengths as function of x_X for CoP. (Unit cell dimensions and other positional parameters from Refs. 7 and 8.)

in the MnP type structure, the physical basis for using Post. 4 to derive expressions for x_X is no longer present. On this background Post. 8 seems to be physically more attractive than the above version of Post. 4.

The scatter in the $T-X$ distances ($\Sigma |(T-X) - (T-X)_{av}|$) can be expressed by x_X . Equated to zero, the differentiated expression will, in principle, give the x_X value corresponding to a minimum scatter in the $T-X$ distances. Unfortunately, the complexity of the expressions prevents a general mathematical solution according to this procedure. However, the problem can be solved numerically for a given set of values for all but x_X of the variables. As an illustration of a practical solution of this type, Fig. 1 presents the variation of $\Sigma |(T-X) - (T-X)_{av}|$ with x_X for the almost "ideal" MnP type structure of CoP. In this case the scatter has a minimum at $x_X = 0.205$, which closely approaches the value given in Post. 9.

The conclusion is accordingly that the postulated minimum scatter in $T-X$ bond lengths is a satisfactory and operative principle for the fixing of x_X in the MnP type structure. Since there is only empirical correlation between bond lengths and energetic parameters for this type of solids, the physical nature of Post. 4 is still somewhat dubious.

Consultation of the structural data for MnP type compounds unveils that nature "mini-

mizes" the scatter in $T-X$ bond distances in an intuitively lucid way. In practice, the two pairs of two-fold degenerate $T-X$ bond distances are often found to be roughly equal (*cf.*, formula No. [II]) and the two remaining $T-X$ bond distances are almost symmetrically located on both sides of "this average". However, the arguments for raising the basis of formula No. [II] to a postulate of the model seem physically less clear-cut than maintaining the whole content of Post. 4.

Although only superficially discussed in Ref. 1, Post. 2 (which is a corollary to Post. 9) was considered a key postulate that, *inter alia*, quantified the parameter x_X from Post. 8. Unfortunately, the simple and intuitive concept of size is particularly ill-defined in rather low-symmetrical atomic arrangements like the MnP type, and the poor specification of this concept in Ref. 1 may have obscured the presentation. Thus, some clarifying comments are appropriate.

Consider the average $T-X$ bond length $(T-X)_{av.} = r_T + r_X$ as being composed of a bonding, average radius r_T for T and r_X for X . (The term radius is used here loosely as a measure of size, or rather as a simple model concept without referring to any specific scale.) If the magnitude of r_X (or r_T) dominates, a close-packed arrangement of X (or T) is expected, and an NiAs (or "anti-NiAs") type structure may emerge. In cases where $r_T \approx r_X$, the prediction of structure type from simple considerations becomes less clear-cut and more assumptions must be included in the model.

Let us assume $r_T \approx r_X$ as a starting point for an "idealized" MnP type structure. On this basis $(T-X)_{av.}$ would match a hypothetical $X-X$ bonding distance. Recalling the physical picture of "the strive" for four $T-T$ contacts as the *initiator* (Post. 3) and the non-bonding character of the shortest $X-X$ distances as the *liminator* (Post. 8) of the MnP type deformation, it seemed natural in Ref. 1 to introduce a 20% increased radius for X (relative to the bonding r_X) to ensure no $X-X$ bonding. The use of $r_T \approx r_X$ and the 20% criterion corresponds roughly to the expression $[(X-X)_{shortest}]^2 = \frac{3}{2}[(T-X)_{av.}]^2$, which is equivalent to formula No. [VI] and on the introduc-

tion of Post. 7 gives $x_X \approx 0.20$, matching the experimental facts.

These considerations, of course, suffer from the weaknesses inherent in all oversimplified models. Using tabulated values for atomic radii, considerations of the MnP type series RuP-RuAs-RuSb would at first sight seem to suggest that the model is totally unrealistic. However, on introducing another simple concept, degree of ionicity, it is natural to claim that RuP is more ionic than RuSb.⁹ On this basis, $r_{Ru}(RuP) < r_{Ru}(RuSb)$ and $[r_P(RuP) - r_P(neutral)]/r_P(neutral) > [r_{Sb}(RuSb) - r_{Sb}(neutral)]/r_{Sb}(neutral)$. This approach also serves to emphasize the limited value of tabulated atomic radii to define *individual* atomic sizes.

It should also be warned against the use of the model to make conclusions on fundamental bonding properties. The significance of the geometrical model lies in singling out Post. 3 as an initiator and Post. 8 as a liminator for the NiAs \rightarrow MnP type deformation. The new data for RuSb and RhSb have not shaken this conclusion.

Acknowledgement. The authors are grateful to Prof. Stig Rundqvist, University of Uppsala for numerous stimulating discussions.

REFERENCES

1. Selte, K. and Kjekshus, A. *Acta Chem. Scand.* 27 (1973) 3195.
2. Hulliger, F. *Struct. Bonding (Berlin)* 4 (1968) 83.
3. Pfisterer, H. and Schubert, K. *Z. Metallkd.* 41 (1950) 358.
4. Holseth, H., Kjekshus, A. and Andresen, A. F. *Acta Chem. Scand.* 24 (1970) 3309.
5. Graeber, J. E., Baughman, R. J. and Morosin, B. *Acta Crystallogr. B* 29 (1973) 1991.
6. Franzen, H. F., Haas, C. and Jellinek, F. *Phys. Rev. B* 10 (1974) 1248.
7. Rundqvist, S. *Acta Chem. Scand.* 16 (1962) 287.
8. Rundqvist, S. and Nawapong, P. C. *Acta Chem. Scand.* 19 (1965) 1006.
9. Kjekshus, A. and Rakke, T. *Struct. Bonding (Berlin)* 19 (1974) 45.

Received November 2, 1976.

Compounds with the Marcasite Type Crystal Structure. XII.

Structural Data for RuP_2 , RuAs_2 , RuSb_2 , OsP_2 , OsAs_2 , and OsSb_2

ARNE KJEKSHUS,^a TROND RAKKE^a and ARNE F. ANDRESEN^b

^a Kjemisk Institutt, Universitetet i Oslo, Blindern, Oslo 3, Norway and ^b Institutt for Atomenergi, Kjeller, Norway

The FeS_2 -*m* type structures of RuP_2 , RuAs_2 , RuSb_2 , OsP_2 , OsAs_2 , and OsSb_2 have been refined by powder neutron diffraction/profile refinement methods, and a brief discussion of structural data for FeS_2 -*m* type compounds is presented.

In the second paper¹ of this series, structural data on a number of binary compounds with the FeS_2 -*m* (*m*=marcasite) type crystal structure were reported. During a continuation² of this study, it became evident that some of the positional parameters given in that paper may be in error (originating from possible shortcomings in the treatment of the X-ray powder diffraction data). Apart from the more "obvious" cases (see Ref. 2) of RuAs_2 and OsP_2 , it is difficult to pick out those of the compounds which may be burdened with significant inaccuracies and it was accordingly decided to reexamine them all, *viz.* RuP_2 , RuAs_2 , RuSb_2 , OsP_2 , OsAs_2 , and OsSb_2 (data for FeAs_2 , NiAs_2 , and NiSb_2 were included in Ref. 2).

EXPERIMENTAL

The compounds RuP_2 , RuAs_2 , RuSb_2 , OsP_2 , OsAs_2 , and OsSb_2 were prepared by heating stoichiometric quantities of the elements [Ru, Os, As, Sb (Johnson, Matthey & Co.), and P (Koch-Light Laboratories); all of purity 99.999%] in evacuated, sealed silica tubes. All neutron diffraction samples were heated at a maximum temperature of 1200 °C for one day, followed by gradual cooling to 600 °C over a period of one week. As demonstrated on small scale samples, this procedure ascertained homogeneity for all, and apart from the antimonides, no improve-

ment in crystallinity could be detected on repeating the heating cycle. For the phosphides and arsenides the present procedure differs from that outlined in Ref. 1 by a substantial increase in maximum temperature. This simple change has thus eliminated the rather time-consuming grinding and reannealing cycles earlier used.¹ The crystallinity of the small scale antimonide samples were found to improve slightly on reannealing at 1200 °C, but weighed against the risk of contaminating the comparatively large scale neutron diffraction samples, the only slight gain in sample perfection was considered insignificant.

Attempts have also been made to prepare (by the sealed silica capsule technique) FeS_2 -*m* type modifications of FeS_2 , CoS_2 , CoSe_2 , NiS_2 , NiSe_2 , NiTe_2 , CuS_2 (from lower chalcogenides and added chalcogen), and RuS_2 , RuSe_2 , RuTe_2 , OsS_2 , OsSe_2 , and OsTe_2 (from the elements). The total heating periods used (so far) amounts to 2–3 years at fixed temperatures in the range 120–240 °C for the sulfides, 220–280 °C for the selenides, and 260–360 °C for the tellurides. Except for RuTe_2 and OsTe_2 all endeavours have, however, been totally in vain; $\text{NiTe} + \text{Te}$ reacted to form the known $\text{Cd}(\text{OH})_2$ type phase, $\text{CuS} + \text{S}$ remained unreacted, and the others reacted (partly or completely) to their FeS_2 -*p* (*p*=pyrite) type modifications without showing any traces of FeS_2 -*m* type phases.

Some properties of the FeS_2 -*m* type modification of OsTe_2 have been reported earlier,^{2–4} and promising indications for its possible preparation in pure form were at hand.⁴ The supplementary information gained up to now can be summarized as follows. The FeS_2 -*m* type modification of OsTe_2 has been obtained only in admixture with the elements or its FeS_2 -*p* type modification depending on both temperature and annealing period. With the reaction periods and temperatures used here (see above), it appears that the FeS_2 -*m* type modification is the first one to be formed from

Table 1. Structural data for RuP₂, OsP₂, RuAs₂, OsAs₂, RuSb₂, and OsSb₂.

Notation	RuP ₂	OsP ₂	RuAs ₂	OsAs ₂	RuSb ₂	OsSb ₂
$a(\text{\AA})$	5.1169(12)	5.1012(14)	5.4279(7)	5.4115(15)	5.9514(10)	5.9411(10)
$b(\text{\AA})$	5.8915(11)	5.9022(13)	6.1834(8)	6.1900(16)	6.6743(12)	6.6873(12)
$c(\text{\AA})$	2.8709(7)	2.9183(8)	2.9685(6)	3.0127(7)	3.1790(7)	3.2109(7)
x	0.1617(7)	0.1634(10)	0.1700(7)	0.1701(9)	0.1812(6)	0.1848(7)
y	0.3727(5)	0.3723(6)	0.3666(5)	0.3671(5)	0.3590(5)	0.3596(6)
$d_1 =$	$T-X(\text{\AA}) \times 4$	2.371(3)	2.468(3)	2.477(4)	2.648(3)	2.639(3)
$d_2 =$	$T-X(\text{\AA}) \times 2$	2.347(3)	2.448(3)	2.452(3)	2.628(3)	2.644(4)
$l =$	$X-X(\text{\AA}) \times 1$	2.234(9)	2.248(12)	2.475(10)	2.869(12)	2.889(11)
$\theta_1 =$	$X-T-X(^{\circ}) \times 4$	87.79(10)	87.7(1)	87.94(10)	87.87(12)	88.34(11)
$\theta_2 = (\varphi_2 =)$	$X-T-X(^{\circ}) \times 4$	92.21(10)	92.3(1)	92.06(10)	92.13(12)	91.72(10)
	$X-T-X(^{\circ}) \times 2$	74.53(7)	75.8(1)	73.94(7)	74.93(9)	73.78(7)
$\varphi_1 =$	$X-T-X(^{\circ}) \times 2$	105.47(7)	104.2(1)	106.06(7)	105.07(9)	106.22(7)
	$T-X-T(^{\circ}) \times 2$	123.61(10)	123.6(1)	125.67(10)	125.35(11)	128.18(10)
$\varphi_2 = (\theta_2 =)$	$T-X-T(^{\circ}) \times 1$	74.53(7)	75.8(1)	73.94(10)	74.93(9)	73.78(7)
	$T-X-X(^{\circ}) \times 2$	109.18(12)	108.9(2)	108.56(12)	108.43(12)	107.83(11)
$\varphi_3 =$	$T-X-X(^{\circ}) \times 1$	111.54(17)	111.4(2)	109.65(16)	109.74(20)	106.88(14)
$\varphi_4 =$						106.00(16)

the elements, and as long as these are present, the FeS_2 - m type modification appears to be stabilized [present values for the unit cell dimensions: $a=5.2804(4)$ Å, $b=6.4018(4)$ Å, and $c=4.0481(3)$ Å]. As the reaction proceeds, the FeS_2 - p type modification of OsTe_2 appears in increasing amounts.

The reaction properties of RuTe_2 seem to be quite similar to those of OsTe_2 , except that its rate of formation is much lower under the same temperature conditions. No earlier report on

the FeS_2 - m type modification of RuTe_2 is found in the literature; its unit cell dimensions are: $a=5.271(1)$ Å, $b=6.387(2)$ Å, and $c=4.038(1)$ Å.

X-Ray powder diffraction data were obtained in a Guinier camera ($\text{CuK}\alpha_1$ radiation, $\lambda=1.54050$ Å; KCl as internal standard, $a=6.2919$ Å) and unit cell dimensions derived by applying the method of least squares. In addition to X-ray (and neutron) diffraction, evidence for sample homogeneity was also obtained by metallographic methods.

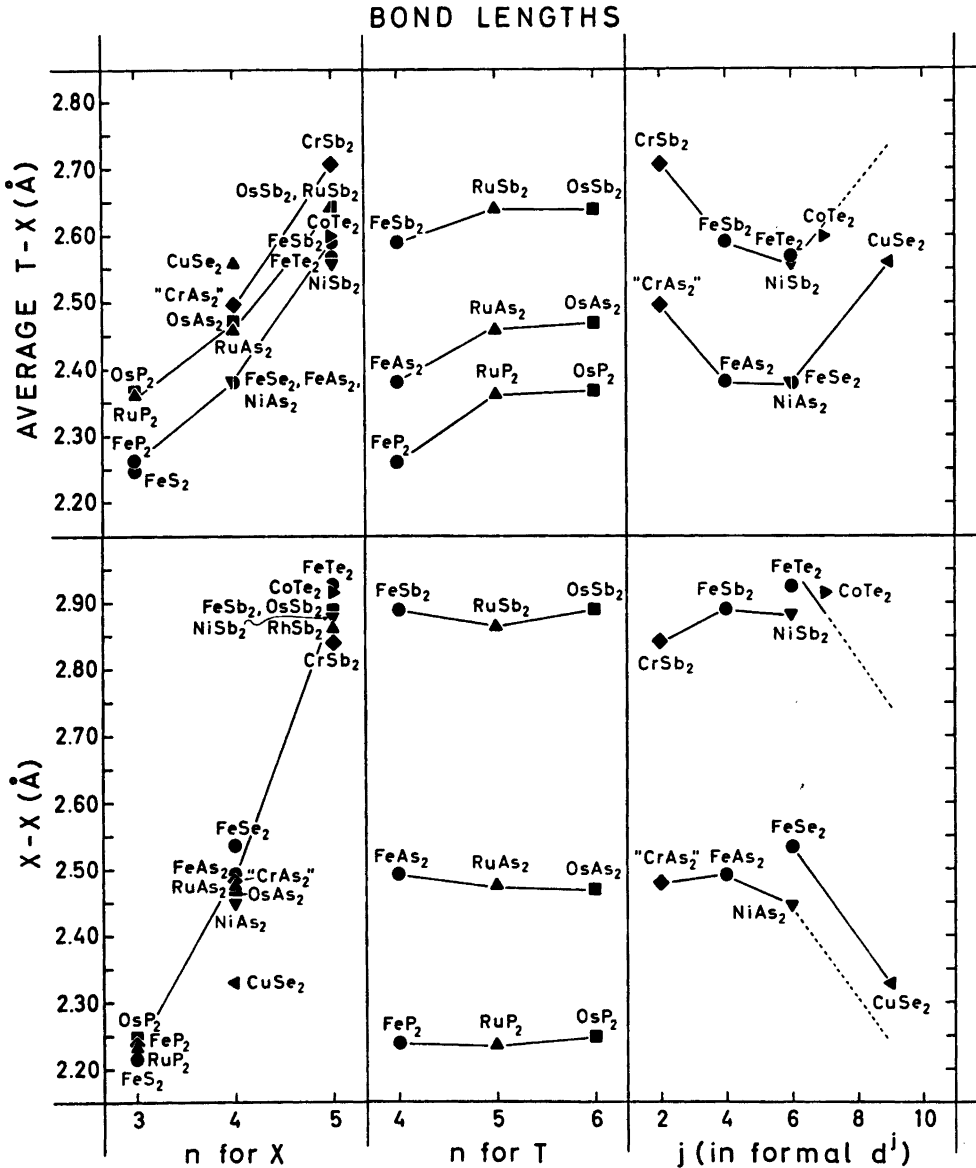


Fig. 1a. Dependence of bond lengths for compounds with FeS_2 - m type structure.

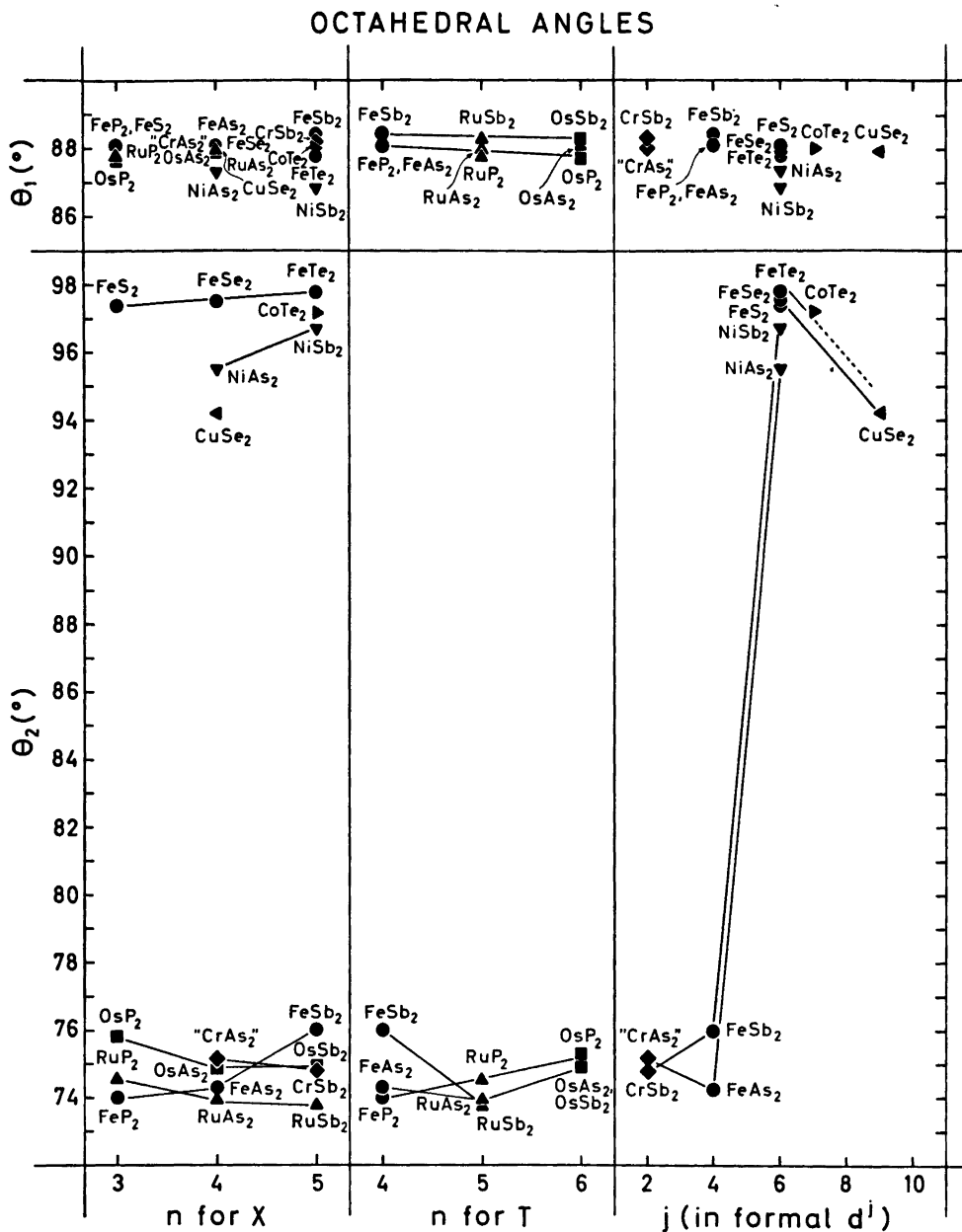


Fig. 1b. Dependence of octahedral angles for compounds with $\text{FeS}_2\text{-}m$ type structure.

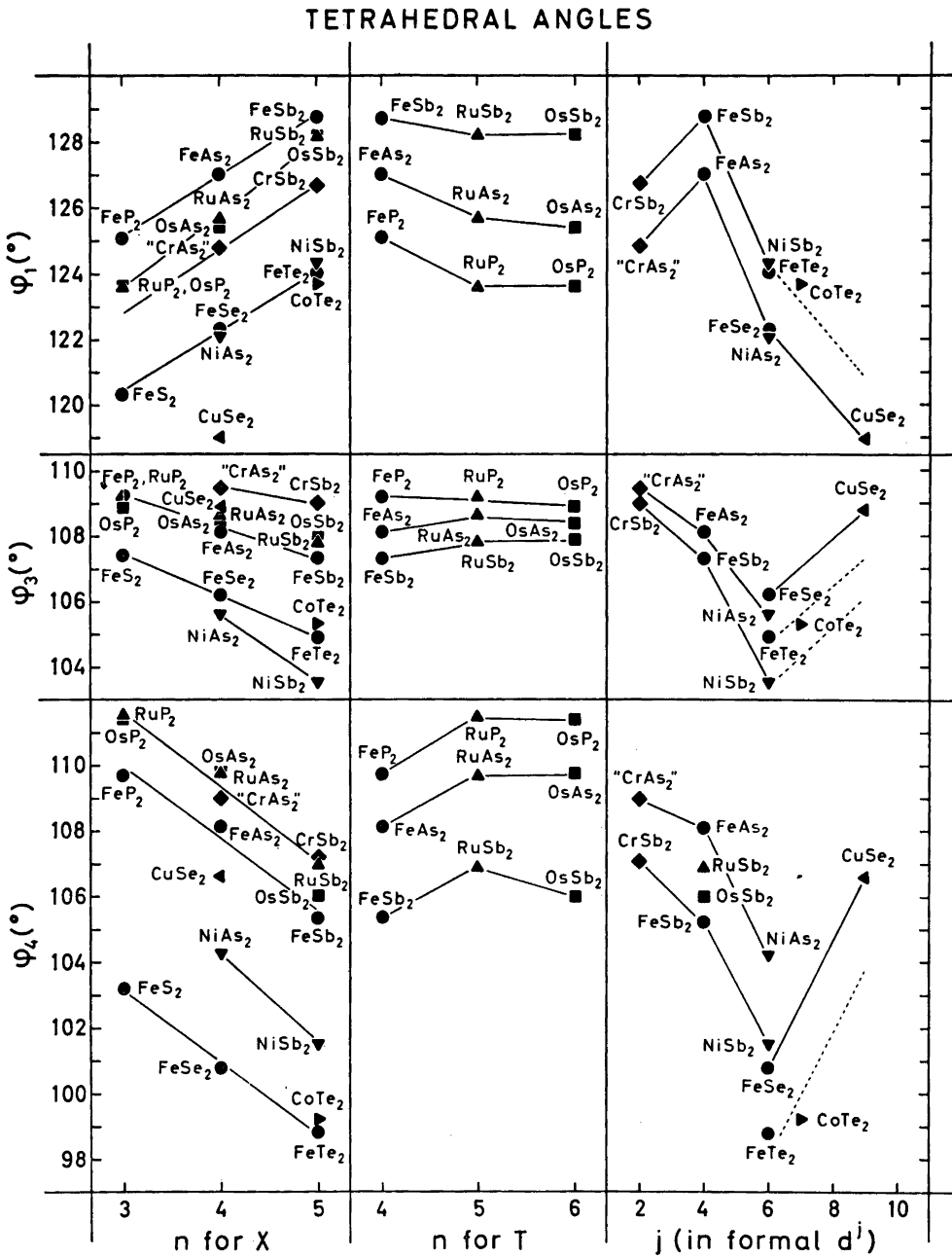


Fig. 1c. Dependence of tetrahedral angles for compounds with $\text{FeS}_2\text{-}m$ type structure.

Powder neutron diffraction data were collected at room temperature using cylindrical sample holders of vanadium. Neutrons of wavelength 1.877 Å were obtained from the Kjeller-reactor JEEP II. The nuclear scattering lengths ($b_{\text{Ru}} = 0.73$, $b_{\text{Os}} = 1.07$, $b_{\text{P}} = 0.51$, $b_{\text{As}} = 0.64$, and $b_{\text{Sb}} = 0.564$, all $\times 10^{-12}$ cm) were taken from Ref. 5. In all cases, the least squares profile refinement programme of Rietveld⁶ was applied in the final fitting of the variable parameters.

RESULTS AND DISCUSSION

The (orthorhombic) unit cell dimensions, positional parameters (x and y), and derived bonding interatomic distances and angles are listed in Table 1. The rather low values for the final neutron diffraction profile reliability factors (ranging between 2.1 and 4.3 %) and circumstantial evidence from a thorough study⁷ of the prototype compound, show that the assumption of space group $Pnmm$ is justified. (For further comments, see Refs. 2 and 7.)

Comparison of the positional parameters in Table 1 with those in Ref. 1 show that highly significant discrepancies occur for RuAs_2 (y) and OsP_2 (x), as singled out in advance.³ The earlier data¹ for RuP_2 (x) and OsSb_2 (x) are also somewhat erroneous. With these corrections, several interesting patterns are seen (Figs. 1 and 2) to emerge from the structural data for binary (TX_2 ; T = transition element, X = pnigogen or chalcogen) FeS_2 - m type compounds (Refs. 2, 7–11 and including unpublished data for “ CrAs_2 ” extrapolated

from $\text{Cr}_{1-x}\text{Fe}_x\text{As}_2$ ¹²). The illustrations do not include data for axes or axial ratios since this is comprehensively covered in Ref. 13.

The thin lines in Fig. 1 connect points of homological (with respect to T or X) series and serve the purpose of focusing attention on certain dependencies on the principal quantum numbers (n) for T or X , or j in formal d^j manifolds of T . Among the trends emerging from Fig. 1, we like to draw attention to the essentially class-wise correlation of the octahedral angle θ_2 , and the remarkable constancy of the octahedral angle θ_1 as opposed to the systematic variations of the tetrahedral angles φ_1 , φ_3 , and φ_4 . (The bond angle notations are defined in Table 1.) In Fig. 1b the behaviour of FeSb_2 with respect to θ_2 breaks the pattern, thus emphasizing once more (*cf.* Ref. 13 and references therein) the somewhat unique character of this compound.

A special variety among the correlations (Fig. 2) is that between the variable positional parameters x and y . This type of structural relationship was briefly taken up in Ref. 2 on what at first sight appears as an essentially proper semi-empirical geometrical basis. A closer examination unveils, however, that this approach³ is marred by some circular logic in the chain of arguments. The approximate, but no means perfect fit between the experimental points and the “empirically averaged” lines for the classes A and B (Fig. 1 in Ref. 2), merely demonstrates that there is a correlation between the structural variables x , y , a/b , and c/b . The correlations emphasized in Fig. 2 are somewhat different in character with approximately parallel lines connecting TX_2 combinations according to their positions in the Periodic System.

The unmistakable message contained in Fig. 2 has encouraged us to start a new search for geometrical conditions on the FeS_2 - m type atomic arrangement. In a reevaluation of geometrical aspects, a more thorough analysis of the FeS_2 - m type atomic architecture must be performed. Suitable starting points are the coordination polyhedra of T and X , but packing features are probably also of importance. An extension of the “ λ -approach” from Ref. 13 may prove useful in this respect.

The term geometrical considerations occurs frequently in the above presentation as well

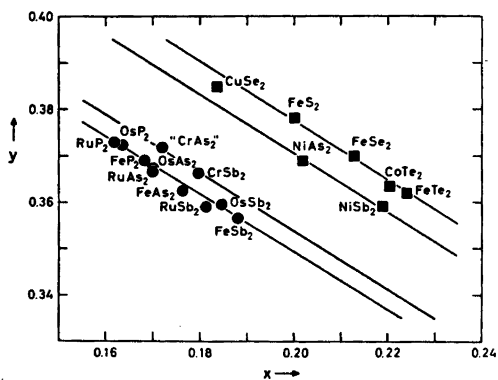


Fig. 2. Empirical correlations of positional parameters for compounds with FeS_2 - m type structure.

as in Ref. 13, and the importance of such considerations lies in that each postulate of geometrical models is expected to have parallel bonding interpretations. Further discussions on geometry and bonding in FeS_2 - m type compounds are postponed to forthcoming papers. Here, we would only like to comment briefly on two important aspects of this matter.

In a recent paper on MnP_4 , Jeitschko and Donohue¹⁴ propose that universal $T-T$ bonding is the stabilizing element in the class A, FeS_2 - m type structure (where, according to them, each T forms two σ and two π $T-T$ half-bonds) and the CoSb_2 type structure (one σ $T-T$ single bond per T). Unfortunately, these authors do not present any arguments in favour of their hypothesis, neither do they discuss arguments for its rejection. (Rejection of the earlier, commonly assumed $T-T$ bonding hypothesis for compounds with the CoSb_2 type structure has already been announced by both Goodenough¹⁵ and two of the present authors¹⁶ and will not be recapitulated here.) Apart from the comparatively short c axes for class A compounds, [ranging from 2.72 Å (FeP_2) to 3.27 Å (CrSb_2)], there is indeed no experimental evidence in favour of a regular type of $T-T$ bonding in these compounds, whereas several indications for the opposite conclusion can be advanced.*

(1) There are two unpaired electrons per Cr atom in CrSb_2 .¹¹

(2) The shortest $T-T$ distances ($=c$) in homological series $TP_2-TAs_2-TSb_2$ and $TS_2-TSe_2-TTe_2$ show consistent and virtually parallel dependencies (cf., e.g., Fig. 3 in Ref. 13) regardless of whether members of the classes A, A/B, or B are considered.

(3) The shortest $T-T$ distances in the class A series $TP_2-TAs_2-TSb_2$ ($T=\text{Fe, Ru, Os}$) vary by about 0.5 Å from P to Sb.

(4) The shortest $T-T$ distances in class A compounds equal the next shortest $X-X$ distances. This observation is particularly relevant for $X=\text{Sb}$ ($c=3.18$ to 3.27 Å) where Sb itself must be regarded as comparatively large

(shortest Sb-Sb for FeS_2 - m type compounds range from 2.84 to 2.89 Å, cf. Fig. 1a).

These and possibly other questions must be accounted for if $T-T$ bonding is to be accepted as the cause of the existence of class A, FeS_2 - m . Goodenough¹⁵ has made a valuable contribution in this connection by pointing out that the secret may be hidden in the $T-X$ bonds. As discussed in Ref. 16, Goodenough's *specialized* interpretation in terms of the enhanced $T-X$ bonding in class A relative to class B is to some extent contradicted by experimental evidence. Pursuing, however, his *general idea* of utilizing (for $T-X$ bonding) a d -orbital, awry-oriented with respect to a regular TX_6 octahedron, a mechanism is at hand for varying the octahedral angle θ_2 (Fig. 1b). According to the FeS_2 - m type geometry, this angle is intimately coupled to the length of the c axis which plays a major role in the assignment of classes.

Acknowledgement. The assistance of cand. mag. Per G. Peterzéns in the neutron diffraction measurements is greatly appreciated.

REFERENCES

- Holseth, H. and Kjekshus, A. *Acta Chem. Scand.* 22 (1968) 3284.
- Kjekshus, A., Rakke, T. and Andresen, A. F. *Acta Chem. Scand. A* 28 (1974) 996.
- Sutarno, Knop, O. and Reid, K. I. G. *Can. J. Chem.* 45 (1967) 1391.
- Kjekshus, A. and Rakke, T. *Acta Chem. Scand. A* 29 (1975) 443.
- The 1976-Compilation of the Neutron Diffraction Commission.*
- Rietveld, H. M. J. *Appl. Cryst.* 2 (1969) 65.
- Brostigen, G., Kjekshus, A. and Rømming, C. *Acta Chem. Scand.* 27 (1973) 2791.
- Dahl, E. *Acta Chem. Scand.* 23 (1969) 2677.
- Holseth, H. and Kjekshus, A. *Acta Chem. Scand.* 23 (1969) 3043.
- Brostigen, G. and Kjekshus, A. *Acta Chem. Scand.* 24 (1970) 1925.
- Holseth, H., Kjekshus, A. and Andresen, A. F. *Acta Chem. Scand.* 24 (1970) 3309.
- Kjekshus, A., Peterzéns, P. G., Rakke, T. and Andresen, A. F. *To be published.*
- Kjekshus, A. and Rakke, T. *Struct. Bonding (Berlin)* 19 (1974) 85.
- Jeitschko, W. and Donohue, P. C. *Acta Crystallogr. B* 31 (1975) 574.
- Goodenough, J. B. *J. Solid State Chem.* 5 (1972) 144.
- Kjekshus, A. and Rakke, T. *Acta Chem. Scand. A* 28 (1974) 1001.

Received November 19, 1976.

* Jeitschko and Donohue are aware of an apparent exception (from their $T-T$ bonding assumption), " $\text{Mo}_{2/3}\text{As}_2$ ", which they try to explain away. However, " $\text{Mo}_{2/3}\text{As}_2$ " is in reality non-existent (confused with FeAs_2 as demonstrated in Ref. 2) and represents no problem in this connection.

A Neutron Powder Diffraction Study of the κ -Phase in the Co-W-C System

A. HÅRSTA, T. JOHANSSON, S. RUNDQVIST and J. O. THOMAS

Institute of Chemistry, University of Uppsala, Box 531, S-751 21 Uppsala, Sweden

The crystal structure of the κ -(Co-W-C) carbide has been refined from neutron powder diffraction data using the Rietveld profile analysis method. The results obtained are as follows: space group $P6_3/mmc$ (No. 194), W(1) in $12k$: $x=0.2038(3)$, $z=0.0682(5)$; W(2) in $6h$: $x=0.5497(4)$; W(3) in $2a$; Co in $6h$: $x=0.8868(9)$; C(1) in $6g$; C(2) in $2c$. The $2c$ position is only 41 % occupied, suggesting the approximate formula $\text{Co}_3\text{W}_{10}\text{C}_{3.4}$. The unit cell dimensions for the sample investigated were: $a=7.8304(4)$ Å, $c=7.8361(6)$ Å.

The occurrence of a hexagonal phase with a composition corresponding approximately to the formula $\text{Co}_3\text{W}_{10}\text{C}_4$ was reported by Rautala and Norton,¹ who denoted this phase by the letter κ . The crystal structure of this carbide was examined by Schönberg² by X-ray powder diffraction methods. He proposed a structure with $P6_3/mmc$ symmetry, involving 12 W on a $12k$ position, 6 W and 6 Co distributed randomly between two $6h$ positions, 6 C on $6g$ and 2 C on $2c$. Pollock and Stadelmaier³ reported phase analytical results indicating a lower carbon content than that corresponding to Schönberg's formula, they thus suggested that the $2c$ position was vacant. In a series of studies, Nowotny, Benesovsky and coworkers⁴⁻⁷ have investigated a large number of phases with crystal structures closely related to that of κ -(Co-W-C). Drawing the analogy with all such phases, Rogl and Nowotny⁷ suggested that the $2a$ position in the κ -(Co-W-C) structure was filled with metal atoms.

In connection with recent studies of the Co-W-C system made by Johansson⁸ it was decided to examine the κ -(Co-W-C) structure more closely using neutron diffraction tech-

niques, particularly in view of the relatively large scattering length for carbon compared with that for tungsten and cobalt. The results of this study are reported in the present paper.

EXPERIMENTAL DETAILS

Preparation. The starting materials for the synthesis of Co-W-C alloys were: tungsten powder from H.C. Starck, Berlin, claimed purity 99.95 %; tungsten monocarbide from H. C. Starck, Berlin, claimed purity 99.9 %; cobalt sponge from Johnson, Matthey & Co. Ltd., London; less than 15 ppm metallic impurities. The components were mixed by wet grinding in benzene in a tungsten carbide ball-mill, pressed into pellets and heated (after evaporation of the benzene) in a graphite tube resistance furnace under a protective atmosphere of argon. The samples were contained in zirconia crucibles and heated at 1750 °C for periods of about 7 h. The sample used for neutron diffraction measurements weighed about 30 g and was carefully ball-milled. An X-ray powder diffraction examination showed the sample to contain traces of $(\text{Co,W})_6\text{C}$ and small amounts of tungsten metal.

X-Ray diffraction. Phase analyses and determinations of unit cell dimensions were made by X-ray powder diffraction. A Hägg-Guinier type camera (Philips XDC 700) with $\text{CrK}\alpha_1$ radiation was used (silicon internal calibration standard: $a=5.431065$ Å).⁹ Unit cell dimensions were refined by the least-squares method using an IBM 1800 computer and a local program CELNE.¹⁰

Neutron diffraction. The neutron powder data were collected at room temperature (~ 298 K) at the R2 reactor, Studsvik, Sweden, using a Ferranti four-circle diffractometer modified to operate as a powder instrument. The reactor beam from a radial channel was passed through a double-crystal monochromator¹¹ using the 220 planes of two copper crystals to give a wavelength of 1.56 Å and a flux

at the specimen of 10^6 neutrons $\text{cm}^{-2} \text{s}^{-1}$. The specimen was contained in a 12 mm diameter vanadium tube of length 4 cm. The volume of powder irradiated was approximately 3.5 cm^3 . The step-scan covered the range $10-103^\circ$ (in 2θ) in steps of 0.08° . Measuring time per point was about 12 min.

The presence of cobalt in the specimen meant that absorption was not negligible (experimental μR was 0.40). No correction for absorption was made, however. The estimated effect of this neglect on the refined value of the overall temperature factor is to increase it from 0.16 to 0.25 \AA^2 . The effect on refined positional and occupancy parameters is likely to be insignificant.

The presence of $(\text{Co}, \text{W})_6\text{C}$ and tungsten impurities resulted in troublesome additional peaks in the profile. The $(\text{Co}, \text{W})_6\text{C}$ peaks were treated by calculating the 2θ regions most seriously affected and removing them from the profile. The tungsten peaks were treated partly in the same way and partly by making a run on pure tungsten and subtracting its estimated contributions from the profile.

STRUCTURE REFINEMENT

The structure refinements were made on an IBM 370/155 computer at the Uppsala Data Center using a local modification NREF¹² of the full-matrix least-squares neutron powder profile analysis program of Rietveld.¹³ The program assumes a Gaussian contribution from each reflection contributing to the profile, and minimizes the quantity $\chi^2 = \sum_i w_i |y_i(\text{obs}) - \frac{1}{c} y_i(\text{calc})|^2$, where w_i is the weighting function applied to y_i , the number of counts at 2θ (after subtraction of background), and c is a scale factor. Three R values are calculated by the program:

$$R_I = \frac{\sum_k |I_k(\text{obs}) - \frac{1}{c} I_k(\text{calc})|}{\sum_k I_k(\text{obs})}$$

$$R_{\text{profile}} = \frac{\sum_i |y_i(\text{obs}) - \frac{1}{c} y_i(\text{calc})|}{\sum_i |y_i(\text{obs})|}$$

$$R_{\text{profile}}(\text{weighted}) = \left[\frac{\sum_i w_i |y_i(\text{obs}) - \frac{1}{c} y_i(\text{calc})|^2}{\sum_i w_i |y_i(\text{obs})|^2} \right]^{\frac{1}{2}}$$

where I_k denotes the integrated intensity of a reflexion k . R_I can be compared with the more familiar $R(F^2)$ of single crystal work.

An initial structure refinement was made using Schönberg's² positional parameters with W in $12k$, $6h$ and $2a$; Co in $6h$ and C in $6g$. The refinement converged with the R values 0.117, 0.163 and 0.166.

In a subsequent series of refinements, the $2c$ position was assumed to be occupied by carbon atoms and the occupancy allowed to refine. The agreement between observed and calculated intensities now improved considerably, with new R values: 0.078, 0.132 and 0.136. The degree of occupation for the $2c$ position was found to be 0.415(17). In further attempts to improve the structural model, the occupancies of the $12k$, $6h$ and $2a$ positions were also refined, but the results indicated no significant deviation from the metal atom distribution assumed initially.

The final structural data are presented in Table 1. These values were obtained from a refinement, where the refined parameters were the following: (a) *profile parameters*: halfwidth parameters (3), 2θ zero-point (1), wavelength (1). (b) *structural parameters*: scale factor (1), positional parameters (4), $2c$ occupancy (1), overall isotropic temperature factor (1). The scattering lengths used were $b_{\text{Co}} = 0.25 \times 10^{-14} \text{ m}$, $b_{\text{W}} = 0.48 \times 10^{-14} \text{ m}$ and $b_{\text{C}} = 0.665 \times 10^{-14} \text{ m}$.¹⁴ The profile fit obtained is shown in Fig. 1.

Table 1. Structure data for κ -(Co-W-C). Space group $P6_3/mmc$ (No. 194); $a = 7.8304(4) \text{ \AA}$, $c = 7.8361(6) \text{ \AA}$. Overall temperature factor $B = 0.16(5) \text{ \AA}^2$.

Atom	Position	x ($y = 2x$)	z	Occupancy
W(1)	$12k$	0.2038(3)	0.0682(5)	1
W(2)	$6h$	0.5497(4)	$\frac{1}{2}$	1
W(3)	$2a$	0	0	1
Co	$6h$	0.8868(9)	$\frac{1}{2}$	1
C(1)	$6g$	$\frac{1}{2}$	0	1
C(2)	$2c$	$\frac{1}{2}$	$\frac{1}{2}$	0.415(17)

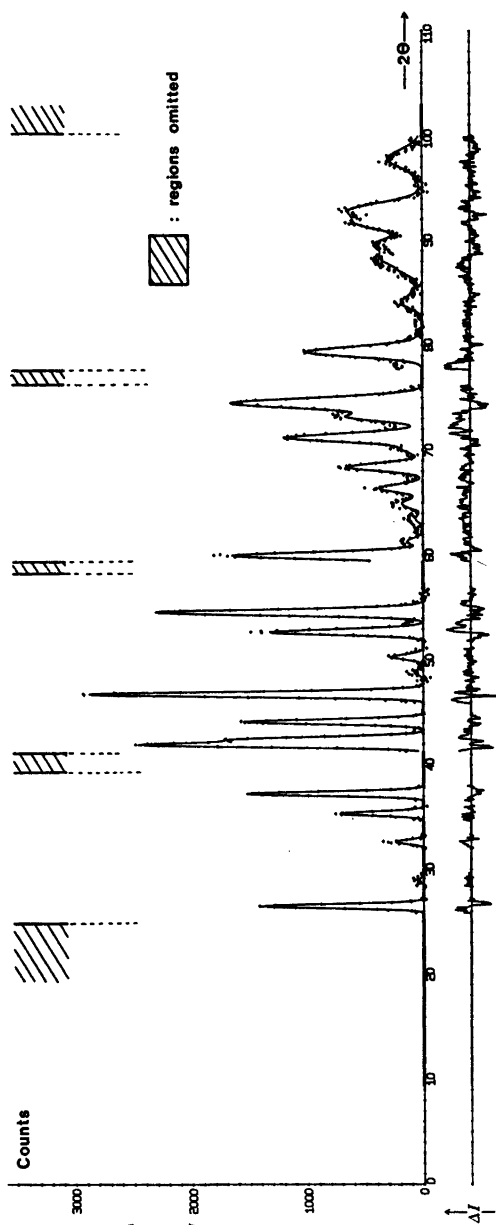


Fig. 1. Neutron powder profile fit for κ -(Co-W-C).

DISCUSSION OF THE STRUCTURE

A projection of the κ -(Co-W-C) structure along the hexagonal axis is shown in Fig. 2. The carbon atoms have only tungsten atoms as their nearest neighbours: in an octahedral

configuration for the $6g$ carbon atoms, and in a trigonal prismatic configuration for the $2c$ carbon atoms. The tungsten atoms situated at $2a$ are surrounded icosahedrally by six $12k$ tungsten atoms and six cobalt atoms. The metal atoms at the $12k$ and $6h$ positions have more irregular coordinations. A list of interatomic distances is given in Table 2.

Although the κ -(Co-W-C) structure has been the subject of much discussion in the past, the only experimental basis was Schönberg's² X-ray powder diffraction analysis reported in 1954. Schönberg succeeded in determining the positional parameters for the $12k$ and the two $6h$ type metal atoms but failed to observe that the $2a$ position is also filled with metal atoms. The missing $2a$ atoms probably forced him to assume a random distribution of cobalt and tungsten atoms on the two $6h$ positions, in order to obtain a reasonable agreement between observed and calculated intensities. It should be pointed out that the analysis of the powder diffraction data is particularly difficult because of the numerous overlaps among the lines, brought about by the nearly equal lengths of the a and the c axes.

As regards the number and distribution of the carbon atoms in the structure, Schönberg's proposal was based solely on considerations of the available space in the unit cell, combined with the value for the carbon content as determined by chemical analysis.

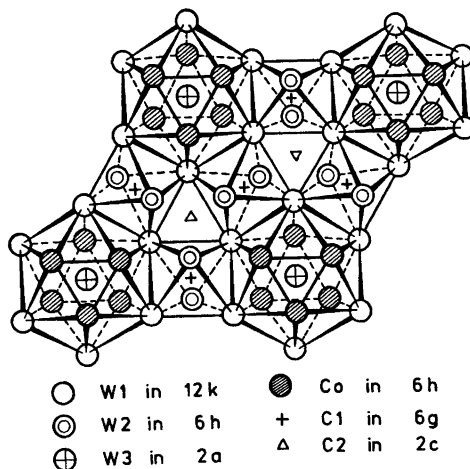


Fig. 2. The structure of κ -(Co-W-C) projected along the hexagonal axis.

Table 2. Interatomic distances (Å) in κ -(Co-W-C). Distances up to 3.8 Å are included. When greater than one, the number of equivalent distances from a central atom to its neighbours precedes the notation for the neighbouring atom.

W(1)–2C(1)	2.124(2)	W(2)–2C(1)	2.072(2)
C(2)	2.262(4)	2Co	2.587(6)
Co	2.780(5)	2W(2)	2.746(10)
2Co	2.790(5)	C(2)	2.935(6)
W(3)	2.815(4)		
W(1)	2.849(9)	W(3)–6Co	2.489(4)
2W(2)	2.928(5)		
2W(1)	2.964(5)	Co–2Co	2.660(10)
2W(2)	3.006(5)	4C(1)	3.334(6)
2W(1)	3.043(5)		
		C(1)–2C(2)	2.991(1)

In a general survey of alloy structures, Kripyakevich^{15,16} pointed out the close relationship between the metal atom lattices in κ -(Co-W-C) and Mn_3Al_{10} ,¹⁷ the icosahedral hole at $2a$ being filled with aluminium atoms in Mn_3Al_{10} but empty in the κ -carbide according to Schönberg. This relationship was further emphasized by Reiffenstein, Nowotny and Benesovsky,⁴ who prepared a number of κ -carbides in quaternary systems of the types Mo-(Mn, Fe, Co, Ni, Cu)-Al-C and W-(Mn, Fe)-Al-C. In the structures of these carbides, Reiffenstein *et al.* assumed that the icosahedral $2a$ position is occupied by aluminium atoms, while the carbon atoms occupy the octahedral $6g$ position, leaving the trigonal prismatic $2c$ position empty. In later studies, Rogl, Nowotny and Benesovsky⁵⁻⁷ discovered the occurrence of κ -type phases composed of only transition metal components in many of the ternary systems {Zr, Hf}-(Mo, W)-{Fe, Co, Ni}. They were also able to identify a number of κ -borides and κ -oxides in the systems {Zr, Hf}, {Mo, W, Re, Os}-B and {Zr, Hf}-{Mo, W, Re}-O. A single crystal structure determination of κ -(Hf-Mo-B) gave the following results:⁸ the $12k$ position is occupied by hafnium atoms, the distribution of hafnium and molybdenum atoms on the two $6h$ positions is completely ordered, molybdenum atoms occupy the $2a$ position, and the boron atoms occupy the $2c$ position. For the κ -phases formed by metallic components only, a distribution of the atoms similar to that in the κ -borides was assumed, with iron, cobalt or nickel replacing the boron atoms on the $2c$ site. This suggestion was supported⁸ by qualitative powder diffraction

intensity data for Hf_3Mo_4Co . The structures of these phases are accordingly close counterparts of the Co_4Al_{10} structure,¹⁸ where, in contrast to Mn_3Al_{10} , the $2c$ position is also filled. For the κ -oxides, on the other hand, Rogl *et al.* suggested that the $2c$ position is empty, and the oxygen atoms occupy only the octahedral $6g$ position.

By analogy with all these κ -phases, Rogl and Nowotny⁷ proposed that the ternary κ -carbides also have a metal lattice of the Mn_3Al_{10} type, with the icosahedral $2a$ hole filled, and an ordered distribution of the two types of metal atom on the two $6h$ sites. As far as the carbon atoms are concerned, Rogl and Nowotny observed that a situation intermediate between the boride and the oxide structures is conceivable, but they favoured a distribution of the carbon atoms on the octahedral $6g$ site exclusively.

The present results are in good agreement with the proposal by Rogl and Nowotny regarding the Mn_3Al_{10} -type metal sublattice. The neutron diffraction data clearly demonstrate that the $2a$ icosahedral holes are filled with tungsten atoms, and the ordered distribution of the tungsten and cobalt atoms on the $6h$ positions is also evident. The ordered distribution provides a near environment of tungsten atoms only about the carbon atoms. This conforms with the well-known rule for carbides in steel and other transition metal alloys: the carbon atoms tend to be associated with those metal atoms which have the lowest group number in the periodic table.

While the neutron data show clearly that the $6g$ position is filled with carbon atoms, the

interpretation of the scattering power associated with the 2c position is less definitive. Assuming carbon atoms in 2c, the scattering power observed corresponds to about 41 % occupation. The structure would then contain carbon atoms in both octahedral and trigonal prismatic coordination simultaneously. This is perhaps not surprising, since octahedral coordination occurs in W_2C , and trigonal prismatic coordination in WC. The W-C distances for the 6g carbon atoms agree closely with those in W_2C , while the W-C distances for carbon atoms in 2c are appreciably larger than those in WC. This difference might be associated with the vacancy formation on the 2c site.

If, on the other hand, the scattering power at 2c were due to cobalt atoms, full occupancy has to be assumed. The corresponding W-Co distances would then be abnormally short, and furthermore, the W/Co atomic ratio in the carbide would be 2.5. In all previous determinations of the W/Co ratio in κ -(Co-W-C),¹⁻³ it has been found to be 3 or larger, and recent microprobe measurements⁸ have given values of the order of 3.5. It is conceivable that higher W/Co ratios might be obtained through a partial W/Co substitution on the 6h cobalt site, but the present neutron diffraction data do not support this hypothesis.

Accordingly, the safest conclusion seems to be that the 2c position is partially occupied by carbon atoms. Although less likely, the possibility of a 2c occupation by a mixture of carbon and cobalt atoms cannot be entirely ruled out, however.

It should be mentioned that κ -(Co-W-C) has a range of homogeneity.⁸ This is indicated by small but significant differences in lattice parameters observed for this carbide between alloys from the various two- and three-phase areas surrounding the κ -phase in the Co-W-C equilibrium diagram. The variations in composition may be connected with a varying carbon atom occupation of 2c, with Co/W substitution in the metal lattice, or perhaps with both mechanisms operating simultaneously. In this context, an interesting observation by Rogl *et al.*⁶ is worth mentioning. For the κ -phases formed between transition metal components only, the unit cell volumes are abnormally small by comparison with the corresponding κ -borides, where iron, cobalt

and nickel atoms have been replaced by boron atoms on the 2c position. Furthermore, the unit cell volumes for iron-, cobalt-, and nickel-containing κ -phases increase in the order mentioned, while a decrease should be expected judging from the normal size for iron, cobalt and nickel atoms. A similar situation occurs among the κ -carbides, where κ -(Fe-W-C)⁸ has a smaller unit cell volume than κ -(Co-W-C).

In order to investigate these problems in more detail, a study of κ -(Fe-W-C) has been started using both diffraction methods and ⁵⁷Fe Mössbauer spectroscopy. The latter technique will hopefully provide additional structural information not accessible by X-ray or neutron diffraction measurements.

Acknowledgement. Financial support from the Swedish Natural Science Research Council is gratefully acknowledged.

REFERENCES

1. Rautala, P. and Norton, J. T. *Trans. AIME* 194 (1952) 1045.
2. Schönberg, N. *Acta Metall.* 2 (1954) 837.
3. Pollock, C. B. and Stadelmaier, H. H. *Metall. Trans.* 1 (1970) 767.
4. Reiffenstein, E., Nowotny, H. and Benesovsky, F. *Monatsh. Chem.* 97 (1966) 499.
5. Rogl, P., Nowotny, H. and Benesovsky, F. *Monatsh. Chem.* 102 (1971) 971.
6. Rogl, P., Nowotny, H. and Benesovsky, F. *Monatsh. Chem.* 104 (1973) 182.
7. Rogl, P. and Nowotny, H. *Monatsh. Chem.* 104 (1973) 1497.
8. Johansson, T. *To be published.*
9. Deslattes, R. D. and Henins, A. *Phys. Rev. Lett.* 31 (1973) 972.
10. Ersson, N. O., University of Uppsala. *Unpublished.*
11. Stedman, R., Almqvist, L., Raunio, G. and Nilsson, G. *Rev. Sci. Instrum.* 40 (1969) 249.
12. Thomas, J. O. Institute of Chemistry, University of Uppsala, Sweden, Publ. No. UUIC-B13-9.
13. Rietveld, H. M. *J. Appl. Crystallogr.* 2 (1969) 65.
14. Bacon, G. E. *Acta Crystallogr. A* 28 (1972) 357.
15. Kripyakevich, P. I. *Zh. Strukt. Khim.* 4 (1963) 117.
16. Kripyakevich, P. I. *Zh. Strukt. Khim.* 4 (1963) 282.
17. Taylor, M. A. *Acta Crystallogr.* 12 (1959) 393.
18. Bradley, A. J. and Cheng, C. S. *Z. Kristallogr. A* 99 (1938) 480.

Received November 26, 1976.

Alkaline Cleavage of β -D-Xylofuranosides

HARRI LÖNNBERG

Department of Chemistry and Biochemistry, University of Turku, SF-20500 Turku, Finland

The rate constants for the hydrolysis of a few 3- and 4-substituted phenyl β -D-xylofuranosides have been measured in aqueous sodium hydroxide solutions of various concentrations. The formal kinetics followed are interpreted to suggest that the alkaline cleavage of these compounds proceeds by a pre-equilibrium formation of an anionic intermediate which undergoes a unimolecular rate-limiting decomposition. The equilibrium constants for the initial ionization and the first-order rate constants for the subsequent heterolysis have been calculated. The effects of the polar properties of the aglycon group on the values of these quantities suggest that the reactive species is the 2-oxyanion of the substrate. The possibility that the rate-limiting step would involve a spontaneous heterolysis of the 2-oxyanion to form a phenoxide and a cyclic oxocarbenium ion is discussed.

Although acetals are normally stable in aqueous base solutions, certain hemicyclic acetals exhibit a marked lability towards alkali. Especially some glycosides are cleaved quite readily under alkaline conditions.¹ The mechanisms for these reactions have been the subject of considerable interest, mainly because simple glycosides are excellent model compounds for the study of the degradation of polysaccharides. For the alkaline hydrolysis of glycopyranosides several tentative mechanisms have been proposed. Compounds with a hydroxyl group at C-2 *trans* to the aglycon group have been repeatedly suggested to react by neighboring group participation of the ionized C-2 hydroxyl function to yield a 1,2-epoxide intermediate, all subsequent reactions being fast.¹⁻⁴ In contrast, the mechanism for the hydrolysis of the corresponding *cis*-1,2-glycosides is more obscure. According to the suggestions made, either C-4 or C-6 oxyanion

can act as an intramolecular catalyst,^{1,3} or a nucleophilic substitution by hydroxide ion may take place at the anomeric or aromatic carbon.^{1,5} For the cleavage of 4-nitrophenyl α -D-glucopyranoside a novel mechanism has been presented, which involves an intramolecular attack by the C-2 oxyanion on C-1 of the phenoxy group.^{6,7}

Glycofuranosides are cleaved by alkali even more rapidly than glycopyranosides, but the experimental data concerning the mechanisms for these reactions are quite limited. Janson and Lindberg⁸ reported the rate constants for the hydrolysis of several methyl aldofuranosides in aqueous 10 % sodium hydroxide solution at 443 K, and suggested that the somewhat higher reactivities of *trans*-1,2-glycosides compared to their *cis*-isomers would be the result of neighboring group participation as in the hydrolysis of glycopyranosides. To elucidate the mechanisms for the alkaline cleavage of aryl aldofuranosides, the hydrolysis of some 3- and 4-substituted phenyl β -D-xylofuranosides has been investigated in this work.

RESULTS AND DISCUSSION

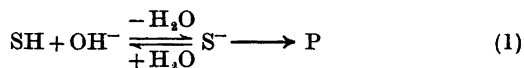
The first-order rate constants for the hydrolysis of the substituted phenyl β -D-xylofuranosides in aqueous sodium hydroxide solutions of various concentrations are collected in Table 1. For all compounds studied the value of the reaction order with respect to base concentration deviates appreciably from unity. For example, in the case of the 4-cyanophenyl derivative the apparent second-order rate constant, $k(\text{obs})/[\text{OH}^-]$, at a hydroxide ion concentration of 0.10 mol dm⁻³ is only half the value obtained in a 0.01 mol dm⁻³ solution, the ionic

Table 1. First-order rate constants ($k/10^{-4} \text{ s}^{-1}$) for the hydrolysis of substituted phenyl β -D-xylofuranosides in aqueous sodium hydroxide solutions of different concentrations ^a at 343.15 K.

OH^- mol dm ⁻³	Substituent in the phenyl group				
	None	4-Chloro	3-Chloro	4-Acetyl	4-Cyano
0.01	0.1379(19)	0.606(4)	1.359(21)	9.95(9)	18.84(19)
0.02	0.278(3)	1.090(18)	2.62(2)	19.96(27)	35.3(3)
0.03	0.397(4)	1.578(15)	3.87(4)	27.9(2)	48.1(6)
0.04	0.530(9)	2.05(3)	5.18(9)	36.1(2)	61.7(8)
0.05	0.639(7)	2.42(3)	5.98(9)	39.4(5)	70.6(10)
0.06	0.739(9)	2.83(2)	6.91(8)	48.4(2)	76.4(8)
0.07	0.862(10)	3.26(3)	7.78(7)	50.4(8)	88.1(10)
0.08	0.953(10)	3.73(3)	8.55(12)	54.1(4)	97.6(8)
0.09	1.030(11)	3.93(5)	8.84(11)	65.4(7)	103.5(14)
0.10	1.140(14)	4.27(5)	9.94(7)	65.6(5)	107.4(12)

^a The ionic strength was adjusted to 0.10 mol dm⁻³ with sodium chloride.

strength of which has been adjusted to 0.10 mol dm⁻³ with sodium chloride (Fig. 1). A difference of this magnitude is far too large to be accounted for by specific salt effects. Addition of sodium chloride in the reaction mixture (0.5 mol dm⁻³), for example, reduced the observed rate constant by less than 10%. The observed deviation from a linear dependence of $k(\text{obs})$ on $[\text{OH}^-]$ rather suggests that the alkaline cleavage of phenyl β -D-xylofuranosides proceeds *via* formation of a kinetically significant intermediate. For instance, a mechanism involving an initial rapid ionization of the substrate (eqn. 1) agrees with the kinetic data in Table 1. The rate-law for this reaction



can be expressed by eqn. (2) where K denotes the equilibrium constant for the formation of

$$\frac{d[\text{P}]}{dt} = \frac{kK[\text{OH}^-][\text{S}]}{1 + K[\text{OH}^-]} \quad (2)$$

the anionic intermediate, S^- , and k stands for the first-order rate constant for the unimolecular decomposition of this species. $[\text{S}]$ is the sum of $[\text{SH}]$ and $[\text{S}^-]$ at any given moment. When the initial substrate concentration is negligible compared to the hydroxide ion concentration, the reaction obeys first-order kinetics, and the observed rate constant, $k(\text{obs})$, is of the form (3). Accordingly, $k(\text{obs})$ is linearly

$$k(\text{obs}) \leq \frac{kK[\text{OH}^-]}{1 + K[\text{OH}^-]} \quad (3)$$

related to $[\text{OH}^-]$ when the product $K[\text{OH}^-]$ is much less than unity, and levels off to a constant value when $K[\text{OH}^-]$ becomes greater than unity. Eqn. (3) can also be written in the form (4). In other words, a plot of $[\text{OH}^-]/k(\text{obs})$ vs. $[\text{OH}^-]$ should yield a straight line if

$$\frac{[\text{OH}^-]}{k(\text{obs})} = \frac{1}{k} [\text{OH}^-] + \frac{1}{kK} \quad (4)$$

the mechanism leading to eqn. (1) is followed. Fig. 2 clearly shows that this is the case in the hydrolysis of 4-cyanophenyl β -D-xylofuranoside

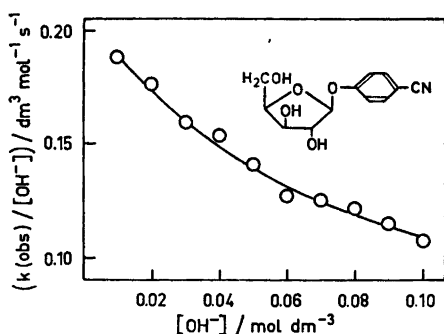


Fig. 1. The apparent second-order rate constants, $k(\text{obs})/[\text{OH}^-]$, at 343.15 K for the alkaline hydrolysis of 4-cyanophenyl β -D-xylofuranoside plotted against the hydroxide ion concentrations of the reaction solution.

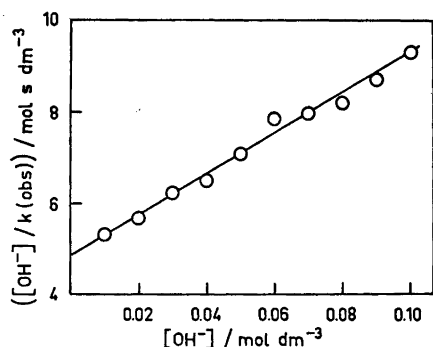


Fig. 2. Reciprocals of the apparent second-order rate constants, $k(\text{obs})/[\text{OH}^-]$, at 343.15 K for the alkaline hydrolysis of 4-cyanophenyl β -D-xylofuranoside plotted against the hydroxide ion concentration of the reaction solution.

side. The other xylosides investigated exhibit a similar kinetic behavior, but the ratio of the slope and intercept of eqn. (4) decreases systematically with the decreasing electronegativity of the aglycon group.

The fact that the formal kinetics of mechanism (1) is followed does not prove, however, that the anionic form of substrate would lie on the reaction pathway. Mechanisms involving a nucleophilic attack of hydroxide ion at the anomeric or aromatic carbon of the unionized substrate (eqn. 5) also lead to a linear relationship between $[\text{OH}^-]/k(\text{obs})$ and $[\text{OH}^-]$ described by eqn. (6). Here K has the same meaning as in eqn. (2), but k denotes the second-order rate constant for the decomposition of SH. However, for the following reasons these



$$\frac{[\text{OH}^-]}{k(\text{obs})} = \frac{K}{k} [\text{OH}^-] + \frac{1}{k} \quad (6)$$

routes seem less probable.

If eqn. (5) were the correct description for the alkaline cleavage of aryl β -D-xylofuranosides, the reciprocal intercepts of plots (6) would give the partial rate constants k . By applying this method to the kinetic data concerning the hydrolysis of the 4-cyanophenyl derivative a value of $0.2 \text{ dm}^3 \text{ mol}^{-1} \text{ s}^{-1}$ is obtained for k at 343.15 K. Obviously a value of this magnitude is far too large to be con-

sistent with an aromatic nucleophilic substitution. For comparison, the second-order rate constants for the hydrolyses of 4-nitrophenyl 2-O-methyl- β -D-galacto- and 2-O-methyl- α -D-mannopyranosides proceeding by this pathway can be estimated to be of the order $10^{-5} \text{ dm}^3 \text{ mol}^{-1} \text{ s}^{-1}$ at this temperature.^{2c} Accordingly, replacement of the leaving 2-O-methyl-glycopyranosyloxy anion by glycofuranosyloxy anion should accelerate the reaction by a factor of 10^4 . This seems highly improbable, since the polar characters and steric requirements of both anions are quite similar. In fact, the rate-enhancing effect should be even greater, because a 4-nitro substituent facilitates nucleophilic attack on C-1 more than a 4-cyano group does. Similar arguments can be presented against the mechanism involving a direct displacement of the substituted phenoxy group by hydroxide ion. Of the glycosides studied, phenyl α -D-glucopyranosides with electropositive or weakly electronegative substituents in the aglycon group have been suggested to react by this mechanism.¹ Their reactivity is, however, low compared to the corresponding β -D-xylofuranosides. For example, the hydrolysis of the unsubstituted derivative exhibits the second-order rate constant of $3 \times 10^{-8} \text{ dm}^3 \text{ mol}^{-1} \text{ s}^{-1}$ at 343.15 K.⁵ For the alkaline cleavage of more reactive *trans*-1,2-glycosides other mechanisms have been proposed. Because it is known that nucleophilic attack on five-membered rings occurs usually about a hundred times faster than on six-membered rings with equal electronic properties and steric hindrances,⁹ a value of $10^{-6} - 10^{-5} \text{ dm}^3 \text{ mol}^{-1} \text{ s}^{-1}$ would be expected at this temperature for the partial rate constant k (eqn. 6) of the hydrolysis of phenyl β -D-xylofuranoside. However, the data in Table 1 give a value of $1.4 \times 10^{-3} \text{ mol}^{-1} \text{ s}^{-1}$. The most obvious explanation for this discrepancy is that the pathway involving nucleophilic attack by hydroxide ion at the anomeric carbon is not the major one in the hydrolysis of aryl β -D-xylofuranosides. Some support for this claim comes from the finding that iodide ion (0.5 mol dm^{-3}) did not exert any rate-enhancing effect on the cleavage of the 4-cyanophenyl derivative, though it sometimes is a more powerful nucleophile than hydroxide ion.¹⁰

On the basis of the preceding discussion it seems probable that the alkaline cleavage of

Table 2. Ionization constants (see eqn. 7) for 3- and 4-substituted phenyl β -D-xylofuranosides in water at 343.15 K and the first-order rate constants for the decomposition of the corresponding 2-oxyanions at the same temperature.

Substituent in the phenyl group	K^a $\text{dm}^3 \text{ mol}^{-1}$	k^a 10^{-3} s^{-1}
None	2.7(2)	0.54(3)
4-Chloro	4.1(4)	1.46(12)
3-Chloro	4.8(5)	3.0(2)
4-Acetyl	6.7(9)	16.3(16)
4-Cyano	9.0(6)	23(1)

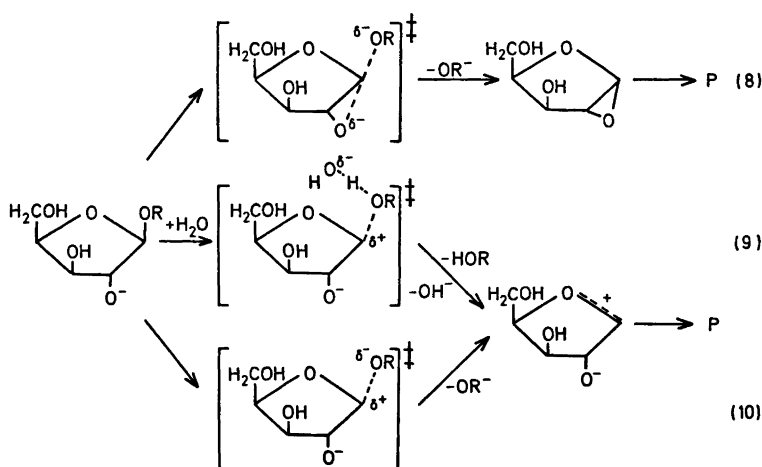
^a Calculated by eqn. (4) from the data in Table 1.

aryl β -D-xylofuranosides would proceed *via* pre-equilibrium formation of an anionic intermediate. One possible way to elucidate the structure of this species is to study the effects that polar substituents in the aglycon group exert on the initial ionization of the substrate. According to eqn. (4) the equilibrium constant, K , for this stage (eqn. 7) is equal to the ratio of the slope and intercept of the plot of $[\text{OH}^-]/K = [\text{S}^-]/[\text{SH}][\text{OH}^-]$ (7)

$k(\text{obs})$ vs. $[\text{OH}^-]$. Table 2 summarizes the results obtained by this method for the β -xylosides studied. They are of the order expected for the dissociation of a hydroxyl group in a carbohydrate molecule.¹¹ Although the experimental errors in the kinetically determined ionization constants are rather large,

it is clearly seen that electron-attracting substituents in the phenoxy group facilitate the pre-equilibrium dissociation of phenyl β -D-xylofuranosides. The only ionizable group in these compounds, the acidity of which would be expected to depend markedly on the polar character of the aglycon group, is the hydroxyl group at C-2. Hence the 2-oxyanion of the substrate appears to be the reactive species. In consistence with this conclusion three kinetically indistinguishable mechanisms can be suggested for the alkaline cleavage of aryl β -D-xylofuranosides. First, neighboring group participation by the ionized hydroxyl group at C-2 may occur, analogous to the hydrolysis of aldopyranosides with a *trans*-1,2-configuration (eqn. 8). Second, water can act as a general acid donating a proton to the glycosidic oxygen atom concerted with carbon-oxygen bond rupture (eqn. 9). Third, the anionic form of substrate may decompose spontaneously to a phenoxide and a cyclic oxo-carbenium ion (eqn. 10).

The first-order rate constants calculated by eqn. (4) for the rate-limiting decomposition of the 2-oxyanions of substituted phenyl β -D-xylofuranosides are collected in Table 2. It is clearly seen that the cleavage is greatly facilitated by electron-attracting substituents in the phenoxy group. Plotting the logarithms of the partial rate constants, k , against the polar substituent constants, σ^- , gives a fairly good linear correlation line with a slope of 1.8 ± 0.1 (Fig. 3). If σ values are used instead, the points



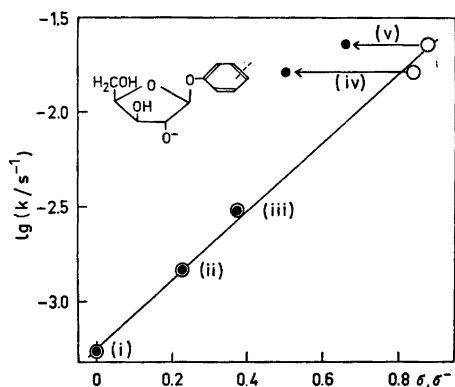


Fig. 3. Heterolysis of the 2-oxyanions of 3- and 4-substituted phenyl β -D-xylofuranosides in water at 343.15 K. Logarithms of the first-order rate constants plotted against the σ (filled circles) and σ^- (open circles) values of the substituents in the phenyl group. Notation: (i) phenyl, (ii) 4-chlorophenyl, (iii) 3-chlorophenyl, (iv) 4-acetylphenyl, and (v) 4-cyanophenyl derivative.

for 4-acetyl and 4-cyano groups fall far above the line the other substituents yield. The need for modified substituent constants, σ^- , to correlate the heterolysis rates, indicates that the reaction occurs with formation of an electron-rich center in direct conjugation with the benzene nucleus. This is what happens if mechanism (8) or (10) is followed. In contrast, no marked change in the resonance interactions between the glycosidic oxygen atom and the benzene ring will take place if the former is protonated by water concerted with the covalent bond fission. For example, the rates for the general acid-catalyzed hydrolysis of 2-(4-substituted phenoxy)tetrahydropyrans correlate with σ rather than with σ^- values.¹² The high positive value of 1.8 for the reaction constant, ρ^- , also argues against mechanism (9). Protonation of the *exo* cyclic oxygen atom concerted with the cleavage of the glycosidic bond would diminish the negative charge developed at this site in the activated complex. Consequently, a lower susceptibility to inductive effects than that observed would be expected.

Mechanisms (8) and (10) cannot be rigorously distinguished with the data indicated above. The fact that 2-aryloxytetrahydrofurans under-

go under alkaline conditions a spontaneous decomposition makes the latter possibility more attractive, however.¹³ The rate constants for these reactions are smaller by a factor of 10–100 than those for the 2-oxyanions of the corresponding β -D-xylofuranosides. A reactivity difference of this order is of what would be expected on the basis of polar inductive effects. When the phenoxy group begins to depart a partial positive charge will develop at the anomeric carbon. The strong electron-donating ability of the ionized hydroxyl group at C-2 increases the electron density at this site leading to a marked stabilization of the transition state. It should be noted, however, that the mechanism involving neighboring group participation by this group has not been rigorously excluded. Moreover, the aim of the preceding discussion is by no means to suggest that mechanism (10) would operate for aldofuranosides with poorer leaving-groups.

EXPERIMENTAL

The aryl β -D-xylofuranosides used in this investigation were obtained in their fully acetylated forms by fusing tetra-*O*-acetyl-D-xylofuranose with appropriate phenols in the presence of *p*-toluenesulfonic acid.¹⁴ Deacetylation of the products with sodium methoxide in methanol gave crude furanoside syrups which were purified by successive crystallizations from ethyl acetate. The melting points, ¹H NMR spectra and elemental analyses for the phenyl, 4-chlorophenyl, and 4-acetylphenyl derivatives are given in Ref. 15. 4-Cyanophenyl β -D-xylofuranoside melted at 383–385 K and gave the following ¹H NMR signals (D₂O): δ 3.6–3.8 (m, 2 H), 4.2–4.5 (m, 3 H), 5.59 (s, 1 H), 6.99 (d, 2 H), 7.50 (d, 2 H). 3-Chlorophenyl β -D-xylofuranoside failed to crystallize. ¹H NMR (D₂O): δ 3.7–3.8 (m, 2 H), 4.3–4.5 (m, 3 H), 5.55 (s, 1 H), 6.9–7.2 (m, 4 H).

Hydrolyses were followed spectrophotometrically at the absorption maxima of the liberated phenoxide ions. The measurements were performed on a Unicam SP 800 spectrophotometer equipped with a scale expansion accessory. The temperature of the cell housing block was kept at 343.15 ± 0.10 K with water circulation from a Lauda thermostat and controlled with a thermoelement. The initial substrate concentration was in the range of 10^{-5} – 10^{-4} mol dm⁻³. The first-order rate constants were calculated by the method of Guggenheim.

Acknowledgements. The financial aid from the Finnish Academy, Division of Science, is gratefully acknowledged.

REFERENCES

1. Capon, B. *Chem. Rev.* 69 (1969) 407.
2. a. McCloskey, C. M. and Coleman, G. H. *J. Org. Chem.* 10 (1945) 184; b. Dyfverman, A. and Lindberg, B. *Acta Chem. Scand.* 4 (1950) 878; c. Ballou, C. E. *Adv. Carbohydr. Chem.* 9 (1954) 59; d. Janson, J. and Lindberg, B. *Acta Chem. Scand.* 13 (1959) 138; e. Gasman, R. C. and Johnson, D. C. *J. Org. Chem.* 31 (1966) 1830.
3. Lai, Y. Z. *Carbohydr. Res.* 24 (1972) 57.
4. DeBruyne, C. K., Van Wijnendaele, F. and Carchon, H. *Carbohydr. Res.* 33 (1974) 75.
5. Hall, A. N., Hollingshead, S. and Rydon, H. N. *J. Chem. Soc.* (1961) 4290.
6. Horton, D. and Luetzow, A. E. *J. Chem. Soc. D* (1971) 79.
7. Tsai, C. S. and Reyes-Zamora, C. J. *Org. Chem.* 37 (1972) 2725.
8. Janson, J. and Lindberg, B. *Acta Chem. Scand.* 14 (1960) 2051.
9. Streitwieser, A., Jr., *Solvolytic Displacement Reactions*, McGraw-Hill, New York 1962, pp. 95–97.
10. Swain, C. G. and Scott, C. B. *J. Am. Chem. Soc.* 75 (1953) 141.
11. a. Michaelis, L. *Ber. Dtsch. Chem. Ges.* 46 (1913) 3683; b. Hirsch, P. and Schlags, R. *Z. Phys. Chem. A* 141 (1929) 387; c. Thamsen, J. *Acta Chem. Scand.* 6 (1952) 270; d. Izatt, R. M., Rytting, J. H., Hansen, L. D. and Christensen, J. J. *J. Am. Chem. Soc.* 88 (1966) 2641; e. Christensen, J. J., Rytting, J. H. and Izatt, R. M. *J. Am. Chem. Soc.* 88 (1966) 5105.
12. Fife, T. H. and Brod, L. H. *J. Am. Chem. Soc.* 92 (1970) 1681.
13. Lönnberg, H. and Pohjola, V. *Acta Chem. Scand. A* 30 (1976) 669.
14. Börjeson, H., Jerkeman, P. and Lindberg, B. *Acta Chem. Scand.* 17 (1963) 1705.
15. Lönnberg, H., Kankaanperä, A. and Haapakka, K. *Carbohydr. Res.* To be published.

Received November 2, 1976.

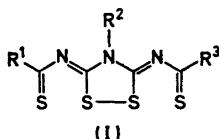
Structures of Linear Multisulfur Systems. XII. The Crystal and Molecular Structure of 3-(*N*-Diisopropylthiocarbamoylimino)-5-(thiobenzimino)-4-methyl-1,2,4-dithiazolidine, C₁₇H₂₂N₄S₄

JORUNN SLETTEN and OLE CHR. LØKKE

Department of Chemistry, University of Bergen, N-5014 Bergen-Univ., Norway

Crystals of the title compound, C₁₇H₂₂N₄S₄, are monoclinic, space group *P*2₁/*c*, with cell dimensions *a* = 10.603(3) Å, *b* = 14.434(2) Å, *c* = 13.866(2) Å, β = 109.60(2)°. 3538 independent reflections were recorded on an off-line four-circle diffractometer employing the θ–2θ scan technique. The structure was solved by the symbolic addition procedure and refined by full-matrix least-squares to an *R* of 0.051. The four sulfur atoms are arranged in a nearly linear row, with S–S distances in the region between a single bond and van der Waals distance; S(1)–S(2) = 2.815(2), S(2)–S(3) = 2.181(2), S(3)–S(4) = 2.620(3) Å.

The present structure determination is part of a program of X-ray crystallographic investigations of linear multisulfur compounds. So far four different symmetrically substituted 1,2,4-



dithiazolidine derivatives of type (I) have been studied.^{1–3} This is the first structure report of an unsymmetrically substituted derivative (R¹ ≠ R³).

EXPERIMENTAL

A sample of the compound was provided by Dr. J. Goerdeler, University of Bonn. Single crystals, deep green in colour, were grown by slow evaporation from a chloroform/light petroleum mixture at room temperature. The crystal used for data collection had dimensions

0.40 × 0.12 × 0.10 mm³ and was mounted along the *a*-axis. The space group was determined from Weissenberg and precession photographs. Cell dimensions were calculated based on diffractometer measurements of the 2θ values [λ(MoKα₁) = 0.70926 Å] for 15 reflections with 2θ > 60° using an ω-scan procedure.⁴ Within a sphere of reflection limited at sin θ/λ = 0.595 (2θ_{max} = 50°) the intensities of 3538 independent reflections were recorded on a four-circle diffractometer using the θ–2θ scan technique and niobium filtered MoKα radiation. Scan ranges were calculated according to the relationship Δ2θ = A + B tan θ,⁵ Δ2θ varying between 1.14° at 2θ = 0° and 1.32° at 2θ = 50°. Two reference reflections, measured for each 50 reflections recorded, indicated no deterioration of the crystal. Standard deviations in the intensities were calculated as σ_I = [σ_c² + (0.014N_{net})²]^{1/2}, where σ_c is the error due to counting statistics, and the “instability factor” of 0.014 were calculated in the data processing program, based on the variation in scale factors. Standard deviations in structure factors were calculated as σ_F = σ_I/2(ILp)^{1/2}. 1566 of the reflections had net counts less than 2σ_c. These reflections were assigned the threshold value of 2σ_c, and were later included in the refinement only if |F_c| > F_{threshold}. Data were corrected for Lorentz and polarization effects and for absorption.

CRYSTAL DATA

C₁₇H₂₂N₄S₄; *M.W.* = 410.65; crystal system monoclinic; space group *P*2₁/*c*; cell dimensions (20°C):
a = 10.603(3) Å, *b* = 14.434(2) Å, *c* = 13.866(2) Å,
 β = 109.60(2)°. *V* = 1999.1(7) Å³, *D_x* = 1.365 g cm⁻³, *D_m* = 1.36(1) g cm⁻³, *Z* = 4, *F*₀₀₀ = 864, μ_{MoKα} = 4.7 cm⁻¹.

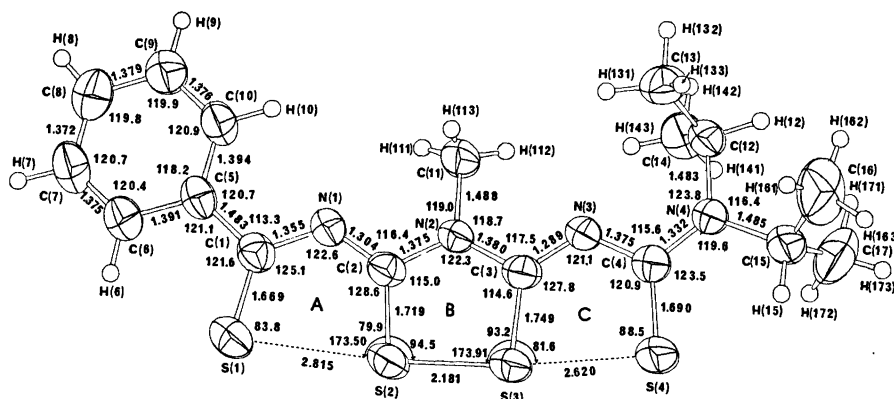


Fig. 1. Intramolecular distances and angles. Standard deviations as calculated from the least-squares inverse matrix are for S-S, S-C and C-N(C) bonds 0.002, 0.004 and 0.005–0.009 Å, respectively. Standard deviations in S-S-S and C-S-S angles are 0.07 and 0.2°; and 0.3–0.5° in angles at C and N. The thermal ellipsoids for non-hydrogen atoms are plotted at the 50 % probability level, hydrogen atoms are plotted with a fixed radius.

Table 1. Fractional coordinates and thermal parameters for non-hydrogen atoms with the corresponding standard deviations in parentheses. Thermal parameters are of the form $T_i = \exp[-2\pi^2(U_{11}h^2a^{*2} + U_{22}k^2b^{*2} + U_{33}l^2c^{*2} + 2U_{12}hka^*b^* + 2U_{13}hla^*c^* + 2U_{23}k lb^*c^*)]$, and the values are multiplied by a factor of 10^4 .

Atom	X/a	Y/b	Z/c	U_{11}	U_{22}	U_{33}	U_{12}	U_{13}	U_{23}
S(1)	0.04311(15)	0.21917(8)	0.56414(10)	1060(12)	493(7)	859(10)	170(7)	465(8)	4(7)
S(2)	0.16626(13)	0.18811(7)	0.41804(9)	878(10)	366(6)	601(8)	79(6)	278(7)	-3(6)
S(3)	0.25500(14)	0.14763(7)	0.30141(9)	1115(12)	363(6)	695(8)	69(7)	459(8)	64(6)
S(4)	0.35187(19)	0.08128(8)	0.16484(11)	2052(19)	452(7)	1050(12)	187(10)	1067(13)	180(7)
N(1)	0.16854(34)	0.05536(19)	0.55415(24)	615(25)	442(19)	495(21)	23(17)	239(19)	-54(16)
N(2)	0.25574(32)	0.01777(19)	0.43584(23)	663(26)	338(17)	493(20)	67(17)	258(19)	30(16)
N(3)	0.33560(33)	-0.03326(19)	0.31147(23)	728(27)	367(17)	507(21)	6(18)	293(20)	-12(16)
N(4)	0.40735(34)	-0.09923(20)	0.18878(23)	736(27)	415(18)	455(20)	18(18)	284(19)	9(15)
C(1)	0.09356(40)	0.11126(25)	0.60047(28)	500(30)	498(24)	526(27)	-42(22)	167(23)	-105(21)
C(2)	0.19085(40)	0.08195(24)	0.47565(28)	542(30)	380(21)	483(25)	-19(21)	148(22)	-46(19)
C(3)	0.28759(41)	0.03461(23)	0.34873(29)	652(33)	381(21)	484(26)	-33(22)	196(24)	-8(19)
C(4)	0.36734(44)	-0.02267(25)	0.22375(30)	802(36)	459(23)	549(28)	4(24)	315(26)	5(21)
C(5)	0.07306(42)	0.06820(27)	0.69122(30)	531(32)	542(26)	473(26)	13(24)	157(24)	-142(22)
C(6)	0.02852(47)	0.12029(29)	0.75787(36)	785(40)	602(29)	620(30)	-18(27)	317(29)	-140(25)
C(7)	0.01396(54)	0.08007(36)	0.84341(40)	957(46)	790(36)	795(38)	54(33)	474(34)	-214(31)
C(8)	0.03976(54)	-0.01243(38)	0.86317(37)	1046(47)	906(39)	653(34)	-19(36)	465(33)	-12(31)
C(9)	0.08047(50)	-0.06585(30)	0.79656(36)	937(43)	622(30)	668(32)	87(29)	375(31)	19(26)
C(10)	0.09786(45)	-0.02581(29)	0.71180(33)	685(36)	576(28)	588(31)	77(26)	274(27)	-103(24)
C(11)	0.28977(50)	-0.07407(27)	0.48665(34)	1108(45)	470(25)	756(33)	264(28)	549(32)	183(24)
C(12)	0.43043(43)	-0.18909(25)	0.24384(29)	594(31)	428(22)	493(26)	-4(23)	197(24)	-63(21)
C(13)	0.30197(47)	-0.23517(28)	0.24254(32)	775(38)	553(27)	717(32)	-152(26)	277(28)	-19(23)
C(14)	0.53564(65)	-0.18336(43)	0.34901(39)	689(44)	691(35)	524(33)	142(35)	140(30)	47(30)
C(15)	0.44328(53)	-0.09495(27)	0.09419(32)	944(42)	491(25)	558(28)	102(27)	358(28)	58(22)
C(16)	0.36714(59)	-0.16938(40)	0.01899(35)	1450(55)	1458(51)	528(32)	-150(44)	383(35)	-326(34)
C(17)	0.59217(64)	-0.10009(38)	0.12013(42)	1031(51)	1213(46)	1088(46)	-53(39)	724(41)	147(37)

STRUCTURE DETERMINATION AND REFINEMENT

The structure was solved by application of the symbolic addition procedure. An *E*-map based

on 283 reflections revealed the eleven atoms of "rings" A+B+C (Fig. 1). The remaining non-hydrogen atoms were localized in a subsequent Fourier map. The structure was refined by full-matrix least-squares, minimizing the

Table 2. Fractional coordinates and thermal parameters for hydrogen atoms with the corresponding standard deviations. Thermal parameters are of the form: $\exp(-8\pi^2 U \sin^2 \theta/\lambda^2)$ and are multiplied by 10^3 .

Atom	X/a	Y/b	Z/c	U
H(6)	0.013(4)	0.189(2)	0.741(2)	72(11)
H(7)	-0.016(4)	0.116(2)	0.893(3)	77(12)
H(8)	0.025(3)	-0.043(2)	0.912(3)	75(12)
H(9)	0.098(3)	-0.132(2)	0.810(2)	68(11)
H(10)	0.132(3)	-0.062(2)	0.668(2)	55(10)
H(111)	0.299(5)	-0.073(3)	0.551(4)	130(16)
H(112)	0.356(5)	-0.100(3)	0.470(3)	119(16)
H(113)	0.217(6)	-0.105(4)	0.464(5)	173(26)
H(12)	0.468(3)	-0.229(2)	0.201(2)	52(10)
H(131)	0.260(4)	-0.207(3)	0.292(3)	83(13)
H(132)	0.317(4)	-0.301(3)	0.272(3)	92(13)
H(133)	0.235(4)	-0.243(3)	0.172(3)	103(13)
H(141)	0.624(6)	-0.155(4)	0.350(4)	145(30)
H(142)	0.561(5)	-0.243(3)	0.378(3)	106(19)
H(143)	0.504(4)	-0.152(3)	0.396(3)	86(17)
H(15)	0.415(3)	-0.036(2)	0.061(3)	57(11)
H(161)	0.260(7)	-0.165(5)	-0.003(5)	225(29)
H(162)	0.401(7)	-0.238(5)	0.038(5)	239(30)
H(163)	0.388(4)	-0.154(3)	-0.040(3)	107(14)
H(171)	0.628(5)	-0.167(4)	0.148(4)	133(19)
H(172)	0.645(7)	-0.047(4)	0.176(6)	218(30)
H(173)	0.622(4)	-0.101(3)	0.069(3)	121(15)

function $\sum w(|F_o| - |F_c|)^2$, where $w = 1/\sigma_F^2$. Anisotropic temperature factors were introduced for the non-hydrogen atoms. Hydrogen atoms were localized from a difference Fourier map, and positional and isotropic thermal parameters were refined. The sulfur atoms exhibit high thermal parameters with pronounced anisotropy. This may possibly indicate disorder in the sulfur chain, hence a model with split sulfur atoms was tested. But during the refinement the partial sulfur atoms in each pair moved constantly closer. Thus in the last refinement cycles only one position was refined for each of the atoms. The final S(4) thermal

parameters are unusually high with the main axis of vibration in a direction almost normal to the plane of rings A + B + C (Fig. 1). A difference map calculated at the end of the refinement showed no peaks around the sulfur atoms above the background level.

The refinement converged at an R ($R = \sum ||F_o| - |F_c|| / \sum |F_o|$) of 0.051, R_w being 0.032 and the standard deviation of an observation of unit weight being 1.71. No sign of secondary extinction was detected at the conclusion of the refinement. Scattering factors used were for C, N and S those of Cromer and Mann,⁶ and for H those of Stewart *et al.*⁷

The final coordinates and thermal parameters are listed in Tables 1 and 2. Lists of observed and calculated structure factors may be obtained from one of the authors (J.S.).

All calculations have been carried out on a UNIVAC 1110 computer. The programs concerning data collection and initial handling of the intensity data have been written by cand. real. K. Maartmann-Moe of this Department. For all other calculations the X-ray 72 system was used.⁸

RESULTS AND DISCUSSION

Intramolecular distances and angles involving non-hydrogen atoms are shown in Fig. 1 and in Table 3. The C-H distances lie in the region 0.86-1.10 Å with a mean value of 0.96 Å for $C(sp^2)$ -H and 0.98 Å for $C(sp^3)$ -H bonds. Standard deviations in the individual C-H bonds are in the range 0.03-0.07 Å. The four sulfur atoms are arranged in an almost linear row, the S-S-S angles being similar to those found in analogous compounds.¹⁻³ The central S-S distance is significantly longer than the S-S bonds generally found in five-membered cyclic disulfides,⁹ and the terminal S-S

Table 3. Bond distances and angles in the isopropyl groups.

Distances	(Å)	Angles	(°)
C(12)-C(13)	1.511(7)	N(4)-C(12)-C(13)	112.7(3)
C(12)-C(14)	1.512(6)	N(4)-C(12)-C(14)	112.9(3)
C(15)-C(16)	1.526(6)	C(13)-C(12)-C(14)	114.0(4)
C(15)-C(17)	1.499(9)	N(4)-C(15)-C(16)	109.9(4)
		N(4)-C(15)-C(17)	110.3(4)
		C(16)-C(15)-C(17)	113.7(5)

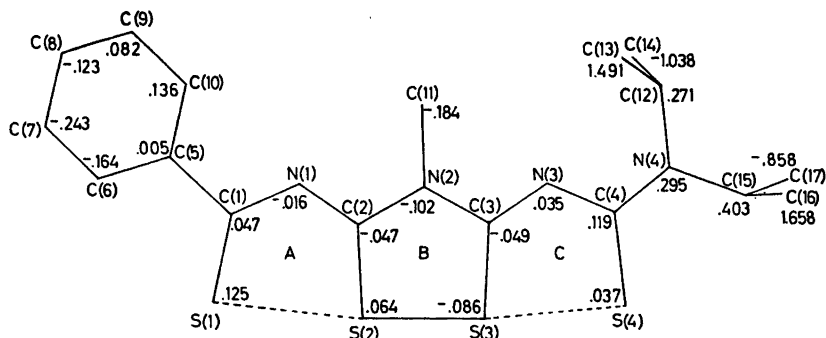


Fig. 2. Atomic deviations from the best least-squares plane through rings A + B + C.

distances are appreciably shorter than van der Waals distance. The bonding along this sulfur sequence may be described in terms of delocalized σ -bonding in a 4-center 6-electron linear system. According to CNDO/2 calculations the energy difference between a sulfur sequence with two-fold symmetry and an asymmetric sulfur sequence is small in this type of compounds.¹⁰ Relatively weak *intra*- as well as *inter*-molecular forces may affect the S–S distances significantly. Hence, it is not surprising that in this unsymmetrically substituted compound a relatively large asymmetry in the sulfur row is found.

The short intramolecular, non-bonding contacts $S(1)\cdots H(6) = 2.62(4)$ Å, $S(4)\cdots H(8) =$

$2.46(4)$ Å and $H(112)\cdots H(143) = 2.28(6)$ Å are of lengths similar to corresponding contacts in the compounds previously studied.^{1,2} In Fig. 2 the molecule is plotted in the best least-squares planes through rings A + B + C. This part of the molecule deviates slightly, but significantly from planarity. The molecule is slightly bent around $S(2) - C(2)$ and $S(3) - C(3)$, the dihedral angles between A and B; A and C; B and C being 3.2, 7.1 and 3.9°, respectively. The angles between the plane of the phenyl group and A is 11.4°.

In Fig. 3 the packing of molecules in the crystal is illustrated. Molecules related by a centre of symmetry (*e.g.* x, y, z and $-x, -y, 1-z$) overlap slightly, such that the phenyl group

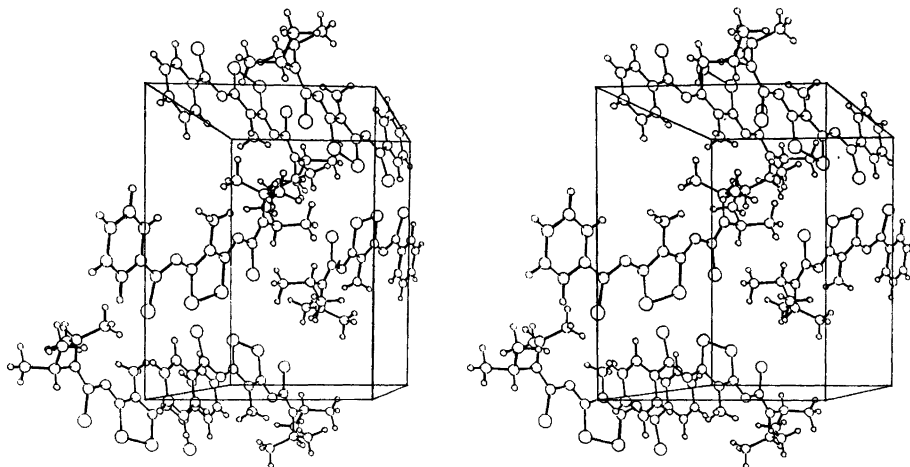


Fig. 3. Stereo drawing showing the molecular packing in the crystal. The *a*-axis runs along the interocular line left to right, the *b*-axis vertically, bottom to top, and the *c**-axis points towards the viewer. Figs. 1 and 3 have been prepared using the ORTEP program.¹¹

of one molecule is situated above ring B of the other molecule at an average distance of 3.5 Å. There are no intermolecular contacts shorter than van der Waals distance.

Acknowledgement. Thanks are due to Professor J. Goerdeler for supplying a sample of the compound.

REFERENCES

1. Sletten, J. *Acta Chem. Scand. A* 28 (1974) 989.
2. Sletten, J. *Acta Chem. Scand. A* 29 (1975) 317.
3. Flippen, J. L. *J. Am. Chem. Soc.* 95 (1973) 6073.
4. Maartmann-Moe, K. *Siemens Review XLI*, Seventh Special Issue "X-Ray and Electron Microscopy News" (1974) 54.
5. Alexander, L. E. and Smith, G. S. *Acta Crystallogr.* 17 (1964) 1195.
6. Cromer, D. and Mann, J. *Acta Crystallogr. A* 24 (1968) 321.
7. Stewart, R. F., Davidson, E. R. and Simpson, W. T. *J. Chem. Phys.* 42 (1965) 3175.
8. The X-Ray System, Version of June 1972; *Technical Report TR-192 of the Computer Science Center*, University of Maryland, June 1972.
9. Hordvik, A. *Quart. Rep. Sulfur Chem.* 5 (1970) 21.
10. Sletten, J. *Acta Chem. Scand. A* 30 (1976) 397.
11. Johnson, C. K. *ORTEP, A Fortran Thermal Ellipsoid Plot Program for Crystal Structure Analysis*, Report ORNL-3794, Oak Ridge National Laboratory, Oak Ridge 1965.

Received December 6, 1976.

The Effect of 4-Methyl and 4-Nitro Substituents on the Reactivity of Benzylic Compounds

TORE THORSTENSON, ROBERT ELIASON * and JON SONGSTAD

Department of Chemistry, University of Bergen, 5014 Bergen-Univ., Norway

The rates of reaction of 4-methylbenzyl halide, benzyl halide and 4-nitrobenzyl halide with various nucleophiles have been determined in acetonitrile.

From the second-order rate constants the rate ratios $k_{(4-Me)}/k_{(4-H)}$ and $k_{(4-NO_2)}/k_{(4-H)}$ have been calculated. These ratios along with some representative values from the literature are presented. The $k_{(4-Me)}/k_{(4-H)}$ ratio varies from 1.2 to 2.3 indicating that the methyl group is rate accelerating for all the reactions. The $k_{(4-NO_2)}/k_{(4-H)}$ ratio varies from 0.28 to 4.7, however, and in addition these ratios are grouped according to the charge of the nucleophile. In general $k_{(4-NO_2)}/k_{(4-H)} > 1$ when the nucleophile is anionic while ≤ 1 when it is uncharged.

These ratios are discussed with respect to recent theories on the prediction of the effect of substituent changes on transition state structures. It is concluded that these rate ratios alone are poor probes for the elucidation of transition state structure.

The Hammett equation is a well-known empirical, linear free energy relationship which correlates structure and reactivity.¹ It has been used extensively to correlate data of benzene derivatives as substrates. There are, however, a number of reactions of 3- or 4-substituted benzylic compounds which show significant deviations from linearity.² In particular non-linear Hammett plots are obtained from simple S_N2 reactions of 3- or 4-substituted benzyl halides. For example, Finckelstein reactions^{3,4} and reactions with thiosulfate ion^{5,6} give U-shaped plots; whereas, L-shaped plots are obtained with Menshutkin reactions⁷ and reactions with triphenylphosphine.⁸

* On leave from Southwest State University, Marshall, Minnesota, USA.

Upon examining Finckelstein and Menshutkin reaction data it was noticed that reactions of uncharged nucleophiles with 4-substituted benzyl halides had a rate ratio $k_{(4-Me)}/k_{(4-H)} > 1$ and a rate ratio $k_{(4-NO_2)}/k_{(4-H)} < 1$. On the other hand reactions of anionic nucleophiles with the same substrates had $k_{(4-Me)}/k_{(4-H)} > 1$, as with uncharged nucleophiles, but had $k_{(4-NO_2)}/k_{(4-H)} > 1$. It thus appeared that the $k_{(4-NO_2)}/k_{(4-H)}$ rate ratios are apparently grouped according to the charge type of the nucleophile.

A study of the S_N2 reaction of 4-substituted benzyl halides in acetonitrile using charged and uncharged nucleophiles was undertaken to test the generality of these groupings.

EXPERIMENTAL

Acetonitrile was purified as reported⁹ and flushed with nitrogen prior to use. The benzyl halides were prepared and purified as previously.⁸ Pyridine and dimethylaniline were purified by standard procedures. Anhydrous tetraphenylarsonium salts of all the ionic nucleophiles were prepared as previously reported¹⁰ and carefully dried under high vacuum. It was assumed that these salts were completely dissociated in acetonitrile.¹¹ Thiourea, Fluka *puriss.*, was crystallized from water and then several times from acetonitrile. Diethyl sulfide, Fluka *purum*, was treated with metallic sodium and twice distilled under reduced pressure.

The rates of reactions utilizing the uncharged nucleophiles were determined by previously described conductance methods.⁸ Rate constants for the diethyl sulfide nucleophile were calculated from the first 15–30 % of reaction and assuming the mobility of the benzyldiethylsulfonium ions to be comparable with those of the benzyltriethylammonium ions.

Table 1. Second-order rate constants for the reactions of 4-substituted benzyl halides (RX) in acetonitrile.

Nucleophile	RX	<i>t</i> /°C	k_2 (l mol ⁻¹ s ⁻¹) ^a		
			4-Me	4-H	4-NO ₂
NNN ⁻	RBr	25	4.7 ± 0.2	2.3 ± 0.1	11.0 ± 0.5
NCS _e ⁻	RBr	25	(2.7 ± 0.1) × 10 ⁻¹	(1.4 ± 0.1) × 10 ⁻¹	(3.3 ± 0.2) × 10 ⁻¹
NCS ⁻	RBr	25	(4.4 ± 0.3) × 10 ⁻²	(2.7 ± 0.1) × 10 ⁻²	(5.4 ± 0.3) × 10 ⁻²
OCN ⁻	RBr	25	(12.9 ± 0.5) × 10 ⁻³	(8.3 ± 0.3) × 10 ⁻³	(20.0 ± 1.0) × 10 ⁻³
(H ₂ N) ₂ CS	RI	25	(6.0 ± 0.2) × 10 ⁻²	(3.4 ± 0.1) × 10 ⁻²	(3.8 ± 0.1) × 10 ⁻²
Et ₂ S	RI	50	(10.0 ± 0.3) × 10 ⁻²	(4.9 ± 0.1) × 10 ⁻³	(1.70 ± 0.05) × 10 ⁻³
Py	RI	50	(22.0 ± 0.5) × 10 ⁻³	(18.0 ± 0.5) × 10 ⁻³	(5.0 ± 0.1) × 10 ⁻³
Me ₂ NPh	RI	50	(32 ± 1) × 10 ⁻³	(15.0 ± 0.5) × 10 ⁻³	(3.8 ± 0.1) × 10 ⁻³

^a The errors are average deviations of the mean.

The rates of the ionic nucleophiles were determined by IR employing liquid IR cells. The reaction solutions were kept in a constant temperature bath, 25.0 ± 0.1 °C, and aliquots were withdrawn periodically. The disappearance of the pseudohalide ion was monitored in the 2100 cm⁻¹ region. The difference in wavenumber for maximum absorption of products and reactants was: RNCO, NCO⁻, ~78 cm⁻¹; RSCN, SCN⁻, 98–100 cm⁻¹; RSeCN, SeCN⁻, 86–88 cm⁻¹; RN₃, N₃⁻, 95–100 cm⁻¹.

RESULTS

The second-order rate constants (k_2) are presented in Table 1. All kinetic measurements were carried out in dry acetonitrile at either 25.0 or 50.0 °C. For reactions involving the uncharged nucleophiles, the nucleophile concentration was kept in large excess, and first-order rate constants were determined from plots of $\log(1/R_\infty - 1/R)$ vs. t where R is the resistance. From k_1 and the nucleophile concentration k_2 could be calculated. The reactions using diethyl sulfide as the nucleophile did not go to completion due to the low carbon basicity of the sulfide; thus, first-order rate constants were obtained from just the first 15–30 % of reaction. When ionic nucleophiles were used, the concentrations of the nucleophile and substrate were equal, and k_2 was obtained directly from plots of $1/C$ vs. t where C is the concentration of the nucleophile.

The $k_{(4-X)}/k_{(4-H)}$ ratios calculated for this study are shown in Table 2 along with some representative values calculated from literature sources. As can be seen, all the $k_{(4-Me)}/k_{(4-H)}$ ratios are > 1 whichever nucleophile

was used. The $k_{(4-NO_2)}/k_{(4-H)}$ ratios are grouped according to nucleophile charge type being > 1 for negatively charged nucleophiles and ≤ 1 for neutral ones. Thiourea, triphenylphosphine and trimorpholinophosphine have $k_{(4-NO_2)}/k_{(4-H)}$ ratios which are close to unity.

DISCUSSION

The detailed mechanism of S_N2 reactions has been, and still is, a matter of controversy.^{12,13} For the sake of discussion here we will adopt the "loose-tight" transition state model of Ko and Parker¹⁴ which may be closest to reality.¹² It has been argued¹⁴ that protic solvents favor "looser" transition states whereas aprotic solvents favor the "tighter" form. Thus, the literature data presented in Table 2 has been limited to dipolar aprotic solvents. The effect of the halogen leaving group on $k_{(4-Me)}/k_{(4-H)}$ and $k_{(4-NO_2)}/k_{(4-H)}$ is shown in Table 3. In general both $k_{(4-Me)}/k_{(4-H)}$ and $k_{(4-NO_2)}/k_{(4-H)}$ decrease as the atomic weight of the halogen decreases, but as can be seen there are notable exceptions. Therefore, some caution must be exercised when attempting to compare reactions with dissimilar leaving groups. The data are discussed with these limitations in mind.

It has been argued^{4-7,15-17} that the sign of the charge on the benzylic carbon atom (C_α) in the transition state is substituent dependent in S_N2 reactions of benzylic systems. The charge changes from positive to negative as the substituent is changed from electron-donating to electron-withdrawing. In a "loose" transition state bond breaking is ahead of bond

Table 2. $k_{(4-X)}/k_{(4-H)}$ ratios for nucleophilic substitution of 4-substituted benzyl halides (RX) in dipolar aprotic solvents at 25 °C unless stated otherwise.

No.	Nucleophile	RX	Solvent	$10^4 k_{2,4-H}$ ($l \text{ mol}^{-1} \text{ s}^{-1}$)	$\frac{k_{(4-Me)}}{k_{(4-H)}}$	$\frac{k_{(4-NO_2)}}{k_{(4-H)}}$	Ref.
1	NNN ⁻	RBr	MeCN	23000	2.04	4.71	24
2	NCS ₆ ⁻	RBr	MeCN	1400	1.93	2.40	24
3	NCS ⁻	RBr	MeCN	270	1.78	2.02	24
4	OCN ⁻	RBr	MeCN	83	1.55	2.40	24
5	Br ⁻	RBr ^a	Me ₂ CO	26.8	2.26	4.19	4
6	Br ⁻	RBr	EDA ^b	7.4	6.16 ^b	11.33	3
7	NCS ⁻	RCl	Me ₂ CO	7.8 ^c	1.40	4.44	25
8	(H ₃ N) ₂ CS	RI	MeCN	340	1.76	1.12	24
9	Et ₃ S	RI	MeCN	49 ^d	2.04	0.34	24
10	Ph ₃ P	RBr	MeCN	21	1.62	1.09	8
11	Mor ₃ P	RBr	MeCN	83	1.45	1.03	8
12	(MeO) ₃ P	RBr	MeCN	0.53 ^d	1.40	0.75	26
13	Ph ₃ As	RBr	MeCN	0.98 ^d	1.75	0.56	8
14	Et ₃ N	RBr	MeCN	68	1.91	0.38	8
15	Me ₂ NPh	RI	MeCN	150 ^d	2.13	0.25	24
16	Py	RI	MeCN	180 ^d	1.22	0.28	24
17	Py	RBr	DMF	8.46	1.51	0.68	27
18	Py	RBr	Me ₂ CO	1.22 ^e	1.65	0.92	28

^a The substrate is α -phenylethyl bromide. ^b Ethylenediacetate solvent. 4-Methoxy substituent. ^c At 65 °C. ^d At 50 °C. ^e At 20 °C.

making, and electron-donating substituents stabilize the developing positive charge plus promote its formation. When bond making is ahead of bond breaking, the transition state is considered "tight" with some negative charge on the C_α. Electron-withdrawing substituents can both stabilize this charge and facilitate its development. Recently, theories¹⁸⁻²⁰ for predicting the effect of substituent changes on transition state geometries have been proposed. In general, one must be able to predict the effect of a substituent perturba-

tion on the parallel and perpendicular normal stretching coordinates in the transition state:

parallel motion: N → ← C L →

perpendicular motion: ← N ← C L →

Parallel motion is along the reaction coordinate, and perpendicular motion is orthogonal to the reaction coordinate. Perturbations which effect parallel motion affect the position along the reaction coordinate in accord with the Hammond postulate.²¹ Perturbations affecting per-

Table 3. Trends in $k_{(4-Me)}/k_{(4-H)}$ and $k_{(4-NO_2)}/k_{(4-H)}$ with leaving group.

Nucleophile	RX	Solvent	<i>t</i> °C	$\frac{k_{(4-Me)}}{k_{(4-H)}}$	$\frac{k_{(4-NO_2)}}{k_{(4-H)}}$	Ref.
Ph ₃ As	RI	MeCN	50	1.86	0.59	8
	RBr			1.75	0.56	
Ph ₃ P	RI	MeCN	25	1.67	0.89	8
	RBr			1.62	1.09	
(MeO) ₃ P	RI	MeCN	50	1.47	0.56	26
	RBr			1.40	0.75	
Py	RBr	MeOH	25	2.88	0.51	27
	RCl			2.37	0.35	
	RBr			1.51	0.68	
Py	RCl	DMF	25	2.55	0.66	27

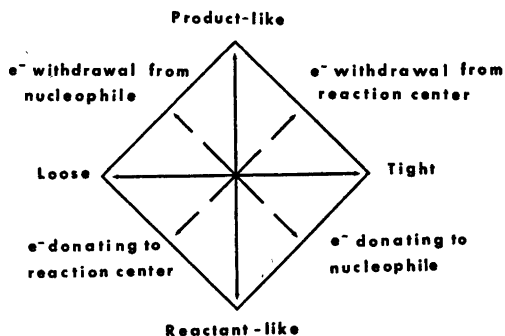


Fig. 1. Pictorial representation of the prediction of substituent effects in S_N2 reactions of benzylic halides.

pendicular motion determine the "tightness" or "looseness" of the transition state. Also, a particular perturbation will affect both the parallel and perpendicular motions. It should be noted that in some cases the effects on these motions oppose each other making even qualitative predictions difficult.²⁰ A summary of the predictions are shown pictorially in Fig. 1. The horizontal and vertical lines refer to the transition state geometries of "loose-tight" (perpendicular motion) and the Hammond postulate (parallel motion), respectively. The dashed diagonal lines refer to perturbation effects on the nucleophile (or leaving group) and on the reaction center (C_α). Thus, an electron-withdrawing substituent attached to the nucleophile can make the transition state both "looser" and more "product-like". However, the prediction of the perturbational effect on C_α , as shown in Fig. 1, applies only when the attacking nucleophile is neutrally charged and the leaving group negatively charged, or when the attacking nucleophile has the same charge but is lighter than the leaving nucleophile. When these conditions are reversed, the reaction center labels must be rotated 90° counter clockwise. The dashed lines should not be taken to imply that a particular perturbation affects both perpendicular and parallel motions equally. The effect on one of the motions may predominate; for example, a transition state may become "tighter" without becoming more or less "product-like".

As can be seen from Table 2 the 4-Me group is rate accelerating, $k_{(4-Me)}/k_{(4-H)} > 1$, which

suggests the development of positive charge on C_α in a "loose" transition state. The small range of the $k_{(4-Me)}/k_{(4-H)}$ ratios compared to four orders of magnitude variation in k_2 also indicates that there is not too much variation in the "looseness" of the transition state. It is interesting to note, however, that the first four entries (1-4) for the charged nucleophiles show a regular decrease in $k_{(4-Me)}/k_{(4-H)}$ with decreasing reactivity. According to the Hammond postulate²¹ the transition state becomes more product like as the reactivity decreases; thus, the decrease in $k_{(4-Me)}/k_{(4-H)}$ could be explained by an increase in bond-making, making the transition state tighter which would reduce the positive charge on the C_α . Evidence from chlorine isotope effects of Grimsrud and Taylor²² support this analysis. It is, therefore, unfortunate that the rest of the data presented in Table 2 is not more amenable to such an analysis.

The most striking feature of the data in Table 2 is the groupings of $k_{(4-NO_2)}/k_{(4-H)}$. All of the anionic nucleophiles have rather large positive $k_{(4-NO_2)}/k_{(4-H)}$ ratios. Two phosphorus nucleophiles and thiourea exhibit only a minimal rate acceleration on going from 4-H to 4- NO_2 substituents: $k_{(4-NO_2)}/k_{(4-H)} \approx 1$. For the rest of the uncharged nucleophiles the reaction rate does decrease upon going from the unsubstituted to the 4-nitro substituted substrate.

The groupings of the $k_{(4-NO_2)}/k_{(4-H)}$ ratios according to nucleophile charge type are in accord with the predictions. Increasing the electron supply at the nucleophile (uncharged to anionic) increases $k_{(4-NO_2)}/k_{(4-H)}$ indicating a shift to "tighter" transition states. In a "tight" transition state the advanced bonding between the nucleophile and the carbon atom would increase the electron density on the carbon. The 4-nitro group in the benzylic system can effectively drain off this excess charge. Anionic nucleophiles, which already have an excess of charge, would be expected to place much more charge on the C_α than uncharged nucleophiles. It is also not unreasonable to expect that while the nitro group stabilizes this charge development, it also encourages it causing the transition state to become "tight" (Fig. 1). The net effect is for the nitro group to really accelerate reactions of the charged nucleophiles. On the other hand un-

charged nucleophiles cannot donate electrons well enough to place bond-making as far ahead of bond-breaking as can charged nucleophiles. As the uncharged nucleophile approaches the C_α , electrons begin to be donated increasing the carbon's electron density. At the same time the nucleophile acquires a partial positive charge; thus, electrons are partially removed from the newly forming bond. This transition state is then not nearly as "tight" as the one involving anionic nucleophiles, in accord with the predictions.

If one looks at the phosphorus and arsenic nucleophiles (Table 2; entries 10–13) an interesting trend in the $k_{(4-NO_2)}/k_{(4-H)}$ ratios will be noticed. The lowest $k_{(4-NO_2)}/k_{(4-H)}$ ratio corresponds to triphenylarsine which is a much weaker base than triphenylphosphine toward both the proton²³ and carbon.⁹ For the phosphorus nucleophiles $k_{(4-NO_2)}/k_{(4-H)}$ increases with phosphorus atom basicity toward carbon as would be predicted⁹ by the decreasing inductive electron-withdrawal of the attached groups. Thus, the increase in $k_{(4-NO_2)}/k_{(4-H)}$ ratios with increasing basicity is in the direction predicted.

Finally, neither $k_{(4-Me)}/k_{(4-H)}$ nor $k_{(4-NO_2)}/k_{(4-H)}$ correlate systematically with the variation in reaction rate between the various reactions or with nucleophile basicity. It appears that these ratios alone are not sensitive enough probes for possible variations in transition state structure. Thus, the data give only general support to theories for predicting changes in transition state geometries caused by substituent effects. The irregularities in the data could possibly be due to specific solvation effects which have not been taken into account.

Acknowledgement. One of us (R. E.) is very grateful to the Royal Norwegian Council for Scientific and Industrial Research (N'NF) for a post-doctoral fellowship.

REFERENCES

1. Hammett, L. P. *Physical Organic Chemistry: Reaction Rates, Equilibria and Mechanisms*, 2nd Ed., McGraw-Hill, London 1970, Chapter 11.
2. Schreck, J. O. *J. Chem. Educ.* 48 (1971) 103.
3. Sugden, S. and Willis, J. B. *J. Chem. Soc.* (1951) 1360.
4. Stein, A. R. *Tetrahedron Lett.* (1974) 4145.
5. Fuchs, R. and Nisbet, A. *J. Am. Chem. Soc.* 81 (1959) 2371.
6. Fuchs, R. and Carlton, D. M. *J. Org. Chem.* 27 (1962) 1520.
7. Swain, C. G. and Langsdorf, W. P., Jr. *J. Am. Chem. Soc.* 73 (1951) 2813.
8. Thorstenson, T. and Songstad, J. *Acta Chem. Scand. A* 30 (1976) 781.
9. Bjorøy, M., Saunders, B. B., Esperås, S. and Songstad, J. *Phosphorus* 6 (1976) 83.
10. Austad, T., Engemyr, L. B. and Songstad, J. *Acta Chem. Scand.* 25 (1971) 3535.
11. Springer, C. H., Coetzee, J. F. and Kay, R. L. *J. Phys. Chem.* 73 (1969) 471.
12. Snee, R. A. *Acc. Chem. Res.* 6 (1973) 46.
13. McLennan, D. J. *Acc. Chem. Res.* 9 (1976) 281.
14. Ko, E. C. F. and Parker, A. J. *J. Am. Chem. Soc.* 90 (1968) 6447.
15. Streitwieser, A., Jr. *Solvolytic Displacement Reactions*, McGraw-Hill, New York 1962.
16. Hudson, R. F. and Klopman, G. *J. Chem. Soc.* (1962) 1062.
17. Klopman, G. and Hudson, R. F. *Helv. Chim. Acta* 44 (1961) 1914.
18. Thornton, E. R. *J. Am. Chem. Soc.* 89 (1967) 2915.
19. Frisone, G. J. and Thornton, E. R. *J. Am. Chem. Soc.* 90 (1968) 1211.
20. Harris, J. C. and Kurz, J. L. *J. Am. Chem. Soc.* 92 (1970) 349.
21. Hammond, G. S. *J. Am. Chem. Soc.* 77 (1955) 334.
22. Grimsrud, E. P. and Taylor, J. W. *J. Am. Chem. Soc.* 92 (1970) 739.
23. Kolling, O. W. and Mawdsley, E. A. *Inorg. Chem.* 9 (1970) 408.
24. This study.
25. Ceccon, A. and Sartori, S. *J. Organomet. Chem.* 50 (1976) 161.
26. Thorstenson, T. and Songstad, J. *Unpublished results*.
27. Haberfeld, P., Nudelman, A., Bloom, A., Romm, R. and Ginsberg, H. *J. Org. Chem.* 36 (1971) 1792.
28. Baker, J. W. *J. Chem. Soc.* (1936) 1448.

Received November 29, 1976.

On the Mechanism of Radical Formation during UV Irradiation of Polar Solutions of Aromatic Molecules at 77 K

JOHAN MOAN

Norsk Hydro's Institute for Cancer Research, The Norwegian Radium Hospital, Montebello, Oslo 3, Norway

Frozen polar solutions of the aromatic amino acids L-tryptophan and L-tyrosine have been exposed to UV-light of wavelengths 254 and 310 nm. The kinetics of radical formation and triplet formation and decay have been studied by ESR methods. A significant fraction of the ejected electrons recombine with their mother ions. When an electron scavenger is present this recombination is prevented, whereby the total radical yield increases. In the absence of scavenger the recombination probability increases with increasing irradiation time.

Furthermore, it is concluded that monophotonic processes do not contribute significantly to radical formation. The radical formation mechanism is biphotonic ionization and the intermediate in all cases studied, except possibly one, is the triplet state. The exception is L-tryptophan irradiated at 310 nm, where the intermediate seems to have shorter lifetime than the triplet state.

Numerous investigations of the mechanisms of photoionization of aromatic molecules have been published. Most authors seem to agree that the ionization process in rigid glasses at low temperatures is biphotonic with the triplet state as an intermediate. However, some authors^{1,2} conclude from their data that monophotonic processes also contribute, notably at the shorter wavelengths. This seems probable since in most cases solvated electrons seem to be formed in monophotonic processes in liquid solutions. If molecules in the triplet state are the only intermediates, the rate of radical production should be proportional to the number of molecules in the triplet state. Hélène *et al.*³ have investigated this in the case of nucleic acid derivatives in an alcohol glass, and their data indicate that there is no proportionality. Thus

we found it worthwhile to investigate this problem more thoroughly.

Model

It can easily be shown⁴ that the number N_s of biphotonic ionization events should follow the equation:

$$N_s = \frac{K_1 C_s \epsilon_M I^2}{k + aI} \left[t - \frac{1}{k + aI} (1 - e^{-(k+aI)t}) \right] \quad (1)$$

where K_1 is a constant, I is the intensity of the UV light, t is the time after onset of the light, k is the rate constant of decay of the intermediate, ϵ_M is the extinction coefficient of the intermediate (related to natural logarithms), C_s is the quantum efficiency for permanent ionization of the intermediate; *i.e.* ionization that results in radicals which are longlived enough to be registered.

$$a = C_s \epsilon_M + C_M \epsilon_0 \quad (2)$$

where ϵ_0 is the extinction coefficient of the ground state and C_M is the quantum efficiency for production of the intermediate state. For a clarifying scheme of the biphotonic ionization model see Fig. 1 in Ref. 4. Eqn. (1) is correct only when a small fraction of the molecules in the ground state is affected. The number of molecules in the metastable state should follow the equation:

$$N_M = \frac{K_1 I}{k + aI} (1 - e^{-(k+aI)t}) \quad (3)$$

If monophotonic processes contribute, eqn. (1) will take the form:

$$N_s = \frac{K_1 C_s \epsilon_M I^2}{k + aI} \left[t - \frac{1}{k + aI} (1 - e^{-(k+aI)t}) \right] + K_2 I t \quad (4)$$

where K_2 is a constant.

Eqn. (1) describes a curve that approaches a straight line as t increases. This line intercepts the t -axis in

$$t_0 = 1/(k + aI) \quad (5)$$

As $t \rightarrow 0$ the slope of the curve approaches 0 while the curve described by eqn. (4) has a slope that approaches $K_2 I$ as $t \rightarrow 0$. Thus by measuring the ionization yield accurately for short irradiation times it can be determined whether monophotonic processes contribute. Furthermore, if the triplet state is the only intermediate the rise time τ_R defined by the equation $N_M = \text{const} (1 - e^{-t/\tau_R})$ should be equal to t_0 . τ_M can easily be measured by either ESR or phosphorescence methods. If monophotonic processes contribute t_0 should be smaller than τ_R according to eqn. (4). Generally, if intermediates with a lifetime different from that of the triplet state are involved t_0 should be different from τ_R .

According to (1) and (3) the following equation is correct when $t \gg t_0$:

$$\frac{dN_s}{dt} = C_s \epsilon_M I N_M \quad (6)$$

Thus, in processes where the triplet state is the only intermediate the rate of radical production is proportional to the number of molecules in the triplet state, provided C_s , the quantum efficiency of radical production by the second quantum, is constant. I and ϵ_M are supposed to be constant. If C_s changes with the irradiation time because of a change in the probability of recombination of shallowly trapped electrons τ_R will also change according to the equation:

$$\tau_R = t_0 = \frac{1}{k + (C_s \epsilon_M + C_M \epsilon_0) I} \quad (7)$$

EXPERIMENTAL

The solvent was a mixture of ethylene glycol and water (EG/H₂O) 1:1 by volume. To this solvent tyrosine or tryptophan of analytical grade from Sigma Chem. Co. was added, usually in a concentration of 2.5×10^{-2} M. CCl₃COONa of analytical grade from Merck was used as an electron scavenger. 100 μ l of sample solution was transferred to quartz ESR tubes and cooled to 77 K by immersion in liquid N₂. The samples were exposed to the light from a 200 W high pressure mercury lamp fitted to a Bausch &

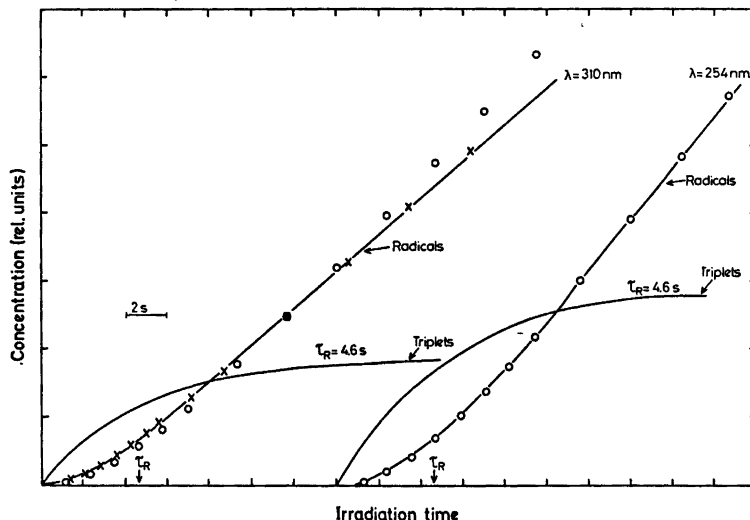


Fig. 1. The yield of radicals and triplets as a function of the exposure time in 2.5×10^{-2} M solution of L-tryptophan in EG/H₂O containing 0.1 M CCl₃COONa as an electron scavenger. The full lines are the experimental curves. O represents curves described by eqn. 1, under the assumption that $t_0 = \tau_R = 4.6$ s. X represents a similar curve with $t_0 = 2.9$ s. The light intensity at 310 nm was adjusted to make τ_R equal at the two wavelengths.

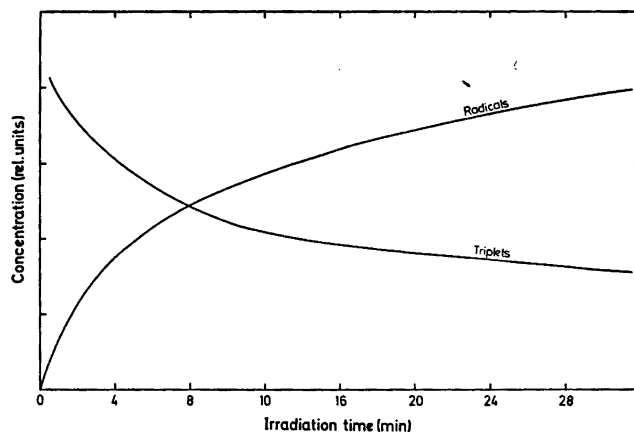


Fig. 2. The yield of radicals and triplets as a function of the exposure time on a longer timescale than in Fig. 1. The wavelength of the UV-light was 310 nm, but similar results were found also at 254 nm.

Lomb grating monochromator. The irradiation took place in the cavity of the ESR spectrometer and the concentration of radicals or molecules in the triplet state could be measured during the irradiation. The light intensities at 254 and 310 nm at full slit widths were, respectively, 10^{-10} and 10^{-9} Einstein/mm² s. The band width was 30 nm.

The ESR spectrometer was an X-band instrument with reflection cavity, operating at 9200 MHz.

RESULTS AND DISCUSSION

In the following experiment we found it necessary to add an electron scavenger since the trapped electrons are readily bleached by the UV light. 0.1 M CCl₃COONa is sufficient to reduce the yield of trapped electrons to less than 5% of that found in the absence of scavengers. The scavenger radicals were unbleachable by the UV-doses used in this work. This was confirmed by exposing an X-irradiated sample of 0.1 M CCl₃COONa in EG/H₂O (which contained the same radicals as an UV irradiated sample) to UV light. It was confirmed that UV irradiation of 0.1 M CCl₃COONa without tyrosine and tryptophan only gave insignificant amounts of radicals, which in no case is of importance for the present results. It was also checked that the presence of oxygen had no influence on the results. Fig. 1 shows the yield *vs.* time curves. It can be seen that the slope of the curve approaches 0 as $t \rightarrow 0$. These curves

can be very accurately reproduced, and it is found that at $t = 15$ s, monophotonic processes contribute less than 5% to the radical production at both wavelengths. Similar results were found also for tyrosine. Corresponding results were obtained in 0.5 M H₂SO₄, except for tryptophan at 254 nm, where the radical production is so slow that curves cannot be meas-

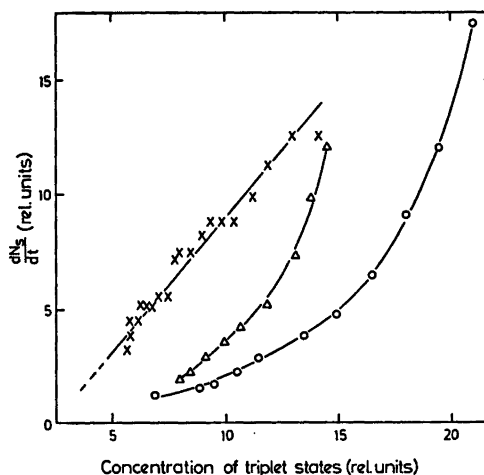


Fig. 3. The rate dN_s/dt of radical production as a function of the concentration of triplet states. ○ 2.5×10^{-2} M L-tryptophan in EG/H₂O containing 0.1 M CCl₃COONa irradiated at 310 nm. Δ, 3×10^{-2} M L-tyrosine in 0.5 M H₂SO₄ 310 nm. ×, data from a work of Hélène *et al.*³ for UV irradiation of 10^{-3} M purine in ethanol.

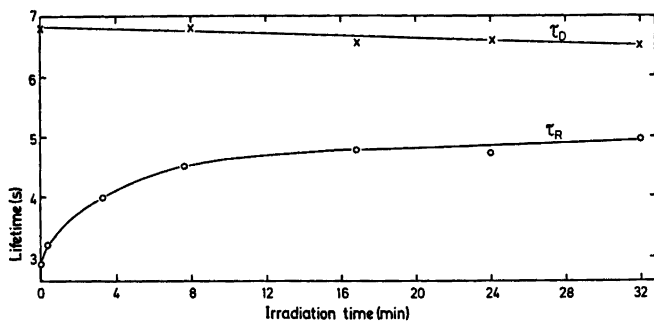


Fig. 4. The rise and decay lifetime of the triplet state of tryptophan as a function of the exposure time at 310 nm. The system is the same as that described under Fig. 1.

ured with sufficient accuracy. Thus in all cases the radical formation goes *via* a metastable intermediate.

Fig. 1 also shows the rise kinetics of the triplet state from which τ_R may be determined. It can be seen that at 254 nm there is excellent agreement between the experimental curve and the curve described by eqn. (1) on the assumption that $\tau_R = t_0$. The same was found for tyrosine at both wavelengths (254 and 310 nm). In the case of tryptophan irradiated with 310 nm light, however, it seems that $t_0 < \tau_R$ (Fig. 1). This may indicate that an intermediate other than the triplet state is involved. This state could be a "semiionized" state of the same type as that proposed by Ottolenghi⁵ to explain biphotonic ionization of aromatic molecules.

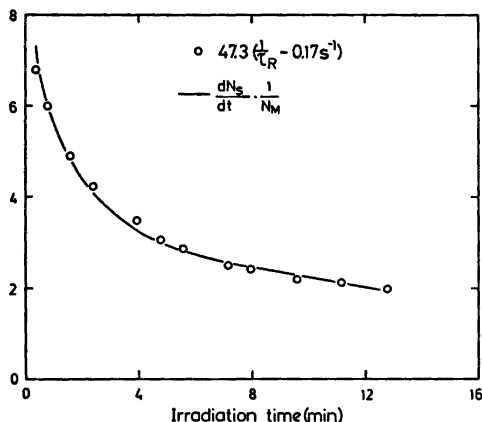


Fig. 5. The full line represents data from Fig. 2. $(dN_s/dt) (1/N_M)$ is plotted as a function of t . The points represent the curve $47.3 (1/\tau_R - 0.17 \text{ s}^{-1})$ i.e. C_s from eqn. 7 with $k + C_M \epsilon_0 I = 0.17 \text{ s}^{-1}$. τ_R is taken from Fig. 4.

Tryptophan has at least two electronic transitions in the wavelength region 250–305 nm.⁶ In principle, therefore, it is possible that one of these transitions populate the "semi-ionized" state while the other does not.

At extended irradiation times the concentration of molecules in the triplet state decreases as shown on Fig. 2. Similar observations were made by Neubacher and Walla⁷ for sensitized ethanol photolysis. The reason for this decrease could be (a) that the accumulation of radicals in the sample causes a quenching of the excited states of tryptophan or (b) that the irradiation results in a destruction of tryptophan molecules. Alternative (a) can be ruled out since X-irradiation of the sample with doses giving considerably larger amounts of radicals than UV irradiation (the same type of radicals are found in the two cases) has no effect on the concentration or lifetime of triplet states induced by UV light. Thus it seems that the UV irradiation causes a permanent destruction of tryptophan molecules.

Provided that the radical production results from triplet absorption and that the constants in eqns. (1) and (3) do not change with the UV dose, one should expect eqn. (6) to be correct for extended irradiation times. (It should be remembered that the same relationship will exist if another metastable state is involved alone or in addition to the triplet state. The number of molecules in such a state will be proportional to the number of molecules in the ground state and therefore also to the number of molecules in the triplet state). Fig. 2 shows that dN_s/dt decreases with t but dN_s/dt is not proportional to N_M as demonstrated in Fig. 3.

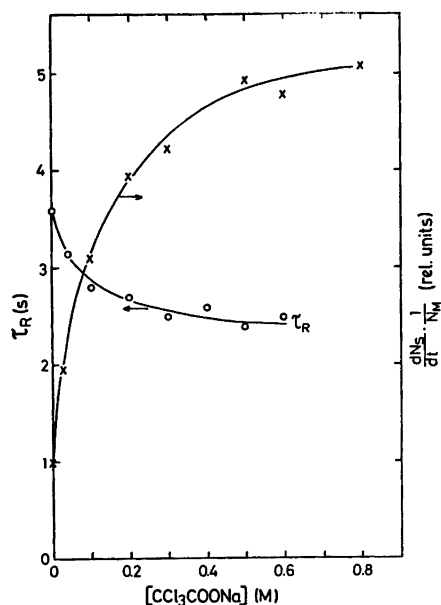


Fig. 6. Rise lifetime of the triplet state (τ_R) and $(dN_s/dt)/(1/N_M)$ as functions of the scavenger concentration. The system is 2.5×10^{-3} M L-tryptophan in EG/H₂O irradiated at 310 nm. The decay lifetime was practically constant (6.7 s) up to 0.6 M. Similar results were found at 254 nm.

In this figure is also shown some data for tyrosine in 0.5 M H₂SO₄ and some data from a work of H el ene *et al.*³ concerning UV irradiation of 10^{-3} M purine in ethanol. Their data show the same tendency though not as pronounced as in the present cases. Analysis of the data of Neubacher and Walla⁷ gives the same result. Thus it seems that this is a general trend being observed at both 310 and 254 nm and in different solvents. The following observation provides an explanation. The rise time τ_R of the triplet state increases with the UV-dose delivered to the sample as shown on Fig. 4. The same is true for t_0 . The decay lifetime of the triplet state does not change measurably. Therefore, the only quantity which may vary in the expression for the rise time [eqn. (7)] is C_s . (This treatment can easily be adapted to two metastable states). Thus C_s decreases with increasing irradiation time. In systems like the present one a significant fraction of the ejected electrons recombine spontaneously. (See below and Ref. 9). Thus C_s is made up of two terms:

$C_s = C_{s,ion}(1 - P_R)$. $C_{s,ion}$ is the initial probability of ionization and P_R is the probability of recombination of an ejected electron. This electron may be in a shallow trap for a short time.

According to eqn. (7) $C_s = \frac{1}{\epsilon_M I} \left(\frac{1}{\tau_R} - k - C_M \epsilon_0 I \right)$. As demonstrated in Fig. 5 the quantity $(1/\tau_R - 0.17 \text{ s}^{-1})$ varies in exactly the same way as $(dN_s/dt)/(1/N_M)$. Thus the model is in correspondence with these data, and it seems that the probability of recombination increases with increasing irradiation time. According to this picture the recombination probability should decrease if the concentration of electron scavenger is increased since the scavenger prevents some of the ejected electrons from recombining. This should cause an increase of C_s and hence a decrease of τ_R [eqn. (7)] and an increase of $(dN_s/dt)/(1/N_M)$. As shown on Fig. 6 the experimental data are in accordance with this. While the decay lifetime was found to be practically constant over the whole concentration range, the rise lifetime decreased markedly. Furthermore, the quantum efficiency of radical formation by the quanta absorbed by the triplet state increased by a factor of about 5 when the scavenger concentration increased from 0 to 0.8 M. This demonstrates that the scavenger prevents recombination.

A problem remaining to be solved is why C_s decreases with increasing irradiation time. The following is just a tentative explanation. In accordance with our earlier results⁹ we find that the total number of radicals in a sample irradiated for 20 s at 310 nm is higher than the number of tryptophan molecules. This means that each tryptophan molecule may give rise to more than one electron. Steen¹⁰ suggested that a tryptophan cation can be neutralized by capturing an electron from the solvent. This seems plausible also in the light of later experiments which indicate that there is almost no tryptophan ion radicals left after UV-irradiation of an ethylene glycol/water glass containing tryptophan.¹¹ Trapped electrons and ethylene glycol radicals are practically the only radicals observed. If this picture is correct, the majority of the tryptophan molecules in the sample will have solvent and scavenger radicals in their neighbourhood. This may reduce the probability of neutralization and therefore increase the probability of recombina-

tion of the ejected electrons. It is also possible that the proximity of tryptophan molecules runs short of scavenger molecules whereby the recombination probability obviously increases with the exposure time.

REFERENCES

1. Pailthorpe, M. T. and Nicholls, C. H. *Photochem. Photobiol.* 15 (1972) 465.
2. Jousot-Dubien, J. and Lesclaux, R. *The Triplet State*, Cambridge Univ. Press, London - New York 1967, p. 197.
3. Hélène, C., Santus, R. and Douzou, P. *Photochem. Photobiol.* 3 (1966) 127.
4. Moan, J. and Steen, H. B. *J. Phys. Chem.* 75 (1971) 2893.
5. Ottolenghi, M. *Chem. Phys. Lett.* 12 (1971) 339.
6. Weber, G. *Biochem. J.* 75 (1960) 335.
7. Neubacher, H. and Walla, W. *Radiat. Environ. Biophys.* 12 (1975) 51.
8. Kaalhus, O. and Moan, J. *Int. J. Radiat. Phys. Chem.* 6 (1975) 222.
9. Moan, J. *Israel J. Chem.* 9 (1971) 637.
10. Steen, H. B. *Photochem. Photobiol.* 9 (1969) 479.
11. Moan, J. and Kaalhus, O. *J. Chem. Phys.* 61 (1974) 3556.

Received October 7, 1976.

The Crystal Structure of V_3As_2

ROLF BERGER

Institute of Chemistry, University of Uppsala, Box 531, S-751 21 Uppsala, Sweden

The crystal structure of V_3As_2 has been determined by means of single-crystal diffractometry. The symmetry is tetragonal, space group $P4/m$, and lattice parameters $a=9.4128$ Å and $c=3.3361$ Å. The structure constitutes a new structure type related to the Ti_3Te_4 type.

Boller and Nowotny¹ assigned the composition V_3As_2 to a phase that was later² proved to be V_4As_3 (orthorhombic), and they also indicated the presence of further phases in this composition range.³ Since they gave no powder data, it is unclear whether their preparations contained V_3As_2 (*vide infra*) or even β - V_4As_3 ⁴ or β - V_5As_3 .⁵ This paper presents a complete single-crystal X-ray determination of the structure of V_3As_2 , showing that the proposed composition and the space-group assignment given earlier⁴ are correct.

EXPERIMENTAL

Preparation. V_3As_2 forms readily in silica-tube syntheses and decomposes at higher temperatures. The formation of V_3As_2 crystal aggregates, together with β - V_5As_3 , was reported earlier.⁵ The crystals, probably formed by a vapour transport process, were severely intergrown, making it difficult to find a single crystal.

Single-crystal diffractometry. A small needle-shaped crystal was selected for the intensity data collection. Its dimensions were $10 \times 12 \times 80$ μm and it was limited by $\{110\}$ and $\{001\}$ faces. The equipment and intensity-collecting procedure is described elsewhere.^{4,5} The part of the reciprocal space covered was limited by $-13 \leq h \leq 13$, $-13 \leq k \leq 13$ and $0 \leq l \leq 4$, corresponding to a maximum in 2θ of 60° . The instrumental and crystal setting stability was checked by remeasuring three reflexions at regular intervals throughout the data collection period. This procedure revealed no drift.

X-Ray powder investigations. The lattice dimensions were determined on powdered crystals using a Guinier-Hägg focussing camera equipped with $\text{CuK}\alpha_1$ radiation. Germanium ($a=5.657906$ Å) was added as an internal calibration standard, and the unit cell dimensions were refined by the method of least squares. Powder intensities were measured densitometrically using a SAAB Mark II film scanner. The powder data, presented for identification purposes, are collected in Table 1.

Numerical calculations. All calculations were performed on IBM 1800 and IBM 370/155 computers using local crystallographic programs.⁶ The calculations included an absorption correction (Gaussian grid) yielding the minimum and maximum transmission factors 0.67 and 0.74 for a linear absorption coefficient of 308 cm^{-1} .

STRUCTURE DETERMINATION

The preliminary Weissenberg and oscillation photographs revealed a primitive tetragonal cell, without any systematic absences among the reflexions. However, the Laue symmetry was either $4/m$ or $4/mmm$ for different crystals. This indicated that some crystals were in fact ideal twins showing false mirror planes, and that the true point group ought to be $4/m$. Unfortunately, this also implied that the absence of a (110) mirrorplane did not exclude the presence of at least some twin character. In fact, one early attempt to solve the structure failed because the data were marred by this effect. In order to avoid twinning, a smaller crystal was eventually selected, which did indeed show a more marked difference between the (hkl) and (khl) reflexions than any of the previously investigated crystals. The most probable space group was $P4/m$ (No. 83), with the atoms situated at $z=0$ and $z=\frac{1}{2}$, which was supported by the short axis and the

Table 1. Powder diffraction data (CrK α_1 radiation) for V₃As₂. Indices (*hkl*) denote both (*hkl*) and (*hkl*) reflexions. Cell dimensions: *a* = 9.4128(3) Å, *c* = 3.3361(2) Å.

<u>hkl</u>	Q $\times 10^5$ (Å ⁻²)		Intensity		<u>hkl</u>	Q $\times 10^5$ (Å ⁻²)		Intensity	
	obs.	calc.	obs.	calc.		obs.	calc.	obs.	calc.
100		1129	-	0	311	20263	20272	50{	32
110		2257	-	0	330	20313	20316		13
200	4510	4515	3	1	420	22579	22573	69	75
210	5637	5643	2	1	321	23661	23658	46	44
001		8985		1	401	27058	27044	4	4
220	9025	9029	35{	25	411	28173	28172		96
101	10111	10114	35{	16	430		28217	102{	12
300	10159	10158		7	500				1
111		11242	-	0	331	29337	29301	13{	4
310	11288	11287	31	26	510		29345		8
201		13500	-	0	421	31551	31558	25	24
211	14620	14628	103{	100	520	32727	32731	33	33
320		14673		3	002	35945	35941	67	67
221	18011	18014	40{	19	440		36117	-	0
400	18063	18059		15	102		37069	-	0
301	19144	19143	80{	80	431			47{	38
410		19187		5	501	37193	37202		10

similar intensity distribution of the *l* = 0 and *l* = 2 zones.

The Patterson sections $P(uv0)$ and $P(uv\frac{1}{2})$ were thus calculated, and a reasonable structure model was derived, consistent with 12 vanadium and 8 arsenic atoms to the cell. The approximate composition was deduced by considering the average atomic volume compared with those of the neighbouring phases. The approximate positional parameters were refined from Fourier syntheses, and eventually a series of full-matrix least-squares refinements was started, based on F in the preliminary stages and finally on F^2 to include reflexions with "negative intensity" values.^{7,8} The atomic scattering factors and dispersion corrections were taken from Ref. 9 and 10, respectively.

The first refinement on an averaged reflexion material with one scale factor, seven isotropic thermal parameters and eight positional parameters converged to $R(F) = 0.031$, the very weakest reflexions being given zero weight (378 reflexions). The introduction of anisotropic thermal parameters gave the residual index $R(F) = 0.023$. The strongest reflexions were systematically weaker than calculated, and therefore an extinction correction according to Coppens and Hamilton¹¹ was performed, neglecting effects of primary beam shape.¹² Since the same extinction occurs only for Friedel-related reflexions, averaging between equivalent non-identical reflexions was no longer permissible. Thirteen reflexions were excluded from the final refinement on F^2 ,

Table 2. Structure data for V₃As₂, including anisotropic thermal parameters U_{ij} ($\times 10^4$) Å². The form of the temperature factor is $\exp[-2\pi(U_{11}h^2 + U_{22}k^2 + 2U_{12}hk)\alpha^2 - 2\pi U_{33}l^2c^*{}^2]$; $U_{13} = U_{23} = 0$. Standard deviations in parentheses. Space group: $P4/m$ (No. 83).

Atom	Position	<i>x</i>	<i>y</i>	<i>z</i>	U_{11}	U_{22}	U_{33}	U_{12}
V(1)	4 <i>k</i>	.13335(9)	.17927(9)	$\frac{1}{2}$	72(4)	53(4)	80(4)	-0(3)
V(2)	4 <i>j</i>	.39694(9)	.28477(9)	0	61(4)	70(4)	66(5)	3(3)
V(3)	2 <i>f</i>	0	$\frac{1}{2}$	$\frac{1}{2}$	76(6)	99(6)	128(7)	26(4)
V(4)	1 <i>d</i>	$\frac{1}{2}$	$\frac{1}{2}$	$\frac{1}{2}$	40(4)	U_{11}	102(9)	0
V(5)	1 <i>a</i>	0	0	0	53(5)	U_{11}	103(9)	0
As(1)	4 <i>k</i>	.24604(5)	.41181(5)	$\frac{1}{2}$	54(2)	54(2)	62(3)	-2(2)
As(2)	4 <i>j</i>	.28481(5)	.03946(5)	0	64(2)	58(2)	60(2)	-2(2)

which yielded $R(F^2)=0.056$ and $R_w(F^2)=0.064$, with the corresponding $R(F)=0.055$ (1834 refl.). The agreement factors are defined below:

$$R(F^n) = \frac{\sum ||F_o^n| - |F_c^n||}{\sum |F_o^n|}$$

$$R_w(F^n) = \left[\frac{\sum w(|F_o^n| - |F_c^n|)^2}{\sum w|F_o^n|^2} \right]^{1/2} \quad n=1,2$$

Here, $w^{-1} = \sigma_c^2 + (p_n|F_o^n|)^2$, where σ_c is the standard deviation of F_o^n based on counting statistics, and p_n ($p_2=0.02$) is an empirical factor to allow for instrumental errors.

Superficially there does not seem to be any gain in the final refining model when comparing the R -values from the different series. However, the very low $R(F)=0.023$ relates to a reduced reflexion material, and intensity thresholds affect the R -value considerably while R_w is less sensitive.^{7,13} As regards the parameters, the result is not significantly different between refinements made on averaged or unaveraged material, but only the latter can be used for the appropriate extinction correction. For the crystal used in this determination, the mean path lengths for X-rays corresponding to equivalent reflexions are approximately the same and would lead to similar extinction corrections within an equivalent set. For comparison only, an extinction correction was performed on an averaged reflexion material. This refinement gave an $R(F^2)$ -value of 0.030 (495 refl.), considerably lower than 0.056 (1834 refl.). This might indicate that the whole material suffers from some twin character of the crystal, the effects of which are reduced in the averaging process. However, a ΔR normal probability plot¹⁴ for the unaveraged material had a slope of 0.97 and an intercept of -0.03 , indicating a fairly random error distribution and appropriate individual weights.

The structure data based on the final F^2 refinement are given in Table 2, while the structure factors can be obtained on request from the author.

DISCUSSION OF THE STRUCTURE

The structure of V_3As_2 constitutes a new structure type. A projection of the structure is shown in Fig. 1b. Its typical features are the metal b.c.c. units and the trigonal prismatic arrangements, both common structural

elements also in α - V_4As_3 ² and β - V_4As_3 ⁴ as well as in other transition metal compounds with phosphorus and arsenic.

The structure of V_3As_2 can be regarded as a "filled" Ti_5Te_4 structure,¹⁵ the latter being

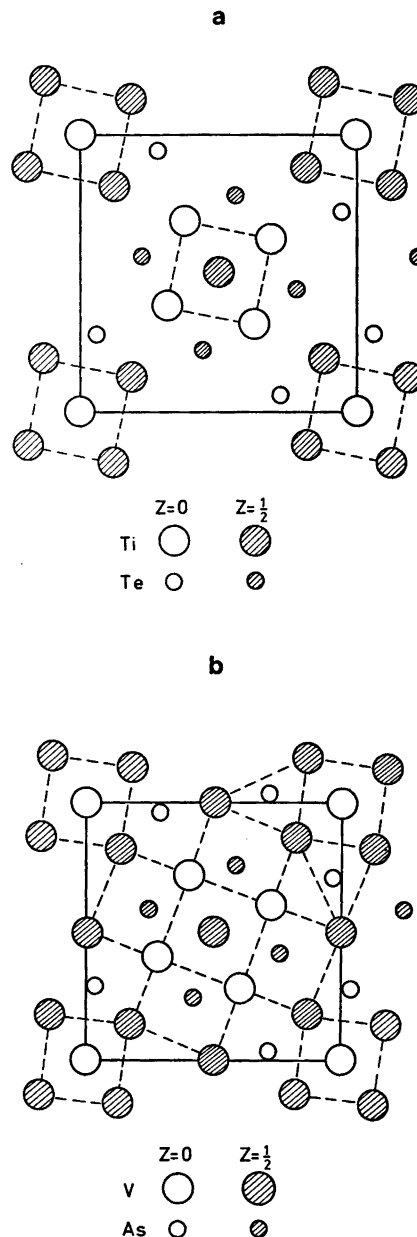


Fig. 1. The structures of (a) Ti_5Te_4 and (b) V_3As_2 projected on (001).

Table 3. Interatomic distances (Å) and coordination in V_3As_2 . Distances shorter than 3.5 Å are listed. Standard deviations in parentheses.

V(1) — As(1)	2.432(1)	V(4) — 4As(1)	2.531(0)
— 2As(2)	2.533(1)	— 8V(2)	2.798(1)
— 2As(2)	2.559(1)	— 2V(4)	3.336(0)
— 2V(5)	2.684(1)		
— 2V(1)	2.974(1)	V(5) — 8V(1)	2.684(1)
— 2V(2)	3.150(1)	— 4As(2)	2.706(0)
— V(3)	3.270(1)	— 2V(5)	3.336(0)
— 2V(1)	3.336(0)		
		As(1) — V(1)	2.432(1)
V(2) — 2As(1)	2.481(1)	— V(3)	2.460(0)
— 2As(1)	2.496(1)	— 2V(2)	2.481(1)
— As(2)	2.539(1)	— 2V(2)	2.496(1)
— 2V(4)	2.798(1)	— V(4)	2.531(0)
— 2V(1)	3.150(1)	— 2As(1)	3.336(0)
— 2V(2)	3.177(1)	— 2As(2)	3.381(1)
— 2V(3)	3.303(1)		
— 2V(2)	3.336(0)	As(2) — 2V(1)	2.533(1)
		— V(2)	2.539(1)
V(3) — 2As(1)	2.460(0)	— 2V(1)	2.559(1)
— 4As(2)	2.650(0)	— 2V(3)	2.650(0)
— 2V(1)	3.270(1)	— V(5)	2.706(0)
— 4V(2)	3.303(1)	— 2As(2)	3.336(0)
— 2V(3)	3.336(0)	— 2As(1)	3.381(1)

depicted in Fig. 1a. V_3As_2 is formally generated by inserting metal atoms in the octahedral voids formed by the non-metal atoms. The symmetry then changes from $I4/m$ to $P4/m$. Among the arsenides, the Ti_5Te_4 structure is adopted by Ta_5As_4 ¹⁶ and Mo_5As_4 .¹⁷ In this context it is interesting to note that, during their attempts to refine the Mo_5As_4 structure, Jensen and Kjekshus invariably found the Laue symmetry $4/mmm$ for their crystals due to twinning.

In view of the relationship between the V_3As_2 and Ti_5As_4 structures, new ternary compounds of the V_3As_2 type, such as $M_3M'X_4$, might possibly be formed by filling up binary Ti_5Te_4 structures with small metal atoms. This would lead to an increase in cell dimensions accompanied by a breakdown of the body-centring. The introduction of iron in Mo_5As_4 yields a unit cell decrease consistent with Mo-Fe substitution.

The interatomic distances in V_3As_2 are presented in Table 3. The V-As distances show no great deviations from those found in the other vanadium arsenides. It may be noted that the intermetallic distances within the non-equivalent b.c.c. units differ significantly, possibly owing to different environments around these units. Thus V(5) has eight vana-

dium neighbours at bonding distances, while V(4) is more tightly bound to its four arsenic neighbours. The thermal anisotropy is rather large for V(4), with relatively small components in the $z = \frac{1}{2}$ plane. This is similar to the situation in $\beta-V_4As_3$,⁴ where essentially the same coordination occurs. Here $U_{11} = 0.0041(2)$, $U_{33} = 0.0035(2)$ and $U_{13} = 0.0005(2)$, all being components in the corresponding plane, while the perpendicular component $U_{22} = 0.0093(3)$. Consequently, it is likely that the thermal parameters for V(4) as given in Table 2 are essentially correct and not the result of biased data.

The composition M_3X_2 is not common among the transition metal arsenides, the only representatives so far being Hf_3As_2 ¹⁸ and Zr_3As_2 ,¹⁹ both of the Hf_3P_2 type.²⁰ This, and also the Cr_3C_2 structure,²¹ are entirely built up of interconnected trigonal prisms, and their anti-types are found among the lanthanide and actinide sulfides.²²⁻²⁴ Anti-types to the V_3As_2 structure would hardly be found among these compounds because of the occurrence of the b.c.c. elements which have no counterpart among sulfide structures.

Acknowledgements. The author thanks Professor I. Olovsson for all the facilities provided and is also grateful to Professor S. Rundqvist

for his helpful comments. This work was financially supported by the Swedish Natural Science Research Council.

REFERENCES

1. Boller, H. and Nowotny, H. *Monatsh. Chem.* 97 (1966) 1053.
2. Yvon, K. and Boller, H. *Monatsh. Chem.* 103 (1972) 1643.
3. Boller, H. and Nowotny, H. *Monatsh. Chem.* 98 (1967) 2127.
4. Berger, R. *Acta Chem. Scand. A* 28 (1974) 771.
5. Berger, R. *Acta Chem. Scand. A* 30 (1976) 363.
6. Lundgren, J.-O., Ed., *Crystallographic Computer Programs*, Institute of Chemistry, University of Uppsala, Uppsala 1975, UUIC-B13-04-2.
7. Hirshfeld, F. L. and Rabinovich, D. *Acta Crystallogr. A* 29 (1973) 510.
8. Wilson, A. J. C. *Acta Crystallogr. A* 32 (1976) 781.
9. Doyle, P. A. and Turner, P. S. *Acta Crystallogr. A* 24 (1968) 390.
10. Cromer, D. T. and Libermann, D. *J. Chem. Phys.* 53 (1970) 1891.
11. Coppens, P. and Hamilton, W. C. *Acta Crystallogr. A* 26 (1970) 71.
12. Urban, J. P. *Acta Crystallogr. A* 32 (1976) 631.
13. Stenkamp, R. E. and Jensen, L. H. *Acta Crystallogr. B* 31 (1975) 1507.
14. *International Tables for X-Ray Crystallography*, Kynoch Press, Birmingham 1974, Vol. IV, p. 293.
15. Grønvold, F., Kjekshus, A. and Raaum, F. *Acta Crystallogr.* 14 (1961) 930.
16. Rundqvist, S., Carlsson, B. and Pontchour, C.-O. *Acta Chem. Scand.* 23 (1969) 2188.
17. Jensen, P. and Kjekshus, A. *Acta Chem. Scand.* 20 (1966) 1309.
18. Rundqvist, S. and Carlsson, B. *Acta Chem. Scand.* 22 (1968) 2395.
19. Carlsson, B., Gölin, M. and Rundqvist, S. *Acta Chem. Scand. A* 30 (1976) 386.
20. Lundström, T. *Acta Chem. Scand.* 22 (1968) 2191.
21. Rundqvist, S. and Runnsjö, G. *Acta Chem. Scand.* 23 (1969) 1191.
22. Sleight, A. W. and Prewitt, C. T. *Inorg. Chem.* 7 (1968) 2282.
23. Range, K.-J. and Leeb, R. *Z. Krist.* 140 (1974) 424.
24. Zachariasen, W. H. *Acta Crystallogr.* 2 (1949) 291.

Received December 1, 1976.

The Crystal and Molecular Structure of 2-*t*-Butyl-6-phenyl-5,6-diaza-1,6a-dithiapentalene, a New Thiathiophthene Analogue

LARS K. HANSEN and KNUT TOMREN

Department of Chemistry, Institute for Mathematical and Physical Sciences, University of Tromsø, Box 790, 9001 Tromsø, Norway

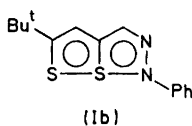
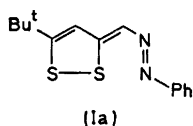
The title compound crystallizes in the monoclinic space group $P2_1/c$ with four molecules in a unit cell of dimensions, $a = 12.483(3)$, $b = 6.134(2)$, $c = 19.388(8)$ Å, and $\beta = 107.35(3)^\circ$.

X-Ray data were collected on a Siemens AED diffractometer using $\text{MoK}\alpha$ radiation and the five-value scan technique. The structure was solved by Patterson methods and refined by full matrix least squares.

The title compound may be described as a 5,6-diaza analogue of 6a-thiathiophthene. The central ring system is planar and the 2-*t*-butyl group and the 6-phenyl group point slightly out of this plane, the phenyl group is twisted 2.5° about the connecting bond N(6)–C(11).

Bond lengths in the central part of the molecule: S(1)–S(6a) = 2.435(1) and S(6a)–N(6) = 1.849(3) Å with the angle S(1)–S(6a)–N(6) = 171.66(9)°, S(1)–C(2) = 1.711(3), S(6a)–C(3a) = 1.735(3), N(6)–N(5) = 1.330(4), C(2)–C(3) = 1.376(5), C(3)–C(3a) = 1.400(4), C(3a)–C(4) = 1.405(5) and C(4)–N(5) = 1.320(4) Å. The connecting bonds C(2)–C(7) and N(6)–C(11) are 1.525(4) and 1.414(4) Å, respectively. The bond lengths have been corrected for libration.

Christie *et al.*^{1,2} have shown that the reaction of 2-*t*-butyl-3-methyl-1,2-dithiolium perchlorate with benzene diazonium fluoroborate yields a compound, which, on the basis of spectral data, may be formulated either as an azo-coupling product of a 1,2-dithole (Ia) or as a diaza analogue of a 6a-thiathiophthene (Ib). An X-ray structure study has been carried out in order to find which formulation would be the correct one.



STRUCTURE ANALYSIS

A sample of the title compound was generously supplied by Reid.^{1,2} The crystals are dark red prisms.

Crystal data.

$\text{C}_{14}\text{H}_{16}\text{N}_2\text{S}_2$ M.W. = 276.41
 Monoclinic, space group $P2_1/c$ with $Z = 4$
 $a = 12.483(3)$ Å, $b = 6.134(2)$ Å, $c = 19.388(8)$ Å,
 $\beta = 107.35(3)^\circ$
 $V = 1417.0$ Å³
 $D_x = 1.296$ g/cm³, $D_m = 1.30$ g/cm³
 $\mu_{\text{MoK}\alpha} = 3.51$ cm⁻¹

Unit cell dimensions and intensity data were measured on a paper-tape controlled Siemens AED diffractometer using $\text{MoK}\alpha$ radiation.

A least squares procedure on the 2θ values of 11 high order reflections, measured at 20°C , gave the cell dimensions quoted above. The crystal used for all X-ray measurements had the dimensions 0.2 mm × 0.4 mm × 0.2 mm in the axial directions.

The intensities of 3092 independent reflections within $\theta = 27^\circ$ were measured by means of the five-value scan technique.³ 1322 of these were regarded as unobserved because their intensities were smaller than the chosen threshold value $2\sigma(I)$.

Corrections for Lorentz and polarization effects were carried out in the usual way. Absorption corrections were considered unnecessary.

Scattering factors from the *International Tables*⁴ were used for sulfur, nitrogen and carbon, and a scattering factor curve given by Stewart *et al.*⁵ was used for hydrogen.

Table 1. Atomic coordinates in fractions of corresponding cell edges. The standard deviations in parentheses refer to the last digits of the respective values.

Atom	<i>x</i>	<i>y</i>	<i>z</i>
S(1)	0.22744(7)	0.25388(14)	0.23276(5)
S(6a)	0.05608(7)	0.12632(13)	0.14571(5)
N(6)	-0.06847(20)	-0.00975(42)	0.08569(14)
C(2)	0.24815(25)	0.01698(51)	0.28011(17)
C(3)	0.16809(27)	-0.14019(56)	0.25636(18)
C(3a)	0.07596(25)	-0.11151(47)	0.19509(17)
C(4)	-0.00861(30)	-0.26229(61)	0.16462(21)
N(5)	-0.08659(23)	-0.20947(44)	0.10452(16)
C(7)	0.35402(26)	-0.01867(55)	0.34289(18)
C(8)	0.40080(51)	0.19870(90)	0.37830(31)
C(9)	0.44080(41)	-0.12446(120)	0.31111(32)
C(10)	0.32947(58)	-0.16938(142)	0.39855(34)
C(11)	-0.13912(25)	0.07984(51)	0.02122(17)
C(12)	-0.23220(30)	-0.03041(69)	-0.02076(22)
C(13)	-0.29910(34)	0.06334(77)	-0.08271(23)
C(14)	-0.27482(32)	0.26629(79)	-0.10432(22)
C(15)	-0.18324(32)	0.37615(72)	-0.06334(20)
C(16)	-0.11518(31)	0.28391(63)	-0.00049(20)
H(3)	0.171(2)	-0.282(5)	0.279(2)
H(4)	-0.011(2)	-0.399(5)	0.184(2)
H(81)	0.467(3)	0.168(6)	0.418(2)
H(82)	0.343(4)	0.245(9)	0.403(3)
H(83)	0.432(4)	0.293(9)	0.334(3)
H(91)	0.459(4)	-0.012(8)	0.280(3)
H(92)	0.393(5)	-0.301(11)	0.298(3)
H(93)	0.506(4)	-0.138(7)	0.350(2)
H(101)	0.394(4)	-0.189(7)	0.434(2)
H(102)	0.279(7)	-0.071(15)	0.414(4)
H(103)	0.314(5)	-0.334(11)	0.376(3)
H(12)	-0.249(3)	-0.164(5)	-0.005(2)
H(13)	-0.366(3)	-0.009(7)	-0.111(2)
H(14)	-0.322(3)	0.336(6)	-0.146(2)
H(15)	-0.160(3)	0.522(6)	-0.077(2)
H(16)	-0.055(3)	0.359(6)	0.028(2)

The sulfur positions were found from a three-dimensional Patterson map, the nitrogen and carbon atoms revealed themselves during subsequent Fouriers, and the hydrogen positions were found from difference maps. The atomic parameters were refined by full matrix least squares (*cf.* Ref. 6) to an *R* of 0.04.

Final atomic coordinates and temperature parameters are listed in Tables 1 and 2, respectively. The final structure factor list is available on request.

Rigid body analyses for the entire molecule as well as for certain parts of the molecule have been carried out according to the method of Schomaker and Trueblood.⁷ The parts of the molecule treated in this way are the central

ring system and the phenyl group plus N(6). The corresponding librational tensors are given in Table 3. One notes from the values there that the libration is rather anisotropic in each case.

All the calculations mentioned above were carried out on the UNIVAC 1110 computer at the University of Bergen. The programs, with a few exceptions, originate from the Weizmann Institute of Science, Rehovoth, Israel.

DISCUSSION

The molecular structure of the title compound with numbering of atoms is shown in Fig. 1.

The central ring system is almost planar. Deviations from a least squares plane through

Table 2. Temperature parameters U_{ij} (\AA^2) for sulfur, nitrogen and carbon, and U (\AA^2) for hydrogen. The expressions used are $\exp\{-2\pi^2(h^2a^{*2}U_{11} + \dots + 2hka^*b^*U_{12} + \dots)\}$ and $\exp\{-8\pi^2U(\sin^2\theta/\lambda^2)\}$. The U_{ij} 's and the U 's are multiplied by 10^4 and 10^3 , respectively. Standard deviations in parentheses refer to the last digits of the respective values.

Atom	U_{11}	U_{22}	U_{33}	U_{12}	U_{23}	U_{13}
S(1)	685(6)	467(5)	738(6)	-97(5)	104(5)	56(4)
S(6a)	585(5)	389(4)	641(5)	-24(4)	24(4)	166(3)
N(6)	527(15)	461(15)	625(17)	-52(13)	-11(14)	192(13)
C(2)	548(19)	471(18)	580(19)	59(16)	47(16)	227(15)
C(3)	598(20)	402(18)	668(22)	24(17)	72(19)	275(18)
C(3a)	520(18)	381(16)	656(20)	1(15)	15(16)	252(15)
C(4)	666(23)	436(20)	779(26)	-76(19)	60(20)	260(20)
N(5)	649(18)	509(17)	747(20)	-140(14)	2(15)	229(16)
C(7)	562(20)	587(21)	616(21)	7(17)	64(19)	179(17)
C(8)	939(37)	1025(39)	951(38)	-18(32)	-110(36)	-108(34)
C(9)	642(29)	1406(53)	1104(40)	370(35)	121(42)	200(30)
C(10)	1088(43)	1490(62)	882(37)	-228(43)	600(42)	-55(33)
C(11)	477(18)	532(20)	578(20)	-12(16)	-75(16)	221(16)
C(12)	609(24)	647(25)	745(26)	-56(21)	-37(23)	198(20)
C(13)	606(25)	908(34)	784(29)	-69(23)	-110(25)	77(22)
C(14)	614(24)	898(31)	663(25)	109(25)	22(26)	112(20)
C(15)	720(25)	711(26)	721(26)	-3(23)	63(24)	193(21)
C(16)	598(22)	668(25)	658(24)	-82(20)	19(21)	104(19)

Atom	U	Atom	U	Atom	U
H(3)	58(9)	H(92)	202(27)	H(12)	59(10)
H(4)	53(9)	H(93)	101(14)	H(13)	105(13)
H(81)	103(14)	H(101)	104(15)	H(14)	93(13)
H(82)	149(23)	H(102)	309(56)	H(15)	93(13)
H(83)	170(22)	H(103)	180(27)	H(16)	80(11)
H(91)	129(20)				

the atoms of this part of the molecule, with triple weight on sulfur, are, S(1) - 0.002, S(6a) 0.014, N(6) - 0.026, C(2) - 0.030, C(3) 0.007, C(3a) 0.022, C(4) 0.016, and N(5) - 0.028 Å. The *t*-butyl and phenyl groups point slightly out of this plane. Thus, C(7) lies - 0.166 Å out of this plane, and the deviations for C(11) and C(14) are - 0.117 and - 0.289 Å, respectively. The phenyl group is twisted 2.5° about the N(6)-C(11) bond. This twist angle was taken as the angle between the normal to the plane through N(6), C(11), C(12), and C(16), and the normal to the plane through N(6), C(11), N(5), and S(6a).

Bond lengths and angles with standard deviations, calculated from the values in Table 1, are listed in Tables 4 and 5, respectively. We realize that a more realistic estimate of the standard deviations might probably be obtained by multiplying those given by a factor of two.⁸

The bond lengths between non-hydrogen atoms have been corrected for rigid body

libration,⁹ and the values l' , l'' and l''' in Table 4 include corrections according to L_1 , L_2 , and L_3 , respectively, cf. Table 3.

Table 3. Rigid body libration tensors for the entire molecule (L_1), the central ring system (L_2), and the phenyl group plus N(6) (L_3).

	Eigenvalues($^\circ$) ²	Eigenvectors (direction cosinus $\times 10^4$ relative to a , b , and c^* , respectively)			
L_1	54.72	-5845	1024	-8049	
	8.74	-6538	-6469	3925	
	6.53	-4805	7557	4450	
L_2	43.77	-5914	-50	-8064	
	6.68	-7653	-3117	5632	
	2.94	-2541	9502	1804	
L_3	67.22	-2128	5179	-8286	
	11.98	-1969	-8533	-4828	
	9.68	-9571	603	2835	

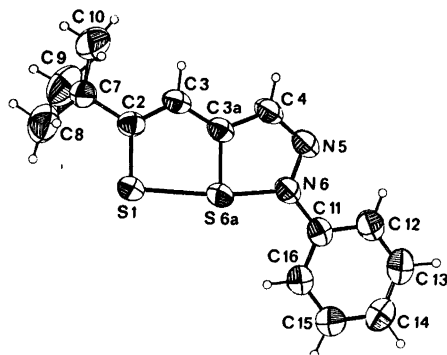


Fig. 1. The 2-*t*-butyl-6-phenyl-5,6-diaza-1,6a-dithiapentalene molecule with numbering of sulfur, nitrogen and carbon atoms. Thermal ellipsoids are shown. The thermal ellipsoids enclose 50 % probability.

One notes that there are only minor differences between the l' and the l'' values, and we have chosen the former to represent the dimensions of the central ring system and the *t*-butyl group. A comparison of the l' and the l''' values show pronounced differences for two of the bonds, namely C(11)–C(12) and C(14)–C(15), the differences are 0.008 and 0.007 Å, respec-

Table 4. Bond lengths l in 2-*t*-butyl-6-phenyl-5,6-diaza-1,6a-dithiapentalene. Standard deviations are given in parentheses. The l' , l'' , and l''' values have been corrected for libration according to the librational tensors L_1 , L_2 , and L_3 , respectively.

Bond	l (Å)	l' (Å)	l'' (Å)	l''' (Å)
S(1)–S(6a)	2.426(1)	2.435	2.431	
S(6a)–N(6)	1.841(3)	1.849	1.846	
S(1)–C(2)	1.697(3)	1.711	1.709	
S(6a)–C(3a)	1.722(3)	1.735	1.733	
N(6)–N(5)	1.317(4)	1.330	1.327	
C(2)–C(3)	1.366(5)	1.376	1.373	
C(3)–C(3a)	1.396(4)	1.400	1.399	
C(3a)–C(4)	1.395(5)	1.405	1.402	
C(4)–N(5)	1.317(4)	1.320	1.319	
C(2)–C(7)	1.522(4)	1.525		
C(7)–C(8)	1.533(6)	1.547		
C(7)–C(9)	1.540(8)	1.555		
C(7)–C(10)	1.520(9)	1.534		
N(6)–C(11)	1.409(4)	1.414		1.414
C(11)–C(12)	1.380(5)	1.387		1.395
C(12)–C(13)	1.369(6)	1.373		1.373
C(13)–C(14)	1.376(7)	1.389		1.388
C(14)–C(15)	1.360(6)	1.367		1.374
C(15)–C(16)	1.382(5)	1.387		1.387
C(16)–C(11)	1.381(5)	1.395		1.394

tively, as compared with the corresponding standard deviations of 0.005 and 0.006 Å. Such differences may be expected when the phenyl group has some additional libration relative to the other part of the molecule.¹⁰ The l''' values were therefore taken to represent the lengths of the C–C bonds of the phenyl group.

The S(1)–S(6a) bond of 2.435(1) Å, *cf.* Table 4, and the S(6a)–N(6) bond of 1.849(3) Å are partial bonds weaker than corresponding single bonds. The former is 16 % longer than the proposed length of 2.10 Å for the S–S single bond in a *cis* planar disulfide group,¹¹ and the latter is 5.7 % longer than the sum of the covalent radii for sulfur and nitrogen, 1.75 Å.¹² Furthermore, in 3,4-diphenyl-6a-thiathiophthene¹³ where the S(1)–S(6a) bond of 2.43 Å is almost equal to that of the present structure, the S(6a)–S(6) bond is 2.24 Å, and thus 6.7 % longer than the corresponding single bond. The

Table 5. Bond angles \angle (ijk) in 2-*t*-butyl-6-phenyl-5,6-diaza-1,6a-dithiapentalene. Standard deviations are given in parentheses.

j	k	\angle (ijk) ^o	
C(2)	S(1)	S(6a)	93.48(10)
S(1)	S(6a)	N(6)	171.66(9)
S(1)	S(6a)	C(3a)	86.30(10)
C(3a)	S(6a)	N(6)	85.52(12)
S(6a)	N(6)	C(11)	124.8(2)
S(6a)	N(6)	N(5)	115.4(2)
N(5)	N(6)	C(11)	119.7(2)
N(6)	N(5)	C(4)	109.4(3)
N(5)	C(4)	C(3a)	118.6(3)
C(4)	C(3a)	S(6a)	111.1(2)
C(4)	C(3a)	C(3)	127.2(3)
S(6a)	C(3a)	C(3)	121.7(2)
C(3a)	C(3)	C(2)	122.1(2)
C(3)	C(2)	S(1)	116.4(2)
C(3)	C(2)	C(7)	122.8(3)
S(1)	C(2)	C(7)	120.8(2)
C(2)	C(7)	C(8)	110.9(3)
C(2)	C(7)	C(9)	106.7(3)
C(2)	C(7)	C(10)	110.1(3)
C(8)	C(7)	C(9)	109.0(4)
C(8)	C(7)	C(10)	110.0(4)
C(9)	C(7)	C(10)	110.0(5)
N(6)	C(11)	C(12)	121.7(3)
N(6)	C(11)	C(16)	119.3(3)
C(12)	C(11)	C(16)	119.0(3)
C(11)	C(12)	C(13)	119.8(3)
C(12)	C(13)	C(14)	121.0(3)
C(13)	C(14)	C(15)	119.6(4)
C(14)	C(15)	C(16)	120.1(4)
C(15)	C(16)	C(11)	120.5(3)

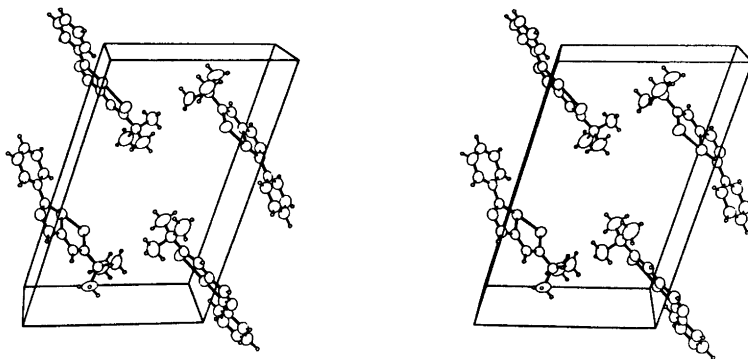


Fig. 2. Stereoview of the molecular packing.

present molecule may therefore be described as a 5,6-diaza analogue of 6a-thiathiophthene.

Another characteristic feature for thiathiophthenes is the difference in length between the central C(3)–C(3a) and C(3a)–C(4) bonds and the terminal C(2)–C(3) and C(4)–C(5) bonds,¹⁴ the former being somewhat longer and the latter somewhat shorter than the aromatic C–C bond in benzene, 1.397 Å. The same structural feature is found in the present molecule. Thus, the lengths of the central C–C bonds are 1.400(4) and 1.405(5) Å, respectively, and the length of the C(2)–C(3) bond is 1.376(5) Å. The C(4)–N(5) bond is found to be 1.320(4) Å as compared with the length of the aromatic C–N bond of 1.340 Å in pyridine.¹⁵

Finally it should be mentioned that the S(6a)–C(3a) bond length of 1.735(3) Å and the S(1)–C(2) bond lengths of 1.711(3) Å agree with the lengths usually found for such bonds in thiathiophthenes,¹⁴ and the N(5)–N(6) bond of 1.330(4) Å fits nicely into this picture.

The connecting bond N(6)–C(11) = 1.414(4) Å has some double bond character, and the phenyl group shows slight quinoid features. Thus, the average length of C(12)–C(13) and C(15)–C(16) is 1.380 Å, while the average length of the other C–C bonds of the phenyl group is 1.388 Å.

A stereoscopic view¹⁶ of the molecular packing in the unit cell is given in Fig. 2. There are no intermolecular contacts shorter than corresponding van der Waals distance.

Acknowledgements. The authors are indebted to Dr. D. H. Reid, Department of Chemistry, The University, St. Andrews, Scotland, for providing a sample of 2-*t*-butyl-6-phenyl-5,6-diaza-1,6a-dithiapentalene. Furthermore we wish to thank

Professor Asbjørn Hordvik for helpful discussions and advice.

REFERENCES

- Christie, R. M., Ingram, A. S., Reid, D. H. and Webster, R. G. *Chem. Commun.* (1973) 92.
- Christie, R. M. and Reid, D. H. *J. Chem. Soc. Perkin Trans. 1* (1976) 228.
- Troughton, P. G. H. *Siemens Review XXXVII* (1970), Fourth Special Issue: X-Ray and Electron Microscopy News.
- International Tables for X-Ray Crystallography*, Kynoch Press, Birmingham 1968, Vol. III, p. 202.
- Stewart, R. F., Davidson, E. R. and Simpson, W. T. *J. Chem. Phys.* 42 (1965) 3175.
- Hordvik, A. and Sæthre, L. J. *Acta Chem. Scand.* 26 (1972) 3114.
- Schomaker, V. and Trueblood, K. N. *Acta Crystallogr. B* 24 (1968) 63.
- Hamilton, W. C. and Abrahams, S. C. *Acta Crystallogr. A* 26 (1970) 18.
- Cruickshank, D. W. J. *Acta Crystallogr.* 9 (1957) 757; 14 (1961) 896.
- Hordvik, A. *Acta Chem. Scand.* 25 (1971) 1583.
- Hordvik, A. *Acta Chem. Scand.* 20 (1966) 1885.
- Pauling, L. *The Nature of the Chemical Bond*, 3rd Ed., Cornell University Press, Ithaca, New York 1960.
- Johnson, P. L. and Paul, I. C. *Chem. Commun.* (1969) 1014; *J. Chem. Soc. Perkin Trans. 2* (1976) 234.
- Hansen, L. K. and Hordvik, A. *Acta Chem. Scand.* 27 (1973) 411.
- Bak, B., Hansen-Nygaard, L. and Rastrup-Andersen, J. *J. Mol. Spectrosc.* 2 (1958) 361.
- Johnson, C. K. *A Fortran Thermal Ellipsoid Plot Program for Crystal Structure Illustrations*, ORNL-3794, Oak Ridge National Laboratory, Oak Ridge 1965.

Received October 26, 1976.

An Electron Diffraction Study of the *anti-gauche* Ratio as a Function of Temperature for Ethylene Chlorohydrin, 2-Chloroethanol

A. ALMENNINGEN, L. FERNHOLT and K. KVESETH

Department of Chemistry, University of Oslo, Blindern, Oslo 3, Norway

In order to investigate the possibility of more accurate determination of energy and entropy differences between conformers using gas electron diffraction techniques, gaseous ethylene chlorohydrin has been studied at five different temperatures (37, 125, 170, 200, and 250 °C). While the less stable *anti* conformer contributes only 6–8 % at the lowest temperature, the gas contains as much as 20–30 % at the highest temperature.

The temperature dependence of the *gauche/anti* ratio (K) is studied by various approaches, including a graphical procedure comparing area ratios on the radial distribution curves.

The best values for the energy and entropy differences between *gauche* and *anti* conformers are $\Delta E = -2.4(2)$ kcal mol⁻¹ and $\Delta S = -2.8(3)$ cal mol⁻¹ deg⁻¹, respectively.*

Earlier studies¹⁻⁷ have demonstrated that the halogenated ethylene hydrins exhibit two co-existing conformers in the gaseous state. At room temperature the *gauche* conformer prevails to the extent that *anti* can hardly be recognized. At higher temperatures the contribution of the *anti* conformer is easily demonstrated by the increase of the O...X peak corresponding to this conformer in the radial distribution curve. The *gauche/anti* ratio (K) may be studied considering K as one of the parameters, in addition to the geometric and vibrational parameters, in a least squares refinement of the intensity curve. This procedure was applied using data obtained at two temperatures in the previous study.¹ The main scope of the present study was to extend the experimental bases by

including data from three more temperatures, and thereby study in detail the influence of the temperature on the part of the radial distribution curves most sensitive to conformational changes.

EXPERIMENTAL AND DATA REDUCTION

The sample of chlorohydrin, obtained from Merck, was used without further purification. In addition to the recordings described in the previous paper¹, electron diffraction photographs were made at three new nozzle temperatures: 125, 170 and 250 (°C), with the Oslo apparatus⁸ under conditions as summarized in Table 1. Selected plates were traced with a microdensitometer, and the data reduced in the usual way,¹⁰ to yield an intensity curve for each plate. The intensities were modified with the function

$$s/|f_{cl}|/|f_0|$$

The theoretical molecular intensities were calculated according to eqn. 11 of Ref. 10. The scattering amplitudes were calculated by the partial wave method,^{10, 11} using Hartree Fock atomic potentials.¹²

The average for each set of plates was calculated, and composites made for each temperature by scaling corresponding pairs of curves and averaging the intensities in the overlap region. Due to the low symmetry of the molecule, reproducible intensity values are obtained in a more limited s -range than normal.

STRUCTURE ANALYSIS

Radial distribution curves (RD-curves) calculated from the corresponding intensities from the 48 cm data by a Fourier transformation,

* 1 cal = 4.184 J.

Table 1. Experimental conditions and photographic plate data.

Temperature (°C)	37	125	170	200	250			
Nozzle-to plate distance (mm)	479.33	260.54	480.72	250.78	480.63	198.78	480.42	250.63
Electron wavelength (Å) ^a	0.064802	0.064846	0.064580	0.064580	0.065580	0.064732	0.064732	0.064598
Range of data (s) ^b	1.5–20.0	5.0–35.0	1.5–18.5	5.0–35.0	1.5–18.5	1.5–20.0	7.0–45.0	1.5–18.5
Data interval (Δs)	0.125	0.250	0.125	0.250	0.125	0.125	0.250	0.125
Number of plates used	4	5	4	7	5	4	4	5
Corresponding curves in Fig. 1	A	B	C	D	E			

^a Determined in separate experiments by calibration to gold. ^b $s = 4\pi\lambda^{-1} \sin \theta$, 2θ is the scattering angle, λ is the electron wavelength

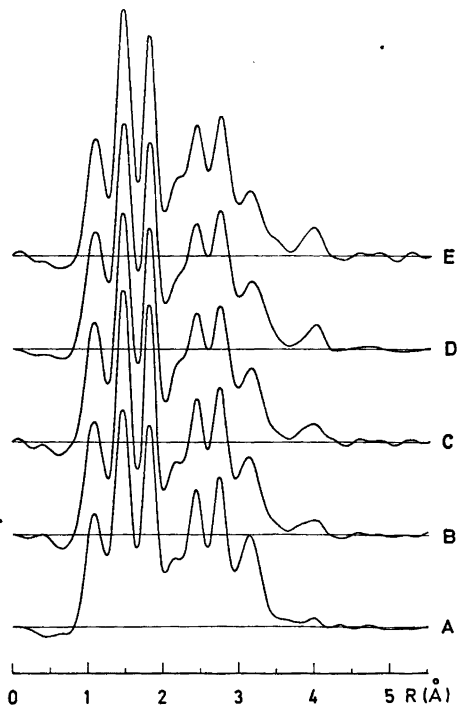


Fig. 1. Experimental radial distribution curves, calculated from the corresponding 48 cm intensity curves with $B = 0.0020 \text{ \AA}^2$.

are shown in Fig. 1. (See Ref. 1 for more detailed discussions.) The five different bond distances contribute to the first three peaks. The peak complex between 2 and 3 Å corresponds to all the non-bonded torsional independent distances. The torsional dependent H...Cl and H...O distances make a negligible contribution to the RD-curves, and the outer complex consists mainly of the torsional dependent O...Cl peaks, at 3.2 Å for *gauche* and 4.0 Å for the *anti* conformer. The area of these two peaks varies with the temperature, and Fig. 1 shows a systematic increase in the peak area at 4.0 Å with the temperature and a corresponding decrease in the *gauche* peak at 3.2 Å.

For practical reasons a theoretical tail was added to the experimental intensities in the outer *s*-region ($s = 18.5 - 45.0 \text{ \AA}^{-1}$) in addition to the theoretical contribution in the inner, unobserved region. Since the vibrational amplitudes for the conformational dependent distances are fairly large ($u(\text{O}\cdots\text{Cl})_a = 0.08$ and $u(\text{O}\cdots\text{Cl})_g = 0.12 - 0.16 \text{ \AA}$), the main contribu-

tions to the total intensity from these distances will be within the experimental s -region of the 48 cm plates. The torsional dependent peaks should therefore be relatively independent of the theoretical contribution added to the experimental intensities.

Because of the similarities between the C-C, C-O and C-H, O-H distances, a mean of these two types and the difference were chosen as geometry parameters in the molecular model.¹ The independent geometry parameters thus used in least squares refinement are $\langle C-C, O \rangle$ (the average of the C-C and C-O

bond), $\Delta(C-C, O)$ (the difference between these two bond lengths), $\langle C, O-H \rangle$, $\Delta(C, O-H)$, $R(C-Cl)$, $\angle CCO$, $\angle CCl$, $\angle HCH$, $\angle COH$ and the torsional angle, ϕ , around the C-C axis. ϕ is defined as 180° in *anti*, and is refined in *gauche* for each temperature.

The torsional independent parameters of the two conformers are assumed to be nearly the same and are therefore put equal. The hydroxyl group has for the sake of simplicity in both conformers been fixed at a *gauche* position with respect to the C-O axis ($\phi' = 60^\circ$), even though an *ab initio* calculation on fluorohydrin¹³ has

Table 2. Molecular parameters. Distances (r_a) and amplitudes (u) in Å, angles (\angle_a) in degrees.

Temp. (°C)	37	125	170 ^a	200	250	^f
$\langle C-C, O \rangle$	1.466(1) ^b	1.465(1)	1.475(1)	1.473(1)	1.464(1)	
$\Delta(C-C, O)$	0.106(2)	0.083(3)	0.10 —	0.106(2)	0.079(4)	
$\langle C, O-H \rangle$	1.063(2)	1.059(3)	1.068(3)	1.067(2)	1.066(3)	
$\Delta(C, O-H)$	0.06 —	0.06 —	0.06 —	0.06 —	0.06 —	
$r(C-Cl)$	1.801(1)	1.796(1)	1.801(1)	1.807(1)	1.794(2)	1.800(2)
$\angle CCl$	110.7(1)	110.5(2)	109.8(2)	109.9(2)	110.9(3)	110.4(2)
$\angle CCO$	113.8(3)	112.0(3)	110.7(3)	110.6(3)	110.5(4)	111.5(6)
$\angle HCH$	108 —	108 —	108 —	108 —	108 —	
$\angle HOC$	125 —	125 —	125 —	125 —	125 —	
ϕ	62.4(6)	66.3(7)	67.9(6)	70.2(8)	70.0(10)	67.3(14)
$r(C-O)$ ^c	1.413(2)	1.424(4)	1.425(1)	1.420(3)	1.424(4)	1.421(2)
$r(C-C)$	1.519(2)	1.507(4)	1.525(1)	1.526(3)	1.504(4)	1.516(2)
$r(C-H)$	1.093(2)	1.089(3)	1.098(3)	1.097(2)	1.096(3)	1.094(2)
$r(O-H)$	1.033(2)	1.029(3)	1.038(3)	1.037(2)	1.036(3)	1.034(2)
$u(C-C)$	0.050 ^e —	0.050 —	0.029(5) ₁ ^d	0.050 —	0.050 —	0.052
$u(C-O)$	0.050 —	0.050 —	0.029(5) ₁	0.050 —	0.050 —	0.051
$u(C-Cl)$	0.052(1)	0.042(2)	0.026(5)	0.050(1)	0.055(2)	0.057
$u(C-H)$	0.090 —	0.090 —	0.090 —	0.090 —	0.090 —	0.078
$u(O-H)$	0.070 —	0.070 —	0.070 —	0.070 —	0.070 —	0.070
$u(C_1 \cdots Cl_9)$	0.061(2)	0.068(2)	0.070(4)	0.080(2)	0.079(3)	0.091
$u(C_3 \cdots O_4)$	0.082(2) ₁	0.067(3) ₁	0.061(4) ₂	0.092(3) ₁	0.078(3) ₁	0.078
$u(Cl_9 \cdots H_7)$	0.106(2) ₁	0.101(3) ₁	0.085(4) ₂	0.116(3) ₁	0.102(3) ₁	0.111
$u(O_4 \cdots H_2)$	0.132(6) ₂	0.094(5) ₂	0.110 —	0.109(6) ₂	0.099(7) ₂	0.105
$u(C_1 \cdots H_5)$	0.132(6) ₂	0.094(5) ₂	0.110 —	0.109(6) ₂	0.099(7) ₂	0.101
$u(C_1 \cdots H_7)$	0.132(6) ₂	0.094(5) ₂	0.110 —	0.109(6) ₂	0.099(7) ₂	0.111
$u(O_4 \cdots Cl_9)_g$	0.125(3)	0.148(5)	0.120 —	0.153(6)	0.169(9)	0.159
$u(Cl_9 \cdots H_2)_g$	0.121(25)	0.056(23)	0.120 —	0.081(26)	0.067(33)	0.113
$u(O_4 \cdots Cl_9)_a$	0.077 —	0.083 —	0.087 —	0.089 —	0.091 —	0.086

^a Data from refinement only on 48 cm data, since 19 cm was not observed. ^b Standard deviations, given in parentheses, are from least squares and do not include estimates of correlation or systematic error. —, parameters which were not refined. ^c Dependent distances calculated from $\langle C-C, O \rangle$, $\Delta(C-C, O)$ and $\langle C, O-H \rangle$, $\Delta(C, O-H)$, respectively. ^d Refined in groups, the suffix number indicates which u 's are in the same groups. ^e Calculated by Cyvin¹⁸ when not refined. ^f Mean of the geometry parameters in the temperature range. Standard deviations, in parentheses, are calculated from the deviations from the mean by $\sigma_{\bar{R}} = [\sum (R_n - \bar{R})^2 / n(n-1)]^{1/2}$, where $n=5$. Calculated u -values for 250 °C.

given $\phi' = 180^\circ$ for the *anti* isomer. Due to low contribution to the total intensity from distances dependent on ϕ' , this assumption will not affect the conclusions of this investigation.

The composition in the gas phase is thus determined from the torsion dependent distances, the O...Cl distance in *gauche* and *anti* being the most important.

In general some of the independent parameters [$\Delta(\text{C}, \text{O}-\text{H})$, $\angle\text{HCH}$ and $\angle\text{COH}$] as well as certain of the vibrational amplitudes did not refine, and were kept at reasonable assigned values.

Table 2 gives the results obtained from refinements at the different temperatures on average composite curves, assuming a reasonable *gauche/anti* ratio, changed by an iterative procedure as the structure analysis proceeded. The lack of molecular symmetry had the largest effect on the 19 cm plates and refinements on 48 cm data have been carried out as well. The overall agreement with the parameters listed in Table 2 was reasonably good.

A simplified valence force field was established for chlorohydrin, applying a program by Gwinn,¹⁴ extended by Stølevik *et al.*¹⁵ to cal-

culate vibrational amplitudes. The force constants (given in Table 3) were chosen from chlorohydrin,⁴ 1,2-dichloroethane,¹⁶ and CH_3-OH ,¹⁷ and slightly modified to get a better agreement with the observed frequencies.³ The small discrepancies in the off-diagonal elements as compared to the forcefield given by Giguère,⁴ are believed to originate mainly from the different numbers of coupling constants included. The calculated vibrational amplitudes (*u*-values) from this force field (given in Table 4) agree excellently with those calculated in *anti* by Cyvin¹⁸ from symmetry coordinates.

Although there are some discrepancies between the assumed *u*-values used in the least squares refinement and the calculated values, we felt that a repeated refinement, based upon the force-field calculations, was not necessary. Since the *u*-values kept constant are insensitive to temperature, as shown in Table 4, the assigned values should not influence the conclusions that may be drawn from the refinements. The unrealistic small *u*-values for the bond distances at 170 °C arise from the short *s*-interval of observations, since that refinement is performed only on 48 cm data.

Table 3. Force constants.^a

Stretch		Interaction	
f_{CC}	4.94	$f_{\text{CC},\text{CCl}}$	0.73
f_{CCl}	3.50	$f_{\text{CC},\text{CO}(\text{anti})}$	0.73
$f_{\text{CO}(\text{anti})}$	4.45	$f_{\text{CH},\text{CH}}$	0.06
f_{CH}	4.91	$f_{\text{CC},\text{CCH}}$	0.26
$f_{\text{OH}(\text{anti})}$	7.49	$f_{\text{CC},\text{CCCl}}$	0.29
$f_{\text{CO}(\text{gauche})}$	5.00	$f_{\text{CC},\text{CCO}}$	0.29
$f_{\text{OH}(\text{gauche})}$	7.33	$f_{\text{CCl},\text{HCCl}}$	0.33
$f_{\text{Cl}\cdots\text{H}(\text{gauche})}$	0.10	$f_{\text{CCl},\text{CCCl}}$	0.55
Bending		$f_{\text{CO},\text{HCO}}$	0.44
f_{CCH}	0.68	$f_{\text{CO},\text{CCO}}$	0.55
f_{HCH}	0.50	$f_{\text{CC},\text{CO}(\text{gauche})}$	0.50
f_{CCCl}	0.75		
f_{HCCl}	0.79		
f_{CCO}	1.09		
f_{HCO}	0.80		
$f_{\text{COH}(\text{anti})}$	0.68		
$f_{\tau(\text{C}-\text{C})}(\text{anti})$	0.10		
$f_{\tau(\text{C}-\text{O})}$	0.03		
$f_{\text{COH}(\text{gauche})}$	0.86		
$f_{\tau(\text{C}-\text{C})}(\text{gauche})$	0.16		

^a Stretching constants in $\text{mdyn } \text{Å}^{-1}$, stretch-bend in mdyn rad^{-1} and bending in $\text{mdyn } \text{Å rad}^{-2}$.

Table 4. Vibrational amplitudes (u), calculated from a valence force field.

	R (Å)	u (Å) 37 °C	125 °C	170 °C	200 °C	250 °C
C—C	1.52	0.050	0.051	0.051	0.052	0.052
C—O	1.42	0.048	0.049	0.050	0.050	0.051
C—Cl	1.80	0.051	0.053	0.054	0.055	0.057
C—H	1.10	0.078	0.078	0.078	0.078	0.078
O—H	1.04	0.070	0.070	0.070	0.070	0.070
C ₁ ...Cl ₉	2.73	0.075	0.082	0.085	0.088	0.091
C ₆ ...O ₄	2.42	0.067	0.072	0.074	0.075	0.078
Cl ₉ ...H ₇	2.40	0.106	0.108	0.109	0.110	0.111
O ₄ ...H ₂	2.07	0.102	0.103	0.103	0.104	0.105
C ₁ ...H ₅	2.19	0.098	0.099	0.099	0.100	0.101
C ₁ ...H ₇	2.15	0.107	0.108	0.109	0.110	0.111
H ₂ ...H ₃	1.78	0.127	0.127	0.128	0.128	0.128
H ₂ ...H ₅	3.04	0.120	0.121	0.121	0.122	0.123
H ₃ ...H ₅	2.57	0.194	0.204	0.210	0.214	0.220
C ₆ ...H ₅	2.83	0.189	0.205	0.213	0.218	0.226
O ₄ ...Cl ₉	3.14	0.125	0.140	0.147	0.151	0.159
O ₄ ...H ₇	2.63	0.155	0.163	0.168	0.171	0.176
O ₄ ...H ₃	3.36	0.103	0.105	0.106	0.107	0.109
Cl ₉ ...H ₂	3.70	0.104	0.108	0.110	0.111	0.113
Cl ₉ ...H ₃	2.85	0.171	0.183	0.189	0.193	0.200
Cl ₉ ...H ₅	2.93	0.191	0.206	0.213	0.218	0.227
H ₆ ...H ₇	3.05	0.310	0.340	0.354	0.364	0.379
H ₅ ...H ₈	3.87	0.168	0.177	0.181	0.184	0.189
H ₂ ...H ₇	2.53	0.169	0.174	0.177	0.179	0.182
H ₂ ...H ₃	2.43	0.165	0.169	0.171	0.173	0.175
O ₄ ...Cl ₉	4.01	0.071	0.077	0.081	0.083	0.086
O ₄ ...H ₇	2.67	0.163	0.175	0.181	0.184	0.191
Cl ₉ ...H ₃	2.90	0.181	0.196	0.204	0.208	0.216
Cl ₉ ...H ₅	4.52	0.174	0.188	0.195	0.199	0.207
H ₅ ...H ₇	2.67	0.280	0.304	0.316	0.324	0.336
H ₅ ...H ₃	3.12	0.328	0.361	0.377	0.388	0.405
H ₂ ...H ₇	3.05	0.128	0.129	0.130	0.130	0.131
H ₂ ...H ₈	2.49	0.180	0.186	0.190	0.192	0.196

Since the aim of the present work is to study the reliability of the deduced thermodynamic functions, a series of computing approaches were tried out. Data reduced from 48 cm plates were studied independently for each temperature, as well as the composites made from various nozzle-to-plate distances. The various approaches may be divided into two types, one based upon conventional least squares refinement, and one based upon area studies of the radial distribution curve.

Because of the rather small percentage of *anti* at low temperatures, in addition to the low symmetry of the molecule, determination of the *gauche/anti* ratio by the conventional least squares method is problematic. We will therefore emphasize the discussion in this work on the second procedure.

The peaks on the RD-curve of particular interest for conformational analysis are those marked W and w in Fig. 2, corresponding to the O...Cl distance in *gauche* and *anti*, respectively. The area under peak w is nearly proportional to the percentage of the *anti* conformer, whereas the peak W is somewhat more complex, due to contributions from other distances.

Fig. 2 presents, for sake of illustration, a theoretical curve based upon a set of well established structure parameters and a chosen, representative, percentage of *anti* (15 %). The line diagram indicates the positions of the interatomic distance, the length of each is a measure of the relative contribution of the corresponding distance to the total area of the radial distribution curve. The solid lines corre-

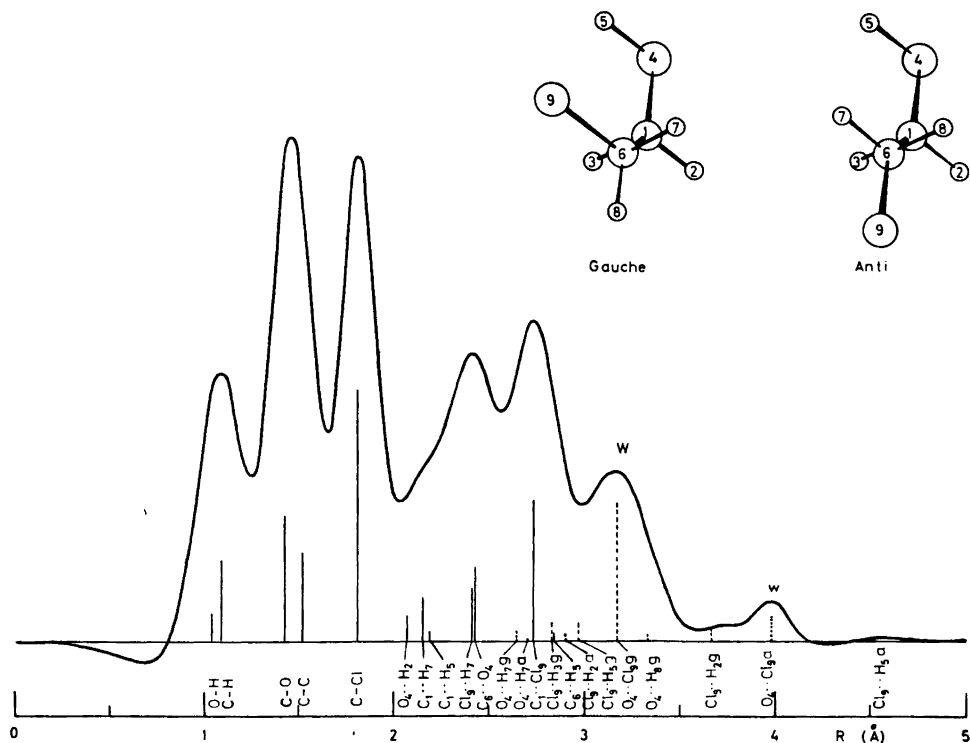


Fig. 2. Theoretical radial distribution curve, calculated from the structural parameters of Table 2 and 15% of *anti*.

spond to those distances which do not vary explicitly with the torsion. The other lines correspond to distances varying with the torsional angle, the dashed ones are *gauche* contributions, the dotted ones *anti*.

The area under the peaks *W* and *w* are designated *WA* and *wA*, respectively. The total area under the RDC-curve is *totA*. *WA* is calculated between 3.1 and 3.6 Å, of *wA* between 3.7 and 4.2 Å and *totA* from 0.8 to 4.2 Å. This type of integration is performed for both experimental and theoretical curves. The theoretical curves are based upon the refined structural parameters of Table 2 and calculated for different *anti/gauche* ratios (5%, 10%, 15% etc. of *anti*). The fractions between the different areas, *WA/wA*, *WA/totA* and *wA/totA* are calculated for both experimental and theoretical data. The experimental *anti/gauche* ratios are determined by comparison between the different area ratios, as a function of the *anti* percentage. The estimated percentages of the

anti conformer are given in Table 5, as well as the thermodynamic quantities.

Inspection of Table 5 reveals some differences between the three outlined approaches. As expected the *WA/totA* values are less able to reproduce the conformational ratio, due to the small percentage change with temperature in this quantity. *WA/wA* and *wA/totA* give nearly identical results, which is quite reasonable because they are essentially the same quantity on different normalization. The discussion in this study is based upon the *WA/wA* values, because we feel that weighting *wA* to the total area (*totA*) will be dominated by the comparatively large value of *totA*, even though *W* (see Fig. 2) is a shoulder in a peak complex and not so easily defined.

Column *f* of Table 2 gives the average values of the geometry parameters in the temperature interval. These values agree excellently with the means presented in the previous paper.¹ Contrary to what is found for halogenated

Table 5. Percentage of *anti* (n_a) and thermodynamic differences.

Temp (°C)	Connected curves			Refined ^a	48 cm curves		
	$\frac{WA}{wA}$	$\frac{WA}{totA}$	$\frac{wA}{totA}$		$\frac{WA}{wA}$	$\frac{WA}{totA}$	$\frac{wA}{totA}$
37	7.10	8.57	6.95	—	6.70	1.50	7.60
125	19.03	15.04	20.55	—	17.30	12.30	19.20
170	—	—	—	—	21.62	17.92	23.10
200	22.65	19.55	23.95	21.2(2.3)	25.43	22.20	27.06
250	28.02	24.08	30.25	25.1(1.2)	30.32	22.60	34.80
ΔE^b (kcal mol ⁻¹)	-2.4(2)	-1.8(1)	-2.6(4)	—	-2.7(1)	-4.7(6)	-2.7(1)
ΔS (cal mol ⁻¹ deg ⁻¹)	-2.8(3)	-1.1(2)	-3.4(9)	—	-3.6(2)	-7.3(16)	-3.9(3)

^a Standard deviations as obtained in the least squares refinement are given in parentheses. ^b For explanations see text.

ethanes, the *gauche* torsional angle for chlorohydrin increases systematically. This indicates that the stabilizing energy of the Cl...H interactions in *gauche* decrease with the temperature.

DISCUSSION

The most interesting results of this investigation are the measurements of the composition as a function of the temperature. If we consider the conformational equilibrium *anti* \rightleftharpoons *gauche*, the difference in energy, $\Delta E = E_g - E_a$, and the difference in entropy, $\Delta S = S_g - S_a$, of the two conformers are obtainable from the effect of the temperature on composition by use of the formula

$$K = \frac{n_g}{n_a} = e^{-(\Delta E - T\Delta S)/RT} = \frac{2Q_g}{\sigma Q_a} e^{-\Delta E^\circ/RT} \quad (1)$$

where n is the percentage of the conformers *gauche* (g) and *anti* (a). Q is the vibrational-rotational partition function, ΔE° is the energy difference between *gauche* and *anti* at the absolute zero point. The factor 2 is the statistical weight from the two identical *gauche* forms, while σ is a statistical weight of the different *anti* forms, arising from the difference in acceptable hydroxy-hydrogen positions in the two conformers. Because of the three nearly identical staggered positions around the C...O axis in *anti*, compared to the one in *gauche* pointing towards the Cl atom to form an internal hydrogen bond, σ is set equal to 3 in this analysis. Even though the calculated partition

functions show a slight temperature dependence of ΔE and ΔS , this effect is fairly small ($RT\partial/\partial T \ln(Q_g/Q_a) = -0.5$ cal mol⁻¹ deg⁻¹), and a straight line is fitted by a least squares method to the $R \ln K$ versus $1/T$ points, giving the mean of ΔE as the slope and ΔS as the intersection of the $R \ln K$ -axis in the actual temperature interval.¹⁹ Selecting the values of column WA/wA , connected curves, of Table 5, the ($R \ln K$, $1/T$) points appear as the Δ given in Fig. 3. The vertical lines give the range of each point as obtained from the different set of values given in Table 5, connected curves. The straight line fit to the WA/wA gave $\Delta E = -2.4(2)$ kcal

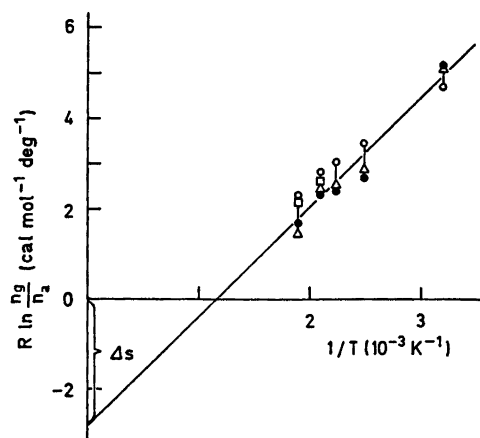


Fig. 3. $R \ln K$ as a function of $1/T$, estimated from the area ratios. Δ , from WA/wA ; \bullet , from $wA/totA$; \circ , from $WA/totA$; \square , refined values.

Table 6. Thermodynamic quantities.^a

	I	II ^b	III
$\Delta E(\text{kcal mol}^{-1})$	-2.4(.2)	-2.4	-2.6(-1.9,0.8)
$\Delta S(\text{cal mol}^{-1} \text{ deg}^{-1})$	-2.8(.3)	-2.2 [-2.08 - (-2.29)]	-2.2
$R \ln (2Q_g/3Q_a)(\text{cal mol}^{-1} \text{ deg}^{-1})$	-2.3	-1.7 [-1.52 - (-1.80)]	
$RT \frac{\partial}{\partial T} (\ln Q_g/Q_a)(\text{cal mol}^{-1} \text{ deg}^{-1})$	-0.5	-0.5 [-0.49 - (-0.56)]	

^a For explanations see text. ^b The values inside the brackets give the temperature variation. $(I_A I_B I_C)_g = 9.956 \times 10^5$ and $(I_A I_B I_C)_a = 8.213 \times 10^5$ a.w.Å.³

mol⁻¹ and $\Delta S = -2.8(3)$ cal mol⁻¹ deg⁻¹ (Table 6, column I). An analysis based on $wA/totalA$ would have changed ΔE insignificantly, whereas ΔS would have decreased to $-3.4(9)$ cal mol⁻¹ deg⁻¹.

The partition functions are calculated from the moments of inertia and vibrational frequencies.¹⁶ The thermodynamic quantities can also be calculated from these, combined with the observed values for the *gauche/anti* ratios (K). These results are presented in column II of Table 6. In column III of that table are presented the results from the previous investigation.¹ (Actually the value given there for the entropy is $\Delta S' = \Delta S - R \ln 2 = -3.6 (-2.5, 1.8)$ cal mol⁻¹ deg⁻¹.)

Table 6 demonstrates the excellent agreement between the electron diffraction results based on WA/wA and the spectroscopic observed frequencies. Under the assumption of a statistical weight of 3 for the *anti* form, the straight line fitted ΔS value corresponds to a torsional frequency in *anti* of 82 cm⁻¹ (observed 115 cm⁻¹ in crystal phase) when the torsion in *gauche* (156 cm⁻¹) is considered as the correct one. A difference well within the error limits of the two methods.

Also the agreement with the estimates in the first paper¹ is reasonable. The conclusions drawn in that investigation are therefore verified. The results may be interpreted in terms of a rather strong intramolecular hydrogen bond favouring the *gauche* conformer.

Compared with the energy differences for fluoro⁷ and bromo⁸ hydrins (less than -2.8 and -1.3 kcal mol⁻¹, respectively), it is demonstrated that the strength of the internal hydrogen bond is between that of H...F and H...Br.

This is contrary to the observations by Buckley *et al.*³ They observe rather more stabilization of the H...Br bond than the H...Cl, the difference in energy is -1.45 and -1.20 kcal mol⁻¹, respectively, as calculated from the intensity difference of the CX bonds (which are the numbers to compare with the electron diffraction results).

The rather large, negative entropy difference between *gauche* and *anti* can be accounted for from the statistical factor of 3 for the essentially equally probable positions of the hydroxyhydrogen in *anti*. Also the conformational entropy difference ($\Delta S_c = \Delta S - R \ln 2/3 = -2.0$ cal mol⁻¹ deg⁻¹), however, is fairly large, about 5 times what is found in 1,2-dichloroethane.¹⁹ This must reflect a higher degree of order in *gauche*, introduced by the formation of the internal hydrogen bond. This estimate of ΔS_c is of course dependent on the assumption of $\sigma = 3$, but a value close to 3 seems reasonable from the theoretical calculations from the partition functions, and the estimate of the torsional frequency in *anti*. σ less than 3 would in fact lead to an even more ordered structure in *gauche*. The large, negative conformational entropy also conflicts with the interpretation of the difference in ΔE obtained from the temperature dependence of the OH and CX bond intensities,³ as due to the presence of a third conformer, a non-hydrogen bonded *gauche* form. This again would introduce a higher degree of statistical disorder in *gauche*, thus making ΔS_c even more negative than the above value of -2.0 cal mol⁻¹ deg⁻¹, which means there is an even higher degree of conformational order in *gauche*. This seems unlikely when the hydrogen bond is formed to a smaller extent.

Acknowledgement. The conformational studies of chlorohydrin were initiated by Professor O. Bastiansen and the authors wish to acknowledge his advice during the refinement procedures, as well as for his valuable discussions and suggestions in the preparation of this manuscript. We are also grateful to the Norwegian Research Council for Science and the Humanities for financial support.

REFERENCES

1. Almenningen, A., Bastiansen, O., Fernholt, L. and Hedberg, K. *Acta Chem. Scand.* 25 (1971) 1946, and references cited therein.
2. Buckley, P., Giguère, P. A. and Yamamoto, D. *Can. J. Chem.* 46 (1968) 2917.
3. Buckley, P., Giguère, P. A. and Schneider, M. *Can. J. Chem.* 47 (1969) 901.
4. Giguère, P. A. and Schneider, M. *Can. J. Chem.* 50 (1972) 152.
5. Azrak, R. G. and Wilson, E. B. *J. Chem. Phys.* 52 (1970) 5299.
6. Buckton, K. S. and Azrak, R. G. *J. Chem. Phys.* 52 (1970) 5652.
7. Hagen, K. and Hedberg, K. *J. Am. Chem. Soc.* 95 (1973) 8263.
8. Hedberg, K. and Samdal, S. *Private communication.*
9. Bastiansen, O., Hassel, O. and Risberg, E. *Acta Chem. Scand.* 9 (1955) 232.
10. Andersen, B., Seip, H. M., Strand, T. G. and Stølevik, R. *Acta Chem. Scand.* 23 (1969) 3224.
11. Peacher, J. and Wills, J. C. *J. Chem. Phys.* 46 (1967) 4809.
12. Strand, T. G. and Bonham, R. A. *J. Chem. Phys.* 46 (1967) 4809.
13. Random, L., Lathan, W. A., Hehre, W. J. and Pople, J. A. *J. Am. Chem. Soc.* 95 (1972) 693.
14. Gwinn, W. D. *J. Chem. Phys.* 55 (1971) 477.
15. Stølevik, R., Seip, H. M. and Cyvin, S. J. *Chem. Phys. Lett.* 15 (1972) 263.
16. Kveseth, K. *Acta Chem. Scand. A* 28 (1974) 482.
17. Ha, T.-K.; Meyer, R. and Güenthard, H. H. *Chem. Phys. Lett.* 22 (1973) 68.
18. Cyvin, S. J. *Private communication.*
19. Kveseth, K. *Acta Chem. Scand. A* 29 (1975) 307.

Received November 24, 1976.

Mechanisms for the Acid-catalyzed Hydrolysis of Some Alkyl Aldofuranosides with *trans*-1,2-Configuration

HARRI LÖNNBERG and ANTERO KULONPÄÄ

Department of Chemistry and Biochemistry, University of Turku, SF-20500 Turku, Finland

The rate constants for the hydrolysis of several alkyl α -D-arabino-, α -D-lyxo-, and β -D-ribofuranosides in aqueous perchloric acid have been measured at different temperatures. The effects of varying the aglycon structure on the hydrolysis rates are interpreted to indicate that α -arabinosides and α -lyxosides are usually hydrolyzed by rate-limiting formation of cyclic oxo-carbenium ions. However, if the aglycon group is strongly electropositive a mechanism involving rate-limiting opening of the five-membered ring may occur. Alkyl β -D-ribofuranosides, with the exception of those carrying highly electronegative substituents in the aglycon group, probably utilize the latter route. The values for the entropy of activation and the rate variations in aqueous perchloric acid—dimethyl sulfoxide solutions of different compositions are interpreted to lend further support for the suggested difference in mechanism.

Whereas the acid-catalyzed hydrolysis of aldopyranosides has been extensively studied in recent years,¹ there have been only a few mechanistic investigations of the corresponding reactions of aldofuranosides.^{2,3} Capon showed that the hydrolysis of methyl aldofuranosides consists of an initial rapid protonation of the substrate and glycosyl-oxygen bond rupture in one of the subsequent steps, but drew no firm conclusions concerning the details of the mechanism.³ In a previous paper one of us suggested that alkyl β -D-xylofuranosides usually react by protonation of the ring-oxygen followed by a unimolecular cleavage of the five-membered ring in the rate-limiting step.⁴ However, a pathway involving protonation of the glycosidic oxygen atom and rate-limiting formation of a cyclic oxo-carbenium ion is probably only slightly less favorable and becomes the major one on going to substrates

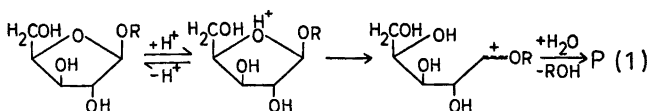
with markedly electronegative aglycon groups. On this basis it does not seem unreasonable that in the hydrolysis of alkyl glycosides of other aldofuranoses the latter mechanism might be followed even when the aglycon group is electropositive. To elucidate the influence of varying the glycon moiety configuration on the relative rates of the reactions described above the hydrolyses of alkyl α -D-arabino-, α -D-lyxo-, and β -D-ribofuranosides have been studied in this work.

EXPERIMENTAL

The alkyl aldofuranosides used in this investigation were obtained by ion exchange chromatography⁵ (Dowex 1X2 resin, mesh 200—400, OH⁻ form) of furanoside-rich syrups prepared by Fischer glycosidation.⁶ The purity of the separated anomers was checked by ¹H NMR spectroscopy (a 60 MHz Perkin-Elmer Model R 10 spectrometer). In each case only one signal in the anomeric proton region (δ 4.7—5.1) was observed indicating the homogeneity of the separated anomers. Many of the products crystallized from ethyl acetate. The melting points and ¹H NMR data are listed in Table 1 together with the specific optical rotations. The kinetic measurements were performed as described earlier.⁴

RESULTS AND DISCUSSION

Scheme 1 describes the mechanism suggested in a previous paper⁴ for the acid-catalyzed hydrolysis of alkyl β -D-xylofuranosides with electropositive or weakly electronegative aglycon groups. The substrate protonated on the ring-oxygen undergoes a rate-limiting heterolysis to form an acyclic oxo-carbenium ion.



Scheme 1.

Table 1. Specific optical rotations (measured in water at 293 K), melting points and ^1H NMR spectra (D_2O ; 306.7 K) for the alkyl aldofuranosides prepared.

$[\alpha]_{\text{D}}^{\text{c}}$ ($^{\circ}$)	M.p. (K)	^1H NMR (δ)
Isopropyl α-D-arabinofuranoside		
+ 102	syrup	1.09 [d, $(\text{CH}_3)_2\text{CH}$], 3.6–3.7 (m, H-5), 3.8–4.0 [m, H-2, H-3, H-4 and $(\text{CH}_3)_2\text{CH}$], 4.99 (d, H-1)
Ethyl α-D-arabinofuranoside		
+ 110	syrup	1.10 (t, CH_3CH_2), 3.4–3.7 (m, H-5 and CH_3CH_2), 3.8–4.0 [m, H-2, H-3 and H-4], 4.90 (d, H-1)
Methyl α-D-arabinofuranoside		
+ 119 ^a	335–338 (hygr.)	3.32 (s, CH_3), 3.6–3.7 (m, H-5), 3.8–4.0 (m, H-2, H-3 and H-4), 4.83 (d, H-1)
2-Methoxyethyl α-D-arabinofuranoside		
+ 99	syrup	3.29 (s, $\text{CH}_3\text{OCH}_2\text{CH}_2$), 3.5–3.7 (m, H-5 and $\text{CH}_3\text{OCH}_2\text{CH}_2$), 3.8–4.0 (m, H-2, H-3 and H-4), 4.93 (d, H-1)
2-Chloroethyl α-D-arabinofuranoside		
+ 77	syrup	3.6–3.8 (m, H-5 and ClCH_2CH_2), 3.8–4.0 (m, H-2, H-3 and H-4), 4.99 (d, H-1)
Isopropyl α-D-lyxofuranoside		
+ 113	362–365	1.11 [d, $(\text{CH}_3)_2\text{CH}$], 3.6–3.8 (m, H-5), 3.9–4.3 [m, H-2, H-3, H-4 and $(\text{CH}_3)_2\text{CH}$], 5.03 (d, H-1)
Methyl α-D-lyxofuranoside		
+ 130 ^b	365–367 ^b	3.35 (s, CH_3), 3.6–3.8 (m, H-5), 3.9–4.3 (m, H-2, H-3, and H-4), 4.86 (d, H-1)
2-Methoxyethyl α-D-lyxofuranoside		
+ 90	syrup	3.27 (s, $\text{CH}_3\text{OCH}_2\text{CH}_2$), 3.5–3.8 (m, H-5 and $\text{CH}_3\text{OCH}_2\text{CH}_2$), 3.9–4.3 (m, H-2, H-3 and H-4), 4.94 (d, H-1)
Isopropyl β-D-ribofuranoside		
– 50	342–343	1.08 [d, $(\text{CH}_3)_2\text{CH}$], 3.6–3.7 (m, H-5), 3.8–4.0 [m, H-2, H-3, H-4 and $(\text{CH}_3)_2\text{CH}$], 4.99 (s, H-1)
Methyl β-D-ribofuranoside		
– 46	syrup ^c	3.30 (s, CH_3), 3.6–3.7 (m, H-5), 3.8–4.0 (m, H-2, H-3 and H-4), 4.81 (s, H-1)
2-Methoxyethyl β-D-ribofuranoside		
– 45	syrup	3.28 (s, $\text{CH}_3\text{OCH}_2\text{CH}_2$), 3.5–3.7 (m, H-5 and $\text{CH}_3\text{OCH}_2\text{CH}_2$), 3.8–4.1 (m, H-2, H-3 and H-4), 4.91 (s, H-1)
2-Chloroethyl β-D-ribofuranoside		
– 40	syrup	3.6–3.8 (m, H-5 and ClCH_2CH_2), 3.8–4.1 (m, H-2, H-3 and H-4), 4.98 (s, H-1)

^a Lit.:⁷ $[\alpha]_{\text{D}} + 123^{\circ}$, m.p. 338–340 K (hygr.). ^b Lit.:⁸ $[\alpha]_{\text{D}} + 131^{\circ}$, m.p. 368–370 K. ^c Lit.:⁹ $[\alpha]_{\text{D}} - 50^{\circ}$, m.p. 353 K.

Table 2. Second-order rate constants at different temperatures and the entropies of activation for the acid-catalyzed hydrolysis of alkyl β -D-ribofuranosides.

$\frac{T}{K}$	k^a $10^3 \text{ dm}^3 \text{ mol}^{-1} \text{ s}^{-1}$	$k(333.15 \text{ K})^b$ $10^3 \text{ dm}^3 \text{ mol}^{-1} \text{ s}^{-1}$	$\Delta S^\ddagger(298.15 \text{ K})$ $\text{J K}^{-1} \text{ mol}^{-1}$
Isopropyl			
312.85	8.38(9)	59.5(24)	-23(9)
317.85	12.85(20)		
322.85	23.3(2)		
327.85	37.6(4)		
332.85	56.3(5)		
Methyl			
312.85	1.034(12)	8.16(7)	-29(2)
317.85	1.768(38)		
322.85	2.99(4)		
327.85	4.93(7)		
332.85	7.84(6)		
2-Methoxyethyl			
332.85	2.83(3)	2.84(11)	-20(9)
337.75	4.53(5)		
342.65	6.93(11)		
347.55	11.08(21)		
352.45	19.12(22)		
2-Chloroethyl			
342.65	3.34(3)	1.189(84)	-14(10)
347.55	5.05(7)		
352.45	7.92(6)		
357.45	13.05(17)		
362.45	22.0(2)		

^a Calculated from the first-order rate constants obtained in 0.10 mol dm⁻³ aqueous perchloric acid.

^b Calculated by the Arrhenius equation from the rate constants at other temperatures.

To determine whether the same pathway is followed in the hydrolysis of the corresponding glycosides of other aldopentoses, the dependences of their hydrolysis rates on the polar properties of the aglycon group were studied. Table 2 records the kinetic data obtained with alkyl β -D-ribofuranosides. The reactivity is considerably decreased with the increasing electron-attracting character of the aglycon group on going from the isopropyl to 2-chloroethyl derivative. This is just what would be expected on the basis of mechanism (1). Electron withdrawal by polar substituents greatly retards the cleavage of the five-membered ring by destabilizing the developing acyclic oxo-carbenium ion, and, owing to the long distance between the ring-oxygen and the aglycon group, exerts only a slight effect on the extent of protonation. As seen from Fig. 1, plotting the logarithms of the rate constants obtained with β -ribosides against the corresponding

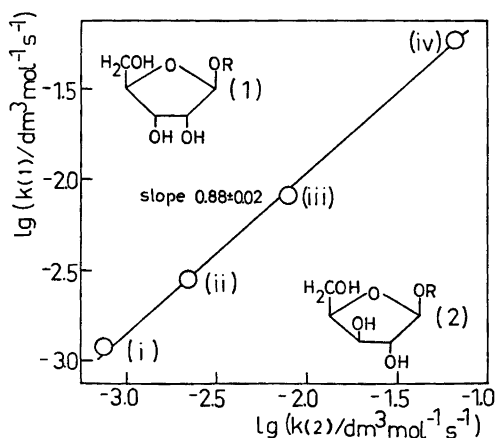
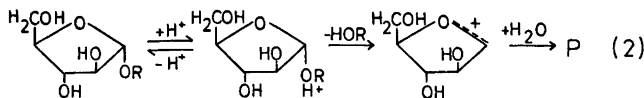


Fig. 1. Comparison of the structural effects in the acid-catalyzed hydrolysis of alkyl β -D-ribofuranosides (1) with those in the hydrolysis of the corresponding β -D-xylofuranosides (2) at 333.15 K. Notation: (i) 2-chloroethyl, (ii) 2-methoxyethyl, (iii) methyl, and (iv) isopropyl derivatives.

Table 3. Second-order rate constants at different temperatures and the entropies of activation for the acid-catalyzed hydrolyses of alkyl α -D-arabino- and α -D-lyxofuranosides.

T K	k^a $10^3 \text{ dm}^3 \text{ mol}^{-1} \text{ s}^{-1}$	$k(333.15 \text{ K})^b$ $10^3 \text{ dm}^3 \text{ mol}^{-1} \text{ s}^{-1}$	$\Delta S^\ddagger(298.15 \text{ K})$ $\text{J K}^{-1} \text{ mol}^{-1}$
α -D-Arabinosides Isopropyl			
347.55	9.75(16)	2.34(15)	-15(8)
352.45	16.12(27)		
357.45	24.1(1)		
362.45	39.0(5)		
Ethyl			
347.55	3.63(4)	0.715(52)	+15(9)
352.45	6.26(6)		
357.45	10.92(10)		
362.45	17.05(33)		
Methyl			
337.75	0.682(8)	0.386(17)	+7(8)
342.65	1.119(8)		
347.55	1.915(19)		
352.45	3.19(3)		
357.45	5.77(6)		
2-Methoxyethyl			
347.55	1.595(23)	0.272(36)	+24(16)
352.45	2.47(3)		
357.45	4.61(6)		
362.45	8.02(11)		
2-Chloroethyl			
347.55	1.822(25)	0.332(7)	+22(3)
352.45	3.18(5)		
357.45	5.38(5)		
362.45	9.27(9)		
α -D-Lyxosides Isopropyl			
317.85	2.13(4)	11.89(42)	-1(9)
327.85	7.15(6)		
337.75	20.0(4)		
347.55	47.6(8)		
Methyl			
322.85	0.571(6)	2.05(2)	+31(4)
327.85	1.049(8)		
332.85	1.981(14)		
337.75	3.56(3)		
2-Methoxyethyl			
332.85	2.18(3)	2.29(4)	+50(4)
337.75	4.17(3)		
342.65	7.47(5)		
347.55	12.98(9)		
352.45	23.8(2)		

^{a,b} See the footnotes in Table 2.



Scheme 2.

values for β -xylofuranosides yields a straight line with a slope close to unity. In other words, the susceptibility to polar inductive effects is in both reactions nearly the same, indicating a constancy of mechanism. As in the xyloside hydrolysis, the values for the entropy of activation are slightly negative in an apparent conflict with the proposed A-1 mechanism. In a previous discussion⁴ we, however, presented evidence for the suggestion that this would be the result of rate-limiting opening of the five-membered ring rather than of the bimolecular nature of the slow step.

In contrast, alkyl α -D-arabino- and α -D-lyxofuranosides exhibit structure-reactivity relationships quite different from that observed for β -xylosides. The second-order rate constants for the hydrolyses of these compounds are given in Table 3 together with the entropies of activation. In both series the reactivity decreases appreciably on going from the isopropyl to methyl derivative but changes little thereafter with the increasing electronegativity of the aglycon group. The latter kind of behavior

argues strongly against mechanism (1). In contrast, it suggests that a mechanism involving rate-limiting formation of a cyclic oxo-carbenium ion (Scheme 2) is followed, as in the hydrolysis of alkyl aldopyranosides.¹ The rate of this reaction would be expected to be relatively insensitive to the polar nature of the aglycon group. Electron-attracting substituents, for example, tend to decrease the basicity of the glycosidic oxygen atom and hence the concentration of the protonated substrate, but at the same time they facilitate the departure of the protonated alkoxy group. For instance, in the hydrolyses of 2-alkoxytetrahydrofurans,¹⁰ 2-alkoxytetrahydropyrans,¹⁰ and several alkyl aldopyranosides,¹¹ shown to proceed *via* a cyclic oxo-carbenium ion, these two influences almost cancel. On this basis it seems probable that of the alkyl α -D-arabino- and α -D-lyxofuranosides studied only isopropyl derivatives would react mainly by mechanism (1), while the others utilize preferably route (2). Mechanisms involving a rate-limiting nucleophilic attack of water at the anomeric

Table 4. First-order rate constants for the hydrolysis of alkyl β -D-ribo- and α -D-arabinofuranosides in water - DMSO mixtures of different compositions containing perchloric acid 0.1 mol dm⁻³.

	Isopropyl β -D-ribose	Methyl β -D-ribose	2-Chloroethyl β -D-ribose	Isopropyl α -D-arabinoside	Methyl α -D-arabinoside	2-Chloroethyl α -D-arabinoside
$x(\text{DMSO})$	$k(342.65 \text{ K})$ 10^{-4} s^{-1}	$k(352.45 \text{ K})$ 10^{-4} s^{-1}	$k(352.45 \text{ K})$ 10^{-4} s^{-1}	$k(352.45 \text{ K})$ 10^{-4} s^{-1}	$k(352.45 \text{ K})$ 10^{-4} s^{-1}	$k(352.45 \text{ K})$ 10^{-4} s^{-1}
0	138.8(89) ^a	46.4(9) ^a	8.32(19) ^a	15.65(26) ^b	3.30(7) ^b	3.16(2) ^b
0.13	55.4(7)		2.81(4)			
0.20		12.97(13)		4.54(6)	1.059(8)	1.045(12)
0.26	26.1(4)		1.470(28)			
0.46		4.29(7)		1.908(3)	0.867(10)	0.878(14)
0.48	14.48(14)		0.896(17)			
0.62	9.10(9)		1.055(17)	2.37(3)	0.930(9)	0.951(13)
0.66		3.13(3)				
0.73	7.66(9)	2.74(5)	1.067(18)	2.68(3)	1.064(13)	1.240(5)
0.87	5.11(7)	2.42(4)	1.168(26)	2.83(3)	1.550(17)	1.767(26)

^a Calculated from the rate constants given in Table 2. ^b Calculated from the rate constants given in Table 3.

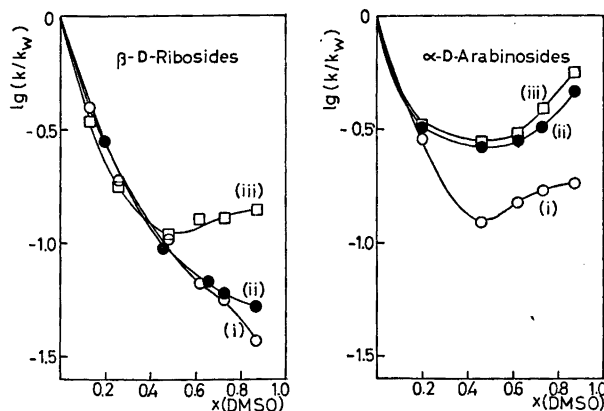


Fig. 2. Rate variations of the acid-catalyzed hydrolyses of alkyl β -D-ribo- and α -D-arabinofuranosides in binary mixtures of water and dimethyl sulfoxide. The values for the first-order rate constants, k and k_w , are given in Table 4. Notation: (i) isopropyl, (ii) methyl, and (iii) 2-chloroethyl derivatives.

carbon concerted with the cleavage of either the *exo* or *endo* cyclic acetal bond would also be expected to exhibit a relatively low susceptibility to the nature of polar substituents in the aglycon group. The fact that the hydrolyses of alkyl α -arabinosides and α -lyxosides are characterized by positive entropies of activation makes, however, these routes less probable.

The influences of solvent composition on the hydrolysis rates of alkyl α -D-arabino- and β -D-ribofuranosides lend some further support for the suggested change in mechanism. Table 4 summarizes the rate constants obtained in binary water-dimethyl sulfoxide mixtures containing perchloric acid 0.10 mol dm^{-3} . The same data are presented in Fig. 2 in terms of the logarithms of the relative rate constants, k/k_w , against the mol fractions of DMSO in reaction solutions. Here k and k_w stand for the first-order rate constants in a given solvent mixture and in water, respectively. Of the compounds studied isopropyl and methyl β -D-ribofuranosides exhibit solvent effects analogous to those reported for the alkyl β -D-xylofuranosides reacting with rate-limiting ring opening.⁴ The relative rate constants, k/k_w , decrease monotonously over the whole range studied. In contrast, the hydrolysis rates of methyl and 2-chloroethyl α -D-arabinofuranosides pass through broad minima in solutions containing approximately equal amounts of water and organic component.

In other words, these reactions respond to changes in solvent composition in roughly the same manner as the hydrolyses of β -xylosides suggested to occur by route (2). The solvent effect curves for isopropyl α -D-arabino- and 2-chloroethyl β -D-ribofuranoside also show broad minima, but the rate-retarding effect of DMSO is in these cases more marked than with methyl and 2-chloroethyl arabinosides. This kind of behavior can be rationalized by assuming that although mechanism (1) prevails in water, the route through a cyclic ion is only slightly less favorable. On the basis of the structure-reactivity relationships indicated above this seems quite feasible for the hydrolyses of these two compounds. Accordingly, route (2) may become the major one in DMSO-rich solutions. The hydrolysis rates would thus experience sharp decreases at low DMSO concentrations, a property suggested to be characteristic for reactions occurring *via* acyclic intermediates, and still go through minima.

In summary, the preceding discussion suggests that the mechanism for the acid-catalyzed hydrolysis of alkyl aldofuranosides depends not only on the polar nature of the aglycon group, but also on the configuration of the glycon moiety. A detailed understanding of the latter factor would, however, require exact knowledge of the conformations of aldofuranosides in water solution.

REFERENCES

1. a. Capon, B. *Chem. Rev.* 69 (1969) 407; b. BeMiller, J. N. *Adv. Carbohydr. Chem.* 22 (1967) 25.
2. a. Blom, J. *Acta Chem. Scand.* 15 (1961) 1667; b. Overend, W. G., Rees, C. W. and Sequeira, J. S. *J. Chem. Soc.* (1962) 3429; c. Capon, B. and Thacker, D. *J. Am. Chem. Soc.* 87 (1965) 4199.
3. Capon, B. and Thacker, D. *J. Chem. Soc. B* (1967) 185.
4. Lönnberg, H., Kankaanperä, A. and Haapakka, K. *Carbohydr. Res. In press.*
5. Austin, P. W., Hardy, F. E., Buchanan, J. G. and Baddiley, J. *J. Chem. Soc.* (1963) 5350.
6. Fischer, E. *Ber. Dtsch. Chem. Ges.* 47 (1914) 1980.
7. Montgomery, E. M. and Hudson, C. S. *J. Am. Chem. Soc.* 59 (1937) 992.
8. Bhattacharya, A. K., Ness, R. K. and Fletcher, H. G., Jr. *J. Org. Chem.* 28 (1963) 428.
9. Augestad, I. and Berner, E. *Acta Chem. Scand.* 10 (1956) 911.
10. Kankaanperä, A. and Miikki, K. *Suom. Kemistil. B* 41 (1968) 42.
11. a. Timell, T. E. *Can. J. Chem.* 42 (1964) 1456; b. DeBruyne, C. K. and Van Wijnendaele, F. *Carbohydr. Res.* 6 (1968) 367; c. BeMiller, J. N. and Doyle, E. R. *Carbohydr. Res.* 20 (1971) 23; d. DeBruyne, C. K. and van der Groen, G. *Carbohydr. Res.* 25 (1972) 59.

Received November 12, 1976.

The Crystal Structure of *N*-(2-Hydroxyethyl)-octadecanamide

BIRGITTA DAHLÉN,* IRMIN PASCHER and STAFFAN SUNDELL

Department of Structural Chemistry, Institute of Medical Biochemistry, University of Göteborg P.O.B. S-400 33 Göteborg 33, Sweden

N-(2-Hydroxyethyl)-octadecanamide (*N*-stearoylethanolamine) crystallizes in the space group *Pc* with the cell constants $a = 47.588$, $b = 4.886$, $c = 8.999$ Å and $\beta = 93.71^\circ$. There are two molecules in the asymmetric unit but parts of the hydrocarbon chains are related by a pseudo centre of symmetry. The molecules are V-shaped (131°) with a bend at the β -carbon atom in the fatty acid chain. The molecules are arranged in double layers and linked together by one $N-H \cdots O$ and one $O-H \cdots O$ hydrogen bond both running in the b axis direction. The chain packing is of the orthorhombic type $O \perp$. The chain axes are tilted by 55.5° to the end group planes.

N-Acylethanolamines of long-chain fatty acids have been isolated from the non-saponifiable lipid fraction of soya lecithin, peanuts and egg yolk.¹ They were later also detected among the lipids of bovine kidney.² It has not so far been established with certainty whether *N*-acylethanolamines as such are essential constituents in cells, or if they are degradation products possibly arising from sphingolipid metabolism^{3,4} or by saponification of unknown precursors. They may in part, also be mere artifacts derived from cephalins during alkaline treatment.⁵

Physicochemical investigations on membrane lipids performed at this Department also include systematical studies of the lipophilic or polar parts of complex lipid molecules. Thus the conformation and molecular packing of, e.g., sphingolipid components such as sphingosine,⁶ tetracosanoylphytyosphingosine⁷ and neuraminic acid⁸ have been established by single crystal work. *N*-Acylethanolamines are of interest in this context as both an amide

bound fatty acid and a hydroxyl group at adjacent carbon atoms of an amino alcohol are characteristic for ceramides which constitute the lipophilic part of all sphingolipids.

CRYSTAL DATA

Molecular formula	$C_{20}H_{41}NO_2$; <i>N</i> -(2-hydroxyethyl)-octadecanamide
Unit cell, monoclinic	$a = 47.588(10)$, $b = 4.886(2)$, $c = 8.999(2)$ Å, $\beta = 93.71(2)^\circ$
<i>V</i>	2088.0 Å ³
Molecular weight	327.55
<i>Z</i>	4
<i>D_c</i>	1.042 g cm ⁻³
λ	1.54051 Å (CuK α_1 radiation)
Systematically absent reflexions	$h0l$ $l = 2n + 1$
Space group	<i>Pc</i>

EXPERIMENTAL

N-(2-Hydroxyethyl)-octadecanamide (*N*-stearoylethanolamine),



was synthesized by selective *N*-acylation of ethanolamine with *p*-nitrophenyloctadecanoate. The compound crystallizes from acetone in elongated prisms which on heating undergo a phase transition at $78 - 84^\circ C$. DPT-diagrams* show an increase of long-spacings from 47.6 to 50.5 Å and a transition of the chain packing from orthorhombic $O \perp$ to hexagonal, indicated by a broad short-spacing line at 4.16 Å. On further heating the crystals melt abruptly at $103.2 - 103.4^\circ C$.

* Diffraction pattern recorded continuously as a function of temperature.

* To whom correspondence should be addressed.

A single crystal with dimensions $0.04 \times 0.44 \times 0.39$ mm was mounted along the b axis. Data were collected on a Picker FACS I automatic diffractometer using graphite monochromated $\text{CuK}\alpha$ radiation. The $\theta-2\theta$ scanning mode was used to measure the reflexions at a scanning rate of 2° min^{-1} and a scan width of 2.75 degrees. 10 s background counts were taken at both ends of the scan range for each reflexion. A total of 2622 reflexions having 2θ less than 110° were recorded. 728 of these intensities were less than 2σ above background and excluded from the calculations.

Corrections for the Lorentz and polarization effects were applied but not for absorption.

STRUCTURE DETERMINATION AND REFINEMENT

The Weissenberg photographs as well as the diffractometer data showed that the crystals were monoclinic with a c -glide plane. However, it was not clear if $0k0$ reflexions with k odd were absent. A Wilson plot was calculated from which it was not possible to decide whether the space group was centric or acentric. The unit cell contained four molecules and initially the space group was assumed to be $P2_1/c$.

From a sharpened three-dimensional Patterson synthesis the carbon chain direction was clearly shown. With the information given in the Patterson map the carbon atoms in the fatty acid chain were located and structure factor and electron density calculations were performed. The R -factor was around 0.5, but the individual agreement between observed and calculated structure factors indicated that the chain was correctly placed. However, it was impossible to locate the rest of the atoms. It was therefore assumed that the molecules crystallized in the acentric space group Pc with two independent molecules in the asymmetric unit. The carbon atoms in the fatty acid chain in the second molecule were given positions as if a symmetry centre existed as it was considered that the deviations from $P2_1/c$ were due to the polar part. From the next few Fourier syntheses the missing atoms were easily located. It was hereby found that only 15 of the atoms of the fatty acid chain were related by the non-crystallographic centre of symmetry and that these atoms corresponded to *different* chain parts in related molecules. After three cycles of block-diagonal refinement

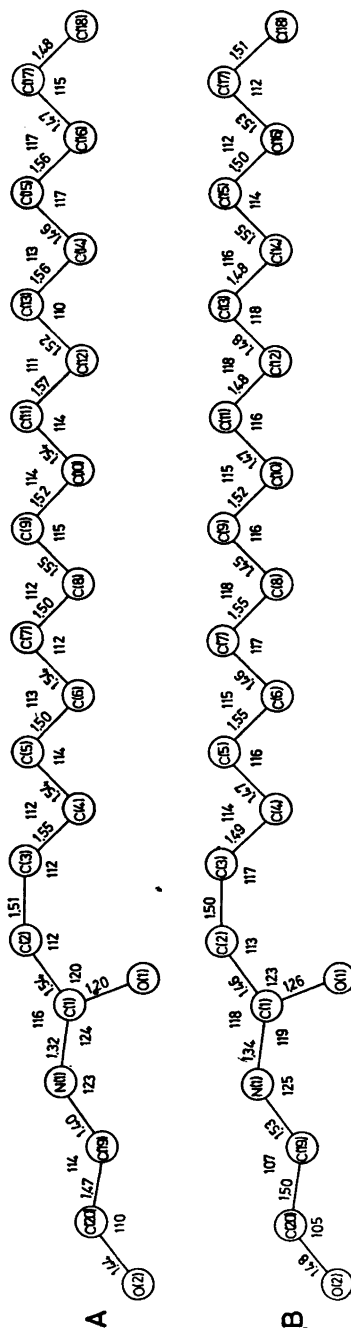


Fig. 1. Bond lengths and angles.

varying the positional parameters and the isotropic temperature factors for all 46 atoms the R -factor was 0.16.

Table 1. Fractional atomic coordinates with standard deviations for the non-hydrogen atoms.

	<i>x</i>	<i>y</i>	<i>z</i>
Molecule A			
C(1)	0.075(1)	0.311(3)	0.445(3)
C(2)	0.097(1)	0.209(3)	0.340(3)
C(3)	0.126(1)	0.328(3)	0.379(3)
C(4)	0.139(1)	0.204(3)	0.525(3)
C(5)	0.169(1)	0.315(3)	0.564(3)
C(6)	0.183(1)	0.196(3)	0.702(3)
C(7)	0.213(1)	0.315(3)	0.739(3)
C(8)	0.227(1)	0.190(3)	0.876(3)
C(9)	0.256(1)	0.314(3)	0.916(3)
C(10)	0.272(1)	0.193(3)	1.053(3)
C(11)	0.301(1)	0.312(3)	1.091(3)
C(12)	0.317(1)	0.189(3)	1.234(3)
C(13)	0.346(1)	0.317(3)	1.261(3)
C(14)	0.362(1)	0.188(3)	1.402(3)
C(15)	0.389(1)	0.309(3)	1.437(3)
C(16)	0.407(1)	0.193(3)	1.574(3)
C(17)	0.435(1)	0.307(3)	1.606(3)
C(18)	0.451(1)	0.196(4)	1.741(3)
C(19)	0.039(1)	0.178(3)	0.606(3)
C(20)	0.011(1)	0.244(4)	0.531(3)
N(1)	0.060(1)	0.120(2)	0.506(3)
O(1)	0.072(1)	0.550(2)	0.470(3)
O(2)	-0.009(1)	0.298(3)	0.641(3)
Molecule B			
C(1)	0.883(1)	0.201(2)	1.369(3)
C(2)	0.862(1)	0.289(2)	1.470(3)
C(3)	0.833(1)	0.185(3)	1.425(3)
C(4)	0.819(1)	0.297(2)	1.284(3)
C(5)	0.791(1)	0.190(2)	1.246(3)
C(6)	0.775(1)	0.309(2)	1.103(3)
C(7)	0.747(1)	0.195(3)	1.068(3)
C(8)	0.730(1)	0.307(3)	0.928(3)
C(9)	0.702(1)	0.196(2)	0.892(3)
C(10)	0.686(1)	0.312(3)	0.754(3)
C(11)	0.658(1)	0.197(2)	0.719(3)
C(12)	0.643(1)	0.309(2)	0.585(3)
C(13)	0.614(1)	0.197(3)	0.543(3)
C(14)	0.599(1)	0.306(3)	0.407(3)
C(15)	0.568(1)	0.196(3)	0.375(3)
C(16)	0.554(1)	0.310(3)	0.236(3)
C(17)	0.524(1)	0.189(4)	0.203(3)
C(18)	0.510(1)	0.309(5)	0.065(3)
C(19)	0.921(1)	0.337(3)	1.200(3)
C(20)	0.948(1)	0.256(4)	1.291(3)
N(1)	0.899(1)	0.393(2)	1.308(3)
O(1)	0.887(1)	-0.047(2)	1.336(3)
O(2)	0.969(1)	0.199(2)	1.182(3)

A Fourier difference synthesis was then calculated from which all hydrogens except H 17 in molecule A (Fig. 1) were located. The

hydrogen atoms were included in the calculations and given the same isotropic temperature factor as the parent atom. Due to the large number of atoms in relation to the number of reflexions only the hydrogen atoms attached to the oxygen and nitrogen atoms were refined. (The positions of the remaining hydrogen atoms were, however, redetermined from a difference map at the end of the refinement).

In the block-diagonal refinement anisotropic temperature factors for all non-hydrogen atoms were used lowering the *R*-value to 0.09. A Fourier difference map now revealed the missing hydrogen atom, whereafter the structure was refined with full matrix methods. At first the two molecules were refined in separate runs due to the large number of parameters. However, as parts of the molecules are related by non-crystallographic symmetry the refinement did not proceed satisfactorily. A bond distance in one molecule is thus too long while the corresponding distance in the second molecule is too short. The parameters were then manually adjusted and for a few cycles all positional parameters were refined simultaneously using the full matrix. This, however, gave similar results as before. The refinement was terminated at an *R*-value of 0.067. Individual distances and angles deviate, for the above mentioned reasons, seemingly considerably from the normal values but this is not significant as the standard deviations are large. No programs allowing constrained refinement were available.

Atomic scattering factors for carbon, nitrogen and oxygen atoms were taken from *International Tables for X-Ray Crystallography*,⁹ while for hydrogen atoms the values given by Stewart, Davidson and Simpson¹⁰ were used.

All calculations have been performed on a Datasab D21-PDP 15 dual computer with the program system developed at this Department.

DESCRIPTION OF THE STRUCTURE

The positional parameters are given in Tables 1, 2 and 3. Interatomic distances and angles are given in Fig. 1 where the atomic numbering is also indicated. The mean C-C bond distance in the fatty acid chain is 1.51 Å and the mean

Table 2. Anisotropic thermal parameters in the form $\exp[-2\pi^2(h^2a^{*2}U_{11} + k^2b^{*2}U_{22} + l^2c^{*2}U_{33} + 2klb^*c^*U_{23} + 2lka^*c^*U_{31} + 2hka^*b^*U_{12})]$. Standard deviations are given in parentheses. All values have been multiplied by 10^3 .

	U_{11}	U_{22}	U_{33}	U_{23}	U_{31}	U_{12}
Molecule A						
C(1)	30(5)	61(6)	26(4)	-11(4)	-7(3)	1(5)
C(2)	41(6)	51(5)	36(4)	10(4)	-20(4)	28(5)
C(3)	31(5)	59(5)	35(4)	23(4)	-6(4)	-1(4)
C(4)	31(6)	66(6)	45(5)	-1(4)	-13(4)	11(5)
C(5)	25(5)	64(6)	40(4)	-9(4)	-5(4)	3(4)
C(6)	30(6)	58(5)	45(5)	-7(4)	-13(4)	26(5)
C(7)	22(5)	44(5)	57(5)	0(4)	2(4)	-7(4)
C(8)	23(5)	50(5)	40(5)	8(4)	-5(4)	-5(4)
C(9)	53(7)	68(6)	22(4)	-15(4)	-4(4)	6(5)
C(10)	54(8)	51(5)	47(5)	2(5)	-8(5)	-14(5)
C(11)	20(5)	62(5)	46(5)	-2(4)	-16(4)	-7(4)
C(12)	67(8)	61(6)	39(5)	-18(4)	-19(5)	6(6)
C(13)	49(7)	57(5)	53(5)	-6(5)	-13(5)	-3(5)
C(14)	35(6)	56(5)	41(5)	-8(4)	-13(4)	-7(4)
C(15)	63(7)	57(5)	50(5)	-2(5)	-12(5)	1(5)
C(16)	82(8)	57(6)	38(5)	2(4)	-15(5)	-9(6)
C(17)	67(6)	67(6)	42(5)	1(5)	-4(4)	-9(5)
C(18)	66(8)	99(9)	71(7)	6(6)	-38(6)	6(7)
C(19)	41(7)	44(5)	63(6)	14(5)	8(5)	-4(5)
C(20)	58(8)	73(7)	58(6)	13(5)	9(6)	8(6)
N(1)	29(4)	30(4)	61(5)	6(4)	5(3)	7(4)
O(1)	68(5)	12(3)	104(5)	-20(3)	8(4)	-10(3)
O(2)	84(6)	68(6)	184(9)	14(6)	65(6)	18(5)
Molecule B						
C(1)	51(5)	9(3)	61(5)	2(3)	-2(4)	1(3)
C(2)	71(6)	37(4)	36(4)	-18(3)	3(4)	-31(4)
C(3)	46(4)	36(4)	45(4)	-6(3)	5(3)	3(3)
C(4)	55(5)	19(3)	38(4)	1(3)	-1(3)	-6(3)
C(5)	59(5)	28(3)	41(4)	11(3)	2(3)	3(3)
C(6)	67(5)	24(3)	43(4)	7(3)	3(4)	-21(3)
C(7)	68(6)	43(4)	31(4)	0(3)	-9(4)	4(4)
C(8)	56(5)	39(4)	47(4)	-5(3)	1(4)	2(4)
C(9)	39(4)	26(3)	51(4)	12(3)	-1(3)	-8(3)
C(10)	31(4)	37(4)	45(4)	2(3)	-6(3)	10(3)
C(11)	67(5)	31(4)	44(4)	8(3)	6(4)	8(4)
C(12)	30(4)	33(3)	51(4)	14(3)	3(3)	-4(3)
C(13)	50(5)	43(4)	37(4)	7(3)	-4(3)	3(3)
C(14)	55(5)	43(4)	55(4)	1(4)	-6(4)	7(4)
C(15)	41(4)	47(4)	55(4)	2(4)	-14(3)	6(4)
C(16)	39(4)	49(4)	66(5)	5(4)	-7(4)	10(4)
C(17)	53(5)	83(7)	81(6)	-5(5)	-24(5)	3(5)
C(18)	53(6)	116(8)	75(6)	8(6)	-11(5)	5(6)
C(19)	82(8)	64(6)	60(5)	-5(4)	-13(5)	14(5)
C(20)	64(6)	82(7)	132(9)	23(6)	31(6)	3(5)
N(1)	73(5)	21(3)	71(4)	-16(3)	17(3)	3(3)
O(1)	76(4)	33(3)	74(3)	6(3)	11(3)	18(3)
O(2)	58(4)	69(5)	109(5)	-5(4)	38(4)	-9(4)

C-C-C angle is 114° . These values are in good agreement with those previously found in long-chain compounds.^{7,11} The mean C-H bond distance is 0.96 \AA and the mean angle

involving hydrogen atoms is 108° . The individual deviations from the average values are quite large as these hydrogen atoms were located from the difference synthesis and their

Table 3. Fractional atomic coordinates and isotropic temperature factors for the hydrogen atoms.

	Molecule A				Molecule B			
	<i>x</i>	<i>y</i>	<i>z</i>	<i>B</i> (Å ²)	<i>x</i>	<i>y</i>	<i>z</i>	<i>B</i> (Å ²)
H(21)	0.096	0.018	0.339	3.5	0.868	0.238	1.584	3.4
H(22)	0.087	0.265	0.248	3.5	0.860	0.482	1.484	3.4
H(31)	0.137	0.290	0.317	3.3	0.835	-0.028	1.421	3.3
H(32)	0.121	0.523	0.406	3.3	0.818	0.214	1.503	3.3
H(41)	0.122	0.248	0.603	3.8	0.816	0.498	1.301	2.9
H(42)	0.138	0.002	0.522	3.8	0.835	0.259	1.223	2.9
H(51)	0.180	0.288	0.495	3.6	0.790	0.001	1.245	3.2
H(52)	0.165	0.497	0.581	3.6	0.776	0.216	1.330	3.2
H(61)	0.164	0.213	0.793	3.8	0.771	0.494	1.124	3.0
H(62)	0.184	0.005	0.698	3.8	0.791	0.280	1.035	3.0
H(71)	0.224	0.298	0.670	3.5	0.746	-0.009	1.065	3.6
H(72)	0.210	0.506	0.760	3.5	0.730	0.204	1.151	3.6
H(81)	0.213	0.216	0.956	3.1	0.728	0.494	0.948	3.8
H(82)	0.227	0.007	0.877	3.1	0.742	0.291	0.872	3.8
H(91)	0.267	0.298	0.852	3.5	0.702	-0.018	0.889	2.9
H(92)	0.253	0.505	0.935	3.5	0.689	0.208	0.973	2.9
H(101)	0.256	0.222	1.333	4.3	0.684	0.497	0.778	2.9
H(102)	0.272	-0.010	1.050	4.3	0.700	0.277	0.692	2.9
H(111)	0.311	0.301	1.018	3.8	0.659	-0.015	0.717	3.5
H(112)	0.297	0.504	1.104	3.8	0.644	0.209	0.807	3.5
H(121)	0.303	0.208	1.301	4.2	0.640	0.504	0.601	3.2
H(122)	0.316	-0.006	1.221	4.2	0.653	0.291	0.519	3.2
H(131)	0.355	0.296	1.192	4.1	0.613	-0.006	0.537	3.4
H(132)	0.342	0.506	1.283	4.1	0.600	0.214	0.633	3.4
H(141)	0.347	0.227	1.486	3.5	0.594	0.483	0.427	4.1
H(142)	0.362	0.003	1.402	3.5	0.608	0.275	0.339	4.1
H(151)	0.402	0.283	1.363	4.3	0.568	0.026	0.371	3.8
H(152)	0.385	0.482	1.452	4.3	0.553	0.223	0.452	3.8
H(161)	0.391	0.220	1.665	4.4	0.549	0.478	0.256	4.2
H(162)	0.406	0.004	1.565	4.4	0.565	0.267	0.161	4.2
H(171)	0.445	0.272	1.538	4.3	0.525	-0.005	0.199	5.5
H(172)	0.430	0.509	1.624	4.3	0.510	0.226	0.284	5.5
H(181)	0.450	-0.003	1.755	6.2	0.518	0.291	-0.009	6.2
H(182)	0.439	0.195	1.831	6.2	0.505	0.475	0.070	6.2
H(183)	0.466	0.271	1.763	6.2	0.489	0.221	0.059	6.2
H(191)	0.044	0.318	0.685	4.3	0.914	0.456	1.148	5.3
H(192)	0.042	0.038	0.678	5.3	0.912	0.192	1.140	5.3
H(201)	0.008	0.027	0.481	5.3	0.944	0.084	1.339	6.7
H(202)	0.011	0.406	0.484	5.3	0.949	0.460	1.343	6.7
H(24)	-0.014(2)	0.085(22)	0.706(10)	8.2(2.4)	0.976(1)	0.340(14)	1.187(7)	1.6(1.6)
H(17)	0.067(2)	-0.019(20)	0.510(10)	2.6(2.6)	0.067(2)	-0.019(16)	0.510(7)	2.6(1.5)

positions never refined. The same mean values were obtained in 13-oxoisostearic acid¹¹ in which case the hydrogen atoms were included in the least-squares refinement.

The molecules are V-shaped with a sharp bend at C(2). The equations for the least-squares plane through the fatty acid chains are given in Table 4, with the out of plane deviations. The chains are planar from C(4) to C(18) within 0.032 and 0.036 Å in molecule A and B, respectively. C(2) and C(3) deviate 0.061–0.093 Å from these planes.

The plane through N(1), O(1), C(1) and C(2) forms an angle with the hydrocarbon chain plane of 84° in both molecules and intersects the ethanol end group plane [the plane through N(1), C(19), C(20) and O(2)] at an angle of 85 and 82° in molecule A and B, respectively. The amide plane is thus almost perpendicular to the carbon chain planes. By this arrangement adjacent amide planes are as close as 3.2 Å. If, on the other hand, the amide planes were parallel to the *ac*-plane, this distance would, of course, be 4.89 Å.

Table 4. The best least-squares planes through the stearoyl chains. The planes are calculated from C(4) to C(18). The plane equations are $-0.9563X + 0.1592Y + 0.2454Z - 0.0285 = 0$ and

$$-0.9556X + 0.1657Y + 0.2439Z + 0.4205 = 0$$

in molecule A and B, respectively. The equations are expressed in terms of the crystal axes.

	Deviations from the plane (Å)	
	Molecule A	Molecule B
C(4)	-0.007	0.036
C(5)	-0.032	0.012
C(6)	-0.004	0.005
C(7)	-0.009	-0.010
C(8)	-0.008	0.001
C(9)	0.023	-0.006
C(10)	0.019	0.008
C(11)	0.018	-0.008
C(12)	0.031	0.006
C(13)	0.018	-0.026
C(14)	-0.010	-0.031
C(15)	0.021	0.027
C(16)	-0.009	-0.001
C(17)	-0.031	0.005
C(18)	-0.021	0.012
C(1)	1.271	-1.190
C(2)	-0.094	0.072
C(3)	-0.074	0.061

The fatty acid chains are tilted by 55.5° towards the methyl end group contact planes and thus allow a good packing at the polar part of the molecules. In unbranched long-chain compounds the corresponding angle is about 60° .¹²

The opening angle formed by the fatty acid chain and the direction of maximum extension of the ethanol end group is about

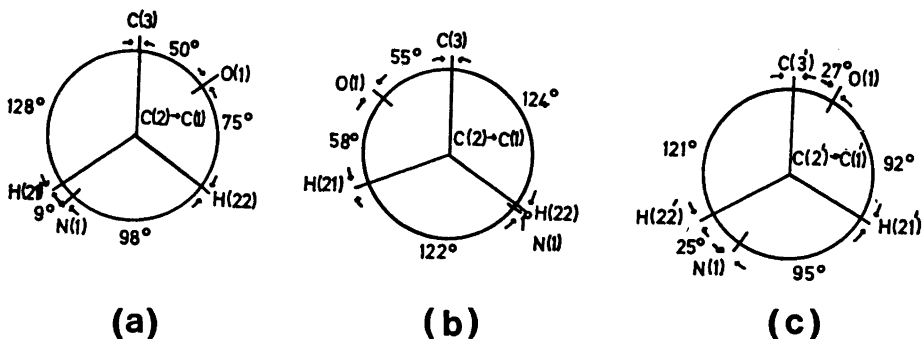


Fig. 2. The conformation around the first bond in the fatty acid chain in (a) molecule A, (b) molecule B in *N*-(2-hydroxyethyl)-octadecanamide, (c) tetracosanoylphytosphingosine.

Table 5. The geometry of the hydrogen bonds.

N(1)A...O(1)A	(0, -1, 0)1 ^a	2.87 Å
N(1)A-H(17)A	(0, 0, 0)1	0.76
H(17)A...O(1)A	(0, -1, 0)1	2.15
N(1)B...O(1)B	(0, 1, 0)1	2.80
N(1)B-H(17)B	(0, 0, 0)1	0.87
H(17)B...O(1)B	(0, 1, 0)1	2.01
O(2)A...O(2)B	(-1, 0, -1)2	2.69
O(2)A...O(2)B	(-1, 1, -1)2	2.72
O(2)A-H(24)A	(0, 0, 0)1	1.22
O(2)A...H(24)B	(-1, 1, -1)2	1.97
O(2)B...H(24)A	(1, -1, 1)2	1.63
O(2)B-H(24)B	(0, 0, 0)1	0.77
O(2)A-H(24)A...O(2)B		141°
O(2)A...H(24)B-O(2)B		164°

^a The numbers in parentheses indicate translations in the directions *a*, *b* and *c*. The 1 or 2 following refer to the equivalent positions *x*, *y*, *z* and *x*, *y*, $\frac{1}{2} + z$.

131° . The molecular conformation at the C(1)-C(2) bond is shown in Fig. 2. As a comparison the torsion angles at the corresponding bond in tetracosanoylphytosphingosine are also given.

The molecular packing projected on the (0 1 0) plane is illustrated in Fig. 3. The molecules are arranged head to head in double layers. They are linked together by two hydrogen bonds running in the *b* axis direction, one connecting molecules within the layers and the other between molecules in different layers. The existence of these hydrogen bonds was also confirmed by the characteristic shifts in the infrared spectrum of the compound in the solid state as compared to that in solution. The geometry around the hydrogen bonds is given in Table 5 and a detailed picture of the

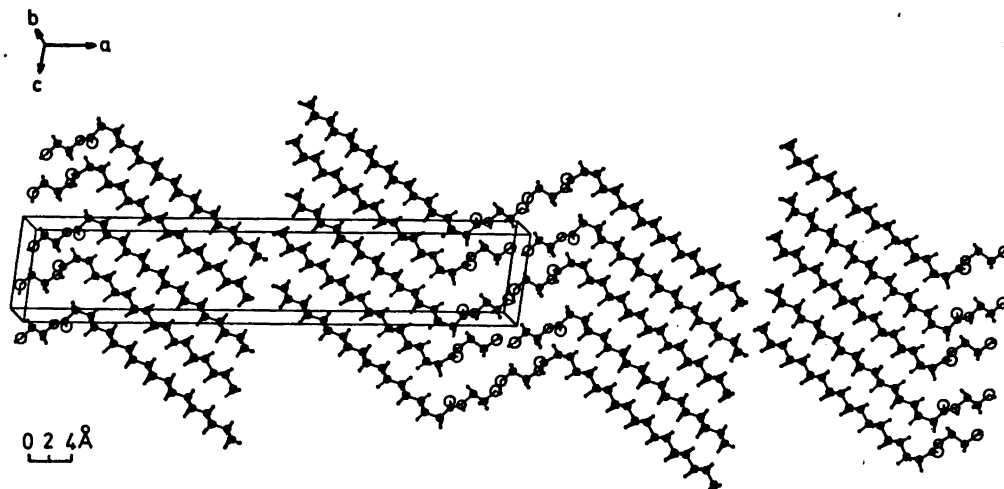


Fig. 3. The molecular packing seen along the *b* axis.

packing at the polar part in Fig. 4. The N···O hydrogen bond distances are 2.87 and 2.80 Å respectively. Reported values for N···O contacts in other long-chain compounds are 2.80 Å in triacetylphingosine¹³ and 2.98 Å in tetra-cosanoylphytosphingosine.

The other hydrogen bond connects the hydroxyl oxygens in molecule A and molecule B so that every oxygen atom takes part in two hydrogen bonds running almost parallel to the *b* axis. A similar arrangement of hydrogen bonded hydroxyl oxygens has been found in 11-bromoundecanol.¹⁴ The O···O contacts are 2.69 and 2.72 Å, respectively, which are in good agreement with those found in tetra-cosanoylphytosphingosine. The arrangement

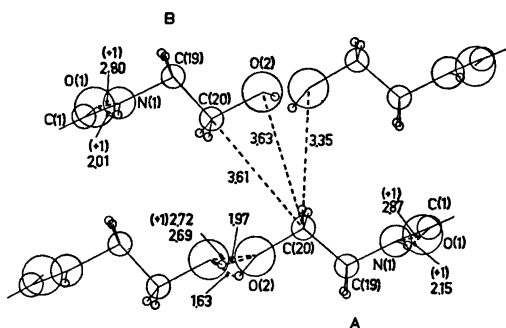


Fig. 4. The polar contact region viewed along the *b* axis with the shorter intermolecular contacts indicated.

in the van der Waals contact planes is shown in Fig. 5. The shortest methyl carbon contact is 3.95 Å. The closest interlayer hydrogen-hydrogen contacts are H(183)A···H(183)B and H(181)A···H(183)B (in the molecule symmetry related by a glide plane) which are 2.83 and 2.85 Å, respectively.

The hydrocarbon chains pack according to the common orthorhombic subcell packing (O₁).¹⁵ The subcell dimensions are *a*_s = 4.89, *b*_s = 7.43, *c*_s = 2.55 Å and the volume per CH₂ group is 23.2 Å³.

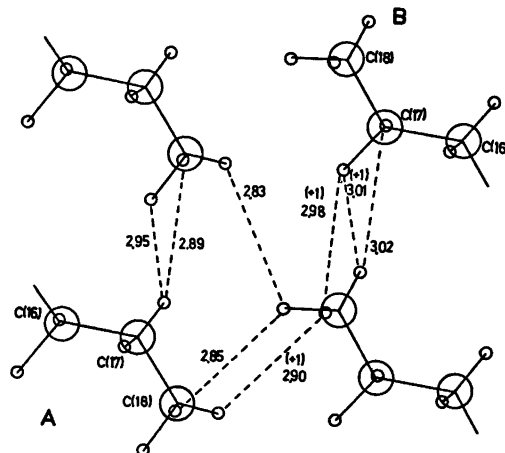


Fig. 5. The methyl end group contacts as seen along the *b* axis with the shorter hydrogen-hydrogen interactions given.

We are grateful to Professor S. Abrahamsson for helpful discussions and Mrs. M. Varju for technical assistance. Grants in support of this Department were obtained from the Swedish Medical Research Council, the Swedish Board for Technical Development, the Wallenberg Foundation and the U.S. Public Health Service (GM-11653).

REFERENCES

1. Kuel, F. A., Jacob, T. A., Ganley, O. H., Ormond, R. E. and Meisinger, M. A. P. *J. Am. Chem. Soc.* 79 (1957) 5577.
2. Karlsson, K.-A., Samuelsson, B. E. and Steen, G. O. *Acta Chem. Scand.* 22 (1968) 2723.
3. Karlsson, K.-A., Samuelsson, B. E. and Steen, G. O. *Acta Chem. Scand.* 21 (1967) 2566.
4. Stoffel, W., Sticht, G. and LeKim, D. *Hoppe-Seyler's Z. Physiol. Chem.* 349 (1968) 1149.
5. Wren, J. J. and Merryfield, D. S. *Biochim. Biophys. Acta* 98 (1965) 589.
6. Nilsson, B. and Pascher, I. *Private communication*.
7. Dahlén, B. and Pascher, I. *Acta Crystallogr. B* 28 (1972) 2396.
8. O'Connell, A. M. *Acta Crystallogr. B* 29 (1973) 2320.
9. *International Tables for X-Ray Crystallography*, Kynoch Press, Birmingham 1962, Vol. III, pp. 201–209.
10. Stewart, R. F., Davidson, E. R. and Simpson, W. T. *J. Chem. Phys.* 42 (1965) 3175.
11. Dahlén, B. *Acta Crystallogr. B* 28 (1972) 2555.
12. von Sydow, E. *Ark. Kemi* 9 (1956) 231.
13. O'Connell, A. M. and Pascher, I. *Acta Crystallogr. B* 25 (1969) 2553.
14. Rosén, L. and Hybl, A. *Acta Crystallogr. B* 28 (1972) 610.
15. Abrahamsson, S., Stållberg-Stenhagen, S. and Stenhagen, E. *Prog. Chem. Fats Other Lipids* 7 (1963) 60.

Received December 1, 1976.

Products of Benzyl Chloride Photolysis in Methanol—Water Mixtures

JOUKO HYÖMÄKI and JOUKO KOSKIKALLIO

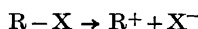
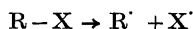
Department of Physical Chemistry, University of Helsinki, Meritullinkatu 1 C, SF-00170 Helsinki 17, Finland

When benzyl chloride was photolysed in methanol–water mixtures at 0 °C the following reaction products were obtained by GLC: benzyl alcohol, benzylmethyl ether, bibenzyl, β -phenylethyl alcohol and small amounts of benzaldehyde. The changes in the relative amounts of different products with changes in the solvent composition are interpreted in terms of a homolytic bond dissociation of singlet excited benzyl chloride followed by two competing reactions: the abstraction of hydrogen from methanol by chlorine atoms and the oxidation of benzyl radical to carbonium ion by chlorine atoms. The final products are then obtained by radical combination reactions and by nucleophilic reactions of the benzyl carbonium ion with solvent molecules.

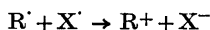
Photolysis of benzyl chloride in gas phase^{1,2} produces benzyl radicals and chlorine atoms. As no toluene has been observed¹ among the products at room temperatures hydrogen abstraction reactions by benzyl radicals are slow compared with radical combination reactions. Chlorine atoms, however, abstract hydrogen atoms forming hydrogen chloride.¹ The benzyl radical has been observed^{3,4} in photolysis of benzyl chloride in solid matrices. Photolysis of benzyl chloride in 1:1 methanol–water mixture⁵ gives products by hydrogen abstraction and combination reactions of the benzyl and chlorine radicals. In addition also benzyl alcohol and methyl benzyl ether were obtained, products which result from photochemical nucleophilic reactions of benzyl chloride with solvent molecules.

A similar competition between two different types of photochemical reactions, radical and nucleophilic reactions, has been observed in photolyses of substituted benzyl acetates^{6–10}

and in photolyses of substituted phenyl esters and phenyl chlorides.^{11,12} These results have been interpreted in terms of two competing primary photodissociation processes, a homolytic and a heterolytic dissociation:



The nucleophiles then react with the carbonium ion R^{+} . In some cases also the excited molecule may react with nucleophiles.¹² It is also possible that the radical X^{\cdot} oxidizes the carbonium radical to a carbonium ion.¹⁰



The quantum yield of photodissociation of benzyl chloride in 1:1 methanol–water mixture is 1.0 and independent of the wavelength of the exciting light and of added oxygen.⁵ The photodissociation is therefore expected to occur from the excited singlet state.

In order to study the mechanism of the photochemical reactions of benzyl chloride we have measured the amounts of different products formed in photolysis of benzyl chloride in methanol–water mixtures.

EXPERIMENTAL

The benzyl chloride, a product of BDH, was purified by vacuum distillation before use.

Non de-aerated benzyl chloride solutions were photolysed with the light of a 100 W medium pressure mercury arc tube in a thermostat at 0 °C. The initial concentration of benzyl chloride was about 4×10^{-2} to 9×10^{-2} mol dm⁻³ except for solutions containing small

Table 1. Products of the photolysis of benzyl chloride in methanol–water mixtures at 0 °C. x is the mol fraction of water in the reaction mixture and c the initial concentration of benzyl chloride.

x H ₂ O	$10^4 c/\text{mol dm}^{-3}$ PhCH ₂ Cl	Mol % of products				
		PhCH ₂ OH	PhCH ₂ OCH ₃	(PhCH ₂) ₂	PhCH ₂ CH ₂ OH	PhCHO
0	766	0	37.8	15.9	44.5	
0.105	806	9.0	38.9	13.0	37.3	
0.197	893	9.5	35.6	13.4	39.8	
0.351	921	11.1	34.3	14.1	38.7	
0.481	920	18.3	32.7	12.3	34.9	
0.585	406	25.6	32.7	11.3	28.8	
0.678	199	34.5	34.5	6.8	22.9	
0.830	42.6	46.2	36.5	7.8	8.9	
0.893	23.2	73.2	15.0	1.3	9.8	0.1
0.950	32.1	87.1	5.2	0.8	5.8	0.9

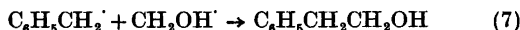
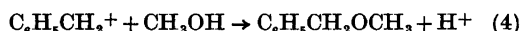
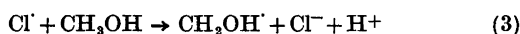
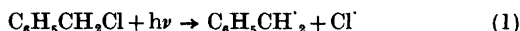
amounts of methanol where lower concentrations of about 1×10^{-3} had to be used. The reaction mixture was analysed by GLC using Carbowax 1540 or 4000 and the products were identified by comparison of their chromatograms with those of known compounds and by mass spectroscopy. A reference sample was kept in the dark at the same temperature and the products of thermal reactions were analysed in the same way and subtracted from the amounts of products obtained in photolysis reactions. These corrections were usually small, of the order of a few per cent of the amounts of products of the photolysis. The results are shown in Table 1.

With different illumination times, which caused from 1 to 16 % of benzyl chloride to decompose, the relative amounts of various products were constant except for a small increase in the relative amount of β -phenylethyl alcohol within the first two per cents of benzyl chloride decomposition. The relative amounts of the products also remained constant as the initial concentration of benzyl chloride was increased from 1.5×10^{-2} to 5.8×10^{-2} mol dm⁻³, except that the amount of β -phenylethyl alcohol increased slightly from 8.2 to 10.2 %. No attempt is made to explain the cause of these small changes. The decreases in the amount of benzyl chloride match well with the sum of the products, and it is therefore likely that all important products of the photolysis of benzyl chloride were detected. The ethylene glycol expected to form in the photolysis could not be detected by GLC, however.

RESULTS AND DISCUSSION

In the present study on the photolysis of benzyl chloride in methanol–water mixtures the following products were obtained: benzyl alcohol, benzylmethyl ether, bibenzyl, β -phenylethyl alcohol and small amounts of benzal-

dehyde (Table 1). In order to explain the observed products we propose the following mechanism:



This mechanism is similar to that proposed by Ichimura and Moi¹ for photolysis of benzyl chloride in gas phase in the presence of an excess of butane. In order to account for the products of nucleophilic reactions we have added the steps 2, 4, and 5.

Chlorine atoms formed by the photodissociation reaction may react in the solvent cage either with methanol by abstracting a hydrogen atom or by oxidizing the benzyl radical to benzyl carbonium ion, reactions 2 and 3, respectively. The relative rates of these two competing reactions can be determined from the ratio of the sum of twice the amount of bibenzyl and β -phenylethyl alcohol and the sum of the amounts of benzyl alcohol and benzylmethyl ether (Table 1 and Fig. 1). This ratio increases linearly as the mol fraction of methanol in water increases from a value

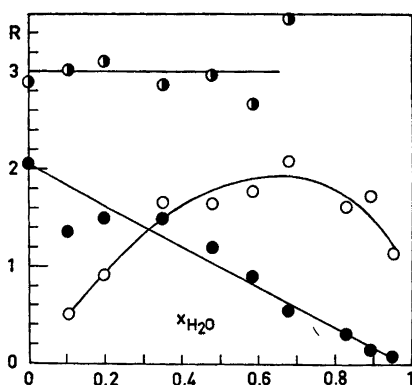
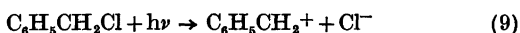


Fig. 1. Relative amounts of products (mol) in photolysis of benzyl chloride in methanol-water mixtures. Half-filled circles: (β -phenylethanol)/(bibenzyl); open circles: (methylbenzyl ether) (water)/(benzyl alcohol) (methanol); filled circles: (β -phenylethanol) + 2 (bibenzyl)/(methylbenzyl ether) + (benzyl alcohol). x is the mol fraction of water in the methanol-water mixtures.

of about zero in pure water to about 2 in pure methanol.

In water all the chlorine atoms formed oxidize the benzyl radicals to benzyl carbonium ions whereas in methanol one third of the chlorine atoms formed oxidize the benzyl radicals and two thirds abstract a proton from methanol molecules. If it is assumed that every chlorine atom reacts within the solvent cage and that in addition to the benzyl radical 8 methanol molecules are within the same minimum distance from the chlorine atom the chlorine atoms would react about 4 times faster with benzyl radicals than with methanol molecules.

The linear relationship of the ratio of two different types of products with the mol fraction of methanol indicates that benzyl radicals are produced in a secondary reaction (2) and not in a primary heterolytic photodissociation reaction (9).



A primary heterolytic photodissociation has been proposed in photolysis of substituted benzyl acetates⁶⁻¹⁰ and substituted phenyl esters.^{11,12} However, no proofs have been given in favour of either reaction (9) or reactions (1)

and (2) for photochemical nucleophilic reactions.

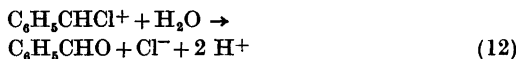
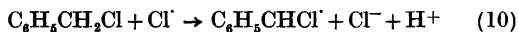
The benzyl radical does not readily abstract hydrogen atoms and if it is not oxidized by chlorine atoms, the benzyl radical combines with another benzyl radical to form bibenzyl or with methanoyl radical to form β -phenylethylalcohol.

The ratio of the two products, β -phenylethyl alcohol and bibenzyl, is approximately constant about 3.0, as shown in Fig. 1. Thus about 60% of the benzyl radicals combine with methanoyl radicals to form β -phenylethyl alcohol, and the rest of the benzyl radicals combine to bibenzyl. If all β -phenylethyl alcohol molecules are formed in the solvent cage this recombination is about 3 times faster than the competing escape of benzyl radicals from the cage in the whole range of methanol-water solvent mixtures. The relatively slow recombination reaction is due to the hydrogen chloride separating the two radicals, benzyl and methanoyl, in the solvent cage.

The benzyl carbonium ion formed in the reaction 2 may react with the nucleophiles chloride ion, water or methanol to form benzyl chloride, benzyl alcohol or benzylmethyl ether. The extent of the re-formation of the starting material, benzyl chloride, cannot be estimated from the present results. The ratio of the two other products, benzylmethyl ether and benzyl alcohol, varies with the solvent composition, as shown in Fig. 1, and a maximum value of about 1.9 is obtained in a solvent mixture where the mol fraction of methanol is about 0.7. The methanolysis reaction of benzyl cation is then about twice as fast as the hydrolysis reaction, whereas the methanolysis of benzyl chloride in the same solvent mixture was found to be about 6.3 times faster than the hydrolysis at 0 °C. There is then less discrimination among the fast nucleophilic reactions of benzyl cation than the slower nucleophilic reactions of benzyl chloride.

In solvent mixtures of low methanol content, small amounts of benzaldehyde were observed in the photolysis of benzyl chloride (Table 1). Small amounts of benzaldehyde has also been observed by electrolytic oxidation of substances which presumably form benzyl radicals as unstable intermediates, e.g. the oxidation of *o*-chlorophenylacetic acid in meth-

anol,¹³ of toluene in acetic acid¹⁴ and of *p*-methoxybenzyl alcohol in methanol.¹⁵ Small amounts of chlorine atoms escaping the cage may oxidize either benzyl chloride or benzyl alcohol to benzaldehyde.



Acknowledgement. The authors wish to record their thanks to the Finnish Academy for financial support.

REFERENCES

1. Ichimura, T. and Moi, Y. *J. Chem. Phys.* 57 (1972) 1677.
2. Boyrakecken, F. and Nicholas, J. E. *J. Chem. Soc. B* (1970) 691.
3. Brockdehurst, B., Porter, G. and Savadotti, M. *Trans. Faraday Soc.* 60 (1964) 2017.
4. Arai, S., Tagawa, S. and Imamura, M. *J. Phys. Chem.* 78 (1974) 519.
5. Ivanov, V. B., Ivanov, V. L. and Kuzmin, M. G. *Zh. Org. Chem.* 9 (1933) 340.
6. Jaeger, D. A. *J. Am. Chem. Soc.* 96 (1974) 6216.
7. Jaeger, D. A. *J. Am. Chem. Soc.* 97 (1975) 903.
8. Jaeger, D. A. *J. Am. Chem. Soc.* 98 (1976) 6401.
9. Saltier, J. *Surv. Prog. Chem.* 2 (1964) 307.
10. Zimmerman, H. E. and Sandel, W. R. *J. Am. Chem. Soc.* 85 (1963) 915, 922.
11. Havinga, E. and Kronenberg, M. E. *Pure Appl. Chem.* 16 (1968) 137.
12. Cornelisse, J. and Havinga, E. *VIII Int. Conference on Photochemistry*, Edmonton 1975.
13. Woolford, R. G. and Liu, W. S. *Can. J. Chem.* 44 (1966) 2783.
14. Ross, S. D., Finkelstein, M. and Petersen, R. C. *J. Am. Chem. Soc.* 89 (1967) 4088.
15. Parker, V. D. and Burgert, B. E. *Tetrahedron Lett.* 20 (1968) 2411.

Received September 13, 1976.

Short Communications

Crystal and Molecular Structure of
Tetra-ammonium *aa'*- μ -Oxobis-
{[*gie'd'*- μ_3 -(*S*)-malato- O^1, O^2, O^4, O^4']-
di- μ -oxobis [dioxomolybdate (VI)]}
Monohydrate. ^{13}C NMR Studies

JAN-ERIC BERG,^a SVANTE BRANDÄNGE,^b
LARS LINDBLOM^b and PER-ERIK WERNER^a

^a Department of Structural Chemistry, Arrhenius Laboratory, University of Stockholm, S-106 91 Stockholm, Sweden and ^b Department of Organic Chemistry, Arrhenius Laboratory, University of Stockholm, S-106 91 Stockholm, Sweden

Molybdate(VI) complexes of optically active α -hydroxy acids were studied polarimetrically as early as at the end of the nineteenth century.¹ More recently, the use of such complexes in determinations of absolute configurations of α -hydroxy acids by CD has been described² and the crystal and molecular structure of $(\text{NH}_4)_4[(\text{MoO}_2)_4\text{O}_3(\text{C}_4\text{H}_3\text{O}_5)_2]\cdot 6\text{H}_2\text{O}$, obtained from malic acid and ammonium molybdate(VI), has been determined.³ This compound, known as ammonium dimolybdomalate, was crystallized from water, but if aqueous ethanol is used instead, a compound corresponding to the formula $(\text{NH}_4)_4[(\text{MoO}_2)_4\text{O}_3(\text{C}_4\text{H}_3\text{O}_5)_2]\cdot \text{H}_2\text{O}$ (*I*) is obtained. The crystal structure of *I* is reported here and also the results of ^{13}C NMR studies which indicate that for the complex in aqueous solution both carboxyl groups of the malic acid are bonded to molybdenum.

X-Ray diffraction studies. No crystals of *I* suitable for single crystal analysis were obtained, but a powder photograph was taken with a focusing Guinier-Hägg camera. Strictly monochromatic $\text{CuK}\alpha_1$ radiation ($\lambda = 1.54051 \text{ \AA}$) was used and potassium chloride was added as an internal standard ($a = 6.2930 \text{ \AA}$ at 25°C). The powder photograph was measured by an automatic film scanner system as described by Malmros and Werner⁴ and 120 integrated intensities were obtained corrected for polarisation, Lorentz and geometrical factors. A monoclinic cell (space group *C*2, $a = 14.572(2) \text{ \AA}$, $b = 10.114(2) \text{ \AA}$, $c = 11.461(2) \text{ \AA}$, $\beta = 121.45(1)^\circ$, cell volume 1441.0 \AA^3 , $Z = 2$, $D_x = 2.10 \text{ g/cm}^3$) was found by a trial-and-error indexing programme (TREOR).^{5,6}

A three-dimensional Patterson function was calculated from the 120 integrated intensities. The two Mo-positions in the asymmetric unit were derived from the Patterson function using space group *C*2. A least squares refinement of the Mo-positions ended with an *R*-value of 0.30. Since no model for the oxygen coordination around the molybdenum atoms could be derived from the integrated intensities, a modified Rietveld profile analysis refinement procedure was applied. The original refinement programme⁷ which was written for neutron diffraction data has been rewritten by Malmros and Thomas⁸ for X-ray Guinier powder data. The use of profile intensities instead of the integrated intensities makes it possible to take full account of the overlaps. An important advantage of using a focusing film camera instead of a powder diffractometer for the determination of diffraction intensities is the high resolution of the diffraction data. The simultaneous collection of intensities from all diffraction angles during the time of exposure is of course of special importance when unstable compounds are dealt with, as in the present structure determination. On the other hand, no accurate atomic positions could be refined from this powder photograph. However, from successive profile refinements and Fourier calculations, a low resolution structure showing the main features of the structure could be obtained. A structure refinement where the positions of 2 Mo, 12 O and 2 N atoms were refined ended with a reliability factor

$$\sum_{hkl} |\sqrt{I}_{\text{obs}} - \sqrt{I}_{\text{calc}}| / \sum_{hkl} \sqrt{I}_{\text{obs}} = 0.11$$

Four carbon atoms were kept in fixed positions and the total number of parameters refined was 51. The refinement, which included 505 reflections, did not completely converge and therefore no accurate positional coordinates with standard deviations can be given. The structure of the anion (Fig. 1) is indistinguishable from that in ammonium dimolybdomalate.³ The main difference between the two structures is found in the packing of the ions in the unit cells. This is obviously an effect of the different contents of crystal water in the two compounds. Full crystallographic details will be published elsewhere.

^{13}C NMR measurements. The CD properties of acidified aqueous solutions containing (–)-malic

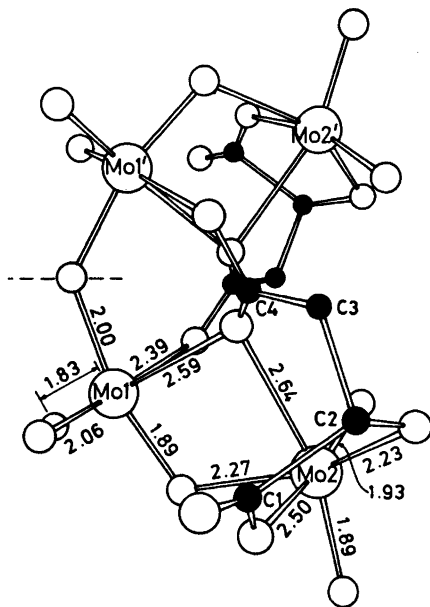


Fig. 1. View of the anion $[(\text{MoO}_2)_2\text{O}_3(\text{C}_4\text{H}_3\text{O}_5)_2]^{4-}$ in the crystal structure of the title compound. E.s.d. in the bond lengths given in the figure are approximately 0.15 Å. The twofold axis is indicated by a dashed line.

acid and molybdate(VI) suggest that both carboxyl groups in the organic acid are involved in the bonding to molybdenum.² The following ¹³C NMR results are in agreement with such bonding. The spectrum of a solution of malic acid and sodium molybdate (2 equiv.) in D₂O [pD = pH (meter reading) + 0.40⁹ = 3.9, dioxane as internal standard, δ_c = 67.4 ppm] does not indicate the presence of more than one complex; four signals were found at δ 184.3, 180.1, 80.3, and 40.4 ppm. Down-field shifts are obtained in going from malic acid to its molybdate complex: C-1 + 5.9 ppm; C-4 + 4.2 ppm (alternatively: C-1 + 1.7 ppm; C-4 + 8.4 ppm); C-2 + 12.1 ppm; C-3 + 0.6 ppm. The fact that the down-field shift of C-4 is larger than that of C-3 indicates that both carboxyl groups of malic acid are bonded to molybdenum. For acetic acid present in the solutions the following values were observed: C-1 + 0.0 ppm; C-2 + 0.2 ppm.

When citric acid was substituted for malic acid three main signals were obtained in the carboxyl region of a spectrum run at 5°C (δ 184.4, 179.5, and 174.8 ppm respectively). This indicates that one of the two β-carboxyl groups bonds to molybdenum whereas the other does not.

Preparation of the complex. Solutions of (-)-malic acid (4.5 g) in water (15 ml) and

ammonium heptamolybdate (4.0 g) in water (25 ml) were prepared with some warming. The solutions were filtered and then combined. Boiling ethanol (185 ml) was added under warming to the aqueous solution. On cooling crystals deposited (2.5 g, 48%). Found: C 10.65; H 2.53; Mo 42.04; N 6.32. Calc. for $(\text{NH}_4)_4[(\text{MoO}_2)_2\text{O}_3(\text{C}_4\text{H}_3\text{O}_5)_2] \cdot \text{H}_2\text{O}$: C 10.53; H 2.65; Mo 42.08; N 6.14. $[\alpha]_{546}^{22} + 245^\circ$ (c 0.65, water). Lit.¹⁰ value for ammonium dimolybdomalate: $[\alpha]_{546} + 239^\circ$ (c 2.8, water).

Acknowledgements. We thank Mr. Bengt Lindqvist for recording the NMR spectra. This work has been supported by the Swedish Natural Science Research Council.

1. *Gmelins Handbuch der Anorg. Chemie* 53 (1935) 330.
2. Voelter, W., Bayer, E., Barth, G., Bunnenberg, E. and Djerassi, C. *Chem. Ber.* 102 (1969) 2003.
3. Porai-Koshits, M. A., Aslanov, L. A., Ivanova, G. V. and Polynova, T. N. *J. Struct. Chem. USSR* 9 (1968) 401.
4. Malmros, G. and Werner, P.-E. *Acta Chem. Scand.* 27 (1973) 493.
5. Werner, P.-E. *Z. Kristallogr.* 120 (1964) 375.
6. Werner, P.-E. *Z. Kristallogr.* 140 (1974) 331.
7. Rietveld, H. M. *J. Appl. Crystallogr.* 2 (1969) 65.
8. Malmros, G. and Thomas, J. O. *J. Appl. Crystallogr. In press.*
9. Glasoe, P. K. and Long, F. A. *J. Phys. Chem.* 64 (1960) 188.
10. Kolli, I. D., Perekalina, Z. B. and Gordeeva, G. A. *Russ. J. Inorg. Chem.* 13 (1968) 388.

Received February 3, 1977.

Lattice Constants of Nb and NbO at Elevated Temperatures

SVEND ERIK RASMUSSEN

Department of Inorganic Chemistry, Aarhus University, DK-8000 Aarhus C, Denmark

As part of attempts to determine phase diagrams of niobium alloys or compounds with germanium and aluminium we determined the lattice constants of pure niobium and of niobium alloys at various temperatures. In the majority of the cases NbO was formed as a thin surface layer, and therefore the lattice constant of this compound was inadvertently determined as well.

Experimental. A Philips high temperature attachment was mounted on a standard powder goniometer. Sample holders of tantalum were used in all runs. As niobium is very reactive at high temperatures, it was not possible to use an internal standard for calibration purposes in the high temperature region. Therefore a calibration valid at room temperature was used at high temperatures too. The ambient atmosphere was a problem. Niobium reacted with residual oxygen even in highly purified helium to form NbO and in some cases also NbO₂, and these oxides were formed at elevated temperatures also in a vacuum of about 10⁻⁴ mmHg. In a few cases, however, we were successful in obtaining a vacuum (~10⁻⁵ mmHg) which was good enough to prevent the formation of niobium oxides during the experiments. Niobium and germanium react slowly to form Nb₃Ge₃ and an Al₁₅ phase at temperatures from 500 °C and onwards. The germanium lines disappear first, whereas the niobium lines persist until the lines of the compounds dominate. NbO was formed too in several of these experiments. Niobium and aluminium reacted qualitatively similarly to niobium and germanium, but in the cases when aluminium was present together with niobium no NbO lines were found. Further information on the formation of niobium-germanium compounds is given separately.¹

Niobium of nominal purity 99.8 % was purchased from Alpha-Inorganics. An analysis by X-ray fluorescence showed no foreign elements heavier than titanium. The lattice constant of niobium was determined at 23 °C, using either germanium or silicon as standard for calibration ($a_{\text{Ge}} = 5.6576 \text{ \AA}$, $a_{\text{Si}} = 5.43054 \text{ \AA}$, $\text{CuK}\alpha_1 = 1.54051 \text{ \AA}$, $\text{CuK}\alpha_2 = 1.54433 \text{ \AA}$). The mean value of a_{Nb} from seven different runs is $a_{\text{Nb}} = 3.3044$, $\sigma = 0.0008 \text{ \AA}$. Temperatures were measured using a W/W₂Re thermocouple.

Discussion. NbO is assumed to have a narrow composition range, and the value of the lattice constant at room temperature found here ($a = 4.210 \text{ \AA}$) is in agreement with values reported by Brauer² ($a = 4.2103 \text{ \AA}$), and by Anderson

and Magnéli³ ($a = 4.210 \text{ \AA}$). NbO appears to be stable in the presence of Nb at 1735 K and at a pressure of 0.5×10^{-4} mmHg. When Ge is present too, NbO appears to be stable up to a temperature of about 1600 K. Al on the other hand appears to act as a better "getter" for oxygen than Nb, and no NbO lines were observed in experiments when Al was added to Nb. The temperature dependence of the lattice constant of NbO is shown in Fig. 1.

Fig. 2 shows the dependence of the lattice constant of Nb on temperature. Earlier data by Edwards, Speiser and Johnston⁴ are shown on the graph as well. These data, obtained by photographic methods, look more accurate than the diffractometer data reported here. The following conclusions may be drawn from the combined available material:

The lattice constant of Nb, at 293 K, is 0.5 % larger in a mixture of Nb and NbO than in a pure Nb sample. Probably the difference is caused by dissolution of oxygen in niobium. The difference in lattice constant between "pure" and oxygen-contaminated Nb decreases with temperature, and extrapolation of the results indicates that the difference disappears at 2400 K. At this temperature oxygen probably does not dissolve in Nb. The graph also shows that the niobium lattice apparently expands less rapidly with temperature when germanium or aluminium is present with niobium. In these cases, however, reactions between niobium and the other elements were taking place slowly and these values do not represent equilibrium values.

Acknowledgements. I wish thank Britta Lundtoft for diligent assistance with the experimental work. The Danish Science Research Council is thanked for a grant covering the cost of the high temperature diffractometer.

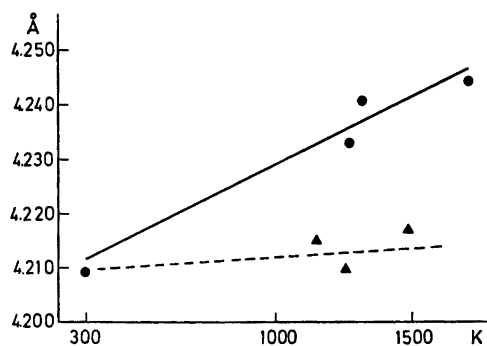


Fig. 1. Dependence of the lattice constant of NbO on temperature. ●, NbO from pure Nb; ▲, NbO in presence of Nb and Ge.

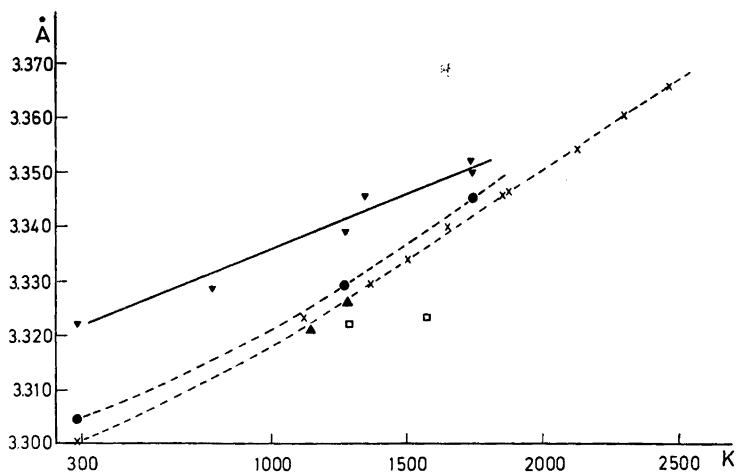


Fig. 2. Dependence of lattice constant of Nb on temperature. ∇ , Nb contaminated with oxygen; \bullet , Nb without oxygen contamination, this paper; \times , Nb according to Ref. 4; \blacktriangle , Nb in the presence of Ge; \square , Nb in the presence of Al.

1. Rasmussen, S. E. *Acta Chem. Scand. A* 31 (1977). *In press*.
2. Brauer, G. *Z. Anorg. Chem.* 248 (1941) 1.
3. Andersson, G. and Magnéli, A. *Acta Chem. Scand.* 11 (1957) 1065.
4. Edwards, J. W., Speiser, R. and Johnston, H. L. *J. Appl. Phys.* 22 (1951) 424.

Received December 2, 1976.

A Reinvestigation of the Hydrolysis of Pentavalent Vanadium

ODD BORGEN, MOHAMED RAFAT MAHMOUD * and INGE SKAUVIK

Division of Physical Chemistry, The University of Trondheim, The Norwegian Institute of Technology, N-7034 Trondheim-NTH, Norway

The hydroxo complexes of pentavalent vanadium in a 1 M perchlorate medium have been reinvestigated by UV-visible spectrophotometric techniques. The acid and alkaline regions were treated separately. The experimental data in the acid region were explained in terms of the following equilibria:



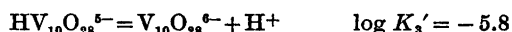
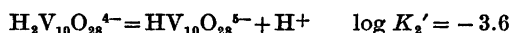
In the alkaline region:



The numerical work was done by factor analysis and least squares refinements, and in addition to the equilibrium constants, molar absorptivities of the individual species have been calculated.

The water chemistry of Group VB metals has been known to be rather complicated. Quite complete discussions of the earlier investigations may be found in the papers by Rosotti and Rosotti,² and Ingri and Brito.⁴ Several workers have attempted to explain the behaviour of vanadium(V) in water, and very early the existence of poly-ions was claimed. However, there was very little agreement be-

tween the workers until the late fifties. Britton and Robinson³ have claimed the existence of the complex $\text{V}_{10}\text{O}_{27}^{4-}$. Several workers have assumed the degree of polymerization to be lower. For instance Düllberg³ chooses the formula $\text{HV}_6\text{O}_{17}^{3-}$. At present the model of Rosotti and Rosotti¹ is generally accepted for the pH-range concerned. These authors have made a study of the system in the acid range by titration curve methods, and explain their data in terms of the equilibria:



In addition to the potentiometric work, absorption spectra in highly acid vanadium solutions were also measured. At the hydrogen ion concentrations in question, VO_2^+ is found to be the only species of significant concentration.

In nearly neutral vanadium solutions, very slow reactions are found to take place. Ingri and Brito⁴ denote this region "the instability gap". The heavy polyvanadates are believed to be broken down to less condensed species in this region. The work of Ingri and Brito is the most important investigation of alkaline vanadium solutions. The following reactions are assumed to take place:



* Present address: Chem. Dept., Faculty of Science, Assiut University, Assiut, Egypt.

Titration curve techniques were applied to obtain these stoichiometries and stability constants, and the investigation mainly covers the pH-range 7.5 to 11. More alkaline solutions have been studied by Newman *et al.*⁵ by spectrometric methods. The presence of HVO_4^{2-} , $\text{V}_2\text{O}_7^{4-}$ and VO_4^{3-} is claimed. For the equilibrium $\text{VO}_4^{3-} + \text{H}_2\text{O} = \text{HVO}_4^{2-} + \text{OH}^-$ a K -value of 0.097 ± 0.005 is given.

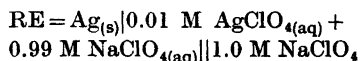
EXPERIMENTAL

The present investigation utilizes UV-visible absorption spectrophotometric data. For reasons caused by the "instability gap" mentioned above, measurements were performed in the acid and alkaline ranges separately. The initial concentrations of the solutions are presented in Tables 3 and 7. Attempts were made to measure the spectra of solutions in the "unstable" range, but these data were not treated quantitatively.

For the measurements in the acid region a Perkin Elmer 137 UV spectrophotometer was utilized. In the alkaline region a Spectronic 710 spectrophotometer was used. In order to perform a proper factor analysis of the absorbance data, the precision of the instruments had to be evaluated. The spectra of acid potassium bichromate solutions of different concentrations were recorded and the residual absorbance errors of the spectrophotometers were estimated using Wernimont's procedure.¹⁰ The investigations showed that the concentration factor was responsible for 99.995 % of the total variance for the Perkin-Elmer instrument, and 99.997 % for the Spectronic instrument, in the range of 0–1.5 absorbance units. The residual 0.005 % and 0.003 %, respectively, were caused by other factors. This corresponds to instrumental residual errors of 0.0034 and 0.0028 absorbance units for the Perkin-Elmer and the Spectronic instrument, respectively. Systematic error sources, like cell imperfections, multiple reflections, imperfect monochromacy and imperfections in the photomultiplier module all contribute to these deviations. We are, however, aware of the fact that the instrumental precision is not invariant. If measurements are made of solutions of high absorbance the error will be greater because of the decreased throughput of light. The refractive index of the liquid and hence the reflectance of the surfaces between the quartz walls and the solutions will be dependent on the wavelength. Such effects will cause the instrumental performance to vary within certain limits. These effects cause difficulties in selecting the number of absorbing components by factor analysis.

In both regions a number of solutions with different $[\text{H}^+]$ and $[\text{V}]$ were prepared, and

their spectra were recorded. The ionic strength for all solutions was kept constant at 1.0 M by adding an appropriate amount of sodium perchlorate, and thus all equilibrium constants evaluated in this investigation are practical constants referring to this ionic strength. In order to avoid interference no buffers were used. $[\text{H}^+]$ was adjusted by addition of HClO_4 and NaOH only, thus assuring the absence of other ions than H^+ , Na^+ , OH^- and ClO_4^- in addition to the several vanadate ions. The perchlorate medium was chosen since the ClO_4^- -ion is known to be a poor complexing agent. The hydroxo complexes are thus assumed to be the only complexes in the solutions. The hydrogen ion concentrations were measured by an Orion 801A pH-meter using a glass electrode in combination with a special reference electrode designed for minimizing the liquid junction potential. This electrode is in principle the same as the one used by Rosotti and Rosotti¹ for measurements in 1 M NaClO_4 -medium:



The inner and outer solutions were connected by a porous glass sinter.

The relation between the measured potential and the hydrogen ion concentration was obtained by titration of NaOH and HClO_4 at ionic strength 1 M, *i.e.* the potentials were measured on solutions with known concentrations of H^+ and OH^- . Certain deviations from Nernst equation behaviour were observed as expected when using a glass electrode. For high and low values of $-\log h$ non-linearity was found, and in the linear range the slope was slightly different from the value predicted from the Nernst equation. At $-\log h = 1.0$ the deviation from the straight line was approximately 12 mV. At $-\log h = 13.0$ a deviation of -20 mV was found. Since this relation is empirical, it is assumed to involve the liquid junction potential and other disturbing factors, and a closer analysis of these phenomena is therefore thought to be unnecessary. It may, however, be mentioned that in the neutral range ($-\log h \approx 7$) the liquid junction potential for an equivalent nitrate electrode is estimated to be 0.06 mV,¹⁴ but that it will increase as $[\text{H}^+]$ or $[\text{OH}^-]$ increases. The titrations were reproducible within limits indicated by a standard deviation of 0.3 mV.

Stability of the solutions was checked by measuring the spectra at intervals of 24 h and comparing the results. In the alkaline range, the solutions were heated to 80 °C for 90 min. This caused the yellow colour of the solution to disappear.⁴ After this all solutions were found to be stable apart from those in the instability gap where the spectra were continuously changing even after two weeks.

INTERPRETATION OF THE DATA

Factor analysis in combination with least squares fitting was used for the interpretation of the experimental data. The basic problem has been to find a model of the system which fits the measured data as well as possible, *i.e.* a least squares fit was performed. For given values of wavelengths and initial concentration, the residual error may be expressed as:

$$s = A - \sum C_i \alpha_i$$

Here A denotes the observed absorbance value while C_i and α_i denote calculated values of concentrations and molar absorptivities. The C_i and α_i values are dependent on certain parameters, *i.e.* the equilibrium constants, and the s -value is then in turn a function of these parameters. Consequently, the sum of squares of residual errors is a function of the equilibrium constants, and may be minimized with respect to these constants. In matrix notation the sum of squares may be expressed by the formula:

$$t = \text{tr}[(A - EC)^T(A - EC)]$$

A is the matrix of observed absorbances, E is the matrix of molar absorptivities and C is the concentration matrix. The E and C matrices may both be unknown. In some cases, however, either the E -matrix or the C -matrix will be known, or perhaps one or more vectors of the E -matrix. In such cases it is desirable to be able to keep the parameters in question invariant during the minimization process. Once the minimization is performed, it may be of interest to obtain a measure of the goodness of the fit. The sum of squares is not very well suited since its numerical value is dependent on the dimensions of the matrices involved. The root mean square (RMS) is, however, better suited. In many cases it may also be of interest to find the standard deviation for each of the single solutions involved. These values should be comparable with the instrumental error. If this is not the case, it is probable that the model chosen is incomplete, or that a false minimum is encountered.

In this work, we have applied, in addition to the least squares fitting, the method of factor analysis.⁷ The essence of this method is

the evaluation of the eigenvalues and eigenvectors of the second moment matrix:⁶

$$M = \frac{1}{n_s} AA^T$$

n_s is the number of solutions investigated. The number of nonzero eigenvalues of this matrix corresponds to the number of linearly independent vectors of the A -matrix. When the necessary allowance is made for experimental error, this number corresponds to the number of absorbing components in the system investigated. This number is naturally of great interest when studying systems where the parameters are generally unknown.

In practice, one eigenvector is assumed initially. The residual standard deviation is then calculated. If the residual standard deviation is greater than the computed instrumental error, one more vector is introduced, and the corresponding residual standard deviation is found. This cycle is repeated until the residual standard deviation is comparable with the instrumental error. The number of eigenvectors needed for this is assumed to be the number of absorbing components in the system. Keeping this in mind, it is clear that uncertainties in the numerical value of the instrumental error will cause problems. Several workers have sought alternative criteria for the vanishing of an eigenvector.^{15,16} Rummel¹⁹ suggests a rather primitive method which, however, has proved to give a fairly correct picture of the systems examined in this work. The point is simply found where the eigenvectors no longer change appreciably as the number of components is increased.

In this work we have made use of two different program systems for the numerical treatment. The first one, MUCO01, is developed by Kankare⁶ and makes use of factor analysis in addition to the least squares techniques. This program has proved to be especially useful when investigating a system where none, or but a few parameters are known beforehand as it has proved to have a quite wide range of convergence with respect to trial parameters. The second program, SQUAD, is designed by Leggett and McBryde.⁸ This program turned out to be superior to MUCO01 on the final refinement stages. Both programs have been modified for the UNIVAC 1108 computer by

the authors. Generally the modifications are minor. A change of a certain importance is, however, applied to SQUAD, where dynamic dimensioning of the matrices has been implemented (Appendix A). The basic principles of the programs are, however, left unchanged, and the reader is referred to the original program descriptions. The well-known program, HALTAFALL, of Ingri, Kakolowicz and Silén,⁹ designed for calculations of equilibrium concentrations has also been used. This program has, however, much wider applications than what has been used in this work. HALTAFALL has also been adapted for the UNIVAC 1108 computer by the authors, and the input structure modified for convenience of use.¹¹ It should be noted that the non-linear refinement routines of the programs MUCO01 and SQUAD require initial guesses of the equilibrium constants and assumptions must be made as to the stoichiometries of the equilibrium systems. The stoichiometric coefficients cannot be determined directly, and difficulties in finding these coefficients are quite common. In practice attempts are made to minimize the RMS-value with respect to stoichiometry as well as the numerical values of the equilibrium constants. In spite of the difficulties, this procedure may be successful in many cases. If the stoichiometries assumed are incorrect, divergence of the refinement may be the result. The method is used with greatest success if a large amount of data of high precision is accessible. In this study, the instruments used have a limited precision, and work is proceeding in this laboratory to develop a high precision computer-controlled spectrophotometer and titration system.

Table 1. Analysis of the second moment matrix for acid vanadate solutions. Instrumental standard deviation is assumed to be 0.0035.

	ROOT	RES.TRACE	RES.S.D.
1	71.194879	.080955	.076043
2	.064320	.016635	.035771
3	.011429	.00506	.020828
4	.003097	.00218	.013844
5	.000862	.001246	.011163
6	.000591	.000655	.008534
7	.000377	.000279	.005904

RESULTS AND DISCUSSION

In the acid range, the analysis of the second moment matrix indicated the presence of two absorbing components in the system assuming the standard error of the spectrophotometer to be 0.0034 absorbance units. This can be seen from Table 1 where the residuals due to increasing numbers of components are presented. In this connection it must be pointed out that for a large part of this investigation 1 mm quartz cells were used. In order to obtain the true absorbance values, it has therefore been necessary to multiply the measured values by 10. Consequently we have had to work with standard errors 10 times as large as the instrument error. On this background it will be seen that two absorbing components are indicated by the factor analysis. However, experience from similar investigations (to be published) has shown that in many cases the model is improved by increasing this number, especially if two or more components resemble each other. This proved to be the case for this set of data where smooth absorbance curves were obtained for four components. It may also be seen from Fig. 3 that four components are indicated by the method of Rummel¹⁹ for the acid vanadium solutions.

After several other attempts, the model of

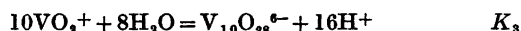
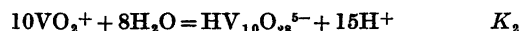
Table 2A. Calculated values for practical equilibrium constants of the system vanadium (V)–H₂O at ionic strength 1.0. (The constants of Rosotti have been expressed as formation constants).

	This work		Rosotti and Rosotti	
	log K	$\sigma(\log K)$	log K	$\sigma(\log K)$
K_1	-7.63	0.14	-6.75	0.15
K_2	-11.57	0.34	-10.35	0.3
K_3	-17.40	1.0	-16.15	0.1

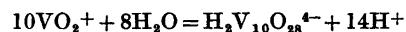
Table 2B. Correlation matrix for the equilibrium constants in the acid range.

	1	2	3
1	1.000	-0.0459	0.6850
2	-0.0459	1.000	-0.1800
3	0.6850	-0.1800	1.000

Rosotti and Rosotti,¹ which corresponds to four absorbing components, was finally assumed, and the corresponding equilibrium constants were calculated. The program systems are so designed that the equilibria most conveniently are presented as follows:



The computed constants are given in Table 2 and compared with the constants of Rosotti and Rosotti. In Table 3 the residual standard deviations of the solutions in question based on this model are presented. A first glance on Table 2 may give an impression of poor agreement between the two investigations. We shall, however, show that differences in the measurement of $[\text{H}^+]$ will cause considerable discrepancies in the calculated constants. The equilibrium



has been examined using HALTAFALL. The connection between the concentration of $\text{H}_2\text{V}_{10}\text{O}_{28}^{4-}$ and $[\text{H}^+]$ has been calculated for a series of numerical values for the equilibrium constant. The result is displayed in Fig. 1. Fig. 2 is based upon this set of graphs. It shows that a change of 0.1 in $-\log h$ will cause a cor-

Table 3. Calculated residuals based upon the best model.

pH	Total conc. of V(V)	Residual standard deviation
1.75	0.00012	0.0204
2.49	0.00012	0.0093
3.00	0.00012	0.0489
3.18	0.00012	0.0592
3.50	0.00012	0.0766
4.10	0.00012	0.0217
4.46	0.00012	0.0132
5.16	0.00012	0.0342
6.12	0.00012	0.0776
1.68	0.001	0.0158
2.54	0.001	0.0454
2.88	0.001	0.0360
3.05	0.001	0.0706
3.63	0.001	0.0213
4.18	0.001	0.0401
4.76	0.001	0.0397
5.57	0.001	0.0524

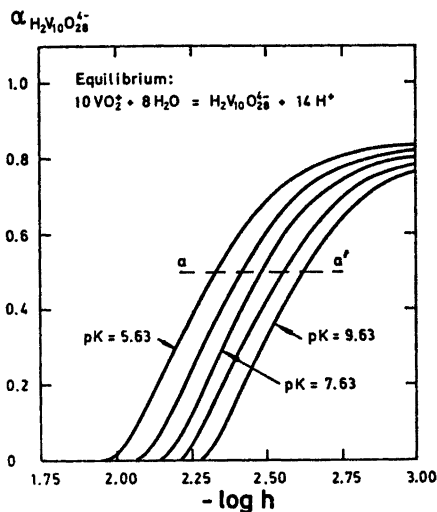


Fig. 1. Relation between $-\log h$ and $\alpha(\text{H}_2\text{V}_{10}\text{O}_{28}^{4-})$ for different values of K_1 . The α -value for a complex is defined as the fraction of the total quantity of vanadium present in the complex. $\alpha=0.5$ is indicated by the dotted line a-a'. Compare Fig. 3B and Fig. 5B.

responding change of approximately 1.4 in the logarithm of the complex constant in the range of main importance. (h denotes hydrogen ion concentration.) The conclusion is that even though an appreciable numerical difference is found between this work and that of Rosotti, the actual concentration distributions are very nearly the same. Besides it might be pointed out that the K -values for the dissociation reactions

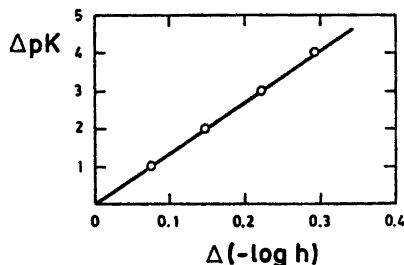
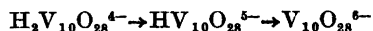


Fig. 2. The uncertainty in the equilibrium constant as a function of the uncertainty in $-\log h$. These values are derived from the line a-a' in Fig. 1.

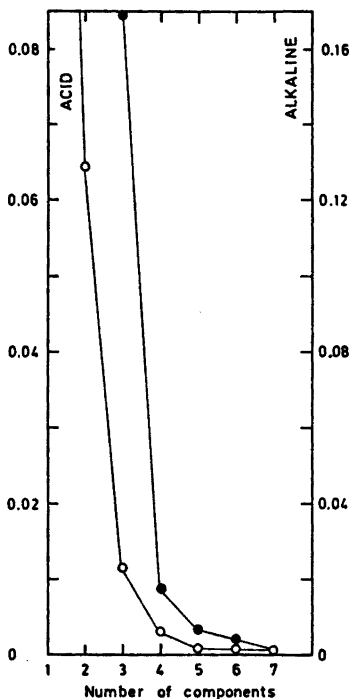


Fig. 3. Eigenvalues of the second moment matrices of the data measured in the acid region (open circles) and in the alkaline region (black dots).

being K_2/K_1 and K_3/K_1 , respectively, agree quite well with the values found by Rosotti. Our values are 3.94 and 5.83, and Rosotti gives the values 3.60 and 5.80, respectively.

In Fig. 4 the connection between $-\log h$ and concentration for the single species is given. The graphs are plotted with aid of HALTAFALL. It may be noted that the concentration of $V_{10}O_{28}^{6-}$ is low within the range studied. This gives as a result a relatively low accuracy of K_3 and the molar absorptivity of the compound. In Table 4 and Fig. 5 the calculated molar absorptivities are presented. VO_2^+ is found to absorb considerably less than the dekanavanadates. Consequently one will expect highly acid solutions to have a weaker colour than solutions of higher $-\log h$. The spectra of $H_2V_{10}O_{28}^{4-}$ and $HV_{10}O_{28}^{5-}$ resemble each other. This may be a source of uncertainty in the values of the complex constants. It should also be pointed out that the values of $\log K_1$ and

Table 4. Calculated molar absorptivities for the vanadates in acid solutions.

$\lambda(\text{nm})$	VO_2^+	$H_2V_{10}O_{28}^{4-}$	$HV_{10}O_{28}^{5-}$	$V_{10}O_{28}^{6-}$
250	2273	69410	74850	37770
260	2013	65440	67620	47090
270	1963	57120	56090	55570
280	1774	46270	45590	46510
290	1565	37270	37390	34270
300	1314	30820	29840	28510
310	1015	26120	25740	25980
320	798	23300	22620	25510
330	691	21740	20450	17850
340	581	21000	18660	16810
350	432	19930	17910	12360
360	311	18430	17590	10050
370	238	17240	16550	6739
380	174	15870	16300	1787
390	144	14580	14810	0

$\log K_3$ are highly correlated, but the refinement converges satisfactorily, nevertheless.

For $-\log h$ -values between 5.5 and 8 instability, or very slow reactions has made numerical work difficult. From $-\log h=8$ and upwards stability was attained, but these solutions had to be heated in order to establish equilibrium. The heating resulted in complete disappearance of the clear yellow colour of the fresh solutions. The same effect could be obtained by storing the solutions for several days. It is reasonable to believe that this fading corresponds to a breakdown of dekanavanadates or other heavy vanadium complexes to more simple species.

The result of the factor analysis of the data obtained in this region is shown in Table 5.

Table 5. Analysis of the second moment matrix for alkaline solutions. Instrumental standard deviation is assumed to be 0.0028.

	ROOT	RES.TRACE	RES.S.D.
1	577.240814	5.404732	.547962
2	5.210184	.194548	.106977
3	.169226	.025322	.039782
4	.017836	.007486	.022340
5	.006976	.000510	.006037
6	.000447	.000063	.002201
7	.000046	.000017	.001188
8	.000017	.000000	.000050

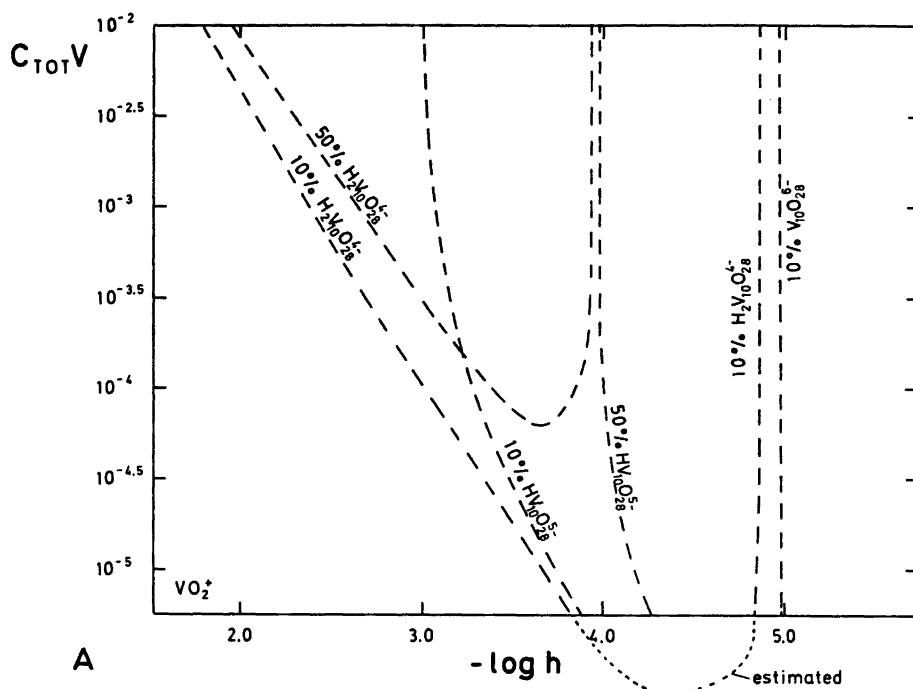


Fig. 4A. Distribution of the dekaavanadates as a function of hydrogen concentration and vanadium concentration. This presentation is similar to the one used by Atkinson and McBryde¹⁷ for portraying the distribution of aquo-complexes of Fe(III).¹⁸ This diagram and those of Figs. 3B, 5A and 5B are calculated by means of HALTAFALL.

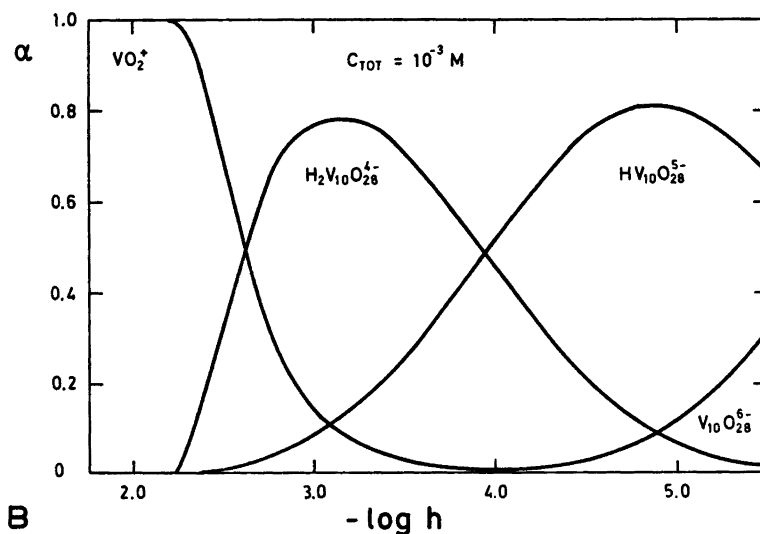


Fig. 4B. Distribution of the dekaavanadates as a function of $-\log h$, the total concentration being kept constant at $10^{-3} M$.

Table 6A. Calculated values for equilibrium constants of the alkaline range of the system vanadium(V)–H₂O.

	This work log K	$\sigma(\log K)$	Ingri and Brito log K	$\sigma(\log K)$	Newman <i>et al.</i> log K	$\sigma(\log K)$
K_4	11.69	0.09	10.82	0.05	—	—
K_5	33.51	0.01	31.78	0.04	—	—
K_6	-12.09	0.01	—	—	-12.99	0.00

Table 6B. Correction matrix for the equilibrium constants in the alkaline range.

	1	2	3
1	1.000	-0.0216	0.2794
2	-0.0216	1.000	-0.1664
3	0.2794	-0.1664	1.000

Assuming the standard error of the instrument to be 0.0028 three absorbing components are indicated, noting that only 1 mm cells have been used for obtaining the data in this region. However, it proved necessary to increase this number by one. Four components are also

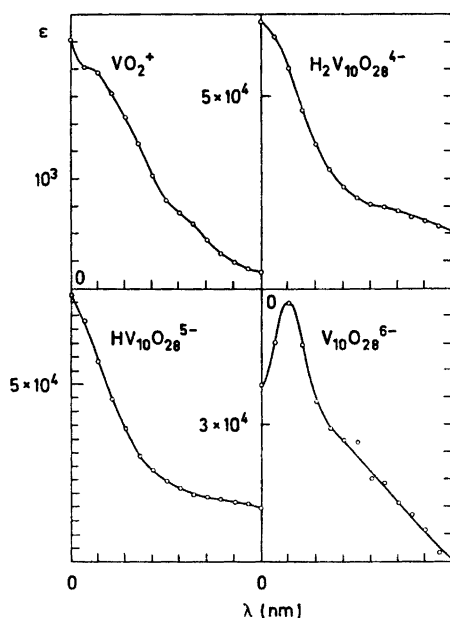
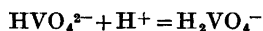


Fig. 5. Spectral characteristics of the species found in acid vanadium solutions. Wavelength range is 250–390 nm.

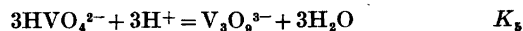
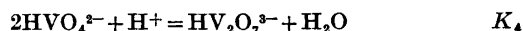
Table 7. Residual errors of alkaline vanadium solutions based upon the best model.

pH	Initial conc. of V	Res. error
7.94	0.001	0.0078
8.13	0.001	0.0193
8.52	0.001	0.0098
9.02	0.001	0.0174
9.41	0.01	0.0212
9.68	0.001	0.0114
10.34	0.001	0.0208
10.76	0.001	0.0153
11.15	0.001	0.0198

indicated by Fig. 3. An attempt of fitting a model with five absorbing components (VO_4^{3-} , HVO_4^{2-} , H_2VO_4^- , $\text{HV}_2\text{O}_7^{3-}$ and $\text{V}_3\text{O}_9^{3-}$) failed completely. When trying to interpret these data, the first assumption was based upon the work of Ingri and Brito.⁴ Since our data covered a greater range of $[\text{H}^+]$ than the data of Ingri and Brito, it was, however, necessary to specify an additional equilibrium for the most alkaline part. We were not able to fit the equilibrium



to the data. The following set of equilibria was found to give the best fit:



The constants calculated are given in Table 6, and the residual errors of the single solutions in Table 7. Comparison is made with the results of Ingri and Brito and Newman *et al.*⁵ In order to make comparison easy, all constants are given as formation constants according to the above equilibria.

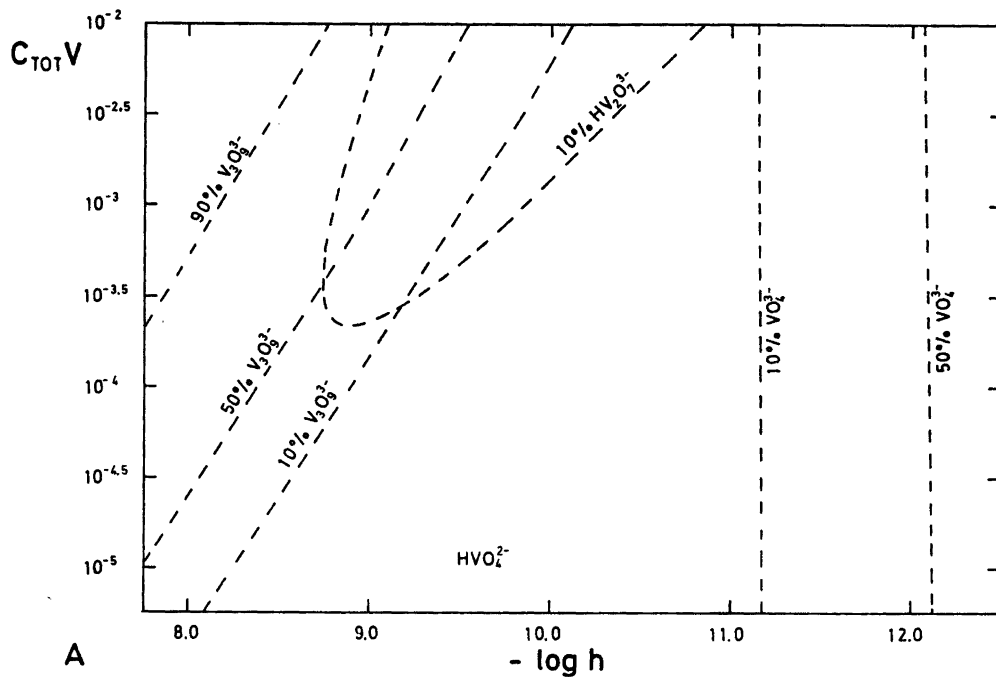


Fig. 6A. Distribution of the alkaline vanadates as a function of $-\log h$ and total concentration of vanadium.

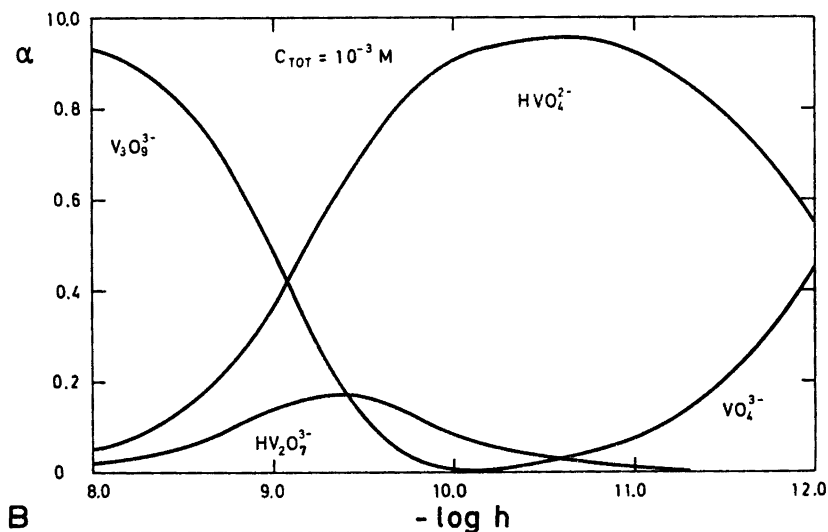


Fig. 6B. Distribution of the alkaline vanadates as a function of $-\log h$. Total vanadium concentration in 10^{-3} M.

Even in this case, the disagreement between this work and that of Ingri and Brito is less than what might be the first impression. It is very important to note that one component

is left out. In order to check the agreement between the two investigations, we have theoretically calculated a titration curve (by means of HALTAFALL) and compared it with the

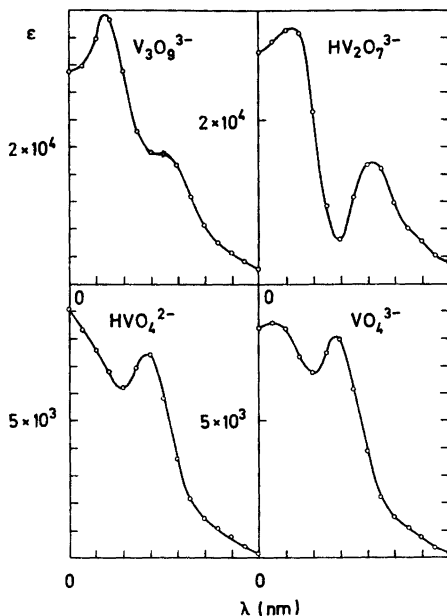


Fig. 7. Spectral characteristics of the alkaline vanadates. Wavelength range is 210–350 nm.

experimental titration curves given in the article of Ingri and Brito. The agreement is, as shown in Fig. 8, satisfactory, taking into ac-

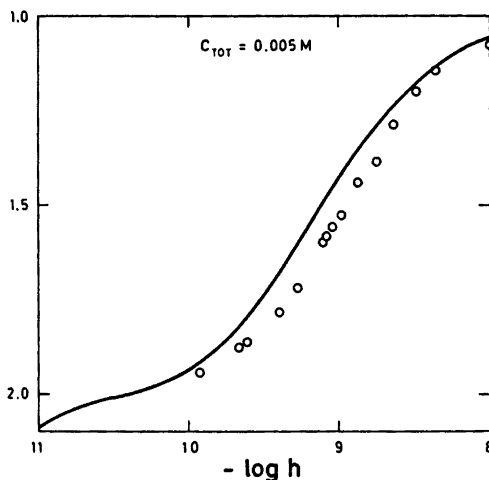


Fig. 8. Theoretical "titration" curve, *i.e.* the average number of protons set free per vanadium, Z , versus $-\log h$ (fully drawn curve). Comparison is made with one experimental titration curve from the work of Ingri and Brito⁴ (open circles).

count that such curves prove sensitive to the species present.

The disagreement between this work and that of Newman *et al.* cannot be readily explained. It should be pointed out, however, that the accuracy of the least squares methods is likely to be higher than that of the simple extrapolation method. This has strikingly been demonstrated by Childs¹² in a recent study. On the other hand the work of Newman *et al.* is based upon a larger amount of data in the $-\log h$ -range in question.

The connection between $-\log h$ and concentration in the alkaline range is presented in Fig. 6. HVO_4^{2-} is found to be the most important component over a large part of the range in fair agreement with Ingri and Brito.

The molar absorptivities for the complexes are presented in Table 8, and graphically in Fig. 7. The spectra are quite different, this being of great advantage when using these methods. It will be seen that none of the species present absorbs appreciably in the visible region, this being the reason for the lack of colour of the solutions.

CONCLUSION

The method of spectrophotometry is well suited for the study of complexation equilibria

Table 8. Calculated molar absorptivities for the vanadates in alkaline solutions.

$\lambda(\text{nm})$	$\text{V}_3\text{O}_9^{3-}$	$\text{HV}_2\text{O}_7^{3-}$	HVO_4^{2-}	VO_4^{3-}
210	30830	23110	9045	8379
220	31770	29460	8302	8555
230	35860	30960	7568	8346
240	38500	30550	6827	7349
250	31140	20920	6219	6758
260	22270	9524	6979	7442
270	19230	5387	7451	8001
280	18930	10570	5806	6151
290	17260	14630	3598	3891
300	12690	14040	2136	2211
310	8658	9948	1462	1501
320	6038	6797	1086	1106
330	4548	5258	748	769
340	3320	3476	431	357
350	2178	2680	178	147
360	1248	1931	701	58
370	524	1445	295	0
380	263	965	85	0
390	114	519	139	0

even in the case of complicated hydrolysis reactions. The least squares techniques represent a powerful tool for the reduction of the relatively large amount of numerical material produced in spectrophotometry. Solutions of relatively low concentrations can be successfully examined by these methods.

In the special case of the hydrolysis of pentavalent vanadium the agreement with the results of potentiometric methods is found to be satisfactory. Moreover it provides valuable information about the absorption characteristics of the individual species present in the solutions.

Acknowledgement. One of the authors (Dr. Mohamed Rafat Mahmoud) wishes to express his gratitude to the Norwegian Agency for International Development (NORAD) for granting him a research fellowship which made his participation in this investigation possible.

REFERENCES

- Rosotti, F. C. and Rosotti, H. *Acta Chem. Scand.* 10 (1956) 957.
- Britton, H. T. S. and Robinson, R. A. *J. Chem. Soc.* (1955) 1932.
- Düllberg, P. *Z. Phys. Chem.* 45 (1903) 129.
- Ingri, N. and Brito, F. *Acta Chem. Scand.* 13 (1959) 1971.
- Newman, L., La Fleur, W. J., Brousaides, F. J. and Ross, A. M. *J. Am. Chem. Soc.* 80 (1958) 4491.
- Kankare, J. J. *Anal. Chem.* 42 (1970) 1322.
- Simmonds, J. L. *J. Opt. Soc. Am.* 53 (1963) 968.
- Legget, D. J. and McBryde, W. A. E. *Anal. Chem.* 47 (1975) 1065.
- Ingri, N., Kakolowicz, W., Sillén, L. G. and Warnqvist, B. *Talanta*, 14 (1967) 1261.
- Wernimont, G. *Anal. Chem.* 39 (1967) 554.
- Borgen, O. and Skauvik, I. *Technical Report 80*, Division of Phys. Chem., The Norwegian Institute of Technology, Trondheim.
- Childs, C. W. *Least squares methods in data analysis*, Austr. Nat. Univ. Comp. Centre. Publ. (1969) pp. 80-86.
- Sperry Rand Corporation: UNIVAC 1100 series NU ALGOL Programmers reference.
- Lindeberg, E. *Technical Report 84*, Division of Phys. Chem., The Norwegian Institute of Technology, Trondheim.
- Hugus, Z. Z. and El-Awady, A. A. *J. Phys. Chem.* 75 (1971) 2954.
- Bulmer, J. T. and Shurvell, H. F. *J. Phys. Chem.* 77 (1973) 256.
- Atkinson, G. F. and McBryde, W. A. E. *J. Chem. Educ.* 38 (1961) 127.
- Acta Chem. Scand. A 31 (1977) No. 5
- Hedström, B. O. A. *Ark. Kemi* 6 (1953) 1.
- Rummel, R. J. *Applied Factor Analysis*, Northwestern University Press, Chicago 1970, p. 361.

APPENDIX A.

DYNAMIC DIMENSIONING OF THE ARRAYS OF SQUAD

The program, SQUAD, is written in FORTRAN IV, and is so constructed that the arrays must be of the exact size required. In the original user's manual for the program, which may be obtained from the authors,⁸ this problem is solved by the method of reassembling the program each time necessary. This step will, however, be inefficient, time-consuming and expensive, especially if the program is often used, with different systems. In our case this solution was unsatisfactory. Fortunately our UNIVAC 1100 computer system permits the use of ALGOL where dynamic dimensioning is performed. Besides, it is permitted to call FORTRAN routines from an ALGOL program, and this is the key to our solution of the problem. A small ALGOL main program is written, whose only task is to dimension the necessary arrays correctly. When the actual main program is called, it is formally treated as an EXTERNAL FORTRAN SUBROUTINE. The small ALGOL "superprogram" has the following form (In the NU ALGOL dialect¹⁸).

```

BEGIN
EXTERNAL FORTRAN PROCEDURE
SQUAD;
INTEGER NUMPH, NBA, NTS, NCV;
INTEGER III, JJJ, NNN;
READ (NUMPH, NBA, NTS, NCV);
III = NBA * NUMPH; JJJ = NCV * 2; NNN =
NTS + 4;
BEGIN
REAL2 ARRAY EQ (1:NNN, 1:NBA), Q(1:
NUMPH, 1:NNN), TS(1:NUMPH, 1:NBA),
SP2(1:III, 1:JJJ), EC(1:4, 1:NBA), STD(1:4, 1:
NBA), B(1:NUMPH, 1:NBA); REAL ARRAY
SPEC(1:NUMPH, 1:NBA), SS1(1:III), SSRSOL
(1:NUMPH);
SQUAD(EQ, Q, TS, SP2, EC, STD,
B, SPEC, SS1, SSRSOL, III, JJJ, NNN, NUMPH,
NBA); END;
END;

```

Received November 12, 1976.

Crystal Structure of 8-Methyl-dihydrothiazolo[3,2-*a*]pyridin-5-one Trihydrate at -160°C

P. GROTH

Department of Chemistry, University of Oslo, Oslo 3, Norway

The crystals are orthorhombic with space group $Pbca$. There are eight formula units in the cell with dimensions $a=6.926(2)\text{ \AA}$, $b=14.172(2)\text{ \AA}$, $c=21.308(6)\text{ \AA}$. The structure was solved by direct methods and refined by full-matrix least-squares technique to $R=3.3\%$ ($R_w=3.5\%$) for 1367 observed reflections (automatic four circle diffractometer). The crystal structure is built up of ribbons of water molecules (parallel to the bc -plane) to pairs of which the pyridinone molecules are attached at both sides by hydrogen bonds of length 2.789 and 2.749 \AA . Between the layers thus formed van der Waals' forces only reside.

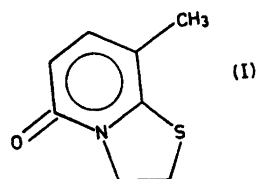
Rearrangement studies in dihydrothiazolo[3,2-*a*]pyridinium salts¹ have yielded a pyridinone,

* All programs used (except those for phase determination and stereoscopic drawing) are included in this reference.

Table 1. Final fractional coordinates and thermal parameters with estimated standard deviations. Expression for anisotropic vibration is: $\exp[-2\pi^2(h^2a^{*2}U_{11} + \dots + 2klb^*c^*U_{23})]$. Hm and Hm_n are bonded to Cm. HWm_n is bonded to OWm.

ATOM	X	Y	Z	U ₁₁	U ₂₂	U ₃₃	U ₁₂	U ₁₃	U ₂₃
S	.66920(3)	.45983(4)	.59883(10)	.0154(3)	.0084(3)	.0238(3)	-.0009(2)	.0016(3)	-.0002(3)
O	.58214(7)	.14631(11)	.68714(26)	.0151(9)	.0158(9)	.0242(9)	-.0028(7)	-.0007(8)	.0029(7)
N	.63279(9)	.26628(13)	.64494(27)	.0126(11)	.0110(9)	.0161(11)	.0005(7)	-.0013(8)	.0001(8)
C1	.68588(18)	.33875(18)	.68138(35)	.0177(12)	.0105(11)	.0187(12)	.0017(9)	.0014(11)	.0004(10)
C2	.69371(12)	.44143(16)	.71887(38)	.0198(14)	.0128(12)	.0233(15)	.0016(10)	.0034(12)	.0007(11)
C3	.67468(11)	.34886(15)	.67851(48)	.0142(13)	.0148(12)	.0199(13)	.0038(10)	.0023(12)	.0002(11)
C4	.63275(11)	.18866(15)	.64897(33)	.0207(14)	.0105(12)	.0115(13)	-.0006(9)	.0048(10)	.0005(10)
C5	.69187(11)	.14569(16)	.68744(37)	.0219(13)	.0096(12)	.0155(13)	.0026(9)	-.0013(11)	.0001(10)
C6	.74311(12)	.19856(17)	.56486(34)	.0143(13)	.0201(14)	.0168(13)	.0047(10)	-.0013(11)	-.0009(11)
C7	.74168(11)	.29789(17)	.56159(32)	.0152(13)	.0169(13)	.0151(13)	.0001(10)	-.0004(11)	.0014(10)
C8	.79887(13)	.35631(20)	.52175(48)	.0166(14)	.0222(15)	.0328(17)	.0025(11)	.0010(13)	.0047(13)
OH1	.44232(9)	.04651(14)	.28381(29)	.0394(11)	.0158(10)	.0208(12)	.0042(8)	-.0068(9)	.0024(9)
OH2	.98732(9)	.33749(12)	.48776(30)	.0179(10)	.0205(10)	.0265(11)	-.0005(8)	.0037(9)	.0016(9)
OH3	.98912(9)	.16147(14)	.52989(32)	.0206(11)	.0167(10)	.0279(12)	-.0033(8)	.0006(9)	.0004(9)

ATOM	X	Y	Z	B	ATOM	X	Y	Z	B
H21	.8661(11)	.4859(17)	.6586(36)	1.2(5)	H22	.6804(11)	.4511(16)	.8565(38)	1.4(5)
H31	.5516(11)	.3393(16)	.5457(39)	1.4(5)	H32	.5492(10)	.3158(15)	.7782(35)	.9(4)
H5	.6932(11)	.0603(18)	.6139(38)	1.7(5)	H6	.7816(12)	.1787(18)	.5356(35)	1.2(5)
H81	.7891(13)	.4193(20)	.4387(41)	2.6(8)	H82	.8292(15)	.3282(22)	.4853(48)	4.1(8)
H83	.8172(12)	.3779(18)	.6324(43)	2.2(8)	HW11	.4285(14)	-.0858(22)	.2924(46)	3.4(8)
HW12	.4384(13)	.8731(20)	.1868(44)	2.2(7)	HW21	.9919(14)	.3482(18)	.3888(42)	2.8(7)
HW22	.9511(13)	.3742(20)	.5861(46)	2.6(7)	HW31	.9286(14)	.1582(21)	.6539(52)	3.3(7)
HW32	.9226(14)	.2864(21)	.4913(43)	2.1(7)					



viz. 8 methyl-dihydrothiazolo[3,2-*a*]pyridin-5-one (I) which is characterized by an unexpectedly low melting point. In order to explore the reason for this, an X-ray crystallographic investigation has been carried out.

The crystals of $\text{C}_7\text{H}_9\text{SON}\cdot 3\text{H}_2\text{O}$ are orthorhombic with cell dimensions $a=6.926(2)\text{ \AA}$, $b=14.172(2)\text{ \AA}$, $c=21.308(6)\text{ \AA}$. The space group is $Pbca$ and there are eight formula units in the unit cell ($D_m=1.38\text{ g cm}^{-3}$, $D_x=1.40\text{ g cm}^{-3}$). Since the compound has a melting

Table 2. Bond distances and angles with estimated standard deviation.

DISTANCE (Å)	DISTANCE (Å)
S - C1 1,749(2)	S - C2 1,826(2)
N - C1 1,372(3)	N - C3 1,482(3)
C2 - C3 1,518(3)	N - C4 1,383(3)
O - C4 1,282(3)	C4 - C5 1,413(3)
C5 - C6 1,371(3)	C6 - C7 1,498(3)
C7 - C1 1,366(3)	C7 - C8 1,498(3)

ANGLE (°)	ANGLE (°)
C1 - S - C2 91,4(1)	S - C2 - C3 106,6(2)
C2 - C3 - N 106,4(2)	C3 - N - C1 115,3(2)
N - C1 - S 112,2(2)	C5 - N - C4 121,3(2)
N - C4 - O 118,7(2)	O - C4 - C5 125,1(2)
N - C4 - C5 119,2(2)	C4 - C5 - C6 121,3(2)
C5 - C6 - C7 122,1(2)	C6 - C7 - C1 116,2(2)
C6 - C7 - C8 122,8(2)	C8 - C7 - C1 121,3(2)
C7 - C1 - N 122,0(2)	C7 - C1 - S 125,7(2)

DISTANCE (Å)	DISTANCE (Å)
O - OH1' 2,789(2)	O - OH2' 2,749(3)
OH1 - OH2' 2,719(3)	OH1 - OH3' 2,798(3)
OH2 - OH3 2,826(3)	OH2 - OH3' 2,817(3)
OH1 - NH11 1,798(31)	OH1 - NH12 1,807(38)
OH2 - NH21 1,761(31)	OH2 - NH22 1,867(32)
OH3 - NH31 1,988(36)	OH3 - NH32 1,746(38)

ANGLE (°)	ANGLE (°)
O - NH11' - OH1' 165(3)	O - NH21' - OH2' 177(3)
OH1 - NH22' - OH2' 177(3)	OH1 - NH12' - OH3' 169(3)
OH2 - NH32 - OH3 175(3)	OH2 - NH31' - OH3' 178(3)

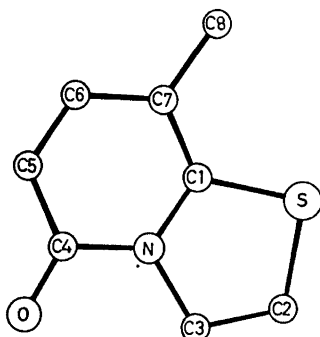


Fig. 1. Schematic drawing of the pyridinone molecule.

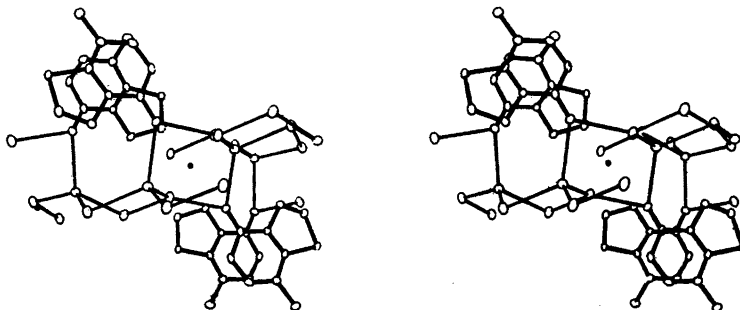


Fig. 2. Stereoscopic view (approximately along [001]) showing the hydrogen bonding network (*b*-axis across the page).

point of about 28 °C the intensities were measured at -160 °C (on a Syntex PI diffractometer with an Enraf-Nonius liquid nitrogen cooling device modified by H. Hope). The radiation was MoK α ($\lambda = 0.71069$ Å) and $2\theta_{\max} = 50^\circ$. With an observed-unobserved cutoff at $2.5 \sigma(I)$, 1367 reflections were recorded as observed. The crystal size was $(0.2 \times 0.3 \times 0.35)$ mm³. No corrections were made for absorption or secondary extinction effects.

The structure was solved by direct methods² and refined by full-matrix least-squares technique.^{3,*} Anisotropic temperature factors were introduced for the heavy atoms. All hydrogen atoms were localized in the difference Fourier map. Atomic form factors were those of Hanson *et al.*⁴ except for hydrogen.⁵ Weights used in least-squares were obtained from the standard deviations in intensities, $\sigma(I)$, taken as

$$\sigma(I) = [C_T + (0.02 C_N)^2]^{1/2}$$

where C_T is the total number of counts and C_N the net count. The final R -value was 3.3 % ($R_w = 3.4$ %) for 1367 observed reflections.

Final fractional coordinates and thermal parameters with estimated standard deviations are given in Table 1. The principal axes of the thermal vibration ellipsoids were calculated from the temperature parameters of Table 1. Maximum r.m.s. amplitudes range from 0.129 to 0.193 Å (corresponding B -values of 1.31 and 2.94 Å²). No rigid-body analysis of translational, librational and screw motion has been carried out.

Bond distances and angles (including hydrogen bonds) are listed in Table 2. The standard deviations, given in parentheses, are estimated

from the correlation matrix of the final least-squares refinement cycle. Fig. 1 is a schematic drawing of the molecule.

The system S, O, N, C1, C3, ..., C8 is planar (to within 0.03 Å) with C2 0.42 Å out of the plane. This puckering of the five-membered ring (and the bond distances and angles as well) agree, within error limits, with the results obtained for *trans*-2-carboxy-5-methyl-dihydrothiazolo[3,2-*a*]pyridinium-3-carboxylate⁶ and *cis*-2,3-(3'-cyclohexanone-1',2'-ylene)-5-methyl-8-ethoxydihydrothiazolo[3,2-*a*]pyridinium bromide.⁷

The crystals contain as much as 24.4 % water (a fact which possibly may be held responsible for the low melting point). The water molecules form a rather complex network of hydrogen bonds. A fragment of this is shown in a stereoscopic drawing⁸ (Fig. 2) where the structure is viewed approximately along [001] (with the *b*-axis across the page) and a centre of symmetry is indicated. The fact that the carbonyl oxygen atom accepts two hydrogen bonds (from OW1 and OW2) is reflected in the C=O bond length of 1.262 Å. As may be seen from Table 2, OW1 and OW3 are involved in three, and OW2 in four hydrogen bonds. Inspection of Fig. 2 shows that O, OW1, and OW2 together with their centro-symmetrically related equivalents constitute chair-formed six-membered rings which are linked together by six water molecule (OW3) bridges. These bridges form condensed five-membered rings and the whole network may be characterized as ribbons of water molecules (parallel to the *bc*-plane) to pairs of which the pyridinone molecules are attached at both sides. Between the layers thus formed van der Waals forces only reside.

Acknowledgement. The author would like to thank cand. real. T. Lærum for preparing the crystals.

REFERENCES

1. Undheim, K. *Personal communication*.
2. Germain, G., Main, P. and Woolfson, M. M. *Acta Crystallogr. A* 27 (1971) 368.
3. Groth, P. *Acta Chem. Scand.* 27 (1973) 1837.
4. Hanson, H. P., Herman, F., Lea, J. D. and Skillman, S. *Acta Crystallogr.* 17 (1964) 1040.

5. Stewart, R. F., Davidson, E. R. and Simpson, W. T. *J. Chem. Phys.* 42 (1965) 3175.
6. Groth, P. *Acta Chem. Scand.* 25 (1971) 118.
7. Groth, P. *Acta Chem. Scand.* 26 (1972) 3131.
8. Johnson, C. K. *ORTEP*, Report ORNL-3795, Oak Ridge National Laboratory, Oak Ridge 1965.

Received December 21, 1976.

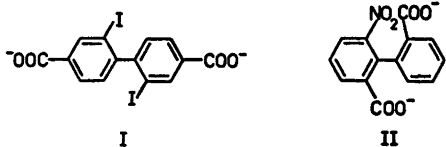
Racemization of Hindered Biphenyls in H₂O and D₂O

NILS-ÅKE BERGMAN and LARS BALTZER

Department of Organic Chemistry, University of Göteborg and Chalmers University of Technology, Fack, S-402 20 Göteborg, Sweden

The solvent isotope effect on the racemization of (+)-2,2'-diiodo-4,4'-dicarboxybiphenyl dianion and (-)-6-nitro-2,2'-dicarboxybiphenyl dianion was found to be about 0 and 8%, respectively, the heavy solvent giving the slower reaction. The effect is discussed in terms of the difference between the fractionation factors of the carboxylate groups in the reactant molecule and those in the activated complex.

According to the generally accepted theory^{1,2} it is possible to interpret the solvent isotope effect in terms of combined contributions from the so-called transfer effect and from what is known as the exchange effect. The former effect may be expressed in terms of a difference in activity coefficients between the isotopic solvents, and the cause of the latter is the fractionation of the isotopic solvent molecules or atoms between solvating and bulk positions. The distinction between these two effects is, however, not really necessary,^{3,4} but it has also been claimed that the transfer effect makes a significant contribution to the solvent isotope effect.⁵



In our search for a model reaction to use in our studies of solvent isotope effects and solvation phenomena in general we have chosen the inversion of optically active biphenyl derivatives which is a simple unimolecular reaction. The rate of the reaction can also be accurately determined by polarimetry.

We now wish to report an investigation of the racemization of (+)-2,2'-diiodo-4,4'-dicarboxybiphenyl dianion (I) and (-)-6-nitro-2,2'-dicarboxybiphenyl dianion (II) in H₂O and D₂O.

As the present reaction involves no catalysing base the only possible fractionation factors are those of the substrate itself in the initial and the transition state. The carboxylate groups present in the two compounds I and II could at least in principle give rise to fractionation although this should be small judging from the results of solvent isotope effect studies on acetate catalysed proton-transfer reactions.⁶⁻⁸ Anyhow, with one of the substrates, I, possible fractionation factors in the transition state should not deviate measurably from the corresponding ones in the initial state because no charged groups are situated at the centre of reaction. Implicit in this conclusion is the assumption that a possible fractionation due to the C—I bond may be neglected due to the rather weak polarity of this bond. Exchange effects should thus be absent for I. The result (Table 1) shows that there cannot be any significant contribution from a transfer effect either provided that the above conclusion is correct, as $k_{\text{obs}}(\text{H}_2\text{O})/k_{\text{obs}}(\text{D}_2\text{O})$ probably equals unity within the limits of the experimental accuracy. The rate enhancement in the last two runs in Table 1 is due to a salt effect.⁹

The other compound used (II) has charged groups at the centre of reaction, but even for this compound the solvent isotope effect is rather weak, $k_{\text{obs}}(\text{H}_2\text{O})/k_{\text{obs}}(\text{D}_2\text{O}) = 1.08$ (Table 2). The situation is, however, somewhat more complicated in this case due to the possible formation of a chelate between the biphenyl dianion and the cation in the solution.¹⁰ The

Table 1. Racemization of (+)-2,2'-diiodo-4,4'-dicarboxybiphenyl dianion (I) in H₂O and D₂O at 25.1 ± 0.1 °C.

Solvent	$k_{\text{obs}}/10^{-4} \text{ s}^{-1} \text{ }^a$	$k_{\text{obs}}(\text{H}_2\text{O})/$ $k_{\text{obs}}(\text{D}_2\text{O})$
H ₂ O	0.920 ± 0.006 ^b	1.010 ± 0.017
D ₂ O	0.911 ± 0.009 ^b	
H ₂ O	1.024 ± 0.005 ^c	1.027 ± 0.012
D ₂ O	0.997 ± 0.008 ^c	

^a Each value is the mean value of two determinations. Errors are maximum deviations from the mean values. ^b Solution was 0.04 M in the sodium salt of compound I. ^c Solution was 0.05 M in the sodium salt of compound I.

dependence of the rate constant on the chelate formation has been investigated¹⁰ and may be expressed by eqn. (1)

$$k_{\text{obs}}/2 = k/(1 + K[\text{M}^+]) \quad (1)$$

where k_{obs} is the observed rate constant, k is the rate constant for inversion, K is the equilibrium constant for the chelate complex formation and $[\text{M}^+]$ is the concentration of Na⁺. The underlying assumption is that inversion takes place only with the non-chelated dianion and not with the complex. This leads to an expres-

Table 2. Racemization of (-)-6-nitro-2,2'-dicarboxybiphenyl dianion (II) in H₂O and D₂O at 59.4 ± 0.1 °C.

Solvent	$k_{\text{obs}}/10^{-4} \text{ s}^{-1}$	$k_{\text{obs}}(\text{H}_2\text{O})/$ $k_{\text{obs}}(\text{D}_2\text{O})$
H ₂ O	0.663 ± 0.007 ^a	1.078 ± 0.037
D ₂ O	0.615 ± 0.014 ^a	
H ₂ O	0.649 ± 0.003 ^b	1.075 ± 0.009
D ₂ O	0.604 ± 0.001 ^b	

^a Mean value of four determinations. Error is the maximum deviation from the mean value. Solution was 0.04 M in the sodium salt of compound II.

^b Mean value of two determinations. Error is the maximum deviation from the mean value. Solution was 0.04 M in the sodium salt of compound II and 0.08 M in sodium chloride.

sion for the observed isotope effect on the racemization [eqn. (2)].

$$k_{\text{obs}}(\text{H}_2\text{O})/k_{\text{obs}}(\text{D}_2\text{O}) = k(\text{H}_2\text{O})/k(\text{D}_2\text{O}) \{ (1 + K(\text{D}_2\text{O})[\text{M}^+]) / (1 + K(\text{H}_2\text{O})[\text{M}^+]) \} \quad (2)$$

that includes two factors, both of which may contribute to the observed effect provided that the equilibrium constant for complex formation is dependent on the isotopic composition of the solvent. If this is the case, the observed isotope effect should vary with $[\text{M}^+]$, and the observed values of $k_{\text{obs}}(\text{H}_2\text{O})/k_{\text{obs}}(\text{D}_2\text{O})$ at $[\text{M}^+] = 0.08 \text{ M}$ and $[\text{M}^+] = 0.16 \text{ M}$ would differ significantly. As can be seen in Table 2, however, they are the same within the experimental accuracy. It is therefore improbable that $K(\text{D}_2\text{O})$ and $K(\text{H}_2\text{O})$ should differ appreciably and thus we attribute the observed effect of 8% to the rate of inversion.

The fractionation factor theory¹ adapted to the present case, neglecting any free-energy transfer terms, leads to eqn. (3).

$$k_{\text{obs}}(\text{H}_2\text{O})/k_{\text{obs}}(\text{D}_2\text{O}) = \prod_{i=1}^m \phi_{\text{R}i} / \prod_{j=1}^p \phi_{\text{T}j} \quad (3)$$

for the limiting rate constant ratio. The symbols $\phi_{\text{R}i}$ and $\phi_{\text{T}j}$ are fractionation factors for the initial state and the transition state, respectively, and m and p are the number of solvating hydrogen atoms in the initial state and the transition state, respectively.

Unfortunately it is not possible to assign definite values to the fractionation factors for either the reactant or the transition state, but it can be of some interest to speculate on the magnitude of them. By assuming for simplicity that all $\phi_{\text{R}i}$ are equal and equal to ϕ_{R} and all $\phi_{\text{T}j}$ are equal and equal to ϕ_{T} eqn. (4) is obtained:

$$k_{\text{obs}}(\text{H}_2\text{O})/k_{\text{obs}}(\text{D}_2\text{O}) = \phi_{\text{R}}^m / \phi_{\text{T}}^p \quad (4)$$

In terms of the magnitude of the observed rate ratio that gives eqn. (5).

$$\phi_{\text{R}}^m / \phi_{\text{T}}^p = 1.08 \quad (5)$$

and hence eqn. (6).

$$\phi_{\text{T}} = \phi_{\text{R}} \left(\frac{\phi_{\text{R}}^{m-p}}{1.08} \right)^{1/p} \quad (6)$$

Provided that $m - p \geq 0$ and $\phi_{\text{R}} < 1$ this gives eqn. (7).

$$\phi_T/\phi_R < 1 \quad (7)$$

It can also be seen that for large values of p , $\phi_T/\phi_R \rightarrow 1$. Qualitatively this can be explained in the following way. It is likely that in the reactant molecule the nitro group and also the carboxylate groups will be coplanar with the rings to which they are attached. This allows charge delocalization from the carboxylate groups into the phenyl rings. In the transition state this is no longer possible due to steric interactions and the result would be less delocalized charges at the carboxylate groups compared to the reactant molecule. The net effect would be a stronger interaction with the solvent in the transition state and hence the fractionation factors in the transition state should be lower than those in the reactant molecule. How much lower depends, as has been shown above, upon the actual values of m and p and the following will clarify the point too.

The value of ϕ_R can be estimated in the following way. Using the derived value of the degenerate activity coefficient for transfer of the acetate ion from H₂O to D₂O, $\gamma_{\text{OAc}} = 1.15$,¹¹ and assuming that each acetate group is solvated by four water molecules an approximate value of the fractionation factor for the water molecules solvating the acetate ion is given by ^{3,4} eqn. (8).

$$\phi_{\text{OAc}} = (1/1.15)^{1/4} = 0.97 \quad (8)$$

Provided that $\phi_R = \phi_{\text{OAc}} = 0.97$ and that each carboxylate group is solvated by four water molecules we have eight sites, in the reactant molecule, each with a fractionation factor of 0.97. For the transition state we assume that the carboxylate group which has to pass the nitro group can be solvated only by two water molecules. In the transition state we thus have six sites each with a fractionation factor of ϕ_T . Using the above formula for ϕ_T we obtain eqn. (9), *i.e.* a very moderate decrease in the

$$\phi_T = 0.97 \left(\frac{0.97^8}{1.08} \right)^{1/6} = 0.95 \quad (9)$$

fractionation factors of the transition state would account for the observed effect of 8% on the reaction rate.

EXPERIMENTAL

The substances I and II were kindly given to us by Dr. Peder Berntsson. The fact that the substances had been stored for about five years gave rise to the question of whether the materials were free of contamination or not. The excellent first-order kinetic behaviour of II did, in spite of a very small quantity of insoluble material on some occasions, suggest that this substance was satisfactory. The substance I, however, was not optically pure since a minor optical activity remained after the completion of reaction. Treatment of the data with the computer program PROGAEXP, assuming a rate equation: $y = Ae^{kt} + A_0$, gave rate constants with high accuracy indicating that the unidentified impurity showed constant optical rotation throughout the reaction and so did not interfere with the kinetics.

The sodium hydroxide solutions were prepared as follows. All but one of the light-water base solutions were prepared by diluting aqueous NaOH from commercially available ampoules to 0.1 M and 0.08 M in volumetric flasks. The additional base solution was prepared from solid sodium hydroxide dissolved in distilled water in a volumetric flask. The heavy-water base solutions were prepared in two ways, either from solid sodium hydroxide or through dilution with D₂O of very concentrated, 4.92 M, light-water bases produced from ampoules, giving H₂O/D₂O mixtures of atom fraction D greater than 0.98. The deuterium oxide used had an atom fraction of D not less than 0.997. For control, some of the base solutions were titrated with a Radiometer TTT 1C automatic titration assembly.

The reaction solutions were prepared by dissolving the proper quantity of solid biphenyl as dicarboxylic acid in 2 ml of a solution containing two equivalents of base. In some runs (Table 2) NaCl was added to change the concentration of Na⁺. The solutions were filtered into the polarimeter cell.

All kinetic runs were performed on a Zeiss Old 5 digital polarimeter using the wavelengths 436 and 546 nm for II and I, respectively, the accuracy in each reading was $\pm 0.001^\circ$. The racemization took place in a 10 cm thermostated polarimeter cell, the temperature of which was controlled by a Hetotherm Ultrathermostat 02 Pt 623 UO together with a Hetofrig cooling bath, type CB6. A Compucorp 425 G Scientist calculator, interfaced on line with the polarimeter, collected polarimeter data and times, and with II it was used to calculate rate constants using a least-squares program.

Acknowledgements. Dr. Peder Berntsson's generous gift of the substances is gratefully acknowledged. We also wish to thank Professor Lars Melander for his interest in this work and for many useful suggestions during the

preparation of the manuscript. One of us (N.-Å. B.) wishes to thank Professor A. J. Kresge for many interesting discussions during a visit at Scarborough College, University of Toronto. Financial support from the Swedish Natural Science Research Council is gratefully acknowledged.

REFERENCES

1. Kresge, A. J. *Pure Appl. Chem.* 8 (1964) 243.
2. Gold, V. *Adv. Phys. Org. Chem.* 7 (1969) 259.
3. Gold, V. *Trans. Faraday Soc.* 64 (1968) 2143.
4. Albery, J. In Caldin, E. F. and Gold, V. Eds., *Proton-Transfer Reactions*, Chapman and Hall, London 1975, Chapter 9.
5. Halevi, E. A. *Israel J. Chem.* 9 (1971) 385, and references given there.
6. Reitz, O. and Kopp, J. *Z. Phys. Chem. (Leipzig) A* 184 (1939) 429.
7. Long, F. A. and Watson, D. *J. Chem. Soc.* (1958) 2019.
8. Hibbert, F. and Long, F. A. *J. Am. Chem. Soc.* 93 (1971) 2836.
9. Berntsson, P., Wanger, M. and Carter, R. E. *Acta Chem. Scand.* 21 (1967) 879.
10. Berntsson, P. and Carter, R. E. *Acta Chem. Scand.* 22 (1968) 2141.
11. Dahlberg, D. B. and Long, F. A. *J. Am. Chem. Soc.* 95 (1973) 3825.

Received December 30, 1976.

Exergy Loss, Dissipation and Entropy Production. Towards a Rational Thermodynamics. II

TORBEN SMITH SØRENSEN

Fysisk-Kemisk Institut, Technical University of Denmark, DK-2800 Lyngby, Denmark

It is shown by application of Brønstedian energetics that the loss of mechanical work (dissipation) by a reversible “cinematographic” reproduction of an irreversible process is equal to the absolute temperature of the standard thermal reservoir from which the compensation entropy is taken times the entropy production during the irreversible process.

Furthermore it is shown that the loss in absolute exergy during an irreversible process in an isolated thermodynamic system is equal to the absolute temperature of the energetic zero-point times the entropy produced.

Examples are given and the difference between energetic zero points and “heat death points” is discussed. The relative exergy for open, stationary flow systems, previously discussed in literature is found to obey similar relations, but the energetic zero points are here arbitrarily chosen and not endogeneously determined by the capacities of the systems, as the case is for the absolute exergy.

In previous publications¹⁻³ I have tried to reconcile Brønstedian and Gibbsian thermodynamics and have shown that Gibbsian thermodynamics may be considered a sub-class within the more general framework of Brønstedian thermodynamics. In order to be in closest possible analogy with the procedures of analytical mechanics, Brønsted's energetics was extended to encompass an *exergy function* being the thermodynamic equivalent of potential energy in mechanics rather than the internal energy. Whereas internal energy is conserved during irreversible transformations in isolated systems, the exergy decreases. Furthermore, the exergy was shown to have an interesting non-additive property, when subsystems were combined into larger systems, whereas the internal energy has to be additive, if the law

of conservation of energy in nature should not be violated.

In the present paper the connection between loss in exergy and entropy production during irreversible processes will be described, and illustrated by simple examples as an introduction to the systematic treatment of multicomponent transport processes in forthcoming papers.

LOSS OF MECHANICAL WORK IN A REVERSIBLE REPRODUCTION OF AN IRREVERSIBLE PROCESS

In Fig. 1 we have depicted an *isolated* thermodynamic system (an energetic universe) which we have subdivided into a *closed* system described by the vectors of potentials and quantities (P, K), a mechanical reservoir (*e.g.* a weight in a gravity field) and a thermal standard reservoir with the fixed absolute temperature T_{st} . We now perform an infinitesimal irreversible process

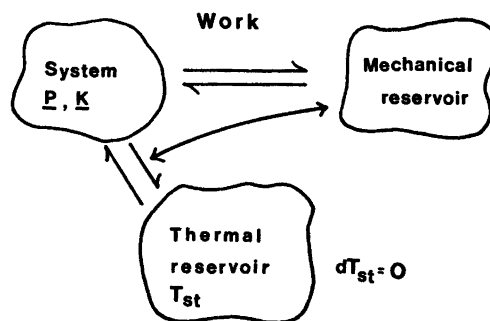


Fig. 1. Closed thermodynamic system in communication with mechanical and thermal reservoir.

$$P, K \rightarrow P + dP, K + dK \quad (1)$$

in the system. According to Brønstedian energetics we have

$$\sum T_i dS_{\text{prod}}^i + \sum_{K \neq S_{\text{prod}}} PdK + dE_{\text{mech}}(\text{irr}) + T_{\text{st}} dS_{\text{st}}(\text{irr}) = 0 \quad (2)$$

The ϕdM terms (ϕ = gravity potential) in the mechanical reservoir have been lumped together in the mechanical potential energy term dE_{mech} and the terms due to produced entropy have been separated out from the PdK -sum for the system. We consider general *polythermal* systems, where the entropy may be produced at many different temperatures (*e.g.* heat conduction).

Consider now a reversible "cinematographic" reproduction of the irreversible process. That means the following: We move around all the quantities inside the closed system in exactly the same way as they move during the irreversible process. We also produce or destruct quantities inside the system (moles of chemical components, interfacial area, but *not* entropy) exactly as in the irreversible process, and make the same supplies from outside ($-dS_{\text{st}}(\text{irr})$) from T_{st} , volume from external volume). But since we make the transformation (1) in a reversible manner, we have no production of entropy, and we have to compensate for that by supplying the *additional* entropy-quantities dS_{ex}^i to the temperature T_i from the standard reservoir by means of reversible Carnot-cycles. We therefore have

$$dS_{\text{prod}}^i(\text{irr}) = dS_{\text{ex}}^i(\text{rev}) \quad (3)$$

Brønsted's work principle applied to the reversible reproduction requires that

$$\sum T_i dS_{\text{ex}}^i + \sum_{K \neq S_{\text{ex}}} PdK + dE_{\text{mech}}(\text{rev}) + T_{\text{st}} dS_{\text{st}}(\text{rev}) = 0 \quad (4)$$

When we speak about a reversible reproduction of the irreversible process we must have

$$\sum_{K \neq S_{\text{ex}}} PdK(\text{rev}) = \sum_{K \neq S_{\text{prod}}} PdK(\text{irr}) \quad (5)$$

and by subtraction of (2) from (4) we obtain

$$dE_{\text{mech}}(\text{rev}) - dE_{\text{mech}}(\text{irr}) = T_{\text{st}} (dS_{\text{st}}^{\text{irr}} - dS_{\text{st}}^{\text{rev}}) \quad (6)$$

The following eqn. must apply

$$dS_{\text{st}}^{\text{irr}} - dS_{\text{st}}^{\text{rev}} = \sum dS_{\text{ex}}^i = dS_{\text{prod}}^{\text{tot}} \quad (7)$$

From (6) and (7) we obtain for the loss of mechanical work by performing the same process irreversibly instead of reversibly

$$dE_{\text{mech}}(\text{rev}) - dE_{\text{mech}}(\text{irr}) = T_{\text{st}} dS_{\text{prod}}^{\text{tot}} \quad (8)$$

Only if T_{st} is equal to the temperature in the system (in case of monothermal systems), is the left hand side of (8) equal to the so-called "loss of work" in Brønsted's terminology. When T_{st} decreases, an increasing amount of the work gained by reversible performance is used again to "elevate" entropy from T_{st} to T_{system} . In the terminology of my previous paper,³ the sum $\sum T_i dS_{\text{prod}}^i$ is equal to the loss of a very special *conditioned exergy*, defined by connecting the T_i -positions in the system with large thermostats of the same temperatures allowing the entropy to flow neutrally between system and thermostats.

A special situation arises when T_{st} tends to zero. As seen by eqn. (8) we will not get additional mechanical work out of the system by reversible performance. This is not so strange, as it might appear in the first place. Formally one cannot see the difference between using a certain amount of mechanical work to elevate entropy reversibly from $T_{\text{st}} \rightarrow 0$ to the local temperature T_i or dissipation of the mechanical work by friction processes at the temperature T_i . The entropy produced at T_i in the latter case is equivalent to the entropy supplied to T_i in the former. A certain manner of mimicking an irreversible process would be to make a reversible reproduction of the process supplying the compensating entropy by dissipating locally the additional mechanical work gained. There will be no difference between the original process and the mimicking process and the work difference (8) has to be zero.

As an example we may consider "simple" heat conduction, which is energetically not so simple as it is usually described in literature.⁴ Consider stationary heat conduction in a rod between the temperatures T_2 and T_1 ($T_2 > T_1$). If we move the amount of entropy δS_{trans} reversibly from T to $T + dT$ (dT may be negative) by means of a Carnot cycle, the mechanical work thus locally gained is $-\delta S_{\text{trans}} dT$. We

now dissipate the work gained at the temperature T (making, e.g., like Count Rumford some canon-boring at the position in question). The produced entropy becomes $\delta S_{\text{prod}} = -\delta S_{\text{trans}} dT/T$. In case of stationary heat conduction the produced entropy joins the entropy transported so we get the differential eqn. for the transported entropy through the rod

$$d\delta S_{\text{trans}} = -\delta S_{\text{trans}} dT/T \quad (9)$$

Separating the variables and solving we obtain

$$T_2 \delta S_{\text{trans}}(2) = T \delta S_{\text{trans}}(T) = T_1 \delta S_{\text{trans}}(1) \quad (10)$$

A "quantity" named heat $= T \delta S_{\text{trans}}$ seems to flow in a conserved manner from T_2 to T_1 . This superficial simplicity has made most thermodynamicists regard "heat" to be the primitive thermal quantity instead of entropy. Heat is, however, in our thermodynamics regarded as a pseudo-quantity. It is only defined in flow systems. Concentration of heat or heat content cannot be defined, whereas entropy is defined both as a stationary and a flowing entity.

LOSS IN ABSOLUTE EXERGY AND ENTROPY PRODUCTION

In Fig. 2 is shown a trajectory in a *thermodynamic phase space* described by an infinitesimal, irreversible process in an *isolated* thermodynamic system from state I (P, K) to state II ($P+dP, K+dK$). The thermodynamic phase space is here macroscopically defined (in contrast to the one used in statistical thermodynamics). We may imagine a space

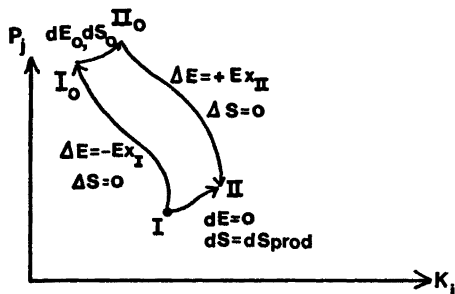


Fig. 2. Trajectory in thermodynamic phase space of an infinitesimal irreversible process and the corresponding energetic zero points.

spanned by orthogonal P - and K -axes for the different localities in our system. When the constraints of the system are known (the constitutive relations) they will not all be necessary, and any sufficient set of P 's and K 's may be selected to span the phase space. Since the process $I \rightarrow II$ happens in an isolated system the change in internal energy $dE=0$ and $dS = dS_{\text{prod}}$.

We now open our system for interaction with an external mechanical reservoir, and extract the exergy from system I, until it reaches its energetic zero point I_0 . It should be emphasized that volume in our energetics is a quantity and a definite volume V_{max} should be allocated to the system, and should be included as regions of vacuum from the beginning, if matter is not spread throughout the system. Due to the definition of exergy in the previous paper we have for the change in internal energy and entropy of the system along the path $I \rightarrow I_0$: $\Delta E = -Ex_I$ and $\Delta S = 0$. Precisely the same can be said of the path $II \rightarrow II_0$, but it is important to notice, that the two energetic zero-points differ infinitesimally, because of the presence of the extra produced entropy in system II. To close the cycle we have therefore to perform the process $I_0 \rightarrow II_0$ with $dE = dE_0$ and the entropy change $dS = dS_0$, which has to be supplied by an external thermal reservoir.

Since E and S are functions of state of the system, we get by considering the closed cycle in Fig. 2

$$dS_0 = dS_{\text{prod}} \quad (11)$$

and

$$Ex_I - Ex_{II} = -dEx = dE_0 \quad (12)$$

At the energetic zero-point the system occupies its maximum volume V_{max} , and the temperature is everywhere the same (T_0) as are all the transport-complex potentials, such as gravi-electro-chemical potentials $\tilde{\mu}_i$. Pressure is not necessarily equalised, for example it varies in a gravity field even at equilibrium. The equalisation of potentials or composed potentials is the case both in I_0 , in II_0 , and in any point of the curve $I_0 \rightarrow II_0$, which may be regarded as intermediary energetic zero-points. The only quantity supplied from outside is entropy, and all the internal quantity transfers, creations

or destructions will be energetically neutral due to the equalisation of potentials or composed potentials. Therefore we have

$$dE_0 = \sum P_0 dK = T_0 dS_0 = T_0 dS_{\text{prod}} \quad (13)$$

Introducing eqn. (13) into eqn. (12) we get the simple, but most important relation for the loss of absolute exergy (for the difference between absolute and relative exergies, see the next section)

$$-dEx = T_0 dS_{\text{prod}} \quad (14)$$

The temperature of the energetic zero-point hides the information on the restricted capacities of the system, which is included in every exergy calculation. The relative nature of the exergy loss is hereby made clear: The lower the temperature of the energetic zero-point the lower the loss of exergy for a given entropy production. In the extreme case, where T_0 approaches zero, no exergy would ever be lost, since the TdS_{prod} may be fully retransformed to mechanical work by reversible transfer of entropy from T to the very small absolute temperature. Also, T_0 depends on what is inside our system, and thus reflects again the non-additivity of exergy discussed in the previous paper.

As a very simple example, consider irreversible "heat" conduction between two identical objects with entropy capacities c independent of temperature. In the previous paper we found the exergy to be

$$Ex = \frac{c}{4} (T_2 - T_1)^2 \quad (15)$$

We consider $T_2 > T_1$ and connect the two objects with a thin heat conducting rod, in which (quasi) stationarity can be assumed at any time. By eqn. (10) we can express the "degree of advancement" of the irreversible process through the integral quantity $S_{\text{trans}}(2)$, which has left the highest temperature. The produced entropy is given by

$$dS_{\text{prod}} = dS_{\text{trans}}(1) - dS_{\text{trans}}(2) = \left(\frac{T_2}{T_1} - 1\right) dS_{\text{trans}}(2) \quad (16)$$

The loss of exergy is given by differentiation of (15) and application of the constitutive relations

$$\begin{aligned} -dEx/dS_{\text{trans}}(2) &= \\ -\frac{c}{2} (T_2 - T_1) &\left(\frac{dT_2}{dS_{\text{trans}}(2)} - \frac{dT_1}{dS_{\text{trans}}(1)}\right) \\ \frac{dS_{\text{trans}}(1)}{dS_{\text{trans}}(2)} &= \frac{1}{2} \frac{(T_1 + T_2)}{2} \left(\frac{T_2}{T_1} - 1\right) \end{aligned} \quad (17)$$

Since the temperature of the energetic zero-point is seen to be the arithmetic mean of T_1 and T_2 by symmetry considerations, we have in (16) and (17) a verification of the relation (14). It should be stressed, that T_0 is *not* equal to the end temperature of the irreversible heat conduction process, which will be in the interval ($T_0|T_2$) due to the greater amount of entropy delivered to the temperature T_1 than removed from the temperature T_2 .

As a somewhat more realistic example take two bodies with *heat* capacities C_1 and C_2 independent of the temperatures T_1 and T_2 . For the exergy in that case we have by the general method given in the previous paper

$$Ex(T_2, T_1) = C_1 T_1 + C_2 T_2 - T_0 \sum C_i \quad (18)$$

with the energetic zero-point

$$T_0 = T_1 C_1 \sum C_i T_2 C_i \sum C_i \quad (19)$$

Doing the analogous differentiation to the one performed in (17) we obtain

$$-dEx/dS_{\text{trans}}(2) = T_2 \left[\left(\frac{T_2}{T_1}\right)^{C_1 \sum C_i} - \left(\frac{T_1}{T_2}\right)^{C_1 \sum C_i} \right] \quad (20)$$

For $dS_{\text{prod}}/dS_{\text{trans}}(2)$ we still have eqn. (16), and eqn. (14) is now easily seen to be obeyed. The temperature reached in the end by the irreversible process – which we shall call the "heat death point" of the system – is given by

$$\begin{aligned} T_{\text{Heat death}} &= T_1 + \frac{C_2}{\sum C_i} (T_2 - T_1) = \\ T_2 - \frac{C_1}{\sum C_i} (T_2 - T_1) \end{aligned} \quad (21)$$

As an illustration we consider equal amounts of the same substance at 0 and 100 °C with the heat capacity taken to be independent of temperature. In Fig. 3 we have shown the irreversible path in a $T_1 - T_2$ phase space when the two substances are connected by a thin conductor. The trajectory of energetic zero-points is also shown. The two trajectories have to meet in the heat death point of the system.

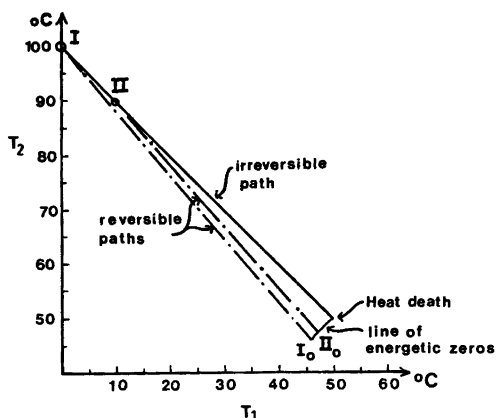


Fig. 3. Heat conduction between equal amounts of the same substance at initial temperatures 0 and 100 °C.

As our last example let us take the irreversible Joule expansion of an ideal gas. Our system consists of an insulated cylinder with piston and volume $V_{\max} = 2V$. The n mol of ideal gas are confined in the volume V with the pressure p and the temperature T . We perform an irreversible expansion δV , whereby (experimentally) the temperature remains constant. We have

$$T \delta S_{\text{prod}} = p \delta V \tag{22}$$

The absolute exergy before the expansion is found by making a reversible, adiabatic expansion of the gas from V to $V_{\max} = 2V$. We obtain

$$T_0(\text{before}) = T \cdot 2^{-R/C_v} \tag{23}$$

and

$$Ex(\text{before}) = nC_v \{T - T_0(\text{before})\} \tag{24}$$

After the expansion δV we have for the energetic zero-point

$$T_0(\text{after}) = T \left(\frac{2V}{(V + \delta V)} \right)^{-R/C_v} = T \cdot 2^{-R/C_v} \left[1 + \frac{R}{C_v} \frac{\delta V}{V} \right] \tag{25}$$

The last equation is obtained by Taylor-expansion of the first. Subtracting the exergy after the expansion (given by the analogous equation to (24) for the exergy before, we obtain for the loss of exergy

$$-dEx = nC_v [T_0(\text{after}) - T_0(\text{before})] = nRT \frac{\delta V}{V} 2^{-R/C_v} = p \delta V \cdot 2^{-R/C_v} \tag{26}$$

and by comparison with (22) and (23) we observe, that eqn. (14) is verified once more. We might have taken our system to include a big thermostat surrounding the cylinder with a temperature T . From the point of view of the irreversible expansion δV , we cannot see any difference, since – as shown by Joule – no entropy is exchanged with the thermostat. The energetic zero-points are very different, however, since they are $(2V, T, p/2)$ before as well as after the infinitesimal expansion. Eqn. (14) holds for that system as well, and the increase in internal energy of the energetic zero-point of the gas cylinder plus the thermostat is exactly $T \delta S_{\text{prod}}$ as required by eqn. (13)

RELATIVE EXERGY FOR STATIONARY FLOW SYSTEMS

To join the exergy concept developed here and in the previous paper with the exergy concept already in use in power and refrigeration technology⁵ and in irreversible thermodynamics,⁶ we consider the stationary flow system visualized in Fig. 4. We shall denote specific quantities (quantities per kg mass) by lower case letters. Thus, w is the useful work (e.g. electric power) exported from the system to the surroundings per kg mass passed through the flow system. The corresponding “heat” from the surroundings to the system is denoted q and is given by

$$q = -T_{\text{env}} \Delta s_{\text{env}} \tag{27}$$

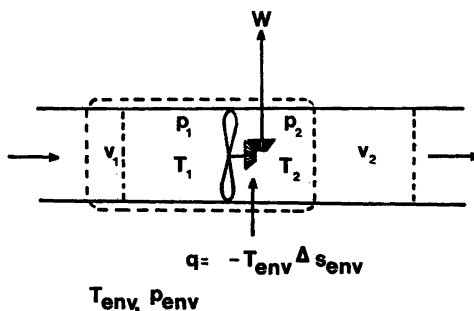


Fig. 4. Generalised Joule-Thomson experiment.

where "env" stands for environment. The system in Fig. 4 is subdivided into three systems: (I) The flowing mass of incoming and outgoing streams + the more or less complex machinery encircled by the broken line. This system follows a specific amount of mass of "fuel" and "smoke" during passage. (II) The surrounding flowing mass. (III) The environments.

We now pass on to energy and entropy balances for the three subsystems in various contexts. For the environment we have for the change in internal energy per kg mass passed

$$\Delta e_{\text{env}} = \Delta e_{\text{III}} = T_{\text{env}} \Delta s_{\text{env}} + w = -q + w \quad (28)$$

The corresponding change in the surrounding flowing mass is

$$\Delta e_{\text{II}} = (-p_1)v_1 - (-p_2)v_2 \quad (29)$$

since the only changes in quantities are the neutral transports of specific volumes between System I and System II. Due to the conservation of energy we have

$$\Delta e_{\text{I}} = e_2 - e_1 = -\Delta e_{\text{II}} - \Delta e_{\text{III}} = q - w - p_2v_2 + p_1v_1 \quad (30)$$

That is - with the usual definition of the enthalpy h - we have

$$w = q - h_2 + h_1 \quad (31)$$

It should be remarked, that in the classical Joule-Thomson experiment, where a real gas is forced through a porous plug, $q = w = 0$ and the process is going on at constant enthalpy.

We shall now carry on a calculation of the specific exergy ex_1 of the incoming stream relative to the surrounding temperature T_{env} and pressure p_{env} . We let all the internal processes, e.g. chemical reactions, come to equilibrium extracting the maximum work by reversible processes. If the temperature and the pressure in the final state are different from $(T_{\text{env}}, p_{\text{env}})$ we move entropy and volume reversibly between the system and the environment until temperature and pressure have been equalized. The outgoing stream is now reduced to a relative exergy $ex_2 = 0$ at $T_2 = T_{\text{env}}$ and $p_2 = p_{\text{env}}$ and the total work delivered $w = ex_1$. This kind of exergy is called relative, since it calls for an arbitrary point of reference

$(T_{\text{env}}, p_{\text{env}})$ and since it does not account for the additional exergy which could be extracted by equalizing the chemical potentials in the outgoing stream and in the environment by mass transfer (exergy of chemical pollution of the environment). We obtain (ref. means values taken at T_{env} and p_{env})

$$w = ex_1 = h_1 - h_{\text{ref}} + q = h_1 - h_{\text{ref}} - T_{\text{env}} \Delta s_{\text{env}} \quad (32)$$

Since

$$\Delta s_{\text{I}} = s_{\text{ref}} - s_1 \quad (33)$$

and

$$\Delta s_{\text{II}} = 0 \quad (34)$$

and entropy is conserved in reversible processes, we obtain

$$\Delta s_{\text{env}} = -(s_{\text{ref}} - s_1) \quad (35)$$

and

$$ex_1 = h_1 - h_{\text{ref}} + T_{\text{env}}(s_{\text{ref}} - s_1) \quad (36)$$

In a process where the maximum work is not extracted we have not $ex_2 = 0$ but ex_2 is given by a formula analogous to (36). Thus, generally, we have for the change in specific relative exergy

$$-\Delta ex_{\text{I}} = ex_1 - ex_2 = -\Delta h_{\text{I}} + T_{\text{env}} \Delta s_{\text{I}} \quad (37)$$

The loss of relative exergy is given by

$$\text{Loss of relative exergy} = -\Delta ex_{\text{I}} - w \quad (38)$$

Using (37) for the change in exergy and (31) for the work we obtain

$$\text{Exergy loss} = T_{\text{env}}(\Delta s_{\text{I}} + \Delta s_{\text{env}}) = T_{\text{env}} \Delta s_{\text{prod}} \quad (39)$$

This formula is the analogue of the expression (14) for the loss in absolute exergy. The difference is, that while the temperature T_0 in eqn. (14) is endogeneously determined by the finite capacities of the isolated energetic system, the environment reference temperature in (39) is just arbitrarily chosen, and the loss in relative exergy is not the complete loss in absolute exergy in the complete energetic universe, since the "pollution exergy" has not been accounted for.

Acknowledgement. The author wishes to express his gratitude to Dr. F. Yssing Hansen from Fysisk-Kemisk Institut for stimulating discussions in connection with the present work.

REFERENCES

1. Sørensen, T. S. *Dan. Kemi* 52 (1971) 138.
2. Sørensen, T. S. *Studier over Fysisk-Kemiske Systemers Statik, Dynamik, Kinetik*, Ph.D. Thesis, Technical University of Denmark, Lyngby 1973.
3. Sørensen, T. S. *Acta Chem. Scand. A* 30 (1976) 555.
4. Brønsted, J. N. *Philos. Mag. Ser. 7* 29 (1940) 449.
5. VDI-Fachgruppe Energietechnik, *Energie und Exergie*, VDI-Verlag, Düsseldorf 1965.
6. Chartier, P., Gross, M. and Spiegler, K. S. *Applications de la thermodynamique du non-equilibre*, Hermann, Paris 1975.

Received October 25, 1976.

The Crystal Structure of Pd₁₅P₂

YVONNE ANDERSSON

Institute of Chemistry, University of Uppsala, Box 531, S-751 21 Uppsala, Sweden

The crystal structure of Pd₁₅P₂ has been determined and refined from 2080 three-dimensional single-crystal X-ray diffractometer data to an $R(\bar{F}^2)$ value of 0.092. The space group is $R\bar{3}$ (No. 148). The hexagonal unit cell, of dimensions $a=7.1067(2)$ Å, $c=17.0867(6)$ Å, contains three formula units. The structure is related geometrically to the α -boron structure.

In the Pd–P system Gullman¹ found a very palladium-rich intermediate phase which forms peritectically at 799 °C and has the approximate composition Pd₅P. In the present paper the results from a crystal structure analysis of this phase are presented. The ideal crystallographic formula is Pd₁₅P₂.

EXPERIMENTAL

Preparation. Starting materials were palladium powder (Heraeus, Germany) with a claimed purity of 99.9 % and red phosphorus of purity greater than 99 %. Polycrystalline Pd₁₅P₂ samples were prepared in exactly the same manner as described by Gullman.¹ To obtain single crystals for X-ray investigations, pressed pellets of well-mixed palladium and phosphorus powder were heated in evacuated silica tubes at 830 °C for two days and 795 °C for five months. In spite of the long heat-treatment the sample contained Pd and Pd₅P in addition to Pd₁₅P₂. Out of the crushed sample good crystals could be obtained, even though they were all of an irregular needle shape.

X-Ray powder investigations. Powder diffraction patterns were obtained with focusing Hagg-Guiner-type cameras using CrK α_1 or CuK α_1 radiation and silicon ($a=5.431065$ Å)² or germanium ($a=5.65806$ Å) as calibration standards. Cell parameters were refined by the least-squares method using the local program CELNE.³ Powder diffraction intensity data were obtained by measuring Hagg-Guiner photographs on an automatic drum densitom-

eter (SAAB model 2), using a method similar to that described by Malmros and Werner.⁴

Single crystal investigations. Single crystal diffraction intensity data were recorded on a Stoe four-circle diffractometer with a graphite monochromator using MoK α radiation. The intensity measurements were made using the ω - 2θ step scan technique, to a maximum in 2θ of 100°. For symmetry control, symmetry-related reflexions were measured in the region $0 \leq 2\theta \leq 40^\circ$ and their hexagonal indices were limited by $-3 \leq h \leq 5$, $-5 \leq k \leq 3$ and $-12 \leq l \leq 12$. For $2\theta > 40^\circ$ the hexagonal indices ranged between $0 \leq h \leq 15$, $-13 \leq k \leq 0$ and $-36 \leq l \leq 36$. Instrumental stability and the crystal setting were checked regularly using three standard reflexions remeasured every 50 reflexions. The weakest of these three, (017), was found to vary somewhat erratically, while the other two remained within expected fluctuations.

Absorption corrections were applied to the single crystal data. The shape of the crystal was approximated to a triangular prism bounded by {111}, {346}, {017}, {116} and {329} planes. The length of the crystal was 0.120 mm and the edges of the triangular cross-sections ranged from 0.033 to 0.057 mm. The minimum and maximum transmission factors were 0.157 and 0.789, using a calculated linear absorption coefficient of 259 cm⁻¹.

The calculations were performed on IBM 370/155 and IBM 1800 computers using crystallographic programs listed in Ref. 5.

STRUCTURE ANALYSIS

The powder diffraction data obtained for Pd₁₅P₂ were in very good agreement with Gullman's¹ Pd₅P results. The Pd₁₅P₂ powder data as obtained in this study are given in Table 1. Using the information from Weissenberg photographs the powder pattern could be indexed with a hexagonal cell of dimensions $a=7.1067(2)$ Å and $c=17.0867(6)$ Å at 25 °C (numbers in parentheses are the calculated standard devia-

Table 1. Powder diffraction data for Pd₁₅P₂. (Guinier-Hägg camera, CuK α ₁ radiation, internal calibration silicon $a = 5.431065$ Å, intensities from film scanner.)

hk l	Q $\times 10^5$ (Å ⁻²)		Intensity		hk l	Q $\times 10^5$ (Å ⁻²)		Intensity	
	obs.	calc.	obs.	calc.		obs.	calc.	obs.	calc.
10 1		2982	-	0	2011	52005	-	0	
00 3		3083	-	0	2310	52732	-	1	
01 2		4010	-	1	2110			0	
11 0		7920	-	0	14 0	55446	55439	28	6
10 4		8120	-	0	41 0			16	
02 1	10896	10902	2	1	35 4	55642	55640	17	5
12 3	11004	11002	-	1	32 4			9	
11 3			-	1	34 8	56243	56241	10	3
01 5	11196	11203	-	1	31 8			3	
20 2	11917	11930	-	0	12 2	57242	57243	22	14
00 6		12331	-	0	1112			3	
02 4		16040	-	0	45 3			9	
23 1			73	73	15 3			3	
21 1	18814	18822	74	27	41 3	58524	58522	14	3
20 5	19125	19123	45	64	14 3			1	
10 7	19432	19423	32	35	25 5	58713	58722	20	4
13 2	19849 ^a	19850	66	12	23 5	59042	59023	23	22
12 2			66	30	40 7	59042	59023	23	22
12 6	20249	20251	75	24	24 9	59431	59424	5	1
11 6			65	65	22 9			6	
30 0	23756	23760	20	23	1311	59932	59925	23	6
23 4			11	0	1211			10	
21 4	23953	23960	11	0	1013		60526	-	0
01 8		24561	-	0	04 8		64161	-	0
03 3			5	5	05 1		66342	-	0
30 3	26846	26842	5	0	35 7			0	
13 5			28	28	32 7		66943	-	0
12 5	27045	27043	24	4	50 2	67380	67369	2	1
02 7	27338	27343	5	5	15 6			0	
00 9	27734	27744	-	0	45 6	67778	67770	5	0
22 0	31659	31680	2	1	41 6			0	
20 8	32482	32481	-	0	14 6			1	
14 1			5	2	0213		68446	-	1
13 1	34665	34662	5	2	1410	68578	68572	8	0
24 3			-	0	1310			5	4
22 3		34762	-	0	0114	69760	69774	5	4
23 7			-	0	33 0		71279	-	0
21 7		35263	-	0	05 4		71480	-	0
12 9			2	2	25 8			9	
11 9		35664	5	1	23 8	72091	72081	14	6
34 2			5	1	3012			6	
31 2		35690	0	0	0312		73082	-	0
03 6			1	1	26 1			0	
30 6	36090	36090	1	0	24 1		74262	-	1
1010	36892	36892	2	2	36 3	74264		4	0
14 4	39798	39800	7	4	33 3		74362	-	1
13 4			7	4	50 5		74562	-	1
13 8			7	4	46 2	75280	75289	20	12
12 8	40396	40401	7	4	42 2			9	
40 1		42582	-	0	3411	75758	75764	8	0
34 5		42882	-	0	3111			5	
31 5			4	4	2313		76366	-	9
04 2	43584	43610	4	4	2113	76401		32	11
24 6			4	0	4010		76491	-	8
22 6	44062	44010	4	1	0015		77067	-	0
0111		44085	3	2	2014	77700	77694	2	3
0210	44809	44812	3	3	26 4			1	
40 4		47720	-	0	24 4		79400	-	3
0012	49307	49323	6	6	2412			4	
35 1			7	3	2212	81020	81002	8	3
32 1		50502	7	3	56 1			5	
04 5	50828	50802	5	4	51 1	82176	82182	4	1
14 7			18	11	46 5			1	
13 7	51087	51103	18	5	42 5	82499	82482	2	2
03 9		51504	3	0	05 7	82801	82783	2	3
30 9			6	1					
25 2	51511		6	1					
23 2		51530	0	0					

a overlapped by Fd.

tions). No significant changes in the unit cell dimensions were observed for different samples.

Weissenberg photographs taken with the crystal rotating about the hexagonal a -axis showed that the rhombohedral condition $-h+k+l=3n$ was obeyed for all reflexions. Since

only a three-fold symmetry was observed, most likely space groups were $R\bar{3}$ and $R\bar{3}$. The cell volume and the approximate composition Pd₉P suggested a unit cell content of about 48 palladium and six phosphorus atoms.

In the preliminary structure analysis, the Harker section $P(u,v,0)$ of the Patterson function indicated $R\bar{3}$ space group symmetry with palladium atoms in two general positions. Space considerations and the Harker section $P(u,0,w)$ indicated two further palladium sites, in $6c$ and $3b$, and one phosphorus site in $6c$. The ideal crystallographic composition should accordingly be Pd₁₅P₂. Since the structure model thus derived appeared quite reasonable from the crystal chemical point of view, least-squares refinements of the parameters were immediately started. The positional parameters, a scale factor and individual isotropic temperature factors were refined using a full-matrix least-squares program.⁵ The atomic scattering factors and the dispersion correction factors were taken from Ref. 6. After three cycles a conventional R -value of 0.106 was obtained based on the 1495 strongest reflexions. Since the structure proposal seemed to be correct, a linear absorption coefficient was calculated, and an absorption correction applied to the observed intensities. In order to correct for extinction effects only reflexions having identical indices were averaged.

A series of least-squares refinements on both F and F^2 were performed. The function minimized was $w(|F_o^n| - |F_c^n|)^2$ with $n=1$ or 2, respectively. Weights were assigned to the reflexions according to the formula $w^{-1} = \sigma^2(F_o^n) + (p_n F_o^n)^2$, where $\sigma^2(F_o^n)$ is based on counting statistics and the empirical factor p_n was set to $p_1=0.02$ and $p_2=0.03$. An isotropic extinction parameter, according to the expression by Coppens and Hamilton⁷ based on approximations introduced by Zachariasen, and anisotropic temperature factors for the palladium atoms was introduced. 32 strong reflexions were assigned zero weight in the refinements because their extinction correction factors did not satisfy the condition for Zachariasen's approximations. The value for the extinction parameter g ⁷ finally obtained was 0.50(5). For the 2080 reflexions refined the following agreement factors were obtained,

Table 2. Structure data for Pd₁₅P₂, including anisotropic thermal parameters β_{ij} (× 10⁶) for the palladium atoms. The form of the temperature factor is exp (−β₁₁h²−β₂₂k²...−2β₁₂hk...).

Atom	Position	x	y	z	β ₁₁	β ₂₂	β ₃₃	β ₁₂	β ₁₃	β ₂₃
Pd(1)	18 f	0.40049(7)	0.28437(7)	0.96339(2)	556(8)	487(8)	61(1)	232(6)	−6(2)	−14(2)
Pd(2)	18 f	0.25807(7)	0.23813(7)	0.79537(2)	488(8)	589(8)	59(1)	274(6)	13(2)	−7(2)
Pd(3)	6 c	0	0	0.07941(4)	542(8)	542(8)	56(2)	271(4)	0	0
Pd(4)	3 b	0	0	1/2	440(10)	440(10)	56(2)	220(5)	0	0
P	6 c	0	0	0.28552(16)	^a					

^a Isotropic temperature factor 0.96(3) (Å²).

$R(F^2) = 0.092$, $R(F) = 0.066$ and $R_w(F^2) = 0.144$, where

$$R(F^m) = \frac{\sum |F_o^m| - |F_c^m|}{\sum |F_o^m|} \text{ and } R_w(F^m) = \left[\frac{\sum w(|F_o^m| - |F_c^m|)^2}{\sum w|F_o^m|^2} \right]^{1/2}$$

In subsequent refinements the occupancy factors were varied but the refinements invariably terminated with insignificant deviations from full occupancy. Experimental errors in the geometrical description of the crystal, together with the very strong absorption, are probably responsible for the comparatively high final values obtained for the agreement factors.

The final structure data obtained are presented in Table 2. A table of observed and calculated structure factors can be obtained from the author on request.

DESCRIPTION AND DISCUSSION OF THE Pd₁₅P₂ STRUCTURE

Calculated interatomic distances are given in Table 3. Each palladium atom coordinates 12–15 palladium and phosphorus neighbours, and the phosphorus atoms have nine palladium neighbours. The structure can be described in terms of slightly distorted icosahedral building elements with six Pd(1) and six Pd(2) atoms at the corners and one Pd(4) atom at the centre. The icosahedra are arranged in nearly the same way as spheres in cubic close-packing.

In the "cubic close-packing" of palladium icosahedra in Pd₁₅P₂, the "octahedral holes" are filled with pairs of Pd(3) atoms and the "tetrahedral holes" with phosphorus atoms.

The "octahedral hole" is illustrated stereoscopically in Fig. 1. It is actually a polyhedron with 18 palladium atoms at the vertices: each

of the surrounding six palladium icosahedra contributing three corner atoms to this polyhedron.

The "tetrahedral hole" is illustrated stereoscopically in Fig. 2. The central phosphorus atom is surrounded by nine palladium neighbours, six of them situated at the corners of a distorted triangular prism, and the remaining three more remotely outside the quadrilateral faces of the prism. This kind of environment

Table 3. Interatomic distances in Pd₁₅P₂ (Å). The maximum standard deviation obtained was 0.0008 Å for Pd–Pd distances and 0.0018 Å for P–Pd distances. Distances shorter than 3.5 Å are listed.

Pd(1)–P	2.263	Pd(3)–3Pd(1)	2.640
Pd(3)	2.640	Pd(3)	2.714
Pd(2)	2.730	3Pd(2)	2.775
Pd(4)	2.825	3Pd(2)	2.940
2Pd(1)	2.828	3Pd(1)	3.219
Pd(2)	2.857		
Pd(2)	2.875	Pd(4)–6Pd(2)	2.710
Pd(1)	2.937	6Pd(1)	2.825
P	2.990		
Pd(2)	3.007	P–3Pd(2)	2.244
2Pd(1)	3.021	3Pd(1)	2.263
Pd(3)	3.219	3Pd(1)	2.990
Pd(2)	3.352		
Pd(2)–P	2.244		
Pd(2)	2.638		
Pd(4)	2.710		
Pd(1)	2.730		
Pd(3)	2.775		
Pd(1)	2.857		
Pd(1)	2.875		
2Pd(2)	2.934		
Pd(3)	2.940		
Pd(1)	3.007		
2Pd(2)	3.061		
Pd(1)	3.352		

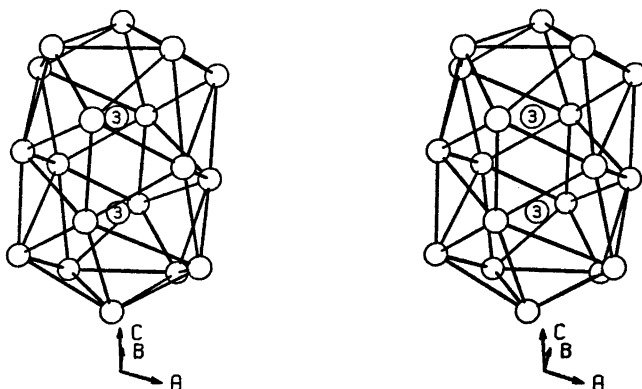


Fig. 1. The "octahedral hole" enclosing the two Pd(3) atoms.

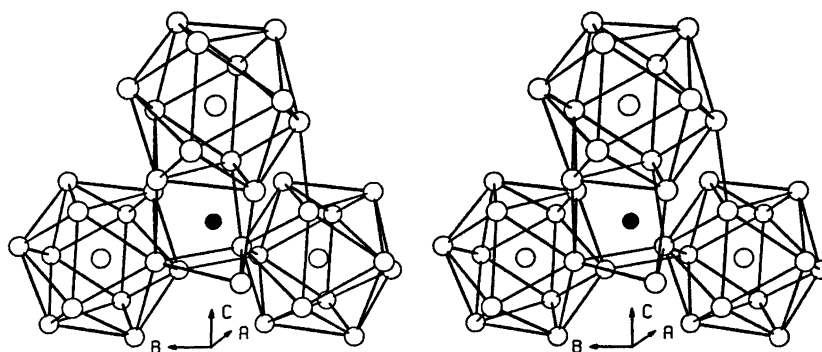


Fig. 2. The "tetrahedral hole" and the environment of the phosphorus atom. For clarity, only one atom of the fourth icosahedron is represented.

of the phosphorus atom is very common in metal-rich transition metal phosphide structures and has been discussed in detail earlier.^{8,9} In particular it occurs¹⁰⁻¹² in the three palladium phosphides Pd_4P , Pd_3P and Pd_6P .

The palladium polyhedron enclosing the central phosphorus atom is built up of the four surrounding palladium icosahedra in the following way. One triangular face of the triangular prism is identical with a triangular face of one of the icosahedra. The second triangular face of the prism is formed by one corner atom from each of the three remaining icosahedra, which also each contribute one of the palladium atoms outside the quadrilateral faces of the prism.

Geometrically, the Pd_{15}P_2 structure is closely related to the rhombohedral α -boron¹³ struc-

ture, where boron icosahedra are packed in a slightly deformed cubic close-packing. Matkovich *et al.*¹⁴ have discussed this kind of packing model in detail. α -Boron crystallizes in space group $R\bar{3}m$ with the hexagonal unit-cell axes $a = 4.908 \text{ \AA}$ and $c = 12.567 \text{ \AA}$.

In interstitial compounds derived from α -boron,^{15,16} for instance B_{12}C_2 and B_{13}C_3 , the "octahedral holes" enclose two to three interstitial atoms, while the "tetrahedral holes" are empty.

Acknowledgements. The author wishes to thank Professor I. Olovsson for all the facilities provided and is deeply indebted to Professor S. Rundqvist for valuable discussions and comments. Financial support from the Swedish Natural Science Research Council is gratefully acknowledged.

REFERENCES

1. Gullman, L.-O. *J. Less-Common Met.* 11 (1966) 157.
2. Deslattes, R. D. and Henins, A. *Phys. Rev. Lett.* 31 (1973) 972.
3. Ersson, N.-O. Institute of Chemistry, University, Uppsala 1973. *Unpublished.*
4. Malmros, G. and Werner, P.-E. *Acta Chem. Scand.* 27 (1973) 493.
5. Lundgren, J.-O., Ed., *Crystallographic Computer Programs*, Institute of Chemistry, University, Uppsala 1975, UUIC-B13-04-2.
6. *International Tables for X-Ray Crystallography*, Kynoch Press, Birmingham 1974, Vol. IV.
7. Coppens, P. and Hamilton, W. C. *Acta Crystallogr. A* 26 (1970) 71.
8. Rundqvist, S. *Ark. Kemi* 20 (1962) 67.
9. Lundström, T. *Ark. Kemi* 31 (1969) 227.
10. Sellberg, B. *Acta Chem. Scand.* 20 (1966) 2179.
11. Rundqvist, S. and Gullman, L.-O. *Acta Chem. Scand.* 14 (1960) 2246.
12. Andersson, Y., Kaewchansilp, V., del Rosario Casteleiro Soto, M. and Rundqvist, S. *Acta Chem. Scand. A* 28 (1974) 797.
13. Decker, B. F. and Kasper, J. S. *Acta Crystallogr.* 12 (1959) 503.
14. Matkovich, V. I., Giese, Jr., R. F. and Economy, J. Z. *Kristallogr.* 122 (1965) 116.
15. Economy, J., Matkovich, V. I. and Giese, Jr., R. F. *Z. Kristallogr.* 122 (1965) 248.
16. Will, G. and Kossobutzki, K. H. *J. Less-Common Met.* 44 (1976) 87.

Received January 3, 1977.

Semi-empirical Expression for Diagonal Torsional Force Constants in Halogenated Propanes and Ethanes

REIDAR STØLEVIK

University of Trondheim, NLHT, Rosenborg, N-7000 Trondheim, Norway

A very simple formula for the diagonal elements within the torsional part of the valence force field in halogenated propanes and ethanes has been proposed. It has been shown, that to a good approximation, the torsional force constant of an ethane-like fragment may be expressed as a sum of six contributions, corresponding to the second order derivatives of the six *gauche* energy interactions.

If the Y,Z atoms of an ethane-like fragment Y'Y''C-CZ'ZZ'' are in nearly staggered positions, then the torsion-angle dependent part of the potential energy (V) is approximately equal to the sum of six Y...Z *gauche* interactions. (Each one of the *gauche* energy terms includes atom-atom interactions as well as bond-bond interactions.)

The torsional force constant ($F_\phi(C-C) = \partial^2 V / \partial \phi^2$) is also expected to be equal to a sum of six contributions, corresponding to the second-order derivatives of the six *gauche* energy terms.

If we consider a propane derivative $R_1-YCY'-R_3$, with Y(Y') equal to H or X (halogen) and $R(CH_3, CH_2X, CHX_2, CX_3)$, we need five different partial force constants (F_{HH}^* , F_{CH}^* , F_{XH}^* , F_{XX}^* , F_{CX}^*) in order to express the total diagonal force constant (F_ϕ).

$$F_\phi = N_{HH} F_{HH}^* + N_{CH} F_{CH}^* + N_{XH} F_{XH}^* + N_{XX} F_{XX}^* + N_{CX} F_{CX}^*$$

N is the number of *gauche* interactions of the types indicated ($\sum N = 6$).

The formula of an ethane derivative R_1-R_3 ($R: CH_3, CH_2X, CHX_2, CX_3$) has only three different terms ($N_{CH} = N_{CX} = 0$).

For $H_3C-CHX-CH_3$ the formula would be $F_\phi(C_1-C_3) = F_\phi(C_2-C_3) = 2F_{HH}^* + 2F_{CH}^* + 2F_{XH}^*$, and for XH_2C-CH_2X we get $F_\phi(anti) = 2F_{HH}^* + 4F_{XH}^*$ and $F_\phi(gauche) = 3F_{HH}^* + 2F_{XH}^* + F_{XX}^*$.

The F^* values may be adjusted in order to reproduce the "experimental" force constants of several molecules. Depending on the number and types of molecules included one will get different sets of F^* values. The set of F^* values presented here reproduce the experimental force constants of 16 related molecules. The average deviation is ca. 10 %, as shown in Table 1. The estimated error limits for most of the experimental values in Table 1 are larger than 10 %.

In adjusting the F^* values, halogenated (X) propanes with parallel C-X bonds on the same side of the CCC skeleton were not included.

The F^* values are: 0.013(HH), 0.017(CH), 0.032(ClH), 0.100(ClCl), and 0.110(CCl) in units of m dyn Å (rad)⁻². The halogenes F, Br, and I may be included in this list. However, the amount of experimental information at present is not as abundant as for chlorinated hydrocarbons. (Useful values for F_{CBr}^* and F_{BrBr}^* are 0.130 and 0.160, respectively, with $F_{BrH}^* \approx F_{ClH}^*$). The list of partial force constants could be extended in order to include molecules containing different kinds of halogenes. (F_{ClBr}^* , F_{ClF}^* , F_{BrF}^* etc.)

Certain limitations of the present model are known for some heavily chlorinated propanes. In the two molecules (X=Cl), $X_2HC-CX_2-CHX_2$ (P6) and $X_3C-CX_2-CX_3$ (P8), the experimental values of the diagonal torsional force constants are 0.86 and 0.36 m dyn Å

Table 1. Diagonal torsional force constants (F_ϕ) for chlorinated ethanes and propanes. $F_\phi(\text{calc.}) = 0.013 N_{\text{HH}} + 0.017 N_{\text{CH}} + 0.032 N_{\text{XH}} + 0.100 N_{\text{XX}} + 0.110 N_{\text{CX}}$, in mdyn Å (rad)⁻².

Molecule (X = Cl)	F_ϕ -value		Conformation	Ref.
	exp.	calc.		
$\text{X}_2\text{C}-\text{CX}_2-\text{CHX}_2(\text{G})$	0.54 ^a	0.50 ^a	G: C_1 symmetry	12
$\text{X}_2\text{HC}-\text{CX}_2-\text{CH}_3(\text{A})$	0.41 ^b	0.48	A: C_s symmetry	11
$\text{X}_2\text{C}-\text{CHX}_2$	0.44 ^c	0.46		9
$\text{X}_2\text{HC}-\text{CHX}-\text{CHX}_2$	0.43 ^a	0.35 ^a	GG(ag)	10
$\text{X}_2\text{C}-\text{CH}_2\text{X}$	0.31 ^d	0.33 ^d		9
$\text{X}_2\text{C}-\text{CH}_2-\text{CHX}_2(\text{G})$	0.32 ^a	0.30 ^a	G: C_1 symmetry	8
$\text{XH}_2\text{C}-\text{CHX}-\text{CH}_2\text{X}$	0.24 ^e	0.23 ^e	mixture ^e	7
$\text{XH}_2\text{C}-\text{CH}_2\text{X}(\text{G})$	0.25	0.19	G: <i>gauche</i>	4
$\text{XH}_2\text{C}-\text{CH}_2-\text{CH}_2\text{X}$	0.17 ^f	0.18 ^f	mixture ^f	6
$\text{H}_3\text{C}-\text{CX}_2-\text{CH}_3$	0.13	0.16		5
$\text{XH}_2\text{C}-\text{CH}_2-\text{CH}_2\text{X}(\text{A})$	0.17	0.15	A: anti	4
$\text{X}_2\text{HC}-\text{CH}_3$	0.14	0.15		3
$\text{H}_3\text{C}-\text{CHX}-\text{CH}_3$	0.13	0.12		2
$\text{XH}_2\text{C}-\text{CH}_3$	0.12	0.12		1
$\text{H}_3\text{C}-\text{CH}_2-\text{CH}_3$	0.078	0.086		1
$\text{H}_3\text{C}-\text{CH}_3$	0.077	0.078		1

^a Average of $F_\phi(C_1-C_2)$ and $F_\phi(C_2-C_3)$. ^b Estimated from $V_0 = 12.9$ kcal/mol and $F_\phi = \frac{9}{2} V_0$. ^c Estimated from $V_0 = 14.2$ kcal/mol. ^d Estimated from $V_0 = 10.0$ kcal/mol. ^e Weighted average of $F_\phi(C_1-C_2)$ and $F_\phi(C_2-C_3)$ for three conformers: 69 % GG(ag), 26 % AG(ga), and 5 % AG(gg). ^f Weighted average of $F_\phi(C_1-C_2)$ and $F_\phi(C_2-C_3)$ for three conformers: 73 % GG, 24 % AG and 3 % AA.

(rad)⁻², respectively, as determined by electron-diffraction works.^{13,14} Although the experimental estimates are quite uncertain (ca. 30 %), the values calculated by the present formula, 0.46 (*P6*) and 0.62 (*P8*), are significantly different from the experimental ones. A rather small value of F_ϕ for *P8* was expected. The stable conformer of *P8* has C_{2v} symmetry¹⁴ corresponding to parallel (1:3) X...X interactions on both sides of the CCC skeleton. The most stable conformer (*GG*) of *P6* has C_2 symmetry¹³ without parallel (1:3) X...X interactions. Therefore the experimental estimates, $F_\phi(P6)$ $F_\phi(P8)$, are reasonable. It is, however, surprising that the calculated F_ϕ values for $\text{X}_2\text{C}-\text{CH}_2-\text{CHX}_2$ and $\text{X}_2\text{C}-\text{CX}_2-\text{CHX}_2$ agree (Table 1) with the experimental ones. The most stable conformer of both molecules possesses one parallel (1:3) X...X interaction.

The limitations pointed out here should be kept in mind. However, for halogenated propanes and related molecules, the most stable conformers usually do not possess parallel (1:3) X...X interactions. It is therefore suggested that the simple formula for F_ϕ is a useful approximation for molecules of the

type Y'YY''C-CZZ'R with Y,Z=H or X (halogen) and R=H,X, -CH₃, -CH₂X, -CHX₂, or -CX₃.

In order to calculate vibrational frequencies, mean amplitudes of vibration, and related quantities for propanes, the torsional interaction force constant ($F_{\phi\phi'} = \partial^2 V / \partial \phi \partial \phi'$) ought to be included in the force field. However, reliable mean amplitudes of vibration may usually be calculated assuming $F_{\phi\phi'} = 0$. (See Refs. 6-8, 10, 12-14). Moreover, the $F_{\phi\phi'}$ values for most halogenated propanes are probably much smaller than the diagonal term (F_ϕ). But a conformer possessing parallel (1:3) X...X interactions may have a $F_{\phi\phi'}$ value which is in magnitude comparable to the F_ϕ value, and most probably negative.^{12,14}

Conformational differences in torsional force constants may be estimated from the simple formula suggested here. For the chlorinated propanes shown in Table 2 the experimental values of the torsional force constants were not available. The calculated values for the heavily chlorinated compounds in Table 2 may deviate as much as 20-30 % from the experimental value, but the average deviation of all F_ϕ values is expected to be ca. 10 %.

Table 2. Diagonal torsional force constants (F_ϕ) predicted for chlorinated propanes ($X=Cl$). (Conformers possessing parallel C-X bonds on the same side of the CCC skeleton were not included.)
 $F_\phi = 0.013N_{HH} + 0.017N_{CH} + 0.032N_{XH} + 0.100N_{XX} + 0.110N_{CX}$

Propane (C ₁ -C ₂ -C ₃)	Conformation	F_ϕ in mdyn Å (rad) ⁻² (C ₁ -C ₂) (C ₂ -C ₃)	
XH ₂ C-CH ₂ -CH ₃	XC-C-C	0.14	0.086
	$\begin{array}{c} X \\ C-C-C \end{array}$	0.20	0.086
XH ₂ C-CHX-CH ₃	$\begin{array}{c} X \\ XC-C-C \end{array}$	0.21	0.12
	$\begin{array}{c} X X \\ C-C-C \end{array}$	0.27	0.12
	$\begin{array}{c} X \\ C-C-C \\ X \end{array}$	0.24	0.12
X ₂ HC-CH ₂ -CH ₃	$\begin{array}{c} X \\ C-C-C \\ X \end{array}$	0.31	0.086
	$\begin{array}{c} XC-C-C \\ X \end{array}$	0.24	0.086
X ₃ C-CH ₂ -CH ₃	$\begin{array}{c} X \\ XC-C-C \\ X \end{array}$	0.35	0.086
X ₂ HC-CH ₃ -CH ₂ X	$\begin{array}{c} X \\ XC-C-C \\ X \end{array}$	0.24	0.20
	$\begin{array}{c} X \\ C-C-CX \\ X \end{array}$	0.31	0.14
	$\begin{array}{c} X \\ XC-C-CX \end{array}$	0.24	0.14
X ₂ C-CHX-CH ₃	$\begin{array}{c} X \\ XC-C-C \\ X \end{array}$	0.32	0.12
	$\begin{array}{c} X X \\ XC-C-C \end{array}$	0.37	0.12
	$\begin{array}{c} X X \\ C-C-C \\ X \end{array}$	0.40	0.12
XH ₂ C-CX ₂ -CH ₃	$\begin{array}{c} X \\ XC-C-C \\ X \end{array}$	0.30	0.16
	$\begin{array}{c} X \\ C-C-C \\ X X \end{array}$	0.32	0.16
X ₃ C-CHX-CH ₃	$\begin{array}{c} X X \\ XC-C-C \\ X \end{array}$	0.48	0.12

Table 2. Continued.

$X_2HC-CHX-CH_2X$	$\begin{array}{c} X \ X \\ C-C-CX \\ X \end{array}$	0.40	0.21
	$\begin{array}{c} X \\ XC-C-CX \\ X \end{array}$	0.32	0.21
	$\begin{array}{c} X \ X \\ XC-C-C \\ X \end{array}$	0.32	0.27
	$\begin{array}{c} X \ X \\ XC-C-CX \\ X \end{array}$	0.37	0.21
	$\begin{array}{c} X \ X \\ XC-C-C \\ X \end{array}$	0.37	0.24
$XH_2C-CX_2-CH_2X$	$\begin{array}{c} X \\ XC-C-CX \\ X \end{array}$	0.30	0.30
	$\begin{array}{c} X \ X \\ C-C-C \\ X \ X \end{array}$	0.32	0.32
	$\begin{array}{c} X \ X \\ XC-C-C \\ X \end{array}$	0.30	0.32
$X_2HC-CH_2-CHX_2$	$\begin{array}{c} X \\ XC-C-CX \\ X \end{array}$	0.24	0.24
$X_2C-CH_2-CH_2X$	$\begin{array}{c} X \\ XC-C-CX \\ X \end{array}$	0.35	0.14
$X_2C-CX_2-CH_2$	$\begin{array}{c} X \ X \\ XC-C-C \\ X \ X \end{array}$	0.62	0.16
$X_2HC-CX_2-CH_2X$	$\begin{array}{c} X \ X \\ C-C-CX \\ X \ X \end{array}$	0.48	0.30
	$\begin{array}{c} X \\ XC-C-CX \\ X \ X \end{array}$	0.46	0.30
	$\begin{array}{c} X \ X \\ XC-C-C \\ X \ X \end{array}$	0.46	0.32
$X_2C-CHX-CH_2X$	$\begin{array}{c} X \\ XC-C-CX \\ X \ X \end{array}$	0.48	0.21
$X_2C-CX_2-CH_2X$	$\begin{array}{c} X \ X \\ XC-C-CX \\ X \ X \end{array}$	0.62	0.30

Using the partial force constants F^*_{BrH} (0.032), F^*_{CBr} (0.130), F^*_{BrBr} (0.160), and the values of F^*_{HH} and F^*_{CH} already given, the F_ϕ values for brominated ethanes and propanes may be estimated, but with less confidence than for the chlorinated compounds.

REFERENCES

1. Moore, W. H., Ching, J. H. C., Warriar, A. V. R. and Krim, S. *Spectrochim. Acta A* 29 (1973) 1847.
2. Cyvin, B. N. and Cyvin, S. J. *Acta Chem. Scand.* 26 (1972) 3943.
3. During, J. R., Sloane, A. E. and Witt, J. D. *J. Phys. Chem.* 76 (1972) 3591.
4. Kveseth, K. *Acta Chem. Scand. A* 28 (1974) 482.
5. Andresen, I. L., Cyvin, S. J., Larsen, B. and Tørset, O. *Acta Chem. Scand.* 25 (1971) 473.
6. Grindheim, S. and Stølevik, R. *Acta Chem. Scand. A* 30 (1976) 625.
7. Farup, P. E. and Stølevik, R. *Acta Chem. Scand. A* 28 (1974) 871.
8. Johnsen, J. P. and Stølevik, R. *Acta Chem. Scand. A* 29 (1975) 457.
9. Allen, G., Brier, P. N. and Lane, G. *Trans. Faraday Soc.* 63 (1967) 824.
10. Grindheim, S. and Stølevik, R. *Acta Chem. Scand. A* 31 (1977) 69.
11. Heatley, F., Allen, G., Hameed, S. and Jones, P. W. *Trans. Faraday Soc.* 68 (1972) 1547.
12. Johnsen, J. P. and Stølevik, R. *Acta Chem. Scand. A* 29 (1975) 201.
13. Fernholt, L. and Stølevik, R. *Acta Chem. Scand. A* 29 (1975) 651.
14. Fernholt, L. and Stølevik, R. *Acta Chem. Scand. A* 28 (1974) 963.

Received December 8, 1976.

The Crystal Structure of 3-Hydroxy-3-isobutyl-2-pyrrolidone-5-carboxylic Acid, Lactam of 4-Hydroxy-4-isobutylglutamic Acid from *Reseda odorata* L.

KAREN KAAS and HILMER SØRENSEN

Chemistry Department, Royal Veterinary and Agricultural University, 40 Thorvaldsensvej, DK-1871 Copenhagen V, Denmark

The relative configuration of 3-hydroxy-3-isobutyl-2-pyrrolidone-5-carboxylic acid has been determined by an X-ray crystal structure analysis. The compound crystallized in space group $P2_12_12_1$ with two molecules in the asymmetric unit. $a = 16.023(3)$ Å, $b = 19.349(7)$ Å, $c = 6.9053(16)$ Å. The structure was solved by direct methods using MULTAN and refined by full-matrix least-squares technique to an R of 0.137 for 645 diffractometer-collected intensities. The absolute configurations of the title compounds were deduced; the configuration of the amino acid and the lactam are 2(*S*),4(*S*) and 3(*S*),5(*S*), respectively.

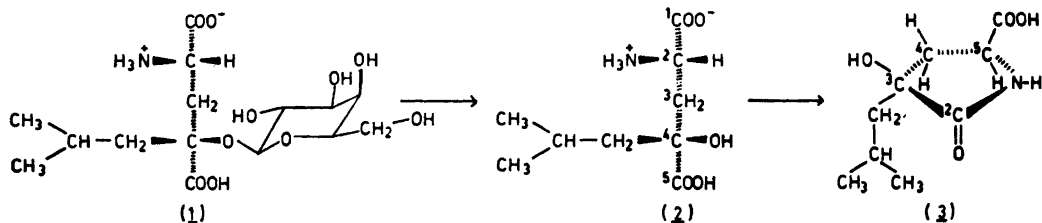
The present structure analysis is part of a series of papers on the 4-substituted glutamic acid derivatives found in nature.^{1,2} From inflorescences of *Reseda odorata* L. 4-(β -D-galactopyranosyloxy)-4-isobutylglutamic acid (*1*) has been isolated in appreciable amounts. Acidic hydrolysis of *1* yields the title compounds 4-hydroxy-4-isobutylglutamic acid (*2*) and 3-hydroxy-3-isobutyl-2-pyrrolidone-5-carboxylic acid (*3*).¹ Recently *2* has been identified as a constituent of *Reseda odorata* L. and the structure has been confirmed by synthesis.³ The con-

figurations of *1*, *2* and *3* have been tentatively proposed on the basis of similarity between ¹H NMR spectra of *2* and the diastereoisomeric 4-hydroxy-4-methylglutamic acids.¹

This paper describes the results obtained from X-ray crystal structure analysis of the lactam *3* produced by acidic hydrolysis of the natural product *1*.

EXPERIMENTAL

The compound used in these investigations was prepared by hydrolysis of the natural product *1*.¹ Most of the crystals from the ether solutions were thin plates. Thicker crystals were composed of several misoriented layers. Even the crystal used for the data collection showed splitting of some reflexions, although its dimensions were only $0.08 \times 0.08 \times 0.43$ mm³. Other recrystallization methods were tried without improvement of the crystal quality. Photographs showed that $h00$ was absent for $h \neq 2n$, $0k0$ for $k \neq 2n$. As all $00l$ reflexions except 002 were absent, it was not possible at this stage to decide whether the space group was $P2_12_12_1$ or $P2_12_12$. Structure solution showed that the first possibility was correct.



Crystal data.

Space group $P2_12_12_1$ (No. 19).
 $a = 16.023(3)$ Å, $b = 19.349(7)$ Å, $c = 6.9053(16)$ Å
 Formula weight 201.22 ($C_9H_{15}NO_4$),
 $Z = 8$, $D_m = 1.25(1)$ g cm $^{-3}$, $D_x = 1.25$ g cm $^{-3}$,
 $V = 2141$ Å 3 ,
 $\mu(\text{MoK}\alpha) = 2.1$ cm $^{-1}$.

The cell dimensions were obtained from least-squares refinement of a series of diffractometer-measured 2θ angles (MoK α , $\lambda = 0.71069$ Å). The density was measured by flotation in a CsCl-solution at 22 °C. $Z = 8$ corresponds to two molecules in the asymmetric unit.

All X-ray data were obtained on a Nonius three-circle automatic diffractometer with graphite-monochromated MoK α radiation. The crystal was mounted on a glass rod and oriented with c along the ϕ -axis of the goniometer. Each reflexion was scanned over a range of 0.6° in both ω and $\theta/2\theta$ scanning mode. Scan speed was 0.3° min $^{-1}$. Background was measured between the axial reflexions and plotted against θ . The background count for each reflexion was interpolated on this curve. A standard reflexion was remeasured after every 25 reflexions. Each of the 1192 independent reflexions in the range $2.5^\circ < \theta < 20.0^\circ$ was measured twice (hkl and $\bar{h}\bar{k}\bar{l}$). The intensities were taken as a sum of

four counts (both ω and $\theta/2\theta$ for each of the symmetry related reflexions) corrected for background. 645 reflexions had intensities greater than 2.5 times their corresponding standard deviations obtained from counting statistics and were considered observed. No absorption correction was applied.

Determination and refinement of the structure.

The structure was solved by direct methods using MULTAN,⁴ which after several attempts gave 24 of the 28 non-hydrogen atoms. Positional and isotropic temperature parameters for the non-hydrogen atoms were refined by full-matrix least-squares technique. For the hydrogen atoms calculated positions were used and isotropic temperature factors were set equal to those of the atoms to which they are bonded. The hydrogen atoms of the hydrogen bonds were placed on the line connecting the bonded atoms. Most of the hydrogen atoms could be detected from a difference electron density map and all hydrogen positions were at points with positive density.

The final R was 0.137 [$R = \sum(|F_o| - |F_c|) / \sum|F_o|$]. (645 reflexions with unit weight were used.) A difference electron density map showed peaks around the non-hydrogen atoms, as if the temperature factors were anisotropic, but all atoms would have the largest value correspond-

Table 1. Final atomic parameters (and e.s.d.'s). Fractional coordinates are $\times 10^3$ and temperature factors Å $^2 \times 10$.

	MOLECULE A				MOLECULE B			
	X	Y	Z	U	X	Y	Z	U
C1	411(2)	603(2)	700(5)	47(9)	20(2)	938(2)	-243(6)	49(10)
C2	230(2)	515(1)	642(4)	24(7)	216(2)	947(1)	-121(5)	31(8)
C3	185(2)	585(1)	680(5)	40(9)	176(2)	895(2)	46(5)	41(9)
C4	259(2)	629(2)	723(5)	53(11)	111(2)	852(1)	-83(5)	37(9)
C5	330(2)	596(2)	637(5)	38(9)	95(2)	900(1)	-259(4)	28(8)
C6	142(2)	604(1)	485(4)	25(8)	236(2)	857(2)	174(6)	55(11)
C7	104(3)	680(2)	476(7)	88(16)	282(3)	797(2)	73(6)	69(12)
C8	37(4)	693(3)	611(10)	183(29)	327(4)	753(3)	232(9)	142(21)
C9	69(4)	682(3)	250(9)	155(24)	340(3)	817(3)	-76(8)	119(19)
N1	305(2)	522(1)	617(4)	29(6)	170(2)	939(1)	-276(4)	39(7)
O1	461(1)	548(1)	719(3)	56(7)	-48(1)	907(1)	-215(3)	54(7)
O2	443(2)	661(1)	753(4)	85(9)	18(1)	1008(1)	-240(4)	65(7)
O3	129(1)	580(1)	839(3)	44(6)	124(1)	944(1)	158(3)	38(6)
O4	187(1)	457(1)	647(3)	44(6)	280(1)	977(1)	-97(3)	36(6)
H(C4)1	267	632	866	52	58	845	-8	37
H(C4)2	250	676	663	53	138	808	-128	37
H(C5)	331	614	500	38	90	871	-376	28
H(C6)1	183	597	377	25	279	889	226	55
H(C6)2	98	569	455	25	207	839	291	55
H(C7)	149	715	494	90	238	767	12	69
H(C8)1	17	741	595	184	358	714	167	140
H(C8)2	-10	660	584	184	369	783	300	140
H(C8)3	58	686	745	184	286	735	326	140
H(C9)1	43	728	222	154	367	775	-133	120
H(C9)2	117	674	158	154	310	843	-180	120
H(C9)3	27	644	230	154	385	847	-18	120
H(N1)	325	491	532	29	186	966	-377	39
H(O1)	518	550	762	56	-102	926	-189	54
H(O3)	79	556	806	44	157	972	242	38

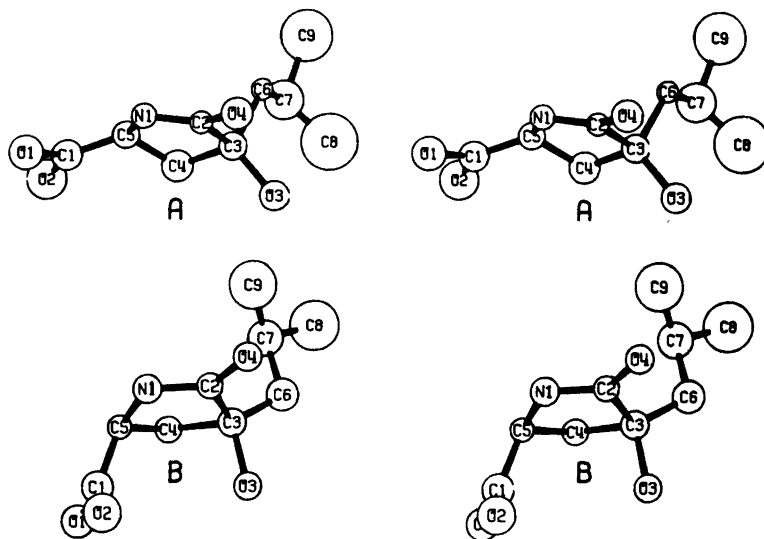


Fig. 1. Stereoscopic drawing of the two crystallographically independent molecules. The hydrogen atoms have been omitted. The thermal ellipsoids enclose 50 % probability. The molecules have been placed individually to allow comparison of the conformations.

ing to vibration in the same direction. The phenomenon is probably due to crystal defects.

The final atomic parameters are listed in Table 1.*

The input tapes for the diffractometer were produced on an IBM 1130 computer by INDIFF.⁵ The remaining calculations were performed on the IBM 370/165 computer at NEUCC, Lundtofte, Denmark. The N.R.C.2. A Picker data reduction programme,⁶ MULTAN,⁴ and the X-RAY System⁷ were used. The drawings were prepared by ORTEP⁸ and the tables by POSTER.⁹

DISCUSSION

The accuracy in the molecular parameters found is low and does not allow a detailed discussion of the structure. The two crystallographically independent molecules named A and B are shown in Fig. 1.

The packing of the molecules in the unit cell is shown in Fig. 2. Six different hydrogen bonds, which involve all NH and OH groups hold the molecules together in double layers perpendicular to *b*, while the non-polar isobutyl groups lay alongside each other. The distances between layers are all greater than the sum of

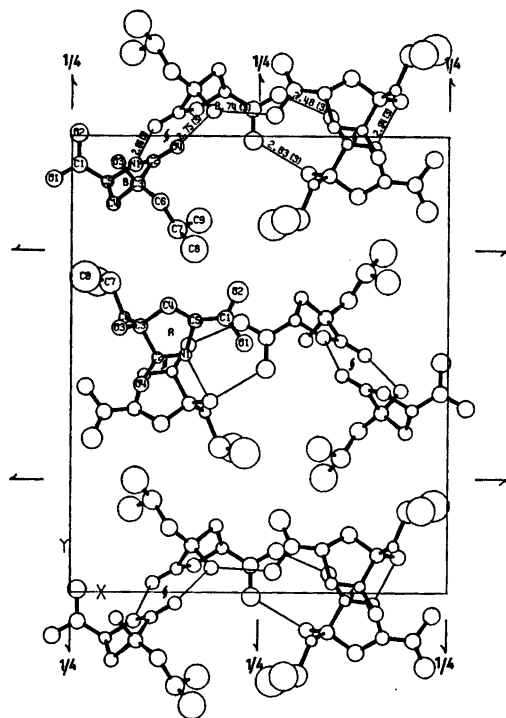


Fig. 2. The crystal structure as seen along the *c* axis. Hydrogen bonds are indicated and their length given.

* Copies of the structure factor table can be obtained from the author on request.

Table 2. Interatomic distances (Å) and angles (°).

DISTANCES			ANGLES		
	A	B		A	B
C1-C5	1.37(5)	1.41(4)	C5-C1-01	121(3)	120(3)
C1-01	1.35(4)	1.26(4)	C5-C1-02	123(3)	122(3)
C1-02	1.28(4)	1.34(4)	01-C1-02	115(3)	118(3)
C2-C3	1.56(4)	1.65(4)	C3-C2-N1	113(2)	106(2)
C2-N1	1.22(4)	1.31(4)	C3-C2-04	119(2)	122(3)
C2-04	1.33(3)	1.19(4)	N1-C2-04	127(3)	131(3)
C3-C4	1.51(5)	1.60(5)	C2-C3-C4	99(2)	100(2)
C3-C6	1.55(4)	1.51(5)	C2-C3-C6	105(2)	117(3)
C3-03	1.42(4)	1.48(4)	C2-C3-03	112(2)	102(2)
C4-C5	1.43(5)	1.56(4)	C4-C3-C6	113(3)	119(3)
C5-N1	1.51(4)	1.42(4)	C4-C3-03	112(3)	105(2)
C6-C7	1.60(5)	1.53(5)	C6-C3-03	114(3)	112(3)
C7-C8	1.45(9)	1.56(7)	C3-C4-C5	107(3)	103(2)
C7-C9	1.65(8)	1.45(7)	C1-C5-C4	125(3)	113(3)
TORSIONAL ANGLES IN THE RING			C1-C5-N1	112(3)	117(3)
N1-C2-C3-C4	-14(3)	11(3)	C4-C5-N1	105(2)	104(2)
C2-C3-C4-C5	22(3)	-23(3)	C3-C6-C7	115(3)	115(3)
C3-C4-C5-N1	-23(3)	29(3)	C6-C7-C8	115(4)	108(4)
C4-C5-N1-C2	14(3)	-25(3)	C6-C7-C9	101(3)	115(3)
C5-N1-C2-C3	0(3)	9(3)	C8-C7-C9	111(5)	110(4)
			C2-N1-C5	111(2)	118(3)

van der Waals radii. The hydrogen bond from the carboxy group in one B molecule to the carbonyl group of an A molecule is rather short, 2.48(3) Å.

The bond lengths and angles together with the torsion angles of the rings are given in Table 2. The rings adopt two different envelope conformations, both with C(4) at the flap of the envelope. The angles between the two planes of the envelope are 25 and -26°, respectively. Consequently, in the molecule A the isobutyl group at C(3) is in axial position, and the C(3)-hydroxy and C(5)-carboxy groups are in equatorial positions. In the molecule B the isobutyl group is in equatorial position and the hydroxy and carboxy groups are in axial positions. The absolute configuration is either 3(*S*),5(*S*) or 3(*R*),5(*R*).

By combination of this result with the knowledge of the 2(*S*)-configuration for 2 the relationship between 3 and 2 reveals that the absolute configuration for 3 is 3(*S*),5(*S*)-3-hydroxy-3-isobutyl-2-pyrrolidone-5-carboxylic acid. Correspondingly 2 has the absolute configuration 2(*S*),4(*S*)-4-hydroxy-4-isobutylglutamic acid and the natural product 1 from *R. odorata* has the configuration 2(*S*),4(*S*)-4-(β-D-galactopyranosyloxy)-4-isobutylglutamic acid. These results differ from the previous tentatively proposed absolute configurations.¹

The previous proposal was made on the basis of comparison of ¹H NMR spectra of 2 and published values for two diastereoisomers of 4-hydroxy-4-methylglutamic acid.¹⁰ The result obtained now raises the question of the validity of this comparison. Another possible explanation for the new result is, however, that the configurations assigned to the diastereoisomeric 4-hydroxy-4-methylglutamic acids should be reversed. Originally 2(*S*),4(*S*) configuration was assigned to optically active 4-hydroxy-4-methylglutamic acid isolated from *Phyllitis scolopendrium* (Aspleniaceae).¹¹ The amino acid was reduced to 4-methylglutamic acid and the configuration assumed to be retained. However, the reduced product was a 9:1 mixture of the two diastereoisomers of 4-methylglutamic acid thus raising doubt on the retention of configuration. The doubt is enhanced since unpublished investigations¹² have demonstrated that both diastereoisomers of 4-hydroxy-4-methylglutamic acid are present in *P. scolopendrium*, and because the rotation reported for the first isolation of 4-hydroxy-4-methylglutamic acid ($[\alpha]_D^{18} - 18.5$ (6 N HCl))¹¹ is different from those later found for both diastereoisomers ($[\alpha]_D^{23} - 8.3$ (0.2 N HCl) and $[\alpha]_D^{23} + 23.2$ (0.2 N HCl)),¹⁰ respectively. Later assignment of configuration to the two diastereoisomers were done on basis of ¹H NMR data and assumptions

about preferred conformations.¹⁰ This method, however, may lead to erroneous results, as the configuration of the diastereoisomers of 3-hydroxy-4-methylglutamic acid which was first proposed on basis of ¹H NMR,¹³ later had to be changed when an X-ray analysis was made.¹⁴

REFERENCES

1. Larsen, P. O., Sørensen, H., Cochran, D. W., Hagaman, E. W. and Wenkert, E. *Phytochemistry* 12 (1973) 1713.
2. Dardenne, G., Casimir, J. and Sørensen, H. *Phytochemistry* 13 (1974) 2195.
3. Kristensen, E. P. and Sørensen, H. *Private communication*.
4. Main, P., Wolfson, M. M., Declercq, I. and Germain, G. *MULTAN, a Computer Programme for the Automatic Solution of Crystal Structures*, Dec. 1974.
5. Sørensen, A. M. *Private communication*.
6. Ahmed, F. R. *N.C.R. 2* revised by Alcock & Sørensen, *World List of Crystallographic Computer Programs*, Utrecht: Oosthoek 1966.
7. Stewart, I. M., Kruger, G. I., Ammon, H. L., Dickenson, C. S. and Hale, C. R. *The X-RAY system*, version of June 1972, Tech. Rep. TR 192, Computer Science Center, University of Maryland, College Park, Maryland.
8. Johnson, C. K. *ORTEP*, Report ORNL-3794, Oak Ridge National Laboratory, Oak Ridge 1965.
9. Kaas, K. *Unpublished*.
10. Alderweireldt, F., Jadot, J., Casimir, J. and Loffet, A. *Biochim. Biophys. Acta* 136 (1967) 89.
11. Blake, J. and Fowden, L. *Biochem. J.* 92 (1964) 136.
12. Meier, L. K. and Sørensen, H. *Private communication*.
13. Dardenne, G. A., Bell, E. A., Nulu, J. R. and Cone, G. *Phytochemistry* 11 (1972) 791.
14. Evrard, G., Durant, F. and Dardenne, G. A. *Cryst. Struct. Commun.* 3 (1974) 65.

Received December 9, 1976.

Hexamethylphosphoramide as Proton Acceptor. Part 2. A Near-infrared Study of Its Heteroassociation with Substituted Phenols

RITVA KUOPIO

School of Pharmacy, University of Helsinki, Fabianinkatu 35, SF-00170 Helsinki 17, Finland

Values of the formation constants K_{11} , frequency shifts $\Delta\nu_{\text{OH}}$ and thermodynamic parameters ΔH , ΔG and ΔS have been determined by near-infrared spectrometry for the hydrogen-bonded acid-base complexes formed between eleven substituted phenols and hexamethylphosphoramide in carbon tetrachloride solution.

The aqueous pK_a values of the substituted phenols vary from 5.3 to 11.7. The values of the spectrometric quantities K_{11} , ΔH and $\Delta\nu_{\text{OH}}$ vary linearly with the acidity of the phenols except where pentahalophenols are the proton donors. In these phenols the OH group seems to be intramolecularly hydrogen bonded to a halogen atom. The + M effect is the obvious reason for the lower values of the spectrometric quantities for the *p*-fluorophenol–hexamethylphosphoramide complex than for the other *p*-halophenol–hexamethylphosphoramide complexes. K_{11} increases more rapidly with the acidity of the proton donor when substituted phenols are the proton donors than when alcohols are the proton donors. The Badger-Bauer relation holds, except for pentahalophenol–hexamethylphosphoramide complexes.

In most cases there are one or more additional hydrogen bonded OH absorption bands, obviously due to the interaction of ν_{OH} (bonded) vibrations with the overtones or combinations of lower frequency vibrations of the proton donor.

In the first part of this series the hydrogen bonding of hexamethylphosphoramide, $[(\text{CH}_3)_2\text{N}]_3\text{PO}$ (HMPA), to ordinary and halogenated alcohols was studied.¹ HMPA was found to be a strong proton acceptor. This property is also evident from Taft's pK_{HB} value.² The base parameter, pK_{HB} , is a measure of the relative strength of the proton acceptor in a hydrogen-bonded complex, and of 117 bases studied, only a few phosphine oxides

have as great pK_{HB} values as HMPA has. Several submaxima were found in the absorption band of the alcohol–HMPA complex when the aqueous pK_a of the alcohol was less than 12.¹

For comparison and also to gain information about the substituent effect, the hydrogen bonding between HMPA and substituted phenols has been studied in the present work. Hexamethylphosphoramide- d_{18} (octadecadeuteriohexamethylphosphoramide, HMPA- d_{18} , $[(\text{CD}_3)_2\text{N}]_3\text{PO}$) has been used in studying the ν_{OH} bands of the complexes in the ν_{CH} region.

EXPERIMENTAL

Chemicals. Hexamethylphosphoramide, hexamethylphosphoramide- d_{18} and carbon tetrachloride were purified as described previously.¹ 2,6-Dimethylphenol (*zur Synthese*, E. Merck AG), 2,6-di-isopropylphenol and 2,6-di-*tert*-butylphenol (Aldrich Chemical Co.) were distilled under vacuum, b.p. 86°C/15 mmHg, 126°C/19 mmHg and 100–101°C/3 mmHg, respectively. *p*-Fluorophenol and pentafluorophenol (*purum*, Fluka AG) were sublimed at atmospheric pressure and dried in a desiccator over P_2O_5 . Pentabromophenol (EGA-Chemie KG) was recrystallized from ethanol and dried in a desiccator over P_2O_5 . *p*-Cresol, *p*-chlorophenol, *p*-bromophenol, pentachlorophenol (*puriss.*, Fluka AG) and phenol and α -naphthol (*pro analysi*, E. Merck AG) were used as received.

Measurements. The near-infrared spectra were recorded on a Beckman DK-2A spectrophotometer. All systems were recorded using the temperatures 0, 15, 25, 40 and 50°C. The concentrations used were about 0.03 M (2,6-di-*tert*-butylphenol) and from 0.0008 to 0.006 M (other phenols), the concentration of hexamethylphosphoramide varying from 0.0005 to 0.3 M depending on the system. The details

Table 1. Spectral data for 1:1 hydrogen-bonded complexes between phenols and HMPA in carbon tetrachloride at 25°C and the pK_a values ⁴⁻⁹ of phenols.

Phenol ^a	K_{11} M ⁻¹	$-\Delta H^\circ$ kJ mol ⁻¹	$-\Delta G^\circ$ kJ mol ⁻¹	$-\Delta S^\circ$ J K ⁻¹ mol ⁻¹	$\Delta\nu_{OH}$ cm ⁻¹	pK_a
1 Phenol	1820	29.9	18.6	37.7	> 464 ^b	9.95
2 <i>p</i> -Cresol	1440	29.9	18.0	40.0	> 460 ^b	10.26
3 α -Naphthol	3200	32.8	20.0	43.1	> 486 ^b	9.34
4 <i>p</i> -BrP	8220	32.9	22.3	35.5	> 496 ^b	9.34
5 <i>p</i> -ClP	8300	33.5	22.3	35.2	> 496 ^b	9.38
6 <i>p</i> -FP	4760	32.3	20.9	38.1	> 478 ^b	9.91
7 PBP	421	24.7	14.9	32.7	> 612 ^b	
8 PCP	1530	26.5	18.2	27.9	> 631 ^b	5.26
9 PFP	26800	35.0	25.2	32.6	> 737 ^b	5.52
10 DMP	126	20.1	12.0	27.2	430	10.63
11 DIPP	88.8	20.3	11.1	30.8	416	11.08
12 DTBP	5.50	12.8	4.23	28.8	444	11.70

^a *p*-BrP = *p*-bromophenol; *p*-ClP = *p*-chlorophenol; *p*-FP = *p*-fluorophenol; PBP = pentabromophenol; PCP = pentachlorophenol; PFP = pentafluorophenol; DMP = 2,6-dimethylphenol; DIPP = 2,6-di-isopropylphenol; DTBP = 2,6-di-*tert*-butylphenol, ^b complex band with several maxima, measured from the first maximum.

of the measuring procedure have been reported earlier.^{3,4}

The K_{11} values were calculated using eqn. (1).³

$$K_{11} = \frac{1 - A/A^\circ}{A/A^\circ [c_B^\circ - c_A^\circ (1 - A/A^\circ)]} \quad (1)$$

c_A° and c_B° are the initial concentrations of the acid and base, respectively, and A° and A are the absorbances at the frequency of the stretching vibration of the free hydroxyl group before and after the complex formation, respectively.

The ΔH values were obtained in the usual way from plots of $\log K_{11}$ against $1/T$ using the method of least squares. The quantities ΔG and ΔS were obtained from eqns. (2) and (3).

$$\Delta G = -RT \ln K_{11} \quad (2)$$

$$\Delta S = (\Delta H - \Delta G)/T \quad (3)$$

The IR spectra were recorded with Perkin Elmer 621 and Perkin Elmer 557 spectrometers under the same conditions as before.¹

The $\Delta\nu_{OH}$ values are estimated to be accurate within ± 5 cm⁻¹, ΔH and ΔG values within ± 2 kJ mol⁻¹, ΔS values within ± 2 J K⁻¹ mol⁻¹ and K_{11} values within 10%.

The non-SI units used were 1 M = 1 mol dm⁻³; 1 mmHg = 133.322 Pa.

RESULTS AND DISCUSSION

The experimental data obtained are presented in Table 1, which also contains the literature values of the aqueous pK_a 's of substituted

phenols. The symbols used for the phenols are explained in a footnote to Table 1.

Variation of the spectrometric quantities with the acidity of phenols. The dependence of $\log K_{11}$ on the acidity is linear except for the pentahalophenol-HMPA complexes, whose K_{11} values are much smaller than expected from their pK_a values (ca. 5) (Fig. 1). K_{11} increases more rapidly with the acidity of the proton donor in substituted phenol-HMPA complexes than in alcohol-HMPA complexes.¹

There are several submaxima in the hydrogen bonded ν_{OH} bands of phenols except 2,6-dialkylphenols. The frequency shifts $\Delta\nu_{OH}$ tabulated in Table 1 are measured from the maximum band nearest the free ν_{OH} band.

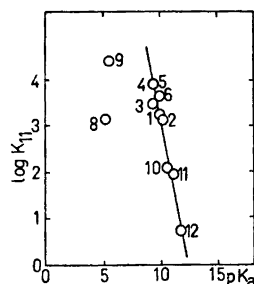


Fig. 1. The plot of $\log K_{11}$ against the pK_a of the phenol for the phenol-HMPA complexes at 25°C.

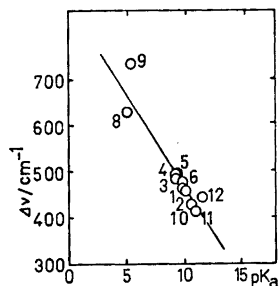


Fig. 2. The plot of $\Delta\nu\text{OH}$ against the pK_a of the phenol for the phenol-HMPA complexes. Temperature ambient. For the $\Delta\nu\text{OH}$ values of the points 8 and 9, see the text.

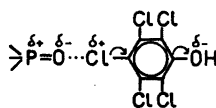
In the case of pentahalophenols the hydrogen bonded νOH bands are very broad, and the $\Delta\nu\text{OH}$ values are therefore only minimum values. In the cases of other phenols the sub-maxima do not seem to shift the top of the bonded νOH band, and $\Delta\nu\text{OH}$ can be regarded as "true" ones (cf. Fig. 4).

The variation of $\Delta\nu\text{OH}$ with the acidity of the proton donor is similar for substituted phenol-HMPA and the halogenated alcohol-HMPA complexes (Fig. 2). The $\Delta\nu\text{OH}$ values of the pentahalophenol-HMPA complexes are not "true" ones, because of the reasons mentioned above and of the intramolecular hydrogen bond between the OH group and the halogen of pentahalophenols. The intramolecular $\Delta\nu\text{OH}$ values of *o*-bromo-, *o*-chloro- and *o*-fluorophenols in CCl_4 are 78, 61 and 18 cm^{-1} , respectively.¹¹ The single νOH stretching vibration bands of pentahalophenols, at 3492 (PBP), 3521 (PCP) and 3577 cm^{-1} (PFP), are due to intramolecular hydrogen bonds. By comparison, the frequencies of νOH for *p*-halophenols are 3610 (*p*-BrP), 3614 (*p*-ClP) and 3618 cm^{-1} (*p*-FP).

In view of the intramolecular hydrogen bonds in pentahalophenols, the great decrease in the equilibrium constant and enthalpy is not surprising. Such a decrease is found also in the *o*-methoxyphenol-dimethyl sulfoxide complex compared with the phenol-dimethyl sulfoxide complex, $\Delta\nu\text{OH}$ being about the same in both cases.¹²

It has been maintained that the anomalies in the equilibrium constants of pentachlorophenol-phosphoryl compound complexes com-

pared with phenol-phosphoryl compound complexes are due to a dipole-dipole association:¹³ Scheme 1.



This kind of association may reduce the acidity of the proton donor or reduce the concentration of the proton acceptor. The solvation of a hydrogen-bonded complex by proton acceptor may also become more specific. On the basis of this study it is impossible to say whether this kind of association exists between HMPA, the P=O bond of which has 50 % ionic character.^{14,15} and pentahalophenols. There are no anomalies in K_{11} values when *p*-halophenols are the proton donors, although these phenols, too, could take part in such a dipole-dipole association.

The mesomeric effect (+*M*) in *p*-halophenols weakens the acidity by the same kind of mechanism as in dipole-dipole association. This acidity-weakening effect is reflected in both the K_{11} and $\Delta\nu\text{OH}$ values. The +*M* effect diminishes in the order $\text{F} > \text{Cl} > \text{Br}$, the effect of chlorine and bromine being almost the same.¹⁶ Thus the *p*-FP-HMPA complex has the smallest K_{11} and $\Delta\nu\text{OH}$ values of the three *p*-halophenol-HMPA complexes.

A steric effect has often been given as the reason for the small values of spectrometric

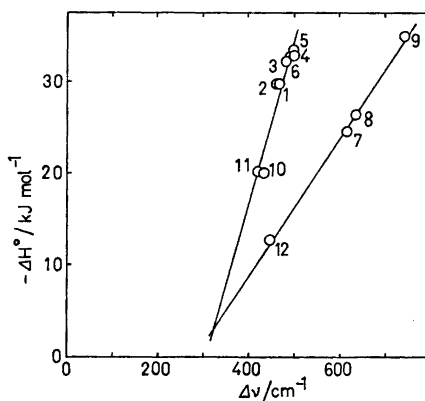


Fig. 3. The plot of $-\Delta H^\circ$ against $\Delta\nu\text{OH}$ for the phenol-HMPA complexes. For the $\Delta\nu\text{OH}$ values of the points 7, 8 and 9, see the text.

quantities obtained when 2,6-di-*tert*-butylphenol hydrogen bonds to proton acceptors.^{17,18} In this study no clear evidence of steric effect is seen. The $\Delta\nu\text{OH}$ value of the DTBP-HMPA complex is rather large compared with the pK_a or ΔH and K_{11} values (Figs. 1–3). But since $\Delta\nu\text{OH}$, on the one hand, and K_{11} or ΔH , on the other, measure different energetic changes in a hydrogen bonded system,¹⁹ it is not surprising that the variations in $\Delta\nu\text{OH}$ do not always correlate with the variations in K_{11} or ΔH .

The Badger-Bauer relation. The more the Badger-Bauer relation, *i.e.*, the linear dependence between ΔH and $\Delta\nu\text{OH}$, has been studied, the more convincing it has become that this relation holds only for a limited number of systems.^{20–23} In this study, where the same proton acceptor is used throughout, the Badger-Bauer relation holds for all but pentahalophenol-HMPA complexes (Fig. 3). The exceptional behaviour of pentahalophenol-HMPA complexes is not surprising in view of the small K_{11} and ΔH values mentioned earlier. It has been stated that in systems, where the proton acceptor is not varied, the Badger-Bauer relation will approximate the truth more closely than in systems where the proton donor is not varied.²³ In the latter case the line should even have a zero intercept.²⁰ When HMPA is the proton acceptor the intercepts are about -55 kJ mol^{-1} (with substituted phenols), 10 kJ mol^{-1} (with halogenated alcohols) and -19 kJ mol^{-1} (with ordinary alcohols), the slope being nearly the same for ordinary alcohol-HMPA and substituted phenol-HMPA complexes and less steep for halogenated alcohol-HMPA complexes.¹

Stymne and coauthors²² found it more satisfactory to plot ΔG than ΔH against $\Delta\nu\text{OH}$, owing to the higher accuracy. In this study, however, the plots are similar.

The double-scale enthalpy equation. The empirical double-scale enthalpy equation $-\Delta H = E_A E_B + C_A C_B$ is useful in predicting the enthalpies of hydrogen bond formation.^{24–27} The meanings of the products $E_A E_B$ and $C_A C_B$ have been explained previously.¹ At present, the parameters E_A and C_A are available only for a few of the phenols studied in this paper.

Table 2 shows the experimental enthalpy values and those calculated from the double-

Table 2. The literature values of the parameters E_A and C_A for phenols, and experimental and calculated (see text) enthalpy values of the phenol-HMPA complexes. The E_B and C_B values of HMPA are 1.52 and 3.55, respectively.

Phenol	E_A	C_A	$-\Delta H^{\circ}_{\text{calc}}$ kJ mol ⁻¹	$-\Delta H^{\circ}_{\text{exp}}$ kJ mol ⁻¹
Phenol	4.33	0.442	34.1	29.9
<i>p</i> -Cresol	4.18	0.404	32.6	29.9
<i>p</i> -BrP	4.34	0.478	34.7	32.9
<i>p</i> -ClP	4.34	0.478	34.7	33.5
<i>p</i> -FP	4.17	0.446	33.1	32.3

scale enthalpy equation. The parameters E_A , E_B , C_A and C_B give the $-\Delta H$ values in the unit kcal mol⁻¹. The agreement between the calculated and experimental enthalpy values is satisfactory for all systems studied.

The form of the hydrogen-bonded complex absorption band. It was found earlier¹ that when HMPA hydrogen bonds to alcohols with pK_a smaller than 12, or to phenol, the νOH absorption band of the complex displays several submaxima. It has been proposed that these are due to Fermi resonance between $\nu\text{OH}(\text{bonded})$ and some combination vibrations of the proton donor.^{28,29} Except for 2,6-dialkylphenol-HMPA complexes, the complex absorption bands of systems studied in this work also display several submaxima. $\Delta\nu\text{OH}$ is therefore measured from the maximum $\nu\text{OH}(\text{bonded})$ band nearest the free νOH band.

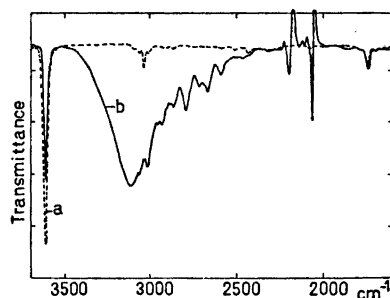


Fig. 4. Illustrative spectra: *a*, for *p*-ClP; and *b*, for the system *p*-ClP-HMPA- d_{18} . Solvent CCl_4 , temperature ambient, 10 mm cells with NaCl windows. Concentrations: *a*, 0.00344 M *p*-ClP (reference CCl_4); *b*, 0.00344 M *p*-ClP + 0.00226 M HMPA- d_{18} (reference 0.00226 M HMPA- d_{18}).

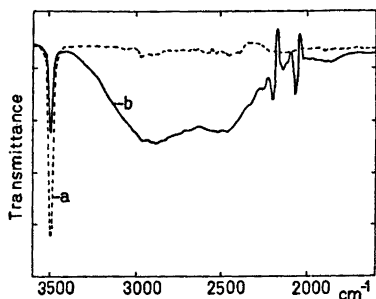


Fig. 5a. Illustrative spectra: *a*, for PBP; and *b*, for the system PBP–HMPA-*d*₁₈. Solvent CCl₄, temperature ambient, 5 mm cells with KBr windows. Concentrations: *a*, 0.00770 M PBP (reference CCl₄); *b*, 0.00770 M PBP + 0.0138 M HMPA-*d*₁₈ (reference 0.0138 M HMPA-*d*₁₈).

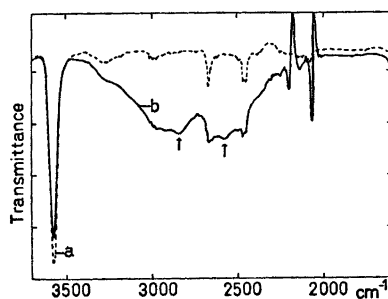


Fig. 5b. Illustrative spectra: *a*, for PFP; and *b*, for the system PFP–HMPA-*d*₁₈. Solvent CCl₄, temperature ambient, 5 mm cells with KBr windows. Concentrations: *a*, 0.00848 M PFP (reference CCl₄); *b*, 0.00848 M PFP + 0.00271 M HMPA-*d*₁₈ (reference 0.00271 M HMPA-*d*₁₈).

The contours of the absorption bands of the *p*-halophenol–HMPA complexes resemble those of the corresponding phenol complex²⁹ in the sense that there are six to nine rather sharp submaxima in both cases (Fig. 4). The negative absorptions in the ν CD vibration area are due to ν CD bands.⁵ On the other hand, the absorption bands of the pentahalophenol–HMPA complexes display only two maxima, the bands being very broad (see Figs. 5a and 5b). An examination of the contour of the complex band of the PFP–HMPA complex is complicated by the absorptions of PFP itself. It is obvious, however, that also in this case there are only two maxima due to hydrogen bonding, the minimum being much lower than

for other pentahalophenol–HMPA complexes. The band contours of pentahalophenol–HMPA complexes resemble those found for pentahalophenol–pyridine and pentahalophenol–triphenylphosphine oxide complexes.⁹ The minimum of the complex absorption band seems to be dependent only on the proton donor. As in the case of phenol,^{28,29} it is obvious that only the vibrations of the proton donor affect the band contour of the complex.

The absorption band of the α -naphthol–HMPA complex consists of many very small and sharp submaxima (Fig. 6). In the case of phenol, ν CC alone or ν CC with δ OH are found to participate in Fermi resonance with the complex absorption band. Thus the large number of C–C vibrations is probably one reason for the presence of many small submaxima in the α -naphthol–HMPA complex band. Although there exist detailed studies on the spectra of some of the substituted phenols studied here (e.g. Refs. 30–32), more work is needed to determine which vibrations are participating in Fermi resonance with the complex absorption bands, or to find other possible reasons for the submaxima of the absorption bands.

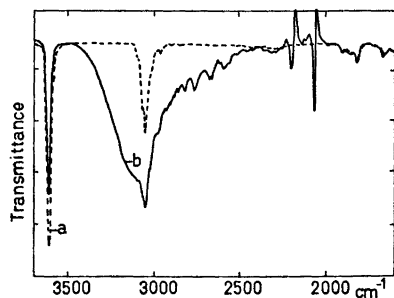


Fig. 6. Illustrative spectra: *a*, for α -naphthol; and *b*, for the system α -naphthol–HMPA-*d*₁₈. Solvent CCl₄, temperature ambient, 10 mm cells with NaCl windows. Concentrations: *a*, 0.00391 M α -naphthol (reference CCl₄); *b*, 0.00391 M α -naphthol + 0.00226 M HMPA-*d*₁₈ (reference 0.00226 M HMPA-*d*₁₈).

Acknowledgements. The author gratefully acknowledges financial support from Jenny and Antti Wihuri Foundation and the Finnish Cultural Foundation.

REFERENCES

1. Kuopio, R., Kivinen, A. and Murto, J. *Acta Chem. Scand. A* 30 (1976) 1.
2. Taft, R. W., Gurka, D., Joris, L., Schleyer, P. von R. and Rakshys, J. W. *J. Am. Chem. Soc.* 91 (1969) 4801.
3. Kivinen, A. and Murto, J. *Suom. Kemistil. B* 40 (1967) 6.
4. Kivinen, A., Murto, J. and Kilpi, L. *Suom. Kemistil. B* 40 (1967) 301.
5. Clotman, D., Van Lerberghe, D. and Zeegers-Huyskens, T. *Spectrochim. Acta A* 26 (1970) 1621.
6. Weast, R. C., Ed., *Handbook of Chemistry and Physics*, 51st Ed., The Chemical Rubber Co., Ohio 1970-1971.
7. Ibbitson, D. A. and Sandall, J. P. B. *J. Chem. Soc.* (1964) 4547.
8. Zeegers-Huyskens, T. *Spectrochim. Acta* 21 (1965) 221.
9. Gramstad, T. and Van Binst, G. *Spectrochim. Acta* 22 (1966) 1681.
10. Nikiforov, G. A. and Ershov, V. V. *Russ. Chem. Rev.* 39 (1970) 644.
11. Baker, A. W. and Shulgin, A. T. *J. Am. Chem. Soc.* 80 (1958) 5358.
12. Spencer, J. N., Robertson, K. S. and Quick, E. E. *J. Phys. Chem.* 78 (1974) 2236.
13. Gramstad, T. *Spectrochim. Acta* 19 (1963) 1363.
14. Bell, J. V., Heisler, J., Tannenbaum, H. and Goldenson, J. *J. Am. Chem. Soc.* 76 (1954) 5185.
15. Larson, L. *Sven. Kem. Tidskr.* 71 (1959) 336.
16. Ingold, C. *Structure and Mechanism in Organic Chemistry*, 2nd Ed., G. Bell and Sons Ltd., London 1969, Chapter XIV.
17. Sousa Lopes, M. C. and Thompson, H. W. *Spectrochim. Acta A* 24 (1968) 1367.
18. Bellamy, L. J., Eglinton, G. and Morman, J. F. *J. Chem. Soc.* (1961) 4762.
19. Lutskii, A. E. *Zh. Strukt. Khim.* 13 (1972) 534.
20. Drago, R. S., O'Bryan, N. and Vogel, G. C. *J. Am. Chem. Soc.* 92 (1970) 3924.
21. Arnett, E. M., Mitchell, E. J. and Murty, T. S. S. R. *J. Am. Chem. Soc.* 96 (1974) 3875.
22. Stymne, B., Stymne, H. and Wettermark, G. *J. Am. Chem. Soc.* 95 (1973) 3490.
23. Rao, C. N. R., Dwivedi, P. C., Ratajczak, H. and Orville-Thomas, W. J. *J. Chem. Soc. Faraday Trans. 2*, 71 (1975) 955.
24. Drago, R. S. and Wayland, B. B. *J. Am. Chem. Soc.* 87 (1965) 3571.
25. Drago, R. S., Vogel, G. C. and Needham, T. E. *J. Am. Chem. Soc.* 93 (1971) 6014.
26. Guidry, R. M. and Drago, R. S. *J. Am. Chem. Soc.* 95 (1973) 759.
27. Slejko, F. L. and Drago, R. S. *J. Am. Chem. Soc.* 95 (1973) 6935.
28. Hall, A. and Wood, J. L. *Spectrochim. Acta A* 23 (1967) 1257.
29. Kivinen, A., Murto, J. and Kuopio, R. *Finn. Chem. Lett.* (1974) 211.
30. Cummings, D. L. and Wood, J. L. *J. Mol. Struct.* 20 (1974) 1.
31. Green, J. H. S., Harrison, D. J. and Kynaston, W. *Spectrochim. Acta A* 27 (1971) 2199.
32. Green, J. H. S., Harrison, D. J. and Stockley, C. P. *J. Mol. Struct.* 33 (1976) 307.

Received December 14, 1976.

A Neutron Diffraction Study of the Crystal Structure of Deuterated Ammonium Tetrachloropalladate(II) at Low and Ambient Temperatures

F. KREBS LARSEN^a and R. W. BERG^b

^a Department of Inorganic Chemistry, Aarhus University, DK-8000 Aarhus C, Denmark and

^b Chemistry Department A, Technical University of Denmark, DK-2800 Lyngby, Denmark

The crystal structure of deuterated ammonium tetrachloropalladate at 125 and 295 K has been studied by neutron diffraction analysis. The results confirm the previously reported X-ray structure; at both temperatures the structure is best described in the tetragonal space group $P4/mmm$. Lattice parameters are $a=b=7.20(1)$ Å, $c=4.21(1)$ Å at 125 K and $a=b=7.22(1)$ Å, $c=4.24(1)$ Å at 295 K. $Z=1$. Full matrix least squares refinements on F^2 converged at $R(F^2, 125\text{ K})=5.2\%$ and $R(F^2, 295\text{ K})=7.7\%$. The $[\text{PdCl}_4]^{2-}$ ions are square planar with Pd—Cl bond lengths of 2.314(4) Å. Deuterium atoms are at both temperatures disordered, corresponding to two equally probable orientations of the ammonium ion with two identical sets of hydrogen bonds N—D...Cl; *i.e.* the ammonium ions in $(\text{ND}_4)_2[\text{PdCl}_4]$ are not freely rotating neither at 125 nor at 295 K. The possibilities of structural distortions at low temperature, as suggested by Adams and Berg from interpretation of low-temperature far infrared spectra, were not substantiated by refinement in space groups less symmetric than $P4/mmm$. It is concluded that if such distortions do occur they must be highly time or space dependent not to appear in the diffraction experiment.

The structural chemistry of palladium(II) and platinum(II) is dominated by the square planar coordination and very few exceptions with minor distortions are known. It was recently suggested by Adams and Berg¹ that $(\text{NH}_4)_2[\text{PdCl}_4]$ should be one such exception according to their interpretation of the low-temperature far infrared spectra of $A_2[\text{PdCl}_4]$ and $A_2[\text{PtCl}_4]$ with $A=\text{K}, \text{NH}_4$ or ND_4 . They had difficulties in interpreting the spectra on the

basis of the known room temperature structures.²⁻⁴ Adams and Berg derived several kinds of lattice distortions which might occur at low temperatures and which might explain the spectra. Since the most pronounced spectral changes on cooling were found in $(\text{NH}_4)_2[\text{PdCl}_4]$, we felt it of interest to investigate the room and low-temperature crystal structure of $(\text{ND}_4)_2[\text{PdCl}_4]$.

EXPERIMENTAL

Crystals of $(\text{ND}_4)_2[\text{PdCl}_4]$ were obtained by repeated re-crystallization of $(\text{NH}_4)_2[\text{PdCl}_4]$ ¹ in heavy water in a desiccator over dry silica gel. The single crystal used for data collection had a volume of 7.2 mm³ ($a \times b \times c \approx 1.6 \times 0.9 \times 5.0$ mm) and was mounted on a Hilger-Ferranti four-circle diffractometer at the Danish Atomic Energy Commission Research Establishment, Risø. The (002) reflection from a Be monochromator crystal provided an incident neutron beam of wavelength 1.070 Å. Data collection was carried out at low temperature, 125 K, achieved in a stream of cold nitrogen gas⁵ and at ambient temperature, 295 K. A neutron structure factor calculation based upon the previously determined X-ray structure^{2,3} was used to select expected stronger reflections for data collection. Bragg intensities were measured with a BF_3 detector using ω -step scan technique. The intensities were integrated in steps of 0.04° over a scan width $\nu=2.0^\circ \text{tg } \theta + 2.4^\circ$. A total of 264 reflections at 125 K and 317 reflections at 295 K were collected within a maximum value of $\sin \theta/\lambda=0.855$. The integrated intensities were evaluated by a method⁶ which divides the step-scanned profile into peak and background in such a way that $\sigma_{\text{count}}(I)/I$ is minimized, where I is the

integrated intensity and $\sigma_{\text{count}}(I)$ its estimated standard deviation based on counting statistics. Two standard reflections (040) and (002) were measured for every 18 reflections and showed an increase in intensity amounting to 1 % over the data collection period both at low and room temperatures. Intensities were corrected for this long term trend and were also corrected for absorption, at first using the linear absorption coefficient $\mu = 0.504 \text{ cm}^{-1}$ calculated for $(\text{ND}_4)_2[\text{PdCl}_4]$ from tabulated mass absorption coefficients and incoherent scattering cross sections,⁷ but later recalculated to $\mu = 0.801 \text{ cm}^{-1}$, when it became evident that deuteration was only partial. The incoherent scattering cross section for the hydrogen nucleus was given the value of 40 barn. The intensities were reduced to squared structure factors, $F_{hkl, \text{obs}}^2$ by application of the inverse Lorentz factor, $\sin 2\theta_{hkl}$. Symmetry related reflections and remeasurements were averaged giving 163 and 169 unrelated structure factors in the low temperature and room temperature data set, respectively. The corresponding internal agreement factors, $R_{\text{int}}(F_{\text{obs}}^2) = \sum |F_{\text{obs}}^2 - \langle F_{\text{obs}}^2 \rangle| / \sum F_{\text{obs}}^2$ were 0.036 and 0.014. In the refinements scattering lengths for Cl and N were those of the Neutron Diffraction Commission,⁸ while for Pd and D they were included as parameters. The resulting values, $b(\text{Pd}, 125 \text{ K}) = 0.51(2) \times 10^{-12} \text{ cm}$ and $b(\text{Pd}, 295 \text{ K}) = 0.51(3) \times 10^{-12} \text{ cm}$ are just significantly different from the tabulated⁸ value of $0.60 \times 10^{-12} \text{ cm}$. For deuterium, $b(\text{D}, 125 \text{ K}) = 0.466(7) \times 10^{-12} \text{ cm}$ and $b(\text{D}, 295 \text{ K}) = 0.428(12) \times 10^{-12} \text{ cm}$ is interpreted as due to partial deuteration of the sample crystal. The degree of deuteration is calculated to a value of 79(1) % using $b(\text{D}) = 0.6672 \times 10^{-12} \text{ cm}$ and $b(\text{H}) = -0.374 \times 10^{-12} \text{ cm}$.

X-Ray film exposures of a crystal cooled by a cryotip mounted on a precession camera

indicated no phase changes as low as 90 K, and no doubling of the tetragonal a axis was observed.

CRYSTAL DATA

$(\text{ND}_4)_2[\text{PdCl}_4]$. M.W. = 292.34 g/mol. Tetragonal. Space group $P4/mmm$ (D_{4h}^{19} , No. 123). $a = b = 7.20(1) \text{ \AA}$ and $c = 4.21(1) \text{ \AA}$ at 125 K, and $a = b = 7.22(1) \text{ \AA}$ and $c = 4.24(1) \text{ \AA}$ at 295 K. $V(125 \text{ K}) = 218.25 \text{ \AA}^3$. $V(295 \text{ K}) = 221.02 \text{ \AA}^3$. $Z = 1$. $D_c(295 \text{ K}) = 2.196 \text{ g/cm}^3$, $D_o = 2.1 \text{ g/cm}^3$ (for the hydrogen compound).³

RESULTS AND DISCUSSION

The structure of the compound $(\text{NH}_4)_2[\text{PdCl}_4]$ was previously^{2,3} solved by means of X-ray film data and refined in space group $P4/mmm$ to give Pd in position a (0,0,0); N in e ($0, \frac{1}{2}, \frac{1}{2}$) and Cl in j ($x, x, 0$) with $x \approx 0.23$.

A difference Fourier map based on the observed neutron structure factors and those calculated from the above structural information showed — for both temperatures — just one predominant peak in the asymmetric unit. The peak is at a general position almost on the line of connection between N and Cl, with distances $\sim 1.00 \text{ \AA}$ from N and $\sim 2.32 \text{ \AA}$ from Cl. The peak is therefore suitable for accommodation of D, but the 16-fold degeneracy of the general position infers fractional occupation (disorder).

Full matrix least-squares refinement of the structure was carried to convergence in space

Table 1. Atomic coordinates expressed as fraction of the cell edges and thermal parameters in $\text{\AA}^2 \times 10^3$. Estimated standard deviations in units of least significant digit are given in parentheses. The temperature factor is of the form $\exp[-2\pi^2(\sum_i \sum_j h_i h_j a_i^* a_j^* U_{ij})]$.

	x/a	y/b	z/c	U_{11}	U_{22}	U_{33}	U_{12}	U_{13}	U_{23}
125 K; $R(F^2) = \sum F_o^2 - k F_c^2 / \sum F_o^2 = 5.2 \%$ (k = scaling multiplier)									
Pd	0.0000	0.0000	0.0000	18(5)	18	15(3)	0	0	0
Cl	0.2266(3)	0.2266	0.0000	25(1)	25	35(1)	-1(1)	0	0
N	0.0000	0.5000	0.5000	36(2)	26(1)	30(1)	0	0	0
D	0.0811(7)	0.4194(6)	0.3581(7)	55(3)	41(2)	45(2)	11(1)	12(2)	-10(2)
295 K; $R(F^2) = 7.7 \%$									
Pd	0.0000	0.0000	0.0000	25(9)	25	26(6)	0	0	0
Cl	0.2266(5)	0.2266	0.0000	34(2)	34	50(2)	-6(1)	0	0
N	0.0000	0.5000	0.5000	57(3)	33(2)	35(2)	0	0	0
D	0.0770(15)	0.4231(14)	0.3601(12)	82(8)	60(6)	69(3)	15(2)	18(5)	-11(4)

Table 2. Distances (Å) and angles (°) for $(ND_4)_2[PdCl_4]$ as refined in space group $P4/mmm$. Distances corrected for riding thermal motion are quoted in italics.

	125 K	295 K
Pd—Cl	2.307(5)	2.307(7)
	<i>2.313(5)</i>	<i>2.315(7)</i>
N—D	1.017(4)	0.980(8)
	<i>1.044(4)</i>	<i>1.023(9)</i>
D—Cl	2.302(5)	2.337(8)
N—Cl	3.312(4)	3.312(4)
Cl—Pd—Cl	90.00	90.00
D—N—D	108.1(4)	106.1(9)
N—D—Cl	171.9(4)	173.0(1.0)

group $P4/mmm$ as well as in the less symmetric space groups suggested by Adams and Berg.¹ A scale factor, an isotropic extinction parameter,⁹ positional and anisotropic thermal parameters were refined by minimizing the expression $\sum w(F_o^2 - F_c^2)^2$, where $w = 1/\sigma^2(F^2)$. For both the low and the room temperature data set there was no significant improvement of fit by

lowering the $P4/mmm-D_{4h}^1$ symmetry and no significant change of atomic positional parameters for nonhydrogen atoms, which means that in all space groups and at both temperatures the $[PdCl_4]$ configuration appears planar within the experimental uncertainty. Final parameters and agreement factors are given in Table 1 and bonded distances and angles in Table 2. A list of structure factors can be obtained upon request. Extinction corrections exceeded 10 % for only two reflections.

The molecular packing and the atomic thermal motion at 125 and 295 K is depicted in Fig. 1 as two stereo pairs of drawings. It is conceivable that the libration of the ammonium ions especially at 295 K are so great that the harmonic approximation applied in the description of the thermal motion is invalidated, which may explain the poorer agreement factor for the presumably better 295 K data set.

The square planar chlorine configuration around Pd makes disorder very plausible. The disorder model of space group $P4/mmm$

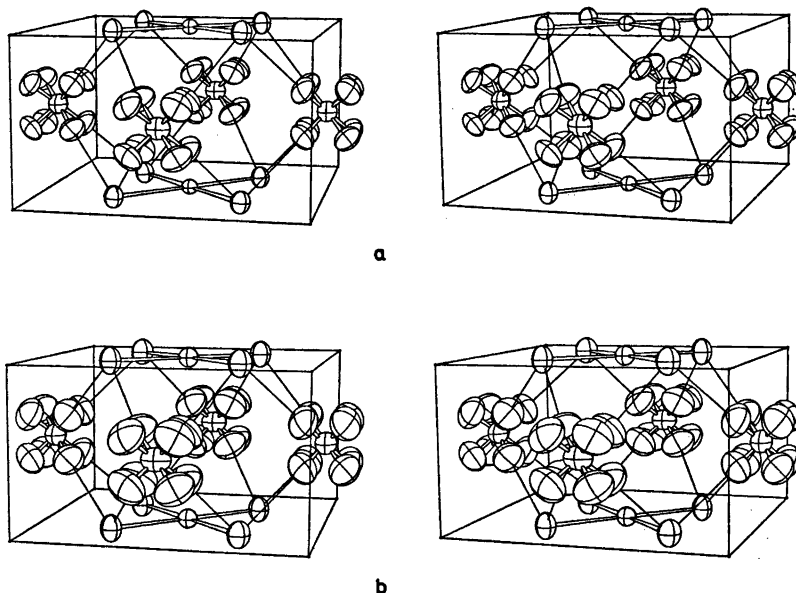


Fig. 1. Stereoscopic view of the molecular packing. The ammonium ion disorder appears as an arrangement of eight deuterium atoms around each nitrogen atom. N—D...Cl hydrogen bonds are shown as single line bonds, while N—D and Pd—Cl bonds are shown as double line bonds. (a) corresponds to the 125 K structure, and (b) to the 295 K structure. 50 % probability ellipsoids are shown.

corresponds to occupation 0.5 of two equally probable orientations of the ammonium ion creating two identical sets of hydrogen bonds $N-D\cdots Cl$ shown as single line bonds in Fig. 1. The hypothesis of disorder was tested in space group $P422$, which allows full occupation of either of the two above-mentioned orientations, and for either model the refinement was poorer at a highly significant level (at 125 K: $R(F)_{D_1}=0.077$, $R(F)_{D_2}=0.075$ as compared to $R(F)_{D_1+D_2}=0.040$ and at 295 K: $R(F)_{D_1}=0.105$, $R(F)_{D_2}=0.123$ as compared to $R(F)_{D_1+D_2}=0.074$). Due to the long counting times involved in diffraction methods, we cannot unambiguously state whether the disorder is static or dynamic, but should it be dynamic the ammonium groups spend little time in the transition phase as evidenced by a smooth final difference Fourier map. Thus, the ammonium ions are not *freely* rotating even at 295 K. This conclusion was also obtained by infrared spectroscopy on NH_3D^+ isotopically diluted crystals of $(NH_4)_2[PdCl_4]$.¹⁰ It seems as if the $N-H\cdots Cl$ hydrogen bonds effectively hinder the rotation. However, our results do not allow a statement on the possibility of any weak correlation between the orientation of neighbouring ammonium ions, which in an instantaneous picture might correspond to the structure having locally adapted to one of the space groups favoured by Adams and Berg.¹ As an example, space group $P42m$ might be the adequate description of a low temperature instantaneous symmetry in ordered microdomains, in which fluctuations in time or space may average to give the overall symmetry $P4/mmm$. This difference in the symmetry deducible from diffraction and spectroscopic techniques is not a unique situation in molecular physics; cf. e.g., the situation in $(NH_4)Br$.^{11,12}

It is in principle possible to test the above speculations on the instantaneous symmetry by checking $(NH_4)_2[PdCl_4]$ crystals for second harmonic generation. If such an effect can be demonstrated at low temperatures, the centre of symmetry is absent.¹³ The experiment is, however impeded¹⁴ by the dark colour of the compound.

REFERENCES

1. Adams, D. M. and Berg, R. W. *J. Chem. Soc. Dalton Trans.* (1976) 52.
2. Dickinson, R. G. *J. Am. Chem. Soc.* **44** (1922) 2404.
3. Bell, J. D., Hall, D. and Waters, T. N. *Acta Crystallogr.* **21** (1966) 440.
4. Mais, R. H. B., Owston, P. G. and Wood, A. M. *Acta Crystallogr.* **B 28** (1972) 393.
5. Merisalo, M., Nielsen, M. H. and Henriksen, K. *Risø Report Series No. 279* (1972).
6. Lehmann, M. S. and Larsen, F. K. *Acta Crystallogr.* **A 30** (1974) 580.
7. *International Tables for X-Ray Crystallography*, Kynoch Press, Birmingham 1968, Vol. III.
8. Bacon, G. E. (for The Neutron Diffraction Commission), *Acta Crystallogr.* **A 28** (1972) 357.
9. Becker, P. J. and Coppens, P. *Acta Crystallogr.* **A 31** (1974) 417.
10. Oxtun, I. A., Knop, O. and Falk, M. *J. Phys. Chem.* **80** (1976) 1212.
11. Wright, R. B. and Wang, C. H. *J. Phys. Chem. Solids* **34** (1973) 787.
12. Geisel, T. and Keller, J. *J. Chem. Phys.* **62** (1975) 3777.
13. Coda, A. and Pandarese, F. *J. Appl. Cryst.* **9** (1976) 193.
14. Vogt, H. II. Physikalisches Institut, Universität Köln. *Private communication.*

Received January 3, 1977.

Microwave Spectrum, Conformation and Structural Parameters of 4-Chloro-1,2-butadiene

FRED KARLSSON, MATS GRANBERG and RAGNAR VESTIN

Department of Physical Chemistry, Arrhenius Laboratory, University of Stockholm, S-104 05 Stockholm, Sweden

The microwave spectrum of 4-chloro-1,2-butadiene has been measured in the region 27 000 – 35 000 MHz. All observed transitions originated from the molecule in the *skew* conformation.

The positions of the chlorine atom and the two terminal allenyl hydrogen atoms were determined by observing the two natural isotopic species: $\text{CH}_2\text{CCHCH}_2^{35}\text{Cl}$ and $\text{CH}_2\text{CCHCH}_2^{37}\text{Cl}$ together with the two deuterated species: $\text{CDHCCHCH}_2^{35}\text{Cl}$ and $\text{CDHCCHCH}_2^{37}\text{Cl}$.

Vibrational satellites were observed and measured for the excited torsional state and a low-lying skeletal bending state.

The substance 4-chloro-1,2-butadiene was first described by Carothers *et al.*¹ as an important intermediate in the synthesis of chloroprene by addition of aqueous hydrogen chloride to vinylacetylene.

It is interesting to compare 4-chloro-1,2-butadiene with 3-chloropropene whose conformational properties have been closely examined by electron diffraction² and spectroscopical methods including microwave,³ infrared⁴ and proton magnetic resonance^{5–7} spectroscopy. The microwave spectroscopical investigation by Hirota⁸ showed clearly the existence of two rotameric forms of 3-chloropropene: *cis* and *skew*. The effect of steric repulsion between the chlorine atom and the vinyl group was demonstrated and vibrational satellites due to torsional states of the *cis* and *skew* form were identified.

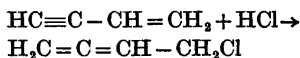
Rondeau and Harrah⁷ developed a simple equation for calculating the population of the *cis* rotamer in 3-halopropene from the coupling constant between the halomethyl protons and

the nearest vinyl proton measured with NMR. From this they determined a relative abundance of 0.16 for the *cis* form of 3-chloropropene, in good agreement with infrared measurements. We used this equation and inserted the derived value for the coupling constant between the chloromethyl protons and the nearest allenyl proton, as measured by Ferguson.⁸ According to these calculations there should be no *cis* form in 4-chloro-1,2-butadiene provided that *cis* and *skew* are the only possible rotamers.

If this is true, it would be interesting to ask why the *cis* form should be more abundant in 3-chloropropene than in 4-chloro-1,2-butadiene. The steric repulsion from an allenyl group is probably stronger than that from a vinyl group. Another possible explanation would be to assume a stabilizing nonbonded interaction between the chlorine atom and the nearest vinyl hydrogen atom for 3-chloropropene in the *cis* form which is not possible in 4-chloro-1,2-butadiene. This kind of interaction has been discussed by Viehe^{9,10} for 1-halo-1,3-butadienes and 1,4-dihalo-1,3-butadienes.

EXPERIMENTAL

4-Chloro-1,2-butadiene was prepared by shaking vinylacetylene with conc. hydrochloric acid in a pressure bottle for 6 h:¹



The sample was isolated by distillation *in vacuo* and finally gas-liquid chromatography at a temperature of 100 °C. The column was

Table 1. Rotational transitions in MHz for four isotopic species of 4-chloro-1,2-butadiene.

J	K_{-1}	K_{+1}	J	K_{-1}	K_{+1}	$\text{CH}_3\text{CCHCH}_2^{35}\text{Cl}$	$\text{CH}_3\text{CCHCH}_2^{37}\text{Cl}$	$\text{CHDCCHCH}_2^{35}\text{Cl}^a$	$\text{CDHCCHCH}_2^{35}\text{Cl}^b$
9	1	9	8	1	8	28249.42	27639.30	27059.20	27255.91
9	0	9	8	0	8	28454.62	27839.69	27242.47	27488.35
9	2	8	8	2	7	28471.55	27855.96	27256.50	27510.13
9	3	7	8	3	6	28480.99	27865.08	27264.70	27520.82
9	2	7	8	2	6	28486.74	27870.43	27268.51	27531.50
9	4	6	8	4	5	28487.27	27871.35	27270.56	27526.30
9	5	5	8	5	4	28496.08	27878.90	27278.69	27534.11
9	6	4	8	6	3	28506.86	27890.81	27288.97	27544.02
9	1	8	8	1	7	28684.89	28064.02	27445.90	27754.95
10	1	10	9	1	9	31386.76	30708.99	30064.51	30282.48
10	0	10	9	0	9	31611.54	30928.45	30265.61	30536.23
10	2	9	9	2	8	31633.75	30949.75	30283.90	30565.26
10	3	8	9	3	7	31645.33	30961.03	30293.82	30578.77
10	4	7	9	4	6	31652.13	30967.84	30300.25	30584.45
10	2	8	9	2	7	31654.50	30969.58	30300.42	30594.50
10	5	6	9	5	5	31661.71	30977.16	30309.19	30593.04
10	6	5	9	6	4	31673.87	30989.23	30320.41	
10	1	9	9	1	8	31870.20	31180.39	30493.94	30836.53
11	1	11	10	1	10	34523.55	33778.05	33069.35	33308.35
11	0	11	10	0	10	34767.03	34015.93	33287.60	33582.30
11	2	10	10	2	9	34795.52	34043.15	33310.87	33619.88
11	3	9	10	3	8	34809.61	34056.82	33322.90	33636.52
11	4	8	10	4	7	34816.75	34063.90	33329.71	33642.42
11	2	9	10	2	8	34823.03	34069.56	33332.79	33658.90
11	5	7	10	5	6	34827.16	34074.31	33339.52	33651.84
11	6	6	10	6	5	34840.49	34087.29	33351.76	33663.67
11	7	5	10	7	4	34856.25	34102.98		
11	1	10	10	1	9	35054.90	34296.28	33541.40	33917.39

^a Deuterium in the position H₂ of Fig. 1. ^b Deuterium in the position H₁ of Fig. 1.

packed with diethylhexylsebacate (15 %) absorbed on Chromosorb. Metallic columns, especially copper, should not be used since the 4-chloro-1,2-butadiene then rearranges to 2-chloro-1,3-butadiene (chloroprene). We used glass columns: length 1.5 m and internal diameter 8 mm.

The deuterated sample of 4-chloro-1,2-butadiene was prepared simply by using deuterated hydrochloric acid in the above reaction. The hydrochlorination of vinylacetylene is believed to be a 1,4-addition, and this was effectively proved by the microwave measurements on the deuterated sample which showed that deuterium only added to the end carbon of the acetylenic group in vinylacetylene.

The microwave spectra were recorded on a Hewlett-Packard model 8460 A R-band spectrometer with a phase stabilized source oscillator. The recordings were made at room temperature and at pressures ranging from 10 to 50 mTorr. The precision of the measured transitions was estimated to be 0.05 MHz.

MICROWAVE SPECTRUM

Most of the lines in the spectrum are gathered in bands at intervals of approximately 3160 MHz. These bands cover almost the whole spectral region. The line abundance and the repeated structure within the bands are mainly due to the low-lying torsional vibration mode.

The observed transitions were all *R*-branch *a*-type transitions with $\Delta J = +1$ and $\Delta K_{-1} = 0$, caused by the *skew* rotamer of 4-chloro-1,2-butadiene behaving as an almost prolate symmetric rotor: see Table 1.

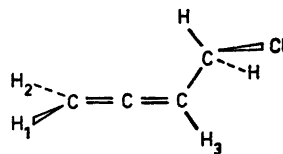


Fig. 1. The model structure of *skew*-4-chloro-1,2-butadiene.

The effect of nuclear quadrupole coupling is observable as a splitting into doublets for transitions with $K_{-1} \geq 4$ and the separation increases with K_{-1} . However, the splitting of these doublets is mainly determined by the nuclear quadrupole coupling constant χ_{aa} and since transitions with $K_{-1} \geq 8$ are obscured by the very dense vibrational bands, it is not possible to calculate χ_{aa} accurately. The values $\chi_{aa} = -30$ MHz for ^{35}Cl and $\chi_{aa} = -24$ MHz for ^{37}Cl are sufficient to account for the observed splittings within the error of measurement.

The lines from the deuterated species were identified and measured with high resolution: see Table 1. The synthesis yields a product with one deuterium atom in the end position of the allenyl group. Due to the skew conformation, this gives two isotopic species in equal amounts with deuterium in the position H_1 or H_2 : see Fig. 1.

The vibrational satellites due to the excited torsional states were measured for $v_1 = 1$ and $v_1 = 2$ for the ^{35}Cl species. Another series of vibrational satellites, probably related to

Table 2. Rotational constants in MHz for four isotopic species of 4-chloro-1,2-butadiene.

	<i>A</i>	<i>B</i>	<i>C</i>
$\text{CH}_2\text{CCHCH}_2\text{ }^{35}\text{Cl}$			
Ground state	15484. \pm 12	1606.07 \pm 0.01	1557.55 \pm 0.01
$v_1 = 1$	15606. \pm 17	1612.84 \pm 0.02	1560.80 \pm 0.02
$v_1 = 2$	15722. \pm 18	1619.59 \pm 0.02	1564.01 \pm 0.02
$v_2 = 1$	15668. \pm 18	1601.19 \pm 0.02	1555.65 \pm 0.02
$\text{CH}_2\text{CCHCH}_2\text{ }^{37}\text{Cl}$			
Ground state	15396. \pm 13	1571.26 \pm 0.01	1523.94 \pm 0.01
$\text{CHDCCHCH}_2\text{ }^{35}\text{Cl}^a$			
Ground state	15296. \pm 16	1535.8 \pm 0.01	1492.75 \pm 0.01
$\text{CDHCCHCH}_2\text{ }^{35}\text{Cl}^b$			
Ground state	14470. \pm 12	1556.25 \pm 0.02	1500.67 \pm 0.02

^a Deuterium in the position H_2 of Fig. 1. ^b Deuterium in the position H_1 of Fig. 1.

Table 3. Centrifugal distortion constants in kHz for four isotopic species of 4-chloro-1,2-butadiene.

	A_J	A_{JK}	δ_J
$\text{CH}_2\text{CCHCH}_2^{35}\text{Cl}$			
Ground state	0.94 ± 0.01	-56.38 ± 0.03	0.19 ± 0.02
$v_1=1$	1.04 ± 0.02	-58.40 ± 0.05	0.23 ± 0.04
$v_1=2$	1.04 ± 0.03	-60.62 ± 0.07	0.22 ± 0.05
$v_2=1$	0.95 ± 0.02	-58.87 ± 0.04	0.17 ± 0.04
$\text{CH}_2\text{CCHCH}_2^{37}\text{Cl}$			
Ground state	0.91 ± 0.01	-55.54 ± 0.03	0.19 ± 0.02
$\text{CHDCCHCH}_2^{35}\text{Cl}^a$			
Ground state	0.84 ± 0.02	-52.24 ± 0.04	0.14 ± 0.03
$\text{CDHCCHCH}_2^{35}\text{Cl}^b$			
Ground state	0.89 ± 0.02	-51.71 ± 0.06	0.17 ± 0.04

^a Deuterium in the position H_2 of Fig. 1. ^b Deuterium in the position H_1 of Fig. 1.

skeletal bending states, were measured for $v_2=1$ for the ^{35}Cl species. Relative intensities of the satellites indicate that the torsional frequency is about $60-70\text{ cm}^{-1}$ and the skeletal bending frequency is about $170-190\text{ cm}^{-1}$. Despite the low precision, these measurements are valuable for identification of the low-lying infrared transitions. This has been demonstrated by Hirota³ who was able to reassign the torsional frequency of *skew*-3-chloropropene originally reported by Radcliff and Wood.⁴

The rotational constants A , B and C , and the three centrifugal distortion parameters A_J , A_{JK} and δ_J were fitted to the observed spectra by the least-squares method: see Tables 2 and 3.

MOLECULAR STRUCTURE

All observed transitions are caused by the *skew* conformer and no lines have been found

that indicate the existence of another possible conformation of 4-chloro-1,2-butadiene. *cis*-4-Chloro-1,2-butadiene, if it exists, is expected to have a rather complicated spectrum mainly composed of Q -branch transitions active through the μ_b dipole moment. This, together with the fact that *skew*-4-chloro-1,2-butadiene has a very rich spectrum covering almost the whole spectral region, makes it hard to find expected contributions from the *cis*-form. In our experience it is not unlikely that even a relative abundance of 10 % might pass unnoticed under these circumstances. Thus the microwave measurements and, in fact, also the above-mentioned calculations using NMR-parameters, do not completely rule out the possibility of other conformers. We think that the best method to prove the absence of other rotamers would be a spectroscopical investigation in the infrared region and this has recently been done by W. C. Harris *et al.*¹¹ Their results

Table 4. Estimated molecular structure of 4-chloro-1,2-butadiene.

Bond length (Å)	Angle (°)
C—C	$\angle\text{C}=\text{C}-\text{C}$
C=C	$\angle\text{C}=\text{C}-\text{H}_1$
C—H ₁	$\angle\text{C}=\text{C}-\text{H}_2$
C—H ₂	$\angle\text{C}-\text{C}-\text{H}_3$
C—H ₃	$\angle\text{C}-\text{C}-\text{H}$ (methylene)
C—H (methylene)	$\angle\text{HCH}$ (methylene)
C—Cl	$\angle\text{C}-\text{C}-\text{Cl}$
	Dihedral angle

Table 5. The absolute values of the coordinates for the chlorine atom and two allenyl hydrogen atoms calculated with Kraitchman's equations and the distance between these atoms compared with the coordinates and the distances from the estimated molecular structure above. Conversion factor 505 374 (MHz) (au Å²).

	Microwave spectroscopy (Å)			Estimated structure (Å)		
Coordinate	Cl	H ₁	H ₂	Cl	H ₁	H ₂
a	1.889	3.164	3.754	1.887	3.154	3.751
b	0.312	1.530	0.218	0.304	1.511	0.181
c	0.018	0.200	0.613	0.048	0.051	0.535
Distance	Cl-H ₁	Cl-H ₂	H ₁ -H ₂	Cl-H ₁	Cl-H ₂	H ₁ -H ₂
r _s	5.202	5.703	1.891	5.184	5.689	1.858

support our conclusion that a single *skew* form of 4-chloro-1,2-butadiene is predominant at ambient temperature.

In order to obtain a good model structure for *skew*-4-chloro-1,2-butadiene we used the distances and angles reported for allene¹² and 3-chloropropene;³ see Table 4. This structure did not fit the measured moments of inertia until we allowed the dihedral angle to change from 122.3°, reported by Hirota³ for 3-chloropropene, to 120.0°. Since all structural parameters contribute to the moments of inertia, this value is of course very sensitive to the values of other parameters. However, after this partial fitting the model was found to be in good agreement even with the Cartesian coordinates of the chlorine atom and the two hydrogen atoms H₁ and H₂: see Table 5. These coordinates were calculated in the principal axis system of the CH₂CCHCH₂³⁵Cl molecule from the change in the moments of inertia on isotopic substitution.^{13,14}

The accuracy of these values as well as the distance parameters obtained from these coordinates are limited due to several reasons. First we must observe that coordinates less than about 0.25 Å derived by this method are always uncertain due to the small change on isotopic substitution. Further, since the observed lines are all *a*-type *R*-branch transitions, it is not possible to determine the value of the moment *I*_a as accurately as the moments *I*_b and *I*_c. Finally vibrational effects always lower the precision especially for the coordinates of the hydrogen atoms.¹⁵ However, it is reason-

able to expect the error of the hydrogen-chlorine distances to be about ±0.01 Å and the error of the hydrogen-hydrogen distances to be about ±0.05 Å.

Acknowledgements. We thank all those who have contributed to this paper and especially Dr. Stig Ljunggren and Dr. Hasse Karlsson for pleasant cooperation and valuable discussions.

REFERENCES

- Carothers, W. H., Berchet, G. J. and Collins, A. M. *J. Am. Chem. Soc.* 54 (1932) 4066.
- Bowen, H. J. M., Gilchrist, A. and Sutton, L. E. *Trans. Faraday Soc.* 51 (1955) 1341.
- Hirota, E. *J. Mol. Spectrosc.* 35 (1970) 9.
- Radcliffe, K. and Wood, J. L. *Trans. Faraday Soc.* 62 (1966) 2038.
- Bothner-By, A. A. and Günther H. *Discuss. Faraday Soc.* 34 (1962) 127.
- Bothner-By, A. A., Castellano, S. S., Ebersole, S. J. and Günther, H. *J. Am. Chem. Soc.* 88 (1966) 2466.
- Rondeau, R. E. and Harrah, L. A. *J. Mol. Spectrosc.* 21 (1966) 332.
- Ferguson, R. C. *J. Phys. Chem.* 68 (1964) 1594.
- Viehe, H. G. *Chem. Ber.* 97 (1964) 598.
- Viehe, H. G. and Franchimont, E. *Chem. Ber.* 97 (1964) 602.
- Harris, W. C., Coe, D. A., Parpart, M. K. and Pyron, R. S. *Private communication.*
- Almenningen, A., Bastiansen, O. and Tretteberg, M. *Acta Chem. Scand.* 13 (1959) 1699.
- Kraitchman, J. *Am. J. Phys.* 21 (1953) 17.
- Costain, C. C. *J. Chem. Phys.* 29 (1958) 864.
- Laurie, V. W. and Herschbach, D. R. *J. Chem. Phys.* 37 (1962) 1687.

Received January 12, 1977.

The Complex Formation between Pb^{2+} and Dicarboxylic Acids $(\text{CH}_2)_n(\text{COOH})_2$ with $n=1-4$

ABBAS HAMMAM,* ÅKE OLIN and PÄR SVANSTRÖM

Institute of Chemistry, University of Uppsala, P.O.B. 531, S-751 21 Uppsala, Sweden

The complex formation between Pb^{2+} and the malonate, succinate, glutarate, and adipate ions (A) has been studied by potentiometric measurements in 1 M $\text{Na}(\text{ClO}_4)$ at 25 °C. The presence of $\text{Pb}(\text{HA})$, $\text{Pb}(\text{HA})_2$, PbA , PbA_2 , and $\text{Pb}(\text{HA})\text{A}$ has been established and the stability constants of the species have been determined. Complexes with three ligands may also be present. It has not been possible to elucidate their compositions with certainty.

In the previous parts of the studies on the complexes formed between Pb^{2+} and dicarboxylate ions the stability constants for the maleate¹ and oxalate² systems have been determined. These investigations have now been extended to include the ligands malonate, succinate, glutarate, and adipate. In what follows these ligands will be denoted by A^{2-} . The $\text{Pb}^{2+}-\text{A}^{2-}$ systems have previously been studied mainly by polarographic measurements. In solutions containing only A^{2-} the complexes PbA , PbA_2 , and PbA_3 have been found by Gaur and Palrecha.³ In addition PbA_4 has been suggested by Maheswari, Jain, Saraswat, and Gaur⁴ to exist in the malonate system. From glass electrode measurements the stability constants of the PbA complexes have been reported by Yasuda, Yamasaki, and Ohtaki.⁵ Little or no attention has been paid to the formation of protonated complexes. Only Lai and Hsieh⁶ have reported on such complexes, *viz.*, PbHA and $\text{Pb}(\text{HA})_2$ in the malonate system.

This work presents the results from potentiometric measurements, where particular care

has been taken to ensure broad concentration ranges in the $\text{H}_2\text{A}-\text{HA}^--\text{A}^{2-}$ systems.

EXPERIMENTAL

Method. The measurements were carried out as a series of potentiometric titrations. In general the total concentration of $\text{Pb}(\text{II})$, B , and the quotient between the total concentration of H^+ , H , and the total concentration of dicarboxylate ion, A , were kept constant during a titration. The concentration of free hydrogen ion, h , and the concentration of Pb^{2+} , b , were measured at 25.0 °C with the cells

$$-\text{glass} \mid \text{Equilibrium solution S} \mid \text{Ref} + \quad (1)$$

$$E_g = E_g^\circ - 59.16 \text{ (mV)} \log(h/M) - E_j \quad (1)$$

$$-\text{Pb-Hg} \mid \text{Equilibrium solution S} \mid \text{Ref} + \quad (11)$$

$$E_{\text{Pb}} = E_{\text{Pb}}^\circ - 29.58 \text{ (mV)} \log(b/M) - E_j \quad (2)$$

The ionic medium has been 1 M $\text{Na}(\text{ClO}_4)$ for all the systems studied. The succinate system has also been investigated in 3 M $\text{Na}(\text{ClO}_4)$. The liquid junction potential, E_j , including the activity factor for H^+ was determined as described earlier¹ and is given by

$$E_j = k[\text{H}^+] + l[\text{H}_2\text{A}] + m[\text{HA}^-] + n[\text{A}^{2-}] \quad (3)$$

where k , l , m , and n are constants.

Apparatus. The potentiometric titrations were performed with an automatic titrator built in this department. All potentials were measured with a digital voltmeter, Data Precision 2520, to ± 0.01 mV. Details on the preparation and stability of the electrodes can be found in Ref. 1. The equilibration of the malonate buffers with lead malonate (s) was performed in the same equipment as used in the investigation of the oxalate system.²

Chemicals and analysis. Malonic acid (Merck zur Synthese) was recrystallized three times

* Present address: Chemistry Department, Faculty of Science, Assiut University, Assiut, Egypt.

from an ether-acetone mixture (1:1) and benzene added to the filtrate to lower the solubility. The formula weight as determined by alkalimetric titration was 104.3 (calc. 104.1). Lead malonate crystals for the solubility measurements were prepared by precipitation from homogeneous solution by addition of small portions of urea during several hours.

Succinic acid (Merck zur Analyse) was recrystallized three times from water and the formula weight found was 118.3 (calc. 118.1).

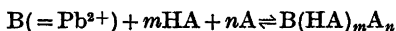
Glutaric acid (Fluka *purum* and Merck "zur Synthese") was purified by repeated recrystallizations from ether-benzene (1:4). The formula weight was 132.3 (calc. 132.1).

Adipic acid (Kebo *purum*) was recrystallized three times from water and the formula weight was found to be 146.3 (calc. 146.1).

Other chemicals were prepared and analysed as described earlier.¹

CALCULATIONS AND RESULTS

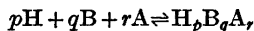
Since both HA^- and A^{2-} can act as ligands the complexes $\text{Pb}_q(\text{HA})_m$, Pb_qA_n , and $\text{Pb}_q(\text{HA})_m\text{A}_n$ will be assumed to form. Due to the small solubility of the lead dicarboxylates the upper limit of the concentration range for Pb(II) was about 1×10^{-3} M. Experiments with different total metal ion concentrations showed that $q = 1$. The stability constant for the reaction



is denoted by

$$\beta_{m,n} = [\text{B}(\text{HA})_m\text{A}_n] b^{-1} [\text{HA}]^{-m} a^{-n} \quad (4)$$

and for the reaction written as



by

$$\beta_{pqr} = [\text{H}_p\text{B}_q\text{A}_r] h^{-p} b^{-q} a^{-r} \quad (q = 0 \text{ or } 1) \quad (5)$$

The total concentration of Pb^{2+} is

$$B = b + \sum_m \sum_n \beta_{m,n} b [\text{HA}]^m a^n \quad (6)$$

and the buffer quotient ϕ is defined by $\phi = [\text{HA}]/a$. The analysis of the measurements was carried out in two steps. Data from solutions with less than 10 % of the perchlorate ions exchanged for the ligands were used in the first step. On the assumption that only complexes with $m+n \leq 2$ are formed eqn. (6) can be written

$$y_1 = (B/b - 1)a^{-1} = \beta_{0,1} + \beta_{1,0}\phi + \beta_{0,2}a + \beta_{1,1}\phi a + \beta_{2,0}\phi^2 a \quad (7)$$

A representative example of the use of eqn. (7) is given in Figs. 1–3 with data from the succinate system. In Fig. 1 y_1 is plotted as a function of a at constant ϕ . Straight lines are obtained indicating that complexes with $m+n \leq 2$ predominate. The intercepts $y_2 = (\beta_{0,1} + \beta_{1,0}\phi)$ and the slopes $y_3 = (\beta_{0,2} + \beta_{1,1}\phi + \beta_{2,0}\phi^2)$ of these lines are plotted as functions of ϕ in Figs. 2 and 3. From these plots, which suggested the existence of $\text{Pb}(\text{HA})$, $\text{Pb}(\text{HA})_2$, PbA , PbA_2 , and $\text{Pb}(\text{HA})\text{A}$ in all the systems

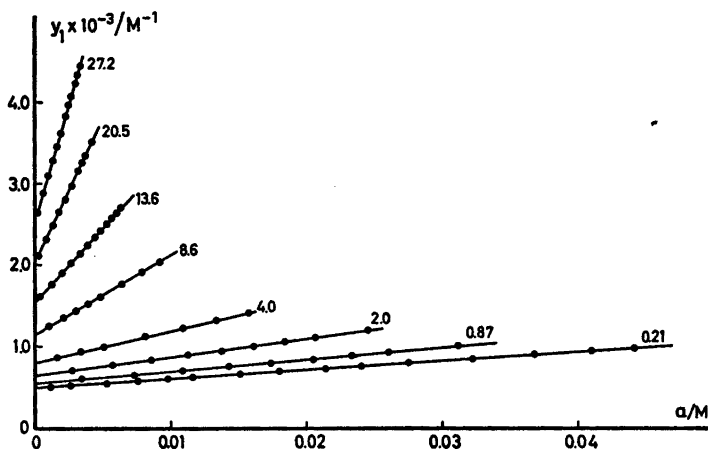


Fig. 1. $y_1 = (B/b - 1)a^{-1}$ plotted as a function of a (see eqn. (7)). Each line refers to a constant value of the buffer quotient $\phi = [\text{HA}]/a$. This value is given in the graph. Only data from solutions where less than 10 % of the perchlorate ions have been exchanged are included.

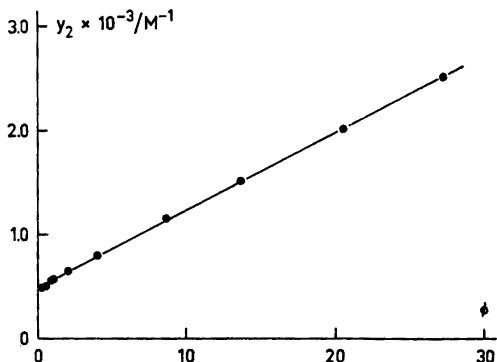


Fig. 2. The y_1 -intercepts, $y_2 = \beta_{0,1} + \beta_{1,0}\phi$, of the lines in Fig. 1 plotted as a function of ϕ . Results for a few buffer quotients not shown in Fig. 1 for clarity are also included.

studied, preliminary values of the stability constants were calculated. These were next refined by the least-squares program Letagrop Vrid, version Etitr,⁷ from 150–200 experimental points.

The data at greater ligand concentrations, corresponding to an exchange of at most 20–25 % of the perchlorate ions for A^{2-} and HA^- , could not be fully explained by the complexes with $m+n \leq 2$. $E_{\text{calc}} - E_{\text{exp}}$ reached about 1 mV at the highest ligand concentrations. Since the effect on the activity coefficients of an exchange of ClO_4^- against A^{2-} is not known and difficult to establish, one is prompted to proceed

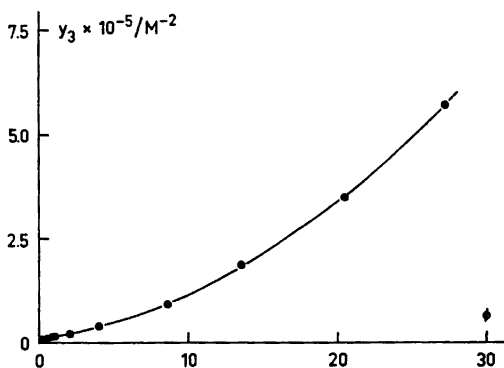


Fig. 3. The slopes, $y_3 = \beta_{0,2} + \beta_{1,1}\phi + \beta_{2,0}\phi^2$, of the lines in Fig. 1 plotted as a function of ϕ . The drawn curve is the polynomial of the second degree fitted to the experimental points by least-squares calculations.

using one of the following hypotheses. Either the deviations are considered to be caused by changes in the activity coefficients or these assumed to be constant and the data explained by inclusion of complexes with $m+n=3$. The truth may well lie between the two assumptions. An attempt has been made to explain the data according to the last mentioned (2nd) hypothesis by inclusion of $\text{Pb}(\text{HA})_3$, PbA_3 , $\text{Pb}(\text{HA})_2\text{A}$, and $\text{Pb}(\text{HA})\text{A}_2$. With all nine complexes present in the model the refinements failed, however. This is not unexpected since the concentrations of the complexes with $m+n=3$ obviously must be small.

As a guidance for further computations the stability constants of the complexes with $m+n=3$ were estimated as follows. $\beta_{0,3}$ and $\beta_{3,0}$ were calculated assuming an invariant ratio between the stepwise stability constants. The constants for the mixed complexes were then estimated on the assumption that the equilibrium constants for the reactions



and



have the statistical value of 27 valid for closely related ligands. With these constants approximate distribution curves were calculated, which for the malonate and succinate systems indicated that PbA_3 and to a lesser extent $\text{Pb}(\text{HA})\text{A}_2$ could be present in the solutions. In the glutarate and adipate systems the concentrations of PbA_3 , $\text{Pb}(\text{HA})_2\text{A}$, and $\text{Pb}(\text{HA})\text{A}_2$ were approximately equal.

The $H^+ - A^{2-}$ systems. $\beta_{1,01}$ and $\beta_{2,01}$ were determined from titrations carried out with $A = 0.010$ and 0.025 M. The results are presented in Table 1. The β -values for malonic and succinic acid are in good agreement with those reported by Dellien and Malmström⁸ and by Schwarzenbach and Szilard.⁹ For the other two acids no constants are available in 1 M NaClO_4 . The stepwise protonation constants of A^{2-} , K_1 and K_2 , have been included in Table 1 to facilitate a comparison with their values in pure water, K_1° and K_2° . $\log K_2$ shows the same increase with the number of CH_2 -groups as does $\log K_2^\circ$. The series of $\log K_1^\circ$ values on the other hand exhibits a maximum at malonic

Table 1. Cumulative and stepwise protonation constants of A^{2-} . The values in pure water, K° , have been taken from Ref. 10. The figures within parentheses are three times the estimated standard deviations from the least-squares calculations.

Acid	$\beta_{101} \times 10^{-6}/M^{-1}$	$\beta_{201} \times 10^{-7}/M^{-2}$	$\log K_2$	$\log K_1$	$\log K_2^\circ$	$\log K_1^\circ$
Oxalic	0.0367 (0.0004)	0.00376 (0.00005)	1.01	3.56	1.271	4.266
Malonic	1.161 (0.003)	4.49 (0.02)	2.59	5.06	2.855	5.696
Succinic	1.317 (0.002)	129.6 (0.3)	3.99	5.12	4.207	5.638
Succinic (3 M NaClO ₄)	3.057 (0.007)	643.0 (1.7)	4.32	5.49		
Glutaric	0.845 (0.004)	132.0 (0.6)	4.19	4.93	4.343	5.272
Adipic	0.878 (0.003)	175.6 (0.1)	4.30	4.94	4.430	5.277

and succinic acid. This maximum also shows up in 1 M NaClO₄.

The malonate system. The measurements were carried out with $B = 5 \times 10^{-4}$ M and the buffers (H/A , A_{\max}/M); 0.17, 0.12; 0.57, 0.23; 0.81, 0.10; 1.47, 0.20. A_{\max} is the highest value of A reached in the titration. The data obtained in the range where $\leq 10\%$ of the ionic medium has been changed could be explained by the formation of PbHA, Pb(HA)₂, PbA, PbA₂, Pb(HA)A and $\sigma(E_{Pb})$ was 0.04 mV. This set of complexes does not satisfactorily account for the data at high ligand concentrations. Inclusion of PbA₃ and Pb(HA)A₂ removes systematic trends in $E_{\text{calc}} - E_{\text{exp}}$ and $\sigma(E_{Pb})$ is 0.03 mV. Addition of only one of these complexes leads to systematic deviations and $\sigma(E_{Pb})$ is 0.08 mV with only PbA₃ added. The low solubility of lead malonate limits the accessible concentration ranges and many titrations were interrupted by seemingly unpredictable precipitations. The solubility product of lead malonate, K_s , was therefore determined by equilibrating buffers with A^{2-} in the concentration range $a = (0.6 - 43) \times 10^{-3}$ M with lead malonate (s) and measuring b by the amalgam electrode. From 8 measurements K_s was found to be $(8.57 \pm 0.10) \times 10^{-8} M^{-2}$. This value shows that the emf measurements have been carried out on supersaturated solutions. This could also

be the case for the other systems investigated but no further determinations of solubility products have been made. The result from the final least-squares refinement is found in Table 2.

The succinate system. The measurements were carried out with $B = 0.5$ and 1.0×10^{-3} M and the buffers; (H/A , A_{\max}/M); 0.17, 0.13; 0.35, 0.17; 0.50, 0.13; 0.79, 0.17; 1.0, 0.20; 1.29, 0.28. This system has been studied more comprehensively than the others, since here the problems associated with the solubilities of the ligand and its lead compounds are less pronounced. The data at low ligand concentrations can be accounted for by the set of complexes with $m+n \leq 2$ and $\sigma(E_{Pb})$ was 0.04 mV. Inclusion of the data at high ligand concentrations necessitated the addition of PbA₃ and Pb(HA)A₂. $\sigma(E_{Pb})$ was 0.04 with both complexes added. With only one of them included, $\sigma(E_{Pb}) > 0.07$ mV.

The evidence for the presence of PbA₃ and Pb(HA)A₂ mainly comes from measurements where a substantial change in the medium has been made. The measurements were therefore repeated in 3 M Na(ClO₄). As in 1 M Na(ClO₄) the data could not be satisfactory explained with the complexes having $m+n \leq 2$ only. With the whole set of complexes found in 1 M Na(ClO₄) $\sigma(E_{Pb})$ was 0.11 mV. Addition of Pb(HA)₂A to the set lowered $\sigma(E_{Pb})$ to 0.06

Table 2. The stability constants, β_{pqr} , of the complexes written as $H_pPb_qA_r$. Three times the estimated standard deviations from the least-squares calculations are given within parentheses.

Acid	β_{111}/M^{-2}	β_{212}/M^{-4}	β_{011}/M^{-1}	β_{012}/M^{-2}	β_{013}/M^{-3}	β_{112}/M^{-3}	β_{113}/M^{-4}
Oxalic ^a	9.7×10^4 (0.9)		1.46×10^4 (0.02)	2.12×10^6 (0.02)			
Malonic	1.60×10^6 (0.03)	3.49×10^{11} (0.19)	6.10×10^3 (0.01)	1.580×10^4 (0.003)	1.45×10^4 (0.04)	1.89×10^8 (0.04)	1.07×10^9 (0.06)
Succinic	9.59×10^6 (0.07)	1.01×10^{13} (0.02)	4.77×10^3 (0.02)	9.76×10^3 (0.12)	7.8×10^3 (1.6)	6.91×10^8 (0.14)	1.57×10^9 (0.26)
Succinic ^b (3 M NaClO ₄)	3.52×10^7 (0.05)	1.46×10^{14} (0.03)	9.12×10^3 (0.08)	2.75×10^4 (0.06)	3.4×10^4 (0.7)	3.54×10^9 (0.10)	9.4×10^9 (1.9)
Glutaric	8.44×10^6 (0.08)	8.24×10^{13} (0.26)	3.21×10^3 (0.04)	5.83×10^3 (0.17)		5.24×10^8 (0.17)	
Adipic	9.78×10^6 (0.03)	1.13×10^{13} (0.01)	2.981×10^2 (0.007)	5.94×10^3 (0.03)		5.71×10^8 (0.05)	

^a Ref. 2. ^b $\beta_{213} = (1.3 \pm 0.2) \times 10^{15}/M^{-5}$.

mV. No evidence for this complex could be found from the data in 1 M Na(ClO₄). Calculations with an estimated value of β_{213} showed that the amount of Pb(HA)₂A is less in 1 M than in 3 M Na(ClO₄) which could be the reason why it is not detected there. The final stability constants are found in Table 2.

The glutarate system. The measurements were carried out with $B = 5 \times 10^{-4}$ M and the buffers; $(H/A, A_{\max}/M)$; 0.19, 0.12; 0.62, 0.20; 1.25, 0.40; 1.69, 0.37; 1.82, 0.12. Again the data at 10 % exchange of ClO₄⁻ could be explained by the set of complexes with $m+n \leq 2$ and $\sigma(E_{Pb})$ was 0.08 mV. At higher ligand concentrations complexes with $m+n=3$ were indicated. It was, however, not possible to establish their compositions. More than one of these complexes must be present since inclusion of only one additional complex in the calculations always resulted in a less satisfactory fit. With two complexes included $\sigma(E_{Pb})$ was always < 0.1 mV and any systematic trend in $E_{\text{calc}} - E_{\text{exp}}$ was less than 0.2 mV. This situation apparently arises because the affinity between Pb²⁺ and A³⁻ decreases as the chain length increases and at the same time the complexing properties of A³⁻ and HA⁻ become more alike. This makes the concentrations of complexes with $m+n=3$ small

and much the same. Calculations based on estimated β -values indicate that the relative amount on any of these complexes does not exceed 5 %. The constants for $m+n \leq 2$ determined from measurements on solutions with < 10 % of the ClO₄⁻ ions exchanged are entered in Table 2.

The adipate system. The measurements were carried out with $B = 5 \times 10^{-4}$ M and the buffers; $(H/A, A_{\max})$; 0.18, 0.13; 0.64, 0.06; 0.78, 0.26; 1.29, 0.22; 1.57, 0.06. The data for less than 10 % exchange of ClO₄⁻ can be explained by the constants in Table 2. $\sigma(E_{Pb})$ was 0.02 mV. In the adipate system the same situation arose as in the glutarate system when the data at high ligand concentrations were analysed. Several combinations of complexes yielded approximately the same $\sigma(E_{Pb}) \approx 0.03 - 0.04$ mV and no definite conclusions could be drawn. In addition there are few data at high ligand concentrations due to restrictions caused by the solubility of adipic acid.

DISCUSSION

In all systems the complexes Pb(HA), Pb(HA)₂, PbA, PbA₂, and Pb(HA)A are well established. The compositions of the complexes with $m+n=3$ are uncertain in the glutarate and

Table 3. The stability constants, $\beta_{m,n}$, of protonated complexes written as $\text{Pb}(\text{HA})_m(\text{A})_n$.

Acid	$\beta_{1,0}/\text{M}^{-1}$	$\beta_{2,0}/\text{M}^{-2}$	$\beta_{1,1}/\text{M}^{-2}$	$\beta_{1,2}/\text{M}^{-3}$
Oxalic	26.5			
Malonic	13.8	26	1.63×10^3	9.22×10^3
Succinic	72.8	582	5.25×10^3	1.19×10^4
Succinic (3 M NaClO_4)	115	1560	1.16×10^4	3.07×10^4
Glutaric	99.9	1150	6.20×10^3	
Adipic	111	1470	6.50×10^3	

adipate systems. Hence no stability constants for such complexes have been entered in Table 2 for these systems. From a practical point of view this is of minor importance since the concentrations of the complexes are small. The procedure proposed in an earlier section to estimate these constants apparently yields fairly good results. The values obtained from the least-squares refinements are quite close to these estimates. It may at this point be apt to restate, that all conclusions regarding complexes with three ligands are based on the loosely-founded assumption of constant activity coefficients even for large changes in the salt background.

Table 3 has been constructed in order to facilitate a discussion of the stabilities of the

complexes formed by HA^- . The relation between $\log \beta_{1,0}$ and $\log K_2$ is linear. $\beta_{1,0}$ for the hydrogen maleate complex also falls on this line. An extrapolation of the line to $\log K_2$ for oxalic acid suggests that $\beta_{1,0}$ for $\text{Pb}(\text{HC}_2\text{O}_4)^+$ should be about 2 M^{-1} . The reported value² is 26.5 M^{-1} , which might indicate that the $-\text{CO}(\text{OH})$ group is partially engaged in the bonding to the metal. The values of $\beta_{0,11} = \beta_{0,1}$ show the normal decrease and levelling off as the chain length of a bidentate ligand increases. The glutarate and adipate ions probably act as monodentate ligands. The $\log \beta_{1,0}$ vs. $\log K_2$ graph suggests that a monodentate ligand with a proton affinity corresponding to $\log K = 5$ would form a 1:1 complex with a stability constant around

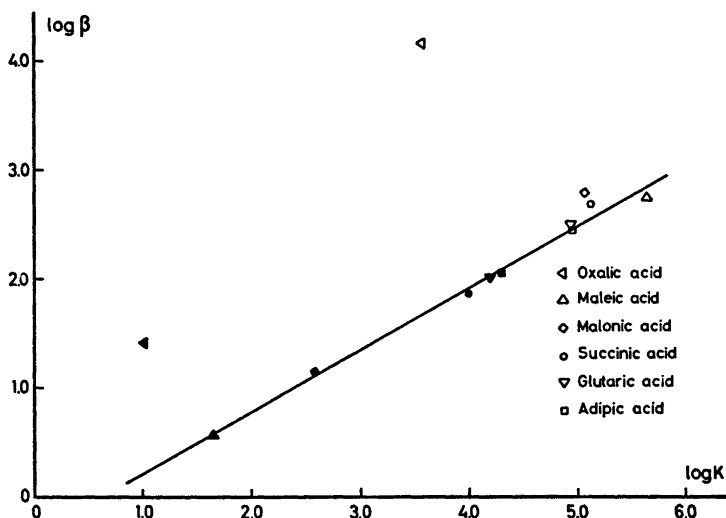


Fig. 4. $\log \beta$ plotted as a function of $\log K$ ($\log \beta_{1,0}$ vs. $\log K_2$ filled and $\log \beta_{0,1}$ vs. $\log K_1$ open symbols). The $\log K_1$ value for malonic acid and values for oxalic acid have been excluded in the calculations of the drawn line.

300 M⁻¹. The observed values are about 300 M⁻¹. It is interesting to note that, with the exception of the oxalate system and $\beta_{0,1}$ for the malonate system, the equation $\log \beta = -0.36 + 0.57 \log K$ predicts to 0.1 logarithmic unit the values of $\log \beta_{1,0}$ and $\log \beta_{0,1}$. See Fig. 4. In the equation $\log K_2$ is used for estimating $\log \beta_{1,0}$ and $\log K_1$ for estimating $\log \beta_{0,1}$. It might be argued that the use of $\log K_1$ overestimates $\beta_{0,1}$ for A²⁻ acting as a monodentate ligand. On account of the symmetry of A²⁻ another reasonable estimate would be $\beta_{0,1}$ (monodentate) $\approx 2\beta_{1,0}$. This estimate also suggests that A²⁻ is largely bound as a monodentate ligand.

Pb(HA)⁺ is a stronger acid than HA⁻ as expected. The exceptional stability of Pb(C₂O₄) makes Pb(HC₂O₄)⁺ an even stronger acid than H₂C₂O₄. The equilibrium constant for Pb(HA)₂ + PbA₂ \rightleftharpoons 2Pb(HA)A varies irregularly between 6.5 and 5 and is thus not far removed from the statistical value for two similar ligands. Using the value 6, $\beta_{1,1}$ for the maleate system becomes 5.6×10^{-2} M⁻¹ and explains why a mixed complex could not be detected in that system.

Acknowledgement. This work has been supported by the Swedish Natural Science Research Council. One of us (A.H.) expresses his gratitude to the International Seminar in Chemistry for a grant.

REFERENCES

1. Olin, Å. and Svanström, P. *Acta Chem. Scand. A* 29 (1975) 849.
2. Hedström, H., Olin, Å., Svanström, P. and Åslin, E. *J. Inorg. Nucl. Chem. In press.*
3. Gaur, J. N. and Palrecha, M. M. *Talanta* 15 (1968) 583.
4. Maheswari, A. K., Jain, D. S., Saraswat, H. C. and Gaur, J. N. *J. Electrochem. Soc. India* 23 (1974) 155.
5. Yasuda, M., Yamasaki, K. and Ohtaki, H. *Bull. Chem. Soc. Jpn.* 33 (1960) 1067.
6. Lai, T. and Hsieh, C. J. *J. Electrochem. Soc.* 112 (1965) 218.
7. Brauner, P., Sillén, L. G. and Whiteker, R. *Ark. Kemi* 31 (1969) 365.
8. Dellien, I. and Grenthe, I. *Acta Chem. Scand.* 25 (1971) 1387.
9. Schwarzenbach, G. and Szilard, I. *Helv. Chim. Acta* 144 (1962) 1223.
10. Robinson, R. A. and Stokes, R. H. *Electrolyte Solutions*, Butterworths, London 1959.

Received January 17, 1977.

Pattern-recognition Search for the Basic Regularities in the Stability of Complex Hydrides. Part 1. A Simplified Model

OLDRICH ŠTROUF^a and SVANTE WOLD^b

^a Institute of Inorganic Chemistry, Czechoslovak Academy of Sciences, 250 68, Rež near Prague, Czechoslovakia and ^b Research Group for Chemometrics, Institute of Chemistry, Umeå University, S-901 87 Umeå, Sweden

The relationship between structural variables and the stability of complex hydrides ABH_nD_{4-n} (A = alkaline atom; B = the Group III B atom; n = number of hydrogen atoms and D non-hydride substituents) is investigated by means of the pattern recognition (PR) method SIMCA.

A learning set consisting of 95 stable and 20 unstable complexes was characterized by 49 structural variables. SIMCA sorted out 28 of these as relevant for the classification of the complexes as stable or unstable.

The resulting relations between these 28 variables for the two classes makes possible a qualitative interpretation of which factors influence the stability of the complexes. The method classifies 75 % of the complexes correctly which is encouraging considering the crudeness of the model.

For inorganic as well as organic chemists, the complex hydrides ABH_nD_{4-n} (A = alkaline metal; B = the metal of the Group III B; n = the number of hydride atoms and D = a substituent other than hydride) represent an interesting and synthetically important group of chemical compounds. Theoretically, the combination of A, B, n and D could give an extremely high number of compounds due to practically unlimited set of the possible substituents D. Nevertheless, numerous empirical facts (see Ref. 1 and references therein) have shown that only some of the complex hydrides are stable, whereas the others exhibit a significant instability.

In this paper, we design a simplified model for the stability of complex hydrides ABH_nD_{4-n} ($n = 1-4$) based on structural data² for A, B and D. For the quantitative interpretation of

these multivariate data we used the SIMCA method, one of the recent pattern recognition (PR) techniques.

PATTERN RECOGNITION

The search for and use of regularities in empirical data has always been of great importance in chemistry. Quantitative methods specifically designed to detect regularities in multivariate data are finding increased use in chemistry under the name of pattern recognition (PR). For reviews, see Kowalski,^{3,4} Jurs and Isenhour,⁵ Redl, Cramer and Berkoff⁶ and others.⁷ The principles of PR can be described as follows:

1. Formulate the problem as a classification problem where objects are to be assigned to one of several classes on the basis of multivariate data observed on these objects (see Fig. 1). In the present application, we wish to classify complex hydrides (the objects) of the general formula ABH_nD_{4-n} as "stable" (class 1) or "unstable" (class 2). Hence, the number of classes, Q , is two.

2. The values of M variables are observed or otherwise defined for a number of objects "known" to belong to the different classes. These objects are called the *training set* or the reference set.

In the present example, each complex hydride is characterised by 49 variables (see below). The training set consists of 95 complexes "known" to be stable and 20 complexes "known" to be unstable.

Object						
Variable	1	2	...	k	...	N
1	y_{11}	y_{12}	...	y_{1k}	...	y_{1N}
2	y_{21}	y_{22}	...	y_{2k}	...	y_{2N}
3	y_{31}	y_{32}	...	y_{3k}	...	y_{3N}
⋮	⋮	⋮	⋮	⋮	⋮	⋮
i	y_{i1}	y_{i2}	...	y_{ik}	...	y_{iN}
⋮	⋮	⋮	⋮	⋮	⋮	⋮
M	y_{M1}	y_{M2}	...	y_{Mk}	...	y_{MN}

Class 1 (reference set 1)
Class Q (reference set Q)
Nonclassified objects

Training set (Learning set)
Test set

Fig. 1. Data used in the analysis of data by pattern recognition methodology.

3. Observe or define the values of the same variables for objects of unknown class assignment (see Fig. 1). These data constitute the *test set*. In the present application, this test set consists of the data for 109 complex hydrides for which information about the stability is rather incomplete or entirely lacking.

4. Find the "common pattern" in each class by analysing the training set by means of a mathematical procedure. We have used the SIMCA method which is specifically designed for chemical pattern recognition.^{8,9}

5. Compare the objects in the test set with the common pattern of each class using the

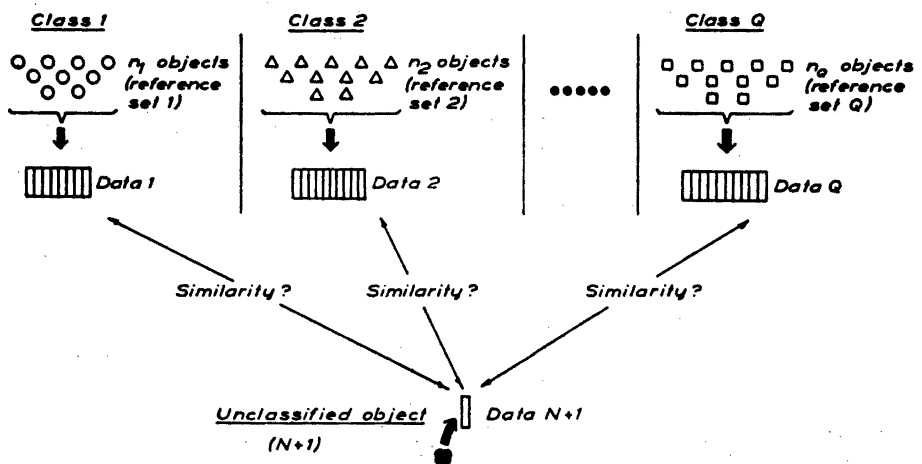


Fig. 2. The principle of pattern recognition as a methodology of assigning an object to the correct class on the basis of the values of M variables measured on the object.

mathematical procedure as a means of comparison. Each object is assigned to the class which shows the greatest similarity with the data of the object (Fig. 2).

Usually, PR methods are used to analyse empirical data such as spectra. In the present context, however, we are interested whether structural information can be used to predict the stability of complex hydrides. The variables used to characterise each hydride are therefore taken to be "theoretical", such as the electronegativity of atom A and the atomic weight of atom B. This use of PR methods to investigate structure reactivity relations has been applied to some extent to problems in biochemistry and pharmacology⁶ but, to our knowledge, not in inorganic chemistry.

THE SIMCA METHOD

The PR method used here is called SIMCA (Simple Modelling Class Analogy). The method is based on the fact that data $y_{ik}^{(q)}$ (see Fig. 1) observed on a group of similar objects (class q) can, provided that a few continuity assumptions are fulfilled, be described by the principal components model^{8,9}

$$y_{ik}^{(q)} = \alpha_i^{(q)} + \sum_{a=1}^A \beta_{ia}^{(q)} \theta_{ak}^{(q)} + \varepsilon_{ik}^{(q)} \quad (1)$$

In eqn. (1), the parameters $\alpha_i^{(q)}$, $\beta_{ia}^{(q)}$ and $\theta_{ak}^{(q)}$ are determined as to make the sum of squared deviations $\varepsilon_{ik}^{(q)}$ minimal. The mathematical method to make this determination for a given matrix of data ($y_{ik}^{(q)}$) is known under the name principal components analysis.

The PR method based on eqn. (1) has the following steps:

A. Given data $y_{ik}^{(q)}$ for the objects in the training set of class q , the parameters in eqn. (1) are determined to minimise the sum of squares deviation (method of least squares).

B. The classification of non-assigned objects (the test set) is then accomplished by fitting the data of each such object (denoted by x_{ij}) to each of the Q class models (index q) with the parameters $\alpha_i^{(q)}$ and $\beta_{ia}^{(q)}$ fixed to the values obtained in step A. This corresponds to one linear regression for each object and each class, i.e. the determination of the coefficients $t_{aj}^{(q)}$ to minimise the residuals $e_{ij}^{(q)}$ in the least squares sense

$$x_{ij} - \alpha_i^{(q)} = \sum_{a=1}^A t_{aj}^{(q)} \beta_{ia}^{(q)} + e_{ij}^{(q)} \quad (2)$$

The object j is assigned to the class for which the residual variance $[s_j^{(q)}]^2$ is the smallest

$$[s_j^{(q)}]^2 = \sum_{i=1}^M \{e_{ij}^{(q)}\}^2 / (M - A) \quad (3)$$

Relevance of variables

The method allows the calculation of the *discrimination power* and the *modelling power* of each variable i . The former is computed as the sum of squared residuals for variable i when all objects in the training set are fitted to the class models of their "own" class divided by the sum of squared residuals for variable i when all objects in the training set are fitted to all other class models. The discrimination power gives valuable information about the importance of each variable for the prediction of the class assignment.

The modelling power of variable is essentially the residual (ε) variance of the variable divided by the variance in the original data (y) of the same variable, both variances computed over all objects in the training set. The modelling power indicates how important a variable is in describing the similarity within the classes.

Selection of variables

One important goal of the data analysis is a reduction of the number of variables. This is particularly important in the present problem since the variables were introduced with little knowledge of their actual relation to the stability of the complexes. Thus, the classification of a variable as relevant or irrelevant also indicates whether it is at all related to the stability of complex hydrides.

However, the selection of relevant variables (or, alternatively, the deletion of irrelevant variables from the set originally chosen) presents fundamental problems. Consider a training set of N objects, each "known" to belong either to class 1 or class 2. Let us then introduce a number of variables by means of which we wish to "explain" the classification of the training set. It is easily realized that *even if we pick these variables completely at random*, we will sooner or later find a variable that is highly correlated

with the classification of the training set. The problem is substantially worse if we also allow combinations of variables to be correlated with the classification.

Hence, it is evident that if we condition the selection of variables on their discrimination power — *i.e.* we search for variables that are highly correlated with the classification of the training set — we must limit the number of original variables. Usually, a ratio between the number of variables and the number of objects in the training set of less than 1 to 10 is recommended.⁴ This would limit the number of variables to 12 in the present case being substantially smaller than we actually have.

However, if we instead condition the selection of the variables on their *modelling power*, the above problem of “contrivedness” is considerably less serious. We then search for variables being highly correlated with several other variables in each class submatrix. The chance of finding such variables in a bunch of random variables is sufficiently small when the number of original variables is of the same order as the average number of objects in each class. In the present case we have, on the average, 57 cases in each class, limiting the number of variables to 50–60, more than the present number of 49. We have, in our selection of variables, gone one step further, deleting only variables showing *both* low discrimination and modelling power, thereby further reducing the change of this selection corresponding to a “random choice”.

Furthermore, the set of retained variables is independently tested in a later step of the analysis (see below, verification). Hence we feel that the deleted variables have little relation to the present classification problem.

In this manner, we have reduced the number of variables for the complex hydrides from 49 to 28, thus obtaining information on which theoretical variables are important for the prediction of the stability of a complex hydride.

Interpretation of the parameters

The values of the parameters $\alpha_i^{(q)}$ and $\beta_{ia}^{(q)}$ in eqn. (1) also give direct information about the “typical pattern” of the data in class q . Thus $\alpha_i^{(q)}$ is the average value of variable i in the

class and $\beta_{ia}^{(q)}$ contain information about the correlation structure. For example, if $\beta_{1a}^{(q)}$ is positive and $\beta_{2a}^{(q)}$ is negative, this tells us that an increase in the first variable can be compensated for by a decrease in the second one. Such information has a direct chemical interpretation as seen below and gives valuable clues to the factors influencing the stability of complex hydrides.

Scaling of data

In order to give each variable the same weight in the initial phase of the analysis, we have followed the usual procedure of subtracting the average of the variable (calculated over all complexes) and dividing by the standard deviation of the same variable. This makes each variable have the mean zero and the variance one. The scaling values used in the analysis of the hydride data are shown in Table 1.

PATTERN RECOGNITION RESULTS

1. *Initial analysis.* To give each variable the same weight in the analysis, the 49 variables were autoscaled^{3,4} to uniform mean and variance by subtraction of the variable mean and division by its standard deviation times $\sqrt{223}$ (values in Table 1).

A SIMCA analysis of the scaled data using $A=5$ in eqn. (1) showed a fair separation of the two training sets. The classification was incorrect for 20 of the 95 “stable” (class 1) and 4 of the 20 “unstable” (class 2) complexes (see Table 2).

Table 1 shows the parameters α_i of the 49 scaled variables for class 1. The values of α_i for class 2 are the same but with opposite sign. These parameters, estimating the mean of each variable within the classes, are of the order 0.02 which is rather small compared to the residual standard deviation after one component in the final analysis, 0.06. Hence, the difference in each variable is insignificant between the two classes, only in combination do they make a contribution to the prediction of the stability of complex hydrides.

2. *Reduction of the number of variables.* By deleting variables with both low modelling and discrimination power, the number of

Table 1. Variables used in the PR analysis. A: Name of variable. B: Mean over all complexes. C: Standard deviation over all complexes. D: Modelling power with A=5, 49 variables. E: Discrimination power, same model. F: α_i for class 1 (stable). G: β_i for class 1, A=1, 28 variables. H: β_i for class 2, A=1, 28 variables.

A	B	C	D	E	F	G	H
1 A, m.p. °C ^a	1184	499	.93	1.1	-.017	--	--
2 A, b.p. °C	1017	244	.88	1.2	-.017	--	--
3 A, density, g/ml ^b	83.5	29.5	.70	1.1	.012	--	--
4 A, atomic radius, Å ^b	188.7	32.3	.96	5.2	.018	.27	.08
5 A, coval. radius, Å ^b	155.0	32.3	.94	5.2	.017	.27	.07
6 A, ionic radius, Å ^b	92.26	30.2	.97	6.0	.017	.27	.08
7 A, 1st ion. energy, kcal/g mol	116.2	10.0	.83	4.0	-.016	-.28	-.06
8 A, electronegativity ^a	9.112	.809	.96	3.5	-.018	-.26	-.08
9 B, m.p. °C ^a	1320	921	.97	4.1	.004	.02	.26
10 B, b.p. °C	2988	778	.98	4.6	.006	.03	.28
11 B, density, g/ml ^b	301.3	169	.80	5.8	-.012	.05	-.34
12 B, atomic, radius, Å ^b	126.7	23.9	.99	4.6	-.008	-.04	-.30
13 B, coval. radius, Å ^b	105.7	20.1	.99	4.4	-.008	-.02	-.32
14 B, ionic radius, Å ^b	40.65	18.7	.98	6.4	-.009	-.01	-.34
15 B, 1st ion. energy, kcal/g mol	158.7	26.1	.96	6.6	.004	.04	.23
16 B, electronegativity ^a	17.13	2.38	.90	9.0	.001	.05	.14
17 D, mol. weight	54.68	37.4	.66	1.6	-.017	-.20	.07
18 D, No. of chain atoms	3.183	2.36	.74	3.1	-.014	-.19	.14
19 D, b.p. of DH at 760 Torr	16.92	138	.89	2.9	-.016	--	--
20 D, density of DH (20 °C)	756.6	455	.89	8.3	-.016	--	--
21 D, π -donor or acceptor (1,0 or -1)	.3348	.733	.57	4.7	-.028	-.08	.07
22 D, No. of subst. on 1st ligand atom	.7768	.896	.84	3.8	.001	-.24	.15
23 D, average electronegat. of these ^a	24.46	3.63	.52	2.1	-.006	--	--
24 D, coval. radius of 1st ligand atom ^c	788.2	214	.78	1.0	.001	--	--
25 D, ionic radius of 1st ligand atom ^b	72.15	17.7	.81	1.2	-.010	--	--
26 D, 1st ion. energy of 1st lig. atom	295.8	32.8	.76	2.0	-.012	--	--
27 D, electronegativ. of 1st lig. atom ^a	29.05	5.48	.83	3.3	-.024	-.19	.18
28 E, corresponding to var. 17	43.18	39.8	.72	2.1	-.008	-.23	.10
29 E, 18	2.509	2.50	.78	3.5	-.006	-.22	.16
30 E, 19	-47.40	167	.88	3.3	-.005	--	--
31 E, 20	604.8	524	.90	4.0	-.007	--	--
32 E, 21	.2768	.631	.63	2.9	-.022	-.07	.10
33 E, 22	.3438	1.08	.86	6.9	-.007	-.29	.16
34 E, 23	23.36	2.96	.63	1.4	-.007	--	--
35 E, 24	675.6	273	.79	2.7	.008	--	--
36 E, 25	62.76	23.5	.83	2.1	.001	--	--
37 E, 26	299.8	28.7	.77	4.0	-.012	--	--
38 E, 27	27.20	5.89	.87	2.1	-.011	-.22	.20
39 F, 17	28.87	37.1	.77	1.4	-.003	-.23	.11
40 F, 18	1.679	2.34	.79	2.9	-.001	-.22	.18
41 F, 19	-116.7	166	.90	2.8	.001	--	--
42 F, 20	426.6	497	.94	5.8	-.001	--	--
43 F, 21	.1741	.528	.64	3.1	-.013	-.07	.13
44 F, 22	-.0804	1.11	.89	5.2	.008	-.26	.16
45 F, 23	22.60	2.67	.69	1.7	-.001	--	--
46 F, 24	559.5	281	.91	3.1	.007	--	--
47 F, 25	52.58	24.1	.94	2.6	.003	--	--
48 F, 26	304.2	24.4	.73	2.7	-.003	--	--
49 F, 27	25.04	5.52	.89	3.1	-.002	-.21	.23

^a Times 10; ^b Times 100; ^c Times 1000.

Table 2. Resulting classification of the hydrides. Prior classification: Compounds 1–95, stable (1); compounds 96–115, unstable (2); compounds 116–224, test set (0). A: Name of hydride. B: Prior classification in verification step. C: Resulting classification with $A=5$ and 49 variables. D: Resulting classification with $A=1$ and 28 variables. E: Resulting classification in the verification step.

A + sign after the resulting class number indicates that the ratio between the standard deviations for the two class models is larger than $\sqrt{2}$.

A	B	C	D	E	A	B	C	D	E
1 LiBH ₄	1	1	1	1	53 LiAlH(OEt) ₃	1	1	2	2
2 LiBH ₃ CH ₃	0	2	1	1	54 LiAlH(OBu-tert) ₃	0	1	2	1
3 LiBH ₂ (2,4,6-PhMe ₃) ₂	1	1+	1	1	55 LiAlH(OPent-tert) ₃	1	1	1	1
4 LiBH ₂ SH ₂	0	2	2	2	56 NaAlH ₄	0	1	1	2
5 LiBHEt ₃	1	1+	1	2	57 NaAlH ₃ (iso-Bu)	1	2+	1	1
6 LiBH(N ₂ C ₃ H ₃) ₃	0	1+	1	1	58 NaAlH ₃ (C≡C-C ₄ H ₉ -n)	0	2	1	1
7 LiBH(N ₂ C ₃ HMe ₂ -3,5) ₃	1	1+	1	1	59 NaAlH ₃ (OBu-tert)	1	2+	2	2
8 LiBH(SMe) ₃	0	2	2	2	60 NaAlH ₂ Me ₂	0	1+	1	1
9 NaBH ₄	1	1+	1+	1+	61 NaAlH ₂ Et ₂	1	1+	1	1
10 NaBH ₃ Et	0	2	1+	1+	62 NaAlH ₃ (n-Pr) ₃	0	1+	1	1
11 NaBH ₃ (n-Pr)	1	2	1+	1+	63 NaAlH ₃ (iso-Bu) ₃	1	1+	1	1
12 NaBH ₃ CN	0	1+	1+	1+	64 NaAlH ₃ (C≡C ₄ H ₉ -n) ₂	0	1+	1	1
13 NaBH ₃ CONHMe	1	1	1	1	65 NaAlH ₃ (OBu-tert) ₂	1	1	2	2
14 NaBH ₂ (2,4,6-PhMe ₃) ₂	0	1+	1	1	66 NaAlH ₃ (OCH ₂ CH ₂ NMe ₂) ₂	0	1	2	1
15 NaBHMe ₃	1	1+	1	1	67 NaAlH ₂ (OCH ₂ CH ₂ OMe) ₂	1	1	2	1
16 NaBHEt ₃	0	1+	1	1	68 NaAlHMe ₃	0	1+	1	1
17 NaBH(n-Pr) ₃	1	1+	1	1	69 NaAlHET ₃	1	1+	1	1
18 NaBH(OMe) ₃	0	2	2+	2+	70 NaAlH(n-Pr) ₃	0	1+	1+	1+
19 NaBH(O-Bu-t) ₃	1	2+	2+	2+	71 NaAlH(iso-Bu) ₃	1	1+	1+	1+
20 NaBH(OOCH ₃) ₃	0	2	2+	2+	72 NaAlHPh ₃	0	1+	1+	1
21 NaBH(OCH ₂ CH ₂ OMe) ₃	1	2+	2+	2+	73 NaAlH(NEt ₂) ₃	1	1	1	1
22 NaBH(N ₂ C ₃ H ₃) ₃	0	1+	1	1	74 NaAlH(OEt) ₃	0	1	2	2
23 NaBHF ₃	1	1+	2+	2	75 NaAlH(OBu-tert) ₃	1	1	2	1
24 NaBH(n-Bu) ₃	0	1+	1	1	76 NaAlH(OCH ₂ CH ₂ NEt ₂) ₃	0	2	1	1
25 NaBH(OPr-iso) ₃	1	2+	2+	2+	77 NaAlH(OCH ₂ CH ₂ OCH ₃) ₃	1	2	2	1
26 NaBH ₃ NMe ₂	0	2	1	1	78 KAlH ₄	0	1+	1+	1+
27 KBH ₄	1	1+	1+	1+	79 KAlH ₂ Me ₂	1	1+	1+	1+
28 KBH ₃ CN	0	1+	1+	1+	80 KAlH ₂ Et ₂	0	1+	1+	1+
29 KBH ₃ CONHMe	1	1+	1+	1+	81 KAlH ₂ (n-Pr) ₂	1	1+	1+	1+
30 KBH ₃ CONMe ₂	0	1+	1+	1+	82 KAlH ₂ (iso-Bu) ₂	0	1+	1+	1+
31 KBH ₃ (COOEt)	1	1	1+	1+	83 KAlHMe ₃	1	1+	1+	1+
32 KBH ₃ F	0	1	1+	1+	84 KAlHEt ₃	0	1+	1+	1+
33 KBH ₂ (N ₂ C ₃ H ₃) ₂	1	1+	1	1	85 KAlH(n-Pr) ₃	1	1+	1+	1+
34 KBHEt ₃	0	1+	1+	1+	86 KAlH(iso-Bu) ₃	0	1+	1+	1+
35 KBH(NC ₄ H ₄) ₃	1	1+	1	1	87 KAlHPh ₃	1	1+	1	1+
36 KBH(N ₂ C ₃ H ₃) ₃	0	1+	1	1	88 KAlHCl ₃	0	2+	1	1
37 KBH(N ₂ C ₃ HMe ₂ -3,5) ₃	1	1+	1	1	89 RbAlH ₄	1	1+	1+	1+
38 RbBH ₄	0	1+	1+	1+	90 CsAlH ₄	0	1+	1+	1+
39 CsBH ₄	1	1+	1+	1+	91 LiGaH ₄	1	2+	2+	2+
40 CsBH(NC ₄ H ₄) ₃	0	1+	1	1+	92 NaGaH ₄	0	2	2	2+
41 LiAlH ₄	1	1	2	2+	93 KGaH ₄	1	1	1+	1
42 LiAlH ₂ Me ₂	0	1+	2	2+	94 RbGaH ₄	0	1+	1+	1+
43 LiAlH ₂ (iso-Bu) ₂	1	1+	2	2	95 CsGaH ₄	1	1+	1+	1+
44 LiAlH ₂ (CN) ₂	0	1	2	2	96 LiBH ₃ SH	0	2	1	1
45 LiAlH ₂ (OMe) ₂	1	2	2	2	97 LiBHMMe ₃	2	1+	1	1
46 LiAlHMe ₃	0	1+	2+	2+	98 LiBH(OMe) ₃	0	1	2+	2+
47 LiAlHET ₃	1	1+	2	2	99 LiBH(OCH ₂ CH ₂ OMe) ₃	2	2	2+	2+
48 LiAlH(iso-Bu) ₃	0	1+	1	1	100 NaBH(OEt) ₃	0	2+	2+	2+
49 LiAlH(C ₅ H ₉ -cyclo) ₃	1	1+	1+	1+	101 NaBH(OCH ₂ CH ₂ NMe ₂) ₃	2	2+	2+	2+
50 LiAlH(C ₇ H ₁₃ -cyclo) ₃	0	1+	1+	1+	102 KBH(OCH ₂ CH ₂ OCH ₃) ₃	0	2	2+	2
51 LiAlHPh ₃	1	1+	1+	1	103 LiAlH ₂ (OC ₃ H ₇ -iso) ₂	2	2	2	2
52 LiAlH(NEt ₂) ₃	0	1	1	1+	104 LiAlH ₂ (OBu-sec) ₂	0	2	2	2

Table 2. Continued.

A	B	C	D	E	A	B	C	D	E
105	LiAlH(OPr-iso) ₃	2	1+	2	1	163	LiAlH ₃ (OC ₁₀ H ₁₉)		2
106	LiAlH(OBu-sec) ₃	0	1	1	1	164	LiAlH ₂ Cl		2+
107	NaAlH ₂ Et	2	2	1	1	165	LiAlH ₂ (Et) ₂		2
108	NaAlH ₂ (OCH ₂ CH ₂ NMe ₂)	0	2+	2	2	166	LiAlH ₂ (Pr-n) ₂		2
109	NaAlH ₂ (OCH ₂ CH ₂ OCH ₃)	2	2+	2	1	167	LiAlH ₂ (C ₆ H ₅ -cyclo) ₂		1
110	NaAlHCl ₂	0	2	2	2	168	LiAlH ₂ (PhMe) ₂		1
111	LiInH ₄	2	2+	2+	2+	169	LiAlH ₂ (OEt) ₂		2
112	LiInHBr ₃	0	2+	2+	2+	170	LiAlH ₂ (OBu-tert) ₂		2
113	LiInHCl ₂	2	2+	2+	2+	171	LiAlH ₂ (OC ₁₀ H ₁₉) ₂		1
114	LiInHI ₃	0	2+	2+	2	172	LiAlH ₂ Cl ₂		2+
115	LiTiH ₄	2	2+	2+	2+	173	LiAlH ₂ Br ₂		2+
116	LiBH ₂ CN				1	174	LiAlH ₂ I ₂		2
117	LiBH ₂ NC ₄ H ₉				1	175	LiAlH(C ₂ H ₅) ₃		1
118	LiBH ₂ OH				2	176	LiAlH(C ₁₀ H ₂₁ -n) ₃		1
119	LiBH ₂ OMe				2	177	LiAlH(NPh ₂) ₃		1+
120	LiBH ₂ OBu-tert				2	178	LiAlH(OMe) ₃		2
121	LiBH(Bu-n) ₃				1	179	LiAlH(OPr-n) ₃		1
122	LiBH ₂ OH ₂				2	180	LiAlH(OBu-n) ₃		1
123	LiBH(Bu-sec) ₃				1	181	LiAlH(C ₆ H ₅ -n) ₃		1
124	LiBH(Bu-iso) ₃				1	182	LiAlH(OC ₆ H ₁₃ -n) ₃		1
125	LiBHPPh ₃				1	183	LiAlH(OC ₆ H ₁₁ -cyclo) ₃		1
126	LiBH(OH) ₃				2+	184	LiAlH(OPh) ₃		1
127	LiBF ₃				2+	185	LiAlHCl ₂		2+
128	NaBH ₂ D				1+	186	LiAlHBr ₂		2+
129	NaBH ₂ (C ₂ H ₅)				1	187	LiAlHI ₂		2
130	NaBH ₂ COOH				1	188	NaAlH ₂ (OMe)		2
131	NaBH ₂ COOMe				1	189	NaAlH ₂ (O-furfuryl)		2
132	NaBH ₂ OH				1	190	NaAlH ₂ (OMe) ₂		2
133	NaBH ₂ (OPh)				1	191	NaAlH ₂ (OEt) ₂		2
134	NaBH ₂ (OPhCl- <i>p</i>)				1	192	NaAlH ₂ (OPr-n) ₂		2
135	NaBH ₂ (OPhCl- <i>m</i>)				1	193	NaAlH ₂ (OPr-iso) ₂		2
136	NaBH ₂ F				1	194	NaAlH ₂ (OPh) ₂		1
137	NaBH ₂ (PMe ₂)				1	195	NaAlH ₂ (OCH ₂ CH ₂ OEt) ₂		2
138	NaBH ₂ (OH) ₂				2	196	NaAlH ₂ - (OCH ₂ CH ₂ OPr-n) ₂		1
139	NaBH ₂ F ₂				2	197	NaAlH ₂ - (OCH ₂ CH ₂ OPr-iso) ₂		2
140	NaBHD ₂				1+	198	NaAlH ₂ - (OCH ₂ CH ₂ OBu-n) ₂		1
141	NaBHPPh ₃				1	199	NaAlH ₂ (OCH ₂ CH ₂ OPh) ₂		1
142	NaBH(OH) ₂				2+	200	NaAlH ₂ - (OCHMeCH ₂ OMe) ₂		2
143	NaBH(OBu-n) ₂				2+	201	NaAlH ₂ - (OCMe ₂ CH ₂ OMe) ₂		2
144	KBH ₃ (NMe ₂)				1+	202	NaAlH ₂ (O(CH ₂) ₄ OMe) ₂		1
145	KBH ₃ (NEt ₂)				1+	203	NaAlH(C ₆ H ₁₁ -cyclo) ₃		1+
146	KBH ₃ (OH)				1+	204	NaAlH(C ₆ H ₅) ₃		1+
147	KBH ₃ (N ₃ C ₃ HMe ₂ -3,5) ₂				1	205	NaAlH(CH ₂ Ph) ₃		1
148	KBH ₃ (OH) ₂				1	206	NaAlH(OMe) ₃		2
149	KBH(Pr-iso) ₃				1	207	NaAlH(OPr-n) ₃		2
150	KBH(Bu-sec) ₃				1	208	NaAlH(OPr-iso) ₃		2
151	KBH(C ₆ H ₁₁ -sec) ₃				1	209	NaAlH(OBu-sec) ₃		2
152	KBH(C ₆ H ₅ -cyclo) ₃				1	210	NaAlH(OPh) ₃		1
153	KBH(C ₆ H ₁₁ -cyclo) ₂				1	211	NaAlH(OCH ₂ CH ₂ OEt) ₃		1
154	KBH(OH) ₃				2	212	NaAlH(OCH ₂ CH ₂ OPh) ₃		1
155	RbBH ₃ (N(Bu-n) ₂)				1	213	NaAlH(OCMe ₂ CH ₂ OMe) ₃		1
156	RbBH ₃ (C ₆ H ₅) ₃				1	214	NaAlH- (OCH ₂ CH ₂ CH ₂ OMe) ₃		1
157	LiAlH ₂ Me				2				
158	LiAlH ₂ Et				2				
159	LiAlH ₂ (C ₂ H ₅)				2				
160	LiAlH ₂ (OMe)				2+				
161	LiAlH ₂ (OEt)				2+				
162	LiAlH ₂ (OBu-tert)				2				

Table 2. Continued.

A	B	C	D	E	A	B	C	D	E
215	NaAlH(O(CH ₂) ₄ OMe) ₃		1		220	CsInH ₄			1+
216	LiGaH ₃ (Me)		2+		221	NaTiH ₄			2+
217	NaInH ₄		2+		222	KTiH ₄			2
218	KInH ₄		1		223	RbTiH ₄			2
219	RbInH ₄		1		224	CsTiH ₄			1

variables was decreased first to 38 and then to 28 variables without an increase in the error rate in the classification of the training set. For the ligands, such variables were deleted which showed low relevance for all three ligands. When further deletions were made, the error rate increased and we therefore stopped at the number of 28 (see Table 1).

3. *Final analysis.* The classification with these 28 variables was essentially the same with $A=5, 4, 3, 2$ and 1 . For simplicity of interpretation we have preferred the results with $A=1$. The resulting parameters β_i for class 1 and 2 are shown in Table 1. The parameters α_i for the retained 28 variables are, naturally, the same as for the 49 variable case. The residual standard deviation with $A=1$ is 0.06.

The classification of the training and test sets with the 28 variables and $A=1$ using the parameters in Table 1 is shown in Table 2; for interpretation, see below.

4. *Verification.* To study the significance of the above classification, we divided the training set into two halves, letting the first half continue being the training set and making the second half constitute the test set with "known answers". These data were then analysed with $A=1$ and the same 28 variables as above. Thus, the parameters α and β were calculated on the basis of the first half only and the classes of complexes in the second half were "predicted" on the basis of these parameters. The results shown in Table 2 are encouraging. The error rate in the classification of the test set was 10 of 47 for the first class and 2 of 10 for the second class. This is significantly better than chance ($\chi^2=19.1, p<0.001$) which indicates that the parameters in Table 2 indeed have a real prediction power for the stability of complex hydrides.

DISCUSSION

Extraction of relevant variables (features). The results of computation show that the variables related to fundamental atomic properties of alkaline metals (atomic, covalent and ionic radii, the first ionization energy and electronegativity) exhibit significantly higher relevance than the variables related to derived properties (melting point, boiling point and density). The relevance of the variables proposed for the metals of the Group III B does not differ markedly in this respect.

The computation extracts five relevant variables for each ligand from eleven variables originally proposed. Three features (molecular weight, number of atoms and number of substituents on the first atom of ligand) represent the bulkiness of the ligand, whereas the remaining two, π -accepting ability and electronegativity, characterize the nature of the first ligand atom. In the formulation of the model we have not included the nature of the atoms of the ligand chain, other than the first one. This might play a role in the classification of some special type of complex hydrides (see below).

Factors influencing the performance of the classification. First, the results of the classification are based on the characterization of the atoms interacting directly with the central atom B. In the present model, the influence of the atoms located further in the chain of a ligand is described only by their bulkiness, not by their nature. Nevertheless, the high correctness of the classification (about 75 %) shows, that important characteristics of the crucial atoms have been included. An increase in the degree of correctness may be expected when the variables for nature of the other ligand atoms are considered (as well as the other additional variables).

Secondly, the correctness of the classification is surprisingly high in spite of the fact that the selection of the hydrides used for training as "stable" and "unstable" is not based on the rigid definition of "stability" and "instability", respectively. The situation in complex hydride chemistry forced us to use as samples such hydrides which were proclaimed by authors on the basis of more or less direct observations as "stable" or "unstable" compounds. But we are not able to check the situation. Often it is difficult to make a decision at all, *e.g.* some hydrides are stable in the solid state and unstable when dissolved in a solvent. But PR is a powerful method for classification of systems with low information level. The present work shows that it is sufficient if the learning set is correctly classified in the majority of cases; the individual details are less important as long as the average contains the correct information.

Furthermore, the correctness of the classification is surprisingly high if we also consider the shortage of "unstable" hydrides for training which may exert a substantial influence on the learning procedure.

Finally, possible errors in the data used and an information noise arising during their working up might also negatively influence the performance of the classification.

The total effect of the above four factors is probably responsible for the main part of about 25 % incorrectness in our classification case.

Note. When only a half of the original training set is used, the percentage of correct classification does not markedly change, but about 10 % of cases are re-classified.

General trends. The simplified model, MODEL-1, reveals some general fundamental trends in "stability" of hydrides ABH_nD_{4-n} as related to the ligand D:

1. The hydrides with ligands attached to the central atom B by means of atom with free electron pair(s) are significantly less stable than those where D are alkyls. The stability of alkoxo derivatives ($D = OR$) might be to some extent overestimated in literature.

2. On the other hand, hydrides with ligands bonded to the atom B by an atom with unsaturated bond are more stable than alkyl hydrides of comparable size. This finding favours the study of hydrides of this type.

3. The hydrides ABH_nD_{4-n} where $A = Li, Na, K$ and B equals boron or aluminium seem to be stable when D is small. Very interesting exceptions in this series are exhibited by $LiAlH_nD_{4-n}$ hydrides which, using our MODEL-1, are "unstable" in the case of small size of D. This is evident, *e.g.*, from the "instability" of the derivatives with $D = CH_3$ and C_2H_5 . The destabilizing effect of small size of the ligands in $LiAlH_nR_{4-n}$ seems to dominate even over the above stabilizing effect 2. The naturally extreme case is $LiAlH_4$ with very small substituents H^- which is classified into class of "unstable" compounds. But this classification can be correct if we consider that $LiAlH_4$ is thermodynamically metastable.¹⁰ Some other ABH_4 are also classified as "unstable" ones (Table 3).

Non-generality of MODEL-1. The classification of hydrides in the training set with some donor atom in an appropriate position in the chain of the ligands is in some cases dubious because of our *a priori* knowledge. Thus, $NaBH(OCH_2CH_2OCH_3)_3$,¹¹ $NaAlH_2(OCH_2CH_2OCH_3)_3$ ¹² and $NaAlH(OCH_2CH_2OCH_3)_3$ ¹² classified as "unstable" are to a significant extent stable. On the other hand, a majority of included items, namely $LiBH(OCH_2CH_2OCH_3)_3$,¹¹ $NaBH(OCH_2CH_2N(CH_3)_2)_3$,¹¹ $KBH(OCH_2CH_2OCH_3)_3$,¹¹ $NaAlH_3(OCH_2CH_2OCH_3)_3$ ¹² and $NaAlH_2(OCH_2CH_2N(CH_3)_2)_3$ ¹² are classified "correctly" as "unstable" hydrides. These facts speak for a non-generality of our MODEL-1 in this respect.

Very interesting is also the classification of the above type of hydrides of "unknown stability". The subset of the hydrides of the general formula $NaAlH_2(O \cdots OR)_2$ (where \cdots represents a carbon chain) is split by the MODEL-1 into "stable" and "unstable" classes, respectively. This classification is evidently

Table 3. Classification of ABH_4 according to the MODEL-1. Hydrides under the border line are classified as "unstable" compounds, otherwise as "stable" ones.

$LiBH_4$	$NaBH_4$	KBH_4	$RbBH_4$	$CsBH_4$
$LiAlH_4$	$NaAlH_4$	$KAlH_4$	$RbAlH_4$	$CsAlH_4$
$LiGaH_4$	$NaGaH_4$	$KGaH_4$	$RbGaH_4$	$CsGaH_4$
$LiInH_4$	$NaInH_4$	$KInH_4$	$RbInH_4$	$CsInH_4$
$LiTlH_4$	$NaTlH_4$	$KTlH_4$	$RbTlH_4$	$CsTlH_4$

sensitive even to very small changes of R. Thus, $\text{NaAlH}_2(\text{OCH}_2\text{CH}_2\text{OC}_2\text{H}_5)_n$,¹⁴ is classified as "stable", whereas very similar $\text{NaAlH}_2(\text{OCH}_2\text{CH}_2\text{OC}_2\text{H}_5)_n$,¹⁵ and $\text{NaAlH}_2(\text{OCH}_2\text{CH}_2\text{OC}_2\text{H}_7\text{-iso})_n$,¹⁴ are classified as "unstable" ones. This fact calls for consideration of some secondary variables for the MODEL-2 as additional ones to the variables representing the effect of a donor atom in the chain of ligand.

The classification of the $\text{NaAlH}(\text{O} \cdots \text{OR})_2$ hydrides as "stable" species is in accordance with the generally found higher stability of these monohydrido derivatives over corresponding dihydrido compounds.

Parameters alpha *

1. Alfa 4, 5 and 6 (for radii) are positive for class 1 and negative for class 2; the average size of metal A is larger for "stable" hydrides than four "unstable" ones.

2. Alfa 7 (for the first ionization energy) is negative for class 1 and positive for class 2; more easily ionizable alkaline metal gives (on average) more stable complex hydrides. This is a natural consequence of point 1 and the correlations in a group in the periodic system.

3. Alfa 8 (for electronegativity) is negative for class 1 and positive for class 2; on average, the complex hydrides with low electronegativity of alkaline metal are relatively more stable than those with high electronegativity. This is also a correlation of the same nature as point 2. Hence, considering the connection between variables 1 through 5 in a group in the periodic system, these variables mainly express the place of atom A in the group.

4. Alfa 11 (for density of the central atom) is negative for class 1 and positive for class 2; this shows that the central metal atoms with low density give generally more stable hydrides than specifically heavier ones.

5. Alfa 32 (π -acceptor ability of the first atom of the second ligand) is negative for class 1 and positive for class 2; the influence of the difference in accepting ability of the first ligand atom is highest for the 2nd ligand and stability is higher in the case of acceptors.

* Only significant parameters were used for interpretation.

Parameters beta *

1. For class 2, the parameters beta 12, 13, 14 (size) for central atoms B are negative, while the parameters beta 27, 38, 49 (electronegativity of the first atom), beta 22, 33, 44 (number of substituents on the first atom) and beta 18, 29, 40 (number of atoms in the chain) for the ligands are positive; thus, a larger atom B can be compensated not only by a less electronegative first atom, but also by a less bulky ligand. In the same way as for atom A, the parameters beta 15 and 16 representing the nature of the central atom B are positive as a consequence of the correlations in the periodic system.

2. For class 1, the parameters beta 4, 5, 6 expressing the size of alkaline metals A are positive, whereas the parameters beta 27, 38, 49, beta 22, 33, 44, beta 18, 29, 40 and beta 17, 28, 39 (molecular weight of D) for ligands are negative; thus, a larger atom A is compensated by a less electronegative first ligand atom as well as by a less bulky ligand.

Further, the negative signs of the parameters beta 7 and 8 for the first ionization energy and electronegativity, representing the nature of the alkaline metals A, show that a decrease in these two factors potentiates the trends found for the ligands.

Conclusion

We feel that PR methodology gives an interesting opportunity to investigate complex structure-reactivity relationships. Considering the crudeness of the present model, exhibited by the rather simple nature of the variables used, the results of the present investigation is encouraging. We are presently working on an extension of MODEL-1 to include more variables and on an extension of the data set to more cases in the training set.

Acknowledgement. We wish to thank Dr. K. Kuchynka from the J. Heyrovský Institute of Physical Chemistry and Electrochemistry in Prague for many stimulating discussions and comments during the chemical formulation of the problem. The project has been supported by the Swedish Natural Science Research Council.

* Only significant parameters were used for interpretation.

REFERENCES

1. Hajos, A. *Komplexe Hydride*. In Kirsten, W., Ed., *Organisch-präparative Methoden*, Band 4, VEB Deutscher Verlag der Wissenschaften, Berlin 1966.
2. Štrouf, O. and Wold, S. *Data Base 1. Stability of Complex Hydrides (MODEL-1)*, Umeå University, Umeå 1977.
3. Kowalski, B. R. *Anal. Chem.* 47 (1975) 1152 A.
4. Kowalski, B. R. In Klopfenstein, C. E. and Wilkins, C. L., Eds., *Computers in Chemical and Biochemical Research*, Vol. 2, Academic, New York 1974.
5. Jurs, P. C. and Isenhour, T. L. *Chemical Applications of Pattern Recognition*, Wiley-Interscience, New York 1975.
6. Redl, G., Cramer, IV, R. D. and Berkoff, C. E. *Chem. Soc. Rev.* 3 (1974) 273.
7. Kanal, L. *IEEE Trans. Inf. Theory* 20 (1974) 697.
8. Wold, S. *Pattern Recognition* 8 (1976) 127.
9. Wold, S. and Sjöström, M. In Chapman, N. B. and Shorter, J., Eds., *Advances in Linear Free Energy Relationships*, Vol. 2, Plenum, London 1977.
10. Ref. 1., p. 80.
11. Sochor, P., Kadlecová, H. and Štrouf, O. *Collect. Czech. Chem. Commun.* 40 (1975) 3177.
12. Čásenský, B., Macháček, J. and Abrham, K. *Collect. Czech. Chem. Commun.* 36 (1971) 2648.
13. Macháček, J., Čásenský, B. and Abrham, K. *Collect. Czech. Chem. Commun.* 38 (1973) 343.
14. Kříž, O., Čásenský, B. and Štrouf, O. *Collect. Czech. Chem. Commun.* 38 (1973) 2076.
15. Čásenský, B., Macháček, J. and Vit, J. *Czech. Pat.* 134 720 (15 Jan. 1970).

Received January 3, 1977.

Effect of Cyclic Polyether on the Base Catalyzed Disproportionation of 1,3-Cyclohexadiene

ALI EL-KHOLY,* E. HAANAES and O. A. ROKSTAD

Laboratory of Industrial Chemistry, The Norwegian Institute of Technology, The University of Trondheim, N-7034 Trondheim-NTH, Norway

The base catalyzed disproportionation of 1,3-cyclohexadiene to benzene and cyclohexene was studied in 1,4-dioxane at 50 °C with potassium *tert*-butylate as catalyst in the presence of varying amounts of 18-crown-6-cyclic polyether. The reaction kinetics showed a second order dependence on the cyclohexadiene concentration. At constant concentration of potassium *tert*-butylate the reaction rate increased moderately when the molar ratio of cyclic polyether to potassium *tert*-butylate was increased up to about one, at higher ratio the rate was almost constant. The increase in rate produced by the cyclic polyether may be explained as a result of complexation of the potassium ion with cyclic polyether, thus, increasing the catalytic activity of potassium *tert*-butylate. The cyclic ether seems to have only a small effect on the hydride transfer reaction step.

Cyclohexadiene and some of its derivatives are known to disproportionate thermally^{1,2} and catalytically over metals,^{3,4} cationic metal complexes^{5,6} and strong bases.^{7,8} The homogeneous base catalyzed disproportionation of 1,3-cyclohexadiene to benzene and cyclohexene was shown to take place quantitatively when the diene was treated with potassium *tert*-butylate in dimethyl sulfoxide.⁹ The isomerization between 1,3- and 1,4-cyclohexadiene was so rapid that either isomer would lead to the same result. In *tert*-butyl alcohol solution only isomerization was observed with no disproportionation. Substituents in the cyclohexadiene ring may decrease⁹ or increase¹⁰ the rate of disproportionation.

The aim of the present work was to study the effect of 18-crown-6-cyclic polyether on the catalytic activity of potassium *tert*-butylate on the disproportionation of 1,3-cyclohexadiene in the low polar solvent, 1,4-dioxane.

The overall reaction is



EXPERIMENTAL

Reagents. 1,4-Dioxane "Zur Analyse" from E. Merck AG. The contaminating peroxides were removed by reduction with sodium metal and small amounts of water. The dioxane was refluxed with sodium metal for 48 h, then distilled under an atmosphere of nitrogen, b.p. 100–101 °C. *tert*-Butyl alcohol "für Chromatographie" from E. Merck AG. 1,3-Cyclohexadiene "pure" from Koch-Light Laboratories. The purity was checked by mass spectrometry and gas chromatography. The gas chromatographic analysis showed that the diene contained about 0.1 % of both benzene and cyclohexene. Potassium metal from Riedel de Haën AG. 18-Crown-6-cyclic polyether from A/S Borregaard, melting point 39–41 °C. The purity was checked by gas chromatography where only one peak was observed. Methanol "zur Analyse" from E. Merck AG. Nitrogen "highly purified" from Norsk Hydro a.s. Nitrogen (including argon) contents higher than 99.99 %, water content less than 0.001 %.

Preparation of catalyst solution. The potassium *tert*-butylate was prepared by reacting a solution of *tert*-butyl alcohol (about 1.0 mol/l) in 1,4-dioxane with an excess of potassium metal. The reaction mixture was then refluxed for 48 h. Traces of hydroxide were allowed to settle, and the solution was kept under nitrogen

* Present address: Chemistry Dept., Faculty of Science, Moharram Bey, Alexandria, Egypt.

atmosphere. The concentration of the stock solution was determined by titration with standardized hydrochloric acid solution. The catalyst solutions for the kinetic runs were prepared by diluting the stock solution with purified 1,4-dioxane to the required concentration. The preparations were carried out in an atmosphere of nitrogen.

Procedure. The disproportionation reaction was carried out in septum bottles with teflon "Mininert" valves (from Precision Sampling Corporation). The required amount of cyclic ether was weighed into the bottle, then 10 ml of potassium *tert*-butylate solution was added. The mixture was kept in a thermostat until it attained the required temperature. The reaction was started by adding 1 ml of 1,3-cyclohexadiene to the mixture and the bottle was vigorously shaken. The entire procedure was performed under nitrogen atmosphere. At different time intervals (using 1 ml syringe) 0.5 ml samples were withdrawn. The samples were quenched by dilution with methanol to the appropriate concentration for spectrophotometric analysis.

The reaction was followed by measuring the UV absorption maximum at 259 nm characteristic for 1,3-cyclohexadiene. These measurements were carried out on a Hilger & Watts H 999 Ultrascan spectrophotometer.

Some samples were also analyzed by gas chromatography. A Perkin Elmer F 33 gas chromatograph was used, equipped with flame ionization detector and a 3 mm column, 4 m long, filled with 13½% bis-2-methoxyethyl adipate and 6½% di(2-ethyl hexyl)sebacate on Chromosorb P, 80–100 mesh.

RESULTS AND DISCUSSION

The disproportionation of 1,3-cyclohexadiene catalyzed by potassium *tert*-butylate in 1,4-dioxane in the presence of 18-crown-6-cyclic polyether was shown by gas chromatographic analysis to give benzene and cyclohexene in a 1:1 molar ratio as the only reaction products even at high conversion. Conversions measured by UV absorption were found to agree well with gas chromatographic analysis. Thus, at high conversion the UV spectrum showed the characteristic absorption for benzene.

The disproportionation of 1,3-cyclohexadiene was found to follow second order kinetics. This is in accordance with the result of Hofman *et al.*⁸ for the base catalyzed reaction in dimethyl sulfoxide at 55 °C. The integrated form of the second order rate equation may be written as

$$(c_0 - c)/c = c_0 kt$$

Acta Chem. Scand. A 31 (1977) No. 5

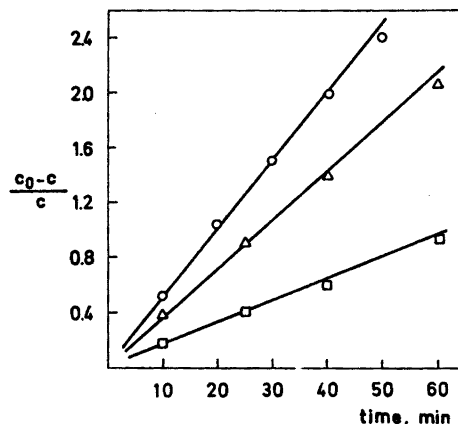


Fig. 1. Second order plots for the base catalyzed disproportionation of 1,3-cyclohexadiene in 1,4-dioxane solution. Temperature 50 °C. Concentration of potassium *tert*-butylate 0.38 mol/l. Concentration of cyclohexadiene at start $c_0 = 0.95$ mol/l. Concentration of 18-crown-6-cyclic polyether: 0.46 mol/l (○), 0.27 mol/l (△), 0.09 mol/l (□).

where c_0 is the initial concentration of 1,3-cyclohexadiene, c is the concentration at time t , and k is the second order rate constant.

Fig. 1 shows examples of the second order plot of the kinetic runs. The second order rate constant was evaluated from the slope of the straight line.

Fig. 2 shows the effect of the cyclic ether concentration on the experimental second order

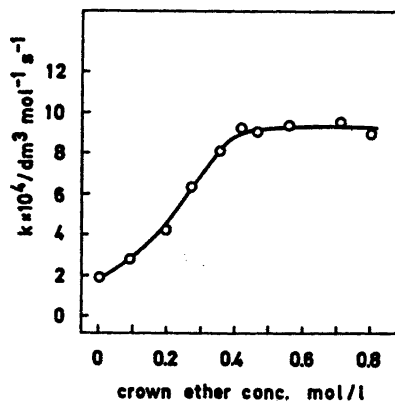


Fig. 2. Effect of the crown ether concentration on the second order rate constant at constant concentration of potassium *tert*-butylate, 0.38 mol/l. Temperature 50 °C.

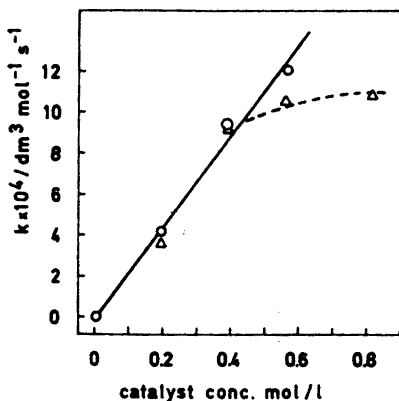
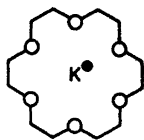


Fig. 3. Effect of the concentration of potassium *tert*-butylate on the second order rate constant at two different concentrations of cyclic polyether: 0.41 mol/l (Δ), 0.55 mol/l (O). Temperature 50 °C.

rate constant at constant concentration of potassium *tert*-butylate of 0.38 mol/l at 50 °C. The rate constant increased with increasing ratio cyclic ether/potassium *tert*-butylate up to a molar ratio close to 1. At higher ratios the rate constant remained almost constant.

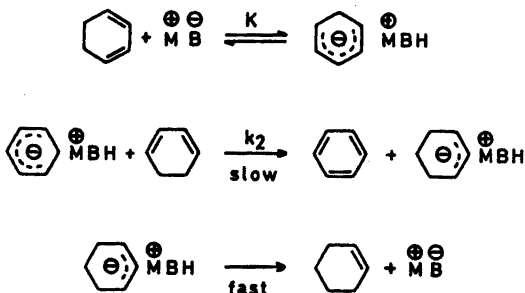
Such a result may be explained by complexation of the alkali metal ion with the macrocyclic polyether,¹¹ leading to an increased activity of the catalyst. The crown ethers are known to fill effectively the coordination sites of alkali metal cations and to convert contact ion pairs into separated ions or separated ion pairs.^{12,13} The upper limit of the reaction rate reached at a molar ratio of cyclic ether/potassium *tert*-butylate of about 1:1 is in accordance with a 1:1 complex between 18-crown-6-cyclic polyether and potassium ions.^{14,15}



In Fig. 3 the experimental second order rate constant is plotted as a function of the concentration of *tert*-butylate at two given concentrations of cyclic ether. There seems to be a linear relationship between the rate constant and the concentration of potassium *tert*-butylate

when the amount of cyclic ether is sufficient to complex all the potassium ions present. The observed increase in rate is less when the concentration of potassium *tert*-butylate was increased above the concentration of cyclic ether. This smaller increase might be due to the smaller catalytic activity of the non-separated ion pairs.

The observed kinetics may be explained by the following mechanism.



which involves carbon-carbon hydride ion transfer as the rate determining step. The proton transfer reaction is supposed to be fast compared to the hydride transfer, and the first step would then be an equilibrium. It is assumed that the carbanion is not free but form an ion pair complex with the cation and the alcohol formed in the first step. The cation may at the same time be strongly complexed to a cyclic polyether molecule as mentioned above.

From the proposed mechanism the following theoretical rate expression is derived

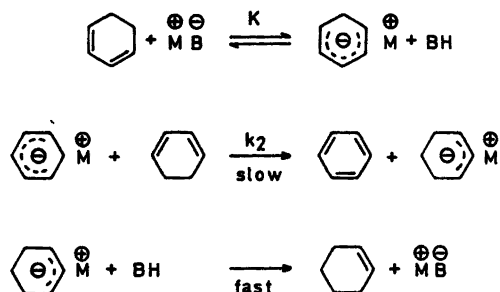
$$r = k_2 K [A]^2 [M B]$$

where k_2 is the rate constant for the second step and K is the equilibrium constant for the first step. $[A]$ is the concentration of cyclo-

hexadiene and $[M B]$ is the concentration of catalyst. The reaction is second order with respect to cyclohexadiene and first order with respect to catalyst as observed.

With potassium *tert*-butylate in dioxane solution the concentration of carbanion is expected to be very small and so also the concentration of *tert*-butyl alcohol formed in the first step. If the solvent or the reactants have not been completely dry, then the water present would

react with the *tert*-butylate forming *tert*-butyl alcohol. In such a case a previously suggested mechanism^{8,10} may explain the observed kinetics for the disproportionation reaction



This mechanism gives the following rate expression

$$r = k_2 K [A]^2 [M^{\oplus} B^{\ominus}] / [B H]$$

If the amount of *tert*-butyl alcohol (BH) formed from moisture present is much higher than the amount formed in the first step, then the concentration of the alcohol [BH] in the denominator may be considered constant, and the rate would be second order with respect to cyclohexadiene and first order with respect to catalyst. In this case the amount of moisture

is supposed to be independent of $[M^{\oplus} B^{\ominus}]$ and $[M^{\oplus} B^{\ominus}] \gg [B H]$.

A similar mechanism was suggested for the reaction in the presence of sodium amide in liquid ammonia.⁷

The role of the cation in hydride transfer reactions in liquid phase is not well understood. The effect of cyclic ether on the hydride transfer step is probably small. The addition of cyclic ether is expected to shift the equilibrium (first step) to the right (K increases) because the *tert*-butylate anion has a more concentrated negative charge than the cyclohexadienyl anion. The effective ionic radius of the latter may therefore be considered larger than that of the former anion. Complexation of the cation with the cyclic ether increases the effective radius of the cation. The effect of increasing the size of the cation on the basicity of the ion pair, and on the cation-anion bond strength is higher with a small than with a large anion.

Acta Chem. Scand. A 31 (1977) No. 5

In base catalyzed isomerization reactions where a proton transfer is rate determining, the effect of cyclic ether on the rate is expected to be very large.¹⁶ In proton abstraction reactions there is a great difference in reactivity between separated ion pairs and contact ion pairs of the base. In this work on the disproportionation of cyclohexadiene, involving a rate determining hydride transfer step, we find only a moderate increase in rate by adding cyclic ether. At a constant base concentration of 0.38 mol/l the rate constant increased only 5 times when the cyclic ether concentration was increased from zero to 0.41 mol/l.

The use of dimethyl sulfoxide as a solvent would be expected to have about the same effect on catalyst activity as addition of crown ether to the dioxane solution. In both cases the catalyst ion pairs are transferred into the separated forms. Interpolation of the data of Hofmann *et al.*⁸ really shows that the rate constant for the disproportionation reaction in dimethyl sulfoxide at 50 °C is about the same as found in dioxane with cyclic polyether added. The small difference (about 25 % higher rate constant in dimethyl sulfoxide) may be attributed to the ability of the sulfoxide to bind strongly alcohols by hydrogen bonding. It is known that cyclohexadiene does not disproportionate in *tert*-butyl alcohol as solvent,⁸ and some *tert*-butyl alcohol is reversibly formed in the first step of the reaction. The failure of 1,3-cyclohexadiene to undergo disproportionation in *tert*-butyl alcohol as a solvent⁸ may be explained by the two effects: (1) Deactivation of the base by hydrogen bonds, and (2) strong solvation of the carbanion with rapid transfer of a proton from the alcohol solvent to the cyclohexadienyl anion.

Acknowledgement. The authors wish to acknowledge the support of this investigation by NORAD. The cyclic polyether used in this work was a generous gift from A/S Borregaard.

REFERENCES

1. Erofeev, B. V., Naumova, S. F. and Tyskalo, L. G. *Dokl. Akad. Nauk Beloruss. SSR* 11 (1967) 911; See *Chem. Abstr.* 68 (1968) 86872.
2. Totani, N., Totani, Y., Kusaka, H. and Matsuo, N. *Seikei Daigaku Kogakubu Kagaku Hokoku* (1972) 1065; see *Chem. Abstr.* 77 (1972) 141693.

3. Freidlin, L. Kh. and Popova, I. L. *Izv. Akad. Nauk SSSR Ser. Khim.* (1968) 1514; see *Chem. Abstr.* 69 (1968) 105590.
4. Freidlin, L. Kh., Popova, I. L. and Dadze, T. P. *Izv. Akad. Nauk SSSR Ser. Khim.* (1972) 2204; see *Chem. Abstr.* 78 (1973) 71065.
5. Mosely, K. and Maitlis, P. M. *Chem. Commun.* (1969) 1156.
6. Green, M. and Kuc, T. A. *J. Chem. Soc. Dalton Trans.* (1972) 832.
7. Mironov, V. A., Fedorovich, A. D. and Akhrem, A. A. *Izv. Akad. SSSR Ser. Khim.* (1974) 1340; see *Chem. Abstr.* 81 (1974) 104814.
8. Hofman, J. E., Argabright, P. A. and Schriesheim, A. *Tetrahedron Lett.* (1964) 1005.
9. Bottini, A. T. and Schear, W. J. *J. Org. Chem.* 30 (1965) 3205.
10. Wyman, D. P. and Song, I. H. *J. Org. Chem.* 32 (1967) 4139.
11. Pedersen, C. J. *J. Am. Chem. Soc.* 89 (1967) 7017.
12. Wong, K. H., Konizer, G. and Smid, J. *J. Am. Chem. Soc.* 92 (1970) 666.
13. Roitman, J. N. and Cram, D. J. *J. Am. Chem. Soc.* 93 (1971) 2231.
14. Pedersen, C. J. *J. Am. Chem. Soc.* 92 (1970) 386.
15. Gray, R. T. and Reinhoudt, D. N. *Tetrahedron Lett.* (1975) 2109.
16. Rokstad, O. A., Ugelstad, J. and Lid, H. *Acta Chem. Scand.* 23 (1969) 782.

Received December 22, 1976.

The Crystal Structure of *O*-Ethyl *S*-(2-Carboxyethyl) Dithiocarbonate

BIRGITTA DAHLÉN

Department of Structural Chemistry, Institute of Medical Biochemistry, University of Göteborg,
P.O.B., S-400 33 Göteborg 33, Sweden

O-Ethyl *S*-(2-carboxyethyl) dithiocarbonate is triclinic (*PI*) with cell dimensions $a = 10.935(13)$, $b = 10.106(7)$, $c = 4.671(5)$ Å, $\alpha = 85.59(10)$, $\beta = 81.87(10)$ and $\gamma = 113.99(9)^\circ$. All intramolecular distances and angles are in agreement with those reported for the two homologues with a hexanoic and dodecanoic fatty acid residue. The molecules are V-shaped as the two homologues but whereas the bend in the latter occurs at the sulfur atom it takes place at the adjacent carbon atom in the title compound. The molecules pack as *Z*-shaped dimers with normal van der Waals contacts.

The title compound belongs to a series of dithiocarbonate fatty acids which have been studied at this Department. These examinations were proposed by Professor A. Fredga of Uppsala University who also provided the crystals for the X-ray work.

Previously the structures of *O*-ethyl *S*-(5-carboxypentyl) dithiocarbonate (ESP)¹ and *O*-ethyl *S*-(11-carboxyundecyl) dithiocarbonate (ESU)² have been determined. This present structure, *O*-ethyl *S*-(2-carboxyethyl) dithiocarbonate, was determined in order to make a comparison with a homologue with a short fatty acid residue.

CRYSTAL DATA

Molecular formula	$C_6H_{10}S_2O_3$
Unit cell, triclinic	$a = 10.935(13)$, $b = 10.106(7)$, $c = 4.671(5)$ Å, $\alpha = 85.59(10)$, $\beta = 81.87(10)$, $\gamma = 113.99(9)^\circ$
<i>V</i>	461.69 Å ³
Molecular weight	194.27
<i>Z</i>	2

D_c	1.397 g cm ⁻³
Space group	<i>P</i> $\bar{1}$
λ	1.54051 Å
μ	47.48 cm ⁻¹ for CuK α radiation

A crystal with dimensions 0.10 × 0.19 × 0.44 mm was mounted along the *c*-axis. Intensity data were collected on a Picker FACS1 automatic diffractometer using the Vanderbilt disc-oriented program system.³ Reflexions were measured up to $2\theta = 120^\circ$ with a total scan width of 2.8° . 10 s background counts were taken on both sides of the peak. 1367 independent reflexions were recorded of which 221 were less than $3\sigma(I)$ and considered as unobserved. Corrections were made for the Lorentz and polarization factors and for absorption and extinction.

STRUCTURE DETERMINATION

The structure was solved with MULTAN 74⁴ with an E_{\min} of 1.4. The set with the highest figure of merit was used for an initial *E*-map which showed the positions of all non-hydrogen atoms.

All heavier atoms were refined with full matrix least-squares using isotropic temperature factors during the first three cycles and thereafter anisotropic ones. The structure refined to an *R*-value of 0.08 and a Fourier difference map now revealed the positions of all the hydrogen atoms. These atoms were included in the refinement using isotropic *B*-values and the structure refined to a final *R*-factor of 0.047. Shift/error values for all atoms, hydrogen atoms

included, were then less than 0.02 with an average value of 0.003. The weighting scheme used during the final stage of the refinement was $\omega = 1/[1 + \{(|F_o| - 5)/5\}^2]$. Atomic scattering factors were taken from Cromer and Mann⁶ except for hydrogen atoms where those of Stewart, Davidson and Simpson⁴ were used. The sulfur atoms were corrected for anomalous dispersion.⁷ A list of the observed and calculated structure factors may be obtained from this Department.

The calculations were performed on a DEC10 computer using the X-Ray System of Crystallographic Programs.⁸ System modifications for the DEC10 were made by Dr. Steve Ernst at University of Pittsburgh and by Dr. Robert Pearson at this Department. Interface routines between X-RAY72 and display programs⁹ have been written by Prof. S. Abrahamsson. They allow a direct inspection of the Fourier output on a graphic display and input of selected

atoms into the structure factor calculation program. By using these routines the time between reading the diffractometer data into the computer and obtaining a structure refined to an *R*-value of 0.08 was less than 2 h.

DESCRIPTION OF THE STRUCTURE

The final atomic parameters are given in Table 1. The atomic numbering and interatomic distances and angles are shown in Figs. 1 and 2.

Intramolecular distances and angles are all in agreement with the corresponding ones found in ESP and ESU. The C-H bonds range from 0.91 to 1.01 Å with a mean value of 0.94 Å. The C-C-H angles are 105–115° with a mean value of 110° and the H-C-H angles are 100–118° with a mean value of 108°.

The conformation of the ethyldithiocarbonate group is very similar to that observed in the two homologues. It is nearly planar (Table 2) with

Table 1. Fractional atomic coordinates and thermal parameters with standard deviations. The anisotropic temperature factors are in the form

$$\exp [-2\pi^2 (h^2 a^{*2} U_{11} + k^2 b^{*2} U_{22} + l^2 c^{*2} U_{33} + 2hka^* b^* U_{12} + 2hla^* c^* U_{13} + 2klb^* c^* U_{23})].$$

	<i>x</i>	<i>y</i>	<i>z</i>	<i>U</i> ₁₁	<i>U</i> ₂₂	<i>U</i> ₃₃	<i>U</i> ₁₂	<i>U</i> ₁₃	<i>U</i> ₂₃
(a) All values have been multiplied by 10 ⁴									
S(1)	3318(1)	3423(1)	6415(2)	509(4)	493(4)	669(5)	242(4)	-67(4)	-163(4)
S(2)	2663(1)	285(1)	5501(2)	610(5)	465(4)	734(5)	241(4)	-42(4)	-92(4)
O(1)	796(3)	4527(3)	7351(6)	826(17)	583(15)	819(17)	404(13)	-373(14)	-269(13)
O(2)	-400(3)	3143(3)	4406(6)	736(17)	551(15)	717(16)	341(13)	-226(14)	-169(12)
O(3)	4786(2)	2715(2)	2939(5)	484(13)	550(13)	643(13)	226(11)	7(11)	-134(11)
C(1)	311(3)	3355(3)	6455(6)	385(15)	526(18)	444(16)	231(14)	8(13)	-90(14)
C(2)	487(3)	2045(4)	7685(8)	496(19)	486(18)	535(19)	218(15)	51(15)	-16(16)
C(3)	1744(4)	2418(4)	8997(7)	650(22)	596(21)	443(17)	347(18)	-28(15)	-63(16)
C(4)	3616(3)	2038(3)	4817(7)	453(17)	507(17)	525(17)	240(14)	-133(14)	-125(14)
C(5)	5314(4)	1836(5)	1239(9)	626(23)	727(24)	663(23)	389(20)	-73(19)	-218(20)
C(6)	6598(5)	2904(7)	-782(14)	592(26)	1088(40)	944(35)	314(27)	60(24)	-306(32)

(b) All values have been multiplied by 10³. The isotropic temperature factors are given as *U*'s.

H(21)	45(3)	144(3)	622(7)	40(7)
H(22)	-33(4)	149(4)	907(8)	65(10)
H(31)	179(4)	157(4)	975(8)	58(10)
H(32)	180(4)	307(4)	1027(9)	65(11)
H(51)	546(4)	123(5)	265(10)	78(12)
H(52)	461(5)	128(5)	28(10)	87(13)
H(61)	638(7)	353(7)	-191(15)	142(27)
H(62)	729(6)	349(6)	38(12)	105(16)
H(63)	702(6)	238(7)	-175(13)	123(19)
H(24)	-55(5)	377(5)	393(10)	76(14)

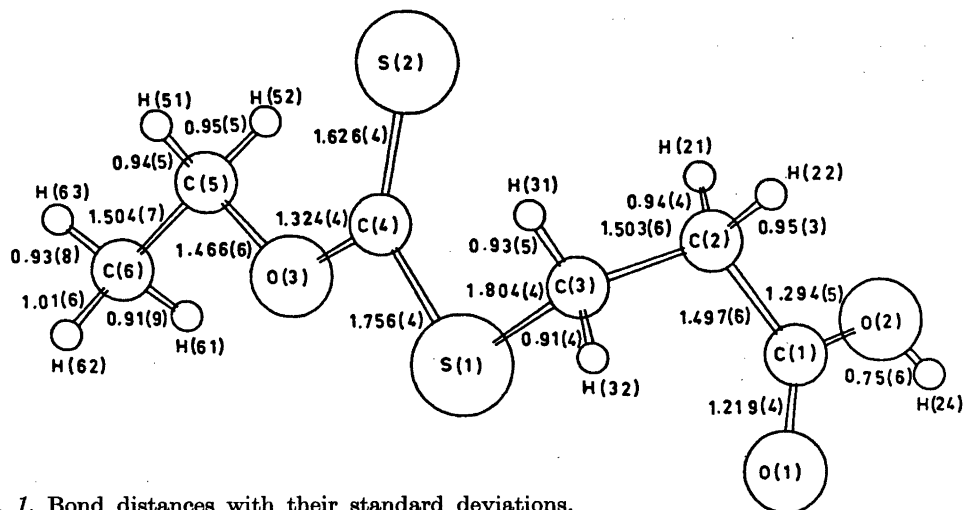


Fig. 1. Bond distances with their standard deviations.

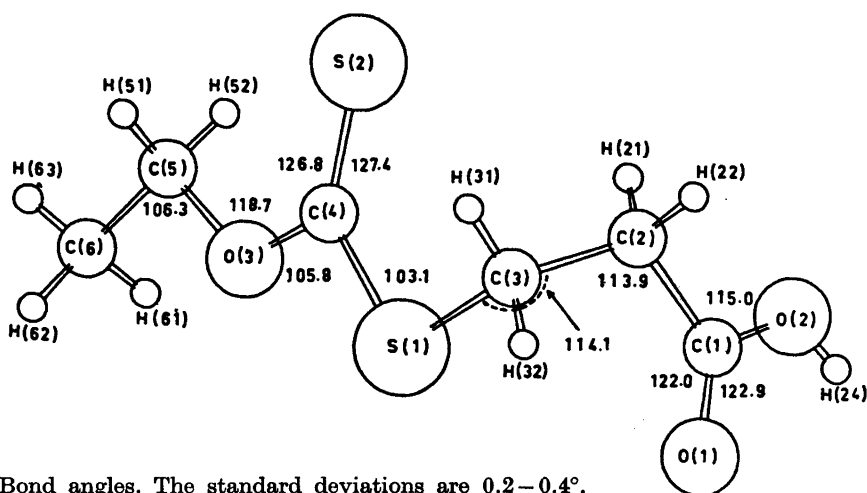


Fig. 2. Bond angles. The standard deviations are 0.2–0.4°.

all atoms within 0.003 Å of the plane through S(1)–S(2)–C(4)–O(3) except C(6) which deviates 0.069 Å. The molecule is V-shaped with a sharp bend at the ω -atom in the hydrocarbon chain. The torsion angle S(1)–C(3)–C(2)–C(1) is 62.3°. The molecules in ESP and ESU are also V-shaped but the bend there occurs at the sulfur atom S(1).

The carboxyl group forms an angle of 25.7° with the plane through the short hydrocarbon chain while these angles are 24.9 and 17.6°, in ESP and ESU respectively.

The molecular packing is shown in a stereoscopic drawing (Fig. 3) and in Fig. 4. The molecules are hydrogen bonded over centres of symmetry to Z-shaped dimers. The planes of the carboxyl groups are separated by 0.148 Å with the two hydrogen atoms halfway (0.07 Å) between these two planes. The O...O and H...O contacts are 2.653(5) and 1.91(6) Å, respectively, and the O–H...O angle is 174(5)°. These values are in agreement with those observed in ESP and ESU and in long chain fatty acids.

Table 2. Distances from some least-squares planes through the molecule.

Atoms defining plane (*)

I C(1), C(2), C(3)

II S(1), S(2), O(3), C(4)

	Distances (Å)	
	I	II
S(1)	1.464	0.001*
S(2)	2.423	0.001*
O(1)	-0.454	-1.863
O(2)	0.502	-3.508
O(3)	3.726	0.001*
C(1)	*	-2.254
C(2)	*	-1.307
C(3)	*	0.042
C(4)	2.633	-0.002*
C(5)	4.897	0.000
C(6)	5.944	-0.069

The dimers are arranged so that rows of parallel carboxyl group planes run in the *c*-axis direction. The rows are enclosed by ethyl end groups pointing towards the centres of the carboxyl group dimers. The shortest ethyl contacts are O(1)···H(62) (2.66 Å) and O(2)···H(63) (2.89 Å).

In order to accommodate the bulky S(2) atom the dimers are translated relative to each other so that S(2) finds space between ethyl groups and carboxyl groups of neighbouring molecules (Fig. 4). S(2) also forms close intramolecular contacts to H(31) (2.72 Å) and to H(52) (2.80 Å) and is furthermore in contact with molecules in the *c*-axis direction with the shortest S···H contacts of 3.23 and 3.32 Å. The shortest methylene group contacts are 2.92 Å in the ethyl end (H(51)···H(51)) and 2.81 Å (H(22)···

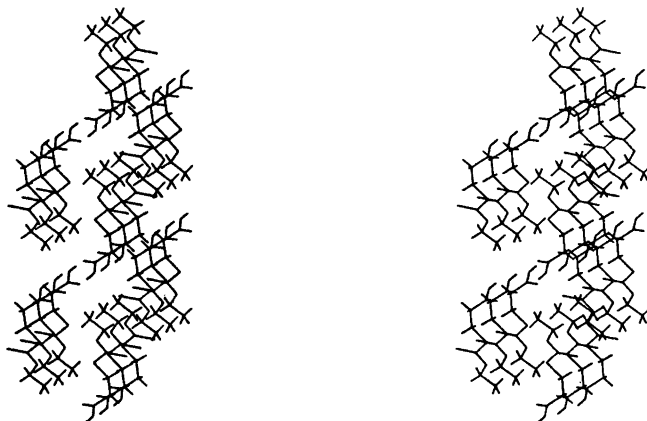


Fig. 3. Stereoscopic drawing.

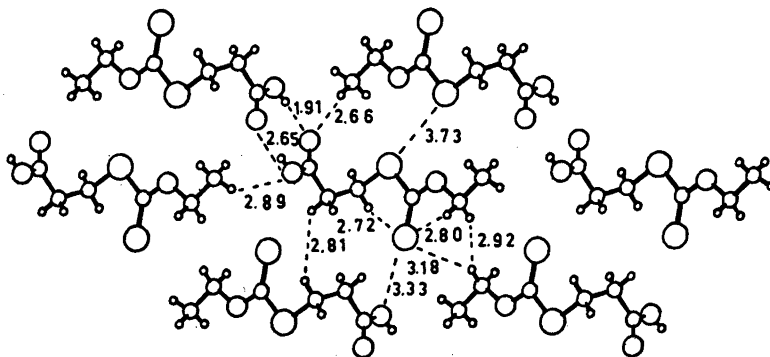


Fig. 4. The molecular packing as seen along the *c*-axis. Important inter- and intramolecular contacts are indicated.

H(31)) in the propionic acid residue. On the more smooth side the molecular separation is determined by the contacts between carbonyl oxygens and methyl ends as mentioned above and by the S(1)...S(1) distance of 3.73 Å.

The packing arrangement is different from that in the two homologues where the carboxyl groups are forced into a hydrocarbon chain matrix and the S(2) atom is accommodated between ethyl end groups.

I wish to thank Professor A. Fredga for providing the crystals, Professor S. Abrahamsson for valuable comments and Mr. M. Lundmark for technical assistance. Grants in support of the Department were obtained from the Swedish Medical Research Council, the Swedish Board for Technical Development, the Wallenberg Foundation and the U.S. Public Health Service (GM-11653).

REFERENCES

1. Abrahamsson, S. and Innes, M. *Acta Crystallogr. B* 30 (1974) 721.
2. Abrahamsson, J. and Pearson, R. *Acta Crystallogr. B* 32 (1976) 2745.
3. Lenhert, P. G. *J. Appl. Crystallogr.* 8 (1975) 568.
4. Declercq, J. P., Germain, G., Main, P. and Woolfson, M. M. *Acta Crystallogr. A* 29 (1973) 231.
5. Cromer, D. T. and Mann, J. B. *Acta Crystallogr. A* 24 (1968) 321.
6. Stewart, R. F., Davidson, E. R. and Simpson, W. T. *J. Chem. Phys.* 42 (1965) 3175.
7. Cromer, D. T. and Liberman, D. *J. Chem. Phys.* 53 (1970) 1891.
8. Stewart, J. M., Kruger, G. J., Ammon, H. L., Dickinson, C. and Hall, S. R. *The X-RAY System, version of June 1972, Tech. Rep. TR-192*, Computer Science Center, Univ. of Maryland, Baltimore 1972.
9. CHEM. Crystal Structure Search Retrieval, DCRT, National Institutes of Health, Bethesda 1974.
10. Dahlén, B., Lundén, B.-M. and Pascher, I. *Acta Crystallogr. B* 32 (1976) 2059.

Received December 16, 1976.

The Crystal and Molecular Structure of 3,4-Dimethyl-6-phenyl-5,6-diaza-1,6a-dithiapentalene

LARS P. DARMO and LARS K. HANSEN

Department of Chemistry, Institute for Mathematical and Physical Sciences, University of Tromsø, Box 790, N-9001 Tromsø, Norway

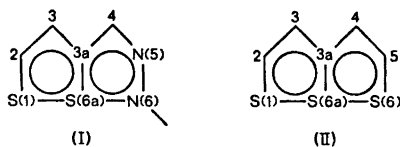
The title compound crystallizes in the monoclinic space group $P2_1/c$ with $Z=4$ and with unit cell dimensions, $a=12.778(2)$, $b=12.172(2)$, $c=7.875(3)$ Å, and $\beta=104.10(2)^\circ$.

X-Ray intensity data were collected on a Siemens AED diffractometer using $\text{MoK}\alpha$ radiation, and the structure was solved by Patterson methods and refined by full matrix least squares.

The molecule is almost planar with the methyl groups in eclipsed orientation, the H—H distances are 2.25(5) Å.

The bond lengths in the central ring system are: S(1)—S(6a)=2.493(1) and S(6a)—N(6)=1.779(2) Å with the angle S(1)—S(6a)—N(6)=174.37(5)°, S(1)—C(2)=1.681(2), S(6a)—C(3a)=1.742(2), N(6)—N(5)=1.324(2), C(2)—C(3)=1.370(2), C(3)—C(3a)=1.418(2), C(3a)—C(4)=1.416(2), and C(4)—N(5)=1.321(2) Å. Corrections for rigid body libration have been applied.

It has been shown through the structure analysis of 2-*t*-butyl-6-phenyl-5,6-diaza-1,6a-dithiapentalene¹ that the 5,6-diaza-1,6a-dithiapentalene system (I) is analogous to the 6a-thiathiophene system (II).²



The lengths of the S—S bonds in 6a-thiathiophenes are influenced by substituents,^{3,4} and the effect of methyl and phenyl groups on the S—S bonding have been found to agree with the results from CNDO/2 calculations.⁵

The degree to which substituents might affect the S—S—N bonding in I was thought to be of

interest, and the present structure study was therefore carried out.

STRUCTURE ANALYSIS

A sample of the title compound was generously supplied by D. H. Reid.^{6,7} The crystals are red needles elongated along *c*.

Crystal data $\text{C}_{11}\text{H}_{11}\text{N}_2\text{S}_2$, M.W=248.37. Monoclinic, space group $P2_1/c$ with $Z=4$ $a=12.778(2)$ Å, $b=12.172(2)$ Å, $c=7.875(3)$ Å, $\beta=104.10(2)^\circ$ $V=1187.9$ Å³ $D_x=1.389$ g/cm³, $D_m=1.385$ g/cm³ $\mu_{\text{MoK}\alpha}=4.10$ cm⁻¹

Unit cell dimensions and intensity data were measured on a paper-tape controlled Siemens AED diffractometer using $\text{MoK}\alpha$ radiation.

The cell dimensions quoted above are the results of a least squares treatment of the 20 values of 18 high order reflections measured at 20 °C.

The intensities of 2789 independent reflections within $\theta=28^\circ$ were measured by means of the five-value scan technique.^{4,8} 2154 of these with intensities greater than $2\sigma(I)$ were regarded as observed. The crystal used for intensity data collection had the dimensions 0.15 mm × 0.3 mm × 0.4 mm in the axial directions.

Corrections for Lorentz and polarization effects were carried out but absorption corrections were considered unnecessary.

Scattering factors for sulfur, nitrogen and carbon were taken from the *International*

Table 1. Atomic coordinates in fractions of corresponding cell edges. The numerical values of the standard deviations in parentheses are chosen to be in the range 3–30.

Atom	<i>x</i>	<i>y</i>	<i>z</i>
S(1)	0.33816(4)	0.02325(4)	0.41899(8)
S(6a)	0.21398(4)	0.17385(4)	0.38069(7)
N(6)	0.13512(11)	0.29047(11)	0.35668(21)
N(5)	0.17992(12)	0.38725(12)	0.36696(22)
C(4)	0.27719(14)	0.37539(14)	0.39481(25)
C(3a)	0.31265(12)	0.26631(14)	0.40714(23)
C(3)	0.41163(13)	0.22896(15)	0.43753(25)
C(2)	0.42826(16)	0.11817(17)	0.44493(29)
C(7)	0.49921(18)	0.30650(22)	0.4622(4)
C(8)	0.33809(22)	0.47978(19)	0.4052(4)
C(9)	0.03116(14)	0.28396(15)	0.32457(26)
C(10)	-0.02495(19)	0.37788(21)	0.3061(4)
C(11)	-0.12560(20)	0.36918(26)	0.2725(4)
C(12)	-0.17217(18)	0.26947(25)	0.2608(4)
C(13)	-0.11705(19)	0.17694(25)	0.2804(4)
C(14)	-0.01552(17)	0.18325(20)	0.3128(4)
H(2)	0.4911(15)	0.0964(16)	0.465(3)
H(10)	0.0092(20)	0.4460(22)	0.312(4)
H(11)	-0.1669(21)	0.4322(24)	0.267(4)
H(12)	-0.2453(18)	0.2652(19)	0.233(3)
H(13)	-0.1484(19)	0.1093(21)	0.275(3)
H(14)	0.0211(19)	0.1224(20)	0.325(3)
H(7,1)	0.4719(19)	0.3608(22)	0.564(3)
H(7,2)	0.5551(16)	0.2634(17)	0.4905(28)
H(7,3)	0.5281(18)	0.3481(18)	0.356(3)
H(8,1)	0.4141(22)	0.4799(20)	0.312(4)
H(8,2)	0.3007(17)	0.5354(19)	0.3854(29)
H(8,3)	0.3522(16)	0.4869(17)	0.5205(29)

Tables,⁹ and the scattering factor curve used for hydrogen was taken from a paper of Stewart *et al.*¹⁰

The structure was solved by the heavy-atom (S) method, and the hydrogen positions were found from difference maps. The atomic parameters were refined by full matrix least squares (see Ref. 11) to an *R* of 0.033.

Final atomic coordinates and temperature parameters are given in Tables 1 and 2. The final structure factor list is available on request.

Rigid body analyses for various parts of the molecule have been carried out according to the method of Schomaker and Trueblood.¹² The parts treated in this way are:

1. The atoms of the fused five-membered rings plus C(7), C(8) and C(9).
2. The phenyl carbons plus N(6).

The corresponding librational tensors L_1 and L_2 are given in Table 3. One sees from the values there that the libration of the phenyl group, L_2 , is more pronounced than the libration of the other part. The eigenvector of L_2 corresponding to the largest libration, 10.9°, is directed roughly along N(6)–C(9)–C(12). The effect of this individual libration of the phenyl group on the “observed” bond lengths is discussed below.

Table 2. Temperature parameters U_{ij} (Å²) for sulfur, nitrogen and carbon, and U (Å²) for hydrogen. The expressions used are $\exp\{-2\pi^2(h^2a^*U_{11} + \dots + 2hka^*b^*U_{12} + \dots)\}$ and $\exp\{-8\pi^2U(\sin^2\theta/\lambda^2)\}$. The numerical value of the standard deviations in parentheses are chosen to be in the range 3–30. The U_{ij} 's and the U 's are multiplied by 10⁴ and 10⁵, respectively.

Atom	U_{11}	U_{22}	U_{33}	U_{12}	U_{23}	U_{13}
S(1)	643(3)	463(3)	73(5)	59(3)	-7(3)	-336(3)
S(6a)	455(3)	410(3)	602(3)	-9(3)	-7(3)	-169(3)
N(6)	499(9)	421(8)	666(12)	19(7)	-6(8)	-200(8)
N(5)	604(10)	406(8)	705(12)	-10(7)	-6(8)	-220(9)
C(4)	520(10)	439(10)	554(13)	-41(9)	-22(9)	-175(9)
C(3a)	468(9)	439(10)	444(11)	-52(8)	-9(9)	-117(9)
C(3)	479(10)	522(12)	509(12)	-18(9)	-2(10)	-151(9)
C(2)	517(12)	615(13)	712(15)	77(10)	-21(12)	-238(11)
C(7)	570(13)	701(16)	853(20)	-90(12)	43(15)	-292(14)
C(8)	793(17)	446(11)	925(21)	-91(12)	7(13)	-377(16)
C(9)	457(10)	525(11)	588(13)	36(9)	-20(10)	-146(9)
C(10)	683(15)	605(14)	1221(24)	85(13)	50(15)	-397(15)
C(11)	674(16)	888(19)	1422(27)	220(16)	64(19)	-449(17)
C(12)	488(12)	1088(21)	959(20)	72(14)	-58(17)	-273(13)
C(13)	624(14)	837(18)	1158(23)	-96(14)	-83(17)	-334(15)
C(14)	614(13)	592(14)	1143(22)	19(11)	-73(14)	-383(14)

Table 2. Continued.

Atom	<i>U</i>	Atom	<i>U</i>
H(2)	69(8)	H(7,1)	108(9)
H(10)	119(10)	H(7,2)	78(6)
H(11)	135(10)	H(7,3)	91(8)
H(12)	102(7)	H(8,1)	121(9)
H(13)	113(9)	H(8,2)	85(8)
H(14)	99(8)	H(8,3)	82(7)

Table 3. Rigid body libration tensors L_1 and L_2 for various parts of the 3,4-dimethyl-6-phenyl-5,6-diaza-1,6a-dithiapentalene molecule.

Eigenvalues	Eigenvectors.	Direction		
cosinus $\times 10^4$ relative to <i>a</i> , <i>b</i> , and <i>c</i> *, respectively				
L_1	19.1 ($^\circ$) ²	-9041	2141	-3698
	6.2	-1786	-9757	-1266
	5.5	-3883	-486	9203
L_2	118.9	-9665	-1547	-2047
	14.2	-2211	980	9703
	10.6	-1302	9831	-1289

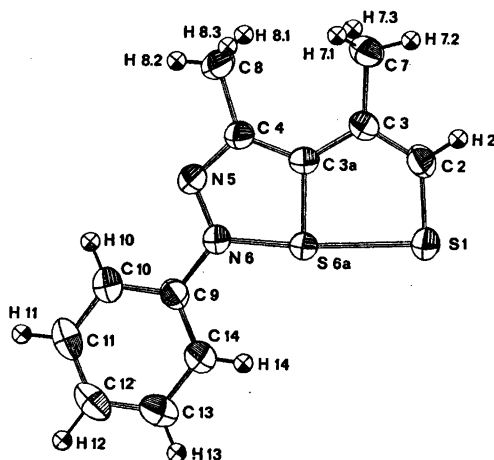


Fig. 1. The 3,4-dimethyl-6-phenyl-5,6-diaza-1,6a-dithiapentalene molecule with numbering of atoms. Thermal ellipsoids are shown. The thermal ellipsoids of the sulfur, nitrogen and carbon atoms enclose 50 % probability.

All the calculations mentioned above were carried out on the UNIVAC 1110 computer at the University of Bergen. The programs with a few exceptions, originate from the Weizmann Institute of Science, Rehovoth, Israel.

DISCUSSION

The molecular structure of the title compound with numbering of atoms is shown in Fig. 1.

The equation for the least squares plane through the atoms of the three rings with triple weight on sulfur is

$$-2.0930x + 0.1246y + 7.2047z = 2.3164$$

where *x*, *y*, and *z* are fractional coordinates. Deviations from the plane are, S(1) -0.004, S(6a) 0.005, N(6) 0.016, C(2) -0.001, C(3) -0.006, C(3a) -0.007, C(4) -0.007, N(5) 0.005, C(7) 0.007, C(8) -0.045, C(9) 0.009, C(10) 0.008, C(11) -0.018, C(12) -0.013, C(13) -0.011, C(14) 0.013 Å. The methyl groups are eclipsed and the H(8,3)-H(7,1) and H(8,1)-H(7,3) distances are both 2.25(5) Å.

Table 4. Bond lengths *l* in 3,4-dimethyl-6-phenyl-5,6-diaza-1,6a-dithiapentalene. Standard deviations are given in parentheses. The l^I and l^{II} values have been corrected for libration according to the librational tensors L_1 and L_2 , respectively. The Δl values correspond to maximum corrections.

Bond	$l(\text{Å})$	$l^I(\text{Å})$	$l^{II}(\text{Å})$	$\Delta l(\text{Å}) \times 10^3$
S(1)-S(6a)	2.487(1)	2.493		6
S(6a)-N(6)	1.774(2)	1.779		5
S(1)-C(2)	1.676(2)	1.681		5
S(6a)-C(3a)	1.737(2)	1.742		5
N(6)-N(5)	1.319(2)	1.324		5
C(2)-C(3)	1.366(2)	1.370		4
C(3)-C(3a)	1.416(2)	1.418		2
C(3a)-C(4)	1.412(2)	1.416		4
C(4)-N(5)	1.318(2)	1.321		3
C(3)-C(7)	1.509(3)	1.514		5
C(4)-C(8)	1.500(3)	1.505		5
N(6)-C(9)	1.411(2)	1.414	1.417	6
C(9)-C(10)	1.373(3)		1.397	24
C(10)-C(11)	1.378(3)		1.383	5
C(11)-C(12)	1.361(4)		1.381	20
C(12)-C(13)	1.354(4)		1.378	24
C(13)-C(14)	1.383(3)		1.388	5
C(14)-C(9)	1.373(3)		1.393	20

Table 5. Bond angles $\angle (ijk)$ in 3,4-dimethyl-6-phenyl-5,6-diaza-1,6a-dithiapentalene. Standard deviations are given in parentheses.

i	j	k	$\angle (ijk)^\circ$
C(2)	S(1)	S(6a)	88.9(1)
S(1)	S(6a)	N(6)	174.4(1)
S(1)	S(6a)	C(3a)	87.9(1)
C(3a)	S(6a)	N(6)	86.5(1)
S(6a)	N(6)	C(9)	123.7(1)
S(6a)	N(6)	N(5)	116.7(1)
N(5)	N(6)	C(9)	120.0(2)
N(6)	N(5)	C(4)	110.5(2)
N(5)	C(4)	C(8)	115.8(2)
N(5)	C(4)	C(3a)	116.3(2)
C(8)	C(4)	C(3a)	127.9(2)
C(4)	C(3a)	S(6a)	110.4(2)
C(4)	C(3a)	C(3)	128.8(2)
S(6a)	C(3a)	C(3)	120.8(2)
C(3a)	C(3)	C(7)	122.5(2)
C(3a)	C(3)	C(2)	118.5(2)
C(7)	C(3)	C(2)	119.0(2)
C(3)	C(2)	S(1)	123.9(2)
N(6)	C(9)	C(10)	120.4(2)
N(6)	C(9)	C(14)	120.1(2)
C(9)	C(10)	C(11)	119.2(2)
C(10)	C(11)	C(12)	121.5(2)
C(11)	C(12)	C(13)	119.2(2)
C(12)	C(13)	C(14)	120.5(2)
C(13)	C(14)	C(9)	120.1(2)
C(14)	C(9)	C(10)	119.5(2)

Bond lengths and angles with standard deviations, calculated from the values in Table 1, are listed in Tables 4 and 5, respectively. We

realize that the standard deviations probably should be multiplied by a factor of two to give a more realistic estimate.¹³

The bond lengths between non-hydrogen atoms have been corrected for libration,¹⁴ the l^I and l^{II} values in Table 4 are corrected according to the libration tensors L_1 and L_2 , respectively. The l^I values are chosen to represent the dimensions of the two fused rings as well as the lengths of the C(3)–C(7) and C(4)–C(8) bonds. For the dimensions of the phenyl group the l^{II} values are supposed to be the more reliable ones. The difference between these and the corresponding l^I values are due to the fact that the phenyl group has some individual libration relative to the other parts of the molecule, *cf.* Table 2. Attention should be drawn to column Δl of Table 4 where the values for C(9)–C(10), C(11)–C(12), C(12)–C(13), and C(14)–C(9) show the degree to which the individual libration of the phenyl group has affected the “observed” bond lengths.

The lengths of the S–C, C–C, N–N, and N–C bonds in the present structure (III) agree with those of the corresponding bonds in the 2-*t*-butyl-derivative (IV).¹ The length of the S–S bond, however, is significantly different in the two structures and so is the length of the S–N bond. This shows that substituents do affect the bonding in the S–S–N sequence of I.

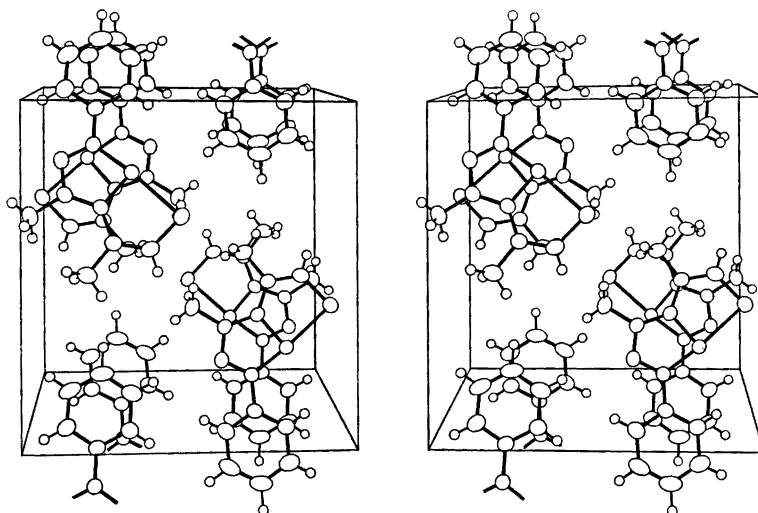
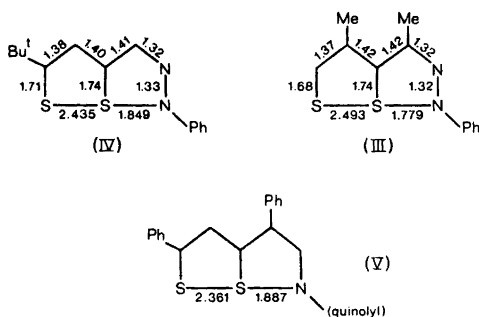


Fig. 2. Stereoview of the molecular packing.



The sums of the S-S and the S-N bond lengths in III, 4.272 Å, and in IV, 4.284 Å, are almost equal and close to the value 4.248 Å for the sum of the corresponding bond lengths in V.¹⁵ The S-N bond in the present structure, 1.779(2) Å, is only 1.7 % greater than the sum of the covalent radii for sulfur and nitrogen, 1.75 Å.^{16,17}

A stereoscopic view¹⁸ of the molecular packing in the unit cell is given in Fig. 2. There are no intermolecular contacts shorter than corresponding van der Waals distances.

Acknowledgements. The authors are indebted to Dr. D. H. Reid, Department of Chemistry, The University, St. Andrews, Scotland, for providing a sample of 3,4-dimethyl-6-phenyl-5,6-diaza-1,6a-dithiapentalene. We also wish to thank Professor Asbjørn Hordvik for helpful discussions.

REFERENCES

- Hansen, L. K. and Tomren, K. *Acta Chem. Scand. A* 31 (1977) 292.
- Hansen, L. K. and Hordvik, A. *Acta Chem. Scand.* 27 (1973) 411.
- Hordvik, A. and Sæthre, L. J. *Israel J. Chem.* 10 (1972) 239.
- Hansen, L. K., Hordvik, A. and Sæthre, L. J. In Sterling, C. J. M., Ed., *Organic Sulphur Chemistry*, Butterworths, London 1975, p. 1.
- Hansen, L. K., Hordvik, A. and Sæthre, L. J. *Chem. Commun.* (1972) 222.
- Christie, R. M., Ingram, A. S., Reid, D. H. and Webster, R. G. *Chem. Commun.* (1973) 92.
- Christie, R. M. and Reid, D. H. *J. Chem. Soc. Perkin Trans. 1* (1976) 228.
- Troughton, P. G. H. *Siemens Review XXXVII* (1970), Fourth Special Issue: X-Ray and Electron Microscopy News.
- International Tables for X-Ray Crystallography*, Kynoch Press, Birmingham 1968, Vol. III, p. 202.

- Stewart, R. F., Davidson, E. R. and Simpson, W. T. *J. Chem. Phys.* 42 (1965) 3175.
- Hordvik, A. and Sæthre, L. J. *Acta Chem. Scand.* 26 (1972) 3114.
- Schomaker, V. and Trueblood, K. N. *Acta Crystallogr. B* 24 (1968) 63.
- Hamilton, W. C. and Abrahams, S. C. *Acta Crystallogr. A* 26 (1970) 18.
- Cruickshank, D. W. J. *Acta Crystallogr.* 9 (1957) 757; 14 (1961) 896.
- Leung, F. and Nyburg, S. C. *Can. J. Chem.* 49 (1971) 167.
- Hordvik, A. *Acta Chem. Scand.* 20 (1966) 1885.
- Pauling, L. *The Nature of the Chemical Bond*, 3rd Ed., Cornell University Press, Ithaca, New York 1960.
- Johnson, C. K. *A Fortran Thermal Ellipsoid Plot Program for Crystal Structure Illustrations*, ORNL-3794, Oak Ridge National Laboratory, Oak Ridge 1965.

Received December 21, 1976.

Effects of Temperature on the ESR Spectra of the Radical Anion of Dihydrophenazine in Trifluoroacetic, Trichloroacetic and Acetic Acids

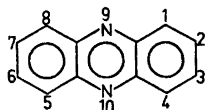
JORMA ELORANTA, IRMA PAANANEN and RAILI KOSKINEN

Department of Chemistry, University of Jyväskylä, Kyllikinkatu 1-3, SF-40100 Jyväskylä 10, Finland

The radical anion of dihydrophenazine was prepared in high vacuum in trifluoroacetic, trichloroacetic and acetic acids. When the temperature was decreased, the triplet with the largest coupling constant in the ESR spectrum disappeared and the intensities of the lines due to the nitrogen nuclei diminished noticeably in all three solvents. The effects are caused by a proton exchange reaction with the solvent.

Under acidic conditions, two protons are transferred to the phenazine molecule and form coordinate bonds with the nitrogens.^{1,2} Based on the UV and visible spectra, moreover, it has been proposed that the proton transfers are consecutive reactions and that a mono-protonated species is formed.³

The aim of this study was to investigate the protonations, the exchange reaction and the possible change in the conformation of the phenazine radical ion. The solvents, trifluoroacetic, trichloroacetic, and acetic acids were chosen in order to determine the possible existence of couplings of the fluorine and chlorine nuclei. In the first two solvents radical cations of some aromatic hydrocarbons have been obtained and the solvents have acted as oxidants.⁴⁻⁶



EXPERIMENTAL

The phenazine was from Fluka AG, the trifluoro- and trichloroacetic acids from Merck

AG, and acetic acid from Riedel-de Haën AG. All products were of analytical grade. The purity of phenazine was tested gas chromatographically.

The samples were prepared in high vacuum in an ampoule made of quartz glass.⁴⁻⁶

The ESR spectra were recorded with Varian model E-12 and E-9 spectrometers equipped with Varian variable temperature regulators. Varian 620/L Spectroscopy 100 computer facilities were used for the spectrum simulation.

The UV and visible spectra were recorded with a Beckman DK-2A spectrometer.

The theoretical spin densities were calculated on the Univac 1108 central computer of the Finnish Universities. Bond lengths taken from Pople and Beveridge⁸ were used in the INDO calculations.⁷

We were unable to prepare the radical of phenazine with tribromoacetic acid. The same results were obtained with and without thallium (III) trifluoroacetate as oxidizing agent, and thus the solvent alone was used as the oxidant.

RESULTS AND DISCUSSION

The formation of coordinate bonds between two protons and the nitrogen atoms in phenazine does not give rise to a radical unless the solvent can act as electron acceptor or donor. For instance, RH_2^{2+} and RH^+ do not give any ESR signal, but $\text{RH}_2^{\cdot+}$ and $\text{R}^{\cdot+}$ have an unpaired electron, the former being an anion radical with π -electron structure and the latter having the structure of a cation radical.

The formation of the dihydrophenazine radical anion (1) and the corresponding radical cation (2) may be written as follows:

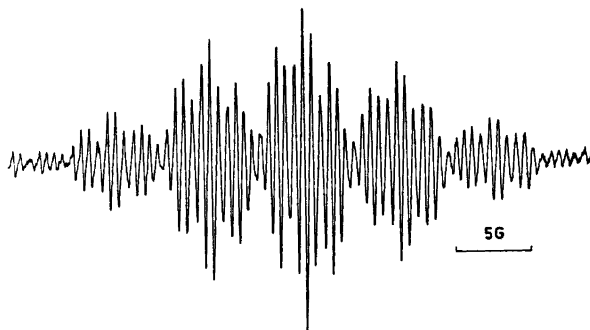


Fig. 1. The ESR spectrum of the radical anion of dihydrophenazine ($\text{RH}_2^{\cdot-}$) in trifluoroacetic acid at 338 K.

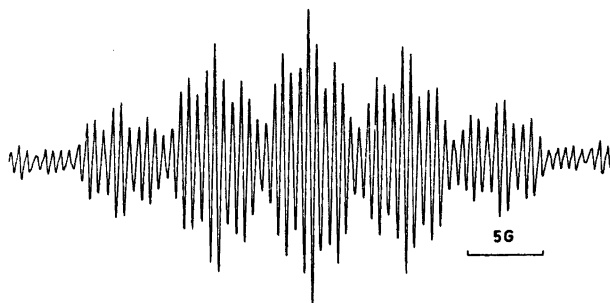
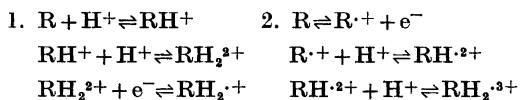


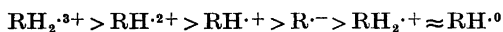
Fig. 2. The simulation of the ESR spectrum in Fig. 1 based on the coupling constants in Table 1 and line width of 0.12 G.



In strong acids like trifluoro- and trichloroacetic acids, radical cations are usually formed from aromatic hydrocarbons.^{5,6}

The radicals $\text{R}^{\cdot-}$ and $\text{RH}^{\cdot0}$ might appear as intermediates during the formation of the radical anion of dihydrophenazine, if the acceptance of the electron were the first stage of the reaction and the acceptance of two protons occurred only thereafter.

INDO calculations of the binding energy give the following order for the energies of the planar radicals:



The energy differences between the radicals are significant except for the last two radicals. According to the INDO calculations, reaction

scheme 2 seems improbable. Fig. 1 shows the ESR spectrum of the radical anion of dihydrophenazine in trifluoroacetic acid at 338 K. Fig. 2 shows the simulation of the same spectrum, based on the coupling constants presented

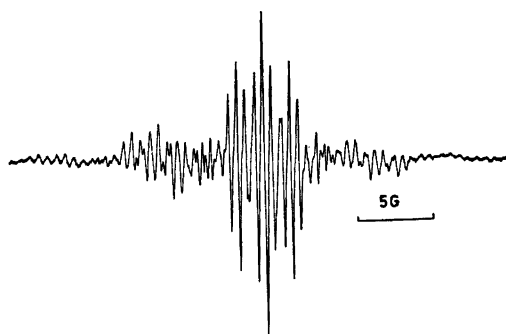


Fig. 3. The ESR spectrum of the radical anion of dihydrophenazine in trifluoroacetic acid at 253 K.

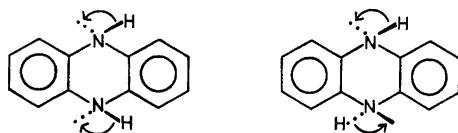
Table 1. Coupling constants (G) of the radical anion of dihydrophenazine. The temperatures are 338, 353 and 323 K, respectively.

Position	CF ₃ COOH	CCl ₃ COOH	CH ₃ COOH	Calculated (INDO)
1,4,5,8	0.53	0.56	0.62	-0.4
2,3,6,7	1.73	1.72	1.71	-0.8
9,10 (N)	6.20	6.12	6.10	7.6
9,10 (H)	6.75	6.70	6.67	-9.3

in Table 1, and Fig. 3 shows the ESR spectrum of the sample at 253 K. In this latter spectrum the innermost peak group has remained practically unchanged, while the outermost peaks have broadened. The higher temperature ESR spectrum of the dihydrophenazine radical anion in trifluoroacetic acid is obtained at room temperature and above. A similar ESR spectrum can be recorded above 353 K in trichloroacetic acid, and above room temperature in acetic acid. Since almost identical ESR spectra are obtained in all three solvents, couplings of the fluorine and chlorine nuclei are excluded.

The coupling constants presented in Table 1 do not differ significantly from those of the radical anion of dihydrophenazine prepared electrolytically in dimethylformamide.²

The broadening of the outermost lines might be due to conformational exchange. The protons in positions 9 and 10 of configuration A are both either axial or equatorial, whereas in configuration B, one is axial and the other equatorial.



Configuration A

Configuration B

The values of the C-N bond in the INDO calculations were 0.137, 0.140 and 0.145 nm, the N-H bond was 0.101 nm and the angle CNH was either 109.47 or 120°.⁸

The INDO calculations assign the minimum energy to the planar molecule when the value 0.140 nm is used for the C-N bond. Further, according to the INDO calculations, the coupling constants in various conformations with A and B do not deviate significantly from the couplings of the planar molecule when the bond lengths 0.140 and 0.145 nm are used. On the other hand, when the bond length of 0.147 nm is used, all coupling constants in the various conformations are changing to such an extent that all lines in the ESR spectrum should broaden, not just the outermost lines. Thus, changes in the conformations, as exhibited by the INDO calculations, do not explain the broadening of the outermost lines in the ESR spectrum.

Fig. 4 shows how the lines of the protons in the phenyl rings split into small doublets (0.06 G). The doublet splitting occurs only at lower temperatures, where the coupling of the protons at positions 9 and 10 can no longer be observed and the lines due to the nitrogen nuclei have broadened.

The magnitude of the second order effect⁹ is only about 0.014 G and the separation of the



Fig. 4. The ESR spectrum of the radical anion of dihydrophenazine in trifluoroacetic acid at 263 K. The lines of the central group are split into small doublets.

modulation side bonds is about 0.036 G for 100 kHz.⁹

Based on energy calculations alone the radical RH^{\cdot} could appear, but the INDO calculations show that its presence would cause considerable changes in all coupling constants. A similar doublet has been observed for the radical cation of pentacene both in trifluoro- and trichloroacetic acids.⁶

The appearance of the doublet is obviously due to the formation of an ion pair between the acid dimer (HAA^-) and the radical ion. Thus the remaining proton of the acid dimer is observed as a doublet in the ESR spectrum, and a proton exchange reaction between it and the protons at the 9,10 positions takes place. At higher temperatures the reaction is so fast that neither the line broadening nor the doublet can be observed.

Shortly after preparation the UV and visible spectra of the same sample in trifluoroacetic acid at room temperature shows peaks at $\lambda(\text{max})$ 385 and 260 nm and after a few hours also at 450 and 430 nm, which are consistent with literature values² and are due to the mono- and diprotonated forms of phenazine. At room temperature, however, the ESR spectrum shows only one radical; hence the monoprotonated form of phenazine is not a radical.

REFERENCES

1. Schieser, D. and Zvirblis, P. *J. Chem. Phys.* **36** (1962) 2237.
2. Barton, B. and Fraenkel, G. *J. Chem. Phys.* **41** (1964) 1455.
3. Bailey, D., Roe, D. and Hercules, D. *J. Am. Chem. Soc.* **90** (1968) 6291.
4. Eloranta, J. and Sippula, A. *Finn. Chem. Lett.* (1975) 170.
5. Eloranta, J. and Ijäs, M. *Finn. Chem. Lett.* (1975) 174.
6. Eloranta, J. and Kolehmainen, S. *Finn. Chem. Lett.* (1976). *In press.*
7. Hase, H. and Schweig, A. *OCPE Program* **261** (1973).
8. Pople, J. and Beveridge, D. *Approximate Molecular Orbital Theory*, McGraw-Hill, New York 1970.
9. Wertz, J. and Bolton, J. *Electron Spin Resonance*, McGraw-Hill, New York 1972, pp. 446, 454.
10. Elson, J. and Kochi, J. *J. Am. Chem. Soc.* **95** (1973) 5061.

Received December 1, 1976.

Short Communication

On Structural and Magnetic Properties of $V_{1-t}Co_tAs$ INGER LISE ANDREASSEN, KARI SELTE
and ARNE KJEKSHUSKjemisk Institutt, Universitetet i Oslo,
Blindern, Oslo 3, Norway

During the course of the present research programme all but one of the pseudo-binary $TAs-T'As$ (T, T' : V, Cr, Mn, Fe, Co) systems with MnP type structure have been studied and reported in this journal. An account of the lacking VAs—CoAs system is given here.

Experimental details concerning purity of elements, preparation of binary and ternary samples (2–4 heat treatments at 600–900 °C for one week, quenching or slow cooling to room temperature), powder X-ray diffraction and magnetic susceptibility measurements are as in Refs. 1 and 2.

Homogeneity ranges and atomic arrangement. An isothermal cross-section of the VAs—CoAs system, as derived for samples quenched from 600 °C, shows (Fig. 1) that this system exhibits a miscibility gap for $0.15 \pm 0.03 \leq t \leq 0.80 \pm 0.03$ of the formula $V_{1-t}Co_tAs$. The limits of the solubility ranges have been determined from the variations in unit cell dimensions with t (Fig. 1) and ascertained by application of the

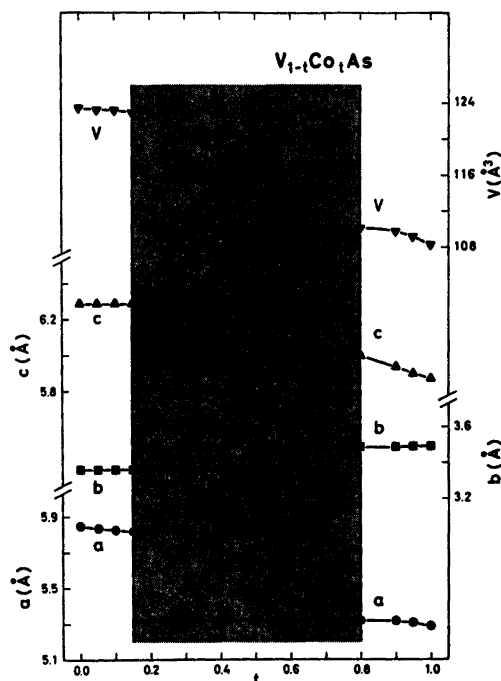


Fig. 1. Room temperature unit cell dimensions of $V_{1-t}Co_tAs$ as functions of t .

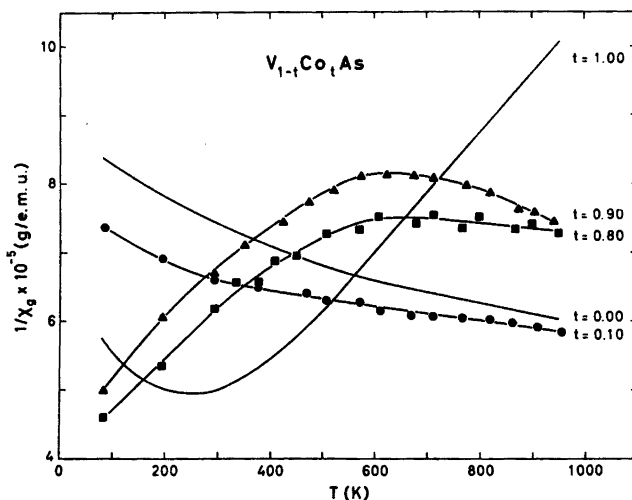


Fig. 2. Reciprocal magnetic susceptibility versus temperature for $V_{1-t}Co_tAs$ samples.

disappearing phase principle to the X-ray data. The diffraction data show that the V and Co atoms are randomly distributed over the metal sub-lattice in an MnP type atomic arrangement.

Magnetic susceptibility. The temperature characteristics of the reciprocal magnetic susceptibility show a consistent trend in their changes with the composition parameter t (Fig. 2). None of the curves satisfies the Curie-Weiss Law, and values for the paramagnetic moment can accordingly not be deduced.

Acknowledgement. This work has received financial support from the Norwegian Research Council for Science and the Humanities.

1. Selte, K. and Kjekshus, A. *Acta Chem. Scand.* 25 (1971) 3277.
2. Selte, K., Kjekshus, A. and Andresen, A. F. *Acta Chem. Scand.* 26 (1972) 4057.

Received February 22, 1977.

Structures of Linear Multisulfur Systems. XIII.

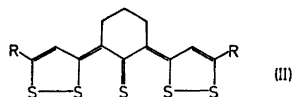
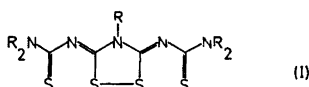
The Crystal and Molecular Structure of 3,5-Bis(*N,N*-diisopropylthiocarbamoylimino)-4-isopropyl-1,2,4-dithiazolidine, C₁₉H₃₅N₅S₄

JORUNN SLETTEN and OLE CHR. LØKKE

Department of Chemistry, University of Bergen, N-5014 Bergen-Univ., Norway

The title compound crystallizes in space group $P\bar{1}$ with a unit cell of dimension $a = 18.726(6)$ Å, $b = 8.204(2)$ Å, $c = 8.794(2)$ Å, $\alpha = 103.08(2)^\circ$, $\beta = 81.81(4)^\circ$, $\gamma = 107.12(2)^\circ$. X-Ray intensity data were recorded on a four-circle diffractometer. The structure was solved by Patterson and Fourier methods and refined by full-matrix least-squares to an R of 0.035. The four sulfur atoms are almost collinearly arranged, the intramolecular S...S distances being 2.729(1), 2.161(1) and 2.721(1) Å, respectively.

A series of compounds containing almost linear sequences of four and five sulfur atoms have been investigated. It has been shown that the S—S σ -bonding in compounds like I and II



may be described in terms of delocalized 4-centre-6-electron bonding and 5-centre-6-electron bonding, respectively.¹ These weak bonds, of lengths between a single bond and van der Waals distance, are easily influenced by *intra*- as well as *inter*-molecular effects. In the present investigation a compound of type I with relatively bulky substituents (R = isopropyl) is studied.

Acta Chem. Scand. A 31 (1977) No. 6

EXPERIMENTAL

The crystals grew as orange prisms from pyridine solution at room temperature. The space group was determined from Weissenberg and precession photographs. A crystal of dimension 0.27 mm \times 0.20 mm \times 0.50 mm mounted along c^* was used throughout the data collection. Cell dimensions were calculated from the 2θ -values [$\lambda(\text{MoK}\alpha) = 0.70926$ Å] of 27 reflections with $2\theta > 36^\circ$ as measured on a four-circle diffractometer with an ω -scan procedure.² The intensities of 4892 unique reflections were recorded on the diffractometer employing the $\theta-2\theta$ scan technique. Scan ranges were calculated according to the Alexander and Smith equation,³ $\Delta 2\theta$ varying between 1.2 and 1.7°. No sign of crystal deterioration was found by remeasuring two reference reflections for every 50 reflections recorded. These measurements were used to bring the data on a common relative scale. Standard deviations in the intensities were evaluated as $\sigma_I = [\sigma_c^2 + (0.01N_{\text{Net}})^2]^{1/2}$, where σ_c is the error due to counting statistics, N_{Net} is the net count of the reflection, and 0.01 is an "instability factor" evaluated from the variation in the reference reflections. 1118 reflections had a net count less than a threshold value of $2\sigma_I$. These reflections were assigned an intensity of $2\sigma_I$ and coded unobserved, and were later included in the refinement only if $|F_{\text{calc}}| > |F_{\text{threshold}}|$. The data were corrected for Lorentz and polarization effects according to standard procedures. Absorption correction was carried out, A^* varying between 1.06 and 1.10.

CRYSTAL DATA

C₁₉H₃₅N₅S₄; M.W. = 461.78; crystal system triclinic; space group $P\bar{1}$ (or $P1$); cell dimen-

Table 1. Final atomic coordinates and thermal parameters with corresponding standard deviations, referring to the last decimal places, in parentheses. Thermal parameters are defined by $T_i = \exp[-2\pi^2(U_{11}h^2a^{*2} + U_{22}k^2b^{*2} + U_{33}l^2c^{*2} + 2U_{12}hka^*b^* + 2U_{13}hla^*c^* + 2U_{23}kbl^*c^*)]$ and are multiplied by a factor of 10^4 .

Atom	X/a	Y/b	Z/c	$U_{11}(\text{Å}^2)$	$U_{22}(\text{Å}^2)$	$U_{33}(\text{Å}^2)$	$U_{12}(\text{Å}^2)$	$U_{13}(\text{Å}^2)$	$U_{23}(\text{Å}^2)$
S(1)	0.38719(4)	0.09664(7)	-0.20895(7)	924(4)	544(3)	917(4)	358(3)	401(3)	432(3)
S(2)	0.30292(3)	0.18728(6)	0.05931(6)	707(3)	345(2)	717(4)	201(2)	127(3)	242(2)
S(3)	0.23265(3)	0.23876(6)	0.27183(6)	786(4)	318(2)	669(3)	233(2)	64(3)	137(2)
S(4)	0.1437(3)	0.27490(6)	0.53991(6)	902(4)	427(3)	631(3)	307(3)	59(3)	42(2)
N(1)	0.41101(8)	-0.21041(18)	-0.21921(18)	543(10)	458(8)	700(11)	209(7)	204(8)	249(8)
N(2)	0.32789(8)	-0.13842(17)	-0.1895(17)	469(9)	376(8)	574(10)	156(7)	91(7)	191(7)
N(3)	0.24817(8)	-0.08083(15)	0.20004(16)	506(9)	288(7)	504(9)	139(6)	56(7)	128(6)
N(4)	0.17653(8)	-0.2738(16)	0.43050(16)	525(9)	359(7)	434(9)	151(7)	-8(7)	50(6)
C(1)	0.10560(8)	-0.1140(17)	0.66481(16)	566(10)	447(8)	394(8)	167(7)	-24(7)	12(7)
C(2)	0.37557(10)	-0.09070(22)	-0.14686(22)	470(11)	415(10)	657(13)	128(8)	82(9)	204(9)
C(3)	0.29498(9)	-0.2518(20)	0.07376(21)	447(11)	323(8)	558(11)	112(8)	1(9)	150(8)
C(4)	0.21544(9)	0.03143(19)	0.31119(20)	480(11)	303(8)	494(11)	120(8)	-63(8)	71(8)
C(5)	0.14090(10)	0.07123(21)	0.54760(20)	514(11)	410(9)	441(10)	133(8)	-99(9)	-4(8)
C(6)	0.39806(11)	-0.38122(23)	-0.17249(23)	609(13)	450(10)	723(14)	262(9)	161(10)	219(9)
C(7)	0.42261(12)	-0.36601(27)	-0.12029(27)	703(15)	684(14)	891(17)	295(12)	-4(12)	299(12)
C(8)	0.31963(12)	-0.49609(24)	-0.19936(26)	692(14)	446(11)	875(16)	137(10)	53(12)	188(11)
C(9)	0.46684(12)	-0.17867(25)	-0.35549(26)	736(15)	578(12)	866(16)	299(11)	362(12)	314(11)
C(10)	0.54470(13)	-0.15927(34)	-0.31372(32)	572(15)	1049(20)	1090(21)	-22(14)	240(14)	33(16)
C(11)	0.44567(13)	-0.31666(34)	-0.50048(28)	804(17)	1185(21)	730(16)	438(15)	113(13)	321(14)
C(12)	0.23677(10)	-0.26482(20)	0.22061(21)	607(12)	283(8)	580(12)	169(8)	130(10)	148(8)
C(13)	0.27428(12)	-0.26827(25)	0.36002(27)	679(14)	499(11)	926(17)	214(10)	-71(12)	303(11)
C(14)	0.15546(11)	-0.36847(22)	0.21412(23)	697(14)	354(10)	608(13)	33(9)	-21(10)	53(9)
C(15)	0.10928(11)	-0.19056(23)	0.66658(21)	713(14)	442(11)	442(11)	210(10)	48(10)	92(9)
C(16)	0.15804(14)	-0.18711(30)	0.79089(27)	970(18)	829(16)	753(16)	362(14)	-157(14)	228(13)
C(17)	0.03205(11)	-0.31530(27)	0.68091(29)	847(17)	529(13)	955(19)	32(12)	-41(14)	83(12)
C(18)	0.06439(11)	0.07061(24)	0.80390(21)	642(13)	565(12)	415(11)	174(10)	6(10)	-32(9)
C(19)	0.11457(13)	0.22878(28)	0.90225(24)	888(17)	750(15)	521(13)	171(13)	-86(12)	-165(11)
	-0.00604(12)	0.10275(30)	0.76331(26)	656(15)	873(16)	762(16)	348(13)	-9(12)	-8(12)

sions: $a=18.726(6)$ Å, $b=8.204(2)$ Å, $c=8.794(2)$ Å, $\alpha=103.08(2)^\circ$, $\beta=81.81(4)^\circ$, $\gamma=107.12(2)^\circ$. $V=1253.5(6)$ Å³, $Z=2$, $D_x=1.224$ gcm⁻³, $D_m=1.22(1)$ gcm⁻³, $F_{000}=496$, $\mu(\text{MoK}\alpha)=3.8$ cm⁻¹.

STRUCTURE DETERMINATION AND REFINEMENT

The distribution of E -values clearly indicated centrosymmetry, thus space group $P\bar{1}$ was tentatively selected. The positions of the four sulfur atoms were derived from a Patterson map. The remaining non-hydrogen atoms were located in two subsequent Fourier maps. Full-matrix least-squares refinement, introducing anisotropic thermal parameters on all atoms

in the final cycles, reduced R to 0.067 ($R = \sum ||F_o| - |F_c|| / \sum |F_o|$). A difference map calculated at this stage revealed the hydrogen atoms, which were included in the refinement with isotropic thermal parameters. The refinement converged at an R of 0.035, the weighted R_w being 0.031. At the end of the refinement correction for secondary extinction was attempted, the correction gave, however, no significant changes in F_c , and was thus abolished. The quantity minimized in the refinement was $\sum w ||F_o| - |F_c||^2$, where $w=1/\sigma_F^2$. Scattering factors for non-hydrogen atoms were taken from Ref. 4, and that for hydrogen was from Ref. 5. Final atomic coordinates and thermal parameters are listed in Tables 1 and 2. Lists

Table 2. Coordinates and thermal parameters of the hydrogen atoms with the corresponding standard deviations. Thermal parameters are defined by $T_i = \exp(-8\pi^2 U \sin^2\theta/\lambda^2)$, and are multiplied by 10³.

Atom	X/a	Y/b	Z/c	U (Å ²)
H(5)	0.4312(9)	-.4359(20)	-.2465(18)	56(5)
H(61)	0.4232(12)	-.4833(28)	0.0027(24)	99(7)
H(62)	0.3902(12)	-.3201(29)	0.0725(25)	106(7)
H(63)	0.4732(12)	-.2895(26)	0.0023(22)	88(7)
H(71)	0.3063(12)	-.5076(27)	-.3095(26)	106(7)
H(72)	0.2824(11)	-.4607(25)	-.1261(23)	87(6)
H(73)	0.3166(11)	-.6157(26)	-.1950(24)	93(7)
H(8)	0.4653(11)	-.0788(25)	-.3770(22)	83(6)
H(91)	0.5531(14)	-.0646(34)	-.2307(32)	143(10)
H(92)	0.5791(13)	-.1344(30)	-.4052(29)	116(8)
H(93)	0.5480(14)	-.2688(35)	-.2938(30)	140(10)
H(101)	0.4523(14)	-.4245(32)	-.4878(28)	124(9)
H(102)	0.4793(12)	-.2861(28)	-.5949(26)	106(8)
H(103)	0.3923(16)	-.3371(35)	-.5232(32)	152(10)
H(11)	0.2635(8)	-.3118(18)	0.1257(17)	42(4)
H(121)	0.3291(12)	-.2053(28)	0.3522(25)	100(7)
H(122)	0.2567(13)	-.2143(30)	0.4572(27)	115(8)
H(123)	0.2743(11)	-.3833(27)	0.3654(23)	92(7)
H(131)	0.1230(11)	-.3333(25)	0.2981(24)	89(7)
H(132)	0.1343(11)	-.3677(25)	0.1157(23)	85(6)
H(133)	0.1530(11)	-.4932(25)	0.2100(22)	84(6)
H(14)	0.1330(9)	-.2245(21)	0.5684(19)	55(5)
H(151)	0.2087(14)	-.1047(33)	0.7807(29)	130(9)
H(152)	0.1359(12)	-.1419(27)	0.8973(24)	99(7)
H(153)	0.1636(12)	-.3033(29)	0.7872(26)	107(8)
H(161)	-.0003(13)	-.3125(31)	0.6099(30)	126(9)
H(162)	0.0035(14)	-.2904(32)	0.7906(30)	129(9)
H(163)	0.0355(11)	-.4319(25)	0.6675(22)	85(6)
H(17)	0.0474(9)	-.0234(21)	0.8643(19)	63(5)
H(181)	0.1622(14)	0.2126(31)	0.9166(29)	127(9)
H(182)	0.0900(13)	0.2503(30)	0.9926(27)	113(8)
H(183)	0.1264(13)	0.3297(30)	0.8564(27)	130(9)
H(191)	-.0375(13)	-.0017(30)	0.7041(26)	115(8)
H(192)	-.0316(13)	0.1453(30)	0.8563(27)	112(8)
H(193)	0.0063(12)	0.2008(29)	0.7030(26)	110(8)

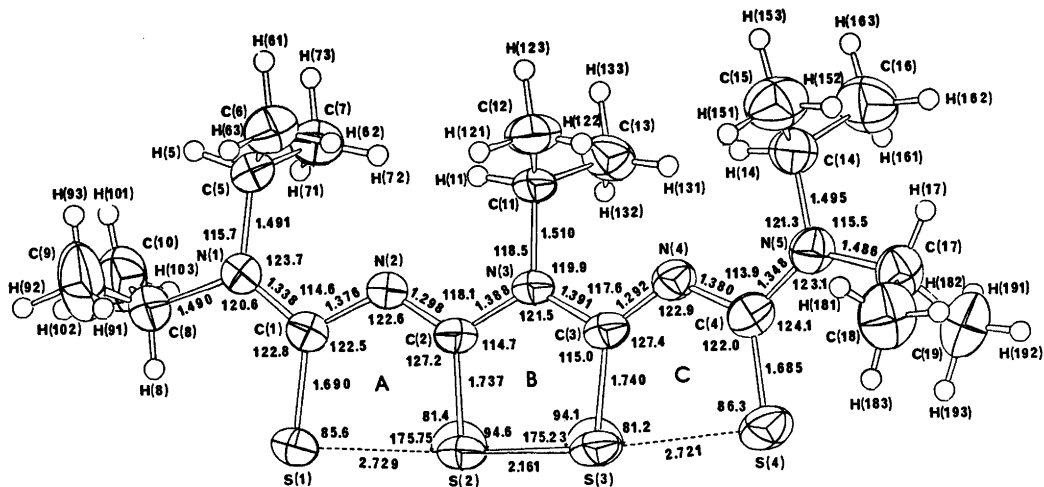


Fig. 1. Bond distances and angles. Standard deviations in S-S, S-C and C-N(C) distances are 0.001, 0.002 and 0.002–0.004 Å, respectively. Standard deviations in angles are: \angle S-S-S 0.03°, \angle C-S-S 0.1°, angles at C and N 0.1–0.2°. The thermal ellipsoids are plotted at the 50 % probability level; hydrogens are plotted with a fixed, arbitrary set radius.

of observed and calculated structure factors may be obtained from one of the authors (JS).

All calculations have been carried out on a UNIVAC 1110 computer utilizing the X-ray 72 system, except when otherwise noted.

RESULTS AND DISCUSSION

Bond distances and angles involving non-hydrogen atoms are shown in Fig. 1 and in Table 3 and 4. The C-H bond lengths are in the range 0.87–1.04 ($\sigma = 0.01$ –0.03) Å with a mean value of 0.97 Å. The four sulfur atoms are arranged in an almost linear row with all

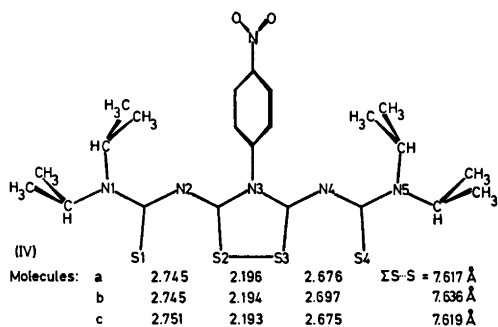
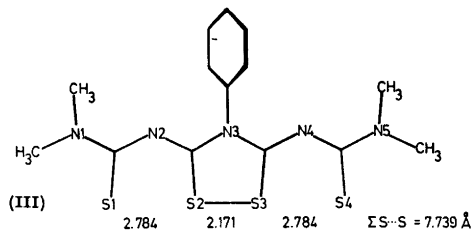
three S...S distances longer than the corresponding bond in isolated cyclic disulfides⁶ and shorter than van der Waals distance. The sulfur sequence has approximately two-fold symmetry. In the analogous derivatives previously studied, symmetrical sulfur rows have been found only when required by crystallographic symmetry.^{7–10} The results of two previous investigations have shown that there is a significantly shorter total S...S sequence in

Table 4. Bond angles in the isopropyl groups.

Table 3. Bond distances in the isopropyl groups.

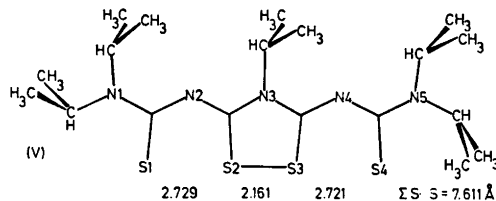
Bond	(Å)
C(5) – C(6)	1.513(3)
C(5) – C(7)	1.511(3)
C(8) – C(9)	1.508(4)
C(8) – C(10)	1.514(3)
C(11) – C(12)	1.507(3)
C(11) – C(13)	1.512(3)
C(14) – C(15)	1.512(4)
C(14) – C(16)	1.513(3)
C(17) – C(18)	1.523(3)
C(17) – C(19)	1.523(4)

Angle	(°)
N(1) – C(5) – C(6)	113.7(1)
N(1) – C(5) – C(7)	111.9(2)
C(6) – C(5) – C(7)	114.5(2)
N(1) – C(8) – C(9)	110.6(2)
N(1) – C(8) – C(10)	112.0(2)
C(9) – C(8) – C(10)	112.3(2)
N(3) – C(11) – C(12)	111.3(1)
N(3) – C(11) – C(13)	111.8(2)
C(12) – C(11) – C(13)	115.7(2)
N(5) – C(14) – C(15)	111.0(1)
N(5) – C(14) – C(16)	111.9(2)
C(15) – C(14) – C(16)	112.7(2)
N(5) – C(17) – C(18)	113.2(2)
N(5) – C(17) – C(19)	112.6(2)
C(18) – C(17) – C(19)	113.7(2)



IV than in III.^{7,9} This might possibly be due to repulsion between the bulky substituent in

the "upper" part of the molecule, squeezing the sulfur atoms together. Introducing an isopropyl substituent at the central nitrogen, N(3), further increases the crowding in the "upper" part of the molecule relative to compound IV. However, the results of the present investigation show that the steric tension has been relieved through a 180° rotation around N-C of the isopropyl groups at N(5), (V),



relative to the orientation in IV, and the total S...S sequence is not significantly shortened as compared to IV. The H...H contacts in the upper part of the molecule are: H(62)...H(11) = 2.37 Å, H(72)...H(11) = 2.31 Å; H(131)...H(14)

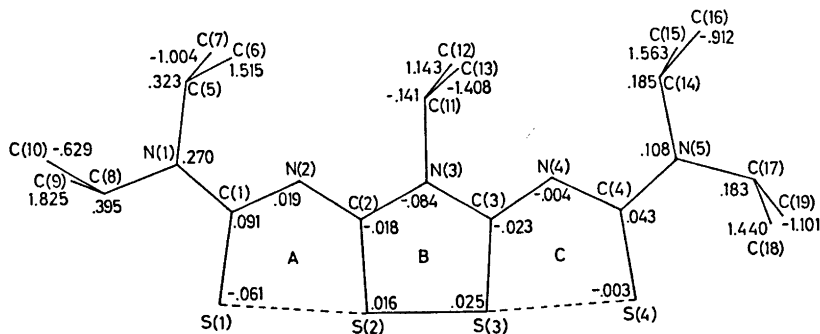


Fig. 2. Atomic deviations from the least-squares plane through rings A + B + C.

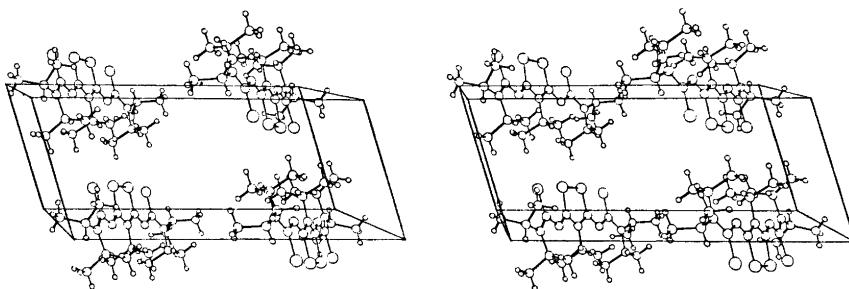


Fig. 3. Stereoscopic view as seen down the c^* -axis; the a -axis runs from left to right, the b -axis from bottom to top.

= 2.36 Å; H(122)···H(14) = 2.37 Å ($\sigma = 0.02 - 0.03$ Å).

Fig. 2 shows the atomic deviations from the best least-squares plane through rings A + B + C. The rings deviate slightly but significantly from planarity; and the substituents at C(1) and C(4) are bent out of the plane to one side, while the N(3) substituent is bent to the opposite side.

In Fig. 3 the three dimensional arrangement of molecules in the crystal is illustrated. There are no intermolecular contacts shorter than van der Waals distance.

Acknowledgement. The authors are indebted to Professor J. Goerdeler, University of Bonn, for providing a sample of the compound.

REFERENCES

1. Sletten, J. *Acta Chem. Scand. A* 30 (1976) 397.
2. Maartmann-Moe, K. *Siemens Review XLI*, Seventh Special Issue, *X-Ray and Electron Microscopy News* (1974) 54.
3. Alexander, L. E. and Smith, G. S. *Acta Crystallogr.* 17 (1964) 1195.
4. Cromer, D. and Mann, J. *Acta Crystallogr. A* 24 (1968) 321.
5. Stewart, R. F., Davidson, E. R. and Simpson, W. T. *J. Chem. Phys.* 42 (1965) 3175.
6. Hordvik, A. *Quart. Rep. Sulfur Chem.* 5 (1970) 21.
7. Flippen, J. L. *J. Am. Chem. Soc.* 95 (1973) 6073.
8. Sletten, J. *Acta Chem. Scand. A* 28 (1974) 989.
9. Sletten, J. *Acta Chem. Scand. A* 29 (1975) 317.
10. Sletten, J. and Løkke, O. C. *Acta Chem. Scand. A* 31 (1977) 271.

Received January 27, 1977.

A Double-bridged Binuclear Chromium(III) Complex with 1,6-Bis(2'-pyridyl)-2,5-diazahexane. Preparation, Resolution and Stereochemistry of the Di- μ -hydroxobis[1,6-bis(2'-pyridyl)-2,5-diazahexane]chromium(III) Ion

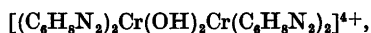
KIRSTEN MICHELSEN

Chemistry Department I (Inorganic Chemistry), University of Copenhagen, H. C. Ørsted Institute, Universitetsparken 5, DK-21000, Copenhagen Ø, Denmark

A new binuclear chromium(III) complex of the double-bridged type $[(C_{14}H_{18}N_4)Cr(OH)_2Cr(C_{14}H_{18}N_4)]^{4+}$, where the tetramine ligand $C_{14}H_{18}N_4 = 1,6$ -bis(2'-pyridyl)-2,5-diazahexane (*N,N'*-bis-(2-methylpyridyl)-1,2-ethanediamine, abbrev. bispicen), has been prepared and resolved into its catoptric forms. As this di- μ -hydroxo complex reacts with hydrochloric acid to α -*cis*- $[Cr(C_{14}H_{18}N_4)Cl_2]^+$, this type of compounds was included in the study. Both the symmetrical α -*cis* and the unsymmetrical β -*cis*-dichloro complex were prepared for the first time and compared with the earlier described cobalt(III) complexes of the same types. The stereochemistry of the complexes was deduced from electronic spectra, CD-spectra, 1H NMR spectra and X-ray powder photographs.

Binuclear chromium(III) complexes with two hydroxo groups as bridging ligands, the so-called diols, have recently attracted much attention because of their kinetic,^{1,2} spectroscopic,³⁻⁶ structural and magnetic properties.⁷⁻¹⁰

In a previous work by the present author,¹¹ the synthesis, resolution and properties of the binuclear ion



where the bidentate ligand $C_6H_8N_2 = 2$ -aminomethylpyridine, were reported. This work concerns di- μ -hydroxo- and *cis*-dichloro complexes of chromium(III) with the related tetradentate ligand $C_{14}H_{18}N_4 = 1,6$ -bis(2'-

pyridyl)-2,5-diazahexane (*N,N'*-bis(2-methylpyridyl)-1,2-ethanediamine, abbrev. bispicen), Fig. 1.

Gibson and McKenzie¹² prepared both the symmetrical α -*cis* and the unsymmetrical β -*cis*-dichloro complexes of cobalt(III) and bispicen and based the structural assignment of the isomers on PMR-spectra. As X-ray powder photographs showed isomorphism between these compounds and the new *cis*-dichloro complexes of chromium(III), an assignment of the configuration of the latter was possible.

EXPERIMENTAL

Reagents. Pyridine-2-carboxaldehyde was purchased from Merck-Schuchardt. *trans*- $[Crpy_4Cl_2]I$ and *trans*- $[Copoly_4Cl_2]Cl \cdot 6H_2O$ were prepared by methods developed by Glerup and Schäffer¹³ and Werner and Feenstra,¹⁴ respectively. All other chemicals were of chemical grade and were used without further purification.

Analyses. The chromium and cobalt analyses were performed on a Perkin Elmer 403 Atomic Absorption Spectrophotometer. The micro-analytical laboratory of this institute carried out the carbon, nitrogen, hydrogen and halogen analyses by standard methods.

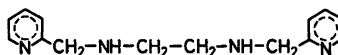


Fig. 1. 1,6-Bis(2'-pyridyl)-2,5-diazahexane, $C_{14}H_{18}N_4$.

Physical measurements. Absorption spectra were recorded on a Cary Model 14 spectrophotometer. The spectra are characterized by their maxima and minima (ϵ, λ), where the molar extinction coefficient ϵ is in units of $l \text{ mol}^{-1} \text{ cm}^{-1}$ and λ is in nm. Circular dichroism was measured on a Roussel-Jouan Dicrographe I. The maxima are given below as $(\Delta\epsilon, \lambda) = [(\epsilon_1 - \epsilon_2), \lambda]$. Optical rotation was measured on a Perkin Elmer Model 141 polarimeter. In all cases the solvent was 0.1 M hydrochloric acid. The X-ray powder photographs were obtained on a camera of the Guinier type with $\text{CuK}\alpha$ radiation. Silicon was used as standard. ^1H NMR spectra were obtained on a Varian Model A-60 spectrometer using $(\text{CD}_3)_2\text{SO}$ as solvent and tetramethylsilane as standard.

Preparations

1. 1,6-Bis(2'-pyridyl)-2,5-diazaheptane (abbrev. bispicen), $\text{C}_{14}\text{H}_{18}\text{N}_4$. The ligand was prepared from pyridine-2-carboxaldehyde (79 g ~ 0.74 mol) and 1,2-ethanediamine (15 g, 0.25 mol) following mainly the method described by Goodwin and Lions,¹⁵ but with the modification that the crude amine was purified before the final distillation. The purification (via the hydrochloride) was performed as follows: The crude amine was dissolved in the fivefold amount of ethanol (99 %); the solution was cooled on ice, and the hydrochloride was precipitated by the addition of conc. hydrochloric acid. Filtering and washing with ethanol. 41 g. The compound was recrystallized by dissolving in 4 M hydrochloric acid (100 ml) and adding of ethanol (600 ml, 99 %). Yield: 31 g (29 %). Anal. $\text{C}_{14}\text{H}_{18}\text{N}_4 \cdot 4\text{HCl} \cdot 2\text{H}_2\text{O}$: C, N, H, Cl. From the pure hydrochloride the amine was liberated with base and isolated and distilled as described before.¹⁵ Yield: ~ 10 g (16–17 %).

2a. α -cis-Dichloro{1,6-bis(2'-pyridyl)-2,5-diazaheptane}cobalt(III) chloride, α -cis- $[\text{Co}(\text{C}_{14}\text{H}_{18}\text{N}_4)\text{Cl}_2]\text{Cl} \cdot 1.33 \text{ H}_2\text{O}$. 4.00 g *trans*- $[\text{Co}(\text{C}_{14}\text{H}_{18}\text{N}_4)\text{Cl}_2]\text{Cl} \cdot 6\text{H}_2\text{O}$ (6.78 mmol) was dissolved in pyridine (80 ml). Heating and stirring. 2.0 ml of bispicen (> 7 mmol) were added dropwise, and a violet precipitate soon appeared. Cooling, filtering and washing with pyridine and acetone. The crude product was dissolved in the necessary amount of hot (80 °C) 4 M hydrochloric acid (10–12 ml). After filtering and cooling of the filtrate on ice, ethanol (500 ml, 99 %) and ether (10 ml) were added to precipitate 2.01 g of blue-violet crystals (69 %). The crystals were recrystallized again with a loss of 10 %. Anal. $[\text{Co}(\text{C}_{14}\text{H}_{18}\text{N}_4)\text{Cl}_2]\text{Cl} \cdot 1.33 \text{ H}_2\text{O}$: Co, C, N, H, Cl. The content of crystal-water was confirmed by thermogravimetry. (ϵ, λ)_{max}: (128, 541.5), (131, 392.5). (ϵ, λ)_{min}: (19, 454), (129, 382). Half-width δ : 3789 cm^{-1} (1. band).

2b. The perchlorate, α -cis- $[\text{Co}(\text{C}_{14}\text{H}_{18}\text{N}_4)\text{Cl}_2]\text{ClO}_4$, was prepared from the chloride (0.60 g 1.39 mmol) by dissolving in 0.1 M hydrochloric acid (6 ml) and adding 2 ml of a 1 M solution of sodium perchlorate. Cooling on ice and filtering. Washing with icewater. Yield: 0.57 g (86 %). Anal. $[\text{Co}(\text{C}_{14}\text{H}_{18}\text{N}_4)\text{Cl}_2]\text{ClO}_4$: Co, C, N, H, Cl. (ϵ, λ)_{max}: (128, 541.5), (132, 392). (ϵ, λ)_{min}: (19, 454), (130, 382).

3. β -cis-Dinitro{1,6-bis(2'-pyridyl)-2,5-diazaheptane}cobalt(III) nitrate, β -cis- $[\text{Co}(\text{C}_{14}\text{H}_{18}\text{N}_4)(\text{NO}_2)_2]\text{NO}_3 \cdot \text{H}_2\text{O}$. The principle in the method, aerial oxidation of Co(II) in the presence of amine and sodium nitrite, was taken from Holtzclaw *et al.*,¹⁶ and was earlier used by the author in the preparation of a similar compound.¹⁷ 4.24 g bispic. $4\text{HCl} \cdot 2\text{H}_2\text{O}$ (10 mmol) was dissolved in 15 ml 2 M sodium hydroxide (30 mmol). Cobalt nitrate, hexahydrate (2.91 g, 10 mmol) and sodium nitrite (1.40 g, 20 mmol) were added, and the solution was oxidized, air being drawn through it for 3 h. Cooling on ice, filtering and washing with ice-water. The yellow compound was recrystallized from boiling water. Washing as above. Yield: 1.3 g (28 %). Anal. $[\text{Co}(\text{C}_{14}\text{H}_{18}\text{N}_4)(\text{NO}_2)_2]\text{NO}_3 \cdot \text{H}_2\text{O}$: Co, C, N, H. (ϵ, λ)_{max}: (334, 446). (ϵ, λ)_{min}: (196, 405).

The mother liquor and all the filtrates from washings and recrystallizations were kept and used for the preparation of β -cis- $[\text{Co}(\text{C}_{14}\text{H}_{18}\text{N}_4)\text{Cl}_2]\text{NO}_3$ (4a).

4a. β -cis-Dichloro{1,6-bis(2'-pyridyl)-2,5-diazaheptane}cobalt(III) nitrate, β -cis- $[\text{Co}(\text{C}_{14}\text{H}_{18}\text{N}_4)\text{Cl}_2]\text{NO}_3 \cdot \frac{1}{2} \text{H}_2\text{O}$. Solid lithium chloride (~ 10 g) was added to the mixed filtrates from the preparation of 3. After 3 days a brick-red precipitate, presumably $[\text{Co}(\text{C}_{14}\text{H}_{18}\text{N}_4)\text{Cl}(\text{NO}_2)]\text{Cl}$ was filtered. Washing with ethanol. Yield: 2.2 g. A slurry of this compound and conc. hydrochloric acid (15 ml) was evaporated to nearly dryness on a boiling water-bath. Cooling on ice and washing on a filter with acetone. The new crude product was dissolved in 1 M hydrochloric acid (15 ml, 35 °C, a few ml of conc. nitric acid was added, and a red compound precipitated. Yield: 1.90 g (43 % based on $\text{Co}(\text{NO}_2)_2 \cdot 6\text{H}_2\text{O}$). Anal. $[\text{Co}(\text{C}_{14}\text{H}_{18}\text{N}_4)\text{Cl}_2]\text{NO}_3 \cdot \frac{1}{2} \text{H}_2\text{O}$: Co, C, N, H, Cl. The content of crystal-water was found by thermogravimetry to be 0.45. (ϵ, λ)_{max}: (158, 532). (ϵ, λ)_{min}: (35, 454.5). Half-width δ : 3278 cm^{-1} .

4b. The dithionate, β -cis- $[\text{Co}(\text{C}_{14}\text{H}_{18}\text{N}_4)\text{Cl}_2]_2 \cdot \text{S}_2\text{O}_8 \cdot 1\frac{1}{2} \text{H}_2\text{O}$, was prepared from the nitrate (0.20 g, 0.45 mmol) by dissolving in water (25 ml) and adding a saturated solution of sodium dithionate, dihydrate (0.20 g). Cooling on ice. The red precipitate was filtered and washed with ice-water and ethanol. Yield: 0.088 g (42 %). Anal. $[\text{Co}(\text{C}_{14}\text{H}_{18}\text{N}_4)\text{Cl}_2]_2 \cdot \text{S}_2\text{O}_8 \cdot 1\frac{1}{2} \text{H}_2\text{O}$: Co, C, N, H, Cl. The content of crystal-water was found by thermogravimetry to be 1.40. In other experiments the compound crystallized with different contents of crystal-water (for instance 2.50). ($\epsilon/2, \lambda$)_{max}: (158, 532). ($\epsilon/2, \lambda$)_{min}: (37, 452.5).

5a. α -*cis*-Dichloro{1,6-bis(2'-pyridyl)-2,5-diazahexane}chromium(III) chloride, α -*cis*-[Cr(C₁₄H₁₈N₄)Cl₂]Cl₃·3H₂O. 1.60 g anhydrous chromium(III) chloride (10 mmol) was suspended in 20 ml dimethyl sulfoxide. During heating and stirring bispicen (2.0 ml ~ 10 mmol) was added slowly causing a violet solid to form. Cooling and filtering. The solid was washed with ethanol and extracted with 1 M hydrochloric acid (35 ml, 90°C). Cooling of the filtrate on ice gave needle-shaped blue-violet crystals, which were washed as above. Yield: 0.97 g of a practically pure product (21%). By a repeated recrystallization 50% of the material was lost. Anal. [Cr(C₁₄H₁₈N₄)Cl₂]Cl₃·3H₂O: Cr, C, N, H, Cl. The content of crystal-water was checked by thermogravimetry. (ϵ, λ)_{max}: (104, 545), (99, 407.5). (ϵ, λ)_{min}: (25, 464), (5, 354). Halfwidth δ : 3334 cm⁻¹. The mother liquor was kept and used for the isolation of β -*cis*-[Cr(C₁₄H₁₈N₄)Cl₂]Cl.

5b. The perchlorate, α -*cis*-[Cr(C₁₄H₁₈N₄)Cl₂]ClO₄, was prepared from the chloride (0.25 g, 0.55 mmol) by dissolving in about 20 ml water (40°C) and adding 1 M sodium perchlorate solution (5 ml). Cooling on ice and filtering. Washing with ice-water. Yield: 0.21 g (82%). Anal. [Cr(C₁₄H₁₈N₄)Cl₂]ClO₄: Cr, C, N, H, Cl. (ϵ, λ)_{max}: (105, 545), (101, 407.5). (ϵ, λ)_{min}: (27, 464), (11, 354).

6a. β -*cis*-Dichloro{1,6-bis(2'-pyridyl)-2,5-diazahexane}chromium(III) nitrate, β -*cis*-[Cr(C₁₄H₁₈N₄)Cl₂]NO₃· $\frac{3}{2}$ H₂O. The mother liquor from the synthesis of the corresponding α -compound (see 5a) was cooled on ice, and ether was added to precipitate a sticky product. This was dissolved in ethanol and reprecipitated with ether. Finally the product was dissolved in water (12 ml, slightly acid, 42°C), and conc. nitric acid was added to the filtrate precipitating a red crystalline nitrate. Washing with ethanol. Yield: 0.20 g (4.5%). Anal. [Cr(C₁₄H₁₈N₄)Cl₂]NO₃· $\frac{3}{2}$ H₂O: Cr, C, N, H, Cl. The content of crystal-water was confirmed by thermogravimetry. (ϵ, λ)_{max}: (131, 538), (100, 407). (ϵ, λ)_{min}: (47, 464.5), (13, 354). Halfwidth, δ : 3698 cm⁻¹.

6b. The dithionate, β -*cis*-[Cr(C₁₄H₁₈N₄)Cl₂]₂S₂O₈·2H₂O, could be prepared from the nitrate and sodium dithionate, but was also obtained by an alternative method. 2.50 g *trans*-[Crpy₂Cl₂]I (4.42 mmol) was suspended in 10–15 ml 2-methoxyethanol. While heating and stirring bispicen (1.0 ml, ~4.4 mmol) was added. After a period of complete dissolution a dark-violet solid (presumably a mixture of α - and β -[Cr(C₁₄H₁₈N₄)Cl₂]I) precipitated. Cooling on ice, filtering and washing with ethanol. 1.15 g. The crude product was treated with freshly prepared silver chloride, and finely pulverized sodium dithionate, dihydrate (0.5 g) was added to the filtrate (~10 ml). Cooling on ice, filtering and washing with ice-water and ethanol. Yield: 0.26 g (13%). Anal. [Cr(C₁₄H₁₈N₄)Cl₂]₂S₂O₈.

2H₂O: Cr, C, N, H, Cl. By thermogravimetry the content of crystal water was found to be 1.85. (ϵ, λ)_{max}: (134, 538), (101, 407). (ϵ, λ)_{min}: (47, 464.5), (19, 355).

7. Di- μ -hydroxobis[{1,6-bis(2'-pyridyl)-2,5-diazahexane}chromium(III)]iodide, [(C₁₄H₁₈N₄)Cr(OH)₂Cr(C₁₄H₁₈N₄)]I₄·3H₂O. 1.00 g [CrBr₂(H₂O)₄]Br·2H₂O (2.50 mmol) was dissolved in 8–10 ml 2-methoxyethanol, and a spatula of zinc powder and 1.0 ml bispic (~4.4 mmol) were stirred in. A red precipitate was filtered after 10 min. Washing with 2-methoxyethanol. The crude product was dissolved in boiling water (~15 ml), and sodium iodide (2 g) and ethanol (15 ml, 99%) were added. Cooling on ice. Filtering and washing with ethanol. Yield: 1.36 g (92%). The practically pure compound was recrystallized from boiling water (15 ml) to give 0.91 g shining, flaky crystals directly and 0.41 g further by addition of sodium iodide (1 g) to the filtrate. Anal. [Cr(C₁₄H₁₈N₄)(OH)₂]₂I₄·3H₂O: Cr, C, N, H, I. (ϵ, λ)_{max}: (197, 534), (150, 385). (ϵ, λ)_{min}: (35, 437), (84, 350).

8a. (-)_D-Di- μ -hydroxobis[{1,6-bis(2'-pyridyl)-2,5-diazahexane}chromium(III)]diantimonyl (+)_D-tartrate diiodide, (-)_D-[(C₁₄H₁₈N₄)Cr(OH)₂Cr(C₁₄H₁₈N₄)]{(+)_D-SbOC₄H₄O₆]₂I₂·11H₂O. [Cr(C₁₄H₁₈N₄)(OH)₂]₂I₄·3H₂O (1.78 g, 1.50 mmol) was dissolved in 20 ml hot water (70°C). Sodium antimonyl (+)_D-tartrate (1.88 g, 6.09 mmol) was dissolved in 10 ml hot water (70°C). The solutions were mixed, gently heated for a moment and then cooled on ice for an hour. By then shining, red crystals had deposited. Filtering and washing, first with a mixture of ethanol and water (50%), finally with ethanol (99%). The compound was recrystallized from boiling water (10 ml). Yield: 1.15 g (47%). Anal. [Cr(C₁₄H₁₈N₄)(OH)₂]₂(SbOC₄H₄O₆)₂I₂·11H₂O: Cr, C, N, H, I. In other experiments the complex crystallized with 6, 7, or 12 mol of crystal-water. (ϵ, λ)_{max}: (196, 534), (151, 385). (ϵ, λ)_{min}: (35, 437), (80, 350). ($\Delta\epsilon, \lambda$)_{max}: (-5.35, 520), (+0.48, 443) (+1.16, 382). The mother liquor was kept and used for the isolation of the (+)_D-form.

8b. (+)_D-Di- μ -hydroxobis[{1,6-bis(2'-pyridyl)-2,5-diazahexane}chromium(III)]antimonyl (+)_D-tartrate, (+)_D-[(C₁₄H₁₈N₄)Cr(OH)₂Cr(C₁₄H₁₈N₄)]{(+)_D-SbOC₄H₄O₆]₂·14H₂O. Ethanol (99%) was added to the mother liquor from 8a to double the volume. The resulting fine precipitate was filtered and washed with a mixture of ethanol and water (50%) and with ethanol (99%). Recrystallization from boiling water (8–9 ml) gave fine, violet crystals, which were washed as above. Yield: 1.12 g (37%). Anal. [Cr(C₁₄H₁₈N₄)(OH)₂]₂(SbOC₄H₄O₆)₂·12H₂O: Cr, C, N, H. (ϵ, λ)_{max}: (196, 534), (151, 385). (ϵ, λ)_{min}: (36, 437), (82, 350). ($\Delta\epsilon, \lambda$)_{max}: (+5.32, 520), (-0.48, 443), (-1.15, 383).

9a. (-)_D-Di- μ -hydroxobis[{1,6-bis(2'-pyridyl)-2,5-diazahexane}chromium(III)]iodide, (-)_D-[(C₁₄H₁₈N₄)Cr(OH)₂Cr(C₁₄H₁₈N₄)]I₄·3H₂O.

(-)_D-[Cr(C₁₄H₁₈N₄)(OH)]₂(+)_D-SbOC₄H₄O₆·I₂·11H₂O (0.83 g, 0.50 mmol) was dissolved in 1 M sodium hydroxide solution (4 ml). Ethanol (100 ml, 99 %) was added dropwise while stirring and cooling to precipitate sodium antimonyl (+)_D-tartrate. Filtering. Then 4 M hydrochloric acid was added to recreate the originally red-violet colour of the diol, and at last sodium iodide (3 g) and a small amount of ascorbic acid were added to precipitate the optically active diol as an iodide. Recrystallization from boiling water (5 ml) with the addition of sodium iodide (1 g) to the filtrate. Washing with ethanol. Yield: 0.447 g (75 %). Anal. [Cr(C₁₄H₁₈N₄)(OH)]₂I₂·3H₂O: Cr, C, N, H, I. (ε, λ)_{max}: (195, 534), (147, 385). (ε, λ)_{min}: (35, 437), (82, 350). (Δε, λ)_{max}: (-5.30, 520), (+0.43, 443), (+1.10, 382).

9b. (+)_D-Di-μ-hydroxobis[1,6-bis-(2'-pyridyl)-2,5-diazaheptane]chromium(III) perchlorate, (+)_D-[Cr(C₁₄H₁₈N₄)₂(OH)₂Cr(C₁₄H₁₈N₄)](ClO₄)₄·4H₂O.

(+)_D-[Cr(C₁₄H₁₈N₄)(OH)]₂(+)_D-SbOC₄H₄O₆·1.14H₂O was dissolved in hot water (8 ml, 70 °C). Sodium perchlorate (1 g) dissolved in water (1 ml) was added. A fluffy precipitate, presumed to be a mixed perchlorate-antimonyl tartrate, immediately appeared. Filtering and washing with ice-water. The compound was dissolved on the filter in boiling water (25 ml). Sodium perchlorate (5 g) was added, and coarse well-shaped crystals appeared on cooling. Recrystallization from boiling water (10 ml) with the addition of sodium perchlorate (1 g) dissolved in water (1 ml). Cooling. Filtering. Washing with ethanol. Yield: 0.197 g (72 %). Anal. [Cr(C₁₄H₁₈N₄)(OH)]₂(ClO₄)₄·4H₂O: Cr, C, N, H, Cl. (ε, λ)_{max}: (197, 534), (150, 385). (ε, λ)_{min}: (36, 437), (78, 350). (Δε, λ)_{max}: (+5.42, 520), (-0.47, 443), (-1.13, 383).

10. (+)_D-α-cis-Dichloro[1,6-bis-(2'-pyridyl)-diazaheptane]chromium(III) perchlorate, (+)_D-α-cis-[Cr(C₁₄H₁₈N₄)Cl₂](ClO₄)₄.

(+)_D-[Cr(C₁₄H₁₈N₄)(OH)]₂(ClO₄)₄·4H₂O (0.245 g, 0.224 mmol) was kept in a stoppered flask with conc. hydrochloric acid (2 ml) for 4 days. By then large violet crystals had formed. They were filtered and washed, first with 1 M sodium perchlorate solution, then with ethanol. Yield: 0.147 g (71 %). (ε, λ)_{max}: (103, 545), (98, 407). (ε, λ)_{min}: (26, 464), (8, 353). (Δε, λ)_{max}: (-1.06, 583), (+1.10, 511), (-0.12, 395).

RESULTS AND DISCUSSION

Synthesis and resolution. Gibson and McKenzie¹² synthesized α-cis-[Co(C₁₄H₁₈N₄)Cl₂]⁺ using the so-called sodium triscarbonatocobaltate(III) as an initial material. We developed another method starting from (trans-[C₁₀py₄Cl₂]Cl₂·6H₂O), which reacted with the amine in an organic medium. β-cis-[Co(C₁₄H₁₈N₄)Cl₂]⁺ was evidently prepared by the same conventional method

in both cases,^{12,16-18} namely by an oxidation with air of the cobalt(II) ion in the presence of amine and sodium nitrite and a subsequent substitution of the nitro groups in the β-cis-dinitro complex formed.

Anhydrous chromium(III) chloride and trans-[C₁₀py₄Cl₂]I react with 2-aminomethylpyridine forming α- and β-cis-[Cr(C₁₄H₁₈N₄)₂Cl₂]⁺, respectively.¹⁹ In the case of 1,6-bis-(2'-pyridyl)-2,5-diazaheptane the same starting materials both gave mixtures of the α- and β-compounds. Differences in solubilities enabled us to separate the compounds, but the final yields were accordingly small.

We have earlier found¹¹ that the di-μ-hydroxobis[bis(2-aminomethylpyridine)chromium(III)] ion could be obtained by the reaction of chromium(III) bromide, hexahydrate and 2-aminomethylpyridine in the presence of chromium(II) or zinc dust. In the present case the method worked equally well, zinc dust being preferred because it was more easily available.

Like the corresponding diols with 2-aminomethylpyridine, 1,10-phenanthroline and 2,2'-bipyridine, the diol with 1,6-bis-(2'-pyridyl)-2,5-diazaheptane could be resolved with sodium antimonyl (+)_D-tartrate as a resolving agent.^{11,5} In all cases the (-)_D-isomer formed the less soluble diastereoisomer. The reaction between the perchlorate of the (+)_D-isomer and conc. hydrochloric acid gave (+)_D-[Cr(C₁₄H₁₈N₄)Cl₂](ClO₄), identified as belonging to the α-type of cis-complexes by means of the absorption spectrum.

Stereochemistry of the cis-dichloro 1,6-bis-(2'-pyridyl)-2,5-diazaheptane-chromium(III) ions. The general formula cis-[M(C₁₄H₁₈N₄)Cl₂]⁺, where M is Co(III) or Cr(III) and C₁₄H₁₈N₄ = 1,6-bis-(2'-pyridyl)-2,5-diazaheptane, theoretically includes two types of geometrical isomers, namely isomers with the symmetrical α-cis configuration (Fig. 2a, b) and isomers with the

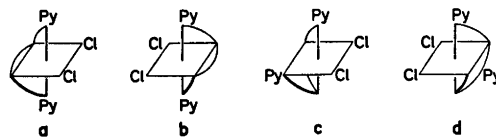


Fig. 2. α- and β-cis-[M(C₁₄H₁₈N₄)Cl₂]⁺. M = Cr(III) or Co(III). Py symbolizes the pyridine nitrogen. a, A (α). b, A' (α). c, A (β). d, A' (β).

Table 1. Data from X-ray powder photographs.

Compound	<i>d</i> -Spacings (Å)
α - <i>cis</i> -[Co(C ₁₄ H ₁₈ N ₄)Cl ₂]ClO ₄	8.98 m, 7.61 s, 7.19 s, 6.69 w, 6.39 s, 5.66 s, 5.62 m, 5.53 m, 5.23 s, 5.08 w, 4.87 s, 4.60 w, 4.40 w, 4.36 w, 4.28 m, 4.23 m, 3.86 m, 3.79 m, 3.69 m, 3.63 s, 3.57 m, 3.49 m, 3.35 w, 3.33 s.
α - <i>cis</i> -[Cr(C ₁₄ H ₁₈ N ₄)Cl ₂]ClO ₄	9.03 m, 7.65 s, 7.19 s, 6.66 w, 6.47 s, 5.67 s, 5.63 s, 5.55 m, 5.25 s, 5.09 w, 4.90 s, 4.61 w, 4.44 w, 4.43 w, 4.31 m, 3.84 s, 3.83 m, 3.66 s, 3.62 s, 3.59 w, 3.50 m, 3.38 m, 3.33 m.
β - <i>cis</i> -[Co(C ₁₄ H ₁₈ N ₄)Cl ₂] ₂ S ₂ O ₈ ·1½H ₂ O	8.30 m, 7.54 s, 6.87 m, 6.75 s, 6.52 w, 6.04 s, 5.39 s, 5.21 m, 5.11 m, 4.87 m, 4.77 w, 4.25 w, 4.21 w, 4.08 m, 3.72 s, 3.49 w.
β - <i>cis</i> -[Cr(C ₁₄ H ₁₈ N ₄)Cl ₂] ₂ S ₂ O ₈ ·2H ₂ O	8.22 m, 7.57 s, 7.03 s, 6.90 m, 6.49 w, 6.04 s, 5.41 s, 5.32 w, 5.23 m, 4.90 m, 4.80 w, 4.25 w, 4.20 w, 4.14 s, 3.82 m, 3.50 s.

Table 2. Electronic spectral parameters from *cis*-dichloro complexes of chromium(III) and cobalt(III) with 2-aminomethylpyridine and 1,6-bis(2'-pyridyl)-2,5-diaza-hexane.

Compound	λ_{\max} nm (1)	ϵ_{\max} (1)	λ_{\max} nm (2)	ϵ_{\max} (2)
α - <i>cis</i> -[Cr(C ₆ H ₈ N ₂) ₂ Cl ₂]Cl·H ₂ O ^a	540.5	97	402	89.5
α - <i>cis</i> -[Cr(C ₁₄ H ₁₈ N ₄)Cl ₂]Cl·3H ₂ O	545	104	407.5	99
β - <i>cis</i> -[Cr(C ₆ H ₈ N ₂) ₂ Cl ₂]I ^a	534	78	405	95
β - <i>cis</i> -[Cr(C ₁₄ H ₁₈ N ₄)Cl ₂]NO ₃ ·½H ₂ O	538	131	407	100
α - <i>cis</i> -[Co(C ₆ H ₈ N ₂) ₂ Cl ₂]Cl·H ₂ O ^b	538.5	136		
α - <i>cis</i> -[Co(C ₁₄ H ₁₈ N ₄)Cl ₂]Cl·1½H ₂ O	541.5	128	392.5	131
β - <i>cis</i> -[Co(C ₆ H ₈ N ₂) ₂ Cl ₂]Cl·2H ₂ O ^b	534	113		
β - <i>cis</i> -[Co(C ₁₄ H ₁₈ N ₄)Cl ₂]NO ₃ ·½H ₂ O	532	158		

^a Ref. 19. ^b Ref. 17.Table 3. CD-spectral parameters for some complexes of chromium(III) with 1,6-bis(2'-pyridyl)-2,5-diaza-hexane (C₁₄H₁₈N₄), 2-aminomethylpyridine (C₆H₈N₂), 1,10-phenanthroline (C₁₂H₈N₂), 2,2'-bipyridine (C₁₀H₈N₂) and 1,2-ethanediamine (C₂H₆N₂).

Compound	Ligand = L	λ_{ex} (1) nm	$\Delta\epsilon_{\text{ex}}$ (1)	λ_{ex} (2) nm	$\Delta\epsilon_{\text{ex}}$ (2)	λ_{ex} (3) nm	$\Delta\epsilon_{\text{ex}}$ (3)	Ref.
(-) _D -[LCr(OH) ₂ CrL] ⁴⁺	C ₁₄ H ₁₈ N ₄			520	-5.30	382	+1.10	
(+) _D -[LCr(OH) ₂ CrL] ⁴⁺	C ₁₄ H ₁₈ N ₄			520	+5.42	383	-1.13	
(-) _D -[L ₂ Cr(OH) ₂ CrL ₂] ⁴⁺	C ₆ H ₈ N ₂	538	+0.37	508	-5.55	376	+1.62	11
$\Delta\Delta$ (-) _D -[L ₂ Cr(OH) ₂ CrL ₂] ⁴⁺	C ₁₂ H ₈ N ₂			~520	~ -6.2	~400	~ +2.6	5
$\Delta\Delta$ (-) _D -[L ₂ Cr(OH) ₂ CrL ₂] ⁴⁺	C ₁₀ H ₈ N ₂	615	+0.18	518	-6.62	402	+0.79	20
(+) _D -[CrLCl ₂] ⁺	C ₁₄ H ₁₈ N ₄	583	-1.06	511	+1.10	395	-0.12	
(+) _D -[CrL ₂ Cl ₂] ⁺	C ₆ H ₈ N ₂	575	-0.66	513	+0.88	409	-0.17	11
Δ (+) _D -[CrL ₂ Cl ₂] ⁺	C ₂ H ₆ N ₂	590	-0.5	520	+0.6	425	+0.25	22

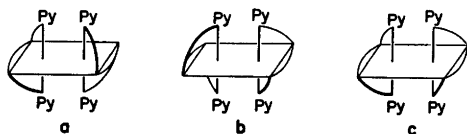


Fig. 3. $[(C_{14}H_{18}N_4)Cr(OH)_2Cr(C_{14}H_{18}N_4)]^{4+}$. a, b and c are the three isomers that can be constructed from two α -*cis*-skeletons. a, Δ (α) Δ (α). b, Δ (α) Δ (α). c, Δ (α) Δ (α).

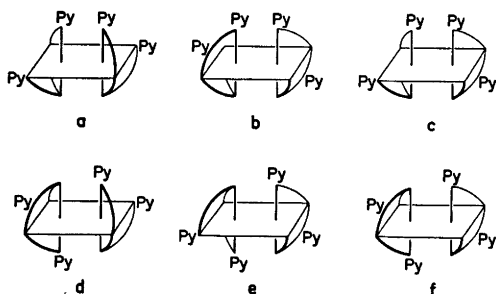


Fig. 4. $[(C_{14}H_{18}N_4)Cr(OH)_2Cr(C_{14}H_{18}N_4)]^{4+}$. a, b, c, d, e and f are the six isomers that can be constructed from two β -*cis*-skeletons. a, Δ (β) Δ (β). b, Δ (β) Δ (β). c, Δ (β) Δ (β). d, Δ (β) Δ (β). e, Δ (β) Δ (β). f, Δ (β) Δ (β).

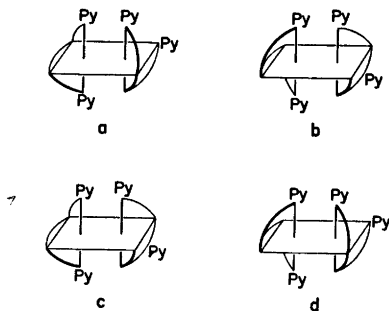


Fig. 5. $[(C_{14}H_{18}N_4)Cr(OH)_2Cr(C_{14}H_{18}N_4)]^{4+}$. a, b, c and d are the four isomers that can be constructed from one α -*cis*-skeleton and one β -*cis*-skeleton. a, Δ (α) Δ (β). b, Δ (α) Δ (β). c, Δ (α) Δ (β). d, Δ (α) Δ (β).

unsymmetrical β -*cis* configuration (Fig. 2c, d). It was possible to isolate racemates of all the predicted compounds and the optically active forms of α -*cis*- $[Cr(C_{14}H_{18}N_4)Cl_2]^+$ (Fig. 2a and b). Gibson and McKenzie¹² assigned the configurations of the cobalt complexes by means of 1H MNR spectra. As we prepared

the α -complex by a totally different method and the β -complex by a slightly different method, we had to repeat the measurements to identify our compounds. Our measurements confirmed the previously found results.

To assign the configurations of the chromium complexes we compared their X-ray powder diffraction patterns with those of the corresponding cobalt complexes. We found strong evidence for isomorphism between blue-violet *cis*- $[Cr(C_{14}H_{18}N_4)Cl_2]ClO_4$ and blue-violet α -*cis*- $[Co(C_{14}H_{18}N_4)Cl_2]ClO_4$ and a reasonable evidence for isomorphism between red-violet *cis*- $[Cr(C_{14}H_{18}N_4)Cl_2]_2S_2O_8 \cdot 2H_2O$ and red-violet β -*cis*- $[Co(C_{14}H_{18}N_4)Cl_2]_2S_2O_8 \cdot 1\frac{1}{2}H_2O$ (Table 1).

Table 2 shows a comparison between the absorption spectra of *cis*- $[M(C_{14}H_{18}N_4)Cl_2]^+$ and *cis*- $[M(C_6H_8N_2)_2Cl_2]^+$ ions, where again $M = Co(III)$ or $Cr(III)$ and $C_6H_8N_2 = 2$ -aminomethylpyridine. We notice the similarity especially regarding the position of the absorption maxima of related compounds.

Stereochemistry of the di- μ -hydroxobis[1,6-(2'-pyridyl)-2,5-diazahexane]chromium(III) ion. The binuclear ion $[(C_{14}H_{18}N_4)Cr(OH)_2Cr(C_{14}H_{18}N_4)]^{4+}$ in principle exists in several isomeric forms. From an α -*cis*-skeleton for instance (Fig. 2 a and b), we can build up a total of three different isomers (Fig. 3 a, b, c). From a β -*cis*-skeleton we can build six different isomers (Fig. 4 a, b, c, d, e, g), and by the combination of an α -*cis*-skeleton and a β -*cis*-skeleton we can build four different isomers (Fig. 5a, b, c). Molecular models indicate, however, that eleven of these thirteen isomers would be grossly hindered sterically. We are thus left with the probability of finding two isomers only, namely the catoptromers shown in Fig. 3a and b.

Our experiments agreed nicely with that. We found one kind of di- μ -hydroxo complex, a racemate that could be resolved, the $(-)_D$ -isomer accounting for 47 % of the starting material.

On the assumption that the acid cleavage reaction of the di- μ -hydroxobis[1,6-bis-(2'-pyridyl)-2,5-diazahexane]chromium(III) ion proceeds with retention of configuration as experienced for diols with 2-aminomethylpyridine,¹¹ 1,10-phenanthroline and 2,2'-bipyridine,^{5,20} the catoptromers (Fig. 3a and b) should react with conc. hydrochloric acid to

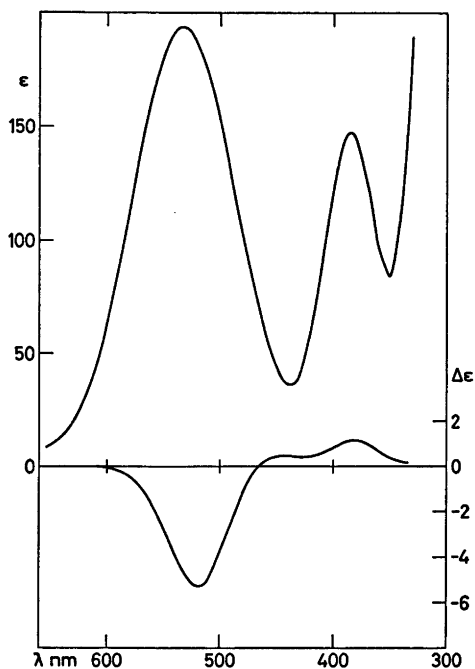


Fig. 6. The absorption spectrum (top) and the circular dichroism spectrum (bottom) of $(-)_D$ - $[(C_{14}H_{18}N_4)Cr(OH)_2Cr(C_{14}H_{18}N_4)]^{4+}$.

form *cis*-dichloro complexes of the symmetrical type shown in Fig. 2a, b. In fact $(+)_D$ - $[(C_{14}H_{18}N_4)Cr(OH)_2Cr(C_{14}H_{18}N_4)](ClO_4)_4 \cdot 4H_2O$ did react solely forming $(+)_D$ - α -*cis*- $[Cr(C_{14}H_{18}N_4)Cl_2]ClO_4$, confirming that our assignments have been correct.

Configuration and optical activity. The absorption and CD spectra of $(-)_D$ - $[(C_{14}H_{18}N_4)Cr(OH)_2Cr(C_{14}H_{18}N_4)]^{4+}$ are shown in Fig. 6, and a comparison with spectral data for corresponding compounds appears in Table 3. If the chirality can be related to the sign of the dominant CD-band in the region of the cubic ${}^4A_{2g} \rightarrow {}^4T_{2g}$ $d-d$ absorption of the chromium(III) ion,²¹ the configurations of $(-)_D$ - and $(+)_D$ - $[(C_{14}H_{18}N_4)Cr(OH)_2Cr(C_{14}H_{18}N_4)]^{4+}$ should be $\Delta\Delta$ and $\Lambda\Lambda$, respectively. Consequently the configuration of $(+)_D$ - α -*cis*- $[Cr(C_{14}H_{18}N_4)Cl_2]^+$ is Λ .

The absorption and CD-spectra of $(+)_D$ - α -*cis*- $[Cr(C_{14}H_{18}N_4)Cl_2]^+$ are shown in Fig. 7, and a comparison with the spectral data for analogous compounds appears in Table 3. The CD-spectrum has the same main features as

Acta Chem. Scand. A 31 (1977) No. 6

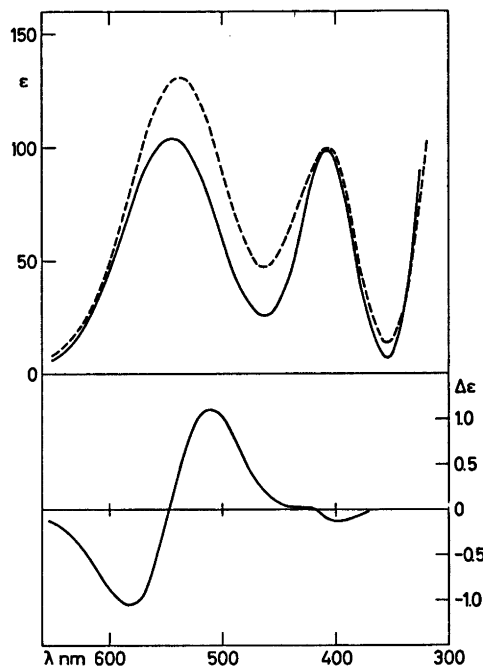


Fig. 7. The absorption spectra (top) of α -*cis*- $[Cr(C_{14}H_{18}N_4)Cl_2]^+$ (—) and β -*cis*- $[Cr(C_{14}H_{18}N_4)Cl_2]^+$ (---) and the circular dichroism spectrum (bottom) of $(+)_D$ - α -*cis*- $[Cr(C_{14}H_{18}N_4)Cl_2]^+$.

the CD-spectra of Λ - $(+)_D$ -*cis*-dichloro complexes of chromium(III) with 2-aminomethylpyridine²¹ and 1,2-ethanediamine²² with a positive, but in this case not dominant, band in the region 510–520 nm.

Acknowledgement. The author is grateful to Karen Margarethe Nielsen for the preparation of 1,6-bis-(2'-pyridyl)-2,5-diazahexane.

REFERENCES

1. Wolcott, S. D. and Hunt, J. B. *Inorg. Chem.* 7 (1968) 755.
2. Springborg, J. and Toftlund, H. *Acta Chem. Scand. A* 30 (1976) 171.
3. Inskoop, R. G. and Benson, M. J. *Inorg. Nucl. Chem.* 20 (1961) 290.
4. Ferraro, J. R., Driver, R., Walker, W. R. and Wosniak, W. *Inorg. Chem.* 6 (1967) 1586.
5. Mason, S. F. and Wood, J. W. *Chem. Commun.* (1968) 1512.
6. Josephsen, J. and Schäffer, C. E. *Acta Chem. Scand.* 24 (1970) 2929.

7. Veal, J. T., Hatfield, W. E. and Hodgson, D. J. *Acta Crystallogr. B* 29 (1973) 12.
8. Earnshaw, A. and Lewis, J. J. *Chem. Soc.* (1961) 396.
9. Morishita, T., Hori, K., Kyono, E. and Tsuchiga, R. *Bull. Chem. Soc. Jpn.* 38 (1965) 1276.
10. Scaringe, R. P., Singh, P., Eckberg, R. P., Hatfield, W. E. and Hodgson, D. J. *Inorg. Chem.* 14 (1975) 1127.
11. Michelsen, K. *Acta Chem. Scand. A* 30 (1976) 521.
12. Gibson, J. G. and McKenzie, E. D. *J. Chem. Soc.* (1971) 1666.
13. Glerup, J. and Schäffer, C. E. *To be published in Inorg. Chem. in 1977-78.*
14. Werner, A. and Feenstra, R. *Ber. Dtsch. Chem. Ges.* 39 (1906) 1538.
15. Goodwin, H. A. and Lions, F. J. *Am. Chem. Soc.* 82 (1960) 5021.
16. Holtzclaw, H. F., Sheetz, D. P. and McCarty, B. D. *Inorg. Synth.* 4 (1953) 176.
17. Michelsen, K. *Acta Chem. Scand.* 26 (1972) 769.
18. Sargeson, A. M. and Searle, G. H. *Inorg. Chem.* 6 (1967) 787.
19. Michelsen, K. *Acta Chem. Scand.* 26 (1972) 1517.
20. Hancock, M. P., Josephsen, J. and Schäffer, C. E. *Acta Chem. Scand. A* 30 (1976) 79.
21. Mason, S. F. *Q. Rev. Chem. Soc.* 17 (1963) 20.
22. McCaffery, A. J., Mason, S. F. and Norman, B. J. *J. Chem. Soc.* (1965) 5094.

Received January 10, 1977.

The Gibbs-Duhem Equation and Equilibrium of Matter in External Fields and Temperature Gradients. Towards a Rational Thermodynamics. III

TORBEN SMITH SØRENSEN

Fysisk-Kemisk Institut, Technical University of Denmark, DK-2800 Lyngby, Denmark.

The possibility of homogeneous integration of the internal energy (E) is considered in connection with a discussion of the proper form of the Gibbs-Duhem equation in thermodynamic systems. It is found that the Gibbs-Duhem equation solely involves variations in "internal" Brønsted-potentials (negative pressure, temperature, chemical potentials, polarising electric or magnetic fields or interfacial tensions) and *not* variations in "external" Brønsted-potentials (electric or gravitational potentials). Equilibrium conditions and overall force balances are established for isothermal systems.

A subdivision of the internal energy (E) of a system into Gibbsian internal energy (U), potential energy (PE) and macroscopic kinetic energy (KE) is considered. The signs of the corresponding time derivatives are seen as important clues to the nature of various types of energy transformations.

Attempts to use equilibrium thermodynamics to describe the partial equilibrium of matter in temperature fields are doomed to failure, since it can be shown on a purely phenomenological basis that "entropies of transport" have nothing to do with partial molar entropies.

The previous papers in the present series have been concerned with the relation between Brønstedian and Gibbsian energetics and the definition and properties of the exergy¹ and with the connection between exergy loss and entropy production.² In this paper we shall take up certain fundamental questions regarding the proper form of the Gibbs-Duhem equation in thermodynamic systems submitted to external fields, a subject which has often led to confusion in the past. We shall make the important distinction between *internal* Brøn-

sted-potentials (*e.g.*, $-p, T, \mu_i$) giving rise to Gibbsian internal energy (U) and *external* potentials (electric and gravitational potentials) giving rise to potential energy (PE). The appropriate equilibrium conditions for matter in isothermal fields are discussed and it is proposed that the sign of the time derivatives dU/dt and dPE/dt together with the sign of the time derivative of the macroscopic kinetic energy (KE) give important information about the physical nature behind the energy transformations taking place in a system.

In the so-called "quasi-thermostatic" methods, equilibrium thermodynamics is used for describing the partial equilibrium of matter in temperature gradients. We shall see that such methods fail to yield a description of the Soret-effect where a composition gradient evolves as a consequence of a difference in temperature. A lot of further evidence is given which shows that "entropies of transport" are purely dynamical quantities which have nothing to do with partial molar entropies. Therefore an entirely new principle of non-equilibrium thermodynamics is called for in order to describe, *e.g.*, the Thomson relation between thermo-electromotoric force and Peltier-entropy transfer.

INTERNAL ENERGY AND GIBBS-DUHEM EQUATION

In the first paper in this series we defined the general internal energy of a thermodynamic system to be

$$E = \sum_i \int_0^{K_i} P_i dK_i \quad (1)$$

If the system is not discrete, but continuous, we may consider a small, fixed region in Cartesian space $\delta\Omega$ with an energy given by

$$\delta E = \sum_i \int_0^{\delta K_i} P_i \delta K_i \quad (2)$$

In general, the values of the potentials at a certain position (x, y, z) will be functions of the concentrations c_K of the quantities at (x, y, z) or *functionals* of the concentration distributions. For example, the electric potential ψ is linked to the charge density (c_q) and the absolute permittivity through the Poisson equation

$$\nabla^2 \psi = - \frac{c_q}{\epsilon} \quad (3)$$

(for application of this equation in problems of electrokinetics and electrolyte diffusion see Refs. 3 and 4). The solution to (3) for a given charge distribution is ⁵

$$\psi_{(x,y,z)} = \frac{1}{4\pi\epsilon} \int_{\Omega} \frac{c_q(x^1, y^1, z^1) dx^1 dy^1 dz^1}{\sqrt{(x-x^1)^2 + (y-y^1)^2 + (z-z^1)^2}} \quad (4)$$

showing that ψ is a functional of $c_q(x, y, z)$.

For the total internal energy in the region Ω occupied by our system, we have

$$E = \int_{\Omega} c_E d\Omega \equiv \int_{\Omega} \frac{\delta E}{\delta \Omega} d\Omega = \int_{\Omega} \left\{ \sum \int_0^{c_K} P dc_K \right\} d\Omega \quad (5)$$

where c_E is the concentration of internal energy. The last expression is obtained using (2) and the definition of concentration of a given quantity K

$$c_K = \frac{\delta K}{\delta \Omega} \quad (6)$$

In case of the quantity being the volume ($K=V$) we have to be aware of not to interchange the meanings of the element of fixed volume in Cartesian space ($\delta\Omega$) and the element of *transported* Brønsted-volume (δV). Filling up, e.g., a jar with water at constant p means that the concentration of Brønsted-volume

added to the water goes from 0 to 1. From eqn. (5) we obtain

$$c_E = \sum \int_0^{c_K} P dc_K \quad (7)$$

and

$$dc_E = \sum P dc_K \quad (8)$$

If – and only if – it is possible to find an integration path for the internal energy where the potentials remain unaltered we have

$$c_E = \sum \left\{ P \int_0^{c_K} dc_K \right\} = \sum P c_K \quad (9)$$

By differentiation of (9) and comparison with (8) we get the general form of Gibbs-Duhem's equation

$$\sum c_K \delta P = 0 \quad (10)$$

Now, in the thermodynamic phases considered by Gibbs (Ref. 29, pp. 55–349) the effect of gravity and electric fields were not considered in any great detail (see pp. 144–150 and pp. 331–333, however). Such a phase characterized by (V, S, n_i) and $(-p, T, \mu_i)$ may be built up isothermally and isobarically and with fixed chemical potentials by adding volume, entropy and moles of different components in the same constant proportions as in the final phase, since the composition will not change during the process of loading. Here we have neglected the contribution to internal energy from the interfacial tension at the boundaries of the considered phase. Thus, we have for the Gibbs-Duhem equation in that particular case

$$-\delta p + c_S \delta T + \sum c_i \delta \mu_i = 0 \quad (11)$$

We may even enlarge our list of quantities with the dielectric polarisation \mathcal{P} and magnetisation \mathcal{M} , if they can be added at constant conjugated potentials, i.e. constant polarising fields \mathcal{E} and \mathcal{H} . This will be the case, when the molar polarisation and magnetisation are unique functions of \mathcal{E} and \mathcal{H} at constant p, T and composition (e.g. a Langevin type of relationship ⁶). In such cases we have the Gibbs-Duhem equation

$$V \delta p - S \delta T + \sum n_i \delta \mu_i + \mathcal{P} \delta \mathcal{E} + \mathcal{M} \delta \mathcal{H} = 0 \quad (12)$$

which may be given in terms of concentrations, if desired. Many multi-phase systems may also be built up at constant potentials. Now we have as further quantities *internal* interfacial area with associated excess surface concentrations and surface entropy, but these surface quantities may often be added in constant proportions to the bulk quantities in such a way that the interfacial tensions (σ) and the surface chemical potentials remain constant. In that way we obtain general Gibbs-Duhem equations such as

$$\sum_{\alpha} \{V^{\alpha} \delta p^{\alpha} - S^{\alpha} \delta T^{\alpha} + \sum_i n_i^{\alpha} \delta \mu_i^{\alpha}\} + \sum_{\alpha\beta} \{A^{\alpha\beta} \delta \sigma^{\alpha\beta} - S^{\alpha\beta} \delta T^{\alpha\beta} + \sum_i \Gamma_i^{\alpha\beta} A^{\alpha\beta} \delta \mu_i^{\alpha\beta}\} = 0 \quad (13)$$

Summation over Greek indices represents summation over phases and double Greek indices over interfaces between phases. Since each bulk phase satisfies separately its own Gibbs-Duhem eqn. (11) we have for the $\alpha\beta$ -interface

$$A^{\alpha\beta} \delta \sigma^{\alpha\beta} - S^{\alpha\beta} \delta T^{\alpha\beta} + \sum_i \Gamma_i^{\alpha\beta} A^{\alpha\beta} \delta \mu_i^{\alpha\beta} = 0 \quad (14)$$

where $S^{\alpha\beta}$ is the excess interfacial entropy and $\Gamma_i^{\alpha\beta}$ the excess interfacial concentration of the i 'th component. Important relations are derived from eqn. (14), e.g. the Gibbs adsorption equation for determining interfacial excess concentrations of surfactants experimentally from interfacial tension/concentration relationships.⁷

Passing now to systems involving *external* fields (electric or gravitational) one might be tempted to generalise the Gibbs-Duhem equation to involve all variations in potentials.

It is therefore a most intriguing question whether or not the expression

$$-\nabla P + c_S \nabla T + \sum_i c_i \nabla \mu_i + c_q \nabla \psi + c_M \nabla \phi \quad (15)$$

equals to zero in continuous media subjected to external gravitational or electric fields (for simplicity we now exclude any dielectric and magnetic polarization). La Mer, Foss and Reiss have claimed such a general Gibbs-Duhem equation to be fulfilled.⁸ However, in a paper (edited by J. Koefoed after the death of Brønsted) Brønsted has presented⁹ a subtle discussion of this matter, which does not confirm the conclusion of La Mer, Foss and Reiss. His arguments become somewhat obscured by the fact that he considers only a single chemical component in equilibrium in a gravitational field, however. Therefore, here we treat the general case of multi-component equilibrium in gravitational and electric fields.

It is easily seen that if the expression (15) is equal to zero and the charge density c_q or the electric field strength $-\nabla \psi$ is equal to zero, there can be no pressure gradients in an isotherm system subjected to gravity forces when the gradients in electro-gravi-chemical potentials vanish

$$\nabla \tilde{\mu}_i = \nabla (\mu_i + z_i F \psi + M_i \phi) = 0 \quad (16)$$

Eqn. (16) is the expression for isothermal equilibrium of matter in gravitational and electric fields, and the same equation is quoted by La Mer, Foss and Reiss. Actually it is just the work principle of Brønsted applied on the virtual displacement of one mol of component i in Cartesian space. We know, however, that there certainly are pressure gradients in gravita-

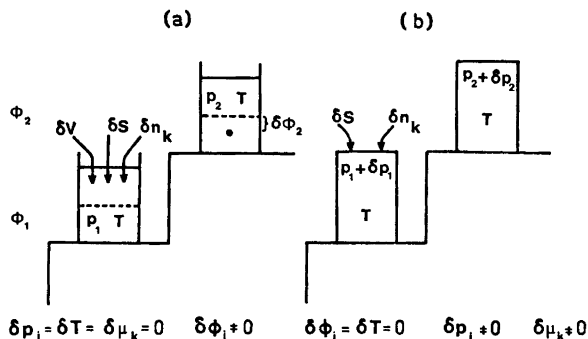


Fig. 1. Different modes of charging a gravity field with matter.

tional systems at equilibrium (hydrostatic pressure), and this can only mean that the "general" Gibbs-Duhem equation is *not* correct.

Since the proofs of the various Gibbs-Duhem equations rely only on the possibility of homogeneous integration of the internal energy into the expression given by eqn. (9), one might wonder, why it is not possible to choose an integration path, where all potentials remain constant, when we change our system with the various quantities. The difficulty is illustrated in Fig. 1. For simplicity we consider a discrete system with two containers mounted at different heights in a gravity field. One can choose *either* to supply Brønsted-volume, entropy and moles of the components together with the molecular masses at fixed temperature and pressure at each position, *or* to supply the moles, the masses and the entropy at equal volumes of the containers. In the first case the volumes in the containers change during the process of filling up the containers and thereby the center of gravity, *i.e.* ϕ , changes in each case, whereas T , p , and the chemical potentials remain constant. In the second case the ϕ 's are constant, but p and the μ 's will vary if dT is chosen to be zero. Thus, it is not possible to choose an integration path with ϕ , ψ , T , p , and the μ 's being simultaneously constants. Therefore, a Gibbs-Duhem equation can only be established for potentials and quantities involved in the traditional (Gibbsian) internal energy which we may designate by the usual symbol U . We have

$$c_U = -p + Tc_S + \sum \mu_i c_i \quad (17a)$$

$$-\nabla p + c_S \nabla T + \sum c_i \nabla \mu_i = 0 \quad (17b)$$

In isothermal external fields $\nabla T = 0$, and when this is introduced in the Gibbs-Duhem eqn. (17b) together with the equilibrium conditions (16) for each component, we obtain the overall force balance on an element of volume

$$-\nabla p = c_M \nabla \phi + c_q \nabla \psi \quad (18)$$

The Gibbsian internal energy U will only be a part of the general internal energy E of a thermodynamic system defined by eqn. (1). Especially we notice – by comparison with the table of quantities and conjugated potentials given in the first paper in this series¹ – that we have neither included electric charge and

heavy mass, nor inertial mass and the conjugated "velocity potential" $v^2/2$ where v is the velocity of the local center of mass. The corresponding contribution to the integral (5) give rise to *potential energy*

$$PE = \int_{\Omega} c_{PE} d\Omega = \int_{\Omega} \left\{ \int_0^q \psi dc_q + \int_0^{c_M} \phi dc_M \right\} d\Omega \quad (19)$$

and macroscopic kinetic energy (*e.g.* hydrodynamic motion)

$$KE = \int_{\Omega} \left(\frac{v^2}{2} c_M \right) d\Omega = \int_{\Omega} \left\{ \int_0^{c_M v} \mathbf{v} \cdot d(c_M \mathbf{v}) \right\} d\Omega \quad (20)$$

The last integral in eqn. (20) corresponds to a bipartition of the "kinetic work" which is often more convenient than $P = v^2/2$ and $K = M$. Here $\mathbf{K} = M\mathbf{v}$, *i.e.* the linear momentum is chosen as a "vectorial quantity". The conjugated "vectorial potential" becomes then the velocity itself. The total internal energy is now the sum of the Gibbsian energy, the potential energy and the kinetic energy

$$E = U + PE + KE \quad (21)$$

In an isolated thermodynamic system $dE/dt = 0$, but that does not mean, obviously, that the three time derivatives are separately zero. On the contrary, the signs of dU/dt , dPE/dt and dKE/dt are important clues to the understanding of the nature of the physical processes going on in the system. Some examples would be illuminating:

1. $dU = dPE = dKE = 0$. Internal, irreversible processes such as "heat" conduction, diffusion processes and chemical reactions.

2. $dU > 0$, $dPE < 0$, $dKE = 0$. "Joule heating" of an electrical resistance.

3. $dU < 0$, $dPE > 0$, $dKE = 0$. Thermoelectric phenomena where electrons (or "positive holes") are taken against the gradient of their electrochemical potential by a flux of entropy.

4. $dU > 0$, $dPE = 0$, $dKE < 0$. Viscous dissipation of hydrodynamic motion.

5. $dU = 0$, $dPE \neq 0$, $dKE \neq 0$. Frictionless Bernoulli (Euler) motion of an incompressible fluid.

6. $dU < 0$, $dPE = 0$, $dKE > 0$. Formation of spontaneous convection cells ("dissipative struc-

tures" in the terminology of Glansdorff and Prigogine¹⁰) at liquid-liquid boundaries due to chemical reactions on the interface¹¹⁻¹³ or due to mass transfer.¹⁴⁻¹⁷

EQUILIBRIUM OF MATTER IN TEMPERATURE GRADIENTS

If we also have gradients of temperature it becomes necessary to modify some of the statements in the previous section concerning the equilibrium of matter. The equilibrium is now a partial equilibrium, since the system *in toto* is not in equilibrium because of the unbalanced flow of entropy (see Ref. 2). However, we may imagine that this entropy has no influence on the quasi-equilibrium condition for component *i*. Instead of (16) we now write

$$\nabla\mu_i + \bar{S}_i\nabla T + z_i F \nabla\psi + M_i \nabla\phi = 0 \quad (22)$$

according to Brønsted's work principle, since we move partial molar entropy (\bar{S}_i) with one mol of component *i* as well as charge $z_i F$ and mass M_i . In the isothermal case this transport is neutral and need not be included in the work principle. Weighting each of the eqns. (22) with c_i and summing we obtain

$$\sum c_i \nabla\mu_i + c_S \nabla T + c_q \nabla\psi + c_M \nabla\phi = 0 \quad (23)$$

and introducing the Gibbs-Duhem eqn. (17b) we recover the overall force balance on an element of volume (18).

Using eqn. (22) to describe equilibrium of conducting electrons in a temperature gradient in a metallic conductor, we have

$$d\mu_e - F d\psi + \bar{S}_e dT = d\tilde{\mu}_e + \bar{S}_e dT = 0 \quad (24)$$

Making a junction between two different conductors - (1) and (2) - with the junction elevated to the temperature $T + \Delta T$, we obtain for the thermo-electromotoric force between the two ends of temperature T

$$\begin{aligned} \text{emf}(1 \rightarrow 2) &= - \left[\frac{\tilde{\mu}_e^{(2)} - \tilde{\mu}_e^{(1)}}{F} \right] \\ &= - \frac{1}{F} \left[\int_T^{T+\Delta T} (\bar{S}_e^{(1)} - \bar{S}_e^{(2)}) dT \right] \end{aligned} \quad (25)$$

since the electrochemical potentials of the electron in the two metals are equal at the

hot junction. Under the assumption of constant partial molar entropy of the electron we obtain approximately

$$\text{emf}(1 \rightarrow 2) \cong - \frac{1}{F} (\bar{S}_e^{(1)} - \bar{S}_e^{(2)}) \Delta T \quad (26)$$

On the other hand, in an experiment where positive current I_q (C/s) is directed from conductor 1 to conductor 2 and the junctions are kept at constant temperatures T and $T + dT$ by means of thermostats, we will have transfer of the following Peltier-entropy per unit time to the "hot" thermostat

$$\frac{dS_{\text{Peltier}}}{dt} = \frac{I_q}{F} (\bar{S}_e^{(2)} - \bar{S}_e^{(1)}) \quad (27)$$

(due to conservation of entropy at the hot junction, the difference between the entropy carried along with the electrons has to be compensated by an entropy exchange with the hot thermostat). Thus, the present "quasi-thermostatic" theory predicts correctly the required relationship between thermo-emf and Peltier heat found by Thomson,^{18,19} since the partial molar entropy of the electron is common for the two experiments.

Thomson himself expressed doubt, however, whether it was correct to use equilibrium thermodynamics to describe virtual displacements of the electron in cases with a "heat" flow. Niels Bohr was probably one of the first to hint that the reversibility of the microscopic Hamiltonian equations of motion was the real physical reason behind Thomson's relations (see Ref. 20, pp. 22, 71 - 75). As is well known, the symmetry to time reversal of time correlation functions of fluctuations in different physical variables was later made a cornerstone in Lars Onsager's proof of the reciprocal relations between transport coefficients,²¹ on which proof the later developed framework of irreversible thermodynamics is resting.²²

It is also possible on a *phenomenological* basis, however, to prove that the quasi-equilibrium condition (22) cannot be correct. For example, Koefoed²³ has once pointed to the fact that experimentally one sometimes finds a definite thermo-emf between two identical single crystals with different orientation. But the partial molar entropy of the electron in a crystal cannot be dependent of orientation, and the emf

should be 0 following (26), if (22) were correct. As another example we may take the thermo-diffusion effect discovered by Ludwig²⁴ and Soret.²⁵ It is an experimental fact that substances in solution in a column with a temperature gradient has a tendency to concentrate somewhat in one end of the column (predominantly the cooler). When we consider a two component system, and thermodiffusion equilibrium has been reached, we have for an uncharged solute (1) according to (22) in a one dimensional T-profile

$$d\mu_1 + \bar{S}_1 dT = 0$$

For systems with no pressure gradients we have $d\mu_1 = -\bar{S}_1 dT + (\partial\mu_1/\partial X)dX$ where X is the mol fraction of component 1, since there is only a single composition variable in a two component system. Combining the two equations we obtain

$$(\partial\mu_1/\partial X)_{T,p} dX = 0$$

which means that $dX = 0$. Thus, assumption of the equilibrium condition (22) for equilibrium of matter under non-isothermal conditions will exclude the possibility of any Soret-effect! We have to replace (22) by eqn. (28)

$$\nabla\mu_1 + S_1^* \nabla T + z_1 F \nabla\psi + M_1 \nabla\phi = 0 \quad (28)$$

where \bar{S}_1^* is the molar "entropy of transport". In anisotropic media we must even take \bar{S}_1^* to be dependent on the chosen direction in space. Since the Gibbs-Duhem eqn. (17b) and the over-all balance of forces (18) still have to be fulfilled, eqn. (23) must still be correct. Weighting each of the eqns. (28) with the concentration c_i and summing, we notice that the following restriction for the entropies of transport has to be respected

$$\sum c_i \bar{S}_i^* = c_S \quad (29)$$

With the new equilibrium condition (28) we have for the Soret-effect in a two component solution

$$\left(\frac{dX}{dT}\right)_{\text{Soret}} = \frac{\bar{S}_1 - \bar{S}_1^*}{(\partial\mu_1/\partial X)_{T,p}} \quad (30)$$

But the entropy of transport is now a purely dynamical quantity without any basis in equilibrium thermodynamics. There is no guarantee that \bar{S}_1^* will be identical under

different experimental conditions. Therefore, the relation between thermo-emf and Peltier-effect must be due to an entirely new principle on non-equilibrium thermodynamics, which may be called "the fourth law of thermodynamics" (expressed for example in Onsager's reciprocal relations).

The measurements of Denbigh and Raumann²⁶⁻²⁸ of the thermo-osmotic pressure differences over rubber membranes exerted by H_2 and CO_2 constitute still another proof that entropies of transport have nothing to do with partial molar entropies. Using (28) for the description of the quasi-equilibrium of the gas dissolved in the rubber membrane we obtain under the assumption of approximately constant \bar{S}^* for the gas through the membrane (small ΔT and Δp)

$$\Delta\mu_{\text{gas in membrane}} + \bar{S}^* \Delta T \cong 0 \quad (31)$$

The difference in chemical potential for the gas is taken between localities just *inside* the two membrane boundaries. Due to local equilibrium the chemical potentials just outside the membrane must be the same. For small ΔT and Δp we have

$$\Delta\mu_{\text{gas}} \cong -\bar{S}_{\text{gas}} \Delta T + \bar{V}_{\text{gas}} \Delta p \quad (32)$$

and combining (31) and (32) we have for the thermo-osmotic pressure

$$\left(\frac{\Delta p}{\Delta T}\right)_{\text{thermo-osmosis}} \cong \frac{\bar{S}_{\text{gas}} - \bar{S}^*}{\bar{V}_{\text{gas}}} \quad (33)$$

If \bar{S}^* were simply the partial molar entropy of the gas dissolved in rubber, eqn. (33) would be nothing more than a simple Clapeyron equation for elevation of the vapor pressure due to an elevation of temperature. The measurements of Denbigh and Raumann show, however, that not only is \bar{S}^* entirely different from the partial molar entropy of the gases dissolved in rubber, but the suspected "entropy of vaporisation" $\bar{S}_{\text{gas}} - \bar{S}^*$ calculated from thermo-osmotic data has even *different signs* for the gases H_2 and CO_2 !

CONCLUSION

Different types of Gibbs-Duhem equations have been investigated. Of particular importance is the statement that electrical and

gravitational potential variations in space must not be included in the Gibbs-Duhem equation.

A division of internal energy of a general thermodynamic system E into Gibbsian internal energy U , potential energy PE and macroscopic kinetic energy KE is made. The signs of dU/dt , dPE/dt and dKE/dt constitute important clues to the physical mechanisms involved in the energy transformations.

The quasi-thermostatic methods of calculation of equilibrium of matter in temperature fields are not correct even on a phenomenological basis. The entropy of transport has nothing to do with the partial molar entropy. It is a purely dynamical quantity, and quantitative relationships between different experiments such as thermo-emf and Peltier-effect are due to an entirely new principle of non-equilibrium thermodynamics, as earlier shown by statistical arguments by Bohr and Onsager. A phenomenological treatment of transport-processes containing Onsager's reciprocal relations as a special case will be presented in a forthcoming paper.

Acknowledgement. The author wishes to express his gratitude to Flemming Yssing Hansen and Jørgen Koefoed for discussions of illuminating value for some of the points of views in the present paper.

REFERENCES

- Sørensen, T. S. *Acta Chem. Scand. A* 30 (1976) 555.
- Sørensen, T. S. *Acta Chem. Scand. A* 31 (1977) 347.
- Sørensen, T. S. and Koefoed, J. *J. Chem. Soc. Faraday Trans. 2*, 70 (1974) 665.
- Sørensen, T. S. and Jensen, K. F. *J. Chem. Soc. Faraday Trans. 2*, 71 (1975) 1805.
- Margenau, H. and Murphy, G. M. *The Mathematics of Physics and Chemistry*, 2nd Ed., D. van Nostrand, Princetown, Toronto, Melbourne, London 1956, Chapter 7, Section 17.
- Langevin, P. *C. R. Acad. Sci.* 140 (1905) 1171.
- Adamson, A. W. *Physical Chemistry of Surfaces*, 2nd Ed., Interscience, New York, London, Sydney 1967, Section II-5A and Section II-6.
- La Mer, V. K., Foss, O. and Reiss, H. *Acta Chem. Scand.* 3 (1949) 1238.
- Brønsted, J. N. *Acta Chem. Scand.* 3 (1949) 1208. (Translated from Danish manuscript after the death of Prof. Brønsted by J. Koefoed).
- Glansdorff, P. and Prigogine, I. *Thermodynamic Theory of Structure, Stability and Fluctuations*, Wiley-Interscience, London, New York, Sydney, Toronto 1971.
- Hennenberg, M., Sørensen, T. S., Steinchen, A. and Sanfeld, A. *J. Chim. Phys.* 72 (1975) 1202.
- Sørensen, T. S., Hennenberg, M., Steinchen, A. and Sanfeld, A. *J. Colloid Interface Sci.* 56 (1976) 191.
- Sørensen, T. S., Hennenberg, M., Steinchen, A. and Sanfeld, A. *Progr. Colloid Polymer Sci.* 61 (1976) 64.
- Sternling, C. V. and Scriven, L. E. *A.I.Ch.E.J.* 5 (1959) 514.
- Orell, A. and Westwater, J. W. *A.I.Ch.E.J.* 8 (1962) 350.
- Hennenberg, M., Sørensen, T. S. and Sanfeld, A. *J. Chem. Soc. Faraday Trans. 2*, 73 (1977) 48.
- Sørensen, T. S., Hennenberg, M. and Sanfeld, A. *J. Colloid Interface Sci. In press.*
- Thomson, W. *Proc. R. Soc. Edinburgh* 3 (1854) 225.
- Brønsted, J. N. *Principer og Problemer i Energetiken*, Københavns Universitets Festskrift, Bianco Luno, København 1946, Chapter VI, Section 4.
- Bohr, N. *Studier over Metallernes Elektron-teori*, Diss., Thaning & Appel, Copenhagen 1911.
- Onsager, L. *Phys. Rev.* 37 (1931) 405; 38 (1931) 2265.
- Prigogine, I. *Etude Thermodynamique des Phénomènes Irreversibles*, Dunod, Paris/Desoer, Liege 1947.
- Koefoed, J. *J. Colloid Sci.* 12 (1957) 131.
- Ludwig, C. *Akad. Wiss. Wien* 20 (1856) 539.
- Soret, C. *Ann. Chim. Phys.* (5) 22 (1881) 293.
- Denbigh, K. G. *Nature* 163 (1949) 60.
- Denbigh, K. G. and Raumann, G. *Nature* 165 (1950) 199.
- Denbigh, K. G. and Raumann, G. *Proc. R. Soc. London Ser. A* 210 (1951) 377, 518.
- Gibbs, J. W. *Scientific Papers, Vol. I*, Dover, New York 1961.

Received December 16, 1976.

A Thermogravimetric Method for Determination of Vapour Pressures Above 10^{-2} Atm. I: Theory

KETIL MOTZFELDT, HALVOR KVANDE and PHILLIP G. WAHLBECK*

Department of Chemistry, The Norwegian Institute of Technology, The University of Trondheim, N-7034 Trondheim-NTH, Norway

Available methods for the determination of vapour pressures at high temperatures appear to leave a demand for an experimentally simple method for the measurement of pressures above the range of molecular flow. A method originating from the early work of Ruff and co-workers is considered for the purpose. In this method, the rate of vapour transport through a capillary is determined as a function of an applied inert-gas pressure at constant furnace temperature. The theory of the method is developed, based on transport equations for a binary gas mixture with gradients in both composition and total pressure. Effects of interdiffusion, viscous flow and thermal transport are considered, and the ranges for dominating influence of each of these effects are delineated. It is shown how computer fitting of the theoretical equation to the experimental data advantageously may be used to determine the equilibrium vapour pressure. Applications to the determination of vapour diffusivity and viscosity also are considered.

The study of vaporization processes forms an important part of high-temperature chemical research. In the present context, vaporization is taken to include all processes whereby gas is evolved from a system of condensed phases, and vapour pressure determinations include the measurement of equilibrium gas pressures in any such system.

For the study of high-temperature systems, the effusion method has been used extensively. The effusion method, however, is based on molecular flow and hence is limited to pressures below *ca.* 10^{-4} atm. The present paper

discusses a method for the higher pressure range (about 10^{-2} to 1 atm), equally applicable at elevated temperatures because the vapour pressure cell employed is comparable to an effusion cell in simplicity.

The chosen method originates from the early work of Ruff *et al.*^{1,2} The substance or system to be investigated is contained in a cell with a narrow capillary opening in the lid. The cell is suspended from a balance into a furnace in an inert-gas atmosphere which initially is at a higher pressure than the equilibrium vapour pressure of the system at the furnace temperature. When the inert-gas pressure is lowered (or the vapour pressure is increased by increasing the temperature), the vapour transport through the opening and hence the rate of mass loss from the cell increase. The enhanced flux particularly is marked when the inert-gas pressure becomes smaller than the equilibrium vapour pressure, and this effect may be used to determine the vapour pressure.

Ruff *et al.*^{1,2} and J. Fischer³ followed the mass change of the cell at constant inert-gas pressure and increasing temperature. From their measurements it was found that a graph of the mass *versus* time or temperature did not exhibit a sharp break at the equilibrium vapour pressure. The situation was not improved substantially by plotting instead the derivative of mass with respect to time (*i.e.*, the rate of mass loss). W. Fischer *et al.*⁴ pointed out the advantages of observing mass changes at constant temperature and decreasing pressure stepwise. However, a really sharp break in the

* Permanent address: Department of Chemistry, Wichita State University, Wichita, Kansas 67208, USA.

curve for rate of mass loss *versus* pressure was not found.

A subsequent theoretical treatment by Wagner⁵ showed that the mentioned curves cannot be expected to give sharp breaks. Wagner gave recommendations as to the best way of performing the experiments, but even so the graphical method for determination of the equilibrium pressure remains unreliable.

It is the purpose of the present paper (1) to develop a consistent theory for the method, (2) to discuss the resulting equation in terms of various assumptions that lead to simpler equations as limiting cases, and (3) to show how a numerical rather than graphical procedure may be used to determine the equilibrium vapour pressure from the experimental observations.

THEORY

A schematic drawing of a suitable cell is shown in Fig. 1. The opening has the shape of a capillary with radius r and length l . The cell is suspended inside a furnace at temperature T . The inert gas is denoted by subscript 1 and the vapour by subscript 2, while subscript f denotes the furnace space and subscript i denotes the interior of the cell. The symbol c denotes concentration, x mol fraction, and P pressure.

The following assumptions are made:

(1) The system is maintained at a steady state, with a net transport \dot{n}_2 (mol/s) of vapour through the capillary, while the net transport of inert gas, $\dot{n}_1 = 0$. The flux $J_2 = \dot{n}_2/(\pi r^2)$.

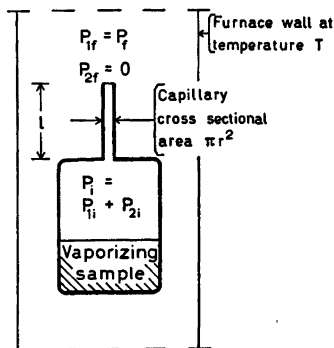


Fig. 1. Schematic diagram of the cell suspended inside the furnace.

(2) At the exit end of the capillary, the vapour dissipates quickly to colder parts of the furnace because of diffusion and convection, so that $x_{1f} = 1$, $x_{2f} = 0$ and $P_{1f} = P_f$, $P_{2f} = 0$.

(3) The capillary is narrow in order to suppress the diffusive flux, and a significant pressure drop may exist through the capillary ($P_i > P_f$). The rate of mass transport is dependent on the rate of viscous flow caused by this pressure drop.

(4) The steady-state evaporation will cause the temperature of the sample to be lower than the observed furnace temperature T , which means that the vapour pressure P_{2i} inside the cell may be lower than the equilibrium vapour pressure P_2° at the temperature T .

As regards assumption (3), Wagner⁵ assumed instead that the pressure remains uniform through the capillary. This assumption limits the applicability of his result to certain experimental conditions, which is the reason why a new treatment appeared to be necessary.

Transport equations for simultaneous diffusion and flow

The first task is to find the correct transport equations for the case of a binary mixture of ideal gases with simultaneous gradients in composition and total pressure. This is a case which appears to have received only occasional attention in the literature. Texts on interdiffusion of gases quite commonly state Fick's first law in terms of gradients in concentration:

$$J_{1d} = -D_{12}(dc_1/dz) \quad (a)^*$$

$$J_{2d} = -D_{21}(dc_2/dz) \quad (b)$$

where D_{12} and D_{21} are the coefficients of interdiffusion for the two gases, and z is the direction of the capillary axis.

An objection to these equations may be raised. Let us introduce the mol fractions $x_1 = c_1/c$, $x_2 = c_2/c$. Rewriting eqn. (a) gives:

$$\begin{aligned} J_{1d} &= -D_{12} \frac{d(cx_1)}{dz} = -D_{12} \left(c \frac{dx_1}{dz} + x_1 \frac{dc}{dz} \right) = \\ &= -\frac{D_{12}}{RT} \left(P \frac{dx_1}{dz} + x_1 \frac{dP}{dz} \right) \quad (c) \end{aligned}$$

* Letters are used here to identify equations which should not be accepted without reservations.

According to Chapman and Cowling⁶ diffusion should be considered as a process caused by a gradient in composition, while flow is a process caused by a gradient in total pressure. It is then apparent that the second term to the right in eqn. (c) does not belong in the expression for the diffusive flux, and therefore eqns. (a) and (b) are not appropriate. The diffusive flux should be expressed in terms of the derivative of the mol fraction.

The total fluxes J_1 and J_2 for the case of gradients in both composition and total pressure may be expressed by the general equations^{7,8}

$$J_1 = -D_{12}c \frac{dx_1}{dz} + cx_1v \quad (1)$$

$$J_2 = -D_{21}c \frac{dx_2}{dz} + cx_2v \quad (2)$$

In these equations, v is the mean molecular velocity in the z direction. In order to derive the correct expression for the velocity v , we will consider first the equations for the special case that the total pressure is uniform.

The case of uniform pressure. The original experimental work of Graham showed that the diffusive fluxes are inversely proportional to the square root of the molecular masses, a result that also may be deduced from a consideration of momentum transfer.⁹ Thus, at uniform pressure $J_{2d} \neq J_{1d}$. The transport equations for this case may be formulated in two ways. One may use equations analogous to eqns. (1) and (2) with $v=0$, using the symbols D_1 and D_2 for the diffusivities to emphasize that they are not equal:

$$J_{1d} = -D_1c(dx_1/dz) \quad (3)$$

$$J_{2d} = -D_2c(dx_2/dz) \quad (4)$$

The diffusivities are related through Graham's law of diffusion:

$$-\frac{J_{1d}}{J_{2d}} = \frac{D_1}{D_2} = \sqrt{\frac{m_2}{m_1}} = \gamma \quad (5)$$

in which m_1 and m_2 are the molecular masses, and the symbol γ has been introduced for brevity of notation.

On the other hand, one may preserve the concept of equal interdiffusion coefficients, that is, $D_{12}=D_{21}=D$. In this case the net transport may be expressed in terms of a mean molecular velocity in the z direction,

designated v_d to indicate that this mean velocity arises from the process of diffusion alone, in the absence of a pressure gradient. Thus, one has

$$J_{1d} = -Dc \frac{dx_1}{dz} + cx_1v_d \quad (6)$$

$$J_{2d} = -Dc \frac{dx_2}{dz} + cx_2v_d \quad (7)$$

The velocity v_d may be calculated by equating the fluxes from eqns. (3) and (6), and from eqns. (4) and (7), introducing also $dx_2/dz = -dx_1/dz$, and substituting eqn. (5). This gives

$$v_d = \frac{D(1-\gamma)}{\gamma + x_1(1-\gamma)} \frac{dx_1}{dz} \quad (8)$$

Introduction of eqn. (8) in eqns. (6) and (7) yields the expressions for the diffusive fluxes at uniform total pressure.

The case of gradients in both composition and total pressure. A gradient in pressure causes a viscous flow (assuming moderate pressure gradients so that turbulence does not occur). The viscous flow may be described in terms of its mean linear velocity v_{visc} . For a straight, cylindrical tube with radius r , this velocity is given by

$$v_{\text{visc}} = -\frac{r^2}{8\eta} \times \frac{dP}{dz} \quad (9)$$

where η is the viscosity of the gas mixture.

The fluxes caused by diffusion and by viscous flow are additive.⁹ This may be expressed by the equations $J_1 = J_{1d} + J_{1\text{visc}}$; $J_2 = J_{2d} + J_{2\text{visc}}$, or by the equivalent statement that the velocity in eqns. (1) and (2) is the sum of two separate contributions:

$$v = v_d + v_{\text{visc}} \quad (10)$$

Substitution of eqn. (10) into eqns. (1) and (2), with v_d given from eqn. (8) and v_{visc} given from eqn. (9), yields the expressions for the fluxes caused by gradients in both composition and total pressure. These equations need not be written for the present purpose.

Application to the vapour pressure method

In the experimental arrangement shown in Fig. 1 at steady state, the net flux is equal to

the mean molecular velocity multiplied by the total concentration. That is,

$$J_2 = cv \quad (11)$$

With $J_1 = 0$ in eqn. (1) we also have

$$cv = cD \frac{d \ln x_1}{dz} \quad (12)$$

From the kinetic theory of gases it is known that the gas diffusivity is inversely proportional to the total pressure, that is

$$DP = D' \quad (13)$$

where D' is a constant at constant temperature.

With substitution of c and J_2 , eqns. (11), (12) and (13) give

$$d \ln x_1 = \frac{RT \dot{n}_2}{\pi r^2 D'} dz \quad (14)$$

Integration between $z = 0$ and $z = l$ yields after some rearrangement:

$$x_{1l} = \exp(-\dot{n}_2/A) \quad (15)$$

The parameter A , which is constant for a given experiment at constant temperature, is defined by

$$A = \frac{\pi r^2 D'}{RTl} \quad (16)$$

The total pressure P_i inside the cell may be expressed in terms of the partial pressures, and we have

$$P_i = \frac{P_{2i}}{1 - \exp(-\dot{n}_2/A)} \quad (17)$$

We now turn to eqn. (11) again. Introduction of eqns. (8), (9) and (10) yields

$$\dot{n}_2 dz = - \frac{\pi r^4}{8RT\eta} P dP + \frac{\pi r^2 D'}{RT} \times \frac{1-\gamma}{\gamma+(1-\gamma)x_1} dx_1 \quad (18)$$

According to the kinetic theory, the viscosity of a gas is independent of pressure, while it is expected to vary with the gas composition. For the latter reason, the value of the viscosity would be expected to vary along the capillary, but we will approximate by the assumption that η is a constant. Eqn. (18) then may be integrated between $z = 0$ and $z = l$, *i.e.*, between $x_1 = x_{1l}$, as given by eqn. (15), and $x_1 = 1$. This gives

$$\dot{n}_2 = \frac{\pi r^4}{16RTl\eta} (P_i^2 - P_f^2) - A \ln [\gamma + (1-\gamma) \exp(-\dot{n}_2/A)] \quad (19)$$

For brevity we define another parameter, constant for a given experiment at constant temperature:

$$C = \frac{\pi r^4}{16RTl\eta} \quad (20)$$

Eqns. (17) and (20) introduced in eqn. (19) give

$$\dot{n}_2 = C \left[\left(\frac{P_{2i}}{1 - \exp(-\dot{n}_2/A)} \right)^2 - P_f^2 \right] - A \ln [\gamma + (1-\gamma) \exp(-\dot{n}_2/A)] \quad (21)$$

The effect of sample cooling

The evaporation requires heat, and the necessary heat flux requires that the sample temperature T_s is slightly lower than the constant furnace temperature T (*cf.* assumption (4) in the introduction). This effect was considered by Wagner.⁵ Assuming a heat transfer coefficient K specific to the given experimental arrangement, one has

$$K(T - T_s) = \dot{n}_2 \Delta H_v$$

where ΔH_v is the molar heat of vaporization of the sample.

The lowered sample temperature causes a lowered vapour pressure in accordance with the Clausius-Clapeyron equation:

$$\ln \frac{P_{2i}}{P_2^\circ} = \frac{\Delta H_v}{R} \left(\frac{1}{T} - \frac{1}{T_s} \right) \cong - \frac{\Delta H_v}{RT^2} (T - T_s)$$

Combination of these two equations yields

$$P_{2i} = P_2^\circ \exp(-\dot{n}_2/B) \quad (22)$$

where the parameter B , a constant for a given experiment at constant temperature, is given by the expression

$$B = KRT^2/\Delta H_v^2 \quad (23)$$

Introducing eqn. (22) in eqn. (21) we get the complete equation for the rate of mass transport:

$$\dot{n}_2 = C \left[\left(\frac{P_2^\circ \exp(-\dot{n}_2/B)}{1 - \exp(-\dot{n}_2/A)} \right)^2 - P_f^2 \right] - A \ln [\gamma + (1-\gamma) \exp(-\dot{n}_2/A)] \quad (24)$$

in which the parameter γ is given by eqn. (5), A by eqn. (16), C by eqn. (20), and B by eqn. (23).

DISCUSSION

An experiment using a thermobalance yields a record of the mass of the cell with sample as a function of time. From the slope of the recorded curve, the rate of mass loss is determined. The inert-gas pressure in the furnace is read on a manometer, and is lowered stepwise in the course of the experiment. Thus, one obtains a set of corresponding values for \dot{n}_2 and P_f , which may be considered as the "knowns" in eqn. (24). For the present we will consider also the parameter $\gamma = (M_2/M_1)^{1/2}$ as known, where M_1 and M_2 are the molecular weights of the inert gas and of the vapour. In a later section we will return to the question of unknown molecular weight of the vapour.

The parameters A , B and C are generally unknown, as is also the vapour pressure P_2° . Thus, there are four unknowns to be determined. The problem may be handled by means of a suitable, non-linear least-squares analysis computer program which fits eqn. (24) to the observed set of data. In this way one obtains the "best" values for the parameters A , B and C , and for P_2° . There is in principle no objection to this procedure. It may happen, however, that eqn. (24) may be fitted to a given set of experimental data with almost equal precision for widely different sets of values for the two parameters B and C . This feature of the equation will be made clear in the discussion to follow. Hence, it is of interest to consider simplifications of eqn. (24) by removal of either B or C .

The course of an experiment roughly may be divided in two parts. At the outset, $P_f > P_2^\circ$, and the mass transport occurs mainly by diffusion of vapour through a higher pressure of inert gas. The rate of mass loss is low and is determined primarily by the value of the parameter A .

In the later stage of the experiment, $P_f < P_2^\circ$, and the rate of mass loss is high. It is determined mainly either by the resistance to viscous flow through the capillary, or by the rate of heat transfer to the sample, or by a combination of both effects. These two effects are

connected with the values of the parameters C and B , respectively. Each of the two limiting cases will be discussed separately.

First case: Viscous flow is rate determining

In this case it is assumed that the sample temperature remains closely equal to the furnace temperature T , so that the vapour pressure inside the cell effectively is maintained at the value P_2° throughout the experiment. Formally this corresponds to an infinite heat transfer coefficient K in eqn. (23). This means an infinite value of B , which makes the exponential in the numerator of eqn. (24) go to unity (that is, eqn. (21) is recovered, with $P_{2f} = P_2^\circ$).

For the purpose of the present discussion it is convenient to express the equation in terms of the ratio P_f/P_2° , which for brevity is denoted by y :

$$\dot{n}_2 = C(P_2^\circ)^2 \left[\left(\frac{1}{1 - \exp(-\dot{n}_2/A)} \right)^2 - y^2 \right] - A \ln [\gamma + (1 - \gamma) \exp(-\dot{n}_2/A)] \quad (25)$$

The behaviour of this equation will be illustrated by graphs of \dot{n}_2 as a function of y . For this purpose a set of arbitrary but reasonable values is chosen for the physical quantities as shown in Table 1, which also gives the corresponding values of the parameters A , C , and γ . The chosen value of M_1 is equal to the atomic weight of argon, while M_2 corresponds roughly to the atomic weight of a metal in the second long period, and the value of the viscosity appears reasonable for a monoatomic metal vapour at the elevated temperature T .

Table 1. Values of constants used for the calculated curves in Fig. 2.

Physical quantities, values chosen	Parameters of eqn. (25), calculated from the chosen physical quantities
$r = 3 \times 10^{-4} \text{ m}$	
$l = 1 \times 10^{-2} \text{ m}$	
$T = 2000 \text{ K}$	$A = 5 \times 10^{-2} \mu\text{mol s}^{-1}$
$D' = D \times P = 30 \text{ N s}^{-1}$	$C = 5 \times 10^{-8} \mu\text{mol s}^{-1} \text{ Pa}^{-2}$
$\eta = 1.1 \times 10^{-4} \text{ N s m}^{-2}$	$\gamma = 1.58$
$M_1 = 40$	
$M_2 = 100$	

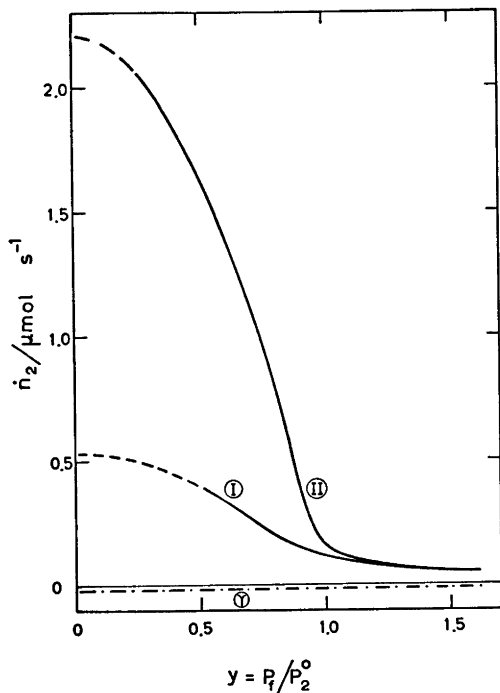


Fig. 2. Curves for the rate of mass loss \dot{n}_2 as a function of y , calculated from eqn. (25) with the parameters given in Table 1. Curve I: $P_2^\circ = 3333 \text{ Pa}$ (=25 Torr); Curve II: $P_2^\circ = 6666 \text{ Pa}$ (=50 Torr); Curve γ : Second term of eqn. (25) plotted separately (closely identical for both vapour pressure values).

Values of \dot{n}_2 have been calculated with these parameter values for two different vapour pressures, and the results are shown as curves I and II in Fig. 2. In addition, the second term of eqn. (25), the " γ term", is plotted separately (bottom curve).

Several features of the graph, Fig. 2, should be noted. First, it is seen that the " γ term" tends toward a small, constant value for $y < 1$, and that this term makes only a minor contribution (in this case, a negative contribution) to the calculated values of \dot{n}_2 . Omission of this term from the equation would move the calculated curves slightly upwards, with hardly any perceptible change in the shape of the curves. This means that the method may be used also without a knowledge of the molecular weight of the vapour. Preferably, one may estimate the molecular weight of the vapour and include the " γ term" on this basis.

It is noted from Fig. 2 also that the rate of mass loss in the diffusion range ($y > 1$) tends toward the same value for both curves, independent of the vapour pressure, owing to the fact that diffusivity is inversely proportional to pressure. In the viscous flow range ($y < 1$), on the other hand, the rate of mass loss is approximately proportional to the square of the vapour pressure, which accounts for the large difference in the two curves.

The calculated curves in Fig. 2 have been drawn to $y=0$ (i.e., $P_f=0$) for the sake of illustration. It should be noted, however, that the theoretical treatment loses validity for P_f less than about 10 Torr, hence the curves are drawn with broken lines below the corresponding y values.

Except for the factor $1/P_2^\circ$ along the abscissa, the curves in Fig. 2 are identical to the curves one would expect to obtain for \dot{n}_2 versus P_f from an experiment for a system with the chosen parameter values. It is seen that graphical, linear extrapolation would appear unreliable since the theoretical curves do not exhibit any extended range of linearity.

Second case: Heat transfer is rate determining

In this case it is assumed that the mass transport occurs by diffusion, with no (or negligible) pressure drop through the capillary. Formally it corresponds to zero viscosity, which means that the parameter C is infinite [cf. eqn. (20)]. It is noted that the first term inside the parenthesis to the left in eqn. (24) is simply P_f^2 , and that for no pressure drop, $P_1 = P_f$, so that the two terms in the parenthesis are equal. This yields directly the equation for this case:

$$P_f = P_2^\circ \frac{\exp(-\dot{n}_2/B)}{1 - \exp(-\dot{n}_2/A)} \quad (26)$$

Eqn. (26) does not appear in Wagner's publication.⁵ In handling the equations he introduced certain simplifying approximations, and arrived at the equation

$$P_f = P_2^\circ (1 + \exp(-\dot{n}_2/A) - \dot{n}_2/B) \quad (27)$$

A numerical check shows that these two equations give closely identical values of \dot{n}_2 for $y = P_f/P_2^\circ < 1$, while the results deviate for

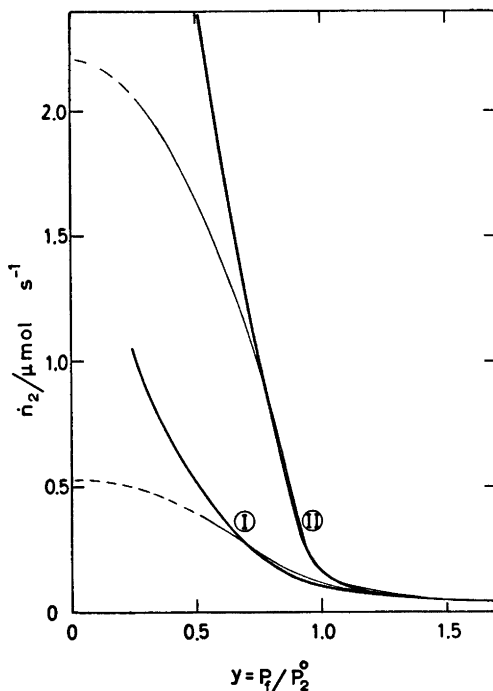


Fig. 3. Comparison of the curves for \dot{n}_2 as a function of y , calculated from eqn. (26) (thick lines) and from eqn. (25) (thin lines, identical to those shown in Fig. 2). Curve I: $P_2^0 = 3333$ Pa, $B = 0.75 \mu\text{mol s}^{-1}$; Curve II: $P_2^0 = 6666$ Pa, $B = 3.50 \mu\text{mol s}^{-1}$.

$y > 1$. Eqn. (26) may be considered the "corrected Wagner equation" and will be discussed here.

We may investigate to what extent eqn. (26) is able to reproduce the curves calculated from eqn. (25) as shown in Fig. 2. The same value of the parameter A is used. As regards pressure, it is seen that eqn. (26) predicts dependence of \dot{n}_2 on the relative pressure y only. Two different values of B thus are needed to match the two curves. It is seen in Fig. 3 that by the use of the values 0.75 and 3.50 $\mu\text{mol s}^{-1}$, the two curves of Fig. 2 are reproduced by eqn. (26) down to y values of about 0.7.

At lower y values, eqn. (26) predicts a steady increase in \dot{n}_2 , and in fact predicts that \dot{n}_2 goes toward infinity when P_i is reduced to zero. This is clearly impossible, and any real, experimental curve would have to bend toward a finite value of \dot{n}_2 due to the restriction im-

posed by the resistance to viscous flow in the capillary.

On the other hand, for y values down to about 0.7, it appears that both eqns. (25) and (26) may be fitted to a given set of experimental data with almost equal precision. A possible consequence is that computer fitting of the complete eqn. (24) may give trouble, because of the relative importance of the two parameters B and C for a given set of experimental data. It is thus of considerable interest to attempt a delineation of the ranges of temperature *etc.*, in which each of the two simplified equations (25) and (26) may be considered valid.

Ranges of validity for the two limiting cases

For this purpose the two equations may be further simplified for $y < 1$. In eqn. (25) the " y term" will be relatively unimportant in this range and may be omitted (*cf.* Fig. 2). Furthermore, for $y < 1$ we have $\dot{n}_2/A \gg 1$ and thus $\exp(-\dot{n}_2/A) \approx 0$. With these approximations eqn. (25) reduces to

$$\dot{n}_2 = C(P_2^0)^2(1 - y^2) \quad (28)$$

Similarly, eqn. (26) is reduced to

$$\dot{n}_2 = -B \ln y \quad (29)$$

A decision between the two models may be reached by comparison of the values of \dot{n}_2 predicted by these two equations for the same experimental conditions. By analogy with chemical kinetics, heat transfer and viscous flow in this case may be considered as consecutive processes, and whichever gives the lower value of \dot{n}_2 represents the rate-determining step.

In order to reach a clear-cut decision we set the ratio of the two predicted values equal to a factor f :

$$\frac{-B \ln y}{C(P_2^0)^2(1 - y^2)} = f \quad (30)$$

The parameter B is proportional to the heat transfer coefficient K , which may be found by assuming heat transfer by radiation:

$$K(T - T_s) = \epsilon \epsilon \sigma (T^4 - T_s^4) \approx 4\epsilon \epsilon \sigma T^3 (T - T_s) \quad (31)$$

in which ϵ is the emissivity, T_s is the temperature, s is the area of the cell surface,

and σ is the Stefan-Boltzmann radiation constant. One may, somewhat arbitrarily, assume a value of 0.5 for the emissivity (alternatively assuming a somewhat higher emissivity combined with a finite resistance to heat flow through the cell wall and the sample). This gives from eqn. (31):

$$K = 2s\sigma T^3 \quad (32)$$

An expression for the enthalpy of vaporization in eqn. (23) is obtained by noting that the molar entropy of vaporization at the boiling point is approximately the same for different substances (Trouton's rule). This may be applied also to a "boiling point" at, e.g., 50 Torr. Thus we have

$$\Delta H_v = T \Delta S_v \quad (33)$$

Introduction of eqns. (20) and (23) in (30), with the substitutions given by eqns. (32) and (33), yields after some rearrangement

$$\frac{T^4}{r^4} = \frac{\pi \Delta S_v^2}{32 R^2 \sigma} \times \frac{(y^2 - 1)}{\ln y} \times \frac{1}{sl\eta} \times (P_2^\circ)^2 f \quad (34)$$

It is chosen to effect a numerical comparison at a value of $y = 0.80$ (cf. Fig. 3). For the entropy of vaporization is assumed $\Delta S_v = 130 \text{ J K}^{-1} \text{ mol}^{-1}$. The viscosity of gases varies with molecular mass, collision diameter, and temperature; we can do nothing better than to assume a constant value $\eta = 5 \times 10^{-5} \text{ N s m}^{-2}$ (roughly corresponding to the viscosity of mercury vapour at 200–300 °C). We assume a cylindrical cell of 2 cm outside diameter and 3 cm height, this gives the surface area $s = 2.5 \times 10^{-3} \text{ m}^2$. The length of the capillary is assumed $l = 1.0 \times 10^{-2} \text{ m}$. With the radiation constant $\sigma = 5.67 \times 10^{-8} \text{ W m}^{-2} \text{ K}^{-4}$, and at a chosen pressure $P_2^\circ = 6666 \text{ Pa}$ (= 50 Torr) eqn. (34) gives

$$T/r = 2.2 \times 10^{-6} f^{1/4} \text{ K m}^{-1} \quad (35)$$

Eqn. (35) indicates a direct proportionality between the capillary radius and the temperature required for the change from heat transfer to viscous flow as the main restraint for the rate of mass transport. It is noted also that the parameters s , l and η enter as fourth root and P_2° as square root in the expression for T/r , which means that eqn. (34) is fairly insensitive to moderate changes in the values of these parameters.

The factor f was introduced in eqn. (30) with the intention that it may be varied over suitable powers of ten. Choosing a value of the capillary radius $r = 0.3 \text{ mm}$ for illustration, one arrives at the following results:

$f = 0.1$	1	10
$T = 371 \text{ K}$	660 K	1173 K

These results may be expressed as follows: At temperatures below 100 °C, heat transfer accounts for more than 9/10 of the restraints to mass loss. In the range 100 to 900 °C heat transfer and viscous flow are both of importance in determining the rate of mass loss, the two effects becoming of equal importance at about 400 °C. Above 900 °C viscous flow represents more than 9/10 of the restraints to mass loss.

Thus, the Wagner model of heat transfer, expressed by eqn. (26), will be strictly valid only at temperatures near room temperature. The viscous flow model, expressed by eqn. (25), will be valid at temperatures above 900 °C. These conclusions are reasonable, since the efficiency of the heat transfer increases rapidly with increasing temperature. Viscosity, on the other hand, increases with temperature for any gas or vapour, which means that the resistance to viscous flow will be less at low temperatures.

The above conclusions are believed to be of fairly general validity for samples with medium and high thermal conductivity. In particular a fine-grained and loosely packed solid powdered sample may have very low thermal conductivity, which, however, may be enhanced by compaction of the powder and subdivision of the compact to coarser pieces. Still it appears advisable in such cases to regard the above conclusions critically, and to perform a similar evaluation from eqn. (30) onwards with the use of numerical values proper to the case at hand, if it is desired to assess the relative importance of heat transfer and viscous flow resistance.

ON THE PRACTICAL APPLICATION OF THE METHOD

Our applications of the method to date include determinations of vapour pressures of various molten salt systems at temperatures around 600 to 1200 °C. The relative merits of

the two simplified eqns. (25) and (26) have been tested by fitting each of these equations to the same set of experimental data, using a non-linear least-squares analysis computer program.¹⁰ It is generally found that the two equations yield nearly the same values for the vapour pressure. This is also to be expected from the proximity of the calculated curves in Fig. 3, as pointed out above. As a consequence, comparison of vapour pressure values obtained from each of the two limiting equations generally will not give information as to which equation is "valid" for the case in hand. Furthermore, when the experimental data have been obtained in a range where resistance to heat transfer and resistance to viscous flow are simultaneously of importance in determining the rate of mass transport, the values obtained separately from eqns. (26) and (25) for the parameters B and C may have little or no physical significance.

From the considerations above, resistance to heat transfer should be particularly significant in experiments at low temperatures. For this effect to be dominating, temperature would have to be so low as to be of little interest in high-temperature chemistry, but effects in the expected direction have been observed in experiments with volatile molecules such as NaAlCl_4 , etc., where the size of the molecule contributes to a low viscosity. On the other hand, resistance to viscous flow should dominate in measurements at high temperatures, in particular for monoatomic metal vapours where the small collision diameter gives a relatively high vapour viscosity. This has been confirmed by determinations of the vapour pressure of silver in the temperature range 1580 to 1860 °C; the experimental curves obtained in this case are very similar to those shown in Fig. 2. (The physical data given in Table 1 were in fact chosen with the silver experiments in mind.)

The most accurate results for the vapour pressures in general are obtained by computer fitting of the complete eqn. (24). This is achieved by use of a more sophisticated computer program,¹¹ which then may yield physically acceptable values for the parameters B and C . The viscosity of the vapour in principle may be determined from the value of C when the exact dimensions of the capillary are known,

cf. eqn. (20). The viscosity value thus obtained, however, will not be very reliable in the general case, since even the best of computer programs will not be able to assess the truly correct values of B and C when both effects are simultaneously of importance. Likewise the interdiffusion coefficient of the vapour and the inert gas may be determined from the value of the parameter A , but again there are sources of error to be considered. Further discussion of the method, including its application to the determination of viscosities and diffusivities, the effect of large difference in molecular weights, and the influence of porous cell materials, will be presented in subsequent communications in conjunction with experimental data.

Acknowledgement. The authors gratefully acknowledge the support by the NATO Research Grants Programme through Grant 836, which made possible the close cooperation of PGW with the two other authors in Trondheim.

REFERENCES

1. Ruff, O. and Bergdahl, B. *Z. Anorg. Allg. Chem.* 106 (1919) 76.
2. Ruff, O. *Z. Angew. Chem.* 42 (1929) 807.
3. Fischer, J. *Z. Anorg. Allg. Chem.* 219 (1934) 367.
4. Fischer, W., Rahlfs, O. and Benze, B. *Z. Anorg. Allg. Chem.* 205 (1932) 1.
5. Wagner, C. *Z. Phys. Chem.* 192 (1943) 85.
6. Chapman, S. and Cowling, T. G. *The Mathematical Theory of Non-Uniform Gases*, 3rd. Ed., Cambridge University Press, New York 1970, p. 97.
7. Present, R. D. *Kinetic Theory of Gases*, McGraw Hill, New York 1958, p. 49.
8. Geankoplis, C. J. *Mass Transport Phenomena*, Holt, Rinehart and Winston, New York 1972, p. 38.
9. Mason, E. A. and Evans, R. B. *J. Chem. Educ.* 46 (1969) 358 and 423.
10. Bakkenes, G. J., Dragt, J. B. and Struch, H. P. *General ALGOL Procedures for the Solution of Least Squares Problems*, RCN Report RCN-35, Petten, The Netherlands 1965.
11. Hertzberg, T. *MODTLP - A General Computer Program for Fitting of Non-Linear Models to Experimental Data*, Chemical Engineering Laboratory, University of Trondheim 1970 (in Norwegian).

Received December 17, 1976.

The Crystal Structure of Cerium(IV) Sulfate Tetrahydrate, Ce(SO₄)₂·4H₂O

OVE LINDGREN

Department of Inorganic Chemistry, Chalmers University of Technology and the University of Göteborg, P.O. Box, S-402 20 Göteborg 5, Sweden

When the common form of Ce(SO₄)₂·4H₂O, space group *Fddd*, is treated hydrothermally with 0.3–1.0 M H₂SO₄, a polymorphic phase, space group *Pnma*, crystallizes. The structure of the latter has been determined from X-ray diffractometer data. The orthorhombic cell has the dimensions $a = 14.5994(17)$ Å, $b = 11.0064(4)$ Å, and $c = 5.6601(5)$ Å; it contains four formula units.

Standard Patterson and Fourier methods were used to solve the structure. Full matrix least-squares refinement based on 1409 reflexions yielded a final *R* of 0.040.

The structure is composed of layers of the empirical formula Ce(SO₄)₂ normal to the *a* axis. The water molecules link the layers together by hydrogen bonds.

Cerium is eight-coordinated by four water molecules and four sulfate oxygen atoms, giving a square antiprismatic configuration. The average Ce—O distance is 2.326 Å (range 2.292–2.388 Å).

A number of cerium(IV) sulfates and a cerium(IV) chromate have been investigated at this Institute.^{1–5} They all contain cerium(IV) ions coordinated by eight oxygen atoms. However, the coordination polyhedra are of different kinds, square antiprisms, a dodecahedron and a bicapped trigonal prism. Usually the compounds have been prepared by hydrothermal hydrolysis with varying acid concentration and at different temperatures. Some of the phases obtained are basic, others neutral.

The compound under investigation is the neutral Ce(SO₄)₂·4H₂O, which seems to be isostructural with U(SO₄)₂·4H₂O.⁶ Some crystallographic data for the cerium compound have been reported⁷ previously, but not a complete structure determination. The present study is

part of a program concerning the type and dimensions of cerium–oxygen polyhedra

EXPERIMENTAL

A saturated solution of Ce(SO₄)₂·4H₂O (space group *Fddd*,⁷ *pro analysi* quality from Merck) in 1.0 M H₂SO₄ was prepared. The solution was divided in five portions, four of them diluted with H₂O in proportions varying from 1:1 to 1:15. About 25 ml of each solution was sealed in a glass tube and heated to 80 °C in an oven for a week. In the tubes containing the more concentrated solutions bright yellow crystals suitable for X-ray work were obtained.

A crystal with the approximate dimensions 0.09 × 0.09 × 0.2 mm was mounted along the needle axis, [001]. Rotation and Weissenberg recordings showed orthorhombic symmetry. The systematic absences were: $hk0$ for $h \neq 2n$ and $0kl$ for $k + l \neq 2n$, which is characteristic of the space groups *Pnma* and *Pn2₁a*.

The cell dimensions were determined from a powder photograph recorded with monochromatized CuK α ₁ radiation in a Guinier camera. Lead nitrate ($a = 7.8566$ Å at 21 °C)⁸ was used as an internal standard. Least-squares refinement of 14 indexed lines gave the following cell constants: $a = 14.5994(17)$ Å, $b = 11.0064(4)$ Å, $c = 5.6601(5)$ Å, and $V = 909.5$ Å³. $Z = 4$ leads to a calculated density of 2.952 g cm⁻³.

Ten layers, $hk0$ to $hk9$, were recorded with graphite monochromatized MoK α radiation on a PAILRED 2-circle diffractometer. The ω scan technique was employed, and measuring times varied from 72 to 120 s for the peaks, while the background intensities were measured in two 24 s periods, one preceding, one following the scan. Reflexions with $\sigma(I)/I > 0.3$ were considered insignificant, $\sigma(I)/I$ defined as $(I_{\text{tot}} + I_{\text{back}})^{1/2} / (I_{\text{tot}} - I_{\text{back}})$. The remaining 1409 independent reflexions were corrected for

Table 1. Atomic coordinates and temperature factors for $\text{Ce}(\text{SO}_4)_2 \cdot 4\text{H}_2\text{O}$. Estimated standard deviations are given in parentheses. The thermal parameters have been multiplied by 10^4 . The temperature factor is of the form $\exp[-2\pi^2(h^2a^{*2}U_{11} + \dots + 2klb^*c^*U_{23})]$.

	<i>x</i>	<i>y</i>	<i>z</i>	U_{11}	U_{22}	U_{33}	U_{12}	U_{13}	U_{23}
Ce	0.17148(3)	0.25	0.12469(9)	91(2)	86(2)	87(2)	0	1(2)	0
S	0.35064(10)	0.05504(13)	0.88347(33)	100(5)	84(5)	111(5)	3(4)	-2(5)	7(5)
O1	0.2606(4)	0.1170(5)	0.9143(10)	170(22)	213(24)	226(28)	39(19)	27(19)	-56(20)
O2	0.3319(4)	0.9230(4)	0.8522(9)	247(22)	111(17)	160(19)	5(18)	4(22)	18(15)
O3	0.4066(4)	0.0691(5)	0.0931(11)	248(25)	144(20)	219(27)	34(19)	-100(21)	22(19)
O4	0.3943(4)	0.1040(5)	0.6713(10)	151(21)	194(23)	209(25)	29(18)	75(18)	73(19)
O5	0.0251(6)	0.25	0.3128(17)	209(36)	122(28)	318(40)	0	160(33)	0
O6	0.2991(5)	0.25	0.3716(17)	149(26)	165(28)	213(29)	0	-46(32)	0
O7	0.0763(4)	0.1249(5)	0.8934(2)	153(21)	216(22)	205(24)	1(17)	-29(20)	-71(22)

Lorentz, polarisation and absorption effects (program: DATAPA⁹). The transmission factors varied from 0.535 to 0.790.

DETERMINATION AND REFINEMENT

To reduce the computation times only half the reflexions were included in all calculations except for the final ones. The major peaks in a Patterson synthesis were all explained as cerium and sulfur vectors assuming the space group to be *Pnma*. A Fourier summation clearly showed seven independent oxygen atoms. Block diagonal refinement (program: BLOCK⁹) was used to adjust the scale factor, the positional and the temperature parameters. In the final refinement, based on all data, the Brookhaven full matrix program LINUS was used. Scattering factors were those of Doyle and Turner,¹⁰ for the uncharged atoms. The effects of anomalous dispersion were neglected since the struc-

ture is centrosymmetric. Weights were calculated according to $w = (10.0 + |F_o| - 0.0025|F_o|^2 + 0.00002|F_o|^3)^{-1}$ leading to a reasonable agreement between w^{-1} and $(|F_o| - |F_c|)^2$ independent of $|F|$. An isotropic secondary extinction parameter and anisotropic temperature factors were included in the refinement and the conventional *R* value dropped to 0.040. A final difference Fourier synthesis showed no significant peaks except fluctuations in the vicinity of cerium. The atomic parameters obtained in the last refinement are listed in Table 1. The structure factor list can be obtained from the author on request.

DESCRIPTION AND DISCUSSION

Fig. 1 illustrates the structures viewed along the *c* axis. Selected interatomic distances and angles are listed in Table 2.

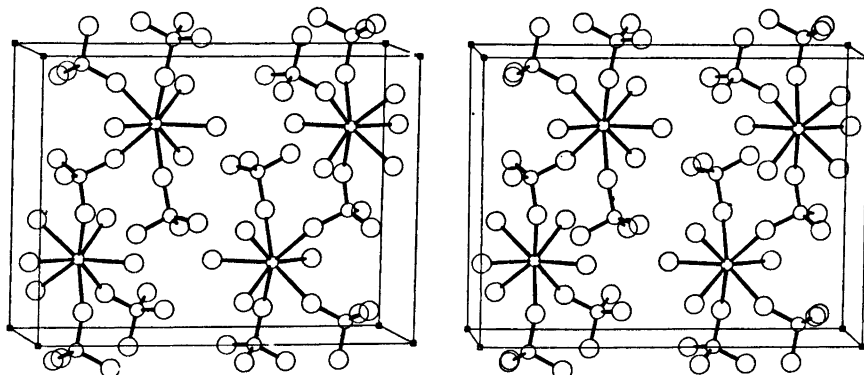


Fig. 1. A stereoscopic drawing of the unit-cell contents viewed approximately along *c*.

Table 2. Interatomic distances (Å) and angles (°).

Antiprism		Sulfate group	
Ce—O1 (2×)	2.292(6)	S—O1	1.491(6)
—O2 (2×)	2.299(5)	—O2	1.490(5)
—O6	2.329(8)	—O3	1.449(6)
—O7 (2×)	2.354(6)	—O4	1.463(6)
—O5	2.388(9)		
Average:	2.326	O1—S—O2	107.3(3)
		O1—S—O3	110.6(3)
O1—O1	2.927(12)	O1—S—O4	108.2(3)
O1—O7 (2×)	2.695(8)	O2—S—O3	107.8(3)
O7—O7	2.754(12)	O2—S—O4	110.0(3)
O2—O5 (2×)	2.835(8)	O3—S—O4	112.8(3)
O2—O6 (2×)	2.701(7)		
O1—O2	2.856(8)		
O1—O6	3.026(10)		
O7—O2	2.970(8)		
O7—O5	2.844(19)		
Hydrogen bond system			
O5—O3 (2×)	2.691(8)	O3—O5—O3	95.5(4)
O6—O4 (2×)	2.719(9)	O4—O6—O4	72.5(3)
O7—O3	2.740(8)	O3—O7—O4	86.5(3)
O7—O4	2.691(8)		

The structure is made up of layers of the composition $\text{Ce}(\text{SO}_4)_2$ normal to the a axis, and the water molecules join these layers by hydrogen bonds. The two sulfate oxygen atoms O3 and O4, which are not bonded to cerium, are at distances varying between 2.691 to 2.740 Å from the water molecules O5, O6 and O7. O5 probably has its hydrogen hydrogens directed towards O3, and O6 towards O4, while O7 has one hydrogen directed towards O3 and one towards O4. Both O3 and O4 thus act as acceptors of two hydrogen bonds.

Cerium is eightfold coordinated by oxygen atoms, four water molecules and four sulfate

oxygens belonging to different sulfate groups. The coordination polyhedron is a somewhat distorted Archimedean square antiprism. The least-squares planes through the square faces form an angle of only 2.3°. One plane has, due to space group symmetry, all four atoms in the same plane while the other formed by the atoms two O2, O5 and O6 shows a minor deviation (0.02 Å) from an ideal plane.

The average Ce—O distance is 2.326 Å, which agrees with those found in related compounds (*cf.* Table 3).

The sulfate group is in contact with two cerium atoms, the other two sulfate oxygens being involved in hydrogen bonding. This is reflected in the deviation from regularity found in the sulfate group. O1 and O2, linked to cerium, are at significantly longer distances from sulfur than O3 and O4. The average S—O and O—O distances in the sulfate group are 1.473 and 2.405 Å.

Cerium sulfate tetrahydrate has two polymorphic forms. The first crystallizes in the space group $Fddd$ and the second in $Pnma$. The analogous uranium compound, reported by Kierkegaard,⁶ has only one form, and it is isomorphous with the $Pnma$ form. Zirconium sulfate tetrahydrate¹² is isomorphous with the $Fddd$ form. However, as described by Singer and Cromer,¹³ the structures of the compounds in $Pnma$ are closely related to those in $Fddd$.

Acknowledgements. The author is very grateful to Professor G. Lundgren for many stimulating discussions during the work. He also wishes to thank Dr. John Wood for revising the English text. This investigation was supported by the Swedish Natural Science Research Council (Contract No. 2318).

Table 3. Coordination polyhedra in cerium(IV) compounds.

Compound	Polyhedron	$\langle \text{Ce—O} \rangle$ Å	Range Å
$\text{Ce}(\text{SO}_4)_2 \cdot 4\text{H}_2\text{O}$	antiprism	2.326	2.292—2.388
CeO_2 ¹¹	cube	2.343	2.343
$\text{Ce}_2\text{O}_4(\text{OH})_4(\text{SO}_4)_2$	antiprism	2.33	2.22—2.39
$\text{CeOSO}_4 \cdot \text{H}_2\text{O}$ ^{1,2}	antiprism	2.364	2.188—2.587
$\text{Ce}_2(\text{OH})_2(\text{H}_2\text{O})_4(\text{SO}_4)_3$ ⁴	dodecahedron	2.328	2.223—2.406
$\text{Ce}(\text{CrO}_4)_2 \cdot 2\text{H}_2\text{O}$ ⁵	bicapped trigonal prism	2.342	2.232—2.575

REFERENCES

1. Lundgren, G. *Ark. Kemi* 6 (1953) 59.
2. Lundgren, G. *Ark. Kemi* 10 (1956) 183.
3. Lindgren, O. *Acta Crystallogr. B* 32 (1976) 3347.
4. Lindgren, O. *Acta Chem. Scand. A* 31 (1977) 163.
5. Lindgren, O. *Acta Chem. Scand. A* 31 (1977) 167.
6. Kierkegaard, P. *Acta Chem. Scand.* 10 (1956) 599.
7. Staritzky, E. and Truitt, A. L. *The Actinide Elements*, NNES, McGraw-Hill, New York 1954, Chapter 19.
8. *International Tables for X-Ray Crystallography*, Kynoch Press, Birmingham 1959.
9. The Program Library of the Dept. of Inorg. Chem., Göteborg.
10. Doyle, P. A. and Turner, P. S. *Acta Crystallogr. A* 24 (1968) 390.
11. Magnéli, A. and Kihlberg, L. *Acta Chem. Scand.* 5 (1951) 578.
12. Singer, J. and Cromer, D. T. *Acta Crystallogr.* 12 (1959) 719.

Received February 4, 1977.

The Crystal Structure of $\text{PrH}_3(\text{SeO}_3)_2(\text{Se}_2\text{O}_5)$, a Compound with Selenite and Diselenite Groups

MARKUS KOSKENLINNA and JUSSI VALKONEN

Department of Chemistry, Helsinki University of Technology, SF-02150 Espoo 15, Finland

The crystal structure of praseodymium trihydrogen biselenite diselenite, $\text{PrH}_3(\text{SeO}_3)_2(\text{Se}_2\text{O}_5)$, has been determined by X-ray methods. The compound crystallizes in the monoclinic space group $P2_1/c$ with $Z=4$. The cell dimensions are $a=12.933(3)$, $b=7.334(2)$, $c=10.811(2)$ Å and $\beta=91.68(1)^\circ$. The structure was solved by direct methods and refined to $R=0.054$.

The compound consists of a two-layered structure parallel to the bc plane in which the diselenite and one of the two non-equivalent selenite groups join the praseodymium atoms into an infinite two-dimensional network. Six diselenite and three selenite O atoms are coordinated to each Pr. Two of the diselenite oxygens around a praseodymium are three-coordinated: one is bonded to one Pr and two Se atoms and the other to one Se and two Pr atoms.

During the crystallization experiments with the isomorphous series $\text{LnH}(\text{SeO}_3)_2 \cdot 2\frac{1}{2}\text{H}_2\text{O}$,¹ tabular crystals containing the lanthanoid and selenium in the molar ratio 1:4 were formed by La and Pr in concentrated solutions of selenous acid. The combination of analytical data leads to two possible formulae for the praseodymium compound, namely $\text{Pr}_2(\text{Se}_2\text{O}_5)_3 \cdot 2\text{H}_2\text{SeO}_3 \cdot \text{H}_2\text{O}$ and $\text{PrH}_3(\text{SeO}_3)_2(\text{Se}_2\text{O}_5)$. A structure determination was initiated to obtain more information on the structural aspects of the compound not previously reported in the literature.

EXPERIMENTAL

Preparation of the compound. The compound was crystallized from 0.1 g of praseodymium hydrogenselenite, prepared as described in Ref. 1, 0.3–0.4 g of SeO_2 and 0.5–0.6 g of H_2O . The mixture was kept in an ampoule at

120–130 °C for 2–4 days, during which time, green, tabular crystals were formed. This method of preparation applied to neodymium did not yield the corresponding compound while lanthanum, under these same conditions, formed isomorphous crystals.

Crystal data. Praseodymium trihydrogen biselenite diselenite, $\text{PrH}_3(\text{SeO}_3)_2(\text{Se}_2\text{O}_5)$, M.W. = 635.73.

Space group $P2_1/c$ (No. 14)
 $a=12.933(3)$ Å $b=7.334(2)$ Å $c=10.811(2)$ Å
 $\beta=91.68(1)^\circ$ $V=1025.0$ Å³
 $Z=4$ $D_{\text{calc}}=4.12$ g/cm³
 $\mu(\text{MoK}\alpha)=188.6$ cm⁻¹

Structure analysis. The X-ray measurements were carried out with a Syntex P2₁ (Fortran-version) automatic diffractometer using the $\theta/2\theta$ scanning technique and graphite monochromatized MoK α radiation. The size of the mounted crystal was 0.3 × 0.3 × 0.1 mm. The scan speed was 1°/min, and the intensity data were collected in the interval $5^\circ < 2\theta < 60^\circ$. The cell dimensions were determined from 14 reflections measured with the diffractometer at 25 °C. The space group was determined to be $P2_1/c$ according to systematic absences in the original intensity data. Reflections for which the net count was greater than four times the respective standard deviation were accepted as observed. With this criterion a total of 1517 independent reflections were obtained.

Absorption correction was made from the ϕ -scan data, after which the Lorentz and polarization corrections were carried out. The positions of the Pr and Se atoms were obtained by direct methods with the computer programs of the X-ray 1976 package;² the atomic scattering factors were taken from the International Tables.³ After four cycles of refinement the value of R was 15.1 %. All the oxygens appeared in the difference Fourier map, and the structure was refined using isotropic temperature factors to an R value of 7.0 %. Final atomic parameters and anisotropic temperature factors were then

Table 1. Atomic coordinates and anisotropic temperature parameters U_{ij} (Å²) in the form $\exp[-2\pi^2(h^2a^{*2}U_{11} + k^2b^{*2}U_{22} + l^2c^{*2}U_{33} + 2hka^*b^*U_{12} + 2hla^*c^*U_{13} + 2klb^*c^*U_{23})]$ with estimated deviations. The values of U_{ij} are multiplied by 10⁴.

Atom	x	y	z	U_{11}	U_{22}	U_{33}	U_{12}	U_{13}	U_{23}
Pr	0.3374(1)	0.9539(1)	0.4487(1)	90(1)	104(4)	74(5)	-10(4)	15(4)	-2(5)
Se1	0.7413(1)	0.0362(3)	0.2115(2)	91(8)	115(9)	134(9)	-13(7)	-1(8)	13(9)
Se2	0.0501(2)	0.9731(3)	0.3467(2)	119(8)	150(10)	208(11)	-27(8)	44(8)	-6(9)
Se3	0.7090(1)	0.5684(3)	0.3922(2)	108(8)	140(9)	97(9)	-16(8)	16(7)	-5(9)
Se4	0.4882(1)	0.8067(3)	0.1706(2)	91(8)	105(8)	106(9)	-16(7)	41(8)	-19(8)
O1	0.7671(11)	0.0799(26)	0.3593(15)	86(65)	404(105)	256(87)	-12(68)	1(65)	129(84)
O2	0.8550(12)	0.9104(22)	0.1842(18)	182(75)	145(77)	555(120)	16(65)	70(82)	-180(84)
O3	0.2209(12)	0.7229(22)	0.3604(16)	162(70)	192(81)	292(89)	-18(63)	50(68)	-136(76)
O4	0.0366(10)	0.6426(23)	0.1040(16)	52(60)	278(87)	319(95)	-6(61)	20(67)	4(79)
O5	0.1546(10)	0.0737(21)	0.3982(16)	62(58)	163(75)	394(97)	35(57)	-105(66)	40(77)
O6	0.0689(14)	0.0458(26)	0.1879(16)	381(98)	282(92)	253(90)	-56(84)	-1(78)	109(86)
O7	0.3333(14)	0.2340(22)	0.0155(17)	385(100)	112(75)	409(108)	74(73)	210(88)	13(80)
O8	0.6645(10)	0.6247(22)	0.2496(15)	53(58)	233(78)	235(81)	-17(57)	15(61)	33(72)
O9	0.3833(11)	0.8875(20)	0.0667(14)	142(67)	186(75)	155(75)	95(60)	-68(61)	-67(67)
O10	0.4275(11)	0.7609(20)	0.3001(15)	163(70)	131(70)	247(83)	-58(59)	155(67)	24(69)
O11	0.4870(10)	0.6080(18)	0.0980(14)	36(53)	166(59)	282(81)	-17(49)	89(60)	-64(62)

Table 2. Selected bond lengths (Å) and bond angles (°) with standard deviations in parentheses.

Pr-O1	2.523(16)	O1-Se1-O2	96.7(8)
Pr-O3	2.443(16)	O1-Se1-O3	103.8(9)
Pr-O5	2.566(14)	O2-Se1-O3	95.4(8)
Pr-O7	2.401(16)		
Pr-O8	2.482(16)	O4-Se2-O5	96.1(7)
Pr-O9	2.865(15)	O4-Se2-O6	97.9(8)
Pr-O10	2.460(15)	O5-Se2-O6	96.7(8)
Pr-O11	2.599(13)		
Pr-O11	2.524(14)	O7-Se3-O8	105.1(8)
		O7-Se3-O9	98.8(8)
Se1-O1	1.654(16)	O8-Se3-O9	101.0(7)
Se1-O2	1.769(16)	O9-Se4-O10	102.9(7)
Se1-O3	1.656(16)	O9-Se4-O11	89.8(7)
		O10-Se4-O11	102.9(7)
Se2-O4	1.766(16)		
Se2-O5	1.624(14)	Se3-O9-Se4	123.8(8)
Se2-O6	1.805(18)		
Se3-O7	1.673(18)		
Se3-O8	1.681(16)		
Se3-O9	1.847(15)		
Se4-O9	1.835(15)		
Se4-O10	1.659(16)		
Se4-O11	1.655(14)		

obtained after four more cycles of refinement; the final value of R was 5.4%. The F_o and F_c listing is available from the authors upon request.

DISCUSSION OF THE STRUCTURE

The atomic coordinates and anisotropic temperature parameters are given in Table 1 and selected interatomic distances and bond angles in Table 2.

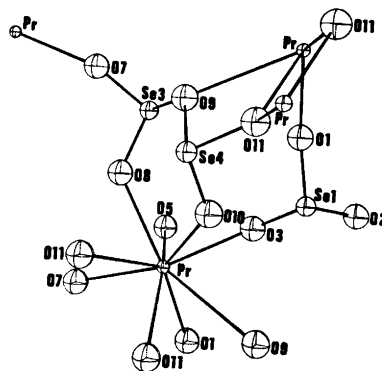


Fig. 1. Bonding scheme of the chain-forming diselenite and selenite groups.

Table 3. A comparison of interatomic distances and bond angles in compounds containing the diselenite ($\text{Se}_2\text{O}_5^{2-}$) ion. O' denotes the oxygen bridging the two selenium atoms.

Compound	Range of Se—O distances (Å)	Range of Se—O' distances (Å)	Range of O—Se—O' angles (°)	Range of Se—O'—Se' angles (°)	Ref.
VSe_2O_5	1.657—1.710	1.768—1.822	96.0—103.4	119.6	5
ZnSe_2O_5	1.658—1.693	1.827	96.3—102.4	121.6	6
MnSe_2O_5	1.644—1.674	1.831	95.9—102.8	121.6	7
CuSe_2O_5	1.668—1.670	1.831	101.4—103.1	122.4	8
$\text{PrH}_3(\text{SeO}_3)_2(\text{Se}_2\text{O}_5)$	1.655—1.681	1.835—1.847	89.8—102.9	123.8	Present work

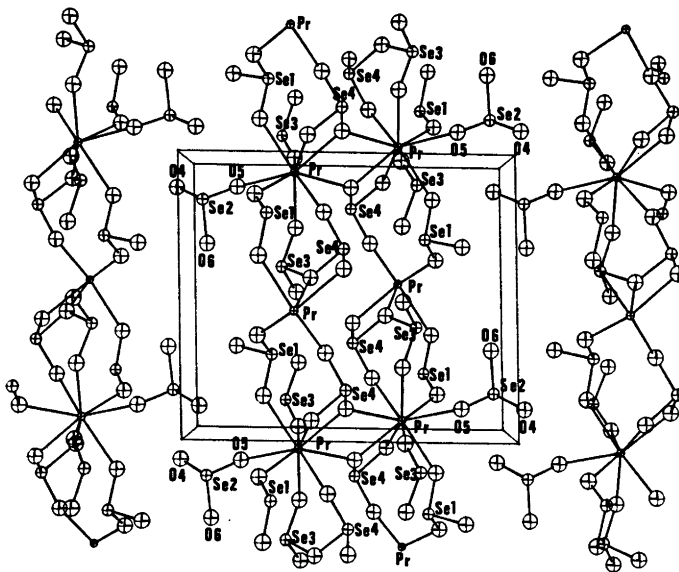


Fig. 2. Perspective view of the double-layer structure of $\text{PrH}_3(\text{SeO}_3)_2(\text{Se}_2\text{O}_5)$ along the b -axis. The unit cell is indicated in the drawing.

There is no water of crystallization in the structure, since all the oxygens belong to either the diselenite or selenite groups. This leads to the formula $\text{PrH}_3(\text{SeO}_3)_2(\text{Se}_2\text{O}_5)$ for the compound. The coordination number of the Pr(III) ion is nine. Six diselenite and three selenite oxygen atoms form a distorted monocapped square antiprism. There are eight oxygens at distances 2.401—2.599 and one, O9, at 2.865 Å. These Pr—O distances are only slightly larger than those in a similar coordination polyhedron within a Pr complex containing both singly and doubly ionized IMDA (IMDA = $\text{HN}(\text{CH}_2\text{COOH})_2$); in this compound the corresponding distances are 2.34—2.58 Å and 2.75

Å.⁴ The “cap” is formed by the oxygen bonding the two seleniums in the diselenite group; it is thus coordinated to three atoms simultaneously. This situation is unique among the diselenites reported so far.⁵⁻⁸

Four praseodymium(III) ions are linked with one diselenite group into a two-dimensional array (see Fig. 1). Two of the five oxygens are coordinated to the same Pr(III) ions, two others to two different Pr(III) ions, and the fifth oxygen is coordinated to two Pr(III) ions simultaneously. Pr(III) ions are situated on two planes parallel to the bc plane, and the result is a two-layered structure, which is essentially held together by the three-coordi-

nated oxygens (see Fig. 2). This double-layer can also be viewed as pairs of edge-sharing coordination polyhedra (the vertices of the common edge being the two O11), which are linked by selenium(IV) ions into a layer network. The layer structure is further strengthened by additional chains formed by the bridging one of the two nonequivalent selenite ligands. The other selenite group does not form a chain-structure, but acts as a monodentate ligand to one Pr(III) ion.

Table 3 compares the diselenite bond distances and angles with those given in Refs. 5–8. The values are compatible with one exception: in the present work one of the angles (O9–Se4–O11) is markedly smaller (89.8°) than the corresponding ones in other compounds. This distortion is probably caused by the unique position held by O11, which is within bonding distance of the selenium in the diselenite group (1.655 Å) as well as of two different Pr(III) ions (2.524 and 2.599 Å).

An interesting phenomenon is observed in the Se–O distances within the selenite groups. If the oxygen is coordinated to Pr(III) ion, the bond length is between 1.624 and 1.656 Å, which is somewhat shorter than usual for selenite ions. In $\text{MnSeO}_3 \cdot 2\text{H}_2\text{O}$ and $\text{CuSeO}_3 \cdot 2\text{H}_2\text{O}$, where all the oxygen atoms of the selenite group are coordinated to the metal, the distances are 1.692–1.713 Å and 1.72–1.78 Å, respectively.^{9,10} If the oxygens are not coordinated to praseodymium, the bond lengths are 1.766–1.805 (see Table 2). This stretching of the Se–O bond can be attributed to the formation of hydrogen bonds, although the positions of the hydrogens could not be identified from the Fourier maps. A similar feature has been observed in crystalline H_2SeO_3 , where the distances were 1.643 and 1.735–1.743 Å for Se–O and Se–OH, respectively.¹¹

REFERENCES

1. Immonen, E., Koskenlinna, M., Niinistö, L. and Pakkanen, T. *Finn. Chem. Lett.* 1976, 67.
2. *The X-Ray System, Version of 1976*, Stewart, J. M., Ed., Technical Report TR-446 of the Computer Science Center, University of Maryland, College Park, Maryland.
3. *International Tables for X-Ray Crystallography*, Kynoch Press, Birmingham 1974, Vol. 4, p. 71.
4. Albertson, J. and Oskarsson, Å. *Acta Chem. Scand. A* 28 (1974) 347.
5. Meunier, P., Bertand, M. and Galy, J. *Acta Crystallogr. B* 30 (1974) 2834.
6. Meunier, P. and Bertand, M. *Acta Crystallogr. B* 30 (1974) 2840.
7. Koskenlinna, M., Niinistö, L. and Valkonen, J. *Acta Chem. Scand. A* 30 (1976) 836.
8. Meunier, P., Svensson, C. and Carpy, A. *Acta Crystallogr. B* 32 (1976) 2664.
9. Koskenlinna, M., Niinistö, L. and Valkonen, J. *Cryst. Struct. Commun.* 5 (1976) 663.
10. Gattow, G. *Acta Crystallogr.* 11 (1958) 377.
11. Larsen, F., Lehman, M. and Søtofte, I. *Acta Chem. Scand.* 25 (1971) 1233.

Received January 14, 1977.

Absorption and Raman Spectra of the Binary Molten Systems MnCl₂-AlCl₃ and MnCl₂-CsCl

WERNER BUES,* LAILA EL-SAYED** and HARALD A. ØYE

Institutt for uorganisk kjemi, Norges tekniske høyskole, Universitetet i Trondheim,
N-7034 Trondheim-NTH, Norway

Molten mixtures of MnCl₂-AlCl₃ and MnCl₂-CsCl have been studied by absorption and Raman spectroscopy. The complete concentration range was covered for mixtures with CsCl while high vapour pressures prevented studies above 30 mol % MnCl₂ in mixtures with AlCl₃. The spectral results are discussed with reference to the decrease in acidity in the series AlCl₃-MnCl₂-CsCl. MnCl₂ is considered to be octahedral in mixtures with AlCl₃ and mainly tetrahedral in mixtures with CsCl. The spectral changes in mixtures with CsCl are attributed to increased Cl-bridging with increasing MnCl₂-content.

As part of our studies on mixtures of covalent and ionic melts,¹⁻⁵ the binary melt systems MnCl₂-AlCl₃ and MnCl₂-CsCl were studied spectrophotometrically. These systems span the transition from the covalent melt AlCl₃, through the partly covalent MnCl₂, to the completely ionic CsCl melt. As Mn²⁺ is spectroscopically active it is possible to detect changes in Mn²⁺ coordination through the changing environments.

The MnCl₂-AlCl₃ system has recently attracted interest because of its role in the Toth-process for aluminium production.^{6,7} The advantage of this process over the existing Bayer-Hall-Heroult process is that the electrolysis step is avoided, with a possible production cost reduction as well as reducing environ-

mental pollution through elimination of fluorides. The crucial step in the process is the manganothermic reduction of AlCl₃:



This reaction results in a solution of MnCl₂ in molten AlCl₃ up to 40 mol %. The present spectroscopic study covers the concentration range which is of importance for the technological process, and the data form the basis of current studies of the process itself in this laboratory.

EXPERIMENTAL

Apparatus. The samples were contained in sealed quartz cells. Optical far U.V. cells (Thermal Syndicate Ltd. Wallsend) with 1 mm pathlength were utilized in the absorption spectroscopic studies of MnCl₂-CsCl except for the mixture with $X_{\text{MnCl}_2} = 0.01$, for which a 1 cm pathlength cell was used. Due to the high pressures generated in the MnCl₂-AlCl₃ systems, cell strength was considered more important than perfect optical quality, consequently 1 cm pathlength cells were made from heavy duty square tubings (Thermal Syndicate Ltd., Wallsend). These tubings have rounded off corners which are essential for pressure endurance.

The cells were placed in a Kanthal-wound furnace with three separate heating elements and a "see-through" channel to transmit a light beam. The heating elements were connected to a EURO THERM (PID) controller, which permitted maintenance of a temperature gradient of less than 2°C over the sample.

A Cary 17H high-temperature absorption spectrophotometer (Cary Instruments, Monrovia, USA) with an optical range 186–2650 nm was used for obtaining the spectra. The

* Anorganisch-Chemisches Institut der Technischen Universität Clausthal, Lehrstuhl B, 3392 Clausthal-Zellerfeld, Bundesrepublik Deutschland.

** Post doctoral fellow. Permanent address: Chemistry Department, Faculty of Science, Alexandria University, Moharem Bay, Alexandria, Egypt.

Cary spectrophotometer was interphased⁸ with a Kennedy 1600 Incremental Tape Recorder, for direct registration of photometric data on computer tape. The computer tape was fed to a UNIVAC 1108 computer which was used for storage of data and for drawing figures on a Kingmatic drawing machine (Kongsberg Våpenfabrikk, Kongsberg, Norway).

The Raman spectra were recorded by a Coderg PHI spectrometer using a pulsed ruby laser with an exciting line 6943 Å. The optical arrangement and the furnace system have been described in detail previously.^{9,10}

Chemicals. To obtain AlCl_3 of satisfactory purity, it was made in the laboratory from 99.999 % Al (Vigeland Brug, Vigeland, Norway) and HCl at 450 °C. The HCl was generated from the reaction of *p.a.* H_2SO_4 with *p.a.* NaCl. We obtained AlCl_3 of high optical quality, with no light scattering silicon particles after two successive sublimation steps. The following precautions were observed:

- Apparatus was scrupulously cleaned;
- The quartz was taken to red heat under vacuum at the final stage;
- Grease was not used in the teflon and quartz parts of the apparatus.

Water-free MnCl_2 was obtained from *p.a.* hydrated MnCl_2 (Merck, Darmstadt, Germany) by treatment with HCl, and gradual heating to above the melting point. In the final step, HCl and then high-purity N_2 were bubbled through the MnCl_2 melt, which was filtered through a quartz frit and sealed into a quartz ampoule.

CsCl *p.a.* (Analar, Hopkin & Williams Ltd.) was recrystallized in distilled water. The purified crystals were heated under vacuum at 400 °C for 2 h, then heated to above the melting point and filtered through a quartz frit.

Procedure. The anhydrous salts were weighed out in a dry box with water content less than 20 ppm. The salts were added to a quartz tube fitted with a quartz filter and an optical cell. The tube with the cell was transferred to a high-vacuum line and, in the case of the MnCl_2 - CsCl system, the mixture was melted above the frit and then filtered into the optical cell, which then was sealed off. Due to the high vapour pressure of AlCl_3 , a slightly different procedure was used for transferring the MnCl_2 - AlCl_3 samples in the cells. The filled tube was first sealed off on the high-vacuum line, well above the frit and the sample. The tube was then placed horizontally in a quartz furnace. When the mixture melted, the furnace was tilted and the melt passed through the filter into the cell under the pressure of aluminium chloride.

All cells were sealed off about 3 cm above the optical zone, in order to have a reservoir where the melt could crystallize. Rupture of the cell by reheating was then prevented by letting the salt crystallize along one wall, not filling any part of the cell completely.

It should be emphasized that the vapour pressure of AlCl_3 rises rapidly with temperature in acidic mixtures ($X_{\text{AlCl}_3} > 0.5$ in mixtures with monovalent chlorides, $X_{\text{AlCl}_3} > 0.66$ in mixtures with divalent chlorides). Such liquids may cause dangerous explosions at elevated temperatures and must be handled behind shields, using appropriate safety measures.

Densities of melts. In order to obtain the concentration in mol/liter and then the molar absorptivities of the spectral transitions, the densities of the samples must be known. The densities of the MnCl_2 - AlCl_3 samples were determined in the optical cell by measuring the height of the melt in the cells with a cathetometer.

RESULTS

Density. The densities (g/cm^3) of MnCl_2 - AlCl_3 -mixtures at 204 °C in the range 0 to 30 mol % MnCl_2 may be represented by the equation:

$$\rho_{204^\circ\text{C}}(\text{MnCl}_2 - \text{AlCl}_3) = 1.208 + 0.934X_{\text{MnCl}_2} + 0.273 X_{\text{MnCl}_2}^2 \quad (2)$$

Standard deviation: 0.009 g/cm^3

For the mixture 30 mol % MnCl_2 - 70 mol % AlCl_3 , the temperature dependence in the range

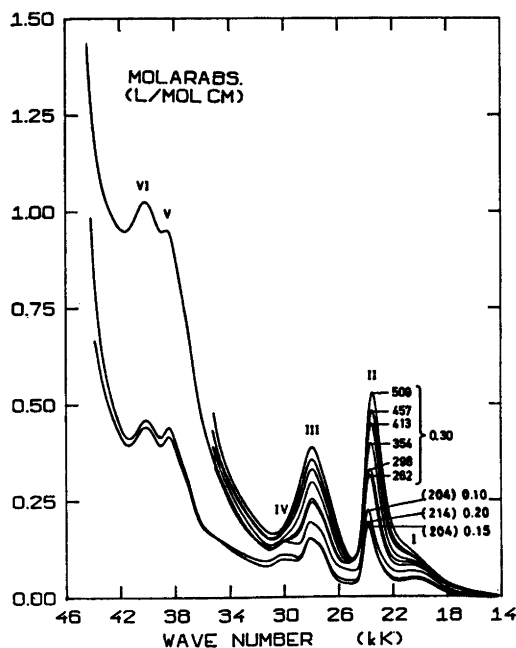


Fig. 1. Absorption spectra of molten MnCl_2 - AlCl_3 mixtures. Temperatures in °C and mol fraction MnCl_2 are given.

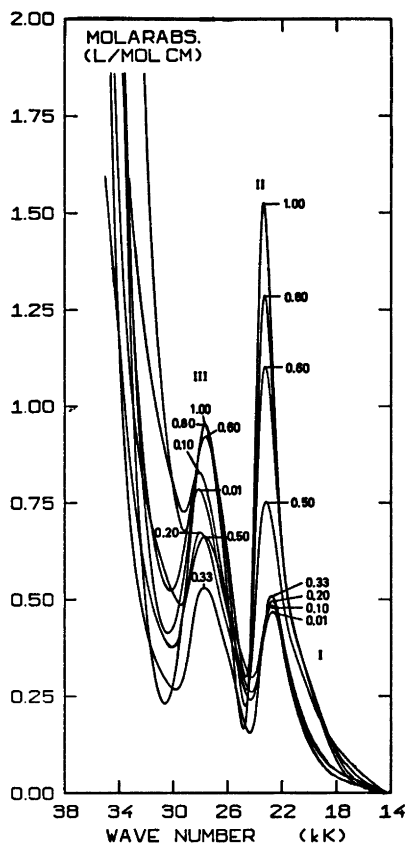


Fig. 2. Absorption spectra of molten $\text{MnCl}_2\text{-CsCl}$ mixtures at 694°C . Mol fraction MnCl_2 is given.

$200^\circ\text{C} < t < 500^\circ\text{C}$ under its own vapour pressure was determined as

$$\rho(30 \text{ mol } \% \text{ MnCl}_2 - 70 \text{ mol } \% \text{ AlCl}_3) = 1.628 - 6.12 \times 10^{-4} (t - 200) - 1.99 \times 10^{-7} (t - 200)^2 \quad (3)$$

Standard deviation: 0.002 g/cm^3 .

The densities of the $\text{MnCl}_2\text{-CsCl}$ mixtures were determined by a hydrostatic weighing method.¹¹

Spectra. The absorption spectra of the molten $\text{MnCl}_2\text{-AlCl}_3$ and $\text{MnCl}_2\text{-CsCl}$ mixtures are given in Figs. 1 and 2, and the locations and magnitudes of the absorption maxima are given in Table 1. Assignments of the spectral transitions are also given. The spectra are computer-drawn from tape.

Acta Chem. Scand. A 31 (1977) No. 6

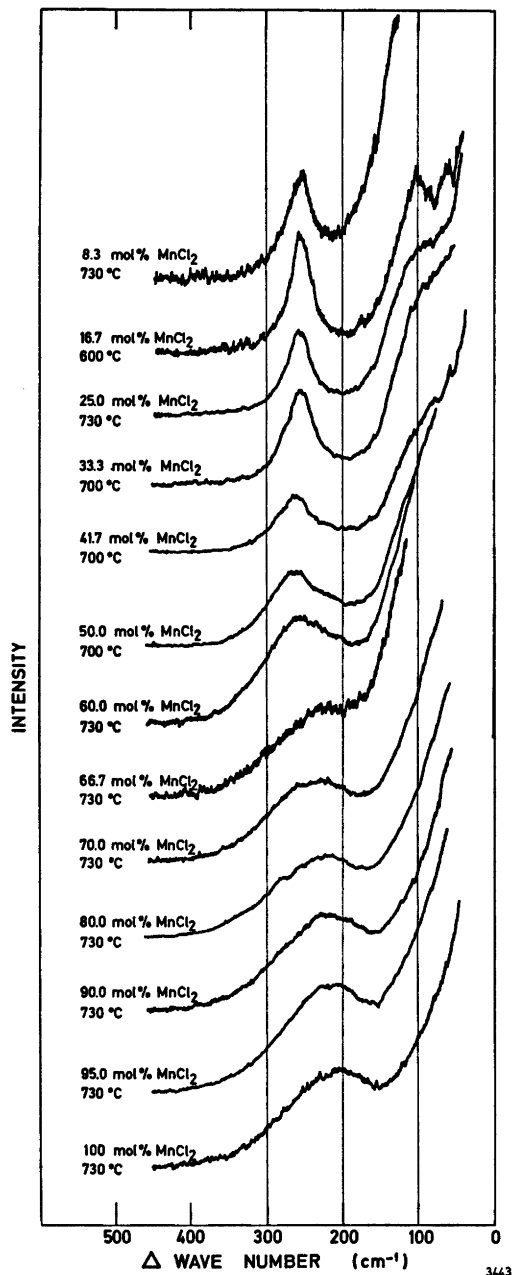


Fig. 3. Raman spectra of molten $\text{MnCl}_2\text{-CsCl}$ mixtures. Optical configuration: Y(X,Y)X .

Figs. 3 and 4 give the Raman spectra of molten $\text{MnCl}_2\text{-CsCl}$ mixtures and of two solid compounds. The spectra were recorded by using

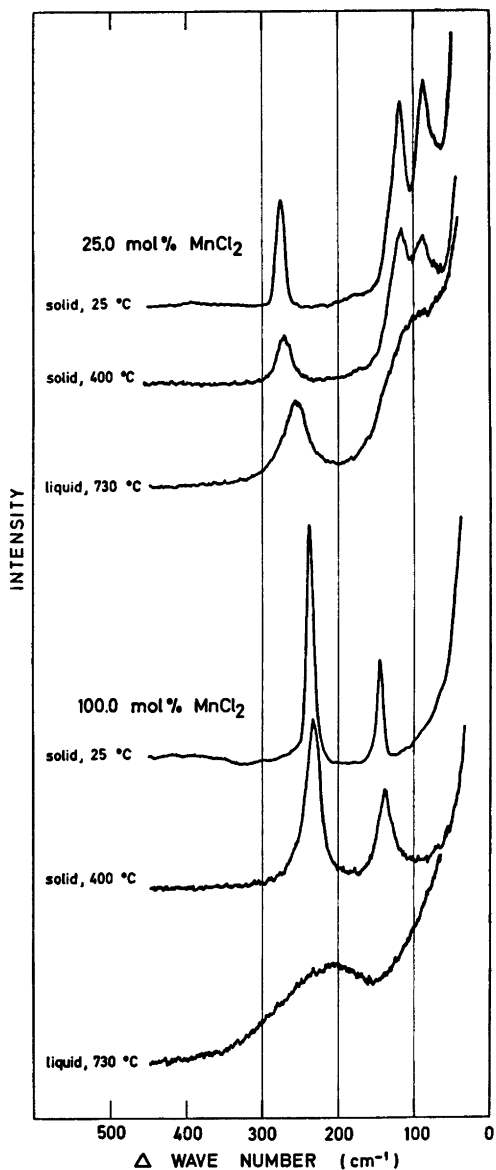


Fig. 4. Raman spectra of the compounds Cs_2MnCl_5 and MnCl_2 in the solid and molten state. Optical configuration: $\text{Y}(\text{X},\text{Y})\text{X}$.

the optical configuration $\text{Y}(\text{X},\text{Y})\text{X}$. Polarization spectra $\text{Y}(\text{X},\text{Z})\text{X}$ revealed that the strong band observed between 200 and 300 cm^{-1} was polarized. Fig. 5 gives the Raman spectrum of a molten mixture of 25 mol % MnCl_2 and 75 mol % AlCl_3 .

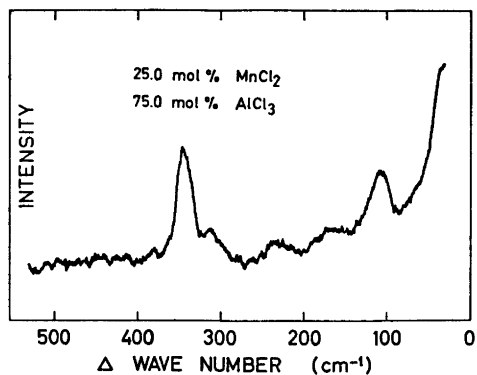


Fig. 5. Raman spectrum of a molten mixture at 250 °C of 25 mol % MnCl_2 and 75 mol % AlCl_3 .

DISCUSSION

The absorption spectra in Fig. 1 can be used to determine the amount of MnCl_2 in the MnCl_2 - AlCl_3 mixtures of potential technical importance. The molar absorptivity is approximately concentration independent, and the absorptivity of the peak at 23.8 kK can be used as a measure of the MnCl_2 content. The slightly higher absolute intensity value of the 5 and 10 mol % MnCl_2 -mixture, as compared with 15 and 20 mol %, is probably due to a higher background absorption caused by the use of imperfect optical cells. The 30 mol % MnCl_2 mixture had to be recorded at a somewhat higher temperature, but when extrapolated down to 204 °C the spectra are considered to be essentially identical to those of the other compositions.

In spite of carefully recorded absorption and Raman spectra, the structural information obtained is limited. This is partly due to the structural insensitivity of the half-filled d -shell of Mn^{2+} and partly due to the fact that Raman spectroscopy mainly gives detailed information when definite species are present. The following structural features can, however, be distinguished.

(a) *Octahedrally coordinated Mn^{2+} .* The absorption spectra of Mn^{2+} in MnCl_2 - AlCl_3 liquid mixtures, $X_{\text{MnCl}_2} \leq 0.30$ (Fig. 1), can be attributed to octahedral coordination of Mn^{2+} in accordance with what was previously proposed for a 5 mol % solution of MnCl_2 in liquid

Table 1. Electronic transitions in the Mn²⁺ in chloride melts. Ground state: ⁶A_{1g}(S).

MnCl ₂ Mol fraction	Temp. °C	Band maxima kK		(Molar absorptivity) l mol ⁻¹ cm ⁻¹					
MnCl ₂ -AlCl ₃									
		I	II	III	IV	V	VI		
0.05 ^a	204	20.61 (0.077)	23.85 (0.23)	28.13 (0.22)	30.30 (0.20)	38.78	40.51		
0.10	204	20.57 (0.068)	23.84 (0.23)	28.11 (0.20)	30.08 (0.15)	38.55	40.18		
0.15	204	20.38 (0.054)	23.85 (0.19)	28.11 (0.16)	30.05 (0.11)	38.47	40.13		
0.20	214	20.42 (0.049)	23.85 (0.20)	28.11 (0.16)	30.07 (0.10)	38.45	40.12		
0.30	262	20.65sh (0.083)	23.75 (0.32)	28.02 (0.25)					
0.30	298		23.70 (0.33)	28.00 (0.25)					
0.30	354		23.66 (0.40)	28.00 (0.30)					
0.30	413		23.62 (0.45)	28.02 (0.33)					
0.30	457		23.57 (0.49)	28.01 (0.36)					
0.30	509		23.54 (0.54)	28.00 (0.39)					
MnCl ₂ -CsCl									
1.00	694	~ 20 sh	23.30 (1.52)	27.63 (0.95)					
0.80	694	~ 20 sh	23.26 (1.29)	27.64 (0.95)					
0.60	694	~ 20 sh	23.15 (1.10)	27.58 (0.92)					
0.50	694	~ 20 sh	23.05 (0.75)	27.58 (0.66)					
0.33	694	~ 20 sh	22.75 (0.51)	27.71 (0.53)					
0.20	694	~ 20 sh	22.66 (0.50)	28.00 (0.68)					
0.10	694	~ 20 sh	22.66 (0.49)	28.09 (0.83)					
0.01	694	~ 20 sh	22.64 (0.47)	28.10 (0.79)					
Assignment of upper energy level. Transitions observed as shoulders given in []		⁴ T _{1g} (G)	⁴ T _{2g} (G) ⁴ E _g ⁴ A _{1g} (G)	⁴ T _{2g} (D) ⁴ E _g (D)	⁴ T _{1g} (P)	⁴ A _{2g} (F) ⁴ T _{1g} (F)	⁴ T _{2g} (F)		
Octahedral Mn ²⁺ , values in kK. ¹³		19.30	[22.70] 23.88	[27.20] 28.14	30.02	38.50	42.70		
Tetrahedral Mn ²⁺ , values in kK. ¹⁴		21.20	[22.40] 23.20	[26.30] 27.10	27.90	~ 38.00 38.30 ^b	39.30 ^b		

^a Taken from chart and not given in Fig. 1 as the computer tape got destroyed. ^b Calculated.

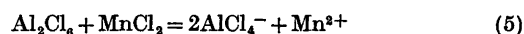
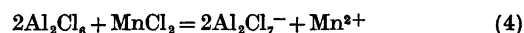
AlCl₃.¹² Except for some deviation for the first ⁴T_{1g}(G) ← ⁶A_{1g}(S) transition, the transitions correspond very closely to those determined by Mehra and Venkateswarlu,¹³ based on the experimental spectra of Mn²⁺ in a KCl host lattice with five transitions appearing as peaks and two as shoulders (Table 1). The increased band intensity with increasing temperature, accompanied by an increased molar absorptivity of the low energy band side, are consistent with a vibronic mechanism generally operative for an octahedral centrosymmetric ligand field.¹⁵

The spectra of Fig. 1 demonstrate that the environment around Mn²⁺ is invariant in the

measured range 0–30 mol % MnCl₂. Severe structural changes do, however, occur for compositions somewhat above 30 mol % MnCl₂, manifested by a steep rise of the melting point.¹⁶

Previous Raman studies have shown the following species to be present as the acidity is increased: AlCl₄⁻, Al₂Cl₇⁻, possibly Al₃Cl₁₀⁻, Al₂Cl₆.^{3,5,17} Al₂Cl₇⁻ is a double tetrahedron with a Cl-bridge.

The acid-base reaction can be written as shown in eqns. (4) and (5):



If the equilibria (4) and (5) are shifted completely to the right, AlCl_3 becomes saturated as AlCl_4^- when the MnCl_2 content is above 33 mol %, corresponding to the stoichiometry $\text{Mn}(\text{AlCl}_4)_2$, and further addition of MnCl_2 does not result in an acid-base reaction. It would have been of great interest to follow the structural changes around 33 mol % spectroscopically, but repeated explosions of the cells, due to high temperatures and pressures, prevented this. In the studied melts Mn^{2+} is considered coordinated octahedrally to AlCl_4^- or Al_2Cl_7^- forming strong ionic bonds.¹⁸

The Raman spectra of MnCl_2 - AlCl_3 mixtures were recorded in order to obtain additional information. The spectra proved generally to be of rather poor quality, and only the best spectrum is shown in Fig. 5, for a mixture containing 25 mol % MnCl_2 and 75 mol % AlCl_3 .

The spectrum is interpreted as follows: A strong peak at 344 cm^{-1} due to Al-Cl stretch in AlCl_4^- and Al_2Cl_6 groupings,² a weak peak at 311 cm^{-1} due to Al-Cl stretch in Al_2Cl_7^- groupings,² a broad band at 233 cm^{-1} probably due to Mn-Cl stretch for Mn^{2+} in octahedral positions, and two broad depolarized bands at 169 and 105 cm^{-1} due to Mn-Cl and Al-Cl bending modes.²

With Mn^{2+} having higher charge over radius ratio than the alkali ions, the Al_2Cl_7^- seems to be destabilized relative to what is observed in AlCl_3 -alkali chloride mixtures.⁵ The spectra do not contradict the model of Mn^{2+} coordinated octahedrally to AlCl_4^- and Al_2Cl_7^- groupings, but overlaps of bands due to AlCl_4^- and Al_2Cl_6 ⁵ and the relative poor spectral quality do prevent a detailed discussion of the structure.

(b) *Tetrahedral MnCl_4^{2-} species.* Although MnCl_2 is a base towards AlCl_3 it can act as an acid towards CsCl , according to eqn. (6):

$$\text{MnCl}_2 + 2\text{CsCl} = \text{MnCl}_4^{2-} + 2\text{Cs}^+ \quad (6)$$

If we assume this system is analogous to the AlCl_3 - MnCl_2 acid-base system with the equilibrium shifted to the right, reaction (6) will be completed when the content of CsCl becomes higher than 66 mol %, corresponding to the stoichiometry of Cs_2MnCl_4 . For stoichiometric reasons MnCl_4^{2-} exists as separate tetrahedral units *only*, above 66 mol % CsCl .

The Raman spectra (Figs. 3 and 4) give strong support for the assumption of formation of separate tetrahedral MnCl_4^{2-} units in mixtures of MnCl_2 with excess CsCl . In Fig. 4 the three upper curves show the spectra of solid Cs_2MnCl_4 where separate MnCl_4^{2-} groupings are present,^{19,20} compared with the spectra of the compound in the molten state. Taking into consideration the observed shift to lower frequencies with temperature and some broadening of peaks in the molten state, a close resemblance between the spectra of the solid and the liquid is demonstrated. Not only the symmetric stretching mode A_1 at 255 cm^{-1} , but also the E and one of the F_2 modes in the region $130-70\text{ cm}^{-1}$ are apparent.

The absorption spectra of MnCl_2 with CsCl in the concentration range $0 < X_{\text{MnCl}_2} \leq 0.33$ (Fig. 2) differ from that of MnCl_2 in AlCl_3 (Fig. 1), but the spectra in mixtures with CsCl are less structured and ligand field spectroscopy gives little aid in characterizing Mn^{2+} as MnCl_4^{2-} . This is more so as the spectra of octahedral¹³ and tetrahedral¹⁴ coordination can be very similar (Table 1).

However, we conclude, based on Raman spectra evidence, that MnCl_4^{2-} is the major species in molten MnCl_2 - CsCl mixtures with excess CsCl . The species MnCl_4^{2-} has also previously been suggested from absorption spectroscopy,²¹ from calorimetry²² and very recently from Raman spectroscopy.²³

(c) *Structural changes in liquid MnCl_2 - CsCl mixtures.* To clarify the structural changes in molten MnCl_2 - CsCl mixtures, we have plotted the location of the two bands that changes most significantly with composition, namely the maximum of the absorption band II (Fig. 2) and the maximum of the Raman symmetric stretching mode (Fig. 3) (Fig. 6).

The observed Raman shifts are qualitatively parallel to those observed in MnCl_2 - KCl by Tanemoto and Nakamura,²³ and also to what is observed for ZnCl_2 -alkali chloride systems.²⁴⁻²⁷

Additional support for the existence of separate MnCl_4^{2-} units in the range $0 < X_{\text{MnCl}_2} \leq 0.33$ is inferred from the graphs in Fig. 6 as the spectra remain unchanged in this region. In fact the shift of the symmetric stretching frequency begins around $X_{\text{MnCl}_2} = 0.33$, where this model starts to be untenable.

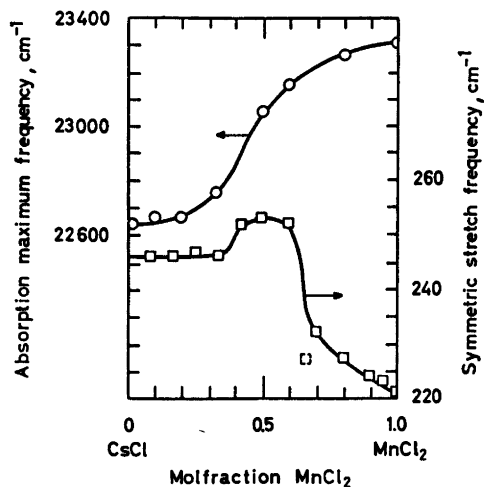


Fig. 6. Band shifts in molten $\text{MnCl}_2\text{-CsCl}$ mixture with composition. O, Maximum of absorption band II (Fig. 2, Table 1); □, maximum of the Raman symmetric stretching frequency (Fig. 3).

As an increase in coordination number generally leads to a lowering of the symmetric stretching frequency, see for instance Ferraro²⁸ who gives empirical rules, the following coordination changes could be expected:

$0 < X_{\text{MnCl}_2} < 0.33$: MnCl_4^{2-} units

$0.33 < X_{\text{MnCl}_2} < 0.50$: MnCl_4^{2-} units \rightarrow MnCl_3^- units

$0.50 < X_{\text{MnCl}_2}$: MnCl_3^- units \rightarrow octahedral coordination in lattice-like structure with Cl-bridging.

This model, however, does not explain readily the S-shaped shift of the location of the absorption band (Fig. 6) and the increased molar absorptivity with increasing MnCl_2 -content (Fig. 2).

An alternate model which in a better way incorporates the absorption spectroscopic results as well, considers the structural changes due to increased Cl-bridging without change of coordination number:

Mainly tetrahedral coordination for all compositions.

$0 < X_{\text{MnCl}_2} < 0.33$: MnCl_4^{2-} units

$0.33 < X_{\text{MnCl}_2} < 0.50$: Linear bridging ($\text{MnCl}_4^{2-} \rightarrow \text{Mn}_2\text{Cl}_7^{2-} \rightarrow \text{Mn}_n\text{Cl}_{3n+1}^{-(n+1)}$)

Acta Chem. Scand. A 31 (1977) No. 6

$0.50 < X_{\text{MnCl}_2}$: Transformation from linear to three-dimensional bridging.

The experimentally observed lowering of the stretching frequency for $X_{\text{MnCl}_2} > 0.6$ is then understood as the effect of three-dimensional bridging retaining the tetrahedral coordination. Linear bridging may, however, not necessarily give a decreased stretching frequency, and the increased stretching frequency for $0.33 < X_{\text{MnCl}_2} < 0.6$ can be explained by the presence of linear polymers. An experimental verification of this point is found by comparison with a similar system: $\text{GaCl}_4^- \text{-Ga}_2\text{Cl}_7^-$. For these ions the central atom is heavier than Cl (as in the case of Mn), and the totally symmetric stretching frequency is shifted from 342 cm^{-1} for GaCl_4^- to 366 cm^{-1} for Ga_2Cl_7^- .¹⁰

The strong shift in the location of the absorption maximum for $0.33 < X_{\text{MnCl}_2} < 0.5$ may then be correlated with a change in the ligand field accompanied by increased linear polymerization. It is also easier to understand the increase in molar absorptivity with increasing content of MnCl_2 (Fig. 2), as due to some distortion of the tetrahedral coordination connected with the three-dimensional bridging rather than transformation to an octahedral coordination where decrease in molar absorptivity generally is expected. This model is suggested in spite of the similarity of the Raman spectra of molten MnCl_2 and solid MnCl_2 where Mn^{2+} is octahedrally coordinated (Fig. 4).

The low viscosity of pure molten MnCl_2 indicates that a three-dimensional bridging may be less complete than in SiO_2 or ZnCl_2 .

In conclusion we would point to the qualitative difference of the Raman spectra in $\text{MnCl}_2\text{-CsCl}$ mixtures above and below 33 mol % MnCl_2 (Fig. 3). The peaks are relatively sharp below 33 mol % MnCl_2 , pointing to isolated MnCl_4^{2-} tetrahedra being the dominating species, while the broadness above 33 mol % probably is a result of several overlapping peaks due to a much more disordered structure.

Acknowledgement. We express our gratitude to The Norwegian Agency for International Development which, by a grant to one of us (Laila El-Sayed), made this work possible. We also gratefully acknowledge the experimental assistance of Mr. Morten Sørli, and "Norges almenvitenskapelige forskningsråd"

for financial support. Mr. D. Grünewald ably assisted with the Raman spectrometer, being financed by a grant from "Die Volkswagenstiftung". Discussions with Dr. M. H. Brooker are also gratefully acknowledged.

REFERENCES

1. Cyvin, S. J., Klæboe, P., Rytter, E. and Øye, H. A. *J. Chem. Phys.* 52 (1970) 2776.
2. Øye, H. A., Rytter, E., Klæboe, P. and Cyvin, S. J. *Acta Chem. Scand.* 25 (1971) 559.
3. Kvaal, T. and Øye, H. A. *Acta Chem. Scand.* 26 (1972) 1647.
4. Øye, H. A. and Bues, W. *Inorg. Nucl. Chem. Lett.* 8. (1972) 31.
5. Rytter, E., Øye, H. A., Cyvin, S. J., Cyvin, B. N. and Klæboe, P. *J. Inorg. Nucl. Chem.* 35 (1973) 1185.
6. Applied Aluminium Research Corporation: Presentation of the Toth Aluminium Production Process 1973, New Orleans, USA.
7. Grjøtheim, K., Krohn, C. and Øye, H. A. *Aluminium* 51 (1975) 697.
8. Borgen, O. and Bruvoll, T., *Technical Report 70*, Institutt for fysikalsk kjemi, Norges tekniske høgskole, Universitetet i Trondheim, Trondheim 1974.
9. Bues, W., Brockner, W. and Grünewald, D. *Spectrochim. Acta A* 28 (1972) 1519.
10. Øye, H. A. and Bues, W. *Acta Chem. Scand. A* 29 (1975) 489.
11. El-Sayed, L. and Øye, H. A. *Acta Chem. Scand. A* 29 (1975) 267.
12. Øye, H. A. and Gruen, D. M. *Inorg. Chem.* 3 (1964) 836.
13. Mehra, A. and Venkateswarlu, P. *J. Chem. Phys.* 45 (1966) 3381.
14. Cotton, F. A., Goodgame, D. M. L. and Goodgame, M. *J. Am. Chem. Soc.* 84 (1962) 167.
15. Ferguson, J. *Progr. Inorg. Chem.* 12 (1970) 159.
16. Levin, E. M., Robbins, C. R. and McMurdie, H. F. *Phase Diagrams for Ceramists 1969 Supplement*, The American Ceramic Soc., Columbus, Ohio 1969.
17. Rytter, E. *Thesis*, No. 26, Institutt for uorganisk kjemi, Norges tekniske høgskole, Universitetet i Trondheim, Trondheim 1974.
18. Anundskås, A. and Øye, H. A. *J. Inorg. Nucl. Chem.* 37 (1975) 1609.
19. Andersen, P. *Resymé*, 9. Nordiske kemikermøde, Aarhus 1956, p. 7.
20. Goodyear, J. and Kennedy, D. J. *Acta Cryst. B* 32 (1976) 631.
21. Sundheim, B. R. and Kukk, M. *Discuss. Faraday Soc.* 32 (1961) 49.
22. Papatheodorou, G. N. and Kleppa, O. J. *Inorg. Nucl. Chem.* 33 (1971) 1249.
23. Tanemoto, K. and Nakamura, T. *Chem. Lett. Jpn.* (1975) 351.
24. Bues, W. *Z. Anorg. Allg. Chem.* 152 (1955) 104.
25. Moyer, J. R., Evans, J. C. and Lo, G. Y.-S. *J. Electrochem. Soc.* 113 (1966) 158.
26. Ellis, R. B. *J. Electrochem. Soc.* 113 (1966) 485.
27. Bues, W. and Brockner, W. *Z. Phys. Chem. N. F.* 88 (1974) 290.
28. Ferraro, J. R. *Low-Frequency Vibrations of Inorganic and Coordination Compounds*, Plenum, New York 1971, Chapter 6.

Received January 28, 1977.

The Crystal Structure of (1*Z*,2*E*)-1,2-Naphthoquinone Dioxime

MATTI NÄSÄKKÄLÄ, HEIKKI SAARINEN, JORMA KORVENRANTA and ELINA NÄSÄKKÄLÄ

Department of Inorganic Chemistry, University of Helsinki, SF-00100 Helsinki 10, Finland

The crystal structure of the title compound has been determined and refined using three-dimensional X-ray diffraction data. The unit cell is monoclinic, $P2_1/c$ (No. 14), with $Z=4$ and cell parameters $a=7.082(12)$, $b=9.046(11)$, $c=13.845(11)$ Å, $\beta=100.2(1)^\circ$. The structure was solved by direct methods and refined by full-matrix least-squares techniques to a final R value of 0.049 for 924 observed reflections. The estimated standard deviations in the bond lengths were in the range 0.004–0.006 Å. The two oxime groups are intramolecularly hydrogen bonded, with the O...N distance of 2.490(5) Å, and the separate molecules are joined together by an intermolecular hydrogen bond of 2.729(4) Å between oxygen atoms of neighbouring oxime groups.

Our studies on 1,2-naphthoquinone monoximes¹ and the metal chelates formed by them,² have led us to investigate the *vicinal* dioxime compounds derived from aromatic nuclei. It is well known that the complex formation ability of the $-C(=NOH)-C(=NOH)-$ group is greatly influenced by the spatial arrangement of the two oxime groups. For instance, the specific action of the grouping towards nickel ions has been attributed to the *anti* isomers of the compounds.³ On the other hand, it has been stated that aromatic rings destroy such action, and no scarlet nickel chelates are formed by the dioximes of 1,2-benzoquinone or 1,2-naphthoquinone,³ for which stable *amphi* configurations could be expected. The relationship between the stability of the isomeric form of the ligand and its capability for complex formation is not, however, very clear-cut.

This paper is a part of our study on the structures of analytically interesting organic ligands and their metal chelates. The present type of compounds has been submitted to investigation since the numerous reports on *vic*-

dioximes and *vic*-dioximates in the literature have mainly been directed to the aliphatic compounds, and information about the chemistry of their aromatic counterparts is very limited; *e.g.* no results from crystal structure studies of such ligands are available.

EXPERIMENTAL

Crystal preparation and analysis. 1,2-Naphthoquinone dioxime was prepared from 1-nitroso-2-naphthol (E. Merck AG) and hydroxylamine hydrochloride. Methanolic solution containing equimolar quantities of 1-nitroso-2-naphthol and hydroxylamine hydrochloride together with a few drops of 2 M HCl was boiled under reflux for 8 h. When the hot solution was poured into excess of water, 1,2-naphthoquinone dioxime and small amounts of the corresponding anhydride compound were precipitated as a light yellow compact mass. The product was purified by dissolving into cold diluted sodium hydroxide solution, filtering off the insoluble anhydride, and reprecipitating the dioxime by adding diluted HCl. 1,2-Naphthoquinone dioxime was recrystallized from warm 1:1 aqueous ethanol from which it separated on gradual cooling as yellow needles; m.p. 163 °C. Anal. $C_{10}H_8O_2N_2$: C, H, N.

Crystal and intensity data. Weissenberg photographs showed that crystals are monoclinic and that the space group, from systematic absences, is $P2_1/c$. The unit cell dimensions were refined using data obtained from powder photographs taken with a Hägg-Guinier camera using $CuK\alpha$ radiation and calcium fluoride as internal standard. The density was determined by the flotation method. Crystal data for $C_{10}H_8O_2N_2$ are:

Space group $P2_1/c$ (No. 14)
 $a=7.082(12)$ Å, $b=9.046(11)$ Å, $c=13.845(11)$ Å
 $\beta=100.2(1)^\circ$, $Z=4$, $D_m=1.44$ g cm⁻³, $D_x=1.432$ g cm⁻³
 $\mu(CuK\alpha)=8.6$ cm⁻¹

Table 1. Fractional atomic coordinates ($\times 10^4$) and anisotropic thermal parameters ($\times 10^3$) for non-hydrogen atoms. Estimated standard deviations are given in parentheses. The anisotropic thermal parameters are of the form $\exp[-2\pi^2(h^2a^{*2}U_{11} + k^2b^{*2}U_{22} + l^2c^{*2}U_{33} + 2hka^*b^*U_{12} + 2hla^*c^*U_{13} + 2klb^*c^*U_{23})]$.

Atom	<i>X/a</i>	<i>Y/b</i>	<i>Z/c</i>	<i>U</i> ₁₁	<i>U</i> ₂₂	<i>U</i> ₃₃	<i>U</i> ₁₂	<i>U</i> ₁₃	<i>U</i> ₂₃
O1	1031(5)	4227(4)	2529(2)	84(2)	58(2)	37(2)	9(2)	7(1)	5(1)
O2	1113(4)	694(3)	4008(2)	75(2)	42(1)	56(2)	0(1)	-1(1)	2(1)
N1	1657(4)	5177(3)	3314(2)	60(2)	52(2)	36(2)	10(2)	10(1)	5(1)
N2	1246(4)	2143(3)	3718(2)	45(2)	41(2)	44(2)	4(1)	4(1)	1(1)
C1	2000(4)	4605(4)	4192(2)	26(2)	46(2)	38(2)	8(1)	9(1)	4(1)
C2	1786(5)	3034(4)	4458(2)	31(2)	44(2)	39(2)	7(1)	9(1)	1(1)
C3	2128(5)	2618(4)	5485(2)	39(2)	49(2)	43(2)	5(2)	5(2)	10(2)
C4	2643(5)	3620(4)	6188(2)	39(2)	61(2)	36(2)	10(2)	5(1)	5(2)
C5	3436(5)	6177(5)	6756(3)	37(2)	68(3)	50(2)	5(2)	2(2)	-12(2)
C6	3661(6)	7639(5)	6562(3)	41(2)	69(3)	71(3)	6(2)	3(2)	-23(2)
C7	3402(6)	8127(5)	5589(3)	41(2)	49(2)	84(3)	2(2)	11(2)	-9(2)
C8	2893(5)	7149(4)	4822(3)	44(2)	49(2)	60(2)	2(2)	11(2)	2(2)
C9	2615(5)	5661(4)	5003(2)	24(2)	49(2)	43(2)	7(1)	8(1)	2(1)
C10	2912(5)	5157(4)	5986(2)	31(2)	55(2)	42(2)	7(2)	6(1)	-2(2)

A crystal with approximate dimensions $0.6 \times 0.4 \times 0.3$ mm was chosen for the data collection. Ni-filtered Cu radiation ($\text{CuK}\alpha$, $\lambda = 1.5418$ Å) and a Stoe-Güttinger diffractometer were used to measure the intensities from the levels $0kl - 6kl$. The total number of reflections was 1349, of which 924 were considered observed, being stronger than $3\sigma(I)$, where $\sigma(I)$ is the standard deviation of the intensity based on counting statistics. The data set was corrected for Lorentz and polarization effects but not for absorption.

Structure determination and refinement. The structure was determined by direct methods, using the X-RAY system (1972).⁴ Scattering factors for the non-hydrogen atoms were taken from Ref. 5 and those for the hydrogen atom from Ref. 6.

The full-matrix least-squares refinement minimizing $\sum w(|F_o| - |F_c|)^2$ was performed with weights $w = 1/(10.0 + |F_o| + 0.0025|F_o|^2)$. The atomic coordinates and temperature factors for the non-hydrogen atoms were refined first isotropically and then anisotropically. The resulting *R* value ($R = \sum ||F_o| - |F_c|| / \sum |F_o|$) was 0.080. A difference Fourier map calculated at this stage showed clearly the positions of all hydrogen atoms. The hydrogen atoms were then included in the subsequent refinement cycles with isotropic thermal parameters. After the last cycle the *R* value for 924 reflections was 0.049.

The atomic coordinates and thermal parameters together with their standard deviations are given for the non-hydrogen atoms in Table 1 and for the hydrogen atoms in Table 2. A list of the observed and calculated structure factors is available on request.

DESCRIPTION AND DISCUSSION OF THE STRUCTURE

The molecular structure of the compound is shown in Fig. 1, where the bond lengths and angles are also given. It can be seen that in the *amphi* configuration of the oxime groups the N1-O1 bond is turned away from the C8 carbon atom. Such orientation is not self-evident since the turning of the 1-oxime group towards the C8 carbon atom has been observed at least in potassium 1,2-naphthoquinone-1-oxime-7-sulfonate monohydrate.¹ The present two oxime C=N [1.304(4) and 1.306(4) Å] and N-O [1.394(4) and 1.379(4) Å] distances are

Table 2. Fractional atomic coordinates ($\times 10^3$) and isotropic thermal parameters ($\times 10^3$) for hydrogen atoms. Estimated standard deviations are given in parentheses.

Atom	<i>X/a</i>	<i>Y/b</i>	<i>Z/c</i>	<i>U</i>
H(O1)	79(7)	325(6)	278(3)	7.4(15)
H(O2)	45(9)	18(7)	346(4)	15.8(23)
H(C3)	192(6)	163(5)	563(3)	7.2(14)
H(C4)	291(6)	329(4)	686(3)	6.0(12)
H(C5)	357(6)	574(4)	745(3)	6.6(12)
H(C6)	396(6)	840(5)	716(3)	8.4(14)
H(C7)	345(7)	924(5)	545(3)	8.5(14)
H(C8)	272(6)	754(4)	414(3)	5.8(11)

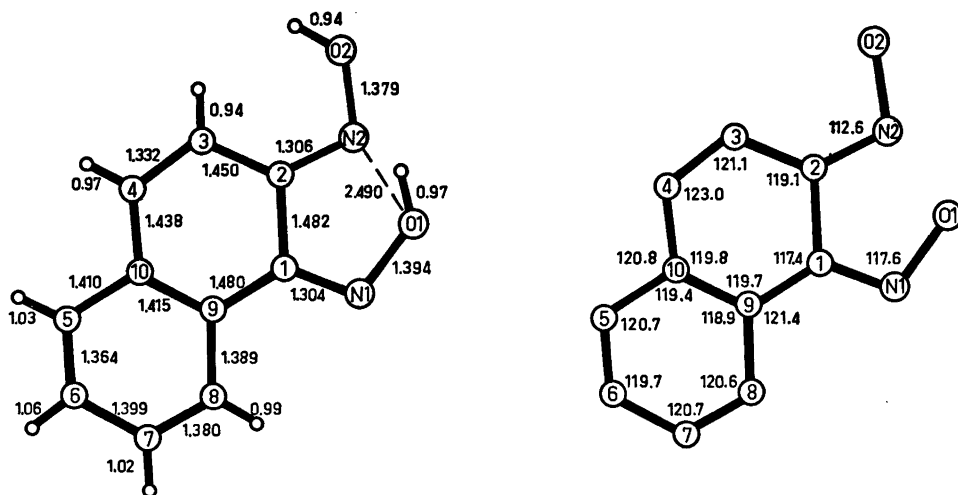


Fig. 1. Schematic representation of the molecule showing bond lengths (Å) and angles ($^{\circ}$). The e.s.d.'s for bond lengths are in the range 0.004–0.006 Å, and for angles, 0.3–0.4 $^{\circ}$.

closely equal. Their values compare well with the corresponding bond lengths found in several other oximes: 1.30 ± 0.02 and 1.38 ± 0.02 Å.⁷

The naphthalene C–C bond lengths are also as expected; the quinonoid nature of the compound is discovered in the short C3–C4 bond [1.332(5) Å], whereas the hexagonal C5–C10 carbon ring has maintained its aromatic character. A similar distribution of the C–C bond lengths has been observed in several 1,2-naphthoquinone monoxime compounds.

A part of the molecular packing is shown in Fig. 2. The structure may be described as built up of infinite serpentine chains of the molecules, running nearly along the *b* axis. The O2–H(O2) and H(O2)···O1($x, y - \frac{1}{2}, -z + \frac{1}{2}$) distances of 0.94(6) and 1.79(6) Å, together with the value of the O2–H(O2)···O1 angle [174(6) $^{\circ}$], indicate that the adjacent molecules are joined together by means of the hydrogen bond from the O2 oxime oxygen to the neighbouring O1 oxime oxygen. The intermolecular O1···O2 distance is 2.729(4) Å. This type of hydrogen bonding is somewhat uncommon, since most of the oximes whose structures are accurately known associate in the solid state via O–H···N hydrogen bond of length about 2.8 Å.⁷

The intramolecular hydrogen-bridged O1···N2 distance in the molecule is 2.490(5) Å. The

position of the H(O1) hydrogen atom can be located at a distance of 0.97(5) Å from the oxygen and 1.63(5) Å from the nitrogen atom, so that the O–H···N angle is 145(4) $^{\circ}$. It was unexpected to find out that comparable intra-

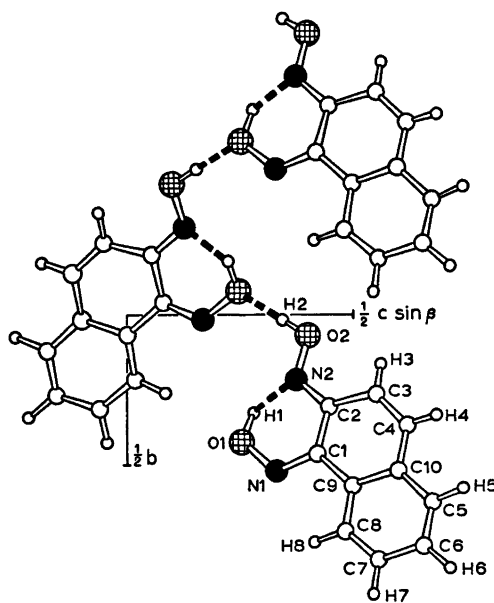


Fig. 2. Partial packing diagram of the compound as viewed down the *a*-axis. The broken lines represent hydrogen bonds.

Table 3. The least-squares plane defined by the naphthalene carbon ring C1–C10. Deviations (Å) of different atoms from the plane are given.

Atom	Distance	Atom	Distance	Atom	Distance
C1	–0.023	C6	–0.020	N1	–0.100
C2	–0.004	C7	0.003	N2	–0.029
C3	0.005	C8	–0.020	O1	–0.163
C4	0.005	C9	0.007	O2	0.022
C5	–0.004	C10	0.011		

molecular hydrogen bonds which involve N and O atoms are hardly available. The present N...O separation is nevertheless quite similar to the comparable O...O bond lengths frequently reported in the literature, *e.g.* 2.473 Å in β -5-propoxy-*o*-quinone-2-oxime.⁸ In such cases symmetrical hydrogen bridges are usually proposed.

The CNO angle in typical oximes is relatively constant around 112–113°.^{1,7} In the present compound the C1–N1–O1 angle is opened up by about 5° from the expected value, while the C2–N2–O2 angle is unaffected. The effect of the intramolecular hydrogen bonding on the planarity of the molecule is also worth noting. The naphthalene carbon ring is relatively planar, the largest deviation from the mean plane being 0.023 Å for the C1 carbon atom. The N2 and O2 atoms lie approximately in the naphthalene mean plane, but the N1 and O1 atoms are markedly displaced from it (Table 3). A further interesting finding is that the outside angle C3–C2–N2 [125.7(3)°] is significantly larger than the inside angle C1–C2–N2 [115.2(3)°], a phenomenon that has been found in several related structures, *e.g.* 1,2-naphthoquinone-2-oxime compounds. It may be noted that almost the same difference is observed between the values of the inside angle C2–C1–N1 [127.0(3)°] and the outside angle C9–C1–N1 [115.6(3)°]. As a whole, it is obvious that the only marked distortions of the geometry and orientation of the present 1,2-oxime groups are associated with the oxime group on the C1 carbon atom.

Acknowledgement. The financial support of the Science Research Council of Finland is gratefully acknowledged.

REFERENCES

- Saarinen, H., Korvenranta, J. and Näsäkkälä, E. *Acta Chem. Scand. A* 31 (1977) 213.
- Saarinen, H., Korvenranta, J. and Näsäkkälä, E. *Finn. Chem. Lett.* (1977). *In press.*
- Feigl, F. *Chemistry of Specific, Selective and Sensitive Reactions*, Academic, New York 1949.
- X-Ray 72, Program System, for X-Ray Crystallography, *Technical Report TR-192 of the Computer Science Center*, University of Maryland, College Park 1972.
- Cromer, D. T. and Mann, J. B. *Acta Crystallogr. A* 24 (1968) 321.
- Stewart, R. F., Davidson, E. and Simpson, W. J. *Chem. Phys.* 42 (1968) 3175.
- Chakravorty, A. *Coord. Chem. Rev.* 13 (1974) 1.
- Romers, C. *Acta Crystallogr.* 17 (1964) 1287.

Received January 31, 1977.

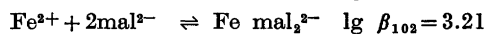
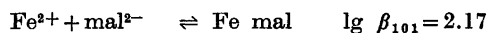
Thermodynamic Properties of Iron Oxalates and Malonates in Perchlorate Medium

INGEMAR DELLIEN

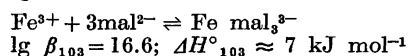
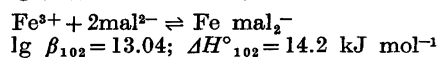
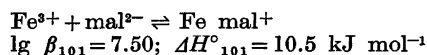
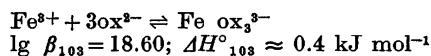
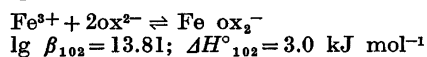
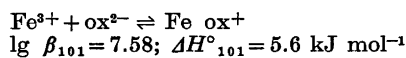
Division of Physical Chemistry 1, Chemical Center, University of Lund, P.O.B. 740, S-220 07 Lund 7, Sweden

Potentiometric measurements at ionic strength 1 M (NaClO₄) and at 25.0 °C have been made to determine the stability constants for the Fe³⁺ malonate complexes, the Fe³⁺ oxalate, and Fe³⁺ malonate complexes. The enthalpies of formation of the ferric oxalate and malonate complexes have been determined calorimetrically.

The Fe²⁺ malonate system was investigated by means of a glass electrode, and equilibrium constants were obtained for the following reactions:



From redox-potential and calorimetric measurements, the following overall equilibrium constants and enthalpy values were calculated:



The complex formation reactions in aqueous solution between iron(II or III) ion and organic ligands derived from saturated mono- or dicarboxylic acids have not been characterized in a satisfactory way. The entries in a comprehensive compilation such as Stability Constants¹ show that several investigations have

resulted in discordant interpretations as to which species that are formed and their stability constants. The main reason for the inconsistent results obtained is probably the complications introduced by the hydrolysis of Fe³⁺ (aq) ion, which makes the interpretation of experimental data difficult.

The ferric ion oxalate system has been the subject of several investigations.²⁻⁶ Deneux *et al.*² have determined stability constants for the complexes Fe(C₂O₄)_n³⁻²ⁿ, where n = 1, 2, and 3. The existence of a hydrogen oxalate complex, FeHC₂O₄²⁺, has been reported once,³ but its formation is questioned by other investigators.^{2,4,5} Several determinations of β₁, the stability constant for the monooxalato complex, are in fair agreement with each other.^{2,4-6} However, values for β₂ and β₃ that differ with about a factor of ten, are reported.^{2,6} In order to resolve these discrepancies, the Fe³⁺ oxalate system was reinvestigated.

The investigations of Deneux *et al.*² and Gordienko *et al.*⁵ disagree upon the malonate system. Deneux *et al.* report a stability constant for the formation of the first malonate complex that is only about 10 % smaller than the corresponding constant for the oxalate system. The trivalent rare earth ion complexes with oxalate ion are more stable than the malonate complexes with a factor of about 20.^{7,8} The values reported by Gordienko *et al.* for the corresponding Fe³⁺ ion complexes follow this pattern, but these investigators also found that the protonated complex FeHCH₂(COO)₂²⁺ is formed in substantial amounts; it would be the dominating ferric

ion complex in the concentration range investigated by Deneux *et al.* Thus, another study of this system is desirable.

In order to calculate stability constants for ferric ion complexes from emf measurements on the $\text{Fe}^{3+}/\text{Fe}^{2+}$ redox couple, the stability constants for the corresponding ferrous ion complexes must be known. The Fe^{2+} oxalate system has been studied by Bottari and Ciavatta,⁹ but no accurate data on Fe^{2+} malonate complexes were available. This system has been investigated here.

There is a nearly complete lack of calorimetric data for complex formation reactions between ferric ion and carboxylate ligands of the type discussed here. Uri¹⁰ has reported $K = 3 \times 10^9 \text{ M}^{-1}$ and $\Delta H^\circ = -0.3 \text{ kcal mol}^{-1}$ for the formation of the monooxalato iron(III) complex, but it is not stated under which conditions these values are supposed to be valid. The enthalpies of formation of the complexes formed in the Fe^{3+} oxalate and malonate systems therefore have been determined.

NOTATIONS

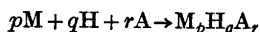
C_M , C_H , and C_A denote the total concentrations of metal ion, free and dissociable hydrogen ions, and ligand ion (oxalate or malonate) respectively. The concentration of free metal ion, hydrogen ion, and ligand ion are denoted m , h , and a , respectively. Ionic charges are usually omitted.

β_{pqr} = the overall stability constant for the complex $\text{M}_p\text{H}_q\text{A}_r$, defined as

$$\beta_{pqr} = [\text{M}_p\text{H}_q\text{A}_r] m^{-p} h^{-q} a^{-r}$$

$$\bar{n} = (C_A - \sum_{j=0}^2 [\text{H}_j\text{A}]) / C_M$$

ΔH°_{pqr} = the standard enthalpy change for the reaction



V = the total volume of the system, $V = V_0 + v$
 V_0 = the initial volume of the titrand solution, S ,
 v = the added volume of the titrator solution, T ,
 Q = the enthalpy change at the addition of T solution.

EXPERIMENTAL

Chemicals used. $\text{Fe}(\text{ClO}_4)_3 \cdot 6\text{H}_2\text{O}$ (Schuchardt, *p.a.*) and $\text{Fe}(\text{ClO}_4)_3 \cdot 6\text{H}_2\text{O}$ (Carl Roth, recrystallized from dilute HClO_4), were used for the preparation of the metal ion solutions. The ferrous perchlorate sample contained about 1% iron as $\text{Fe}(\text{III})$. Stock solutions of $\text{Fe}(\text{ClO}_4)_3$ were reduced with H_2S prior to use, after which treatment $[\text{Fe}(\text{III})] \leq 2 \times 10^{-5} \text{ M}$, as estimated from the reaction with KSCN solution. The iron content was determined by titration with KMnO_4 and the hydrogen ion content by a cation exchange procedure. All other chemicals used were of reagent grade and purified prior to use, when necessary. The measurements were made under nitrogen, which had passed through wash bottles with a $\text{Cr}(\text{II})$ solution and 1 M NaClO_4 .

Potentiometric measurements. The emf E of galvanic cells of the types given in Scheme 1 were measured. (A denotes either oxalate or malonate ion). In addition, sodium perchlorate was added to the solutions to make the total concentration of ionic equivalents, $I' = \frac{1}{2} (\sum c_i |z_i|)$, equal to 1.00 M. (As the concentration of polyvalent ions was rather low, also the formal ionic strength, $I = \frac{1}{2} (\sum c_i z_i^2)$, is close to 1.00 M). The pH measurements on the Fe^{3+} malonate system were made with a Jena glass electrode of the "Thalamid" type, while a bright platinum foil (area $\sim 11 \text{ cm}^2$) was used in the redox measurements. The Ag, AgCl electrodes were prepared according to Brown.¹¹ The emf values were measured to 0.1 mV with a digital Orion 801 voltmeter. The reproducibility of the emf values was usually within 0.2 mV. However, the last points of series 3, Table 1, were only reproducible to within 0.5 mV. The equilibration time for these points was also considerably longer (5–20 min) than for the other points, which equilibrated practically instantaneously. This might be caused by hydrolysis, due to a local excess of the titrator and subsequent slow equilibration of the hydrolyzed species. The final solutions are stable and remain clear for at least several

Ag, AgCl (s)	0.02500 M	1.00 M	$C_{\text{Fe}^{3+}}$	$\text{Fe}(\text{ClO}_4)_3$	Glass electrode or Pt (s)
	NaCl		$C_{\text{Fe}^{2+}}$	$\text{Fe}(\text{ClO}_4)_2$	
	0.975 M	NaClO ₄	$C_{\text{H}_2\text{A}}$	H_2A	
	NaClO ₄		$C_{\text{Na}_2\text{A}}$	Na_2A	
				C_{HClO_4}	

Scheme 1.

Table 1. Some experimental data for the Fe^{3+} malonate system. The results are given as v/ml , E/mV . The S and T solutions contain sodium perchlorate to make the total concentration of ionic equivalents equal to 1.00 M.

Series 1. S: $C_{\text{H}} = 148.5 \text{ mM}$, $C_{\text{Fe(III)}} = 5.88 \text{ mM}$, $C_{\text{Fe(II)}} = 5.26 \text{ mM}$, $C_{\text{A}} = 0$; T: $C_{\text{H}} = 338.0 \text{ mM}$, $C_{\text{Fe(III)}} = 5.88 \text{ mM}$, $C_{\text{Fe(II)}} = 5.26 \text{ mM}$, $C_{\text{A}} = 99.62 \text{ mM}$; $V_0 = 21 \text{ ml}$, $E_0 = 402.7 \text{ mV}$.

0.25, 404.5; 1, 402.5; 2, 400.1; 3.5, 397.1; 5, 394.7; 7, 392.1; 9, 390.0; 11.5, 387.8; 15, 385.6; 17, 384.5; 22, 382.4.

Series 2. S: $C_{\text{H}} = 148.5 \text{ mM}$, $C_{\text{Fe(III)}} = 12.35 \text{ mM}$, $C_{\text{Fe(II)}} = 11.21 \text{ mM}$, $C_{\text{A}} = 0$; T: $C_{\text{H}} = 419.3 \text{ mM}$, $C_{\text{Fe(III)}} = 12.35 \text{ mM}$, $C_{\text{Fe(II)}} = 11.21 \text{ mM}$, $C_{\text{A}} = 149.6 \text{ mM}$; $V_0 = 25 \text{ ml}$, $E_0 = 401.3 \text{ mV}$.

0.5, 402.2; 1, 400.6; 1.5, 399.2; 2, 397.8; 3.25, 394.9; 5, 391.6; 7, 388.5; 9.5, 385.5; 11, 384.0; 14, 381.4; 18, 378.8; 24, 375.8.

Series 3. S: $C_{\text{H}} = 33.30 \text{ mM}$, $C_{\text{Fe(III)}} = 3.430 \text{ mM}$, $C_{\text{Fe(II)}} = 3.115 \text{ mM}$, $C_{\text{A}} = 0$; T: $C_{\text{H}} = 99.2 \text{ mM}$, $C_{\text{Fe(III)}} = C_{\text{Fe(II)}} = 0$, $C_{\text{A}} = 99.6 \text{ mM}$; $V_0 = 24 \text{ ml}$, $E_0 = 410.4 \text{ mV}$.

0.2, 407.4; 0.6, 398.8; 1, 390.2; 1.5, 380.1; 2, 370.7; 2.6, 360.3; 3.4, 347.5; 4.2, 335.4; 5, 323.6; 5.8, 311.8; 6.6, 300.1; 7.5, 286.6; 8.5, 271.2; 9.5, 255.2; 10.75, 235.3; 12.25, 212.1; 13.5, 194.1; 15, 174.1; 16.5, 156.1; 18, 139.2.

months. The degree of stability and reproducibility obtained in these experiments is about the same as reported in many earlier investigations of this type, but is far better than found by Deneux *et al.*

The measurements on the Fe^{2+} malonate system have been made with great variations of the ratio $C_{\text{H}}/C_{\text{A}}$ and of C_{M} in the solutions, so that the formation of protonated or polynuclear species could be detected. Some of the measurements were made in poorly buffered solutions at such high pH values that possibly present Fe^{3+} should be strongly hydrolyzed or bound to malonate ion, thus causing a considerable error in the determination of the concentration of free ligand ion from the emf readings. To prevent that any oxidation from the ferrous to the ferric state occurred during the measurements, all solutions were swept free from dissolved oxygen prior to use. The measured emf values have been corrected for liquid junction potentials as described earlier.⁷

The measurements on the Fe^{3+} malonate system has been made in the following way. The titrand contains Fe^{3+} and perchloric acid and the titrant was a malonate buffer. In a series of titrations, the concentration free hydrogen ion, h , has been kept approximately constant, $h \approx 50 \text{ mM}$, while C_{M} has been varied. The measurements have then been performed

at another constant h -value, $h \approx 150 \text{ mM}$. One series (number 3 in Table 1) has been performed at lower h -values. Table 1 contains some of the experimental data, the complete data can be obtained from the author.

For the Fe^{3+} oxalate system, the preliminary results showed a fair agreement with the results of Deneux *et al.* and a detailed investigation was considered unnecessary. Two titrations were made and gave 36 experimental points. To retard the photochemical decomposition of Fe(III) in oxalate solutions, the solutions were kept in dark during the measurements.

The calorimetric measurements were performed as titrations. Two types of titrations were made: either a ferric ion solution was titrated with an oxalate (malonate) buffer, or the buffer solution was titrated with the metal ion solution. In this way solutions with \bar{n} values up to 2.8 (for the oxalate system) or up to 2.2 (for the malonate system) have been investigated. Other details of the procedure have been described earlier.^{12,13}

CALCULATIONS AND RESULTS

Potentiometric measurements

i. The Fe^{2+} malonate system. The stability constants for this system have been calculated from the experimentally determined values of v/ml and E/mV by the least squares procedure "Letagrop Vrid",¹⁴ and also by standard graphical procedures. The data were described by assuming the existence of two Fe^{2+} malonate complexes, FeA and FeA_2^{2-} , with the following stability constants:

$$\beta_{101} = (1.49 \pm 0.05) \times 10^3 \text{ M}^{-1}$$

$$\beta_{102} = (1.62 \pm 0.20) \times 10^3 \text{ M}^{-2}$$

(The errors here and in the following are equal to 3σ , where σ denotes the standard deviation). 111 experimental points were included in the calculation, and the standard deviation in the error carrying variable $C_{\text{H}}/C_{\text{A}}$ was equal to 3.8×10^{-3} , which indicates that the experimental values are quite satisfactorily described by the calculated constants. Some experimental and calculated \bar{n} vs. $-\lg(a/\text{M})$ values are shown in Fig. 1.

The assumption that an acid complex with the composition FeHA^+ is formed does not improve the fit between experimental and calculated values, and the corresponding stability constant β_{111} is not significantly positive. It is possible to give an estimate of the max-

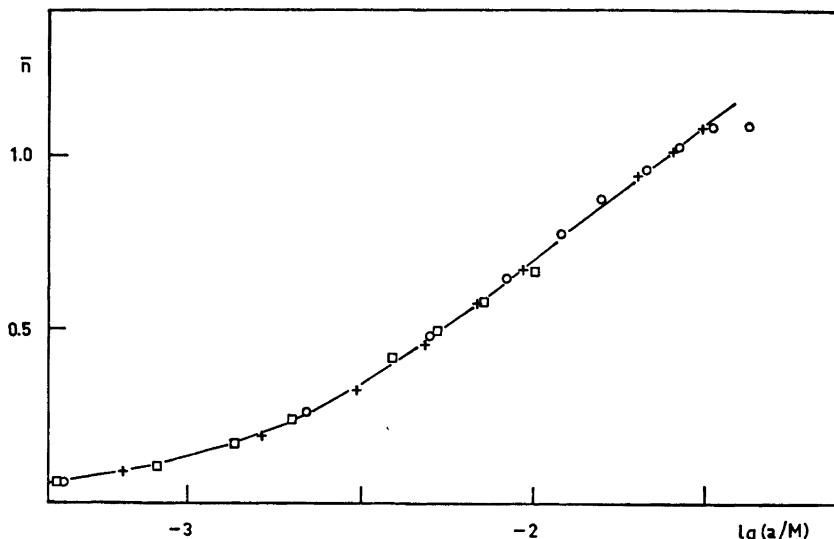


Fig. 1. Experimental \bar{n} vs. $-\lg(a/M)$ data for the Fe^{2+} malonate system. The curve has been calculated with the stability constants given in the text.

Symbol	Solution S C_H/mM	C_M/mM	C_A/mM	Solution T C_H/mM	C_M/mM	C_A/mM
○	16.2	14.2	0	114	0	255
+	32.4	28.4	0	114	0	255
□	16.2	14.2	0	147	0	198

imum value of β_{111} , and both the least squares calculations and graphical evaluations indicate that β_{111} is less than $2 \times 10^5 \text{ M}^{-2}$. There is no indication of the formation of polynuclear species.

ii. *The Fe^{3+} oxalate system.* As the available "Letagrop" program is not adopted for this type of four component systems, a computer program that calculated E/mV values from values of total concentrations and stability constants was written. The stability constants were varied until the best fit between calculated and observed E/mV values was obtained, that is, the error square sum $\sum(E_{\text{calc}} - E_{\text{obs}})^2$ was minimized, where the summation is over all experimental values.

Although the measurements have been designed so that the hydrolysis of ferric ion should be small in the solutions studied, the formation of FeOH^{2+} and $\text{Fe}_2(\text{OH})_2^{4+}$ has been accounted for by using the hydrolysis constants

$$\beta_{1-10} = 1.5 \times 10^{-3} \text{ M}$$

$$\beta_{2-20} = 1.9 \times 10^{-3} \text{ M}^2$$

The value for β_{1-10} is an average of several values quoted in Stability Constants,¹ and β_{2-20} is from Milburn, as cited by Sillén.¹ The stability constants for the Fe^{2+} oxalate system must be known; the values of Bottari and Ciavatta have been used.⁹

The following stability constants for the proton oxalate complexes in 1 M NaClO_4 were taken from Moorhead and Sutin:⁴

$$\beta_{011} = 3.58 \times 10^3 \text{ M}^{-1}$$

$$\beta_{021} = 4.27 \times 10^4 \text{ M}^{-2}$$

The calculations on 36 experimental points from two titration series gave the following stability constants for the formation of the Fe^{3+} oxalate complexes:

$$\beta_{101} = (3.83 \pm 0.15) \times 10^7 \text{ M}^{-1};$$

$$\lg(\beta_{101}/\text{M}^{-1}) = 7.58$$

$$\beta_{102} = (6.4 \pm 0.3) \times 10^{13} \text{ M}^{-2};$$

$$\lg(\beta_{102}/\text{M}^{-2}) = 13.81$$

$$\beta_{103} = (4.6 \pm 0.6) \times 10^{18} \text{ M}^{-3};$$

$$\lg(\beta_{103}/\text{M}^{-3}) = 18.66$$

The standard deviation in the emf E was 0.2 mV.

iii. The Fe³⁺ malonate system. Table 1 gives some of the experimental data for this system. The calculations on this system were performed in the same way as for the oxalates. (The stability constants for the proton malonate complexes were taken from Ref. 7). It is also possible to use a graphical method, due to Fronæus,¹⁵ on each set of titrations at a (nearly) constant value of the concentration free hydrogen ion, h , but at various C_M values. The value of β_{101} obtained in this way was in precise agreement with the value obtained from the numerical procedure. The value of β_{101} was calculated from each titration series. Each set of measurements at constant h but at various C_M values could be described with one value of β_{101} , which indicates that the formation of polynuclear species is negligible in the concentration range studied. If an acid complex is formed, *e.g.* FeHA^{2+} , one expects the calculated stability constant, β_{101}^* , to vary linearly with h :

$$\beta_{101}^* = \beta_{101} + h\beta_{111} \quad (1)$$

The value obtained, $\beta_{101}^* = (3.14 \pm 0.04) \times 10^7 \text{ M}^{-1}$, describes the measurements, in which h varied from about 40 mM to 150 mM, and no systematic variation of β_{101}^* with h was observed. If eqn. (1) is applied, an "extreme" interpretation of the findings is that $\beta_{101} = 3.08 \times 10^7 \text{ M}^{-1}$ and $\beta_{111} = 7 \times 10^6 \text{ M}^{-2}$. This value of β_{111} thus represents the upper limit of β_{111} that is reconcilable with the experimental data, but the data are best described by the following three stability constants:

$$\beta_{101} = (3.14 \pm 0.04) \times 10^7 \text{ M}^{-1};$$

$$\lg(\beta_{101}/\text{M}^{-1}) = 7.50$$

$$\beta_{102} = (1.09 \pm 0.06) \times 10^{13} \text{ M}^{-2};$$

$$\lg(\beta_{102}/\text{M}^{-2}) = 13.04$$

$$\beta_{103} = (4 \pm 2) \times 10^{18} \text{ M}^{-3};$$

$$\lg(\beta_{103}/\text{M}^{-3}) = 16.6$$

The values are based on in all 16 series with 356 experimental points. The standard
Acta Chem. Scand. A 31 (1977) No. 6

deviation in the emf E was 0.15 mV.

The error in β_{103} is considerable, due to the lower reproducibility of the measured emf values in solutions with high \bar{n} values, and also because the highest \bar{n} value obtained is only 2.1.

Schaap *et al.* have polarographically obtained a value for the ratio of the dissociation constants of the tris(malonato)ferrate(III) ion and the bis(malonato)ferrate(II) ion.¹⁶ Combining this number with the stability constant for the bis(malonato)ferrate(II) ion obtained in this work leads to $\beta_{103} = (5.1 \pm 1.3) \times 10^{16} \text{ M}^{-3}$ for the formation of $\text{Fe}[\text{CH}_2(\text{COO})_2]_3^{3-}$.

Calorimetric measurements

All enthalpy values have been calculated with the least squares program "Letagrop Kalle" from the experimental (v/ml , Q/J) values. The overall enthalpies of protonation of malonate ion at 25 °C in 1 M NaClO_4 are known,¹³ while the corresponding values for the oxalate system were determined. From 11 experimental points, the following values were calculated:

$$\Delta H^\circ_{011} = (4.0 \pm 0.2) \text{ kJ mol}^{-1}$$

$$\Delta H^\circ_{021} = (5.2 \pm 0.9) \text{ kJ mol}^{-1}$$

The enthalpy of hydrolysis of Fe^{3+} in 1 M NaClO_4 has not been determined, but Arnek has calculated $\Delta H^\circ_{1-10} = (46.0 \pm 7.5) \text{ kJ mol}^{-1}$ and $\Delta H^\circ_{2-20} = 41.8 \text{ kJ mol}^{-1}$ from Schlyter's measurements in 3 M NaClO_4 .¹⁷ Some ΔH°_{1-10} values within the limits given by Arnek were tried and the best fit was obtained with $\Delta H^\circ_{1-10} = 38 \text{ kJ mol}^{-1}$. The formation of $\text{Fe}_2(\text{OH})_2^{4+}$ is small in the solutions used and no variation of ΔH°_{2-20} was tried. The calculated overall enthalpy values are listed in Table 2, together with ΔH° and ΔS° values.

The obtained values for the standard deviation in Q are of the same magnitude as obtained earlier with this type of equipment.¹³ The error in the enthalpy of formation of $\text{Fe}(\text{mal})_3^{3-}$ is especially great, mainly due to the fact that the maximum \bar{n} value in the solutions used is as low as 2.2.

DISCUSSION

A direct comparison of the stability constants obtained here for the Fe^{2+} malonate

Table 2. The overall enthalpy, Gibbs energy, and entropy changes for the formation of Fe³⁺ oxalate and malonate complexes. The number of experimental points and the standard deviation in the Q values in the calorimetric measurements are given. The uncertainties are equal to three times the standard deviations.

Reaction	Number of experimental points	Standard deviation in Q/J	ΔH° kJ mol ⁻¹	$-\Delta G^\circ$ kJ mol ⁻¹	ΔS° J K ⁻¹ mol ⁻¹
Fe ³⁺ + ox ²⁻ → Fe ox ⁺	17	0.09	6.3 ± 0.9	43.28 ± 0.10	166 ± 3
Fe ³⁺ + 2ox ²⁻ → Fe ox ₂ ⁻			3.7 ± 1.8	78.80 ± 0.12	277 ± 6
Fe ³⁺ + 3ox ²⁻ → Fe ox ₃ ³⁻			0.4 ± 1.3	106.5 ± 0.3	359 ± 4
Fe ³⁺ + mal ²⁻ → Fe mal ⁺	20	0.05	11.3 ± 0.2	42.79 ± 0.03	181.4 ± 0.7
Fe ³⁺ + 2mal ²⁻ → Fe mal ₂ ⁻			14.4 ± 0.7	74.41 ± 0.14	298 ± 2
Fe ³⁺ + 3mal ²⁻ → Fe mal ₃ ³⁻			9.8 ± 7.3	94.8 ± 1.7	351 ± 25

complexes with the data of Nancollas *et al.*^{18,19} is not possible, as their data refer to a very low ionic strength. However, the first Fe³⁺ oxalate complex is 5.0 kJ/mol more stable than the malonate complex, which value is intermediate between the corresponding values for the Mn²⁺ and Co²⁺ complexes. The result also conforms to the general observation that oxalate complexes are more stable than the corresponding malonates.

Hydrogen malonate ion complexing has been observed with the trivalent lanthanoid ions,⁷

but not with the divalent transition metal ions. The lanthanoid-hydrogen malonate complexes are somewhat less stable than the corresponding acetate complexes. The upper limit for β_{111} found here corresponds to an equilibrium constant for the equilibrium between Fe³⁺ ion and hydrogen malonate ion of less than 1.8 M⁻¹. The β_1 value for the Fe³⁺ acetate complex is 2.1 M⁻¹ (at 20 °C).²⁰

The stability constants of the ferric ion oxalate and malonate complexes are collected in Table 3, together with some literature values.

Table 3. Some values of stability constants of iron(III) with oxalate, malonate and succinate ion at 25 °C.

lg (β_{101}/M^{-1})	lg (β_{102}/M^{-2})	lg (β_{103}/M^{-3})	Ionic strength	Ref.
Oxalate				
7.58	13.81	18.66	1 M NaClO ₄	This work
7.54	14.59	20.0	0.5 M NaNO ₃ ^a	6
7.59	—	—	1 M NaClO ₄	4
7.53	13.64	18.49	0.5 M LiClO ₄	2
7.56	—	—	1 M NaClO ₄	5
—	—	18.54 ^b	~1 M NaClO ₄	16
Malonate				
7.50	13.04	16.6	1 M NaClO ₄	This work
7.46	—	—	0.5 M LiClO ₄	2
—	—	16.7 ^c	~1 M NaClO ₄	16
6.54, lg(β_{111}/M^{-2}) = 7.59	—	—	1 M NaClO ₄	5
Succinate				
6.52	—	—	1 M NaClO ₄ ^a	22
6.88	—	—	0.5 M LiClO ₄	2

^a Temperature not given. ^b Calculated with auxiliary data from Ref. 9. ^c Calculated with auxiliary data from this paper.

The agreement is good, with one exception: the results of Gordienko *et al.* on the Fe^{2+} malonate system. It should be noted that Gordienko's acidity constants for malonic acid differ considerably from the results of two other investigations.^{7,21} It also seems unlikely that protonated complexes, as FeHA^{2+} , should be formed in the malonate system but not in the succinate system.²² It thus seems probable that Gordienko's measurements on the malonate system are beset with some systematic error.

The lanthanoid acetate complexes are about 1–2 kJ mol^{-1} more stable than the corresponding hydrogen malonate complexes. This difference is much greater, at least 7 kJ mol^{-1} , for the corresponding ferric ion complexes.

It has also been shown that the strength of the acid MHA^{2+} steadily increases as the radius of the lanthanoid ion M^{3+} decreases. This behaviour has been described in simple electrostatic terms.⁷ The upper limit of β_{111} for FeHA^{2+} determined here shows that FeHA^{2+} is a much stronger acid than the lanthanoid hydrogen malonates, in keeping with the smaller size of the iron(III) ion. It is suggested that this finding indicates that the malonate ion has a very strong tendency to form a chelate complex with ferric ion. It is noteworthy that the ferric monooxalate complex is only 0.5 kJ mol^{-1} more stable than the malonate complex. The trivalent rare earth oxalate complexes are about 7 kJ/mol more stable than the malonates.

The ratios of the stepwise stability constants are different for the oxalates and malonates: K_1/K_2 and K_2/K_3 are equal to 23 for the oxalates and 92 for the malonates. This increased difficulty for the formation of the higher malonate complexes as compared to the oxalates might be caused by different geometrical requirements of the bulkier malonate ion. Structural data would be of interest for a more detailed discussion, but only the structure of $\text{K}_3[\text{Fe ox}_3] \cdot 3\text{H}_2\text{O}$ is known at present.²³

It can be seen from Table 2 that the stepwise enthalpy changes become less positive for the higher complexes. The ferric ion malonate complexes are similar to the rare earth malonates in this respect. The complexes are stabilized by the large positive entropy changes, due to the liberation of water molecules from the metal ion. The stepwise entropy changes

become less positive for the higher complexes, which can be described as caused by the coordinated water molecules being less firmly bound in a higher complex than in a lower.

REFERENCES

1. Sillén, L. G. and Martell, A. E., Eds., *Stability Constants of Metal-ion Complexes*, Chem. Soc. Spec. Publ. Nos. 17 (1964) and 25 (1971).
2. Deneux, M., Meilleur, R. and Benoit, R. L. *Can. J. Chem.* 46 (1968) 1383.
3. Bauer, R. F. and Smith, W. M. *Can. J. Chem.* 43 (1965) 2755.
4. Moorhead, E. G. and Sutin, N. *Inorg. Chem.* 5 (1966) 1866.
5. Gordienko, V. I., Mikhailyuk, Yu. I. and Sidorenko, V. I. *Russ. J. Gen. Chem.* 41 (1971) 501.
6. Paramonova, V. I., Kereichuk, A. S. and Chizhov, A. V. *Radiochimia* 5 (1963) 63.
7. Dellien, I. and Grenthe, I. *Acta Chem. Scand.* 25 (1971) 1387.
8. Grenthe, I., Gårdhammar, G. and Rundcrantz, E. *Acta Chem. Scand.* 23 (1969) 93.
9. Bottari, E. and Ciavatta, L. *Gazz. Chim. Ital.* 95 (1965) 908.
10. Uri, N. *Chem. Rev.* 50 (1952) 375.
11. Brown, A. S. *J. Am. Chem. Soc.* 56 (1934) 646.
12. Grenthe, I., Ots, H. and Ginstrup, O. *Acta Chem. Scand.* 24 (1970) 1067.
13. Dellien, I. *Acta Chem. Scand.* 27 (1973) 733.
14. Arnek, R., Sillén, L. G. and Wahlberg, O. *Ark. Kemi* 31 (1968) 353.
15. Fronæus, S. *Komplexsystem hos koppar*, Diss., C. W. K. Gleerups Förlag, Lund 1948.
16. Schaap, W. B., Laitinen, H. A. and Bailar, J. C. *J. Am. Chem. Soc.* 76 (1954) 5868.
17. Arnek, R. *Ark. Kemi* 32 (1970) 55.
18. McAuley, A., Nancollas, G. H. and Torrance, K. *J. Inorg. Nucl. Chem.* 28 (1966) 917.
19. McAuley, A., Nancollas, G. H. and Torrance, K. *Inorg. Chem.* 6 (1967) 136.
20. Perrin, D. D. *J. Chem. Soc.* (1959) 1710.
21. Szilard, I. *Protonierte Metallkomplexe mehrzähliger Liganden*, Diss., ETH, Juris-Verlag, Zürich 1961.
22. Kereichuk, A. S. and Pobegai, R. S. *Vestn. Leningr. Univ., Ser. Fiz. Khim.* (1975) 122; *Chem. Abstr.* 83 (1975) 33716e.
23. Herpin, P. *Bull. Soc. Fr. Mineral. Cristallogr.* 81 (1958) 245.

Received February 23, 1977.

The Crystal and Molecular Structure of 2,2'-Diaminodiphenyl at $-165\text{ }^{\circ}\text{C}$

TOR OTTERSEN

Department of Chemistry, University of Oslo, Oslo 3, Norway

The structure of the title compound has been determined by X-ray crystallographic methods using 2406 observed reflections collected by counter methods at $-165\text{ }^{\circ}\text{C}$. The compound crystallizes in the space group $C2/c$ with four molecules per unit cell with a crystallographically determined twofold axis through the central carbon-carbon bond of the molecules. The structure model was refined to a conventional R of 0.045. In order to remove the influence of the asphericity of the valence electron densities all reflections with $\sin \theta/\lambda < 0.65\text{ \AA}^{-1}$ were excluded from the final refinements of the nonhydrogen atoms leaving 1353 F_{obs} 's ($R = 0.034$, $R_w = 0.040$). The angle between the planes of the phenyl rings is 58.2° with the amino groups *syn*. The determining factor in the configuration is probably the *intra*-molecular $\text{N}\cdots\text{N}$ hydrogen bond with $\text{N}\cdots\text{N}$ distance $2.933(1)\text{ \AA}$. The hydrogen arrangement in the amino groups is disordered such that each nitrogen is either donor in an *intra*-molecular hydrogen bond and acceptor in an *inter*-molecular hydrogen bond or *vice versa*. The bond lengths and bond angles in the phenyl rings indicate significant deformations of the ring.

Structure investigations of 2,2'-disubstituted biphenyls in the gas¹⁻³ and crystalline³⁻⁶ states have shown the preferred conformation to be *syn*, with the rotation angle between the ring planes (ϕ) varying from 60° in 2,2'-difluorobiphenyl¹ to 86° in 4,4'-diamino-2,2'-dimethylbiphenyl⁶ ($\phi = 0$ for *syn*-periplanar). The value of ϕ found for 2,2'-dichlorobiphenyl³ is about 70° both in the crystalline and gaseous state and a similar value ($\phi = 72^{\circ}$) was obtained for 4,4'-diamino-2,2'-dichlorobiphenyl.⁵ This value of ϕ gives a relatively short *intra*-molecular $\text{Cl}-\text{Cl}'$ distance of about 3.42 \AA which leads to small deformations in the molecule,³ an opening of the $\text{Cl}'-\text{Cl}-\text{C}2$ angles to 123.0°

and the $\text{C}2-\text{Cl}$ bond is bent 2.3° out of the plane of the phenyl ring. The energies involved in these deformations are probably small, similar deformations were also found in the crystal structure investigations of 3,3'-dimethyl-⁷ and 3,3'-dichloro-4,4'-diaminobiphenyl.⁸

The preferred *syn* conformation of the 2,2'-disubstituted biphenyls imply that van der Waals type interactions between the substituents must play a dominant part in the conformational structure of biphenyls. In support of this are the *trans* conformations found in the crystal structure investigations of the two 3,3'-disubstituted biphenyls.^{7,8} In these cases the deciding factors must be the conjugation over the $\text{C}1-\text{C}1'$ bond, interactions between the hydrogens at the 2, 2', 6 and 6' positions and packing effects. The rotation barrier in biphenyl is small, *ab initio* calculations⁹ indicated a minimum of $\phi = 32^{\circ}$, 1.2 kcal/mol lower than for $\phi = 0$ and 4.5 kcal/mol lower than for $\phi = 90^{\circ}$. A ϕ of about 42° was obtained in the electron diffraction studies of gaseous biphenyl^{10,11} whereas a planar structure was found in the crystal structure investigation.¹²

In order to gain more information on the conformations of biphenyls a crystal structure investigation of 2,2'-diaminobiphenyl was carried out. The factor controlling the conformation in this case should be the probable formation of an *intra*-molecular $\text{N}\cdots\text{N}$ hydrogen bond.

EXPERIMENTAL

An approximately cube-shaped crystal with edges of about 0.4 mm was mounted on a computer-controlled Syntex PI four-circle dif-

fractometer with scintillation detector and equipped with incident-beam graphite monochromatized MoK α -radiation and a modified Enraf-Nonius low-temperature device (liquid N₂). The temperature at crystal site was -165 °C. The axial solutions from the angular coordinates of fifteen reflections implied a monoclinic system. The systematic absences found in a fast low-angle datacollection were those of space group *Cc* or *C2/c*, and the cell volume indicated four molecules in the unit cell. The later structure determination showed the space group to be *C2/c*. Unit cell dimensions were determined by a least-squares treatment of fifteen reflections with 2θ -values between 40 and 45°.

Three-dimensional intensity data were recorded using the ω - 2θ scanning mode with scan speed variable from 3 to 12° min⁻¹ depending on the intensity of the reflection as determined by the counts in a 2 s scan over the reflection. Scan area was from [$2\theta(\alpha_1) - 0.8^\circ$] to [$2\theta(\alpha_2) + 1.1^\circ$] and background counting time was equal to 0.7 \times scan time. Reflections with 2θ -values larger than 45° which had integrated counts of less than 10 cps determined in the 2 s scan were not recorded. The variations in the intensities of three standard reflections which were remeasured after every 60 reflections were random and accordingly no corrections were applied to the intensity data for these variations.

The estimated standard deviations were taken as the square root of the total counts with a 2 % addition of the net intensity for experimental uncertainties. Of the 2729 symmetry-independent reflections recorded ($2\theta_{\max} = 90^\circ$), 2406 had intensities larger than twice their standard deviations. These were regarded as "observed" reflections and the remaining were excluded from the refinements. The intensities were corrected for Lorentz and polarization effects. The computer program used, as well as programs subsequently employed, is part of a local assembly of computer programs for CYBER-74 which is described in Ref. 13.

The atomic scattering factors used were those calculated by Doyle and Turner¹⁴ for nitrogen and carbon and of Stewart *et al.*¹⁵ for hydrogen.

CRYSTAL DATA

2,2'-Diaminobiphenyl, C₁₂H₁₂N₂, *M* = 184.21 amu, space group: *C2/c*, cell dimensions at -165 °C: *a* = 19.463(4) Å, *b* = 6.211(1) Å, *c* = 8.305(2) Å, β = 104.93°(2), *V* = 970.0(3) Å³, *Z* = 4, *D*_{calc} = 1.261 g cm⁻³, *F*(000) = 392.

STRUCTURE DETERMINATION AND REFINEMENTS

The phase problem was solved by the MULTAN program assembly¹⁶ in combination

with the use of negative quartets,¹⁷ assuming the centrosymmetric space group *C2/c* which requires the molecule to possess a two-fold axis of symmetry.

The structure model was refined with isotropic temperature factors to a conventional *R* of 0.14. At this point anisotropic temperature factors were introduced for the nonhydrogen atoms. Least-squares refinements lowered *R* to 0.07 and *R*_w to 0.12. The factor minimized was $\sum w\Delta F^2$ with $w = 1/\sigma(F_{\text{obs}})$. A difference Fourier synthesis revealed the positions of the six hydrogen atoms. The four hydrogens bonded to the phenyl ring and one of the hydrogens of the amino-group showed up as the five highest peaks in the difference map (peak heights: 0.8–0.6 e Å⁻³), whereas the second hydrogen of the amino-group was distributed between two positions (peak heights: 0.4 e Å⁻³), one where it participated in an *intra*-molecular hydrogen bond and one where it participated in an *inter*-molecular hydrogen bond. The twofold symmetry requires this hydrogen to be equally distributed between the two positions. The hydrogens, five with weights of 1 and two with weights of 1/2, were included in the refinements. Final least-squares refinement of all positional parameters, anisotropic thermal parameters for nonhydrogen atoms and isotropic thermal parameters for hydrogen atoms converged to an *R* of 0.045 and an *R*_w of 0.060.

In order to remove the influence of the asphericity of the valence electrons on the atomic parameters refinements were carried out with a $\sin \theta/\lambda$ minimum cutoff of 0.65 Å⁻¹, leaving 1353 *F*_{obs}'s. Earlier structure determinations^{18,19} have implied that the asphericity of the electron densities has no effect on carbon and nitrogen parameters when this cutoff is used. Least-squares refinement of all parameters involving nonhydrogen atoms converged to an *R* of 0.034, an *R*_w of 0.040 and an *R*_t for the total data set of 0.043. The exclusion of low-angle data in the refinement resulted in significant changes, in the order of 0.002–0.005 Å, in the bond lengths.

Final atomic parameters for nonhydrogen atoms are listed in Table 1 together with those obtained for the hydrogen atoms in the refinement using all data. A list of observed and calculated structure factors is available from the author upon request. Standard deviations

Table 1. Fractional atomic coordinates and thermal parameters with estimated standard deviations. The anisotropic temperature factor is given by: $\exp \{-2\pi^2[U_{11}(a^*h)^2 + \dots + 2U_{23}(b^*c^*hd)]\}$.

Atom	x	y	z	U11	U22	U33	U12	U13	U23
C1	.03879(3)	.20678(7)	.25503(5)	.0178(2)	.0115(2)	.0140(2)	-.0008(1)	-.0004(1)	.0005(1)
C2	.08444(3)	.37382(8)	.33432(6)	.0230(3)	.0154(2)	.0130(2)	-.0052(2)	.0016(1)	-.0001(1)
C3	.15707(4)	.36210(13)	.34192(8)	.0243(3)	.0317(3)	.0201(2)	-.0128(2)	.0069(2)	-.0055(2)
C4	.18470(4)	.18918(18)	.27228(11)	.0218(3)	.0433(4)	.0275(3)	-.0930(3)	.0092(2)	-.0101(3)
C5	.14027(4)	.02356(12)	.19450(8)	.0208(3)	.0287(3)	.0226(2)	.0009(2)	.0048(2)	-.0037(2)
C6	.06817(3)	.03328(8)	.18810(6)	.0190(2)	.0146(2)	.0178(2)	.0014(1)	.0009(1)	-.0004(1)
N7	.05719(4)	.54854(8)	.40452(6)	.0319(3)	.0161(2)	.0168(2)	-.0072(2)	.0066(2)	-.0049(1)
Atom	x	y	z	B	Atom	x	x	z	B
H3	.1901(6)	.4846(19)	.4006(16)	3.2(2)	H4	.2358(6)	.1845(20)	.2794(16)	3.5(2)
H5	.1583(6)	-.1004(20)	.7444(15)	2.8(2)	H6	.0350(5)	-.0841(17)	.1330(12)	1.8(2)
H71	.0914(7)	.6457(21)	.4621(17)	3.7(3)	H72A	.0165(9)	.5232(30)	.4530(23)	1.4(3)
H72B	.0240(11)	.6097(34)	.3289(27)	2.3(4)					

in molecular parameters were calculated from the correlation matrix ignoring standard deviations in cell parameters.

DISCUSSION

Bond lengths and bond angles are listed in Fig. 1 where the numbering of the atoms is indicated, and deviations from planarity are given in Table 2. A view of the molecule as seen along the C1-C1' bond is given in Fig. 2. Each phenyl ring is planar with the nitrogen atom in the ring plane, whereas in 2,2'-dichlorobiphenyl³ the C2-Cl bond was bent 2.3° out of the ring plane. The angle between the ring planes is 58.2°. In addition to a rotation around the central C1-C1' bond the rings are bent relative to each other, as showed by the difference in the two torsional angles C2-C1-C1'-C2' [59.79°(8)] and C6-C1-C1'-C6 [56.17°(9)], and the configuration around C1 is slightly nonplanar with C1 0.013 Å out of the plane through C2, C6 and C1'. The two C1'-C1-C2 angles are opened to 122.15° which gives a nonlinear C4-C1-C1'-C4' arrangement as can be seen in Fig. 2, in agreement with the results found for 2,2'-dichlorobiphenyl.³

The factor determining the configuration of the 2,2'-diaminobiphenyl molecule must be the *intra*-molecular N...N hydrogen bond. The hydrogen arrangement around the aminogroups is disordered (see Figs. 1 and 2), such that each nitrogen atom is either donor in an *intra*-molecular hydrogen bond (N-H72B...N, N...N: 2.933(1) Å, ∠N-H...N: 143°) and acceptor in an *inter*-molecular hydrogen bond (N...H72A-N, in position: -x, 1-y, 1-z, N...N: 3.107(1) Å, ∠N...H-N: 170°) or

Table 2. Deviations, Dev., (Å × 10³) from a least-squares plane through the six atoms in the phenyl ring.

Atom	Dev.	Atom	Dev.	Atom	Dev.
C1	-6	C6	7	H5	-7
C2	0	N7	4	H6	9
C3	4	C1'	15	H71	81
C4	-2	H3	12	H72A	475
C5	-3	H4	2	H72B	-680

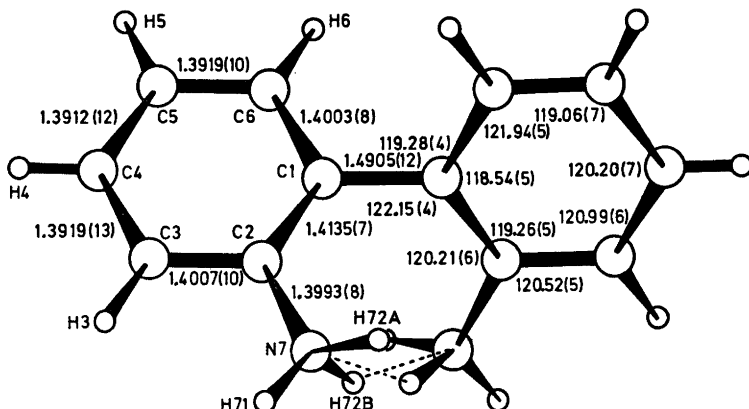


Fig. 1. Bond lengths (Å) and bond angles (°) with estimated standard deviations in the last digit of the corresponding number. The disordered *intra*-molecular hydrogen bond is indicated by broken lines. The results for the heavy atoms are based on the parameters obtained in the refinement using only high-angle data. The three C-N-H angles are: C2-N7-H71 114.8°; C2-N7-H72A 118.4°; C2-N7-H72B 109.3°.

vice versa. Each molecule has one *intra*-molecular hydrogen bond and participates in two *inter*-molecular hydrogen bonds, in one as a donor and in one as an acceptor.

The phenyl ring angles deviate significantly from 120°, the C2-C1-C6 angle is closed in agreement with results found for other biphenyls,^{3,7,8,12,20} although the value found in the present case (118.54°) is significantly larger than those found in 2,2'-dichlorobiphenyl³ (116.2°) and in biphenyl²⁰ (117.4°, corrected for thermal vibration effects). The relatively small angles found in other biphenyls may in part be due to both thermal vibration effects and the shifts of the atomic positions towards the center of the phenyl ring caused by the asphericity of the electron density. The closing of the C2-C1-C6 angle is probably caused by the conjugation over the C1-C1' bond (double bond character: 0.15). Similarly the closing of the C1-C2-C3 angle must be caused by the participation of the amino group in the conjugated system. Studies of acetamide and related systems²¹ have shown that the O-C-C angle decreases with decreasing double bond character of the C-O bond and increasing double bond character of the C-N bond. The C2-N7 bond in the present case is short with a double bond character of 0.33 assuming N7 to be *sp*²-

hybridized, and the C1-C2 bond [1.4135(7) Å] is significantly longer than the standard benzene bond length of 1.396 Å. The conjugation over N7-C2-C1-C1'-C2'-N7' is probably enhanced by the hydrogen bonding.²¹ The closing of the C6-C1-C2 and C1-C2-C3 angles and the lengthening of (*i.e.* decreased

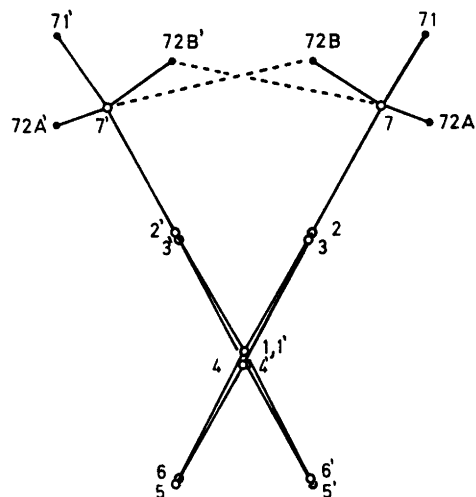


Fig. 2. 2,2'-Diaminobiphenyl as seen along the central carbon-carbon bond. The disordered *intra*-molecular hydrogen bond is indicated by broken lines.

conjugation over) the C1–C2 bond lead to the other deformations in the phenyl ring (see Fig. 1).

Acknowledgement. The author wants to thank Dr. Carsten Christophersen for supplying crystals and Døsent Christian Rømming for helpful discussions.

REFERENCES

1. Bastiansen, O. and Smedvik, L. *Acta Chem. Scand.* 8 (1954) 1593.
2. Bastiansen, O. *Acta Chem. Scand.* 4 (1950) 926.
3. Rømming, C., Seip, H. M. and Aanesen-Øymo, I.-M. *Acta Chem. Scand. A* 28 (1974) 507.
4. Fowweather, F. and Hargreaves, A. *Acta Crystallogr.* 3 (1950) 81.
5. Smare, D. L. *Acta Crystallogr.* 1 (1948) 150.
6. Fowweather, F. *Acta Crystallogr.* 5 (1952) 820.
7. Chawdury, S. A., Hargreaves, A. and Sullivan, R. A. L. *Acta Crystallogr. B* 24 (1968) 1222.
8. Chawdury, S. A., Hargreaves, A. and Rizvi, S. H. *Acta Crystallogr. B* 24 (1968) 1633.
9. Almlöf, J. *Chem. Phys.* 6 (1974) 135.
10. Bastiansen, O. *Acta Chem. Scand.* 3 (1949) 408.
11. Almenningen, A. and Bastiansen, O. *K. Nor. Vidensk. Selsk. Skr.* (1958) No. 4.
12. Trotter, J. *Acta Crystallogr.* 14 (1961) 1135.
13. Groth, P. *Acta Chem. Scand.* 27 (1973) 1837.
14. Doyle, P. A. and Turner, P. S. *Acta Crystallogr. A* 24 (1968) 390.
15. Stewart, R. F., Davidson, E. R. and Simpson, W. T. *J. Chem. Phys.* 42 (1965) 3175.
16. Germain, G., Main, P. and Woolfson, M. M. *Acta Crystallogr. A* 27 (1971) 368.
17. De Titta, G. T., Edmonds, J. W., Langs, D. A. and Hauptman, H. *Acta Crystallogr. A* 31 (1975) 472.
18. Stevens, E. D. and Hope, H. *Acta Crystallogr. A* 31 (1975) 494.
19. Hope, H. and Ottersen, T. *Acta Crystallogr. B*. Submitted for publication.
20. Robertson, G. B. *Nature (London)* 191 (1961) 593.
21. Ottersen, T. *Adv. Mol. Rel. Proc.* 9 (1976) 105.

Received March 15, 1977.

The Crystal and Molecular Structure of 5-Nitrososalicylic Acid

H. J. TALBERG

Department of Chemistry, University of Oslo, Oslo 3, Norway

The crystal and molecular structure of 5-nitrososalicylic acid has been determined from X-ray diffraction data collected at -165°C and refined by least squares methods. The space group is $P2_1/n$ with cell dimensions $a = 22.829(2)$ Å, $b = 8.028(1)$ Å, $c = 3.6696(4)$ Å and $\beta = 91.07(1)^{\circ}$ at -165°C . The final R factor was 5.1% and the estimated standard deviations in bond lengths are in the range 0.002–0.003 Å and in angles 0.2° . The C–NO and the N–O bond lengths are found to be, respectively, much longer (0.067 Å) and much shorter (0.059 Å) than those of the *p*-nitrosophenolate anion. Other bond lengths and angles resemble closely those of salicylic acid and 5-sulfosalicylic acid di- and trihydrate. The slight deviations found seem to be consistent with a less pronounced *ortho* quinonoid structure in 5-nitrososalicylic acid than in these compounds.

The present structure investigation of 5-nitrososalicylic acid (I) is part of a series of investigations of *C*-nitroso compounds. Previously the oxime tautomer of *p*-nitrosophenol (II) and three of its salts¹ and the compound *N,N*-dimethyl-*p*-nitrosoaniline and *N,N,N',N'*-tetramethyl-1,5-diamino-4-nitrosobenzene (III)² have been investigated.

The title compound forms crystals having the characteristic blue colour of *C*-nitroso compounds. This indicates that it is one of the few *para* nitrosophenols which can be isolated.³ In solution these compounds participate in a rapid equilibrium with their oxime tautomer and in most cases only the oxime tautomer crystallizes from the solution. Probably stabilization by internal hydrogen bonding causes (I) and not its oxime tautomer to form crystals (see Ref. 3 and references therein).

The investigation of the *p*-nitrosophenolate anion and (III) confirmed previous IR-studies which indicated that the ω_{NO} wave number

is much lower than that of a "pure" NO double bond. The bond number has been found to be as low as 1.5–1.7 in both compounds, and extended conjugation gives the molecules a very pronounced quinonoid appearance. As to (I) however, the IR-KBr- ω_{NO} wave number (1480 cm^{-1}) seems to be in the normal range ($1560\text{--}1480\text{ cm}^{-1}$). It was therefore decided to carry out a structure determination of (I) in order to compare the degree of conjugation in this molecule with that of the other compounds investigated.

EXPERIMENTAL

The title compound was derived from salicylic acid by nitrosation.⁴ Recrystallization from toluene gave green needle shaped crystals suited for X-ray work. Also some azur coloured tabular monoclinic crystals were obtained ($V = 830\text{ Å}^3$), probably a monohydrate of (I). All the data were collected and the unit cell constants determined using a crystal of dimensions $0.60 \times 0.16 \times 0.08\text{ mm}$. Apart from the following details the experimental conditions were as those described in Ref. 2. The temperature at the crystal site was -165°C . The scan limits were $2\theta(\alpha_1) - 1.2^{\circ}$ and $2\theta(\alpha_2) + 1.2^{\circ}$ and a quadrant of reciprocal space was examined. Out of 2272 unique reflections measured 1448 had intensities larger than $2.5\sigma(I)$ where $\sigma(I)$ is the estimated standard deviation of the intensity based on counting statistics adding 2% uncertainty due to experimental fluctuations.

The atomic scattering factors for the heavy atoms were those of Doyle and Turner⁵ and for hydrogen those of Stewart *et al.*⁶ Core and valence electron scattering factors used in an *L*-shell refinement were those given by Stewart.⁷ All programs except for the ORTEP program (Ref. 8 in Ref. 1) and the MULTAN program⁶ applied during the structure investigation are described in Ref. 9.

Table 1. Fractional atomic coordinates and thermal parameters. The anisotropic temperature factors are expressed as: $\exp[-2\pi^2(h^2a^{*2}U_{11} + \dots + 2klb^*c^*U_{23})]$. Estimated standard deviations in parentheses.

ATOM	x	y	z	U ₁₁	U ₂₂	U ₃₃	U ₁₂	U ₁₃	U ₂₃
O2	0.17728(6)	0.86428(18)	1.23519(48)	0.0122(7)	0.0144(7)	0.0323(10)	0.0014(6)	-0.0032(7)	-0.0080(7)
O5	0.15285(6)	0.15579(19)	0.59201(52)	0.0225(7)	0.0176(8)	0.0421(11)	0.0038(6)	-0.0018(8)	-0.0111(8)
O71	0.00595(6)	0.77907(19)	0.83405(51)	0.0113(6)	0.0158(7)	0.0358(10)	0.0034(6)	-0.0061(7)	-0.0070(7)
O72	0.06644(6)	0.95502(17)	1.13367(45)	0.0149(6)	0.0135(7)	0.0303(9)	0.0022(5)	-0.0028(7)	-0.0057(7)
H5	0.11344(7)	0.25982(22)	0.62185(57)	0.0191(8)	0.0153(9)	0.0255(10)	0.0007(7)	0.0003(8)	-0.0049(8)
C1	0.10188(8)	0.68968(24)	0.95744(57)	0.0111(8)	0.0117(9)	0.0156(11)	0.0009(6)	-0.0014(8)	-0.0007(8)
C2	0.15994(8)	0.72085(23)	1.08051(61)	0.0144(9)	0.0128(9)	0.0142(10)	-0.0010(7)	-0.0018(8)	-0.0019(8)
C3	0.20328(8)	0.59799(25)	1.04711(63)	0.0112(8)	0.0169(9)	0.0186(11)	0.0005(7)	-0.0003(8)	-0.0023(9)
C4	0.18981(8)	0.44687(25)	0.89693(60)	0.0122(8)	0.0150(9)	0.0181(11)	0.0038(7)	-0.0005(8)	-0.0014(9)
C5	0.13193(8)	0.41361(24)	0.78057(59)	0.0150(8)	0.0110(9)	0.0156(11)	0.0004(7)	-0.0017(8)	-0.0012(9)
C6	0.08883(8)	0.53350(24)	0.81013(61)	0.0113(8)	0.0144(9)	0.0173(11)	-0.0005(7)	-0.0013(8)	-0.0010(9)
C7	0.05683(8)	0.81979(24)	0.98513(62)	0.0136(9)	0.0153(9)	0.0178(11)	0.0014(7)	0.0011(8)	-0.0003(9)

ATOM	x	y	z	B	ATOM	x	y	z	B
H2	0.1506(9)	0.9218(29)	1.2640(70)	1.8(5)	H3	0.2417(8)	0.6231(25)	1.1280(61)	1.1(4)
H4	0.2184(8)	0.3564(25)	0.8706(62)	1.1(4)	H6	0.0501(8)	0.5106(23)	0.7301(63)	1.1(4)
H71	-0.0152(10)	0.8552(32)	0.8512(86)	3.2(6)					

CRYSTAL DATA

5-Nitrososalicylic acid or 1-carboxy-2-hydroxy-5-nitrosobenzene, $C_7H_5O_4N$, monoclinic, space group $P2_1/n$ (No. 14). Dimensions of the unit cell at -165°C : $a = 22.829(2)$ Å, $b = 8.028(1)$ Å, $c = 3.6696(4)$ Å, $\beta = 91.07(1)^\circ$, $V = 672.4$ Å³, $M = 167.12$, $F(000) = 344$, $D_{\text{calc}}(-165^\circ\text{C}) = 1.651$ g cm⁻³, $Z = 4$.

STRUCTURE DETERMINATION

The structure was determined by direct methods^{8,9} and refined by full matrix least squares techniques. Including only heavy atoms anisotropic refinement yielded a conventional R factor of 0.069. At this stage a difference Fourier map revealing the positions of all the hydrogen atoms was calculated. The refinement including all atoms and all observed reflections [with (I) greater than $2.5\sigma(I)$] converged with $R = 0.051$, a weighted R_w factor of 0.046 and a goodness of fit S of 1.73. Using 1018 reflections with $\sin \theta/\lambda$ greater than 0.45 the refinement yielded $R = 0.055$, $R_w = 0.049$ and $S = 1.26$. Disregarding valence electron scattering the C-N, C-O bonds and the N-O bond became shorter while the C-C bonds became longer. The shifts were in the range 0.001–0.007 Å. Apart from the C-N bond similar shifts have been observed previ-

ously for the *p*-nitrosophenolate ion¹ and for (III).² Only parameters obtained from the refinement with all the observed reflections will be discussed in the following as this enables a direct comparison of (I) with the previously investigated compounds in this series.

A list of structure amplitudes is available from the author. Final parameters from the refinement with all the observed reflections are given in Table 1.

Magnitudes and directions of the principal axes of the vibrational ellipsoids are indicated in Fig. 1. A rigid body analysis of the entire

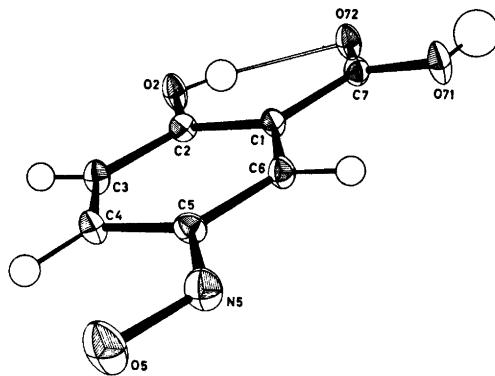


Fig. 1. 50% probability ellipsoids and numbering of atoms.

Table 2. Bond lengths (Å) and angles (°).

Bond lengths. (Libration corrected bond lengths are given in the second row).					
O5-N5	1.234(2)	1.235	C1-C2	1.415(3)	1.418
O71-C7	1.319(2)	1.321	C2-C3	1.404(3)	1.406
O72-C7	1.233(2)	1.234	C3-C4	1.365(3)	1.367
O2-C2	1.340(2)	1.342	C4-C5	1.407(3)	1.409
N5-C5	1.426(2)	1.428	C5-C6	1.382(3)	1.384
C7-C1	1.471(3)	1.473	C6-C1	1.395(3)	1.398
Bond angles					
O71-C7-O72	123.5(2)		N5-C5-C4	123.9(2)	
O72-C7-C1	122.5(2)		N5-C5-C6	115.4(2)	
O71-C7-C1	114.0(2)		C1-C2-C3	120.4(2)	
O5-N5-C5	114.3(2)		C2-C3-C4	120.4(2)	
C7-C1-C2	120.3(2)		C3-C4-C5	119.7(2)	
C7-C1-C6	121.4(2)		C4-C5-C6	120.7(2)	
O2-C2-C3	115.9(2)		C5-C6-C1	120.6(2)	
O2-C2-C1	123.7(2)		C6-C1-C2	118.3(2)	
Distances and angles involving hydrogen atoms					
	O-H	H...O	O...O	O-H...O	C-O-H
O2-H...O72	0.77(2)	1.99(2)	2.653(2)	144(2)	110.2(1.8)
O2-H...O5(2)		2.23(2)	2.744(2)	125(2)	
O71-H...O72(b)	0.78(3)	1.92(3)	2.704(2)	177(3)	108.2(1.9)
	C-H		C-C-H		C-C-H
C3-H	0.94(2)	C2-C3-H	118.4(1.3)	C4-C3-H	121.2(1.3)
C4-H	0.98(2)	C3-C4-H	123.4(1.3)	C5-C4-H	116.9(1.2)
C6-H	0.94(2)	C5-C6-H	120.3(1.2)	C1-C6-H	119.2(1.2)
Intermolecular contacts			Torsion angles		
O72...O5(a)	3.032		O72-C7-C1-C6	177.2(2)	
O71...N5(c)	3.187		O5-N5-C5-C4	-0.3(3)	
			O5-N5-C5-C6	178.7(2)	
			H-O2-C2-C3	-174(2)	
Symmetry code					
(a): $x, y+1, z+1$, (b): $-x, -y+2, -z+2$, (c): $-x, -y+1, -z+1$					

molecule shows a good agreement between observed and calculated vibration tensor elements ($\Delta U = 0.0015 \text{ \AA}^2$). The r.m.s. eigenvalues of T are 0.11, 0.11 and 0.10 Å and of L 3.6, 2.6 and 1.3°. Adjusting the coordinates according to this libration, shifts in the bond lengths from 0.001 to 0.003 Å were obtained.

Bond lengths and angles are given in Table 2. The estimated standard deviations were derived from the final correlation matrix of the least squares refinement.

A final difference Fourier map of the molecule in the benzene ring plane is shown in Fig. 5. The map was calculated in the same manner as for the *p*-nitrosophenolate ions.¹ The pat-

tern of the residual peaks resembling closely that of the anions¹ (location in the middle of the bonds and at lone pair positions) indicates that only small systematic errors influence the structural results.

Using the data in the range 0.0–0.65 Å⁻¹ for $\sin \theta/\lambda$ an *L*-shell refinement⁷ gives $R = 0.045$, $R_w = 0.039$ and $S = 1.71$. The adjusted⁷ gross atomic populations are shown in Fig. 3 together with results from an INDO calculation.

DISCUSSION

The location of the hydrogen atoms in the difference Fourier map and the subsequent

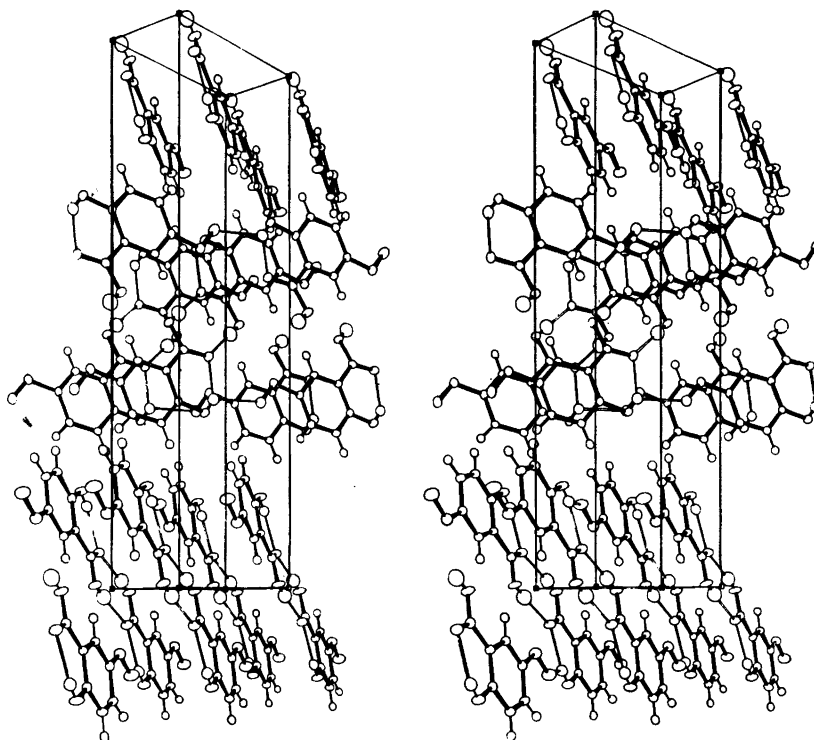


Fig. 2. A stereoscopic illustration of the structure.

refinement leave no doubt about the compound being 5-nitrososalicylic acid and not its oxime tautomer. It is further clear that, as in salicylic acid there is an intramolecular hydrogen bond. Also, and in conformity with most other carboxylic acids, (I), does form a centrosymmetric hydrogen bonded dimer. Fig. 2 shows that these dimers form layers parallel to (011). There seems to be only weak van der Waals forces between the layers. The short translation along c gives a separation between molecular planes of 3.34 Å. Fig. 3 shows the projection of a molecule onto the neighbouring molecular plane along the plane normal. Apparently the positively charged heavy atoms (C2, C4, C6, C7 and N5) are in contact with negatively charged atoms (O2, C3, C1, O72 and C5). The interplanar spacing is, however, by no means especially short considering the temperature,¹⁰ and it seems unlikely that these interactions should influence the degree of conjugation in the molecule to any appreciable extent (contrary to what apparently is the case for N,N -dimeth-

ylnitrosamine¹¹). Dimers approximately in the same plane have contact with each other through the hydroxyl group at C2 and the nitroso group. Probably the interaction is the weaker part of an asymmetric bifurcated hydrogen bond ($O\cdots O$: 2.744 Å, $O\cdots H$: 2.23 Å and $O-H\cdots O$: 125°).¹² Then 5-nitrososalicylic acid conforms with the oxime tautomer of p -nitrosophenol in that the proton involved in the tautomerism is bonded to both the nitroso and the phenoxide oxygen atom. It is tempting to relate the weaker interaction in the present case to the vanishingly small amount of the oxime form present in solution.

The intramolecular hydrogen bond (the stronger part of the bifurcated H-bond) is found to be slightly longer than that of salicylic acid (IV)^{13,14} and nearly identical to that of 5-sulfosalicylic acid di- (V)¹⁵ and trihydrate.¹⁶ In these compounds bifurcated H-bonds are not present. As accentuation of the *ortho* quinonoid element in the π resonance hybrid probably strengthens the H-bond, 5-substitu-

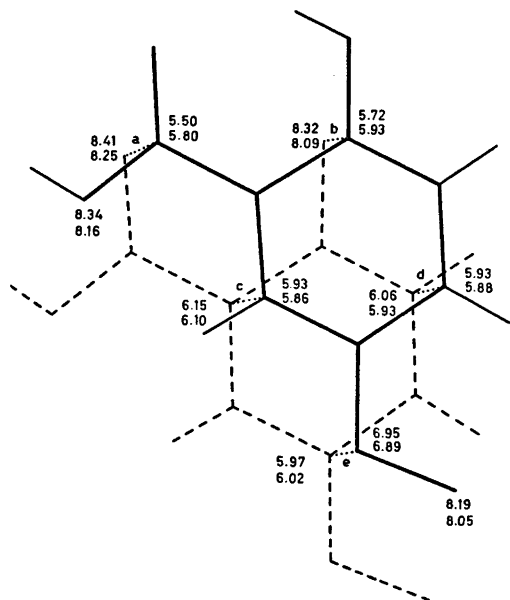


Fig. 3. The projection of a molecule onto the neighbouring molecular plane along the plane normal and the calculated (upper line) and experimental (lower line) gross atomic populations. The letters denote intermolecular contacts: $a=3.319$ Å, $b=3.339$ Å, $c=3.389$ Å, $d=3.366$ Å and $e=3.359$ Å.

ents promoting a *para* quinonoid structure to the displacement of an *ortho* quinonoid structure should weaken the H-bond. Also the forming of a bifurcated H-bond arrangement

Table 3. Deviation (Å) of atoms from least squares planes. Atoms defining the planes are marked with an asterisk.

O2	0.0319	
O5	-0.0217	
O71	-0.1547	-0.0009*
O72	0.0349	-0.0011*
N5	0.0006	
C1	-0.0081*	-0.0011*
C2	0.0056*	
C3	0.0025*	
C4	-0.0081*	
C5	0.0055*	
C6	0.0027*	
C7	-0.0351	0.0038*
H1	-0.195	-0.031
H2	0.111	
H3	-0.002	
H4	0.001	
H6	0.006	

probably weakens this bond.¹⁷ This may be the cause of a slightly longer O2...O72 separation in (I) than in (IV).

As may be seen from Table 3 the benzene ring and the carboxyl group are both planar within the accuracy of the experiment. The angle between these two fragments is 5.07° or somewhat larger than the corresponding angle in (IV)¹³ (1.1°). The phenolic hydrogen atom deviates 0.11 Å from the ring plane and to the same side as its acceptor atoms. Probably the somewhat larger torsion angle about the C-COOH bond in (I) than in (IV) may be due to the H2...O5 hydrogen bond.

The torsion angle about the C-NO bond is only 1.07° . Nitrosation of (IV) in the 5-position apparently introduces only a slight *para* quinonoid element as the benzene ring of (I) definitely has the same *ortho* quinonoid appearance as that of (IV). Fig. 4 shows a comparison between observed and calculated (INDO) differences in bond lengths between (I) and (IV).¹³ Only the sign of the differences are comparable since the calculations have been based on the found geometry of (I) for both compounds. In this respect there is a good correspondence between experiment and theory. Benzene ring bonds approximately parallel to the C5-X (X=H,NO) bond seem to be slightly shorter while the other C-C

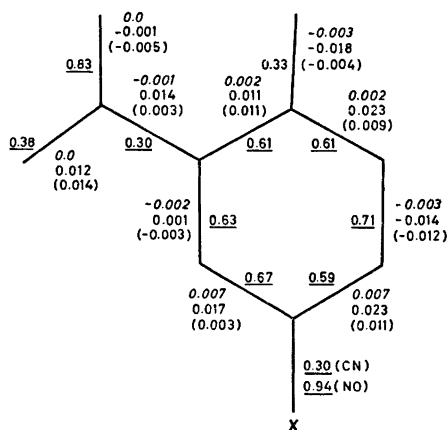


Fig. 4. Underlined figures are (INDO) π -bond orders for (I). The figures in the rows are calculated (upper line) and observed (middle line) bond length differences between (I) and (IV) and observed bond length differences between (I) and (V) (lower line).

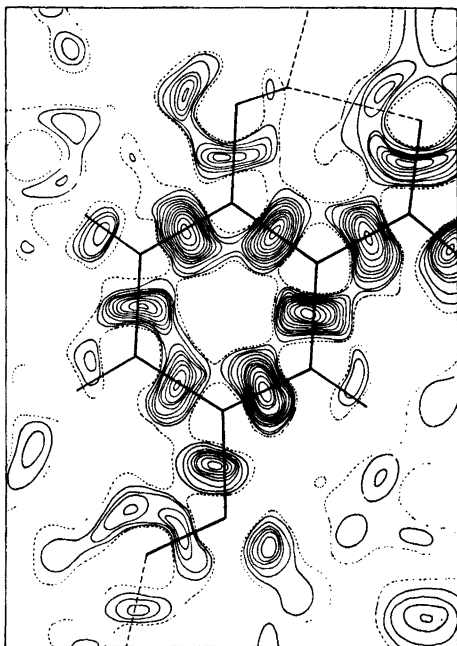


Fig. 5. Final difference Fourier synthesis in the least squares plane through the ring atoms. The zero line is dotted and the difference between the contours is $0.05 \text{ e}\text{\AA}^{-1}$.

bonds are somewhat longer in (I) than in (V). Accordingly the C2–OH bond is slightly shorter in (I) than in (IV). Then substitution at the 5-position by a nitroso group apparently introduces a *para* quinonoid element to the displacement of some of the *ortho* quinonoid element present in the π system of the benzene ring of salicylic acid. However, only some of the observed shifts are formally significant. Comparing (I) and 5-sulfosalicylic acid dihydrate (V)¹⁵ one finds four significant and one probably significant difference in the range $0.009\text{--}0.014 \text{ \AA}$. The differences are consistent with a slightly less *ortho* quinonoid structure in (I) than in (V).¹⁶

Both the C–N bond and the C2–O bond are found to be much longer than the corresponding bonds in the *p*-nitrosophenolate ions. Comparing with the anion of the magnesium salt one finds that the C–N bond is 0.067 \AA and the C–O bond 0.059 \AA longer in (I) than in the anion.¹ If one assumes that the C–O bond is slightly longer and the C–N bond

length practically unchanged after decarboxylation of (I) it is possible to estimate roughly a point for *p*-nitrosophenol in the plot of Fig. 5 in Ref. 1. From the resulting plot of the C–O bond length against the C–N bond length in *p*-nitrosophenol, its oxime tautomer and the *p*-nitrosophenolate anions one gets the impression that there is *not* a linear relationship between the two bond lengths as previously thought.¹

The C–N bond length [$1.426(2) \text{ \AA}$] is also much longer than the corresponding bond length in (III) [$1.372(2) \text{ \AA}$]. In accordance with this the N–O bond length [$1.234(2) \text{ \AA}$] is much shorter than that of the *p*-nitrosophenolate ions and (III) [$1.276(2) \text{ \AA}$]. The two nitroso group bond lengths are, however, about 0.03 \AA shorter/longer than that of a “pure” $C(sp^2)\text{--}N(sp^2)/N=O$ single/double bond.¹⁸ This then confirms the spectroscopic indication of a somewhat long although “normal” N–O bond in 5-nitrososalicylic acid.

It is interesting to note that the point for (I) in the plot of N–O bond lengths against C–N bond lengths in Fig. 6, Ref. 1 lies nearly exactly on the graph of $R_{NO} = R_{NO}^\circ + k/(R_{CO} - R_{CO}^\circ)$ where $R_{NO} = 1.150 \text{ \AA}$, $R_{CN}^\circ = 1.233 \text{ \AA}$ and $k = 0.016 \text{ \AA}^2$. This is also the case for a new point for trifluoronitrosomethane (VI) which has recently been investigated by microwave spectroscopy.¹⁹ Inserting the values observed for R_{CN} [$= 1.512(16) \text{ \AA}$ in (VI)] one gets $R_{NO}^{\text{calc}} = 1.233 \text{ \AA}$ for (I) and $R_{NO}^{\text{calc}} = 1.207 \text{ \AA}$ for (VI). These values are not different from those observed [$R_{NO} = 1.198(4) \text{ \AA}$ in (VI)].

It is further noteworthy that (I) and (VI) which both have less conjugation over the C–N–O fragment than the nitrosates¹ and (III) also have substantially smaller CNO angles than those latter compounds; $114.3(2)^\circ$ for (I) and $112.4(3)^\circ$ for (VI) compared with values in the range $116\text{--}117^\circ$.¹

The exocyclic angles at the carbon atom bonded to the NO group resemble closely those of the *p*-nitrosophenolate ions and those of *p*-benzoquinone monoxime. As to the ring angles and the other exocyclic angles they resemble closely those of (V). Probably the minor deviations found (less than 1.5°) may be attributed to the crowded situation arising when substituting a NO group for a SO_3^- group.

The *trans* conformation about the C-N bond with respect to the *meta* position (to C5) carrying the carboxyl group is possibly adopted because it gives less crowding than the corresponding *cis* conformation.

REFERENCES

1. Talberg, H. J. *Acta Chem. Scand. A* 31 (1977) 37.
2. Talberg, H. J. *Acta Chem. Scand. A* 30 (1976) 829.
3. Uffman, H. *Z. Naturforsch. Teil B* 22 (1967) 491.
4. Gulinov, V. G. *J. Chem. Ind. (Moscow)* 5 (1923) 225; see *Chem. Abstr.* 22 (1928) 3648.
5. Doyle, P. A. and Turner, P. S. *Acta Crystallogr. A* 24 (1970) 2232.
6. Stewart, R. F., Davidson, E. R. and Simpson, W. T. *J. Chem. Phys.* 42 (1965) 3175.
7. Stewart, R. F. *J. Chem. Phys.* 53 (1970) 205.
8. Germain, G., Main, P. and Woolfson, M. M. *Acta Crystallogr. A* 27 (1971) 368.
9. Groth, P. *Acta Chem. Scand.* 27 (1973) 1837.
10. Semmingsen, D. *Acta Chem. Scand. A* 30 (1976) 808.
11. Krebs, B. and Mandt, J. *Chem. Ber.* 108 (1975) 1130.
12. Olovsson, I. and Jönsson, P. G. In Schuster, P., Zundel, G. and Sandorty, C., Eds., *The Hydrogen Bond*, Nort-Holland Publishing Company, Amsterdam, New York and Oxford 1976, Vol. II, p. 408.
13. Sundaralingam, M. and Jensen, L. H. *Acta Crystallogr.* 18 (1965) 1053.
14. Bacon, G. E. and Jude, R. J. *Z. Kristallogr.* 138 (1973) 19.
15. Attig, R. *Cryst. Struct. Commun.* 5 (1976) 223.
16. Mootz, D. and Fayos, J. *Acta Crystallogr. B* 26 (1970) 2046.
17. Furberg, S. and Schwitters, B. *Acta Chem. Scand. B* 31 (1977) 313.
18. Fischer-Hjalmars, I. and Sundbom, M. *Acta Chem. Scand.* 22 (1968) 2237.
19. Turner, P. H. and Cox, A. P. *Chem. Phys. Lett.* 39 (1976) 585.

Received March 15, 1977.

Microwave Spectrum of 2-Nitrothiophene

W. RALOWSKI and S. LJUNGGREN

Department of Physical Chemistry, The Royal Institute of Technology, S-100 44 Stockholm 70, Sweden

The microwave spectrum of 2-nitrothiophene has been studied in the frequency region 18 000–26 500 MHz. The rotational transitions of the ground state and the first four torsionally excited states have been assigned. The molecule has been shown to be planar in the equilibrium conformation. The first torsional frequency and the barrier to internal rotation of the nitro group have also been estimated.

The present work reports a microwave spectroscopic investigation of 2-nitrothiophene and is an extension of the recently published article on 3-nitrothiophene.¹ As in our previous work the aim of the present study was to determine the equilibrium conformation of the molecule and to estimate the torsional frequency and the barrier to internal rotation of the nitro group.

EXPERIMENTAL

The sample of 2-nitrothiophene was purchased from Ega-Chemie KG and used without further purification. Microwave spectra were recorded at room temperature in the frequency region 18–26.5 GHz using a Hewlett-Packard 8460A spectrometer. Sample pressures ranged between 15 and 70 mTorr.

MICROWAVE SPECTRUM AND ROTATIONAL CONSTANTS

The rotational transitions of the ground state of 2-nitrothiophene (*cf.* Fig. 1) were assigned together with four vibrational satellites with regularly decreasing intensities. Since the torsional vibration of the nitro group is expected to be the lowest frequency vibration, the observed satellites were assigned to this mode.

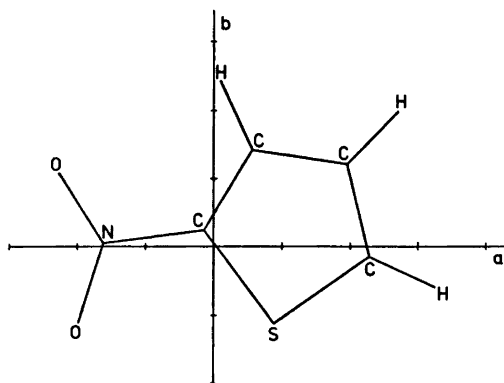


Fig. 1. 2-Nitrothiophene.

The measured and calculated transition frequencies of the ground state are listed in Table 1. The measured transition frequencies of the four assigned torsionally excited states are obtainable upon request from the authors. Only *R*-branch *a*-type transitions of the common ³²S species were identified in the spectrum. The rotational constants, calculated by a least squares method, are presented in Table 2. Since the agreement between the measured and calculated frequencies was good, the centrifugal distortion coefficients were not included in the fit. Table 2 contains also moments of inertia and inertial defects for all vibrational species.

RESULTS AND DISCUSSION

The expected planarity of the molecule of 2-nitrothiophene is clearly demonstrated by the small negative value ($\Delta = -0.164 \text{ amu \AA}^2$) of the inertial defect in the ground state (*cf.* Table 2) and an equally small but positive

Table 1. Rotational transitions (MHz) of 2-nitrothiophene in the ground state.

Transition	ν_{obs}^a	$\nu_{\text{obs}} - \nu_{\text{calc}}$	Transition	ν_{obs}^a	$\nu_{\text{obs}} - \nu_{\text{calc}}$
$8_{1,8} \leftarrow 7_{1,7}$	18 437.50	-0.01	$10_{1,10} \leftarrow 9_{1,9}$	22 815.05	0.00
$7_{3,5} \leftarrow 6_{3,4}$	18 467.80	0.20	$10_{0,10} \leftarrow 9_{0,9}$	22 843.14	0.03
$7_{4,4} \leftarrow 6_{4,3}$	18 500.85	0.19	$9_{9,2} \leftarrow 8_{9,1}$	23 640.13	-0.15
$8_{0,8} \leftarrow 7_{0,7}$	18 533.01	0.07			
$7_{1,6} \leftarrow 6_{1,5}$	18 770.68	-0.06	$9_{7,3} \leftarrow 8_{7,2}$	23 673.87	-0.05
$7_{3,4} \leftarrow 6_{3,3}$	18 948.44	0.01			
$7_{2,5} \leftarrow 6_{2,4}$	19 629.87	0.09	$9_{7,2} \leftarrow 8_{7,1}$	23 823.73	0.05
$8_{2,7} \leftarrow 7_{2,6}$	20 202.28	0.11	$9_{5,4} \leftarrow 8_{5,3}$	23 896.39	0.15
$9_{1,9} \leftarrow 8_{1,8}$	20 630.59	-0.03	$9_{4,6} \leftarrow 8_{4,5}$	24 104.46	-0.02
$9_{0,9} \leftarrow 8_{0,8}$	20 683.34	0.02	$9_{5,4} \leftarrow 8_{5,3}$	24 965.22	0.00
$8_{7,2} \leftarrow 7_{7,1}$	21 017.16	0.04	$9_{3,6} \leftarrow 8_{3,5}$	24 994.37	-0.01
$8_{7,1} \leftarrow 7_{7,0}$	21 035.86	0.04	$11_{1,11} \leftarrow 10_{1,10}$	25 092.03	-0.01
$8_{1,7} \leftarrow 7_{1,6}$	21 054.08	0.09	$9_{2,7} \leftarrow 8_{2,6}$	25 285.35	-0.04
$8_{6,3} \leftarrow 7_{6,2}$	21 079.13	0.11	$10_{1,9} \leftarrow 9_{1,8}$	26 171.52	-0.06
$8_{6,2} \leftarrow 7_{6,1}$	21 287.40	0.01	$10_{3,8} \leftarrow 9_{3,7}$	26 263.48	-0.17
$8_{3,6} \leftarrow 7_{3,5}$	21 930.62	0.05	$10_{2,9} \leftarrow 9_{2,8}$	26 294.92	-0.10
$8_{4,4} \leftarrow 7_{4,3}$	22 421.78	0.05	$10_{3,2} \leftarrow 9_{3,1}$	26 341.24	-0.06
$8_{3,5} \leftarrow 7_{3,4}$	22 534.68	0.11	$10_{7,4} \leftarrow 9_{7,3}$		-0.09
$9_{2,8} \leftarrow 8_{2,7}$			$10_{7,3} \leftarrow 9_{7,2}$		

^a ± 0.05 MHz.

 Table 2. Rotational constants (MHz), moments of inertia (amu \AA^2) and inertial defects (amu \AA^2) of 2-nitrothiophene in the ground and torsionally excited states.^a

	$v=0^b$	$v=1$	$v=2$	$v=3$	$v=4$
<i>A</i>	3818.49(8)	3817.72(9)	3816.81(13)	3816.21(14)	3815.49(11)
<i>B</i>	1518.602(3)	1515.521(3)	1512.447(5)	1509.399(5)	1506.351(4)
<i>C</i>	1086.887(3)	1087.777(3)	1088.672(4)	1089.566(4)	1090.473(3)
<i>I</i> _a	132.350	132.376	132.408	132.429	132.454
<i>I</i> _b	332.790	333.467	334.145	334.819	335.497
<i>I</i> _c	464.976	464.595	464.213	463.832	463.447
Δ	-0.164	-1.248	-2.340	-3.416	-4.504

^a The uncertainties represent one standard deviation. ^b $\kappa = -0.6839$.

value ($\Delta = +0.38$ amu \AA^2) of the extrapolated inertial defect for the hypothetical torsionless state. The planarity is also demonstrated by the linear variation of the rotational constants *B* and *C* with the torsional quantum number (the variation of the constant *A* has not been considered because of its large standard deviation).

This linear variation as well as the linear variation of the inertial defect with the torsional quantum number, indicate that the torsional mode of vibration of the nitro group is

harmonic (or nearly harmonic). We could thus estimate the first torsional frequency using the well-known formula:²

$$\nu_t = \frac{\hbar}{2\pi^2 c} \frac{1}{\Delta_0 - \Delta_1}$$

where the torsional frequency (ν_t) was calculated from the change of the inertial defect between the ground and the first torsionally excited states. Inserting the values of Δ_0 and Δ_1 from Table 2 we obtained $\nu_t = 62$ cm⁻¹.

Unfortunately this value is in less than perfect agreement with the value of the torsional frequency, obtained from relative intensity measurements. These measurements, performed on 10 line pairs at room temperature, gave an intensity ratio of 0.65 ± 0.08 between the first vibrational satellite and the ground state lines. This ratio corresponds to a vibrational frequency $\nu_t = 90 \pm 20 \text{ cm}^{-1}$.

Of the two estimates, higher credibility should be given to the value obtained from the inertial defect variation in view of the fairly harmonic character of the torsional vibration, and the very approximate intensity measurements.

No comparable data are available since no far infra-red investigation on 2-nitrothiophene has yet been reported. The estimated value of the torsional frequency of the nitro group in 2-nitrothiophene, reported in this paper, lies between the corresponding torsional frequencies of nitrobenzene³ and nitroethylene.⁴

Since the torsional frequency is known, the height of the barrier hindering the rotation of the nitro group could be estimated, using the theory of Fateley *et al.*⁵ The results presented in this article yielded only an order of magnitude estimate of the height of the barrier. Approximate calculation gave a value of 20 kJ/mol.

Acknowledgements. This work was supported by the Swedish Natural Science Research Council (NFR). Part of the equipment was financed with a donation from the Knut and Alice Wallenberg Foundation.

REFERENCES

1. Isvén, M. K., Ralowski, W. M. and Ljunggren, S. O. *Chem. Phys. Lett.* **47** (1977) 294.
2. Hanyu, Y., Britt, C. O. and Boggs, J. E. *J. Chem. Phys.* **45** (1966) 4725.
3. Hög, J. H. *Ph. D. Thesis*, University of Copenhagen, Copenhagen 1971.
4. Meyer, R., Gammeter, A., Smith, P., Kühne, H., Nösberger, P. and Günthard, H. *J. Mol. Spectrosc.* **46** (1973) 397.
5. Fateley, W. G., Harris, R. K., Miller, F. A. and Witkowski, R. E. *Spectrochim. Acta* **21** (1965) 231.

Received January 24, 1977.

The Crystal Structure and Absolute Configuration of (+)_D-Tris-[-(-)_D-1-(2-pyridyl)ethylamine]cobalt(III) Perchlorate Dihydrate

EVA BANG

Department I, Inorganic Chemistry, H.C. Ørsted Institute University of Copenhagen,
Universitetsparken 5, DK-2100, Copenhagen Ø, Denmark

The absolute configuration and the conformations of the complex ion in (+)_D-[Co{(-)_D-1-(2-pyridyl)ethylamine}] (ClO₄)₂·2H₂O has been determined to be $\Lambda\delta\delta\delta$ by means of X-ray investigations (MoK α and CuK α). The absolute configuration of the ligand was determined to be *S*. The crystals were monoclinic, space group *P*2₁, $a = 9.416(4)$, $b = 18.122(6)$, $c = 9.129(3)$ Å, $\beta = 92.16^\circ$; $Z = 2$.

The ligand has the pyridine ring tilted against the plane defined by the cobalt atom and the two nitrogen atoms of the ligand. The torsion angles in the 5-membered ring are 20–30°, and the methyl group is close to an equatorial position. The perchlorate ions are disordered. 3438 independent reflexions from diffractometer data were used in the refinement. The final *R*-value was 0.085.

Three different isomers together with their enantiomers of the optically active tris complexes of (-)_D- and (+)_D-[1-2-pyridyl)ethylamine] and Co(III) have recently been isolated.¹ The X-ray structure investigation reported here has been taken up to elucidate the correctness of assignment based upon NMR spectra, circular dichroism spectra and absorption spectra.

EXPERIMENTAL

The crystals were provided by K. Michelsen and belonged to the group described as the first band on the Sephadex column.¹ Thermogravimetric analyses showed two molecules of H₂O per complex.

The crystals were flat, brownish-red needles (*b* needle axis) and were assigned to space group *P*2₁ through Weissenberg and precession photographs. Intensity data were collected on

a Picker FACS-1 diffractometer with graphite-monochromated MoK α (λ 0.7107 Å) radiation. The measurements were carried out in the $\theta - 2\theta$ mode. The scan rate was 1°/min, the scan range 1.5° and increasing with 2θ . The background counts were made for 20 s at each end of the scan range.

From the 4291 reflexions recorded, 3438 independent reflexions for which $0.06 < \sin \theta / \lambda \leq 0.65$ were retained having $I / \sigma(I) > 1.5$. $\sigma(I)$ is the standard deviation of the intensity calculated from counting statistics. The crystal size was $0.48 \times 0.08 \times 0.12$ mm³. No correction for absorption was applied. Data for centrosymmetric reflexions selected from the Weissenberg diagrams were collected on the diffractometer with monochromatic CuK α (λ 1.5418 Å) radiation and used in the determination of the absolute configuration. The same crystal was used in both diffractometer experiments. The cell dimensions were refined from powder diagrams obtained from a Hägg-Guinier camera and CuK α radiation (λ 1.5405 Å), Si as internal standard.

The X-ray system² was used in the crystal structure analyses and the Ortep II³ for the illustrations.

CRYSTAL DATA

CoC₂₁N₆H₃₄Cl₃O₁₄; Monoclinic, *P*2₁;
 $a = 9.416(4)$, $b = 18.122(6)$, $c = 9.129(3)$ Å, $\beta = 92.16(3)^\circ$, $Z = 2$; $\mu(\text{MoK}\alpha) = 9.2$ cm⁻¹; $D_x = 1.621$, $D_m = 1.61$ gcm⁻³.

SOLUTION OF THE STRUCTURE

The cobalt, three chlorine and two nitrogen atoms were found through a combination of Patterson and direct methods (Multan). The

Table 1. Fractional atomic coordinates ($\times 10^4$), anisotropic thermal parameters ($\text{\AA}^2 \times 10^3$). The anisotropic temperature factor is of the form $T = \exp [-2\pi^2(U_{11}h^2a^{*2} + \dots + 2U_{12}hka^*b^* + \dots)]$.

	<i>x</i>	<i>y</i>	<i>z</i>	U_{11}	U_{22}	U_{33}	U_{12}	U_{13}	U_{23}
Co	0539(1)	0000	7178(1)	2.67(7)	2.93(8)	2.12(7)	0.01(6)	0.06(4)	.02(5)
N1	7900(9)	4596(4)	3959(8)	4.1(5)	3.2(5)	2.1(4)	0.1(1)	-0.4(3)	-0.1(3)
N2	0434(9)	4107(5)	3634(10)	3.6(5)	3.3(4)	3.5(4)	-0.1(4)	0.7(4)	-0.0(3)
N3	9652(9)	0584(5)	5613(8)	3.5(4)	3.2(4)	2.4(4)	0.1(4)	-0.1(3)	-0.1(3)
N4	8872(9)	0289(5)	8241(9)	2.9(4)	4.8(5)	2.4(4)	-0.8(4)	0.1(3)	-0.2(4)
N5	1648(9)	0791(5)	8030(9)	3.5(4)	3.5(4)	4.1(5)	2.5(4)	0.1(3)	0.8(4)
N6	8689(9)	4434(5)	1106(9)	4.1(5)	4.1(5)	3.8(5)	2.3(4)	0.0(3)	-0.1(4)
C1	6690(10)	4967(9)	4289(10)	2.9(4)	5.2(5)	3.4(4)	0.0(6)	0.2(3)	0.4(6)
C2	5623(13)	4648(8)	5037(12)	5.1(7)	5.7(8)	3.2(5)	0.6(6)	0.1(5)	0.0(5)
C3	5772(14)	3942(8)	5517(14)	4.9(7)	6.0(8)	5.3(7)	1.0(6)	1.1(6)	0.8(7)
C4	7026(13)	3550(8)	5278(13)	5.0(7)	5.3(7)	4.4(6)	0.8(6)	1.6(5)	0.1(6)
C5	8052(11)	3901(6)	4466(11)	3.7(5)	3.7(6)	3.0(6)	0.8(5)	-0.2(4)	0.1(4)
C6	9422(12)	3521(6)	4030(12)	4.6(6)	3.5(6)	3.5(5)	0.1(5)	0.6(5)	0.2(5)
C7	0064(15)	3024(8)	5275(16)	6.0(8)	4.9(8)	6.9(9)	-1.3(7)	1.0(7)	-1.5(7)
C8	0289(12)	0802(6)	4387(11)	4.6(6)	4.1(6)	2.8(5)	0.3(5)	0.0(4)	-0.6(4)
C9	9565(16)	1223(8)	3292(13)	7.1(9)	5.4(8)	3.2(6)	0.6(7)	-0.6(5)	-0.7(5)
C10	8167(15)	1428(8)	3531(15)	6.4(8)	4.7(7)	5.3(7)	-0.2(6)	-1.8(6)	-1.8(6)
C11	7517(13)	1204(8)	4825(14)	4.6(7)	5.0(8)	5.4(7)	-0.6(6)	-1.1(6)	-1.4(5)
C12	8314(12)	0758(6)	5819(11)	4.0(5)	3.3(5)	3.4(5)	0.0(5)	-0.9(4)	0.1(4)
C13	7628(11)	0431(7)	2835(13)	2.8(5)	5.0(7)	4.4(6)	-0.2(5)	0.1(4)	-0.5(5)
C14	6483(13)	0870(9)	7861(15)	4.1(8)	7.8(9)	5.7(8)	-1.5(7)	1.3(6)	0.9(7)
C15	1917(14)	1438(7)	7426(12)	6.3(8)	3.8(6)	3.9(6)	0.9(6)	0.9(5)	0.7(5)
C16	2802(15)	1965(8)	8093(15)	6.3(8)	4.8(8)	5.6(8)	0.8(6)	1.1(6)	1.3(6)
C17	3483(17)	1901(9)	9480(16)	7.1(9)	6.6(9)	5.9(8)	2.0(8)	0.9(7)	3.1(8)
C18	3138(14)	1145(9)	0110(13)	5.5(7)	6.9(9)	3.7(6)	0.3(7)	-0.0(5)	1.7(6)
C19	2209(12)	0653(7)	9381(12)	3.9(6)	5.1(7)	3.4(5)	0.6(5)	0.6(4)	0.8(5)
C20	1671(11)	0035(9)	0112(10)	5.4(6)	5.6(7)	3.0(5)	0.9(8)	-0.3(4)	-0.1(7)
C21	7343(19)	4631(10)	8698(16)	9.3(9)	8.7(1.0)	4.5(7)	2.2(9)	-2.3(7)	0.4(8)
Cl1	3920(3)	2103(2)	3770(3)	4.8(2)	6.1(2)	4.4(2)	0.5(2)	0.3(1)	-0.9(1)
Cl2	8878(4)	2451(2)	9674(4)	8.3(2)	5.1(2)	4.3(2)	-0.9(2)	1.1(2)	0.0(1)
Cl3	2565(4)	4457(2)	7961(3)	6.4(2)	4.9(2)	3.8(2)	-0.9(2)	0.7(1)	-0.1(1)
<i>U</i>									
O1	2550(12)	3679(6)	1515(12)	7.2(2)					
O2	5907(14)	3728(8)	1534(14)	9.3(3)					
O3	5020(13)	2233(7)	2799(13)	8.3(3)					
O4	3783(18)	1348(10)	3917(18)	12.2(5)					
O5	4298(20)	2330(13)	5044(23)	16.1(7)					
O6	2627(20)	2274(12)	3155(2)	15.2(6)					
O7	9398(12)	1717(6)	9817(12)	7.8(3)					
O8	7672(21)	2547(11)	0584(2)	14.9(6)					
O9	9878(20)	2960(11)	0229(21)	13.8(6)					
O10	8422(21)	2608(12)	8341(22)	15.6(6)					
O11	6453(14)	0048(10)	1692(15)	10.7(4)					
O12	1333(14)	4568(8)	8708(15)	9.6(4)					
O13	2283(11)	4481(6)	6401(11)	6.8(2)					
O14	3226(12)	3786(7)	8342(13)	7.6(3)					

rest of the complex and the water molecules could be located from electron density maps using a weighting scheme for the structure factors according to Sim.⁴ Those oxygen atoms from the perchlorate ions which later showed

good contact to the amine groups were also found in these maps. The rest of the oxygen atoms were taken from difference Fourier syntheses and showed disorder. The structure was refined isotropically to an *R* factor 0.11.

Table 2. Determination of absolute configuration.

<i>h</i>	<i>k</i>	<i>l</i>	<i>F</i> _o	<i>F</i> _c	<i>h</i>	<i>k</i>	<i>l</i>	<i>F</i> _o	<i>F</i> _c
0	2	0	52.2	58.2	1	6	$\bar{2}$	29.9	29.5
0	2	0	50.8	54.7	$\bar{1}$	$\bar{6}$	2	20.8	20.4
0	4	0	78.2	104.1	1	7	$\bar{2}$	12.1	13.4
0	4	0	87.1	115.1	$\bar{1}$	$\bar{7}$	2	4.5	5.2
0	5	2	32.5	31.8	1	10	1	20.8	20.7
0	5	2	34.5	37.2	$\bar{1}$	$\bar{10}$	$\bar{1}$	20.1	20.5
0	6	0	24.5	40.7	1	11	1	11.5	6.2
0	6	0	23.2	37.5	$\bar{1}$	$\bar{11}$	$\bar{1}$	20.9	17.4
0	8	0	57.6	77.6	2	6	1	64.1	61.0
0	8	0	64.5	86.6	$\bar{2}$	$\bar{6}$	$\bar{1}$	70.8	66.2
0	9	$\bar{1}$	14.5	6.6	4	5	1	41.0	29.6
0	9	1	19.8	15.4	$\bar{5}$	$\bar{5}$	$\bar{1}$	36.5	27.4
0	10	0	13.3	22.1	4	11	0	30.8	30.9
0	10	0	23.1	26.8	$\bar{4}$	$\bar{11}$	0	23.2	25.5
0	12	0	4.5	9.2	6	2	0	21.2	16.5
0	12	0	16.5	16.5	$\bar{6}$	$\bar{2}$	0	26.4	21.4
0	14	$\bar{3}$	17.6	18.3	7	1	0	32.5	26.1
0	14	3	22.3	23.0	$\bar{7}$	$\bar{1}$	0	33.9	28.3
1	6	2	73.8	70.2					
$\bar{1}$	$\bar{6}$	$\bar{2}$	80.3	77.9					

After refining anisotropically for all atoms except the oxygens the *R* factor was 0.085.

No further refining or determination of the hydrogen positions were attempted because of the disorder of the perchlorate ions. Atomic parameters are given in Table 1. A list of ob-

served and calculated structure factors can be obtained from the author on request.

The intensity measurements with CuK α -radiation determined the choice of absolute configuration. A list of observed and calculated structure factors for these calculations is given in Table 2.

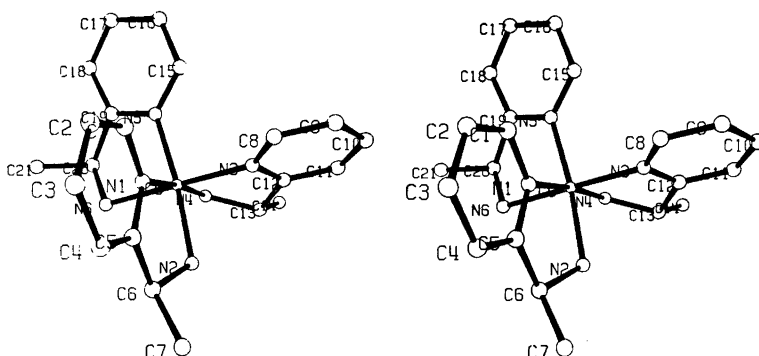


Fig. 1. Stereoscopic view of the complex ion (+)_D(Co(-)_D{1-(2-pyridyl)ethylamine}₃.

Table 3. Bond lengths (Å).

Co-N1	1.972(8)	N5-C15	1.323(15)
Co-N2	1.989(9)	N5-C19	1.346(14)
Co-N3	1.941(8)	C15-C16	1.392(18)
Co-N4	1.948(8)	C16-C17	1.428(16)
Co-N5	1.922(9)	C17-C18	1.366(22)
Co-N6	1.987(9)	C18-C19	1.400(18)
		C19-C20	1.510(20)
N1-C1	1.366(13)	C20-N6	1.500(20)
N1-C5	1.348(14)	C20-C21	1.527(16)
C1-C2	1.364(16)		
C2-C3	1.358(20)	C11-O3	1.408(12)
C3-C4	1.402(19)	C11-O4	1.383(18)
C4-C5	1.394(17)	C11-O5	1.271(19)
C5-C6	1.527(15)	C11-O6	1.358(19)
C6-N2	1.481(14)		
C6-C7	1.555(18)	C12-O7	1.423(12)
		C12-O8	1.443(19)
N3-C9	1.348(13)	C12-O9	1.400(19)
N3-C12	1.319(13)	C12-O10	1.306(19)
C8-C9	1.413(17)		
C9-C10	1.392(19)	C13-O11	1.442(16)
C10-C11	1.411(20)	C13-O12	1.383(14)
C11-C12	1.410(17)	C13-O13	1.440(10)
C12-C13	1.528(15)	C13-O14	1.404(12)
C13-N4	1.521(18)		
C13-C14	1.501(13)		

DESCRIPTION OF THE STRUCTURE

As expected the complex ion is facial and the configuration is $\Lambda\delta\delta\delta$ (Fig. 1) in accordance with the assumptions made in Ref. 1. The absolute chirality of the ligand $(-)_D$ -1-(2-pyridyl)ethylamine is *S*. The atomic distances and angles are given in Tables 3 and 4.

The distances from the atoms in each pyridine ring to the best plane through the ring do not exceed 0.02 Å. The distances from the cobalt atom to these planes vary from 0.03 to 0.15 Å. For each ligand the pyridine ring is tilted to the same side against the plane of the cobalt atom and the two nitrogen atoms of the ligand. The tilt angles, characterized by the nitrogen atom of the pyridine ring to which they belong, are: N1 15°, N3 16°, N5 13°. The carbon atoms of the five-membered rings are both on the same side of the cobalt-nitrogen plane defined above. The methyl groups are not far from being equatorial. The distances from the plane are: C5, 0.26, C6 0.56, C7-0.04 Å; C12 0.27, C13 0.61, C14 0.32 Å; C19 0.19, C20 0.61, C21 0.30 Å. The angles between the normal to the cobalt nitrogen plane and the C-C bond to

Table 4. Selected angles (°).

N1-Co-N2	81.0(3)	C8-N3-C12	120.4(9)
N1-Co-N3	97.1(3)	N3-C8-C9	121.8(10)
N1-Co-N4	173.1(4)	C-C9-C10	117.8(11)
N1-Co-N5	94.9(3)	C9-C10-C11	119.8(12)
N1-Co-N6	88.0(4)	C10-C11-C12	117.8(11)
N2-Co-N3	89.4(4)	C11-C12-N3	122.2(10)
N2-Co-N4	92.1(4)	C11-C12-C13	120.6(9)
N2-Co-N5	173.6(4)	N3-C12-C13	117.2(9)
N2-Co-N6	91.4(4)	C12-C13-N4	104.3(8)
N3-Co-N4	83.6(3)	C12-C13-C14	117.8(10)
N3-Co-N5	95.9(4)	N4-C13-C14	111.3(9)
N3-Co-N6	174.9(4)		
N4-Co-N5	91.9(4)	C15-N5-C19	118.2(9)
N4-Co-N6	91.4(3)	N5-C15-C16	123.1(12)
N5-Co-N6	83.6(3)	C15-C16-C17	119.1(12)
		C16-C17-C18	116.6(13)
C1-N1-C5	117.6(9)	C17-C18-C19	120.6(12)
N1-C1-C2	122.5(12)	N5-C19-C20	115.6(10)
C1-C2-C3	119.5(12)	C18-C19-N5	122.2(11)
C2-C3-C4	120.3(12)	C18-C19-C20	121.9(10)
C3-C4-C5	117.2(12)	N6-C20-C21	112.8(13)
C4-C5-N1	122.8(10)	C19-C20-C21	115.9(11)
N1-C5-C6	114.3(9)	C19-C20-N6	105.8(8)
C4-C5-C6	122.8(10)		
C5-C6-N2	107.3(8)		
C5-C6-C1	110.9(9)		
N2-C6-C7	112.3(9)		

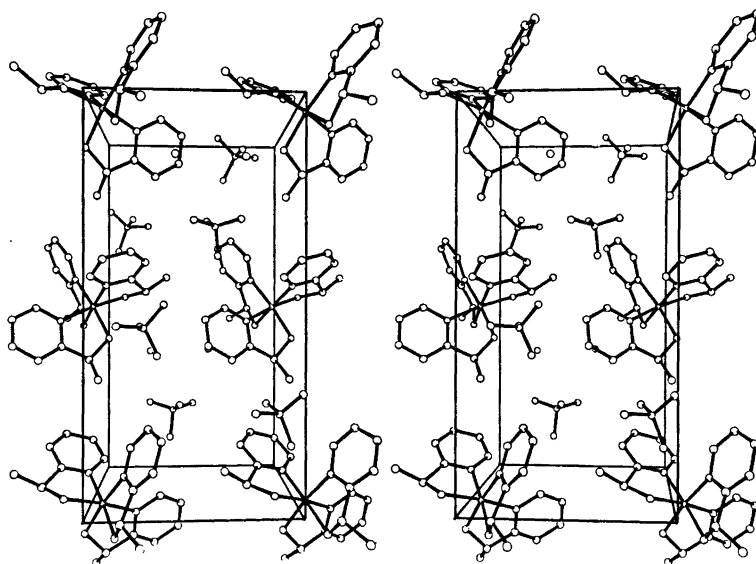


Fig. 2. Stereoscopic view of the cell perpendicular to the *ab* plane.

Table 5. Relevant interatomic distances less than 3.30 Å outside the complex cation.

O1-N2	2.93(1)	O2-N1	3.25(1)	N2-O13	3.09(1)
O1-N4	3.22(1)	O2-N6	2.95(2)	N3-O13	3.23(1)
O1-O2	3.16(2)	O2-O3	3.07(2)	N4-O7	2.99(2)
O1-O6	2.95(2)	O2-O8	2.86(2)	N5-O7	3.20(1)
O1-O9	3.03(2)			N6-O9	3.02(2)
O1-O12	3.20(2)				
O1-O14	3.00(2)				

the methyl group are for C6-C7 67°, for C13-C14 77° and for C20-C21 78°.

The torsion angles for the five-membered rings are N1-C5-C6-N2 20°, N3-C12-C13-N4 26° and N5-C19-C20-N6 31°. The octahedral angles in the five-membered rings are 81-84°, between bonds to pyridine rings 94-97° and the rest 88-92°.

The unit cell is shown in Fig. 2, the intermolecular distances in Table 5 and the distances for the perchlorate ions in Table 3. The oxygens of the perchlorate ions are as mentioned partly disordered and the variations in distances and angles found here are not unusual. We find from a survey of 22 structures of perchlorate salts published in recent years that more than 50 % of these showed perchlorate ion disorder.

CONCLUSIONS

The theoretical work of Corey and Bailar⁵ indicated that the most stable conformation of the coordinated 1,2-propanediamine in *tris* complexes is that with the methyl group in the equatorial position. This is in accord with the stereospecificity displayed by optically active propanediamine in the formation of such complexes.⁶ An equatorial methyl group was found in the structures of the facial species of (+)₅₈₉-[Co(Rpn)₃][Co(CN)₆·2H₂O and (-)₅₈₉-[Co(Rpn)₃][Br₃],^{7,8} and the angles between the bonds to the methyl groups and the normal to the cobalt nitrogen plane varied from 74 to 81°.

These investigations were followed up on Co(III) complexes^{9,10} where optically active

propanediamine forms a part of a more complex ligand, and in one such species one of the methyl groups was found to be axial. It follows that an equatorial orientation of the methyl group cannot automatically be assumed in structure assignment, especially not in the case of a rather inflexible ligand such as 1-(2-pyridyl)ethylamine.

The meridional form of *tris*(1-(2-pyridyl)ethylamine)cobalt(III) theoretically occurs as 16 isomers for each of the two enantiomeric ligands. In the case of the facial complex only eight isomers are possible for each enantiomeric ligand. This therefore gives the possibility of 24 ($\times 2$) isomers in the crystalline state.

As mentioned previously only three ($\times 2$) isomers could be prepared.¹ In the spectroscopic assignment of a facial structure to one of these the existence of a 3-fold axis was also assumed. However, the 3-fold symmetry is absent in the crystalline state. The $\Delta S\delta\delta\delta$ structure was assigned on the basis of spectral data in agreement with the X-ray results. The assignment of $\Delta S\lambda\lambda\lambda$ configuration to the second isolated facial isomer then followed automatically.

The configurational assignment of the third isomer is more problematical. If we assume the same general features for the ligands as found in the present structure we then have the $\Delta\lambda\lambda\lambda$ and $\Delta\delta\delta\delta$ structures for the meridional case with no great differences in steric interactions. The stability may be improved if the methyl group can adopt the axial orientation. It appears that these problems can only be solved satisfactorily by further X-ray investigations.

REFERENCES

1. Michelsen, K. *Acta Chem. Scand. A* 28 (1974) 428.
2. Stewart, J. M. *et al.*, *The X-RAY System 1972*, Technical Report 92, Computer Science Center, University of Maryland.
3. Johnson, C. K. *Ortep: A Fortran Ellipsoid Plot Program for Crystal Structure Illustrations*, Report ORNL-3794, Sec. Rev., Oak Ridge National Laboratory, Oak Ridge 1970.
4. Sim, G. A. *Acta Crystallogr.* 13 (1960) 511.
5. Corey, E. J. and Bailar, J. C. *J. Am. Chem. Soc.* 81 (1959) 2620.
6. Harnung, S. E., Kallesøe, S., Sargeson, A. M. and Schäffer, C. E. *Acta Chem. Scand. A* 28 (1974) 385.

7. Kuroda, R. and Saito, Y. *Acta Crystallogr. B* 30 (1974) 2126.
8. Kuroda, R., Shimanouchi, N. and Saito, Y. *Acta Crystallogr. B* 31 (1975) 931.
9. Kobayashi, A., Marumo, F. and Saito, Y. *Acta Crystallogr. B* 30 (1974) 1495.
10. Toriumi, K. and Saito, Y. *Acta Crystallogr. B* 31 (1975) 1247.

Received February 23, 1977.

The Crystal Structure of a Tetranuclear Nickel(II) Cluster Compound, $\text{Ni}_4(\text{OH})_4[\text{C}_6\text{H}_9(\text{NH}_2)_3]_4(\text{NO}_3)_4(\text{H}_2\text{O})_7$

BENGT AURIVILLIUS

Division of Inorganic Chemistry 2, Chemical Center, The Lund Institute of Technology, P.O. Box 740, S-220 07 Lund 7, Sweden

Crystals of $\text{Ni}_4(\text{OH})_4[\text{C}_6\text{H}_9(\text{NH}_2)_3]_4(\text{NO}_3)_4(\text{H}_2\text{O})_7$ are monoclinic, space group $P2_1/m$ with the cell parameters $a = 11.542(6)$, $b = 14.204(1)$, $c = 15.372(12)$ Å, $\beta = 99.22(6)^\circ$ (Hägg-Guinier powder diffractogram), $V = 2487.6$ Å³ and $Z = 2$. The crystal structure has been determined from Patterson and Fourier methods and refined by least-squares to $R = 0.064$ based on 4054 independent reflections (X-ray counter intensities).

The nickel atoms form clusters of four tetrahedrally arranged atoms each with interatomic distances varying between 3.16 and 3.20 Å. The shortest distance between nickel atoms belonging to different clusters is 9.02 Å. The Ni^{2+} and OH^- ions form a cubane-like structure with Ni—O distances of 2.07—2.10 Å.

The compound is an example of a complex between a metal atom and a stereo-specific ligand. The actual ligand, 1,3,5-triamino(*aaa*)-cyclohexane, and its nickel complex were first synthesized by Schwarzenbach and Egli, Zürich. 1,3,5-Triamino(*aaa*)-cyclohexane, denoted "tach" in this paper, has been used by Schwarzenbach¹ and Egli as a complexing agent. In "tach" the three NH_2 -groups form an approximately equilateral triangle with the side 3.0 Å. "Tach" in this way offers three fixed ligands for octahedrally coordinated ions like Co(II), Ni(II) and Cu(II). The remaining three ligands of the octahedron may be supplied by OH^- ions. "Tach" acts here, according to Schwarzenbach as a stereo-specific ligand. The present investigation was started to elucidate the geometry of a complex ion containing per each nickel atom one OH^- ion and one "tach" molecule. The single crystals used for the structure determination were kindly supplied by G. Schwarzenbach.

EXPERIMENTAL

Crystal data. $\text{Ni}_4(\text{OH})_4[\text{C}_6\text{H}_9(\text{NH}_2)_3]_4(\text{NO}_3)_4(\text{H}_2\text{O})_7$, F.W. 1193.8. Space group $P2_1/m$ (No. 11); $a = 11.505(6)$, $b = 14.203(1)$, $c = 15.309(12)$ Å, $\beta = 99.24(6)^\circ$ (single-crystal diffractometer, $\text{MoK}\alpha$, 30 reflections); $a = 11.542(6)$, $b = 14.204(1)$, $c = 15.372(12)$ Å, $\beta = 99.22(6)^\circ$, $V = 2487.6$ Å³ (Guinier-Hägg powder diffractogram, $\text{CuK}\alpha_1$, 21 single indexed reflections). $D_m = 1.6$ g cm⁻³ (by flotation), $Z = 2$, $D_x = 1.594$ g cm⁻³, $\mu = 15.80$ cm⁻¹ ($\text{MoK}\alpha$).

The dimensions of the monoclinic unit cell were determined from least-squares analyses of the angular positions of 30 reflections registered on a single crystal diffractometer as well as of $\sin^2\theta$ values recorded in a Guinier-Hägg focussing camera with $\text{CuK}\alpha_1$ radiation ($\lambda = 1.54051$ Å) using KCl ($a = 6.2930$ Å at 22 °C)

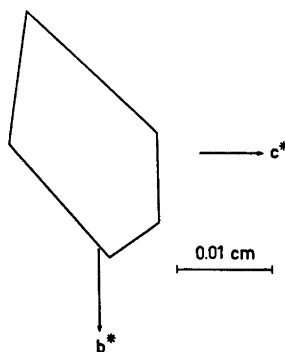


Fig. 1. Section perpendicular to the crystallographic a -axis of the single crystal used for the data collection. The directions of the reciprocal b^* - and c^* -axes are indicated.

as an internal standard. Slightly different values of the cell parameters were obtained, the largest deviation between the values being about 4σ . The discrepancy may partly be due to $\text{MoK}\alpha_1$ and $\text{MoK}\alpha_2$ not being resolved for the angles used, partly to systematic errors in the θ -values. The cell dimensions obtained from the powder diffractogram have been used consistently in this paper.

The blue transparent single crystal used had the form of an oblique prism with its edges extending along the a -axis and its basal planes lying in the bc -plane. The length of the prism parallel to the a -axis was 0.204 mm. A section through the prism at right angles to the a -axis (the b^*c^* -plane) is shown in Fig. 1. An approximate absorption correction was made on the basis of this drawing; the transmission factors varying between 0.76 and 0.85.

Preliminary Weissenberg photographs showed that the symmetry was monoclinic and that the only systematically missing reflections were $0k0$ with $k=2n+1$, indicating the space groups $P2_1$ (No. 4) and $P2_1/m$ (No. 11).

Intensity data were collected on a computer-controlled four-circle diffractometer (CAD-4) equipped with a graphite monochromator ($\text{MoK}\alpha$, $\lambda=0.70930$ Å). The $\omega-2\theta$ scan technique was used with a scan interval $\Delta\omega=(0.70+0.50 \tan \theta)^\circ$. The background was measured for one quarter of the scan time at each end of the interval. In the range $3^\circ < \theta < 35^\circ$ 6164 independent reflections were recorded. The intensities of two control reflections were measured at regular intervals (124 times each). Based on these 248 values a scaling polynomial for the intensities was found, $I_{\text{corr}}=I_{\text{obs}}(1-0.2785 \times 10^{-3}h)$, where h (hours) is the time of exposure of the crystal. Out of the 6164 reflections, 1412 had zero or negative intensities and were therefore deleted. A further 698 reflections were given zero weight as $\sigma(I)/I > 3.09$. A total of 4054 reflections were used for the subsequent calculations after their

intensities were corrected for Lorentz, polarization and absorption effects.

STRUCTURE DETERMINATION AND REFINEMENT

Assuming space group $P2_1/m$ all large maxima in a three-dimensional Patterson function could be explained as resulting from nickel-nickel vectors. Subsequent difference Fourier maps revealed the remaining non-hydrogen atoms. The parameters obtained were refined by least-squares calculations using anisotropic temperature factors for the nickel atoms and isotropic ones for the others. The function minimized was $\sum w_i(|F_o| - |F_c|)^2$, where $w_i^{-1} = \sigma^2(|F_o|^2)/4|F_o|^2 + 0.004|F_o|^2 + 5.0$. The final refinement converged at $R=0.064$ and $R_w=0.091$ (4054 independent reflections). The averages of $w_i(|F_o| - |F_c|)^2$ were approximately constant as a function of both $|F_o|$ and $\sin \theta$. The value of S , defined by $[\sum w_i(|F_o| - |F_c|)^2/(m-n)]^{1/2}$, where m and n are the numbers of observations and parameters varied, was 0.91. The form factors were those of the neutral atoms given by Hanson *et al.*³

Final positional and thermal parameters are given in Table 1. Lists of observed and calculated structure amplitudes are available from the author on request. As the structure so arrived at looked reasonable and as the thermal parameters were normal, no effort was made to refine the structure in space group $P2_1$. The positions of the hydrogen atoms were not determined.

Table 1. Final positional and thermal parameters for $\text{Ni}_4(\text{OH})_4(\text{C}_6\text{H}_{15}\text{N}_3)_4(\text{NO}_3)_4(\text{H}_2\text{O})_7$. Anisotropic temperature factors have been used for the nickel atoms and isotropic ones for the others. The expressions used for the temperature coefficients are $\exp[-2\pi^2(U_{11}h^2a^{*2} + U_{22}k^2b^{*2} + U_{33}l^2c^{*2} + 2U_{12}hka^*b^* + 2U_{13}hla^*c^* + 2U_{23}klb^*c^*)]$ and $\exp[-8\pi^2U(\sin^2\theta)/\lambda^2]$, respectively. The thermal parameters are in units 10^3 \AA^2 . Estimated standard deviations are given in parentheses. For U_{ij} see below.

Atom	x	y	z	U
Ni(1)	0.17135(6)	0.13864(5)	0.26150(4)	(2.17)
Ni(2)	0.40977(9)	$\frac{1}{4}$	0.32133(6)	(2.22)
Ni(3)	0.28806(9)	$\frac{1}{4}$	0.11933(6)	(2.10)
<i>OH⁻ ions</i>				
O(1)	0.3356(3)	0.1556(3)	0.2226(2)	2.58(8)
O(2)	0.2377(5)	$\frac{1}{4}$	0.3436(4)	2.71(11)
O(3)	0.1329(5)	$\frac{1}{4}$	0.1739(3)	2.47(11)

Table 1. Continued.

"Tach" molecule 1 bonded to Ni(1)

N(11)	0.0085(5)	0.1374(4)	0.3073(3)	3.58(11)
N(12)	0.1013(5)	0.0365(4)	0.1657(3)	3.61(11)
N(13)	0.2317(5)	0.0279(4)	0.3491(3)	3.55(11)
C(11)	-0.0433(6)	0.0431(5)	0.3209(4)	3.92(14)
C(12)	-0.0728(6)	-0.0096(5)	0.2332(4)	4.23(15)
C(13)	0.0360(6)	-0.0437(5)	0.1967(4)	3.72(14)
C(14)	0.1170(6)	-0.1006(5)	0.2662(4)	4.17(15)
C(15)	0.1476(6)	-0.0502(5)	0.3556(4)	3.84(14)
C(16)	0.0382(6)	-0.0138(5)	0.3888(4)	3.99(15)

"Tach" molecule 2 bonded to Ni(2)

N(21)	0.4684(5)	0.1470(4)	0.4179(3)	3.39(11)
N(22)	0.5796(7)	$\frac{1}{4}$	0.2839(5)	3.7(2)
C(21)	0.5877(6)	0.1607(5)	0.4734(4)	3.68(14)
C(22)	0.6814(6)	0.1609(5)	0.4141(4)	3.98(15)
C(23)	0.6826(8)	$\frac{1}{4}$	0.3586(6)	3.8(2)
C(24)	0.5884(9)	$\frac{1}{4}$	0.5273(6)	4.2(2)

"Tach" molecule 3 bonded to Ni(3)

N(31)	0.2290(5)	0.1480(4)	0.0220(3)	3.57(11)
N(32)	0.4551(6)	$\frac{1}{4}$	0.0807(5)	3.20(15)
C(31)	0.2645(6)	0.1609(5)	-0.0672(4)	3.56(13)
C(32)	0.3984(6)	0.1608(5)	-0.0589(4)	4.14(15)
C(33)	0.4559(8)	$\frac{1}{4}$	-0.0175(6)	3.4(2)
C(34)	0.2109(9)	$\frac{1}{4}$	-0.1112(6)	4.0(2)

Nitrate ions

N(4)	0.4684(7)	0.0415(6)	0.7347(5)	6.5(2)
O(41)	0.3648(8)	0.0487(6)	0.7312(5)	10.0(2)
O(42)	0.5126(8)	0.0569(6)	0.6694(6)	10.3(3)
O(43)	0.5229(8)	0.0101(6)	0.8040(6)	10.2(2)
N(5)	0.9025(9)	$\frac{1}{4}$	0.9841(6)	5.5(2)
O(51)	0.7980(9)	$\frac{1}{4}$	0.9412(6)	7.3(2)
O(52)	0.9489(6)	0.1740(4)	1.0031(4)	7.7(2)
N(6)	0.0379(8)	$\frac{1}{4}$	0.5494(6)	4.6(2)
O(61)	0.0843(12)	$\frac{1}{4}$	0.4855(9)	10.8(4)
O(62)	-0.0664(12)	$\frac{1}{4}$	0.5468(8)	10.4(4)
O(63)	0.0969(10)	$\frac{1}{4}$	0.6205(7)	9.0(3)

Water molecules

O(W1)	0.8176(8)	$\frac{1}{4}$	0.1713(6)	6.5(2)
O(W2)	0.7042(6)	0.0655(5)	0.9398(4)	7.5(2)
O(W3)	0.6569(6)	0.0988(5)	0.1168(4)	7.7(2)
O(W4)	0.2846(6)	0.1135(5)	0.5414(4)	7.3(2)

Anisotropic thermal parameters for the nickel atoms

Atom	U_{11}	U_{22}	U_{33}	U_{12}	U_{13}	U_{23}
Ni(1)	2.07(4)	2.26(4)	2.21(3)	-0.17(3)	0.32(3)	0.17(3)
Ni(2)	1.91(5)	2.74(5)	2.03(5)	0	0.07(4)	0
Ni(3)	2.23(5)	2.31(5)	1.80(5)	0	0.36(4)	0

Table 2. Selected interatomic distances (Å) and angles (°) in the crystal structure of $\text{Ni}_4(\text{OH})_4 \cdot (\text{C}_6\text{H}_{15}\text{N}_3)_4(\text{NO}_3)_4(\text{H}_2\text{O})_7$. The sign ' denotes atoms symmetry related to those given in Table 1.

Ni-Ni distances < 9.00 Å		Ni-O(OH ⁻) distances < 3.50 Å	
Ni(1)-Ni(3)	3.168(2)	Ni(1)-O(3)	2.079(3)
Ni(1)-Ni(1')	3.164(1)	Ni(1)-O(1)	2.091(4)
Ni(1)-Ni(2)	3.180(2)	Ni(1)-O(2)	2.091(4)
Ni(2)-Ni(3)	3.196(3)		
		Ni(2)-O(2)	2.068(6)
		Ni(2)-O(1)	2.102(4) 2 ×
		Ni(3)-O(1)	2.083(4) 2 ×
		Ni(3)-O(3)	2.096(6)
Ni-N(NH ₂) distances < 3.50 Å			
Ni(1)-N(11)	2.110(5)		
Ni(1)-N(13)	2.114(5)		
Ni(1)-N(12)	2.132(5)		
Ni(2)-N(21)	2.117(5) 2 ×		
Ni(2)-N(22)	2.129(8)		
Ni(3)-N(32)	2.106(7)		
Ni(3)-N(31)	2.116(5) 2 ×		
The cubane-like clusters $\text{Ni}_4(\text{OH})_4^{4+}$			
O-Ni-O		Ni-O-Ni	
O(2)-Ni(1)-O(3)	80.5(2)	Ni(1)-O(1)-Ni(2)	98.6(2)
O(2)-Ni(1)-O(1)	79.9(2)	Ni(1)-O(1)-Ni(3)	98.8(2)
O(3)-Ni(1)-O(1)	80.6(2)	Ni(2)-O(1)-Ni(3)	99.6(2)
O(2)-Ni(2)-O(1)	80.1(2)	Ni(1)-O(2)-Ni(1')	98.3(2)
O(2)-Ni(2)-O(1')	80.1(2)	Ni(1)-O(2)-Ni(2)	99.7(2)
O(1)-Ni(2)-O(1')	79.3(2)	Ni(1')-O(2)-Ni(2)	99.7(2)
O(1)-Ni(3)-O(1')	80.1(2)	Ni(1)-O(3)-Ni(1')	99.1(2)
O(1)-Ni(3)-O(3)	80.4(2)	Ni(1)-O(3)-Ni(3)	98.7(2)
O(1')-Ni(3)-O(3)	80.4(2)	Ni(1')-O(3)-Ni(3)	98.7(2)
The "tach" molecules			
Molecule 1			
C(11)-C(12)	1.530(10)	C(16)-C(11)-C(12)	111.7(6)
C(12)-C(13)	1.534(10)	C(11)-C(12)-C(13)	113.4(6)
C(13)-C(14)	1.532(10)	C(12)-C(13)-C(14)	110.8(5)
C(14)-C(15)	1.540(9)	C(13)-C(14)-C(15)	113.8(6)
C(15)-C(16)	1.525(9)	C(14)-C(15)-C(16)	111.9(6)
C(16)-C(11)	1.521(9)	C(15)-C(16)-C(11)	113.9(5)
C(11)-N(11)	1.495(9)	C(12)-C(11)-N(11)	110.6(5)
C(13)-N(12)	1.487(9)	C(16)-C(11)-N(11)	110.7(5)
C(15)-N(13)	1.488(9)	C(12)-C(13)-N(12)	111.2(5)
		C(14)-C(13)-N(12)	110.1(5)
		C(14)-C(15)-N(13)	110.3(5)
		C(16)-C(15)-N(13)	110.7(5)
Molecule 2			
C(21)-C(22)	1.523(9) 2 ×	C(21)-C(24)-C(21')	113.8(8)
C(22)-C(23)	1.527(9) 2 ×	C(24)-C(21)-C(22)	112.5(6) 2 ×
C(21)-C(24)	1.514(8) 2 ×	C(21)-C(22)-C(23)	114.0(6) 2 ×
		C(22)-C(23)-C(22')	111.8(8)

Table 2. Continued.

C(21)–N(21)	1.512(8)	2 ×	C(24)–C(21)–N(21)	110.0(6)	2 ×
C(23)–N(22)	1.515(12)		C(22)–C(21)–N(21)	109.4(5)	2 ×
			C(22)–C(23)–N(22)	110.3(5)	2 ×
Molecule 3					
C(31)–C(32)	1.530(9)	2 ×	C(31)–C(34)–C(31')	112.8(8)	
C(31)–C(34)	1.520(8)	2 ×	C(34)–C(31)–C(32)	111.8(6)	2 ×
C(32)–C(33)	1.522(9)	2 ×	C(31)–C(32)–C(33)	113.6(6)	2 ×
			C(32)–C(33)–C(32')	112.7(8)	
C(31)–N(31)	1.504(8)	2 ×	C(32)–C(31)–N(31)	110.1(5)	2 ×
C(33)–N(32)	1.511(11)		C(34)–C(31)–N(31)	110.9(6)	2 ×
			C(32)–C(33)–N(32)	110.2(5)	2 ×
The nitrate ions					
Ion 1					
N(4)–O(41)	1.192(12)		O(41)–N(4)–O(42)	119.8(9)	
N(4)–O(42)	1.218(12)		O(41)–N(4)–O(43)	116.1(9)	
N(4)–O(43)	1.230(12)		O(42)–N(4)–O(43)	123.7(9)	
Ion 2					
N(5)–O(51)	1.279(14)		O(52)–N(5)–O(52')	124.5(1.1)	
N(5)–O(52)	1.220(8)	2 ×	O(52)–N(5)–O(51)	117.7(5)	2 ×
Ion 3					
N(6)–O(61)	1.191(16)		O(61)–N(6)–O(62)	123.7(1.2)	
N(6)–O(62)	1.199(16)		O(61)–N(6)–O(63)	119.3(1.2)	
N(6)–O(63)	1.192(14)		O(62)–N(6)–O(63)	116.9(1.1)	
Possible hydrogen bond contacts < 3.00 Å					
O(W2)–O(43)	2.821(11)		O(W2)–O(W3)	2.898(10)	
O(51)–O(W2)	2.835(8)	2 ×	O(1)–O(43)	2.931(10)	
O(W1)–O(W3)	2.873(9)	2 ×	O(43)–O(W3)	2.999(11)	

DESCRIPTION AND DISCUSSION OF THE STRUCTURE

The coordination of nickel. The three-dimensional Patterson function, the symmetry, the

cell volume and the observed density showed that the unit cell contains eight nickel atoms. The determination of the structure (the non-hydrogen atoms) made clear that the unit cell content is two formula units $\text{Ni}_4(\text{OH})_4$.

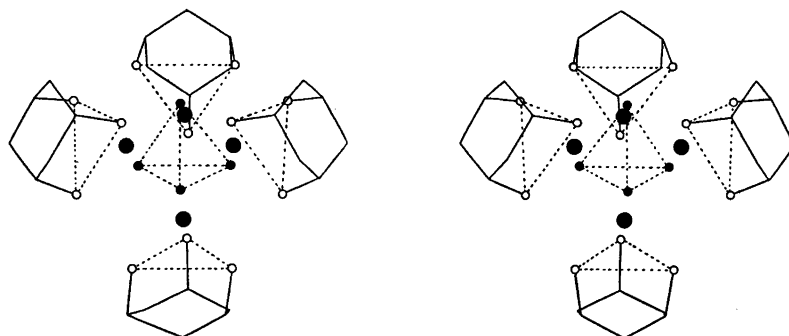


Fig. 2. Stereo view of one complex ion $\text{Ni}_4(\text{OH})_4(\text{C}_6\text{H}_{16}\text{N}_3)_4^{4+}$. Large filled circles denote nickel atoms, small filled ones hydroxide ions and empty ones amino groups. The $(\text{OH})_4$ tetrahedron is marked out by dotted lines. Dotted lines are also drawn between nitrogen atoms bonded to the same nickel atom.

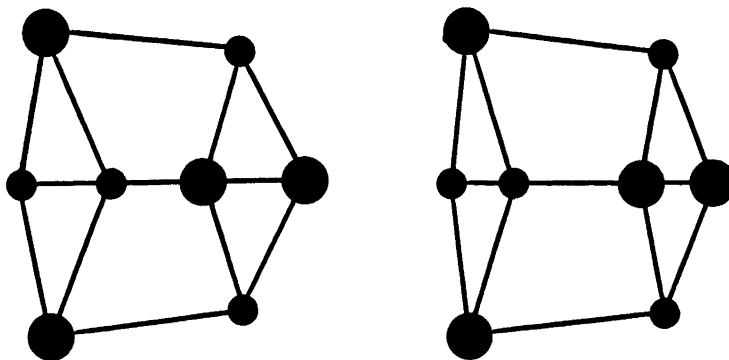


Fig. 3a. Stereo view of the cubane-like structure of $\text{Ni}_4(\text{OH})_4^{4+}$ in the present compound. Large filled circles denote nickel atoms and small ones hydroxide ions. $\text{Ni}-\text{O}(\text{OH}^-)$ bonds are shown by full lines.

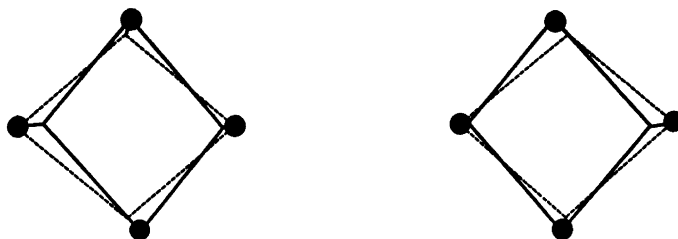


Fig. 3b. Stereo view of the cubane-like structure of the $\text{Ni}_4(\text{OCH}_3)_4^{4+}$ ion in $\text{Ni}_4(\text{OCH}_3)_4(\text{acac})_4(\text{CH}_3\text{OH})_4$. The circles indicate nickel atoms. Full and dotted lines indicate $\text{Ni}-\text{O}(\text{OCH}_3^-)$ bonds.

$(\text{C}_6\text{H}_{15}\text{N}_3)_4(\text{NO}_3)_4(\text{H}_2\text{O})_7$, a composition which was not unreasonable with respect to the stability measurements performed by Schwarzenbach.¹

Four and four of the nickel atoms form clusters, the atoms arranged in form of nearly regular tetrahedra, *cf.* Table 2 and Fig. 2. Within the tetrahedra the $\text{Ni}-\text{Ni}$ distances vary between 3.168(2) and 3.196(3) Å, whereas the shortest distance between Ni atoms belonging to different tetrahedra is 9.016(8) Å.

The hydroxide oxygen atoms $\text{O}(\text{OH}^-)$ also form nearly regular tetrahedra (Fig. 2) with distances $\text{O}-\text{O}$ varying between 2.682(8) and 2.697(8) Å (the $\text{O}-\text{O}$ distances are not listed in Table 2).

The nickel atoms and the $\text{O}(\text{OH}^-)$ atoms form together a cubane-like structure (Fig. 3a). Distances and angles within the "cube" are given in Table 2. None of the six planes defining the "cube" is, however, exactly planar. The deviations of the atoms from the respective

best planes range between 0.08 and 0.09 Å. Within the "cube" the $\text{Ni}-\text{O}-\text{Ni}$ angles vary between 98.3(2) and 99.7(2)°, whereas the $\text{O}-\text{Ni}-\text{O}$ angles vary between 79.3(2) and 80.6(2)°.

The nickel atoms are octahedrally coordinated by three hydroxide oxygen atoms $\text{O}(\text{OH}^-)$ and three amino nitrogen atoms $\text{N}(\text{NH}_2)$. The $\text{Ni}-\text{O}(\text{OH}^-)$ distances vary between 2.068(6) and 2.102(4) Å and the $\text{Ni}-\text{N}(\text{NH}_2)$ distances between 2.106(7) and 2.132(5) Å. The distances are normal as compared to the values 2.085(2) and 2.11(4) Å, respectively, given in the International Tables.²

The same kind of nickel tetramer as found here has previously been described for tetrakis- $[(\mu_3\text{-methoxy-2,4-pentanedionato-methanol})\text{-nickel(II)}]$, $\text{Ni}_4(\text{OCH}_3)_4(\text{acac})_4(\text{CH}_3\text{OH})_4$.⁴ Both in this compound and in the present one the $\text{Ni}-\text{Ni}$ distances are slightly larger than 3 Å. There is thus no reason to assume metal-metal bonding. The cubane-like structure of the

Table 3. Comparison between mean values of distances (Å) and angles (°) in 1,3,5-triamino(*aaa*)-cyclohexane, "tach", and cyclohexylammonium chloride.⁵ The *e.s.d.*'s given in parentheses refer to one single measurement.

	C-C	C-N	C-C-C	C-C-N
"Tach" molecule 1	1.530(10)	1.490(9)	112.6(6)	110.7(5)
"Tach" molecule 2	1.521(9)	1.513(12)	113.1(8)	109.9(6)
"Tach" molecule 3	1.524(9)	1.506(11)	112.7(8)	110.4(6)
Cyclohexylammonium chloride	1.515(10)	1.488(8)	111.4(5)	110.0(5)

acetylacetonate nickel(II) tetramer (Fig. 3b) is somewhat less deformed than the corresponding part in the present compound. The magnetic properties of the acetylacetonate nickel(II) tetramer have been investigated by Martin and coworkers.⁴ Similar investigations on Ni "tach" are in progress.⁵

The "tach" molecules. The "tach" molecules contain the cyclohexane rings in the *chair* conformation. Three crystallographically different "tach" molecules occur in the unit cell. For two of them (molecules 2 and 3, *cf.* Table 2) the four carbon atoms forming the bottom of the chair lie by symmetry in one plane; for the third (molecule 1) their maximum deviations from the best plane are 0.01 Å. The "tach" molecules are thus not twisted. All distances and angles in the molecules are normal as compared to corresponding values in cyclohexylammonium chloride⁶ (Table 3).

Possible hydrogen bonds. As mentioned earlier the positions of the hydrogen atoms were not determined. Possible hydrogen bond contacts

shorter than 3.00 Å are given in Table 2 and indicated by dotted lines in Fig. 4. As seen from the drawing there are no short N-H...O or N-H...N bonds. The unit cell contains eight nitrate ions, denoted ions 1, 2 and 3, and 14 water molecules, denoted O(W1), O(W2), O(W3) and O(W4) (*cf.* Table 2). Two nitrate ions (ion 3) and four water molecules O(W4) have no short contacts O-H...O. On the other hand four nitrate ions (ion 1) and two nitrate ions (ion 2) may be linked by two water molecules O(W1), four O(W2) and four O(W3) by hydrogen bonds O-H...O.

The nitrate oxygen O(43) (ion 1) may also be linked to the hydroxide oxygen atoms O(1) of Ni₄(OH)₄⁴⁺ and in this way the tetramers will occur in pairs joined *via* hydrogen bonds.

Acknowledgement. The author wishes to thank Dr. Karin Aurivillius for valuable discussions. This investigation has been financially supported by grants from the Swedish Natural Science Research Council.

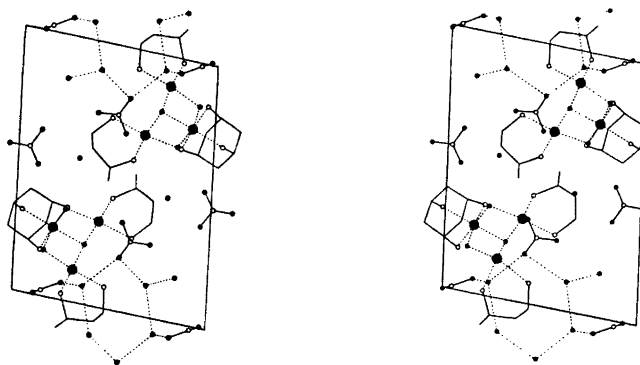


Fig. 4. Stereo view of the content of one unit cell of Ni₄(OH)₄(C₆H₁₅N₃)₄(NO₃)₄(H₂O)₇. Large filled circles indicate nickel atoms, small filled ones oxygen atoms and small open ones nitrogen atoms. Dotted lines indicate Ni-O(OH⁻) bonds as well as possible hydrogen bonds.

REFERENCES

1. Schwarzenbach, G. *Private communication*.
2. Hanson, H. P., Herman, F., Lea, I. D. and Skillman, S. *Acta Crystallogr. 17* (1964) 1940.
3. *International Tables for X-Ray Crystallography*, Kynoch Press, Birmingham 1962, Vol. 3, p. 269.
4. Bertrand, J. A., Ginsberg, A. P., Kaplan, R. J., Kirkwood, C. E., Martin, R. L. and Sherwood, R. C. *Inorg. Chem. 10* (1971) 240.
5. Martin, R. L. *Private communication*.
6. Rao, S. T. and Sundralingam, M. *Acta Crystallogr. B 25* (1969) 2509.

Received February 16, 1977.

A Neutron Diffraction Investigation on a Crystal of α -Mo₂C

A. NØRLUND CHRISTENSEN

Department of Inorganic Chemistry, Aarhus University, DK-8000 Aarhus C, Denmark

The crystal structure of α -Mo₂C was refined in space group *Pbcn* (No. 60) from neutron diffraction single crystal data. The unit cell $a = 4.732(2)$ Å, $b = 6.037(3)$ Å, $c = 5.204(2)$ Å, has $Z = 4$. The carbon atoms are partly ordered in the structure. Each carbon atom is coordinated with six molybdenum atoms in an octahedron. Each molybdenum atom is coordinated with three carbon atoms arranged in a triangle with the molybdenum atom placed approximately in the centre. α -Mo₂C has a superstructure. It is most likely a modulation of the carbon sublattice that yields the superstructure.

Some of the carbides and nitrides of the group IV, V, and VI transition metals have structures with the metal atoms either in face centered cubic or in hexagonal close packings. The carbon or nitrogen atoms are placed in the octahedral holes of the structures. Two structures are known for molybdenum carbide. β -Mo₂C has a hexagonal structure with the metal atoms in a hexagonal close packing and with the carbon atoms arranged statistically in the octahedral holes of the structure. (The number of holes is twice the number of carbon atoms). The structure of α -Mo₂C is orthorhombic. The packing of the metal atoms is of the hexagonal close packing type, but is deformed to an orthorhombic symmetry, and the carbon atoms are ordered in the structure.¹ The crystal structure of α -Mo₂C was studied by Parthé and Sadagopan¹ by neutron diffraction powder techniques.

Single crystals of α -Mo₂C have been made using floating zone crystal growth methods.² A preliminary X-ray crystallographic investigation of such a single crystal showed the diffraction pattern of α -Mo₂C to have strong reflections that were indexed with an orthorhombic unit cell *abc* of the same size as that

reported previously,¹ and some rather weak reflections that were indexed with an orthorhombic unit cell with $a_s = a$, $b_s = 2b$, and $c_s = 4c$.² The compound has thus a superstructure, that is assumed to arise from a small modulation of the crystal structure.¹ This paper is concerned with the structure of α -Mo₂C and the nature of the modulation of the structure that results in the occurrence of the superstructure. This could be due to a partial ordering of the carbon atoms in the octahedral sites available, or could be due to a modulation of the atomic positions of the carbon and/or the molybdenum sublattices.

EXPERIMENTAL

The preparation of single crystals of α -Mo₂C is reported elsewhere.² A Guinier powder pattern was taken of the compound with germanium, $a = 6.6576$ Å, as an internal standard. The powder pattern was indexed with an orthorhombic unit cell with $a = 4.732(2)$ Å, $b = 6.037(3)$ Å, $c = 5.204(2)$ Å, see Table 1. No superstructure reflections could be observed in the X-ray powder pattern but were visible on Weissenberg and precession photographs.²

The neutron diffraction data were measured at an automatic four-circle diffractometer at DR3, Risø, using 1.07 Å neutrons and a standard $\omega - 2\theta$ scan technique.³ A single crystal of α -Mo₂C with a volume of 2.04 mm³ and linear dimensions in the range 0.8 to 1.8 mm was used in measuring a total of 1557 reflections. The diffraction data were reduced using a standard procedure,⁴ resulting in a total of 301 independent reflections with $I > 3\sigma(I)$. Of these reflections 87 belonged to the small cell and only 214 of the reflections were superstructure reflections. A total of 195 of the superstructure reflections had intensities between $3\sigma(I)$ and $4\sigma(I)$. The reflections were corrected for absorption ($\mu = 11.6$ cm⁻¹).

Table 1. X-Ray powder pattern of α -Mo₂C, $a = 4.732(2)$ Å, $b = 6.037(3)$ Å, $c = 5.204(2)$ Å.

d_{obs}	d_{calc}	h k l	I_{obs}
2.613	2.611	0 2 1	m
2.604	2.602	0 0 2	m
2.369	2.366	2 0 0	m
2.290	2.286	1 2 1	s
2.282	2.280	1 0 2	m
1.754	1.753	2 2 1	s
1.751	1.750	2 0 2	m
1.509	1.509	0 4 0	m
1.504	1.504	0 2 3	s
1.351	1.349	3 0 2	m
1.306	1.305	0 4 2	w
1.301	1.301	0 0 4	w
1.272	1.272	2 4 0	m
1.269	1.269	2 2 3	m
1.258	1.258	1 4 2	m
1.254	1.254	1 0 4	m
1.182	1.183	4 0 0	w

s: strong, m: medium, w: weak

The structure of Mo₂C was refined using only reflections belonging to the small cell. The program LINUS⁵ was used to compare observed and calculated intensities. The neutron scattering lengths used for Mo and C were (in units of 10⁻¹² cm) 0.688 and 0.6648, respectively.⁶

Refinement of the structure of the small cell. The observed reflections correspond to the space group *Pbcn* (No. 60). As starting values in the refinement the following set of atomic coordinates from the structure of α -Mo₂C described by Parthé and Sadagopan were used.¹ Mo1 in site 8d at (0.25, 0.125, 0.083) and C1 in

site 4c at (0, 0.375, 0.25). The number of parameters refined was: one scale factor, four positional parameters and two isotropic temperature factor parameters, giving a total of seven parameters. This model of the structure refined to a conventional *R*-value of 7.6 %, see Table 2. Fourier and difference Fourier maps phased on this model showed, however, that the structure was not completely ordered with respect to the carbon atoms but had less mass density at the atomic site listed in Table 2 than corresponding to the multiplicity 0.5 and had additional mass density at the position (0, 0.87, 0.25). A model with only partly ordered carbon atoms was introduced. A total of nine parameters was refined: one scale factor, five positional parameters, an isotropic temperature factor parameter for Mo and two multiplicity parameters for the carbon atoms. This model of the structure refined to a conventional *R*-value of 6.4 %, see Table 2. The isotropic temperature factor parameters of the carbon atoms were not refined as they were strongly correlated with the multiplicity parameters.

Refinement of the structure of the superlattice. The reflections observed for the large cell corresponds to the space group *P2₁2₁2₁* (No. 19). A Patterson function made with the superstructure reflections only showed that these reflections had scattering contributions from atoms arranged in a h.c.p. type packing that could be the atoms in the carbon sublattice. The asymmetric unit in the superstructure cell contains eight formula units. A refinement of all positional, thermal and multiplicity parameters and a scale factor would involve 145 parameters, and many of these would be strongly correlated. Refinements showed as expected that the limited number of observed intensities, 301 reflections, was insufficient for a determination of the parameter of the superstructure. Fourier maps showed, however, that the superstructure was due to a modulation of the partial ordering of the carbon atoms found for the structure described in the small cell.

Table 2. Atomic coordinates for the structure of α -Mo₂C.

Atom	Multiplicity	x	y	z	$B(\text{Å}^2)$
<i>R</i> = 7.6 %					
Mo1	1.0	0.252(5)	0.124(9)	0.083(1)	0.68(6)
C1	0.5	0	0.376(9)	0.25	0.71(9)
<i>R</i> = 6.4 % ^a					
Mo1	1.0	0.249(5)	0.130(12)	0.083(1)	0.71(7)
C1	0.10(6)	0	0.355(73)	0.25	0.70
C2	0.41(6)	0	0.866(17)	0.25	0.70

^a The list of observed and calculated structure factors is available on request.

CONCLUSION

The investigation of the crystal structure of α -Mo₂C shows that the structure is orthorhombic of the type reported previously.¹ The specimen investigated had only a partial ordering of the carbon atoms in the structure and its X-ray and neutron diffraction pattern had superstructure reflections. It is most likely that the superstructure is due to a modulation of the atomic arrangement in the carbon sublattice. The partial ordering of the carbon atoms in the structure could only be found by Fourier methods and could not be elucidated from neutron diffraction powder data.¹

The phase α -Mo₂C is obtained on cooling from the phase β -Mo₂C and an ordering of the carbon atoms in the lattice is involved in this phase transition. For the sample investigated this ordering has not been complete, and this has resulted in a crystal with a superstructure.

The interatomic distances in the structure show Mo–C distances from 2.00(2) to 2.22(2) Å.

Acknowledgements. I am indebted to Mr. M. H. Nielsen, Mrs. R. G. Hazell and Mr. F. K. Larsen for assistance in data collection and reduction.

REFERENCES

1. Parthé, E. and Sadagopan, V. *Acta Crystallogr.* 16 (1963) 202.
2. Christensen, A. N. *J. Crystal Growth* 33 (1976) 58.
3. Lehmann, M. S., Larsen, F. K., Poulsen, F. R., Christensen, A. N. and Rasmussen, S. E. *Acta Chem. Scand.* 24 (1970) 1662.
4. Lehmann, M. S. and Larsen, F. K. *Acta Crystallogr. A* 30 (1974) 580.
5. Busing, W. R., Martin, K. O. and Levy, H. A. *ORFLS, A Fortran Crystallographic Least Squares Program*, Report ORNL-TM-305, Oak Ridge National Laboratory, Oak Ridge 1962, *LINUS* is a 1971 version of *ORFLS*.
6. Shull, C. G. *Coherent Neutron Scattering Amplitudes*, Massachusetts Institute of Technology, Cambridge, Mass. 1972.

Received March 7, 1977.

Short Communications

The Crystal Structure of (1*Z*,2*E*)-1,2-Naphthoquinone Dioxime. A New Modification

HEIKKI SAARINEN, MATTI NÄSÄKKÄLÄ, JORMA KORVENRANTA and ELINA NÄSÄKKÄLÄ

Department of Inorganic Chemistry, University of Helsinki, SF-00100 Helsinki 10, Finland

In a recent report we described the crystal and molecular structure of (1*Z*,2*E*)-1,2-naphthoquinone dioxime.¹ We have since noticed that minor changes in the recrystallization procedure yield a crystallographically different form of the compound. Because it seemed possible that a new configuration of the oxime groups had been established, an X-ray structure analysis of the new crystals was undertaken.

The new modification (=B) was obtained from the raw product of 1,2-naphthoquinone dioxime¹ on recrystallization from 75% aqueous ethanol; m.p. 165 °C. Anal. C₁₀H₈O₂N₂: C, H, N. The yellow-brown tabular crystals are monoclinic with the following crystal data: $a =$

11.993(10), $b = 11.078(10)$, $c = 13.632(12)$ Å, $\beta = 98.60(7)^\circ$, $Z = 8$, $D_m = 1.42$ g cm⁻³, $D_x = 1.396$ g cm⁻³ and $\mu(\text{MoK}\alpha) = 2.4$ cm⁻¹. The space group, from systematic absences and statistical tests, is $C2/c$ (No. 15).

The intensity data were collected with a Syntex P2₁ diffractometer using graphite monochromated Mo radiation (MoK α , $\lambda = 0.7107$ Å) and the $\theta - 2\theta$ scan technique. Out of a total of 2054 reflections having 2θ less than 60°, 960 with $I > 2\sigma(I)$ were regarded as observed. No

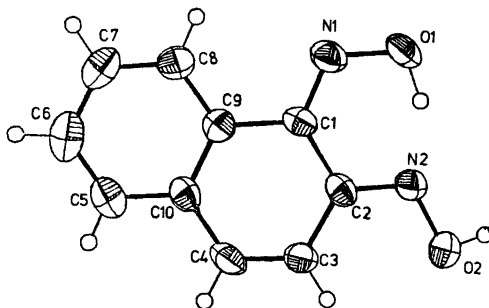


Fig. 1. Numbering and 50% probability ellipsoids of the atoms.

Table 1. Fractional coordinates ($\times 10^4$) and anisotropic thermal parameters^a ($\times 10^3$) for non-hydrogen atoms.

Atom	X/a	Y/b	Z/c	U_{11}	U_{22}	U_{33}	U_{12}	U_{13}	U_{23}
C1	2041(4)	2907(4)	6333(3)	32(2)	37(2)	37(2)	5(2)	-2(2)	-8(2)
C2	1346(4)	1795(4)	6242(3)	37(2)	38(2)	33(2)	9(2)	0(2)	-1(2)
C3	434(4)	1682(4)	5408(4)	38(3)	35(2)	52(3)	-1(2)	-7(2)	-1(2)
C4	256(4)	2540(5)	4715(4)	42(3)	52(3)	44(3)	6(2)	-14(2)	-4(2)
C5	712(5)	4498(5)	3987(4)	51(3)	63(4)	41(3)	11(3)	4(2)	7(3)
C6	1345(5)	5524(5)	4004(5)	71(4)	52(3)	64(4)	16(3)	28(3)	17(3)
C7	2233(5)	5715(5)	4786(4)	63(4)	37(3)	72(4)	-3(3)	22(3)	2(3)
C8	2459(4)	4876(4)	5529(4)	53(3)	41(3)	47(3)	-4(2)	2(2)	-7(2)
C9	1811(4)	3828(4)	5528(3)	40(2)	31(2)	39(2)	6(2)	6(2)	-6(2)
C10	923(4)	3626(4)	4742(3)	39(2)	40(2)	36(2)	9(2)	2(2)	0(2)
N1	2837(4)	3171(4)	7070(3)	53(2)	42(2)	45(2)	1(2)	-10(2)	-8(2)
N2	1603(3)	971(3)	6919(3)	43(2)	36(2)	43(2)	-2(2)	-3(2)	0(2)
O1	3088(4)	2326(4)	7826(3)	78(3)	54(2)	48(2)	-7(2)	-30(2)	3(2)
O2	928(3)	-45(3)	6780(3)	59(2)	43(2)	61(2)	-6(2)	-4(2)	14(2)

^a The anisotropic thermal parameters are of the form $\exp[-2\pi^2(h^2a^{*2}U_{11} + \dots + 2klb^*c^*U_{23})]$.

Table 2. Fractional coordinates ($\times 10^3$) and isotropic thermal parameters ($\times 10^3$) for the hydrogen atoms.

Atom	X/a	Y/b	Z/c	U
H(O1)	255(6)	168(6)	764(5)	9.8(22)
H(O2)	127(5)	-47(6)	722(5)	9.1(22)
H(C3)	30(4)	97(4)	535(3)	3.4(12)
H(C4)	-29(4)	244(4)	419(3)	3.8(12)
H(C5)	13(4)	435(4)	351(3)	4.2(13)
H(C6)	129(6)	613(6)	349(5)	9.9(23)
H(C7)	268(5)	642(5)	481(4)	6.9(17)
H(C8)	305(4)	503(4)	603(3)	4.1(12)

correction for absorption was carried out (crystal size $0.3 \times 0.3 \times 0.15$ mm). The methods of solving and refining the structure were the same as in Ref. 1. The weighting parameters used in the calculations were: $a=40.0$ and $b=0.04$. An R value of 8.5% was achieved by refining the non-hydrogen atoms anisotropically. All hydrogen atoms were then located from a difference Fourier map and included in the subsequent least-squares cycles with isotropic temperature factors. The final R value for 960 reflections was 5.3%. Atomic coordinates and thermal parameters are listed in Tables 1 and 2.

The structure of the molecule is visualized in Fig. 1. The interatomic distances and angles

together with the respective values of the former modification ($=A$) are listed in Table 3. The observed C-H and O-H bond lengths not seen in Table 3 vary from 0.82 to 0.97 Å, the respective standard deviations falling between 0.04 and 0.07 Å.

The two modifications have the same (1*Z*,2*E*)-configuration of the oxime groups and the differences between the corresponding bond lengths and angles are not significant. The similarity between the intramolecular hydrogen bonds in A and B is also obvious: the observed O1...N2 distances are 2.490(5) and 2.508(5) Å, respectively. The differences between the crystal forms of the two modifications arise rather from a different packing of the molecules in the structure. In B the molecules are linked together by a hydrogen bond [2.804(5) Å] from the O2 oxime oxygen to the N1 ($-x + \frac{1}{2}, y - \frac{1}{2}, z + \frac{1}{2}$) nitrogen atom, whereas in A the same H(O2) was accepted by a neighbouring oxime oxygen.

A list of the observed and calculated structure factors is available on request.

Acknowledgement. The financial support of the Science Research Council of Finland is gratefully acknowledged.

1. Näsäkkälä, M., Saarinen, H., Korvenranta, J. and Näsäkkälä, E. *Acta Chem. Scand. A* 31 (1977) 469.

Received March 21, 1977.

Table 3. Intramolecular distances (Å) and angles ($^\circ$) of the different modifications of (1*Z*,2*E*)-1,2-naphthoquinone dioxime. Standard deviations in bond lengths and angles are in the range 0.004–0.006 Å and 0.3–0.4 $^\circ$ for modification A, and 0.005–0.008 Å and 0.3–0.5 $^\circ$ for B.

Distance	Modification		Angle	Modification	
	A	B		A	B
C1–C2	1.482	1.482	C1–C2–C3	119.1	118.9
C1–C9	1.480	1.494	C2–C3–C4	121.3	120.8
C2–C3	1.450	1.460	C3–C4–C10	123.0	123.1
C3–C4	1.332	1.334	C4–C10–C9	119.8	120.3
C4–C10	1.438	1.443	C5–C10–C9	119.4	118.7
C5–C6	1.364	1.365	C5–C6–C7	119.7	119.6
C5–C10	1.410	1.407	C6–C5–C10	120.7	121.4
C6–C7	1.399	1.405	C6–C7–C8	120.7	120.2
C7–C8	1.380	1.372	C7–C8–C9	120.6	120.9
C8–C9	1.389	1.397	C8–C9–C10	118.9	119.3
C9–C10	1.415	1.411	C9–C1–C2	117.4	117.8
C1–N1	1.304	1.311	C10–C9–C1	119.7	119.1
C2–N2	1.306	1.302	C9–C1–N1	115.6	116.4
N1–O1	1.394	1.391	C2–C1–N1	127.0	125.8
N2–O2	1.379	1.382	C1–N1–O1	117.6	118.0
O1–N2	2.490	2.508	C1–C2–N2	115.2	116.9
			C3–C2–N2	125.7	124.3
			C2–N2–O2	112.6	113.6

Crystallographic Data on New Arsenides and Antimonides of Titanium and Scandium

ROLF BERGER

Institute of Chemistry, University of Uppsala,
Box 531, S-751 21 Uppsala, Sweden

In the course of a study of the vanadium arsenides, the common technique of performing syntheses in evacuated silica tubes was supplemented with arc-melting. Some aspects of these two methods have been discussed earlier.¹ In view of the fact that the arc-melting technique often reveals phases not obtainable in silica tube syntheses, it was considered worthwhile to extend this supplementary method to other related systems.

Starting materials. The elements used for the syntheses were titanium (Koch-Light Ltd., 99.95%), scandium (Rare Earths Prod., 99.99%), arsenic (Koch-Light Ltd., 99.9999%) and antimony (Johnson & Matthey, 99.9999%). The figures indicate the claimed purity. The actual purity is probably slightly lower, primarily owing to the presence of oxide films. As_2O_3 was removed from the elemental arsenic by vacuum sublimation, but the other elements were not treated for impurities before the syntheses.

X-Ray equipment and methods. The phase analyses were based on powder diffraction, using Guinier-Hägg focussing cameras equipped with $CuK\alpha_1$ radiation ($\lambda = 1.540598 \text{ \AA}$). Silicon ($a = 5.431065 \text{ \AA}$)² or germanium ($a = 5.657906 \text{ \AA}$)³ were used as primary internal calibration standards. Cell parameters refined by the least-squares method are presented together with other crystallographic data in Table 1.

The Ti-As system. TiAs (TiP type) was formed by reacting the elements in a silica tube at 900 °C for 7 days. The powdered product was compressed to a pellet and melted in an arc furnace in a protective argon atmosphere. Additional lines formed on the corresponding powder photograph, since the melting caused an uncontrolled but intentional loss of arsenic from the sample. The same method was used for preparing $\beta\text{-V}_4\text{As}_3$ from VAs.⁴ The cell dimensions of TiAs showed no significant deviation from those obtained from the single-phase starting product and were in good agreement with those reported by Łukaszewicz and Trzebiatowski.⁵ There was no sign of $\beta\text{-TiAs}$ of the NiAs type, which was assumed by Bachmayer *et al.* to be stable on the metal-rich side or to be a high-temperature phase.⁶ Neither were there any indications as to stacking disorder, since all TiAs lines were sharp. The additional lines were indexed on a body-centred cubic cell. The new compound is assigned the composition Ti_4As_3 , an analogue existing in

the Ti-P system.⁷ Preliminary investigations using less pure starting materials did not yield Ti_4As_3 , but instead the hexagonal phase reported by Boller and Nowotny,⁸ and assigned the composition Ti_5As_3 . This difference might be due to the stabilizing effect of a contaminant. The formation of ternary compounds with the Mn_3Si_2 -type structure ("Nowotny phases") requires only minute amounts of nitrogen, carbon or oxygen; it is therefore often difficult to ascertain whether the presence of these phases corresponds to thermodynamic stability in the binary system. A moderate addition of titanium to the two-phase product made the TiAs phase disappear. In addition to the Ti_4As_3 lines that remained, the resulting product showed new diffraction lines. A few of these, very weak and blurred, belonged to the Mn_3Si_2 -type phase, while the rest could be indexed on a primitive orthorhombic cell of the same magnitude as those of the two high-temperature V_4As_3 polymorphs.⁹ This new phase is probably isostructural with $\gamma\text{-V}_4As_3$ ($\beta\text{-Yb}_3Sb_3$ type¹⁰). It cannot be inferred with certainty whether the $Ti_{11}P$ phase reported by Snell⁷ also belongs to this class of compounds, but the cell dimensions and the powder line indices do not contradict such a hypothesis. Still more metal-rich specimens indicated the presence of further phases in the system. One powder pattern was interpreted as belonging to Ti_5As_3 , isostructural with Ti_3P . Again there is an obvious similarity between the Ti-As and the Ti-P systems. The phase analysis is far from complete, and one must bear in mind that the arc-melting technique creates conditions where it is difficult to attain equilibrium.

The Sc-As system. ScAs (NaCl type) was synthesized in a silica tube at 900 °C for 4 days. Powder diffraction showed the presence of Sc_2O_3 in minute amounts, its strongest lines being detected as weak traces. The cell parameter of ScAs was compatible with that given by Brixner.¹¹ The method of arc-melting the monoarsenide was used to obtain a phase containing less arsenic. The cell parameters of ScAs in this two-phase region did not differ significantly from that of the initial monoarsenide. The lines of the new phase were indexed on a primitive tetragonal cell. Its volume suggests a cell content of 20 atoms, and it is likely that the new compound has the composition Sc_3As_2 , being isostructural with V_3As_2 .¹² Preliminary intensity calculations suggest that this might very well be the case. The cell dimensions of Sc_3As_2 were refined, ScAs being used as a secondary internal standard. There exist still further phases in the system, and one was confirmed as being identical with a tetragonal phase found by Rundqvist and Nyarko.¹³ Their crystallographic data are given in Table 1. The exact composition of this phase is unknown; it is approximately 70 atomic % Sc, and the cell volume indicates about 80 atoms to the cell. A literature search for a

Table 1. Crystallographic data of phases obtained in the present study. Cell dimensions in Å units with standard deviations in parentheses.

Phase	Space group	Structure type	Cell dimensions	Internal standard	No. of reflexions
TiAs	$P6_3/mmc$	TiP	$a = 3.6419(2)$ $c = 12.055(1)$	Ge	25
Ti ₄ As ₃	$I\bar{4}3d$	<i>anti</i> -Th ₃ P ₄	$a = 7.6795(2)$	Ge	15
Ti ₅ As ₃	$Pnma$	β -Yb ₅ Sb ₃	$a = 9.8521(4)$ $b = 7.7363(11)$ $c = 6.7232(4)$	Ti ₄ As ₃	63
Ti ₃ As	$P4_2/n$	Ti ₃ P	$a = 10.1618(2)$ $c = 5.1098(2)$	Si	75
ScAs	$Fm\bar{3}m$	NaCl	$a = 5.4640(2)$	Ge	9
Sc ₃ As ₂	$P4/m$	V ₃ As ₂	$a = 10.3755(3)$ $c = 3.8064(2)$	ScAs	58
Sc _{2,3} As	$I4/mmm$	—	$a = 14.3743(9)$ $c = 8.0257(6)$	Si	60
Ti ₅ Sb ₃	$Pnma$	β -Yb ₅ Sb ₃	$a = 10.2173(5)$ $b = 8.3281(5)$ $c = 7.1459(4)$	Ge	76
ScSb	$Fm\bar{3}m$	NaCl	$a = 5.8517(4)$	Ge	10
Sc ₅ Sb ₃	$Pnma$	β -Yb ₅ Sb ₃	$a = 11.0792(8)$ $b = 8.7126(5)$ $c = 7.6272(5)$	Si	102
Sc ₂ Sb	$P4/nmm$	Cu ₂ Sb	$a = 4.2049(2)$ $c = 7.7902(4)$	Ge	38

report on an isostructural phase was not successful.

The Ti-Sb system. Kjekshus *et al.*¹⁴ reported an orthorhombic phase of the approximate composition Ti_{1.7}Sb. The cell parameters indicated that this phase might be assigned the formula Ti₅Sb₃ and be related to either the β -Yb₅Sb₃ type¹⁰ or the Y₅Bi₃ type.^{9,15} In their paper, Kjekshus *et al.* stated that the only systematic extinctions occurred for the $hk0$ reflexions when $h = 2n + 1$. This is not compatible with either of the two suggested structure types which, with the similar axis setting, respectively belong to the $Pnma$ and $Pcmn$ space groups. However, investigations of single crystals from a sample obtained by arc-melting titanium and antimony in the atomic ratio 5:3 clearly showed that the space-group assignment ought rather to be $Pnma$ (or $Pn2_1a$) with an axis setting corresponding to β -Yb₅Sb₃. The compound obtained is obviously identical with that found by Kjekshus *et al.*, despite the differences in our indexing of high-angle lines.

A single-crystal structure determination has been started, and the preliminary results support this structure hypothesis.

The Sc-Sb system. As is often the case with compounds of the Group V non-metals with Sc, Y or the rare-earth elements, only the 1:1 compound has been reported.¹¹ On arc-melting the elements in a ratio corresponding to Sc_{1.2}Sb, a phase mixture was obtained. One phase was identified as ScSb, its cell parameter being not very different from that reported by Brixner.¹¹ The remaining lines were not indexed. Heat-treatment in a silica tube at 950 °C for 7 days yielded a new pattern, which still contained lines attributed to ScSb. The remainder could be indexed on a primitive orthorhombic cell. On the basis of atomic volume considerations including comparisons with the Y-Sb system,¹⁶ the cell volume agreed very well with a content of 32 atoms. It is likely that this phase is also of the β -Yb₅Sb₃ type. The indexing of the powder lines is similar to that of Ti₅Sb₃. No single-crystal data are available as yet.

In the metal-rich region there also exists a phase indexable on a primitive tetragonal cell. This compound seems to be isostructural with Cu_2Sb . No corresponding phase was found in the Y-Sb system.¹⁶ The specimens initially showed a silvery lustre, but tended to turn dark on long exposure to air, probably because of the formation of a superficial oxide film.

1. Berger, R. *Acta Chem. Scand. A* 29 (1975) 641.
2. Deslattes, R. D. and Henins, A. *Phys. Rev. Lett.* 31 (1973) 972.
3. Baker, J. F. C. and Hart, M. *Acta Crystallogr. A* 31 (1975) 364.
4. Berger, R. *Acta Chem. Scand. A* 28 (1974) 771.
5. Łukaszewicz, K. and Trzebiatowski, W. *Bull. Acad. Pol. Sci. Ser. C2* (1954) 277.
6. Bachmayer, K., Nowotny, H. and Kohl, A. *Monatsh. Chem.* 86 (1955) 39.
7. Snell, P.-O. *Acta Chem. Scand.* 22 (1968) 1942.
8. Boller, H. and Nowotny, H. *Monatsh. Chem.* 96 (1965) 565.
9. Berger, R. *Acta Chem. Scand. A* 30 (1976) 363.
10. Brunton, G. D. and Steinfink, H. *Inorg. Chem.* 10 (1971) 2301.
11. Brixner, L. H. *J. Inorg. Nucl. Chem.* 15 (1960) 199.
12. Berger, R. *Acta Chem. Scand. A* 31 (1977) 287.
13. Rundqvist, S. and Nyarko, D. G. University of Uppsala (1970). *Unpublished*.
14. Kjekshus, A., Grønvold, F. and Thorbjørnsen, J. *Acta Chem. Scand.* 16 (1962) 1493.
15. Wang, Yu, Gabe, E., Calvert, L. D. and Taylor, J. B. *Acta Crystallogr. B* 32 (1976) 1440.
16. Schmidt, F. A. and McMasters, O. D. *J. Less-Common Met.* 21 (1970) 415.

Received April 28, 1977.

High Temperature Studies of Marcasite and Arsenopyrite Type Compounds

ARNE KJEKSHUS and TROND RAKKE

Kjemisk Institutt, Universitetet i Oslo, Blindern, Oslo 3, Norway

High temperature investigations by X-ray diffraction, DTA, and quenching experiments have been carried out on FeAs_2 , FeSb_2 , CoAs_2 , CoSb_2 , RhAs_2 , RhSb_2 , RhBi_2 , IrAs_2 , IrSb_2 , $\text{Fe}_{0.5}\text{Ni}_{0.5}\text{As}_2$, $\text{Fe}_{0.5}\text{Ni}_{0.5}\text{Sb}_2$, NiAs_2 , and NiSb_2 . The thermal properties of these compounds are discussed in relation to the arsenopyrite *versus* marcasite type structure.

Some two hundred binary and ternary transition metal (T) compounds of the main group V and VI elements (X) take the structure types FeS_2 - p (p = pyrite), FeS_2 - m (m = marcasite) and/or FeAsS (arsenopyrite; binary prototype CoSb_2). A substantial amount of the literature on the subject covers geological aspects or deals with various properties of individual compounds. However, an additional interest stems from their apparent suitability as model substances for bonding considerations. This interest may be based on several motives, their simplicity in atomic architecture and mutual structural resemblance (*cf.*, *e.g.*, Refs. 1, 2, and references therein) being probably the most important.

Features of the relations between the FeS_2 - p and FeS_2 - m types are presented in recent communications.^{1,3} The structural resemblance between the CoSb_2 and FeS_2 - m types is even more pronounced, and the former can be regarded as a slightly distorted variant of the latter. For the translational symmetry of the lattice the actual deformations are so small that prior to 1955, binary representatives of the CoSb_2 type were erroneously classified among the FeS_2 - m type compounds. The

atomic arrangements correspond similarly⁴ and transitions between the two structure types may accordingly be expected as functions of composition, temperature, and/or pressure. In fact, gradual transitions from the CoSb_2 to the FeS_2 - m type have been accomplished in ternary series $T_t\text{Co}_{1-t}\text{X}_2$ ($T = \text{Fe, Ni}$; $X = \text{As, Sb}$)^{2,5,6} as a function of the compositional parameter t .

At normal temperatures and pressures, binary CoSb_2 type compounds have exclusively been found for Co, Rh, and Ir in combination with P, As, Sb, or Bi. This apparent constraint on the CoSb_2 type structure compared with the widespread occurrence (in relation to the Periodic System) of compounds with the FeS_2 - p and FeS_2 - m types, provokes the question of what happens to the CoSb_2 type at higher temperatures. An answer to this question could also provide further insight into the occurrence of the various classes A, A/B, and B (*vide infra*) of the FeS_2 - m type. Elaboration of the latter point has led to a parallel study of representative FeS_2 - m type compounds. Thus, the compounds subject to this study are:

A(FeS_2 - m): FeAs_2 , FeSb_2
 B(FeS_2 - m): NiAs_2 , NiSb_2
 A/B(FeS_2 - m): $\text{Fe}_{0.5}\text{Ni}_{0.5}\text{As}_2$, $\text{Fe}_{0.5}\text{Ni}_{0.5}\text{Sb}_2$
 A/B(CoSb_2): CoAs_2 , CoSb_2 , RhAs_2 , RhSb_2 ,
 RhBi_2 , IrAs_2 , IrSb_2

where the assigned classifications (see Ref. 7) relate to the room temperature, unit cell proportions.

EXPERIMENTAL

The first preparational step consisted in heating appropriate amounts of the respective elements [turnings from 99.99+ % Fe, 99.999 % Co, and 99.995 % Ni rods, 99.99 % Rh and 99.99 % Ir powders (all from Johnson, Matthey & Co.), 99.999 % As and 99.9995 % Sb (Koch-Light Laboratories), and 99.99+ % Bi (American Smelting and Refining Co.)] in evacuated, sealed silica tubes. The FeAs_2 and NiAs_2 (*viz.* β - NiAs_2) samples were treated as described previously⁸ [the "low temperature" modification, α - NiAs_2 , was readily made by a 2×14 days reaction period (intervening crushing) from $\text{NiAs} + \text{As}$ at 550 °C], but for the preparations of the other compounds, some modifications of earlier procedures were adopted.

The alterations introduced for FeSb_2 , CoSb_2 , and NiSb_2 consisted in the initial preparations of the phases FeSb , CoSb , and NiSb by high temperature (1200–1000 °C) treatments. The samples were ground to fine powders, appropriate amounts of Sb added, and subsequently annealed once (CoSb_2) or twice (intervening crushing) at 700 (FeSb_2), 900 (CoSb_2), or 600 °C (NiSb_2). The FeSb_2 and CoSb_2 samples were slowly cooled to 600 °C. These simple alterations have thus eliminated the rather time-consuming grinding and annealing cycles earlier used.^{4,9}

CoAs_2 , RhAs_2 , RhSb_2 , IrAs_2 , and IrSb_2 were made essentially as described in Ref. 4. On turning to higher maximum temperatures, *viz.* 1000 (CoAs_2) or 1200 °C, the overall annealing periods and number of intervening crushings could be reduced appreciably (to 2×2 days). All samples were slowly cooled to 600 °C.

RhBi_2 was obtained after reaction at 750 °C (2 days), followed by grinding and annealing at 400 °C (1 month). Renewed attempts to prepare CoBi_2 and IrBi_2 (*cf.* Ref. 10) were in vain as also reported in, *e.g.*, Ref. 4.

The ternary samples, $\text{Fe}_{0.5}\text{Ni}_{0.5}\text{As}_2$ and $\text{Fe}_{0.5}\text{Ni}_{0.5}\text{Sb}_2$, were made from the binary end members. $\text{Fe}_{0.5}\text{Ni}_{0.5}\text{As}_2$ is readily made by two successive annealings at 740 °C, followed by slow cooling to 600 °C. $\text{Fe}_{0.5}\text{Ni}_{0.5}\text{Sb}_2$ is, however, somewhat more difficult to make. The maximum temperature in the annealing process must not exceed 640 °C (*vide infra*) and equilibrium is attained rather slowly below this temperature. Of the numerous attempts to prepare pure $\text{Fe}_{0.5}\text{Ni}_{0.5}\text{Sb}_2$, none of the samples could be handled identically with respect to annealing time and number of intervening crushings. Further work on the synthetic and other properties of the Fe–Ni–Sb system is in progress.

The temperature of the furnaces surrounding the specimens was kept constant to within ± 0.5 °C during the annealing processes, using Getrosist (Philips) temperature regulators and Frigistor reference chambers for the cold points of the Pt/Pt-Rh thermocouples. The recorded

annealing and quenching temperatures were measured separately with calibrated Pt/Pt-Rh thermocouples. The silica capsules were made as short as possible in order to minimize effects of thermal gradients in the furnaces, and thin-walled ampoules were utilized for quenching experiments in order to ensure fast cooling rates. The quenching experiments were performed with or without shattering the silica ampoules (depending on the quenching rate required) when brought into contact with ice-water.

Room temperature X-ray powder diffraction data were obtained in a Guinier camera ($\text{CuK}\alpha_1$ radiation, KCl as internal standard) and unit cell dimensions derived by applying the method of least squares. All samples were also examined by metallographic methods.

DTA data were collected with a Mettler Recording Vacuum Thermoanalyzer, using ~60 mg samples in sealed silica crucibles (Pd powder as reference). High temperature X-ray powder photographs were obtained in a Unicam camera ($\text{CuK}\alpha$ radiation) with the samples sealed in thin-walled silica capillaries. The temperature of the furnace surrounding the specimen was kept constant to within ± 5 °C during the exposures. The Pt/Pt-Rh thermocouples of the furnace were calibrated with a standard sample (Ag) in the range 22 to 900 °C. The Guinier data were used to correct the Unicam photographs and least squares refinements were subsequently applied.

A General Electric powder X-ray diffractometer ($\text{CuK}\alpha$ radiation, diamond powder as internal standard) with cryostat attachment was used to collect X-ray powder data below room temperature.

RESULTS AND DISCUSSION

(i). FeAs_2 , FeSb_2 , NiAs_2 , and NiSb_2 . The high temperature X-ray diffraction data (Fig. 1) show that the FeS_2 -*m* type structures of FeAs_2 , FeSb_2 , β - NiAs_2 , and NiSb_2 persist until the samples decompose peritectically according to $\text{TX}_2 \rightarrow \text{TX} + \text{liq.}$, where TX represents phases with NiAs/MnP type structure. The actual temperatures for these reactions are 1014 ± 7 , 745 ± 4 , 852 ± 5 , and 620 ± 2 °C for FeAs_2 , FeSb_2 , NiAs_2 , and NiSb_2 , respectively, as determined by DTA and quenching experiments.

For FeSb_2 and NiSb_2 these results are in agreement with those reported in Refs. 11, 12. (Redetermined values for the temperature of the eutectic between TSb_2 and Sb are 628 ± 2 and 616 ± 2 °C for $T = \text{Fe}$ and Ni, respectively.) The results for FeAs_2 and NiAs_2 are, on the

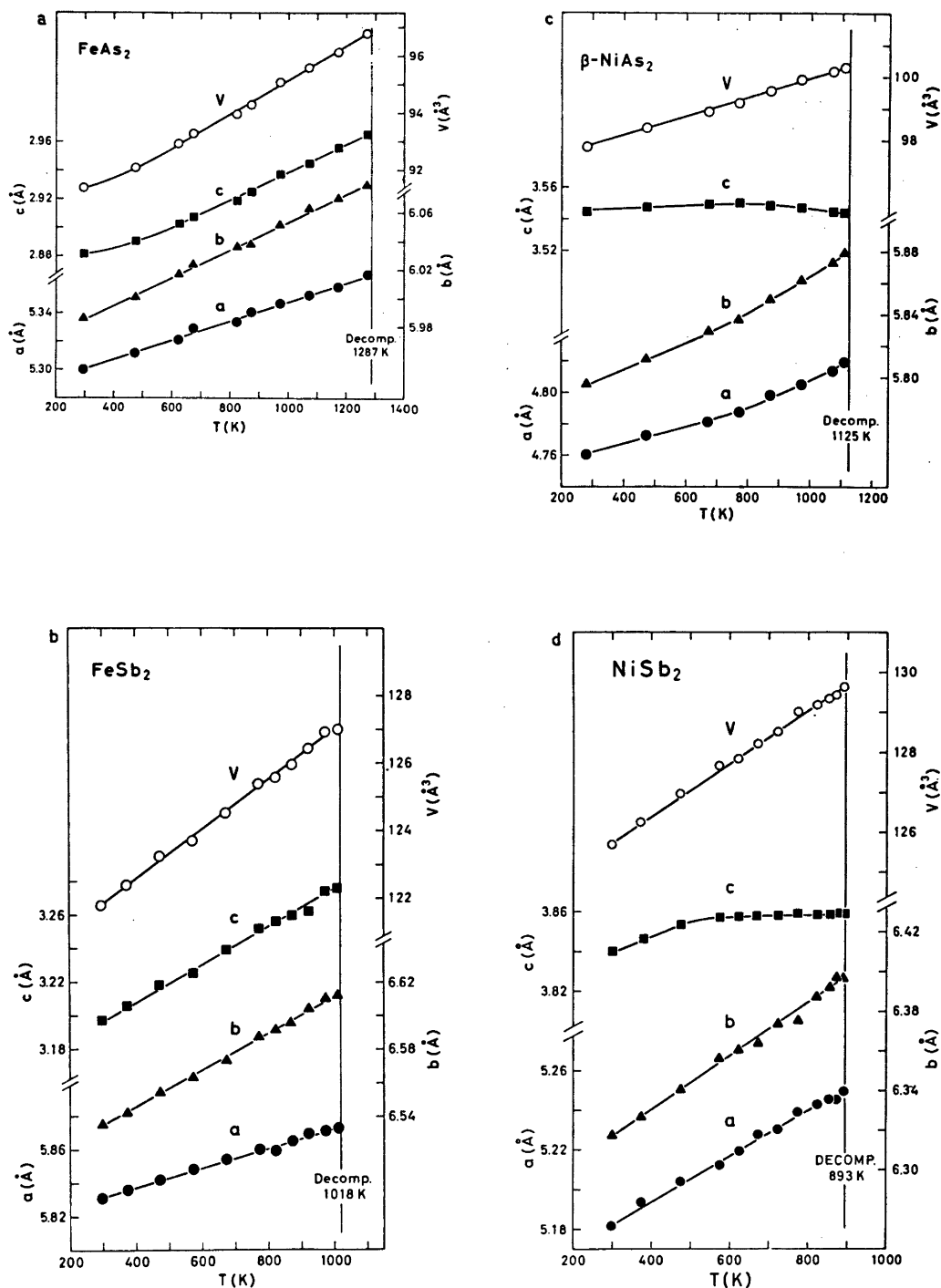


Fig. 1. Thermal expansion of: (a) FeAs₂, (b) FeSb₂, (c) β -NiAs₂ and (d) NiSb₂.

other hand, at variance. The reported¹² temperature for the decomposition of FeAs_2 is in agreement with the present determination, but the interpretation differs: melting *versus* peritectic reaction. As a support for peritectic reaction, FeAs is detectable on the high temperature X-ray diagrams taken above 1014 °C. For NiAs_2 , the temperature 852 °C is interpreted in Ref. 12 as representing an eutectic between NiAs and NiAs_2 , and it is also reported that NiAs_2 decomposes (melts) above 1040 °C. According to the present results, NiAs_2 disappears at 852 °C, leaving NiAs and liquid. The equilibrium vapour pressures at these high temperatures disturb the sensitivity of the methods and further investigations are needed to find the cause of the discrepancy between Ref. 12 and the present results.

The only minor thermal effect on the c axes for the two class B type compounds, $\beta\text{-NiAs}_2$ and NiSb_2 , is notable. The fact that

the thermal expansion of c is considerably less than for a and b has also been observed³ for other class B, FeS_2 - m type compounds (particularly for FeSe_2 and FeTe_2). The class A compounds exhibit, on the other hand, comparable thermal expansions for all axes.

Quenching experiments (followed by room temperature X-ray analyses) from selected temperatures on samples with different nominal compositions, show that the unit cell dimensions are invariant both with respect to temperature and compositions. Hence (using also inferences from Ref. 9), we conclude that the compounds exhibit no appreciable ranges of homogeneity on either side of the TX_2 composition.

Below the temperatures of decomposition (see above), quenched samples demonstrated various degrees of "partial decompositions" $\text{TX}_2(\text{s}) \rightleftharpoons \text{TX}(\text{s}) + \text{X}(\text{g})$. This is particularly noticeable for NiAs_2 which, moreover, also exhibits an $\alpha \rightleftharpoons \beta$ transition (cf. Refs. 13, 14;

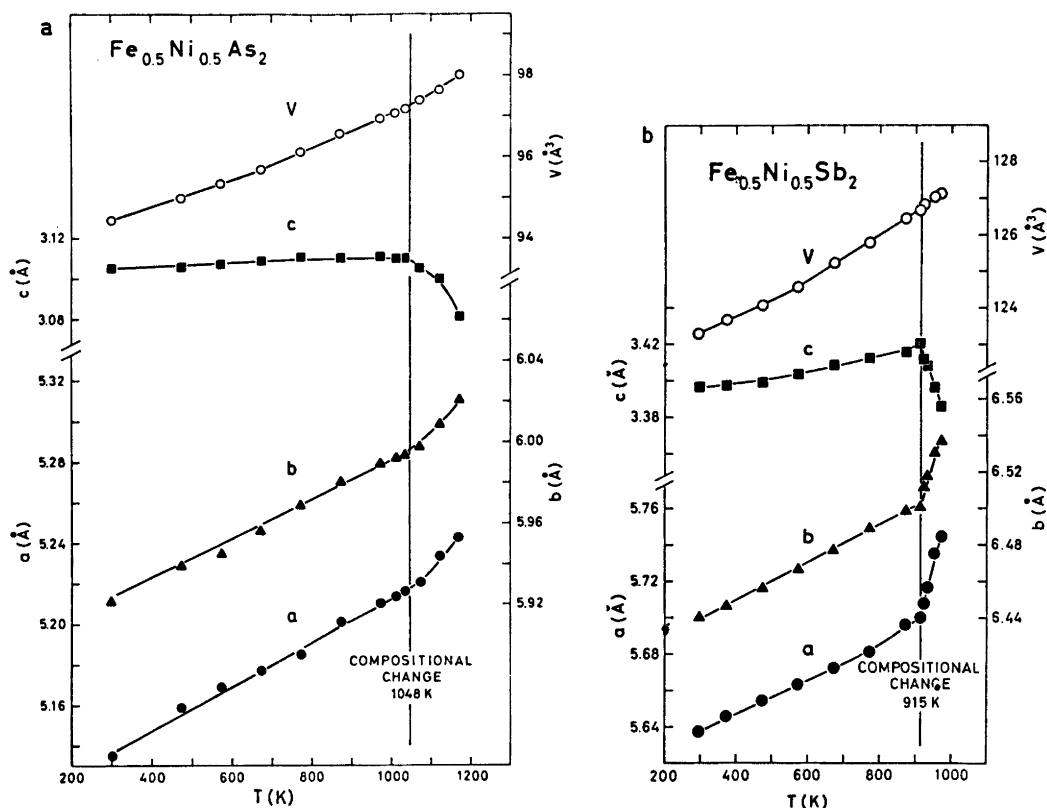


Fig. 2. Unit cell dimensions of: (a) $\text{Fe}_{0.5}\text{Ni}_{0.5}\text{As}_2$ and (b) $\text{Fe}_{0.5}\text{Ni}_{0.5}\text{Sb}_2$ as functions of temperature.

a third, high pressure-high temperature induced, modification with the FeS_2 - p type structure is also known^{15,16}). The reaction $\beta \rightarrow \alpha$ is so slow even at 560 °C that, once β - NiAs_2 is formed it persists with no detectable changes (at 560 °C) up to ~60 days before the first traces of α - NiAs_2 [orthorhombic; $a = 5.772(2)$, $b = 5.834(2)$, and $c = 11.420(7)$ Å] is detectable. Conversely, the reaction $\alpha \rightarrow \beta$ is also kinetically hampered below 600 °C, whereas complete conversion is rapidly attained above 640 °C. A number of quenching experiments on α - and β - NiAs_2 between 560 and 590 °C establish the transformation temperature as 580 ± 4 °C. (The conversion rate for $\beta \rightarrow \alpha$ can be accelerated by adding excess As to β - NiAs_2 , thus suggesting that the reaction is not of the solid state type but involves the vapour phase, cf. Ref. 3.)

Inspired by the existence of α - NiAs_2 , long term syntheses of NiSb_2 (from $\text{NiSb} + \text{Sb}$) at selected temperatures down to 300 °C were performed with no success in detecting a corresponding modification for NiSb_2 .

(ii). $\text{Fe}_{0.5}\text{Ni}_{0.5}\text{As}_2$ and $\text{Fe}_{0.5}\text{Ni}_{0.5}\text{Sb}_2$. Data for the class A/B, FeS_2 - m type representatives $\text{Fe}_{0.5}\text{Ni}_{0.5}\text{As}_2$ and $\text{Fe}_{0.5}\text{Ni}_{0.5}\text{Sb}_2$ are presented in Fig. 2, which show that their c axes (like for class B) expand only slightly below 775 and 642 °C, respectively. Above these temperatures, changes of composition occur according to $\text{Fe}_{0.5}\text{Ni}_{0.5}\text{X}_2 \rightarrow \text{Fe}_{1-t}\text{Ni}_t\text{X}_2 + \text{“NiX”} + \text{liq}$. The notation “NiX” refers to an Ni-rich phase with NiAs like structure, whose composition (judged from data for quenched samples) changes with temperature. There may be a variable Fe content and/or a variable T to X ratio for “NiX”, but studies of the FeAs – NiAs and FeSb – NiSb series are needed to resolve this question.

The compositional changes for $\text{Fe}_{0.5}\text{Ni}_{0.5}\text{X}_2$ are, on the other hand, comparatively easy to follow as a function of temperature. Fig. 3 shows the unit cell dimensions of these phases in the samples quenched from various temperatures T_q . By comparison with unit cell dimensions for the $\text{Fe}_{1-t}\text{Ni}_t\text{X}_2$ phases,^{2,5,6} it is evident that a gradual decrease of Ni-content occurs with increasing T_q (no indications of non-stoichiometry of these ternary phases being found; suggesting that the problem may be regarded as “pseudo-binary”). The complete disappearance (as judged from X-ray diffraction and metallo-

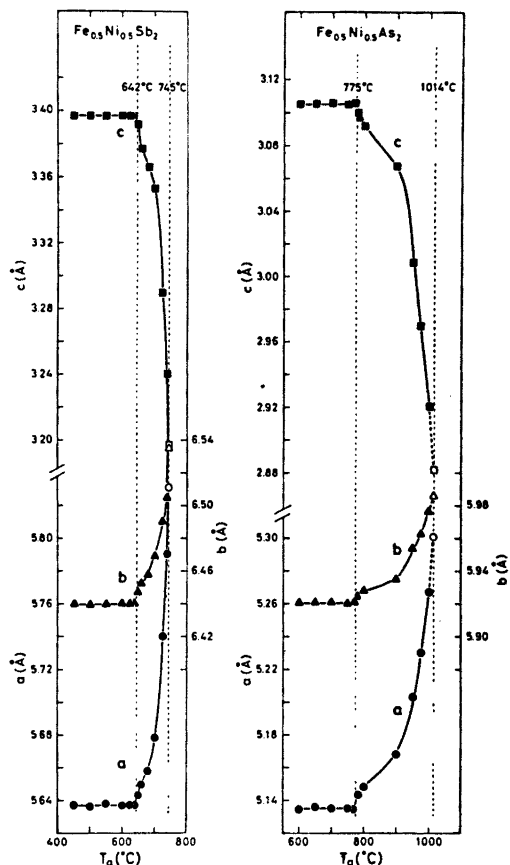
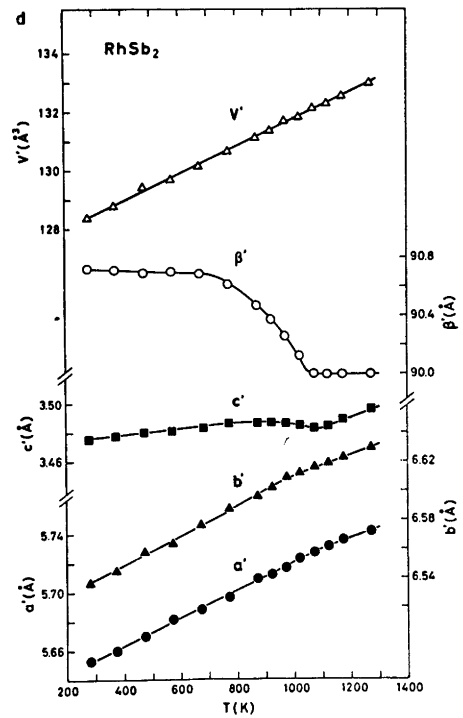
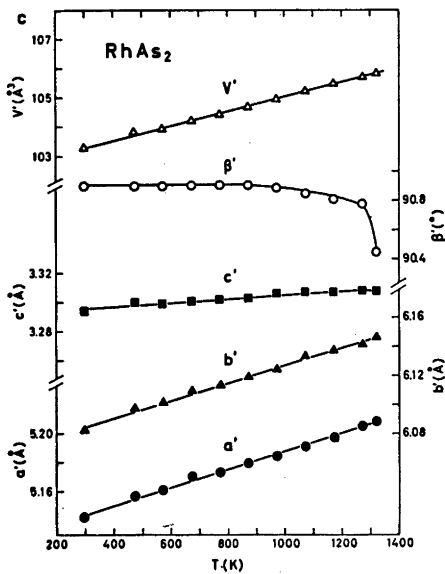
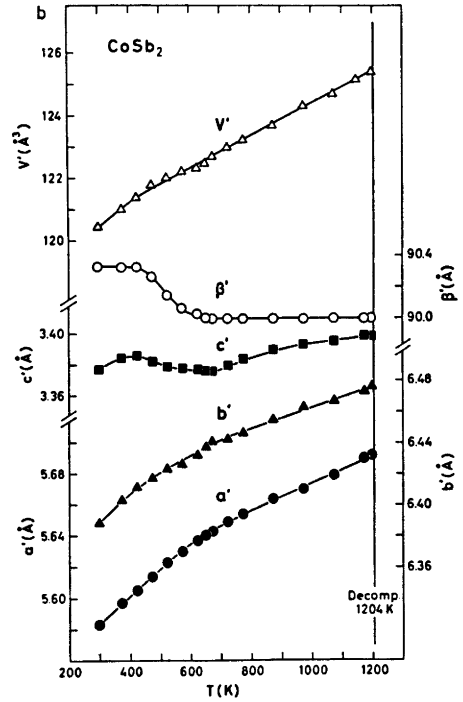
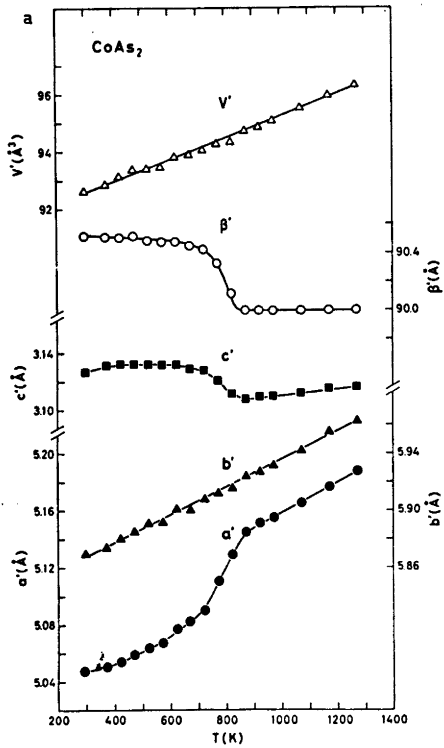


Fig. 3. Room temperature unit cell dimensions for samples of $\text{Fe}_{0.5}\text{Ni}_{0.5}\text{As}_2$ and $\text{Fe}_{0.5}\text{Ni}_{0.5}\text{Sb}_2$ quenched from various temperatures T_q .

graphic examinations of quenched samples, high temperature X-ray diffraction and DTA) of the FeS_2 - m type phases occurs at 1014 and 745 °C for $X = \text{As}$ and Sb , respectively. (Due to the disturbingly high As pressure, the uncertainty is larger for $\text{Fe}_{1-t}\text{Ni}_t\text{As}_2$ than for $\text{Fe}_{1-t}\text{Ni}_t\text{Sb}_2$.) This fact and the trends for the unit cell dimensions (Fig. 3) strongly suggest that just before the final decomposition, the approximately pure FeX_2 remains.

The mutual substitution of one kind of atom for another is usually expected to increase with increasing temperature and this has also been suggested for $\text{Fe}_{1-t}\text{Ni}_t\text{As}_2$.⁵ Our results show that this cannot be the case and a more detailed reexamination of the phase relation-



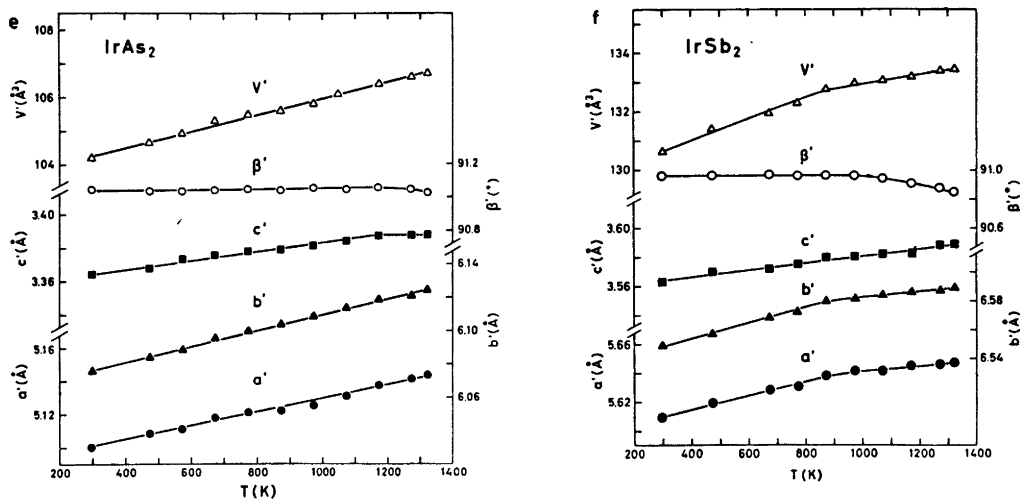


Fig. 4. Pseudo FeS_2 - m type unit cell dimensions versus temperature for (a) CoAs_2 , (b) CoSb_2 , (c) RhAs_2 , (d) RhSb_2 , (e) IrAs_2 , and (f) IrSb_2 .

ships (as a function of temperature) for $\text{Fe}_{1-x}\text{Ni}_x\text{X}_2$ ($X = \text{As}, \text{Sb}$) is called for.

(iii). CoAs_2 , CoSb_2 , RhAs_2 , RhSb_2 , IrAs_2 , and IrSb_2 . The scope of the present high temperature X-ray study included, originally, all binary compounds with the CoSb_2 type structure. Preliminary attempts showed that the samples of RhP_2 and IrP_2^* were difficult to load into the silica capillaries, and examination of these compounds was postponed towards the end of the programme. For reasons given in section *v* they were, however, finally dismissed.

The indexing and reduction of the X-ray diffraction data for CoSb_2 type compounds were performed in terms of their true monoclinic unit cells [\mathbf{a}_{AP} , \mathbf{b}_{AP} , \mathbf{c}_{AP} ; (β_{AP})], but in order to facilitate comparison with the FeS_2 - m type compounds, their pseudo FeS_2 - m type cells [$\mathbf{a}' = (\mathbf{a}_{\text{AP}} - \mathbf{c}_{\text{AP}})/2$, $\mathbf{b}' = \mathbf{b}_{\text{AP}}$, $\mathbf{c}' = (\mathbf{a}_{\text{AP}} + \mathbf{c}_{\text{AP}})/2$; (β')] are conveniently used in the following presentation.

As evident from Fig. 4, CoAs_2 , CoSb_2 , and RhSb_2 apparently exhibit transformations from monoclinic to orthorhombic symmetry at 870, 650, and 1070 K, respectively; uncertainties being difficult to estimate (*vide infra*). RhAs_2 ,

IrAs_2 , and IrSb_2 maintain the monoclinic symmetry up to the maximum temperature (~ 1300 K) of examination. (The peritectic decomposition of CoSb_2 at $931 \pm 5^\circ \text{C}$ is significantly higher in temperature than reported in Ref. 17. This is also the case for CoSb_3 which undergoes the peritectic decomposition at $876 \pm 5^\circ \text{C}$ according to the present finding.)

The gradual structural changes as a function of temperature for the compounds under consideration are completely reproducible and do not vary, *e.g.*, with the heating procedure of the samples in the X-ray equipment. Quenching experiments confirm that no appreciable ranges of homogeneity can exist for these TX_2 compounds.⁴ The crystalline perfection of samples quenched from temperatures where the high temperature X-ray data show that the orthorhombic symmetry prevails, is compatible with data for samples quenched from the monoclinic temperature region. (The orthorhombic state of these samples is not quenchable.) Hence, non-equilibrium crystal imperfections cannot be the cause of the observed gradual changes for CoAs_2 , CoSb_2 , and RhSb_2 . The results in Fig. 4 must therefore imply that these compounds undergo phase transitions of second or higher order (see *v*). An anomaly in the thermal expansion curves of c is a common feature for all these transitions.

* Attempted syntheses of CoP_2 failed, the reaction product being invariably CoP and CoP_3 .

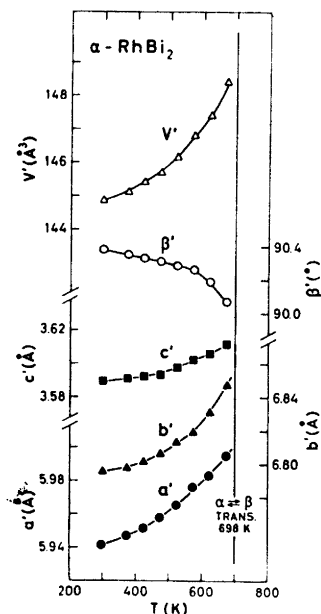


Fig. 5. Pseudo FeS_2 - m type unit cell dimensions for α - RhBi_2 as function of temperature.

(iv). RhBi_2 . The $\alpha \rightleftharpoons \beta$ transition in RhBi_2 ($\alpha \rightarrow \beta$ detectable on DTA, β - RhBi_2 quenchable) is established at 425 ± 3 °C (from DTA and quenching experiments). Peritectic decomposition of β - RhBi_2 to RhBi (NiAs type structure) and liquid occurs at 778 ± 4 °C. These results are in perfect agreement with those in Ref. 12.

The thermal expansion of α - RhBi_2 (Fig. 5) reveals that β' gradually approaches 90°. Despite numerous additional X-ray photographs taken around 425 °C, the condition $\beta' = 90^\circ$ was never observed. The thermal expansion of c for α - RhBi_2 differs from those for CoAs_2 , CoSb_2 , and RhSb_2 in that the former compound shows no anomaly. Hence, we conclude that the first order phase change $\alpha \rightarrow \beta$ occurs (just) before the structure becomes orthorhombic. Knowledge about the actual atomic arrangement of β - RhBi_2 will be needed in order to understand the reason for this odd behaviour.

The structure of β - RhBi_2 has been approached,^{18,19} but the single crystal data obtained so far have apparently been so poor that the problem remains unsolved. In fact, we were unable to index our X-ray powder data on the basis of the monoclinic unit cell

dimensions reported in Refs. 18, 19. Since β - RhBi_2 is quenchable, we intend to give the problem continued attention.

(v). $\text{CoSb}_2 \rightleftharpoons \text{FeS}_2$ - m type transformations. The transformations referred to in section iii almost certainly reflect transitions between the CoSb_2 and FeS_2 - m type structures. Unequivocal confirmation of crystallographic changes is difficult in these cases due to the close structural relationship. The angle β' of the pseudo-cell gradually approaches 90° and ultimately, the exact fulfillment of $\beta' = 90^\circ$ becomes virtually indistinguishable from the approximate satisfaction of this condition. Apart from the splitting of certain reflections when $\beta' \neq 90^\circ$, the CoSb_2 type diffraction pattern differs from that of FeS_2 - m also by additional reflections. The intensity of these reflections diminishes rapidly when β' becomes nearly 90°, and their possible presence or absence are even more difficult to detect than the degree of overlap between reflections. The somewhat low quality of the high temperature X-ray powder intensity data prevented clarification of this question through structural refinements. However, semi-quantitative calculations and comparison with relative intensities for CoAs_2 versus $\text{Fe}_{0.5}\text{Ni}_{0.5}\text{As}_2$ and CoSb_2 versus $\text{Fe}_{0.5}\text{Ni}_{0.5}\text{Sb}_2$ show that the FeS_2 - m type is at least a very good approximation to the high temperature structures of CoAs_2 and CoSb_2 . We believe that the same applies to RhSb_2 .

The $\text{CoSb}_2 \rightleftharpoons \text{FeS}_2$ - m type transition may accordingly be regarded as experimentally well established for CoAs_2 , CoSb_2 , and RhSb_2 . The fact that these transitions are of second or higher order contradicts the prediction of Goodenough²⁰ and emphasizes an important distinction between the $\text{CoSb}_2 \rightleftharpoons \text{FeS}_2$ - m and $\text{VO}_2 \rightleftharpoons \text{TiO}_2$ - r (r =rutile) type transitions.

It appears appropriate to ask why RhAs_2 , (α - RhBi_2), IrAs_2 , and IrSb_2 do not show corresponding $\text{CoSb}_2 \rightleftharpoons \text{FeS}_2$ - m type transitions. The answer to this question is clearly hidden in the parameters (including those specifying the thermal movements of the atoms) which describe the distortion of the CoSb_2 type relative to the FeS_2 - m type structure. Since both structure types comprise a number of parameters (see vi), it is difficult to find a satisfactory, general approach to this problem. However, β' can probably be regarded as a parameter

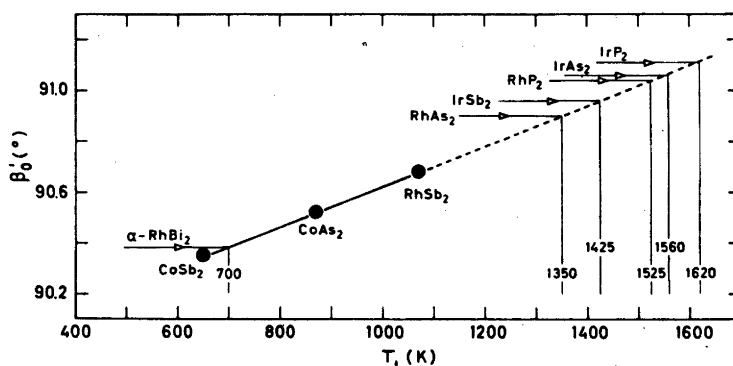


Fig. 6. Room temperature values β'_0 versus $\text{CoSb}_2 \rightleftharpoons \text{FeS}_2$ - m type transition temperature T_1 for CoAs_2 , CoSb_2 , and RhSb_2 .

describing the average degree of distortion between the CoSb_2 and FeS_2 - m type structures. In line with this, Fig. 6 shows a linear empirical correlation between the $\text{CoSb}_2 \rightleftharpoons \text{FeS}_2$ - m type transition temperature T_1 (for CoAs_2 , CoSb_2 , and RhSb_2) and the room temperature values β'_0 of β' . Assuming that this correlation applies to all compounds with the CoSb_2 type structure, α - RhBi_2 should undergo the $\text{CoSb}_2 \rightleftharpoons \text{FeS}_2$ - m type transition at about 700 K (*i.e.* very nearly at the same temperature as found for the $\alpha \rightleftharpoons \beta$ transition). According to the same correlation, the remaining CoSb_2 type compounds should transform to the FeS_2 - m type above 1300 K. This was, in fact, the reason why RhP_2 and IrP_2 were finally dismissed from the high temperature X-ray programme (*vide supra*).

In the same way that compounds possessing the CoSb_2 type structure at room temperature convert to the FeS_2 - m type at higher temperatures, it is feasible (but less likely) that those of the latter type could show the opposite transition at lower temperatures. Thus, FeAs_2 , NiAs_2 , NiSb_2 , $\text{Fe}_{0.5}\text{Ni}_{0.5}\text{As}_2$, and $\text{Fe}_{0.5}\text{Ni}_{0.5}\text{Sb}_2$ were examined by X-ray diffraction down to 4 K. None of the X-ray diagrams gave, however, indication of (partial or complete) FeS_2 - $m \rightarrow \text{CoSb}_2$ type transformation. This finding concurs with previous results for CrSb_2 and FeSb_2 .²¹ Again the somewhat unique character (*viz.* in relation to the Periodic System) of CoSb_2 type compounds is evident.

(vi). *The CoSb_2 versus the FeS_2 - m type structure.* A complete structural description of a crystalline solid involves specification of

positions and movements of the atoms relative to each other. Although this problem can be approached in several ways, the conventional crystallographic scheme entirely dominates the field. (A discussion of the CoSb_2 and FeS_2 - m type geometry in terms of alternative variables will be presented in a forthcoming paper.) Following the traditional scheme, a geometrical description of the FeS_2 - m type structure [space group $Pn\bar{m}$; T in 2(a), X in 4(g)] requires the knowledge of three axes (a , b , c) and two positional parameters (x , y), whereas the CoSb_2 type [space group $P2_1/c$; $4T$, $4X_I$, and $4X_{II}$ in 4(e)] demands three axes (a_{AP} , b_{AP} , c_{AP}), one angle (β_{AP}), and nine positional parameters (x_T , y_T , z_T , x_I , y_I , z_I , x_{II} , y_{II} , z_{II}).

Since the space group of the CoSb_2 type is a subgroup of that for the FeS_2 - m type, the latter can be converted to a CoSb_2 type setting with a_{AP} ($=c_{AP}$), b_{AP} , and β_{AP} specifying the unit cell, and $x_T = 1/4$, $y_T = 0$, $z_T = 1/4$, $x_I = 1/4 + x/2$, $y_I = y$, $z_I = 1/4 - x/2$, $x_{II} = 1/4 - x/2$, $y_{II} = 1 - y$, and $z_{II} = 1/4 + x/2$ for the positional parameters. Hence, the CoSb_2 versus FeS_2 - m type coordinate relationship can, in terms of the distortion parameters Δx_T , Δy_T , *etc.*, be expressed as

$$T: \quad x_T = 1/4 + \Delta x_T, \quad y_T = \Delta y_T, \quad z_T = 1/4 + \Delta z_T$$

$$X_I: \quad x_I = 1/4 + x/2 + \Delta x_I, \quad y_I = y + \Delta y_I, \quad z_I = 1/4 - x/2 + \Delta z_I$$

$$X_{II}: \quad x_{II} = 1/4 - x/2 + \Delta x_{II}, \quad y_{II} = 1 - y + \Delta y_{II}, \quad z_{II} = 1/4 + x/2 + \Delta z_{II}$$

In order to judge the magnitude of these distortion parameters, sufficiently accurate values for the positional parameters of class A/B, FeS_2 - m and CoSb_2 type compounds are

required. According to Ref. 22, x and y vary systematically within the FeS_{2-m} type family. The natural class A/B, FeS_{2-m} type candidates for such a comparison would be $\text{Fe}_{0.5}\text{Ni}_{0.5}\text{As}_2$ and $\text{Fe}_{0.5}\text{Ni}_{0.5}\text{Sb}_2$ (not yet structurally refined), or the Ru-Pd and Os-Pt analogues (could apparently not be prepared¹⁴). In the lack of experimental data, it may be argued that average values for FeAs_2 , versus NiAs_2 , and FeSb_2 , versus NiSb_2 , will provide useful approximations. (Some support for this assumption is to be found in the approximately linear relationships between x , y and the compositional parameter t in the series $\text{Cr}_{1-t}\text{Fe}_t\text{As}_2$, and $\text{Cr}_{1-t}\text{Fe}_t\text{Sb}_2$.²³).

The degree of reliability of the structure determinations for the CoSb_2 type compounds represents another concern. The large number of positional parameters to be determined makes the results⁴ from powder diffraction data unreliable for RhP_2 , RhAs_2 , IrP_2 , and IrAs_2 . The structural data for CoSb_2 , RhSb_2 , α -

RhBi_2 , and IrSb_2 are indeed obtained by single crystal methods,²⁴ but the results are apparently not of sufficient quality to justify comparative analyses. One is therefore left with CoAs_2 ⁴ as the only suitable candidate.

A schematic presentation of the relationship between the FeS_{2-m} and CoSb_2 type structures is shown in Fig. 7. The projection shows the positions of the T and X atoms in the FeS_{2-m} type arrangement (assumed for $\text{Fe}_{0.5}\text{Ni}_{0.5}\text{As}_2$, *vide supra*), whereas the lengths and directions of the arrows give their main displacements in the CoSb_2 type cell of CoAs_2 (displacements along the projection axis are negligible). The illustration shows that the X atoms are shifted mainly along $\pm(\mathbf{a}-\mathbf{c})$, whereas the T atoms approximately along $\pm(\mathbf{a}/5-\mathbf{c})$. The magnitude of each T displacement is about twice that of each X . (For CoAs_2 , versus $\text{Fe}_{0.5}\text{Ni}_{0.5}\text{As}_2$, $\Delta x_T = 0.02$, $\Delta y_T = 0.00$, $\Delta z_T = 0.03$, $\Delta x_I = \Delta x_{II} = 0.00$, $\Delta y_I = \Delta y_{II} = 0.00$, $\Delta z_I = \Delta z_{II} = 0.02$. Similar relations appear to apply to the CoSb_2 type

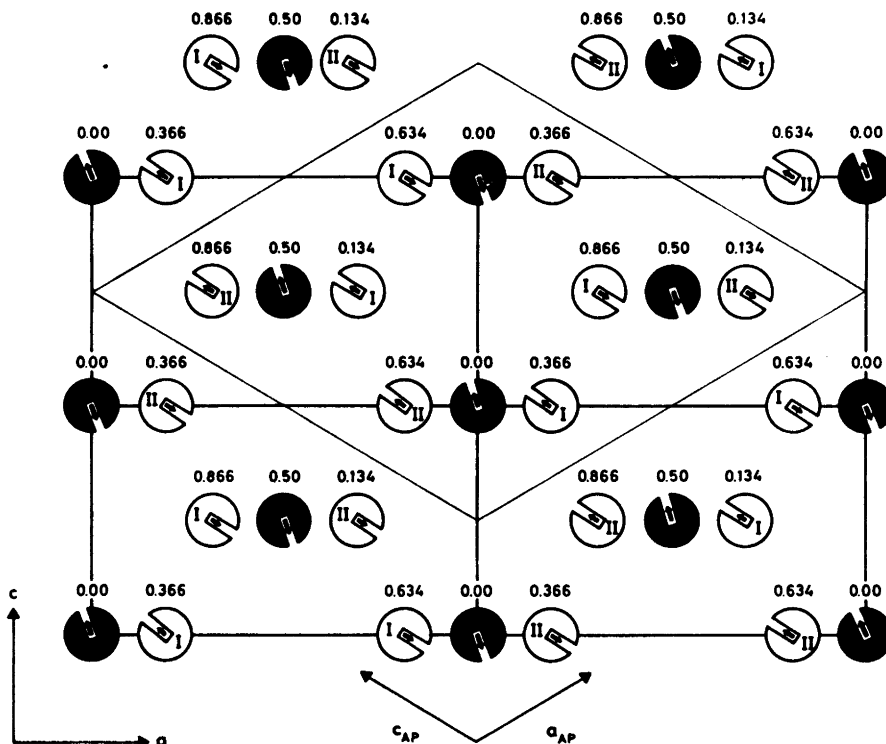


Fig. 7. Relationship between the FeS_{2-m} and CoSb_2 type structures. Filled and open circles represent T and X atoms, respectively, in class A/B, FeS_{2-m} type arrangement. Lengths and directions of arrows give displacements in order to obtain CoSb_2 type atomic arrangement.

antimonides *versus* $\text{Fe}_{0.5}\text{Ni}_{0.5}\text{Sb}_2$.) The net effect of the displacements is that the average $T-X$ distance is kept approximately constant during the transition. A consistent trend is, however, observed in the shifts such that the six approximately equal $T-X$ distances in the FeS_2 - m type structure are split into three shorter ($T-X_I$) and three longer ($T-X_{II}$) distances in the CoSb_2 type (see *viii*).

The FeS_2 - $m \rightleftharpoons \text{CoSb}_2$ type transition (and possibly other transitions originating from the FeS_2 - m type structure) can be described in

terms of the Landau theory.²⁵ However, a general treatment of this problem is more complicated than for the $\text{NiAs} \rightleftharpoons \text{MnP}$ or $\text{NiAs} \rightleftharpoons \text{NbS}$ type transitions,²⁶ due to the variable positional parameters of the FeS_2 - m type as opposed to the variable-free NiAs type (in this respect).

(*vii*). *Axial ratios.* Due to differences in absolute dimensions, thermal expansion data are often difficult to compare. In order to facilitate comparison, axial ratios are frequently consulted. For compounds with the FeS_2 - m

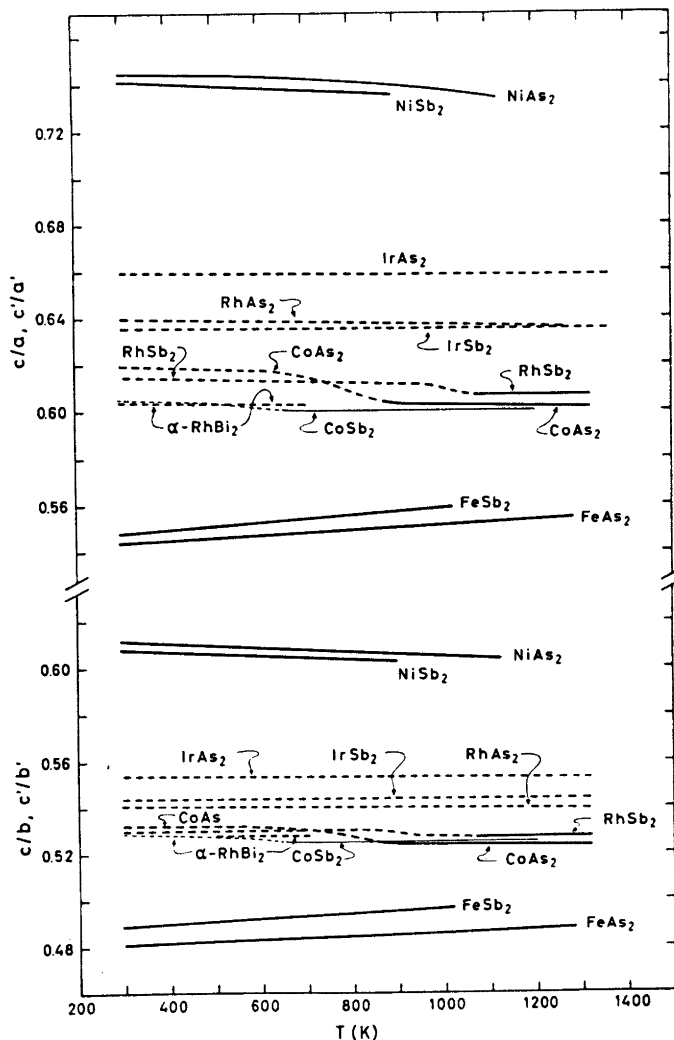


Fig. 8. Axial ratios c/a , c/b and c'/a' , c'/b' versus temperature for FeS_2 - m and CoSb_2 type compounds, respectively. Broken and solid curves correspond to CoSb_2 and FeS_2 - m type regions, respectively.

(and CoSb_2) type structure(s), axial ratios have an additional important function in providing the basis for division of the compounds into the classes A, B, and A/B (*vide supra*).

Fig. 8 shows the temperature variation in axial ratios c/a (c'/a') and c/b (c'/b') for the compounds under investigation. Evidently, the class A representatives FeAs_2 and FeSb_2 , exhibit increasing c/a and c/b with increasing temperature, whereas the opposite trend prevails for the class B members $\beta\text{-NiAs}_2$ and NiSb_2 (*cf.* also the results for class B, $\text{FeS}_2\text{-}m$ type chalcogenides in Ref. 3). The class A/B, $\text{FeS}_2\text{-}m$ type compounds $\text{Fe}_{0.5}\text{Ni}_{0.5}\text{As}_2$ and $\text{Fe}_{0.5}\text{Ni}_{0.5}\text{Sb}_2$ exhibit c/a , c/b values of 0.605, 0.525 and 0.603, 0.528, respectively, at room temperature and decreases only slightly with increasing temperature (these compounds are, for clarity, not included in Fig. 8). The same applies to the CoSb_2 type compounds (class A/B) well below T_1 (see *v*) for all members and also from just above T_1 for CoAs_2 , CoSb_2 , and RhSb_2 .

The approximate temperature independence of axial ratios for class A/B, $\text{FeS}_2\text{-}m$ or CoSb_2 type compounds (neglecting in this connection the $\text{CoSb}_2 \rightleftharpoons \text{FeS}_2\text{-}m$ type transition regions) is consistent with the increasing and decreasing axial ratios with temperature for the classes A and B, respectively, and also with the idea of class A/B as a "mixture" of the classes A and B (see *viii*). A common decrease in axial ratios is, however, observed in the $\text{CoSb}_2 \rightleftharpoons \text{FeS}_2\text{-}m$ type transition regions for CoAs_2 , CoSb_2 , and RhSb_2 . (This finding is not a consequence of our neglect to correct c'/a' and c'/b' for $\beta' \neq 90^\circ$ which amounts to a rather minor effect in these cases.) Generalizing from the relative magnitude of the observed decreases for CoAs_2 and CoSb_2 , the changes in axial ratios during the $\text{CoSb}_2 \rightleftharpoons \text{FeS}_2\text{-}m$ type transitions should be successively smaller (for fixed T atoms) along the sequence: phosphides, arsenides, antimonides, bismuthides. Although the $\alpha \rightleftharpoons \beta$ transition for RhBi_2 complicates the situation, it is worth noting that the above observation is consistent with the absence of an anomaly in c (see *iii* and *iv*) and/or a beginning decrease in axial ratios for this compound. Similarly, this finding may also shed new light on the scatter in the room temperature axial ratios for the CoSb_2 type compounds: [0.604

($\alpha\text{-RhBi}_2$) $\leq c'/a' \leq 0.680$ (IrP_2), 0.528 ($\alpha\text{-RhBi}_2$) $\leq c'/b' \leq 0.563$ (IrP_2)], which may be considerably reduced on referring to their (real or hypothetical) $\text{FeS}_2\text{-}m$ type modifications.

(*viii*). *Further aspects.* Previous discussions concerning the relationship between the CoSb_2 and $\text{FeS}_2\text{-}m$ type structures have focused attention on that effect of the distortion which produces alternately shorter and longer $T\text{-}T$ distances along c' . This "pair formation" and the formal d^5 manifold attributed to T for the CoSb_2 type compounds have led a number of workers in the field (*cf.* Refs. 4, 7, 27, and references therein) to suggest that localized, normal $T\text{-}T$ σ -bonds are the stabilizing element of the CoSb_2 type structure. The rejection of this hypothesis is discussed in Refs. 2, 20 and a few relevant remarks will be made here.

With the attention still focused on the T atoms, it is recognized that six of the twelve $X\text{-}T\text{-}X$ angles for CoSb_2 type compounds show some resemblance to the octahedral angles for class A, $\text{FeS}_2\text{-}m$ type compounds, whereas the other six correspond with those in class B.

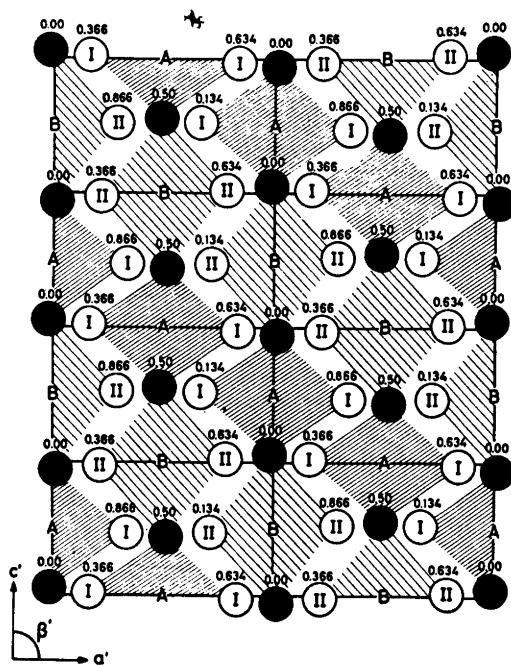


Fig. 9. Arrangement of classes A and B $\text{FeS}_2\text{-}m$ type fragments in the CoSb_2 type structure.

However, a simpler and closer similarity between the CoSb_2 and the two FeS_2 - m type classes emerges when attention is shifted to the two crystallographically non-equivalent X_{I} and X_{II} atoms in the CoSb_2 type structure. The immediate coordination ($3T$ and $1X_{\text{II}}$) of X_{I} resembles that for the X atoms in class A, whereas the neighbours ($3T$ and $1X_{\text{I}}$) of X_{II} are arranged as in class B. This aspect is illustrated in Fig. 9, where a distinct pattern of four-membered A and B clusters is evident.

In this pictorial way, the CoSb_2 type structure occurs as a natural consequence of mixing equal amounts of structural elements from the FeS_2 - m type classes A and B. This interpretation lends support to the use of the notation A/B also for the CoSb_2 type and reduces in a way the cause of the existence of this structure type to the effects responsible for the distinction between the FeS_2 - m type classes A and B. Referring to our discussion in Ref. 22 (where we conclude that there is indeed no experimental evidence in favour of a regular type of $T-T$ bonding in class A, FeS_2 - m type compounds) this observation makes it even more unlikely that the CoSb_2 type should be stabilized by normal, localized $T-T$ σ -bonds. This conclusion is also supported by the observed thermal contraction of c for CoAs_2 , CoSb_2 , and RhSb_2 (Fig. 4) during their $\text{CoSb}_2 \rightleftharpoons \text{FeS}_2$ - m type transitions. If $T-T$ bonds had been present in their CoSb_2 type modifications, the opposite result with an increased c would have been expected through relaxation of these bonds.

Without specifying the bonding situation in the FeS_2 - m and CoSb_2 type structures, it seems that the variation in bonding character of the $X-T$ ($T-X$) bonds (*cf.* Ref. 22; the points being elaborated further in a forthcoming paper) is responsible for the occurrence of their different variants A, B, and A/B. The distinct A and B pattern in the CoSb_2 type class A/B (Fig. 9) shows that the effects in question occur in a regular, ordered manner, as opposed to the disordered distribution of bonding characteristics in the FeS_2 - m type class A/B. On this basis, it is only natural that CoSb_2 type compounds transform gradually to the class A/B, FeS_2 - m type structure at higher temperatures by increasing disordering of bonding characteristics.

REFERENCES

1. Kjekshus, A. and Rakke, T. *Struct. Bonding (Berlin)* 19 (1974) 85.
2. Kjekshus, A. and Rakke, T. *Acta Chem. Scand. A* 28 (1974) 1001.
3. Kjekshus, A. and Rakke, T. *Acta Chem. Scand. A* 29 (1975) 443.
4. Kjekshus, A. *Acta Chem. Scand.* 25 (1971) 411.
5. Roseboom, E. H. *Am. Mineral.* 48 (1963) 271.
6. Bjerkelund, E. and Kjekshus, A. *Acta Chem. Scand.* 24 (1970) 3317.
7. Brostigen, G. and Kjekshus, A. *Acta Chem. Scand.* 24 (1970) 2983.
8. Kjekshus, A., Rakke, T. and Andresen, A. F. *Acta Chem. Scand. A* 28 (1974) 996.
9. Holseth, H. and Kjekshus, A. *Acta Chem. Scand.* 22 (1968) 3273.
10. Zhuravlev, N. N. and Smirnova, E. M. *Sov. Phys. Crystallogr.* 10 (1966) 694.
11. Hansen, M. and Anderko, K. *Constitution of Binary Alloys*, McGraw-Hill, New York 1958.
12. Shunk, F. A. *Constitution of Binary Alloys, Second Supplement*, McGraw-Hill, New York 1969.
13. Yund, R. A. *Econ. Geol.* 56 (1961) 1273.
14. Bennett, S. L. and Heyding, R. D. *Can. J. Chem.* 44 (1966) 3017.
15. Donohue, P. C., Bither, T. A. and Young, H. S. *Inorg. Chem.* 7 (1968) 998.
16. Munson, R. A. *Inorg. Chem.* 7 (1968) 389.
17. Elliott, R. P. *Constitution of Binary Alloys, First Supplement*, McGraw-Hill, New York 1965.
18. Zhuravlev, N. N. and Zhdanov, G. S. *Soviet Phys. JETP* 1 (1955) 91.
19. Kuz'min, R. N. and Zhuravlev, N. N. *Sov. Phys. Crystallogr.* 6 (1961) 209.
20. Goodenough, J. B. *J. Solid State Chem.* 5 (1972) 144.
21. Holseth, H., Kjekshus, A. and Andresen, A. F. *Acta Chem. Scand.* 24 (1970) 3309.
22. Kjekshus, A., Rakke, T. and Andresen, A. F. *Acta Chem. Scand. A* 31 (1977) 253.
23. Kjekshus, A., Peterzéns, P. G., Rakke, T. and Andresen, A. F. *To be published*.
24. Zhdanov, G. S. and Kuz'min, R. N. *Sov. Phys. Crystallogr.* 6 (1962) 704.
25. Landau, L. D. and Lifshitz, E. M. *Statistical Physics*, Pergamon, London 1969.
26. Franzen, H. F., Haas, C. and Jelinek, F. *Phys. Rev. B* 10 (1974) 1248.
27. Jeitschko, W. and Donohue, P. C. *Acta Crystallogr. B* 31 (1975) 574.

Received March 31, 1977.

An Estimate of the Effect of Series Termination on Deformation Density Peak Heights *

M. S. LEHMANN^a and P. COPPENS^b

^a Institut Laue-Langevin, B.P.n° 156X, 38042-Grenoble Cédex, France and ^b Department of Chemistry, State University of New York, Buffalo, New York 14214, U.S.A.

An expression is derived which describes the reduction in height of a Gaussian shaped peak in a deformation electron density map as a function of the data cut-off limit. It is found that for a given reduction in peak height the data collection limit is inversely proportional to the peak width at infinite resolution. The expression provides a test for the completeness of the data set. It also allows an estimate of the number of reflections to be collected to achieve a required minimum ratio of observed peak height to peak height at infinite resolution. The dependence of the thermal smearing function on temperature within the harmonic approximation is used for an estimate of the maximum data collection temperature, using the criterion that the width of the peak at rest should exceed the width of the thermal smearing function. Results are illustrated with examples from a recent charge density study of *p*-nitro-pyridine *N*-oxide carried out at 30 K.

Several studies of the charge density in crystals have become available in recent years. They employ a combination of X-ray data with either neutron or very high order X-ray data. Results are often expressed as deformation density maps in which spherical neutral atoms with positional and thermal parameters from the neutron or high order experiment are subtracted from the experimental density.

The principal features of such maps are the overlap or bond density peaks located between covalently bound atoms and density near terminal atoms, which is commonly associated with lone pair electrons. Each peak may be

described by its position, its height and shape. In first approximation the peak *positions* are expected to be relatively insensitive to the details of systematic corrections for effects such as absorption, extinction or series termination. This justifies qualitative interpretation of the maps in the familiar terms of chemical bonding theory. But the quantitative information inherent in the height and shape of the maxima requires a more careful analysis of all effects which influence the final results. The purpose of the present discussion is an estimate of the relation between the cut-off limit in data collection and the experimental peak heights as well as the condition this relation imposes on the completeness of the data set.

The effect of Fourier series termination on the peak height. If data are collected up to a maximum value of $S_{\max} = (2 \sin \theta/\lambda)_{\max}$, the effective scattering factor corresponding to a peak in the deformation density can be described as

$$f'(S) = f(S) \cdot R(S)$$

with the resolution function *R* defined as

$$R(S) = \begin{cases} 1 & \text{for } S \leq S_{\max} \\ 0 & \text{for } S_{\max} < S \end{cases}$$

The density corresponds to the Fourier transform

$$\varrho'(r) = \mathcal{F}[f'] = \mathcal{F}[f \cdot R] = \varrho * \mathcal{F}[R] \quad (1)$$

where $\varrho(r) = \mathcal{F}[f(S)]$ is the density at infinite resolution, and where * indicates a convolution between two functions.

* An account of this work was given at the 9th Nordic Structural Chemistry Meeting, Odense, Denmark, January 1976.

$\mathcal{F}[R(S)] = C(r)$ is easily derived and is given by¹

$$C(r) = 4\pi S_{\max}^3 (\sin m - m \cos m) / m^3$$

with

$$m = 2\pi S_{\max} r$$

The form of the peak in the difference density is less easy to predict. For a discussion of the general behaviour of the peak we have chosen here an isotropic Gaussian distribution function

$$\varrho(r) = \varrho(0) \exp(-r^2/2\sigma_T^2)$$

where $\varrho(0)$, the maximum, is defined by

$$\varrho(0) = P / (2\pi)^{3/2} \sigma_T^3 \tag{2}$$

and where P is the number of electrons in the peak. The distribution parameter σ_T describes the width of the thermally smeared density. If both the thermal smearing function and the unsmearred density can be assumed to be of Gaussian nature, σ_T can be expressed as

$$\sigma_T^2 = \sigma^2 + u^2 \tag{3}$$

where σ and u are the distribution parameters for the density and the thermal smearing function, respectively.

As S_{\max} increases $C(r)$ will approach a δ -type function. Thus as more and more data are included in the calculation $\varrho'(r)$ approaches $\varrho(r)$, the peak height increases, and the observed σ_T' decreases. The changes in $\varrho'(0)$ and σ_T' are observed from a series of calculations with increasing S_{\max} , but as $\varrho'(0)$ varies more rapidly than σ_T' , following the relationship $d\varrho'(0)/\varrho'(0) \simeq -3d\sigma_T'/\sigma_T'$, we will focus our attention on the expected value of $\varrho'(0)$ for a given S_{\max} . From (1) we get

$$\varrho'(0) = \int_0^\infty \varrho(r) C(r) dr$$

Both $\varrho(r)$ and $C(r)$ are spherically symmetric, the elementary volume dr becomes $4\pi r^2 dr$, leading to

$$\varrho'(0) = \frac{2\varrho(0)}{\pi} \int_0^\infty \{\exp(-r^2/2\sigma_T^2) (\sin 2\pi S_{\max} r - 2\pi S_{\max} r \cos 2\pi S_{\max} r) / r\} dr \tag{4a}$$

which can be written as (see Appendix)

$$\varrho'(0) = \varrho(0) \frac{4}{\sqrt{\pi}} \int_0^\infty t^2 \exp(-t^2) dt = \varrho(0) \phi(\nu) \tag{4b}$$

Table 1. Values of $\alpha = \phi(\nu_\alpha) = \frac{4}{\sqrt{\pi}} \int_0^{\nu_\alpha} t^2 e^{-t^2} dt$ for a series of ν_α .

ν_α	$\phi(\nu_\alpha)$
1.088	0.50
1.214	0.60
1.354	0.70
1.433	0.75
1.524	0.80
1.631	0.85
1.768	0.90
1.977	0.95
2.381	0.99

with

$$\nu = 2\frac{1}{2}\pi S_{\max} \sigma_T$$

The function $\phi(\nu)$ has a sigmoidal behaviour. Table 1 gives $\phi(\nu_\alpha) = \alpha$ for a series of values of ν_α , while Fig. 1 shows $\varrho'(0)/\varrho(0) = \alpha$ as a function of S_{\max} for a series of values of σ_T .

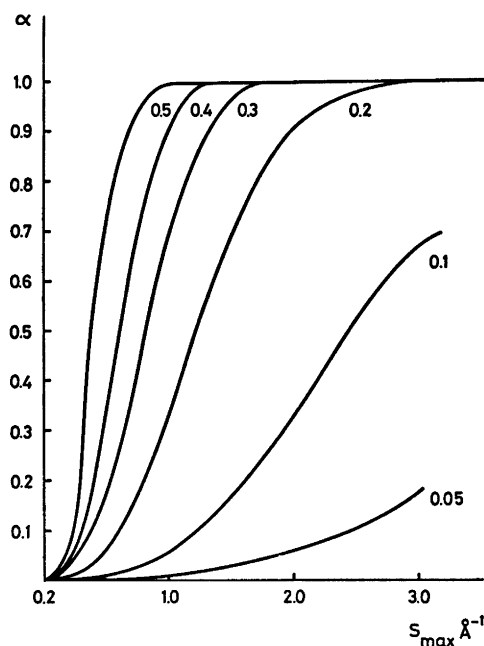


Fig. 1. The ratio between the peak height at resolution S_{\max} and at infinity, $\varrho'(0)/\varrho(0) = \alpha$, as a function of S_{\max} for a series of values of the distribution parameter σ_T (given on the plot in Å). Very sharp peaks with $\sigma_T < 0.20$ Å will produce scattering beyond the Mo radiation limit.

Expression (4b) can be used to estimate the reduction in peak height due to finite resolution.

As an example of such calculations we will use observations from combined X-ray and neutron studies of *p*-nitropyridine-*N*-oxide carried out at 30 K.³ X-Ray data³ were measured up to $S_{\max} = 2.0 \text{ \AA}^{-1}$, and deformation densities were calculated for $S_{\max} = 1.3, 1.5, 1.7$ and 2.0 \AA^{-1} . The peak heights of all bonding densities were averaged for each value of S_{\max} and a similar calculation was carried out for the lone pair densities. Fig. 2 shows the behaviour of the two types of densities. Functions of the type given in (4b) were now fitted to the points by a least squares procedure in which $\rho(0)$ and σ_T were varied. For simplicity all points were given equal weight and correlations between points were neglected despite the fact that the points are based on overlapping sets of reflections. The resultant curves are also shown in Fig. 2. The values obtained were for the bonding density $\sigma_T = 0.22(3) \text{ \AA}$ and $\rho(0) = 0.61(3) \text{ e/\AA}^3$ and for the lone pair density $\sigma_T = 0.17(5) \text{ \AA}$ and $\rho(0) = 0.80(6) \text{ e/\AA}^3$.

The figure indicates, that the resolution is sufficient for an adequate description of bonding densities, but the lone pair densities would require data to at least an S_{\max} of approximately 2.3 \AA^{-1} .

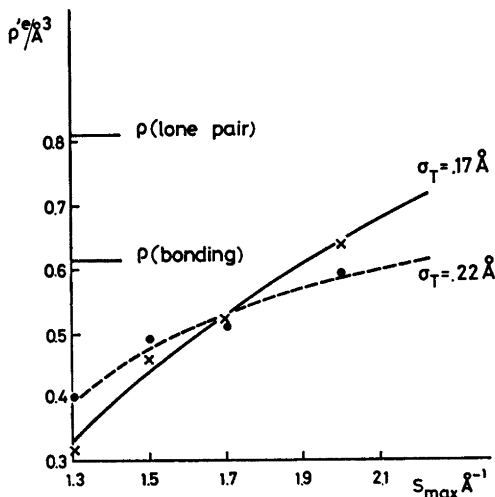


Fig. 2. The peak value of the bonding density (\times) and lone pair density (\bullet) as a function of S_{\max} for *p*-nitropyridine-*N*-oxide. Points are mean values for a given resolution. Limits for infinite resolution are indicated.

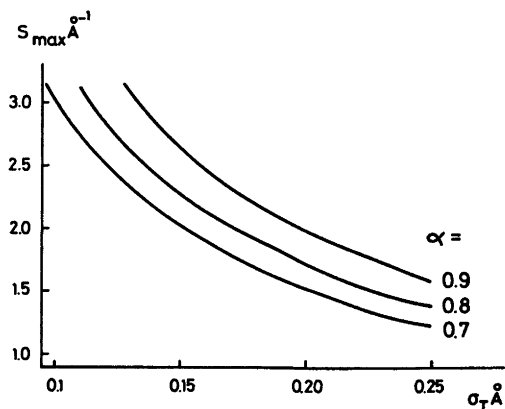


Fig. 3. Desired resolution, S_{\max} , as a function of the distribution parameter for the thermally smeared peak, σ_T . Curves are given for various values of $\alpha = \rho'(0)/\rho(0)$. $\rho'(0)$ is the observed peak height, $\rho(0)$ the peak height for infinite resolution.

Using expression (2) we can estimate the integrated density in the peaks, which is found to be 0.10 e and 0.06 e for bonding and lone pairs, respectively, again under the assumption of isotropic density distributions. If the value of σ_T is known approximately, expression (4b) may be used to estimate the desired resolution. Fig. 3 shows S_{\max} as a function of σ_T for a series of values of the ratio α . For the example discussed for which $\sigma_T = 0.17 \text{ \AA}$ data would have to be collected up to $S_{\max} = 2.3 \text{ \AA}^{-1}$, if we had required that the lone pair peak should attain 90% of the value for infinite resolution.

Conditions imposed on measurement temperature and necessary number of reflection data. The distribution parameter σ_T consists of two contributions as indicated by (3), the width σ of the electron distribution at rest, and a width, u , due to the thermal smearing. When the electron density is to be studied u is generally of little interest, and to reduce its magnitude measurements are frequently carried out at low temperatures. The behaviour of u with temperature in the harmonic approximation and assuming that the molecule in question moves as a rigid body is given by

$$u^2 = \frac{\hbar}{8\pi^2 M \omega_T} \coth \frac{\hbar \omega_T}{2kT} + d^2 \frac{\hbar}{8\pi^2 I \omega_L} \coth \frac{\hbar \omega_L}{2kT} \quad (5)$$

where the first term describes the translational motion with frequency ω_T and the second term gives the librational motion for an atom at distance d from the center of libration. M and I are mass and moment of inertia, respectively. If we express the variables in atomic mass units, Å, cm^{-1} and K, the two quantities involved, $h/8\pi^2$ and $h/2k$ have values of 16.86 Å² a.m.u. cm^{-1} and 0.719 K/ cm^{-1} , respectively.

Assuming that $\omega/T < 0.75 \text{ cm}^{-1}/\text{K}$, we introduce an error of less than 10 % by setting $\coth(h\omega/2kT) = 2kT/h\omega$ and the expression (5) for the mean square displacement of a given atom becomes

$$u^2 = \frac{kT}{4\pi^2 M \omega^2}$$

with

$$\frac{1}{\omega^2} = \frac{1}{\omega_T^2} + d^2 \frac{M}{I} \frac{1}{\omega_L^2}$$

So the thermal motion for a given atom as a function of temperature can be approximately described as a translation with frequency ω , which can be fixed from a room temperature observation of the mean square displacement, u_0^2 .

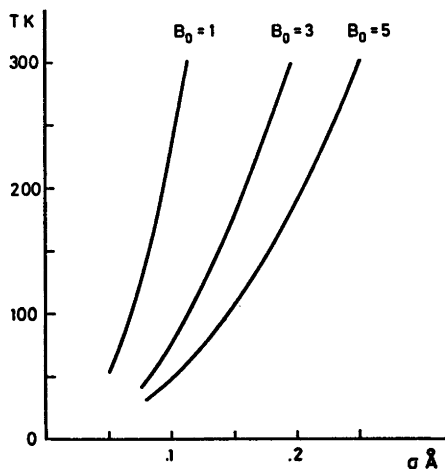


Fig. 4. Relationship between σ , the distribution parameter of the electron density at rest, and the measurement temperature, T , according to the condition, that $\sigma = u$, where u is the atomic root mean square thermal displacement. For the condition $\sigma > u$ the curves indicate the maximum possible measurement temperature. The isotropic temperature factors indicated on the figure are observations at 300 K.

Acta Chem. Scand. A 31 (1977) No. 7

To make sure, that σ is not negligible compared to u a reasonable requirement would be, that u is less than σ which fixes the measurement temperature condition as

$$\sigma^2 \geq \frac{kT}{4\pi^2 M \omega^2} = \frac{B_0 T}{8\pi^2 T_0}$$

with $B_0 = 8\pi^2 u_0^2$, the isotropic temperature factor, determined at room temperature T_0 . Fig. 4 shows T as a function of σ for the condition $\sigma = u$ for a series of B_0 values fixing T_0 to 300 K. Taking again as an example the *p*-nitropyridine-*N*-oxide, we find, that at 30 K the mean u^2 for the oxygen atoms is 0.0093 Å². For the lone pair electrons σ_T^2 equals 0.0289 Å² which gives $\sigma = 0.14$ Å. The mean B_0 for oxygen at room temperature is 4.9 Å² so according to the above criterium that $\sigma > u$ the measurement should be made at a temperature below 95 K.

In general σ is of course not known before completion of the analysis but approximate values may be obtained from theoretical chemical calculations, or from comparable molecules which have been studied previously.

If σ is known it is possible to estimate the number of unique reflections required to obtain a given $\alpha = \rho'(0)/\rho(0)$ for a specific atom, assuming that the thermal behaviour at some temperature, normally room temperature, is known. We consider a primitive centrosymmetric space group for which in general the number of asymmetric units per unit cell Z equals the number of equivalent reflection in a form. The minimal number of unique reflections is then

$$n = \frac{1}{Z} \frac{4}{3} \pi S_{\max}^3 V = \frac{1}{Z} \frac{4}{3} \pi S_{\max}^3 \frac{MZ}{D} = \frac{4}{3} \pi S_{\max}^3 \frac{M}{D}$$

where V is the volume of the unit cell, M is the mass of the molecule, and D is the density of the material. Introducing $\nu_\alpha = 2\frac{1}{3}\pi S_{\max}^3 \sigma_T$ where ν_α is defined in Table 1 we get

$$n = \frac{2\frac{1}{3}\nu_\alpha^3 M}{3\pi^2 D \sigma_T^3}$$

With σ_T from expression (3) and (5), n can be estimated.

We take again the above discussed example, and use the calculated σ_T to estimate n for observation of bonding and lone pair density. For this compound $M = 140$ a.m.u. and $D = 1.6$

g/cm³. If we require, that $\alpha=0.9$ we find that 1800 unique reflections are needed if the bonding density, and 3900 if the lone pair density is to be observed at 90 % peak height.

CONCLUSIONS

Though subtraction of the unperturbed spherical atom in a deformation density map leads to a considerable reduction in series termination effects, incompleteness of the data set cannot be ignored when a quantitative interpretation of the charge density is made. One approach followed by Rees and Mitschler⁴ and by Stevens and Coppens⁵ is to introduce series termination (and thermal smearing) into the theoretical density maps. The assumption of a Gaussian peak shape gives an estimate of the effects involved. It is obvious that in all cases extension of the data set leads to an increase in resolution but the improvement becomes less important as thermal motion increases. The use of a Gaussian peak shape in the discussion ignores details of the charge distribution which may become observable with shorter wavelengths or at lower temperatures. Nevertheless it leads to a tractable expression which is in reasonable agreement with the very-low temperature observations on *p*-nitropyridine *N*-oxide.

APPENDIX

Using formulas 861.22 and 861.20 in Tables of Integrals and other Mathematical Data (Dwight, 1961)⁶ (4a) can be written

$$\rho'(0) = 2\rho(0)\left[\frac{1}{2} \operatorname{erf}(\nu) - \frac{1}{\sqrt{\pi}} \nu \exp(-\nu^2)\right] \quad (\text{A1})$$

with $\nu = 2\frac{1}{2}\pi S_{\max}\sigma$

Applying the relationship

$$uv]_0^\nu = \int_0^\nu u dv + \int_0^\nu v du$$

with $u = \frac{t}{\sqrt{\pi}}$, $v = \exp(-t^2)$ gives

$$\frac{1}{2} \operatorname{erf}(\nu) - \frac{\nu}{\sqrt{\pi}} \exp(-\nu^2) = \frac{2}{\sqrt{\pi}} \int_0^\nu t^2 \exp(-t^2) dt$$

which, inserted in (A1) leads to

$$\rho'(0) = \rho(0) \frac{\sqrt{\pi}}{4} \int_0^\nu t^2 \exp(-t^2) dt$$

REFERENCES

1. James, R. W. *Acta Crystallogr. I* (1948) 132.
2. Coppens, P. and Lehmann, M. S. *Acta Crystallogr. B* 32 (1976) 1777.
3. Wang, V., Blessing, R. H., Ross, F. K. and Coppens, P. *Acta Crystallogr. B* 32 (1976) 572.
4. Rees, B. and Mitschler, A. J. *Am. Chem. Soc.* (1976). *In press*.
5. Stevens, E. D. and Coppens, P. Submitted to *J. Am. Chem. Soc.* (1976).
6. Dwight, H. B. *Tables of Integrals and Other Mathematical Data*, Macmillan, New York 1961.

Received January 17, 1977.

Luminescence Spectra of Some Ruthenium(II) Complexes

RONALD A. KRAUSE^a and C. J. BALLHAUSEN^b

^a The Department of Chemistry, University of Connecticut, Storrs, Ct. 06268, U.S.A. and

^b Chemical Laboratory IV, Department of Physical Chemistry, H.C. Ørsted Institute, DK-2100 Copenhagen Ø, Denmark

Luminescence spectra and luminescence lifetimes have been obtained for several ruthenium(II) complexes in rigid glasses at 77 K. Complexes which have been studied are $[\text{Ru}(\text{dipy})(\text{py})_4]^{2+}$, *cis*- and *trans*- $[\text{Ru}(\text{dipy})_2(\text{py})_2]^{2+}$, *cis*- and *trans*- $[\text{Ru}(\text{dipy})(\text{py})_2(\text{phen})]^{2+}$, $[\text{Ru}(\text{dipy})(\text{phen})_2]^{2+}$, $[\text{Ru}(\text{dipy})(\text{py})_3\text{en}]^{2+}$, $[\text{Ru}(\text{dipy})(\text{py})_3(\text{PMA})]^{2+}$, $[\text{Ru}(\text{dipy})(\text{PMA})_2]^{2+}$, $[\text{Ru}(\text{dipy})(\text{py})_2(\text{PEA})]^{2+}$, $[\text{Ru}(\text{dipy})(\text{py})_2(\text{NH}_3)_2]^{2+}$ and $[\text{Ru}(\text{dipy})(\text{py})_3\text{Cl}]^+$ (dipy = 2,2'-dipyridyl, py = pyridine, phen = 1,10-phenanthroline, en = ethylenediamine, PMA = 2-aminomethylpyridine, and PEA = 2-aminoethylpyridine).

With two exceptions the emission spectra are all very similar with band maxima near 17 000 and 16 000 cm^{-1} . $[\text{Ru}(\text{dipy})(\text{PMA})_2]^{2+}$ and $[\text{Ru}(\text{dipy})(\text{py})_2(\text{NH}_3)_2]^{2+}$ exhibited "anomalous" spectra showing different intensity ratios. The spectra are all classified as ligand $\pi^* \rightarrow$ metal *d* charge transfer type. Lifetimes are all near 10 μs ; several of the decay curves showed a deviation from first order behaviour indicating a weak coupling between the ligands.

Since 1959 when Paris and Brandt reported the first observation of luminescence from a ruthenium(II) complex¹ there have been a number of papers published dealing with this topic. Most of these reports, with only a few exceptions, involved ruthenium(II) complexes containing 2,2'-dipyridyl (or the essentially identical ligand, 1,10-phenanthroline). Unfortunately, the luminescence research which has been reported to date covers a range of complexes with very little ligand, or structural, variety and few conclusions may be drawn regarding qualitative relationships. To obtain luminescence data on a broader range of complexes we have initiated the present research.

Since several ruthenium(II) complexes containing two or three dipyritydyls are known to

emit it was felt wise to start at this point. We have varied the coligands making several complexes based on the parent compound¹ $[\text{Ru}(\text{dipy})(\text{py})_4]^{2+}$. Phosphorescence spectra and luminescence lifetimes at 77 K are reported here.

EXPERIMENTAL

Complexes were prepared as already described.²

Luminescence measurements were made on samples dissolved in an ethyleneglycol; water glass (2:1) (approx. 10^{-3} M) in quartz tubes immersed in liquid nitrogen. Excitation was with the 3371 Å line of an Avco nitrogen laser firing at 100 pulses per second. A filter in the laser beam (Jena UG-11) removed higher orders. Emission from the sample was focused through appropriate lenses onto the entrance slit (slit width approximately 100 μ) of a Jarrell Ash 0.5 meter monochromator. The light from the monochromator went directly into an EM1-95580A photomultiplier (S-20 response). PMT output went to a Keithley 414S picoammeter and then to an appropriate recorder. Spectra are uncorrected.

Lifetimes were determined by sending the signal from the PMT into a Tektronix type 454 oscilloscope which functioned as a 10:1 pre-amplifier; this output went into a PAR Boxcar Integrator (Model 160) using a 0.5 μs aperture time and an appropriate time base (generally 20 or 50 μs). Triggering of the boxcar was by means of a presignal from the laser signal generator; the cable for the trigger signal also went to the oscilloscope for triggering, where it was terminated in a 50 ω load resistor. Output from the boxcar went through a voltage divider into a recorder.

In order to avoid saturation of the PMT and consequent distortion of the luminescence decay curves it was found to be necessary to adjust the monochromator slit width so that

Table 1. Emission maxima and lifetimes at 77 K.

Compound	ν_1 (in 1000 cm)	ν_2	ν_3	τ_1 (in μ s)	τ_2^a
[Ru(dipy)(py) ₄](ClO ₄) ₂	17.1	16.0		10.9 ^b	9.8 ^b
<i>cis</i> -[Ru(dipy) ₂ (py) ₂](ClO ₄) ₂	17.2	16.0		11.4 ^b	10.3 ^b
<i>trans</i> -[Ru(dipy) ₂ (py) ₂](ClO ₄) ₂	17.1	15.9		10.6 ^b	10.4 ^b
<i>cis</i> -[Ru(dipy)(py) ₂ (phen)](ClO ₄) ₂	17.3	16.2		14.8	13.2 ^b
<i>trans</i> -[Ru(dipy)(py) ₂ (phen)](ClO ₄) ₂	17.0	15.9		8.0 ^b	8 ^b
[Ru(dipy)(phen) ₂](ClO ₄) ₂	17.4	16.1	16.5	15.8	15.1
[Ru(dipy)(py) ₂ en](ClO ₄) ₂	17.2	15.8		10.9 ^b	9.8 ^b
[Ru(dipy)(py) ₂ PMA](ClO ₄) ₂	17.2	16.1	16.4	10.6 ^b	10.2 ^b
[Ru(dipy)(PMA) ₂](ClO ₄) ₂	16.3	15.4	17.4	9.0 ^c	7.8 ^c
[Ru(dipy)(py) ₂ (PEA)](ClO ₄) ₂	17.2	16.0		11.3 ^b	9.6 ^b
[Ru(dipy)(py) ₃ Cl](ClO ₄)	17.2	15.7		10.5	^c
[Ru(dipy)(py) ₂ (NH ₃) ₂](ClO ₄) ₂	16.0	17.2	15.0	^c	9.3

^a ν_1 most intense; ν_3 weakly resolved, shoulder, or very weak. τ_1 is the emission lifetime at ν_1 . ^b First order decay plot shows some curvature, with initial slope generally within 25 % of the least squares value. ^c First order decay plot nonlinear.

the maximum signal reaching the boxcar was less than 370 mV. These slit widths were all near 100 μ .

Least squares analysis was applied to the data to determine the lifetime value, assuming first order decay.

RESULTS AND DISCUSSION

As first suggested by Paris and Brandt¹ all of the emission spectra are most likely of the charge transfer type, ligand $\pi^* \rightarrow t_2$ metal orbital. Thus the emission spectrum reflects the properties of the low lying excited charge transfer states and the vibrational spectrum associated with the ground electronic state.

The lifetimes of the excited states are approximately 10 μ s. An interesting feature emerges in that the first order decay plots of a number of the emission peaks deviate from linearity, most only slightly but several to a great extent (Table 1). This could be caused by several factors, one of which is the possibility of a manifold of decaying excited states in thermal equilibrium. Harrigan and Crosby³ have suggested such a condition from a study of Ru(dipy)₃²⁺ and two related complexes. Recently, Hager and Crosby⁴ studied computer fit temperature dependence data and presented a model involving at least three closely lying emitting excited states. Lifetimes of 10 μ s are rather short for spin-singlet \rightarrow spin-triplet transitions and quite long for singlet \rightarrow

singlet transitions. In accord with the proposal of Crosby, Hipps and Elfring⁵ we take it that the spin-orbit coupling has done away with *S* as a good quantum number for the excited states.

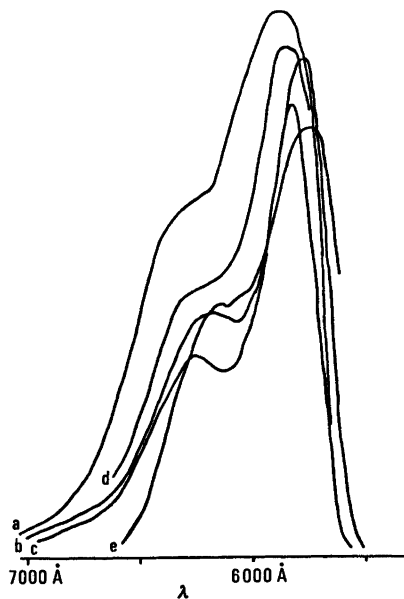


Fig. 1. Emission spectra in ethylene glycol-water glass at 77 K. (Intensities offset for clarity). a, *trans*-[Ru(dipy)(py)₂(phen)](ClO₄)₂; b, *cis*-[Ru(dipy)(py)₂(phen)](ClO₄)₂; c, *cis*-[Ru(dipy)₂(py)₂](ClO₄)₂; d, *trans*-[Ru(dipy)₂(py)₂](ClO₄)₂; e, [Ru(dipy)(phen)₂](ClO₄)₂.

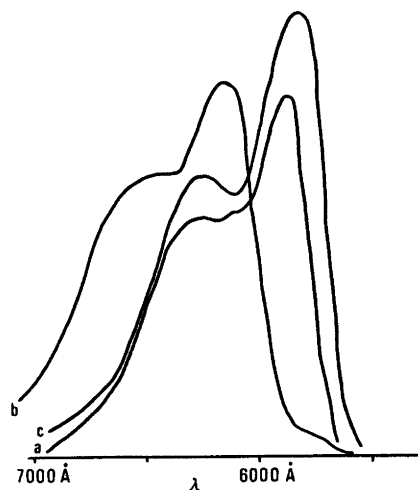


Fig. 2. Emission spectra in ethylene glycol-water glass at 77 K. (Intensities offset for clarity). a, $[\text{Ru}(\text{dipy})(\text{py})_2\text{PMA}](\text{ClO}_4)_2$; b, $[\text{Ru}(\text{dipy})(\text{PMA})_2](\text{ClO}_4)_2$; c, $[\text{Ru}(\text{dipy})(\text{py})_2\text{PEA}](\text{ClO}_4)_2$.

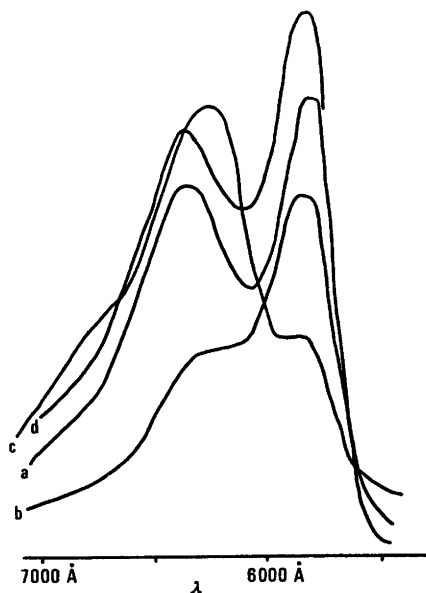


Fig. 3. Emission spectra in ethylene glycol-water glass at 77 K. (Intensities offset for clarity). a, $[\text{Ru}(\text{dipy})(\text{py})_2\text{en}](\text{ClO}_4)_2$; b, $[\text{Ru}(\text{dipy})(\text{py})_4](\text{ClO}_4)_2$; c, $[\text{Ru}(\text{dipy})(\text{py})_2(\text{NH}_3)_2](\text{ClO}_4)_2$; d, $[\text{Ru}(\text{dipy})(\text{py})_3\text{Cl}](\text{ClO}_4)_2$.

With two exceptions the emission spectra reflecting the ground state vibrations of the complexes under study are all very much alike. They are characterized by a band near $17\,000\text{ cm}^{-1}$ and a second, weaker band at $16\,000\text{ cm}^{-1}$. In two cases a third component is visible between the two major peaks. The two *cis-trans* pairs are very much alike in band position, band shape, and relative intensities. Replacing one aromatic amine group with the aliphatic NH_2 of PMA or PEA leaves the basic emission spectrum relatively unchanged. Replacing two aromatic amine groups with one ethylenediamine is also without effect.

Two of the spectra are anomalous in that they depart from the form of those of the other ten compounds. $[\text{Ru}(\text{dipy})(\text{PMA})_2](\text{ClO}_4)_2$ has an emission which is red shifted by about 1000 cm^{-1} from the other complexes. $[\text{Ru}(\text{dipy})(\text{py})_2(\text{NH}_3)_2](\text{ClO}_4)_2$ has a different shape to its emission spectrum, the highest energy band being of lower intensity than the principle peak at $16\,000\text{ cm}^{-1}$.

Most of the ruthenium(II) complexes which have been observed to emit contain dipyriddy or phenanthroline. The few exceptions are the complex with tripyridyl^{6,7} a complex with di(quinolyl)pyridine⁸ (although both of these really would be expected to be identical with dipyriddy), ruthenocene⁹ and possibly¹⁰ $[\text{Ru}(\phi_2\text{PCH}_2\text{CH}_2\text{P}\phi_2)]\text{Cl}_2$ (later workers could not detect emission from this compound¹¹). Klassen *et al.*⁸ did however observe a case of apparent steric influence in that the lifetime of the di(quinolyl)pyridine complex was significantly reduced below that of the tripyridyl compound ($4.7\text{ vs. }10.7\ \mu\text{s}$).

With an electronic excitation into one of the π ligand systems a competition between three processes occurs. The molecule can revert to its ground state *via* a radiationless transition, it can emit from the lowest excited state of the ligand in question or the excitation can spread out over the entire π network of all three ligands before the system goes back to the ground state. It is clear that when the electronic coupling is weak, and the excitation remains localized the emission spectrum will be rather unaffected by the unexcited ligands. If on the other hand the electronic coupling is strong and a delocalization is the dominant

ing process an entirely new situation is met with.

Both of these extremes have been reported previously. Halper and DeArmond¹² in a study of some rhodium(III) complexes observed a nonlinear decay and concluded multiple emissions, from localized triplets, to be the cause. Recently Crosby and Elfring¹³ concurred with this; however, in the same study these latter authors concluded there to be strong ligand-ligand electronic coupling in a set of ruthenium(II) complexes.

The accumulated evidence in the present study points toward a weak coupling. With the excited state being primarily a spin-triplet the energy transfer from one ligand to another is a slow process, and the excitation remains localized for many periods of ligand vibrations. The majority of emission spectra from mixed complexes should in this case be observed as superpositions of bands from their "parent" species. The existence of a weak coupling from one ligand to another produces a second channel for relaxation which again will lead to a non-linear decay law. Hence the majority of the investigated complexes are seen to fall in the weak coupling limit. For the complexes which fall outside this general pattern more detailed spectra than can be obtained at liquid nitrogen temperatures would be needed in order to settle the nature of the electronic couplings between the ligands.

One final comment on our results is pertinent; that is the dependence of emission properties on molecular geometry. While the *cis* and *trans* isomers of $[\text{Ru}(\text{dipy})_2(\text{py})_2]^{2+}$ are nearly identical in emission lifetimes and presumably have the same electronic symmetry, the *cis* and *trans* isomers of $[\text{Ru}(\text{dipy})(\text{py})_2(\text{phen})]^{2+}$ show considerably different lifetimes. At this point it is difficult to conclude the exact meaning of this, but further studies, of a wide variety of compounds, is certainly called for.

REFERENCES

1. Paris, J. P. and Brandt, W. W. *J. Am. Chem. Soc.* **81** (1959) 5001.
2. Krause, R. A. *Inorg. Chim. Acta* **22** (1977) 209.
3. Harrigan, R. W. and Crosby, G. A. *J. Chem. Phys.* **59** (1973) 3468.
4. Hager, G. D. and Crosby, G. A. *J. Am. Chem. Soc.* **97** (1975) 7031.
5. Crosby, G. A., Hipps, K. W. and Elfring, W. H., Jr. *J. Am. Chem. Soc.* **96** (1974) 629.
6. Klassen, D. M. and Crosby, G. A. *J. Chem. Phys.* **48** (1968) 1853.
7. Fink, D. W. and Ohnesorge, W. E. *J. Am. Chem. Soc.* **91** (1969) 4995.
8. Klassen, D. M., Hudson, C. W. and Shaddix, E. L. *Inorg. Chem.* **14** (1975) 2733.
9. Crosby, G. A., Hager, G. D., Hipps, K. W. and Stone, M. L. *Chem. Phys. Lett.* **28** (1974) 497.
10. Klassen, D. M. and Crosby, G. A. *J. Mol. Spectrosc.* **25** (1968) 398.
11. Arnold, G. S., Klotz, W. L., Halper, W. and DeArmond, M. K. *Chem. Phys. Lett.* **19** (1973) 546.
12. Halper, W. and DeArmond, M. K. *J. Luminescence* **5** (1972) 225.
13. Crosby, G. A. and Elfring, W. H., Jr. *J. Phys. Chem.* **80** (1976) 2206.

Received March 14, 1977.

Solvent Effects and Activation Parameters for the Isotopic Exchange Reaction between Lithium Bromide and Butyl Bromide in Acetone—Water Mixtures

ALLAN HOLMGREN

Department of Physical Chemistry, University of Umeå, S-901 87, Umeå, Sweden

The effect of minute amounts of water (≤ 1.5 wt.-%) in acetone on the kinetics of the isotopic exchange between lithium bromide and butyl bromide has been investigated over a range of temperatures (15–35 °C) using ^{82}Br as a radioactive indicator. The observed rapid decrease in the specific rate of exchange with increasing concentration of water in the solvent mixture is interpreted in terms of preferential solvation of the bromide ion. Activation parameters, ΔG^\ddagger , ΔH^\ddagger , and ΔS^\ddagger have been calculated. The inhibitory effect of the protic constituent on the exchange reaction is reflected in a decreasing entropy of activation with increasing water concentration rather than in an increasing enthalpy of activation. Transfer activity coefficients for the transfer of bromide ions from pure to aqueous acetone have been estimated from the kinetic data and are used together with ion-pair association for lithium bromide to obtain information about solvation of the ion-pairs.

Preferential solvation of bromide ions in aqueous acetone at 25 °C was studied kinetically in a previous investigation¹ by following the exchange of radiobromide between lithium bromide and butyl bromide in acetone containing from 0.005 to 1.5 wt.-% of water. For these low concentrations of water, the macroscopic permittivity of the solvent mixtures used to carry out the exchange reaction remains almost constant; in addition self-association of the water molecules is minimized. The protic constituent of the solvent mixture was found to inhibit the exchange reaction very strongly. Addition of 1.5 wt.-% of water to anhydrous acetone decreased the specific reaction rate by a factor of 5.

The aim of the present research was to obtain more detailed insight into the various factors influencing the kinetics of the exchange reaction discussed above. To that end the kinetic measurements have now been extended to cover a range of temperatures, *viz.* from 15 to 35 °C.

EXPERIMENTAL

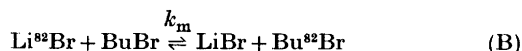
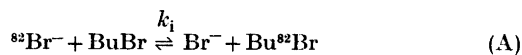
Acetone (Merck, *p.a.*) and water were purified according to Ref. 1. The density of the purified acetone was $0.7843 \text{ kg dm}^{-3}$ at 25 °C. Acetone–water solvent mixtures were prepared by weight at 25 °C. The reactants, *i.e.* butyl bromide (Fluka, *puriss.*) and lithium bromide (Fluka, *suprapur*), were purified according to Ref. 1. Radioactive lithium bromide, Li^{82}Br , was prepared by neutron irradiation of known amounts of inactive lithium bromide in the R 2 reactor of the Swedish Atomic Energy Company, Studsvik, Sweden. The irradiated salt was dissolved in a known volume of the solvent mixture.

The time dependence of the exchange reaction was followed by anodic deposition of bromide on silver electrodes.^{2,3} The anodic current density was chosen⁴ to yield 100 % current efficiency with respect to the electrode reaction, $\text{Ag} + \text{Br}^- \rightarrow \text{AgBr} + \text{e}^-$. The radioactivity of each electrode was measured by means of a proportional counter. The usual corrections for deadtime losses, backgrounds counts, and decay were applied to the counting rates.

The rate of exchange, R , was calculated by means of the McKay equation⁵ using the method of least squares.

RESULTS AND DISCUSSION

According to the Acree hypothesis,⁶ the overall exchange reaction studied may be separated into the following two reactions,



where k_i and k_m are the rate constants for the two different exchange reactions involving free and paired bromide ions, respectively.

The Acree equation for the observed second-order rate constant, k , may be expressed,

$$k = k_i\alpha + k_m(1 - \alpha) \quad (1)$$

where α is the degree of dissociation of the ion-pairs. Hence, application of eqn. (1) to the kinetic data requires access to ion-pair association constants, K_A , of lithium bromide in the various acetone-water solvent mixtures investigated.

The association constants listed in Table 1 were evaluated from electrical conductance data^{7,8} using the conductance equation of Fuoss and Hsia^{9,10} in the form of Fernández-Prini.¹¹ The Debye-Hückel equation¹² for the mean activity coefficient of free ions was used. The method of calculating K_A has been described.¹³

Table 1, in which ϵ is the permittivity of the solvent and q is the Bjerrum radius,¹⁴ reveals that the association constant is rather insensi-

Table 1. Association constants for lithium bromide in acetone-water mixtures.⁸

water conc. wt.-%	ϵ	$q \times 10^{10}$ m	K_A/M^{-1} $r=q$	$r=q/2$
15 °C				
0.005	21.62	13.41	3424	3344
0.055	21.66	13.39	2990	2905
0.106	21.69	13.37	2814	2739
1.505	22.45	12.92	1697	1635
25 °C				
0.005	20.7	13.54	4160	4073
0.055	20.75	13.51	3695	3610
0.106	20.8	13.47	3413	3334
1.505	21.3	13.16	1758	1698
35 °C				
0.005	19.65	13.80	4513	4404
0.055	19.67	13.79	4168	4080
0.106	19.68	13.78	3918	3830
1.505	20.40	13.29	1852	1780

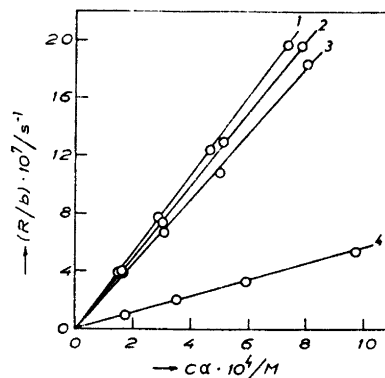


Fig. 1. Graphs of R/b vs. $c\alpha$ for the isotopic exchange between lithium bromide and butyl bromide in acetone-water mixtures at 15 °C. The curves 1-4 represent data for solvent mixtures containing 0.005, 0.055, 0.106 and 1.505 wt.-% water, respectively.

tive to the value of the distance parameter, r , the maximum centre-to-centre distance between the ions in the ion-pair. For a given solvent mixture the values of K_A corresponding to $r=q$ and $r=q/2$, respectively, differ only slightly. Because of this fact, and because the rate constant, k_i , is rather insensitive to moderate changes in K_A , as will be shown below, the distance parameter may be set equal to the Bjerrum radius.

The total rate of exchange, R , may be written

$$R = k_1b + kbc \quad (2)$$

where k_1 is the first-order rate constant, b is the concentration of the organic bromide and c is the concentration of the inorganic bromide.

According to eqns. (1) and (2) a plot of R/b vs. $c\alpha$ should yield a straight line with intercept k_1 and slope k_i , if $\alpha=1$ and/or if $k_m=0$. A straight line was fitted to the experimental points by means of the relative deviation least squares method.¹⁵ Representative graphs of R/b vs. $c\alpha$ are illustrated in Fig. 1. Within experimental errors all curves pass through the origin, indicating no observable contribution of S_N1 exchange to the reaction rate. Hence, the term k_1b in eqn. (2) may be omitted and the observed second-order rate constant k represented by the expression,

$$k = R/(bc) \quad (3)$$

Table 2. Kinetic data for exchange of ^{82}Br between lithium bromide and butyl bromide in acetone-water mixtures at 15.0 °C.

$b \times 10^3$ M	$c \times 10^4$ M	$R \times 10^8$ M s ⁻¹	$k \times 10^4$ M ⁻¹ s ⁻¹	α
0.005 wt-% water				
5.649	20.18	11.116	9.751	0.3658
5.752	10.20	7.0874	12.08	0.4598
5.740	5.014	4.4610	15.50	0.5686
6.101	2.116	2.3870	18.49	0.7033
0.055 wt-% water				
5.674	20.51	11.056	9.500	0.3843
5.117	10.96	6.5785	11.73	0.4721
5.677	5.195	4.1554	14.09	0.5870
5.697	2.236	2.3018	18.07	0.7171
0.106 wt-% water				
5.694	20.48	10.459	8.969	0.3939
5.708	10.20	6.1540	10.57	0.4932
5.690	5.070	3.7676	13.06	0.6015
5.701	2.266	2.1948	16.99	0.7248
1.505 wt-% water				
5.737	20.36	3.0498	2.611	0.4761
5.739	10.21	1.8762	3.201	0.5801
5.711	5.134	1.1763	4.012	0.6854
5.722	2.133	0.55032	4.509	0.8059

The results of the kinetic measurements are summarized in Tables 2–3, in which the degree of dissociation, α , of the ionic reactant is included.

In accord with eqn. (1) rate constants, k_i and k_m , were evaluated by fitting straight lines to the experimental points of k/α vs. $(1-\alpha)/\alpha$ using the relative deviation least squares method. Calculations of this kind were performed using values of K_A corresponding to $r=q$ and $r=q/2$, respectively. The results are listed in Table 4.

The values of k_i at 25 °C in Table 4, reevaluated from kinetic data previously reported,¹ deviate by less than 1 % from the corresponding values of k_i in Ref. 1, in which α values according to the Fuoss-Onsager equation¹⁶ from 1957 were used. The compilation in Table 4 reveals that the values of k_i obtained using association constants, K_A , corresponding to $r=q$ and $r=q/2$, respectively, differ insignificantly.

The derived values for the ion-pair rate constant, k_m , have not been tabulated. In all in-

stances the k_m values are close to zero. The maximum value of k_m/k_i , obtained for acetone containing 0.055 wt-% water at 25 °C with r set equal to q , amounts to 4 %. Hence the lithium bromide ion-pairs might be regarded as non-reactive species although some reservation should be attached to this statement because it has not been possible to correct for the presence of any (small) kinetic salt effect.

From the data in Table 4 and from Table 3 in Ref. 1 it is apparent that the S_N2 exchange of bromide between lithium bromide and butyl bromide is much faster in anhydrous acetone than in the acetone-water solvent mixtures. The major reason for this retarding effect on the free ion-molecule reaction, when the protic component is added to the system, would be the property of water as a hydrogen-bond donor. Since the bromide ion behaves like a Lewis base (nucleophile) it forms a hydrogen bond with the protic component. This interaction would be stronger than the interaction between the bromide ion and acetone molecules.

For a reaction like (A) in a mixed solvent of acetone and water it would be a competition

Table 3. Kinetic data for exchange of ^{82}Br between lithium bromide and butyl bromide in acetone-water mixture at 35.0 °C.

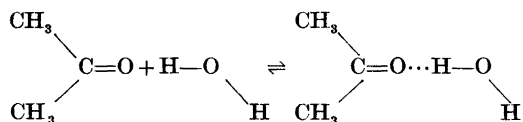
$b \times 10^2$ M	$c \times 10^4$ M	$R \times 10^8$ M s ⁻¹	$k \times 10^4$ M ⁻¹ s ⁻¹	α
0.005 wt-% water				
5.161	19.61	68.730	67.91	0.3309
5.165	9.905	43.557	85.14	0.4201
5.178	4.869	27.329	108.4	0.5261
5.221	2.052	15.095	140.9	0.6629
0.055 wt-% water				
5.153	19.78	67.169	65.90	0.3411
5.118	4.929	26.437	104.8	0.5381
5.144	2.066	14.251	134.1	0.6753
0.106 wt-% water				
5.111	9.936	42.211	83.12	0.4428
5.092	4.995	25.765	101.3	0.5469
5.144	2.116	13.932	128.0	0.6821
1.505 wt-% water				
5.163	19.79	22.949	22.46	0.4675
5.164	9.919	13.814	26.97	0.5711
5.198	4.987	8.5803	33.10	0.6766
5.193	2.082	3.9863	36.87	0.7981

Table 4. Rate constants, k_i , for the exchange of bromine between lithium bromide and butyl bromide in acetone-water mixtures at 15, 25 and 35 °C.^a

Water conc. wt.-%	$k_i \times 10^4 / s^{-1}$ 15 °C	25 °C	35 °C
	$r = q$		
0.005	26.62 ± 0.65	78.15 ± 0.40	212.1 ± 4.3
0.055	24.77 ± 0.71	70.37 ± 1.65	199.0 ± 2.2
0.106	22.66 ± 1.30	68.04 ± 1.51	186.7 ± 3.3
1.505	5.772 ± 0.187	16.61 ± 0.21	46.83 ± 1.46
	$r = q/2$		
0.005	26.57 ± 0.65	78.00 ± 0.40	211.5 ± 4.3
0.055	24.72 ± 0.71	70.22 ± 1.63	198.7 ± 2.3
0.106	22.64 ± 1.29	67.92 ± 1.49	186.4 ± 3.3
1.505	5.762 ± 0.186	16.59 ± 0.21	46.74 ± 1.45

^a The values of k_i at 25 °C were evaluated from the experimental data reported in Ref. 1.

between the different components of the reaction mixture for the hydrogen bonds donated by water. These interactions, *e.g.* that between acetone and water,¹⁷



would be of importance for the rate of the exchange reaction studied. The competition between acetone and water molecules for the bromide ions may be represented by the solvation equilibrium (*cf.* Ref. 1),



according to which we assume that each bromide ion is solvated by either n molecules of acetone ("A") or by $(n-m)$ molecules of acetone and m molecules of water ("W").

According to a spectroscopic investigation of Parker and Brody,¹⁸ the solvation of anions by hydrogen-bond donating solvents has more the character of a general interaction than a specific interaction involving stoichiometric hydrogen-bonded species. In contrast, investigations of Kolthoff and Chantooni^{19,20} on the hydration of ions in aqueous acetonitrile indicate that there are specific 1:1 and 1:2 interactions between ions and water.

Whatever the true picture of the solvation of ions, we will use the equilibrium (C) to cal-

culate overall values of the solvation equilibrium constant, K , and the solvation number m . Following the derivation in Ref. 1 the thermodynamic equilibrium constant, K_{th} , for the equilibrium (C) may be written,

$$K_{\text{th}} = \frac{[\text{Br}^- \text{A}_{n-m} \text{W}_m] [\text{A}]^m}{[\text{Br}^- \text{A}_n] [\text{W}]^m} \times \Phi \quad (4)$$

where square brackets denote molar concentrations and Φ is the activity coefficient ratio for the species involved. On the assumption that the activity coefficient ratio, Φ , does not vary with the composition of the solvent we have,

$$K_{\text{th}}/\Phi = K = \frac{[\text{Br}^- \text{A}_{n-m} \text{W}_m] [\text{A}]^m}{[\text{Br}^- \text{A}_n] [\text{W}]^m} \quad (5)$$

in which the constant, K , may be estimated from our kinetic data.

Using the results of eqns. (1-2), which indicate that both k_1 and k_m may be omitted, and using the stoichiometric condition for bromide ions we obtain the following equation¹

$$\frac{k_A - k_i}{k_i - k_{\text{AW}}} = K \left(\frac{[\text{W}]}{[\text{A}]} \right)^m \quad (6)$$

where k_A is the second-order rate constant for the exchange of bromide and k_{AW} is the rate constant for the corresponding exchange reaction involving $\text{Br}^- \text{A}_{n-m} \text{W}_m$.

For low concentrations of water in the solvent mixture, $k_i \gg k_{\text{AW}}$. Hence, eqn. (6) may be expressed,

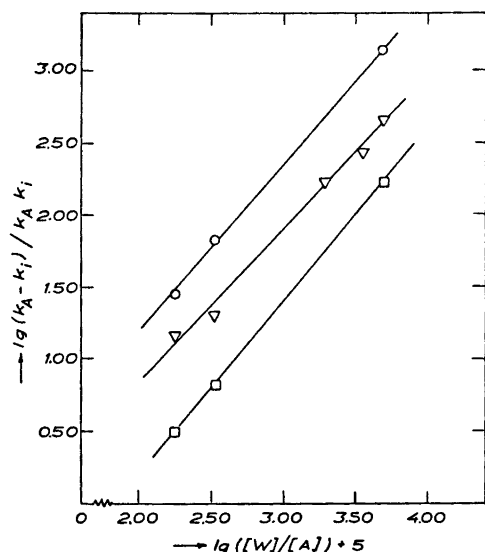


Fig. 2. Graphs according to eqn. 7 for the isotopic exchange between lithium bromide and butyl bromide in acetone-water mixtures at 15 °C (O), 25 °C (∇) and 35 °C (□). Data at 25 °C are obtained from Ref. 1. In the computation of m and K at 25 °C one point (acetone containing 0.3 wt-% water) was omitted.

$$\lg \frac{k_A - k_i}{k_i k_A} = m \lg \frac{[W]}{[A]} + \lg \frac{K}{k_A} \quad (7)$$

Using the method of least squares, eqn. (7) was applied to the kinetic data in Table 4 and in Table 3 of Ref. 1. Graphical representations of eqn. (7) are shown in Fig. 2.

From the slopes and intercepts of the three lines in this figure values of m and K , for solvation of the bromide ion in the acetone-water mixtures investigated at 15, 25 and 35 °C, were obtained. The results are summarized in Table 5, where errors quoted are standard deviations.

Table 5. Over-all solvation constants, K , and over-all solvation numbers, m , for the equilibria (C) and (D) at different temperatures.

t °C	m	K (C)	(D)
15	1.16 ± 0.03	119	5.8
25	1.09 ± 0.06	92	5.4
35	1.20 ± 0.02	132	5.9

If water as a hydrogen bond donor is assumed to solvate the bromide ion much more strongly than acetone, the solvation equilibrium (D) may be used to calculate m and K .



On the assumption expressed by (D), the following equation may be deduced,

$$\lg \frac{k_A - k_i}{k_i k_A} = m \lg [W] + \lg \frac{K}{k_A} \quad (8)$$

As may be seen from Table 5, the values of K calculated by means of eqn. (8) are lower than the K -values obtained by means of eqn. (7), but the values of m are unchanged.

According to Table 5 the overall number of water molecules associated to the bromide ion is close to 1.

With $m=1$, eqn. (7) may be rewritten,

$$\frac{1}{k_i} = \frac{1}{k_A} + \frac{K [W]}{k_A [A]} \quad (9)$$

Application of this expression to the kinetic data in Table 4 using the relative deviation least squares method yields $K=76$, 73, and 75 at 15, 25, and 35 °C, respectively. Comparison of these values with the corresponding figures in Table 5 indicates that the value of the equilibrium constant, K , is rather sensitive to the value of the overall solvation number, m .

Equilibrium (D) with $m=1$, yields $K=5.7$, 5.1 and 5.7 at 15, 25, and 35 °C, respectively.

According to the transition state theory²¹⁻²³ the temperature dependence of the rate constant, k_i , in eqn. (1) may be written

$$\ln k_i = \ln \frac{kT}{h} + \frac{\Delta S^\ddagger}{R} - \frac{\Delta H^\ddagger}{RT} \quad (10)$$

where k is Boltzmann's constant, T is the absolute temperature, h is Planck's constant, R is the gas constant, ΔH^\ddagger is the standard enthalpy of activation, and ΔS^\ddagger is the standard entropy of activation. By means of the definition of the Arrhenius activation energy, E_a , eqn. (10) may be written in the form

$$\ln k_i = \ln \frac{kT}{h} + 1 + \frac{\Delta S^\ddagger}{R} - \frac{E_a}{RT} \quad (11)$$

Eqn. (11) was fitted to the kinetic data, referring to $r=q$ in Table 4, according to the method of least squares. Graphs of $\ln k_i$ vs. T^{-1}

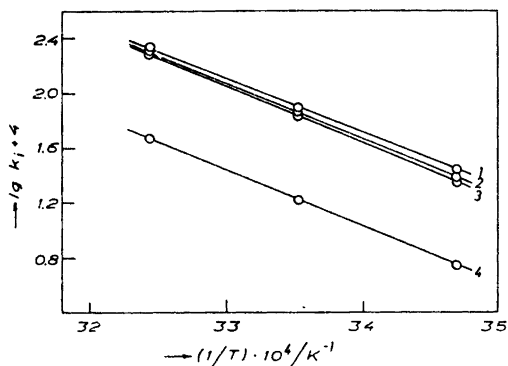


Fig. 3. Temperature dependence of k_i on solvent composition according to eqn. (11). The curves 1–4 represent data for solvent mixtures containing 0.005, 0.055, 0.106 and 1.505 % water by weight, respectively.

are shown in Fig. 3. From the equation of these straight lines we obtain the activation parameters summarized in Table 6, where errors quoted are estimated standard deviations.

When considering the effect of increasing concentration of protic component on the reaction rate, one must consider the changes in solvation of the reactants and the transition state, *i.e.* the changes in Gibbs' free energy of each of these species with solvent composition. According to Table 6, the increase in ΔG^\ddagger amounts to 3.8 kJ mol⁻¹ when the concentration of water in the solvent mixture is increased from 0.005 to 1.5 wt-%. This implies that the solvation of the reactants increases as compared with the solvation of the activated complex.

It seems reasonable to assume that the solvation of butyl bromide should decrease rather than increase with increasing water concentra-

Table 6. Thermodynamic data for the exchange of ⁸²Br between lithium bromide and butyl bromide in aqueous acetone at 25.0 °C.

Water conc. wt-%	ΔG^\ddagger kJ mol ⁻¹	ΔH^\ddagger kJ mol ⁻¹	ΔS^\ddagger J K ⁻¹ mol ⁻¹
0.005	85.0	74.1 ± 0.2	-36.7 ± 0.1
0.055	85.3	74.4 ± 1.4	-36.4 ± 0.8
0.106	85.4	75.4 ± 0.4	-33.7 ± 0.2
1.505	88.9	74.8 ± 1.0	-47.2 ± 0.8

tion of the solvent mixture. Hence, the increase in solvation of the reactants would depend almost entirely on solvation of the anion.

In the activated complex, the negative charge originally located on one bromide ion is distributed on two bromide ions. Hence, formation of the activated complex is accompanied by a reduction in the charge density reducing the ability to form hydrogen bonds. For the acetone–water mixtures with water concentration ≤ 0.1 wt-% (Table 6), $-\Delta S^\ddagger \approx 34-37$ J K⁻¹ mol⁻¹, *i.e.* approximately constant. At 1.5 wt-% water, the activation entropy has decreased to -47 J K⁻¹ mol⁻¹. These data indicate that, for the solvent mixture containing 1.5 wt-% water, the activated complex represents a higher order relative to the reactants than does the transition state in pure acetone.

Comparison of the values of ΔH^\ddagger and ΔS^\ddagger in Table 6 reveals that the entropy of activation is of major importance for the increase in Gibbs' free energy of activation, when the water content of the solvent mixtures is increased from 0.005 to 1.5 wt-%.

Several authors have demonstrated that in reactions of type (A) substitution of a protic solvent for an aprotic one decreases the specific reaction rate. There is strong evidence²⁴⁻²⁵ that an increase in the enthalpy of activation, rather than a decrease in the entropy of activation, is responsible for this change. Comparison with the results of the present investigation suggests that the relative importance of ΔH^\ddagger and ΔS^\ddagger in protic-aprotic solvent mixtures changes gradually with the composition of the solvent.

The influence of ionic strength on the rate of reaction (A) may be represented by the Brønsted-Bjerrum equation,

$$k = k^\circ \frac{(\gamma_{\text{Br}^-})(\gamma_{\text{BuBr}})}{\gamma^\ddagger} \quad (12)$$

where γ is the activity coefficient and \ddagger stands for the activated complex.

In discussing solvation the following type of activity coefficient has been defined, *cf.* Refs. 27–28 and references therein,

$$(\mu_i^\circ)_S = (\mu_i^\circ)_R + RT \ln \gamma_{t,i} \quad (13)$$

where S stands for any solvent or mixture of solvents, R stands for a selected reference sol-

vent, and $\gamma_{t,i}$ is the transfer activity coefficient, which reflects the change in chemical potential of a solute, i , on transfer from a reference solvent to another solvent. When transfer activity coefficients are applied to reaction rates by means of the absolute rate theory, an equation similar to eqn. (12), but in terms of transfer activity coefficients, is obtained.

If we use transfer activity coefficients for the systems investigated in this research, the effect of solvent on the rate of the exchange reaction studied may be written,²⁸

$$(k_i)_{AW} = (k_i)_A \frac{(\gamma_{t,Br^-})(\gamma_{t,BuBr})}{\gamma_{t,\ddagger}} \quad (14)$$

where AW and A denote aqueous and pure acetone, respectively.

Upon application of eqn. (13) to reaction (A), the difference in chemical potential between transition state and reactants may be written,

$$(\Delta G^\ddagger)_{AW} = (\Delta G^\ddagger)_A + RT \ln \frac{\gamma_{t,\ddagger}}{(\gamma_{t,Br^-})(\gamma_{t,BuBr})} \quad (15)$$

According to eqns. (14) and (15) we have,

$$(\Delta G^\ddagger_t)_{A \rightarrow AW} = -RT \ln \frac{(k_i)_{AW}}{(k_i)_A} \quad (16)$$

where $(\Delta G^\ddagger_t)_{A \rightarrow AW}$ is the difference in Gibbs' free energy of activation for reaction (A) in aqueous and pure acetone, respectively.

Application of a thermodynamic cycle to reaction (A) in pure acetone and in aqueous acetone yields,

$$\begin{aligned} (\Delta G^\ddagger_t)_{A \rightarrow AW} &= (\Delta G^\ddagger_t)_{A \rightarrow AW} - \\ &(\Delta G^\ddagger_{t,BuBr})_{A \rightarrow AW} - (\Delta G^\ddagger_{t,Br^-})_{A \rightarrow AW} \end{aligned} \quad (17)$$

Eqn. (17) may be reduced to,

$$(\Delta G^\ddagger_t)_{A \rightarrow AW} = -(\Delta G^\ddagger_{t,Br^-})_{A \rightarrow AW} \quad (18)$$

if we assume that $(\Delta G^\ddagger_{t,\ddagger})_{A \rightarrow AW} = (\Delta G^\ddagger_{t,BuBr})_{A \rightarrow AW}$

which may be a crude approximation because butyl bromide is a neutral molecule but the activated complex is negatively charged. Since the activated complex would be more strongly solvated than the butyl bromide reactant molecule, the effect of solvation on the transfer activity coefficients listed for the bromide ion (Table 7), would be underestimated, which may be seen from eqn. (14).

Using the above-mentioned approximation, comparison of eqns. (15-18) reveals that,

$$(\Delta G^\ddagger_{t,Br^-})_{A \rightarrow AW} = RT \ln \frac{(k_i)_{AW}}{(k_i)_A} = RT \ln \gamma_{t,Br^-} \quad (19)$$

If we further assume that the solvation of bromide ions due to hydrogen bond formation is of major importance²⁸ for the retardation of the observed reaction rate, eqn. (19) gives an estimate of the transfer activity coefficient, γ_{t,Br^-} , referring to hydrogen-bond formation.

Transfer activity coefficients derived from kinetic data may be used together with ion-pair association constants, K_A , to obtain some information concerning changes in solvation of the lithium bromide ion-pairs when transferred from pure acetone to a mixture of acetone and water.

From the equilibrium



in pure and aqueous acetone, respectively, we may write,

$$(\mu^\circ_{LiBr})_A - (\mu^\circ_{Li^+})_A - (\mu^\circ_{Br^-})_A = -RT \ln (K_A)_A \quad (20 a)$$

$$(\mu^\circ_{LiBr})_{AW} - (\mu^\circ_{Li^+})_{AW} - (\mu^\circ_{Br^-})_{AW} = -RT \ln (K_A)_{AW} \quad (20 b)$$

Table 7. Estimated values of transfer activity coefficients according to eqns. (19) and (21).

Water conc. wt.-%	$(\gamma_{t,Br^-})_{A \rightarrow AW}$	$(K_A)_{AW}/(K_A)_A$	$\frac{(\gamma_{t,Li^+})_{A \rightarrow AW}}{(\gamma_{t,LiBr})_{A \rightarrow AW}}$
0.005	1	1	1
0.055	0.89	0.89	1
0.106	0.80	0.82	1
1.505	0.22	0.42	2

which, according to eqn. (13), yields,

$$\frac{(K_A)_{AW}}{(K_A)_A} = \frac{(\gamma_{t, Li^+})(\gamma_{t, Br^-})}{\gamma_{t, LiBr}} \quad (21)$$

where $(K_A)_{AW}$ and $(K_A)_A$ are the ion-pair association constants of lithium bromide in aqueous and anhydrous acetone, respectively.

Using the values of K_A at 25 °C in Table 1 and values of k_i/k_A according to eqn. (9) with $K=73$, the data in Table 7 were derived from eqns. (19) and (21). According to these data the activity coefficient ratio, $\gamma_{t, Li^+}/\gamma_{t, LiBr}$, is approximately equal to unity for water concentrations of 0.1 wt-% or less. At 1.5 wt-% water the ratio has increased by a factor of 2. One reason for this effect may be an increased solvation of lithium bromide ion-pairs in the aqueous solvent mixture as compared with the pure solvent.

Acknowledgements. The author thanks Dr. Per Beronius for valuable discussions, for suggesting improvements of the manuscript, and for access to unpublished data. Financial assistance by the Swedish Natural Science Research Council is gratefully acknowledged.

1. Holmgren, A. and Beronius, P. *Acta Chem. Scand.* 26 (1972) 3881.
2. Beronius, P. *Acta Chem. Scand.* 15 (1961) 1151.
3. Beronius, P., Isacson, U. and Nilsson, A.-M. *Acta Chem. Scand.* 24 (1970) 189.
4. Beronius, P. *Trans. R. Inst. Technol., Stockholm* 1963, No. 213.
5. McKay, H. A. C. *J. Am. Chem. Soc.* 65 (1943) 702.
6. Acree, S. F. *Am. Chem. J.* 48 (1912) 352.
7. Nilsson, A.-M. and Beronius, P. *Z. Phys. Chem. (Frankfurt am Main)* 79 (1972) 83.
8. Beronius, P. *Unpublished.*
9. Fuoss, R. M. and Hsia, K.-L. *Proc. Natl. Acad. Sci. U.S.A.* 57 (1967) 1550.
10. Fuoss, R. M. and Hsia, K.-L. *Proc. Natl. Acad. Sci. U.S.A.* 58 (1968) 1818.
11. Fernández-Prini, R. *Trans. Faraday Soc.* 65 (1969) 3311.
12. Robinson, R. A. and Stokes, R. H. *Electrolyte Solutions*, Butterworths, London 1965, p. 229.
13. Beronius, P. *Acta Chem. Scand.* A 28 (1974) 77.
14. Bjerrum, N. K. *Dan. Vidensk. Selsk. Mat.-Fys. Medd.* 7 (1926) No. 9.
15. Hald, A. *Statistical Theory with Engineering Applications*, Wiley, New York 1965, pp. 551–557.
16. Fuoss, R. M. and Onsager, L. *J. Phys. Chem.* 61 (1957) 668.

17. Becker, E. D. *Spectrochim. Acta* 17 (1961) 436.
18. Parker, A. J. and Brody, D. *J. Chem. Soc.* (1963) 4061.
19. Chantooni, M. K., Jr. and Kolthoff, I. M. *J. Am. Chem. Soc.* 89 (1967) 1582.
20. Kolthoff, I. M. and Chantooni, M. K., Jr. *J. Am. Chem. Soc.* 89 (1967) 2521.
21. Eyring, H. *J. Chem. Phys.* 3 (1935) 107.
22. Evans, M. G. and Polanyi, M. *Trans. Faraday Soc.* 31 (1935) 875.
23. Glasstone, S., Laidler, K. J. and Eyring, H. *The Theory of Rate Processes*, McGraw, New York 1941.
24. Alexander, R., Ko, E. C. F., Parker, A. J. and Broxton, T. J. *J. Am. Chem. Soc.* 90 (1968) 5049.
25. Moelwyn-Hughes, E. A. *Trans. Faraday Soc.* 45 (1949) 167.
26. Swart, E. R. and Le Roux, L. J. *J. Chem. Soc.* (1957) 406.
27. Trémillon, B. *Chemistry in Non-Aqueous Solvents*, D. Reidel Publishing Company, Dordrecht, Holland 1974, Chapter V.
28. Parker, A. J. *J. Chem. Soc. A* (1966) 220.

Received February 22, 1977.

Preparation and Reactions of a Coordinatively Unsaturated Surface Compound of Iron(II) on Silica Gel

BERND REBENSTORF

Division of Inorganic Chemistry I, Chemical Center, University of Lund, Box 740, S-220 07 Lund 7, Sweden

The preparation of a coordinatively unsaturated surface compound of iron(II) on silica gel is described. CO, C₂H₄, NO and O₂ are adsorbed by this surface compound at room temperature with colour change. Stoichiometric measurements are explained on the basis that one (CO, C₂H₄) or two ligands (NO) can be adsorbed by one iron(II) surface ion, which is thought to be connected to the silica gel by two oxygen ligands. The oligomerization of C₂H₄ to benzene is catalysed at room temperature, but polymerization of C₂H₄ was not observed.

Up to now two coordinatively unsaturated surface compounds have been observed, which consist of transition metal ions on silica gel with the oxidation number two and which are thought to be connected to the silica gel surface by two oxygen ligands. These are the surface compounds of chromium(II)¹ and cobalt(II).² In this article a third member of the group is described and its properties are compared with those of the known compounds.

EXPERIMENTAL

When not explicitly mentioned below, the experimental conditions were in general the same as those described in Ref. 2.

For impregnation a solution of iron(II) chloride in water was added to the purified silica gel "Merck 7733" and dried at 120 °C in vacuum. The impregnated silica gel was heated in a quartz tube under vacuum to a final pressure of 10⁻² Torr at the special temperature mentioned below. These operations were performed with exclusion of air.

Iron(II) was analysed after oxidation to iron(III) with peroxodisulfate solution in water by determining the absorption at 458 nm of the

thiocyanate complex in dilute hydrochloric acid. The error was within 2 %.

The reflectance spectra were recorded at room temperature on a Beckman DK 2 spectrophotometer equipped with a reflectance attachment. Magnesium oxide was used as a reference sample and the absorbance was calculated according to the Kubelka-Munk function.³

RESULTS

Vacuum heat treatment of the impregnated silica gel up to 1000 °C changes the colour of the samples only in a minor respect from nearly white to light grey, while water and, between 200 and 500 °C, hydrochloric acid are lost. The reflectance spectra* of selected samples with pretreatment temperatures of 200, 500 and 1000 °C show only small peaks in the NIR region (Fig. 1); for instance after vacuum heat treatment at 1000 °C two maxima at 7.6 and 12.0 kK are observed. If CO or C₂H₄ are added (20 °C/760 Torr) to a sample with such a pretreatment the colour changes to blue green or blue, respectively, and comparably intense bands are observed in the reflectance spectra (Fig. 2). This behaviour is thought to be strong indication of a coordinatively unsaturated surface compound of iron(II) on silica gel.

Adding water to this compound does not change the colour significantly (Fig. 2/3). Exposure of the coordinatively unsaturated compound to air or O₂ changes the colour immediately to brown (Fig. 2/4), but the colour

* Two sharp peaks at 7.3 and 4.5 kK belong to overtones or combination vibrations of the SiOH surface groups.

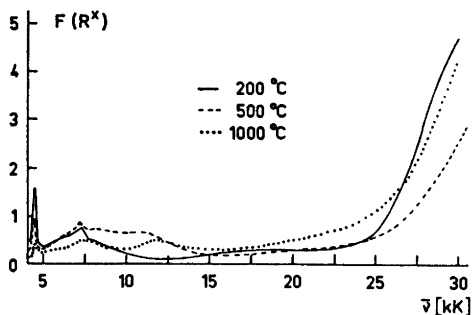


Fig. 1. Reflectance spectra of iron-containing silica gel with vacuum heat treatment at 200, 500 and 1000 °C, respectively [0.7 % iron(II)].

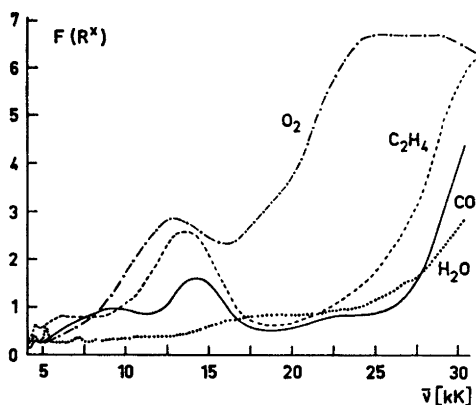


Fig. 2. Reflectance spectra of iron-containing silica gel [0.7 % iron(II), pretreatment: 1000 °C] with CO , C_2H_4 , O_2 and H_2O , respectively, adsorbed at 20 °C.

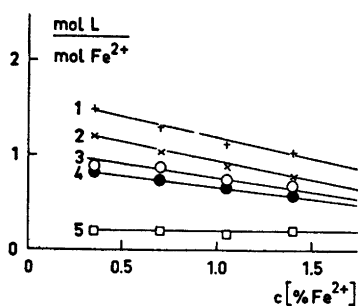


Fig. 3. Adsorption of NO , CO , C_2H_4 and O_2 at 0 °C on iron-containing silica gel with different iron(II) concentrations (pretreatment: 1000 °C). Curve 1, NO , 1 Torr; 2, CO , 760 Torr; 3, C_2H_4 , 1 Torr; 4, CO , 1 Torr; 5, O_2 , 1 Torr.

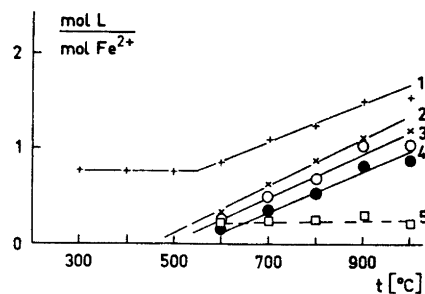


Fig. 4. Effect of pretreatment temperature on the adsorption of NO , CO , C_2H_4 and O_2 at 0 °C on the iron-containing silica gel [0.35 % iron(II)]. Curves 1 – 5, see legend to Fig. 3.

change is reversed again to light grey if water is added or if the compound is in contact with moisture. After a few days exposure to air this sample becomes yellow, obviously due to the oxidation to iron(III). If NO is added to the coordinatively unsaturated surface compound the colour becomes black and changes again, if O_2 is added, to yellow.

NO and O_2 react also with samples pretreated only at temperatures between 200 and 500 °C but in this case the colours are different (NO : green) and with O_2 , addition of water gives a yellow sample.

Gravimetric determination of the ligand/iron(II) ratio (Fig. 3) shows the same concentration effect as was observed with cobalt(II) on silica gel,* with the difference that O_2 is adsorbed to the same relative amount at all concentrations. Up to 90 % of this O_2 can be removed by heating the sample to 300 °C under vacuum. On the basis of Fig. 3 the stoichiometric ratio of CO or C_2H_4 to iron(II), under conditions similar to those at which the reflectance spectra were recorded (20 °C, 760 Torr, 0.7 % iron(II)), is assumed to be 1:1.* From the corresponding ratio of 1.5:1 for adsorbed NO at low iron concentrations at least half of the iron(II) surface ions are thought to have each two molecules NO adsorbed. Adsorbed CO , C_2H_4 or NO can be removed under the same conditions as O_2 .

Investigation of the pretreatment temperature effect (Figs. 4 and 5) showed that adsorp-

* However, the application of lower temperatures at the same pressure may lead to a ratio of 2:1 or even higher.

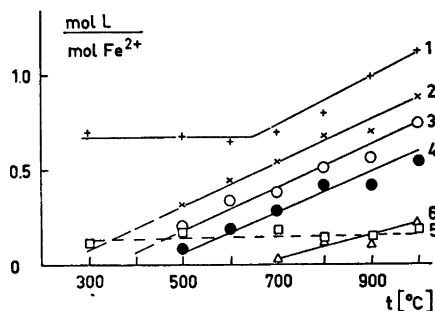


Fig. 5. The same as Fig. 4 but with different iron content [1.05 % iron(II)]. Curves 1–5, see legend to Fig. 3. Curve 6, N_2 , 760 Torr.

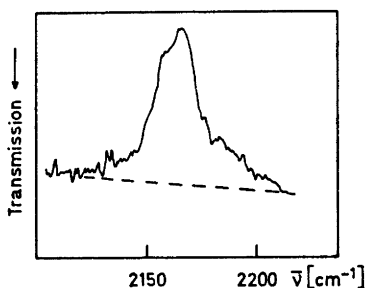


Fig. 6. IR spectrum of adsorbed CO [iron(II) content: 0.7 %, pretreatment: 1000 °C].

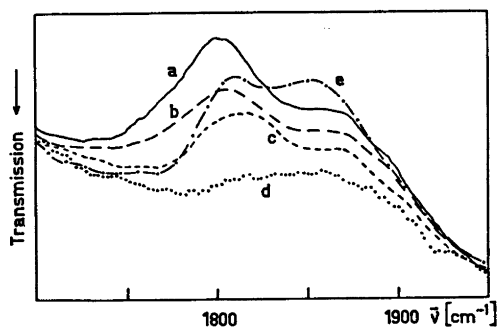


Fig. 7. IR spectra of adsorbed NO [iron(II) content: 0.7 %; a, b, c, d; pretreatment at 1000 °C; e: pretreatment at 300 °C] evacuated at a: 20, b: 100, c: 200, d: 400, e: 20 °C.

tion of CO and C_2H_4 at 0 °C begins when pretreatment temperatures of about 400 °C are used, while N_2 adsorption (Fig. 5) begins only after pretreatment at temperatures higher than 600 °C and is obviously much weaker than that

of CO or C_2H_4 . The NO adsorption decreases with decreasing temperature of the pretreatment to only approximately half of its value at 1000 °C and then remains constant from 500 down to 200 °C. The stoichiometric ratio of NO to iron(II) is then rather 1:1. No effect of the pretreatment temperature on the O_2 adsorption was observed (Fig. 5).

Gravimetric measurements showed also that adsorbed NO reacts at room temperature with O_2 to give adsorbed NO_2 with an accompanying colour change from black to yellow. The same reaction was observed with chromium(II) on silica gel.⁴

CO adsorbed by the coordinatively unsaturated iron(II) surface compound (pretreatment temperature: 1000 °C) shows an IR absorption band at 2165 cm^{-1} (Fig. 6). NO adsorbed by the same surface compound has two bands at 1802 and 1870 cm^{-1} (Fig. 7a and b) when evacuated (1 Torr) at 20 or 100 °C before the IR measurements and two bands at 1815 and 1865 cm^{-1} when evacuated at 200 °C (Fig. 7c). Evacuation at 400 °C desorbs all NO and gives the baseline (Fig. 7d). The fact that two IR bands exist also at higher evacuation temperatures (100 and 200 °C) is an indication that either two NO molecules or none are adsorbed. On this basis the angle between the two NO molecules can be calculated according to Beck *et al.*⁵ from the intensities of the IR absorptions. This calculation gives a value of approximately 130° for a sample with adsorbed NO evacuated at 20 °C.

If a low pretreatment temperature (300 °C) is used for the preparation of the sample, adsorbed NO gives two IR bands at 1810 and 1855 cm^{-1} (Fig. 7e) possibly due to two different adsorption sites and not to two adsorbed NO molecules at one iron(II) surface ion.

As in the case of cobalt(II)² and in contrast to chromium(II)¹ C_2H_4 is not polymerised by the coordinatively unsaturated iron(II) surface compound at room temperature and 760 Torr pressure. C_2H_2 is oligomerised to benzene by all three surface compounds.

DISCUSSION

In general the model for the reactions during the preparation of the coordinatively unsaturated cobalt(II) surface compound² applies also to the iron(II) surface compound. During the

impregnation the hexaaquo iron(II) ion is physisorbed at the silica gel surface and subsequently loses water when heated to 200 °C in vacuum to give the tetraaquo ion. Between 200 and 500 °C the anion combines with a proton from a silanol surface group to give hydrochloric acid. The iron(II) ion is bonded to the silica gel surface by two oxygen ligands and two water molecules are left adsorbed to the iron, which is now four coordinated with pseudo square planar or more exactly C_{2v} symmetry. During heating to 1000 °C the adsorbed water is lost to give the coordinatively unsaturated iron(II) compound with the coordination number two and C_{2v} symmetry.

Both the four coordinated compounds have free coordination sites where NO or O₂ can be adsorbed. However, only the two coordinated surface compounds can adsorb CO, C₂H₄ and, very weakly, N₂.

This model for the coordinatively unsaturated surface compound of iron(II) is the same as that proposed for chromium(II)⁶ and cobalt(II),² so there should be a number of comparable properties. For instance all three compounds adsorb CO or C₂H₄ at room temperature and 760 Torr with, in the case of CO, an IR vibration at higher wave-numbers than gaseous CO. This is an indication of electron donation from the CO coupled with weak back donation from the metal and is caused by the relatively high oxidation number of the metal ion. Perhaps the siloxane bond between the silica gel surface and the metal ion is also influencing this.

All three surface compounds bind C₂H₄ a little stronger than CO and adsorb two molecules NO at room temperature which have two IR absorptions at lower wave-numbers than the gaseous NO. The oligomerization of C₂H₂ to benzene was mentioned before.

Beside this general correspondence between the three surface compounds there are some special similarities in the reflectance spectra of chromium(II)⁷ and iron(II) compounds. Both the coordinatively unsaturated surface compounds absorb at 7.6 and 12.0 kK, after adsorbing one molecular CO per metal ion they both have maxima at 8.7 and 13.8 kK and also the reflectance spectra after adsorption of one molecule C₂H₄ or in the case of chromium(II) of an olefin⁸ equal each other.

This astonishing behaviour can easily be understood by applying the electron hole formalism of ligand field theory, which predicts that a d^4 electronic system [chromium(II)] should have comparable spectra to a d^6 system [iron(II)]. However, there is a difference in the stability of the ligand adsorption, which is for instance expressed by the weaker N₂ adsorption of iron(II) compared to chromium(II) and which is the cause of the difference in the IR spectra of adsorbed CO [chromium(II): 2186 cm⁻¹; iron(II): 2165 cm⁻¹].

Acknowledgement. This work was made possible by a stipend from the Deutsche Forschungsgemeinschaft. The author thanks Dr. R. Larsson for valuable discussions.

REFERENCES

1. Krauss, H. L. and Stach, H. *Z. Anorg. Allg. Chem.* 366 (1969) 34.
2. Rebenstorf, B. *Acta Chem. Scand. A* 31 (1977) 208.
3. Kubelka, P. and Munk, F. *Z. Techn. Physik* 12 (1931) 593.
4. Krauss, H. L. and Weisser, B. *Z. Anorg. Allg. Chem.* 412 (1975) 82.
5. Beck, W., Melnikoff, A. and Stahl, R. *Chem. Ber.* 99 (1966) 3721.
6. Krauss, H. L. *Proc. Int. Congr. Catal.* 5th, 1972, 1 (1973) 207.
7. Krauss, H. L., Rebenstorf, B., Westphal, U. and Schneeweiss, D. In Delmon, B., Jacobs, P. A. and Poncelet, G., Eds., *Preparation of Catalysts*, Elsevier, Amsterdam 1976, p. 489.
8. Westphal, U. Freie Universität Berlin. *Private communication.*

Received February 16, 1977.

Alternative Routes in Hydroxide Ion-catalyzed Hydrogen Isotope Exchange of Unsymmetrical Ketones

ALPO KANKAANPERÄ, LEENA OINONEN and PENTTI SALOMAA †

Department of Chemistry and Biochemistry, University of Turku, 20500 Turku 50, Finland

The hydroxide ion-catalyzed detritiation of a number of unsymmetrical ketones has been studied in water at 298.15 K. The hydrogen isotope exchange takes place in the α -positions. The rate coefficients for both of these parallel reactions have been calculated. On the basis of these kinetic results the contributions of alternative routes in different base-catalyzed reactions of ketones can be estimated.

Base-catalyzed reactions of ketones has been the subject of numerous kinetic studies.^{1,2} Especially halogenation, deuteration, and racemisation reactions have been thoroughly studied. It has been suggested that in all of these cases the proton abstraction from the ketone is the rate-limiting step of the reaction.^{1,2} Although an alternative rate-limiting step has been proposed for the halogenation of some aliphatic ketones,³ a recent study⁴ reveals that this assumption is less probable. Only little information is available on the relative reactivities of alternative acidic sites. The base-catalyzed deuteration of unsymmetrical ketones has previously been studied⁵ but most of these papers concern only the deuteration of 2-butanone.^{5a,b,f,g,i} In addition the accuracy which has been obtained by the NMR method is insufficient for detailed studies. Partly this is due to secondary isotope effects which lead to deviations from the first-order kinetics. A more exact information on the relative reactivities of the alternative acidic sites is, however, important. Therefore the detritiation of unsymmetrical ketones — CH_2COCH_3 and $>\text{CHCOCH}_3$ was subjected to a thorough kinetic study.

EXPERIMENTAL

Labeling. Most of the ketones used in the kinetic measurements were products of Fluka AG; 1-phenyl-1-buten-3-one was purchased from British Drug House. The ethyl *tert*-butyl ketone used in the kinetic measurements was prepared by Taskinen.⁶ 1-Methoxy-2-propanone was synthesized by the following method:⁷ A solution of 225 g of concentrated sulfuric acid in 58 g of water was dropped into a solution of 188 g of sodium dichromate and 101 g of 1-methoxy-2-propanol in 100 cm³ of water during 6 h with vigorous stirring. During the addition the temperature of the reaction mixture was kept at 293–298 K. Leaving the solution overnight the ketone was extracted into diethyl ether. The ethereal solution was dried with potassium carbonate, the ether removed in vacuum and the ketone purified by distillation. B.p. 387–388 K. ¹H NMR δ 3.80 (2 H), 3.35 (3 H), 2.05 (3 H).

In the tritium labeling 10 cm³ of a ketone was stirred with 30 cm³ of 0.1 mol dm⁻³ sodium hydroxide and about 1 mm³ of tritiated water at room temperature from 20 to 50 h depending on the substrate. The activity of the tritiated water (The Radiochemical Centre) was 10⁷ s⁻¹ mm⁻³. In most cases the aqueous solution and the ketone were immiscible and therefore the reaction mixture was shaken vigorously to emulsify the two phases and thus increase the rate of isotope exchange reaction. After labeling the ketone was extracted into diethyl ether with three portions of 20 cm³. The efficiency of the extraction was increased by salting out the ketone from the aqueous solution with sodium chloride. The ethereal solutions were dried over magnesium sulfate, the ether removed in vacuum and the ketone distilled. The purity of the product was controlled by NMR spectroscopy. The extent of labeling was studied with a Wallac 8100 scintillation counter and 1 mm³ samples from the various ketones were found to give activities between 200 and 2000 s⁻¹. In the tritiation of 1-phenyl-1-buten-3-one the

above-mentioned procedure was slightly modified: The solid ketone (10 g) was dissolved in 10 cm³ of diethyl ether and the solution was stirred vigorously with 30 cm³ of 0.1 mol dm⁻³ sodium hydroxide and 2 mm³ of tritiated water for 80 h at room temperature. The ketone was extracted into diethyl ether with three portions of 20 cm³ and the ethereal solution was dried over magnesium sulfate. After the ether had been evaporated the ketone was crystallized from benzene. In some cases the labeling was performed in dimethyl sulfoxide-water mixtures ($x_{\text{DMSO}} = 0.8 - 0.9$) with tetramethylammonium hydroxide (0.01 mol dm⁻³) as catalyst. Under these conditions the labeling takes place in one phase and, additionally, the relatively high basicity of this medium⁸ favors the hydrogen isotope exchange reaction. After tritiation the labeled product was extracted into pentane and distilled.

Kinetic measurements. Kinetic measurements were performed in water at 298.15 ± 0.05 K with 0.1 mol cm⁻³ sodium hydroxide as the catalyst. 85 cm³ of the sodium hydroxide solution was thermostated to the desired temperature and 0.04–0.2 cm³ of the labeled substrate was added. After vigorous shaking the first sample was taken with a 5 cm³ semi-automatic pipet. The content of the pipet was added to 2 cm³ of 0.3 mol dm⁻³ sulfuric acid to stop the reaction. The solution was saturated with disodium hydrogen phosphate and the ketone was extracted into 10 cm³ of anisole. The 5 cm³ samples taken from the organic layer were transferred to the vials of a scintillation counter with 10 cm³ of the scintillation liquid (10 g of diphenyloxazole and 0.25 g of *p*-bis(*o*-methylstyryl)benzene in 2.5 dm³ of toluene). The decrease in the activity of the ketone was followed with the Wallac 8100 scintillation counter. 10 to 15 samples were withdrawn from each kinetic run. The final samples were taken after ten half lives. The first-order rate coefficients were calculated from eqn. (1)

$$k = \frac{1}{t} \ln \frac{N_0 - N_\infty}{N_t - N_\infty} \quad (1)$$

where t denotes the time calculated from the withdrawal of the first sample and N_0 , N_t , and N_∞ are the measured count rates for the first sample, for the sample taken at time t , and for the final sample, respectively. In most cases the ketone contained, however, alternative exchangeable α -hydrogens and therefore the above-mentioned procedure was slightly modified. The labeled substrate (0.1–0.2 cm³) was added to 180 cm³ of 0.1 mol dm⁻³ aqueous sodium hydroxide and first 4–5 samples were withdrawn as fast as possible in order to extrapolate the count rates to the beginning of the reaction. During the progress of the reaction about 30 samples were withdrawn. The first-order rate coefficients, k_a and

k_b , for the parallel reactions were calculated by eqn. (2) on a Univac 1108 computer using

$$\frac{N_0 - N_t}{N_0 - N_\infty} = x_a(1 - e^{-k_a t}) + (1 - x_a)(1 - e^{-k_b t}) \quad (2)$$

the method of least squares.⁹ In eqn. (2) x_a denotes the mol fraction of tritium in the more acidic site of the ketone, k_a the first-order rate coefficient for the detritiation of the more acidic α -hydrogen and k_b the corresponding rate coefficient for the detritiation of the less acidic α -hydrogen. Notations N are as in eqn. (1) except N_0 which is the extrapolated count rate at the beginning of the reaction.

RESULTS AND DISCUSSION

On the basis of the present kinetic data the fraction of tritium in the alternative acidic sites of the labeled ketones was calculated and the results are collected in Table 1. It can be concluded that the x_a -values (mol fraction of tritium in the more acidic α -hydrogen) give in most cases the fractions of tritium in the methyl group. Only the phenyl and the methoxy group in compounds 10 and 12 are more electronegative than are the hydrogen atoms in the methyl group. It is thus reasonable to assume that only in these two cases the methylene hydrogens are more acidic than those in the alternative methyl group. Qualitative evidence for this assumption can be obtained by studying the alternative hydrogen exchange reaction, the deuteration of ketones. The results from these measurements really reveal that only for compounds 10 and 12 the deuteration of the methyl group takes place with a slower rate than that of the methylene group. If the tritiation of unsymmetrical ketones had led to an equilibrium roughly a statistical distribution between the alternative α -hydrogens is to be expected. For compounds 2, 4, 5, 6, and 7 the x_a -values in Table 1 are really seen to be in accordance with the statistical values 0.75 or 0.60 within the limits of experimental errors. For compounds 3, 9, 10, and 12 the measured x_a -values are slightly higher than can be expected on the basis of the amount of exchangeable hydrogen atoms, but the distribution of tritium is, however, in favor of the more acidic site of the substrate as a result of kinetic control. With the exception of compounds 5 and 6 the conformity

Table 1. Detritiation of unsymmetrical ketones RCOCH_3 in 0.1 mol dm^{-3} aqueous sodium hydroxide at 298.15 K.

No.	RCOCH_3 R	x_a^a	$k_a/10^{-4} \text{ s}^{-1}^b$	$k_b/10^{-4} \text{ s}^{-1}^c$
1	$(\text{CH}_3)_3\text{C}$	—	0.961 0.972	—
2	$(\text{CH}_3)_2\text{CH}$	0.664 0.735 0.703	1.88 1.73 1.78	0.250 0.159 0.175
3	$(\text{CH}_3)_3\text{CCH}_2$	0.724 0.797	2.29 2.19	0.989 0.841
4	$\text{CH}_3(\text{CH}_2)_3$	0.600 0.600	1.58 1.63	1.14 1.09
5	$(\text{CH}_3)_2\text{CHCH}_2$	0.722 0.570	1.87 2.20	0.633 0.857
6	$\text{CH}_3(\text{CH}_2)_2$	0.667 0.524	1.59 1.74	0.957 1.034
7	CH_3CH_2	0.600 0.600	1.52 1.38	1.18 1.38
8	CH_3	—	2.19	—
9	$\text{Ph}-\text{CH}_2\text{CH}_2$	0.743 0.785 0.675	3.58 3.41 3.65	2.04 1.99 2.15
10	$\text{Ph}-\text{CH}_2$	0.570 0.574	81.6 85.1	3.85 3.91
11	$\text{Ph}-\text{CH}=\text{CH}$	— ^d	3.58 3.53	—
12	CH_3OCH_2	0.463 0.477	8.74 9.00	5.45 5.60
13	Ph	— —	5.75 5.72	—

^a x_a = mol fraction of tritium in the more acidic site of the substrate. ^b k_a = first-order rate coefficient for the detritiation from the more acidic site of the substrate. ^c k_b = first-order rate coefficient for the detritiation from the less acidic site of the substrate. ^d The isotope exchange in the CH-group was negligible in the used conditions.

Table 2. Second-order rate coefficients for the detritiation of ketones RCOCH_3^* , at 298 K.

No.	RCOCH_3 R	σ^*_R	$k_{\text{CH}_3}/10^{-3} \text{ mol}^{-1} \text{ dm}^3 \text{ s}^{-1}$
1	$(\text{CH}_3)_3\text{C}$	-0.320	0.966
2	$(\text{CH}_3)_2\text{CH}$	-0.200	1.80
3	$(\text{CH}_3)_3\text{CCH}_2$	-0.140	2.24
4	$\text{CH}_3(\text{CH}_2)_3$	-0.130	1.61
5	$(\text{CH}_3)_2\text{CHCH}_2$	-0.125	2.03
6	$\text{CH}_3(\text{CH}_2)_2$	-0.115	1.70
7	CH_3CH_2	-0.100	1.45
8	CH_3	0.000	2.19
9	$\text{Ph}-\text{CH}_2\text{CH}_2$	+0.080	3.54
10	$\text{Ph}-\text{CH}_2$	+0.225	3.87
11	$\text{Ph}-\text{CH}=\text{CH}$	+0.410	3.55
12	CH_3OCH_2	+0.520	5.52
13	Ph	+0.600	5.73

of the parallel α_a -values is seen to be satisfactory, since the evaluation of the three parameters from a single run requires high accuracy in the kinetic experiments. The best results were obtained when the rate coefficients for parallel reactions differ substantially as shown in previous studies⁷ for the detritiation of methyl benzyl ketone (compound 10).

As discussed above the faster of the alternative detritiation reactions is that of the methyl group with exception of compounds 10 and 12, in which the methylene hydrogens are more acidic. The accuracy of the measured k_a -values is seen to be satisfactory, since the difference between the parallel k_a -values is less than ten per cent with exception of compound 5. Also the parallel k_b -values are seen to be almost equal with the exception of compounds 2, 3, and 5. In the case of acetophenone the present kinetic data can be compared with the results in previous studies. The second-order rate coefficient, $0.00574 \text{ mol}^{-1} \text{ dm}^3 \text{ s}^{-1}$, calculated from the first-order rate coefficients in Table 1 is in good agreement with the values of $0.0058 \text{ mol}^{-1} \text{ dm}^3 \text{ s}^{-1}$ (Ref. 10) and $0.0054 \text{ mol}^{-1} \text{ dm}^3 \text{ s}^{-1}$ (Ref. 11).

Detritiation of the methyl group. On the basis of the present kinetic data structural effects in reaction (3), in which the detritiation takes



place from the methyl group of an unsymmetrical ketone, can be discussed. The second-order rate coefficients k_{CH_3} (Table 2) for this reaction were calculated from the k_a -values in Table 1 by dividing the first-order rate coefficients with the hydroxide ion concentration. As discussed above in the case of compounds 10 and 12 the k_{CH_3} -values must be calculated from the first-order rate coefficients k_b in Table 1. When the logarithms of the rate coefficients k_{CH_3} are plotted against the σ^* -values¹² of the α -substituent a linear correlation is observed (Fig. 1). When the slope of this plot was calculated by the method of least squares the kinetic data for the detritiation of the phenyl and styryl substituted derivatives (compounds 11 and 13) were neglected since resonance effects may be operative in these reactions. From the kinetic data for eleven ketones the relationship (4)

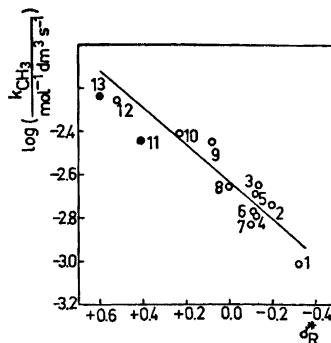
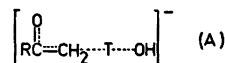


Fig. 1. Plot of the logarithms of rate coefficients of detritiation for RCOCH_3 against substituent constant σ^*_R . The numbers of the compounds refer to Table 2. Compounds 11 and 13 (filled circles) were neglected when the correlation line was plotted.

was obtained. The rate coefficients for the detritiation reactions of the phenyl and styryl

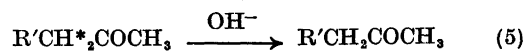
$$\log k_{\text{CH}_3} = (0.862 \pm 0.117)\sigma^*_R - (2.639 \pm 0.026) \quad (4)$$

substituted derivatives are seen to differ only slightly from the linear free energy correlation; this reflects that the stabilization due to the conjugation of the carbonyl group and the



aromatic ring (R =phenyl in scheme A) has diminished only slightly in the attainment of the transition state A of reaction (3).

Detritiation of the methylene group. On the basis of the present kinetic data structural effects in the detritiation of the methylene hydrogens can be discussed. In the case of compounds 3–10 and 12 in Table 1 detritiation from the methyl and methylene group are parallel reactions and as mentioned above the lower of the measured rate coefficients is that of the detritiation of the methylene group except for compounds 10 and 12. The second-order rate coefficients for reaction (5) are collected in Table 3. When the logarithms of these



rate coefficients are plotted against the σ^* -values of the substituents attached at the methylene

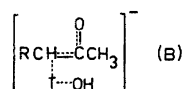
Table 3. Second-order rate coefficients for the detritiation of ketones $R'CH_2COCH_3$ at 298 K.

No.	$R'CH_2COCH_3$ R'	$\sigma^*_{R'}$	$k_{CH_3}/10^{-3} \text{ mol}^{-1} \text{ dm}^3 \text{ s}^{-1}$
3	$(CH_3)_2C$	-0.320	0.914
4	$CH_3(CH_2)_2$	-0.115	1.11
5	$(CH_3)_2CH$	-0.200	0.745
6	CH_3CH_2	-0.100	0.996
7	CH_3	0.000	1.28
8	H	+0.490	2.19
9	Ph- CH_2	+0.225	2.06
10	Ph	+0.600	83.3
12	CH_2O	+1.46	8.87

group (Fig. 2) a linear correlation is observed when the phenyl substituted derivative is excluded. The slope of this plot was calculated from the kinetic data by the method of least squares (eqn. 6). Although only inductive polar effects are seen to be operative in the detritia-

$$\log k_{CH_3} = (0.588 \pm 0.043)\sigma^*_{R'} - (2.908 \pm 0.024) \quad (6)$$

tion of the above-mentioned compounds resonance effects cannot be excluded. It can be seen (Fig. 2) that the phenyl substituted derivative reacts with a rate which is markedly higher (by a factor of about 30) than might be expected on the basis of inductive polar effects only. The accelerating effect of this substituent must be due to resonance effects since in the transition state (B) the phenyl



group (R' = phenyl) is in conjugation with the partial double bond system.

On the basis of the obtained linear free energy correlations (4) and (6) rate coefficients for the detritiation of α -methyl and α -methylene hydrogens in different unsymmetrical ketones can be estimated. The measured rate coefficients can also be applied in the determination of the pK_a -values of different acidic sites of ketones.¹³

Acknowledgement. Grants for support of this work from the Finnish Academy, Division of Sciences, are gratefully acknowledged.

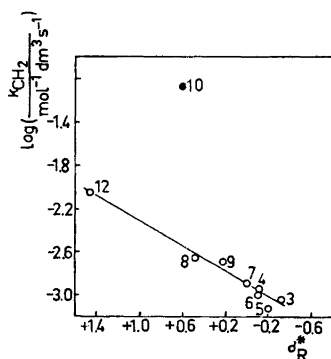


Fig. 2. Plot of the logarithms of rate coefficients in detritiation of $R'CH_2COCH_3$ against substituent constants $\sigma^*_{R'}$. The numbers refer to Table 3. Compound 10 (filled circle) was neglected when the correlation line was plotted.

REFERENCES

- Gould, E. *Mechanism and Structure in Organic Chemistry*, Holt, Reinhardt and Winston, New York 1959, p. 372.
- Bell, R. P. *The Proton in Chemistry*, 2nd Ed., Chapman and Hall, London 1973, p. 171.
- Rappe, C. *Acta Chem. Scand.* 20 (1966) 1721; 21 (1967) 857, 1823; 22 (1968) 219.
- Swain, C. G. and Dunlop, R. P. *J. Am. Chem. Soc.* 94 (1972) 7204.
- a. Rappe, C. *Acta Chem. Scand.* 20 (1966) 2236, 2305; b. Warkentin, J. and Tee, O. S. *Chem. Commun.* 7 (1966) 190; c. Botner-By, A. A. and Sun, C. *J. Org. Chem.* 32 (1967) 492; d. Rappe, C. and Sachs, W. H. *J. Org. Chem.* 32 (1967) 4127; e. Rappe, C. and Sachs, W. H. *Tetrahedron* 24 (1968) 6287; f. Warkentin, J. and Cox, R. A. *J. Org. Chem.* 33 (1968) 1301; g. Rappe, C. *Acta Chem. Scand.* 23 (1969) 2305; h. Hine, J.,

- Hampton, G. and Menon, B. C. *J. Am. Chem. Soc.* 89 (1967) 2664; i. Warkentin, J. and Tee, O. S. *J. Am. Chem. Soc.* 88 (1966) 5540.
6. Taskinen, E. *Unpublished results.*
 7. Marinella, R. P. and Leech, J. L. *J. Am. Chem. Soc.* 71 (1949) 3558.
 8. Jones, J. R. *The Ionisation of Carbon Acids*, Academic, London 1973, p. 92.
 9. Kankaanperä, A., Oinonen, L. and Salomaa, P. *Acta Chem. Scand. A* 29 (1975) 153.
 10. Jones, J. R. and Stewart, R. *J. Chem. Soc. B* (1967) 1173.
 11. Jones, J. R., Marks, R. E. and Subba Rao, S. C. *Trans. Faraday Soc.* 63 (1967) 111.
 12. Taft, Jr., R. W. *J. Am. Chem. Soc.* 75 (1953) 4231.
 13. Kankaanperä, A., Salomaa, P., Oinonen, L. and Mattsen, M. *Finn. Chem. Lett. In press.*

Received April 19, 1977.

Electron-diffraction Study of Gaseous Tricyclo[4.1.0.0^{1,3}]heptane

ZUZANA SMITH,^a BIRGIT ANDERSEN^b and STANLEY BUNCE^c

^a Department of Chemistry, University of Oslo, Oslo 3, Norway, ^b Norwegian Research Council for Science and the Humanities, Institute for Studies in Research and Higher Education, Oslo 1, Norway and ^c Department of Chemistry, Rensselaer Polytechnic Institute, Troy, New York, U.S.A.

The molecular structure of tricyclo[4.1.0.0^{1,3}]heptane has been studied by gas-phase electron diffraction. Under the assumption of C_2 symmetry, the electron-diffraction analysis led to the following values for the principal parameters: $r_a(C1-C2)=1.465(7)$ Å, $r_a(C1-C3)=1.519(25)$ Å, $r_a(C2-C3)=1.526(10)$ Å, $r_a(C3-C4)=1.521(30)$ Å, $r_a(C4-C5)=1.572(14)$ Å, $r_a(C-H)_{av}=1.107(2)$ Å, $\angle C2C1C7=162.4(18)^\circ$, and the average angle of the five-membered ring $\angle(CCC)=105.1(2)^\circ$. The values in parentheses are standard deviations.

Tricyclo[4.1.0.0^{1,3}]heptane (TCH) contains highly-strained spiropentane bridged by a dimethylene grouping (see Fig. 1). One can also view the molecule as cyclopentane with two fused cyclopropane rings. The compound was first synthesized by Skattebøl,¹ and its thermal isomerization was investigated by Frey *et al.*² The present study was initiated to obtain infor-

mation concerning the gas-phase structure of TCH in order to gain a better understanding of the strain effects in this molecule.

EXPERIMENT AND DATA PROCESSING

A sample of tricyclo[4.1.0.0^{1,3}]heptane was obtained from Prof. L. Skattebøl, University of Oslo. Gas chromatographic analysis (10 % OV 17, a 50 % phenylsilicone, in a glass column at 50–150 °C) indicated a maximum of 6.3 % impurity, but it was believed that some thermal rearrangement occurred. The NMR spectrum (Varian HA100) showed a small amount of olefin; integration, based on an assumed 1,2,6-heptatriene structure for the impurity,¹ indicated 3.3 %. It was used without further purification. The diffraction diagrams were recorded with the Oslo apparatus³ on 24 × 6 cm Scientica 34B50 plates at a nozzle temperature of about 20 °C. Four plates exposed at a camera distance of 480.65 mm and four at 200.65 mm were selected for the structural analysis. The electron wavelength was determined from gold-foil diffraction patterns and adjusted by 0.1 % to 0.06464 Å by calibration with the diffraction patterns of gaseous benzene.

The optical densities were recorded while oscillating the plates, and the experimental intensities were treated in the usual way.⁴ They were leveled by using the elastic scattering factors calculated by the partial-wave method,⁵ based upon the analytical HF potential for a C-atom⁶ and using the best electron density of bonded hydrogen for H.⁷ The inelastic scattering factors used were those of Tavard *et al.*⁸

The experimental backgrounds were drawn by hand for each plate, and the average molecular intensities were calculated for each set of plates using the modification function $s/|f_C|^2$.⁴ The final background correction of 20 cm data was made on the modified intensities for each plate. The intensity ranges for the two sets of data were 2.0–19.25 and 7.25–42.25 Å⁻¹ with increments in s of 0.125 and 0.25 Å⁻¹, respec-

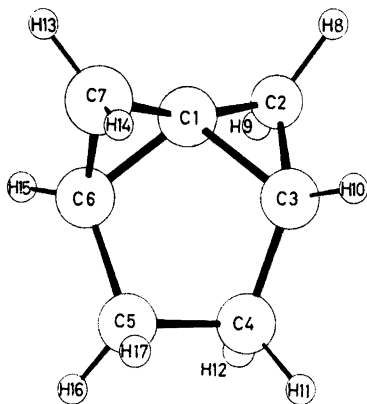


Fig. 1. Tricyclo[4.1.0.0^{1,3}]heptane. The numbering of the atoms is indicated.

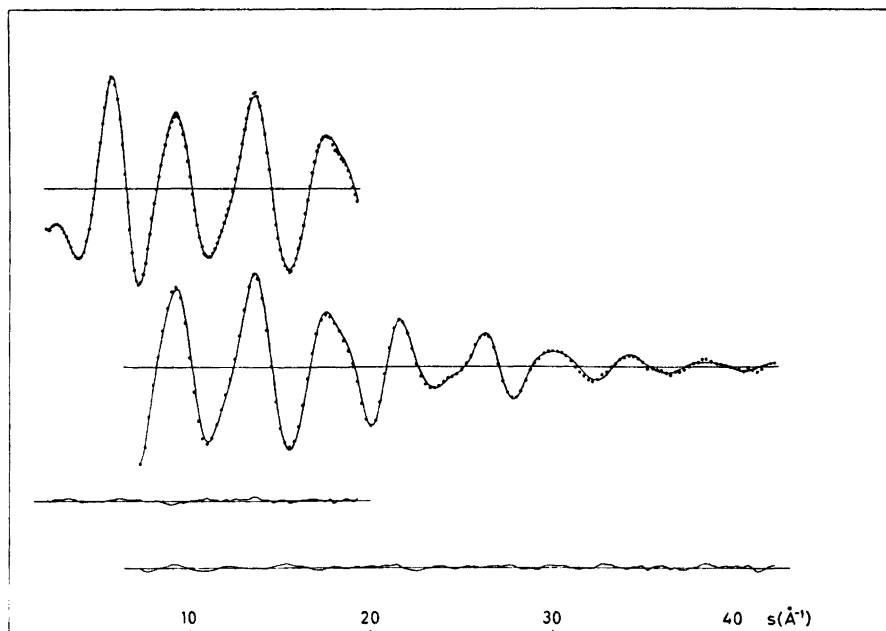


Fig. 2. The experimental intensity data (dots) for tricyclo[4.1.0.0^{1,2}]heptane from the 48 cm and the 20 cm camera distances. The solid line corresponds to the calculated molecular intensities, while the lower curves represent the difference between the experimental and the calculated intensities.

tively (Fig. 2). The radial distribution function calculated by the Fourier transformation of composite molecular intensity⁴ is shown in Fig. 3.

ANALYSIS OF DATA

Structural parameters were derived by a least-squares analysis of the molecular intensities under the following assumptions (for numbering of the atoms see Fig. 1):

- (1) The molecule has C_2 symmetry.
- (2) All C-H bond lengths are equal.
- (3) The HC_iH plane is perpendicular to the CC_iC plane and the bisectors of the HC_iH and CC_iC angles are colinear. ($i=2, 4, 5, 7$).
- (4) All the CC_jH angles are equal for $j=3, 6$.
- (5) The vibrational amplitudes, l , and the perpendicular amplitude correction coefficients, K , (see Table 1) were calculated by normal coordinate analysis,⁹ using Hildebrandt's program,¹⁰ on the basis of an estimated set of Urey-Bradley force-field parameters. The force

constants were derived from those in hydrocarbons such as cyclohexane¹¹ and are listed in Table 2. The l -values for the C-C bond distances and the C...C non-bonded distances (with the exception of $l(\text{C2}-\text{C5})$, which was refined separately) were refined in two groups,⁴ keeping the differences within each group at the calculated values. The l -values for the non-bonded C...H and H...H distances were maintained at the calculated values.

Under the above assumptions the structure is described by eleven parameters. The following parameters were used: $r(\text{C1}-\text{C2})$, $r(\text{C1}-\text{C3})$, $\Delta r = r(\text{C2}-\text{C3}) - r(\text{C1}-\text{C2})$, $r(\text{C3}-\text{C4})$, $r(\text{C4}-\text{C5})$, $r(\text{C}-\text{H})$, $\angle \text{C6C1C3}$, $\angle \text{HC4H}$, angle γ (the angle between the C6-C1-C3 and C1-C2-C3 planes), and ϕ_3 (the dihedral angle C3C4-C5C6).

The interpretation of the main features of the radial distribution curve was straightforward. The peaks at about 1.1 Å and 1.5 Å represent the C-H and C-C bond distances. The shoulder at 2.2 Å is formed by contributions of the C...H non-bonded distances, the

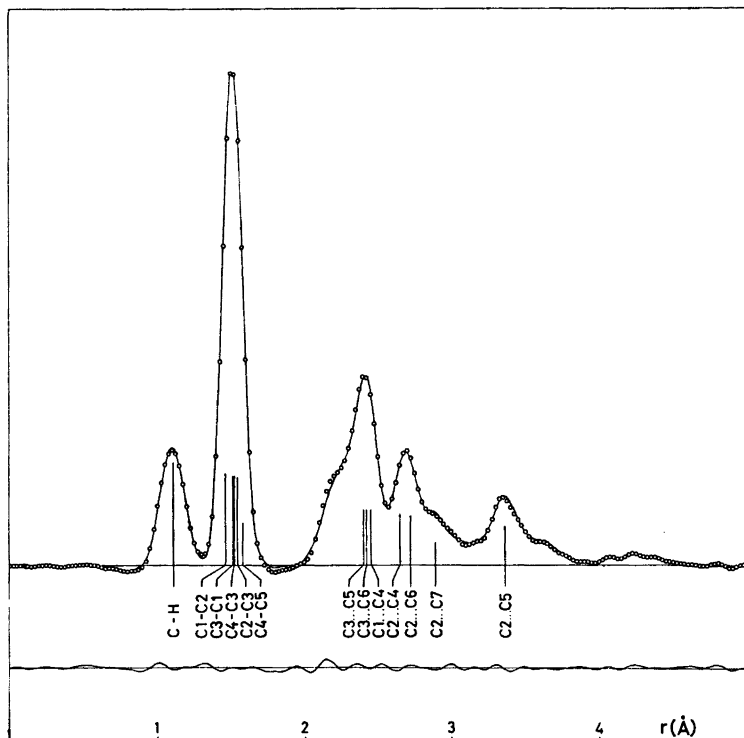


Fig. 3. Experimental (circles) and calculated (solid line) radial distribution curves for tricyclo-[4.1.0.0^{1,3}]heptane. The lower curve represents the difference between the experimental and calculated curves. The position and approximate areas of the most important interatomic distances are indicated. Damping factor $\exp(-0.0002 s^2)$ was used.

Table 1. Mean amplitudes of vibration, l , and perpendicular amplitude correction coefficients, K (in Å), calculated from assumed force-field.

Parameter	l	K	Parameter	l	K
C1-C2	0.051	0.003	C1...H11	0.10	0.006
C1-C3	0.052	0.002	C1...H12	0.13	0.006
C2-C3	0.051	0.003	C2...H11	0.11	0.006
C3-C4	0.052	0.003	C2...H12	0.15	0.007
C4-C5	0.052	0.003	C4...H8	0.11	0.006
C-H	0.078	0.018	C4...H9	0.14	0.007
C1...C4	0.060	0.001	C5...H8	0.10	0.004
C3...C5	0.065	0.001	C5...H9	0.13	0.005
C3...C6	0.061	0.001	C5...H10	0.13	0.005
C2...C4	0.068	0.002	C6...H8	0.10	0.006
C2...C6	0.066	0.001	C6...H9	0.14	0.006
C2...C7	0.062	0.002	C6...H10	0.12	0.005
C2...C5	0.069	0.001	C6...H11	0.10	0.006
C1...H8	0.10	0.010	C6...H12	0.14	0.006
C3...H8	0.10	0.010	C7...H8	0.12	0.006
C1...H10	0.10	0.009	C7...H9	0.12	0.006
C2...H10	0.10	0.010	C7...H10	0.15	0.005
C4...H10	0.10	0.010	C7...H11	0.12	0.004
C3...H11	0.11	0.010	C7...H12	0.13	0.004
C5...H11	0.11	0.010			

Table 2. Assumed force-field parameters for tricyclo[4.1.0.0^{1,3}]heptane.^a The number of contributions of each type is given in parentheses.

$K(\text{C}-\text{C})$	2.3(9)	$F(\text{C}-\text{C}-\text{C})$	0.34(10)
$K(\text{C}-\text{H})$	4.1(10)	$F(\text{H}-\text{C}-\text{C})$	0.53(22)
$H(\text{C}-\text{C}-\text{C})$	0.6(16)	$F(\text{H}-\text{C}-\text{H})$	0.18(4)
$H(\text{H}-\text{C}-\text{C})$	0.3(22)	$Y(\text{C}-\text{C})$	0.11(9)
$H(\text{H}-\text{C}-\text{H})$	0.5(4)		

^a The stretching constants, K , and non-bonded stretching constants, F , are in mdyn Å⁻¹, bending constants, H , and torsional constant, Y , in mdyn Å rad⁻².

Table 3. Structural parameters^a for tricyclo[4.1.0.0^{1,3}]heptane.

Parameter	$r_a(\text{Å})$	$l(\text{Å})$	
C1-C2	1.465(7)	0.054	(4) ^b
C1-C3	1.519(25)	0.055	
C2-C3	1.526(10)	0.054	
C3-C4	1.521(30)	0.055	
C4-C5	1.572(14)	0.055	
C-H	1.107(2)	0.077(2)	(5)
C1...C4	2.45(2)	0.062	
C3...C5	2.41(2)	0.067	
C3...C6	2.42(1)	0.063	
C2...C4	2.66(1)	0.070	
C2...C6	2.72(1)	0.068	
C2...C7	2.89(1)	0.064	
C2...C5	3.363(4)	0.073(3)	
(C-C) average	1.514(2)		

Angles (in degrees)

$\angle \text{C2C1C3}$	61.5(5)
$\angle \text{C1C3C2}$	57.5(7)
$\angle \text{C2C1C7}$	162.4(18)
γ^c	50.9(5)
$\angle (\text{CCC})^d$	105.1(2)
$\angle \text{C6C1C3}$	105.7(26)
$\angle \text{C1C3C4}$	107.5(13)
$\angle \text{C3C4C5}$	102.3(30)
$\phi_1(\text{C6C1}-\text{C3C4})$	12.5(5)
$\phi_2(\text{C1C3}-\text{C4C5})$	31.4(12)
$\phi_3(\text{C3C4}-\text{C5C6})$	37.9(14)
$\angle \text{HC2H}$	106.3(8)
$\angle \text{HC4H}$	108.4(13)

^a For the definition of r_a see Ref. 12. Parenthesized values are estimates of uncertainties, which are the standard deviations. See text for details. The asymmetry constants were (in 10⁻⁶ Å³): $k(\text{CC})=2.0$, $k(\text{CH})=10.0$, and zero for non-bonded distances. ^b The indicated l -values were refined in groups. ^c Angle between the planes C1-C3-C6 and C1-C2-C3. ^d Average CCC angle in the five-membered ring.

peak at 2.4 Å by the non-bonded C...C distances of the five-membered ring, the peak at 2.7 Å by non-bonded C...C distances of the type C2...C4, and C2...C6, the shoulder at 2.9 Å is mainly formed by the C2...C7 distance and the peak at 3.4 Å by the C2...C5 distance.

There are five different C-C bonds in this molecule, which all contribute to one peak in the radial distribution curve. In order to improve the convergence in the least-squares refinements, it was necessary to apply a correction factor of 0.3 in order to decrease the calculated shift, δx . The applied shift in cycle i , $\delta x_i'$, was given by $\delta x_i' = 0.3 \delta x_i$ (for more details see Ref. 4). It was determined that the minimum thus found was independent of the input parameters in the least-squares analysis.

The vibrational amplitudes of the C-C bond distances were refined in a group,⁴ and values 0.003 Å higher than the calculated ones were obtained. When these vibrational amplitudes were held at the calculated values, the standard deviations of the other parameters decreased by half, and the values of the parameters changed by no more than one standard deviation. The difference in the parameters was insignificant, regardless of whether the calculated shrinkage correction was included in the analysis of the data or not.

The final parameters are shown in Table 3, and the correlation coefficients larger than 0.5 in Table 4. A conventional diagonal weight matrix⁴ was used in the least-squares refinements, and the constants for the weighting scheme are shown in Table 5. The standard deviations for the distance parameters and vibrational amplitudes were corrected for data correlation¹³ by multiplying the standard deviations, σ_{LS} , obtained from the least-squares refinement by a factor F . (For definition see Ref. 13, eqn. 11.28. For the bond distances listed in Table 3, factor F was about 1.8). $\sigma = [F^2 \sigma_{\text{LS}}^2 + (0.001r)^2]^{\frac{1}{2}}$. The term involving r provides an estimate of possible systematic error. The standard deviations for the angles were corrected by $\sigma = 1.5 \sigma_{\text{LS}}$.

DISCUSSION

Bicyclo[3.1.0]hexane, which lacks one of the fused cyclopropane rings of TCH, has an "envelope" conformation (C_s symmetry), as

Table 4. Correlation coefficients whose absolute value is greater than 0.5.

	$\angle C6C1C3$	ϕ_3	γ	$\angle HC4H$	$r(C1C3)$	$r(C1C2)$	Δr	$r(C3C4)$	$r(C4C5)$
γ									
$\angle HC4H$									
$\angle HC2H$									
$r(C1C3)$	-0.99			-0.89	-0.58				
$r(C1C2)$	0.81			0.63	0.72	-0.81			
Δr	-0.66	0.61		-0.65	0.64	-0.89			
$r(C3C4)$	0.95			0.75	0.61	-0.95	0.87	-0.83	
$r(C4C5)$	-0.67				0.64	-0.79	0.87	-0.82	
$l(C1C3)$	0.64				0.63	-0.62	0.89	-0.92	0.77
$l(C1C4)$	0.95			0.89	0.51	-0.95	0.70	0.84	-0.51

Table 5. Constants of the weighting scheme.⁴

Data	48 cm	20 cm
s_1 (in \AA^{-1})	4.5	7.5
s_2 (in \AA^{-1})	18.5	40.0
w_1	0.25	0.05
w_2	0.05	0.02

shown by microwave spectroscopy¹⁴ and by X-ray diffraction of an *N*-brosylamine derivative.¹⁵ The envelope conformation is much strained in TCH and it is not surprising that this work gives evidence only of the "half-chair" structure shown.

Despite attempting many initial combinations of different C-C distances and CCC angles, only one minimum in the least-squares analysis was found. The high correlation among parameters is reflected in their large standard deviations. The unusual features in the TCH are the very large C2C1C7 angle (162°) compared to spiropentane¹⁶ (137.2°) and the long C4-C5 distance, 1.57 \AA .

For comparison, the parameters determined for spiropentane¹⁶ were the following (for numbering of atoms see Fig. 4): $r(C1-C3) = 1.469(1)$ \AA , $r(C1-C2) = 1.519(3)$ \AA and $\angle C1C3C4 = 137.2^\circ$. In TCH, $r(C1-C2)$ and $r(C2-C3)$ are found about the same length as in spiropentane. The shortest bonds $r(C1-C2)$ and $r(C1-C7)$ have an included angle of 162° , and must be considered to have almost *sp* hybridization of the central carbon atom. The fact that $r(C1-C2)$ is so short might well be attributed to the large measure of *s*-character.

According to the Suernam and Harmony hypothesis,^{17,18} saturated small rings in different polycyclic hydrocarbons "have a certain fixed amount of electron density for C-C bonding which will be distributed around the ring in a manner which is appropriate to achieve the minimum energy configuration". As a consequence the average bond lengths of a given sized ring are fairly constant even though the individual bond lengths in the ring vary. In TCH the average C-C bond lengths (1.503 \AA) agree well with cyclopropane, 1.510(2) \AA .¹⁹ The agreement is actually better than in spiropentane,¹⁶ for which the average C-C bond length in the 3-membered ring is much shorter, 1.487 \AA .

The bond distance $r(C4-C5)$, whose length was found to be 1.57 \AA , is significantly longer than the similar bond in cyclopentane,²⁰ $r(C-C) = 1.546(1)$ \AA . A similar trend is found

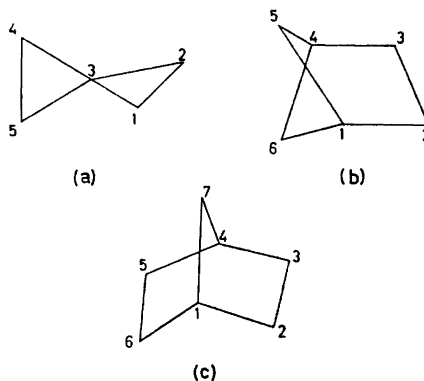


Fig. 4. Numbering of atoms in (a) spiropentane, (b) bicyclo[2.1.1]hexane and (c) norbornane.

in norbornane,²¹ where the corresponding distance $r(\text{C2}-\text{C3})$ is 1.557(25) Å. In bicyclo[2.1.1]hexane²² however, $r(\text{C1}-\text{C2})$ was found to be 1.544(5) Å, and $r(\text{C2}-\text{C3})$ was 1.513(15) Å, which show just the opposite trend. However, other authors²³ report only the average value of these distances, as does Fukuyama *et al.*²⁴ in 5-thiabicyclo[2.1.1]hexane, because these two parameters are highly correlated in those molecules. In TCH the correlation coefficient between $r(\text{C4}-\text{C5})$ and $r(\text{C3}-\text{C4})$ is -0.82 if the l -values of C-C bond distances are varied; however, if they are not refined, the correlation coefficient of these two distances is only 0.35. The average bond length of the cyclopentane ring in TCH is 1.530(14), in comparison to 1.546(1) in cyclopentane itself.²⁰

On the other hand, it is interesting that the average CCC bond angle of the five-membered ring and the torsional angles are quite similar to those in cyclopentane.²⁰ The average CCC angle in cyclopentane was 104.5° and the torsional angles for conformer with C_2 symmetry were 13.2, 34.3 and 42.3°.

Acknowledgement. We would like to thank Dr. H. M. Seip for helpful discussions regarding this manuscript, Prof. L. Skattebøl for providing the sample for this study, Prof. H. Matsuura for his recommendation of the force field, Cand. real. A. Almenningen for taking the electron-diffraction diagrams, and Mr. H. Volden for his technical assistance. The financial support for this research was provided, in part, by the Royal Norwegian Council for Scientific and Industrial Research (NTNF).

REFERENCES

1. Skattebøl, L. *J. Org. Chem.* **31** (1966) 2789.
2. Frey, H. M., Hopkins, R. G. and Skattebøl, L. *J. Chem. Soc.* (1971) 539.
3. Bastiansen, O., Hassel, O. and Risberg, E. *Acta Chem. Scand.* **9** (1955) 232.
4. Andersen, B., Seip, H. M., Strand, T. G. and Stølevik, R. *Acta Chem. Scand.* **23** (1969) 3224.
5. Yates, A. C. *Comput. Phys. Commun.* **2** (1971) 175.
6. Strand, T. G. and Bonham, R. A. *J. Chem. Phys.* **40** (1964) 1686.
7. Stewart, R. F., Davidson, E. R. and Simpson, W. T. *J. Chem. Phys.* **42** (1965) 3175.
8. Tavard, C., Nicolas, D. and Rouault, M. *J. Chim. Phys.* **64** (1967) 540.
9. Gwinn, W. D. *J. Chem. Phys.* **55** (1971) 477.
10. Hildebrandt, R. L. Dept. of Chem., North Dakota State Univ., Fargo.
11. Takahashi, H. and Shimanouchi, T. *J. Mol. Spectrosc.* **13** (1964) 43.
12. Kuchitsu, K. and Cyvin, S. J. In Cyvin, S. J., Ed., *Molecular Structures and Vibrations*, Elsevier, Amsterdam 1972, Chapter 12.
13. Seip, H. M. and Stølevik, R. *Ibid.* Chapter 11.
14. Cook, R. L. and Malloy, T. B., Jr. *J. Am. Chem. Soc.* **96** (1974) 1703.
15. Grostic, M. F., Duchamp, D. J. and Chidester, C. G. *J. Org. Chem.* **36** (1971) 2929.
16. Dallinga, G., van der Draai, R. K. and Toneman, L. H. *Recl. Trav. Chim. Pays-Bas* **87** (1968) 897.
17. Suenram, R. D. and Harmony, M. D. *J. Chem. Phys.* **56** (1972) 3837.
18. Suenram, R. D. *J. Am. Chem. Soc.* **97** (1975) 4869.
19. Bastiansen, O., Fritsch, F. N. and Hedberg, K. *Acta Crystallogr.* **17** (1964) 538.
20. Adams, W. J., Geise, H. J. and Bartell, L. S. *J. Am. Chem. Soc.* **92** (1970) 5013.
21. Yokozeki, A. and Kuchitsu, K. *Bull. Chem. Soc. Jpn.* **44** (1971) 2356.
22. Chiang, J. F. *J. Am. Chem. Soc.* **93** (1971) 5044.
23. Dallinga, G. and Toneman, L. H. *Recl. Trav. Chim. Pays-Bas* **86** (1967) 171.
24. Fukuyama, T., Oyanagi, K. and Kuchitsu, K. *Bull. Chem. Soc. Jpn.* **49** (1976) 638.

Received January 28, 1977.

Infrared, Matrix Infrared and Raman Spectra of Trifluoro-*tert*-butyl Alcohol and Vibrational Assignment

JOUKO KORPPI-TOMMOLA

Department of Physical Chemistry, University of Helsinki, Meritullinkatu 1 C, SF-00170 Helsinki 17, Finland

Infrared spectra of trifluoro-*tert*-butyl alcohol and its OD derivative have been studied in the gaseous and liquid states, in solution, and in argon, krypton and nitrogen matrices. The Raman spectra of the pure liquids and CCl₄ and H₂O solutions have also been recorded. Only one conformer appears to be present in all phases studied. Assignments of vibrational bands are made. A frequency of 82 cm⁻¹ is tentatively suggested for the CF₃ torsion. The associates of trifluoro-*tert*-butyl alcohol seem to be mostly dimers in dilute solutions and in dilute matrices.

A few investigations of trifluoromethyl alcohols have been reported in the literature. Barnes *et al.* found a pattern of several satellite bands on either side of the $\nu(\text{OH})$ band of 2,2,2-trifluoro ethanol (TFE) in the infrared spectrum of the vapour.¹ Vibrational assignments given for TFE^{1,2} and 1,1,1-trifluoro-2-propanol (TFP)³ reveal marked couplings of the fundamental vibrations in the region from 1300 to 900 cm⁻¹. Several association studies of trifluoromethyl alcohols in CCl₄ solutions⁴⁻⁶ and in matrices^{1,3} reveal the existence of the $\nu(\text{OH})$ end group band of a dimer in the spectra and the minor degree of association of the fluoro-alcohols as compared with the corresponding alkanols. Since molecular vibrations⁷ and association⁸ of *tert*-butyl alcohol (2-methyl-2-propanol, TB) have recently been studied in this laboratory, it was of interest to study the spectra of the corresponding trifluoro alcohol, 2-trifluoromethyl-2-propanol (trifluoro-*tert*-butyl alcohol, TFTB).

EXPERIMENTAL

TFTB was purchased from Pierce Chemical Co., Rockford, Ill., and purified by fractional distillation.⁹ The OD derivative was synthesized simply by shaking the alcohol with D₂O, collecting the alcohol layer (TFTB and D₂O are only partly miscible) and distilling the fraction over D₂SO₄. After repeating the procedure four or five times, the product was more than 95 % isotopically pure.

The infrared spectra were recorded on Perkin-Elmer 125, 180 and 621 spectrometers in the wavenumber regions from 5000 to 3000 cm⁻¹, from 500 to 50 cm⁻¹ and from 4000 to 200 cm⁻¹, respectively. The wavenumber scales were calibrated using atmospheric water vapour spectra. The usual equipment was used to record the vapour and liquid spectra. The windows of the cells were of CsI or KBr. In the far infrared region, polyethylene windows and a 1 m gas cell were used.

The matrix isolation system used has been described elsewhere.³ The temperature of the CsI deposition window was kept at about 9 K during the recording of the spectra. During the depositions the temperature was raised to 15 K for argon and to 13 K for nitrogen matrices. Throughout the experiments the deposition rates were about 5 mmol/h of gas mixture. The pressures of the alcohol and the matrix gas were measured with a mercury manometer. The matrix to absorber (M/A) ratio was varied between 2000 and 20.

The Raman spectra were recorded on a Jarrell-Ash 25-305 spectrometer with the 488 nm line of an argon ion laser as the exciting line. During all measurements the spectral slit width was kept constant (at about 2.5 cm⁻¹). A multipass cell and 90 degree excitation were used for liquid and solution samples.

The positions of the infrared and Raman bands are believed to be correct to ± 2 cm⁻¹. The frequency differences between sharp peaks were found to be reproducible to 0.5 cm⁻¹ in

Table 1. The observed infrared and Raman frequencies (cm^{-1}) of $(\text{CF}_3)(\text{CH}_3)_2\text{COH}$ (fundamental regions).

Vapour	Argon matrix IR ^a	Nitrogen matrix IR ^a	Raman liquid ^b	Fundamental	Tentative Assignments ^c
3647 sh			3621 (2)	} ν_1	$\nu(\text{OH})$ ν_1 , end group
3639 m	3624 m	3617 m	3613 (2)		
3632 sh	3609 sh	3600 sh			
3215 vw			3230 (1)	} ν_2	$\nu_6 + \nu_{35}$ $\nu(\text{CH}_3)$
3013 sh	3012 w	3013 w			
3006 s	3006 w	3006 sh	3003 (30)	} ν_3	$\nu(\text{CH}_3)$
2999 sh		2996 sh			
2992 sh	2992 w	2992 w		} ν_4	$\nu(\text{CH}_3)$
	2964 sh	2968 sh	2959 (as)		
2957 m	2954 w	2956 w	2943 (35)		
	2935 br	2925 br	2923 (as)	} ν_5	$\nu(\text{CH}_3)$
2898 br	2898 sh		2883 (18)		
			2786 (2)	} ν_6	$2\nu_8$ $\nu(\text{CH}_3)$
			2741 (2)		
1485 m	1483 w	1483 w	1464 (6)		
1476 m	1476 vw	1476 sh		} ν_8	$\delta(\text{CH}_3)$
	1471 w	1473 w	1447 (6)		
	1462 sh	1464 sh		} ν_{10}	$\delta(\text{CH}_3)$ $\nu_{20} + \nu_{32}$ $\nu_{24} + \nu_{27}$ $\nu_{18} + \nu_{38}$
	1451 vw	1453 vw			
	1418 vw	1423 vw			
1404 sh				} ν_{11}	$\delta(\text{CH}_3)$
1398 s	1394 m	1396 m	1400 (1)		
1391 sh	1388 vw			} ν_{12}	$\nu_{18} + \nu_{38}$ $\delta(\text{CH}_3)$
	1381 sh	1383 m			
1383 s	1379 m	1382 sh		} ν_{13}	$\delta(\text{OH})$
	1358 vw	1357 sh			
1352 m	1348 m	1355 w		} ν_{14}	$\nu_{22} + \nu_{32}$ $\nu_{25} + \nu_{38}$ $\delta(\text{CH}_3)$
1341 as		1350 w			
	1334 vw	1338 vw		} ν_{15}	$\nu_{24} + \nu_{30}$ $\nu(\text{CCC})$
1327 sh	1328 vw	1332 w	1323 (2)		
1321 s	1319 m	1322 s		} ν_{16}	$\nu_{24} + \nu_{32}$ $\nu(\text{CCC})$
1316 sh	1310 vw	1314 vw	1210 (3)		
	1224 w	1224 w		} ν_{17}	$\nu_{24} + \nu_{33}$ $2\nu_{28}$
	1219 vw	1220 sh	1200 (3)		
	1213 w	1215 sh		} ν_{18}	$\nu_{28} + \nu_{30}$ $\nu(\text{CF}_2)$
	1209 sh	1212 w			
1199 sh	1199 sh	1201 sh		} ν_{19}	$\nu_{28} + \nu_{37}$ $\nu(\text{CF}_2)$
1189 vs	1195 vs	1197 s	1170 (1)		
1182 vs	1192 vs	1191 vs		} ν_{20}	$2\nu_{28}$ $\nu(\text{CF}_2)$ $\nu_{24} + \nu_{36}$
	1182 m	1184 s	1135 (1)		
	1173 vs	1173 vs		} ν_{21}	$\nu(\text{CO})$ $\nu_{24} + \nu_{38}$ $\nu_{25} + \nu_{32}$
	1162 m	1165 s			
1150 sh	1149 sh	1149 sh		} ν_{22}	$\rho(\text{CH}_3)$ $\nu_{25} + \nu_{38}$ $\rho(\text{CH}_3)$
1145 vs	1140 vs	1140 vs	1003 (1)		
	1132 vw	1133 vw		} ν_{23}	$\rho(\text{CH}_3)$
	1118 vw	1120 sh			
1123 sh	1113 sh	1119 vs		} ν_{24}	$\rho(\text{CH}_3)$
1116 s	1112 vs	1114 m			
	1109 vs	1111 w		} ν_{25}	$\rho(\text{CH}_3)$
	1102 vw	1108 sh			
1011 sh				} ν_{26}	$\rho(\text{CH}_3)$
1004 w	1000 w	1001 w	1003 (1)		
989 sh	985 sh			} ν_{27}	$\rho(\text{CH}_3)$
981 s	979 s	982 s	981 (5)		
973 sh		979 m		} ν_{28}	$\rho(\text{CH}_3)$
	940 vw	940 vw	945 (2)		

Table 1. Continued.

881 sh				}	ν_{24}	$\rho(\text{CH}_3)$
875 w	870 w	872 w	872 (11)			
868 sh		870 w		}	ν_{25}	$\nu(\text{CCC})$
764 sh	756 sh		754 (99)			
756 w	753 w	755 w		}	ν_{26}	$\delta(\text{CF}_3)$
749 sh			603 (13)			
608 sh	600 m	601 m		}	ν_{27}	$\delta(\text{CF}_3)$
602 s			584 (8)			
595 sh		582 w	575 w	}	ν_{28}	$\delta(\text{CF}_3)$
582 m	581 w		578 (8)			
575 m	574 w			}	ν_{29}	$\delta(\text{CCO})$
477 sh	468 sh	469 w	476 (1)			
469 m	464 w			}	ν_{30}	$\delta(\text{CCO})$
463 sh			446 (1)			
444 vw	445 sh	441 w	446 (1)	}	ν_{31}	$\delta(\text{CCC})$
439 vw	440 vw	357 m	372 (5)			
358 sh	358 vw	351 w	357 (8)	}	ν_{32}	$\delta(\text{CCC})$
351 m	351 w		341 (9)			
345 sh				}	ν_{33}	$\delta(\text{CCC})$
337 m	339 vw	391 m				
316 sh	307 s	384 sh		}	ν_{34}	$\tau(\text{OH})$
309 s	303 vs	375 s				
302 sh		310 vw		}	ν_{35}	$\rho(\text{CF}_3)$
254 w	260 vw		261 (< 1)			
238 w	240 vw	242 vw	241 (1)	}	$\nu_{36,37}$	$\tau(\text{CH}_3)$
			81 br			
				}	ν_{38}	$\rho(\text{CF}_3)$
				}	ν_{39}	$\tau(\text{CF}_3)$

^a Intensities refer to matrices with large M/A ratios. ^b Relative intensities are given in parenthesis. ^c The assignments of combination bands should be understood as informative only. ^d FR refers to Fermi resonance.

the matrix spectra. The non-SI units used are $1 \text{ \AA} = 10^{-10} \text{ m}$ and $1 \text{ amu} = 1.660 \times 10^{-27} \text{ kg}$.

RESULTS AND DISCUSSION

TFTB has 39 normal modes of vibration, of which three are hydroxyl, 18 methyl, nine trifluoromethyl and nine skeletal modes. All Raman bands should be more or less polarized if we assume C_1 symmetry for the molecule. The most important results and tentative assignments are given in Table 1. Detailed spectroscopic data for the deuterio alcohol (TFTB-OD), including argon and nitrogen matrix spectra, are obtainable from the author on request.

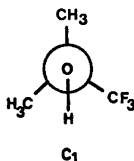


Fig. 1. The conformer of TFTB.

Acta Chem. Scand. A 31 (1977) No. 7

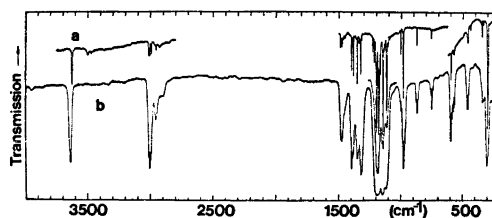


Fig. 2. IR spectra of TFTB. (a) argon matrix, M/A = 2000, 15 μmol ; (b) vapour spectrum, 1 m cuvette with CsI windows, pressures 1.5 and < 0.5 mmHg.

The principal moments of inertia were calculated for the conformer shown in Fig. 1 with the CH_3 and CF_3 groups in staggered positions with respect to the carbon skeleton. The following structural parameters were used: $r(\text{CC}) = 1.537$, $r(\text{CH}) = 1.096$, $r(\text{CF}) = 1.334$, $r(\text{CO}) = 1.427$, $r(\text{OH}) = 0.956 \text{ \AA}$; $\angle(\text{COH}) = 109^\circ$ and all other angles tetrahedral.¹⁰⁻¹² These parameters put the centre of mass almost at the halfway point of the C— CF_3 bond and give principal moments of $I_A = 196$, $I_B = 274$ and

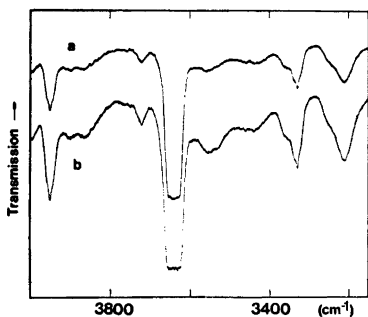


Fig. 3. The OH stretching region in the IR spectrum of TFTB vapour. 1 m gas cuvette with CsI windows, pressures (a) 30 and (b) 52 mmHg.

$I_C = 277 \text{ amu \AA}^2$. The A-axis of the molecule is very close and almost parallel to the C-CF₃ bond. The molecule is nearly a prolate symmetric top. The band contours in the infrared spectrum of the TFTB vapour, however, are more or less of hybrid type.

Hydroxyl fundamentals. Since the spectra of TFTB in vapour, in dilute matrices (Fig. 2) and in dilute solutions show a singlet hydroxyl stretching band, it is likely that the alcohol has only one conformer in these phases. We propose a structure with the hydroxyl group slightly rotated towards the CF₃ group (Fig. 1).

The infrared spectrum of the TFTB vapour shows two bands, which are found to appear symmetrically on both sides of the $\nu(\text{OH})$ band (Fig. 3). These bands give the sum and difference frequencies of 312 and 308 cm⁻¹, respectively. A frequency of 309 cm⁻¹ is found for the hydroxyl torsion elsewhere in the spectrum. The band at 3720 cm⁻¹ (Fig. 3) is probably the $\nu(\text{OH}) + \tau(\text{CF}_3)$ satellite, giving the frequency of 81 cm⁻¹ for the CF₃ torsion. The corresponding difference band is obviously engulfed by the dimer association band at 3555 cm⁻¹.

The $\nu(\text{OH})$ dimer bands of TFTB are at 3555 cm⁻¹ in the vapour (Fig. 3), at about 3500 cm⁻¹ in dilute argon matrices, between 3500 and 3440 cm⁻¹ in dilute nitrogen matrices (Fig. 4) and at about 3495 cm⁻¹ in dilute CCl₄ solutions. Polymer bands are seen in the spectra as the concentration of the alcohol is increased. For TFTB in solution and in matrices we propose two groups of associates, dimers and polymers. Additionally, a considerable fraction of 'linear'

dimers seems to be present in matrices, as indicated by the intensities of the separate 'dimer end group' absorptions¹³ found in all matrix spectra (Fig. 4).

Several authors have found couplings of the $\delta(\text{OH})$ vibration of ordinary^{7,14} and fluoro-alcohols.^{2,3} For TFTB the bands at 1109 and 1348 cm⁻¹ (argon matrix frequencies) shift considerably on OH deuteration. Both bands behave in a way that is typical of $\delta(\text{OH})$ bands in matrices. However, the frequency of the former is too low for a pure $\delta(\text{OH})$ vibration. All matrix spectra show a $\delta(\text{OD})$ band at about 914 cm⁻¹ and a new weak band at 1264 cm⁻¹ for TFTB-OD. The latter band appears more clearly in the Raman spectra of the liquid. Analogous to *tert*-butyl alcohol,⁷ it is suggested that a coupling occurs between the $\delta(\text{OH})$ and $\nu(\text{CO})$ vibrations for TFTB, as well.

The intense bands at 309 and 303 cm⁻¹ in the infrared spectra of TFTB in the vapour state and in argon matrices, respectively, (Fig. 2) are assigned to the hydroxyl torsion. The nitrogen matrix frequency of the torsion is about 70 cm⁻¹ higher than the corresponding argon and krypton matrix frequencies, which seems to be typical of many aliphatic alcohols.³

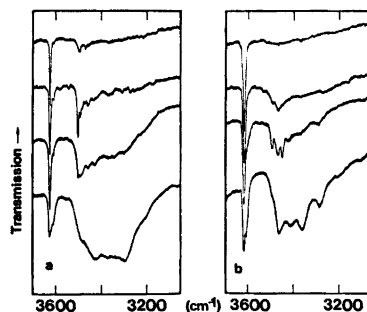


Fig. 4. IR matrix spectra of TFTB in the $\nu(\text{OH})$ region. Features on the left (a) are reproduced from argon matrix spectra, M/A ratios from top to bottom: 2000 (12 μmol), 500 (20 μmol), 200 (70 μmol) and 50 (28 μmol). Features on the right (b) are reproduced from nitrogen matrix spectra, M/A ratios from top to bottom: 2000 (25 μmol), 200 (20 μmol), 200 (20 μmol) and 50 (20 μmol). The third curve from the top on the right is recorded from the M/A=200 matrix after warming the matrix to 30 K for 4 min and cooling back to about 9 K. The numbers in the parentheses indicate the amount of deposited TFTB.

The isotopic shift ratio $\tau(\text{OH})/\tau(\text{OD})$, which is 1.25 in the vapour spectrum, 1.21 in argon and 1.32 in nitrogen matrix spectra, is not transferable from argon to nitrogen matrix frequencies or *vice versa*. In the liquid, there is a broad $\tau(\text{OH})$ association band at 620 cm^{-1} , which is shifted to 470 cm^{-1} on OH deuteration.

Other fundamentals. The group frequency approximation seems to be satisfactorily valid for TFTB. However, the assignments given in Table 1 should be taken as tentative only.

In the Raman spectra of liquid TFTB the two bands at 2786 and 2741 cm^{-1} are most probably the overtones of the CH_3 deformations. Since these bands are on the lower frequency side of the methyl stretching bands, a slight Fermi interaction may occur between the overtones and the stretchings.¹⁵ The feature at 260 cm^{-1} in the Raman spectrum of liquid TFTB is assigned to the methyl torsions. *tert*-Butyl alcohol shows a similar type of band at about 270 cm^{-1} , which is shifted to 190 cm^{-1} in the spectrum of the corresponding CH_3 deuterated alcohol.⁷

The bands, assigned to CF_3 stretching, appear with very low intensity in the Raman spectra but are very strong in the infrared (Fig. 2). The bands at about 600 , 582 and 575 cm^{-1} , which are not present in the spectra of *tert*-butyl alcohol and are well separated from other vibrational bands of TFTB, are assigned to the CF_3 deformations.

The frequency of the broad shoulder at 81 cm^{-1} in the Raman spectrum of the liquid is suitable for the CF_3 torsion. To obtain further support for this assignment, far infrared spectra of TFTB vapour were recorded. In spite of some instrumental difficulties, evidence of a broad band at about 85 cm^{-1} was obtained. Since a value of 81 cm^{-1} was obtained from one of the $\nu(\text{OH})$ sum bands (for the fundamental frequency), it is likely that the CF_3 torsion frequency of TFTB is about 82 cm^{-1} . The value is markedly larger than has been reported for CF_3COCl ¹⁶ (45 cm^{-1}) and for CF_3CHO ¹⁷ (55 cm^{-1}), markedly smaller than that for $\text{CF}_3\text{CH}_2\text{OH}$ ¹ (120 cm^{-1}), but of the same order of magnitude as those given for $\text{CF}_3\text{CHOHCH}_3$ ³ (75 cm^{-1}) and $(\text{CF}_3)_3\text{COH}$ ¹⁸ (70 cm^{-1}).

The coupling of the CO stretching mode has been discussed above. The strongest Raman band of TFTB at 755 cm^{-1} is assigned to the symmetrical CCC stretching mode. The strong Raman band at 339 cm^{-1} is probably due to the symmetric CCC bending vibration.

Acknowledgements. The author gratefully acknowledges financial support from the Emil Aaltonen Foundation and the Science Research Council of Finland. The encouragement and advice of Assoc. Prof. Juhani Murto, Ph.D., during the course of the work has been much appreciated.

REFERENCES

1. Barnes, A. J., Hallam, H. E. and Jones, D. *Proc. R. Soc. London A* 335 (1973) 97.
2. Travert, J. and Lavalley, J. C. *Spectrochim. Acta Part A* 32 (1976) 637.
3. Murto, J., Kivinen, A., Edelmänn, K. and Hassinen, E. *Spectrochim. Acta Part A* 31 (1975) 479.
4. Krueger, P. J. and Mettee, H. D. *Can. J. Chem.* 42 (1964) 340.
5. Kivinen, A. and Murto, J. *Suom. Kemistil. B* 40 (1967) 6.
6. Kivinen, A., Murto, J., Korppi-Tommola, J. and Kuopio, R. *Acta Chem. Scand.* 26 (1972) 904.
7. Korppi-Tommola, J. *Spectrochim. Acta. In press.*
8. Korppi-Tommola, J. *J. Mol. Struct.* 40 (1977) 13.
9. Murto, J., Kivinen, A., Kivimaa, S. and Laakso, R. *Suom. Kemistil. B* 40 (1967) 250.
10. Venkateswarlu, P. and Cordy, W. *J. Chem. Phys.* 23 (1955) 1200.
11. Barum, W., Günther, H., Umbrecht, H. and Zeil, W. *Z. Phys. Chem. Frankfurt am Main* 93 (1974) 247.
12. Stølevik, R. and Thom, E. *Acta Chem. Scand.* 25 (1971) 3205.
13. Hallam, H. E., Ed., *Vibrational Spectroscopy of Trapped Species*, Wiley, London 1973.
14. Barnes, A. J. and Hallam, H. E. *Trans. Faraday Soc.* 66 (1970) 1920, 1931.
15. Lavalley, J. C. and Sheppard, N. *Spectrochim. Acta Part A* 28 (1972) 2091.
16. Berney, C. V. *Spectrochim. Acta* 21 (1965) 1809.
17. Berney, C. V. *Spectrochim. Acta Part A* 25 (1969) 793.
18. Murto, J., Kivinen, A., Korppi-Tommola, J., Viitala, R. and Hyömäki, J. *Acta Chem. Scand.* 27 (1973) 107.

Received January 12, 1977.

Infrared, Matrix Infrared and Raman Spectra of Hexafluoro-*tert*-butyl Alcohol and Vibrational Assignment

JOUKO KORPPI-TOMMOLA

Department of Physical Chemistry, University of Helsinki, Meritullinkatu 1 C, SF-00170 Helsinki 17, Finland

Infrared spectra are reported for hexafluoro-*tert*-butyl alcohol and its OD derivative in gaseous, liquid and solid states, in CCl₄ solution and in argon, krypton and nitrogen matrices. The Raman spectra of the liquids and CCl₄ solutions have also been recorded. Two conformers are found in the vapour and liquid states and in CCl₄ solution, while in matrices, two species appear only for the deuterio-alcohol in solid nitrogen. A vibrational assignment is given for the conformer present in most phases. The alcohol dimers seem to have open-chain (non-cyclic) structures in matrices. A non-bonded interaction is proposed as the origin of the end group bands in the matrix spectra of halogenated alcohols.

To complete our study of the conformations, molecular vibrations and association of *tert*-butyl alcohol and a series of its fluorine derivatives, we have recorded infrared and Raman spectra of hexafluoro-*tert*-butyl alcohol (2-methyl-1,1,1,3,3,3-hexafluoro-2-propanol, HFTB). The molecular vibrations¹ and association² of *tert*-butyl alcohol (2-methyl-2-propanol, TB) and infrared and Raman spectra of trifluoro-*tert*-butyl alcohol³ (2-trifluoro-methyl-2-propanol, TFTB) and perfluoro-*tert*-butyl alcohol (PFTB)⁴ have recently been reported.

Hexafluoro-2-propanol (HFP) and hexafluoro-*tert*-butyl alcohol are closely related compounds. Since the conformational isomerism⁵ and the vibrational spectra⁶ of the former have already been studied, it is of interest to see whether the conformers and the association characteristics of the two alcohols are similar.

EXPERIMENTAL

HFTB was purchased from Pierce Chemical Co., Rockford, Ill., and purified by fractional distillation.⁷ The OD derivative was synthesized by shaking the alcohol with D₂O, collecting the alcohol layer (HFTB and D₂O are only partly miscible) and distilling the fraction over D₂SO₄. After repeating the procedure four or five times the product was more than 95 % isotopically pure.

The infrared spectra were recorded with Perkin-Elmer 180 and 621 spectrometers in the wavenumber regions from 500 to 50 cm⁻¹ and from 4000 to 200 cm⁻¹, respectively.¹ Matrix spectra were obtained in the same way, as previously reported,^{3,8} varying the matrix to absorber (M/A) ratio from 5000 to 20. The Raman spectra were recorded with a Jarrell-Ash spectrometer with the 488 nm line of an argon ion laser as the exciting line.¹ Throughout the experiments the spectral slit width was kept constant at about 2.5 cm⁻¹. Standard 90 degree excitation was used for most measurements.

RESULTS AND DISCUSSION

HFTB has 39 modes of vibration, 22 of species *a'* and 17 of species *a''* assuming the point group C_s. All vibrations are infrared and Raman active, the *a'* species showing polarized bands in the Raman spectra. The most important spectral results and tentative assignments are given in Table 1. A Raman spectrum of liquid HFTB is shown in Fig. 1. Detailed spectroscopic data for HFTB-OD, including the results from argon and nitrogen matrix spectra, are available from the author on request.

Conformations. In the vapour phase, the infrared spectrum of HFTB in the $\nu(\text{OH})$ region

Table 1. The observed infrared and Raman frequencies (cm⁻¹) of (CF₃)₂(CH₃)COH (fundamental regions).

Vapour	Argon matrix IR ^a	Nitrogen matrix IR ^a	Raman liquid ^b	Fund. and species	Tentative assignments ^c		
3656 w		3624 vw	3638 (1) p	ν_1, a'	$\nu(\text{OH}), C_1$ conformer		
3629 sh		3586 as		ν_1, a'	$\nu(\text{OH}), C_s$ conformer		
3624 s	3604 s	3583 s	3610 (2) p				
3617 sh		3579 s					
			3230 (<1) dp		$\nu_{02} + \nu_{36}$		
3035 sh				ν_{23}, a''	$\nu(\text{CH}_3)$		
3028 w	3024 vw	3026 vw	3025 (12) dp				
2973 w	2969 vw	2970 vw	2969 (40) p			ν_2, a'	$\nu(\text{CH}_3)$
2907 vw			2908 (6) p			ν_3, a'	$\nu(\text{CH}_3)$
			2769 (2) p		$2\nu_5$ FR with ν_2		
1469 sh	1474 vw	1478 vw		ν_{24}, a''	$\nu_{25} + \nu_{37}$		
1465 m	1464 sh	1465 sh					
1459 m	1460 m	1462 m	1468 (4) dp			$\nu_{13} + \nu_{30}$	$\delta(\text{CH}_3)$
1455 sh	1457 sh					$\nu_{28} + \nu_{34}$	$\delta(\text{CH}_3)$
1449 sh	1448 w	1451 w		ν_4, a'	$\delta(\text{CH}_3)$		
1398 m	1395 w	1398 w	1400 (2) p	ν_5, a'	$\delta(\text{CH}_3)$		
	1392 sh				$\nu_{10} + \nu_{37}$		
	1389 vw	1392 w			$\nu_{13} + \nu_{14}$		
1375 sh	1371 vw				$\nu_{13} + \nu_{31}$		
	1366 sh	1377 w		ν_6, a'	$\nu_{11} + \nu_{20}$		
1369 m	1365 w	1375 sh	1375 (<1) p				
	1319 as	1329 vw		ν_7, a'	$\delta(\text{OH})$		
1315 s	1316 vs	1318 vs	1316 (2) p				
	1309 sh	1311 as			$\nu_{12} + \nu_{34}$		
	1300 sh	1303 sh		ν_8, a'	$\nu(\text{CF}_3)$		
1294 s	1291 vs	1294 s	1295 (3) p				
	1283 w	1290 s			$\nu_{11} + \nu_{37}$		
	1271 sh	1267 w			$\nu_{13} + \nu_{32}$		
	1265 w	1262 w			$\nu(\text{CF}_3) + \delta(\text{OH})$		
	1237 vs	1238 s	1240 (as)	ν_{25}, a''	$\nu_{12} + \nu_{18}$		
1239 sh	1229 vs	1230 vs	1225 (3) dp				
1233 vs	1224 vs	1224 vs		ν_{26}, a''	$\nu_{13} + \nu_{16}$		
	1217 sh	1216 sh		ν_{27}, a''	$2\nu_{14}$		
	1214 sh	1213 sh			$2\nu_{31}$		
	1203 vw	1200 w			$\nu_{16} + \nu_{30}$		
	1197 vw	1197 sh			$\nu_{12} + \nu_{36}$		
	1194 w				$\nu_{18} + \nu_{29}$		
1187 sh	1181 m	1182 vs		ν_9, a'	$\nu_{12} + \nu_{37}$		
1182 vs	1178 vs	1180 vs	1180 (sh) p				
	1174 sh	1173 sh			$\nu(\text{CF}_3)$		
	1162 sh	1164 vw		ν_{10}, a'	$\nu_{14} + \nu_{32}$		
1163 sh	1158 s	1158 s	1160 (1) dp				
1101 sh	1113 vw	1111 vw	1109 (as)		$\nu(\text{CCC})$		
1098 vs	1092 vs	1092 vs	1090 (1) dp	ν_{28}, a''	$\nu_{13} + \nu_{35}$		
1093 sh	1086 w			ν_{11}, a'	$\nu(\text{CF}_3)$		
1082 sh	1076 s	1082 s	1080 (as)				
	1062 sh	1067 sh			$\nu_{13} + \nu_{18}$		
	1061 w				$\nu(\text{CO}) + \delta(\text{OH})$		
		964 as	961 (as)		$2\nu_{32}$		
		961 w	957 (4) p	ν_{12}, a'	$\nu_{30} + \nu_{34}$		
961 m	958 m	957 sh					
956 sh					$\varrho(\text{CH}_3)$		
880 sh				ν_{29}, a''	$\nu_{31} + \nu_{35}$		
876 m	873 w	875 m	877 (1) dp				
872 sh		869 sh			$\nu_{16} + \nu_{34}$		
P769 sh					$\varrho(\text{CH}_3)$		
Q765 w					$\nu_{16} + \nu_{17}$		
Q763 w	762 w	763 w	766 (99) p	ν_{13}, a'	$\nu(\text{CCC})$		

Table 1. Continued.

R758 sh						
P707 sh						
Q702 s	700 s	701 s	705 (1) dp	}	ν_{30}, a''	$\delta(\text{CF}_3)$
R698 sh	698 sh					$\nu_{32} + \nu_{37}$
638 sh				}	ν_{14}, a'	$\delta(\text{CF}_3)$
633 m	629 w	631 w	636 (12) p			$\nu_{21} + \nu_{33}$
624 sh	617 sh	622 sh		}	ν_{15}, a'	$\delta(\text{CF}_3)$
613 w	609 vw	608 vw	613 (7) dp			ν_{31}, a''
606 sh						$\nu_{34} + \nu_{37}$
P539 sh				}	ν_{32}, a''	$\delta(\text{CF}_3)$
Q534 m	533 w	534 w	540 (2) dp			
R530				}	ν_{16}, a'	$\delta(\text{CF}_3)$
517 sh						ν_{33}, a''
512 m	512 m	513 m	520 (6) p	}	ν_{34}, a''	$\tau(\text{OH})$
464 m	464 w	465 m	467 (1) dp			
457 sh				}	ν_{17}, a'	$\delta(\text{CCO})$
367 s	365 sh	454 s	369 (7) dp			ν_{35}, a''
315 w	363 s	443 m	356 (9) dp	}	ν_{18}, a'	$\delta(\text{CCC})$
		432 sh				ν_{19}, a'
	358 sh	362 w	369 (7) dp	}	ν_{20}, a'	$\rho(\text{CF}_3)$
349 m	348 m	353 vw	356 (9) dp			ν_{36}, a''
P336 sh				}	ν_{37}, a''	$\rho(\text{CF}_3)$
Q330 s	329 m	331 vw	336 (sh)			ν_{38}, a''
R325 sh	324 sh	326 vw	330 (17) p	}	ν_{31}, a'	$\rho(\text{CF}_3)$
293 sh						ν_{38}, a''
289 vw	288 vw	289 vw	294 (1) dp	}	ν_{38}, a''	$\tau(\text{CF}_3)$ and ν_{22}, a'
286 sh						
249 vw	245 vw	247 vw	247 (< 1)	}	ν_{38}, a''	$\tau(\text{CF}_3)$ and ν_{22}, a'
235 vw	235 vw	235 vw				
			221 (< 1)	}	ν_{38}, a''	$\tau(\text{CF}_3)$ and ν_{22}, a'
170 d_{vw}			173 (1) p			
91 d_{br}			102 (br)			

^a The intensities refer to matrices with large M/A ratios. ^b Relative intensities are given in parenthesis. The letters p or dp after the parenthesis refer to depolarization ratios. ^c The assignments of combination bands should be taken as informative only. ^d From far-infrared spectrum (Perkin-Elmer 180 spectrometer and 1 m gas cell with polyethylene windows were used).

shows two bands at 3656 and 3624 cm^{-1} , the latter being more intense, (Fig. 2a). From the variation in the ratio of the integrated intensities of these bands as a function of temperature (from 300 to 453 K) an enthalpy difference of 6.8 kJ mol^{-1} is derived. For dilute CCl_4 solutions a doublet is found at 3610 and 3583 cm^{-1} , (Fig.

2b) and for the pure liquid at 3638 and 3610 cm^{-1} , (Fig. 1) in the infrared and Raman spectra. In the solid state no $\nu(\text{OH})$ monomer bands were observed. Monomeric HFTB exhibits only one $\nu(\text{OH})$ band at 3604 cm^{-1} in argon matrices, three closely spaced bands at 3586, 3583 and 3579 cm^{-1} in nitrogen matrices

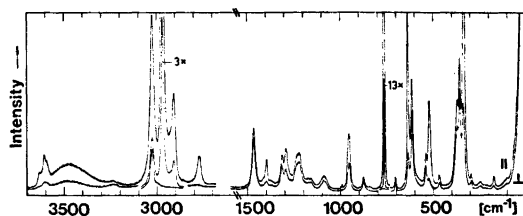


Fig. 1. Raman spectrum of liquid HFTB. Multipass cuvette; 488 nm exciting line; slits 2.5 cm^{-1} .

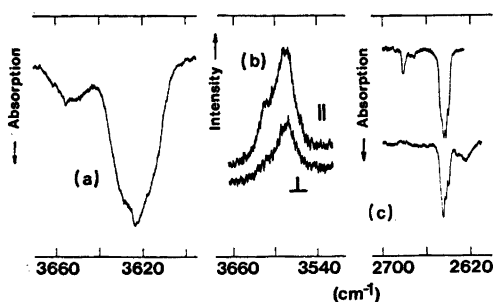


Fig. 2. The $\nu(\text{OH})$ band of HFTB in several spectra. (a) Infrared vapour spectrum; (b) Raman spectrum of 4% (w/w) CCl_4 solution; (c) OD alcohol in nitrogen matrices M/A = 1000, 15 μmol deposited. Lower curve is recorded after warming the matrix to 30 K for a few minutes and recooling to 9 K.

and two bands at 3598 and 3590 cm^{-1} in krypton matrices.

To explain our spectroscopic results in the $\nu(\text{OH})$ region for HFTB in the vapour and liquid states and in CCl_4 solution, two conformers, with structures shown in Fig. 3, are proposed. Comparison with the spectra of TFTB³ (for the C_1 conformer) and of PFTB⁴ (for the C_s conformer) suggest that the higher frequency $\nu(\text{OH})$ band is due to a conformer having the OH group interacting with only one CF_3 group (Fig. 3b), while the lower frequency band is due to a conformer stabilized by the interactions of the two CF_3 groups, (Fig. 3a). The intensity variations of the two $\nu(\text{OH})$ bands with temperature indicate that the C_s conformer has a more stable structure than the C_1 conformer in the vapour phase. Assuming that the lower frequency absorption is due to the C_s conformer in all phases and the higher frequency absorption is due to the C_1 conformer, the C_s conformer seems to be dominant in the vapour phase and in CCl_4 solution and the only conformer present in matrices (a frequency

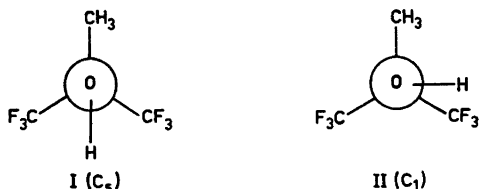


Fig. 3. The conformers of HFTB.

Acta Chem. Scand. A 31 (1977) No. 7

shift of about 20 cm^{-1} from vapour phase to argon or krypton matrices is normal for a $\nu(\text{OH})$ band⁵). Since only one conformer of HFTB seems to be present in matrices, the conversion of the C_1 conformer, apparently present in the vapour phase, must occur either when the molecules strike the matrix during deposition or immediately after deposition.^{9,10}

In contrast to HFP⁹ and HCP⁹ (hexachloro-2-propanol) in dilute nitrogen matrices, where two groups of $\nu(\text{OH})$ absorptions have been reported, HFTB shows only one such group, most probably due to C_s conformers. The fine structure of the $\nu(\text{OH})$ band of HFTB in krypton or nitrogen matrices may be explained in terms of two conformers with structures close to the C_s conformer (*cf.* Ref. 5). The additional peaks in nitrogen matrix spectra, as indicated by their behaviour on temperature cycling, may arise from different trapping sites (Fig. 2c).

Though HFTB shows only one group of $\nu(\text{OH})$ bands in dilute nitrogen matrices, two such groups are found for HFTB-OD. The higher frequency bands are at 2681 and 2672 cm^{-1} and the lower frequency bands at 2648, 2645, 2643 and 2640 cm^{-1} (Fig. 2c). As the M/A ratio is decreased to about 50, the fine structure disappears and only two bands are found at 2681 and 2645 cm^{-1} , respectively (Fig. 4a). On warming the matrix, the higher frequency band disappears from the spectra more rapidly than the lower frequency band, while at the same time dimer bands increase in intensity (Figs.

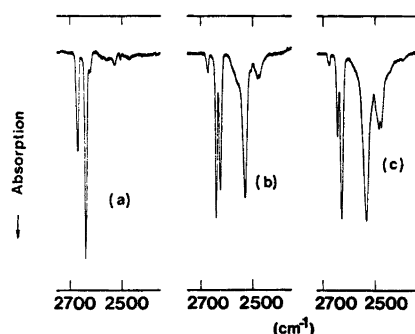


Fig. 4. Association bands of HFTB-OD in nitrogen matrices. (a) M/A = 50, 1 μmol deposited; (b) recorded after warming the (a) matrix to 24 K for 5 min and recooling to 9 K; (c) recorded after warming the (b) matrix to 35 K for 6 min and recooling to 9 K.

2c and 4). Accordingly, it seems likely that HFTB-OD has two conformers in nitrogen matrices. Assuming our conformational assignments for HFTB to be valid also for HFTB-OD in nitrogen matrices, the C_1 conformer seems to associate more readily than the C_s conformer.

Molecular vibrations. The assignments given in Table 1 are based on the infrared frequencies found in dilute matrices, where only the C_s conformer seems to be present. Since the matrix spectra are very complicated in the region from 1500 to 1000 cm^{-1} , the assignments should be taken as tentative only.

In very dilute matrices ($M/A \approx 5000$), most of the infrared bands of HFTB do not appear. However, six intense bands are found in the spectra in the region from 1350 to 1050 cm^{-1} . These undoubtedly involve the six CF_3 stretching modes (Table 1).⁵ The bands at 1365, 1295 and 1076 cm^{-1} (argon matrix frequencies) are sensitive to diffusion in the matrix and are shifted considerably on OH deuteration. Two of them, assigned to CF_3 stretching (1295 cm^{-1}) and to CO stretching (1076 cm^{-1}), in fact arise from mixed vibrations involving the OH bending. The hydroxyl bending bands at 1365 and 897 cm^{-1} for HFTB and HFTB-OD, respectively, give an isotopic shift ratio of 1.52. This also indicates that some coupling of OH bending with other modes occurs. The frequencies of the monomer $\delta(\text{OH})$ bands seem to increase from 1328 cm^{-1} for TB,¹ to 1348 cm^{-1} for TFTB³ and to 1382 cm^{-1} for PFTB⁴ (argon matrix frequencies) as the fluorine content of the *tert*-butyl alcohol is increased.

The infrared spectrum of HFTB vapour shows one band at 367 cm^{-1} , while HFTB-OD shows two bands at 271 and 232 cm^{-1} due to the hydroxyl torsion. In the latter case, it is tempting to assign the bands to the C_s and C_1 conformers, respectively. In argon and krypton matrices the $\tau(\text{OH})$ bands are singlets, with a shoulder on the high-frequency sides. The $\tau(\text{OD})$ frequency is about 270 cm^{-1} in both matrices. Three closely spaced $\tau(\text{OH})$ bands are found for HFTB in nitrogen matrices (Table 1), while HFTB-OD shows only two clearly separated bands at 364 and 318 cm^{-1} due to the torsion. For HFTB in nitrogen matrices the $\tau(\text{OH})$ frequencies seem to be about 90 cm^{-1} higher than the corresponding argon or krypton matrix frequencies (*cf.* Refs. 3 and 8).

In the Raman spectra of liquid HFTB and HFTB-OD, two intense and polarized bands at 766 and 330 cm^{-1} are assigned to symmetric skeletal stretching and bending bands, respectively. The band at 2770 cm^{-1} for both liquids is probably due to the overtone $2\delta(\text{CH}_3)$ in weak Fermi resonance with one of the CH_3 stretching modes (Fig. 1).^{1,3}

A study of the sum and difference bands of the $\nu(\text{OH})$ band gives the fundamental frequencies of 89 cm^{-1} for the CF_3 torsion, 238 cm^{-1} for a CF_3 rocking, 330 and 349 cm^{-1} for CCC bending modes and 367 cm^{-1} for the hydroxyl torsion, the difference bands being at 3535, 3386, 3294, 3276 and 3258 cm^{-1} in the infrared spectra of the HFTB vapour, respectively (1 m gas cell and pressures from 20 to 50 mmHg were used). The corresponding sum bands were also detected in the spectra.

For HFTB-OD in nitrogen matrices the bands at 1344, 1216, 1082, 925, 853 and 318 cm^{-1} show intensity changes parallel to the higher frequency $\nu(\text{OD})$ band on warming the matrix. These bands are assigned to the C_1 conformer. The fundamental frequencies for the C_s conformer in nitrogen matrices seem to be almost the same for HFTB and HFTB-OD.

Association. HFTB has a lower tendency for association than TFTB³ or TB,² but is certainly more associated than PFTB^{4,11} in the liquid state. Hence the degree of association decreases as the fluorine content of the alcohol increases, as is usual for halogenated alcohols.

No association bands were detected for HFTB in the vapour phase. However, HFTB in matrices shows sharp association bands in the $\nu(\text{OH})$ region. A spectrum of HFTB-OD in nitrogen matrices ($M/A = 50$) is shown in Fig. 4. Two monomer bands at 2681 and 2645 cm^{-1} are found in the spectrum and practically no association bands appear immediately after deposition (Fig. 4a). After warming the matrix to 25 K and recooling to 9 K the band at 2681 cm^{-1} decreases in intensity and a tiny feature at 2624 cm^{-1} on the foot of the 2645 cm^{-1} band together with a dimer band at 2531 cm^{-1} increase simultaneously in intensity (the ratio of the peak heights is almost 1:1, Fig. 4b). On further warming the band at 2645 cm^{-1} decreases in intensity, while the bands at 2624 and 2531 cm^{-1} become the strongest bands in the region (Fig. 4c). An additional dimer band

Table 2. Infrared frequencies (cm^{-1}) of hydroxyl stretching bands of HFTB and HFTB-OD in several phases.

Species	Vapour	Argon matrix	Nitrogen matrix	Liquid	Solid (196 K)	
C_1 conformer	3656	—	—	3632	—	} $\nu(\text{OH})$
C_s conformer	3624	3604	3579	3604	—	
Free OH of associate	—	3590	3555	3591	3582	
Dimer	—	3475	3450	—	—	
Dimer	—	3445	3415	3455	—	
Dimer	—	3375	3335	—	3375	
C_1 conformer	2696	—	2681	2683	—	
C_s conformer	2676	2659	2645	2662	—	
Free OD of associate	—	2649	2624	2654	—	
Dimer	—	2575	2553	2575	—	
Dimer	—	2550	2531	—	2507	
Dimer	—	2495	2480	—	2381	

IR frequencies for the $\nu(\text{OH})$ band of HFTB in dilute CCl_4 solutions are 3610 (C_1 conformer), 3583 (C_s conformer) and 3500 cm^{-1} (dimer).

at 2480 cm^{-1} appears in the spectrum. The above picture is valid for HFTB and HFTB-OD in all matrices studied, with the exception that two monomer bands are found for HFTB-OD in nitrogen only and that a third, very sharp dimer band with highest frequency of all dimer bands (for HFTB-OD at 2553 cm^{-1} in nitrogen) appears in the spectra at M/A ratios near 200 (Table 2).

Detection of a separate $\nu(\text{OH})$ end group absorption at 2624 cm^{-1} for HFTB-OD in nitrogen suggests open chain (non-cyclic) structures for HFTB dimers. End group bands have been observed also for TFTB³ and PFTB,⁸ while TB² does not show such bands in the matrix spectra. Since the dimers of the fluorinated *tert*-butyl alcohols apparently have open-chain structures, there is no reason to believe that TB dimers should have basically different structures (*i.e.* cyclic, *cf.* Ref. 2). Accordingly, the association bands of HFTB in matrices are assigned using the dimer models proposed for TB.² The sharp dimer band with the highest frequency (at 2553 cm^{-1} for HFTB-OD in nitrogen) is assigned to the C_s dimer, while the two 'main' dimer absorptions (at 2531 and 2480 cm^{-1} for HFTB-OD in nitrogen) are assigned to C_1 dimers, both proposed models having an open chain structure. It may be mentioned that the dimers of HFTB show more definite structures than those of HFP⁵ in matrices.

In the liquid state and solution Raman spectra, an end group band is detected in addition to the monomer $\nu(\text{OH})$ bands of the C_s and C_1 conformers (Fig. 1). Since dimers seem to be the only associates of HFTB in matrices, the proportion of dimers must be considerable also in the liquid and solid states, and in solution.¹¹

The origin of the $\nu(\text{OH})$ end group bands. Dimer end group bands have not been reported for methanol,¹² ethanol¹² and *tert*-butyl alcohol² in matrices, though the dimer concentrations present would have presumed it. Open chain dimer structures have been proposed for all the above-mentioned alcohols in matrices. On the other hand, the existence of the $\nu(\text{OH})$ end group bands for the fluorinated alcohols TFP (1,1,1-trifluoro-2-propanol),⁸ HFP,⁵ hexafluoro-2,2-propanediol,¹³ TFTB,³ HFTB (Fig. 4) and PFTB⁸ is well established, the bands being shifted to lower frequencies from the monomer $\nu(\text{OH})$ band as the fluorine content of the alcohol is increased. We propose a non-bonded interaction between the acceptor hydroxyl group and the donor skeleton as the origin of the end group bands of halogenated alcohols. The interaction in question is small for ordinary alcohols.

Acknowledgements. The author gratefully acknowledges financial support from the Science Research Council of Finland.

REFERENCES

1. Korppi-Tommola, J. *Spectrochim. Acta. In press.*
2. Korppi-Tommola, J. *J. Mol. Struct.* **40** (1977) 13.
3. Korppi-Tommola, J. *Acta Chem. Scand. A* **31** (1977) 563.
4. Murto, J., Kivinen, A., Korppi-Tommola, J., Viitala, R. and Hyömäki, J. *Acta Chem. Scand.* **27** (1973) 107.
5. Barnes, A. J. and Murto, J. *J. Chem. Soc. Faraday Trans. 2*, **68** (1972) 1642.
6. Murto, J., Kivinen, A., Viitala, R. and Hyömäki, J. *Spectrochim. Acta Part A* **29** (1973) 1121.
7. Murto, J., Kivinen, A., Kivimaa, S. and Laakso, R. *Suom. Kemistil. B* **40** (1967) 250.
8. Murto, J., Kivinen, A., Edelmann, K. and Hassinen, E. *Spectrochim. Acta Part A* **31** (1975) 479.
9. Murto, J., Kivinen, A., Räsänen, M. and Perttilä, M. *Spectrochim. Acta Part A* **33** (1977) 291.
10. Barnes, A. J. and Whittle, G. C. Paper presented at the XIIth European Congress on Molecular Spectroscopy, Strasbourg 1975.
11. Kivinen, A., Murto, J., Korppi-Tommola, J. and Kuopio, R. *Acta Chem. Scand.* **26** (1972) 904.
12. Barnes, A. J. and Hallam, H. E. *Trans. Faraday Soc.* **66** (1970) 1920, 1931.
13. Murto, J., Kivinen, A., Manninen, A. and Perttilä, M. *Spectrochim. Acta Part A* **31** (1975) 217.

Received January 12, 1977.

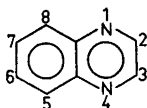
The EPR Spectra of Radical Ions Generated from Quinoxaline in Trifluoro- and Deuteriotrifluoroacetic Acid

JORMA ELORANTA and RAILI KOSKINEN

Department of Chemistry, University of Jyväskylä, Kyllinkatu 1—3, SF-40100 Jyväskylä 10, Finland

The triplet (7.50 G) appearing in the EPR spectrum of the radical anion of dihydroquinoxaline in trifluoroacetic acid at room temperature is barely observable at 253 K. In deuteriotrifluoroacetic acid, a quintet (1.18 G) appears in the EPR spectrum in place of the triplet. When quinoxaline was oxidized with thallium(III) trifluoroacetate at 253 K, a radical was obtained, but it was destroyed when the temperature was raised.

In acidic solvents, nitrogen-containing aromatic molecules tend to attach a proton coordinately to the free electron pair on nitrogen.



If two protons are attached to the radical anion of quinoxaline, denoted here $R^{\cdot-}$, the radical ion $RH_2^{\cdot+}$ is obtained.¹ Since the π -electron structure of $RH_2^{\cdot+}$ is similar to that of $R^{\cdot-}$, $RH_2^{\cdot+}$ should be called the radical anion of dihydroquinoxaline (despite the positive charge).

The purpose of this work was the chemical assignment of the coupling constants of the protons attached to quinoxaline by comparing the EPR spectra obtained in trifluoroacetic and deuteriotrifluoroacetic acids. Decreasing the temperature affects the rate of the proton exchange reaction with the solvent and should be seen as line broadening in the EPR spectrum.

We also sought to prepare the cation radical of quinoxaline, using thallium(III) trifluoroacetate² as oxidizing agent.

Furthermore, we wished to compare the experimental coupling constants with the coupling constants obtained with INDO³ and GEOMIN⁴ calculations. (In the GEOMIN program the molecular geometry is optimized with respect to the total energy.)

EXPERIMENTAL

The samples were prepared in high vacuum and the ampoule used was made of quartz glass.⁵

Thallium(III) trifluoroacetate, trifluoroacetic acid and deuteriotrifluoroacetic acid were Merck products (for spectroscopy). Quinoxaline was a product of Fluka AG (laboratory grade) and was purified by gas chromatography.

The EPR spectra were recorded with Varian E-9 and E-12 spectrometers equipped with variable temperature controls and connected to Varian 620/L SS-100 computer facilities.

The spin density calculations and the simulations of the spectra were carried out on the UNIVAC 1108 central computer for Finnish universities.

Bond lengths according to Pople and Beveridge⁶ were used in the INDO calculations. They were also used as the initial data in optimizing the molecular geometry with the GEOMIN program.

RESULTS AND DISCUSSION

In Figs. 1, 2 and 3 we see the EPR spectrum of $RH_2^{\cdot+}$ in trifluoroacetic acid at room temperature and at 253 K, respectively. The triplet caused by the protons in positions 1 and 4 (7.50 G) appearing in the room temperature spectrum is broadened at the lower temperature. The quintet caused by the nitrogens (6.72

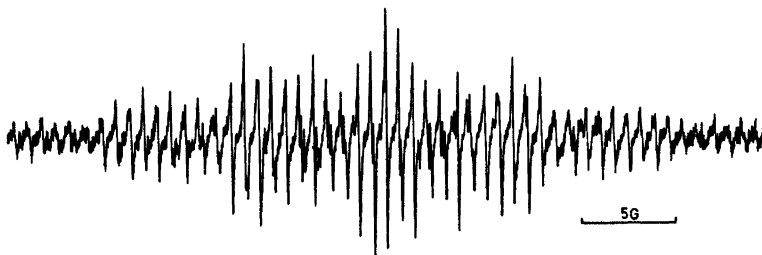


Fig. 1. The EPR spectrum of the radical anion of dihydroquinoxaline ($\text{RH}_2\cdot^+$) in trifluoroacetic acid at room temperature.



Fig. 2. The simulated EPR spectrum of the anion of Fig. 1 (based on Table 1 and the line width of 0.08 G).

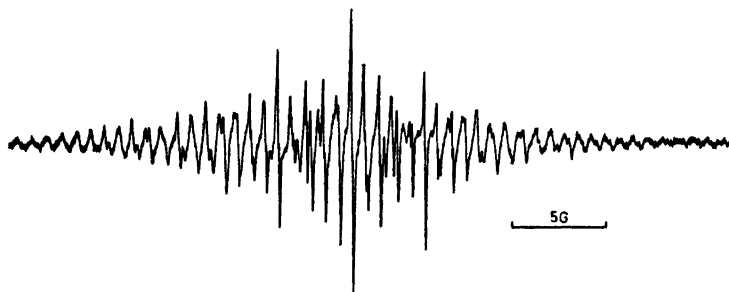


Fig. 3. The EPR spectrum of the radical anion of dihydroquinoxaline ($\text{RH}_2\cdot^+$) in trifluoroacetic acid at 253 K.

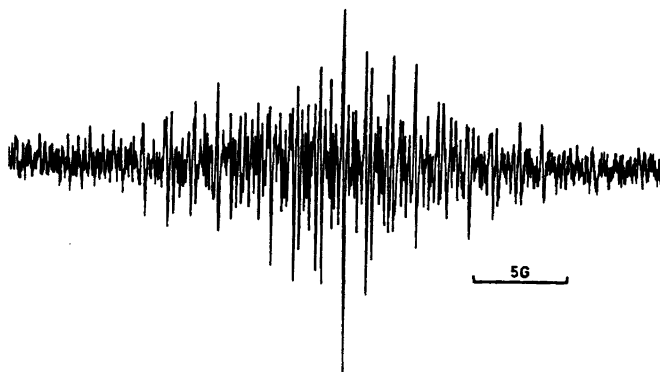


Fig. 4. The EPR spectrum of the radical anion of dideterioquinoxaline ($\text{RD}_2\cdot^+$) in deuterio-trifluoroacetic acid at room temperature.

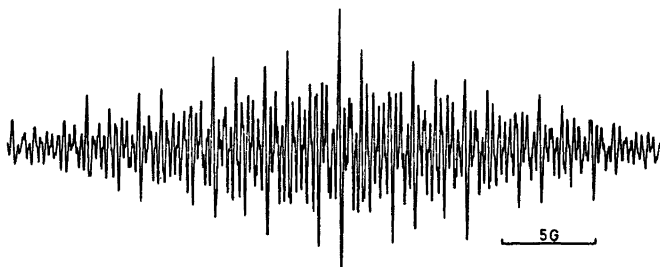


Fig. 5. The simulated EPR spectrum of the anion of Fig. 4 (based on Table 1 and the line width 0.08 G).



Fig. 6. The EPR spectrum of the radical ion generated from quinoxaline in trifluoroacetic acid with thallium(III) trifluoroacetate as oxidizing agent at 261 K.

G) is also clearly broadened at the lower temperature. This line broadening is due to proton exchange reactions with the solvent. The other coupling constants are only slightly disturbed by proton exchange reactions. The rate of the reactions at room temperature is so high that the triplet appears with its normal intensity in the EPR spectrum.

When deuteriotrifluoroacetic acid is used as solvent (Figs. 4 and 5), the proton triplet of 7.50 G does not appear in the EPR spectrum even at room temperature and a new quintet of 1.18 due to deuterium appears instead. Since $g_N(D)/g_N(H) = 0.1535$, we can calculate $a_D = 0.1535 \times 7.50 \text{ G} = 1.15 \text{ G}$, which is in good agreement with the experimental coupling constant.

No line broadening is observed in the EPR spectrum of the radical anion of dideuterioquinoxaline over the temperature range 253–300 K.

Phenazine⁵ exhibits identical well-resolved EPR spectra in trifluoroacetic and trichloroacetic acids, whereas quinoxaline gives only a poorly resolved spectrum in the latter solvent. No EPR spectrum was obtained from quinoxaline in acetic acid. Attempts were made to prepare the cation radical of quinoxaline with thallium(III) trifluoroacetate in trifluoroacetic

acid. The radical obtained was stable for only a few hours when the temperature was kept below 263 K, and was destroyed when the temperature was raised.

The following coupling constants are observed in the EPR spectra of the radical (Figs. 6 and 7): one triplet $a(N) = 30.4 \text{ G}$ and two quartets $a(H) = 4.9 \text{ G}$ and $a(H) = 1.1 \text{ G}$. Neither a coupling of the other nitrogen nor of thallium ($I_N = 1/2$) is observed. If a complex of thallium and the radical cation of quinoxaline had formed, the π -electron structure of the radical ion would be different. The assignment of the coupling constant for the Tl-complex cannot be made with INDO calculations for orbital limitations. After the decomposition of the radical when the temperature increases, no

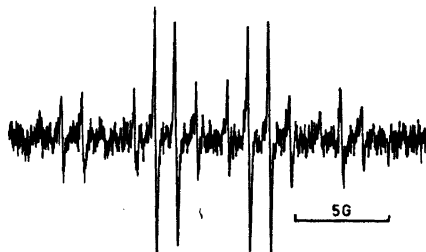


Fig. 7. Enlargement of the line group appearing in the middle of Fig. 6.

Table 1. The coupling constants (G) of the radical anions of dihydroquinoxaline and dideuterioquinoxaline.

Position	RH ₂ [•] + CF ₃ COOH		INDO	GEOMIN	RD ₂ [•] + CF ₃ COOD
	Room temp.	253 K			
1,4 (N)	6.72	6.72	7.5	7.7	6.68
1,4 (H)	7.50	—	-10.1	-11.1	—
1,4 (D)	—	—	—	—	1.18
2, 3	3.80	3.85	-2.3	-2.0	3.93
5, 8	0.70	0.65	-0.5	-0.52	0.66
6, 7	1.48	1.48	-0.7	-0.53	1.46

Table 2. Bond lengths (nm) of the radical anion of dihydroquinoxaline as used with INDO and calculated with GEOMIN.

	1-2	2-3	1-9	9-10	5-10	5-6	6-7	1(N)-11(H)
INDO	0.137	0.140	0.137	0.140	0.140	0.140	0.140	0.1015
GEOMIN	0.1369	0.1365	0.1399	0.1414	0.1405	0.1379	0.1399	0.10712

radical anion of dihydroquinoxaline is formed.

INDO calculations with standard bond lengths⁶ gave the following order for the energies of the radicals: RH^{•+} > RH^{•0} > RH₂^{•+}. Thus, according to the calculations, RH₂^{•+} has the most stable structure.

GEOMIN calculations lowered the total energy of the dihydroquinoxaline radical anion by about 25 kJ/mol during the optimization of the bond lengths (Table 2), but the coupling constants were not better than the INDO values (Table 1).

REFERENCES

1. Barton, B. and Fraenkel, G. *J. Chem. Phys.* **41** (1964) 1455.
2. Elson, J. and Kochi, J. *J. Am. Chem. Soc.* **95** (1973) 5061.
3. Hase, H. and Schweig, A. *QCPE Program* **261** (1973).
4. Purcell, K. and Zapata, J. *QCPE Program* **312** (1976).
5. Eloranta, J., Paananen, I. and Koskinen, R. *Acta Chem. Scand. A* **31** (1977) 417.
6. Pople, J. and Beveridge, D. *Approximate Molecular Orbital Theory*, McGraw-Hill, New York 1970.

Received January 17, 1977.

The Crystal Structure of $\text{NaVO}_3 \cdot 1.89\text{H}_2\text{O}$

ARNE BJÖRNBERG and BRITT HEDMAN

Department of Inorganic Chemistry, University of Umeå, S-901 87 Umeå, Sweden

The crystal structure of $\text{NaVO}_3 \cdot 1.89\text{H}_2\text{O}$ has been determined from three-dimensional X-ray diffraction data collected with a PAILRED diffractometer using $\text{MoK}\alpha$ -radiation. The crystals are monoclinic, space group $P2_1/a$ (No. 14), with unit cell dimensions $a = 16.756(2)$ Å, $b = 3.6391(3)$ Å, $c = 8.023(1)$ Å, $\beta = 111.18(1)^\circ$ and the cell contains four formula units. Refinement by full-matrix least-squares methods using anisotropic thermal parameters resulted in a final R -value of 0.023, based on 1307 independent reflexions.

In the structure each vanadium atom is surrounded by five oxygen atoms forming a distorted trigonal bipyramid. Each bipyramid shares two edges forming continuous chains parallel with the y -axis. The chains are held

together in the z direction by $\text{O}-\text{Na}-\text{O}$ bridges

and in the x direction by hydrogen bonds involving the water molecules. One of the two water positions is only partly occupied with an occupancy factor of 0.89(1). The $\text{V}-\text{O}$ distances are 1.643(1) and 1.653(1) Å for unshared oxygen atoms and 1.882(3), 1.923(3) and 1.988(1) Å for shared oxygens, while the $\text{Na}-\text{O}$ and $\text{Na}-\text{O}_w$ distances vary between 2.37 and 2.46 Å.

Numerous attempts have been made to determine which ions are present in vanadate solutions at different pH-values. Aqueous equilibrium studies using potentiometric methods have indicated that the pH-range 0–14 can be divided into different regions depending on the composition of the species. A critical review of the equilibrium studies and the species found has recently been given by Baes and Mesmer.¹ One of the regions, the metavanadate region ($6 \lesssim \text{pH} \lesssim 9$), is very complicated to investigate with these methods, due to slow equilibria and low solubility. The general formula of the metavanadates $(\text{VO}_3^-)_n$ has been established, however, and two anions,

$\text{V}_3\text{O}_9^{3-}$ and $\text{V}_4\text{O}_{12}^{4-}$, have been suggested.^{2–4} Work is at present in progress at this department to further establish equilibria and dominating species in this region.⁵

Parallel with these investigations, crystallization experiments followed by X-ray structure investigations have been performed in order to support the results of the equilibrium studies. However, with Na^+ , K^+ , Ca^{2+} , Sr^{2+} or NH_4^+ as cations only structures with infinite metavanadate chains are found. Crystals containing the $\text{V}_3\text{O}_9^{3-}$ or $\text{V}_4\text{O}_{12}^{4-}$ anions have so far not been obtained from aqueous solutions, but by dissolution of V_2O_5 in an ethanolic tetrabutylammonium hydroxide solution followed by recrystallization in acetone on addition of benzene, the compound $[\text{N}(\text{C}_4\text{H}_9)_4]_3\text{HV}_4\text{O}_{12}$ has recently been isolated.⁶ The structure determination was not completed, but the structure of the V_4O_{12} group is similar to that of the tetrametaphosphate ion, $\text{P}_4\text{O}_{12}^{4-}$.⁷

The subject of the present investigation is the crystal structure of a sodium metavanadate, $\text{NaVO}_3 \cdot 1.89\text{H}_2\text{O}$, which is of interest for the systematic studies of vanadates in our department. Apart from information on the metavanadate chains the crystal structure can explain the non-stoichiometry for the water of crystallization. This compound has been referred to as $\text{NaVO}_3 \cdot 1.9\text{H}_2\text{O}$ by Lukács and Strusievici⁸ (powder diffraction, IR, DTA), but usually it has been assigned the composition $\text{NaVO}_3 \cdot 2\text{H}_2\text{O}$.⁹

EXPERIMENTAL

Crystal preparation and analyses. In a typical preparation 0.455 g of V_2O_5 was dissolved in 100 ml of 0.060 M NaOH giving an average charge per vanadium, (z), equal to -1.2 . Then

0.001 mol of perchloric acid was added, raising the z value to -1.0 (the same as in the metavanadate anions, $(\text{VO}_3^-)_n$). After a few days (sometimes weeks) of slow evaporation at room temperature, white or colourless acicular crystals were formed, often grown together forming a thistle-like arrangement. The crystals are unstable in air and during the X-ray exposures they were enclosed, together with part of the mother liquor, in a sealed Lindemann capillary.

The contents of Na (by atomic emission) and V (by reduction with $\text{Fe}(\text{NH}_4)_2(\text{SO}_4)_2$, addition of H_3PO_4 and titration with MnO_4^-) were determined, the analyses being performed at the Analytical Laboratory, Boliden AB, Skelleftehamn. Found: (weight %) Na 14.3; V 32.6. Calc. for $\text{NaVO}_3 \cdot 1.89\text{H}_2\text{O}$: Na 14.7; V 32.7. Water analysis was performed with the Penfield method¹⁰ and gave 21.4% H_2O (calc. 21.8%). The water analysis gives the formula $\text{NaVO}_3 \cdot 1.86\text{H}_2\text{O}$, which is in fair agreement with the occupancy factor refined from X-ray data.

Crystal data. Preliminary Weissenberg and precession photographs showed the crystal system to be monoclinic. Systematic extinctions $h0l$, $h=2n+1$ and $0k0$, $k=2n+1$ uniquely determined the space group as $P2_1/a$. However, all hkl ($k \neq 0$) reflexions with $h=2n+1$ were very weak, indicating the structure to be very close to space group $P2_1/m$ with a sub-cell where $a=8.378$ Å. As can be seen from Table 1, the y -coordinates of all non-hydrogen atoms are close to $1/4$.

The unit cell dimensions were refined by least-squares methods¹¹ from powder photographs taken with a Guinier-Hägg camera using $\text{CuK}\alpha$ -radiation ($\lambda=1.54051$ Å) and with $\text{Pb}(\text{NO}_3)_2$ as internal standard ($a[\text{Pb}(\text{NO}_3)_2]=7.8575$ Å, 25°C). The density of the crystals was determined by flotation in a bromoform/carbon tetrachloride solution.

$\text{NaVO}_3 \cdot 1.89\text{H}_2\text{O}$
Space group $P2_1/a$, (No. 14), all atoms in $4(e)$:
 $\pm(x, y, z; 1/2+x, 1/2-y, z)$
 $a=16.756(2)$ Å, $b=3.6391(3)$ Å, $c=8.023(1)$ Å,
 $\beta=111.18(1)^\circ$, $V=456.2$ Å³, F.W.=155.98,
 $Z=4$, $D_m=2.28(1)$ g cm⁻³, $D_x=2.27$ g cm⁻³,
 $\mu(\text{MoK}\alpha)=23.15$ cm⁻¹

Collection and reduction of intensity data. The structure was solved from a preliminary data set, collected with equi-inclination Weissenberg film methods, using $\text{CuK}\alpha$ -radiation ($\lambda=1.5418$ Å). The intensities of 398 independent reflexions from the layers $h0l-h2l$ were estimated visually. In order to obtain more accurate intensity values for the weak $h=2n+1$ reflexions and determine the full structure, three-dimensional intensity data were collected at 25°C with a Philips PAILRED linear diffractometer using $\text{MoK}\alpha$ -radiation ($\lambda=0.71069$ Å) monochromatized with a graphite monochromator. A crystal of approximate dimensions $0.10 \times 0.18 \times 0.15$ mm was mounted and rotated along

the y -axis, which was parallel with the 0.18 mm edge. A total of 1584 unique reflexions were scanned in the layers $h0l-h6l$ and within $(\sin \theta)/\lambda=0.86$ Å⁻¹. The measurements were made with scan speed 1° min⁻¹ and background time 40 s at the beginning and end of the interval.

Reflexions with a relative statistical error $^{12} \Delta I_o/I_o$ greater than 0.5 were omitted leaving a total of 1325 reflexions. The intensities were corrected for Lorentz and polarization effects, and absorption correction was applied ($\mu=23.15$ cm⁻¹) using a $4 \times 8 \times 6$ Gaussian grid. The transmission factor varied between 0.721 and 0.822.

STRUCTURE DETERMINATION AND REFINEMENT

Since all reflexions with $h=2n+1$ were very weak, the structure, when first determined from film data, was based on the sub-cell with $a=8.378$ Å and space group $P2_1/m$. The vanadium atomic position was found from a three-dimensional Patterson synthesis, and routine heavy-atom methods revealed the non-hydrogen atoms, all atoms being in position $2(e)$. This structure was refined with isotropic thermal parameter to an R -value of 0.156.

With diffractometer data, including the weak $h=2n+1$ reflexions, the a parameter was doubled to 16.756 Å changing the space group to $P2_1/a$. The refinements were started with the film-data parameters, and with isotropic temperature factors they converged at $R=0.101$. The refinements were then continued with anisotropic thermal parameters resulting in an R -value of 0.036.

A difference Fourier synthesis showed a weak negative peak at the same position as one of the water oxygens. The occupancy factor for this atom was therefore refined resulting in a value of 0.89(1), which is in fair agreement with the result of the water analysis.

From a difference Fourier synthesis based on the 372 reflexions with $(\sin \theta)/\lambda < 0.5$ Å⁻¹ two peaks around Aq1 were found, while near the partly occupied Aq2 position, only one well-defined peak appeared. These three peaks were taken as hydrogen atoms and included in the refinements. The β_{22} parameter for Aq2 is abnormally large and may well include the effects from an unresolved second hydrogen atom. Attempts to split the Aq2 position into

two partly occupied oxygen atomic positions, as well as into one oxygen and one hydrogen atomic position caused the refinements to diverge.

Since for the strongest reflexions F_c was greater than F_o , an isotropic secondary extinction parameter was included as described by Coppens and Hamilton,¹³ this parameter receiving a value of $g' = 0.77(4)$. The refinements finally converged with an R -value of 0.023, R being defined as $\sum ||F_o| - |F_c|| / \sum |F_o|$ and with $\sum w_i (|F_o| - |F_c|)^2$ as the function minimized. A weighting scheme according to Cruickshank¹⁴ was applied, $w = (a + |F_o| + c|F_o|^2 + d|F_o|^3)^{-1}$, with $a = 600$, $c = 0.2133$ and $d = 0.008$. In the last cycle of refinement the parameter shifts were less than 0.25σ for all non-hydrogen atoms.

The atomic scattering factors used for V³⁺, O, O⁻, Na⁺ and H were those given by International Tables, Vol IV.¹⁵ Account was taken of the real and imaginary parts of the anomalous dispersion correction. The computations were

performed with a CDC 3300 computer at the University of Umeå, with programs given in Ref. 11.

Final atomic positional and thermal parameters are given in Tables 1 and 2. A list of observed and calculated structure factors can be obtained from the authors on request.

DESCRIPTION AND DISCUSSION OF THE STRUCTURE

The structure is built up from continuous chains, parallel with the y -axis, consisting of vanadium-oxygen trigonal bipyramids sharing edges. These chains are held together in

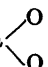
the z -direction by O—Na  bridges. The coordination around the sodium atoms is octahedral, with three vanadate oxygens and three water oxygens coordinated to each sodium atom. The layers thus formed are held

Table 1. The fractional atomic coordinates and, for the hydrogen atoms, the isotropic temperature factors (Å^2). The estimated standard deviations are given in parentheses.

	x	y	z	B
V	0.03783(2)	0.2455(2)	0.16781(3)	
O1	0.00071(8)	0.2510(10)	0.3327(1)	
O2	0.14265(9)	0.2780(10)	0.2540(2)	
O3	0.98668(9)	0.2479(8)	0.9023(1)	
Na	0.09375(5)	0.2520(7)	0.6478(1)	
Aq1	0.32282(8)	0.2581(14)	0.4108(2)	
Aq2	0.18965(16)	0.2423(23)	0.9491(3)	
H1	0.272(2)	0.198(13)	0.369(4)	2.8(7)
H2	0.333(2)	0.201(15)	0.511(5)	3.8(8)
H3	0.167(4)	0.361(23)	0.018(9)	7.8(19)

Table 2. The final anisotropic thermal parameters ($\times 10^4$) with their estimated standard deviations ($\times 10^4$) in parentheses. The parameters are calculated according to the formula $\exp[-(h^2\beta_{11} + k^2\beta_{22} + l^2\beta_{33} + 2hk\beta_{12} + 2hl\beta_{13} + 2kl\beta_{23})]$.

	β_{11}	β_{22}	β_{33}	β_{12}	β_{13}	β_{23}
V	14(0)	149(1)	35(0)	11(1)	7(0)	3(2)
O1	22(0)	295(7)	60(1)	-8(7)	20(1)	12(13)
O2	15(0)	474(17)	97(2)	-12(3)	11(1)	-25(7)
O3	40(1)	156(6)	43(1)	3(6)	7(1)	59(9)
Na	22(0)	378(6)	119(1)	24(4)	9(0)	-8(9)
Aq1	18(0)	650(13)	90(2)	-10(7)	12(1)	15(16)
Aq2	31(1)	3841(110)	120(4)	117(20)	29(2)	187(39)

together in the x -direction by hydrogen bonds, which accounts for the extremely good (100) cleavage.

The vanadium-oxygen arrangement. As can be seen from Fig. 1, each vanadium atom is surrounded by five oxygen atoms in a distorted trigonal bipyramidal arrangement. The interatomic V–O distances are longer (1.88–1.99 Å) to the three oxygen atoms which are shared between two or three vanadium atoms, than to the two unshared oxygens (1.64–1.65 Å). The apexes of the trigonal bipyramid are out of line with the vanadium atom; the O3–V–O3 angle is $145.54(7)^\circ$. As can be seen from Table 1, the vanadium atom is not in the same plane as the three equatorial oxygen atoms. All atoms slightly offset from $y=1/4$, thus giving rise to the weak $h=2n+1$ reflexions. In $\text{KVO}_3 \cdot \text{H}_2\text{O}$ ¹⁶ all atoms are in $z=1/4$ as a result of the space group symmetry ($Pnam$) and the vanadium atom in that compound lies in the plane of the oxygen atoms. The trigonal bipyramids share edges to form chains parallel with the y -axis. The V–V distances within the chain are 3.096(1) and 3.134(1) Å.

The results show that the vanadate chains in this structure look very much like those reported in $\text{KVO}_3 \cdot \text{H}_2\text{O}$,¹⁶ $\text{Ca}(\text{VO}_3)_2 \cdot 4\text{H}_2\text{O}$ ¹⁷ and $\text{Sr}(\text{VO}_3)_2 \cdot 4\text{H}_2\text{O}$.¹⁸

There seem to be two distinctly different kinds of five-coordinated vanadium, one being trigonal bipyramidal as in $\text{NaVO}_3 \cdot 1.89\text{H}_2\text{O}$ or $\text{KVO}_3 \cdot \text{H}_2\text{O}$, and one square pyramidal, e.g. in CsV_3O_8 .¹⁹ The two configurations can most easily be distinguished by the V–O distances. In the trigonal bipyramid, there are two short (<1.68 Å) and three long (>1.85 Å) bonds,

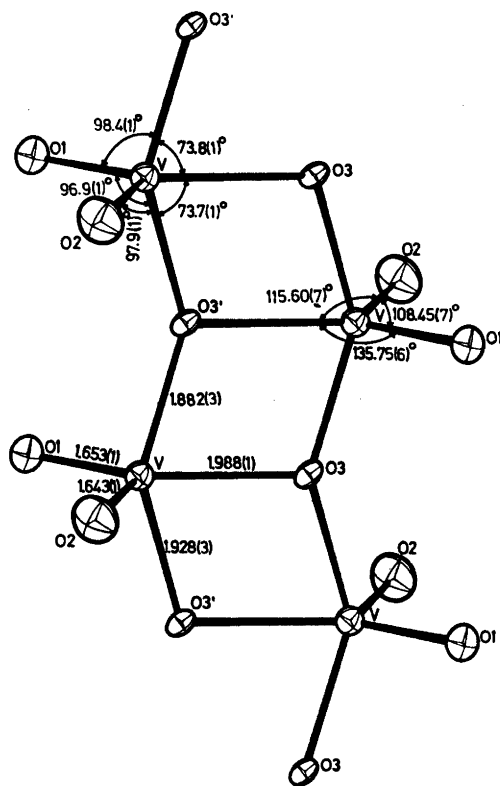


Fig. 1. The vanadium-oxygen coordination. The interatomic distances (Å) and angles ($^\circ$) are given, with the e.s.d.'s in parentheses referring to the last decimal place given. The angle O3'–V–O2 from the top O3' atom is $106.2(1)^\circ$. The thermal ellipsoids are scaled to enclose 50 % probability.²¹

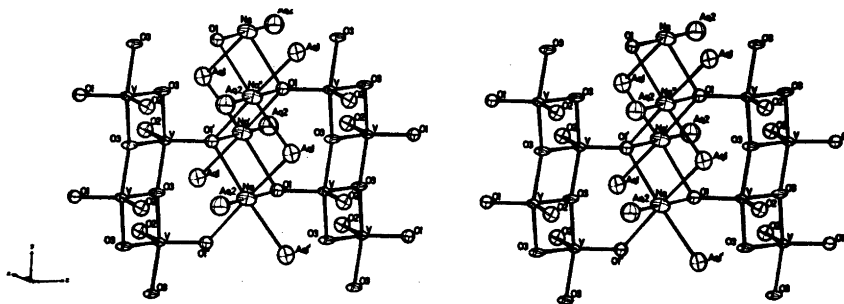


Fig. 2. A stereoscopic view of the layer structure created by vanadium-oxygen-sodium. The thermal ellipsoids are scaled to enclose 50 % probability,²¹ except for Aq2, which is drawn as a sphere of radius 0.22 Å. The magnitude of the real β_{22} would cause Aq2 to obscure large parts of the drawing.

Table 3. Distances (Å) and angles (°) within the $\text{NaO}_3(\text{H}_2\text{O})_3$ octahedra. The designation of the atoms refers to the bottom octahedron in Fig. 2. The estimated standard deviations are given in parentheses and refer to the last decimal place given.

Na—Aq1	2.458(4)	Na—O1'	2.445(3)
Na—Aq1'	2.425(4)	Na—O1''	2.462(3)
Na—O1	2.444(1)	Na—Aq2	2.371(3)
Na—Na''	3.6391(3)		
Na—Na'	3.671(3)		
Na'—Na''	3.656(3)		
O1'—Na—O1''	95.74(5)	O1—Na—O1'	83.19(9)
O1''—Na—Aq1'	83.69(13)	O1—Na—O1''	83.11(9)
Aq1'—Na—Aq1	96.36(6)	O1—Na—Aq1'	89.74(9)
Aq1—Na—O1'	83.34(13)	O1—Na—Aq1	89.87(9)
Aq2—Na—O1'	99.30(17)		
Aq2—Na—O1''	97.96(17)	Aq2—Na—O1	177.16(11)
Aq2—Na—Aq1'	87.76(16)		
Aq2—Na—Aq1	89.05(17)		

while in the square pyramid there are one short apical bond and four long (1.75–2.00 Å) bonds. Distances and angles within the vanadate chain are given in Fig. 1.

The sodium-oxygen arrangement. The Na^+ -ion coordinates six oxygen atoms in an octahedral arrangement, which can be written $\text{NaO}_3(\text{H}_2\text{O})_3$. These octahedra are linked together by sharing edges to form continuous double chains in between and parallel with the vanadate chains.

The oxygen atoms shared with vanadium are always O1, the bridge between two vanadium atoms being $\text{V}-\text{O1} \begin{matrix} \text{Na} \\ \text{Na} \end{matrix} \text{O1}-\text{V}$. The water

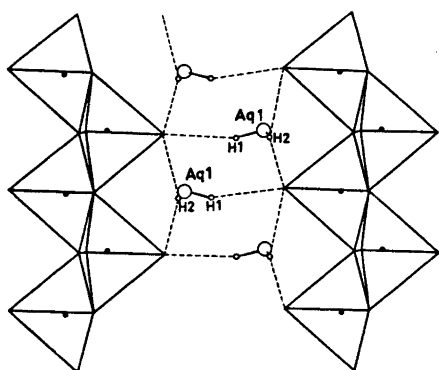


Fig. 3. A projection along [001] showing the hydrogen bonds from Aq1. The left-hand chain is related to the right-hand chain by a $1/2, 0, 1$ translation. The positions of the vanadium atoms are indicated by black dots.

Acta Chem. Scand. A 31 (1977) No. 7

molecules in an octahedron are two Aq1, both bonded to two Na^+ -ions, and one Aq2 which is bonded to only one Na^+ . A detail of the resulting layer structure is shown in Fig. 2. The octahedra are not very far from regular, with Na—O distances varying between 2.37 and 2.46 Å. Distances and angles within the sodium-oxygen octahedra are given in Table 3.

Hydrogen bonding. The layers mentioned above are held together by hydrogen bonds from water molecules to O2, which for spatial reasons is the only oxygen atom available

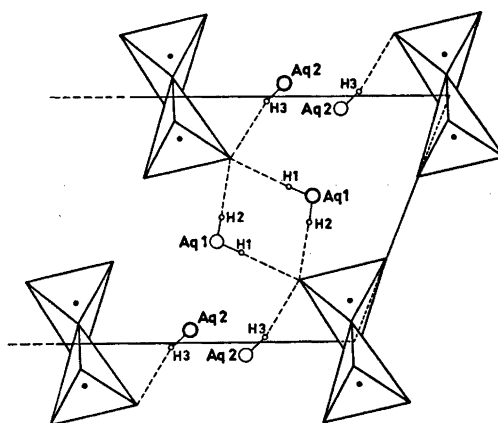


Fig. 4. A projection along [010] showing the hydrogen bonds. Aq atoms with heavy contours are situated in $y \sim 3/4$, Aq atoms with light contours are in $y \sim 1/4$. The positions of the vanadium atoms are indicated by black dots.

Table 4. Hydrogen bond and O–H distances (Å). The designation of the atoms refers to Figs. 3 and 4. The estimated standard deviations are given in parentheses and refer to the last decimal place given.

O–O		O–H	
Aq1–H1···O2	2.821(2)	Aq1–H1	0.83(4)
		Aq1–H2	0.79(4)
Aq1–H2	3.081(4)	Aq2–H3	0.88(7)
\ O2			
/ O2'	3.165(4)		
Aq2–H3···O2	2.830(3)		

for hydrogen bonding. Aq1 participates in an ordinary hydrogen bond Aq1–H1···O2 with bond length 2.821(2) Å, and in what seems to

be a bifurcated bond Aq1–H2 $\begin{matrix} \diagup O2 \\ \diagdown O2' \end{matrix}$. Aq2 is

less tightly bonded to the vanadate oxygen atoms with only one atom (O2) within hydrogen bond distance. However, every Aq2 atom has another two Aq2's at distances of 2.622(4) Å. This suggests hydrogen bonds, but as described above, it has not been possible to determine the position of the hydrogen atom. It seems highly probable that it should be located close to a line Aq2–Aq2'.

Since Aq2 is bonded to the vanadate chains via one hydrogen atom only, this could be the explanation of why Aq2 alone accounts for the nonstoichiometry of the crystal.²⁰

Hydrogen bonds are shown in Figs. 3 and 4, and hydrogen bond distances are given in Table 4.

Acknowledgements. We thank Professor Nils Ingri for much valuable advice, for his great interest and for all the facilities placed at our disposal. Thanks are also due to Dr. Lage Pettersson for much valuable help. The English of the paper has been corrected by Dr. Michael Sharp. The work forms part of a program financially supported by the Swedish Natural Science Research Council.

REFERENCES

1. Baes, C. F., Jr. and Mesmer, R. E. *The Hydrolysis of Cations*, Wiley, New York 1976.
2. Ingri, N. and Brito, F. *Acta Chem. Scand.* 13 (1959) 1971.

3. Brito, F. *An. Quim. B* 62 (1966) 123.
4. Ingri, N., Brito, F. and Sillén, L. G. *Acta Chem. Scand.* 18 (1964) 1557.
5. Pettersson, L. *Private communication*.
6. Fuchs, J., Mahjour, S. and Pickardt, J. *Angew. Chem.* 88 (1976) 385.
7. Hilmer, W. *Acta Crystallogr.* 17 (1964) 1063.
8. Lukács, I. and Strusievici, C. Z. *Anorg. Allg. Chem.* 315 (1962) 323.
9. Perraud, J. *Rev. Chim. Miner.* 11 (1976) 302.
10. Penfield, S. L. *Am. J. Sci.* 48 (1894) 30.
11. Antti, B.-M. *Acta Chem. Scand. A* 30 (1976) 24.
12. Antti, B.-M. *Acta Chem. Scand.* 27 (1973) 3513.
13. Coppens, P. and Hamilton, W. C. *Acta Crystallogr. A* 26 (1970) 71.
14. Cruickshank, D. W. J. *Computing Methods in Crystallography*, Pergamon, London 1965, p. 114.
15. *International Tables for X-Ray Crystallography*, Kynoch Press, Birmingham 1974, Vol. IV.
16. Evans, H. T., Jr. *Z. Kristallogr.* 114 (1960) 257.
17. Ahmed, F. R. and Barnes, W. H. *Can. Miner.* 8 (1962) 713.
18. Sedlacek, P. and Dornberger-Schiff, K. *Acta Crystallogr.* 18 (1965) 407.
19. Evans, H. T., Jr. and Block, S. *Inorg. Chem.* 5 (1966) 1808.
20. Pletnev, R. N., Gorshkov, V. V. and Ivakin, A. A. *Russ. J. Inorg. Chem.* 21 (2) (1976) 178.
21. Johnson, C. K. *ORTEP*, Report ORNL-3794, Oak Ridge National Laboratory, Oak Ridge 1965.

Received April 19, 1977.

Transfer of Individual Ions from H₂O to D₂O. Gibbs Energy of Transfer of Dimethylmaleate Ion

ANTTI VESALA and JUHO-PERTTI JALAVA

Department of Chemistry and Biochemistry, University of Turku, SF-20500 Turku 50, Finland

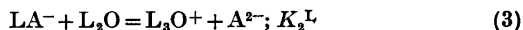
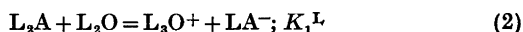
The Gibbs energy of transfer of dimethylmaleate ion from light to heavy water was determined using appropriate assumptions. This determination comprised the measurements of the first and second acidity constants of dimethylmaleic acid and the dehydration constant of the acid both in H₂O and D₂O. The evaluation of the transfer free energy of dimethylmaleate ion from H₂O to D₂O was based on the separation of transfer and exchange effects in the equilibria of dimethylmaleic acid dissociation in light and heavy water. The contributions of cations Ag⁺ and Ba²⁺ to the Gibbs energy of transfer were estimated on the basis of the solubilities of silver and barium dimethylmaleates in H₂O and D₂O.

The thermodynamics of transfer of solutes from one solvent to another gives valuable information about the structure of the solutions. Considering electrolytes as solutes, the assignment of the Gibbs energy of transfer to contributions of individual ions can be made using appropriate extrathermodynamic assumptions.¹ Most common methods of evaluation, in this context, are the tetraphenylarsonium—tetraphenylboride, the large anion—large molecule, the large cation—large molecule assumptions and the modifications of the Born equation. Furthermore, depending on the solutes in question some special ways to estimate these ionic contributions are available.

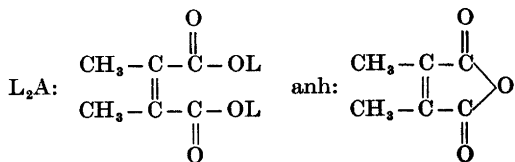
Taking the H₂O—D₂O system as an example, the most reliable results, perhaps, have been obtained by using certain specific procedures. One among the first methods of estimation was to pay no attention to the contribution of cations in the Gibbs energy of transfer.² One useful assumption is to neglect the Gibbs energy of transfer of the L₂O⁺ ion (L=H or D) from

light to heavy water.³ This assumption seems reasonable considering the structural features of the system. The other method is to apply suitable acid—base equilibria in H₂O and D₂O.⁴ These equilibria must be abnormal in the sense that the isotopic exchange effects can be eliminated from the equations derived for the total isotope effect. This method has been successfully applied to carbonic and sulfurous acids to evaluate the Gibbs energy of transfer of carbonate and sulfite ions.⁴ To determine the Gibbs energy of transfer of dimethylmaleate ion we shall apply a similar method.

Three equilibria (1)–(3) exist for dimethylmaleic acid



in water. In these three equations the abbreviations presented below are used. It must also be noticed that L denotes either H or D. From



the derived equations for the isotope effects of the equilibrium constants, the isotopic fractionating factors, ϕ_1 for L₂A and ϕ_2 for LA⁻, can be eliminated. Assuming the Gibbs energy of transfer to be zero for the L₂O⁺ ion, the transfer effect for the dianion, A²⁻, can be evaluated. The generally accepted value of 0.69

(with three significant figures 0.686)⁴ for l , the isotopic fractionating factor of the L_3O^+ ion, is needed in the calculations.^{5a} To get the cationic contributions to the Gibbs energy of transfer, the solubilities of silver and barium dimethylmaleates in light and heavy water were measured.

EXPERIMENTAL

Reagents. Heavy water with a deuterium mol fraction of 0.998 was purchased from Norsk Hydro. Light water was distilled water. Both waters were boiled under reduced pressure to eliminate dissolved gases. The dimethylmaleic anhydride was a *purissimum* product delivered by Fluka AG. Its purity was found to be (99.8 ± 0.4) % when titrated against a standard solution of NaOH. The preparation of the silver and barium salts of dimethylmaleic acid was carried out by first synthesizing potassium dimethylmaleate. From it and $AgNO_3$ and $BaCl_2$ the wanted salts could be precipitated in water solution.⁶⁻⁸ The purities were 100.0 % for the silver salt determined by ignition and weighing, and 99.6 % for the barium salt determined by titration of the anion.

The other reagents were of analytical grade and were used as received.

Methods. The dehydration constant of dimethylmaleic acid was determined kinetically by the method described by Ebersson.⁹ The kinetics were followed by a Unicam UV Spectrophotometer SP 1700 using a wavelength of 256 nm where the anhydride has its maximum absorption.

If the rate constant for the forward reaction (1) is denoted by k_1 and that for the reverse reaction, k_{-1} , the observed rate constant can be presented by eqn. (4). Here c_L denotes the lyonium ion concentration. The dehydration

$$k_{\text{exp}} = k_{-1} + \frac{k_1}{1 + K_1^L(1/c_L) + K_1^L K_2^L(1/c_L)^2} \quad (4)$$

constant, K_d^L , can be expressed by the aid of the rate constants as k_1/k_{-1} . It can be concluded on the basis of eqn. (4) that $k_{\text{exp}} = k_{-1}$ when c_L is sufficiently low. For calculations eqn. (4) can be modified to a more suitable form (5). The approximative value for $1/K_d^L$ can be evaluated

$$\frac{1}{(k_{\text{exp}}/k_{-1}) - 1} = \frac{1}{K_d^L} + \frac{K_1^L}{K_d^L(1/c_L)} + \frac{K_1^L K_2^L}{K_d^L(1/c_L)^2} \quad (5)$$

by determining k_{exp} when the lyonium concentration is relatively high. The best value for k_{-1} is then calculated from eqn. (5) using an iterative procedure. The ionic strength of the buffer solutions which regulated c_L was 0.0100

mol dm^{-3} . Adjusting the ionic strength did not affect the results more than did experimental errors.

The first acidity constant of dimethylmaleic acid was determined by the method of potentiostatic titration. A more detailed description of the method has been presented earlier.^{10,11} The measurable (apparent) first acidity constant has, owing to the dehydration equilibrium, the form expressed by eqn. (6). It was our aim to determine both the first and the

$$K_1^L(\text{app}) = K_1^L/(1 + K_d^L) \quad (6)$$

second acidity constants by potentiostatic titration. However, the accuracy of the method was not sufficiently high in the region of the second constant. Therefore, the first constant was determined considering the acid as monobasic with the degree of deprotonation having values between 0.15 and 0.38. The highest value of the ionic strength in the measurements was about 0.012 mol dm^{-3} at the end of the titration. The titration mixture contained 0.0100 mol dm^{-3} of KCl.

The second acidity constant was determined by measuring the pL values of buffer solutions prepared of NaOH solution and the acid. The procedure was similar to that applied earlier.¹² The ionic strength of the buffers with different acid/anion ratios was regulated to 0.0100 mol dm^{-3} both in H_2O and D_2O . The value given by the fifty-fifty buffer was chosen to be used in further calculations. The deuterium oxide correction for the glass electrode was that presented earlier.¹² The measurements were carried out on a digital pH-meter constructed in our laboratory using a combined glass silver-silver chloride electrode by Metrohm.

The solubilities were determined in sealed conical flasks kept in a thermostated water bath. The flasks were covered to prevent the possible decomposition of solutes by light. A Lauda thermostat was employed to control the temperature within 298.15 ± 0.10 K in all measurements (including those of the equilibrium constants). The contents of the flasks could be stirred with a magnetic stirrer. The time for equilibration was 10 days. The samples were taken through a glass wool layer by a pipette, transferred to weighing glasses, weighed and analyzed. The methods of analysis of the amounts of solutes were as follows. The total amount of acid and anhydride was obtained by potentiometric titration with a standard solution of NaOH. A sample of barium dimethylmaleate solution was evaporated and the residue weighed. The weighed samples of silver dimethylmaleate solutions were titrated potentiometrically using a standard NaI solution and silver and mercurous sulfate electrodes.

The activity corrections for the constants, i.e. for the acidity constants and the solubility products, were made by the Debye-Hückel extrapolation (7). In this equation the symbols

$$-\log y_{\pm} = \frac{z_+ z_- A I^{1/2}}{1 + (Ba) I^{1/2}} \quad (7)$$

have their usual definitions. Constant A has values of 0.5107 and 0.5140 in H₂O and D₂O, respectively. Ionic size parameter (Ba) has a value of 1.65 for the barium salt and 1.24 for the silver salt in both waters.¹³ The effect of the activity corrections was greatest on the solubility product of barium dimethylmaleate. In the other cases it could have been omitted. Where solely nonelectrolytes were handled, as in the calculations of dehydration constants, activity corrections were unnecessary.

RESULTS AND DISCUSSION

In the determination of the dehydration constants, K_d^L , the obtained first-order rate constants k_{exp} in H₂O and D₂O, respectively, are presented in Table 1. Applying the mean values in Table 1 the data were set to follow eqn. (5) by the aid of a program of least squares on a Wang 2200 computer. The obtained constants for eqn. (5) are reported in Table 2.

The apparent first acidity constants of dimethylmaleic acid in light and heavy water are collected in Table 3. The method of calculations was similar to that described earlier.¹⁰ The second acidity constants of the acid are presented in Table 4 and the measured solubility data in Table 5.

The constants determined in this work are in good agreement with those reported earlier. Koskikallio reports for K_d^H a value of 3.2 at 293 K and for pK_1^H that of 3.2 at 313 K.¹⁴ Ebersson gives the values 5.3 for K_d^H and 3.0 for pK_1^H at 293 K.⁹

When equilibria (1)–(3) take place in light and heavy water the following equations, considering the isotopic exchange and medium, *i.e.* the transfer effects, are obtained:¹⁵

$$\frac{K_d^H}{K_d^D} = \phi_1^3 F_d \quad (8)$$

$$\frac{K_1^H}{K_1^D} = \frac{K_1^H(\text{app})}{K_1^D(\text{app})} \frac{(1 + K_d^H)}{(1 + K_d^D)} = l^{-3} \phi_2^{-1} \phi_1^2 F_1 \quad (9)$$

$$\frac{K_2^H}{K_2^D} = l^{-3} \phi_2 F_2 \quad (10)$$

In the equations l is the isotopic fractionating factor for the L₂O⁺ ion, ϕ_1 and ϕ_2 are the fractionating factors for L₂A and LA⁻, respec-

Table 1. The observed first-order rate constants k_{exp} in H₂O and D₂O measured in various buffer solutions and at 298.15 K.

pL	H ₂ O $k_{\text{exp}}/(\text{ks})^{-1}$	D ₂ O $k_{\text{exp}}/(\text{ks})^{-1}$
	Buffer: LCl	
2.00	26.49(12) ^a	13.86(3) ^a
2.00	27.15(10)	13.93(4)
2.00	26.82(15)	13.65(4)
	26.82 ^b	13.81 ^b
	Buffer: Formic acid – formate	
3.00	17.54(4)	
3.00	17.49(6)	
3.00	17.34(6)	
	17.46 ^b	
3.30	12.68(6)	10.40(4)
3.30	12.75(4)	10.27(3)
3.30		10.37(4)
	12.71 ^b	10.35 ^b
3.50	10.53(4)	8.96(3)
3.50	10.26(4)	8.87(2)
3.50	10.45(3)	8.96(3)
	10.41 ^b	8.93 ^b
3.70	8.83(3)	7.60(1)
3.70	8.76(4)	7.64(3)
3.70	8.83(2)	
	8.81 ^b	7.62 ^b
3.90	7.29(5)	6.21(2)
3.90	7.57(4)	6.28(2)
3.90	7.78(3)	6.30(2)
	7.55 ^b	6.26 ^b
4.00	6.93(6)	5.58(2)
4.00	7.24(3)	5.58(2)
4.00	7.13(3)	5.59(2)
	7.10 ^b	5.58 ^b
4.10	6.69(2)	5.02(2)
4.10	6.74(5)	5.03(3)
4.10	6.64(2)	4.89(2)
	6.69 ^b	4.98 ^b
4.20	6.49(3)	4.52(2)
4.20	6.23(3)	4.57(2)
4.20	6.46(2)	4.44(2)
	6.37 ^b	4.53 ^b
	Buffer: Acetic acid – acetate	
5.20	5.17(3)	
5.20	5.14(1)	
5.20	5.23(1)	
	5.18 ^b	
5.80		2.13(1)
5.80		2.08(1)
5.80		2.14(1)
		2.12 ^b

^a Standard errors in parentheses. ^b Mean values.

tively. The transfer terms include the transfer effects according to the following scheme:

F_d contains the transfer of
(1) L₂A from H₂O to D₂O

Table 2. The parameters calculated from eqn. (5) in H₂O and D₂O at 298.15 K.

Parameter	H ₂ O	D ₂ O
k_{-1} , ks ⁻¹	5.043	2.098
$1/K_d^L$	0.2017(38)	0.1735(18)
K_1^L/K_d^L , mmol m ⁻³	[227.5(13)]	[40.81(58)]
$K_1^L K_2^L/K_d^L$, mmol ² m ⁻⁶	[-22.53(8367)]	[197.7(353)]
corr. coeff.	0.99994	0.9998
K_d^L	4.958	5.764

Table 3. The apparent first acidity constants of dimethylmaleic acid in H₂O and D₂O determined by potentiostatic titration at 298.15 K.

H ₂ O Z^a	I^b /mol m ⁻³	pK ₁ ^H (app)	D ₂ O Z^a	I^b /mol m ⁻³	pK ₁ ^D (app)
0.2518	10.94	4.071	0.1678	10.59	4.565
0.2821	10.99	4.051	0.1909	10.62	4.566
0.3157	11.03	4.057	0.2269	10.68	4.572
0.3171	11.03	4.053			
0.3651	11.10	4.075			
		[4.061(7)] ^c			[4.568(3)] ^c

^a Degree of deprotonation. ^b Average ionic strength. ^c Mean values with their standard errors.

Table 4. The second acidity constants of dimethylmaleic acid in H₂O and D₂O determined by buffer method at 298.15 K.

Buffer ratio ($c_{LA^-}/c_{A^{2-}}$)	pK ₂ ^H	pK ₂ ^D
0.250	6.036	6.636
0.500	6.010 ^a	6.606 ^a
0.750	6.010	6.617

^a Used in further calculations.

(2) anH from D₂O to H₂O

F_1 contains the transfer of

(1) L₂A from H₂O to D₂O

(2) LA⁻ from D₂O to H₂O

(3) L₃O⁺ from D₂O to H₂O

F_2 contains the transfer of

(1) LA⁻ from H₂O to D₂O

(2) A²⁻ from D₂O to H₂O

(3) L₃O⁺ from D₂O to H₂O

Assuming ideal conditions (this is justified, since the ionic strength lies in the magnitude of 0.01 mol dm⁻³ and since we are studying

differences) the F terms can be presented by eqns. (11)–(13) where c_H and c_D stand for concentrations in H₂O and D₂O, respectively. It must be noticed that the concentration ratios

$$F_d = (c_D/c_H)_{L_2A} (c_H/c_D)_{anH} \quad (11)$$

$$F_1 = (c_D/c_H)_{LA^-} (c_H/c_D)_{LA^-} (c_H/c_D)_{L_3O^+} \quad (12)$$

$$F_2 = (c_D/c_H)_{LA^-} (c_H/c_D)_{A^{2-}} (c_H/c_D)_{L_3O^+} \quad (13)$$

in equations (11)–(13) ought to be replaced by the corresponding (inverse) ratios of activity coefficients.¹⁵ Here the above presentation is, however, practical because of the ideality assumption. Another assumption made in this work is that the transfer effects have similar magnitudes despite the isomeric isotopic form of the molecule transferred. This assumption seems to be valid, since the transferred molecules are relatively large. The explanations for the validity of this assumption for the L₃O⁺ ion have been analyzed by Salomaa.³

The fractionating factors ϕ_1 and ϕ_2 can be eliminated from eqns. (8), (9), and (10) by simple operations to give eqn. (14). The product of the F terms, which gives the total transfer effect, can be presented with the aid of eqns.

Table 5. Solubilities of dimethylmaleic acid + anhydride, silver dimethylmaleate and barium dimethylmaleate in H₂O and D₂O at 298.15 K.

H ₂ O s/10 ⁻³ mol dm ⁻³	pK _s ^H	D ₂ O s/10 ⁻³ mol dm ⁻³	pK _s ^D
Acid + anhydride			
36.87		32.91	
36.93		32.86	
36.90 ^a		32.88 ^a	
Ag ₂ A			
1.758		1.492	
1.757		1.499	
1.758 ^a	7.6621	1.496 ^a	7.8731
	7.6717 ^b		7.8819 ^b
BaA			
36.26		24.00	
36.00		23.84	
36.19		24.00	
36.19 ^a	2.8828	23.95 ^a	3.2414
	3.8389 ^b		4.0856 ^b

^a Mean values. ^b Extrapolated to zero ionic strength.

$$\frac{K_1^H(\text{app})}{K_1^D(\text{app})} \times \frac{(1+K_d^H)}{(1+K_d^D)} \times \frac{K_2^H}{K_2^D} \times \frac{K_d^D}{K_d^H} = l^{-2} F_d^{-1} F_1 F_2 \quad (14)$$

(11)–(13). By performing cancellations and assuming that $(c_H/c_D)_{\text{L}_2\text{O}^+} = 1$, eqn. (15) is obtained. The main source for the transfer

$$F_d^{-1} F_1 F_2 = (c_D/c_H)_{\text{anh}} (c_H/c_D)_{\text{A}^{2-}} \quad (15)$$

effect would thus be the transfer of the anhydride from H₂O to D₂O and that of the dimethylmaleate ion from D₂O to H₂O.

Finally, the transfer effect (16) for the dianion, A²⁻, is obtained with the aid of eqns. (14) and (15).

$$(c_D/c_H)_{\text{A}^{2-}} = (c_D/c_H)_{\text{anh}} l^{-6} \times \left[\frac{K_1^H(\text{app})}{K_1^D(\text{app})} \frac{(1+K_d^H)}{(1+K_d^D)} \frac{K_2^H}{K_2^D} \frac{K_d^D}{K_d^H} \right]^{-1} \quad (16)$$

The Gibbs energies of transfers which were calculated with the aid of Tables 2, 3, 4, and 5 and eqn. (16) are reported in Table 6. It must be noticed that the value for $(c_D/c_H)_{\text{anh}}$ was calculated by the aid of the total acid–anhydride solubility, the respective dehydration, and the first acidity constants.

Qualitatively the standard Gibbs energies reported in Table 6 for individual ions confirm the earlier observations, *viz.* that univalent cations have transfer energies from light to heavy water which are slightly positive while

the energies for divalent cations are somewhat higher.^{5b} Anions have Gibbs energies which are generally higher than those for cations.^{5b} This agrees well with the fact that anions necessarily interact with isotopically different hydrogen atoms in H₂O and D₂O, while cations interact with similar oxygen atoms in both solvents. That the Gibbs energies of transfer of divalent cations are higher than those for monovalent cations may depend on their greater densities of charge, which force the water molecules to reorient in a higher degree than happens in the solutions of monovalent cations. The Gibbs energies of transfer for nonelectrolytes are either negative or positive depending on the polarity of their molecules or on the number of polar sites in their molecules.^{16,17} The magnitude of

Table 6. The standard Gibbs energies of transfer of some dimethylmaleic acid derivatives from H₂O to D₂O at 298.15 K.

Compound	$\Delta G_t^\circ/\text{J mol}^{-1}$
Anhydride	292
Dimethylmaleate ion (= A ²⁻)	975
Ag ₂ A	1200
BaA	1408
Ag ⁺	112
Ba ²⁺	433

the transfer free energy for the anhydride is reasonable considering the polar oxygen atoms in the anhydride molecule. The ΔG_t^θ values obtained here for Ag^+ and Ba^{2+} ions are lower than the values estimated earlier for these ions by applying inorganic salts and different assumptions. These earlier values range from 200 J mol^{-1} to 500 J mol^{-1} for the Ag^+ ion.¹⁸⁻²⁰ For the Ba^{2+} ion the value of 470 J mol^{-1} has been reported.²¹

The influence of the assumptions on the results is difficult to estimate. However, if the L_3O^+ ion would have a fixed transfer energy, it might be slightly positive. That would cause a certain increase in the value of the transfer energy of the A^{2-} ion. This brings about a decrease in the values of Gibbs energies of transfer for cations. This may be possible but hardly reliable. When thinking of the ideality assumption, we can only conclude that its influences are negligible compared to the experimental errors. This is because we are studying differences and both solvents greatly resemble each other.

There may be a systematic error in the obtained results that makes both cationic contributions a little lower than the earlier values. The standard errors which are evaluated on statistical basis range from 10 J mol^{-1} (Ag_2A) to 90 J mol^{-1} (Ba^{2+} ion). Of course, these experimental errors in this somewhat complicated procedure can be one reason for differences. The system itself is also different from that by which the earlier results have been determined. It can be thought that the differences rise from some specific details of this complicated inorganic-organic solute-solvent system. For instance, the calculation of the Gibbs energy of transfer for the anhydride is carried out on a generalized basis. In reality, the whole equilibrium (1) with the isotopic exchange reaction is transferred from light to heavy water. This may cause a certain unreliability in the estimated value of $(c_D/c_H)_{\text{anh}}$. It can hardly be assumed that the transfer effects of the acid and the anhydride would be of equal magnitude, because their structures differ distinctly. The exchange effect contributes a portion to this which is difficult to estimate. The relatively large activity corrections for the solubility product of BaA may be the cause to some extent of the unreliability of the obtained values. However,

making these corrections certainly increases the accuracy. Finally, it must be concluded that the procedure gives fairly good estimates of the ionic contributions of the Gibbs energy of transfer from light to heavy water.

It would be interesting to determine the Gibbs energies of transfer for alkali metal salts of dimethylmaleic acid, because the thermodynamics of transfer of alkali metal cations nowadays lies on a relatively firm basis. Great difficulties are encountered when choosing the method of determination, because the solubilities of the salts in question are too high for the saturated solutions to be assumed ideal.

REFERENCES

1. Parker, A. J. *Chem. Rev.* 69 (1969) 7.
2. Salomaa, P. and Aalto, V. *Acta Chem. Scand.* 20 (1966) 2035.
3. Salomaa, P. *Acta Chem. Scand.* 25 (1971) 365.
4. Salomaa, P., Vesala, A. and Vesala, S. *Acta Chem. Scand.* 23 (1969) 2107.
5. Albery, J. In Caldin, E. E. and Gold, V., Eds., *Proton Transfer Reactions*, Chapman and Hall, London 1975, Chapter 9; a. p. 279; b. p. 283.
6. Roser, W. *Ber. Dtsch. Chem. Ges.* 15 (1882) 1318.
7. Rach, C. *Justus Liebigs Ann. Chem.* 234 (1886) 44.
8. Parker, G. *Justus Liebigs Ann. Chem.* 267 (1892) 204.
9. Ebersson, L. *Acta Chem. Scand.* 18 (1964) 1276.
10. Kankare, J. J. *Anal. Chem.* 44 (1972) 2376.
11. Vesala, A. and Salomaa, E. *Acta Chem. Scand.* A 30 (1976) 277.
12. Salomaa, P., Schaleger, L. and Long, F. A. *J. Am. Chem. Soc.* 86 (1964) 1.
13. Kielland, J. *J. Am. Chem. Soc.* 59 (1937) 1675.
14. Koskikallio, J. *Suom. Kemistil. B* 29 (1956) 5.
15. Salomaa, P. *Acta Chem. Scand.* 23 (1969) 2095.
16. Vesala, A. *Acta Chem. Scand.* A 28 (1974) 839.
17. Vesala, A. and Kaikkonen, J. *Acta Chem. Scand.* A 30 (1976) 453.
18. Ramette, R. W. and Dratz, E. A. *J. Phys. Chem.* 67 (1963) 940.
19. Ramette, R. W. and Spencer, J. B. *J. Phys. Chem.* 67 (1963) 943.
20. Hein, F. and Bähr, G. *Z. Phys. Chem. Abt. B* 28 (1937) 270.
21. Kellomäki, A. *Ann. Acad. Sci. Fenn. Ser. A* 2 (1972) 40.

Received March 24, 1977.

The Crystal Structure of Sodium Cerium(III) Sulfate Hydrate, $\text{NaCe}(\text{SO}_4)_2 \cdot \text{H}_2\text{O}$

OVE LINDGREN

Department of Inorganic Chemistry, Chalmers University of Technology and the University of Göteborg, P.O. Box, S-402 20 Göteborg 5, Sweden

The crystal structure of $\text{NaCe}(\text{SO}_4)_2 \cdot \text{H}_2\text{O}$ has been determined from three-dimensional X-ray diffractometer data. The crystals are trigonal, space group $P\bar{3},21$, with $a = 7.0134(14)$ Å, $c = 12.920(3)$ Å and $Z = 3$. The positions of the non-hydrogen atoms were evaluated from Patterson and electron density maps. Full matrix least squares refinement based on 574 reflexions yielded a final R value of 0.047.

A three-dimensional network is formed by the linking of cerium atoms and sulfate groups. The voids that remain are occupied by sodium ions and water molecules.

Cerium is coordinated by nine oxygen atoms, one water molecule and eight sulfate oxygens.

The coordination polyhedron can be described as a pentagonal bipyramid with the axial bonds each consisting of two bonds to sulfate groups acting as bidentate ligands. The Ce—O bond distances are in the range 2.477—2.584 Å with the average 2.534 Å.

In order to study cerium(IV)—oxygen polyhedra a number of structures¹⁻⁵ of solid phases in the system CeO_2 — SO_3 — H_2O have been determined at this Institute. Attempts have also been made to prepare mixed Ce(III)—Ce(IV) sulfates and a structure determination of such a compound is in progress.⁶

In connection with the latter project a structure investigation of the title compound, *viz.* $\text{NaCe}(\text{SO}_4)_2 \cdot \text{H}_2\text{O}$, has been undertaken.

EXPERIMENTAL

Freshly precipitated $\text{Ce}(\text{OH})_3$ was dissolved in 0.5 M H_2SO_4 and mixed with an aqueous solution of Na_2SO_4 in approximate molar ratios 1:1. About 25 ml of the solution was transferred to a thickwalled glass tube. This was sealed and heated to 230 °C in an oven for a week. A

large number of microcrystals were obtained and in addition some transparent hexagonal prisms of suitable size for single crystal investigation. A Guinier recording showed the microcrystals to be part of the same solid phase.

A crystal of approximate dimensions $0.2 \times 0.2 \times 0.25$ mm was mounted along a on a Weissenberg camera and the zero, first and second layer-lines were recorded. Reflexions of the types h,k,l ; $k,h,-l$; $k,-h-k,l$; $h+k,-k,l$; $h+k,-h,-l$ and $h,-h-k,-l$ proved to have the same intensities implying that the crystal has trigonal symmetry. The only reflexions systematically absent were $00l$ for $l \neq 3n$. The space group is thus uniquely determined to be $P\bar{3},21$ (or its enantiomorph $P3_1,21$).

Cell constants were obtained from a Guinier diagram using monochromatized $\text{CuK}\alpha$ radiation and $\text{Pb}(\text{NO}_3)_2$ ($a = 7.8566$ Å at 21 °C)⁷ as an internal standard. A least squares refinement of 12 indexed lines (program: POWDER⁸) resulted in the following lattice parameters: $a = 7.0134(14)$ Å and $c = 12.920(3)$ Å. Assuming $Z = 3$ the calculated density $D_x = 3.378$ g cm⁻³.

The crystal chosen for the preliminary Weissenberg studies was transferred to a PAILRED single crystal diffractometer. Nine layers, $0kl-8kl$, were registered with graphite monochromatized $\text{MoK}\alpha$ radiation. 574 reflexions were retained when an observed/unobserved cutoff at $3.0 \sigma(I)$ was employed. The intensities were reduced to structure factors by application of Lorentz and polarisation factors but no absorption correction was made.

STRUCTURE DETERMINATION AND REFINEMENT

The coordinates of the cerium and sulfur atoms were deduced from the Patterson function. A Fourier synthesis phased from these atoms showed the positions of the other atoms. The structure was refined by the least squares

Table 1. Atomic coordinates and temperature factors for $\text{NaCe}(\text{SO}_4)_2 \cdot \text{H}_2\text{O}$. Estimated standard deviations are given in parentheses. The thermal parameters have been multiplied by 10^4 for Ce, Na and S and by 10^3 for O. The temperature factor is of the form $\exp[-2\pi^2(h^2a^{*2}U_{11} + \dots + klb^*c^*U_{23})]$.

	<i>x</i>	<i>y</i>	<i>z</i>	U_{11}	U_{22}	U_{33}	U_{12}	U_{13}	U_{23}
Ce	0	0.43323(16)	1/6	102(6)	139(13)	65(3)	139(0)	-10(10)	-21(0)
Na	0.4711(14)	0	1/3	266(38)	27(40)	210(34)	27(0)	17(34)	34(0)
S	0.5592(6)	0.5470(6)	0.2542(2)	131(15)	163(15)	79(9)	165(32)	-32(24)	-9(21)
O1	0.7566(16)	0.5909(17)	0.1926(8)	15(5)	12(5)	15(4)	6(8)	5(7)	-6(7)
O2	0.3827(22)	0.5049(21)	0.1819(8)	21(6)	27(7)	15(4)	22(11)	3(9)	1(9)
O3	0.4938(18)	0.3589(21)	0.3263(7)	16(5)	27(6)	12(4)	28(9)	-5(7)	-6(8)
O4	0.6111(16)	0.7406(16)	0.3194(7)	21(5)	13(4)	8(3)	16(8)	3(6)	7(7)
O5	0	0.0674(35)	1/6	39(17)	16(16)	97(20)	16(0)	-10(23)	-21(0)

program LALS.⁹ In the later cycles, anisotropic temperature factors were introduced. Weights were calculated according to the formula: $w = (30 + |F_o| + 0.003|F_o|^2)^{-1}$, which led to a reasonable agreement between w^{-1} and $(|F_o| - |F_c|)^2$ independent of $|F_o|$. The scattering factors for Ce, S, O and Na^+ were taken from Cromer and Waber.¹⁰ When the shifts were considerably less than the estimated standard deviations, the *R* value (conventional) had converged to 0.047. A difference Fourier map showed no significant peaks, except for some fluctuations in the vicinity of the heavy atoms. The final coordinates and anisotropic thermal

parameters are listed in Table 1. A listing of observed and calculated structure factors may be obtained from the author on request.

DESCRIPTION AND DISCUSSION

Coordination numbers (CN) from six to twelve have been established in lanthanoid compounds but nine and eight coordination appear most frequently. Previous studies of trivalent cerium sulfates^{11,12} show CN=9 and the preferred polyhedron seems to be a tri-capped trigonal prism, D_{3h} .

Table 2. Selected distances (Å) and angles (°) for $\text{NaCe}(\text{SO}_4)_2 \cdot \text{H}_2\text{O}$.

Ce-O1 (2 ×)	2.477(10)	O5-O1' (2 ×)	2.914(23)
O2 (2 ×)	2.479(13)	O2 (2 ×)	2.902(19)
O3 (2 ×)	2.584(10)	O4 (2 ×)	3.050(17)
O4 (2 ×)	2.578(9)		
O5	2.566(24)	O1-S-O2	107.9(6)
Average:	2.534	O1-S-O3	111.1(6)
Na-O1 (2 ×)	2.870(11)	O1-S-O4	109.7(6)
O2 (2 ×)	2.536(11)	O2-S-O3	111.6(7)
O3 (2 ×)	2.443(14)	O2-S-O4	110.2(7)
O4 (2 ×)	2.468(12)	O3-S-O4	106.4(6)
S-O1	1.490(11)	Five membered ring around cerium	
O2	1.458(13)	O1-Ce-O1	75.5(5)
O3	1.488(12)	O1-Ce-O2 (2 ×)	73.7(4)
O4	1.480(10)	O2-Ce-O5 (2 ×)	70.2(3)
Average:	1.479		
Deviations from the least squares plane (cf. Fig. 1)			
Ce	0.00	O2	0.21
O1	-0.33	O2'	-0.21
O1'	0.33	O5	0.00

In the present structure also, cerium is coordinated by nine oxygen atoms; eight of these are sulfate oxygen atoms and one a water molecule. Four oxygen atoms belonging to different sulfate groups and the water molecule form a puckered five member ring around cerium perpendicular to the c axis. Two oxygen atoms belonging to the same sulfate group are coordinated above this ring, with a further two from a second sulfate group coordinated below. The latter, axial oxygen atoms, are at approximately right angles to each other. Thus, in the equatorial bonds the

sulfate groups act as unidentate ligands and in the axial directions as bidentate ligands. The deviations from the least squares plane through the pentagon are found at the end of Table 2. The cerium atom was included in the calculation of the "best" plane. The coordination polyhedron with the atom-numbering system used in this report is shown in Fig. 1.

In the coordination sphere the nine Ce—O distances vary from 2.477 to 2.584 Å and the average value is 2.53 Å, in agreement with those found in $\text{Ce}_2(\text{SO}_4)_3 \cdot 9\text{H}_2\text{O}$:¹¹ 2.51 Å, in $\text{Na}_2\text{Ce}(\text{C}_2\text{H}_4\text{O}_4)_3 \cdot 9\text{H}_2\text{O}$:¹³ 2.52 Å and in $\text{Ce}_2(\text{C}_2\text{O}_4)_3$

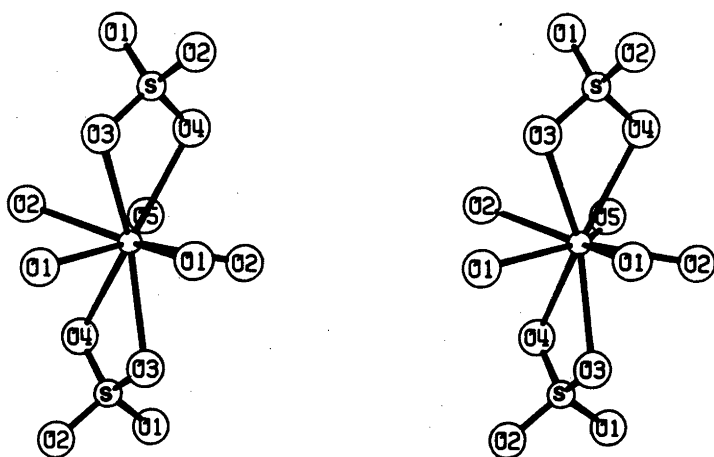


Fig. 1. A stereo view of the coordination polyhedron.

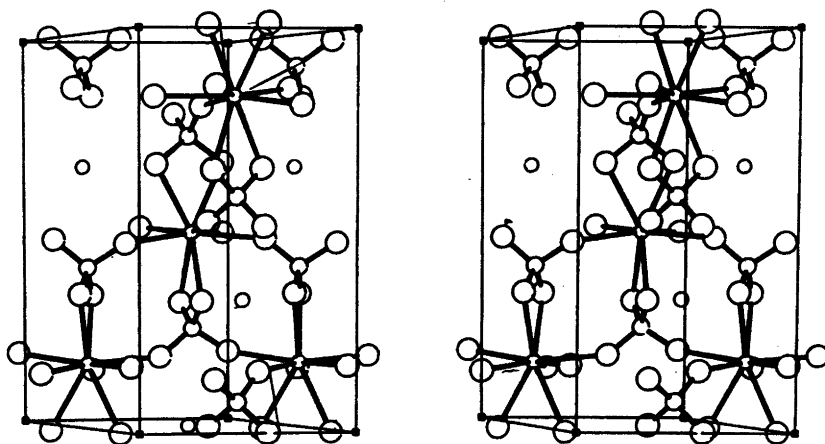


Fig. 2. A stereo drawing of the structure viewed approximately in the b -direction. The longest axis is the c axis.

$\cdot 10\text{H}_2\text{O}$:¹⁴ 2.55 Å. Selected distances and angles are given in Table 2.

The structure is built up by Ce atoms joined by sulfate groups forming a three-dimensional network. This can be described in the following way. The sulfur atom has its x and y parameters almost equal which causes the six sulfur atoms in a unit cell to appear in pairs and defining three axes perpendicular to the xy plane. On approximately the same axes, between the sulfate groups, Na and Ce atoms alternate in filling the vacancies. A remaining void in the structure is occupied by a water molecule which completes the nine-coordination of cerium. A stereo view of the structure is shown in Fig. 2.

Na is surrounded by six oxygen atoms in the range 2.443 Å–2.536 Å and another two at distances 2.870 Å. All eight oxygen atoms belong to sulfate groups. The coordination polyhedron does not permit a simple description.

The sulfate group is fairly regular, the angles being in the range 106.4–111.6°. However, the distance S–O₂ is short, only 1.458 Å, while the other S–O distances are in the range 1.480–1.490 Å. Admittedly shorter S–O distances (in sulfate groups) have been reported but then only for terminal bonds. A conceivable explanation is that in this structure all four oxygen atoms are involved in bonds to cerium. These bonds are strong and add further geometrical constraints to the tetrahedron, deforming it somewhat. It should be remembered, however, that the difference in the bond lengths is just at the limit of significance (about three times the e. s. d.). In spite of the distortion, the average S–O bond length, 1.479 Å, is close to the usual average value.

The water molecule, O5, has four short distances to the sulfate oxygens, two to each of O1 and O2. The two O1 atoms are neighbours in the five-membered ring around cerium, whereas O5 belongs to an adjacent ring.

Hydrogen bonds are probably directed away from the cerium atom, eliminating the O5–O2 interaction. Possible hydrogen bonds are thus two O5–O1, 2.914 Å, the O1–O5–O1 angle being 63°.

Acknowledgements. The author would like to thank Professor Georg Lundgren for encouraging and valuable discussions concerning

this work. Sincere thanks are also due to Dr. John Wood, who revised the English of this article.

This work has been financially supported by the Swedish Natural Science Research Council (Contract No. 2318).

REFERENCES

1. Lundgren, G. *Ark. Kemi* 6 (1953) 59.
2. Lundgren, G. *Ark. Kemi* 10 (1956) 183.
3. Lindgren, O. *Acta Crystallogr. B* 32 (1976) 3347.
4. Lindgren, O. *Acta Chem. Scand. A* 31 (1977) 163.
5. Lindgren, O. *Acta Chem. Scand. A* 31 (1977) 453.
6. Lindgren, O. *To be published.*
7. *International Tables for X-Ray Crystallography*, Kynoch Press, Birmingham 1959.
8. Lindqvist, O. and Wengelin, F. *Ark. Kemi* 28 (1967) 179.
9. The Program Library of the Dept. of Inorg. Chem., Göteborg.
10. Cromer, D. T. and Waber, J. T. *Acta Crystallogr.* 18 (1965) 104.
11. Dereigne, A. and Pannetier, G. *Bull. Soc. Chim. Fr.* (1968) 174.
12. Dereigne, A., Manoli, J.-M., Pannetier, G. and Herpin, P. *Bull. Soc. Fr. Minéral. Cristallogr.* 95 (1972) 269.
13. Elding, I. *Acta Chem. Scand. A* 30 (1976) 649.
14. Ollendorff, W. and Weigel, F. *Inorg. Nucl. Chem. Lett.* 5 (1969) 263.

Received March 21, 1977.

Semiempirical Calculations of Spin-spin Coupling Constants.

A Comparison of some Parametrizations

A. TARPØ, H. BILDSØE and K. SCHAUMBURG

Chemical Laboratory V, University of Copenhagen, The H. C. Ørsted Institute, 5 Universitetsparken, DK-2100 Copenhagen Ø, Denmark

The CNDO/2 and INDO semiempirical calculation schemes have been used to obtain correlation diagrams between experimental and calculated spin-spin coupling constants through one, two and three bonds in molecules at equilibrium geometries. The calculation scheme included a variable screening in the Slater atomic orbitals depending on electron populations. The CNDO, INDO parametrizations suggested by Boyd have been used to evaluate molecular orbitals and energies for calculation of spin-spin coupling constants.

Since the first semiempirical calculations of spin-spin coupling constants were published by Karplus and Anderson¹ and by McConnell² a large number of applications of the sum over states (SOS) method has been published. However, first the development of CNDO/2 and INDO by Pople *et al.*³ indicated that within modest computational requirements the calculations would provide sensible results.⁴ The results obtained by the SOS method were refined by inclusion of configuration interaction⁵ and by including spin-spin and spin-orbit contributions.⁴ Alternatively to this method Pople *et al.* later introduced the finite perturbation method.⁶ Also with this method acceptable predictions could be established, and it was for several types of spin-spin couplings found to be superior to the SOS method.

Simultaneous with the semiempirical calculations *ab initio* type of calculations were developed primarily for small systems.⁷ It was, however, found that the greatly improved wave functions did not produce equally better numerical results for the spin-spin coupling constants. In most calculations it has been

found that the dominating term is the Fermi contact term, in coupling calculations involving hydrogen it is the only one. In 1971 Jeu⁸ mentioned that the mathematical expression for the Fermi contact term is an approximation to the real relativistic equation and that it is only valid to first order in the theory of perturbation. Later Wooley⁹ presented a critical discussion of the same problem and concluded that "one cannot give a precise meaning to the idea of spin-spin coupling within a molecule". In view of the controversial state of interpretation and due to the significantly higher cost of *ab initio* calculations it therefore seems obvious that semiempirical calculations still will be valuable for some time.

In the non relativistic approximation used the Fermi contact term depends on the electron density at the site of the nucleus, $\langle \psi^2(0) \rangle$. This term has been handled in three different manners. The basis set used in CNDO/2 and INDO calculations of spin-spin coupling constants is Slater type orbitals, where the functions are evaluated to reproduce the experimental values for atomic energy levels in X-ray studies and atomic and ion radii.¹⁰ For this type the behaviour near the center position of the nucleus is known to be poor for the orbitals $2s$, $3s$ etc. So alternatively the integral, $\langle \psi^2(0) \rangle$ can be handled as a semiempirical parameter, the value of which depends only on the nature of the atom.⁸ The third approach is to use the mathematical expression for the integral and evaluate $\langle \psi^2(0) \rangle$ after an improvement of the basis set.¹¹ In this expression the exponential factor in the radial part

of the orbital appears. The exponential factor can be chosen as a fixed value, which only depends on the nature of the atom, or one can use a value, which depends both on the atom and the molecule. However, it has been found that the integral is rather sensitive to variation in the exponential factor.¹² When scaled, exponential factors are used in the calculation of the Fermi contact term, a logical extension would be to introduce a scaling of the atomic orbitals in the SCF scale itself and finally apply them in the calculation of the spin-spin coupling constants. This idea has been investigated as one of the parametrizations below.

It has been found by several authors¹³ that the spin-spin coupling constants calculated depend strongly on the molecular geometry used. To provide a consistent set of geometries Pople *et al.*³ have suggested use of standard bond lengths and angles. Alternatively calculations have been published¹¹ where experimental geometries were used. Both methods reflect the reluctance towards use of the minimal energy configuration that might be determined within the CNDO/2 and INDO method itself. This reflects the unrealistic geometries that in some papers have been found by energy minimization using the two methods.¹⁴

We found that conceptually it would be attractive if a semiempirical method would exist that allowed fairly good estimates of geometries and at the same time lead to acceptable values for spin-spin coupling constants.

In a number of papers^{15,16} Whitehead and coworkers have developed a modification of the CNDO and INDO methods with the aim of providing a route to more realistic estimates of geometries. One of the programs is described in Ref. 16a, in the thesis of Boyd^{16d} and some private communications. The method has been extensively applied for estimates of geometries and mechanistic reaction pathways by Snyder *et al.*¹⁷ as well as Boyd.^{16b,16c} From these papers it can be concluded that capability of estimating geometries is significantly improved. The energy minimized geometries are in general very close to the experimental data. In the present paper we have investigated how the CNDO/B¹⁸ and INDO/B¹⁸ methods are reflected in the calculation of spin-spin coupling constants.

THEORY AND CALCULATION

In the CNDO/2 and INDO calculations reported in the following section the parametrization is identical with the one given by Pople,³ Santry⁴ and Segal.^{14a}

In the two methods presented by Boyd¹⁶ the parametrizations differ substantially. The basis set is *s* and *p* Slater orbitals, but for hydrogen the exponent factor is 1.0, whereas 1.2 is used by Pople.

Overlap integrals are calculated explicitly.

The repulsion integrals, γ_{AB} , have been introduced according to the formula given by Ohno,¹⁶

$$\gamma_{AB} = \frac{1}{(R_{AB}^2 + \alpha^2)^2}, \text{ where } \alpha = \frac{2}{\gamma_{AA}^* + \gamma_{BB}^*}$$

the * means the atomic limit.^{15a}

The one center Coulomb integrals are determined as reported by Sichel and Whitehead^{15a} based on spectroscopic data previously given by Hinze and Jaffé.¹⁹

While the parametrization by Pople allows calculations involving third period atoms for CNDO/2 and involving hydrogen and second period for INDO, Boyd's parametrization of the CNDO approximation is rather sporadic, but that of the INDO is complete. Calculations using the two schemes were carried out until the energy minimization showed consistency better than 10^{-6} a.u.

It has previously been found that configuration interaction including the single excited states leads to improvement in the calculated spin-spin coupling constants.⁵ For the small molecules selected here it has been possible to perform this calculation.

The use of variable electron density at the site of the nucleus, $\langle \psi^2(0) \rangle$, was introduced as a scaling mechanism by Towl and Schaumburg.¹¹ This first order correction for unequal charge distribution did not require any modification of the SCF calculation. In the present case we have introduced a self-consistent electro-negativity type of scaling²⁰ but for all sorts of valence electrons, whereby the atomic orbitals in the basis set are scaled according to eqns. (2)–(4). The iterative scheme has been modified such that consistency for eqns. (2)–(4) was obtained as well as a minimum energy for that particular set of AO's.

For hydrogen:

$$\xi = 1.2(1.0 - 0.3(P_H - 1.0)) \quad (2)$$

For second period atoms:

$$\xi = (Z_A - 1.7 - 0.35(P_A - 1.0))/2 \quad (3)$$

For third period atoms:

$$\xi = (Z_A - 8.8 - 0.35(P_A - 1.0))/3 \quad (4)$$

Where ξ is the exponential factor in the radial part of Slater type orbitals, Z_A is the atomic number, and P_A is the electron population on the atom A.

It was not obvious to us what convergence properties such a calculation scheme would possess if any. Experimentally it was found that the iterative scheme would converge leading to exponential factor constant within 10^{-4} charge unit within 6–8 cycles.

The calculation of coupling constant was, irrespective of the choice of the preceding options, performed using the sum over states method (SOS) using the perturbing Hamiltonian given by Towl and Schaumburg¹¹ including spin-spin and spin-orbit contributions.

In the formula the electron densities at the site of the nuclei still appear as a factor. It is therefore possible to apply yet one alternative set of parameters, since Clementi and Raymond¹² have published a set of optimized values for the exponential factors based on *ab initio* calculations.

The possible parametrizations based on the options above are represented in Table 1.

To be able to compare the values of the spin-spin coupling constants calculated in the different manners all the calculations were carried out using the experimentally determined geometries of the molecules.

The programs used in the calculations were a symmetry adopted version of the program used by Towl and Schaumburg¹¹ and programs used by Boyd and Snyder.^{16,17} The calculations were carried out on an IBM 370/165.

RESULTS AND DISCUSSION

The molecules chosen for the present comparison have been selected according to three criteria. Firstly, the experimental geometry

Acta Chem. Scand. A 31 (1977) No. 7

Table 1. An inventory of the 24 calculation schemes used. FD means that the electron density only depends on the nature of the atom. VD means that the electron density both depends on the nature of the atom and on the molecule. DI means diagonal approximation, *i.e.* no configuration interaction.

	The approximation of CNDO				The approximation of INDO			
	Without CI		With CI		Without CI		With CI	
	Using FD	Using VD	Using FD	Using VD	Using FD	Using VD	Using FD	Using VD
With the parametrization of Pople	CNDO/2 with DI and FD	CNDO/2 with DI and VD	CNDO/2 with CI and FD	CNDO/2 with CI and VD	INDO with DI and FD	INDO with DI and VD	INDO with CI and FD	INDO with CI and VD
With the parametrization of Pople and scaling (V.O.)	CNDO/2 with V.O., DI and FD	CNDO/2 with V.O., DI and VD	CNDO/2 with V.O., CI and FD	CNDO/2 with V.O., CI and VD	INDO with V.O., DI and FD	INDO with V.O., DI and VD	INDO with V.O., CI and FD	INDO with V.O., CI and VD
With the parametrization of Boyd	CNDO/B with DI and FD	CNDO/B with DI and VD	CNDO/B with CI and FD	CNDO/B with CI and VD	INDO/B with DI and FD	INDO/B with DI and VD	INDO/B with CI and FD	INDO/B with CI and VD

Table 2. Calculated and experimental values for ${}^1K_{\text{AH}}$. All the values are to be multiplied by 10^{30} cm^{-3} .

	CNDO/2		CNDO/2 with V.O.		CNDO/B		INDO		INDO with V.O.		INDO/B		Exp. values for ${}^1K_{\text{AH}}$	Refs. to exp. for ${}^1K_{\text{AH}}$ geom.	
	DI	CI	DI	CI	DI	CI	DI	CI	DI	CI	DI	CI			
BH_4^-	13.84	16.31	12.93	14.97	24.12	29.26	13.94	17.86	13.03	16.37	23.38	34.76	20.95	44	25
VD	10.80	12.73	10.00	11.58	19.53	23.69	11.05	14.15	10.27	12.90	18.49	27.50			
CH_4	22.71	26.48	22.68	26.45	32.30	38.65	22.61	29.71	22.64	29.76	32.05	50.36	41.41	46	26
VD	23.31	27.19	23.28	27.15	32.69	39.01	23.50	30.88	23.52	30.92	32.04	50.34			
CH_3F	25.89	31.24	26.07	31.72		B	26.39	35.10	26.70	35.97	41.12	62.21	49.40	49	31
VD	28.67	34.59	28.81	35.05			29.80	39.64	30.06	40.49	48.97	74.07			
$\text{H}_2\text{C}=\text{CH}_2$	27.96	35.74	27.88	35.65	39.36	51.71	27.88	38.54	27.90	38.56	40.58	64.47	51.75	59	40
VD	28.97	37.02	28.88	36.93	40.98	53.83	28.80	39.81	28.82	39.84	42.31	67.22			
$\text{H}_2\text{C}=\text{C}=\text{CH}_2$	27.32	37.02	27.34	37.03	42.31	58.50	27.37	39.99	27.41	39.99	42.51	69.30	55.72	62	42
VD	28.04	38.01	28.08	38.03	43.43	60.04	28.12	41.08	28.16	41.08	43.59	71.07			
NH_3^+	32.93	37.64	33.11	38.56	43.31	49.21	32.40	42.90	32.70	44.17	39.30	59.96	60.80	47	27
VD	42.43	48.49	42.79	49.84	51.54	58.57	42.05	55.67	42.53	57.45	49.29	75.20			
CH_2F_2	30.84	37.95	31.12	39.01		B	32.73	42.94	33.19	44.73	59.65	83.92	61.12	49	34
VD	36.59	45.03	36.75	46.06			39.72	52.12	40.04	53.95	81.13	114.13			
$\text{H}_2\text{C}=\text{N}=\text{N}$	36.74	46.49	36.90	46.35	57.96	60.32	37.79	49.80	37.92	49.61	56.99	63.64	(±)64.64	55	35
VD	36.34	45.98	36.61	45.98	63.61	66.19	37.18	49.00	37.44	48.98	56.74	63.36			
CHF_3	39.38	47.47	39.65	49.25		B	43.71	55.53	44.51	58.39	107.44	135.00	79.21	49	32
VD	49.69	60.16	49.74	61.77			56.39	71.65	57.08	74.88	163.98	206.04			
$\text{HC}\equiv\text{CH}$	49.18	60.37	48.72	60.00	72.27	91.36	49.53	63.05	49.15	62.77	75.64	102.16	82.49	59	41
VD	52.58	64.54	52.05	64.09	80.25	101.45	52.67	67.06	52.23	66.70	84.01	113.46			
RMS	3.64	3.40	3.19	2.65	5.70	6.52	3.91	2.25	3.46	1.47	6.66	6.78		I	
Error	4.61	2.43	4.56	2.67	4.27	4.35	4.39	3.55	4.37	4.10	4.32	5.71			
RMS	4.32	4.56	3.86	3.50		B	3.47	2.52	2.98	1.34	8.91	8.70		II	
Error	3.87	2.05	3.82	2.25			4.28	3.49	4.36	4.21	10.76	10.71			

Explanations of symbols used in Tables 1-8. A. The value of this spin-spin coupling constant is not calculated because it cannot be derived in a meaningful way with method DI. B. The value is not calculated because of the sporadic parametrization of CNDO/B. ^a This coupling is a *cis* coupling. ^b This coupling is a *trans* coupling. ^c This coupling is transmitted via a nitrogen atom. ^d This coupling constant is ${}^2K_{\text{HH}}$ in pyridazine, where the hydrogens are in *ortho* and *meta* positions to the nearest nitrogen. ^e This coupling constant is ${}^2K_{\text{HH}}$ in pyridazine, where the hydrogens are in *meta* and *para* positions to the nitrogens. ^f This coupling constant is of the type ${}^2K_{\text{NH}}$. ^g This coupling constant is of the type ${}^2K_{\text{FH}}$. ^h This coupling is ${}^2K_{\text{HH}}$ between the hydrogens in positions 2 and 3. ⁱ This coupling is ${}^2K_{\text{HH}}$ between the hydrogens in positions 3 and 4. ^j The RMS errors are calculated on the basis of the coupling constants which can be calculated in all the CNDO/B methods. ^k The RMS errors are calculated on the basis of the coupling constants which can be calculated in all methods but the CNDO/B methods. ^l As I, but only for methods using CI. ^m As II, but only for methods using CI.

When a sign of a coupling constant is not established experimentally, then a sign is chosen, which to a lesser degree alters the correlation between calculated and experimentally determined spin-spin coupling constants.

should be accurately known, since the calculated values for the coupling constants are depending on the geometries and since these variations for the different calculation schemes are not well known. Secondly, the experimental data for the spin-spin coupling constants should be well determined in magnitude as well as sign. Thirdly, a wide variety of compounds with regard to elements and chemical bonding should be covered in order to make the evaluation as general as possible. In order to bring the data on a common scale it has been chosen to report the reduced spin-spin coupling constants $K_{AB} = 4\pi^2 \cdot J_{AB}/(h\gamma_A\gamma_B)$ as has become usual in recent papers (K_{AB} in cm^{-3} and J_{AB} in Hz). γ is the gyromagnetic ratio.

The large number of K_{AB} that have been calculated will not be treated as one group, but separated into classes according to criteria given below:

The importance of mechanism. It can be expected that coupling between two protons only involving Fermi contact term might display a type of correlation between experimental and calculated values different from what is found in the case of coupling between two second period atoms.

The importance of basis set. It can be expected that this will influence the coupling between protons and second period atoms in a way different from two protons. For inter proton coupling it has been found by Kowalewski²² that the size of the basis set is very important for the obtained numerical results. Furthermore it can be seen²² that an increase in basis set does not influence inter proton coupling over different numbers of valence bonds equally. It would therefore be likely that semiempirical calculations would only show an acceptable correlation to experiments if the data are further subdivided into classes ${}^nK_{AB}$ depending on n .

${}^1K_{AH}$. In Table 2 and Fig. 1 results obtained for ${}^1K_{AH}$, $A \neq H$ are reported. For all the methods investigated good correlations can be established between the calculated and experimental values.

When the strong dependence on ξ is taken into account, it is surprising to observe that only minor changes are introduced by the variable orbital exponent modification, V.O.

The values obtained by the Boyd methods are considerably larger, but the correlation

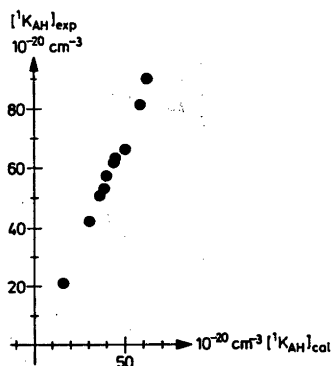


Fig. 1. One of the correlations between calculated and experimentally determined spin-spin coupling constants is shown for the type of coupling ${}^1K_{AH}$. The calculation scheme used is: INDO with V.O., CI and FD.

has not improved. The best result was obtained using the INDO method with V.O., CI and FD leading to the formula:

$${}^1K_{AH} = 1.32({}^1K_{AH})_{\text{calc}} + 1.21 \times 10^{20} \text{ cm}^{-3}$$

$$\text{RMS error: } 1.3 \times 10^{20} \text{ cm}^{-3}$$

${}^1K_{AB}$. In Table 3 and Fig. 2 data for the ${}^1K_{AB}$, $A, B \neq H$, coupling are reported. The range spanned by the experimental data is from $(-195.95 \text{ to } 183.57)10^{20} \text{ cm}^{-3}$. The Boyd parametrization of the CNDO approximation has not been completed for fluorine interaction with other atoms, and here the column is omitted. Since charge distribution in, e.g., CF_4

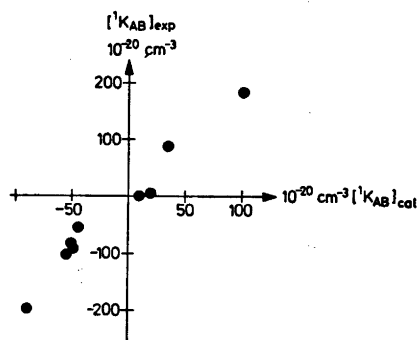


Fig. 2. One of the correlations between calculated and experimentally determined spin-spin coupling constants is shown for the type of coupling ${}^1K_{AB}$. The calculation scheme used is: INDO with V.O., CI and VD.

Table 3. Calculated and experimental values for ${}^1K_{AB}$. All the values are to be multiplied by 10^{20} cm^{-3} .

	CNDO/2		CNDO/2 with V.O.		INDO		INDO with V.O.		INDO/B		Exp. values for ${}^1K_{BB}$	Refs. to exp. for ${}^1K_{BB}$ geom.
	DI	CI	DI	CI	DI	CI	DI	CI	DI	CI		
NF ₃	FD -54.27	-59.19	-51.96	-55.89	-72.16	-80.50	-66.12	-73.65	-167.79	-171.11	-195.95	54 33
	VD -64.42	-70.68	-61.49	-66.60	-87.03	-97.46	-79.36	-88.81	-217.79	-222.24		
CHF ₃	FD -14.86	-22.72	-18.54	-26.04	-33.32	-36.68	-37.93	-41.56	-107.12	-100.04		
	VD -18.68	-28.79	-23.01	-32.48	-44.50	-49.02	-49.36	-54.13	-161.78	-150.99	-96.55	49 32
CF ₄	FD -2.64	-12.81	-9.05	-19.52	-19.95	-25.65	-27.65	-35.41	-57.16	-52.65		
	VD -3.13	-16.96	-11.62	-25.51	-28.14	-36.27	-37.85	-48.60	-95.75	-88.02	-91.23	49 29
CH ₂ F ₂	FD -20.75	-26.62	-22.62	-33.09	-38.30	-39.69	-40.04	-41.74	-103.88	-95.68		
	VD -24.57	-31.65	-26.22	-38.07	-47.58	-49.36	-48.95	-51.11	-138.33	-127.37	-82.64	49 34
CH ₃ F	FD -19.77	-25.70	-19.94	-26.18	-36.16	-37.85	-37.44	-38.51	-88.56	-80.79		
	VD -21.98	-28.54	-23.15	-29.01	-41.54	-43.48	-42.79	-44.02	-100.67	-91.89	-55.44	49 31
BF ₃	FD 19.17	17.85	14.65	13.31	11.88	13.75	6.22	7.58	5.11	10.71	1.32	48 28
	VD 24.73	23.07	18.52	16.88	16.33	18.89	8.43	10.24	9.17	18.79		
BF ₃	FD 32.56	29.95	23.71	20.66	23.06	24.93	12.38	13.25	14.41	21.53	4.14	50 30
	VD 45.48	41.94	32.48	28.44	33.58	36.34	17.75	19.03	26.10	38.80		
H ₂ C=CH ₂	FD 29.27	30.01	29.70	30.45	27.59	33.09	27.48	32.99	-8.32	12.99	89.06	52 40
	VD 30.94	31.72	31.41	32.19	29.86	35.79	29.75	35.68	-7.68	13.38		
HC≡CH	FD 96.17	98.20	98.00	100.10	91.18	98.47	92.71	99.99	59.44	85.68	183.57	52 41
	VD 97.46	99.54	99.45	101.60	93.07	100.55	94.76	102.24	56.15	81.32		
RMS	FD 30.94	28.02	27.22	25.54	26.60	23.34	24.39	20.71	42.93	35.65		
Error	VD 34.35	30.42	26.84	24.35	28.86	26.25	23.09	20.04	46.04	41.72		

Table 4. Calculated and experimental values for ${}^2K_{\text{HH}}$. All the values are to be multiplied by 10^{20} cm^{-3} . For explanation of A, I, II, III and IV see below Table 2.

		INDO with V.O.		INDO/B		Exp. values for ${}^2K_{\text{HH}}$	Refs. to exp. for ${}^2K_{\text{HH}}$	geom.
		DI	CI	DI	CI			
CH_4	FD		-0.13		-1.38	-1.033	45	26
	VD	A	-0.12	A	-1.53			
NH_4^+	FD		-0.16		-1.46	-0.922	47	27
	VD	A	-0.25	A	-2.59			
BH_4^-	FD		0.024		1.25	-0.871	44	25
	VD	A	0.016	A	0.84			
CH_3F	FD		0.35		1.27	-0.800	51	31
	VD	A	0.34	A	1.27			
H_2O	FD	0.27	-0.19	0.72	-0.50	-0.600	57	37
	VD	0.35	-0.26	1.14	-0.80			
$\text{H}_2\text{C}=\text{CF}_2$	FD	0.43	0.43	0.85	0.58	(+) 0.400	56	36
	VD	0.48	0.48	1.09	0.74			
$\text{H}_2\text{C}=\text{CH}_2$	FD	0.74	0.83	2.42	2.33	0.192	52	40
	VD	0.74	0.82	2.67	2.58			
HCONH_2	FD	0.93	1.20	1.60	0.97	0.192	63	43
	VD	1.17	1.51	2.39	1.46			
$\text{H}_2\text{C}=\overset{+}{\text{N}}=\overset{-}{\text{N}}$	FD	0.96	1.11	2.20	2.05	+ 0.380	55	35
	VD	1.02	1.19	2.76	2.57			
RMS	FD	0.054	0.013	0.126	0.114		I	
Error	VD	0.107	0.028	0.057	0.077			
RMS	FD	0.084	0.131	0.151	0.175		II	
Error	VD	0.172	0.172	0.088	0.139			
RMS	FD		0.169		0.314		III	
Error	VD	A	0.188	A	0.281			
RMS	FD		0.199		0.361		IV	
Error	VD	A	0.226	A	0.323			

is significantly different from neutrality some effect of the V.O. method is observed, but still it remains smaller than the effect of CI. How-

ever, both are small compared to the changes from the CNDO/2 and INDO to the INDO/B method. The best method is again INDO with V.O. and CI but VD:

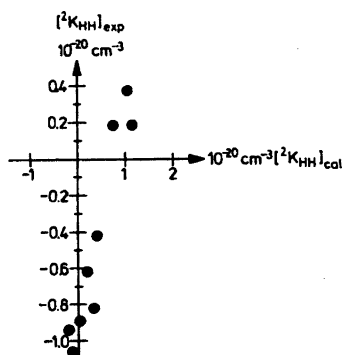


Fig. 3. One of the correlations between calculated and experimentally determined spin-spin coupling constants is shown for the type of coupling ${}^2K_{\text{HH}}$. The calculations scheme used is: INDO with V.O., CI and FD.

$${}^1K_{\text{AB}} = 1.85({}^1K_{\text{AB}})_{\text{calc}} - 2.47 \times 10^{20} \text{ cm}^{-3}$$

RMS error: $20.0 \times 10^{20} \text{ cm}^{-3}$

${}^2K_{\text{HH}}$. Table 4 and Fig. 3 reproduce the data observed for geminal proton coupling, ${}^2K_{\text{HH}}$. They have in many previous calculations been found most difficult to calculate. The present results do not differ from previous results in this respect. It is possible to establish a reasonable correlation but again the Pople parametrization is superior to the method of Boyd. Again the best result is obtained using INDO with V.O., CI and FD:

$${}^2K_{\text{HH}} = 0.92({}^2K_{\text{HH}})_{\text{calc}} - 0.78 \times 10^{20} \text{ cm}^{-3}$$

RMS error: $0.2 \times 10^{20} \text{ cm}^{-3}$

Table 5. In this table it is shown that not all properties are calculated in a meaningful way, when the calculation scheme includes the DI method (without CI). The results quoted below for models I, II and III, see Fig. 4, are obtained using the CNDO/2 method without CI and with FD.

Energy in unit of a.u.						
Model	Total-	Electronic-		Bonding		
I } II } III }	-10.11369014	-19.629820		-1.39377553		
Valence electronic population of atom						
Model	C	H				
I } II } III }	4.04933	0.98767				
Spin-spin coupling constants in Hz						
Model	J_{CH_1}	J_{CH_2}	J_{CH_3}	J_{CH_4}		
I } II } III }	68.5522	68.5522	68.5522	68.5522		
Model	$J_{\text{H}_1\text{H}_2}$	$J_{\text{H}_1\text{H}_3}$	$J_{\text{H}_1\text{H}_4}$	$J_{\text{H}_2\text{H}_3}$	$J_{\text{H}_2\text{H}_4}$	$J_{\text{H}_3\text{H}_4}$
I	1.5255	1.7824	1.2592	-1.2350	0.7088	0.7677
II	0.4415	0.4006	1.4865	0.4612	1.3111	0.1246
III	1.6659	2.5196	1.2740	0.3221	0.2025	1.3370

Table 6. Calculated and experimental values for ${}^3K_{\text{HH}}$. All values are to be multiplied by 10^{20} cm^{-3} . For explanation of I, II, a, b, c, d, e, h and i see below Table 2.

		INDO with V.O.		INDO/B		Exp. values for ${}^3K_{\text{HH}}$	Refs. to exp. for ${}^3K_{\text{HH}}$	geom.
		DI	CI	DI	CI			
<i>cis</i>	FD	0.15	0.19	0.67	0.55	+0.167 (-)	56	36
FHC=CHF	VD	0.15	0.20	0.62	0.59			
HCONH ₂ , a	FD	0.19	0.29	-0.73	-0.35	0.175	63	43
	VD	0.19	0.30	-0.86	-0.41			
Pyrrole h	FD	0.14	0.15	0.005	-0.088	0.225	58	39
	VD	0.14	0.14	0.005	-0.088			
Pyrrole i	FD	0.14	0.35	-0.27	-0.17	0.279	58	39
	VD	0.13	0.34	-0.30	-0.19			
Pyridazine d	FD	0.41	0.65	-0.074	0.044	0.421	55	38
	VD	0.39	0.62	-0.079	0.047			
Pyridazine e	FD	0.56	0.83	0.012	0.31	0.685	55	38
	VD	0.55	0.81	0.013	0.34			
HC≡CH	FD	0.91	1.03	4.29	4.92	0.816	52	41
	VD	1.00	1.13	5.48	6.29			
H ₂ C=CH ₂ , a	FD	0.78	1.01	0.47	0.69	0.958	52	40
	VD	0.78	1.00	0.51	0.77			
HCONH ₂ , b	FD	1.55	2.57	4.29	5.89	1.158	63	43
	VD	1.64	2.71	5.13	7.05			
H ₂ C=CH ₂ , b	FD	2.14	2.73	4.88	6.52	1.591	52	40
	VD	2.13	2.71	5.38	7.20			
RMS	FD	0.101	0.112	0.274	0.247		I	
Error	VD	0.105	0.107	0.295	0.269			
RMS	FD	0.108	0.153	0.265	0.242		II	
Error	VD	0.115	0.163	0.279	0.258			

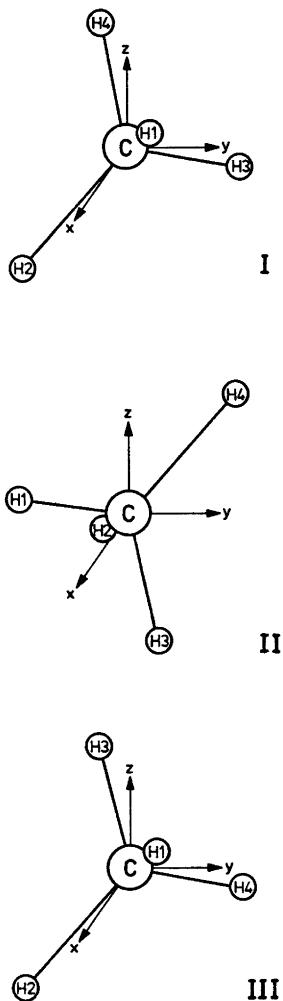


Fig. 4. This figure shows a methane molecule placed in three different manners in a coordinate system ($a = 0.63164 \text{ \AA}$). For each of the three sets of coordinates calculations are performed using the method CNDO/2 without CI but with FD. The results are shown in Table 5.

Model I: The coordinates are for C: (0,0,0); H1: (a, a, a); H2: ($a, -a, -a$); H3: ($-a, a, -a$); H4: ($-a, -a, a$).

Model II: The coordinates are for C: (0,0,0); H1: ($a, -a, a$); H2: ($-a, -a, -a$); H3: ($a, a, -a$); H4: ($-a, a, a$).

Model III: The coordinates are for C: (0,0,0); H1: (a, a, a); H2: ($a, -a, -a$); H3: ($-a, -a, a$); H4: ($-a, a, -a$).

Acta Chem. Scand. A 31 (1977) No. 7

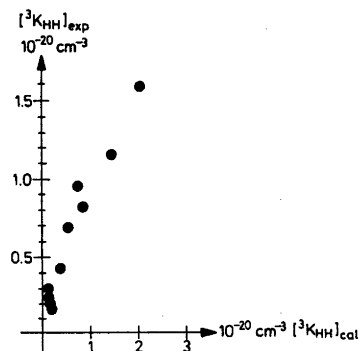


Fig. 5. One of the correlations between calculated and experimentally determined spin-spin coupling constants is shown for the ${}^3K_{HH}$ type of coupling. The calculation scheme used is: INDO without CI and with FD.

In this case the results obtained without CI are not reported in the table. This is due to the fundamental defect in the CNDO and INDO methods in handling degenerate orbitals. This was first pointed out by Ditchfield and Murrell²³ and later mentioned by Pouzard *et al.*²⁴

In calculations reported by Murrell the degenerate molecular orbitals were chosen in such a way that all triplet excited states arising from a degenerate configuration had the same energy.²³ This procedure seems somewhat arbitrary since these energies are not invariant under coordinate transformations.

In Table 5 and Fig. 4 data for CH_4 in three different coordinate systems are quoted.

No problem is encountered in calculations employing CI since the resulting wavefunctions for the triplet excited states are projected into the irreducible species of the molecular point group.

${}^3K_{HH}$. Most geometrical considerations have been focused on ${}^3K_{HH}$. In Table 6 and Fig. 5 the results obtained for vicinal coupling constants are reported. For this coupling the Boyd methods show definitely poor performance, since the RMS error is two times bigger than the ones found in the Pople parametrization. The best correlation was found for the INDO. The correlation is slightly better in the case without CI than with CI, but the difference is insignificant. The calculated relationship is given as (in the method INDO without CI and with FD):

Table 7. Calculated and experimental values for ${}^2K_{AH}$. All the values are to be multiplied by 10^{20} cm^{-3} . For explanation of I, II, *f* and *g* see below Table 2.

		INDO with V.O.		INDO/B		Exp. values for ${}^2K_{AH}$	Refs. to exp. for	
		DI	CI	DI	CI		${}^2K_{AH}$	geom.
$\text{H}_2\text{C}=\text{CH}_2$	FD	0.61	-0.41	2.66	-0.24	-0.80	60	40
	VD	0.63	-0.42	2.78	-0.25			
Pyrrole <i>f</i>	FD	1.30	2.07	5.51	6.31	+ (-) 3.72	58	39
	VD	1.32	2.10	5.64	6.46			
CH_3F	FD	0.77	0.20	1.09	0.91	4.12	53	31
	VD	0.75	0.20	1.04	0.87			
CH_2F_2	FD	0.59	0.41	2.13	2.31	4.46	53	34
	VD	0.57	0.40	1.96	2.13			
<i>cis</i>	FD	0.24	0.55	1.48	2.33	6.43	56	36
HFC=CFH <i>g</i>	VD	0.24	0.55	1.49	2.34			
CHF_3	FD	1.36	1.24	8.12	8.77	6.99	53	32
	VD	1.31	1.20	7.38	7.97			
Pyridazine	FD	6.33	10.45	8.34	12.54	9.90	55	38
	<i>f</i> VD	6.26	10.34	8.61	12.95			
HCONH_2 <i>f</i>	FD	5.19	7.97	23.38	25.13	11.90	63	43
	VD	4.75	7.30	20.28	21.80			
$\text{HC}\equiv\text{CH}$	FD	2.42	2.31	9.95	8.66	16.33	60	41
	VD	2.58	2.46	11.05	9.62			
RMS	FD	5.57	5.87	1.20	4.23	I		
Error	VD	5.47	5.82	0.69	3.93			
RMS	FD	3.83	3.99	3.66	3.60	II		
Error	VD	3.79	3.98	3.37	3.34			

Table 8. Calculated and experimental values for ${}^3K_{AH}$. All values are to be multiplied by 10^{20} cm^{-3} . For explanation of I, II, *a*, *b*, *c* and *f* see below Table 2.

		INDO with V.O.		INDO/B		Exp. values for ${}^3K_{AH}$	Refs. to exp. for	
		DI	CI	DI	CI		${}^3K_{AH}$	geom.
$\text{H}_2\text{C}=\text{CF}_2$ <i>a</i>	FD	0.80	0.70	1.16	-0.33	0.06	56	36
	VD	0.83	0.74	1.26	-0.35			
$\text{H}_2\text{C}=\text{N}=\text{N}$	FD	0.02	0.14	-0.42	0.09	+ (-) 0.90	55	35
	VD	0.02	0.15	-0.46	0.10			
Pyridazine	FD	-0.70	-0.36	-0.53	-1.04	0.92	55	38
	<i>f</i> VD	-0.70	-0.36	-0.56	-1.09			
<i>cis</i>	FD	2.08	2.10	4.45	5.54	1.81	56	36
HFC=CFH	VD	2.09	2.11	4.47	5.58			
$\text{H}_2\text{C}=\text{CF}_2$ <i>b</i>	FD	2.21	2.48	6.02	7.61	3.00	56	36
	VD	2.31	2.59	6.53	8.26			
Pyridazine	FD	0.42	0.35	0.14	-0.54	3.04	55	38
	<i>c, f</i> VD	0.42	0.34	0.14	-0.56			
Pyrrole <i>f</i>	FD	4.52	6.37	5.93	8.37	+ (-) 4.43	58	39
	VD	4.61	6.48	6.12	8.63			
RMS	FD	0.69	0.79	0.75	0.89	I		
Error	VD	0.69	0.79	0.75	0.89			
RMS	FD	0.93	0.90	1.07	0.99	II		
Error	VD	0.93	0.90	1.07	0.99			

$${}^3K_{\text{HH}} = 0.69({}^3K_{\text{HH}})_{\text{cal}} + 0.16 \times 10^{20} \text{ cm}^{-3}$$

$$\text{RMS error: } 0.1 \times 10^{20} \text{ cm}^{-3}$$

${}^2K_{\text{AH}}, {}^3K_{\text{AH}}$. Recently considerable interest has been given to K_{AH} with $A = {}^{13}\text{C}, {}^{15}\text{N}, {}^{31}\text{P}$ etc. In Table 7 data are given for ${}^2K_{\text{AH}}$ and in Table 8 for ${}^3K_{\text{AH}}$. The Boyd parametrization again reduces the number of data available in CNDO/B. Also for these two types of coupling constants is it possible to obtain a reasonable correlation, but the RMS errors are not acceptable.

In the test molecules a number of ${}^4K_{\text{HH}}$ coupling constants are available, but the correlations obtainable are not sufficiently accurate to warrant any predictions.

CONCLUSION

Based on a selected set of molecules it seems unlikely that the parametrization introduced by Boyd, Sichel and Whitehead will serve as an attractive alternative to CNDO/2 and INDO calculations with conventional parametrization. The use of the concept of variable orbital exponents can be incorporated in an iterative scheme with stable convergence behaviour. The result obtained is not substantially different from the standard calculation but a marginal improvement is found when the correlation of experimental and calculated results are considered. In all cases but one the CI improves the correlations. For systems having n fold symmetry axis, $n > 3$, it is necessary to introduce a procedure that yields symmetry adapted excited states in order to obtain well defined results.

Acknowledgements. The authors express their gratitude for computational facilities at their disposal at NEUCC (Northern Europe University Computing Center), Copenhagen.

REFERENCES

- Karplus, M. and Anderson, D. H. *J. Chem. Phys.* 30 (1954) 6.
- McConnell, H. M. *J. Chem. Phys.* 24 (1956) 460.
- Pople, J. A. and Beveridge, D. L. *Approximate Molecular Orbital Theory*, McGraw-Hill, New York 1970.
- Pople, J. A. and Santry, D. P. *Mol. Phys.* 8 (1964) 1.
- a. Armour, E. A. G. and Stone, A. J. *Proc. R. Soc. London Ser. A* 302 (1967) 25; b. Ditchfield, R. *Mol. Phys.* 17 (1969) 33.
- a. Pople, J. A., McIver, J. W., Jr. and Ostlund, N. S. *J. Chem. Phys.* 49 (1968) 2960; b. Pople, J. A., McIver, J. W., Jr. and Ostlund, N. S. *J. Chem. Phys.* 49 (1968) 2965.
- Kowalewski, J., Roos, B., Siegbahn, P. and Vestin, R. *Chem. Phys.* 3 (1974) 70, and references therein.
- de Jeu, W. H. *Mol. Phys.* 20 (1971) 573.
- Wooley, R. G. *Mol. Phys.* 30 (1975) 649.
- Hirschfelder, J. O. and Wahl, A. C. In Löwdin, P. O., Ed., *Quantum Theory of Atoms, Molecules and the Solid State*, Academic, London, New York 1966, p. 217.
- Towl, A. D. C. and Schaumburg, K. *Mol. Phys.* 22 (1971) 49.
- Barbier, C. and Berthier, G. *Theor. Chim. Acta* 14 (1969) 71.
- a. Kowalewski, J., Roos, B., Siegbahn, P. and Vestin, R. *Chem. Phys.* 9 (1975) 29; b. Murrell, J. N., Turpin, M. A. and Ditchfield, R. *Mol. Phys.* 18 (1970) 271.
- a. Segal, G. A. *J. Chem. Phys.* 47 (1967) 1876; b. Groppen, O. and Seip, H. M. *Chem. Phys. Lett.* 11 (1971) 445.
- a. Sichel, J. M. and Whitehead, M. A. *Theor. Chim. Acta* 7 (1967) 32; b. Sichel, J. M. and Whitehead, M. A. *Theor. Chim. Acta* 11 (1968) 220; c. Sichel, J. M. and Whitehead, M. A. *Theor. Chim. Acta* 11 (1968) 239; d. Sichel, J. M. and Whitehead, M. A. *Theor. Chim. Acta* 11 (1968) 254; e. Sichel, J. M. and Whitehead, M. A. *Theor. Chim. Acta* 11 (1968) 263.
- a. Boyd, R. J. and Whitehead, M. A. *J. Chem. Soc. Dalton Trans.* (1972) 73; b. Boyd, R. J. and Whitehead, M. A. *J. Chem. Soc. Dalton Trans.* (1972) 78; c. Boyd, R. J. and Whitehead, M. A. *J. Chem. Soc. Dalton Trans.* (1972) 81; d. Boyd, R. J. *Diss. Abstr. Int. B* 32 (1972) 3875.
- a. Snyder, J. P. *Tetrahedron Lett.* (1972) 2451; b. Snyder, J. P., Boyd, R. J. and Whitehead, M. A. *Tetrahedron Lett.* (1972) 4347.
- Ohno, K. *Theor. Chim. Acta* 2 (1964) 219.
- a. Hinze, J. and Jaffé, H. H. *J. Am. Chem. Soc.* 84 (1962) 540; b. Hinze, J. and Jaffé, H. H. *J. Phys. Chem.* 67 (1963) 1501.
- Brown, R. D. and Heffernan, M. L. *Trans. Faraday Soc.* 54 (1958) 757.
- Clementi, E. and Raimondi, D. L. *J. Chem. Phys.* 38 (1963) 2686.
- Kowalewski, J. *Chem. Commun. Univ. Stockholm* 14 (1974).
- Ditchfield, R. and Murrell, J. N. *Mol. Phys.* 14 (1968) 481.
- Pouzard, G., Rajzmann, M., Bodot, H. and Pujol, L. *Org. Magn. Reson.* 5 (1973) 209.

25. Ford, P. T. and Richards, R. E. *Discuss. Faraday Soc.* 19 (1955) 230.
26. Herranz, J. and Stoicheff, B. P. *J. Mol. Spectrosc.* 10 (1963) 448.
27. Ibers, J. A. and Stevenson, D. P. *J. Chem. Phys.* 28 (1958) 929.
28. Pendred, D. and Richards, R. E. *Trans. Faraday Soc.* 51 (1955) 468.
29. Thornton, C. *Diss. Abstr.* 14 (1954) 604.
30. Nielsen, A. H. *J. Chem. Phys.* 22 (1954) 659.
31. Andersen, F. A., Bak, B. and Brodersen, S. *J. Chem. Phys.* 24 (1956) 989.
32. Gordy, W. *J. Chem. Phys.* 20 (1952) 605.
33. Schomaker, V. and Lu, C. S. *J. Am. Chem. Soc.* 72 (1950) 1182.
34. Hirota, E., Tanaka, T., Sakahibara, K., Ohashi, Y. and Morino, Y. *J. Mol. Spectrosc.* 34 (1970) 222.
35. Sheridan, J. *Advances in Molecular Spectroscopy*, Pergamon, London 1962, p. 139.
36. Laurie, V. W. and Pence, D. T. *J. Chem. Phys.* 38 (1963) 2693.
37. Benedict, W. S., Gailar, N. and Plyler, E. K. *J. Chem. Phys.* 24 (1956) 1139.
38. Innes, K. K. and Lacos, R. M. *J. Mol. Spectrosc.* 24 (1967) 247.
39. Nygaard, L., Nielsen, J. T., Kirchheiner, J., Maltesen, G., Rastrup-Andersen, J. and Sørensen, G. O. *J. Mol. Struct.* 3 (1969) 491.
40. Kuchitsu, K. *J. Chem. Phys.* 49 (1968) 4456.
41. Lafferty, W. J., Plyhn, E. K. and Tidwell, E. D. *J. Chem. Phys.* 37 (1968) 1981.
42. Maki, A. G. and Toth, R. A. *J. Mol. Spectrosc.* 17 (1965) 136.
43. Hirota, E. *J. Mol. Spectrosc.* 49 (1974) 251.
44. Pedersen, J., Schaumburg, K. and Tarpø A. *Unpublished works.*
45. Meinzer, R. A. *Thesis*, University of Illinois, Chicago 1965.
46. Muller, N. and Pritchard, D. E. *J. Chem. Phys.* 31 (1959) 768.
47. McFarlane, W. and Dean, R. R. *J. Chem. Soc. A* (1968) 1535.
48. Chambers, R. P., Clark, H. C., Reevers, L. W. and Willis, C. J. *Can. J. Chem.* 39 (1961) 258.
49. Frankis, S. G. *J. Phys. Chem.* 67 (1963) 752.
50. Coyle, T. D. and Stone, F. G. A. *J. Chem. Phys.* 32 (1960) 1892.
51. Kaplan, F. K. and Roberts, J. D. *J. Am. Chem. Soc.* 83 (1961) 4666.
52. Graham, D. M. and Holloway, C. E. *Can. J. Chem.* 41 (1963) 2114.
53. Muller, N. and Carr, D. T. *J. Phys. Chem.* 67 (1963) 112.
54. Muettterties, E. L. and Phillips, W. D. *J. Am. Chem. Soc.* 81 (1959) 1084.
55. Jacobsen, J. P., Schaumburg, K. and Nielsen, J. T. *J. Magn. Reson.* 13 (1974) 372.
56. Flynn, G. W., Matsushima, M., Balde-schwieler, J. D. and Craig, N. C. *J. Chem. Phys.* 38 (1963) 2295.
57. Holmes, J. R., Kivelson, D. and Drinkard, W. C. *J. Chem. Phys.* 37 (1962) 150.
58. Rahkamaa, E. *Mol. Phys.* 19 (1970) 727.
59. Lynden-Bell, R. M. and Sheppard, N. *Proc. R. Soc. London Ser. A* 269 (1962) 385.
60. Barbier, C. and Berthier, G. *Theor. Chim. Acta* 14 (1969) 71.
61. Whipple, E. B., Goldstein, J. H. and Ste-ward, W. E. *J. Am. Chem. Soc.* 81 (1959) 4761.
62. Goldstein, J. H. and Reddy, G. S. *J. Chem. Phys.* 36 (1962) 2644.
63. Chunk, R. J., Gillies, D. G. and Randall, E. W. *Mol. Phys.* 16 (1969) 121.

Received March 9, 1977.

Short Communications

Refinement of the Acetamide Hemihydrobromide Crystal Structure at -160°C

P. GROTH

Department of Chemistry, University of Oslo, Oslo 3, Norway

The crystal structure of acetamide hemihydrobromide, $(\text{CH}_3\text{CONH}_2)_2 \cdot \text{HBr}$, was determined (at room temperature) in 1969 by film methods.¹ However, the accuracy of that investigation was relatively poor, and in particular the hydrogen atoms could not be localized. With the main purpose of trying to establish whether the short intermolecular $\text{O}\cdots\text{O}'$ hydrogen bond is symmetrical or not, a redetermination has been carried out at -160°C .

The crystals belong to the monoclinic system with space group $P2_1/n$, cell dimensions $a = 6.443(2) \text{ \AA}$, $b = 8.632(3) \text{ \AA}$, $c = 7.979(3) \text{ \AA}$, $\beta = 112.40(3)^{\circ}$, and $Z = 2$ ($D_m = 1.59 \text{ g cm}^{-3}$, $D_x = 1.61 \text{ g cm}^{-3}$).

With $2\theta_{\text{max}} = 50^{\circ}$ and $\text{MoK}\alpha$ -radiation 1584 independent reflections were measured on an automatic four circle diffractometer at -160°C . Using an observed-unobserved cutoff at $2.5\sigma(I)$, 1165 reflections were recorded as observed. The crystal size was $(0.2 \times 0.2 \times 0.15) \text{ mm}^3$ and no absorption corrections were applied ($\mu = 52.5 \text{ cm}^{-1}$).

The structure was solved by the heavy atom method and refined by full-matrix least-squares technique.^{2*} Hydrogen atom positions were

* All programs used (except for ORTEP) are included in this reference.

localized in a difference Fourier map. Anisotropic temperature factors were introduced for the non-hydrogen atoms and weights in least-squares were calculated from the standard deviations in intensities, $\sigma(I)$, taken as

$$\sigma(I) = [C_T + (0.02 C_N)^2]^{\frac{1}{2}}$$

where C_T is the total number of counts and C_N the net count.

The hydrogen atom HO, being localized at a position close to that of Table 1, was refined with multiplicity factor 0.5. No shifts towards the centre of inversion (to give a more symmetric hydrogen bond) occurred. When forcing it closer to the centre of symmetry and refining, the B -value increased rapidly.

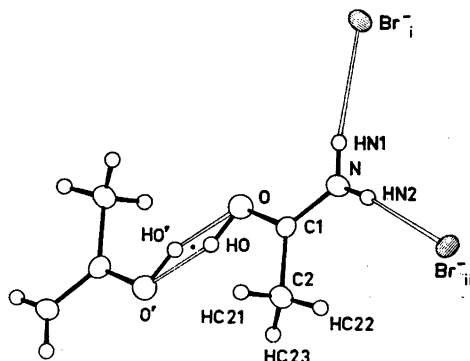


Fig. 1. Schematic drawing showing the numbering of atoms. The atoms labelled HO and HO' correspond to 'half' hydrogen atoms.

Table 1. Final fractional coordinates and thermal parameters with estimated standard deviations. The expression for anisotropic vibration is $\exp[-2\pi^2(h^2a^{*2}U_{11} + \dots + 2klb^*c^*U_{23})]$.

ATOM	X	Y	Z	U11	U22	U33	U12	U13	U23
Br-	.00000	.00000	.00000	.0167(2)	.0177(2)	.0211(2)	.0032(2)	.0031(1)	-.0027(2)
O	.15649(42)	.00581(29)	.52625(35)	.0176(11)	.0231(12)	.0277(13)	-.0011(10)	.0029(10)	.0014(10)
N	.51908(49)	-.13548(35)	.67936(42)	.0187(13)	.0184(13)	.0246(14)	-.0002(10)	.0057(11)	.0033(11)
C1	.34592(54)	.04414(39)	.63842(47)	.0185(14)	.0173(13)	.0205(15)	.0010(11)	.0081(12)	-.0012(11)
C2	.37232(62)	-.11047(43)	.72921(55)	.0210(15)	.0200(16)	.0303(18)	-.0014(13)	.0110(14)	.0031(14)
ATOM	X	Y	Z	B	ATOM	X	Y	Z	B
HO	.064(17)	.005(11)	.520(14)	2.5(21)	HN1	.593(9)	.229(6)	.639(7)	3.3(12)
HN2	.644(8)	-.189(6)	.752(7)	2.6(11)	MC21	.310(8)	-.193(5)	.648(7)	2.0(11)
HC22	.521(8)	-.135(5)	.794(6)	1.2(9)	MC23	.286(8)	-.100(6)	.002(6)	3.4(11)

Table 2. Bond distances and angles with estimated standard deviations. i: $\frac{1}{2} + x$, $\frac{1}{2} + y$, $\frac{1}{2} + z$. ii: $1 + x$, y , $1 + z$. Values from the earlier investigation are also included.

Distance	(Å)	(Å)	Distance	(Å)	(Å)
O - C1	1.264(4)	1.27(9)	N - C1	1.307(4)	1.35(11)
C1 - C2	1.497(5)	1.56(12)	N...Br ⁻ _{ii}	3.388(3)	3.41(8)
N...Br ⁻ _i	3.439(3)	3.41(8)	O...O'	2.438(5)	2.48
O - HO	0.93(8)		N - HN1	0.86(5)	
N - HN2	0.83(5)		C2 - HC21	0.94(5)	
C2 - HC22	0.92(4)		C2 - HC23	0.95(5)	
HO...O'	1.55(9)		HN1...Br ⁻ _i	2.59(5)	
HN2...Br ⁻ _{ii}	2.57(5)				
Angle	(°)	(°)	Angle	(°)	(°)
O - C1 - N	119.7(3)	117(1)	O - C1 - C2	121.3(3)	123(1)
N - C1 - C2	119.0(3)	118(1)	C1 - N...Br ⁻ _{ii}	115.6(2)	114(1)
C1 - N...Br ⁻ _i	123.8(2)	114(1)	C1 - O...O'	116.0(2)	113(1)
C1 - O - HO	103(7)		C1 - N - HN1	120(3)	
C1 - N - HN2	122(4)		HN1 - N - HN2	118(3)	
C1 - C2 - HC21	114(3)		C1 - C2 - HC22	112(3)	
C1 - C2 - HC23	103(3)		HC21 - C2 - HC22	107(4)	
HC21 - C2 - HC23	107(4)		HC22 - C2 - HC23	114(4)	
O - HO...O'	159(11)		N - HN1...Br ⁻ _i	172(5)	
N - HN2...Br ⁻ _{ii}	171(5)				

The form factors used were those of Doyle *et al.*³ except for hydrogen.⁴ The final *R*-value was 4.5 % (*R*_w = 4.9 %) for 1165 observed reflections.

Final fractional coordinates and thermal parameters are listed in Table 1. From the thermal parameters of this table the principal axes of the thermal vibration ellipsoids for the non-hydrogen atoms were calculated. Maximum r.m.s. amplitudes range from 0.145 to 0.185 Å (corresponding *B*-values are 1.65 and 2.70 Å²). Bond distances and angles with

estimated standard deviations (calculated from the correlation matrix of the final least-squares refinement cycle) are given in Table 2. Fig. 1 is a schematic drawing showing the numbering of atoms, and the stereoscopic illustration of Fig. 2 indicates the hydrogen bonding system.

The refining scheme for HO mentioned above strongly suggests that the O...O' hydrogen bond of length 2.438(5) Å is in fact asymmetric. However, the uncertainty in the proton position is large, and the degree of asymmetry is not significantly larger than that of a corre-

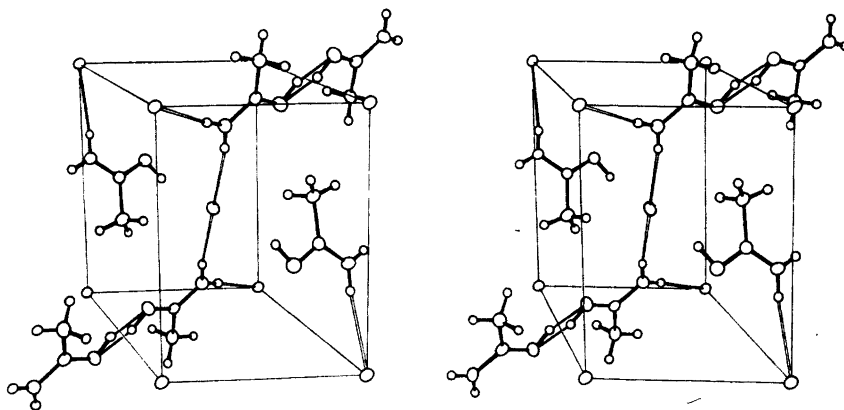


Fig. 2. Stereoscopic illustration showing the hydrogen bonding system [Johnson, C. K. ORTEP ORNL-3794, Oak Ridge National Laboratory, Oak Ridge 1965]. *a*-axis is across, *b*-axis down the page.

spondingly short intramolecular hydrogen bond in the enol form of 5,6-diacetyl-2,9-dimethyl-4,7-decanedione,⁵ where $O \cdots O' = 2.439(1)$ Å, $O-HO = 1.08(2)$ Å, and $HO \cdots O = 1.42(2)$ Å.

Bond distances and angles of the acetamide molecule in the present structure may be compared with those of a recent low temperature crystal structure redetermination of the separate molecule.⁶ The $C1-N$ bond of the present compound ($1.307(4)$ Å) is somewhat shorter than that of acetamide itself ($1.330(1)$ Å), and the angle $C2-C1-N$ is more open ($119.0(3)^\circ$; $116.8(1)^\circ$). As to be expected, the $C1-O$ bond is elongated ($1.264(4)$ Å; $1.247(1)$ Å). No other geometrical parameters show significant differences. The four non-hydrogen atoms are coplanar to within 0.008 Å.

The two $N \cdots Br^-$ distances of length $3.388(3)$ Å and $3.439(3)$ Å are normal for hydrobromides of this type,⁷ and the $N-HN \cdots Br^-$ bonds are, within error limits, linear.

1. Wiemann, J., Gillier-Pandrau, M., Thoai, N. and Beauté, C. *Bull. Soc. Chim. Fr.* (1969) 2147.
2. Groth, P. *Acta Chem. Scand.* 27 (1973) 1837.
3. Doyle, P. A. and Turner, P. S. *Acta Crystallogr. A* 24 (1968) 392.
4. Stewart, R. F., Davidson, E. R. and Simpson, W. T. *J. Chem. Phys.* 43 (1965) 3175.
5. Groth, P. and Semmingsen, D. *Acta Chem. Scand. B* 30 (1976) 737.
6. Ottersen, T., Hope, H. and Almlöf, J. *To be published.*
7. Ernst, S. R. and Cagle, Jr., F. W. *Acta Crystallogr. B* 29 (1973) 1543.

Received June 20, 1977.

On the Properties of a Tricenter Iron(II)dicobalt(III) Coordination Compound

SVEN BAGGER

Chemistry Department A, The Technical University of Denmark, Building 207, DK-2800 Lyngby, Denmark

In a previous study¹ a novel tricenter compound, $K_2\{[Co(L-his)_2]_2Fe(CN)_6\} \cdot nH_2O$ ($n=0-10$), was isolated. It was synthesized in aqueous solution from bis(histidinato)cobalt(II) and hexacyanoiron(III).

The available evidence¹ from IR and ¹³C NMR data indicates a structure as shown in Fig. 1. Two carboxylate groups are uncoordinated and the three metal centers are connected through cyano bridges.

For a more complete structural characterization an X-ray structure determination is desirable.

Several attempts by use of standard techniques² have been made to grow large crystals for this purpose. However, the crystals tend to grow in sheet-like colonies of parallel thin needles and it has not been possible to obtain a satisfactory single crystal.

The ion $[(L-his)_2Co.NC.Fe(CN)_6.CN.Co(L-his)_2]^{2-}$ formally has the metal ion sequence Co(III), Fe(II), Co(III) and is abbreviated $[III,II,III]^{2-}$ in the following.

The possible existence of the corresponding oxidation states $[III,III,III]^{1-}$, $[II,II,III]^{3-}$, and $[II,II,II]^{4-}$ has been investigated.

For this purpose a spectro-electrochemical thin-layer cell with an optically transparent electrode^{3,4} was applied. A micromesh gold net operates as the working electrode in a three-electrode voltammetric circuit. The cell allows controlled potential electrolysis experiments to be performed in the sample compartment of a Cary 11 spectrophotometer with simultaneous recording of absorption spectra.

When an aqueous solution of $[III,II,III]^{2-}$ is oxidized at potentials between 750 and 950 mV (*vs.* N.H.E.) spectrum b in Fig. 2 is obtained. A subsequent reduction at -50 mV

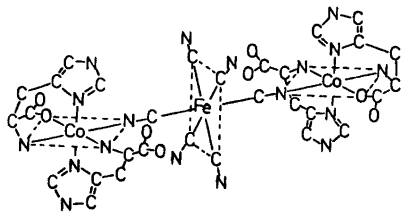


Fig. 1. Hypothetical structure of the iron-dicobalt complex based upon the available evidence. (Hydrogen atoms omitted.)

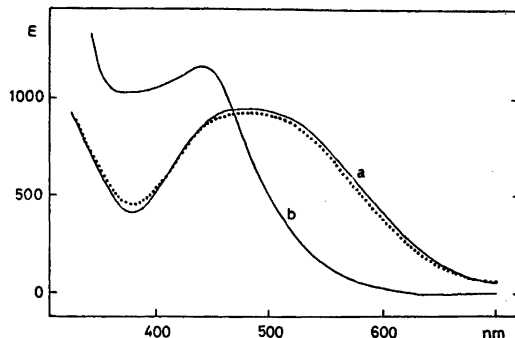


Fig. 2. a. Spectrum of $[III,II,III]^{2-}$; original (full drawn) and regenerated (dotted). b. Spectrum of oxidized $[III,II,III]^{2-}$. The concentration is 10^{-3} M in aqueous 0.5 M sodium perchlorate. $t=25.0^\circ C$. Path length 0.019 cm. ϵ is given in $dm^3 mol^{-1} cm^{-1}$.

(*vs.* N.H.E.) regenerates the spectrum of $[III,II,III]^{2-}$. An analysis of the current *vs.* time curves shows that one-electron reactions take place. The spectrum b of $[III,III,III]^{1-}$ is stable at least for several minutes, which means that this oxidation state is relatively robust.

After reduction of $[III,II,III]^{2-}$ it is not possible to regenerate the original spectrum by oxidation. This is in accordance with the expected lability of $[II,II,III]^{3-}$ and $[II,II,II]^{4-}$. Rapid dissociation takes place after their formation.

A potentiometric semimicro titration with cerium(IV) of an air-dried sample of $K_2\{[Co(L-his)_2]_2Fe(CN)_6\} \cdot nH_2O$ in acid solution yielded an equivalent weight of 1182 (average of 1178, 1166, 1177, and 1207). This corresponds to $n=10$. It has been observed that the crystals can lose and take up water of crystallisation without deteriorating.

1. Bagger, S. and Gibson, K. *Acta Chem. Scand.* 27 (1973) 3227.
2. Stout, G. H. and Jensen, L. H. *X-Ray Structure Determination*, The Macmillan Company, London 1968, Chapter 4.
3. Murray, R. W., Heineman, W. R. and O'Dom, G. W. *Anal. Chem.* 39 (1967) 1666.
4. Glauser, R., Hauser, U., Herren, F., Ludi, A., Roder, P., Schmidt, E., Siegenthaler, H. and Wenk, F. *J. Am. Chem. Soc.* 95 (1973) 8457.

Received June 27, 1977.

Jahn-Teller Distortions in the Structure of Manganese(III) Selenite Trihydrate, $\text{Mn}_2(\text{SeO}_3)_3 \cdot 3\text{H}_2\text{O}$

MARKUS KOSKENLINNA and JUSSI VALKONEN

Department of Chemistry, Helsinki University of Technology, Otaniemi, SF-02150 Espoo 15, Finland

The crystal structure of manganese(III) selenite trihydrate, $\text{Mn}_2(\text{SeO}_3)_3 \cdot 3\text{H}_2\text{O}$, has been determined by X-ray methods. The compound is monoclinic, and belongs to the space group $P2_1/c$ (No. 14) with $Z=4$. The crystal axes are $a=7.751(3)$ Å, $b=10.330(4)$ Å and $c=13.429(7)$ Å and the angle $\beta=92.74(3)^\circ$. The structure was solved by direct methods and refined to $R=0.043$.

The three non-equivalent manganese atoms are octahedrally coordinated, and the coordination polyhedra exhibit Jahn-Teller distortions. All the octahedra are tetragonally elongated, and two of the three non-equivalent octahedra have an additional small axial distortion in the equatorial plane. Each selenium atom bridges three different MnO_6 -octahedra, linking them into a three-dimensional network. The bonding scheme of the selenium is pyramidal and the bond lengths and angles are within the normal ranges.

In our earlier studies on divalent manganese selenites we described the relatively small and irregular distortions of the MnO_6 -octahedra within the compounds $\text{MnSeO}_3 \cdot \text{D}_2\text{O}$ and $\text{MnSeO}_3 \cdot 2\text{H}_2\text{O}$.^{1,2} In divalent manganese ion the d -electron density is spherically distributed and does not contribute to the possible distortions of the coordination polyhedra. As a result, the MnO_6 octahedron may be quite regular in some compounds as in MnSe_2O_8 , where the differences in bond lengths are statistically insignificant.³ In this respect divalent manganese greatly differs from trivalent manganese, which is expected to exhibit distortions of the Jahn-Teller type in octahedral coordination owing to its high-spin d^4 -configuration.

In the light of these studies it was considered interesting to see the effect of Jahn-Teller forces on the structure of manganese selenites.

We therefore sought to prepare crystals of the selenite compounds of trivalent manganese. In this communication we describe the preparation and crystal structure of manganese(III) selenite trihydrate, $\text{Mn}_2(\text{SeO}_3)_3 \cdot 3\text{H}_2\text{O}$.

EXPERIMENTAL

The compound was crystallized from a suspension of freshly precipitated hydrated manganese dioxide and concentrated selenous acid. 1.0 mol/dm³ selenous acid was added upon the manganese dioxide in the molar ratio 4:1 and the suspension was placed in a steel reactor with Teflon lining. The temperature was maintained at 100–140 °C for 2–4 days. Under these conditions, well-developed, lustrous, dark-brown prisms of $\text{Mn}_2(\text{SeO}_3)_3 \cdot 3\text{H}_2\text{O}$ were grown. In the preparations, reagents of analytical grade were used.

The X-ray intensity data were recorded on a Syntex $P2_1$ (fortran-version) automatic diffractometer with graphite monochromatized $\text{MoK}\alpha$ -radiation. Reflections with 2θ values between 5 and 60° were recorded using the $\theta-2\theta$ scan technique and a scan speed of 1°/min. The unit cell was determined by measuring the positional parameters of 17 independent reflections with the diffractometer and the cell dimensions refined by the method of least-squares. The unit cell was monoclinic with dimensions $a=7.751(3)$ Å, $b=10.330(4)$ Å, $c=13.429(7)$ Å and $\beta=92.74(3)^\circ$. The systematic absences in the original intensity data indicated the space group $P2_1/c$ (No. 14). There were four formula units in the unit cell. The calculated and measured (flotation) densities were 3.37 and 3.4 g cm⁻³, respectively. With the criterion $I > 4\sigma(I)$ a total of 1839 independent reflections were obtained and used in the subsequent calculations. Lorentz and polarization corrections were applied and the empirical absorption correction ($\mu=123.9$ cm⁻¹) was made on the basis of the ϕ -scan data.

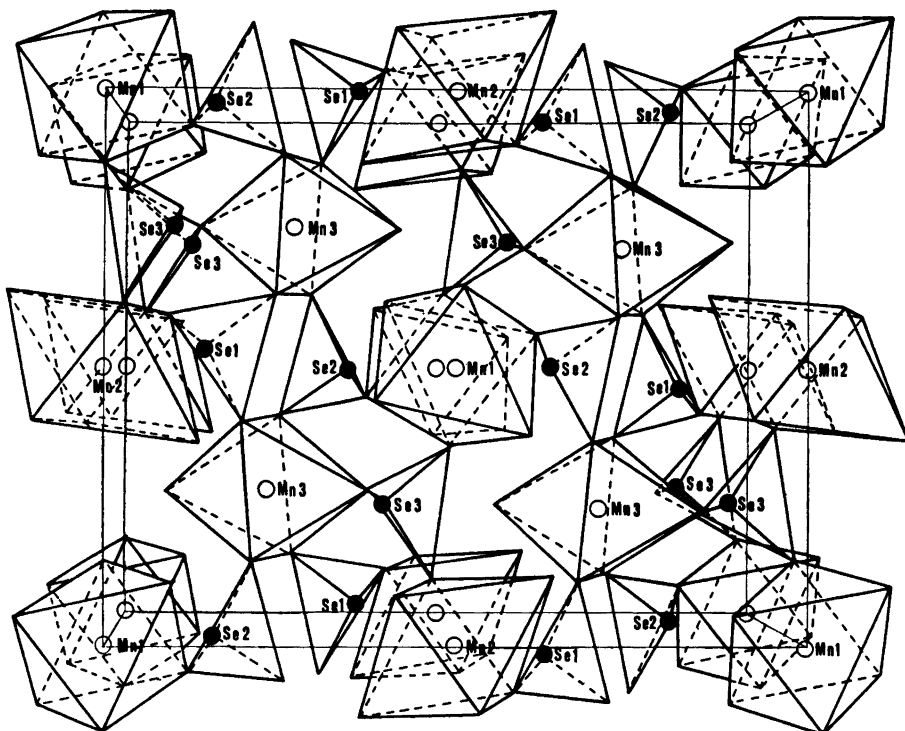


Fig. 1. Perspective view of the unit cell packing of $Mn_3(SeO_3)_3 \cdot 3H_2O$ along the b -axis.

Table 1. Final positional and thermal parameters with their estimated standard deviations in parentheses. The anisotropic parameters are multiplied by 10^4 ; they are of the form: $\exp[-2\pi^2(h^2a^{*2}U_{11} + k^2b^{*2}U_{22} + l^2c^{*2}U_{33} + 2hka^*b^*U_{12} + 2hla^*c^*U_{13} + 2klb^*c^*U_{23})]$.

Atom	x	y	z	U_{11}	U_{22}	U_{33}	U_{12}	U_{13}	U_{23}
Mn1	0	0.5	0.5	111(11)	69(11)	141(12)	29(9)	-66(9)	-15(10)
Mn2	0	0.5	0	125(12)	63(11)	152(12)	18(9)	-55(10)	-25(10)
Mn3	.5405(2)	.7677(2)	.2700(1)	102(8)	36(7)	131(8)	-1(6)	-46(6)	-6(6)
Se1	.6498(1)	.0386(1)	.3642(1)	137(5)	69(5)	146(5)	0(4)	-41(4)	5(4)
Se2	.6691(1)	.4965(1)	.3515(1)	138(5)	75(5)	145(5)	7(4)	-40(4)	-3(4)
Se3	.1734(1)	.2490(1)	.3978(1)	130(5)	88(5)	138(5)	4(4)	-34(4)	1(4)
O1	.2856(11)	.3990(8)	.1950(7)	125(39)	89(37)	248(47)	-5(31)	-7(34)	74(34)
O2	.3674(11)	.6350(8)	.2413(6)	188(44)	139(40)	144(43)	-53(34)	-14(34)	-29(33)
O3	.1547(11)	.5949(8)	.0904(7)	191(44)	99(39)	270(51)	52(33)	-145(38)	-20(36)
O4	.6325(11)	.4027(8)	.2454(6)	173(42)	101(37)	135(41)	-18(32)	-31(33)	-9(32)
O5	.7191(11)	.6394(8)	.2935(7)	135(41)	75(37)	232(46)	-33(30)	-48(35)	25(33)
O6	.8722(12)	.4396(8)	.3814(7)	233(47)	106(40)	257(49)	117(34)	-141(39)	-71(35)
O7	.8137(11)	.6075(8)	.0328(7)	181(44)	155(42)	188(45)	9(35)	-38(36)	-78(35)
O8	.6112(10)	.7704(8)	.1179(6)	84(40)	190(43)	189(43)	53(33)	6(31)	20(35)
O9	.1512(12)	.3566(9)	.4937(7)	259(50)	187(44)	139(43)	83(37)	-45(37)	-93(35)
O10	1.9453(12)	.3669(9)	.1365(7)	214(47)	215(47)	253(51)	-64(38)	-16(39)	43(39)
O11	.4578(12)	.7623(10)	.4289(7)	210(45)	350(55)	180(45)	3(42)	-67(36)	34(42)
O12	.8407(13)	.1212(9)	.1000(8)	302(55)	203(49)	328(56)	17(42)	-16(46)	-50(42)

The structure was resolved and refined with the aid of the crystallographic computer program X-Ray 1976.⁴ For the scattering factors neutral atoms were presumed and their values were taken from the International Tables.⁵ The positions of the manganese and selenium atoms were obtained by direct methods from the *E*-map calculated with 343 *E*-values bigger than 1.4. After refinement of these the value of *R* was 27.3 %. The positions of all the oxygens were found in the corresponding difference-Fourier map. The structure was then refined with isotropic temperature factors to an *R* value of 6.7 %. With anisotropic temperature factors using block-diagonal refinement the value of *R* was reduced to 4.3 %. The *F*_o and *F*_c listing is available from the authors upon request.

DISCUSSION

Final atomic coordinates and anisotropic temperature factors are given in Table 1. The

manganese atoms labelled Mn(1) and Mn(2) are in two-fold special positions. The oxygen atoms O(1)–O(9) are all bonded to one of the three selenium atoms and O(10)–O(12) are due to water of crystallization. Selected bond distances and angles are given in Table 2.

The three non-equivalent manganese atoms are octahedrally coordinated by oxygens. The coordination polyhedra are in each case strongly distorted. Since the Mn–O bond lengths fall roughly into two classes, comprising four short and two longer distances, the distortion is mainly tetragonal elongation. Around Mn(1) and Mn(2) there are three pairs of identical Mn–O bonds on opposite sides of the manganese atoms and, as a further consequence of the two manganese atoms being in special positions, the angle O–Mn–O for each of these pairs is exactly 180°. The bond lengths

Table 2. Selected interatomic distances (Å) and bond angles (°) and their estimated standard deviations.

2 × Mn1–O6	1.938(9) ^{i,ii}	Se1–O1	1.728(8) ⁱⁱⁱ
2 × Mn1–O9	1.893(9) ^{i,ii}	Se1–O2	1.731(9) ⁱⁱⁱ
2 × Mn1–O12	2.248(10) ^{iii,iv}	Se1–O3	1.708(9) ⁱⁱⁱ
2 × Mn2–O3	1.932(9) ^{i,ii}	Se2–O4	1.735(8) ⁱ
2 × Mn2–O7	1.891(9) ^{i,ii}	Se2–O5	1.721(8) ⁱ
2 × Mn2–O10	2.346(10) ^{i,ii}	Se2–O6	1.710(9) ⁱ
Mn3–O1	1.954(8) ⁱⁱⁱ	Se3–O7	1.734(9) ⁱⁱⁱ
Mn3–O2	1.944(9) ⁱ	Se3–O8	1.707(8) ⁱⁱⁱ
Mn3–O4	1.939(8) ⁱⁱⁱ	Se3–O9	1.717(9) ⁱ
Mn3–O5	1.932(8) ⁱ		
Mn3–O8	2.140(9) ⁱ	O1 ⁱⁱⁱ –Se1–O2 ⁱⁱⁱ	96.9(4)
Mn3–O11	2.258(9) ⁱ	O1 ⁱⁱⁱ –Se1–O3 ⁱⁱⁱ	100.1(4)
		O2 ⁱⁱⁱ –Se1–O3 ⁱⁱⁱ	97.4(4)
O6 ⁱ –Mn1–O6 ⁱⁱ	180.0(4)	O4 ⁱ –Se2–O5 ⁱ	98.0(4)
O9 ⁱ –Mn1–O9 ⁱⁱ	180.0(4)	O4 ⁱ –Se2–O6 ⁱ	96.5(4)
O12 ⁱⁱⁱ –Mn1–O12 ^{iv}	180.0(4)	O5 ⁱ –Se2–O6 ⁱ	100.1(4)
O6 ⁱ –Mn1–O9 ⁱ	90.3(4)		
O6 ⁱ –Mn1–O12 ^{iv}	92.2(4)	O7 ⁱⁱⁱ –Se3–O8 ⁱⁱⁱ	98.3(4)
O9 ⁱ –Mn1–O12 ^{iv}	87.1(4)	O7 ⁱⁱⁱ –Se3–O9 ⁱ	98.5(4)
		O8 ⁱⁱⁱ –Se3–O9 ⁱ	98.2(4)
O3 ⁱ –Mn2–O3 ⁱⁱ	180.0(4)	O1 ⁱⁱⁱ –Mn3–O2 ⁱ	177.3(4)
O7 ⁱ –Mn2–O7 ⁱⁱ	180.0(4)	O4 ⁱⁱⁱ –Mn3–O5 ⁱ	176.1(4)
O10 ⁱ –Mn2–O10 ⁱⁱ	180.0(4)	O8 ⁱ –Mn3–O11 ⁱ	178.2(3)
O3 ⁱ –Mn2–O7 ⁱⁱ	89.2(4)	O1 ⁱⁱⁱ –Mn3–O11 ⁱ	90.6(4)
O3 ⁱ –Mn2–O10 ⁱ	86.3(4)	O2 ⁱ –Mn3–O5 ⁱ	91.8(4)
O7 ⁱ –Mn2–O10 ⁱⁱ	90.4(4)	O4 ⁱⁱⁱ –Mn3–O8 ⁱ	95.5(3)

The superscripts denote the symmetry operations:

- i *x, y, z*
- ii $\bar{x}, \bar{y}, \bar{z}$
- iii $\bar{x}, 1/2 + y, 1/2 - z$
- iv $x, 1/2 - y, 1/2 + z$

of the two Mn—O bond pairs in the equatorial planes of the two octahedra are almost equal; they differ by only 0.045 Å and 0.042 Å, a distance, which must be considered statistically significant ($> 4\sigma$ in both cases), however.

The mean length of the four shorter Mn(3)—O bonds is 1.942 Å. Since the difference between the extreme values of the four shorter bonds is less than 3σ , the differences between these bonds are statistically insignificant. The two axial bond lengths differ markedly from each other. The reason for this is probably that the oxygen O(11) farther from Mn(3) is contributed by a water molecule, while O(8), the other axially bonded oxygen belongs to a selenite group.

It can be concluded that the distortion of the coordination polyhedra is mainly tetragonal, but in the case of Mn(1) and Mn(2) there is a further, distinctly smaller axial distortion in the equatorial plane. Thus, it appears that the coordination octahedra around Mn(1) and Mn(2) are orthorhombically distorted. An orthorhombically distorted MnO_6 -octahedron has recently been detected in tris(tropolonato)manganese(III), $\text{Mn}(\text{O}_2\text{C}_6\text{H}_7)_3$, in which one of the two nonequivalent MnO_6 -octahedra had three pairs of bond lengths, and their weighted means were 2.051(16), 1.990(5) and 1.944(8) Å.⁶

The MnO_6 -octahedra are considerably elongated as can be seen by comparing to some other Mn(III) compounds. In $\text{Mn}(\text{O}_2\text{C}_7\text{H}_5)_3$, the range of Mn—O bonds is 1.925(10)—2.110(10) Å and in tris(2,4-pentanedionato)manganese(III), $\text{Mn}(\text{O}_2\text{C}_5\text{H}_7)_3$, the range is from 1.931(10) to 2.020(7) Å.⁷ In anhydrous manganic acetate, $\text{Mn}_2\text{O}(\text{OAc})_6 \cdot \text{AcOH} \cdot \text{OAc}$, a compound of trivalent manganese containing also a distorted MnO_6 -octahedron, the range is 1.85(4)—2.24(4) Å.⁸

It must be emphasized, however, that it is difficult to estimate how large a portion of the distortion is due to the Jahn-Teller forces, since the hydrogen bonds have an effect on the distortion, too. In both $\text{Mn}(1)\text{O}_6$ and $\text{Mn}(2)\text{O}_6$ the two cap oxygens of the octahedron are contributed by water molecules, and the longest of the Mn—O bonds in $\text{Mn}(3)\text{O}_6$ which is formed with the oxygen of a water molecule, is of the same magnitude as the long bonds in $\text{Mn}(1)\text{O}_6$ and $\text{Mn}(2)\text{O}_6$. The oxygen (O8) of the other long bond belongs to the selenite

group, and the bond length is noticeably shorter. It is only slightly larger than the corresponding bonds in $\text{Mn}(\text{O}_2\text{C}_7\text{H}_5)_3$ and $\text{Mn}(\text{O}_2\text{C}_5\text{H}_7)_3$.

The bonds in the selenite groups are slightly longer than those in manganese(II) selenites.¹⁻³ The mean of the bond angles is also somewhat smaller. All the three nonequivalent selenite groups act as bridging ligands between three manganese atoms.

REFERENCES

1. Koskenlinna, M. and Valkonen, *Acta Chem. Scand. A* 31 (1977). *In press*.
2. Koskenlinna, M., Niinistö, L. and Valkonen, *J. Cryst. Struct. Commun.* 5 (1976) 663.
3. Koskenlinna, M., Niinistö, L. and Valkonen, *J. Acta Chem. Scand. A* 30 (1976) 836.
4. The X-Ray System, Version of 1976, Steward, J. M., Ed., *Technical Report TR-446 of the Computer Science Center*, University of Maryland, College Park, Maryland.
5. *International Tables for X-Ray Crystallography*, Kynoch Press, Birmingham 1974, Vol. 4, p. 72.
6. Avdeef, A., Costamagna, J. and Fachler, J. P. *Inorg. Chem.* 13 (1974) 1854.
7. Fachler, J. P. and Avdeef, A. *Inorg. Chem.* 13 (1974) 1864.
8. Hessel, L. W. and Romers, C. *Recl. Trav. Chim. Pays-Bas* 88 (1969) 545.

Received April 19, 1977.

Thermodynamics of Metal Complex Formation in Aqueous Solution. XII. Equilibrium Measurements on the Copper(I) Bromide, Iodide and Thiocyanate Systems

STEN AHRLAND and BERNT TAGESSON

Inorganic Chemistry 1, Chemical Center, University of Lund, P.O.B. 740, S-220 07 Lund, Sweden

The bromide, iodide and thiocyanate complexes of copper(I) have been studied in aqueous solution at 25 °C, in a sodium perchlorate medium of ionic strength $I = 5$ M. Both potentiometric and solubility measurements have been performed. At low metal concentrations, mononuclear complexes predominate. The solubilities of the complexes decrease and the stabilities increase in the order bromide, iodide, thiocyanate. For iodide and thiocyanate, but not for bromide, a fourth complex is formed within the available concentration range. At higher metal concentration, polynuclear complexes exist in appreciable concentrations.

Copper(I) seems to be the only oxidation state of a first row transition element showing typical class (b) behaviour, characterized *inter alia* by the halide affinity sequence $F^- \ll Cl^- < Br^- < I^-$ in aqueous solution.^{1,5} The complex formation of an acceptor in such a unique position is of special interest. The hydrated copper(I) ion disproportionates almost completely, except at extremely low concentrations. Copper(I) is therefore stable in aqueous solution only in the presence of ligands forming strong complexes. The thiocyanate ion and all the halide ions with the exception of the fluoride ion belong to this group, see *e.g.* Ref. 3. Their complex formation has in fact been studied since the beginning of the century⁴ but due to the severe experimental difficulties many points have nevertheless remained obscure. It therefore seemed worthwhile to reinvestigate the systems. The first results of these studies, concerning copper(I) chloride, were published some years

ago.⁵ In this paper, the bromide, iodide and thiocyanate equilibria are discussed.

The chief method of measurement was the potentiometric determination of the free central ion concentration $[Cu^+]$ by means of a copper amalgam electrode. From these measurements both the stability constants and the solubility products were obtained. To check these results some solubility measurements have also been performed.

In the present systems, complexes beyond the second one are formed in appreciable amounts only at fairly high ligand concentrations. In order to cover also these equilibria, a medium of high ionic strength has to be used. The measurements have therefore been performed at $I = 5$ M with sodium perchlorate as supplementary neutral salt. This choice also allows a direct comparison with the previous measurements of copper(I) chloride,⁵ silver(I) halide⁶⁻⁹ and silver(I) thiocyanate¹⁰ complexes performed in the same, or almost the same, medium.

The lower limit of the ligand concentration is set by the low solubility of the neutral complexes CuL . As soon as these constitute an appreciable part of the copper(I) present in the solution, the total solubility becomes too low for potentiometric measurements. Even when solubility measurements are used, solutions containing much of the copper(I) as CuL are difficult to reach. The final lower limit for the ligand concentration is determined by the disproportionation reaction (*cf.* Ref. 5).

On account of this disproportionation, the potentiometric determination of the equilibrium

constants of the copper(I) system cannot take place according to the standard procedure. The formal standard potential E°_I of the couple $\text{Cu}^+/\text{Cu}(\text{Hg})$ cannot be directly measured. It has to be calculated *via* the disproportionation constant K and the formal standard potential E°_{II} of the couple $\text{Cu}^{2+}/\text{Cu}(\text{Hg})$. The latter quantity can be directly measured only in acidic solutions where the hydrolysis of copper(II) does not interfere. For the chloride system measured previously, and also for the present bromide measurements, an 0.1 M acid medium has therefore been chosen, brought about by an appropriate substitution of perchloric acid for sodium perchlorate. On account of the decomposition of acid thiocyanate solutions, and the rapid oxidation of acid iodide solutions, an acid medium is unsuitable in these cases. Neutral solutions have therefore been used, and the appropriate value of E°_{II} found by an extrapolation procedure; *cf.* Procedure. All measurements have been performed at 25 °C.

CALCULATIONS

Potentiometric measurements. The emf of the cell (I) given in Scheme 1 can be written ($[\text{M}] = [\text{Cu}^+]$):

$$E_I = E^{\circ}_I - (RT/F) \ln [\text{M}] \quad (1)$$

As has already been pointed out, E°_I cannot be measured directly, on account of the disproportionation of Cu^+ taking place in solutions without a stabilizing ligand. The value of E°_I can be found, however, from the formula:⁵

$$E^{\circ}_I = (RT/2F) \ln K - E^{\circ}_{II} \quad (2)$$

where K is the disproportionation constant:

$$K = [\text{M}]^2/[\text{M}]_{II} \quad ([\text{M}]_{II} = [\text{Cu}^{2+}]) \quad (3)$$

which is known for the medium used,⁵ while E°_{II} is determined by means of the cell (II) given in Scheme 1 with the emf:

$$E_{II} = E^{\circ}_{II} + (RT/2F) \ln [\text{M}]_{II} \quad (4)$$

As $[\text{M}]_{II}$ is known, E°_{II} can be calculated, and hence E°_I from eqn. (2). From eqn. (2), $[\text{M}]$ is then found, and as C_M is known from the added amount of copper(I), the function $C_M/[\text{M}]$ needed for the preliminary graphical evaluation of the stability constants can be calculated.

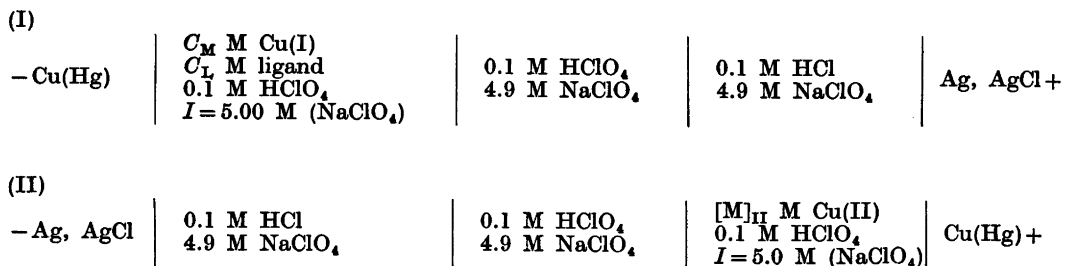
The information about the composition and the stability of the complexes obtained by this graphical treatment is then fed into the computer program EMK (*cf.* Ref. 11) which yields the final refined values of the equilibrium constants.

The formulas used for the graphical evaluation have been derived before^{12,13} and only a brief summary will be given here. If only mononuclear complexes are formed, $C_M/[\text{M}]$ will be a function of the free ligand concentration $[\text{L}]$ only:

$$C_M/[\text{M}] = X = 1 + \sum_{j=1}^N \beta_j [\text{L}]^j \quad (5)$$

In this case, the functions $C_L(C_M)$ for constant X are straight lines with the intercepts $C_L = [\text{L}]$ and the slopes equal to the ligand number $\bar{n} = (C_L - [\text{L}])/C_M$. X is thus obtained as a function of $[\text{L}]$ and from this function the stability constants can be calculated.

If polynuclear complexes are formed as well, the curves $C_L(C_M)$ are no longer straight lines with the slopes \bar{n} . Extrapolation to $C_M = 0$ will nevertheless yield corresponding values of $[\text{L}]$ and X and hence the mononuclear constants β_j , just as before.¹² The slopes at the point of intersection, *i.e.* at $C_M = 0$, are $< \bar{n}$,



Scheme 1.

however, and the difference is often very considerable. This is so in the case of copper(I) iodide and thiocyanate which certainly indicates that appreciable amounts of polynuclear complexes are formed in these systems.

The program EMK in the version used here is able to compute simultaneously both mononuclear and dinuclear complexes. When polynuclear complexes are indicated by the graphical evaluation, various plausible dinuclear complexes, or combinations of such complexes, have been fed into the program, beside the mononuclear complexes already identified. The best values are found by minimizing the error square sum

$$U(\beta_j, \bar{n}) = \sum_{i=1}^N w_i (E_{M,i,calc} - E_{M,i})^2 \quad (6)$$

$$\text{where } E_M = (RT/F) \ln C_M/[M] \quad (7)$$

and the weighting term $w_i = 1$.

For both iodide and thiocyanate, the introduction of one single dinuclear complex makes $U(\beta_j, \bar{n})$ so low that the deviations between measured and calculated values of E_M are clearly within the experimental error. A more sophisticated interpretation of the experimental data is therefore neither necessary nor possible.

Solubility measurements. In order to extend the potentiometric measurements to as low values of \bar{n} as possible some series were performed in such a way that the value of $[L]$ decreased during the series until finally a precipitate CuL formed. As indicated by the attainment of a constant emf, equilibrium between the solution and the solid phase was reached within a few hours; cf. Procedure. From these solutions, the total solubilities S of the various copper(I) systems, as a function of $[L]$, could be determined, as could also the solubility products K_s of CuL(s). By combining these determinations, several of the constants β_j can be calculated from measurements which are independent of the previously measured emf's.

The values of S were found from analyses of the equilibrium solutions, as described in Procedure. The corresponding values of $[L]$ were calculated from

$$[L] = C_L - (\bar{n} - 1)S - C_M \quad (8)$$

where C_L and C_M denote the stoichiometric concentrations added, whether still in solution or precipitated. As the correction term $(\bar{n} - 1)S$ never exceeds a few per cent of C_L , a sufficiently accurate value of \bar{n} can be estimated from the potentiometric measurements. It also turns out that the values of $[L]$ thus obtained are not changed appreciably if \bar{n} is instead calculated from the solubility function, as described previously.⁵ As $[M]$ is directly measured (eqn. 1),

$$K_s = [M][L] \quad (9)$$

can be calculated once $[L]$ is known.

From the solubility function $S([L])$ it cannot be discerned whether polynuclear complexes are formed or not, for the inherent reason that the method does not allow various values of C_M (i.e. S) for a fixed value of C_L . In these systems where the solid phases are composed CuL, the number of such entities present in the complexes remains unknown.^{12,14} Generally, the evaluation of $S([L])$ would only yield sums of constants for complexes of the same charge. For the present systems, however, the potentiometric measurements prove that only mononuclear complexes exist in appreciable amounts in the concentration range where the solubility measurements are performed. Consequently, $S([L])$ is of the simple form

$$S = K_s[L]^{-1}X \quad (10)$$

At first, the constants $K_s\beta_j$ are obtained and from these β_j can be found as K_s is known. The evaluation is performed numerically by a least-squares program.

Immediate information about the predominating complexes is obtained from the slopes of the solubility curves $\log S(\log [L])$ which for the present solid phases of the composition CuL are $\bar{n} - 1$ (cf. Ref. 14).

EXPERIMENTAL

Chemicals and analysis. Copper(I) bromide, copper(I) iodide and copper(I) thiocyanate (BDH) were used without further purification. Traces of copper(II) present (<2%) were reduced by treating the copper(I) solutions with copper amalgam.

Sodium perchlorate (Fluka) was purified by recrystallisation between 140 °C and 110 °C. The crystals were dried at 140 °C.

Sodium bromide (Malinckrodt *p.a.*), *sodium iodide* (Merck *p.a.*) and *sodium thiocyanate* (Malinckrodt *p.a.*) were used without further purification. The stock solutions were analyzed argentometrically, with dichlorofluorescein as indicator.

Copper amalgam containing $\approx 3\%$ copper was prepared by electrolyzing a copper(II) perchlorate solution with a mercury pool as cathode. At room temperature, a two-phase amalgam is formed between 0.0032 and 24.1% copper.^{15,16} Within this range, the potential will be independent of the composition, and the exact concentration of copper is therefore unimportant.⁵ A high copper content should be avoided, however, as the amalgam then becomes inconveniently stiff. The amalgam was stored under 0.1 M perchloric acid. Prior to use it was washed with dilute perchloric acid to remove traces of copper(II).

Analysis. The copper(I) solutions were oxidized and the concentration of copper(II) then determined spectrophotometrically by means of the cuprizone complex.¹⁷ For bromide and iodide, the oxidation was brought about by concentrated perchloric acid. The samples were then evaporated to dryness in order to remove the halide and the excess acid. A maximum molar absorptivity $\epsilon = 16\,360\text{ M}^{-1}\text{ cm}^{-1}$ was found at 600 nm, as compared with $\epsilon = 16\,520\text{ M}^{-1}\text{ cm}^{-1}$ quoted in the original investigation.¹⁷ For thiocyanate this technique was not possible due to the decomposition of thiocyanate in acid solution. Instead the samples were diluted and then oxidized by air. The analysis was then carried out in 0.5 M sodium thiocyanate solution, where slight variations in the thiocyanate concentration did not influence the absorbance. For this solution a maximum absorbance of $\epsilon = 16\,550\text{ M}^{-1}\text{ cm}^{-1}$ was found at 600 nm.

Apparatus. The emf's were measured by means of a "Norma Präz. Kompensationsapp. Mod 54" combined with a Kipp galvanometer allowing a precision of 0.01 mV. The silver-silver chloride electrodes were prepared according to Brown.¹⁸ The electrode solutions, in vessels of the Ingold type, were kept at $25.0 \pm 0.1\text{ }^\circ\text{C}$ by means of water circulating in an outer jacket. The ligand solutions were added from a Methrohm piston burette.

Procedure. The measurements for determination of E°_{II} were arranged as titrations where a copper(II) solution was titrated into the initial sodium perchlorate solution. The measurements for the iodide and thiocyanate systems had to be performed in neutral solutions where, however, the value of E°_{II} cannot be directly measured; cf. Introduction. Instead it was obtained by measuring cell II at different acidities in the right hand half-cell and subsequent extrapolation to zero acidity. For $[\text{H}^+] = 0.1\text{ M}$, $E^\circ_{\text{II}} = 107.2 \pm 0.4\text{ mV}$, while for $[\text{H}^+] = 0.01\text{ M}$ the value of E°_{II} was 2.6 mV higher. Hence for a neutral solution $E^\circ_{\text{II}} =$

$110.1 \pm 0.4\text{ mV}$. These values are the mean of about 15 determinations of E_{II} within the range $0.5 \lesssim [\text{M}]_{\text{II}} \lesssim 25\text{ mM}$. The values of E°_{II} could be reproduced within $\pm 0.3\text{ mV}$, and they did not depend upon $[\text{M}]_{\text{II}}$, which means that the copper amalgam electrodes behaved according to Nernst's law.

With the value of E°_{II} thus found and with $K = (1.13 \pm 0.13) \times 10^{-8}\text{ (M)}$, eqn. (2) yields $E^\circ_{\text{I}} = -286.0 \pm 1.5\text{ mV}$ for neutral solution and $E^\circ_{\text{I}} = -283.1 \pm 1.5\text{ mV}$ for $[\text{H}^+] = 0.1\text{ M}$.

In the main measurements, solutions of the left half-cell of cell I were obtained by adding $v\text{ cm}^3$ of a solution T to $V_0\text{ cm}^3$ of a solution S. Two different titration series were performed on each system using either (a) $T' = 4.9\text{ M NaBr}$, 0.1 M HClO_4 , or 5 M NaI if $L = \text{I}$ or SCN ; or (b) $T'' = 4.9\text{ M NaClO}_4$, 0.1 M HClO_4 (if $L = \text{Br}$), or 5 M NaClO_4 (if $L = \text{I}$ or SCN).

The solution S had the composition: $C_M\text{ M Cu(I)ClO}_4$; $C_L\text{ M NaL}$, $L = \text{Cl, Br or SCN}$; $I = 5\text{ M}$ by means of NaClO_4 , or, if $L = \text{Br, NaClO}_4 + 0.1\text{ M HClO}_4$. The S-solutions were prepared by dissolving copper(I) halide or thiocyanate in a ligand solution of a concentration high enough to ensure complete dissolution. Before adding the copper(I) halide, or thiocyanate, the solutions were made free from oxygen by nitrogen bubbling for about 30 min. Traces of copper(II) in this solution were reduced by shaking the solution overnight with copper amalgam under nitrogen. Before the transfer to the Ingold vessel the absence of copper(II) was checked by a negative cuprizone test. At the same time samples were withdrawn which after oxidation were used to determine the total copper concentration by cuprizone, as outlined in Analysis. Oxygen-free nitrogen was continuously bubbling through the left half-cell of cell I, in order to mix the solutions and prevent oxidation. The T-solutions were also freed from oxygen by nitrogen bubbling. In order to obtain the right vapour pressure, the nitrogen was passed through 5 M NaClO_4 before entering the solutions.

Titration series with solution T' were performed with at least three different initial concentrations of copper(I), ranging from 1 to 20 mM, in the S-solutions. Constant values of the emf's were reached within 5 min. Each series was repeated at least once, and the reproducibility was found to be within $\pm 0.3\text{ mV}$. At the end of some series, samples were withdrawn for direct analytical determination by cuprizone both of copper(II) and total copper content. In no case was copper(II) found and the total copper concentration had not changed significantly from that calculated from the initial one, from which follows that no oxidation of copper(I) or copper amalgam had taken place.

The titration series with solutions T'' were performed with at least five different initial copper(I) concentrations, ranging from 1 to 25 mM. These titrations were performed in the

same way as the T' titrations until copper(I) halide, or thiocyanate, began to precipitate. Equilibrium between the saturated copper(I) ligand solution and the precipitated solid CuL was attained about four hours after the precipitate had started to form, as indicated by the establishment of a stable emf. The equilibrium potentials remained very constant drifting $\lesssim 0.3$ mV in two days. Due to the fairly slow attainment of the heterogeneous equilibrium, the titrations were not continued once a precipitate had formed. When equilibrium had been reached, samples were taken to determine the solubility S . The samples were filtered through a glass filter G4 and then analyzed by the cuprizone method.

MEASUREMENTS AND RESULTS

Potentiometric measurements. The emf's for a random selection of points are shown in Figs. 1, 2 and 3. Complete potentiometric data are obtainable from the authors.

The stability constants calculated from the potentiometric data by means of the least-squares EMK program are shown in Table 1. The mononuclear constants found by the graphical evaluations of the bromide, iodide and thiocyanate systems did not deviate significantly from the numerical constants listed in Table 1.

Copper(I) chloride. The constants of the chloride system have been recalculated by means of the EMK program. The new values, of β_2 and β_3 , differ from the previous ones, evaluated graphically,⁵ by amounts just outside

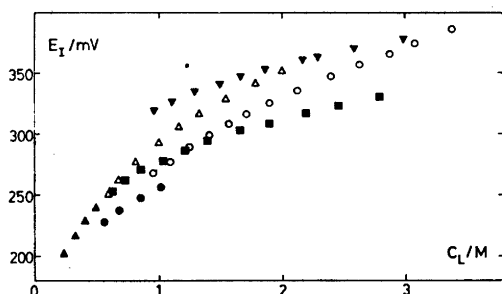


Fig. 1. Copper(I) bromide. A random selection of the measured emfs E_I . Filled and open symbols refer to titrations with 5.0 M sodium perchlorate (emf decreasing) and 5.0 M sodium halide (emf increasing), respectively. The initial and final copper(I) concentrations are (mM): ∇ 5.25, 1.70; \triangle 5.67, 3.85; \blacktriangle 6.19, 3.02; \circ 12.7, 5.08; \bullet 22.9, 12.7; \blacksquare 27.9, 6.00.

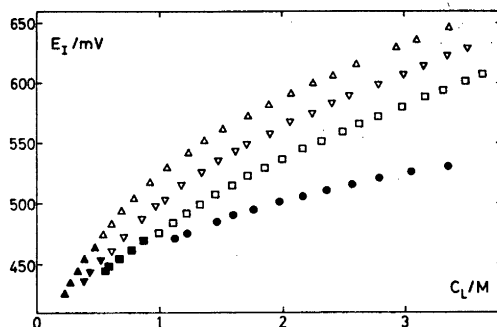


Fig. 2. Copper(I) iodide. A random selection of the measured emfs E_I (cf. Fig. 1). The initial and final copper(I) concentrations are (mM): \blacktriangle 0.72, 0.34; \triangle 0.71, 0.26; ∇ 1.50, 1.08; ∇ 1.76, 0.59; \blacksquare 4.00, 2.56; \square 4.56, 1.52; \bullet 23.8, 7.93.

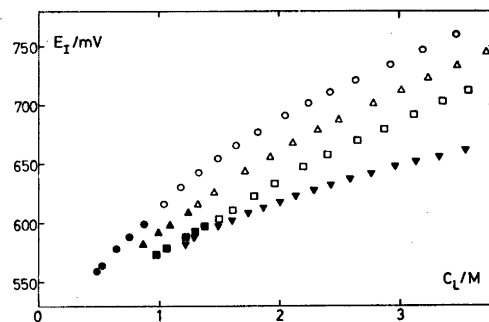


Fig. 3. Copper(I) thiocyanate. A random selection of the emfs E_I (cf. Fig. 1). The initial and final copper(I) concentrations are (mM): \bullet 0.96, 0.54; \circ 0.92, 0.35; \blacktriangle 2.48, 1.71; \triangle 2.44, 0.83; \blacksquare 5.63, 3.98; \square 6.18, 2.47; ∇ 18.3, 6.23.

the random errors; Table 1. The value of the dinuclear constant β_{42} , previously determined by a combination of potentiometric and solubility measurements,⁵ has been nicely confirmed by the present calculation which involved only the potentiometric data.

Copper(I) bromide. The functions $C_M/[M](C_L)$ calculated from the family of functions $E_I(C_L)$ plotted in Fig. 1 do not vary significantly between the series of different copper(I) concentrations. Consequently, within the limits of random errors, $[L] \approx C_L$. For the further calculations, the mean of the C_L -values found for each $C_M/[M]$ was therefore taken as $[L]$. From this follows that the curves $C_L(C_M)$ ($C_M/[M] = \text{constant}$) have no defined slopes.

Table 1. The overall stability constants β_j and the solubility products K_s for the copper(I) systems. The limits of error correspond to three standard deviations, as obtained by the computer or as estimated.

	Chloride Graphical	Chloride Numerical	Bromide	Iodide	Thiocyanate
<i>A. Potentiometric measurements</i>					
β_2/M^{-2}	$(1.00 \pm 0.05) \times 10^6$	$(1.14 \pm 0.06) \times 10^6$	$(1.89 \pm 0.25) \times 10^6$	$(4.8 \pm 3.7) \times 10^8$	
β_3/M^{-3}	$(0.97 \pm 0.05) \times 10^6$	$(0.87 \pm 0.04) \times 10^6$	$(2.80 \pm 0.05) \times 10^7$	$(2.70 \pm 0.11) \times 10^{10}$	$(4.01 \pm 0.15) \times 10^{11}$
β_4/M^{-4}				$(2.50 \pm 0.30) \times 10^9$	$(10.51 \pm 0.12) \times 10^{11}$
β_{23}/M^{-5}	$(12 \pm 5) \times 10^{13}$	$(8.8 \pm 3.5) \times 10^{13}$			
β_{23}/M^{-7}				$(10.0 \pm 1.2) \times 10^{21}$	$(2.17 \pm 0.30) \times 10^{24}$
K_d/M^{-1}	12 ± 6^a	7 ± 4^a		14 ± 2^b	14 ± 2^b
<i>B. Solubility measurements</i>					
K_s/M^3	$(4.2 \pm 0.3) \times 10^{-8}$		$(1.30 \pm 0.06) \times 10^{-9}$	$(1.92 \pm 0.06) \times 10^{-13}$	$(1.71 \pm 0.16) \times 10^{-15}$
β_2/M^{-2}			$(1.5 \pm 1.0) \times 10^6$		
β_3/M^{-3}			$(3.0 \pm 0.5) \times 10^7$	$(2.8 \pm 0.4) \times 10^{10}$	$(5.4 \pm 1.6) \times 10^{11}$
β_4/M^{-4}				$(7.9 \pm 7.4) \times 10^9$	$(10.8 \pm 1.6) \times 10^{11}$

^a $K_d = \beta_{23}/\beta_2^2$ is the constant for dimerization according to $2 \text{Cu}_2\text{L}_2 \rightleftharpoons \text{CuL}_4^{2-}$.

^b $K_d = \beta_{23}/\beta_3^2$ is the constant for dimerization according to $2 \text{Cu}_2\text{L}_3 \rightleftharpoons \text{CuL}_6^{4-}$.

Consequently, no information can be obtained about the possible existence of polynuclear complexes. The graphical evaluation indicated that the second and the third mononuclear complex were formed within the range covered. These were also the only complexes found in the subsequent numerical calculation. For the stability constant of the first complex no significant value was found, $\beta_1 = (0 \pm 0.13) \times 10^6 \text{ M}^{-1}$. As expected from the graphical evaluation, tests with dinuclear complexes, *viz.* $\text{Cu}_2\text{Br}_2^{2-}$ and $\text{Cu}_2\text{Br}_4^{4-}$, did not give a better fit. This difference from the other systems might, however, at least partly be due to the fact that the random errors are evidently somewhat larger for the bromide system. *Per se*, a formation of polynuclear complexes is of course plausible also in this system, though probably to a lower degree than for iodide or thiocyanate, *cf.* the corresponding silver(I) systems.⁷⁻¹⁰

Copper(I) iodide. For this system the functions $C_M/[M](C_L)$ calculated from the family of functions $E_I(C_L)$, Fig. 2, varied significantly with C_M . The functions $C_L(C_M)(C_M/[M] = \text{constant})$ were fairly well-defined lines, yielding [L] by extrapolation to $C_M = 0$. Their slopes were negative, however, varying between -1 and -8 . These values are evidently much lower than \bar{n} , indicating that polynuclear complexes are formed in appreciable amounts. Graphically,

the second, third and fourth mononuclear complexes are indicated. In the numerical calculation, various dinuclear complexes have been introduced besides the mononuclear ones. The best fit is found with $\text{Cu}_2\text{I}_4^{4-}$, with an error square sum $\approx 25\%$ of that found by the calculation involving only mononuclear complexes.

Copper(I) thiocyanate. Also in this system the functions $C_M/[M](C_L)$ calculated from $E_I(C_L)$, Fig. 3, varied significantly with C_M . The functions $C_L(C_M)(C_M/[M] = \text{constant})$ are again well-defined lines, yielding [L] by extrapolation. The slopes are ≈ 1 , *i.e.* much higher than in the iodide system: Still they are evidently much lower than \bar{n} , indicating the formation of considerable amounts of polynuclear complexes also in this system. Graphically, only the third and fourth mononuclear complexes were found. This was confirmed by the numerical calculations which yielded $\beta_2 = (0 \pm 0.21) \times 10^{11} \text{ M}^{-2}$. Introduction of the dinuclear complex $\text{Cu}_2(\text{SCN})_6^{4-}$, in addition to CuL_3^{2-} and CuL_4^{2-} , reduces the error square sum to $\approx 16\%$ of that obtained for only mononuclear complexes. Introduction of $\text{Cu}_2(\text{SCN})_5^{5-}$ results in an even better fit ($\approx 13\%$ of the mononuclear sum). A value of $\beta_{73} = (9.8 \pm 1.1) \times 10^{24}$ was obtained while β_3 and β_4 remained much the same as in Table 1A.

Considering the rather unlikely configuration of a complex $\text{Cu}_2(\text{SCN})_7^{4-}$ and the slight difference in fit between the two dinuclear complexes tried, we think $\text{Cu}_2(\text{SCN})_6^{4-}$ the most plausible alternative, especially as the analogous $\text{Cu}_2\text{I}_6^{4-}$ seems the best one to adopt in the iodide system.

Solubility measurements. From the corresponding values of S and $[\text{L}]$ determined as described in Procedure, the solubility curves $\log S(\log [\text{L}])$ presented in Fig. 4 have been calculated for the systems investigated. The potentiometric measurements indicate that for no point in the solubility measurements have the amounts of polynuclear complexes exceeded 5 % of the total copper(I) concentration. For most points the figure is in fact $< 2\%$. Consequently, eqn. (10) applies within the limits of error, and the constants directly found are $K_s\beta_j$. The slopes of the solubility curves confirm that for the bromide system only the second and third complexes, for the iodide and thiocyanate systems only the third and fourth complexes, are present in appreciable amounts. With the values of K_s determined as described in Solubility measurements, the values of β_j can be found immediately, Table 1B. For the bromide and iodide systems only the values of β_3 are in fact significant, while for the thiocyanate system a value of β_4 is also obtained. This is to be expected, as the third complex strongly predominates in the concentration ranges used for the bromide and iodide measurements, while large amounts of the fourth complex are present in the case of the thiocyanate,

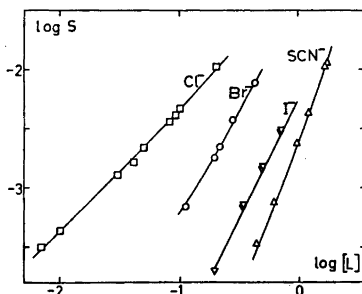


Fig. 4. The solubility curves of the copper(I) halide and thiocyanate systems. The points refer to the solubilities directly measured, while the full-drawn curves have been calculated from the stability constants and the solubility products listed in Table 2.

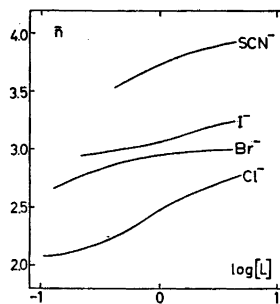


Fig. 5. The complex formation functions of the copper(I) systems, as calculated from the constants listed in Table 2.

cf. Fig. 5. In so far as significant values of β_j are obtained from the solubility measurements, they agree very well with those obtained potentiometrically which are thus confirmed; *cf.* Table 1. The precision is far better with the latter method, however, as is evident from the random errors of β_j listed. This is why those values have been used in the following discussion. The differences between these values and a weighted mean of the constants found by the two methods are in any case insignificant.

COMPARISON WITH PREVIOUS WORK, DISCUSSION

In Table 2, the results of the present studies are compared to those found in earlier investigations. The table also lists the constants found for the analogous silver systems.

A direct comparison between the various results presupposes, of course, that the constants have been determined under the same, or at least similar, conditions. For the copper(I) chloride system this was the case in some instances. A reasonable agreement was indeed found, at least for the principal constants.⁵ For the bromide system, only one investigation¹⁰ has been performed under conditions somewhat similar to ours. If the presently determined value of K_s is applied, the values of β_2 and β_3 resulting from that investigation agree reasonably well with the present ones, Table 2. Moreover, polynuclear complexes have been proved not to exist in the solutions studied which is also in accordance with our result. No less than three investigations²⁰⁻²²

Table 2. Mononuclear halide and thiocyanate complexes of copper(I) and silver(I). Stepwise (K_j) and overall (β_j) stability constants of the complexes ML_j , and solubility products (K_s) of the solids ML .

L	$\log K_j$				$\log \beta_j$			pK_s	t (°C)	I (M)	Ref.	
	1	2	3	4	2	3	4					
<i>Copper(I)</i>												
Cl ⁻			-0.12		6.06	5.94		7.38	25	5	5	
Br ⁻			1.17		6.28	7.45		8.89			<i>a</i>	
I ⁻			~1.7	-1.03	~8.7	10.43	9.40	12.72			<i>a</i>	
SCN ⁻				0.43		11.60	12.03	14.77			<i>a</i>	
Cl ⁻					5.31			6.50	25	0	3	
Br ⁻					5.04			7.38	19	var.	4	
					5.92			8.28	25	0	3	
		1.01			6.47 ^b	7.48 ^b			25	2	19	
I ⁻					8.19			11.30	19	var.	4	
					8.85			11.96	25	0	3	
			0.35				9.38	9.73	25	5	20	
		0.71			9.03	9.74		12.03	20	0.6	21	
								9.85	20	4	21	
					9.68			9.44	20	3.9	22	
SCN ⁻								13.40	25	0	3	
			0.18				9.90	10.09	12.73	20	var.	28
		-0.10	-0.42		11.00	10.90	10.48		25	5	20	
<i>Silver(I)</i>												
Cl ⁻	3.08	2.32	0.75	-0.85	5.40	6.15	5.30	10.10	25	5	6	
Br ⁻	4.22	3.00	1.88	0.11	7.22	9.10	9.21	12.62	25	5	7	
I ⁻			2.85	0.72	10.35	13.20	13.92	16.35	25	4	8,9	
	6.58	5.16	1.94	-0.6	11.74	13.68	~13.1	16.60	18	0	27	
SCN ⁻	4.59	3.70	1.77	1.20	8.29	10.06	11.26	12.11	25	4	10	

^a This study. ^b Calculated from their $K_s\beta_j$ -values by means of our $pK_s=8.89$.

of the iodide system have been performed at conditions similar to ours, all by means of solubility measurements. The results of these investigations do not agree very well, nor have they been confirmed by the present measurements. One reason for this is certainly that the earlier investigators have not taken polynuclear complexes into account in solutions where they exist in considerable amounts, another that values of K_s have been applied that are not valid in the medium actually used. As to the thiocyanate system, one investigation has been performed under conditions similar to ours (though in a nitrate medium), by mean of solubility measurements.²⁰ The results seem doubtful for the same reasons as quoted in the case of the iodide system. Evidently they do not agree with the present ones.

The values of K_s presently found for $I=5$ M are throughout considerably smaller than those

valid at $I=0$, Table 2. The difference is about the same for all the halides and seemingly somewhat larger for the thiocyanate.

The typical (*b*)-behaviour is certainly the most prominent feature of the halide complex formation of copper(I); Table 2. All the stability constants increase in the order $Cl^- < Br^- < I^-$. The differences between the various halides are throughout smaller than for silver(I), however. As might be expected from its position in a higher period, this acceptor has an even stronger (*b*)-character than copper(I).²⁴

With copper(I), thiocyanate forms complexes which are even stronger than the iodide complexes, in striking difference to silver(I), where the iodide complexes are considerably stronger than the thiocyanate ones. The complexes formed by copper(I) with the latter ligand are even more stable than the corresponding silver complexes. Being typical (*b*)-acceptors, both copper(I) and silver(I) certainly coordinate

the thiocyanate ion *via* its sulfur end.^{25,26} Evidently, copper(I) prefers the heavy chalcogen sulfur as donor atom in relation to the heavy halides in a much higher degree than does silver(I).

For both copper(I) and silver(I), the solubility products decrease as the stability constants increase. The increase of the latter is not sufficient to compensate for the decrease of the former, however, so in solutions of a certain solubility *S* of copper(I) the proportion of higher complexes increases strongly in the sequence $\text{Cl}^- < \text{Br}^- < \text{I}^- < \text{SCN}^-$. At the lowest solubilities measured here, the second complex predominated in the chloride and is still prominent in the bromide system while for iodide it can just be proved to exist. In the thiocyanate system, no complex below the third one can be discerned.

For the silver(I) halide systems, the solubility products are throughout smaller relative to the stability constants than for copper(I). Consequently, the solubilities are even lower. A rather complete determination of the stability constants has nevertheless been possible by solubility measurements, as even very low solubilities of silver(I) can be measured radiometrically.^{6,7,9,27} For copper such measurements are not feasible as no suitable active isotope exists.

The higher halide complexes in the copper(I) systems are formed only reluctantly so that even at the highest halide concentrations available a fourth complex does not exist at all in the chloride and bromide systems, and only in relatively minor amounts in the iodide system. In contrast to this, the fourth complex is the most prominent species in the whole range of thiocyanate concentrations employed and at the highest concentration it is completely predominating. These conditions are clearly illustrated by the complex formation curves drawn in Fig. 5.

In the silver(I) halide systems the highest complexes are formed much more readily. The values of K_3 and K_4 are throughout considerably higher for the silver(I) systems; Table 2. This applies also to the chloride system where the lower complexes are less stable than the corresponding copper(I) complexes. A similar behaviour is also found for thiocyanate. While the value of β_3 is higher for copper(I)

than for silver(I), the opposite is true for K_4 . Within the same range of halide concentrations as in the present investigation, appreciable amounts of the fourth complex are formed in all the silver(I) systems.

The dinuclear complex $\text{M}_2\text{L}_6^{4-}$ postulated to exist in the copper(I) iodide and thiocyanate systems has also been found in the corresponding silver systems.^{9,10} In these, higher complexes of the series $\text{Ag}_n\text{L}_{2n+2}^{(n+2)-}$ are seemingly also formed, while no such complexes are indicated in the corresponding copper(I) systems. This may be because the concentrations of copper(I) in the present measurements never exceeded 25 mM, which is much less than the concentrations of silver(I) in those solutions, where the polynuclear silver complexes have been found. Also the existence of $\text{Ag}_2\text{Br}_6^{4-}$ has been claimed, although the stability constant could not be calculated.⁷ The corresponding copper(I) complex might well be found at higher concentrations of copper(I) than those used here.

Acknowledgement. This work is part of a program sponsored by the Swedish Natural Science Research Council whose support is most gratefully acknowledged.

REFERENCES

1. Ahrland, S., Chatt, J. and Davies, N. R. *Chem. Rev.* 12 (1958) 265; also in Pearson, R. G., Ed., *Hard and Soft Acids and Bases*, Dowden, Hutchinson and Ross, Stroudsburg, Pa. 1973, p. 28.
2. Pearson, R. G. *J. Chem. Educ.* 45 (1968) 581, 643.
3. Latimer, W. M. *The Oxidation States of the Elements and their Properties in Aqueous Solutions*, 2nd Ed., Prentice-Hall, Englewood Cliffs, N. J. 1952, p. 183.
4. Bodländer, G. and Störbeck, O. *Z. Anorg. Chem.* 31 (1902) 1, 458.
5. Ahrland, S. and Rawsthorne, J. *Acta Chem. Scand.* 24 (1970) 157.
6. Berne, E. and Leden, I. *Sven. Kem. Tidskr.* 65 (1953) 88.
7. Berne, E. and Leden, I. *Z. Naturforsch. Teil A* 8 (1953) 719.
8. Leden, I. and Parck, C. *Acta Chem. Scand.* 10 (1956) 535.
9. Leden, I. *Acta Chem. Scand.* 10 (1956) 540, 812.
10. Leden, I. and Nilsson, R. *Z. Naturforsch. Teil A* 10 (1955) 67.
11. Ahrland, S. and Björk, N.-O. *Acta Chem. Scand. A* 30 (1976) 249.

12. Fronæus, S. In Jonassen, H. B. and Weissberger, A., Eds., *Technique of Inorg. Chem.*, Interscience, New York, London 1963, Vol. 1, Chapter 1.
13. Ahrland, S., Chatt, J., Davies, N. R. and Williams, A. A. *J. Chem. Soc.* (1958) 264.
14. Johansson, L. *Coord. Chem. Rev.* 3 (1968) 293.
15. Tammann, G. and Kollmann, K. *Z. Anorg. Chem.* 143 (1925) 357.
16. Tammann, G. and Stassfurth, T. *Z. Anorg. Chem.* 160 (1927) 246.
17. Wetlesen, C. U. *Anal. Chim. Acta* 16 (1957) 268.
18. Brown, A. S. *J. Am. Chem. Soc.* 56 (1934) 646.
19. Peters, D. G. and Caldwell, R. L. *Inorg. Chem.* 6 (1967) 1478.
20. Fridman, Ya.D. and Sarbaev, Dzh.S. *Russ. J. Inorg. Chem.* 4 (1959) 835.
21. Golub, A. M., Sazhienko, S. M. and Romanenko, *Ukrain. Khim. Zh.* 28 (1962) 561 (as cited in Ref. 23).
22. Gyunner, E. A. and Yakhkind, N. D. *Russ. J. Inorg. Chem.* 13 (1968) 1420 (as corrected in Ref. 23).
23. Sillén, L. G. and Martell, A. E. *Stability Constants of Metal-Ion Complexes*, Chemical Society, London 1964 and 1971 (Special Publications Nos. 17 and 25).
24. Ahrland, S. *Struct. Bonding (Berlin)* 1 (1966) 207.
25. Bailey, R. A., Kozak, S. L., Michelsen, T. M. and Mills, W. N. *Coord. Chem. Rev.* 6 (1971) 407.
26. Kullberg, L. *Acta Chem. Scand. A* 28 (1974) 979.
27. Lieser, K. H. *Z. Anorg. Chem.* 292 (1957) 97.
28. Golub, A. M. *Zh. Neorg. Khim.* 1 (1956) 2517 (as cited in Ref. 23).

Received May 11, 1977.

Thermodynamics of Metal Complex Formation in Aqueous Solution. XIII. Enthalpy Measurements on Copper(I) and Silver(I) Halide Systems

STEN AHRLAND, BERNT TAGESSON and DINKO TUHTAR

Inorganic Chemistry 1, Chemical Center, University of Lund, P.O.B. 740, S-220 07 Lund, Sweden

In the silver(I) chloride and bromide systems the thermodynamic functions in aqueous solution have been determined for the reactions $\text{Ag}^+ + j\text{L}^- \rightarrow \text{AgL}_j^{(j-1)-}$, $j=3$ and 4 , and also for the precipitation reactions $\text{Ag}^+ + \text{L}^- \rightarrow \text{AgL}(s)$. In the copper(I) halide systems, the corresponding functions have not been possible to determine. Some interesting information about the thermodynamics of these systems has nevertheless been gained, as the functions referring to the reactions $\text{CuCl}_2^- + \text{Cl}^- \rightarrow \text{CuCl}_3^{2-}$ and $\text{CuL}_3' + 3\text{L}'' \rightarrow \text{CuL}_3'' + 3\text{L}'$, $\text{L} = \text{Cl}^-$, Br^- and I^- , have been determined. These results have been achieved by the investigation of several types of reactions, performed by various calorimetric techniques. The data refer to a perchlorate medium of an ionic strength $I=5$ M, at 25°C .

As is expected for these interactions between soft acceptors and soft donors the complexes are all enthalpy stabilized, while the entropy term counteracts their formation. For both silver(I) and copper(I), the formation reactions become more exothermic as the ligand becomes softer, *i.e.* in the sequence $\text{Cl}^- < \text{Br}^- < \text{I}^-$. This is of course also the order of increasing stability of the complexes. Although increasingly unfavourable, the entropy term evidently cannot neutralize the stabilizing influence exerted by the enthalpy term in the order mentioned.

In order to elucidate the nature of the coordinate bond in metal complexes, it is useful to know all the thermodynamic functions involved in the formation reactions.¹⁻³ The free energy changes $\Delta G^\circ_{\beta j}$ can be calculated from the stability constants β_j :

$$\Delta G^\circ_{\beta j} = -RT \ln \beta_j \quad (1)$$

If the enthalpy changes, $\Delta H^\circ_{\beta j}$, are measured, the entropy changes $\Delta S^\circ_{\beta j}$ can finally be calculated from

$$\Delta G^\circ_{\beta j} = \Delta H^\circ_{\beta j} - T \Delta S^\circ_{\beta j} \quad (2)$$

The enthalpy changes can be obtained, either calorimetrically, or from the temperature coefficients of the stability constants. The calorimetric method is generally much to be preferred as it is both more precise and more accurate.⁴⁻⁶ With modern calorimeters, measuring precisely even quite small amounts of heat (≈ 0.5 J), the calorimetric method also works with small amounts of reactants, *i.e.* at fairly low concentrations. Nevertheless, the concentration necessary for a calorimetric measurement are still much larger than those demanded by many methods used for the determination of stability constants.^{6,7} This is of course a restriction on the calorimetric determination of $\Delta H^\circ_{\beta j}$, which has proved rather serious for the systems investigated here.

The aim of the present investigation is to determine the thermodynamic functions for the formation of the halide complexes of copper(I) and silver(I) in aqueous solution, as far as this is experimentally possible. The stability constants for most of the complexes involved have been determined previously. Moreover, for all systems except silver(I) iodide, measurements exist for identical conditions, *i.e.* for a perchlorate medium of ionic strength $I=5$ M, at 25°C .⁸ The present measurements of $\Delta H^\circ_{\beta j}$ therefore refer to these conditions. As before, sodium perchlorate is used as a

supplementary salt. In all the present measurements, however, a minor part of the medium, *viz.* 0.1 M, is perchloric acid. The compelling reason is that such an acidity is necessary for some of the reactions employed. The choice of 0.1 M perchloric acid was natural as the recent determination of the stabilities of the copper(I) chloride and bromide complexes refer to that medium.

A medium of high ionic strength is in fact necessary for the calorimetric measurements as sufficiently high solubilities are reached only at fairly high ligand concentrations.

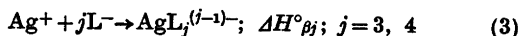
For copper(I), the disproportionation taking place in aqueous solution,⁹ in the absence of stabilizing ligands, prevents all measurements involving the use of solutions of the hydrated metal ion. A direct determination of $\Delta H^\circ_{\beta_j}$ is therefore not feasible and this of course further severely restricts the scope of the investigation as will be demonstrated. As a consequence, the results achieved for the copper(I) systems are not at all as extensive as those achieved for the corresponding silver(I) systems, where this last complication does not exist.

THE REACTIONS INVESTIGATED CALORIMETRICALLY

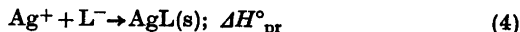
Two essentially different techniques have been used for the calorimetric measurements. In the first one, portions of a solution T, containing silver(I) or copper(I), is titrated into a solution S in the calorimeter vessel. In the second one, a solid silver(I) or copper(I) compound is dissolved in the solution present in the calorimeter.

In the titration experiments involving silver(I), T has been a pure perchlorate solution while S contains various concentrations of chloride or bromide. Iodide and thiocyanate have so far been avoided, as the complex formation reactions are rather more complicated in these systems, involving large amounts of polynuclear complexes even at fairly low concentrations.^{11,12} As long as the concentration of chloride, or bromide, is sufficiently high, and that of silver(I) sufficiently low, formation of complexes $\text{AgL}_j^{(j-1)-}$ takes place in the solution. As the silver(I) concentration increases, precipitation of $\text{AgL}(s)$ occurs. This happens sooner, the lower the concentration

of ligand chosen. From the measurements in homogeneous solution enthalpy changes referring to the reactions

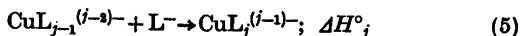


can be calculated and from the measurements involving precipitation, the enthalpy change of



The total halide concentration C_{L} is so high that it is not appreciably changed by the amounts of $\text{AgL}(s)$ actually precipitated. Once the solubility product has been reached, practically all Ag^+ added therefore reacts according to eqn. (4), and the amount of $\text{AgL}(s)$ formed can easily be calculated. Moreover, reactions according to eqn. (3) cannot take place to any appreciable extent. The whole of the reaction heat measured thus applies to eqn. (4).

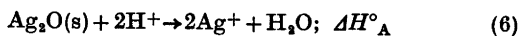
In the case of copper(I), on the other hand, T has had a very high concentration of ligand, in order to protect copper(I) from disproportionation, while S has either been the pure perchlorate medium, or a ligand solution of fairly low concentration. During the titration, $[\text{L}]$ decreases so that in principle the enthalpy change for



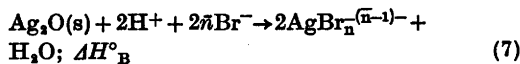
can be determined. In practice, however, it is only possible to investigate the third step of the chloride system. In the bromide and iodide systems, the variation of the ligand number \bar{n} is too slight in the range of ligand concentrations available and for the thiocyanate system, the solubility is too low for reliable calorimetric measurements.⁸

The experiments involving the solution of solid silver(I) compounds have been confined to the bromide system, where the conditions seemed especially favourable. The solubility is fairly high and yet polynuclear complexes are formed only in minor amounts.¹²

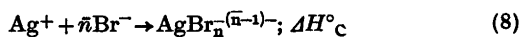
In the first set of experiments, silver(I) oxide has been dissolved in the pure perchlorate medium



as well as in a strong bromide solution ($C_{\text{L}} = 4.9 \text{ M}$), with an acidity = 0.1 M

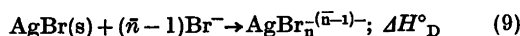


Evidently [(7) - (6)]/2 results in



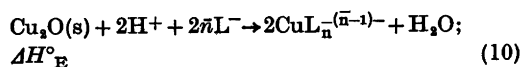
The free bromide concentration $[\text{L}^-] \simeq C_{\text{L}}$ and as the stability constants are also known, \bar{n} can be calculated.¹² The value is in fact just below 4, viz. 3.87. The value of $\Delta H^\circ_{\text{A}}$ found in the titration experiments can confidently be used for the small correction needed in order to transform the value of $\Delta H^\circ_{\text{C}}$ found into a value of ΔH_{β_4} , to be compared with that determined as described above.

In the second solution experiment, silver bromide has been dissolved in the 4.9 M bromide solution



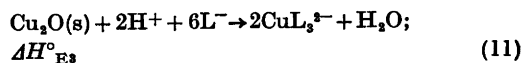
Evidently, (9) + (4) = (8) (if $\text{L}^- = \text{Br}^-$) and $\Delta H^\circ_{\text{C}} = \Delta H^\circ_{\text{D}} + \Delta H^\circ_{\text{pr}}$. With the same small correction as before, using $\Delta H^\circ_{\text{A}}$, a value of $\Delta H^\circ_{\beta_4}$ is again obtained, to be compared with the two previous ones.

In the case of copper(I), a reaction corresponding to eqn. (6) is not possible. The counterpart of eqn. (7) has been studied, however



and moreover for $\text{L}^- = \text{Cl}^-, \text{Br}^-, \text{I}^-$. No measurements involving SCN^- have been attempted, as this ligand slowly disintegrates in acid solutions, with the formation of CN^- , which might cause difficulties, considering the extreme affinity of CN^- for copper(I).

For Cl^- , $[\text{L}] \simeq C_{\text{L}} = 4.9 \text{ M}$ which means $\bar{n} = 2.77$. The complex CuCl_3^{2-} thus predominates although CuCl_2^- is still present in fairly large amounts. As $\Delta H^\circ_{\beta_3}$ of the chloride system has been determined by titration calorimetry, however, the change referring to the formation of the third complex can be calculated.



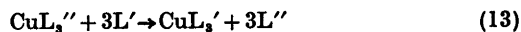
For bromide, $C_{\text{L}} = 4 \text{ M}$. The choice between that value and the somewhat higher 4.9 M does not matter,⁸ as in any case $\bar{n} \simeq 3$. Within the limits of error, the value measured thus

actually refers to eqn. (11). For iodide, $C_{\text{L}} = 4 \text{ M}$ corresponds⁸ to a value of $\bar{n} = 3.27$. In this case, no data are available from titration experiments to bring about that correction to $\bar{n} = 3$ which is necessary in order to ensure a direct comparison with the results found for the other halides. Instead, the measurement has been repeated at the lowest iodide concentration that still produces a sufficiently rapid solution, viz. $C_{\text{M}} = 2.5 \text{ M}$, corresponding to $\bar{n} = 3.18$. From the values of $\Delta H^\circ_{\text{E}}$ found at the two values of \bar{n} , a reasonable value of $\Delta H^\circ_{\text{E}_3}$ can be estimated.

Once the values of $\Delta H^\circ_{\text{E}_3}$ are known for the various systems, the differences

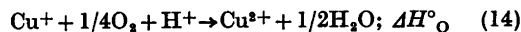
$$[\Delta H^\circ_{\text{E}_3}(\text{L}') - \Delta H^\circ_{\text{E}_3}(\text{L}'')]/2 = \Delta H^\circ_{\beta_3}(\text{L}') - \Delta H^\circ_{\beta_3}(\text{L}'') \quad (12)$$

can be calculated. These differences between the enthalpy changes accompanying the formation of analogous complexes of the three halide ions are highly informative. They refer to the heats evolved in the substitution reactions (charges omitted)

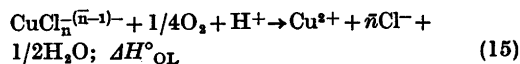


It would of course be even more interesting to know the absolute values of $\Delta H^\circ_{\beta_3}$, but all attempts to arrive at these have so far failed in spite of strenuous efforts.

The first attempt at this was measuring the reaction corresponding to eqn. (6) in a concentrated solution of copper(II), which would ensure the highest possible concentration of Cu^+ in solution. This process was slow and erratic. The second attempt tried to utilize the oxidation reactions



and



Also the heats measured in these cases, and especially for eqn. (14), were not reproducible enough for the purpose intended.

EXPERIMENTAL

Chemicals. Red copper(I) oxide was prepared according to Brauer¹³ (p. 755). Electrolytic

analysis for total copper gave 86.5 % Cu(I) + Cu(II). Titrimetric analysis with cerium(IV) gave 86.1 % Cu(I). Theoretically, the compound should contain 88.8 % Cu(I). The low copper content is most probably due to moisture which cannot be removed by heating, however, as the oxide will then decompose. The contamination due to Cu(II) is in any case slight which is the important fact.

Silver oxide was also prepared according to Brauer¹³ (p. 771). Electrolytic analysis gave 93.0 % Ag (theoretically 93.09 %).

Hydrochloric acid and THAM [tris(hydroxymethyl)aminomethane] used for testing the solution calorimeter were of analytical grade.

Sodium perchlorate (Fluka) was mostly used without further purification. A purified⁸ preparation was necessary only for those solutions that must not contain even a trace of halide, i.e. the pure silver perchlorate solutions.

The copper(I) and the ligand solutions were prepared and analyzed as described,⁸ while silver perchlorate solution was prepared by neutralizing silver oxide with perchloric acid.

Titration calorimetry. The calorimeter is that developed by Grenthe *et al.*¹⁴ For shorter periods ($\lesssim 1$ h, sufficient for the measurement of one experimental point), the temperature of the precision thermostat surrounding the calorimeter stayed constant within $\pm 2 \times 10^{-4}$ °C. The room temperature had to be kept at 25.0 ± 0.2 °C.

In the silver measurements the tube delivering the solution T had its tip above the surface of the solution S, as the tip was clogged if immersed. To make sure that only a tiny droplet could possibly stay out of the solution S, a very thin-walled capillary tip was used.

The copper(I) solutions had to be very carefully protected against air. During the whole titration, nitrogen was therefore bubbled through the solution in the calorimeter vessel. In order to get the right vapour pressure and temperature, the gas was bubbled through 5 M sodium perchlorate and then passed through a heat exchanger, placed in the precision thermostat, before entering the calorimeter solution.

Initially 100 cm³ of solution S was equilibrated in the calorimeter which takes ≈ 2 h. The temperature was adjusted so that a steady increase was obtained during the fore-period. Portions of solution T (at most 4 cm³) were then added from a piston burette at a rate of 1 cm³/min. All additions were made at a special "addition temperature" defined as the temperature where mixing of identical solutions causes no change of the temperature. Between each portion added, the calorimeter was cooled, or heated, back to approximately the initial temperature before a new cycle was started.

The titrations were repeated at least once. For heats of the common magnitude of 5 J, the reproducibility was around 1 %, for larger heats the relative error was smaller, for smaller heats larger.

The heat equivalent of the calorimetric system,¹⁴ obtained by electric calibration, was a linear function of the volume added: $\epsilon_V = 2.182 + 2.162 \times 10^{-2}(V - 100)$ J/°C for all solutions of $I = 5$ M (cf. also Ref. 15).

For all calculations referring to titrations performed in homogenous solution, the computer program "Kalori"¹⁶ was used. The errors given in Tables 2 and 3 are three standard deviations, as given by the program.

Heats of dilution. These must be determined in order to obtain the true heats of reaction from the heats actually measured. The determinations are performed by titrations analogous to those just described, but with only one of the reactants present (see, e.g., Ref. 15).

With the range of concentration used, up to 60 mM silver(I) perchlorate, the heat of dilution of Ag⁺ is quite negligible. Likewise, up to the highest concentration of copper(I) used, 65 mM, no measureable heat effect is found when a copper(I) chloride solution of $C_L = 4.9$ M is added to a copper-free chloride solution of the same concentration.

In the present measurements, the concentrations of anions are extraordinarily high, almost 100 times higher than those of silver(I) or copper(I). This applies both to the perchlorate

Table 1. The heats of dilution, in J, of sodium perchlorate and chloride, when a solution T is added into a solution S. All solutions contain 0.1 M HClO₄. Initial volume 100.0 cm³.

Added volume of T/cm ³	S: 1.96 M NaBr	4.9 M NaBr	4.9 M NaCl	4.9 M NaClO ₄	4.9 M NaClO ₄
	T: 4.9 M NaClO ₄	4.9 M NaClO ₄	4.9 M NaClO ₄	4.9 M NaCl	3.9 M NaCl
3	-0.50	-9.96	-5.45	-0.68	+0.41
6	-0.45	-8.96	-4.58	-0.94	+0.23
9	-0.41	-8.13	-4.06	-1.07	+0.12
12		-7.40	-3.56	-1.18	-0.02
15		-6.74	-3.15	-1.28	-0.10
18		-6.16	-2.76		
21		-5.62			

and the halide ions. In some series, the dilution might therefore be very drastic. Consequently, considerable heat effects might be expected and are in fact also found, Table 1. Very striking is, however, that the heat of dilution found when a concentrated, *i.e.* 5 M, perchlorate solution is added to a chloride solution of about the same concentration is much higher than that of the opposite process, *i.e.* addition of chloride to perchlorate. The heat evolved at the addition of perchlorate to bromide is even larger than at the addition to chloride, and the difference is considerable; Table 1. Evidently, the ion solvation in these concentrated solutions differs very much from that in dilute solutions and depends strongly on the properties of the individual ions.

In extreme cases, the correction due to the heat of dilution is almost half of the value actually measured but generally it is much smaller, often $\approx 10\%$.

Reaction solution calorimetry. This calorimeter was also of the isothermal jacket type. Essentially, the design of Sunner and Wadsö¹⁷ has been followed. As the reactions studied here proceeded too slowly in a calorimeter of the original design, however, some modifications have been introduced in order to achieve a better contact between the reacting phases. It was observed that after the ampoule containing the solid phase had been broken, the heavy solid stayed at the bottom of the vessel where the stirring was not very efficient. This was improved by modifying the construction in such a way that the stirrer could be fixed in a lowered position, close to the bottom of the vessel, once the ampoule had been broken. The stirring was further made more efficient

by fixing eight blades on the stirrer, each of an area $\approx 10\text{ mm}^2$. Four of these blades were in the upper part of the solution acting as a left hand screw forcing the liquid down, four were close to the bottom, acting as a right hand screw forcing the liquid upwards. With this arrangement, the solids were dissolved in 15 to 20 min which allows a good measurement. A difficulty with this very efficient stirring was, however, that the circulation of glass fragments from the broken ampoule caused an irregular evolution of friction heat that could not be tolerated. This problem was solved by fastening a platinum net (0.3 mm wire, 0.7×0.7 mm meshes) along the inside of the calorimeter gold-vessel. In this net the fragments were caught. The net should not extend to the bottom of the vessel as this interferes with the stirring of the solid. Instead it is designed like a standing trough with the end ≈ 7 mm above the bottom. With this arrangement, the heat produced in connexion with ampoule breaking was no more than $\Delta H_{\text{br}} = -0.06 \pm 0.03$ J. This value was found by breaking empty ampoules, as the mean of five experiments.

The ampoules used for introducing the solid were of the standard LKB type. The filling with Cu_2O was performed in a nitrogen atmosphere. In these experiments, nitrogen was also bubbled through the solution during the reaction. After the ampoule had been broken, the stirrer was moved up and down three times in order to make it easier to catch the glass fragments before it was finally fixed in the lowered position. In other respects, the experiments were conducted as described before.⁹

The electric calibration gave $\epsilon = 2.035\text{ J}/\Omega$ for 90 ml of a solution of $I = 5\text{ M}$.

Table 2. The silver chloride and bromide systems. Stability constant and thermodynamic functions of the reactions $\text{Ag}^+ + j\text{L}^- \rightarrow \text{AgL}_j^{1-j}$ and $\text{AgL}_3^{2-} + \text{L}^- \rightarrow \text{AgL}_4^{3-}$.

Ligand \rightarrow	j	Cl^-	Br^-
β_j/M^{-j}	3	$(14.0 \pm 1.0) \times 10^5$ ^a	1.2×10^9 ^b
	4	$(2.1 \pm 0.5) \times 10^5$ ^a	1.6×10^9 ^b
$-\Delta G^\circ_{\beta j}/\text{kJ mol}^{-1}$	3	35.1 ± 0.2	51.8
	4	30.6 ± 0.7	52.6
$-\Delta H^\circ_{\beta j}/\text{kJ mol}^{-1}$	3	39.2 ± 4.8	54.6 ± 5.2
	4	62.0 ± 8.4	79.6 ± 1.1
$-\Delta S^\circ_{\beta j}/\text{J mol}^{-1}\text{ K}^{-1}$	3	14 ± 16	9 ± 18
	4	105 ± 29	91 ± 4
$-\Delta G^\circ_4/\text{kJ mol}^{-1}$		-4.5 ± 0.7	0.7
$-\Delta H^\circ_4/\text{kJ mol}^{-1}$		23 ± 10	25 ± 6
$-\Delta S^\circ_4/\text{J mol}^{-1}\text{ K}^{-1}$		92 ± 33	82 ± 18

^a Ref. 20. ^b Ref. 12.

Table 3. The solubility products and the thermodynamic functions for the precipitation of silver halide complexes, at 25 °C.

I^-	Cl^-	Br^-	Cl^-	Br^-	I^-
I	5^a	5^a	0^b	0^b	0^b
K_s	M^3	$(1.14 \pm 0.06)10^{-10}^c$	$(2.20 \pm 0.010)10^{-13}^d$		
$-\Delta G_{pr}^\circ$	kJ mol^{-1}	56.76 ± 0.14	72.26 ± 0.12	55.65	70.21
$-\Delta H_{pr}^\circ$	kJ mol^{-1}	62.7 ± 0.9	80.0 ± 0.5	65.7	84.8
$-\Delta S_{pr}^\circ$	$\text{JK}^{-1} \text{mol}^{-1}$	20 ± 3	26 ± 2	33.8	49.0

^a Present work. ^b Ref. 21. ^c From values of K_s determined ²⁰ at $I = 5 \text{ M}$ and $1 < [Cl^-] < 2.5 \text{ M}$. ^d From values of K_s determined ¹³ at $I = 5 \text{ M}$ and $1 < [Br^-] < 2.5 \text{ M}$.

The accuracy of the calorimeter was tested by dissolving varying amounts (60–150 mg) of THAM in 90 cm³ 0.100 M hydrochloric acid. A value of $-\Delta H = 29.77 \pm 0.11 \text{ kJ/mol}$ was found, in perfect agreement with the value considered as the "best" one,¹⁹ $-\Delta H = 29.75 \text{ kJ/mol}$.

RESULTS

Silver (I) complexes. The results of the homogeneous titrations are shown in Table 2. For the chloride system, the values of $\Delta H^\circ_{\beta_j}$ are unfortunately not very precise. This is due to the slight variation of \bar{n} within the range of C_L available and, in the case of $\Delta H^\circ_{\beta_4}$, also to the poor precision ²⁰ of β_4 . The lowest value of C_L compatible with a sufficiently high solubility is $\approx 1.9 \text{ M}$, corresponding to $\bar{n} = 3.22$, while even at the highest value of C_L used, 4.6 M, the value of \bar{n} reached is not higher than 3.40. For the bromide systems, where it is possible to use a value of C_L as low as $\approx 0.5 \text{ M}$, the conditions are more favourable.^{10,8} This lower limit of C_L corresponds to $\bar{n} = 3.37$ while at the upper limit of $C_L = 4.9 \text{ M}$, $\bar{n} = 3.86$. Consequently, the precision of $\Delta H^\circ_{\beta_4}$ is quite good while that of $\Delta H^\circ_{\beta_3}$ is still mediocre. The precision of the values of $\Delta S^\circ_{\beta_j}$ follows, of course, the same pattern, Table 2.

In the range of concentrations investigated here, the values of $\Delta H^\circ_{\beta_j}$ are independent of C_M . Consequently, no polynuclear complexes are formed.

The results of the heterogeneous titrations are in Table 3. In the case of chloride, the value of ΔH°_{pr} is the mean of seven experiments. In each, $\approx 30 \mu\text{mol}$ of Ag^+ is added to a 2 M chloride solution, already in equilibrium with

$AgCl(s)$ [cf. eqn. (4)]. In the case of bromide, four experiments were performed by adding $\approx 90 \mu\text{mol}$ Ag^+ to a 2 M bromide solution, and four by adding $\approx 30 \mu\text{mol}$ Ag^+ to a 1 M bromide solution. The value of ΔH°_{pr} is the mean of all eight experiments. As the precipitation reactions are simple and complete and the values of K_s well-known, all the thermodynamic functions can be calculated with a rather high degree of precision.

The thermodynamics of the precipitation of the silver halides has been frequently studied in the past. Recently, a very careful determination of ΔH°_{pr} for $AgCl$, $AgBr$ and AgI has been performed by Wagman and Kilday.²¹ With a reaction solution calorimeter, they measured the heats of transforming $AgNO_3(s)$ into $AgL(s)$ by means of potassium halide solutions and also the heats of the reciprocal reactions, transforming $KL(s)$ into $AgL(s)$ by means of a silver nitrate solution. Combined with the heats of solution of $AgNO_3(s)$ and $KL(s)$, respectively, which were also measured, these heats of transformation yield ΔH°_{pr} . Very nearly the same values are obtained by the two approaches. The values are corrected to $I = 0$. Values of ΔG°_{pr} at $I = 0$ are selected and corresponding values of ΔS°_{pr} calculated. The functions thus found are listed in Table 3. The differences between the values of ΔH°_{pr} determined at $I = 0$ and 5 M are modest, $\approx 4 \text{ kJ mol}^{-1}$ for both the chloride and the bromide system.

Wagman and Kilday also give an extensive survey of previous investigations of the thermodynamics of silver halide precipitation. These include the classical calorimetric measurements of ΔH°_{pr} by Berthelot^{22,23} and by Thomsen,²⁴ and also the very early potentiometric deter-

Table 4. Silver bromide system. Determination of $\Delta H^\circ_{\beta_4}$, by reaction solution calorimetry. Values of ΔH° in kJ mol⁻¹.

Solid	$-\Delta H^\circ_A$	$-\Delta H^\circ_B$	$-H^\circ_C$	$-H^\circ_{\beta_4}$
Ag ₂ O	54.7 ± 1.3	213.8 ± 1.5	79.5 ± 1.4	82.8 ± 2.2
AgBr		$\Delta H^\circ_D = 3.9 \pm 0.5$	76.1 ± 1.0	79.3 ± 1.8

minations of ΔG°_{pr} by Goodwin,²⁵ all resulting in values close to those accepted today.

In Table 4, the results of the solution of Ag₂O(s) and AgBr(s) are presented. In the case of Ag₂O, both ΔH°_A and ΔH°_B are the mean values of six experiments where 65 to 200 μmol have been dissolved in 0.1 M acid, or in 4.9 M bromide solution of an acidity = 0.1 M, respectively. In the case of AgBr, ΔH°_D is the mean of five experiments where 130 to 370 μmol have been dissolved in the bromide solution. As the value of ΔH°_{pr} refers to the formation of wet AgBr(s), the values actually measured at the solution of dry AgBr(s) have been corrected for the enthalpy of wetting. The correction is quite small, however, *viz.* -0.45 ± 0.06 kJ mol⁻¹. Moreover, as $\bar{n} = 3.87$ is so close to 4, the correction from ΔH°_C to $\Delta H^\circ_{\beta_4}$ does not introduce any large error, in spite of the rather large error of ΔH°_4 , Table 2.

For the bromide system, the value of $\Delta H^\circ_{\beta_4}$ has thus been determined by three different

calorimetric methods. The results agree in a very satisfactory manner, Table 5. A somewhat higher precision is achieved by titration than by solution calorimetry, but the difference is by no means large. The modified reaction solution calorimeter works well and is evidently able to handle also reactions which are too slow for the old design.

As pointed out earlier, the slightly soluble silver halide systems are not especially well suited to calorimetric work. Indeed they exemplify systems where determination of the thermodynamic functions by means of the temperature coefficient method might be competitive. Such an investigation of the silver bromide system has in fact recently been performed.²⁶ The results, referring to a 4.6 M sodium nitrate medium, are also listed in Table 5. As might be expected the drastic qualitative change of the medium markedly influences the stability constants. Much the same value of $\Delta H^\circ_{\beta_3}$ is found as in the present

Table 5. The silver(I) bromide system. Comparison of the thermodynamic functions found by different methods, at 25 °C.

	<i>j</i>	Present work			Ref. 26
		<i>a</i>	<i>b</i>	<i>c</i>	<i>d</i>
$-\Delta G^\circ_{\beta_j}/\text{kJ mol}^{-1}$	2				42.6
	3	51.8 ^e	<i>f</i>	<i>f</i>	45.0
	4	52.5 ^e	<i>f</i>	<i>f</i>	48.6
$-\Delta H^\circ_{\beta_j}/\text{kJ mol}^{-1}$	2				44
	3	54.6 ± 5.2			54
	4	79.6 ± 1.1	82.8 ± 2.2	79.3 ± 1.8	67
$-\Delta S^\circ_{\beta_j}/\text{J mol}^{-1} \text{K}^{-1}$	2				5
	3	9 ± 18			30
	4	91 ± 4	101 ± 8	90 ± 7	62

^a Titration calorimetry. ^b Solution of Ag₂O(s). ^c Solution of AgBr(s) combined with precipitation of AgBr(s). ^d In 4.6 M NaNO₃; from the temperature coefficient of β_j . ^e Ref. 12. ^f The same values of ΔG_{β_j} (see note e) have been used for all calculations referring to the present work.

Table 6. Copper(I) chloride system. The thermodynamic functions for the reaction $\text{CuCl}_2 + \text{Cl}^- \rightarrow \text{CuCl}_3^{2-}$, at 25 °C.

$I \rightarrow$	5^a	5^b	2^b
K_3 , M^{-1}	0.76 ± 0.10	1.3	2.6
$-\Delta G^\circ$, kJ mol^{-1}	-0.7 ± 0.2	0.7	2.4
$-\Delta H^\circ$, kJ mol^{-1}	19.9 ± 0.7	7.7	11.2
$-\Delta S^\circ$, $\text{J K}^{-1} \text{mol}^{-1}$	69 ± 3	23	30

^a Present work, sodium chloride-perchlorate medium, acidity = 0.1 M. ^b Ref. 27, hydrochloric-perchloric acid medium.

investigation while the value of $\Delta H^\circ_{\beta_4}$ differs considerably.

Copper(I) complexes. Titration calorimetry has been possible only in the case of the chloride system, cf. eqn. (5). The value of C_L has been varied between 0.49 and 4.87 M, corresponding to a variation of \bar{n} between 2.23 and 2.77. With the seemingly reliable value of K_3 available,⁸ the data allow the calculation of a good value of ΔH°_3 , listed in Table 6, together with the corresponding values of ΔG°_3 and ΔS°_3 .

Within the range of C_M used ΔH°_3 is independent of C_M which implies that the formation of polynuclear complexes is insignificant at these concentrations of copper(I). This is in accordance with the results of the stability measurements.⁹

Recently,¹⁷ values of ΔH°_3 for the copper(I) chloride system have also been determined by dissolving $\text{CuCl}_2(\text{s})$ in hydrochloric acid of varying concentration, at 15, 25 and 35 °C. Media of $I = 2, 3, 4$ and 5 are brought about by means of perchloric acid. Values of ΔG°_3 are selected for the various media and temperatures used, and corresponding values of ΔS°_3 calculated. In Table 6, the values referring to $I = 2$ M and 5 M, at 25 °C, have been listed. They differ considerably from our results. Partly, this is certainly due to the large qualitative difference of medium. It might also be, however, that the values of K_3 selected are not the most probable ones. If so, the values of ΔH°_3 might easily get rather far off the mark, as they are quite sensitive to changes in the values of K_3 .

The results of the solution of $\text{Cu}_2\text{O}(\text{s})$ are presented in Table 7. Each value of ΔH°_E is the mean of four or five determinations. In the

chloride and bromide solutions, 70 to 280 μmol have been dissolved in each experiment, in the iodide solutions only 30 to 60 μmol . Less oxide was used in the latter case in order to avoid the formation of polynuclear complexes which are formed more readily in the iodide system.⁸ In the present solutions, their concentrations should be $< 2\%$. That only insignificant amounts are formed is also proved by the fact that the values of ΔH°_E found are independent of C_M .

For the chloride system, the precise value of ΔH°_3 obtained by titration calorimetry permits the calculation of a good value of ΔH°_{E3} . As to the bromide system, $\bar{n} \approx 3$ and consequently $\Delta H^\circ_E \approx \Delta H^\circ_{E3}$. Also this quantity has a small random error. For the iodide system, finally, the random errors are so large that no significant difference was found between the values of ΔH°_E measured at $\bar{n} = 3.18$ and 3.27 . This shows, on the other hand, that ΔH°_{E3} must have much the same value, admittedly only within the fairly wide limits of error.

From the values of ΔH°_{E3} thus found, the differences $\Delta H^\circ_{\beta_3}(\text{L}') - \Delta H^\circ_{\beta_3}(\text{L}'')$ have been calculated [eqn. (12)]. As the corresponding differences $\Delta G^\circ_{\beta_3}(\text{L}') - \Delta G^\circ_{\beta_3}(\text{L}'')$ are known

Table 7. Copper(I) halide systems. Dissolution of $\text{Cu}_2\text{O}(\text{s})$ in acid halide solutions.

L^-	C_L/M	\bar{n}	$-\Delta H^\circ_E/\text{kJ mol}^{-1}$	$-\Delta H^\circ_{E3}/\text{kJ mol}^{-1}$
Cl^-	4.88	2.77	50.8 ± 1.2	57.7 ± 1.4
Br^-	3.98	2.98	80.8 ± 0.5	81 ± 1
I^-	4.00	3.27	156.7 ± 2.5	156 ± 5
	2.50	3.18	156.9 ± 3.5	

Table 8. The copper(I) halide systems. The differences between the thermodynamic functions for the reactions $\text{Cu}^+ + 3\text{L}^- \rightarrow \text{CuL}_3^{2-}$, $\text{L} = \text{Cl}^-, \text{Br}^-, \text{I}^-$. The values refer to ligand substitution according to $\text{CuL}_3'' + 3\text{L}' \rightarrow \text{CuL}_3' + 3\text{L}''$.

	$\text{L}' = \text{Br}^-$ $\text{L}'' = \text{Cl}^-$	$\text{L}' = \text{I}^-$ $\text{L}'' = \text{Br}^-$
$\Delta G^\circ_{\beta_3}(\text{L}') - \Delta G^\circ_{\beta_3}(\text{L}'')/\text{kJ mol}^{-1}$	-8.61 ± 0.13	-17.03 ± 0.12
$\Delta H^\circ_{\beta_3}(\text{L}') - \Delta H^\circ_{\beta_3}(\text{L}'')/\text{kJ mol}^{-1}$	-12 ± 1	-38 ± 3
$\Delta S^\circ_{\beta_3}(\text{L}') - \Delta S^\circ_{\beta_3}(\text{L}'')/\text{J mol}^{-1} \text{K}^{-1}$	-11 ± 3	-69 ± 10

from the stability measurements, $\Delta S^\circ_{\beta_3}(\text{L}') - \Delta S^\circ_{\beta_3}(\text{L}'')$ can also be calculated. The values found have been listed in Table 8.

DISCUSSION AND CONCLUSIONS

All the reactions studied involving the formation of halide complexes of silver(I) and copper(I) in aqueous solution are without exception exothermic; Tables 2, 5 and 6. Though the data are not complete, it can further be safely assumed that the enthalpy changes become more negative in the order $\text{Cl}^- < \text{Br}^- < \text{I}^-$, cf. Tables 2 and 8. Also the precipitation of the silver halides follow the same pattern, Table 3. This behaviour is certainly to be expected for interactions taking place in aqueous solution between soft metal ions, like the present ones, and the heavy halides, the softness of which increases in the order mentioned. The thermodynamics indicates that the bonds are markedly covalent, and the covalent character is strengthened as the ligand becomes softer.^{29,1,2}

The entropy changes are also all negative which means that they counteract the complex formation, as well as the precipitation of solid halides, Tables 2, 3, 5 and 6. This is because these monovalent metal ions are so poorly hydrated that the order of the systems is improved by the complex formation, and by the precipitation of crystalline solids. The entropy changes generally become more unfavourable as the ligand increases in size and consequently, becomes less strongly hydrated,²⁸ Tables 3 and 8. At the formation of the third and fourth chloride and bromide complexes of silver(I), however, the entropy changes are practically the same for both ligands, Table 2.

Also when the entropy changes become more negative in the usual sequence this does not at all compensate the simultaneous decrease of

the enthalpies. On the balance, a considerable net increase of the stabilities takes place⁸ in the order $\text{Cl}^- < \text{Br}^- < \text{I}^-$, although of course markedly smaller than would follow from the enthalpy changes alone.

Unfortunately, a comparison between the enthalpy changes of analogous reactions of silver(I) and copper(I) is possible only in one case, viz. between the values of $\Delta H^\circ_{\beta_3}(\text{Br}) - \Delta H^\circ_{\beta_3}(\text{Cl})$, characterizing the reaction of eqn. (13). The values found are for silver(I) -15 ± 10 kJ and for copper(I) -12 ± 1 kJ, Tables 2 and 8. The experimental error of the silver value is large enough to cover a significant difference between the two acceptors but evidently not a very large one. For the divalent d^{10} acceptor mercury(II), with coordinating properties similar to silver(I) and copper(I), this difference is significantly more negative,³⁰ viz. -35 ± 7 kJ, at $I = 3$ M and 25°C . This trend is even more obvious at the formation of the highest complexes ML_4 which can be studied in the case of silver(I) and mercury(II). The values of $\Delta H_{\beta_4}(\text{Br}) - \Delta H_{\beta_4}(\text{Cl})$ are -18 ± 9 kJ (Table 2) and -47 ± 3 kJ, respectively.³⁰

Acknowledgement. We gratefully acknowledge the generous support given to this work by the Swedish Natural Science Research Council.

REFERENCES

1. Ahrland, S. *Struct. Bonding (Berlin)* 5 (1968) 118.
2. Ahrland, S. *Struct. Bonding (Berlin)* 15 (1973) 167.
3. Schwarzenbach, G. *Pure Appl. Chem.* 24 (1970) 307.
4. McAuley, A. and Nancollas, G. *J. Chem. Soc.* (1963) 989.
5. Choppin, G. R. and Schneider, J. K. *J. Inorg. Nucl. Chem.* 32 (1970) 3283.
6. de Carvalho, R. G. and Choppin, G. R. *J. Inorg. Nucl. Chem.* 29 (1967) 725, 737.

7. Ahrland, S. In Lagowski, J. J., Ed., *The Chemistry of Non-Aqueous Solvents*, Academic, New York 1977, Vol. 5.
8. Ahrland, S. and Tagesson, B. *Acta Chem. Scand. A* 31 (1977) 615.
9. Ahrland, S. and Rawsthorne, J. *Acta Chem. Scand.* 24 (1970) 157.
10. Leden, I. *Acta Chem. Scand.* 10 (1956) 540, 812.
11. Leden, I. and Nilsson, R. *Z. Naturforsch. Teil A* 10 (1955) 67.
12. Berne, E. and Leden, I. *Z. Naturforsch. Teil A* 8 (1953) 719.
13. Brauer, G. *Handbuch der preparativen anorganischen Chemie*, Enke, Stuttgart 1954.
14. Grenthe, I., Ots, H. and Ginstrup, O. *Acta Chem. Scand.* 24 (1970) 1067.
15. Ahrland, S. and Kullberg, L. *Acta Chem. Scand.* 25 (1971) 3471.
16. Karlsson, R. and Kullberg, L. *Chem. Scr.* 9 (1976) 54.
17. Sunner, S. and Wadsö, I. *Science Tools* 13 (1966) 1.
18. Kullberg, L. *Acta Chem. Scand. A* 28 (1974) 979.
19. Hill, J. O., Öjelund, G. and Wadsö, I. *J. Chem. Thermodyn.* 1 (1969) 11.
20. Leden, I. *Sven. Kem. Tidskr.* 64 (1952) 249.
21. Wagman, D. D. and Kilday, M. V. *J. Res. Natl. Bur. Stand. Sect. A* 77 (1973) 569.
22. Berthelot, M. *Ann. Chim. Phys.* [5] 4 (1875) 160.
23. Berthelot, M. *C. R. Acad. Sci.* 93 (1881) 870.
24. Thomsen, J. *Thermochemical Investigations*, Barth, Leipzig 1883, Vol. 3.
25. Goodwin, H. M. *Z. Phys. Chem.* 13 (1894) 577.
26. Pouradier, J. and Pailliotet, A. *C. R. Acad. Sci. Ser. C* 280 (1975) 1049.
27. Vasil'ev, V. P. and Kunin, B. T. *Russ. J. Inorg. Chem.* 20 (1975) 1050.
28. Morris, D. F. C. *Struct. Bonding (Berlin)* 4 (1968) 63.
29. Ahrland, S. *Helv. Chim. Acta* 50 (1966) 306.
30. Arnek, R. *Ark. Kemi* 26 (1965) 531.

Received May 11, 1977.

The Disordered Structure of Ammonium Pentafluoroperoxotitanate(IV), $(\text{NH}_4)_3[\text{TiF}_5(\text{O}_2)]$

ROLF STOMBERG and ING-BRITT SVENSSON

Department of Inorganic Chemistry, Chalmers University of Technology and University of Göteborg, P.O. Box, S-402 20 Göteborg 5, Sweden

Ammonium pentafluoroperoxotitanate(IV) has a disordered structure at room temperature for which a possible model is suggested. This model is based on single crystal X-ray diffraction data collected by the integrating Weissenberg film method. The crystals are cubic, space group $Fm\bar{3}m$, with $a = 9.231(5)$ Å, $V = 787(1)$ Å³ and $Z = 4$. Least squares refinement of the structural parameters yielded a final R -value of 0.058, based on 68 independent reflexions. The average distance between titanium and the ligand atoms is 1.94(2) Å. The data are consistent with a statistically oriented pentagonal bipyramidal complex anion, and three ammonium ions, one of which is also statistically oriented.

The structure of $(\text{NH}_4)_3[\text{TiF}_5(\text{O}_2)]$ has been studied as part of an investigation on transition metal peroxo complexes. From powder data,¹ Peyronel suggested that the structure was disordered and could be described in a similar way as that used by Hampson and Pauling² for $(\text{NH}_4)_3[\text{ZrF}_7]$, *i.e.* with $[\text{TiF}_5(\text{O}_2)]^{3-}$ as a capped octahedron. Since the space group is $Fm\bar{3}m$ it is evident that an ordered structure is impossible. The model proposed by Peyronel is, however, not the only possible one. In fact, a transition metal peroxo complex with mono-capped octahedral symmetry is highly unlikely in view of existing knowledge concerning the structures of such compounds. Instead, a pentagonal bipyramidal arrangement of ligand atoms seems more natural. In a re-investigation³ of $(\text{NH}_4)_3[\text{ZrF}_7]$, the $[\text{ZrF}_7]^{3-}$ ion has been shown to have a pentagonal bipyramidal configuration. The present investigation was undertaken in order to elucidate the structure of the $[\text{TiF}_5(\text{O}_2)]^{3-}$ ion.

EXPERIMENTAL

The compound was prepared according to Piccini,⁴ whose method gave small, pale yellow octahedral crystals. The intensity data were collected with an integrating Weissenberg camera using $\text{CuK}\alpha$ radiation. A total of 68 independent reflexions were recorded by the multiple film method. The intensities of the reflexions were estimated visually and corrected for Lorentz and polarization effects but not for absorption and extinction.

A powder photograph of the substance, taken with $\text{CuK}\alpha$ radiation in a Guinier camera with lead nitrate as internal standard, was used to determine the cell dimensions accurately. Observed and calculated d -values are given in Table 1. All calculations were performed at the Göteborg Universities' Computing Centre using an IBM 360/65 computer and a set of crystallographic programs in use at Göteborg. The atomic scattering factors used in the calculation of structure factors were taken from Cromer and Waber.⁵

Table 1. Observed lines in the powder photograph of $(\text{NH}_4)_3[\text{TiF}_5(\text{O}_2)]$ at room temperature registered with $\text{CuK}\alpha$ radiation, using lead nitrate ($a = 7.8566$ Å) as internal standard.

d_o	d_c	$h k l$	I_o
5.334	5.325	1 1 1	vs
4.618	4.611	2 0 0	s
3.261	3.261	2 2 0	s
2.6635	2.6625	2 2 2	vw
2.3064	2.3059	4 0 0	s
2.0607	2.0624	4 2 0	w
1.8824	1.8828	4 2 2	m
1.7762	1.7751	5 1 1	m
		3 3 3	
1.6298	1.6305	4 4 0	w

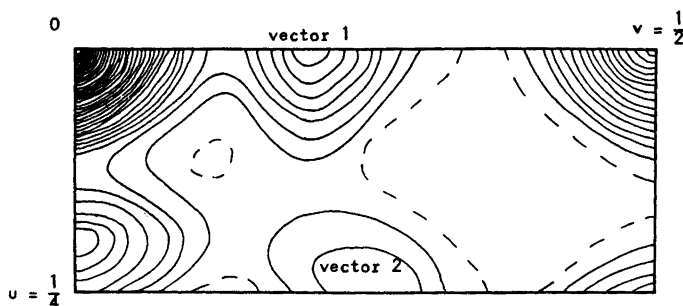


Fig. 1. The Patterson function $P(uvw)$ at $w=0$.

CRYSTAL DATA

$(\text{NH}_4)_3[\text{TiF}_6(\text{O}_2)]$; $M = 229.0 \text{ g mol}^{-1}$
 Cubic, $Fm\bar{3}m$ (No. 225), $Z = 4$
 $a = 9.231(5) \text{ \AA}$ (Peyronel;¹ $a = 9.20 \text{ \AA}$)
 $V = 787(1) \text{ \AA}^3$
 $D_c = 1.934 \text{ g cm}^{-3}$
 $\mu(\text{CuK}\alpha) = 103 \text{ cm}^{-1}$

A list of observed and calculated structure factors is available from the author R.S. on request.

STRUCTURE DETERMINATION

The unit cell contains four formula units. The four titanium atoms thus might occupy the positions $4a$ of space group $Fm\bar{3}m$. The Patterson function ought to resemble the structure since vectors involving the titanium atoms will appear at atomic positions if the titanium atoms are not disordered and thus occupy the positions $4a$. The Patterson function (the section at $w=0$ is given in Fig. 1) showed two crystallographically independent diffuse peaks at about 2 \AA from the origin, which were interpreted as Ti-F and Ti-O vectors. Fluorine and oxygen atoms thus occupy two positions (denoted by 1 and 2) of the type $0yz$. Vectors at $\frac{1}{2}00$ and $\frac{1}{4}\frac{1}{4}\frac{1}{4}$ were interpreted as Ti-N(1) and Ti-N(2) vectors. The data could not be analysed in terms of ordered fluorine and oxygen atoms. Furthermore, since it was evident that it would not be possible to distinguish between oxygen and fluorine, all atoms coordinated to titanium were treated as fluorine atoms (F(1) and F(2), respectively). The disordered fluorine and oxygen electron

distribution was accounted for in the calculated structure factors by introducing partial fluorine atoms within the disordered peaks in such a way that the observed peak shapes were reproduced. Since the ratio between the heights of the Patterson peaks 1 and 2 is about 2.5 and there is a total of twenty-eight oxygen and fluorine atoms, vector 1 was accounted for by twenty partial fluorine (and oxygen) atoms F(1) in positions $96j$ of space group $Fm\bar{3}m$ while vector 2 was taken to be due to eight partial fluorine (and oxygen) atoms F(2), also in positions $96j$.

A least-squares refinement was undertaken at this stage. After three cycles of refinement the R -value was 0.083. Both an electron density map and a difference map were calculated. The latter showed the hydrogen atoms H(1) and H(2) bonded to N(1) and N(2), respectively. Since there were six peaks around N(1) it was apparent that the hydrogen atoms H(1) were also disordered. Introduction of these hydrogen atoms, with appropriate occupancy factors, into the least-squares refinement reduced the R -value to 0.058 after three more cycles. The temperature parameters of the hydrogen atoms were kept constant and were given the value $B = 5.0 \text{ \AA}^2$. All shifts were less than 10 % of the corresponding standard deviations after the last cycle. The results from the refinement were checked by calculating a three-dimensional electron density difference map. This showed only small residual maxima, the largest maximum having a magnitude of about 5 % of the height of a nitrogen peak in the F_0 -synthesis. The atomic parameters are given in Table 2.

Table 2. Atomic coordinates, expressed as fractions of the cell edges, and isotropic thermal parameters for $(\text{NH}_4)_3[\text{TiF}_5(\text{O}_2)]$. Space group $Fm\bar{3}m$, $Z=4$. The numbers in parentheses are the standard deviations of the last significant figures. The temperature factor = $\exp(-B \sin^2 \theta/\lambda^2)$. The thermal parameters of the hydrogen atoms were assigned the value 5.0 \AA^2 and were not refined. Note that F(1) and F(2) include the oxygen atoms as well.

Atom	Position	Occupancy factor	x	y	z	B
Ti	4a	1	0	0	0	3.07(9)
N(1)	4b	1	$\frac{1}{2}$	$\frac{1}{2}$	$\frac{1}{2}$	4.9(7)
N(2)	8c	1	$\frac{1}{4}$	$\frac{1}{4}$	$\frac{1}{4}$	5.0(3)
F(1)	96j	0.208	0	0.046(1)	0.205(1)	4.9(3)
F(2)	96j	0.083	0	0.112(3)	0.180(3)	5.4(6)
H(1)	24e	0.667	0.388(13)	0	0	5.0
H(2)	32f	1	0.185(6)	0.185(6)	0.185(6)	5.0

DISCUSSION

The capped octahedron model proposed by Hampson and Pauling for ammonium heptafluorozirconate and applied to ammonium pentafluoroperoxotitanate by Peyronel is without doubt incorrect since this requires fluorine and oxygen atoms along the [111] direction and a slight disorder of the heavy atoms. These conditions were not observed. Instead, the many partial fluorine and oxygen sites are consistent with a disordered orientation of an ordered pentagonal bipyramidal arrangement of ligands (Fig. 2) such as that found in the ion $[\text{NbF}_5(\text{O}_2)]^{2-}$.

The observed interatomic distances

Ti—F(1)	1.938(14) Å
Ti—F(2)	1.959(39) Å
N(1)—H(1)	1.03(12) Å
N(2)—H(2)	1.04(9) Å

are very probable, which is a further indication of the correctness of the structure.

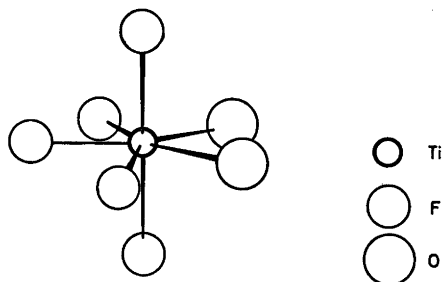


Fig. 2. The ion $[\text{TiF}_5(\text{O}_2)]^{2-}$.

Acta Chem. Scand. A 31 (1977) No. 8

REFERENCES

1. Peyronel, G. *Gazz. Chim. Ital.* 71 (1941) 620.
2. Hampson, G. C. and Pauling, L. *J. Am. Chem. Soc.* 60 (1938) 2702.
3. Hurst, H. J. and Taylor, J. C. *Acta Crystallogr. B* 26 (1970) 417.
4. Piccini, A. *Z. Anorg. Allg. Chem.* 10 (1895) 438.
5. Cromer, D. T. and Waber, J. T. *Acta Crystallogr.* 18 (1965) 104.
6. Stomberg, R. *To be published.*

Received April 27, 1977.

Crystal Structure of Manganese(III) Hydrogen Selenite Diselenite, $\text{MnH}(\text{SeO}_3)(\text{Se}_2\text{O}_5)$

MARKUS KOSKENLINNA and JUSSI VALKONEN

Department of Chemistry, Helsinki University of Technology, Otaniemi, SF-02150 Espoo 15, Finland

The crystal structure of manganese(III) hydrogen selenite diselenite, $\text{MnH}(\text{SeO}_3)(\text{Se}_2\text{O}_5)$, has been determined by X-ray methods. The compound is monoclinic, and belongs to the space group $P2_1/n$ with $Z=4$. The cell dimensions are $a=7.451(2)$ Å, $b=12.583(4)$ Å, $c=7.575(2)$ Å and $\beta=92.82(2)^\circ$. The structure was solved by direct methods, and refined to $R=0.035$.

The MnO_6 -octahedron is distorted by Jahn-Teller forces, with Mn—O bonds ranging from 1.916 Å to 2.179 Å. The compound contains both selenite and diselenite groups, which act as bridging ligands between two and three Mn atoms, respectively. The Se—O bonds range between 1.662 and 1.776 Å in the selenite and between 1.664 and 1.803 Å in the diselenite group.

The structural features of Mn(III) compounds are of interest because of the high spin d^4 -configuration leading to Jahn-Teller distortions of the coordination polyhedron around the central atom. As a part of our studies on the manganese selenites we described the preparation and structure of $\text{Mn}_2(\text{SeO}_3)_3 \cdot 3\text{H}_2\text{O}$, a compound having tetragonally elongated MnO_6 -octahedra.¹ Recently it was found that a praseodymium compound with both a selenite and a diselenite group as a ligand could be prepared.² We report now the preparation and structure of $\text{MnH}(\text{SeO}_3)(\text{Se}_2\text{O}_5)$.

EXPERIMENTAL

Manganese(III) hydrogen selenite diselenite, $\text{MnH}(\text{SeO}_3)(\text{Se}_2\text{O}_5)$, was prepared in two stages. First, freshly precipitated, hydrated manganese dioxide and a concentrated solution (1 mol/dm³) of selenous acid were placed in a steel reactor with Teflon lining, and the

suspension was held at 140 °C for 1–3 weeks. A red, amorphous manganese selenite precipitation was obtained. This was filtered off and placed a second time in the reactor at 140 °C, with an excess of 1 mol/dm³ selenous acid. The tightness of the sealing of the reactor was so adjusted that all the water was able to escape within 2–3 days and thus the SeO_2 concentration was gradually increased. When the resulting white mass consisting mainly of SeO_2 was extracted with water, the dark-red, lustrous, well-developed prisms of $\text{MnH}(\text{SeO}_3)(\text{Se}_2\text{O}_5)$ remained in the residue.

The intensities of 1366 reflections with $I > 3\sigma$ (I) were measured between $5^\circ < 2\theta < 55^\circ$ in a θ – 2θ scan, using a Syntex $P2_1$ (fortran version) automatic four-circle diffractometer and graphite monochromatized $\text{MoK}\alpha$ -radiation. The scan speed was $2^\circ/\text{min}$. The size of the crystal was approximately $0.2 \times 0.2 \times 0.2$ mm³. The unit cell dimensions were obtained by measuring 25 independent reflections from the random-orientation rotation photograph and centering their positional parameters with the diffractometer. The unit cell dimensions for the selected set of axes are, after least-squares treatment $a=7.451(2)$ Å, $b=12.583(4)$ Å, $c=7.575(2)$ Å and $\beta=92.82(2)^\circ$ and the unit cell belongs to the space group $P2_1/n$ according to the systematic absences $h0l$ with $h+l=2n+1$ and $0k0$ with $k=2n+1$. Calculated density for the crystals was 3.94 g/cm³. There are four formula units in the unit cell. Lorentz, polarization and empirical absorption corrections (from the ϕ -scan data, $\mu=170.5$ cm⁻¹) were applied to the data.

Neutral atoms were presumed in the solving and refinement of the structure and the values for their scattering factors were obtained from the International Tables.³ All the calculations were performed on a Univac 1108 computer using the X-Ray 1976 program package.⁴ The structure was solved by direct methods with 208 E -values bigger than 1.4. The E -map gave the sites of the Se and Mn atoms. These were then refined to an R of 17.9 %, and the subse-

Table 1. Atomic coordinates and anisotropic temperature coefficients with their estimated standard deviations. The temperature coefficients are of the form $\exp[-2\pi^2(h^2a^{*2}U_{11} + k^2b^{*2}U_{22} + l^2c^{*2}U_{33} + 2hka^*b^*U_{12} + 2hla^*c^*U_{13} + 2klb^*c^*U_{23})]$, and have been multiplied by 10⁴.

Atom	<i>x</i>	<i>y</i>	<i>z</i>	<i>U</i> ₁₁	<i>U</i> ₂₂	<i>U</i> ₃₃	<i>U</i> ₁₂	<i>U</i> ₁₃	<i>U</i> ₂₃
Mn	.4387(2)	.6792(1)	.3055(2)	80(6)	53(6)	68(6)	6(5)	15(5)	5(5)
Se1	.0520(1)	.7988(1)	.3869(1)	107(4)	84(4)	90(4)	18(3)	27(3)	10(3)
Se2	.0668(1)	.6330(1)	.0677(1)	109(4)	85(4)	94(4)	-13(3)	5(3)	-1(3)
Se3	.7258(1)	.5148(1)	.4281(1)	109(1)	78(4)	128(4)	11(3)	16(3)	7(3)
O1	.5337(9)	.7647(6)	.0780(8)	187(36)	128(34)	95(31)	-53(28)	48(26)	-25(26)
O2	.2742(9)	.7930(6)	.3440(9)	121(32)	107(32)	189(34)	-8(27)	47(26)	-19(28)
O3	.2667(9)	.5970(6)	.1577(10)	139(34)	117(33)	204(36)	27(27)	-11(28)	8(28)
O4	.6222(9)	.7603(6)	.4510(9)	115(32)	181(35)	97(31)	48(27)	15(25)	42(27)
O5	.8891(10)	.0720(6)	.2466(9)	178(35)	165(36)	87(31)	-59(29)	47(26)	21(27)
O6	.6099(10)	.4040(6)	.4583(9)	198(36)	107(33)	143(33)	34(28)	54(27)	79(27)
O7	.6001(11)	.9606(6)	.1963(11)	247(42)	155(38)	328(45)	-57(32)	148(35)	-82(33)
O8	.5384(10)	.1930(6)	.2511(9)	158(34)	268(42)	129(33)	50(31)	67(27)	46(31)

Table 2. Selected bond distances (Å) and angles (°). The estimated standard deviations are in parentheses.

Mn-O1	2.179(7)	Se1-O1	1.664(7)	O1-Se1-O2	105.5(3)
Mn-O2	1.916(7)	Se1-O2	1.705(7)	O1-Se1-O8	96.1(3)
Mn-O3	1.956(7)	Se1-O8	1.803(8)	O2-Se1-O8	101.3(3)
Mn-O4	1.994(7)	Se2-O8	1.781(8)	O8-Se2-O3	102.6(3)
Mn-O5	1.916(7)	Se2-O3	1.670(7)	O8-Se2-O4	101.4(4)
Mn-O6	2.119(7)	Se2-O4	1.671(7)	O3-Se2-O4	101.3(3)
				Se1-O8-Se2	126.4(4)
O1-Mn-O6	170.8(3)	Se3-O5	1.700(7)		
O2-Mn-O5	175.7(3)	Se3-O6	1.662(7)	O5-Se3-O6	102.5(3)
O3-Mn-O4	177.7(3)	Se3-O7	1.776(8)	O5-Se3-O7	95.9(4)
O1-Mn-O3	92.2(3)			O6-Se3-O7	98.6(4)
O4-Mn-O5	91.5(3)				
O2-Mn-O6	95.9(3)				

quent difference Fourier map revealed the sites of all the O atoms. After refinement with isotropic temperature factors the value of *R* was 4.3 %, and with anisotropic temperature factors, after block-diagonal refinement, 3.5 %.

The $|F_o|$ and $|F_c|$ listing is available from the authors upon request.

DISCUSSION

The atomic coordinates and anisotropic temperature coefficients are given in Table 1. The seleniums Se1 and Se2 belong to a diselenite ion and Se3 to a selenite ion. In Table 2 some characteristic bond lengths and angles are given.

The compound contains both selenite and diselenite groups. One of the Se-O bonds in the selenite group is significantly longer, 1.776(8)

Å, than the other two, suggesting a hydrogen bridge. Similar stretching was detected in PrH₃(SeO₃)₂(Se₂O₇), in which the Se-O bonds of the two non-equivalent selenite groups lie in the range 1.624(14)–1.656(16) Å and 1.766(16)–1.805(18) Å for Se-O and Se-OH bonds, respectively.³ The selenite group acts as a bridging ligand between two Mn atoms, and the Se links the apical oxygen of one octahedron to the equatorial oxygen of another.

The geometry of the diselenite group is like that of several other diselenite compounds. However, the bonds to the oxygen bridging the two Se atoms are slightly shorter than usual: 1.781(8) and 1.803(8) Å, compared with 1.835 and 1.847 Å in PrH₃(SeO₃)₂(Se₂O₇), 1.831 Å in MnSe₂O₆, 1.831 Å in CuSe₂O₆, 1.768 and 1.822 Å in VSe₂O₆ and 1.827 Å in

$\text{ZnSe}_2\text{O}_6^{2-}$.⁵⁻⁸ The ion is also less bent than usual. The angle $\text{Se1}-\text{O8}-\text{Se2}$ is $126.4(4)^\circ$, which may well be a consequence of the short $\text{Se}-\text{O}$ bond lengths: if the angle were 120° , the $\text{Se}-\text{O}$ bonds would be of the order 1.84 \AA , with a fixed $\text{Se1}-\text{Se2}$ distance. In the other diselenites the corresponding bond angles range between 119.6 and 123.8° . Four of the oxygens in the $\text{Se}_2\text{O}_6^{2-}$ -ion are within bonding distance of three Mn atoms, and the ion acts as a bridging ligand between them (*cf.* Fig. 1). Two of the oxygens are coordinated to the same Mn , and are on the equatorial plane of the octahedron. The third oxygen, O2 , is on the equatorial plane of another MnO_6 -octahedron, and the fourth one, O1 , forms the apical oxygen of yet another MnO_6 -octahedron. Thus, the two apical oxygens of the octahedron are from different groups, one being contributed by the diselenite group and the other by the selenite group. One of the equatorial oxygens, O5 , is also different from the others: it belongs to a selenite group, while the other three belong to diselenite groups. These differences are reflected in the $\text{Mn}-\text{O}$ distances.

The coordination polyhedron around Mn is distorted as expected. Two of the $\text{Mn}-\text{O}$ bond distances are noticeably larger than the

other four. Since the difference between the extreme values within the four shorter bond distances is more than 11 times the corresponding estimated standard deviation, they are not statistically of equal length. The bonds can be arranged into pairs of like magnitude (O1 and O6 , O3 and O4 , O2 and O5) with the bonds of each pair situated on opposite sides of the central atoms. The distorted polyhedron thus approximates an orthorhombically distorted octahedron.

The distorted MnO_6 -octahedra in $\text{Mn}_2(\text{SeO}_3)_3 \cdot 3\text{H}_2\text{O}$ offer an interesting comparison. One of the three non-equivalent octahedra is tetragonally elongated and two are orthorhombically distorted. The range of bond lengths in the equatorial plane is $1.891(9)-1.938(9) \text{ \AA}$ and in the axial direction, when the apical oxygens are contributed by water molecules, $2.248(10)-2.346(10) \text{ \AA}$.⁹ It is most interesting to note that the one apical oxygen belonging to a selenite group has a shorter $\text{Mn}-\text{O}$ bond length of $2.140(9) \text{ \AA}$, a value quite compatible with those obtained in the present work ($2.119(7)-2.179(7) \text{ \AA}$). Thus, in $\text{Mn}_2(\text{SeO}_3)_3 \cdot 3\text{H}_2\text{O}$, hydrogen bond formation stretches the $\text{Mn}-\text{O}$ bonds in the axial direction markedly.

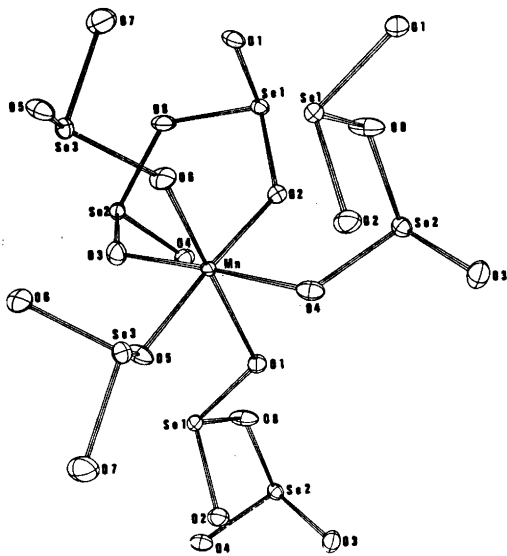


Fig. 1. Bonding scheme of selenite and diselenite groups in $\text{MnH}(\text{SeO}_3)$ (Se_2O_6).

REFERENCES

1. Koskenlinna, M. and Valkonen, J. *Acta Chem. Scand. A* 31 (1977) 611.
2. Koskenlinna, M. and Valkonen, J. *Acta Chem. Scand. A* 31 (1977) 453.
3. *International Tables for X-Ray Crystallography*, Kynoch Press, Birmingham 1974, Vol. 4, p. 72.
4. The X-Ray System, Version of 1976, Steward, J. M. Ed., *Technical Report TR-446 of the Computer Science Center*, University of Maryland, College Park, Maryland.
5. Koskenlinna, M., Niinistö, L. and Valkonen, J. *Acta Chem. Scand. A* 30 (1976) 836.
6. Meunier, P., Svensson, C. and Carpy, A. *Acta Crystallogr. B* 32 (1976) 2664.
7. Meunier, P., Bertand, M. and Galy, J. *Acta Crystallogr. B* 30 (1974) 2834.
8. Meunier, P. and Bertand, M. *Acta Crystallogr. B* 30 (1974) 2840.

Received May 9, 1977.

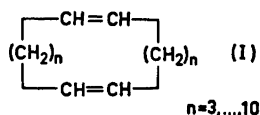
Crystal Conformation of *cis,cis*-1,2,11,12-Tetrakis-trimethylsiloxycycloeikosadien-1,11 at $-160\text{ }^{\circ}\text{C}$

P. GROTH

Department of Chemistry, University of Oslo, Oslo 3, Norway

The crystals of $\text{C}_{32}\text{H}_{68}\text{O}_4\text{Si}_4$ belong to the monoclinic system with space group $P2_1/n$, cell dimensions $a = 8.439(3)\text{ \AA}$, $b = 26.909(16)\text{ \AA}$, $c = 17.326(8)\text{ \AA}$, $\beta = 96.70(4)^\circ$, and four molecules in the unit cell. The structure was solved by direct methods and refined by full-matrix least-squares technique to a final weighted R -value of 5.1% (conventional $R = 5.9\%$) for 3464 observed reflections collected at $-160\text{ }^{\circ}\text{C}$ on an automatic four circle X-ray diffractometer. The conformation of the 20-membered ring may be described in terms of a pseudo two-fold axis of rotation and two "corner" atoms. Two additional "corners" are created by the *cis* double bonds.

The thermodynamic equilibria between the *trans,trans*-, *cis,trans*-, and *cis,cis*-isomers of symmetrical cycloalkadienes with the general formula I have been studied by Dale and



Moussebois.¹ For $n = 5, 7$ and 9 there are strong preferences for the *trans,trans*-isomers, while no

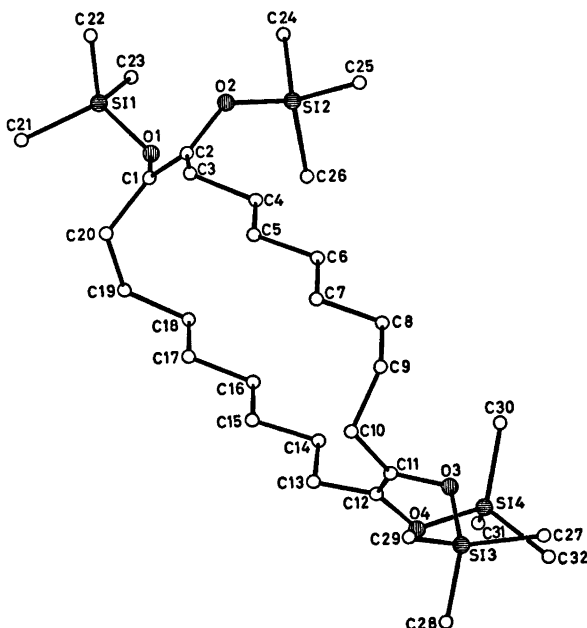


Fig. 1. Schematic drawing of the molecule.

such effects are observed for the 16- and 20-membered rings ($n=6$ and 8). In order to obtain detailed conformational information, the crystal structure of *cis,cis*-1,2,11,12-tetrakis(trimethylsilyloxy)cycloicosadien-1,11, illustrating the case $n=8$, has been determined.

The crystals of $C_{38}H_{68}O_4Si_4$ belong to the monoclinic system with space group $P2_1/n$, cell dimensions $a=8.439(3)$ Å, $b=26.909(16)$ Å, $c=17.326(8)$ Å, $\beta=96.70(4)^\circ$, and $Z=4$ ($D_m=1.04$ g cm $^{-3}$, $D_x=1.06$ g cm $^{-3}$). Data were collected at -160° C on an automatic four circle

Table 1. Final fractional coordinates and thermal parameters with estimated standard deviations. The expression for anisotropic vibration is $\exp[-2\pi^2(h^2a^{*2}U11 + \dots + 2klb^*c^*U23)]$. Hmn is bonded to Cm.

ATOM	X	Y	Z	U11	U22	U33	U12	U13	U23
H11	.3042(16)	.4520(6)	.00304(9)	.0296(7)	.0193(9)	.0153(9)	-.0024(7)	-.0037(6)	.0000(7)
H12	.2760(17)	.6042(6)	.1777(3)	.0343(7)	.0177(9)	.0225(10)	.0049(7)	-.0063(7)	-.0007(8)
H13	1.2166(16)	.7257(6)	.7943(9)	.0278(7)	.0201(9)	.0201(10)	.0018(7)	-.0064(7)	-.0036(8)
H14	1.2166(16)	.7470(6)	.0420(9)	.0293(7)	.0192(9)	.0225(9)	-.0039(7)	-.0025(6)	.0042(8)
O1	.4215(23)	.4924(12)	.1359(19)	.0317(17)	.0242(22)	.0152(21)	.0011(13)	-.0014(15)	.0018(17)
O2	.2875(36)	.5525(12)	.2275(19)	.0258(17)	.0216(21)	.0250(24)	.0021(15)	-.0017(16)	-.0019(18)
O3	1.0041(23)	.7197(12)	.7120(19)	.0324(16)	.0202(21)	.0190(24)	.0000(15)	-.0020(15)	-.0043(18)
O4	1.2510(37)	.6930(12)	.5636(20)	.0335(18)	.0188(21)	.0253(22)	.0012(15)	.0011(16)	.0032(19)
C1	.4836(25)	.4904(18)	.2185(29)	.0282(25)	.0196(31)	.0161(33)	.0025(23)	-.0031(23)	.0022(26)
C2	.3747(29)	.5224(18)	.2615(29)	.0245(24)	.0160(31)	.0204(35)	.0038(23)	-.0033(23)	.0036(26)
C3	.3950(54)	.5226(19)	.3489(29)	.0280(25)	.0277(35)	.0200(33)	.0019(24)	.0010(23)	-.0024(27)
C4	.4074(58)	.5713(21)	.0339(27)	.0337(30)	.0208(34)	.0209(34)	.0029(26)	.0012(24)	-.0011(29)
C5	.0140(55)	.5709(20)	.4405(31)	.0306(26)	.0239(34)	.0295(37)	.0009(24)	.0005(25)	.0016(29)
C6	.0071(54)	.6207(19)	.0014(28)	.0324(26)	.0203(30)	.0167(32)	.0003(24)	-.0033(23)	-.0011(26)
C7	.6414(55)	.6186(20)	.0008(30)	.0327(26)	.0233(37)	.0194(33)	.0007(25)	-.0027(24)	.0019(29)
C8	.0071(54)	.6699(20)	.0104(31)	.0346(27)	.0206(37)	.0247(36)	.0016(25)	-.0034(24)	-.0002(29)
C9	.7795(57)	.6670(20)	.7015(30)	.0319(26)	.0336(36)	.0204(34)	.0022(26)	.0022(24)	-.0030(29)
C10	.9428(56)	.6429(20)	.1105(30)	.0312(27)	.0336(37)	.0160(33)	.0024(25)	.0045(23)	.0031(28)
C11	1.0600(52)	.6732(20)	.6710(30)	.0256(25)	.0237(30)	.0166(33)	.0041(23)	.0000(24)	.0001(28)
C12	1.1420(53)	.6615(18)	.6167(30)	.0274(25)	.0186(33)	.0209(36)	.0000(23)	-.0047(25)	.0021(28)
C13	1.2711(53)	.6721(18)	.5721(29)	.0320(25)	.0176(33)	.0244(33)	.0002(24)	.0002(24)	.0018(26)
C14	1.0515(56)	.6173(20)	.4874(30)	.0370(27)	.0277(36)	.0196(33)	.0035(25)	.0009(24)	-.0011(27)
C15	1.0064(55)	.6656(19)	.4523(30)	.0320(26)	.0177(33)	.0265(35)	.0007(23)	.0010(24)	-.0021(27)
C16	.9410(56)	.6677(20)	.3654(31)	.0344(27)	.0264(35)	.0240(35)	.0046(24)	.0025(24)	.0003(27)
C17	.0007(55)	.6711(20)	.3352(30)	.0312(26)	.0223(34)	.0265(35)	.0010(24)	-.0042(24)	.0050(28)
C18	.0162(54)	.6185(19)	.2494(30)	.0297(25)	.0243(33)	.0223(34)	.0022(23)	.0034(23)	.0028(27)
C19	.7457(57)	.4684(19)	.2188(30)	.0340(27)	.0251(34)	.0217(34)	.0078(24)	-.0019(25)	.0013(27)
C20	.0064(55)	.4500(20)	.2470(32)	.0313(25)	.0254(33)	.0180(32)	.0019(24)	.0003(23)	-.0013(27)
C21	.1117(54)	.4473(24)	.1249(34)	.0624(37)	.0490(44)	.0322(40)	.0015(34)	-.0031(31)	-.0010(34)
C22	.3083(75)	.3050(23)	.0007(36)	.0728(38)	.0393(41)	.0388(42)	.0091(34)	.0246(34)	-.0145(34)
C23	.2737(89)	.4784(21)	.0181(31)	.0370(28)	.0366(38)	.0281(36)	.0018(26)	.0015(26)	-.0041(29)
C24	1.1360(77)	.6087(23)	.0073(37)	.0714(39)	.0361(41)	.0474(44)	.0006(34)	-.0239(35)	.0045(38)
C25	.4081(66)	.6140(21)	.1578(35)	.0562(34)	.0295(38)	.0455(42)	.0102(29)	.0000(31)	-.0056(33)
C26	.2149(63)	.6574(20)	.2346(34)	.0485(32)	.0265(37)	.0426(42)	.0043(27)	-.0033(29)	.0007(31)
C27	1.1633(60)	.6665(21)	.7732(32)	.0391(28)	.0393(39)	.0277(37)	.0007(27)	.0065(26)	-.0001(30)
C28	1.4283(81)	.7120(21)	.7642(34)	.0391(29)	.0383(39)	.0307(40)	.0010(27)	-.0003(28)	-.0005(32)
C29	1.1090(67)	.7932(22)	.0215(34)	.0542(34)	.0431(42)	.0340(38)	.0043(30)	-.0060(30)	-.0113(33)
C30	1.2021(68)	.7416(21)	.4400(34)	.0555(32)	.0341(39)	.0378(40)	.0046(30)	.0003(29)	.0006(32)
C31	1.0000(60)	.7600(19)	.5094(31)	.0445(29)	.0236(35)	.0201(35)	.0092(25)	-.0064(26)	.0129(28)
C32	1.3310(63)	.7050(20)	.0000(35)	.0460(31)	.0190(35)	.0013(35)	.0006(27)	-.0052(30)	.0091(31)
ATOM	X	Y	Z	B	ATOM	X	Y	Z	B
H31	.4637(46)	.4967(16)	.3683(24)	.8(9)	H32	.2907(48)	.5143(16)	.3662(25)	.4(9)
H33	.3597(62)	.6906(20)	.3657(32)	4.6(14)	H34	.5475(49)	.5798(16)	.3539(26)	1.0(19)
H35	.6019(49)	.5402(17)	.4775(26)	1.4(10)	H36	.4281(56)	.5591(19)	.4946(28)	2.2(12)
H37	.4778(60)	.6442(17)	.4966(26)	1.0(10)	H38	.6572(48)	.6355(16)	.4728(25)	1.0(10)
H39	.7425(48)	.6018(17)	.5857(26)	1.0(10)	H40	.5617(59)	.6028(19)	.6159(29)	2.4(12)
H41	.0976(60)	.6923(17)	.6118(25)	9.1(10)	H42	.7692(53)	.6889(18)	.5846(27)	2.5(11)
H43	.7100(49)	.6512(16)	.7370(26)	1.5(10)	H44	.7867(46)	.7082(15)	.7266(24)	1.7(9)
H45	.9310(50)	.6892(17)	.6078(26)	1.5(10)	H46	.9817(59)	.6374(19)	.7670(30)	3.0(13)
H47	1.0070(49)	.5876(16)	.6023(25)	1.6(10)	H48	1.2322(47)	.6018(16)	.5721(25)	1.3(9)
H49	1.1268(62)	.6362(18)	.4579(27)	1.6(11)	H50	.9483(57)	.6373(19)	.4865(29)	2.0(12)
H51	.9209(64)	.5534(19)	.4846(28)	1.9(11)	H52	1.1895(49)	.5403(17)	.4600(26)	1.0(10)
H53	1.0279(44)	.5780(15)	.3354(24)	1.0(9)	H54	.8647(47)	.5898(16)	.3601(25)	1.6(10)
H55	.7800(61)	.5868(17)	.3655(27)	2.5(10)	H56	.9724(49)	.4981(16)	.3468(26)	1.7(10)
H57	.9029(49)	.5289(16)	.2202(26)	6.1(10)	H58	.7163(62)	.5437(19)	.2429(31)	3.4(13)
H59	.6273(57)	.4426(15)	.2339(30)	2.5(12)	H60	.7405(57)	.4700(18)	.1631(30)	3.0(12)
H61	.5902(44)	.4498(15)	.3065(24)	4(9)	H62	.5602(54)	.4213(17)	.0291(28)	2.4(11)
H63	.0606(49)	.4796(17)	.1251(26)	1.0(10)	H64	.0373(72)	.4150(21)	.2226(34)	5.9(16)
H65	1.2397(70)	.4398(23)	.1757(34)	6.1(16)	H66	.5073(51)	.3950(17)	.0702(27)	2.4(10)
H67	.3512(64)	.3671(25)	.0464(40)	7.2(19)	H68	.4029(54)	.3775(18)	.1302(28)	2.3(11)
H69	.2311(60)	.5108(20)	-.0172(31)	2.4(13)	H70	.3713(63)	.4063(20)	-.0341(33)	3.7(13)
H71	.2132(66)	.4568(21)	-.0466(32)	4.0(15)	H72	.0336(64)	.5097(18)	.0000(27)	4.2(11)
H73	1.2297(64)	.6282(21)	.0000(32)	4.3(14)	H74	.0336(64)	.5097(18)	.0000(27)	4.2(11)
H75	.5219(52)	.5697(17)	.1271(27)	1.9(11)	H76	.1738(78)	.5788(24)	.8553(38)	7.5(18)
H77	.4803(66)	.6497(21)	.1920(34)	4.2(15)	H78	.5478(53)	.5212(28)	.2044(32)	4.0(13)
H79	.2051(74)	.6552(23)	.2782(30)	5.2(17)	H80	.1859(58)	.0055(17)	.2416(26)	2.3(11)
H81	1.0583(61)	.6846(20)	.6785(32)	2.4(13)	H82	.2381(68)	.6808(21)	.2095(34)	3.7(14)
H83	1.2309(63)	.6966(18)	.9215(27)	2.5(11)	H84	1.1931(65)	.6532(21)	.8644(33)	2.4(14)
H85	1.4723(46)	.7385(16)	.7431(25)	3.7(9)	H86	1.0613(57)	.7140(19)	.8249(29)	5.1(12)
H87	1.2253(55)	.8114(18)	.7805(29)	2.6(11)	H88	1.4329(54)	.6011(17)	.7829(28)	3.3(11)
H89	1.2501(66)	.8001(22)	.8707(34)	5.0(15)	H90	1.0074(62)	.7079(20)	.8283(31)	2.2(13)
H91	1.2309(56)	.7155(18)	.4115(29)	4.7(11)	H92	1.4111(48)	.7329(16)	.4551(26)	4.9(10)
H93	.9327(64)	.7360(20)	.4962(33)	3.7(14)	H94	1.2657(53)	.7732(18)	.4100(28)	3.2(11)
H95	.9033(53)	.7896(18)	.5091(28)	2.1(11)	H96	.9462(57)	.7612(49)	.5804(29)	4.1(12)
H97	1.4453(52)	.7877(17)	.6021(27)	4.9(11)	H98	1.2769(54)	.8002(17)	.6463(28)	3.0(11)
					H100	1.3298(77)	.8288(23)	.3720(37)	3.3(10)

Table 2. Bond distances, bond angles and dihedral angles with estimated standard deviations

DISTANCE	(Å)	DISTANCE	(Å)
Si1 - O1	1.659(3)	Si2 - O2	1.663(4)
Si3 - O3	1.662(3)	Si4 - O4	1.662(4)
Si1 - C23	1.854(6)	Si1 - C22	1.857(6)
Si1 - C25	1.856(6)	Si2 - C24	1.858(6)
Si2 - C27	1.858(6)	Si3 - C28	1.859(6)
Si3 - C29	1.857(6)	Si4 - C30	1.853(6)
Si4 - C31	1.848(6)	Si4 - C32	1.855(6)
O1 - C1	1.410(6)	O2 - C2	1.386(6)
O3 - C11	1.402(6)	O4 - C12	1.387(6)
C1 - C2	1.326(7)	C11 - C12	1.319(7)
C2 - C3	1.505(7)	C3 - C4	1.538(7)
C4 - C5	1.532(7)	C5 - C6	1.505(7)
C6 - C7	1.540(7)	C7 - C8	1.538(7)
C8 - C9	1.524(7)	C9 - C10	1.528(7)
C10 - C11	1.587(7)	C12 - C13	1.589(7)
C13 - C14	1.533(7)	C14 - C15	1.525(7)
C15 - C16	1.542(7)	C16 - C17	1.510(7)
C17 - C18	1.522(7)	C18 - C19	1.538(7)
C19 - C20	1.528(7)	C20 - C1	1.509(7)

ANGLE	(°)	ANGLE	(°)
O1 - Si1 - C21	109.4(2)	O1 - Si1 - C22	111.5(2)
O1 - Si1 - C23	106.1(2)	C21 - Si1 - C22	109.7(3)
C21 - Si1 - C23	111.8(3)	C22 - Si1 - C23	106.4(3)
O2 - Si2 - C24	106.8(2)	O2 - Si2 - C25	111.4(2)
O2 - Si2 - C26	108.6(2)	C24 - Si2 - C25	112.0(3)
C24 - Si2 - C26	108.4(3)	C25 - Si2 - C26	109.4(3)
O3 - Si3 - C27	111.8(2)	O3 - Si3 - C28	118.0(2)
O3 - Si3 - C29	104.8(2)	C27 - Si3 - C28	109.0(3)
C27 - Si3 - C29	109.3(3)	C28 - Si3 - C29	111.9(3)
O4 - Si4 - C30	107.2(2)	O4 - Si4 - C31	110.7(2)
O4 - Si4 - C32	109.0(2)	C30 - Si4 - C31	109.9(3)
C30 - Si4 - C32	108.3(3)	C31 - Si4 - C32	111.6(3)
Si1 - O1 - C1	124.2(3)	Si2 - O2 - C2	129.6(3)
Si3 - O3 - C11	122.6(3)	Si4 - O4 - C12	127.0(3)
O1 - C1 - C2	120.9(4)	O1 - C1 - C20	119.3(4)
C2 - C1 - C20	113.7(4)	O2 - C2 - C1	121.3(4)
O3 - C11 - C10	113.1(4)	C1 - C2 - C3	125.7(4)
O3 - C11 - C12	113.1(4)	O3 - C11 - C12	120.0(5)
C10 - C11 - C12	126.7(5)	O4 - C12 - C11	122.2(5)
O4 - C12 - C11	111.5(4)	C11 - C12 - C13	126.3(5)
C2 - C3 - C4	113.7(4)	C3 - C4 - C5	112.4(5)
C4 - C5 - C6	112.5(5)	C5 - C6 - C7	113.6(4)
C6 - C7 - C8	112.5(4)	C7 - C8 - C9	112.9(5)
C8 - C9 - C10	114.9(5)	C9 - C10 - C11	113.0(4)
C12 - C13 - C14	115.4(4)	C13 - C14 - C15	111.9(4)
C14 - C15 - C16	114.6(4)	C15 - C16 - C17	113.0(4)
C16 - C17 - C18	113.2(5)	C17 - C18 - C19	113.8(4)
C18 - C19 - C20	114.8(5)	C19 - C20 - C1	113.0(4)

DIHEDRAL ANGLE	(°)
C1 - C2 - C3 - C4	116.7(6)
C2 - C3 - C4 - C5	-166.5(4)
C3 - C4 - C5 - C6	-177.0(4)
C4 - C5 - C6 - C7	-173.9(4)
C5 - C6 - C7 - C8	178.9(4)
C6 - C7 - C8 - C9	-176.8(4)
C7 - C8 - C9 - C10	89.7(6)
C8 - C9 - C10 - C11	78.1(6)
C9 - C10 - C11 - C12	-113.7(6)
C10 - C11 - C12 - C13	-5.4(8)
C11 - C12 - C13 - C14	114.7(6)
C12 - C13 - C14 - C15	-167.3(4)
C13 - C14 - C15 - C16	-178.0(4)
C14 - C15 - C16 - C17	-173.5(4)
C15 - C16 - C17 - C18	-179.8(4)
C16 - C17 - C18 - C19	-176.8(4)
C17 - C18 - C19 - C20	71.9(5)
C18 - C19 - C20 - C1	64.9(6)
C19 - C20 - C1 - C2	-115.6(6)
C20 - C1 - C2 - C3	-3.0(8)

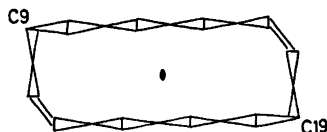
nique.** The positions of methylene hydrogen atoms were calculated while those of the methyl groups were localized in a difference Fourier map. Anisotropic temperature factors were introduced for Si, O and C atoms and weights in least squares were calculated from the standard deviations in intensities, $\sigma(I)$, taken as $\sigma(I) = [C_T + (0.02C_N)^2]^{1/2}$

where C_T is the total number of counts and C_N the net count. The final weighted R -value was 5.1% (conventional $R = 5.9\%$) for 3464 observed reflections. The form factors used were those of Hanson *et al.*⁴ except for hydrogen.⁵

Final fractional coordinates and thermal parameters are given in Table 1. The principal axes of thermal vibration ellipsoids were calculated from the temperature parameters of this table, and the maximum r.m.s. amplitudes range from 0.175 to 0.316 Å (corresponding B -values 2.42 and 7.88 Å²). Due to the size of the molecule no rigid-body analysis has been carried out.

Bond distances and angles and dihedral angles are listed in Table 2. Fig. 1 is a schematic drawing of the molecule indicating the numbering of atoms.

The conformation of the 20-membered ring may be described in terms of a pseudo two-fold axis of rotation (approximately parallel to [01 $\bar{1}$] and two "corner" atoms (C9 and C19):



Two additional corners are effectively created by the *cis* double bonds.

The average Si - O bond distance of 1.662 Å seems to be somewhat longer than that of 17 β -trimethylsiloxy-4-androsten-3-one (silandron)⁶ [1.623(7) Å]. Within error limits the Si - C bond length (mean value 1.856 Å) agrees with the corresponding value of silandron [1.87(1) Å] and with the more accurate average Si - C bond distance in 2,6-*cis*-diphenylhexamethylcyclo-tetrasiloxane⁷ of 1.851 Å. C - C bond lengths

* All programs used (except those for phase determination) are included in this reference.

diffractometer (MoK α -radiation). Using an observed-unobserved cutoff at $2\sigma(I)$, 3464 reflections were recorded as observed. No corrections for absorption or secondary extinction were applied (crystal size $0.3 \times 0.2 \times 0.3$ mm³).

The structure was solved by direct methods⁸ and refined by full-matrix least-squares tech-

and bond angles have normal values. The only short H—H contacts are H31···H201 (1.94 Å) and H101···H131 (2.06 Å).

A list of observed and calculated structure factors is available from the author.

Acknowledgements. The author would like to thank cand.real. T. Ledaal for supplying the crystals.

REFERENCES

1. Dale, J. and Moussebois, C. *J. Chem. Soc. C* (1966) 264.
2. Germain, G., Main, P. and Woolfson, M. M. *Acta Crystallogr. A* 27 (1971) 368.
3. Groth, P. *Acta Chem. Scand.* 27 (1973) 1837.
4. Hanson, H. P., Herman, F., Lea, J. D. and Skillman, S. *Acta Crystallogr.* 17 (1964) 1040.
5. Stewart, R. F., Davidson, E. R. and Simpson, W. T. *J. Chem. Phys.* 43 (1965) 3175.
6. Weeks, C. M., Hauptman, H. and Norton, D. A. *Cryst. Struct. Commun.* 1 (1972) 79.
7. Carlström, D. and Falkenberg, G. *Acta Chem. Scand.* 27 (1973) 1203.

Received April 19, 1977.

Preparation and Properties of Some Bis(triphenylphosphine)-iminium Salts, $[(\text{Ph}_3\text{P})_2\text{N}]\text{X}$

ARVE MARTINSEN and JON SONGSTAD

Department of Chemistry, University of Bergen, N-5014 Bergen-Univ., Norway

A number of bis(triphenylphosphine)iminium salts, $[(\text{Ph}_3\text{P})_2\text{N}]\text{X}$, abbreviated $[\text{PNP}]\text{X}$, of small inorganic ions have been prepared. All the salts, except the fluoride, can be prepared from the easily available $[\text{PNP}]^+\text{-chloride}$ by precipitation with excess alkali metal salts in water.

The salts are simple to purify and are non-hygroscopic. Their solubilities in a number of dipolar aprotic solvents suggest that the $[\text{PNP}]^+$ -cation is a valuable alternative to the usually employed onium cations for synthetic and kinetic studies in this class of solvents.

In recent years various tetraorganoammonium, phosphonium and arsonium cations in addition to numerous crown ether complexes of the alkali metal cations have been used extensively as counter ions.¹⁻⁵ Salts of these ions may be both very soluble and well dissociated in a number of aprotic solvents^{6,7} allowing reactions to be performed homogeneously and even to be studied kinetically.⁸ The weakly polarizing effect to these cations allows the isolation of a number of salts of anions which otherwise would not be possible; for a review, cf. Ref. 2.

Unfortunately, these cations have their disadvantages; difficulties in preparing various salts in their pure states,⁹ solubility and hygroscopicity of their salts,^{9,10} the ability of some of these cations to catalyze oxidation reactions,^{11,12} and, in the case of Ph_4P^+ , Ph_4As^+ and especially crown ethers, their exorbitant cost.

As part of a program to study the solution behaviour and structural properties of certain inorganic anions we have synthesized a number of salts of the bis(triphenylphosphine)iminium

cation, $[(\text{Ph}_3\text{P})_2\text{N}]^+$,¹³ abbreviated $[\text{PNP}]^+$.^{*} We offer our results as proof of the utility and facility of $[\text{PNP}]^+$ as a valuable counter ion.

Preparation of $[\text{PNP}]^+$ -salts. $[\text{PNP}]^+\text{-chloride}$, which serves as the starting material for the preparation of the various $[\text{PNP}]^+$ -salts, can now be readily obtained in high yield, > 90 %.¹⁵ It is the experience of these authors that it is considerably simpler to prepare this compound than Ph_4PCl and Ph_4AsCl . Although $[\text{PNP}]\text{Cl}$ is prepared from the rather costly triphenylphosphine and the maximum total conversion into $[\text{PNP}]\text{Cl}$ is only ~60 % (3 mol of Ph_3P yield 1 mol of $[\text{PNP}]\text{Cl}$ ¹⁵), this compound should compare favourably with Ph_4PCl and Ph_4AsCl with regard to cost.

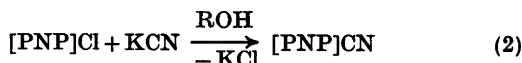
Part of the facility by which $[\text{PNP}]^+$ -salts can be employed comes from the fact that a salt of a desired anion, X^- , can be rapidly obtained in high yield, > 80 %, by precipitation with excess alkali metal salts, MX , in warm water according to eqn. 1:

* The bis(triphenylphosphine)iminium ion is the usual name for this ion, but since this ion is fundamentally not an iminium ion, various names have been suggested: The bistrisphenylphosphinenitride ion,¹⁴ the μ -nitrido-bis(triphenylphosphorus) (1+) ion,¹⁵ the bis(triphenylphosphoranylidene)ammonium ion,¹⁶ the bis(triphenylphosphoranylidene)iminium ion,¹⁷ and the hexaphenyldiphosphazanium ion.¹⁸ *Chemical Abstracts* recommends "triphenyl-(*P,P,P*-triphenylphosphine imidato-*N*)phosphorus (1+)", a name which is not particularly handy. To avoid confusion we will only use $[\text{PNP}]^+$. Some authors have used the abbreviation PPN^+ , but since this formulation may indicate that the positive charge resides on the nitrogen atom, which is not the case,¹⁹ this abbreviation should be avoided.

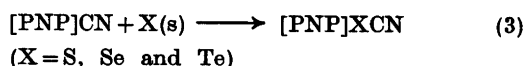


The cause for this simple anion exchange procedure is that most $[\text{PNP}]^+$ -salts, except the fluoride, have only a limited solubility in water at room temperature while $[\text{PNP}]\text{Cl}$ is exceptionally soluble in warm water, ~ 100 g/l at 80°C . Even at 25°C is the solubility of $[\text{PNP}]\text{Cl}$ considerable, 7.1 g/l, as judged from the UV spectrum of a saturated aqueous solution.

The cyanide, $[\text{PNP}]\text{CN}$, may also be prepared according to eqn. 1. However, in order to avoid co-precipitation of the fairly insoluble hydroxide, the cyanide can only be precipitated slowly from dilute solutions. This compound is therefore easier to prepare from the chloride and excess potassium cyanide in dry methanol or ethanol taking advantage of the high solubility of $[\text{PNP}]^+$ -salts in this class of solvents; eqn. 2:



From the cyanide, the thiocyanate, the selenocyanate and the tellurocyanate are easily prepared in acetone or acetonitrile according to eqn. 3:

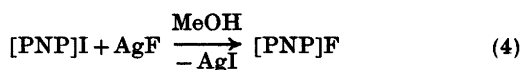


The thiocyanate and the selenocyanate may be prepared as well according to eqns. 1 and 2.

The procedure depicted by eqn. 2 is especially convenient for the synthesis of small quantities of the cyanide. Thus, from the costly potassium ^{13}C cyanide a high molecular weight

^{13}C cyanide is readily available. With the $[\text{PNP}]^+ - ^{13}\text{C}$ cyanide in hand, the corresponding thiocyanate, selenocyanate and tellurocyanate can be prepared as depicted by eqn. 3. In Table 1 are listed the ν_{XCN} in the 2000–2200 cm^{-1} region for the ^{13}C and the ^{13}C pseudo-halide ions.

The fluoride, $[\text{PNP}]\text{F}$, cannot be prepared from $[\text{PNP}]\text{Cl}$ and excess potassium fluoride, eqn. 1. Upon cooling of the reaction mixture only a highly viscous solution is obtained. However, from the iodide and silver fluoride in methanol, the nicely crystalline fluoride can be obtained in high yield, eqn. 4:



Properties of $[\text{PNP}]^+$ -salts. In Table 2 are listed the various $[\text{PNP}]^+$ -salts prepared in the present study. All the salts have rather sharp and well-defined melting points or decomposition temperatures. In recent years a number of $[\text{PNP}]^+$ -salts have been prepared, notably salts of heavy metal carbonyl ions,^{15,22–24} but also of anions of carboxylic acids²⁵ and various main group inorganic anions.^{26–28} Several X-ray structure determinations have been performed; for a survey of references, cf. Ref. 29. When considering the range of anions with which the $[\text{PNP}]^+$ -cation makes stable and well-crystalline salts, the versatile nature of this ion as a counter ion in synthesis seems well established.

The success of this ion as a counter ion for the preparation of stable salts seems to be due to two factors. The positive charge of the cation is well distributed in the triphenylphosphine moieties¹⁹ causing this cation to have a negligible polarizing effect. In this respect this cation should be comparable with other bulky onium cations, notably the tetraphenylphosphonium cation, Ph_4P^+ , and the tetraphenylarsonium cation, Ph_4As^+ . The major advantage of the $[\text{PNP}]^+$ -cation, however, comes from its apparently exceptional hydrophobic nature causing all known salts of this cation to be non-hygroscopic. No decomposition of potentially unstable anions will thus be initiated by the presence of polarizing water molecules. A number of Ph_4P^+ - and Ph_4As^+ -salts are well-known to readily pick up 1 to 3 mol of water.^{10,20}

Table 1. IR data of $\text{X}[^{12}\text{C}]\text{CN}^-$ and $\text{X}[^{13}\text{C}]\text{CN}^-$ in acetonitrile (X = S, se and Te).

	ν_{max} cm^{-1} ^a	$\Delta\nu_{\frac{1}{2}}$ cm^{-1} ^b	$A \times 10^{-4}$ $\text{M}^{-1} \text{cm}^{-2}$ ^b
$\text{S}[^{12}\text{C}]\text{CN}^-$	2058	12	4.1
$\text{S}[^{13}\text{C}]\text{CN}^-$	2011		
$\text{Se}[^{12}\text{C}]\text{CN}^-$	2067	10	2.2
$\text{Se}[^{13}\text{C}]\text{CN}^-$	2021		
$\text{Te}[^{12}\text{C}]\text{CN}^-$	2081	12	1.8
$\text{Te}[^{13}\text{C}]\text{CN}^-$	2034		

^a $\pm 1 \text{ cm}^{-1}$, ^b Ref. 20.

Table 2. Melting points and analytical data for some [PNP]⁺-salts.

	M.p. °C	Found (Calc.) %
Cl ⁻	273–274 (268–270 ¹⁵)	
Br ⁻	253–255 (256 ²¹)	
I ⁻	252–254 (254 ²¹)	
F ⁻	177–178	C: 77.88 (77.55), H: 5.62 (5.42)
SO ₄ ²⁻	258–261	N: 2.67 (2.51)
S ₂ O ₃ ²⁻	210–212 (dec.)	N: 2.55 (2.39), S: 2.67 (2.73)
MnO ₄ ⁻	~155 (dec. violently)	N: 2.11 (2.36), S: 5.37 (5.39)
CrO ₄ ²⁻	234–235 (dec.)	N: 2.29 (2.35)
ClO ₄ ⁻	259–261 (264–266 ¹⁴)	
NO ₃ ⁻	225–226	N: 4.37 (4.79)
NO ₂ ⁻	233–234 (232 ²¹)	
N ₃ ^{- a}	214–215 (214–216 ¹⁴)	
Ac ⁻	114–115	C: 77.32 (76.37), N: 6.03 (5.57)
CN ⁻	212–214	N: 2.13 (2.34)
OCN ^{- a}	203–204	C: 78.12 (78.70), H: 5.49 (5.36)
SCN ^{- a}	187–188	N: 4.96 (4.47)
SeCN ^{- a}	182–185 (dec.)	N: 4.37 (4.79)
TeCN ^{- a}	190–193 (dec.)	C: 64.72 (64.20), H: 4.18 (4.37)
		N: 3.55 (4.05)

^a Determined by liquid IR in acetonitrile in the 2000–2200 cm⁻¹ range to be >98 % pure.³⁰

Several of the salts listed in Table 2 may be purified by crystallization from water. Although [PNP]⁺-salts generally do not crystallize with crystal water, (one known example, with the squarate²⁵), it is our experience that the removal of surface water in high vacuum at elevated temperature is quite time-consuming. Furthermore, some of the [PNP]⁺-salts, the bromide, the selenocyanate and especially the iodide, are not sufficiently soluble in water to apply this solvent as a convenient crystallization agent. (1 l of boiling water dissolves less than 1 g [PNP]I and the solubility product of this salt at 25.0 °C is only 3.0 × 10⁻⁹ M², 0.035 g/l). It is therefore recommended that an organic solvent be applied as crystallization agent whereby traces of co-precipitated alkali metal salts are removed as well. Acetone seems to be the best choice, even though only the iodide and the tellurocyanate of the compounds listed in Table 2 can be recovered from this solvent alone without excessive losses. No evidence for solvated acetone in any of the synthesized [PNP]⁺-salts could be found; [PNP]⁺-salts are known to crystallize as solvates from organic solvents like chloro-

benzene,³⁰ acetonitrile,³⁰ benzonitrile,³¹ and dichloromethane.¹⁵

The [PNP]⁺-salts are generally very soluble in the usual dipolar aprotic solvents; acetone, acetonitrile, dimethyl sulfoxide, dimethylformamide, benzyl cyanide, nitromethane and nitrobenzene. Actually, their solubilities in most dipolar aprotic solvents prevent these solvents alone to be used as crystallization agents. Due to their considerable solubility in this class of solvents [PNP]⁺-salts may therefore serve as convenient sources of anions in substitution reactions (the nucleophilic anions), in salt-effect studies (the non-nucleophilic anions), in elimination reactions³² (the fluoride) and in oxydation reactions³³ (the chromate and the permanganate). The [PNP]⁺-salts are even very soluble in 1,1,2,2-tetrachloroethane and in dichloromethane. However, care should be exercised when employing dichloromethane since the most nucleophilic anions, notably the selenocyanate ion and the azide ion, react fairly rapidly with this solvent.³⁴ For this reason, [PNP]TeCN decomposes rapidly when dissolved in dichloromethane.

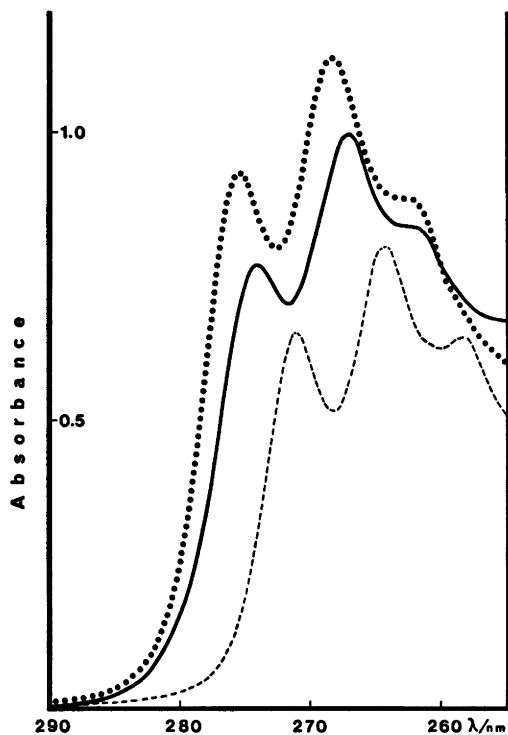


Fig. 1. UV spectra of 2.5×10^{-4} M solutions of [PNP]Cl (—), Ph_4AsCl (---) and $\text{Ph}_4\text{P}^+\text{Cl}^-$ (---) in acetonitrile in the 255–290 nm region. Path-length, 1 cm.

Stability of the [PNP]⁺-cation. The [PNP]⁺-cation seems to be completely unaffected by molecular oxygen and does not seem to be attacked by strong nucleophiles, e.g. the cyanide ion, in dry dipolar aprotic solvents. With ionic cyanide in moist acetone, however, a very slow decomposition takes place at reflux temperature. Presumably, the cation is very slowly attacked by the hydroxide ions present and triphenylphosphine oxide, Ph_3PO , is formed (see Experimental). It has previously been shown that

the [PNP]⁺-cation is attacked only very slowly by a warm concentrated solution of sodium hydroxide.²¹

Toward mineral acids the [PNP]⁺-cation is reported to be completely stable.²¹ No decomposition of [PNP]⁺-salts seems to take place during drying at elevated temperatures. The stability of the [PNP]⁺-cation may thus equal that of the Ph_4As^+ -cation. Since the Ph_4P^+ -cation is known to be decomposed rapidly by hydroxide ions,²⁵ Ph_4P^+ -salts of anions of weak acids, e.g. Ph_4PCN , are difficult to synthesize and can only be used in scrupulously dried aprotic solvents.

Spectral characteristics of the [PNP]⁺-cation. In Fig. 1 is shown the UV spectra of 2.5×10^{-4} M solutions in acetonitrile of [PNP]Cl, Ph_4AsCl and $\text{Ph}_4\text{P}^+\text{Cl}^-$ in the 255–290 nm region. The three spectra are in principle quite similar exhibiting three main peaks. In Table 3 are listed the absorption maxima positions together with the molar absorptivities (ϵ). The Ph_4P^+ -cation is clearly the most absorbing one; the [PNP]⁺-cation being intermediate. Above 300 nm the absorption due to the [PNP]⁺-cation is negligible. Below 250 nm the [PNP]⁺-cation is by far the most absorbing one of the three ions. Measurements in water on [PNP]Cl showed a slight blue-shift, 0.3–0.4 nm, but with unaltered extinction coefficients.

The IR spectrum of the [PNP]⁺-cation shows strong absorptions at 803, 995, 1115, 1250(broad), 1440 and 1490 cm^{-1} in addition to the usual aromatic absorptions in the 650–750 and 3050 cm^{-1} regions. No attempt was made to assign the various peaks. The cation appears transparent in the 810–970 cm^{-1} region and in the 1650–3000 cm^{-1} region.

The ¹H NMR spectrum of the [PNP]⁺-cation consists of a complex multiplet in the benzene region while the ³¹P NMR spectrum consists of a singlet at –22.3 ppm vs. phosphoric acid.¹⁵

Table 3. Absorption maxima positions (λ) and molar absorptivities, ϵ , of [PNP]Cl, Ph_4AsCl and $\text{Ph}_4\text{P}^+\text{Cl}^-$ in acetonitrile in the 255–290 nm region.

	λ_1	$\epsilon \times 10^{-3}$	λ_2	$\epsilon \times 10^{-3}$	λ_3	$\epsilon \times 10^{-3}$	$\lambda(\epsilon < 100)$
[PNP]Cl	262.3	3.35	267.4	4.01	274.3	3.10	287.5
Ph_4AsCl	258.4	2.44	264.6	3.06	271.4	2.48	285
$\text{Ph}_4\text{P}^+\text{Cl}^-$	263.0	3.21	268.6	4.38	275.7	3.60	291

EXPERIMENTAL

Acetonitrile was purified as previously reported.⁴ Acetone, *p.a.*, absolute methanol and ethanol were used without further purification, 1,1,2,2-Tetrachlorethane, benzene and diethyl ether were dried and purified according to standard procedures. All solvents were flushed with dry nitrogen prior to use.

The potassium and sodium salts were of analytical grade and used without further purification except potassium cyanide, potassium thiocyanate and potassium selenocyanate which were recrystallized and carefully dried prior to use. Potassium [¹³C]cyanide, 90.5 % enriched, was used as received from British Oxygen Co., Ltd.

[PNP]Cl was prepared as described by Ruff and Schlientz¹⁵ and finally crystallized twice from acetone/diethyl ether.

Preparation of [PNP]X. General procedure. (Except for X = F, CN and TeCN). [PNP]Cl, 1 to 2 g, was dissolved in a minimum amount of warm water, 60–80 °C, 25–40 ml, and the warm concentrated solution of KX or NaX, 5–10 g, was then added under constant stirring. (Boiling water frequently caused the product to separate as an oil). The reaction mixture was set aside at 0 °C for 1 h and filtered. The product was dissolved in acetonitrile (traces of water were removed azeotropically with benzene) and finally crystallized from acetone/diethyl ether (ethanol for the thiosulfate).

In the case of the acetate, the chromate, the sulfate and the nitrate, the precipitation procedure in water had to be repeated once to obtain chloride-free products. The chromate was both times precipitated with a sodium chromate solution which was 0.02 M in sodium hydroxide. In the final crystallization of [PNP]₂CrO₄ acetone containing 2 % triethylamine was used to avoid a trace of darkening of the crystals.

[PNP]CN. *In water, eqn. 1.* To 1.4 g [PNP]Cl, dissolved in 100 ml water was added a solution of 5 g KCN in 25 ml water. The solution was stirred at room temperature for 10 min and set aside for 24 h at 0 °C. Yield of [PNP]CN, 1.15 g, 82 %. *In methanol, eqn. 2.* 2.3 g [PNP]Cl and 0.29 g KCN were dissolved in 25 ml warm methanol. After 2–3 h at 0 °C the precipitated potassium chloride was removed by filtration. To ensure a complete removal of ionic chloride this treatment was repeated with 0.1 g KCN. Yield from acetone/diethyl ether, 1.94 g, 85 %.

All operations with [PNP]CN in acetone or acetonitrile were carefully performed under nitrogen. If oxygen was allowed to enter, a yellow to orange solution was slowly obtained and the IR in the 2000–2200 cm⁻¹ region suggested that ionic cyanate among other products had been formed.

[PNP]TeCN. To 0.40 g [PNP]CN in 20 ml acetone was added 0.5 g black tellurium powder and the reaction mixture heated to 50 °C for

30 min. After filtration the tellurocyanate was precipitated with diethyl ether and finally crystallized from acetone. Yield 0.30 g, 65 %. The thiocyanate and the selenocyanate were prepared in a similar way in close to quantitative yield.

[PNP][¹³C]CN. To 0.85 g [PNP]Cl in 10 ml methanol was added 0.10 g potassium [¹³C]cyanide (5 % excess of cyanide). An additional amount of 0.01 g of the cyanide was added after the first crop of potassium chloride had been removed. Yield 0.72 g.

[PNP]F. 2.0 g [PNP]I in 25 ml methanol and an equivalent amount of AgF was stirred at 40 °C for 2 h. After filtration an additional amount of 0.1 g AgF was added. The reaction solution was repeatedly (six times) evaporated to dryness and redissolved in methanol and filtered until a clear colourless solution was obtained when the residue was dissolved in acetone or methanol. Yield from acetone/diethyl ether, 1.30 g, 60 %. An acidified solution of this salt did not give any precipitate with potassium chloride or silver nitrate.

Attempted decomposition experiments. (1) [PNP]Cl and molecular oxygen in acetone. 0.3 g [PNP]Cl in 25 ml acetone was kept at ~50 °C and flushed with oxygen for 2 h. No colouring of the solution was observed and the UV of the solution did not suggest that any decomposition had taken place. (2) [PNP]CN in acetonitrile. 0.3 g [PNP]CN in 25 ml acetonitrile, flushed with nitrogen, was kept at ~50 °C for 2 h. A faint yellow colour of the solution developed, presumably due to traces of oxygen having been present. No decomposition products could be detected. (3) [PNP]CN in acetone/H₂O (acetone/D₂O). 0.3 g [PNP]CN, dissolved in 10 ml acetone and 1 ml H₂O (D₂O), was refluxed for 3 h in a nitrogen stream. The yellowish solution was evaporated to dryness and treated with benzene. The benzene extract gave 0.015 g of a brownish, sticky residue. IR indicated that this residue was partly a [PNP]⁺-salt, but a broad peak in the 1200 cm⁻¹ region indicated that some triphenylphosphine oxide, maximum 0.010 g, had been formed. No peaks due to NH (ND) could be detected.

Instrumental. The IR measurements were performed with a Unicam SP 200 Infrared Spectrophotometer. The measurements on the pseudohalide ions were performed in acetonitrile employing liquid IR cells with a path length of 0.1 cm. The UV measurements were performed with a Varian-Techtron UV-VIS Spectrophotometer, Model 635, employing matched 1 cm quartz cells.

The melting points were determined by a Gallenkamp melting point apparatus. The melting points are corrected.

REFERENCES

1. Parker, A. J. *Chem. Rev.* 69 (1969) 1.
2. Basolo, F. *Coord. Chem. Rev.* 3 (1968) 213.
3. Dockx, J. *Synthesis* (1973) 441.
4. Martinsen, A., Austad, T. and Songstad, J. *Acta Chem. Scand. A* 29 (1975) 661.
5. Pedersen, C. J. and Frensdorff, H. K. *Angew. Chem.* 84 (1972) 16.
6. Savedoff, L. V. *J. Am. Chem. Soc.* 88 (1966) 664.
7. Springer, C. H., Coetzee, J. F. and Kay, R. L. *J. Phys. Chem.* 73 (1969) 471.
8. Austad, T., Engemyr, L. B. and Songstad, J. *Acta Chem. Scand.* 25 (1971) 3535.
9. Makosza, M. and Bialecka, E. *Synth. Commun.* 6 (1976) 313.
10. Loach K. W. *Anal. Chim. Acta* 44 (1969) 323.
11. Ohkubo, K. and Kanaeda, H. *Bull. Chem. Soc. Jpn.* 45 (1972) 11; 322.
12. van Tilborg, W. J. M. *Tetrahedron* 31 (1975) 2841.
13. Appel, R. and Haus, A. *Chem. Ber.* 93 (1960) 405.
14. Cookson, R. C. and Hughes, A. N. *J. Chem. Soc.* (1963) 6061.
15. Ruff, J. K. and Schlientz, W. J. *Inorg. Synth.* 15 (1974) 84.
16. Rave, T. V. *J. Org. Chem.* 32 (1967) 3461.
17. Glidewell, G. J. *J. Inorg. Nucl. Chem.* 38 (1976) 669.
18. Emsley, J. and Hall, D. *The Chemistry of Phosphorus*, Harper & Row, London 1976, p. 380.
19. Schwartz, W. E., Jr., Ruff, J. K. and Hercules, D. M. *J. Am. Chem. Soc.* 94 (1972) 5227.
20. Austad, T., Songstad, J. and Åse, K. *Acta Chem. Scand.* 25 (1971) 331.
21. Appel, R. and Hauss, A. *Z. Anorg. Allg. Chem.* 311 (1961) 290.
22. Ruff, J. K. *Inorg. Chem.* 7 (1968) 1818; 1821.
23. Ruff, J. K. and King, R. B. *Inorg. Chem.* 8 (1969) 180.
24. Handy, L. B., Ruff, J. K. and Dahl, L. F. *J. Am. Chem. Soc.* 92 (1970) 7327.
25. Patton, E. V. and West, R. *J. Phys. Chem.* 77 (1973) 2652.
26. Appel, R. and Siegemund, G. *Z. Anorg. Allg. Chem.* 361 (1968) 203.
27. Wiberg, N., Schwenk, G. and Schmid, M. *Chem. Ber.* 105 (1972) 1209.
28. Wynne, K. J., Pearson, P. S., Newton, M. G. and Golen, J. *Inorg. Chem.* 11 (1972) 1192.
29. Wilson, R. D. and Bau, R. *J. Am. Chem. Soc.* 96 (1974) 7601.
30. Finn, P. A., King, M. S., Kilty, P. A. and McCarley, R. E. *J. Am. Chem. Soc.* 97 (1975) 220.
31. Douglas, W. and Ruff, J. K. *J. Organomet. Chem.* 65 (1974) 65.
32. Hayami, J., Uno, N. and Kaji, A. *Tetrahedron Lett.* (1968) 1385.
33. Cardillo, G., Orena, M. and Sandri, S. *Chem. Commun.* (1976) 190.
34. Thorstenson, T. and Songstad, J. *To be published.*
35. Aksnes, G. and Songstad, J. *Acta Chem. Scand.* 16 (1962) 1426.

Received April 22, 1977.

Geometric and Optical Isomerism in Cobalt(III) and Chromium(III) Tris Complexes of *cis*-1,2-Cyclohexanediamine

HANS TOFTLUND^a and TROELS LAIER^b

^a Department of Chemistry, University of Odense, DK-5000 Odense, Denmark and ^b Chemistry Department, Royal Veterinary and Agricultural University, DK-1871 Copenhagen V, Denmark

The tris *cis*-1,2-cyclohexanediamine complexes of cobalt(III) and chromium(III) have been prepared and the four possible isomers *mer-Δ*, *mer-Λ*, *fac-Δ* and *fac-Λ* have been isolated and characterized. The equilibrium between the isomers of the cobalt(III) complex has been established at 90 °C. The identification of the isomers have been performed on the basis of the electronic, the circular dichroism, ESR and ¹³C NMR spectra.

When a bidentate ligand, with two dissymmetric centers of opposite chirality (*R,S*) and a mirror plane as *cis*-1,2-cyclohexanediamine, (*cis*-chxn), coordinates as part of a tris complex, geometric isomers are possible for each optical enantiomers. Tris complexes with three such ligands are named *facial* (*fac*) and *meridional* (*mer*) referring to the spatial arrangement of the dissymmetric centers. The possibility of this type of isomerism has been mentioned by Woldbye^{1,2} and Tapscott.³ The first detection and separation of *fac* and *mer* isomers was performed by Toftlund and Pedersen.⁴ The tris(*meso*-2,3-butanediamine) cobalt(III) and tris(*meso*-2,4-pentanediamine) cobalt(III) complexes have been separated in the four possible isomers by Kojima *et al.*^{5,6} In the present paper separation and characterization of the four isomers for both [Co(*cis*-chxn)₃]³⁺ and [Cr(*cis*-chxn)₃]³⁺ will be presented. The designation of configuration is, in accordance with IUPAC,⁷ based upon the edges of the octahedron spanned by the chelate rings. The three pairs of edges form three pairs of skew lines describing screws of the same type, either right-handed (*Δ*) or left-handed (*Λ*).

Each chelate ring may exist in one of two conformations designated as *tel* or *ob*, depending on whether the C—C bond in the chelate ring is almost parallel or oblique to the (pseudo) three-fold axis (Fig. 1).

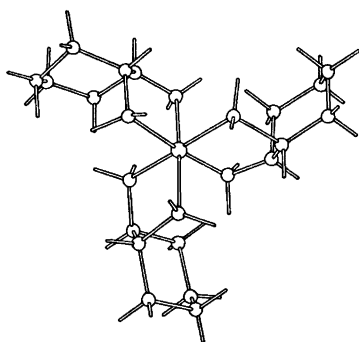
EXPERIMENTAL

Preparations

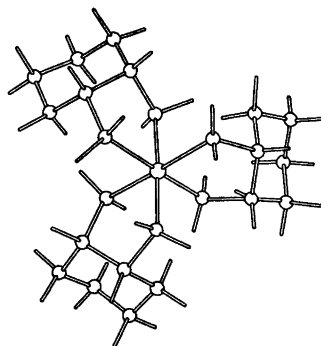
cis-1,2-Cyclohexanediamine. The starting material, purchased from Wolf and Kaaber Farum, contains 51 % of *trans*-, 48 % of *cis*-1,2-cyclohexanediamine and 1 % of 1,6-hexanediamine. The *trans*-1,2-cyclohexanediamine (\pm chxn) was resolved from the crude diamine (240 ml, 2.0 mol) according to Galsbøl *et al.*⁸ The residue after removal of (–)chxn and (+)chxn, contained *ca.* 90 % *cis*-chxn and *ca.* 10 % *trans*-chxn. This residue was heated to 80 °C, and dropwise addition of sulfuric acid (60 ml 9 M) with stirring and cooling precipitated *cis*-chxn.H₂SO₄ (46 g). The crystals were filtered off and dropwise addition of ethanol (150 ml) to the filtrate precipitated 30 g more. No *trans*-chxn could be detected by ¹H NMR in this product.

The *cis*-chxn was liberated from *cis*-chxn.H₂SO₄ (73 g) with potassium hydroxide according to Galsbøl *et al.*⁸ The diamine was distilled under nitrogen. Yield 26 g (11 % from the crude amine), b.p. 58–60 °C/1 Torr, m.p. 6 °C.

Tris(*cis*-1,2-cyclohexanediamine)cobalt(III) chloride [Co(*cis*-chxn)₃]Cl₃. To a solution of *trans*-[Copy₄Cl₂]Cl₆H₂O (8 g 13.3 mmol) in 2-methoxyethanol (25 ml) was dropwise added *cis*-1,2-cyclohexanediamine (5 g 43.8 mmol) at 25 °C. After addition of lithium chloride, (3 g) a few drops of conc. hydrochloric acid and a 1:1 v/v mixture of absolute ethanol and ether (10 ml) the orange chloride precipitated during 3 h at 0 °C. The tris complex was filtered off

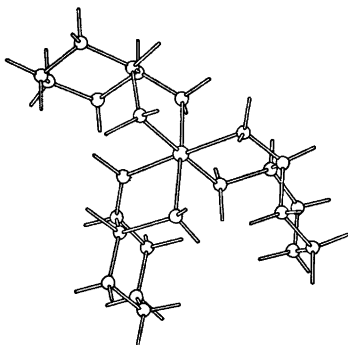


$\text{fac-}\Delta\text{-l}e\ell_3\text{-[Co(cis-chxn)}_3\text{]}^{3+}$

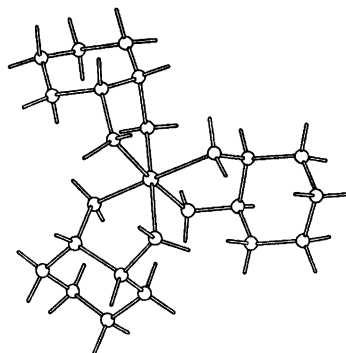


$\text{fac-}\Delta\text{-ob}_3\text{-[Co(cis-chxn)}_3\text{]}^{3+}$

Fig. 1a and 1b. The $le\ell_3$ and ob_3 conformers of $\text{fac-}\Delta\text{-[Co(cis-chxn)}_3\text{]}^{3+}$ viewed along the 3-fold axis



$\text{mer-}\Delta\text{-l}e\ell_3\text{-[Co(cis-chxn)}_3\text{]}^{3+}$



$\text{mer-}\Delta\text{-ob}_3\text{-[Co(cis-chxn)}_3\text{]}^{3+}$

Fig. 1c and 1d. The $le\ell_3$ and ob_3 conformers of $\text{mer-}\Delta\text{-[Co(cis-chxn)}_3\text{]}^{3+}$ viewed along the pseudo-3-fold axis.

and washed twice with 8 ml portions of a 1:1 v/v mixture of abs. ethanol and ether. Yield: 6.3 g (93 %).

Tris(cis-1,2-cyclohexanediamine)chromium(III) chloride, $[\text{Cr(cis-chxn)}_3]\text{Cl}_3$. *cis-1,2-Cyclohexanediamine* (5 g, 44 mmol) and *trichlorotris(pyridine)chromium(III)* (3.5 g, 8.8 mmol) was added to absolute ethanol (50 ml) (dried over molecular sieves) in a 250 ml flask provided with a reflux condenser fitted with a KOH-tube. The mixture was refluxed for 24 h. After 2 h precipitation of yellow-orange crystals commenced. The solution was filtered and the precipitate was washed twice with absolute ethanol. Yield 3.6 g (82 %) of crude $[\text{Cr(cis-chxn)}_3]\text{Cl}_3$.

Separation of the isomers

mer- and fac-Tris(cis-1,2-cyclohexanediamine)cobalt(III) bromide and perchlorate. Separation

of the isomers was done on SP-Sephadex C-25 cation exchange resin using 0.19 M potassium sodium (+)-tartrate as an eluent. A good separation into three bands was obtained; 1. *mer-Δ* 2. *mer-Δ-fac-Δ* and 3. *fac-Δ*. The three fractions were diluted, resorbed on new columns, washed with water and eluted with 0.5 M sodium perchlorate (1st fraction) or with 1 M lithium bromide (2nd and 3rd fractions). The eluates were concentrated by evaporation on a vacuum rotary evaporator and by cooling in ice the complex salts precipitated as orange crystals. The products were reprecipitated from water with saturated sodium perchlorate or saturated sodium bromide. From 1.0 g crude $[\text{Co(cis-chxn)}_3]\text{Cl}_3$ we obtained 0.31 g (1st fraction *ca.* 30 %) of *mer-Δ*. {Anal. $[\text{Co}(\text{C}_6\text{H}_{14}\text{N}_2)_3](\text{ClO}_4)_3$: Co, C, H, N, Cl} and 0.20 g (3rd fraction *ca.* 20 %) of *fac-Δ*. Anal. $[\text{Co}(\text{C}_6\text{H}_{14}\text{N}_2)_3]\text{Br}_3 \cdot 2\text{H}_2\text{O}$: Co, C, H, N, Br. *mer- and fac-Tris(cis-1,2-cyclohexanediamine)chromium(III) perchlorate.* Separation of

the *facial* and *meridional* isomers was done on SP-Sephadex C-25 cation exchange resin using 0.15 M disodium hydrogenphosphate as an eluent.

The *facial* and *meridional* isomers were resorbed on a new column and separated into their optical enantiomers using 0.2 M disodium tartrate. Finally all four isomers were resorbed on a new column and eluted with 0.5 M sodium perchlorate; the eluates were concentrated by evaporation on a vacuum rotary evaporator, whereby most of the complexes separated as yellow crystals. All separations were performed in the dark at 5 °C to prevent hydrolysis.

The products were reprecipitated from water with 60 % perchloric acid. From 2.0 g crude $[\text{Cr}(\text{cis-chxn})_3]\text{Cl}_3$ we obtained 0.50 g of each of the *facial* enantiomers and 0.15 g of each of the *meridional* ones. Anal. $[\text{Cr}(\text{C}_6\text{H}_{14}\text{N}_2)_3](\text{ClO}_4)_3 \cdot 2\text{H}_2\text{O}$; Cr, C, H, N, Cl.

Determination of the relative equilibrium constants. *fac*- $[\text{Co}(\text{cis-chxn})_3]^{3+}$ (100 mg, 0.7 mmol) was dissolved in water (10 ml). *cis*-chxn.2HCl (17.5 mg, 0.1 mmol) was added and pH was adjusted to 7 with 0.1 M sodium hydroxide. Charcoal (Medicinsk A, Struers) (10 mg) was added and the mixture was heated to 90 °C. The mixture was stirred mechanically and the temperature was kept constant for 15 min. The equilibrium was quenched with 0.1 M HCl (4 ml) and the mixture was filtered. After dilution to 100 ml the *fac* and *mer* isomers were separated on an SP-Sephadex-C-25 cation exchanger by elution with a 0.25 M sodium (+)-tartratoantimonate (III) solution and the contents of cobalt were measured in each fraction by atomic absorption.

Measurements

Absorption and circular dichroism spectra were measured with a Cary 14 Spectrophotometer and a Jouan Dichrographe 2B. The cobalt(III) and chromium(III) concentrations were determined by atomic absorption with a Beckman 1248 Atomic Absorption Spectrophotometer. Proton-decoupled 15.03 MHz ^{13}C NMR spectra were measured with a JEOL FX-60 NMR Spectrometer. The ESR measurements were done at 9.115 GHz using a JEOL JES-ME-IX spectrometer.

RESULTS AND DISCUSSIONS

Preparations. As the *cis*-1,2-cyclohexanediamine is a rather poor ligand, the conventional method of preparation of *tris*-diamine-cobalt(III) complexes by oxidation of a cobalt(II) diamine mixture with molecular oxygen was unsuccessful. Instead we obtained an almost quantitative yield from the reaction

between *trans*- $[\text{Co}(\text{py})_2\text{Cl}]\text{Cl}$ and the diamine in 2-methoxyethanol solution.

The *tris-cis*-1,2-cyclohexanediamine chromium(III) chloride was prepared from trichlorotris(pyridine)chromium(III) and the diamine in absolute ethanol. In this preparation even very small amounts of water in the diamine or the absolute ethanol resulted in the formation of a violet product, presumably a diol.

Separation. All separations of the geometrical isomers and the enantiomers were done by chromatography using SP-Sephadex C-25 cation exchange resin and a suitable eluant. $[\text{Co}(\text{cis-chxn})_3]^{3+}$ could be separated into both its geometrical isomers and its enantiomers using 0.19 M disodium (+)-tartrate, *mer-Δ* being eluted first. The geometrical isomers and the enantiomers of $[\text{Cr}(\text{cis-chxn})_3]^{3+}$ could be separated using 0.15 M disodium hydrogenphosphate and 0.2 M disodium (+)-tartrate successively. With phosphate *fac* was eluted first and with (+)-tartrate *Δ* was eluted first. In addition the geometrical isomers of $[\text{Co}(\text{cis-chxn})_3]^{3+}$ could be separated using 0.25 M sodium (+)-tartratoantimonate(III) the fractions appeared in the order: 1st fraction *mer* and 2nd fraction *fac* as for $[\text{Co}(\text{meso-bn})_3]^{3+}$ and $[\text{Co}(\text{meso-ptn})_3]^{3+}$.^{5,6}

NMR Spectra. The ^1H NMR spectrum of *cis*-1,2-cyclohexanediamine has two rather broad peaks at δ 1.45 and 2.80. The *trans*-1,2-cyclohexanediamine has three multiplets around δ 1.20, 1.70 and 2.35. The peaks at 2.80 and 2.35, due to the methine protons, do not overlap each other; thus it is possible to measure the relative amounts of *cis* and *trans*-chxn in a mixture with accuracy. The ^1H NMR spectra of the two geometrical isomers of Co(III) consist of many overlapping lines and are similar, so an identification on this ground is not possible. On the other hand the proton decoupled 15.03 MHz ^{13}C NMR spectra (Fig. 2) distinguish clearly between the two isomers. As the *facial* isomer has three equivalent chelate rings each with six magnetically nonequivalent carbon atoms one would expect to find six lines as indeed are observed for one of the isomers. The assignment is obtained from the gated ^1H -coupled ^{13}C spectrum which shows two doublets for the lines at 56 ppm and 58 ppm and four triplets for the remaining C atoms.

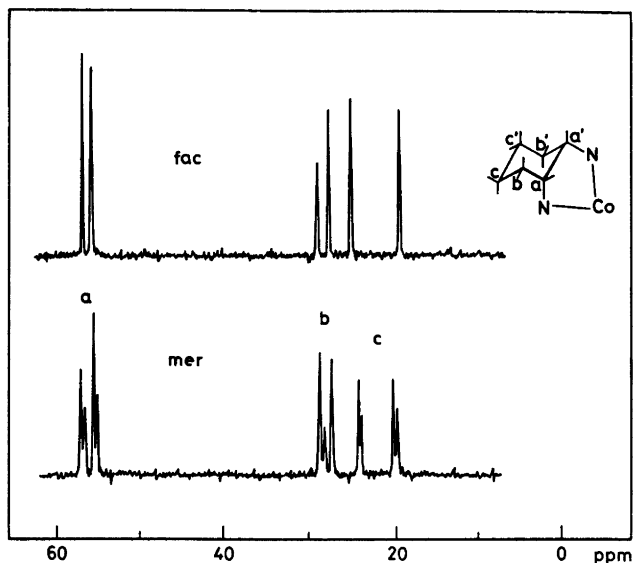


Fig. 2. The 15.03 MHz ^{13}C NMR spectra of *fac*- and *mer*- Δ -[Co(*cis*-chxn) $_3$] $^{3+}$ in D_2O .

The other isomer exhibits a complicated spectrum with at least 11 lines. Theoretically one would expect 18 lines for the *mer*-isomer. The ^{13}C NMR spectrum of the free *cis*-1,2-cyclohexanediamine at 30 °C consists of three sharp lines, whereas the spectrum at -50 °C shows six broad lines, indicating that the ring inversion in the cyclohexanering, at 30 °C, is rapid compared with the ^{13}C frequency. The splitting of the a, b and c carbon signals in the *fac* isomer of [Co(*cis*-chxn) $_3$] $^{3+}$ is caused by the interaction of one cyclohexane ring with the other two chelate rings as this interaction is asymmetric in any point of the inversion. Hence the ring inversion in the complexes too are rapid at room temperature and it is impossible to isolate the *tel*- and *ob*- conformers (eight *mer*- and four *fac*-enantiomeric pairs).

ESR Spectra. The ESR spectra of the two geometrical isomers of Cr(III) in frozen solution are shown in Fig. 3. Because of the great similarity the assignment is difficult to achieve. The spectrum of isomer *a* has larger line widths and the $-\frac{3}{2} \rightarrow \frac{3}{2}$ (*z*) transition at 1100 G has gained intensity and moved slightly upfield relative to the spectrum of complex *b*. This suggests that *a* has a larger *E* value than *b* and most probably is the *mer*-isomer.

The salts. The identification of the isomers is supported by the fact that the *fac* isomers form the least soluble salts.

It is remarkable that the Cr(III) and Co(III) complexes do not form isomorphous salts, thus co-crystallization could not be detected by ESR measurements. One possible explanation of this fact could be that the Cr(III) and Co(III) complexes have different conformations (at least in the solid state).

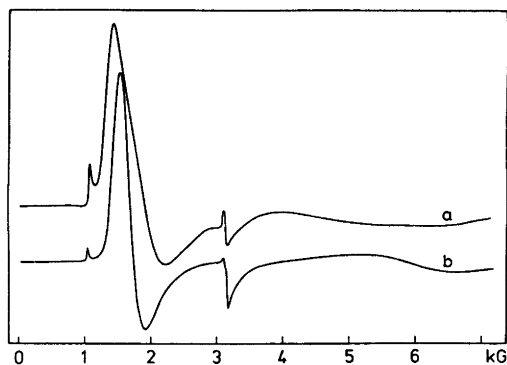


Fig. 3. The ESR spectra of the *mer* (a) and *fac* (b) isomers of Δ -[Cr(*cis*-chxn) $_3$] $^{3+}$ in frozen solution (DMF, H_2O , CH_3OH glass 1:1:2 at -150 °C).

Table 1.

Isomer	Abs		CD		
	ν_{\max} (ϵ)	ν_{\max}^a (ϵ) ^b	ν_{ext} ($\epsilon_1 - \epsilon_d$)	ν_{ext}^a ($\epsilon_1 - \epsilon_d$)	ν_{ext} ($\epsilon_1 - \epsilon_d$)
<i>Δ</i> - <i>mer</i> -[Co(<i>cis</i> -chxn) ₃] ³⁺	20.79 (106.6)	28.74 (102.1)	20.02 (-2.89)	27.21 (-0.159)	35.97 +0.63
<i>Δ</i> - <i>fac</i> -[Co(<i>cis</i> -chxn) ₃] ³⁺	20.88 (99.6)	28.99 (92.8)	20.04 (-2.45)	27.66 (-0.211)	35.71 +0.39
<i>Δ</i> - <i>mer</i> -[Cr(<i>cis</i> -chxn) ₃] ³⁺	21.28 (93.9)	27.89 (79.0)	21.79 (-2.78)	28.01 (+0.21)	
<i>Δ</i> - <i>fac</i> -[Cr(<i>cis</i> -chxn) ₃] ³⁺	21.19 (89.4)	27.78 (74.6)	21.65 (-2.38)	27.93 (+0.15)	30.58 (-0.014)

^a ν_{\max} and ν_{ext} in units of 1000 cm⁻¹. ^b ϵ in units of l mol⁻¹ cm⁻¹.

Absorption and circular dichroism spectra. The spectral data are listed in Table 1 and Figs. 4 and 5. The absorption spectra of the *mer* isomers are a little more intense than the *fac* isomers for both Cr(III) and Co(III). And the positions of the maxima are red-shifted for both isomers relative to the tris-*trans*-1,2-cyclohexanediamine complexes,⁹ indicating greater steric strain in the former.¹⁰ The CD spectra of the two geometric isomers,

mer and *fac*, are similar in shape, but the band intensities of the former are slightly higher than those of the latter, as for the corresponding *meso*-2,4-pentanediamine⁵ and *cis*-1,2-cyclopentanediamine complexes,⁴ but in contrast to the *meso*-2,3-butanediamine complex.⁵ It is interesting that the 2nd band in the CD spectrum of *mer*-[Co(*cis*-chxn)₃]³⁺ is split in two components; it suggests a larger distortion than in the *fac* isomer. The enantiomers with

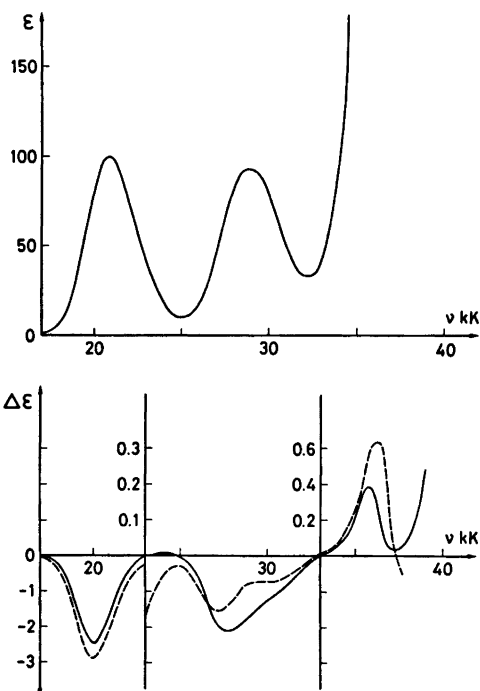


Fig. 4. *a*. Absorption spectrum of *fac*- Δ -[Co(*cis*-chxn)₃]³⁺. *b*. CD spectra of the *fac*- (—) and *mer*- (---) isomers of Δ -[Co(*cis*-chxn)₃]³⁺.

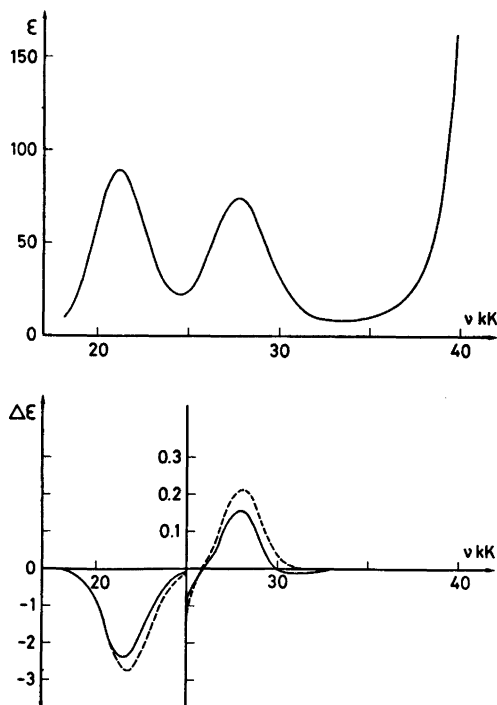


Fig. 5. *a*. Absorption spectrum of *fac*- Δ -[Cr(*cis*-chxn)₃]³⁺. *b*. CD spectra of the *fac*- (—) and *mer*- (---) isomers of Δ -[Cr(*cis*-chxn)₃]³⁺.

positive main deflections in the first ligand band we assign as Δ .^{9,11,12}

Formation ratio. If the relative abundances of the geometric isomers were governed by statistical consideration alone, the ratio of the *mer* isomer to the *fac* isomer should be 3:1; but Dreiding models indicate a little more steric interaction in the *mer*- than in the *fac*-isomer, Fig 1. Kojima *et al.* found the *mer/fac* ratio 1.4 for $[\text{Co}(\text{mbn})_3]^{3+}$ and 1.5 for $[\text{Co}(\text{meso-ptn})_3]^{3+}$, but these figures may be uncertain as no equilibration of the isomers was performed. In the present work the crude $[\text{Co}(\text{cis-chxn})_3]\text{Cl}_3$ was separated in the geometrical isomers and the *fac* isomer equilibrated with charcoal at 90 °C according to Harnung.⁹

We found the *mer/fac* ratio to be 1.43. The enthalpy of the transition *fac*→*mer*, after accounting for the statistical entropy contribution is $\Delta H^\circ = 0.54$ kcal/mol at 90 °C.

REFERENCES

1. Woldbye, F. *Studier over optisk aktivitet*, Diss., Copenhagen 1969, p. 186.
2. Niketic, S. R. and Woldbye, F. *Acta Chem. Scand.* 27 (1973) 3811.
3. Tapscott, R. E. *Inorg. Chem.* 14 (1975) 216.
4. Toftlund, H. and Pedersen, E. *Acta Chem. Scand.* 26 (1972) 4019.
5. Kojima, M., Funaki, H., Yoskikawa, Y. and Yamasaki, K. *Bull. Chem. Soc. Jpn.* 48 (1975) 2801.
6. Kojima, M. and Fujita, J. *Chem. Lett.* (1976) 429.
7. *Inorg. Chem.* 9 (1970) 1.
8. Galsbøl, F., Steenbøl, P. and Sørensen, B. S. *Acta Chem. Scand.* 26 (1972) 3605.
9. Harnung, S. E., Sørensen, B. S., Creaser, I. (neé Olsen), Maegaard, H., Phenninger, U. and Schäffer, C. E. *Acta Chem. Scand.* *In press.*
10. Schäffer, C. E. *Proc. R. Soc. London A* 297 (1967) 96.
11. Saito, Y. *Pure Appl. Chem.* 17 (1968) 21.
12. Harnung, S. E. and Laier, T. *Acta Chem. Scand.* *In press.*

Received April 28, 1977.

Nickel(II) Complexes of Thiohydrazonates. I

J. GABEL, ERIK LARSEN and P. TRINDERUP *

Chemistry Department I, The H.C. Ørsted Institute, Universitetsparken 5,
DK-2100 Copenhagen Ø, Denmark

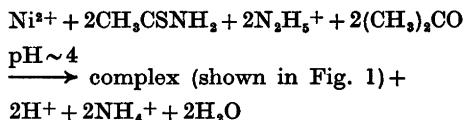
Dedicated to Professor K. A. Jensen on his 70th birthday

New condensation products of aliphatic thiohydrazides and mono- and diketones have been synthesized as ligands in nickel(II) inner complexes. These complexes have been characterized by means of ^1H NMR, UV-VIS spectroscopy and cyclic voltametry. The protonated complexes may exist at high acidities in solutions of low water activity but the free ligands are not stable. For comparison some nickel(II) complexes of thiosemicarbazonates were prepared as well.

Complexes of thiosemicarbazides and of thiosemicarbazonates were first described by K. A. Jensen in 1934, and in 1952 he investigated nickel(II) complexes of the closely related thio-benzhydrazide.¹⁻⁴ Another homologous ligand, *e.g.* thioacetylhydrazide, could not be isolated and accordingly no complexes were made.⁵ However, it was recently found that bis(thiohydrazidato)nickel(II) is formed from thioacetamide, hydrazinium ions and nickel(II) ions at $\text{pH} \sim 4$.⁶

While attempting to grow crystals of this complex for a single crystal X-ray diffraction investigation, it was found that this compound when dissolved in dimethyl sulfoxide, reacts at room temperature for months with acetone forming a red crystalline product very distinctly different from the starting material. Chemical analysis indicated that a template reaction analogous to that discovered by Curtis⁷ could have taken place or that a complex of acetone thioacetylhydrazone (*cf.* Fig. 1) had been formed. The latter explanation turned out to be correct,

and a series of compounds has been prepared by analogous condensations. However, it became evident that it is not necessary first to isolate bis(thioacetylhydrazidato)nickel(II) in order to obtain the condensation products. Aqueous mixtures of thioacetamide, hydrazine and a suitable ketone enters with nickel(II) ions into template reactions and the non-electrolyte products can readily be isolated. For acetone the reaction scheme is



Complexes of thiosemicarbazonates and their anions closely related to compounds investigated in this work have for some time been studied with the main emphasis on either the antitumor activity shown by some copper(II) derivatives⁸ or on the fascinating ability for some of the reaction products to exist in many oxidation states. The field has recently been reviewed by Campbell.⁹ The present preparative investigation has been undertaken to clarify the stereochemistry of thioacetylhydrazonato nickel(II) complexes by means of spectroscopy and

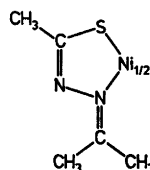


Fig. 1.

* Present address: Northern European University Computing Center, Technical University of Denmark, DK-2800 Lyngby, Denmark.

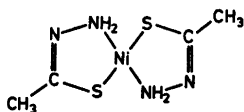


Fig. 2.

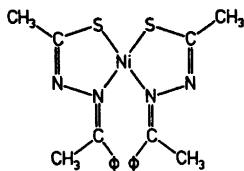


Fig. 3.

X-ray diffraction. So far, the crystal and molecular structure of bis(thioacetylthioacetimidato)nickel(II)⁶ and bis(acetophenone thioacetimidato)nickel(II)¹⁰ have been published (Figs. 2 and 3).

EXPERIMENTAL

Starting materials. Bis(thioacetylthioacetimidato)nickel(II) and bis(thiophenylacetylthioacetimidato)nickel(II) were prepared as previously described,⁶ while bis(thiosemicarbazidato)nickel(II) was prepared according to Jensen and Rancke-Madsen.³ Phenylacetthiamide was prepared according to Berntsen¹¹ and Kindler.¹² Anal. C_8H_9NS : C, H, N, S. Reagents were commercial chemicals of analytical grade.

Physical measurements. Absorption spectra were measured with Cary 14 and Perkin Elmer IR 337 spectrophotometers, diffuse reflectance spectra with a Spectronic 505, and ¹H NMR spectra with Varian A-60, A-100 and Bruker X90 spectrographs using TMS as internal standard. Polarographic data were obtained using a three electrode polarograph constructed by Dr. E. Pedersen in this laboratory, with a Beckman 19001 Pt electrode as working electrode, a Pt wire as auxiliary electrode, and a Metrohm EA 429 Ag/AgCl reference electrode with a salt bridge consisting of a 0.2 M $(n-C_4H_9)_4NClO_4$ solution in dimethylformamide saturated with $(n-C_4H_9)_4NCl$. Reported $E_{1/2}$ values are in V relative to aqueous SCE.

Complexes. All complexes prepared were characterized by chemical analysis, ¹H NMR and absorption spectra and checked for small amounts of impurities by thin layer chromatography normally using chloroform as the solvent and silica gel as the stationary phase. Melting points given below are uncorrected.

The abbreviations used are: thioacetylthioacetimidato = tahH, phenylacetthioacetimidato = pathH, thiosemicarbazidato = tscH, and 2,4-

pentandione = acacH. A condensation product of a thiohydrazide and a ketone is denoted by means of parentheses including the abbreviation for the thiohydrazide and the name of the ketone.

Preparations. In general, two methods of preparation are possible. In the first method solutions in suitable solvents of nickel acetate, hydrazine hydrate, the thiamide, and the ketone are mixed and refluxed, whereupon the complex precipitates. In the second method, the ketone is condensed with the nickel thiohydrazide complex either in a homogeneous reaction using dimethyl sulfoxide (DMSO) as the solvent, or in a heterogeneous reaction usually with ethanol as the solvent. It may be necessary to catalyze the reaction by adding a drop of 12 M hydrochloric acid. For most of the complexes with thiosemicarbazones as ligands a third method of preparation is available. This involves the preparation of the ligand by a standard procedure, followed by reaction with nickel(II) by adding an ethanol solution of the ligand to an ammoniacal solution of an equivalent amount of nickel. The methods of preparation mentioned below are those found to yield the purest product.

[Ni(tah acetone)₂]. In the first method 9.0 g (0.035 mol) of nickel acetate tetrahydrate, 5.0 g (0.067 mol) of thioacetamide, 3.5 ml (0.07 mol) of hydrazine hydrate, and 25 ml (0.34 mol) of acetone were dissolved in a mixture of 25 ml of glacial acetic acid and 125 ml of water. The mixture was refluxed for 24 h. After cooling, the solid was filtered off, washed with water and ethanol, and dried in air. Yield: 9.0 g (82 %). The crude product was dissolved in 1 l of chloroform, and the solution was filtered and evaporated to 1/10 of the original volume. The recrystallization was repeated once or twice.

According to the second method the complex was prepared in a homogeneous reaction by dissolving 2.0 g (0.0084 mol) of [Ni(tah)₂] in 100 ml of DMSO and adding 100 ml (0.84 mol) of acetone. After refluxing for 24 h the mixture was cooled to room temperature, the solid filtered off, and washed with ethanol. Yield: 1.75 g. By adding 100 ml of water to the mother liquor, further 0.5 g was isolated (total yield: 85 %).

The product was a violet microcrystalline powder m.p. 290–291 °C with decomposition. (Found: C 37.80; H 5.74; N 17.92; S 20.04. Calc. for $C_{10}H_{16}N_4NiS_2$: C 37.89; H 5.68; N 17.68; S 20.21).

[Ni(path acetone)₂]. This complex is prepared in the same way as the corresponding thio-derivative. The small plates obtained exhibited pleochroism with colour changes from red to green, and melted unsharply at 190–196 °C. Anal. $C_{22}H_{26}N_4NiS_2$: C, H, N, S, Ni.

[Ni(tsc acetone)₂]. The compound was best prepared from [Ni(tsc)₂] according to the second method in a homogeneous reaction with DMSO as the solvent. The light brown, crystalline

powder was recrystallized from 2-ethoxyethanol. M.p. 236–237°C with decomposition. Anal. $C_8H_{14}N_6NiS_2$: C, H, N, S.

[Ni(tah butanone)₂]. A solution of 2.4 g (0.010 mol) of [Ni(tah)₂] and 5 ml (0.055 mol) of 2-butanone in 50 ml of DMSO was heated at 100°C for 1.5 h, whereupon 10 ml of water was added. After cooling to room temperature, the mixture was filtered and the precipitate washed with small portions of ethanol. After drying at 50°C the yield was 1.0 g (29%) of small, violet plates melting at 178–180°C. TLC revealed that three isomers had formed. By column chromatography on silica gel with 5% ethyl acetate in benzene as eluent one isomer could be obtained rather pure. (Found: C 41.00; H 6.56; N 15.78; S 18.59. Calc. for $C_{12}H_{22}N_4NiS_2$: C 41.77; H 6.38; N 16.26; S 18.57).

[Ni(path butanone)₂]. The preparation is analogous to that of the corresponding tah derivative. The small, violet crystals melted unsharply at 91–94°C. Anal. $C_{24}H_{30}N_4NiS_2$: C, H, N, Ni, S.

[Ni(tsc butanone)₂]. To a solution of 5 g (0.017 mol) of nickel nitrate hexahydrate in 200 ml of water a slight excess of conc. ammonia was added, and the resulting solution was mixed with a solution of 5 g (0.034 mol) of butanone thiosemicarbazone in 750 ml of hot methanol. After standing overnight, the precipitate was filtered off, washed with water and ethanol, and dried. Yield 4.8 g (41%) dark brown thin plates m.p. 218.5–220°C. Soxhlet extraction with CH_3CN did not improve the purity of the product, but produced small red-brown crystals. (Found: C 33.95; H 3.94; N 24.35; Ni 16.81; S 17.90. Calc. for $C_{10}H_{20}N_4NiS_2$: C 34.59; H 5.82; N 24.21; Ni 16.91; S 18.47).

[Ni(tah acetophenone)₂]. Both methods mentioned first were used successfully to prepare this complex. The crystals obtained are irregularly shaped polyhedra, exhibiting pleochroism with colour changes from red to green. Unsharp m.p. at 258–262°C. TLC on silica gel and aluminium oxide with a variety of eluents failed to prove the existence of more than one isomer. Anal. $C_{26}H_{22}N_4NiS_2$: C, H, N, S.

[Ni(path acetophenone)₂]. A mixture of 3 g (0.0074 mol) of [Ni(path)₂]. H_2O and 5 ml (0.042 mol) of acetophenone in 100 ml of 96% ethanol, to which 3 drops of 12 M HCl was added, was refluxed for 24 h. After cooling to –10°C the reaction mixture was filtered, and the precipitate washed with small amounts of ethanol. After drying in vacuum over NaOH pellets, the yield was 2.9 g of a brown crystalline powder. The crude product was extracted with 250 ml of boiling 96% ethanol and filtered. Next the filtrate was cooled to –10°C, and the first formed crystals were filtered off and dried in air. Yield: 0.2 g (5%) of brown crystals melting at 209–210°C. (Found: C 64.55; H 4.98; N 9.22; Ni 9.73; S 10.80. Calc. for $C_{32}H_{30}N_4NiS_2$: C 64.76; H 5.11; N 9.44; Ni 9.89; S 10.80).

[Ni(tsc acetophenone)₂]. The complex was prepared by mixing an ammoniacal solution of nickel nitrate and a solution of acetophenone thiosemicarbazone in methanol. The product was purified by Soxhlet extraction with acetonitrile for 24 h. The small, black crystals melted at about 270°C with decomposition. Anal. $C_{18}H_{20}N_6NiS_2$: C, H, N, Ni, S.

[Ni(tah₂ butanedione)]. A solution containing 9.0 g (0.035 mol) of nickel acetate, 5.0 g (0.067 mol) of thioacetamide, 3.5 ml (0.07 mol) of hydrazine hydrate in a mixture of 25 ml of glacial acetic acid and 125 ml of water was refluxed for 15 min. whereupon a solution of 3.5 ml (0.040 mol) of butanedione in 50 ml of ethanol was added slowly. It is of importance for the purity of the product not to introduce the solution too rapidly. The mixture was refluxed for 2 h, allowed to cool to room temperature, and filtered. The crude product was washed with ethanol and recrystallized from chloroform. Yield: 9.3 g (96%) of small, dark, violet crystals, which decomposed above 250°C without melting. (Found: C 33.04; H 4.16; N 19.38; S 22.29. Calc. for $C_8H_{12}N_4NiS_2$: C 33.48; H 4.19; N 19.53; S 22.32).

[Ni(path₂ butanedione)]. The preparation is the same as for the tah derivative. The intense red, almost black crystals melted at 253–254°C with decomposition. (Found: C 54.75; H 4.63; N 12.85; Ni 13.13; S 14.39. Calc. for $C_{20}H_{20}N_4NiS_2$: C 54.67; H 4.59; N 12.76; Ni 13.37; S 14.60).

[Ni(tsc₂ butanedione)]. The second method was followed using 10.0 g (0.031 mol) of [Ni(tsc)₂] and 5.0 ml (0.057 mol) of butanedione dissolved in 50 ml of DMSO. The mixture was kept at 100°C for 6 h and then allowed to stand overnight at room temperature. The crude product was filtered off, washed with ethanol, and recrystallized from 100 ml of DMSO. The yield was 5.0 g (42%) of small green crystals which did not melt below 330°C. (Found: C 25.15; H 3.80; N 28.51; S 22.40. Calc. for $C_6H_{10}N_4NiS_2$: C 24.92; H 3.49; N 29.08; S 22.18).

[Ni(tah₂ benzil)]. A slurry of 9.0 g (0.035 mol) of nickel acetate, 5.0 g (0.067 mol) of thioacetamide, 3.5 ml (0.07 mol) of hydrazine hydrate, and 7.4 g (0.035 mol) of benzil in 275 ml of 96% ethanol was refluxed for 24 h. After cooling and filtering, the solid was washed thoroughly with ethanol and acetone. The crude product (7.7 g) was recrystallized from chloroform, giving 3.1 g (22%) of green needles. M.p.; 272°C with decomposition. (Found: C 52.19; H 3.94; N 13.88; Ni 14.28; S 15.16. Calc. for $C_{16}H_{16}N_4NiS_2$: C 53.58; H 3.92; N 13.63; Ni 14.28; S 15.60).

[Ni(path₂ benzil)]. A mixture of 3.7 g (0.0091 mol) of [Ni(path)₂]. H_2O and 2.0 g (0.0095 mol) of benzil in 150 ml of 96% ethanol containing 0.5 ml of 12 M HCl, was refluxed for 4 days. The hot mixture was filtered, and the solid washed with ethanol. After drying, 4.4 g of crude product was obtained. For purification 2.0 g of this was extracted with 150 ml of boiling tetra-

hydrofuran. The solution was filtered and the filtrate evaporated to 25 ml. After cooling to 0°C, the solid was filtered off, and dried in air. Yield: 0.3 g of small, dark green crystals melting at 249–251°C with decomposition. (Found: C 63.65; H 4.37; N 9.83; Ni 10.10; S 11.47. Calc. for $C_8H_{24}N_4NiS_2$: C 63.95; H 4.30; N 9.95; Ni 10.42; S 11.38).

[Ni(tsc₂ benzil)]. The complex was prepared in the same way as the corresponding path derivative using DMSO as the solvent. The crude product was Soxhlet extracted with acetone yielding dark, red crystals. (Found: C 47.40; H 3.87; N 18.97; S 14.24. Calc. for $C_{14}H_{41}N_6NiS_2$: C 46.51; H 3.42; N 20.34; S 14.21).

[Ni(tah₂ acacH)]. A slurry of 4 g (0.017 mol) of [Ni(tah₂)₂] and 15 ml (0.15 mol) of 2,4-pentanedione in 150 ml of 50% ethanol was refluxed for 4 h and then cooled to 5°C. The solid was filtered off, washed with water and dried in vacuum over conc. H_2SO_4 . The yield was 4.7 g (80%) of a fairly pure product corresponding to the composition [Ni(tah₂ acacH)]. C_2H_5OH . The complex could be purified by Soxhlet extraction with ethanol, preferably under an atmosphere of nitrogen since the complex tended to oxidize somewhat when wet. (Found: C 37.95; H 5.81; N 16.42; S 18.52. Calc. for $C_{11}H_{20}N_4NiS_2$: C 38.05; H 5.82; N 16.14; S 18.47). The solvent of crystallization could easily be removed by heating at 100°C for 3 h in a vacuum. The red-brown crystals thus obtained melted unsharply at about 300°C with decomposition. (Found: C 36.00; H 4.72; N 18.72; S 21.23. Calc. for $C_9H_{14}N_4NiS_2$: C 35.90; H 4.70; N 18.61; S 21.30).

[Ni(path₂ acacH)]. The compound was prepared analogously to [Ni(tah₂ acacH)], but the chocolate-brown crystals obtained did not contain solvent of crystallization. M.p. 203–205.5°C. (Found: C 55.85; H 5.04; N 12.36; S 14.38. Calc. for $C_{21}H_{32}N_4NiS_2$: C 55.65; H 4.89; N 12.36; S 14.15).

[Ni(tsc₂ acacH)]. The preparation of this complex is the same as that given for the corresponding tah derivative. However, since the compound is easily oxidized by atmospheric oxygen all preparations were performed under an atmosphere of nitrogen. The product was light brown and fairly stable in air when perfectly dry. (Found: C 27.71; H 4.04; N 27.88; S 19.83. Calc. for $C_7H_{12}N_6NiS_2$: C 27.74; H 4.00; N 27.74; S 19.37).

(*n*- C_4H_9)₄N[Ni(tah₂ acac)]. 6.5 g (0.019 mol) of [Ni(tah₂ acacH)]. C_2H_5OH was dissolved in 70 ml of 0.6 M NaOH, and after filtration a solution of 6.5 g (0.019 mol) of tetrabutylammonium perchlorate in 600 ml of acetone was added. The mixture was evaporated to a volume of 150 ml and then cooled at –10°C for 2 h. The precipitate was filtered off and dried in vacuum over conc. H_2SO_4 . Yield: 8.0 g (78%) of orange-red plates melting at 143–144°C. (Found: C 55.25; H 9.42; N 13.04; S 11.50. Calc. for $C_{25}H_{40}N_6NiS_2$: C 55.33; H 9.12; N 12.91; S 11.82).

(*n*- C_4H_9)₄N[Ni(path₂ acac)]. To a filtered solution of 0.95 g (0.0021 mol) of [Ni(path₂ acacH)] in a mixture of 3 ml 40% aqueous tetrabutylammonium hydroxide (0.0046 mol) and 20 ml of ethanol was added another solution containing 1.0 g (0.0029 mol) of tetrabutylammonium perchlorate in 100 ml of acetone. The solution was evaporated until crystals began to separate and then kept at –10°C overnight. The product was filtered off, washed with water, and dried in vacuum over conc. H_2SO_4 . Yield: 1.1 g (74%) of a reddish-brown crystalline powder melting at 135.5–136.5°C. (Found: C 63.80; H 7.23; N 10.12; S 9.54. Calc. for $C_{25}H_{37}N_6NiS_2$: C 63.95; H 8.29; N 10.08; S 9.23).

(*n*- C_4H_9)₄[Ni(tsc₂ acac)]. This complex is prepared analogously to the corresponding tah derivative using [Ni(tsc₂ acacH)] as the starting material, and all operations were carried out under an atmosphere of nitrogen. Even when dry this compound was oxidized rapidly in the air forming a dark, green product. (Found: C 48.34; H 8.08; N 17.91. Calc. for $C_{23}H_{47}N_6NiS_2$: C 50.72; H 8.72; N 18.01).

[Ni(tah₂ 2,5-hexanedione)]. To a suspension of 10.0 g (0.042 mol) of [Ni(tah₂)₂] in 200 ml of 50% ethanol was added 11.0 g (0.097 mol) of 2,5-hexanedione, and the mixture was refluxed for 12 h. After cooling to room temperature 200 ml of water was added, and the mixture was kept at 5°C overnight. The precipitate was filtered off, washed with water, and dried in vacuum over conc. H_2SO_4 . Yield: 9.5 g (72%) of brown crystalline powder. The crude product was purified by Soxhlet extraction with ethanol under an atmosphere of nitrogen. M.p. 190.5–192.5°C. (Found: C 37.95; H 5.16; N 17.68; Ni 19.16; S 20.20. Calc. for $C_{10}H_{16}N_4NiS_2$: C 38.11; H 5.12; N 17.78; Ni 18.63; S 20.35).

[Ni(path 2,5-hexanedione)]. The complex was prepared in the same way as the corresponding tah derivative. The brown-red crystal plates melted at 139–140°C. Anal. $C_{22}H_{24}N_4NiS_2$: C, H, N, S.

[Ni(tsc 2,5-hexanedione)]. The ligand was prepared separately and added to an ammoniacal solution of nickel. After stirring overnight the solid was filtered off, washed with water and dried. Yield: 15 g (94%). The product was purified by Soxhlet extraction with ethanol. The red-violet crystals melted at 297–298°C with decomposition. (Found: C 30.37; H 4.72; N 26.30; S 20.23. Calc. for $C_6H_{14}N_6NiS_2$: C 30.30; H 4.46; N 26.51; S 20.22).

[Ni(tah₂ acacO)] = (5,7-dimethyl-6-oxo-3,4,8,9-tetraazaundeca-2,4,7,9-tetraene-2,10-dithiolato-*N*³,*N*⁸,*S*,*S'*)nickel(II). A suspension of 4.0 g (0.0012 mol) of [Ni(tah₂ acacH)]. C_2H_5OH and 8.0 g (0.08 mol) of powdered calcium carbonate in 400 ml of water was stirred and refluxed under an atmosphere of nitrogen for 24 h. The mixture was filtered and a brisk current of air was drawn through the red filtrate for 4 days at room temperature. An olive-green precipitate

formed, and it was extracted with four 250 ml portions of toluene. After drying with 50 g of anhydrous magnesium sulfate and filtering, the toluene phase was evaporated to dryness, and the solid extracted with 200 ml of boiling acetone. After filtering the green solution was kept at -10°C overnight. The product was filtered off and dried in vacuum over conc. H_2SO_4 . Yield: 0.5 g (14%) of dark green needles. M.p. $263-265^{\circ}\text{C}$ with decomposition. (Found: C 34.30; H 3.96; N 17.82; S 20.07. Calc. for $\text{C}_9\text{H}_{12}\text{N}_4\text{NiOS}_2$: C 34.31; H 3.85; N 17.76; S 20.35).

Attempts to prepare the corresponding path and tsc compounds were unsuccessful.

$[\text{Ni}(\text{tah}_2, 3\text{-methyl-2,4-pentanedione})]$. 3-Methyl-2,4-pentanedione was prepared by adding first 37 g (0.37 mol) of 2,4-pentanedione and then 52 g (0.37 mol) of methyl iodide to a chilled solution of 8.5 g (0.37 mol) of sodium metal in 85 g of ethanol, refluxing the mixture for 36 h, cooling to -10°C , and adding 250 ml of ether to precipitate the sodium iodide formed. The ether was distilled off, and one third of the resulting solution (70 ml, containing 0.125 mol of 3-methyl-2,4-pentanedione) was refluxed with 24.0 g (0.10 mol) of $[\text{Ni}(\text{tah})_2]$ for 2 days. After cooling to -10°C the solid was filtered off, washed with ethanol, and dried in air. Yield: 23.5 g of red-brown powder. This was purified by double extraction with ethanol, the second time under an atmosphere of nitrogen. Red-brown crystals were obtained melting at $238-240^{\circ}\text{C}$ with decomposition. The product was not quite pure but attempts to purify it were unsuccessful. (Found: C 36.81; H 5.25; N 17.73; Ni 17.60; S 19.75. Calc. for $\text{C}_{19}\text{H}_{16}\text{N}_4\text{NiS}_2$: C 38.11; H 5.13; N 17.78; Ni 18.63; S 20.35).

During a search for another preparative route to the above complex a compound of composition $[\text{Ni}(\text{tah}_2, \text{acacH})]\cdot\text{CH}_3\text{I}$ was isolated: A mixture of 5 g (0.0092 mol) of $(n\text{-C}_4\text{H}_9)_3\text{N}[\text{Ni}(\text{tah}_2, \text{acac})]$ and 6 g (0.042 mol) of methyl iodide in 75 ml of ethanol was refluxed for 3 days. After cooling to -10°C the solid was filtered off, washed with a small portion of ethanol, and dried in air. Yield: 3.5 g (86%) of a brown-red powder which did not melt below 330°C . Recrystallization from a variety of solvents invariably led to loss of iodine. (Found: C 26.94; H 3.85; I 28.42; N 13.33; S 14.6. Calc. for $\text{C}_{10}\text{H}_{17}\text{IN}_4\text{NiS}_2$: C 27.11; H 3.88; I 28.64; N 12.65; S 14.47).

$[\text{Ni}(\text{tsc CH}_3\text{COC}_6\text{H}_4\text{-4-SO}_2\text{Na})_2]\cdot 4\text{H}_2\text{O}$. 31.0 g (0.105 mol) of the sodium salt of 4-sulfoacetophenone thiosemicarbazone and 12.5 g (0.053 mol) of nickel chloride hexahydrate were dissolved in 250 ml of water, and a solution of 25 g (0.62 mol) of sodium hydroxide in 25 ml of water was added with stirring. After stirring overnight the mixture was centrifuged, and the solid was washed with water until the colour of the washings changed from yellow to red. The precipitate was extracted with 1 l of hot water, and the red solution was filtered and

evaporated to a volume of 500 ml. The precipitate was removed by centrifugation, washed with acetone, and dried at 75°C . Yield: 15.4 g (46%) of a dull-green powder. (Found: C 29.81; H 3.66; N 11.85; Na 6.40; Ni 8.6; S 17.63. Calc. for $\text{C}_{18}\text{H}_{18}\text{N}_6\text{Na}_2\text{NiO}_6\text{S}_4\cdot 4\text{H}_2\text{O}$: C 30.05; H 3.65; N 11.68; Na 6.39; Ni 8.16; S 17.83).

RESULTS

UV and VIS spectra of a representative series of compounds in aprotic and acid (F_3CCOOH) media are collected in Table I. Generally one or two weak absorption components in the visible region were found which can be ascribed to $d-d$ transitions. The remainder of the spectrum consists of broad uncharacteristic bands reaching $\epsilon = (5-30) \times 10^3$. The ^1H NMR spectra are relatively simple because couplings are absent in nearly all the cases studied.

The electrochemical behaviour in dimethylformamide (0.2 M in $(n\text{-C}_4\text{H}_9)_4\text{NClO}_4$) of all the compounds have been investigated by cyclic voltametry. It was essential to add activated Al_2O_3 (Woelm neutral alumina) to the solutions in the cell to eliminate protic impurities. Table 2 summarizes the obtained results.

DISCUSSION

The compounds described in the experimental section are all made very easily using template reactions. The thioacylhydrazides are unknown except for those having tertiary α -carbon atoms, and likewise the ketone thioacylhydrazones are unknown. It is therefore interesting that it is possible to trap these hydrazones as their nickel(II) inner complexes. When the complexes precipitate from aqueous solution their stability might be due to their insolubility in water. However, the complexes may be prepared in a homogeneous solution in dimethylsulfoxide and they are generally soluble in polar organic solvents. We thus conclude that the chelation stabilizes the ligand system. In conc. sulfuric acid and in trifluoroacetic acid the complexes are soluble as protonated species. These solutions gave intensely coloured precipitates with conc. perchloric acid, and solutions of zirconium(IV) chloride and antimony(V) chloride in 12 M hydrochloric acid. These precipitates, however, could not be washed or dried without yielding the neutral (and usually differently coloured) complexes. Thus, although the protonated

Table 1. Electronic spectra of nickel complexes given at maximum (or as shoulders) in 10^3 cm^{-1} with molar absorptivity in parenthesis.

Complex	Solvent ^a	
[Ni(tah) ₂] ^b	DMF	16.4(45), 22.7(135)sh, 23.4(139), 26.2(99)sh, 27.3(130)sh
[Ni(tah) ₂] ^c	DMF	15.7(386), 21.7(195)sh, 24.7(246)
[Ni(tah) ₂] ^d		14.5, 17.8, 23.2
[Ni(tah acetone) ₂]	CHCl ₃	16.7(120)sh, 19.4(250), 28.0(5000)sh, 35.5(19700)sh, 37.0(20800)
[Ni(tah acetophenone) ₂]	MeCN	18.7(250), 26.2(6000), 41.0(33800)
[Ni(tah ₂ butanedione)]	CHCl ₃	15.9(250)sh, 16.8(335), 25.0(2200)sh, 27.4(4500), 35.4(10900)
[Ni(tsc ₂ butanedione)]	DMSO	15.1(495), 16.7(430)sh, 25.1(11500), 31.5(7500)sh,
[Ni(tah ₂ acacH)]	MeCN	19.5(230), 24.0(10600), 32.3(7700), 36.4(15100), 40.8(28400)
Bu ₄ N[Ni(tah ₂ acac)]	MeCN	19.5(235), 25.0(11300), 34.3(7500)sh, 40.0(27000)sh, 44.9(31200)
[Ni(tah ₂ acacO)]	MeCN	16.0(340), 19.2(220)sh, 28.8(10050), 32.8(8500), 41.0(20600), 45.6(24000)
[Ni(tah ₂ 2,5-hexanedione)]	MeCN	16.4(57)sh, 21.1(253), 36.4(2380)sh, 37.5(13300), 41.7(11920)
[Ni(tah acetophenone) ₂]	TFAA	17.6(42), 24.1(440)sh, 33.5(8050)
[Ni(tsc acetophenone) ₂]	TFAA	17.2(97), 20.8(41)sh, 29.4(3800)sh, 40.0(72900)
[Ni(tah ₂ butanedione)]	TFAA	17.6(300), 25.5(1030)sh, 28.5(2500)sh, 31.0(4700)
[Ni(tah ₂ acacH)]	TFAA	19.5(99), 24.1(6100), 25.4(3900)sh, 27.2(3100), 31.4(5700)
[Ni(tah ₂ acacO)]	TFAA	18.2(650), 19.3(660), 30.9(10150), 33.5(9600)

^a The solvents used are DMF dimethylformamide, MeCN acetonitrile, DMSO dimethyl sulfoxide, TFAA trifluoroacetic acid and chloroform. ^b Extrapolated back to time of dissolution. ^c 30 min after dissolution. ^d Diffuse reflectance spectrum.

Table 2. Half wave potentials from cyclic voltametry in dimethylformamide at 10 °C.

Complex	$E^{\circ}_{\frac{1}{2}}$ V	Peak separation mV	Sweep rate mV/s
Ni(tah acetone) ₂	-1.21	90	20
[Ni(path acetone) ₂]	-1.16	190	100
Ni(tsc acetone) ₂	-1.31	310	100
[Ni(tah acetophenone) ₂]	-1.17	108	25
[Ni(path acetophenone) ₂]	-1.12	160	5
[Ni(tsc acetophenone) ₂]	-1.26	105	5
[Ni(tah ₂ butanedione)]	-0.66	80	10
	-1.58	80	10
[Ni(path ₂ butanedione)]	-0.65	130	100
	-1.53	185	200
[Ni(tsc ₂ butanedione)]	-1.28	80	40
	-1.85	95	40
[Ni(bth ₂ butanedione)] ^a	-0.53		
	-1.24		
[Ni(tah ₂ benzil)]	-0.42	80	20
	-1.34	90	20
[Ni(tsc ₂ benzil)]	-1.05	105	15
	-1.64	112	15
[Ni(tah ₂ acacH)]	no reduction waves observed		
[Ni(tah ₂ acacO)]	-0.35	171	80
	-1.15	irr.	
[Ni(tah ₂ 2,5-hexanedione)]	-1.34	80	4
[Ni(tsc 2,5-hexanedione)]	-1.41	145	100
[Ni(tsc 3-hexene-2,5-dione)] ^b	-1.22		

^a Recorded in dimethyl sulfoxide. bth = C₆H₅C(S) = N - N =. See Ref. 22. ^b Ref. 20.

species are analogous to the acid nickel(II) complexes of thiosemicarbazones, they are much weaker bases. The latter kind of complexes have been investigated by X-ray diffraction¹³ and spectroscopy.^{14,15} It seems established that the complexes are five coordinated in the solid but six coordinated in methanol solutions. From the near-IR bands (Table 1) it seems reasonable to conclude that the thioacylhydrazone nickel complexes behave similarly to the thiosemicarbazone nickel complexes. Bähr^{16,17} has earlier prepared nickel(II) complexes of thiosemicarbazones, and the preparations given here are in some cases easier. For derivatives of diketones like acetylacetone where the thiosemicarbazone is unknown the reported methods of preparation seem to be of general utility.

The planar inner complexes of monoketone derivatives can give rise to *cis-trans* isomerism. Bis(thioacetylhydrazidato)-nickel(II)⁶ (cf. Fig. 2) is known to assume the *trans*-form like bis(thiosemicarbazidato)nickel(II),¹⁸ but bis(acetophenone thioacetylhydrazonato)nickel(II) was found to have a structure which may be described as a tetrahedrally distorted *cis* planar complex having the phenyl groups in a *syn* configuration (Fig. 3). The electronic spectra reported in Table 1 seem to indicate that also the inner complexes of acetone thioacylhydrazides are *cis* complexes. The diffuse reflectance spectrum of *trans* [Ni(tah)₂] shows maxima at 14.5, 17.8 and 23.2 kK. The compound is soluble in dimethyl sulfoxide and dimethylformamide, however, in these solvents the absorption spectrum varies with time presumably because of *trans-cis* rearrangement or extension of the coordination number. Extrapolations to time of dissolution in DMF indicate absorption maxima at 13.4, 15.4 and 23.5 kK. These values are significantly different from the absorption shown by [Ni(tah acetone)₂] (16.7 (Sh) and 19.4 kK) in a variety of solvents and on this basis the latter complex is believed to be *cis*. The same conclusion is reached for the butanone derivative. The rather large variation in the position of the maxima for these *cis* complexes and for [Ni(tah acetophenone)₂] may reflect the variation of the deviation from co-planarity of the two ligands or the difference in conjugation of the acetophenone derivative compared to the aliphatic derivatives.

Acta Chem. Scand. A 31 (1977) No. 8

Thin layer and column chromatography and the ¹H NMR spectra show that [Ni(tah acetophenone)₂] exists as only one isomer whereas the product derived from butanone consists of three isomers. Thus it is also demonstrated that the inner complexes are robust in organic solvents as chloroform and benzene used in these experiments. The number of isomers formed by the butanone derivatives can be explained as the *syn*, *anti* and *amphi* forms of either the *cis* or the *trans* complex. If the assignment of the *cis* planar configuration based on the electronic spectra is correct, it seems that the determining factor in the *cis-trans* isomerism must be the bulkiness of the sulfur atoms and the substantial van der Waal interactions possible in the *cis* complex. This phenomenon was observed¹⁰ for [Ni(tah acetophenone)₂].

The ¹H NMR spectra of the compounds with the structures shown in Figs. 3, 4, and 6 show a number of peaks corresponding to the presence of a twofold axis of symmetry in each molecule. For [Ni(tah₂ acacH)] the low solubility in CDCl₃ is a problem, and this complex because of its acid character could in principle have a nitrogen bound proton judged from the acid character of the compound. The complex derived from 3-methyl-2,4-pentanedione was therefore prepared for ¹H NMR spectroscopy. The spectrum shows a signal for a methyl group split into a doublet (*J* = 7.5 Hz) and this proves that the methyl group and the acid proton are bound to the same carbon atom.

The colour variation within the series [Ni(tah acetone)₂] (reddish-violet), [Ni(tah₂ butanedi-one)] (green), [Ni(tah₂ acacH)] (yellow) and [Ni(tah₂ acacO)] (green), Figs. 4–6 indicate that the degree of conjugation plays a large role for the spectral properties. The bands in the visible region attributable to the *d-d* transitions are rather similar for [Ni(tah acetone)₂] and [Ni(tah₂ acacH)] in accordance with the proposed *cis* structure for the former complex. The smaller *d-d* transition energies for

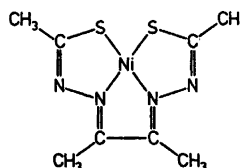


Fig. 4.

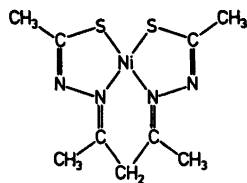


Fig. 5.

[Ni(tah₂ butanedione)] (16–17 kK) than for [Ni(tah₂ acacH)] (19 kK) reflects the smaller difference between the σ^* and π^* d -orbitals in the complex of the most conjugated ligand.

In view of the common *cis* configuration, the largest structural difference arises in the different planarity of the ligand systems. Only the conjugated ligands can be expected to form planar complexes in which the ligand π orbitals have maximum overlap with the d_{π} orbitals. In [Ni(tah acetophenone)₂] the two planes defined by S–C=N–N form an angle of 19°. Some deviation from planarity is expected for [Ni(tah acetone)₂] for steric reasons but since [Ni(tah₂ acacH)] has a very similar spectral behaviour in the visible region one may conclude that the d_{π} -ligand $_{\pi}$ overlaps are roughly equal. The latter compound is soluble in base, and salts containing the anion have been isolated. In not too basic solvents [Ni(tah₂ acacH)] or its anion is oxidized by air forming a green complex of the structure shown in Fig. 6. The presence of a ketone group has been established by IR absorption. The compound exhibits a C=O band at 1655 cm⁻¹ which compares favourably with the 1663 cm⁻¹ band found¹⁸ for $\Delta^1,4$ -androstadienedione-3,17. The corresponding [Ni(tsc₂ acacH)] is much more easily oxidized but the solubility properties of the oxidized compound has so far hindered its isolation.

Electrochemistry. McCleverty *et al.* have reported on the electrochemical properties of

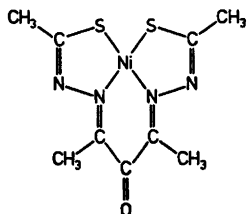


Fig. 6.

eleven nickel complexes of diketone bithiosemicarbazones.²⁰ These authors found generally two one-electron reduction steps at *ca.* -1 and -2 V. The rather small variation in $E_{1/2}$ values (~ 0.2 V) was explained by various substitutional effects and the degree of conjugation in the chelate system. In Table 2 are shown the reduction potentials for a series of thiohydrazone complexes in *N,N*-dimethylformamide measured by cyclic voltametry. We have found the procedure of Hammerich and Parker²¹ for removal of impurities with alumina very useful since with this technique it was easier to obtain reversible voltamograms for the second reduction.

From Table 2 it is evident that the acyl derivatives are more easily reduced than the corresponding thiosemicarbazones. The monoketone derivatives have reduction potentials more or less uninfluenced by substituents on the carbonyl carbon and the α -carbon of the acyl radical. For the complexes derived from the diketones butanedione and benzil there is a dramatic difference in the $E_{1/2}$ values while again the tah and path derivatives have nearly the same reduction potentials.

The acetylacetone derivatives [Ni(tah₂ acacH)] and [Ni(path₂ acacH)] give irreversible waves probably because of reactions involving a proton from the methylene group. The anions obtained as the tetrabutylammonium salts gave better voltamograms but they were still not quite reversible.

REFERENCES

1. Jensen, K. A. *Z. Anorg. Allg. Chem.* **221** (1934) 11.
2. Jensen, K. A. and Rancke-Madsen, E. *Z. Anorg. Allg. Chem.* **219** (1934) 243.
3. Jensen, K. A. *Z. Anorg. Allg. Chem.* **229** (1936) 265.
4. Jensen, K. A. and Miquel, J. F. *Acta Chem. Scand.* **6** (1952) 189.
5. Jensen, K. A. and Pedersen, C. *Acta Chem. Scand.* **15** (1961) 1097.
6. Larsen, E., Trinderup, P., Olsen, B. and Watson, K. J. *Acta Chem. Scand.* **24** (1970) 261.
7. Curtis, N. F. *J. Chem. Soc.* (1960) 4409.
8. Liebermeister, K. *Z. Naturforsch. Teil B* **5** (1950) 79.
9. Campbell, M. J. M. *Coord. Chem. Rev.* **15** (1975) 279.
10. Larsen, S. *Acta Chem. Scand. A* **28** (1974) 779.

11. Berntsen, A. *Justus Liebigs Ann. Chem.* 184 (1877) 293.
12. Kindler, K. *Justus Liebigs Ann. Chem.* 431 (1923) 203.
13. Mathew, M., Palenik, G. J. and Clark, G. R. *Inorg. Chem.* 12 (1973) 446.
14. Malik, M. A. and Philips, D. J. *Aust. J. Chem.* 28 (1975) 305.
15. Beechcroft, B., Campbell, M. J. M. and Grzeskowiak, R. *J. Inorg. Nucl. Chem.* 36 (1974) 55.
16. Bähr, G. *Z. Anorg. Allg. Chem.* 278 (1955) 136.
17. Bähr, G. *Z. Anorg. Allg. Chem.* 280 (1955) 161.
18. Cavalca, L., Nardelli, M. and Fava, G. *Acta Crystallogr.* 15 (1962) 1139.
19. Jones, R. N., Humphries, P. and Dobriner, K. *J. Am. Chem. Soc.* 72 (1950) 956.
20. Bailey, N. A., Hule, S. E., Jones, C. J. and McCleverty, J. A. *Chem. Commun.* (1970) 124.
21. Hammerich, O. and Parker, V. C. *Electrochim. Acta* 18 (1973) 537.
22. Holm, R. H., Balch, A. L., Davidson, A., Maki, A. H. and Berry, T. E. *J. Am. Chem. Soc.* 89 (1967) 2866.

Received April 20, 1977.

Comparable *ab initio* Calculated Energies of HCNS, CNSH, NCSH and HNCS. Optimized Geometries and Dipole Moments

B. BAK,^a J. J. CHRISTIANSEN,^b O. J. NIELSEN^a and H. SVANHOLT^a

^a Chemical Laboratory V, H. C. Ørsted Institutet, DK-2100 Copenhagen, Denmark and ^b Department of Chemistry, Royal Danish School of Educational Studies, Emdrupvej 115 B, DK-2400 Copenhagen, Denmark

Dedicated to Professor K. A. Jensen on his 70th birthday

Energies of geometry optimized models of HCNS (−490.15344 hartrees), CNSH (−490.17332 hartrees), NCSH (−490.20453 hartrees), and HNCS (−490.21238 hartrees) have been calculated *ab initio* by LCAO-MO-SCF technique applying a $4s,1p$ (H); $7s,3p$ (N); $7s,3p$ (C); $10s,6p,1d$ (S) basis set. Within the framework of this basis the most stable species is HNCS while HCNS (0.05894 hartrees), CNSH (0.03906 hartrees), and NCSH (0.00785 hartrees) are of higher energy as quoted parenthetically. Only at *ca.* 2000 °C NCSH may coexist. At 700 °C $\text{HC}=\text{N}-\text{S}-\text{CO}-\text{O}$ or

1,3,4-oxathiazol-2-one pyrolyzes to HNCS while a product in which the atomic sequence had been conserved would be HCNS, thiofulminic acid. Predicted dipole moments in Debye units are *ca.* 5 for HCNS and *ca.* 3 for the remaining structural isomers.

When the five-membered ring compound $\text{HC}=\text{N}-\text{S}-\text{CO}-\text{O}$, 1,3,4-oxathiazol-2-one (I)¹

is pyrolyzed on a quartz surface at 700 °C and $p \approx 0.02$ mmHg for *ca.* 30 s it dissociates into HNCS (II) and CO₂. We have identified II by means of its well-known microwave spectrum^{2,3} by pumping the products of pyrolysis continuously through a microwave cell. Also, pyrolysis products were collected for 3–4 h on a cooled (liq. N₂) KBr-disc. An infrared spectrum was obtained verifying the presence of II⁴ without, however, excluding the presence of hitherto unknown HCNS. A mass spectrum of the products showed dominating peaks for CO₂ and HCN. While work on necessary improvements of the experimental technique

is in progress we have found it useful to produce *ab initio* estimates of the energies of the title compounds, simultaneously optimizing their structures. The energy calculations will determine relative stabilities. Optimized geometries and calculated dipole moments will assist in the search for spectra of HCNS, CNSH and NCSH whether of terrestrial or interstellar origin. These species have not yet been prepared, whereas infrared and microwave spectra of HNCS are known.^{2–4} The difference between the experimental and the *ab initio* calculated structure of HNCS is informative as to the reliability of the calculated structures of the three remaining isomers (Fig. 1). Errors of ± 0.02 Å may be implied due to basis set imperfection.

CALCULATIONS

All calculations were of conventional LCAO-MO-SCF type, the program system MOLECULE⁵ being applied. Orbital exponents of the basis functions for C, N and S have been taken from Ref. 5. The orbital exponents for H were those of Huzinaga⁶ multiplied by 1.25.

Fig. 1 summarizes energies and optimized structures. Data from (CH₃)₂S,⁷ CH₃SH,⁸ CH₃NCS,⁹ and CH₃SCN⁹ were used as start parameters. The changes necessary to produce minimum energy (= 'geometry optimization') were slight. In the case of HNCS differences between calculated and experimental geometry

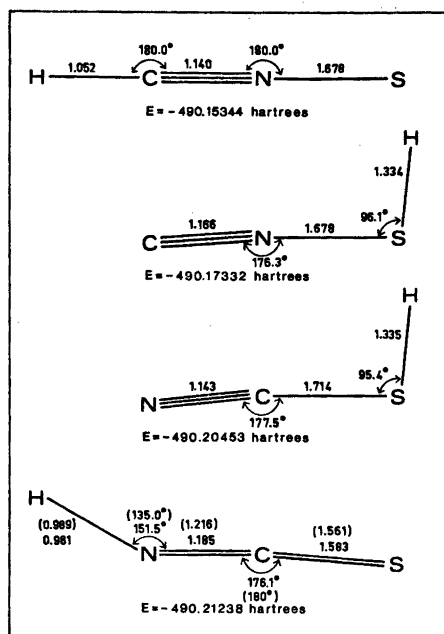


Fig. 1. Optimized structures (distances in Å) and energies of HCNS, CNSH, NCSH and HCNS. Experimental structure of HCNS in parentheses. 1 hartree = 627.5 kcal mol⁻¹.

may be seen from Fig. 1. They are probably of the same order of magnitude for all structural isomers.

Calculated dipole moments and their corresponding μ_a -components ('a' being an inertial axis) are reported in Table 1 with rotational constants A, B, C for all calculated structures.

Table 1. Calculated total dipole moments (μ) and components along inertial "a"-axis (μ_a) (in Debye units) for HCNS, CNSH, NCSH, and HCNS. Rotational constants A, B, C (in MHz).

	HCNS	CNSH	NCSH	HCNS
μ	5.38	3.05	3.41	3.14
μ_a	5.38	2.83	3.19	2.91 ^a
A	—	259610	294591	2889304 ^b
B	5857	6277	5765	5828 ^b
C	5857	6147	5655	5816 ^b

^a Experimental $\mu_a = 1.72$ Debye. ^b Necessarily different from experimental (ground state) value (A = 1483000, B = 5883, C = 5846).

DISCUSSION

As seen from Fig. 1. molecular energy decreases in the order HCNS, CNSH, NCSH and HCNS. This is in harmony with the fact that HCNS is the only hitherto available structural isomer. Also, the sequence $\mathcal{E}(\text{CNSH}) > \mathcal{E}(\text{NCSH})$ (energy \mathcal{E}) is expected. The energy relations suggest that primarily released HCNS, in which the atomic sequence of parental I has been conserved, reorganizes to HCNS. It is energetically possible that this happens step-wise through metastable CNSH and NCSH. Clearly, if species other than HCNS are wanted their formation must take place under non-equilibrium conditions. Such as low temperature, 'flash' heating etc.

Within the framework of the applied 4s, 1p (H); 7s, 3p (N); 7s, 3p (C); 10 s, 6p, 1d (S) Gaussian type basis set, hypothetical HCNS was found to be linear. The three remaining species possess slightly bent CNS or NCS groups in a conformation *trans* to H. However, it should be noted that these features have not been finally established until larger basis sets have been used. This general phenomenon is well illustrated in a recent publication¹⁰ on HCNO, NCOH, and HNCO. So the calculated structures must be considered *preliminary* (Fig. 1).

From an *experimental* point of view the choice between a linear or a non-linear NCS group in HCNS is also difficult since the experimentally well-established difference between the rotational constants B and C may not entirely be due to off-line hydrogen (deuterium). Table 2 shows that a model in which NCS has been bent by 4° (as suggested by the *ab initio* treatment) can reproduce the experimental values for B and C if the angle HNC is changed by only 2°. This is not to suggest that this latter model is preferable for H(D)NCS considering, for example, that a large amplitude motion of H is involved.

In a series of calculations, S of HCNS (*ab initio* model) was moved from +4° (*trans*) through 0 to -4° while establishing hydrogen positions corresponding to minimum molecular energy as a function of the angle HNC and the H-N distance. It was found that H and S pass the N≡C axis simultaneously. The energy at linear conformation was calculated

Table 2. Experimental rotational constants B and C (a) in MHz of HNCS and DNCS and rotational constants of models b , c and d .

	a	b	c	d
B				
HNCS	5883	5870	5867	5875
DNCS	5501	5489	5479	5492
C				
HNCS	5846	5840	5839	5845
DNCS	5445	5440	5436	5445

^a Experimental.^{2,3} ^b Recalculated from exp. parameters in (), Fig. 1. ^c As for b , but NCS bent by 4° (*trans* to H). ^d As for c , but diminishing the angle HNC by 2°.

as being 86 cm⁻¹ higher than for the "natural" bent molecule. The height of this barrier is of interest to spectroscopists. However, our calculated value only represents a crude estimate.

Parental HC=N-S-CO-O has also been a target in photolysis. Identified products were CO₂, HCN, OCS, and HNCO.¹¹ It is worth noting that the quanta of radiation involved in the present pyrolytic experiment are an order of magnitude smaller than quanta in the visible-ultraviolet region.

Acknowledgement. Thanks are due to the Danish Research Council for Natural Sciences for supporting this work. We are indebted to Arne Holm for suggesting the pyrolysis of 1,3,4-oxathiazol-2-one and for providing samples of this compound. Thanks are due to Helge Johansen, Chem. Lab. B, The Technical University of Denmark, for his constant help and advice.

REFERENCES

1. Holm, A. *Unpublished preparation*. Chem. Lab. II, The H. C. Ørsted Institute, Copenhagen.
2. Kewley, R., Sastry, K. V. L. N. and Winnewisser, M. *J. Mol. Spectrosc.* 10 (1963) 418.
3. Yamada, K., Winnewisser, G., Winnewisser, M., Szalanski, L. B. and Gerry, M. C. L. *J. Mol. Spectrosc.* 64 (1977) 401.
4. Draper, G. R. and Werner, R. L. *J. Mol. Spectrosc.* 50 (1974) 369.
5. Roos, B. and Siegbahn, P. *Theor. Chim. Acta* 17 (1970) 209.

6. Huzinaga, S. *J. Chem. Phys.* 42 (1965) 1293.
7. Pierce, L. and Hayashi, M. *J. Chem. Phys.* 35 (1961) 479.
8. Kojima, T. and Nishikawa, T. *J. Phys. Soc. Jpn.* 12 (1957) 680.
9. Lett, R. G. and Flygare, W. H. *J. Chem. Phys.* 47 (1967) 4730.
10. McLean, A. D., Loew, G. H. and Berkowitz, D. S. *J. Mol. Spectrosc.* 64 (1977) 184.
11. Holm, A. *Private communication*.
12. Beard, C. I. and Dailey, B. P. *J. Chem. Phys.* 18 (1950) 1437.

Received April 29, 1977.

About the Crystal Structure of Cesium Cadmium Tribromide and Some Observations on Crystals of Cesium Cadmium Trichloride

CHR. KNAKKERGAARD MØLLER

Department of Chemistry, Odense University, DK-5000 Odense, Denmark

Dedicated to Professor K. A. Jensen on his 70th birthday

CsCdBr_3 forms hexagonal, optically positive crystals which contain infinite polyions $(\text{CdBr}_3^-)_n$. The polyions consist of face sharing, nearly regular CdBr_3^{4-} -octahedra stacked along the *c*-axis. The crystals are isomorphous to those of RbNiCl_3 . The existence of a cubic perovskite form of CsCdBr_3 cannot be verified. A pure perovskite form of CsCdCl_3 is stable at room temperature while a hexagonal form with a structure different from that of CsCdBr_3 is stable at elevated temperatures.

Compounds of the composition M(I)M(II)X_3 , where X is a halogen and M a metal often form crystals where the M(II) -atoms are octahedrally surrounded by X-atoms.¹ The octahedra may share corners, edges or faces of which examples are represented by CsCdCl_3 , (cubic perovskite structure)^{2,3} RbCdBr_3 , (orthorhombic)⁴ and RbNiCl_3 , (hexagonal),⁵ respectively. CsCdBr_3 might be expected to have a structure similar to that of CsCdCl_3 , and it has been reported to have a cubic perovskite structure with $a = 5.33$ Å.⁶ However, the density calculated on this basis is too high, 5.38 g/cm³, which is even higher than that of CsHgBr_3 . Hence a reinvestigation of cesium cadmium bromide was considered worthwhile.

EXPERIMENTAL

Crystals of composition CsCdBr_3 were prepared by precipitation from aqueous solutions, e.g. by adding to 3.5 ml of water at room temperature 1.0 ml saturated CdBr_2 -solution and 0.5 ml saturated CsBr -solution. The crystals were lath-shaped with pointed ends. Under the

polarizing microscope they showed extinction parallel to their length and they appeared to be hexagonal and uniaxial positive, but with a rather low birefringence.

Determination of Br after Volhard and EDTA-titration of Cd showed that the crystals contained 49.9 % Br and 23.2 % Cd. (Calc. for CsCdBr_3 : 49.4 % Br and 23.2 % Cd).

X-Ray (Guinier) powder diagrams were taken of crystals which were precipitated under very varied conditions, but they all showed the same pattern.

In order to find the conditions where the cubic form of CsCdBr_3 might be stable a series of solutions of CsBr or of CdBr_2 were prepared and to each of them crystals of the previously prepared CsCdBr_3 were added to form saturated solutions. The suspensions of the crystals were kept agitated in a thermostat for several days at certain well defined temperatures. For each temperature the equilibrium concentrations of Br and Cd were determined by Volhard and EDTA-titration, respectively, and the crystals in each suspension were examined optically and by X-rays (Guinier diagrams). They turned out always to be of the original, hexagonal type so that no new crystal phase was formed.

The ratio of the increase in molal concentration of Br to the increase in molal concentration of Cd, $\Delta m(\text{Br})/\Delta m(\text{Cd})$, on going from one temperature to a higher one was determined for each suspension (Table 1). This ratio is close to 3.0 indicating that the crystals dissolve (nearly) congruently in these solutions.

Guinier diagrams of $\text{CsBr} + \text{CdBr}_2 \cdot 4\text{H}_2\text{O}$ fused together in the stoichiometric ratio 1:1 show that the same crystalline product of CsCdBr_3 is obtained as from precipitation. Hence the formation of a cubic perovskite of CsCdBr_3 can not be confirmed from these experiments.

Crystals of composition CsCdCl_3 were obtained by fusing CsCl and $\text{CdCl}_2 \cdot 2\frac{1}{2}\text{H}_2\text{O}$ together in the correct stoichiometric proportion.

Table 1. Molal concentrations of Br and Cd in aqueous solutions in equilibrium with crystals of CsCdBr₃ at three different temperatures.

Solvent	21.0 °C		24.1 °C		29.1 °C		$\frac{\Delta m(\text{Br})}{\Delta m(\text{Cd})}$
	<i>m</i> (Br)	<i>m</i> (Cd)	<i>m</i> (Br)	<i>m</i> (Cd)	<i>m</i> (Br)	<i>m</i> (Cd)	
Pure water	0.807	0.265	0.883	0.293	1.015	0.336	2.9 ₃
0.05 M CsBr	0.782	0.242	0.858	0.273	0.982	0.311	2.8 ₃
0.10 M CsBr	0.743	0.217	0.836	0.248	0.960	0.299	2.7 ₀
0.25 M CsBr	0.716	0.167	0.822	0.197	0.934	0.243	2.8 ₃
0.50 M CsBr	0.793	0.119	0.885	0.153	0.988	0.189	2.8 ₅
1.00 M CsBr	1.199	0.103	1.257	0.128	1.380	0.168	2.8 ₅
0.05 M CdBr ₂	0.850	0.287	0.911	0.315	1.023	0.354	2.6 ₅
0.10 M CdBr ₂	0.884	0.308	0.956	0.336	1.085	0.385	2.7 ₀
0.25 M CdBr ₂	1.022	0.406	1.112	0.454	1.205	0.474	2.7 ₅
0.50 M CdBr ₂	1.372	0.612	1.460	0.639	1.552	0.683 ₀	2.7 ₀
1.00 M CdBr ₂	2.277	1.086	2.343	1.111	2.449	1.149 ₀	2.7 ₀

X-Ray (Guinier) powder diagram of the reaction product could be indexed unambiguously on a hexagonal cell with $a = 7.41_1$ Å and $c = 18.45_4$ Å.^{3,5}

On mixing dilute aqueous solutions of CsCl and CdCl₂ (e.g. 1 ml saturated CsCl-solution and 1 ml saturated CdCl₂-solution in 10 ml water) a white crystalline, birefringent precipitate results. The X-ray powder diagram of this has lines in common with that of CsCdCl₃ prepared by fusion, but in addition some other lines also. A precipitate of composition CsCdCl₃ was left for about three months in the mother-liquor. Then it was observed that the precipitate had lost its birefringence. An X-ray powder diagram revealed that the precipitate now consisted of crystals with ideal cubic perovskite structure with $a = 5.23_4$ Å. Thus the perovskite structure is the form of CsCdCl₃ which is stable at room temperature. On heating crystals of CsCdCl₃ having perovskite structure to about 230 °C they gradually became birefringent, and X-ray powder diagrams of the crushed crystals showed that both the cubic and the hexagonal forms were present. The transformation in the solid state appears to be very sluggish and may even commence at about 110 °C. Thus CsCdCl₃ is truly dimorphic.

X-Ray investigation of CsCdBr₃. A single crystal (0.8 × 0.2 × 0.2 mm³) of CsCdBr₃

grown from aqueous solution was examined by X-rays on a Weissenberg goniometer and on a precession instrument (CuK α -radiation). It was found to be hexagonal with the *c*-axis parallel to the goniometer axis. The values obtained for *a* and *c* were used for indexing Guinier diagrams of a crystalline powder of CsCdBr₃ and refined values could be obtained for the axes: $a = 7.68_1$ Å, $c = 6.72_0$ Å. On the assumption that the molar volumes of CsBr and CdBr₂ are approximately additive the unit cell is found to contain two units of formula CsCdBr₃. Calculated density is 4.68₅ g/cm³.

The Weissenberg photographs of the first and the third layer lines ($l = 1$ and $l = 3$) were nearly identical (apart from geometric distortion). They were generally weaker than the zeroth and second layer lines, which had many more reflections, and were definitely different from these. Also, the latter two were mutually different. Reflections of the type $h h 2\bar{h}l$ were only observed for $l = 2n$. These observations comply with the space group $P6_3/mmc - D_{6h}^{3*}$ with the two sets of metal atoms in special positions "a" and "d", the 6 bromine atoms in special positions "h",⁷ (see Table 2).

Using a calibrated scale intensities were visually estimated for the zeroth and the first layer line and $|F|^2$ -values were obtained after Lorentz

Table 2. Atomic positions in hexagonal CsCdBr₃.

2Cd:	0,0,0;	0,0, $\frac{1}{2}$.	
2Cs:	$\frac{2}{3}, \frac{1}{3}, \frac{1}{2}$;	$\frac{1}{3}, \frac{2}{3}, \frac{1}{2}$.	
6Br:	$x, 2x, \frac{1}{2}$	$2\bar{x}, \bar{x}, \frac{1}{2}$;	$x, \bar{x}, \frac{1}{2}$;
	$\bar{x}, 2\bar{x}, \frac{1}{2}$;	$2x, x, \frac{1}{2}$;	$\bar{x}, x, \frac{1}{2}$;
	$x = \frac{1}{3} = 0.167$		

Table 3. Some interatomic distances (Å) between nearest neighbours and angles (°) in hexagonal CsCdBr₃, *z*-parameters indicated.

Cs($\frac{1}{3}$) - 6Br($\frac{1}{2}$)	4.03
Cs($\frac{1}{3}$) - 6Br($\frac{1}{2}$)	3.84
Cd(0) - 6Br($\pm \frac{1}{2}$)	2.78
Cd(0) - Cd($\frac{1}{2}$)	3.36
Br($\frac{1}{2}$) - Br($\frac{1}{2}$) [†]	3.94
\angle Br($\frac{1}{2}$) - Cd(0) - Br($\frac{1}{2}$)	87.3
\angle Br($\frac{1}{2}$) - Cd(0) - Br($\frac{1}{2}$)	92.7

Table 4. Comparison of Cd-X- and Cd-Cd-distances in different cadmium halogen compounds.

Compound	Cd-X Å	Sum of ionic radii ¹⁰ Å	Cd-Cd Å	Octahedra
K ₂ CdCl ₆ (hex) ⁹	2.63	2.78	7.45	isolated
CsCdCl ₃ (cub) ³	2.62	2.78	5.23	sharing corners
CsCdCl ₃ (hex) ^{3,8}	2.64;2.59	2.78	3.23	sharing faces ^a
CsCdBr ₃ (hex)	2.78	2.92	3.36	sharing faces
RbCdBr ₃ (o-rh) ⁴	2.63-2.87	2.92	4.15	sharing edges

^a Face-sharing as well as corner-sharing occurs in these crystals.

and polarisation corrections had been applied.

The value of the parameter α was obtained from a kind of bounded projection of the Patterson function based on the first layer line only.

Structure factor amplitudes $|F|_{\text{calc}}$ were calculated on the basis of the atomic positions given in Table 2 and atomic scattering factors from Ref. 7. The observed $|F|_{\text{obs}}$ were brought on the same scale and stripped of absorption and isotropic temperature factor.* Leaving out three strong reflections which appear definitely to have been measured too low, a reliability index $R=0.16$ was obtained for the zeroth and first layer line together. Refinement did not seem appropriate with the present intensity data, but even so the value for the parameter α is presumably fairly accurate.

Representative interatomic distances and "bond angles" calculated on the basis of the atomic positions in Table 2 are given in Table 3. They are presumably accurate to ± 0.05 Å and 1° , respectively. CsCdBr₃ is thus seen to be isostructural with RbNiCl₃⁵ but not with hexagonal CsCdCl₃^{3,8}

DISCUSSION

In the crystals of CsCdBr₃ Cd is surrounded by 6 Br-atoms in nearly regular octahedral arrangement. These octahedra are stacked on top of one another along the *c*-axis, sharing the faces which are perpendicular to the *c*-axis. In this way linear polynuclear ions (CdBr₃)_n result which may explain the positive birefringence and the relatively low solubility. The octahedra appear to be slightly elongated along the $\bar{3}$ -axis coinciding with the *c*-axis.

CdX₆-octahedra occur in other cadmium halogen compounds of which some examples are given in Table 4. The Cd-X-distances in these

crystals are shorter than the sum of the ionic radii of Cd²⁺ and X⁻,¹⁰ which may indicate either that the accepted ionic radius for Cd²⁺ is too long or that the shortening is due to complex formation. Accepting the latter point of view it does not seem valid to maintain that ionic radii can be deduced from crystals with the perovskite structure which often have been considered to be "ionic".

On the contrary, it may be more helpful to regard the perovskite structure as the result of the formation of a three-dimensional polynuclear complex ion consisting of CdX₆-octahedra sharing corners with the other metal ions

Table 5. Comparison of observed and calculated *d*-values for CsCdBr₃. CuK α -radiation, $\lambda=1.5418$ Å.

<i>d</i> _o Å	<i>d</i> _c Å	Indices <i>hkl</i>	<i>I</i> _o ^a
6.67 ₂	6.65 ₂	100	vs
4.74 ₀	4.73 ₀	101	m-w
3.842	3.841	110	m-s
3.364	3.363	002	m-s
3.328	3.326	200	m-w
3.005	3.001	102	s
2.983	2.982	201	vs
2.531 ₃	2.530 ₂	112	m-w
2.515 ₁	2.514 ₃	210	m
2.365 ₀	2.364 ₀	202	vs
2.355 ₆	2.355 ₃	211	vw
2.217 ₁	2.217 ₄	300	m-w
2.123 ₄	2.124 ₃	103	vw?
2.012 ₇	2.013 ₇	212	m-s
1.919 ₃	1.920 ₃	220	m-s
1.857 ₇	1.859 ₁	203	m-s
1.843 ₆	1.845 ₀	310	vw
1.680 ₈	1.681 ₆	004	m-s
1.666 ₃	1.667 ₆	222	m

* A table of calculated and observed structure factors can be obtained from the author.

^a Estimated intensity.

(e.g. Cs⁺) trapped in the resulting interstices. This would be in analogy to the one-dimensional polynuclear complex ions (CdBr₃⁻)_n built up of face-sharing octahedra in CsCdBr₃ or edge-sharing ones in RbCdBr₃. The isolated octahedra are then represented in K₄CdCl₆.

Similar considerations could presumably be applied to many oxides with the perovskite structure.

Acknowledgement. I am very indebted to Professor, dr.phil. R. W. Asmussen for the loan of his private Weissenberg goniometer used for this work.

REFERENCES

1. Ting-I Li, Stucky, G. D. and McPherson, G. L. *Acta Crystallogr. B* 29 (1973) 1330.
2. Ferrari, A. and Baroni, A. *Rend. Accad. Lincei* 6 (1927) 418.
3. Siegel, S. and Gebert, E. *Acta Crystallogr.* 17 (1964) 790.
4. Natarajan Iyer, M., Faggiani, R. and Brown, I. D. *Acta Crystallogr. B* 33 (1977) 127.
5. Asmussen, R. W., Larsen, T. K. and Soling, H. *Acta Chem. Scand.* 23 (1969) 2055.
6. Natta, G. and Passerini, L. *Gazz. Chim. Ital.* 58 (1928) 472.
7. *International Tables for X-Ray Crystallography*, Kynoch Press, Birmingham 1965, Vols. I–III.
8. Chang, Jin Rong, McPherson, G. L. and Atwood, J. L. *Inorg. Chem.* 14 (1975) 3079.
9. Bergerhoff, G. and Schmitz-Dumont, O. *Z. Anorg. Allg. Chem.* 284 (1956) 10.
10. Landolt-Börnstein, I Band, Teil 4 (1955) 523.

Received April 20, 1977.

A Contribution to Our Knowledge of Weak Chloro Complex Formation by Copper(II) in Aqueous Chloride Solutions

JANNIK BJERRUM^a and L. H. SKIBSTED^b

^a Chemistry Dept. I, Inorganic Chemistry, H. C. Ørsted Institute, University of Copenhagen, DK-2100 Copenhagen Ø, Denmark and ^b Chemistry Dept., Royal Veterinary and Agricultural University, DK-1871 Copenhagen V, Denmark

Dedicated to Professor K. A. Jensen on his 70th birthday

The problems involved in obtaining both stability constants and extinction coefficients from spectrophotometric measurements are discussed in relation to a recently published study of the copper(II) chloride system. The results of this latter study do not agree well with those obtained previously by one of the present authors and we have therefore made some supplementary measurements and re-calculated the data.

In the case of strong metal ion complex formation with rapid equilibrium adjustment the concentration stability constants can usually be determined with a high degree of accuracy by potentiometric methods when the measurements are performed in the presence of a high concentration of an inert salt and low concentrations of the reacting species. However, these experimental conditions cannot be fulfilled in the case of weak complex formation which takes place first at high concentrations of the complex forming electrolyte. In such cases spectrophotometric methods provide the best means of studying complex formation.

It is usually possible to distinguish between inner- and outer-sphere complex formation when the metal ion complexes in question give rise to ligand-field absorption bands, but on the other hand it is a hard test of the data to try to determine stability constants as well as extinction coefficients in the general case where the absorption is a cumulative property of all the complexes present. This can some-

times be done by separating the determination of the constants and the extinction coefficients, and such separate determination is possible using the Principle of Corresponding Solutions for complexes of average stability by varying both the metal and the ligand concentrations.^{1,2} However, this procedure has been superseded by modern computer techniques. One has a much better chance of obtaining reliable results in those special cases where the optical method permits the direct determination of the concentration of one of the complexes present over a certain range of ligand concentrations. Such data provide a firm basis for calculation, but if the composition of the salt medium is changed by more than about 10 % it is not possible to calculate the concentration stability constants with any high degree of certainty.³ Therefore in cases in which very weak complex formation in aqueous solution is involved it is often preferable to study the system using solutions in which the salt medium is provided by varying concentrations of the complex-forming electrolyte itself, and with the introduction of crude activity corrections under simplifying conditions. Studies of this kind, which give rough information about the activity stability constants have been performed by the present authors⁴⁻⁶ for the case of weak chloro complex formation in aqueous solutions of copper(II) and cobalt(II) ions, where the formation of the tetrachloro complexes is first complete in solutions with chloride concentrations ≥ 10 M.

THE STABILITY CONSTANTS OF THE CHLORO COPPER(II) COMPLEXES

One stimulus for the present study was a recent publication by Schwing-Weill,^{7,8} in which she has calculated stability constants and extinction coefficients for the four chloro copper(II) complexes from spectrophotometric data measured for a 5 M mixed NaCl and NaClO₄ medium.

A complete bibliography of copper(II) chloride stability constants determined up to 1969 is to be found in *Tables of Stability Constants*,⁹ and some of the more reliable spectrophotometric data including recently published results are given in Table 1. Spectrophotometric methods usually give reliable values of the products $K_n \epsilon_n$ of the consecutive constants and corresponding extinction coefficients, but are not well suited to determination of these quantities individually for very strong or very weak complexes. The values for K_1 and ϵ_1 in 1 M HClO₄ given by three different authors¹²⁻¹⁴ (Table 1) show this clearly; it should be noted that the product $K_1 \epsilon_1$ is not far from being constant. Näsänen¹⁰ has determined K_1 in mixed solutions of CuCl₂ and LiClO₄ and corrected to ionic strength zero by the use of Debye-Hückel expressions with two empirically determined parameters. However, subsequent complex formation was not taken into consideration.^{12,13} Libus¹¹ has determined K_1 at ionic strength zero from measurements in mixtures of Cu(ClO₄)₂ and Mg(ClO₄)₂ to which only minute amounts of NaCl are added. Both of these authors' results agree reasonably well with the results of Bjerrum^{4,5} who was able to determine the concentration of CuCl₂²⁻ and approximate values for all of the four consecutive constants by employing simplified assumptions about the activity coefficients in concentrated chloride solutions in which the salt medium is provided by varying concentrations of the complex-forming electrolyte itself. The values given in Table 1 are those corresponding to the use of the activity expression^{4,5} $\log F = -0.5 + B[Cl^-]$, where B was adapted to the experimental data with the following values for the various chloride media: HCl 0.20, LiCl 0.23, MgCl₂ 0.18 and CaCl₂ 0.18. Schwing-Weill^{7,8} has calculated values for the four copper(II) chloride stability constants, as well

Table 1. A selection of estimated consecutive stability constants (K_n) and molar extinction coefficients for the monochloro (ϵ_1) and dichloro complex (ϵ_2) in aqueous copper(II) solutions at $\sim 25^\circ\text{C}$.

Medium	K_1	K_2	K_3	K_4	$\epsilon_1(250)$	$\epsilon_1(272)$	$\epsilon_2(250)$	Ref.
0 corr	~ 1	~ 0.4	~ 0.06	~ 0.01	-	-	-	4,5
0 corr	1.11					1478		10
0 corr	1.63 ± 0.15					1115 ± 80		11
1 M H(Cl,ClO ₄)	1.30 ± 0.03	0.23 ± 0.15			~ 1000	~ 316		12
1 M H(Cl,ClO ₄)	0.27				3800			13
1 M H(Cl,ClO ₄)	2.3 ± 0.4	0.72 ± 0.9			530	~ 186	1620	14
5 M Na(Cl,ClO ₄)	4	1.2	0.42	0.12	1042		2424	7,8
4 M Na(Cl,ClO ₄)	1.3 ± 0.1							15
6 M Na(Cl,ClO ₄)	1.85 ± 0.2							15
5 M Na(Cl,ClO ₄)	1.5	0.42	0.14	0.036	2705		2002	This paper

Table 2. Extinction coefficients of copper(II) chloride at 436 nm in weakly acid 5 M NaCl – NaClO₄ solutions at 25 °C.

C_{CuCl_2}	C_{NaCl}	C_{NaClO_4}	$C_{\text{Cl}^-} + C_{\text{ClO}_4^-}$	$[\text{Cl}^-]$	ϵ_{436}	$\alpha_4 = \epsilon_{436}/308$
0.0943	0.943	3.774	5.00	1.043	1.317	0.0043
0.0943	1.887	2.830	5.00	1.944	4.03	0.0131
0.0943	2.830	1.887	5.00	2.859	7.38	0.0239
0.0943	3.774	0.994	5.00	3.780	10.5	0.0336
0.02433	5.00	—	5.05	4.997	15.8	0.0513
0.01218	5.00	—	5.02	4.998	15.6	0.0507

as corresponding extinction coefficients, from spectrophotometric measurements in a salt medium varying from 5 M NaClO₄ to 5 M NaCl. Thus the ionic strength has been kept constant, but this gives no guarantee for proportionality between activity and concentration of the species involved in such strong salt solutions. The estimated stability constants, together with values for ϵ_1 and ϵ_2 at 250 nm, are tabulated in Table 1. Schwing-Weill calculates a suspiciously low value for the extinction coefficient of the tetrachloro complex at 400 nm ($\alpha_4 = 216$). For comparison it can be mentioned that a 0.0008 M CuCl₂ solution in saturated CaCl₂ at 400 nm has $\epsilon = 950$ (see Experimental). It was therefore thought worthwhile to examine whether more detailed information could be obtained when Schwing-Weill's data were employed together with the basis for Bjerrum's^{4,5} determination of the constants, *viz.* that the tetrachloro complex is the only species absorbing at the wavelength of the blue mercury line (436 nm) at chloride concentrations higher than 3 M. The degree of formation of the tetrachloro complex $\alpha_4 = [\text{CuCl}_4^{2-}]/C_{\text{Cu}}$ can then be calculated directly from the expression

$$\alpha_4 = \epsilon_{436}/\epsilon_{436}^\circ$$

where ϵ_{436}° is the limiting extinction coefficient for $[\text{Cl}^-] \geq 12$ M. We have taken ϵ_{436}° to be 308, the value measured for saturated CaCl₂ solutions (see Experimental).

Schwing-Weill has made no measurements at 436 nm and we have therefore made some supplementary measurements with the 5 M salt medium at this wavelength. The results are shown in Table 2. In Table 3 $\epsilon_{436}/\epsilon_{436}^\circ$ (interpolated to "round-number" chloride ion concentrations) is compared with the values of

α_4 and \bar{n} one calculates from the stability constants presented in Table 1. The quantity $\epsilon_{436}/\epsilon_{436}^\circ$ is seen to be much smaller than α_4 calculated with Schwing-Weill's stability constants, in spite of the fact that owing to absorption of the lower complexes it must be larger than the latter. The set of constants proposed by us in Table 1, with K_1 chosen to be 1.5 M⁻¹, is selected as giving more reasonable values for α_4 with the tacit assumption that the system has a characteristic coordination number 4 and a nearly constant ligand effect, although this cannot be regarded as certain.¹⁸ The ligand effect¹⁸ is defined as follows:

$$L_{n,n+1} = \log (K_n/K_{n+1}) - S_{n,n+1}$$

where $S_{n,n+1} = \log \{(4-n+1)(n+1)/(4-n)n\}$ is the statistical effect in the case of characteristic coordination number four and monodentate ligands. Our set has been chosen to have $L_{1,2} = L_{2,3} = 0.13$ and $L_{3,4} = 0.15$. The values of α_4 and \bar{n} corresponding to these constants are shown in Table 3, and it is obvious that this set of constants is adapted to fulfill the condition that $\epsilon_{436}/\epsilon_{436}^\circ$ is equal to α_4 in 4–5 M chloride

Table 3. Comparison of the values of $\epsilon_{436}/\epsilon_{436}^\circ$ in 5 M Na(Cl,ClO₄) with values of α_4 and \bar{n} calculated from the sets of stability constants given in Table 1.

$[\text{Cl}^-]$	$\epsilon_{436}/\epsilon_{436}^\circ$	Schwing-Weill ^{7,8}		This paper	
		α_4	\bar{n}	α_4	\bar{n}
1	0.0040	0.0195	1.69	0.00098	0.94
2	0.0137	0.078	2.28	0.0070	1.42
3	0.0254	0.147	2.60	0.0186	1.74
4	0.0360	0.213	2.81	0.0345	1.97
5	0.0510	0.272	2.97	0.0532	2.14

Table 4. Calculated molar extinction coefficients for the intermediate chloro copper(II) complexes.

$\lambda(\text{nm})$	ϵ_1	ϵ_2	ϵ_3
230	1241 ± 7	1257 ± 35	2372 ± 66
250	2705 ± 7	2002 ± 34	2810 ± 71
280	563 ± 2	3150 ± 23	1636 ± 60
360	0.3 ± 0.4	116 ± 4	54 ± 12
380	-0.4 ± 0.3	53 ± 3	81 ± 14
756	23.6 ± 0.1	34.6 ± 0.3	32.4 ± 0.6

solutions. It is also in agreement with what should be expected^{4,5} that $\epsilon_{436}/\epsilon_{436}^\circ$ gives too high values for α_4 for solutions with chloride concentrations smaller than ~ 3 M, for which the absorption of the lower complexes cannot be neglected. The \bar{n} -values, which are considerably smaller than those calculated from Schwing-Weill's constants, have been used to correct the total chloride concentrations to concentrations of free chloride in the cases where such a correction is necessary.

THE EXTINCTION COEFFICIENTS OF THE CHLORO COPPER(II) COMPLEXES

From the spectrophotometric data reported by Schwing-Weill^{7,8} we have calculated the extinction coefficients ϵ_1 , ϵ_2 and ϵ_3 of the intermediate chloro complexes. The calculation using the modified stability constants makes use of values of the extinction coefficients for the tetrachloro complex which have been equated with those given in Table 5 for copper(II) chloride in 6–7 M calcium chloride solution. This calculation of the extinction coefficients for the three intermediate chloro complexes from chosen values for the stability constants entails the solution of linear equations and was carried out by the method of least squares. The results are given in Table 4. The rather low uncertainty assigned to the extinction coefficients calculated in this way merely reflects the fact that the uncertainties in the stability constants in this case have not been taken into account.

Fig. 1 shows the directly measured spectrum for the tetrachloro complex and the estimated spectra for the mono-, di- and trichloro com-

plexes; the latter have been drawn through the few calculated points with a considerable degree of uncertainty. The spectra are very similar and therefore difficult to resolve, and it is clear that the best wavelength range in which to study the formation of the tetrachloro complex is that used earlier by Bjerrum^{4,5} close to 400 nm where the absorption of the other chloro complexes is negligible.

The UV absorption bands of the chloro copper(II) complexes are of the electron transfer type and as such are more sensitive to the environment¹⁷ than is the case with ligand field bands. Thus it is characteristic that the molar extinction coefficient at 436 nm has the following limiting values: 308 in 6.5 M CaCl_2 , 308 in 5 M MgCl_2 , 416 in 12 M LiCl and 537 in 13 M HCl .⁵ This pronounced medium effect renders the choice of correct values of the extinction coefficients for the tetrachloro complex in 5 M NaCl somewhat uncertain, but we believe that only a relatively small error is introduced by equating them with the nearly constant values for CaCl_2 solutions with chloride concentrations between 12 and 14 M. The weak ligand-field band in infrared is less influenced by changes in the salt medium, but chloro complex formation causes such

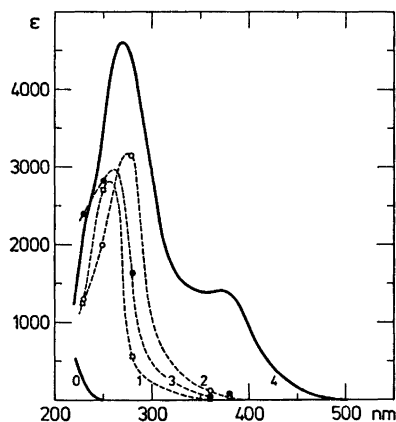


Fig. 1. The UV spectra of the four chloro-copper(II) complexes. The numbers on the curves indicate the number of Cl^- per Cu(II) ion. The full curve 4 represents the directly measured absorption curve for a 6.5 M CaCl_2 solution, and the curve 0 for that of the aqua copper(II) ion. The points marked on the dashed curves correspond to the values of ϵ_1 (\square), ϵ_2 (\circ), and ϵ_3 (\bullet) in Table 4.

Table 5. Molar extinction coefficients for CuCl_4^{2-} in 6.2 M CaCl_2 .

nm	ϵ	nm	ϵ
230	2188	560	0.25
250	3488	600	0.95
270	4613	660	5.7
280	4356	700	16.2
300	2906	740	33.5
320	1750	756	42.4
340	1456	780	57.6
360	1394	820	83.4
380	1394	860	105.2
400	950	900	119
436	308	940	125
460	99	960	126
500	7.85		

small changes in this band that it is hardly possible to use it as a basis for a calculation of the stability constants. Estimated values for the extinction coefficients of the intermediate chloro complexes at 756 nm are shown in Table 4 and data for the absorption of the tetrachloro complex are quoted in Table 5.

The conclusion of this paper is that attempts to obtain quantitative results in studies of consecutive weak complex formation in solution necessitate the use of many approximations, and studies of such systems can therefore be expected to give only semiquantitative results.

EXPERIMENTAL

The solutions used for spectrophotometric measurements were prepared from analyzed stock solutions. The water used was doubly-distilled, and all chemicals were of analytical grade.

Spectrophotometric measurements were made on a Zeiss DMR 21 recording spectrophotometer with a cell-holder thermostated at 25 °C. Extinction coefficients quoted are corrected for the absorption of the medium. Quartz cells (1 cm and 5 cm) were used and the concentrations of CuCl_2 varied from 0.0002 M to 0.1 M, depending on the magnitude of the absorption. The values obtained for the molar extinction coefficients of CuCl_4^{2-} in 6.2 M CaCl_2 are given in Table 5.

Acknowledgements. The authors are most grateful to Ole Mønsted for helpful advice concerning the computer calculations and to Dr. Martin Hancock for revising the English manuscript.

REFERENCES

1. Bjerrum, J. K. *Dan. Vidensk. Selsk., Mat.-Fys. Medd.* 21 (1944) No. 4.
2. Bjerrum, J. *Acta Chem. Scand.* 18 (1964) 843.
3. Bjerrum, J. *Trans. R. Inst. Technol. Stockholm* 253 (1972).
4. Bjerrum, J. *Kem. Maanedst. Nord. Handelsbl. Kem. Ind.* 26 (1945) 24.
5. Bjerrum, J. K. *Dan. Vidensk. Selsk., Mat.-Fys. Medd.* 22 (1946) No. 18.
6. Bjerrum, J., Halonin, A. S. and Skibsted, L. H. *Acta Chem. Scand. A* 29 (1975) 326.
7. Schwing-Weill, M.-J. *Bull. Soc. Chim. Fr.* (1973) 823.
8. Khan, M. A. and Schwing-Weill, M.-J. *Inorg. Chem.* 15 (1976) 2202.
9. Sillén, L. G. and Martell, A. E. *Stability Constants, Chem. Soc. Spec. Publ. No. 17* (1964), and *Supplement No. 25* (1970).
10. Näsänen, R. *Acta Chem. Scand.* 4 (1950) 140.
11. Libus, Z. *Inorg. Chem.* 12 (1973) 2974.
12. McConnell, H. and Davidson, N. *J. Am. Chem. Soc.* 72 (1950) 3164.
13. Kruh, R. *J. Am. Chem. Soc.* 76 (1954) 4865.
14. Carlsson, B. and Wettermark, G. *J. Inorg. Nucl. Chem.* 38 (1975) 1525.
15. Koneva, T. N. and Fedorov, V. A. *Russ. J. Inorg. Chem.* 21 (1976) 616.
16. Bjerrum, J. *Metal Ammine Formation in Aqueous Solution*, 2nd Ed., P. Haase and Son, Copenhagen 1957.
17. Bjerrum, J., Adamson, A. W. and Bostrup, O. *Acta Chem. Scand.* 10 (1956) 329.
18. Wasson, J. R., Hall, J. W., Richardson, H. W. and Hatfield, W. E. *Inorg. Chem.* 16 (1977) 458.

Received April 20, 1977.

Rhodium(III) Complexes of the *trans*- and *cis*-Bis(1,3-diaminopropane) Series

MARTIN PAUL HANCOCK

Dept. of General and Organic Chemistry, University of Copenhagen, H.C. Ørsted Institute, Universitetsparken 5, DK-2100 Copenhagen Ø, Denmark

Dedicated to Professor K. A. Jensen on his 70th birthday

The complexes *trans*- and *cis*-[RhX₂(tn)₂]⁺ (X = Cl or Br; tn = 1,3-diaminopropane) have been prepared from RhCl₃·3H₂O by a controlled-pH method. In the presence of small amounts of sodium borohydride the dominant product, the *trans* isomer, undergoes a rapid reaction with oxalate ion in boiling aqueous solution to give the chelated oxalato species [Rh(ox)(tn)₂]⁺ in high yield, and the latter reacts cleanly and stereoretentively with boiling aqueous HX (X = Cl or Br) to give the *cis*-dihalo complexes *cis*-[RhX₂(tn)₂]⁺. The latter reaction sequence constitutes a more satisfactory synthesis of *cis*-[RhCl₂(tn)₂]⁺ than the direct preparation from RhCl₃·3H₂O. The *trans* isomer of [RhBr₂(tn)₂]⁺ is obtained in good yield from the reaction between *trans*-[RhCl₂(tn)₂]⁺ and bromide ion in aqueous solution under reflux.

The new complexes have been isolated and purified as the perchlorate salts and their geometry established from a comparison of their ligand-field absorption spectra with those of the bis(1,2-diaminoethane) and tetraammine analogues.

Five-membered chelate ring bis(diamine) complexes of rhodium(III) with 1,2-diaminoethane (ethylenediamine, en)¹ and various *C*- or *N*-methyl substituted 1,2-diaminoethanes¹⁻⁴ have been known for some time and a number of them have been of key importance in studies of the substitutional behaviour of rhodium(III) complexes in solution.^{5,6} No attention appears to have been paid, however, to analogous complexes containing six-membered diamine chelate rings. The present paper describes the synthesis, characterisation and interconversion

of some *trans*- and *cis*-bis(diamine)rhodium(III) complexes of the latter type with the ligand 1,3-diaminopropane (trimethylenediamine, tn).

EXPERIMENTAL

Materials. RhCl₃·3H₂O was supplied by Johnson-Matthey Ltd. and 1,3-diaminopropane by Fluka. 1,3-Diaminopropane dihydrochloride was prepared by slow addition of a slight excess of a 1:1 (v/v) solution of conc. hydrochloric acid in ethanol to a 1:1 (v/v) ethanolic solution of 1,3-diaminopropane. The diamine solution was cooled in an ice-bath during the addition of the acid. After leaving the mixture to stand for 30 min at 0 °C, the white crystals were filtered off, washed with 96 % ethanol and dried by air suction. The product was recrystallised by dissolving it in conc. hydrochloric acid and slowly adding an excess of 96 % ethanol to the stirred, filtered solution. The crystals were then filtered off and washed and dried as before. Anal. C₃H₁₁N₃Cl₂: C, H, N.

All other chemicals were of reagent grade and were used without further purification. **Analyses.** Microanalyses for carbon, hydrogen, nitrogen and halogen were performed by the microanalytical laboratory of this department, using standard methods.

Spectra. Absorption spectra in the wavelength region 600–250 nm were recorded using a Cary Model 14 spectrophotometer. Characterising data for absorption maxima, minima or shoulders (sh) in Table I are given with the wavelength λ in nm and the molar absorbance ε in l mol⁻¹ cm⁻¹. Water was used as solvent in all cases.

Synthesis of new complexes. 1. *trans*-Dichlorobis(1,3-diaminopropane)rhodium(III) perchlorate, *trans*-[RhCl₂(tn)₂]ClO₄·RhCl₃·3H₂O (5.26 g, 20 mmol) and 1,3-diaminopropane dihydro-

chloride (5.88 g, 40 mmol) were dissolved in water (100 ml) and 2 M NaOH (20 ml, 40 mmol) was then added to the deep red solution. The resulting brick-red suspension was heated under reflux with vigorous magnetic stirring, giving a clear cherry-red solution. 2 M NaOH (ca. 20 ml) was then added, *via* the reflux condenser, in small aliquots (ca. 1 ml) over a period of about 10 min. The pH of the boiling solution was tested at intervals (universal indicator paper) and addition of NaOH was ceased when the pH was steady at ca. 7. The resulting dirty orange-yellow solution was suction filtered while still hot through a fine porosity sintered glass funnel (to remove some rhodium metal) and the clear, golden-yellow filtrate was treated with 70 % HClO₄ (30 ml), at which point orange-yellow crystals rapidly began to form. After leaving the mixture to stand overnight at room temperature the crystals were isolated by suction filtration on a fine porosity sinter, washed with ice-cold 25 % HClO₄ and then 96 % ethanol (CAUTION!*), and dried by air suction. The product was recrystallised by dissolving it on the filter in the minimum volume of boiling water, filtering the solution and adding 70 % HClO₄ (10 ml) to the filtrate which had been reheated to boiling point. The solution was then left to stand overnight, and the long orange-yellow needles were filtered off and washed and dried as before. Yield 3.15 g (37 %). Anal. [Rh(C₃H₁₀N₂)₂Cl₂]ClO₄: C, H, N, Cl.

2. *cis*-Dichlorobis(1,3-diaminopropane)rhodium(III) perchlorate dihydrate, *cis*-[RhCl₂(tn)₂]ClO₄·2H₂O. Isolation from the mother-liquor remaining after removal of the *trans* isomer. The mother-liquor from prep. 1 (above) was treated with a further quantity of 70 % HClO₄ (20 ml) and then kept in a deep-freezer at ca. -15 °C for 4 d, during which time a pale yellow precipitate of the crude *cis* isomer was deposited. The latter was removed by suction filtration and washed and dried as in prep. 1. The product was recrystallised twice from the minimum volume of boiling water containing a few drops of 4 M HCl by adding a hot solution of LiClO₄·3H₂O (1 g) in water (5 ml) and then keeping the solution in a refrigerator (ca. 5 °C) for several days. The lemon-yellow crystals were filtered off, washed with 96 % ethanol and dried by air suction. Yield 0.65 g (7 %). Anal. [Rh(C₃H₁₀N₂)₂Cl₂]ClO₄·2H₂O: C, H, N, Cl.

A more satisfactory synthesis of this isomer is provided by the reaction of [Rh(ox)(tn)₂]⁺ with HCl (prep. 5, below).

3. *trans*-Dibromobis(1,3-diaminopropane)rhodium(III) perchlorate, *trans*-[RhBr₂(tn)₂]ClO₄. A solution of *trans*-[RhCl₂(tn)₂]ClO₄ (1.15 g, 2.73 mmol) and NaBr (5.0 g, 48.6 mmol)

in water (50 ml) was heated under reflux for 3 h. The resulting orange-red solution was treated while hot with a hot solution of LiClO₄·3H₂O (3 g) in water (5 ml) and was then kept in a refrigerator overnight. The orange crystals were filtered off, washed with 96 % ethanol and dried by air suction. The crude product was then again heated under reflux with NaBr (5 g) in water (35 ml) for 2 h and the hot solution treated with 70 % HClO₄ (12 ml) and kept overnight in a refrigerator. The orange crystals were isolated by filtration and recrystallised, washed and dried as for the *trans*-dichloro perchlorate (prep. 1). Yield 0.80 g (57 %). Anal. [Rh(C₃H₁₀N₂)₂Br₂]ClO₄: C, H, N.

4. *Bis*(1,3-diaminopropane)oxalatorhodium(III) perchlorate 2½ hydrate, [Rh(ox)(tn)₂]ClO₄·2½H₂O. A mixture of *trans*-[RhCl₂(tn)₂]ClO₄ (0.60 g, 1.42 mmol) and sodium oxalate (0.40 g, 2.98 mmol) in water (50 ml) was heated to boiling. After the solution had boiled for ca. 2 min a small speck of sodium borohydride was added, whereupon an immediate reaction occurred, the mixture darkening owing to the formation of a small amount of rhodium metal. Two further specks of sodium borohydride were added at 1 min intervals and the solution was then heated under reflux for 5 min. The hot solution was filtered through a fine porosity sintered glass funnel and the pale yellow filtrate was cooled to ca. 35 °C. Addition of 70 % HClO₄ (3 ml) and subsequent cooling in a refrigerator for 2 d resulted in the formation of long, pale yellow needles which were isolated by filtration, washed with a little ice-cold water and then 96 % ethanol, and dried by air suction. The product was recrystallised from boiling water (40 ml) by adding a hot solution of LiClO₄·3H₂O (4 g) in water (10 ml) and then keeping the solution in a refrigerator for 24 h. The crystals were filtered off and washed and dried as before. Yield 0.46 g (67 %). Anal. [Rh(C₃H₁₀N₂)₂(C₂O₄)ClO₄·2½H₂O: C, H, N, Cl.

5. *cis*-[RhCl₂(tn)₂]ClO₄·2H₂O. Preparation from [Rh(ox)(tn)₂]ClO₄·2½H₂O. [Rh(ox)(tn)₂]ClO₄·2½H₂O (0.50 g, 1.03 mmol) was boiled for 1 min with 4 M HCl (15 ml). The hot lemon-yellow solution was treated with 70 % HClO₄ (2 ml) and then kept in a refrigerator for 3 d. The crystals were isolated by filtration, washed with 96 % ethanol (CAUTION!*) and dried by air suction.

The product was recrystallised from boiling water (25 ml) as described in prep. 2. Yield 0.38 g (80 %).

Anal. [Rh(C₃H₁₀N₂)₂Cl₂]ClO₄·2H₂O: C, H, N, Cl.

The electronic absorption spectrum of the complex (Table 1) was identical with that of the product from prep. 2.

6. *cis*-Dibromobis(1,3-diaminopropane)rhodium(III) perchlorate 1½ hydrate, *cis*-

* To obviate any risk of explosion the suction flask should be emptied of perchloric acid washings and rinsed with water before the ethanol washing is performed.

* See footnote to prep. 1.

$[\text{RhBr}_2(\text{tn})_2]\text{ClO}_4 \cdot 1\frac{1}{2}\text{H}_2\text{O}$. This complex was prepared in the same way as the *cis*-dichloro analogue (prep. 5), using $[\text{Rh}(\text{ox})(\text{tn})_2]\text{ClO}_4 \cdot 2\frac{1}{2}\text{H}_2\text{O}$ (0.50 g) and 5 M HBr (15 ml). After adding 70 % HClO_4 (5 ml) and allowing the solution to cool it was then kept in a deep-freezer at ca. -20°C for several days. The resulting orange crystals were filtered off, washed with 96 % ethanol (CAUTION!*) and dried by air suction. The product was then recrystallised, washed and dried as in prep. 5. Yield 0.37 g (67 %).

Anal. $[\text{Rh}(\text{C}_3\text{H}_{10}\text{N}_2)_2\text{Br}_2]\text{ClO}_4 \cdot 1\frac{1}{2}\text{H}_2\text{O}$: C, H, N.

RESULTS AND DISCUSSION

The complexes *trans*- and *cis*- $[\text{RhCl}_2(\text{tn})_2]^+$, the former of which is an excellent starting material for the synthesis of the other bis(tn) complexes described here, were prepared by an extension of the method of Johnson and Basolo¹ for the synthesis of the *trans* and *cis* isomers of $[\text{RhCl}_2(\text{en})_2]^+$, involving the gradual addition of base to a boiling aqueous solution containing rhodium trichloride trihydrate and the stoichiometric quantity of half-neutralised diamine dihydrochloride until the pH of the reaction mixture is steady at ca. 7. Both isomers were isolated as the perchlorate salts after addition of concentrated perchloric acid. The perchlorate salt of the *trans* isomer crystallises rapidly from the hot reaction mixture, whereas that of the *cis* isomer is only obtained, in low yield, after prolonged cooling of the mother-liquor. The yields of the two isomers prepared by this method are comparable to those of the analogous bis(en) complexes (isolated as their nitrate salts),¹ even though the formation of a certain amount of rhodium metal is observed during the synthesis of the 1,3-propanediamine complexes.

The low yield of *cis* isomer obtained as described above, together with the fact that several recrystallisations are necessary to ensure that the product is free from traces of the *trans* isomer, made it desirable to devise a better procedure for the synthesis of the former. In keeping with results obtained in earlier work with the bis(1,2-diaminoethane)-rhodium(III) system⁷ it was found that sodium borohydride promotes the rapid reaction of *trans*- $[\text{RhCl}_2(\text{tn})_2]^+$ with oxalate ion in boiling aqueous solution to give the chelated oxalato complex $[\text{Rh}(\text{ox})(\text{tn})_2]^+$. The latter can be isolated

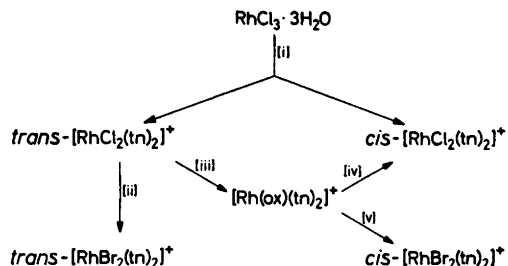


Fig. 1. Reaction scheme for synthesis and interconversion of bis(tn) rhodium(III) complexes. [i], 2 mol tn.2HCl + gradual addition of NaOH to boiling solution; [ii], excess Br^- + reflux; [iii], oxalate ion + trace NaBH_4 + boiling; [iv] + [v], aqueous HX (X = Cl or Br) + boiling.

and purified in high yield as the perchlorate salt and is a convenient precursor for the synthesis of other *cis*-bis(1,3-diaminopropane) rhodium(III) complexes since, by analogy with $[\text{Rh}(\text{ox})(\text{en})_2]^+$ ⁷ and $[\text{Rh}(\text{ox})(\text{NH}_3)_4]^+$,⁸ it reacts rapidly and stereoretentively with boiling aqueous hydrohalic acid HX (X = Cl or Br) to give *cis*- $[\text{RhX}_2(\text{tn})_2]^+$.

The *trans* isomer of $[\text{RhBr}_2(\text{tn})_2]^+$ may be prepared by the reaction of *trans*- $[\text{RhCl}_2(\text{tn})_2]^+$ with bromide ion (excess) in aqueous solution under reflux and isolated in high yield as the perchlorate.

The initial synthetic- and subsequent interconversion reactions employed in the present work are summarised in Fig. 1.

The geometric configuration of *trans*- and *cis*- $[\text{RhX}_2(\text{tn})_2]^+$ (X = Cl or Br) is assigned on the basis of a comparison of their ligand-field absorption spectra with those of the known bis(1,2-diaminoethane) and tetraammine analogues (Table 1). The spectrum of $[\text{Rh}(\text{ox})(\text{tn})_2]^+$ (which necessarily has the *cis* configuration) is, as expected, very similar to those of $[\text{Rh}(\text{ox})(\text{en})_2]^+$ and $[\text{Rh}(\text{ox})(\text{NH}_3)_4]^+$ (Table 1).

Recent work^{12,13} on the kinetics and the steric course of base hydrolysis of *trans*- $[\text{RhCl}_2(\text{en})_2]^+$ has revealed a rate-law of the form: $k_{\text{obs}} = k_1 + k_2[\text{OH}^-]$. Appreciable *trans* → *cis* isomerisation, which is otherwise very rare in rhodium(III) systems of this type, occurs at moderately high pH and is apparently associated with the second-order pathway.¹² With this in mind a kinetic study of the base hydrolysis behaviour of *trans*- $[\text{RhCl}_2(\text{tn})_2]^+$ is currently in progress.¹⁴

Table 1. Ligand-field spectra of *trans*- and *cis*-bis(1,3-diaminopropane)rhodium(III) complexes and some related chromophores.

Complex	λ_{\max}	λ_{\min}	ϵ_{\max}	ϵ_{\min}	Ref.
<i>trans</i> -[RhCl ₂ (tn) ₂] ⁺	418,	289	80,	136	This work
<i>trans</i> -[RhCl ₂ (en) ₂] ⁺	406,	286	75,	130	1
	406,	286	84,	130	9
<i>trans</i> -[RhCl ₂ (NH ₃) ₄] ⁺	415,	293	74,	85	10
<i>cis</i> -[RhCl ₂ (tn) ₂] ⁺	<i>ca.</i> 387(sh),	353,	<i>ca.</i> 89,	123,	This work
<i>cis</i> -[RhCl ₂ (en) ₂] ⁺		352,		156,	1
		352,		195,	7
		360,		126,	8
<i>cis</i> -[RhCl ₂ (NH ₃) ₄] ⁺	441,	<i>ca.</i> 342(sh),	119,	3170	This work
<i>trans</i> -[RhBr ₂ (tn) ₂] ⁺	426,	281	100,	1800	1
<i>trans</i> -[RhBr ₂ (en) ₂] ⁺	428,	276	107,	2720	9
	441,	276	111,	<i>ca.</i> 2700	10
<i>trans</i> -[RhBr ₂ (NH ₃) ₄] ⁺	<i>ca.</i> 405(sh),	<i>ca.</i> 280(sh)	<i>ca.</i> 125,	<i>ca.</i> 1140	This work
<i>cis</i> -[RhBr ₂ (tn) ₂] ⁺		<i>ca.</i> 278(sh)	158,	210,	1
<i>cis</i> -[RhBr ₂ (en) ₂] ⁺		276(sh)	260,	900	7
		280(sh)	170,	<i>ca.</i> 940	8
		<i>ca.</i> 275(sh)			This work
<i>cis</i> -[RhBr ₂ (NH ₃) ₄] ⁺	329	307	172	142	11
[Rh(ox)(tn) ₂] ⁺	325		260		11
[Rh(ox)(en) ₂] ⁺	325		270		7
[Rh(ox)(NH ₃) ₄] ⁺	333		167		8

REFERENCES

1. Johnson, S. A. and Basolo, F. *Inorg. Chem.* **1** (1962) 925.
2. Hall, S. K. and Douglas, B. E. *Inorg. Chem.* **7** (1968) 533.
3. Watt, G. W. and Alexander, P. W. *J. Am. Chem. Soc.* **89** (1967) 1814.
4. Hancock, M. P., Heaton, B. T. and Vaughan, D. H. *J. Chem. Soc. Dalton Trans.* (1976) 931.
5. Johnson, S. A., Basolo, F. and Pearson, R. G. *J. Am. Chem. Soc.* **85** (1963) 1741.
6. Poš, A. J. and Shaw, K. *J. Chem. Soc. A* (1970) 393, and references therein.
7. Addison, A. W., Gillard, R. D., Sheridan, P. S. and Tipping, L. R. H. *J. Chem. Soc. Dalton Trans.* (1974) 709.
8. Hancock, M. P. *Acta Chem. Scand. A* **29** (1975) 468.
9. Burgess, C., Hartley, F. R. and Rogers, D. E. *Inorg. Chim. Acta* **13** (1975) 35.
10. Poš, A. J. and Twigg, M. V. *Can. J. Chem.* **50** (1972) 1089.
11. Dasgupta, T. P., Milburn, R. M. and Damrauer, L. *Inorg. Chem.* **9** (1970) 2789.
12. Poš, A. and Vuik, C. *J. Chem. Soc. Dalton Trans.* (1976) 661.
13. Hancock, M. P., Heaton, B. T. and Vaughan, D. H. *To be published.*
14. Vaughan, D. H. *Personal communication.*

Received April 20, 1977.

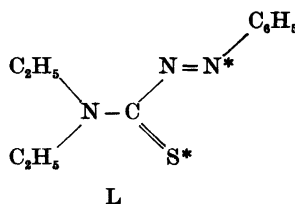
Nonplanar Electron Transfer Complexes. II.¹ The Chemistry of Four Cu—N₂S₂^z Complexes Derived from Copper-bis-*N,N*-diethylphenylazothioformamide

KLAUS BECHGAARD

Department of General and Organic Chemistry, University of Copenhagen, The H.C. Ørsted Institute, DK-2100 Copenhagen, Denmark

Dedicated to Professor K. A. Jensen on his 70th birthday

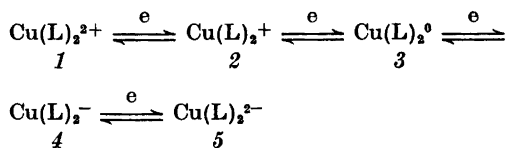
The existence of a series of five electron transfer complexes derived from nonplanar copper-bis-*N,N*-diethylphenylazothioformamide, has been demonstrated by cyclic voltammetry and coulometric techniques. The obtained magnetic, spectral and structural data suggest that four of the Cu—N₂S₂^z complexes can be described as simple Cu(II) or Cu(I) compounds coordinated by neutral or radical anion ligands.



Relatively few investigations of copper-containing electron transfer complexes have been published. Apart from copper bis-dithiolenes, in which only the Cu—S₄⁻ and Cu—S₄²⁻ species are stable,^{2,3} two series of the general type Cu—N₂S₂^z have been described. In both systems a tetradentate ligand was used. Holm *et al.*⁴ investigated copper-diacetyl-bis-thiobenzhydrazonate and demonstrated the existence of two discrete species, while Warren *et al.*⁵ demonstrated the existence of a four-membered series in a similar system. In both cases only the neutral species, Cu—N₂S₂⁰, was isolated and investigated, and was described as being planar with a ²B₂(d⁹) ground state.

Phenylazothioformamides, which have proven useful ligands in the preparation of new electron transfer series,^{1,6,7} form stable copper compounds.⁸ The present paper describes results obtained for copper complexes derived from *N,N*-diethylphenylazothioformamide (L).

The first of these copper compounds to be obtained⁶ was the neutral bis complex, Cu(L)₂⁰(3), which proved to be one of a series of five electron transfer species (1)–(5):

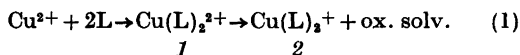


Two members of this series have been isolated, two were generated in solution, while the dinegative couple (5) could only be demonstrated by cyclic voltammetry. Additionally, results obtained for double salts of 2 are presented.

It is the purpose of the present work to document the existence of the series in question, to present results obtained for individual species, and to discuss the structural and electronic characteristics of this new electron transfer series.

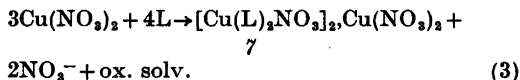
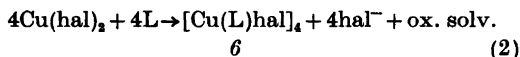
RESULTS

Preparation. The neutral member (3) of the series was prepared by quinone oxidation of the corresponding bis-thiosemicarbazidate. This preparation has been reported in detail elsewhere.⁶ The monocationic complex (2) was prepared by treatment of 1 mol of $\text{Cu}(\text{BF}_4)_2$ in water with 2 mol of L dissolved in ethanol. The product first formed is 1, which is reduced rapidly by the solvent to give 2. Eqn. 1 summarizes the reactions:



$\text{Cu}(\text{L})_2^+$ was isolated as the tetrafluoroborate, which crystallizes from acetone-ether (1:1) with precisely 1 mol of acetone per copper atom. It was shown by thermogravimetry that the "crystal acetone" is given off at temperatures higher than 80 °C.

The necessity of using BF_4^- as counter ion is illustrated by the formation of products such as (6) and (7), when other cupric salts are used (eqns. 2 and 3).



These two examples demonstrate that the system Cu-L exhibits some tendency to

cluster or double salt formation. Compound 6 has been prepared previously by a different procedure.⁶

The dicationic complex (1) was generated by electrolysis of 2 in methylene chloride at a fairly positive potential ($E_1 = +1.3$ V vs. SCE). This is in accord with the observation that 1 is so easily reduced by labile solvents. However, methylene chloride solutions of 1 are stable when protected from moisture.

The monoanion (4) was generated by electrolytic reduction of 3 in either methylene chloride or acetonitrile. The solutions are stable when protected from oxygen and moisture. Attempts to prepare the dianion (5) either electrolytically or by Na-Hg reduction of 3 were, however, unsuccessful.

Electrochemical evidence for the existence of the electron transfer complexes (1)–(5). CH_2Cl_2 . The solution equilibria established as a consequence of reduction or oxidation of (2) are illustrated by the cyclic voltammogram of Fig. 1. In the cathodic scan starting at A, 2 is reduced to 3 at R_2 in a reversible process. Coulometric reduction⁸ uses precisely 1 F/mol and 3 can be reoxidized to 2 in nearly 100 % yield. The peak separation $R_2 - O_2$ is approximately 100 mV, slightly larger than the 60 mV required for a reversible one-electron transfer. This is due, however, to the use of a relatively low concentration of depolarizer (0.1 M); increasing the concentration of the latter or changing the solvent to acetonitrile improved

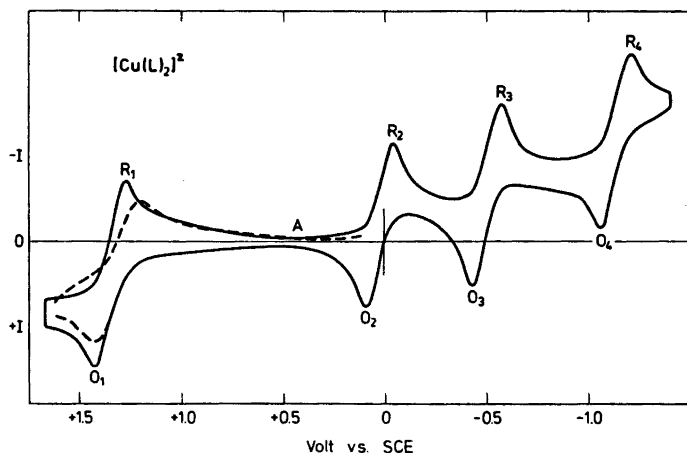


Fig. 1. Cyclic voltammogram of $\text{Cu}(\text{L})_2^{2+}$ in CH_2Cl_2 at 298 K (full line). At 248 K (broken line).

Table 1. Voltammetry of $\text{Cu}(\text{L})_2^+$ in CH_2Cl_2 and CH_3CN .

Compound	Solvent ^b	Peak potentials ^a							
		O ₁	R ₁	O ₂	R ₂	O ₃	R ₃	O ₄	R ₄
$\text{Cu}(\text{L})_2^+$	CH_2Cl_2	+1.34	+1.24	+0.05	-0.05	-0.48	-0.59	-1.14	-1.24
$\text{Cu}(\text{L})_2^+$	CH_3CN	-	-	-0.06	-0.12	-0.53	-0.59	-1.18	-1.24

^a Volts vs. SCE. Platinum button electrode, sweep rate 200 mV/s. ^b Depolarizer Bu_4NBF_4 (0.1 M).

the voltammograms. However, owing to the presence of trace amount of water in the depolarizer it was convenient to use low concentrations. The peak current ratio is 1:1. There thus seems to be no doubt that 3 is formed by reversible one-electron reduction of 2. At the more negative potential R_3 , 3 is reduced to 4. Again the criteria of reversible electron transfer are fulfilled and 4 is stable under the conditions employed. At an even more negative potential R_4 , 4 is reduced to 5 reversibly. 5 is stable within the time scale of cyclic voltammetry but decomposes on allowing the solution to stand.

In the anodic scan starting at A, 2 is oxidized to 1 at O_1 in a quasi-reversible process. Coulometric oxidation of 2 uses precisely 1 F/mol and 1 can be reduced back to 2 quantitatively. The peak current ratio is 1:1, but the peak separation $R_1 - O_1$ turns out to be temperature dependent, as illustrated in Fig. 1. Although the peak separation at 298 K is 100 mV, it is larger than 250 mV at 243 K. This behaviour is unique for the couple $R_1 - O_1$, and strongly suggests that although the redox reaction is chemically reversible, the electron transfer is followed by another process, probably a structural change (see below). The latter process must clearly proceed at rates compatible with the voltammetric technique, since the

voltammograms change so drastically on lowering the temperature.

CH_3CN . In acetonitrile the three reversible couples $R_2 - O_2$, $R_3 - O_3$ and $R_4 - O_4$ established in the investigation in CH_2Cl_2 are again apparent. However, it was not possible to achieve reversibility of the couple $R_1 - O_1$, since trace amounts of water or other nucleophiles immediately destroy 1.

To summarize, the results obtained clearly demonstrate the existence of a five-membered series of electron transfer complexes but they also indicate that a reversible chemical change occurs on going from 2 to 1.

Structure

$\text{Cu}(\text{L})_2^0$, (3). It has been shown by X-ray powder diffraction that 3 is isostructural with the analogous nickel compound, $\text{Ni}(\text{L})_2^0$. The metal atom in $\text{Ni}(\text{L})_2^0$ was shown⁹ to be sited in a distorted tetrahedral N_2S_2 coordination sphere. Due to the isostructurality it is thus reasonable to conclude that $\text{Cu}(\text{L})_2^0$ has a closely similar coordination geometry.

Thus, $\text{Cu}(\text{L})_2^0$, like $\text{Ni}(\text{L})_2^0$, is a member of a series of electron transfer complexes, in which at least one member is nonplanar.

ESR and magnetic susceptibility. Results are collected in Tables 2 and 3. The ESR spectrum

Table 2. ESR results

Compound	Medium	$\langle g \rangle$	Frozen solution			a_{Cu} gauss
			g_1	g_2	g_3	
$\text{Cu}(\text{L})_2^0$	2-Me-THF	-	... 2.001 ^a ...			20
$\text{Cu}(\text{L})_2^{2+}$	CH_2Cl_2	2.06 ^b	$g_{\perp} = 2.01$, $g_{\parallel} = 2.16$			$a_{\parallel} = 137$

^a No resolvable anisotropy. ^b Calc. from g_{\perp} and g_{\parallel} .

Table 3. Magnetic susceptibility.

Compound	T K	χ^a egs/mol	μ_{eff} BM
Cu(L) ₂ ⁰	80	458 × 10 ⁻⁵	1.71
	203	181 × 10 ⁻⁵	1.72
	300	122 × 10 ⁻⁵	1.71

^a Faraday method. Diam. correction - 26 × 10⁻⁵ egs/mol.

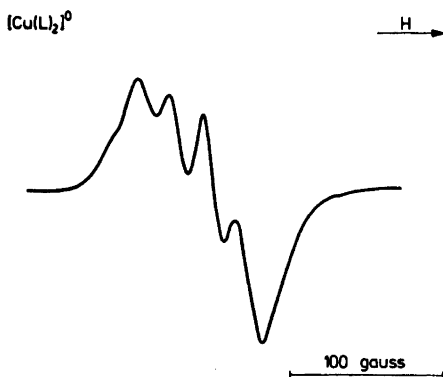


Fig. 2. X-Band ESR spectrum of Cu(L)₂⁰ in 2-Me-THF at 77 K.

Table 4. Electronic spectral data for Cu(L)₂^z in CH₂Cl₂.

Complex	λ_{max} nm	ϵ^a
Cu(L) ₂ ²⁺	530 sh	1 400
	490	4 100
	380	7 400
	332	25 700
Cu(L) ₂ ⁺	695	7 700
	359	29 400
Cu(L) ₂ ⁰	790	5 400
	531	6 500
	510 sh	6 370
	362	27 300
	330 sh	22 000
Cu(L) ₂ ⁻	505	7 200
	471	7 400
	380	32 100
	294	18 700

^a Uncorrected for underlying absorptions.

reported for *1* was recorded in a frozen methylene chloride solution containing Bu₄NBF₄ (0.1 M) at liquid nitrogen temperature; at the latter temperature a microcrystalline matrix is formed. Owing to the instability of *1* spectra of *1* at room temperature were not recorded. The ESR spectrum quoted for *3* is that recorded for 2-Me-THF solutions (10⁻³–10⁻⁵ M). *3* exhibits no solution spectrum at room temperature, indicating that an effective relaxation mechanism is operating. However, at 77 K, at which 2-Me-THF forms a glass, the characteristic spectrum shown in Fig. 2 is observed. Compounds *2* and *4* appear to be diamagnetic, since no spectra were observed even at low temperature.

The magnetic susceptibility of powdered samples of *3* was determined in the temperature range 80–278 K.

Electronic spectra of *2* and *3* were recorded for solutions in dry methylene chloride, while the spectra of *1* and *4* were recorded for methylene chloride solutions containing Bu₄NBF₄ (0.1 M). Spectral parameters are given in Table 4.

DISCUSSION

Cu(L)₂²⁺ (*1*). The rather anodic potential (+1.3 V vs. SCE) at which *1* is formed probably excludes the possibility of isolating *1* as a pure salt. However, stable CH₂Cl₂ solutions can be prepared. The ESR spectrum of (*3*) in frozen CH₂Cl₂ exhibits an axial or near axial *g*-tensor, which is characteristic of Cu(II), *d*⁹, in a planar or octahedral (BF₄⁻ or solvent) environment.¹⁰⁻¹² The spectrum cannot be rationalized in terms of tetrahedral coordination, which would lead to a rhombic *g*-tensor.^{13,14} Likewise, the observed electrochemical irreversibility of the couple R₁-O₁ at low temperature indicates that the oxidation of Cu(L)₂⁺ to give Cu(L)₂²⁺ is followed by another transformation which could very well be a flattening of the tetrahedron to give planar Cu-N₂S₂. It therefore seems reasonable to describe Cu(L)₂²⁺ in simple terms as Cu(II), *d*⁹, coordinated by two closed shell azothioformamide ligands in a planar arrangement. This situation, in which members of a series of electron transfer complexes have different geometries [Cu(L)₂⁰ is tetrahedral], has to the present authors' knowledge not been described elsewhere.

$\text{Cu}(\text{L})_2^+$ (2). The one-electron relationship between 1 and 2 is obviously most simply explained as reduction of Cu(II) to Cu(I). A similar case, in which a Cu(II)-bis-thiosemicarbazone is spontaneously reduced by the solvent, has been described previously.¹⁵ $\text{Cu}(\text{L})_2\text{BF}_4$ is diamagnetic and can be described as Cu(I), d^{10} , with azothioformamide ligands in a tetrahedral arrangement, since all known tetra-coordinated Cu(I) compounds are tetrahedral.¹⁶

$\text{Cu}(\text{L})_2^+$ is isoelectronic with the previously described $\text{Ni}(\text{L})_2^0$, for which a simple model of the bonding was proposed. If this model is used in the description of $\text{Cu}(\text{L})_2^+$ as Cu(I), d^{10} , the π^* orbitals of the ligands must be interchanged with d_{xy} . A similar interchange has been used to explain the observed differences in the properties of planar isoelectronic nickel and copper bis-dithiolenes.⁴

The two compounds 6 and 7 (eqns. 2 and 3) are variants of $\text{Cu}(\text{L})_2^+$. 7 exhibits $\mu_{\text{eff}} = 1.8$ BM per 3 Cu atoms at 300 K in the solid state and both behave like $\text{Cu}(\text{L})_2^+$ in solution (electronic spectra and cyclic voltammetry). It is therefore reasonable to describe both as double salts of $\text{Cu}(\text{L})_2^+$, presumably formed because crystal packing of $\text{Cu}(\text{L})_2^+$ and various counter ions leave open spaces in the structure.

$\text{Cu}(\text{L})_2^0$ (3). X-Ray diffraction data indicate strongly that this species is tetrahedral. μ_{eff} of the solid is 1.72 BM at temperatures between 80–300 K, indicating that spin-orbit coupling effects are small. This is fully supported by the ESR results. The observed isotropic g -tensor is in accordance with a simple description which places the unpaired spin in a ligand π^* orbital of minimal metal character. Similar observations have been described for planar Cu-phthalocyanine compounds.¹⁷ The Cu hyperfine splitting ($a_{\text{Cu}} = 20$ gauss) for $\text{Cu}(\text{L})_2^0$ is as far as is known the smallest observed for any copper compound. This further supports the proposal that the odd-electron orbital is of predominantly π^* character and that the observed splitting is of a similar origin to alkali-metal induced splittings observed for aromatic anion radicals.¹⁸

The weak inflection in the $m_1 = -\frac{3}{2}$ component of the ESR spectrum (Fig. 2) is tentatively assigned to the presence of different copper isotopes, in accordance with what is usually seen when isotopically impure copper is used.

$\text{Cu}(\text{L})_2^0$ is isoelectronic with $\text{Ni}(\text{L})_2^+$, for which weak but resolvable g -tensor anisotropy was observed.¹ By analogy with $\text{Cu}(\text{L})_2^+$ and $\text{Ni}(\text{L})_2^0$ the simple bonding model proposed for the nickel compounds¹ is again useful for the copper compound if π^* and d_{xy} are interchanged.

$\text{Cu}(\text{L})_2^0$ exhibits no ESR signal in solution at room temperature, indicating that an effective relaxation mechanism is operating. Degeneracy or near degeneracy of π^* (a) and π^* (b) could provide such a mechanism.¹⁹

On a simple basis $\text{Cu}(\text{L})_2^0$ is reasonably described as Cu(I), d^{10} , with one neutral and one radical anion ligand. The low energy transition of $\text{Cu}(\text{L})_2^+$ at 695 nm is probably an M→L transition; in $\text{Cu}(\text{L})_2^0$ it moves to lower energy as more anion character is transferred to the ligand.

$\text{Cu}(\text{L})_2^-$ (4). If the π^* orbitals of $\text{Cu}(\text{L})_2^0$ are degenerate or near degenerate the one-electron reduction might lead to 3B or 1A ground states of equal energy. The isoelectronic $\text{Zn}(\text{L})_2^0$ is an example of such a system.⁶

$\text{Cu}(\text{L})_2^-$ solutions are unfortunately rather unstable and the experimental results therefore few. For $\text{Cu}(\text{L})_2^-$ in frozen CH_2Cl_2 at 77 K 1A rather than 3B is indicated since no ESR spectrum is observed. However, since 3B $\text{Cu}(\text{L})_2^-$ might possess effective relaxation mechanisms line broadening could occur. Attempts to isolate solid $\text{Cu}(\text{L})_2^-$ as the sodium salt were unsuccessful and no magnetic susceptibility results were obtained.

$\text{Cu}(\text{L})_2^{2-}$ (5). The only experimental evidence for the existence of this species is provided by the cyclic voltammetry results. No further data were obtained.

EXPERIMENTAL

Equipment and experimental techniques are described in Ref. 1.

$\text{Cu}(\text{L})_2(\text{BF}_4)$. 10 ml of a 0.5 M aqueous solution of $\text{Cu}(\text{BF}_4)_2$ were added to a solution of 2.2 g of *N,N*-diethylphenylazothioformamide (0.01 mol) in 40 ml abs. ethanol. The solution was heated under reflux for 10 min. The solution was filtered and cooled in ice, and the precipitate was collected and dried. Soxhlet extraction with 100 ml ether–acetone (2:1) yielded $\text{Cu}(\text{L})_2\text{BF}_4 \cdot (\text{CH}_3)_2\text{CO}$. After drying for 6 h at 80 °C dark green crystals were obtained in yields of 60–80%. M.p. not well defined. Aanal. $\text{C}_{22}\text{H}_{30}\text{N}_4\text{BCuF}_4\text{S}_2$: C, H, N.

REFERENCES

1. Bechgaard, K. *Acta Chem. Scand. A* 28 (1974) 185.
2. Williams, R., Billig, E., Waters, J. H. and Gray, H. B. *J. Am. Chem. Soc.* 88 (1966) 43.
3. Maki, A. H., Edelstein, N., Davidson, A. and Holm, R. H. *J. Am. Chem. Soc.* 86 (1964) 4580.
4. Holm, R. H., Balch, A. L., Davidson, A., Maki, A. H. and Berry, T. E. *J. Am. Chem. Soc.* 89 (1967) 2866.
5. Warren, L. E., Horner, S. M. and Hatfield, W. E. *J. Am. Chem. Soc.* 94 (1972) 6392.
6. Jensen, K. A., Bechgaard, K. and Pedersen, C. T. *Acta Chem. Scand.* 26 (1972) 2913.
7. Forbes, C. E., Gold, A. and Holm, R. H. *Inorg. Chem.* 10 (1971) 2479.
8. Parker, V. D. *Acta Chem. Scand.* 24 (1970) 2768.
9. Hazell, R. G. *Acta Chem. Scand. A* 30 (1976) 322.
10. Maki, A. H. and McGarvey, B. R. *J. Chem. Phys.* 29 (1958) 31.
11. Kivelson, D. and Neiman, R. *J. Chem. Phys.* 35 (1961) 149.
12. Wiersema, A. K. and Windle, J. J. *J. Phys. Chem.* 68 (1964) 2316.
13. Fritz, H. P., Golla, B. M. and Keller, H. J. *Z. Naturforsch.* 216 (1966) 1015.
14. Kuska, H. A. and Rogers, M. T. In *Radical Ions*, Interscience, N.Y. 1968, p. 696.
15. Ablov, A. V. and Gerbelev, N. V. *Russ. J. Inorg. Chem. (Eng. Ed.)* 9 (1964) 46.
16. Hatfield, W. E. and Whyman, R. *Transition Met. Chem.* 5 (1969) 47.
17. Guzy, C. M., Raynon, J. B., Stodulski, L. D. and Symonds, M. C. R. *J. Chem. Soc. A* (1969) 997.
18. Karplus, M. and Fraenkel, G. K. *J. Chem. Phys.* 35 (1961) 1312.
19. Fritz, H. P., Golla, B. M., Keller, H. J. and Schwartzhaus, K. E. *Z. Naturforsch.* 216 (1966) 725.

Received May 26, 1977.

The Crystal Structure of Tetraaqua(1,2-naphthoquinone-1-oximato-6-sulfonate)nickel(II) Sesquihydrate: $[\text{Ni}(\text{H}_2\text{O})_4(\text{C}_{10}\text{H}_5\text{NO}_5\text{S})] \cdot 1\frac{1}{2}\text{H}_2\text{O}$

JORMA KORVENRANTA, HEIKKI SAARINEN and ELINA NÄSÄKKÄLÄ

Department of Inorganic Chemistry, University of Helsinki, SF-00100 Helsinki 10, Finland

The crystal structure of the title compound has been determined from X-ray data. The space group is $C2/c$, $Z=8$, $a=28.895(15)$, $b=10.637(4)$, $c=9.831(4)$ Å, $\beta=91.97(5)^\circ$. The structure was solved by direct methods and refined by least-squares procedures to a final R value of 0.062 for 1467 observed reflections. The estimated standard deviation in the bond lengths for the non-hydrogen atoms was in the range 0.005–0.012 Å. In the structure the octahedron around nickel consists of one nitrogen and one oxygen atom from the ligand, and of four aqua water oxygens.

In the course of our structural studies on 1,2-nitronaphthols (\rightleftharpoons 1,2-naphthoquinone monoximes) and the metal complexes formed by them we have recently characterized a number of compounds by X-ray methods.^{1,2} The title compound has been specially selected for analysis in order to ascertain the way in which divalent nickel coordinates to such chelating agents. Nickel as the central metal ion and 1-nitroso-2-naphthol-6-sulfonic acid anion as the ligand are both new in this series of investigations.

EXPERIMENTAL

Crystal preparation. The complex was obtained by addition of an aqueous solution of $\text{NiSO}_4 \cdot 6\text{H}_2\text{O}$ (1 mol equiv.) to a hot aqueous solution of sodium 1-nitroso-2-naphthol-6-sulfonate (1 mol equiv., prepared from sodium 2-naphthol-6-sulfonate on nitrosation³). The crude product that separated on cooling was dissolved into water, from which the dark brown crystals were formed on gradual cooling during two weeks. Anal. C, H, N, S, Ni.

Crystal and intensity data. Weissenberg photographs indicated monoclinic symmetry. Systematic absences were characteristic for the space groups Cc (No. 9) and $C2/c$ (No. 15), but the space group Cc was excluded on the basis of statistical tests favouring a centrosymmetric structure. The unit cell dimensions were determined from powder photographs taken with a Hagg-Guinier camera, with $\text{CuK}\alpha$ radiation and calcium fluoride ($a=5.4630$ Å) as an internal standard. The cell parameters were refined by a least-squares program. The density was determined by the flotation method. Crystal data for $[\text{Ni}(\text{H}_2\text{O})_4(\text{C}_{10}\text{H}_5\text{NO}_5\text{S})] \cdot 1\frac{1}{2}\text{H}_2\text{O}$ are: Space group: $C2/c$
 $a=28.895(15)$ Å, $b=10.637(4)$ Å, $c=9.831(4)$ Å
 $\beta=91.97(5)^\circ$, $Z=8$, $D_m=1.79$ g cm⁻³, $D_x=1.799$ g cm⁻³, $\mu(\text{CuK}\alpha)=35.8$ cm⁻¹

The crystals were unstable in the X-ray beam and decomposed after a couple of days. The intensities from levels $h0l-h4l$ and $h5l-h8l$ were measured from two separate crystals, both with approximate dimensions $0.3 \times 0.4 \times 0.3$ mm. The data were collected with a Stoe-Güttinger diffractometer using Ni-filtered Cu radiation ($\text{CuK}\alpha$, $\lambda=1.5418$ Å). The total number of reflections was 2137, of which the 1467 stronger than $3\sigma(I)$ were considered observed. The data set was corrected for Lorentz and polarization effects but not for absorption.

Structure determination. Attempts to solve the structure by direct methods with the X-RAY 76 program system⁴ were not successful but initial coordinates for 17 non-hydrogen atoms were obtained from an E map by use of the MULTAN 74 program.⁵ The positions of the remaining non-hydrogen atoms were found from a difference map. At last a difference Fourier synthesis revealed the positions of the hydrogen atoms.

The final refinement was carried out by full-matrix least-squares methods, with anisotropic temperature factors for the non-hydrogen atoms and the fixed value ($B=2.9$ Å²) for the

Table 1. Fractional atomic coordinates for the non-hydrogen atoms.

Atom	X/a	Y/b	Z/c	Atom	X/a	Y/b	Z/c
C1	0.1885(3)	0.3266(9)	0.3270(8)	O2	0.1302(2)	0.4112(6)	0.4625(5)
C2	0.1733(3)	0.3971(8)	0.4394(8)	O3	0.0307(2)	0.4199(6)	0.3879(6)
C3	0.2074(3)	0.4551(10)	0.5288(7)	O4	0.0537(2)	0.2760(6)	0.1287(5)
C4	0.2526(3)	0.4488(9)	0.5013(8)	O5	0.0721(2)	0.1811(6)	0.4020(6)
C5	0.3160(3)	0.3844(9)	0.3574(8)	O6	0.0980(3)	0.5097(6)	0.2074(6)
C6	0.3325(3)	0.3200(8)	0.2443(8)	O7	0.5233(2)	0.4613(7)	0.6286(7)
C7	0.3004(3)	0.2488(9)	0.1616(8)	O8	0.0000	0.3545(9)	0.7500
C8	0.2544(3)	0.2468(10)	0.1885(8)	S	0.3905(1)	0.3304(2)	0.1954(2)
C9	0.2370(3)	0.3164(8)	0.2996(8)	O9	0.4190(2)	0.3328(7)	0.3213(5)
C10	0.2693(3)	0.3823(9)	0.3832(8)	O10	0.3938(2)	0.4434(7)	0.1165(6)
N	0.1515(2)	0.2780(8)	0.2509(6)	O11	0.3995(2)	0.2164(7)	0.1174(6)
O1	0.1586(2)	0.2048(7)	0.1530(6)	Ni	0.0894(1)	0.3424(1)	0.3039(1)

hydrogen atoms. The weighting scheme was $w = 1/(60.0 + |F_o| + 0.05|F_o|^2)$. Atomic scattering factors for the non-hydrogen and hydrogen atoms were taken from Refs. 6 and 7, respectively, and the dispersion corrections ($\Delta f'$, $\Delta f''$) were applied for Ni and S.⁸ The final R value was 0.062 for 1467 observed reflections.

The atomic coordinates for the non-hydrogen atoms are given in Table 1 and for hydrogen atoms in Table 2. Lists of the structure factors and thermal parameters are available on request from the authors.

DESCRIPTION OF THE STRUCTURE

The complex molecule is visualized in Fig. 1 where the bond lengths are also shown. The

Table 2. Fractional atomic coordinates for the hydrogen atoms.

Atom	X/a	Y/b	Z/c
H(C3)	0.203(3)	0.495(9)	0.601(8)
H(C4)	0.277(3)	0.504(9)	0.570(8)
H(C5)	0.342(3)	0.435(8)	0.419(8)
H(C7)	0.315(3)	0.198(8)	0.071(8)
H(C8)	0.232(3)	0.185(8)	0.136(9)
H1(O3)	0.133(3)	0.486(8)	0.334(8)
H2(O3)	0.005(3)	0.366(9)	0.394(9)
H1(O4)	0.034(3)	0.153(8)	0.114(9)
H2(O4)	0.061(3)	0.309(8)	0.055(9)
H1(O5)	0.091(3)	0.087(9)	0.405(9)
H2(O5)	0.076(3)	0.189(9)	0.452(9)
H1(O6)	0.101(3)	0.528(9)	0.157(9)
H2(O6)	0.097(3)	0.578(9)	0.250(9)
H1(O7)	0.548(3)	0.526(9)	0.648(8)
H2(O7)	0.509(3)	0.486(9)	0.570(8)
H1(O8)	0.023(3)	0.323(9)	0.727(8)

bond angles can be found in Table 3. It can be seen from the figure that the coordination octahedron around nickel is formed of one nitrogen and one oxygen atom from the ligand, and of the four aqua water oxygens. The chelate ring is thus five-membered, which is consistent with the copper(II) and zinc(II) chelates of the isomeric nitrosophthal ligands studied previously.^{1,2} The five Ni—O distances, ranging from 2.036(7) to 2.099(6) Å, are somewhat longer than the Ni—N distance 2.007(7) Å, which together with the respective O—Ni—O and O—Ni—N angles (Table 3) display the expected distortions from true octahedron.

As in the earlier reported 1:1 copper complex of 2-nitroso-1-naphthol-4-sulfonic acid,⁹ the electrically neutral complex molecule is a zwitter-

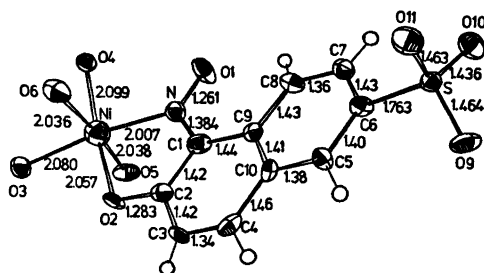


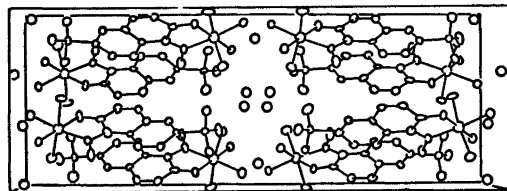
Fig. 1. ORTEP drawing of the complex molecule including bond lengths. The thermal ellipsoids are drawn at the 50% probability level. The e.s.d.'s for the C—C bonds are 0.011–0.012 Å and for the rest of the bonds 0.005–0.009 Å. The observed C—H and O—H bond lengths are 0.86–1.14 Å and 0.54–1.44 Å, respectively, the average e.s.d. being 0.09 Å.

Table 3. Bond angles ($^\circ$) and their standard deviations.

The nickel environment			
N-Ni-O2	79.8(2)	O2-Ni-O4	88.0(2)
N-Ni-O3	170.5(2)	O3-Ni-O4	94.3(2)
N-Ni-O4	95.2(2)	O3-Ni-O5	86.0(3)
N-Ni-O5	94.1(3)	O3-Ni-O6	87.3(3)
N-Ni-O6	93.0(3)	O4-Ni-O5	89.1(2)
O2-Ni-O3	90.7(2)	O4-Ni-O6	88.6(3)
O2-Ni-O4	173.8(2)	O5-Ni-O6	172.7(3)
O2-Ni-O5	94.8(2)		
The ligand molecule			
C2-C1-C9	121.0(7)	C8-C9-C10	117.5(7)
C2-C1-N	111.4(7)	C4-C10-C5	119.4(8)
C9-C1-N	127.6(8)	C4-C10-C9	118.5(7)
C1-C2-C3	118.2(8)	C5-C10-C9	122.2(8)
C1-C2-O2	121.9(7)	C1-N-O1	120.0(6)
C3-C2-O2	119.9(7)	C5-C6-S	122.5(6)
C2-C3-C4	121.6(8)	C7-C6-S	118.8(6)
C3-C4-C10	121.7(8)	C6-S-O9	106.5(3)
C6-C5-C10	120.0(8)	C6-S-O10	106.4(4)
C5-C6-C7	118.6(7)	C6-S-O11	106.3(4)
C6-C7-C8	121.0(8)	O9-S-O10	113.3(4)
C7-C8-C9	120.8(8)	O9-S-O11	110.6(4)
C1-C9-C8	123.6(7)	O10-S-O11	113.2(4)
C1-C9-C10	118.8(7)		

Table 4. Possible hydrogen bonding.

X-H...Y	Position of acceptor atom			X...Y	X-H...Y
O3-H1(O3)...O8	-x	1-y	1-z	2.88	159
O3-H2(O3)...O4	-x	y	$\frac{1}{2}$ -z	2.88	167
O4-H1(O4)...O7	$-\frac{1}{2}+x$	$\frac{1}{2}-y$	$-\frac{1}{2}+z$	2.67	164
O4-H2(O4)...O11	$\frac{1}{2}-x$	$\frac{1}{2}-y$	-z	2.81	143
O5-H1(O5)...O10	$\frac{1}{2}-x$	$-\frac{1}{2}+y$	$\frac{1}{2}-z$	2.73	164
O5-H2(O5)...O9	$\frac{1}{2}-x$	$\frac{1}{2}-y$	1-z	2.72	162
O6-H1(O6)...O2	x	1-y	$-\frac{1}{2}+z$	2.74	166
O6-H2(O6)...O11	$\frac{1}{2}-x$	$\frac{1}{2}+y$	$\frac{1}{2}-z$	2.79	167
O7-H1(O7)...O9	1-x	1-y	1-z	2.79	167
O7-H2(O7)...O7	1-x	y	$1\frac{1}{2}-z$	2.78	169

Fig. 2. Molecular packing looking down the *c* axis.

terion type of compound, being composed of the positive nickel part and negative sulfonate part. The unit cell packing illustrated in Fig. 2 indicates that the structure may be described as built up from pairs of such zwitterions. The orientation of the molecules within the pairs is typically dipolar: the similarly charged parts of the dipoles repel and oppositely charged parts attract each other.

The decisive features for the packing arise from hydrogen bond formation. As the hydrogen atoms in the structure could be located only with relatively low accuracy (*cf.* Fig. 1), some of the hydrogen bonding details are partly uncertain. It is probable, however, that bonding between the molecules of the aforementioned pairs is effected by an aqua water molecule which donates a hydrogen bond to the adjacent sulfonate oxygen, and the separate pairs are chiefly connected through hydrogen bonds from aqua waters to sulfonate oxygens and to the oxygens of the "free" water molecules. In this way the aqua waters of separate complex pairs are joined together in the direction of the *a* axis *via* the water molecule in the special position. It is further evident that the remaining "free" waters in the structure are also hydrogen bonded to each other. The proposed hydrogen bonds which are mostly of medium strength, varying from 2.7 to 2.9 Å, are collected in Table 4.

In the previous studies we have indicated that uncoordinated 1,2-nitrosonaphthols exist in their tautomeric 1,2-naphthoquinone oxime forms in the solid state.¹ Comparison of the bond lengths and angles of ligands in "free" and copper and zinc coordinated states has shown some systematic changes to occur upon coordination, but the quinonoid nature is still important in describing the structure of the metal complex. As the characteristic C—N, N—O, and C3—C4 bond distances of the present molecule (Fig. 1) do not significantly differ from those previously found for the copper and zinc chelates of this type of ligand,^{1,2} the designation of the complex as naphthoquinone oximate has been preferred to the alternative nitrosonaphtholato.

Acknowledgement. The financial support of the Science Research Council of Finland is gratefully acknowledged.

REFERENCES

1. Saarinen, H., Korvenranta, J. and Näsäkkälä, E. *Acta Chem. Scand. A* 31 (1977) 213.
2. Saarinen, H., Korvenranta, J. and Näsäkkälä, E. *Finn. Chem. Lett.* (1977) 155.
3. Mäkitie, O. and Saarinen, H. *Anal. Chim. Acta* 46 (1969) 314.
4. X-Ray 76, Program System for X-Ray Crystallography, *Technical Report TR-446 of the Computer Science Center*, University of Maryland.
5. Main P., Woolfson, M. M., Lessinger, L., Germain, G. and Declercq, J.-P. MÜLTAN 74, A System of Computer Programmes for the Automatic Solution of Crystal Structures from X-Ray Diffraction Data.
6. Cromer, D. T. and Mann, J. B. *Acta Crystallogr. A* 24 (1968) 321.
7. Stewart, R. F., Davidson, E. and Simpson, W. *J. Chem. Phys.* 42 (1968) 3175.
8. *International Tables for X-Ray Crystallography*, Kynoch Press, Birmingham 1974, Vol. IV, p. 149.
9. Korvenranta, J. and Saarinen, H. *Finn. Chem. Lett.* (1975) 314.

Received May 9, 1977.

The Crystal Structure of a Tetrameric Copper(II) Complex of 2-[(3-Aminopropyl)amino]ethanol: $[\text{Cu}_4(\text{C}_5\text{H}_{13}\text{N}_2\text{O})_4](\text{NO}_3)_4 \cdot 2\text{H}_2\text{O}$

KARI NIEMINEN

Department of Inorganic Chemistry, University of Helsinki, SF-00100 Helsinki 10, Finland

The crystal structure of tetrakis- μ_3 -{2-[(3-aminopropyl)amino]ethanolato}-tetracopper(II) tetraniolate dihydrate, $[\text{Cu}_4(\text{C}_5\text{H}_{13}\text{N}_2\text{O})_4](\text{NO}_3)_4 \cdot 2\text{H}_2\text{O}$, has been determined by three-dimensional X-ray methods. The compound crystallizes in the monoclinic space group $C2/c$ with unit cell dimensions $a = 27.312(15)$, $b = 20.936(13)$, $c = 17.519(9)$ Å, $\beta = 128.82(3)^\circ$, and $Z = 8$. The intensity data were collected with a four-circle automated diffractometer. The positions of copper(II) ions and the oxygen atoms of 2-[(3-aminopropyl)amino]ethanols were determined by direct methods and the other non-hydrogen atoms by Fourier syntheses. The structure was refined by block-diagonal least-squares methods to an R value of 0.070 ($R_w = 0.101$) on the basis of 3400 independent reflections. The complex has a tetranuclear cubane-type structure. The four copper(II) ions, with interatomic distances 3.224–3.433 Å, are connected by oxygen bridges. The Cu–O distances vary between 1.937 and 2.633 Å. The cation $[\text{Cu}_4(\text{C}_5\text{H}_{13}\text{N}_2\text{O})_4]^{4+}$ has S_4 pseudosymmetry. These tetranuclear units are joined by NO_3 groups and between these chains there are bridges formed by water molecules and nitrate ions. Each copper(II) ion has a distorted octahedral (4+2)-coordination. The equatorial interatomic distances (mean values): Cu(i)–N(i1) 1.99 Å, Cu(i)–N(i2) 2.02 Å, Cu(i)–O(i) 1.95 Å and Cu(i)–O(j) 1.98 Å are coordination bond values and the axial Cu–O distances 2.59 and 2.70 Å correspond to semicoordination bonds.

The reactions of 2-[(3-aminopropyl)amino]ethanol (HL) with copper(II) salts in methanol solution yield crystalline one-to-one complexes according to analysis.^{1,2} On the basis of the crystal structure of $\text{CuLCl} \cdot \text{H}_2\text{O}$ ($\text{L} = 2\text{-}[(3\text{-aminopropyl)amino]ethanolato}^-$) and ESR spectrometric studies, these complexes have evidently tetrameric structures.^{3,4} The present investigation was undertaken in order to

study the possible tetrameric structure of the complex $\text{CuLNO}_3 \cdot \frac{1}{2}\text{H}_2\text{O}$.

EXPERIMENTAL

The preparation and crystal data. The preparation and crystal data of the compound have been published earlier.¹ Cell dimensions were obtained with a Syntex P2₁ automated four-circle diffractometer by a least-squares refinement of setting angles for 20 well-centered reflections. The radiation was $\text{MoK}\alpha$ ($\lambda = 0.7107$ Å) monochromatized by graphite. The cell dimensions were $a = 27.312(15)$ Å, $b = 20.936(13)$ Å, $c = 17.519(9)$ Å, $\beta = 128.82(3)^\circ$, volume $V = 7805(7)$ Å³, and there were eight formula units in each cell. Of the two possible space groups, Cc (No. 9) and $C2/c$ (No. 15), the latter was found to describe the structure sufficiently well as far as the complexes are concerned.

Intensity data. The crystal selected for data collection was a plate with approximate dimensions $0.5 \times 0.4 \times 0.1$ mm. Intensities were collected by scanning in 2θ (scan speed varied between 2.93 and 29.30° min⁻¹, scan range was 1.0°, and 2θ varied between 5 and 50°). Of the 6059 reflections considered, 3400 had $F_o > 4.0\sigma(F_o)$, and these were regarded as observed. Data were corrected for Lorentz and polarization effects and also for absorption from ϕ -scan data [$\mu(\text{MoK}\alpha) = 23.2$ cm⁻¹]. The standard reflection measured periodically during the data collection varied about $\pm 8\%$, but showed no systematic increase or decrease.

Structure determination and refinement. The structure was solved by direct methods and Fourier techniques. In the calculations of F_c , atomic scattering factors computed from numerical Hartree-Fock wave functions were used for all atoms.⁵ The effects of anomalous dispersion of copper were included in the calculations and the values of $\Delta f' = 0.30$ and $\Delta f'' = 1.35$ were taken from International Tables for X-Ray Crystallography.⁶

Table 1. Fractional atomic coordinates ($\times 10^4$) and thermal parameters a ($\times 10^3$). Estimated standard deviations are given in parentheses.

Atom	X/a	Y/b	Z/c	U_{11}/U_{10}	U_{22}	U_{33}	U_{12}	U_{13}	U_{23}
Cu(1)	214(1)	-2273(2)	105(1)	28(1)	31(1)	35(1)	8(1)	21(1)	10(1)
Cu(2)	1134(1)	-3045(1)	359(1)	32(1)	33(1)	29(1)	8(1)	19(1)	4(1)
Cu(3)	1767(1)	-1854(1)	1849(1)	31(1)	25(1)	39(1)	1(1)	25(1)	4(1)
Cu(4)	1156(1)	-3060(1)	2121(1)	33(1)	26(1)	30(1)	0(1)	21(1)	4(1)
O(1)	897(4)	-2215(4)	21(6)	31(5)	31(5)	37(5)	10(4)	24(4)	15(4)
O(2)	1879(4)	-2766(4)	1712(6)	28(5)	27(5)	36(5)	2(4)	22(4)	-5(4)
O(3)	1131(4)	-2113(4)	1960(6)	34(5)	21(4)	34(5)	6(3)	24(4)	0(4)
O(4)	541(4)	-3123(4)	700(6)	32(4)	22(4)	43(5)	-8(4)	27(4)	6(4)
N(11)	-452(5)	-2281(5)	257(10)	45(7)	27(6)	82(9)	12(5)	55(7)	12(6)
N(12)	-153(5)	-1512(5)	-813(8)	37(6)	22(6)	49(7)	19(5)	27(6)	29(5)
N(21)	755(5)	-3397(6)	-1009(8)	44(7)	58(8)	27(6)	10(6)	20(6)	-1(5)
N(22)	1964(5)	-3764(5)	848(8)	41(6)	25(6)	42(6)	6(5)	29(6)	8(5)
N(31)	2367(5)	-1562(5)	1643(9)	29(6)	40(7)	60(8)	1(5)	34(6)	6(6)
N(32)	1708(5)	-995(5)	2301(8)	38(6)	17(5)	44(6)	-7(4)	24(6)	-4(5)
N(41)	1840(5)	-3045(6)	3581(7)	44(7)	43(7)	25(6)	6(5)	20(5)	10(5)
N(42)	928(5)	-3981(5)	2129(7)	31(6)	24(6)	31(6)	8(4)	20(5)	8(4)
C(11)	-695(7)	-1635(7)	300(12)	49(9)	48(9)	66(10)	11(7)	41(9)	21(8)
C(12)	-979(7)	-1249(8)	-643(12)	56(10)	61(11)	69(11)	30(8)	48(9)	32(9)
C(13)	-452(8)	-983(7)	-665(11)	61(10)	40(9)	47(9)	13(7)	31(8)	14(7)
C(14)	338(6)	-1273(8)	-862(11)	35(8)	58(10)	59(9)	22(7)	33(8)	26(8)
C(15)	709(6)	-1833(7)	-793(10)	39(8)	42(8)	46(8)	18(6)	35(7)	28(7)
C(21)	676(9)	-4112(8)	-1043(13)	89(14)	47(10)	62(11)	19(9)	36(11)	-9(9)
C(22)	1300(9)	-4465(8)	-624(13)	93(14)	42(10)	53(10)	5(9)	32(10)	-17(8)
C(23)	1742(7)	-4436(7)	489(13)	44(9)	42(9)	71(12)	6(7)	34(9)	-14(8)
C(24)	2394(6)	-3752(6)	1940(11)	32(7)	33(8)	63(10)	17(6)	33(7)	13(7)
C(25)	2496(6)	-3050(6)	2246(9)	31(7)	39(8)	36(7)	17(6)	22(6)	11(6)
C(31)	2279(7)	-891(7)	1245(12)	56(9)	35(8)	71(11)	4(7)	49(9)	16(7)
C(32)	2281(7)	-363(6)	1874(11)	56(9)	18(7)	60(10)	-17(6)	35(8)	-2(6)
C(33)	1710(6)	-393(6)	1836(10)	41(8)	26(7)	42(8)	3(6)	20(7)	0(6)
C(34)	1129(8)	-1028(7)	2250(12)	78(11)	37(8)	75(11)	-20(8)	65(10)	-20(8)
C(35)	1094(6)	-1672(7)	2538(10)	38(8)	44(8)	44(8)	-5(6)	29(7)	2(7)
C(41)	2229(7)	-3628(7)	4051(10)	50(9)	52(9)	26(7)	11(7)	14(7)	22(7)
C(42)	1824(8)	-4223(8)	3863(11)	79(12)	47(9)	45(9)	-8(8)	42(9)	1(7)
C(43)	1404(7)	-4470(7)	2790(11)	56(9)	36(8)	60(9)	26(7)	43(8)	23(7)
C(44)	520(6)	-4225(6)	1090(10)	32(7)	29(7)	36(7)	-2(6)	17(6)	-6(6)
C(45)	104(7)	-3654(7)	417(10)	48(8)	35(8)	35(8)	7(7)	22(7)	10(6)
O(111)	-474(5)	-2875(6)	-1723(11)	32(6)	76(9)	108(11)	-4(6)	32(7)	-17(8)
N(111)	-977(6)	-3118(7)	-2084(10)	43(7)	66(9)	57(8)	-5(7)	27(7)	-10(7)
O(112)	-1251(6)	-2991(7)	-1769(10)	65(8)	108(11)	80(9)	-5(8)	47(8)	-26(8)
O(113)	-1144(12)	-3545(14)	-2629(20)	238(26)	289(32)	261(29)	-189(25)	220(26)	-213(27)
O(211)	2151(10)	-2521(11)	141(17)	182(19)	164(19)	215(23)	-89(16)	172(20)	-45(16)
N(211) ^b	2444(52)	-2548(58)	-129(80)	85(12)					
O(212) ^b	2393(18)	-1848(17)	-156(33)	146(30)	133(29)	240(43)	22(24)	175(34)	61(28)
O(311)	2647(6)	-1983(7)	3778(9)	57(8)	99(11)	58(8)	-26(7)	18(7)	-5(7)
N(311)	3136(6)	-1722(7)	4377(10)	51(8)	82(10)	63(9)	14(7)	44(7)	-5(7)
O(312)	3127(9)	-1125(7)	4177(11)	158(16)	73(10)	84(10)	-24(11)	59(11)	-1(9)
O(313)	3593(7)	-1903(9)	5159(10)	74(9)	171(17)	57(8)	76(10)	23(7)	22(9)
O(411)	294(6)	-2862(5)	2296(9)	76(8)	52(7)	104(10)	4(6)	80(8)	9(6)
N(411)	0(-)	-3166(8)	2500(-)	38(4)					
O(412)	0(-)	-3763(7)	2500(-)	51(4)					
O(511)	1024(8)	-415(11)	-1565(18)	87(12)	134(17)	211(24)	-27(12)	58(14)	53(16)
N(511)	1528(10)	-96(11)	-940(15)	114(15)	133(18)	86(13)	25(13)	62(12)	39(12)
O(512)	1952(10)	-213(14)	-896(17)	118(15)	309(33)	152(19)	27(18)	103(15)	30(19)
O(513)	1524(12)	359(12)	-451(17)	200(22)	131(19)	134(18)	2(17)	90(17)	7(15)
O(6)	1289(9)	-1463(11)	-2116(12)	112(13)	181(20)	81(11)	-1(13)	63(11)	-9(12)
O(7)	0(-)	471(26)	-2500(-)	270(21)					
O(8) ^b	3823(20)	-599(23)	3906(33)	167(16)					

^a The anisotropic thermal parameters are of the form $\exp[-2\pi^2(h^2a^{*2}U_{11} + k^2b^{*2}U_{22} + l^2c^{*2}U_{33} + 2hka^*b^*U_{12} + 2hla^*c^*U_{13} + 2klb^*c^*U_{23})]$. ^b Population parameter 0.5.

The 322 reflections having $|E_o| \geq 1.50$ were used to calculate an F_o statistical map from which the positions of the copper atoms and the four oxygen atoms in the ethanolato groups were located. With these atoms, isotropic thermal parameters and unit weights, the R value after one cycle was 0.329 ($R = \sum ||F_o| - |F_c|| / \sum |F_o|$). The other non-hydrogen atoms were located from successive Fourier syntheses. One oxygen atom and the nitrogen atom of one NO₃⁻ ion and the oxygen atom of one water molecule are located on the *two-fold* axis. Near the special position (1/4, 1/4, 1/2) there is a disordered NO₃⁻ ion. The nitrogen atom and one oxygen atom of this NO₃⁻ ion are situated in two positions, with the population parameter 0.5. All the other atoms occupy general positions.

According to the analysis there are two water molecules in the asymmetric unit. Because there is one water molecule in a general position and a half molecule in a special position, there must be another half molecule in a special position or in a general position with the population parameter 0.5. In the difference-Fourier map the only noticeable maximum 1.12 e Å⁻³ is at the general position (0.3823, -0.0599, 0.3906), and the other half of the water molecule is located in that position.

Atomic coordinates were refined by block-diagonal least-squares techniques to an R value of 0.070 ($R_w = 0.101$, with the weighting scheme $w = 1/(35.0 + |F_o| + 0.031 |F_o|^2)$). Isotropic thermal parameters were used for the four atoms located in the special positions and for O(8), and anisotropic thermal parameters for all the other atoms. The computations were performed on a UNIVAC 1108 computer using the X-Ray 72 program system.⁷ The figures were drawn by a Honeywell GE 635 computer using the Perspect graphic program.⁸

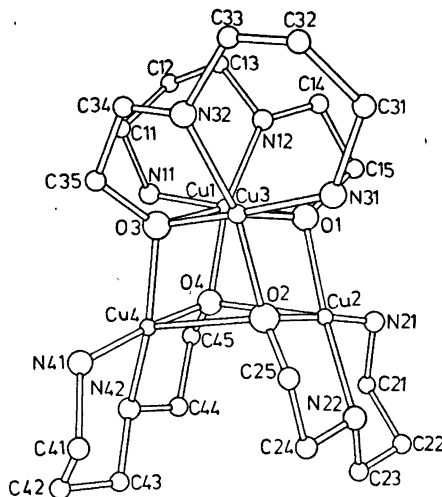


Fig. 1. Perspective view of the cation [Cu₄(C₅H₁₃N₂O)₄]⁴⁺.

RESULTS AND DISCUSSION

The atomic coordinates and thermal parameters with their standard deviations are given in Table 1. A list of observed and calculated structure factors is obtainable from the author. The structure consists of tetrameric units formed by four copper(II) ions and four deprotonated 2-[(3-aminopropyl)amino]ethanols (Fig. 1). The array of copper(II) ions is roughly tetrahedral having interatomic distances Cu...Cu 3.224–3.443 Å (Table 2). Two of the

Table 2. Interatomic distances (Å), bond lengths (Å) and bond angles (°) for the tetranuclear unit Cu₄O₄. Estimated standard deviations are given in parentheses.

Cu(1)···Cu(2)	3.233(3)	O(1)–Cu(1)–O(3)	82.5(4)	Cu(1)–O(1)–Cu(2)	110.2(5)
Cu(1)···Cu(3)	3.443(2)	O(1)–Cu(1)–O(4)	87.7(4)	Cu(1)–O(1)–Cu(3)	95.9(5)
Cu(1)···Cu(4)	3.227(2)	O(3)–Cu(1)–O(4)	72.1(3)	Cu(2)–O(1)–Cu(3)	88.5(2)
Cu(2)···Cu(3)	3.249(2)	O(1)–Cu(2)–O(2)	87.6(4)	Cu(2)–O(2)–Cu(3)	112.4(4)
Cu(2)···Cu(4)	3.411(3)	O(1)–Cu(2)–O(4)	72.0(4)	Cu(2)–O(2)–Cu(4)	97.7(4)
Cu(3)···Cu(4)	3.224(3)	O(2)–Cu(2)–O(4)	81.3(4)	Cu(3)–O(2)–Cu(4)	89.7(5)
Cu(1)–O(1)	1.967(13)	O(1)–Cu(3)–O(2)	70.4(3)	Cu(1)–O(3)–Cu(3)	97.6(5)
Cu(1)–O(3)	2.596(7)	O(1)–Cu(3)–O(3)	81.9(4)	Cu(1)–O(3)–Cu(4)	88.2(3)
Cu(1)–O(4)	1.971(8)	O(2)–Cu(3)–O(3)	87.6(4)	Cu(3)–O(3)–Cu(4)	109.7(5)
Cu(2)–O(1)	1.977(9)	O(2)–Cu(4)–O(3)	71.7(4)	Cu(1)–O(4)–Cu(2)	89.3(4)
Cu(2)–O(2)	1.937(8)	O(2)–Cu(4)–O(4)	81.8(4)	Cu(1)–O(4)–Cu(4)	110.9(4)
Cu(2)–O(4)	2.587(13)	O(3)–Cu(4)–O(4)	87.8(3)	Cu(2)–O(4)–Cu(4)	96.6(4)
Cu(3)–O(1)	2.633(8)				
Cu(3)–O(2)	1.972(9)				
Cu(3)–O(3)	1.944(13)				
Cu(4)–O(2)	2.561(13)				
Cu(4)–O(3)	2.000(8)				
Cu(4)–O(4)	1.947(8)				

Table 3. The equations of least-squares planes for Cu_4O_4 , the distances (\AA) of some atoms from these planes, and the angles ($^\circ$) between the planes. Equations of the planes are expressed as $PX + QY + RZ = S$ in direct space.

Plane 1: Cu(1), Cu(3), O(1), O(3)
 $-4.92X + 20.24Y - 0.49Z = -4.82$
 Cu(1) 0.107, Cu(3) 0.107, O(1) -0.106, O(3) -0.109

Plane 2: Cu(1), Cu(2), O(1), O(4)
 $2.83X + 7.70Y + 11.48Z = -1.50$
 Cu(1) -0.069, Cu(2) -0.055, O(1) 0.073, O(4) 0.052

Plane 3: Cu(1), Cu(4), O(3), O(4)
 $27.05X - 0.11Y - 12.76Z = 0.53$
 Cu(1) -0.058, Cu(4) -0.073, O(3) 0.053, O(4) 0.078

Plane 4: Cu(3), Cu(4), O(2), O(3)
 $4.57X + 0.46Y + 11.61Z = 2.79$
 Cu(3) 0.085, Cu(4) 0.067, O(2) -0.064, O(3) -0.089

Plane 5: Cu(2), Cu(3), O(1), O(2)
 $25.43X + 6.57Y - 12.77Z = 0.85$
 Cu(2) 0.077, Cu(3) 0.060, O(1) -0.055, O(2) -0.082

Plane 6: Cu(2), Cu(4), O(2), O(4)
 $-5.13X + 20.23Y - 0.34Z = -6.74$
 Cu(2) -0.119, Cu(4) -0.119, O(2) 0.120, O(4) 0.118

Angles ($^\circ$) between the planes:

Plane	2	3	4	5	6
1	80.2	80.9	79.2	80.3	0.5
2		88.4	20.6	87.7	80.0
3			88.3	18.9	80.4
4				88.8	79.4
5					80.7

Table 4. The equations of least-squares planes through the atoms N(i1), N(i2), O(i) and O(j), and the distances (\AA) of some atoms from these planes. Equations of the planes are expressed as $PX + QY + RZ = S$ in direct space.

Plane 1: N(11), N(12), O(1), O(4)
 $1.54X + 10.98Y + 10.97Z = -2.43$
 N(11) 0.136, N(12) -0.147, O(1) 0.159, O(4) -0.148
 Cu(1) 0.081, O(3) 2.435, O(111) -2.691

Plane 2: N(21), N(22), O(2), O(1)
 $23.59X + 9.77Y - 12.09Z = -0.20$
 N(21) -0.117, N(22) 0.130, O(2) -0.141, O(1) 0.128
 Cu(2) -0.063, O(4) -2.421, O(211) 2.641

Plane 3: N(31), N(32), O(3), O(2)
 $4.60X - 3.35Y + 11.43Z = 3.61$
 N(31) -0.124, N(32) 0.135, O(3) -0.146, O(2) 0.135
 Cu(3) -0.067, O(1) -2.434, O(311) 2.586

Plane 4: N(41), N(42), O(4), O(3)
 $26.69X - 3.96Y - 12.02Z = 1.66$
 N(41) 0.151, N(42) -0.167, O(4) 0.178, O(3) -0.163
 Cu(4) 0.087, O(2) 2.391, O(411) -2.503

distances are noticeably longer than the other four. The copper(II) ions are bridged by an approximately tetrahedral array of oxygen atoms, forming the cubane-type structure Cu₄O₄. The limiting planes of this cube and the angles between the planes are calculated and shown in Table 3. The structure of the array is similar to that of the chloride salt of this cation⁸ and resembles the structures of the copper(II) compound of the Schiff base of aminoethanol and acetylacetone,⁹ chloro(2-diethylaminoethanolato)copper(II),^{10,11} and chloro-, and γ -bromo(2-dibutylaminoethanolato)copper(II).¹² However, the difference between the shortest and longest interatomic copper(II) ion distances is smaller in the present cation than in those just mentioned, so that the coupling in the present compound can be thought to have more tetranuclear character. The unit Cu₄O₄ has S₄ pseudosymmetry, and the whole cation [Cu₄(C₅H₁₃N₂O)₄]⁴⁺ has approximately this symmetry too.

The coordination around the copper(II) ions is distorted octahedral (4+2)-coordination. The two nitrogen atoms and the oxygen atom of one amine (i) and the oxygen atom of another amine (j) lie almost in a plane with the cop-

per(II) ion. The least-squares planes through the nitrogen and oxygen atoms are calculated and are given in Table 4. The copper(II) ions are situated 0.063–0.087 Å from the planes toward the oxygen atom of the third amine (k). The bond distances (Tables 2 and 5) in the plane correspond to typical coordination bonds: (mean values) Cu(i)–N(i1) 1.99 Å, Cu(i)–N(i2) 2.02 Å, Cu(i)–O(i) 1.95 Å and Cu(i)–O(j) 1.98 Å. The apices of the octahedron are occupied by the oxygen atom of the third amine, having an interatomic distance 2.59 Å (mean value), and an oxygen atom of the NO₃ group having the Cu(i)–O(i11) distance 2.70 Å (mean value). These longer distances can be considered semicoordination bonds and they are in agreement with the bond extension in the axial direction of copper(II) octahedral coordination.¹³ The coordination of the copper(II) ion in this cation differs from the coordinations in other compounds described earlier, where it is bipyramidal (3+2)-coordination with two oxygen atoms in axial positions and a nitrogen atom and two oxygen atoms of different ligands in equatorial positions or distorted square pyramidal coordination.^{9–12}

The amine configuration is similar to that of

Table 5. Bond lengths (Å) between the atoms in the amine rings and in the NO₃ ions. The shortest interatomic distances (Å) from the oxygens of water molecules to other atoms. Estimated standard deviations are given in parentheses.

	i=1	i=2	i=3	i=4	i=5
Cu(i)–N(i1)	1.99(2)	2.01(1)	1.98(2)	2.01(1)	
Cu(i)–N(i2)	2.03(1)	2.03(1)	2.01(1)	2.03(1)	
N(i1)–C(i1)	1.53(2)	1.51(2)	1.52(2)	1.48(2)	
C(i1)–C(i2)	1.54(3)	1.56(3)	1.56(3)	1.56(3)	
C(i2)–C(i3)	1.56(3)	1.52(2)	1.52(3)	1.55(2)	
C(i3)–N(i2)	1.49(2)	1.50(2)	1.50(2)	1.48(2)	
N(i2)–C(i4)	1.48(3)	1.49(2)	1.53(3)	1.51(2)	
C(i4)–C(i5)	1.50(2)	1.53(2)	1.46(2)	1.56(2)	
C(i5)–O(i)	1.42(2)	1.45(2)	1.42(2)	1.47(2)	
Cu(i)–O(i11)	2.80(2)	2.72(3)	2.66(1)	2.59(2)	
N(i11)–O(i11)	1.21(2)	1.16(18)	1.19(2)	1.24(2)	1.28(3)
N(i11)–O(i12)	1.21(3)	1.47(13) ^a	1.29(2)	1.25(2)	1.14(4)
N(i11)–O(i13)	1.17(3)	1.13(17)	1.20(2)	1.24(2)	1.29(4)
O(6)···O(511)	2.67(4)				
O(6)···O(212)	2.92(4)				
O(7)···O(511)	2.86(4)				
O(8)···O(312)	2.49(7)				

^a The interatomic distance O(212) [1/2–x, 1/2–y, z]···N(211) is 1.33 Å and the distance N(211)···N(211) [1/2–x, 1/2–y, z] is 0.40 Å.

Table 6. Bond angles ($^{\circ}$) in the amine rings and in the NO_3 ions. The interatomic angles ($^{\circ}$) from the oxygens water molecules. Estimated standard deviations are given in parentheses.

	i = 1	i = 2	i = 3	i = 4	i = 5
N(i1)–Cu(i)–N(i2)	94.2(6)	93.2(5)	94.3(6)	92.9(4)	
N(i1)–Cu(i)–O(i)	175.9(4)	175.9(5)	175.9(4)	175.0(6)	
N(i1)–Cu(i)–O(j)	94.5(5) ^{j=3}	96.1(5) ^{j=4}	94.9(5) ^{j=1}	95.0(4) ^{j=2}	
N(i1)–Cu(i)–O(k)	94.1(5) ^{k=4}	95.2(4) ^{k=1}	93.9(5) ^{k=2}	94.9(4) ^{k=3}	
N(i1)–Cu(i)–O(i11)	97.8(5)	94.6(7)	94.1(5)	92.0(6)	
N(i2)–Cu(i)–O(i)	84.9(5)	84.8(4)	85.0(5)	85.5(4)	
N(i2)–Cu(i)–O(j)	120.0(3) ^{j=3}	117.8(5) ^{j=4}	120.1(3) ^{j=1}	121.6(5) ^{j=2}	
N(i2)–Cu(i)–O(k)	164.6(5) ^{k=4}	166.4(4) ^{k=1}	165.9(5) ^{k=2}	163.9(5) ^{k=3}	
N(i2)–Cu(i)–O(i11)	78.6(4)	78.7(6)	79.8(4)	81.1(5)	
O(i)–Cu(i)–O(i11)	86.0(5)	89.0(6)	89.8(5)	92.4(5)	
O(j)–Cu(i)–O(i11)	156.9(3) ^{j=3}	159.6(6) ^{j=4}	157.3(4) ^{j=1}	155.6(3) ^{j=2}	
O(k)–Cu(i)–O(i11)	87.5(4) ^{k=4}	89.8(6) ^{k=1}	88.3(4) ^{k=2}	84.5(5) ^{k=3}	
Cu(i)–N(i1)–C(i1)	117.3(12)	113.4(10)	117.3(12)	117.6(9)	
N(i1)–C(i1)–C(i2)	110.7(18)	111.5(17)	113.7(17)	112.0(13)	
C(i1)–C(i2)–C(i3)	111.1(13)	110.0(20)	113.0(12)	114.2(17)	
C(i2)–C(i3)–N(i2)	110.6(13)	111.2(14)	111.2(11)	109.8(13)	
C(i3)–N(i2)–Cu(i)	119.8(12)	120.3(9)	120.7(12)	122.6(8)	
Cu(i)–N(i2)–C(i4)	107.3(8)	107.9(10)	105.8(8)	108.2(9)	
C(i3)–N(i2)–C(i4)	111.9(12)	109.8(11)	111.1(11)	109.4(11)	
N(i2)–C(i4)–C(i5)	108.6(13)	106.8(11)	108.2(14)	106.8(11)	
C(i4)–C(i5)–O(i)	108.8(16)	106.6(9)	107.6(17)	105.8(10)	
C(i5)–O(i)–Cu(i)	110.3(9)	110.9(9)	111.0(9)	110.5(9)	
C(i5)–O(i)–Cu(j)	124.5(11) ^{j=3}	121.8(7) ^{j=3}	123.8(10) ^{j=4}	120.0(7) ^{j=1}	
C(i5)–O(i)–Cu(k)	122.9(7) ^{k=3}	120.7(9) ^{k=4}	122.2(6) ^{k=1}	126.1(10) ^{k=2}	
Cu(i)–O(i11)–N(i11)	121(2)	151(6) ^a	134(1)	139(1)	
O(i11)–N(i11)–O(i12)	120(2)	84(9) ^a	113(1)	121(1)	116(3)
O(i11)–N(i11)–O(i13)	119(3)	160(10) ^a	130(2)	118(2)	120(3)
O(i12)–N(i11)–O(i13)	120(2)	87(9) ^a	116(1)	121(1)	123(3)
O(212)···O(6)···O(511)	97(1)				
O(511)···O(7)···O(511) ^b	99(–)				

^a Disordered. ^b Equivalent position $\bar{x}, y, 1/2 - z$.

tetrameric $\{2-[(3\text{-aminopropyl})\text{amino}]\text{ethanolato}\}\text{copper(II) chloride monohydrate}$.³ The bond lengths (Table 5) in both amine rings are typical single bond values, and the (3-aminopropyl)amino ring has chair conformation. Both the bond length and angles (Table 6) are in agreement with those of (3-aminopropyl)amines reported earlier.¹⁴ The mean value of the bond angles around the oxygen atom is 109° . This corresponds to sp^3 hybridization. The coordination is rather distorted, however.

The bond lengths and angles for NO_3 groups are shown in Tables 5 and 6. These values are normal except those for the disordered $\text{NO}_3(2)$. Three types of NO_3 groups can be distinguished. $\text{NO}_3(2)$ and $\text{NO}_3(4)$ are located in special positions $(0, -0.3166, 1/4)$ and

$(1/4, -1/4, 0)$, having the $\text{Cu}(i) - \text{O}(i11)$ distance 2.65 \AA (mean value). These NO_3 groups form bridges between tetrameric $[\text{Cu}_4(\text{C}_5\text{H}_{13}\text{N}_2\text{O})_4]^{4+}$ units in the direction $\vec{a} - \vec{c}$. $\text{NO}_3(1)$ and $\text{NO}_3(3)$ are semicoordinated to copper(II) ions, having the mean value $\text{Cu}(i) - \text{O}(i11)$ distance 2.73 \AA . There is a possible hydrogen bond from the atom $\text{O}(312)$ to the lattice water molecule $\text{O}(8)$ [$\text{O}(312) \cdots \text{O}(8)$ 2.49 \AA]. $\text{NO}_3(5)$ is probably joined to the structure through hydrogen bonds. Oxygen atom $\text{O}(6)$ is at a distance 2.67 \AA from oxygen atom $\text{O}(511)$ and at a distance 2.92 \AA from oxygen atom $\text{O}(212)$, and the angle $\text{O}(511) \cdots \text{O}(6) \cdots \text{O}(212)$ is 97° . Thus water (6) joins together $\text{NO}_3(2)$ and $\text{NO}_3(5)$ groups. Oxygen atom $\text{O}(7)$ is located on the *two*-fold axis. The interatomic

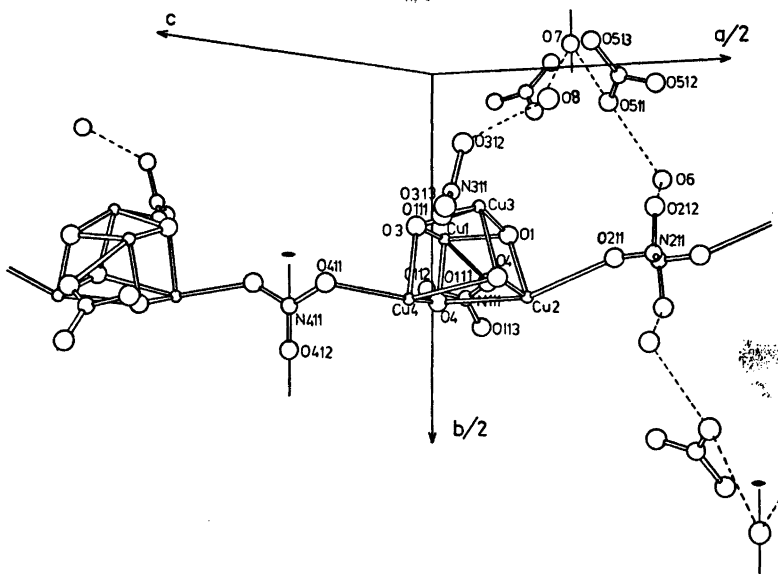


Fig. 2. Perspective view of the chain.

O(7)···O(511) distances are 2.86 Å and the angle O(511)···O(7)···O(511)' is 99°, which values probably indicate hydrogen bonds. The bridges formed by water molecules and nitrate ions join {[Cu₄(C₅H₁₃N₂O)₄](NO₃)₄}_n⁺ chains together in the direction $\vec{a} + \vec{c}$. A view of the chain is shown in Fig. 2 (the amine rings are omitted for clarity).

Acknowledgement. The financial support of the E. J. Sariola Foundation is gratefully acknowledged.

REFERENCES

1. Näsänen, R., Luukkonen, E., Kalmi, H. and Nieminen, K. *Suom. Kemistil. B* 44 (1971) 327.
2. Nieminen, K. and Pajunen, S. *Suom. Kemistil. B* 45 (1972) 391.
3. Pajunen, A. and Nieminen, K. *Finn. Chem. Lett.* (1975) 67.
4. Ishimura, Y., Nonaka, Y., Nishida, Y. and Kida, S. *Bull. Chem. Soc. Jpn.* 46 (1973) 3728.
5. Cromer, D. and Mann, J. *Acta Crystallogr. A* 24 (1968) 321.
6. *International Tables for X-Ray Crystallography*, Kynoch Press, Birmingham 1962, Vol. 3, Table 3.3.2C.
7. Stewart, J. M., Ed., *The X-Ray System, Version of June 1972*, Technical Report

TR-192, Computer Science Center, University of Maryland 1972, College Park 1972.

8. Kantola, P. and Nieminen, K. *Unpublished results.*
9. Bertland, J. and Kelley, J. *Inorg. Chim. Acta* 4 (1970) 203.
10. Haase, W. *Chem. Ber.* 106 (1973) 3132.
11. Dixon Estes, E. and Hodgson, D. *Inorg. Chem.* 14 (1975) 334.
12. von Mergehenn, R., Haase, W. and Allmann, R. *Acta Crystallogr. B* 31 (1975) 1847.
13. Pauling, L. *The Nature of the Chemical Bond*, 3rd. Ed., Cornell University Press, Ithaca 1960, p. 160.
14. Orama, O. *Ann. Acad. Sci. Fenn. Ser. A II* 180 (1976), and references cited therein concerning (3-aminopropyl)amines.

Received March 24, 1977.

Short Communications

Nuclear Magnetic Resonance Studies on Aromatic Compounds. Part II. ^{13}C and ^1H NMR Spectra of 1-Hydroxy-4-sulfo-2-naphthoic AcidLAURI H. LAJUNEN ^a and
KAUKO RÄISÄNEN ^b^a Department of Chemistry and ^b Department of Physics, University of Oulu, SF-90100 Oulu 10, Finland

The ^{13}C NMR spectra of the following aromatic monosulfo-substituted *o*-hydroxy carboxylic acids have been reported in part I of this series:¹ 3-hydroxy-4-sulfo-2-naphthoic (342HSN), 3-hydroxy-5-sulfo-2-naphthoic (352HSN), 3-hydroxy-7-sulfo-2-naphthoic (372HSN), and 5-sulfosalicylic (5SSA) acid. A pure monomeric ^{13}C NMR spectrum could be recorded for all carboxylic acids studied except 352HSN, which was found to be partly in dimeric form in concentrated D_2O solutions. We have now completed our investigations of this type of *o*-hydroxy carboxylic acids, and report here our findings for 1-hydroxy-4-sulfo-2-naphthoic acid (142HSN). The ^1H NMR spectrum of this compound is recorded in order to verify the analysis of the ^{13}C spectrum.

Experimental. 1-Hydroxy-4-sulfo-2-naphthoic acid was prepared by sulfonation of 1-hydroxy-2-naphthoic acid with an ice-cold mixture consisting of two parts of 20% fuming H_2SO_4 and three parts of conc. H_2SO_4 , followed by

heating to 60 °C.² The acid was converted to its monosodium salt with NaCl and the product was recrystallized several times from hot water.

Apparatus and methods. The ^{13}C and ^1H NMR spectra of 142HSN were determined on a concentrated solution (10 mg/ml) with a Jeol JNM-FX100 FT-spectrometer operating in DQD mode and at 25.06 MHz. The ^{13}C NMR spectrum was recorded with proton noise-decoupling to assess chemical shifts, and without proton noise-decoupling to assess coupling constants. In both cases the recording parameters were: spectral width 5 kHz with 16k memory points; pulse width, 10 μs ; number of pulses accumulated, about 4000. Both the normal and decoupled ^1H NMR spectra were recorded in DQD mode and at 99.6 MHz. The recording parameters were: spectral width 1 kHz for recording the whole spectrum and 200 Hz with 16k memory points for the aromatic range of the spectrum; pulse width, 12 μs ; number of pulses accumulated in the normal ^1H NMR spectrum, about 30.

The protons H-5, H-6, H-7, and H-8 of the present compound form an ABCD system. With this system as a basis, the theoretical spectrum was calculated with the program LAOCN3³ on a Univac 1108 computer. The theoretical line shapes were calculated with the program PLOTTI (a program made in this laboratory), which is based on the Lorentzian shape function. The proton H-3 was neglected in the theoretical calculations because the couplings from this proton to the other protons are smaller than the half-widths of the lines in the spectrum. All the measurements were carried out in D_2O

Table 1. ^{13}C Chemical shifts of 142HSN relative to the external standard TMS at 298 K, and one- and three-bond carbon—proton couplings ($^1J_{\text{CH}}$ and $^3J_{\text{CH}}$). The chemical shifts of naphthalene are included in the table for comparison.⁶ The coupling constants are absolute values.

Compound	Chemical shifts (ppm)										
	C-1	C-2	C-3	C-4	C-5	C-6	C-7	C-8	C-9	C-10	C-11
Naphthalene	128.10	125.95	125.95	128.10	128.10	125.95	125.95	128.10	133.70	133.70	—
142HSN	163.45	105.40	127.10	132.60	127.60	124.90	126.10	131.80	125.80	131.80	173.65

$^1J_{\text{C}_8\text{H}} = 166.6$ Hz, $^1J_{\text{C}_6\text{H}} = 164.8$ Hz, $^1J_{\text{C}_6\text{H}} = 166.3$ Hz, $^1J_{\text{C}_7\text{H}} = 166.0$ Hz, $^1J_{\text{C}_8\text{H}} = 164.2$ Hz, $^3J_{\text{C}_1-\text{sH}} = ^3J_{\text{C}_9-\text{tH}} = ^3J_{\text{C}_1-\text{sH}} = 7.9$ Hz, $^3J_{\text{C}_1-\text{sH}} = 9.1$ Hz, $^3J_{\text{C}_5-\text{rH}} = ^3J_{\text{C}_7-\text{sH}} = 9.2$ Hz, $^3J_{\text{C}_6-\text{sH}} = ^3J_{\text{C}_8-\text{sH}} = 8.0$ Hz, $^3J_{\text{C}_9-\text{sH}} = ^3J_{\text{C}_9-\text{rH}} = ^3J_{\text{C}_{10}-\text{sH}} = ^3J_{\text{C}_{10}-\text{sH}} = 6.7$ Hz.

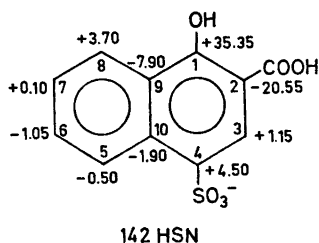


Fig. 1. The differences between the chemical shifts (in ppm) for the ^{13}C nuclei of 142HSN relative to naphthalene.

solution at 298 K, and TMS was used as an external standard for the chemical shifts. No corrections of the chemical shifts were made.

Results and discussion. The chemical shifts of the ^{13}C nuclei of 142HSN and naphthalene are given in Table 1. The changes of the chemical shifts of the corresponding carbon atoms of 142HSN do not differ significantly from those observed for the related compounds of our earlier study (Fig. 1).¹ The difference between

the chemical shift of 142HSN and that of naphthalene for the carbon C-8 is positive, whereas the corresponding difference for all the other derivatives of 1-naphthol studied in this series is negative.^{4,5} The difference between the chemical shifts for the carbon C-4 is also opposite in sign (being 4.50 ppm) to the differences for the 1-naphthol derivatives.^{4,5}

The one-bond carbon-proton couplings of 142HSN (Table 1) are between 164.2 and 166.6 Hz, and the three-bond couplings of the carbons C-1, C-3, C-4, C-5, C-6, C-7, and C-8 to the hydrogen nuclei between 8 and 9 Hz. The three-bond couplings of the bridge-end ^{13}C nuclei are about 6.7 Hz.

The recorded and calculated ^1H spectra of 142HSN are presented in Fig. 2 and the observed chemical shifts and couplings in Table 2. It is especially notable that the proton H-8 appears at lower field than the proton H-5. The positions of the corresponding ^{13}C nuclei are quite similar with respect to one another and the changes in the chemical shifts of the protons at C-6 and C-7 are similar in sign to those of the carbons C-6 and C-7, respectively.

The long-range proton couplings J_{35} must be smaller than 0.3 Hz, because the half-width

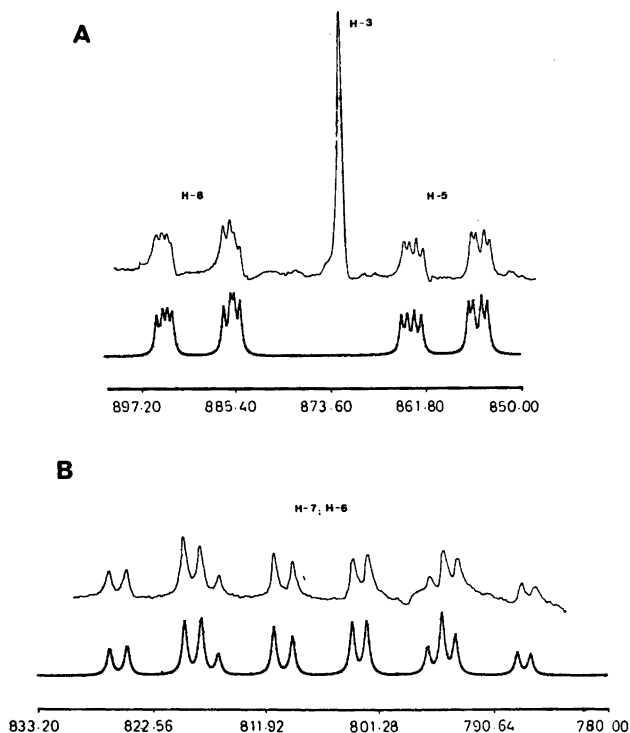


Fig. 2. The recorded ^1H spectrum (above) and calculated ^1H spectrum (below) of 142HSN. In A the protons H-5 and H-8, and in B the protons H-6 and H-7. The chemical shifts are presented in a Hz-scale relative to TMS.

Table 2. The chemical shifts (Hz) relative to the external standard TMS at 298 K and the proton-proton couplings of 142HSN derived by iteration from the 100 MHz ^1H spectrum. The coupling constants are absolute values.

H-3	H-5	H-6	H-7	H-8
872.3	859.6	795.4	817.9	890.3

$J_{56} = 8.5$ Hz, $J_{57} = 1.3$ Hz, $J_{58} = 0.7$ Hz,
 $J_{67} = 8.4$ Hz, $J_{68} = 1.7$ Hz, $J_{78} = 8.2$ Hz.

of the lines in the recorded ^1H spectrum of 142HSN is about 0.3 Hz. The rest of the proton-proton couplings are of about the same size as in other aromatic compounds.⁷

1. Räsänen, K. and Lajunen, L. H. J. *Org. Magn. Reson. In press.* Part I.
2. König, K. *Ber. Dtsch. Chem. Ges.* 22 (1889) 787.
3. Castellano, S. and Bothner-By, A. A. *J. Chem. Phys.* 41 (1964) 3863.
4. Räsänen, K. and Lajunen, L. H. J. *Z. Naturforsch. Teil B* 32 (1977) 818. Part IV.
5. Lajunen, L. H. J. and Räsänen, K. *To be published.* Part V.
6. Alger, T. D., Grant, D. M. and Paul, E. G. *J. Am. Chem. Soc.* 88 (1966) 5397.
7. Levy, G. C. *Top. Carbon-13 NMR Spectrosc.* 1 (1975) 54.

Received June 30, 1977.

Electrical Conductivities of Polyazophenylene Based Amorphous Carbon

BARBRO LÖFGREN,^a JORMA RAUTAVUORI^b
and PERTTI TÖRMÄLÄ^b

^a Department of Wood and Polymer Chemistry, University of Helsinki, Malminkatu 20, SF-00100 Helsinki 10, Finland and ^b Institute of Materials Science, Tampere University of Technology, SF-33101 Tampere 10, Finland

It has been known for many years that certain thermosetting polymers pyrolyze to form disordered nongraphitizing carbons with glass-like properties. However, because of the large volume of gaseous decomposition products which were evolved during the reaction, these carbons were generally quite porous. About fifteen years ago it was found that carbon with very low gas permeability, glass-like isotropic properties, high temperature stability, and chemical inertness can be achieved by slow carbonization of the precursor polymer under carefully controlled conditions in the solid state.¹⁻⁵ Amorphous and ordered carbons (*e.g.* carbon fibers) are bringing about a revolution in the field of materials and composites because of their unique chemical, thermal or mechanical properties.⁶

In an earlier study we found that polyazophenylenes can be pyrolyzed to amorphous carbon by heating to 1000 °C in an inert atmosphere.⁷ Polyazophenylenes are semiconducting polymers.⁸ Therefore we have studied the effect of carbonization on the conductivity of these polymers.

Experimental. The studied polymers, poly(2,4-diaminotoluene), I, ($M_n = 62\,800$) and poly(2,5-diaminotoluene), II, ($M_n = 36\,800$) were prepared by oxidative coupling.⁹ The molecular weights were determined by titration of the residual amine groups with perchloric acid in glacial acetic acid. The polymers were thermally stable up to 400 °C, measured by DSC (Differential Scanning Calorimetry).

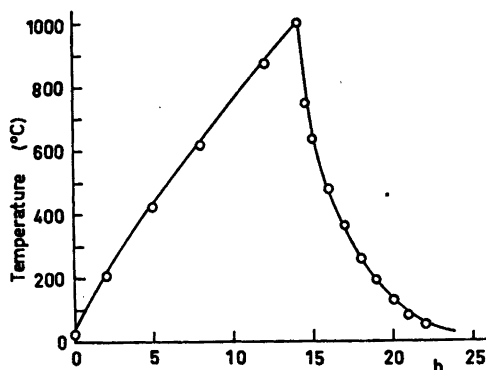
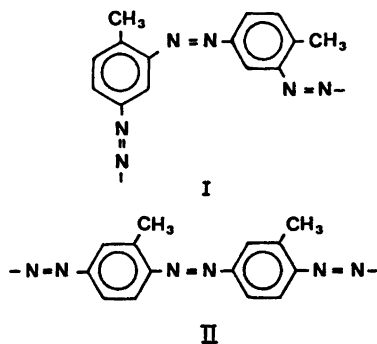


Fig. 1. The heat-treatment diagram.

The polymers were powdered and examined as molded pellets. Pellets (13 mm diameter and 1–2 mm thick) were molded at pressures up to 30 MPa. The pellets were carbonized in a tube furnace by heating to 1000 °C in nitrogen atmosphere. The heat treatment diagram is given in Fig. 1. The yield of carbon was $56 \pm 0.1\%$ in each case.

The pellets were equipped with silver paint electrodes for conductivity measurements. The conductivity measurements were performed in vacuum using an electrometer, and the conductivity was studied as a function of temperature.

X-Ray diagrams were taken of carbon samples to detect any traces of graphite. The

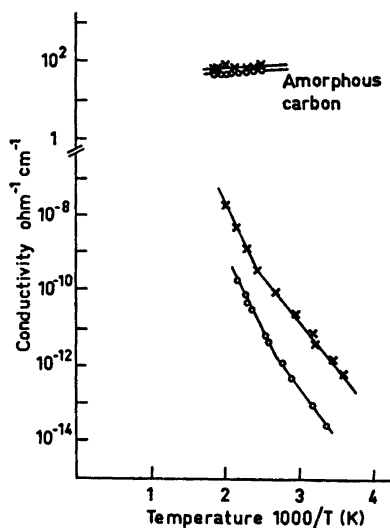


Fig. 2. Conductivity as a function of temperature. \times , poly(2,4-diaminotoluene); \circ , poly(2,5-diaminotoluene).

reflections of graphite were totally absent. Therefore it was concluded that the samples were amorphous by nature.

Results and discussion. The conductivity σ as a function of temperature is shown in Fig. 2 for polyazophenylenes⁸ and corresponding amorphous carbon. Fig. 2 shows that the heat-treatment of polyazophenylenes significantly enhanced the electrical conductivity, and also changed the conductivity behaviour. Before the heat-treatment the conductivity increased with increasing test temperature as for conventional semiconductors. The conduction mechanism in polyazophenylenes have been described^{8,10} in terms of a thermally activated rotational movement of polymer molecules or parts of polymer molecules and a non-activated tunnelling process, according to the theory originally presented by Gutmann.¹¹

The electrical conductivity of polyazophenylenes after being heat-treated at 1000 °C shows a similar behaviour to that of graphite,¹² as the conductivity decreases with increasing test temperature, indicating that the scattering process mainly is thermal. In the resistivity map,¹³ shown in Fig. 3, the electrical resistivity of amorphous carbon is compared with the resistivity of various types of graphite in direction parallel to layer planes on grain. That the amorphous carbon has a resistivity several orders of magnitude higher than the various types of graphite is due to the turbostratic structure of amorphous carbon.

It is known that the turbostratic structure of phenolic resin carbon consists of small graphite-like lamellae (diameter 15–50 Å) which are strongly disturbed by structural de-

fects (such as vacancies, dislocations, kinks and jogs). These lamellae are strongly twisted and distorted in relation to each other.⁸ Fig. 3 indicates that the degree of order and the resistivity of carbon are inversely proportional to each others. Because the resistivities of poly-(diaminotoluene) carbons are somewhat higher than the resistivity of phenolic resin carbon it can be concluded that poly(diaminotoluene) carbons have a still more distorted structure than phenolic resin carbons.

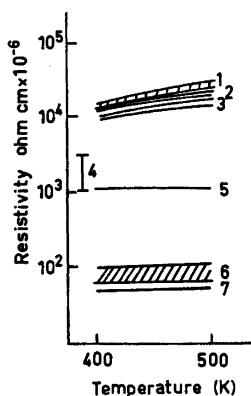


Fig. 3. Resistivity of polyazophenylenes based amorphous carbon, phenolic resin carbon,⁷ and various types of graphite. 1, poly(2,4-diaminotoluene) carbon; 2, poly(2,5-diaminotoluene) carbon; 3, phenolic resin carbon; 4, amorphous carbon; 5, manufactured graphite; 6, pyrolytic filaments annealed to 3000–3200 °C; 7, single crystal graphite.

1. Davidson, H. W. *Brit. Pat.* 860 342 (1961).
2. Yamada, S. and Sato, M. *Nature* 193 (1962) 261.
3. Fitzer, E., Schäfer, W. and Yamada, S. *Carbon* 7 (1969) 643.
4. Fitzer, E. and Schäfer, W. *Carbon* 8 (1970) 353.
5. Fitzer, E., Müller, K. and Schäfer, W. In Walker, P. L., Ed., *Chemistry and Physics of Carbon*, Dekker, New York 1971, p. 237.
6. McKee, D. W. *Annu. Rev. Mater. Sci.* 3 (1973) 195.
7. Rautavuori, J. and Törmälä, P. *Unpublished results*.
8. Heleskivi, J. and Löfgren, B. *J. Polym. Sci. Part A-2* 10 (1972) 747.
9. Sandholm (Löfgren), B., Selin, J.-F. and Lindberg, J. *J. Suom. Kemistil. B* 42 (1969) 421.
10. Löfgren, B., Sipilä, R. and Heleskivi, J. *J. Polym. Sci. Polymer Phys. Ed.* 12 (1974) 1547.
11. Gutman, F. *Jpn. J. Appl. Phys.* 8 (1969) 1417.
12. Spain, I. L. In Walker, P. L., Ed., *Chemistry and Physics of Carbon*, Dekker, New York 1971, p. 1.
13. Lozier, W. W. and Manofsky, M. B. In Kriegel, W. W. and Palmour, H., Eds., *Mechanical Properties of Engineering Ceramics*, Interscience, New York 1961, p. 451.

Received April 27, 1977.

Metal Complexes with Mixed Ligands. II. The Formation of Ternary Mononuclear and Polynuclear Mercury(II) Complexes in the System $\text{Hg}^{2+}-\text{Cl}^{-}-\text{OH}^{-}$. A Potentiometric Study in 3.0 M (Na)ClO₄, Cl Media

STAFFAN SJÖBERG

Department of Inorganic Chemistry, University of Umeå, S-901 87 Umeå, Sweden

The hydrolytic equilibria of the different $\text{HgCl}_n^{(2-n)}$ species, $n=0, 1, 2, 3$ and 4, have been investigated within the range $-9 \leq \log [\text{H}^+] \leq -1$. The measurements have been performed as potentiometric (glass electrode) titrations in 3.0 M (Na)ClO₄, Cl media at 25 °C. The measurements can be divided into series in which the ratio total chloride concentration/total mercury(II) concentration has been kept constant at values 0, 1/3, 1/2, 2/3, 1, 2. In two series the chloride excess over the HgCl_2 level was kept at 0.1 and 3.0 M, respectively. Data have been analysed using the least squares program LETAGROPVRID. Besides pure binary hydrolytic species, HgOH^+ , $\text{Hg}(\text{OH})_2$ and $\text{Hg}_2(\text{OH})_2^{3+}$ and unhydrolyzed mercury(II)-chloride complexes, $\text{HgCl}_n^{(2-n)+}$, $n=1, 2, 3$ and 4, all data could be explained with the ternary complexes HgOHCl , $\text{Hg}_2\text{OHCl}_2^+$ and $\text{Hg}_3(\text{OH})_2\text{Cl}^{3+}$.

In a series of investigations in progress in this department, aqueous equilibria and complex formation in metal ion systems, containing three or four reacting components, are under extensive investigations. Our main interest is focused on the formation of ternary complexes and particularly towards those containing OH^{-} . The systems under study are: $\text{M}-\text{OH}^{-}-\text{L}$, $\text{M}-\text{OH}^{-}-\text{Cl}^{-}$ and $\text{M}-\text{OH}^{-}-\text{L}-\text{Cl}^{-}$, where M stands for the metal ions Ni^{2+} , Cu^{2+} , Zn^{2+} , Hg^{2+} and L for imidazole, $\text{C}_3\text{H}_4\text{N}_2$.

The aim of the present paper is to give and discuss the results obtained in the three components system $\text{Hg}^{2+}-\text{OH}^{-}-\text{Cl}^{-}$.

PREVIOUS STUDIES

The system $\text{Hg}^{2+}-\text{OH}^{-}$. The hydrolytic equilibria in Hg^{2+} -solutions have been extensively investigated by means of a great number of methods.¹⁻⁹ In 1952 Hietanen and Sillén² made accurate emf-measurements using glass and redox electrodes in 0.5 M (Na)ClO₄ medium. With the total mercury(II) concentration, B , ranging from 0.001 to 0.015 M, they found the hydrolytic species to be HgOH^+ and $\text{Hg}(\text{OH})_2$ with $\log K_a(\text{Hg}^{2+}) = -3.70$ and $\log K_a(\text{HgOH}^+) = -2.60$. In order to find out whether polynuclear complexes exist in hydrolyzed Hg^{2+} -solutions, Ahlberg³ (1962) extended the measurements to more concentrated solutions ($0.0025 \leq B \leq 1.3$ M). As ionic medium she used 3 M (Na) ClO₄, 3 M (Mg)ClO₄ and 3 M (Ca)ClO₄. Ahlberg concluded that in addition to the previously found mononuclear complexes HgOH^+ and $\text{Hg}(\text{OH})_2$, polynuclear complexes also exist. At B -values 0.1, 0.5 and 1.0 M and within the $-\log h$ range 0.3–2.0 the complexes $\text{Hg}_2\text{OH}^{3+}$, $\text{Hg}_2(\text{OH})_2^{2+}$ and $\text{Hg}_4(\text{OH})_3^{5+}$ were found.

X-Ray scattering measurements on hydrolyzed mercury(II) perchlorate solution have been performed by Johansson.⁴ It was concluded that polynuclear complexes are formed, and besides binuclear, trinuclear rather than tetranuclear complexes were proposed. By comparing the result of the solution X-ray measurements with the crystal structure of the solid pha-

ses $\text{Hg}_5\text{O}_2(\text{OH})_2(\text{ClO}_4)_4(\text{H}_2\text{O})_x$ (triclinic),¹⁰ $\text{Hg}_2\text{O}_4(\text{OH})_2(\text{ClO}_4)_4$ (orthorhombic)¹¹ and $\text{Hg}_2\text{O}(\text{OH})\text{ClO}_4$ (monoclinic),¹⁶ Johansson could also derive possible structures for some hydrolysis complexes of mercury(II) in solution.

The system $\text{Hg}^{2+} - \text{Cl}^-$. It is well-known that Hg^{2+} forms a series of mononuclear complexes $\text{HgCl}_n^{(2-n)+}$, with $n = 1, 2, 3$ and 4 ,¹ (see Table 1) and these equilibria have been investigated in water solutions using potentiometric, calorimetric, solubility and extraction methods.

The formation of polynuclear $\text{Hg}^{2+} - \text{Cl}^-$ complexes was claimed by Linhart¹⁵ in 1915. He concluded, by measuring the distribution of HgCl_2 between a water and benzene phase, that the species Hg_2Cl_4 , Hg_2Cl_5^- and $\text{Hg}_2\text{Cl}_6^{2-}$ were formed. However, in solutions with the HgCl_2 concentration less than 0.2 M, Ciavatta¹⁶ found no evidence for the formation of polynuclear complexes. Recently Sandström¹⁷ has shown that in concentrated solutions ($B \geq 0.5$ M) with a Cl/Hg mol ratio around three, polynuclear complexes occur. His X-ray diffraction as well as Raman data were explained by assuming the dominating complex to be tri- and tetranuclear with double chlorine bridges between the mercury atoms.

The system $\text{Hg}^{2+} - \text{Cl}^- - \text{OH}^-$. Studies of the hydrolytic equilibria of the $\text{HgCl}_n^{(2-n)+}$ -species seem to have been restricted to the HgCl_2 -complex.¹⁸⁻²¹ Recent careful work in Ciavattas¹⁶ laboratory on the hydrolysis of HgCl_2 in 1.0 M (Na)ClO₄ medium has shown that the hydrolytic species HgOHCl and $\text{Hg}(\text{OH})_2$ predominate in a concentration range 0.005–0.2 M in HgCl_2 . This equilibrium model was also reported by

Partridge *et al.*²² in 1965, valid at zero ionic strength. Hydrolytic equilibria in solutions containing HgCl^+ , HgCl_2^- and HgCl_4^{2-} do not seem to have been investigated.

The crystal structure of several mercury(II) oxide chlorides have been determined by the single crystal X-ray method.²²⁻²⁷ In these structures, mercury and oxygen usually form endless chains or networks of different geometries. In Hg_3OCl_4 , however,²⁴ trinuclear pyramidal ions $\text{OHg}_3\text{Cl}_3^+$ and chloride ions form the structure. Another trinuclear complex $\text{SO}_4 - \text{Hg} - \text{OH} - \text{Hg} - \text{OH} - \text{Hg} - \text{SO}_4$ (zigzag form) exists as isolated units in the compound $\text{Hg}(\text{OH})_2 \cdot 2\text{HgSO}_4$.²⁸ In $\text{HgO} \cdot \text{Hg}(\text{CN})_2$ ²⁹ dinuclear molecules $\text{Hg}_2\text{O}(\text{CN})_2$ are the building elements.

No investigation dealing with the structure of an $\text{Hg}_7(\text{OH})_6\text{Cl}_7$ complex in water solutions has yet been reported.

EXPERIMENTAL

Chemicals and analysis. Sodium chloride (Merck *p.a.*) was dried at 200 °C and used without further purification. Fresh chloride solutions were always used in the measurements to avoid the contamination by bacteria.

Sodium perchlorate, perchloric acid and sodium hydroxide were prepared and analyzed as described earlier.³⁰

Mercury(II) perchlorate was prepared by dissolving a weighed amount of HgO (Merck *p.a.*) in a known excess of standardized HClO_4 . It was checked that no opalescence appeared due to the formation of Hg_2Cl_2 upon adding an excess of Cl^- .

Mercury(II) chloride (Merck *p.a.*) was recrystallized from water and dried over H_2SO_4

Table 1. Previously published results $\log K_n$ ($\text{HgCl}_{n-1}^{(3-n)+} + \text{Cl}^- \rightleftharpoons \text{HgCl}_n^{(2-n)+}$) valid at 25 °C.

Method	Medium, M	$\log K_1$	$\log K_2$	$\log K_1K_2$	$\log K_3$	$\log K_4$	Ref.
red. Hg	0.5 (NaClO ₄)	6.74	6.48	13.22	0.85	1.00	12
dis	0.5 (NaClO ₄)	6.74	6.48	13.22	0.95	1.05	42, 12
sp	0.5 NaClO ₄				0.66	1.10	43
red. Hg	1.0 (NaClO ₄)	6.72	6.51	13.23	1.00	0.97	13
red. Hg	3.0 (Na)ClO ₄	7.07	6.91	13.98	0.75	1.38	14
		± 0.15	± 0.15		± 0.12	± 0.06	
cal	3.0 (Na)ClO ₄				1.08	1.09	14
					± 0.21	± 0.24	
gl	3.0 (Na)ClO ₄ , Cl	7.22	6.78	14.00	1.07	1.07	This work
		± 0.03	± 0.05		± 0.03	± 0.05	

in a vacuum desiccator. Small amounts (less than 0.1 %) of insoluble products, probably Hg_2Cl_2 , were filtered off before use. The mercury content was analyzed gravimetrically as HgS and was about 0.2 % less than that expected from the amount weighed. Solutions of known HgCl_2 concentration were prepared by dissolving the solid according to its formula weight.

Determination of H . The analytical H^+ -concentration, H , (calculated over the 0-level HgCl_2 , Cl^- and H_2O) must be known very accurately in order to obtain reliable results. Of course all test solutions have been prepared by mixing reagents with known H . As long as the quotient (total chloride concentration, Y)/(total mercury(II) concentration, B) ≥ 2 , the value of H could be controlled using Gran extrapolation method.³¹ At quotients $Y/B < 2$, the complex formation starts at $-1 > \log[\text{H}^+] > -3$ and no accurate determination of H can be made with this method. However, in separate experiments, NaCl was added to suppress the hydrolytic equilibria and H could be determined as above. All test solutions were analyzed and controlled in this way.

Apparatus. The thermostat, cell arrangement and experimental details of the emf measurements were fully described earlier.^{30,32} The electrodes used were of the type Beckman No. 40498 and Ingold NS201. In order to check their reliability, usually two electrodes were immersed in the equilibrium solution during the titration. If a drift in the difference between the measured emf values was found to exceed 0.2 mV, these experimental points were not included in the calculations. Emf values stable to within 0.01–0.02 mV were reached within 15–20 min.

Method. The measurements were carried out as a series of potentiometric titrations at 25 °C. The solutions were made to contain $[\text{ClO}_4^-] + X = 3.0 \text{ M}$, where X is the chloride excess over HgCl_2 . This medium will enable us to use and compare the results obtained in previous investigations concerning the chloride complex formation (Arnek¹⁴) and hydrolytic equilibria of Hg^{2+} (Ahlberg³). The solutions had the general composition $B \text{ M Hg}^{2+}$, $H \text{ M H}^+$, $Y \text{ M Cl}^-$, $([\text{ClO}_4^-] + Y - 2B - H) \text{ M Na}^+$ and 3.0 M ClO_4^- , ($X \leq 0$) or $(3.0 - X) \text{ M ClO}_4^-$ ($X \geq 0$). In general B and Y were kept constant in each of the titrations. These can be divided into series in which the ratios Y/B have been kept constant. The free hydrogen ion concentration, h , was varied by adding H^+ or OH^- and determined by measuring the emf of the cell $-\text{RE}|\text{equilibrium solution}|\text{glass electrode} + \text{The same reference half cell (RE)}$ as before was used.³¹ The emf in mV of this cell may be written

$$E = E_0 + 59.157 \log h + E_j \quad (1)$$

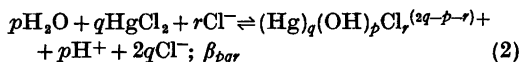
where $E_j = -16.7 \text{ h mV}^{33}$ has been used.

Acta Chem. Scand. A 31 (1977) No. 9

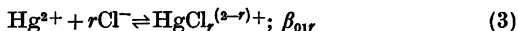
In the present investigation changes in E_0 were observed, especially when working with high B ($B \geq 0.04 \text{ M}$). Within the concentration range $B \leq 0.320 \text{ M}$, the change in E_0 was 12.0 mV M^{-1} at $[\text{H}^+] \sim 0.1 \text{ M}$. To find out whether this change is dependent on $[\text{H}^+]$, additional measurements were performed in which data in the form $E(B)_{[\text{H}^+]}$ were collected. The measurements were performed at $[\text{H}^+] = 0.4$ and 0.7 M respectively with B ranging from 0 to 1.0 M . In these measurements the change in E_0 due to B was 10.4 ± 0.1 and $10.5 \pm 0.1 \text{ mV M}^{-1}$, respectively; thus a slightly lower value compared with that obtained at $[\text{H}^+] = 0.1 \text{ M}$ was obtained. This may indicate that at this H^+ -level, complex formation occurs to some extent at high B , however, the effects expressed in mV are less than $\sim 0.2 \text{ mV}$ for the highest B -value (0.160 M) investigated.

The dependence of E_0 due to the total concentration of Cl^- and HgCl_2 was also investigated. Within the ranges $0 \leq X \leq 3.0 \text{ M}$ (with $[\text{ClO}_4^-] + X = 3.0 \text{ M}$) and $0 \leq [\text{HgCl}_2] \leq 0.100 \text{ M}$ the values found were $0 \pm 0.1 \text{ mV M}^{-1}$ and $-3.0 \pm 0.5 \text{ mV M}^{-1}$, respectively. Thus the concentration scale for H^+ does not seem to have changed although the amount of ClO_4^- ions has been completely changed to Cl^- ions.

We will assume the presence of 3-component equilibria of the general form

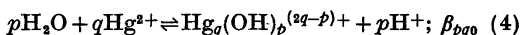


Besides the 3-component equilibria in (2) we have first to consider (i) the complex formation between Hg^{2+} and Cl^- according to



where $r = 1, 2, 3$ and 4 .

(ii) the hydrolysis of Hg^{2+}



with pq -combinations as determined in this

investigation: 1,1, 2,1 and 2,2 (see below).

Data treatment. The refinement of constants and the error calculations were performed with the least squares program LETAGROPVRID,³⁴ version ETITR.³⁵ On treating the emf data the error squares sums $U = \sum (Z_{\text{calc}} - Z)^2$, where $Z = h - H/B$, were minimized. The standard deviations are defined and calculated according to Sillén.³⁶ The computation was performed on a CD 3300 computer.

DATA, CALCULATIONS AND RESULTS

The evaluation of the different equilibria in the system $\text{Hg}^{2+} - \text{Cl}^- - \text{OH}^-$ will be much simplified if it can be divided into smaller

systems in which the number of equilibria is reduced. The different "subsystems" chosen in the present investigation were:

- (1) the hydrolysis of HgCl_2 at $X = 0$ M,
- (2) the hydrolysis of HgCl_4^{2-} at $X = 3.0$ M,
- (3) the hydrolytic equilibria in solutions containing mixtures of HgCl_2 , HgCl_3^- and HgCl_4^{2-} ,
- (4) the hydrolysis of Hg^{2+} at $Y = 0$ M,
- (5) the hydrolytic equilibria in solutions containing mixtures of Hg^{2+} , HgCl^+ and HgCl_2 , e.g. $0 < Y/B < 2$.

The results obtained will now be discussed in detail.

(1) *Hydrolysis of HgCl_2 in 3.0 M (Na)ClO₄.*

When dissolving HgCl_2 in an acid solution, where the hydrolysis is suppressed, HgCl_2 becomes the dominating mercury(II)-chloride complex, while less than 1 % of B is transformed to HgCl^+ , HgCl_3^- and HgCl_4^{2-} species (cf. Fig. 1).

Values of B ranging from 0.0025 to 0.100 M were investigated. Measurements with $B > 0.1$ M could not be realized due to the limited solubility of HgCl_2 in 3 M NaClO_4 medium. The available $\log h$ range was $-7 \lesssim \log h \lesssim -4$ giving $Z \lesssim 0.6$. As is seen in Fig. 2, where $Z(\log h)_B$ curves are plotted, B increases with decreasing $\log h$ at a given Z -value. This indicates that Cl^- is set free in the hydrolysis reactions. From the different Z -curves it was found that $(\Delta \log B / \Delta \log h)_Z = -1$ for $B < 0.01$ M.

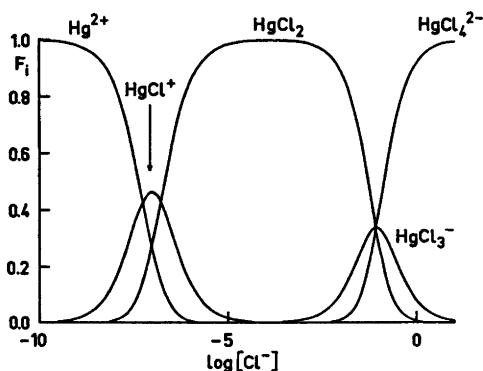


Fig. 1. Distribution diagram $F_i(\log[\text{Cl}^-])_B$. F_i is defined as the ratio between mercury(II) in a species and total mercury(II), B . The final proposed constants given in Table 5 have been used in the calculation.

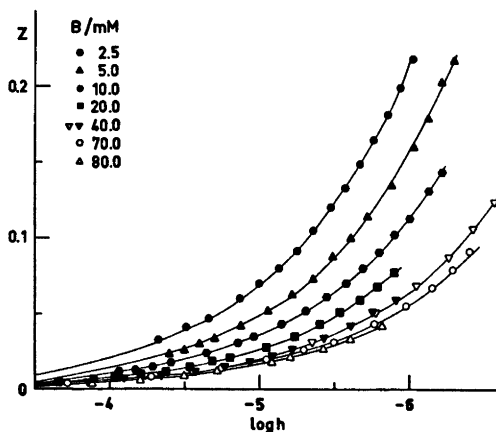
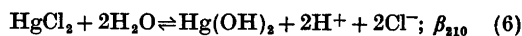
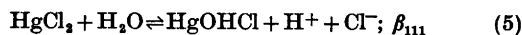


Fig. 2. A part of experimental data plotted as curves $Z(\log h)_B$ for $X = 0$ M. Open symbols are obtained in forward titrations (decreasing $\log h$) and filled in reverse titrations. The full curves have been calculated with the set of proposed constants in Table 5.

This indicates reactions of the type:



By assuming the concentrations of Hg^{2+} , HgCl^+ , HgCl_3^- , HgCl_4^{2-} and HgOH^+ to be negligible compared with the concentration of HgCl_2 , Z is given by

$$Z = \frac{([\text{HgOHCl}] + 2[\text{Hg}(\text{OH})_2])}{([\text{HgCl}_2] + [\text{HgOHCl}] + [\text{Hg}(\text{OH})_2])} = \frac{(\beta_{111}h^{-1}x^{-1} + 2\beta_{210}h^{-2}x^{-2})}{(1 + \beta_{111}h^{-1}x^{-1} + \beta_{210}h^{-2}x^{-2})} \quad (7)$$

i.e. Z is solely a function of h and x . As BZ is equal to the amount of Cl^- set free, x can now be calculated by using the relation

$$x = x_{Z=0} + BZ \quad (8)$$

The experimental $Z(\log h)_B$ -data were now recalculated in the form $Z(-\log h - \log x)_B$. Data with $B \leq 0.01$ M were plotted in this form (see Fig. 3) giving coinciding curves, indicating that the proposed equilibria in (5) and (6) predominate. These curves were superimposed on plots of normalized functions $Z(\log v)_B$, where

$$Z = \frac{(v + 2uv^2)}{(1 + v + uv^2)}$$

$$\log v = \log \beta_{111} - \log h - \log x; \log u = \log \beta_{210} - 2 \log \beta_{111}$$

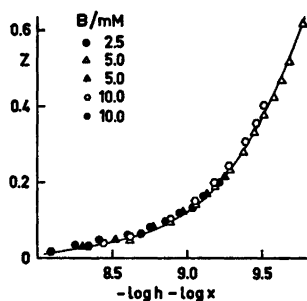


Fig. 3. Experimental data plotted as curves $Z(-\log h - \log x)_B$ for $X=0$ M and $B \leq 0.01$ M. The full curve has been calculated with the set of proposed constants in Table 5.

The best fit was obtained with $\log \beta_{111} = -9.90 \pm 0.05$ and $\log \beta_{210} = -20.20 \pm 0.10$. At $B > 0.01$ M ($\Delta \log B / \Delta \log h$) $_Z > -1$ and the different $Z(-\log h, -\log x)_B$ -curves no longer coincide, indicating that another complex(es) must be included in the equilibrium model. Assuming the potentiometrically determined equilibrium constants given by Arnek for the formation of HgCl_3^- and HgCl_4^{2-} to be correct, systematic deviations were found at high B . In order to determine whether ternary polynuclear complexes are present, a *pqr* analysis was performed. The best fit was obtained with the complex $\text{Hg}_3(\text{OH})_3\text{Cl}^{2+}$ giving $\sigma(Z) \times 1000 = 1.3$, but the complexes Hg_2OHCl_3 , $\text{Hg}_2(\text{OH})_2\text{Cl}^+$ and $\text{Hg}_3(\text{OH})_2\text{Cl}_3^+$ could explain data as well (all giving $\sigma(Z) \times 1000 = 1.4$). However, it was also found that a change in the equilibrium constant for HgCl_3^- by 0.3 logarithmic units ($\log \beta_{013} = 1.08 \pm 0.03$) gave a fit as good as with any polynuclear complex (see Table 2). This value is in good agreement with that reported by Arnek from his calorimetric measurements ($\log \beta_{013} = 1.08 \pm 0.21$).

Supplementary measurements were now performed with a slight excess Cl^- ($X=0.001-0.003$ M). Calculations, given in Table 2, show that at this level $\log \beta_{013} = 1.07 \pm 0.04$, while a change of about 0.2 log units was found in the equilibrium constant for the polynuclear complexes mentioned above. Thus it is reasonable to assume the "polynuclear effect" to be caused by a too small value in β_{013} . Measurement at $X=0.100$ M will also confirm this (see below).

Table 2. Results of graphical and LETAGROP calculations concerning the complexes formed and defined according to the equilibria: $p\text{H}_2\text{O} + q\text{HgCl}_2 + r\text{Cl}^- \rightleftharpoons \text{Hg}_p(\text{OH})_q\text{Cl}_r^{(2q-p-r)+} + p\text{H}^+ + 2q\text{Cl}^-$; β_{pqr} . The errors 3σ ($\log \beta_{pqr}$) are given (in parentheses) when the corresponding equilibrium constant has been varied.

No. of titr./ No. of points	Y/mM	HgOHCl $\log \beta_{111}$	Hg(OH) $_2$ $\log \beta_{210}$	HgCl $_3^-$ $\log \beta_{013}$	HgCl $_4^{2-}$ $\log \beta_{014}$	HgCl $^+$ $\log \beta_{011}$	Hg $^{2+}$ $\log \beta_{010}$	$\sigma(Z)$ $\times 1000$	Remarks
17/337	2B	-9.90(6)	-20.20(10)	-	-	-	-	1.9	graphical $X=0.001-0.003$ M $B \leq 10$ mM $B \leq 10$ mM $B \leq 10$ mM $B \leq 10$ mM graphical $B \leq 10$ mM Arnek (pot.) Arnek (cal.)
9/132	2B+X	-9.91(1)	-20.18(2)	1.08(3)	-	-	-	0.7	
7/118	2B+100	-9.94(2)	-20.19(3)	1.07(3)	-	-	-	1.7	
2/30	B/3	-9.90(1)	-20.22(2)	1.07(4)	2.14(4)	-6.83(9)	-14.01(4)	3.3	
3/66	B/2	-9.83(1)	-20.26(3)	1.07	2.14	-6.82(6)	-14.01(2)	4.5	
2/44	2B/3	-9.84(1)	-20.26(1)	1.07	2.14	-6.83(3)	-14.01(2)	2.5	
5/97	B	-9.94(3)	-20.22(2)	1.07	2.14	-6.78(2)	-13.99(2)	3.0	
	B/3-B	-9.84(1)	-20.27(2)	1.07	2.14	-6.91	-13.98	-	
	B/3-B	-9.90(5)	-20.23	1.07	2.14	-6.78(1)	-14.01(11)	4.6	
12/237	B/3-B	-9.86(1)	-20.24(1)	1.07	2.13(6)	-6.91(5)	-13.98(15)	-	
				1.08(21)	2.17(9)	-	-	-	

(2) *Hydrolysis of HgCl₄²⁻ in 3.0 M (Na)Cl.* Some measurements were performed with $X = 3.0$ M. At this chloride level HgCl₄²⁻ is the predominating Hg²⁺-Cl⁻ complex (cf. Fig. 1). For $B \leq 0.010$ M, Z reached a maximum value of ~ 0.1 , and the complex formation was suppressed to $\log h < -10.5$. It was found that these experimental data could not be explained by assuming HgOHCl to be the main hydrolytic species. The experimental difficulties at this high pH are great. Since reliable results cannot be obtained with the glass electrode, we find it unwise to try to explain the effects as caused by complex formation.

(3) *Hydrolysis of HgCl₂ + HgCl₃⁻ + HgCl₄²⁻ mixtures.* To attempt to evaluate the hydrolytic species formed from HgCl₃⁻ and HgCl₄²⁻, measurements were performed at a constant chloride level $X = 0.100$ M.

In the measurements, B ranged from 0.005 to 0.100 M, $-9 \leq \log h \leq -6$ giving $Z \lesssim 0.6$.

A calculation based upon the equilibrium model found at $X = 0 - 0.003$ M gave the result given in Table 2. $\log \beta_{013} = 1.07 \pm 0.04$ is a value in very good agreement with that found at $X = 0$ and $\log \beta_{014} = 2.14 \pm 0.04$ can be compared with Arneks 2.13 ± 0.06 (red. Hg) and 2.17 ± 0.09 (cal.). The constants $\log \beta_{111}$ and $\log \beta_{210}$ were found to be -9.90 ± 0.01 and -20.22 ± 0.02 , values in good agreement with those obtained at the lower chloride level. The complexes

HgCl₂OH⁻, HgCl₃OH²⁻, HgCl₂(OH)₂²⁻ and HgCl(OH)₂⁻ were also tested, but without any significant improvement.

We may thus conclude by summarizing that in solutions of HgCl₂, HgCl₃⁻ and HgCl₄²⁻, the predominating hydrolytic species within the $\log h$ range -4 to -9 , are HgOHCl and Hg(OH)₂.

(4) *Hydrolysis of Hg²⁺ in 3.0 M (Na)ClO₄.* Before investigating the hydrolysis reactions in solutions containing HgCl⁺, some titrations were performed in order to check the equilibrium model in hydrolyzed Hg²⁺-solutions, reported by Ahlberg.³

The concentration ranges studied were $0.005 \leq B \leq 0.160$ M, $-5 \leq \log h \leq -1$, with $Z \leq 2.00$. With $B \leq 0.010$ M experimental data could be explained with the complexes HgOH⁺ ($\log \beta_{110} = 3.58 \pm 0.02$) and Hg(OH)₂ ($\log \beta_{210} = 6.228 \pm 0.004$). These equilibrium constants are in good agreement with those reported by Ahlberg.

In the polynuclear range ($B > 0.01$ M) a pq -analysis showed that all experimental data could be explained by assuming Hg₂(OH)₂²⁺ to be the only polynuclear complex. A good fit was obtained with $\log \beta_{22} = -4.84 \pm 0.02$ giving $\sigma(Z) \times 1000 = 1.5$. Attempts were also made to add the complex Hg₂OH³⁺, which has been proposed by Ahlberg (see Table 3). However, a great uncertainty in β_{12} was always obtained

Table 3. Results of LETAGROP calculations concerning the complexes formed in hydrolyzed Hg²⁺-ClO₄⁻ solutions. The stability constants β_{pq} are defined according to $q\text{Hg}^{2+} + p\text{H}_2\text{O} \rightleftharpoons \text{Hg}_q(\text{OH})_p^{(2q-p)+} + p\text{H}^+$; β_{pq} Ranges 1 and 2 refer to data with $0.0025 \leq B \leq 0.010$ M and $0.010 \leq B \leq 0.160$ M, respectively. In some calculations E_0 for the glass electrode was covaried with one or two stability constants. ΔE_0 is defined as $E_0(\text{exp}) - E_0(\text{calc})$. In the lower half of the table some LETAGROP calculations have been made on $Z(\log h)_B$ -data (3.0 M (Na)ClO₄ medium) published by Ahlberg.³

Range	$\sigma(Z)$ $\times 1000$	$\log(\beta_{11} \pm 3\sigma)$	$\log(\beta_{21} \pm 3\sigma)$	$\log(\beta_{12} \pm 3\sigma)$	$\log(\beta_{22} \pm 3\sigma)q$	Rem.
1 (63 points)	4.9	-3.58(2)	-6.228(4)	-	-	
2 (92 points)	4.5	-3.58	-6.228	-2.60(5)	-	
	3.2	-3.58	-6.228	-2.51(5)	-	^a
	2.5	-3.58	-6.228	-	-4.81(2)	
	1.5	-3.58	-6.228	-	-4.84(2)	^b
	1.5	-3.58	-6.228	-3.38(31)	-4.89(7)	^c
$B = 0.1$ M	0.9	-3.55	-6.21	-2.66(8)	-5.41(4)	
	3.0	-3.55	-6.21	-	-4.88(9)	$\Delta E_0 = 0.15$ mV

^a $\Delta E_0 = 0.55, 1.29, 0.01, 0.04, 0.04, 0.98$ mV. ^b $\Delta E_0 = -0.15, -0.36, -0.04, -0.27, -0.18, -0.08$ mV. ^c $\Delta E_0 = -0.04, -0.10, -0.04, -0.23, -0.14, -0.09$ mV.

and the error squares sum was not significantly lowered. This seems to indicate that if $\text{Hg}_2\text{OH}^{3+}$ is formed, it exists only in small amounts (<1% of B), within the concentration range investigated.

As no primary $E(H)_B$ data were given by Ahlberg, it was difficult to test different assumptions concerning the complexes found. Calculations based upon her published $Z(\log h)_B$ data will always be affected by the fact that E_0 of the glass electrode was determined under the assumption that the complex $\text{Hg}_2\text{OH}^{3+}$ was formed with $\log \beta_{12} = -2.70$. As a consequence, Z as well as $\log h$, are to some extent dependent on the refined value in E_0 .

However, some calculations have been performed on her $Z(\log h)_B$ data with $B = 0.1$ M (see Table 3). As can be seen from this table, a calculation where $\text{Hg}_2(\text{OH})_2^{2+}$ was assumed to be the only polynuclear complex, gave $\log \beta_{22} = -4.88 \pm 0.09$ (cf. the value -4.84 ± 0.02 obtained in this work) with $\sigma(Z) \times 1000 = 3.0$ and a correction in E_0 of 0.15 mV. As a fairly good explanation is obtained and the result is in accordance with that obtained in the present investigation, we will, in the following calculations, assume $\text{Hg}_2(\text{OH})_2^{2+}$ to be the only polynuclear complex within the concentration ranges investigated.

(5) *Hydrolysis of $\text{Hg}^{2+} + \text{HgCl}^+ + \text{HgCl}_2$ mixtures.* For solutions, in which $Y/B < 2$, the amount of HgCl^+ at equilibrium is at most about 50% of B (see Fig. 1). This means that at these ratios the hydrolysis of Hg^{2+} and HgCl_2 must be accounted for as well.

The ratios $Y/B = 0.5$ and 1.0 were at first investigated. However, it was later found that to obtain a full understanding of the equilibrium situation at high B , the data range had to be extended to include $Y/B = 1/3$ and $2/3$ as well (see below).

The following concentration ranges were investigated: $0.0025 \leq B \leq 0.160$ M and $-8 \lesssim \log h \lesssim -1$, with $Z \lesssim 2 - Y/B$. With $B \leq 0.010$ M, the experimental $Z(\log h)_{Y/B}$ -curves were found to coincide up to $Z = 2 - Y/B$. Coinciding curves indicate a complex of composition HgOHCl , which can be shown as follows. Assuming that the concentration of HgCl_3^- , HgCl_4^{2-} and Cl^- may be neglected in the range studied, the following expression will hold taking Hg^{2+} , Cl^- , H_2O as 0-point.

$$Y/B = ([\text{HgCl}^+] + 2[\text{HgCl}_2] + [\text{HgOHCl}]) / ([\text{Hg}^{2+}] + [\text{HgOH}^+] + [\text{Hg}(\text{OH})_2] + [\text{HgCl}^+] + [\text{HgOHCl}] + [\text{HgCl}_2]) \quad (9)$$

$$Z = ([\text{HgOH}^+] + 2[\text{Hg}(\text{OH})_2] + [\text{HgOHCl}]) / ([\text{Hg}^{2+}] + [\text{HgOH}^+] + [\text{Hg}(\text{OH})_2] + [\text{HgCl}^+] + [\text{HgOHCl}] + [\text{HgCl}_2]) \quad (10)$$

Taking the expression for $[\text{HgCl}_2]$ from (9), and inserting in (10), we have after rearrangement:

$$Z = ([\text{HgOH}^+] + 2[\text{Hg}(\text{OH})_2] + [\text{HgOHCl}]) (2 - Y/B) / (2([\text{Hg}^{2+}] + [\text{HgOH}^+] + [\text{Hg}(\text{OH})_2] + [\text{HgCl}^+] + [\text{HgClOH}]) = (\beta_{110}h^{-1} + 2\beta_{210}h^{-2} + \beta_{111}h^{-1}x)(2 - Y/B) / (2(1 + \beta_{110}h^{-1} + \beta_{210}h^{-2}) + \beta_{011}x + \beta_{111}h^{-1}x) \quad (11)$$

Thus at high pH, Z will reach a limiting value $2 - Y/B$. Furthermore, Z is a function of h , x and Y/B . From (9) it can easily be shown that x is a function of h and Y/B , i.e. Z depends only on h and Y/B . (The derivation of eqn. (11) has earlier been given by Ahlberg and Leden in Ref. 41).

By assuming different values of β_{111} , taking β_{110} , β_{210} from $Y/B = 0$, β_{011} and β_{012} according to Arnek, one may calculate sets of Z -curves by means of the computer program HALTA-FALL,³⁷ or SOLGASWATER.⁴⁵ Curve fitting gave the results given in Table 2. In the LETAGROP calculations β_{011} and β_{012} as well as β_{111} and β_{210} were refined and the results are given in the same table.

As can be seen from Fig. 4, a narrow Z -range, $Z > 2 - Y/B$, is obtained at low B ($B \leq 0.005$ M).

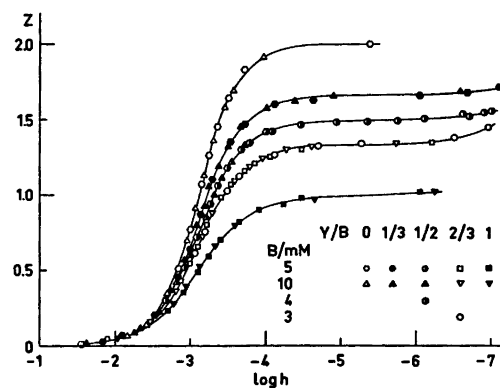


Fig. 4. Experimental data plotted as curves $Z(\log h)_B$ for quotients $Y/B = 0, 1/3, 1/2, 2/3$ and 1.

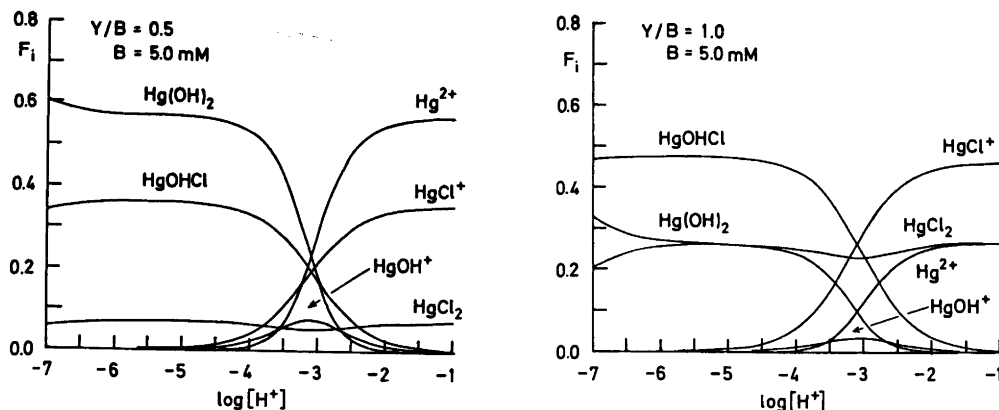


Fig. 5. Distribution diagrams $F_i(\log h)_B$ for $Y/B = 1/2$ (a) and 1 (b).

Within this range it was found that reproducible and reversible equilibria were obtained only in hydrolyzed solutions, which were allowed to stand for several weeks. Otherwise effects, probable due to slow precipitation reactions, were observed.

Distribution diagrams are given in Fig. 5.

With $B > 0.010 \text{ M}$ systematic deviations from the mononuclear curves were observed indicating the existence of polynuclear hydrolytic species. As the deviations could not be explained with the binary $\text{Hg}_2(\text{OH})_2^{2+}$ -complex, ternary polynuclear complexes $\text{Hg}_q(\text{OH})_p\text{Cl}_r$ must be formed. Experimental $Z(\log h)_{Y/B,B}$ -curves are given in Fig. 6, showing the onset of the complex formation to be at $\log h \sim -1$, which means that there is no suitable range available for calibration of the glass electrode. Instead E_0 was estimated from the most acidic points in the titrations ($\log h \lesssim -1$), and was then usually covaried with the tested equilibrium model in the LETAGROP-calculations.

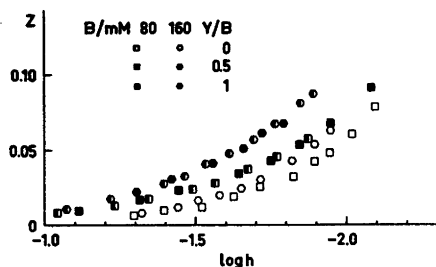


Fig. 6. A part of experimental data $Z(\log h)_B$ for quotients $Y/B = 0, 1/2$ and 1.

In the final equilibrium model, the difference E_0 (estimated) - E_0 (refined) never exceeded 0.2 mV.

With experimental data from ratios $Y/B = 0.5$ and 1.0 available, the search for the ternary polynuclear complexes was started with a pqr -

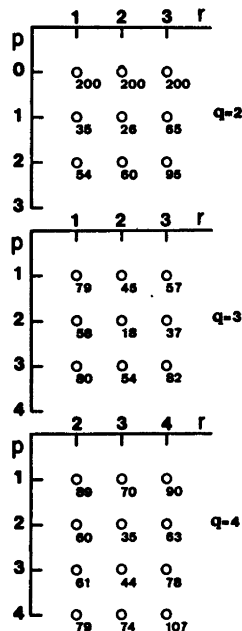


Fig. 7. Result of a pqr -analysis in the polynuclear range with $Y/B = 1/2$ and 1. Lowest error squares sums ($U_{\min} \times 10^{-4}$) are plotted as a function of various pqr -sets with $q = 1, 2$ and 3. p, q and r stand for the number of OH^- , Hg^{2+} and Cl^- in the complexes.

analysis. In this search, the formation constants refined in the LETAGROP calculations on data from the mononuclear range, were assumed to be correct and no attempts were made to refine them further. In this analysis different *pqr*-combinations were systematically tested, and the results are given in Fig. 7. The two "best" complexes found were $\text{Hg}_2(\text{OH})\text{Cl}_2^+$ with $\log \beta_{122} = -15.25 \pm 0.04$, $\sigma(Z) \times 1000 = 4.2$ and $\text{Hg}_3(\text{OH})_2\text{Cl}_2^{2+}$ with $\log \beta_{232} = -29.94 \pm 0.04$, $\sigma(Z) \times 1000 = 3.6$. However, after a closer look at the residuals $Z_{\text{calc}} - Z_{\text{exp}}$, systematic trends were found, indicating that another complex(es) must be taken into account. As in the *pqr*-analysis, tetranuclear species were not found to give as good improvement of data as binuclear and trinuclear ternary complexes, pairs of *pqr* triplets with $q = 2$ and 3 have been tested. As n species will yield $n(n-1)/2$ combinations, n had to be reduced to save computer time, and the following species were picked out from the *pqr*-analysis: $\text{Hg}_2(\text{OH})\text{Cl}^{2+}$, $\text{Hg}_2(\text{OH})\text{Cl}_2^+$, $\text{Hg}_2(\text{OH})_2\text{Cl}^+$, $\text{Hg}_2(\text{OH})_2\text{Cl}_2$, $\text{Hg}_2(\text{OH})_2\text{Cl}^{2+}$, $\text{Hg}_3(\text{OH})_2\text{Cl}_2^{2+}$ and $\text{Hg}_3(\text{OH})_2\text{Cl}_3^+$. The "best"

combinations out of the 21 that can be formed of these 7 species, are given in Table 4. Thus the "best" explanation is given by the combination $\text{Hg}_2(\text{OH})\text{Cl}_2^+$ and $\text{Hg}_3(\text{OH})_2\text{Cl}^{2+}$ ($U = 330$, $\sigma(Z) \times 1000 = 1.3$). Another combination with a somewhat higher error squares sum ($U = 490$, $\sigma(Z) \times 1000 = 1.6$) is found for the combination $\text{Hg}_2(\text{OH})\text{Cl}^{2+}$ and $\text{Hg}_3(\text{OH})_2\text{Cl}_3^+$. In these two combinations, the nuclearity and ratio OH/Hg are the same, and thus well established, while the difference is found in the Cl/Hg ratio. To obtain a more distinct answer to what combination is the "best", the ratios $Y/B = 1/3$ and $2/3$ were investigated in addition. By comparing the residuals given in Fig. 8, the combination $\text{Hg}_2(\text{OH})\text{Cl}_2^+ + \text{Hg}_3(\text{OH})_2\text{Cl}^{2+}$ shows no systematic trend within the experimental uncertainty and the fit is better at each ratio studied (especially at $Y/B = 1/3$) compared with the $\text{Hg}_2(\text{OH})\text{Cl}^{2+} + \text{Hg}_3(\text{OH})_2\text{Cl}_3^+$ -combination. Some measurements were performed at constant Z and B , where the ratio Y/B was varied between 0 and 2 in order to check whether additional effects are found in the range $1 \leq Y/B < 2$.

Table 4. Results of calculations for some different assumptions concerning the ternary polynuclear complexes formed at (a) $Y/B = 1/2$ and 1 (9 titrations 209 points) and (b) $Y/B = 1/3$, $1/2$, $2/3$ and 1 (17 titrations 359 points). In the calculations pairs of *pqr* triplets were tested and binary and ternary (mononuclear) constants given in Table 5 were not varied. The constants β_{pqr} are defined as in Table 2. In the calculations \bar{E}_0 has been refined together with the stability constants.

$U \times 10^{-3}$	$\sigma(Z) \times 1000$	Complex-combination	$\log(\beta_{pqr} \pm 3\sigma)$
(a)			
0.33	1.3	$\text{Hg}_2\text{Cl}_2\text{OH}^+$ $\text{Hg}_3\text{Cl}(\text{OH})_2^{3+}$	-15.26(2) -37.78(4)
0.49	1.6	$\text{Hg}_2\text{ClOH}^{2+}$ $\text{Hg}_3\text{Cl}_3(\text{OH})_2^+$	-22.55(3) -23.14(4)
1.23	2.5	$\text{Hg}_2\text{Cl}_3(\text{OH})_2^+$ $\text{Hg}_3\text{Cl}(\text{OH})_2^{3+}$	-22.94(4) -37.60(5)
1.95	3.1	$\text{Hg}_2\text{Cl}_3(\text{OH})_2^{2+}$ $\text{Hg}_2\text{Cl}_2(\text{OH})_2$	-30.05(5) -18.12(2)
2.07	3.1	$\text{Hg}_2\text{Cl}(\text{OH})_2^{3+}$ $\text{Hg}_3\text{Cl}_2\text{OH}^+$	-37.80(4) -15.29(4)
(b)			
0.61	1.3	$\text{Hg}_2\text{Cl}_2\text{OH}^+$ $\text{Hg}_2\text{Cl}(\text{OH})_2^{3+}$	-15.25(1) -37.79(2)
0.81	1.6	Hg_2ClOH^+ $\text{Hg}_3\text{Cl}_3(\text{OH})_2^{3+}$	-22.55(2) -23.15(3)

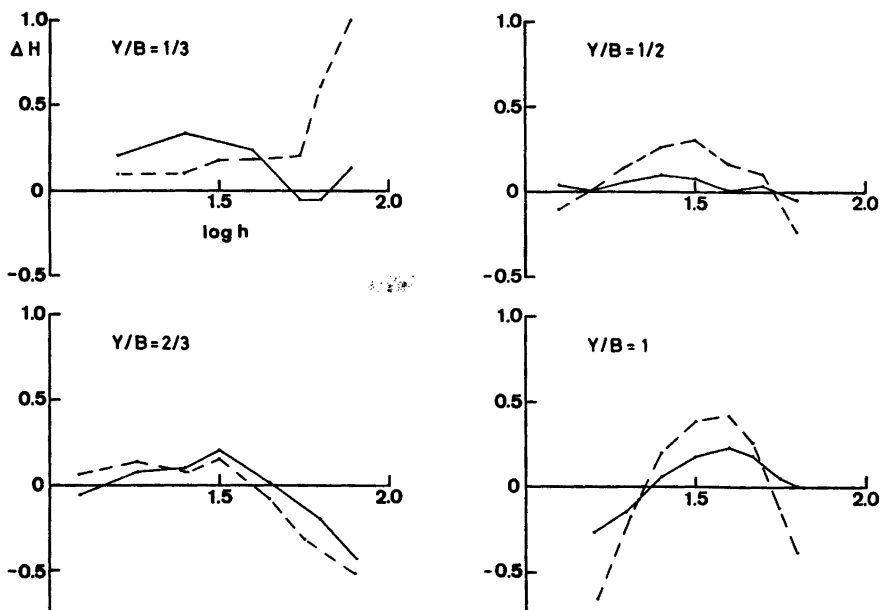


Fig. 8. Residual plots $H = (H_{\text{calc}} - H_{\text{exp}})$ mM at Y/B ratios 1/3, 1/2, 2/3 and 1 with $B = 0.16$ M. Broken and full lines show residuals by assuming the ternary polynuclear complexes to be $\text{Hg}_2\text{OHCl}_2^+ + \text{Hg}_3(\text{OH})_2\text{Cl}_3^+$ and $\text{Hg}_2\text{OHCl}_2^+ + \text{Hg}_3(\text{OH})_2\text{Cl}_3^+$, respectively. Proposed constants for binary and ternary (mononuclear) complexes given in Table 5 were used and not varied in the calculations.

As no additional species seem to be formed in this range, no separate investigations were undertaken. Thus within the range $0 < Y/B < 2$ the ternary polynuclear complexes formed, $\text{Hg}_2\text{OHCl}_2^+$ and $\text{Hg}_3(\text{OH})_2\text{Cl}_3^+$, are proposed with $\log \beta_{123} = -15.25 \pm 0.01$ and $\log \beta_{231} = 37.79 \pm 0.02$ giving $\sigma(Z) \times 1000 = 1.3$. Thus a good explanation of experimental data is obtained and if other ternary species are present

(e.g. $\text{Hg}_3(\text{OH})_2\text{Cl}_3^+$) they are formed in very small amounts.

DISCUSSION

In the present investigation equilibrium constants for the formation of binary $\text{Hg}^{2+} - \text{Cl}^-$, $\text{Hg}^{2+} - \text{OH}^-$ as well as ternary $\text{Hg}^{2+} - \text{Cl}^- - \text{OH}^-$ complexes have been determined,

Table 5. Proposed complexes with formation constants defined according to the equilibria given in the table.

Equilibria	$\log (\beta \pm 3\sigma)$
$\text{Hg}^{2+} + \text{H}_2\text{O} \rightleftharpoons \text{HgOH}^+ + \text{H}^+$	- 3.58(2)
$2\text{Hg}^{2+} + 2\text{H}_2\text{O} \rightleftharpoons \text{Hg}_2(\text{OH})_2^{2+} + 2\text{H}^+$	- 4.84(2)
$\text{HgCl}_2 + \text{H}_2\text{O} \rightleftharpoons \text{HgClOH} + \text{H}^+ + \text{Cl}^-$	- 9.87(2)
$\text{HgCl}_2 + 2\text{H}_2\text{O} \rightleftharpoons \text{Hg}(\text{OH})_2 + 2\text{H}^+ + 2\text{Cl}^-$	- 20.24(2)
$2\text{HgCl}_2 + \text{H}_2\text{O} \rightleftharpoons \text{Hg}_2\text{Cl}_2\text{OH}^+ + 2\text{Cl}^- + \text{H}^+$	- 15.25(1)
$3\text{HgCl}_2 + 2\text{H}_2\text{O} \rightleftharpoons \text{Hg}_3\text{Cl}(\text{OH})_2^{3+} + 2\text{H}^+ + 5\text{Cl}^-$	- 37.79(2)
$\text{HgCl}_2 \rightleftharpoons \text{HgCl}^+ + \text{Cl}^-$	- 6.78(5)
$\text{HgCl}_2 \rightleftharpoons \text{Hg}^{2+} + 2\text{Cl}^-$	- 14.00(3)
$\text{HgCl}_2 + \text{Cl}^- \rightleftharpoons \text{HgCl}_3^-$	1.07(3)
$\text{HgCl}_2 + 2\text{Cl}^- \rightleftharpoons \text{HgCl}_4^{2-}$	2.14(5)

and in all 10 different equilibrium constants have been evaluated. As the free H^+ -concentration was the only measured quantity, it was found necessary to investigate as wide concentration ranges as possible in B and Y and at the same time to cover the most interesting ratios Y/B . A total of approximately 150 titrations were performed including ~ 3000 experimental points. (In this estimate, data for controls of reversibility and reproducibility have been included). A complete list of experimental data is available from this department.

As can be seen from Table 5, the standard deviations of the proposed complexes are low ($3\sigma(\log \beta_{pqr}) \leq 0.05$) and the complexes may thus be considered as well determined.

The formation constants of the binary $HgCl_n^{(2-n)+}$ -species were determined indirectly in hydrolyzed $Hg^{2+} - Cl^-$ solutions using solely a glass-electrode. As can be seen from Table 2, where results from each ratio Y/B investigated are summarized, no systematic trend in these constants is found and they all fall within its limits of error. By comparing these constants with those reported by Arnek (see Table 1), the agreement is very good in K_1, K_2, K_3 and K_4 (cal.), while a difference of 0.1 logarithmic unit in $\log K_1$ and $\log K_2$ is found. However, the difference lies within the limits of error given by Arnek. In $Y/B > 0$ ratios studied, both $HgOHCl$ and $Hg(OH)_2$ have been identified with equilibrium constants given in Table 2. There seems to be a small difference in the formation constant for $HgOHCl$, depending on whether Y/B is greater than 2 or not. At $Y/B \geq 2$, $\log \beta_{HgOHCl} = -9.91 \pm 0.01$, while at $Y/B < 2$ a higher value -9.86 ± 0.01 is found. A corresponding difference in $\log \beta_{Hg(OH)_2}$ can be seen with values -20.20 ± 0.02 ($Y/B \geq 2$) and -20.24 ± 0.01 ($Y/B < 2$). Although this difference is slightly greater than the error limits, it probably is not significant, especially when the number of constants that have been determined is taken into account. Furthermore, by comparing $\beta_{Hg(OH)_2}$, determined in a pure Hg^{2+} -solution where $Y/B = 0$ with solution where $Y/B > 0$, the agreement is very satisfactory and is consistent with a value reported by Ahlberg.³

The formation of polynuclear hydrolytic species must be taken into consideration in solutions with ratios $Y/B < 2$. In Fig. 9 a distribution diagram $(Y/B)_{\log h, B}$ is given. According

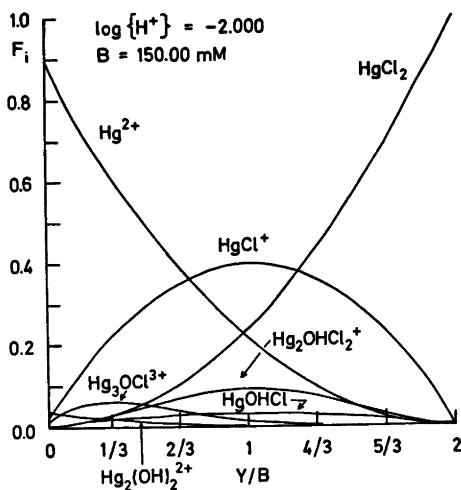
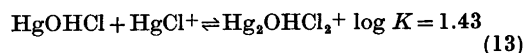
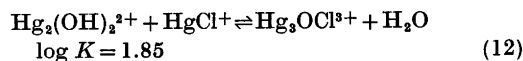


Fig. 9. Distribution diagrams $F_i(Y/B)_{\log h, B}$.

to this diagram, it seems reasonable to assume $Hg_3(OH)_2Cl^{3+}$ and $Hg_2OHCl_2^+$ to be formed according to the reactions



As mentioned earlier, isolated units $Hg_3OCl_3^+$ have been found in the solid state. Detectable amounts of this complex in solution with $1 \leq Y/B \leq 2$ have not been found. However, a possible mechanism for its formation could be $HgOHCl + Hg_2OHCl_2^+ \rightleftharpoons Hg_3OCl_3^+ + H_2O$ (14)

It is interesting to note that in aqueous solutions of methylmercury, the hydrolytic species CH_3HgOH and $(CH_3Hg)_2OH^+$ have been identified from pH-titration data (Schwarzenbach and Schellenberg³⁸), from Raman measurements (Woodward *et al.*³⁹) and from proton magnetic resonance (1H NMR) studies by Rabenstein and coworkers.⁴⁰ In a recent investigation Rabenstein *et al.*⁴² have extended the concentration range of CH_3Hg^+ up to 0.51 M and from both Raman and 1H NMR measurements they found that in a supersaturated solution with respect to $[(CH_3Hg)_2O]ClO_4$, the $(CH_3Hg)_3O^+$ -cation is detectable in small amounts. They found

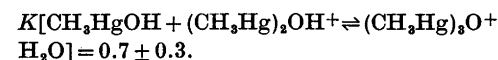
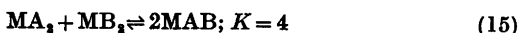


Table 6. Acidity constants of some mercury(II)-species.

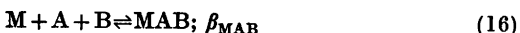
Complex	$-\log K_a$	Ref.
Hg^{2+}	3.6	This work, 2, 3
HgOH^+	2.7	This work, 2, 2
HgCl^+	3.1	This work, 16, 41
HgBr^+	3.5	41
HgI^+	4.0	41

In Table 6 acidity constants are given for some mercury(II) complexes with ligand H_2O , OH^- , Cl^- , Br^- and I^- . It can be seen that $\text{p}K_a(\text{HgCl}^+) = 3.09$ is in good agreement with the value 3.05 obtained by Ciavatta in 1.0 M NaClO_4 -medium. Furthermore, both HgOH^+ and HgCl^+ are stronger acids than Hg^{2+} . The higher chloride species HgCl_2 , HgCl_3^- and HgCl_4^{2-} are found not to give rise to appreciable amounts of hydrolysis products in the $\log h$ range investigated ($\log h > -9$). Although one water molecule around the mercury ion is replaced by a hydroxide or a chloride ion, the tendency to hydrolyze is still appreciable. However, when the species $\text{Hg}(\text{OH})_2$, HgOHCl , HgCl_2 , HgCl_3^- and HgCl_4^{2-} are formed, water molecules far from the Hg^{2+} -ion are available to split off protons and the acidity constants diminish greatly (cf. $\text{p}K_a[\text{Hg}(\text{OH})_2] \sim 15$ according to Garrett and Hirschler⁸).

If statistical reasons alone determine the formation of the complex MAB, the equilibrium constant of the reaction



should have the value 4. However, it has been found convenient to define the equilibria



for which the statistical value of the stability constants is easily calculated by using the equation

$$\beta_{\text{MAB}} = 2(\beta_{\text{MA}}\beta_{\text{MB}})^{1/2} \quad (17)$$

This equation can be derived from (15) and (16). Using $\log \beta_{\text{HgCl}_2} = 14.00$, $\log \beta_{\text{Hg}(\text{OH})_2} = 22.21$ and $\log K_w = -14.22$, a statistical value of the stability constants β_{HgClOH} has been calculated. The calculated value $10 \exp(18.40)$

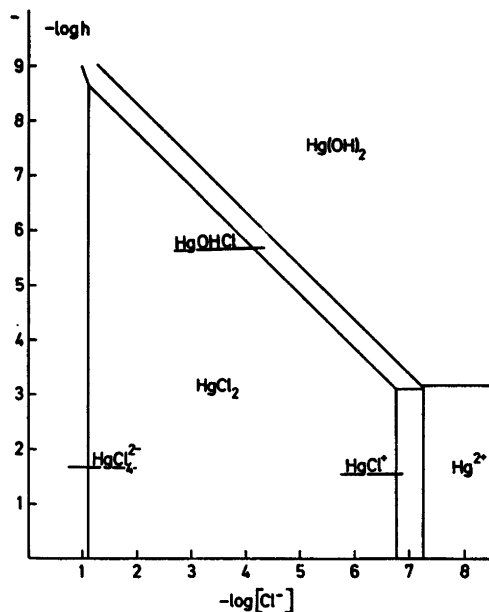


Fig. 10. Predominance area diagram. The composition of the mononuclear species predominating in a certain $\log h - \log [\text{Cl}^-]$ area is shown. The lines have been calculated by using the constants of Table 5.

M^{-2} is close to the experimental value $10 \exp(18.53) \text{ M}^{-2}$, indicating that HgOHCl is formed almost statistically. The same has been found by Ahlberg,^{41,44} concerning the formation of $\text{Hg}(\text{OH})\text{Br}$ and $\text{Hg}(\text{OH})\text{I}$.

In Fig. 10 an attempt is made to illustrate the various equilibria by showing the $(\log h - \log [\text{Cl}^-])$ areas in which a given species predominates.

Acknowledgements. I thank Professor Nils Ingri for much valuable advice, for his great interest, and for all the facilities placed at my disposal. Thanks are also due to Lab.ing. Agneta Nordin for valuable help with the experimental part of the potentiometric measurements. The English of the present paper has been corrected by Dr. Michael Sharp. The work forms part of a program financially supported by the Swedish Natural Science Research Council.

REFERENCES

- Sillén, L. G. and Martell, A. E. (compilers) *Stability Constants, Chem. Soc. London, Spec. Publ. No. 17 (1964) and No. 25 (1971)*.
- Hietanen, S. and Sillén, L. G. *Acta Chem. Scand.* 6 (1952) 747.

3. Ahlberg, I. *Acta Chem. Scand.* 16 (1962) 887.
4. Hayek, E. *Monatsh. Chem.* 85 (1954) 472.
5. Garrett, A. B. and Howell, W. W. *J. Am. Chem. Soc.* 61 (1939) 1730.
6. Garrett, A. B. and Hirschler, A. E. *J. Am. Chem. Soc.* 60 (1938) 299.
7. Dyrssen, D. and Tyrrell, V. *Acta Chem. Scand.* 15 (1961) 393; 1622.
8. Johansson, G. *Acta Chem. Scand.* 25 (1971) 2787.
9. Panthaleon van Eck, C. L., Wolter, H. B. M. and Jaspers, W. J. M. *Recl. Trav. Chim. Pays-Bas* 75 (1956) 802.
10. Johansson, G. *Acta Chem. Scand.* 25 (1971) 1905.
11. Johansson, G. *Acta Chem. Scand.* 25 (1971) 2799.
12. Sillén, L. G. *Acta Chem. Scand.* 3 (1949) 539.
13. Ciavatta, L. and Grimaldi, M. J. *Inorg. Nucl. Chem. Lett.* 30 (1968) 197.
14. Arnek, R. *Ark. Kemi* 24 (1965) 531.
15. Linhart, G. A. *J. Am. Chem. Soc.* 37 (1915) 259; 38 (1916) 1272.
16. Ciavatta, L. and Grimaldi, M. J. *Inorg. Nucl. Chem. Lett.* 30 (1968) 563.
17. Sandström, M. *Acta Chem. Scand. A* 31 (1977) 141.
18. Luther, R. *Z. Phys. Chem.* 47 (1904) 107.
19. Carriere, E. and Lafitte, M. *Bull. Soc. Chim. Fr.* 12 (1945) 833.
20. Carrière, E., Guiter, H. and Lafitte, M. *Bull. Soc. Chim. Fr.* 15 (1945) 23.
21. Damm, K. and Weiss, A. *Z. Naturforsch.* 106 (1955) 534.
22. Partridge, J. A., Izatt, R. M. and Christensen, J. J. *J. Chem. Soc.* (1965) 4231.
23. Gmelin-Kraut, *Handbuch der anorganischen Chemie*, Heidelberg 1914, 679.
24. Aurivillius, K. *Ark. Kemi* 22 (1964) 537.
25. Aurivillius, K. and Stålhandske, C. *Acta Crystallogr. B* 30 (1974) 1907.
26. Aurivillius, K. *Acta Chem. Scand.* 8 (1954) 523.
27. Aurivillius, K. and Stålhandske, C. *To be published.*
28. Björnlund, G. *Acta Chem. Scand. A* 28 (1974) 169.
29. Šćavnićar, S. *Z. Kristallogr.* 118 (1963) 248.
30. Sjöberg, S. *Acta Chem. Scand.* 25 (1971) 2149.
31. Gran, G. *Acta Chem. Scand.* 4 (1950) 559.
32. Sjöberg, S. *Acta Chem. Scand.* 27 (1973) 3721.
33. Biedermann, G. and Sillén, L. G. *Ark. Kemi* 5 (1953) 425.
34. Ingri, N. and Sillén, L. G. *Ark. Kemi* 23 (1964) 97.
35. Arnek, R., Sillén, L. G. and Wahlberg, O. *Ark. Kemi* 31 (1969) 353; Brauner, P., Sillén, L. G. and Whiteker, R. *Ark. Kemi* 31 (1969) 365.
36. Sillén, L. G. *Acta Chem. Scand.* 16 (1962) 159; Sillén, L. G. and Warnqvist, B. *Ark. Kemi* 31 (1969) 341.
37. Ingri, N., Kakolowicz, W., Sillén, L. G. and Warnqvist, B. *Talanta* 14 (1967) 1261.
38. Schwarzenbach, G. and Schellenberg, M. *Helv. Chim. Acta* 48 (1965) 28.
39. Clarke, J. H. R. and Woodward, L. A. *Trans. Faraday Soc.* 62 (1966) 3022; Goggin, P. L. and Woodward, L. A. *Trans. Faraday Soc.* 56 (1960) 1591; Goggin, P. L. and Woodward, L. A. *Trans. Faraday Soc.* 58 (1962) 1495.
40. Rabenstein, D. L., Evans, C. A., Tourangeau, M. C. and Fairhurst, M. *Anal. Chem.* 47 (1975) 338.
41. Ahlberg, I. and Leden, I. *Trans. R. Inst. Technol. Stockholm* 249 (1972) 17.
42. Marcus, Y. *Acta Chem. Scand.* 11 (1957) 599.
43. Panthaleon van Eck, C. L. *Thesis*. Leiden 1958.
44. Ahlberg, I. *Acta Chem. Scand.* 27 (1973) 3003.
45. Eriksson, G. *To be published.*
46. Johansson, G. and Hansen, E. *Acta Chem. Scand.* 26 (1972) 796.

Received March 8, 1977.

Metal Complexes with Mixed Ligands. 12. A Potentiometric Study of the Systems Hg^{2+} —Imidazole, Hg^{2+} — OH^- —Imidazole and Hg^{2+} — Cl^- —Imidazole in 3.0 M (Na)ClO₄, Cl Media

STAFFAN SJÖBERG

Department of Inorganic Chemistry, University of Umeå, S-901 87 Umeå, Sweden

Four component equilibria between mercury(II), imidazole ($\text{C}_3\text{H}_4\text{N}_2$; L) OH^- and Cl^- have been studied at 25 °C by means of emf titrations using a glass electrode. The measurements were performed in media consisting of mixtures of 3.0 M (Na)ClO₄ and 3.0 M (Na)Cl with $0 \leq [\text{Cl}^-] \leq 3.0$ M. Besides pure binary species HgL^{2+} and HgL_2^{2+} , all data could be explained with the ternary complexes HgClL^+ , HgCl_2L , HgCl_3L^- and HgCl_4^{2-} . The formation of a mixed hydroxo complex $\text{Hg}(\text{OH})\text{L}^+$ has also been established. The equilibrium constants determined are collected in Table 4. Data have been analysed with the least squares computer program LETA-GROPVRID.

In a preceding publication,⁵ equilibria in hydrolyzed mercury(II) chloride solutions were reported. Besides pure binary hydrolytic complexes, HgOH^+ , $\text{Hg}(\text{OH})_2$ and $\text{Hg}_2(\text{OH})_2^{2+}$ and unhydrolyzed $\text{HgCl}_n^{(2-n)+}$ ($n = 1, 2, 3, 4$) species, experimental data were explained with the ternary complexes HgOHCl , $\text{Hg}_2\text{OHCl}_2^+$ and $\text{Hg}_3(\text{OH})_2\text{Cl}^{2+}$. The aim of the present investigation is to determine

the composition of the complexes formed in the system Hg^{2+} —imidazole (L)— OH^- — Cl^- .

PREVIOUS STUDIES

The literature concerning aqueous mercury(II) imidazoles indicates that two mononuclear species, HgL^{2+} and HgL_2^{2+} , should be formed (see Table 1). Brooks and Davidson¹ performed some potentiometric titrations (0.15 M NaClO₄, 27 °C) using both a mercury-mercury(II) and a glass electrode. They concluded that the principal complex formed is HgL_2^{2+} while HgL^{2+} , for which no stability constant was evaluated, seemed to be present only in small amounts. Recently Marsicano *et al.*² [0.5 M (Na)ClO₄, 25 °C] evaluated from titration calorimetric measurements, formation constants for both HgL^{2+} and HgL_2^{2+} . The investigation by Smith³ yielded very low values of the formation constants (*cf.* Table 1), which most certainly is due to the ionic medium consisting of 0.058 M KCl. As mercury(II) in this medium

Table 1. Earlier studies on mercury(II)—imidazoles. The constants are defined according to the equilibria: $\text{Hg}^{2+} + n\text{L} \rightleftharpoons \text{HgL}_n^{2+}$; β_n

Temp. °C	Medium	Method	$\log(\beta_1 + 3\sigma)$	$\log(\beta_2 + 3\sigma)$	Ref.
27	0.15(Na)ClO ₄	pot. (gl. Hg)	—	18.74	1
25	0.5(Na)ClO ₄	cal.	9.64(35)	18.29(21)	2
25	0.058 KCl	pot. (gl.)	3.57	6.95	3
25	3.0(Na)ClO ₄	pot. (gl.)	9.18(12)	18.19(2)	This work

exists as chloride complexes, the equilibrium constants given are not true stability constants, but rather "conditional" constants.

Any attempt to try to find $\text{Hg}^{2+} - \text{OH}^- - \text{L}$ or $\text{Hg}^{2+} - \text{Cl}^- - \text{L}$ species has not been reported.

EXPERIMENTAL

Chemicals and analysis. All solutions used were prepared and analysed as described earlier.^{4,5}

Apparatus. The thermostat, cell arrangement and experimental details for the emf measurements are fully described in Refs. 4 and 5.

Method. The measurements were carried out as potentiometric titrations at 25 °C. The titration procedures used were similar to those described earlier.

The equilibrium solutions were made to contain $[\text{ClO}_4^-] + X = 3.0 \text{ M}$. X is defined as the total chloride concentration over the HgCl_2 level. The solutions had the general composition: $B \text{ M HgCl}_2$, $C \text{ M HL}^+$, $H \text{ M H}^+$, $X \text{ M Cl}^-$, $([\text{ClO}_4^-] + X - C - H) \text{ M Na}^+$ and $3.0 - X \text{ M ClO}_4^-$. B and C are the total concentrations of mercury(II) and imidazole, and H stands for the total concentration of protons, calculated over the 0-level HgCl_2 , HL^+ , Cl^- and H_2O .

The free hydrogen ion concentration, h , was determined according to the relation

$$E = E_0 + 59.157 \log h + E_j \quad (1)$$

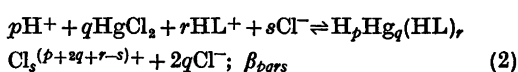
The liquid junction potential E_j was expected to be caused mainly by the presence of H^+ . In 3.0 M NaClO_4 and 3.0 M NaCl $E_j = -16.7 \text{ h mV}^{12}$ and -17.0 h mV ,⁸ respectively, have been used. In solutions where $3.0 < X < 0 \text{ M}$ a value of $E_j = -16.7 \text{ h mV}$ has been used.

To find out whether the replacement of ClO_4^- to Cl^- or the reverse, will change the concentration scale for H^+ , some supplementary titrations were performed. In these $B = C = 0$ and h was either kept constant or varied, while X ranged from 0 to 3.0 M. It was found that E_0 of the glass electrode did not change by more than $\pm 0.1 \text{ mV M}^{-1}$ of exchanged anion. Thus the concentration scale of H^+ does not seem to be affected by the change of chloride ions in the ionic medium.

Most of the titrations were started with a calibration of the glass electrode using those acidic points where hydrolysis and complex formation can be neglected. This calibration thus gives E_0 and E_j , and H could be controlled by using Gran's extrapolation method.⁷ However, with $X = 0$, the complex formation starts at $\log h > -3$, and no accurate determinations of both E_0 and H can be made. Instead E_0 was estimated from the most acidic points in the titrations, and H was controlled in separate experiments by the addition of NaCl (to

suppress the complex formation between HgCl_2 and L) as described earlier.⁸

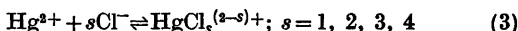
We will assume the presence of 4-component equilibria of the general form:



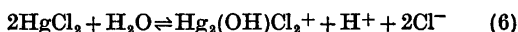
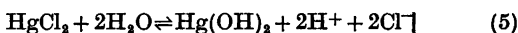
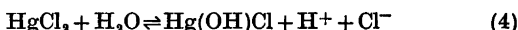
It will be convenient to write complexes where $-p=r$ as $\text{Hg}_q\text{L}_n\text{Cl}_s$ and the stability constants as β_{nqs} , which is used throughout in this paper whenever possible.

Besides the four component equilibria in (2) we have to take into account,

(i) the complex formation between Hg^{2+} and Cl^- according to



(ii) the hydrolysis of these chloride complexes which with $\log h > -9$ is explained by the following equilibria:

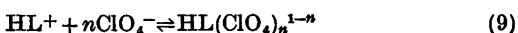


(iii) the proton imidazole equilibrium:



which has been found to be dependent on the composition of the ionic medium; e.g. $\log K_a(\text{HL}^+) = -7.913$ and -7.635 in 3.0 M $(\text{Na})\text{ClO}_4$ and 3.0 M $(\text{Na})\text{Cl}$,⁸ respectively. Equilibrium constants for reactions (3)–(7) have been determined in earlier investigations⁸ and will be assumed to be known.

$K_a(\text{HL}^+)_X$ in mixed media with $[\text{ClO}_4^-] + X = 3.0 \text{ M}$. In separate measurements this acidity constant was determined at $X = 0.1, 0.2, 0.4, 0.5, 0.75, 1.0$ and 1.5 M with the results given in Table 2. According to this table there is a steady increase in K_a with increasing X . As a hypothesis we will try to explain this tendency as caused by complex formation. Calculations on the collected experimental data showed that two alternative explanations were possible. Either by assuming the perchlorate ion to form complexes with the imidazolium ion or speciation between the imidazole molecule and chloride ions. Letagrop calculations showed that a satisfactory fit was obtained by assuming the equilibria



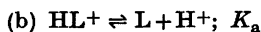
with $\log \beta(\text{HLCIO}_4) = -0.57 \pm 0.01$, $\log \beta[\text{HL}(\text{ClO}_4)_2^-] = -1.63 \pm 0.08$ and $\log K_a(\text{HL})^+ = -7.636 \pm 0.002$.

Table 2. Results of LETAGROP calculations on the system $H^+ - HL^+ - Cl^-$. The complexes formed at different levels of X were defined either according to



with $n=0, 1, 2$

or according to



In the last column under (b) a calculated value of K_a is given, in which the relation

$$K_a(\text{calc}) = \beta_{100}x^0 + \beta_{101}x^1 + \beta_{102}x^2$$

has been employed. In the calculation $x = X$ has been used, which seems reasonable as the change in x due to the complex formation with L is small.

(a)

No. of titr./ No. of points	X/M	$\sigma(Z) \times 1000$	$\log(\beta_{100} \pm 3\sigma)$	$\log(\beta_{101} \pm 3\sigma)$	$\log(\beta_{102} \pm 3\sigma)$
14/317	0.0–3.0	2.2	–7.940(2)	–8.641(16)	–9.279(26)

(b)

X/M	$\sigma(Z) \times 1000$	$-\log(K_a \pm 3\sigma)$	$-\log K_a(\text{calc.})$
0		7.913(1) ^a	7.940
0.1	2.2	7.927(4)	7.931
0.2	1.9	7.922(5)	7.921
0.4	2.0	7.907(3)	7.903
0.5	2.7	7.894(2)	7.889
0.75	2.3	7.865(3)	7.863
1.0	1.5	7.845(1)	7.844
1.5	2.6	7.794(4)	7.792
3.0		7.637(2) ^b	7.635

^a Value taken from Ref. 4. ^b Value taken from Ref. 8.

Alternatively it was found that the equilibria



with equilibrium constants given in Table 2, equally well could explain the experimental data.

Whether $HL^+ - ClO_4^-$ and/or $L - Cl^-$ complexes are formed is difficult to predict from the type of measurements performed in this work. As these complexes are very weak, we can put $x = X$ and $[ClO_4^-] = [ClO_4^-]_{\text{tot}}$ as a good approximation. This means that interpretation of the four-component equilibria as defined under (2) are independent of whether equilibria (9) or (10)–(11) are introduced in the equilibrium model. However, to restrict the number of components to four, corrections for the medium dependence of $K_a(HL^+)$ will be made by means of equilibria (10)–(11) (see below).

Data treatment. For the case when only complexes of the general type $Hg_qL_r^{2q+}$ are formed, e.g. when $-p=r$ in (1), \bar{n} is defined as the average ligand number and is given by

$$\bar{n} = (h - H - K_w h^{-1} - [L])/B \quad (12)$$

where K_w is the ionic product of water. In the present study the term $K_w h^{-1}$ can be neglected. $[L]$ can be calculated from the relation

$$[L] = K_a h^{-1} [HL^+] = K_a h^{-1} [C - (h - H)] \quad (13)$$

In cases with $-p \neq r$ it can easily be shown that

$$[HL^+] \neq C - (h - H) \quad (14)$$

and apparent values of \bar{n} and $[L]$ are obtained. These parameters are now calculated only to test how poorly a set of experimental data fits a series of complexes $Hg_qL_r^{2q+}$.

When ternary species $Hg^{2+} - Cl^- - L$ are formed \bar{n} can be calculated in two ways. When

measurements have been performed at constant levels of X , $[L]$ can be calculated either by the use of the "conditional" acidity constant of HL^+ valid at the X -level in question, or by assuming the value of K_a valid in 3.0 M $(Na)ClO_4$ to be the "true" acidity constant. In the latter case complex formation between L and Cl^- is assumed to occur and \bar{n} is now given by

$$\bar{n} = (h - H - [L] - [LCl^-] - [LCl_2^{2-}])/B \quad (15)$$

where $[L]$ is given by (13) and $[LCl^-]$ and $[LCl_2^{2-}]$ are calculated according to

$$[LCl^-] = \beta_{101}h^{-1}x[HL^+] = \beta_{101}h^{-1}x(C + H - h) \quad (16)$$

$$[LCl_2^{2-}] = \beta_{102}h^{-1}x^2[HL^+] = \beta_{102}h^{-1}x^2(C + H - h) \quad (17)$$

The same \bar{n} is now obtained independently of whether the "conditional" or the "true" value of $K_a(HL^+)$ has been used. However, a difference in $\log [L]$ is obtained equal to the difference between the logarithms of the two acidity constants.

The search for the "best" model was performed by using the least squares computer program LETAGROPVRID⁹ (version ETITR¹⁰). The error squares sum $U = \sum(Z_{\text{calc}} - Z_{\text{exp}})^2$ was minimized, where $Z = h - H/C$. The standard deviations were defined and calculated according to Sillén.¹¹ The computation was performed on a CD 3300 computer.

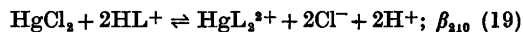
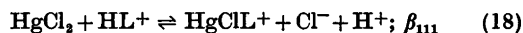
DATA, CALCULATIONS AND RESULTS

The complex formation between $HgCl_2$ and imidazole in a 3.0 M $(Na)ClO_4$ medium was at first investigated. These measurements yielded formation constants for $HgClL^+$, HgL_2^{2+} and $Hg(OH)L^+$. When $HgCl_2$ was dissolved in 3.0 M $(Na)Cl$ medium, $HgCl_4^{2-}$ becomes the dominating mercury(II)-chloride complex, and the complex formation with imidazole was strongly suppressed. It was also found that if these experimental data were to be explained assuming the same equilibrium model as was found at the $HgCl_2$ level, a change in the equilibrium constant for $HgClL^+$ by a factor ~ 500 was observed. This great difference is an indication that additional complexes must be formed upon increasing the chloride content in the ionic medium, *i.e.* when $HgCl_3^-$ and $HgCl_4^{2-}$ are formed.

Supplementary measurements were now performed at different chloride concentrations, X , with $[ClO_4^-] + X = 3.0$ M. The results ob-

tained at the different levels of X will now be discussed in detail.

$HgCl_2 + L$ in 3.0 M $(Na)ClO_4$. Complex formation between $HgCl_2$ and L was at first investigated. Experimental data have been collected covering the following concentration ranges: $0.0025 \leq B \leq 0.080$ M, $0.00125 \leq C \leq 0.320$ M, with $\bar{n} \leq 2$ and $-\log h \lesssim 7.2$. In each titration the quotients C/B were kept constant and had values 0.25, 0.5, 1, 2, 4, 8, 16, 32 and 64. A total of 30 ($B-C$) combinations were investigated. Parts of these experimental data are visualized in Figs. 1 and 3 in the form of Bjerrum plots $\bar{n}(\log [L])$. It was found (*cf.* Fig. 1) that for different quotients C/B , different curves were obtained. Furthermore, the space between the different curves was constant, giving $(\Delta \log B / \Delta \log [L])\bar{n} = +1$ within the concentration ranges studied. This indicates reactions of the type



By assuming the amount of the species Hg^{2+} , $HgCl^+$, $HgCl_3^-$ and $HgCl_4^{2-}$ to be negligible, \bar{n} is given by

$$\bar{n} = ([HgClL^+] + 2[HgL_2^{2+}]) / ([HgCl_2] + [HgClL^+] + [HgL_2^{2+}]) = (\beta_{111}h^{-1}cx^{-1} + 2\beta_{210}h^{-2}c^2x^{-2}) / (1 + \beta_{111}h^{-1}cx^{-1} + \beta_{210}h^{-2}c^2x^{-2}) \quad (20)$$

Thus \bar{n} is a function of both x and $[L]$ ($= K_a h^{-1}c$). The amount of Cl^- set free according to

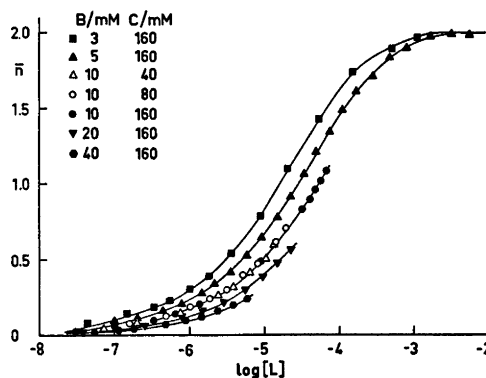


Fig. 1. A part of experimental data plotted as curves $\bar{n}(\log [L])$ for $X = 0$ M. The full curves have been calculated with the set of constants given in Table 4.

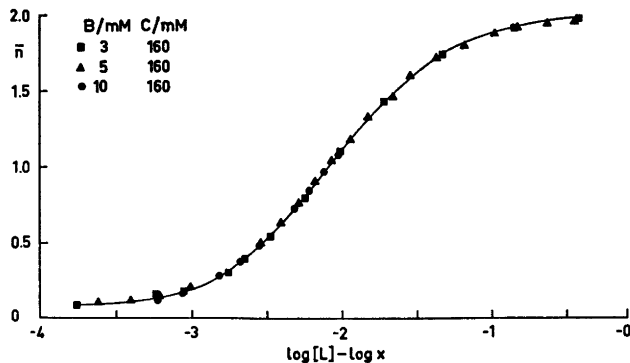


Fig. 2. A part of experimental data plotted as curves $\bar{n}(\log[L] - \log x)$ for $X = 0$ M. The full curve has been calculated with values of β_{111} and β_{210} given in Table 4.

equilibria (18) and (19) can be calculated and is equal to $B\bar{n}$, thus giving $x = [\text{Cl}^-]_{\bar{n}=0} + B\bar{n}$. This means that experimental data can now be recalculated in the form $\bar{n}(\log[L] - \log x)$. Data with $C/B > 8$ were plotted in this form (Fig. 2) giving coinciding curves, indicating that the main equilibria are given by (18) and (19). These curves could be superimposed on plots of normalized curves $\bar{n}(\log v)_u$

$$\bar{n} = (v + 2uv^2)/(1 + v + uv^2) \quad (21)$$

where $\log v = \log \beta_{111} + [\log L] - \log x - \log K_a$
and $\log u = \log \beta_{210} - 2 \log \beta_{111}$

The best fit was obtained with $\log \beta_{111} = -5.50 \pm 0.05$ and $\log \beta_{210} = -11.55 \pm 0.05$. A

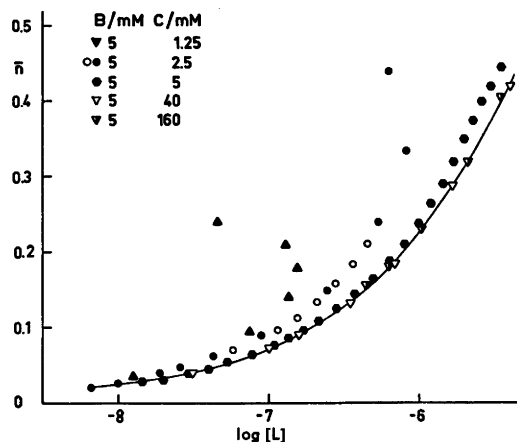


Fig. 3. A part of experimental data with $X = 0$ M plotted as curves $\bar{n}(\log[L])$ for C/B ratios 1/4, 1/2, 1, 8 and 32. The full curve has been calculated with values of β_{111} and β_{210} given in Table 4.

LETAGROP calculation yielded $\log \beta_{111} = -5.531 \pm 0.013$ and $\log \beta_{210} = -11.537 \pm 0.017$ with $\sigma(Z) \times 1000 = 0.6$.

At quotients $C/B < 4$ and $B < 0.020$ M, systematic deviations from the $\bar{n}(\log[L])_B$ curves were observed (see Fig. 3), which indicates that additional complex(es) to those previously found must be present. Among a number of species which were tested, the $\text{Hg}(\text{OH})\text{L}$ complex was found to give the "best" explanation to the experimental data with $\log \beta_{210} = -14.30 \pm 0.02$ and $\sigma(Z) \times 1000 = 3.4$ (see Table 3a).

HgCl₂ + L in 3.0 M (Na)Cl. To determine whether ternary species like $\text{HgCl}_m\text{L}^{2-m}$ ($m \geq 2$) and $\text{HgCl}_n\text{L}_2^{2-n}$ ($n \geq 1$), and eventual quaternary species $\text{Hg}^{2+} - \text{OH}^- - \text{Cl}^- - \text{L}$, exist, the chloride excess, X , was increased to 3.0 M.

At this high chloride concentration HgCl_4^{2-} is the predominating complex. The following concentration ranges have been investigated: $0.0025 \leq B \leq 0.080$ M, $0.005 \leq C \leq 0.320$ M and $-8.0 \leq \log h \leq -5.5$. The quotients C/B ranged from 0.25 to 64, yielding 53 ($B-C$) combinations.

With $C \leq 0.080$ M and $C/B \leq 8$ coinciding $\bar{n}(\log[L])$ curves were obtained independently of B and C (see Fig. 4). These data could be explained very well by assuming a mono-nuclear complex with one imidazole molecule coordinated to the mercury(II) atom. As the variation in x is very small, the number of chloride ions, coordinated in this complex, cannot be obtained.

However, an equilibrium constant for the formation of HgClL^+ , was calculated giving

Table 3a. Results of graphical and LETAGROP calculations. The errors $3\sigma(\log \beta_{pqrs})$ are given when the corresponding equilibrium constant has been varied. In the calculations constants for equilibria (3)–(8) have been taken from Ref. 5. $X=0$ M.

No. of titr./ No. of points	$\sigma(Z) \times 1000$	HgClL ⁺ $\log(\beta_{111} \pm 3\sigma)$	HgL ₂ ²⁺ $\log(\beta_{210} \pm 3\sigma)$	Hg(OH)L ⁺ $\log(\beta_{210} \pm 3\sigma)$	Rem.
15/190	0.6	-5.50(5) -5.53(1)	-11.55(5) -11.54(2)		graph.
7/52	3.4	-5.53	-11.54	-14.30(2)	

Table 3b. Calculations given in this table have been performed by assuming formation constants for the species HgClL⁺ and HgL₂²⁺ given in Table 3a, to be known. Furthermore the value of K_a taken from Table 2b has been used.

No. of titr./ No. of points	X/M	$\sigma(Z) \times 1000$	HgCl ₂ L $\log(\beta_{112} \pm 3\sigma)$	HgCl ₃ L ⁻ $\log(\beta_{113} \pm 3\sigma)$
7/75	0.1	1.0	-4.46(3)	-
	0.1	1.0		-3.45(3)
	0.1	0.3 ^a	-4.81(3)	-3.81 ^b
4/39	0.2	0.6	-4.38(3)	
	0.2	0.6		-3.67(2)
	0.2	0.5	-4.85(7)	-3.81
7/68	0.4	0.5	-4.15(1)	
	0.4	0.5		-3.74(1)
	0.75	0.3	-3.96(1)	
3/27	0.75	0.3		-3.83(1)
	0.75	0.3		
4/44	1.5	0.9	-3.65(2)	
	1.5	0.9		-3.82(2)
9/42	3.0	1.1	-3.30(1)	
	3.0	1.1		-3.77(1)

^a A calculation based upon data with $\bar{n} \lesssim 0.2$. ^b An average value of $\log \beta_{113}$ taken from data with $X \geq 0.75$ M.

Table 3c. In the calculations presented in this table, equilibria (8)–(10), with equilibrium constants given in Table 2a, have been included. R denotes a rejected complex.

X/M	$\sigma(Z) \times 1000$	HgCl ₂ L $\log(\beta_{112} \pm 3\sigma)$	HgCl ₃ L ⁻ $\log(\beta_{113} \pm 3\sigma)$	HgClL ₂ ⁺ $\log(\beta_{211} \pm 3\sigma)$	HgCl ₂ L ₂ $\log(\beta_{212} \pm 3\sigma)$	Points
0.75, 1.5, 3.0	1.4	-	-3.79(1)	-	-	113
0.1, 0.2, 0.4 ^a	0.9	-4.81(4)	-3.79	-	-	139
0.1, 0.2, 0.4 ^b	1.0	-4.81	-3.79	-10.84(10)	R	191
	1.3	-4.81	-3.79	-	10.26(19)	

^a $\bar{n} \lesssim 0.3$. ^b In these calculations data ($X, \log h$), have been included.

$\log \beta_{111} = -2.84 \pm 0.01$ and $\sigma(Z) \times 1000 = 1.7$, which can be compared with $\log \beta_{111} = -5.53 \pm 0.01$ obtained at $X=0$ M. The great difference, which is about 2.7 logarithmic units, cannot be due to so called "medium effects". Instead it seems more likely that the difference is

caused by an incorrect assumption concerning the equilibrium model at $X=3.0$ M. This indicates that formation of species like HgCl₂L and/or HgCl₃L⁻ are possible.

Although low values in B with $C/B=0.25$, 0.5, 1 and 2 were investigated, no indications

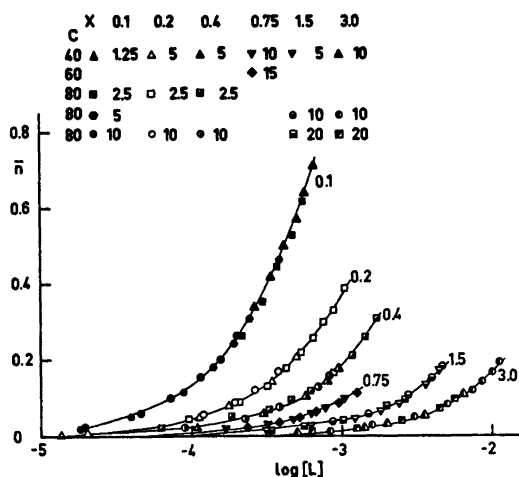


Fig. 4. "Mononuclear" $\bar{n}(\log[L])$ curves at constant levels of X ($=0.1, 0.2, 0.4, 0.75, 1.5$ and 3.0 M). The full curves have been calculated with constants for the binary $\text{Hg}^{2+} - \text{Cl}^-$ species from Ref. 5, the acidity constant of imidazolium from Table 2b and the set of constants proposed in Table 4. The concentrations are given in M (X), mM (C and B). B -values are given to the right of each symbol.

of any quaternary complex $\text{Hg}^{2+} - \text{OH}^- - \text{L} - \text{Cl}^-$ were found. At high ratios C/B , $8 \leq C/B \leq 64$, \bar{n} seems to be dependent on B and C . An analysis of these data indicates formation of acidic complexes of the type $\text{HgCl}_x\text{L}_y(\text{HL})_z^{2-x+z}$. The results and discussions of these complexes will be given in a forthcoming paper.

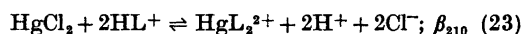
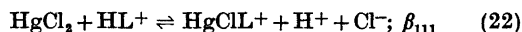
HgCl₂ + L in mixed media, with $[\text{ClO}_4^-] + X = 3.0$ M. To attempt to explain the great differences in the formation constants for HgClL^+ found at levels with $X = 0$ and 3.0 , respectively, supplementary measurements were performed. These can be divided into series in which X has been kept constant at levels with $X = 0.1, 0.2, 0.4, 0.75$ and 1.5 M. In another series X was varied by adding chloride ions to solutions where $Z = 0.7$ and 1.2 , respectively. The concentration ranges investigated were $0.00125 \leq B \leq 0.040$ M, $0.040 \leq C \leq 0.160$ M with $4 \leq C/B \leq 32$ and $3 < -\log h < 8$.

The average ligand number \bar{n} was calculated according to eqn. (12) by using the "conditional" constant for $K_a(\text{HL}^+)$, valid at the X -level in question (cf. eqn. (13)).

Plots $\bar{n}(\log[L])_x$ are given in Fig. 4. This figure clearly shows that the complex formation is systematically suppressed with increasing X . As the curves coincide at each level of X , mononuclear complexes HgCl_xL_y are formed. Furthermore, the amount of soluble complexes seems to decrease with increasing X .

These experimental data have been treated in two ways: (i) separate calculations at each level of X , and the "conditional" acidity constant of imidazolium (see Table 2) was used; (ii) calculations where all X -levels are treated together, including data in the form $(X, \log h)_x$. In these calculations the binary $\text{L} - \text{Cl}^-$ equilibria were included in the equilibrium models.

(i) *Data at constant X.* The equilibria



were established from data with $X = 0$ and the calculated values of β_{111} and β_{210} were assumed to be correct. As the curves $\bar{n}(\log[L])_x$ coincide, mononuclear complexes are formed. For data with $\bar{n} \lesssim 0.2$, the species HgCl_2L and HgCl_3L^- were tested one at a time. The results of these calculations are given in Table 3b.

We will now compare the equilibrium constants β_{112} and β_{113} obtained at each level of X . As can be seen from Table 3b, $\log \beta_{112}$ increases from -4.46 ($X = 0.1$ M) to -3.30 ($X = 3.0$ M). On the other hand $\log \beta_{113}$ yields a nearly constant value with $X = 0.4, 0.75, 1.5$ and 3.0 M ($-3.74, -3.83, -3.82, -3.77$). This seems to indicate that HgCl_3L^- is the predominating ternary complex within this concentration range.

With $X < 0.4$ M, β_{113} increases with decreasing X , which could be explained by assuming the calculated constant to represent a sum of two constants, i.e. β_{112} and β_{113} . To test this hypothesis, some additional calculations were performed at $X = 0.1$ and 0.2 M. In these HgCl_3L^- with $\log \beta_{113} = -3.81$ (average value from $X = 0.75, 1.5$ and 3.0) was included in the equilibrium model. The values of $\log(\beta_{112} \pm 3\sigma)$ found were -4.81 ± 0.03 and -4.85 ± 0.07 , respectively. Thus these calculations showed that experimental data $(Z, \log h)_x$, $X = 0.1$,

0.2, 0.4, 0.75, 1.5 and 3.0 M, can fully be explained by assuming the ternary species HgCl_2L and HgCl_2L^- to exist in addition to HgClL^+ . Data with $\bar{n} > 0.5$ was reached within a rather limited range in X (see Fig. 4). However, within this range there were indications of species $\text{HgCl}_n\text{L}_2^{2-n}$, $n > 0$. Evaluation of formation constants for these complexes will be described below.

(ii) *Data with $0 < X < 3.0$ M.* As pointed out earlier, the concentration scale for protons does not seem to change within this concentration range in X . Therefore data $(Z, \log h)_x$ and $(X, \log h)_z$ were treated together. The same equilibrium model as was found under (i) was tested. The question now is whether the same model and the same equilibrium constants are obtained upon treating the experimental data in this way. All calculations are given in Table 3c.

At first β_{111} was determined from data with $X \geq 0.75$ M, where HgCl_2^{2-} is the predominating binary $\text{Hg}^{2+} - \text{Cl}^-$ complex. This calculation yielded $\log \beta_{111} = -3.79 \pm 0.01$ with $\sigma(Z) \times 1000 = 1.4$. This value is in very good accordance with the average value -3.81 ± 0.04 obtained under (i). The calculated value of $\log \beta_{112}$, derived from data with $X \leq 0.4$ M, was -4.81 ± 0.04 (cf. -4.83 ± 0.04 from (i)). Thus the agreement is good between the formation constants as determined under (i) and (ii).

Concerning eventual complexes $\text{HgCl}_n\text{L}_2^{2-n}$, with $n \geq 0$, data with $\bar{n} > 0.5$ were included. In addition to HgL_2^{2+} , the species HgClL_2^+ and HgCl_2L_2 were tested, with the results given in Table 3c. It was found that each of these complexes could explain data equally well, however in a covariation of β_{211} and β_{212} , β_{212} came out as zero. Thus it seems as if the concentration range in X , within which high \bar{n} values are obtained, should be too small to favour the formation of HgCl_2L_2 .

Hg²⁺ + L in 3.0 M (Na)ClO₄. Attempts have been made to determine the formation constant of HgL^{2+} . Since low ratios C/B must favour the formation of this complex, the titrations were performed in such a way as to increase C/B within each titration, yielding $0 \leq C/B \leq 5$. B was varied within the limits $0.003 \leq B \leq 0.010$ M and to avoid precipitation the available $\log h$ range was restricted to $\log h > -3.1$. In the calculations the formation

constant for HgL_2^{2+} was assumed to be known, as it is well determined from data with $X = 0$. Within the concentration ranges investigated HgOH^+ and $\text{Hg}(\text{OH})_2$ are formed to some extent, as imidazole was added to partly hydrolyzed solutions ($Z \lesssim 0.10$). Thus, besides the eventual formation of HgL^{2+} , there is reason to believe that the complex $\text{Hg}(\text{OH})\text{L}^+$ should be formed too. A good fit to experimental data was obtained ($\sigma(H) \times 1000 = 0.09$) with

$$\log \beta(\text{Hg}^{2+} + \text{HL}^+ \rightleftharpoons \text{HgL}^{2+} + \text{H}^+) = 1.24 \pm 0.12 \text{ and}$$

$$\log \beta(\text{Hg}^{2+} + \text{HL}^+ + \text{H}_2\text{O} \rightleftharpoons \text{Hg}(\text{OH})\text{L}^+ + 2\text{H}^+) = -0.10 \pm 0.07,$$

a value which can be compared with -0.30 obtained from data with $X = 0$.

DISCUSSION

In all, approximately 150 potentiometric titrations (including ~4000 experimental points) have been performed in this investigation.* However, as the calculations on this four-component system were very time consuming, the number of experimental data in the calculations have been reduced. It has been shown that when imidazole is added successively to mercury(II) chloride solutions, binary $\text{Hg}^{2+} - \text{L}$ as well as ternary $\text{Hg}^{2+} - \text{Cl}^- - \text{L}$ and $\text{Hg}^{2+} - \text{OH}^- - \text{L}$ complexes are formed. As can be seen from Table 4, the three standard deviations of the formation constants are low and the complexes may thus be considered as well determined.

The results obtained seem to indicate that each of the species Hg^{2+} , HgCl^+ , HgCl_2 and HgCl_3^- form complexes with an imidazole molecule in the solution and the following equilibria could be established



with $\log K = 9.18, 9.18, 3.15$ and 3.08 , respectively. Thus each of the species Hg^{2+} , HgCl^+ ,

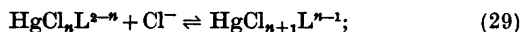
* A complete list of the experimental data is available from this Department.

Table 4. Proposed complexes with formation constants defined according to the equilibria given in the table.

Equilibria	$\log(\beta \pm 3\sigma)$
$\text{Hg}^{2+} + \text{HL}^+ \rightleftharpoons \text{HgL}^{3+} + \text{H}^+$	1.24(12)
$\text{HgCl}_2 + \text{HL}^+ \rightleftharpoons \text{HgClL}^+ + \text{H}^+ + \text{Cl}^-$	-5.53(1)
$\text{HgCl}_2 + 2\text{HL}^+ \rightleftharpoons \text{HgL}_2^{3+} + 2\text{H}^+ + 2\text{Cl}^-$	-11.54(2)
$\text{HgCl}_2 + \text{HL}^+ \rightleftharpoons \text{Hg}(\text{OH})\text{L}^+ + 2\text{H}^+ + 2\text{Cl}^-$	-14.30(2)
$\text{HgCl}_2 + \text{HL}^+ \rightleftharpoons \text{HgCl}_2\text{L}^+ + \text{H}^+$	-4.81(4)
$\text{HgCl}_2 + \text{HL}^+ + \text{Cl}^- \rightleftharpoons \text{HgCl}_2\text{L}^- + \text{H}^+$	-3.79(1)
$\text{HgCl}_2 + 2\text{HL}^+ \rightleftharpoons \text{HgClL}_2^+ + 2\text{H}^+ + \text{Cl}^-$	-10.84(10)

HgCl_2 and HgCl_2^- forms stronger complexes with the imidazole molecule than with the chloride ion, for which the corresponding values are 7.22, 6.78, 1.07 and 1.07.⁵

Alternatively the results may be interpreted as a series of stepwise reactions according to



with $n=0, 1$ and 2 . The stability constants for these reactions are given in Table 5. In this table other stepwise reactions, found in the different binary as well as ternary systems, are also given.

In addition to mono- and dicoordinated species Hg^{2+} forms with Cl^- and L ternary species which are 3- and 4-coordinated. According to Table 5 a sharp decrease in the stepwise constants is observed upon increasing the coordination number above 2. This effect is assumed to be due to a change in configuration, from linear 2-coordinated to tetrahedral or square planar 4-coordinated species. Furthermore, the stepwise constants defining the uptake of a chloride ion to form 3- and 4-coordinated complexes, is of the same mag-

nitude independently of whether the reactant is a binary $\text{Hg}^{2+} - \text{Cl}^-$, $\text{Hg}^{2+} - \text{L}$ or a ternary $\text{Hg}^{2+} - \text{L} - \text{Cl}^-$ complex.

Thus it seems plausible to estimate

$$\log K(\text{HgClL}_2^+ + \text{Cl}^- \rightleftharpoons \text{HgCl}_2\text{L}_2) \sim 1.0$$

according to this finding.

As an attempt to illustrate the stability of the various $\text{Hg}^{2+} - \text{Cl}^- - \text{L}$ complexes, a predominance area diagram is given in Fig. 5.

At low ratios $0 < C/B < 4$ a mixed hydroxo complex $\text{Hg}(\text{OH})\text{L}^+$ is formed. It was found that with $X=0$, the maximum amount of $\text{Hg}(\text{OH})\text{L}^+$ is about 10 % of B , while in a perchlorate solution of Hg^{2+} this complex predominates within certain C/B ranges (cf. Fig. 6) and is formed to about 60 % of B .

Although it is impossible from potentiometric data to decide whether this complex really is a $\text{Hg}(\text{OH})\text{L}^+$ or a $\text{HgC}_3\text{H}_3\text{N}_3^+$ complex, we find the first alternative more probable. This is because

(i) in the equilibrium solutions, where effects due to this complex were observed, the hydrolytic species HgOH^+ and $\text{Hg}(\text{OH})_2$ are formed in significant amounts.

Table 5. Some stepwise reactions with constants calculated by means of formation constants proposed in Table 4 (this work), Table 5 (Ref. 5) and $-\log K_w = 14.22$.¹⁷ The different reactions are defining the stepwise uptake of ligands Cl^- , OH^- and L and should be read horizontally. (Example: $\text{HgCl}^+ 6.78 \text{ HgCl}_2$ stands for $\text{HgCl}^+ + \text{Cl}^- \rightleftharpoons \text{HgCl}_2$ with $\log K = 6.78$).

Hg^{2+}	7.22	HgCl^+	6.78	HgCl_2	1.07	HgCl_2^-	1.07	HgCl_4^{2-}
Hg^{2+}	9.18	HgL^{3+}	7.23	HgClL	0.72	HgCl_2L	1.02	HgCl_2L^-
Hg^{2+}	9.18	HgL^{2+}	9.01	HgL_2	0.70	HgClL_2^+	1.0 ^a	HgCl_2L_2
Hg^{2+}	9.18	HgL^{2+}	12.68	$\text{Hg}(\text{OH})\text{L}^+$				
Hg^{2+}	10.64	HgOH^+	11.56	$\text{Hg}(\text{OH})_2$				
Hg^{2+}	7.22	HgCl^+	11.17	$\text{Hg}(\text{OH})\text{Cl}$				
Hg^{2+}	10.64	HgOH^+	7.71	$\text{Hg}(\text{OH})\text{Cl}$				

^a Estimated value.

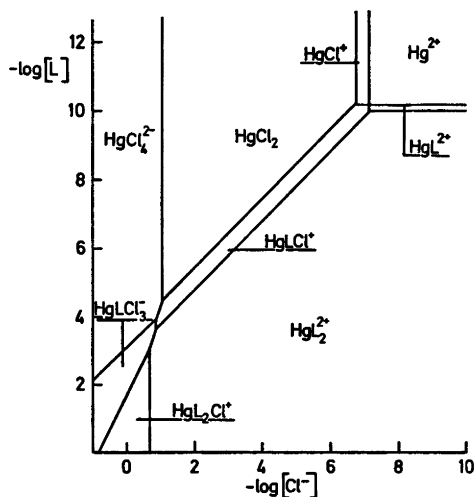
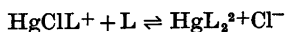
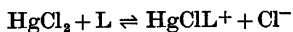
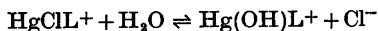


Fig. 5. Predominance area diagram. The composition of the different $Hg^{2+}-Cl-L$ species predominating in a certain $\log[L] - \log[Cl^-]$ area is shown. Along the lines the concentrations of the two adjacent species are equal. In the corner points three species prevail to the same extent. The lines have been calculated by using the constants of Table 5.

(ii) the stepwise equilibria



are well determined and it seems reasonable to assume a similar mechanism



(iii) two coordinated mercury(II) species as a rule are very stable, which favours the hydroxo complex.

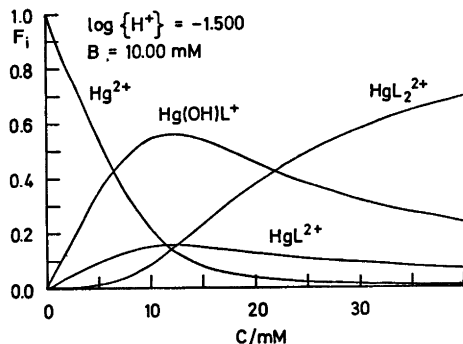


Fig. 6. Distribution diagrams $F_i(C)_{\log A, B}$.

The acidity constant of HgL^{2+} has been calculated to amount to $\log K_a(HgL^{2+}) = -1.54$. Thus this complex is an acid of appreciable strength, stronger than $HgOH^+$, $HgCl^+$ and Hg^{2+} as well, for which the acidity constants are -2.65 , -3.05 and -3.58 , respectively. Thus the introduction of a ligand Cl^- , OH^- or L will increase the acidity of the mercury(II) ion. This is in accordance with earlier findings in the systems $M-L-OH^-$. With $M = Cu^{2+}$,⁹ Ni^{2+} ¹³ and Zn^{2+} ¹⁴ the values found were: $\log K_a(ML^{2+})$, $\log K_a(M^{2+})$; -7.18 , -8.0 ; -9.19 , ≤ -10.5 ; -8.92 , -9.25 , respectively.

Assuming that statistical reasons alone determine the formation of $HgClL^+$ and $Hg(OH)L^+$, equilibrium constants have been calculated according to the formula

$$\beta_{HgL} = 2(\beta_{HgL^{2+}} \cdot \beta_{HgL})^{1/2}$$

Using $\log \beta_{HgL^{2+}} = 18.19$, $\log \beta_{HgL} = 14.00$, $\log \beta_{Hg(OH)} = 22.21$

and $-\log K_w = 14.22$,¹⁷ the calculated values were $\log \beta_{HgL^+} = 16.41$, which is very close to the experimental value of 16.38.

For $Hg(OH)L^+$ the calculated statistical value of $\log \beta_{Hg(OH)L^+}$ is 20.42 compared with 21.90 found experimentally. This great difference between the experimental and statistical value indicates, that the probability of forming $Hg(OH)L^+$ is determined by an entropy as well as by an enthalpy change.

It is interesting to note that the ternary species $Hg(OH)Cl$, $Hg(OH)Br$ ¹⁵ and $Hg(OH)I$ ¹⁶ are formed almost statistically. This seems to indicate that eventual species $HgLBr^+$ and $HgLI^+$ should be formed statistically as in the case with $HgClL^+$.

By comparing the few literature values reported concerning stability constants in the mercury(II)-imidazole system, (see Table 1) great discrepancies are found. However, the formation constants for both HgL^{2+} and HgL_2^{2+} as reported by Marsicano *et al.*² are in rather good accordance with the values deduced in this work.

Acknowledgements. I wish to thank Professor Nils Ingri for much valuable advice, for his great interest, and for all the facilities placed at my disposal. Thanks are also due to Lab.ing. Agneta Nordin for valuable help with some of the measurements. The English of the present paper has been corrected by Dr. Michael

Sharp. The work forms part of a program financially supported by the Swedish Natural Science Research Council.

REFERENCES

1. Brooks, P. and Davidson, N. *J. Am. Chem. Soc.* **82** (1960) 2118.
2. Marsicano, F., Hancock, R. D. and Finkelstein, N. P. *Private communications*.
3. Smith, J. C. *Diss.*, Kansas State Univ., Lawrence 1961.
4. Sjöberg, S. *Acta Chem. Scand.* **25** (1971) 2149.
5. Sjöberg, S. *Acta Chem. Scand. A* **31** (1977) 705.
6. Biedermann, G. and Sillén, L. G. *Ark. Kemi* **5** (1953) 425.
7. Gran, G. *Acta Chem. Scand.* **4** (1950) 559.
8. Sjöberg, S. *Acta Chem. Scand.* **27** (1973) 3721.
9. Ingri, N. and Sillén, L. G. *Ark. Kemi* **23** (1964) 97.
10. Arnek, R., Sillén, L. G. and Wahlberg, O. *Ark. Kemi* **31** (1969) 353; Brauner, P., Sillén, L. G. and Whiteker, R. *Ark. Kemi* **31** (1969) 365.
11. Sillén, L. G. *Acta Chem. Scand.* **16** (1962) 159; Sillén, L. G. and Warnqvist, B. *Ark. Kemi* **31** (1969) 341.
12. Biedermann, G. and Sillén, L. G. *Ark. Kemi* **5** (1953) 425.
13. Forsling, W. and Sjöberg, S. *Acta Chem. Scand. A* **29** (1975) 569.
14. Forsling, W. *Private communications*.
15. Ahlberg, I. and Leden, I. *Trans. R. Inst. Technol. Stockholm* **249** (1972) 17.
16. Ahlberg, I. *Acta Chem. Scand.* **27** (1973) 3003.
17. Ingri, N., Lagerström, G., Frydman, M. and Sillén, L. G. *Acta Chem. Scand.* **11** (1957) 1034.

Received March 8, 1977.

Metal Complexes with Mixed Ligands. 13. A Combined Potentiometric and Spectrophotometric Study of the Systems Cu^{2+} —Imidazole, Cu^{2+} — OH^- —Imidazole and Cu^{2+} — Cl^- —Imidazole in 3.0 M $(\text{Na})\text{ClO}_4$, Cl Media

STAFFAN SJÖBERG

Department of Inorganic Chemistry, University of Umeå, S-901 87 Umeå, Sweden

Equilibria between copper(II), imidazole ($\text{C}_3\text{H}_4\text{N}_2$; L), OH^- and Cl^- were studied at 25 °C by means of a combined potentiometric (glass electrode) and spectrophotometric method. The measurements were performed in media consisting of 3.0 M $(\text{Na})\text{ClO}_4$, 3.0 M $(\text{Na})\text{Cl}$ and mixtures of these two with $0 \leq [\text{Cl}^-] \leq 3.0$ M. Besides pure binary species CuL_n^{2+} , with $n = 1, 2, 3$ and 4, data could be explained with the ternary complexes $\text{Cu}(\text{OH})\text{L}^+$, $\text{Cu}_2(\text{OH})_2\text{L}_2^{2+}$ and $\text{Cu}_2(\text{OH})_2\text{L}_4^{2+}$ in addition to the ternary chloro species CuLCl^+ , CuLCl_2 , CuL_2Cl^+ , CuL_2Cl_2 and CuL_3Cl^+ . Formation constants as well as molar absorption coefficients for the different species were evaluated within the wavelength range 450–750 nm. Data were analyzed with the least squares computer program LETA-GROPVRID.

In parts 1¹ and 7² of this series, equilibria in the system Cu^{2+} — OH^- —imidazole (L) were studied at 25 °C in the media 3.0 M $(\text{Na})\text{ClO}_4$, 3.0 M $(\text{Na})\text{Cl}$ and 5.0 M $(\text{Na})\text{Cl}$. The results showed that besides a series of mononuclear CuL_n^{2+} complexes with $n = 1, \dots, 6$, the ternary species $\text{Cu}(\text{OH})\text{L}^+$, $\text{Cu}_2(\text{OH})_2\text{L}_2^{2+}$ and $\text{Cu}_2(\text{OH})_2\text{L}_4^{2+}$ were formed. By comparing the results obtained in 3.0 M $(\text{Na})\text{ClO}_4$ and 3.0 M $(\text{Na})\text{Cl}$ media, indications for the formation of ternary Cu^{2+} — $\text{C}_3\text{H}_4\text{N}_2$ — Cl^- complexes were also found.

The aim of the present investigation was to confirm the results obtained from these emf-investigations by employing a spectrophotometric method in which both $\log [\text{H}^+]$ and absorbance values are measured. Furthermore,

in an attempt to determine formation of eventual ternary Cu^{2+} — $\text{C}_3\text{H}_4\text{N}_2$ — Cl^- complexes, measurements were performed in media consisting of mixtures of 3.0 M $(\text{Na})\text{ClO}_4$ and 3.0 M $(\text{Na})\text{Cl}$ with $0 \leq [\text{Cl}^-] \leq 3.0$ M. The results of these investigations are discussed below.

EXPERIMENTAL

Chemicals and analysis. All solutions used were prepared and analyzed as described earlier.^{1,2}

Apparatus. The cell arrangement and experimental details of the emf measurements are fully described in Refs. 1 and 2.

The spectrophotometer used was a Heath model 721 single beam instrument with an automatic sample-reference changer combined with an automated potentiometric titrator. A sample cell of flow-through type with a path length of 1.001 cm (HELLMA, type OS) was used. Wavelengths greater than 750 nm were not investigated due to the low sensitivity of the photo cell within this wavelength range. A detailed description of the automated potentiometric and spectrophotometric titration system will be given in a forthcoming paper by Ginstrup, Lyhamn and Ingri.³

Method. The present study was carried out as a series of titrations in which both emf and absorbance values were measured. The measurements were performed at 25 °C and were divided into series in which the ionic medium consisted of 3.0 M $(\text{Na})\text{ClO}_4$, 3.0 M $(\text{Na})\text{Cl}$ or mixtures of these two. In the titrations the total concentrations of copper(II), B , and imidazole, C , were either kept constant or varied, while the ratio C/B was always held constant. The total concentration of hydrogen

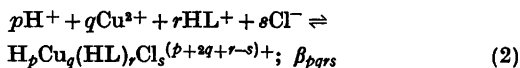
ions, H , was calculated over the zero level Cu^{2+} , $\text{C}_3\text{H}_5\text{N}_2^+$ and H_2O and the free hydrogen ion concentration, h , was varied by addition of H^+ and measured with a glass electrode. h was determined according to the relation:

$$E = E_0 + 59.157 \log h + E_j \quad (1)$$

where E_0 is a constant determined in acid solutions where complex formation could be neglected. In some cases E_0 was determined in solutions of known Z -values ($Z = (h - H)/B$). The liquid junction potential, $E_j = -16.7h$ mV was used in 3.0 M $(\text{Na})\text{ClO}_4$,⁴ 3.0 M $(\text{Na})\text{Cl}$ ⁵ as well as in mixtures of these two media. It has earlier been shown⁵ that within the concentration range $0 \leq X \leq 3.0$ M with $[\text{ClO}_4^-] + X = 3.0$ M the concentration scale for H^+ remains constant. No change in E_0 could be found on replacing ClO_4^- by Cl^- or *vice versa*. X stands for the total concentration of chloride ions.

The combined emf and spectrophotometric measurements were performed so that for each titration point the emf was measured until equilibrium was obtained and then the transmittance, T , was recorded at a number of different wavelengths ($N\lambda$). As reference a 3.0 M NaClO_4 or 3.0 M NaCl solution was used. The relation between the absorbance, OD , and the concentrations, c_i , of the various absorbing species is given by the equation: $OD = l \sum \epsilon_i c_i$ where ϵ_i is the molar absorption coefficient for the absorbing species i at the wavelength λ . The spectrophotometric measurements thus give data (OD , $\log h$, H , B , C , X) $N\lambda$, (after recalculating T to OD).

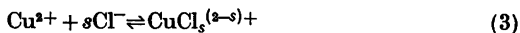
We assume the presence of four-component equilibria of the general form:



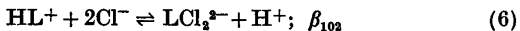
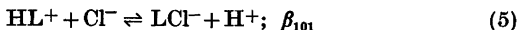
It is convenient to write complexes where $-p = r$ as $\text{Cu}_q\text{L}_p\text{Cl}_s$ and the stability constants as β_{nqs} . This terminology is used throughout this paper whenever possible.

Besides the four-component equilibria in (2) we have:

(i) the complex formation between Cu^{2+} and Cl^- :

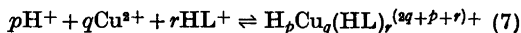


(ii) the imidazole equilibria, which within the concentration range $0 \leq X \leq 3.0$ M with $[\text{ClO}_4^-] + X = 3.0$ M are⁶



with $\log K_a = -7.940$, $\log \beta_{101} = -8.641$ and $\log \beta_{102} = -9.279$.

(iii) the copper(II) imidazole equilibria



with equilibrium constants given in Table 1. In the present study hydrolytic equilibria of the copper(II) ion could be neglected.

Equilibria (3)–(7) were determined in separate investigations and are assumed to be known in calculations concerning the four-component equilibria.

Data treatment. In the evaluation of the experimental data, the LETAGROP⁶ version ETITR⁷ was applied to the emf-data, and the error squares sum $U = \sum (Z_{\text{calc}} - Z_C)^2$, where $Z_C = (h - H)/C$ was minimized. In calculations on the combined emf and spectrophotometric data, the LETAGROP version TITRERSPEFO⁸ was used, and $U = \sum (OD_{\text{calc}} - OD)^2$ was minimized.

At the present time this program is unable to treat a four-component system. However, it will be possible to reduce the four-component system $\text{H}^+ - \text{Cu}^{2+} - \text{C}_3\text{H}_5\text{N}_2^+ - \text{Cl}^-$ to the three-component system $\text{C}_3\text{H}_5\text{N}_2^+ - \text{Cu}^{2+} - \text{Cl}^-$ under the assumption that $-p = r$ in (2) *i.e.* only complexes of the type $\text{Cu}_q\text{L}_p\text{Cl}_s^{(2q-s)+}$ are formed. With this assumption $[\text{L}]$ can be calculated using the relation

$$[\text{L}] = k_a h^{-1} [\text{HL}^+] = k_a h^{-1} [C - (h - H)] \quad (8)$$

Thus as input to the program data in the form (OD , $\log[\text{L}]$, B , X) $N\lambda$ are given instead of (OD , $\log h$, B , C , X) $N\lambda$.

The different standard deviations given, $3\sigma(\log\beta)$ and $\sigma(\epsilon)$, were defined and calculated according to Sillén.⁹ The computation was performed on a CD 3300 computer.

DATA, CALCULATIONS AND RESULTS

The complex formation between copper(II) and imidazole has already been investigated in 3.0 M $(\text{Na})\text{ClO}_4$ and 3.0 M $(\text{Na})\text{Cl}$ media, by using the emf-titration method. Results of these measurements are found in Refs. 1 and 2. In an attempt to confirm the different binary $\text{Cu}^{2+} - \text{L}$ as well as ternary $\text{Cu}^{2+} - \text{OH}^- - \text{L}$ complexes proposed, spectrophotometric measurements in which both $\log h$ and absorbance were measured, were performed. In addition the formation of ternary $\text{Cu}^{2+} - \text{L} - \text{Cl}^-$ complexes was investigated by employing this combined emf and spectrophotometric method. The results obtained in the different investigations are given below.

(i) *Copper(II) imidazoles in 3.0 M (Na)ClO₄ medium.* In all 11 different titrations, including

186 titration points, were performed. As 16 different wavelengths, ranging from 450 to 750 nm, with 20 nm interval were investigated 2976 measured absorbance values were collected. The following concentration ranges were investigated: $0.004 \leq B \leq 0.020$ M, $0.025 \leq C \leq 0.320$ M, $3.0 \leq -\log h \leq 6.7$ with $C/B = 2.5, 3.5, 8, 16, 32, \text{ and } 64$. With $C/B \geq 8$ a series of mononuclear CuL_n^{2+} species was found to predominate, while with $C/B < 4$ the ternary complexes $\text{Cu}(\text{OH})\text{L}^+$, $\text{Cu}_2(\text{OH})_2\text{L}_2^{2+}$ and $\text{Cu}_2(\text{OH})_2\text{L}_4^{2+}$ are formed in addition. A part of the experimental data is visualized as $\bar{n}(\log[\text{L}])$ plots² in Fig. 1.

In the LETAGROP (TITRERSPEFO) calculations data with $C/B \geq 8$ were at first treated. The calculations were started with formation constants for the species CuL_n^{2+} , with $n = 1, 2, 3$ and 4 taken from Ref. 2. Molar absorption coefficients ϵ_{n1n} for each of the different copper(II) species were then calculated and it was found that a satisfactory fit to the experimental data was obtained. In the subsequent calculations, data with $0 \leq \bar{n} \leq 1.5$ were treated and β_{-111} , β_{-212} , ϵ_{-111} and ϵ_{-212} were covaried, while β_{-313} , β_{-414} , ϵ_{-313} , and ϵ_{-414} were kept constant. The results of this calculation are given in Table 1. In a similar way data with $1.5 \leq \bar{n} \leq 3.5$ were treated: β_{-313} ,

β_{-414} , ϵ_{-313} and ϵ_{-414} were covaried while the new refined values of β_{-111} , β_{-212} , ϵ_{-111} and ϵ_{-212} were kept constant.

As can be seen from Table 1 the values of the different β_{-n1n} constants were obtained with very low errors [$3\sigma(\log \beta_{-n1n}) \leq 0.03$] and they are in agreement with those obtained from the emf-investigation.

Data with $C/B < 4$, where the ternary $\text{Cu}^{2+} - \text{L} - \text{OH}^-$ complexes are formed, were treated as follows: With knowledge of the formation constants of these species molar absorption coefficients at each wavelength investigated could be calculated. As the amounts of $\text{Cu}(\text{OH})\text{L}^+$, $\text{Cu}_2(\text{OH})_2\text{L}_2^{2+}$ are less than 10 % of B within the C/B ratios studied, ϵ_{-211} and ϵ_{-422} were obtained with relatively high errors and no attempts were made to refine their formation constants. However, the formation constant of $\text{Cu}_2(\text{OH})_2\text{L}_4^{2+}$ was varied in one calculation giving $\log \beta_{-424} = -27.08 \pm 0.07$ which can be compared with the value -27.18 ± 0.02 obtained in the emf-investigation.

Molar absorption coefficients of the different $\text{Cu}^{2+} - \text{L}$ and $\text{Cu}^{2+} - \text{L} - \text{OH}^-$ complexes are given in Table 2.

(ii) *Copper(II) imidazoles in 3.0 M (Na)Cl medium.* 5 different titrations yielding 77 titration points were performed, the following $B(C)$ combinations were investigated 4(242), 10(151), 20(151), 20(302), 42(302) mM, respectively, with $3.0 \leq -\log h \leq 6.7$. These experimental data are visualized as an $\bar{n}(\log[\text{L}])$ plot in Fig. 1. The same wavelength ranges as in (i) were covered, thus yielding 1232 absorbance values. The calculations were performed as under (i) and the formation constants are given in Table 1. Molar absorption coefficients are visualized in Fig. 2b. Formation constants as well as molar absorption coefficients determined in this medium are "conditional" as in the different species chloride ions most probably are coordinated. This is strongly indicated by comparing the spectra for the different mononuclear $\text{Cu}^{2+} - \text{L}$ species given in Figs 2a and 2b. As can be seen from these figures the chloride medium appears to cause a shift of the absorption maximum to higher wavelengths and an increase of the molar absorbance for each of the species Cu^{2+} , CuL^{2+} , CuL_2^{2+} and CuL_3^{2+} was found, while the spectrum of CuL_4^{2+} was almost identical in the two media.

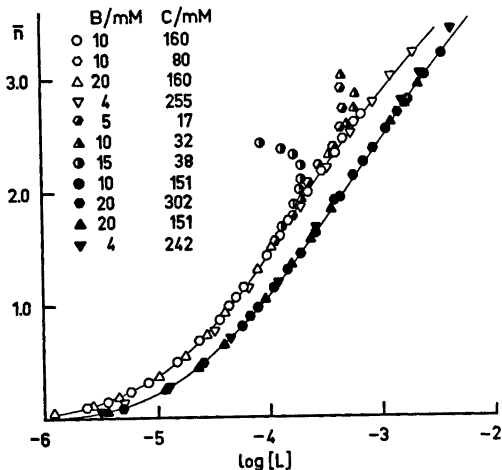


Fig. 1. Parts of experimental data plotted as curves $\bar{n}(\log[\text{L}])$ in 3.0 M $(\text{Na})\text{ClO}_4$ (left) and $(\text{Na})\text{Cl}$ (right) media. The full curves were calculated with the set of constants given in Table 1 (emf + spect.):

Table 1. Results of LETAGROP calculations concerning the equilibria: $pH^+ + qCu^{2+} + rC_3H_5N_3^+ \rightleftharpoons H_pCu_q(C_3H_5N_3^+)_r(p+qr+r^2)^+$.

Medium	Method	$\log(\beta_{\text{par}} \pm 3\sigma)$						Remark
		-111	-212	-313	-414	-211	-422	-624
3.0 M (Na)ClO ₄	emf	-3.27(3)	-7.23(3)	-11.82(4)	-17.04(4)	-10.44(6)	-17.90(7)	-27.18(2)
	emf + spect.	-3.28(3)	-7.24(3)	-11.82	-17.04	-	-	-
	emf + spect.	-3.28	-7.24	-11.80(2)	-17.18(1)	-	-	-
3.0 M (Na)Cl	emf	-3.24(2)	-7.21(1)	-11.85(2)	-17.17(2)	-10.44	-17.90	-27.08(7)
	emf + spect.	-3.21(1)	-7.20(2)	-11.85	-17.17	-	-	-
	emf + spect.	-3.21	-7.20	-11.84(2)	-17.13(1)	-	-	-

^a This work.Table 2. Molar absorption coefficients for different copper(II) complexes in 3.0 M (Na)ClO₄ medium (L=C₃H₅N₃).

λ/nm	Cu ²⁺	CuL ²⁺	CuL ₂ ²⁺	CuL ₃ ²⁺	CuL ₄ ²⁺	Cu(OH)L ⁺	Cu ₂ (OH) ₂ L ₂ ²⁺	Cu ₃ (OH) ₃ L ₃ ²⁺	$\sigma(OD) \times 10^3$
450	0.1(1)	0.1(1)	0.0(4)	0.6(2)	2.4(11)	-	-	-	1
470	0.1(1)	0.1(1)	0.1(1)	1.0(2)	9.6(10)	-	-	-	1
490	0.1(1)	0.1(1)	0.6(1)	2.9(2)	20.2(10)	-	-	-	1
510	0.1(1)	0.1(1)	1.7(2)	6.5(2)	34.8(10)	-	-	-	1
530	0.2(2)	0.4(1)	3.2(2)	13.1(2)	48.7(14)	0.0(9)	18.5(14)	49.2(21)	2
550	0.3(2)	0.9(1)	6.0(2)	21.6(2)	59.4(16)	0.0(11)	33.9(11)	65.8(17)	2
570	0.5(3)	1.9(1)	10.1(2)	30.9(3)	61.9(20)	0.0(11)	54.6(11)	80.3(17)	2
590	0.8(3)	3.4(1)	15.5(2)	38.1(3)	62.2(20)	6.6(13)	57.2(32)	97.2(22)	3
610	1.3(2)	5.7(1)	21.0(1)	43.4(3)	55.7(19)	16.6(20)	52.3(48)	108.0(33)	2
630	1.9(1)	8.3(1)	26.2(1)	44.9(3)	49.4(22)	19.5(21)	57.5(49)	107.7(33)	3
650	3.0(1)	11.5(1)	29.9(2)	43.7(3)	42.9(22)	23.1(16)	68.1(38)	94.5(26)	2
670	4.3(1)	14.5(1)	32.1(1)	40.8(3)	38.3(19)	32.6(20)	53.0(47)	88.1(32)	2
690	5.9(1)	17.0(1)	32.8(1)	37.4(3)	32.2(19)	30.7(17)	51.4(41)	77.2(28)	2
710	7.5(1)	18.7(1)	32.3(1)	33.3(3)	27.2(17)	30.5(24)	46.3(58)	67.6(40)	2
730	9.0(1)	19.9(1)	30.6(2)	29.7(3)	24.4(19)	31.2(14)	32.6(32)	47.2(40)	2
750	10.3(2)	20.2(1)	29.0(1)	26.4(3)	19.6(16)	24.9(24)	20.6(58)	39.7(22)	2

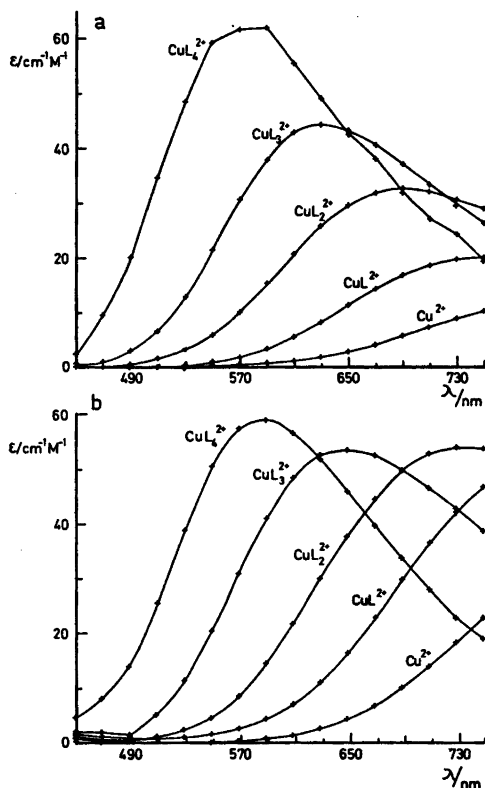


Fig. 2. Molar absorption coefficients, ϵ $\text{cm}^{-1} \text{M}^{-1}$, as a function of the wavelength, λ nm, plotted for the mononuclear complexes CuL_n^{2+} with $n=0, 1, 2, 3$ and 4 . (a) 3.0 M (Na)ClO_4 and (b) 3.0 M (Na)Cl medium.

These pronounced spectral changes indicate that ternary complexes, in which up to three imidazole molecules are coordinated, are formed.

(iii) *Copper(II) chlorides in mixtures of 3.0 M (Na)ClO₄ and 3.0 M (Na)Cl media.* In an attempt to determine formation constants of different $\text{Cu}^{2+} - \text{Cl}^-$ equilibria, titrations were performed at a constant acidity level ($[\text{H}^+] = 0.01 \text{ M}$), where eventual hydrolysis reactions could be neglected. 5 different titrations were performed yielding 66 titration points and 1056 absorbance values. The concentration ranges investigated were $0.010 \leq B \leq 0.040 \text{ M}$ and $0 \leq X \leq 3.0 \text{ M}$. The calculations showed that within the concentration ranges investigated formation of the complexes CuCl^+ and CuCl_2 could be established. $K(\text{Cu}^{2+} + \text{Cl}^- \rightleftharpoons \text{CuCl}^+) = 0.99 \pm 0.15 \text{ M}^{-1}$ and $K(\text{CuCl}^+ + \text{Cl}^- \rightleftharpoons \text{CuCl}_2) = 0.40 \pm 0.06 \text{ M}^{-1}$ are values in good agreement with those reported by Bjerrum,¹⁰ Lister *et al.*¹¹ and McConell *et al.*¹² The standard deviation $\sigma(OD)$ at the different wavelengths ranged from 0.001 to 0.003, thus a good fit to experimental data at each wavelength studied was obtained.

(iv) *Copper(II) imidazoles in mixtures of 3.0 M (Na)ClO₄ and 3.0 M (Na)Cl.* For determining the formation of ternary $\text{Cu}^{2+} - \text{C}_2\text{H}_4\text{N}_2 - \text{Cl}^-$ complexes measurements were performed in the four-component system $\text{H}^+ - \text{Cu}^{2+} - \text{C}_2\text{H}_4\text{N}_2^+ - \text{Cl}^-$. In the measurements the concentration ranges $0.003 \leq B \leq 0.02 \text{ M}$, $0.04 \leq C \leq 0.3 \text{ M}$, $0 \leq X \leq 3.0 \text{ M}$ and $3.9 \leq -\log h \leq 6.5$ were investigated. The measurements were performed at different constant levels of Z ($Z=0.5, 1.3, 1.5, 2.5$ and 4.2) and X was varied by the addition of a solution where $X=3.0 \text{ M}$ to a solution where $[\text{ClO}_4^-]=3.0 \text{ M}$ or *vice versa*. In this way it was possible to cover the range $0 \leq X \leq 3.0 \text{ M}$. H , B and C were either kept constant or varied in the measurement. The experiments thus give data $(OD, \log h, H, B, C, X)_{N\lambda}$. In the LETAGROP calculations the two data sets $(\log h, H, B, C, X)$ and $(OD, \log[L], B, X)_{N\lambda}$ were treated separately in order to assess their consistency.

In these calculations equilibria (3)–(7) were assumed to be known and no attempts were made to adjust their equilibrium constants.

(log h, H, B, C, X) data. 13 different titrations including 197 experimental points were treated in the LETAGROP calculations. The ternary complexes CuLCl^+ , CuLCl_2 , CuL_2Cl^+ , CuL_2Cl_2 and CuL_3Cl^+ were included in the equilibrium model. A final covariation of formation constants for all these species, showed that a very good fit to experimental data was obtained giving $\sigma(Z_C) \times 1000 = 1.8$ (cf. Table 3). In one calculation formation constants for CuCl^+ and CuCl_2 were covaried with β_{111} and β_{112} on data with $Z \leq 1.3$. This calculation gave $\beta_{011} = 1.20 \pm 0.03 \text{ M}^{-1}$ and $\beta_{012} = 0.25 \pm 0.005 \text{ M}^{-2}$, values which can be compared with $0.99 \pm 0.15 \text{ M}^{-1}$ and $0.40 \pm 0.06 \text{ M}^{-2}$, respectively, obtained from the spectrophotometric investigation.

($OD, \log[L], B, X$)_{Nλ} data. To confirm formation of the different ternary species, the combined emf and spectrophotometric data were treated. 9 different titrations including 164 titration points and 1312 absorbance values

Table 3. Results of LETAGROP calculations concerning formation of ternary $\text{Cu}^{2+} - \text{L}(\text{C}_3\text{H}_4\text{N}_2) - \text{Cl}^-$ complexes. The equilibria are defined according to: $\text{Cu}^{2+} + n\text{HL} + s\text{Cl}^- = \text{CuL}_n\text{Cl}_s^{(2-s)+} + n\text{H}^+$; β_{n1s} . The errors 3σ ($\log \beta_{n1s}$) are given when the corresponding equilibrium constant has been varied.

$\sigma(Z) \times 10^3$	CuCl^+ $\log(\beta_{011} \pm 3\sigma)$	CuCl_2 $\log(\beta_{012} \pm 3\sigma)$	CuLCl^+ $\log(\beta_{111} \pm 3\sigma)$	CuLCl_2 $\log(\beta_{112} \pm 3\sigma)$	CuL_2Cl^+ $\log(\beta_{211} \pm 3\sigma)$	CuL_2Cl_2 $\log(\beta_{212} \pm 3\sigma)$	CuL_3Cl^+ $\log(\beta_{311} \pm 3\sigma)$	Remark
1.8	0.00 ^a	-0.40 ^a	-3.19(3)	-3.88(11)	-7.50(5)	-7.54(3)	-11.56(2)	$0 \leq Z \leq 4.3$
0.3	0.08(1)	-0.60(3)	-3.16(1)	-3.88(1)	-7.50	-7.54	-11.56	$0 \leq Z \leq 1.3$
0.002 ^c	0.000	-0.40	-3.15(1)	-3.92(7)	-7.50	-7.54	-11.56	^b

^a Values from a separate spectrophotometric investigation. ^b A calculation based upon (OD, $\log[\text{C}_3\text{H}_4\text{N}_2]$, B, X)_{N1} data. ^c $\sigma(\text{OD})$.

were treated in the calculations. As the addition of chloride ions to a copper(II) imidazole solution was found to displace the absorption spectra to higher wavelengths, 8 different wavelengths ranging from 610 to 750 nm were investigated. The concentrations ranges were mainly the same as given under (iv) except that solutions with $Z=1.3$ and 4.2 were not investigated.

By assuming the different $\text{Cu}^{2+} - \text{Cl}^-$ and $\text{Cu}^{2+} - \text{L}$ equilibria with formation constants and molar absorption coefficients as obtained under (iii) and (i) to be known the following calculations were performed: the different ternary $\text{Cu}^{2+} - \text{L} - \text{Cl}^-$ complexes, with their formation constants as obtained from calculations on the emf data, were included in the equilibrium model. This calculation showed that a satisfactory fit to experimental data was obtained. $\sigma(\text{OD})$ at each wavelength varied between 0.001 and 0.003 and any discrepancies within the wavelength range investigated could not be found, which is in support of the equilibrium model proposed.

The molar absorption coefficients of the ternary complexes are given in Table 4.

DISCUSSION

The combined emf and spectrophotometric titration technique, in which both $\log h$ and absorbance values were measured, was found to yield accurate and extensive experimental data in a convenient way. In this study 30 different titrations, including 527 titration points and approximately 6500 absorbance values, were treated. As approximately 250 different parameters (molar absorption coefficients for each absorbing species at each wavelength plus a number of formation constants) were determined, it seems necessary to collect this vast data amount. Unless automated titration procedures are available this collecting of data is unrealistic.*

With regard to the results of the different investigations, there is very good agreement between formation constants of the different CuL_n^{2+} complexes with $n=1, 2, 3$ and 4, as

* A complete list of the experimental data, including the spectrophotometric data, is available from this Department.

Table 4. Molar absorption coefficients for different $\text{Cu}^{2+} - \text{C}_3\text{H}_4\text{N}_2 - \text{Cl}^-$ complexes obtained in a LETAGROP calculation ($\text{L} = \text{C}_3\text{H}_4\text{N}_2$).

λ/nm	$\varepsilon \pm \sigma(\varepsilon)/\text{cm}^{-1} \text{M}^{-1}$		CuLCl^+	CuLCl_2	CuL_2Cl^+	CuL_2Cl_2	CuL_3Cl^+	$\sigma(OD) \times 10^3$
	CuCl^+	CuCl_2						
610	1.4(0)	1.4(0)	6.6(3)	3.8(9)	11.4(19)	23.1(7)	45.7(6)	3
630	2.7(0)	2.4(0)	10.6(4)	11.3(2)	17.7(25)	30.0(10)	49.5(8)	3
650	4.4(1)	4.4(1)	14.7(3)	20.0(7)	24.5(16)	37.7(6)	50.1(5)	2
670	6.9(0)	7.2(0)	18.8(2)	34.1(7)	30.7(15)	44.4(6)	48.0(5)	2
690	9.9(0)	11.3(1)	22.7(2)	49.8(7)	32.4(14)	50.7(6)	44.9(5)	2
710	13.4(1)	16.5(1)	25.5(2)	66.8(7)	31.8(15)	55.5(6)	41.7(5)	2
730	16.8(1)	22.6(1)	27.6(3)	83.3(8)	30.7(16)	57.6(6)	37.6(5)	2
750	19.9(1)	29.2(1)	28.4(3)	95.8(9)	30.5(20)	58.2(8)	34.1(7)	3

evaluated in this study compared with those reported from the emf investigations^{1,2} (cf. Table 1). The standard deviations of the constants valid in 3.0 M (Na)ClO₄ and 3.0 M (Na)Cl media are less than 0.03 logarithmic units, values which are of the same magnitude as those obtained in the emf investigations. Thus it may be concluded that the combined emf and spectrophotometric measurements strongly support the complexes and complex constants earlier proposed.

The formation of ternary $\text{Cu}^{2+} - \text{L} - \text{OH}^-$ complexes were also investigated by this spectrophotometric method. The agreement in $\log \beta_{-624}$ as obtained in this study (-27.08 ± 0.07) compared with the value earlier proposed² (-27.18 ± 0.02) is satisfactory and confirms the existence of the $\text{Cu}_2(\text{OH})_2\text{L}_4^{2+}$ complex.

The formation of binary $\text{Cu}^{2+} - \text{Cl}^-$ and ternary $\text{Cu}^{2+} - \text{L} - \text{Cl}^-$ complexes was also studied. Within the concentration range $0 \leq X \leq 3.0$ M, the binary CuCl^+ and CuCl_2 as well as the ternary CuLCl^+ , CuLCl_2 , CuL_2Cl^+ , CuL_2Cl_2 and CuL_3Cl^+ complexes were evaluated with formation constants given in Table 3. According to this Table $3\sigma(\log \beta_{\text{ms}}) \leq 0.05$ and the equilibria must be considered as well-determined. Distributions of the different complexes are visualized in Figs. 3a–3c. As can be seen from these diagrams the ternary $\text{Cu}^{2+} - \text{L} - \text{Cl}^-$ complexes are formed to about 15–60 % of B, with the two- and four-coordinated species dominating.

The results obtained can be interpreted as series of stepwise reactions in which chloride ions are successively coordinated to a CuL_n^{2+} .

Table 5. Some stepwise reactions with constants (K or $\log K$) calculated by means of formation constants given in Ref. 2 and Table 4. The different reactions define the stepwise uptake of ligands (a) $\text{C}_3\text{H}_4\text{N}_2(\text{L})$ and (b) Cl^- , and are to be read horizontally. ($\text{CuLCl}^+ + 3.62 \text{ CuL}_2\text{Cl}^+$ stands for $\text{CuLCl}^+ + \text{L} \rightleftharpoons \text{CuL}_2\text{Cl}^+$ with $\log K = 3.62$).

(a)	$\log K$		$\log K$		$\log K$	
Cu^{2+}	4.65	CuL^{2+}	3.95	CuL_2^{2+}	3.32	CuL_3^{2+}
CuCl^+	4.75	CuLCl^+	3.62	CuL_2Cl^+	3.89	CuL_3Cl^+
CuCl_2	4.46	CuLCl_2	3.98	CuL_2Cl_2		
(b)	K		K			
Cu^{2+}	0.99	CuCl^+	0.40	CuCl_2		
CuL^{2+}	1.04	CuLCl^+	0.40	CuLCl_2		
CuL_2^{2+}	0.51	CuL_2Cl^+	0.94	CuL_2Cl_2		
CuL_3^{2+}	1.90	CuL_3Cl^+				

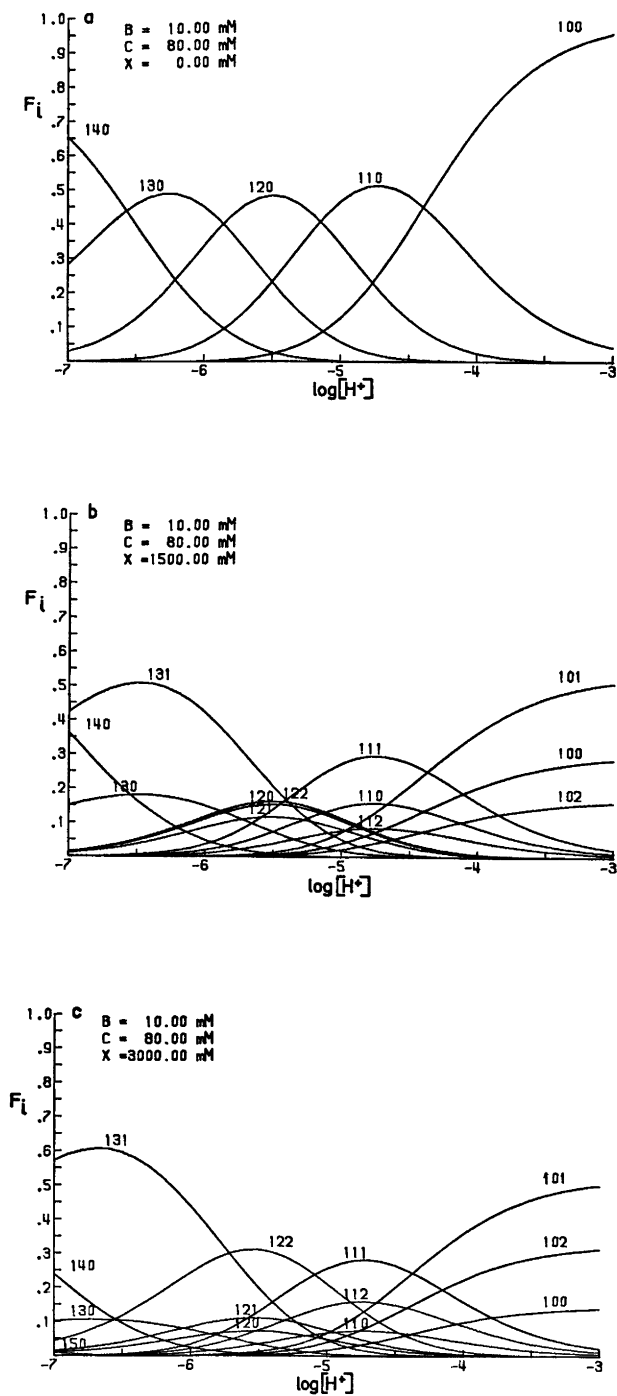


Fig. 3. Distribution diagrams $F_i(\log h)_{B,C,X}$ for the different copper(II) imidazole complexes. The computer program SOLGASWATER¹⁷ was used in the calculations. The figures denote the number of Cu^{2+} , $C_3H_4N_2$, and Cl^- in the complexes.

core with $n=0, 1, 2$ and 3 or alternatively as imidazole molecules coordinated to a $\text{CuCl}_n^{(2-n)+}$ core with $n=0, 1, 2$. Stepwise constants of these reactions are given in Table 5.

According to this table the successive uptake of an imidazole molecule proceeds easily irrespective of whether the core is Cu^{2+} , CuCl^+ or CuCl_2 . A similar trend was found in the $\text{Hg}^{2+}-\text{C}_3\text{H}_4\text{N}_2-\text{Cl}^-$ system,⁵ *i.e.* $K(\text{Hg}^{2+} + \text{C}_3\text{H}_4\text{N}_2 \rightleftharpoons \text{HgC}_3\text{H}_4\text{N}_2^{2+}) \approx K(\text{HgCl}^+ + \text{C}_3\text{H}_4\text{N}_2 \rightleftharpoons \text{HgClC}_3\text{H}_4\text{N}_2)$ and $K(\text{HgCl}_2 + \text{C}_3\text{H}_4\text{N}_2 \rightleftharpoons \text{HgCl}_2\text{C}_3\text{H}_4\text{N}_2) \approx K(\text{HgCl}_2^- + \text{C}_3\text{H}_4\text{N}_2 \rightleftharpoons \text{HgCl}_2\text{C}_3\text{H}_4\text{N}_2^-)$. In the Ni^{2+} -system¹³ this relation was also found concerning formation of $\text{NiC}_3\text{H}_4\text{N}_2^{2+}$ and $\text{NiClC}_3\text{H}_4\text{N}_2^+$.

From Table 5 it can also be seen that chloride ions approximately coordinate the Cu^{2+} -ion as easily as the different $\text{Cu}^{2+}-\text{L}$ complexes.

These findings indicate that approximate stepwise constants defining formation of these ternary species should be given by the corresponding binary $\text{Cu}^{2+}-\text{L}$ or $\text{Cu}^{2+}-\text{Cl}^-$ constants. These findings are also valid in the Hg^{2+} - and Ni^{2+} -systems.

The spectrophotometric investigations not only confirmed results obtained in the different emf investigations, but also provided characteristic optical spectra for each of the different copper(II) species. As the wavelength range was restricted to $\lambda \leq 750$ nm complete

optical spectra of all species, especially the ternary $\text{Cu}^{2+}-\text{L}-\text{Cl}^-$ species were not obtained. However, complementary measurements with $\lambda > 750$ nm are planned.

The wavelength (λ_{max}) where absorption maxima (ϵ_{max}) for some copper(II) complexes were found are given in Table 6. As can be seen from this table the strength of the ligand field increases (λ_{max} decreases) with the number of imidazole molecules coordinated in the different CuL_n^{2+} complexes ($n=0, 1, 2, 3$ and 4).

Furthermore ϵ_{max} also increases with n . These findings are consistent with results obtained from other systems in which nitrogen containing ligands are successively coordinated to the copper(II) ion.^{12,15}

With regard to the spectra of the different $\text{Cu}^{2+}-\text{L}-\text{OH}^-$ complexes $\lambda_{\text{max}}=610$ nm and $\epsilon_{\text{max}}=108$ $\text{cm}^{-1} \text{M}^{-1}$ were found for the $\text{Cu}_2(\text{OH})_2\text{L}_4^{2+}$ complex. These values are consistent with those reported by Harris *et al.*¹⁶ for $\text{Cu}_2(\text{OH})_2\text{L}_2^{2+}$ complexes with $\text{L}=2,2'$ -bipyridyl and 1,10-phenanthroline. They found $\lambda_{\text{max}}=620$ nm and $\epsilon_{\text{max}}=97$ $\text{cm}^{-1} \text{M}^{-1}$ with 2,2'-bipyridyl and $\lambda_{\text{max}}=630$ nm and $\epsilon_{\text{max}}=105$ $\text{cm}^{-1} \text{M}^{-1}$ with 1,10 phenanthroline as ligands.

Some common features may also be derived concerning the spectra of the different $\text{Cu}^{2+}-\text{L}-\text{Cl}^-$ complexes. The uptake of chloride ions to a CuL_n^{2+} complex with $n=0, 1, 2$, and 3 yields an increase in λ_{max} as well as in ϵ_{max} . Before a detailed discussion of the spectra of these complexes can be made it is necessary to extend the measurement to include data with $\lambda > 750$ nm. However, it may finally be concluded that the strength of the ligand field increases within the series $\text{C}_3\text{H}_4\text{N}_2 > \text{H}_2\text{O} > \text{Cl}^-$, which is in accordance with the spectrochemical series.

Acknowledgements. I thank Professor Nils Ingri for much valuable advice, for his great interest and for all the facilities placed at my disposal. Many thanks are also due to Fil. lic. Lennart Lyhamn for valuable help with the computer calculations. The English of the present paper has been corrected by Dr. Michael Sharp. The work forms part of a program financially supported by the Swedish Natural Science Research Council.

Table 6. The wavelength, λ_{max} , with corresponding molar absorption maximum, ϵ_{max} for different copper(II) complexes. The uncertainty in λ_{max} and ϵ_{max} is estimated to 10 nm and 1 $\text{cm}^{-1} \text{M}^{-1}$, respectively. $\text{L}=\text{C}_3\text{H}_4\text{N}_2$.

Complex	λ_{max}	$\epsilon_{\text{max}}/\text{cm}^{-1} \text{M}^{-1}$
Cu^{2+}	800 ^a	11
CuL^{2+}	750 ^a	21
CuL_2^{2+}	690	33
CuL_3^{2+}	630	45
CuL_4^{2+}	580	62
$\text{Cu}(\text{OH})\text{L}^+$	—	—
$\text{Cu}_2(\text{OH})_2\text{L}_2^{2+}$	650	68
$\text{Cu}_2(\text{OH})_2\text{L}_4^{2+}$	610	108
CuLCl^+	≥ 750	29
CuLCl_2	—	—
CuL_2Cl^+	700	33
CuL_2Cl_2	≥ 750	58
CuL_3Cl^+	650	50

^a Value taken from Ref. 1.

REFERENCES

1. Sjöberg, S. *Acta Chem. Scand.* 25 (1971) 2149.
2. Sjöberg, S. *Acta Chem. Scand.* 27 (1973) 3721.
3. Ginstруп, O., Lyhamn, L. and Ingri, N. *To be published.*
4. Biedermann, G. and Sillén, L. G. *Ark. Kemi* 5 (1953) 425.
5. Sjöberg, S. *Acta Chem Scand. A* 31 (1977) 718.
6. Ingri, N. and Sillén, L. G. *Ark. Kemi* 23 (1964) 97.
7. Arnek, R., Sillén, L. G. and Wahlberg, O. *Ark. Kemi* 31 (1969) 353; Brauner, P., Sillén, L. G. and Whiteker, R. *Ark. Kemi* 31 (1969) 365.
8. Lyhamn, L. *Chem. Scr.* 10 (1976) 49.
9. Sillén, L. G. *Acta Chem. Scand.* 16 (1962) 159; Sillén, L. G. and Warnqvist, B. *Ark. Kemi* 31 (1969) 341.
10. Bjerrum, J. K. *Dan. Vidensk. Selsk. Mat. Fys. Medd.* 22 (1946) No. 18.
11. Lister, M. W. and Rosenblum, P. *Can. J. Chem.* 38 (1960) 1827.
12. McConnell, H. and Davidson, N. *J. Am. Chem. Soc.* 72 (1950) 3164.
13. Forsling, W. *To be published.*
14. Hay, R. W. and Porter, L. J. *Aust. J. Chem.* 20 (1967) 675.
15. Bjerrum, J. K. *Dan. Vidensk. Selsk. Mat. Fys. Medd.* 10 (1932) 50.
16. Harris, C. M., Sinn, E., Walker, W. R. and Woolliams, P. R. *Aust. J. Chem.* 21 (1968) 631.
17. Eriksson, G. *To be published.*

Received March 8, 1977.

Kinetics and Equilibria for the Solvolysis of Lactaldehyde in Aqueous Solution

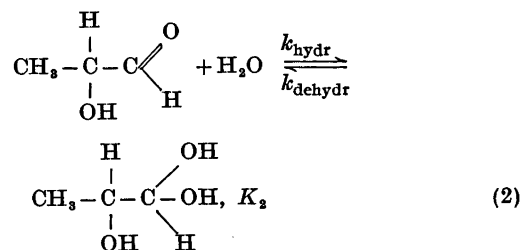
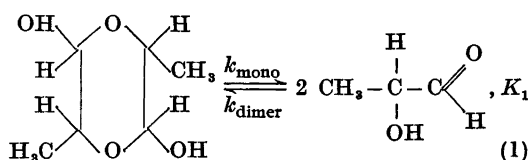
H. NIELSEN and P. E. SØRENSEN

Chemistry Department A, The Technical University of Denmark, Building 207, DK-2800 Lyngby, Denmark

Kinetics and equilibria have been studied for aqueous solutions of lactaldehyde (2-hydroxypropionaldehyde) at 298.2 K by UV spectrophotometry, a pH-stat technique and NMR spectroscopy. Rate constants for the water-, H^+ - and HO^- -catalysed hydration/dehydration reaction are reported as well as kinetic data for the H^+ -catalysed monomerization of the dimeric compound. An equilibrated solution of lactaldehyde in water contains largely the dimer and the hydrated monomer. The monomer is found to be approximately 96 % hydrated at equilibrium.

Simple sugars such as glycolaldehyde (2-hydroxyacetaldehyde), lactaldehyde (2-hydroxypropionaldehyde) and 1,3-dihydroxyacetone may be important intermediates in many metabolic reactions in biological systems. Thus, it was suggested and shown by Hough and Jones¹ that the methyl pentose sugars which are common in nature can be obtained from aldol condensation of two triose units, lactaldehyde and dihydroxyacetone, particularly in the presence of an enzyme such as aldolase. As each of these sugars can undergo various types of spontaneous as well as acid-base catalysed reactions, *e.g.* dimerization, keto-enol conversion and hydration, in aqueous solution, it is of considerable interest to study the kinetic and thermodynamic behaviour of such compounds for a better understanding of their biological role. Such investigations were carried out recently for glycolaldehyde² and the present paper presents results from a similar study of lactaldehyde. The equilibria between the three dominating forms of lactaldehyde in aqueous solution, the dimer, the monomer, and the

hydrated monomer, are presented in eqns. (1) and (2).



where k and K denote rate and equilibrium constants, respectively.

EXPERIMENTAL

DL-Lactaldehyde was synthesised according to the procedure described by Hough and Jones¹ with the only modification that pyruvaldehyde dimethyl acetal (FLUKA, 'pract.') was used as starting material instead of the butyl compound, which is not commercially available. Lactaldehyde is a white crystalline compound, the kinetic behaviour of which is very similar in nature to that of glycolaldehyde² and of dihydroxyacetone,³ and therefore appears in its dimeric form. Elemental analysis gave 48.7 % C and 8.1 % H (theoretical: 48.6 and 8.2 %).

Semicarbazide hydrochloride or hydroxylammonium chloride (both BDH, AnalaR) were used as scavengers for determining dehydration rate constants for the hydrate at selected pH-

values below 6.5. These experiments were carried out spectrophotometrically on a Beckman M24 instrument by following the reaction products (Schiff bases) at 225 and 214 nm, respectively, as described earlier.² At pH-values above 6.5 sulfite buffers ($\text{Na}_2\text{SO}_3 \cdot 7\text{H}_2\text{O}$, BDH, AnalaR and $\text{Na}_2\text{S}_2\text{O}_5$, Riedel-de Haën, 'für Analyse') were efficient scavengers in connection with a pH-stat technique (Radiometer).³

NMR spectra for solutions of lactaldehyde in D_2O (Stohler, 99.8 %) and in dioxane (Merck, reinst) were recorded on a Varian A-60D instrument. To obtain appreciable amounts of lactaldehyde monomer for investigation of rates of hydration of this compound a 1 M solution in dioxane was heated under reflux for approximately 4 h.² Small samples of this solution (rapidly cooled) were injected by a microsyringe into aqueous acetate buffer (glacial acetic acid, BDH, lab. reag., distilled and $\text{CH}_3\text{COONa} \cdot 3\text{H}_2\text{O}$, Riedel-de Haën, 'für Analyse'), equimolar solution, and the decrease in absorption, due to the disappearance of the free carbonyl group, was followed spectrophotometrically at 275 nm. Complete mixing took 5–10 s and this technique was sufficiently rapid despite the fact that the reaction is rather fast ($t_{1/2} \approx 5$ s) and the total change in absorbance only about 0.25. The H^+ -catalysed monomerization of dimeric lactaldehyde in freshly prepared 0.1 M aqueous solution was also followed at this wavelength (hydrochloric acid, Merck, Titrisol). This procedure is possible because a small proportion (≈ 4 %, see later) of the monomer is still present in its unhydrated form at equilibrium.

NaCl (Riedel-de Haën, 'für Analyse') was used for adjusting ionic strength and redistilled water was used throughout. For the experiments where sulfite was used as a scavenger the solutions were kept free from carbon dioxide and oxygen by a stream of O_2 -free nitrogen. All kinetic experiments were carried out at 298.2 ± 0.2 K.

RESULTS AND DISCUSSION

NMR Measurements. Spectra of an equilibrated solution (5 %, 298.2 K) of lactaldehyde in D_2O gave two doublets at δ 1.14–1.25 and 1.11–1.22 deriving from the methyl group in the dimer and the hydrated monomer, respectively. The intensity of the signals indicated a 45/55 % mixture of these two species and they undoubtedly represent almost 100 % (see later) of the total concentration of the compound as no low field signal, deriving from the carbonyl proton of the free aldehyde, was observed with certainty. However, after heat-

ing of lactaldehyde in dioxane as described in the experimental section the NMR spectrum shows a pronounced peak at δ 8.79 indicating the presence of a considerable amount of the monomeric unhydrated species in this solution.

Hydration experiments. Injection of 25, 50, and 75 mm³, respectively, of this solution in 1 cm³ of a 10^{-2} M (total) solution of acetate buffer ($I=0.1$, pH=4.60) in 1 cm silica cells gave first order kinetic curves when the decrease of the carbonyl absorption was followed at 275 nm and the following rate constants [$k_{\text{hydr}} + k_{\text{dehydr}}$ in eqn. (2)] were obtained (mean values of two experiments): 0.146, 0.138 and 0.130 s⁻¹. A simple extrapolation to pure aqueous solution gives a value of 0.150 ± 0.005 s⁻¹ for this constant. Because of the rather low concentration of the buffer, catalytic effects have been ignored and it was observed that no measureable pH-change took place as a result of the injections. The fact that first order kinetics was observed in the present case indicates that only the hydration reaction is followed and not the dimerization, the rate of which would show a second order dependence on carbonyl concentration.

Dehydration experiments. As found from NMR measurements an equilibrated solution of lactaldehyde in water contains both hydrated monomer and the dimer and the kinetic curves obtained from scavenger experiments therefore reflect two parallel reactions, the dehydration and the monomerization, leading to the same reaction product. We have analysed the kinetic data by fitting these (least squares computer program) to an expression of the type $Y = X_1(1 - e^{-k_1 t} - e^{-k_2 t}) + X_2$, where Y represents some linear function of concentration of the reaction products followed, X_1 and X_2 are constants and k_1 and k_2 denote the observed first order rate constants for dehydration and monomerization, respectively. From this analysis it becomes clear that one of these rate constants is only a few per cent of the other, and that the kinetic curves therefore deviate only slightly from first order behaviour. The smaller value can clearly be ascribed to the less mobile monomerization process and is therefore k_2 . It could only be determined with little accuracy but it was found to be of the same order of magnitude as a value determined from a separate investigation of the mono-

merization reaction (see below). Throughout the pH-range investigated good linearity was observed when $k_1 = k_{\text{dehydr}}^{\text{obs}}$ was plotted against total scavenger concentration, *i.e.* $k_{\text{dehydr}}^{\text{obs}} = k_{\text{dehydr}}^{\circ} + k_{\text{scavenger}} [\text{scavenger}]$. Such simple behaviour may prove the efficiency of the applied scavenger substances. Values of $k_{\text{dehydr}}^{\circ}$ as a function of pH are given in Table 1. The catalytic activity of the various scavenger substances was not studied in detail but general acid-base catalysis was observed in all cases in agreement with results from studies of

similar systems.^{2,4} Quantitative information about specific catalysis by H^+ and HO^- ions is obtained from the data in Table 1 if $k_{\text{dehydr}}^{\circ}$ is plotted against the concentrations of these two species, respectively. These plots show good linearity and $k_{\text{dehydr}}^{\text{H}}$ and $k_{\text{dehydr}}^{\text{HO}}$ are found to be 3.4 and $7.5 \times 10^3 \text{ dm}^3 \text{ mol}^{-1} \text{ s}^{-1}$, respectively, which values seem reasonable compared to 8.3 and $6 \times 10^3 \text{ dm}^3 \text{ mol}^{-1} \text{ s}^{-1}$ found for glycolaldehyde.² It appears that $k_{\text{dehydr}}^{\circ}$ is practically independent of pH in the range 4–7 and equal to $(6.3 \pm 0.5) \times 10^{-3} \text{ s}^{-1}$ (mean

Table 1. Rate constants for the dehydration ($k_{\text{dehydr}}^{\circ}$) of lactaldehyde in aqueous solution as a function of pH ($I=0.10$, 298.2 K). Concentrations in mol dm^{-3} , rate constants in s^{-1} .

pH measured	Scavenger (conc. range) ^b	$[\text{H}^+] \times 10^3$ ^c	$[\text{HO}^-] \times 10^7$ ^d	$k_{\text{dehydr}}^{\circ} \times 10^3$
2.00 ^a	semicarbazide (0.05–0.25)	12.7		51(2)
2.90	semicarbazide (0.02–0.10)	1.52		10(2)
3.65	semicarbazide (0.02–0.10)	0.270		8.9(3)
4.20	semicarbazide (0.02–0.10)	0.0760		7.2(2)
5.00	semicarbazide (0.02–0.10)	0.0121		6.8(2)
6.00	hydroxylamine (0.01–0.04)	—	—	6.3(2)
6.65	sulfite (0.005–0.025)		0.588	4.3(9)
7.38	sulfite (0.005–0.025)		3.09	6.8(6)
7.58	sulfite (0.005–0.025)		5.00	8.4(3)
7.75	sulfite (0.005–0.025)		7.00	10.4(2)
8.02	sulfite (0.005–0.030)		13.8	14.5(5)
8.33	sulfite (0.005–0.035)		28.1	26(1)

^a $I=0.25$. ^b Total concentrations. ^c $[\text{H}^+] = \frac{10^{-\text{pH}}}{f_{\text{H}^+}}$, $f_{\text{H}^+}=0.83$ ($I=0.10$), $f_{\text{H}^+}=0.79$ ($I=0.25$) (Ref. 7).

^d $[\text{HO}^-] = \frac{10^{\text{pH}-\text{p}K_{\text{H}_2\text{O}}}}{f_{\text{HO}^-}}$, $f_{\text{HO}^-}=0.76$ ($I=0.10$) (Ref. 7).

Table 2. Rate constants for the monomerization of lactaldehyde in aqueous solution as a function of $[H^+]$ ($I = 0.10$, 298.2 K). Concentrations in mol dm^{-3} , rate constants in s^{-1} .

$C_{\text{HCl}}([H^+])$	$k_{\text{mono}}^{\text{obs}} \times 10^4$
0.02	2.17(2)
0.04	4.00(1)
0.06	4.42(3)
0.08	7.53(1)
0.10	9.25(1)
0.12 ^a	11.10(5)

^a $I = 0.12$.

value). This value can be ascribed to the pure water catalysed reaction and is comparable with, e.g., $9.6 \times 10^{-3} \text{ s}^{-1}$ for glycolaldehyde and with values for a series of aliphatic carbonyl compounds, the dehydration of which is not subject to intramolecular catalysis.⁴

Monomerization. Kinetic results from the H^+ -catalysed monomerization of the dimer of lactaldehyde are given in Table 2. The kinetic curves obtained as described in the experimental section were of first order ($\ln|A_{\text{eq}} - A|$ against time) and $k_{\text{mono}}^{\text{H}}$ and k_{mono}° were found to be $(9.0 \pm 0.2) \times 10^{-3} \text{ dm}^3 \text{ mol}^{-1} \text{ s}^{-1}$ and $(2.7 \pm 0.9) \times 10^{-5} \text{ s}^{-1}$ from the slope and intersection respectively, of a plot of $k_{\text{mono}}^{\text{obs}}$ against $[H^+]$. These rate constants are seen to be considerably smaller than the corresponding values for the dehydration reaction but of a similar order of magnitude as found by Bell and Baughan for the monomerization of dihydroxyacetone.⁵ Each value observed for $k_{\text{mono}}^{\text{obs}}$ is actually a sum of the forward and backward reaction rate constants in eqn. (1) (the hydration reaction assumed to be much faster than the dimerization) but as we have observed good agreement between k_{mono}° determined by the method above and values for this constant estimated from the scavenger experiments (see previous paragraph) the contribution from dimerization is presumably small and water itself operates as a sufficiently good scavenger for the monomerization process.

Equilibrium constants. K_2 for eqn. (2) is obtained by combining $k_{\text{hydr}}^{\text{obs}} = k_{\text{hydr}}^{\circ} + k_{\text{dehydr}}^{\circ} = 0.150 \text{ s}^{-1}$ and $k_{\text{dehydr}}^{\circ} = 6.3 \times 10^{-3} \text{ s}^{-1}$, i.e., $K_2 = k_{\text{hydr}}^{\circ} / k_{\text{dehydr}}^{\circ}$ is found to be 23 corre-

sponding to approximately 96 % hydration of lactaldehyde in aqueous solution. This relatively high degree of hydration explains why no signals from the free carbonyl group is observed in the NMR spectrum of lactaldehyde in aqueous solutions of moderate concentrations.

The corresponding equilibrium constant for glycolaldehyde reported earlier,² indicating 90 % hydration of this compound, is probably too low. A large extrapolation from a 50 % water/dioxane mixture was used to obtain $k_{\text{hydr}}^{\text{obs}}$ in pure water and this may not be well justified because it relies on constant reaction orders with respect to water over a large range of water concentrations. These reaction orders have recently been shown to vary considerably with water concentration⁶ and we have shown that application of the procedure for obtaining $k_{\text{hydr}}^{\text{obs}}$ as described in the present paper, to glycolaldehyde leads to higher values for the degree of hydration of this compound in agreement with the result found by applying an empirical expression correlating equilibrium constants with Tafts polar and steric substituent parameters.³

REFERENCES

- Hough, L. and Jones, J. K. N. *J. Chem. Soc.* (1952) 4052.
- Sørensen, P. E. *Acta Chem. Scand.* 26 (1972) 3357.
- Bell, R. P. and Hirst, J. P. H. *J. Chem. Soc.* (1939) 1777.
- Sørensen, P. E., Bruhn, K. and Lindeløv, F. *Acta Chem. Scand. A* 28 (1974) 162.
- Bell, R. P. and Baughan, E. C. *J. Chem. Soc.* (1937) 1947.
- Sørensen, P. E. *Acta Chem. Scand. A* 30 (1976) 673.
- Kielland, J. *J. Am. Chem. Soc.* 59 (1937) 1675.

Received May 4, 1977.

The Crystal and Molecular Structure of *N,N*-Diethyl-*p*-nitrosoaniline

HANS JØRGEN TALBERG

Department of Chemistry, University of Oslo, Oslo 3, Norway

The crystal and molecular structure of *N,N*-diethyl-*p*-nitrosoaniline has been determined from X-ray diffraction data collected at -165°C and refined by least-squares methods. The space group is $P2_1/n$ with cell dimensions $a = 14.339(5)$ Å, $b = 9.921(2)$ Å, $c = 13.670(4)$ Å and $\beta = 87.16(2)^{\circ}$ at -165°C . The final R factor was 5.6%. The asymmetric unit contains two molecules which are slightly different as to the conformation in the diethylamino groups. Slight disordering in the nitroso groups gives an "average" molecular structure having near C_2 symmetry. Apparently the disorder does not prevent elucidation of physically meaningful bond lengths and angles in the diethylaminophenyl part of the molecule. This seems also to be the case for the nitroso group in one of the molecules when refining with "high" angle data. The molecular structure is consistent with a strong charge displacement from the diethylamino group to the nitroso group.

The present structure investigation of *N,N*-diethyl-*p*-nitrosoaniline (I) is part of a series of investigations of *C*-nitroso compounds. Previously the oxime tautomer of *p*-nitrosophenol and three of its salts (Ref. 1 and references therein), 5-nitrososalicylic acid,² *N,N*-dimethyl-*p*-nitrosoaniline (II)³ and its hydrochloride (III),⁴ and the compound *N,N,N',N'*-tetramethyl-1,5-diamino-4-nitrosobenzene (IV)⁵ have been investigated.

In the hydrochloride (III) the nitroso oxygen atom is protonated and the molecule has a pronounced *para* quinonoid structure (oxime form).⁴ This indicates a strong basic character of the nitroso group in the *p*-nitrosoanilines and keeps with the fact that these compounds often react as *para* quinonoid zwitterions.⁶ Noteworthy is the hydrolysis giving an amine and

a salt of *p*-nitrosophenol. The fact that additional base is not required for the condensation with reactive methylene groups [(II) is a reagent for these] giving anils is another outstanding evidence for the basic character (Ref. 6, p. 278). For (IV) a similar *intra*-molecular condensation yielding a benzimidazole severely obstructs isolation. The investigation of this compound showed the N—O bond to be much longer than a "pure" NO double bond [1.276(2) Å]. The X-ray study of the methyl analog to the title compound, *i.e.* (II), showed the crystal to be disordered. Owing to this the structural results do only give indications as to the degree of *intra*-molecular charge displacement.³

EXPERIMENTAL

Suitable prismatic crystals were obtained by sublimation using a "cold finger". A preliminary film investigation at room temperature showed monoclinic symmetry, space group $P2_1/n$ and unit cell dimensions deviating a few per cent from those determined at liquid nitrogen temperature.

All the data were collected and the unit cell constants determined using a well developed crystal of dimensions $0.50 \times 0.10 \times 0.10$ mm³. Apart from the following details the experimental conditions were as those described in Ref. 5.

The temperature at the crystal site was -165°C . The scan limits were $2\theta(\alpha_1) - 1.0^{\circ}$ and $2\theta(\alpha_2) + 1.0^{\circ}$ and a quadrant of reciprocal space was examined. Reflections up to 60° in 2θ were measured and only those having integrated counts larger than a preset value during a 2 s scan over the peak. Out of 2588 unique reflections measured 1835 had intensities larger than $2.5\sigma(I)$ where $\sigma(I)$ is the estimated standard deviation of the intensity based on counting statistics adding 2% uncertainty due to

experimental fluctuations. The atomic scattering factors for the heavy atoms were those of Doyle and Turner⁷ and for hydrogen those of Stewart *et al.*⁸ All programs except for the ORTEP program (Ref. 11 in Ref. 5) and the MULTAN program⁹ applied during the investigation are described in Ref. 10.

CRYSTAL DATA

N,N-Diethyl-*p*-nitrosoaniline, $C_{10}H_{14}N_2O$, monoclinic, space group $P2_1/n$ (No. 14). Dimensions of the unit cell at -165°C : $a = 14.339(5)$ Å, $b = 9.921(2)$ Å, $c = 13.670(4)$ Å and $\beta = 87.16(2)^\circ$; $V = 1944.3$ Å³, $M = 178.24$, $F(000) = 768$, $D_{\text{calc}} (-165^\circ\text{C}) = 1.218$ g cm⁻³, $Z = 8$.

STRUCTURE DETERMINATION

The structure was determined by direct methods.^{9,10} Using an ordered model anisotropic full matrix least-squares refinement with the heavy atoms yielded a conventional R factor of 11%. At this stage hydrogen atoms were included. Their parameters refined smoothly starting from values estimated from stereochemical considerations. The refinement with all the observed reflections and all the atoms converged after a few cycles (alternately refining different groups) yielding $R = 0.075$ a weighted R_w factor of 0.064 and a goodness of fit S of 2.2. The estimated standard deviations (e.s.d.'s) in the bond lengths were in the range 0.005–0.009 Å and all bond lengths and angles but those involving the nitroso group atoms seemed reasonable. The C–NO and the N–O bond lengths, however, were respectively astonishingly long and unreasonably short in both molecules in the asymmetric unit (molecule A and molecule B). In molecule A the separations were 1.475(7) and 1.212(6) Å and in molecule B 1.585(9) and 1.153(7) Å for, respectively, the C–NO and the N–O bond length. In a subsequent Fourier synthesis the C–NO bond lengths became "normal": 1.385 Å for molecule A and 1.405 Å for molecule B.

A difference Fourier map was then calculated using "high angle" parameters and a low angle data set (above and below 0.40 in $\sin \theta/\lambda$). The map showed two residual peaks of about 1 eÅ⁻³ whose positions were related to those of the oxygen atoms by a 2-fold rotation about a line through the atoms C1, C4 and N1. Inte-

gration over several peaks in Fourier maps indicated that the oxygen atom is situated with an occupational factor of 0.27 for molecule B and 0.19 for molecule A in this other position, O4*. These figures were obtained assuming gross atomic charges of 8.25 e at O4 and 6.95 e at N4 in both molecules.

By analogy with other monomeric nitrosobenzenes investigated it was assumed that (I) has unequal exocyclic angles at C4 (usually differing 7–10°). It was therefore decided to modify the model by including both an O4* and a N4* pseudo atom. Their initial positional parameters were estimated from stereochemical considerations. In the first refinement cycles with the disordered model the multiplicities cited were used, and all atoms were included (alternately). The nitroso group atoms were treated isotropically. This was also the case in a subsequent refinement varying (without constraint) only the parameters for O4, N4 and the pseudo atoms. Different occupational factors were tried in a regular manner and the best R factors were obtained with 0.160 for the pseudo atoms in molecule A (0.840 for O4A and N4A) and 0.278 for the pseudo atoms in molecule B (0.722 for O4B and N4B). Using these occupational factors also the most reasonable temperature factors and structural results were obtained (reasonable in the sense that the results for A or B resembled closely those for A* or B*). In the remaining refinement these occupational factors and the parameters arrived at for the pseudo atoms were retained. The latter was considered appropriate as a separate refinement with isotropic pseudo atoms and anisotropic heavy atoms of molecule B yielded unreasonable temperature factors for the nitroso group atoms. Treating the O4 and the N4 atoms anisotropically the final refinement (alternately refining different groups) converged yielding a R , R_w and S factor being significantly¹¹ smaller than that obtained for the ordered model: $R = 0.56$, $R_w = 0.047$ and $S = 1.69$. Final parameters are given in Table 1 and 2.

Magnitudes and directions of the principal axes of the vibrational ellipsoids are indicated in Fig. 1. A rigid body analysis of the entire molecule shows a fairly good agreement between observed and calculated vibrational tensor elements: $\Delta U_{\text{rms}} = 0.0038$ Å² for molecule

Table 1. Fractional atomic coordinates and thermal parameters for the non-hydrogen atoms. The temperature factors are expressed as: $\exp[-2\pi^2(h^2a^{*2}U_{11} + \dots + 2klb^*c^*U_{23})]$. Estimated standard deviations in parentheses.

ATOM	x	y	z	U ₁₁	U ₂₂	U ₃₃	U ₁₂	U ₁₃	U ₂₃
O4A	.38366(21)	.81511(32)	-.06229(24)	.0488(28)	.0395(22)	.0369(21)	.0024(17)	-.0114(17)	-.0029(18)
N1A	.57749(18)	.79159(31)	.28643(28)	.0228(17)	.0239(17)	.0208(17)	-.0012(16)	-.0050(14)	-.0018(15)
N4A	.28286(28)	.79861(42)	.02780(31)	.0562(27)	.0368(27)	.0365(26)	.0013(23)	-.0043(22)	.0042(24)
C1A	.68834(24)	.79488(36)	.21618(25)	.0261(21)	.0142(20)	.0226(21)	-.0015(18)	-.0037(17)	-.0048(18)
C2A	.62852(24)	.81353(37)	.11429(25)	.0293(22)	.0284(25)	.0177(20)	.0027(18)	-.0005(17)	.0024(18)
C3A	.48741(26)	.81653(34)	.05838(25)	.0389(24)	.0193(23)	.0288(21)	.0044(18)	-.0003(19)	.0016(17)
C4A	.36886(25)	.80046(38)	.00387(27)	.0272(22)	.0288(23)	.0314(24)	.0069(19)	-.0115(19)	-.0016(19)
C5A	.34368(25)	.78147(39)	.18263(28)	.0228(20)	.0267(23)	.0358(24)	-.0001(20)	-.0023(18)	.0013(22)
C6A	.41383(23)	.77868(37)	.24847(25)	.0255(21)	.0212(20)	.0262(21)	.0002(19)	-.0002(17)	.0005(19)
C7A	.67648(24)	.79716(39)	.24615(26)	.0225(20)	.0327(23)	.0282(22)	.0033(20)	-.0053(17)	.0015(20)
C8A	.58893(25)	.78171(40)	.38615(25)	.0375(23)	.0293(22)	.0126(19)	-.0031(21)	-.0023(16)	.0018(19)
C9A	.71186(26)	.84855(40)	.23189(30)	.0332(24)	.0344(25)	.0436(27)	-.0091(21)	-.0038(20)	.0006(22)
C10A	.85318(27)	.83619(38)	.42144(27)	.0538(28)	.0236(22)	.0225(21)	.0013(21)	-.0039(20)	.0006(19)
O4B	.18688(25)	.80733(45)	-.09534(28)	.0361(24)	.0527(28)	.0586(27)	.0001(23)	-.0053(20)	-.0059(25)
N1B	.49264(19)	.77985(38)	.19213(20)	.0276(18)	.0146(16)	.0227(17)	.0021(16)	-.0064(15)	-.0025(15)
N4B	.14898(31)	.31384(49)	-.07186(32)	.0293(27)	.0388(33)	.0356(29)	-.0011(24)	.0028(24)	.0007(25)
C1B	.38718(24)	.28226(39)	.12994(25)	.0246(20)	.0237(21)	.0179(19)	-.0025(25)	-.0019(17)	-.0001(19)
C6B	.38708(24)	.40527(37)	.00789(26)	.0243(22)	.0261(24)	.0271(22)	.0039(18)	-.0044(19)	.0014(19)
C5B	.88871(26)	.40747(40)	.02813(28)	.0257(24)	.0364(28)	.0299(25)	.0058(20)	.0001(20)	.0053(21)
C4B	.21104(25)	.28876(58)	-.00124(26)	.0179(20)	.0501(29)	.0196(22)	.0044(24)	-.0040(17)	-.0041(23)
C3B	.23948(26)	.16887(41)	.03884(28)	.0224(22)	.0428(28)	.0268(23)	-.0007(19)	.0004(19)	-.0157(21)
C2B	.38895(25)	.16889(37)	.18386(29)	.0262(22)	.0258(22)	.0328(23)	-.0028(18)	.0018(19)	-.0042(19)
C5B	.4722(27)	.8439(37)	.22334(27)	.039(25)	.0239(24)	.0277(23)	.0045(20)	-.0188(20)	-.0002(19)
C7B	.46206(25)	.15356(36)	.25373(27)	.0314(23)	.0211(22)	.0262(22)	.0068(19)	-.0007(19)	.0015(19)
C10B	.85197(26)	.44426(39)	.15287(38)	.0317(24)	.0273(24)	.0492(27)	-.0033(19)	-.0158(21)	-.0038(22)
C9B	.48089(27)	.11583(39)	.32813(27)	.0486(26)	.0295(23)	.0256(23)	.0118(21)	-.0056(20)	.0024(19)

Table 2. Fractional atomic coordinates and isotropic thermal parameters (\AA^2) for the hydrogen atoms and the nitroso group atoms in their less preferred sites. Estimated standard deviations in parentheses.

Atom	x	y	z	B
H2A	0.5914(21)	0.8286(29)	0.0845(22)	1.6(7)
H3A	0.4780(21)	0.8300(31)	-0.0159(25)	2.1(8)
H5A	0.2751(21)	0.7688(31)	0.2080(21)	2.1(7)
H6A	0.3944(19)	0.7642(30)	0.3187(21)	1.4(7)
H71A	0.7090(21)	0.7521(29)	0.2975(22)	1.6(7)
H72A	0.6894(21)	0.7406(32)	0.1814(24)	2.5(8)
H81A	0.6092(25)	0.8287(35)	0.4203(24)	3.0(9)
H82A	0.4971(22)	0.8367(32)	0.4102(25)	2.5(8)
H91A	0.7789(25)	0.9388(34)	0.2069(25)	3.3(9)
H92A	0.7027(25)	1.0001(38)	0.2935(29)	4.1(1.0)
H93A	0.6767(25)	0.9885(36)	0.1814(27)	3.8(1.0)
H101A	0.5389(22)	0.6348(36)	0.4910(28)	3.3(9)
H102A	0.6094(23)	0.5820(34)	0.3967(24)	2.6(9)
H103A	0.4986(25)	0.5932(35)	0.3945(26)	3.5(1.0)
H2B	0.3278(21)	0.0787(34)	0.1296(23)	1.9(8)
H3B	0.2105(20)	0.0851(30)	0.0220(21)	1.2(7)
H5B	0.2356(23)	0.4911(33)	-0.0084(25)	2.6(8)
H6B	0.3523(22)	0.4908(33)	0.1050(23)	2.1(8)
H71B	0.5318(22)	0.1733(29)	0.2512(22)	1.9(7)
H72B	0.4612(20)	0.4612(31)	0.1838(22)	1.5(7)
H81B	0.4959(23)	0.3875(35)	0.2811(26)	2.7(9)
H82B	0.4225(19)	0.4772(31)	0.2372(20)	1.1(7)
H91B	0.4054(25)	0.1902(34)	0.3742(24)	2.4(8)
H92B	0.4420(25)	0.0480(40)	0.3656(27)	4.0(1.0)
H93B	0.3440(29)	0.0816(40)	0.3231(29)	5.2(1.2)
H101B	0.5978(23)	0.3767(37)	0.1354(25)	3.0(9)
H102B	0.5838(25)	0.5267(39)	0.1799(27)	4.2(1.0)
H103B	0.5309(24)	0.4725(36)	0.0863(27)	3.3(9)
O4A*	0.2277(13)	0.8027(18)	0.0219(13)	3.9(4)
N4A*	0.3130(14)	0.8099(22)	-0.0026(18)	2.1(4)
O4B*	0.1086(07)	0.3704(11)	-0.0964(07)	3.4(2)
N4B*	0.1381(11)	0.2606(16)	-0.0620(11)	3.0(3)

A and $\Delta U_{\text{rms}} = 0.0044 \text{ \AA}^2$ for molecule B. Exclusion of the terminal methyl carbon atoms did not improve the agreement while this was the case when excluding the O4 and N4 atoms ($\Delta U_{\text{rms}} = 0.0025 \text{ \AA}^2$ for both molecules). For the entire molecule the r.m.s. "eigenvalues" of T are 0.17, 0.15 and 0.13 \AA^2 as to molecule A and 0.17, 0.16 and 0.14 \AA^2 for molecule B while the r.m.s. "eigenvalues" of L are 2.9, 2.2 and 1.8° for molecule A and 3.2, 2.1 and 1.3° for molecule B.

Disregard of low angle scattering has a marked shortening effect on the C4-N4 bond

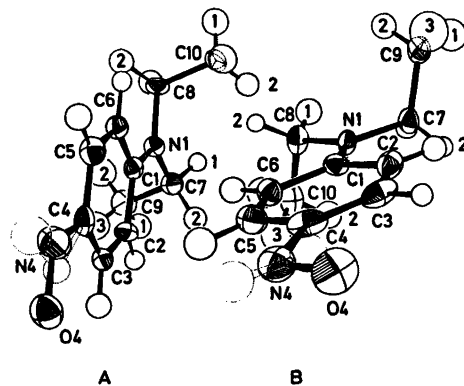


Fig. 1. 50 % probability ellipsoids and numbering of atoms. The pseudo atoms are dotted.

Table 3. The dependency upon the inner cutoff value of $\sin \theta/\lambda$ for the bond lengths (Å) and angles (°) involving the O4 and the N4 atom. The estimated standard deviations are in parentheses.

Data set	O4-N4	N4-C4	O4-N4-C4	N4-C4-C5
Molecule A				
1	1.253(5)	1.437(5)	110.9(4)	111.8(4)
2	1.254(5)	1.432(5)	111.2(4)	112.1(3)
3	1.255(6)	1.406(7)	112.4(4)	112.6(4)
4	1.269(11)	1.382(11)	112.6(6)	112.7(6)
Molecule B				
1	1.216(5)	1.458(6)	109.9(4)	112.0(4)
2	1.217(6)	1.451(6)	110.3(4)	112.2(4)
3	1.221(8)	1.432(7)	111.0(5)	112.0(5)
4	1.225(13)	1.417(9)	111.7(8)	111.0(7)

Data set	$\sin \theta/\lambda$ range	Number of reflections	Scale factor	$R \times 100$	$R_w \times 100$	S
1	0.0-0.7	1835	0.656	5.6	4.7	1.7
2	0.2-0.7	1712	0.642	5.8	4.8	1.5
3	0.3-0.7	1446	0.659	6.1	5.2	1.4
4	0.4-0.7	1029	0.684	6.3	5.3	1.3

length and a widening effect on the C4-N4-O4 angle. This can be seen from Table 3 where values from several refinements using different inner cutoff values for $\sin \theta/\lambda$ are listed. The contribution from the valence-electrons to the total integrated scattering of nitrogen decreases from about 30 to less than 10 % when excluding data below 0.4 in $\sin \theta/\lambda$ ($B_{iso} = 2.5 \text{ \AA}^2$). Then, the error in the positional parameters resulting from the extended "overlap" of the valence-electron clouds of N4 and N4* is

probably less using only data above 0.4 in $\sin \theta/\lambda$ than when using all the data.

Bond lengths and angles involving the non-hydrogen atoms are given in Table 4. The e.s.d.'s were obtained from the correlation matrix of the final refinement cycle with these atoms. The C-H bond lengths obtained are in the range 0.89-1.07 Å with e.s.d.'s of 0.03 Å. Deviations of atoms from least-squares planes are given in Table 5.

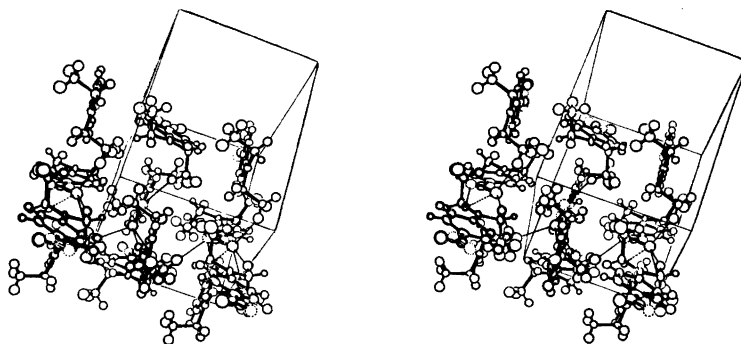


Fig. 2. A stereoscopic illustration of the structure. The shortest O...H contacts are indicated by fine lines.

Table 4. Bond lengths (Å) and angles (°).

	A	B		A	B
In the diethylaminophenyl part					
N1-C1	1.358(4)	1.345(4)	C1-C2	1.420(5)	1.425(5)
N1-C7	1.473(4)	1.480(4)	C2-C3	1.376(5)	1.372(5)
N1-C8	1.460(4)	1.469(4)	C3-C4	1.386(5)	1.393(5)
C7-C9	1.519(5)	1.520(5)	C4-C5	1.393(5)	1.397(5)
C8-C10	1.523(5)	1.512(5)	C5-C6	1.375(5)	1.360(5)
			C6-C1	1.425(5)	1.426(5)
C1-N1-C7	121.1(3)	122.9(3)	C1-C2-C3	120.3(3)	120.8(4)
C1-N1-C8	122.7(3)	121.8(3)	C2-C3-C4	121.2(3)	120.8(4)
C7-N1-C8	116.3(3)	115.4(3)	C3-C4-C5	119.5(3)	119.2(3)
N1-C7-C9	112.7(3)	111.5(3)	C4-C5-C6	120.7(3)	121.1(4)
N1-C8-C10	112.4(3)	112.3(3)	C5-C6-C1	120.6(3)	121.0(4)
N1-C1-C2	121.2(3)	121.8(4)	C6-C1-C2	117.7(3)	117.1(3)
N1-C1-C6	121.1(3)	121.1(4)			
In the nitroso group of molecule A by use of Data set 4					
O4-N4	1.27(1)		O4-N4-C4	112.6(6)	
N4-C4	1.38(1)		N4-C4-C3	129.1(6)	
			N4-C4-C5	112.7(6)	
In the nitroso group with atoms in the less preferred position					
O4*-N4*	1.25(2)	1.27(2)	O4*-N4*-C4	109(1)	109(1)
N4*-C4	1.42(1)	1.41(1)			
In the nitroso group when refining with all atoms in molecule B including the pseudo atoms O4* and N4*					
O4-N4	1.220(14)		O4*-N4*	1.27(4)	
N4-C4	1.435(19)		N4*-C4	1.43(4)	

Table 5. Deviations (Å) of atoms from a least-squares plane defined by the benzene ring atoms.

Atom	A	B
O4	-0.024	0.102
N1	-0.003	0.009
N4	-0.016	0.028
C1	0.002	0.002
C2	-0.003	-0.011
C3	0.002	0.008
C4	0.000	0.004
C5	-0.001	-0.013
C6	0.002	0.009
C7	-0.114	0.081
C8	0.092	-0.054
C9	1.230	-1.304
C10	-1.273	1.312
O4*	0.08	-0.08
N4*	0.01	-0.01

DISCUSSION

Fig. 2 shows the packing of molecules in the crystal. All intermolecular contacts, including those involving the pseudo atoms, are of van der Waals type. Each of the two independent molecules form chains by lying head to tail along the *n*-glides. An approximately linear NC-H...O contact (3.450 and 3.390 Å for, respectively, the A and B molecule with oxygen in its preferred site) constitutes the link between the molecules in the chains and it seems as if this contact has an orienting effect on the packing along the chains.

The type of disorder in the present structure parallels that found in the crystals of *N,N*-dimethyl-*p*-nitrosoaniline (II) in that the nitroso group atoms occupy two positions related by twofold rotational symmetry about the line through N1, C1 and C4. This similarity is proba-

bly a consequence of the similar packing pattern for (I) and (II) with only van der Waals contacts⁸ to the nitroso group in both its orientations. However, whereas there is no preference for one of the orientations in (II) this is the case for both the molecules of (I). It seems as if the NO group experiences a discriminating difference between its possible types of environment in the latter case. Sterically the difference between the two immediate surroundings consists in fewer contacts to hydrogen atoms and a less regular coordination of these in the less preferred site. However, because of the long range effect of the coulombic and dispersion forces there are four types of environment which should be considered: both, only one (two types) and none of the NO groups having the preferred orientation. These four possibilities correspond to the four ordered structures AB, A*B, AB* and A*B* composing the disordered structure. The portion (*p*) of the individual structure type in the crystal is within the range 0.72–0.56 for AB, 0.28–0.12 for AB* and 0.16–0.0 for A*B and A*B* (or 0.60, 0.24, 0.12 and 0.04, respectively, if $p_{AB}/p_{AB^*} = p_{A^*B}/p_{A^*B^*}$). If this is a distribution resulting from dynamic disorder at the temperature of formation of the crystal (85 °C) the energy difference between for example AB and AB* is at least about 0.5 kcal/mol. Any difference between calculated packing energies is less than 0.10 kcal/mol using the Kitaigorodsky universal potential¹³ for the dispersion energy and the expression $(kq_iq_j/r_{ij})\exp(r_{ij}^0 - r_{ij})$ (Ref. 13) for the Coulomb energy. As it is rather unlikely the disorder being dynamic at temperatures appreciably below the melting point this indicates that the observed distribution is mainly a result of other factors. The calculated dispersion energies amounts to –14.4 to –14.5 kcal/mol and the Coulomb energies to 1.0–1.2 kcal/mol. In the expression for the Coulomb energy *k* is a constant (332.1 kcal/mol erg), *q* is the net atomic charge from INDO calculations based upon the found molecular geometry (gross atomic populations in Table 6) and *r*⁰ is the equilibrium *inter*-molecular distance.¹³

The molecular structure. Both the benzene rings and both the C1N1(C7)C8 fragments are planar within the accuracy of the experiment. The amino nitrogen atoms do not deviate

Table 6. Gross atomic populations from INDO calculations based upon the geometry of molecule A.

O4	8.21	C6	6.08
N1	7.17	C7	5.83
N4	6.95	C8	5.82
C1	5.82	C9	5.99
C2	6.07	C10	6.00
C3	5.94	H(C _{ar})	1.01
C4	5.97	H(C7, C8)	1.04
C5	5.96	H(C9, C10)	1.00

significantly from the ring plane and the twist about the Et₂N–C bonds is only a few degrees. The nitroso group atoms of molecule A and the N4B atom seem to be in the ring plane while the deviation of the O4B atom is probably large enough as to be considered significant. The methyl carbon atoms deviate nearly maximally (within the frames set by normal ethyl group geometry) to either side of the C1N1(C7)C8-plane in both molecules. This conformation is similar to that of the *N,N*-diethyl-anilino moiety of a pyrazoline dye (V)¹⁴ and is probably that which gives least crowding. Fig. 3 shows that the difference between the two independent molecules as to their conformation are only of the order of a few degrees. It is noteworthy however that it seems to be connected to the NC–H...O contacts mentioned above.

Apart from the C–NO and the N–O bond length there are not any formally significant differences between corresponding bond lengths in the two molecules. Neither are there any significant differences between chemically equivalent bond lengths within the two molecules. This is taken to indicate that these bond lengths are physically meaningful and influenced negligibly by the disorder.

A comparison of (I) and the *para* substituted *N,N*-dialkylanilines (V) and methyl orange¹⁵ shows that these three compounds have very similar bond lengths. Probably this similarity is due to a nearly equal electron-accepting ability of the *para* substituents (a 4-imino-2-pyrazolin-5-one group in (V) and an azophenyl group in methyl orange). This is confirmed by comparing (I) and the compound *p*-dimethyl-amino-phenyl-diphenylphosphine (VI)¹⁶ where a weakly electron-accepting PPh₂ group is in

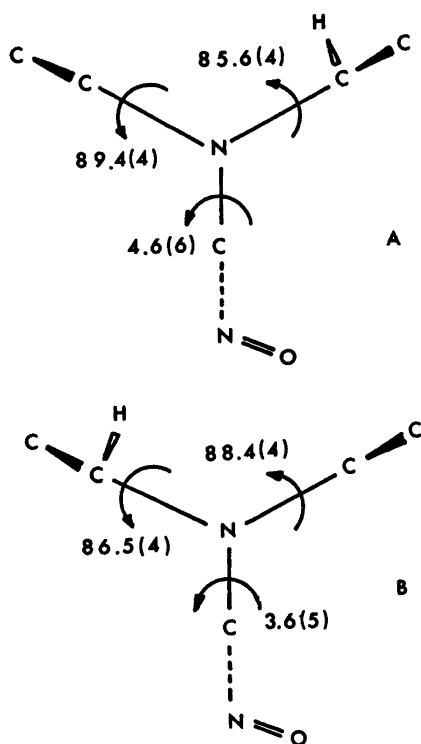


Fig. 3. Dihedral angles in the diethylamino groups. The protons shown are those involved in the NC-H...O contacts mentioned in the text.

para position to the dialkylamino group. Most C-C bond lengths in (I) deviate about 0.02 Å from corresponding bond lengths in (VI) which seem to be of only one type (the mean value is 1.393 Å with an e.s.d. of 0.004 Å which is identical to the e.s.d. in the separate bond lengths). In (I), (V) and methyl orange the bond lengths are of three types (the mean value for both molecules of (I) is 1.396 Å with an e.s.d. of 0.022 Å for A and an e.s.d. of 0.027 Å for B); two being 0.02–0.03 Å longer, two being 0.02–0.03 Å shorter and two being very similar to the benzene separation. The two former and the two latter bonds are adjacent to respectively the R₂N-C bond and the C-NX bond [X=O for (I), X=N for methyl orange and X=C for (V)]. In consistency with this the R₂N-C bond length in (I), (V) [1.355(2) Å] and methyl orange [1.365(6) Å] is about 0.02–0.03 Å shorter than that in (VI) [1.380(3)

Å]. For all the dialkylanilines mentioned the amino-nitrogen atom is trigonally hybridized and the twist about the N-C_{ar} bond of only a few degrees.

Considering the inductive effect of the NO group the major cause of shorter C-C4 bonds than C-C1 bonds it seems as if a *para* quinonoid element is contributing appreciably to the π -resonance in (I). The INDO calculations mentioned above yielded π -bond orders being consistent with a lesser contribution of this element than actually observed: N1-C1: 0.40, C1-C2(6): 0.59, C2(6)-C3(5): 0.70, C3(5)-C4: 0.62, C4-N4: 0.31 and N-O: 0.93. The gross atomic populations calculated (in Table 6) indicate about equal net charge on the oxygen atom and the amino nitrogen atom. However, it seems probable that the oxygen atom actually is appreciably more negative than the amino nitrogen atom as the calculated dipole moment is substantially smaller than that measured in inert solution (5.1 D compared with 7.23 D). Possibly this discrepancy between theory and experiment may be attributed to the inadequacy of the one-electron configuration description of the molecular ground state used in the calculations.

The differences between corresponding bond lengths in (I) and the hydrochloride of (II) resemble closely those between the *p*-nitrosophenolate anions and *p*-benzoquinone monoxime.¹ They are, however, generally slightly larger than in the latter case.

The bond angles except for those involving the nitroso group atoms are very similar to those of (V). Owing to this similarity and the close resemblance of corresponding bond lengths in the diethylaminophenyl part of (I) and (V) it seems reasonable that also the C4-N bond lengths of the two compounds resemble each other. And this is the case if one considers the bond length in molecule A obtained by use of "high" angle data in the refinement [1.374(3) Å for (V) compared with 1.38(1) Å for (I)]. This bond length is also very similar to that in *N,N,N',N'*-tetramethyl-1,5-diamino-4-nitrosobenzene, (IV), [1.372(2) Å]; in consistency with the resemblance of the N-O bond lengths in (I) and (IV) [1.276(2) Å in (IV) compared with 1.27(1) Å for (I)].

It is worth mentioning that the N-O bond length from this investigation (1.27 Å) is very

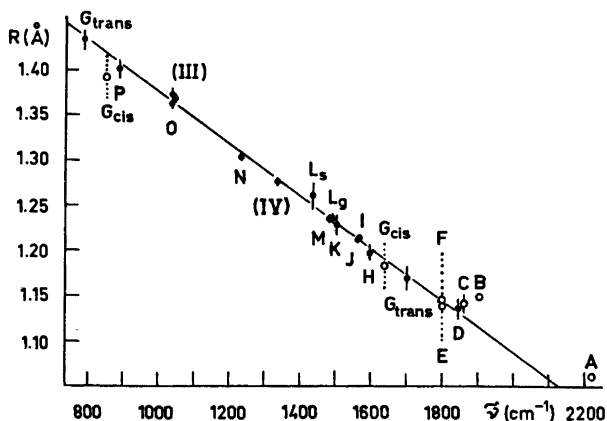


Fig. 4. A plot of the N—O bond length R and the wave number $\tilde{\nu}$ of the ω normal mode involving essentially the NO group in the compounds NO^+ (A),¹⁷ NO (B),¹⁷ N_2O_3 (C),¹⁷ FNO (D),^{19, 17} ClNO (E),¹⁷ BrNO (F),¹⁷ HNO_2 (G),^{18, 17} CF_3NO (H),^{19, 6} CH_3NO (I),^{19, 6} HNO (J),^{20, 21} NCNO (K),^{20, 22} Me_2NNO (L),^{20, 23, 24} 5-nitrososalicylic acid (M),² (IV),^{5, 25} sodium *p*-nitrosophenolate trihydrate (N) (Ref. within Ref. 1), (III),^{4, 25} *p*-benzoquinone monoxime (O) (Ref. within Ref. 1 and Ref. 25), formaldoxime (P).^{20, 26} The least-squares line shown is for the ●-points (2.5σ in R indicated with bars).

similar to an R_{NO} value obtained using IR spectroscopy and correlation of N—O bond lengths with the wave number of the normal ω mode involving essentially the NO group. The plot of R_{NO} against ω_{NO} in Fig. 4 shows a remarkable linearity between the two magnitudes if one excludes the points for NO^+ , NO and N_2O_3 (the confidence factor is 0.99). The least-squares line shown has the slope $-2.90 \times 10^4 \text{ \AA}^2$ and the intercept 1.667 Å. Assuming inaccuracy only in R_{NO} with a mean e.s.d. of 0.003 Å the e.s.d. in the slope is $3 \times 10^3 \text{ \AA}^2$ and in the intercept 0.004 Å. The KBr-IR spectrum of (I) is very similar to that of (II) and using the assignment of Knieriem²⁵ for (II) the wave number for ω_{NO} is set to 1380 cm^{-1} . Insertion of this value in the equation for the least-squares line gives the value 1.265 Å for R_{NO} in (I).

REFERENCES

1. Talberg, H. J. *Acta Chem. Scand. A* 31 (1977) 37.
2. Talberg, H. J. *Acta Chem. Scand. A* 31 (1977) 485.
3. Rømming, C. and Talberg, H. J. *Acta Chem. Scand.* 27 (1973) 2246.
4. Drangfelt, O. and Rømming, C. *Acta Chem. Scand. A* 28 (1974) 593.
5. Talberg, H. J. *Acta Chem. Scand. A* 30 (1976) 829.
6. Patai, S. In Feuer, H., Ed., *The Chemistry of the Nitro and Nitroso Groups*, Interscience, New York 1969, Part 1.
7. Doyle, P. A. and Turner, P. S. *Acta Crystallogr. A* 24 (1970) 2232.
8. Stewart, R. F., Davidson, E. R. and Simpson, W. T. *J. Chem. Phys.* 53 (1970) 205.
9. Germain, G., Main, P. and Woolfson, M. M. *Acta Crystallogr. A* 27 (1971) 368.
10. Groth, P. *Acta Chem. Scand.* 27 (1973) 1837.
11. Hamilton, W. C. *Acta Crystallogr.* 18 (1965) 502.
12. Kitaigorodsky, A. I. *Molecular Crystals and Molecules*, Academic, New York and London 1973, p. 388.
13. Skorczyk, R. *Acta Crystallogr. A* 32 (1976) 447.
14. Smith, D. L. and Barret, E. K. *Acta Crystallogr. B* 27 (1971) 2043.
15. Hanson, A. W. *Acta Crystallogr. B* 29 (1973) 454.
16. Dreissig, W. and Pleith, K. *Z. Kristallogr.* 135 (1972) 17.
17. Brittain, A. H., Cox, A. P. and Kuczkowski, R. L. *Trans. Faraday Soc.* 65 (1969) 1963.
18. Cox, A. P., Brittain, A. H. and Finnigan, D. J. *Trans. Faraday Soc.* 67 (1971) 2179.
19. Turner, P. H. and Cox, A. P. *Chem. Phys. Lett.* (1976) 585.
20. Landolt-Börnstein, *Numerical Data and Functional Relationships in Science and Technology*, New Series Vol. 7, Springer, Berlin, Heidelberg and New York 1976.

21. Stals, J. *Rev. Pure Appl. Chem.* 20 (1970) 1.
22. Dorko, E. A. and Buelow, L. *J. Chem. Phys.* 62 (1975) 1869.
23. Krebs, B. and Mandt, J. *Chem. Ber.* 108 (1975) 1130.
24. Rademacher, P. and Lüttke, W. *Spectrochim. Acta Part A* 27 (1971) 715.
25. Knieriem, B. *Thesis*, Göttingen 1972.
26. Califano, S. and Lüttke, W. *Z. Phys. Chem.* 6 (1956) 83.

Received May 4, 1977.

The Crystal Structure of Manganese(II) Selenite Monodeuterate

MARKUS KOSKENLINNA and JUSSI VALKONEN

Department of Chemistry, Helsinki University of Technology, Otaniemi SF-02150 Espoo 15, Finland

The crystal structure of manganese(II) selenite monodeuterate, $\text{MnSeO}_3 \cdot \text{D}_2\text{O}$, has been determined by X-ray methods. The compound is orthorhombic with crystal axes $a = 13.179(6)$ Å, $b = 5.826(4)$ Å and $c = 4.933(3)$ Å. It has four formula units in the unit cell, and belongs to the space group $Pnma$ (No. 62).

The structure consists of layers of distorted MnO_6 -octahedra with four shared vertices. The Mn–O distances range from 2.135 to 2.310 Å. The selenium atoms are situated in the cavities within the network, and the bonding scheme of the selenium is the main reason for the distortion of the octahedra. Each octahedron is tilted at an angle of 119.8° with respect to the four neighbouring octahedra.

Several compounds of the system $\text{MnO} - \text{SeO}_3 - \text{H}_2\text{O}$ are known. Recently the compounds MnSeO_3 , $\text{MnSeO}_3 \cdot 2\text{H}_2\text{O}$ and MnSe_2O_5 have been prepared and described.^{1–3} In all of these the manganese atom is octahedrally coordinated, and in the case of MnSeO_3 and $\text{MnSeO}_3 \cdot 2\text{H}_2\text{O}$ the coordination polyhedron is considerably distorted. This is somewhat unexpected since the $t_{2g}^3 e_g^2$ configuration of the Mn^{2+} ion implies a spherically distributed d -electron density around the metal ion, which in turn would favour regular octahedra in the solid state.

The structure of MnSeO_3 can be described in terms of MnO_6 -octahedra with shared vertices and selenium(IV) ions in the cavities thus formed. In $\text{MnSeO}_3 \cdot 2\text{H}_2\text{O}$, on the other hand, the MnO_6 -polyhedra are joined by the selenium (IV) ions into a three-dimensional network. In connection with our studies on manganese selenites we have now prepared the monodeuterate, $\text{MnSeO}_3 \cdot \text{D}_2\text{O}$, and have undertaken its structural characterization to throw more light on the coordination of divalent manganese in selenite compounds.

EXPERIMENTAL

A solution of 1 mol/dm³ potassium selenite was added dropwise to a solution of 1 mol/dm³ manganese sulfate until the precipitation of manganese as a selenite hydrate was complete. After this, selenous acid (1 mol/dm³) was added slowly with vigorous stirring until the precipitate just dissolved at $\text{pH} = 4.2 \pm 0.2$. The solution was then kept at $80 - 95^\circ\text{C}$ for 16–24 h. Flat, needle-shaped crystals with a pink tint were formed. All the preparations were made in heavy water, since the crystals thus obtained were larger. The crystals showed a great tendency to split into sheets if gently touched under microscopic investigation.

For recording of the X-ray data, a Syntex P2₁ (Fortran-version) automatic diffractometer and graphite monochromatized $\text{MoK}\alpha$ -radiation were used. Unit cell dimensions were obtained by measuring 14 independent reflections with the diffractometer after which they were refined by least-squares methods. The axes were $a = 13.179(6)$ Å, $b = 5.826(4)$ Å and $c = 4.933(3)$ Å. The space group was deduced from the original intensity data to be $Pnma$ (No. 62). There are four formula units in the cell, and calculated and measured (flotation) densities were 3.51 and 3.5 g cm⁻³, respectively.

Intensity data for 560 independent reflections were collected at the interval $5^\circ < 2\theta < 60^\circ$ using the $\theta - 2\theta$ scanning technique and 1°/min scan speed. Of these reflections, 500 were taken as observed with the criterion of $I > 2\sigma(I)$. Lorentz, polarization and empirical absorption corrections were applied ($\mu = 127.4$ cm⁻¹). The size of the crystal was $0.1 \times 0.1 \times 0.15$ mm.

The scattering factors for all the atoms were taken from the International Tables.⁴ The positions of Se and Mn were obtained by direct methods with the computer program package X-Ray 1976, which was used also in the refinement of the structure.⁵ In the final cycles of block-diagonal refinement, anisotropic temperature coefficients were used, and the value of R was reduced to 0.066. The F_o and F_c listing is available from the authors upon request.

Table 1. Atomic coordinates and thermal parameters with estimated standard deviations for the atoms. The anisotropic temperature coefficients are of the form: $\exp[-2\pi^2(U_{11}h^2a^{*2} + U_{22}k^2b^{*2} + U_{33}l^2c^{*2} + 2U_{12}hka^*b^* + 2U_{13}hla^*c^* + 2U_{23}k lb^*c^*)]$; The values of U_{ij} are multiplied by 10^4 .

Atom	<i>x</i>	<i>y</i>	<i>z</i>	U_{11}	U_{22}	U_{33}	U_{12}	U_{13}	U_{23}
Mn	0.7683(2)	0.2500	0.3985(5)	219(11)	161(10)	86(10)	0	-6(9)	0
Se	0.4018(1)	0.7500	0.0247(3)	148(6)	179(6)	89(6)	0	7(6)	0
O1	0.3632(9)	0.7500	0.3489(22)	261(57)	194(53)	81(47)	0	46(45)	0
O2	0.1671(6)	0.0303(14)	0.3824(15)	231(34)	155(36)	115(33)	23(33)	23(30)	26(30)
O3	0.8908(9)	0.2500	0.0918(24)	253(59)	204(55)	209(61)	0	31(51)	0

Table 2. Bond distances (Å) and angles (°) with estimated standard deviations.^a

Mn—O1	2.135(12)	Se—O1	1.678(11)
Mn—O2 ^{i,iii}	2.135(8) (2 ×)	Se—O2 ^{i,iii}	1.720(8) (2 ×)
Mn—O2 ^{ii,iv}	2.310(8) (2 ×)		
Mn—O3	2.212(13)		
		O1—Se—O2 ^{i,iii}	103.2(4) (2 ×)
		O2—Se—O2 ^{i,iii}	96.2(4)

^a The superscripts denote the following symmetry operations:

- i *x, y, z*
- ii $1/2 - x, 1/2 + y, 1/2 + z$
- iii $x, 1/2 - y, z$
- iv $1/2 - x, -y, 1/2 + z$

DISCUSSION

The atomic coordinates and anisotropic temperature factors are given in Table 1. As can be seen, the manganese, selenium and two of the three oxygens are located in special positions. The oxygen labelled O3 belongs to the water molecule.

The structure consists of MnO₆-octahedra joined by four shared equatorial vertices into a layer network (cf. Fig. 1). The equatorial oxygens (O2) are three-coordinated, with bond lengths to the selenium and two manganese atoms of 1.720(8), 2.135(8) and 2.310(8) Å, respectively. These values coincide well with those in other manganese selenites (cf. Table 3). The bond arrangement of the oxygens is pyramidal, and the bond angles are 119.8(4), 125.0(4) and 97.9(4)° for the angles Mn—O2—Mn', Mn—O2—Se and Se—O2—Mn', respectively.

Each MnO₆-octahedron is tilted with respect to the four neighbouring ones. The tilt angle is extraordinarily large, the angle Mn—O2—Mn' deviating from 180° by 60.2°. In this respect the structure of MnSeO₃.D₂O is similar to

anhydrous manganese(II) selenite, which can also be described in terms of MnO₆-octahedra.¹ The number of shared vertices in this case is six, but the octahedra are tilted, and there are two different tilt angles of 121.7 and 127.6°.

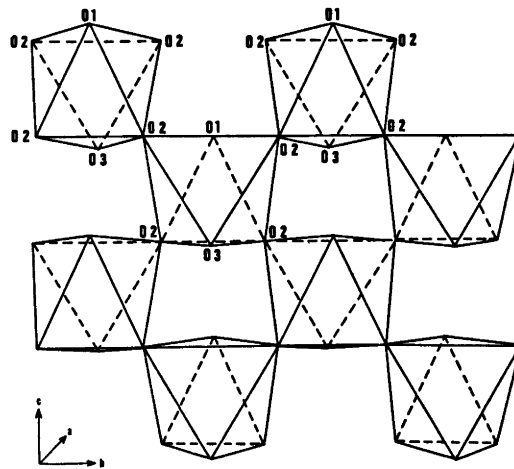


Fig. 1. A layer of tilted MnO₆-octahedra in MnSeO₃.D₂O.

Table 3. Manganese-oxygen and selenium-oxygen bond lengths (Å) selenium-oxygen bond angles (°) with standard deviations in manganese(II) selenites.

Compound	Range of Mn—O bond lengths	Range of Se—O bond lengths	Range of O—Se—O bond angles	Ref.
MnSeO ₃	2.172–2.281	1.710–1.716	95.3–103.5	1
MnSeO ₃ ·D ₂ O	2.135(12)–2.310(8)	1.678(11)–1.710(8)	96.2(4)–103.2(4)	Present work
MnSeO ₃ ·2H ₂ O	2.189(2)–2.278(2)	1.692(2)–1.713(2)	100.4(1)–101.7(1)	2
MnSe ₂ O ₅	2.179(14)–2.206(16)	1.644(14)–1.831(9)	95.9(6)–102.8(6)	3

In regular octahedra, if the edge length of the octahedron is accepted as the minimum value for the distance between the caps of two octahedra with a shared vertex, the maximum value for the deviation from 180° is, for geometric reasons, 48.2°. The fact that the tilt angle in the present case exceeds this by 12° reflects the significant distortion of the coordination polyhedron. The variations of the edge lengths of the octahedron (*cf.* Fig. 2) clearly express this distortion. The irregularity of the distortion is striking, and it cannot be solely identified as one or the other of the two common forms of distortion encountered in octahedral coordination (tetragonal/trigonal elongation or contraction). The irregularity is mainly caused by one markedly shorter edge length (2.560 Å) as compared with the others in the octahedron (2.954–3.313 Å, *cf.* Fig. 2) It is worthwhile to note that this edge length appears between the two equatorial oxygens O2 which are bonded to the same selenium atom. The Mn—O bond lengths are also stretched, to 2.310(8) Å in both cases. It can be concluded that the main reason for these

anomalies is the tendency of the selenite group to maintain its geometry in the compound.

The selenium atoms are bonded to two equatorial oxygens (O2) of one and the cap oxygen (O1) of another octahedron (*cf.* Fig. 2). The bond lengths are normal as compared with the values observed in other manganese selenites (*cf.* Table 3). The bond angles in the selenite group agree with those of the anhydrous MnSeO₃.

The contribution of the water molecule to the distortion is somewhat difficult to judge. In MnSeO₃ no water molecules are present and in MnSeO₃·D₂O the distance Mn—O3 (which could be assumed to stretch due to hydrogen bonds) is 2.212(13) Å, representing almost the mean of the shortest and longest Mn—O bond lengths in the compound. However, in MnSeO₃·2H₂O, which also has a distorted MnO₆ octahedron, the longest bonds are found between the divalent manganese and the two water oxygens. The most regular octahedron seems to be found in the diselenite compound.

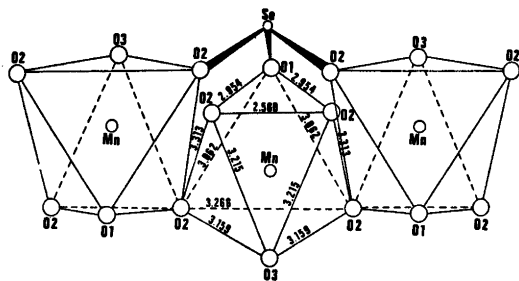


Fig. 2. The pyramidal bond arrangement of selenium(IV) and the distorted MnO₆ octahedron with edge lengths. The *a*-axis is vertical, the *b*-axis horizontal and the *c*-axis perpendicular to the figure plane.

REFERENCES

1. Kohn, K., Inoue, K., Florie, O. and Akimoto, S.-I. *J. Solid State Chem.* 18 (1976) 27.
2. Koskenlinna, M., Niinistö, L. and Valkonen, J. *Cryst. Struct. Commun.* 5 (1976) 663.
3. Koskenlinna, M., Niinistö, L. and Valkonen, J. *Acta Chem. Scand. A* 30 (1976) 836.
4. *International Tables for X-Ray Crystallography*, Kynoch Press, Birmingham 1974, Vol. 4, p. 72.
5. Stewart, J. M., Ed., *The X-Ray System, Version of 1976*, Technical Report TR-466 of the Computer Science Center, University of Maryland, College Park.
6. Wells, A. F. *Structural Inorganic Chemistry*, Clarendon Press, Oxford 1975, p. 157.

Received March 9, 1977.

Pyrolytic Production and Microwave Spectra of Light and Heavy *N*-Methylmethylenimine

B. BAK, N. W. LARSEN and H. SVANHOLT

Chemical Laboratory V, H.C. Ørsted Institutet, DK-2100 Copenhagen, Denmark

$\text{CH}_2=\text{N}-\text{CH}_3$ (I), *N*-methylmethylenimine, and $\text{CD}_2=\text{N}-\text{CD}_3$ (II) have been produced by pyrolysis of $(\text{CH}_3)_2\text{NH}$ and $(\text{CD}_3)_2\text{ND}$, respectively, on a quartz surface at 950°C and $p \approx 30$ mTorr. I and II were identified by their microwave spectra (12.5–40 GHz). 16 transitions in addition to 12 found in earlier work were assigned to $\text{CH}_2=\text{N}-\text{CH}_3$. 28 transitions were assigned to $\text{CD}_2=\text{N}-\text{CD}_3$. Rotational and centrifugal distortion constants were calculated for both species.

In recent attempts to identify interstellar molecules it has become necessary to produce 'suspect' species in the laboratory. One example of this is $\text{CH}_2=\text{NH}$, methylenimine.¹ Primarily, only *spectra* of such compounds are wanted so that bulk production is unnecessary. Methylenimine has been obtained by pyrolysis of methylamine and identified by its microwave (m.w.) spectrum.¹ In consequence, interstellar m.w. radiation due to methylenimine has been safely identified.² Generally, in the search for interstellar species experience has shown that *methyl* derivatives of small hydrogen-containing molecules are likely to occur.³ Thus, for $\text{CH}_2=\text{NH}$, future identification of *cis*, *trans* $\text{CH}_3-\text{CH}=\text{NH}$ and of $\text{CH}_2=\text{N}-\text{CH}_3$ (I) is not unlikely. $\text{CH}_3-\text{CH}=\text{NH}$ has already been produced by pyrolysis of ethylamine.⁴ Earlier, I has been prepared from $[\text{CH}_2=\text{N}-\text{CH}_3]_3$ by decomposition on $\text{Al}_2\text{O}_3, \text{SiO}_2$ at 425°C .⁵ 12 m.w. transitions were measured.⁵ We wanted to see if easy production of I from $(\text{CH}_3)_2\text{NH}$ by pyrolysis would be possible. If so, we wanted to measure a larger number of m.w. transitions to get rotational and centrifugal distortion constants of high precision. A study of the m.w. spectrum of II formed by pyrolysis of $(\text{CD}_3)_2\text{ND}$

soon proved to be a useful pre-stage to a final analysis of the m.w. spectrum of I. The resulting rotational constants of II add to our knowledge of the structure of *N*-methylmethylenimine^{5,6} but a discussion of this is not given in this paper.

EXPERIMENTAL

5 g quantities of commercial $(\text{CH}_3)_2\text{NH}$ (III) and $(\text{CD}_3)_2\text{NH}$ (IV) were repeatedly distilled at -80°C and *ca.* 2 Torr, collecting fractions of constant pressure. Parts of the samples were repeatedly exchanged by 99.5% D_2O at -10°C to produce $(\text{CH}_3)_2\text{ND}$ (V) and $(\text{CD}_3)_2\text{ND}$ (VI). To obtain dry gases III–VI for pyrolysis, samples were taken at -80°C where $p(\text{H}_2\text{O})=0.4$ mTorr. Before gases were admitted to the pyrolysis zone, a 20 cm long quartz tube of i.d. 9 mm, their pressure was reduced to ~ 50 mTorr. At the chosen pumping speed the gases were carried through the electrically heated tube in *ca.* 30 s and directly admitted to the cell of a conventional Stark-modulated m.w. spectrometer. The cell was kept at -30°C , the entrance and exit pressures being of the order 20 and 10 mTorr, respectively. The consumption of 'parent' compound (III–VI) was of the order 0.1 mg/h.

In an experiment a m.w. line of medium intensity and well-separated from other lines of, say, III was repeatedly scanned while the temperature of the quartz tube was raised. Typically, the line intensity remained constant up to $800-850^\circ\text{C}$, then started to decrease to *ca.* $\frac{1}{2}$ intensity at 950°C . When pyrolyzing gases of III 'new' lines turned out to be lines from $\text{CH}_2=\text{N}-\text{CH}_3$ (I), $\text{CH}_2=\text{NH}$, NH_3 and HCN. The m.w. region scanned by us was 17.5–40 GHz. Here, positions of lines from NH_3 , ND_3 , HCN and DCN are well-known while positions of lines from $\text{CH}_2=\text{NH}$ and $\text{CD}_2=\text{ND}$ had to be calculated ignoring centrifugal distortion.¹ A large portion of 'new'

lines was discarded in this way. Positive identification of lines from I and II was based on precalculated relative intensities, Stark-lobe positions, and ^{14}N -quadrupole coupling patterns, all available by using data from Ref. 5.

Pyrolysis of III at 950°C produced I as expected. Four transitions below 40 GHz earlier found by Sastry and Curl⁵ were identified. It was found that complete separation of Stark lobes occurred at an electric field intensity $>1000\text{ V cm}^{-1}$. The measured intensity of these 4 lines proved very useful in further identification of lines in the spectra of I and II.

ASSIGNMENT

Observation of m.w. lines from I and II was sometimes questionable due to, for example, strong 'parental' lines. However, both III and V form I by pyrolysis. So, a spectral 'background' of III could be replaced by a background of V and *vice versa* wherever necessary. Following the identification of 4 lines in the

m.w. spectrum of I (as mentioned above) we proceeded to pyrolyze IV (or VI) to II ($\text{CD}_3=\text{N}-\text{CD}_3$). For I and II with a barrier to CH_3 and CD_3 torsion of ca. 2 kcal mol^{-1} ⁵ so-called *A,E*-splitting is expected. For II, a preliminary calculation based on the barrier of 1970 cal mol^{-1} from Ref. 5 showed this splitting to be $<1\text{ MHz}$ for transitions observed by us ($17.5-40\text{ GHz}$) with $J < 10$, $K_{-1} < 3$. Thus, the first 10 transitions of Table 1 may be considered a group of firmly established 'A' components (coinciding with *E*'s). Any further assigned *A*-component ($J > 10$) must be agreeable with this group within the framework of a rigid rotor Hamiltonian including centrifugal distortion. Also, for $J > 9-10$, *E*-components may split further, while the *A*-components remain single and, therefore, of the larger intensity. Using these two criteria as further guides in the assignment 18 further *A*-components were assigned. Table 1 reviews the total number of transitions assigned, their

Table 1. Number and type of transitions (17.5–40 GHz) measured. Maximum rotational quantum number J_{max} involved. ROTFIT r.m.s. deviations in the analysis of microwave spectra of $\text{CD}_3-\text{N}=\text{CD}_3$ and $\text{CH}_3-\text{N}=\text{CH}_3$.

	R-type	Q-type	P-type	J_{max}	ROTFIT r.m.s. deviations (MHz)
$\text{CD}_3-\text{N}=\text{CD}_3$	14	6	8	28	0.2498
$\text{CH}_3-\text{N}=\text{CH}_3$	11	0	8	20	0.2125

Table 2. Rotational constants *A, B, C* in MHz for $\text{CH}_3-\text{N}=\text{CH}_3$ and $\text{CD}_3-\text{N}=\text{CD}_3$. Quartic distortion constants Δ_J , Δ_{JK} , Δ_K , δ_j and δ_{jk} in kHz. Sextic constants H_K and H_{KJ} in Hz. Asymmetry parameter κ . Both sets correspond to observed *A*-components.

	$\text{CH}_3-\text{N}=\text{CH}_3$	$\text{CD}_3-\text{N}=\text{CD}_3$
<i>A</i>	$52\,527.265 \pm 0.12^a$	$34\,577.274 \pm 0.11$
<i>B</i>	$10\,666.1008 \pm 0.029^a$	$8\,161.0836 \pm 0.027$
<i>C</i>	$9\,377.3587 \pm 0.023^a$	$7\,191.1612 \pm 0.029$
Δ_J	6.566 ± 0.75	3.354 ± 0.38
Δ_{JK}	$-18.327 \pm 11.$	11.294 ± 4.6
Δ_K	$1\,041.818 \pm 17.$	125.885 ± 4.1
δ_j	1.3334 ± 0.068	0.8779 ± 0.085
δ_{jk}	-45.788 ± 1.1	-59.730 ± 3.7
H_K	$3\,820.34 \pm 270.$	
H_{KJ}	$176.72 \pm 25.$	
κ	-0.94026675	-0.92916684

^a Ref. 5 has $A = 52\,523.75 \pm 1.2\text{ MHz}$, $B = 10\,666.13 \pm 0.3\text{ MHz}$, and $C = 9\,377.19 \pm 0.3\text{ MHz}$.

Table 3. Observed and calculated (SEM-4)^a frequencies of ν_A and ν_E components (MHz) in the microwave spectrum of CH₃-N=CH₂ corresponding to a methyl group torsional barrier of 2007 cal/mol^d and an angle between the symmetry-axis of CH₃ and the *a*-axis of the entire molecule of 27.52°.^d

Transition $J_{K-1K+1} \rightarrow J'_{K'-1K'+1}$	ν_A		$\nu_A - \nu_E$	
	Obs.	Calc.	Obs.	Calc.
1 _{0,1} - 1 _{1,0}	43 148.91	43 147.56	18.00	18.76
2 _{0,2} - 2 _{1,1}	44 467.25	44 466.25	19.50	19.57
3 _{0,3} - 3 _{1,2}	46 499.28	46 498.99	20.2	19.95
4 _{0,4} - 4 _{1,3}	49 309.25	49 310.22	19.7	20.30
2 _{1,2} - 3 _{0,3}	19 411.78	19 411.82	-19.0	-18.86
3 _{1,3} - 4 _{0,4}	41 113.35	41 114.17	-18.0	-17.96
4 _{1,3} - 3 _{2,2}	40 963.98	40 964.85	68.4	68.19
6 _{2,5} - 7 _{1,6}	30 183.3	30 183.43 ^c	-47.3	-47.5
9 _{2,7} - 8 _{3,6}	^b	25 053.36 ^c		66.0
9 _{2,8} - 8 _{3,6}	34 460.8	34 461.53 ^c	45.0	44.4
9 _{2,7} - 10 _{1,10}	26 501.4	26 501.40 ^c	-49.9	-51.9
10 _{2,8} - 11 _{1,11}	34 556.3	34 556.50 ^c	-49.9	-51.8
10 _{2,8} - 11 _{2,9}	22 191.8	22 191.65 ^c	-62.0	-53.0
11 _{3,8} - 12 _{2,11}	20 047.5	20 047.20 ^c	-52.2	-45.7

^a Internal rotation program valid for any symmetry of the frame and top, N. W. Larsen and Th. Pedersen (to be published). ^b Probably hidden under a very intense NH₃-absorption line at 25056 MHz. ^c Calculated from the data in Table 2, left column. ^d Ref. 5 has a barrier of 1970 ± 25 cal/mol and an angle of 29.9 ± 1°.

type and the r.m.s. deviation at a ROTFIT fit.⁷ The complete list of measured frequencies is available on request. The corresponding rotational and centrifugal distortion constants are reported in Table 2 (right column).

Finally the more complicated m.w. spectrum of I was assigned (Table 3). The first seven transitions were taken from Ref. 5 ($J \leq 4$). This group was increased by the following seven *A*, *E* transitions of Table 3 as identified by the positions of the *A*-components (fitted to a rigid rotor/centrifugal distortion Hamiltonian) and *A*, *E*-splittings (calculated by means of the computer-program 'SEM-4'; see footnote *a* in Table 3). Assignment of the remaining 9 *A*-components ($J, K_{-1} \geq 12, 3$) was performed as for II but with distortion terms up to the sixth power in \hat{P} (H_K and $H_{KJ} \pm 0$). Observed *A*-components are available on request. Rotational and centrifugal distortion constants of I are given in Table 2 (left column).

DISCUSSION

A rigid molecular model of II derived from the rigid model of I (see Fig. 1), presented in Ref. 5, by replacing all hydrogen atoms by

deuterium has $A = 34810$ MHz, $B = 8169$ MHz, and $C = 7219$ MHz. The values found here are (Table 2) $A_{\text{exp}} = 34577$ MHz, $B_{\text{exp}} = 8161$ MHz, and $C_{\text{exp}} = 7191$ MHz. Generally for several isotopic species (like I and II) agreement between experimental rotational constants and rotational constants of a rigid model is not to

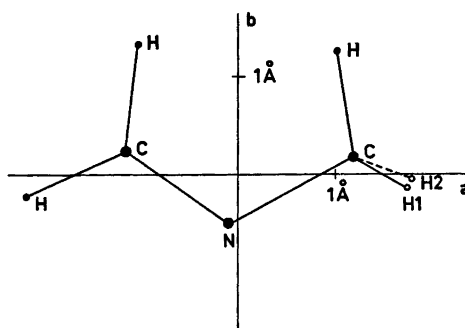


Fig. 1. Position of atoms in *N*-methylmethyl-enimine (I) in its principal axes system (point group C_s). Atoms in and outside the *ab* plane represented by ● and ○, respectively. H1 above and H2 below the *ab* plane. A rigid model (C_s) has 12 geometric parameters. For assumed threefold symmetry of CH₃ (axis N-C) the model has 9 parameters.

be expected. Furthermore the non-rigidity of I and II will add to this disagreement. However, in view of the large number of assumed geometric parameters it is, so far, of little use to discuss the nature and magnitude of the disagreement found.

In the search for interstellar $\text{CH}_3-\text{N}=\text{CH}_2$ observation of emission lines at frequencies higher than 40 GHz may be necessary. The spectroscopic constants derived in this paper (Table 2) should facilitate this.

REFERENCES

1. Johnson, D. R. and Lovas, F. J. *Chem. Phys. Lett.* 15 (1972) 65.
2. Godfrey, P. D., Brown, R. D., Robinson, B. J. and Sinclair, M. W. *Astrophys. Lett.* 13 (1973) 119.
3. Winnewisser, G., Mezger, P. G. and Breuer, H. D. *Interstellar Molecules*. In *Fortschr. Chem. Forsch.* 44 (1973).
4. Lovas, F. J., Clark, F. O. and Tiemann, E. *J. Chem. Phys.* 62 (1975) 1925.
5. Sastry, K. V. L. N. and Curl, R. F., Jr. *J. Chem. Phys.* 41 (1964) 77.
6. Yardley, J. T., Hinze, J. and Curl, R. F., Jr. *J. Chem. Phys.* 41 (1964) 2562.
7. Sørensen, G. O. This laboratory 1975.

Received June 1, 1977.

Metal Complexes With Mixed Ligands. 14. A Potentiometric Study of the Systems Zn^{2+} —Imidazole and Zn^{2+} —OH⁻—Imidazole in 3.0 M (Na)ClO₄ and 3.0 M (Na)Cl

WILLIS FORSLING

Department of Inorganic Chemistry, University of Umeå, S-901 87 Umeå, Sweden

Three component equilibria between zinc(II), imidazole (C₃H₄N₂; L) and OH⁻ have been studied by means of emf titrations at 25 °C in two media 3.0 M (Na)ClO₄ and 3.0 M (Na)Cl using a glass electrode. The total zinc, *B*, and the total imidazole, *C*, have been varied within the limits 0.0025 ≤ *B* ≤ 0.075 M and 0.0025 ≤ *C* ≤ 0.295 M and the ratios *C/B* between 0.25 ≤ *C/B* ≤ 45. At the highest *C/B*-ratios data can be explained solely with step-wise metal complexes ZnL_{*n*}²⁺ *n* = 1, 2, 3, 4 and the following log β_{*n*}-values could be determined: log β₁ = 2.92, log β₂ = 4.93, log β₃ = 8.77 and log β₄ = 11.41 in 3.0 M (Na)ClO₄ and log β₁ = 3.12, log β₂ = 5.64, log β₃ = 7.66 and log β₄ = 9.04 in 3.0 M (Na)Cl. At the lowest *C/B*-ratios ternary hydroxo-imidazoles Zn(OH)L₃⁺ and Zn₂(OH)L₃²⁺ in 3.0 M (Na)ClO₄ and Zn(OH)L⁺ and Zn₂(OH)L₂²⁺ in 3.0 M (Na)Cl also seem to be formed. The equilibrium constants with standard deviations (3σ) are given in Table 4. Data have been analyzed with the least squares computer program LETAGROPVRID.

In preceding papers of this series the three-component equilibria in the systems copper(II)–imidazole–OH⁻^{3,7,12} and nickel(II)–imidazole–OH⁻⁴ have been investigated. Besides the metal complexes ML_{*n*}²⁺, *n* = 1, 2, 3, 4, ternary complexes were also formed. In the copper system data clearly indicated the formation of Cu₂(OH)₂L₂²⁺, Cu₂(OH)₂L₄²⁺ and Cu(OH)L⁺ and in the nickel system Ni(OH)L⁺.

In the binary zinc(II)–OH⁻^{13,41} system the hydroxy complexes are Zn₂OH³⁺ and ZnOH⁺. One would then expect hydroxoimidazoles of the types Zn₂(OH)L₂²⁺ and Zn(OH)L_{*y*}⁺. The present investigation was made to determine whether such ternary complexes exist in the zinc(II)–imidazole–OH⁻ system.

In previous studies of zinc(II)–imidazole complexes no experimental attempts seem to have been made to find hydroxoimidazoles. Earlier data indicated that only ZnL_{*n*}²⁺ should be formed (see Table 1).

EXPERIMENTAL

Chemicals and analysis. Stock solutions of sodium chloride and sodium perchlorate were prepared and analyzed as described earlier.⁴ The dilute *hydrochloric and perchloric acids* and the stock solutions of *imidazolium*, HL⁺, were prepared and standardized as earlier.⁴ Dilute *sodium hydroxide* was prepared from "oljelut" (50 % NaOH and 50 % H₂O) and standardized against acid or hydrazine sulfate. Stock solutions of *zinc chloride* and *zinc perchlorate* were prepared by dissolving carefully washed zinc pellets in hydrochloric and perchloric acids and analyzed for zinc by titration with EDTA and analyzed for [H⁺] by titration with a hydroxide solution using a Gran plot.² The differences in concentrations between analyzed and expected value were always less than 0.2 %.

Apparatus. The thermostat, cell arrangement and electrodes were described earlier.^{4,12} The potentiometric titrations were performed with an automatic system for precise emf titrations, a system constructed and built at this institute by O. Ginstrup.⁶

METHOD

Method. The titration procedures used were similar to those described in earlier papers.^{3,4} During the titrations the total concentrations of zinc, *B*, and imidazole, *C*, were kept either constant or varied. In general each titration was performed at a constant *C/B*-ratio. The free hydrogen ion concentration, *h*, was varied

Table 1. Values of the gross stability constants of zinc(II)–imidazole complexes collected for comparison from the literature. Temperature 25 °C; potentiometric method.

Ref.	Medium	pK_a	$\log \beta_1$	$\log \beta_2$	$\log \beta_3$	$\log \beta_4$
19	0.16 ^a NaNO ₃	7.11	2.58	4.95	7.18	9.20
20	0.16		2.57	4.93	7.15	9.16
21	0.16	7.08	2.52	4.84	7.18	9.21
22	0.15 ^b		2.6			
1	0.058 (KCl)		3.15	6.10		
23	0.2 KNO ₃	7.12	2.13			
24	0.5 NH ₄ NO ₃		2.29– 2.46	4.65– 4.72	6.87– 7.15	9.08– 9.11
18	0.25 (Na)ClO ₄	7.052	2.588	4.424		
18	0.5 (Na)ClO ₄	7.125	2.618		7.596	10.041
18	1 (Na)ClO ₄	7.287	2.663	4.451		10.292
18	2 (Na)ClO ₄	7.575	2.745		8.253	10.919
18	4 (Na)ClO ₄	8.176	3.441			
This work	3 (Na)ClO ₄	7.914	2.916	4.925	8.77	11.417
This work	3 (Na)Cl	7.646	3.123	5.641	7.66	9.04

^a 24 °C. ^b Distribution method.

by adding hydroxide ions or hydrogen ions and measured with a glass electrode. To check their reliability often two electrodes were immersed in the same equilibrium solution. The change in the differences between the emf values was not allowed to exceed 0.2 mV. A constant ionic medium of 3.0 M (Na)ClO₄ or 3.0 M (Na)Cl was used in order to avoid activity coefficient variations. The reproducibility and reversibility of equilibria were tested by performing both forward (increasing $-\log h$) and backward (decreasing $-\log h$) titrations. To check the reversibility at low C/B quotients dilution experiments were carried out. Special efforts were made to cover as great a part of the concentration range as possible. Owing to the formation of precipitates, the available $-\log h$ range was restricted to an upper limit of 6–8.5. An account of these precipitates will be published in a forthcoming paper.¹⁶ The total concentrations (initial concentrations) of B and C were varied within the limits $0.0025 \leq B \leq 0.043$ M, $0.0025 \leq C \leq 0.143$ M in 3.0 M (Na)Cl and $0.0025 \leq B \leq 0.075$ M, $0.0025 \leq C < 0.295$ M in 3.0 M (Na)ClO₄. A greater concentration range was studied in the perchlorate medium because of the fact that in the 3.0 M (Na)Cl medium much of the total zinc, B , occurs as the

complexes ZnCl₃⁻¹⁷ and perhaps even ZnCl₄²⁻. At high zinc concentrations so much chloride is bound in the complex that the medium is changed and that will influence the proton imidazole equilibrium. The change in pK_a is about 0.02 for 0.1 M change in the chloride medium. The following quotients C/B were studied: 0.5, 0.6, 0.7, 0.8, 1, 1.4, 1.6, 1.8, 2, 2.2, 2.8, 3.4, 3.9, 5.6, 7.7 and 10.5 in 3.0 M (Na)Cl, and 0.6, 0.9, 1, 1.1, 1.3, 1.35, 1.5, 1.8, 2.2, 3, 4, 5.4, 6, 11 and 44.9 in 3.0 M (Na)ClO₄.

Calibrations and assumptions in connection with the use of the glass electrode were the same as described earlier.¹³

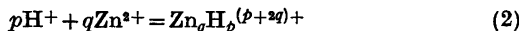
The mathematical analysis of data was performed with the least squares computer program LETAGROPVRID⁹ (version ETITR).¹⁰ On treating the emf data the error squares sum $U = \sum (Z_{\text{exp}} - Z_{\text{calc}})^2$ was minimized, where $Z = (h - H)/C$. The standard deviations were defined and calculated according to Sillén.¹¹ The computation was performed on a CD 3300 computer.

Concerning the binary proton imidazole equilibrium



we will make use of the results obtained from separate experiments. For reaction (1) we found $\log(K_a \pm 3\sigma)$ to be -7.646 ± 0.002 in 3.0 M (Na)Cl and -7.914 ± 0.002 in 3.0 M (Na)ClO₄.

For the binary hydrolysis equilibria



we used the results obtained by Schorsch¹⁴ (3.0 M (Na)Cl) and Biedermann¹⁵ (3.0 M (Li)ClO₄). The investigations both of Schorsch and Biedermann clearly show that the main species in a hydrolyzed Zn²⁺-solution is Zn₂OH²⁺ and the following $\log \beta_{-12}$ -values were reported: -7.50 (3.0 M (Na)Cl) and -8.7 (3.0 M (Li)ClO₄). In the chloride medium the complex ZnOH⁺ with $\log \beta_{-11} = -9.25$ was also reported. These binary equilibria were assumed to be exactly known and all effects above this level will be treated as being caused by binary ZnL_n²⁺ and ternary species.

DATA, CALCULATIONS AND RESULTS

The data were visualized by making a Bjerrum plot $\bar{n}(\log [L])$. This plot is shown in Fig 1. It is seen from the plot that for quotients $C/B \geq 4$ the function $\bar{n}(\log [L])$ seems to be independent of B and C thus indicating the formation of a series of stepwise metal complexes ZnL_n²⁺.

A Letagrop analysis showed that data in both media fulfilling these conditions could be well explained with the complexes ZnL²⁺, ZnL₂²⁺, ZnL₃²⁺ and ZnL₄²⁺. The analysis ended at a $\sigma(Z)$ of 0.002 in both media and must be considered as a very good explanation. The data included in the analysis consist of around 300 experimental points distributed over 15 BC-combinations. The best equilibrium constants with the corresponding standard deviations obtained in these analysis are given in Table 4 calculation denoted 1. The residuals $\Delta Z = Z_{\text{exp}} - Z_{\text{calc}}$ after best fit are given together with experimental data in Table 4.

Data 2. These data cover the ranges $0.0025 \leq B \leq 0.043$ M, $0.0028 \leq C \leq 0.072$ M in 3.0 M (Na)Cl and $0.0025 \leq B \leq 0.070$ M, $0.0075 \leq C \leq 0.118$ M in 3.0 M (Na)ClO₄, $1 < -\log h \leq 8$ and $0.25 \leq C/B \leq 5$. In the search for the ternary hydrolytic species it was assumed that the binary species ZnL_n²⁺ were known and that the equilibrium constants had the values given above.

The search was started with a *pqr* analysis (systematic testing of *pqr*-complexes) in the

Acta Chem. Scand. A 31 (1977) No. 9

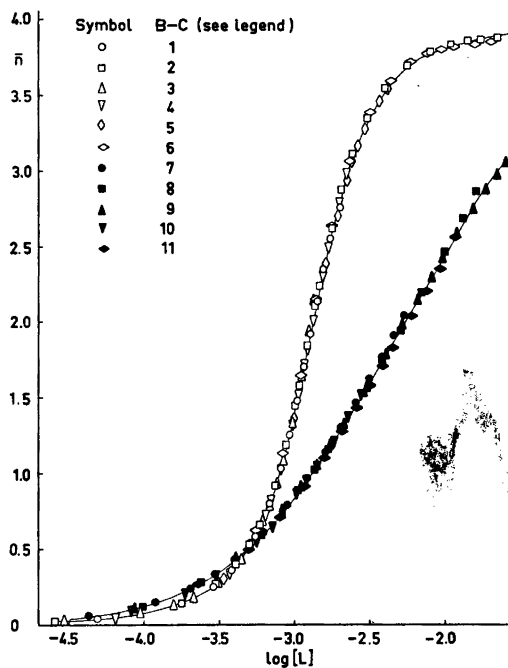


Fig. 1. Experimental data plotted as curves $\bar{n}(\log [L])$ for high C/B ratios ($3 \leq C/B < 45$) and high C concentrations. Open symbols mark titrations in 3 M (Na)ClO₄ and dark symbols 3 M (Na)Cl. The figure also gives a comparison between the strength of complexation in the two media. The symbols stand for the following B and C in mM (start concentrations). 1, 35.4–6.57; 2, 185–16.9; 3, 118–39.3; 4, 118–19.7; 5, 58.9–9.86; 6, 147–3.28; 7, 85.9–25.5; 8, 82.7–10.7; 9, 107–10.2; 10, 17.2–5.11; 11, 41.4–5.36. In order to make the figure clear only a few titrations have been plotted. The full curves have been calculated with a set of proposed constants in Table 4.

3.0 M (Na)Cl medium where the effects are greater. The results of the analysis with the best fitting species are given in Table 2. It is seen from these calculations that the lowest error squares sum for one complex is obtained for Zn(OH)L⁺. Assuming two species, the best combination is Zn(OH)L⁺ and Zn₂(OH)L₂²⁺. The data could also be fairly well explained with the species Zn(OH)L⁺ and Zn₂(OH)L²⁺.

In the 3.0 M (Na)ClO₄ medium the effects are not collected around $\bar{n} = 1$ as in the chloride medium, but cover $1 \leq \bar{n} < 3$. This means that probably at least two ternary complexes with different C/B -ratios exist. In the systematic

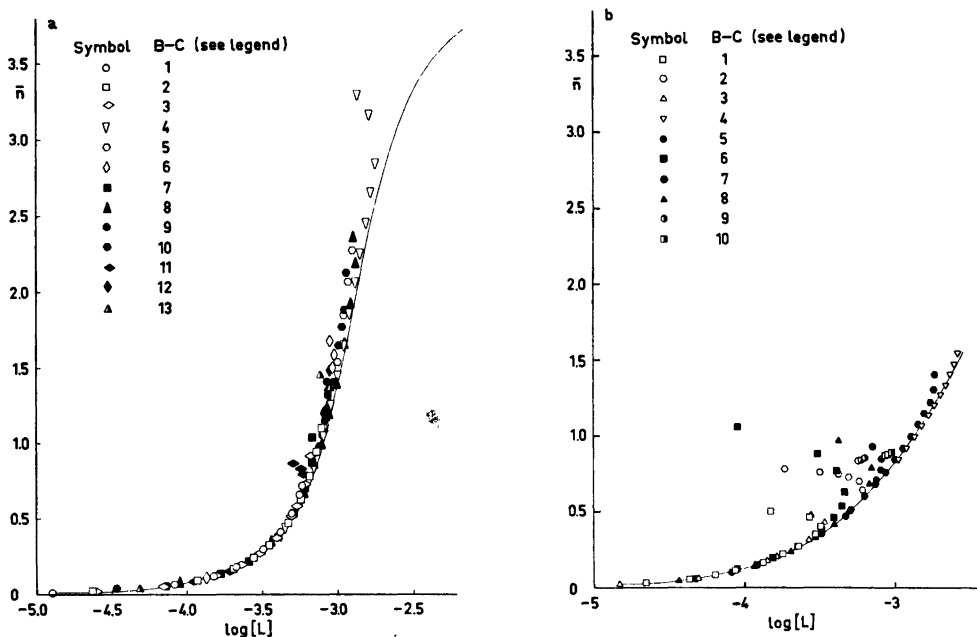


Fig. 2. Experimental data plotted as curves $\bar{n}(\log [L])$ for low C/B ratios ($0.5 \leq C/B \leq 4$). The symbols stand for the following B and C in mM (start concentrations).

a. 3 M (Na)ClO₄ medium. 1, 8.18–5.56; 2, 17.7–9.85; 3, 22.1–16.4; 4, 80.0–20.0; 5, 18.5–4.63; 6, 45.2–20.3; 7, 55.6–42.8; 8, 64.2–21.5; 9, 76.0–41.4; 10, 10.6–2.64; 11, 67.3–67.4; 12, 22.6–10.1; 13, 89.4–50.2.

b. 3 M (Na)Cl medium. 1, 9.74–18.5; 2, 23.2–29.0; 3, 18.4–34.9; 4, 14.1–5.09; 5, 11.4–10.2; 6, 2.85–2.55; 7, 11.4–5.10; 8, 5.70–5.10; 9, 24.3–25.9; 10, 42.8–39.7.

Only a few titrations have been plotted. The full curves have been calculated with the set of proposed constants for the series ZnL_n^{2+} given in Table 4.

Table 2. Data 2. Results of LETAGROP calculations for some different assumptions concerning the ternary complexes formed in 3 M (Na)Cl medium. In the calculations the binary constants for the species ZnL_n^{2+} given in Table 4 and the hydrolysis constants given by Schorsch have not been varied. The constants β_{pqr} are defined according to $pH^+ + Zn^{2+} + rHL^+ \rightleftharpoons (H^+)_p(Zn^{2+})_q(HL^+)_r/\beta_{pqr}$. The errors given are $3\sigma(\log \beta_{pqr})$. The results under the line refer to titrations where $C/B < 1$ and the amounts of the ternary species are especially high.

Number of titr./ number of points	p, q, r	$\log(\beta_{pqr} \pm 3\sigma)$	p, q, r	$\log(\beta_{pqr} \pm 3\sigma)$	$\sigma(Z)$ $\times 1000$	$U/10^3$
18/304						1110
18/304	–2,1,1	–13.19(3)			6.8	140
18/304	–3,1,2	–17.85(6)			11.2	377
18/304			–2,2,1	–10.95(3)	7.2	158
18/304			–3,2,2	–15.47(3)	7.1	151
18/304	–2,1,1	–13.44(5)	–2,2,1	–11.24(6)	4.1	51.3
18/304	–2,1,1	–13.43(5)	–3,2,2	–15.75(6)	3.9	46.9
18/304	–2,1,1	–13.45(9)	–4,2,2	–23.57(10)	5.3	83.8
9/154	–2,1,1	–13.44	–2,2,1	–11.23(4)	3.7	20.6
9/154	–2,1,1	–13.44	–3,2,2	–15.71(3)	3.4	17.5

Table 3. Data 2. Results of LETAGROP calculations in 3 M (Na)ClO₄. No variation of the constants of the binary species ZnL_n²⁺ given in Table 4 and the hydrolysis constants given by Biedermann have been made. The constants β_{pqr} are refined in Table 2. The errors are 3σ(log β_{pqr}). The results under the line correspond to the calculations where the amounts of the binuclear ternary complexes are expected to be as high as possible.

Number of titr./ number of points	<i>p,q,r</i>	log(β _{pqr} ± 3σ)	<i>p,q,r</i>	log(β _{pqr} ± 3σ)	σ(Z) × 1000	U/10
21/385						4270
21/385	-2,1,1	-13.07(4)			5.1	1010
21/385	-3,1,2	-17.90(3)			4.1	629
21/385	-4,1,3	-22.81(3)			4.6	813
21/385			-4,2,3	-20.67(5)	5.8	1273
21/385			-5,2,4	-25.45(4)	5.2	1006
21/385			-6,2,5	-30.33(4)	5.3	1036
21/385	-3,1,2	-18.06(5)	-5,2,4	-25.82(9)	3.0	356
21/385	-3,1,2	-18.06(5)	-6,2,5	-30.67(8)	3.0	342
21/385	-3,1,2	-18.03(5)	-4,2,3	-21.06(9)	3.3	406
21/385	-3,1,2	-18.00(4)	-7,2,6	-35.70(9)	3.2	388
21/385	-4,1,3	-23.01(5)	-5,2,4	-25.73(6)	3.0	333
21/385	-4,1,3	-22.97(4)	-4,2,3	-20.94(5)	2.8	294
21/385	-4,1,3	-22.94(3)	-3,2,2	-16.18(5)	2.8	310
21/385	-4,1,3	-23.03(9)	-2,1,1	-13.38(10)	3.9	573
21/385	-2,1,1	-13.22(4)	-7,2,6	-35.55(6)	3.3	420
21/385	-3,2,2	-16.11(8)	-7,2,6	-35.50(8)	4.9	907
21/385	-3,2,2	-16.33(16)	-6,2,5	-30.47(8)	5.0	928
21/385	-4,2,3	-21.04(17)	-6,2,5	-30.51(11)	5.0	934
21/385	-4,2,3	-20.84(8)	-7,2,6	-35.57(11)	4.8	893
2/33	-4,1,3	-22.90(2)			2.7	
10/198	-4,1,3	-22.90	-3,2,2	-16.22(5)	2.6	130
10/198	-4,1,3	-22.90	-4,2,3	-20.99(4)	2.3	102

testing of *pqr*-complexes the lowest error squares sum, assuming one complex, was obtained for Zn(OH)L₂⁺. However, the remaining effects indicated that this species must be considered as an average of two or more other species. Assuming two complexes the best fit was obtained for Zn(OH)L₃⁺ and Zn₂(OH)L₃²⁺ (see Table 3). However, nearly the same error squares sum was obtained for the combination of Zn(OH)L₃⁺ and Zn₂(OH)L₂³⁺. An attempt to select one of the two combinations was made in the following way. The equilibrium constant for the complex Zn(OH)L₃⁺ was determined in titrations where *C/B*=4 and the amounts of other ternary complexes are low (about 1 %). In a titration set where the amounts of the binuclear ternary species are expected to be as high as possible the two complexes Zn₂(OH)L₂³⁺ and Zn₃(OH)L₃³⁺ were subsequently tested (see Table 3). Once more the species Zn₂(OH)L₃²⁺ was obtained with the lowest error squares sum and this complex is therefore proposed to be the best complement

to the mononuclear species Zn(OH)L₃⁺. However, the amounts of the binuclear species are low (5–6 %) and more information would perhaps be obtained in a less concentrated ionic medium, where the solubility is probably greater.

In order to visualize the amounts of the ternary species at some typical concentrations and *C/B*-ratios, we have collected a set of distribution diagrams which are shown in Fig. 3.

DISCUSSION

The present emf investigation has given evidence for the existence of the hydrolyzed zinc imidazole complexes Zn(OH)L⁺, Zn(OH)L₃⁺ and Zn₂(OH)L₂³⁺ together with a series of stepwise metal complexes ZnL_n²⁺, *n*=1, 2, 3, 4, and it has also indicated the formation of Zn₂(OH)L₃²⁺. The composition of the ternary complexes seems to indicate the close connection between these species and

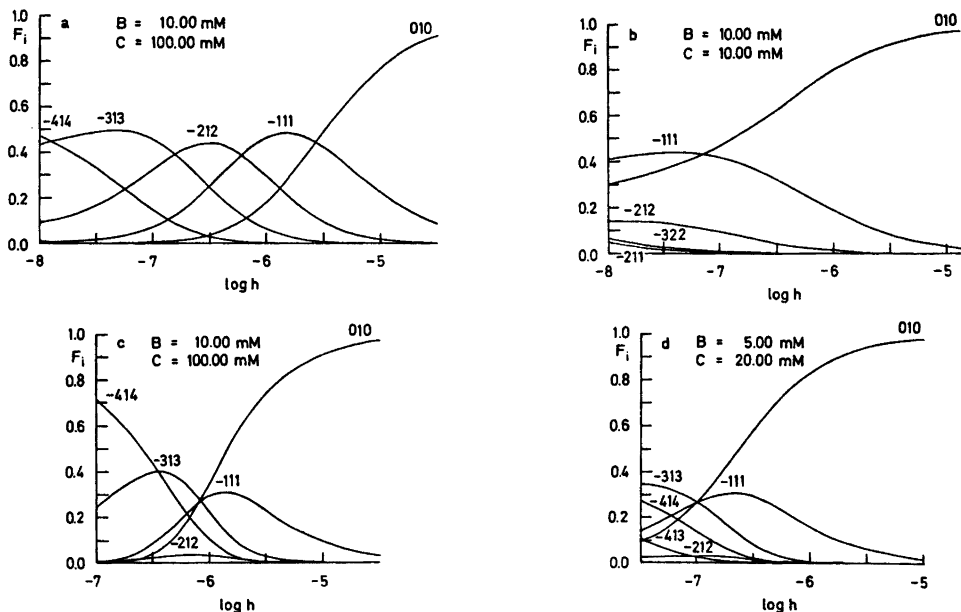
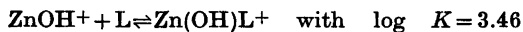
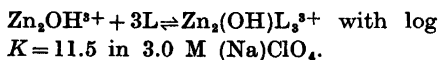
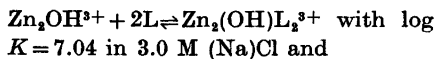


Fig. 3. Distribution diagrams $F_i(\log h)_{BC}$ in 3 M (Na)ClO₄ (a and b) and 3 M (Na)Cl (c and d). F_i is defined as the ratio between zinc(II) in the species and total zinc(II). The calculations have been performed using a version of the computer program SOLGAS³⁸ valid for equilibria in solution and equipped with a plotting procedure (Gunnar Eriksson, to be published).

the binary hydroxo zinc complexes ZnOH⁺ and Zn₂OH³⁺. Thus it was possible to establish the following equilibria:



and



The hydrolyzed zinc ion seems to be a stronger complexing agent than the corresponding hydrated zinc ion because $\text{Zn}^{2+} + \text{L} \rightleftharpoons \text{ZnL}^{2+}$ with $\log K = 3.12$ in 3.0 M (Na)Cl.

It is also possible to compare the acidities (tendency to hydrolyze) of the species $\text{Zn}(\text{H}_2\text{O})_x^{2+}$ and $\text{Zn}(\text{H}_2\text{O})_y\text{L}^{2+}$ in the chloride medium. It is found that $\log K_a(\text{ZnL}^{2+}) > \log K_a(\text{Zn}^{2+})$. The actual values of $\log K_a$ are -8.92 and -9.25 , respectively. It seems that the introduction of an imidazole ligand increases the acidity of the zinc ion. The same effect

is observed in the copper(II),⁷ nickel(II),⁴ silver(I)³⁷ and mercury(II)₄³⁸ imidazole systems. An OH⁻ group together with an L molecule may equally well be interpreted as an imidazolate group $\text{C}_3\text{H}_3\text{N}_2^-$. Thus the complexes proposed could also be $\text{ZnC}_3\text{H}_3\text{N}_2^+$, $\text{Zn}(\text{C}_3\text{H}_3\text{N}_2)\text{L}_2^+$, $\text{Zn}_2(\text{C}_3\text{H}_3\text{N}_2)\text{L}^{3+}$ and $\text{Zn}_2(\text{C}_3\text{H}_3\text{N}_2)\text{L}_2^{3+}$. However, the close connection between the binary hydrolysis and the ternary complexes in this and other metal imidazole systems makes the presence of a hydroxide group in the complexes more probable.

A comparison of the behavior of the zinc system in the two media 3.0 M (Na)ClO₄ and 3.0 M (Na)Cl is interesting. Concerning the binary zinc(II)–OH⁻ system the complexation is much stronger in the chloride medium [$\log \beta_{-12} = -7.50$ in 3.0 M (Na)Cl and $\log \beta_{-12} = -8.7$ in 3.0 M (Li)ClO₄]. Furthermore the species ZnOH⁺ (e.g. for example ZnOHCl_2^{2-}) is found only in the chloride medium. This is probably due to the fact that in 3.0 M (Na)Cl at least 88 % of total zinc, B, is obtained as the tetrahedral complex $\text{ZnCl}_3(\text{H}_2\text{O})^{-17,35}$ and perhaps

Table 4. Results of the final covariations of binary and ternary constants in the two media investigated. When no $3\sigma(\log\beta_{pqr})$, is given, the formation constant has not been varied. The constants β_{pqr} are defined in Table 2.

Number of sets/ number of points	Medium	$\log\beta_{-01}$	$\log\beta_{-111} \pm 3\sigma$	$\log\beta_{-212} \pm 3\sigma$	$\log\beta_{-313} \pm 3\sigma$	$\log\beta_{-414} \pm 3\sigma$	$\log\beta_{-515} \pm 3\sigma$	$\log\beta_{-323} \pm 3\sigma$	$\log\beta_{-413} \pm 3\sigma$	$\log\beta_{-423} \pm 3\sigma$	(Z)
16/268	3.0 M (Na)Cl	-7.646	-4.523(4)	-	9.651(7)	-15.28(2)	-21.55(5)	-	-	-	0.002
18/304	3.0 M (Na)Cl	-7.646	-4.523	-	9.651	-15.28	-21.55	-13.44(5)	-15.75(6)	-	0.004
13/294	3.0 M (Na)ClO ₄	-7.914	-4.998(6)	-10.90(6)	-14.969(6)	-20.25(1)	-	-	-	-	0.002
21/385	3.0 M (Na)ClO ₄	-7.914	-4.998	-10.90	-14.969	-20.25	-	-22.97(4)	-20.94(5)	-	0.003

even as $ZnCl_4^{2-}$, but in the perchlorate medium zinc occurs as the octahedral complex $Zn(H_2O)_6^{2+}$. The association between zinc(II) and ClO_4^- is supposed to be negligible. The distance Zn-O in the tetrahedral complexes is about 1.96 Å as for example in the structures of $KZnCl_3 \cdot 2H_2O$,²⁵ $Zn_3(OH)_3Cl_2 \cdot H_2O$,²⁶ $Zn_3(OH)_3(NO_3)_2 \cdot 2H_2O$ ²⁷ and $Zn(OH)_2$,²⁸ but the corresponding distance in the octahedral complexes is about 2.10–2.13 Å as in $Zn(NO_3)_2 \cdot 6H_2O$,²⁹ $Zn_3(OH)_3(NO_3)_2 \cdot 2H_2O$ ²⁷ and in the X-ray investigation of an aqueous solution of $Zn(H_2O)_6^{2+}$.³⁰ The shorter distance Zn-O in the tetrahedral configuration makes the water protons more acidic and thus the complexation of zinc(II)-OH⁻ stronger.

The complexation of zinc(II)-L is also different in the two media. In 3.0 M (Na)Cl the stepwise stability constants $ZnL_{n-1}^{2+} + L \rightleftharpoons ZnL_n^{2+}$ $n=1, 2, 3, 4$ are $\log K_1=3.12$, $\log K_2=2.52$, $\log K_3=2.02$ and $\log K_4=1.37$.

In 3.0 M (Na)ClO₄ the corresponding constants are $\log K_1=2.92$, $\log K_2=2.01$, $\log K_3=3.84$ and $\log K_4=2.64$.

In 3.0 M (Na)Cl the ZnL_n^{2+} series could be well explained with a two parameter approximation of the type $K_{n+1}=K_0k^n$ with $\log K_0=3.126$ and $\log k=-0.57$. In the 3.0 M (Na)ClO₄ medium this is not possible probably due to a shift from octahedral to tetrahedral configuration at the second step. This configuration shift is also proposed by Ahrland *et al.*^{15,34,35} in several other zinc(II) systems.

The configuration shift in the perchlorate medium with the corresponding changes of the differences

	Octahedral (Å)	Tetrahedral (Å)
Zn-O	2.10–2.13	1.95–1.96
Zn-N	2.15–2.25	2.00–2.01 ^{31,32}
Zn-Cl	2.50–2.60	2.25–2.30 ^{33,32}

will of course influence the occurrence of the ternary zinc(II)-imidazole-OH⁻ complexes.

This investigation indicated that the ternary complexes mainly occur in the tetrahedral form. In 3.0 M (Na)ClO₄ medium the ternary complexes are obtained at higher \bar{n} -values than in the 3.0 M (Na)Cl medium, corresponding to a higher C/B ratio in the species. This is in good agreement with the statement above.

[Compare the species $Zn(OH)L^+$ in 3.0 M (Na)Cl and $Zn(OH)L_3^+$ in 3.0 M (Na)ClO₄]. An emf investigation of the four component equilibria zinc(II)–imidazole–OH⁻–Cl⁻ in 3.0 M (NaClO₄) is completed and will soon be published.

A calorimetric study of the zinc(II)–imidazole–OH⁻ system is planned.

Acknowledgements. I thank Professor Nils Ingri for much valuable advice, for his great interest and for all the facilities placed at my disposal. Thanks are also due to Fil. Dr. Staffan Sjöberg for many helpful discussions. The English of the present paper has been corrected by Dr. Michael Sharp. The work forms part of a program financially supported by the Swedish Natural Science Research Council.

REFERENCES

- Sillén, L. G. and Martell, A. E. (compilers), *Stability Constants, Chem. Soc. London Spec. Publ. No. 17* (1964) and *No. 25* (1971.)
- Gran, G. *Acta Chem. Scand.* **4** (1950) 559.
- Sjöberg, S. *Acta Chem. Scand.* **27** (1973) 3721.
- Forsling, W. and Sjöberg, S. *Acta Chem. Scand.* **A 29** (1975) 569.
- Forsling, W., Hietanen, S. and Sillén, L. G. *Acta Chem. Scand.* **6** (1952) 901.
- Ginstrup, O. *Chem. Instrum.* **4** (1973) 141.
- Sjöberg, S. *Acta Chem. Scand.* **26** (1971) 2149.
- Ingri, N., Kakalowics, W., Sillén, L. G. and Warnqvist, B. *Talanta* **14** (1967) 1261.
- Ingri, N. and Sillén, L. G. *Ark. Kemi* **23** (1964) 97.
- Arnek, R., Sillén, L. G. and Wahlberg, O. *Ark. Kemi* **31** (1969) 353; Brauner, P., Sillén, L. G. and Whiteker, R. *Ark. Kemi* **31** (1969) 365.
- Sillén, L. G. *Acta Chem. Scand.* **16** (1962) 159; Sillén, L. G. and Warnqvist, B. *Ark. Kemi* **31** (1969) 341.
- Sjöberg, S. *Diss.*, University of Umeå, Umeå 1976.
- Biedermann, G. *Proc. 7ICC* (Stockholm-Uppsala June 1962), Abstracts.
- Schorsch, G. *Bull. Soc. Chim. Fr.* (1965) 988.
- Avsar, E. *Diss.* University of Lund, Lund 1975.
- Forsling, W. To be published.
- Sillén, L. G. and Liljeqvist, B. *Sven. Kem. Tidskr.* **56** (1944) 85.
- Lumme, P. and Virtanen, P. *Acta Chem. Scand.* **A 28** (1974) 1055.
- Edsall, J. T., Felsenfeld, G., Goodman, D. S. and Gurd, F. R. N. *J. Am. Chem. Soc.* **75** (1954) 3054.
- Nozaki, Y., Gurd, F. R. N., Chen, R. F. and Edsall, J. T. *J. Am. Chem. Soc.* **79** (1957) 2123.
- Koltun, W. L., Kexter, R. N., Clark, R. F. and Gurd, F. R. N. *J. Am. Chem. Soc.* **80** (1958) 4188.
- Schutert, J. L., Lind, E. L., Westfall, W. M., Pleger, R. and Li, N. C. *J. Am. Chem. Soc.* **80** (1958) 4799.
- Chakravorty, A. and Cotton, F. A. *J. Phys. Chem.* **67** (1963) 2878.
- Berthon, G. and Luca, C. *Chimie Anal. Paris* **53** 10 oct. 1971.
- Brehler, B. and Siisse, P. *Naturwissenschaften* **50** (1963) 517.
- Allman, R. *Z. Kristallogr.* **126** (1968) 417.
- Stählin, W. and Oswald, H. R. *Acta Crystallogr.* **B 26** (1970) 860.
- Wells, H. G. *Structural Inorganic Chemistry*, 4th Ed., Oxford University Press 1975, p. 522.
- Ferrari, A., Braibanti, A., Manotti Lanfredi, A. M. and Tripicchio, A. *Acta Crystallogr.* **22** (1967) 240.
- Bol, W., Gerrits, G. J. A. and Panthaleon van Eck, C. L. *J. Appl. Crystallogr.* **3** (1970) 486.
- Sandmark, C. and Brändén, C-I. *Acta Chem. Scand.* **21** (1967) 993.
- Lundberg, B. K. S. *Acta Crystallogr.* **21** (1966) 901.
- Forsberg, H. E. and Nowacki, W. *Acta Chem. Scand.* **13** (1959) 1049.
- Björk, N.-O. *Diss.*, University of Lund, Lund 1975.
- Ahrland, S. *Struct. Bonding (Berlin)* **15** (1973) 167.
- Eriksson, G. *Acta Chem. Scand.* **25** (1971) 2651.
- Granberg, I. *Private communications.*
- Sjöberg, S. *Acta Chem. Scand.* **A 31** (1977) 718.
- Bear, C. A., Duggan, K. A. and Freeman, H. C. *Acta Crystallogr.* **B 31** (1975) 2713.

Received March 8, 1977.

The Crystal Structure of Sodium Cholesteryl Sulfate Dihydrate

IRMIN PASCHER and STAFFAN SUNDELL

Dept. of Structural Chemistry, Institute of Medical Biochemistry, University of Göteborg,
P.O.B. S-400 33 Göteborg, Sweden

Sodium cholesteryl sulfate crystallizes as the dihydrate in space group $P1$ with $a=6.296$, $b=6.238$, $c=40.813$ Å, $\alpha=88.94$, $\beta=89.51$ and $\gamma=107.44^\circ$. The unit cell contains two independent molecules with their main conformational difference in the side chain. The molecules are arranged tail to tail in a double layer. Three regions with different lateral interactions exist. In the polar part each sodium ion is roughly octahedrally surrounded by oxygen atoms, four belonging to sulfate groups and two belonging to water of crystallization. The steroid part is in van der Waals contact only with other steroid skeleta. In the third region only side chains interact. Due to the bulkiness of the steroid part the side chains are left with unusually large space which causes disorder and/or large thermal vibrations. The lateral arrangement of the steroid skeleta is of interest as it resembles in geometry and cross sectional area the hybrid packing modes of hydrocarbon chains.

The existence of cholesteryl sulfate in animal tissues and fluids has been known for several years. Minor amounts have been identified in adrenal glands,¹ in kidney, liver, plasma, urine and bile² and in blood and gallstone.³ A relatively high concentration in faeces suggested a role as a metabolite of cholesterol.² Recently, however, cholesteryl sulfate was shown to be an abundant constituent of the brushborder membrane of intestine (K.-A. Karlsson, unpublished). Its occurrence in faeces therefore appears more likely to be due to the rapid turnover of these membranes.

This type of steroid sulfate has also been identified as one of the major lipid components in the starfish *Asterias rubens*.^{4,5} The high amount of 1.3 mg per g dry weight in different tissues also here suggests a function as a membrane constituent.

In several vertebrate tissues an interesting correlation between the concentration of cerebroside sulfate (sulfatide) and the $\text{Na}^+ - \text{K}^+ - \text{ATPase}$ activity was found suggesting this sulfolipid to be involved in the sodium transport across the plasma membrane.^{6,7} Similarly, cholesteryl sulfate may participate in ion transport, especially as other sulfolipids have not been found in the starfish.

This marine organism has a vascular system for motion and progression. The fluid pressure in this hydraulic system is thought to be regulated by osmotic principles by means of a potassium pump.⁸ The demand of a potassium pump and presence of cholesteryl sulfate support the hypothesis that sulfolipids may function as ion receptors in sodium-potassium transport across membranes.

It is therefore of interest to investigate the properties of these sulfolipids and their significance for membrane structure and function. The phase behaviour of cholesteryl sulfate and phosphate in pure form and in presence of water has been determined.⁹ In the case of the phosphate a remarkable lamellar long range order was observed in the aqueous gel phase. Further structural information on sulfolipids has been obtained by the X-ray analysis of sodium dodecyl sulfate.¹⁰

EXPERIMENTAL

Cholesteryl sulfate (cholesteryl- 3β -sulfate) was synthesized according to Sobel *et al.*¹¹ and converted into its sodium salt on an ion exchange column. Crystals were obtained from a 1 % solution in 95 % ethanol as thin elongated plates.

A crystal with the dimensions $0.25 \times 0.54 \times 0.02$ mm was used for data collection on a Picker FACS I diffractometer.¹² The reflexions were measured by a $\theta - 2\theta$ step scan with 20 steps of 0.13° each. The counting time for each step was 2 s. Background counts of 10 s were taken at each side of the peak. 3439 independent reflexions in the 2θ range $3 - 100^\circ$ were measured. 2582 reflexions with intensities greater than $2\sigma(I)$ were considered observed. For these reflexions corrections for Lorentz and polarization effects were made.

CRYSTAL DATA

Molecular formula: $C_{27}H_{45}SO_4Na \cdot 2H_2O$.Crystal system: triclinic. Space group: $P1$.Unit cell: $a = 6.296(11)$, $b = 6.238(14)$, $c = 40.813(67)$ Å, $\alpha = 88.94(3)$, $\beta = 89.51(2)$, $\gamma = 107.44(2)^\circ$. $V = 1529$ Å³, $M = 524.74$, $Z = 2$, $D_c = 1.14$ g cm⁻³, $\lambda = 1.5405$ Å (CuK α radiation), $\mu = 13.8$ cm⁻¹.

Systematic absences: None.

Table 1. Fractional coordinates and thermal parameters ($\times 10^3$) with estimated standard deviations in parentheses. The isotropic and anisotropic thermal parameters are in the form $-\frac{8\pi}{3}U(\sin^2\theta/\lambda^2)$ and $\exp -2\pi^2(h^2a^{*2}U_{11} + \dots + 2kl2b^*c^*U_{23})$, respectively.

Atom	x	y	z	U or U ₁₁	U ₂₂	U ₃₃	U ₁₂	U ₁₃	U ₂₃
Na(1)	0.7039(17)	0.4426(18)	0.0322(3)	27(5)	46(6)	48(6)	20(5)	1(5)	-8(5)
Na(2)	0.2073(17)	0.4589(20)	0.9704(3)	26(6)	62(7)	50(7)	25(5)	-5(5)	-4(6)
O(1)	0.8865(17)	0.8270(34)	0.0454(7)	55(14)	39(13)	129(22)	22(11)	-19(14)	-16(13)
O(2)	0.5488(33)	0.0578(33)	0.0264(6)	45(13)	48(13)	83(17)	23(11)	3(12)	-9(12)
O(3)	0.3937(37)	0.8546(33)	0.9596(6)	66(14)	45(13)	80(16)	29(11)	-7(12)	-20(12)
O(4)	0.0538(35)	0.0760(32)	0.9782(6)	49(13)	29(12)	109(19)	2(10)	-8(13)	0(12)

Molecule A

S(1)	0.2390(11)	0.4963(12)	0.0571(2)	18(3)	35(4)	39(4)	16(3)	-4(3)	0(3)
O(11)	0.3309(29)	0.5111(29)	0.0252(5)	27(10)	36(11)	58(12)	11(9)	-22(9)	10(9)
O(12)	0.0034(28)	0.3471(31)	0.0596(5)	20(10)	49(12)	53(13)	8(9)	0(9)	6(10)
O(13)	0.2692(29)	0.7058(31)	0.0715(5)	30(10)	50(12)	52(13)	18(9)	-5(9)	15(10)
O(14)	0.3878(29)	0.3709(33)	0.0771(4)	34(11)	67(14)	34(11)	33(10)	-1(8)	-11(10)
C(1)	0.2787(43)	0.2011(49)	0.1661(8)	23(16)	49(19)	68(23)	18(14)	8(15)	10(16)
C(2)	0.2349(51)	0.1749(60)	0.1285(8)	38(19)	79(25)	62(24)	24(18)	3(17)	1(19)
C(3)	0.3956(42)	0.3814(50)	0.1115(7)	22(15)	65(21)	45(19)	29(15)	-12(13)	7(16)
C(4)	0.6525(40)	0.3907(55)	0.1186(7)	8(14)	87(24)	40(19)	11(15)	5(12)	7(16)
C(5)	0.6851(40)	0.3903(47)	0.1555(7)	14(14)	47(18)	65(22)	23(13)	11(13)	10(15)
C(6)	0.8590(43)	0.5553(50)	0.1674(8)	22(15)	54(19)	65(23)	21(14)	-8(15)	-9(16)
C(7)	0.9205(41)	0.5680(48)	0.2029(7)	18(14)	55(19)	50(20)	14(14)	-1(13)	12(15)
C(8)	0.7998(37)	0.3432(40)	0.2232(7)	9(12)	24(15)	47(17)	-5(11)	15(12)	0(13)
C(9)	0.5484(42)	0.2606(52)	0.2135(7)	17(14)	67(21)	42(19)	13(14)	-8(13)	13(16)
C(10)	0.5292(36)	0.2103(43)	0.1768(7)	3(12)	40(17)	47(19)	0(11)	-5(12)	7(13)
C(11)	0.4180(47)	0.0725(52)	0.2365(8)	32(17)	55(21)	65(23)	6(16)	-3(16)	-2(17)
C(12)	0.4526(47)	0.1116(55)	0.2736(8)	29(16)	69(23)	57(22)	13(15)	9(15)	-17(17)
C(13)	0.7053(44)	0.1928(51)	0.2835(7)	32(16)	65(20)	28(16)	22(15)	-9(13)	-8(14)
C(14)	0.8117(45)	0.4057(54)	0.2599(7)	28(16)	68(21)	41(18)	10(15)	-4(14)	6(16)
C(15)	1.0428(49)	0.5002(55)	0.2747(8)	39(19)	59(21)	60(22)	-4(16)	-31(16)	-22(17)
C(16)	1.0037(57)	0.4591(63)	0.3119(9)	54(22)	85(27)	64(25)	18(20)	-26(18)	2(20)
C(17)	0.7538(59)	0.3172(65)	0.3189(9)	63(24)	88(28)	55(23)	5(21)	-24(19)	-24(20)
C(18)	0.5601(48)	-0.0330(54)	0.1698(9)	33(18)	62(22)	77(24)	21(16)	-15(16)	-14(18)
C(19)	0.8002(46)	-0.0067(47)	0.2792(7)	40(17)	42(18)	46(19)	15(15)	-5(15)	-1(15)
C(20)	0.7216(78)	0.1509(59)	0.3482(8)	125(37)	85(29)	34(20)	-37(26)	-14(22)	27(20)
C(21)	0.4868(86)	0.0037(90)	0.3528(9)	126(39)	153(45)	37(23)	-33(34)	-7(23)	58(26)
C(22)	0.7984(101)	0.3389(106)	0.3798(12)	154(51)	179(58)	73(33)	-22(43)	20(32)	77(36)
C(23)	0.8181(118)	0.1863(114)	0.4101(17)	155(23)					
C(24)	1.0282(285)	0.3600(312)	0.4337(47)	389(83)					
C(25)	0.9966(204)	0.1791(260)	0.4623(32)	274(50)					
C(26)	0.9407(305)	-0.0637(339)	0.4666(44)	408(88)					
C(27)	1.1462(385)	0.3423(363)	0.4903(54)	482(107)					

Table 1. Continued.

Atom	x	y	z	U or U11	U22	U33	U12	U13	U23
<u>Molecule B</u>									
S(1)	0.7487(11)	0.5286(12)	0.9460(2)	24(3)	35(4)	44(4)	18(3)	8(3)	-2(3)
O(11)	0.8380(33)	0.5263(33)	0.9784(6)	43(12)	48(13)	79(15)	22(10)	29(11)	-6(11)
O(12)	0.5272(27)	0.3823(30)	0.9420(5)	20(9)	42(12)	63(13)	13(9)	1(9)	-4(10)
O(13)	0.7749(30)	0.7498(33)	0.9336(5)	28(11)	60(14)	68(14)	14(10)	8(10)	-10(11)
O(14)	0.9169(26)	0.4364(30)	0.9249(4)	18(9)	57(12)	37(11)	25(9)	11(8)	-6(9)
C(1)	1.0644(48)	0.5388(45)	0.8354(7)	44(18)	28(16)	57(21)	7(14)	9(15)	5(14)
C(2)	1.0720(44)	0.5761(47)	0.8718(7)	35(17)	51(19)	30(17)	4(15)	-28(13)	-13(14)
C(3)	0.8800(39)	0.4147(43)	0.8907(7)	12(13)	28(15)	66(20)	18(12)	-2(13)	6(14)
C(4)	0.8594(49)	0.1613(52)	0.8821(8)	43(19)	58(22)	56(21)	23(17)	8(16)	16(17)
C(5)	0.8593(51)	0.1316(50)	0.8463(8)	45(19)	35(18)	61(21)	21(16)	7(16)	27(16)
C(6)	0.7013(56)	-0.0427(61)	0.8333(10)	43(20)	62(24)	97(30)	27(20)	7(19)	25(21)
C(7)	0.6744(49)	-0.1082(53)	0.7957(8)	37(19)	54(21)	66(24)	0(16)	7(17)	12(17)
C(8)	0.8863(42)	0.0224(48)	0.7769(7)	23(15)	47(18)	49(18)	21(13)	6(13)	3(14)
C(9)	0.9743(39)	0.2712(42)	0.7877(7)	16(14)	30(15)	49(18)	4(12)	1(12)	-14(13)
C(10)	1.0440(39)	0.2937(46)	0.8257(7)	9(13)	43(17)	56(19)	3(12)	5(13)	0(14)
C(11)	1.1777(55)	0.4102(54)	0.7641(8)	58(22)	53(21)	65(23)	16(17)	-3(18)	-10(18)
C(12)	1.1122(45)	0.3772(48)	0.7259(7)	32(16)	45(19)	49(19)	10(14)	-6(14)	-6(15)
C(13)	1.0367(50)	0.1347(49)	0.7174(8)	43(18)	41(19)	69(23)	13(15)	25(16)	-6(16)
C(14)	0.8283(45)	0.0172(55)	0.7406(7)	23(16)	78(24)	41(19)	7(16)	10(14)	-3(17)
C(15)	0.7269(46)	-0.2136(53)	0.7268(9)	25(17)	58(22)	72(25)	2(15)	5(16)	-32(19)
C(16)	0.7714(58)	-0.1779(72)	0.6910(13)	36(21)	89(32)	145(44)	2(21)	-7(24)	-54(29)
C(17)	0.9129(66)	0.0695(68)	0.6843(8)	86(28)	95(30)	34(20)	13(24)	2(18)	-25(19)
C(18)	1.2706(42)	0.2484(50)	0.8312(9)	11(14)	45(19)	99(26)	3(13)	-20(15)	-8(17)
C(19)	1.2267(55)	0.0138(69)	0.7217(9)	44(20)	115(32)	62(23)	40(21)	4(17)	-10(21)
C(20)	1.0683(70)	0.1114(74)	0.6521(10)	83(30)	93(32)	82(30)	-16(25)	-34(24)	-31(25)
C(21)	1.2052(90)	0.3585(101)	0.6487(9)	140(44)	183(54)	22(21)	-16(39)	31(24)	10(26)
C(22)	0.9073(121)	0.0561(102)	0.6207(9)	274(78)	173(54)	15(22)	-63(52)	11(32)	-50(27)
C(23)	0.7909(229)	0.2327(221)	0.5999(31)	306(56)					
C(24)	0.6465(191)	0.0415(187)	0.5813(27)	262(47)					
C(25)	0.6213(345)	0.2079(376)	0.5526(50)	433(106)					
C(26)	0.6893(271)	0.4394(317)	0.5461(39)	371(78)					
C(27)	0.4935(241)	-0.0082(229)	0.5278(33)	316(58)					

STRUCTURE DETERMINATION AND REFINEMENT

From a sharpened three-dimensional Patterson function the peak corresponding to the S-S vector was easily found. At a distance of about 1.4 Å from this peak there were eight peaks which could be separated into two groups. Each group contained four likely S-O vectors consistent with the known geometry of the sulfate group. The positions of atoms of the two sulfate groups thus determined were used as a first phasing model. In subsequent Fourier syntheses all non-hydrogen atoms except those belonging to the outer part of the side chains C(23)-C(27) in the two independent molecules were found. At this stage two cycles of block diagonal refinement with isotropic temperature factors were performed which

reduced the R -value from 0.26 to 0.16. From a Fourier and a difference synthesis a reasonable suggestion for the location of the missing part of the side chains was obtained. The refinement now again continued with anisotropic temperature factors. The last located atoms of the side chains, however, were given isotropic temperature factors. After five cycles using the full matrix the refinement converged at $R=0.118$ and $R_w=0.129$. The weight assigned to each reflexion¹³ was:

$$1/[1 + (F_o - 2.7F_{\min})^2 / (4.2F_{\min})^2]$$

Most bond distances and angles of the side chains did not improve and the temperature factor of some atoms became large. This indicates that disorder and/or considerable thermal motion exists in the side chain region. A

difference Fourier of this region contained some fairly weak peaks. From their positions, however, no model for a possible disorder could be deduced. The form factors used were those given by Cromer and Mann.¹⁴ All calculations were performed on a DEC 10 computer system using the X-RAY 72 program system.¹⁵

DESCRIPTION AND DISCUSSION OF THE STRUCTURE

The atomic parameters are listed in Table I. A list of final observed and calculated structure

factors can be obtained from this Department. The numbering of atoms and the bond distances and angles of the two cholesterol sulfate molecules A and B are shown in Figs. 1 and 2. These values are as expected considering the high standard deviations. The geometry of the cholesterol skeleton is in agreement with that observed in other cholesterol derivatives.¹⁶⁻²⁰ The two independent molecules differ in their conformation about the C(20)-C(22) bond (Fig. 3).

Fig. 4 shows the tail to tail packing of cholesterol sulfate molecules in a double layer ar-

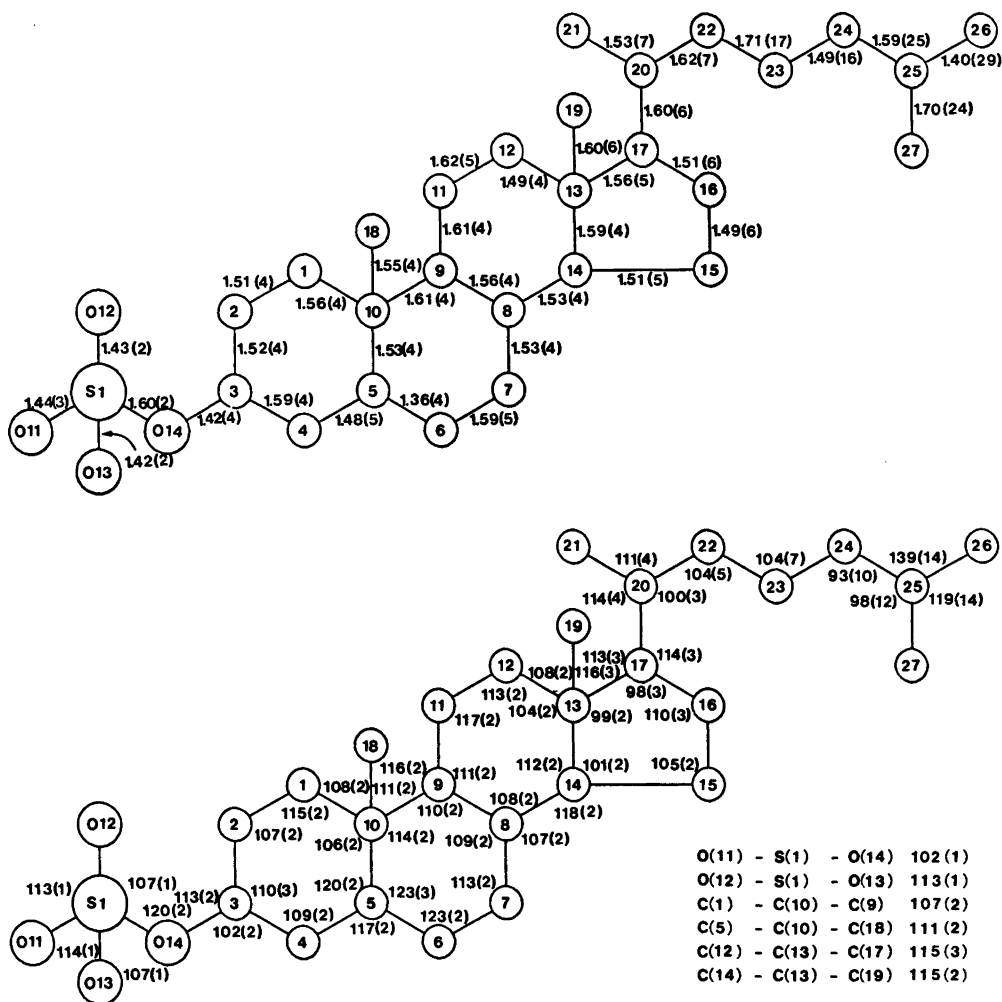


Fig. 1. Atom numbering and bond distances (Å) and angles (°) of molecule A. Estimated standard deviations are given in parentheses.

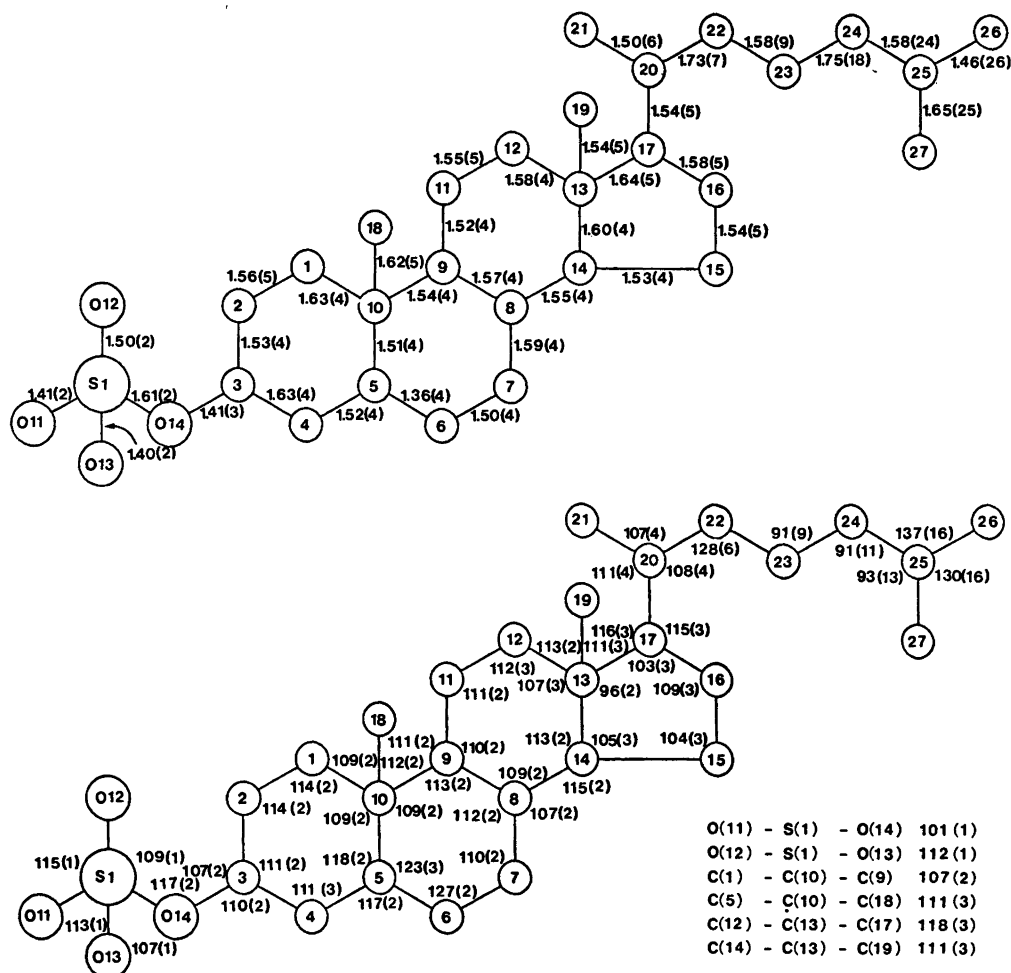


Fig. 2. Atom numbering and bond distances (Å) and angles (°) of molecule B. Estimated standard deviations are given in parentheses.

rangement. The two halves of the double layer are not identical in that each half contains only

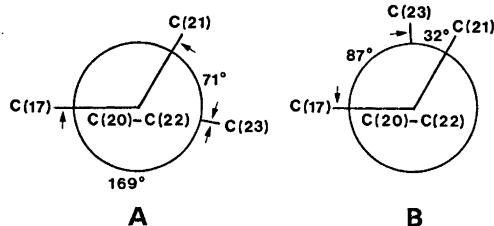


Fig. 3. The molecular conformation about the bond C(20)-C(22) in molecules A and B.

one type of the two independent molecules. Both molecules are tilted 75° towards the layer boundary.

The sulfate groups, the rigid steroid skeletons and the branched hydrocarbon side chains form three regions with different packing character within the double layer.

The sulfur atoms and sodium ions lie close to a plane parallel to the *ac*-face. Each sodium atom is roughly octahedrally surrounded by six oxygens at distances between 2.31 and 2.63 Å (Table 2). Four of these belong to the sulfate groups and lie approximately in one plane while the two other oxygens belong to water

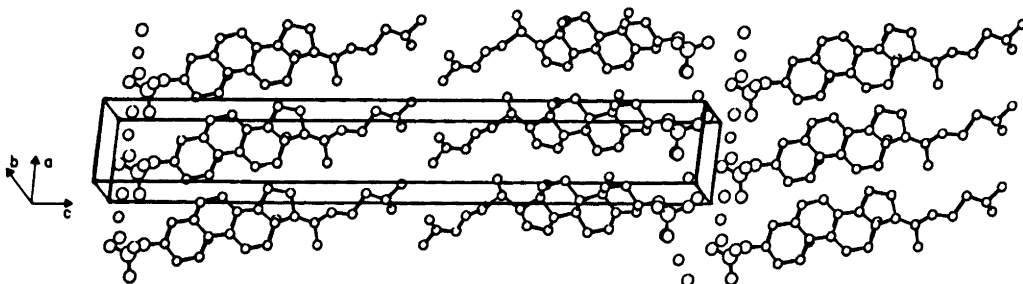


Fig. 4. The molecule arrangement of cholesterol sulfate.

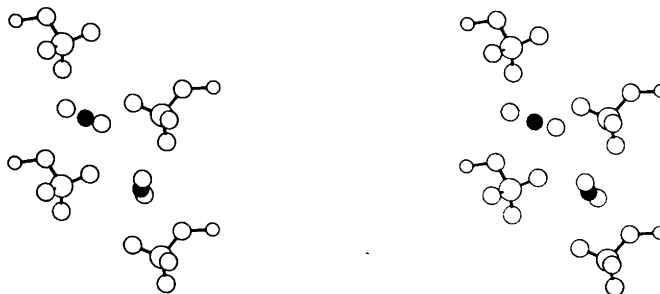


Fig. 5. Stereoscopic view of the polar region.

molecules. The polar region is visualized stereographically in Fig. 5 and torsion angles about the ester bond are shown in Fig. 6. Short intermolecular oxygen-oxygen distances are given in Table 3. All of these involve water molecules and may represent hydrogen bonds.

Table 2. Sodium oxygen distances (Å) less than 3.5 Å and their estimated standard deviations ($\times 10^2$).

Na(1)–O(1)	(0,0,0) ^a	2.40(3)
Na(1)–O(2)	(0,0,0)	2.32(3)
Na(1)–O(A11)	(0,0,0)	2.53(3)
Na(1)–O(A12)	(1,0,0)	2.42(3)
Na(1)–O(A14)	(0,0,0)	2.63(2)
Na(1)–O(B11)	(0,0,-1)	2.34(3)
Na(2)–O(3)	(0,0,0)	2.42(3)
Na(2)–O(4)	(0,0,0)	2.31(3)
Na(2)–O(A11)	(0,0,1)	2.37(2)
Na(2)–O(B11)	(-1,0,0)	2.50(3)
Na(2)–O(B12)	(0,0,0)	2.49(3)
Na(2)–O(B14)	(-1,0,0)	2.59(2)

^a The figures within parentheses indicate translations in the directions *a*, *b* and *c* of the second atom.

The lateral packing of the steroid skeleta is different from that found in other cholesterol derivatives. In cholesterol esters^{18,19} the skeleta pack laterally in a double row arrangement in which the projecting methyl groups face each other and can interdigitate due to a displacement of the steroid skeleta in the direction of their maximum extension. In cholesterol sulfate the skeleta pack in single rows only. In Fig. 7 this lateral arrangement is shown for molecule A (the packing of molecule B is similar). The methyl groups project into the space between two skeleta of the adjacent row. This arrangement also differs from that of the

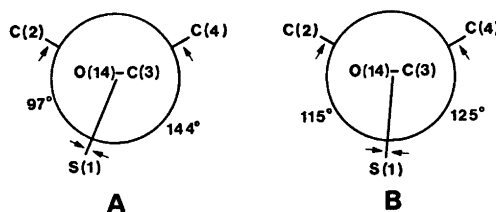


Fig. 6. The molecular conformation about the bond O(14)–C(3) in molecules A and B.

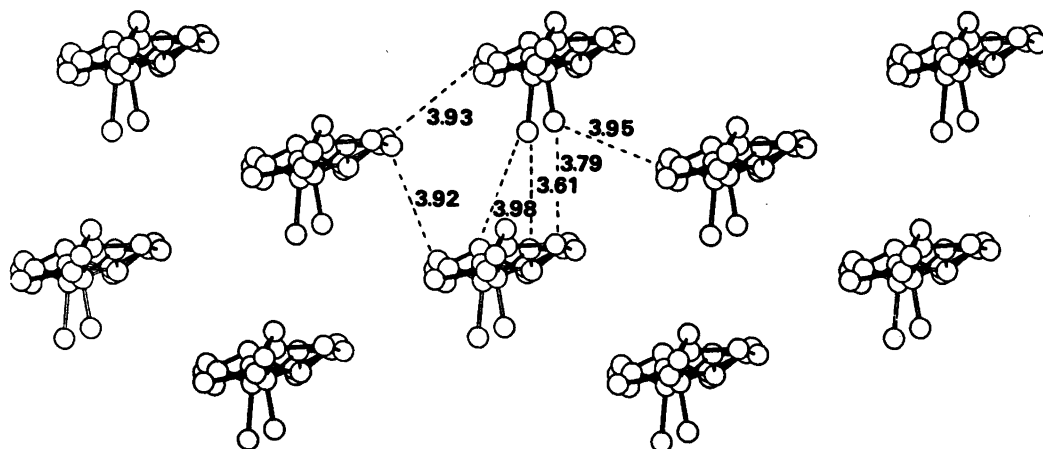


Fig. 7. The lateral arrangement of the steroid skeleta of molecule A.

cholesteryl esters in that adjacent skeleta show only a small mutual displacement in their direction of maximum extension. Both types of lateral packing are about equally effective with a cross sectional area of 37 \AA^2 per molecule.

These packing requirements of the bulky steroid groups leave the side chains with unusually large space. This no doubt explains the observed disorder and/or large thermal vibrations in the chain packing region. Though the skeleta planes of molecule A and B have different orientation in the unit cell their side chains become roughly parallel due to conformational differences about the C(20–C(22) bond (Fig. 3).

The side chains tilt by an angle of approximately 60° towards the layer boundary. The

Table 3. Intramolecular oxygen-oxygen distances (\AA) less than 3.2 \AA and their estimated standard deviations ($\times 10^2$).

O(A12)---O(1)	(-1, -1, 0) ^a	3.17(4)
O(A13)---O(1)	(-1, 0, 0)	2.94(4)
O(A13)---O(2)	(0, 1, 0)	2.96(3)
O(B13)---O(3)	(0, 0, 0)	2.87(4)
O(B13)---O(4)	(1, 1, 0)	2.93(3)
O(1)---O(2)	(0, 1, 0)	3.00(4)
O(1)---O(4)	(1, 1, -1)	3.14(4)
O(2)---O(3)	(0, -1, -1)	3.07(3)
O(3)---O(4)	(0, 1, 0)	2.97(4)

^a The figures within parentheses indicate translations in the directions *a*, *b* and *c* of the second atom.

lateral distance between the chains then corresponds to a cross section area of about 35 \AA^2 per chain which can be compared with a value of 21 \AA^2 for hexagonal α -phase adopted by many long-chain compounds near their melting point. In cholesteryl iodide¹⁶ and in 7-bromo-cholesteryl-bromide¹⁷ the side chains pack more effectively being in contact also with the sterol skeleta.

The arrangement of the steroid skeleta of cholesteryl sulfate appears to be of interest when considering the copacking of cholesterol and long chain lipids in biological membranes. Recent single crystal analyses of a cholesteryl ester,¹⁸ phosphatidylethanolamine²¹ and cerebroside²² have shown that the hydrocarbon chains of these complex lipids arrange according to earlier unknown hybrid packing modes. These chain matrices have a striking resemblance in geometry and cross sectional area with the cholesterol packing pattern in cholesteryl sulfate which in principle allows a random replacement of a cholesterol molecule by two hydrocarbon chains of a complex lipid.²³

Acknowledgements. We wish to thank Prof. S. Abrahamsson for valuable discussions and advice. Grants in support of this Department were obtained from the Swedish Medical Research Council, the Swedish Board for Technical Development, the Wallenberg Foundation and the U.S. Public Health Service (G.M.-11653).

REFERENCES

1. Drayer, N. M., Roberts, K. D., Bandi, I. and Lieberman, S. *J. Biol. Chem.* **239** (1964) 3112.
2. Moser, H. W., Moser, A. B. and Orr, J. C. *Biochim. Biophys. Acta* **116** (1966) 146.
3. Drayer, N. M. and Lieberman, S. *Biochem. Biophys. Res. Commun.* **18** (1965) 126.
4. Björkman, L. R., Karlsson, K.-A., Pascher, I. and Samuelsson, B. E. *Biochim. Biophys. Acta* **270** (1972) 260.
5. Björkman, L. R., Karlsson, K.-A. and Nilsson, K. *Comp. Biochem. Physiol. B* **43** (1972) 409.
6. Karlsson, K.-A., Samuelsson, B. E. and Steen, G. O. *J. Membr. Biol.* **5** (1971) 169.
7. Karlsson, K.-A., Samuelsson, B. E. and Steen, G. O. *Eur. J. Biochem.* **46** (1974) 243.
8. Binyon, J. J. *Mar. Biol. Assoc. U.K.* **44** (1964) 577.
9. Abrahamsson, J., Abrahamsson, S., Hellquist, B., Larsson, K., Pascher, I. and Sundell, S. *Chem. Phys. Lipids* **19** (1977) 213.
10. Sundell, S. *Acta Chem. Scand. A* **31** (1977) *In press*.
11. Sobel, A. E., Dreker, I. J. and Natelson, S. *J. Biol. Chem.* **115** (1936) 381.
12. Lenhert, P. G. *J. Appl. Crystallogr.* **8** (1975) 568.
13. Mills, O. S. and Rollet, J. S. *Computing Methods and the Phase Problem in X-Ray Crystal Analysis* Pergamon, London 1961, pp. 107–124.
14. Cromer, D. T. and Mann, J. B. *Acta Crystallogr. A* **24** (1968) 321.
15. Stewart, J. M. *et al.* *The X-Ray System 1972*, Technical Report TR-192, Computer Science Center, University of Maryland, College Park.
16. Carlisle, C. H. and Crowfoot, D. *Proc. R. Soc. (London) Ser. A.* **184** (1945) 64.
17. Bürki H. and Nowacki W. *Z. Kristallogr.* **108** (1956) 206.
18. Craven, B. M. and DeTitta, G. T. *J. Chem. Soc. Perkin Trans. 2* (1976) 814.
19. Abrahamsson, S. and Dahlén, B. *Chem. Phys. Lipids.* **20** (1977) 43.
20. Craven, B. M. *Nature* **260** (1976) 727.
21. Hitchcock, P. B., Mason, R., Thomas K. M. and Shipley G. G. *Proc. Natl. Acad. Sci. U.S.A.* **71** (1974) 3036.
22. Pascher I. and Sundell S. *Chem. Phys. Lipids* **20** (1977) 175.
23. Abrahamsson, S., Dahlén, B., Löfgren, H., Pascher, I. and Sundell, S. In Abrahamsson, S. and Pascher, I., Eds., *Structure of Biological Membranes*, Plenum, New York 1977, pp. 1–23.

Received May 23, 1977.

Thermodynamics of Complex Formation in Dimethyl Sulfoxide with Ligands Coordinating *via* N, P, As, Sb, or Bi.

I. Silver Complexes

STEN AHRLAND,^a TORSTEN BERG^b and PER TRINDERUP^c

^a Inorganic Chemistry 1, Chemical Center, University of Lund, P.O.B. 740, S-220 07 Lund, Sweden, ^b Chemistry Department 1, Inorganic Chemistry, H. C. Ørsted Institute, University of Copenhagen, DK-2100 Copenhagen Ø, Denmark and ^c NEUCC, Building 305, Technical University of Denmark, DK-2800 Lyngby, Denmark

The thermodynamics of the complex formation between silver(I) and the triphenyl compounds Ph_3X (X = N, P, As, Sb or Bi) has been studied in dimethyl sulfoxide (DMSO) at 25°C. The ionic strength of the solutions was maintained at 0.1 with ammonium perchlorate. The stability constants have been determined potentiometrically, using silver electrodes, and the enthalpy changes calorimetrically.

The stability constants found confirm quantitatively the affinity sequence $\text{N} \ll \text{P} > \text{As} > \text{Sb} > \text{Bi}$ previously inferred from largely qualitative observations on complex formation between soft acceptors and ligands coordinating *via* group V donor atoms. In the phosphine, arsine and stibine systems coordination of up to three ligands is found in solution, the mono- and tris(ligand) complexes predominating strongly over their neighbours. Coordination of a fourth ligand cannot be detected in solution, although solids of composition $[\text{Ag}(\text{Ph}_3\text{X})_4]\text{ClO}_4$ (X = P, As or Sb) precipitate at high ligand concentrations. In the case of the amine and bismuthine systems, the complex formation is so weak that only the mono-complex is detected.

All the strong complexes are heavily enthalpy stabilized whereas the entropy contributions counteract the complex formation, generally quite strongly. The enthalpy and entropy changes for the consecutive steps in the various systems vary in a most interesting manner which apparently reflects a gradual change in the character of the donor to acceptor bond.

As is evident from numerous preparative studies,¹ ligands coordinating *via* phosphorus, arsenic and antimony behave as typically soft donors in that they form strong complexes

with typically soft acceptors while their affinities for other acceptors are quite weak. Quantitative studies of equilibria involving such ligands are rare, however, for several reasons. Unlike ammonia and the simple amines, the homologous compounds of phosphorus, arsenic and antimony are extremely sensitive to oxidation. They are also increasingly thermally unstable in the order mentioned² and are moreover often highly toxic. In these respects, however, the trialkyl and triaryl derivatives have the least unfavourable properties, the triphenyl compounds in particular being easy to handle. At ordinary temperatures the latter are stable non-volatile solids. This is also the case for triphenyl bismuthine, so that this donor can also be included in the investigation. Unfortunately the triphenyl compounds are essentially insoluble in water, a problem which has been a severe hindrance to quantitative equilibrium studies since the techniques used for such investigations have been developed primarily for aqueous media. Early approaches to this problem involved modifying the ligands so as to render them sufficiently soluble in water. In the case of the triphenyl compounds this can be achieved by sulfonation.³ A related method which has been applied to triethylphosphine is the replacement of one alkyl group with an alcoholic substituent.⁴ Interesting results have indeed been obtained by this type of approach²⁻⁴ but modification of the ligands in this manner is a time-consuming and rather

troublesome procedure which moreover does not lead to analogous compounds for all the various donor atoms. Still more unsatisfactory is the fact that no such modification has ever been achieved for antimony or bismuth. In addition, the solubilities attained are often too low for the calorimetric measurements which are necessary for a complete determination of the thermodynamics of the complex formation.

The other possible approach to this problem which has been adopted in the present investigation is to change the solvent to meet the needs of the systems of complexes to be investigated. The ligands to be used here are not soluble in water because the strong hydrogen bonding between the water molecules virtually prevents any solvation of the ligands. In a less well-structured solvent, on the other hand, where the specific interactions between the solvent molecules are much weaker, the formation of ligand solvates becomes possible. Many ligands which are not soluble in water will therefore be soluble in such solvents. A really useful solvent has, however, to possess a number of additional important properties: It must be a good solvent not only for the ligands but also for the metal ion acceptors to be investigated and for the complexes formed. Suitable inert salts must also be soluble in order to provide the necessary ionic medium. Generally, its dielectric constant ϵ must not be too low since otherwise the purely electrostatic interactions might overshadow the specific acceptor-donor interactions which are of prime interest; for the present ligands, which are uncharged and have low dipole moments, this condition should not be very critical, however. Finally the solvent should have a suitable liquid range and be reasonably easy to handle.

All these conditions are fulfilled by dimethyl sulfoxide, DMSO. In this aprotic solvent, in which there is no hydrogen bonding, the triphenyl compounds Ph_3X ($\text{X}=\text{N}$, P , As or Sb or Bi) are all soluble. The reactions of a complete series of analogous ligands coordinating *via* group V donor atoms can thus be compared. Furthermore, all the metal ions which have been investigated so far are adequately solvated by DMSO. The solvation is in fact without exception considerably stronger than in wa-

ter.⁹⁻¹² This also applies^{10,11} to Ag^+ which has been selected as the first acceptor to be studied in the present series of investigations. The silver complexes formed by the present ligands are soluble in DMSO except for the fact that the species $\text{Ag}(\text{Ph}_3\text{X})_4^+$ ($\text{X}=\text{P}$, As or Sb), which are formed at high ligand concentrations, are all precipitated as perchlorates in the medium used. These perchlorates are also precipitated from ethanol and diethyl ether media and they appear in fact to have low solubility in most solvents.^{13,14} Other non-complexing anions, *e.g.* BF_4^- , NO_3^- and BrO_3^- , also give salts of low solubility with these cations.^{13,14} The physical properties of DMSO are favourable. Its melting point is 18.55°C and it is thus suitable for measurements at the standard temperature of 25°C at which it has a vapour pressure of only 0.599 Torr.¹⁵ The boiling point of DMSO is 189°C at 760 Torr and the dielectric constant ϵ is quite high, *viz.* 46.4 at 25°C.¹⁶

The stability of a complex is the net result of many different interactions between the various species involved. These are reflected in changes in both the enthalpy and the entropy of the system when the complex is formed. In order to elucidate as far as possible the various factors influencing the reaction it is necessary to find out how the changes in enthalpy and entropy contribute to the net free energy change.^{12,17,18} This is achieved by determination of both the stability constant, K_j , and the heat of formation, ΔH_j° , for each consecutive step, thereby permitting the calculation of all the thermodynamic functions according to eqn. (1).

$$-RT \ln K_j = \Delta G_j^\circ = \Delta H_j^\circ - T \Delta S_j^\circ \quad (1)$$

For the present systems, K_j and ΔH_j° have been determined in separate measurements. The values of K_j have been found potentiometrically, using silver electrodes, whereas the values of ΔH_j° have been measured calorimetrically. The results obtained by the use of these two separate methods are generally both more accurate and more precise than those obtained from measurements of the variation of K_j with temperature.¹⁹⁻²¹ Provided that certain conditions are fulfilled it is possible in principle to determine both K_j and ΔH_j° from calorimetric measurements.^{22,23} For simple systems, the precision of such determinations

is generally good.^{24,25} For more complex systems, however, the thermodynamic conditions have to be rather exceptional if reasonable precision is to be achieved.²⁶⁻²⁸ The present systems are not well suited to such simultaneous determination of K_j and ΔH_j° and consequently only the results of the separate determinations are tabulated and discussed here.

The ionic strength in the present measurements was maintained at 0.1 using ammonium perchlorate. This medium has been used in other investigations of metal complex equilibria in DMSO.¹² The use of media of the same ionic strength containing the related tetraethylammonium perchlorate is also common.¹² A perchlorate medium of ionic strength much higher than 0.1 was not suitable in the present case since it tends to bring about the precipitation of the rather insoluble $\text{Ag}(\text{Ph}_3\text{X})_4\text{ClO}_4$ species at an early stage of the complex formation.

EXPERIMENTAL

Chemicals. The silver and ammonium perchlorates, triphenylamine, -phosphine, -arsine, -stibine and -bismuthine were commercial products of analytical grade and were used without further purification. The ammonium perchlorate was dried at 110°C and the other reagents were dried at room temperature *in vacuo* over 4 Å molecular sieves.

The DMSO was purified by distillation under reduced pressure over calcium hydride and the distillate was stored in a dark bottle over molecular sieves. This solution contained less than 0.05% water as determined by a modified Karl Fischer titration method.²⁹

Solutions. The silver perchlorate solutions were prepared from anhydrous AgClO_4 and DMSO and the ionic strength adjusted to 0.1 M with anhydrous ammonium perchlorate. The exact silver content was determined by potentiometric titration with chloride. The solutions were stable for several weeks.

The ligand solutions were prepared by weighing an exact amount of the ligand and adding ammonium perchlorate (to give ionic strength 0.1 M) and anhydrous DMSO. These solutions were prepared daily since the ligands are slowly oxidized by DMSO. The stability of the Ph_3X ligands in this medium decreases in the sequence P, As, Sb and Bi. A solution of Ph_3Bi was only stable for about one hour but even the Ph_3P solutions deteriorated markedly in a few days, contrary to what has been reported in the literature.³⁰

Unfortunately, molecular sieves could not be added to minimise water contamination

of these solutions since they caused concentration changes as a result of adsorption. Consequently the water concentration was somewhat higher than in the pure solvent, typically 0.3%.

Potentiometric measurements. The silver electrodes were prepared as follows: platinum wire electrodes were immersed in an aqueous suspension of freshly prepared hydrated silver oxide. The electrodes were then placed in an electric oven and heated gradually to $\approx 400^\circ\text{C}$ over a period of 2 h. They were maintained at that temperature for 6 h and then cooled slowly to room temperature.³¹

Electrode vessels of the Ingold type were used for the electrode solutions: one for the reaction vessel and two for the reference electrodes. The solutions were maintained at a temperature of $25.0 \pm 0.1^\circ\text{C}$ by the flow of water from a pumping thermostat through outer jackets around the vessels. Potential measurements were made with an Eldorado 1820 potentiometer.

The manipulations and measurements were performed in a dry box containing molecular sieves (4 Å) to remove traces of water. Dry, oxygen free nitrogen saturated with DMSO vapour, was bubbled through the solutions in the electrode vessels in order to exclude moisture and prevent oxidation. The gas stream also provided efficient stirring in the vessels.

Procedure. The reaction vessel initially contained V cm³ silver perchlorate solution of concentration C_M' . The reference electrode vessel also contained this solution. To the reaction vessel were added portions of ligand solution, of concentration C_L . The emf measured is associated both with the complex formation and the dilution of the silver solution in the reaction vessel.³ When v cm³ of ligand solution have been added the total silver concentration has decreased to $C_M = C_M' V / (V + v)$. If the concentration of free silver ions is denoted by $[M]$, the emf E in this point may be expressed as eqn. (2), where the first term

$$E = \frac{RT}{F} \log_e \frac{C_M}{[M]} + \frac{RT}{F} \log_e \frac{V+v}{v} \quad (2)$$

is associated with the complex formation and the second with the dilution. In the phosphine, amine and stibine systems, where strong complexes are formed, the dilution term is small relative to the term for complex formation.

Owing to the limited stability of the triphenylbismuthine ligand in DMSO measurements on this system were made using fresh solutions for each point instead of the titration technique.

Two electrodes in the reaction solution and two reference electrodes were used. When the same potential within 0.1 mV was read between the electrodes pairwise it was taken as an indication that equilibrium had been reached. This was normally achieved within 15 min.

Titration series were performed for 3 or 4 values of C_M' and each series was repeated at least twice. The reproducibility was generally better than 0.2 mV except at the highest values of \bar{n} where it was ≈ 1 mV.

The calculation of the stability constants was performed using a least squares computer program described previously.³²

Calorimetric measurements. A titration calorimeter of the isothermal jacket type described by Ots³³ was employed. To allow work with DMSO solutions, the experimental arrangement was modified so that all parts in contact with the solvent were made of gold, glass, teflon or silicone rubber. The inner gold vessel, which holds 100 cm³, was inserted in an outer can completely immersed in an LKB precision thermostatted water bath, maintaining the temperature at 25.000 ± 0.001 °C. For shorter periods, however, the temperature normally remained constant within $\pm 2 \times 10^{-4}$ °C. The room temperature was maintained at 25.0 ± 0.1 °C.

Procedure. The calorimetric titrations were performed as described by Ahrland and Björk.²⁷ For each system, 5–10 titration series were performed. In most of these, ligand solutions T with $C_L = 100$ mM were titrated into silver ion solutions S with C_M' varying from ≈ 2 mM to ≈ 10 mM. In other series silver ion solutions T of ≈ 40 mM were titrated into ligand solutions S of ≈ 25 mM or ≈ 100 mM.

The experimental heat changes were corrected for heats of dilution which were determined separately.²⁷ The latter were quite small for both the silver perchlorate and the ligand solutions.

The least squares program "KALORI"^{34,35} was employed for the enthalpy and entropy calculations.

RESULTS

The quantities calculated directly from the potentiometric and calorimetric measurements are β_j and $\Delta H\beta_j^\circ$, respectively, referring to the

overall reactions $\text{Ag}^+ + jL \rightleftharpoons \text{AgL}_j^+$. The values found are listed in Table 1, with errors corresponding to three times the standard deviations as given by the computer. The precision is much better for β_j than for $\Delta H\beta_j^\circ$. Within the three systems where extensive complex formation takes place, the magnitude of the errors generally increases in the order $\text{P} < \text{As} < \text{Sb}$. This may reflect the decreasing stability of the ligand in solution. In all cases, however, the values obtained permit the calculation of reasonably precise values of the stability constants and the thermodynamic functions referring to the consecutive steps. These quantities are listed in Table 2. The full experimental data can be obtained from the authors upon request. Previously studied silver(I) systems involving modified phosphine or arsine ligands in aqueous solution^{3,4} are also included in the table for comparison purposes.

DISCUSSION

Stabilities of complexes examined. The affinity of the soft acceptor Ag^+ for the present group V donors generally follows the sequence $\text{N} \ll \text{P} > \text{As} > \text{Sb} > \text{Bi}$ (Table 2). This indeed confirms the stability sequence postulated as early as 1958 on the basis of the rather few and largely qualitative data then available.³⁶ The evidence in the case of Sb was at that time very sparse, and for Bi no complexes containing Bi as donor atom had in fact ever been prepared. Since then further preparative work has been done,³ including the preparation¹⁴ of the perchlorate of the silver(I) bismuthine complex AgPh_3Bi^+ . This work has certainly strengthened

Table 1. Overall stability constants (β_j/M^{-j}) and enthalpy changes ($\Delta H\beta_j^\circ/\text{kJ mol}^{-1}$) calculated for the complexes formed between silver(I) and ligands Ph_3X in DMSO. The errors correspond to three standard deviations. Ionic medium 0.1 M NH_4ClO_4 ; 25 °C.

X→	N	P	As	Sb	Bi
$\log \beta_1$	0.19(14)	6.58(2)	3.56(1)	3.16(2)	0.80(8)
$\log \beta_2$		10.73(3)	5.37(3)	4.62(11)	
$\log \beta_3$		13.17(2)	6.68(6)	6.06(12)	
$-\Delta H\beta_1^\circ$	1(1)	51.8(7)	34.1(8)	32.1(10)	0.5(5)
$-\Delta H\beta_2^\circ$		89.9(10)	52.4(23)	40.7(45)	
$-\Delta H\beta_3^\circ$		126.2(14)	98.8(37)	97.8(35)	

Table 2. Equilibrium constants (K_j/M^{-1}) and thermodynamics for the stepwise formation of complexes between silver(I) and ligands coordinating *via* N-group donors in DMSO and in water, at 25 °C (C (Dop 22 °C). ΔG_j° , ΔH_j° /kJ mol⁻¹; ΔS_j° /JK⁻¹ mol⁻¹.

X→	DMSO; ligands Ph ₃ X; 0.1 M NH ₄ ClO ₄					Water		
	N	P	As	Sb	Bi	Dpm ^a	Dop ^b	Asm ^a
log K_1	0.19	6.58	3.56	3.16	0.80	8.15	11.83	5.36
log K_2		4.15	1.81	1.45		5.95	9.02	
log K_3		2.44	1.31	1.45		5.40	4.86	
K_1/K_2		269	56	51		160	650	
K_2/K_3		52	3.2	1.0		3.5	14500	
$-\Delta G_1^\circ$	1.1	37.6	20.3	18.1	4.6	46.5	66.8	30.6
$-\Delta G_2^\circ$		23.7	10.4	8.3		34.0	51.0	
$-\Delta G_3^\circ$		13.9	7.5	8.3		30.8	27.4	
$-\Delta H_1^\circ$	1	51.8	34.5	32.1	0.5		80.8	
$-\Delta H_2^\circ$		38.1	19.4	8.6			69.0	
$-\Delta H_3^\circ$		36.3	44.5	57.1			38.1	
$-\Delta S_1^\circ$	0	48	48	47	-14		47	
$-\Delta S_2^\circ$		48	30	1			60	
$-\Delta S_3^\circ$		75	124	164			36	
$-\Delta G_{\beta_3}^\circ$		75.2	38.1	34.6		111.3	145.2	
$-\Delta H_{\beta_3}^\circ$		126.2	98.4	97.8			187.9	
$-\Delta S_{\beta_3}^\circ$		171	202	212			143	

^a Ref. 3; Dpm=Ph₂PC₆H₄SO₃⁻(*m*-); 0.1 M NaClO₄; Asm=As(C₆H₄SO₃⁻)₃³⁻(*m*-); 0.2 M NaClO₄. ^b Ref. 4; Dop=Et₂PCH₂CH₂OH; 1 M KNO₃.

the view that the above affinity sequence is valid generally for soft acceptors but the present study seems to provide the first quantitative confirmation of these observations.

This study shows, on the other hand, that the affinity differences between two consecutive group V donors with a given acceptor vary greatly as one descends in group V. The phosphine complexes are far more stable than the arsine complexes, while the latter do not differ very much in stability from the stibine complexes. An exception to the general sequence is the fact that the value of K_3 is somewhat higher for the stibine than for the arsine system. Between the stibine and the bismuthine complex the difference in stability is again very large. The affinity of Ph₃Bi for Ag⁺ is, like that of Ph₃N, so low that only the mono(ligand) complex is formed even at the highest ligand concentrations obtainable.

A very interesting feature displayed by all the three systems in which the complex formation proceeds beyond the first step is that the mono- and tris(ligand) complexes are particularly stable relative to their neighbours. The bis(ligand) complex, which is so prominent in most silver(I) systems both in protic and

aprotic solvents,^{12,37} plays a rather subordinate part here. No appreciable amounts of the tetrakis(ligand) complexes are formed in any of the systems within the range of ligand concentrations used.

The above features are clearly illustrated by the complex formation curves drawn in Fig. 1. These functions give the ligand number, \bar{n} , defined as the average number of ligands per acceptor ion, as a function of the free ligand concentration, [L]. The wide range of existence of the mono-complex is evident from the marked

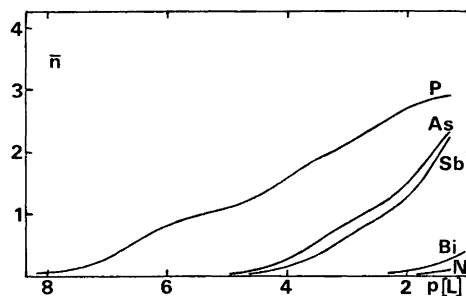


Fig. 1. The complex formation curves of the systems Ag⁺-Ph₃X, X=N, P, As, Sb, Bi, in DMSO. Medium 0.1 M NH₄ClO₄; 25 °C.

inflexions at $\bar{n}=1$ for the three systems in which strong complexes are formed. Only for the phosphine system can an inflexion at all be discerned at $\bar{n}=2$. For this system, \bar{n} seems to approach a limiting value of 3 without any visible tendency to exceed this value.

These features are also reflected in the values of the ratios K_j/K_{j+1} (Table 2). If the complex formation were statistical, the ratios between the consecutive stability constants would be (if tetrahedral coordination ($N=4$) is assumed):³⁸ $K_1/K_2 = 8/3$; $K_2/K_3 = 9/4$ and $K_3/K_4 = 8/3$. For systems such as the present ones, for which specific interactions are clearly prominent, the actual ratios are generally far from the statistical ones. The values of K_1/K_2 are indeed much larger, and also much larger than K_3/K_4 . In this respect, as in others, the phosphine system stands out from the arsine and stibine systems in having much larger values of both the ratios mentioned. Again, the differences between the arsine and stibine systems seem slight. Since no values of K_4 can be determined the ratios K_3/K_4 cannot be calculated. On the reasonable assumption, however, that in the phosphine system a concentration of the tetrakis-complex amounting to $\approx 10\%$ of the total would at least be detected, the value of K_3/K_4 must be $\gtrsim 270$, *i.e.* at least as large as K_1/K_2 . For the amine and stibine systems, for which \bar{n} reaches only 2.4 and 2.3, respectively, an analogous estimate is of little significance.

As already mentioned, perchlorates of composition $\text{Ag}(\text{Ph}_3\text{X})_4\text{ClO}_4$ ($\text{X} = \text{P}, \text{As}$ or Sb) are precipitated on addition of excess ligand, the arsine and stibine species being precipitated rather more easily than the phosphine compound. Preliminary structural investigations of the precipitates show that they are all isostructural,³⁹ the ligands being tetrahedrally coordinated to Ag^+ . This does not mean, however, that the ligands are also tetrahedrally disposed in the preceding complexes. The marked stop at $\bar{n}=3$ found in the phosphine system might well be indicative of a change of coordination geometry accompanying the formation of the tetrakis complex. A trigonal planar configuration for the complex $(\text{ToI}_3\text{P})_3\text{Ag}^+$ ($\text{ToI} = p\text{-tolyl}$) has in fact been inferred⁴⁰ from NMR measurements on dichloromethane solutions. Moreover, in solid phosphine halido

complexes of copper(I)⁴¹ and gold(I),⁴² *viz.* $(\text{Ph}_3\text{P})_2\text{CuBr}$ and $(\text{Ph}_3\text{P})_2\text{AuCl}$ (both of which crystallize with $1/2 \text{C}_6\text{H}_6$), this configuration has been unequivocally demonstrated by full X-ray structure determinations. The same is true also for the complex $(\text{Ph}_3\text{P})_3\text{Pt}$ formed by the d^{10} acceptor platinum(0).⁴³ It is therefore probable that the complex $(\text{Ph}_3\text{P})_3\text{Ag}^+$ in DMSO solution has the same configuration. The same may also apply to the corresponding arsine and stibine complexes, although in the absence of structural data for analogous systems of this type this prediction is less well-founded.

The silver(I) complexes formed by the ligands Ph_3P and Ph_3As in DMSO are considerably less stable than those formed by the sulfonated phosphine, Dpm, and sulfonated arsine, Asm, in water (see Table 2), in spite of the fact that the sulfonation would be expected to weaken the donor properties of the ligands. This lower stability in DMSO is undoubtedly due mainly to the stronger solvation of Ag^+ in this solvent, reflected in the very negative value of the enthalpy of transfer for Ag^+ between water and DMSO,¹¹ $\Delta H_{\text{tr}}^\circ (\text{W} \rightarrow \text{DMSO}) = -54 \text{ kJ mol}^{-1}$. Owing to the stronger donating properties of the aliphatic phosphine Dop, the silver(I) complex formed by this ligand in aqueous solution are even stronger than those formed by the aromatic Dpm.

As in the present system, the mono- and tris-(ligand) complexes predominate in the sulfonated aromatic phosphine system in aqueous solution. No tetrakis-complex is detected within the range of $[\text{L}]$ available, which implies that $K_3/K_4 \gtrsim 4000$. For the sulfonated arsine Asm, the mono-complex has an even wider range of existence, no further complex formation being detected. This indicates that $K_1/K_2 \gtrsim 20\,000$. The aliphatic phosphine, Dop, behaves similarly in so far as both the mono- and the tris-complex have unusually wide ranges of existence with a ratio $K_3/K_4 \gtrsim 4000$. In this latter system, however, the bis(ligand) complex is predominant, and the qualitative picture is thus reminiscent of that for most other silver(I) systems.

Thermodynamic functions. The formation of phosphine, arsine and stibine complexes of silver(I) is strongly exothermic, both in DMSO and in aqueous solution (Table 2). This is to be expected in view of the strong covalency of the

Ag-X bond (X=P, As, Sb) and the weak solvation, especially of the ligands. The weak solvation also results in unfavourable entropy contributions, however, so that the stabilities of the complexes are lower than would be expected *per se* in view of the very considerable enthalpy decreases. The value of $-\Delta H_{\beta_3}^\circ$ referring to the formation of the highest complex actually found in the solutions, decreases in the order P > As > Sb, reflecting decreasing strength of the Ag-X bond, while the value of $-\Delta S_{\beta_3}^\circ$ increases in the same order, reflecting the increasing steric restrictions on the ligands as they become more bulky. For both $\Delta H_{\beta_3}^\circ$ and $\Delta S_{\beta_3}^\circ$, however, the really significant jump is between P and As, while the differences between the As and Sb systems are quite small, especially in the case of $\Delta H_{\beta_3}^\circ$.

Whereas the formation of the highest complexes from the solvated Ag^+ ion and Ph_3X are characterized by thermodynamic functions which can be fairly easily interpreted in terms of bond strength, solvation and conformation, this is not the case for the individual complex formation steps. For these, a very intricate but also very consistent pattern is found (Table 2). Most interesting is the observation that the very similar stabilities of the triphenylarsine and -stibine complexes in DMSO are the net result of very different enthalpy and entropy contributions which largely compensate each other. Moreover, for both these ligands, the second step is characterized by enthalpy contributions which are less favourable and by entropy terms which are more favourable than those for the neighbouring steps. This trait is particularly apparent for the stibine system. A gradual change in the covalent character of the Ag-X bond with the donor atom X is undoubtedly one of the main causes of the variations observed. At present, however, it seems wise to postpone any elaborate interpretation until experimental data have also been gathered for other acceptors which are capable of coordinating these donors.

The weak complex formation between silver(I) and the ligands Ph_3N and Ph_3Bi is characterized by low values of both ΔH_1° and ΔS_1° (Table 2). Evidently, these reactions involve only very modest changes in bond strength and structural ordering.

Acknowledgement. This work was initiated during the stay of one of us (S.A.) as visiting professor at the University of Copenhagen 1974. The generosity and hospitality of the University is most gratefully acknowledged.

Valuable support has also been received from the Swedish Natural Science Research Council.

The authors are further much indebted to Professor Jannik Bjerrum for help given in many ways.

Finally we wish to thank Dr. M. P. Hancock for his painstaking work with our English manuscript.

REFERENCES

1. McAuliffe, C. A., Ed., *Transition Metal Complexes of Phosphorus, Arsenic and Antimony Ligands*, Macmillan, London and Basingstoke 1973.
2. Doak, G. O. and Freedman, L. D. *Organometallic Compounds of Arsenic, Antimony and Bismuth*, Wiley-Interscience, New York 1970.
3. Ahrlund, S., Chatt, J., Davies, N. R. and Williams, A. A. *J. Chem. Soc.* (1958) 276.
4. Meier, M. *Phosphinokomplexe von Metallen*, Diss., Nr. 3988, Eidgenössische Technische Hochschule, Zürich 1967.
5. Salvesen, B. and Bjerrum, J. *Acta Chem. Scand.* 16 (1962) 735.
6. George, R. and Bjerrum, J. *Acta Chem. Scand.* 22 (1968) 497.
7. Hawkins, C. J., Mønsted, O. and Bjerrum, J. *Acta Chem. Scand.* 24 (1970) 1059.
8. Chang, J. C. and Bjerrum, J. *Acta Chem. Scand.* 26 (1972) 815.
9. Krishnan, C. V. and Friedman, H. L. *J. Phys. Chem.* 73 (1969) 3934.
10. Le Démezet, M. *Bull. Soc. Chim. Fr.* (1970) 4550.
11. Cox, B. G. and Parker, A. J. *J. Am. Chem. Soc.* 95 (1973) 402.
12. Ahrlund, S. In Lagowski, J. J., Ed., *The Chemistry of Non-aqueous Solvents*, Academic, London and New York, Vol. 5, Chapter 1. *In press.*
13. Cotton, F. A. and Goodgame, D. M. L. *J. Chem. Soc.* (1960) 5267.
14. Nuttall, R. H., Roberts, E. R. and Sharp, D. W. A. *J. Chem. Soc.* (1962) 2854.
15. Lam, S. Y. and Benoit, R. L. *Can. J. Chem.* 52 (1974) 718.
16. Martin, D. and Hauthal, H. G. *Dimethyl Sulphoxide*, van Nostrand Reinhold, Wokingham, Berks. 1975.
17. Ahrlund, S. *Struct. Bonding (Berlin)* 15 (1973) 167.
18. Schwarzenbach, G. *Pure Appl. Chem.* 24 (1970) 307.
19. McAuley, A. and Nancollas, G. *J. Chem. Soc.* (1963) 989.

20. Carvalho, R. G. and Choppin, G. R. *J. Inorg. Nucl. Chem.* 29 (1967) 737.
21. Choppin, G. R. and Schneider, J. K. *J. Inorg. Nucl. Chem.* 32 (1970) 3283.
22. Christensen, J. J., Ruckman, J., Eatough, D. J. and Izatt, R. M. *Thermochim. Acta* 3 (1972) 203.
23. Eatough, D. J., Christensen, J. J. and Izatt, R. M. *Thermochim. Acta* 3 (1972) 219.
24. Eatough, D. J., Izatt, R. M. and Christensen, J. J. *Thermochim. Acta* 3 (1972) 233.
25. Ahrland, S. and Kullberg, L. *Acta Chem. Scand.* 25 (1971) 3677.
26. Ahrland, S., Avsar, E. and Kullberg, L. *Acta Chem. Scand. A* 28 (1974) 855.
27. Ahrland, S. and Björk, N.-O. *Acta Chem. Scand. A* 30 (1976) 257.
28. Ahrland, S., Björk, N.-O. and Portanova, R. *Acta Chem. Scand. A* 30 (1976) 270.
29. Karlsson, R. and Karrman, K. J. *Talanta* 18 (1971) 459.
30. Amonoo-Neizer, E. H., Ray, S. K., Shaw, R. A. and Smith, B. C. *J. Chem. Soc.* (1965) 4296.
31. Lewis, G. N. *J. Am. Chem. Soc.* 28 (1906) 154.
32. Trinderup, P. *Acta Chem. Scand. A* 30 (1976) 47.
33. Ots, H. *Acta Chem. Scand.* 26 (1972) 3810.
34. Karlsson, R. and Kullberg, L. *Chem. Scr.* 9 (1976) 54.
35. Kullberg, L. *Acta Chem. Scand. A* 28 (1974) 829.
36. Ahrland, S., Chatt, J. and Davies, N. R. *Q. Rev. Chem. Soc.* 12 (1958) 265.
37. Sillén, L. G. and Martell, A. E. *Stability Constants of Metal-ion Complexes*, Spec. Publ. Nos. 17 and 25, Chemical Society, London 1964, 1971.
38. Bjerrum, J. *Metal Ammine Formation in Aqueous Solution*, Diss., Københavns Universitet, Copenhagen 1940.
39. Cassel, A. *Personal communication*.
40. Muetterties, E. L. and Aleganti, C. W. *J. Am. Chem. Soc.* 92 (1970) 4114.
41. Davis, P. H., Belford, R. L. and Paul, I. C. *Inorg. Chem.* 12 (1973) 213.
42. Baenziger, N. C., Dittmore, K. M. and Doyle, J. R. *Inorg. Chem.* 13 (1974) 805.
43. Albano, V., Bellon, P. L. and Scatturin, V. *Chem. Commun.* (1966) 507.

Received June 3, 1977.

Metal Complexes with Mixed Ligands. 15. A Potentiometric Study of the System $\text{Zn}^{2+} - \text{Cl}^- - \text{Imidazole}$ in 3.0 M $(\text{Na})\text{ClO}_4, \text{Cl}$ Media

WILLIS FORSLING

Department of Inorganic Chemistry, University of Umeå, S-901 87 Umeå, Sweden

Four component equilibria between zinc(II), imidazole ($\text{C}_3\text{H}_4\text{N}_2$; L), OH^- and Cl^- were studied by means of emf titrations at 25 °C in 3.0 M $(\text{Na})\text{ClO}_4, \text{Cl}$ using a glass electrode. The total zinc, B , the total imidazole, C , and the total chloride, X , were varied within the limits $0.005 \leq B \leq 0.025$ M, $0.040 \leq C \leq 0.185$ M and $0 \leq X \leq 3.0$ M and the ratios C/B between $3.4 \leq C/B \leq 36.2$. In addition to the stepwise metal complexes ZnL_n^{2+} $n=1, 2, 3, 4$, data can be explained with the following ternary complexes: ZnClL_n^+ $n=1, 2, 3, 4, 5$, ZnCl_2L_2 and ZnCl_3L^- . The equilibrium constants are given in Table 1. Data were analyzed with the least squares computer program LETAGROPVRID.

In part 14 of this series the three-component equilibria in the system zinc(II)–imidazole– OH^- in 3.0 M $(\text{Na})\text{ClO}_4$ and 3.0 M $(\text{Na})\text{Cl}$ were investigated using a glass electrode at 25 °C. It was found that in both media at high quotients ($C/B > 4$) only stepwise metal complexes ZnL_n^{2+} were formed. The equilibrium constants are $\log K_1 = 2.92$, $\log K_2 = 2.01$, $\log K_3 = 3.84$ and $\log K_4 = 2.64$ in 3.0 M $(\text{Na})\text{ClO}_4$ and $\log K_1 = 3.12$, $\log K_2 = 2.52$, $\log K_3 = 2.02$ and $\log K_4 = 1.37$ in 3.0 M $(\text{Na})\text{Cl}$.¹

Thus the complexation in the two media is different. In the chloride medium the ZnL_n^{2+} series can be well explained with a two-parameter approximation of the type $K_{n+1} = K_0 k^n$, $n=0, 1, 2, 3$, with $\log K_0 = 3.126$ and $\log k = -0.57$. This is not possible in the perchlorate medium, probably due to a coordination shift at the second step. The values of K_1 and K_2 are also greater in the chloride medium in spite

of the fact that no correction for chloro complexes has been made. This behaviour can be explained by the fact that in 3.0 M $(\text{Na})\text{Cl}$ at least 90 % of the total zinc is obtained in the complex ZnCl_3^{-2} or even ZnCl_4^{2-} , which already has a tetrahedral configuration. In this case the complexation with imidazole implies a stepwise exchange of the chloride ions around the zinc ion for imidazole molecules without any coordination shift.

This model for complexation signifies the existence of the ternary complexes ZnLCl_3^- , ZnL_2Cl_2 and ZnL_3Cl^+ . Since the binary zinc(II)–chloro complexes besides ZnCl_3^- are ZnCl^+ and ZnCl_2^2 one would also expect other ternary complexes of the types ZnL_2Cl^+ , ZnL_3Cl_2 and $\text{ZnL}_2\text{Cl}_3^-$ at other chloride concentration levels.

Another interesting difference in the two media concerns the crystalline phases. In the chloride medium two different crystalline phases have been found corresponding to the formulae $\text{ZnL}_2\text{Cl}_2^2$ and $\text{ZnL}_4\text{Cl}_2 \cdot 4\text{H}_2\text{O}$.⁷ In the former crystal the configuration around zinc is tetrahedral and in the latter octahedral. In the perchlorate medium no octahedral complex is found but only the tetrahedral $\text{ZnL}_4(\text{ClO}_4)_2$.⁵ Thus the chloride ions seem to make the formation of the octahedral complex ZnL_6^{2+} easier.

The purpose of the present study was to investigate the zinc(II)–imidazole–chloro system and to confirm the formation of ternary $\text{Zn}^{2+} - \text{L} - \text{Cl}^-$ complexes.

EXPERIMENTAL

Chemicals and analysis. All solutions used were prepared and analyzed as described earlier.¹

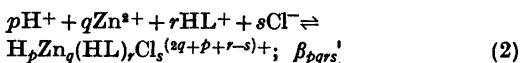
Apparatus. The cell arrangement and experimental details of the emf measurements are fully described earlier.⁶

Method. The titrations were performed as potentiometric titrations at 25 °C similarly to those described in earlier papers.^{6,7} The equilibrium solutions were made to contain $[\text{ClO}_4^-] + X = 3.0 \text{ M}$, where X is the chloride concentration. The general compositions of the solutions were: $B \text{ mM Zn}^{2+}$, $C \text{ mM C}_3\text{H}_5\text{N}_3^+$, $H \text{ mM H}^+$, $X \text{ mM Cl}^-$ ($[\text{ClO}_4^-] + X - C - H - 2B$) mM Na^+ and $3000 - X \text{ mM ClO}_4^-$. In the titrations the total concentrations of zinc(II), B , and imidazole, C , were varied, while the ratio C/B was always held constant. The total concentration of hydrogen ions, H , was calculated over the zero level, Zn^{2+} , HL^+ and H_2O and the free hydrogen ion concentration, h , was varied by addition of OH^- and measured with a glass electrode. h was determined according to the relation

$$E = E_0 + 59.157 \log h + E_j \quad (1)$$

where E_0 is a constant determined in acid solutions where complex formation could be neglected. The liquid junction potential $E_j = -16.7 h \text{ mV}$ was used in 3.0 M (Na)ClO_4 , 3.0 M (Na)Cl as well as in mixtures of these two media. It has earlier been shown by Sjöberg⁷ that within the concentration range $0 \leq X \leq 3.0 \text{ M}$ with $[\text{ClO}_4^-] + X = 3.0 \text{ M}$ the concentration scale for H^+ remains constant. No change in E_0 could be found on replacing ClO_4^- by Cl^- or *vice versa*.

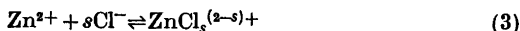
We will assume the presence of four-component equilibria of the general form



It is convenient to write complexes where $-p=r$ as $\text{Zn}_q\text{L}_r\text{Cl}_s^{(2q-s)+}$ and the stability constants as β_{nqs} . This terminology is used throughout this paper.

In addition to the four-component equilibria in (2) we have

(i) the complex formation between Zn^{2+} and Cl^-



(ii) the imidazole equilibria, which within the concentration range $0 \leq X \leq 3.0 \text{ M}$ with $[\text{ClO}_4^-] + X = 3.0 \text{ M}$ are

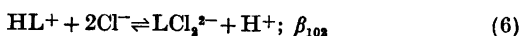
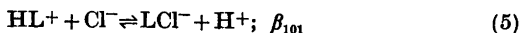
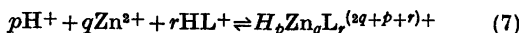


Table 1. Results of the final LETAGROP calculations giving the formation constants for the "best fitting" complexes. The Roman numerals in brackets refer to the different data sets mentioned in the text. The formation constants are related according to the reaction $p\text{L} + \text{Zn}^{2+} + r\text{Cl}^- \rightleftharpoons \text{L}_p\text{Zn}_q\text{Cl}_r^{(2q-r)+}$, where L stands for $\text{C}_3\text{H}_5\text{N}_3^+$. When no 3 ($\log \beta_{pqrs}$) is given, the formation constant has not been varied.

No. of titr./ No. of points	$\sigma(C-c) \times 1000$	ZnCl^+ $\log(\beta_{011}) \pm 3\sigma$	ZnCl_2 $\log(\beta_{012}) \pm 3\sigma$	ZnCl_3^- $\log(\beta_{013}) \pm 3\sigma$	ZnL_2Cl^+ $\log(\beta_{211}) \pm 3\sigma$	ZnL_3Cl^+ $\log(\beta_{212}) \pm 3\sigma$	ZnL_4Cl^+ $\log(\beta_{213}) \pm 3\sigma$	ZnL_5Cl^+ $\log(\beta_{214}) \pm 3\sigma$	$\text{ZnL}_6\text{Cl}_2^-$ $\log(\beta_{215}) \pm 3\sigma$	$\text{ZnL}_7\text{Cl}_3^-$ $\log(\beta_{216}) \pm 3\sigma$	$\text{ZnL}_8\text{Cl}_4^-$ $\log(\beta_{217}) \pm 3\sigma$
13/201 (I)	0.11	-0.19	-0.60	0.15	5.97	9.59	3.60	6.93	3.60	6.93	6.93
14/235 (II)	0.18	-0.19	-0.60	0.15	5.97	9.58	3.60	6.93	3.60	6.93	6.93
11/80 (III)	0.06	-0.19	-0.60	0.15	5.97	9.59	3.44	6.95	3.59	6.95	6.95
11/80 (III)	0.06	-0.25	-0.65	0.133	5.97	9.58	3.38	6.92	3.58	6.92	6.92
8/35	0.07	-0.19	-0.60	0.15	5.97	9.58	3.43	6.95	3.60	6.95	6.95

with $\log k_a = -7.940$, $\log \beta_{101} = -8.641$ and $\log \beta_{102} = -9.279.7$

(iii) the zinc(II) imidazole equilibria



with equilibrium constants given in Table 1. In the present study hydrolytic equilibria of the zinc(II) ion as well as formation of ternary zinc(II)–OH[−]–imidazole complexes could be neglected.

Equilibria (3)–(7) were determined in separate investigations and are assumed to be known in calculations concerning the four-component equilibria.

Data treatment. It is possible to reduce the four-component system $\text{H}^+ - \text{Zn}^{2+} - \text{HL}^+ - \text{Cl}^-$ to the three-component system $\text{L} - \text{Zn}^{2+} - \text{Cl}^-$ under the assumption that $-p=r$ in eqn. (2), which means that only complexes of the type $\text{Zn}_q\text{L}_p\text{Cl}_s^{(2q-s)+}$ are formed. With this assumption [L] can be calculated according to the relation

$$[\text{L}] = k_a h^{-1} [\text{HL}^+] = k_a h^{-1} [C - (h - H)] \quad (8)$$

where k_a is the acidity constant of HL^+ in 3.0 M (Na)ClO₄. Thus as input to the computer, data in the form (C , $\log[\text{L}]$, B , X) are given instead of (H , $\log h$, B , C , X). This was done to save computer time, which is considerably greater with four components.

The mathematical analysis were performed with the least squares computer program LETAGROPVRID⁸ (version ETITR⁹). On treating the emf data the error squares sum $U = \sum (A_{\text{calc}} - A_{\text{exp}})^2$ was minimized, where A denotes $C-c$, i.e. the total imidazole concentration not obtained as HL^+ . The standard deviations were defined and calculated according to Sillén.¹⁰ The computation was performed on a CDC 3300 computer.

DATA, CALCULATIONS AND RESULTS

The complex formation between zinc(II) and imidazole has already been investigated in 3.0 M (Na)ClO₄ and 3.0 M (Na)Cl media by using the emf-titration method. Results of these measurements are found in Ref. 1.

The binary zinc(II)–Cl[−] system in 3.0 M (Na)ClO₄ has been investigated by Liljeqvist and Sillén² by potentiometric titrations using a zinc amalgam electrode. Their data comprises the chloride concentration range $0 \leq [\text{Cl}^-] \leq 0.9$ M with the dominating species ZnCl^+ , ZnCl_2 and ZnCl_3^- . Since in this investigation the chloride concentration range is increased to $0 \leq [\text{Cl}^-] \leq 3.0$ M, special attention must be paid to the eventual formation of ZnCl_4^{2-} .

Particularly at low \bar{n} -values where the concentrations of the binary $\text{ZnCl}_3^{(2-s)+}$ -complexes are high, appreciable amounts of ZnCl_4^{2-} would influence the calculations. Thus in this region two different data sets were arranged. One data set comprises the chloride concentrations $0 \leq [\text{Cl}^-] \leq 1.0$ M and the other set $0 \leq [\text{Cl}^-] \leq 3.0$ M. No significant differences either in the model or the formation constants were obtained in the calculations. The results are given for comparison in Table 1. Furthermore the species ZnCl_4^{2-} was rejected by the computer in all the calculations.

In the search for the ternary zinc(II)–imidazole–Cl[−] species it was assumed that the binary complexes were exactly known and that the equilibrium constants had the values given in Ref. 1 and Ref. 2, respectively. However, a final covariation of the binary complexes, together with the ternary complexes, was made to determine whether any ternary species would be eliminated by a small variation of the binary ones (see below).

Many titrations were performed at a constant X -level ($X=0, 0.5, 1, 3$; $[\text{ClO}_4^-] + X = 3.0$ M; $X = [\text{Cl}^-]$). In these cases $[\text{C}_3\text{H}_4\text{N}_2]$ can be calculated either by use of the conditional acidity constant of $\text{C}_3\text{H}_7\text{N}_2^+$ valid at the actual X -level or by assuming the value of k_a valid in 3.0 M (Na)ClO₄ to be the genuine acidity constant. Thus the constants at the different X -levels are a result of complex formation between L and Cl[−] and \bar{n} is given by

$$\bar{n} = (h - H - [\text{L}] - [\text{LCl}^-] - [\text{LCl}_2^{2-}]) / B \quad (9)$$

where [L] is given by (8) and $[\text{LCl}^-]$ and $[\text{LCl}_2^{2-}]$ are calculated according to

$$[\text{LCl}^-] = \beta_{101} h^{-1} X [\text{HL}^+] = \beta_{101} h^{-1} X (C + H - h) \quad (10)$$

$$[\text{LCl}_2^{2-}] = \beta_{102} h^{-1} X^2 [\text{HL}^+] = \beta_{102} h^{-1} X^2 (C + H - h) \quad (11)$$

The same \bar{n} is now obtained independently of whether the conditional or the complex formation model above has been used.

The calculated quantities \bar{n} and $\log[\text{L}]$, visualized as Bjerrum plots in Fig. 1, are calculated using the conditional acidity constant. As seen from the plot, the complexation is stronger in the mixed chloride media at low \bar{n} -values ($\bar{n} < 2$) in spite of the fact that no

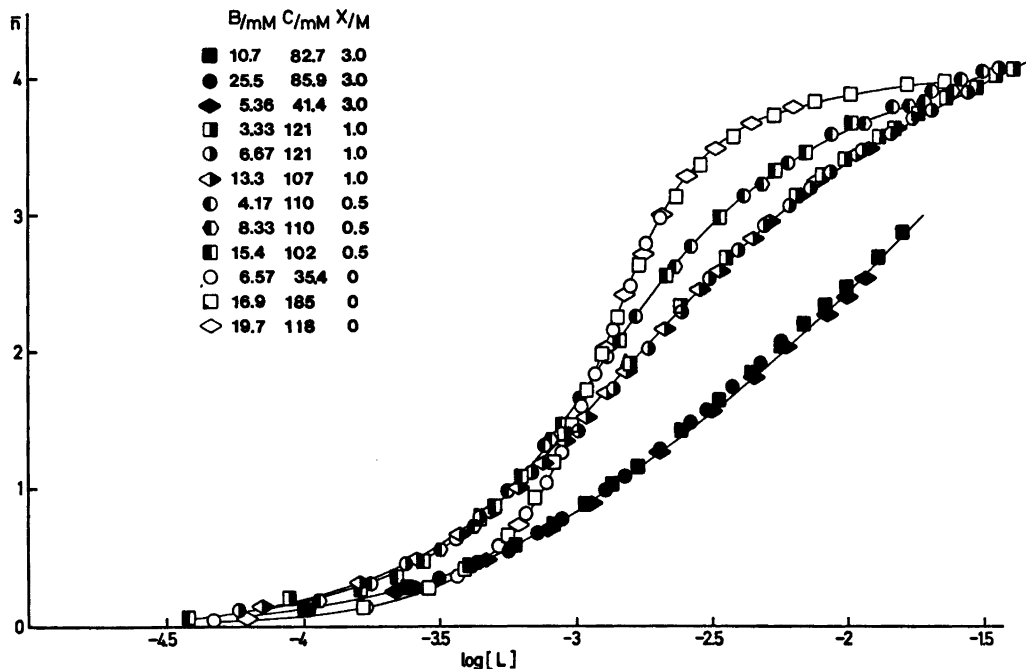


Fig. 1. Parts of experimental data plotted as curves $\bar{n}(\log[L])$ in the mixed 3.0 M (Na)ClO₄, Cl media. The full curves were calculated with the set of constants given in Table 1.

correction for zinc(II)-chloro-complexes has been made. These conditions must be due to the formation of ternary zinc(II)-imidazole-Cl⁻ complexes and furthermore at least one of the species ZnCl⁺, ZnCl₂ and ZnCl₃⁻ has to be a stronger complexing agent to imidazole than the corresponding hydrated zinc(II) ion. Owing to the limited space in the data program for the number of formation constants, the LETAGROP calculations were divided into three parts, which partly overlapped each other.* The first part, Data I, comprises data where $0 \leq \bar{n} \leq 2$ and $0 \leq X \leq 3$. These data consist of 13 titrations with 201 titration points. The titrations were performed both at constant X-values ($X=0.5, 1, 3$) and as dilution experiments at constant \bar{n} -values. In these experiments we titrated a solution in 3.0 M (Na)ClO₄ with 3.0 M (Na)Cl medium or *vice versa*. The actual \bar{n} -values were about 0.5, 1, 1.25 and 1.75. In this part the ternary zinc(II)-L-Cl⁻ species with $\bar{n} < 4$ (less than

four imidazole, molecules bound per zinc) were determined. The best explanation was obtained with the complexes ZnLCl₃⁻, ZnL₂Cl₃, ZnLCl⁺, ZnL₂Cl⁺ and ZnL₃Cl⁺. Other species were either rejected by the computer as ZnL₂Cl₃⁻, ZnL₃Cl₂ and ZnL₃Cl₃⁻ or did not lower the error squares sum to any appreciable extent as ZnLCl₂. In a final covariation all the "fitting" complexes were allowed to compete and the result of this computer calculations is given in Table 1. All the species except ZnL₂Cl⁺ were obtained with very low standard deviations ($3\sigma \leq 0.04$). The relatively high error in the formation constant of the species ZnL₂Cl⁺ ($3\sigma=0.16$) is explained by the smaller amounts of this complex. The calculation ended at a $\sigma(A)=0.11$. This corresponds to an error of 0.11 mM in the total imidazole concentration not obtained as HL⁺. The second part, Data II, consists of data where $\bar{n} \geq 2$ and $0 \leq X \leq 3$. It consists of 14 titrations with 235 titration points. Similar dilution experiments as above were performed at \bar{n} about 2.75, 3 and 3.75.

When treating these data all formation constants from the first part except for the

* A list of experimental data is available from this Department.

Table 2. Some stepwise reactions with constants calculated by means of formation constants given in Ref. 1 and Table 1. The different reactions define the stepwise uptake of ligands. (a) $C_3H_4N_2$ (L) and (b) Cl^- , are to be read horizontally ($ZnL_2Cl^+ + 3.61 ZnL_3Cl^+$ stands for $ZnL_2Cl^+ + L \rightleftharpoons ZnL_3Cl^+$ with $\log K = 3.61$).

	log K		log K		log K		log K		log K
(a)									
Zn^{2+}	2.93	ZnL^{2+}	2.00	ZnL_2^{2+}	3.79	ZnL_3^{2+}	2.82	ZnL_4^{2+}	
$ZnCl^+$	3.64	$ZnLCl^+$	2.52	ZnL_2Cl^+	3.61	ZnL_3Cl^+	1.38	ZnL_4Cl^+	1.83
$ZnCl_3^-$	3.45	$ZnLCl_3^-$							
(b)									
Zn^{2+}	-0.19	$ZnCl^+$	-0.41	$ZnCl_2$	0.75	$ZnCl_3^-$			
ZnL^{2+}	0.56	$ZnLCl^+$							
ZnL_2^{2+}	1.01	ZnL_2Cl^+	0.96	ZnL_2Cl_2					
ZnL_3^{2+}	0.84	ZnL_3Cl^+							
ZnL_4^{2+}	-0.61	ZnL_4Cl^+							

species ZnL_3Cl^+ were kept constant. Once more the complexes ZnL_3Cl_2 and $ZnL_3Cl_3^-$ were rejected by the computer. The species ZnL_4Cl_2 was rejected by a covariation with the species ZnL_4^{2+} and ZnL_4Cl^+ .

Thus the "best fit" was obtained with the ternary species ZnL_3Cl^+ , ZnL_4Cl^+ , ZnL_5Cl^+ together with the binary species ZnL_4^{2+} . The result of the final covariation is shown in Table 2. The calculation ended at $\sigma(A) = 0.18$. In Data III, which consists of 11 titrations and 80 titration points where $\bar{n} < 0.7$, the formation constants of the binary species $ZnCl^+$, $ZnCl_2$ and $ZnCl_3^-$ were varied together with the ternary ones. This calculation confirmed the results from the other parts and also gave values of the binary constants in an indirect way. These values were in a very good agreement with those determined by Sillén. The results are given in Table 1. In order to visualize the amounts of the ternary species at some typical X-levels, we have collected a set of distribution diagrams, which are shown in Fig. 2. These diagrams show that the ternary zinc(II)-chloro-imidazole species are generally obtained in great amounts even at proportionally low total chloride concentration levels. For instance, at the chloride concentration level of sea water (~ 0.5 M Cl^- , even if, in this investigation, the total ionic medium is 3.0 M by addition of $NaClO_4$) the ternary species $ZnLCl^+$, ZnL_2Cl_2 and ZnL_3Cl^+ together

with the binary ZnL_4^{2+} are dominating in spite of the fact that the amounts of the binary zinc(II)-chloro complexes are rather low.

As mentioned earlier, special calculations with $[Cl^-] \leq 1.0$ M were performed in the range $\bar{n} < 0.7$ to estimate the importance of small amounts of the complex $ZnCl_4^{2-}$. These data consist of 8 titrations with 35 titration points and the results are given in Table 1.

DISCUSSION

The present emf investigation has strongly confirmed the existence of ternary zinc(II)-imidazole- Cl^- complexes. The dominating species besides the series ZnL_nCl^+ , $n = 1 \dots 5$, are the complexes $ZnLCl_3^-$ and ZnL_2Cl_2 .

Concerning the ZnL_nCl^+ series, the results can be interpreted as stepwise reactions in which imidazole molecules are successively coordinated to a $ZnCl^+$ core or alternatively as chloride ions coordinated to ZnL_n^{2+} core with $n = 0, 1, 2, 3, 4, 5$. Stepwise constants of these reactions are given in Table 2. As for the ZnL_n^{2+} series it is not possible to explain ZnL_nCl^+ series by a two parameter approximation of the type $K_{n+1} = K_0 k^n$. The $\log K_n$ -values are given in Table 2 and the low values for the quotients $K_2/K_3 = 0.07$ and $K_4/K_5 = 0.35$ indicate coordination shifts at the second and fourth step. The first shift is probably obtained from octahedral to tetrahedral coordination

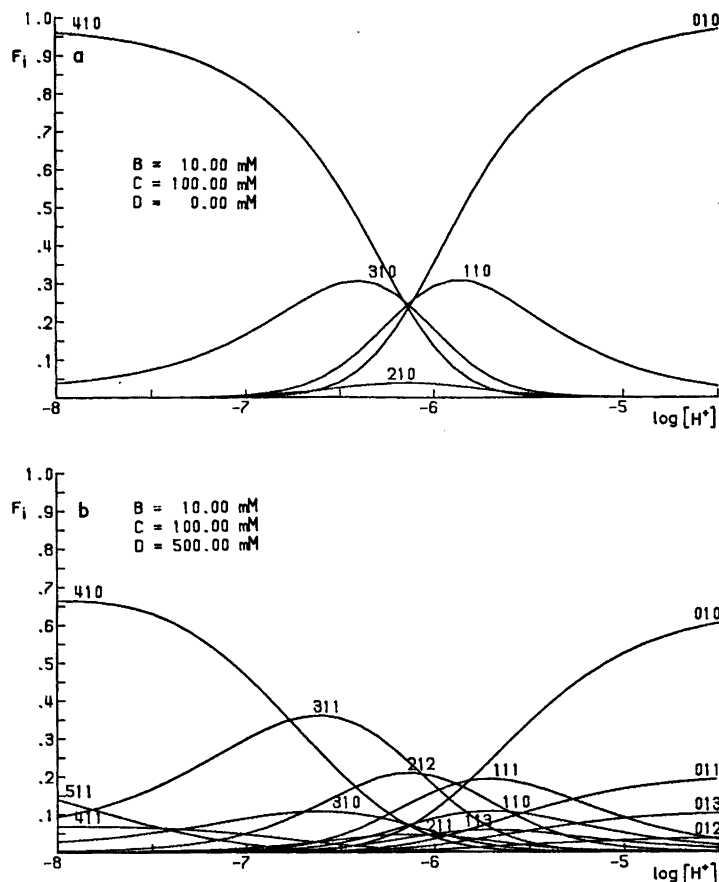
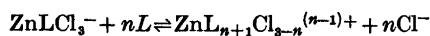


Fig. 2. Distribution diagrams $F_i(\log h)_{B,C,X}$ for the different zinc(II)-imidazole complexes. The computer program SOLGAS-WATER¹² was used in the calculations. The figures denote the number of $C_3H_4N_2$, Zn^{2+} and Cl^- in the complexes.

and the second in the reverse direction. Thus the chloride ions seem to take part in the coordination shift back to octahedral coordination at the fourth step. A tetrahedral series is built up from the $ZnCl_3^-$ core according to



$n=1, 2, 3$, with values of $\log K=3.33, 2.66$ and 1.98 . This series is very well explained with a two parameter approximation of the type $K_{n+1}=K_0k^n$ with $\log K_0=3.33$ and $\log k=-0.67$.

Comparing the reactions $Zn^{2+}+L \rightleftharpoons ZnL^{2+}$ with $\log K_1=2.93$ and $ZnCl^++L \rightleftharpoons ZnLCl^+$ with $\log K=3.64$ it is obvious that $ZnCl^+$,

as $ZnOH^+$, is a stronger complexing agent to imidazole than the hydrated zinc(II)-ion. The same properties have been found in the corresponding investigations of the copper(II)-⁷ and nickel(II)-¹¹ imidazole- Cl^- systems with $\log K(M^{2+}+L \rightleftharpoons ML^{2+})=4.65$ (Cu^{2+}) and 3.37 (Ni^{2+}), respectively compared to $\log K(MCl^++L \rightleftharpoons MLCl^+)=4.75$ (Cu^{2+}) and 3.65 (Ni^{2+}).

In the distribution diagrams it is easily seen that the even coordination numbers 2, 4, 6 are usually favoured compared to the odd numbers 1, 3 and 5. At chloride concentration levels less than 1.0 M many coexisting complexes make the distribution diagrams rather complicated,

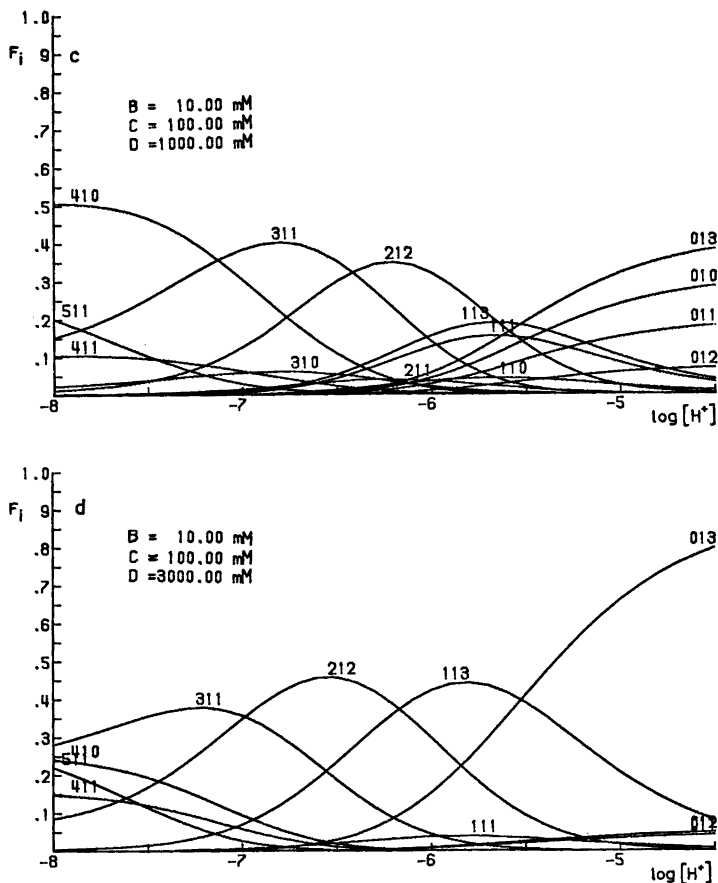


Fig. 2. c and d.

but in 3.0 M (Na)Cl medium the diagram is again quite simple with a few strongly dominating species. Thus the main complexes are $Zn(H_2O)Cl_3^-$, $ZnLCl_3^-$, ZnL_2Cl_2 and ZnL_3Cl^+ , which accounts for the good explanation of data with the two-parameter approximation model in this medium. As seen from the plot $\bar{n}(\log[L])$ the complexation starts at $\log[L] \sim -4.5$. That leads to the fact that at the natural concentrations of sea water ($[Zn^{2+}]_{tot} \leq 10^{-7} \text{ M}$, $[NH_4^+]_{tot} \sim [Amino\ acids]_{tot} \leq 10^{-5.4} \text{ M}$) the amounts of the ternary species are very low. The dominating complexes in this case seem to be the hydrated zinc(II)-ion and the binary $ZnCl_3^{(2-)-}$.

Concerning the crystalline phases, powder X-ray investigations of the precipitates from the different mixed media were made. In the 3.0 M (Na)Cl medium no phases other than

those earlier X-ray investigated, ZnL_2Cl_2 and $ZnL_3Cl \cdot 4H_2O$, were found. In the 3.0 M (Na)ClO₄ medium ($[Cl] = 0$) the phase $ZnL_4(ClO_4)_2$ was identified together with a new phase not yet examined. This new phase was also found in some of the mixed media with low chloride concentrations.

Acknowledgements. I thank Professor Nils Ingri for much valuable advice, for his great interest and for all the facilities placed at my disposal. Thanks are also due to Dr. Gun Ivarsson for valuable help with some of the measurements and the X-ray powder investigation. I also wish to thank Dr. Staffan Sjöberg for many helpful discussions and valuable comments on the manuscript. The English of the present paper has been corrected by Dr. Michael Sharp. The work forms part of a program financially supported by the Swedish Natural Science Research Council.

REFERENCES

1. Forsling, W. *Acta Chem. Scand. A* 31 (1977) 759.
2. Sillén, L. G. and Liljeqvist, B. *Sven. Kem. Tidskr.* 56 (1944) 85.
3. Lundberg, B. K. S. *Acta Crystallogr.* 21 (1966) 901.
4. Sandmark, C. and Brändén, C-I. *Acta Chem. Scand.* 21 (1967) 993.
5. Bear, C. A., Duggan, K. A. and Freeman, H. C. *Acta Crystallogr. B* 31 (1975).
6. Forsling, W. and Sjöberg, S. *Acta Chem. Scand. A* 29 (1975) 569.
7. Sjöberg, S. *Diss.*, University of Umeå, Umeå 1976.
8. Ingri, N. and Sillén, L. G. *Ark. Kemi* 23 (1964) 97.
9. Arnek, R., Sillén, L. G. and Wahlberg, O. *Ark. Kemi* 31 (1969) 353; Brauner, P., Sillén, L. G. and Whiteker, R. *Ark. Kemi* 31 (1969) 365.
10. Sillén, L. G. *Acta Chem. Scand.* 16 (1962) 159; Sillén, L. G. and Warnqvist, B. *Ark Kemi* 31 (1969) 341.
11. Forsling, W. *To be published.*
12. Eriksson, G. *To be published.*

Received March 8, 1977.

Centrifugal Distortion in Thietane

C. J. NIELSEN

Department of Chemistry, University of Oslo, Oslo 3, Norway

The microwave spectrum of thietane (trimethylene sulfide) has been remeasured for the $v=0, 1$ states of the puckering vibration in the region 8 to 40 GHz. New high- J Q-branch transitions have been assigned.

The spectrum has been interpreted using an effective two-level vibration-rotation Hamiltonian including quartic and sextic centrifugal distortion constants.

In the last decade there has been considerable interest in the microwave spectra of small ring compounds with a low-frequency out-of-plane vibration.¹⁻⁷ These investigations have mainly been concerned with determining the anharmonic potential for this vibration from the vibrational dependence of the rotational constants. Little attention has, however, been paid to the centrifugal distortion and the additional information that can be extracted from the corresponding constants.

Recently, Creswell and Mills⁸ have investigated the spectra of oxetane and deuterated species using an effective Hamiltonian for each of the puckering vibrational states. The distortion constants found show the same zig-zag dependence of the puckering quantum number as the rotational constants. This could be explained in terms of the double minimum potential for this vibration.

In thietane the separation between the $v=0, 1$ levels of the puckering vibration is approximately 8230 MHz¹ and nearly equal rotational and distortion constants are expected for these states.

The present work was also motivated by recent results on cyanamide- d_3 , where centrifugal distortion is essential for describing the observed spectrum.⁸

EXPERIMENTAL

The sample of thietane was a commercial product from Fluka AG, which was further purified by vacuum distillation. The spectrum was recorded on a Hewlett-Packard 8460A MRR spectrometer in Copenhagen. Sample temperatures varied from -40 to 25°C at pressures less than $10\ \mu$. Frequencies were measured to ± 0.05 MHz.

EFFECTIVE HAMILTONIAN

Angular momentum, arising from the large-amplitude puckering motion, enters into the Hamiltonian, to a first order approximation, in two terms,⁹ $L_b J_b$ and $\mu_{ac}(J_a J_c + J_c J_a)$. L_b contains the b component of internal angular momentum. The ambiguity of these vibration-rotation interactions was first noticed by Harris *et al.*¹ who pointed out that the two terms are physically equivalent. Further, the angular momentum from the vibration can be distributed in any ratio between L_b and μ_{ac} depending only on the axis system chosen for developing the Hamiltonian. This relationship was later formulated by Pickett.¹⁰

Thus, it is not possible at the same time to define a molecule-fixed rotating axis system and determine both interaction constants. It is necessary to fix either L_b or μ_{ac} and the most reasonable choice is the limit, $\mu_{ac}=0$ or $L_b=0$. The first choice corresponds to the principal axis system (PAS), the second, denoted as the reduced axis system (RAS),¹⁰ is close to the better-known Eckart system. Transformation between the two limiting systems is merely equivalent to a dynamic rotation about the b -axis,

$$H_{\text{RAS}} = \exp[i\theta(Q)J_b] H_{\text{PAS}} \exp[-i\theta(Q)J_b]$$

Q being the large-amplitude coordinate and $\theta(Q)$ some well-defined operator.

In thietane the $v=0, 1$ states of the puckering vibration are well separated from the rest of the vibrational energy levels in the molecule. By projecting the total vibration-rotation Hamiltonian into the subspace consisting of this doublet it is possible to produce an effective two-level rotational Hamiltonian. Further reduction of the Hamiltonian to a form containing only five quartic and seven sextic distortion constants for each state is necessary before fitting the data.

In this work, the observed spectrum was fitted to the following reduced Hamiltonian

$$H_{\text{red}} = |0\rangle\langle 0| (H_r^{(0)} + H_d^{(0)}) |0\rangle\langle 0| + |1\rangle\langle 1| (H_r^{(1)} + H_d^{(1)}) \\ + W_{01} |1\rangle\langle 0| + |0\rangle\langle 1| + |1\rangle\langle 1| H_c |0\rangle\langle 0|$$

$$H_r^{(v)} = X^{(v)} J_x^2 + Y^{(v)} J_y^2 + Z^{(v)} J_z^2$$

$$H_d^{(v)} = \{\text{Watson quartic and sextic distortion}\}^{(v)}$$

$$W_{01} = \langle 1|H_{\text{vib}}^0|0\rangle - \langle 0|H_{\text{vib}}^0|1\rangle$$

$$H_c = \mu_{yz}(J_y J_z + J_x J_y) \text{ or } L_x J_x$$

RESULTS

In order to establish the most suitable coordinate system for developing the Hamiltonian all reported data on similar molecules were used. There was, however, no reliable evidence in favour of either system.

On the basis of the more accurate measurements on thietane, it soon became evident that the RAS system was superior to the PAS system. It was found that the Hamiltonian converged more rapidly if developed in the RAS system. Even in calculations based on transitions with J less than 6, where centrifugal distortion normally can be ignored, there was a marked difference in the goodness of the fit. Hence the RAS system was used in the later calculations.

The final assignment was then based on prediction, on Stark effect and on frequency fitting. A total of 169 transitions with J up to 50 was measured. It was found necessary to consider sextic centrifugal distortion in order to get a reasonable fit. Only one sextic constant could be determined for each state with significance. The least correlation between parameters was found using h_{JK} .

The derived parameters are given in Table 1. A list of frequencies and the correlation matrix is available from the author upon request.

Simultaneously with this work Wieser and Mills of the University of Reading have inves-

Table 1. Derived parameter (RAS) for the $v=0, 1$ states of the puckering vibration in thietane. Rotational constants (A, B, C), energy difference (W_{01}), coupling constant (μ_{yz}) and standard deviation (σ) in MHz. Quartic distortion constants ($\Delta J, \Delta_{JK}, \Delta_K, \delta J, \delta_K$) in kHz. Sextic distortion constant (h_{JK}) in Hz. Numbers in parentheses represent one standard deviation.

	$v=0$	$v=1$
A	10107.2018 (16)	10107.5431 (13)
B	6670.1426 (11)	6670.0768 (11)
C	4443.6175 (11)	4444.2911 (11)
ΔJ	2.386 (19)	2.388 (20)
Δ_{JK}	-2.171 (60)	-2.113 (49)
Δ_K	6.69 (10)	6.769 (90)
δJ	0.6119 (44)	0.599 (30)
δ_K	2.085 (33)	1.954 (31)
h_{JK}	0.0943 (37)	0.0757 (19)
<hr/>		
	$W_{01} = 8231.961 (15)$	$\mu_{yz} = 121.3323 (40)$
	$\sigma = 0.019$	

tigated the MW spectra of thietane and several deuterated species including the higher excited states of the puckering vibration. A detailed analysis of the vibrational dependence of the centrifugal distortion constants will be given by these authors.

Acknowledgement. The author would like to thank the staff of Chemical Laboratory V, University of Copenhagen, for the use of their equipment. A special thanks to Dr. G. O. Sørensen for helpful discussions and programming aid.

REFERENCES

- Harris, D. O., Harrington, H. W., Luntz, A. C. and Gwinn, W. D. *J. Chem. Phys.* **44** (1966) 3467.
- Chan, S. I., Borgers, T. R., Russell, J. W., Strauss, H. L. and Gwinn, W. D. *J. Chem. Phys.* **44** (1966) 1103.
- Creswell, R. A. and Mills, I. M. *J. Mol. Spectrosc.* **52** (1974) 392.
- Petit, M. G., Gibson, J. S. and Harris, D. O. *J. Chem. Phys.* **53** (1970) 3408.
- Luntz, A. C. *J. Chem. Phys.* **50** (1969) 1109.
- Pringle, W. C., Jr. *J. Chem. Phys.* **54** (1971) 4979.
- Scharpen, L. H. and Laurie, V. W. *J. Chem. Phys.* **49** (1968) 3041.
- Tyler, J. K. *Private communication.*
- Lide, D. R. Jr. *J. Mol. Spectrosc.* **8** (1962) 142.
- Pickett, H. M. *J. Chem. Phys.* **56** (1972) 1715.

Received May 5, 1977.

Short Communications

The Protolytic Properties of Iron(III)-EDTA Complexes in Weakly Alkaline Solution and the Solubility Product of Iron(III) Hydroxide

HANS HENRIK CHRISTENSEN and
OLE K. BORGGAAARD

Royal Veterinary and Agricultural University,
Chemistry Department, Thorvaldsensvej 40,
DK-1871 Copenhagen V, Denmark

As part of an investigation of the feasibility of performing selective extraction of amorphous iron(III) hydroxide mixed with crystalline iron(III) compounds by means of EDTA solutions (EDTA, ethylenediamine-*N,N,N',N'*-tetraacetic acid H_4Y), it was found necessary to reinvestigate the protolytic properties of iron(III)-EDTA in the pH range 6–11 and the solubility product of iron(III) hydroxide. This note presents the acid dissociation constants K_1 ($HY^{3-} \rightleftharpoons H^+ + Y^{4-}$) and K_2 ($H_2Y^{2-} \rightleftharpoons HY^{3-} + H^+$), the constants of the iron(III)-EDTA-hydroxo complexes, and the solubility product of iron(III) hydroxide aged one day determined at ionic strength 1.0 (KNO_3) and 25 °C.

All chemicals were *pro analysis* or of similar purity, and the water was deionized. The pH-meter used was calibrated by means of standard buffer solutions. All the constants given in this paper are mixed constants (*i.e.* molar concentrations except H^+ and OH^- which are activities).

The acid dissociation constants of EDTA. Different solutions of EDTA (Titriplex II, Merck dissolved in KOH solutions) with the ionic strength adjusted to 1.0 (KNO_3) were titrated with 1.000 M KOH solution at 25.0 °C. The constants calculated from these experiments were: $pK_1 = 9.98 \pm 0.02$ and $pK_2 = 6.298 \pm 0.005$ at 25 °C and ionic strength 1.0 in good agreement with the figures of Andereg ¹ ($pK_1 = 9.95$ and $pK_2 = 6.26$ at 20 °C and ionic strength 1.0 (KCl)).

Iron(III)-EDTA-hydroxo complexes. According to Schwarzenbach and Heller ² iron(III)-EDTA forms a monohydroxo complex ($pK_{FeY}^H = 7.49$: $FeY^- + H_2O \rightleftharpoons FeYOH^{2-} + H^+$) and a dihydroxo complex ($pK_{FeYO}^H = 9.41$: $FeYOH^{2-} + H_2O \rightleftharpoons FeY(OH)_2^{3-} + H^+$). The existence of the monohydroxo complex has been

confirmed by others ^{3,4} together with the occurrence of its dimer. The existence of the dihydroxo complex has, however, to the best of our knowledge not been confirmed. In order to calculate the solubility product of iron(III) hydroxide from dissolution experiments with EDTA ⁵ or to calculate the total iron(III) concentration in an EDTA solution in contact with iron(III) hydroxide, ⁶ it is important to know whether the dihydroxo complex exists or not in weakly alkaline solution. In an attempt to solve this problem solutions containing iron(III) nitrate and EDTA and adjusted to ionic strength 1.0 (KNO_3) were titrated with 1.000 M KOH at 25.0 °C. An excess of EDTA was added to some solutions to increase the pH range before precipitation of iron(III) hydroxide. The iron(III)/EDTA ratios ranged from 1.0 to 0.125.

Fig. 1 shows the titration curves for a solution (a) containing iron(III) plus an excess

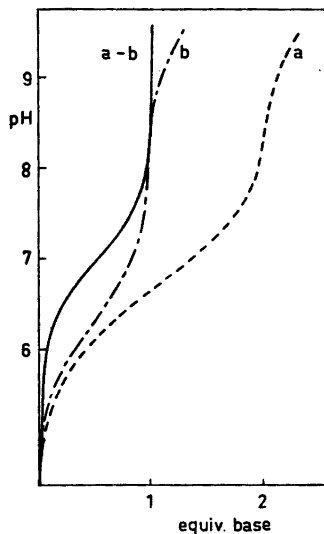


Fig. 1. Titration curves for solutions containing: (a) 2×10^{-2} M iron(III) and 4×10^{-2} M EDTA; (b) 2×10^{-2} M EDTA. (a–b) is the difference between curve (a) and (b) corresponding to the titration of a 2×10^{-2} M iron(III)-EDTA solution. Temperature 25.0 °C and ionic strength 1.0 (KNO_3).

of EDTA and a solution (b) containing only EDTA. The third curve (a-b) in Fig. 1 is the difference between these two curves and corresponds to the titration curve obtained by the titration of an equimolar solution of iron(III) and EDTA. It may be seen that the curve (a-b) has an inflection at $\text{pH} \sim 7$ corresponding to the monohydroxo complex, but up to $\text{pH} \sim 9.5$ no further inflections occur. All the other titration curves showed a similar pattern. This indicates that the $\text{p}K_{\text{FeYOH}^{\text{H}}} = 9.41^2$ for the reaction $\text{FeYOH}^{2-} + \text{H}_2\text{O} \rightleftharpoons \text{FeY(OH)}_2^{\text{H}} + \text{H}^+$ is too low and that the dihydroxo complex may be ignored in weakly alkaline solution. $\text{p}K_{\text{FeY}^{\text{H}}}$ and the equilibrium constant for the dimerization of the monohydroxo complex ($K_{\text{d}}: 2\text{FeYOH}^{2-} \rightleftharpoons (\text{FeYOH})_2^{4-}$) were calculated from the titration curves. $\text{p}K_{\text{FeY}^{\text{H}}} = 7.48$ and $\text{p}K_{\text{d}} = -2.6$ at 25°C and ionic strength 1.0 (KNO_3) in good agreement with the literature.^{3,3,4,7} Thus, Schwarzenbach and Heller² found $\text{p}K_{\text{FeY}^{\text{H}}} = 7.49$ at 20°C and ionic strength 0.1 (KCl), Gustavson and Martell³ $\text{p}K_{\text{FeY}^{\text{H}}} = 7.58$ and $\text{p}K_{\text{d}} = -2.8$ at 25°C and ionic strength 1.0 (KCl), Schugar *et al.*⁴ $\text{p}K_{\text{d}} = -2.53$ at 26°C and ionic strength 1.0 (NaClO_4), and McLendon *et al.*⁷ $\text{p}K_{\text{d}} = -2.5$ at 25°C and ionic strength 0.5 (ammonia buffer).

The solubility product of iron(III) hydroxide. The figures given in the literature⁸ for the solubility product of iron(III) hydroxide differ from $10^{-35.5}$ to $10^{-39.4}$. Iron(III) hydroxide is thermodynamically unstable compared with crystalline iron(III) oxide hydroxides and oxides and suspensions of iron(III) hydroxide in water turn into these compounds on ageing.

It was our intention to determine the solubility product of X-ray amorphous iron(III) hydroxide, *i.e.* before crystalline iron(III) compounds were formed. Therefore, different solutions were prepared containing iron(III) and EDTA with pH at the time of preparation in the range 9.5 to 11 and the ionic strength adjusted to 1.0 (KNO_3). All the solutions were supersaturated and iron(III) hydroxide started to settle out immediately. The suspensions were aged at 25.0°C and the pH and the iron(III) concentration in solution were determined from time to time after centrifugation. The iron(III) concentration was determined by atomic absorption spectrophotometry. Some of the precipitates were washed several times with ethanol and acetone and X-rayed (Ni-filtered $\text{CuK}\alpha$). As crystalline iron(III) compounds (goethite and/or hematite) appeared after a few days of ageing, it was decided to use only the measurements from suspensions aged one day. From these measurements combined with the acid dissociation constants of EDTA, and the stability constant for the normal,⁹ the monohydroxo, and the monohydroxo dimer complexes of iron(III)-EDTA, the solubility product may be calculated as $10^{-38.4 \pm 0.2}$ at ionic strength 1.0 (KNO_3) and

25°C . This figure agrees quite well with the more recently published values in the literature.^{5,8} The solubility product of iron(III) hydroxide was also calculated by taking into account the stability constant of the iron(III)-EDTA-dihydroxo² complex besides the above-mentioned constants. These calculations gave figures which decreased as a function of pH supporting further evidence to the statement that the stability constant of the iron(III)-EDTA-dihydroxo complex given by Schwarzenbach and Heller² is incorrect.

1. Anderegg, G. *Helv. Chim. Acta* 50 (1967) 2333.
2. Schwarzenbach, G. and Heller, J. *Helv. Chim. Acta* 34 (1951) 576.
3. Gustavson, R. L. and Martell, A. E. *J. Phys. Chem.* 67 (1963) 576.
4. Schugar, H. J., Hubbard, A. T., Anson, F. C. and Gray, H. B. *J. Am. Chem. Soc.* 91 (1969) 71.
5. Borggaard, O. K. *J. Soil Sci.* 27 (1976) 478.
6. Borggaard, O. K. *Acta Agric. Scand.* 26 (1976) 144.
7. McLendon, G., Motekaitis, R. J. and Martell, A. E. *Inorg. Chem.* 15 (1976) 2306.
8. Vlek, P. L. G., Blom, T. J. M., Beek, J. and Lindsay, W. L. *Proc. Soil Sci. Soc. Am.* 38 (1974) 429.
9. Bottari, E. and Anderegg, G. *Helv. Chim. Acta* 50 (1967) 2349.

Received July 11, 1977.

Molecular Structure and Composition of Gaseous Methyl Formate as Determined by Electron Diffraction

QUANG SHEN

Department of Chemistry, University of Trondheim, NLHT, Rosenborg, N-7000 Trondheim, Norway

If one disregards the orientation of the methyl group, methyl formate can exist in two forms, *syn* and *anti* derived about the C1–O4 single bond (Fig. 1). The molecular structure has been studied at room temperature by electron diffraction¹ and microwave spectroscopy² and in both investigations no evidence for the presence of other than the *syn* form was found. The object of the present study at an elevated temperature of 200 °C was to look for the possible presence of a second conformer.

The sample of methyl formate (>98 %; Fluka) was checked by gas chromatography before use. The diffraction experiment was carried out at a nozzle temperature of 200 °C in the Oslo Balzers apparatus,³ with an electron wavelength of 0.05859 Å and nozzle-to-plate distances of 499.20 and 249.36 mm. Three plates from the long and four plates from the short distance were selected for analysis. Data covered the s ranges 1.25–15.25 (long distance) and 5.00–29.75 (short distance) in intervals $\Delta s = 0.25$. Smooth hand-drawn back-

ground curves were subtracted from the reduced data to yield intensity curves.

The structural analysis was carried out in the usual way.⁴ Refinements of the structure were done by the method of least squares based on the two intensity curves in the form $sI_m(s)$ using a unit weight matrix. The geometrical parameters were $r(\text{C}=\text{O})$, $r(\text{C}-\text{H}_m)$ ($\text{H}_m =$

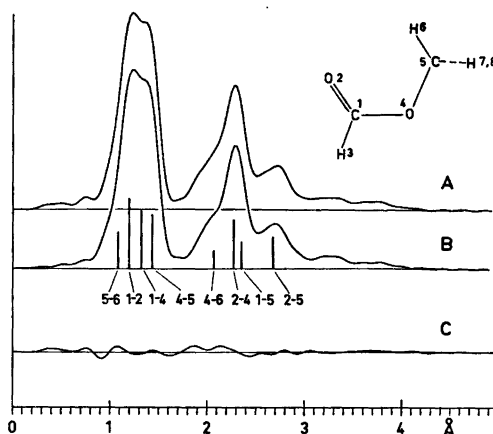


Fig. 1. Experimental (A), theoretical (B) and difference (C) radial distribution curves for methyl formate with $B = 0.0020$. The lengths of the vertical bars are proportional to the weights of the distances.

Table 1. Final results for methyl formate^a.

Parameter	r_a	l	Parameter	θ/r_a	l
C–H _m	1.081(20)	0.077	$\angle \text{O}=\text{C}-\text{O}$	126.8(16)	
C=O	1.206(5)		$\angle \text{O}-\text{C}-\text{H}$	109.3	
$\langle \text{C}-\text{O} \rangle$	1.393(5)		$\angle \text{C}-\text{O}-\text{C}$	114.3(16)	
$\Delta \text{C}-\text{O}$	0.104(7)		$\angle \text{O}-\text{C}-\text{H}_m$	110.2(28)	
C–H	1.101	0.077	τ	60.0	
R^b	0.13		δ	0.0	
Other distances and amplitude parameters					
C=O	1.206(5)	0.027	C5...O2	2.683(23)	0.114(20)
C1–O4	1.341(7)	0.035	C5...H3	3.292(17)	0.104
O4–C5	1.445(5)	0.040	H3...H6	3.630(44)	0.193
O2...H3	2.036(18)	0.090	H3...H7	4.074(32)	0.143
O4...H3	1.997(6)	0.092	O2...H6	2.667(46)	0.38
O4...H5	2.082(32)	0.103	O2...H7	3.748(28)	0.127
O2...O4	2.279(10)	0.057	C1...H6	2.627(43)	0.219
C1...C5	2.341(25)	0.076	C1...H7	3.259(30)	0.106
H7...H6	1.758(54)	0.128			

^a Distances (r_a) and amplitudes (l) in Å; angles in degrees. Bracketed values were refined as groups. Values in parentheses are 2σ . Values with no errors associated are not refined. ^b $R = [\sum w_i \Delta_i^2 / \sum w_i I_i(\text{obs})^2]^{1/2}$, where $\Delta_i = I_i(\text{obs}) - I_i(\text{calc})$.

proton on the methyl group), $\langle C-O \rangle = (r_{14} + r_{45})/2$, $\Delta(C-O) = r_{45} - r_{14}$, $r(C-H) = 1.101$ Å (assumed), $\angle C-O-C$, $\angle H_m-C-O$, $\tau(H_m-C-O-C) = 60^\circ$ (assumed, where 0° is as when a C-H bond is eclipsed with C1-O4), and $\delta(O=C-O-C) = 0.0$ (assumed, with 0° taken as planar *syn*). The above assumptions were taken from the microwave results² and were verified by test refinements. For example, $\tau = 0.0$ gave worse agreement than $\tau = 60^\circ$, and a rough refined value for $\angle O-C-H$ was found to be $107 \pm 10^\circ$.

From the appearance of the radial distribution curve (Fig. 1), it was clear that refinements of more than a few amplitudes of vibration were impossible. Accordingly amplitudes were calculated⁵ from a rough force field similar to those reported for methyl formate⁶ and ethyl formate⁷ chosen to fit the reported frequencies.⁸ These calculated amplitude values

were used whenever refinements were not feasible. In cases where several amplitude parameters were grouped together their differences as indicated by the calculated values were maintained. For details, see the final results of least squares refinement summarized in Table 1. The corresponding correlation matrix is given in Table 2.

The experimental radial distribution curve (Fig. 1) was found to be in good agreement with a model consisting of only the planar *syn* conformer. The radial distribution curve corresponding to the final model is also shown in Fig. 1. If an *anti* conformer were to be present in appreciable amounts the shape of the curve in the region $r \approx 2.7$ Å would be less prominent, and that in the region $r \approx 3.5$ Å more prominent due to conversion of the O2...C5 distance from *syn* to *anti*. Calculations testing the allowable amount of an *anti* conformer led to a result

Table 2. Correlation matrix for the parameters of methyl formate^{a,b}

r_1	r_2	r_3	r_4	$\angle 1$	$\angle 2$	$\angle 3$	l_{12}	l_{23}	l_{24}	l_{25}
100	69	50	-58	-53	22	-33	27	2	-41	-13
	100	68	-73	-74	34	-32	40	1	-44	-11
		100	-47	-71	24	-37	49	5	-38	-12
			100	61	-28	20	-59	16	32	8
				100	-69	50	-42	-5	71	6
					100	-25	14	-11	-70	-14
						100	-23	4	30	6
							100	32	-12	-5
								100	14	-6
									100	5
										100

^a Distances (r_n) and mean amplitudes of vibration (l) in Å, angles in degrees. ^b Standard deviations from least squares are $r_1 = C-H_m(0.0072)$, $r_2 = C=O(0.0016)$, $r_3 = \langle C-O \rangle(0.0016)$, $r_4 = \Delta(C-O)$ (0.0024), $\angle 1 = \angle O=C-O(0.567)$, $\angle 2 = \angle C-O-C(0.586)$, $\angle 3 = \angle O-C-H_m(1.008)$, $l_{12}(0.0022)$, $l_{23}(0.0059)$, $l_{24}(0.0031)$, $l_{25}(0.0069)$.

Table 3. Bond distances (Å) and angles ($^\circ$) for methyl formate.

Parameter	E. D.	Microwave	E. D.
C-H _m	1.081(20)	1.086(15)	—
C=O	1.206(5)	1.200(10)	1.22(3)
C1-O4	1.341(7)	1.334(10)	1.37(4)
C4-C5	1.445(5)	1.437(10)	1.47(4)
C-H	1.101	1.101(10)	—
$\angle O=C-O$	126.8(1.6)	125.8(1.0)	123(4)
$\angle O-C-H$	109.3	109.3(1.0)	—
$\angle C-O-C$	114.3(1.6)	114.8(1.0)	112(4)
$\angle O-C-H_m$	110.2(2.8)	108	—
τ	60.0	60.0	—
δ	0	0	0-20
Ref.	This work	2	1

of 0–15%. The theoretical radial distribution curve corresponding to 15% *anti* conformer was also found to be in poorer agreement with the experimental one than the curve for a model based on only the *syn* conformer. We concluded that there is no evidence for the presence of a second conformer.

The results from our present study compared very well with the earlier electron diffraction¹ and microwave² works (see Table 3). Comparison with the recent electron diffraction work on dimethyl carbonate (CH₃OCOOCH₃)⁹ showed no substantial difference between values of comparable parameters. In both the formate and carbonate only comparable conformers *syn* and *syn-syn* were found.

It is of interest to compare two structurally related molecules like methyl formate and methylvinyl ether.¹⁰ The C(sp²)-O bond is longer by 0.02 Å in the ether than in the formate and the C-O-C value is 4° greater in the ether. Also, in contrast to methyl formate, two conformers (73% *syn* and 27% *anti*) are observed for methylvinyl ether at 210 °C. Assuming that the entropy differences of conformers are similar, these results are in agreement with the *ab initio* molecular orbital calculations¹¹ showing the *anti* form to be 4–8 kcal mol⁻¹ above the *syn* form in methyl formate while the *anti* form is only 1–2 kcal mol⁻¹ above the *syn* form in methylvinyl ether (1 kcal = 4.184 kJ).

Acknowledgement. The author would like to express his appreciation to Siv. ing. Ragnhild Seip for taking the electron diffraction photographs.

- O'Gorman, J. M., Shand, W., Jr. and Schomaker, V. *J. Am. Chem. Soc.* 72 (1950) 4222.
- Curl, R. F. *J. Chem. Phys.* 30 (1959) 1529.
- Bastiansan, O., Graber, R. and Wegmann, L. *Balzer's High Vacuum Report* 25 (1969) 1.
- Hagen, K. and Hedberg, K. *J. Am. Chem. Soc.* 95 (1973) 1003, and reference cited therein.
- Cyvin, S. J. *Molecular Vibrations and Mean Squares Amplitudes*, Universitetsforlaget, Oslo and Elsevier, Amsterdam 1968.
- Susi, H. and Scherer, J. R. *Spectrochim. Acta A* 25 (1969) 1243.
- Charles, S. W., Jones, G. I. L., Owen, N. L., Cyvin, S. J. and Cyvin, B. N. *J. Mol. Struct.* 16 (1973) 225.
- Harris, W. C., Coe, D. A. and George, W. O. *Spectrochim. Acta A* 32 (1976) 1.
- Mijlhoff, F. C. *J. Mol. Struct.* 36 (1977) 334.
- Samdal, S. and Seip, H. M. *J. Mol. Struct.* 28 (1975) 193.
- John, I. G. and Radom, L. *J. Mol. Struct.* 36 (1977) 133.

Received June 22, 1977.

Acta Chem. Scand. A 31 (1977) No. 9

The Coefficients for Isothermal Transport. II. Cation Exchange Membrane and Electrodes Reversible to One of the Cations

SIGNE KJELSTRUP RATKJE

Laboratory of Physical Chemistry, The Norwegian Institute of Technology, The University of Trondheim, N-7034 Trondheim-NTH, Norway

A rigorous thermodynamic description of electrolyte transport across a membrane has been given in a previous publication by Førland, Førland and Ratkje.¹ Specific for their presentation is that the number and kind of components used to describe the system, conform with the phase rule. The presentation deals only with measurable quantities. This ensures an independent choice of forces in the flux equations.

When restrictions such as selectivity of the membrane and of the electrodes are imposed on the mass and charge transfer, relations between the phenomenological coefficients of the flux-force system may be developed.^{1,2} Relations were obtained for anion electrodes and a cation selective membrane.¹ This communication is a supplement to the previous work. The effect of substituting anion electrodes by cation electrodes is investigated. Information of the relative size of the phenomenological coefficients is developed.

Transports in an ion exchange membrane placed between electrodes reversible to a cation. The number of mass fluxes in a transport system of n components is $(n-1)$, the flux of the n 'th component being chosen as the zero reference.¹ With an electric current passing through the system there are independent forces. In the Førland-Ratkje formalism these are the $(n-1)$ gradients in chemical potential and the gradient in electric potential.¹ The fluxes J_i are linear combinations of the forces X_j :

$$J_i = \sum_{j=1}^n L_{ij} X_j \quad (1)$$

When the fluxes are linearly dependent

$$\sum_{i=1}^n \alpha_i J_i = 0 \quad (2)$$

general relations between the phenomenological coefficients have been developed.^{1,2}

$$\sum_{i=1}^n \alpha_i L_{ij} = 0 \quad j = 1, \dots, n \quad (3)$$

α_i , $i = 1, \dots, n$, are coefficients giving the interdependency.

of 0–15%. The theoretical radial distribution curve corresponding to 15% *anti* conformer was also found to be in poorer agreement with the experimental one than the curve for a model based on only the *syn* conformer. We concluded that there is no evidence for the presence of a second conformer.

The results from our present study compared very well with the earlier electron diffraction¹ and microwave² works (see Table 3). Comparison with the recent electron diffraction work on dimethyl carbonate (CH₃OCOOCH₃)⁹ showed no substantial difference between values of comparable parameters. In both the formate and carbonate only comparable conformers *syn* and *syn-syn* were found.

It is of interest to compare two structurally related molecules like methyl formate and methylvinyl ether.¹⁰ The C(sp²)-O bond is longer by 0.02 Å in the ether than in the formate and the C-O-C value is 4° greater in the ether. Also, in contrast to methyl formate, two conformers (73% *syn* and 27% *anti*) are observed for methylvinyl ether at 210 °C. Assuming that the entropy differences of conformers are similar, these results are in agreement with the *ab initio* molecular orbital calculations¹¹ showing the *anti* form to be 4–8 kcal mol⁻¹ above the *syn* form in methyl formate while the *anti* form is only 1–2 kcal mol⁻¹ above the *syn* form in methylvinyl ether (1 kcal = 4.184 kJ).

Acknowledgement. The author would like to express his appreciation to Siv. ing. Ragnhild Seip for taking the electron diffraction photographs.

- O'Gorman, J. M., Shand, W., Jr. and Schomaker, V. *J. Am. Chem. Soc.* 72 (1950) 4222.
- Curl, R. F. *J. Chem. Phys.* 30 (1959) 1529.
- Bastiansan, O., Graber, R. and Wegmann, L. *Balzer's High Vacuum Report* 25 (1969) 1.
- Hagen, K. and Hedberg, K. *J. Am. Chem. Soc.* 95 (1973) 1003, and reference cited therein.
- Cyvin, S. J. *Molecular Vibrations and Mean Squares Amplitudes*, Universitetsforlaget, Oslo and Elsevier, Amsterdam 1968.
- Susi, H. and Scherer, J. R. *Spectrochim. Acta A* 25 (1969) 1243.
- Charles, S. W., Jones, G. I. L., Owen, N. L., Cyvin, S. J. and Cyvin, B. N. *J. Mol. Struct.* 16 (1973) 225.
- Harris, W. C., Coe, D. A. and George, W. O. *Spectrochim. Acta A* 32 (1976) 1.
- Mijlhoff, F. C. *J. Mol. Struct.* 36 (1977) 334.
- Samdal, S. and Seip, H. M. *J. Mol. Struct.* 28 (1975) 193.
- John, I. G. and Radom, L. *J. Mol. Struct.* 36 (1977) 133.

Received June 22, 1977.

Acta Chem. Scand. A 31 (1977) No. 9

The Coefficients for Isothermal Transport. II. Cation Exchange Membrane and Electrodes Reversible to One of the Cations

SIGNE KJELSTRUP RATKJE

Laboratory of Physical Chemistry, The Norwegian Institute of Technology, The University of Trondheim, N-7034 Trondheim-NTH, Norway

A rigorous thermodynamic description of electrolyte transport across a membrane has been given in a previous publication by Førland, Førland and Ratkje.¹ Specific for their presentation is that the number and kind of components used to describe the system, conform with the phase rule. The presentation deals only with measurable quantities. This ensures an independent choice of forces in the flux equations.

When restrictions such as selectivity of the membrane and of the electrodes are imposed on the mass and charge transfer, relations between the phenomenological coefficients of the flux-force system may be developed.^{1,2} Relations were obtained for anion electrodes and a cation selective membrane.¹ This communication is a supplement to the previous work. The effect of substituting anion electrodes by cation electrodes is investigated. Information of the relative size of the phenomenological coefficients is developed.

Transports in an ion exchange membrane placed between electrodes reversible to a cation. The number of mass fluxes in a transport system of n components is $(n-1)$, the flux of the n 'th component being chosen as the zero reference.¹ With an electric current passing through the system there are independent forces. In the Førland-Ratkje formalism these are the $(n-1)$ gradients in chemical potential and the gradient in electric potential.¹ The fluxes J_i are linear combinations of the forces X_j :

$$J_i = \sum_{j=1}^n L_{ij} X_j \quad (1)$$

When the fluxes are linearly dependent

$$\sum_{i=1}^n \alpha_i J_i = 0 \quad (2)$$

general relations between the phenomenological coefficients have been developed.^{1,2}

$$\sum_{i=1}^n \alpha_i L_{ij} = 0 \quad j = 1, \dots, n \quad (3)$$

α_i , $i=1, \dots, n$, are coefficients giving the interdependency.

Consider as an example the transport of the components HCl, NaCl and H₂O with reference to the membrane component HM. The membrane is conducting cations only. The system which includes electrodes reversible to the H⁺-ion, is illustrated in Fig. 1.

When anion reversible electrodes are chosen, an electrolyte flux is defined by the flux of the cation of a component. In the present case, with a common anion Cl⁻ and cation reversible electrodes, the total flux of electrolytes, $J_{\text{HCl}} + J_{\text{NaCl}}$, is defined by the flux of Cl⁻. As no current is carried by Cl⁻ the linear dependency among the fluxes is

$$J_{\text{HCl}} + J_{\text{NaCl}} = 0 \quad (4)$$

Eqn. (4) corresponds to (2) with $\alpha_1 = \alpha_2 = 1$ and $\alpha_3 = \alpha_4 = 0$. The relations between the phenomenological coefficients are thus

$$L_{11}' + L_{21}' = 0 \quad i = 1, \dots, 4 \quad (5)$$

The coefficients are primed to indicate that cation reversible electrodes are used. The physical meaning of eqn. (4) or (5) is that the transport of charge in one direction across the membrane is balanced by a charge transport in the opposite direction. This is obviously so when no net current is passing (simple interdiffusion) but due to the specific choice of electrodes the statement is also true for $I \neq 0$ in this macroscopic description where J_{HCl} includes the transfer of H⁺ via the electrodes.

For comparison, the relations (3) are for the same system with chloride reversible electrodes¹ (indicated by unprimed coefficients)

$$L_{11} + L_{21} = L_{41} \quad i = 1, \dots, 4 \quad (6)$$

While $L_{12}' \leq 0$, from eqn. (5) and the requirement $L_{41} \geq 0$, L_{12} need not be negative from eqn. (6). The transport of HCl and NaCl do not balance when current is passed. The excess transfer of say H⁺ relative to Na⁺ in one direction is compensated by the electrode yield of Cl⁻ to achieve electroneutrality in each compartment.

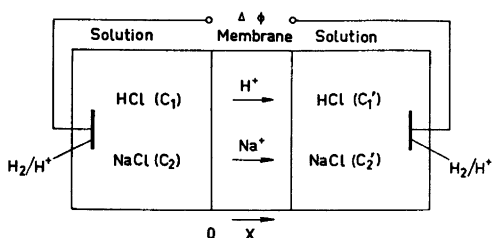


Fig. 1. A cation exchange membrane separating two solutions of HCl and NaCl. The electrodes are reversible to the H⁺-ion.

The description given above for selective cation transport across membranes is redundant, due to eqn. (2). But as the cation restricted transport is a limiting case of the general case allowing passage also of anions, it may be useful to keep the redundant equation system (1). This is because the redundant coefficient sets of L_{ij} and L_{ij}' are subject to the restrictions (3) which will give a limit behaviour of nonredundant coefficient sets, as shown below:

We have previously¹ defined the electrode independent diffusion coefficients l_{ij} which are related to L_{ij} by

$$l_{ij} = L_{ij} - (L_{nj}L_{in})/L_{nn} \quad (7)$$

In our case of cation selective membrane transport the diffusion coefficients obey

$$l_{11} + l_{21} = 0 \quad i = 1, \dots \quad (8)$$

From eqns. (7-8) and the general restriction $l_{ii} \geq 0$ we have

$$l_{12} = L_{12} - \frac{L_{14}L_{24}}{L_{44}} = L_{12} - t_1 t_2 L_{44} \leq 0 \quad (9)$$

t_1 and t_2 are electric transference numbers of the component 1 and 2, respectively. t_i is defined by (see Ref. 1 for details)

$$t_i = L_{i4}/L_{44} \quad i = 1, 2 \quad (10)$$

As $t_1 + t_2 = 1$ or $t_i \leq 1$ we have from eqn. (9)

$$L_{12} \leq 0.25 L_{44} \quad (11)$$

$$L_{i4} \leq L_{44} \quad i = 1, 2 \quad (12)$$

By inserting eqns. (11) and (12) into (6) one obtains

$$L_{11} \leq 0.75 L_{44} \quad i = 1, 2 \quad (13)$$

Conclusion. The relations which can be developed between the phenomenological coefficients for ion-selective membrane transport from a rigorous thermodynamic description, are electrode dependent, but permit a detailed analysis of the system on the macroscopic phenomenological level. They furthermore provide experimental testing criteria for the single phenomenological coefficients, as limits for their behaviour can be developed.

Acknowledgement. Valuable discussions with T. Førland are greatly acknowledged.

1. Førland, K. S., Førland, T. and Ratkje, S. K. *Acta Chem. Scand. A* 31 (1977) 47.
2. DeGroot, S. R. and Mazur, P. *Nonequilibrium Thermodynamics*, Interscience, New York 1962, p. 67.

Received May 2, 1977.

The Crystal Structure of Sodium Dodecylsulfate

STAFFAN SUNDELL

Dept. of Structural Chemistry, Institute of Medical Biochemistry, University of Göteborg,
P.O.B., S-400 33 Göteborg, Sweden

Sodium dodecylsulfate ($\text{CH}_3(\text{CH}_2)_{11}\text{OSO}_3^-\text{Na}^+$) which has been studied as a model sulfolipid is monoclinic ($C2/c$) with $a = 78.69$, $b = 10.22$, $c = 16.41$ Å, $\beta = 98.28^\circ$. The unit cell contains 32 molecules and in addition 4 molecules of water. The lipid molecules are arranged tail to tail in double layers. Favourable electrostatic interactions within the polar region are achieved by an alternating 2 Å displacement of adjacent molecules perpendicular to the layer plane. This arrangement of the polar head groups determines the lateral packing of the molecules and leaves the hydrocarbon chains with about 10 % larger cross section area than usual in solid state chain packing arrangements. Still the hydrocarbon chains are fully extended and only slightly tilted (79°) to the layer plane. The chain packing, however, is irregular and can be described as an intermediate between the orthorhombic $O1$ and the hexagonal chain packing mode.

A variety of complex sulfolipids have been isolated from different organisms.¹ For sulfatide (cerebroside sulfate), the dominating sulfolipid in vertebrates, an interesting correlation with $\text{Na}^+ - \text{K}^+$ ATPase has been shown.² Other sulfolipids like lactosylceramide sulfate of kidney,³ the sulfate ester of 2,3-di-*O*-phytanil-1-*O*-triglycosyl-L-glycerol of halophilic bacteria,⁴ the plant sulfolipid 6-sulfo-quinovosyl-diglycerid⁵ have similar structures in their polar parts and may have the same biological function as sulfatide. In the sea star *Asterias rubens* large amounts of cholesteryl sulfate were detected while other types of common sulfolipids were missing.⁶ This finding suggests that also cholesteryl sulfate may participate in ion transport phenomena. In our structural studies of membrane lipids we have started X-ray work on sulfatides and cholesteryl sulfate. Sodium dodecylsulfate (SDS) has been included in this

study as it represents a simple alkyl sulfate. Alkyl sulfates and chloroalkyl sulfates have been found in nature in phytoflagellates.⁷ The molecular arrangement and phase behaviour of SDS is also of interest with regard to its role as an important detergent.

EXPERIMENTAL

The synthetic sodium dodecylsulfate used in this study was shown by gas chromatographic analysis to contain dodecanol with a purity of better than 99 %. Single crystals were obtained as thin plates from a chloroform-methanol (9:1, v:v) solution on slow evaporation.

The intensity data were collected on a Picker FACS I automatic diffractometer⁸ using graphite monochromated $\text{CuK}\alpha$ radiation. The crystal used had the dimensions $0.36 \times 0.32 \times 0.03$ mm. The $\theta - 2\theta$ scanning mode was used with a scan speed of 1 degree/min and a scan width of 2.5° plus a dispersion term. On each side of the reflexion the background level was determined from 10 s counts. After every 50th reflexion, three standards were measured in order to make a correction for the decaying scattering power of the crystal. It was found at the end of the measurement that the standard reflexions had decreased in intensity to about 70 % of the original values. 5841 independent reflexions were measured. 3666 of these were considered observed [$I > 4\sigma(I)$] and used in the analysis. The intensities were corrected for Lorentz, polarization and absorption effects. No extinction correction was made.

CRYSTAL DATA

Molecular formula: $\text{CH}_3(\text{CH}_2)_{11}\text{OSO}_3^-\text{Na}^+ \cdot 1/8\text{H}_2\text{O}$. Crystal system: monoclinic. Space group: $C2/c$. Unit cell: $a = 78.69(26)$, $b = 10.220(22)$, $c = 16.410(45)$ Å, $\beta = 98.28(8)^\circ$, $V = 13060$ Å³, $M = 289.73$, $Z = 32$, $D_c = 1.19$ g

cm^{-3} , $D_m = 1.18 \text{ g cm}^{-3}$, $\lambda = 1.54051 \text{ \AA}$ ($\text{CuK}\alpha_1$ radiation), $\mu = 20.1 \text{ cm}^{-1}$.

Systematic absences: $hkl: h + k = 2n + 1$
 $h0l: l = 2n + 1$.

STRUCTURE DETERMINATION AND REFINEMENT

As there are four heavy atoms in the asymmetric unit the solution of the Patterson series was not straight-forward. However, a vector set was selected which appeared to define the positions of three sulfur atoms. The phases of one of these atoms were used for a Fourier synthesis, which showed that the two other sulfur positions had been correctly determined from the Patterson function. The following two Fourier syntheses – the first based on the phases of the three sulfur atoms – revealed the structure of the whole polar region including a peak that could only represent a crystal water oxygen. At this stage the R -value was 0.32. After three cycles of block diagonal refinement using anisotropic temperature factors for the sulfur, sodium and oxygen atoms the R -value had dropped to 0.25. An electron density and a difference synthesis were then

calculated. In both cases the carbon atoms of the chains were poorly resolved. The resolution was nevertheless sufficient near the polar regions to determine the direction of the chains and the tilt of the zigzag planes to the ac -plane. One chain (2) (Fig. 2) was better defined than the others. About a quarter of the carbon atoms were incorporated in the next structure factor calculation. In the following three Fourier syntheses the remaining carbons were successively included to give the best fit to the electron density. Anisotropic temperature factors were assigned to the carbon atoms but after a few cycles of refinement many of the U_{ij} values of atoms belonging to chain (1), (3) and (4) had become unrealistically high. The refinement was then restarted with isotropic temperature factors for the carbons in chains (1), (3) and (4), while anisotropic ones were still used in chain (2). The structure was refined by six cycles of full matrix refinement to $R = 0.103$ and $R_w = 0.118$. The temperature factors for the carbons of chains (1), (2) and (3) became very large (on the average 26 \AA^2). The poor resolution of these atoms was also clear from the electron density map (Fig. 1). Finally a check of the space group choice was made.

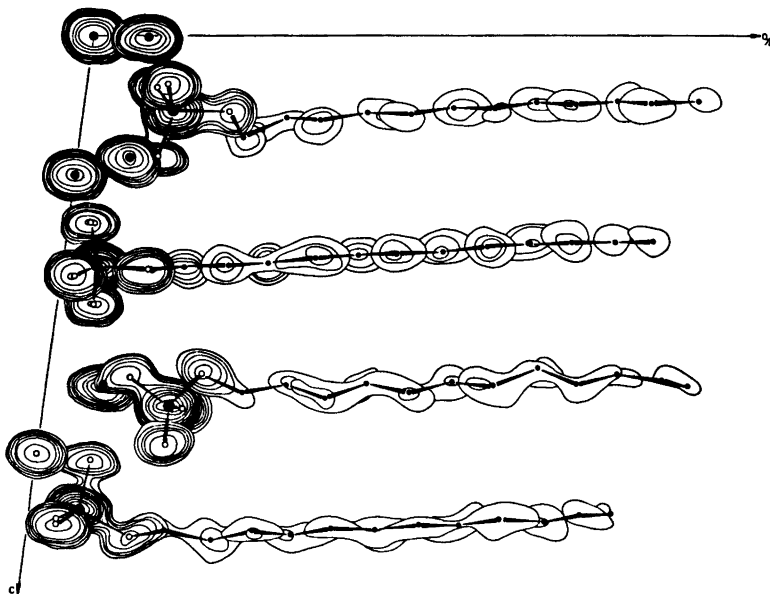


Fig. 1. Composite electron map of one asymmetric unit $(0,0,0)$, $(1/4,1/2,1)$. Contours are drawn at intervals of 1.5, 2.0, 2.5, 3.0, 4.0, 6.0, 8.0, 10.0, 12.0, 14.0, 16.0 and 18.0 e/\AA^3 .

The structure was solved as before starting with the phases of one sulfur atom but this time in *Cc*. The resulting atom positions, however, did not differ significantly from the centrosymmetrically related positions in *C2/c*. The form factors used were those given in *International Tables for X-Ray Crystallography*.⁹ All calculations were performed on a DEC 10 computer using the X-RAY 72 program

system.¹⁰ The weight assigned to each observation¹¹ in the least-squares refinement was:

$$w = 1/[1 + (|F_o| - 5.6F_{\min})^2 / (11.1F_{\min})^2]$$

DESCRIPTION AND DISCUSSION OF THE STRUCTURE

Lists of observed and calculated structure factors can be obtained from this Department.

Table 1. Fractional coordinates and thermal parameters ($\times 10^3$) with estimated standard deviations in parentheses. The isotropic and anisotropic thermal parameters are in the form $\exp -8\pi U(\sin^2\theta/\lambda^2)$ and $\exp -2\pi^2(h^2a^{*2}U_{11} + \dots + 2kl2b^*c^*U_{23})$, respectively.

Atom	x	y	z	U or U11	U22	U33	U12	U13	U23
Na(11)	0.0000(-)	0.0000(-)	0.0000(-)	95(7)	22(3)	23(3)	3(4)	11(3)	3(2)
Na(12)	0.0000(-)	0.0590(6)	0.2500(-)	93(7)	31(3)	21(3)	0(-)	7(3)	0(-)
Na(2)	0.0208(1)	0.4134(4)	0.0019(2)	96(5)	26(2)	23(2)	-2(3)	7(2)	0(2)
Na(3)	0.0200(1)	0.3628(4)	0.2197(3)	102(5)	37(3)	45(3)	-2(3)	22(3)	-6(2)
Na(4)	0.0216(1)	0.2111(4)	0.6279(2)	91(5)	37(3)	23(2)	-6(3)	10(2)	0(2)
O(5)	0.0000(-)	0.4832(9)	0.7500(-)	98(12)	24(6)	21(5)	0(-)	9(6)	0(-)
S(1)	0.0338(1)	0.1239(3)	0.1348(2)	66(3)	23(2)	25(1)	5(2)	6(2)	-1(1)
O(11)	0.0302(1)	0.2400(8)	0.0878(5)	98(9)	39(5)	56(5)	6(5)	12(5)	10(4)
O(12)	0.0261(1)	0.0117(7)	0.0954(5)	130(10)	23(4)	53(5)	-11(5)	1(5)	-6(4)
O(13)	0.0301(1)	0.1383(9)	0.2170(4)	121(10)	63(6)	34(5)	27(6)	9(5)	-6(4)
O(14)	0.0531(1)	0.1104(9)	0.1383(6)	96(10)	54(6)	88(7)	0(6)	8(6)	7(5)
C(11)	0.0617(3)	0.0089(24)	0.1837(14)	155(9)					
C(12)	0.0776(5)	-0.0420(35)	0.1571(20)	239(15)					
C(13)	0.0923(4)	0.0315(29)	0.1547(17)	191(11)					
C(14)	0.1089(4)	-0.0469(31)	0.1478(18)	220(13)					
C(15)	0.1234(4)	0.0265(34)	0.1435(19)	224(13)					
C(16)	0.1387(5)	-0.0416(33)	0.1310(19)	211(13)					
C(17)	0.1532(4)	0.0397(34)	0.1321(19)	226(14)					
C(18)	0.1700(5)	-0.0422(34)	0.1273(19)	224(14)					
C(19)	0.1856(6)	0.0376(42)	0.1311(23)	270(18)					
C(110)	0.2014(7)	-0.0414(47)	0.1201(27)	293(21)					
C(111)	0.2158(9)	0.0359(59)	0.1273(34)	393(29)					
C(112)	0.2309(7)	-0.0271(54)	0.1173(29)	350(26)					
S(2)	0.0135(1)	0.2945(3)	0.4187(1)	57(3)	23(1)	14(1)	-4(2)	7(1)	-1(1)
O(21)	0.0081(1)	0.2428(7)	0.3369(4)	117(9)	28(4)	15(4)	5(5)	9(4)	-3(3)
O(22)	0.0047(1)	0.4124(7)	0.4334(4)	94(8)	25(4)	27(4)	-14(5)	14(4)	-1(3)
O(23)	0.0136(1)	0.1993(7)	0.4826(4)	98(8)	32(4)	20(4)	-7(5)	5(4)	5(3)
O(24)	0.0319(1)	0.3404(8)	0.4203(4)	44(7)	59(5)	44(4)	12(5)	11(4)	5(4)
C(21)	0.0462(2)	0.2532(17)	0.4202(8)	44(14)	120(14)	61(9)	35(11)	0(8)	8(9)
C(22)	0.0631(3)	0.3205(21)	0.4160(10)	94(18)	147(19)	87(12)	-15(15)	5(11)	4(12)
C(23)	0.0772(3)	0.2286(18)	0.4106(10)	111(20)	105(14)	100(13)	-3(14)	32(13)	-1(11)
C(24)	0.0937(3)	0.3024(20)	0.4036(11)	104(20)	125(16)	118(15)	-3(15)	28(13)	3(13)
C(25)	0.1086(3)	0.2210(24)	0.3986(13)	55(20)	171(21)	150(18)	-3(17)	1(14)	-3(16)
C(26)	0.1259(4)	0.2896(28)	0.3947(14)	75(27)	187(26)	161(21)	25(21)	17(17)	4(18)
C(27)	0.1413(4)	0.2144(26)	0.3874(15)	90(26)	170(23)	181(23)	0(19)	34(18)	-12(18)
C(28)	0.1581(4)	0.2821(31)	0.3881(16)	144(28)	220(31)	183(24)	-31(24)	72(20)	-2(22)
C(29)	0.1731(4)	0.2108(31)	0.3754(18)	139(28)	207(30)	235(29)	-21(23)	60(22)	-17(24)
C(210)	0.1888(4)	0.2829(37)	0.3769(19)	58(31)	300(41)	263(33)	15(27)	49(24)	1(29)
C(211)	0.2039(5)	0.2116(46)	0.3716(23)	59(41)	334(52)	351(45)	3(33)	77(32)	0(36)
C(212)	0.2196(5)	0.2773(47)	0.3684(24)	106(37)	390(57)	357(49)	19(36)	100(32)	34(41)

Table 1. Continued.

Atom	x	y	z	U or U11	U22	U33	U12	U13	U23
S(3)	0.0469(1)	0.4389(3)	0.6647(2)	94(4)	35(2)	39(2)	-5(2)	4(2)	0(1)
O(31)	0.0306(2)	0.4471(9)	0.6135(6)	145(12)	63(6)	69(7)	5(7)	3(7)	1(5)
O(32)	0.0468(2)	0.5130(9)	0.7373(5)	139(11)	69(7)	56(6)	-7(7)	11(6)	-20(5)
O(33)	0.0517(2)	0.3057(9)	0.6758(6)	132(11)	54(6)	90(7)	24(7)	23(7)	17(6)
O(34)	0.0583(2)	0.5087(13)	0.6103(8)	222(17)	122(11)	141(11)	-64(12)	98(11)	-51(9)
C(31)	0.0735(3)	0.5769(27)	0.6488(15)	181(11)					
C(32)	0.0876(4)	0.4967(30)	0.6299(17)	203(11)					
C(33)	0.1042(4)	0.5526(29)	0.6547(17)	189(11)					
C(34)	0.1198(5)	0.4854(35)	0.6327(20)	242(14)					
C(35)	0.1360(4)	0.5508(28)	0.6477(16)	194(11)					
C(36)	0.1519(5)	0.4759(36)	0.6270(20)	239(15)					
C(37)	0.1678(6)	0.5423(41)	0.6418(23)	268(18)					
C(38)	0.1828(6)	0.4695(41)	0.6168(23)	268(17)					
C(39)	0.1993(7)	0.5398(47)	0.6350(26)	299(21)					
C(310)	0.2138(7)	0.4659(49)	0.6099(27)	317(22)					
C(311)	0.2303(9)	0.5484(66)	0.6244(38)	436(34)					
C(312)	0.2421(9)	0.4419(73)	0.6239(40)	449(41)					
S(4)	0.0186(1)	0.1847(3)	0.8508(2)	73(3)	27(2)	17(1)	-4(2)	5(2)	-3(1)
O(41)	0.0204(1)	0.1838(8)	0.7649(4)	117(8)	71(6)	17(4)	-3(6)	22(5)	0(4)
O(42)	0.0100(1)	0.0738(8)	0.8748(4)	147(11)	34(5)	35(5)	-17(6)	17(5)	3(4)
O(43)	0.0116(1)	0.3007(8)	0.8766(5)	164(11)	33(5)	33(5)	4(6)	18(5)	5(4)
O(44)	0.0376(2)	0.1678(15)	0.9010(6)	126(12)	236(15)	43(6)	-50(11)	14(7)	6(8)
C(41)	0.0528(4)	0.2436(27)	0.8968(15)	172(10)					
C(42)	0.0683(4)	0.1776(29)	0.9080(16)	191(11)					
C(43)	0.0821(4)	0.2675(31)	0.8961(18)	216(12)					
C(44)	0.0991(3)	0.2105(27)	0.9010(16)	186(11)					
C(45)	0.1145(4)	0.2813(32)	0.8885(19)	230(13)					
C(46)	0.1302(4)	0.2127(32)	0.8975(19)	229(14)					
C(47)	0.1462(4)	0.2817(35)	0.8817(21)	255(15)					
C(48)	0.1614(4)	0.2107(33)	0.8918(19)	235(14)					
C(49)	0.1759(5)	0.2832(38)	0.8713(22)	264(17)					
C(410)	0.1924(6)	0.2269(42)	0.8840(24)	286(19)					
C(411)	0.2072(6)	0.2874(48)	0.8604(27)	336(23)					
C(412)	0.2234(7)	0.2272(49)	0.8668(28)	342(24)					

Table 2. Average interatomic distances and angles with standard deviations in parentheses.

Distance	Å	Angle	Degrees
S-O(1)	1.44(1)	O(1)-S-O(2)	112.2(0.5)
S-O(2)	1.42(1)	O(1)-S-O(3)	112.2(0.5)
S-O(3)	1.42(1)	O(1)-S-O(4)	104.8(0.6)
S-O(4)	1.55(1)	O(2)-S-O(3)	113.6(0.6)
O(4)-C(1)	1.43(2)	O(2)-S-O(4)	105.4(0.6)
C(1)-C(2)	1.43(4)	O(3)-S-O(4)	108.6(0.6)
C(2)-C(3)	1.44(4)	O(4)-C(1)-C(2)	113.4(2.0)
C(3)-C(4)	1.51(4)	C(1)-C(2)-C(3)	115.3(2.4)
C(4)-C(5)	1.43(4)	C(2)-C(3)-C(4)	115.5(2.4)
C(5)-C(6)	1.48(4)	C(3)-C(4)-C(5)	118.8(2.5)
C(6)-C(7)	1.44(5)	C(4)-C(5)-C(6)	117.8(2.7)
C(7)-C(8)	1.49(5)	C(5)-C(6)-C(7)	117.8(2.8)
C(8)-C(9)	1.46(5)	C(6)-C(7)-C(8)	116.2(3.0)
C(9)-C(10)	1.46(6)	C(7)-C(8)-C(9)	115.6(3.1)
C(10)-C(11)	1.44(7)	C(8)-C(9)-C(10)	115.9(3.5)
C(11)-C(12)	1.41(8)	C(9)-C(10)-C(11)	115.8(4.0)
		C(10)-C(11)-C(12)	114.2(4.8)

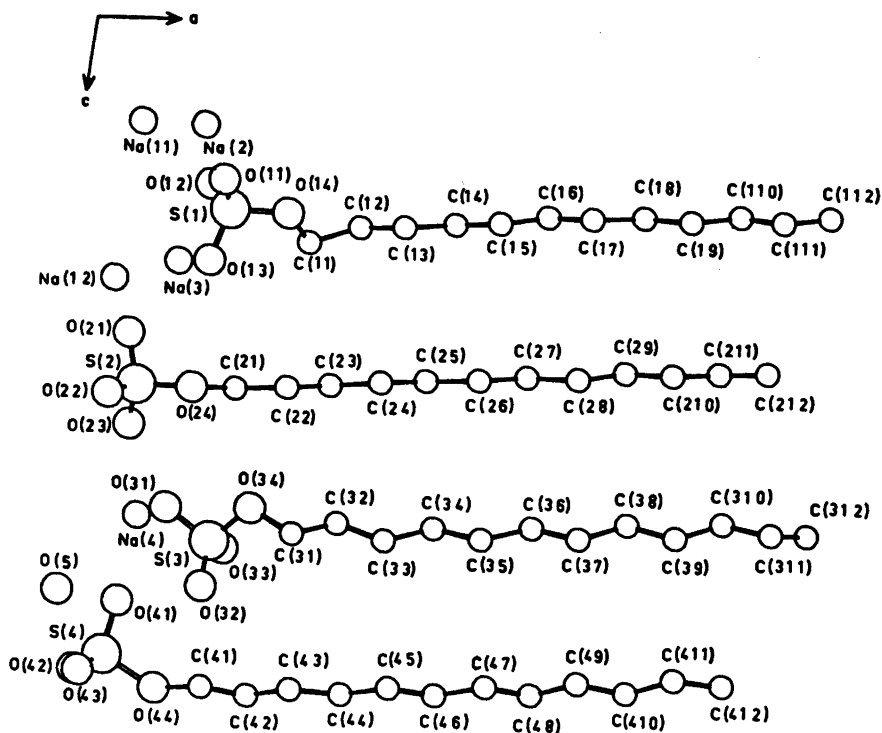


Fig. 2. The numbering of atoms. The first figure of the atom index gives the number of the molecule.

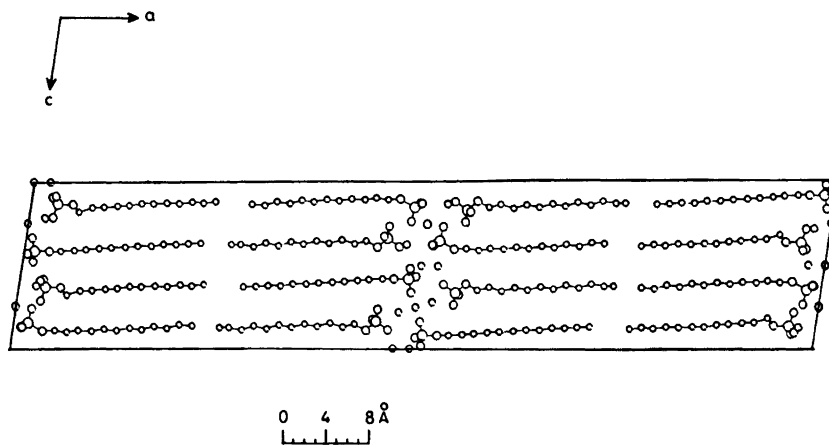


Fig. 3. The molecular arrangement of SDS viewed along the b -axis.

The final atomic parameters are listed in Table 1 and average interatomic parameters are listed in Table 2. The numbering of the atoms is shown in Fig. 2. The structure is built up of double layers of molecules in a tail

to tail arrangement (Fig. 3). The carbon chain axes are tilted 79° to the layer plane.

The polar part. The sulfate head groups of adjacent molecules are alternatingly displaced by about 2 \AA in direction of the a -axis. The

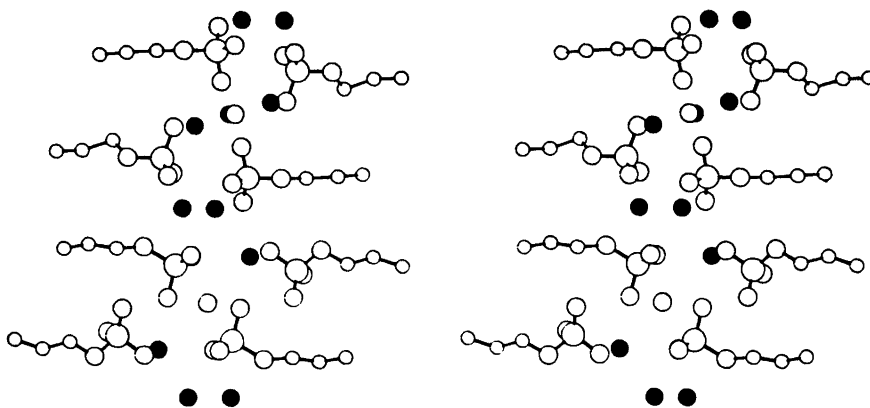


Fig. 4. Stereogram of the polar region.

rippled structure thereby produced allows favourable electrostatic interaction within the polar region as sodium ions become distributed between sulfate groups both within each layer and between opposite layers. A stereo drawing of the polar region is shown in Fig. 4. The average S-O distance and O-S-O angle excluding those containing the ester oxygen are 1.43 Å and 112.7°. The corresponding

values for the ester oxygen are 1.54 Å and 106.0°. The sodium ions Na(11) and Na(12) situated in special positions are coordinated by six oxygens each, forming a distorted octahedron (Fig. 5). The Na-O distance intervals are 2.34–2.42 and 2.39–2.63 Å, respectively.

Na(2) is surrounded by five oxygens at a distance between 2.32 and 2.40 Å where the O-Na-O angles deviate less than 16° from

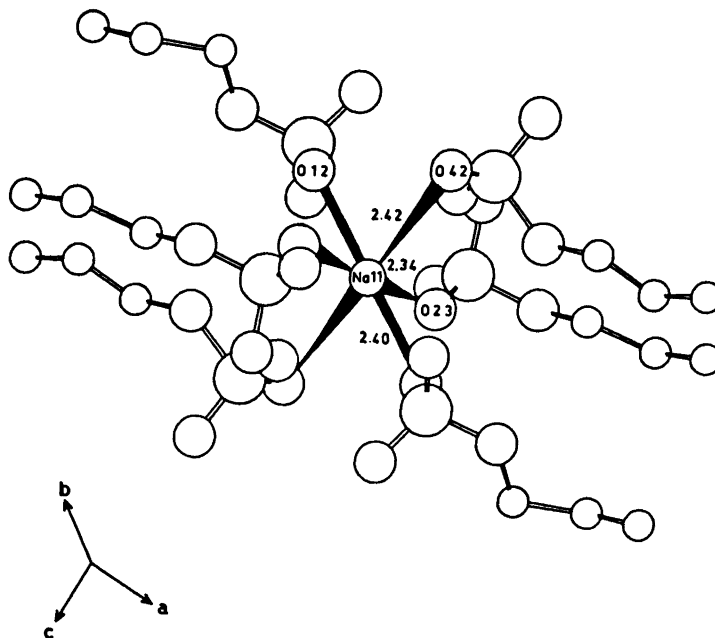


Fig. 5. The environment of Na(11).

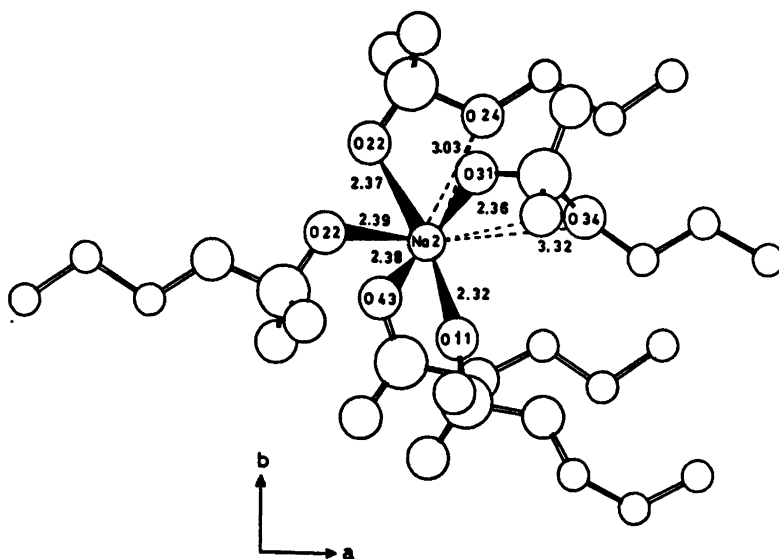


Fig. 6. The environment of Na(2) viewed along the *c*-axis.

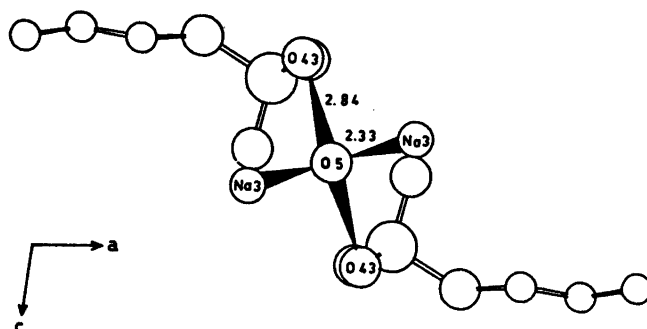


Fig. 7. The environment of the crystal water oxygen O(5) viewed along the *b*-axis.

those of a regular octahedron. In the vicinity of the sixth corner of the octahedron there are two oxygens at 3.03 and 3.32 Å from the sodium ion (Fig. 6). A similar oxygen arrangement is also found around Na(3) and Na(4). The Na-O distance intervals for the five closest oxygens are in the latter cases 2.30–2.57 and 2.28–2.57 Å respectively. For Na(3) the distances to the two more remote oxygens are 2.72 and 2.82 Å while for Na(4) the distances are 2.76 and 2.85 Å.

The crystal water oxygen O(5) placed on a twofold axis is hydrogen bonded to O(43) and its symmetry equivalent generated by the

twofold axis (Fig. 7). The O...O distance is 2.84 Å and the O-O-O angle 98.0°. The lone pair valence orbitals point towards Na(3) and its symmetry equivalent, the Na-O distance being 2.33 Å and Na-O-Na angle 95.0°. A list of sodium-oxygen distances is given in Table 3.

The non-polar part. The strong ionic forces and the hydrogen bond system in the polar region dominate the molecular structure to the extent that the hydrocarbon chains cannot adopt any of the common side packing arrangements with optimum van der Waals interactions.^{12,13} Despite the alternating dis-

Table 3. Sodium-oxygen distances (Å) less than 3.5 Å and their estimated standard deviations.

Na(11)	O(12)	(0,0,0)1 ^a	2.40(1)
Na(11)	O(12)	(0,0,0)2	2.40(1)
Na(11)	O(23)	(0,0,0)3	2.34(1)
Na(11)	O(23)	(0,0,-1)4	2.34(1)
Na(11)	O(42)	(0,0,-1)1	2.42(1)
Na(11)	O(42)	(0,0,1)2	2.42(1)
Na(12)	O(13)	(0,0,0)1	2.63(1)
Na(12)	O(13)	(0,0,0)3	2.63(1)
Na(12)	O(21)	(0,0,0)1	2.39(1)
Na(12)	O(21)	(0,0,0)3	2.39(1)
Na(12)	O(41)	(0,0,1)2	2.95(1)
Na(12)	O(41)	(0,0,-1)4	2.95(1)
Na(12)	O(42)	(0,0,1)2	2.49(1)
Na(12)	O(42)	(0,0,-1)4	2.49(1)
Na(2)	O(11)	(0,0,0)1	2.32(1)
Na(2)	O(22)	(0,0,0)3	2.40(1)
Na(2)	O(22)	(0,1,-1)4	2.37(1)
Na(2)	O(24)	(0,1,-1)4	3.03(1)
Na(2)	O(31)	(0,1,-1)4	2.36(1)
Na(2)	O(34)	(0,1,-1)4	3.31(2)
Na(2)	O(43)	(0,0,-1)1	2.38(1)
Na(2)	O(44)	(0,0,-1)1	3.38(2)
Na(3)	O(11)	(0,0,0)1	2.72(1)
Na(3)	O(13)	(0,0,0)1	2.43(1)
Na(3)	O(21)	(0,0,0)1	2.57(1)
Na(3)	O(21)	(0,0,0)3	2.58(1)
Na(3)	O(22)	(0,0,0)3	2.99(1)
Na(3)	O(24)	(0,0,0)1	3.30(1)
Na(3)	O(31)	(0,1,-1)4	2.82(1)
Na(3)	O(32)	(0,1,-1)4	2.44(1)
Na(3)	O(5)	(0,0,1)2	2.33(1)
Na(4)	O(12)	(0,0,0)4	2.38(1)
Na(4)	O(23)	(0,0,0)1	2.38(1)
Na(4)	O(31)	(0,0,0)1	2.53(1)
Na(4)	O(33)	(0,0,0)1	2.57(1)
Na(4)	O(41)	(0,0,0)1	2.28(1)
Na(4)	O(42)	(0,0,1)3	2.85(1)
Na(4)	O(43)	(0,0,1)3	2.76(1)

^a The figures within parentheses indicate translations in the directions *a*, *b* and *c* of the second atom and the last figure to the equivalent position. 1: *x*, *y*, *z*; 2: \bar{x} , \bar{y} , \bar{z} ; 3: \bar{x} , *y*, $1/2-z$; 4: *x*, \bar{y} , $1/2+z$.

placement of adjacent molecules the area occupied per sulfate group is larger than the cross section area normally required by a hydrocarbon chain in the solid state. The chains are only slightly tilted and the average area per chain is 20.9 Å² compared with a value of about 19 Å² for the common orthorhombic chain packing O1. Only in the hexagonal chain arrangement which is often adopted near the melting point chains pack as cylindrical rods with a cross section of 21.1 Å. The chains in SDS must, however, be considered to

be in an intermediate state between O1 and the hexagonal packing (Fig. 8) as the symmetry along the chain axis is still clearly twofold.

The chains in SDS are too irregular to allow any formal subcell description of the arrangement. On the other hand, all attempts to use an idealized model for the chains have resulted in a higher *R*-value and/or too close contacts between hydrogen atoms when included at their expected positions. This indicates that the chain structure reported here – though very unusual – must be essentially correct.

As the space available for each chain is large, high thermal vibrations and disorder is expected. This is also indicated by the short average C–C distance of 1.45 Å and the large carbon valence angles of 116° with estimated standard deviations ($s = [(\sum_N(\bar{X}_N - X^2/N - 1)]^{1/2}$) 0.05 Å and 5.2°, respectively. The normal values for long chains are around 1.51 Å and 114°, respectively. The molecular arrangement of SDS is interesting in connection with biological lipid systems such as the cell membranes. In these it is generally concluded that the polar regions of lipid bilayers can have a fairly ordered arrangement whereas the carbon chains are in a more fluid state. The present analysis shows that the rigid arrangement of the polar head groups leaves the hydrocarbon chains with 10 % more space than normally required in the solid state, thereby allowing disorder and high thermal motion in the hydrocarbon matrix. On heating SDS undergoes a phase transition at 85 °C which is accompanied by a layer thickness decrease of 5 Å and a change to hexagonal chain packing as indicated in the powder diagram by a single short-spacing line at 4.28 Å.

The decrease in lamellar thickness can be explained by a change in tilt of the hydrocarbon chains from 79° to about 60°. However, this tilt and the hexagonal chain packing require an increase of the molecular area in the *ac*-plane from 20.9 to approximately 24.5 Å. This suggests that the transition to the high temperature phase involves a change of the sulfate groups from a rippled to a planar arrangement.

Acknowledgements. I wish to thank Prof. S. Abrahamsson, Drs. S. Aleby and I. Pascher, who also provided the crystals, for their en-

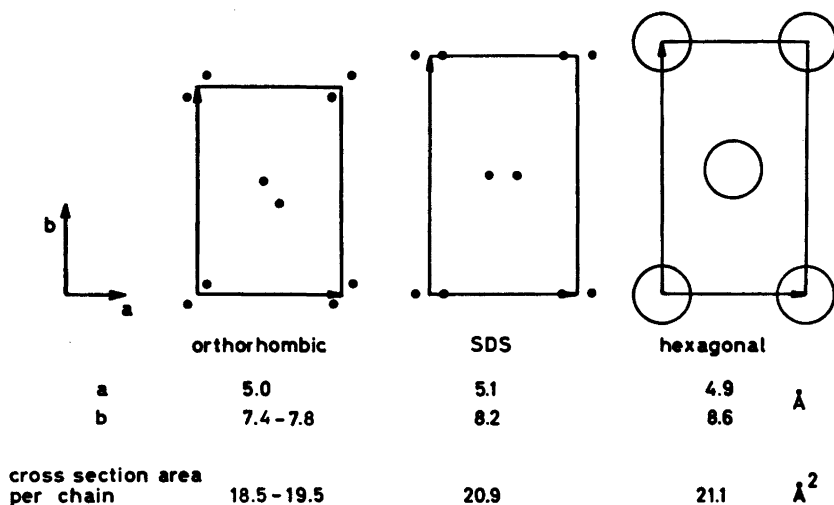


Fig. 8. The idealized subcell of SDS compared with an orthorhombic and a hexagonal subcell.

couragement and advice. I also wish to thank Mrs. M. Innes for technical assistance. Grants in support of this Department were obtained from the Swedish Medical Research Council, the Swedish Board for Technical Development, the Wallenberg Foundation and the U.S. Public Health Service (G. M.-11653).

Crystal Analysis, Pergamon, London 1961, pp. 107-124.

- Abrahamsson, S., Ställberg-Stenhagen, S. and Stenhagen, E. *Prog. Chem. Fats Other Lipids* 7 (1963) 59.
- Abrahamsson, S., Dahlén, B., Löfgren, H. and Pascher, I. *Prog. Chem. Fats Other Lipids*. In press.

Received May 23, 1977.

REFERENCES

- Haines, T. *Prog. Chem. Fats Other Lipids* 11 (1971) 297.
- Karlsson, K.-A., Samuelsson, B. E. and Steen, G. O. *Eur. J. Biochem.* 46 (1974) 243.
- Mårtensson, E. *Biochim. Biophys. Acta* 116 (1966) 521.
- Kates, M. and Deroo, P. W. *J. Lipid Res.* 14 (1973) 438.
- Miyano, M. and Bensson, A. A. *J. Am. Chem. Soc.* 84 (1962) 57.
- Björkman, L. R., Karlsson, K.-A., Pascher, I. and Samuelsson, B. E. *Biochim. Biophys. Acta* 270 (1972) 260.
- Mayers, G. L. and Haines, T. H. *Biochemistry* 6 (1967) 1665.
- Lenhert, P. G. *J. Appl. Crystallogr.* 8 (1975) 568.
- International Tables for X-Ray Crystallography*, Kynoch Press, Birmingham 1962, Vol. III, pp. 201-209.
- Stewart, J. M. et al. *The X-Ray System 1972*, Technical Report TR-192, Computer Science Center, University of Maryland, College Park.
- Mills, O. S. and Rollet, J. S. *Computing Methods and the Phase Problem in X-Ray*

The Crystal and Molecular Structure of Hexahydro-1,2-dimethyl-3,6-pyridazinedione at -165°C

TOR OTTERSEN and ULLA SØRENSEN *

Department of Chemistry, University of Oslo, Oslo 3, Norway

The crystal and molecular structure of the title compound, $\text{C}_8\text{H}_{10}\text{N}_2\text{O}_2$, has been determined using 3284 reflections above background level collected at -165°C . The crystals are monoclinic, space group $C2/c$ with cell dimensions $a = 19.107(5) \text{ \AA}$, $b = 6.099(2) \text{ \AA}$, $c = 12.893(3) \text{ \AA}$, $\beta = 113.59^{\circ}(2)$. The structure model was refined to an R of 0.056. In order to reduce the influence of valence electron asphericity on the structural parameters low-angle data were excluded from the final refinements. The heavy atom parameters converged to their final values for a minimum $\sin \theta/\lambda$ cutoff of 0.65 \AA^{-1} , leaving 1840 reflections used in the refinement, the R -factor obtained is 0.037. The molecule has a "twisted boat" conformation with close to C_2 symmetry. Compared with hexahydro-3,6-pyridazinedione the loss of hydrogen bonding leads to a lengthening of the $\text{C}-\text{N}$ bonds by about 0.020 \AA and a shortening of the $\text{C}=\text{O}$ bonds by about 0.019 \AA .

The structure determination of hexahydro-1,2-dimethyl-3,6-pyridazinedione (HDMP) is part of a series of structure investigations of 3,6-pyridazinediones and related compounds, of which part of the purpose is to study the effect of hydrogen bonding on the peptide linkage, the $\text{N}-\text{C}=\text{O}$ fragment. The experimental results have been complemented by a series of theoretical studies using hydrogen-bonded complexes of formamide as model systems (for a review see Ref. 1).

In the crystal structure of hexahydro-3,6-pyridazinedione² the molecules are bound together by $\text{N}-\text{H}\cdots\text{O}$ hydrogen bonds such

* On leave from: Department of General and Organic Chemistry, University of Copenhagen, H. C. Ørsted Institute, DK-2100 Copenhagen, Denmark.

that each $\text{N}-\text{C}=\text{O}$ fragment participates in two intermolecular hydrogen bonds around a center of symmetry forming hydrogen-bonded dimers of the type found for formamide.³ The structure of hexahydro-3,6-pyridazinedione has recently been reinvestigated using a more extensive data set in order to study the deformation electron densities.⁴ In order to get further quantitative results on the effect of hydrogen bonding on the peptide linkage, *i.e.* the changes in molecular parameters induced by the formation of hydrogen bonds, it was of interest to study a hexahydro-3,6-pyridazinedione which was not involved in hydrogen bonding. In the unreduced 3,6-pyridazinediones the possibility of hydrogen bonding has been deliberately eliminated by successive methyl substitution of the hydrogen atoms bonded to the nitrogen and oxygen atoms, and a similar approach could be used for hexahydro-3,6-pyridazinedione. The results from a series of structure determinations of some simple amides in the gaseous state,⁵⁻⁸ imply that introduction of a methyl group at the nitrogen atom has little or no effect on the $\text{C}-\text{N}$ bond length, whereas a small lengthening ($\sim 0.005 \text{ \AA}$) of the $\text{C}=\text{O}$ bond is indicated. A structure determination of HDMP was, therefore, carried out.

EXPERIMENTAL

1,2-Dimethyl-3,6-pyridazinedione was synthesized by the method of Eichenberger *et al.*⁹ and reduced¹⁰ to give HDMP. The product was recrystallized in ethanol. The crystals grew as platy needles.

Oscillation and Weissenberg photographs indicated monoclinic symmetry and the system-

atic absences were those characteristic of the space group $C2/c$. The density indicated eight molecules in the unit cell.

A computer-controlled Syntex P1 four-circle diffractometer with graphite-monochromatized $MoK\alpha$ radiation and equipped with a modified Enraf-Nonius liquid nitrogen cooling device was utilized in the determination of unit cell parameters and the collection of intensity data. Cell constants were determined by a least-squares treatment of the angular coordinates of fifteen reflections with 2θ -values between 40 and 45°. The temperature at crystal site was -165°C.

Three-dimensional intensity data were recorded using the $\omega-2\theta$ scanning mode with scan speed variable from 2 to 6° min⁻¹, depending on the peak intensity of the reflection. Background counting time was equal to 0.7 × scan time. All reflections with 2θ -values less than 55° were recorded using a crystal of dimensions 0.2 × 0.2 × 0.5 mm. Due to icing this crystal was lost and a crystal of dimensions 0.2 × 0.2 × 0.4 mm was used in the recording of reflections with 2θ -values larger than 55°. Of these only those which had integrated counts larger than 5 cps determined in a 2 s scan over the reflection were recorded. The intensities of three standard reflections which were remeasured after every sixty reflections were essentially constant throughout each recording run. The intensities of these reflections were used in scaling the two data sets to a common scale.

The estimated standard deviations were taken as the square root of the total counts with a 2% addition for experimental uncertainties. Of the 3632 reflections measured ($2\theta_{max} = 80^\circ$), 3284 had intensities larger than twice their standard deviations. These were regarded as observed, whereas the remaining were excluded from further calculations. The intensities were corrected for Lorentz and polarization effects. The computer program used, as well as programs subsequently employed, is part of a local assembly of computer programs for CYBER-74 which is described in Ref. 11.

The atomic scattering factors used were those of Doyle and Turner¹² for oxygen, nitrogen, and carbon, and of Stewart *et al.*¹³ for hydrogen.

CRYSTAL DATA

Hexahydro-1,2-dimethyl-3,6-pyridazinedione, $C_8H_{10}N_2O_2$, $M = 142.15$ amu. Space group $C2/c$, cell dimensions at -165°C: $a = 19.107(5)$ Å, $b = 6.099(2)$ Å, $c = 12.893(3)$ Å, $\beta = 113.59^\circ(2)$, $V = 1376.9(6)$ Å³. D_{obs} (floatation, 19°C) = 1.36 g cm⁻³, $Z = 8$, $D_{calc} = 1.371$ g cm⁻³. $F(000) = 608$.

STRUCTURE DETERMINATION AND REFINEMENTS

The phase problem was solved by the MULTAN¹⁴ program assembly. The heavy atom structure model was refined with anisotropic temperature factors to a conventional R of 0.08. The hydrogen atoms were found as the ten largest peaks in a difference Fourier synthesis calculated using this structure model. These were included in the refinement with isotropic temperature factors. Full-matrix least-squares refinement of all positional and thermal parameters converged to an R of 0.056 and a weighted R_w of 0.068. The "goodness of fit" (G) ($\{[\sum(F_o - |F_c|)^2]/(m-s)\}^{1/2}$) is 3.48.

In order to remove the influence of the valence electron asphericity on the structural parameters the low-angle data were excluded from the final refinements. Full-matrix least-squares refinements of all parameters involving the heavy atoms were performed with minimum $\sin \theta/\lambda$ -cutoffs of 0.50, 0.65 and 0.75 Å⁻¹. The

Table 1. Fractional atomic coordinates and thermal parameters with estimated standard deviations. The anisotropic temperature factor is given by: $\exp\{-2\pi^2[U_{11}(a^*h)^2 + \dots + 2U_{23}(b^*c^*kl)]\}$.

ATOM	X	Y	Z	U11	U22	U33	U12	U13	U23
O1	.6997(4)	.5372(11)	.4285(5)	.0234(2)	.0225(2)	.0198(2)	.0089(2)	.0097(2)	-.0046(2)
O2	.5694(4)	1.1167(10)	.4861(5)	.0264(2)	.0198(2)	.0219(2)	.0024(2)	.0109(2)	-.0034(2)
N1	.6188(4)	.7758(10)	.6833(5)	.0224(2)	.0173(2)	.0158(2)	.0025(2)	.0094(2)	.0020(1)
N2	.6553(3)	.6318(10)	.5624(4)	.0202(2)	.0170(2)	.0143(2)	.0029(1)	.0066(1)	.0015(1)
C3	.6623(4)	.6636(10)	.4656(5)	.0179(2)	.0173(2)	.0143(2)	-.0013(2)	.0059(1)	-.0015(1)
C4	.6624(4)	.8401(12)	.3096(5)	.0200(2)	.0235(3)	.0137(2)	.0025(2)	.0062(2)	.0024(2)
C5	.6220(4)	1.0387(11)	.4687(5)	.0224(2)	.0175(2)	.0199(2)	.0006(2)	.0050(2)	.0031(2)
C6	.6013(4)	.9067(10)	.5660(5)	.0188(2)	.0164(2)	.0158(2)	.0002(2)	.0057(1)	-.0005(1)
C7	.6761(5)	.6762(14)	.6682(7)	.0329(3)	.0247(3)	.0222(2)	.0020(2)	.0177(2)	.0046(2)
C8	.7181(5)	.5051(12)	.6487(6)	.0251(3)	.0197(2)	.0180(2)	.0040(2)	.0061(2)	.0032(2)

ATOM	X	Y	Z	B	ATOM	X	Y	Z	B
H41	.6149(8)	.6609(20)	.3255(13)	2.0(3)	H42	.5496(8)	.8007(24)	.3685(12)	1.7(3)
H51	.6709(8)	1.0635(24)	.4950(12)	1.8(3)	H52	.5973(9)	1.1672(26)	.4327(13)	2.2(3)
H71	.6405(9)	.7800(27)	.0707(13)	2.5(3)	H72	.5523(10)	.5465(32)	.6343(15)	3.0(3)
H73	.6120(10)	.6351(30)	.7438(16)	3.7(4)	H81	.7598(10)	.6051(29)	.6973(14)	3.0(3)
H82	.7340(10)	.4025(29)	.6142(15)	3.0(3)	H83	.6952(10)	.4308(32)	.6926(16)	3.0(3)

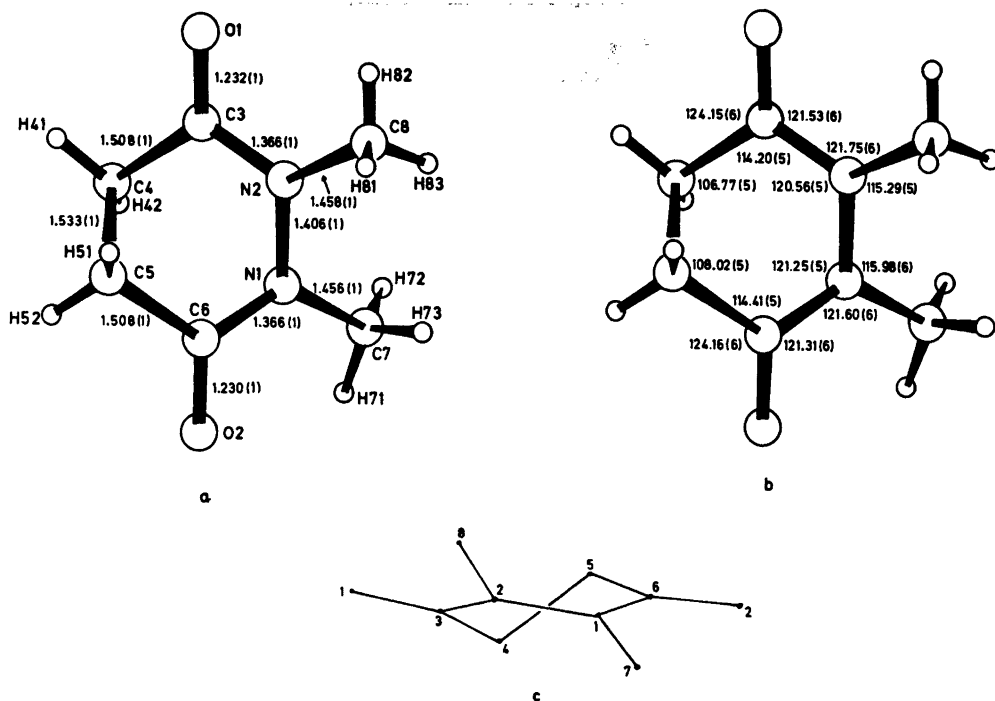


Fig. 1. (a) Bond lengths (Å) corrected for thermal libration effects. (b) Bond angles (°). (c) A view of the molecule as seen in the least-squares plane calculated using all nonhydrogen atoms.

number of reflections in the refinement, final R , R_w and G factors are as follows: cutoff 0.50 \AA^{-1} : 2598, 0.050, 0.054, 2.22; cutoff 0.65 \AA^{-1} : 1840, 0.037, 0.036, 1.18; cutoff 0.75 \AA^{-1} : 1172, 0.039, 0.038, 1.07. The heavy atom parameters converged to their final values for the 0.65 \AA^{-1} cutoff in agreement with the refinement of hexamethylenetetramine,¹⁵ although this cutoff is lower than that of 0.75 \AA^{-1} found for similar compounds (hexahydro-3,6-pyridazinedione,⁴ diformylhydrazine¹⁶ and carbonylhydrazide¹⁷). Atomic parameters for nonhydrogen atoms obtained in the refinement with a minimum $\sin \theta/\lambda$ cutoff of 0.65 \AA^{-1} are listed in Table 1, together with the parameters found for hydrogen atoms in the refinement using all data. A list of observed and calculated structure factors is available from the authors upon request.

The r.m.s. difference between the observed U_{ij} 's and those calculated from the "rigid-body" model¹⁸ is 0.0007 \AA^2 , which indicates that the molecule may be regarded as a rigid

body. The atomic positions were accordingly corrected for the vibrational motion. The eigenvalues of T are 0.14 , 0.12 and 0.11 \AA^2 , and the r.m.s. librational amplitudes are 3.1 , 2.1 and 1.7° .

DISCUSSION

Bond lengths and bond angles are listed in Fig. 1 where also the numbering of the atoms is indicated. The lengths of corresponding bonds are equal, the maximum deviations being 0.002 \AA between $N1-C7$ and $N2-C8$, and between $C3-O1$ and $C6-O2$. On the other hand, there are significant differences in corresponding bond angles. The $C4-C5-C6$ and $N2-N1-C6$ angles are opened by about 1.3° compared with, respectively, the $C5-C4-C3$ and $N1-N2-C6$ angles. These angular differences are probably coupled to the differences in the torsional angles around the $N2-C3$ and $N1-C6$ bonds and the $C3-C4$ and $C5-C6$ bonds. (Torsional angles are listed in Table 2). The

Table 2. Selected torsional angles ($^{\circ}$), the angles are positive in a right-hand screw.

Angle	($^{\circ}$)	Angle	($^{\circ}$)
C6-N1-N2-C3	-29.73(9)	C3-C4-C5-C6	-64.07(7)
N1-N2-C3-C4	-0.49(9)	C5-C6-N1-N2	7.80(8)
C8-N2-C3-C4	-162.07(6)	C5-C6-N1-C7	-159.36(7)
N2-C3-C4-C5	45.71(7)	C4-C5-C6-N1	38.31(7)
O1-C3-C4-C5	-130.35(7)	C4-C5-C6-O2	-137.71(7)
C7-N1-N2-C3	138.12(7)	C6-N1-N2-C8	132.98(6)
N1-N2-C3-O1	175.68(6)	O2-C6-N1-N2	-176.06(7)

corresponding torsional angles N1-N2-C3-C4 and C5-C6-N1-N2, and the angles N2-C3-C4-C5 and C4-C5-C6-N1 differ by about 7.3° . The molecule has a "twisted boat" conformation with roughly C_2 symmetry, the twofold axis passing through the midpoints of the N1-N2, and C4-C5 bonds, in agreement with the conformation found for hexahydro-3,6-pyridazinedione^{3,4} (a view of HDMP as seen along the twofold axis is given in Fig. 1c).

A comparison of the lengths found for the C-O and C-N bonds in HDMP and hexahydro-3,6-pyridazinedione clearly shows the effect of hydrogen bonding on the conjugation over the N-C=O fragment. The formation of the one N-H...O hydrogen bond found in hexahydro-3,6-pyridazinedione⁴ leads to a shortened C-N bond [1.346(1) Å] and a lengthened C-O bond [1.245(1) Å]. Taking into consideration the lengthening of about 0.005 Å of the C-O bond induced by introducing a methyl group at the nitrogen atom (see Ref. 1 for a discussion of this), the formation of one N-H...O bond leads to a lengthening of the C-O bond by about 0.019 Å and a shortening of the C-N bond by about 0.020 Å. These values are in good agreement with those found for the unreduced 3,6-pyridazinediones,¹ (0.015 Å and 0.025 Å, respectively). However, both for these unreduced compounds and for the simple amides,¹ which have two N-H...O bonds, the results obtained imply that the shortening of the C-N bond is significantly larger than the corresponding lengthening of the C-O bond. Theoretical calculations (see Ref. 1 for a review) have shown that the increased conjugation over the N-C=O fragment induced by hydrogen bonding is caused by a transfer of σ -electronic charge from the oxygen to the nitrogen atom

via the hydrogen bond which is counteracted by a greater participation of the nitrogen lone pair in the conjugated system. This greater participation of the nitrogen lone pair affects the whole ring system in the semiaromatic 3,6-pyridazinediones whereas in the hexahydro-3,6-pyridazinediones the effect is mainly found in the N-C=O fragments. This difference in the two systems may be a reason for the difference in the effect on the N-C and C-O bonds, although more data is clearly necessary on the reduced system.

The loss of hydrogen bonding in HDMP compared with hexahydro-3,6-pyridazinedione,⁴ i.e. the reduced conjugation over the N-C=O fragments, leads to some changes in the molecule. The N-N bond is lengthened from 1.398(1) to 1.406(1) Å, and the torsional angle C3-N2-N1-C6 has increased from $25.6(2)^{\circ}$ in hexahydro-3,6-pyridazinedione to $29.73(9)^{\circ}$ in HDMP. An increase is also found in the C6-C5-C4-C3 angle from $56.3(2)$ to $64.07(7)^{\circ}$. The configurations around C3, C6 and around the nitrogen atoms are also affected by the decrease in conjugation, the C3 and C6 atoms

Table 3. Deviations from least-squares planes ($\text{\AA} \times 10^3$). The deviations for those atoms used to define a plane are given in italicized numbers.

Atom	Plane A	Atom	Plane B
O1	6	O2	6
N2	6	N1	6
C3	-21	C6	-21
C4	6	C5	6
C5	1 093	C4	951
N1	65	N2	108
C7	-782	C8	1 051

are found 0.027 Å out of the plane through, respectively, O1, N2 and C4, and O2, N1 and C5 (see Table 3), whereas this value is only 0.005 Å in hexahydro-3,6-pyridazinedione. The results also show much less planarity around the nitrogen atoms in HDMP than in hexahydro-3,6-pyridazinedione implying a larger degree of sp^3 -hybridization of the nitrogens.

All *intra*-ring bond angles in HDMP have decreased compared with those found for hexahydro-3,6-pyridazinedione, the changes vary from 0.25° (N1–C6–C5) to 3.1° (C3–C4–C5). The largest angular differences are found in the *exo*-cyclic angles around the nitrogen atoms, in hexahydro-3,6-pyridazinedione the N–N–H1 angle is 125(4)° and the C–N–H1 angle is 113(4)°, whereas in HDMP the angles N1–N2–C8 and N2–N1–C7 are 115.98(6) and 115.29(5)°, respectively and the C3–N2–C8 and C6–N1–C7 are 121.75(6) and 121.60(6)°. These differences may be caused by the involvement of H1 in the hydrogen bond.

The shortest intermolecular contacts are of normal van der Waals lengths.

REFERENCES

- Ottersen, T. *Adv. Mol. Relaxation Processes* 9 (1976) 105.
- Ottersen, T. *Acta Chem. Scand. A* 29 (1975) 690.
- Ottersen, T. *Acta Chem. Scand. A* 29 (1975) 939.
- Ottersen, T. and Almlöf, J. *Acta Chem. Scand. A. In press.*
- Kitano, M. and Kuchitsu, K. *Bull. Chem. Soc. Jpn.* 46 (1973) 3048.
- Kitano, M., Fukuyama, T. and Kuchitsu, K. *Bull. Chem. Soc. Jpn.* 46 (1973) 348.
- Kitano, M. and Kuchitsu, K. *Bull. Chem. Soc. Jpn.* 47 (1974) 67.
- Kitano, M. and Kuchitsu, K. *Bull. Chem. Soc. Jpn.* 47 (1974) 631.
- Eichenberger, K., Staehelin, A. and Druey, J. *Helv. Chim. Acta* 37 (1954) 837.
- Feuer, H., Bachman, G. B. and White, E. M. *J. Am. Chem. Soc.* 73 (1951) 4716.
- Groth, P. *Acta Chem. Scand.* 27 (1973) 1837.
- Doyle, P. A. and Turner, P. S. *Acta Crystallogr. A* 24 (1968) 390.
- Stewart, R. F., Davidson, E. R. and Simpson, W. T. *J. Chem. Phys.* 42 (1965) 3175.
- Germain, G., Main, P. and Woolfson, M. M. *Acta Crystallogr. A* 27 (1971) 368.
- Stevens, E. D. and Hope, H. *Acta Crystallogr. A* 31 (1975) 494.
- Hope, H. and Ottersen, T. *To be published.*
- Ottersen, T. and Hope, H. *To be published.*
- Shoemaker, V. and Trueblood, K. N. *Acta Crystallogr. B* 24 (1968) 63.

Received June 21, 1977.

The Position of 2,2'-Bipyridine and 1,10-Phenanthroline in the Spectrochemical Series

JENS JOSEPHSEN * and CLAUD ERIK SCHÄFFER

Department I, Inorganic Chemistry, H. C. Ørsted Institute, University of Copenhagen, Universitetsparken 5, DK-2100 Copenhagen Ø, Denmark

Dedicated to Professor K. A. Jensen on his 70th birthday

New mixed-ligand complex ions $[M(\text{III})-(\text{NH}_3)_{6-2a}(\text{N-N})_a]^{3+}$ ($M = \text{Cr}$ and Co ; $(\text{N-N}) = \text{bipy}$ and phen ; $a = 1$ and 2) have been prepared in mixtures, separated chromatographically and isolated as perchlorates. Comparative ligand field spectral studies (within the expanded radial function model) of these complexes and of relevant $\text{Ni}(\text{II})$ complexes reported in the literature reveal, in consensus with literature, that the heteroaromatic ligands (N-N) lie above the amines in the spectrochemical series when the central ions are $\text{Co}(\text{III})$ and $\text{Ni}(\text{II})$. However, contrary to literature conclusions, the opposite relationship is found for $\text{Cr}(\text{III})$. Certain irregularities found between the spectra of corresponding $\text{Cr}(\text{III})$ and $\text{Co}(\text{III})$ complexes invite the conclusion that the cyanide ion as a ligand gives rise to pronouncedly more π -back-bonding when bound to $\text{Co}(\text{III})$ than when bound to $\text{Cr}(\text{III})$, and the same is found to be true for the (N-N) -ligands, but to a much lesser extent. From $\text{tris}(\text{N-N})\text{Ni}(\text{II})$ complexes it appears that the (N-N) -ligands lie below ammonia in the nephelauxetic series, and they lie below ethylenediamine in the hyperchromic series when the central ions are $\text{Cr}(\text{III})$ or $\text{Co}(\text{III})$.

Various consequences of the approximately Gaussian shape of absorption bands are discussed and the empirical average environment rule is shown for $A_i \rightarrow T_j$ transitions (i and j independently taking on the values 1 or 2) of cubic complexes with small low-symmetry perturbations to be derivable under the assumptions about a pure cubic parentage of the excited level and about equal heights and widths of band components.

I. INTRODUCTION

The spectrochemical series¹ of ligands was originally purely empirical and listed the ligands X^{z-} in the order of increasing energy of the so-called first absorption band of $[\text{Co}(\text{NH}_3)_6X]^{(3-z)+}$ complexes. This band situated at about $20\,000\text{ cm}^{-1}$ was later assigned^{2,3} as the transition ${}^1A_{1g}(O_h) \rightarrow {}^1T_{1g}(O_h)$. The same series was obtained analogously on the basis of other complexes⁴ such as $[\text{Co en}_2 X_2]^{(2-z)+}$.

The experimental results⁵ further showed that the molar absorptivities ϵ_{max} for both the first and the second absorption band varied with X^{z-} even much more than did the energies.

This variation was the same for the above two types of complexes and on this basis a so-called *hyperchromic series*⁵ was established.

When ligand field theory began to be used for the interpretation of absorption spectra, the expanded radial function model* was applied to these complexes, and it became clear that the spectrochemical series could be interpreted³ as a series of increasing values of this model's empirical parameter Δ defined by

$$\Delta = h[\epsilon_g(O_h)] - h[\epsilon_{2g}(O_h)] \quad (1)$$

when referring to regularly octahedral complexes. Δ was at the time³ often called $10Dq$. When Δ is given a sub-index X^{z-} , $\Delta_{X^{z-}}$ refers

* The expanded radial function model⁶ is a symmetry-based semi-empirical model which takes empirical parameters for the ligand field as well as for the interelectronic repulsion.

* On leave from Roskilde University, P.O. Box 260, DK-4000 Roskilde, Denmark.

to the $[\text{CoX}_6]^{(3-6x)+}$ complex. $h[\gamma(O_k)]$ of eqn. 1 is the one-electron energy of the expanded radial function model associated with the d orbital spanning the irreducible representation γ of the octahedral group O_h . This interpretation of the spectrochemical series in terms of the empirical parameter Δ made it possible to study the series also for other metal ions and such studies soon led to the discovery⁷ that the series of ligands was essentially the same for all central ions for which it could be studied.

The spectrochemical properties of the ligands 2,2'-bipyridine (bipy) and 1,10-phenanthroline (phen) are only known⁸ with certainty for nickel(II) as the central ion. In this case the heteroaromatic ligands both lie *ca.* 12 % above ammonia and *ca.* 5 % above ethylenediamine in the Δ -series, their relative position being a little uncertain as further discussed in section V in connection with Table 3. When bound to cobalt(III) in tris-complexes bipy and phen are also above ammonia and ethylenediamine in the spectrochemical series⁹⁻¹¹ as will be discussed in the present paper, but for chromium(III) there is a lack of agreement on this point. Some authors¹² have assigned shoulders at 22 000 and 23 000 cm^{-1} in the complexes $[\text{Cr bipy}_3]^{3+}$ and $[\text{Cr phen}_3]^{3+}$, respectively, as the ${}^4A_{2g} \rightarrow {}^4T_{2g}(O_h)$ transition whose energy is a direct measure of Δ . Other authors¹³ concluded that Δ for $[\text{Cr bipy}_3]^{3+}$ is 23400 cm^{-1} and the present authors¹⁴ gave some indication based upon the spectra of di- μ -hydroxo complexes that both these ligands have Δ -values which are smaller than or comparable to that of ethylenediamine.

The purpose of the present paper is to further elucidate this problem. New mixed-ligand chromium(III) and cobalt(III) complexes containing ammonia and bipy or phen (the latter two ligands being designated in the following by the common symbol N-N) have been prepared and their spectra studied to provide quantitative information concerning the Δ values for these heteroaromatic ligands and thereby their positions in the spectrochemical series for chromium(III) and cobalt(III).

II. ATTEMPTS AT A CHEMICAL INTERPRETATION OF Δ

It was early realized¹⁵ that the symmetry properties of the d -orbitals might give some

understanding of the physical background for the ligand field parameter Δ of eqn. (1). Thus the e_g orbitals are able to form σ -bonds (but not π -bonds) with the ligands and the t_{2g} orbitals can form π -bonds (but not σ -bonds). In molecular orbital language Δ for most ligands could then be interpreted as the difference between a σ -antibonding and a π -antibonding action from the filled ligand orbitals on the d orbitals as expressed by the equation

$$\Delta = \Delta\sigma - \Delta\pi \quad (2)$$

For special ligands,¹⁶ the so-called π -acceptor ligands, with low lying empty or only partially filled orbitals, a π -bonding action could also be present and this could then give a positive contribution to the value of Δ . These considerations are generalized in the semi-empirical angular overlap model,^{17,18} which may be considered a zeroth order molecular orbital model.

With the interpretation of Δ expressed in eqn. (2) the fact that the spectrochemical series hardly depends on the central ion⁷ is perhaps acceptable for ligands without π -acceptor properties and it is also acceptable that Δ increases with the oxidation state of the metal ion, as illustrated by the following d^3 examples:¹⁹⁻²¹

$$\Delta([\text{MnF}_6]^{3-})/\Delta([\text{CrF}_6]^{3-}) = 21\,800/15\,200 = 1.43 \quad (3)$$

$$\Delta([\text{Cr}(\text{H}_2\text{O})_6]^{3+})/\Delta([\text{V}(\text{H}_2\text{O})_6]^{3+}) = 17\,400/12\,400 = 1.40$$

But for π -acceptor ligands the lower oxidation state would have to obtain the larger positive contribution to Δ from π -back donation (*i.e.* charge transfer from the central ion to the ligand), and therefore for such ligands irregularities in the spectrochemical series would be expected to occur at least when metal ions with the same electron configuration but different oxidation states were compared. Actually the fact that the d^5 system $[\text{Mn}(\text{CN})_6]^{3-}$ is colourless and thus has no ligand field bands in the visible region was early taken as evidence²² that the ligand CN^- which potentially belongs to the π -acceptor class also effectively does so.

The reasoning can be represented as follows. From eqn. (3) it is seen that Δ is reduced by

a factor of approximately 1.4 as the oxidation state is reduced from 4 to 3 and from 3 to 2. If one assumes the same factor of reduction on going from oxidation state 2 to 1 and if one further assumes that the same factor applies to the ratios between the wave numbers σ_1 of the first spin-allowed absorption band ${}^1A_{1g} \rightarrow {}^1T_{1g}(O_h)$ of d^8 systems (cf Table 1) then it is possible on the basis of σ_1 for $[\text{Co}(\text{CN})_6]^{3-}$ ($32\,200\text{ cm}^{-1}$) to predict a value of $16\,000\text{ cm}^{-1}$ for $[\text{Mn}(\text{CN})_6]^{5-}$. The lack of colour of this complex, however, places a lower limit of $26\,000\text{ cm}^{-1}$ on the experimental quantity σ_1 , and the conclusion is that considerable π -back-bonding has taken place.

Ligand field data are scarce for π -acceptor ligands, particularly for low oxidation states of the central ion, since these often have their ligand field bands covered^{10,11} by backward electron transfer bands, e.g. $[\text{Fe phen}_3]^{2+}$. Recently, however, some ligand field data for chromium(III) pyridine complexes could be interpreted using a net negative angular overlap model π -parameter²³ corresponding to weak net backward π -bonding in exactly the sense that we have discussed here.

It is interesting in this context to compare (Table 1) data for d^3 and low-spin d^6 systems, the latter of which belongs to the class of

complexes which obeys the so-called noble gas rule by having the number of σ -donated electrons and the number of metal electrons adding up to the number of electrons of krypton. It is seen from Table 1 that the ratio $\Delta(\text{Co})/\Delta(\text{Cr})$ is fairly constant for the ligands without π -acceptor character while the Δ value for CN^- is relatively much higher for the d^6 system. This is a piece of ligand field theoretical evidence for the amusing fact that the noble gas rule, which in its formulation is only concerned with σ -electrons from the ligands, has energetic consequences only when these same ligands are also π -acceptors.

It is always tempting to try to assess how far such chemical reasoning about parameters of physical models makes sense.

In the present case one might reason as follows. Δ is not as fundamental a parameter as its constituents $\Delta\sigma$ and $\Delta\pi$ of eqn. (2). Therefore the fact that $\Delta(\text{Co})/\Delta(\text{Cr})$ is a constant for ligands with vanishing or small and positive $\Delta\pi$ parameter values²³ makes it likely that the following relation is approximately valid for these ligands:

$$\frac{\Delta(\text{Co})}{\Delta(\text{Cr})} = \frac{\Delta\sigma(\text{Co})}{\Delta\sigma(\text{Cr})} = \frac{\Delta\pi(\text{Co})}{\Delta\pi(\text{Cr})} \cong 1.05; C = 4B \quad (4)$$

Table 1. Values of the wavenumbers²³ (in kK units) of the maxima of the first spin-allowed absorption bands for some octahedral chromium(III) complexes [assignment: ${}^4A_{2g} \rightarrow {}^4T_{2g}(O_h)$] and cobalt(III) complexes [assignment: ${}^1A_{1g} \rightarrow {}^1T_{1g}(O_h)$]. For chromium(III) this wavenumber is a direct measure of Δ , eqn. (1), while for cobalt(III) a correction has to be made. Knowing the position also of the maximum of the second spin-allowed absorption band, ${}^1A_{1g} \rightarrow {}^1T_{2g}(O_h)$, and the ratio between the Racah parameters C and B , this correction can be calculated using the d^6 energy matrices of the expanded radial function model, given by Tanabe and Sugano.²⁴ The ratio mentioned is not known but is likely to lie in the region between 4 and 5.5. The table clearly shows that even though the numerical value of Δ does depend on the choice of the ratio C/B neither the spectrochemical series nor the trend of energy ratios between corresponding cobalt and chromium quantities (the last three rows of the table) are influenced by this choice. It is remarkable that the semi-theoretical ratios of the last two rows are no better than the purely empirical ratio between the wavenumbers, given in the third from last row. The value 21.10 kK for $\sigma_1([\text{Co}(\text{NH}_3)_6]^{3+})$ used in connection with eqn. (8) was measured here using the same instrument as that used for the other cobalt complexes.

$X^{3-} =$	H_2O	$\text{C}_2\text{O}_4^{2-}$	NH_3	en	CN^-
$\sigma_1([\text{CrX}_6]^{3-x})$	17.40	17.48	21.50	21.90	26.60
$\sigma_1([\text{CoX}_6]^{3-x})$	16.50	16.60	21.20	21.55	32.00
$\Delta([\text{CoX}_6]^{3-x}); C = 4B$	18.16	18.02	22.87	23.17	33.45
$\Delta([\text{CoX}_6]^{3-x}); C = 5.5B$	18.76	18.54	23.48	23.75	33.98
$\sigma_1([\text{CoX}_6]^{3-x})/\sigma_1([\text{CrX}_6]^{3-x})$	0.95	0.95	0.97	0.98	1.20
$\Delta([\text{CoX}_6]^{3-x})/\Delta([\text{CrX}_6]^{3-x}); C = 4B$	1.04	1.03	1.06	1.06	1.26
$\Delta([\text{CoX}_6]^{3-x})/\Delta([\text{CrX}_6]^{3-x}); C = 5.5B$	1.08	1.06	1.09	1.08	1.28

The value 1.05 (Table 1) of eqn. (4) is a lower limit for the ratio $\Delta\sigma_{\text{CN}-(\text{Co})}/\Delta\sigma_{\text{CN}-(\text{Cr})}$, since the extra π -stabilization in $[\text{Co}(\text{CN})_6]^{3-}$ as a secondary effect would increase $\Delta\sigma_{\text{CN}-(\text{Co})}$ relative to $\Delta\sigma_{\text{CN}-(\text{Cr})}$. If, however, one assumes $\Delta\sigma_{\text{CN}-(\text{Co})}/\Delta\sigma_{\text{CN}-(\text{Cr})} = 1.05$ the quantity $\delta_{\pi\text{CN}^-} = \Delta\pi_{\text{CN}-(\text{Co})} - \Delta\pi_{\text{CN}-(\text{Cr})}$ can be estimated. If $\Delta\pi_{\text{CN}-(\text{Cr})}$ is known $\delta_{\pi\text{CN}^-}$ can within the assumptions be calculated exactly, but it turns out that $\delta_{\pi\text{CN}^-}$ varies very little with $\Delta\pi_{\text{CN}-(\text{Cr})}$. For example, for $\Delta\pi_{\text{CN}-(\text{Cr})} = 0$ and $\Delta\pi_{\text{CN}-(\text{Cr})} = -4$ values for $\delta_{\pi\text{CN}^-}$ of -5.5 and -5.7 kK are found, respectively. It further turns out that these $\delta_{\pi\text{CN}^-}$ values are lower limits (*i.e.* upper limits for the absolute values) when 1.05 is a lower limit to $\Delta\sigma_{\text{CN}-(\text{Co})}/\Delta\sigma_{\text{CN}-(\text{Cr})}$. In conclusion the difference 6.9 kK between the Δ values referring to $[\text{Co}(\text{CN})_6]^{3-}$ and $[\text{Cr}(\text{CN})_6]^{3-}$ can then be interpreted as due to differences in $\Delta\sigma$ and $\Delta\pi$ values of $\delta_{\pi\text{CN}^-} = 1.3$ kK and $\delta_{\pi\text{CN}^-} = -5.6$ kK, where both numbers represent lower limits.

III. THE AVERAGE ENVIRONMENT RULE AND GAUSSIAN SHAPE OF ABSORPTION BANDS

In the introduction it was mentioned that the spectrochemical series originally was established¹ for $[\text{Co}(\text{NH}_3)_6\text{X}]^{(3-x)+}$ -type complexes and later rationalized² using the expanded radial function model by reference to cubic complexes of $[\text{CoX}_6]^{(3-6x)+}$ -type.

Although historically it did not happen so straight-forwardly one may say to-day that this interrelation of spectra for quite different molecules which could never have been theoretically predicted to be possible, was based upon the approximate validity of the empirical rule²⁴ called the Average Environment Rule.

This rule may be formulated as follows: a given broad absorption band for a mixed-ligand complex $[\text{MX}_a\text{Y}_b]^{(n-ax-by)+}$ (with $a+b=6$), based upon the octahedron, n being the oxidation state of the central ion M, has a maximum position whose wave-number σ is given by

$$\sigma([\text{MX}_a\text{Y}_b]^{(n-ax-by)+}) = (\alpha/6)\sigma([\text{MX}_6]^{(n-6x)+}) + (b/6)\sigma([\text{MY}_6]^{(n-6y)+}) \quad (5)$$

or, in other words, is a weighted average of the maxima for the cubic complexes $[\text{MX}_6]^{(n-6x)+}$ and $[\text{MY}_6]^{(n-6y)+}$.

The absorption bands, for which the empirical average environment rule was established, always arise from transitions from orbitally non-degenerate ground levels to excited levels which in octahedral symmetry are orbitally triply degenerate. For the lower symmetry complex there is no longer the symmetry requirement that the three components be degenerate and the average environment rule therefore somehow implies that the observed curve can be considered a sum of the components. This is the basic idea behind curve analysis procedures. Particularly for chromium-(III) and cobalt(III) complexes the band shape can often be represented approximately by Gaussian error curves using the wavelength λ as the independent²⁵ variable. This gives the functional expression

$$\varepsilon = \varepsilon_0 \times \exp - [(\lambda - \lambda_0)/(\delta/2(\ln 2)^{1/2})]^2 \quad (6)$$

where the maximum is at $(\lambda_0, \varepsilon_0)$ and δ is the full half width of the band.

It is useful for the qualitative interpretation of absorption spectra to note a few of the properties^{26,27} of a sum of two Gaussians. Firstly, Gaussians with the same positions and half widths add up to a Gaussian with the same values of these parameters and with a height which is the sum of the heights of the components. Secondly, two Gaussians with the same height and the same half width δ can be removed²⁶ as far as $\delta/(2 \ln 2)^{1/2} = 0.85 \delta$ away from each other before their sum curve exhibits a minimum. Thirdly, this separation requirement increases when the heights of the component Gaussians are different. When, for example, the height ratio is 2:1 for two Gaussians of the same widths a minimum does not occur between them until their separation is about 1.15 δ , at a separation of 0.85 δ a shoulder just becomes visible and at a separation of 0.5 δ the sum curve looks to the eye completely symmetrical. Fourthly, when a narrow Gaussian is added to a broad one the narrow one makes itself the more conspicuous of them, even when it has a low intensity. This latter point is illustrated in Fig. 1 which shows analyses of the red tail of the absorption spectra of $[\text{Cr}(\text{NH}_3)_4(\text{N-N})]^{3+}$ complexes. The foot from the ultraviolet has been represented by an exponential function which for practical purposes is very similar to the lower part of

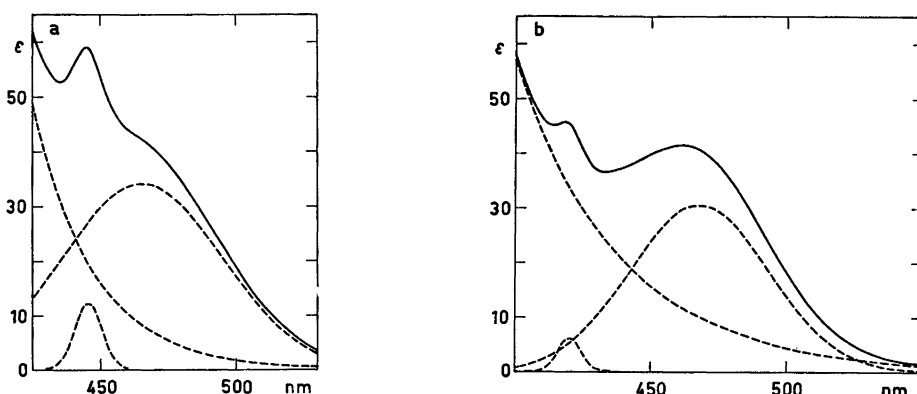


Fig. 1. The red feet of the absorption spectra of $[\text{Cr}(\text{NH}_3)_4\text{bipy}]^{3+}$ (a) and $[\text{Cr}(\text{NH}_3)_4\text{phen}]^{3+}$ (b), (full lines). Each experimental curve was represented by a set of points (λ, ϵ) which was analyzed by non-linear regression modelling it as a sum (broken lines) of two Gaussians of the form

$$\epsilon_0 \times \exp - [(\lambda - \lambda_0)/(\delta/2(\ln 2)^{1/2})]^2 \text{ and one exponential of the form } h \times \exp - [(\lambda - \lambda_t)/(\delta/2(\ln 2)^{1/2})]$$

the latter function in order to account for the absorption toward the ultraviolet. λ_t is the lowest λ value of the (λ, ϵ) set chosen. The value λ_0 belonging to the broader Gaussian associated with each set refers to the ${}^4A_{2g} \rightarrow {}^4T_{2g}(O_h)$ transition and has in nanometers the values 465.5 ± 2.2 and 467.8 ± 0.2 for the two complexes, respectively, but the standard deviations should be taken *cum grano salis* because the experimental curve is rather badly represented by the model.

a Gaussian. It is noteworthy that even though the ratio between the areas of the large and the small Gaussians is 16 and 30 for the bipy and phen complexes, respectively, the small bands are quite conspicuous. This is because in each case the small band is quite narrow, its width being about 1/6 of that of its broad neighbour.

The qualitative assumption involved here is that an absorption curve can be considered a sum of its electronic components, each one independently provided with width, and the further assumption that these individual components have an approximately Gaussian shape. All the qualitative conclusions which can be drawn on the basis of these assumptions are, apparently without exception, borne out by experiments.

We note the approximate expression for the position of the maximum of the sum curve of ν Gaussians of equal half width and at small separations

$$\nu_0 = \frac{\sum \nu_i \epsilon_i}{\sum \epsilon_i} \quad (7)$$

ν_0 is here the wave number position of the maximum of the sum curve whose components'

maxima are given by the coordinates (ν_i, ϵ_i) . This expression will be referred to in the following.

IV. RESULTS

1. Cobalt(III) complexes. The position of bipy and phen in the spectrochemical series above ethylenediamine has been considered clear^{10,11} for some time for cobalt(III) complexes. Particularly in the case of bipy $[\text{Co}(\text{bipy})_3]^{3+}$ exhibits a rather well-isolated (Fig. 2) band $(\lambda_{\text{max}}, \epsilon_{\text{max}}) = (449, 69.5)$, assigned as ${}^1A_{1g} \rightarrow {}^1T_{1g}(O_h)$, to be compared with the figures (465, 84) for $[\text{Co}(\text{en})_3]^{3+}$. However, the $[\text{Co}(\text{phen})_3]^{3+}$ complex in this region only exhibits a shoulder on a steep rise in absorption toward the ultraviolet (Fig. 2). For both complexes it is true that intense absorption lies quite near these presumed ligand field bands but recalling the situation with $[\text{Co}(\text{NO}_2)_6]^{3-}$, one has to be careful. This ion has $(\lambda_{\text{max}}, \epsilon_{\text{max}}) = (484, 219)$ in this region,²⁸ *i.e.* its maximum is considerably red-shifted relative to that of $[\text{Co}(\text{en})_3]^{3+}$, even though mixed

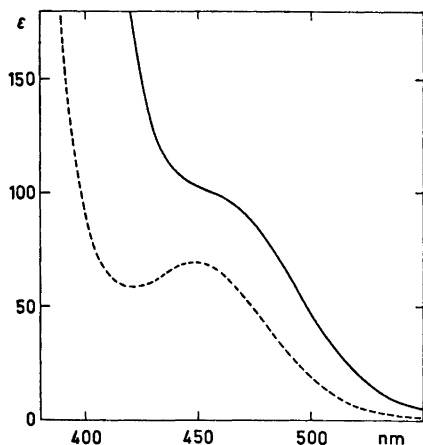


Fig. 2. Visible absorption spectra of $[\text{Co}(\text{N-N})_3]^{3+}$ complexes. Part of the spectra (λ, ϵ) were analyzed as described in the legend to Fig. 1, here modelling the (λ, ϵ) set as a sum of one Gaussian and one exponential, the latter referring to the ${}^1A_{1g} \rightarrow {}^1T_{1g}(O_h)$ transition.

... N-N=bipy. Analyzing the spectrum in the interval $400 \leq \lambda \leq 530$ nm gave (λ_0, ϵ_0) = $(450.9 \pm 0.3, 67.0 \pm 0.2)$. — N-N=phen. Here the analysis was done in two λ -intervals, $425 \leq \lambda \leq 550$ nm and $425 \leq \lambda \leq 535$ nm giving the results for the Gaussians (λ_0, ϵ_0) = $(457.9 \pm 1.3, 92.4 \pm 1.8)$ and $(459.6 \pm 0.9, 90.5 \pm 1.4)$, respectively. The mean of these two λ_0 -values, 459.0 ± 0.7 nm, was used to compare with the results calculated on the basis of the mixed complexes (eqn. 8).

complexes containing NO_2^- together with ethylenediamine and ammonia, by the average environment rule, clearly place the nitro ligand above ethylenediamine in the spectro-

chemical series. This unusual red-shift found²⁸ in $[\text{Co}(\text{NO}_2)_6]^{3-}$ could of course be caused by the chemistry, *i.e.* $[\text{Co}(\text{NO}_2)_6]^{3-}$ not being present in the solution measured, or some of the NO_2^- ligands being coordinated through oxygen. However, we are not aware of any additional evidence for this and we find it a much more likely explanation that the d^8 level ${}^1T_{1g}$ has been mixed with electron transfer levels or excited levels of the ligands, both of which mechanisms would have to shift the lower energy mixed level toward lower energy. A mechanism of a similar kind might well be at work also in $[\text{Co}(\text{bipy})_3]^{3+}$ and $[\text{Co}(\text{phen})_3]^{3+}$ in which case the wavenumber position of the pure ligand field transition, ${}^1A_{1g} \rightarrow {}^1T_{1g}(O_h)$, might have been underestimated.

In order to clear up such uncertainties as to the spectrochemical parameters for bipy and phen the spectra of mixed complexes of the type $[\text{Co}(\text{NH}_3)_{6-2a}(\text{N-N})_a]^{3+}$ have been measured in this region. The results are given in Table 2.

All the spectra resemble that of $[\text{Co}(\text{bipy})_3]^{3+}$ of Fig. 2. However, the band in the 455 nm region is in all cases better isolated because the steep rise in absorption moves toward the ultraviolet as the number of ammonia molecules increases within the complex ions. This can clearly be seen from the positions and absorptivities of the minima given in Table 2.

Introducing the known quantity $\sigma_1([\text{Co}(\text{NH}_3)_6]^{3+}) = 21\,100 \text{ cm}^{-1}$ and using the average environment rule on the mixed complexes, one obtains for each individual (N-N)-ligand two linear equations to determine the quantity $\sigma_1([\text{Co}(\text{N-N})_a]^{3+})$. For example, for $[\text{Co}(\text{NH}_3)_4(\text{bipy})_2]^{3+}$ the equation is

Table 2. Spectral data for $[\text{Co}(\text{NH}_3)_{6-2a}(\text{N-N})_a]^{3+}$ complexes. σ_1 is the wavenumber of the maximum of the ${}^1A_{1g} \rightarrow {}^1T_{1g}(O_h)$ transition, σ_{min} that of the minimum before the rise in absorption toward the UV. See fig. 2. The ϵ quantities are the corresponding molar absorptivities.

	σ_1	ϵ_1	σ_{min}	ϵ_{min}
$[\text{Co}(\text{bipy})_3]^{3+}$	22 270	69.5	23 750	58.5
$[\text{Co}(\text{NH}_3)_4(\text{bipy})_2]^{3+}$	21 880	68.0	25 130	20.0
$[\text{Co}(\text{NH}_3)_5(\text{bipy})]^{3+}$	21 440	62.5	25 510	9.5
$[\text{Co}(\text{NH}_3)_4(\text{phen})_2]^{3+}$	21 670	72.5	24 180	37.5
$[\text{Co}(\text{NH}_3)_5(\text{phen})]^{3+}$	21 340	61.5	25 160	12.0

$$\sigma_1([\text{Co}(\text{NH}_3)_4\text{bipy}]^{3+}) = \frac{2}{3} \times 21\,100 + \frac{1}{3} \sigma_1([\text{Co bipy}_3]^{3+})$$

corresponding to eqn. (5). Weighting the two equations equally the data from the four last rows of Table 2 give the calculated quantities σ

$$\begin{aligned} \sigma_1([\text{Co bipy}_3]^{3+}) &= 22\,200 \pm 100 \quad \text{and} \\ \sigma_1([\text{Co phen}_3]^{3+}) &= 21\,890 \pm 100 \end{aligned} \quad (8)$$

to be compared with the quantities $22\,180 \pm 20$ and $21\,790 \pm 40$ obtained from Gaussian analyses of the spectra of the *tris*-complexes themselves (see text to Fig. 2).

The mixed complexes under consideration all have the symmetry C_2 so that one would predict from symmetry that the band of cubic parentage ${}^1A_{1g} \rightarrow {}^1T_{1g}(O_h)$ would split into three components. Obviously these components lie close to one another as compared with their half-widths and this is the reason why no splitting is observed (*cf.* Section III). It is interesting to note that the assumptions that the levels have a pure cubic parentage²⁰ and that the components can be represented by Gaussians with the same heights and widths lead to results (eqn. 7) identical to those obtained using the empirical average environment rule (eqn. 5). It is for our present complexes, because of the small splittings, immaterial whether we assume Gaussians as a function of wavenumber or as a function of wavelength.

It should be stressed that the fact that the empirical average environment rule apparently works so well does not allow the conclusion that these assumptions about components are meaningful. On the other hand, it does make such concepts as hidden components and additivity of these attractive until it is actually proved that they are misleading.

2. Chromium(III) complexes. For the *tris*-(N-N)chromium(III) complexes a steep absorption toward the ultraviolet presents problems which from an interpretation point of view are similar to those for cobalt(III), though, in a quantitative sense, they are the more serious for chromium and from a physical point of view probably of a quite different origin.

Also here the spectra of the mixed ammonia-(N-N) complexes have been studied and are depicted and described in Figs. 3 and 1.

In the spectrum of the complex $[\text{Cr}(\text{NH}_3)_4\text{phen}]^{3+}$ (Fig. 3) there is a narrow peak at 420 nm, which, when looked at from a component additivity point of view (Fig. 1), is far too narrow to be assigned as the first spin-allowed ligand field band ${}^4A_{2g} \rightarrow {}^4T_{2g}$ that we are looking for. Even though its position does not exclude the alternative assignment ${}^4A_{2g} \rightarrow {}^2T_{2g}$ we believe that its intensity is too high for this assignment in view of the fact that it lies too far away from the spin-allowed transitions which, as we shall see below, are expected to lie quite close to those of the $[\text{Cr}(\text{NH}_3)_6]^{3+}$ complex which has $\lambda_{\text{max}}({}^4A_{2g} \rightarrow {}^4T_{2g}) = 465$ nm and $\lambda_{\text{max}}({}^4A_{2g} \rightarrow {}^2T_{1g}) = 351$ nm. Further, the narrow band under discussion appears to have analogs with a successively enhanced intensity in the complexes $[\text{Cr}(\text{NH}_3)_2\text{phen}_2]^{3+}$ and $[\text{Cr phen}_3]^{3+}$. Its analog at 425 nm in $[\text{Cr phen}_3]^{3+}$ was previously assigned¹² as the ${}^4A_{2g} \rightarrow {}^4T_{2g}$ ligand field band, but our present evidence is that this band is completely covered in the $[\text{Cr phen}_3]^{3+}$ complex. A quite nicely separated maximum at 462 nm in the spectrum of the $[\text{Cr}(\text{NH}_3)_4\text{phen}]^{3+}$ complex and a shoulder in that of $[\text{Cr}(\text{NH}_3)_2\text{phen}_2]^{3+}$ are associated by us with the ligand field assignment ${}^4A_{2g} \rightarrow {}^4T_{2g}$ which is consistent not only with their widths but also reasonably well with their molar absorptivities.

From our own previous work²⁰ it is known that bipy and phen lie close to one another in the hyperchromic series mentioned in section I both being pronouncedly below ethylenediamine. As an example of this one may mention that the ϵ_{max} values for the *cis*-complexes $[\text{Cr en}_2\text{F}_2]^{3+}$, $[\text{Cr bipy}_2\text{F}_2]^{3+}$, $[\text{Cr phen}_2\text{F}_2]^{3+}$ and $[\text{Cr}(\text{NH}_3)_4\text{F}_2]^{3+}$ are 75, 49, 47, and 42, respectively. Recalling that ϵ_{max} for $[\text{Cr}(\text{NH}_3)_6]^{3+}$ is 40 one immediately sees that the assignment of the first maximum of $[\text{Cr}(\text{NH}_3)_4\text{phen}]^{3+}$ is quite reasonable from a molar absorptivity point of view although the Gaussian analyses would place them below ammonia hyperchromically.

This intensity point of view gives us also the clue to the chromium(III) bipyridine systems. Here the steep rise in absorption toward the ultraviolet is even more serious and even in the $[\text{Cr}(\text{NH}_3)_4\text{bipy}]^{3+}$ complex no ligand field band appears with a separate maximum (Fig. 3). On the other hand with the results from the

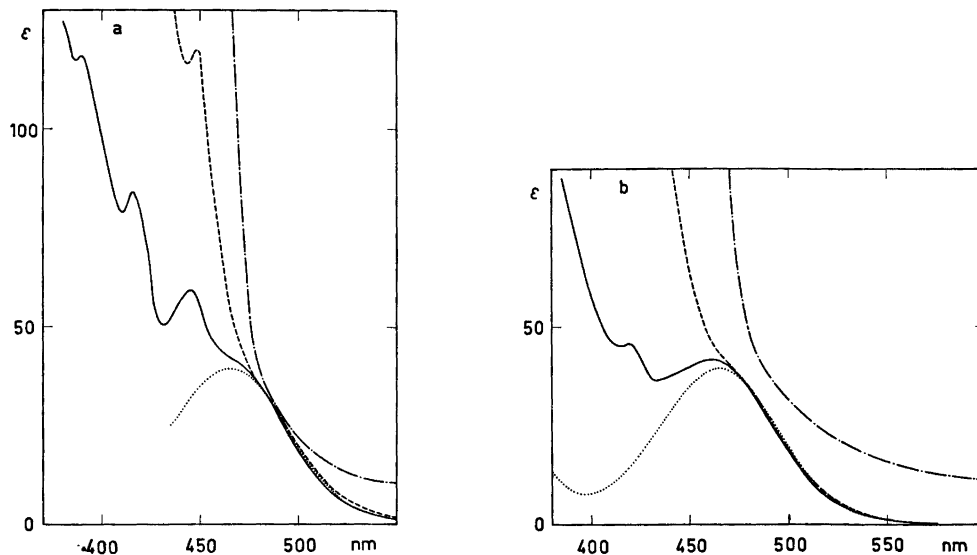


Fig. 3. Visible absorption spectra of $[\text{Cr}(\text{NH}_3)_{6-2a}(\text{N}-\text{N})_a]^{3+}$ complexes. ..., $a=0$; —, $a=1$; ---, $a=2$; - · - ·, $a=3$.

(a) $(\text{N}-\text{N}) = \text{bipy}$. The pattern consisting of three maxima shown for $a=1$ at 445, 415, and 390 nm is also found as maxima for $a=2$ and in this case at 450, 420, and 395 nm. For $a=3$ the apparently analogous transitions appear as two shoulders at about 455 and 425 and one maximum at 400 nm.

(b) $(\text{N}-\text{N}) = \text{phen}$. A maximum analogous to that shown for $a=1$ at 420 nm is found as shoulders around 423 and 425 nm for $a=2$ and $a=3$, respectively.

Thus a red-shift of both these patterns, characteristic for chromium(III) complexes with bipy and phen, respectively, is observed when the number of the ligands $(\text{N}-\text{N})$ increases.

phen system in mind it is quite clear that the shoulder at about 460 nm fulfils the requirements for the ${}^4A_{1g} \rightarrow {}^4T_{2g}$ ligand field transition both with respect to width and molar absorptivity (Fig. 1). It may further be noted that the weakly indicated shoulder at almost the same wave-length in the spectrum of the $[\text{Cr}(\text{NH}_3)_2\text{bipy}_2]^{3+}$ complex supports the assignment.

Previous authors when assigning the ${}^4A_{1g} \rightarrow {}^4T_{2g}$ ligand field transition in $[\text{Cr bipy}_3]^{3+}$ have chosen either the longest wave-length shoulder¹² at 455 nm or an average¹³ of the three narrow bands, 425 nm. We believe that these assignments are out of the question alone because of their small widths (see here Fig. 1). Further evidence is that the three narrow bands occur in all three bipy complexes and apparently have an intensity that increases with the number of bipy molecules in the complex (see text to Fig. 3).

The Gaussian analyses (Fig. 1) make it possible to estimate the positions of the maxima corresponding to the ${}^4A_{1g} \rightarrow {}^4T_{2g}(O_h)$ transitions in the $[\text{Cr}(\text{NH}_3)_4(\text{N}-\text{N})]^{3+}$ complexes for both $(\text{N}-\text{N})$ -ligands and when these estimates are combined with $\sigma_1([\text{Cr}(\text{NH}_3)_6]^{3+}) = 21\,500 \text{ cm}^{-1}$, according to eqn. (5) the following results are obtained

$$\begin{aligned} \sigma_1([\text{Cr bipy}_3]^{3+}) &= 21\,440 \pm 300 \text{ cm}^{-1} \\ \sigma_1([\text{Cr phen}_3]^{3+}) &= 21\,140 \pm 30 \text{ cm}^{-1} \end{aligned} \quad (9)$$

where the standard deviations given, as required by eqn. (5), are three times those found by the Gaussian analyses of Fig. 1. As stated previously they should, however, be taken with a certain reservation.

V. DISCUSSION

Until the present time bipyridine and phenanthroline have only been placed in the spectro-

Table 3. Experimental ^a and calculated values for the wave-numbers σ_1 , σ_2 , and σ_3 , of the three spin-allowed transitions of nickel complexes treated using the expanded radial function model ⁶ for cubic complexes. For $[\text{Ni}(\text{NH}_3)_6]^{2+}$ and $[\text{Ni en}_3]^{2+}$ a least squares treatment with equal weighting has been used and the two resulting independent empirical parameters Δ [eqn. (1)] and B [the Racah parameter] are given together with the field strength parameter ³¹ $\Sigma = \Delta/B$. For the complexes with the heteroaromatic ligands σ_3 is not observable and the calculation has no degrees of freedom, and therefore only represents a non-linear transformation of the experimental wave-numbers into the set of empirical parameters using the energy matrices of the model. The calculated σ values have in these cases been given in parentheses. Numbers in kK (except last column).

	σ_1	σ_2	σ_3	Δ	B	Σ	
$[\text{Ni}(\text{NH}_3)_6]^{2+}$	10.80	17.50	28.20	10.89	0.864	12.60	exp
	10.89	17.40	28.20				calc.
$[\text{Ni en}_3]^{2+}$	11.60	18.35	29.00	11.65	0.825	14.13	exp
	11.65	18.28	29.03				calc.
$[\text{Ni bipy}_3]^{2+}$	12.10	19.20		12.10	0.917	13.19	exp
	(12.10)	(19.20)		12.20	0.879	13.88	calc.
	(12.20)	(19.20)					calc.
$[\text{Ni phen}_3]^{2+}$	12.20	19.30		12.20	0.908	13.44	exp
	(12.20)	(19.30)					calc.

chemical series with the central ion nickel(II). Jørgensen ⁸ measured the nickel(II) tris complexes with these ligands and obtained values for the wavenumbers σ_1 and σ_2 of the two lowest energy spin-allowed transitions which assigned cubically are ${}^3A_{2g} \rightarrow {}^3T_{2g}(O_h)$ and ${}^3A_{2g} \rightarrow {}^3T_{1g}(O_h)$. The third band of wave-number σ_3 , corresponding to ${}^3A_{2g} \rightarrow {}^3T_{1g}(O_h)$, was not observable because of absorption of other origin than $d-d$ transitions in this region. Jørgensen's values for σ_1 are estimates which are made uncertain by the observed mixing of the 1E_g and ${}^3T_{2g}$ excited states. Even the order of the two ligands (bipy < phen) is not quite certain, being based mainly upon the fact that such an inequality applies to the σ_2 values. In Table 3 we give Jørgensen's experimental results and estimations including also his values for $[\text{Ni}(\text{NH}_3)_6]^{2+}$ and $[\text{Ni en}_3]^{2+}$. For these two latter ions we have used the wavenumbers of all three spin-allowed transitions to determine the two independent empirical parameters Δ and B placing ammonia and ethylenediamine in their usual order in the spectrochemical and nephelauxetic series. In addition to the derived empirical parameter, the field strength parameter, ³¹ $\Sigma = \Delta/B$, which alone is responsible for the extent to which

the cubic subconfigurations are mixed, or for that matter, the extent to which the gaseous multiplet terms 3F and 3P are mixed, has been given. For the $[\text{Ni}(\text{N-N})_3]^{2+}$ complexes σ_1 and σ_2 have been used to calculate the same parameters. It is a consequence of the expanded radial function model ⁶ that $(\partial\sigma_2/\partial B)_\Delta = 3.2$ for $\Sigma = 13$. Therefore the fact that σ_2 is found to be 100 cm^{-1} higher for $[\text{Ni phen}_3]^{2+}$ than for $[\text{Ni bipy}_3]^{2+}$ need not imply that Δ is also higher but can alternatively be explained by Δ being the same but B being about 30 cm^{-1} higher. In this connection the experimental fact that the minimum between the first and the second spin-allowed transitions is blue-shifted by more than 100 cm^{-1} on going from $[\text{Ni phen}_3]^{2+}$ to $[\text{Ni bipy}_3]^{2+}$, has made us include an estimation of 12.2 kK for σ_1 for $[\text{Ni bipy}_3]^{2+}$ as an alternative to the value 12.1 kK, given by Jørgensen. These numbers are, of course, in themselves not very important but Table 3 shows clearly that all the empirical parameters are only good to within a few per cent. Therefore the two ligands (N-N) cannot be distinguished parametrically but it is probably safe to place them relative to ammonia and ethylenediamine at three different places in the three semi-empirical series

$$\begin{array}{l}
 \Delta \quad \text{NH}_3 < \text{en} < \text{N-N} \\
 B_0 - B \quad \text{N-N} < \text{NH}_3 < \text{en} \\
 \Sigma \quad \text{NH}_3 < \text{N-N} < \text{en}
 \end{array} \quad (10)$$

where B_0 is the Racah parameter of the gaseous nickel(II) ion. It has to our knowledge not been noted before that the N-N ligands are less nephelauxetic than ammonia and ethylenediamine. It is, however, not too surprising in view of their low position in the hyperchromic series.

Turning our attention now to cobalt(III) and comparing the σ_1 values of the expression (8) with $\sigma_1([\text{Co}(\text{NH}_3)_6]^{3+}) = 21\,100 \text{ cm}^{-1}$ and $\sigma_1([\text{Co en}_3]^{3+}) = 21\,500 \text{ cm}^{-1}$ we see that both bipy and phen give rise to σ_1 -values above that of ethylenediamine. Using the same correction $\Delta - \sigma_1$ as that for $[\text{Co en}_3]^{3+}$ (Table 1) we obtain

$$\begin{array}{l}
 \Delta([\text{Co bipy}_3]^{3+}) = 23\,800; \Delta([\text{Co phen}_3]^{3+}) = \\
 23\,500; C/B = 4 \text{ or}
 \end{array} \quad (11)$$

$$\begin{array}{l}
 \Delta([\text{Co bipy}_3]^{3+}) = 24\,400; \Delta([\text{Co phen}_3]^{3+}) = \\
 24\,100; C/B = 5.5
 \end{array}$$

to be compared with the values for other complexes of cobalt(III) given in Table 1. The spectrochemical series for cobalt(III) then is

$$\Delta \quad \text{NH}_3 < \text{en} < \text{phen} < \text{bipy}$$

where the relative position of bipy and phen is small but significant and also in agreement with our recent findings³⁰ based upon *cis*-bis(N-N) complexes.

For chromium(III) the situation is different. While for cobalt(III) the average environment rule was checked simultaneously with providing the estimates of σ_1 values for the tris-(N-N) complexes, this is not so for chromium(III). Here we have had to rely on the validity of this rule which on the other hand is more likely to be true for chromium(III) than for cobalt(III) using the π back-bonding argument (see below). The results obtained for chromium(III) place both heteroaromatic ligands with certainty below ethylenediamine in the Δ series

$$\Delta \quad \text{phen} < \text{bipy} \lesssim \text{NH}_3 < \text{en}$$

but the position relative to ammonia is less certain in view of the uncertainties associated

with the curve analysis procedures (Fig. 1). However, the relative position of the two (N-N) ligands is in agreement with the results suggested³⁰ by the spectra of *cis*-bis(N-N) chromium(III) complexes.

Comparing σ_1 values for corresponding systems of cobalt(III) and chromium(III) by calculating their ratios (eqns. 8 and 9) one obtains

$$\sigma_1([\text{Co bipy}_3]^{3+})/\sigma_1([\text{Cr bipy}_3]^{3+}) = 1.04 \pm 0.02$$

$$\sigma_1([\text{Co phen}_3]^{3+})/\sigma_1([\text{Cr phen}_3]^{3+}) = 1.04 \pm 0.01$$

Even though the standard deviations here do not have their proper significance, it is clear that the ratios obtained place these ligands in the region outside the first four ligands of Table 1 whose corresponding ratios are 0.963 ± 0.015 .

Comparing the Δ values (for $C/B=4$) for cobalt(III) (N-N) complexes (eqn. 11) with those for chromium(III) (eqn. 9) it is seen that for both (N-N) ligands $\Delta(\text{Co})$ is 2.4 kK higher than $\Delta(\text{Cr})$. Using the same assumptions and arguments as those presented at the end of Section II for the ligand CN^- it is possible to separate this Δ difference into a σ and a π component. The results are

$$\delta_{\sigma(\text{N-N})} = \Delta_{\sigma(\text{N-N})}(\text{Co}) - \Delta_{\sigma(\text{N-N})}(\text{Cr}) = 1.0 \text{ kK}$$

$$\delta_{\pi(\text{N-N})} = \Delta_{\pi(\text{N-N})}(\text{Co}) - \Delta_{\pi(\text{N-N})}(\text{Cr}) = -1.4 \text{ kK}$$

and, as with the CN^- complexes, the values both represent lower limits.

We see through this discussion that there is ligand field theoretical evidence for weak π back-bonding in these complexes, though much weaker than in cyanide complexes. The qualitative arguments for ligand field evidence for π acceptor properties discussed in section II and quantitatively documented in Table 1, are based upon a comparison of d^6 and d^3 systems. In previous work³² concerned with pyridine complexes of chromium(III) the higher acidity of $[\text{Co py}_4(\text{H}_2\text{O})_2]^{3+}$ as compared with $[\text{Cr py}_4(\text{H}_2\text{O})_2]^{3+}$ was also taken as evidence for cobalt(III) being the better donor of π -electrons.

From infrared evidence it is well-known that carbon mono-oxide molecules, at least when several of them are bound to the same metal ion, show a certain mutual limiting influence

upon each other in the sense that their π back-bonding can be enhanced by replacing, for example, three out of six carbon mono-oxide molecules by one molecule such as diethylene-triamine which is unable to act as a π acceptor. Having had trouble with the interpretation of the spectra of *cis*-bis(N-N) complexes, which we published³⁰ without comments, we had expected in our work a similar mutual influence upon the σ_1 values, which would have made the average environment rule break down in such a way that the $\sigma_1([\text{Co}(\text{N-N})_a]^{3+})$ values calculated from the mixed complexes should be higher the lower the number of (N-N) molecules in the complexes. However, this does not seem to be the case, at least not when the other ligands are ammonia molecules, and the results of the present paper thus provide no evidence for the breakdown of the additive¹⁸ ligand field.

VI. EXPERIMENTAL

Analyses and absorption spectra. C, H, N and Cl analyses were carried out by the micro-analytical laboratory of this institute, using standard procedures. Absorption spectra of aqueous solutions (10^{-3} M in hydrochloric acid) of the compounds were recorded using either a Cary Model 118 spectrophotometer (chromium(III) complexes) or a Beckman Model Acta III spectrophotometer (cobalt(III) complexes).

Preparations

1. *Chromium(III) complexes.* *cis*- $[\text{Cr}(\text{NH}_3)_2\text{bipy}_2](\text{ClO}_4)_3$, $[\text{Cr}(\text{NH}_3)_4\text{bipy}](\text{ClO}_4)_3 \cdot \text{H}_2\text{O}$, *cis*- $[\text{Cr}(\text{NH}_3)_2\text{phen}_2](\text{ClO}_4)_3 \cdot 3\text{H}_2\text{O}$, and $[\text{Cr}(\text{NH}_3)_4\text{phen}](\text{ClO}_4)_3 \cdot \frac{1}{2}\text{H}_2\text{O}$.

Crude *cis*-dibromobis(N-N)chromium(III) bromide³⁰ (3 g), dried at 110°C for several hours, was treated with liquid ammonia (100 ml) in a steel autoclave at room temperature overnight. Excess ammonia was allowed to evaporate at 1 atm in the air, and the moist brownish product was dissolved in water and neutralized with hydrochloric acid. The components of this yellow solution were separated on a column of Sephadex C 25 using a solution which was 0.3 M in lithium chloride and 0.01 M in hydrochloric acid as the eluent. The first red fraction was discarded and the following yellow fractions of first $[\text{Cr}(\text{NH}_3)_2(\text{N-N})_2]^{3+}$ and then $[\text{Cr}(\text{NH}_3)_4(\text{N-N})]^{3+}$ (10–20% and 30–40% of initial chromium, respectively) were collected. Each such eluate fraction was treated in the following way: it was diluted 5 times with water and

stirred with about 5 times the calculated amount of Sephadex C 25 for one hour, when the yellow Sephadex was filtered off from the colourless solution, washed with water, and placed on the top of a new short column containing about 5 times as much Sephadex as the yellow top layer. Elution with 0.2 M sodium acetate, adjusted to pH~7 with acetic acid forced red hydroxo complexes through the column preceding the slowly moving yellow complex. After the impurities had been removed, the complex was taken out using 5 M lithium chloride and crystallised directly in the eluate as perchlorate by the addition of lithium perchlorate trihydrate (2–5 g) followed by cooling at 0°C. The yellow perchlorate was washed with ethanol and dried in the air. All the compounds were analysed for Cr, C, H, N, and Cl. The absorption spectra are depicted in Fig. 3.

2. *Cobalt(III) complexes.* $[\text{Cobipy}_2](\text{ClO}_4)_3 \cdot 3\text{H}_2\text{O}$, *cis*- $[\text{Co}(\text{NH}_3)_2\text{bipy}_2](\text{ClO}_4)_3 \cdot 2\text{H}_2\text{O}$, $[\text{Co}(\text{NH}_3)_4\text{bipy}](\text{ClO}_4)_3 \cdot \frac{1}{2}\text{H}_2\text{O}$, $[\text{Cophen}_2](\text{ClO}_4)_3 \cdot 2\text{H}_2\text{O}$, *cis*- $[\text{Co}(\text{NH}_3)_2\text{phen}_2](\text{ClO}_4)_3 \cdot \text{H}_2\text{O}$, and $[\text{Co}(\text{NH}_3)_4\text{phen}](\text{ClO}_4)_3$.

cis-Dichlorobis(N-N)cobalt(III) chloride³⁰ (2 g) was stirred at room temperature for a couple of hours with a solution (20 ml) which contained ammonium chloride (4.5 M) and ammonia (1.5 M) and to which charcoal (0.2 g) had been added. The charcoal was filtered off and the components of the yellow filtrate were separated on a column of Sephadex C 25 using a solution which was 0.4 M in lithium chloride and 0.01 M in hydrochloric acid as the eluent, the procedure being otherwise identical to that described for the chromium complexes. However, with the cobalt complexes the cleaning procedure with sodium acetate was found to be unnecessary. The first minor red band was discarded and three yellow bands of $[\text{Co}(\text{NH}_3)_{6-2a}(\text{N-N})_a]^{3+}$ ($a=3, 2,$ and 1) were collected in the same order as with the corresponding chromium complexes, *i.e.* that of decreasing a (about 20, 50 and 20% for $a=3, 2,$ and 1 , respectively, of initial cobalt). For crystallization, the addition of a little water to the concentrated eluate (5 M in lithium chloride) was found to improve the yield. Recrystallization from dilute perchloric acid (50→0°C) gave in all cases the pure perchlorate salt (anal Co, C, H, N, and Cl). The spectral data are given in Table 2 and Fig. 2.

Acknowledgement. The authors would like to thank Ole Mønsted for adapting his general minimization computer programs for our curve-analytical problems. Further thanks are due to Brigitte Søndergaard Sørensen, who participated in the experimental work on the cobalt complexes.

REFERENCES

1. Tsuchida, R. *Bull. Chem. Soc. Jpn.* 13 (1938) 388.
2. Orgel, L. E. *J. Chem. Soc.* (1952) 4756.
3. Orgel, L. E. *J. Chem. Phys.* 23 (1955) 1004.
4. Kuroya, H. and Tsuchida, R. *Bull. Chem. Soc. Jpn.* 15 (1940) 427.
5. Yamada, S. and Tsuchida, R. *Bull. Chem. Soc. Jpn.* 26 (1953) 15.
6. Jørgensen, C. K. *Discuss. Faraday Soc.* 26 (1958) 110.
7. Jørgensen, C. K. *Prog. Inorg. Chem.* 4 (1962) 73.
8. Jørgensen, C. K. *Acta Chem. Scand.* 9 (1955) 1362.
9. Yamasaki, K. *Bull. Chem. Soc. Jpn.* 13 (1938) 538.
10. Császár, J. and Horváth, E. *Acta Chim. Acad. Sci. Hung.* 24 (1960) 259.
11. Császár, J. *Acta Chim. Acad. Sci. Hung.* 24 (1960) 55.
12. Schläfer, H. L., Gausmann, H. and Witzke, H. *J. Chem. Phys.* 46 (1967) 1423.
13. König, E. and Herzog, S. *J. Inorg. Nucl. Chem.* 32 (1970) 585.
14. Josephsen, J. and Schäffer, C. E. *Acta Chem. Scand.* 24 (1970) 2929.
15. Van Vleck, J. H. *J. Chem. Phys.* 3 (1935) 807.
16. Orgel, L. E. *J. Chem. Phys.* 23 (1955) 1819.
17. Schäffer, C. E. and Jørgensen, C. K. *Mol. Phys.* 9 (1965) 401.
18. Schäffer, C. E. *Struct. Bonding (Berlin)* 14 (1973) 69.
19. Jørgensen, C. K. *Acta Chem. Scand.* 12 (1958) 1539.
20. Schäffer, C. E. *J. Inorg. Nucl. Chem.* 8 (1958) 149.
21. Jørgensen, C. K. *Acta Chem. Scand.* 12 (1958) 1537.
22. Schäffer, C. E. *J. Inorg. Nucl. Chem.* 8 (1958) 148.
23. Glerup, J., Mønsted, O. and Schäffer, C. E. *Inorg. Chem.* 15 (1976) 1399.
24. Bostrup, O. and Jørgensen, C. K. *Acta Chem. Scand.* 11 (1957) 1223.
25. Mead, A. *Trans. Faraday Soc.* 30 (1934) 1055.
26. Schäffer, C. E. *Symposium on the Structure and Properties of Coordination Compounds*, Bratislava, September 1964.
27. Schäffer, C. E. *Proc. 8th I.C.C.C.*, Gutmann, V., Ed., Vienna 1964, p. 77.
28. Tsuchida, R. and Kashimoto S. *Bull. Chem. Soc. Jpn.* 11 (1936) 785.
29. Schäffer, C. E. In Price, W. C., Chissick, S. S. and Ravensdale, T., *Wave Mechanics - The First Fifty Years*, Butterworths, London 1973, Chapter 12, Fig. 1.
30. Hancock, M. P., Josephsen, J. and Schäffer, C. E. *Acta Chem. Scand. A* 30 (1976) 79.
31. Schäffer, C. E. *Proc. R. Soc. London A* 297 (1967) 96.
32. Glerup, J. and Schäffer, C. E. *Unpublished work.*
33. The experimental data given in this table were measured by one of the authors (C.S.) in 1955 and have later been used in various ^{7,85} places.
34. Tanabe, Y. and Sugano, S. *J. Phys. Soc. Jpn.* 9 (1954) 753.
35. Griffith, J. S. *The Theory of Transition Metal Ions*, Cambridge Univ. Press, London, New York 1961.

Received May 24, 1977.

Nickel(II) Complexes of Thiohydrazonates. II. The Crystal and Molecular Structure of [Butanedione di(phenylacetthiohydrazone)]nickel(II)

FLEMMING HANSEN and SINE LARSEN

Chemical Laboratory IV, University of Copenhagen, The H.C. Ørsted Institute, Universitetsparken 5, DK-2100 Copenhagen Ø, Denmark

Dedicated to Professor K. A. Jensen on his 70th birthday

The crystal structure of the title compound has been determined by X-ray diffraction methods using diffractometer data. The crystals are monoclinic, space group $P2_1/a$, $Z=4$, with unit cell dimensions $a=14.202 \text{ \AA}$, $b=9.754 \text{ \AA}$, $c=13.620 \text{ \AA}$, $\beta=93^\circ 35'$. The final least squares refinement based on the 4080 observed reflections gave a unit weighted residual of 0.044.

The structure shows that the nickel atom has a planar coordination. The phenyl groups stick out on each side of the coordination plane. Apart from the phenyl groups the molecule possesses a pseudo twofold axis of symmetry. Strain within the tetradentate ligand causes the coordination angles and distances to be somewhat different from those found in other *cis* Ni—S complexes.

The ligand contains a series of alternating single and double bonds but the conjugation has only a slight effect on the observed bond lengths.

The synthesis and spectroscopic characterization of a series of nickel complexes with mono- or diketone thioacetylhydrazones have been described in a preceding paper.¹ The organic ligands have previously been unknown and it seems that the apparently unstable molecules are stabilized as nickel(II) complexes.

One of these compounds has already been studied structurally, namely bis(acetophenone thioacetylhydrazonato)nickel(II).² This complex has a tetrahedrally distorted *cis* planar configuration and the phenyl groups are in a *syn* arrangement.

The equivalent complexes made from diketones are bound to have a *cis* configuration and one could anticipate that the backbone of the ligand would be considerably more planar than

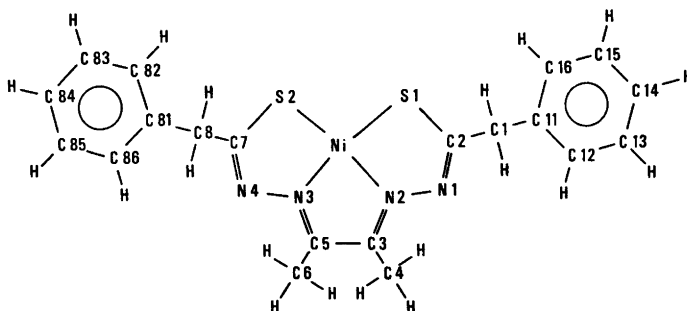


Fig. 1. A schematic drawing of [butanedione di(phenylacetthiohydrazone)]nickel(II), $[\text{Ni}(\text{path})_2\text{-diac}]$, illustrating the atomic labelling.

the equivalent monoketone complex. To obtain structural information about these complexes the crystal structure analysis was undertaken of [butanedione di(phenylacetthiohydrazonato)nickel(II), [Ni(path)₂diac]. From the schematic drawing of this compound shown in Fig. 1, the ligand can be seen to contain alternating double and single bonds and it could be expected that conjugation within the ligand would affect its bond lengths. The crystals of the equivalent acetic acid derivatives are twinned and to avoid this complication the structure analysis was performed for the equivalent phenylacetic acid derivative.

EXPERIMENTAL

A sample of [butanedione di(phenylacetthiohydrazonato)nickel(II)] was supplied by Erik Larsen. This compound crystallizes as intensely coloured rhombic prisms. In polarized light they are red when the electric vector is parallel to the rhombic face. X-Ray diffraction photographs showed that the crystals are monoclinic. The space group is uniquely determined to be $P2_1/a$ from the systematically absent reflections. The density of the crystals was measured by flotation in bromobenzene.

A single crystal 0.11 mm thick and 0.43 by 0.36 mm along the rhombic diagonals was used for the data collection and for the accurate determination of unit cell parameters, using $MoK\alpha$ radiation and a graphite monochromator. The setting angles for 14 relatively high angle reflections were optimized automatically on a Picker FACS-1 diffractometer and these angles were used in a least squares refinement of the unit cell parameters and the orientation matrix. The intensity data were collected by operating the diffractometer in a $\theta - 2\theta$ scan mode at a scan rate of 1° min in 2θ . The scan range was symmetrical and increased with 2θ following the expression $\Delta 2\theta_{sc} = 3.8^\circ + 0.629 \tan \theta$.

Background counts were made for 20 s at each end of the scan range. The intensities of three standard reflections measured after every 40 reflections indicated that no deterioration or misalignment of the crystal had occurred during the data collection. The relative intensities were measured for all the independent reflections where $2.4^\circ \leq 2\theta \leq 60^\circ$. Of the 5733 reflections obtained 4080 had $I/\sigma(I) \geq 2.5$, where $\sigma(I)$ is the standard derivation of the intensity calculated from counting statistics. The data was corrected for Lorentz and polarization effects, but not for absorption.

For the crystallographic calculations use was made of the following computer programs: The Vanderbilt System³ for all diffractometer operations, a local modification of the program

NRC-2Å⁴ for data reduction, ORTEP II⁵ for the illustrations, and the X-Ray System⁶ for the crystal structure analysis.

The atomic scattering factors used in the calculations were those given by Cromer and Mann⁷ using the values for the uncharged atoms, except for hydrogen where the scattering factor calculated by Stewart *et al.*⁸ was employed. The anomalous dispersion corrections added to the scattering factors for nickel and sulfur were those given by Cromer and Liebermann.⁹

CRYSTAL DATA

[Butanedione di(phenylacetthiohydrazonato)nickel(II); C₂₀H₂₀N₄S₂Ni; M = 439.3. Monoclinic, $a = 14.802(9)$ Å, $b = 9.754(6)$ Å, $c = 13.620(8)$ Å, $\beta = 93^\circ 35'(2)$; $V = 1962.6$ Å³; $d_{obs} = 1.49$ g/cm³; $Z = 4$; $d_{calc} = 1.486$ g/cm³. $\mu(MoK\alpha) = 12.08$ cm⁻¹, $F(000) = 912$. Systematically absent reflections: $h0l$ when h odd, $0k0$ when k odd; spacegroup $P2_1/a$ (C_{2h}^5 , No. 14). Developed faces are $\{110\}$ and $\{001\}$.

Table 1. Final coordinates for the non-hydrogen atoms. The estimated standard deviations are given in parenthesis. The labelling corresponds to Fig. 1.

Atom	<i>x</i>	<i>y</i>	<i>z</i>
Ni ¹	0.12215(2)	0.09917(3)	0.53572(2)
S1 ¹	0.14942(5)	0.30505(7)	0.48941(5)
S2 ¹	0.08576(6)	0.12828(7)	0.68479(5)
N1 ¹	0.1756(2)	0.1339(2)	0.3384(2)
N2 ¹	0.1512(2)	0.0429(2)	0.4117(2)
N3 ¹	0.1039(1)	-0.0867(2)	0.5551(2)
N4 ¹	0.0760(2)	-0.1420(2)	0.6419(2)
C1 ¹	0.1958(2)	0.3708(3)	0.2994(2)
C2 ¹	0.1737(2)	0.2581(3)	0.3705(2)
C3 ¹	0.1490(2)	-0.0882(3)	0.3954(2)
C4 ¹	0.1724(3)	-0.1565(4)	0.3028(2)
C5 ¹	0.1203(2)	-0.1669(2)	0.4816(2)
C6 ¹	0.1102(3)	-0.3179(3)	0.4818(3)
C7 ¹	0.0654(2)	-0.0456(3)	0.7061(2)
C8 ¹	0.0309(2)	-0.0876(4)	0.8035(2)
C11 ¹	0.1135(2)	0.4372(3)	0.2470(2)
C12 ¹	0.1256(3)	0.5110(4)	0.1614(2)
C13 ¹	0.0522(4)	0.5732(4)	0.1114(3)
C14 ¹	-0.0325(4)	0.5635(4)	0.1461(3)
C15 ¹	-0.0446(3)	0.4933(4)	0.2303(3)
C16 ¹	0.0280(2)	0.4303(3)	0.2807(3)
C81 ¹	0.0895(2)	-0.0456(3)	0.8928(2)
C82 ¹	0.1496(3)	-0.1374(4)	0.9385(2)
C83 ¹	0.2012(3)	-0.1000(5)	1.0227(3)
C84 ¹	0.1928(3)	0.0292(6)	1.0618(3)
C85 ¹	0.1330(4)	0.1205(5)	1.0170(3)
C86 ¹	0.0816(3)	0.0823(4)	0.9340(3)

Table 2. Final thermal parameters, u_{ij} , in units of $\text{\AA}^2 \times 10^4$ for the heavier atoms. The expression for the temperature factor is $\exp\{-2\pi^2(u_{11}h^2a^{*2} + u_{22}k^2b^{*2} + u_{33}l^2c^{*2} + 2u_{12}hka^*b^* + 2u_{13}hla^*c^* + 2u_{23}k lb^*c^*)\}$. The estimated standard deviations are given in parenthesis.

Atom	u_{11}	u_{22}	u_{33}	u_{12}	u_{13}	u_{23}
Ni	325(1)	232(1)	317(1)	-1(1)	14(1)	-4(1)
S1	468(4)	258(3)	426(3)	-38(3)	9(3)	11(2)
S2	558(4)	338(3)	362(3)	-29(3)	89(3)	-48(3)
N1	422(13)	373(11)	341(11)	0(10)	32(9)	74(9)
N2	372(12)	280(9)	316(10)	-2(9)	10(9)	21(8)
N3	352(11)	250(9)	357(10)	-34(8)	22(8)	26(8)
N4	396(12)	323(10)	371(11)	-57(9)	48(9)	28(9)
C1	420(16)	403(15)	513(17)	-66(13)	48(13)	153(13)
C2	338(14)	340(12)	392(13)	-13(11)	-8(10)	63(10)
C3	364(13)	296(12)	343(12)	33(11)	-12(10)	-36(10)
C4	622(22)	431(16)	398(15)	99(16)	69(15)	-65(13)
C5	348(13)	239(11)	391(13)	-12(10)	0(10)	-30(9)
C6	525(19)	259(12)	598(19)	-38(13)	55(16)	-72(12)
C7	343(14)	412(13)	356(12)	-55(11)	29(10)	27(11)
C8	503(18)	574(20)	385(14)	-139(16)	96(12)	44(13)
C11	523(17)	252(11)	367(13)	-58(11)	-31(12)	25(9)
C12	732(25)	516(19)	445(16)	23(17)	74(16)	129(14)
C13	1075(38)	666(25)	540(21)	103(24)	-72(22)	265(18)
C14	817(31)	569(22)	806(28)	112(21)	-267(24)	184(20)
C15	507(22)	556(21)	875(28)	10(18)	-142(20)	145(19)
C16	471(18)	471(17)	590(19)	-64(14)	-44(14)	184(14)
C81	440(16)	426(14)	329(12)	-34(12)	123(11)	41(11)
C82	642(23)	569(20)	472(17)	68(17)	126(16)	65(15)
C83	627(24)	990(34)	516(20)	76(24)	-1(17)	209(22)
C83	849(31)	1046(36)	399(17)	-403(28)	4(19)	96(21)
C85	1129(37)	591(23)	470(19)	-279(24)	184(22)	-83(16)
C86	771(25)	431(17)	472(17)	-13(17)	117(16)	23(13)

Table 3. Positional parameters and isotropic temperature factors for the hydrogen atoms. The temperature factors are $\exp\{-8\pi^2 U \sin^2 \theta/\lambda^2\}$. Standard deviations are in parenthesis.

Atom	x	y	z	$U \times 10^3 \text{\AA}^2$
H1(C1)	0.233(2)	0.329(3)	0.251(2)	5(1)
H2(C1)	0.226(3)	0.442(4)	0.340(2)	6(1)
H1(C4)	0.122(3)	-0.203(4)	0.277(3)	8(1)
H2(C4)	0.189(4)	-0.087(6)	0.249(4)	12(2)
H3(C4)	0.221(3)	-0.209(5)	0.312(3)	7(1)
H1(C6)	0.065(4)	-0.342(5)	0.434(4)	10(2)
H2(C6)	0.153(3)	-0.360(5)	0.444(3)	9(1)
H3(C6)	0.107(4)	-0.353(6)	0.554(4)	12(2)
H1(C8)	0.025(3)	-0.187(4)	0.800(2)	7(1)
H2(C8)	-0.029(3)	-0.044(4)	0.805(3)	6(1)
H(C12)	0.187(3)	0.512(5)	0.139(3)	8(1)
H(C13)	0.441(3)	0.129(5)	0.953(3)	7(1)
H(C14)	0.079(3)	0.396(4)	0.889(3)	7(1)
H(C15)	-0.098(4)	0.486(6)	0.252(4)	11(2)
H(C16)	0.018(3)	0.378(4)	0.338(3)	7(1)
H(C82)	0.157(3)	-0.217(4)	-0.091(3)	6(1)
H(C83)	0.241(3)	-0.174(5)	0.055(3)	9(1)
H(C84)	0.231(4)	0.059(6)	0.118(4)	11(2)
H(C85)	0.122(3)	0.206(5)	0.045(3)	8(1)
H(C86)	0.035(3)	0.141(5)	0.908(3)	9(1)

STRUCTURE DETERMINATION AND REFINEMENT

The position of the nickel atom was deduced from the three dimensional Patterson function and the positions for the other non-hydrogen atoms were located from two successive Fourier syntheses.

The structure has been refined by the method of least squares, minimizing $R = \sum w(|F_o| - K|F_c|)^2$ using the 4080 observed reflections. Initially a unit weighted full matrix refinement of the scalefactor, the atomic parameters and individually isotropic temperature factors, was performed. Later when anisotropic temperature factors were introduced a block diagonal refinement was used. After this refinement had converged, a calculated difference Fourier showed peaks in all the expected positions for the hydrogen atoms of the structure. Positional and isotropic temperature factors for the hydrogen atoms were included in the final cycles of the least squares refinement. The weights were $w = 1/(A\sigma(F)^2 + BF + CF^2 + D \sin \theta)$. The numerical values for the coefficients, A , B , C and D were derived by minimizing $S = \sum_{i=1}^{NREF} p_i \log p_i$, where $p_i = (w_i |\Delta F_i|^2) / \sum_{i=1}^{NREF} w_i |\Delta F_i|^2$

with respect to the parameters in the weighting function. NREF is the number of reflections. This method is described and programmed by Kurt Nielsen¹⁰ and it has resulted in the following values: $A = 3.84$, $B = 0.0649$, $C = 0.0004$, $D = -2.05$.

After convergence of this refinement, the maximum shift for the parameters was 0.025σ and the unit weighted and weighted residuals were 4.4 and 5.1 %, respectively.

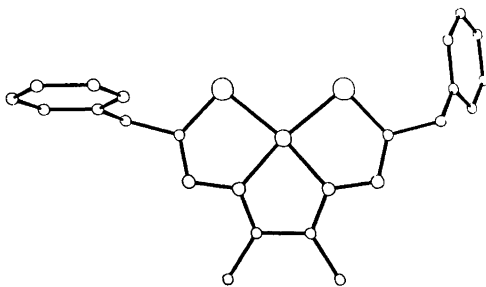


Fig. 2. ORTEP drawing of the molecule seen perpendicular to the coordination plane.

Table 4. Distances (Å) from the least squares plane. The atoms marked with an asterisk are those defining the least squares plane.

Atom	Plane I	Atom	Plane I
Ni	0.005*	C8	-0.10
S1	0.02*	C11	-1.49
S2	0.02*	C12	-1.71
N1	-0.01*	C13	-2.96
N2	0.00*	C14	-4.00
N3	-0.01*	C15	-3.80
N4	-0.02*	C16	-2.54
C1	-0.09	C81	1.00
C2	-0.03*	C82	2.09
C3	0.03*	C83	3.09
C4	0.07	C84	3.00
C5	0.02*	C85	1.92
C6	0.02	C86	0.93
C7	-0.02*		

Table 5. Bond lengths (Å) in [Ni(path)₂diac]. Standard deviations in parenthesis.

Ni-S1	2.150(1)	Ni-S2	2.152(1)
Ni-N2	1.852(2)	Ni-N3	1.854(2)
S1-C2	1.743(3)	S2-C7	1.750(3)
C2-N1	1.289(4)	C7-N4	1.301(4)
N1-N2	1.400(3)	N3-N4	1.386(3)
C2-C1	1.514(4)	C7-C8	1.507(4)
N2-C3	1.298(3)	N3-C5	1.305(3)
C3-C4	1.486(4)	C5-C6	1.481(4)
C1-C11	1.517(4)	C8-C81	1.507(4)
C11-C12	1.391(4)	C81-C82	1.382(5)
C12-C13	1.385(7)	C82-C83	1.387(6)
C13-C14	1.370(8)	C83-C84	1.377(8)
C14-C15	1.356(7)	C84-C85	1.372(7)
C15-C16	1.383(6)	C85-C86	1.374(6)
C16-C11	1.376(5)	C86-C81	1.375(5)
C3-C5	1.486(4)		
C1-H1(C1)	0.97(3)	C8-H1(C8)	0.97(4)
C1-H2(C1)	0.99(4)	C8-H2(C8)	0.98(4)
C12-H(C12)	0.98(5)	C82-H(C82)	0.89(4)
C13-H(C13)	1.04(4)	C83-H(C83)	1.02(5)
C14-H(C14)	0.90(4)	C84-H(C84)	0.96(5)
C15-H(C15)	0.87(6)	C85-H(C85)	0.93(5)
C16-H(C16)	0.95(4)	C86-H(C86)	0.95(5)
C4-H1(C4)	0.92(4)	C6-H1(C6)	0.94(5)
C4-H2(C4)	1.04(6)	C6-H2(C6)	0.94(5)
C4-H3(C4)	0.88(4)	C6-H3(C6)	1.04(6)

The final atomic parameters are listed in Tables 1-3. A list of observed and calculated structure amplitudes may be obtained from the authors upon request.

Table 6. Selected bond angles ($^{\circ}$) in $[\text{Ni}(\text{path})_2\text{diac}]$.

S2-Ni-S1	102.49(3)	N3-Ni-N2	83.33(10)
S1-Ni-N2	87.18(7)	S2-Ni-N3	87.00(7)
Ni-S1-C2	94.6(1)	Ni-S2-C7	94.8(1)
S1-C2-C1	117.9(2)	S2-C7-C8	118.7(2)
S1-C2-N1	124.9(2)	S2-C7-N4	124.1(2)
C1-C2-N1	117.1(2)	C8-C7-N4	117.2(3)
C2-N1-N2	110.0(2)	C7-N4-N3	110.3(2)
N1-N2-Ni	123.2(2)	N4-N3-Ni	123.7(2)
N1-N2-C3	120.5(2)	N4-N3-C5	120.1(2)
Ni-N2-C3	116.3(2)	Ni-N3-C5	116.2(2)
N2-C3-C5	112.3(2)	N3-C5-C3	111.9(2)
N2-C3-C4	125.6(3)	N3-C5-C6	124.8(3)
C4-C3-C5	122.2(2)	C6-C5-C3	123.3(2)
C2-C1-C11	114.4(3)	C7-C8-C81	115.3(3)
C1-C11-C12	118.3(3)	C8-C81-C82	120.6(3)
C1-C11-C16	123.4(3)	C8-C81-C86	121.1(3)
C16-C11-C12	118.3(3)	C86-C81-C82	118.2(3)
C11-C12-C13	120.0(4)	C81-C82-C83	120.5(4)
C12-C13-C14	120.4(4)	C82-C83-C84	120.1(4)
C13-C14-C15	119.9(4)	C83-C84-C85	119.6(3)
C14-C15-C16	120.3(4)	C84-C85-C86	119.9(4)
C15-C16-C11	121.0(3)	C85-C86-C81	121.6(4)

DESCRIPTION AND DISCUSSION OF THE STRUCTURE

The overall molecular structure is illustrated by the ORTEP drawing shown in Fig. 2. Except for the phenyl groups the molecule is planar. The calculation of a least squares plane confirms this, see Table 4. The phenyl groups lie on either side of the plane of the ligand. The planes of the phenyl groups, C11 to C16 and C81 to C86 form angles of 60 and 76° , respectively, with the coordination plane.

Bond angles and bond lengths are shown in Tables 5 and 6. A comparison of the values for

the two equivalent halves of the molecules shows that there are no significant differences. Thus, apart from the phenyl groups the molecule has a pseudo twofold axis of symmetry in agreement with ^1H NMR spectra of the complex in solution.¹

The related complex derived from acetophenone has a tetrahedrally distorted planar configuration, the angle between the two ligand planes being 19° , and it crystallizes with the nickel atom on a crystallographic twofold axis.²

There are interesting similarities and differences between the two structures. The angles,

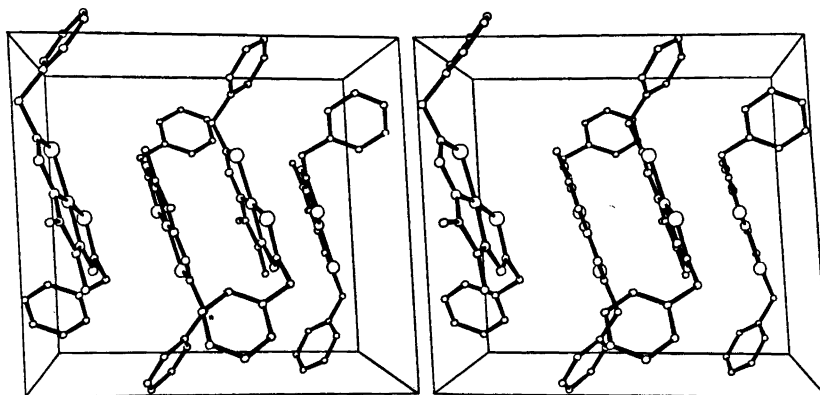


Fig. 3. Stereo pair showing the packing viewed along the b axis.

S-Ni-S and N-Ni-N, in the present structure are grossly different from the angles found in the equivalent acetophenone complex and other *cis*-nickel sulfur complexes.^{2,13} The S-Ni-S angle is 10° larger (102.5° compared to 92°) and similarly the N-Ni-N angle is 10° smaller. This significant change in the coordination angles is due to a considerable steric strain within the tetradentate ligand. Model building indicates that this strain may also cause the observed shortening of the Ni-N distances in this complex derived from diacetyl. The average Ni-N distance is 1.851 Å compared to 1.935 Å found in the equivalent acetophenone complex. The Ni-S distances, however, are virtually identical in the two structures (2.15 Å).

There are no significant differences between corresponding bonds within the ligands of the two structures. The C-N bond lengths in [Ni(path)₂diac] have values ranging from 1.289 to 1.305 Å as compared with the value 1.28 Å for the length of a C-N double bond.¹⁴ The N-N bonds average to 1.393 Å in the present structure and to 1.423 Å in the acetophenone complex.²

In the crystal structures of nickel thiosemicarbazide complexes¹²⁻¹⁴ and of [sulfato bis-(thiocarbonohydrazide-*N,S*)]copper(II) tetrahydrate,¹⁵ which contains coordinated hydrazine groups, the values for the N-N bond lengths vary from 1.406 to 1.436 Å. From the above it may be concluded that the system of conjugated double bonds in the ligand only causes small deviations from the accepted values for single and double bonds.

The molecular packing in the crystal is determined by van der Waals interactions as illustrated in Fig. 3. The molecules are arranged with the coordination planes nearly parallel to the *b*-axis.

REFERENCES

- Gabel, J., Larsen, E. and Trinderup, P. *Acta Chem. Scand. A* 31 (1977) 657.
- Larsen, S. *Acta Chem. Scand. A* 28 (1974) 779.
- Lehnert, P. G. *J. Appl. Crystallogr.* 8 (1975) 568.
- Ahmed, F. R. *N.R.C. Crystallographic Program System*, National Research Council, Ottawa 1968.

- Johnson, C. K. ORTEP: *A Fortran Ellipsoid Plot Program for Crystal Structure Illustrations*, Report ORNL-3794, Second Rev., Oak Ridge National Laboratory, Oak Ridge 1970.
- Stewart, J. M., Ed., *The X-Ray System 1972*, Technical Report Tr-192, Computer Science Center, University of Maryland, College Park.
- Cromer, D. and Mann, J. B. *Acta Crystallogr. A* 24 (1968) 321.
- Stewart, R. F., Davidson, E. R. and Simpson, W. T. *J. Chem. Phys.* 42 (1965) 3175.
- Cromer, D. and Liebermann, D. J. *J. Chem. Phys.* 53 (1970) 1891.
- Nielsen, K. *Acta Crystallogr. A* 33 (1977). *In press.*
- Pauling, L. *The Nature of the Chemical Bond*, 3rd Ed., Cornell University Press, Ithaca, N.Y. 1960.
- Hazell, R. G. *Acta Chem. Scand.* 22 (1968) 2809.
- Hazell, R. G. *Acta Chem. Scand.* 22 (1968) 2171.
- Hazell, R. G. *Acta Chem. Scand.* 26 (1972) 1365.
- Bigoli, F., Pellinghelli, M. A., Tiripicchio A. and Camellini, M. T. *Acta Crystallogr. B* 31 (1975) 55.

Received April 20, 1977.

Explicit Expression for the Relaxation Spectrum of a Model with Infinitely Many Coupled Chemical Reactions. II

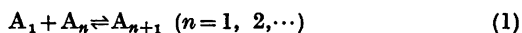
OLE J. HEILMANN

Kemisk Laboratorium III, H.C. Ørsted Institutet, DK-2100 Copenhagen Ø, Denmark

Dedicated to Professor K. A. Jensen on his 70th birthday

In the first article of this series the explicit expression for the relaxation spectrum of the polymerization reaction $A_1 + A_n \rightleftharpoons A_{n+1}$ ($n = 1, 2, \dots$) was found under the assumption that all reactions had the same values of the thermodynamic and kinetic parameters. In the present article the method is generalized to allow the first reaction to deviate from the following reactions. The result does not show any surprising features compared to what would have been expected on the basis of the first article. But the new result is more directly applicable to actual experimental situations.

In the first article¹ (hereafter referred to as I) of this series the following reaction scheme for formation of polymers was considered:



An exact expression for the relaxation spectrum was found under the assumption that all the reactions behaved identically; *i.e.* that the reactions have identical values of the thermodynamic and kinetic parameters. In the present article the result is generalized to cover the case where the first reaction is allowed to be different.

In principle, the method can be generalized to cover the case where the m first reactions deviate from the remaining reactions. But the computations become extremely tedious in the general case, and the resulting expressions are so complicated that they will probably be of very limited value. Also, the present generalization is sufficient to cover several models suggested by experimentalists as realistic models for actual physical systems.

Acta Chem. Scand. A 31 (1977) No. 10

We assume the following reaction scheme (eqns. 2, 3).



If $\nu_0 = 0$ and $n \geq 2$ we have a polymerization which starts by the formation of an n -mer; if $n = 2$ we have the same reaction scheme as in eqn. (1) (taking $A_m = C_m$), while the case where n is somewhat larger ($n \sim 10$) might be considered as a model for micelle formation (this particular model with all reactions in eqn. (3) behaving identically does not appear to have been used in interpreting experiments on micelle formation kinetics, but rather similar models are discussed for example by Zana *et al.*²).

The possibility, $\nu_0 = 1$, will occur for formation of clusters of the solvent molecules (A_1) around a solute molecule (B); an example would be the structuring of water molecules around dissolved alcohol molecules (see for example the review article by Blandamer and Waddington³ and the more recent article on ethanol-water mixtures by Bruun *et al.*⁴).

BASIC NOTATION

The notation will follow the notation of I and the reader is referred to this article (in particular its section II) for the meaning of the vectors \mathbf{f} and \mathbf{h} , the matrix \mathbf{A} and the reaction rates g_j^2 ($j = 1, n+1, n+2, \dots$).

Here we use k_1 for the forward and k_{-1} for the backward rate constant for the reaction (2), and k_+ for the forward and k_- for the backward rate constant for (3). The corresponding equilibrium constants are

$$K_1 = k_1/k_{-1} \quad (4)$$

and

$$K = k_+/k_- \quad (5)$$

\mathbf{e}_j will denote the j 'th unit vector and $\mathbf{e}^{(i)}$ the vector (superscript T stands for transposing; vectors are supposed to be column vectors):

$$\mathbf{e}^{(1)T} = \{0, 1, 1, \dots\} \quad (6)$$

The vectors \mathbf{f} and \mathbf{h} can then be written

$$\mathbf{f} = f_1 \mathbf{e}_1 + f \mathbf{e}^{(1)} \quad (7)$$

$$\mathbf{h} = h_1 \mathbf{e}_1 + h \mathbf{e}^{(1)} \quad (8)$$

The mol fraction of B is denoted x_b ; x_1 stands for the mol fraction of A_1 and x_j ($j = n, n+1, \dots$) stands for the mol fraction of C_j . As in I we introduce the parameter ϕ :

$$\phi = Kx_1 \quad (9)$$

and find

$$x_j = x_n \phi^{j-n}, \quad j = n, n+1, \dots \quad (10)$$

We choose the unit of time to make k_- equal to one and write

$$\kappa_1 = k_{-1}/k_- \quad (11)$$

The rate of reaction, g_1^2 , corresponding to the reaction in (2) is given by

$$g_1^2 = \kappa_1 x_n \quad (12a)$$

while the rate of reaction, g_{m+1}^2 , corresponding to the reaction in (3) is given by

$$g_{m+1}^2 = x_n \phi^{m-n+1} \quad (12b)$$

The matrix \mathbf{A} is divided in two parts as in I:

$$\mathbf{A} = \mathbf{A}' + \mathbf{A}'' \quad (13)$$

where the elements of \mathbf{A}'' are

$$a''_{j,j} = 1 + \phi, \quad j = 2, 3, \dots \quad (14a)$$

$$a''_{j,j+1} = a''_{j+1,j} = -\phi^{\frac{1}{2}}, \quad j = 2, 3, \dots \quad (14b)$$

$$a_{i,j} = 0, \quad |i-j| \geq 2 \quad (14c)$$

$$a_{1,j} = a_{j,1} = 0, \quad j = 1, 2, \dots \quad (14d)$$

and the matrix \mathbf{A}' is given by

$$\mathbf{A}' = c_1 \mathbf{e}_1 \mathbf{e}_1^T + c_2 (\mathbf{e}_1 \mathbf{y}^T + \mathbf{y} \mathbf{e}_1^T) + c_3 \mathbf{y} \mathbf{y}^T + \kappa_1 (\nu_0^2 x_n / x_b + 1) \mathbf{e}_1 \mathbf{e}_1^T - (\kappa_1 \phi)^{\frac{1}{2}} (\mathbf{e}_1 \mathbf{e}_2^T + \mathbf{e}_2 \mathbf{e}_1^T) \quad (15)$$

In eqn. (15) we have introduced the following new symbols:

$$c_1 = \kappa_1 x_n (h_1^2 + n^2 / x_1 - (n + \nu_0 - 1)^2) \quad (16a)$$

$$c_2 = (\kappa_1 \phi)^{\frac{1}{2}} x_n (h h_1 + n / x_1 - (n + \nu_0 - 1)) \quad (16b)$$

$$c_3 = \phi x_n (h^2 + 1 / x_1 - 1) \quad (16c)$$

$$\mathbf{y}^T = \{0, 1, \phi^{\frac{1}{2}}, \phi, \phi^{3/2}, \dots\} \quad (17)$$

A SIMILARITY TRANSFORMATION

The method used in I consists of two steps. First the matrix \mathbf{A} is transformed into tridiagonal form by Lanczos' tridiagonalization algorithm, and then the complex susceptibility $\kappa(\omega)$ is computed as function of the frequency ω by a continued fraction expansion from the tridiagonal form. Here we shall keep the principles of the second step unchanged, while we shall find it more profitable to use another point of view on the first step.

The first step in I can alternatively be considered as a transformation to a new basis set which has been obtained by applying a Schmidt orthogonalization to the sequence of vectors $\mathbf{y}_1, \mathbf{e}_1, \mathbf{e}_2, \dots$, where

$$\mathbf{y}_1^T = \{1, \phi^{\frac{1}{2}}, \phi, \dots\}$$

The fact that in the present case the first reaction is different from the following reactions suggests that one should apply the Schmidt orthogonalization to the sequence

$$\mathbf{b}'_1, \mathbf{e}_1, \mathbf{e}_2, \dots, \text{ with } \mathbf{b}'_1 = \alpha \mathbf{e}_1 + \mathbf{y} \quad (18)$$

The parameter, α , is determined by the requirement that the vector \mathbf{b}'_1 should be parallel to the vector \mathbf{Gf} of eqn. (10) in I; this choice secures that we can still find $\kappa(\omega)$ by just computing the (1,1)-element of the inverse of the matrix $\mathbf{C} + i\omega I$ where \mathbf{C} is the matrix given by eqn. (25) below. The desired value of α is

$$\alpha = (f_1/f) (\kappa_1/\phi)^{\frac{1}{2}} \quad (19)$$

The Schmidt orthogonalization yields the following orthogonal vectors (besides \mathbf{b}'_1):

$$\mathbf{b}'_2 = \mathbf{e}_1 - \alpha(1 - \phi)\mathbf{y} \quad (20)$$

and for $j > 2$:

$$\mathbf{b}'_j = (1 - \phi) \sum_{k=2}^{j-2} \{\phi^{(k-2)/2} \mathbf{e}_k - \mathbf{y}\} + \phi^{(j-3)/2} \mathbf{e}_{j-1} \quad (21)$$

From this set we derive the orthonormal set, $\mathbf{b}_j (j = 1, 2, \dots)$:

$$\mathbf{b}_j = \pi_j \mathbf{b}'_j \quad (22)$$

$$\pi_1 = \{(1 - \phi) / [1 + \alpha^2(1 - \phi)]\}^{1/2} \quad (23a)$$

$$\pi_2 = \{1 + \alpha^2(1 - \phi)\}^{-1/2} \quad (23b)$$

$$\pi_j = \phi^{-(j-2)/2}, j = 3, 4, \dots \quad (23c)$$

Let \mathbf{B} be the matrix whose columns are the vectors $\mathbf{b}_1, \mathbf{b}_2, \dots$; then \mathbf{B} is unitary:

$$\mathbf{B}^T \mathbf{B} = \mathbf{I} \quad (24)$$

and we introduce the transformed matrix, \mathbf{C} , by

$$\mathbf{C} = \mathbf{B}^T \mathbf{A} \mathbf{B} \quad (25)$$

Since \mathbf{A} is real and symmetric and \mathbf{B} is real and unitary, then \mathbf{C} is real and symmetric. The partition of \mathbf{A} in \mathbf{A}' and \mathbf{A}'' carries over to \mathbf{C} :

$$\mathbf{C} = \mathbf{C}^{(1)} + \mathbf{C}^{(2)} \quad (26)$$

$$\mathbf{C}^{(1)} = \mathbf{B}^T \mathbf{A}' \mathbf{B}, \quad \mathbf{C}^{(2)} = \mathbf{B}^T \mathbf{A}'' \mathbf{B} \quad (27)$$

By straight forward though tedious computations we find the following expressions for the elements of $\mathbf{C}^{(1)}$ and $\mathbf{C}^{(2)}$:

$$c^{(1)}_{11} = \pi_1^2 \alpha^2 c_1 + 2\pi_1^2 (1 - \phi)^{-1} \alpha c_2 + \pi_1^2 (1 - \phi)^{-2} c_3 + \kappa_1 \pi_1^2 \alpha^2 (v_0^2 x_n / x_b + 1) - 2(\kappa_1 \phi)^{1/2} \pi_1^2 \alpha \quad (28)$$

$$c^{(1)}_{12} = (1 - \phi)^{1/2} \pi_2^2 \alpha c_1 + \{(1 - \phi)^{-1/2} - \alpha^2 (1 - \phi)^{1/2}\} \pi_2^2 c_2 - \alpha (1 - \phi)^{-1/2} \pi_2^2 c_3 + (1 - \phi)^{1/2} \pi_2^2 \alpha \kappa_1 (v_0^2 x_n / x_b + 1) - \{(1 - \phi)^{1/2} - \alpha^2 (1 - \phi)^{3/2}\} \pi_2^2 (\kappa_1 \phi)^{1/2} \quad (29)$$

$$c^{(1)}_{13} = -\phi \alpha \kappa_1^{1/2} \pi_1 \quad (30)$$

$$c^{(1)}_{22} = \pi_2^2 c_1 - 2\pi_2^2 \alpha c_2 + \pi_2^2 \alpha^2 c_3 + \pi_2^2 \kappa_1 (v_0^2 x_n / x_b + 1) + 2\pi_2^2 (\kappa_1 \phi)^{1/2} \alpha (1 - \phi) \quad (31)$$

$$c^{(1)}_{23} = -\pi_2 \kappa_1^{1/2} \phi \quad (32)$$

$$c^{(1)}_{ij} = 0 \text{ if } i > 3 \text{ or } j > 3 \text{ or } i = j = 3 \quad (33)$$

$$c^{(2)}_{11} = \pi_1^2 \quad (34)$$

$$c^{(2)}_{12} = -(1 - \phi)^{3/2} \pi_2^2 \quad (35)$$

$$c^{(2)}_{13} = \pi_1 \phi^{1/2} \quad (36)$$

$$c^{(2)}_{22} = \alpha^2 (1 - \phi)^2 \pi_2^2 \quad (37)$$

$$c^{(2)}_{23} = -\alpha (1 - \phi) \phi^{1/2} \pi_2 \quad (38)$$

$$c^{(2)}_{jj} = 1 + \phi, j \geq 3 \quad (39)$$

$$c^{(2)}_{j,j+1} = -\phi^{1/2}, j \geq 3 \quad (40)$$

$$c^{(2)}_{1,j} = 0, j \geq 4 \quad (41a)$$

$$c^{(2)}_{j,j+i} = 0, j \geq 2, i \geq 2 \quad (41b)$$

The elements of \mathbf{C} are then given by

$$c_{i,j} = c^{(1)}_{i,j} + c^{(2)}_{i,j} \quad (42)$$

Note that \mathbf{C} is tridiagonal except for the fact that $c_{13} = c_{31}$ is different from zero:

$$c_{13} = \pi_1 \phi^{1/2} (1 - \kappa_1 f_1 / f) \quad (43)$$

A CONTINUED FRACTION EXPANSION

As in I the complex susceptibility, $\kappa(\omega)$ is, given by

$$\kappa(\omega) = (f^2 x_n \phi \pi_1^{-2}) \eta(\omega) \quad (44)$$

where $\eta(\omega)$ is the (1,1)-element of $(\mathbf{C} + i\omega \mathbf{I})^{-1}$. If \mathbf{C}_j is the $j \times j$ matrix consisting of the first j columns and rows of \mathbf{C} and \mathbf{I}_j is the $j \times j$ unit matrix, then we can define $\eta_j(\omega)$ as the (1,1)-element of $(\mathbf{C}_j + i\omega \mathbf{I}_j)^{-1}$ and obtain $\eta(\omega)$ as the limit for $j \rightarrow \infty$ of $\eta_j(\omega)$. By the standard rule for calculating the inverse matrix $\eta_j(\omega)$ is given as the ratio between two determinants

$$\eta_j(\omega) = P_j(\omega) / Q_j(\omega) \quad (45)$$

$$P_j(\omega) = \text{Det}(\mathbf{C}'_{j-1} + i\omega \mathbf{I}_{j-1}) \quad (46)$$

$$Q_j(\omega) = \text{Det}(\mathbf{C}_j + i\omega \mathbf{I}_j) \quad (47)$$

where \mathbf{C}'_{j-1} is obtained from \mathbf{C}_j by deleting the first row and column.

From the almost tridiagonal form of \mathbf{C} follows that for $j \geq 4$ both P_j and Q_j fulfil the recurrence relation

$$R_j(\omega) = (1 + \phi + i\omega) R_{j-1}(\omega) - \phi R_{j-2}(\omega) \quad (48)$$

If we introduce

$$x = \frac{1}{2}(1 + \phi + i\omega) / \sqrt{\phi} \quad (49)$$

then we can determine coefficients a_1, a_2, a_3 and a_4 such that for all $j \geq 2$

$$P_j(\omega) = \phi^{(j-2)/2} (a_1 U_j(x) + a_2 T_j(x)) \quad (50)$$

$$Q_j(\omega) = \phi^{(j-2)/2} (a_3 U_j(x) + a_4 T_j(x)) \quad (51)$$

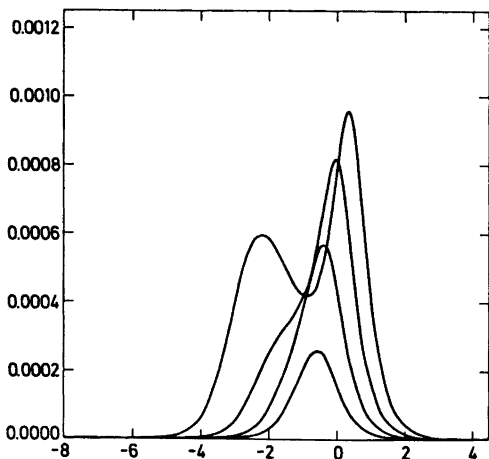


Fig. 1. The imaginary part of $\kappa(\omega)$ as a function of $\log_{10}(\omega)$ for the parameters specified in eqn. (61) and $\kappa_1=1$, $f_1/f=1$. The four curves correspond in increasing order to $y=0.002$, 0.005, 0.02 and 0.1.

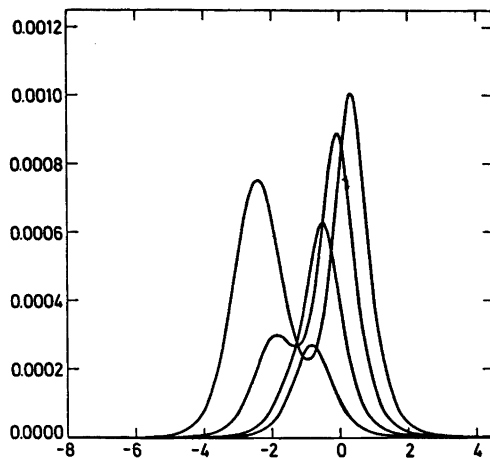


Fig. 2. The imaginary part of $\kappa(\omega)$ as a function of $\log_{10}(\omega)$ for the parameters specified in eqn. (61) and $\kappa_1=0.1$, $f_1/f=1$. The four curves correspond in increasing order to $y=0.002$, 0.005, 0.02 and 0.1.

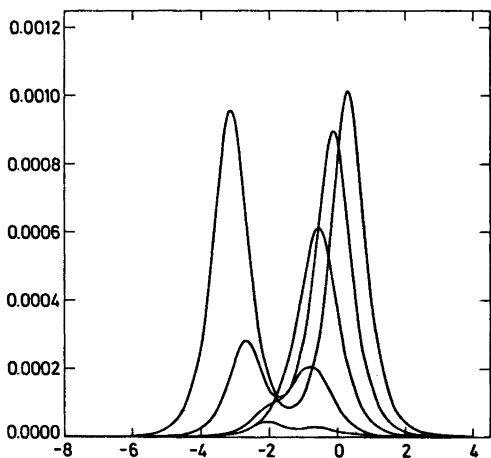


Fig. 3. The imaginary part of $\kappa(\omega)$ as a function of $\log_{10}(\omega)$ for the parameters specified in eqn. (61) and $\kappa_1=0.01$, $f_1/f=1$. The five curves correspond to $y=0.001$, 0.002, 0.005, 0.02 and 0.1. They can be identified by the fact that the right peak increases monotonously with y . The curve for $y=0.005$ only has one peak.

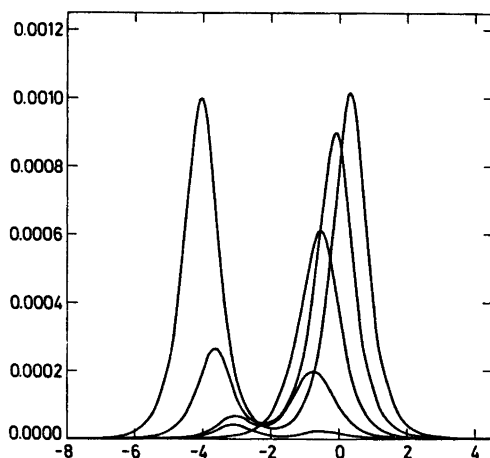


Fig. 4. The imaginary part of $\kappa(\omega)$ as a function of $\log_{10}(\omega)$ for the parameters specified in eqn. (61) and $\kappa_1=0.001$, $f_1/f=1$. The five curves correspond to $y=0.001$, 0.002, 0.005, 0.02 and 0.1. The right peak increases monotonously with y ; the left peak also appears to increase with y , except for $y=0.005$ where it does not exist.

where U_j and T_j are the Tschebyscheff polynomials

$$T_j(x) = \cos(jv) \quad (52)$$

$$U_j(x) = \sin[(j+1)v]/\sin v \quad (53)$$

$$\cos v = x \quad (54)$$

In fact, we have

$$a_1 = \phi^{-\frac{1}{2}} P_3(\omega)/x - P_2(\omega) \quad (55)$$

$$a_2 = 2P_2(\omega) - \phi^{-\frac{1}{2}} P_3(\omega)/x \quad (56)$$

$$a_3 = \phi^{-\frac{1}{2}} Q_3(\omega)/x - Q_2(\omega) \quad (57)$$

$$a_4 = 2Q_2(\omega) - \phi^{-\frac{1}{2}} Q_3(\omega)/x \quad (58)$$

Eqn. (54) can be solved for e^{iv}

$$e^{iv} = x + \sqrt{x^2 - 1} \quad (59)$$

If the sign of square root is defined by the convention that the real part of the square root should have the same sign as the real part of x , then e^{iv} is an analytic function of x outside a cut in the complex x -plane from -1 to 1 along the real axis and e^{iv} is numerically larger than one in this region. It is then a trivial matter to take the limit $j \rightarrow \infty$ and obtain

$$\eta(\omega) = \left\{ (a_1 + \frac{1}{2}a_2)e^{iv} - \frac{1}{2}a_2e^{-iv} \right\} / \left\{ (a_3 + \frac{1}{2}a_4)e^{iv} - \frac{1}{2}a_4e^{-iv} \right\}$$

or

$$\eta(\omega) = \{P_3(\omega) - \phi^{\frac{1}{2}}P_2(\omega)(x - \sqrt{x^2 - 1})\} / \{Q_3(\omega) - \phi^{\frac{1}{2}}Q_2(\omega)(x - \sqrt{x^2 - 1})\} \quad (60)$$

DISCUSSION

The computation of the real and the imaginary part of $\kappa(\omega)$ from eqns. (44), (60), (46) and (47) together with the equations of the earlier sections is in principle straight forward on a high speed computer as long as the necessary care is exercised to ensure that the programming is free of errors.

Since there are many free parameters, then the number of principally different cases is presumably large and we shall not try to be exhaustive, but rather show a few examples which take their origin in an actual application of the present model in the interpretation of experiments. The case we shall use is the ultrasonic absorption by a solution of *N*-methyl acetamide in carbon tetrachloride for which Rassing⁵⁻⁶ found that the following choice of parameters would fit the experiments

$$n = 2, \nu_0 = 0, K_1 = 46, K = 460, h = h_1 = 2 \quad (61)$$

$$\kappa_1 = 1, f_1/f = 1 \quad (62)$$

(the values of k_- and f only influences the scaling so we keep them equal to one). The computations by Rassing⁵ were done by cutting the matrix **A** down to a finite size and apply a numerical diagonalization; when these computations were compared with results obtained by using the formulas of the present article no significant deviations were found.

Acta Chem. Scand. A 31 (1977) No. 10

In the examples we are going to consider we keep the parameters given in eqn. (61) fixed while we vary the two parameters given in eqn. (62). In all the cases we give plots which show the imaginary part of $\kappa(\omega)$ as a function of $\log_{10}(\omega)$ for various values of the brutto mol fraction of monomers, y ; i.e. the mol fraction of monomers if one assumes complete dissociation:

$$y = \sum_{j=1}^{\infty} jx_j / (1 + \sum_{j=2}^{\infty} (j-1)x_j) \quad (63)$$

The figures 1-4 show the effect of lowering κ_1 from 1 to 0.001 while f_1/f is kept fixed at 1. At the two highest values of κ_1 one has the same picture as in I; i.e. a single peak which separates into two peaks as the mol fraction increases. The peak at the high frequencies corresponds to the isolated eigenvalue which was discussed in I, while the peak at the lower frequencies corresponds to the continuous part of the spectrum of **A**. When κ_1 gets sufficiently small, then the rate of the reaction



deviates sufficiently from the rate of the other reactions to make this reaction appear as an isolated peak at low mol fraction. This has the interesting effect of making the peak at low frequencies raise at low and high mol fractions while it disappears at intermediate mol fractions.

The figures 5-8 show the effect of changing f_1/f while κ_1 is kept constant at 0.001. At low values of f_1/f ($f_1/f = 0.5$, Fig. 5) and high values of f_1/f ($f_1/f = 4$, Fig. 8) both peaks increase monotonously with the mol fractions, and the peak at low frequencies eventually becomes dominant. At $f_1/f = 1$ (Fig. 4) and $f_1/f = 3$ (Fig. 7) we have the above-mentioned "up-down-up" behaviour for the peak at low frequencies and the peaks have equal height at the highest mol fraction. Finally, in Fig. 6 at $f_1/f = 2$ ($=n$) the left peak shows an "up-down" behaviour and disappears totally at the highest mol fraction; except for the lowest mol fraction, the right peak dominates.

The very drastic changes in the pictures when f_1/f is changed carry an important message to persons who want to compare the results of different experimental situations.

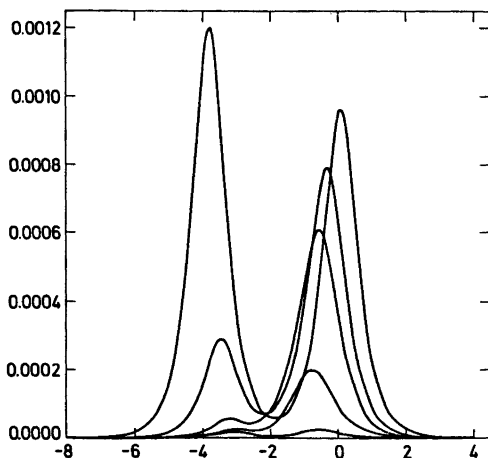


Fig. 5. The imaginary part of $\kappa(\omega)$ as a function of $\log_{10}(\omega)$ for the parameters specified in eqn. (61) and $\kappa_1=0.001$, $f_1/f=0.5$. The five curves correspond to $y=0.001$, 0.002, 0.005, 0.01 and 0.04. Both peaks increase with y .

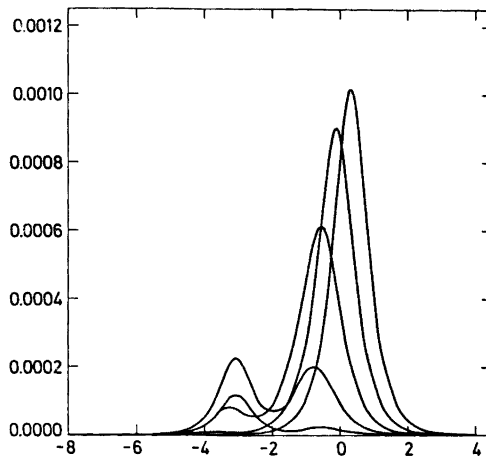


Fig. 6. The imaginary part of $\kappa(\omega)$ as a function of $\log_{10}(\omega)$ for the parameters specified in eqn. (61) and $\kappa_1=0.001$, $f_1/f=2$. The five curves correspond to $y=0.001$, 0.002, 0.005, 0.02 and 0.1. The right peak increases with y . The three highest values of the left correspond in decreasing order to $y=0.002$, 0.001 and 0.005.

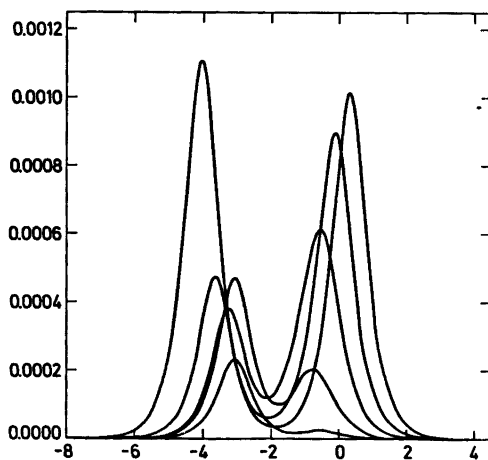


Fig. 7. The imaginary part of $\kappa(\omega)$ as a function of $\log_{10}(\omega)$ for the parameters specified in eqn. (61) and $\kappa_1=0.001$, $f_1/f=3$. The five curves correspond to $y=0.001$, 0.002, 0.005, 0.02 and 0.1. The right peak increases with y . For the left peak the curves are in order of increasing height: $y=0.001$, $y=0.005$, $y=0.002$ (left) and $y=0.02$ (right), $y=0.1$.

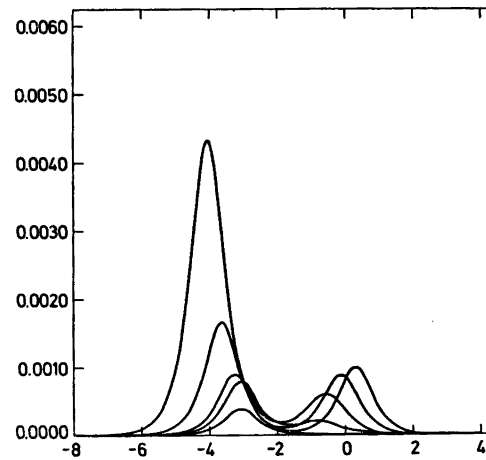


Fig. 8. The imaginary part of $\kappa(\omega)$ as a function of $\log_{10}(\omega)$ for the parameters specified in eqn. (61) and $\kappa_1=0.001$, $f_1/f=4$. The five curves correspond to $y=0.001$, 0.002, 0.005, 0.02, 0.1. Both peaks increase with y .

When the experimental set-up is changed this will only cause minor changes in the matrix **A** (stemming from the changes in the vector **h** which seems to be rather unimportant); therefore, the eigenvalues and eigenvectors can be considered as essentially the same for all experiments. But the vector **f** which may be said to represent the measurement can easily be imagined to change significantly. As can be seen from Figs. 5–8 this can cause the peaks of the relaxation spectrum to show very different behaviour; a fact which is often assumed to occur only as a result of experimental errors.

REFERENCES

1. Heilmann, O. J. *Adv. Mol. Relaxation Processes* 8 (1976) 155.
2. Lang, J., Tondre, C., Zana, R., Bauer, R., Hoffmann, H. and Ulbricht, W. *J. Phys. Chem.* 79 (1975) 276.
3. Blandamer, M. J. and Waddington, D. *Adv. Mol. Relaxation Processes* 2 (1970) 1.
4. Bruun, S. G., Sørensen, P. G. and Hvidt, A. *Acta Chem. Scand. A* 28 (1974) 1047.
5. Rassing, J. *Acta Chem. Scand.* 25 (1971) 1418.
6. Rassing, J. *Hydrogenbindingskinetik og Relaksationsspektrometri*, Thesis, København 1971.

Received May 6, 1977.

The Complex Formation between Pb^{2+} , Ca^{2+} and Some Pentoses

LARS-GÖSTA EKSTRÖM and ÅKE OLIN

Institute of Chemistry, University of Uppsala, P.O.B. 531, S-751 21 Uppsala, Sweden

The complex formation between Pb^{2+} , Ca^{2+} and arabinose, ribose, and xylose has been studied by emf measurements. Results obtained at different ionic strengths have been compared with those from NMR measurements. It is concluded that the more detailed information obtained from NMR spectra at high concentrations is also applicable at low concentrations. The emf measurements have also confirmed that the presence of an *ax-eq-ax* or a *cis-cis-cis* sequence of hydroxyl groups is necessary for a significant complex formation to occur.

Weak interactions have long been known to exist between carbohydrates or cyclitols and metal ions in neutral and acid aqueous solution.¹ Quantitative studies of these interactions have been made by Angyal *et al.*^{2,3} using 1H NMR spectroscopy and stability constants have been determined for a large number of carbohydrate complexes especially with the alkaline earth metal ions.

For the complex formation to occur to a significant extent, three vicinal hydroxyl groups either in an *ax-eq-ax* sequence on a six-membered ring or in a *cis-cis* sequence on a five-membered ring must be present. The conclusions reached from 1H NMR spectroscopy about the nature of the binding site have been confirmed by Andrasko and Forsén⁴ from measurement of the spin-lattice relaxation time of ^{23}Na in aqueous carbohydrate and inositol solutions. Practical use of the complex formation has been made in preparative work.⁵

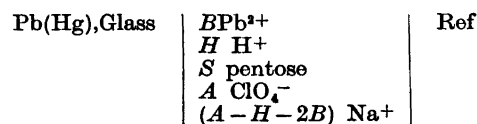
The NMR measurements have to be carried out with comparatively high concentrations of metal ion and carbohydrate (0.5–2 mol/dm³). In the present investigation the complex formation has been studied at low concentrations with the emf technique. By carrying out

measurements at different ionic strengths it would then be possible to establish if values of stability constants determined at high concentrations are applicable at low concentrations. As models in these studies Pb^{2+} -pentose interactions have been used. Some measurements with Ca^{2+} employing the competition technique have also been included in this investigation.

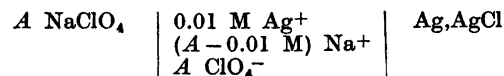
Emf methods have been little used previously. Angyal and Hickman⁶ have employed a divalent ion-sensitive electrode to investigate the complex formation between Ca^{2+} , Sr^{2+} , and Ba^{2+} and *epi*- and *cis*-inositol.

EXPERIMENTAL

Method. The interaction between Pb^{2+} and the carbohydrate was studied at 25.0(1) °C by measurements of the cells



The reference electrode was



The emfs of the cells may be written

$$E_{Pb} = E_{Pb}^\circ - 29.58 \ (mV) \lg (b/M) - 29.58 \ (mV) \lg (y_{Pb^{2+}}) - E_j \quad (I)$$

$$E_g = E_g^\circ - 59.16 \ (mV) \lg (h/M) - 59.16 \ (mV) \lg (y_{H^+}) - E_j \quad (II)$$

Capital letters denote total concentrations whereas small letters are used for the corresponding free concentrations. The activity

coefficient, y , refers to activity scales where $y=1$ in the pure ionic medium. The test solutions were prepared by the titration technique and in an experiment B and H were kept constant usually at 1×10^{-3} and 5×10^{-3} M, respectively. S was varied from 0 to 0.09 M. The influence of the sodium perchlorate used as salt background was followed by making measurements at the $(\text{Na})\text{ClO}_4$ concentrations 0.025, 0.050, 0.100, 0.250, 0.500, and 1.000 M. Some experiments were also made in 0.1 M $(\text{C}_2\text{H}_5)_4\text{NClO}_4$ in order to study the effect of a qualitative change in the medium.

In the experiments with Ca^{2+} , S was kept constant at 0.1 M and the total concentration of Ca^{2+} , C , was varied from 0 to 0.15 M. Measurements were performed in 1 M $(\text{Na})\text{ClO}_4$ only.

Chemicals. Sodium, calcium, lead and silver perchlorates, and perchloric acid solutions were prepared and analysed as described in Refs. 7 and 8.

Tetraethylammonium perchlorate was prepared by neutralizing a hot 20 % water solution of tetraethylammonium hydroxide (Kebo, *purum*) with perchloric acid. The product was recrystallized twice from methanol. The crystals were dried and stored over silica gel in a desiccator.

L(+)-Arabinose (Merck, für die Mikrobiologie), D(-)-ribose, and D(+)-xylose (both Merck, für biochemische Zwecke) were purified by recrystallization after treatment with activated charcoal. Aqueous ethanol was used for recrystallization of arabinose and xylose and aqueous 1-propanol for ribose. The crystals were dried and stored over silica gel in a vacuum desiccator. The purification of the chemicals was repeated until the emf measurements on the products from two consecutive recrystallizations gave the same result. The analytical hydrogen ion concentrations in solutions of the pentoses were found from potentiometric titrations with dilute perchloric acid. Gran extrapolations were used for the determination of the equivalence point.

Lead amalgam was prepared by dissolving lead metal (Merck, silberfrei) in mercury (Kebo, *puriss*, twice distilled). The amalgam (0.1 % Pb) was stored under 0.1 M HClO_4 in a N_2 atmosphere. Ribose was deuterated for the NMR measurements by dissolving it in D_2O (99.7 %, Ciba-Geigy) and evaporating the solvent under vacuum. This was repeated twice. CaCl_2 and $\text{Pb}(\text{NO}_3)_2$ were dried at 200 °C for 20 h. $\text{Pb}(\text{ClO}_4)_2$ was obtained from the stock solution in H_2O . The water was driven off under an infrared lamp and the evaporation was repeated twice with D_2O .

Apparatus. The titrations were carried out with an automatic titrator. The salt bridge, electrodes, and other experimental details were essentially the same as in Ref. 8. All potentials were measured to ± 0.01 mV. Since the changes in the measured potentials are small particular care was taken to exclude oxygen

from the measuring system. All solutions were thus continuously flushed with oxygen-free argon. All plastic tubing from the buret was mantled and nitrogen passed between the inner and outer tube in order to prevent oxygen from diffusing through the walls of the inner tubing.

The NMR spectra were recorded on a JEOL JNM-FX100 spectrometer at 24 °C. Chemical shifts were measured from sodium 3-(trimethylsilyl)propionate as internal standard.

DATA TREATMENT, RESULTS AND DISCUSSION

Lead complexes. The data from the main series of measurements in which Pb^{2+} complexes were studied will be treated first. H^+ does not interact with the pentoses, *i.e.* $h=H$. Then

$$\Delta E_g = E_g(s=S) - E_g(s=0) = E_j(s=0) - E_j(s=S) - 59.16 \lg(y_{\text{H}^+}) \quad (1)$$

will be a measure of the changes in the liquid junction potential and the activity coefficient for H^+ upon addition of the pentose. The solution with $s=0$ is chosen as the standard state for each perchlorate concentration. In the same way ΔE_{Pb} can be calculated. $\text{Lg}(y_{\text{Pb}^{2+}})$ will then include any specific interaction between Pb^{2+} and the carbohydrate.

ΔE_g and ΔE_{Pb} were found to be independent of B (1×10^{-3} M $\leq B \leq 5 \times 10^{-3}$ M) and H (2×10^{-3} M $\leq H \leq 10 \times 10^{-3}$ M). Furthermore the same values were obtained whether s was increased or decreased during a titration, indicating that any interactions occurring are reversible.

In Fig. 1 the results in 1 M $(\text{Na})\text{ClO}_4$ are shown. These are typical for all concentrations of the ionic media except 0.025 M. ΔE_g decreases and ΔE_{Pb} increases to a good approximation linearly with the carbohydrate concentration. The slopes of these lines, which are virtually independent of A , are presented in Table 1.

If complex formation occurs E_{Pb} must increase with S . This is found to be the case but only to a small extent except for the D-ribose system. When stability constants are calculated from data obtained in a constant ionic medium it is generally assumed that the activity factors are constant. E_g would then be a measure of the change in the liquid junc-

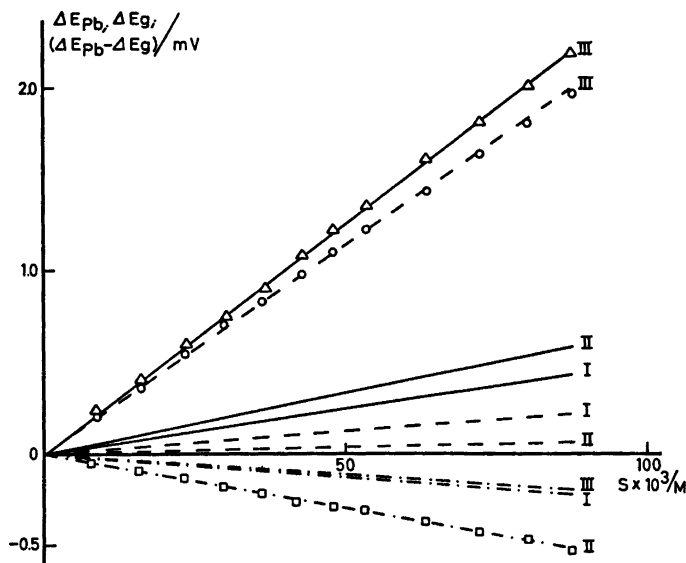


Fig. 1. The changes in the potential of the glass electrode (ΔE_g - - -), and the lead amalgam electrode (ΔE_{Pb} - · - ·) and $\Delta E = \Delta E_{Pb} - \Delta E_g$ (—) as a function of the concentration of the pentose, S , in 1 M (Na) ClO_4 . The lines for L-arabinose, D-xylose, and D-ribose are identified by the symbols I, II, and III, respectively. For clarity the experimental points have in general been left out.

Table 1. Summary of the results from the emf measurements on the Pb^{2+} complexation.

A M	L-Arabinose			D-Xylose			D-Ribose		
	$d\Delta E_g/dS$ mV M ⁻¹	$d\Delta E_{Pb}/dS$ mV M ⁻¹	β M ⁻¹	$d\Delta E_g/dS$ mV M ⁻¹	$d\Delta E_{Pb}/dS$ mV M ⁻¹	β M ⁻¹	$d\Delta E_g/dS$ mV M ⁻¹	$d\Delta E_{Pb}/dS$ mV M ⁻¹	β M ⁻¹
1.000	-2.5	2.4	0.38	-6.0	0.6	0.51	-2.3	22.6	1.94
0.500	-1.5	3.5	0.39	-4.2	0.0	0.34	-1.7	22.4	1.88
0.250	-1.9	3.4	0.41	-4.8	0.1	0.38	-2.0	21.3	1.81
0.100	-1.9	2.9	0.37	-4.7	0.5	0.40	-2.9	21.7	1.91
0.050	-1.2	4.2	0.42	-4.8	0.8	0.44	-2.7	21.7	1.90
0.025	^a	^a	0.41	^a	^a	0.40	^a	^a	1.88
0.100 ^b	-1.5	4.0	0.43	-5.9	-0.6	0.43	-2.6	22.6	1.96

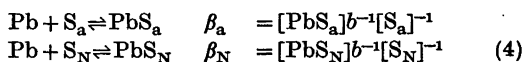
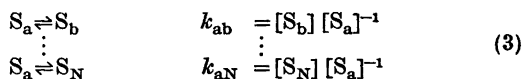
^a In 0.025 M NaClO_4 , E_g and E_{Pb} did not vary linearly with S . The difference $\Delta E_{Pb} - \Delta E_g$ was, however, a linear function of S . ^b in 0.1 M $(\text{C}_2\text{H}_5)_4\text{NClO}_4$.

tion. Since E_j has the same value in (I) and (II) combination of the expressions for ΔE_g and ΔE_{Pb} yields

$$\Delta E_{Pb} = \Delta E_g + 29.58 \lg (B/b) + 29.58 \lg (y_{\text{H}^+} / y_{\text{Pb}^{2+}}) \quad (2)$$

In solution the pentose is present in a number of forms which will be denoted S_a, S_b, \dots, S_N and assumed to form the 1:1 complexes

$\text{PbS}_a, \text{PbS}_b, \dots, \text{PbS}_N$. Charges have been omitted for convenience. Between the various species the following equilibria exist



Activity factors have been left out since they may be expected largely to cancel and for uncharged species to be almost constant.

The total concentrations can be written

$$S = \sum[S_n] + \sum[PbS_n] \quad (5a)$$

$$B = b + \sum[PbS_n] \quad (5b)$$

Combination of eqns. (3), (4), and (5) yields

$$B = b[1 + \sum(\beta_n k_{an}[S_a]); k_{aa} = 1 \quad (6)$$

and from eqns. (5a), (5b), and (3)

$$[S_a] = (S - B + b) (\sum k_{an})^{-1} \approx S (\sum k_{an})^{-1} \quad (7)$$

where the approximate expression is valid when the complex formation is weak. Inserting eqns. (6) and (7) in (2) and differentiating the resulting expression in the case of weak complex formation yields

$$d(\Delta E_{Pb})/dS - d(\Delta E_g)/dS = \Phi \approx 29.58 (\ln 10)^{-1} (\sum \beta_n k_{an}) (\sum k_{an})^{-1} + 29.58 d[\lg(y_{H^+}^2/y_{Pb^{2+}})]/dS \quad (8)$$

The experimental results are thus in accord with eqn. (8) if the activity factors are constant or $\lg(y_{H^+}^2/y_{Pb^{2+}})$ varies linearly with S . Emf measurements evidently cannot be used to find the stability constants of the complexes formed by the individual forms of the carbohydrate. Instead a "mixed" constant, $\beta = \sum \beta_n k_{an} / \sum k_{an}$, is obtained. The values of this constant calculated from eqn. (8) for the three carbohydrates, neglecting the last term, are given in Table 1. The constant for D-ribose is five times larger than the constants for L-arabinose and D-xylose, which are small and have the same value within the limits of the experimental error. There is no significant variation of the constants with the concentration of $(Na)ClO_4$. This is a common result for complex formation with neutral ligands.⁹ It also indicates a negligible interaction between Na^+ and the carbohydrates. This was confirmed by measurements in 0.1 M $(C_2H_5)_4NClO_4$ which led to the same β -values as the measurements in $NaClO_4$.

Calcium complexes. When treating the data from the competition measurements it will be found convenient to let the symbols carry an index [d_1, d_2] in order to indicate the compositions of the equilibrium solutions in cell (I) and (II). The first position in the index refers

to the absence ($d_1=0$) or presence ($d_1=1$) of Ca^{2+} . In the same way $d_2=0$ and $d_2=1$ denote the absence or presence of pentose.

With no pentose present the changes of the emf's of cell (I) and (II) upon addition of Ca^{2+} can be written

$$\Delta E_g[1,0] = E_g[1,0] - E_g[0,0] = \Delta E_j[1,0] - 59.15 \lg y_{H^+}[1,0] \quad (9)$$

$$\Delta E_{Pb}[0,0] = E_{Pb}[1,0] - E_{Pb}[0,0] = \Delta E_j[1,0] - 29.58 \lg y_{Pb^{2+}}[1,0] \quad (10)$$

where $\Delta E_j[1,0] = E_j[0,0] - E_j[1,0]$, and the solution with $c=0$ has been chosen as the standard state. The ratio $y_{H^+}^2[1,0]/y_{Pb^{2+}}[1,0]$ can be found from

$$\Delta E[1,0] = \Delta E_{Pb}[1,0] - \Delta E_g[1,0] = 29.58 \lg (y_{H^+}^2[1,0]/y_{Pb^{2+}}[1,0]) \quad (11)$$

In the presence of pentose the corresponding changes on addition of Ca^{2+} are

$$\Delta E_g[1,1] = \Delta E_j[1,1] - 59.15 \lg y_{H^+}[1,1] \quad (12)$$

$$\Delta E_{Pb}[1,1] = \Delta E_j[1,1] + 29.58 \lg (b[0,1]/b[1,1]) - 29.58 \lg y_{Pb^{2+}}[1,1] \quad (13)$$

and

$$\Delta E[1,1] = 29.58 \lg (b[0,1]/b[1,1]) + 29.58 \lg (y_{H^+}^2[1,1]/y_{Pb^{2+}}[1,1]) \quad (14)$$

On the assumption that the quotients of the activity coefficients in Equations (11) and (14) are equal, one obtains

$$\Delta E = \Delta E[1,1] - \Delta E[1,0] = 29.58 \lg (b[0,1]/b[1,1]) \quad (15)$$

When only 1:1 complexes are formed the expressions for the mass balances and equilibria yield the following equation for calculating b .

$$b^3(\beta_1\beta_2 - \beta_1^2) + b^2(\beta_1\beta_2S - \beta_1^2S - \beta_1 + \beta_2 + \beta_1^2B - 2\beta_1\beta_2B - \beta_1\beta_2C) + b(-\beta_1\beta_2BS + \beta_1B - 2\beta_2B + \beta_1\beta_2B^2 + \beta_1\beta_2BC) + \beta_2B^2 = 0 \quad (16)$$

The stability constants $\beta_1 = \beta_{Pb}$ and $\beta_2 = \beta_{Ca}$ are mixed constants as previously defined.

The value of β_{Ca} can be found by minimizing the error function $X = \sum (\Delta E_{exp} - \Delta E_{calc})^2$. ΔE_{calc} is obtained from the right-hand side of eqn. (15) with $b[0,1]$ and $b[1,1]$ calculated from eqn. (16). Since ΔE_{exp} may be beset by a systematic error from the measurements of the reference potentials $E_g[0,0]$, $E_g[1,0]$, $E_{Pb}[0,0]$,

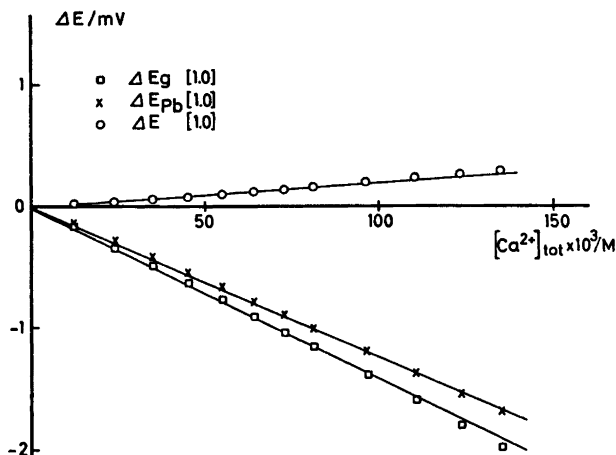


Fig. 2. The changes in the potential of the glass electrode (ΔE_g) and the lead amalgam electrode (ΔE_{Pb}) upon exchange of Na^+ against Ca^{2+} in 1 M (Na) ClO_4 . $\Delta E = \Delta E_{Pb} - \Delta E_g$.

and $E_{Pb}[1,0]$ a parameter, ε , has been added to ΔE_{calc} in order to allow for this situation.

Fig. 2 presents results from the titrations with $S=0$. $\Delta E_g[1,0]$ and $\Delta E_{Pb}[1,0]$ vary linearly with c . The slopes of the lines are not very different. The change in $y_{H^+}[1,0]/y_{Pb^{2+}}[1,0]$ is therefore small, when Na^+ in the background electrolyte is exchanged for Ca^{2+} .

The results in the presence of a pentose are shown in Fig. 3. ΔE for L-arabinose or D-xylose is very small. This is the expected result,

since β_{Pb} is small ($\approx 0.5 \text{ M}^{-1}$). ΔE for D-ribose is large enough to permit a calculation of β_{Ca} . The minimum in X was found by systematic variations of β_{Ca} and ε . From 4 titrations the mean value and the standard deviation of β_{Ca} was found to be $1.6(3) \text{ M}^{-1}$. The ε -values were 0.02 mV or less.

Discussion and comparison with NMR data.

The results of the present measurements agree qualitatively with those obtained from other kinds of measurements. D-Ribose has an

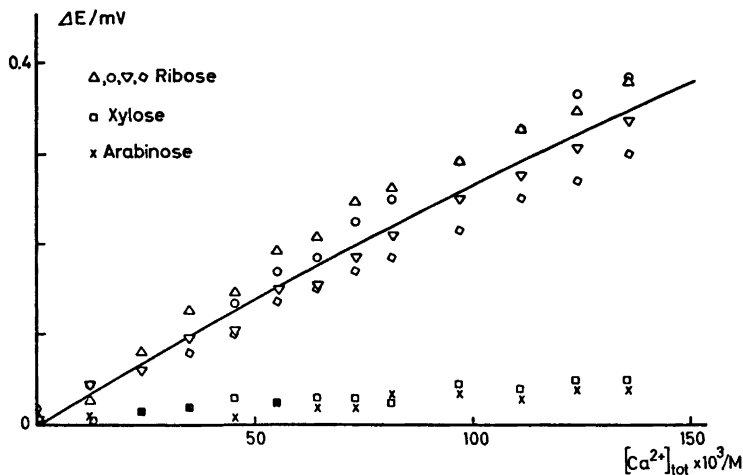


Fig. 3. ΔE defined by Equation (15) as a function of $[\text{Ca}^{2+}]$. The drawn curve represents calculated ΔE values for $\beta_{Ca} = 1.6 \text{ M}^{-1}$.

ax-eq-ax sequence of hydroxyl groups in the α -pyranose form and in the *1C* conformation of the β -pyranose form. A *cis-cis* sequence is present in the α -furanose form. L-Arabinose and D-xylose exist almost exclusively in pyranose forms which lack the *ax-eq-ax* sequence and the stability constants for these carbohydrates are expected to be small as observed.

Angyal² reports that no substantial change in the NMR spectrum of D-arabinose was observed on addition of calcium chloride. If it is assumed that arabinose and xylose do not form complexes the last term in eqn. (8) can be estimated from the Φ -values for these carbohydrates. Φ is independent of the NaClO₄ concentration and its mean value is 5 ± 1 mV M⁻¹ for both compounds. Substituting this figure in eqn. (8) the stability constant for ribose is found to drop from 1.9 to 1.5 M⁻¹. Calculated as a percentage the difference is large between the two values of β_{Pb} and reflects the difficulties in estimating stability constants in weakly interacting systems.^{10,11} The last value might be too small, since it is unlikely that the interaction would be wholly dependent on the presence of one hydroxyl group to complete an *ax-eq-ax* sequence.

In order to obtain more information on this point some experiments were also done with simple alcohols. It was then found that addition of monools and diols with nonadjacent OH-groups resulted in negative values of Φ . Hence these alcohols decrease $y_{H^+}/y_{Pb^{2+}}$.

Diols with vicinal OH-groups and glycerol on the other hand yielded positive values of Φ , the value for glycerol being the greatest and about the same as that for arabinose and xylose. There is thus qualitative agreement between the results of these experiments and the expected order of the strength of the interaction between the metal ion and the alcohols.

Angyal² has determined the stability constants for the complexes between Ca²⁺ and the various forms of D-ribose from NMR spectra. From his results the mixed constant β_{Ca} can be calculated to be 2.0 M⁻¹, which compares quite well with our figure. The mixed constant defined in eqn. (8) was computed from

$$\beta = \frac{\sum \beta_n k_{an} / \sum k_{an} = \sum \beta_n [S_n] / \sum [S_n]}{\sum \beta_n p_n / 100} \quad (9)$$

Table 2. Chemical shifts and coupling constants for anomeric protons of ribose, and the equilibrium compositions of ribose solutions and the equilibrium constants calculated on the basis of these compositions.

	Pyranose		Furanose	
	α	β	α	β
0.5 M ribose				
δ	4.86	4.93	5.4	5.25
J/Hz	2.2	6.3	—	1.3
%	21.6	57.6	6.6	14.2
0.5 M ribose + 1.5 M CaCl ₂				
δ	4.99	5.13	5.50	5.31
J/Hz	2.2	3.9	4.0	—
%	43.4	41.7	10.9	3.9
β_n/M^{-1}	5.5	1.4	4.4	^a
0.5 M ribose + 1.0 M Pb(ClO ₄) ₂				
δ	5.02	5.12	5.48	5.28
J/Hz	1.7	4.2	4.3	—
%	43.7	43.2	7.9	5.2
β_n/M^{-1}	6.7	1.5	3.4	^a
0.5 M ribose + 1.0 M Pb(NO ₃) ₂				
δ	5.0	5.07	5.47	5.29
J/Hz	1.7	4.6	—	—
%	34.1	52.2	7.5	6.3
β_n/M^{-1}	3.5	1.4	2.2	^a

^a Assumed not to form complexes.

where p_n is the percentage of the n 'th form of the pentose. No constants are available for the Pb²⁺ complexes and these were therefore determined from NMR spectra as outlined in Ref. 2. The results are entered in Table 2. The data for the pure ribose solution and the constants for the calcium complexes agree well with those reported in Ref. 2. The value of the mixed constant is 2.5 M⁻¹ with Pb(ClO₄)₂ and 1.7 M⁻¹ with Pb(NO₃)₂ and thus about the same as found by the emf method. The smaller value found in nitrate medium probably reflects the fact that Pb²⁺ is complexed by NO₃⁻.¹² Complexation — in this case by acetate ions — is probably the reason why the constant for the Pb²⁺-D-allose complex is considerably smaller than for the corresponding alkaline earth metal complexes.²

The results of the present investigation suggest that stability constants for carbohydrate complexes determined at high concentrations are also applicable at low concentrations,

but the small values of the constants make it unlikely that metal ion-carbohydrate interactions are of much importance in, for instance, biological systems.

Acknowledgements. Dr P. Ahlberg and Mrs C. Engdahl are thanked for their generous help with the NMR measurements. This work has been supported by the Swedish Natural Science Research Council.

REFERENCES

1. Rendleman, J. A., Jr. *Adv. Carbohydr. Chem.* 21 (1966) 209.
2. Angyal, S. J. *Aust. J. Chem.* 25 (1972) 1957.
3. Angyal, S. J. *Pure Appl. Chem.* 35 (1973) 131.
4. Andrasko, J. and Forsén, S. *Biochem. Biophys. Res. Commun.* 52 (1973) 233.
5. Evans, M. E. and Angyal, S. J. *Carbohydr. Res.* 25 (1972) 43.
6. Angyal, S. J. and Hickman, R. J. *Aust. J. Chem.* 28 (1975) 1279.
7. Carell, B. and Olin, Å. *Acta Chem. Scand.* 15 (1961) 727.
8. Olin, Å. and Svanström, P. *Acta Chem. Scand. A* 29 (1975) 849.
9. Bjerrum, J. *Metal Ammine Formation in Aqueous Solution*, Diss., P. Haase and Son, Copenhagen 1941.
10. Bjerrum, J. *Trans. Royal Inst. Tech. Stockholm No. 253* (1972) 69.
11. Hindman, J. C. and Sullivan, J. C. In Martell, A. E., Ed., *Coordination Chemistry*, Vol. 1, ACS Monograph 168, Van Nostrand Reinhold Company, New York 1971.
12. *Stability Constants*, The Chemical Society, London, Spec. Publ. Nos. 17 (1964) and 25 (1971).

Received June 22, 1977.

NMR Studies on Cyclic Arsenites. ^{13}C NMR Spectra of Seventeen 1,3,2-Dioxarsenanes

DAGFINN W. AKSNES

Department of Chemistry, University of Bergen, Allégaten 70, N-5014 Bergen-Univ., Norway

^{13}C chemical shifts have been measured for five 2-substituted 1,3,2-dioxarsenanes and twelve of their ring-substituted methyl derivatives. A variety of general trends are observed in the ^{13}C NMR data and a comparison with related heterocyclic systems has been made.

The substituent at arsenic has a marked influence on the ring carbon shieldings. By comparing compounds differing only in the 2-substituent it is seen that the shielding at C(4,6) increases in the series Ph, Br, Cl, OPh, and OMe. However, the shift effect of these substituents except Ph, on the C(5) carbon is opposite that for C(4,6).

On the introduction of an equatorial 4- or 6-methyl group the ring carbon atoms experience lowfield α_e , β_e , and γ_e shifts of 5.6–6.2, 6.5–6.6, and 0.2–0.5 ppm, respectively. An axial 6-methyl group produces similar deshielding effects at the α and β carbons whereas the γ carbon is shielded. 5-*gem*-Dimethyl substitution produces significantly smaller lowfield shifts than substitution at C(6).

The ^{13}C nucleus of a single equatorial methyl group at C(4,6) resonates near 24 ppm from TMS regardless of the substituent at arsenic. Furthermore, the ^{13}C signal of an axial methyl group appears downfield from the signal of an equatorial methyl group.

Recently increasing attention has been paid to ^{13}C NMR spectra of various heterocyclic ring systems.¹ The reported ^{13}C NMR studies on 1,3-dioxanes,^{2,3} trimethylene sulfites^{4,5} and 1,3,2-dioxaphosphorinanes^{6–8} which are of particular relevance to this work, constitute a very useful addition to previous ^1H NMR studies.

In favourable cases^{4,9} ^{13}C chemical shifts are an order of magnitude more sensitive to steric factors than ^1H chemical shifts. Furthermore, quite often certain substituent trends are sufficiently well defined that even relatively small shielding differences offer valuable as-

sistance in signal identification and may lead to definitive stereochemical assignments.^{1–4,9}

As part of our NMR studies on cyclic arsenites we have investigated the ^{13}C NMR spectra of a series of 1,3,2-dioxarsenanes. Previous NMR studies^{10–14} have been confined to proton spectra and the present paper reports the first ^{13}C NMR investigation on these compounds.

EXPERIMENTAL

The syntheses of the cyclic arsenites have been described in previous papers.^{12–14}

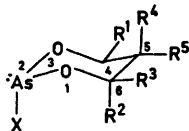
The seventeen compounds were examined in deuteriochloroform solutions (ca. 30 % v/v) at ambient probe temperature. A small amount of TMS was added to the samples and used as internal standard whereas deuteriochloroform served as internal ^2H lock signal source.

The ^{13}C NMR spectra of all compounds except III and XV, were recorded in 10 mm o.d. tubes on a Jeol FX 60 spectrometer operating at 15.04 MHz. The ^{13}C NMR spectra of III and XV were run in 5 mm o.d. tubes at 25.05 MHz on a Jeol FX 100 spectrometer. A spectral width of 2.5 or 4 kHz and a data memory size of 8 K were used.

Off-resonance decoupling was used for the purpose of signal identification.

RESULTS AND DISCUSSION

The studied compounds and the obtained ^{13}C chemical shift data are summarized in Table 1. The ^{13}C chemical shifts were obtained under proton-noise decoupling conditions. The assignment of the resonance signals due to C(4) and C(6) followed from the downfield inductive effect of the ring oxygen atoms and intensity considerations. For the methyl compounds off-

Table 1. ^{13}C NMR chemical shifts (ppm from TMS) of 1,3,2-dioxarsenanes measured in deuteriochloroform solution.

Compound	Substituents X	R ¹ ^a	C(4)	C(5)	C(6)	4-Me ^c	5-Me	6-Me	2-OMe
I	Cl		62.85	30.32	62.85				
II	Br		64.26	30.21	64.26				
III	OMe		61.30	31.19	61.30				49.80
IV	OPh		62.01	30.65	62.01				
V	Ph		64.45	34.05	64.45				
VI	Cl		69.07	36.84	63.28	23.65			
VII	OMe	R ¹ = Me	67.01	37.73	61.81	23.96			
VIII	OPh		67.64	37.29	62.18	23.91			49.80
IX	Cl	R ¹ = R ³ = Me	69.67	43.89	69.67	23.63		23.63 (eq)	
X	OMe		66.16	44.87	66.16	24.74		24.74 (eq)	49.15
XI ^b	Cl	R ¹ = R ² = Me	67.72	39.93	67.72	23.57		23.57 (ax)	
XII	OMe		62.46	41.43	68.44	23.89		24.22 (ax)	49.61
XIII	Cl	R ¹ = R ³ = R ⁵ = Me	65.85	46.20	77.58	23.84		33.07 (ax)	
XIV	OMe		62.94	48.01	74.59	24.11		28.33 (eq)	49.43
XV ^b	Cl	R ⁴ = R ⁵ = Me	71.99	32.94	71.99		22.14 (ax)		
XVI	OMe		70.63	33.27	70.63		22.14 (eq)		49.83
XVII	OPh		71.15	33.01	71.15		21.90 (eq)		
							22.81 (ax)		
						21.77 (eq)			

^a R¹ = H unless otherwise stated. ^b The observed chemical shifts are the result of rapid exchange of chlorine. ^c The 4-methyl group is equatorial.

resonance decoupling together with empirically established trends of methyl substitution on carbon resonances,^{3,9,15} aided the signal assignments.

The empirical approach used in this work is similar to the methods applied in ^{13}C NMR spectroscopy by many authors to rationalize, if not always to explain, experimental results. A variety of general trends can be observed in the data of Table 1, and a comparison with similar data for the related phosphites,⁶⁻⁸ sulfites^{4,5} and dioxanes^{2,3} should be made.

Previous ^1H NMR studies¹¹⁻¹⁴ have shown that the 1,3,2-dioxarsenane ring has a chair conformation and that the preferred orientation of the 2-substituent at arsenic is axial. Furthermore, Arbuzov *et al.* report,¹⁶ in a study based on measurements of dipole moments and Kerr constants, that the As-Cl

bond is axial in 2-chloro-4-methyl-1,3,2-dioxarsenane. Supporting evidence for a predominantly axial orientation of the 2-methoxy group is found in the remarkably similar ^{13}C chemical shift values observed for this group in the 2-methoxy-1,3,2-dioxarsenanes and their axially 2-substituted phosphorus analogues.⁷ (The ^{13}C signal of the $P\text{-OCH}_3$ group appears *ca.* 1 ppm upfield in the equatorially substituted stereoisomer).

The substituent at arsenic has a marked influence on the ring carbon shieldings. By comparing compounds differing only in the 2-substituent it is seen that the shielding at C(4) and C(6) increases in the series Ph, Br, Cl, OPh, and OMe. An axially oriented substituent at arsenic is *gauche* related to the C(4,6) carbon atoms and should give rise to a maximal γ effect.^{9,15} However, the steric γ ef-

Table 2. ¹³C NMR chemical shifts of α , β , and γ ring carbons in methyl substituted 2-chloro-, 2-methoxy- and 2-phenoxy-1,3,2-dioxarsenanes relative to the unsubstituted parent compounds (possessing the same 2-substituent).

Compound	Substituents ^a	$\Delta C(4)$	$\Delta C(5)$	$\Delta C(6)$
VI	2-Cl-4-Me	6.2	6.5	0.4
VII	2-OMe-4-Me	5.7	6.5	0.5
VIII	2-OPh-4-Me	5.6	6.6	0.2
IX	2-Cl-4,6- <i>cis</i> -di-Me	6.8	13.6	6.8
X	2-OMe-4,6- <i>cis</i> -diMe	4.9	13.7	4.9
XI	2-Cl-4,6- <i>trans</i> -diMe	4.9	9.6	4.9
XII	2-OMe-4,6- <i>trans</i> -diMe	1.2	10.2	7.1
XIII	2-Cl-4,6,6-triMe	3.0	15.9	14.7
XIV	2-OMe-4,6,6-triMe	1.6	16.8	13.3
XV	2-Cl-5,5-diMe	9.1	2.6	9.1
XVI	2-OMe-5,5-diMe	9.3	2.1	9.3
XVII	2-OPh-5,5-diMe	9.1	2.4	9.1

^a The 4-methyl group is equatorial.

fect cannot account for the large downfield shifts produced by phenyl and bromine in comparison with methoxy.

The phenyl group produces a significant downfield shift on C(5) as well. In contrast, all the other 2-substituents give rise to a shift effect on C(5) opposite that for C(4,6). The relatively small ¹³C chemical shift range measured for C(5) can be largely ascribed to the remote δ effect.^{15,17}

The chemical shift effect of methyl substitution is obtained by comparing the ¹³C chemical shifts of the methyl derivatives with the corresponding parent compounds (Table 2).

On the introduction of an equatorial 4-methyl group to the basic ring system the C(4), C(5), and C(6) ring carbon atoms of compounds VI–VIII experience α_e , β_e , and γ_e deshielding effects of 5.6–6.2, 6.5–6.6, and 0.2–0.5 ppm, respectively. Similar α_e deshielding effects of an equatorial 4-methyl group have been reported for 1,3-dioxane (7.3 ppm),³ trimethylene sulfite (6.7–7.0 ppm)^{4,5} and methyl cyclohexanes (6.0 ppm).¹⁵

The *ca.* 6.5 ppm β_e deshielding effect on C(5) in the 4-methyl substituted arsenanes VI–VIII is again similar to the 7.3 ppm downfield shift observed in the corresponding 1,3-dioxane³ and trimethylene sulfite.^{4,5} Mason¹⁸ has proposed that a diamagnetic term comparable in

magnitude to the paramagnetic terms is contributing to the α carbon shifts. This is a possible explanation of why the α_e and β_e shifts are roughly equal in magnitude.

The observed downfield shifts for IX and X are similar to those reported for the analogous 4,6-*cis*-dimethyl substituted 2-methoxy-1,3,2-dioxaphosphorinane⁷ and trimethylene sulfite.⁴ The results for these related ring systems indicate when compared with the corresponding mono-4-methyl substituted derivatives, that the shift effect of the two equatorial methyl groups is roughly additive as expected.

The ¹³C NMR shifts for XI and XV show that a process which leads to exchange of the nuclear magnetic environments of the asymmetric C(4,6) ring carbons and/or methyl carbons, is taking place. In accordance with previous ¹H NMR results,^{12,14,19} this process is believed to be an intermolecular chlorine exchange.

The observed α_a and β_a deshielding effects of the axial 6-methyl group in XII are consistent with similar results for the related sulfites ($\alpha_a \approx 6-14$ and $\beta_a \approx 5$ ppm).⁴ Replacement of both hydrogen atoms on C(6) by methyl shifts the C(6) resonance downfield by *ca.* 14 ppm in the trimethyl derivatives XIII and XIV, as compared with 33.5 ppm in the corresponding sulfite (axial S=O).⁴ In 1,3-dioxanes³ and cyclohexanes,¹⁵ however, *gem*-dimethyl substitution produces a significantly smaller downfield shift on the α carbon (*ca.* 4 ppm).

It is interesting to note that C(4) of compounds XI–XIV is shielded by 2–4 ppm relative to the corresponding 4,6-*cis*-dimethyl derivatives IX and X. Similar upfield shifts have also been observed for similarly substituted sulfites⁴ and dioxanes.³ We believe, in agreement with Buchanan *et al.*⁴ that steric interactions between the axial methyl group on C(6) and the axial hydrogen atom on C(4) are likely to be causing this shielding (γ effect).

It is notable that the α carbon bearing the axial methyl group suffers a considerably larger downfield shift in the arsenites and sulfites as compared with dioxanes and cyclohexanes. However, the β and γ ring carbons appear to be similarly affected by the axial methyl group in these four six-membered ring systems.

The ¹³C NMR data for compounds XV–XVII and 2-methoxy-5,5-dimethyl-1,3,2-dioxaphos-

phorinane⁷ show that *gem*-dimethyl substitution at C(5) produces a significantly smaller shift effect than substitution at C(4,6). This observation may be a reflection of the much less hindered environments of C(5) compared with C(4,6).

Apparently the ¹³C nucleus of a single equatorial methyl group at C(4) or C(6) resonates near 24 ppm (from TMS) regardless of the substituent at arsenic.

The ¹³C signal of an axial methyl group at C(6) appears downfield from the signal of an equatorial methyl group at C(4,6) in XII–XIV and the analogous sulfites.⁴ The remote δ effect^{9,17} is probably responsible for this downfield shift.

Similarly, the ¹³C signal of an axial methyl on C(5) appears at lower field than the geminal equatorial methyl signal in XVI and XVII and the corresponding phosphites⁷ and dioxanes.³ This is, however, the reverse of what is observed in methyl cyclohexanes¹⁵ (upfield γ effect). In the three series of heterocyclic compounds the axial methyl group at C(5) has no *syn*-axial hydrogen atoms with which to interact but rather appears to be deshielded by the ring oxygen atoms. Similar shielding effects are apparently operating on the methyl protons as well since the proton signal of the axial methyl group appears downfield for the equatorial methyl signal in these heterocyclic compounds.^{13,14,19–21}

Acknowledgements. The author is indebted to Mrs. Grete Wöien, Chemical Institute, University of Oslo, and førsteamanuensis Jostein Krane, Department of Chemistry, University of Trondheim, for their assistance in recording the ¹³C NMR spectra.

REFERENCES

- See, for example, Eliel, E. L., Bailey, W. F., Kopp, L. D., Willer, R. L., Grant, D. M., Bertrand, R., Christensen, K. A., Dalling, D. K., Duch, M. W., Wenkert, E., Schell, F. M. and Cochran, D. W. *J. Am. Chem. Soc.* **97** (1975) 322, and references therein.
- Jones, A. J., Eliel, E. L., Grant, D. M., Knoeber, M. C. and Bailey, W. F. *J. Am. Chem. Soc.* **93** (1971) 4772.
- Kellie, G. M. and Riddell, F. G. *J. Chem. Soc. B* (1971) 1030.
- Buchanan, G. W., Stothers, J. B. and Wood, G. *Can. J. Chem.* **51** (1973) 3746.
- Albriktsen, P. *Acta Chem. Scand.* **27** (1973) 3889.
- Bentrude, W. G., Yee, K. C., Bertrand, R. D. and Grant, D. M. *J. Am. Chem. Soc.* **93** (1971) 797.
- Haemers, M., Ottinger, R., Zimmermann, D. and Reisse, J. *Tetrahedron* **29** (1973) 3539.
- Bentrude, W. G. and Tan, H.-W. *J. Am. Chem. Soc.* **95** (1973) 4666.
- Stothers, J. B. *Carbon-13 NMR Spectroscopy*, Academic, New York 1972; Levy, G. C. and Nelson, G. L. *Carbon-13 Nuclear Magnetic Resonance for Organic Chemists*, Wiley, New York 1972.
- Aksnes, D. W. and Vikane, O. *Acta Chem. Scand.* **26** (1972) 4170.
- Samitov, Y. Y., Taceeva, N. K., Chadaeva, N. A. and Kamai, C. H. *Chemistry of Heterocyclic Compounds*, (Russian) 1973, No. 4, p. 457.
- Aksnes, D. W. *Acta Chem. Scand. A* **28** (1974) 1175.
- Aksnes, D. W. and Tøgersen, S. *Acta Chem. Scand. A* **29** (1975) 376.
- Aksnes, D. W., Andersen, J. and Bergesen, K. *Acta Chem. Scand. A* **30** (1976) 327.
- Dalling, D. K. and Grant, D. M. *J. Am. Chem. Soc.* **89** (1967) 6612; **94** (1972) 5318.
- Arbuzov, B. A., Anonimova, I. V., Vul'fson, S. G., Yuldasheva, L. K., Chadaeva, N. A. and Vereshchagin, A. N. *Phosphorus* **5** (1974) 17.
- Grover, S. H., Guthrie, J. P., Stothers, J. B. and Tan, C. T. *J. Magn. Reson.* **10** (1973) 227.
- Mason, J. *J. Chem. Soc. A* (1971) 1038.
- White, D. W., Bertrand, R. D., McEwen, G. K. and Verkade, J. G. *J. Am. Chem. Soc.* **92** (1970) 7125.
- Maroni, P. and Gorrichon, J.-P. *Bull. Soc. Chim. Fr.* (1972) 785.
- Cazaux, L. and Maroni, P. *Bull. Soc. Chim. Fr.* (1972) 773.

Received June 13, 1977.

Solvation and Ion-pair Formation of Lithium Bromide in Acetone-methanol and Acetone-ethanol Mixtures Studied by Reaction Kinetics

ALLAN HOLMGREN and PER BERONIUS

Division of Physical Chemistry, University of Umeå, S 901 87 Umeå, Sweden

Kinetic data at 25 °C for the exchange of bromine between lithium bromide and butyl bromide in acetone-methanol and acetone-ethanol mixtures containing between 0.1 and 1.0 wt-% of the hydroxylic compound are reported. The data have been analyzed by means of the McKay and Acree equations. The exchange appears to be of S_N2-type. The second-order rate constant for the exchange between free bromide ions and the organic bromide decreases strongly with increasing concentration of the hydroxylic constituent of the solvent medium. Ion-pairs of lithium bromide have been found to be kinetically inactive. The dependence of the kinetics on the composition of the solvent mixture is discussed in terms of preferential solvation of the ionic bromide. Transfer activity coefficients, estimated from the kinetic data, are used to obtain information about solvation of lithium bromide ion-pairs in the solvent mixtures investigated.

The kinetics of the exchange of ⁸²Br between butyl bromide and lithium bromide in acetone-water mixtures was studied in earlier investigations.^{1,2} The water present in the solvent was found to have a strong inhibitory effect on the exchange reaction. This effect was interpreted as a difference in solvation of the activated complex and the reactants caused by hydrogen bond formation.

The main purpose of the present investigation was to study how the same exchange reaction is affected upon substituting the water in the solvent mixture by methanol and ethanol, respectively.

Measurements were performed at several different lithium bromide concentrations be-

tween 2×10^{-4} and 8×10^{-3} M. The concentration of the protic component in the solvent mixture varied between 0.1 and 1.0 wt-%. At these low concentrations of protic component in acetone, the self-association of hydroxylic molecules is minimized and the macroscopic permittivity is retained at almost a constant value.

EXPERIMENTAL

The acetone used (Merck, *p.a.*) was purified according to Ref. 1. Its density at 25 °C was 0.7843 kg dm⁻³.

Methanol (Merck, *p.a.*) was dried over a molecular sieve (Fischer Sci. Co. type 4 A) and fractionally distilled in a Widmer column. The same procedure was used to purify "absolute" ethanol (99.9 %).

After purification the densities of methanol and ethanol were 0.7867 kg dm⁻³ and 0.7851 kg dm⁻³, respectively.

Solvent mixtures of acetone-methanol and acetone-ethanol were prepared by weight at 25 °C.

Butyl bromide (Fluka, *puriss*) was dried over phosphorus pentoxide and fractionally distilled.

Lithium bromide (Fluka, *suprapur*) was dried at 200 °C for 6 h and cooled in a vacuum desiccator.

The method employed to convert inactive lithium bromide to radiobromide and the preparation of solutions of lithium radiobromide of different concentrations has been reported.¹

The course of the exchange reaction was followed electroanalytically by anodic deposition of bromide on silver electrodes according to Refs. 3–4.

The electrode reaction, $\text{Ag} + \text{Br}^- \rightarrow \text{AgBr} + \text{e}^-$, was investigated with respect to the dependence

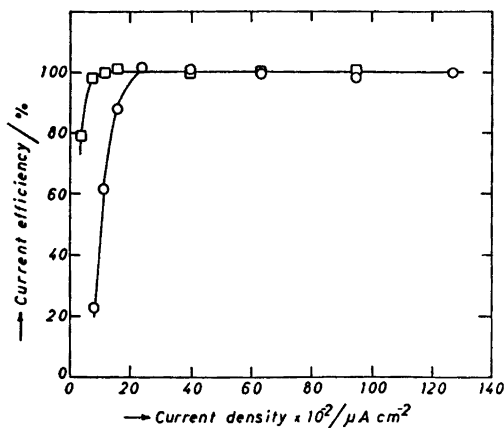


Fig. 1. Graphs of current efficiency vs. current density for 5.1×10^{-4} M (squares) and 2.04×10^{-3} M (open circles) solutions of lithium bromide in acetone containing 0.1 wt-% methanol at 25°C.

of the current efficiency on the current density. Fig. 1 representatively illustrates how the shape of the current efficiency-current density curve depends on the concentration of lithium bromide at constant solvent composition (acetone-methanol containing 0.1 wt-% of the hydroxylic constituent).

RESULTS AND DISCUSSION

The kinetic data were analyzed by means of the McKay equation⁵ using the method of least squares. The results are summarized in Tables 1–2, in which the second-order rate constant, k , is defined by the expression,

$$k = R/(bc) \quad (1)$$

where R is the total rate of exchange, b is the concentration of butyl bromide, and c is the concentration of lithium bromide.

The degree of dissociation of the inorganic bromide, α , was calculated from ion-pair association constants, K_A , of lithium bromide in the various solvent mixtures investigated.

The association constants listed in Table 3 were evaluated from electrical conductance data^{6,7} by means of the Fuoss-Hsia conductance equation^{8,9} in the form developed by Fernandez-Prini.¹⁰ The mean activity coefficient of free ions was evaluated from the Debye-Hückel equation.¹¹

Table 1. Kinetic data for the exchange of ^{82}Br between lithium bromide and butyl bromide in acetone-methanol mixtures at 25.0°C.

$b \times 10^3$ M	$c \times 10^4$ M	$R \times 10^6$ M s ⁻¹	$k \times 10^4$ M ⁻¹ s ⁻¹	α
0.10 wt-% CH ₃ OH				
5.087	76.64	56.570	14.51	0.2239
5.087	19.71	25.898	25.83	0.3693
5.046	9.975	14.869	29.54	0.4634
5.106	4.731	8.9862	37.20	0.5780
5.108	2.091	4.5126	42.25	0.7051
0.30 wt-% CH ₃ OH				
5.125	79.34	47.778	11.75	0.2493
5.132	39.18	29.336	14.59	0.3228
5.101	20.39	18.961	18.23	0.4046
5.136	9.841	11.721	23.19	0.5094
5.087	5.109	6.9964	26.92	0.6110
5.110	1.960	3.1830	31.78	0.7546
1.00 wt-% CH ₃ OH				
4.878	77.60	32.826	8.672	0.3133
5.089	39.41	18.598	9.273	0.3948
5.076	19.81	12.911	12.84	0.4900
5.106	4.608	4.5175	19.20	0.7097

Table 2. Kinetic data for the exchange of ^{82}Br between lithium bromide and butyl bromide in acetone-ethanol mixtures at 25.0°C.

$b \times 10^3$ M	$c \times 10^4$ M	$R \times 10^6$ M s ⁻¹	$k \times 10^4$ M ⁻¹ s ⁻¹	α
0.30 wt-% C ₂ H ₅ OH				
5.047	65.55	49.261	14.89	0.2402
5.172	43.89	38.454	16.94	0.2793
5.067	22.19	25.017	22.25	0.3575
5.632	11.04	16.630	26.75	0.4523
5.163	5.538	9.4842	33.17	0.5571
5.077	2.273	4.5952	39.82	0.6962
0.60 wt-% C ₂ H ₅ OH				
5.317	45.63	30.812	12.70	0.2975
4.958	30.22	21.531	14.37	0.3448
5.692	14.98	16.550	19.41	0.4373
5.458	7.561	9.3266	22.60	0.5391
5.119	3.746	5.2753	27.51	0.6488
5.002	1.548	2.5560	33.01	0.7776
1.00 wt-% C ₂ H ₅ OH				
5.083	80.22	37.701	9.246	0.2603
5.140	42.64	29.807	13.60	0.3274
5.145	21.34	16.733	15.24	0.4148
5.153	10.59	9.8390	18.03	0.5162
5.032	5.323	5.9812	22.33	0.6225
5.200	2.115	3.0003	27.29	0.7594

Table 3. Permittivities and conductance parameters for lithium bromide in acetone-methanol⁶ and acetone-ethanol⁷ mixtures at 25°C. The values of K_A for acetone-methanol as solvent have been reevaluated (see text) from conductance data in Ref. 6.

Hydroxylic conc. wt-%	ϵ	K_A M^{-1}	$r \times 10^{10}$ m
Methanol			
—	20.7	4160	13.54
0.10	20.6	3436	13.60
0.30	20.6	2664	13.60
1.00	20.7	1640	13.54
Ethanol			
0.30	20.6	3361	13.60
0.60	20.6	2830	13.60
1.00	20.6	2407	13.60

The ion-pair association constant, and hence the rate constants k_i and k_m , were found to be only slightly sensitive to the maximum center-to-center distance, r , between the ions in the ion-pair within the range $q/2 \leq r \leq q$, where q is the Bjerrum radius.¹² The association constants in Table 3, corresponding to $r=q$, were used in evaluating the α -values listed in Tables 1–2.

If the exchange of bromine between the organic and inorganic bromides is a mixed S_N1-S_N2 reaction and if the contribution of ion-pairs of lithium bromide to the reaction rate is negligible, the latter may be expressed,

$$R = k_1 b + k_i b c \alpha \quad (2)$$

where k_1 is the first-order rate constant, k_i is the second-order rate constant for the exchange of free bromide ions, and α is the degree of dissociation of the ion-pairs.

According to eqn. (2) a graph of R/b vs. $c\alpha$ should yield a straight line with intercept equal to k_1 .

Graphs of this kind are shown in Figs. 2–3. All lines pass within experimental error through the origin indicating no significant S_N1 contribution to the reaction rate. Hence the exchange mechanism is considered to be of S_N2 -type.

If the ion-pairs contribute to the rate of exchange a term, $k_m b c (1-\alpha)$, where k_m is the second-order rate constant for the exchange of bromide between butyl bromide and lithium

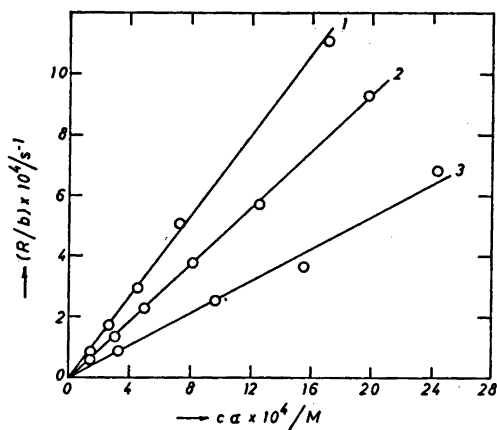


Fig. 2. Graphs of R/b vs. $c\alpha$ for the exchange of bromine between lithium bromide and butyl bromide in acetone-methanol mixtures at 25°C. The curves 1–3 refer to solvent mixtures containing 0.1, 0.3 and 1.0 wt-% methanol, respectively.

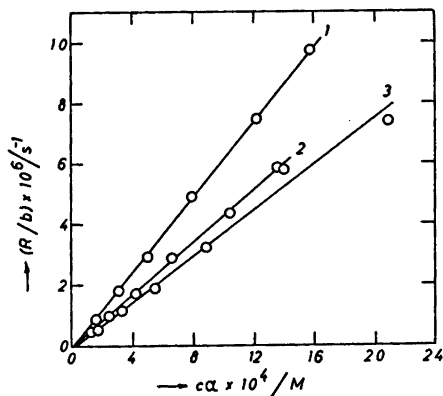


Fig. 3. Graphs of R/b vs. $c\alpha$ according to eqn. (2) for the same exchange reaction as in Fig. 2, in acetone-ethanol mixtures at 25°C. The curves 1–3 refer to solvent mixtures containing 0.3, 0.6 and 1.0 wt-% ethanol, respectively.

bromide ion-pairs, should be added to the right-hand side of eqn. (2). Combination of eqn. (1) with k_1 set equal to zero, and the extended form of eqn. (2) yields,

$$k/\alpha = k_i + k_m(1-\alpha)/\alpha \quad (3)$$

which is the Acree equation.¹³

Rate constants, k_i and k_m , derived from eqn. (3) by means of a relative deviation least squares treatment¹⁴ of the kinetic data in

Table 4. Rate constants for reactions of ions and ion-pairs, k_i and k_m , respectively, for the same systems as in Tables 2 and 3.

Hydroxylic conc. wt-%	$k_i \times 10^4$ $M^{-1} s^{-1}$	$k_m \times 10^4$ $M^{-1} s^{-1}$
Methanol		
—	78.15 ± 0.40^a	1.0 ± 0.2^a
0.10	62.7 ± 2.9	1.2 ± 3.8
0.30	42.8 ± 0.7	1.4 ± 0.4
1.00	26.2 ± 2.5	-0.05 ± 1.73
Ethanol		
0.30	57.7 ± 1.0	1.5 ± 0.5
0.60	42.6 ± 0.8	0.03 ± 0.59
1.00	35.6 ± 1.9	0.8 ± 1.2

^a Data from Ref. 2.

Tables 1–2, are summarized in Table 4 in which the corresponding rate constants for pure acetone as solvent medium are included. The errors listed in this table and elsewhere are standard deviations.

The rapid decrease in rate of exchange between the organic bromide and bromide ions with increasing concentration of methanol and ethanol, respectively, is illustrated in Fig. 4, where the corresponding graph for acetone-water solvent mixtures is included.

According to Fig. 4 the effectiveness of the protic component as inhibitor for the exchange reaction decreases in the following order:

Methanol > ethanol > water

The order between ethanol and water is the same as that found by Leary and Kahn,¹⁵ who investigated the effect of various protic components in acetone on the kinetics of the exchange of radiiodine between potassium iodide and benzyl iodides. The order between methanol and ethanol indicates that the ionic reactant is more strongly solvated by methanol than by ethanol. The same order has been reported by Becker,¹⁶ who investigated hydrogen-bonding in several alcohol-base systems by means of infrared spectroscopy.

Free energies of formation of 1:1 hydrogen-bonded complexes between acetone-methanol and acetone-ethanol were found to be -1.5 and -0.5 kJ mol⁻¹, respectively.

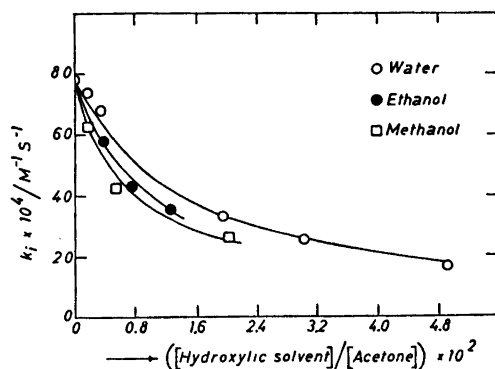
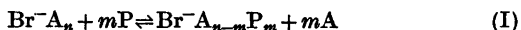


Fig. 4. The variation of k_i with solvent composition as calculated from eqn. (8).

The decrease in rate of the exchange reaction with increasing concentration of the protic component may be qualitatively explained by the ability of the hydroxylic constituent to form hydrogen bonds. This would result in a decrease in Gibbs' free energy of activation for the exchange reaction, in the following order:

Acetone-methanol > acetone-ethanol > acetone-water > acetone

If we assume that unpaired bromide ions in a solution of acetone containing a protic component of low concentration are solvated by either n molecules of acetone ("A") or by $(n-m)$ molecules of acetone and m molecules of protic component ("P"), we are concerned with the solvation equilibrium (I), cf. Ref. 2.



Following the derivation in Ref. 2, the overall equilibrium constant, K , for the equilibrium (I) may be written as eqn. (4), and the rate of

$$K = \frac{[\text{Br}^- \text{A}_{n-m} \text{P}_m][\text{A}]^m}{[\text{Br}^- \text{A}_n][\text{P}]^m} \quad (4)$$

exchange may be expressed as eqn. (5), where

$$R = k_A b [\text{Br}^- \text{A}_n] + k_{AP} b [\text{Br}^- \text{A}_{n-m} \text{P}_m] \quad (5)$$

k_A is the rate constant for exchange of bromine between $\text{Br}^- \text{A}_n$ and butyl bromide and k_{AP} is the rate constant for the corresponding exchange reaction involving $\text{Br}^- \text{A}_{n-m} \text{P}_m$.

Using the results of eqns. (2-3), which indicate that the terms containing k_1 and k_m may be omitted, together with the stoichiometric condition for bromide ions [eqn. (6)],

$$[\text{Br}^-]_{\text{tot}} = [\text{Br}^- \text{A}_n] + [\text{Br}^- \text{A}_{n-m} \text{P}_m] \quad (6)$$

we obtain upon combining eqns. (4-6) eqn. (7).

$$\lg \frac{k_A - k_i}{k_i k_A} = m \lg \frac{[\text{P}]}{[\text{A}]} + \lg \frac{K}{k_A} \quad (7)$$

A condition for eqn. (7) to be valid is that the concentration of the protic component in the solvent mixtures is sufficiently low to keep $k_i \gg k_{\text{AP}}$.

Eqn. (7) was fitted to the kinetic data in Table 4 according to the method of least squares. The equation of the straight lines yielded the overall values $m = 0.90 \pm 0.11$ and $m = 1.02 \pm 0.15$ for the bromide ion in acetone containing methanol and ethanol, respectively. For the solvation equilibrium involving bromide ions in acetone-water mixtures² at 25°C, the value of m is 1.09 ± 0.06 . According to these calculations the overall number of hydroxylic molecules associated with each bromide ion is close to one for the range of concentrations of hydroxylic compound investigated.

If m is set equal to one, eqn. (7) may conveniently be rewritten [eqn. (8)].

$$\frac{1}{k_i} = \frac{1}{k_A} + \frac{K}{k_A} \frac{[\text{P}]}{[\text{A}]} \quad (8)$$

To evaluate K , eqn. (8) was fitted to values of $1/k_i$ vs. $[\text{P}]/[\text{A}]$ using the relative deviation least squares method. For the acetone-methanol and acetone-ethanol systems this procedure yielded $K = 110$ and $K = 98$, respectively. Compare these values with the figure, $K = 73$, for the corresponding equilibrium in acetone-water.¹

If the hydroxylic compound as a hydrogen-bond donor solvates the bromide ion much more strongly than acetone, the solvation equilibrium (II) may be used to calculate m and K . The numerical values of m



calculated on this assumption are the same as those calculated for equilibrium (I). With $m = 1$ equilibrium (II) yields $K = 7.3$ and 8.2

for the acetone-ethanol and acetone-methanol systems, respectively.

In a previous paper² transfer activity coefficients were used to obtain information about changes in ion-pair solvation when small amounts of water were added to anhydrous acetone.

The transfer activity coefficient is defined¹⁷⁻¹⁸ in eqn. (9), where $(\mu_i^0)_S$ stands for the standard

$$(\mu_i^0)_S = (\mu_i^0)_R + RT \ln \gamma_{i,i} \quad (9)$$

chemical potential of a solute, "i", in any solvent, "S", $(\mu_i^0)_R$ is the corresponding quantity in the selected reference solvent, "R". R is the gas constant, T is the absolute temperature, and $\gamma_{i,i}$ is the transfer activity coefficient.

Following the derivation in Ref. 2, the effect of solvent on the rate of the exchange reaction concerned may be written as eqn. (10), where

$$\frac{(k_i)_P}{(k_i)_A} = \frac{(\gamma_{i,\text{Br}^-}) (\gamma_{i,\text{BuBr}})}{\gamma_{i,\ddagger}} \quad (10)$$

"P" and "A" denote solvent mixture and pure acetone, respectively, and \ddagger stands for the activated complex. According to the theory of absolute reaction rate,¹⁹⁻²¹

$$(\Delta G_i^{\ddagger})_{A \rightarrow P} = -RT \ln [(k_i)_P / (k_i)_A] \quad (11)$$

where $(\Delta G_i^{\ddagger})_{A \rightarrow P}$ is the difference in Gibbs' free energy of activation for the exchange reaction in pure acetone and in acetone containing a protic component.

On the reasonable assumption that $\gamma_{i,\text{BuBr}} \geq \gamma_{i,\ddagger}$ a comparison of eqns. (10) and (11) reveals that

$$\gamma_{i,\text{Br}^-} \leq (k_i)_P / (k_i)_A \quad (12)$$

Application of a thermodynamic cycle to the association equilibrium (III) in pure acetone



and in the corresponding protic-aprotic solvent mixture and use of the relation $\Delta G^0 = -RT \ln K$, yields eqn. (13),

$$\frac{(K_A)_P}{(K_A)_A} = \frac{(\gamma_{i,\text{Li}^+}) (\gamma_{i,\text{Br}^-})}{\gamma_{i,\text{LiBr}}} \quad (13)$$

where $(K_A)_A$ is the ion-pair association constants of lithium bromide in pure acetone and $(K_A)_P$

Table 5. Transfer activity coefficients at 25°C according to eqns. (12) and (13).

Hydroxylic conc. wt-%	$(\gamma_{i,Br^-})_{A \rightarrow P}$	$(K_A)_P / (K_A)_A$	$(\gamma_{i,Li^+})_{A \rightarrow P} / (\gamma_{i,LiBr})_{A \rightarrow P}$
Methanol			
0.10	0.80	0.83	1
0.30	0.55	0.64	1.2
1.00	0.33	0.39	1.2
Ethanol			
0.30	0.74	0.81	1.1
0.60	0.54	0.68	1.3
1.00	0.46	0.58	1.3

is the corresponding quantity referring to the solvent mixture.

Using the values of K_A and k_i at 25°C in Tables 3 and 4 the figures listed in Table 5 were derived from eqns. (12) and (13).

According to these data there is a tendency for the activity coefficient ratio $(\gamma_{i,Li^+})_{A \rightarrow P} / (\gamma_{i,LiBr})_{A \rightarrow P}$ to increase with increasing concentration of the protic component. This may be due to increasing solvation of the lithium bromide ion-pairs. If the solvation of the lithium ion increases with the concentration of the protic component, the values listed in the last column of Table 5 would be an underestimation of the effect of solvation on the ion-pairs.

Acknowledgements. The authors thank Miss Eva Borg for technical assistance and the Swedish Natural Science Research Council for financial support.

REFERENCES

- Holmgren, A. and Beronius, P. *Acta Chem. Scand.* 26 (1972) 3881.
- Holmgren, A. *Acta Chem. Scand. A* 31 (1977) 539.
- Beronius, P. *Acta Chem. Scand.* 15 (1961) 1151.
- Beronius, P., Isacsson, U. and Nilsson, A.-M. *Acta Chem. Scand.* 24 (1970) 189.
- McKay, H. A. C. *J. Am. Chem. Soc.* 65 (1943) 702.
- Nilsson, A.-M. *Acta Chem. Scand.* 27 (1973) 2722.
- Beronius, P. *Unpublished.*
- Fuoss, R. M. and Hsia, K.-L. *Proc. Natl. Acad. Sci. U.S.A.* 57 (1967) 1550.
- Fuoss, R. M. and Hsia, K.-L. *Proc. Natl. Acad. Sci. U.S.A.* 58 (1968) 1818.
- Fernández-Prini, R. *Trans. Faraday Soc.* 65 (1969) 3311.
- Robinson, R. A. and Stokes, R. H. *Electrolyte Solutions*, Butterworths, London 1965, p. 229.
- Bjerrum, N. K. *Dan. Vidensk. Selsk. Mat. Fys. Medd.* 7 (1926) No. 9.
- Acree, S. F. *Am. Chem. J.* 48 (1912) 352.
- Hald, A. *Statistical Theory with Engineering Applications*, Wiley, New York 1965, p. 551.
- Leary, J. A. and Kahn, M. J. *Am. Chem. Soc.* 81 (1959) 4173.
- Becker, E. D. *Spectrochim. Acta* 17 (1961) 436.
- Trémillon, B. *Chemistry in Non-Aqueous Solvents*, D. Reidel Publishing Company, Dordrecht, Holland 1974, Chapter 5.
- Parker, A. J. *J. Chem. Soc. A* (1966) 220.
- Eyring, H. *J. Chem. Phys.* 3 (1935) 107.
- Evans, M. G. and Polanyi, M. *Trans. Faraday Soc.* 31 (1935) 875.
- Glasstone, S., Laidler, K. J. and Eyring, H. *The Theory of Rate Processes*, McGraw Hill, New York 1941.

Received June 13, 1977.

The Crystal and Molecular Structure of 2-Diisopropylamino-4-methyl-6-phenyl-3,4,6-triaza-1,6a-dithiapentalenylium-5-thiolate, $C_{16}H_{22}N_4S_3$

LARS KR. HANSEN

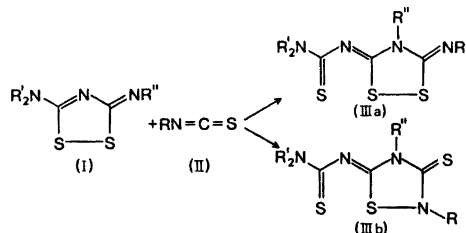
Department of Chemistry, Institute of Mathematical and Physical Sciences, University of Tromsø, Box 790, N-9001 Tromsø, Norway

The title compound crystallizes in the monoclinic space group $P2_1/c$ with $Z=4$ and unit cell dimensions, $a=9.675(2)$, $b=15.054(3)$, $c=12.788(3)$ Å, and $\beta=92.37(2)^\circ$. The structure was solved by direct methods and refined by full matrix least squares to a final R of 0.041.

Each of the two five-membered rings in the central ring system is planar with an angle of 3.7° between the normals of the two planes. The 6-phenyl group is twisted 45° about the connecting bond $N(6)-C(7)$.

The bond lengths in the central ring system are: $S(1)-S(6a)=2.447(1)$ and $S(6a)-N(6)=1.863(2)$ Å with the angle $S(1)-S(6a)-N(6)=168.99(8)^\circ$, $S(1)-C(2)=1.715(3)$, $S(6a)-C(3a)=1.746(3)$, $N(6)-C(5)=1.338(3)$, $C(2)-N(3)=1.363(3)$, $N(3)-C(3a)=1.302(3)$, $C(3a)-N(4)=1.368$, and $N(4)-C(5)=1.398(3)$ Å. Corrections for rigid body libration have been applied. The X-ray investigation shows that the molecule is a 6-aza-1,6a-dithiapentalene derivative.

It is known that 5-(dialkylamino)-3-(alkyl- or arylimino)-1,2,4-dithiazoles (I) forms adducts with 1,3-dipolarophiles (isocyanates, isothiocyanates or carbon disulfide), but there has been some controversy about the structural formula of these adducts. With isothiocyanate (II) for example the two isomers (IIIa) and (IIIb) may be formed.^{5,6}



On the basis of ^1H NMR spectra Goerdeler first assigned formula (IIIb) to the adduct with $\text{R}'=\text{CH}(\text{CH}_3)_2$, $\text{R}''=\text{CH}_3$ and $\text{R}=\text{C}_6\text{H}_5$.^{1,2} Then later, on the basis of UV and ^{13}C NMR data formula (IIIa) was assigned.³ In the meantime Oliver *et al.* published the syntheses of some similar compounds for which formula (IIIa) was proposed ($\text{R}'=\text{CH}_3$, $\text{R}''=\text{CH}_3$, C_6H_5 , $\text{R}=\text{CH}_3$, C_6H_5).⁴ The structures of two adducts with $\text{R}=(\text{CH}_3)_2\text{NCS}-$ have been studied by X-ray methods and are shown to be of the (IIIa) type.^{5,6}

The present X-ray study has been carried out in order to establish which of the forms (IIIa) or (IIIb) is the correct one for an adduct formed with a "simple" isothiocyanate like $\text{C}_6\text{H}_5\text{N}=\text{C}=\text{S}$. Further, information about the bonding in the possible linear sequences $\text{S}\cdots\text{S}-\text{S}$ or $\text{S}\cdots\text{S}-\text{N}$ was of interest.

STRUCTURE ANALYSIS

A sample of the title compound, consisting of colourless, prismatic crystals was provided by Dr. J. Goerdeler, University of Bonn.³ The crystal used for all X-ray measurements was mounted parallel to the crystallographic a -axis. The dimensions of the crystal were $0.65 \text{ mm} \times 0.33 \text{ mm} \times 0.28 \text{ mm}$ along $[100]$, $[011]$, and $[0\bar{1}\bar{1}]$, respectively.

Crystal data

$C_{16}H_{22}N_4S_3$; M.W. = 366.57

Monoclinic, space group $P2_1/c$ with $Z=4$

$a = 9.675(2) \text{ \AA}$, $b = 15.054(3) \text{ \AA}$, $c = 12.788(3) \text{ \AA}$
 $\beta = 92.37(2)^\circ$
 $V = 1860.9(8) \text{ \AA}^3$
 $D_x = 1.308 \text{ g/cm}^3$, $D_m = 1.30 \text{ g/cm}^3$
 $\mu(\text{MoK}\alpha) = 3.92 \text{ cm}^{-1}$, $F_{000} = 776$

The cell dimensions were calculated from diffractometer measurements of the setting angles for 12 reflections with $2\theta > 39^\circ$.

The intensities of 4528 independent reflections within $2\theta = 55^\circ$ were recorded on a Picker FACS-1 automatic diffractometer using $\theta - 2\theta$ scan and niobium filtered MoK α radiation. All measurements were made at 20°C . Scan ranges were calculated according to the relationship $\Delta\theta = 1.2 + 0.692 \text{ tg } \theta$,⁷ where 0.692 is a dispersion correction for molybdenum radiation. A scan speed of 2° min^{-1} in 2θ was used with the background recorded 20 s at each side of the reflections.

3314 reflections with net intensity I greater than $2\sigma(I)$ were regarded as observed, $\sigma(I)$ being defined as $\{\sigma_N^2 + (0.01N_{\text{net}})^2\}^{1/2}$ where the last term accounts for a 1% instrumental

instability. σ_N is the statistical counting error and N_{net} the net peak count. 1214 reflections had net counts less than $2\sigma(I)$. These reflections were given a threshold value of $2\sigma(I)$ and were later included in the refinement only if $|F_{\text{calc}}| > F_{\text{threshold}}$.

Corrections for Lorentz and polarization effects were carried out in the usual way. Absorption corrections were considered unnecessary.

The structure was solved by direct methods. This process was carried out with the X-RAY 72 programs NORMSF, SINGEN and PHASE.⁸ 262 phases with $E > 1.80$ were generated, and these phases were used to calculate an E map. All the non-hydrogen atoms except C(18) and C(21) were found from this E map, and structure factors calculated from the coordinates of these 21 atoms resulted in an R factor of 0.23 ($R = \sum ||F_o| - |F_c|| / \sum |F_o|$). A subsequent Fourier map revealed the two remaining carbon atoms, and the hydrogen positions were found from a difference map. The atomic parameters were refined by full matrix least squares

Table 1. Atomic coordinates and temperature parameters U_{ij} (\AA^2) for the sulfur, nitrogen and carbon atoms. The temperature factor is $\exp\{-2\pi^2(h^2a^{*2}U_{11} + \dots + 2hka^*b^*U_{13} + \dots)\}$. The U_{ij} 's are multiplied by 10^4 .

Atom	x	y	z	U_{11}	U_{22}	U_{33}	U_{12}	U_{13}	U_{23}
S(1)	0.11757(11)	0.41860(5)	0.23233(6)	971(7)	393(4)	535(4)	161(4)	-312(4)	-82(3)
S(6a)	0.26094(8)	0.36953(4)	0.30296(5)	602(4)	321(3)	404(3)	39(3)	-104(3)	-17(2)
N(6)	0.37007(24)	0.35508(14)	0.50468(15)	537(13)	382(11)	355(10)	23(10)	-75(10)	33(9)
C(2)	0.10413(29)	0.52268(17)	0.28452(20)	514(16)	304(13)	433(13)	39(12)	-46(12)	9(11)
N(3)	0.15735(24)	0.53871(13)	0.38255(16)	544(13)	332(10)	402(11)	39(10)	-34(10)	11(8)
C(2a)	0.22957(28)	0.47621(16)	0.42901(18)	493(15)	331(12)	363(12)	-35(11)	2(11)	-1(9)
H(4)	0.29096(25)	0.49167(14)	0.52508(15)	588(14)	345(11)	354(11)	-1(10)	-49(10)	-4(8)
C(5)	0.37656(29)	0.42528(17)	0.56018(19)	493(15)	425(13)	368(12)	-36(12)	-9(11)	28(10)
C(7)	0.43295(28)	0.27085(17)	0.52300(20)	458(14)	367(13)	465(14)	6(11)	-101(12)	27(11)
C(8)	0.49457(31)	0.22867(19)	0.44093(21)	557(17)	465(15)	484(15)	-1(13)	-71(13)	-27(12)
C(9)	0.55084(35)	0.14479(21)	0.45608(26)	630(20)	548(10)	710(20)	104(16)	-76(16)	-170(15)
C(10)	0.54757(37)	0.10442(20)	0.55259(29)	700(22)	410(15)	869(24)	93(15)	-275(19)	22(15)
C(11)	0.48421(37)	0.14569(21)	0.63330(26)	706(22)	519(17)	679(20)	33(16)	-124(17)	176(15)
C(12)	0.42505(32)	0.22840(21)	0.61902(22)	584(18)	502(16)	496(15)	59(14)	-27(13)	108(12)
S(13)	0.46988(9)	0.43850(6)	0.67930(6)	653(5)	631(5)	429(4)	-17(4)	-152(3)	-34(3)
C(14)	0.27097(39)	0.57730(19)	0.57654(23)	935(25)	417(15)	517(16)	54(16)	-131(17)	-121(13)
H(15)	0.04437(25)	0.59030(14)	0.23335(17)	569(14)	372(11)	456(12)	51(10)	-66(11)	35(9)
C(16)	0.03440(31)	0.68092(17)	0.28017(22)	526(16)	363(13)	558(16)	29(12)	-10(13)	60(12)
C(17)	-0.05696(37)	0.68048(21)	0.37264(27)	717(22)	513(17)	768(21)	95(16)	227(18)	-43(16)
C(18)	0.17415(36)	0.72430(21)	0.30009(27)	656(21)	483(17)	789(22)	-06(16)	22(17)	10(15)
C(19)	-0.01451(36)	0.57885(20)	0.12522(23)	729(21)	491(16)	509(16)	97(15)	-177(15)	45(13)
C(20)	-0.16774(42)	0.59680(34)	0.11721(33)	639(24)	1397(41)	871(28)	-74(26)	-248(21)	-73(27)
C(21)	0.06111(73)	0.63533(56)	0.05002(35)	1132(44)	1675(62)	475(21)	-355(42)	-115(24)	194(29)

Table 2. Atomic coordinates and isotropic thermal parameters U (\AA^2) for the hydrogen atoms. The temperature factor is $\exp\{-8\pi^2 U(\sin^2\theta/\lambda^2)\}$. The U 's are multiplied by 10^3 .

Atom	x	y	z	U	Atom	x	y	z	U
H(8)	0.4953(29)	0.2563(18)	0.3773(20)	53(8)	H(173)	-0.1463(42)	0.6358(27)	0.3615(29)	114(14)
H(9)	0.5951(31)	0.1209(19)	0.4000(22)	67(9)	H(181)	0.2265(38)	0.6966(25)	0.3593(28)	101(12)
H(10)	0.5871(35)	0.0490(22)	0.5640(25)	87(11)	H(182)	0.2339(36)	0.7172(23)	0.2427(27)	86(11)
H(11)	0.4721(33)	0.1165(21)	0.7029(23)	77(10)	H(183)	0.1627(36)	0.7828(23)	0.3187(26)	87(11)
H(12)	0.3818(33)	0.2571(21)	0.6717(24)	80(10)	H(19)	-0.0004(36)	0.5188(22)	0.1084(25)	89(11)
H(141)	0.3081(38)	0.5746(23)	0.6410(27)	91(11)	H(201)	-0.2002(37)	0.5866(24)	0.0474(28)	96(12)
H(142)	0.1607(45)	0.5792(27)	0.5917(30)	125(15)	H(202)	-0.2081(45)	0.5602(30)	0.1723(33)	140(15)
H(143)	0.3032(40)	0.6226(25)	0.5356(28)	111(13)	H(203)	-0.1978(56)	0.6541(37)	0.1473(40)	203(21)
H(16)	-0.0145(26)	0.7141(16)	0.2259(18)	40(7)	H(211)	0.0616(60)	0.7006(36)	0.0676(40)	153(24)
H(171)	-0.0821(35)	0.7318(22)	0.3941(24)	81(11)	H(212)	0.0344(43)	0.6234(27)	-0.0189(33)	100(14)
H(172)	-0.0182(37)	0.6476(23)	0.4371(25)	87(11)	H(213)	0.1554(65)	0.6282(44)	0.0608(46)	183(28)

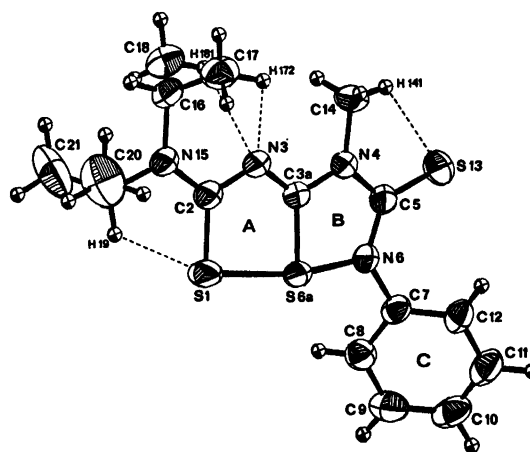


Fig. 1. ORTEP²⁰ drawing of the title compound with the numbering of the atoms in the molecule. Thermal ellipsoids for the non-hydrogen atoms are drawn at the 50% probability level. Note that carbon atom C(19) is concealed by C(20).

Table 3. Rigid body libration tensors L_1 and L_2 for various parts of the molecule.

	Eigenvalues ($^\circ$) ²	Eigenvectors ^a		
L_1	26.9	-5574	7729	-3031
	5.2	-6700	-6344	-3856
	1.6	-4903	-118	8715
L_2	46.7	4734	-5840	6594
	7.1	1346	-6918	-7094
	2.8	8705	4245	-2490

^a Direction cosinus $\times 10$ relative to a , b , and c^* , respectively.

(X-RAY 72 program CRYLSQ).⁶ With anisotropic temperature factor coefficients for all atoms except hydrogen, the final R factor is 0.041. The weighted R is 0.041. The function minimized in the refinement was $\sum w(|F_o| - \frac{1}{k}|F_c|)^2$, where $w = 1/\sigma_F^2$. At the end of the refinement the average shift/error ratio was 0.17. No indication of secondary extinction was observed. The scattering factors used for sulfur, nitrogen and carbon were those of Doyle and Turner⁹ and for hydrogen the scattering factor curve of Stewart *et al.*¹⁰ was used. Final atomic coordinates and temperature parameters are listed in Tables 1 and 2. The final structure

factor list is available from the author on request.

Rigid body analyses for various parts of the molecule have been carried out according to the method of Schomaker and Trueblood.¹¹ The parts of the molecule treated in this way are, the central ring system plus C(7), S(13), C(14), N(15), C(16) and C(19), and the phenyl group plus N(6). The corresponding librational tensors L_1 and L_2 respectively, are given in Table 3.

All the calculations were carried out on the UNIVAC 1110 computer at the University of Bergen.

DISCUSSION

Fig. 1 shows the structure of the title compound and the numbering of the atoms in the molecule. It is verified that the molecule is a 6-aza-1,6a-dithiapentalene derivative (IIIb) and not a 1,6,6a-trithiapentalene derivative (IIIa).

Table 4. Bond lengths (l) in 2-diisopropylamino-4-methyl-6-phenyl-3,4,6-triaza-1,6a-dithiapentalenylium-5-thiolate. The μ^I and μ^{II} values have been corrected for libration according to the librational tensors L_1 and L_2 , respectively.

Bond	$l(\text{\AA})$	$\mu^I(\text{\AA})$	$\mu^{II}(\text{\AA})$
S(1)–S(6a)	2.441(1)	2.447	
S(6a)–N(6)	1.857(2)	1.863	
S(1)–C(2)	1.710(3)	1.715	
S(6a)–C(3a)	1.742(3)	1.746	
N(6)–C(5)	1.333(3)	1.338	
C(2)–N(3)	1.357(3)	1.363	
N(3)–C(3a)	1.301(3)	1.302	
C(3a)–N(4)	1.362(3)	1.368	
N(4)–C(5)	1.397(3)	1.398	
C(5)–S(13)	1.664(3)	1.670	
N(6)–C(7)	1.422(3)	1.423	1.426
C(7)–C(8)	1.383(4)		1.393
C(8)–C(9)	1.386(4)		1.391
C(9)–C(10)	1.377(5)		1.382
C(10)–C(11)	1.371(5)		1.381
C(11)–C(12)	1.379(4)		1.384
C(12)–C(7)	1.389(4)		1.394
N(4)–C(14)	1.464(4)	1.468	
C(2)–N(15)	1.329(3)	1.331	
N(15)–C(16)	1.495(3)	1.499	
N(15)–C(19)	1.484(4)	1.490	
C(16)–C(17)	1.505(5)		
C(16)–C(18)	1.514(5)		
C(19)–C(20)	1.506(5)		
C(19)–C(21)	1.497(7)		

Calculations of least squares planes through the rings A, B and C, cf. Fig. 1, show that these rings are planar within the error. The angle between the normals of the planes of A and B is 3.7°. The substituents C(7), S(13) and C(14) lie slightly out of plane B, -0.08 , 0.11 and -0.05 Å, respectively; and N(15), C(16) and C(19) are 0.18 , 0.25 and 0.28 Å, respectively, out of plane A. The phenyl group C is twisted 45° about the connecting bond N(6)–C(7), with the atoms N(6), C(7) and C(10) -0.00 , -0.08 and -0.26 Å, respectively, out of plane B.

Table 5. Bond angles $\angle(ijk)$ in 2-diisopropylamino-4-methyl-6-phenyl-3,4,6-triaza-1,6a-dithiapentalenylium-5-thiolate.

i	j	k	$\angle(ijk)^\circ$
C(2)	S(1)	S(6a)	91.10(9)
S(1)	S(6a)	N(6)	168.99(8)
S(1)	S(6a)	C(3a)	83.48(8)
C(3a)	S(6a)	N(6)	85.73(11)
S(6a)	N(6)	C(7)	117.9(2)
S(6a)	N(6)	C(5)	115.4(2)
C(5)	N(6)	C(7)	126.7(2)
N(6)	C(5)	S(13)	128.7(2)
N(6)	C(5)	N(4)	108.3(2)
S(13)	C(5)	N(4)	122.9(2)
C(5)	N(4)	C(14)	122.7(2)
C(5)	N(4)	C(3a)	117.6(2)
C(14)	N(4)	C(3a)	119.7(2)
N(4)	C(3a)	S(6a)	112.8(2)
N(4)	C(3a)	N(3)	119.6(2)
S(6a)	C(3a)	N(3)	127.6(2)
C(3a)	N(3)	C(2)	118.0(2)
N(3)	C(2)	N(15)	117.3(2)
S(1)	C(2)	N(3)	119.4(2)
S(1)	C(2)	N(15)	123.2(2)
C(2)	N(15)	C(16)	122.4(2)
C(2)	N(15)	C(19)	120.8(2)
N(15)	C(16)	C(17)	111.2(2)
N(15)	C(16)	C(18)	112.9(2)
N(15)	C(19)	C(20)	112.4(3)
N(15)	C(19)	C(21)	110.7(3)
C(17)	C(16)	C(18)	114.8(3)
C(16)	N(15)	C(19)	116.8(2)
C(20)	C(19)	C(21)	111.1(4)
N(6)	C(7)	C(8)	118.7(2)
N(6)	C(7)	C(12)	121.1(2)
C(8)	C(7)	C(12)	120.1(2)
C(7)	C(8)	C(9)	119.4(3)
C(8)	C(9)	C(10)	120.3(3)
C(9)	C(10)	C(11)	120.2(3)
C(10)	C(11)	C(12)	120.4(3)
C(11)	C(12)	C(7)	119.6(3)

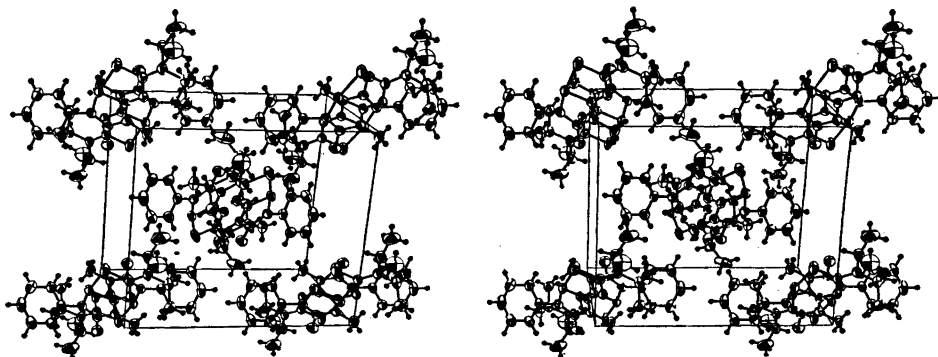


Fig. 2. A stereoscopic view of the arrangement of the molecules in the unit cell.

Bond lengths and angles for non-hydrogen atoms in the present structure as calculated from the positional parameters in Table 1, are listed in Tables 4 and 5. The standard deviations given for the bond lengths and angles are based on the standard deviations in positional parameters from the least squares refinement. According to Hamilton and Abrahams¹⁸ a more realistic estimate of the standard deviations would probably be obtained by multiplying those given by a factor of two.

The bond lengths between non-hydrogen atoms, with the exceptions of the C–C bonds in the isopropyl groups, have been corrected for libration, *cf.* Table 4. The U and U^{II} values are corrected according to the librational tensors L_1 and L_3 , respectively. The U values are chosen to represent the central ring system as well as the lengths of the C(5)–S(13), N(4)–C(14), C(2)–N(15), N(15)–C(16) and N(15)–C(19) bonds. For the dimensions of the phenyl group the U^{II} values have been used.

The S(1)–S(6a) bond in the present structure is 2.447(1) Å and the S(6a)–N(6) bond is 1.863(2) Å. These lengths are compatible with those found in two other 6-phenyl-6-aza-1,6a-dithiapentalenes.^{13,14} In 2-*t*-butyl-6-phenyl-5,6-diaza-1,6a-dithiapentalene¹³ the bond distances are S(1)–S(6a)=2.426(1) and S(6a)–N(6)=1.841(2) Å, and in 3,4-dimethyl-6-phenyl-5,6-diaza-1,6a-dithiapentalene¹⁴ the corresponding bonds are 2.487(1) and 1.774(1) Å, respectively.

The S–S bond in the present structure is 0.34 Å longer than the accepted single bond distance of 2.10 Å,¹⁵ but appreciable shorter than the van der Waals contact of 3.40 Å.^{16,17}

The S–N bond is 0.11 Å longer than the S–N single bond of 1.75 Å.¹⁸

The sum of the S(1)–S(6a) and the S(6a)–N(6) bond length is 4.30 Å. This value is 11.7% longer than the sum of the two single bond distances (3.85 Å) and in good agreement with what has been found for analogous compounds.¹⁹ The S–C(sp^3) and N–C(sp^3) bond distances are all in the region between single bonds and double bonds, indicating π -conjugation throughout the system.

The C–H bond lengths all lie in the region 0.86 to 1.10 Å with a mean value of 0.96 Å. The mean value for the C(sp^2)–H and the C(sp^3)–H bonds is 0.94 and 0.96 Å, respectively. Standard deviations in the individual C–H distances range from 0.02 to 0.06 Å. The standard deviation of the mean value is 0.06 Å.

The bond angles involving hydrogen atoms in the phenyl group range from 116 to 124°, with a mean value of 120°. The standard deviation in the individual C–C–H angles is 2° and that of the mean value is 3°. The bond angles involving hydrogen atoms in the methyl group and the isopropyl groups range from 94 to 117° with standard deviations ranging from 1 to 5°. The mean value is 109° with a standard deviation of 6°.

There are a few short intramolecular S \cdots H and N \cdots H distances in the molecule. S(1) \cdots H(19)=2.44(3) Å, S(13) \cdots H(14)=2.61(4) Å, N(3) \cdots H(181)=2.49(4) Å and N(3) \cdots H(172)=2.48(4) Å, respectively, *cf.* Fig. 1. Atom H(19) lies only 0.03 Å out of the plane through S(1), C(2), N(15) and C(19),

while H(141) lies -0.10 \AA out of the plane through S(13), C(5), N(4) and C(14). These two short contacts as well as the two contacts N(3) \cdots H(181) and N(3) \cdots H(172) seem to contribute to the conformation of the methyl group and the two isopropyl groups in the solid state.

There are no intermolecular contacts shorter than van der Waals distances. A stereoscopic view of the arrangement of molecules in the unit cell is given in Fig. 2.²⁰

Acknowledgement. The author wishes to thank Dr. J. Goerdeler, University of Bonn, for supplying a sample of the title compound. He also wishes to thank Tech. lic. J. Hjortås, Institutt for Røntgenteknikk, The University of Trondheim, for assistance with the data collection, and Prof. A. Hordvik, this University, for helpful comments and advice.

REFERENCES

- Goerdeler, J. and Ulmen, J. *Chem. Ber.* 105 (1972) 1568.
- Goerdeler, J. Lecture held at The 4th. Int. Congress of Heterocyclic Chemistry, Salt Lake City 1973.
- Goerdeler, J. *Private communication.*
- Oliver, J. E. and Brown, R. T. *J. Org. Chem.* 39 (1974) 2228.
- Oliver, J. E., Flippen, J. L. and Karle, J. *Chem. Commun.* (1972) 1153.
- Flippen, J. L. *J. Am. Chem. Soc.* 95 (1973) 6073.
- Alexander, L. E. and Smith, G. S. *Acta Crystallogr.* 17 (1964) 1195.
- X-RAY Program System (1972)*. Version of June 1972, Technical Report Tr-192 of the Computer Science Center, Univ. of Maryland, College Park.
- Doyle, P. A. and Turner, P. S. *Acta Crystallogr. A* 24 (1968) 390.
- Stewart, R. F., Davidson, E. R. and Simpson, W. T. *J. Chem. Phys.* 42 (1965) 3175.
- Schomaker, V. and Trueblood, K. N. *Acta Crystallogr. B* 24 (1968) 63.
- Hamilton, W. C. and Abrahams, S. C. *Acta Crystallogr. A* 26 (1970) 18.
- Hansen, L. K. and Tomren, K. *Acta Chem. Scand. A* 31 (1977) 292.
- Darmo, L. P. and Hansen, L. K. *Acta Chem. Scand. A* 31 (1977) 412.
- Hordvik, A. *Quart. Rep. Sulfur Chem.* 5 (1970) 21.
- Sletten, J. *Acta Chem. Scand.* 25 (1971) 3577.
- Sletten, J. *Doctoral thesis*, Univ. of Bergen 1976, p. 19.
- Pauling, L. *The Nature of the Chemical Bond*, 3rd Ed., Cornell University Press, Ithaca, New York 1960.
- Hordvik, A. and Sæthre, L. *J. Israel J. Chem.* 10 (1972) 239.
- Johnson, C. K. *ORTEP-II: A Fortran Thermal-Ellipsoid Plot Program For Crystal Structure Illustrations*, Report ORNL-3794, Oak Ridge National Laboratory, Oak Ridge 1971.

Received June 22, 1977.

Preparation, Composition and Solid State Investigations of TiN, ZrN, NbN and Compounds from the Pseudobinary Systems NbN-NbC, NbN-TiC and NbN-TiN

A. NØRLUND CHRISTENSEN ^a and S. FREGERSLEV ^b

^a Department of Inorganic Chemistry, Aarhus University, DK-8000 Aarhus C, Denmark and ^b Department of Geology, Aarhus University, DK-8000 Aarhus C, Denmark

Single crystals of the cubic phases TiN, ZrN, δ -NbN and of compounds from the pseudobinary systems NbN-NbC, NbN-TiC, and NbN-TiN were obtained by zone melting, zone annealing and annealing of the metals and metal carbides in nitrogen gas of 2 MPa. Single crystals of the tetragonal phase γ -NbN were obtained in a similar way by annealing of niobium.

The nitrides are non-stoichiometric. TiN was obtained in the composition range TiN_{0.99} to TiN_{0.50}, ZrN in the range ZrN_{1.00} to ZrN_{0.43}, and the niobium nitrides were obtained in the composition range NbN_{0.90} to NbN_{0.69}. The compounds from the pseudobinary systems have up to 35 % vacant sites in the nitrogen-carbon sublattice. TiN and ZrN have only vacant sites in the nitrogen sublattice. A correlation is found between the unit cell parameters for titanium nitride and zirconium nitride and the nitrogen-metal ratios.

The carbides and nitrides of the group IV, V, and VI transition metals have high melting points, and metallic properties such as appreciable thermal and electrical conductivity and metallic lustre. The compounds are hard and brittle. Such properties are not often found in conjunction with appreciable electrical conductivity for refractory materials. Some of the nitrides, all with the sodium chloride structure, are superconductors with moderate to high transition temperatures, the values for T_c are: TiN, 5 K; ZrN, 10K; and δ -NbN, 17.3 K.¹ The generally accepted mechanism for superconductivity is the electron-phonon interaction and it is therefore of great interest to understand the phonon spectra of these compounds.

Inelastic neutron scattering experiments show for some of these transition metal compounds an appreciable difference in the phonon dispersion curves between the compounds that are superconductors and those that are not.²⁻⁵ The anomalies in the phonon dispersion curves are assumed to be due to the strong electron-phonon interactions.

A high temperature crystal growth program was started with the intention to develop reproducible growth methods for the transition metal carbides and nitrides and to make single crystals of these materials available for elastic and inelastic neutron scattering experiments and for other physical investigations. Due to the refractory nature of these compounds, the floating zone crystal growth technique was assumed to be the only method by which large single crystals could be obtained. Growth of transition metal carbides has been reported previously,⁶ and large single crystals of titanium carbide have recently been produced using the floating zone technique.⁷⁻⁹ The preparation of large crystals of the nitrides has not previously been reported in the literature, but has now succeeded during this crystal growth project.^{8,9}

The purpose of this paper is to describe the preparation and characterization of crystals of the compounds TiN, ZrN, γ -NbN, δ -NbN, and of compounds from the pseudobinary systems NbN-NbC, NbN-TiC, and NbN-TiN. All these compounds can exist over a rather broad composition range and are normally obtained as non-stoichiometric phases. In the

following the formulae TiN, ZrN, etc. will be used for the non-stoichiometric compounds.

EXPERIMENTAL

Sample preparation and X-ray technique. The crystal growth furnace used was an ADL MP furnace¹⁰ designed to operate at gas pressures up to 2 MPa. The power supply for the furnace was a 30 kW induction generator¹¹ that operated at 200 kHz. The starting materials were solid rods of the pure metals (Ti and Zr) and powders of the elements and the carbides (Nb, Ti, NbC, TiC). Rods for zone melting experiments were pressed isostatically from powders.⁹ The nitrogen used was 99.99% pure (Dansk Ilt- og Brintfabrik, Copenhagen).

X-Ray diffraction techniques, including Laue back reflection, precession and Guinier powder photography, and optical metallography have been used to characterize the crystals produced. Guinier powder patterns were obtained on all melted and annealed samples using $\text{CuK}\alpha_1$ radiation, $\lambda = 1.54051 \text{ \AA}$, or $\text{CoK}\alpha_1$ radiation, $\lambda = 1.78892 \text{ \AA}$, with sodium chloride $a_{\text{NaCl}} = 5.6389 \text{ \AA}$, or germanium $a_{\text{Ge}} = 5.6576 \text{ \AA}$, as internal standards. The specimens were sectioned with a water-cooled diamond cut-off wheel, and the samples were then lapped on a cast iron lap with 400 mesh powder of boron carbide. The lapping was sufficient to make the grain structure of the specimens visible.

TiN. Zone melting of polycrystalline rods of titanium nitride in an ambient nitrogen gas pressure of 2 MPa could not be used in the preparation of single crystals of the compound. The rods expanded and became covered with a porous polycrystalline surface layer and a considerable evaporation started from the heated part of the rod before a molten zone was formed.⁹ At temperatures of approximately 3000 K cracks were formed in the surface layer, and through the cracks melted material could be observed. Zone annealing of rods of titanium metal in an ambient nitrogen gas pressure of 2 MPa proved to be a successful method for the preparation of single crystals of titanium nitride. The procedure for a zone annealing is similar to that of a zone melting. A hot zone, and not a molten zone, travels through the specimen at low speed. Large crystal grains are formed during this annealing process. By this method titanium nitride was formed from titanium and nitrogen and the crystals were obtained in one experimental operation. Typical values for the temperature of the heated zone are the range 2000–2800 K, and an ambient nitrogen gas pressure of 1–2 MPa was normally applied. The crystals had the highest nitrogen content when made at high temperatures and gas pressures. The nitrogen content of the crystals can be raised by annealing of small volumes of single crystals, approximately 0.5 cm^3 , in ambient nitrogen pressures of 2 MPa and

temperatures in the range 2800–2900 K for long periods of time, 65–76 h.

ZrN. The main difficulties in the floating zone growth of crystals of ZrN from polycrystalline rods of zirconium nitride were the same as met in the crystal growth of TiN from polycrystalline rods of titanium nitride. A considerable evaporation of ZrN started from the hot, heated part of the specimen before a molten zone was formed, and a porous polycrystalline surface layer of ZrN developed at high temperatures. Through cracks in this surface layer it was possible to observe melted material. — Single crystals of ZrN could be made by zone annealing of zirconium metal in nitrogen gas at 1–2 MPa and temperatures in the range 2000–2800 K. The crystals had the highest nitrogen content when made at the highest accessible temperatures and gas pressures, and specimens with a composition close to the stoichiometric composition could be made by this method.

NbN. When δ -NbN was zone melted in ambient nitrogen gas pressures of up to 2 MPa specimens were obtained that contained β -Nb₂N and γ -NbN in a lamella structure.¹² In the zone melting nitrogen gas was released from the molten zone. The average composition of a specimen zone melted at an ambient nitrogen gas pressure of 2 MPa was NbN_{0.99(1)} and the feed rod for the zone melting had the composition NbN_{1.0}. When a solid bar of niobium metal was annealed in an ambient nitrogen gas pressure of 2 MPa at 2100 K for 110 h a specimen containing twinned crystals of γ -NbN was obtained. The composition of this specimen was NbN_{0.77(1)}. Single crystals of δ -NbN were obtained by annealing of small volumes of single crystals of γ -NbN, approximately 0.5 cm^3 , in ambient nitrogen gas pressures of up to 2 MPa and temperatures in the range 2100–2200 K for long periods of time, 90–110 h. A single crystal of δ -NbN made by this method had the composition NbN_{0.90(1)}.

Compounds from the pseudobinary systems, NbN-NbC, NbN-TiC, and NbN-TiN. Compounds from these pseudobinary systems could be made by zone melting in ambient nitrogen gas pressures of 1–2 MPa. In most cases specimens containing cubic single crystals of only one phase were obtained.

Analysis. Determination of the unit cell parameter a showed that the values for a varied within the specimens and also from specimen to specimen in a systematic way, depending upon the experimental conditions used in the crystal growth of the specimens. The variation in a follows the variation in the composition of the metal nitride. The compound TiN_x can exist over a large composition range and an empirical relation between the unit cell parameter a and the ratio N/Ti has been reported.¹³ The unit cell parameter is increasing with increasing values of x . As the specimens

showed a systematic variation of a from the surface regions to the centre parts of the specimens, corresponding to a composition gradient, and as nitrogen in TiN cannot be converted quantitatively to NH_3 and determined by this method, it was decided to use the microprobe analysis technique in the determination of the composition and the composition gradients in the specimens of TiN_x . The microprobe analyses were made on a Jeol JXA 50A microprobe operating at an accelerating voltage of 15 kV and a sample current of about 30 nA. Corrections for absorption were made using the procedure of Springer.¹⁴ The titanium contents were determined using 99.99% Ti and rutile, TiO_2 , as standards, and the nitrogen contents were obtained as differences, assuming

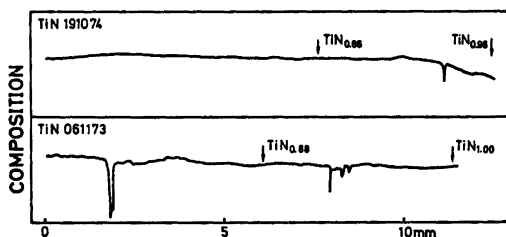


Fig. 1. Composition gradient in two specimens of TiN obtained by scanning along a diameter of a cross sectional slice of the specimens. The composition indicates the metal concentration. The discontinuities in the curves are due to cracks and scratches in the specimens.

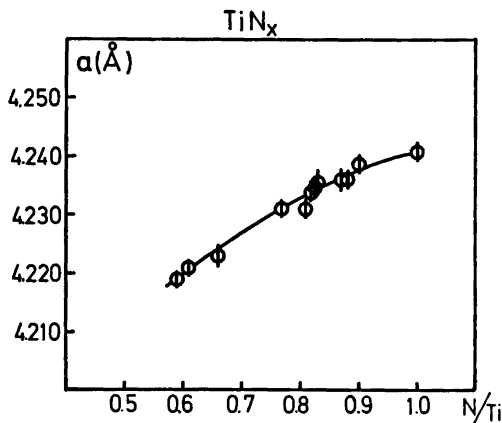


Fig. 2. Correlation between the ratio N/Ti and the unit cell parameter a in TiN_x . The bars indicate the standard deviation on a . Ehrlich¹³ has reported the values $a=4.213 \text{ \AA}$ for $\text{N/Ti}=0.5$ and $a=4.234 \text{ \AA}$ for $\text{N/Ti}=1.0$. The value for $a=4.240(1) \text{ \AA}$ at the stoichiometric composition is thus higher than the value published previously.

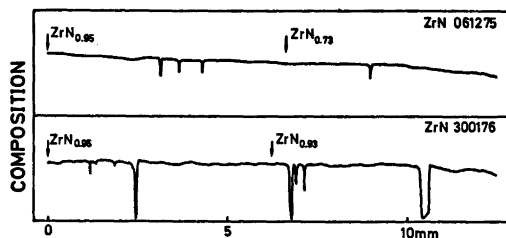


Fig. 3. Composition gradient in two specimens of ZrN obtained by scanning along a diameter of a cross sectional slice of the specimens.

that the specimens contained only the two elements titanium and nitrogen. Fig. 1 illustrates the concentration gradients of two specimens of TiN obtained by scanning along a diameter of a cross sectional slice of the specimens.

The composition of the centre parts of the specimens where the concentration gradients were less pronounced was also determined by gravimetical analysis. TiN_x was converted quantitatively to TiO_2 by ignition in air at 1000°C . The samples were placed in Pt-crucibles and kept in an electric furnace for approximately 1 h. Fig. 2 shows the variation in the unit cell parameter a with the composition.

The composition of the specimens of ZrN was also determined by the microprobe analysis technique as described for TiN. In this case 99.99% Zr was used as a standard. The nature of the concentration gradients for two specimens is shown in Fig. 3. Gravimetical analysis were made of the centre parts of the

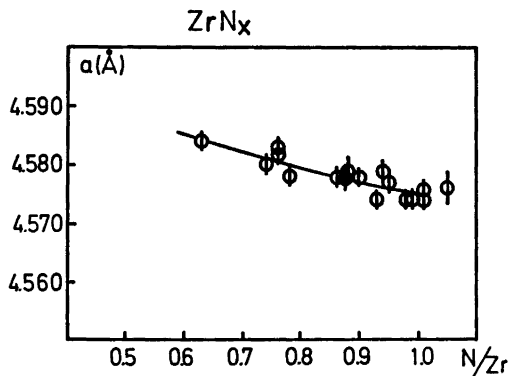


Fig. 4. Correlation between the ratio N/Zr and the unit cell parameter a in ZrN_x . The bars indicate the standard deviation on a . Rudy and Benesovsky¹⁵ have reported the value $a=4.577 \text{ \AA}$ for $\text{N/Zr}=1.0$ and $a=4.584 \text{ \AA}$ for $\text{N/Zr}=0.5$. The values for the unit cell parameter obtained in this investigation are in acceptable agreement with the values reported previously.¹⁵

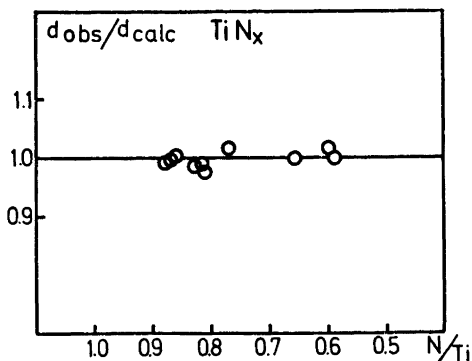


Fig. 5. Display of $d_{\text{obs}}/d_{\text{calc}}$ vs. x in TiN_x . The standard deviation on $d_{\text{obs}}/d_{\text{calc}}$ is 0.004. At the stoichiometric composition Ehrlich¹⁵ found 4% of the lattice sites unoccupied. This is in disagreement with the findings of the present work.

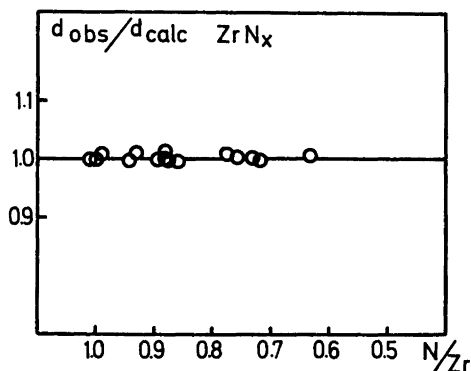


Fig. 6. Display of $d_{\text{obs}}/d_{\text{calc}}$ vs. x in ZrN_x . Standard deviations on $d_{\text{obs}}/d_{\text{calc}}$ are 0.003. At approximately $\text{ZrN}_{1.0}$ the data of Straumanis, Faunce and James¹⁶ indicate both sublattices contain vacancies. The present work does not support this hypothesis.

specimens. ZrN_x was converted quantitatively to ZrO_2 by ignition in the air at 1180°C. Fig. 4 shows the variation in the unit cell parameter a with the composition.

The composition of the specimens of niobium nitride was determined gravimetrically by ignition in air at 1000°C. NbN_x is by this treatment converted quantitatively to Nb_2O_5 .

The compounds from the pseudobinary systems NbN-NbC, NbN-TiC, and NbN-TiN were analyzed using the microprobe analysis technique. As standards were used 99.99% Nb, 99.99% Ti and TiC and ZrN with known compositions. The specimens were analyzed for Nb, Ti, C, and N. Gravimetric analyses were also made. (Taking into consideration that the chemical analyses give an average composition of a relatively large volume and the microprobe analyses give compositions of very small volumes of the specimens and often reveal composition fluctuations in the specimens, the two methods of analyses give results in acceptable agreement with each other).

Density determinations. The densities of the

compounds were measured by the method of Archimedes. The densities of the samples of TiN_x and ZrN_x were calculated using values for the composition from the chemical analysis and the unit cell parameter, and assuming that the unit cell contained four formula units of TiN_x or ZrN_x . Figs. 5 and 6 are displays of the ratios between observed and calculated densities vs. the ratios N/Ti and N/Zr, respectively. The densities of the compounds from the pseudobinary systems were calculated in the same way, assuming four formula units in the unit cell.

Magnetic properties. The magnetization of samples of TiN_x and ZrN_x was measured at temperatures from 75–300 K using the Faraday method. The samples were placed in a flow cryostat cooled with liquid nitrogen, and the magnetization was recorded with an electrobalance. The magnetic field was calibrated using Mohr's salt, $(\text{NH}_4)_2\text{Fe}(\text{SO}_4)_2 \cdot 6\text{H}_2\text{O}$, $\chi_g = 32.2 \times 10^{-6}$, as a standard. The magnetization varied only 8% over the temperature range investigated. The magnetic data at 300 K for TiN_x and ZrN_x are listed in Table 1.

Table 1. Magnetic data^a for TiN_x and ZrN_x .

Compound	χ_{mol}^{-1}	Compound	χ_{mol}^{-1}	Compound	χ_{mol}^{-1}
$\text{TiN}_{0.99}$	142.8	$\text{TiN}_{0.82}$	19.3	$\text{TiN}_{0.59}$	24.8
$\text{TiN}_{0.90}$	37.9	$\text{TiN}_{0.77}$	32.6	$\text{ZrN}_{0.88}$	50.0
$\text{TiN}_{0.87}$	43.2	$\text{TiN}_{0.66}$	18.0	$\text{ZrN}_{0.88}$	38.4
$\text{TiN}_{0.83}$	32.7	$\text{TiN}_{0.61}$	33.5	$\text{ZrN}_{0.72}$	18.3

^a χ_{mol}^{-1} determined for magnetic field 3000 Gauss.

RESULTS AND DISCUSSION

The investigation shows that large single crystals can be made of TiN, ZrN, of the niobium nitrides γ -NbN and δ -NbN, and of compounds from the pseudobinary systems NbN-TiC, NbN-TiN, and NbN-NbC. These compounds from the pseudobinary systems can be obtained by the floating zone crystal growth technique. Large single crystals of vanadium nitride, VN, can also be made by this growth method.¹⁷ Single crystals of TiN and ZrN are made by the zone annealing technique. The annealing technique was applied in the preparation of crystals of γ -NbN and δ -NbN. This method was also used to increase the nitrogen content in specimens of TiN and ZrN made by the zone annealing technique.

Specimens of TiN and ZrN prepared by the zone annealing method show a composition gradient from the surface to the centre of the rods. This composition gradient can be determined by the microprobe analysis method and by chemical analysis. The surface layers have higher nitrogen contents than the centre regions. The nitrides are formed in the solid state and the formation is governed by diffusion of nitrogen from the surface layers to the centre regions of the rods. Many specimens had a yellow colour of the surface layers and a metallic white colour of the centre regions corresponding to compositions close to the stoichiometric compositions of the surface layers and composition far from stoichiometry of the centre regions.

The composition of the specimens of TiN and ZrN is dependent upon the preparative parameters temperature, time and nitrogen gas pressure. Specimens kept at the highest temperatures and gas pressures for the longest periods of time had the highest nitrogen contents. TiN was obtained as single crystals within the composition range TiN_{0.99} to TiN_{0.99}, and ZrN was obtained as single crystals within the composition range ZrN_{1.00} to ZrN_{0.93}.

Empirical relations have been found between the unit cell parameter a and the composition for TiN _{x} and ZrN _{x} (see Figs. 2 and 4). The parameter a for TiN _{x} is increasing with increasing values for x . From the crystal structure of ϵ -TaN¹⁸ the radius for N of 0.708(3) Å in a metal nitride is obtained. This is in good

agreement with previously reported values of 0.71 Å.¹⁹ For a metal nitride with the NaCl structure the densest packing is obtained when $r_N/r_M = 0.4142$, or when $r_M = 1.71$ Å. With increasing values of x the unit cell parameter a should increase when $r_M < 1.71$ Å, in that case the volume of a vacant site would be smaller than that of a nitrogen atom. This is the case for Ti, $r = 1.467$ Å, as well as for Zr, $r = 1.597$ Å (values listed for coordination number 12 in Ref. 1). The effect is observed for TiN _{x} but not for ZrN _{x} . It is assumed that the metal nitride has an appreciable metal-nitrogen bonding contribution to the chemical bonds of the compounds. When the nitrogen content is increased in ZrN _{x} the number of Zr-N bonds is increased and if this type of interaction is comparable with or even stronger than the Zr-Zr and the N-N interactions, the lattice will contract. This effect is apparently dominating over the vacancy filling effect of the nitrogen sublattice in ZrN _{x} . The heat of formation of ZrN is numerically larger than that of TiN.¹ It is thus tempting to assume that ZrN has stronger bonds than TiN.

For compounds showing superconductivity at low temperatures, it is normally found that the transition temperature T_c has its highest value for specimens with a stoichiometric composition, and the values of T_c fall with an increasing deviation from the stoichiometric composition. For the compounds TiN _{x} and ZrN _{x} with the sodium chloride structure it is evident that non-stoichiometric TiN _{x} and ZrN _{x} with $x < 1.0$ will have vacant lattice points on the nitrogen sublattice. The metal sublattice may be filled, or may have vacant lattice positions as well. In the compound TiO it is found that each of the two sublattices have 15.5 % vacant lattice sites for the stoichiometric composition Ti_{1.0}O_{1.0}.²⁰ This is due to an ordering of the vacant sites in the two sublattices so the symmetry of the crystal is changed from cubic to monoclinic. TiO shows no superconductivity at low temperatures. For TiN it is likely that the two sublattices are filled when the compound has the stoichiometric composition. This can be made probable by making a comparison of observed and calculated densities. The densities for the samples of TiN _{x} were calculated using the values for the composition and the unit cell

parameter, and assuming that the unit cell contained four formula units of TiN_x . This corresponds to a filled titanium sublattice and a nitrogen sublattice with vacant sites. Fig. 5 is a display of the ratios between observed and calculated densities *vs.* the ratios N/Ti . This shows that the values for $d_{\text{obs}}/d_{\text{calc}}$ cluster round the value 1.0 in the composition range investigated. It is thus most likely that the two sublattices in TiN are filled at the stoichiometric composition $\text{Ti}_{1.0}\text{N}_{1.0}$.

The densities for the specimens of ZrN_x were also calculated using the values for the composition obtained from the chemical analysis and the unit cell parameter, and assuming that the unit cell contained four formula units of ZrN_x . This corresponds to a filled zirconium sublattice and a nitrogen sublattice with vacant sites. Fig. 6 is a display of the ratios between observed and calculated densities *vs.* the ratio N/Zr . This shows that the values for $d_{\text{obs}}/d_{\text{calc}}$ cluster around the value 1.0 in the composition range investigated. It is thus most likely that the two sublattices in ZrN are filled at the stoichiometric composition $\text{Zr}_{1.0}\text{N}_{1.0}$. The superconductivity of the two stoichiometric nitrides TiN and ZrN also supports the assumption that the metal sublattices are filled at the stoichiometric compositions.

The investigation of the magnetic properties of TiN and ZrN shows that the compounds have field dependent values for X_{mol}^{-1} . A tendency is observed for increasing values of X_{mol}^{-1} with increasing values of the ratio N/M , but the data does not give a clear picture of this relation between X_{mol}^{-1} and N/M . The large scatter in the data may be due to different contents of paramagnetic impurities in the specimens. (The nitrides were prepared from metals obtained from different suppliers).

The zone melting experiments on $\delta\text{-NbN}$ with an almost stoichiometric composition all resulted in specimens containing $\gamma\text{-NbN}$ and $\beta\text{-Nb}_2\text{N}$. By increasing the ambient nitrogen gas pressure to 2 MPa it was possible to reduce the quantity of $\beta\text{-Nb}_2\text{N}$ in the specimens considerably compared with the content of $\beta\text{-Nb}_2\text{N}$ in specimens made by zone melting with nitrogen gas pressures less than 0.5 MPa. However, by increasing the nitrogen gas pressure to 2 MPa it was not possible to obtain specimens of pure $\gamma\text{-NbN}$, as these specimens

always contained a minor quantity of $\beta\text{-Nb}_2\text{N}$. The zone melting growth technique was thus not adequate for the preparation of the pure phases $\delta\text{-NbN}$, $\gamma\text{-NbN}$, and $\beta\text{-Nb}_2\text{N}$. This is in contrast to the zone melting of sintered rods of $\delta\text{-VN}$ in an ambient gas pressure of 2 MPa, that gave single crystals of $\delta\text{-VN}$ with compositions in the range $\text{VN}_{0.74}$ to $\text{VN}_{0.86}$.¹⁷ Zone melting of sintered rods of $\delta\text{-VN}$ in an ambient nitrogen gas pressure of 1 MPa yielded specimens containing $\beta\text{-V}_2\text{N}$ and $\delta\text{-VN}$ in a lamella structure.²¹ An ambient nitrogen gas pressure of 2 MPa is thus sufficient to keep the composition of a melt of vanadium nitride within a composition range where $\delta\text{-VN}$ is the stable solid phase but is insufficient to keep the composition of a melt of niobium nitride within a composition range where $\delta\text{-NbN}$ is the stable solid phase.

Annealing of niobium or niobium nitride in pure nitrogen at temperatures over 2000 °C resulted in the formation of the pure phase $\gamma\text{-NbN}$. However, the crystals of $\gamma\text{-NbN}$ in the specimens were twinned. Annealing of small samples of $\gamma\text{-NbN}$ (volumes approximately 0.5 cm³) at 2100–2200 °C and ambient nitrogen gas pressures of up to 2 MPa for long periods of time, approximately 100 h, resulted in an increase of the nitrogen content of the specimens. Cubic single crystals of $\delta\text{-NbN}$ formed in this annealing growth process could be cooled to room temperature without undergoing the phase transition¹² to $\gamma\text{-NbN}$. The fast cooling from temperatures above 1800 °C that was used in the formation of polycrystalline rods of $\delta\text{-NbN}$ ²² could thus also be used in the formation of single crystals of $\delta\text{-NbN}$. In one annealing experiment where the specimen had a volume of approximately 1 cm³ a single crystal of $\gamma\text{-NbN}$ was obtained. The annealing time used for this experiment has possibly been too short to insure a sufficiently high nitrogen content in the specimen to avoid the phase transition from $\delta\text{-NbN}$ to $\gamma\text{-NbN}$ during the cooling process.

Typical values for the composition of niobium nitrides obtained by the different preparative methods are listed in Table 2.

Single crystals of compounds belonging to the pseudobinary systems NbN-TiC , NbN-TiN , and NbN-NbC have been made using the floating zone crystal growth technique. Results

Table 2. Composition and unit cell parameters of niobium nitrides. (Standard deviations in parentheses).

Method of preparation	N ₂ gas pressure in MPa	Temp. in °C	Time h	Composition from chemical analysis	Product	Unit cell parameter in Å
Zone melting of δ-NbN	1.95	>2100	13	NbN _{0.89(1)}	γ-NbN	a = 4.380(1) ^a c = 4.303(1)
					β-Nb ₂ N	a = 5.279(2) c = 4.990(2) a = 4.392(2) ^a c = 4.317(3)
Annealing of Nb in N ₂	2.00	2100	112	NbN _{0.77(1)}	γ-NbN	a = 4.377(1)
Annealing of γ-NbN in N ₂	2.00	2100	96	NbN _{0.80(1)}	δ-NbN	a = 4.377(1)
Fast reaction between Nb and N ₂ (Ref. 18)	2.00	>1800	20 20 s	NbN _{0.88(2)} ^b	δ-NbN	a = 4.394(3)

^a Small unit cell used. ^b From neutron diffraction.

 Table 3. Composition, unit cell parameters and densities of single crystals from NbN-MeX systems.^c

Exp. No.	Composition from analysis	Unit cell parameter in Å	d _{obs} g cm ⁻³	d _{calc} ^b g cm ⁻³	d _{obs} /d _{calc}
1.	Nb _{0.84} Ti _{0.16} N _{0.87} C _{0.10} □ _{0.23}	4.360(2)	7.566	7.716	0.981
2.	Nb _{0.83} Ti _{0.17} N _{0.81} C _{0.10} □ _{0.29}	4.362(2)	7.612	7.602	1.001
3.	Nb _{0.83} Ti _{0.17} N _{0.70} □ _{0.30}	4.361(2)	7.751	7.612	1.018
4.	Nb _{0.91} Ti _{0.09} N _{0.87} C _{0.11} □ _{0.32}	4.380(2)	7.826	7.759	1.009
5.	Nb _{0.83} Ti _{0.17} N _{0.85} C _{0.05} □ _{0.30}	4.336(3)	7.637	7.737	0.987
6.	Nb _{0.85} Ti _{0.15} N _{0.83} C _{0.10} □ _{0.27}	4.358(2)	7.523	7.718	0.975
7.	Nb _{0.83} Ti _{0.17} N _{0.78} □ _{0.22}	4.343(2)	7.809	7.731	1.010
8.	Nb _{0.83} Ti _{0.17} N _{0.77} C _{0.05} □ _{0.18}	4.346(1)	7.857	7.819	1.005
9.	Nb _{1.00} N _{0.86} C _{0.14} □ _{0.30}	4.397(2)	8.011	8.003	1.001
10.	Nb _{1.00} N _{0.85} C _{0.13} □ _{0.32}	4.388(3)	8.034	8.032	1.000
		a = 4.390(1) ^a			
11.	Nb _{1.00} N _{0.72} C _{0.03} □ _{0.25}	c = 4.331(1)	8.155	8.224	0.992
12.	Nb _{1.00} N _{0.88} C _{0.07} □ _{0.35}	4.380(1)	8.135	8.052	1.010
13.	Nb _{1.00} N _{0.88} C _{0.10} □ _{0.32}	4.393(2)	8.053	8.009	1.006
14.	Nb _{1.00} N _{0.82} C _{0.16} □ _{0.32}	4.403(1)	7.971	7.945	1.003
15.	Nb _{1.00} N _{0.81} C _{0.17} □ _{0.32}	4.406(2)	7.909	7.927	0.998
16.	Nb _{1.00} N _{0.81} C _{0.19} □ _{0.30}	4.420(2)	7.885	7.871	1.002

^a Tetragonal. ^b Calculated from chemical and microprobe analysis. ^c Standard deviations of a in parentheses. Typical values of standard deviations for d_{obs}, d_{calc}, and d_{obs}/d_{calc} are 0.015, 0.015, and 0.003, respectively.

of these growth experiments are listed in Table 3. Growth experiments resulted in samples containing single crystals. Systems containing niobium nitride and niobium carbide or other transition metal carbides and nitrides have been reported to have compounds with moderate to high transition temperatures for super-

conductivity. For compounds from the systems NbN-TiC and NbN-NbC reported values are: (NbN)_{0.8}(TiC)_{0.2}, 18.0 K; and (NbN)_{0.7}(NbC)_{0.3}, 17.8 K.¹

By addition of transition metal carbides and nitrides to NbN it has thus been possible to obtain cubic phases, and the phase transition

observed for pure niobium nitride from δ -NbN to γ -NbN on cooling is thus suppressed. For the pseudobinary system NbN-NbC it was found that zone melting of a specimen with the nominal composition Nb_{1.0}N_{0.9}C_{0.1} resulted in a sample of a tetragonal phase with unit cell parameters similar to the unit cell parameters of γ -NbN. For the systems addition of NbC, TiC, and TiN in a quantity corresponding to a mol fraction of 0.2 was sufficient to insure the formation of cubic crystals. It is assumed that the high values for T_c are connected with the cubic structure of these materials and increasing values of T_c should be expected for specimens with compositions approaching the stoichiometric composition. The results of chemical analysis, microprobe analysis and density determinations listed in Table 3 indicate that the crystals of these compounds are non-stoichiometric, and it is most likely that the nitrogen-carbon sublattice has up to 35 % vacant sites, with the metal sublattice being filled.

Investigations of the superconducting properties of single crystals obtained in this crystal growth project are planned, and the results will be published elsewhere. Measurements of the phonon dispersion curves for TiN,²³ ZrN,²⁴ VN, and δ -NbN are in progress.

Acknowledgements. We are indebted to "Statens naturvidenskabelige Forskningsråd" for the use of the Faraday magnetometer, and to Mr. N. J. Hansen for valuable technical assistance.

REFERENCES

- Toth, L. E. *Transition Metal Carbides and Nitrides*, Academic, New York and London 1971.
- Smith, H. G. and Gläser, W. *Phys. Rev. Lett.* 25 (1970) 1611.
- Smith, H. G. *Phys. Rev. Lett.* 29 (1972) 353.
- Weber, W. *Phys. Rev. B* 8 (1973) 5082.
- Weber, W. *Phys. Rev. B* 8 (1973) 5093.
- Haggerty, J. S., Lee, D. W. and Wenckus, J. F. *Preparation and Characterization of High Quality Single Crystal Refractory Metal Borides and Carbides*, Technical report AFML-TR-68-228, Wright-Patterson Air Force Base, Ohio 1969.
- Christensen, A. N. *15de Nordiska Kemistmötet, Resuméer*, p. 20, Tammerfors 1974.
- Christensen, A. N. *10th Int. Congr. Crystallography, Collected Abstracts*, Amsterdam 1975, p. S 209.
- Christensen, A. N. *J. Crystal Growth* 33 (1976) 99.
- Arthur D. Little, Inc., 20 Acorn Park, Cambridge, Mass. 02140, U.S.A.
- Fritz Hüttinger Elektronik GmbH, 78 Freiburg, Germany.
- Christensen, A. N. *Acta Chem. Scand. A* 30 (1976) 219.
- Ehrlich, P. *Z. Anorg. Allg. Chem.* 259 (1949) 1.
- Springer, G. *Fortschr. Mineral.* 45 (1967) 103.
- Rudy, E. and Benesovsky, F. *Monatsh. Chem.* 92 (1961) 415.
- Straumanis, M. E., Faunce, C. A. and James, W. J. *Inorg. Chem.* 5 (1966) 2027.
- Christensen, A. N. and Roedhammer, P. *J. Crystal Growth* 38 (1977) 281.
- Christensen, A. N. and Lebech, B. *Acta Crystallogr. B. Paper submitted 1977.*
- Hägg, G. *Z. Phys. Chem. Abt. B* 6 (1929) 221.
- Andersson, S., Collén, B., Kuylenstierna, U. and Magnéli, A. *Acta Chem. Scand.* 11 (1957) 1641.
- Billingham, J., Bell, P. S. and Lewis, M. H. *J. Crystal Growth* 13/14 (1972) 693.
- Christensen, A. N. *Acta Chem Scand. A* 31 (1977) 77.
- Kress, W., Roedhammer, P., Bilz, H., Teuchert, W. D. and Christensen, A. N. *J. Phys. C. Submitted 1977.*
- Dietrich, O. W. and Christensen, A. N. In *Physical Department Annual Report, Risø Report No. 352, Risø 1977*, pp. 22-24.

Received June 22, 1977.

Ionic Association and Ion-Solvent Interactions. The Conductance of Lithium Bromide in Acetone-Water Mixtures at 15—35 °C

PER BERONIUS

Department of Physical Chemistry, University of Umeå, S-901 87 Umeå, Sweden

The electrical conductance of lithium bromide in several aqueous acetone mixtures containing from 5×10^{-3} to 20 wt-% water at 15, 25, and 35 °C has been studied. The data were treated by means of the conductance equation of Fuoss and Hsia in the form of Fernández-Prini to obtain the ion pair association constant, K_A , and the limiting molar conductivity, Λ_0 . The minimum center-to-center distance of the ions in the ion pair, derived according to the Gilkerson-Fuoss and Bjerrum theories, and the solvation energies of the free ions relative to the ion pair varies with the composition of the solvent mixture. The heat of activation, ΔH_0^\ddagger , for migration of free ions, obtained from the temperature dependence of Λ_0 , increases with increasing proportion of water in the solvent.

The dependence of reaction rate on solvent composition for nucleophilic substitution reactions in mixed solvents may give information concerning preferential solvation of ionic species. In recent investigations ^{1,2} of this kind the kinetics of the halogen exchange between lithium bromide and butyl bromide in acetone-water mixtures were investigated over the temperature range 15–35 °C.

Under the prevailing conditions lithium bromide is subject to significant ion pair formation which affects the overall reaction rate because of different reactivities of anionic nucleophile (Br^-) and ion paired nucleophile (Li^+Br^-). To separate the observed rate constant of the overall exchange reaction into the different rate constants of the two exchange reactions involving free and paired bromide ions, respectively, precise knowledge of the extent of ion pair formation was required. To obtain the information sought the electrical conductance measurements previously performed ³ at 25 °C were extended to 15 and 35 °C. The objective of the present paper is to discuss the results of these measurements.

EXPERIMENTAL

Lithium bromide (Merck, *suprapur*), acetone (Merck, *pro analysi*), and water were treated as before.³ Solutions were prepared by weight. The determinations of densities, ρ_0 , viscosities, η , and permittivities, ϵ , of mixtures of acetone and water have been described.³ The results of these determinations are given in Table 1.

Table 1. Properties of acetone-water mixtures at 15 and 35 °C.

Water conc. wt-%	ρ_0 g cm ⁻³	η cP	ϵ	ρ_0 g cm ⁻³	η cP	ϵ
	15 °C			35 °C		
0.005	0.79565	0.331	21.62	0.77275	0.273	19.65
0.10	0.79600	0.332	21.69	0.77311	0.274	19.68
0.30	0.79663	0.334	21.79	0.77366	0.275	19.80
1.00	0.79867	0.341	22.19	0.77590	0.280	20.17
2.00	0.80166	0.352	22.75	0.77890	0.287	20.67
5.00	0.81076	0.393	24.51	0.78820	0.315	22.23
10.0	0.82561	0.483	27.33	0.80345	0.371	24.82
20.0	0.85352	0.722	33.05	0.83218	0.514	30.12

For each solvent mixture the density, ρ , of the most concentrated solution of lithium bromide was determined. Densities of less concentrated solutions were calculated assuming a linear relationship,³

$$\rho = \rho_0 + Am \quad (1)$$

where m is the molality of lithium bromide. The value of the constant, A , was found to be of the order $0.06 - 0.08 \text{ kg}^2 \text{ mol}^{-1} \text{ dm}^{-3}$.

Electrolytic conductivities of acetone-water mixtures and of lithium bromide solutions were measured by means of a Leeds and Northrup 4866 conductivity bridge. A modified version³ of a Daggett-Bair-Kraus conductivity cell,⁴ provided with a Hawes-Kay salt cup dispensing device^{5,6} was used. A detailed account of the equipment and of the performance of the measurements has been reported.³

RESULTS AND CALCULATIONS

Molar conductivities, Λ , corrected for the conductivity of the solvent, and the corresponding concentrations, c , of lithium bromide in eight different acetone-water mixtures at 15 and 35 °C are quoted in Tables 2 and 3.

The conductance data were analyzed by means of the equation of Fuoss and Hsia^{7,8} in the form of Fernández-Prini.⁹ For pair-wise associated electrolytes the molar conductivity may be expressed,

$$\Lambda = \alpha[\Lambda_0 - S(\alpha)^{1/2} + E\alpha^{10} \log(\alpha) + J_1\alpha - J_2(\alpha)^{3/2}] \quad (2)$$

where α is the degree of dissociation of the salt, S and E are coefficients¹⁰ which depend upon

Table 2. Electrical conductance data for lithium bromide in acetone-water mixtures at 15 °C.

Run A		Run B		Run A		Run B	
$c \times 10^4$ M	Λ $\text{cm}^2 \Omega^{-1}$ mol^{-1}	$c \times 10^4$ M	Λ $\text{cm}^2 \Omega^{-1}$ mol^{-1}	$c \times 10^4$ M	Λ $\text{cm}^2 \Omega^{-1}$ mol^{-1}	$c \times 10^4$ M	Λ $\text{cm}^2 \Omega^{-1}$ mol^{-1}
0.005 wt-% water				2.00 wt-% water			
1.1920	134.53	1.0412	137.58	2.7461	113.09	1.0093	128.65
3.1873	108.07	4.0179	101.58	5.6086	98.086	2.4356	115.23
6.5803	87.706	10.555	75.216	11.095	82.505	4.9259	100.99
12.758	70.504	17.843	62.599	16.952	72.917	10.169	84.63
20.443	59.588	26.954	53.787	24.057	65.265	15.648	74.715
28.940	52.364	38.710	46.883	37.924	55.899	24.641	64.754
41.452	45.662	40.571	46.052			38.016	55.849
0.10 wt-% water				5.00 wt-% water			
1.2269	136.28	1.3841	133.41	1.0834	111.48	1.1236	111.26
3.4179	110.15	3.5519	108.98	2.2247	105.88	2.4261	105.10
7.0930	90.048	7.2003	89.576	4.5525	97.970	4.6602	97.675
14.938	70.732	15.008	70.629	9.6218	87.035	9.7262	86.881
23.150	60.639	22.720	61.003	15.113	79.404	15.040	79.398
35.782	51.669	34.160	52.542	24.306	70.926	23.626	71.385
52.117	44.797	42.096	48.573	37.456	63.093	36.731	63.413
0.30 wt-% water				10.0 wt-% water			
1.0765	138.84	1.0031	140.36	0.98596	89.346	0.82645	89.655
2.5750	118.60	2.5991	118.46	4.7092	82.754	3.7321	84.059
4.8420	101.92	4.8536	101.87	9.6429	77.451	8.7821	78.234
8.9427	85.496	9.4336	84.102	14.678	73.532	14.224	73.736
16.944	69.445	17.235	69.050	23.053	68.700	23.143	68.592
25.971	59.767	25.801	59.915	35.967	63.388	36.544	63.135
31.177	55.925	37.733	52.112				
1.00 wt-% water				20.0 wt-% water			
3.3508	109.99	1.1905	131.68	0.99431	65.658	1.1065	65.539
6.6958	92.805	3.0811	111.80	2.1059	64.702	2.3999	64.515
13.538	75.389	6.3078	94.188	4.2132	63.318	4.3273	63.264
21.090	65.075	12.691	76.860	8.7446	61.364	8.4286	61.453
29.591	57.785	19.908	66.317	13.210	59.821	13.448	59.738
43.681	50.094	28.330	58.647	21.939	57.527	26.252	56.601
		40.927	51.275	33.865	55.170	35.467	54.845

Table 3. Electrical conductance data for lithium bromide in acetone-water mixtures at 35 °C.

Run A		Run B		Run A		Run B	
$c \times 10^4$ M	Λ $\text{cm}^2 \Omega^{-1}$ mol^{-1}	$c \times 10^4$ M	Λ $\text{cm}^2 \Omega^{-1}$ mol^{-1}	$c \times 10^4$ M	Λ $\text{cm}^2 \Omega^{-1}$ mol^{-1}	$c \times 10^4$ M	Λ $\text{cm}^2 \Omega^{-1}$ mol^{-1}
0.005 wt-% water				2.00 wt-% water			
2.5812	126.69	2.0369	134.79	1.0167	158.76	2.2820	142.89
4.8959	105.03	3.8790	112.79	2.3477	142.06	4.2343	127.26
9.0956	85.558	6.9233	93.899	4.6173	124.88	8.4508	107.93
15.846	70.062	13.200	74.962	9.1748	105.54	14.706	92.169
24.761	59.181	23.129	60.776	15.574	90.548	23.259	79.688
37.415	50.393	36.317	51.013	24.187	78.642	35.632	68.870
0.10 wt-% water				5.00 wt-% water			
0.98592	161.89	1.1803	156.77	0.92678	145.74	0.83810	146.26
1.9739	140.31	2.6627	130.41	2.1883	136.71	2.0229	137.71
3.7329	118.95	4.7856	110.64	4.1592	126.99	3.9390	127.90
8.6198	91.747	9.3381	89.282	8.1880	113.96	8.0380	114.29
15.977	73.906	16.675	72.786	14.588	101.13	14.296	101.58
25.181	62.437	27.454	60.423	23.828	89.624	23.431	90.022
39.236	52.655	40.959	51.773	36.209	79.784	35.569	80.201
0.30 wt-% water				10.0 wt-% water			
0.84161	168.28	0.81647	168.68	1.0584	121.79	0.94340	122.20
2.3324	139.32	2.3303	139.32	2.3754	117.61	2.4169	117.44
4.7272	116.20	4.6339	116.79	4.4901	112.74	4.3395	113.08
9.7394	93.080	8.8837	95.876	8.6754	105.83	8.1853	106.44
15.469	79.526	16.165	78.293	15.708	97.845	14.598	98.882
25.176	66.707	26.023	65.877	24.793	90.719	23.486	91.575
39.216	56.446	40.258	55.871	37.012	83.919	36.684	84.053
1.00 wt-% water				20.0 wt-% water			
1.0460	162.09	1.1945	159.17	0.90058	96.052	0.86462	96.134
2.4568	140.61	2.5975	139.12	2.1879	94.269	2.0497	94.481
4.1008	125.49	4.7345	121.18	4.2901	92.239	3.9714	92.535
7.9431	105.29	8.8696	101.94	8.3246	89.335	7.7610	89.746
14.124	88.147	15.531	85.455	14.899	85.952	13.650	86.556
22.130	75.743	24.411	73.190	24.209	82.390	23.137	82.767
34.388	64.666	36.578	63.208	37.159	78.671	35.845	79.021

Λ_0 , η , ϵ , and the absolute temperature, T , while the coefficients J_1 and J_2 depend, in addition, upon the maximum center-to-center distance, R , between the ions in the ion pair.^{11,12}

The association constant for the equilibrium between free and paired ions is defined by the expression,

$$K_A = (1 - \alpha)/(c\gamma^2\alpha^2) \quad (3)$$

where γ is the mean molar activity coefficient of free ions, which was calculated using the Debye-Hückel equation,

$$^{10}\log \gamma = -A(c\alpha)^{1/2}/[1 + BR(c\alpha)^{1/2}] \quad (4)$$

where A and B are functions of ϵ and T .

Using eqns. (2-4) the values of Λ_0 and K_A which minimize $\sigma(\Lambda)$, the standard deviation between measured and calculated Λ -values, were determined as a function of the distance parameter, R , using a computer program described.¹³ Typical examples of the dependence of Λ_0 and K_A on R are shown in Fig. 1.

In most instances the curve obtained upon plotting $\sigma(\Lambda)$ vs. R was found to exhibit two minima for two quite different values of R , cf. Fig. 2.

This behaviour, which is not uncommon as has been recently demonstrated,¹⁴ indicates that the condition, $\sigma(\Lambda) = \text{minimum}$, is not useful as criterion of "best set" conductance parameters.

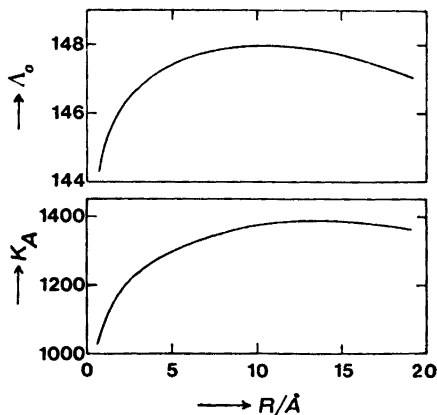


Fig. 1. Dependence of Λ_0 and K_A on the distance parameter, R , for LiBr in aqueous acetone (2 wt-% H_2O) at 15°C.

Since there exists at present no method of determining the value of R uniquely, this distance parameter will in the following be set equal to the Bjerrum radius, q , which for univalent electrolytes is given by the expression,

$$q = e^2/2ekT \quad (5)$$

where e is the electronic charge and k is Boltzmann's constant.¹⁵

A compilation of the values derived for Λ_0 , K_A , and $\sigma(\lambda)$ for this choice of R is given in Table 4. The relative standard deviations in Λ_0 and K_A were usually less than 0.2 and 0.5 %, respectively. The values of K_A obtained indicate that association to pairs increases with temperature.

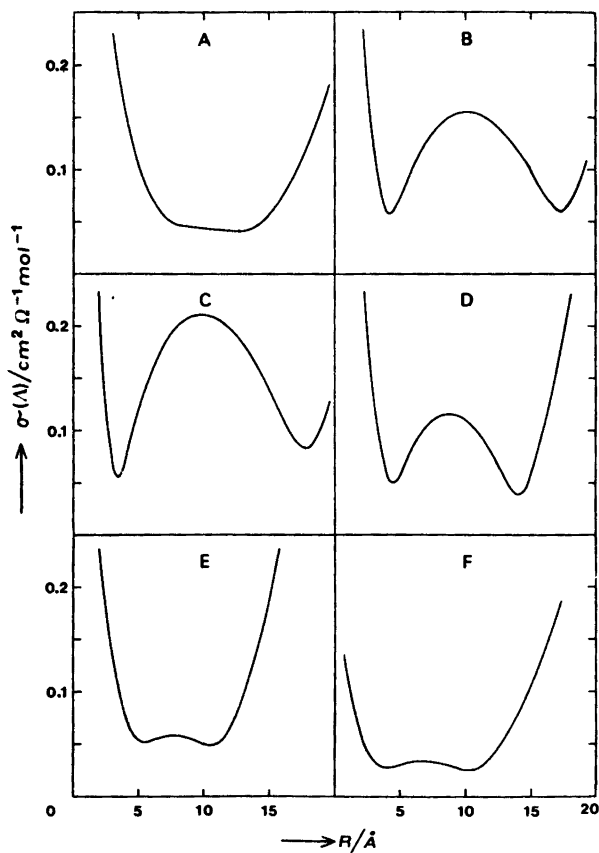


Fig. 2. Dependence of $\sigma(\lambda)$ on the distance parameter, R , for LiBr in aqueous acetone at 15°C. The curves A – F refer to solvent mixtures containing 0.3, 1, 2, 5, 10, and 20 wt-% H_2O , respectively.

Table 4. Conductance parameters for lithium bromide in acetone-water mixtures.

Water conc. wt.-%	q Å	A_0 $\text{cm}^2 \Omega^{-1} \text{mol}^{-1}$	K_A M^{-1}	$\sigma(A)$ $\text{cm}^2 \Omega^{-1} \text{mol}^{-1}$
15 °C				
0.005	13.41	177.0	3 424	0.10
0.10	13.37	174.4	2 813	0.07
0.30	13.31	171.3	2 503	0.04
1.00	13.07	160.4	2 018	0.13
2.00	12.74	147.9	1 385	0.19
5.00	11.83	120.8	516	0.08
10.0	10.61	93.5	171	0.05
20.0	8.77	67.6	42	0.03
25 °C				
0.005	13.54	194.3	4 160	0.11
0.10	13.47	192.7	3 413	0.08
0.30	13.47	189.9	2 839	0.06
1.00	13.22	179.8	2 163	0.17
2.00	12.79	165.7	1 449	0.29
5.00	12.03	138.4	552	0.19
10.0	10.74	110.1	186	0.07
20.0	8.87	82.5	47	0.05
35 °C				
0.005	13.80	211.0	4 513	0.10
0.10	13.78	211.0	3 918	0.10
0.30	13.69	206.9	3 163	0.10
1.00	13.44	196.4	2 230	0.09
2.00	13.12	184.2	1 534	0.19
5.00	12.20	157.4	603	0.10
10.0	10.92	128.1	205	0.04
20.0	9.00	98.8	52	0.02

DISCUSSION

Taking into account solvent-ion and solvent-ion pair interaction energies, Gilkerson¹⁶ arrived at the following equation for the ion pair association constant,

$$K_A = (2\pi\mu kT/h^2)^{-3/2} (g\nu\bar{\sigma})^{-1} \exp(E_s/RT) \exp(Ne^2/\epsilon a RT) \quad (6)$$

where R = gas constant and N = Avogadro's number. The other symbols are explained in the original paper.¹⁶

Eqn. (6) contains three adjustable parameters: the minimum distance, a , between the charges in the ion pair; the difference, E_s , between solvent-ion and solvent-ion pair interaction energies ($E_s = E_+ + E_- - E_{\pm}$); and $(g\nu\bar{\sigma})$ which is a function of the free volumes available to the ions and the ion pair.

Later a transformation was made from Gilkerson's free-volume approach¹⁶ by grafting

a specific solvation term¹⁷ to Fuoss' hard sphere in a continuum model¹⁸ resulting in the expression:

$$K_A = (4\pi N a^3 / 3000) \exp(E_s/RT) \exp(Ne^2/\epsilon a RT) \quad (7)$$

The logarithmic form of this equation indicates that a straight line should be obtained upon plotting $\ln K_A$ vs. $1/\epsilon$ at constant temperature provided that a and E_s are independent of the composition of the solvent mixture. However, the graphs shown in Fig. 3 for the systems concerned exhibit significant curvature which increases with decreasing proportion of the protic component.

For a given composition of the solvent mixture (a and E_s constant) the minimum center-to-center distance between the ions in the ion pair may be calculated from the derivative,

$$\frac{d \ln K_A}{d(1/\epsilon)} = \frac{Ne^2}{a RT} \quad (8)$$

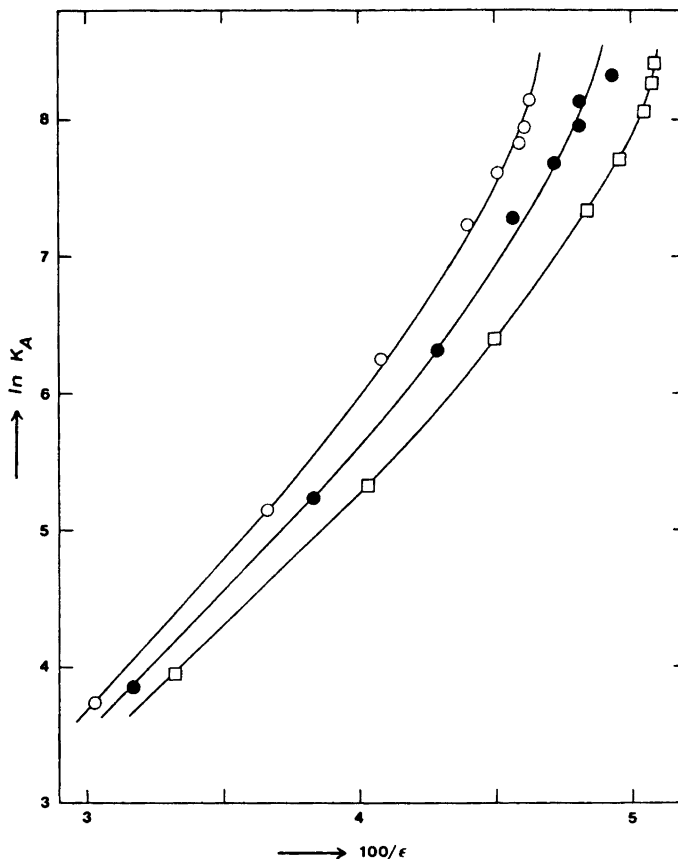


Fig. 3. Graphs of $\ln K_A$ vs. $100/\epsilon$ for LiBr in aqueous acetone at 15 °C (open circles), 25 °C (full circles), and 35 °C (squares).

obtained from eqn. (7). Values of a according to eqn. (7) were calculated from the slopes of the curves in Fig. 3 at four different concentrations of water in the solvent mixture, viz. 0.3, 2, 5, and 20 wt-%.

The values of a obtained for the three different temperatures investigated are given in the next to last column of Table 5 in which the corresponding values derived from the Bjerrum equation,¹⁵

$$K_A = \frac{4\pi N}{1000} \int_a^q r^2 \exp\left(\frac{e^2}{\epsilon k T r}\right) dr \quad (9)$$

are included in the second column. The following conclusions may be drawn.

For a given composition of the solvent mixture the minimum center-to-center distance

between the ions in the ion pair appears to be independent of temperature. According to the Gilkerson-Fuoss equation, eqn. (7), the average values of a at the three different temperatures investigated amount to 1.1, 1.8, 2.1, and 2.7 Å for the solvent mixtures containing 0.3, 2, 5, and 20 wt-% water, respectively. The corresponding average values of a according to Bjerrum's equation, eqn. (9), are 2.1, 2.2, 2.3, and 2.9 Å. These values of a , being in most instances less than the crystal radii sum of Li^+ and Br^- (2.6 Å), obviously underestimate the minimum center-to-center distance between the ions in the ion pair.

The trend of the a values to decrease with decreasing proportions of water in the solvent mixture may possibly be taken as evidence that the character of Li^+Br^- as solvent separated

Table 5. Parameters according to eqns. (7) and (9) for LiBr in aqueous acetone.

Water conc. wt.-%	a , eqn. (9) Å	a , eqn. (7) Å	E_s kJ mol ⁻¹
15 °C			
0.3	2.11	1.12	-24.4
2.0	2.22	1.79	-6.9
5.0	2.34	2.13	-2.9
20.0	2.94	2.63	+0.4
25 °C			
0.3	2.12	1.20	-22.3
2.0	2.24	1.81	-7.0
5.0	2.34	2.06	-3.8
20.0	2.85	2.71	+0.7
35 °C			
0.3	2.15	1.03	-32.3
2.0	2.24	1.82	-7.4
5.0	2.36	2.11	-3.6
20.0	2.81	2.80	+1.1

ion pair decreases with decreasing concentration of the protic constituent.

The values of E_s in Table 5 suggest that the difference in solvation energies of the ions and the ion pair decreases with increasing proportions of water in the solvent mixture. For acetone containing 0.3 wt.-% water E_s is of the order -20 to -30 kJ mol⁻¹. The negative value of E_s indicates that the solvent-ion pair interaction term, E_{\pm} , is greater than the solvation interaction terms, ($E_+ + E_-$). For the solvent mixture containing 20 wt.-% water E_s is close to zero for all three temperatures studied indicating approximately equal solvation energies for the ion pair and the free ions.

On the assumption that the ions migrate through the liquid by successive jumps from one equilibrium position to another and that a characteristic free energy of activation, ΔG_{oi}^{\ddagger} , is required for each jump the limiting molar conductivity of i-ions may be expressed,¹⁹

$$\lambda_{oi} = \frac{1}{6} \frac{zeF}{h} L_i^3 \exp\left(-\frac{\Delta G_{oi}^{\ddagger}}{RT}\right) \quad (10)$$

where L_i is the jump distance. The other notations in eqn. (10) have their usual significance.

Differentiation of the logarithmic form of eqn. (10) with respect to temperature at constant pressure and use of the relations,¹⁹

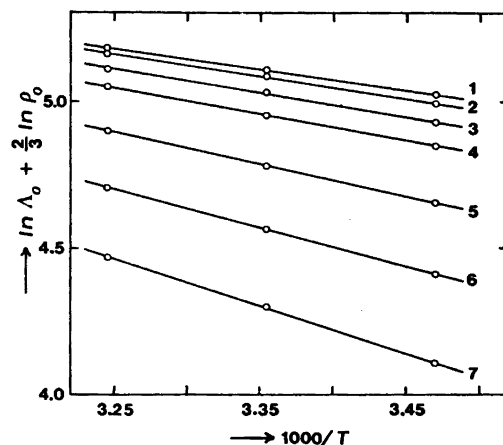


Fig. 4. Graphs according to eqn. (13) for LiBr in aqueous acetone. The straight lines 1-7 refer to solvent mixtures containing 0.005, 0.3, 1, 2, 5, 10, and 20 wt.-% H₂O.

$$\left(\frac{\partial \ln L_i}{\partial T}\right)_P = \frac{1}{3} \left(\frac{\partial \ln V}{\partial T}\right)_P = -\frac{1}{3} \left(\frac{\partial \ln \rho_0}{\partial T}\right)_P \quad (11)$$

results in the following expression,

$$\Delta H_{oi}^{\ddagger} = RT^2 \left(\frac{\partial \ln \lambda_{oi}}{\partial T}\right)_P + \frac{2}{3} RT^2 \left(\frac{\partial \ln \rho_0}{\partial T}\right)_P \quad (12)$$

where ΔH_{oi}^{\ddagger} is the enthalpy change referring to the unit displacement (one jump) of one mol of ions.

Provided that the transport numbers, t_i and t_j , do not change significantly with temperature the integrated form of eqn. (12) may be written,

$$\ln \lambda_0 + \frac{2}{3} \ln \rho_0 = -\frac{\Delta H_0^{\ddagger}}{RT} + B \quad (13)$$

where $\Delta H_0^{\ddagger} = t_i \Delta H_{oi}^{\ddagger} + t_j \Delta H_{oj}^{\ddagger}$ and B is an integration constant, cf. Ref. 20.

Graphs according to eqn. (13) for lithium bromide in several aqueous acetone mixtures are shown in Fig. 4. For the temperature interval studied no temperature dependence of the heat of activation can be detected. Application of eqn. (13) to the experimental data using the method of least squares yields the values of ΔH_0^{\ddagger} quoted in Table 6.

It is found that ΔH_0^{\ddagger} increases with increasing proportions of water in the solvent mixture, viz. from 6 kJ mol⁻¹ for anhydrous acetone to 13 kJ mol⁻¹ for acetone containing 20 wt.-%

Table 6. Dependence of ΔH_0^\ddagger according to eqn. (13) on solvent composition of LiBr in aqueous acetone.

Water conc. wt.-%	ΔH_0^\ddagger kJ mol ⁻¹
0.005	5.8
0.10	6.3
0.30	6.2
1.00	6.8
2.00	7.4
5.00	9.1
10.0	11.0
20.0	13.4

15. Bjerrum, N. K. *Dan. Vidensk. Selsk., Mat.-Fys. Medd.* 7 (1926) No. 9.
16. Gilkerson, W. R. *J. Chem. Phys.* 25 (1956) 1199.
17. Sadek, H. and Fuoss, R. M. *J. Am. Chem. Soc.* 81 (1959) 4507.
18. Fuoss, R. M. *J. Am. Chem. Soc.* 80 (1958) 5059.
19. Brummer, S. B. and Hills, G. J. *Trans. Faraday Soc.* 57 (1961) 1816.
20. Barthel, J., Wachter, R. and Knerr, M. *Electrochim. Acta* 16 (1971) 723.
21. Harned, H. S. and Owen, B. B. *The Physical Chemistry of Electrolytic Solutions*, 3rd Ed., Reinhold, New York 1964, p. 234.

Received June 30, 1977

water. Compare $\Delta H_0^\ddagger = 15$ kJ mol⁻¹ for lithium bromide in water at 25 °C. This value was calculated from the temperature dependence of Λ_0 obtained from limiting molar conductivities and transport numbers for LiCl and KBr.²¹

Acknowledgements. The author thanks Mrs. Margareta Ögren for technical assistance and the Swedish Natural Science Research Council for financial support.

REFERENCES

1. Holmgren, A. and Beronius, P. *Acta Chem. Scand.* 26 (1972) 3881.
2. Holmgren, A. *Acta Chem. Scand. A* 31 (1977) 539.
3. Nilsson, A.-M. and Beronius, P. *Z. Phys. Chem. Frankfurt am Main* 79 (1972) 83.
4. Daggett, H. M., Bair, E. J. and Kraus, C. A. *J. Am. Chem. Soc.* 73 (1951) 799.
5. Hawes, J. L. and Kay, R. L. *J. Phys. Chem.* 69 (1965) 2420.
6. Kay, R. L., Hales, B. J. and Cunningham, G. P. *J. Phys. Chem.* 71 (1967) 3925.
7. Fuoss, R. M. and Hsia, K.-L. *Proc. Natl. Acad. Sci. U.S.A.* 57 (1967) 1550.
8. Fuoss, R. M. and Hsia, K.-L. *Proc. Natl. Acad. Sci. U.S.A.* 58 (1968) 1818.
9. Fernández-Prini, R. *Trans. Faraday Soc.* 65 (1969) 3311.
10. Fuoss, R. M. and Accascina, F. *Electrolytic Conductance*, Interscience, New York 1959.
11. Justice, J.-C. *Electrochim. Acta* 16 (1971) 701.
12. Barthel, J., Justice, J.-C. and Wachter, R. *Z. Phys. Chem. Frankfurt am Main* 84 (1973) 100.
13. Beronius, P. *Acta Chem. Scand. A* 28 (1974) 77.
14. Beronius, P. *Acta Chem. Scand. A* 30 (1976) 115.

Catalysis by Coordinatively Unsaturated Surface Compounds of Chromium(II), Iron(II), Cobalt(II) and Nickel(II) on Silica Gel.

I. Decomposition of NO and NO Reduction by CO

BERND REBENSTORF, LENNART LARSSON and RAGNAR LARSSON

Division of Inorganic Chemistry 1, Chemical Center, University of Lund, Box 740, S-220 07 Lund 7, Sweden

The coordinatively unsaturated surface compounds of chromium(II), iron(II), cobalt(II) and nickel(II) on silica gel catalyse the reduction of NO by CO and, with the exception of chromium(II), the decomposition of NO. The catalytic activity increases from nickel(II) to chromium(II) (reduction) and from nickel(II) to iron(II) (decomposition). During the reduction of NO by CO, N₂O is produced at lower and N₂ at higher temperatures. On the basis that NO is chemisorbed by these surface compounds a reaction model is set up, in which the coordinatively unsaturated surface compounds act as the catalytic center. This model is supported by the poisoning effect of water and by the fact that iron(II) samples with low pretreatment temperatures (300 and 500 °C) have no catalytic activity.

The four coordinatively unsaturated surface compounds of chromium(II),¹ iron(II),² cobalt(II)³ and nickel(II)⁴ on silica gel can each adsorb two molecules NO per metal ion at room temperature.⁵ This observation indicates that these surface compounds might be catalytically active, as the first step in any catalytic reaction involving nitric oxide must be the chemisorption of NO.⁶

The strong interest in catalytic removal of nitrogen oxides from automotive exhaust gases⁷ has made us concentrate our investigation on two reactions. The first is the decomposition of NO to N₂ and O₂, the second is the reduction of NO by CO to N₂ (and CO₂). From these investigations we also hope to obtain some understanding of the role of the electronic structure of the metal ion for the catalytic activity in the series of coordinatively unsaturated surface compounds.

EXPERIMENTAL

The chromium(II) surface compound was prepared by impregnating purified⁸ silica gel "Merck 7733" (specific surface area approximately 600 m²/g) with a solution of chromium(VI) oxide in water, drying this mixture at 120 °C in air and afterwards heating it in vacuum to 800 °C in a quartz tube. At that temperature oxygen was applied to the sample, which was then cooled down to 400 °C. After evacuation the chromium(VI) surface compound was reduced by CO. The samples of the coordinatively unsaturated surface compound of chromium(II) on silica gel so produced had obviously the same activity as those described in Ref. 8; for instance chemiluminescence during reaction with O₂ or the colour change from green to blue on adsorption of N₂ was the same as described there. The chromium concentration in the sample was 0.6 %.

The preparations of the coordinatively unsaturated iron(II) and cobalt(II) surface compounds on silica gel have been described previously^{2,3} and the corresponding nickel(II) compound was prepared in the same way as that of cobalt(II).³ The iron content of the samples was 0.7 %, while the cobalt(II) and nickel(II) contents were 0.6 %.

To perform the catalytic reactions the samples were placed in a column with an inner diameter of 8 mm and a heated length of 200 mm. The gases NO or NO/CO were dried by molecular sieve and phosphorus pentoxide before passing over the sample with a speed of 10 ml/h. In the NO decomposition experiments NO₂ was removed from the produced gas mixture by moist potassium hydroxide⁹ and the remaining NO and the catalytically produced N₂ and N₂O determined with a Perkin-Elmer F 17 gas chromatograph. The separation column was filled with molecular sieve 13 X, mesh 45/60. The error of these measurements was within

3 %. In the case of the NO reduction by CO the gases N_2 , N_2O , NO and CO were determined.

RESULTS

NO decomposition. During an examination of the decomposition of NO five reactions have to be taken into consideration:

1. $2NO \rightarrow N_2 + O_2$
2. $2NO \rightarrow N_2O + 1/2O_2$
3. $N_2O \rightarrow N_2 + 1/2O_2$
4. $2NO + O_2 \rightleftharpoons 2NO_2$
5. $2NO_2 \rightleftharpoons 2N_2O_4$

The equilibrium of reactions 4 and 5 are shifted to the right only at relatively low temperatures, so that the gas mixture in the column contains only NO, N_2 and perhaps N_2O at the temperatures where catalytic activity was observed.

The catalytic decomposition of NO takes place on the coordinatively unsaturated surface compounds of iron(II), cobalt(II) and nickel(II) at temperatures higher than 300 °C and is most effective with the iron(II) surface compound, as is shown in Fig. 1. With this surface compound a maximum conversion of 75 % was reached at 750 °C (Fig. 2).

In contrast to these three surface compounds no catalytic activity was observed with the chromium(II) surface compound. However, the

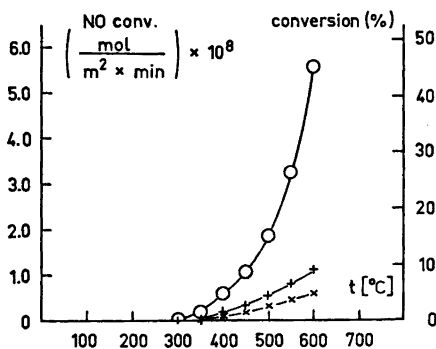


Fig. 1. Decomposition of NO over iron(II), cobalt(II) and nickel(II) on silica gel as a function of temperature. O, 0.7 % Fe; +, 0.6 % Co; x, 0.6 % Ni.

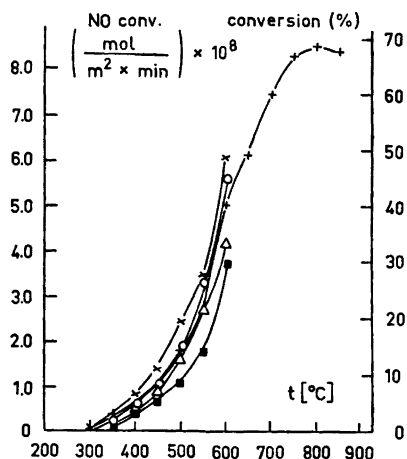


Fig. 2. Decomposition of NO over samples with different iron(II) concentrations on silica gel as a function of temperature. x, 1.4 % Fe; +, 1.05 % Fe; O, 0.7 % Fe; Δ, 0.35 % Fe; ■, 0.175 % Fe.

production of N_2O and a small quantity of N_2 was observed between 150 and 250 °C. The N_2O may be produced according to reaction 2 in the above reaction list. In this case the accompanying O_2 is a strong poison for the chromium(II) surface compound, because the O_2 oxidises the chromium(II) to chromium(VI).^{1,8} Only small amounts of N_2O and N_2 are produced by the surface compounds of iron(II), cobalt(II) and nickel(II) between 150 and 300 °C.

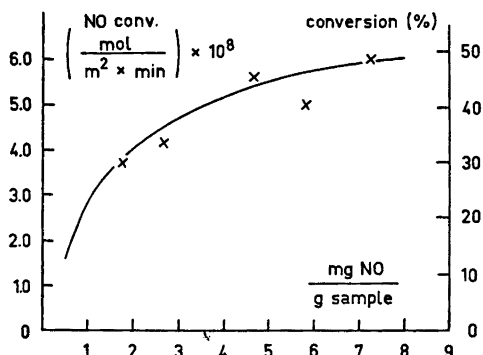


Fig. 3. Decomposition of NO at 500 °C over samples with different iron(II) concentrations on silica gel versus NO adsorption at 0 °C and vacuum (1 Torr).

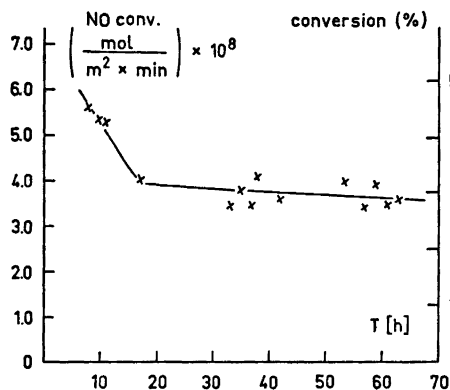


Fig. 4. Decomposition of NO at 600 °C over 0.7 % iron(II) on silica gel versus time.

The effect of different iron(II) concentrations on the conversion rate of the catalytic decomposition of NO is relatively small (Fig. 2). Obviously there exists no linear relation between the rate of the catalytic conversion of NO and the NO adsorption of samples with different iron(II) content (Fig. 3). A possible explanation of the latter two effects may lie in a slow diffusion of the gas molecules to and away from the catalytic sites since the mean pore diameter of the silica gel used here is relatively small (60 Å). Another explanation may be that only some of the surface iron(II) ions, which adsorb NO, are catalytically active.

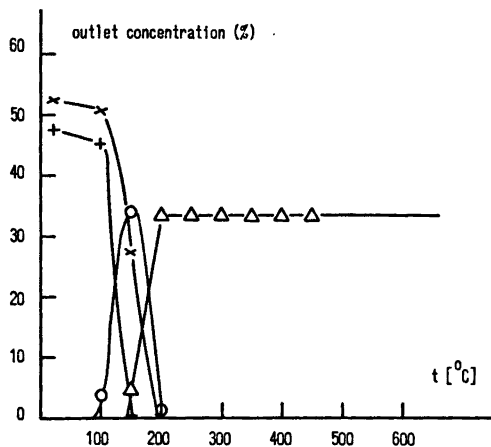


Fig. 5. NO reduction by CO over chromium(II) on silica gel versus temperature. x, CO; +, NO; O, N₂O; Δ, N₂.

When run a long time, as shown in Fig. 4, the rate of decomposition of NO decreases over a period of approximately ten hours and remains constant afterwards at nearly half the value of the original conversion rate. If samples of iron(II) on silica gel, which were pretreated in vacuum at only 500 °C and not at 1000 °C as used before, were applied, no catalytic conversion of NO was detected up to 600 °C. It was also found that water is a strong poison for the above reaction. If it is assumed that only the coordinatively unsaturated iron(II) ions are the catalytically active centers the last two observations support the reaction scheme² put forward for the preparation of this species. There are no observations limiting this conclusion to iron(II) only and so it may be extended to cobalt(II) and nickel(II).

NO reduction by CO. Three reactions can be involved in the catalytic reduction of NO by CO:

1. $2\text{NO} + 2\text{CO} \rightarrow \text{N}_2 + 2\text{CO}_2$
2. $2\text{NO} + \text{CO} \rightarrow \text{N}_2\text{O} + \text{CO}_2$
3. $\text{N}_2\text{O} + \text{CO} \rightarrow \text{N}_2 + \text{CO}_2$

As shown in the Figs. 5–8 N₂O is produced in the beginning of the reduction at relatively low temperatures and is replaced as a reaction product at higher temperatures by N₂. The catalytic activity decreases from chromium(II) to nickel(II), as indicated by the increase in the

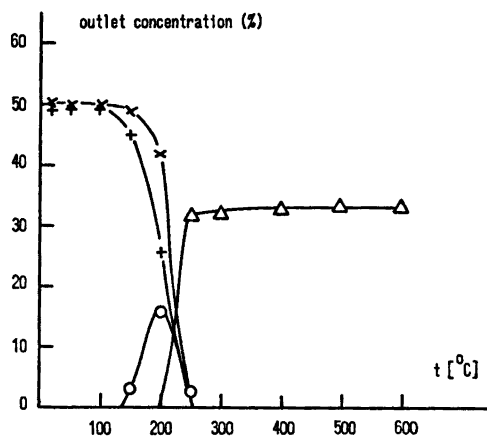


Fig. 6. NO reduction by CO over iron(II) on silica gel versus temperature. x, CO; +, NO; O, N₂O; Δ, N₂.

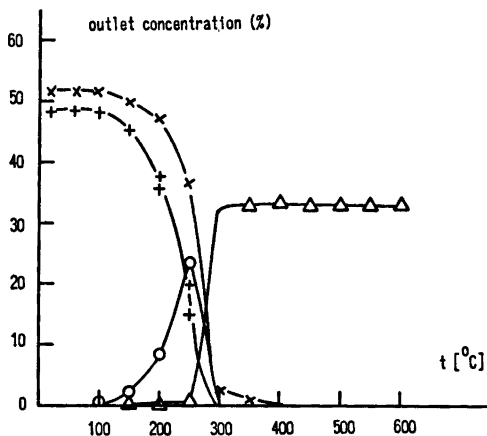


Fig. 7. NO reduction by CO over cobalt(II) on silica gel versus temperature. x, CO; +, NO; O, N₂O; Δ, N₂.

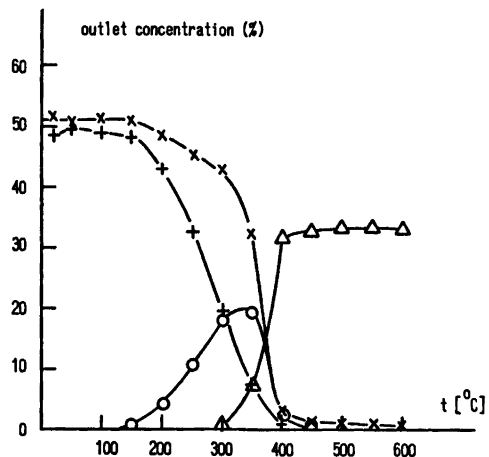


Fig. 8. NO reduction by CO over nickel(II) on silica gel versus temperature. x, CO; +, NO; O, N₂O; Δ, N₂.

temperature of the N₂O maximum and by the increase in the temperature of complete conversion of N₂. The decrease in the catalytic activity observed on going from iron(II) to nickel(II) is approximately the same as that during the catalytic decomposition of NO. It was observed that, after heating the samples to 600 °C under the catalytic process conditions, the temperature of the N₂O maximum and that of complete conversion to N₂ is about 50

°C higher than before in the case of iron(II), cobalt(II) and nickel(II). This temperature shift was not observed with chromium(II).

It was found that water is a strong poison for the catalytic reduction of NO by CO. As Figs. 9 and 10 show, the catalytic activity in this reaction decreases, when iron(II) on silica gel is heated to only 500 °C in vacuum and vanishes if a pretreatment temperature of 300 °C is used. In the latter case it is interesting

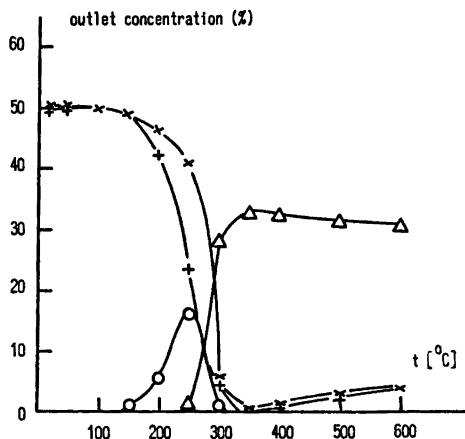


Fig. 9. NO reduction by CO over iron(II) on silica gel (pretreatment temperature 500 °C) versus temperature. x, CO; +, NO; O, N₂O; Δ, N₂.

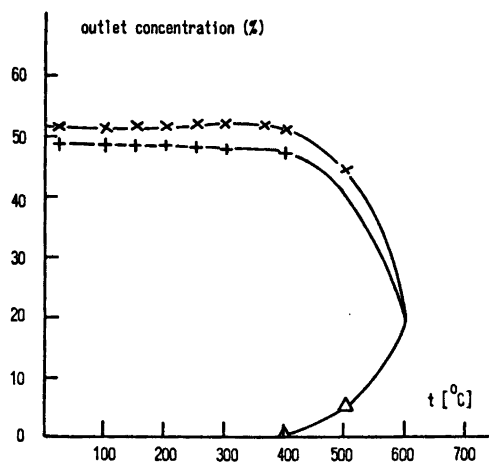


Fig. 10. NO reduction by CO over iron(II) on silica gel (pretreatment temperature 300 °C) versus temperature. x, CO; +, NO; Δ, N₂.

Table 1. Results of IR measurements on NO adsorbed by coordinatively unsaturated transition metal ions on silica gel.

Transition metal ion	$\bar{\nu}_a(\text{NO})$ (cm^{-1})	$\bar{\nu}_s(\text{NO})$ (cm^{-1})	$\frac{\bar{\nu}_a(\text{NO}) + \bar{\nu}_s(\text{NO})}{2}$ (cm^{-1})	Angle between NO's ($^\circ$)
Chromium(II) ^{5b}	1747	1865	1806	126 ^a
Iron(II) ³	1802	1870	1836	130
Cobalt(II) ³	1797	1875	1836	110
Nickel(II) ⁴	1832	1878	1855	99

^a This angle was calculated from the intensity ratio reported by Zecchina *et al.*¹³

that, when some water is stripped off the iron(II) surface compound at temperatures higher than 300 °C, not N₂O but N₂ is the product of the catalytic reduction of NO. A comparison of the results given in Figs. 6, 9 and 10 indicates that during the last treatment more or less the same catalytic center is produced as with the vacuum heat treatment at 1000 °C described in Ref. 2. This leads again to the conclusion that only the coordinatively unsaturated iron(II) surface compound can be the catalytic center. It is assumed that this conclusion can again be extended to the other three surface compounds used in the above experiments.

DISCUSSION

It was noted above that the four coordinatively unsaturated surface compounds of chromium(II), iron(II), cobalt(II) and nickel(II) on silica gel each adsorb two molecules NO per surface metal ion.⁵ As Table 1 shows all four surface compounds have two IR bands, the separation of which decreases from chromium(II) to nickel(II). The arithmetic mean value of the two IR absorptions increases in that direction. The angle between the two adsorbed NO molecules, as calculated from the intensities of the IR bands,¹⁰ decreases in the same direction. Indeed at high temperatures there exists some evidence that either two molecules or none are bound to the metal surface ion.^{3,11a} Furthermore, attention should be directed towards the observations of Zecchina *et al.*¹³ that some additional molecules (but not NO) can be adsorbed to the bis-NO surface complex, at least at low temperatures. This

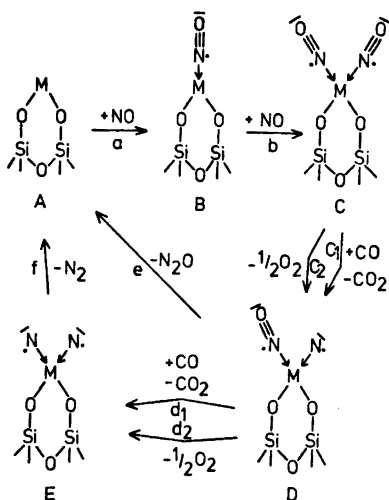
is an indication of a possible five-coordination complex at the reduction (*cf.* below).

In order to discuss the bond between the adsorbed NO and the metal surface ion, a coordinative bonding is very likely, as NO wavenumbers between 1700 and 1870 cm^{-1} are assigned to such a chemisorption.¹³ Because the unpaired electron occupies an antibonding π^* orbital, increasing the electron density of the N–O bond will decrease the bond strength and the frequency of the NO stretching vibration. If the electron density is decreased the bond strength and the wavenumber of the NO vibration will increase. In our case of NO adsorbed at the coordinatively unsaturated surface compounds the arithmetic mean value decreases from nickel(II) to chromium(II) indicating an increase in electron density at the N–O bond and an increasing electron donation from the metal ion.

This effect is in contrast to the number of *d*-electrons, which decreases from nickel(II) (*d*⁸) to chromium(II) (*d*⁴). However, a parallel effect between the ease of losing electrons (exemplified by the charge transfer spectra of the aqueous complexes, *cf.* Dainton¹⁴) and the back bonding can be stated.

A reaction mechanism of the catalytic decomposition of NO and the catalytic reduction of NO by CO should contain the reaction steps shown in the scheme. Some of these steps were pointed out before by other authors.¹¹

The reactions *c*₁ and *d*₁ may use the above-mentioned additional free coordination site at the transition metal ion, the fifth, as the four others are used by two oxygen ligands from the surface of the silica gel and by two nitrogen ligands, respectively. The structures



D and E may be stabilised through two effects. One is a "back-bonding" from a metal d -orbital to an empty orbital of the N atom. We presuppose an sp^3 hybridization in the discussion, but perhaps other orbital combinations may be better. This effect will follow the trend discussed above, *i.e.* Cr, Fe, Co and Ni. The second effect is the formation of a three-center N-M-N bond housing the odd electrons of the nitrogen atoms.

This model allows us to understand how the two nitrogen atoms can leave the complex as an N-N unit. The larger the part of the three-center bond that is dominated by the s -orbital contribution, the larger is the N-N bonding and the closer the two atoms will approach each other.

Stabilising the intermediate reaction states D and E would decrease the activation energies of the reactions c and d and result in an enhancement of the catalytic reactions in the direction from nickel(II) to chromium(II). The same effect may be expected from the decreasing N-O bond strength, because that will make it more easy, on one side for the CO to attack the chemisorbed NO and on the other side for the N-O bond to be split.

From the scheme it can also be concluded that the production of N_2O or N_2 will depend on the relation of the two rates of reactions e and d_(1,2). If reaction e is faster than reaction d N_2O will be produced, in the reverse case

N_2 , and if both reaction rates are equal N_2O and N_2 will be produced in the same amount.

Comparing the discussion of the scheme with the observed reactions makes some additional remarks necessary. The decomposition of NO over chromium(II) on silica gel can be explained by the assumption that structure D in this case is very much stabilised and so much N_2O and so little N_2 are observed. As mentioned before the chromium(II) surface compound is destroyed during this reaction by the produced O_2 . The fact that only a little N_2O is produced by the surface compounds of iron(II), cobalt(II) and nickel(II) at low temperatures in the decomposition of NO may be similarly explained by assuming that structure E in this case is more stabilised than structure D. This means that at the same time as the molecular bonds between N and O and the coordinative bonds between the metal and the adsorbed NO are weakened and at last split, new bonds between the oxygen atoms and the two nitrogen atoms are built. In such a case there would be no place for the building of N_2O .

Comparing the results from the catalytic reduction of NO by CO with the scheme, shows more straight-forward agreement, than in the above case. So the question may be asked if the proposed mechanism can also be applied to the catalytic reduction of NO by CO over transition metal oxides.⁶ On one hand the N_2O at lower and the N_2 production at higher temperatures agree well with our observations. On the other hand there are no experimental results to support a model, like the coordinatively unsaturated surface compound as proposed here, describing a catalytic center of the decomposition of NO and of the catalytic reduction of NO by CO.

In the above scheme N_2O is not an intermediate reaction product, in contrast to ideas put forward in Ref. 6. Such an assumption seems not to be necessary. However, to be sure further experiments, especially with N_2O , should be performed.

Acknowledgement. This work has been financially supported by the Swedish Board of Technical Development and by the Deutsche Forschungsgemeinschaft. The latter agency has given a grant to one of us (B.R.), which made it possible for him to work in Sweden.

REFERENCES

1. Krauss, H. L. and Stach, H. Z. *Anorg. Allg. Chem.* 366 (1969) 34.
2. Rebenstorf, B. *Acta Chem. Scand. A* 31 (1977) 547.
3. Rebenstorf, B. *Acta Chem. Scand. A* 31 (1977) 208.
4. Rebenstorf, B. *Unpublished results.*
5. a. Krauss, H. L. and Weisser, B. Z. *Anorg. Allg. Chem.* 412 (1975) 82; b. Zecchina, A., Garrone, E., Morterra, C. and Coluccia, S. *J. Phys. Chem.* 79 (1975) 978; c. For NO adsorbed on iron(II), cobalt(II) and nickel(II) see Refs. 2, 3 and 4.
6. Shelef, M. and Kummer, J. T. *AIChE Symp. Ser. No. 115*, 67 (1971) 74.
7. a. Weigert, W. M. and Koberstein, E. *Angew. Chem.* 88 (1976) 657; b. McEvoy, J. E., Ed., *Catalysts for the Control of Automotive Pollutants*, *Adv. Chem. Ser.*, American Chemical Society, Washington, D. C. 1975, USA.
8. Krauss, H. L., Rebenstorf, B. and Westphal, U. Z. *Anorg. Allg. Chem.* 414 (1975) 97.
9. Winter, E. R. S. *J. Catal.* 22 (1971) 158.
10. Beck, W., Melnikoff, A. and Stahl, R. *Chem. Ber.* 99 (1966) 3721.
11. a. Shih, S. S., Shihabi, D. S. and Squires, R. G. *Preprints of the Sixth International Congress on Catalysis, B* 36; b. Eisenberg, R. and Meyer, C. D. *Acc. Chem. Res.* 8 (1975) 26.
12. Zecchina, A., Garrone, E., Ghiotti, G. and Coluccia, S. *J. Phys. Chem.* 79 (1975) 984.
13. a. Terenin, A. N. and Roev, L. N. *Actes Congr. Int. Catal. 2nd, 1960, 2*, (1961) 2188; b. Terenin, A. and Roev, L. *Spectrochim. Acta* 15 (1959) 946; c. Little, C. H. *Infrared Spectra of Adsorbed Species*, Academic, London, New York 1966.
14. Dainton, F. S. *J. Chem. Soc.* (1952) 1953.

Received June 22, 1977.

The Vibrational Spectra and Force Constants of the Tellurocyanate Ion (TeCN^-)

PETER KLÆBOE,^a CLAUD J. NIELSEN^a and JON SONGSTAD^b

^a Department of Chemistry, University of Oslo, Oslo 3, Norway and ^b Department of Chemistry, University of Bergen, N-5014 Bergen, Norway

The infrared spectra of crystalline samples of $(\text{C}_6\text{H}_5)_4\text{PTeCN}$ (I), $(\text{C}_6\text{H}_5)_4\text{AsTeCN}$ (II) and $[(\text{C}_6\text{H}_5)_3\text{P}]_2\text{NTeCN}$ (III) including the ^{13}C isotopic species of I and II were recorded in the region $4000 - 180 \text{ cm}^{-1}$ as potassium iodide and polyethylene pellets and as Nujol mulls. Raman spectra of the crystalline compounds were obtained while III was also studied in acetonitrile and acetone solution: Spectra of the cyanide salts of the cations $(\text{C}_6\text{H}_5)_4\text{P}^+$, $(\text{C}_6\text{H}_5)_4\text{As}^+$ and $[(\text{C}_6\text{H}_5)_3\text{P}]_2\text{N}^+$ were also recorded.

The three fundamental frequencies of the TeCN^- ion were assigned. A general valence force field for I was calculated employing the ^{13}C data. The force constants are compared with those reported for the OCN^- , SCN^- and SeCN^- ions.

The vibrational spectra of the cyanate ion, NCO^- , the thiocyanate ion, NCS^- and the selenocyanate ion, NCSe^- , have been the subject of considerable study in recent years.¹⁻⁵ Structural data together with spectroscopic studies on ^{13}C -enriched species have permitted the calculation of force constants for these ions.

With regard to the tellurocyanate ion, TeCN^- considerably less is known. The chemical evidence indicates that the tellurium-carbon bond is very weak and salts of this ion can only be prepared with large, non-polarizing cations.⁶

In a previous IR study on the tellurocyanate ion, tetramethylammonium, Me_4N^+ , and tetraphenylarsonium, Ph_4As^+ , salts were employed.⁷ However, difficulties arose due to the fact that Me_4NTeCN was very unstable while Ph_4AsTeCN was not sufficiently soluble to permit solution spectra to be recorded.

Recently, the bis(triphenylphosphine)-iminium tellurocyanate, $[(\text{C}_6\text{H}_5)_3\text{P}]_2\text{NTeCN}$, was

prepared⁸ and this salt is quite soluble in both acetone and acetonitrile. Furthermore, the molecular structure of this salt has been solved by X-ray crystallographic methods.⁹ With the exact structural parameters on hand, together with the possibility of recording both the IR and Raman spectra of the ^{12}C - and ^{13}C -tellurocyanates, the vibrational spectra of the tellurocyanate ion could be obtained. Force constants for the last member in the XCN^- -series could thus be calculated.

EXPERIMENTAL

The syntheses of the three tellurocyanates $(\text{C}_6\text{H}_5)_4\text{PTeCN}$ (I), $(\text{C}_6\text{H}_5)_4\text{AsTeCN}$ (II) and $[(\text{C}_6\text{H}_5)_3\text{P}]_2\text{NTeCN}$ (III) as well as the corresponding cyanides $(\text{C}_6\text{H}_5)_4\text{PCN}$, $(\text{C}_6\text{H}_5)_4\text{AsCN}$ and $[(\text{C}_6\text{H}_5)_3\text{P}]_2\text{NCN}$ have been described in earlier papers.^{6,8} The ^{13}C enriched samples of I and II were prepared from 90.5% ^{13}C -enriched KCN, used as received from British Oxygen Co, Ltd. All the compounds used in the present study were recrystallized from deoxygenated acetone, *p.a.*, prior to use.

Infrared spectra of the samples were recorded in the region $4000 - 180 \text{ cm}^{-1}$ on Perkin-Elmer models 225 and 180 spectrometers as Nujol mulls, KBr and polyethylene pellets. Raman spectra were obtained on a Cary 81 spectrometer excited by argon ion (CRL 52 G) and helium neon (Spectra Physics 125 A) lasers and on a Coderg model T 800 spectrometer combined with a Spectra Physics model 170-03 argon ion laser. None of the compounds I–III were stable when excited by the 5145 or 4880 Å argon ion laser beams, but decomposed slowly resulting in increased fluorescence. Reasonably good spectra were recorded with a spinning cell holder and a laser power below 40 mW. The best Raman spectra were obtained with the 6328 Å helium neon laser line. Attempts to

record the Raman spectra in saturated acetonitrile or acetone solutions were made, but only III gave reasonably successful solution spectra.

The fundamental frequencies of the counterions were determined by recording the IR and Raman spectra of the following compounds: $(C_6H_5)_4PCN$ (Ia), $(C_6H_5)_4AsCN$ (IIa) and $[(C_6H_5)_3P]_2NCN$ (IIIa) by the same procedure as the tellurocyanates I, II and III. The isotopic wave number shifts of I and II were recorded with large dispersion on the same charts using identical spectral parameter settings.

RESULTS

Because of their large size the counterions in the three present tellurocyanates all have very complicated vibrational spectra with a large number of vibrational bands. The tellurocyanate ions, on the other hand, have only three fundamental frequencies. By comparing the spectra of I, II and III with those of Ia, IIa and IIIa, respectively, we were able to determine the counterion spectra with considerable certainty, since the IR and Raman spectra were practically identical. The spectral differences were caused by the tellurocyanate ions, and the $TeCN^-$ vibrational modes could therefore be detected.

For I and II the ^{13}C isotopic species were available and the fundamentals of the tellurocyanate ion could be determined with complete certainty as the three vibrational bands which showed isotopic shifts. The complete lists of IR and Raman bands for compounds I, II and III have not been given for the sake of brevity. For II our data were essentially identical to those of our earlier paper.⁷ The IR and Raman bands assigned to

the tellurocyanate ion in compounds I, II and III as well as in the isotopic species are listed in Table 1. Our earlier assignments⁷ for the tellurocyanate fundamentals were essentially confirmed. However, for II the present data reveal that ν_2 is associated with the IR band at 353 cm^{-1} (350 cm^{-1} in Raman) rather than the neighbouring band at 359 cm^{-1} (360 cm^{-1} in Raman) assigned previously.⁷ The latter band belonged to the counterion since it was present in the spectrum of compound IIa and showed no isotopic shift.

For III we had no ^{13}C isotopic molecule available, but the tellurocyanate modes were assigned with the aid of the data from I and II. As apparent from Table 1 both ν_2 and ν_3 of III showed factor group splitting in the IR Nujol spectrum, whereas only one band for each fundamental was observed in Raman. In acetonitrile solution (Raman) the bands were slightly displaced from the solid state frequencies. Our assignments were supported by the polarization measurements in which ν_1 and ν_2 were definitely polarized while ν_3 appeared depolarized.

The bands assigned to the three fundamentals were situated at nearly the same wave numbers in the spectra of all three compounds. Also, the isotopic frequency shifts were nearly identical in I and II. Therefore, it can be concluded that the tellurocyanate ions in the three compounds have practically identical bonding energies. Moreover the crystal lattices of the compounds probably do not perturb the vibrations of the tellurocyanate ions significantly although correlation splitting was observed in the spectrum of III.

Table 1. Fundamental frequencies for the tellurocyanate ions.^a

$(C_6H_5)_4PTeCN$, I		$(C_6H_5)_4AsTeCN$, II		$[(C_6H_5)_3P]_2NTeCN$, III			Assignments
IR Nujol	Raman solid	IR Nujol	Raman solid	IR Nujol	Raman solid	Raman CH_3CN sol.	
2080 s	2079 s	2076 s	2080 s	2075 s	2078 s	2086 s,P	ν_1 ^{12}C Σ^+
2034 s	2034 s	2031 s	2033 s				ν_1 ^{13}C Σ^+
458 w	460 w	458 m	458 w	463 m } 449 m }	457 m	451 m,P	ν_2 ^{12}C Σ^+
451 w	453 w	~450 w	451 w				ν_2 ^{13}C Σ^+
349 vw	350 vw	353 m	350 w	360 w } 348 w }	365 w	365 w,D?	ν_3 ^{12}C Π
338 vw	340 vw	343 m	340 w				ν_3 ^{13}C Π

^a Abbreviations: s, strong; m, medium; w, weak; v, very; P, polarized and D, depolarized.

Table 2. Force constants (mdyn/Å) derived for the tellurocyanate ion (I).

Freq.	¹² C	¹³ C
1	2080	2034
2	458	451
3	349	338

Force const.	Set A ^a	Set B ^b
f_{11}	15.62	16.57
f_{22}	2.81	2.69
f_{12}	0	0.83
f_{33}	0.14	0.14

^a Set A, from ¹²C data, f_{12} defined as zero. ^b Set B, from ¹²C and ¹³C data.

Force constant calculations. The tellurocyanate ion is linear (as apparent from the X-ray crystallographic study⁹ of III), like the lighter homologues OCN⁻, SCN⁻ and SeCN⁻. From the two stretching modes ν_1 and ν_2 of species Σ^+ the diagonal stretching force constants f_{11} and f_{22} can easily be determined if the interaction term f_{12} is neglected. The force constant f_{33} is unequivocally determined from the bending mode ν_3 of species Π . The Te-C and C-N distances, 2.05 and 1.13 Å, respectively, determined in the X-ray study⁹ were used in the calculations. An initial set of force constants were adopted and by an iteration procedure the set A of Table 2 was determined using the assigned frequencies for the parent molecule I, chosen because the experimental data were most reliable for this compound. Adding the observed frequencies for the ¹³C

species yields just sufficient information to determine the complete valence force field, in view of the product rule. Two solutions arise, but only one, set B of Table 2, is physically reasonable.

The calculated force constants for the tellurocyanate ion agree remarkably well with the values predicted by Greenwood *et al.*¹¹ Also, the values clearly demonstrate the reduced X-C (X≡O, S, Se, Te) bond strengths in the series X-C=N¹⁻⁵ as apparent from Table 3. Comparison can also be made with the very precisely determined force constants for the halocyanides by Ruoff.¹⁰

Acknowledgement. P. K. wishes to acknowledge the hospitality of Professor W. Zeil, Tübingen, in whose laboratory parts of the work was done. Financial support was obtained from NTNf and NAVF.

REFERENCES

- Maki, A. and Decius, J. C. *J. Chem. Phys.* 31 (1959) 772; Schettino, V. and Hisatsune, I. C. *J. Chem. Phys.* 52 (1970) 9.
- Jones, L. H. *J. Chem. Phys.* 25 (1956) 1069.
- Jones, L. H. *J. Chem. Phys.* 28 (1958) 1234.
- Bürger, H. and Schmid, W. *Z. Anorg. Allg. Chem.* 388 (1972) 67.
- Ti, S. S. and Kettle, S. F. A. *Spectrochim. Acta* 32 A (1976) 1765.
- Austad, T., Songstad, J. and Åse, K. *Acta Chem. Scand.* 25 (1971) 331.
- Ellestad, O. H., Klæboe, P. and Songstad, J. *Acta Chem. Scand.* 26 (1972) 1724.
- Martinsen, A. and Songstad, J. *Acta Chem. Scand.* A 31 (1977) 645.
- Foust, A. and Songstad, J. *To be published.*
- Ruoff, A. *Spectrochim. Acta* 26 A (1970) 545.
- Greenwood, N. N., Little, R. and Sprague, M. J. *J. Chem. Soc.* (1964) 1292.

Received June 30, 1977.

Table 3. Comparison between force constants (mdyn/Å) for the homologue series XCN (X=O, S, Se, Te).

Force const.	K(OCN) ^a	K(SCN) ^b	K(SeCN) ^c	(C ₄ H ₅) ₄ PTeCN ^d
f_{11}	15.42	15.95	15.97	16.57
f_{22}	11.46	5.18	3.75	2.69
f_{12}	1.15	0.9	0.88	0.83
f_{33}	0.51	0.31	0.22	0.15

^a Ref. 1. ^b Ref. 2. ^c Ref. 4. ^d This work.

Short Communications

Effect of Crown Ethers on the Racemization of 2-Phenylpropionitrile in Methanol and Ethanol

NILS-ÅKE BERGMAN and INGER KÄLLSSON

Department of Organic Chemistry, University of Göteborg and Chalmers University of Technology, Fack, S- 402 20 Göteborg, Sweden

In a previous investigation of the racemization of 2-phenylpropionitrile in methanol¹ a small increase in the second-order rate constant (obtained by dividing the observed rate constant by the corresponding base concentration) with the base (sodium methoxide) concentration was found over the investigated interval (2.8–10.8 mM at 25 °C). It was suggested that this increase in the rate constant could be due to the existence of sodium methoxide ion pairs more efficient as catalysts than the non-ionpaired methoxide ions. We now wish to report some experimental facts which contradict the suggested explanation.

Our intention was to use a complexing agent for the sodium ions to decrease the concentration of possible sodium methoxide ion pairs. The most powerful complexing agents for alkali cations known are the cryptates.² The complex constant for formation of the sodium complex with 2,2,1-cryptate (4,7,13,16,21-pentaoxa-1,10-diazabicyclo[8,8,5]tricosane) is $10^{5.4}$ M⁻¹ in methanol at 25 °C.² Unfortunately, this compound racemized 2-phenylpropionitrile in methanol³ and could not be used as a complexing agent in the sodium methoxide solutions.

However, it turned out that it was possible to use another type of complexing agents, namely some macrocyclic polyethers, the crown ethers. Since the first investigation by Pedersen⁴ crown ethers have been used to clarify the role of ion pairs in mechanisms of organic reactions as well as in synthetic applications. Two recent reviews on the properties and applications of crown ethers have been published recently.^{5,6}

The properties of the crown ethers can be changed by altering the size of the macrocyclic ring and also by introducing different side groups on it.⁵ We have used two different crown ethers: 18-crown-6 (1,4,7,10,13,16-hexaoxacyclooctadecane) and 15-crown-5 (1,4,7,10,13-pentaoxacyclopentadecane). The equilibrium con-

stant for the formation of the sodium complex with 18-crown-6 in methanol is $10^{4.32}$ M⁻¹.⁷ The corresponding equilibrium constant for 15-crown-5 has not been measured as far as we know.

The magnitude of the complex constant has previously been assumed to be correlated to the similarity between the ionic diameter of the cation and the hole size in the crown ether.⁷ In such a case 15-crown-5 should be somewhat better for sodium than 18-crown-6. Such a correlation is somewhat doubtful, however, but in any case it is plausible that the complex constant for 15-crown-5 should be of the same order of magnitude as for 18-crown-6. In a methanolic solution of sodium methoxide and an excess of crown ether the fraction of non-complexed sodium ions should thus be negligible.

Table 1 gives the results of the racemization of 2-phenylpropionitrile in methanol with added 18-crown-6. As can be seen, no difference exists in the observed rate before and after 18-crown-6 has been added. The crown ether has been added in excess and the result is the same irrespective of the degree of excess (last row in Table 1).

Table 1. Racemization rates for 2-phenylpropionitrile in methanol with sodium methoxide as base with and without the presence of 18-crown-6. Concentration of substrate 0.12 M. Temperature 24.93 ± 0.05 °C.

[Base]/mM ^a	[18-crown-6]/mM	$k_{\text{obs}}/10^{-4}$ s ⁻¹ ^b
2.70	—	5.11
2.70 ^c	37.8	5.18
5.61	—	12.2
5.61 ^c	60.5	12.4
34.8	—	85
34.8 ^c	41.6–87.0	85

^a The estimated error in the base concentration is less than 5%. ^b Mean value obtained from two or three runs. Maximum deviation from the mean value is less than 1.7%. ^c The run with crown ether present was done using base solution from the same batch as for the one without crown ether.

Table 2. Effect of added 15-crown-5 on the alkoxide-catalysed racemization rate of 2-phenylpropionitrile in methanol and ethanol. Concentration of substrate 0.12 M. Temperature 25.00 ± 0.05 °C.

[Base]/mM ^a	[15-crown-5]/mM	$k_{\text{obs}}/10^{-4} \text{ s}^{-1}$
Methanol/methoxide		
4.10	—	8.23 ^b
4.10 ^c	6.5	8.54 ^b
24.5	—	58.2 ^b
24.5 ^c	35.1	62.5 ^b
Ethanol/ethoxide		
3.1	—	153 ^d
3.1 ^c	5	168 ^d

^a The estimated error in the base concentration is less than 5%. ^b Each value is obtained from only one run. ^c The run with crown ether present was done using base solution from the same batch as for the one without crown ether. ^d Mean value from two runs. Maximum deviation from the mean value is 2%.

The results obtained with 15-crown-5 (Table 2) are similar although a slight increase in k_{obs} was observed upon addition of 15-crown-5 at least at the highest base concentration in methanol. In no case was a decrease in k_{obs} observed upon addition of crown ethers which ought to be the case if the sodium methoxide ion pairs were more reactive than the non-ionpaired methoxide ions. Thus there is no evidence supporting the idea that the change in the second-order rate constant with base concentration should be due to a more reactive sodium methoxide ion pair.

The very small effect (if any) on k_{obs} upon addition of crown ethers could be due to a very low concentration of sodium methoxide ion pairs at these rather low base concentrations. The association constant for sodium methoxide in methanol is not known with any high accuracy but some conductometric measurements at very low sodium methoxide concentrations ($3-13 \times 10^{-4}$ M) indicate that it should be close to zero or rather small ($7.5 \pm 7.9 \text{ M}^{-1}$).⁸

Sodium ethoxide in ethanol has a much larger association constant ($102 \pm 8 \text{ M}^{-1}$).⁸ It is therefore interesting to see that the rate of proton abstraction from 2-phenylpropionitrile is increased by about 10% when 15-crown-5 is added to a 3.1 mM sodium ethoxide solution (Table 2). This indicates that the free ethoxide ions are more effective as catalysts in the abstraction than are the ion pairs.

Experimental. The experimental procedure has been described before.¹ The crown ethers were commercial samples from FLUKA AG and were used without any purification. Commercial 99.5% spectrographic ethanol was dried over CaH_2 and distilled and handled in the same way as methanol.¹

Acknowledgements. We wish to thank Professor Lars Melander for his interest and for many constructive discussions concerning the present work. The kindness of Dr. Per Beronius to bring some references to our attention is gratefully acknowledged. Financial support from the Swedish Natural Science Research Council is also gratefully acknowledged.

- Bergman, N.-Å. and Källsson, I. *Acta Chem. Scand. A* 30 (1976) 411.
- Lehn, J. M. and Sauvage, J. P. *J. Am. Chem. Soc.* 97 (1975) 6700.
- Källsson, I. *Unpublished results.*
- Pedersen, C. J. *J. Am. Chem. Soc.* 89 (1967) 7017.
- Christensen, J. J., Eatough, D. J. and Izatt, R. M. *Chem. Rev.* 74 (1974) 351.
- Knipe, A. C. *J. Chem. Educ.* 1976 618.
- Frénsdorff, H. K. *J. Am. Chem. Soc.* 93 (1971) 600.
- Barthel, J., Justice, J.-C. and Wachter, R. *Z. Phys. Chem. Frankfurt am Main* 84 (1973) 100.

Received August 18, 1977.

Structure Refinement of Ti_5Sb_3 from Single-crystal Data

ROLF BERGER

Institute of Chemistry, University of Uppsala,
Box 531, S-751 21 Uppsala, Sweden

In a previous paper, crystallographic data on new arsenides and antimonides of titanium and scandium were presented.¹ It was claimed that the β - Yb_5Sb_3 structure type² is represented in the Sc-Sb, Ti-Sb, Ti-As and probably also in the Ti-P systems. The author was then unaware of the work by Steinmetz *et al.*,³ who, on the basis of powder diffraction data, showed that Ti_5Sb_3 crystallizes with this structure. The present report confirms their findings, but their positional parameters, which were derived from less extensive data, have had to be revised in the light of the single-crystal data.

Experimental. Titanium (Koch-Light Laboratories Ltd., 99.95 %) and antimony (Johnson Matthey Chemicals Ltd., 99.9999 %) were reacted by arc-melting to give a single phase sample.⁴ A single crystal fragment was picked from the debris of the crushed alloy for the X-ray intensity measurement.

A Stoe-Philips four-circle diffractometer was used for collecting the data, the ω - 2θ step scan technique being employed. The reflexions were measured within the intervals $0 \leq h \leq 15$, $-9 \leq k \leq 12$ and $-8 \leq l \leq 10$, corresponding to an upper angular limit of $2\theta = 66^\circ$. Three test reflexions were monitored at regular intervals to check the stability. The measurement also included those reflexions systematically absent according to the $Pnma$ space-group assignment. The intensities of these reflexions never exceeded two standard deviations, which supports the proposal of $Pnma$ symmetry^{1,3} and contradicts the suggestion by Kjekshus *et al.*⁴

The crystal used for the data collection was rather small and of an irregular shape. In the course of examination by scanning electron microscopy for obtaining a good geometrical description of it, the crystal was unfortunately lost. Accordingly, no appropriate correction for absorption could be performed. In view of the small size of the crystal — maximum cross section $50 \mu m$ — together with a linear absorption coefficient of 192 cm^{-1} , the general effects of neglecting this correction are small. Nevertheless, systematic errors occur, since — owing to the irregular shape of the crystal — some groups of reflexions are likely to be more affected than the average. After the systematically absent reflexions had been rejected, the intensities were averaged and corrected for Lp effects. A series of structure refinements was started, using a full-matrix least-squares method. Space-group symmetry $Pnma$ was assumed, supported by a zero moment plot. The positional parameters of β - Yb_5Sb_3 were adopted as

starting values for the coordinates. The initial refinement involved 1 scale factor, 14 positional parameters and 6 isotropic temperature factors. The atomic scattering factors⁵ were corrected for anomalous dispersion.⁶

The quantity minimized was $\sum w(|F_o^n| - |F_c^n|)^2$ with $n=1$ or $n=2$ for refinement on F and F^2 , respectively. The agreement indices found in the text are defined as:

$$R(F^n) = \sum ||F_o^n| - |F_c^n|| / \sum |F_o^n|$$

$$\text{and } R_w(F^n) = [\sum w(|F_o^n| - |F_c^n|)^2 / \sum w|F_o^n|^2]^{1/2}; \\ n = 1, 2.$$

Here, w denotes the individual weight of each reflexion and is defined by the expression:

$$w^{-1} = \sigma_c^2 + (p|F_o^n|)^2.$$

σ_c is the standard deviation of F^n based on counting statistics, while the other term modifies the weight to account for other errors. The value of p was selected to give an even weighting scheme.

The first refinement — on F , to suppress divergence — yielded higher temperature factors than expected. Another disturbing feature was that F_o was consistently lower than F_c for the low-angle reflexions where k was odd. Since the $8d$ atoms give only small contributions to these reflexions when $y \sim 0$, it was considered likely that the effects could be accounted for by thermal anisotropy if the electron density is very different in the b direction as compared with that in the ac plane. However, the introduction of anisotropic thermal parameters did not create any considerable drop in the R -value.

Another attempt was then made at refining the occupancy of the atoms with the highest temperature factors, the $8d$ titanium and the $4c$ antimony, respectively. The occupancy of the antimony was refined to 92 %, causing a small drop in the R -value. The actual values of the occupancy and the anisotropic thermal parameters probably reflect systematic errors to a great extent. The abnormally high temperature factors as well as the disturbing k -index dependence remained. It is possible that the observed errors are due to the neglect of an absorption correction or to some kind of disorder in the crystal.

The refinement on F cannot cover reflexions with randomly occurring negative values for the intensities, and hence the data tend to be somewhat biased as compared with an F^2 refinement.^{7,8} The final refinement on F^2 , including all the reflexions, gave the R -values (1205 refl.):

$$R(F^2) = 0.087, R_w(F^2) = 0.12 \text{ and } R(F) = 0.088.$$

A ΔR plot gave a fairly straight line for the ranked deviates in the range ± 2 around the

mean. It had a slope of 0.67 and an intercept of -0.03 .

The positional parameters were not especially sensitive to the different modes of refinement and are presented in Table 1. The cell dimensions were determined from powder photographs.¹

Table 1. Crystallographic data of Ti_5Sb_3 . Cell dimensions: $a=10.2173(5)$ Å, $b=8.3281(5)$ Å, $c=7.1459(4)$ Å. Space group $Pnma$ (No. 62), $Z=4$.

Atom	Position	x	y	z
Ti(1)	8d	0.05705(20)	0.05823(27)	0.20174(28)
Ti(2)	4c	0.23539(26)	1/4	0.81717(39)
Ti(3)	4c	0.28158(29)	1/4	0.33160(40)
Ti(4)	4c	0.00533(23)	1/4	0.52152(38)
Sb(1)	8d	0.32279(7)	0.49075(8)	0.06612(9)
Sb(2)	4c	0.47625(11)	1/4	0.58965(15)

Table 2. Interatomic distances in Ti_5Sb_3 , less than 3.8 Å.

Ti(1)–Sb(2)	2.710(2)	Ti(4)–Sb(2)	2.794(3)
Sb(2)	2.751(2)	2Sb(1)	2.801(2)
Ti(4)	2.838(3)	2Sb(1)	2.809(2)
Sb(1)	2.912(2)	2Ti(1)	2.838(3)
Sb(1)	2.933(2)	Ti(2)	2.989(4)
Sb(1)	2.941(2)	Ti(3)	3.132(4)
Ti(3)	2.945(3)	Ti(2)	3.160(4)
Ti(1)	3.194(5)	2Ti(1)	3.302(3)
Ti(3)	3.245(3)	Ti(3)	3.405(4)
Ti(1)	3.258(4)		
Ti(4)	3.302(3)	Sb(1)–Ti(3)	2.792(2)
Ti(2)	3.430(3)	Ti(4)	2.801(2)
Ti(2)	3.664(4)	Ti(4)	2.809(2)
Ti(2)–Sb(2)	2.730(3)	Ti(2)	2.825(2)
2Sb(1)	2.825(2)	Ti(2)	2.869(2)
2Sb(1)	2.869(2)	Ti(1)	2.912(2)
Sb(2)	2.949(3)	Ti(1)	2.933(2)
Ti(4)	2.989(4)	Ti(3)	2.934(2)
Ti(4)	3.160(4)	Ti(1)	2.941(2)
2Ti(1)	3.430(3)	Ti(1)	2.941(2)
Ti(3)	3.502(4)	Sb(2)	3.745(1)
2Ti(1)	3.664(3)	Sb(1)	3.746(1)
Ti(3)	3.706(4)		
Ti(3)–Sb(2)	2.712(3)	Sb(2)–2Ti(1)	2.710(2)
2Sb(1)	2.792(2)	Ti(3)	2.712(3)
2Sb(1)	2.934(2)	Ti(2)	2.730(3)
2Ti(1)	2.945(3)	2Ti(1)	2.751(2)
Ti(4)	3.132(4)	Ti(4)	2.794(3)
2Ti(1)	3.245(3)	Ti(2)	2.949(3)
Ti(4)	3.405(4)	2Sb(1)	3.745(1)
Ti(2)	3.502(4)		
Ti(2)	3.706(4)		

Result and discussion. The single-crystal refinement confirms that Ti_5Sb_3 belongs to the β - Yb_5Sb_3 structure type. The positional parameters of Table 1 differ from those reported by Steinmetz *et al.*,³ and are much more accurate. Owing to the systematic errors encountered in the refinements, the individual thermal parameters are not very reliable and are therefore not presented.

From Table 2, where the interatomic distances are given, it emerges that the 4c antimony tends to be surrounded by eight neighbours, while the 8d antimony clearly coordinates nine metal atoms. The former arrangement is that of a slightly distorted bisphenoid (dodecahedron), and the latter can be described as a triangular prism with one additional atom outside each rectangular face of the prism (tetrakaidecahedron). The coordination of the metal atoms around the non-metal is thus somewhat different from the situation in the isostructural compounds β - Yb_5Sb_3 ,³ Ca_5Sb_3 ,⁹ and Ca_5Bi_3 .¹⁰ In these compounds, the coordination number is seven for the 4c non-metal atom and eight or seven for the 8d. It would be very interesting to compare the coordination numbers within the series Ti_5As_3 ,¹ γ - V_5As_3 ,¹¹ and Cr_5As_3 ,¹¹ but no data are yet available for any of these compounds. The situation in Yb_5Bi_3 ,¹² is probably similar to that in β - Yb_5Sb_3 .

Acknowledgement. Financial support by the Swedish Natural Science Research Council is gratefully acknowledged.

- Berger, R. *Acta Chem. Scand. A* 31 (1977) 514.
- Brunton, G. D. and Steinfink, H. *Inorg. Chem.* 10 (1971) 2301.
- Steinmetz, J., Malaman, B. and Roques, B. *C.R. Acad. Sci. C* 284 (1977) 499.
- Kjekshus, A., Grønvald, F. and Thorbjørnsen, J. *Acta Chem. Scand.* 16 (1962) 1493.
- International Tables for X-Ray Crystallography*, Kynoch Press, Birmingham 1974. Vol. 4, p. 71.
- Ibid.*, Vol. 4, p. 148.
- Hirshfeld, F. L. and Rabinovich, D. *Acta Crystallogr. A* 29 (1973) 510.
- Wilson, A. J. C. *Acta Crystallogr. A* 32 (1976) 781.
- Martinez-Ripoll, M. and Brauer, G. *Acta Crystallogr. B* 30 (1974) 1083.
- Martinez-Ripoll, M., Haase, A. and Brauer, G. *Acta Crystallogr. B* 30 (1974) 2004.
- Berger, R. *Acta Chem. Scand. A* 30 (1976) 363.
- Calvert, L. D., Division of Chemistry, National Research Council Canada, Ottawa (1977). *Private communication*.

Received September 26, 1977.

Brønstedian Energetics and the Basic Kinetic Process

TORBEN KNUDSEN

Instituttet for Silikatindustri, Danmarks Tekniske Højskole, Bygning 204, DK-2800 Lyngby, Denmark

Reading the article entitled "Brønstedian Energetics, Classical Thermodynamics and the Exergy" by Torben Smith Sørensen in this journal¹ provided me with great pleasure and excited the old feeling of enthusiasm for this ingenious construction called energetics, with its substantial didactic value. It is my hope, that this article might work in the direction of promoting the Brønsted scheme of thermodynamics on levels of education within physical chemistry.

In the definition of the kinetic conjugated potential and quantity Sørensen suggests the couple $v^2/2$ and M , being the velocity raised to the second power and mass, respectively. This definition seems to me in bad agreement with the purely thermodynamic conjugated pairs (S, T) , $(V, -P)$ and (n_i, μ_i) as defined by Brønsted. Instead the pair v and p should be chosen, being velocity and momentum, which to my mind constitutes a consistent analogy to the Brønstedian pairs of conjugated potentials and quantities.

To see this, let us consider an example of a mechanical system of a simple but explanatory kind. Two bodies 1 and 2 interact with the mutual force F and change their momenta p_1 and p_2 by dp_1 and dp_2 in the time elapse dt . The dp 's are governed by the equation:

$$dp_1 + dp_2 = 0 \quad (1)$$

being the principle of conservation of momentum. This equation is suggestive of the choice of quantity (in the sense of Brønsted) consistent with the Brønsted scheme. If we define dp according to:

$$dp = dp_1 = -dp_2 \quad (2)$$

dp will constitute a small part of a quantity p , transported from body 2 to body 1. This is an important property of a Brønsted quantity, that it should be transportable in a basic process, conserving its magnitude.

The choice of potential should be such, that the work done by the system by the transport of the quantity, should be expressible in the form:

$$(\text{Work done}) = \Delta(\text{potential}) \times (\text{transported quantity})$$

Now the choice of potential is obvious from the other fundamental relation of mechanics:

$$v_1 dp_1 + v_2 dp_2 = F ds \quad (3)$$

stating the conservation of kinetic plus potential energy for this conservative system. ds is here the distance between the particles. Inserting (2) into (3) the analogy to the Brønsted scheme is apparent:

$$(v_1 - v_2) dp = F ds \quad (4)$$

By treating the right hand side of (4) in analogy with the conjugated pairs $(V, -P)$ or (A, γ) , where V is volume, P pressure, A interfacial area and γ interfacial tension, the content of the whole equation can be interpreted in the terminology of Brønsted: The kinetic basic process coupled to the mechanical basic process communicates work, by transport of momentum between velocities v_1 and v_2 in the kinetic basic process, and transport of distance between F and zero force in the mechanical basic process.

It is interesting to see, that the concept of mass takes the meaning of capacity in the presented formulation of the fundamental laws of mechanics. The kinetic capacity is derived from the expression:

$$C_{\text{kin}} = \partial p / \partial v \quad (5)$$

in analogy with the purely thermodynamic capacities. One might speculate whether the introduction of the concept mass in textbooks of mechanics as a capacity, would tend to ease the conceptual jump to relativistic mechanics, when leaning on this analogy to thermodynamical capacities, which are known to be functions of the potentials of the system.

The kinetic energy term for the single body will appear in analogy with the energetic scheme:

$$dE = (\text{potential}) \times d(\text{quantity}) \quad (6)$$

$$\text{as } dE_{\text{kin}} = v C_{\text{kin}} dv = d(v^2/2) C_{\text{kin}}$$

It may be stated, that the coupling between the kinetic and the mechanical basis process described here constitutes the microscopical principle of the second law of thermodynamics. This particular coupling differs namely substantially from the coupling between purely thermodynamic basic processes. A thermal and a spatial basic process for instance can be brought in static equilibrium with each other, and a reversible communication of work between the two can be conceived as an indefinitely slow transport of quantities in their potentials, which can be stopped and reversed by principally no exertion of work from outside. In contrast to this stands any coupling in which the kinetic basic process is taking part. This kind of coupling can never be brought to static equilibrium, and will end up vibrating or be-

ing directional in the sense of given priority to kinetic energy at the expense of any form of potential energy. Time's arrow points in the direction of kinetic chaos.

1. Sørensen, T. S. *Acta Chem. Scand. A* 30 (1976) 555.

Received September 19, 1977.

Rational Thermodynamics and Mechanics

TORBEN SMITH SØRENSEN

Fysisk-Kemisk Institut, Technical University of Denmark, DK-2800 Lyngby, Denmark

In the short communication "Brønstedian Energetics and the Basic Kinetic Process"¹ Torben Knudsen criticises my choice of $v^2/2$ and M as the potential and the quantity in the basic kinetic process in mechanics.² He argues that it would be better to choose momentum \mathbf{p} as the conserved quantity and velocity as the conjugated potential. I perfectly agree with this objection, since I had already some qualms about it when I wrote that \mathbf{p} and \mathbf{v} is a more convenient bipartition of the kinetic energy than the pair chosen in Table 1, Ref. 2. This was written in connection with eqn. (20) in the paper No. III in the series "Towards a Rational Thermodynamics".³

It is not true — as states Knudsen — that conservation in itself is a fundamental property of a Brønsted quantity. Moles are not conserved in chemical reactions, interfacial area is not conserved in emulsification process and entropy not in irreversible processes, just to take some examples. Also, the heavy mass is just as conserved as momentum in classical mechanics. However, \mathbf{p} and \mathbf{v} is a better choice, since the analogy between momentum transport in velocity gradients in viscous processes, charge transport in electric fields, entropy transport in temperature gradients and so on is much more clearly put forward, as well as

the differences: momentum transport is a tensorial process in contrast to the "normal" vectorial transport processes or scalar chemical processes. With respect to the transition to relativistic mechanics, I would like to point out the pages 95 to 110 in my Ph. D. dissertation⁴ where I have sketched the outlines of a general thermodynamic systems theory. Similar attempts were at the same time and independently made by Oster, Perelson and Katchalsky⁵ and by Karin Beyer.⁶ Especially, one observes in Table 2, p. 98 in Ref. 4, that the basic difference between classical mechanics and relativistic mechanics is that the constitutive relation between momentum and velocity is non-linear in the latter, and therefore there is a difference between kinetic energy and coenergy in relativistic mechanics, but not in classical mechanics. Whenever a difference, the coenergy turns out to be the fundamental energy-function to be used *e.g.*, in Hamilton's variational principle, see also Lanczos' monography.⁷

Finally, I do not quite agree with the statement of Knudsen, that any coupling in which the basic kinetic process is taking part stands in contrast to reversible couplings between other Brønstedian basic processes, since it can never be brought to any static equilibrium. Purely mechanical systems with no dissipative elements are just examples of static equilibrium between potential forces and inertial forces, as expressed in the principle of d'Alembert.⁷ The earth revolving around the sun is a system in perfect thermodynamic equilibrium (tidal effects neglected): reversible coupling between the gravitational basic process and the kinetic basic process is taking place and the system is neutrally stable (in the Liapounov sense) to external disturbances. The fact that time explicitly enters the kinetic potential (velocity) should not obscure this fundamental analogy to other reversible couplings between Brønsted's basic processes.

1. Knudsen, T. *Acta Chem. Scand. A* 31 (1977) 891.
2. Sørensen, T. S. *Acta Chem. Scand. A* 30 (1976) 555.
3. Sørensen, T. S. *Acta Chem. Scand. A* 31 (1977) 437.
4. Sørensen, T. S. *Studier over Fysisk-Kemiske Systemers Statik, Dynamik, Kinetik*, Ph. D. Thesis, Technical University of Denmark, Lyngby 1973.
5. Oster, G. F., Perelson, A. S. and Katchalsky, A. Q. *Rev. Biophys.* 6 (1973) 1.
6. Beyer, K. *Entropi og Biologiske Økosystemer*, Prisopgave i Fysik, University of Copenhagen 1972.
7. Lanczos, C. *The Variational Principles of Mechanics*, 3rd Ed., University of Toronto Press, Toronto 1966.

Received October 3, 1977.

ing directional in the sense of given priority to kinetic energy at the expense of any form of potential energy. Time's arrow points in the direction of kinetic chaos.

1. Sørensen, T. S. *Acta Chem. Scand. A* 30 (1976) 555.

Received September 19, 1977.

Rational Thermodynamics and Mechanics

TORBEN SMITH SØRENSEN

Fysisk-Kemisk Institut, Technical University of Denmark, DK-2800 Lyngby, Denmark

In the short communication "Brønstedian Energetics and the Basic Kinetic Process"¹ Torben Knudsen criticises my choice of $v^2/2$ and M as the potential and the quantity in the basic kinetic process in mechanics.² He argues that it would be better to choose momentum \mathbf{p} as the conserved quantity and velocity as the conjugated potential. I perfectly agree with this objection, since I had already some qualms about it when I wrote that \mathbf{p} and \mathbf{v} is a more convenient bipartition of the kinetic energy than the pair chosen in Table 1, Ref. 2. This was written in connection with eqn. (20) in the paper No. III in the series "Towards a Rational Thermodynamics".³

It is not true — as states Knudsen — that conservation in itself is a fundamental property of a Brønsted quantity. Moles are not conserved in chemical reactions, interfacial area is not conserved in emulsification process and entropy not in irreversible processes, just to take some examples. Also, the heavy mass is just as conserved as momentum in classical mechanics. However, \mathbf{p} and \mathbf{v} is a better choice, since the analogy between momentum transport in velocity gradients in viscous processes, charge transport in electric fields, entropy transport in temperature gradients and so on is much more clearly put forward, as well as

the differences: momentum transport is a tensorial process in contrast to the "normal" vectorial transport processes or scalar chemical processes. With respect to the transition to relativistic mechanics, I would like to point out the pages 95 to 110 in my Ph. D. dissertation⁴ where I have sketched the outlines of a general thermodynamic systems theory. Similar attempts were at the same time and independently made by Oster, Perelson and Katchalsky⁵ and by Karin Beyer.⁶ Especially, one observes in Table 2, p. 98 in Ref. 4, that the basic difference between classical mechanics and relativistic mechanics is that the constitutive relation between momentum and velocity is non-linear in the latter, and therefore there is a difference between kinetic energy and coenergy in relativistic mechanics, but not in classical mechanics. Whenever a difference, the coenergy turns out to be the fundamental energy-function to be used *e.g.*, in Hamilton's variational principle, see also Lanczos' monography.⁷

Finally, I do not quite agree with the statement of Knudsen, that any coupling in which the basic kinetic process is taking part stands in contrast to reversible couplings between other Brønstedian basic processes, since it can never be brought to any static equilibrium. Purely mechanical systems with no dissipative elements are just examples of static equilibrium between potential forces and inertial forces, as expressed in the principle of d'Alembert.⁷ The earth revolving around the sun is a system in perfect thermodynamic equilibrium (tidal effects neglected): reversible coupling between the gravitational basic process and the kinetic basic process is taking place and the system is neutrally stable (in the Liapounov sense) to external disturbances. The fact that time explicitly enters the kinetic potential (velocity) should not obscure this fundamental analogy to other reversible couplings between Brønsted's basic processes.

1. Knudsen, T. *Acta Chem. Scand. A* 31 (1977) 891.
2. Sørensen, T. S. *Acta Chem. Scand. A* 30 (1976) 555.
3. Sørensen, T. S. *Acta Chem. Scand. A* 31 (1977) 437.
4. Sørensen, T. S. *Studier over Fysisk-Kemiske Systemers Statik, Dynamik, Kinetik*, Ph. D. Thesis, Technical University of Denmark, Lyngby 1973.
5. Oster, G. F., Perelson, A. S. and Katchalsky, A. Q. *Rev. Biophys.* 6 (1973) 1.
6. Beyer, K. *Entropi og Biologiske Økosystemer*, Prisopgave i Fysik, University of Copenhagen 1972.
7. Lanczos, C. *The Variational Principles of Mechanics*, 3rd Ed., University of Toronto Press, Toronto 1966.

Received October 3, 1977.